On demand

[E] Poster | U (Union)：Union

[U-02] Assessment and Accountability of Scientific Knowledge Creation

convener:Michiyo SHIMAMURA(Japan Agency for Marine-Earth Science and Technology), Yasuhiro Yamanaka(Faculty of Environmental Earth Science, Hokkaido University), Kiyoshi Suyehiro(Japan Agency for Marine-Earth Science and Technology), Brooks Hanson(American Geophysical Union)

[U02-P01] Let's start the discussion of the international tuning of research assessment in earth science to create a culture and indicators of “creation of knowledge”

*Yasuhiro Yamanaka[1], Michiyo SHIMAMURA[2], Kiyoshi Suyehiro[2] (1.Faculty of Environmental Earth Science, Hokkaido University, 2. Japan Agency for Marine-Earth Science and Technology)

[E] Poster | U (Union)：Union

[U-03] Sustainable global groundwater management for human security

convener:Yoshihide Wada(International Institute for Applied Systems Analysis), Makoto Taniguchi(Research Institute for Humanity and Nature)

[U03-P01] **Estimating yield is key to obtaining global material flux via the submarine groundwater discharge**

*Chen-Tung Arthur Chen[1,2], Ting-Hsuan Huang[1], Hon-Kit Lui[1], JING ZHANG[3] (1.National Sun Yat Sen University, 2.Zhejiang University, 3.University of Toyama)

[U03-P02] Quantitative assessment of the impacts of sustainable irrigation on global bioenergy production

*Zhipin Ai[1], Naota Hanasaki[1] (1.National Institute for Environmental Studies, Japan)

[U03-P03] Integrated structural, geophysical and hydrogeological approaches for sustainable groundwater resources in Precambrian basement rock terranes, India

*Rudra Mohan Pradhan[1], Tapas Kumar Biswal[1] (1.Department of Earth Sciences, Indian Institute of Technology Bombay, India)

[E] Poster | U (Union)：Union

[U-04] International Efforts Supporting Global Navigation Satellite System-Enhanced Tsunami Early Warning

convener:Rundle John B(University of California Davis), Kazuyoshi Nanjo(University of Shizuoka), Eiichi Fukuyama(Kyoto University / National Research Institute for Earth Science and Disaster Resilience)

[U04-P01] **GNSS total electron content for ionospheric tsunami early warning**

Tien-Chi Liu[1], Katsumi Hattori[2], *JANN-YENQ Liu[3,4,5], CHIYEN LIN[3,4], Yu-Lin Tsai[1], Tso-Ren Wu[1] (1.Graduate Institute of Hydrological and Oceanic Sciences, National Central University, Taiwan, 2.Graduate School of Science, Chiba University, Japan, 3.Center for Astronautical Physics and Engineering, National Central University, Taiwan, 4.Department of Space Science and Engineering, National Central University, Taiwan, 5.Center for Space and Remote Sensing Research, National Central University, Taiwan)

[E] Poster | U (Union)：Union

[U-05] Advanced understanding of Quaternary and Anthropocene hydroclimate changes in East Asia

convener:Chuan-Chou Shen(High-Precision Mass Spectrometry and Environment Change Laboratory, Department of Geosciences, National Taiwan University), Yusuke Yokoyama(Atmosphere and Ocean Research Institute, University of Tokyo), Kaoru Kubota(Graduate School of Human Development and Environment, Kobe University), Li Lo(Department of Geosciences, National Taiwan University)

[U05-P01] Precessionally Paced Foraminifera-bound Nitrogen Isotope Variations in the Solomon Sea Influenced by Eastern Equatorial Pacific Upwelling Intensity

★Invited Papers

*Haojia Abby Ren[1], Wei-Ning Fang[1], Yi-Chi Chen[1], Kuo-Yen Wei[1], Chuan-Chou Shen[1] (1.National Taiwan University)

[U05-P02] Annual record of boron isotopes of massive *Porites* coral skeleton from Chichijima Island in the western North Pacific

*Kaoru Kubota[1], Ryo Nakano[2], Masafumi MURAYAMA[2], Tsuyoshi Ishikawa[1], Yusuke Yokoyama[3], Atsushi Suzuki[4] (1.Kochi Institute for Core Sample Research, JAMSTEC, 2.Faculty of Agriculture and Marine Science, Graduate School of Integrated Arts and Sciences, Kochi University, 3.Atmosphere and Ocean Research Institute, The University of Tokyo, 4.Geological Survey of Japan, National Institute of Advanced Industrial Science and Technology)

[U05-P03] Gauging Quaternary Sea Level Changes using various sea level indicators and GIA model

*Yusuke Yokoyama[1], Anthony Purcell[2], Takeshige Ishiwa[3] (1.Atmosphere and Ocean Research Institute, University of Tokyo, 2.Research School of Earth Sciences, The Australian National University, 3.National Institute of Polar Research)

[U05-P04] Sea-level change in Tongatapu, the Kingdom of Tonga for the last 3000 years based on local marine reservoir effect and geophysical modeling

*Naoto Fukuyo[1,2], Anthony Purcell[3], Geoffrey Clark[4], Phillip Parton[4], Yusuke Yokoyama[1,2] (1.Atmosphere and Ocean Research Institute, The University of Tokyo, 2.Department of Earth and Planetary Sciences, Faculty of Science, The University of Tokyo, 3.Research School of Earth Sciences, The Australian National University, 4.College of Asia and the Pacific, Australian National University)

[U05-P05] High-resolution Holocene records of a stalagmite from maritime Japan

*Shota Amekawa[1], Akihiro Kano[1], Kenji Kashiwagi[2], Taiki Mori[3], Fumito Shiraishi[4], Chuan-Chou Shen[5,6,7] (1.Graduate School of Science, The University of Tokyo, 2.Department of Environmental Biology and Chemistry, Faculty of Science, University of Toyama, 3.Graduate School of Integrated Sciences for Global Society, Kyushu University, 4.Department of Earth and Planetary Systems Science, Graduate School of Science, Hiroshima University, 5.High-precision Mass Spectrometry and Environment Change Laboratory (HISPEC), Department of Geosciences, National Taiwan University, 6.Global Change Research Center, National Taiwan University, 7.Research Center for Future Earth, National Taiwan University)

[U05-P06] Mg/Ca and stable oxygen isotopes of individual foraminifera in the tropics: Climate variability or ecology?

★Invited Papers

*Sze Ling Ho[1], Jeroen Groeneveld[2,3], Andreas Mackensen[4], Mahyar Mohtadi[3], Thomas Laepple[2] (1.Institute of Oceanography, National Taiwan University, 10617 Taipei, Taiwan, 2.Alfred Wegener Institute, Helmholtz Center for Polar and Marine Research, Telegrafenberg A45, D-14473 Potsdam, Germany, 3.MARUM-Center for Marine Environmental Sciences, University of Bremen, Klagenfurter Strasse 2-4, D-28359 Bremen, Germany, 4.Alfred Wegener Institute, Helmholtz Center for Polar and Marine Research, Am Alten Hafen 26, D-27568 Bremerhaven, Germany)

[U05-P07] Insight to Western Pacific circulation from coral skeletal radiocarbon

*Shoko Hirabayashi[1,2,3], Yusuke Yokoyama[2,3], Atsushi Suzuki[4], Tezer Esat[5], Yosuke Miyairi[2], Takahiro Aze[2], Fernando Siringan[6], Yasuo Maeda[7], Hironobu Kan[1] (1.Faculty of Social and Cultural Studies, Kyushu University, 2.Atmosphere and Ocean Research Institute, The University of Tokyo, 3.Department of Earth and Planetary Science, Graduate School of Science, The University of Tokyo, 4.Geological Survey of Japan, National Institute of Advanced Industrial Science and Technology (AIST), 5.Research School of Earth Sciences, The Australian National University, 6.Marine Science Institute, University of the Philippines, 7.Institute of Natural and Environmental Sciences, University of Hyogo)

[U05-P08] Surface productivity and potential terrestrial ecology system in the central Okhotsk Sea during the middle-early Pleistocene

*Li Lo[1], Lukas Smik[2], Simon T. Belt[2] (1.Department of Geosciences, National Taiwan University, 2.School of Geography, Earth and Environmental Sciences, University of Plymouth)

[U05-P09] **Lake water distribution derived from surface water oxygen and hydrogen isotopes around Fuji Five Lakes**

*Ota Kosuke[1,2], Yusuke Yokoyama[1,2], Yosuke Miyairi[2], Shinya Yamamoto[3], Toshihiro Miyajima[2] (1.University of Tokyo, 2.Atmosphere and Ocean Research Institute, The University of Tokyo, 3.Mount Fuji Research Institute, Yamanashi Prefectural Government,)

[U05-P10] Carbon and oxygen isotopes and ^{14}C age of travertine and spring water in NW Iran

*Yubo Zhang[1], Yoshihiro Asahara[1], Masayo Minami[2], Masaki kaneko[1], Hadi Amin-Rasouli[3], Hossein Azizi[3] (1.Graduate School of Environmental Studies, Nagoya Univercity , 2.Institute for Space Earth Environmental Research, Nagoya University, 3.University of Kurdistan)

[E] Poster | U (Union)：Union

[U-10] Linking Education and Research Communities in Geosciences: Engaging the Public and Local Communities

convener:Vincent Tong(University College London), Takashi Oguchi(Center for Spatial Information Science, The University of Tokyo), Renee M Clary(Mississippi State University), Keiko Kuge(Department of Geophysics, Graduate School of Science, Kyoto University)

[U10-P01] Activities of the Committee for School Education, Seismological Society of Japan: Communicating with educators

*Makoto Yamano[1], Ken'ichi Arai[2], Akihiko Ito[3], Yasuyuki Kano[1], Osamu Kuwano[4], Masashige Minamishima[5], Ayako Misawa[6], Eiichi Misawa[7], Hiroo Nemoto[8], Akiko Sato[9], Nobuyuki Yamada[10] (1.The University of Tokyo, 2.Sakae Higashi High School, 3.Utsunomiya University, 4.JAMSTEC, 5.Tokyo Metropolitan High School of Ryogoku, 6.Shizuoka Prefectural Shizuoka Senior High School, 7.Chiba Prefectural Keiyo Senior High School, 8.Ritsumeikan University, 9.Hiratsuka City Nakahara Junior High School, 10.Kochi University)

[U10-P02] Activities of Education and Outreach by the Seismological Society of Japan

*Keiko Kuge[1], Takashi Furumura[2], Mitsuyuki Hoshiba[3], Naoji Koizumi[4], Kazuyuki Nakagawa[5], Masayuki Obayashi[6], Shin'ichi Sakai[2], Katsuhiko Shiomi[7], Keiichi Tadokoro[8], Satoru Tanaka[6], Hiroshi Tsuruoka[2], Takahiko Uchide[9], Makoto Yamano[2] (1.Department of Geophysics, Graduate School of Science, Kyoto University, 2.Earthquake Research Institute, The University of Tokyo, 3.Meterological Research Institute, 4.School of Environmental Science, The University of Shiga Prefecture, 5.Jiji Press, 6.Japan Agency for Marine-Earth Science and Technology, 7.National Research Institute for Earth Science and Disaster Resilience, 8.Earthquake and Volcano Research Center, Nagoya University, 9.Geological Survey of Japan, National Institute of Advanced Industrial Science and Technology)

[U10-P03] 20th Children's Summer School on Seismology and Volcanology in the Tango Peninsula, Japan

*Yasuyuki Kano[1], 20th School Children's Summer Course on Seismology and Volcanology (1.Earthquake Research Institute, The University of Tokyo)

[U10-P04] Development of e-learning materials for GIS exercises in Japan and their outcomes

*Hiroyuki Yamauchi[1], Takashi Oguchi[2], Yuichi S. Hayakawa[3,2], Toshikazu Seto[2] (1.Department of Natural Environmental Studies, Graduate School of Frontier Sciences, The University of Tokyo, 2.Center for Spatial Information Science, The University of Tokyo, 3.Environmental Geography, Faculty of Environmental Earth Science, Hokkaido University)

[U10-P06] Enhancing the impact of sustainability research and education: Distributed leadership as a guiding model

*Vincent Tong[1] (1.University College London)

[E] Poster | U (Union)：Union

[U-20] "Open Colloquium" Exploring the Earth's interior using cutting edge science and technology

convener:Hiroko Watanabe(Research Center for Neutrino Science, Tohoku University), William F McDonough(Department of Earth Science and Research Center for Neutrino Science, Tohoku University, Sendai, Miyagi 980-8578, Japan), Kenta Ueki(Japan Agency for Marine-Earth Science and Technology), Eiichiro Araki(Japan Agency for Marine-Earth Science and Technology)

[U20-P01] **Study of Ocean Bottom Detector for observation of geo-neutrinos from mantle**

*Taichi Sakai[1], Kunio Inoue[1], Hiroko Watanabe[1], William F McDonough[2,3], Kenta Ueki[4], Natsue Abe[4], Noriaki Sakurai[4], Masanori Kyo[4], Eiichiro Araki[4], Takafumi Kasaya[4], Hiroshi Yoshida[4] (1.Tohoku university,Research Center for Neutrino Science, 2.Tohoku university, 3.University of Maryland, 4.JAMSTEC)

[E] Poster | U (Union)：Union

[U-22] Environmental drivers and impacts of the evolving COVID-19 pandemic

convener:Benjamin F Zaitchik(Johns Hopkins University), Teppei J Yasunari(Arctic Research Center, Hokkaido University)

[U22-P01] Learning from the war against the Corona epidemic to ensure the availability of drinking water

*SHUBHAM TIWARI[1] (1.Indian Institute of Technology Roorkee)

[U22-P02] Integrate NASA Remote Sensing Data into your COVID-19 Research with our new Data Pathfinder

*Cynthia Hall[1], Kevin Ward[2] (1.NASA Goddard Space Flight Center, 2.NASA Earth Science Data Systems)

[U22-P03] Is the impact of COVID-19 modulated by well-water arsenic in rural Bangladesh? Setting a baseline.

*Alexander van Geen[1], Prabhat Barnwal[2], Yiqian Wang[2], Nishat Jui[3], Shabib Raihan[3], Ashraful Haque[3] (1.Columbia University of New York, 2.Michigan State University, 3.Innovations for Poverty Action, Bangladesh)

[U22-P04] The Spatial Pattern of Coronavirus Disease 2019 in China over Four Periods

*ZILAI ZHENG[1] (1.Graduate School of Life and Environmental Sciences, University of Tsukuba)

[U22-P05] Consequences of modeling assumptions and scope of analysis on connections between meteorology and COVID-19

*Gaige Hunter Kerr[1], Hamada Badr[2], Lauren Gardner[3], Javier Perez-Saez[4], Benjamin F Zaitchik[2] (1.George Washington University, 2.Department of Earth and Planetary Sciences, Johns Hopkins University, 3.Department of Civil and Systems Engineering, Johns Hopkins University, 4.Department of Epidemiology, Johns Hopkins Bloomberg School of Public Health)

[U22-P06] Limited Regional Aerosol Changes Despite Unprecedented NO2 Decline During the February Coronavirus Shutdown in China

*Michael S S Diamond[1], Robert Wood[1] (1.University of Washington Seattle)

[U22-P07] Will the pandemic of COVID-19 change climate?: tests using MIROC-ES2L earth system model

*Rumi Ohgaito[1], Michio Kawamiya[1], Tomohiro Hajima[1], Ken'ichi Matsumoto[1,2] (1.Japan Agency for Marine-Earth Science and Technology, 2.Nagasaki University)

[U22-P08] Using mathematical models to assess the number of total deaths and deaths per 10000 people from the COVID-19 epidemic

*Qingqing Sun[1], Chunyi Wang[2] (1.Tianjin University, 2.Mathematics Faculty, University of Waterloo)

[U22-P09] Global early warning system by Complex-Envelope (CE) Processing of Seismic Waves

*Rudolf Unger[1] (1.Delft University of Technology)

[U22-P10] **A possible role of environmental arsenic against COVID-19**

*Satadal Das[1], Milan Sengupta[2], Rathin Chakraborty[3] (1.peerless hospital and b. k. roy research centre, kolkata, india, 2.D. N. De H. Medical College, Kolkata, India., 3.Dr.Bholanath Chakravarty Integrated Medical Research & Treatment Centre, Howrah,West Bengal, India.)

[E] Poster | U (Union)：Union

[U-23] New challenges to diversity, equality and inclusion under COVID-19

convener:Chiaki T. Oguchi(Institute for Environmental Science and Technology, Graduate School of Science and Engineering, Saitama University), Rie Hori, S.(Department of Earth Science, Faculty of Science, Ehime University), Claudia Jesus-Rydin(European Research Council), Hodaka Kawahata(Atmosphere Ocean Research Institute, the University of Tokyo)

[U23-P01] GEOLATINAS: embracing, empowering, and inspiring Latinas in Geoscience

*Angela Meneses-Gutierrez[1,2,3], Rocío Caballero-Gill[4,3], Adriana Crisóstomo-Figueroa[7,3], Clara Rodriguez[8,3], Carolina Villarraga Morales[3], Grisel Jiménez Soto[5,3], Natalia A. Cifuentes[6,3] (1.Institute for Advanced Research, Nagoya University, Japan, 2. Disaster Mitigation Research Center, Nagoya University, Japan, 3.GeoLatinas, 4.George Mason University, USA, 5.South East Asia Carbonate Research Laboratory, Universiti Teknologi PETRONAS, Malaysia , 6.Department of Geosciences and Environment, National University of Colombia (Medellin), Colombia, 7.University of Leeds, Leeds, UK, 8.Petronas, Mexico)

[U23-P02] **How the COVID-19 Response Opens Broader Viewpoints for Promoting Inclusive Conferences in the Earth and Space Sciences**

*Beverly Smith-Keiling[1], Andreas Keiking[2] (1.University of Minnesota Twin Cities, 2.University of California-Berkeley)

[U23-P03] How to empower diversity, equality and inclusion for risk management in the COVID-19 Era

*Megumi Sugimoto[1] (1.Kyushu University)

[U23-P04] The Effect of COVID-19 on AGU Journal Authors by Gender and Geographical Location

*Paige Rene Wooden[1], Brooks Hanson[1] (1.American Geophysical Union)

[E] Poster | P (Space and Planetary Sciences)：P-PS Planetary Sciences

[P-PS01] Outer Solar System Exploration Today, and Tomorrow

convener:Jun Kimura(Osaka University), Kunio M. Sayanagi(Hampton University), Fuminori Tsuchiya(Planetary Plasma and Atmospheric Research Center, Graduate School of Science, Tohoku University), Steven Douglas Vance(NASA Jet Propulsion Laboratory, California Institute of Technology)

[PPS01-P01] Pluto's surface albedo distribution and its evolution due to sublimation and condensation of ices

Hisashi Matsui[1], *Jun Kimura[1] (1.Osaka University)

[PPS01-P02] A low-energy energetic neutral atom analyzer (PEP/JNA) for JUICE mission

*Kazushi Asamura[1], Manabu Shimoyama[2], Yoshifumi Futaana[2], Yoshizumi Miyoshi[3], Takeshi Sakanoi[4], Yoshifumi Saito[1] (1.Institute of Space and Astronautical Science, Japan Aerospace Exploration Agency, 2.Swedish Institute of Space Physics, 3.Nagoya University, 4.Tohoku University)

[PPS01-P03] The Ganymede Laser Altimeter (GALA) for the JUICE mission – overview and current status

*Enya Keigo[1], Masanori Kobayashi[2], Jun Kimura[3], Noriyuki Namiki[4], Hiroshi Araki[4], Hirotomo Noda[4], Shoko Oshigami[1], Shingo Kashima[4], Shin Utsunomiya[4], Ko Ishibashi[2], Masanobu Ozaki[1], Takahide Mizuno[1], Yoshifumi Saito[1], Kazuyuki Touhara[1], Shunichi Kamata[5], Koji Matsumoto[4], Kiyoshi Kuramoto[5], Sho Sasaki[3], Satoru Iwamura[6], Yoshiaki Matsumoto[7], Masayuki Fujii[8], Naofumi Fujishiro[9], Yuki Sato[10], Takeshi Yokozawa[10], Tsutomu Numata[10], Satoko mizumoto[10], Hiroyuki Mizuno[10], Akihiko Sawamura[10], Kazuo Tanimoto[10], Hisato Imai[11], Hiroyuki Nakagawa[11], Okiharu Kirino[11], Hussmann Hauke[12], Kay Lingenauber[12], Reinald Kallenbach[12], Christian Althaus[12], Simone DelTogno[12], Thomas Behnke[12], Christian Huettig [12] (1.ISAS, 2.CIT, 3.Osaka Univ., 4.NAOJ, 5.Hokkaido Univ., 6.MRJ, 7.PTIJ, 8.FAM Science, 9.Astro-Opt, 10.Meisei Electric, 11.Cristal Optics, 12.DLR)

[PPS01-P04] Tidally heated convection and the occurrence of melting in icy satellites: application to Europa

*Kenny Vilella[1], Gael Choblet[2], Wei-En Tsao[3], Frederic Deschamps[3] (1.Hokkaido University, 2.LPG Nantes, 3.Institute of Earth Sciences, Academia Sinica)

[PPS01-P05] Measurements of Saturn's Zonal Wind from Voyager Images using Modern Cloud-Tracking Method

*Justin Garland[1], Kunio M. Sayanagi[1], Jacob L. Gunnarson[1], John J. Blalock[2,1] (1.Hampton University, 2.USGS Astrogeology Science Center)

[PPS01-P06] Inhibition of moist convection in the atmospheres of Jovian planets: the case of NH4SH formation by chemical reaction of NH3 and H2S

*Ko-ichiro SUGIYAMA[1], Kensuke Nakajima[2], Kiyoshi Kuramoto[3], Yoshi-Yuki Hayashi[4] (1.National Institute of Technology, Matsue College, 2.Kyushu University, 3.Hokkaido University, 4.Kobe University)

[PPS01-P07] Detectability of water plumes on icy moons with Earth-orbiting UV telescope

*Ryoichi Koga[1], Fuminori Tsuchiya[1], Go Murakami[3], Kazuo Yoshioka[2], Masato Kagitani[1], Tomoki Kimura[1], Atsushi Yamazaki[3], Ichiro Yoshikawa[2], Hajime Kita[3], Masaki Kuwabara[3] (1.Tohoku University, 2.The University of Tokyo, 3.JAXA/ISAS)

[PPS01-P08] **Development of a radial diffusion model of Jovian inner magnetospheric plasma transportation for a comparison with HISAKI data**

*Kazuki Yamaguchi[1], Takeshi Sakanoi[1], Fuminori Tsuchiya[1], Masato Kagitani[1], Tomoki Kimura[2], Ryoichi Koga[1], Reina Hikida[3] (1.Tohoku university, 2.Frontier Research Institute for Interdisciplinary Sciences, Tohoku University, 3.Department of Earth and Planetary Science, Graduate School of Science, Tokyo University)

[PPS01-P09] Light Curve of Jupiter's UV Aurora and Io Plasma Torus after 2016 Obtained from Hisaki EXCEED

*Hajime Kita[1], Tomoki Kimura[2], Fuminori Tsuchiya[2], Go Murakami[1], Atsushi Yamazaki[1], Ryoichi Koga[2], Reina Hikida[3], Kazuo Yoshioka[3], Ichiro Yoshikawa[3] (1.Institute of Space and Astronautical Science, Japan Aerospace Exploration Agency , 2.Tohoku Univ., 3.The University of Tokyo)

[PPS01-P10] Laboratory demonstration of cryogenic-specific reddish coloration with cryoplasma

*Noritaka Sakakibara[1], Yu Yu Phua[1], Tsuyohito Ito[1], Kazuo Terashima[1] (1.The University of Tokyo)

[E] Poster | P (Space and Planetary Sciences)：P-PS Planetary Sciences

[P-PS02] Lunar Science and Exploration

convener:Masaki N Nishino(Japan Aerospace Exploration Agency, Institute of Space and Astronautical Science), Masahiro KAYAMA(Department of General Systems Studies, Graduate School of Arts and Sciences, The University of Tokyo), Hiroshi Nagaoka(Japan Aerospace Exploration Agency), Yusuke Nakauchi(Japan Aerospace Exploration Agency)

[PPS02-P01] Cause of boulder falls near a lobate scarp on the Moon: source estimate based on the attenuation relation of peak ground accelerations

*Ayame Ikeda[1], Hiroyuki Kumagai[1], Tomokatsu Morota[2] (1.Graduate School of Environmental Studies, Nagoya University, 2.Department of Earth and Planetary Science, The University of Tokyo)

[PPS02-P02] The lunar tidal dissipation energy by the Earth-moon tide

*Ryuichiro Tanaka[1], Satoshi Kaneshima[2] (1.Department of Earth and Planetary Sciences, Graduate School of Science, Kyushu University, 2.Department of Earth and Planetary Sciences, Faculty of Science, Kyushu University)

[PPS02-P03] The heterogeneity of lunar plasma environment and its influences on lunar surface hydration

*Huizi Wang[1], Jiang Zhang[1], Quanqi Shi[1,2], Yoshifumi Saito[3], Ying Ye[1] (1.Shandong Key Laboratory of Optical Astronomy and Solar-Terrestrial Environment, School of Space Science and Physics, Institute of Space Sciences, Shandong University, Weihai, Shandong, China., 2.State Key Laboratory of Space Weather, National Space Science Center (NSSC), Chinese Academy of Sciences, Beijing, China, 3.Institute of Space and Astronautical Science, Japan Aerospace Exploration Agency, Sagamihara, Japan.)

[PPS02-P04] **Phase boundary and kinetics of moganite-coesite phase transition at high-pressure and high-temperature: implications for an impact event and trace of water on the Moon**

*Shin Ozawa[1], Masahiro KAYAMA[1,2], Tatsuya Sakamaki[1], Tomonori Ohashi[1], Akio Suzuki[1] (1.Department of Earth Science, Graduate School of Science, Tohoku University, 2.Department of General Systems Studies, Graduate School of Arts and Sciences, The University of Tokyo)

[PPS02-P05] Evaluating the thickness and stratigraphy of ejecta materials at the Chang'e-4 landing site

*Luyuan Xu[1], Xunyu Zhang[1], Le Qiao[2] (1.State Key Laboratory of Lunar and Planetary Sciences, Macau University of Science and Technology, 2.Shandong Provincial Key Laboratory of Optical Astronomy and Solar-Terrestrial Environment, Shandong University, Weihai)

[PPS02-P06] An explaination of the origin of Davy Crater Chain on the Moon other than impacts of fragments comprising a comet

Akiya Saito[1,2], *Junichi Haruyama[1], Wataru Miyake[2] (1.Japan Aerospace Exploration Agency, 2.Tokay University)

[PPS02-P07] UZUME: A Lunar Lava Tube Exploration of Japan

*Junichi Haruyama[1] (1.Japan Aerospace Exploration Agency)

[PPS02-P08] On magnetic field observation in and near a lunar pit for understanding magnetic history of the Moon

*Hisayoshi Shimizu[1] (1.Earthquake Research Institute, University of Tokyo)

[PPS02-P09] Radiation dose and protection by a lunar hole and lava tube

*Masayuki Naito[1], Nobuyuki Hasebe[2], Satoshi Kodaira[1], Yoshiharu Amano[2], Junichi Haruyama[3] (1.National Institutes for Quantum and Radiological Scinence and Technology, 2.Waseda University, 3.JAXA)

[PPS02-P10] Breadboard Model of Bionic Legged Robot for Lunar Lava Cave Exploration

*LIANG CHEN[1] (1.Ashikaga University)

[PPS02-P11] Study of lunar 3-D terrain mapping using both the camera and the LIDAR loaded on the rover

*Ryuhei Yamada[1], Yuichi Yaguch[1], Keitaro Naruse[1] (1.The University of Aizu, Department of Computer Science and Engineering)

[PPS02-P12] **Characterizing Sites for Landed Lunar Missions with NASA's Moon Trek Portal**

*Emily Law[1], Brian Hamilton Day[2] (1.Jet Propulsion Laboratory, 2.Ames Research Center)

[PPS02-P13] Development of a compact LIBS instrument for future lunar explorations: a feasibility study using lunar meteorites

*Akinojo Ogura[1], Yuichiro Cho[2], Naoki Yamamoto[1], Koki Yumoto[2], Takafumi Niihara[3], Shingo Kameda[4], Seiji Sugita[2], Takahide Mizuno[5] (1.Department of Earth and Planetary Physics, University of Tokyo, 2.Department of Earth and Planetary Science, University of Tokyo, 3.Department of Systems Innovation, University of Tokyo, 4.School of Science, Rikkyo University, 5.Institute of Space and Astronautical Science, Japan Aerospace Exploration Agency)

[PPS02-P14] **Preparation status of Multi-Band Camera onboard SLIM lander**

*Kazuto Saiki[1], Makiko Ohtake[2], Yusuke Nakauchi[2], Hiroaki Shiraishi[2], Chikatoshi Honda[3], Hiroyuki Sato[2], Yoshiaki Ishihara[4], Takao Maeda[5], Chihiro Yamanaka[1], Hiroshi Nagaoka[2] (1.Graduate School of Science, Osaka University, 2.Japan Aerospace Exploration Agency, 3.University of Aizu, 4.National Institute for Environmental Studies, 5.Chuo University)

[PPS02-P15] The search for whistler-mode chorus emissions related to the Moon using ARTEMIS

*Wataru Sawaguchi[1], Yuki Harada[1], Satoshi Kurita[2] (1.Graduate School of Science, Kyoto University, 2.RISH, Kyoto University)

[E] Poster | P (Space and Planetary Sciences)：P-PS Planetary Sciences

[P-PS03] High-pressure phases in shocked meteorites: key to understanding impact events on parent asteroids

convener:Kishan Tiwari(Indian Institute of Technology Kharagpur)

[PPS03-P01] Thermal infrared measurement of impact in laboratory experiment

*Tetsuya Fukuhara[1], Shinsuke Abe[2], Masahisa Yanagisawa, Ryota Fuse[2], Naoya Sakatani[3] (1.Rikkyo University, 2.Nihon University, 3.JAXA/ISAS)

[E] Poster | P (Space and Planetary Sciences)：P-PS Planetary Sciences

[P-PS04] Regolith Science

convener:Koji Wada(Planetary Exploration Research Center, Chiba Institute of Technology), Akiko Nakamura(Graduate School of Science, Kobe University), Patrick Michel(Universite Cote D Azur Observatoire De La Cote D Azur CNRS Laboratoire Lagrange), Kevin John Walsh(Southwest Research Institute Boulder)

[PPS04-P01] Laboratory penetration experiments conducted at low effective gravity II

*Akiko Nakamura[1], Junpei Nakahata[2], Yuuya Nagaashi[1] (1.Graduate School of Science, Kobe University, 2.Faculty of Science, Kobe University)

[PPS04-P02] Experimental study of high-velocity impacts into granular material in reduced gravity

*Masato Kiuchi[1], Takaya Okamoto[1], Sunao Hasegawa[1], Akiko Nakamura[2] (1.Japan aerospace exploration agency, Institute of space and astronautical science, 2.Graduate School of Science, Kobe University)

[PPS04-P03] A Tentative Numerical Study on the Effect of Aspect Ratio of Cylindrical Projectile on Crater Morphology using iSALE code

*Yuri Shimaki[1] (1.Institute of Space and Astronautical Science, Japan Aerospace Exploration Agency)

[PPS04-P05] Automated Identification of Particles in Rock Gravel of Small Bodies

*Yuta Shimizu[1], Hideaki Miyamoto[1] (1.University of Tokyo)

[PPS04-P06] Development of lunar regolith simulants based on previous lunar explorations

*Takemura Tomohiro[1], Takafumi Niihara[1], Hideaki Miyamoto[1] (1.The University of Tokyo)

[PPS04-P07] **Estimation of abrasion rates of regolith particles on Itokawa and the Moon based on abration experiments.**

*Akira Tsuchiyama[1], Hirotaka Yamaguchi[2], Akiko Nakamura[3] (1.Research Organization of Science and Technology, Ritsumeikan University, 2.Graduate School of Science, Kyoto University, 3.Graduate School of Science, Kobe University)

[E] Poster | P (Space and Planetary Sciences)：P-PS Planetary Sciences

[P-PS05] Planetary Seismic Exploration-From InSight and Apollo to Future Missions-

convener:Taichi Kawamura(Institut de Physique du Globe de Paris), Takeshi Tsuji(Department of Earth Resources Engineering, Kyushu University), Ralph Lorenz(Johns Hopkins University Applied Physics Laboratory), William Bruce Banerdt(Jet Propulsion Laboratory)

[PPS05-P01] Estimation of the lunar near-surface effects on Moonquake waves amplification.

*Mohamed Amrouche[1], Renee Weber[2] (1.Schlumberger., 2.NASA Marshall Space Flight Center.)

[PPS05-P02] Scattering properties near Apollo 12 landing site inferred from numerical simulation of seismic wave propagation

*Keisuke Onodera[1,2], Taichi Kawamura[1], Satoshi Tanaka[3], Yoshiaki Ishihara[4], Takuto Maeda[5] (1.University of Paris/Institut de Physique du Globe de Paris, 2.The Graduate University for Advanced Studies (SOKENDAI), 3.Institute of Space and Astronautical Science/Japan Aerospace Exploration Agency, 4.National Institute for Environmental Studies, 5.Hirosaki University)

[PPS05-P03] **INSIGHT SEIS data and dataless dynamic production.**

*Taoufik GABSI[1], Philippe Lognonne[1], Constanza Pardo[1], Charles Yana[2], Eric Beucler[3], John Clinton[4], Vincent Conejero[1], Taïchi Kawamura[1], Gregory Sainton[1], Tanguy Nebut[1], Clément Perrin[1], Matthieu Plasman[1], Simon Stähler[4], Renee Weber[5], Bruce W Banerdt[7], Nobuaki Fuji[1], Sébastien de Raucourt[1], Eléonore Stutzmann[1], Rudolf Widmer-Schnidrig[6] (1.Institut de Physique du Globe de Paris , France, 2.Centre National des Etudes Spatialles, France, 3.Laboratoire de planétologie et géodynamique Nantes Université, France, 4.ETH, Zürich, Switzerland, 5.NASA Marshall Space Flight Center, USA, 6.Universität Stuttgart, Stuttgart, Germany, 7. Jet Propulsion Laboratory, NASA, USA)

[PPS05-P05] **Comparison of attenuation and scattering of Lunar and Martian structures**

*Sabrina Menina[1], Taichi Kawamura[1], Ludovic Margerin[2], Mélanie Drilleau[1], Philippe Henri Lognonné[1], Marie Calvet[2], Marc Monnereau[2] (1.Institut de Physique du Globe de Paris, 2.Institut de Recherche en Astrophysique et Planétologie (IRAP), Toulouse, France)

[PPS05-P06] Orbital Remote sensing seismology on Venus: the VAMOS concept.

*Philippe Henri Lognonné[1], Attila Komjathy[2], Siddharth Krishnamoorthy[2], Raphael F. Garcia[3], Balthasar Kenda[1], Brian M. Sutin[2] (1.Université de Paris, Institut de physique du globe de Paris, CNRS, 2.Jet Propulsion Laboratory, California Institute of Technology, Pasadena, CA 91109, USA, 3.Institut Supérieur de l'Aéronautique et de l'Espace SUPAERO, 10 Avenue Edouard Belin, 31400 Toulouse, France)

[E] Poster | P (Space and Planetary Sciences)：P-PS Planetary Sciences

[P-PS06] Science of Venus: Venus Express, Akatsuki, and beyond

convener:Takehiko Satoh(Institute of Space and Astronautical Science, Japan Aerospace Exploration Agency), Kevin McGouldrick(University of Colorado Boulder), Hideo Sagawa(Kyoto Sangyo University), Thomas Widemann(Observatoire De Paris)

[PPS06-P01] Polarimetry of Venus upper atmosphere with a new single-shot type polarimeter

*Takehiko Satoh[1,2], Masato Kagitani[3], Takeshi Sakanoi[3], Takao M. Sato[4], James O'Donoghue[1] (1.Institute of Space and Astronautical Science, Japan Aerospace Exploration Agency, 2.Department of Space and Astronautical Science, The Graduate University for Advanced Studies, SOKENDAI, 3.Faculty of Science, Tohoku University, 4.Space Information Center, Hokkaido Information University)

[PPS06-P02] Venus's Atmospheric Features in UV as Viewed from Ground-Based Observations

*Ryan M. McCabe[1], Kunio M. Sayanagi[1], John J. Blalock[1], Jacob L. Gunnarson[1], Javier Peralta[2], Candace L. Gray[4], Kevin McGouldrick[5], Takeshi Imamura[2], Shigeto Watanabe[3], Yeon Joo Lee[6] (1.Hampton University, 2.Institute of Space and Astronautical Sciences, JAXA, 3.Department of Earth and Planetary Sciences, Hokkaido Univ., Japan, 4.Apache Point Observatory , Sunspot, NM, 5.LASP, Univ. of Colorado Boulder, 6.Technical University of Berlin, Germany)

[PPS06-P03] 3-D Thermal Structure of the Venus Atmosphere Obtained by Akatsuki/LIR

*Masahiro Akiba[1], Makoto Taguchi[2], Tetsuya Fukuhara[2], Takeshi Imamura[3], Toru Kouyama[4], Takao M. Sato[5] (1.Rikkyo graduate School, 2.Rikkyo University, 3.The University of Tokyo, 4.National Institute of Advanced Industrial Science and Technology, 5.Hokkaido Information University)

[PPS06-P04] An uppermost haze layer above 100 km found over Venus by the SOIR onboard Venus Express

*Seiko Takagi[1], Arnaud Mahieux[2], Valérie Wilquet[2], Séverine Robert[2], Ann Carine Vandaele[2], Naomoto Iwagami (1.Hokkaido University, Graduate School of Science, 2.Belgian Institute for Space Aeronomy)

[PPS06-P05] **Variations in the activities of planetary-scale waves at the Venusian cloud top observed by Akatsuki UVI**

★Invited Papers

*Masataka Imai[1], Toru Kouyama[1], Atsushi Yamazaki[2], Shigeto Watanabe[3], Manabu Yamada[4], Shin-ya Murakami[2], Takeshi Imamura[5], Takehiko Satoh[2], Masato Nakamura[2], Kazunori Ogohara[6], Takeshi Horinouchi[7] (1.Advanced Industrial Science and Technology, 2.Institute of Space and Astronautical Science, 3.Hokkaido Information University, 4.Chiba Institute of Technology, 5.The University of Tokyo, 6.The University of Shiga Prefecture, 7.Hokkaido University)

[PPS06-P06] The global variation of Venus cloud investigated from AKATSUKI 1-μm camera

*Seiko Takagi[1], Naomoto Iwagami (1.Hokkaido University, Graduate School of Science)

[PPS06-P07] **Cosmic rays and high energetic particles at Venus: Analysis of triggered pulse events detected by Akatsuki/LAC**

*Masataka Imai[1], Yukihiro Takahashi[2], Ralph Lorenz[3], Mitsuteru Sato[2] (1.National Institute of Advanced Industrial Science and Technology, 2.Hokkaido University, 3.Johns Hopkins University Applied Physics Laboratory)

[PPS06-P08] Ground-based Observation of planetary lightning flashes by using Photomultiplier tube

*Tatsuharu Ono[1], Yukihiro Takahashi[1], Mitsuteru Sato[1], Shigeto Watanabe[1], Seiko Takagi[1], Masataka Imai[2] (1.Department of Cosmosciences, Graduate School of Science, Hokkaido University, 2.National Institute of Advanced Industrial Science and Technology)

[PPS06-P09] Observation of the Venusian Lower Atmosphere in the 1.7 μm Band by Near-infrared Echelle Spectrometer onboard PIRKA Telescope in Nayoro Observatory

Daiki Tsukiyama[1], *Hiroyuki Maezawa[1], Atsushi Nishimura[1], Masataka Imai[4], Hidenori Takahashi[2], Masuo Tanaka[2], Yukihiro Takahashi[3], Mitsuteru Sato[3], Seiko Takagi[3], Shin-ichiro Okumura[5], Yeon Joo Lee[6] (1.Department of Physical Science Osaka Prefecture University, 2.Institute of Astronomy, School of Science, The University of Tokyo, 3.Hokkaido University, Graduate School of Science, 4.The National Institute of Advanced Industrial Science and Technology, 5.Japan Spaceguard Association, 6.Technical University of Berlin)

[PPS06-P10] A sensitivity study of the radiative-convective equilibrium temperature profile in Venus atmosphere

★Invited Papers

*Miho Sekiguchi[1], Masahiro Takagi[2], Hideo Sagawa[2], Yoshihisa Matsuda[3] (1.Tokyo University of Marine Science and Technology, 2.Kyoto Sangyo University, 3.Tokyo Gakugei University)

[PPS06-P11] Meridional distribution of CO on Venus

*Shinya Kuwayama[1], George HASHIMOTO[1] (1.Okayama University)

[PPS06-P12] Trials toward first Venus analysis product by data assimilation of Akatsuki observation

★Invited Papers

*Yukiko Fujisawa[1], Shin-ya Murakami[2], Norihiko Sugimoto[1], Masahiro Takagi[3], Takeshi Imamura[4], Takeshi Horinouchi[5], George HASHIMOTO[6], Masaki Ishiwatari[5], Takeshi Enomoto[7], Takemasa Miyoshi[8], Yoshi-Yuki Hayashi[9] (1.Keio University, 2.JAXA, 3.Kyoto Sangyo University, 4.Tokyo University, 5.Hokkaido University, 6.Okayama University, 7.Disaster prevention Research Institute, Kyoto University, 8.RIKEN, 9.Kobe University)

[PPS06-P13] Dynamics of Decadal Sulfur Dioxide Variability in Venus' Atmosphere with a Simple Model

*Pushkar Kopparla[1], Ashwin Seshadri[2], Takeshi Imamura[1], Yeon Joo Lee[3], Javier Peralta[4] (1.University of Tokyo, 2.Indian Institute of Science, 3.Technical University of Berlin, 4.ISAS JAXA)

[E] Poster | P (Space and Planetary Sciences)：P-PS Planetary Sciences

[P-PS07] Solar System Small Bodies: Explorations of Ryugu, Bennu, and the Solar System at Large

convener:Taishi Nakamoto(Tokyo Institute of Technology), Tatsuaki Okada(Institute of Space and Astronautical Science, Japan Aerospace Exploration Agency), Dante S Lauretta(University of Arizona), Masateru Ishiguro(Department of Physics and Astronomy, Seoul National University)

[PPS07-P01] Tests and rehearsals for curation of samples returned from asteroid Ryugu by Hayabusa2 spacecraft

*Toru Yada[1], Masanao Abe[1], Aiko Nakato[1], Kasumi Yogata[1], Akiko Miyazaki[1], Tatsuaki Okada[1], Masahiro Nishimura[1], Kazuya Kumagai[2], Miwa Yoshitake[1], Shizuho Furuya[1], Ayako Iwamae[2], Tasuku Hayashi[1], Daiki Yamamoto[1], Shogo Tachibana[1,3], Tomohiro Usui[1], Hisayoshi Yurimoto[1,4] (1.Japan Aerospace Exploration Agency, 2.Marine Works Japan, 3.University of Tokyo, 4.Hokkaido University)

[PPS07-P02] **Soluble organic matter in Ryugu: The first rehearsal analysis**

*Hiroshi Naraoka[1], Yoshinori Takano[2], Nanako O. Ogawa[2], Minako Hashiguchi[1], Hannah L. McLain[3], Eric T. Parker[3], Kenji Hamase[1], Francois-Régis Orthous-Daunay[4], Junko Isa[4], Dan Aoki[5], Kazuhiko Fukushima[5], Philip Schmitt-Kopplin[6], Jason P. Dworkin[3], SOM Analysis Team (1.Kyushu University, Japan, 2.Japan Agency for Marine-Earth Science Technology, Japan, 3.NASA Goddard Space Flight Center, USA, 4.Université Grenoble Alpes, France, 5.Nagoya University, Japan, 6.Helmholtz Zentrum Muenchen, Germany)

[PPS07-P03] Visible Wavelength Normal Albedo Map of Ryugu Derived by Hayabusa2 Optical Navigation Camera

*Yasuhiro Yokota[1,2], Rie Honda[2], Eri Tatsumi[3,4,5], Deborah Domingue[6], Stefanus E. Schröder[7], Moe Matsuoka[1], Seiji Sugita[5], Tomokatsu Morota[5,8], Shingo Kameda[9], Toru Kouyama[10], Hidehiko Suzuki[11], Manabu Yamada[12], Naoya Sakatani[1], Chikatoshi Honda[13], Masahiko Hayakawa[1], Kazuo Yoshioka[5], Yuichiro Cho[5], Hirotaka Sawada[1], Kazunori Ogawa[1,14] (1.ISAS/JAXA, 2.Kochi Univ., Japan, 3.Instituto de Astrofisica de Canarias, Spain, 4.Univ. of La Laguna, Spain, 5.Univ. of Tokyo, Japan, 6.Planetary Science Institute, USA, 7.DLR, Germany, 8.Nagoya Univ., Japan, 9.Rikkyo Univ., Japan, 10.AIST, Japan, 11.Meiji Univ., Japan, 12.Chiba Inst. Tech, Japan, 13.Univ. of Aizu, Japan, 14.Kobe Univ., Japan)

[PPS07-P04] Change in boulder surface spectra on asteroid Ryugu induced by touchdown operations of Hayabusa2

*Yudai Takai[1], Seiji Sugita[1], Rie Honda[2], Tomokatsu Morota[1], Shingo Kameda[3], ERI TATSUMI[4], Yuichiro Cho[1], Kazuo Yoshioka[1], Hirotaka Sawada[5], yokota yasuhiro[5], Naoya Sakatani[5], Masahiko Hayakawa[5], Moe Matsuoka[5], Manabu Yamada[6], Toru Kouyama[7], Hidehiko Suzuki[8], Chikatoshi Honda[9], Kazunori Ogawa[5] (1.University of Tokyo, 2.Kochi University, 3.Rikkyo University, 4.University of La Laguna, 5.JAXA, 6.Chiba Institute of Technology, 7.National Institute of Advanced Industrial Science and Technology, 8.Meiji University, 9.The University of Aizu)

[PPS07-P05] The Surface Roughness of (162173) Ryugu based on the Topography from HAYABUSA2 Laser Altimeter (LIDAR)

*Shinsuke Abe[1], Noriyuki Namiki[2], Koji Matsumoto[2], Hirotomo Noda[2], Hiroki Senshu[3], Naru Hirata[4], Hirohide Demura[4] (1.Department of Aerospace Engineering, College of Science and Technology, Nihon University, 2.National Astronomical Observatory of Japan, 3.Planetary Exploration Research Center, Chiba Institute of Technology, 4.The University of Aizu)

[PPS07-P06] Estimation based on analysis of boulder motion of bulk density of the boulders on the surface of Ryugu at touchdown operation

*Kousuke Kitsunai[1], Shingo Kameda[1], ERI TATSUMI[2], Naoya Sakatani[3], Shogo Tachibana[4], Osamu Mori[3], Seiji Sugita[4], Rie Honda[5], Tomokatsu Morota[4], yokota yasuhiro[3], Toru Kouyama[6], Hidehiko Suzuki[7], Manabu Yamada[8], Chikatoshi Honda[9], Masahiko Hayakawa[3], Kazuo Yoshioka[4], Yuichiro Cho[4] (1.Rikkyo University, 2.IAC, 3.JAXA/ISAS, 4.University of Tokyo, 5.Kochi University, 6.AIST, 7.Meiji University, 8.Chiba Inst. Tech, 9.University of Aizu)

[PPS07-P07] **East-west asymmetric crater ejecta on Ryugu**

*Naoyuki Hirata[1], Noriyuki Namiki[2] (1.Kobe University, 2.National Astronomical Observatory of Japan)

[PPS07-P08] Crack orientation of surface boulders on Ryugu

*Sho Sasaki[1], Shiho Kanda[1], Hiroshi Kikuchi[2], Tatsuhiro Michikami[3], Tomokatsu Morota[4], Chikatoshi Honda[5], Hideaki Miyamoto[6,7], Ryodo Hemmi[7], Seiji Sugita[4], Eri Tatsumi[8], Masanori Kanamaru[1], Naoya Sakatani[2], Sei-ichiro

Watanabe[9], Noriyuki Namiki[10], Terunori Irie[9], Patrick Michel[11], Masatoshi Hirabayashi[12], Naru Hirata[5], Tomoki Nakamura[13], Takaaki Noguchi[14], Takahiro Hiroi[15], Koji Matsumoto[10], Hirotomo Noda[10], Shingo Kameda[16], Toru Kouyama[17], Hidehiko Suzuki[18], Manabu Yamada[19], Rie Honda[20], Yuichiro Cho[4], Kazuo Yoshioka[4], Masahiko Hayakawa[2], Moe Matsuoka[2], Hirotaka Sawada[2], Yokota Yasuhiro[20], Makoto Yoshikawa[2] (1.Department of Earth and Space Sciences, School of Science, Osaka University, 2.ISAS/JAXA, 3.Faculty of Engineering, Kindai University, 4.Department of Earth and Planetary Science, The University of Tokyo, 5.The University of Aizu, 6.School of Engineering, The University of Tokyo, 7.The University Museum, The University of Tokyo, 8.Instituto de Astrofisica de Canarias, 9.Division of Earth and Planetary Sciences, Nagoya University, 10.RISE Project, National Astronomical Observatory of Japan, 11.Observatoire De La Cote D'Azur, 12.Auburn University, 13.Department of Earth and Planetary Materials Sciences, Tohoku University, 14.Department of Arts and Science, Kyushu University, 15.Brown University, 16.Department of Physics, Rikkyo University, 17.National Institute of Advanced Industrial Science and Technology, 18.Department of Physics, Meiji University, 19.Planetary Exploration Research Center, Chiba Institute of Technology, 20.Department of Science and Technology, Kochi University)

[PPS07-P09] Temperature variations of boulders on Ryugu observed in Hayabusa2 decent operations

*Ayumu Ohsugi[1], Naoya Sakatani[2], Yuri Shimaki[2], Hiroki Senshu[3], Takehiko Arai[4], Hirohide Demura[5], Satoshi Tanaka[2], Tetsuya Fukuhara[6], Tatsuaki Okada[1,2] (1.The University of Tokyo, 2.Institute of Space and Astronautical Science, Japan Aerospace Exploration Agency, 3.Planetary Exploration Research Center, Chiba Institute of Technology, 4.Faculty of Engineering, Department of Innovative Engineering, Division of Systems and Information Engineering, Ashikaga University, 5.Department of Computer Science and Engineering, University of Aizu, 6.Department of Physics, College of Science, Rikkyo University)

[PPS07-P10] **Evaluation of Surface Temperature Variation on Asteroid Ryugu caused by Space Weathering**

*Takehiko Arai[1], Tatsuaki Okada[2], Satoshi Tanaka[2], Tetsuya Fukuhara[3], Hirohide Demura[4], Naoya Sakatani[2], Toru Kouyama[5], Yuri Shimaki[2], Hiroki Senshu[6], Tomohiko Sekiguchi[7], Jun Takita[8] (1.Ashikaga University, 2.Japan Aerospace Exploration Agency, 3.Rikkyo University, 4.The University of Aizu, 5.National Institute of Advanced Industrial Science and Technology, 6.Chiba Institute of Technology, 7.Hokkaido University of Education, 8.Hokkaido Kitami Hokuto High School)

[PPS07-P11] The effects of porosity of surface materials on the reflectance spectra of C-type asteroids

*Eiichi Kagawa[1], Tomoki Nakamura[1], Kana Amano[1], Lucie Riu[2], Moe Matauoka[2], Osamu Sasaki[3] (1.Department of Earth and Planetary Materials Sciences, Faculty of Science, Tohoku University, 2.Institute of Space and Astronautial Siences/Japan Aerospace Exploration Agency, 3.The Tohoku University Museum)

[PPS07-P12] Evidence of Boulder Mass Movement in the Northern Latitudes of Asteroid Bennu and Implications for its Surface Evolution

*Yuhui Tang[1], Dante S Lauretta[1], Ronald Ballouz[1], Daniella DellaGiustina[1], Carina Bennet[1] (1.University of Arizona)

[PPS07-P13] Q-type asteroids: possibility of having non-fresh weathered surfaces without fine particles

*Sunao Hasegawa[1], Takahiro Hiroi[2], Katsuhito Ohtsuka[3], Masateru Ishiguro[4], Daisuke Kuroda[5], Takashi Ito[6], Sho Sasaki[7] (1.Japan Aerospace Exploration Agency, 2.Brown University, 3.Tokyo Meteor Network, 4.Seoul National University, 5.Kyoto University, 6.National Astronomical Observatory of Japan, 7.Osaka University)

[PPS07-P14] Three-dimensional tracking of various sized glass beads ejected from crater formed by high-velocity impact

*Hatsune Okawa[1], Minami Yasui[1], Masahiko Arakawa[1], Sunao Hasegawa[2], Yusaku Yokota[1], Yuya Yamamoto[1] (1.Graduate School of Science, Kobe University, 2.Japan Aerospase Exploration Agency, Institute of Space and Astronautical Science)

[PPS07-P15] Effects of surface topography on ejecta growth and crater formation process

*Yusaku Yokota[1], Masahiko Arakawa[1], Minami Yasui[1], Yuya Yamamoto[1], Hatsune Okawa[1], Sunao Hasegawa[2] (1.Graduate School of Science, Kobe University, 2.Japan Aerospace Exploration Agency)

[PPS07-P16] Heating effects on the structures and elemental ratios of IOM in Jbilet Winselwan and Y 793321 CM chondrites

*Ryota Ichimura[1], Yoshihiro Furukawa[1], Tomoki Nakamura[1], Megumi Matsumoto[1], Mariko Ando (1.Department of Earth and Planetary Materials Sciences, Faculty of Science, Tohoku University)

[PPS07-P17] Survival of organic materials during atmospheric entry of micrometeorites

*Masayuki Uesugi[1], Motoo Ito[2], Naotaka Tomioka[2], Yu Kodama[3], Takuji Ohigashi[4], Hayato Yuzawa[4], Kentaro Uesugi[1], Akira Yamaguchi[5], Naoya Imae[5], Naoki Shirai[6], Yuzuru Karouji[7], Aiko Nakato[7], Kasumi Yogata[7], Kaori Hirahara[8], Ikuya Sakurai[9], Toru Yada[7], Masanao Abe[7] (1.Japan synchrotron radiation research institute, 2.Kochi institute for Core Sample Research JAMSTEC, 3.Marine Works Japan Ltd., 4.UVSOR Institute for Molecular Science, 5.National institute of Polar Research, 6.Tokyo metropolitan university, 7.Japan aerospace exploration agency, 8.Osaka University, 9.Nagoya University)

[PPS07-P18] Near-Earth Asteroid Survey with Tomo-e Gozen

*Ryou Ohsawa[1], Jin Beniyama[1], Shigeyuki Sako[1], Seitaro Urakawa[2], Shin-ichiro Okumura[2], Jun-ichi Watanabe[3], Makoto Yoshikawa[4], Tomoki Morokuma[1], Tomo-e Gozen collaboration (1.Institute of Astronomy, Graduate School of Science, The University of Tokyo, 2.Japan Spaceguard Association, 3.National Astronomical Observatory of Japan, 4.JAXA Institute of Space and Astronautical Science)

[PPS07-P19] Phase curves of >20,000 small solar system bodies obtained by the Tomo-e Gozen transient survey

*Fumi Yoshida[1], Takashi Ito[2], Seitaro Urakawa[3], Tsuyoshi Terai[4], Nozomu Tominaga[5], Tomoki Morokuma[6], Shigeyuki Sako[6], Ryou Ohsawa[6], Masaomi Tanaka[7], Ryo Hamasaki[5], Tomo-e Gozen collaboration (1.Planetary Exploration Research Center, Chiba Institute of Technology, 2.National Astronomical Observatory of Japan, Center for Computational Astrophysics, 3.Japan Spaceguard Assosication, Bisei Spaceguard Center, 4.National Astronomical Observatory of Japan, Subaru Telescope, 5.Konan University, 6.University of Tokyo, 7.Tohoku University)

[PPS07-P20] Size distribution of Jupiter's Trojan asteroids in the L5 swarm obtained by the Subaru/Hyper Suprime-Cam

Kotomi Uehata[1], *Tsuyoshi Terai[2], Keiji Ohtsuki[1], Fumi Yoshida[3] (1.Graduate School of Science, Kobe University, 2.Subaru Telescope, National Astronomical Observatory of Japan, National Institutes of Natural Sciences, 3.Planetary Exploration Research Center, Chiba Institute of Technology)

[PPS07-P21] Measurement of Size Distribution of Cold Classical Trans-Neptunian Objects

*Tsuyoshi Terai[1], Fumi Yoshida[2], Keiji Ohtsuki[3] (1.Subaru Telescope, National Astronomical Observatory of Japan, National Institutes of Natural Sciences, 2.Planetary Exploration Research Center, Chiba Institute of Technology, 3.Graduate School of Science, Kobe University)

[PPS07-P22] Comparison of original orbits of Oort Cloud new comets given in various catalogues

*Takashi Ito[1], Arika Higuchi[1] (1.National Astronomical Observatory of Japan, National Institutes of Natural Science)

[PPS07-P23] Observational campaigns of (3200) Phaethon in 2017-2019

*Fumi Yoshida[1], Tomoko Arai[1], Ko Ishibashi[1], Peng Hong[1], Ryo Ishimaru[1], Takaya Okamoto[2], Jun-ichi Watanabe[3], DESTINY+ collaborators (1.Planetary Exploration Research Center, Chiba Institute of Technology, 2.Institute of Space and Astronautical Science, 3.National Astronomical Observatory of Japan)

[PPS07-P24] Flyby Observation of Asteroid (3200) Phaethon to Be Conducted by Cameras onboard DESTINY$^+$ Spacecraft

*Ko Ishibashi[1], Peng Hong[1], Takaya Okamoto[2], Takahiro Ishimaru[2], Shunsuke Sato[2], Manabu Yamada[1], Osamu Okudaira[1], Tomoko Arai[1], Fumi Yoshida[1], Shingo Kameda[3], Masato Kagitani[4], Takahiro Iwata[2], Tatsuaki Okada[2], Takeshi Takashima[2] (1.Chiba Institute of Technology, 2.Japan Aerospace Exploration Agency, 3.Rikkyo University, 4.Tohoku Universtiy)

[PPS07-P25] Imaging experiment simulating DESTINY$^+$ flyby exploration

*Peng Hong[1], Ko Ishibashi[1], Takaya Okamoto[2], Osamu Okudaira[1] (1.Planetary Exploration Research Center, Chiba Institute of Technology, 2.Institute of Space and Astronautical Science, Japan Aerospace Exploration Agency)

[PPS07-P26] Modeling of an Ejecta Cloud in the Vicinity of Asteroid (3200) Phaethon: A Predicton for the Detection of Ejecta Dust by the DESTINY+ Dust Analyzer (DDA)

*Hiroshi Kimura[1], Masanori Kobayashi[1], Koji Wada[1], Tomoko Arai[1], Hiroki Senshu[1], Ko Ishibashi[1], Takayuki Hirai[1], Fumi Yoshida[1], Peng Hong[1] (1.PERC/Chitec)

[PPS07-P27] Development and ground calibration strategy of DESTINY$^+$ Dust Analyzer

*Takayuki Hirai[1], Masanori Kobayashi[1], Tomoko Arai[1], Hiroshi Kimura[1], Ralf Srama[2], Harald Krueger[3], Hikaru Yabuta[5], Motoo Ito[6], Mario Trieloff[4], Sho Sasaki[7], Tomoki Nakamura[8], Hajime Yano[9] (1.Chiba Institute of Technology, Planetary Exploration Research Center, 2.University of Stuttgart, 3.Max Planck Institute for Solar System Research,

4.Heidelberg University, 5.Hiroshima University, 6.Japan Agency for Marine-Earth Science and Technology, 7.Osaka University, 8.Tohoku University, 9.Japan Aerospace Exploration Agency)

[PPS07-P28] **Visualization and Analysis of Data from Small-Body Missions with NASA's Solar System Treks Portals**

*Brian Hamilton Day[1], Emily Law[2], NASA Solar System Treks Team -[2] (1.NASA Ames Research Center, 2.NASA Jet Propulsion Laboratory)

[PPS07-P29] Comet Interceptor mission: an overview and an expected contribution from Japan

*Satoshi Kasahara[1], Shingo Kameda[2], Kazuo Yoshioka[1], Ayako Matsuoka[3], Hideyo Kawakita[4], Shinnaka Yoshiharu[4], Jun-ichi Watanabe[5], Yoshifumi Saito[6], Ryu Funase[1,6], Ozaki Naoya[6] (1.The university of Tokyo, 2.Rikkyo University, 3.Kyoto University, 4.Kyoto Sangyo University, 5.National Astronomical Observatory of Japan, 6.Institute of Space and Astronautical Science)

[PPS07-P30] **Thermal Infrared Multi-band Imager for the Hera Mission**

*Tatsuaki Okada[1,2], Tetsuya Fukuhara[3], Satoshi Tanaka[1], Takehiko Arai[4], Naoya Sakatani[1], Yuri Shimaki[1], Hiroki Senshu[5], Hirohide Demura[6], Toru Kouyama[7], Tomohiko Sekiguchi[8], Sunao Hasegawa[1], Makoto Yoshikawa[1] (1.Institute of Space and Astronautical Science, Japan Aerospace Exploration Agency, 2.University of Tokyo, 3.Rikkyo University, 4.Ashikaga University, 5.Chiba Institute of Technology, 6.University of Aizu, 7.National Institute of Advanced Industrial Science and Technology, 8.Hokkaido University of Education)

[PPS07-P31] **Janus: A NASA SIMPLEx mission to explore two NEO Binary Asteroids**

*Daniel Jay Scheeres[1], J W McMahon[1], E B Bierhaus[2], J Wood[2], L A.M. Benner[3], C Hartzell[4], P Hayne[1], R Jedicke[5], J Hopkins[2], L Le Corre[6], S Naidu[3], P Pravec[7], M Ravine[8] (1.University of Colorado Boulder, 2.Lockheed Martin, 3.JPL, 4.University of Maryland, 5.University of Hawaii, 6.Planetary Science Institute, 7.Astronomical Institute of the Academy of Sciences, Czech Republic, 8.Malin Space Science Systems)

[PPS07-P32] Time evolution of the Jacobi integral of the elliptic restricted three-body problem

*Arika Higuchi[1] (1.National Astronomical Observatory in Japan)

[PPS07-P33] Planetesimal Formation by Collisional Growth of Dust Aggregates in Disk Formation Phase

Ryohei Ozaki[1], *Taishi Nakamoto[1] (1.Tokyo Institute of Technology)

[E] Poster | P (Space and Planetary Sciences)：P-PS Planetary Sciences

[P-PS08] Mars and Mars system: results from a broad spectrum of Mars studies and aspects for future missions

convener:Hideaki Miyamoto(University of Tokyo), Tomohiro Usui(Japan Aerospace Exploration Agency), Yuki Harada(Kyoto University), Sushil K Atreya(University of Michigan Ann Arbor)

[PPS08-P01] Experimental study on thermal properties of high porosity particles for understanding physical properties of Phobos surface

*Amiko Takano[1], Naoya Sakatani[1], Hideaki Miyamoto[2], Tomohiro Usui[1], Takafumi Niihara[2], Bernadett Pál[3], Takahiro Iwata[1] (1.Japan Aerospace Exploration Agency, 2.University of Tokyo, 3.Hungarian Academy of Sciences)

[PPS08-P02] Near-infrared Hyperspectral Imager MacrOmega on MMX to Observe Martian System: Its Observation Plans and Development

*Takahiro Iwata[1], Hiromu Nakagawa[2], Tomoki Nakamura[2], Jean-Pierre Bibring [3], Cedric Pilorget [3], Vincent Hamm[3], Fuminori Tsuchiya[2], Lucie Riu[1], Moe Matsuoka[1], Hiroyuki Kurokawa[4] (1.Institute of Space and Astronautical Science, Japan Aerospace Exploration Agency, 2.Tohoku University, 3.Institut d'Astrophysique Spatiale, Université Paris-Sud, 4.Tokyo Institute of Technology)

[PPS08-P03] Shape modeling strategy for MMX

*Koji Matsumoto[1], Toru Kouyama[2], Naru Hirata[3], Hitoshi Ikeda[4], Hiroki Senshu[5] (1.RISE Project, National Astronomical Observatory of Japan, 2.National Institute of Advanced Industrial Science and Technology, 3.University of Aizu, 4.Japan Aerospace Exploration Agency, 5.Chiba Institute of Technology)

[PPS08-P04] Restoration of highest-resolution images of Phobos observed by the High-Resolution Stereo Camera (HRSC) onboard Mars Express

*Ryodo Hemmi[1], Hiroshi Kikuchi[2] (1.The Universit Museum, The University of Tokyo, 2.Institute of Space and Astronautical Science, Japan Aerospace Exploration Agency)

[PPS08-P05] Re-impacts from the craters residing at the deepest location generating the blue units on Phobos

*Hiroshi Kikuchi[1] (1.Japan Aerospace Exploration Agency)

[PPS08-P06] Mars and Earth - distinct inner Solar System products

*Takashi Yoshizaki[1], William F McDonough[1,2] (1.Tohoku University, 2.University of Maryland, College Park)

[PPS08-P07] Examination of the similarity between crack patterns due to dry fracture on the ground and heat-shrink polygons on Mars

*Chihiro Uemura[1], Takahiro Iwata[1,2], Akio Nakahara[3], Tomohiro Usui[2], Yosuke Matsuo[3], Rina Noguchi[2] (1.SOKENDAI, 2.ISAS/JAXA, 3.Nihion Univ.)

[PPS08-P08] Search of shallow subsurface reflectors in Chryse and Acidalia Planitiae on Mars

*Aina Oura[1], Yasumasa Kasaba[1], Atsushi Kumamoto[1], Rina Noguchi[2], Ken Ishiyama[3], Fuminori Tsuchiya[1], Tomohiro Usui[2], Chihiro Uemura[4] (1.Tohoku University, 2.ISAS/JAXA, 3.National Institute of Technology, Tsuruoka College, 4.Sokendai)

[PPS08-P09] Development of subsurface radar for future Mars, the Moon, and asteroid explorations

*Atsushi Kumamoto[1], Hideaki Miyamoto[2], Toshiyuki Nishibori[3], Fuminori Tsuchiya[1], Ken Ishiyama[4] (1.Department of Geophysics, Graduate School of Science, Tohoku University, 2.University of Tokyo, 3.JAXA, 4.Tsuruoka College, National Institute of Technology)

[PPS08-P10] Increase in trivalent iron elution amount and iron compounds from fayalite by ultraviolet C

*Nobuo Komori[1] (1.The United Graduate School of Education Tokyo Gakugei University)

[PPS08-P11] Introduction of the highest resolution image to the Mars Web-GIS “RedAce ” to study the local and detailed surface environment

*Hiroshi Sakai[1], Hayashi Yohei[2], Hironori Fukuchi[1], Yuya Matsubara[3], Yoshiko Ogawa[1] (1.The University of Aizu, 2.National Observatory of Japan, 3.The University of Aizu(Now NTTDocomo Inc.))

[PPS08-P12] **Estimation of dust optical depth observed by MGS/TES from visible images observed by MGS/MOC using a convolutional neural network**

*Karin miyabe[1], Kazunori Ogohara[1] (1.Graduate school of the University of Shiga Prefecture)

[PPS08-P13] Survey of dayside reconnection signatures at Mars with MAVEN

*Yuki Harada[1], Jasper S. Halekas[2], Gina A. DiBraccio[3], Shaosui Xu[4], Suranga Ruhunusiri[2], Takuya Hara[4], Jared Espley[3], James P McFadden[4], David L Mitchell[4], Christian Mazelle[5] (1.Graduate School of Science, Kyoto University, 2.Department of Physics and Astronomy, University of Iowa, 3.NASA Goddard Space Flight Center, 4.Space Sciences Laboratory, University of California, Berkeley, 5.IRAP, University of Toulouse, CNRS, UPS, CNES)

[PPS08-P14] **Seasonal variation of neutral and ion compositions in the Martian upper atmosphere observed by MAVEN/NGIMS**

*Nao Yoshida[1], Naoki Terada[1], Hiromu Nakagawa[1], Dave A Brain[2] (1.Dep. Geophysics Graduate School of Science Tohoku University, 2.LASP, University of Colorado)

[E] Poster | P (Space and Planetary Sciences)：P-EM Solar-Terrestrial Sciences, Space Electromagnetism & Space Environment

[P-EM11] Heliosphere and Interplanetary Space

convener:Kazumasa Iwai(Institute for Space–Earth Environmental Research (ISEE), Nagoya University), Yasuhiro Nariyuki(Faculty of Education, University of Toyama), Ken Tsubouchi(University of Electro-Communications), Masaki N(Japan Aerospace Exploration Agency, Institute of Space and Astronautical Science)

[PEM11-P01] Measurement of solar wind density distribution using dispersion measures of Crab pulsar

*Maeda Ryuya[1], Munetoshi Tokumaru[1], Kaito Tawara[1], Toshio Terasawa[2], Kazuhiro Takafuji[3] (1.Institute for Space-Earth Environmental Research, Nagoya University, 2.Inter-University Research Institute Corporation, National Institutes of Natural Sciences, National Astronomical Observatory of Japan, 3.Japan Aerospace Exploration Agency)

[PEM11-P02] Occurrence dependence on solar activity cycle for type III radio bursts based on the automatic detection analyses

*Yuichiro Seki[1], Hiroaki Misawa[1], Fuminori Tsuchiya[1], Takahiro Obara[1], Tatsuya Fujimoto[1] (1.Tohoku University)

[PEM11-P03] The characteristics of type III solar radio bursts in ^{3}He-rich impulsive solar energetic particle phenomena

*Tatsuya Fujimoto[1], Hiroaki Misawa[1], Fuminori Tsuchiya[1], Takahiro Obara[1] (1.Tohoku University)

[PEM11-P04] Relationship between solar energetic particles and spectral fine structures of metric type II radio bursts

*Hiroaki Misawa[1], Fuminori Tsuchiya[1], Takahiro Obara[1], Tatsuya Fujimoto[1] (1.Planetary Plasma and Atmospheric Research Center, Graduate School of Science, Tohoku University)

[PEM11-P05] Spectral Structures of Type II Solar Radio Bursts and Solar Energetic Particles

*Kazumasa Iwai[1], Seiji Yashiro[2], Nariaki Nitta[3], Yuki Kubo[4] (1.Institute for Space–Earth Environmental Research (ISEE), Nagoya University, 2.The Catholic University of America/NASA GSFC, 3.Lockheed Martin Advanced Technology Center, 4.National Institute of Information and Communications Technology)

[PEM11-P06] Stellar flare of a close binary system during the NICER-Hisaki Observing Campaign 2018-2019

*Tomoki Kimura[1], Wataru Iwakiri[2], Atsushi Yamazaki[3], Go Murakami[3], Fuminori Tsuchiya[4], Kazuo Yoshioka[5], Hajime Kita[3], Masaki Kuwabara[3], Shin Toriumi[3] (1.Frontier Research Institute for Interdisciplinary Sciences, Tohoku University, Sendai, Japan, 2.Faculty of Science and Engineering, Chuo University, Tokyo, Japan, 3.Institute of Space and Astronautical Science, Japan Aerospace Exploration Agency, Sagamihara, Japan, 4.Planetary Plasma and Atmospheric Research Center, Tohoku University, Sendai, Japan, 5.Department of Complexity Science and Engineering, University of Tokyo, Kashiwa, Japan)

[PEM11-P07] 5-season's optical observations of neutral helium distribution in interplanetary space by Hisaki

*Atsushi Yamazaki[1], Go Murakami[1], Kazuo Yoshioka[2], Tomoki Kimura[3], Fuminori Tsuchiya[4], Masato Kagitani[4], Takeshi Sakanoi[4], Naoki Terada[5], Yasumasa Kasaba[6], Ichiro Yoshikawa[7] (1.Institute of Space and Astronautical Science / Japan Aerospace Exploration Agency, 2.Graduate School of frontier Science, The University of Tokyo, 3.Tohoku University, 4.Planetary Plasma and Atmospheric Research Center, Graduate School of Science, Tohoku University, 5.Graduate School of Science, Tohoku University, 6.Planetary Plasma and Atmospheric Research Center, Tohoku University, 7.The University of Tokyo)

[PEM11-P08] **Group movement by magnetic coupling of high-speed protons running side by side in the chromosphere of the Sun**

*Shinji Karasawa[1] (1.Miyagi National College of Technology Professor emeritus)

[E] Poster | P (Space and Planetary Sciences)：P-EM Solar-Terrestrial Sciences, Space Electromagnetism & Space Environment

[P-EM12] Coupling Processes in the Atmosphere-Ionosphere System

convener:Huixin Liu(Earth and Planetary Science Division, Kyushu University SERC, Kyushu University), Yuichi Otsuka(Institute for Space-Earth Environmental Research, Nagoya University), Yue Deng(University of Texas at Arlington), Loren Chang(Institute of Space Science, National Central University)

[PEM12-P01] LOW IONOSPHERE AS A SOURCE OF REMOTE SENSING

*ALEXEI DMITRIEV[1,2], S.O. Adamson[3], A.A. Berlin[4], Y.A. Dyakov[5], L.V. Eppelbaum[6], G.V. Golubkov[3,5], A.A. Lushnikov[6], M.I. Manzhelii[7], M.G. Golubkov[3] (1.Institute of Space Science and Engineering, National Central University, Jungli City, Taiwan, 2.Skobeltsyn Institute of Nuclear Physics, Lomonosov Moscow State University, Moscow, Russia, 3.Semenov Federal Research Center for Chemical Physics, Russian Academy of Sciences, Moscow 119991, Russian Federation , 4.Department of Earth Sciences, Tel Aviv University, Tel Aviv 69978, Israel, 5.National Research Center “Kurchatov Institute”, Moscow 123182, Russian Federation, 6.Geophysical Center, Russian Academy of Sciences, Moscow 119296, Russian Federation, 7.Center for Chemical Physics of Atmosphere, Moscow 119991, Russian Federation)

[PEM12-P02] Relationship between Na layer and CNA variations observed over Syowa, Antarctic

*Takuo T. Tsuda[1], Ryo Tozu[1], Kyogo Takizawa[1], Yoshimasa Tanaka[2], Takuya Kawahara[3], Mitsumu K. Ejiri[2], Takanori Nishiyama[2], Takuji Nakamura[2] (1.University of Electro-Communications, 2.National Institute of Polar Research, 3.Shinshu University)

[PEM12-P03] Occurrence feature of plasma bubble observed in mid-latitudes during geomagnetic storms using GNSS-TEC data

*Sori Takuya[1], Yuichi Otsuka[1], Atsuki Shinbori[1], Takuya Tsugawa[2], Michi Nishioka[2] (1.Institute for Space-Earth Environmental Research, Nagoya University, 2.National Institute of Information and Communications Technology)

[PEM12-P04] Three-dimensional ionospheric simulation of the Es layer: Physical mechanism of the sporadic appearance

*Satoshi Andoh[1], Akinori Saito[1], Hiroyuki Shinagawa[2], Mitsumu K. Ejiri[3], Shinichi Miyazaki[1] (1.Graduate School of Science, Kyoto University, 2.National Institute of Information and Communications Technology, 3.National Institute of Polar Research)

[PEM12-P05] Time and height variability of Fe-layer in the Mesosphere and the Lower Thermosphere region at Syowa Station, Antarctica (69.0°S, 39.6°E) based on a resonance scattering lidar measurements in two winter seasons

*Takanori Nishiyama[1,2], Mitsumu K. Ejiri[1,2], Takuo T. Tsuda[3], Katsuhiko Tsuno[4], Toru Takahashi[5], Makoto Abo[6], Takuya Kawahara[7], Takayo Ogawa[4], Satoshi Wada[4], Takuji Nakamura[1,2] (1.National Institute of Polar Research, 2.The Graduate University for Advanced Studies, SOKENDAI, 3.The University of Electro- Communications, 4.RIKEN, 5.University of Oslo, 6.Tokyo Metropolitan University, 7.Shinshu University)

[PEM12-P06] Analysis of VLF Band Waves near the Sq Current System observed by S-310-44 Sounding Rocket

*Taketoshi Miyake[1], Ryuichiro Nakamura[1], Keigo Ishisaka[1], Takumi Abe[2], Atsushi Kumamoto[3], Makoto Tanaka[4] (1.Department of Electrical and Computer Engineering, Faculty of Engineering, Toyama Prefectural University, 2.Japan Aerospace Exploration Agency Institute of Space and Astronautical Science Department of Solar System Sciences, 3.Department of Geophysics, Graduate School of Science, Tohoku University, 4.Tokai University, ICT Education Center)

[PEM12-P07] Monte Carlo simulation of solar EUV scattering by oxygen ions

*Shin ya Nakano[1], Yuta Hozumi[2], Akinori Saito[3] (1.The Institute of Statistical Mathematics, 2.University of Electro-Communications, 3.Department of Geophysics, Graduate School of Science, Kyoto University)

[PEM12-P08] Automatic detection of Spread-F on ionogram using Machine Learning

*Shimizu Junji[1], Hiroyuki Nakata[1], Hiroyo Ohya[1], Toshiaki Takano (1.Graduate School of Engineering, Chiba University)

[PEM12-P09] Examination of the ionospheric perturbations propagation associated with H-IIA rocket launchings

*Junpei Yamazaki[1], Hiroyuki Nakata[2], Hiroyo Ohya[2], Toshiaki Takano[2], Keisuke Hosokawa[3] (1.Graduate School of Science and Engineering, Chiba University, 2.Graduate School of Engineering, Chiba University, 3.Department of

Communication Engineering and Information, University of Electro-Communications)

[PEM12-P10] Spatial and temporal distributions of atmospheric gravity wave potential energy evaluated using ERA-5 temperature data over the equatorial latitudes

*Shih-Sian Yang[1], Chen-Jeih Pan[1], Uma Das[2], Chian-Chiau Lin[3] (1.National Central University, Jhongli, Taoyuan 32001, Taiwan, 2.Department of Physics, Indian Institute of Information Technology, India, 3.Environmental Research and Information Center, Chang Jung Christian University, Taiwan)

[PEM12-P11] Atmospheric wave propagation observed by GNSS-TEC: Fireball explosion and atmospheric mode

*Ai Matsushita[1], Kosuke Heki[1] (1.Hokkaido University Graduate School of Science)

[PEM12-P12] Investigation of the climatology and long-term variations of the stratospheric Kelvin waves using ERA-Interim

*Chen-Jeih Pan[1], Shih-Sian Yang[1], Uma Das[2], Wei-Sheng Chen[1] (1.Institute of Space Science, National Central University, Taiwan, 2.Department of Physics, Indian Institute of Information Technology, India)

[PEM12-P13] **Statistical study of seasonal dependence of MSTID occurrence and propagation velocity using the SuperDARN Hokkaido East HF radar**

*Wataru Hazeyama[1], Nozomu Nishitani[1], Tomoaki Hori[1] (1.Institute for Space-Earth Environmental Reseach)

[PEM12-P14] First simultaneous observation of nighttime medium-scale traveling ionospheric disturbance (MSTID) by a ground airglow imager and the Arase satellite in the inner magnetosphere

*Kouki Kawai[1], Kazuo Shiokawa[1], Yuichi Otsuka[1], Yoshiya Kasahara[2], Fuminori Tsuchiya[3], Ayako Matsuoka[4], Yasumasa Kasaba[3], Kazushi Asamura[4], Satoshi Kasahara[6], Yoshizumi Miyoshi[1], Shin-ichiro Oyama[1,7,8], Yoichi Kazama[5] (1.Institute for Space-Earth Environmental Research, Nagoya Univ, Japan, 2.Kanazawa Univ, Japan, 3.Tohoku Univ, Japan, 4.Japan Aerospace Exploration Agency, 5.Academia Sinica, 6.Tokyo Univ, Japan, 7.Oulu Univ, Finland, 8.National Institute od polar Research)

[PEM12-P15] Study of variations in the D-region ionosphere after the 2016 Kumamoto earthquakes using VLF/LF transmitter signals

*Tekkan Akashi[1], Hiroyo Ohya[2], Hiroyuki Nakata[2], Fuminori Tsuchiya[3] (1.Graduate School of Science and Engineering, Chiba University, 2.Graduate School of Engineering, Chiba University, 3.Graduate School of Science, Tohoku University)

[PEM12-P16] Analysis of source and generation mechanism of atmospheric gravity waves and MSITDs observed in airglow images in Hawaii

*Hideto Naito[1], Kazuo Shiokawa[1], Yuichi Otsuka[1], Takeshi Sakanoi[2], Akinori Saito[3], Takuji Nakamura[4] (1.Nagoya University, 2.Tohoku University, 3.Kyoto University, 4.National Institute of Polar Research)

[PEM12-P17] Solar flare effects of the D-region ionosphere using daytime tweek atmospherics and VLF/LF standard radio waves

*Kodai Yamanobe[1], Hiroyo Ohya[1], Hiroyuki Nakata[1], Kazuo Shiokawa[2], Fuminori Tsuchiya[3], Kozo Yamashita[4], Yukihiro Takahashi[5] (1.Chiba Univ., 2.Nagoya Univ., 3.Tohoku Univ., 4.Ashikaga Univ., 5.Hokkaido Univ.)

[PEM12-P18] **The spatial structures and seasonal variations of the polar mesospheric clouds seen from the meteorological satellite Himawari-8**

*Yuta Hozumi[1], Takuo T. Tsuda[1], Kento Kawaura[1], Yoshiaki Ando[1], Keisuke Hosokawa[1], Hidehiko Suzuki[2], Takuji Nakamura[3], Ken T. Murata[4] (1.University of Electro-Communications, 2.Meiji University, 3.National Institute of Polar Research, 4.National Institute of Information and Communications Technology)

[PEM12-P19] Fireball-associated variations in the D-region ionosphere observed using VLF/LF transmitter signals

*Takeru Suzuki[1], Hiroyo Ohya[2], Fuminori Tsuchiya[3], Kazuo Shiokawa[4], Hiroyuki Nakata[2] (1.Graduate School of Science and Engineering, Chiba University, 2.Graduate School of Engineering, Chiba University, 3.Graduate School of Science, Tohoku University, 4.Institute for Space-Earth Environmental Research, Nagoya University)

[PEM12-P20] Calcium ion layer observed with resonance scattering lidar at Syowa Station

*Mitsumu K. Ejiri[1,2], Takanori Nishiyama[1,2], Takuo T. Tsuda[3], Makoto Abo[4], Katsuhiko Tsuno[5], Takuya Kawahara[6], Takayo Ogawa[5], Satoshi Wada[5], Takuji Nakamura[1,2] (1.National Institute of Polar Research, 2.The Graduate

University for Advanced Studies, SOKENDAI, 3.The University of Electro-Communications, 4.Tokyo Metropolitan University, 5.RIKEN, RAP, 6.Shinshu University Faculty of Engineering)

[PEM12-P21] **Generation and movement of equatorial plasma bubbles: Roles of vertical plasma drifts, seeding perturbations, and geomagnetic storms**

*Chaosong Huang[1] (1.Air Force Research Laboratory Albuquerque)

[PEM12-P22] Variations of the Earth's magnetic field during fall of the Tunguska and Chelyabinsk bolides: analogies and differences

*Ravil Rakhmatulin[1] (1.Institute of Solar-Terrestrial Physics, SB RAS)

[PEM12-P23] Atmospheric-ionospheric vertical coupling study focusing on the quasi-6-day oscillation in Sq-EEJ current system

*Takayama Kumi[1], Yasunobu Miyoshi[1], Akimasa Yoshikawa[1] (1.Kyushu University)

[PEM12-P24] Investigating of cusp heating process by using chemical releases of Ba/Sr: Initial result of CHI rocket experiment

*Taro Watanabe[1], Yoshihiro Kakinami[2], Masa-yuki Yamamoto[1], Miguel Larsen[3], Mark Conde[4], Takao M. Sato[2], Yuuichi Kaga[2], Takako Kaga[2] (1.Kochi University of Technology, 2.Hokkaido Information University, 3.Clemson University, 4.University of Alaska Fairbanks)

[PEM12-P25] Characterization of counter electrojet current according to specific time frame in Southeast Asian sector

*Nur Izzati Mohd Rosli[1], Nurul Shazana Abdul Hamid[1], Mardina Abdullah[1], Akimasa Yoshikawa[2], Teiji Uozumi[2] (1.Universiti Kebangsaan Malaysia, 2.Kyushu University)

[PEM12-P26] Characterizing ionospheric irregularities with GEONET

*Guanyi Ma[1], Qi Li[1], Takashi Maruyama[2,1], Jinghua Li[1], Qingtao Wan[1], Xiaolan Wang[1], Jiangtao Fan[1], Jie Zhang[1] (1.National Astronomical Observatories, Chinese Academy of Sciences, 2.National Institute of Information and Communications Technology)

[PEM12-P27] Imaging observation of Ionospheric Field Aligned Irregularities by the PANSY radar at Antarctic Syowa Station

*Daisuke Kagawa[1], Taishi Hashimoto[2], Akinori Saito[1], Koji Nishimura[2], Masaki Tsutsumi[2], Toru Sato[3], Kaoru Sato[4] (1.Graduate School of Science, Kyoto University, 2.National Institute of Polar Research, 3.Graduate School of Informatics, Kyoto University, 4.Graduate School of Science, Tokyo University)

[PEM12-P28] Vertical profile of ionospheric disturbances associated with Tohoku Earthquake using GPS occultation observation

*Hiroyuki Nakata[1], Yuto Imae[2], Toshiaki Takano[1], Hiroyo Ohya[1] (1.Graduate School of Engineering, Chiba University, 2.Department of Electrical and Electronics Engineering, Faculty of Engineering, Chiba University)

[PEM12-P29] **Statistical study of the growth rates of medium-scale traveling ionospheric disturbances observed with GNSS-TEC**

*Takafumi Ikeda[1], Akinori Saito[1], Takuya Tsugawa[2] (1.Department of Geophysics, Graduate School of Science, Kyoto University, 2.National Institute of Information and Communications Technology)

[PEM12-P30] Retrieval of the Mesosphere and Lower Thermosphere (MLT) physical and chemical properties with the proposed Superconducting Submillimeter-Wave Limb-Emission Sounder 2 (SMILES-2)

*Philippe Baron[1], Satoshi Ochiai[1], Hideo Sagawa[2], Akinori Saito[3], Takatoshi Sakazaki[3], Masato Shiotani[3], Makoto Suzuki[4] (1.National Institute of Information and Communications Technology, 2.Kyoto Sangyo University, 3.Kyoto University, 4.Japan Aerospace Exploration Agency)

[PEM12-P31] Formation of a Ring-Like Region of Increased Electron Temperature in the Subauroral Ionosphere in Winter

Innokentiy Alexeevich Golikov[1], Artem Yurevich Gololobov[2], *Ilia Ilyich Varlamov[1,2] (1.Yu.G.Shafer Institute of Cosmophysical Research and Aeronomy (IKFIA), Siberian Branch of the Russian Academy of Sciences, 2.M. K. Ammosov Northeastern Federal University (NEFU),)

[PEM12-P32] Magnetic Field Measurement in the Ionosphere by using 2U-size CubeSat

*Kentarou Kitamura[1], Kazumasa Imai[2], Taku Takada[2], Manabu Shinohara[3], Makoto Wakabayashi[4], Masahiro Tokumitsu[5] (1.NIT, Tokuyama College, 2.NIT, Kochi College, 3.NIT, Kagoshima College, 4.NIT, Niihama College, 5.NIT, Yonago College)

[PEM12-P33] Observations of night time Sporadic-E layer by HF Doppler sounder network: association with Medium-Scale Traveling Ionospheric Disturbance (MSTID)

*Ryo Matsushima [1], Keisuke Hosokawa[1], Jun Sakai[1], Mitsumu K Ejiri[2], Michi Nishioka[3], Takuya Tsugawa[3] (1.The University of Electro-Communications, 2.National Institute of Polar Research, 3.National Institute of Information and Communications Technology)

[PEM12-P34] SMILES-2, satellite mission for observation of the stratosphere, mesosphere, and lower thermosphere with THz receivers

*Satoshi Ochiai[1], Philippe Baron[1], Yoshihisa Irimajiri[1], Akira Kawakami[1], Toshiyuki Nishibori[2], Makoto Suzuki[2], Yoshinori Uzawa[3], Yasunori Fujii[3], Hiroyuki Maezawa[4], Akinori Saito[5], Takatoshi Sakazaki[5], Masato Shiotani[5] (1.National Institute of Information and Communications Technology, 2.Japan Aerospace Exploration Agency, 3.National Astronomical Observatory of Japan, 4.Osaka Prefecture University, 5.Kyoto University)

[PEM12-P37] Numerical study of the internal mesh structure for ion drift velocity analyzer on sounding rocket

*Ryuto Hashiba[1], Takumi Abe[2] (1.Graduate School of Science, Hokkaido University, 2.Institute of Space and Astronautical Science, Japan Aerospace Exploration Agency)

[PEM12-P38] **Using a Software Defined Radio to Receive the FORMOSAT-7 RF Beacon and Derive the Total Electron Content**

*Tsai-Ju Yu[1], Loren C. Chang[1], Jann-Yenq Liu[1], Tung-Yuan Hsiao[2] (1.Graduate Institute of Space Science and Engineering, National Central University, Taoyuan City, Taiwan, 2.Accelerator Laboratory, Nuclear Science and Technology Development Center, National Tsing Hua University, Hsinchu, Taiwan)

[PEM12-P39] Neutral and ion dynamics seen in GAIA with variable high-latitude input

*Chihiro Tao[1], Hidekatsu Jin[1], Hiroyuki Shinagawa[1], Yasunobu Miyoshi[2], Hitoshi Fujiwara[3] (1.National Institute of Information and Communications Technology, 2.Department of Earth and Planetary Sciences, Kyushu University, 3.Faculty of Science and Technology, Seikei University)

[PEM12-P41] Time-dependent responses of the neutral mass density to magnetospheric energy inputs into the cusp region in the thermosphere

*Tomokazu Oigawa[1], Hiroyuki Shinagawa[2], Satoshi Taguchi[1] (1.Department of Geophysics, Graduate School of Science, Kyoto University, 2.National Institute of Information and Communications Technology)

[PEM12-P42] 2-dimentional FDTD simulation about spatial structure change of sporadic E layer

*takuto tawaki[1], Taketoshi Miyake[1] (1.Toyama prefectural university)

[PEM12-P43] **Atmospheric density variations observed by GOCE**

*Nakayama Sayuka [1], Liu Huixin[1] (1.Earth and planetary science division,Kyushu university,Japan)

[PEM12-P44] revision and data assimilation of a whole atmosphere-ionoshere model GAIA

*Hidekatsu Jin[1], Yasunobu Miyoshi[2], Chihiro Tao[1], Hiroyuki Shinagawa[1], Hitoshi Fujiwara[3] (1.National Institude of Information and Communications Technology, 2.Kyushu university, 3.Seikei university)

[PEM12-P45] Overview of Vertical Incidence Pulsed Ionospheric Radar 2 (VIPIR2) observation in Japan

*Michi Nishioka[1], Hideo MAENO[1], Hiroyuki YAMAKAWA[1], Takumi Kondo[1], Takuya Tsugawa[1], Mamoru Ishii[1] (1.National Institute of Information and Communications Technology)

[E] Poster | P (Space and Planetary Sciences)：P-EM Solar-Terrestrial Sciences, Space Electromagnetism & Space Environment

[P-EM13] Dynamics of Magnetosphere and Ionosphere

convener:Aoi Nakamizo(Applied Electromagnetic Research Institute, National Institute of Information and Communications Technology), Mitsunori Ozaki(Faculty of Electrical and Computer Engineering, Institute of Science and Engineering, Kanazawa University), Akiko Fujimoto(Kyushu Institute of Technology), Yuka Sato(Nippon Institute of Technology)

[PEM13-P01] Overview of electron number density and plasma wave observations by SS-520-3 NEI/PWM

*Atsushi Kumamoto[1], Yuto Katoh[1], Hirotsugu Kojima[2], Keigo Ishisaka[3] (1.Department of Geophysics, Graduate School of Science, Tohoku University, 2.Research Institute for Sustainable Humanosphere, Kyoto University, 3.Toyama Prefectural University)

[PEM13-P02] Geomagnetic N+/O+ variation in the Ring Current Observed by the Arase (ERG) Satellite

*Koichiro Tsuda[1], Shoichiro Yokota[1], Satoshi Kasahara[2], Kunihiro Keika[3], Tomoaki Hori[4], Yoshizumi Miyoshi[4], Iku Shinohara[5], Kentaro Terada[1] (1.Department of Earth and Space Science, Graduate School of Science, Osaka University, 2.The University of Tokyo, 3.Department of Earth and Planetary science, Guraduate School of Science, The University of Tokyo, 4.Institute for Space-Earth Environment Research, Nagoya University, 5.Japan Aerospace Exploration Agency/Institute of Space and Astronautical Science)

[PEM13-P03] Precipitation Loss of Radiation Belt Electrons by Two-band Plasmaspheric Hiss Waves

*Zhaoguo He[1] (1.Sun Yat-sen University)

[PEM13-P04] On the possible scenario of MeV electrons at the plasma sheet boundary

*Iku Shinohara[1], Nagai Tsugunobu[1], Takefumi Mitani[1], Nana Higashio[2], Satoshi Kasahara[3], Yoichi Kazama[4], Shiang-Yu Wang[4], Sunny Tam[5], Ayako Matsuoka[1], Kazushi Asamura[1], Shoichiro Yokota[6], Takeshi Takashima[1], Yoshizumi Miyoshi[7] (1.Japan Aerospace Exploration Agency/Institute of Space and Astronautical Science, 2.Japan Aerospace Exploration Agency, 3.University of Tokyo, 4.ASIAA, 5.NCKU, 6.Osaka University, 7.Nagoya University/Institute for Space-Earth Environmental Research)

[PEM13-P05] PARM-HEP Observation of Microburst Precipitation over Pulsating Aurora

*Taku Namekawa[1,2], Takefumi Mitani[1], Kazushi Asamura[1], Yoshizumi Miyoshi[3], Keisuke Hosokawa[4], Yasunobu Ogawa[5], Shinji Saito[6], Yoshifumi Saito[1] (1.Japan Aerospace Exploration Agency, 2.The University of Tokyo, 3.Nagoya University, 4.The University of Electro-Communications, 5.National Institute of Polar Research, 6.National Institute of Information and Communications Technology)

[PEM13-P06] Plasma waves causing 20 Hz intensity modulation of pulsating aurora

*Herbert Akihito Uchida[1], Ryuho Kataoka[2,1], Kiyoka Murase[1], Shoya Matsuda[3], Yoshiya Kasahara[4], Masafumi Shoji[5], Yoshizumi Miyoshi[5], Iku Shinohara[3], Ayako Matsuoka[3], Satoshi Kurita[5], Keisuke Hosokawa[6] (1.The Graduate University for Advanced Studies, 2.National Institute of Polar Research, 3.Institute of Space and Astronautical Science, 4.Kanazawa University, 5.Institute for Space–Earth Environmental Research, 6.The University of Electro-Communications)

[PEM13-P07] Relationship between ECH waves, ionospheric F-region ionization and pulsating aurora based on ground-based optical, EISCAT and Arase satellite observations

*Mizuki Fukizawa[1], Takeshi Sakanoi[1], Yasunobu Ogawa[2], Keisuke Hosokawa[3], Yoshiya Kasahara[4], Shoya Matsuda[5], Ayako Matsuoka[6] (1.Planetary Plasma and Atmospheric Research Center, Graduate School of Science, Tohoku University, 2.National Institute of Polar Research, 3.Department of Communication Engineering and Informatics, University of Electro-Communications, 4.Information Media Center, Kanazawa University, 5.Institute of Space and Astronautical Science/Japan Aerospace Exploration Agency, 6.Research Division for Space Plasma, Institute of Space and Astronautical Science, Japan Aerospace Exploration Agency)

[PEM13-P09] Simultaneous ground-satellite observation of dayside pulsating aurora

*Shumpei Abe[1], Keisuke Hosokawa[1], Yasunobu Ogawa[2] (1.The University of Electro-Communications, 2.National Institute of Polar Research)

[PEM13-P10] Characteristics of periodicity of the dayside pulsating aurora and its response to solar wind obtained by multi-wavelength all-sky cameras at South Pole Station

*Miki Kawamura[1], Takeshi Sakanoi[1], Mizuki Fukizawa[1], Naoshi Yagi[1], Yusuke Ebihara[2], Tetsuo Motoba[3], Akira Kadokura[4], Yasunobu Ogawa[4] (1.Tohoku University, 2.Research Institute for Sustainable Humanosphere, Kyouto

University, 3.Nagoya University, 4.National Institute of Polar Research)

[PEM13-P11] Latitudinal distributions of magnetic variations in the near-earth magnetosphere during substorm

*Shun Imajo[1], Masahito Nose[1], Mari Aida[2], Nana Higashio[2], Haruhisa Matsumoto[2], Kiyokazu Koga[2], Akimasa Yoshikawa[3], Yoshizumi Miyoshi[1] (1.Institute for Space-Earth Environmental Research, Nagoya University, 2.Japan Aerospace eXploration Agency, 3.ICSWSE, Kyushu University)

[PEM13-P12] If Pi2 is onset indicator of substorms, what triggers Pi2s?

*Osuke Saka[1] (1.Office Geophysik)

[PEM13-P13] Time evolution of aurora structures associated with inverted-V electron distributions

*Morio Tanaka[1], Satoshi Taguchi[1], Keisuke Hosokawa[2] (1.Department of Geophysics, Graduate school of science, Kyoto University, 2.Department of Communication Engineering and Informatics, University of Electro-Communications)

[PEM13-P14] Automatic Classification of Auroral videos based on 3D-CNN

*Toru Mikuriya[1], Akiko Fujimoto[1], Yoshizumi Miyoshi[2], Yasunobu Ogawa[3], Keisuke Hosokawa[4] (1.Kyushu Institute of Technology, 2.Nagoya University, 3.National Institute of Polar Research, 4.The University of Electro-Communications)

[PEM13-P15] Spectral investigations on short-wavelength infrared aurora and airglow (0.9-1.6 μm): Ground-based observations in the both polar regions and developments of 2-D imaging spectrograph with high resolutions

*Takanori Nishiyama[1,2], Makoto Taguchi[3], Masato Kagitani[4], Yasunobu Ogawa[1,2], Hidehiko Suzuki[5], Takeshi Sakanoi[4], Fuminori Tsuchiya[4], Peter Dalin[6], Urban Brändström[6] (1.National Institute of Polar Research, 2.The Graduate University for Advanced Studies, SOKENDAI, 3.Rikkyo University, 4.Tohoku University, 5.Meiji University, 6.Swedish Institute of Space Physics)

[PEM13-P16] “Great Wall” seen in the omega band: full-color digital camera observation from the International Space Station

*Sota Nanjo[1], Natsuo Sato[2], Yuta Hozumi[1], Keisuke Hosokawa[1], Ryuho Kataoka[2,3], Yoshizumi Miyoshi[4], Shin-ichiro Oyama[2,4,5], Mitsunori Ozaki[6], Kazuo Shiokawa[4], Satoshi Kurita[4] (1.The University of Electro-Communications, 2.National Institute of Polar Research, 3.Department of Polar Science, School of Multidisciplinary Sciences, SOKENDAI, The Graduate University for Advanced Studies, 4.Institute for Space-Earth Environmental Research, Nagoya University, 5.Ionospheric Physics Research Unit, University of Oulu, 6.Graduate School of Natural Science and Technology, Kanazawa University)

[PEM13-P17] A tool to diagnose magnetosphere under northward IMF conditions: Simultaneous detections of TPA and omega-band aurora

*Motoharu Nowada[1] (1.Shandong Provincial Key Laboratory of Optical Astronomy and Solar-Terrestrial Environment, Institute of Space Sciences, Shandong University, Weihai)

[PEM13-P18] Transient and localized field-aligned current in the cusp region associated with the Sudden Commencement

*Shigeru Fujita[1] (1.Meteorological College, Japan Meteorological Agency/ Nationa Institute of Polar Research)

[PEM13-P19] Existence of the Region1 field-aligned current system for zero interplanetary magnetic field

*Tsubasa Hashimoto[1], Masakazu Watanabe[2], Ryuho Kataoka[3], Shigeru Fujita[4], Takashi Tanaka[5] (1.Department of Earth and Planetary Sciences, Graduate School of Science, Kyushu University, 2.Department of Earth and Planetary Sciences, Faculty of Science, Kyushu University, 3.National Institute of Polar Research, 4.Meteorological College, Japan Meteorological Agency/ National Institute of Polar Research, 5.International Center for Space Weather Science and Education)

[PEM13-P20] A Modified Magnetosphere-Ionosphere Coupling Model by Including the Hall Effects due to Thinning of the Near-Earth Plasma Sheet

*Pai-Sheng Wang[1], Ling-Hsiao Lyu[1] (1.Institute of Space Science and Engineering, National Central University, Taoyuan, Taiwan)

[PEM13-P21] **Alfvénic disturbances generated by the ionospheric polarization and the convection reversal in the magnetosphere**

*Aoi Nakamizo[1], Akimasa Yoshikawa[2], Shinichi Ohtani[3], Takashi Tanaka[2] (1.Applied Electromagnetic Research Institute, National Institute of Information and Communications Technology, 2.Faculty of Science, Kyushu University, 3.The Johns Hopkins University Applied Physics Laboratory)

[PEM13-P22] **Near-earth plasma environment and injection simulated by global magnetosphere model with precession of magnetic axis**

*Aoi Nakamizo[1], Yasubumi Kubota[1], Tsutomu Nagatsuma[1], Takashi Tanaka[2] (1.Applied Electromagnetic Research Institute, National Institute of Information and Communications Technology, 2.Faculty of Science, Kyushu University)

[PEM13-P23] Automatic identification of FLR events in VLOS data of multiple SuperDARN radars

*Hideaki Kawano[1,2], Akira Sessai Yukimatu[3,4], Nozomu Nishitani[5], Yoshimasa Tanaka[3,4], Satoko Saita[6], Tomoaki Hori[5] (1.Department of Earth and Planetary Sciences, Kyushu University, 2.ICSWSE, Kyushu University, 3.National Institute of Polar Research, 4.SOKENDAI, 5.ISEE, Nagoya University, 6.Kitakyushu College)

[PEM13-P24] Statistical study of SAPS occurrence characteristics using the SuperDARN HOkkaido Pair of (HOP) HF Radars

*Kento Oya[1], Nozomu Nishitani[1], Tomoaki Hori[1] (1.Institute for Space-Earth Environmental Research, Nagoya University)

[PEM13-P25] Ion precipitation in the cusp for stably northward IMF: Seasonal dependence

*Haruto Koike[1], Satoshi Taguchi[1] (1.Department of Geophysics, Graduate School of Science, Kyoto University)

[PEM13-P26] Hemispheric Asymmetry of the Vertical Ion Drifts at Dawn Observed by DMSP

*Mohan Liu[1], Xiao-Xin Zhang[1], Fei He[2], Wenbin Wang[3] (1.National Satellite Meteorological Center, 2.Institute of Geology and Geophysics, Chinese Academy of Sciences, 3.High Altitude Observatory, National Center for Atmospheric Research)

[PEM13-P28] Ground-based observations of MF/HF auroral radio emissions at three stations

*Yuka Sato[1,2], Atsushi Kumamoto[2], Yuto Katoh[2], Yasunobu Ogawa[3], Akira Kadokura[3], Atsuki Shinbori[4] (1.Nippon Institute of Technology, 2.Graduate school of Science, Tohoku University, 3.National Institute of Polar Research, 4.Institute for Space-Earth Environmental Research, Nagoya University)

[PEM13-P29] Application of Magneto-Impedance Sensor to Geomagnetic Field Measurements for Constructing Distributed Arrays of Small Instruments (DASI)

*Nomura Hiroshi[1], Masahito Nosé[1], Hitoshi Aoyama[2], Takeshi Kawano[2], Masafumi Hirahara[1] (1.Institute for Space-Earth Environmental Research, Nagoya University, 2.Aichi Steel Corporation)

[E] Poster | P (Space and Planetary Sciences)：P-EM Solar-Terrestrial Sciences, Space Electromagnetism & Space Environment

[P-EM14] Frontiers in solar physics

convener:Shinsuke Imada(Institute for Space-Earth Environmental Research, Nagoya University), Alphonse Sterling(NASA/MSFC), Takaaki Yokoyama(School of Science, University of Tokyo), Toshifumi Shimizu(Institute of Space and Astronautical Science, JAXA)

[PEM14-P01] Prediction of sunspot number and latitude distribution using machine learning

*Kento Michiwaki[1], Shinsuke Imada[1], Yoshizumi Miyoshi[1] (1.Institute for Space-Earth Environmental Research, Nagoya University)

[PEM14-P02] Image analysis of sunspot drawings in Dalton minimum(the early 1800s) and reproduction of magnetograms from sunspot drawings by using machine learning.

*SHOMA UNEME[1], Shinsuke Imada[1], Hisashi hayakawa[2], Lee Harim[3], Moon Yongjae[3], Park Eunsu[3], Yoshizumi Miyoshi[1] (1.nagoya university institutive for Space Earth for enviornmental research, 2.Osaka University School of Letters , 3.School of Space Research, Kyung Hee University)

[PEM14-P03] Solar surface flow around the cycle 24 minimum

*Kengo Matoba[1], Shinsuke Imada[1] (1.Institute for Space-Earth Environmental Research, Nagoya University)

[PEM14-P04] Impact of morphological asymmetry in a sunspot group on the solar cycle prediction

★Invited Papers

*Haruhisa Iijima[1], Hideyuki Hotta[2], Shinsuke Imada[1] (1.Institute for Space-Earth Environmental Research, Nagoya University, 2.Faculty of Science, Chiba University)

[PEM14-P05] Thermal non-equilibrium plasma during a solar flare

*Shinsuke Imada[1] (1.Institute for Space-Earth Environmental Research, Nagoya University)

[PEM14-P06] Hall MHD calculation of magnetic reconnection assuming coronal heating

*Kyohei Murakami[1], Shinsuke Imada[1], Haruhisa Iijima[1], Yoshizumi Miyoshi[1] (1.Nagoya University Institute for Space-Earth Environmental)

[PEM14-P07] Statistical investigation of magnetic and temperature properties of white-light flares

*Kyoko Watanabe[1], Kosuke Tsuruda[1], Satoshi Masuda[2], Sam Krucker[2,3,4] (1.National Defense Academy of Japan, 2.Institute for Space-Earth Environmental Research, Nagoya University, 3.University of Applied Sciences Northwestern Switzerland, 4.UC Berkeley)

[PEM14-P08] Validation of EUV dynamic spectra and their impact on the ionosphere

★Invited Papers

*Shohei Nishimoto[1], Kyoko Watanabe[1], Shinsuke Imada[2], Toshiki Kawai[2], Tomoko Kawate[3], Hidekatsu Jin[5], Kyoung-Sun Lee[4] (1.National Defense Academy, 2.Institune for Space-Earth Environmental Research, Nagoya University, 3.Institute of Space and Astronautical Science, Japan Aerospace Exploration Agency, 4.Center for Space Plasma and Aeronomic Research, University of Alabama in Huntsville, 5.National Institute of Information and Communications Technology)

[PEM14-P09] Recent and Upcoming Studies of Solar Coronal Jets

*Alphonse Sterling[1], Ronald Moore[2,1], Navdeep Panesar[3,4] (1.NASA/MSFC, 2.U of Alabama Huntsville, 3.LMSAL, 4.Baeri)

[PEM14-P11] Perspective of simulation studies for the Solar-C_EUVST science

*Takaaki Yokoyama[1], Shinsuke Imada[2], Haruhisa Iijima[2], Shin Toriumi[3] (1.School of Science, The University of Tokyo, 2.Institute for Space-Earth Environmental Research, Nagoya University, 3.Institute of Space and Aeronautical Science, JAXA)

[E] Poster | P (Space and Planetary Sciences)：P-EM Solar-Terrestrial Sciences, Space Electromagnetism & Space Environment

[P-EM15] Plasma Theory and Simulation

convener:Seiji Zenitani(Kobe University), Fan Guo(Los Alamos National Laboratory), Takayuki Umeda(Institute for Space-Earth Environmental Research, Nagoya University), Takanobu Amano(Department of Earth and Planetary Science, University of Tokyo), Yasuhiro Nariyuki(Faculty of Education, University of Toyama)

[PEM15-P01] Full particle-in-cell simulation of the interaction between two plasmas for laboratory experiments on the generation of magnetized collisionless shocks with high-power lasers

*Takayuki Umeda[1], Ryo Yamazaki[2], Yutaka Ohira[3] (1.Institute for Space-Earth Environmental Research, Nagoya University, 2.Aoyama Gakuin University, 3.The University of Tokyo)

[PEM15-P02] PIC simulation on non-linear development of lower hybrid waves instabilities driven by energetic ions with a ring-like velocity distribution: the comparison of initial value problems and energetic-ion injection models.

*Tsubasa Kotani[1], Mieko Toida[2], Toseo Moritaka[2], Satoshi Taguchi[1] (1.Department of Geophysics, Graduate School of Science, Kyoto University, 2.National Institute for Fusion Science)

[PEM15-P03] A comparison of relativistic particle integrators in a fast magnetized flow (2)

*Seiji Zenitani[1], Tsunehiko Kato[2] (1.Kobe University, 2.National Astronomical Observatory of Japan)

[PEM15-P04] Particle Simulation of Triggered Emissions from Large Amplitude Whistler-mode Waves

*Takeshi Nogi[1], Satoko Nakamura[1,2], Yoshiharu Omura[1] (1.Reserch Institute for Sustainable Humanosphere, Kyoto University, 2.Institute for Space-Earth Environmental Research, Nagoya University)

[PEM15-P05] Electromagnetic particle simulation of whistler mode triggered emissions in the equatorial magnetosphere

*Yuya Fujiwara[1], Yoshiharu Omura[1], Takeshi Nogi[1], Yikai Hsieh[1], Satoko Nakamura[1,2] (1.Research Institute for Sustainable Humanosphere, Kyoto University, 2.Institute for Space-Earth Environmental Research, Nagoya University)

[PEM15-P06] Study of the Pitch Angle Scattering of Small Pitch Angle Electrons by Coherent Whistler-Mode Waves

*Genki Ishizawa[1], Yuto Katoh[1], Masahiro Kitahara[1], Atsushi Kumamoto[1], Tomoki Kimura[1,2], Yohei Kawazura[1,2] (1. Department of Geophysics Graduated School of Science Tohoku university , 2.Frontier Research Institute for Interdisciplinary Sciences Tohoku University)

[PEM15-P07] Development of numerical code of the electron transport equation with spectral method

*Takuma Katou[1], Takanobu Amano[1] (1.The University of Tokyo)

[PEM15-P08] Vlasov solver using rational Chebyshev function

*Taiki Jikei[1], Takanobu Amano[1] (1.The University of Tokyo)

[PEM15-P09] A Multistate Low-dissipation Advection Upstream Splitting Method for Ideal Magnetohydrodynamics

*Takashi Minoshima[1], Keiichi Kitamura[2], Takahiro Miyoshi[3] (1.Center for Mathematical Science and Advanced Technology, Japan Agency for Marine-Earth Science and Technology, 2.Yokohama National University, 3.Hiroshima University)

[PEM15-P10] On the rate of electron injection at collisionless shocks

*Takanobu Amano[1] (1.Department of Earth and Planetary Science, University of Tokyo)

[PEM15-P11] A Study of Evolutions of Growth Rates and the Most Unstable Modes in the Events of Sub-magnetosonic Kelvin-Helmholtz Instabilities in an MHD plasma

*Chun-Yen Hsu[1], Ling-Hsiao Lyu[1] (1.Institute of Space Science and Engineering, National Central University, Taoyuan, Taiwan)

[PEM15-P12] Structure formation in chiral magnetohydrodynamics: Effect of background magnetic field

*Takahiro Miyoshi[1] (1.Hiroshima University)

[PEM15-P13] Synchrotron maser emission and associated particle acceleration in relativistic shocks

*Masanori Iwamoto[1], Takanobu Amano[2], Masahiro Hoshino[2], Yosuke Matsumoto[3] (1.Interdisciplinary Graduate School of Engineering Sciences, Kyushu University, 2.Graduate School of Science, The University of Tokyo, 3.Graduate School of Science, Chiba University)

[E] Poster | P (Space and Planetary Sciences)：P-EM Solar-Terrestrial Sciences, Space Electromagnetism & Space Environment

[P-EM16] Magnetospheric Multi Scale (MMS) mission: Accomplishments and Future Plans

convener:Yoshifumi Saito(Solar System Science Division, Institute of Space and Astronautical Science, Japan Aerospace Exploration Agency), James L Burch(Southwest Research Institute), Barbara L Giles(NASA Goddard Space Flight Center), Hiroshi Hasegawa(Institute of Space and Astronautical Science, Japan Aerospace Exploration Agency)

[PEM16-P01] Magnetic island formation in reconnecting electron-scale current sheet: MMS observations in the magnetotail

*Hiroshi Hasegawa[1], Richard E. Denton[2], Rumi Nakamura[3], Kevin J. Genestreti[4], Takuma Nakamura[3], Kyoung Joo Hwang[5], Narges Ahmadi[6], Tai D. Phan[7], Roy B. Torbert[4], Jim L. Burch[5], Barbara L. Giles[8], Dan J. Gershman[8], Christopher T. Russell[9], Robert J. Strangeway[9], Per Arne Lindqvist[10], Yuri V. Khotyaintsev[11], Robert E. Ergun[6], Yoshifumi Saito[1] (1.Institute of Space and Astronautical Science, Japan Aerospace Exploration Agency, 2.Dartmouth College, 3.Space Research Institute, Austrian Academy of Science, 4.University of New Hampshire, 5.Southwest Research Institute, 6.University of Colorado, 7.Space Sciences Laboratory, University of California Berkeley, 8.NASA Goddard Space Flight Ceter, 9.University of California Los Angeles, 10.Royal Institute of Technology, 11.Swedish Institute of Space Physics)

[PEM16-P02] Multi-spacecraft observations of cold-dense plasma sheet under northward IMF

*Masaki N Nishino[1], Yoshifumi Saito[1], Iku Shinohara[1], Tsugunobu Nagai[1], Kazushi Asamura[1], Yoichi Kazama[2], Shiang-Yu Wang[2], Sunny Wing-Yee Tam[3], Ayako Matsuoka[1], Yoshizumi Miyoshi[4], Barbara L Giles[5], Christopher T Russell[6], Daniel J Gershman[7], Benoit Lavraud[8], Yukinaga Miyashita[9] (1.Japan Aerospace Exploration Agency, Institute of Space and Astronautical Science, 2.Institute of Astronomy and Astrophysics, Academia Sinica, Taiwan, 3.Institute of Space and Plasma Sciences, National Cheng Kung University, Taiwan, 4.Institute for Space-Earth Environmental Research, Nagoya University, 5.NASA, Goddard Space Flight Center, 6.University of California, Los Angeles, 7.University of Maryland, College Park, 8.Institut de Recherche en Astrophysique et Planétologie, 9.Korean Astronomy and Space Science Institute)

[PEM16-P03] Uncertainties on Fields Gradients and Propagation Velocities Estimated From Multi-Spacecraft Missions

*Gerard Marcel CHANTEUR[1] (1.CNRS & Sorbonne Université, Laboratoire de Physique des Plasma)

[PEM16-P04] PIC simulation of electron acceleration at quasi-perpendicular collisionless shock: Application to Earth's bow shock

*Fumiko Otsuka[1], Shuichi Matsukiyo[2], Mitsuo Oka[3] (1.NIT, Kurume College, 2.ESST, Kyushu Univ., 3.UC Berkeley)

[E] Poster | P (Space and Planetary Sciences)：P-EM Solar-Terrestrial Sciences, Space Electromagnetism & Space Environment

[P-EM17] Space Weather and Space Climate

convener:Ryuho Kataoka(National Institute of Polar Research), Antti A Pulkkinen(NASA Goddard Space Flight Center), Kanya Kusano(Institute for Space-Earth Environmental Research, Nagoya University), Kaori Sakaguchi(National Institute of Information and Communications Technology)

[PEM17-P01] Preparedness for extreme space weather events

*Mamoru Ishii[1], Daikou Shiota[1], Chihiro Tao[1] (1.National Institute of Information and Communications Technology)

[PEM17-P02] Value of forecast: forecast verification in user's perspective

*Yuki Kubo[1] (1.National Institute of Information and Communications Technology)

[PEM17-P03] Statistical analysis of short-wave fadeout toward extreme event estimation for space weather hazardous map of Japan

*Chihiro Tao[1], Michi Nishioka[1], Takuya Tsugawa[1], Daikou Shiota[1], Susumu Saito[2], Kyoko Watanabe[3], Mamoru Ishii[1] (1.National Institute of Information and Communications Technology, 2.Electronic Navigation Research Institute, 3.National Defense Academy)

[PEM17-P04] Effect of equatorial plasma bubbles on midlatitude region

*Tatsuhiro Yokoyama[1], Hiroyuki Shinagawa[2], Yuichi Otsuka[3] (1.Research Institute for Sustainable Humanosphere, Kyoto University, 2.National Institute of Information and Communications Technology, 3.Institute for Space-Earth Environmental Research, Nagoya University)

[PEM17-P05] Calculation of the ray paths and propagation times of HF radio waves in the simulator of HF-START project.

*Ryo Nakao[1], Hiroyuki Nakata[2], Kornyanat Hozumi[3], Takuya Tsugawa[3], Susumu Saito[4], Hiroyo Ohya[2], Toshiaki Takano[2], Mamoru Ishii[3] (1.Graduate School of Engineerings, Chiba University, 2.Graduate School of Engineering, Chiba University, 3.National Institute of Information and Communications Technology, 4.Electronic Navigation Research Institute)

[PEM17-P06] Characteristics of F-region irregularities near a northern anomaly crest during the rising half of solar cycle 23

Hsin-Hua Wu[1], Pei-Yu Chen[1], *Chien-Chih Lee[1] (1.Department of Applied Geomatics, Chien Hsin University of Science and Technology)

[PEM17-P07] Variations of thermospheric mass density probed from satellite orbit change

*Wataru Miyake[1] (1.Tokai University)

[PEM17-P09] Influence of the solar wind on El Nino

*Kazuyoshi Yamashita[1] (1.Yokohama National University, Graduate School of Env. & Inf. Sciences)

[PEM17-P10] Development of Space Environment Customized Risk Estimation for Satellite (SECURES)

*Tsutomu Nagatsuma[1], Haruhisa Matsumoto[2], Kiyokazu Koga[2], Masao Nakamura[3], Aoi Nakamizo[1], Yasubumi Kubota[1], Yoshizumi Miyoshi[4] (1.National Institute of Information and Communications Technology, 2.Japan Aerospace Exploration Agency, 3.Osaka Prefecture University, 4.Nagoya Unibersity)

[PEM17-P11] Spacecraft surface charging and discharging risk estimation method around geosynchronous altitude

*Masao Nakamura[1], Hirotaka Maeda[1], Tsutomu Nagatsuma[2], Mamoru Ishii[2] (1.Osaka Prefecture University, 2.NICT)

[PEM17-P12] Study of IMF By dependence of plasma injection position using real-time magnetosphere simulation data

*Yasubumi Kubota[1], Aoi Nakamizo[1], Kaori Sakaguchi[1], Tsutomu Nagatsuma[1], Mitsue Den[1], Yuki Kubo[1], Takashi Tanaka[1,2] (1.National Institute of Information and Communications Technology, 2.Kyushu University)

[PEM17-P14] Multi point measurements of geomagnetically induced currents in the Chugoku region

*Kumiko K. Hashimoto[1], Kentarou Kitamura[2], Takashi Kikuchi[3], Yusuke Ebihara[4] (1.Kibi International University, 2.National Institute of Technology, Tokuyama College, 3.Nagoya University, 4.Kyoto University)

[PEM17-P15] SuperDARN future plan in terms of Planning of phase X 6-year project of Japanese Antarctic Research Expedition and beyond

*Akira Sessai Yukimatu[1,2] (1.National Institute of Polar Research, 2.SOKENDAI)

[PEM17-P16] Study of dependence of solar flare induced SuperDARN Doppler velocity on X-ray intensity, SZA and season

*Tomoya Takada[1], Nozomu Nishitani[1], Tomoaki Hori[1] (1.Institute for Space-Earth Environmental Research)

[PEM17-P17] Summary of the five-year extended observations of Nobeyama Radioheliograph

*Satoshi Masuda[1] (1.Institute for Space-Earth Environmental Research, Nagoya University)

[PEM17-P18] Phesant tail aurora: The oldest record of astronomical phenomenon in Japan

*Ryuho Kataoka[1], Kazuaki Yamamoto[2], Yasunori Fujiwara[1], Kozue Shiomi[1], Nobuo Kokubun[1] (1.National Institute of Polar Research, 2.National Institute of Japanese Literature)

[PEM17-P19] Plasma waves causing relativistic electron precipitation events at International Space Station

*Ryuho Kataoka[1], CALET Collaboration, Arase Collaboration (1.National Institute of Polar Research)

[PEM17-P20] Investigation of the Relation Between Magnetospheric Activity and Solar Wind Parameters Based on Potential Learning

*Ryozo Kitajima[1], Motoharu Nowada[2], Ryotaro Kamimura[3] (1.Dept. Engineering, Tokyo Polytechnic University, Kanagawa, Japan, 2.Shandong Provincial Key Laboratory of Optical Astronomy and Solar-Terrestrial Environment, Institute of Space Sciences, Shandong University, Weihai, P. R. China, 3.IT Education Center, Tokai University, Kanagawa, Japan)

[PEM17-P21] Cosmic Ray Intensity Increase Associated with Slow Coronal Mass Ejection

*Wataru Kihara[1], Chihiro Kato[1], Kazuoki Munakata[1], Yukino Ko[1], Ryuho Kataoka[2], Akira Kadokura[2], the GMDN collaborations - (1.Department of Physics, Shinshu University, 2.National Institute of Polar Research)

[PEM17-P22] Study on the global occurrence characteristics of Pc2 pulsation with the 10Hz data of the MAGDAS9 system

*Taisei Kabasawa[1], Akimasa Yoshikawa[2], Teiji Uozumi[3], Akiko Fujimoto[4], Shuji Abe[3] (1.Kyushu University, 2.Department of Earth and Planetary Science, Kyushu University, 3.International center for space weather science and education, Kyushu university, 4.Department of information technology, Kyushu Institute of Technology)

[PEM17-P23] Data assimilation of radiation belt electrons using the DREAM code and multiple spacecraft data of Arase, Himawari, and GPS

*Kaori Sakaguchi[1], Andrew Walker[2], Sophie Graf[2], Reinhard Friedel[2], Takefumi Mitani[3], Nana Higashio[3], Takeshi Takashima[3], Tsutomu Nagatsuma[1], Mamoru Ishii[1] (1.National Institute of Information and Communications Technology, 2.Los Alamos National Laboratory, 3.Japan Aerospace Exploration Agency)

[E] Poster | P (Space and Planetary Sciences)：P-EM Solar-Terrestrial Sciences, Space Electromagnetism & Space Environment

[P-EM18] Study of coupling processes in solar-terrestrial system

convener:Mamoru Yamamoto(Research Institute for Sustainable Humanosphere, Kyoto University), Yasunobu Ogawa(National Institute of Polar Research), Satonori Nozawa(Institute for Space-Earth Environmental Research, Nagoya University), Akimasa Yoshikawa(Department of Earth and Planetary Sciences, Kyushu University)

[PEM18-P01] Development of Software-Defined Multichannel Receiver for Equatorial Atmosphere Radar (EAR)

*Hiroyuki Hashiguchi[1], Nor Azlan Bin Mohd Aris -[1], Mamoru Yamamoto[1] (1.Research Institute for Sustainable Humanosphere, Kyoto University)

[PEM18-P02] Observation of ozone vertical mixing due to KH instability in tropical tropopause layer

*Momoko Hashino[1], Hiroyuki Hashiguchi[1], Richard Wilson[2], Shin-Ya Ogino[3], Junko Suzuki[3] (1.Research Institute for Sustainable Humanosphere, Kyoto University, 2.LATMOS/IPSL, Sorbonne Université, 3.Japan Agency for Marine-Earth Science and Technology)

[PEM18-P03] Study of daily and seasonal variation of the equatorial ionization anomaly in Asia based on satellite-ground beacon experiment

*Mamoru Yamamoto[1], Yuki Sakamoto[1], Kornyanat Hozumi[2] (1.Research Institute for Sustainable Humanosphere, Kyoto University, 2.National Institute of Information and Communications Technology)

[PEM18-P04] Development of transmitter and antenna on board of sounding rocket for the TEC measurement

*Koki Kurokawa[1], Mamoru Yamamoto[1] (1.Research Institute for Sustainable Humanosphere, Kyoto University)

[PEM18-P05] Ionospheric observations by Equatorial Atmosphere Radar during annular eclipse in December 2019

*Rieko Takagi[1], Tatsuhiro Yokoyama[1], Mamoru Yamamoto[1], Kornyanat Hozumi[2] (1.Research Institute for Sustainable Humanosphere, Kyoto University, 2.National Institute of Information and Communications Technology)

[PEM18-P06] Upgrade of equatorial plasma bubble simulation toward coupling with GAIA model

*Taichi Komoto[1], Tatsuhiro Yokoyama[1], Hiroyuki Shinagawa[2] (1.Research Institute for Sustainable Humanosphere, 2.National Institute of Information and Communications Technology)

[PEM18-P07] Long-term statistical analysis of the ionospheric observation with the MU radar

*Tatsuhiro Yokoyama[1], Masanori Ueno[1], Mamoru Yamamoto[1] (1.Research Institute for Sustainable Humanosphere, Kyoto University)

[PEM18-P08] **Space weather modelling of the dayside polar ionosphere and thermosphere**

*Hitoshi Fujiwara[1], Yasunobu Miyoshi[2], Satonori Nozawa[3], Yasunobu Ogawa[4], Hidekatsu Jin[5], Chihiro Tao[5], Hiroyuki Shinagawa[5] (1.Faculty of Science and Technology, Seikei University, 2.Department of Earth and Planetary Sciences, Kyushu University, Japan, 3.Institute for Space-Earth Environmental Research, Nagoya University, Japan, 4.National Institute of Polar Research, Japan, 5.National Institute of Communication Technology, Japan)

[PEM18-P09] Network observations of aurora and airglow with low-cost multi-wavelength imager system

*Yasunobu Ogawa[1], Akira Kadokura[1], Yoshimasa Tanaka[1] (1.National Institute of Polar Research)

[PEM18-P10] A pulsating aurora event observed by an optical spectrograph at Tromsø, Norway

*Takuo T. Tsuda[1], Chengyu Li[1], Keisuke Hosokawa[1], Satonori Nozawa[2], Tetsuya Kawabata[2], Akira Mizuno[2], Shin-ichiro Oyama[2], Junichi Kurihara[3] (1.University of Electro-Communications, 2.Nagoya University, 3.Hokkaido University)

[PEM18-P11] Study of atmospheric stability in the polar upper mesosphere and lower thermosphere above Tromsø by using sodium LIDAR data

*Sakiho Maeda[1], Satonori Nozawa[1], Takuya Kawahara[2], Norihito Saito[3], Takuo T. Tsuda[4], Satoshi Wada[3], Toru Takahashi[5], Tetsuya Kawabata[1], Chris Hall[6] (1.Institute for Space-Earth Environmental Research, Nagoya University,

2.Faculty of Engineering, Shinshu University, 3.RIKEN Center for Advanced Photonics, RIKEN, 4.The University of Electro-Communications, 5.Department of Physics, University of Olso, 6.UiT The Arctic University of Norway)

[PEM18-P12] Observational evaluation of temperature/wind perturbations associated with small-scale AGWs : Parameterisation and validation of wave structures

*Shin Suzuki[1], Satonori Nozawa[2] (1.Faculty of Regional Policy, Aichi University, 2.ISEE, Nagoya University)

[PEM18-P13] Development of SDR-based scintillation detector system integrated with MAGDAS project

*Akiko Fujimoto[1], Shuji Abe[2], Akimasa Yoshikawa[2] (1.Kyushu Institute of Technology, 2.Kyushu University)

[PEM18-P14] Recent and future activities of ICSWSE and MAGDAS project

*Shuji Abe[1], Akiko Fujimoto[2], Teiji Uozumi[1], Akimasa Yoshikawa[1,3] (1.International Center for Space Weather Science and Education, Japan, 2.Kyushu Institute of Technology, Japan, 3.Department of Earth and Planetary Sciences, Kyushu University, Japan)

[PEM18-P16] Day-to-day Variability of Field-Aligned Irregularities Occurrence in Nighttime F-region Ionosphere over Equatorial Atmosphere Radar : A Combinatorics Analysis

*Dyah Rahayu Martiningrum[1], Mamoru Yamamoto[2], Rezy Pradipta[3] (1.National Institute of Aeronautics and Space - LAPAN, Indonesia, 2.Research Institute for Sustainable Humanosphere (RISH), Kyoto University, Japan, 3.Institute for Scientific Research, Boston College, Chestnut Hill, MA, United States)

[E] Poster | P (Space and Planetary Sciences)：P-EM Solar-Terrestrial Sciences, Space Electromagnetism & Space Environment

[P-EM19] Dynamics of the Inner Magnetospheric System

convener:Kunihiro Keika(Department of Earth and Planetary Science, Graduate School of Science, The University of Tokyo), Aleksandr Y Ukhorskiy(Johns Hopkins University Applied Physics Laboratory), Yoshizumi Miyoshi(Institute for Space-Earth Environmental Research, Nagoya University), Lynn M Kistler(University of New Hampshire Main Campus)

[PEM19-P01] Numerical simulation on energetic electron precipitations by chorus waves

*Yoshiki Ito[1], Shinji Saito[2], Yoshizumi Miyoshi[1] (1.Nagoya University, ISEE, 2.National Institute of Information ans Communications Technology)

[PEM19-P02] A pipeline for comprehensive tracking of pulsating patches in All-Sky Imager data

*Riku Nomiyama[1], Yoshizumi Miyoshi[2], Kohei Toyama[2], Yasunobu Ogawa[3], Keisuke Hosokawa[4], Terumasa Tokunaga[1] (1.Kyushu Institute of Technology, 2.Institute for Space-Earth Environmental Research, Nagoya University, 3.National Institute of Polar Research, 4.Department of Communication Engineering and Informatics, University of Electro-Communications)

[PEM19-P03] Estimation of precipitating electron energy of pulsating aurora by multiwavelength aurora optical observation

*Kohei Toyama[1], Yoshizumi Miyoshi[1], Satoshi Kurita[1], Keisuke Hosokawa[2], Yasunobu Ogawa[3], Shin-ichiro Oyama[1], Satonori Nozawa[1] (1.Institute for Space-Earth Environmental Research, Nagoya University, 2.Department of Communication Engineering Informatics,Univarsity Electro-Communications, 3.National Institute of Polar Research)

[PEM19-P04] Observation plan of pulsating aurora by the multi-spectral auroral camera on the LAMP rocket

Naoshi Yagi[1], *Takeshi Sakanoi[1], Miki Kawamura[1], Kazushi Asamura[2], Yoshizumi Miyoshi[3], Keisuke Hosokawa[4], Sarah L Jones[5], Marc Lessard[6] (1.Planetary Plasma and Atmospheric Research Center, Graduate School of Science, Tohoku University, 2.ISAS/JAXA, 3.ISEE, Nagoya University, 4.Graduate School of Informatics and Engineering, The University of Electro-Communications, 5.Goddard Space Flight Center, NASA, 6.University of New Hampshire)

[PEM19-P05] Statistical study of EMIC waves and energetic electron precipitation: ground-based magnetometer and subionospheric VLF/LF radio measurements at subauroral latitude

*Asuka Hirai[1], Fuminori Tsuchiya[1], Takahiro Obara[1], Yasumasa Kasaba[1], Yuto Katoh[2], Hiroaki Misawa[1], Kazuo Shiokawa[3], Yoshizumi Miyoshi[3], Satoshi Kurita[3], Chae-Woo Jun[3], Martin G Connors[4] (1.Planetary Plasma and Atmospheric Research Center, Graduate School of Science, Tohoku Univ. , 2.Department of Geophysics, Graduate School of Science, Tohoku University, 3.Institute for Space-Earth Environmental Research, Nagoya University, 4.Athabasca University)

[PEM19-P06] First simultaneous observation of the isolated proton aurora at subauroral latitudes by a highly sensitive all-sky camera and the Van Allen Probes satellite

*Kohki Nakamura[1], Kazuo Shiokawa[1], Yuichi Otsuka[1], Atsuki Shinbori[1], Martin G Connors[2], Geoff Reeves[4], Charles Smith[3] (1.Institute for Space-Earth Environmental Research, 2.Athabasca Univ., 3.New Hampshire Univ., 4.Los Alamos National Laboratory)

[PEM19-P07] Modulation of Pc1 wave ducting by equatorial plasma bubbles

*Hyangpyo Kim[1], Kazuo Shiokawa[1], Jaeheung Park[2,3], Yoshizumi Miyoshi[1], Junga Hwang[2,3], Akira Kadokura[4] (1.Institute for Space-Earth Environmental Research, Nagoya University, Nagoya, Japan, 2.Korea Astronomy and Space science Institute, Daejeon, South Korea, 3.Korea University of Science and Technology, Daejeon, South Korea, 4.Space and Upper Atmospheric Sciences, National Institute of Polar Research, Tokyo, Japan)

[PEM19-P08] Modulation of energetic electron distribution caused by toroidal mode ULF waves in association with periodic enhancement of chorus emissions

Atsuhiro Ono[1], *Yuto Katoh[1], Mariko Teramoto[2], Atsushi Kumamoto[1], Fuminori Tsuchiya[1], Yoshiya Kasahara[3], Shoya Matsuda[4], Ayako Matsuoka[4], Satoshi Kasahara[5], Shoichiro Yokota[7], Kunihiro Keika[5], Takefumi Mitani[4], Tomoaki Hori[6], Yoshizumi Miyoshi[6], Iku Shinohara[4] (1.Department of Geophysics, Graduate School of Science, Tohoku University, 2.Kyutech, 3.Kanazawa University, 4.ISAS/JAXA, 5.The University of Tokyo, 6.Nagoya University, 7.Osaka Univ.)

[PEM19-P10] **Comparative study of magnetic field and ion flux variations in inner magnetosphere during magnetic storms using Arase observations and RAM-SCB simulations**

*Sandeep Kumar[1], Yoshizumi Miyoshi[1], Vania Jordanova[2], Ayako Matsuoka[3], Kazushi Asamura[3], Shoichiro Yokota[4], Satoshi Kasahara[5], Kunihiro Keika[5], Tomoaki Hori[1], Iku Shinohara[3] (1.ISEE, Nagoya University, Japan, 2.Los Alamos National Laboratory, USA, 3.ISAS/JAXA, Japan, 4.Osaka University, Japan, 5.University of Tokyo, Japan)

[PEM19-P11] **Observational study on mass and charge dependence of plasma energization in the inner magnetosphere and near-Earth magnetotail**

*Kunihiro Keika[1], Satoshi Kasahara[1], Shoichiro Yokota[2], Masahiro Hoshino[1], Kanako Seki[1], Takanobu Amano[1], Lynn M Kistler[3], Masahito Nose[4], Yoshizumi Miyoshi[4], Tomoaki Hori[4], Iku Shinohara[5] (1.Graduate School of Science, The University of Tokyo , 2.Graduate School of Science, Osaka University, 3.University of New Hampshire, 4.Institute for Space-Earth Environmental Research, Nagoya University, 5.Institute of Space and Astronautical Science, Japan Aerospace Exploration Agency)

[PEM19-P12] Improvement of detector response matrices of the high-energy electron experiments (HEP) onboard the Arase satellite

*Takefumi Mitani[1], PARK INCHUN[2], Tomoaki Hori[2], Takeshi Takashima[1], Satoshi Kasahara[3], Satoshi Kurita[2], Mariko Teramoto[4], Nana Higashio[1], Yoshizumi Miyoshi[2], Iku Shinohara[1] (1.Japan Aerospace Exploration Agency, 2.Nagoya University, 3.The University of Tokyo, 4.Kyushu Institute of Technology)

[PEM19-P13] Inter-channel normalization and energy spectrum correction of the high-energy electron experiments (HEP) onboard the Arase satellite

*Tomoaki Hori[1], Takefumi Mitani[2], Takeshi Takashima[2], InChun Park[1], Satoshi Kurita[1], Mariko Teramoto[3], Nana Higashio[4], Satoshi Kasahara[5], Shoichiro Yokota[6], Yoshizumi Miyoshi[1], Iku Shinohara[2] (1.Institute for Space-Earth Environmental Research, Nagoya University, 2.JAXA/ISAS, 3.Kyushu Inst. of Tech., 4.JAXA, 5.The Univ. of Tokyo, 6.Osaka Univ.)

[PEM19-P14] Evaluation of response characteristics of the XEP onboard the Arase spacecraft

*Kohei Ueda[1], Takefumi Mitani[2], Nana Higashio[3], Shoichiro Yokota[1], Takeshi Takashima[2], Yoshizumi Miyoshi[4], Iku Shinohara[2], Kentaro Terada[1] (1.Osaka University, 2.Japan Aerospace Exploration Agency/Institute of Space and Astronautical Science, 3. Japan Aerospace Exploration Agency, 4.Nagoya University/Institute for Space-Earth Environment Research)

[PEM19-P15] The observational study for high energy particles below L=2.1 using Hisaki

*Kazuo Yoshioka[1], Ichiro Yoshikawa[1], Atsushi Yamazaki[2], Go Murakami[2], Hajime Kita[2], Fuminori Tsuchiya[3], Tomoki Kimura[4], Yoshizumi Miyoshi[5], Satoshi Kurita[5], Mariko Teramoto[6] (1.Graduate School of frontier Science, The University of Tokyo, 2.Institute of Space and Astronautical Science / Japan Aerospace Exploration Agency, 3.Planetary Plasma and Atmospheric Research Center, Graduate School of Science, Tohoku University, 4.Tohoku University, 5.Institute for Space-Earth Environmental Research, Nagoya University, 6.Kyushu Institute of Technology)

[PEM19-P16] Calibration of waveform data measured by the electric sensors on board the Arase satellite

*Yoshiya Kasahara[1], Hiroyuki Nishizawa[1], Shoya Matsuda[2], Hirotsugu Kojima[3], Fuminori Tsuchiya[4], Atsushi Kumamoto[4], Yasumasa Kasaba[4], Ayako Matsuoka[2] (1.Kanazawa University, 2.ISAS/JAXA, 3.Kyoto University, 4.Tohoku University)

[PEM19-P17] Machine learning classification of low frequency waves observed by Arase satellite

*Shun Amano[1], Taketoshi Miyake[1], Yoshiya Kasahara[2] (1.Toyama prefectural university , 2.Kanazawa university)

[PEM19-P18] Evaluation of Automatic Determined UHR Frequencies by a Convolutional Neural Network

*Shoya Matsuda[1], Tatsuhito Hasegawa[2], Atsushi Kumamoto[3], Fuminori Tsuchiya[3], Yoshiya Kasahara[4], Yoshizumi Miyoshi[5], Yasumasa Kasaba[3], Ayako Matsuoka[1], Iku Shinohara[1] (1.Institute of Space and Astronautical Science/Japan Aerospace Exploration Agency, 2.University of Fukui, 3.Tohoku University, 4.Kanazawa University, 5.Nagoya University)

[E] Poster | P (Space and Planetary Sciences)：P-EM Solar-Terrestrial Sciences, Space Electromagnetism & Space Environment

[P-EM20] Recent Advances in Ionosphere Observation and Modeling through New Observation Opportunities

convener:CHIYEN LIN(Center for Astronautical Physics and Engineering, National Central University, TAIWAN), Yen-Jung Wu(Space Sciences Laboratory, University of California, Berkeley), Yang-Yi Sun(China University of Geosciences), Charles Lin(Department of Earth Sciences, National Cheng Kung University)

[PEM20-P01] Compact Ionospheric Probe for CubeSat-based Science Missions

*Chi-Kuang Chao[1,2] (1.Graduate Institute of Space Science, National Central University, 2.Center for Astronautical Physics and Engineering, National Central University)

[PEM20-P02] Global Ion Density Distributions Observed by Advanced Ionospheric Probe Onboard FORMOSAT-5 Satellite

Pei-Cii Hong[1], *Chi-Kuang Chao[1,2] (1.Graduate Institute of Space Science and Engineering, National Central University, 2.Center for Astronautical Physics and Engineering, National Central University)

[PEM20-P03] **Ionospheric responses on the 21 August 2017 solar eclipse by using three-dimensional GNSS tomography**

*Chia-Hung Chen[1], Charles Lin[1], Akinori Saito[2], Mamoru Yamamoto[3], Susumu Saito[4] (1.Department of Earth Sciences, National Cheng Kung University, 2.Department of Geophysics, Graduate School of Science, Kyoto University, 3.Research Institute for Sustainable Humanosphere, Kyoto University, 4.Electronic Navigation Research Institute, National Institute of Maritime, Port, and Aviation Technology)

[PEM20-P04] **Traveling Ionospheric Disturbances Triggered by Typhoon Hagibis (2019)**

*Yu-Chen Cheng[1], Charles Lin[1], Shih-Ping Chen[1], Min-Yang Chou[2] (1.Department of Earth Science, National Cheng Kung University, Tainan, Taiwan, 2.COSMIC Program Office, University Corporation for Atmospheric Research Boulder, CO, USA)

[PEM20-P05] Study of Medium-Scale Traveling Ionospheric Disturbances in Low-Latitude Ionosphere Using an Automatic Algorithm

*Pin-Hsuan Cheng[1], Charles Lin[1], Hanli Liu[2] (1.Department of Earth Sciences, National Cheng Kung University, 2.University Corporation For Atmospheric Research)

[PEM20-P06] Short-term Variabilities of Wave-3 and 4 Structures in the Low-latitude Ionosphere

*Jia-Ting Lin[1], Charles Lin[1], CHIYEN LIN[2,3], P. K. Pedatella[1], Nicholas M Pedatella[4,5] (1.Department of Earth Sciences, National Cheng Kung University, Taiwan, 2.Center for Astronautical Physics and Engineering, National Central University, Taoyuan, Taiwan, 3.Graduate Institute of Space Science, National Central University, Taoyuan, Taiwan, 4.High Altitude Observatory, National Center for Atmospheric Research, Boulder, CO, USA, 5.COSMIC Program Office, University Corporation for Atmospheric Research, Boulder, CO, USA)

[PEM20-P07] Taiwan Radio Occultation Process System (TROPS) : Preliminary results of ionospheric products

*Wen-Hao Yeh[1], Cheng-Yung Huang[1], Kun-Lin Chen[1], Tzu-Pang Tseng[2], Hsu-Hui Ho[3], Jing-Mei Wu[4], Jyun-Ying Huang[3], Hsiu-Wen Li[4], Ching-Chieh Lin[3] (1.National Space Organization, National Applied Research Laboratories, Taiwan, 2.Geoscience Australia, Australia, 3.Taiwan Analysis Center for COSMIC, Central Weather Bureau, Taiwan, 4.GPS Science and Application Research Center, National Central University, Taiwan)

[PEM20-P08] GNSS observation of ionospheric variation due to perturbations near the Earth’s surface

*Yang-Yi Sun[1] (1.China University of Geosciences (Wuhan))

[PEM20-P09] A multi-directional particle detector on HXMT

*Hong Guo Shen

[PEM20-P10] New observations of the total electron content over Ho Chi Minh City

*Tam Dao[1,2], Minh Huy Le[3], Brett A Carter[1], Que Le[2] (1.SPACE Research Centre, School of Science, RMIT University, Australia, 2.Department of Physics, International University, Vietnam, 3.Institute of Geophysics, Vietnam Academy of Science and Technology (VAST), Vietnam)

[E] Poster | P (Space and Planetary Sciences)：P-EM Solar-Terrestrial Sciences, Space Electromagnetism & Space Environment

[P-EM21] Surprises from the Subauroral Zone: Synthesizing Ground and Space-Based Observations and Theory

convener:Connors Martin G(Athabasca University), Kazuo Shiokawa(Institute for Space-Earth Environmental Research, Nagoya University)

[PEM21-P01] Subauroral-zone surprises obtained from the PWING project

*Kazuo Shiokawa[1], Martin G Connors[2] (1.Institute for Space-Earth Environmental Research, Nagoya University, 2.Athabasca University)

[PEM21-P02] The pulsating aurora of January 27, 2017 as observed by e-POP, NOAA spacecraft, and ground assets

*Martin G Connors[1], Andrew W Yau[2], Kazuo Shiokawa[3], Claudia Martinez Calderon[3], Xinlin Li[4] (1.Athabasca University, 2.University of Calgary, 3.Nagoya University, 4.University of Colorado)

[PEM21-P03] SAR arc at 68^{o} geomagnetic (71^{o} geographic) North for Kp = 0+

*Shin-ichiro Oyama[1,2,3], Atsuki Shinbori[1], Anita Aikio[2], Heikki Vanhamaki[2], Yasunobu Ogawa[3], Mirjam Kellinsalmi[4], Tero Raita[2], Mike Rietveld[5], Kazuo Shiokawa[1], Ilkka Virtanen[2], Lei Cai[6], Abiyot Workayehu[2], Marcus Pedersen[2], Kirsti Kauristie[4], Boris Kozelov[7], Andrei Demekhov[7] (1.Institute for Space-Earth Environmental Research, Nagoya University, Japan, 2.Space Physics and Astronomy Research Unit, University of Oulu, Finland, 3.National Institute of Polar Research, Japan, 4.Finnish Meteorological Institute, Finland, 5.EISCAT, Norway, 6.KTH Royal Institute of Technology, Sweden, 7.Polar Geophysical Institute, Russia)

[PEM21-P04] Simultaneous observation of detachment of a bright Stable Auroral Red (SAR) arc by a ground-based camera and the Arase satellite on 4 November 2019

*Yudai Inaba[1], Kazuo Shiokawa[1], Shin-ichiro Oyama[1,9,10], Yuichi Otsuka[1], Atsuki Shinbori[1], Yoshizumi Miyoshi[1], Yoichi Kazama[2], Shiang-Yu Wang[2], Sunny W.T. Tam[3], Tzu-Fang Chang[3], Bo-Jhou Wang[2], Kazushi Asamura[4], Shoichiro Yokota[5], Satoshi Kasahara[6], Kunihiro Keika[6], Tomoaki Hori[1], Ayako Matsuoka[4], Yoshiya Kasahara[7], Atsushi Kumamoto[8], Shoya Matsuda[4], Yasumasa Kasaba[8], Masafumi Shoji[1], Iku Shinohara[4] (1.Institute for Space-Earth Environmental Research, 2.Academia Sinica Institute of Astronomy and Astrophysics, Taipei, Taiwan, 3. Institute of Space and Plasma Sciences, National Cheng Kung University, Tainan, Taiwan, 4.JAXA, 5.Osaka Univ., 6.Univ. Tokyo, 7.Kanazawa Univ., 8.Tohoku Univ., 9.Univ. of Oulu, Finland, 10.National Institute of Polar Research)

[PEM21-P05] Spatial-temporal variations of the SAPS structure with recurrent period of a few minutes observed by the SuperDARN HOP radars

*Nozomu Nishitani[1], Tomoaki Hori[1], Mariko Teramoto[2] (1.Institute for Space-Earth Environmental Research, Nagoya University, 2.Kyushu Institute of Technology)

[PEM21-P06] New curiosities observed from ground-based data: KHF-VLF Emissions

*Claudia Martinez Calderon[1], Jyrki Manninen[2], Tauno Turunen[2] (1.Institute for Space-Earth Environmental Research, Nagoya University, 2.Sodankylä Geophysical Observatory, University of Oulu, Sodankylä)

[E] Poster | P (Space and Planetary Sciences)：P-AE Astronomy & Extrasolar Bodies

[P-AE22] Exoplanets

convener:Masahiro Ikoma(Department of Earth and Planetary Science, The University of Tokyo), Norio Narita(The University of Tokyo), Yuka Fujii(National Astronomical Observatory of Japan)

[PAE22-P01] Climate for land planets

*Takanori Kodama[1] (1.University of Bordeaux)

[PAE22-P02] The Numerical Simulation for Detecting Atmospheric Oxygen on Exoplanets Around M and K Stars.

*Toru Muraoka[1], Osada Naoya[1], Shingo Kameda[1], Go Murakami[2], Norio Narita[3], Masahiro Ikoma[4], Hitoshi Fujiwara[5] (1.Rikkyo University, 2.Institute of Astronomical Science, Japan Aeronomy Exploration Agency, 3.National Astronomical Observatory of Japan, 4.Tokyo University, 5.Seikei University)

[PAE22-P03] Prevalence and extent of magma oceans in rocky bodies

Diogo Lourenço[1,2], *Matthieu Laneuville[1] (1.Earth-Life Science Institute, Tokyo Institute of Technology, 2.University of Califorinia, Berkeley)

[PAE22-P04] Exploring Super-Earth Surfaces: Albedo of Near-Airless Magma Ocean Planets and Topography

*Yuichi Ito[1], Darius Modirrousta-Galian[2,3], Giuseppina Micela[2] (1. University College London, 2.INAF - Osservatorio Astronomico di Palermo, 3.University of Palermo)

[PAE22-P06] How does the nodal precession affect observations of hot Jupiters around A-type stars?

*Noriharu Watanabe[1], Norio Narita[2] (1.The Graduate University for Advanced Studies, SOKENDAI, 2.Astrobiology Center)

[PAE22-P07] **WASP-76 b: A Tale of Two Spectra**

*Billy Nelson Edwards[1], Quentin Changeat[1], Robin Baeyens[2], Angelos Tsiaras[1], Ingo Waldmann[1] (1.University College London , 2.Instituut voor Sterrenkunde, KU-Leuven)

[PAE22-P08] A feasibility study on the detection of molecular species in exoplanet atmospheres by high-resolution transmission spectroscopy with SPICA/SMI

*Kawauchi Kiyoe[1], Yui Kawashima[2], Teruyuki Hirano[3], Yuka Fujii[4], Taro Matsuo[5], Kazumasa Ohno[3], Ayaka Okuya[3] (1.University of Tokyo, 2.SRON - Netherlands Institute for Space Research, 3.Tokyo Institute of technology, 4.Earth-Life Science Institute, Tokyo Institute of technology, 5.Nagoya University)

[PAE22-P09] Characterizing exoplanets with low-frequency radio observations

*Yuka Fujii[1], Keitaro Takahashi[2], Tomoki Kimura[3], Jun Hashimoto[4], Yuhiko Aoyama[5], Yuta Shiohira[2], Yuka Terada[6], Hajime Kita[7], Fuminori Tsuchiya[3], SKA-JP planet team (1.Earth-Life Science Institute, Tokyo Institute of Technology, 2.Kumamoto University, 3.Tohoku University, 4.National Astronomical Observatory of Japan, 5.Tsinghua University, 6.University of Tokyo, 7.Institute of Space and Astronautical Science, Japan Aerospace Exploration Agency)

[PAE22-P10] The evolution outcome of the planetary systems predicted from the observed protoplanetary disk of HL Tau

*Shijie Wang[1], Kazuhiro Kanagawa[1], Toshinori Hayashi[1], Yasushi Suto[1] (1.University of Tokyo)

[PAE22-P11] Stability of resonant trapping of planetesimals during the migration of a giant planet

*Sho Shibata[1], Masahiro Ikoma[1] (1.Graduate School of Science, The University of Tokyo)

[PAE22-P12] **Variety of Planets from the Outer Edge of the Inner Hole**

*Masahiro Morikawa[1], Suzuka Amaya[1] (1.Department of Physics, Ochanomizu University)

[PAE22-P13] Orbital evolution of close-in super-Earths via atmospheric escape

*Naho Fujita[1], Yasunori Hori[2], Takanori Sasaki[1] (1.Department of Astronomy, Kyoto University, 2.Astrobiology Center, National Institutes of Natural Sciences)

[PAE22-P14] Bayesian inference of occurrence rates of super-Earths in systems with cold-Jupiters around low-mass stars

*Masahiro Ogihara[1], Hiroki Harakawa[2] (1.National Astronomical Observatory of Japan, 2.Subaru Telescope)

[PAE22-P15] Filling in the gaps: imputing the missing properties of exoplanets with machine learning

*Elizabeth Tasker[1], Matthieu Laneuville[2], Nicholas Guttenberg[2] (1.Institute of Space and Astronautical Science (ISAS), JAXA, 2.Earth-Life Science Institute (ELSI), Tokyo Institute of Technology)

[E] Poster | P (Space and Planetary Sciences)：P-CG Complex & General

[P-CG23] Shock responses of planetary materials elucidated from meteorites and laboratory experiments

convener:Takuo Okuchi(Institute for Planetary Materials, Okayama University), Toshimori Sekine(Center for High Pressure Science and Technology Advanced Research), Naotaka Tomioka(Kochi Institute for Core Sample Research, Japan Agency for Marine-Earth Science and Technology)

[PCG23-P01] Nanofragmentation as potential marks of multiple low-velocity impacts in carbonaceous chondrites

*Balazs Bradak[1], Yusuke Seto[2], Akos Kereszturi[3,4], Martin Chadima[5], Masayuki Hyodo[6] (1.Department of Physics, University of Burgos, Burgos, Spain, 2.Department of Planetology, Kobe University, Kobe, Japan, 3.Konkoly Thege Miklos Astronomical Institute, Research Centre for Astronomy and Earth Sciences, MTA Centre for Excellence, Budapest, Hungary, 4.European Astrobiology Institute, virtual institute hosted by the European Science Foundation, Strasbourg, France, 5.AGICO Inc., Brno, Czech Republic, , 6.Research Center for Inland Seas, Kobe University, Kobe, Japan)

[PCG23-P02] *In-situ* observations of shock-induced dehydration of goethite

*Tsubasa Tobase[1], Huijeong Hwang[2], Yongjae Lee[2], Takuo Okuchi[3], Toshimori Sekine[1,4] (1.Center for High Pressure Science and Technology Advanced Research, 2.Department of Earth System Sciences, Yonsei University, 3.Institute of Planetary Materials, Okayama University, 4.Graduate School of Engineering, Osaka University)

[PCG23-P03] Gekko XII experiment on magnetized collisionless shock

*Shuichi Matsukiyo[1], Takumi Higuchi[2], Hiroo Murakami[2], Youichi Sakawa[3], Taichi Morita[1], Kentaro Tomita[1], Ryo Yamazaki[4], Takayoshi Sano[3], Yasuhiro Kuramitsu[5], Shuta J Tanaka[4], Natsuki Ishizaka[4], Shin Kakuchi[4], Shuto Sei[4], Kei Sugiyama[4], Masato Ota[3], Shunsuke Egashira[3], Tomohiro Izumi[3], Kentaro Sakai[5], Takumi Minami[5], Hiroki Nishioka[2], Mariko Takagi[2], Takuto Kojima[2], Kento Aihara[4], Shota Kanbayashi[4], Sara Tomita[4], Yoshiharu Nakagawa[3], Takahiro Nishimoto[5], Masaki Takano[5] (1.Faculty of Engineering Sciences, Kyushu University, 2.Interdisciplinary Graduate School of Engineering Sciences, Kyushu University, 3.Institute of Laser Engineering, Osaka University, 4.Department of Physics and Mathematics, Aoyama Gakuin University, 5.Graduate School of Engineering, Osaka University)

[PCG23-P04] Laser-driven shock compression experiments of synthetic wadsleyite and ringwoodite crystals

*Takuo Okuchi[1], Narangoo Purevjav[1], Norimasa Ozaki[2], Takayoshi Sano[3], Yuhei Umeda[2], Ryosuke Kodama[2,3] (1.Institute for Planetary Materials, Okayama University, 2.Graduate School of Engineering, Osaka University, 3.Institute of Laser Engineering, Osaka University)

[PCG23-P05] *In situ* observation of phase transition behavior of shocked baddeleyite

*Sota Takagi[1,2], Atsushi Kyono[1], Shunsuke Nozawa[2], Nobuaki Kawai[3], Koji Inukai[4], Ryo Fukaya[2], Nobumasa Funamori[2], Shin-ichi Adachi[2], Kouhei Ichiyanagi[2] (1.University of Tsukuba, 2.KEK, 3.Kumamoto University, 4.Noritake Co., Limited)

[PCG23-P06] Dynamic behavior of calcite under planetary impact condition

★Invited Papers

*Yuhei Umeda[1,2], Keiya Fukui[1], Toshimori Sekine[3,1], Marco Guaruaglini[4], Alessandra Benuzzi-Mounaix[4], Nobuki Kamimura[1], Kento Katagiri[1], Ryosuke Kodama[1,2], Takeshi Matsuoka[1], Kohei Miyanishi[5], Alessandra Ravasio[4], Takayoshi Sano[2], Norimasa Ozaki[1,2] (1.Graduate School of Engineering, Osaka University, 2.Institute of Laser Engineering, Osaka University, 3.Center for High Pressure Science & Technology Advanced Research, 4.Ecole Polytechnique, 5.Riken, Spring-8, SACLA)

[E] Poster | P (Space and Planetary Sciences)：P-CG Complex & General

[P-CG24] Future missions and instrumentation for space and planetary science

convener:Kazuo Yoshioka(Graduate School of frontier Science, The University of Tokyo), Satoshi Kasahara(The university of Tokyo), Kazunori Ogawa(Japan Aerospace Exploration Agency), Mitsunori Ozaki(Faculty of Electrical and Computer Engineering, Institute of Science and Engineering, Kanazawa University)

[PCG24-P01] Stray-Light Analysis and Improvement Method of Wide-Angle Multiband Camera OROCHI onboard MMX

*Ryota Fuse[1], Keigo Enya[2], Shingo Kameda[3], Hiroki Kato[3], Masanobu Ozaki[2], Ko Ishibashi[4], Toru Kouyama[5], Shinsuke Abe[1] (1.Nihon University, 2.Japan Aerospace Exploration Agency, 3.Rikkyo University, 4.Chiba Institute of Technology, 5.National Institute of Advanced Industrial Science and Technology)

[PCG24-P02] Organizational framework for scientific studies and instruments in Martian Moons Exploration (MMX) mission

*Kazunori Ogawa[1], Koji Wada[2], Tomohiro Usui[1], Shingo Kameda[3], Tomoki Nakamura[4], Kiyoshi Kuramoto[5], Jean-Pierre Bibring[6], Masaki Fujimoto[1], Hidenori Genda[7], Jörn Helbert[8], Naru Hirata[9], Takeshi Imamura[10], Yasuhiro Kawakatsu[1], Masanori Kobayashi[2], Hiroki Kusano[11], David Lawrence[12], Koji Matsumoto[13], Patrick Michel[14], Hideaki Miyamoto[10], Hiromu Nakagawa[4], Hisashi Otake[1], Sara Russell[15], Sho Sasaki[16], Hirotaka Sawada[1], Hiroki Senshu[2], Naoki Terada[4], Stephan Ulamec[8], Sei-ichiro WATANABE[17], Shoichiro Yokota[16] (1.Japan Aerospace Exploration Agency, 2.Chiba Institute of Technology, 3.Rikkyo University, 4.Tohoku University, 5.Hokkaido University, 6.Université de Paris-Sud, 7.Tokyo Institute of Technology, 8.Deutsches Zentrums für Luft- und Raumfahrt, 9.Aizu University, 10.The University of Tokyo, 11.National Institutes for Quantum and Radiological Science and Technology, 12.The Johns Hopkins University, 13.National Astronomical Observatory of Japan, 14.Observatoire de la Côte d'Azur, 15.Natural History Museum, 16.Osaka University, 17.Nagoya University)

[PCG24-P03] Design of Small Ion Mass Spectorometer for Comet Interceptor Mission

*Rurie Mizuno[1], Satoshi Kasahara[1] (1.The university of Tokyo)

[PCG24-P04] An international multi-point space exploration mission for intergrated observations in the space-Earth coupling system

*Masafumi Hirahara[1], Masatoshi Yamauchi[2], Yoshifumi Saito[3], Hirotsugu Kojima[4], Kazushi Asamura[3], Takeshi Sakanoi[6], Yoshizumi Miyoshi[1], Naritoshi Kitamura[5] (1.Institute of Space-Earth Environmental Research, Nagoya University, 2.Swedish Institute of Space Physics, 3.Institute of Space and Astronautical Science, Japan Aerospace Exploration Agency, 4.Research Institute for Sustainable Humanosphere, Kyoto University, 5.Graduate School of Science, The University of Tokyo, 6.Graduate School of Science, Tohoku University)

[PCG24-P05] Auroral imaging at visible and far-ultra-violet wavelengths for the future polar orbiting satellite mission FACTORS

*Takeshi Sakanoi[1], Masafumi Hirahara[2], Yoshizumi Miyoshi[2], Kazushi Asamura[3], Keisuke Hosokawa[4], Yoshifumi Saito[3], Hirotsugu Kojima[5], Naritoshi Kitamura[7], Mizuki Fukizawa[1], Shin-ichiro Oyama[2], Takuo T. Tsuda[4], Akinori Saito[6], Harald Frey[8], Nick Shneider[9] (1.Planetary Plasma and Atmospheric Research Center, Graduate School of Science, Tohoku University, 2.ISEE, Nagoya University, 3.ISAS/JAXA, 4.School of Informatics and Engineering, The University of Electro-Communications, 5.RISH, Kyoto University, 6.Graduate Shool of Science, Kyoto University, 7.Graduate Shool of Science, The University of Tokyo, 8.SSL, University of California, Berkeley, 9.LASP, University of Colorado Boulder)

[PCG24-P06] Design of electric field measurements in the future mission FACTORS targeting transverse ion acceleration in the terrestrial polar magnetosphere

*Hirotsugu Kojima[1], Naritoshi Kitamura[2], Koji Shibuya[1], Ibuki Fukasawa[1], Yasumasa Kasaba[3], Masafumi Hirahara[4], Yoshiya Kasahara[5], Yohei Miyake[8], Hideyuki Usui[6], Kazushi Asamura[7], Yoshifumi Saito[7] (1.Research institute for sustainable humanosphere, Kyoto University, 2.Graduate School of Science, University of Tokyo, 3.Planetary Plasma and Atmospheric Research Center, Graduate School of Science, Tohoku University, 4.Institute for Space–Earth Environmental Research, Nagoya University, 5.Advanced Research Center for Space Science and Technology, Kanazawa University, 6.Graduate School of System Informatics, Kobe University, 7.Institute of Space and Astronautical Science, Japan Aerospace Exploration Agency, 8.Education Center on Computational Science and Engineering, Kobe University)

[PCG24-P07] Investigation of requirements for regolith thrusters

*Noruji MUTO[1], Necmi Cihan ORGER[1], Jose Rodrigo CORDOVA-ALARCON[1], Kazuhiro Toyoda[1], Mengu Cho[1] (1.Kyushu Institute of Technology)

[PCG24-P08] Attitude Control System for Kanazawa-SAT3 Microsatellite

*Yuki Yasuda[1], Kohei Fujiki[1], Takuya Nakashima[1], Tomohiko Imachi[1], Satoshi Yagitani[1], Yoshiya Kasahara[1], Daisuke Yonetoku[1], Tatsuya Sawano[1], Makoto Arimoto[1] (1.Kanazawa University)

[PCG24-P09] Microsatellite Development and Education of Space Science and Technology at Kanazawa University

*Tomohiko Imachi[1], Satoshi Yagitani[1], Daisuke Yonetoku[1], Yoshiya Kasahara[1], Tatsuya Sawano[1], Makoto Arimoto[1], Kei Sano[1], Yoshitaka Goto[1], Mitsunori Ozaki[1], Ryuichi Fujimoto[1] (1.Kanazawa University)

[PCG24-P10] S Band and UHF Band Communication Systems for Kanazawa-SAT3 Microsatellite

*Koyo Ina[1], Mayuko Tachiya[1], Teruya Minamoto[1], Tomohiko Imachi[1], Satoshi Yagitani[1], Yoshitaka Goto[1], Daisuke Yonetoku[1], Yoshiya Kasahara[1], Tatsuya Sawano[1], Makoto Arimoto[1] (1.Kanazawa University)

[PCG24-P11] Development of ASIC for energetic electron detector for future planetary explorations

*Shin Sugo[1], Satoshi Kasahara[1], Hirokazu Ikeda[2], Hirotsugu Kojima[3], Takahiro Zushi[4], Motoyuki Kikukawa[3], Kazushi Asamura[2] (1.The University of Tokyo, 2.Institute of Space and Astronautical Science, 3.Research institute for sustainable humanosphere, Kyoto University, 4.National Institute of Technology, Nara College)

[PCG24-P12] Development and Integration of the High-Speed Current Detection Circuits in Particle Sensors Dedicated to Wave-Particle Interaction Analyzer

*Motoyuki Kikukawa[1], Hirotsugu Kojima[1], Kazushi Asamura[2], Yoshifumi Saito[2] (1.Research Institute for Sustainable Humanosphere, Kyoto University, 2.Institute of Space and Astronautical Science)

[PCG24-P13] Development of the wideband analog integrated circuit for plasma wave receivers

*Shoya Nakao[1], Takahiro Zushi[1], Hirotsugu Kojima[2] (1.National Institute of Technology, Nara College, 2.Kyoto University)

[PCG24-P14] Basic study on search coil magnetometer for improving magnetic sensitivity

*Yohei Yamaka[1], Yuya Tokunaga[1], Mitsunori Ozaki[1], Satoshi Yagitani[1] (1.Kanazawa University)

[PCG24-P15] Development of an instrument to measure ion drift velocity and density in the ionosphere

*Takumi Abe[1], Shigeto Watanabe[2], Akinori Saito[3], Ryuto Hashiba[4] (1.Japan Aerospace Exploration Agency, Institute of Space and Astronautical Science Department of Solar System Sciences, 2.Hokkaido Information University, 3.Kyoto University, Graduate School of Science, 4.Hokkaido Universiity)

[PCG24-P16] Satellite-to-satellite radio occultation for the exploration of planetary atmospheres

*Takeshi Imamura[1], Hiroki Ando[2], Norihiko Sugimoto[4], Hideo Sagawa[2], Masahiro Takagi[2], Katsuyuki Noguchi[8], Kazunori Ogohara[7], Atsushi Yamazaki[9], Takahiro Iwata[9], Tomotaka Yamamoto[3], Satoshi Ikari[3], Yosuke Kawabata[3], Shoko Sano[3], Yukiko Fujisawa[4], Ryu Funase[3], Mutsuko Morimoto[4], Mirai Abe[6], Asako Hosono[5] (1.Graduate School of Frontier Sciences, The University of Tokyo, 2.Faculty of Science, Kyoto Sangyo University, 3.Department of Aeronautics and Astronautics, The University of Tokyo, 4.Department of Physics, Keio University, 5.Toshimagaoka Women High School, 6.Faculty of Law, Keio University, 7.School of Engineering, The University of Shiga Prefecture, 8.Department of Information and Computer Sciences, Nara Women's University, 9.Institute of Space and Astronautical Science, Japan Aerospace Exploration Agency)

[PCG24-P17] Life-signature Detection fluorescence Microscope (LDM)

*Enya Keigo[1], Yoshitaka - Yoshimura[2], Satoshi - Sasaki[3], Akihiko - Yamagishi[1,4], Atsuo - Miyakawa[4], Eiichi - Imai[5], Hajime - Mita[7], Takehiko Satoh[1], Kensei - Kobayashi[6], Yoko - Kebukawa[6], Tomoka - Okada[6], Hikaru - Yabuta[8], Takeshi - Naganuma[8], Tomoiro - Usui[1], Kazuhisa - Fujita[1] (1.Institute of Space and Astronautical Science, 2.Tamagawa University, 3.Tokyo University of Technology, 4.Tokyo University of Pharmacy and Life Science, 5.Nagaoka University of Technology, 6.Yokohama National University, 7.Fukuoka Institute of Technology, 8.Hiroshima University)

[PCG24-P18] Development of a near-infrared high-resolution Echelle spectrograph ESPRIT for planetary atmospheric observations

*Ayumu Kambara[1], Takeshi Sakanoi[1], Masato Kagitani[1], Yasumasa Kasaba[1], Aya Otomo[1], Yasuhiro Hirahara[2] (1.Planetary Plasma and Atmospheric Research Center, Graduate School of Science, Tohoku University, 2.Graduate School of Environmental Studies, Nagoya University)

[PCG24-P19] Development of the absorption cell filters for remote D/H observation

*Masaki Kuwabara[1], Kazuo Yoshioka[2], Makoto Taguchi[3], Takuya Kawahara[4], Shingo Kameda[3] (1.JAXA, 2.The Univ. of Tokyo, 3.Rikkyo Univ., 4.Shinshu Univ.)

[E] Poster | P (Space and Planetary Sciences)：P-CG Complex & General

[P-CG25] Planetary Magnetosphere, Ionosphere, and Atmosphere

convener:Kanako Seki(Graduate School of Science, University of Tokyo), Takeshi Imamura(Graduate School of Frontier Sciences, The University of Tokyo), Hiroyuki Maezawa(Department of Physical Science Osaka Prefecture University), Naoki Terada(Graduate School of Science, Tohoku University)

[PCG25-P01] Estimation of the drift rate and intensity of Neptune’s storm by Pirika telescope

*Yuuki Sato[1], Yukihiro Takahashi[1], Mitsuteru Sato[1], Seiko Takagi[1], Masataka Imai[2], Tatsuharu Ono[1] (1.Graduate School of Science, Hokkaido University, 2.National Institute of Advanced Industrial Science and Technology)

[PCG25-P02] Multi spectral observation of changes in Uranus' cloud obtained by Pirka telescope

*Haruki Sugiyama[1], Yukihiro Takahashi[1], Mitsuteru Sato[1], Seiko Takagi[1], Yuuki Sato[1], Tatsuharu Ono[1], Shuntaro Yokota[1] (1.Hokkaido University)

[PCG25-P03] Parameter experiments of climates of various planets by the use of a general circulation model

*Yoshi-Yuki Hayashi[1], Yoshiyuki O. Takahashi[1], Masaki Ishiwatari[2], Kensuke Nakajima[3], George HASHIMOTO[4] (1.Department of Planetology/CPS, Graduate School of Science, Kobe University, 2.Department of Cosmosciences, Graduate school of Science, Hokkaido University, 3.Department of Earth and Planetary Sciences,Flculty of Sciences,Kyushu University, 4.Department of Earth Sciences, Faculty of Science, Okayama University)

[PCG25-P04] The influence of carbon escape on the evolution of the Martian atmosphere

Ryosuke Yagi[1], *Naoki Terada[1], Shungo Koyama[1], Takeshi Kuroda[1], Hiromu Nakagawa[1], Isao Murata[1], Yasumasa Kasaba[1] (1.Graduate School of Science, Tohoku University)

[PCG25-P05] Radiative Transport Simulations for 0.4 - 1.9 THz Band Heterodyne Spectroscopy of Martian Atmospheric Trace Gases

*Yuki Hamaguchi[1], Hiroyuki Maezawa[1], Hideo Sagawa[2] (1.Osaka Prefecture University, 2.Kyoto Sangyo University)

[E] Poster | A (Atmospheric and Hydrospheric Sciences)：A-AS Atmospheric Sciences, Meteorology & Atmospheric Environment

[A-AS01] High performance computing for next generation weather, climate, and environmental sciences

convener:Hiromu Seko(Meteorological Research Institute), Takemasa Miyoshi(RIKEN), Chihiro Kodama(Japan Agency for Marine-Earth Science and Technology), Masayuki Takigawa(Japan Agency for Marine-Earth Science and Technology)

[AAS01-P01] Ultra-high Resolution Numerical Weather Simulation and Dependency of Simulated Convective Cells on Model Resolutions

*Tsutao OIZUMI[1,2], Kazuo Saito[1,3,2], Duc Le[1,2], Junshi Ito[3,2] (1.The Japan Meteorological Business Support Center, 2.Meteorological Research Institute, 3.The Atmosphere and Ocean Research Institute)

[AAS01-P02] The Assimilation of Dual Phased Array Weather Radar Observations to Short-range Convective Forecasts

*James David Taylor[1], Guo-Yuan Lien[3], Shinsuke Satoh[2], Takemasa Miyoshi[1] (1.RIKEN Research center for computational science, 2.NICT National Institute of Information and Communications Technology, 3.Central Weather Bureau)

[AAS01-P03] Toward assimilation of dense and frequent 3-D lightning location data on a severe local rainfall forecast

★Invited Papers

*Yasumitsu Maejima[1], Tomoo Ushio[2], Takemasa Miyoshi[1] (1.RIKEN Center for Computational Science, 2.Graduate School of Engineering, Osaka University)

[AAS01-P04] Simulation of fog in Tokyo Bay: the role of atmosphere-ocean-river interaction

★Invited Papers

*Kohei Takatama[1], Takemasa Miyoshi[1] (1.RIKEN)

[AAS01-P05] **The ensemble Kalman inversion and its application into estimating parameters of a distributed rainfall-runoff model**

*Le Duc[1,2] (1.JMBSC, 2.MRI)

[AAS01-P06] **Retrieval of hygroscopic growth factor of uniformly mixed aerosol particles based on immune evolution algorithm**

*Zhicha Zhang[1,2], Changjian Ni[1,2] (1.Chengdu University of Information Technology, 2.Plateau Atmospheres and Environment Key Laboratory of Sichuan Province)

[AAS01-P07] A scale-aware PBL scheme: for the unified simulation in mesoscale and global circulation models

*Wei Wei[1] (1.Chinese Academy of Meteorological Sciences)

[AAS01-P08] The resent progress of the weather forecast system based on the NICAM-LETKF assimilation system

★Invited Papers

*Ying-Wen Chen[1], Koji Terasaki[2], Shunji Kotsuki[3], Kaya Kanemaru[4], Masaki Satoh[1], Takemasa Miyoshi[2], Takuji Kubota[5] (1.Atmospheric and Ocean Research Institute, The University of Tokyo , 2.Center for Computational Science, RIKEN, 3.Chiba University, 4.National Institute of Information and Communications Technology, 5.Japan Aerospace Exploration Agency)

[E] Poster | A (Atmospheric and Hydrospheric Sciences)：A-AS Atmospheric Sciences, Meteorology & Atmospheric Environment

[A-AS02] Abnormal weathers and disasters in urban environments in East Asia related to climate change

convener:Masaru Inatsu(Faculty of Science, Hokkaido University), Yukari Takayabu(Atmosphere and Ocean Research Institute, the University of Tokyo)

[AAS02-P01] Drawing Storylines of Extraordinary Weather Phenomena around Japan in Changing Climate

*Yukari Takayabu[1], Hisashi Nakamura[2], Takeshi Horinouchi[3], Tosiyuki Nakaegawa[4], Seita Emori[5] (1.Atmosphere and Ocean Research Institute, the University of Tokyo, 2.Research Center for Advanced Science and Technology, the University of Tokyo, 3.Hokkaido University, 4.Meteorological Research Institute, JMA, 5.National Institute for Environmental Studies)

[AAS02-P02] Climate change adaptation to disaster in urban areas

*Masaru Inatsu[1], Kusaka Hiroyuki[2], Takemi Tetsuya[3] (1.Faculty of Science, Hokkaido University, 2.Center for Computer Sciences, Tsukuba University, 3.Disaster Prevention Center, Kyoto University)

[AAS02-P03] Assessing the impacts of typhoons on extreme winds in densely-built urban districts

*Tetsuya Takemi[1], Guangdong Duan[1], Kumi Nakamae[1] (1.Disaster Prevention Research Institute, Kyoto University)

[AAS02-P04] A strategy towards the Japan regional reanalysis to protect our lives, properties and the social infra-structure under the changing climate

*Kenichi Kuma[1], Toshiki Iwasaki[2], Hisashi Nakamura[1] (1.Research Center for Advanced Science and Technology, The University of Tokyo, 2.Department of Geophysics. Graduate School of Science. Tohoku University)

[AAS02-P05] Impacts of climate change on heavy wet snowfall in Japan: differences among wether patterns

*Masamichi Ohba[1], Soichiro Sugimoto[1] (1.Central Research Institute of Electric Power Industry)

[AAS02-P06] An application of the detection method for atmospheric fronts to a large ensemble climate data

*Maki Miyamoto[1], Tomohito Tomohito[1] (1.Hokkaido University)

[AAS02-P07] Diurnal Variability of Urban Heat Island Intensity in Metro Manila, Philippines: An Initial Investigation

*John Asaula Manalo[1,2], Jun Matsumoto[1,3] (1.Department of Geography, Graduate School of Urban Environmental Sciences, Tokyo Metropolitan University, 2.Climatology and Agrometeorology Division, Philippine Atmospheric Geophysical and Astronomical Services Administration, Quezon City, Philippines, 3.Department of Coupled Ocean-Atmosphere-Land Processes Research, JAMSTEC, Yokosuka, Japan)

[AAS02-P08] Land suitability evaluation for agricultural cropland in the Dornod province, Mongolia using Remote Sensing and GIS tools

*Tsolmon Renchin[1], Bayanjargal Darkhijav[1], Davaajargal Jargalsaikhan[2], Enkhjargal Natsagdorj[3], Batbayar Ganchudur[1] (1.National University of Mongolia, Mongolia, 2.Institute of Mathematics and Digital technology Mongolian Academy of Sciences, Mongolia , 3.Dept. of Geography, Ghent University, Ghent, Belgium)

[E] Poster | A (Atmospheric and Hydrospheric Sciences)：A-AS Atmospheric Sciences, Meteorology & Atmospheric Environment

[A-AS03] Atmospheric Chemistry in Highly Polluted Environments

convener:Hongliang Zhang(Fudan University), Jianlin Hu(NUIST Nanjing University of Information Science and Technology), Jia Xing(Tsinghua University), Siyu Chen(Lanzhou University)

[AAS03-P01] Significant contributions of upwind sources to ground-level ozone in the North China Plain

*Hongliang Zhang[1,2], Kaiyu Chen[2], Pengfei Wang[2], Siyu Wang[1], Peng Wang[3], Qi Ying[4], Jianlin Hu[5] (1.Fudan Univ., 2.LSU, 3.HKPU, 4.TAMU, 5.NUIST)

[AAS03-P02] **How much do emissions from China affect Northeast Asia?**

*Hongliang Zhang[1,2], Pengfei Wang[2], Chun Cheng[3], Yele Sun[3] (1.Fudan Univ., 2.LSU, 3.IAP, CAS)

[AAS03-P03] **Modeling analysis of the spatiotemporal distribution characteristics of the atmospheric ultrafine particle in North China Plain and Yangtze River Delta of China in 2016**

Yanhong Zhu[1], *Jianlin Hu[1] (1.NUIST Nanjing University of Information Science and Technology)

[AAS03-P04] **Impact of land-use changes on biogenic emissions and formation of ozone and secondary organic aerosols in China from 2013 to 2017**

*JinLong Ma[1], Yu Wang[1], Peng Wang[2], hongliang Zhang[1] (1.Fudan University, 2.The Hong Kong Polytechnic University)

[AAS03-P05] Long term trends in air pollution in China

*Shengqiang Zhu[1], Siyu Wang[1], Zhihao Shi[2], Fei Ye[2], Jianlin Hu[2], Hongliang Zhang[1] (1.Fudan University, 2.Nanjing University of Information Science & Technology)

[AAS03-P06] **Improving ozone simulation and understanding its adverse effects in India**

*Mengyuan Zhang[1], Siyu Wang[1], Kaiyu Chen, Xue Qiao, Sri Harsha Kota, Hongliang Zhang[1] (1.Fudan University)

[AAS03-P07] **Comparison of the SAPRC18 and SAPRC11 photochemical mechanisms for ozone simulation in China**

*Yu Wang[1], JinLong Ma[1], Peng Wang[2], Hongliang Zhang[1] (1.Fudan University, 2.The Hong Kong Polytechnic University)

[AAS03-P08] **Contribution of biogenic sources to secondary organic aerosol in summertime in Shaanxi, China**

*Yong Xu[1], Hongliang Zhang[2], Dexiang Wang[3] (1. Yangzhou University, 2.Fudan University, 3.Northwest A&F University)

[AAS03-P09] **Preliminary study on physical and chemical properties of dust**

*Yuan Luo[1], Siyu Chen[1] (1.Lanzhou university)

[AAS03-P10] Associations of fine particulate matter and health burdens in Handan city

*aifang gao[1,2,3,4,5,6], junyi wang[1], jianfei luo[1], aiguo li[1], jingyi li[4,5,6], Hongliang Zhang (1.School of Water Resources and Environment, Hebei GEO University, 2.Hebei Province Collaborative Innovation Center for Sustainable Utilization of Water Resources and Optimization of Industrial Structure , 3.Hebei Province Key Laboratory of Sustained Utilization and Development of Water Resources, 4.Jiangsu Key Laboratory of Atmospheric Environment Monitoring and Pollution Control, 5.Collaborative Innovation Center of Atmospheric Environment and Equipment Technology, 6.Nanjing University of Information Science & Technology)

[AAS03-P11] Data assimilation of lidar-derived aerosol extinction coefficients and its application in China

*Zengliang Zang[1], Xiaobin Pan[1], Yanfei Liang[1], Wei You[1], Yiwen Hu[1] (1.National University of Defense Technology)

[AAS03-P12] The effectiveness of the Air Pollution Prevention and Control Action Plan on the air quality and human health during 2013-2017 in China

Dian Ding[1], *Jia Xing[1], Shuxiao Wang[1] (1.Tsinghua University)

[AAS03-P13] Modeling the source-receptor relationships in highly polluted regions

*Jia Xing[1], Dian Ding[1], Shuxiao Wang[1], Jim Kelly[2], Carey Jang[2], Yun Zhu[3] (1.Tsinghua University, 2.U.S. Environmental Protection Agency, 3.South China University of Technology)

[AAS03-P14] **Opposite Role of H_2SO_4 Formation Pathway on Secondary Organic Aerosol Formation Derived from Ethyl Ethacrylate Ozonolysis**

*Peng Zhang[1] (1.Rcees)

[AAS03-P15] **Investigating the performance of satellite-based models in estimating the surface $PM_{2.5}$ over China**

*Siwei Li[1], Lechao Dong[1], Jie Yang[1], Wenxuan Shi[1] (1.Wuhan University)

[AAS03-P16] Tiramisu snow and the weakening of surface albedo

Siyu Chen[1], *Hongru Bi[1] (1.Lanzhou University)

[AAS03-P17] Diurnal variations and source apportionment of ozone at the summit of Mount Huang, a rural site in Eastern China

*Jinhui Gao[1] (1.Southern university for science and technology)

[AAS03-P18] **Optical Properties and Molecular Compositions of Atmospheric Brown Carbon in Nanjing, East China**

*Junjun Deng[1], Xinfeng Wang[2], Wei Hu[1], Libin Wu[1], Pingqing Fu[1] (1.Institute of Surface-Earth System Science, Tianjin University, 2.Environment Research Institute, Shandong University, Jinan 250100, China)

[AAS03-P19] **Quantification of household emissions in non-attainment cities of Punjab, India**

Arpit Katiyar[1], Jagriti Suneja[1], Mukesh Khare[1], Arvind K Nema[1], *Sri Harsha Kota[1] (1.Indian Institute of Technology Delhi)

[AAS03-P20] Regional Source Apportionment of Summertime Ozone and Its Precursors in the Megacities of Beijing and Shanghai using a Source-Oriented Chemical Transport Model

*Peng Wang[1], Tao Wang[1], Qi Ying[2] (1.the Hong Kong Polytechnic University, 2.Texas A&M University)

[E] Poster | A (Atmospheric and Hydrospheric Sciences)：A-AS Atmospheric Sciences, Meteorology & Atmospheric Environment

[A-AS04] Formation of Air Pollution and Its Interactions with Weather/Climate

convener:Yang Yang(Nanjing University of Information Science & Technology), Meng Gao(State Key Laboratory of Environmental and Biological Analysis), Guangxing Lin(Pacific Northwest National Laboratory)

[AAS04-P01] **Seasonal distribution and vertical structure of different types of aerosols in southwest China observed from CALIPSO**

*Tingting Liao[1], Zhengwu Ouyang[1], Bihan Wang[1], Ke Gui[2] (1.Chengdu University of Information Technology, 2.Key Laboratory of Atmospheric Chemistry (LAC), Chinese Academy of Meteorological Sciences)

[AAS04-P02] Estimation of biogenic VOC emissions and their corresponding impact on ozone and secondary organic aerosol formation in China

*Xianyu Yang[1] (1.Chengdu university of information technology)

[AAS04-P03] Characteristics of Severe Air Pollution in Jiangsu Province and its Relationship with Meteorological Conditions under Cold Air

*Lu Cao[1,2], Duanyang Liu[1,2], Peng Zhou[3], Wenlian Yan[2], Chen Hao[2] (1.Key Laboratory of Transportation Meteorology, 2.Jiangsu Meteorological Observatory, 3.Nanjing Meteorological Bureau)

[AAS04-P04] **Spatiotemporal variations of recent NO_2 concentrations and anthropogenic and meteorological drivers over typical urban agglomerations in China**

*Yang Shen[1], Fei Jiang[1] (1.Nanjing University)

[AAS04-P05] Sub-seasonal seesaw of PM2.5 over the North China Plain in autumn and early winter

*Lian Xue[1] (1.Nanjing University)

[AAS04-P06] Transport of Ozone Pollution Over the East China Sea and the Yellow Sea: a Case Study in Coastal Cities in Eastern China

*Yanhua Zheng[1], Fei Jiang[1], Shuzhuang Feng[1], Zhe Cai[2] (1.Nanjing Univ., 2.Nanjing CLIMBLUE Technology co.LTD)

[E] Poster | A (Atmospheric and Hydrospheric Sciences)：A-AS Atmospheric Sciences, Meteorology & Atmospheric Environment

[A-AS05] Large-scale moisture and organized cloud systems

convener:Hiroaki Miura(The University of Tokyo), Atsushi Hamada(University of Toyama), Satoru Yokoi(Japan Agency for Marine-Earth Science and Technology), Masaki Satoh(Atmosphere and Ocean Research Institute, The University of Tokyo)

[AAS05-P01] Inversion and Preliminary Validation for Global Cloud Classification and Cloud Phase Products of Fengyun-3D in CMA-NSMC

★Invited Papers

*Bo Li[1,2], Ruixia Liu[1,2] (1.China Meteorological Administration, 2.National Satellite Meteorological Center)

[AAS05-P02] An Initiation Process of TD-type Disturbances under an Influence of Upper-Level Troughs

*Yuya Hamaguchi[1,2], Yukari Takayabu[1] (1.Atmosphere and Ocean Research Institute, The University of Tokyo, 2.Department of Earth and Planetary Science, The University of Tokyo)

[AAS05-P03] Numerical Study on the Diurnal Cycle of Precipitation Observed near the West Coast of Sumatra Island

*Mamiko Terada[1], Hiroaki Miura[1] (1. The University of Tokyo)

[AAS05-P04] A statistical study on precipitation characteristics coupled with equatorial Kelvin waves and equatorial Rossby waves.

*Yuhi Nakamura[1], Yukari Takayabu[1] (1.Department of Earth and Planetary Science, School of Science / Division of Climate System Research, Atmosphere and Ocean Research Institute, The University of Tokyo)

[AAS05-P05] **Gravity wave response to convective heating and its importance to understanding the weak temperature gradient approximation and its limitation**

★Invited Papers

*Ching-Shu Hung[1], Hiroaki Miura[1] (1.The University of Tokyo)

[E] Poster | A (Atmospheric and Hydrospheric Sciences)：A-AS Atmospheric Sciences, Meteorology & Atmospheric Environment

[A-AS06] Advances in Tropical Cyclone Research: Past, Present, and Future

convener:Yoshiaki Miyamoto(Faculty of Environment and Information Studies, Keio University), Sachie Kanada(Nagoya University), Akiyoshi Wada(Department of Typhoon and Severe Weather Research, Meteorological Research Institute), Kosuke Ito(University of the Ryukyus)

[AAS06-P01] Increased severe landfall typhoons in China since 2004

*Cai Yao[1,2], zhixiang Xiao[1], Song Yang[2,3], Xiaoli Luo[4] (1.Guangxi Institute of Meteorological Sciences, Nanning , China, 2.Southern Marine Science and Engineering Guangdong Laboratory (Zhuhai), Zhuhai , China, 3.School of Atmospheric Sciences, and Guangdong Province Key Laboratory for Climate Change and Natural Disaster Studies, Sun Yat-sen University, Guangzhou, China, 4.Guangxi Weather Service Center, Nanning, China)

[AAS06-P02] Perspective on Landfalling Frequency and Genesis Location Variations of Southern China Typhoon During Peak Summer

*Chengyang Zhang[1], Chundi Hu[2,3,4], Gang Huang[4], Cai Yao[1], Zhihai Zheng[5], Song Yang[2,3,6], Dake Chen[3,7] (1.Climate Center & Guangxi Institute of Meteorological Sciences, Guangxi Meteorological Bureau, Nanning, China, 2.School of Atmospheric Sciences & Guangdong Province Key Laboratory for Climate Change and Natural Disaster Studies, Sun Yat-sen University, Zhuhai, China, 3.Southern Marine Science and Engineering Guangdong Laboratory (Zhuhai), Zhuhai, China, 4.State Key Laboratory of Numerical Modeling for Atmospheric Sciences and Geophysical Fluid Dynamics, Institute of Atmospheric Physics, Chinese Academy of Sciences, Beijing, China, 5.Laboratory for Climate Studies, National Climate Center, China Meteorological Administration, Beijing, China, 6.Institute of Earth Climate and Environment System, Sun Yat-sen University, Guangzhou, China, 7.State Key Laboratory of Satellite Ocean Environment Dynamics, Second Institute of Oceanography, Ministry of Natural Resources, Hangzhou, China)

[AAS06-P04] **Analysis of Multi-scale Circulation Characteristics Affecting the Multiple Tropical Cyclogenesis in Midsummer of 2018**

*JIANYUN GAO[1], LIJUN YOU[2] (1.Fujian Institute of Meteorological Sciences, 2.Fujian Climate center)

[AAS06-P05] **Improvement of Prediction Accuracy of 3-second gust caused by Typhoon – FDDA and High Resolution SST -**

*Woosik Jung[1] (1.INJE University, Department of Atmospheric Environment Information Engineering, Gimhae, Republic of Korea)

[AAS06-P06] **Improvement of Prediction Accuracy of 3-second gust caused by Typhoon – Meteorological Input Data : GDAPS, RDAPS, GFS -**

*Woosik Jung[1] (1.INJE University, Department of Atmospheric Environment Information Engineering, Gimhae, Republic of Korea)

[AAS06-P07] **Improvement of Prediction Accuracy of 3-second gust caused by Typhoon – Soil Data : GDAPS SOIL, GFS SOIL -**

*Woosik Jung[1] (1.INJE University, Department of Atmospheric Environment Information Engineering, Gimhae, Republic of Korea)

[AAS06-P08] **Autumn Typhoon on the Korean Peninsula - Comparison of Past and Present**

*Woosik Jung[1], Hana Na[1] (1.INJE University, Department of Atmospheric Environment Information Engineering, Gimhae, Republic of Korea)

[AAS06-P09] **Water vapor transport associated with remote precipitation caused by typhoon in autumn season**

*Shinichi Kodama[1], Masaki Satoh[1] (1.Atmosphere and Ocean Research Institute, Univ. of Tokyo)

[AAS06-P10] The impact of lower stratospheric temperature change on Typhoon

*Kenta Kobayashi[1], Nawo Eguchi[1], Kosuke Ito[2] (1.Interdisciplinary Graduate School of Engineering Science, Kyushu University , 2.Faculty of Science, University of the Ryukyus)

[AAS06-P13] Sensitivity Experiments of Relative Humidity Assimilation on Typhoon Lan (2017)

Jaedeok Lee[1], *Kosuke Ito[1], Chun-Chieh Wu[2] (1.University of the Ryukyus, 2.National Taiwan University)

[AAS06-P14] **Role of VHTs and Helical flow organization in the formation of Tropical Cyclogenesis over North Indian Ocean**

*EMMANUEL RONGMIE[1,4], Medha Deshpande[2], Mano Kranthi Ganadhi[1], Sopan Tukaram Ingle[3], Phani Murali krishna[2] (1.Research Scholar in Indian Institute of Tropical Meteorology Pune, 2.Scientist D in Indian Institute of Tropical Meteorology Pune, 3.Professor and Director in K.B.C. North Maharashtra University, Jalgaon, 4.North Maharashtra University, Jalgaon)

[AAS06-P15] **Monthly Variation and Spatial Distribution of Quadrant Tropical Cyclone Size in the Western North Pacific**

*Tonghua Su[4], Wei Hong[1], Yulan Zheng[2], Bin Chen[3], Xiaoqing Ke[5] (1.Fujian Meteorological Observatory of of China Meteorological Administration, 2.Fujian Meteorological Information Center of China Meteorological Administration, 3.Electric Power Research Institute of State Grid Fujian Electric Power Company, 4.Fujian Climate Center of China Meteorological Administration, 5.Fujian Meteorological Service Center of China Meteorological Administration)

[E] Poster | A (Atmospheric and Hydrospheric Sciences)：A-AS Atmospheric Sciences, Meteorology & Atmospheric Environment

[A-AS07] Atmospheric Chemistry

convener:Naoko Saitoh(Center for Environmental Remote Sensing), Tomoki Nakayama(Graduate School of Fisheries and Environmental Sciences, Nagasaki University), Sakae Toyoda(Department of Chemical Science and Engineering, Tokyo Institute of Technology), Risa Uchida(Japan Automobile Research Institute)

[AAS07-P01] **Top-down estimation of terrestrial CO_2 flux in Northern Eurasia**

*Tomoko Shirai[1], Misa Ishizawa[2], Motoki Sasakawa[1], Akihiko Ito[1], Toshinobu Machida[1], Shamil Maksyutov[1] (1.National Institute for Environmental Studies, 2.Environment and Climate Change Canada)

[AAS07-P02] **Recent stagnation of CH_4 emission growth from East Asia based on the analysis of synoptic variations of atmospheric CH_4 and CO_2 observed at Hateruma Island**

*Yasunori Tohjima[1], Jiye Zeng[1], Akihiko Ito[1], Naveen Chandra[2], Yosuke Niwa[1], Hitoshi Mukai[1], Tomoko Shirai[1], Motoki Sasakawa[1], Prabir Patra[2], Toshinobu Machida[1] (1.National Institute for Environmental Studies, 2.Japan Agency for Marine-Earth Science and Technology)

[AAS07-P03] **Spatio-temporal variations of atmospheric methane concentrations over Japan: Data analysis of governmental monitoring and TROPOMI satellite from air pollution research viewpoint**

*Yugo Kanaya[1] (1.Research Institute for Global Change, Japan Agency for Marine-Earth Science and Technology)

[AAS07-P04] Variations of surface ocean pCO_2 and air-sea CO_2 fluxes in the Western Pacific Ocean

*Wataru Konarita[1], Shinji Morimoto[1], Shuji Aoki[1] (1.Center for Atmospheric and Oceanic Studies, Graduate School of Science, Tohoku University)

[AAS07-P05] In-situ and continuous observation of atmospheric N_2O and CO concentrations at Syowa Station, Antarctica.

*Shogo Akai[1], Shinji Morimoto[1], Wei Li[1], Daisuke Goto[2], Shuji Aoki[1] (1.Graduate School of Science, Tohoku University, 2.National Institute of Polar Research)

[AAS07-P06] Seasonal variations in the atmospheric Ar/N_2 ratio observed at ground-based stations in Japan and Antarctica and its application to an evaluation of the air-sea heat flux

*Shigeyuki Ishidoya[1], Kentaro Ishijima[2], Satoshi Sugawara[3], Yosuke Niwa[4], Yasunori Tohjima[4], Daisuke Goto[5], Kazuhiro Tsuboi[2], Shohei Murayama[1], Nobuyuki Aoki[1], Takashi Maki[2], Taichu Y Tanaka[2], Takashi Nakamura[6] (1.National Instutite of Advanced Industrial Science and Technology (AIST), 2.Meteorological Research Institute, 3.Miyagi University of Education, 4.National Institute for Environmental Studies, 5.National Institute of Polar Research, 6.Japan Meteorological Agency)

[AAS07-P07] Development of a new ISEE Chemical Lagrangian Model to elucidate the atmospheric composition changes in the mesosphere

*Tomoo Nagahama[1], Shingo Nakanishi[2], Fujita Ken[2], Tac Nakajima[1], Akira Mizuno[1] (1.Institute for Space-Earth Environmental Research, Nagoya University, 2.Graduate School of Science, Nagoya University)

[AAS07-P08] Analysis of the mesospheric ozone enhancement event in the Arctic winter with a new ISEE Chemical Lagrangian Model

*Fujita Ken[1], Tomoo Nagahama[2], Shingo Nakanishi[1] (1.Graduate School of Science, Nagoya University, 2.Institute for Space-Earth Environmental Research, Nagoya University)

[AAS07-P09] Short-term variations of HCl and HF trends observed with FTIR at Tsukuba

*Isao Murata[1], Yoshihiro Tomikawa[2,3], Isamu Morino[4], Hideaki Nakajima[4], Hideharu Akiyoshi[4] (1.Graduate School of Environmental Studies, Tohoku University, 2.National Institute of Polar Research, 3.The Graduate University for Advanced Studies, SOKENDAI , 4.National Institute for Environmental Studies)

[AAS07-P11] **Impact of HFCs on stratospheric ozone and temperature as simulated by chemistry-climate models**

*Hideharu Akiyoshi[1], Eric Dupuy[1], Yousuke Yamashita[2,1] (1.National Institute for Environmental Studies, 2.Japan Agency for Marine-Earth Science and Technology)

[AAS07-P12] ODS and GHG dependence of total ozone at mid- and high latitudes indicated by multi-ensemble simulations using MIROC3.2 and MIROC5 chemistry-climate models

*Hideharu Akiyoshi[1], Masanao Kadowaki[2], Yousuke Yamashita[3,1], Eric Dupuy[1], Toshiharu Nagatomo[1] (1.National Institute for Environmental Studies, 2.Japan Atomic Energy Agency, 3.Japan Agency for Marine-Earth Science and Technology)

[AAS07-P13] A modeling study on the roles of cloud distribution in global tropospheric chemistry: detailed evaluation of clouds in a chemistry climate model (MIROC-CHASER)

*Ryoki Matsuda[1], Kengo Sudo[1,2] (1.Graduate School of Environmental Studies, Nagoya University , 2.Japan Marine-Earth Science and Technology)

[AAS07-P14] Impacts of tropospheric bromine and iodine on global tropospheric ozone: a modeling study using CHASER

*Takashi Sekiya[1], Yugo Kanaya[1], Kengo Sudo[2,1], Fumikazu Taketani[1], Maki Noguchi Aita[1], Akitomo Yamamoto[1], Yoko Iwamoto[3], Katsuhiro Kawamoto[4] (1.Japan Agency for Marine-Earth Science and Technology, 2.Graduate School of Environmental Studies, Nagoya University, 3.Graduate School of Integrated Sciences for Life, Hiroshima University, 4.Graduate School of Maritime Sciences, Kobe University)

[AAS07-P15] **The weekday/weekend ozone differences induced by the emissions change in Guangzhou megacity of China**

*Yu Zou[1] (1.Institute of Tropical and Marine Meteorology, CMA,Guangzhou,China)

[AAS07-P16] **A Study on the Optimization of 3D Expressions for the Analysis of Local Scale Meteorological and Air Quality Information**

*Woosik Jung[1], Gunwoo Kim[1] (1.INJE University, Department of Atmospheric Environment Information Engineering, Gimhae, Republic of Korea)

[AAS07-P17] Validation of tropospheric NO_2 column density data observed by TROPOMI: Comparison with 4AZ-MAXDOAS

*Hikaru Saito[1], Hitoshi Irie[1] (1.University of Chiba)

[AAS07-P18] **Chemical composition of atmospheric aerosols over Jakarta megacity**

*Masahide Nishihashi[1], Hitoshi Mukai[1], Yukio Terao[1], Shigeru Hashimoto[1], Rizaldi Boer[2], Muhammad Ardiansyah[2], Bregas Budianto[2], Adi Rakhman[2], Gito Sugih Immanuel[2], Rudi Nugroho[3], Nawa Suwedi[3], Anies Marufatin[3], Muhammad Agus Salim[3], Dodo Gunawan[4], Eka Suharguniyawan[4], Asep Firman Ilahi[4], Muharam Syam Nugraha[4], Ronald Christian Wattimena[4], Bayu Feriaji[4], Qoriana Maulani[4] (1.National Institute for Environmental Studies, 2.IPB University, Indonesia, 3.Agency for the Assessment and Application of Technology (BPPT), Indonesia, 4.Meteorological, Climatological, and Geophysical Agency (BMKG), Indonesia)

[AAS07-P19] Seasonal Variation of Wet Deposition of Black Carbon in Arctic Alaska

*Tatsuhiro Mori[1], Yutaka Kondo[2], Sho Ohata[3,4], Yongjing Zhao[5], Puna Ram Sinha[6], Naga Oshima[7], Hitoshi MATSUI[8], Nobuhiro Moteki[9], Makoto Koike[9] (1.Tokyo University of Science, 2.National Institute of Polar Research, 3.Institute for Space–Earth Environmental Research, Nagoya University, 4.Institute for Advanced Research, Nagoya University, 5.Air Quality Research Center, University of California-Davis, 6.Department of Earth and Space Sciences, Indian Institute of Space Science and Technology, 7.Meteorological Research Institute, 8.Graduate School of Environmental Studies, Nagoya University, 9.Graduate School of Science, The University of Tokyo)

[AAS07-P20] Investigation of wet removal rate of black carbon in East Asia: A perspective from airmass pathways

*Yongjoo Choi[1], Yugo Kanaya[1], Masayuki Takigawa[1], Chunmao Zhu[1], Seung-Myung Park[2], Atsushi Matsuki[3], Yasuhiro Sadanaga[4], Sang-Woo Kim[5], Xiaole PAN[6] (1.Japan Agency for Marine-Earth Science and Technology, Japan, 2.National Institute of Environmental Research, Korea, 3.Kanazawa University, Japan, 4.Osaka Prefecture University, Japan, 5.Seoul National University, Korea, 6.Chinese Academy of Sciences, China)

[AAS07-P21] Light absorption properties of organic aerosols at Fukue Island in 2018 spring

*Chunmao Zhu[1], Takuma Miyakawa[1], Hitoshi Irie[2], Fumikazu Taketani[1], Yugo Kanaya[1] (1.Japan Agency for Marine-Earth Science and Technology, 2.Chiba University)

[AAS07-P22] **Can a global chemistry climate model reproduce interannual variabilities and trends of depositions of sulfate, nitrate, and ammonium preserved in the Southeastern Greenland Dome ice core?**

*Kengo Sudo[1,2], Hinako Shiratsuchi[1], Yoshinori Iizuka[3] (1.Graduate School of Environmental Studies, Nagoya University, 2.Japan Agency for Marine-Earth Science and Technology (JAMSTEC), 3.Institute of Low Temperature Science, Hokaido University)

[AAS07-P23] **Evaluation of GCOM-C aerosol products using ground-based sky radiometer observations**

*Hossain Mohammed Syedul Hoque[1], Hitoshi Irie[1], Alessandro Damiani[1], Mashiro Momoi[1] (1.Center for Environmental Remote Sensing (CEReS), Chiba University)

[AAS07-P24] Atmospheric sulfate formation pathways over the past 60 years constrained by a global chemical transport model

*Shohei Hattori[1], Becky Alexander[2], Sakiko Ishino[3], Shuting Zhai[2] (1.Department of Chemical Science and Engineering, School of Materials and Chemical Technology, Tokyo Institute of Technology, 2.Department of Atmospheric Sciences, University of Washington, Seattle WA 98195-1640, USA, 3.National Institute of Polar Research, Research Organization of Information and Systems, Tokyo 190-8518, Japan)

[AAS07-P25] High-temporal-resolution elemental characterization of fine-mode aerosols in springtime Asian outflow: Emission and removal characteristics, and comparison with model simulation

*Takuma Miyakawa[1], Akinori Ito[1], Chunmao Zhu[1], Yugo Kanaya[1] (1.Japan Agency for Marine-Earth Science and Technology)

[AAS07-P26] **Comparison of compositional characteristics of aerosol and rainwater samples collected in Nagoya**

*Wei Chenran[1], Sonia Afsana[1], Qingcai Chen[2], Dhananjay Kumar Deshmukh[3], Kimitaka Kawamura[3], Michihiro Mochida[1,4] (1.Graduate School of Environmental Studies, Nagoya University, Nagoya, Japan, 2.School of Environmental Science and Engineering, Shaanxi University of Science and Technology, Xi'an, China, 3.Chubu Institute for Advanced Studies, Chubu University, Kasugai, Japan, 4.Institute for Space-Earth Environmental Research, Nagoya University, Nagoya, Japan)

[AAS07-P27] Formation processes of dimers measured in α-pinene secondary organic aerosol particles

*Kei Sato[1], Sathiyamurthi Ramasamy[1], Satoshi Inomata[1], Shinichi Enami[1], Yu Morino[1] (1.National Institute for Environmental Studies)

[AAS07-P28] Nitric acid gas captured in quasi-liquid layers on ice surfaces

*Ken Nagashima[1], Josée Maurais[2], Ken-ichiro Murata[1], Yoshinori Furukawa[1], Patrick Ayotte[2], Gen Sazaki[1] (1.The Institute of Low Temperature Science, Hokkaido University, 2.Université de Sherbrooke, Québec, Canada)

[AAS07-P29] Five-years seasonal variations of nitrogen and triple oxygen isotopic compositions of atmospheric nitrate at Noto Peninsula, Japan

*Kazuki Kamezaki[1], Shohei Hattori[1], Atsushi Matsuki[2], Naohiro Yoshida[1,3] (1.Department of Chemical Science and Engineering, School of Materials and Chemical Technology, Tokyo Institute of Technology, 2.Institute of Nature and Environmental Technology, Kanazawa University, 3.Earth-Life Science Institute)

[AAS07-P30] **Impacts of ship emissions on atmospheric particulate matter and gaseous components over the Seto Inland Sea areas**

*Moe Tauchi[1], Katsuhiro Kawamoto[2], Kazuyo Yamaji[1], Ryohei Nakatsubo[3], Yoshie Oshita[3], Yasuyuki Itano[4] (1.Kobe University, 2.Takamatsu Local Meteorological office, 3.Hyogo Prefectural Institute of Environmental Sciences, 4.Osaka City Research Center of Environmental Science)

[AAS07-P31] Spatiotemporal variations of NO_2 over Fukuoka Japan, observed by multiple MAX-DOAS and 3-D coherent Doppler lidar

*Hironobu Ueki[1], Hisahiro Takashima[2], Martina Michaela Friedrich[3] (1.Fukuoka university graduate school, 2.Fukuoka university, 3.Belgian Institute for Space Aeronomy)

[E] Poster | A (Atmospheric and Hydrospheric Sciences)：A-AS Atmospheric Sciences, Meteorology & Atmospheric Environment

[A-AS08] Stratosphere-troposphere interaction

convener:Takatoshi Sakazaki(Graduate School of Science, Kyoto University), Takenari Kinoshita(Japan Agency for Marine-Earth Science and Technology), Pu Lin(Princeton University/NOAA Geophysical Fluid Dynamics Laboratory), Peter Hitchcock(Cornell University)

[AAS08-P01] **Representation of the Equatorial Stratopause Semiannual Oscillation in Global Atmospheric Reanalyses**

*Yoshio Kawatani[1], Toshihiko Hirooka[2], Kevin Hamilton[3], Anne K. Smith[4], Masatomo Fujiwara[5] (1.Japan Agency for Marine-Earth Science and Technology, 2.Faculty of Science, Kyushu University, 3.International Pacific Research Center, University of Hawaii, 4.National Center for Atmospheric Research, 5.Faculty of Environmental Earth Science, Hokkaido University)

[AAS08-P02] Laplace's Atmosphere: An Array of Ringing Modes Discovered in Global Reanalysis Data

*Takatoshi Sakazaki[1], Kevin Hamilton[2] (1.Graduate School of Science, Kyoto University, 2.International Pacific Research Center and Department of Atmospheric Sciences, University of Hawai'i at Manoa)

[AAS08-P03] Bias correction of satellite multi-sensor total column ozone datasets and their merged ozone dataset

*Hiroaki Naoe[1], Takanori Matsumoto[2], Keisuke Ueno[3], Takashi Maki[1], Makoto Deushi[1], Ayako Takeuchi[2,4] (1.Meteorological Research Institute, 2.Japan Meteorological Agency, 3.Japan Meteorological Agency, Aerological Observatory, 4.Ministry of Land, Infrastructure, Transport and Tourism)

[AAS08-P04] **Relationship between the Boreal Summer Intra-seasonal Oscillation and the Stratospheric Quasi-Biennial Oscillation**

*Yayoi Harada[1] (1.Meteorological Research Institute)

[AAS08-P05] A statistical analysis of the turbulent kinetic energy dissipation rate estimated from the PMWE spectral width in the Antarctic

*Masashi Kohma[1], Kaoru Sato[1], Koji Nishimura[2], Masaki Tsutsumi[2], Toru Sato[3] (1.Department of Earth and Planet Science, Graduate School of Science, The University of Tokyo, 2.National Institute of Polar Research and The Graduate University for Advanced Studies (SOKENDAI), Tokyo, Japan, 3.Institute for Liberal Arts and Sciences, Kyoto University, Kyoto, Japan)

[AAS08-P06] Influence of stratospheric dynamics on tropical convection and equatorial waves

*Nawo Eguchi[1], Tomoe Nasuno[2], Kunihiko Kodera[3] (1.Kyushu University, 2.Japan Agency for Marine-Earth Science and Technology, 3.Meteorological Research Institute)

[AAS08-P07] The impact of stratosphere to troposphere: raising model top from 5hPa to 0.1hPa of GRAPES_GFS (weather model)

*Yong Su[1] (1.Yong Su)

[AAS08-P08] **Parametrization of tropical coastal nonstationary gravity waves robustizing QBO**

*Manabu D. Yamanaka[1] (1.Research Institute for Humanity and Nature / Professor Emeritus of Kobe University)

[AAS08-P10] Height-dependent expression for the energy flux of equatorial waves: exact and approximate versions for unified model diagnosis

*Hidenori AIKI[1,2], Fukutomi Yoshiki[1], Yuki Kanno[2], Tomomichi Ogata[2], Takahiro Toyoda[3], Hideyuki Nakano[3] (1.Nagoya University, 2.Japan Agency for Marine-Earth Science and Technology, 3.Meteorological Research Institute)

[AAS08-P11] CCMI stratospheric trends in relation to the stratospheric shrinkage

*Michal Zak[1], Petr Pisoft[1], Petr Sacha[1,2] (1.Dept. of Atmospheric Physics, Faculty of Mathematics and Physics, Charles University, Prague, Czech Republic, 2.Inst. of Meteorology, University of Natural Resources and Life Sciences, Vienna, Austria)

[AAS08-P12] A study of wave activities and ozone fluctuations around the Maritime Continent during YMC-BSM 2018

*Takenari Kinoshita[1], Junko Suzuki[1], Shin-Ya Ogino[1], Ryuichi Shirooka[1] (1.Japan Agency for Marine-Earth Science and Technology)

[AAS08-P13] **Traveling Planetary Waves in the Northern Hemisphere Winter Middle Atmosphere**

*Koki Iwao[1], Toshihiko Hirooka[2] (1.National Institute of Technology, Kumamoto College, 2.Kyushu University)

[AAS08-P14] Impact of Satellite Observations on Forecasting Sudden Stratospheric Warmings

*Shunsuke Noguchi[1,2], Yuhji Kuroda[2,3], Hitoshi Mukougawa[4], Ryo Mizuta[2], Chiaki Kobayashi[2] (1.Japan Agency for Marine-Earth Science and Technology, 2.Meteorological Research Institute, 3.Meteorological College, 4.Kyoto University)

[E] Poster | A (Atmospheric and Hydrospheric Sciences)：A-AS Atmospheric Sciences, Meteorology & Atmospheric Environment

[A-AS09] Cloud-Resolving Model Simulations for Climate and Weather Studies

convener:Toshihisa Matsui(NASA Goddard Space Flight Center), Masaki Satoh(Atmosphere and Ocean Research Institute, The University of Tokyo), Wei-Kuo Tao(NASA Goddard Space Flight Center)

[AAS09-P01] Polarimetric Radar Characteristics of Simulated and Observed Intense Convective Cores for a Midlatitude Continental and Tropical Maritime Environment

*Toshihisa Matsui[1,2], Brenda Dolan[3], Takamichi Iguchi[1,2], Steven A. Rutledge[3], Wei-Kuo Tao[1], Stephen Lang[1,4] (1.NASA Goddard Space Flight Center, 2.ESSIC University of Maryland, 3.Colorado State University, 4.Science Systems and Applications, Inc)

[AAS09-P03] Videosonde and HYVIS cloud particle imaging radiosondes: Carrier frequency migration from 1680 to 400 MHz

*Norio Nagahama[1], Kensaku Shimizu[1], Takuji Sugidachi[1], Kenji Yamaguchi[1], Kenji Suzuki[2], Fujiwara Masatomo[3] (1.meisei electric co.,ltd., 2.Graduate School of Sciences and Technology for Innovation, Yamaguchi University, 3.Faculty of Environmental Earth Science, Hokkaido University)

[E] Poster | A (Atmospheric and Hydrospheric Sciences)：A-AS Atmospheric Sciences, Meteorology & Atmospheric Environment

[A-AS10] Land-Atmosphere interactions and precipitation variations over the Asian monsoon region.

convener:Hiroshi G. Takahashi(Department of Geography, Tokyo Metropolitan University), Hirokazu Endo(Meteorological Research Institute, Japan Meteorological Agency), Shiori Sugimoto(JAMSTEC Japan Agency for Marine-Earth Science and Technology), Hatsuki Fujinami(Nagoya University)

[AAS10-P01] **Spatial differences of the Tibetan Plateau monsoon and its application**

*Shaobo Zhang[1], Xianyu Yang[1], Yong Zhao[1] (1.Chengdu University of Information Technology)

[AAS10-P02] The concurrent effects of the South Asian monsoon and Tibetan plateau monsoon on summer rainfall in Tarim Basin of China

*YONG ZHAO[1], XIAOJING YU[2] (1.Chengdu University of Information Technology, 2.Institute of Desert Meteorology, CMA)

[AAS10-P03] Numerical simulations of precipitation in high altitude Himalaya mountainous area by using JMA-NHM

*Akihiro Hashimoto[1], Masashi Niwano[1], Hatsuki Fujinami[2], Akiko Sakai[3], Koji Fujita[3] (1.Meteorological Research Institute, Japan Meteorological Agency, 2.Institute for Space-Earth Environmental Research, Nagoya University, 3.Graduate School of Environmental studies, Nagoya University)

[AAS10-P04] Moisture sources of summer precipitation over eastern China during 1979–2009: A Lagrangian transient simulation

*QIN HU[1] (1.Chengdu University of Information Technology)

[AAS10-P05] **Study on the severe weather caused by mesoscale convective system on the Meiyu front in northwestern Taiwan**

*LI-ZHEN SU[1], Jou-Ping Hou[1], Ba-Xiu Wei[2] (1.Chung Cheng Institute of Technology National Defense University, 2.Air Force Weather Wing)

[AAS10-P06] **Long-term trends and interannual variability in precipitation over Vietnam during 1984-2016**

*Hoa Thi Thanh Pham[1], Hiroshi G. Takahashi[1] (1.Department of Geography, Tokyo Metropolitan University)

[AAS10-P07] Recent increase of rain-on-snow events and rain proportion in north-eastern Japan

*Alexander Brandt[1,2], Maximo Larry Lopez Caceres[1] (1.Yamagata University, 2.United Graduate School of Agricultural Scienes (UGAS))

[AAS10-P08] Regional snowfall and precipitation distributions in a Japan-Sea side of central Japan associated with low-frequency variabilities in the Eurasian and East Asian regions

*Akira Yamazaki[1], Meiji Honda[2], Hiroaki Kawase[3] (1.Application Laboratory, Japan Agency for Marine-Earth Science and Technology, 2.Niigata University, 3.Meteorological Research Institute, Japan Mereorological Agency)

[AAS10-P09] Quantitative identification of moisture sources over the Tibetan Plateau and the relationship between thermal forcing and moisture transport

*Chen Pan[1,2,3,4], Bin Zhu[3,4], Zhiming Kang[1,2] (1.Jiangsu Meteorological Observatory, Nanjing, China, 2.Key Laboratory of Transportation Meteorology, China Meteorological Administration, Nanjing, China, 3.Key Laboratory for Aerosol-Cloud-Precipitation of China Meteorological Administration, Nanjing University of Information Science & Technology, Nanjing, China, 4.Collaborative Innovation Center on Forecast and Evaluation of Meteorological Disasters, Nanjing University of Information Science & Technology, Nanjing, China)

[AAS10-P10] **Multi-scale convection system simulation during Meiyu season in Taiwan**

*Yi Hao Liao[1], Jou-Ping Hou[1], Yu-De Wu[2] (1.Department of Environmental Information and Engineering, CCIT, National Defense University, 2.Air Force Weather Wing)

[AAS10-P11] Responses of rainfall characteristics to the land surface conditions over the wet Asian monsoon region

*Hiroshi G. Takahashi[1] (1.Department of Geography, Tokyo Metropolitan University)

[AAS10-P12] Analysis of Characteristics and Causes of Meiyu over the Yangtze–Huai River Basin in 2019

*Ruoyun Niu[1] (1.National Meteorological Center, China Meteorological Administration)

[AAS10-P13] Similarities and differences of summer persistent heavy rainfall and atmospheric circulation characteristics in the middle and lower reaches of the Yangtze River between 2016 and 1998

*Xiaolin ZHAO[1] (1.National Meteorological Centre, China Meteorological Administration)

[AAS10-P14] **Characteristics of the Precipitation Diurnal Variation over Jiangsu, Eastern China during Warm Season**

*Xiyu Mu[1], Qi Xu[2], Yang Wu[3], Anning Huang[3] (1.Key Laboratory of Transportation Meteorology of CMA; Jiangsu Institute of Meteorological Sciences; Nanjing Joint Institute for Atmospheric Sciences, 2.Jiangsu Air Traffic Management Branch Bureau of CAAC, 3.School of Atmospheric Sciences, Nanjing University)

[AAS10-P15] Frequency of noon/afternoon convective precipitation dominates on wet surface conditions over Indian summer monsoon region

*Rakesh Teja Konduru[1], Hiroshi G. Takahashi[1] (1.Department of Geography, Tokyo Metropolitan University)

[AAS10-P17] Modification of near-surface temperature over East Asia associated with local-scale paddy irrigation

*Shiori Sugimoto[1], Hiroshi G. Takahashi[2], Sekiyama Hirosato[2,3] (1.JAMSTEC Japan Agency for Marine-Earth Science and Technology, 2.Tokyo Metropolitan University, 3.Japan Meteorological Agency)

[AAS10-P18] **The freeze-thaw cycle and key parameters in a Tibetan Plateau lake using LAKE2.0 model and field observation**

*Zhaoguo Li[1], Shihua Lyu[2], Lijuan Wen[1], Lin Zhao[1], Xianhong Meng[1], Yinhuan Ao[1] (1.Northwest Institute of Eco-Environment and Resources, Chinese Academy of Sciences, 2.School of Atmospheric Sciences, Chengdu University of Information Technology)

[AAS10-P19] **Numerical simulation of the climate effect of high-altitude lakes on the Tibetan Plateau**

*Yinhuan Ao[1], Shihua Lyu[2], Zhaoguo Li[1] (1.Northwest Institute of Eco-Environment and Resources, Chinese Academy of Sciences, 2.School of Atmospheric Sciences, Chengdu University of Information Technology)

[AAS10-P20] Impacts of four land-use products on the simulation of land surface temperature in East China

*Yongjie Pan[1] (1.Northwest Institute of Eco-Environment and Resources, Chinese Academy of Sciences)

[AAS10-P21] **Topographic and resolution impact on the monsoon rainfall in dynamical downscaling simulation**

*Yoshiyuki Kajikawa[1,2], Tsuyoshi Yamaura[1,2] (1.Research Center for Urban Safety and Security, Kobe University, 2.RIKEN Center for Computational Science)

[E] Poster | A (Atmospheric and Hydrospheric Sciences)：A-AS Atmospheric Sciences, Meteorology & Atmospheric Environment

[A-AS11] Aerosol impacts on air quality, climate system, and our society

convener:Teppei J Yasunari(Arctic Research Center, Hokkaido University), Kyu-Myong Kim(NASA Goddard Space Flight Center), Hongbin Yu(NASA Goddard Space Flight Center), Toshihiko Takemura(Research Institute for Applied Mechanics, Kyushu University)

[AAS11-P01] The impact of urbanization and consumption patterns on China's Black Carbon emissions — Based on SDA and IO Analysis

*Zhongci Deng[1], Xiaoling Zhang[1], Ping Kang[1] (1.School of Atmospheric Sciences, Chengdu University of Information Technology, China)

[AAS11-P02] **Size-resolved hygroscopic behaviour of submicron aerosols in a megacity of Sichuan Basin**

*Liang Yuan[1] (1.Chengdu University of Information Technology)

[AAS11-P04] Comparison of absorption coefficient and black carbon concentration at Byeongcheon, South Korea using Tricolor absorption photometer (TAP) and Multiangle absorption photometer (MAAP)

*Jeonghoon Lee[1] (1.KOREATECH)

[AAS11-P05] $PM_{2.5}$ vertical concentration observations using a drone based on comparison of $PM_{2.5}$ concentration data with small sensor and atmospheric environment measurement station data

*Takashi Chiba[1], Masatsugu Kodate[1], Osamu Kiguchi[1], Makoto Inoue[1], Hirokazu Madokoro[2], Takeshi Nagayosi[1] (1.Faculty of Bioresource Sciences, Akita Prefectural University, 2.Faculty of Systems Science and Technology, Akita Prefectural University)

[AAS11-P06] **Long-term measurements of aerosol physical properties in the Noto Peninsula**

*Seiji Kubota[1], Alessia Nicosia[2], Yoko Iwamoto[3], Naoki Kaneyasu[4], Ayumi Iwata[5], Hiroshi Tsurumaru[6], Atsushi Matsuki[2] (1.Graduate School of Natural Science and Technology, Kanazawa University, 2.Institute of Nature and Environment Technology, Kanazawa University, 3.Graduate School of Biosphere Science, Hiroshima University, 4.Atmospheric Environment Research Group, National Institute of Advanced Industrial Science and Technology, 5.Department of Applied Chemistry, Faculty of Science and Technology, Keio University, 6.Tokyo Metropolitan Research Institute for Environmental Protection)

[AAS11-P07] Recurrent Neural Network (RNN), Long short-term memory (LSTM) for Aerosol Optical Depth (AOD) using NASA's MERRA-2 Reanalysis

*Mohammed Ezzat Magooda[1], Muhammed Eltahan[2], Karim Moharm[3] (1.Aerospace Engineering Dept, Cairo Univ., Cairo, Egypt, 2.Institute of Bio-Geosciences (IBG-3, Agrosphere), Forschungszentrum Jülich, Jülich, Germany, 3.Electrical Engineering Dept., Alexandria University, Alexandria, Egypt)

[AAS11-P08] Development of SCALE-Chem and its application for regional simulation targeting on urban area and mountain area of Japan

*Makiko Nakata[1], Mizuo Kajino[2], Yousuke Sato[3,4], Hisashi Yashiro[5,4], Itaru Sano[1], Sonoyo Mukai[6] (1.Kindai University, 2.Meteorological Research Institute, 3.Faculty of Science, Department of Earth and Planetary Sciences, Hokkaido University, 4.RIKEN Center for Computational Science, 5.National Center for Environmental Studies, 6.The Kyoto College of Graduate Studies for Informatics)

[AAS11-P09] Regional trends of combustion aerosol and dust in recent decades: a satellite-model integrated analysis

*Hongbin Yu[1], Yang Yang[2], Hailong Wang[1], Qian Tan[3,4], Mian Chin[1], Robert Levy[1], Lorraine Remer[5], Steven Smith[2], Tianle Yuan[1,5], Yingxi Shi[1,5], Zhibo Zhang[5], Qianqian Song[5], Paul Ginoux[6] (1.NASA Goddard Space Flight Center, 2.Pacific Northwest National Laboratory, 3.Bay Area Environmental Research Institute, 4.NASA Ames Research Center, 5.University oof Maryland Baltimore County, 6.NOAA GFDL)

[AAS11-P10] Development of a regime-dependent autoconversion parameterization using satellite observations

*Tomoki Hirata[1], Takuro Michibata[2], Toshihiko Takemura[2] (1.Interdisciplinary Graduate School of Engineering Sciences, Kyushu University, 2.RIAM Research Institute for Applied Mechanics)

[AAS11-P11] Aerosol data assimilation experiment using GCOM-C SGLI aerosol product

*Taichu Y Tanaka[1], Keiya Yumimoto[3,1], Mayumi Yoshida[2], Hiroshi Murakami[2], Takashi M. Nagao[4], Megumi Okata[2] (1.Meteorological Research Institute, Japan Meteorological Agency, 2.Earth Observation Research Center, Japan Aerospace Exploration Agency, 3.Research Institute for Applied Mechanics, Kyushu University, 4.Atmosphere and Ocean Research Institute, The University of Tokyo)

[AAS11-P12] A study on the effects of sulfate aerosols on ocean circulation and the consequent atmospheric feedback

*Yuki Kusakabe[1], Toshihiko Takemura[2] (1.Interdisciplinary Graduate School of Engineering Sciences, Kyushu University, 2.Research Institute for Applied Mechanics, Kyushu University)

[AAS11-P13] Surface air temperature response to large-scale volcanic eruptions and its relationship with ENSO

*Sho Kitabayashi[1], Hiroshi G. Takahashi[1] (1.Tokyo Metropolitan University)

[E] Poster | A (Atmospheric and Hydrospheric Sciences)：A-AS Atmospheric Sciences, Meteorology & Atmospheric Environment

[A-AS12] Weather and climate extremes in East Asian monsoon system: mechanism, predictability, and projection

convener:JinHo Yoon(GIST Gwangju Institute of Science and Technology), Shih-Yu (Simon) Wang(Utah State University), Hyungjun Kim(The Univ. of Tokyo)

[AAS12-P01] **The study on the dynamic influence factors of the interdecadal variability of the subtropical high in the Western Pacific Ocean based on the information flow method**

*Mei Hong[1], Ren Zhang[1], Kefeng Liu[1], Liang Zhao[1], Jingjing Ge[2] (1. National University of Defence Technology, 2.The 31110 troop of PLA)

[AAS12-P03] **Characteristics and Formation of a Synoptic Situation Causing Sudden Turning of Mesoscale Convective Systems over South China**

*Zhaoming Liang[1], Ying Liu[1], Jinfang Yin[1] (1.Chinese Academy of Meteorological Sciences)

[AAS12-P04] Large-Scale Circulation Anomalies Associated with Extreme Heat in South Korea and Southern–Central Japan

*Ke Xu[1] (1. Institute of Atmospheric Physics, Chinese Academy of Sciences)

[AAS12-P05] A Synoptic Assessment of Climate Models' Representation of Summer Precipitation Extremes over East China

*Yi Deng[1], Yang Hu[2], Zhimin Zhou[2] (1.Georgia Institute of Technology, Atlanta, Georgia, United States, 2.Institute of Heavy Rain, China Meteorological Administration, Wuhan, China)

[AAS12-P06] Comparison of the East Asian Summer Monsoon Activities Represented by Clouds and Precipitation

*Yunying Li[1], Yun Jia[1] (1.College of Meteorology and Oceanography, National University of Defense Technology, China)

[AAS12-P07] **Impact of the recant warming of the surrounding ocean on the heavy rain event of July 2018 in Japan**

*ATSUYOSHI MANDA[1], Satoshi Iizuka[2], Hisashi Nakamura[3], Takafumi Miyasaka[4,5,3] (1.Mie University, 2.National Research Institute for Earth Science and Disaster Resilience, 3.The University of Tokyo, 4.Japan Meteorological Business Support Center, 5.Meteorological Research Institute)

[AAS12-P08] The effects of boundary layer processes on snowfall in Yanqing Zone of 2022 Winter Olympic Games

*BO YU[1], Jia DU[1], Ruixin LIU[1], Yujue LIU[2], Ziming LI[3], Luyang XU[1] (1.Beijing Municipal Weather Forecast Center, 2.Institute of Urban Meteorology, China Meteorology Administration, 3.Environmental Meteorology Forecast Center of Beijing-Tianjin-Hebei)

[AAS12-P09] MJO Effects on the Formation and Subseasonal Predictability of Record-breaking Northeast Asian Heatwave in the Summer of 2018

*Pang-Chi Hsu[1], Yitian Qian[1], Hiroyuki Murakami[2] (1.Nanjing University of Information Science & Technology, 2.NOAA/GFDL)

[AAS12-P10] Causes of Inter-decadal Increase in Intraseasonal Rainfall Variability over Southern China around Early 1990s

*Lu Wang[1], Tim Li[2,1], Yifeng Cheng[1] (1.Nanjing University of Information Science and Technology, Nanjing, 210044, China, 2.University of Hawaii, Honolulu, HI 96822, USA)

[AAS12-P11] Consecutive extreme flooding and heat wave in Japan: Are they becoming a norm?

*JinHo Yoon[1], Shih-Yu (Simon) Wang[2], Hyungjun Kim[3], Jeehoon Jeong[1] (1.GIST Gwangju Institute of Science and Technology, 2.Utah State University, 3.University of Tokyo)

[AAS12-P12] Consecutive compound extremes of flood and heatwave within East Asia Summer Monsoon Lifecycle

*Hyungjun Kim[1], Gavin Madakumbura[2], Shih-Yu (Simon) Wang[3], JinHo Yoon[4] (1.The Univ. of Tokyo, 2.University of California, Los Angeles, 3.Utah State University, 4.Gwangju Institute of Science and Technology)

[E] Poster | A (Atmospheric and Hydrospheric Sciences)：A-AS Atmospheric Sciences, Meteorology & Atmospheric Environment

[A-AS13] New particle formation and its impacts on atmospheric chemistry

convener:Jun Zheng(Nanjing University of Information Science and Technology), Lin Wang(Fudan University)

[AAS13-P01] **Formation of sulfuric acid clusters governed by a combined effect of dimethylamine and condensation sink in polluted northern China**

Yiqun Lu[1], Gan Yang[1], Yiliang Liu[1], Yuwei Wang[1], *Lin Wang[1] (1.Fudan University)

[AAS13-P02] Role of water molecule in aerosol nucleation and air-water interface reaction: quantum chemical and molecular dynamic simulation

*Fei Xu[1] (1.Shandong University)

[AAS13-P03] The Cloud Condensation Nuclei (CCN) activity during the New Particle Formation (NPF) events in the mountain region of China inland

*Mingfu Cai[1,2], Baoling Liang[1], Qibin Sun[1], Bin Yuan[2], Min Shao[2], Haobo Tan[3], Lihong Ren[4], Jun Zhao[1,5] (1.Institue for Environmental and Climate Research, Jinan University, 2.School of Atmospheric Sciences, Sun Yat-sen University, 3.Institute of Tropical and Marine Meteorology/Guangdong Provincial Key Laboratory of Regional Numerical Weather Prediction, CMA, 4.Atmospheric Chemistry and Aerosol Research Division, Chinese Research Academy of Environmental Science, 5.Southern Laboratory of Ocean Science and Engineering (Guangdong, Zhuhai), Zhuhai)

[AAS13-P04] **Nucleation events within an industrial zone in the YRD region of China**

*Jun Zheng[1], Yan Ma[1], Dongsen Yang[1] (1.Nanjing University of Information Science and Technology)

[AAS13-P05] Effects of SO2 on secondary organic aerosol generated from photooxidation of toluene

*Weigang Wang[1] (1.Institute of Chemistry,Chinese Academy of Sciences)

[E] Poster | A (Atmospheric and Hydrospheric Sciences)：A-AS Atmospheric Sciences, Meteorology & Atmospheric Environment

[A-AS14] Extreme Events: Observations and Modeling

convener:Sridhara Nayak(Disaster Prevention Research Institute, Kyoto University), JAGABANDHU PANDA(National Institute of Technology Rourkela)

[AAS14-P01] Heat Wave Identification Using an Operational Weather Model and Analog Ensemble

*Alon Sidel[1], Weiming Hu[1], Martina Calovi[1], Guido Cervone[1,2] (1.The Pennsylvania State University, 2.National Center for Atmospheric Research)

[AAS14-P02] **Assimilation radar reflectivity to improve the simulation of a squall line case**

*Linlin Zheng[1,2], Xuexing Qiu[1] (1.Anhui Meteorological Observatory, 2.Anhui Institute of Meteorological Sciences)

[AAS14-P03] Characteristics of **Low-level Jets** in *Tianjin* with a Wind Profile Radar during 2015-2016

*Bingui Wu[1,2], Zongfei Li[1,2], Tingting Ju[3] (1.Tianjin Key Labarotory of Marine Meteorology, China, 2.Tianjin Meteorological Bureau, China, 3.Institute of Navigation College, Dalian Maritime University, China)

[AAS14-P04] Climate change impacts on extreme rainfall and their differences between weather patterns

*Masamichi Ohba[1], Soichiro Sugimoto[1] (1.Central Research Institute of Electric Power Industry)

[AAS14-P05] **Spatial and Temporal Variation of Thermodynamic Indices in Relation to Pre-Monsoon Thunderstorms over Tripura, India**

*Rajesh Kumar Sahu[1], Bhishma Tyagi[1] (1.National Institute of Technology Rourkela, Odisha, India)

[AAS14-P06] **Probabilistic Forecast of Extreme High Temperature in Extended Period with the Bayesian Model Averaging**

*Wei Zhang[1], Jianyun Gao[1], Qiaozhen Lai[2], Yanzhen Chi[3], Tonghua Su[4] (1.Fujian Institute of Meteorological Sciences, Fuzhou, China, 2.Longyan Meteorological Bureau, Longyan, China, 3.Xiamen Meteorological Bureau, Xiamen, China, 4.Fujian Climate Center, Fuzhou, China)

[AAS14-P07] **Introduction of CLoud Analysis and Ingestion System(CLAIS)**

*Ruixia Liu[1], Bingyun Yang[1], Wen Hui[1] (1.China Meteorological Administration)

[AAS14-P08] **Verification of multiple-Doppler-radar derived vertical velocity using profiler data**

*Yi-An CHEN[1,2] (1.Yu-Chieng LIOU , 2.Jou-Ping Hou)

[AAS14-P09] Characteristics of the diurnal variations flood period precipitation in Anhui during the last 30
years

*chun liu[1] (1.ANHUI METEOROLOGY SERVICE)

[AAS14-P10] **Understanding the impact of soil moisture variations on temperature extremes over the Indian region**

*Naresh Govind Ganeshi[1,2], Milind Mujumdar[1], R Krishnan[1], Mangesh Goswami[1,3], Yuhei Takaya[4], Toru Terao[5] (1.Centre for Climate Change Research, Indian Institute of Tropical Meteorology, Pune, India, 2.Department of Atmospheric and Space Sciences, Savitribai Phule Pune University, Pune, India, 3.Kavayitri Bahinabai Chaudhari North Maharashtra University, Pune, India, 4.Meteorological Research Institute, Climate Research Department, Ibaraki, Japan, 5.Faculty of Education, Kagawa University, Kagawa, Japan)

[AAS14-P11] Diurnal Variations of Low-Level Winds and Precipitation Response to Large-Scale Circulations during a Heavy Rainfall Event

*Wenxin Zeng[1], Guixing Chen[1], Yu Du[1], Zhiping Wen[2] (1.School of Atmospheric Sciences, Sun Yat-sen University, 2.Department of Atmospheric and Oceanic Sciences, and Institute of Atmospheric Sciences, Fudan University)

[AAS14-P12] **Extreme weather in the context of solar wind coupling to the magnetosphere-ionosphere-atmosphere system**

*Paul Prikryl[1,2], Vojto Rušin[3], Pavel Šťastný[4], Maroš Turňa[4], Martina Zeleňáková[5] (1.Physics Department University of New Brunswick, Canada, 2.Geomagnetic Laboratory Natural Resources Canada, 3.Astronomical Institute, Slovak

Academy of Sciences, Slovakia, 4.Slovak Hydrometeorological Institute, Slovakia, 5.Technical University of Košice, Slovakia)

[AAS14-P13] Increasing strength of typhoons in the Northwest Pacific Ocean in the recent years and their influencing seasonal factors

*Ravi Shankar Pandey[1], Yuei-An Liou[1] (1.National Central University)

[AAS14-P14] **High space resolution atmospheric simulation of severe regional precipitation and vehicle strain mode**

*Jou Ping Hou[1], Zan-Han Huang[1], Qun-Yu Fan[1] (1.Chung Cheng Institute of Technology)

[AAS14-P15] Variations of Daily Precipitation Extremes over Xinjiang Province, China

*MINGGANG LI[1], YONG ZHAO[1] (1.Chengdu University of Information Technology)

[AAS14-P16] Relevance of Background Error Statistics for Variational Radar Assimilation System

*THIRUVENGADAM PADMANABHAN[1], INDU J[1,2], SUBIMAL GHOSH[1,2] (1.Department of Civil Engineering, Indian Institute of Technology Bombay, Mumbai 400076, India., 2.Interdisciplinary Centre for Climate Studies, Indian Institute of Technology Bombay, Mumbai 400076, India.)

[AAS14-P19] Analysis of Hydroclimatic Extremes over Narmada Basin under Climate Change

*SABYASACHI SWAIN[1], SURENDRA KUMAR MISHRA[1], ASHISH PANDEY[1] (1.Indian Institute of Technology Roorkee)

[AAS14-P21] **Flashfloods and landslides along the foothills of the Himalayas: their precursors, dynamics and thermodynamics**

*Anu Gupta[1], Jun Matsumoto[1] (1.Tokyo Metropolitan University, Tokyo)

[AAS14-P22] Standardized Variability Index (SVI) : A multiscale index to assess the variability of precipitation

*Ravi kumar Guntu[1], Ankit Agarwal[1] (1.Department of Hydrology, Indian Institute of Technology Roorkee, 247667, India)

[E] Poster | A (Atmospheric and Hydrospheric Sciences)：A-OS Ocean Sciences & Ocean Environment

[A-OS16] Ocean renewable energy: resource, impacts and technologies

convener:Bahareh Kamranzad(The Hakubi Center for Advanced Research/Graduate School of Advanced Integrated Studies in Human Survivability, Kyoto University), Simon P Neill(Bangor University), Zhaoqing Yang(Pacific Northwest National Laboratory)

[AOS16-P01] On the coastal ocean modelling assessment of tidal stream and range energy resources

★Invited Papers

*Athanasios Angeloudis[1], Lucas Mackie[2], Daniel Stephen Coles[2], Anastasia Fragkou[1], Stephan C Kramer[2], Matthew D Piggott[2] (1.School of Engineering, Institute for Infrastructure and the Environment, University of Edinburgh, 2.Department of Earth Science and Engineering, Imperial College London)

[AOS16-P02] Feedbacks between tidal energy extraction and physical processes

★Invited Papers

*Simon P Neill[1], Peter Robins[1], Matthew Lewis[1] (1.Bangor Univ.)

[AOS16-P03] Climate Change Impact on Offshore Wind Energy Resources in Japan

*Masamichi Ohba[1] (1.Central Research Institute of Electric Power Industry)

[AOS16-P04] Sustainability of wave energy potential in Japan

*Bahareh Kamranzad[1] (1.The Hakubi Center for Advanced Research/Graduate School of Advanced Integrated Studies in Human Survivability, Kyoto University)

[AOS16-P05] **The effect of future climate-related variabilities of tropical monsoons in the Indian Ocean on wave energy resource around Sri Lanka**

*Bahareh Kamranzad[1], Pravin Maduwantha[3], Harsha Rathnasooriya[3], Kasun De Silva[3], Harshinie Karunarathna[2] (1.The Hakubi Center for Advanced Research/Graduate School of Advanced Integrated Studies in Human Survivability, Kyoto University, 2.Zienkiewicz Centre for Computational Engineering, College of Engineering, Bay Campus, Swansea University, 3.Department of Civil Engineering, University of Moratuwa)

[E] Poster | A (Atmospheric and Hydrospheric Sciences)：A-OS Ocean Sciences & Ocean Environment

[A-OS17] Climate variability and predictability on subseasonal to decadal timescales

convener:Takashi Mochizuki(Department of Earth and Planetary Sciences, Kyushu University), V Ramaswamy(NOAA GFDL), Yushi Morioka(Japan Agency for Marine-Earth Science and Technology)

[AOS17-P01] Predictability of two flavors of El Nino and statistical downscaling by SVD analysis using the MIROC5 seasonal prediction system

★Invited Papers

*Yukiko Imada[1], Hiroaki Tatebe[2], Masayoshi Ishii[1], Yoshimitsu Chikamoto[6], Masato Mori[4], Miki Arai[2], Shinjiro Kanae[5], Masahiro Watanabe[3], Masahide Kimoto[3] (1.Meteorological Research Institute, Japan Meteorological Agency, 2.Japan Agency for Marine-Earth Science and Technology, 3.Atmosphere and Ocean Research Institute, the University of Tokyo, 4.Research Center for Advanced Science and Technology, the University of Tokyo, 5.Tokyo Institute of Technology, 6.University of Utah)

[AOS17-P02] Parameter sensitivity analysis for predicting two types of El Niño with an intermediate coupled model

*Haibo Chen[1,2,3] (1.CAS Key Laboratory of Ocean Circulation and Waves, Institute of Oceanology, Chinese Academy of Sciences, 2.Pilot National Laboratory for Marine Science and Technology, 3.Center for Ocean Mega-Science, Chinese Academy of Sciences)

[AOS17-P03] Interannual Salinity Variability Associated with the Central Pacific and Eastern Pacific El Niños in the Tropical Pacific

*Hai Zhi[1] (1. Nanjing University of Information Science and Technology, Nanjing, China)

[AOS17-P04] Forecast of summer precipitation in the Yangtze River Valley based on South China Sea springtime sea surface salinity

*LILI ZENG[1], Raymond W. Schmitt[2], Laifang Li[3], Qiang Wang[1] (1.State Key Laboratory of Tropical Oceanography (LTO), South China Sea Institute of Oceanology, Chinese Academy of Sciences, 2.Physical Oceanography Department, Woods Hole Oceanographic Instituti, 3.Earth and Ocean Sciences, Nicholas School of the Environment, Duke University)

[AOS17-P05] Scale-dependent effects on ENSO induced by ocean chlorophyll due to interannual variability and tropical instability waves

*Rong-Hua Zhang[1] (1.Institute of Oceanology, Chinese Academy of Sciences)

[AOS17-P06] Responses of the subseasonal to seasonal atmospheric variability to the recent Pacific SST anomaly

*Tomoe Nasuno[1], Masuo Nakano[1], Hiroyuki Murakami[2], Kazuyoshi Kikuchi[3] (1.Japan Agency for Marine-Earth Science and Technology, 2.Geophysical Fluid Dynamics Laboratory , 3.International Pacific Research Center)

[AOS17-P07] Intraseasonal Variability over the Arabian Sea and Its Impact on the Indian Summer Monsoon Onset

*Jing Cha[1], Yun Qiu[1], Xinyu Lin[1], Fuwen Qiu[1] (1.TIO, MNR)

[AOS17-P08] Zonal Displacement of the Western North Pacific Subtropical High from Early to Late Summer

*Xiao Dong[1], Chao He[2], Renping Lin[1] (1.Institute of Atmospheric Physics, Chinese Academy of Sciences, 2.Institute for Environmental and Climate Research, Jinan University, Guangzhou, China)

[AOS17-P09] Impacts of the Indian Ocean Dipole on Sea Level and Gyre Circulation of the Western Tropical Pacific Ocean

*Jing Duan[1,2,3], Yuanlong Li[1,2,3], Lei Zhang[4], Fan Wang[1,2,3] (1.Institute of Oceanology, Chinese Academy of Sciences, 2.Function Laboratory for Ocean Dynamics and Climate, Qingdao National Laboratory for Marine Science and Technology, 3.Center for Ocean Mega-Science, Chinese Academy of Sciences, 4.Department of Atmospheric and Oceanic Sciences, University of Colorado)

[AOS17-P10] Predictability study on the seasonal reduction of the upstream Kuroshio transport and related targeted observation application.

*Kun Zhang[1,2] (1.Institute of Oceanology, Chinese Academy of Sciences, 2.Center for Ocean Mega-Science, Chinese Academy of Sciences)

[AOS17-P11] Remote and local processes controlling decadal sea-ice variability in the Weddell Sea

*Yushi Morioka[1], Swadhin Behera[1] (1.Japan Agency for Marine-Earth Science and Technology)

[AOS17-P12] **Can tropical Pacific winds enhance the footprint of the Interdecadal Pacific Oscillation on the upper-ocean heat content in the South China Sea?**

*Fuan Xiao[1], Dongxiao Wang[2] (1.Guangzhou Univ., 2.Sun Yat-sen Univ.)

[AOS17-P13] The Atlantic SST influences on the Pacific subdecadal variability

*Takashi Mochizuki[1,2], Masahiro Watanabe[3], Masahide Kimoto[3] (1.Department of Earth and Planetary Sciences, Kyushu University, 2.Japan Agency for Marine-Earth Science and Technology, 3.Atmosphere and Ocean Research Institute, The University of Tokyo)

[AOS17-P14] **An evaluation of the Decadal Climate Prediction Experiments by the BCC_CSM Model**

*Yongjie Fang[1], Tongwen Wu[1], Xiaoge Xin[1] (1.National Climate Center, Chinese Meteorological Administration)

[E] Poster | A (Atmospheric and Hydrospheric Sciences)：A-OS Ocean Sciences & Ocean Environment

[A-OS19] Marine ecosystems and biogeochemical cycles: theory, observation and modeling

convener:Takafumi Hirata(Arctic Research Center, Hokkaido University), Shin-ichi Ito(Atmosphere and Ocean Research Institute, The University of Tokyo), Enrique N Curchitser(Rutgers University New Brunswick), Eileen E Hofmann(Old Dominion University)

[AOS19-P01] A modeling study of early diagenesis using an ocean sediment model

*Hidetaka Kobayashi[1], Akira Oka[1] (1.Atmosphere and Ocean Research Institute, The University of Tokyo)

[AOS19-P02] **A simulation on seasonal variation of bottom oxygen in the Bohai Sea**

*Haiyan Zhang[1], Hao Wei[1], Liang Zhao[2] (1.Tianjing University, 2.Tianjin University of Science & Technology)

[AOS19-P03] Particulate organic carbon fluxes of the upper ocean response to typhoons in the northern South China Sea

*CHUNG-YU CHIANG[1], Yun Hsuan Lu[1], Yung-Yen Shih[1] (1.R.O.C NAVAL ACADEMY Dept. of Applied Science)

[AOS19-P04] **Mid-latitude Winter Carbon Export Is Missed Using Prescribed BCG-Argo Sampling ProtocolsAbstract**

*Xiaogang Xing[1], Mark Wells[2], Shuangling Chen[1], Yunwei Yan[1], Fei Chai[1,2] (1.Second Institute of Oceanography, MNR, China, 2.University of Maine, US)

[AOS19-P05] **Effects on ocean biology induced by El Niño-accompanied positive freshwater flux anomalies in the tropical Pacific**

*Feng Tian[1,2,3,4], Rong-Hua Zhang[1,2,3,4], Xiujun Wang[5] (1.Institute of Oceanology, Chinese Academy of Sciences, 2.Pilot National Laboratory for Marine Science and Technology, Qingdao, 3.Center for Ocean Mega-Science, Chinese Academy of Sciences, 4.University of Chinese Academy of Sciences, Beijing , 5.College of Global Change and Earth System Science, Beijing Normal University, and Joint Center for Global Change Studies, Beijing)

[AOS19-P06] Spatial and temporal variability of biological carbon pump in the northern South China Sea

*Jia-Jang Hung[1], Zong-Ying Lin, Ching-Han Tung, Shao-Hung Peng, Yen-Hui Lin (1.Department of Oceanography, National Sun Yat Sen University, Kaohsiung, Taiwan)

[AOS19-P07] Seasonal and Inter-annual variability of chlorophyll-*a* in the Gulf of Thailand

*Dudsadee Leenawarat[1], Anukul Buranapratheprat[2], Joji Ishizaka[3] (1.Graduate School of Environmental Studies, Nagoya University, 2.Department of Aquatic Science, Faculty of Science, Burapha University, Thailand , 3.Institute for Space-Earth Environmental Research, Nagoya University, Japan)

[AOS19-P08] **Comparison of spatiotemporal variety between *in-situ* and remote surface chlorophyll in the northern South China Sea**

*Yun Hsuan Lu[1], Ko Mei Lin[1], Yung Yen Shin[1] (1.Department of Applied Science, R.O.C Naval Academy)

[AOS19-P09] Effects of the Kuroshio meander on phytoplankton in Japanese waters as observed by satellite remote sensing

Satoshi Kitaoka[2], *Takafumi Hirata[1], Keiko Sato[1] (1.Arctic Research Center, Hokkaido University, 2.Faculty of Environmental Earth Science)

[AOS19-P10] Declining catch of Japanese sandeels

*Shin-ichi Ito[1] (1.Atmosphere and Ocean Research Institute, The University of Tokyo)

[AOS19-P11] Comparative study on respiration of Japanese anchovy (*Engraulis japonicus*) around Japan

*Shin-ichi Ito[1], Chenying Guo[1], Megumi Enomoto[1], Tomoya Aono[1], Michio Yoneda[2], Michiya Matsuyama[3], Takashi Kitagawa[1], Motomitsu Takahashi[2] (1.Atmosphere and Ocean Research Institute, The University of Tokyo, 2.Fisheries Research and Education Agency Japan, 3.Kyushu University)

[AOS19-P12] Estimation of migratory routes of Japanese sardine in the Tsushima Warm Current area by combining the microscale stable isotopic analysis of otoliths and a data assimilation mode

*Tomoya Aono[1,2], Tatsuya Sakamoto[2,3], Tohya Yasuda[4,3], Motomitsu Takahashi[3], Toyoho Ishimura[1] (1.National Institute of Technology, Ibaraki College, 2.Atmosphere and Ocean Research Institute, The University of Tokyo,

3.Seikai Nat. Fish. Res. Inst., 4.Nat. Res. Inst. Fish. Sci.)

[AOS19-P13] The transition of the experienced environment of jack mackerel in the East China Sea

*Tomihiko Higuchi[1], Motomitsu Takahashi[2], Kotaro Shirai[1], Shin-ichi Ito[1] (1.Atmosphere and Ocean Research Institute, The University of Tokyo, 2.Seikai National Fisheries Research Institute, FRA)

[AOS19-P14] Discussion on future collaboration

*Shin-ichi Ito[1], Takafumi Hirata[2] (1.Atmosphere and Ocean Research Institute, The University of Tokyo, 2.Hokkaido University)

[AOS19-P15] **Interannual salinity variability in the Western Tropical Pacific and along the Kuroshio**

*Chevarria Saravia Ricardo[1], Daniel Andres Lizarbe[1], Takeyoshi Nagai[2] (1.National Agrarian University La Molina, 2.Tokyo University of Marine Science and Technology)

[AOS19-P16] Phytoplankton blooms along the Kuroshio due to the Large Meander

*Lizarbe Andres Daniel[1], Ricardo Saravia Chevarria[1], Takeyoshi Nagai[2], Takafumi Hirata[3] (1.National Agrarian University La Molina, 2.Tokyo University of Marine Science and Technology, 3.Hokkaido University)

[E] Poster | A (Atmospheric and Hydrospheric Sciences)：A-OS Ocean Sciences & Ocean Environment

[A-OS20] Coastal physical processes associated with mixing, eddies, and internal waves

convener:Taira Nagai(Graduate School of Science, The University of Tokyo), Eisuke Tsutsumi(Atmosphere and Ocean Research Institute, The University of Tokyo), Eiji Masunaga(Ibaraki University)

[AOS20-P01] Water exchange between the Bohai and Yellow Seas in response to high winds in winter

*Chao Ma[1,3], Xia Ju[2,3], Xiuquan Wan[1,3] (1.Ocean Univ. China, 2.Inst. Oceanog. 1, MNR, 3.Pilot Natl. Lab. Marine Sci. & Technol.)

[AOS20-P02] Eddy Induced Transport of Saline Kuroshio Water Into the Northern South China Sea

*Tao Xing[1,2], Yikai Yang[2] (1.MLR Key Laboratory of Marine Mineral Resources, Guangzhou Marine Geological Survey, 2.South China Sea Institute of Oceanology, Chinese Academy of Sciences)

[AOS20-P03] A temperature description of vortex street around the Green Island off the eastern coast of Taiwan

*Chia-Ying Ho[1], Hung-Jen Lee[1] (1.National Taiwan Ocean University)

[AOS20-P04] Summertime Upwelling in the Central South China Sea: Interannual Variability and Associated Dynamics

*Yi-Chia Hsin[1], Mai-Han Ngo[1] (1.Academia Sinica)

[E] Poster | A (Atmospheric and Hydrospheric Sciences)：A-OS Ocean Sciences & Ocean Environment

[A-OS21] Dynamics of oceanic and atmospheric waves, vortices, and circulations

convener:Yuki Tanaka(Fukui Prefectural University), Ryo Furue(APL/JAMSTEC), Yukiharu Hisaki(University of the Ryukyus), Norihiko Sugimoto(Keio University, Department of Physics)

[AOS21-P01] Data Assimilation of the Venus Atmosphere to Reproduce Planetary-scale Wave

*Yukiko Fujisawa[1], Mimo Shirasaka[2], Norihiko Sugimoto[1], Asako Hosono[3], Mirai Abe[1], Hiroki Ando[4], Masahiro Takagi[4], Masaru Yamamoto[5] (1.Keio University, 2.Seisen Senior High School, 3.Toshimagaoka Women High School, 4.Kyoto Sangyo University, 5.Research Institute for Applied Mechanics, Kyushu University)

[AOS21-P02] The study for designing the future Venus atmosphere observing mission of radio occultation measurement among small satellites using data assimilation

*Asako Hosono[1], Yukiko Fujisawa[2], Norihiko Sugimoto[2], Mirai Abe[2], Yukako Kikuchi[3], Tomotaka Yamamoto[4], Yosuke Kawabata[4], Satoshi Ikari[4], Hiroki Ando[5], Masahiro Takagi[5], Itziar Garate Lopez[6], Sebastien Lebonnois[7], Chi Ao[8] (1.Toshimagaoka Women High School, 2.Keio University, 3.Yokohama Futaba High School, 4.Tokyo University, 5.Kyoto Sangyo University, 6.Euskal Herriko Unibertsitatea, 7.Sorbonne Universite, 8.Jet Propulsion Laboratory)

[AOS21-P03] Verification of wave prediction model by drifting buoy observations

*Yukiharu Hisaki[1] (1.University of the Ryukyus)

[AOS21-P04] Size distribution of marine microplastics: A statistical mechanics approach

*Kunihiro Aoki[1], Ryo Furue[1] (1.Japan Agency for Marine Earth Science and Technology)

[AOS21-P05] Interannual modulation of intraseasonal wave activity over the equatorial Indian Ocean

*Tomomichi Ogata[1] (1.JAMSTEC Application Lab)

[AOS21-P06] On the statistics of deep zonal jets in the eastern North Pacific in an ensemble of eddy-resolving ocean general circulation model runs

*Ryo Furue[1], Masami Nonaka[1], Hideharu Sasaki[1] (1.APL/JAMSTEC)

[AOS21-P07] Predictability of interannual-to-decadal variability in eddy activity in the Kuroshio Extension

★Invited Papers

*Masami Nonaka[1], Hideharu Sasaki[1], Bunmei Taguchi[2], Niklas Schneider[3] (1.Application Laboratory, Japan Agency for Marine-Earth Science and Technology, 2.University of Toyama, 3.IPRC, University of Toyama)

[AOS21-P08] Surface water pathways in the subtropical-subarctic intergyre frontal zone of the western North Pacific

*Hatsumi Nishikawa[1], Humio Mitsudera[1], Takeshi Okunishi[2], Shin-ichi Ito[3], Taku Wagawa[4], Daisuke Hasegawa[2], Toru Miyama[5], Hitoshi Kaneko[3] (1.Institute of Low Temperature Science, Hokkaido University, 2.Tohoku National Fisheries Research Institute, 3.Atmosphere and Ocean Research Institute, The University of Tokyo, 4.Japan Sea National Fisheries Research Institute, 5.Japan Agency for Marine-Earth Science and Technology)

[AOS21-P09] Genesis of Spiciness Anomaly in the Northeast Pacific

*Yongqing Guo[1], Meng Wei[2] (1.Zhejiang Ocean University, 2.First Institute of Oceanography, Ministry of Natural Resources of the People's Republic of China)

[AOS21-P10] **Intensified Deep Ocean Variability Induced by Topographic Rossby Waves at the Pacific Yap-Mariana Junction**

*Qiang Ma[1], Jianing Wang[1], Fan Wang[1], Yilong Lyu[1] (1.Institute of Oceanology, Chinese Academy of Sciences)

[AOS21-P11] Direct measurements of near-surface upwelling and vertical heat flux in marginal ice zone of the Canada Basin, Arctic Ocean

*EunYae Son[1], Yusuke Kawaguchi[2] (1.Graduate School of Frontier Sciences, University of Tokyo, 2.Atmosphere and Ocean Research Institute, The University of Tokyo)

[AOS21-P12] Symmetric and Mixed Layer Instability at a Sharp Ocean Front

*Yuki Tanaka[1] (1.Graduate School of Science, The University of Tokyo)

[AOS21-P14] Reconstruct the 1970 Bhola Cyclone and Analysis the Effects of Cyclone Track and Tide to the Flooding Area

*Po-Sen Tseng[1], Tso-Ren Wu[1], CHIA-CHUN HSU[1], Chun-Wei Lin[1], Shun-Chun Chunag[1], Mei-Hui Chunag[1] (1.Graduate Institute of Hydrological and Oceanic Sciences, Nation Central University)

[AOS21-P15] Reconstruct the 1845 Kouhu Storm Surge Event with Ensemble Method

*CHIA-CHUN HSU[1], Tso-Ren Wu[1], Po-Sen Tseng[1], Shu-Chun Chuang[1], Chun-Wei Lin[1], Mei-Hui Chuang[1] (1.Graduate Institute of Hydrological and Oceanic Sciences, National Central University)

[AOS21-P16] Coastal Geographic Surveying Result on Gyoam beach in South Korea by Integrated Coastal Zone Management

*DongSeob Song[1] (1.Kangwon National University)

[E] Poster | A (Atmospheric and Hydrospheric Sciences)：A-OS Ocean Sciences & Ocean Environment

[A-OS22] Physical, chemical and biological processes and variability in the Indian Ocean

convener:Yukio Masumoto(Graduate School of Science, The University of Tokyo), Hiroaki Saito(Atmosphere and Ocean Research Institute, The University of Tokyo)

[AOS22-P01] IndOOS-2: A Roadmap to Better Observations of the Rapidly Warming Indian Ocean

Lisa M Beal[1], Jérôme Vialard[2], Matthew K Roxy[3], *Motoki Nagura[4] (1.Rosenstiel School of Marine and Atmospheric Science, University of Miami, 2.Institut de Recherche pour le Développement (IRD)/LOCEAN, 3.Indian Institute of Tropical Meteorology (IITM), 4.Japan Agency for Marine-Earth Science and Technology)

[AOS22-P02] The imprint of climate variability on the Maritime Continent surface ocean biology

*Eko Siswanto[1], Takanori Horii[1], Iskhaq Iskandar[2], Jonson Lumban Gaol[3], Riza Yuliratno Setiawan[4] (1.Japan Agency for Marine-Earth Science and Technology, 2.Sriwijaya University, 3.IPB University, 4.Gadjah Mada University)

[AOS22-P03] Particulate organic carbon distribution and primary production of Java-Sumatra upwelling system of Eastern Indian Ocean

*Edwards Taufiqurrahman[1], A'an Johan Wahyudi[1] (1.Research Center for Oceanography - Indonesian Institute of Sciences)

[AOS22-P04] The Pathways and Timescales of Indonesian Throughflow

*ISKANDAR MOCHAMAD RIZA[1], Toshio Suga[1], Kelvin John Richards[2], Hideharu Sasaki[3] (1.Graduate School of Sciences, Tohoku University, 2.International Pacific Research Center, University of Hawaii, 3.Application Laboratory, Japan Agency for Marine-Earth Science and Technology)

[AOS22-P05] Observation in the Java-Sumatra upwelling region during positive IOD in 2019

*Iwao Ueki[1] (1.JAMSTEC Japan Agency for Marine-Earth Science and Technology)

[AOS22-P06] A role of eastward-propagating intraseasonal oscillation in controlling coastal upwelling southwest of Sumatra

*Takanori Horii[1], Iwao Ueki[1] (1.Global Ocean Observation Research Center, Japan Agency for Marine-Earth Science and Technology (JAMSTEC))

[AOS22-P07] Distribution and isotopic composition of N_2O in the eastern Indian Ocean

*Sakae Toyoda[1], Kotaro Terajima[1], Naohiro Yoshida[2], Chisato Yoshikawa[3], Akiko Makabe[4], Fuminori Hashihama[5], Hiroshi Ogawa[6] (1.School of Materials and Chemical Technology, Tokyo Institute of Technology, 2.Earth-Life Science Institute, Tokyo Institute of Technology, 3.Research Institute for Marine Resources Utilization, Japan Agency for Marine-Earth Science and Technology, 4.Institute for Extra-cutting-edge Science and Technology Avant-garde Research (X-star), Japan Agency for Marine-Earth Science and Technology, 5.Department of Ocean Sciences, Tokyo University of Marine Science and Technology, 6.Atmosphere and Ocean Research Institute, The University of Tokyo)

[AOS22-P08] Nitrate isotopes in the Bay of Bengal

*Chisato Yoshikawa[1], Akiko Makabe[1], Yohei Matsui[1], Sakae Toyoda[2], Makio Honda[1], Naohiko Ohkouchi[1] (1.Japan Agency for Marine-Earth Science and Technology, 2.Tokyo Institute of Technology)

[E] Poster | A (Atmospheric and Hydrospheric Sciences)：A-OS Ocean Sciences & Ocean Environment

[A-OS23] Atlantic climate variability, and its global impacts and predictability

convener:Ingo Richter(JAMSTEC Japan Agency for Marine-Earth Science and Technology), Hiroki Tokinaga(Research Institute for Applied Mechanics, Kyushu University), Andrea Taschetto(University of New South Wales), Noel S Keenlyside(Geophysical Institute Bergen)

[AOS23-P01] **An evaluation of the performance of CMIP6 models in the tropical Atlantic: mean state, variability, and remote impacts**

*Ingo Richter[1], Hiroki Tokinaga[2] (1.JAMSTEC Japan Agency for Marine-Earth Science and Technology, 2.Kyushu University, Kasuga, Fukuoka, Japan)

[AOS23-P02] Decadal variability of the Benguela Niño/Niña

*Hiroki Tokinaga[1] (1.Research Institute for Applied Mechanics, Kyushu University)

[AOS23-P03] Climate change in the tropical Atlantic

*Noel S Keenlyside[1], Lander Crespo[1], Shunya Koseki[1], Ingo Richter[2], Lea Svendsen[1] (1.Geophysical Institute, University of Bergen and Bjerknes Centre for Climate Research, Norway, 2.JAMSTEC, Japan)

[AOS23-P04] The extraordinary Atlantic Nino of 2019/2020

*Ingo Richter[1] (1.JAMSTEC Japan Agency for Marine-Earth Science and Technology)

[AOS23-P05] Impact of springtime cross-equatorial SST gradient on the Atlantic Niño/Niña

Takaaki Yokoi[1], *Hiroki Tokinaga[1] (1.Research Institute for Applied Mechanics, Kyushu University)

[AOS23-P06] Investigating South American monsoon during mid-Pliocene

*Andrea Taschetto[1], Gabriel Pontes[2], Ilana Wainer[2], Alex Sen Gupta[1] (1.Climate Change Research Centre and ARC Centre for Excellence in Climate Extremes, University of New South Wales, Australia, 2.Department of Physical Oceanography, University of São Paulo, Brazil)

[E] Poster | A (Atmospheric and Hydrospheric Sciences)：A-OS Ocean Sciences & Ocean Environment

[A-OS24] Exploring new frontiers of oceanic mixing research in the next decade

convener:Toshiyuki Hibiya(Department of Earth and Planetary Science, Graduate School of Science, University of Tokyo), Ichiro Yasuda(Atmosphere and Ocean Research Institute, The University of Tokyo), Lakshmi Kantha(Aerospace Engineering Sciences, University of Colorado, Boulder, Colorado, USA)

[AOS24-P01] Synchronized interdecadal periodic variations behind regime shifts in Pacific Decadal Oscillation

*Masaki Hamamoto[1], Ichiro Yasuda[1] (1.Atmosphere and Ocean Research Institute, The University of Tokyo)

[AOS24-P02] Role of the vertical mixing in the bottom water warming in a new ocean state estimate using tidally induced mixing parameterization

*Satoshi Osafune[1], Shuhei Masuda[1], Nozomi Sugiura[1], Toshimasa Doi[1], Tadashi Hemmi[1] (1.Japan Agency for Marine-Earth Science and Technology)

[AOS24-P03] Global distribution of the ocean vertical diffusivity derived from an ocean tracer inverse model approach

*Akira Oka[1] (1.Atmosphere and Ocean Research Institute, The University of Tokyo)

[AOS24-P05] A theoretical and observational study of the vertical decay scale of tidal mixing over rough seafloor topography

Takahiro Yanagimachi[1], *Toshiyuki Hibiya[1] (1.Department of Earth and Planetary Science, Graduate School of Science, University of Tokyo)

[AOS24-P07] Estimation of energy source of near-inertial oscillations observed at abyssal depths in Main Gap of the Emperor Seamount Chain

*Daigo Yanagimoto[1] (1.Atmosphere and Ocean Research Institute University of Tokyo)

[AOS24-P08] Characteristics of Vertically Propagating Near-inertial Internal Waves in the Japan Sea Excited in Northern Area

*Akie Sakai[1], Tomoharu Senjyu[2], Kosuke Mori[3], Takahiro Endo[2] (1.Department of Earth System Science and Technology, Interdisciplinary Graduate School of Engineering Sciences, Kyushu University, 2.Research Institute for Applied Mechanics, Kyushu University, 3.Okinawa Marine Science Support Section, Okinawa Institute of Science and Technology Graduate University)

[AOS24-P09] Near-inertial shear and widespread intensified thermocline mixing in a seasonally stratified shelf sea

*Wei Yang[1] (1.Tianjin University)

[AOS24-P10] The estimation of the vertical mixing in double diffusive favorable regions of the Indian Ocean by CTD-attached microstructure measurement

*Yusuke Sasaki[1], Ichiro Yasuda[1], Katsuro Katsumata[2], Shinya Kouketsu[2], Hiroshi Uchida[2] (1.Atmosphere and Ocean Research Institute, The University of Tokyo, 2. Japan Agency of Marine-Earth Science and Technology)

[AOS24-P11] Turbulence, internal waves, and associated nutrient supply caused by the Kuroshio southeast of Kyushu

*Duran Gomez Silvana Gloria[1], Takeyoshi Nagai[2] (1.Graduate School of Tokyo University of Marine Science and Technology, 2.Tokyo University of Marine Science and Technology)

[AOS24-P12] Revisit of typhoon's effect on biogeochemistry in the western Pacific subtropical-oligotrophic region

*Makio Honda[1], Yutaka Yoshikawa[2] (1.Japan Agency for Marine-Earth Science and Technology, 2.Kyoto University)

[AOS24-P13] Study on the vertical mixing and nutrient supply off the east coast of the Kamchatka

*kimura shino[1] (1.The Univercity of Tokyo)

[AOS24-P14] Reproduction of Iron-rich Intermediate Water in the Subarctic North Pacific by High-resolution Biogeochemical Model

*Hatsumi Nishikawa[1], Humio Mitsudera[1] (1.Institute of Low Temperature Science, Hokkaido University)

[AOS24-P15] Role of tidal mixing on biogeochemical cycling in the northwestern North Pacific

*Kazuhiro Misumi[1], Tsubono Takaki[2], Daisuke Tsumune[2] (1.Planning Group, Central Research Institute of Electric Power Industry, 2.Environmental Science Research Laboratory, Central Research Institute of Electric Power Industry)

[AOS24-P16] Interannual variations in primary productivity in the North Pacific western subarctic gyre (WSG), assessed by using settling particle delta N-15

*Yoshihisa Mino[1], Makio Honda[2], Fujiki Tetsuichi[2], Minoru Kitamura[2], Naomi Harada[2] (1.Nagoya University, 2.Japan Agency for Marine-Earth Science and Technology)

[AOS24-P17] Seasonal dynamics of zooplankton at station K2, NW Pacific, reconstructed from archived ADCP data

*Minoru Kitamura[1], Motoyo Itho[1] (1.Japan Agency for Marine-Earth Science and Technology)

[AOS24-P18] Variations in egg production rates of *Calanus sinicus* (Copepoda: Calanoida) estimated by gonad morphology

*Kiyotaka Hidaka[1], Shinji Shimode[2], Takashi Fushima[2] (1.Japan Fisheries Research and Education Agency, 2.Yokohama National University)

[E] Poster | A (Atmospheric and Hydrospheric Sciences)：A-OS Ocean Sciences & Ocean Environment

[A-OS25] Continental-Oceanic Mutual Interaction: Planetary scale Material Circulation

convener:Yosuke Alexandre Yamashiki(Earth & Planetary Water Resources Assessment Laboratory Graduate School of Advanced Integrated Studies in Human Survivability Kyoto University), Yukio Masumoto(Graduate School of Science, The University of Tokyo), Swadhin Behera(Climate Variation Predictability and Applicability Research Group, Application Laboratory, JAMSTEC, 3173-25 Showa-machi, Yokohama 236-0001), Takanori Sasaki(Department of Astronomy, Kyoto University)

[AOS25-P01] Ionizing Radiation at the Martian Surface during Young and Current Sun

*Yosuke Alexandre Yamashiki[1], Hiroyuki Maehara[2], Vladimir Airapetian[3], Yuta Notsu[4], Tatsuhiko Sato[5] (1.Earth & Planetary Water Resources Assessment Laboratory Graduate School of Advanced Integrated Studies in Human Survivability Kyoto University, 2.Okayama Branch Office, Subaru Telescope, National Astronomical Observatory of Japan, 3.NASA/GSFC, 4.Laboratory for Atmospheric and Space Physics, University of Colorado Boulder, 5.Nuclear Science and Engineering Center, Japan Atomic Energy Agency (JAEA),)

[AOS25-P02] The internal ocean in a closure environment

*Hiroaki Sato[1], Tomomi Kubo[1], Ami Hashimoto[1], Hayate Hirai[1], Yusaku Miyashita[1], Yosuke Alexandre Yamashiki[3], Katie Morgan[2] (1.Kyoto University, 2.University of Arizona, 3.Graduate School of Advanced Integrated Studies in Human Survivability Kyoto University)

[AOS25-P03] **Japanese small water supply facility and depopulation**

*Sayaka Hori[1] (1.Kyoto University)

[AOS25-P04] A Method to Forecast Extreme River Discharges from Typhoon Hagibis 2019 and Western Japan Floods 2018

*Josko Troselj[1], Han Soo Lee[1] (1.Graduate School for International Development and Cooperation, Hiroshima University)

[AOS25-P05] Scientific illustration and Computer Graphics of exoplanets in *Exo* Kyoto's extrasolar planet catalog

*Nami Kimura[1], Yosuke Alexandre Yamashiki[1], Hiroaki Sato[1] (1.Kyoto University)

[AOS25-P06] Methodology for Recognizing Marine Creature by Using Neural Network Based Image Recognition in Shirahama Area: Example of *Dendronephthya gigantea*

*Okamura Shin[1], Yamashiki Yosuke[1] (1.Graduate School of Advanced Integrated Studies in Human Survivability Kyoto University)

[AOS25-P07] Continental-Oceanic Material and Non-Material Interaction: Investigating Methodologies for Heterogenous Dataset Integration

*Andrea Yuri Flores Urushima[1], Yosuke Alexandre Yamashiki[1], Takeshi Ise[1], Yoh Yamashita[1] (1.Kyoto University)

[AOS25-P08] Toward a global SPH simulation of an icy moon with internal ocean

*keiya murashima[1], Takanori Sasaki[1], Natsuki Hosono[2], Yosuke Alexandre Yamashiki[1] (1.Kyoto University, 2.Japan Agency for Marine-Earth Science and Technology)

[E] Poster | A (Atmospheric and Hydrospheric Sciences)：A-HW Hydrology & Water Environment

[A-HW30] Hydrology & Water Environment

convener:Ayumi Kotani(Graduate School of Bioagricultural Sciences, Nagoya University), Takeshi Hayashi(Faculty of Education and Human Studies, Akita University), Keisuke Fukushi(Institute of Nature & Environmental Technology, Kanazawa University), Masahiro Tanoue(School of Engineering, The University of Tokyo)

[AHW30-P01] Impact of climate change on the surface water balance and groundwater level in the Kurobe River basin, Japan

*Takuya Matsuura[1], TEBAKARI TAICHI[1] (1.Toyama prefectural University)

[AHW30-P02] **Assessment of the precipitation characteristics and identification of urban flooding hotspots for an Indian satellite town**

*Osheen Mehta[1], Mitthan Lal Kansal[1] (1.Indian Institute of Technology Roorkee)

[AHW30-P03] Dynamics of terrestrial water storage in three major river basins over Peninsular India

*Abhishek .[1], Tsuyoshi Kinouchi[2] (1.Indian Institute of Technology Roorkee, 2.Tokyo Institute of Technology)

[AHW30-P04] Comparing constant dispersivity with scale-dependent one: for heated water injection case

*Ye-Chen Lin[1], Hund-Der Yeh[1] (1.National Chiao Tung University)

[AHW30-P05] **Similarities and differences among ten global water models in modelling water use**

*Camelia Eliza Telteu[1], Hannes Müller Schmied [1,2], Wim Thiery [3], Guoyong Leng [4], Peter Burek [5], Xingcai Liu [4], Julien Eric Stanislas Boulange [6], Lauren Paige Seaby[7], Manolis Grillakis[8], Yusuke Satoh [6], Oldrich Rakovec[9], Tobias Stacke[10], Jinfeng Chang[11,5], Niko Wanders[12], Harsh Lovekumar Shah [13], Ganquan Mao[14], Aristeidis Koutroulis [8], Yadu Pokhrel [15], Luis Samaniego [9], Yoshihide Wada [5], Vimal Mishra [13], Junguo Liu [14], Petra Döll [1,2], Simon Newland Gosling [16], Jacob Schewe [7], Fang Zhao [17] (1.Institute of Physical Geography, Goethe University Frankfurt, Frankfurt am Main, Germany, 2.Senckenberg Leibniz Biodiversity and Climate Research Center, Frankfurt am Main, Germany, 3.Department of Hydrology and Hydraulic Engineering, Vrije Universiteit Brussel, Brussels, Belgium, 4.Key Laboratory of Water Cycle and Related Land Surface Processes, Institute of Geographic Sciences and Natural Resources Research, Chinese Academy of Sciences, Beijing, China, 5.International Institute for Applied Systems Analysis, Laxenburg, Austria , 6.National Institute for Environmental Studies, Tsukuba, Japan , 7.Potsdam Institute for Climate Impact Research, Potsdam, Germany , 8.School of Environmental Engineering, Technical University of Crete, Chania, Greece , 9.Helmholtz Centre for Environmental Research, Leipzig, Germany , 10.Institute of Coastal Research, Helmholtz-Zentrum Geesthacht, Geesthacht, Germany, 11.Laboratoire des Sciences du Climat et de l'Environnement, Gif-sur-Yvette, France, 12.Department of Physical Geography, Utrecht University, Utrecht, the Netherlands, 13.Indian Institute of Technology Gandhinagar, Palaj, Gandhinagar, India, 14.School of Environmental Science and Engineering, Southern University of Science and Technology, Shenzhen, China , 15.Department of Civil and Environmental Engineering, Michigan State University, East Lansing, Michigan, United States of America , 16.School of Geography, University of Nottingham, Nottingham, United Kingdom of Great Britain and Northern Ireland, 17.School of Geographic Sciences, East China Normal University, Shanghai, China)

[AHW30-P06] Discussion on the correlation between professional characteristics and willingness to pay for ecosystem services

*Li-chun Peng[1], Yu-pin Lin[1], Wan-yu Lien[1] (1.National Taiwan University)

[AHW30-P07] Seasonal variability of stable isotopes in precipitation over Indonesia observed for 2010-2018

*Kimpei Ichiyanagi[1], Takayuki Uesugi[1], Rusmawan Suwarman[2], Halda Aditya Belgaman[3], Masahiro TANOUE[4] (1.Kumamoto University, 2.Bandung Institute of Technology, 3.Badan Pengkajian dan Penerapan Teknologi, 4.Shibaura Institute of Technology)

[AHW30-P08] Finding the optimal time for the integration in Lagrangian analysis for the best estimation of moisture sources.

*Raquel Nieto[1], Luis Gimeno[1] (1.University of Vigo)

[AHW30-P09] ATMOSPHERIC MOISTURE SOURCES ASSOCIATED WITH EXTREME PRECIPITATION DURING THE PEAK PRECIPITATION MONTH

*Luis Gimeno[1], Marta Vazquez[1,2,3], Raquel NIETO [1], Margarida Liberato[2,3] (1.Environmental Physics Laboratory (EPhysLab), CIM-UVigo, Universidade de Vigo, Ourense, Spain, 2.Instituto Dom Luiz (IDL), Faculdade de Ciências,

Universidade de Lisboa, 1749-016 Lisboa, Portugal, 3.Escola de Ciências e Tecnologia, Universidade de Trás-os-Montes e Alto Douro, Vila Real, Portugal)

[AHW30-P10] SEASONAL VARIATION OF DISSOLVED TRACE ELEMNTS IN LAKE KIBA-GATA

*Ariunsanaa BATERDENE[1], Seiya NAGAO[2], Keisuke Fukushi[2], Kohei Sakaguchi[1], Tetsuya Matsunaka[2] (1.Graduate School of Natural Science and Technology Kanazawa University, 2.Institute of Nature and Environmental Technology, Kanazawa University)

[AHW30-P12] Study on the origin of hot spring water using the deep part of Inubohsaki Onsen's core.

*Satoko Tezuka[1], Mana Kamata[1] (1.Chiba Institute of science)

[AHW30-P13] *Lysimeter experiments to assess the influence of afforested vegetation on effective infiltration and recharge in a semi- arid area*

*Zaiyong Zhang[1], Wenke Wang[1], Chengcheng Gong[1], Harrie-Jan Hendricks Franssen[2], Philip Brunner[3] (1.Chang'an University, 2.Agrosphere (IBG-3), Forschungszentrum Jülich GmbH, Jülich, Germany, 3.Center for Hydrogeology and Geothermics, (CHYN), University of Neuchatel, Switzerland)

[AHW30-P14] Development of a Multi-function Water Depth Sensor in the Irrigated Paddy Fields for Water Resource Management and Precision Agriculture

*Chun-Yen KUO[1] (1.National United University)

[AHW30-P15] Dynamic calibration of tipping-bucket rain gauges and flow meters for precise measurements of rainfall partitioning

*Shin'ichi Iida[1], Takanori Shimizu[1], Yoshinori Shinohara[2], Tomo'omi Kumagai[3], Darryl E. Carlyle-Moses[4], Delphis F. Levia[5] (1.Forestry and Forest Products Research Institute, 2.University of Miyazaki, 3.University of Tokyo, 4.Thompson Rivers University, 5.University of Delaware)

[AHW30-P16] Understory biomass measurement based on SfM data by a manual low-flying drone under the canopy

*Yupan Zhang[1], Yuichi Onda[1], Xinchao Sun[2], Takashi Gomi[3] (1.Center for Research on Isotopes and Environmental Dynamics, University of Tsukuba, Ibaraki, Japan, 2.Institute of Surface-Earth System Science, Tianjin University, Tianjin , PR China, 3.Department of International Environmental and Agricultural Science, Tokyo University of Agriculture and Technology, Tokyo , Japan)

[AHW30-P17] Seasonal changes in the canopy water balance of Japanese plantation forest

*Linh Thuy Pham[1], Yuichi Onda[1], Xinchao Sun[2], Sean Andrew Hudson[1], Janice Elaine Hudson[1], Yupan Zhang[1], Chiu Wei Chen[3] (1.University of Tsukuba, 2.Tianjin University, 3.Tokyo University of Agriculture and Technology)

[E] Poster | A (Atmospheric and Hydrospheric Sciences)：A-HW Hydrology & Water Environment

[A-HW31] Surface and subsurface hydrologic models: From uncertainty analysis to water management

convener:Tomochika Tokunaga(Department of Environment Systems, University of Tokyo), Rene Therrien(Laval University), Philip Brunner(Center for Hydrogeology and Geothermics, University of Neuchatel), Jiaqi Liu(The University of Tokyo)

[AHW31-P01] A method for estimating large scale groundwater recharge depending on forest management practice.

*Sean Hudson[1], Yuichi Onda[2], Takashi Gomi[3], Chen-wei Chiu[3], Yosuke Adachi[1] (1.University of Tsukuba, Faculty of Life and Environmental Sciences, 2.University of Tsukuba, Center for Research in Isotopes and Environmental Dynamics, 3.Tokyo University of Agriculture and Technology, Graduate School of Agriculture, Department of International Environmental and Agricultural Sciences)

[AHW31-P02] Developing a new data assimilation technique based on polynomial chaos expansion theory for hydrologic prediction

*Jongho Kim[1], Vinh Ngoc Tran[1] (1.University of Ulsan)

[AHW31-P03] Junction angles of river channels in uplifted basins and the effect of contributing area: Model experiments and comparison with natural cases

*Ryosei Hirosaki[1] (1.Graduate school of science and technology, Kanazawa University)

[AHW31-P04] **Quantifying uncertainty in soil hydraulic parameters for the dual porosity model using null-space Monte Carlo method - implications for uncertainty in potential groundwater recharge estimation**

*Sakambari Padhi[1], R Rangarajan[2], Tomochika Tokunaga[1], Philip Brunner[3] (1.The University of Tokyo, Japan, 2.CSIR-NGRI, India, 3.University of Neuchatel, Switzerland)

[AHW31-P05] Impacts of earthquake-induced surface elevation changes on flooding: a case example from Mobara area, Japan

*Mao Ouyang[1], Ito Yuka[1], Tomochika Tokunaga[1] (1.The University of Tokyo)

[AHW31-P06] Modeling of tsunami-induced seawater intrusion into unconfined coastal aquifers: uncertainties analysis and water management

*Jiaqi Liu[1], Tomochika Tokunaga[1] (1.The University of Tokyo)

[AHW31-P07] **Groundwater level fluctuations and land use changes in the basaltic aquifer of Narmada basin (Central India)**

*Sakshi Ramesh Shiradhonkar[1], Tomochika Tokunaga[1] (1.Department of Environment Systems, University of Tokyo)

[AHW31-P08] Estimation of stemflow using forest inventory data and funneling ratio for Japanese cedar and Japanese cypress plantations

*Seonghun Jeong[1], Kyoichi Otsuki[2], Yoshinori Shinohara[3], Akio Inoue[4], Ryuji Ichihashi[5] (1.Graduate School of Bioresources and Bioenvironmental Sciences, Kyushu University, 2.Kasuya Research Forest, Kyushu University, 3.Faculty of Agriculture, University of Miyazaki, 4.Faculty of Agriculture, Kindai University, 5.Shiiba Research Forest, Kyushu University)

[E] Poster | A (Atmospheric and Hydrospheric Sciences)：A-HW Hydrology & Water Environment

[A-HW32] Material transportation and cycling in aquatic ecosystems; from headwaters to coastal areas

convener:Syuhei Ban(The University of Shiga Prefecture), Adina Paytan(University of California Santa Cruz), Takahiro Hosono(Faculty of Advanced Science and Technology, Kumamoto University), Morihiro Maeda(Okayama University)

[AHW32-P01] Estimates of hydrological, thermal and chemical budgets of Okama Crater Lake, Zao Volcano, Japan: A preliminary study

*Kazuhisa A. Chikita[1], Akio Goto[2], Jun Okada[3], Satoshi Miura[4], Mare Yamamoto[4] (1.Arctic Research Center, Hokkaido University, 2.Center for Northeast Asian Studies, Tohoku University, 3.Volcanology Research Department, Meteorological Research Institute, , 4.Research Center for Prediction of Earthquakes and Volcanic Eruptions, Faculty of Science, Tohoku University)

[AHW32-P02] How the precipitation to the catchment effect on the lake water level using depth meter moored in north Lake Biwa

*Maho Iwaki[1], Kazuhide Hayakawa[2], Naoshige Goto[3] (1.Lake Biwa Museum, 2.Lake Biwa Environmental Research Institute, 3.The University of Shiga Prefecture)

[AHW32-P03] Observation for the spatial variation of lacustrine groundwater discharge (LGD) in the northern basin of Lake Biwa by multi-layer measurement of radon (^{222}Rn)

*Mitsuyo Saito[1], Shin-ichi Onodera[2], Yusuke Tomozawa[2], Kunyang Wang[2], Syuhei Ban[3], Noboru Okuda[4] (1.Graduate School of Environmental and Life Science, Okayama University, 2.Graduate School of Integrated Arts and Sciences, Hiroshima University, 3.School of Environmental Sciences, The University of Shiga Prefecture, 4.Research Institute for Humanity and Nature)

[AHW32-P04] Effects of disturbance events on primary production in the northern basin of Lake Biwa

*Naoshige Goto[1], Maho Iwaki[2], Shuhei Ban[1], Kazuhide Hayakawa[3] (1.The University of Shiga Prefecture, 2.Lake Biwa Museum, 3.Lake Biwa Environmental Research Institute)

[AHW32-P05] Estimation of lake water circulation mechanism in Lake Tazawa based on Physico-chemical characteristics

*Arata Katamura[1], Takeshi Hayashi[2], Daizo Ishiyama[1], Yasumasa Ogawa[1] (1.Graduate School of International Resource Sciences, Akita University, 2.Faculty of Education and Human Studies, Akita University)

[AHW32-P06] **Impact of Nishi-Nihon Big Storm in 2018 on nutrient discharge in a Seto Inland Sea Catchment: example in Takahashi River**

*Shin-ichi Onodera[1], Mitsuyo Saito[2], Yusuke Tomozawa[1], Toru Takeuchi[3] (1.Graduate School of Integrated and Arts Sciences, Hiroshima University, 2.Okayama University, 3.Fujita Geology Co.)

[AHW32-P07] **Ammonium sources in rural coastal aquifer using integrated water quality parameters: chemical, biological, and environmental isotopes**

*Anna Fadliah Rusydi[1,5], Mitsuyo Saito[2], Seiichiro Ioka[3], Morihiro Maeda[2], Fujio Hyodo[4], Rizka Maria[5], Shin-ichi Onodera[1] (1.Graduate School of Integrated Arts and Sciences, Hiroshima University, Japan, 2.Graduate School of Environmental and Life Sciences, Okayama University, Japan, 3.Institute of Regional Innovation, Hirosaki University, Japan, 4.Research Core for Interdisciplinary Sciences, Okayama University, 5.Research Center for Geotechnology, Indonesian Institute of Sciences, Indonesia)

[AHW32-P08] **Long-term Estimation on Nitrogen flux in the Yamato River Basin Influenced by the Construction of Sewerage Treatment Systems**

*Kunyang Wang[1], Shin-ichi Onodera[1], Mitsuyo Saito[2], Yuta Shimizu[3] (1.Graduate School of Integrated Arts and Science, Hiroshima University, 2.Faculty of Environmental Science and Technology, Okayama University, 3.National Agriculture and Food Research Organization)

[AHW32-P09] Characteristic of spatial distribution on nitrate shallow aquifer in a citrus watershed

*Yuta Shimizu[1], Kenji Matsumori[1] (1.Western Region Agricultural Research Center, National Agriculture and Food Research Organization)

[AHW32-P10] **Nitrate and Phosphate Contamination of Groundwater in Small and Steep Sedimentary Rock Island**

*Sharon Bih Kimbi[1], Shingo Nozaki[1], Shin-ichi Onodera[1], Kunyang Wang[1], Yusuke Tomozawa[1] (1.Graduate School of Integrate Arts and Sciences, Hiroshima University)

[AHW32-P11] Phosphorus in groundwater in the coastal area of Mataram, Lombok Island, Indonesia

*Seiichiro Ioka[1], Shin-ichi Onodera[2], Mitsuyo Saito[3], Anna Fadliah Rusydi[2,4], Sachi Wakasa[1] (1.Institute of Regional Innovation, Hirosaki University, Japan, 2.Graduate School of Integrated Arts and Sciences, Hiroshima University, Japan, 3.Graduate School of Environmental and Life Sciences, Okayama University, Japan, 4.Research Center for Geotechnology, Indonesian Institute of Sciences, Indonesia)

[AHW32-P12] Distribution of phosphate oxygen isotope in boring core samples for evaluation of phosphorus cycling in groundwater

*Takuya Ishida[1], Yusuke Tomozawa[2], Xin Liu[3], Jun Qian[3], Mitsuyo Saito[4], Shin-ichi Onodera[2], Noboru Okuda[1], Syuhei Ban[3] (1.Research Institute for Humanity and Nature, 2.Hiroshima Univ., 3.The Univ. of Shiga Pref., 4.Okayama Univ.)

[AHW32-P13] Bulk precipitation and throughfall depositions of atmospheric nitrogen and sulfur in forests surrounding the Tokyo metropolitan area

*Yuko Itoh[1], Masahiro Kobayashi[1], Toru Okamoto[1], Akihiro Imaya[2] (1.Forestry and Forest Products Research Institute, Japan, 2.Japan International Research Center for Agricultural Sciences)

[AHW32-P14] Numerical modeling of nutrient transport in the Ise Bay basin

*Taichi Matsuura[1], Yasuhiro Tawara[1], Susumu Saita[1], Takafumi Yoshida[1], Tetsunori Inoue[2] (1.Geosphere Environmental Technology Corp., 2.Port and Airport Research Institute)

[AHW32-P16] Influence of Material Supply and Human Intervention from Mt. Kusatsu-Shirane Volcano on the Surrounding Water Environment

*Yoshihiro Igari[1], Koji Kodera[2], Kazuki Asami[1] (1.Hosei University Graduate School, 2.Hosei University)

[AHW32-P17] Spatial distributions in groundwater (SGD) and nutrient discharge on tidal flat with the area of around 100m square in a small and steep island, western Japan

*Shingo Nozaki[1], Shin-ichi Onodera[2], Yusuke Tomozawa[2], Mitsuyo Saito[3] (1. Graduate school of integrate arts and sciences,Hiroshima University, 2.Graduate school of integrate arts and sciences,Hiroshima University, 3.Graduate school of Environmental and Life science, Okayama University)

[AHW32-P18] Estimation of unsteady confined groundwater flow with river water intrusion in coastal alluvial plain during a large flood.

*Yusuke Tomozawa[1], Shin-ichi Onodera[1], Mitsuyo Saito[2], Tohru TAKEUCHI[3], Yutaka MARUYAMA, Koichi Kitaoka[4] (1.Graduate School of Integrated Arts and Sciences Hiroshima University, 2.Graduate School of Environmental and Life Science, Okayama University, 3.Fujita Geology Co., Ltd., 4.Okayama University of Scienece)

[AHW32-P19] Establishment and evaluation of a method to reconstruct the past snow fall and winter monsoon intensity based on the inter-annual variabilities of river discharges in Hokkaido, northern Japan

*Airi Maruyama[1], Tomohisa Irino[1] (1.Biogeochemistry Course, Earth System Science, Faculty of Environmental Earth Science, Hokkaido University)

[AHW32-P20] Classification analysis of coastal seaweed beds using UAV and Near-Infrared camera

*Akimitsu Shiraishi[1], Mitsuyo Saito[1], Akira Hama[2], Shin-ichi Onodera[3], Toru Iwata[1] (1.Graduate School of Environmental Science, Okayama University, 2.College of Education, Yokohama National University, 3.Graduate School of Integrated Arts and Sciences, Hiroshima University)

[AHW32-P21] Biogeochemical pathways of critical environmental contaminants (PTTE, POPs) in the rhizospheric soil-plant system

*Hideyuki Inui[1], Vladimir Beskoski[2], Mikael Motelica-Heino[3] (1.Kobe University, 2.University of Belgrade, 3.University of Orléans)

[AHW32-P22] Study on water quality composition and its change in Ishigaki Island

*Masato Oda[1], Koji Kodera[1], Atsuki Sato[1] (1.Hosei University, faculty of literature ,Geography)

[AHW32-P23] **Effects of sugarcane growth on hydrological elements and sediment yield**

*Yang Cao[1], Shin-ichi Onodera[2], Mitsuyo Saito[3], Hide Omae[4], Yoshiko Iizumi[5] (1.Nanjing Institute of Geography and Limnology, Chinese Academy of Sciences, 2.Hiroshima University, 3.Okayama University, 4.Tropical Agriculture Research Front (TARF), Japan International Research Center for Agricultural Sciences (JIRCAS), 5.Nihon University)

[AHW32-P24] Field measurement and numerical simulation of water flux in a forest soil

*Masahiro Kobayashi[1] (1.Forestry and Forest Products Research Institute)

[AHW32-P25] Hydrogen and oxygen stable isotopic mapping that allows us to investigate water cycle regimes over Japanese Island

*Shota Nakauchi[1], Takahiro Hosono[1], Kimpei Ichiyanagi[1] (1.Kumamoto University)

[AHW32-P26] Estimation of discharge at small forest watersheds in Ibaraki Prefecture by using the SWAT model

*Naohiro Imamura[1], Naoyuki Yamashita[1], Masahiro Kobayashi[1], Takanori Shimizu[1], Shinji Sawano[1], Koji Tamai[1], Shin'ichi Iida[1], Naoki Kabeya[1], Yoshio Tsuboyama[1] (1.Forestry and Forest Products Research Institute)

[E] Poster | A (Atmospheric and Hydrospheric Sciences)：A-HW Hydrology & Water Environment

[A-HW33] Prediction of water and sediment dynamics from small to large scales

convener:Yoshiyuki Yokoo(Fukushima University), Yuko Asano(The University of Tokyo)

[AHW33-P01] Quantitative evaluation of sediment dynamics caused by extreme rainfall events in August 2016 in the Pankenushi River, Hokkaido, northern Japan

*Hiromi Akita[1], Shigeru Mizugaki[1], Yasuhiro Murakami[1] (1.Civil Engineering Research Institute for Cold Region)

[AHW33-P02] Evaluation of suspended sediment sources at the basin scale: a case study of coastal basin, Hokkaido, northern Japan

*Shigeru Mizugaki[1], Junichi Ohtsuka[1], Yasuhiro Murakami[1], Hiromi Akita[1], Atsushi Tanise[1], Masa-aki Murayama[1] (1.Civil Engineering Research Institute for Cold Region, PWRI)

[AHW33-P03] Dependency of watershed-scale rainwater storage on watershed-area at the occurrence times of slope failures: a preliminary investigation in Japan

*Hikaru Satou[1], Yoshiyuki Yokoo[2], Chris Leong[2] (1.Graduate School of Symbiotic Systems Science, Fukushima University, 2.Faculty of Symbiotic Systems Science, Fukushima University)

[AHW33-P04] Sediment dynamics after the 1973 landslide event in mountain watersheds of Hokkaido, Japan

*Takashi Koi[1], Yasutaka Tanaka[1] (1.Center for Natural Hazards Research, Hokkaido University)

[AHW33-P05] Factors controlling concentration of dissolved ^{90}Sr and ^{137}Cs in river water in the Chernobyl exclusion zone.

*Matsushita Koki[1], Yasunori Igarashi[2], Yuichi Onda[1], Yoshifumi Wakiyama[2], Alexei Konoplev[2], Gennady Laptev[3], Sergii Obrizan[4], Volodymyr Demianovych[4], Mark Zheleznyak[2] (1.Tsukuba University, 2.Institute of Environmental Radioactivity at Fukushima University, 3.Ukrainian Hydrometeorological Institute, 4.Chernobyl Ecocentre, State Agency of Ukraine on Exclusion Zone Management)

[AHW33-P06] Explication the effect of thinning on suspended sediment runoff in a cypress and cedar plantation forest by end-member mixing analysis using Fukushima-derived Cs-137, Cs-134 and Pb-210ex

*Motosuke Kinoshita[1], Yuichi Onda[2], Soo Youn Nam[3], Hiroaki Kato[2], Takashi Gomi[3], Chen-wei Chiu[3], Keisuke Taniguchi[4] (1.University of Tsukuba, 2.Center for Research in Isotopes and Environmental Dynamics, University of TSUKUBA, 3.Tokyo University of Agriculture and Technology Institute of Agriculture Division of International Environmental and Agricultural Science, 4.Fukushima Prefectural Centre for Environmental Creation)

[E] Poster | A (Atmospheric and Hydrospheric Sciences)：A-HW Hydrology & Water Environment

[A-HW37] Interdisciplinary approach to support climate change adaptation measures in regional scale

convener:TEBAKARI TAICHI(Toyama Prefectural University), Yadu Pokhrel(Michigan State University), Masashi Kiguchi(University of Tokyo), Sompratana Ritphring(Kasetsart University)

[AHW37-P01] **International Interdisciplinary Collaboration Essential to Linking the Changing Antarctic Ice Sheets with Global Coastlines**

*Robin Elizabeth Bell[1] (1.Lamont Doherty Earth Observatory of Columbia University)

[AHW37-P02] Development of climate change-related data accumulation system in Thailand

*Masashi Kiguchi[1], Chaiporn Jaikaeo[2], Eiji Ikoma[1] (1.The University of Tokyo, 2.Kasetsart University)

[AHW37-P03] Development of future climate scenario based on multi GCMs of CMIP5 and rain gridded data observed by multi-agencies in Thailand

*Masashi Kiguchi[1], Ruthaikarn BUAPHEAN[2], Aphantree YUTTAPHAN[2], Boonlert ARCHEVARAHUPROK[2], Eiji IKOMA[1], Taikan OKI[1,3] (1.The University of Tokyo, 2.Thai Meteorological Department, 3.United Nation University)

[AHW37-P04] Interannual variability of timing of monsoon-onset in South East Asia

*Ryosuke Kato[1], Tomohito Yamada[2] (1.Hokkaido university graduate school of engineering, 2.Hokkaido university faculty of engineering)

[AHW37-P05] Deep learning for seasonal to sub-seasonal rainfall prediction in Chaophraya river basin

*Kiyoharu Hasegawa[1], Shinjiro Kanae[1] (1.Toyko Institute of Technology)

[AHW37-P06] Seasonal precipitation forecast model in wet and dry seasons using global monthly surface temperature by deep learning

*Shingo Zenkoji[1], Taichi Tebakari[1], Kazutoshi Sakakibara[1] (1.Toyama Prefecural University)

[AHW37-P07] Using weather pattern recognition to classify and predict summertime heavy rainfall occurrence over the Upper Nan river basin, northwestern Thailand

*Ryosuke Kato[1], Dzung Nguyen-Le[2], Tomohito Yamada[2] (1.Hokkaido university graduate school of engineering, 2.Hokkaido university faculty of engineering)

[AHW37-P08] Impact of Rainfall on Urban Traffic Flow based on Probe Vehicle Data in Bangkok

*Tsuyoshi Takano[1], Hiroyoshi Morita[1], Shinichiro Nakamura[2], Miyazaki Hiroyuki[3], Wasan Pattara-atikom[4], Napaporn Piamsa-nga[5] (1.Nippon Engineering Consultants Co., Ltd, 2.Nagoya Univ., 3.Asian Institute of Technology, 4.National Electronics and Computer Technology Center, 5.Kasetsart Univ.)

[AHW37-P09] Investigation of Extreme Flood Changes in the Mekong River Basin Using +4K Climate Simulation

*Sophal Try[1], Shigenobu Tanaka[1], Kenji Tanaka[1], Takahiro Sayama[1], Chantha Oeurng[2] (1.Kyoto University, 2.Institute of Technology of Cambodia)

[AHW37-P10] Climate change and land use change impact assessment on flood and inundation in a river basin in Sumatra island in Indonesia

*Kodai Yamamoto[1], Takahiro Sayama[2], Apip Apip[3] (1.Graduate School of Engineering, Kyoto University, 2.Disaster Prevention Research Institute, 3.Research Center of Limnology, Indonesian Institute of Sciences)

[AHW37-P11] AN ASSESSMENT OF RESERVOIR OPERATION POTENTIAL FOR FLOW REGULATION IN THE CHAO PHRAYA RIVER BASIN

*SARITHA PADIYEDATH GOPALAN[1], Naota Hanasaki[1] (1.National Institute for Environmental Studies)

[AHW37-P12] Regional climate change impact on water quality in the lower Chao Phraya River, Thailand

Taichi Tebakari[1], Sanit Wongsa[2], *Horiuchi Yusuke[1] (1.Toyama Prefectural University, 2.King Mongkut's University)

[AHW37-P13] Research on the current thermal energy budget of land surface by continuous observation of near-surface ground temperature in Kanto Plain, Japan

*Osamu Matsubayashi[1], Hideki Hamamoto[2], Sachio Ehara[3] (1.National Institute of Advanced Industrial Science and Technology, 2.Center for Environmental Science in Saitama, 3.Institute for Geothermal Information)

[AHW37-P14] **Good Practices for Climate Change Adaptation in Agricultural Sector, Thailand**

*KOSHI YOSHIDA[1] (1.Ibaraki University)

[AHW37-P15] **Evaluation of salinity effects on rice production in farmers' fields in Ban Phai, Khon Kaen, Thailand**

*YI YANG[1], Rongling Ye[1], Thanyaluck Nontasri[2], Mallika Srisutham[2], Supranee Sritumboon[3], Masayasu Maki[4], KOSHI YOSHIDA[5], Kazuo Oki[6], Koki Homma[1] (1.tohoku university, 2.Khon Kaen Univ., Thailand, 3.LDD, Thailand, 4.Fukushima Univ., 5.Ibaraki Univ., 6.Univ. Tokyo)

[AHW37-P16] Calibration of cultivar parameters of SIMRIW-RS (rice simulation model for remote sensing) for the rice growth monitoring in Thailand

*Koki Homma[1], Mongkol Raksapatcharawong[2], Watcharee Veerakachen[2], Peerapon Prompitakporn[2], Masayasu Maki[3], Kazuo Oki[4] (1.Tohoku University, 2.Kasesart University, 3.Fukushima University, 4.The University of Tokyo)

[AHW37-P18] Farmers' perception of climate change induced drought in the Northeast Thailand

*Miki Nodera[1], Keigo Noda[1], Koshi Yoshida[2], Mallika Srisutham[3] (1.Gifu University, 2.Ibaraki University, 3.Khon Kaen University)

[AHW37-P19] **Research on farmers' awareness of adaptation to climate change and its information collection and sharing in rural area in Thailand**

*Kyoko Matsumoto[1], Mallika Srisutham[2], Supranee Sritumboon[3], Sompratana Ritphring[4], Masashi Kiguchi[1], Taikan Oki[5] (1.Institute of Industrial Science, The University of Tokyo, 2.Facutly of Agriculture, Khonkaen University, 3.Land Development Department, 4.Faculty of Engineering, Kasetsart University, 5.Institute for Future Initiatives, The University of Tokyo)

[E] Poster | A (Atmospheric and Hydrospheric Sciences)：A-CC Cryospheric Sciences & Cold District Environment

[A-CC38] Ice cores and paleoenvironmental modeling

convener:Ayako Abe-Ouchi(Atmosphere and Ocean Research Institute, The University of Tokyo), Ryu Uemura(Nagoya University), Kenji Kawamura(National Institute of Polar Research, Research Organization of Information and Systems), Nozomu Takeuchi(Chiba University)

[ACC38-P02] **Compositions of dust and sea salts in the Dome C and Dome Fuji ice cores from Last Glacial Maximum to early Holocene based on ice-sublimation and single-particle measurements**

*Ikumi Oyabu[1], Yoshinori Iizuka[2], Kenji Kawamura[1,3,4], Eric Wolff[5], Mirko Severi[6], Rumi Ohgaito[4], Ayako Abe-Ouchi[7,1,4], Margareta Hansson[8] (1.National Institute of Polar Research, Research Organization of Information and Systems, 2.Institute of Low Temperature Science, Hokkaido University, 3.Department of Polar Science, The Graduate University of Advanced Studies (SOKENDAI), 4.Japan Agency for Marine Science and Technology (JAMSTEC), 5.Department of Earth Sciences, University of Cambridge, 6.Department of Chemistry “Ugo Schiff”, University of Florence, 7.Atmosphere Ocean Research Institte, University of Tokyo, 8.Department of Physical Geography, Stockholm University)

[ACC38-P03] Evolution in geometry of firn in ice sheets detected by dielectric anisotropy

*Shuji Fujita[1,2], Kotaro FUKUI[3], Mikihiro Hirabayashi[1], Iizuka Yoshinori[4], Sumito Matoba[4], Atsushi Miyamoto[5], Takeshi Saito[4], Hideaki Motoyama[1,2], Toshitaka Suzuki[6] (1.National Institute of Polar Research, Research Organization of Information and Systems(ROIS), 2.SOKENDAI, Japan, 3.Tateyama Caldera Sabo Museum, Japan, 4.ILTS, Hokkaido Univ., Japan, 5.Hokkaido Univ., Japan, 6.Yamagata Univ., Japan)

[ACC38-P04] Dielectric anisotropy measurement of Dome Fuji ice core and implications for crystal orientation fabric development

*Tomotaka Saruya[1], Shuji Fujita[1,2] (1.National Institute of Polar Research, 2.The Graduate University for Advanced Studies)

[ACC38-P05] Development of a numerical ice-sheet model for simulation of summit dynamics

*Fuyuki SAITO[1], Ayako Abe-Ouchi[2,1], Takashi Obase[2] (1.Japan Agency for Marine-Earth Science and Technology, 2.Atmosphere Ocean Research Institute, Univ. of Tokyo)

[ACC38-P06] Layering, densification and bubble close-off of firn at a new site near Dome Fuji, East Antarctica

*Ryo Inoue[1], Shuji Fujita[2,1], Kenji Kawamura[2,1,3], Fumio Nakazawa[2,1], Ikumi Oyabu[2] (1.The Graduate University for Advanced Studies, SOKENDAI, 2.National Institute of Polar Research, 3.JAMSTEC)

[ACC38-P08] PMIP4/CMIP6 Last Interglacial simulations using different versions of MIROC, with and without vegetation feedback

*Ryouta O'ishi[1], Wing-Le Chan[1], Ayako Abe-Ouchi[1,2,3], Sam Sherriff-Tadano[1], Rumi Ohgaito[3] (1.Atmosphere and Ocean Research Institute, the Universitoy of Tokyo, 2.National Institute of Polar Research, 3.Japan Agency for Marine-Earth Science and Technology)

[ACC38-P09] Response of convective systems to changes in orbital forcing of the last interglacial

*Minoru Chikira[1], Yohei Yamada[2], Ayako Abe-Ouchi[1], Masaki Satoh[1] (1.The University of Tokyo, Atmosphere and Ocean Research Institute, 2.Japan Agency for Marine-Earth Science and Technology)

[E] Poster | A (Atmospheric and Hydrospheric Sciences)：A-GE Geological & Soil Environment

[A-GE40] Subsurface Mass Transport and Environmental Assessment

convener:Hirotaka Saito(Department of Ecoregion Science, Tokyo University of Agriculture and Technology), Shoichiro Hamamoto(Department of Biological and Environmental Engineering, The University of Tokyo), Yuki Kojima(Department of Civil Engineering, Gifu University), Yasushi Mori(Graduate School of Environmental and Life Science, Okayama University)

[AGE40-P01] Environmental Impact Assessment of Open Loop Geothermal Heat Pump System in Gifu City, Central Japan

★Invited Papers

*Randa Permanda[1], Tomoyuki Ohtani[1] (1.Gifu University)

[AGE40-P02] Estimation of correlation between soil organic matter and soil components using neural network

*Masaki Kiyohiro[1], Yasushi Mori[1], Yutaro Yamamoto[1] (1.Okayama University Graduate school of Environmental and Life Science)

[AGE40-P03] Fracture domain of granite based on orientation analysis and its relation to water conducting fractures: an example from the “-500m access/research gallery-North” of the Mizunami Underground Research Laboratory

*Koji Shimada[1], Masakazu Niwa[1], Ryuji Takeuchi[1], Kenji Amano[1] (1.Japan Atomic Energy Agency)

[AGE40-P04] Effects of Moisture Content on Soil Water and Ion Movements in the Vicinity of Soybean Roots

*Rui Nakasone[1], Shoichiro Hamamoto[1], Naoto Nihei[2], Taku Nishimura[1] (1.Graduate School of Agricultural and Life Sciences, the University of Tokyo, 2.Fukusima University)

[AGE40-P05] The effect of gas emission from organic matter on the stability of rice terraces structure

*Yasushi Mori[1], Mayuka Kashi[1], Tomoyo Kurozumi[1], Hiroaki Somura[1], Milagros Ong How[2] (1.Graduate School of Environmental and Life Science, Okayama University, 2.Global Harvester)

[AGE40-P06] **Effects of Macropore Structures on Agricultural Soil’s Greenhouse Gases Emission**

*Thanh Long Bui[1], Yasushi Mori[1] (1.Graduate School of Environmental and Life Science, Okayama University)

[AGE40-P07] **Interaction between Nano-Bubbles and Colloidal Particles in Saturated Porous Media under Flowing Condition**

Takuya Sugimoto[1], *Shoichiro Hamamoto[1], Taku Nishimura[1] (1.Department of Biological and Environmental Engineering, The University of Tokyo)

[AGE40-P08] Numerical Analysis of the Effects of Capillary Barrier under Subsurface Drip Irrigation to Improve Water-use Efficiency

*Koichi Noguchi[1], Hirotaka Saito[1] (1.Tokyo University of Agriculture and Technology)

[AGE40-P09] Deformation analysis of fill dams due to level 2 earthquakes using PIV

*Mai Masutani[1], Tomotaka Sato[2], Hirotaka Saito[3], Yuji Kohgo[2] (1.Graduate School of Agriculture, Tokyo University of Agriculture and Technology, 2.United Graduate School of Agricultural Science, Tokyo University of Agriculture and Technology, 3.Department of Ecoregion Science, Tokyo University of Agriculture and Technology)

[AGE40-P10] **An observation of swelling behavior and microstructural change for granulated bentonite mixtures under controlled relative humidity**

*Mazhar Nazir[1], Akihiro Matsuno[1], Takeshi Saito[1], Ken Kawamoto[1] (1.Graduate School of Science and Engineering, Saitama University)

[E] Poster | A (Atmospheric and Hydrospheric Sciences)：A-GE Geological & Soil Environment

[A-GE41] Energy-Environment-Water Nexus and Sustainable Development

convener:Ming Zhang(Institute for Geo-Resources and Environment, Geological Survey of Japan, AIST), Yonghong Hao(Tianjin Normal University), Jet-Chau Wen(National Yunlin University of Science and Technology), Ken Kawamoto(Graduate School of Science and Engineering, Saitama University)

[AGE41-P01] **Season Effect of the Operation of IPCC Reactor on Solar Photocatalysis of Phenol Wastewater**

*Wen-Shiuh Kuo[1], An-Chi Chen[1] (1.National United University, Taiwan)

[AGE41-P02] Solar photocatalysis of MeO wastewater with metal@TiO_2 film

*Ting-Yu Zeng[1], Ling-Syuan Tzeng[1], Wen-Shiuh Kuo[1] (1.National United University, Taiwan.)

[AGE41-P03] **Effects of fine content on mechanical properties of recycled concrete aggregates for unbound road base materials in Vietnam**

*Thai Hong Nam[1], Akira Kato[1], Takeshi Saito[1], Ken Kawamoto[1] (1.Graduate School of Science and Engineering, Saitama University)

[AGE41-P04] Development of filtering materials for removing heavy metals utilizing industrial by-products

*Akito Ujiie[1], Buddhika Bandara[1], Akihiro Matsuno[1], Takeshi Saitou[1], Ken Kawamoto[1] (1.Saitama university)

[AGE41-P05] Effects of Silicic Acid on Arsenite Leaching from Spent Calcium-Based Arsenic Adsorbents

*Hajime Sugita[1], Terumi Oguma[1], Ming Zhang[1], Junko Hara[1], Yoshishige Kawabe[1] (1.National Institute of Advanced Industrial Science and Technology)

[E] Poster | A (Atmospheric and Hydrospheric Sciences)：A-GE Geological & Soil Environment

[A-GE42] Interactions between Earth Critical Zone Hydrogeological Processes and Ecosystem

convener:Wang Wenke(Chang'an University), Yaqian Zhao(Xian University of Technology), Jet-Chau Wen(National Yunlin University of Science and Technology), Ming Zhang(Institute for Geo-Resources and Environment, Geological Survey of Japan, AIST)

[AGE42-P01] **The Impact of LSTM Network Structure on Flood Process Simulation and Forecast Period: A Case Study of the Middle Yellow River**

★Invited Papers

*Caihong Hu[1] (1.school of water conservancy science and engineering, zhengzhou university, Zhengzhou city, Henan Province, P.R.China, 450001)

[AGE42-P02] **CHARACTERIZATION OF WATER RETENTION AND HYDRAULIC CONDUCTIVITY PROPERTIES FOR GRADED RECYCLED AGGREGATES BLENDED WITH AUTOCLAVED AERATED CONCRETE GRAINS IN VIETNAM**

*Nam Pham Van[1], Akira KATO[1], Akihiro MATSUNO[1], Hoang Giang NGUYEN[2], Van Tuan NGUYEN[2], Takeshi SAITO[1], Ken KAWAMOTO[1,2] (1.Graduate School of Science and Engineering, Saitama University, Japan, 2.National University of Civil Engineering, Vietnam)

[AGE42-P03] **UTILIZATION OF CONSTRUCTION aND DEMOLITION WASTE (CDW) AND INDUSTRIAL BY-PRODUCTS(IBPS) AS LOW-COST LIMING AGENTS FOR NEUTRALIZATION OF SOIL ACIDITY**

*Isiri Upeksha Nagasinghe[1], Takeshi Saito[1], Akihiro Matsuno[1], Akira Kato[1], Ken Kawamoto[1] (1.Department of Civil and Environmental Engineering, Graduate School of Science and Engineering, Saitama University, Japan)

[AGE42-P04] Estimation of Coastal Aquifer Properties Using Multiple-Frequency Ocean Tides

*Ming Zhang[1], Ling Yang[2], Yonghong Hao[2], Zhixue Zhao[2], Tongke Wang[2] (1.Institute for Geo-Resources and Environment, Geological Survey of Japan, AIST, 2.Tianjin Normal University)

[E] Poster | A (Atmospheric and Hydrospheric Sciences)：A-GE Geological & Soil Environment

[A-GE43] Extending Hydropedology- -in memory of Professor Henry Lin

convener:Kosuke Noborio(Meiji University), Yasushi Mori(Graduate School of Environmental and Life Science, Okayama University)

[AGE43-P01] History of Hydropedology and perspectives

*Kosuke Noborio[1] (1.Meiji University)

[AGE43-P02] Simulation of Water Harvesting with a Sand Ditch using WASH_2D

*Haruyuki Fujimaki[1], Majed Abu-Zreig[1] (1.Arid Land Research Center, Tottori University)

[AGE43-P03] Hydraulic properties of clay loam paddy soils in Japan.

*Taku Nishimura[1], Shoichiro Hamamoto[1] (1.Deptartment of Biological and Environmental Engineering, Graduate School of Agricultural and Life Sciences, University of Tokyo)

[AGE43-P04] **Cosmic-Ray Neutron Sensing for Measuring Soil Water Content at Area Wide Scale: Case Study at IAEA and Future Collaboration**

★Invited Papers

*Ammar Wahbi[1], Trenton Franz[2], Hami Said Ahmed[3], Lee Kheng Heng[3], Peter Strauss[4], Hisashi Tsujimoto[1], Haruyuki Fujimaki[1] (1.Arid Land Research Center, Tottori Univeristy, Tottori, Japan, 2.School of Natural Resources, University of Nebraska-Lincoln, Nebraska, USA, 3.Soil and Water Management & Crop Nutrition Subprogramme, Joint FAO/IAEA Division of Nuclear Techniques in Food and Agriculture, International Atomic Energy Agency, Vienna, Austria, 4.Institute for Land and Water Management Research, Federal Agency for Water Management Austria, 3252 Petzenkirchen, Austria)

[AGE43-P05] Relationship between GPS signal and soil volume moisture content / electrical conductivity

*Natsumi Naganuma[1], Shinsuke Aoki[2], Tetsushi Ikegami[3], Kosuke Noborio[4] (1.Graduate School of Agriculture, Meiji University, 2.Institute of Soil, Water, and Environmental SciencesAgricultural Research, The Volcani Center, 3.School of Science and Technology, Meiji University, 4.School of Agriculture, Meiji University)

[AGE43-P06] Reviewing the EC Temperature Calibration Equations and Tracing Two Dimensional Distribution of Soil Nutrients.

*Yuki Sunakawa[1], Satoko Fujita[2], Yuki Ito[3], Shinsuke Aoki[4], Kosuke Noborio[2] (1.Graduate School of Agriculture, Meiji University , 2.School of Agriculture, Meiji University, 3.Gilat Research Center, Agricultural Research Organization, Israel, 4.Institute of Soil, Water, and Environmental Sciences Agricultural Research, The Volcani Center, Israel)

[AGE43-P07] Case study of current status and issues of new entrant apple farmers in Nagano Prefecture

*Takamitsu Kai[1] (1.Meiji University)

[E] Poster | A (Atmospheric and Hydrospheric Sciences)：A-CG Complex & General

[A-CG44] Extratropical oceans and atmosphere

convener:Youichi Kamae(Faculty of Life and Environmental Sciences, University of Tsukuba), Toyama Katsuya(Meteorological Research Institute), Hyodae Seo(Woods Hole Oceanographic Institution), Yoshi N(Hokkaido University)

[ACG44-P01] Seasonality and Regional Characteristics of Sea-Surface Wind Responses to Mesoscale SST Features assessed by Transfer Functions

*Ryusuke Masunaga[1], Niklas Schneider[1] (1.International Pacific Research Center, University of Hawaii)

[ACG44-P02] Ocean warming patterns and heavy rainfall over East Asia associated with atmospheric rivers

*Youichi Kamae[1], Wei Mei[2] (1.Faculty of Life and Environmental Sciences, University of Tsukuba, 2.University of North Carolina at Chapel Hill)

[ACG44-P03] Predictability of 2019 stratospheric sudden warming in the Southern Hemisphere and its impact of surface weather

*Hiroaki Naoe[1], Chiaki Kobayashi[1], Yayoi Harada[1], Yukiko Imada[1], Shuhei Maeda[1], Toshihiko Hirooka[2] (1.Meteorological Research Institute, 2.Kyusyu University)

[ACG44-P04] Interaction between a typhoon moving westward in western Japan and a cold vortex

*Mine Taisei[1], Yoshihiro Tachibana[1] (1.Faculty of Bioresources, Mie University)

[ACG44-P05] On the maintenance mechanisms for the wintertime subtropical high over the South Indian Ocean

*Ayumu Miyamoto[1], Hisashi Nakamura[1], Takafumi Miyasaka[1,2], Yu Kosaka[1], Bunmei Taguchi[3], Kazuaki Nishii[4] (1.Research Center for Advanced Science and Technology, The University of Tokyo, 2.Japan Meteorological Business Support Center, 3.School of Sustainable Design, University of Toyama, 4.Graduate School of Bioresources, Mie University)

[ACG44-P06] Surface velocity variation of the Kuroshio-Kuroshio Extension system -its relations with local monsoon winds-

*YUXIANG QIAO[1], Hirohiko Nakamura[2], Kako Shinichiro[3], Ayako Nishina[2] (1.The United Graduate School of Agricultural Sciences, Kagoshima University, 2.Faculty of Fisheries, Kagoshima University, 3.Graduate School of Science and Engineering, Kagoshima University)

[ACG44-P07] The potential impact of the 2014-2016 marine heat wave over the North Pacific on the atmosphere

*Kazuaki Nishii[1], Bunmei Taguchi[2], Hisashi Nakamura[3] (1.Graduate School of Bioresources, Mie University, 2. Faculty of Sustainable Design, University of Toyama, 3.Research Center for Advanced Science and Technology, The University of Tokyo)

[E] Poster | A (Atmospheric and Hydrospheric Sciences)：A-CG Complex & General

[A-CG45] Multi-scale ocean-atmosphere interaction in the tropical Indo-Pacific region

convener:Yu Kosaka(Research Center for Advanced Science and Technology, University of Tokyo), Sang-Wook Yeh(Hanyang University), Takanori Horii(Research and Development Center for Global Change (RCGC), Strategic Research and Development Area, Japan Agency for Marine-Earth Science and Technology (JAMSTEC)), Hiroki Tokinaga(Disaster Prevention Research Institute, Kyoto University)

[ACG45-P01] Diurnal cycles of precipitation and lightning in the tropics observed by TRMM3G68, GSMaP, LIS, and WWLLN

★Invited Papers

*Shoshiro Minobe[1], Jun Hyock Park[1], Katrina S. Virts[2] (1.Graduate School of Science, Hokkaido University, 2.The University of Alabama in Huntsville)

[ACG45-P02] Intermodel diversity in the impact of tropical volcanic eruptions on ENSO

*Masamichi Ohba[1] (1.Central Research Institute of Electric Power Industry)

[ACG45-P03] Revisiting the ENSO impact on the Indian Ocean SST based on the combined linear regression

*Lianyi Zhang[1,2,3], Yan DU[1,2], Tomoki Tozuka[3], Shoichiro Kido[3] (1.South China Sea Institute of Oceanology, Chinese Academy of Sciences, 2.University of Chinese Academy of Sciences, Chinese Academy of Sciences, 3.The University of Tokyo)

[ACG45-P04] Assessments of salinity impacts on SST using a linear inverse model

★Invited Papers

*Shoichiro Kido[1], Tomoki Tozuka[1] (1.Graduate School of Science, The University of Tokyo)

[ACG45-P05] The relationship between the boreal summer intraseasonal oscillation and the Pacific-Japan pattern

*Ayako Seiki[1], Yu Kosaka[2], Satoru Yokoi[1] (1.Japan Agency for Marine-Earth Science and Technology, 2.Research Center for Advanced Science and Technology, The university of Tokyo)

[ACG45-P06] The Impact of IOD on rainfall over Spain

*Sourabh Shrivastava[1], Saji Hameed[1] (1.University of Aizu)

[ACG45-P07] How Large-Scale Circulations Integratedly Influence Precipitation in the Source Region of the Yangtze River,China

*Yiheng Du[1], Dong An[1], Ronny Berndtsson[1] (1.Lund University)

[ACG45-P08] Summertime climate anomalies in Asia and the Northwestern Pacific induced by ENSO: Dependence on ENSO's phase transition

*Yu Kosaka[1], Daiki Kado[1] (1.Research Center for Advanced Science and Technology, University of Tokyo)

[E] Poster | A (Atmospheric and Hydrospheric Sciences)：A-CG Complex & General

[A-CG46] Atmospheric deposition impact on Terrestrial and marine Ecosystems

convener:Eyal Rahav(Israel Oceanographicand Limnological Research), Adina Paytan(University of California Santa Cruz)

[ACG46-P01] The hitchhike's guide to bacterial transport: the role of viable dust-borne microbes deposition into marine environments

*Eyal Rahav[1], Barak Herut[1], Adina Paytan[2] (1.Israel Oceanographic and Limnological Research, Haifa 31080, Israel, 2.Institute of Marine Science, University of California, Santa Cruz, CA, 95064, USA)

[E] Poster | A (Atmospheric and Hydrospheric Sciences)：A-CG Complex & General

[A-CG47] Global Carbon Cycle Observation and Analysis

convener:Kazuhito Ichii(Chiba University), Prabir Patra(Research Institute for Global Change, JAMSTEC), Forrest M. Hoffman(Oak Ridge National Laboratory), Makoto Saito(National Institute of Environmental Studies)

[ACG47-P02] Preliminary results for GOSAT-2 Level 4 global surface fluxes

*Makoto Saito[1], Yosuke Niwa[1], Tazu Saeki[1], Kazutaka Murakami[1], Richao Cong[1], Tatsuya Miyauchi[1], Hisashi Yashiro[1], Tomohiro Shiraishi[1], Ryuichi Hirata[1], Yukio Yoshida[1], Isamu Morino[1], Hibiki M Noda[1], Hirofumi Ohyama[1], Akihide Kamei[1], Tsuneo Matsunaga[1] (1.National Institute of Environmental Studies)

[ACG47-P03] Toward a long-term global inversion of atmospheric CO_2 for elucidating seasonal and interannual variations of natural carbon fluxes

*Yosuke Niwa[1] (1.National Institute for Environmental Studies)

[ACG47-P04] INVERSION ESTIMATES OF METHANE EMISSION IN EAST, SOUTH AND SOUTHEAST ASIA IN 2010-2017 USING GOSAT AND GROUND-BASED OBSERVATIONS

*Fenjuan Wang[1,2], Shamil S Maksyutov[1], Rajesh Janardanan[1], Aki Tsuruta[3], Akihiko Ito[1], Isamu Morino[1], Yukio Yoshida[1], Johannes W. Kaiser[4], Greet Janssens Maenhout[5], Ed Dlugokencky[6], Ivan Mammarella[7], Jost V. Lavric[8], Tsuneo Matsunaga[1] (1.NIES National Institute of Environmental Studies, 2.Department of Climate Change, National Climate Center, 3.Finnish Meteorological Institute, 4.Deutscher Wetterdienst, 5.European Commission Joint Research Centre, 6.Earth System Research Laboratory, NOAA, 7.University of Helsinki, 8.Max Planck Institute for Biogeochemistry)

[ACG47-P05] Refinement of a diagnostic terrestrial ecosystem model using AsiaFlux network data toward GCOM-C SGLI GPP/NPP product

*LI JIAWEI[1], Kazuhito Ichii[1], Hideki Kobayashi[2], Wei Yang[1] (1.Chiba University, 2.Japan Agency for Marine-Earch Science and Technology)

[ACG47-P06] In-situ observation of greenhouse-gas flux at proglacial grounds of a glacier – preliminary result for Gulkana Glacier, Alaska-

*Keiko Konya[1], Go Iwahana[3,2], Tetsuo Sueyoshi[4], Tomoaki Morishita[5] (1.Japan Agency for Marine-Earth Science and Technology, 2.Universitry of Alaska, Fairbanks, 3.Hokkaido university, 4.Ninational Institute of Polar Research, 5.Forestry and Forest Products Research Institute)

[ACG47-P07] Testing machine-learning methods toward improvement of terrestrial CO2 flux estimations

*Zhiyan Liu[1], Kazuhito Ichii[1] (1.Center for Environmental Remote Sensing Chiba University, Chiba University)

[E] Poster | A (Atmospheric and Hydrospheric Sciences)：A-CG Complex & General

[A-CG48] Projection and detection of global environmental change

convener:Michio Kawamiya(Japan Agency for Marine-Earth Science and Technology), Kaoru Tachiiri(Japan Agency for Marine-Earth Science and Technology), Hiroaki Tatebe(Japan Agency for Marine-Earth Science and Technology), V Ramaswamy(NOAA GFDL)

[ACG48-P01] Methodology of probabilistic climate projections for the assessment of climate change mitigation pathways

*Junichi Tsutsui[1] (1.Central Research Institute of Electric Power Industry)

[ACG48-P02] Improvement in runoff reproducibility of a land surface model and its implications for the energy-water balances on land

*Kumiko TAKATA[1], Naota Hanasaki[1] (1.Center for Climate Change Adaptation, National Institute for Environmental Studies)

[ACG48-P03] **Impact of volcanic eruption on surface climate in VolMIP experiments by MIROC-ES2L**

*Manabu Abe[1], Tomohiro Hajima[1] (1.Japan Agency for Marine-Earth Science and Technology)

[ACG48-P04] Effect on the Earth system of realizing a 1.5 °C warming climate target after overshooting to the 2 °C level

*Kaoru Tachiiri[1], Diego Silva Herran[2], Xuanming Su[1], Michio Kawamiya[1] (1.Japan Agency for Marine-Earth Science and Technology, 2.National Institute for Environmental Studies)

[E] Poster | A (Atmospheric and Hydrospheric Sciences)：A-CG Complex & General

[A-CG49] Greenhouse Gas Monitoring from Space: Current Capabilities, Challenges, and Future Needs

convener:kurosu thomas p(Jet Propulsion Laboratory, California Institute of Technology), Annmarie Eldering(Jet Propulsion Laboratory), Akihiko Kuze(Japan Aerospace Exploration Agency), Tsuneo Matsunaga(Center for Global Environmental Research and Satellite Observation Center, National Institute for Environmental Studies)

[ACG49-P01] A high-resolution CO_2 inverse modeling using observations from the global ground-based monitoring network and the GOSAT satellite

*Shamil Maksyutov[1], Rajesh Janardanan[1], Tomohiro Oda[2], Makoto Saito[1], Yukio Yoshida[1], Johannes W Kaiser[3], Vinu Valsala[4], Edward Dlugokencky[5], Tsuneo Matsunaga[1] (1.National Institute for Environmental Studies, Tsukuba, Japan, 2.USRA/NASA GSFC, Greenbelt, USA, 3.DWD, Offenbach, Germany, 4.Indian Institute for Tropical Meteorology, Pune, India, 5.Global Monitoring Division, NOAA, Boulder, USA)

[ACG49-P02] GOSAT series product validation with TCCON, Sky radiometer and lidar data

*TRIEU THI NGOC TRAN[1], Isamu Morino[1], Osamu Uchino[1], Yukitomo Tsutsumi[1], Tetsu Sakai[2], Tomohiro Nagai[2], Akihiro Yamazaki[2], Hiroshi Okumura[3], Kouhei Arai[3], Ben Liley[4] (1.National Institute for Environmental Studies (NIES), Tsukuba, Japan, 2.Meteorological Research Institute, Japan Meteorological Agency, Tsukuba, Japan, 3.Graduate school of Science and Engineering, Saga University, Saga, Japan, 4.National Institute of Water and Atmospheric Research, Lauder, New Zealand)

[ACG49-P03] Observations of the Tropical Land Biosphere response to the 2015-2016 El Niño with the Orbiting Carbon Observatory-2 (OCO-2) and Greenhouse gases Observing SATellite (GOSAT)

*David Crisp[1] (1.Jet Propulsion Laboratory, California Institute of Technology)

[ACG49-P04] Global and local flux estimation of carbon dioxide and methane by GOSAT satellites

*Akihiko Kuze[1], Nobuhiro Kikuchi[1], Hiroshi Suto[1], Kei Shiomi[1], Fumie Kataoka[2] (1.Japan Aerospace Exploration Agency, 2.Remote Sensing Technology Center of Japan)

[E] Poster | A (Atmospheric and Hydrospheric Sciences)：A-CG Complex & General

[A-CG50] Earth & Environmental Sciences and Artificial Intelligence

convener:Tomohiko Tomita(Faculty of Advanced Science and Technology, Kumamoto University), Shigeki Hosoda(Japan Marine-Earth Science and Technology), Ken-ichi Fukui(Osaka University), Satoshi Ono(Kagoshima University)

[ACG50-P01] A precipitation prediction using an artificial neural network model based on observation time series data

He Zhang[1], Naoki Matsumoto[1], *Tomohiko Tomita[2] (1.Graduate School of Science and Technology, Kumamoto University, 2.Faculty of Advanced Science and Technology, Kumamoto University)

[ACG50-P02] Climate Prediction by Using Periodic Convolutional Recurrent Network

*Ekasit Phermphoonphiphat[1], Tomohiko Tomita[2], Masayuki Numao[1], Ken-ichi Fukui[1] (1.Osaka University, 2.Kumamoto University)

[ACG50-P03] K-means clustering of Argo profiles for identifying circulation patterns

*Nozomi Sugiura[1] (1.Japan Agency of Marine-Earth Science and Technology)

[ACG50-P04] A Preliminary Study on Algo Float Trajectory Prediction using Multimodal Convolutional LSTM

*Serina Higashi[1], Takahiro Kinoshita[1], Shigeki Hosoda[3], Ken-ichi Fukui[2], Satoshi Ono[1] (1.Kagoshima University, 2.Osaka University, 3.Japan Marine-Earth Science and Technology)

[E] Poster | A (Atmospheric and Hydrospheric Sciences)：A-CG Complex & General

[A-CG51] Satellite Earth Environment Observation

convener:Riko Oki(Japan Aerospace Exploration Agency), Yoshiaki HONDA(Center for Environmental Remote Sensing, Chiba University), Yukari Takayabu(Atmosphere and Ocean Research Institute, the University of Tokyo), Tsuneo Matsunaga(Center for Global Environmental Research and Satellite Observation Center, National Institute for Environmental Studies)

[ACG51-P01] Australian bushfire captured by AHI/Himawari-8 and SGLI/GCOM-C

*Yukio Kurihara[1], Kazuhisa Tanada[1], Hiroshi Murakami[1], Misako Kachi[1] (1.Japan Aerospace Exploration Agency / Earth Observation Research Center)

[ACG51-P02] Detecting the Kuroshio-induced island vortices observed from GCOM-C and Himawari-8 data

*Po-Chun Hsu[1], Chung-Ru Ho[1] (1.Department of Marine Environmental Informatics , National Taiwan Ocean University)

[ACG51-P03] **Variability of groundwater storage in Northern India using the GRACE**

*Amit K Singh[1], M Saravanan[2], Swetabh Patel[3] (1.School of Environmental Sciences, Jawaharlal Nehru University,New Delhi, 2.College of Health Science,Mekelle University, Ethiopia, 3.Department of Agronomy,Iowa State University USA)

[ACG51-P04] The characteristics of precipitation and anvil cloud detected by GPM/DPR

*Koichi Toyoshima[1], Hitoshi Hirose[2], Atsushi Higuchi[1] (1.Center for Environmental Remote Sensing, Chiba University, 2.JAXA EORC)

[ACG51-P05] Improvement for infrared rainfall estimation algorithm of GSMaP using machine learning

*Hitoshi Hirose[1], Takuji Kubota[1], Atsushi Higuchi[2], Koichi Toyoshima[2], Shoichi Shige[3], Tomoo Ushio[4], Tomoaki Mega[4] (1.Japan Aerospace Exploration Agency, 2.Center for Environmental Remote Sensing, Chiba university, 3.Department of Science, Kyoto University, 4.Department of Engineering, Osaka University)

[ACG51-P06] Sensitivity experiment of aerosol models in aerosol retrieval algorithm and comparison with ground-based observation using GOSAT/CAI and GOSAT-2/CAI-2 data

*Makiko Hashimoto[1], Hideaki Takenaka[1], Chong Shi[1], Teruyuki Nakajima[1] (1.Japan Aerospace Explortion Agency)

[ACG51-P07] High resolution Motion Vector for the GSMaP MVK

*Tomoaki Mega[1], Tomoo Ushio[1] (1.Osaka Univ.)

[ACG51-P08] Validation of GSMaP toward practical hydrological use over Vietnam: basin-scale validation and estimation of accuracy with time lapse from microwave observation

*Masato I. Nodzu[1], Jun Matsumoto[1,2], Thanh Ngo-Duc[3], Long Trinh-Tuan[3], Tri Truong-Duc[4] (1.Tokyo Metropolitan University, 2.Japan Agency for Marine-Earth Science and Technology, 3.University of Science and Technology of Hanoi, Vietnam Academy of Science and Technology, 4.Ministry of Natural Resources and Environment, Vietnam)

[ACG51-P09] Cloud and aerosol discrimination algorithm for EarthCARE/ATLID lidar

*Eiji Oikawa[1], Hajime Okamoto[1], Tomoaki Nishizawa[2], Kaori Sato[1], Rei Kudo[3] (1.Research Institute for Applied Mechanics, Kyushu University, 2.National Institute for Environmental Studies, 3.Meteorological Research Institute, Japan Meteorological Agency)

[ACG51-P10] **Climate and air pollution impact on wheat crop over Eastern Indo Gangetic Plains of India**

*geetika sonkar[1] (1.Banaras Hindu University)

[ACG51-P11] Orverview of Earth Clouds, Aerosols and Radiation Explorer (EarthCARE) projects

*Takahashi Chikako[1], Riko Oki[1], Takuji Kubota[1], Maki Kikuchi[1], Yuichiro Hagihara[1], Mayumi YOSHIDA[1] (1.Japan Aerospace Exploration Agency)

[ACG51-P12] Sources of countercurrent in northeastern Taiwan

*Chen-Chen Ho[1], Po-Chun Hsu[1], Ching-Yuan Lu[1], Chung-Ru Ho[1] (1.Department of Marine Environmental Informatics, National Taiwan Ocean University)

[ACG51-P13] **An improved procedure for estimation of propagation distance of tweek atmospherics**

*Masafumi Kanno[1], Hiroyo Ohya[2], Kazuo Shiokawa[3], Hiroyuki Nakata[2], Toshiaki Takano[2] (1. Graduate School of Science and Engineering, Chiba University, 2.Graduate School of Engineering, Chiba University, 3.Institute for Space-Earth Environmental Research, Nagoya University)

[ACG51-P14] Current status of the calibration for the GPM DPR

*Takeshi Masaki[1], Toshio Iguchi[2], Kaya Kanemaru[3], Kinji Furukawa[4], Naofumi Yoshida[1], Takuji Kubota[5], Riko Oki[5] (1.Remote Sensing Technology Center of Japan , 2.Earth System Science Interdisciplinary Center, University of Maryland, 3.National Institute of Information and Communications Technology, 4.Satellite Applications and Operations Center, Japan Aerospace Exploration Agency, 5.Earth Observation Research Center, Japan Aerospace Exploration Agency)

[ACG51-P15] Observing Simulation System Experiment for Future Small Precipitation Radar Constellation: Impact on GSMaP Accuracy

*Yamaji Moeka[1], Takuji Kubota[1] (1.Japan Aerospace Exploration Agency (JAXA))

[ACG51-P17] **Calibration of INSAT-3D meteorological satellite imager visible channel using Moon**

*Shailesh Parihar[1], A.K. Mitra, R. Bhatla[1] (1.Banaras Hindu University, Varanasi, India)

[E] Poster | A (Atmospheric and Hydrospheric Sciences)：A-CG Complex & General

[A-CG52] Large Ensemble Modeling Approaches as Tools for Climate and Impacts Research

convener:Rodgers Keith Bradley(IBS Center for Climate Physics), Shoshiro Minobe(Graduate School of Science, Hokkaido University), Hideo Shiogama(Center for Global Environmental Research, National Institute for Environmental Studies), Ryo Mizuta(Meteorological Research Institute)

[ACG52-P01] Increase in Rain-on-Snow events in Japan as projected by large ensemble of regional climate simulations

*Masamichi Ohba[1], Hiroaki Kawase[2] (1.Central Research Institute of Electric Power Industry, 2.Meteorological Research Institute)

[ACG52-P02] Projected changes in extreme precipitation in a 60-km AGCM large ensemble and their dependence on return periods

*Ryo Mizuta[1], Hirokazu Endo[1] (1.Meteorological Research Institute)

[ACG52-P03] Detection and Analysis of Tropical Cyclones in the d4pdf Mega-ensemble Projection

*Adrean Webb[1], Tomoya Shimura[1], Nobuhito Mori[1] (1.Kyoto University, Disaster Prevention Research Institute, Coastal Disaster Research)

[ACG52-P04] ESM-projected global change in the indices of extreme weather using the TR3S method of bias-correction

*Martin Gomez-Garcia[1], Akiko Matsumura[1], Daikichi Ogawada[1] (1.Nippon Koei Co., Ltd. Research and Development Center)

[ACG52-P05] **Droughts, fires and fire emissions of CO_2 and $PM_{2.5}$ in equatorial Asia due to historical and future climate changes**

*Hideo Shiogama[1] (1.Center for Global Environmental Research, National Institute for Environmental Studies)

[ACG52-P06] Future change in phytoplankton phenology simulated by large ensemble experiment

*Ryohei Yamaguchi[1], Keith Rodgers[1,2], Karl J Stein[1,2], Axel Timmermann[1,2], John P Dunne[3], Richard D Slater[4], Sarah Schlunegger[4] (1.IBS Center for Climate Physics, 2.Pusan National University, 3.NOAA Geophysical Fluid Dynamics Laboratory, 4.Princeton University)

[ACG52-P07] Seasonality Constraints on the rate of Pteropod Habitat Compression under 21st Century Climate Change

*Keith Bradley Rodgers[1,2], Sarah Schlunegger[3], Richard Slater[3], Burke Hales[4] (1.IBS Center for Climate Physics, 2.Pusan National University, 3.AOS Program, Princeton University, 4.Oregon State University)

[E] Poster | A (Atmospheric and Hydrospheric Sciences)：A-CG Complex & General

[A-CG53] Terrestrial monitoring using new-generation geostationary satellites

convener:Yuhei Yamamoto(Center for Environmental Remote Sensing, Chiba University), Yunyue Yu(NOAA National Environmental Satellite, Data, and Information Service), Tomoaki Miura(Univ Hawaii), Kazuhito Ichii(Chiba University)

[ACG53-P01] Evaluation of Estimated precipitation product by machine learning method using Himawari 8

*Koichi Toyoshima[1], Hitoshi Hirose[2], Atsushi Higuchi[1] (1.Center for Environmental Remote Sensing, Chiba University, 2.JAXA EORC)

[ACG53-P02] Development and application of land surface products using Himawari-8 AHI

*Kazuhito Ichii[1], Yuhei Yamamoto[1], Kodai Hayashi[1] (1.Chiba University)

[ACG53-P03] Monitoring seasonal variations in vegetation activities over Southeast Asia using Himawari-8

*Kodai Hayashi[1], Kazuhito Ichii[1], Yuhei Yamamoto[1] (1.Chiba University)

[ACG53-P04] Analysis of the spatial variations in the phenology of deciduous broadleaf forests in Japan with Himawari-8 NDVI hyper-temporal signatures

*Tomoaki Miura[1], Shin Nagai[2] (1.University of Hawaii at Manoa, 2.JAMSTEC)

[E] Poster | H (Human Geosciences)：H-GM Geomorphology

[H-GM02] Geomorphology

convener:Tsuyoshi Hattanji(Faculty of Life and Environmental Sciences, University of Tsukuba), Masayuki Seto(Fukushima Future Center for Regional Revitalization, Fukushima University)

[HGM02-P01] Bank erosion owing to tidal currents and its impact on village distribution in the Sittaung River estuary, Myanmar

*Naoko Nagumo[1], Daisuke Harada[1], Tanjir Saif Ahmed[1,2], Shinji Egashira[1] (1.International Centre for Water Hazard and Risk Management, Public Works Research Institute, 2.National Graduate Institute for Policy Studies)

[HGM02-P02] Grain size and OSL dating of river bank dune deposits: an example from the Kiso River, central Japan

*Kazuaki Hori[1], Kohei Ohata[1], Yuji Ishii[2,3] (1.Nagoya Univ., 2.JSPS, 3.AIST)

[HGM02-P03] Topographic development process of bedrock river: model experiment

*Yuta Takase[1], Noritaka Endo[1] (1.Kanazawa University)

[HGM02-P04] Patterns of slopes and geological structure in the Atsuma River catchment, Hokkaido

*Takahisa Furuichi[1,2], Seiji Yanai[3], Tomoya Hayakawa[4] (1.Miyagi University of Education, 2.University of the Sunshine Coast, 3.Ishikawa Prefectural University, 4.Nippon Koei, Co. Ltd.)

[HGM02-P05] Radiocarbon-based Chronology of Valley Head Deposits: A Case Study of Landslide Scars in Hofu, Yamaguchi Prefecture

Takatoshi Kawano[1], *Tsuyoshi Hattanji[2], Takahisa Furuichi[3], Shoji Doshida[4], Yasushi Tanaka[5] (1.Graduate School of Life and Environmental Sciences, University of Tsukuba, 2.Faculty of Life and Environmental Sciences, University of Tsukuba, 3.Miyagi University of Education, 4.National Research Institute of Fire and Disaster, 5.Komazawa University)

[HGM02-P06] Impact of Understory Coverage and Tree Height on Sediment Transport Activity in Tenryu Artificial Forest, Japan

*Kautsar Qurratul Aini Binti Mahyudin[1], Fumitoshi Imaizumi[1] (1.Shizuoka University)

[E] Poster | H (Human Geosciences)：H-QR Quaternary research

[H-QR04] Innovative Applications of Trapped-Charge Dating to Quaternary Geochronology

convener:Toru Tamura(Institute of Geology and Geoinformation Geological Survey of Japan, AIST), Shin Toyoda(Department of Applied Physics, Faculty of Science, Okayama University of Science), Yuji Ishii(National Institute of Advanced Industrial Science and Technology), Sumiko Tsukamoto(Leibniz Institute for Applied Geophysics)

[HQR04-P01] Optically stimulated luminescence (OSL) dating using quartz extracted from loess as archeo-sediments of Paleolithic site

*Yorinao Shitaoka[1] (1.Department of Environment System, Faculty of Geo-environmental Science, Rissho University)

[HQR04-P02] Luminescence dating and age correction of marine terrace deposits in Kamikita Coastal Plain and Shimokita Peninsula, northeastern Japan

*Kazumi Ito[1], Toru Tamura[1] (1.Geological Survey of Japan, AIST)

[HQR04-P03] Comparison of luminescence readers using post-Infrared Infrared stimulated luminescence of K-feldspar from last interglacial marine terrace deposits

*Hayashizaki Ryo[1], Eiji Nakata[1] (1.Central Research Institute of Electric Power Industry)

[HQR04-P04] **Late Quaternary loess accumulation at the Rudak section in Uzbekistan, central Asia: Chronology and palaeoclimate implications**

★Invited Papers

*Jingran Zhang[1], Xinying Zhou[2], Hao Long[3] (1.Nanjing Normal Univ., 2.IVPP, CAS, 3.NIGLAS)

[HQR04-P05] Dating of hydrothermal silicified sediments by thermoluminescence

*Naoya Obata[3,1], Takashi Goto[4,1], Chitaro Gouzu[1], Jun-ichiro Ishibashi[2], Shin Toyoda[3] (1.Hiruzen Institute for Geology and Chronology Co., Ltd., 2.Kyushu University, 3.Okayama University of Science, 4.Fuji Geological Institute)

[HQR04-P06] Applications of trapped-charge dating techniques to hydrothermal mineral deposits collected from active seafloor hydrothermal fields

*Jun-ichiro Ishibashi[1], Naru Tsukamoto[1], Yusuke Okazaki[1], Taisei Fujiwara[2], Naoya Obata[2], Takashi Goto[2], Chitaro Gouzu[2], Shin Toyoda[3] (1.Department of Earth and Planetary Sciences, Faculty of Science, Kyushu University, 2.Hiruzen Institute for Geology and Chronology, 3.Okayama University of Science)

[HQR04-P07] **Luminescence dating of the late Quaternary terrestrial-marine interaction sedimentary history of the north Jiangsu coastal plain and the Yangtze River delta in China**

*Lei Gao[1], Hao Long[1], Toru Tamura[2] (1.Nanjing Institute of Geography and Limnology, Chinese Academy of Sciences, 2.Geological Survey of Japan, National Institute of Advanced Industrial Science and Technology)

[HQR04-P08] Composite chronology of Paleolithic sites in Jebel Qalkha revealed by pIRIR dating

Risako Kida[1], *Toru Tamura[2], Seiji Kadowaki[1] (1.Nagoya University Museum, Nagoya University, 2.Institute of Geology and Geoinformation Geological Survey of Japan, AIST)

[E] Poster | H (Human Geosciences)：H-DS Disaster geosciences

[H-DS08] Tsunami and tsunami forecast

convener:Hiroaki Tsushima(Meteorological Research Institute, Japan Meteorological Agency), Tatsuya Kubota(National Research Institute for Earth Science and Disaster Resilience)

[HDS08-P01] Probabilistic Hazard Assessment of Tsunami due to Large Earthquakes along the Nankai Trough

*Kazuhiro Ichijo[1], Yutaka Hayashi[1], Yasuyuki Kawazoe[2], Fumihiko Imamura[3], Hisashi Suito[1] (1.Ministry of Education, Culture, Sports, Science and Technology, 2.Japan Meteorological Agency, 3.International Research Institute of Disaster Science, Tohoku University)

[HDS08-P02] Characterized earthquake fault models along the Nankai Trough for probabilistic tsunami hazard assessment

*Kenji Hirata[1], Tadashi Kito[2], Nobuhiko Toyama[2], Hiroyuki Fujiwara[1], Hiromitsu Nakamura[1], Nobuyuki Morikawa[1], DOHI YUJI[1], Hisanori Matsuyama[2], Kenshi Ohshima[2], Yasuhiro Murata[3], Ryu Saito[3], Mariko Korenaga[4], Yuta Abe[4] (1.National Research Institue for Earth Science and Diaster Prevention, 2.OYO corporation, 3.KKC, 4.CTC)

[HDS08-P03] Tsunami simulations for probabilistic tsunami hazard assessment in the Nankai Trough

*Ryu Saito[1], Kenshi Ohshima[2], Tadashi Kito[2], Yasuhiro Murata[1], Tomoyuki Shibuki[1], Mariko Korenaga[3], Yuji Dohi[4], Hiromitsu Nakamura[4], Kenji Hirata[4], Hiroyuki Fujiwara[4] (1.KOKUSAI KOGYO CO., LTD, 2.OYO Corporation, 3.CTC (ITOCHU Techno-Solutions Corporation), 4.NIED (National Research Institute for Earth Science and Disaster Resilience))

[HDS08-P04] Probabilistic Tsunami Hazard Assessment for Nankai Trough:Weight Ratio and Results of PTHA

*Yuta Abe[1], Mariko Korenaga[1], Shinichi Akiyama[1], Teppei Ono[1], Hiroyuki Fujiwara[2], Kenji Hirata[2], Hiromitsu Nakamura[2], Tadashi Kito[3], Yasuhiro Murata[4] (1.ITOCHU Techno-Solutions Corporation, 2.National Research Institute for Earth Science and Disaster Resilience, 3.OYO Corporation, 4.Kokusai Kogyo Co., Ltd.)

[HDS08-P05] Consideration of tsunami source generated in the Hyuga-nada region in 1662

*Kei Ioki[1], Yusuke Yamashita[2], Yoshihiro Kase[3] (1.Geological Survey of Japan, National Institute of Advanced Industrial Science and Technology, 2.Disaster Prevention Research Institute, Kyoto University, 3.Geological Survey of Hokkaido, Hokkaido Research Organization)

[HDS08-P06] Source of the 1923 great Kanto earthquake explaining observed tsunami waveforms

*Yumi Nakadai[1], Yuichiro Tanioka[1] (1.Hokkaido University)

[HDS08-P07] Volcanic tsunami earthquakes repeating at submarine calderas (2): Kinematic source modeling of the 2015 Torishima earthquake

*Osamu Sandanbata[1], Shingo Watada[1], Kenji Satake[1], Hiroo Kanamori[2], Luis Rivera[3], Zhongwen Zhan[2] (1.Earthquake Research Institute, the University of Tokyo, 2.California Institute of Technology, 3.Université de Strasbourg, CNRS, IPGS UMR 7516, F-67000 Strasbourg)

[HDS08-P08] Sliding direction of the landslide that caused the 1998 Papua New Guinea tsunami

*Akio Katsumata[1], Yasuhiro Yoshida[2], Kenji Nakata[1], Kenichi Fujita[3], Masayuki Tanaka[1], Koji Tamaribuchi[1], Takahito Nishimiya[1], Akio Kobayashi[1] (1.Meteorological Research Institute, Japan Meteorological Agency, 2.Meteorological College, Japan Meteorological Agency, 3.Geospatial Information Authority of Japan)

[HDS08-P09] Simulation of reflected tsunami wave caused by the three cases of earthquake off Fukushima prefecture

*Kenji Nakata[1], Takeyasu Yamamoto[1] (1.Meteorological Research Institute, Japan Meteorological Agency)

[HDS08-P10] Real-Time Tsunami Detection Based on Ensemble Empirical Mode Decomposition

*Yuchen Wang[1], Kenji Satake[1], Takuto Maeda[2], Masanao Shinohara[1], Shin'ichi Sakai[1] (1.Earthquake Research Institute, University of Tokyo, 2.Graduate School of Science and Technology, Hirosaki University)

[HDS08-P11] Early estimation of tsunami height from near-fault ocean bottom pressure records: Comparison of DONET and S-net data

*Ayumu Mizutani[1], Kiyoshi Yomogida[1] (1.Graduate School of Science, Hokkaido University)

[HDS08-P13] Analytic solutions of seismic tsunamis' initial waveforms: a mathematical study

*Chi-Min Liu[1] (1.Department of Civil Engineering, Chienkuo Technology University)

[HDS08-P14] Predictions of tsunamis caused by possible outer-rise earthquakes in the Japan Trench

*Toshitaka Baba[1], Naotaka YAMAMOTO CHIKASADA[2], Yasuyuki Nakamura[3], Gou Fujie[3], Koichiro Obana[3], Seiichi Miura[3], Shuichi Kodaira[3] (1.Graduate School of Social Science and Technology, Tokushima University, 2.NIED, 3.JAMSTEC)

[HDS08-P15] Influence of coastal structures on probabilistic tsunami inundation assessments

*Toru Takeda[1], Toshitaka Baba[2], Tsuneo Ohsumi[3], Hiroyuki Fujiwara[4] (1.Graduate School of Advanced Science and Technology Education Department of Intelligent Mechanical Systems Engineering Construction Creative System Engineering Course, Tokushima University, 2.Graduate School of Science and Technology, Tokushima University, 3.National Research Institute for Earth Science and Disaster Prevention , 4.National Research Institute for Earth Science and Disaster Prevention)

[HDS08-P16] Simulations of sediment movement for tsunami deposits in Kamoda Pond along the Nankai Trough

*Takuya Saito[1], Toru Takeda[1], Kei Yamashita[2], Toshitaka Baba[3] (1.Graduate School of Advanced Science and Technology Education Department of Intelligent Mechanical Systems Engineering Construction Creative System Engineering Course, Tokushima University, 2.International Research Institute of Disaster Science, 3.Graduate School of Science and Technology, Tokushima University)

[E] Poster | H (Human Geosciences)：H-DS Disaster geosciences

[H-DS09] Landslides and related phenomena

convener:Masahiro Chigira(Disaster Prevention Research Institute, Kyoto University), Fumitoshi Imaizumi(Faculty of Agriculture, Shizuoka University), Gonghui Wang(Disaster Prevention Research Institute, Kyoto University)

[HDS09-P01] A new method for landslide extraction using optical and SAR images

*Yuga Kumagai[1], Masaru Fujita[2], Yasukuni Okubo[2], Kiichiro Kawamura[1] (1.Yamaguchi University, 2.Japan Space Systems)

[HDS09-P02] Landslides caused by the 2018 Hokkaido Iburi-tobu earthquake - Shallow slides of tephra deposits and deep-sheeted bedrock slides -

*Makoto Kaneko[1], Norio Oyagi[1], Hiroshi, P. Sato[2], Yusuke Muramiya[1] (1.Fukada Geological Institute, 2.College of Humanities and Sciences, Nihon University)

[HDS09-P03] **The geomorphic characteristics of landslides induced by The 2018 Eastern Iburi earthquake, Hokkaido**

★Invited Papers

*Rasis Putra Ritonga[1], Takashi Gomi[2,4], Hefryan Sukma Kharismalatri[2], Rozaqqa Noviandi[3], Yoshiharu Ishikawa[4] (1.United Graduate School of Agricultural Science, Tokyo University of Agriculture and Technology, 2.Institute of Global Innovation Research, Tokyo University of Agriculture and Technology, 3.International Environmental and Agricultural Science, Tokyo University of Agriculture and Technology, 4.Graduate School of Agriculture, Tokyo University of Agriculture and Technology)

[HDS09-P04] Relationship between the subsurface structure and the deformation area accompanied with the 2018 Hokkaido Eastern Iburi earthquake in a fill in Atsuma town, Hokkaido

*Issei Doi[1], Ryokei Azuma[2], Yuki Maenaka[2], Toshitaka Kamai[1] (1.Disaster Prevention Research Institute, 2.Faculty of Technology, Osaka Institute of Technology)

[HDS09-P05] Seismic site response of tephra slope: a case study for the landslides triggered by the 2018 Hokkaido Eastern Iburi Earthquake

*Gonghui Wang[1], Ning Ma[2], Issei Doi[1], Gen Furuya[3], Naoki Watanabe[4], Satoshi Ishimaru[5], Hiromichi Koyasu[5] (1.Kyoto University, 2.Southwest Jiaotong University, 3.Toyama Prefectural University, 4.Niigata University, 5.Hokkaido Research Organization)

[HDS09-P06] Microtremor Survey and Spectrum Analysis of a Coseismic Landslide: a Case Study in Subao Village, Ningxia, China

*Xiaobo LI[1,2], Jingshan BO[1], Issei DOI[2], Gonghui WANG[2], Toshitaka KAMAI[2] (1.Institute of Disaster Prevention, China Earthquake Adiministration, 2.Disaster Prevention Research Institute, Kyoto Unviersity)

[HDS09-P07] **Pore structure characteristics of wide-grading loose soils in the Wenchuan earthquake area**

*Yifei Cui[1], Chaoxu Guo[2] (1.State Key Laboratory of Hydroscience and Engineering, Tsinghua University, 2.Fujian Academy of Building Research, Co.LTD., Fujian Key Laboratory of Green Building Technology)

[HDS09-P08] Seismic Response of Rock Wedges under Dynamic Loading Revealed by Shaking Table Test

*Hung-Hui Li[1], Chi-Chieh Chen[1], Chang-Liang Chun[1], Ming-Han Lin[1], Chen-Shi Ping[1] (1.Chung-Cheng Institute of Technology, National Defense University of Taiwan)

[HDS09-P09] Seismic Response of Dip-Slope with Various Roughness of Weakness Revealed by Shaking Table Test

Wen-Zhang Chen [1], Ming-Han Lin[1], KAI-YANG LIN[1], *Hung-Hui Li[1] (1.Chung-Cheng Institute of Technology, National Defense University of Taiwan)

[HDS09-P10] Analytical solutions for submarine avalanche entraining/detraining process

*Yi Ping Lu[1], Chi-Yao Hung[1] (1.National Chung Hsing University)

[HDS09-P11] Slope failure - debris flow events in rhyolitic and granitic areas in Hiroshima triggered by 2018 torrential rainfall and its implications for disaster risk reduction – a quantitative approach by photogrammetry and field survey

*Toshihiko Sugai[1], Kunnga Mergen[1], Natsuki Sasaki[1], Sako Hasegawa[1], Shoichiro Uchiyama[2] (1.Department of Natural Environmental Studies, Institute of Environmental Studies, Graduate School of Frontier Science, The University of Tokyo, 2. National Research Institute for Earth Science and Disaster Resilience)

[HDS09-P12] **The effect of rainfall event characteristics on event-based landslide susceptibility map**

*Chun-Yi Wu[1], Chiao-Ling Hsueh[1], Sheng-Yu Lin[1] (1.Department of Soil and Water Conservation, National Chung Hsing University)

[HDS09-P13] Non-plastic fines content effect on the initiation and movement of rainfall-induced landslides in small flume tests

*Chao HUANG[1], Gonghui Wang[2] (1.Division of Earth and Planetary Sciences, Graduate School of Science, Kyoto University, 2.Disaster Prevention Research Institute, Kyoto University, Kyoto, Japan)

[HDS09-P14] **The influence of the orientation of weak planes on slope deformation**

*Chao-Yu Wang[1], Kuang-Tsung Chang[1] (1.National Chung Hsing University)

[HDS09-P15] Can we detect the acceleration of long-term gravitational deformation on steep slopes before catastrophic events? -A case study on two large-scale rapid landslides in Kii peninsular, Japan-

*Teruyuki Kikuchi[1], Norio Oyagi[2], Makoto Kaneko[2], Koki Sakita[3], Teruyoshi Hatano[4] (1.JP-Design. co. ltd., 2.Fukada Geological Institute, 3.Okayama University, 4.Electric Power Development Co., Ltd)

[HDS09-P16] Long-term distribution and evolution of landslide in the landslide-prone watershed: A case study in the Chishan river upstream watershed in Taiwan

*Chengyi Lin[1], Chunuhung WU[1] (1.Feng Chia University)

[HDS09-P17] A decade analysis of landslide distribution in the dense-landslide watersheds in Taiwan

*Chengyi Lin[1], Chunuhng WU[1] (1.Feng Chia University)

[HDS09-P18] **Study of Seeding Amount of Vegetation Pellets**

*Hung-Yen Hu[1], Guo-Zhang Michael Song[1], Shin-Hwei Lin[1], Kai-Chi Hsu[1] (1.National Chung-Hsing university, department of soil and water conservation)

[E] Poster | H (Human Geosciences)：H-DS Disaster geosciences

[H-DS10] Natural hazard impacts on human society, economics and technological systems

convener:ELENA PETROVA(Lomonosov Moscow State University, Faculty of Geography), Hajime Matsushima(Research Faculty of Agriculture, Hokkaido University)

[HDS10-P01] **The 2019 Activity of Kamchatkan and Kurile Islands Volcanoes and Danger to Aviation**

*Olga Girina[1], Dmitry Melnikov[1], Alexander Manevich[1], Anton Nuzhdaev[1], Elena Petrova[2] (1.Institute of Volcanology and Seismology, Far East Division, Russian Academy of Sciences, 2.Lomonosov Moscow State University, Geography Faculty, Russia)

[HDS10-P02] Annual and monthly risk assessment of typhoon disasters in China based on the information diffusion method.

*ge GAO[1], Dapeng Huang[1], Shanshan Zhao[1] (1.NCC, China)

[HDS10-P03] Study on the state of damage and the geographic distribution of flood damages in Japan from 2008 to 2017

*fumeng Zhang[1], Katsunori Furuya[1] (1.Chiba Univercity)

[HDS10-P04] A Research about the role of Eco-DRR: Ecosystem-based Disaster Risk Reduction in landscape design in Asian Cities

*Minghui Tang[1], Naoko Fujita[1] (1.University of Tsukuba)

[HDS10-P05] Impact of Climate Change on Socio-Economically Weaker Section in India

*Ruhma Khan[1], Jahangeer -[2] (1.Jamia Millia Islamia University, New Delhi , India, 2.University of Nebraska Lincoln USA)

[HDS10-P06] Cultural ecosystem services of green infrastructure: the comparison between Russia and Japan

*ELENA PETROVA[1], Hajime Matsushima[2], Anastasia Petrova[3], Yury Semenov[4] (1.Lomonosov Moscow State University, Faculty of Geography, 2.Hokkaido University, 3.Institute of Oriental Sudies of the Russian Academy of Sciences, 4.Sochava Institute of Geography, Siberian Branch of the Russian Academy of Sciences)

[HDS10-P07] **The Reconstruction Assistance from Kumamoto Earthquake by the Grassland Conservation Volunteers in the Aso National Park**

★Invited Papers

*REIKO MACHIDA[1] (1.TOKYO UNIVERSITY OF AGRICULTURE)

[HDS10-P08] Drought, War, and Cannibalism in Northern China in History

*Harry F Lee[1] (1.The Chinese University of Hong Kong)

[HDS10-P09] Design and evaluation of effective methods of green infrastructure for municipalities

*Shan Liu[1], Naoko Fujita[1] (1.University of Tsukuba)

[E] Poster | H (Human Geosciences)：H-DS Disaster geosciences

[H-DS11] Subaqueous Landslides and Their Anthropogenic Impact for Coastal Regions

convener:Yujin Kitamura(Department of Earth and Environmental Sciences, Graduate School of Science and Engineering, Kagoshima University), Kiichiro Kawamura(Yamaguchi University)

[HDS11-P01] Numerical Simulation of Submarine Landslide Tsunami due to the 1929 Grand Banks Earthquake

*Tatsuya Nakagaki[1], Yuichiro Tanioka[1] (1.Hokkaido University)

[HDS11-P02] Trial and error estimation of the initial sea surface deformation of the tsunami caused by the 2009 Suruga Bay earthquake

*Masahiro Kurozumi[1], Toshitaka Baba[2] (1.Tokushima University Graduate School of Frontier Sciences, 2.Tokushima University Graduate School of Industrial Science and Engineering)

[HDS11-P03] Effect of cohesion between sedimentary layers on water film formation in submarine landslides

*Shogo Kawakita[1], Daisuke Asahina[2], Takato Takemura[3], Hinako Hosono[3], Keiji Kitajima[4] (1.Graduate School of Science and Technology, Nihon Univ., 2.National Institute of Advanced Industrial Science and Technology, 3.College of Humanities and Sciences, Nihon Univ., 4.College of Science and Technology, Nihon Univ.)

[E] Poster | H (Human Geosciences)：H-TT Technology & Techniques

[H-TT14] Geographic Information Systems and Cartography

convener:Takashi Oguchi(Center for Spatial Information Science, The University of Tokyo), Yoshiki Wakabayashi(Graduate School of Urban Environmental Sciences, Tokyo Metropolitan University), Yuei-An Liou(National Central University), Ronald C. Estoque(National Institute for Environmental Studies, Japan)

[HTT14-P01] Evaluation of seismic wave amplifications in the mountainous area with a temporary seismic network in Totsukawa Village

★Invited Papers

*Chi-Wen Chen[1,2], Masato Sato[1], Ryuji Yamada[1], Tomoyuki Iida[1,2] (1.National Research Institute for Earth Science and Disaster Resilience, 2.The University of Tokyo)

[HTT14-P02] **Landslide Detection from Remote Sensing Imagery Based on SPP-PCANet**

*Yimei Wei[1], Takashi Oguchi[2] (1.The University of Tokyo, 2.Center for Spatial Information Science, The University of Tokyo)

[HTT14-P03] **GIS-based frequency ratio, logistic regression and artificial neural network models for landslide susceptibility analysis in central Shenzhen, South China**

*DI LU[2], Takashi Oguchi[1] (1.Center for Spatial Information Science, The University of Tokyo, 2.The University of Tokyo)

[HTT14-P04] **Analysis of Morphometric Parameters and Precipitation Characteristics for Landslides Using GIS**

*Toshikazu Fukuba[1], Takashi Oguchi[2] (1.Department of Earth and Planetary Environmental Science, The University of Tokyo, 2.Center for Spatial Information Science)

[HTT14-P05] **GIS and remote sensing applied to topographic analyses of hilly and mountainous communities, Nishi-Awa, Japan**

★Invited Papers

*Roxanne Lai[1], Takashi Oguchi[1] (1.University of Tokyo)

[HTT14-P07] Development of e-learning materials for high school education on topography using GIS

*Hiroyuki Yamauchi[1], Takashi Oguchi[2] (1.Department of Natural Environmental Studies, Graduate School of Frontier Sciences, The University of Tokyo, 2.Center for Spatial information Science, The University of Tokyo)

[HTT14-P08] An Improved Mosaicking Algorithm for UAV Photographs of Vegetated Areas

*Zijin Wang[1], Takashi Oguchi[2] (1.Department of Natural Environmental Studies, Graduate School of Frontier Science, The University of Tokyo, 2.Center for Spatial Information Science, The University of Tokyo)

[HTT14-P09] Surge event of Alakesayi Glacier, West Kunlun Shan, based on remote sensing data

*Qiqi MA[1], Takashi OGUCHI[2,1] (1.Dept. of Natural Environmental Studies, Graduate School of Frontier Sciences, The University of Tokyo, 2.Center for Spatial Information Science, Division of Spatial Information Analysis, The University of Tokyo)

[HTT14-P10] Remote Sensing-Based Urban Heat Risk Assessment in Philippine Cities

★Invited Papers

*Ronald C. Estoque[1], Makoto Ooba[1], Xerxes T. Seposo[2], Takuya Togawa[1], Yasuaki Hijioka[1], Kiyoshi Takahashi[1], Shogo Nakamura[1] (1.National Institute for Environmental Studies, Japan, 2.Nagasaki University, Japan)

[E] Poster | H (Human Geosciences)：H-TT Technology & Techniques

[H-TT15] Environmental Remote Sensing

convener:Wei Yang(Chiba University), Akihiko Kondoh(Center for Environmental Remote Sensing, Chiba University), Carolynne Hultquist(Columbia University), Elena Sava(US Army Corps of Engineers Geospatial Research Laboratory), Guido Cervone(Pennsylvania State University Main Campus)

[HTT15-P01] **Impacts of urbanization on the local thermal environment in Central America**

*Son Thanh Nguyen[1], Chi-Farn Chen[1], Cheng-Ru Chen[1] (1.Center for Space and Remote Sensing Research, National Central University, Zhongli District, Taoyuan City 32001, TAIWAN)

[HTT15-P03] Generation of the GCOM-C land surface phenology product: Algorithm development and performance evaluation

*MENGYU LI[1], Wei Yang[2], Akihiko Kondoh[2] (1.Graduate School of Science and Engineering, Chiba University, 2.Center for Environmental Remote Sensing, Chiba University)

[HTT15-P04] **Monitoring macrophyte phenology in Lake Inba-numa, Japan based on Sentinel-2 images**

*HU LIANG[1] (1.Chiba University, Graduate School of Science and Engineering, Center for Environmental Remote Sensing)

[HTT15-P06] **Detecting Urban Growth Using Remote Sensing and GIS Techniques in Taoyuan City, Taiwan**

*Cheng-Ru Chen[1,2], Chi-Farn Chen[1], Thanh-Son Nguyen[1] (1.CSRSR,NCU, 2.CLVSC)

[HTT15-P07] **Evaluation and comparison of *Karenia mikimotoi* detection in the Seto-Inland Sea by remote sensing**

*Zhenjia Zhou[1], Joji Ishizaka[2] (1.GSES, Nagoya Univ., 2.ISEE, Nagoya Univ.)

[HTT15-P08] Spectro-polarimetric BRF measurements of the desert sand with multispectral LCTF camera

*Begzsuren Tumendemberel[1], Yukihiro Takahashi[1], Junichi Kurihara[1], Tetsuro Ishida, Nobuyasu Naruse[2], Ahmad Shaqeer[1] (1.Hokkaido University, Department of Cosmosciences, Graduate School of Science, Kita 10-Nishi 8, Kita-ku, Sapporo, Hokkaido 060-0810, 2.Division of Physics Dept. of Fundamental Bioscience, Faculty of Medicine, Shiga University of Medical Science ZIP: 520-2192 Seta, Tsukinowa-cho, Otsu, Shiga, JAPAN)

[HTT15-P09] Mirror Reflection Measurement of Leaves from Different Environmental Stresses

*Garid Zorigoo[1], Begzsuren Tumendemberel[1], Yukihiro Takahashi[1] (1.Department of Cosmosciences, Graduate School of Science, Hokkaido University)

[E] Poster | H (Human Geosciences)：H-CG Complex & General

[H-CG21] International Comparison of Landscape Appreciation

convener:yoji aoki(Open University of Japan)

[HCG21-P01] Sightseeing image of Asakusa based on Foreign Tourist Preference

*Xie Zijiao[1], saraswati Sisriany[1], Wang Huixin [1], Zhao Yuqing [1], Oka Masaya [1], Kobayashi Kumiko [1], Furuya Katsunori[1] (1.Chiba University)

[HCG21-P02] Study on the Influence of Japanese Traditional Garden and Culture on Japanese People's Perception of Residential Garden

*Zhendong Liu[1], Tingyu Lu[1], Heyan Jiang[1], Junhei Watanabe[2], Fumeng Zhang[1], Zhi Li[1], Yingming Mao[1], Dibyanti Dibyanti Danniswari[1], Pratiwi Prita Indah[1], Katsunori Furuya[1] (1.Graduate School of Horticulture, Chiba University, 2.Faculty of Horticulture, Chiba University)

[HCG21-P04] **An attempt to manage both rural landscape conservation and tourism development**

*Kojima Shusaku[1], Megumi Aso[2] (1.Graduate School of Tokyo University of Agriculture, 2.Community-reactivating cooperator squard of Miyaki town)

[HCG21-P05] **Appreciations of Japanese landscapes by the western visitors arrived (1549-1858)**

*yoji aoki[1], Fumihiro Konta[2] (1.Open University of Japan, 2.National Science Museum)

[HCG21-P06] Trends of the methods of landscape presentation in the landscape appreciation test from 1967 to 1987

*yoji aoki[1] (1.Open University of Japan)

[E] Poster | H (Human Geosciences)：H-CG Complex & General

[H-CG22] Deltas and estuaries: multidisciplinary analyses of complex river-mouth systems

convener:Yoshiki Saito(Estuary Research Center, Shimane University), David L Dettman(University of Arizona), Kazuaki Hori(Department of Geography, Graduate School of Environmental Studies, Nagoya University)

[HCG22-P01] Numerical estimation of Holocene paleowave changes in an estuarine environment: case of Tokyo Bay, central Japan

*Katsuto Uehara[1] (1.Kyushu University)

[HCG22-P02] **Channel deformation of the lower Mississippi and Yangtze Rivers – Implications for future backwater zone studies**

*Yi-Jun Xu[1], Maotian Li[2], Zhongyuan Chen[2], Bo Wang[1], Shuwei Zheng[3], Weiguo Zhang[2] (1.Louisiana State University, 2.East China Normal University, 3.Shandong Normal University)

[HCG22-P03] Offset in radiocarbon ages between marine bioclast and terrestrial plant pairs in the Holocene sediments along the Pacific coasts around Japan

*Nakanishi Toshimichi[1], Futoshi Nanayama[2], Kazuaki Hori[3], Yuichi Niwa[4], Junko Komatsubara[5], Akihisa Kitamura[6], Wan Hong[7] (1.Japan Atomic Energy Agency, 2.AIST/Kumamoto Univ., 3.Nagoya Univ., 4.Chuo Univ., 5.AIST, 6.Shizuoka Univ., 7.KIGAM)

[E] Poster | H (Human Geosciences)：H-CG Complex & General

[H-CG23] Earth surface processes related to deposition, erosion and sediment transport

convener:Koji Seike(Geological Survey of Japan, AIST), Masayuki Ikeda(University of Tokyo), Hideko Takayanagi(Institute of Geology and Paleontology, Graduate School of Science, Tohoku University), Hajime Naruse(Department of Geology and Mineralogy, Graduate School of Science, Kyoto University)

[HCG23-P01] **Wind Dynamic Process and Ecological Effect in Sand Barrier Environment of Mu Us Sandy land**

*Hongyue Li[1,2], Hasi -[1,2], Jie Yin[1,2] (1.School of Natural Resources,Beijing Normal Univ., 2.Faculty of Geographical Science,Beijing Normal Univ.)

[HCG23-P02] **Comparison of Roughness-Cover Models for bedrock bed with Experimental Observations**

*Jagriti Mishra[1], Takuya Inoue[1] (1.Civil Engineering Research Institute for Cold Region)

[HCG23-P03] Paleosols distributed in marine terraces in the Goshogawara area, Aomori Prefecture, Northeast Japan

*Aya Omata[1], Kohki Yoshida[2] (1.Division of Science and Technology, Graduate School of Shinshu University, 2.Department of Geology, Faculty of Science, Shinshu University)

[HCG23-P04] **Effects of soil moisture variation on rainfall infiltration and erosion of the badland soil in Taiwan**

*po yuan Chou[1], Yung-Chieh Wang[1] (1.National Chung Hsing University)

[HCG23-P05] Forced regression deposits during MIS 5c and 5a observed in the Iioka marine terrace (the Pleistocene Katori Formation, central Japan)

*Hiroko Okazaki[1], Hiroomi Nakazato[2], Toru Tamura[3], Kazumi Ito[3], Masakazu Nara[4] (1.Division of Earth Science, Natural History and Institute, Chiba, 2.Institute for Rural Engineering, NARO, 3.Institute of Geology and Geoinformation Geological Survey of Japan, AIST, 4.Sciences Unit, Natural Sciences Cluster, Research and Education Faculty, Kochi University)

[E] Poster | H (Human Geosciences)：H-CG Complex & General

[H-CG24] Enhancing Integrated Research for Sustainable Future - a human geoscience perspective

convener:Yukio Himiyama(Emeritus Professor, Hokkaido University of Education), Takeshi Sakurai(Graduate School of Agricultural and Life Sciences, The University of Tokyo), Akihiko Kondoh(Center for Environmental Remote Sensing, Chiba University)

[HCG24-P01] **Pattern of Electricity Consumption in Consecutive Hot Days with respect to Microclimate, a case study of Taipei city**

*Po Yu Chen[1], Jehn-Yih Juang[1,2] (1.International Degree Program in Climate Change and Sustainable Development, National Taiwan University, Taiwan(R.O.C.), 2.Department of Geography, National Taiwan University, Taiwan(R.O.C.))

[HCG24-P02] Biodiversity and ecosystem functioning under different land management regimes -Case study in grazing lands in northern Ethiopia

*Keiichi Kimura[1], Akito Kono[1], Shigdaf Mekuriaw[2], Yeshambel Mekuriaw[3], Misganaw Wale[3], Asaminew Tassewe[3], Okuro Toshiya[1] (1.Graduate School of Agricultural and Life Sciences, The University of Tokyo, 2.Arid Land Research Center, Tottori University, 3.Bahir Dar University)

[HCG24-P03] Simulating the Spatial Flow of Carbon Sequestration Service: A Case Study of Tumen River Watershed

*Jian ZHANG[1], Shizuka HASHIMOTO[1], Weihong ZHU[2], Toshiya OKURO[1] (1. The University of Tokyo, 2.The Yanbian University)

[HCG24-P04] Measuring Urban Sustainability Using Spatial and Socio-Economic Factor and the Impact on Planning Policies in a Rapidly Urbanizing Area

*Anoraga Jatayu[1], Ernan Rustiadi[2,3], Didit Okta Pribadi[4,3] (1.Regional and Rural Development Planning Science Study Program, 2.IPB University, 3.Center for Regional Systems, Analysis, Planning and Development, 4.Research Center for Plant Conservation and Botanic Garden, Indonesian Institute of Science)

[E] Poster | H (Human Geosciences)：H-CG Complex & General

[H-CG25] Turbidity current: generation, morphodynamics and deposits

convener:Hajime Naruse(Department of Geology and Mineralogy, Graduate School of Science, Kyoto University), Robert Michael Dorrell(University of Hull), Miwa Yokokawa(Osaka Institute of Technology)

[HCG25-P01] Inverse Analysis of Experimental Scale Turbidity Currents by Deep Learning Neural Network

*Cai Zhirong[1], Hajime Naruse[1] (1.Kyoto University)

[HCG25-P02] Dynamic stratification enables auto-suspension and thus the ultra-long run-out of sediment-laden buoyancy driven flows

*Robert Michael Dorrell[1] (1.University of Hull)

[HCG25-P03] Dynamics of turbidity currents influenced by tidal flows

*Justine Poppeschi[1], Hajime Naruse[1], Robert Michael Dorrell[2] (1.Kyoto University, 2.University of Hull)

[HCG25-P04] Evaluation of plant-fragment concentration system in the turbiditic sequence by terrigenous biomarker analysis of sediments from the Kawabata Formation, Yubari area, central Hokkaido, Japan.

*Muhammad Adam Ismail[1], Hiroyasu Asahi[1], Satoshi Furota[3], Ken Sawada[2] (1.Graduate School of Science, Hokkaido University, 2.Department of Earth and Planetary Sciences, Faculty of Science, Hokkaido University, 3.Geological Survey of Japan, National Institute of Advanced Industrial Science and Technology)

[HCG25-P05] Grain fabric analysis of massive sandstone beds of the Upper Cretaceous Himenoura Group distributed in Amakusa-Kamishima Island, Kyushu, Southwestern Japan by Deep Learning Convolutional Neural Network

*Sayo Ishii[1], Hajime Naruse[1] (1.Department of Geology and Mineralogy, Graduate School of Science, Kyoto University)

[HCG25-P06] Revisiting the meandering channel developed in the Okinawa Trough

*Takeshi Matsumoto[1], Yasuhiro Morii[2], Nobuhiro Yamawaki[2], Itaru Aizawa[2], Sota Hoshina[2], Tsukasa Kinoshita[2] (1.Faculty of Science, University of the Ryukyus, 2.Faculty of Fisheries, Nagasaki University)

[HCG25-P07] Cyclic steps inside submarine canyon and in canyon-fan transition zone: Numerical experiments by 2D shallow-water model of turbidity currents

*Hajime Naruse[1] (1.Department of Geology and Mineralogy, Graduate School of Science, Kyoto University)

[HCG25-P08] Sedimentary facies related to supercritical-flow bedforms in foreset slopes of middle Pleistocene Gilbert-type delta, central Japan

*Hiroko Okazaki[1] (1.Division of Earth Science, Natural History and Institute, Chiba)

[E] Poster | S (Solid Earth Sciences)：S-GD Geodesy

[S-GD01] Geodetic Infrastructure for Monitoring the Dynamic Earth: The Global Geodetic Observing System

convener:Basara Miyahara(GSI of Japan), Richard S Gross(NASA Jet Propulsion Laboratory)

[SGD01-P01] The International VLBI Service and Its Role in GGOS

*Hiroshi Munekane[1], Dirk Behrend[2], Nancy Wolfe Kotary[3] (1.Geospatial Information Aurhotiry of Japan, 2.NVI, Inc., 3.MIT Haystack Observatory)

[SGD01-P03] DORIS: 30 years of success in precise orbit determination and ground station positioning

*Frank G Lemoine[1], Guilhem Moreaux[2], Jérôme Saunier[3], Pascale Ferrage[4], Laurent Soudarin[2], Koichiro Doi[5] (1.NASA Goddard Space Flight Center, Greenbelt, Maryland, U.S.A., 2.Collecte Localisation Satellites, Ramonville Saint-Agne, France, 3.Institut National de l'Information Géographique et Forestière, St-Mandé, France, 4.Centre National d'Etudes Spatiales, Toulouse, France, 5.National Institute of Polar Research, Tachikawa-City, Tokyo, Japan)

[SGD01-P04] The International Gravity Field Service (IGFS) and its contributions to the GGOS infrastructure

Riccardo Barzaghi[1], George S Vergos[2], *Basara Miyahara[3] (1.Politecnico di Milano, 2.Aristotle University of Thessaloniki, 3.GSI of Japan)

[SGD01-P05] Activities of the Ishioka VLBI Station as a VGOS station

*Haruka Ueshiba[1], Tomokazu Nakakuki[1], Saho Matsumoto[1], Nobuhiro Ishikura[1], Michiko Umei[1], Kyonosuke Hayashi[1], Toru Yutsudo[1], Tadao Kikkawa[1], Hiroshi Munekane[1] (1.GSI of Japan)

[SGD01-P06] Satellite Laser Ranging and GNSS observations in the Shimosato Hydrographic Observatory, Japan

*Shun-ichi Watanabe[1], Noritsune Seo[2], Yuto Nakamura[1], Yusuke Yokota[3], Hiroko Fukura[4] (1.Hydrographic and Oceanographic Department, Japan Coast Guard, 2.Shimosato Hydrographic Observatory, 5th Regional Coast Guard Headquarters, Japan Coast Guard, 3.Institute of Industrial Science, University of Tokyo, 4.8th Regional Coast Guard Headquarters, Japan Coast Guard)

[SGD01-P07] Current Status and Prospect of GEONET, Japanese dense GNSS network

*Takayuki Miyazaki[1], Koki Kumagai[1] (1.GSI of Japan)

[SGD01-P09] **Crustal Deformation Measurements in Himachal Himalaya: A New Evidence of Extensional Tectonics**

*Yogendra Sharma[1], Sumanta Pasari[1], Kuo En Ching[2], Onkar Dikshit[3], Javed N Malik[3] (1.Birla Institute of Technology and Science, Pilani, 2.National Cheng Kung University, Taiwan, 3.IIT Kanpur)

[SGD01-P10] Crustal deformation by the 2019 Typhoon Hagibis: High time-resolution study

*Wei Zhan[1], Kosuke Heki[2] (1.The First Monitoring and Application Center, China Earthquake Administration, 2.Department of Natural History Sciences, Hokkaido University)

[SGD01-P11] Analyzing the Tropospheric Delay Estimates on Global Navigation Satellite Systems (GNSS) with Precise Point Positioning (PPP) Services using the goGPS software.

*Syachrul Arief[1], Kosuke Heki[1], Andrea Gatti[2], Eugenio Realini[2] (1.Hokkaido University - Sapporo, Japan, 2.Geomatics Research and Development s.r.l. - Lomazzo, Italy)

[SGD01-P12] Development of novel ground-based microwave radiometer for earth science -results of the first measurements-

*Ryuichi Ichikawa[1], Hideki Ujihara[1], Shinsuke Satoh[1], Yusaku Ohta[2], Basara Miyahara[3], Hiroshi Munekane[3], Taketo Nagasaki[4], Osamu Tajima[5], Kentaro Araki[6], Takuya Tajiri[6], Hiroshi Takiguchi[7], Takeshi Matsushima[8], Nobuo Matsushima[9], Tatsuya Momotani[10], Kenji Utsunomiya[10] (1.National Institute of Information and Communications Technology, 2.Tohoku University, 3.Geospatial Information Authority of Japan, 4.RIKEN, 5.Kyoto University, 6.Meteorological Research Institute, JMA, 7.Japan Aerospace eXploration Agency, 8.Kyushu University, 9.National Institute of Advanced Industrial Science and Technology, 10.Japan Weather Association)

[SGD01-P13] Use Delay-Doppler Map Made by Oceanic Reflected GPS Signal to Evaluate Ocean Surface Wind

*Wen-Hao Yeh[1], Yung-Fu Tsai[1], Chen-Tsung Lin[1], Hwa Chien[2], Lin Zhang [2] (1.National Space Organization, National Applied Research Laboratories, Taiwan, 2.Institute of Hydrological & Oceanic Sciences, National Central University, Taiwan)

[E] Poster | S (Solid Earth Sciences)：S-SS Seismology

[S-SS03] Seismological advances in the ocean

convener:Takashi Tonegawa(Research and Development center for Earthquake and Tsunami, Japan Agency for Marine-Earth Science and Technology), Takeshi Akuhara(Earthquake Research Institute, University of Tokyo), Pascal Audet(University of Ottawa), Taka'aki Taira(Berkeley Seismological Laboratory, University of California, Berkeley)

[SSS03-P02] Incoming directions of broadband infragravity waves observed at the central part of the Pacific Ocean

*Takashi Tonegawa[1], Kiwamu Nishida[2], Yoshio Fukao[1] (1.Research Institute for Marine Geodynamics, Japan Agency for Marine-Earth Science and Technology, 2.Earthquake Research Institute, The University of Tokyo)

[SSS03-P04] Structure of the northern Hikurangi margin from receiver functions using broadband OBS data from the HOBITSS experiment

*Pascal Audet[1], Martha K Savage[2], Anne Sheehan[3], Kimihiro Mochizuki[4] (1.University of Ottawa, 2.Victoria University of Wellington, 3.University of Colorado at Boulder, 4.University of Tokyo)

[SSS03-P05] Seismic interferometry analyses of teleseismic coda waves on a dense network of permanent ocean bottom seismometers (S-net) offshore Honshu, Japan

★Invited Papers

*Tomoya Takano[1,2], Florent Brenguier[1], Pierre Boue[1], Ryota Takagi[3], Kaoru Sawazaki[4], Tetsuya Takeda[4], Yosuke Aoki[2], Kiwamu Nishida[2] (1.Institut des Sciences de la Terre, Univ. Grenoble Alpes, 2.Earthquake Research Institute, The University of Tokyo, 3.Research Center for Prediction of Earthquakes and Volcanic Eruptions, Graduate School of Science, Tohoku University, 4.NIED)

[SSS03-P06] “N”-shaped Y/X coda spectral ratio observed for in-line type OBS of S-net and ETMC

*Kaoru Sawazaki[1], Takeshi Nakamura[1] (1.National Research Institute for Earth Science and Disaster Resilience)

[SSS03-P07] Spatiotemporal Variations of PM Excitation in the Northern Okinawa Trough Revealed by OBS Array

*Chih-Chieh Chien[6], Ying-Nien Chen[3], Yuancheng Gung[6], Ban-Yuan Kuo[1], Shu-Huei Hung[6], Eh Tan[1], Kate Huihsuan Chen[5], Shuichi Kodaira[2], Yasushi Ishihara[2], Mamoru Nakamura[8], Chau-Chang Wang[4,7], Ching-Ren Lin[1] (1.Academia Sinica, Taipei, Taiwan, 2.Japan Agency for Marine-Earth Science and Technology, Yokohama, Japan, 3.National Chung Cheng University, Chiayi, Taiwan, 4.National Sun Yat-sen University, Kaohsiung, Taiwan, 5.National Taiwan Normal University, Taipei, Taiwan, 6.National Taiwan University, Taipei, Taiwan, 7.Taiwan Ocean Research Institute, National Applied Research Laboratories, Kaohsiung, Taiwan, 8.University of the Ryukyus, Okinawa, Japan)

[SSS03-P08] Rayleigh wave ellipticity estimated from earthquake and noise cross-correlations of OBS data: Effect of ocean and sedimentary layers.

*Shun Fukushima[1], Kiyoshi Yomogida[2] (1.Hokkaido University,Graduate school of Science,Department of Natural History Sciences,Seismology Laboratory , 2.Department of Earth and Planetary Dynamics, Graduate School of Science, Hokkaido University)

[SSS03-P09] A Temporal Variation of Auto-correlation Function Calculated from Ocean Bottom Seismometers off Miyagi Prefecture

*Miyuu Uemura[1], Yoshihiro Ito[2], Kazuaki Ohta[3], Ryota Hino[4], Masanao Shinohara[5] (1.Graduate School of Science, Kyoto University, 2.Disaster Prevention Research Institute, Kyoto University, 3.National Research Institute for Earth Science and Disaster Resilience, 4.Graduate School of Science, Tohoku University, 5.Earthquake Research Institute, University of Tokyo)

[SSS03-P10] Similar earthquake activity in the northern part of the Ryukyu subduction zone observed by onshore and offshore seismic data

*Yukihiro Nakatani[1], Hiroshi Yakiwara[1], Shuichiro Hirano[2], Reiji Kobayashi[2], Hiroki Miyamachi[2], Shigeru Nakao[2], Yusuke Yamashita[3], Kazunari Uchida[4], Takeshi Matsushima[4], Hiroshi Shimizu[4], Kazuo Nakahigashi[5], Tomoaki Yamada[6], Hideji Abe[7], Masanao Shinohara[7] (1.Nansei-Toko Observatory for Earthquakes and Volcanoes, Kagoshima University, 2.Graduate School of Science and Engineering, Kagoshima University, 3.Disaster Prevention Research Institute, Kyoto University, 4.Institute of Seismology and Volcanology, Faculty of Science, Kyushu University, 5.Tokyo University of Marine Science and Technology, 6.Japan Meteorological Agency, 7.Earthquake Research Institute, the University of Tokyo)

[SSS03-P11] Spatiotemporal distribution of fin whale signals in northeast Japan

*Takeshi Nakamura[1], Ryoichi Iwase[2] (1.National Research Institute for Earth Science and Disaster Resilience, 2.Japan Agency for Marine-Earth Science and Technology)

[E] Poster | S (Solid Earth Sciences)：S-SS Seismology

[S-SS04] Strong Ground Motion and Earthquake Disaster

convener:Kazuhiro Somei(Geo-Research Institute), Yasuhiro Matsumoto(Kozo Keikaku Engineering)

[SSS04-P01] Toward to construction of strong-motion database for seismic hazard assessment in Japan

*Nobuyuki Morikawa[1], Hiroyuki Fujiwara[1], Asako Iwaki[1], Takahiro Maeda[1], Hisahiko Kubo[1], Shin Aoi[1], Kenichi Kato[2], Yusuke Tomozawa[2], Fumino Suzuki[2], Toshiaki Sato[3], Toru Ishii[3], Naomi Shimazu[3], Jun'ichi Miyakoshi[3], Atsuko Oana[3], Hongjun Si[4], Toshihiko Hayakawa[5], Takayuki Hayashi[6], Natsuki Kishida[6], Saburoh Midorikawa[7] (1.National Research Institute for Earth Science and Disaster Resilience, 2.Kobori Research Complex Inc., 3.Ohsaki Research Institute Inc., 4.Seismological Research Institute Inc., 5.Mitsubishi Space Software Co., Ltd., 6.Tokio Marine & Nichido Risk Consulting Co., Ltd., 7.Tokyo Institute of Technology)

[SSS04-P02] **Tilt and rotational motions during the strong shaking**

*Toshimi Satoh[1] (1.Shimizu Corporation)

[SSS04-P03] Analysis of pulse-like waves observed in the eastern part of Fukushima Prefecture during the 2011 Tohoku earthquake

*Tomiichi Uetake[1], Kazuhito Hikima[1], Akihito Shimmura[1], Masatoshi Fujioka[1], Ryosuke Sugimoto[1] (1.Tokyo Electric Power Company Holdings)

[SSS04-P04] **Ground Motion Estimation from the Initial P Wave of the Great Earthquake**

*Zijun WANG[1], Boming ZHAO[1], Takao KAGAWA[2], Masanori HORIKE[3] (1.Beijing Jiaotong University, 2.Tottori University , 3.Hanshin Consultants Co., Ltd.)

[SSS04-P05] **Damage Hazard Caused by the Great Earthquake Ground Motion**

*Boming ZHAO[1], Zijun WANG[1], Takao KAGAWA[2], Masanori HORIKE[3] (1.Beijing Jiaotong University, 2.Tottori University, 3.Hanshin Consultants Co., Ltd.)

[SSS04-P06] Disaster mainly of stone torii by the Yamagata Offshore Earthquake in 2019

*Takayuki Kawabe[1] (1.Ex. Faculty of Education, Arts and Sciences, Yamagata University)

[SSS04-P07] Source inversion using empirical Green's functions for the 2019 Off Yamagata earthquake (Mj 6.7)

*Yoshiaki Shiba[1] (1.Central Research Institute of Electric Power Industry)

[SSS04-P08] Source rupture process and strong motion generation areas for the 2018 Hokkaido Eastern Iburi earthquake

*Kazuhiro Somei[1], Ken Miyakoshi[1], Yujia Guo[1] (1.Geo-Research Institute)

[SSS04-P09] Conjugate fault model of the 2018 Anchorage, Alaska, intraplate earthquake (M_W 7.1) based on strong-motion waveform inversion

*Yujia Guo[1], Ken Miyakoshi[1], Masato Tsurugi[1] (1.Geo-Research Institute)

[SSS04-P11] An idea to extract effective fault size from a slip distribution estimated by inversion analysis

*Kazuhito Hikima[1], Akihiro Shimmura[1] (1.Tokyo Electric Power Company Holdings, Inc.)

[SSS04-P12] Estimation of subsurface structure based on microtremor and gravity observation in Shigaku area, Mt. Sanbe, Shimane Prefecture, Japan

*Tatsuya Noguchi[1], Yutaro Itohara[1], Mayuko Kuya[1], Isamu Nishimura[2], Takao Kagawa[1] (1.Faculty of Engineering, Tottori University, 2.Graduate School of Engineering, Tottori University)

[SSS04-P13] Estimation of Subsurface Structure and Ground Motion Characteristics in the Damaged Areas of the 2016 Central Tottori Prefecture Earthquake

*Isamu Nishimura[1], Tatsuya Noguchi[2], Takao Kagawa[2] (1.Tottori Univercity Graduate School of Engineering, Department of Management of Social Systems and Civil Engineering, Civil Engineering Course, 2.Tottori Univercity Graduate School of Engineering)

[SSS04-P14] CMP-SPAC and SPAC microtremor array surveys around Tegano active fault, Gifu, Japan

*Masayuki Yoshimi[1], Haruhiko Suzuki[2] (1.Geological Survey of Japan, AIST, 2.Oyo Corporation)

[SSS04-P15] Improvement of Accuracy to Estimate Phase Velocity using Arbitrary Shape Arrays with Extra Observation Sites

*Huan Zhang[1], Kahori Iiyama[1], Hitoshi Morikawa[1] (1.Tokyo Institute of Technology)

[SSS04-P16] Site Classification Method in Microtremor Array Exploration Using a Supervised Machine Learning

*Takumi Hayashida[1] (1.International Institute of Seismology and Earthquake Engineering, Building Research Institute)

[SSS04-P17] **Verification for the Deep Sedimentary Velocity Structure in the Kathmandu Valley using Receiver Function Analysis**

*Michiko Shigefuji[1], Nobuo Takai[2], Subeg Bijukchhen[3] (1.Kyushu University, 2.Hokkaido University, 3.Khwopa Engineering College, Nepal)

[SSS04-P18] Detect of Underground Velocity Discontinuity by Autocorrelation of Strong Motion Data in the Osaka and Kyoto Basins

*Shuta Fukutome[1], Kimiyuki Asano[1], Tomotaka Iwata[1] (1.Disaster Prevention Research Institute, Kyoto University)

[SSS04-P19] **CONSTRUCTION OF SHALLOW AND DEEP LAYERS COMBINED MODEL IN THE KANTO REGION, JAPAN**

*Hiroaki Yamanaka[1], Yoko Tono[2], Shigeki Senna[3], Masahiro Ohbuchi[4], Hiroyuki Fujiwara[3] (1.Interdisciplinary Graduate School of Science and Engineering,Tokyo institute of Technology, 2. Earthquake Research Institute, University of Tokyo, 3.National Research Institute for Earth Science and Disaster Resilience, 4.Ministry of Education, Culture, Sports, Science and Technology)

[SSS04-P20] Estimation of earthquake ground motions at MeSO-net stations

*Atsushi Wakai[1], Shigeki Senna[1], Atsushi Shimizu[1] (1.National Research Institute for Earth Science and Disaster Resilience)

[SSS04-P21] Modeling of subsurface velocity structure from seismic bedrock to ground surface based on array microtremor observation in Aso area

*Shigeki Senna[1], Atsushi Wakai[1], Atsushi Yatagai[2], Yoshiaki Inagaki[2], Hisanori Matsuyama[2], Hiroyuki Fujiwara[1] (1.National Research Institute for Earth Science and Disaster Resilience, 2.OYO Corp)

[SSS04-P22] The examination of liquafaction damage rate by recent earthquakes

*Shigeki Senna[1], Kyoko Ozawa[1] (1.National Research Institute for Earth Science and Disaster Resilience)

[SSS04-P23] **Ground Motion Estimation by using Microtremor H/V Spectral Ratio**

*Guan-Yu Chen[1], Che-Min Lin[2], Kuo-Liang Wen[1] (1.Department of Earth Science, National Central University, Taoyuan, Taiwan, 2.National Center for Research on Earthquake Engineering, Taipei, Taiwan)

[SSS04-P24] ISNL- - an new parameter of soil nonlinearity used for Taiwan and New Zealand earthquake

*Kao Ching[1], Huang Jyun-Yan[2], Wen Kuo-Liang [2] (1.National Central University, 2.National Center for Research on Earthquake Engineering)

[SSS04-P25] Assessment of the liquefaction risk at Re-liquefied site

*CHIH-SHENG KU[1], Yun-Ling Hsieh[1], Po-Wei Cheng[1] (1.I-SHOU University)

[SSS04-P26] Experimental Study on Dynamic Shear Modulus of Cohesive Soil in Beijing Plain

*Yi Fang, Guoxing Chen, Yanju Peng, Yuejun Lyu

[E] Poster | S (Solid Earth Sciences)：S-SS Seismology

[S-SS05] Innovative data analysis methods for characterization of seismicity

convener:Francesco Grigoli(ETH Zurich Swiss Federal Institute of Technology Zurich), Bogdan Enescu(Department of Geophysics, Kyoto University), Aitaro Kato(Earthquake Research Institute, the University of Tokyo), Yosuke Aoki(Earthquake Research Institute, University of Tokyo)

[SSS05-P01] **Erecting and Observation Data of Broadband Seismic Array in Haiyuan- Liupanshan Fault Zone, Ningxia, China**

*Guofu luo[1], Heqin - Ma[1] (1.Earthquake Administration of Ningxia Hui Autonomous Region)

[SSS05-P02] Energy release patterns and shaking effects of earthquakes in the Japan Trench: A Hilbert-Huang Transform approach

*Swapnil Mache[1], Kusala Rajendran[1] (1.Indian Institute of Science, Bangalore)

[SSS05-P03] The 2019 September 15th Stigliano natural seismic sequence revealed by a local network designed for induced seismicity monitoring

*Chiara Cocorullo[1], Giancarlo Graci[2], Stefano Limonta[1], Alexander Garcia[3], Thomas Braun[3], Francesco Grigoli[4] (1.SolGeo srl, 2.TOTAL E&P ITALIA, 3.INGV, 4.ETH-Zurich, Swiss Seismological Service)

[SSS05-P04] The systematic spatial bias pattern of earthquakes related to tectonic heterogeneity

*Yijun Zhang[1] (1.Southwest JiaoTong University)

[SSS05-P05] Location of seismic events with a single station using Distance Geometry Solvers

*Francesco Grigoli[1], William L Ellsworth[2], Miao Zhang[3], Simone Cesca[4], Claudio Satriano[5], Mostafa Mousavi[2], Gregory C Beroza[2], Stefan Wiemer[1] (1.ETH-Zurich, Switzerland, 2.Stanford University, United States, 3.Dalhousie University, Halifax, Canada, 4.GFZ-Potsdam, Germany, 5.IPGP-Paris, France)

[SSS05-P06] Evaluation of deep-neural-network-based seismic arrival-time picking method for S-net data

*Rintaroh Suzuki[1], Naoki Uchida[1], Weiqiang Zhu[2], Gregory C Beroza[2] (1.Research Center for Prediction of Earthquakes and Volcanic Eruptions Graduate School of Science, Tohoku University, 2.Department of Geophysics, Stanford University)

[E] Poster | S (Solid Earth Sciences)：S-SS Seismology

[S-SS06] Active faults and Paleoseismology

convener:Hisao Kondo(Geological Survey of Japan, National Institute of Advanced Industrial Science and Technology), Mamoru Koarai(Earth Science course, College of Science, Ibaraki University), Takashi OGAMI(National Institute of Advanced Industrial Science and Technology), Yoshiki Sato(Advanced Industrial Science and Technology, Geological Survey of Japan)

[SSS06-P01] Active tectonics of the northern Banda Arc, eastern Indonesia: a preliminary geomorphic mapping

*Adi Patria[1,3], Hiroyuki Tsutsumi[2], Danny Hilman Natawidjaja[3] (1.Graduate School of Science and Engineering, Doshisha University, 2.Department of Environmental Systems Science, Doshisha University, 3.RC for Geotechnology, Indonesian Institute of Sciences (LIPI))

[SSS06-P02] Paleoseismological studies along the un-ruptured southern segment of Yokote Basin Fault Zone, northeast Japan

*SHREYA Arora[1], Hisao Kondo[1] (1.Geological Survey of Japan, National Institute of Advanced Industrial Science and Technology)

[SSS06-P03] Parametric study on ground surface deformation forming pull-apart basin

*Hidetaka Saomoto[1] (1.National Institute of Advanced Industrial Science and Technology)

[SSS06-P04] S wave seismic reflection survey on the Shikano fault appeared in the 1943 Tottori earthquake

*Takao Kagawa[1], Tatsuya Noguchi[1], Koji Yamada[2], Tetsuya Takemoto[2] (1.Tottori University Graduate School of Engineering, 2.Hanshin Consultants Co., Ltd.)

[SSS06-P05] Offset streams across active faults in Chugoku region in the southwestern Japan

*Takashi Azuma[1] (1.National Institute of Advanced Industrial Science and Technology)

[SSS06-P06] Change in stress with seismic cycles in coherent and mélange units in the Cretaceous Shimanto Belt, SW Japan

*Makoto Hashiguchi[1], Yoshitaka Hashimoto[1] (1.Kochi University)

[E] Poster | S (Solid Earth Sciences)：S-SS Seismology

[S-SS07] Earthquake prediction and forecast+pre-earthquake geoscientific changes(TBD)

convener:Masayuki Obayashi(Japan Agency for Marine-Earth Science and Technology), Toshitaka Baba(Graduate School of Science and Technology, Tokushima University), Chi-Yu King(Retired)

[SSS07-P01] Long-term level and temperature changes in groundwater at the frontier land zone for impending great earthquakes at the Nankai trough, southwest Japan
- Recent anomalous changes, possible great earthquake precursors -

*Tameshige Tsukuda[1] (1.none)

[SSS07-P02] **Application of different statistical tools to investigate radon time-series data for earthquake precursory studies in Taiwan**

*Vivek Walia[1], Arvind Kumar[1], Ching-Chou Fu[2], Shih-Jung Lin[1], Cheng-Horng Lin[1,2] (1.National Center for Research on Earthquake Engineering, NARL, Taipei, Taiwan , 2.Institute of Earth Sciences, Academia Sinica, Taiwan)

[SSS07-P03] Correlations of earthquake properties with geomagnetic ULF precursor characteristics over multiple events

*Muhammad Khairul Adib Muhammad Yusof[1], Mardina Abdullah[1,2], Nurul Shazana Abdul Hamid[1,3], Suaidi Ahadi[4], Akimasa Yoshikawa[5] (1.Space Science Center, Institute of Climate Change, Universiti Kebangsaan Malaysia, Malaysia, 2.Department of Electrical, Electronic and Systems Engineering, Faculty of Engineering and Built Environment, Universiti Kebangsaan Malaysia, Malaysia, 3.Department of Applied Physics, Faculty of Science and Technology, Universiti Kebangsaan Malaysia, Malaysia, 4.Department of Geophysics, Indonesian Agency for Meteorology, Climatology and Geophysics, Jakarta, Indonesia, 5.International Center for Space Weather Science and Education, Kyushu University, Fukuoka 812-8581)

[SSS07-P04] Recent Advances in Earthquakes Relocation and Probabilistic Seismic Hazard Assessment for Risk Mitigation and Planning in West Africa

*Umar Afegbua Kadiri[1], Tahir Abubakar Yakubu[1], Friday Ezomo, Brassnavy Manzunzu (1.Centre for Geodesy and Geodynamics Toro)

[SSS07-P05] Ionosphere Magnetic Field Precursor Anomalies Extraction Associated with 2016 Ecuador Earthquake using NMF

*Mengxuan Fan[1], Kaiguang Zhu[1], Xiaodan He[1], Kaiyan Li[1], Dedalo Marchetti[2], Chengquan Chi[1], ZINING YU[1] (1.Jilin University, 2.National Institute of Geophysics and Volcanology)

[E] Poster | S (Solid Earth Sciences)：S-SS Seismology

[S-SS08] Statistical seismology and underlying physical processes

convener:Yasuhiro Yoshida(Meteorological College, Japan Meteorological Agency)

[SSS08-P01] Stress induced from large earthquakes since 1900 and temporal b value change in Nankai trough

Junhyung Lee[1], Ilgoo Kim[1], *Tae-Kyung Hong[1] (1.Department of Earth System Sciences, Yonsei University)

[SSS08-P02] Microseismicity distribution and inferred fault geometry beneath the western Marmara Sea, Turkey, deduced from long-term ocean bottom seismographic observations

*Yojiro Yamamoto[1], Dogan Kalafat[2], Ali Pinar[2], Narumi Takahashi[3,1], Zeynep Coskun[2], Remzi Polat[2], Haluk Ozener[2], Yoshiyuki Kaneda[4,1] (1.Japan Agency for Marine-Earth Science and Technology, 2.KOERI, Bogaziti University, 3.National Research Institute for Earth Science and Disaster Resilience, 4.Kagawa University)

[SSS08-P03] Spatio-temporal characteristics of seismicity in the source region of the 2011 Tohoku earthquake

*MEITONG DUAN[1], Takuji Yamada[1], Jun Kawahara[1] (1.IBRAKI University)

[E] Poster | S (Solid Earth Sciences)：S-SS Seismology

[S-SS09] INDUCED AND TRIGGERED SEISMICITY: CASE STUDIES, MONITORING AND MODELING TECHNIQUES

convener:Luca Urpi, Yusuke Mukuhira(Institute of Fluid Science, Tohoku University), Bogdan Enescu(Department of Geophysics, Kyoto University), Francesco Grigoli(ETH Zurich Swiss Federal Institute of Technology Zurich)

[SSS09-P01] **Investigation of the physical link between the injection induced seismicity and information from borehole logging**

*Yusuke Mukuhira[1], Martin Ziegler[2], Takatoshi Ito[1], Hiroshi Asanuma[3], Markus O Häring[4] (1.Institute of Fluid Science, Tohoku University, 2.Department of Earth Sciences, Engineering Geology, ETH Zurich, 3.AIST, 4.Häring GeoProject)

[SSS09-P03] **Estimation of focal mechanisms of large number of induced seismicity to understand fracture system in the geothermal reservoir**

*Kangnan Yan[1,2], Yusuke Mukuhira[1], Takatoshi Ito[1], Yinhui Zuo[2], Hiroshi Asanuma[3], Markus O Häring[4] (1.Institute of Fluid Science, Tohoku University, 2.State Key Laboratory of Oil and Gas Geology and Exploitation, Chengdu University of Technology, 3.Fukushima Renewable Energy Institute (FREA), National Institute of Advanced Industrial Science and Technology (AIST), 4.Häring GeoProject)

[SSS09-P04] Source Mechanism and triggering process for the April 12th and 13th 2014 earthquake doublet in the Solomon Islands

*Calvin Luiramo Qwana[1], Masatoshi Miyazawa[1], James Mori[1] (1.Disaster Prevention Research Institute Kyoto University)

[SSS09-P05] Ultra-microearthquakes observed at Mizunami Underground Research Laboratory

*Osamu Murakami[1], Yasuhiro Asai[1], Hiroshi Ishii[1] (1.Tono Rearch Institute of Earthquake Science, Association for the Development of Earthquake Prediction)

[SSS09-P06] Seismoelectromagnetic conversions generated by a double-couple source in partially saturated media.

*Sheldon Dwight Warden[1], Pascal Sailhac[2], Stéphane Garambois[3] (1.Hyperion Geophysical Services, 7 rue de Châtenois, 67100, Strasbourg, France., 2.GEOPS (Geosciences Paris Sud), Université de Paris Saclay, 15 Rue Georges Clemenceau, 91400, Orsay, France., 3.ISTerre (Institut des Sciences de la Terre), Université de Grenoble Alpes, 1381 rue de la piscine, 38400, Saint Martin d'Heres, France.)

[SSS09-P07] Investigation of the pore pressure sensitivity toward ocean loading influence from seismic ambient noise monitoring

*Rezkia Dewi Andajani[1], Takeshi Tsuji[1,2] (1.Department of Earth Resources Engineering, Kyushu University , 2.International Institute for Carbon-Neutral Energy Research, Kyushu University)

[SSS09-P08] **The character of the Focal mechanisms with Kagan angles in Japan area for the extended 2-D ETAS model**

*Maita Eri[1], Jiancang Zhuang (1.SOKENDAI)

[E] Poster | S (Solid Earth Sciences)：S-SS Seismology

[S-SS10] Rethinking PSHA

convener:Naoshi Hirata(National Research Institute for Earth Science and Disaster Resilience), Danijel Schorlemmer(GFZ German Research Centre for Geosciences), Matt Gerstenberger(GNS Science), Kuo-Fong Ma(Institute of Geophysics, National Central University, Taiwan, ROC)

[E] Poster | S (Solid Earth Sciences)：S-EM Earth's Electromagnetism

[S-EM18] Paleomagnetism and rock magnetism applied to solving geological and geophysical problems

convener:Martin Chadima(Institute of Geology of the Czech Academy of Sciences), Balazs Bradak(University of Burgos, Spain), Daniel Pastor-Galan(Center for North East Asian Studies, Tohoku University), Myriam Annie Claire Kars(Center for Advanced Marine Core Research)

[SEM18-P01] Anisoft – Advanced Treatment Of Magnetic Anisotropy Data

*Martin Chadima[1,2] (1.Institute of Geology of the Czech Academy of Sciences, Prague, Czech Republic, 2.AGICO Ltd., Brno, Czech Republic, e-mail: chadima@agico.cz)

[SEM18-P02] Anisotropy of out-of-phase magnetic susceptibility as an alternative proxy for lattice preferred orientation of graphite

*Martin Chadima[1,2], Frantisek Hrouda[2,3], Josef Jezek[3], Štěpánka Mrázová[4], Michal Poňavič[4] (1.Institute of Geology of the Czech Academy of Sciences, Prague, Czech Republic, 2.AGICO, Brno, Czech Republic, 3.Faculty of Science, Charles University, Prague, Czech Republic, 4.Czech Geological Survey, Prague, Czech Republic)

[SEM18-P03] Magnetic fabric of anthropogenic ash horizons in cave sediment succession

*Balazs Bradak[1], Ángel Carrancho Alonso[1], Ángela Herrejon Lagunilla[1], Juan J. Villalain Santamaria[1], Carolina Mallol[2,3], Gilbert Tostevin[4], Gilliane F. Monnier[4], Goran Pajović[5], Mile Baković[6], Nikola Borovinić[6] (1.Paleomagnetic Laboratory, Department of Physics, Burgos University, Spain, 2.UDI de Prehistoria, Arqueología e Historia Antigua, Facultad de Geografía e Historia, Universidad de La Laguna, La Laguna, Spain. , 3.Archaeological Micromorphology and Biomarker Research Lab, University of La Laguna, La 10 Laguna, Spain., 4.Department of Anthropology, University of Minnesota Twin Cities, United States, 5.National Museum of Montenegro, Cetinje, Montenegro, 6.Center for Conservation and Archaeology of Montenegro)

[SEM18-P04] Bacterial magnetosome morphology in Hiroshima Bay sediments

*Noriko Kawamura[1], Kengo Hiyamizu[2], Toshitsugu Yamazaki[3] (1.Japan Coast Guard Academy, 2.Japan Coast Guard, 3. Atmosphere and Ocean Research Institute, The University of Tokyo)

[SEM18-P05] FORC-PCA analyses of red clay in the Pacific

*Toshitsugu Yamazaki[1], Wei Fu[1], Takaya Shimono[2], Yoichi Usui[3] (1.Atmosphere and Ocean Research Institute, The University of Tokyo, 2.Meiji University, 3.Japan Agency for Marine-Earth Science and Technology)

[SEM18-P06] A new $^{40}Ar/^{39}Ar$ age and magnetostratigraphy of the Afro-Arabian Large Igneous Province in the Lima-Limo section erupted in Oligocene

*Yutaka Yoshimura[1], Osamu Ishizuka[2], Toshitsugu Yamazaki[1], Yuhji Yamamoto[3], Hyeon-Seon Ahn[4], Tesfaye Kidane[5], Yo-ichiro Otofuji[6], Naoto Ishikawa[7] (1.Atmosphere and Ocean Research Institute, The University of Tokyo, 2.National Institute of Advanced Industrial Science and Technology, 3.Center for Advanced Marine Core Research , Kochi Univ., 4.Korea Institute of Geoscience & Mineral Resources, 5.School of Agricultural, Earth, and Environmental Sciences, University of KwaZulu Natal, 6.Institute of Geohistory, 7.School of Sustainable Design, University of Toyama)

[SEM18-P07] PRELIMINARY ARCHAEOMAGNETIC STUDY IN THE ARCHAEOLOGICAL SITE OF GRAKLIANI (REPUBLIC OF GEORGIA)

*Manuel Calvo-Rathert[1,5], Natalia Garcia-Redondo[1], Angel Carrancho[2], Avto Gogichaishvili[3], Vakhtang Licheli[4] (1.Departamento de Fisica, EPS, Universidad de Burgos, Burgos, Spain , 2.Departamento de Historia, Geografía y Comunicación, Universidad de Burgos, Burgos, Spain., 3.Servicio Arqueomagnetico Nacional – Instituto de Geofisica, Universidad Nacional Autonoma de Mexico, Morelia, Mexico, 4.Institute of Archaeology, Ivane Javakhishvili Tbilisi State University, Tbilisi, Georgia., 5.Hawaii Institute of Geophysics and Planetology, University of Hawaii at Manoa, Honolulu, Hawaii, United States)

[SEM18-P08] Paleomagnetism.org 2.0: an online multiplatform, open source and FAIR paleomagnetic data management software

Mathijs Koymans[2], *Daniel Pastor-Galan[1], Douwe van Hinsbergen[2], Bram Vaes[2], Cor Langereis[2] (1.Center for North East Asian Studies, Tohoku University, 2.Utrecht University)

[SEM18-P09] Brunhes and Matuyama Chron Paleosecular variation study from dated lava flows erupted from West Maui, Hawaii, USA.

*Emilio Herrero-Bervera[1] (1.University of Hawaii at Manoa)

[SEM18-P10] Centennial-resolution terrestrial climatostratigraphy and Matuyama-Brunhes transition from a loess sequence in China

*Masayuki Hyodo[1], Kenta Banjo[2], Tianshui Yang[3], Shigehiro Katoh[6], Shi Meinan[3], Yuki Yasuda[4], Jun-ichi Fukuda[1], Masako Miki[2], Balázs Bradák[5] (1.Research Center for Inland Seas, Kobe University, 2.Department of Planetology, Kobe University, 3.China University of Geosciences, 4.Institute of Seismology and Volcanology, Hokkaido University, 5.Department of Physics, EPS, University of Burgos, 6.Museum of Nature and Human Activities, Hyogo)

[SEM18-P12] **Paleomagnetism of sediment cores taken from the Ontong-Java plateau: for better understanding of the role of biogenic magnetite in geomagnetic paleointensity recording**

*Jiaxi Li [1] (1.Atmosphere and Ocean Research Institute, The University of Tokyo)

[SEM18-P13] **New paleomagnetic data from of Late Cretaceous volcanics of the northern part of the Okhotsk-Chukotka volcanic belt**

*Aleksandr Pasenko[1], Ivan Lebedev[1], Florian Lhuillier[2], Baha Eid[2], Vladimir Pavlov[1] (1.The Schmidt Institute of Physics of the Earth of the Russian Academy of Sciences, Moscow, Russia, 2.Department of Earth and Environmental Sciences, Ludwig Maximilians University, Munich, Germany)

[E] Poster | S (Solid Earth Sciences)：S-EM Earth's Electromagnetism

[S-EM19] Earth and planetary magnetism: Observations, modeling, and implications on dynamics and evolution

convener:Hirokuni Oda(Institute of Geology and Geoinformation, Geological Survey of Japan, AIST), Futoshi Takahashi(Faculty of Sciences, Kyushu University), Courtney Jean Sprain(University of Florida), Yoichi Usui(Japan Agency for Marine-Earth Science and Technology)

[SEM19-P01] Magnetic survey for buried old kilns with paleomagnetic and rock magnetic interpretation

*Tadahiro Hatakeyama[1,2], Yu Kitahara[3], Nobutatsu Mochizuki[4], Yorinao Shitaoka[5], Kenji Kanegae[6], Hirotsugu Matsusaki[7], Naoko Nakamura[8] (1.Information Processing Center, Okayama University of Science, 2.Graduate School of Biosphere-Geosphere Science, Okayama University of Science, 3.Graduate School of Social and Cultural Studies, Kyushu University, 4.Faculty of Advanced Science and Technology, Kumamoto University, 5.Faculty of Geo-Environmental Science, Rissho University, 6.Archaeological Museum, The International University of Kagoshima, 7.Education Board, Ibusuki City, 8.Research Center for Archaeology, Kagoshima University)

[SEM19-P02] Paleomagnetic study on the transitionally magnetized volcanic rocks from the Tahaa Island, French Polynesia

*Yuhji Yamamoto[1], Kenneth A Hoffman[2], Myriam Annie Claire Kars[1] (1.Center for Advanced Marine Core Research, Kochi University, 2.California Polytechnic State University)

[SEM19-P03] High resolution paleomagnetic secular variation records from Lake Biwa and its implications on core dynamics

*Hirokuni Oda[1], Yuhji Yamamoto[2], Yoshio Inouchi[3] (1.Institute of Geology and Geoinformation, Geological Survey of Japan, AIST, 2.Kochi University, 3.Waseda University)

[SEM19-P04] Paleomagnetism around the Cretaceous-Paleogene boundary in the Pacific red clay

*Yoichi Usui[1], Toshitsugu Yamazaki[2], Junichiro Ohta[3,4,1], Honami Sato[4], Akira Ishikawa[5] (1.Japan Agency for Marine-Earth Science and Technology, 2.Atmosphere and Ocean Research Institute, The University of Tokyo, 3.FRCER, The University of Tokyo, 4.ORCeNG, Chiba Institute of Technology, 5.Department of Earth and Planetary Sciences, Tokyo Institute of Technology)

[SEM19-P05] Avalonia, get bent! Paleomagnetism from SW Iberia confirms the Greater Cantabrian Orocline

Bruno Daniel Leite Mendes[2], *Daniel Pastor-Galan[1], Mark J. Dekkers[2], Wout Krijgsman[2] (1.Center for North East Asian Studies, Tohoku University, 2.Paleomagnetic Laboratory 'Fort Hoofddijk', Utrecht University)

[SEM19-P06] The Magnetics Information Consortium (MagIC) Data Repository: Status and Future Evolution

*Catherine Constable[1], Nicholas Jarboe[1], Rupert Minnett[2], Anthony A.P. Koppers[3], Lisa Tauxe[1], Lori Jonestrask[1] (1.Scripps Institution of Ocenaography, University of California San Diego, 2.Cogense Inc., 3.Oregon State University)

[SEM19-P08] Assessing the robustness of long-term field variations in the palaeomagnetic record

*Courtney Jean Sprain[1,2], Andrew J. Biggin[2], Richard K. Bono[2], Chris Davies[3], Greig Paterson[2], Louise Hawkins[2], Lauri J. Pesonen[4], Pavel Doubrovine[5], Toni Veikkolainen[6], Aleksey Smirnov[7], Elisa Piispa[8], Evgeniy Kulakov[5], Siim Ots[9], Luke Fairchild[10] (1.Department of Geological Sciences, University of Florida, Gainesville, FL, USA, 2.Department of Earth, Ocean and Ecological Sciences, University of Liverpool, UK, 3.School of Earth and Environment, University of Leeds, Leeds, UK, 4.Physics Department, University of Helsinki, Finland, FI-00014, Finland, 5.Centre for Earth Evolution and Dynamics, University of Oslo, Norway, 6.Department of Geosciences and Geography, University of Helsinki, Finland, 7.Department of Geological and Mining Engineering and Sciences and Department of Physics, Michigan Technological University, Houghton, MI, USA, 8.School of Earth Sciences, Energy and Environment, Yachay Tech, Ibarra, Ecuador, 9.Department of Geology, University of Tartu, Estonia, 10.Department of Earth and Planetary Sciences, University of California, Berkeley, CA, USA)

[SEM19-P09] Inferring geomagnetic secular variation using MHD/kinematic dynamo modeling with data assimilation

*Futoshi Takahashi[1], Shin ya Nakano[2], Takuto Minami[3], Hinami Taniguchi[4], Ryosuke Nakashima[4], Masaki Matsushima[5], Hisayoshi Shimizu[6], Hiroaki TOH[7] (1.Faculty of Sciences, Kyushu University, 2.The Institute of Statistical Mathematics, 3.Division of Frontier Planetology, Department of Planetology, Graduate School of Science, Kobe University, 4.Graduate School of Science, Kyushu University, 5.Department of Earth and Planetary Sciences,

School of Science, Tokyo Institute of Technology, 6.Earthquake Research Institute, University of Tokyo, 7.Data Analysis Center for Geomagnetism and Space Magnetism, Graduate School of Science, Kyoto University)

[SEM19-P10] Influence of high electrical conductivity heterogeneity at the bottom of the mantle on generation of 2007 geomagnetic jerk

*Hisayoshi Shimizu[1] (1.Earthquake Research Institute, University of Tokyo)

[SEM19-P11] The Elsasser number dependence of core surface flow models and its implications for long-term changes in core dynamics

*Masaki Matsushima[1] (1.Department of Earth and Planetary Sciences, School of Science, Tokyo Institute of Technology)

[SEM19-P12] A modern interpretation of magnetic instability

*Ataru Sakuraba[1] (1.Department of Earth and Planetary Science, University of Tokyo)

[E] Poster | S (Solid Earth Sciences)：S-EM Earth's Electromagnetism

[S-EM20] Electric and Electromagnetic survey technologies and the scientific achievements: Recent advances

convener:Kiyoshi Baba(Earthquake Research Institute, The University of Tokyo), Tada-nori Goto(Graduate School of Life Science, University of Hyogo), Toshihiro Uchida(National Institute of Advanced Industrial Science and Technology), Toru Mogi(Faculty of Science, Tokyo Institute of Technology)

[SEM20-P01] A tensor measurement with simultaneously transmitted Electromagnetic Accurately Controlled, Routinely Operated Signal System: utilization of distortionless response tensor

*Kuo Hsuan Tseng[1], Yasuo Ogawa[2] (1.Tokyo Institute of Technology, 2.Volcanic Fluid Research Center, Tokyo Institute of Technology)

[SEM20-P02] Pseudo 3-D resistivity model for Geomagnetic Induced Current (GIC) based on 3-D seismic velocity structure

*Tada-nori Goto[1], Kota Hori[1] (1.Graduate School of Life Science, University of Hyogo)

[SEM20-P03] Sensitivity of local electromagnetic response functions from Sq field to the electrical conductivity in the upper mantle

*Xiaoli WAN[1,2], Hisayoshi Shimizu[2], Hisashi Utada[2] (1.Tongji Univ., 2.Earthquake Research Institute, the Univ. of Tokyo)

[SEM20-P04] The sparse inversion of the magnetic data to recover subsurface blocky structures.

*Mitsuru Utsugi[1] (1.Aso Volcanological Laboratory, Institute for Geothermal Sciences, Graduate School of Science, Kyoto University)

[SEM20-P05] Understanding Unzen volcano magmatic system by broadband Magnetotelluric observation

*Agnis Triahadini[1], Koki Aizawa[2], Keita Chiba[2], Kanta Miyano[1], Yuto Yamamoto[1], Kazunari Uchida[2], Tasuku Hashimoto[1] (1.Department of Earth and Planetary Sciences Graduate School of Science Kyushu University, 2.Institute of Seismology and Volcanology Faculty of Science Kyushu University)

[E] Poster | S (Solid Earth Sciences)：S-IT Science of the Earth's Interior & Techtonophysics

[S-IT23] Property and role of liquids inside terrestrial planets

convener:Tatsuya Sakamaki(Department of Earth Science, Tohoku University), Yoichi Nakajima(Kumamoto University, Priority Organization for Innovation and Excellence)

[SIT23-P03] Effect of water on the structure of sodium silicate melts under pressure

*Tomonori Ohashi[1], Tatsuya Sakamaki[1], Ken-ichi Funakoshi[2], Miki Muranushi[1], Chikara Shito[1,3], Osamu Ikeda[1], Yuki Shibazaki[4], Akio Suzuki[1] (1.Tohoku Univ., 2.CROSS, 3.Univ. Tokyo, 4.NIMS)

[SIT23-P04] Nitrogen in the core from sound velocity measurements of liquid Fe-N at high pressure

*Asaki Iwamoto[1], Yoichi Nakajima[1,2], Daisuke Kinoshita[1], Yasuhiro Kuwayama[2,3], Kei Hirose[3], Daisuke Ishikawa[2,4], Alfred Q.R. Baron[2] (1.Kumamoto University, 2.RIKEN MDL, 3.The University of Tokyo, 4.JASRI)

[SIT23-P05] Sound velocity of liquid Fe-P alloy at high pressure

*Yoichi Nakajima[1,2], Daisuke Kinoshita[3], Yasuhiro Kuwayama[4], Kei Hirose[5,4], Asaki Iwamoto[3], Daisuke Ishikawa[6], Alfred Q.R. Baron[2] (1.POIE, Kumamoto Univ., 2.RIKEN MDL, 3.Grad. School Sci. Tech., Kumamoto Univ., 4.Dept. Earth Planet. Sci., Univ. Tokyo , 5.ELSI, Tokyo Tech. , 6.JASRI)

[E] Poster | S (Solid Earth Sciences)：S-IT Science of the Earth's Interior & Techtonophysics

[S-IT24] MAGMA AND FLUID TRANSPORT IN THE EARTH'S INTERIOR

convener:Bjorn Mysen(Geophysical Laboratory, Carnegie Inst. Washington), Eiji Ohtani(Department of Earth and Planetary Materials Science, Graduate School of Science, Tohoku University), Dapeng Zhao(Department of Geophysics, Tohoku University), Michihiko Nakamura(Division of Earth and Planetary Materials Science, Department of Earth Science, Graduate School of Science, Tohoku University)

[SIT24-P01] Viscosity of silicate network phase-separating from aqueous fluid

*Takehito Koyama[1] (1.Institute of Industrial Science, the University of Tokyo)

[SIT24-P02] Structure and density of H_2O-rich Mg_2SiO_4 melts at high pressure from *ab initio* simulations

*Gerd Steinle-Neumann[1], Liang Yuan[1,2], Akio Suzuki[2] (1.Bayerisches Geoinstitut, Universitaet Bayreuth, 2.Department of Earth Science, Tohoku University)

[SIT24-P03] A three-dimensional electrical conductivity model of the crust beneath the southern Tohoku district, NE Japan

Aoi Motoyama[1], *Masahiro Ichiki[1], Yasuo Ogawa[2], Makoto Uyeshima[3], Koichi Asamori[4], Toshihiro Uchida[5], Takao Koyama[3], Shin'ya Sakanaka[3,6], Hideaki Hase[3,8], Koki Aizawa[3,7], Yusuke Yamaya[3,5] (1.Graduate School of Science, Tohoku University, 2.School of Science, Tokyo Institute of Technology, 3.Earthquake Research Institute, The University of Tokyo, 4.Tono Geoscience Center, Japan Atomic Energy Agency, 5.National Institute of Advanced Industrial Science and Technology, 6.Graduate School of International Resource Science, Akita University, 7.Graduate School of Science, Kyushu University, 8.Geothermal Energy and Development Co. Ltd.)

[SIT24-P04] **Experimental constraint on the fluid connectivity in an olivine–H_2O–CO_2–NaCl system in subduction zones**

*Yongsheng HUANG[1], Takayuki Nakatani[1], Michihiko Nakamura[1], Catherine McCammon[2] (1.Graduate School of Science, Tohoku University, 2.Bayerisches Geoinstitut, University of Bayreuth)

[SIT24-P05] **Anomalous structural dynamics of basaltic melt at mantle conditions: Implications for superplumes and magma oceans**

*Arnab Majumdar[1], Min Wu[2,1], Yuanming Pan[1], Toshiaki IITAKA[3], John S Tse[1] (1.University of Saskatchewan, 2.Zhejiang University of Technology, 3.RIKEN)

[E] Poster | S (Solid Earth Sciences)：S-IT Science of the Earth's Interior & Techtonophysics

[S-IT25] Structure and Dynamics of Earth and Planetary Mantles

convener:Takashi Yoshino(Institute for Planetary Materials, Okayama University), Takashi Nakagawa(Department of Earth Sciences, The University of Hong Kong), Dapeng Zhao(Department of Geophysics, Tohoku University)

[SIT25-P01] **Origin** of **Plate Tectonics**,Why did Plate Tectonics occur **only on Earth**?
Why is there a Deep Ocean Floor and Seawater **only on Earth**?
Mystery (**Driving Force** and **Origin of Pacific Rim Back-Arc Basin**).
we challenge Them All !

*Akira Taneko[1] (1.SEED SCIENCE Lab.)

[SIT25-P02] The viscosity structure of the low-viscosity zone of the Moon derived from the tidal response

*Yanxia Tan[1], Yuji Harada[1] (1.State Key Laboratory of Lunar and Planetary Sciences, Macau University of Science and Technology)

[SIT25-P05] 2D Visco-elasto-plastic numerical modeling of buckling and uplift on passive margin under compression: implications for topography of SE Korea and the East Sea (Japan Sea)

*Seok-Hyeon Do[1] (1.Kangwon National University)

[SIT25-P06] **Development of 3-D Lagrangian Free Subduction Model: Implications for Surface Process of the Earth**

*Jae-Yoon Keum[1], Byung-Dal So[1] (1.Kangwon National University)

[SIT25-P07] **Application of Parker-Oldenburg Algorithm to map Moho Discontinuity using Gravity Data in Western North America Cordillera**

*Mohammad Shehata[1,2], Hideki Mizunaga[2] (1.Department of Geology, Faculty of Science, Port Said University, Egypt, 2.Department of Earth Resources Engineering, Faculty of Engineering, Kyushu University, Japan)

[SIT25-P08] Multi-mode surface wave phase speed distribution in North America

*Hitoshi Matsuzawa[1], Kazunori Yoshizawa[2], Fan-Chi Lin[3] (1.Graduate School of Science, Hokkaido University, 2.Faculty of Science, Hokkaido University, 3.The University of Utah)

[SIT25-P09] Mapping azimuthal anisotropy in the Australasian upper mantle with multi-mode surface waves

*Kazunori Yoshizawa[1,2], Yuka Nishimura[2] (1.Faculty of Science, Hokkaido University, 2.Graduate School of Science, Hokkaido University)

[SIT25-P10] **Upper mantle anisotropy beneath Sri Lanka region using shear-wave splitting analysis**

*Shivam Chandra[1] (1.Undergraduate student member)

[SIT25-P11] Lattice preferred orientation of akimotoite deformed in the D111 Kawai-type multianvil apparatus

*Longli Guan[1], Daisuke Yamazaki[1], Noriyoshi Tsujino[1] (1.Institute for Planetary Materials, Okayama University, Misasa, Japan)

[SIT25-P12] Mantle discontinuities oceanward of the Krile - Honshu slab

*Masayuki Obayashi[1], Junko Yoshimitsu[1], Yoshio Fukao[1] (1.Japan Agency for Marine-Earth Science and Technology)

[SIT25-P13] Tomography Model Using Singular Value Decomposition

*Jun Su[1,2], Christine Houser[2], John William Hernlund[2] (1.Department of Earth and Planetary Sciences, Tokyo Institute of Technology, 2.Earth-Life Science Institute)

[SIT25-P14] **Whole-mantle P-wave tomography beneath East Asia**

*Yu Katayama[1], Dapeng Zhao[1], Genti Toyokuni[1] (1.Research Center for Prediction of Earthquakes and Volcanic Eruptions, Graduate School of Science, Tohoku University)

[SIT25-P15] **Seebeck coefficient measurement of olivine by dual heating system and its application to the redox kinetics of the subducted slabs**

*Ran Wang[1], Takashi Yoshino[1] (1.Institute for Planetary Materials, Okayama University)

[SIT25-P16] High-pressure generation to 150 GPa in multianvil apparatus using the 6-8-2 system with nano-polycrystalline diamond anvils.

*Takehiro Kunimoto[1], Masayuki Nishi[1], Tetsuo Irifune[1] (1.Geodynamics Research Center)

[E] Poster | S (Solid Earth Sciences)：S-IT Science of the Earth's Interior & Techtonophysics

[S-IT26] Interaction and Coevolution of the Core and Mantle in the Earth and Planets

convener:Kenji Ohta(Department of Earth and Planetary Sciences, Tokyo Institute of Technology), Tsuyoshi Iizuka(University of Tokyo), Kenji Kawai(Department of Earth and Planetary Science, School of Science, University of Tokyo), Taku Tsuchiya(Geodynamics Research Center, Ehime University)

[SIT26-P01] **Density of Fe^{3+}-bearing magma at high pressure**

Rintaro Ban[1], *Akio Suzuki[1], Tatsuya Sakamaki[1] (1.Department of Earth Science, Graduate School of Science, Tohoku University)

[SIT26-P02] Quantitative evaluation of the geochemical correlation length within the single granitic body, toward the error estimation of geoneutrino flux from the Japanese crust

*Kenta Ueki[1], Minami Kazuki[2], Akimichi Taketa[2], Tsuyoshi Iizuka[3], Sanshiro Enomoto[4], Nozomu Takeuchi[2], Hiroyuki Tanaka[2] (1.Japan Agency for Marine-Earth Science and Technology, 2.Earthquake Research Institute, the University of Tokyo, 3.Department of Earth and Planetary Science, The University of Tokyo, 4.University of Washington, Department of physics)

[SIT26-P03] Re-evaluation of thermal data in the Japanese Islands for better estimation of the temperature structure in the crust

*Makoto Yamano[1], Akiko Tanaka[2], Hideki Hamamoto[3], Shusaku Goto[2], Takumi Matsumoto[4] (1.Earthq. Res. Inst., Univ. Tokyo, 2.Geol. Surv. Japan, AIST, 3.Center Environ. Sci. Saitama, 4.Nat. Res. Inst. Earth Sci. Disaster Resilience)

[SIT26-P04] Outer core flows and dynamo induced by heterogeneous growth of the inner core of the Earth

*Shin-ichi Takehiro[1], Youhei SASAKI[2] (1.Research Institute for Mathematical Sciences, Kyoto University, 2.Department of Architecture/Institute of Fundamental Sciences, Setsunan University)

[SIT26-P05] Seismic structure near the inner core boundary in the north polar region

*Toshiki Ohtaki[1], Satoru Tanaka[2], Satoshi Kaneshima[3], Weerachai Siripunvaraporn[4,5], Songkhun Boonchaisuk[5,6], Sutthipong Noisagool[4,5], Kenji Kawai[7], Taewoon Kim[2], Yuki Suzuki[7], Yasushi Ishihara[2], Koji MIYAKAWA[8], Nozomu Takeuchi[8], Hitoshi Kawakatsu[8] (1.Geological Survey of Japan, National Institute of Advanced Industrial Science and Technology (AIST), 2.Japan Agency for Marine-Earth Science and Technology (JAMSTEC), 3.Department of Earth and Planetary Sciences, Faculty of Sciences, Kyushu University, 4.Faculty of Science, Mahidol University, Kingdom of Thailand, 5.ThEP Center, Commission on Higher Education, Kingdom of Thailand, 6.Geoscience Program, Mahidol University, Kingdom of Thailand, 7.Graduate School of Science, University of Tokyo, 8.Earthquake Research Institute, University of Tokyo)

[SIT26-P06] Deformation experiments of lower mantle minerals using D111 type press

*Noriyoshi Tsujino[1], Daisuke Yamazaki[1], Yu Nishihara[2] (1.Institute for Planetary Materials, Okayama University, 2.GRC, Ehime University)

[SIT26-P07] **Chromium isotopes of basalts from the Ontong Java Plateau and Samoan Ocean Islands: Implications for the core-mantle interaction**

*Yuki Hibiya[1], Tsuyoshi Iizuka[2], Katsuhiko Suzuki[1], Shigekazu Yoneda[3] (1.Japan Agency for Marine-Earth Science and Technology, 2.The University of Tokyo, 3.National Museum of Nature and Science)

[SIT26-P08] The tungsten isotopic compositions of kimberlites: constraints on material circulation in the deep Earth

*Otaro Kobayashi[1], Tsuyoshi Iizuka[1], Hatsuki Enomoto[1] (1.Department of Earth and Planetary Science, Graduate School of Science, The University of Tokyo)

[SIT26-P09] In situ X-ray and neutron diffraction studies of hcp iron hydride

*Sho Kakizawa[1,2], Hiroyuki Kagi[2], Chikara Shito[2], Hiroyuki Saitoh[3], Yuji Higo[4], Yoshinori Tange[4], Asami Sano-Furukawa[5], Takanori Hattori[5], Katsutoshi Aoki[2] (1.Hiroshima University, 2.Geochemical Research Center, The University of Tokyo, 3.National Institutes for Quantum Radiological Science and Technology, 4.Japan Synchrotron Radiation Research Institute, 5.J-PARC center, Japan Atomic Energy Agency)

[SIT26-P10] ***Ab initio* lattice thermal conductivity of (Mg,Fe)O ferropericlase at the deepest mantle**

*Haruhiko Dekura[1], Taku Tsuchiya[1] (1.Geodynamics Research Center, Ehime University)

[SIT26-P11] Soft Core-Mantle Boundary: A Mechanism for Chemical Interactions Between the Core and Mantle

*Kang Wei Lim[1], Irene Bonati[1], Scott D Hull[2], John W Hernlund[1] (1.Earth-Life Science Institute, Tokyo Institute of Technology, 2.Earth and Environmental Sciences, University of Rochester)

[SIT26-P12] **Electrical conductivity measurement of water-bearing bridgmanite using an externally heated diamond anvil cell**

*Yoshiyuki Okuda[1], Kenji Ohta[1], Yu Nishihara[2], Hiroyuki Kagi[3], Kei Hirose[3,4] (1.Tokyo Institute of Technology, 2.Ehime University, 3.University of Toyko, 4.Earth-Life Science Institute)

[SIT26-P13] Mechanisms of the post-perovskite transformation in $NaNiF_3$

Koyumi Yamashita[1], *Tomoaki Kubo[1], Yoshinori Tange[2], Yuji Higo[2] (1.Kyushu Univ., 2.JASRI)

[E] Poster | S (Solid Earth Sciences)：S-IT Science of the Earth's Interior & Techtonophysics

[S-IT27] Oceanic lithosphere and asthenosphere

convener:Nozomu Takeuchi(Earthquake Research Institute, University of Tokyo), Ban-Yuan Kuo(Institute of Earth Sciences, Academia Sinica), Rob L Evans(Woods Hole Oceanographic Institution), Younghee Kim(Seoul National University)

[SIT27-P01] The Oldest Array: Japan-Korea Pacific Array collaboration to study the lithosphere-asthenosphere system below the oldest part of the Pacific Ocean

*Hajime Shiobara[1], Hisashi Utada[1], Seung-Sep Kim[2], YoungHee Kim[3], Kiyoshi Baba[1], Takehi Isse[1], Hogyum Kim[3], HyeJeong Kim[1], Hiroko Sugioka[4], Nozomu Takeuchi[1], Yuki Kawano[1], Hitoshi Kawakatsu[1], Sang-Mook Lee[3], Onboard scientists of 2018/2019 Oldest cruises (1.Ocean Hemisphere Research Center, Earthquake Research Institute, University of Tokyo, 2.Chungnam National University, 3.Seoul National University, 4.Kobe University)

[SIT27-P02] The Electrical Conductivity Structure of The Oldest Pacific: Preliminary Results from Magnetotelluric Observation Data of Pacific Array, Oldest-1

*Hogyum Kim[1], Kiyoshi Baba[2], Hisashi Utada[2], Sang-Mook Lee[1], Hitoshi Kawakatsu[2], YoungHee Kim[1] (1.School of Earth and Environmental Sciences, Seoul National University, 2.Earthquake Research Institute, The University of Tokyo)

[SIT27-P03] P Velocity Heterogeneities in the Upper Mantle beneath the Northwestern Pacific

*Nozomu Takeuchi[1], Hitoshi Kawakatsu[1], Hajime Shiobara[1], Takehi Isse[1], Hiroko Sugioka[2], Aki Ito[3], Hisashi Utada[1] (1.Earthquake Research Institute, University of Tokyo, 2.Kobe University, 3.JAMSTEC)

[SIT27-P04] Seismic velocity structure beneath the oldest region of the Pacific ocean basin from multiscale finite-frequency traveltime tomography

*Hyunsun Kang[1], Younghee Kim[1], Shu-Huei Hung[2], Pei-Ying Patty Lin[3], Takehi Isse[4], Hajime Shiobara[4], Hitoshi Kawakatsu[4], Sang-Mook Lee[1], Hisashi Utada[4], Nozomu Takeuchi[4] (1.Seoul National University, 2.National Taiwan University, 3.National Taiwan Normal University, 4.Earthquake Research Institute, The University of Tokyo)

[E] Poster | S (Solid Earth Sciences)：S-IT Science of the Earth's Interior & Techtonophysics

[S-IT28] Mantle dynamic from thermochemical imaging from observable to numerical modeling

convener:Walid Ben Mansour(Macquarie University), Yosuke Aoki(Earthquake Research Institute, University of Tokyo)

[SIT28-P01] Constraints on the composition of LLSVPs from seismic properties of lower mantle minerals

*Kenny Vilella[1], Thomas Bodin[2], Charles-Edouard Boukare[3], Frederic Deschamps[4], James Badro[5], Maxim Ballmer[6], Yang Li[7] (1.Hokkaido University, 2.Laboratoire de Geologie de Lyon, 3.Ecole Polytechnique Federale de Lausanne, 4.Institute of Earth Sciences, Academia Sinica, 5.Institut de Physique du Globe de Paris, 6.ETH Zurich, 7.Institute of Geology and Geophysics, Chinese Academy of Science)

[E] Poster | S (Solid Earth Sciences)：S-IT Science of the Earth's Interior & Techtonophysics

[S-IT29] New perspectives on East Asia geodynamics

convener:Jonny Wu(University of Houston), Asuka Yamaguchi(Atomosphere and Ocean Research Institute, The University of Tokyo), Kyoko Okino(Atmosphere and Ocean Research Institute, The University of Tokyo), Timothy B Byrne(University of Connecticut)

[SIT29-P02] Early Miocene zircon U-Pb ages in the Hidaka Supergroup of the Tomuraushi area, Hokkaido : Ridge subduction or marginal basin magmatism?

*Michiru Inoue[1], Hayato Ueda[1] (1.Department of Geology, Niigata University)

[SIT29-P03] Subduction and exhumation history of the early metamorphic rocks of southern Kamuikotan Zone, Hokkaido, Japan.

*Yuki Furukawa[1], Hayato Ueda[1], Megumi Ozawa[2] (1.Niigata University, 2.Asano Taiseikiso Engineering Corporation)

[SIT29-P04] Examination of hiterland based on clastic rock composition and zircon U-Pb age in the Nikoro Group, Tokoro Belt

*Komei Nara[1], Yuta Akutsu[2], Hayato Ueda[1] (1.Niigata University, 2.Kowa co.Ltd)

[SIT29-P05] Zircon U-Pb ages and felsic volcanic clasts in the Lower Cretaceous Rebun Group, Hokkaido

*Nozomu Suzuki[1], yusuke Sugiyama, Hayato Ueda[1] (1.Niigata University)

[SIT29-P06] Paleozoic accretionary complex in the Khangai-Khentei belt, central Mongolia, and stratigraphy of Devonian chert

*Tomohito Nakano[1], Yukio Isozaki[2], Uyanga Bold[2], Otgonbaatar D[3], Yukiyasu Tsutsumi[4] (1.Department of Earth and Planetary Science, The University of Tokyo, 2.Department of Earth Science and Astronomy, Multi-disciplinary Sciences - General Systems Studies, Graduate School of Arts and Sciences, The University of Tokyo, 3.Institute of Paleontology and Geology, Mongolian Academy of Science, 4.Department of Geology and Paleontology, National Museum of Nature and Science)

[SIT29-P07] Tectono-depositional evolution of the Mio-Pleistocene forearc basin on the Boso Peninsula, central Japan

*Nana Kamiya[1], Yuzuru Yamamoto[2], Masayuki Utsunomiya[3], Feng Zhang[4], Weiren Lin[1] (1.Graduate School of Engineering, Kyoto University, 2.Kobe University, 3.AIST, 4.Nagoya Institute of Technology)

[SIT29-P08] Preliminary Study on the Crustal Deformation along Sagaing Fault in Myanmar by using GNSS data

*Tha Zin Htet Tin[1,2], Takuya NISHIMURA[3], Manabu Hashimoto[3], Eric Lindsey[4], Myo Thant[2,5] (1.Graduate School of Science, Kyoto University, 2.Department of Geology, University of Yangon, Myanmar, 3.Disaster Prevention Research Institute, Kyoto University, 4.Earth Observatory of Singapore, Nanyang Technological University, Singapore, 5.Myanmar Earthquake Committee)

[SIT29-P09] Evidence for Late Mesozoic intraoceanic subduction offshore NE Asia from mantle convection and geoid models

*Lorenzo Colli[1], Jonny Wu[1], Yi-An Lin[1] (1.University of Houston)

[SIT29-P10] Brittle-Plastic Structures Provide Constraints on the Rapid Exhumation of the Central Range: Taiwan

*Lauren Donati[1], Lindsey Aman[1], Susan Adams[1], Jonathan C Lewis[1] (1.Indiana University of Pennsylvania)

[SIT29-P11] Where are the proto-South China Sea slabs? SE Asian plate tectonics and mantle flow history from global mantle convection modeling

*Yi-An Lin[1], Lorenzo Colli[1], Jonny Wu[1] (1.University of Houston)

[E] Poster | S (Solid Earth Sciences)：S-IT Science of the Earth's Interior & Techtonophysics

[S-IT30] Tectonic collision systems in continents and oceans

convener:Ling Bai(ITP Institute of Tibetan Plateau Research, Chinese Academy of Sciences), James Mori(Earthquake Hazards Division, Disaster Prevention Research Institute, Kyoto University), Xiaodong Song(University of Illinois at Urbana-Champaign), Yuzo Ishikawa(The National Institute of Advanced Industrial Science and Technology)

[SIT30-P01] **Upper mantle deformation of the Terror Rift and northern Transantarctic Mountains in Antarctica: Insight from P-wave anisotropic tomography**

★Invited Papers

*heng zhang[1] (1.Institute of Tibetan Plateau Research, Chinese Academy of Sciences)

[SIT30-P02] **Source parameters of the 2019 Ms6.3 Medog earthquake in the southeastern Tibetan plateau and its tectonic implications**

*Guohui Li[1,2], Ling Bai[1], Lin Ding[1], Bowen Song[1,3,4], Yong Jiang[1,4] (1.Key Laboratory of Continental Collision and Plateau Uplift, Institute of Tibetan Plateau Research, Center for Excellence in Tibetan Plateau Earth Sciences, Chinese Academy of Sciences, 2.Institute of Earthquake forecasting, China Earthquake Administration, 3.Geophysical Exploration Center , China Earthquake Administration, 4.University of Chinese Academy of Sciences)

[SIT30-P03] **Crustal and mantle velocity structures of the Sulawesi Island from multi-scale seismic tomography.**

*Bagus Adi Wibowo[1,2], Ling Bai[2], Supriyanto Rohadi[1], Muzli -[1], Andry Syaly Sembiring[1], Rahmat Triyono[1], Muhamad Sadly[1], Suko Prayitno Adi[1] (1.Meteorological, Climatological, and Geophysical Agency, Indonesia, 2.ITP Insitute of Tibetan Plateau Research, Chinese Academy of Sciences, China)

[SIT30-P04] **Forearc basin development at the Northern Andes – southern boundary transform fault: Progreso basin, SW Ecuador**

*Carlos Alberto Aizprua Luna[1,2,3], Cesar Witt[2] (1.Department of Geosciences and Petroleum, Norwegian University of science and Technology (NTNU), Trondheim, Norway , 2.Univ. Lille, CNRS, Univ. Littoral Côte d'Opale, UMR 8187, LOG, Laboratoire d'Océanologie et de Géosciences, F 59000 Lille, France, 3.Facultad de Ingeniería en Ciencias de la Tierra, Escuela Superior Politécnica del Litoral, Campus Gustavo Galindo – km 30.5 vía perimetral, Guayaquil, Ecuador)

[SIT30-P05] Seismic anisotropy in the deep continental upper mantle beneath Tibetan Plateau

*Cheng-Chien Peng[1,2], Ban-Yuan Kuo[2], Eric Debayle[3], Ling-Yun Chiao[1] (1.IONTU Institute of Oceanography National Taiwan University, 2. Institute of Earth Sciences Academia Sinica, 3.Laboratoire de Géologie de Lyon, Université Claude Bernard Lyon 1)

[SIT30-P06] Shear velocity structure of the crust and lithospheric mantle beneath Taiwan from teleseismic Rayleigh-wave tomography

*Ayush Goyal[1], Shu-Huei Hung[1] (1.Department of Geosciences, National Taiwan University)

[E] Poster | S (Solid Earth Sciences)：S-IT Science of the Earth's Interior & Techtonophysics

[S-IT31] Planetary cores: Structure, formation, and evolution

convener:Hidenori Terasaki(Faculty of Science, Okayama University), Eiji Ohtani(Department of Earth and Planetary Materials Science, Graduate School of Science, Tohoku University), Gerd Steinle-Neumann(Bayerisches Geoinstitut, Universitaet Bayreuth), William F McDonough(Department of Earth Science and Research Center for Neutrino Science, Tohoku University, Sendai, Miyagi 980-8578, Japan)

[SIT31-P01] Sound velocity measurement of Fe-Ni-Si alloys at high pressure and high temperature

*Daijo Ikuta[1], Eiji Ohtani[1], Hiroshi Fukui[2,3], Hiroshi Uchiyama[4], Satoshi Tsutsui[4], Baron Alfred[3] (1.Department of Earth Science, Tohoku University, 2.Department of Material Science, University of Hyogo, 3.RIKEN, 4.JASRI)

[SIT31-P02] Mercury core size constrained from elastic properties of Fe-Ni-S-Si liquid

Iori Yamada[1], *Hidenori Terasaki[1], Ryo Tsuruoka[1], Asaka Kamiya[1], Tadashi Kondo[1], Yoshinori Tange[2], Yuji Higo[2] (1.Graduate School of Science, Osaka University, 2.JASRI)

[SIT31-P03] **Metal-silicate partitioning of carbon at the core formation**

*Yutaro Tsutsumi[1], Naoya Sakamoto[2], Kei Hirose[3], Shunpei Yokoo[1], Shoh Tagawa[4], Hisayoshi Yurimoto[5] (1.The University of Tokyo, 2.Creative Research Institution, Hokkaido University, 3.Earth-Life Science Institute, Tokyo Institute of Technology, 4.Department of Earth and Planetary Science, The University of Tokyo, 5.Department of Natural History Sciences, Hokkaido University)

[SIT31-P04] Thermodynamic analysis of density of Fe-Ni-S melts at high pressure

*Satoru Urakawa[1], Hidenori Terasaki[2], Akihiko Machida[3] (1.Department of Earth Sciences, Okayama University, 2.Department of Earth and Space Science, Osaka University, 3.QST)

[SIT31-P05] Possibility of percolation of Fe-S melts in asteroids

*Takumi Miura[1], Hidenori Terasaki[1], Tadashi Kondo[1] (1.Department of Earth and Space Science, Graduate School of Science, Osaka University)

[SIT31-P06] **Effect of Isostatic Rebound on Lithosphere in the Discrete Element Method Simulation**

*Soojung An[1] (1.Kangwon National University)

[E] Poster | S (Solid Earth Sciences)：S-IT Science of the Earth's Interior & Techtonophysics

[S-IT32] Do plumes exist?

convener:Hidehisa Mashima(Center for Obsidian and Lithic Studies, Meiji University), Gillian R Foulger(Durham University), Dapeng Zhao(Department of Geophysics, Tohoku University)

[SIT32-P02] **Origin of the Caroline Plateau/Seamount Chain from a short lived mantle plume**

*Guoliang Zhang[1,3], Ji Zhang[1,2], Shuai Wang[1,2] (1.Institute of Oceanology, Chinese Academy of Sciences, 2.University of Chinese Academy of Sciences, 3. Center for Ocean Mega-Science, Chinese Academy of Sciences)

[SIT32-P03] Meteorite Impact Origin of ***Mantle Plumes*** Growing Downward by ***Mantle Depletion of Volatiles*** Not Convection From CMB

*Hermann G. W. Burchard[1] (1.Oklahoma State University)

[SIT32-P04] Genesis of high-Ni olivine phenocrysts of the Dali picrites in the Central Emeishan large igneous province

★Invited Papers

*Wenchang Cai[1], Zhaochong Zhang[1], Jiang Zhu[2], M. Santosh[1,3], Ronghao Pan[1] (1. China University of Geosciences, Beijing, China, 2.Yunnan Institute of Geological Sciences, Kunming,, China, 3.Department of Earth Sciences, University of Adelaide, Australia)

[SIT32-P05] Continental crust in the ocean

*Gillian R Foulger[1] (1.Durham University)

[SIT32-P06] The magma system beneath Changbaishan Volcano, China: an insight from magnetotellurics imaging

*Wule Lin[1], Xiangyun Hu[1], Bo Yang[1] (1.Hubei subsurface Multi-Scale Imaging Key Laboratory, Institute of Geophysics and Geomatics, China University of Geosciences)

[SIT32-P07] Evidence for the strike-slip opening of the Japan Sea

*Hidehisa Mashima[1] (1.Center for Obsidian and Lithic Studies, Meiji University)

[SIT32-P08] **Genesis of high-Ni olivine phenocrysts of the Dali picrites in the Emeishan large igneous province, SW China.**

*Wenchang Cai[1], Zhaochong Zhang[1], Jiang Zhu[1,2], M. Santosh[1,3], Ronghao Pan[1] (1. China University of Geosciences, Beijing, China, 2.Yunnan Institute of Geological Sciences, Kunming, China, 3.Department of Earth Sciences, University of Adelaide, Australia)

[E] Poster | S (Solid Earth Sciences)：S-GL Geology

[S-GL33] Geologic structure and tectonic history of East Asia and Japanese Islands

convener:Jun Hosoi(Geological Survey of Japan, Institute of Geology and Geoinformation, AIST), Makoto Otsubo(Geological Survey of Japan, Research Institute of Earthquake and Volcano Geology)

[SGL33-P01] **Deformation characteristics and metamorphic temperature of the high-pressure terrace of the Taiwan orogeny**

*Han Chun Lin[1], Yuan Hsi Lee[1], Lucas Manuel Ortinez Mesalles[1], Jian Cheng Lee[2] (1.Department of Earth and Environmental Sciences, National Chung-Cheng University, Taiwan, 2.Institute of Earth Sciences, Academia Sinica, Taiwan)

[SGL33-P02] Zircon U-Pb Ages from sandstones of the Muro Accretionary sequence in the Shimanto Superbelt, Kii Peninsula, Southwestern Japan

*Takanori Bessho[1], Hiroyuki Suzuki[2], Toshiya Yamamoto[3], Tohru Danhara[4], Hideki Iwano[4], Takafumi Hirata[5] (1.Department of Geosciences Osaka City University, 2.Nanki Kumano Jeopark Center, 3.Tanabe Highschool, 4.Kyoto Fissin-Track Co., Ltd., 5.Tokyo University)

[SGL33-P03] Geochemical characteristics of metamorphic and igneous rocks from the Hida belt: whole-rock major and trace elements, and multiple S isotope compositions

*Raiki Yamada[1], Shinnosuke Aoyama[2], Ouchi Wataru[1], Toshiro Takahashi[1], Satish Kumar M.[1] (1.Niigata University, 2.Yokohama National University)

[SGL33-P04] **Identification of the source caldera for the Pliocene pyroclastic flow deposit in NE Japan based on apatite trace-element compositions**

*Reishi Takashima[1], Haruka Kusakawa[2], Yuji Orihashi[3], Hiroshi Nishi[1] (1.Tohoku University, 2.Chichibu Taiheiyo Cement Co. Ltd. , 3.Hirosaki University)

[SGL33-P05] New age constraints and tectonic significance of the early Miocene sediments in the Hidaka Belt around Tomuraushi area, central Hokkaido, Japan

*Futoshi Nanayama[1,2], Mahito Watanabe[1], Toru Yamasaki[1], Hideki Iwano[3], Tohru Danhara[3], Takafumi Hirata[4] (1.Geological Survey of Japan, AIST, 2.CWMD, Kumamoto University, 3.Kyoto Fission-Track Co. Ltd, 4.The University of Tokyo)

[SGL33-P06] Provenance of the Yezo forearc basin in Northeast Japan from detrital zircon U–Pb age spectra

*Koh Kubomi[1], Shin-ichi Sano[2], Minami Murakami[3], Hiroto Ota[1], Mitsuhiro Nagata[1], Koshi Yamamoto[4], Shigeru Otoh[2] (1.Graduate School of Science and Engineering, University of Toyama, 2.Academic Assembly, Faculty of Sustainable Design, University of Toyama, 3.OYO Corporation, 4.Graduate School of Environmental Studies, Nagoya University)

[SGL33-P07] Tectonics of the Miocene Median Tectonic Line in the west of Ina-Valley, central Japan

*Akira Ono[1] (1.None)

[SGL33-P08] On the paleocurrent of the Miocene Goto Group in Fukue Island, Nagasaki Prefecture

*Yuta Ikebata[1], Shoichi Kiyokawa[1] (1.Department of Earth and Planetary Sciences, Graduate School of Science, Kyushu University)

[SGL33-P09] **North-South extension and compression juring the Japan Sea opening in the Amakusa, western Kyushu, Japan**

*Kentaro Ushimaru[1], Atsushi Yamaji[1] (1.Division of Earth and Planetary Sciences, Graduate School of Science, Kyoto University)

[SGL33-P10] Visualization of a high-strain shear zone based on a field survey for minor faults: A case study of southern Kyushu, Japan

*Akira Goto[1], Koji Shimada[1], Masakazu Niwa[1], Shuji Terusawa[2] (1.Japan Atomic Energy Agency, 2.OYO Corporation)

[SGL33-P11] Structural position of the Akiyoshi Limestone in the Permian accretionary complex of the Akiyoshi Belt, Southwest Japan

*Koji Wakita[1], Hokuto Obara[2], Takanori Nakagawa (1.Yamaguchi University Community Future Center, 2.Mine Akiyoshidai Karst Plateau Geopark Promotion Council)

[SGL33-P12] **Deformation characteristics and metamorphic temperature of the high-pressure terrace of the Taiwan orogeny**

*Han Chun Lin[1], Yuan Hsi Lee[1], Lucas Mesalles[1], Jian Cheng Lee[2] (1.Department of Earth and Environmental Sciences, National Chung-Cheng University, 2.Institute of Earth Sciences, Academia Sinica, Taiwan)

[E] Poster | S (Solid Earth Sciences)：S-RD Resources, Mineral Deposit & Resource Exploration

[S-RD35] Mineral Resources for Society: Ore deposit formation and exploration

convener:Yasushi Watanabe(Faculty of International Resource Sciences, Akita University), Kotaro Yonezu(Deaprtment of Earth Resources Engineering, Faculty of Engineering, Kyushu University)

[SRD35-P01] Heavy mineral sands ore deposits in Somaliland (Southern Gulf of Aden) coastal areas

*Awul Mohamud Ibrahm[1], Mohammed Ali[2] (1.Burao University, 2.Khalifa University of Science and Technology)

[SRD35-P02] **Economic potential of red earth deposits in the north and northwestern coastal belt of Sri Lanka**

*W.L.A.C.I. Weedagama [1,2], N.W.B. Balasooriya[2], Atula Senaratne[2], Bhathiya Athurupana[2], Rohana Chandrajith[2], Nadeesha H. Koralegedara[2] (1.Post Graduate Institute of Science, University of Peradeniya, Peradeniya, Sri lanka, 2.Department of Geology, University of Perdeniya, Peradeniya, Sri Lanka)

[SRD35-P03] Mineralogy and sulfur isotopic compositions of the Mowana vein-type copper deposit, Northeastern, Botswana

*AMOGELANG KOOGANNE[1], Akira Imai[2], Ryohei Takahashi[1], Andrea Agangi[1] (1.Akita University, 2.Kyushu University)

[SRD35-P04] Potential for Iron Oxide-Apatite Deposit and Iron Oxide-Copper-Gold Deposit in Japan: A new paradigm beyond current metallogeny

*Hiroyasu Murakami[1], Atsushi MIYASHITA[2] (1.Waseda University, 2.Seikei University)

[E] Poster | S (Solid Earth Sciences)：S-MP Mineralogy & Petrology

[S-MP36] Physics and Chemistry of Minerals

convener:Seiji Kamada(Frontier Research Institute for Interdisciplinary Sciences, Tohoku University), Masahiro KAYAMA(Department of General Systems Studies, Graduate School of Arts and Sciences, The University of Tokyo)

[SMP36-P01] Chemical and optical evaluation of zircon synthesized by Li-Mo flux method

*Masahiro KAYAMA[1], Das Kaushik[2], Yuta Tsuchiya[3] (1.Department of General Systems Studies, Graduate School of Arts and Sciences, The University of Tokyo, 2.Department of Earth and Planetary Systems Science, Hiroshima University, 3.Department of Biosphere-Geosphere Science, Okayama University of Science)

[SMP36-P02] Geological study around Strontian mine considered from zeolite and galena.

*Yuki Inoue[1], Mana Yasui[2], Hiroshi Hagiya[1], Atsushi Yamazaki[3] (1.Tokyo City University , 2.Waseda Research Institute for Science and Engineering, 3.Department of Resources and Environmental Engineering, School of Creative Science and Engineering, Waseda University)

[SMP36-P03] The influence of OH content on elastic constants of single-crystal topaz studied via sphere-resonance method

*Kako Aradachi[1], Tohru Watanabe[1], Morihisa Hamada[2] (1.University of Toyama, 2.Japan Agency for Marine-Earth Science and Technology)

[SMP36-P04] Structural changes of diatomaceous earth by heat treatment

*Naoya Sasaki[1,2], Akane Arasuna[1], Masayuki Okuno[1] (1.Kanazawa University, 2.Industrial Research Institute of Ishikawa)

[SMP36-P05] Density and elastic properties of liquid gallium using externally heated diamond anvil cell

*Ryo Tsuruoka[1], Hidenori Terasaki[1], Seiji Kamada[2,3], Fumiya Maeda[3], Tadashi Kondo[1], Iori Yamada[1], Satoru Urakawa[4], Akira Yoneda[5], Naohisa Hirao[6], Saori I. Kawaguchi[6], Akihiko Machida[7] (1.Department of Earth and Space Science, Graduate School of Science, Osaka University, 2.Frontier Research Institute for Interdisciplinary Sciences, Tohoku University, 3.Department of Earth and Planetary Materials Science, Graduate School of Science, Tohoku University, 4.Department of Earth Sciences, Okayama University, 5.Institute for Planetary Materials, Okayama University, 6.JASRI, 7.QST)

[SMP36-P06] Nano-polycrystalline diamond synthesized through the decomposition of stearic acid under high pressure and high temperature condition

*Hideaki Kawamura[1], Hiroaki Ohfuji[1] (1.Geodynamics Research Center, Ehime University)

[SMP36-P07] The magnetite-maghemite-hematite transformation

*Ibuki Kinebuchi[1], Atsushi Kyono[1], Yoshinari Sano[1] (1.University of Tsukuba)

[SMP36-P08] Effect of pressure on the band gap and the Seebeck coefficient of silicon

*Hitoshi Gomi[1], Ran Wang[2], Takashi Yoshino[2] (1.Tokyo Institute of Technology, 2.Okayama University)

[SMP36-P09] Density measurement of magmas under high pressure by the sink/float method

*Akio Suzuki[1] (1.Department of Earth Science, Graduate School of Science, Tohoku University)

[SMP36-P10] Twinning in wadsleyite

Nobuyoshi Miyajima[1], Johannes Buchen[1,2], *Takaaki Kawazoe[1,3] (1.Bayerisches Geoinstitut, University of Bayreuth, 2.Division of Geological and Planetary Sciences, California Institute of Technology, 3.Department of Earth and Planetary Systems Science, Hiroshima University)

[SMP36-P11] Melting experiments in the system $MgSiO_3$-SiO_2 at 13 GPa

*Takuya Moriguti[1], Akira Yoneda[1], Eiji Ito[1] (1.Institute for Planetary Materials, Okayama University)

[E] Poster | S (Solid Earth Sciences)：S-MP Mineralogy & Petrology

[S-MP37] Supercontinents and crustal evolution

convener:Madhusoodhan Satish-Kumar(Department of Geology, Faculty of Science, Niigata University), Krishnan Sajeev(Centre for Earth Sciences, Indian Institute of Science), Tomokazu Hokada(National Institute of Polar Research), Yasuhito Osanai(Division of Evolution of Earth Environments, Faculty of Social and Cultural Studies, Kyushu University)

[SMP37-P01] **Subdivision of the Lützow-Holm Complex in East Antarctica**

*Tomokazu Hokada[1,2], Daniel J. Dunkley[1], Kazuyuki Shiraishi[1,2], Yoshikuni Hiroi[3,1], Yoichi Motoyoshi[1,2] (1.National Institute of Polar Research, 2.The Graduate University for Advanced Studies, SOKENDAI, 3.Chiba University)

[SMP37-P02] Detrital zircon geochronology of the Limpopo Complex, southern Africa: Implications for Neoarchean to Paleoproterozoic collisional events

Taeko Uehara[1], *Toshiaki Tsunogae[1,2], Thembiso Otladisang Basupi[1], Yukiyasu Tsutsumi[3] (1.The University of Tsukuba, 2.University of Johannesburg, 3.National Museum of Nature and Science)

[SMP37-P03] Multiple sulfur isotope geochemistry of the Precambrian mafic dyke swarms in the Dharwar craton, South India.

*Silpa Ammini Sasidharan[1], Madhusoodhan Satish-Kumar[1] (1.Department of Geology, Faculty of Science, Niigata University)

[SMP37-P04] **Signatures of poly-phase deformation and an upper amphibolite metamorphism from garnet bearing schists of Askot Klippe, Kumaun Himalayas**

*Prakash Chandra Arya[1], Krishnan Sajeev[1] (1.Indian Institute of Science)

[SMP37-P05] Sr-Nd isotopic evidence for juvenile components and extensively reworked ancient crustal materials in the Vijayan Complex, Sri Lanka

*M A Sanjeewa P K Malaviarachchi[1], Madhusoodhan Satish-Kumar[2], Toshiro Takahashi[2] (1.Department of Geology, Faculty of Science, University of Peradeniya, Sri Lanka, 2.Department of Geology, Faculty of Science, Niigata University, Japan)

[SMP37-P06] Geochemical characteristics of mafic and felsic igneous rocks (1.9-1.75 Ga) in the Lesser Himalaya: Regional variation and its implications for tectonic setting

*Ryuichi Shinjo[1], Tomoki Amuro[1], Kohei Oura[1], Kazuya Oshiro[1], Shiro Tahara[1], Harutaka Sakai[2] (1.Department of Physics and Earth Sciences, University of the Ryukyus, 2.Department of Geology and Mineralogy, Kyoto University)

[SMP37-P07] A Tarim-North India connection in northern Gondwana related to final closure of the Proto-Tethys Ocean: Constraints from provenance of early Paleozoic sedimentary rocks in the Altyn Tagh orogen

*Qian Liu[1,2], Toshiaki Tsunogae[2,3], Guochun Zhao[4,5] (1.JSPS, 2.Tsukuba Univ. , 3.Johannesburg Univ. , 4.HKU, 5.Northwest Univ.)

[SMP37-P08] Native iron and serpentinization of peridotite, Oshika Village, Nagano Prefecture, Japan

*Yuya Takeda[1], Seiichiro Uehara[2] (1.Department of Earth and Planetary Science, Graduate School of Science, Kyushu University, 2.Department of Earth and Planetary Science, Faculty of Science, Kyushu University)

[E] Poster | S (Solid Earth Sciences)：S-MP Mineralogy & Petrology

[S-MP38] Deformed rocks, Metamorphic rocks and Tectonics

convener:Yoshihiro Nakamura(Geological Survey of Japan, National Institute of Advanced Industrial Science and Technology), Yumiko Harigane(Geological Survey of Japan, National Institute of Advanced Industrial Science and Technology (AIST))

[SMP38-P01] Metamorphism and geochronology of garnet amphibolite from the Beishan Orogen, southern Central Asian Orogenic Belt: Constraints from P-T path and zircon U-Pb dating

*Wenbin Kang[1], Wei Li[1] (1.State Key Laboratory of Continental Dynamics, Department of Geology, Northwest University, Xi'an 710069, China)

[SMP38-P02] Field evidence and mineral assemblage of eclogite from the Khungui zone, Zavkhan terrane, Western Mongolia

*Manzshir Bayarbold[1], Atsushi Okamoto[1], OTGONBAYAR DANDAR[1], Masaoki Uno[1], Noriyoshi Tsuchiya[1] (1.Graduate School of Environmental Studies, Tohoku University)

[SMP38-P03] Eclogite-to-granulite transition in the Ufipa Complex (Tanzania): Pressure—Temperature—time paths of a Pan-African continental collision zone

*Morita Isamu[1], Tatsuki Tsujimori[1], Nelson Boniface[2], Kennet E Flores[3], Shogo Aoki[4], Kazumasa Aoki[4] (1.Tohoku University, 2.University of Dar es Salaam, 3.Brooklyn College of the City University of New York, 4.Okayama University of Science)

[SMP38-P04] **Geochemistry, Pressure-Temperature conditions and tectonic setting of the amphibolite from the southern part of Motloutse Complex, eastern Botswana**

*Thembiso Otladisang Basupi[1], Toshiaki Tsunogae (1.Graduate of Life and Environmental Sciences, University of Tsukuba)

[SMP38-P05] **Crystal Preferred Orientation Development of Secondary Olivine Formed by Hydration of Orthopyroxene: Implication to Anisotropy of Shallow Mantle Wedge during Initiation Stage of Subduction**

*OTGONBAYAR DANDAR[1], Atsushi Okamoto[1], Takayoshi Nagaya[2], Masaoki Uno[1], Noriyoshi Tsuchiya[1] (1.Graduate School of Environmental Studies, Tohoku University, 2.Graduate School of Science, University of Tokyo)

[SMP38-P07] **Crustal fracturing and brecciation processes in middle crust associated with granitoid intrusions in Sør Rondane Mountains, East Antarctica**

*Tatsuya Takemori[1], Masaoki Uno[1], SATISH KUMAR[2], Noriyoshi Tsuchiya[1], Atsushi Okamoto[1] (1.Tohoku University, 2.Niigata University)

[SMP38-P08] Multiple timings of high-grade garnet-forming metamorphism from Sør Rondane Mountains, East Antarctica

*Fumiko Higashino[1], Tetsuo Kawakami[2], Shuhei Sakata[3], Takafumi Hirata[3] (1.Faculty of Science, Okayama University of Science, 2.Kyoto University, 3.The University of Tokyo)

[SMP38-P09] **Thermal modeling for "Hot-on-cold" thrusting: Thermal structure during orogenic movement at the western boundary of Eastern Ghats Belt, India**

*Fumihiko Sato[1], Tomoeki Nakakuki[1], Kaushik Das[1] (1.Hiroshima University)

[SMP38-P10] Fluid-rock interaction and formation of high-grade metamorphic rocks in the Trivandrum Block, southern India

*Nishi Ayumi[1] (1.Faculty of Life and Environmental Sciences, University of Tsukuba)

[SMP38-P11] Structural geology of Hidaka Metamorphic Belt in the Mt.Nozuka and Mt.Rakko area, Hokkaido,JAPAN -Growth process and mechanism of the Cenozoic continental crust-

*Moeko Kanno[1], Tsuyoshi Toyoshima[2], Hayato Ueda[2] (1.Graduate school of Science and Technology, Environmental Science and Technology,Earth science, 2.Niigata University, Faculty of Science,Department Geology)

[SMP38-P13] **Raman carbonaceous material thermometry applied to mapping the thermal structure of contact metamorphic domains in the Hongusan area, central Japan incorporating the effects of widespread detrital carbonaceous material**

*Ken Yamaoka[1], Simon Richard Wallis[1], Akira Miyake[2], Yui Kouketsu[3] (1.The University of Tokyo, 2.Aichi University of Education, 3.Nagoya University)

[SMP38-P14] Raman parameters of carbonaceous material estimated from fully-automatic spectral fitting method and their relation to vitrinite reflectance

*Shunya Kaneki[1], Yoshihiro Nakamura[2], Yui Kouketsu[3], Hideki Mukoyoshi[4] (1.Disaster Prevention Research Institute, Kyoto University, 2.Geological Survey of Japan, National Institute of Advancecd Industrial Science and Technology, 3.Graduate School of Environmental Studies, Nagoya University, 4.Graduate School of Science and Engineering, Shimane University)

[SMP38-P15] Raman spectroscopy of quartz eclogite in the Sanbagawa metamorphic belt: Potential of Raman geobarometry using kyanite-quartz system

*Yuki Tomioka[1], Yui Kouketsu[1], Tomoki Taguchi[2] (1.Nagoya University, 2.Kyoto University)

[SMP38-P16] The R.G. Coleman Cazadero Collection: A preliminary sample description for systematic curation

*Oka Hiroki[1], Tatsuki Tsujimori[1] (1.Tohoku University)

[SMP38-P17] The Microstructure and Composition of Picrolitic Antigorite Veins in Serpentinites from the High-P Metamorphic Yuli Belt in Eastern Taiwan

*Ilona Talvikki Sakaguchi[1], Yui Kouketsu[1], Chin-Ho Tsai[2], Dominikus Deka Dewangga [2], Katsuyoshi Michibayashi[1] (1.Nagoya University, 2.National Dong Hwa University)

[SMP38-P18] Estimation of P-T history of amphibolite tectonic blocks in serpentinite mélange of Kamuikotan metamorphic rocks

*Yuto Kimura[1], Toru Takeshita[1] (1.Department of Natural History Sciences, Graduate School of Science, Hokkaido University)

[SMP38-P19] Datolite in the high-pressure marble from the Eastern Iratsu body of the Sanbagawa metamorphic belt

*Kenta Yoshida[1], Sota Niki[2], Hikaru Sawada[1,2], Ryosuke Oyanagi[1] (1.Japan Agency for Marine-earth Science and Technology, 2.Geochemical Research Center, The University of Tokyo)

[SMP38-P20] The occurrence of jadeite in the ultramafic body discovered in the Sanbagawa belt, Shibukawa region, central Japan

*Hikaru Shioya[1], Katsuyoshi Michibayashi[1], Yui Kouketsu[1], Masaki Enami[1] (1.Nagoya University)

[SMP38-P21] Geochronology of the Yorii metamorphic rocks on the Kanto Mountains - Extension of the Abukuma metamorphic rocks to Southwest Japan.

Shota Matsunaga [2], *Atsushi MIYASHITA[1], Tatsuki Tsujimori[2], Kazumasa Aoki[3], Shogo Aoki[3] (1.Seikei University, 2.Tohoku University, 3.Okayama University of Science)

[SMP38-P22] Geology, deformation, and metamorphism of high-grade Shimanto accretionary complex in Kerama Islands, Okinawa, Ryukyu arc

*Ippei Yamamoto[1], Kenichiro Tani[2], Yui Kouketsu[3], Rina Fukuchi[1], Hiroaki Koge[4], Asuka Yamaguchi[1] (1.Atmosphere and Ocean Research Institute, The University of Tokyo, 2.National Museum of Nature and Science, 3.Nagoya University, 4.National Institute of Advanced Industrial Science and Technology)

[E] Poster | S (Solid Earth Sciences)：S-MP Mineralogy & Petrology

[S-MP39] Oceanic and Continental Subduction Processes

convener:REHMAN Hafiz Ur(Department of Earth and Environmental Sciences, Graduate School of Science and Engineering, Kagoshima University), Tatsuki Tsujimori(Tohoku University), Kazuaki Okamoto(Faculty of Education, Saitama University)

[SMP39-P01] Deeply subducted Jurassic ridge hydrothermal ore deposit -case study from the Sanbagawa eclogite-amphibolite-blueschist-

Yuki Wakabayashi[1], *Yukari Otsuka[1], Kazuaki Okamoto[1] (1.Saitama University)

[SMP39-P02] Metasomatic and metamorphic signature of the MORB in the Shimanto belt

*Yuka Mikami[1], Kazuaki Okamoto[1] (1.Saitama University)

[SMP39-P03] New titanite U–Pb age of so-called 'Inishi-type' calcareous rock from the Hida Belt: Constraints on timing of the carbonate–silicate rock interaction during a collision

*Hironobu Harada[1], Tatsuki Tsujimori[1], Shogo Aoki[2], Kazumasa Aoki[2] (1.Tohoku Univesity, 2.Okayama Univerity of Science)

[SMP39-P04] Stable isotope study of carbonate associated with antigorite serpentinite: O–C isotope characterization of a textually zoned calcite rock from the Itoigawa–Omi area, Japan

*Toshiaki Komata[1], Tatsuki Tsujimori[1], Hideko Takayanagi[1], Yasufumi Iryu[1] (1.Tohoku University)

[SMP39-P07] The Miocene Kaikomagatake granitoid pluton in the Izu collision zone, central Japan: its petrogenesis, emplacement depth and exhumation history

*Satoshi SAITO[1] (1.Graduate School of Science and Engineering, Ehime University)

[SMP39-P08] Whole-rock chemical composition of the granitoids in Ryoke belt, Takanawa Peninsula, northwest Shikoku, southwest Japan

*Kazuya Shimooka[1], Satoshi SAITO[1], Kenichiro Tani[2], Toshiro Takahashi[3] (1.Graduate School of Science and Engineering, Ehime University, 2.National Museum of Nature and Science, 3.Graduate School of Science and Technology, NiigataUniversity)

[SMP39-P09] Pressure-to-depth conversion models for metamorphic rocks: review and application

*Arthur Bauville[1], Philippe Yamato[2] (1.Center for Mathematical Science and Advanced Technology, JAMSTEC, 2.University of Rennes 1, France)

[SMP39-P10] Late Paleozoic-early Mesozoic magmatism in Delgerkhaan region, Central Mongolia: constraints from the zircon U-Pb age and geochemistry

*Ariuntsetseg Ganbat[1], Tatsuki Tsujimori[1,2], Chimedtseren Anaad[3], Munkhtsengel Baatar[3], Inna Safonova[4,5] (1.Department of Earth Science, Graduate School of Science, Tohoku University, Sendai, Japan, 2.Center for Northeast Asian Studies, Tohoku University, Sendai, Japan, 3.Mongolian University of Science and Technology, Ulaanbaatar, Mongolia , 4.Novosibirsk State University, Novosibirsk, Russia, 5.Sobolev Institute of Geology and Mineralogy, SB RAS, Novosibirsk, Russia)

[E] Poster | S (Solid Earth Sciences)：S-MP Mineralogy & Petrology

[S-MP40] Thermal structure of subduction zones: modeling and the rock record

convener:Simon Richard Wallis(The University of Tokyo), Takayoshi Nagaya(Graduate School of Science, The University of Tokyo), Shoichi Yoshioka(Research Center for Urban Safety and Security, Kobe University)

[SMP40-P01] Brucite as a major phase in the shallow mantle wedge

*Takayoshi Nagaya[1], Simon Richard Wallis[1], Kazuhiro Kawahara[2], Shunsuke Endo[3], Hiroshi Mori[4], Yoshihiro Asahara[5] (1.Graduate School of Science, The University of Tokyo, 2.Japan Oil, Gas and Metals National Corporation, 3.Shimane University, 4.Shinshu University, 5.Nagoya University)

[SMP40-P02] Development of high fluid pressure at the base of the shallow mantle wedge due to presence of an antigorite shear zone

*Simon Richard Wallis[1], Mari Yokota[1,2] (1.The University of Tokyo, 2.Nagoya University)

[SMP40-P03] Mineralogy and structure of the shallow mantle wedge: evidence from seismic anisotropy in the Ryukyu Arc and structural petrological studies

*Takayoshi Nagaya[1], Simon Richard Wallis[1], Andrew Walker[2], James Wookey[3], Kazuhiko Ishii[4], Michael Kendall[5] (1.Graduate School of Science, The University of Tokyo, 2.University of Leeds, 3.University of Bristol, 4.Osaka Prefecture University, 5.University of Oxford)

[SMP40-P04] Low-pressure type metamorphic rocks from No-jima Island, Yamaguchi Prefecture

*ZEJIN LU[1] (1.Graduate School of Science and Engineering for Innovation, Yamaguchi University)

[E] Poster | S (Solid Earth Sciences)：S-VC Volcanology

[S-VC41] Timescales of magmatism: from genesis to eruption

convener:Chamberlain Katy Jane(University of Derby), Iona McIntosh(Japan Agency for Marine-Earth Science and Technology), Kenichiro Tani(Department of Geology and Paleontology, National Museum of Nature and Science), Akihiko Tomiya(Geological Survey of Japan, National Institute of Advanced Industrial Science and Technology)

[SVC41-P01] **Magma mixing triggering eruption of deep rhyolite at Ascension Island, south Atlantic**

*Katy Jane Chamberlain[1], Jenni Barclay[2], Katie Preece[3], Richard J Brown[4], Iona McIntosh[5], E IMF[6] (1.ESRC, School of Environmental Sciences, University of Derby, Derby, DE22 1GB, UKUniversity of Derby, 2.School of Environmental Sciences, University of East Anglia, Norwich, NR4 7TJ, UK, 3.Department of Geography, College of Science, Swansea University, Swansea, SA2 8PP, UK., 4.Department of Earth Sciences, Durham University, Durham, DH1 3LE, UK, 5.Institute for Marine Geodynamics, Japan Agency for Marine Earth Science and Technology, Yokosuka 237-0061, Japan, 6.Edinburgh Ion Microprobe Facility, University of Edinburgh, Edinburgh, EH9 3FE, UK)

[SVC41-P02] The August 2019 Eruption of Volcano 0403-091: timescales of pumice raft formation and evolution during dispersal

*Iona McIntosh[1], Isobel Yeo[2], Scott Bryan[3], Matthew Dunbabin[3], Kenichiro Tani[4], Patrick Collins[5] (1.Japan Agency for Marine-Earth Science and Technology, 2.National Oceanography Centre Southampton, UK, 3.Queensland University of Technology, Australia, 4.National Museum of Nature and Science, Japan, 5.Queens University Belfast, UK)

[SVC41-P03] Magma plumbing system at Zao volcano, NE Japan: time scales of magmatic processes revealed by chemical zoning in orthopyroxene phenocrysts

*Motohiro Sato[1], Masao Ban[1] (1.Graduate School of Science and Technology, Yamagata University)

[SVC41-P04] Discovery of Quaternary volcanism in southern Sakhalin

*Kenichiro Tani[1], Hiroshi Kawabata[2], Osamu Ishizuka[3], Takashi Sano[1], Alexey Yu. Martynov[4] (1.National Museum of Nature and Science, 2.Kochi University, 3.Geological Survey of Japan/AIST, 4.Far East Geological Institute, Russian Academy of Sciences)

[SVC41-P05] Timescales of magmatic processes related to the AD 2000 eruptions at Miyakejima, Japan

*Chris Conway[1], Nobuo Geshi[1], Yumiko Harigane[1], Genji Saito[1], Akihiko Tomiya[1] (1.Geological Survey of Japan)

[SVC41-P06] **Boninite ascent rates constrained using chromite crystal chemistry: Observations of experimental products applied to the extrusive sequence of the Troodos Ophiolite**

*Daniel Coulthard[1], Georg F Zellmer[1], Sebastien Jego[2], Akihiko Tomiya[3] (1.Volcanic Risk Solutions, Massey University, Palmerston North, New Zealand, 2.Institut des Sciences de la Terre d'Orleans, Centre National de la Recherche Scientifique, Universite d'Orleans, Orleans, France, 3.Geological Survey of Japan, Advanced Institute of Science and Technology, Tsukuba, Japan)

[SVC41-P07] Novel approach for olivine-hosted melt inclusion corrections and its application to northern Japan tephras.

*Raimundo Brahm[1], Georg F Zellmer[1], Takeshi Kuritani[2], Naoya Sakamoto[3], Daniel Coulthard[1], Mitsuhiro Nakagawa[2], Eiichi Sato[4], Hisayoshi Yurimoto[3] (1.VRS, Massey Univ., 2.Grad. School of Sc., Hokkaido Univ., 3.IIL, CRI, Hokkaido Univ., 4.Hokkaido Univ. of Educ.)

[E] Poster | S (Solid Earth Sciences)：S-VC Volcanology

[S-VC42] Dynamics of volcanic eruptions and their physical and chemical processes

convener:Atsuko Namiki(Graduate School of Integrated Arts and Sciences, Hiroshima University), Christian Huber(Brown University), Michael Manga(University of California Berkeley), Yujiro Suzuki(Earthquake Research Institute, The University of Tokyo)

[SVC42-P01] A Model Experiment of Fracture Induced Long-Period Events: Injection of Pressurized Gas Into a Viscoelastic Rock Analog

*Atsuko Namiki[1], Makoto Takahashi[1], Ryo Tsutsui[1] (1.School of Integrated Arts and Sciences, Hiroshima University)

[SVC42-P02] Multi-parameter observations at Shikabe geyser and unique changes in interval between eruptions

*Ayuta Tsuge[1], Hiroshi Aoyama[1], Masayoshi Ichiyanagi[1] (1.Institute of Seismology and Volcanology, Faculty of Science, Hokkaido University)

[SVC42-P03] A new model of buoyancy-driven bubble coalescence with deformation effect

*Takafumi Maruishi[1], Atsushi Toramaru[2] (1.Department of Earth and Planetary Sciences, Graduate School of Sciences, Kyushu University, 2.Department of Earth and Planetary Sciences, Faculty of Sciences, Kyushu University)

[SVC42-P05] Experimental validation of a two-layer model for pyroclastic density currents

*Hiroyuki A. Shimizu[1], Takehiro Koyaguchi[2], Yujiro J. Suzuki[2], Brosch Ermanno[3], Gert Lube[3] (1.National Research Institute for Earth Science and Disaster Resilience, 2.Earthquake Research Institute, The University of Tokyo, 3.Massey University)

[SVC42-P06] **Numerical simulation of ballistic trajectories based on wind tunnel experiments**

*Kae Tsunematsu[1] (1.Yamagata University)

[SVC42-P07] Excitation of airwave by a bubble bursting in particle-bearing fluids : regime transitions and implications for basaltic volcanic eruptions

*Ikuro Sumita[1], Kana Hashimoto[2] (1.Geosciences and Civil Engineering, Institute of Science and Engineering, Kanazawa University, 2.Graduate School of Natural Science and Technology, Kanazawa University)

[SVC42-P08] Ash fall observation using 2D-Video Disdrometer

*Eiichi Sato[1], Masato Iguchi[2] (1.Meteorological Research Institute, 2.Kyoto Univ.)

[SVC42-P09] An attempt at quantification of starting eruption cloud at Sakurajima volcano

*Taishi Yamada[1], Masato Iguchi[1], Eisuke Fujita[2] (1.Sakurajima Volcano Research Center, Disaster Prevention Research Institute, Kyoto University, 2.National Research Institute for Earth Science and Disaster Resilience)

[SVC42-P10] Temperature dependence of titanomagnetite composition in a titanohematite-free silicic magma

*Naoki Araya[1], Michihiko Nakamura[1] (1.Department of Earth Science, Graduate School of Science, Tohoku University)

[SVC42-P11] **STRATIGRAPHY AND CHARACTERISTICS OF CALDERA II DEPOSITS, BATUR VOLCANIC COMPLEX, BALI, INDONESIA**

*Rahajeng Ardinni Noor[1], Atsushi Toramaru[1], Agung Harijoko[2,3], Haryo Edi Wibowo[2], Tomoharu Miyamoto[1], Mitsuru Okuno[4] (1.Department of Earth and Planetary Sciences, Faculty of Sciences, Kyushu University, 2.Department of Geological Engineering, Universitas Gadjah Mada, Indonesia, 3.Disaster Studies Center, Universitas Gadjah Mada, Indonesia, 4.Department of Earth System Science, Faculty of Science, Fukuoka University, Japan)

[SVC42-P12] Factors affecting the sequence of the Plinian eruption inferred from rock texture and physical properties - an example of the 1783 eruption, Asama volcano, Japan

*Tatsuki Mizuno[1], Fukashi Maeno[1], ATSUSHI YASUDA[1] (1.Earthquake Research Institute, Department of Earth and Planetary Science, University of Tokyo)

[SVC42-P13] Thermal history of pyroclasts reflecting the structure of eruption clouds: Application of textural analysis of pyrrhotite oxidation

*Keiko Matsumoto[1] (1.Geological Survey of Japan, The National Institute of Advanced Industrial Science and Technology)

[SVC42-P14] Intermittent ascent of aphyric andesitic melts revealed by cryptic micro-antecryst textures

*Charline Lormand[1], Georg F Zellmer[1], Naoya Sakamoto[2], Geoff Kilgour[3], Teresa Ubide[4], Hisayoshi Yurimoto[2], Alan Palmer[5], Karoly Nemeth[1], Yoshiyuki Iizuka[6], Anja Moebis[5] (1.School of Agriculture and Environment, Volcanic Risk Solutions, Massey University, PO Box 11222, Palmerston North 4442, New Zealand, 2.Isotope Imaging Laboratory, Natural History Sciences, Hokkaido University, Sapporo 060-0810, Japan, 3.GNS Science, Wairakei Research Centre, Private Bag 2000, Taupo 3352, New Zealand, 4.School of Earth and Environmental Sciences, The University of Queensland, Brisbane, QLD 4072, Australia , 5.School of Agriculture and Environment, Department of Soil Science, Massey University, PO Box 11222, Palmerston North 4442, New Zealand , 6.Institute of Earth Sciences, Academia Sinica, 128 Academia Road Sec. 2, Nankang, Taipei 11529, Taiwan)

[E] Poster | S (Solid Earth Sciences)：S-VC Volcanology

[S-VC43] Magma crystallization, fragmentation, and their roles on volcanic eruption

convener:Takahiro Miwa(National research institute for earth science and disaster prevention), Satoshi Okumura(Division of Earth and Planetary Materials Science, Department of Earth Science, Graduate School of Science, Tohoku University), Pranabendu Moitra(University of Arizona)

[SVC43-P01] Estimating the parameter to determine bubble - crystal interaction styles

*Ikeda Kyoko[1], Atsushi Toramaru[1] (1.Kyushu University, Department of Earth and Planetary Science)

[SVC43-P02] Effects of equilibrium crystallization on conduit flow dynamics during the 1986 eruption at Izu-Oshima volcano

*Tomofumi Kozono[1], Hidemi Ishibashi[2], Satoshi Okumura[3], Takahiro Miwa[4] (1.Department of Geophysics, Graduate School of Science, Tohoku University, 2.Department of Geoscience, Faculty of Science, Shizuoka University, 3.Department of Earth Science, Graduate School of Science, Tohoku University, 4.National Research Institute for Earth Science and Disaster Resilience)

[SVC43-P03] Experimental study on groundmass crystallization of the Izu-Oshima 1986 B basaltic andesite magma during conduit ascent

Ryoya Oida[2,3], *Hidemi Ishibashi[1], Akihiko Tomiya[3], Masashi Ushioda[3], Natsumi Hokanishi[4], Atsushi Yasuda[4] (1.Faculty of Science, Shizuoka University, 2.Graduate School of Integrated Science and Technology, Shizuoka University, 3.GSJ, AIST, 4.Univ. Tokyo, ERI)

[SVC43-P04] Effect of superheating on decompression-induced crystallization of hydrous rhyodacite magma: An experimental study

*Kazuhisa Matsumoto[1], Satoshi Okumura[1], Akihiko Tomiya[2] (1.Division of Earth and Planetaly Materials Science, Department of Earth Science, Graduate School of Science, Tohoku University, 2.Geological Survey of Japan, National Institute of Advanced Industrial Science and Technology)

[SVC43-P05] Analog experiment on vesiculation by crystallization with H_2O-KCl-CO_2

*Shiho Fujimura[1], Atsushi Toramaru[1] (1.Kyushu University)

[SVC43-P06] Deep Crystallization of Tholeiitic Melt: Insights from Manguao Basalt, Palawan, Philippines

*James Cesar Avisado Refran[1], Tsukasa Ohba[1], Carlo Arcilla, Takashi Hoshide[1], Ma. Ines Rosana Balangue-Tarriela (1.Akita University)

[SVC43-P07] Relationship between the change of eruption style and the rock texture of ejecta during the Shinmoe-dake 2018 eruption, Kirishima, Japan

*Sayaka Shohata[1], Fukashi Maeno[2], Yuki Suzuki[3], ATSUSHI YASUDA[2], Natsumi Hokanishi[2] (1.Department of Earth and Planetary Science, School of Science, The University of Tokyo, 2.Earthquake Research Institute, The University of Tokyo, 3.Faculty of Education and Integrated Arts & Sciences, Waseda University)

[SVC43-P08] Stratigraphy and Unit Determination of Ranau Tuff in Sumatra, Indonesia

*Rachmi Mustika Pertiwi Putri Gunawan[1], Atsushi Toramaru[1], Tomoharu Miyamoto[1] (1.Department of Earth and Planetary Sciences, Kyushu University, Fukuoka, Japan)

[SVC43-P09] 3D crystal size distributions of pyroxene nanolites based on nanoX-ray CT analyses

*Shota Okumura[1], Mayumi Mujin[2], Akira Tsuchiyama[3,4], Akira Miyake[1] (1.Department of Geology and Mineralogy, Graduate School of Science, Kyoto University, 2.Division of Earth and Planetary Materials Science, Department of Earth Science, Tohoku University, 3.Research Organization of Science and Technology, Ritsumeikan University, 4.Guangzhou Institute of Geochemistry, Chinese Academy of Sciences)

[SVC43-P10] Pre-eruptive Magma Condition of Tondano Caldera I: Domato Tuff, Minahasa, NE Sulawesi, Indonesia

*Tabegra Disando[1], Atsushi Toramaru[1] (1.Department of Earth and Planetary Sciences, Kyushu University, Fukuoka, Japan)

[SVC43-P11] **Magma fracturing, oxidation and nanolite crystallization processes during silicic magma eruption: Implication from textural and chemical analyses on oxidized obsidian**

*Kyohei Sano[1], Eiichi Sato[2] (1.Graduate School of Regional Resource Management, University of Hyogo, 2.Faculty of Liberal Arts and Sciences, Osaka Prefecture University)

[SVC43-P12] Redox state and nanolite crystallization of erupting magma during ash forming eruption at Bromo Volcano, Indonesia

*Takahiro Miwa[1], Hidemi Ishibashi[2], Masato Iguchi[3], Genji Saito[4], ATSUSHI YASUDA[5], Natsumi Hokanishi[5] (1.National research institute for earth science and disaster resilience, 2.Shizuoka University, 3.DPRI, Kyoto University, 4.AIST, 5.ERI, University of Tokyo)

[E] Poster | S (Solid Earth Sciences)：S-GC Geochemistry

[S-GC48] Volatiles in the Earth - from Surface to Deep Mantle

convener:Takeshi Hanyu(Japan Agency for Marine-Earth Science and Technology, Research Institute for Marine Geodynamics), Gray E Bebout(Lehigh University), Hirochika Sumino(Department of Basic Science, Graduate School of Arts and Sciences, The University of Tokyo), Yuji Sano(Division of Ocean and Earth Systems, Atmosphere and Ocean Research Institute, University of Tokyo)

[SGC48-P01] **Helium isotopic signature of the plate boundary suture in an active arc-continent collision**

*Ai-ti Chen[1,2], Yuji Sano[1], Timothy B Byrne[3], Naoto Takahata[1], Tsanyao Frank Yang[2], Yunshuen Wang[4], Chuan-Chou Shen[2] (1.Univ. of Tokyo, 2.National Taiwan Univ., 3.Univ. of Connecticut, 4.Central Geological Survey)

[SGC48-P02] ^{4}He/U-Th dating of pore waters from Quaternary sediments of the Swiss Midland

★Invited Papers

*Yama Tomonaga[1], Edith Horstmann[1], Gaudenz Deplazes[2], Rolf Kipfer[1] (1.Swiss Federal Institute of Aquatic Science and Technology (Eawag), 2.National Cooperative for the Disposal of Radioactive Waste (Nagra))

[SGC48-P03] Noble gas composition in hot spring gas in Shikine Island, Izu–Bonin volcanic arc, Japan

*Kotaro Toyama[1], Hirochika Sumino[1], Muga Yaguchi[2], Takeshi Ohba[3], Takashi Toyofuku[4], Shigeki Wada[5] (1.The University of Tokyo, 2.Meteorological Research Institute, 3.Tokai Univ., 4.JAMSTEC, 5.Shimoda Marine Research Center, University of Tsukuba)

[SGC48-P04] Helium and CO_2 fluxes in Wakamiko caldera

*Ma. Teresa Escobar[1], Naoto Takahata[1], Kotaro Shirai[1], Takanori Kagoshima[1], Kentaro Tanaka[1], Hajime Obata[1], Yuji Sano[1] (1.Atmosphere and Ocean Research Institute University of Tokyo)

[SGC48-P05] Noble gas isotope compositions of mafic phenocrysts in the Stage 3 lavas of Kusatsu-Shirane Volcano

★Invited Papers

*Nobuko Kametani[1,2], Hirochika Sumino[3], Kenta Ueki[4], Morihisa Hamada[4], Yasuo Ishizaki[5] (1.Graduate School of Science and Engineering, University of Toyama, 2.Mount Fuji Research Institute Yamanashi Prefectural Government, 3.Department of Basic Science, Graduate School of Arts and Sciences, The University of Tokyo, 4.Research Institute for Marine Geodynamics, Japan Agency for Marine-Earth Science and Technology, 5.Faculty of Sustainable Design, University of Toyama)

[SGC48-P06] **The complex melt–fluid–rock interaction history of a dismembered cumulate dunite from eastern Singhbhum Craton, India**

*Tushar Mouli Chakraborti[1], Arijit Ray[2], Gautam Kumar Deb[2] (1.Hiroshima Univ., 2.Presidency Univ.)

[SGC48-P07] SIMS sensitivity factors of ^{2}H and $^{16}O^{2}H$ relative to ^{18}O in spinel-structured oxides

*Georg F Zellmer[1], Naoya Sakamoto[2], Minami Kuroda[3], Isao Sakaguchi[4], Hisayoshi Yurimoto[2,5] (1.Massey University, 2.Hokkaido University, 3.AIST, 4.National Institute of Material Sciences, 5.Japan Aerospace Exploration Agency)

[E] Poster | S (Solid Earth Sciences)：S-TT Technology & Techniques

[S-TT50] Synthetic Aperture Radar and its application

convener:Yohei Kinoshita(University of Tsukuba), Yu Morishita(Geospatial Information Authority of Japan), Shoko Kobayashi(Tamagawa University), Takahiro Abe(Earth Observation Research Center, Japan Aerospace Exploration Agency)

[STT50-P01] Development of InSAR tropospheric phase delay correction system at MRI (4th report)

*Satoshi Okuyama[1], Shinobu Ando[1], Toshiki Shimbori[1] (1.Meteorological Research Institute)

[STT50-P02] Progress for detecting surface displacement associated with 2018 Boso SSE by ALOS-2 ScanSAR interferometry

*Yohei Kinoshita[1] (1.University of Tsukuba)

[STT50-P03] Interseismic crustal deformation along the Xianshuihe Fault System, Western China, detected by ALOS-2 ScanSAR interferometry

*XUEMEI WANG[1], Youichiro Takada[2] (1.Department of Natural History Sciences, Graduate School of Science, Hokkaido University, 2.Department of Earth and Planetary Sciences, Hokkaido University)

[STT50-P04] Estimation of crustal deformation at Azumayama volcano during Aug. 2014 – Oct. 2019 by using InSAR in comparison with GNSS

*Takehiro Arai[1], Yoshiko Ogawa[1], Yasuhiro Hisada[1], Hirohide Demura[1], Taku Ozawa[2], Satoshi Miura[3] (1.The University of Aizu, 2.Graduate school of Science and Faculty of Science, Tohoku Univeristy, 3.National Research Institute for Earth Science and Disaster Resilience)

[STT50-P05] Extraction of topographic changes associated with the 2018 eruption and tsunami of Krakatau volcano using time-series SAR

*Daiki Inano[1], Hodaka Okazaki[1], Masanobu Shimada[1] (1.Tokyo Denki University)

[STT50-P06] Land subsidence prediction in Beijing plain using machine learning methods

*Yuyi Wang[1], Yun Pan[1] (1.Capital normal university)

[STT50-P07] Estimation of velocity distribution of Shirase Glacier derived from SAR data obtained by ERS-1/2 tandem mission (2)

*Koichiro Doi[1,2], Yuichi Aoyama[1,2], Kazuki Nakamura[3], Tsutomu Yamanokuchi[4], Kazuo Shibuya[1] (1.National Institute of Polar Research, 2.The Graduate University for Advanced Studies, SOKENDAI, 3.College of Engineering, Nihon University, 4.Remote Sensing Technology Center)

[STT50-P08] Evaluation of inundation area extraction method for the 2018 Western Japan heavy rainfall using PALSAR-2

*Hasatani Ryuta[1], Hiroto Nagai[2] (1.Waseda Univ School of Creative Science and Engineering, 2.Waseda Univ School of Education)

[STT50-P09] Integration of ALOS PALSAR and Landsat-7 ETM+ data for buried lineaments extraction at the Farafra Oasis, Egypt

*Noha Ismail Medhat[1,2], M.-Y Yamamoto[1], K. Mansour[2], A.M Abbas[2], M. Abdel Zaher[2] (1.Kochi University of Technology, 185, Miyanokuchi, Tosayamada, Kami, Kochi, 782-8502, Japan, 2.National Research Institute of Astronomy and Geophysics, Helwan, Cairo 11421, Egypt)

[STT50-P10] Development of multi-type portable radar interferometer for volcano observation

Taku Ozawa[1], *Yuji Himematsu[1] (1.National Research Institute for Earth Science and Disaster Resilience)

[STT50-P11] An Open-Source InSAR Time Series Analysis Package LiCSBAS and Its Application

*Yu Morishita[1,2], Milan Lazecky [2], Tim J. Wright [2], Jonathan R. Weiss [3,2], Yasser Maghsoudi [2], John R. Elliott [2], Andy Hooper [2] (1.Geospatial Information Authority of Japan, 2.University of Leeds, 3.University of Potsdam)

[E] Poster | S (Solid Earth Sciences)：S-TT Technology & Techniques

[S-TT51] seismic monitoring and processing system

convener:Takahiro Maeda(National Research Institute for Earth Science and Disaster Resilience)

[STT51-P01] Acquisition and application of offshore W-VSP in deep gas field in East China Sea basin

*Shunli Gao[1], Senqing Hu[1], Jun Zhao[1] (1.China National Offshore Oil Corporation (CNOOC), China Limited-Shanghai)

[STT51-P02] Study on the cause of the misalignment of the incidence azimuth of the air gun signal at the S-net station estimated from particle motion

*Ryoichi Iwase[1] (1.National Research and Development Agency, Japan Agency for Marine-Earth Science and Technology)

[STT51-P03] Analysis of Seismic Waves from Continuous and Controlled Seismic Signal System in Kyushu Area

*Ryosuke Matsuura[1], Tatsunori Ikeda[2,3], Takeshi Tsuji[1,2,3], Koshun Yamaoka[4] (1.Cooperative Program for Resources Engineering, Kyushu University, 2.Department of Earth Resources Engineering, Kyushu University, 3.International Institute for Carbon-Neutral Energy Research (I2CNER), Kyushu University, 4.Earthquake and Volcano Research Center, Graduate School of Environmental Studies, Nagoya University)

[STT51-P04] Development of seismic waveform monitor application by JAVA

*Masayoshi Ichiyanagi[1], Hiroaki Takahashi[1] (1.Institute of Seismology and Volcanology, Graduate School of Science, Hokkaido University)

[STT51-P05] Yet another module for reading WIN format data in ObsPy

*Shigeki Nakagawa[1], Aitaro Kato[1] (1.Earthquake Research Institute, the University of Tokyo)

[STT51-P07] Calibration of broadband seismographs based on the teleseismic records

*Takeshi Kimura[1] (1.National Research Institute for Earth Science and Disaster Resilience)

[STT51-P09] DEVELOPMENT OF CLOUD-TYPE MICROTREMOR OBSERVATION SYSTEM

*Shigeki Senna[1], Atsushi Wakai[1] (1.National Research Institute for Earth Science and Disaster Resilience)

[STT51-P10] Development of underground structure information analysis cloud system

*Shigeki Senna[1] (1.National Research Institute for Earth Science and Disaster Resilience)

[E] Poster | S (Solid Earth Sciences)：S-TT Technology & Techniques

[S-TT52] Seismic Big Data Analysis Based on the State-of-the-Art of Bayesian Statistics

convener:Hiromichi Nagao(Earthquake Research Institute, The University of Tokyo), Aitaro Kato(Earthquake Research Institute, the University of Tokyo), Keisuke Yano(The University of Tokyo, Graduate School of Information Science and Technology), Takahiro Shiina(Earthquake Research Institute, The University of Tokyo)

[STT52-P01] Comprehensive analysis of deep low-frequency earthquakes in 52 regions all over Japan

*Ryo Kurihara[1], Kazushige Obara[1] (1.Earthquake Research Institute, The University of Tokyo)

[STT52-P02] An application of reversible-jump MCMC method for simultaneous determinations of 1-D velocity structures and hypocenters around a fault (I): Formulation

*Masayuki Kano[1], Takahiro Shiina[2] (1.Graduate school of science, Tohoku University, 2.Earthquake Research Institute, The University of Tokyo)

[STT52-P03] An application of reversible-jump MCMC method for simultaneous determinations of 1-D velocity structures and hypocenters around a fault (II): Synthetic analyses

*Takahiro Shiina[1], Masayuki Kano[2] (1.Earthquake Research Institute, The University of Tokyo, 2.Graduate School of Science, Tohoku University)

[STT52-P04] A Bayesian seismic tomography adapted to discontinuities

*Sumito Kurata[1], Naoya Takakura[1], Keisuke Yano[1], Fumiyasu Komaki[1] (1.Graduate School of Information Science and Technology, The University of Tokyo)

[STT52-P05] Multi-mode surface wave tomography with trans-dimensional hierarchical Bayesian inversion: application to Australia

*Kazunori Yoshizawa[1,2], Toru Taira[2] (1.Faculty of Science, Hokkaido University, 2.Graduate School of Science, Hokkaido University)

[STT52-P06] Twin Experiment of 4DVar Capable of Uncertainty Quantification Based on Seismic Wavefield Propagation

*Hiromichi Nagao[1,2], Shin-ichi Ito[1,2], Masayuki Kano[3], Mitsuru Matsumura[4] (1.Earthquake Research Institute, The University of Tokyo, 2.Graduate School of Information Science and Technology, The University of Tokyo, 3.Graduate School of Science, Tohoku University, 4.CJS Inc.)

[STT52-P07] On the Optimum Solutions of Bayesian Inversions

*Daisuke Sato[1], Yukitoshi Fukahata[1] (1.Disaster Prevention Research Institute, Kyoto University)

[STT52-P08] Towards application of data-driven sparse sensor placement technique developed in fluid mechanics to seismology

*Takayuki Nagata[1], Keigo Yamada[1], Yuji Saito[1], Taku Nonomura[1], Keisuke Asai[1] (1.Tohoku University)

[E] Poster | S (Solid Earth Sciences)：S-TT Technology & Techniques

[S-TT53] Airborne surveys and monitoring of the Earth

convener:Shigekazu Kusumoto(Graduate School of Science and Engineering for Research, University of Toyama), Takao Koyama(Earthquake Research Institute, The University of Tokyo), Yuji Mitsuhata(AdvancedIndustrial Science and Technology), Shigeo Okuma(Geological Survey of Japan, National Institute of Advanced Industrial Science and Technology (AIST))

[STT53-P01] Repeated droneborne magnetic survey in Iwoyama, Kirishima volcano

*Takao Koyama[1], Atsushi Watanabe[1], Takayuki Kaneko[1], Takao Ohminato[1], Yoshiaki HONDA[2] (1.Earthquake Research Institute, The University of Tokyo, 2.Center for Environmental Remote Sensing, Chiba University)

[STT53-P02] Utilization of Beta Angle for Detecting Edges in Potential Field Methods

*Tamer Mahmoud Ragab Farag[1,2], Remon Aziz[3,2], Hidiki Mizunaga[1] (1.Exploration Geophysics lab, Earth Resources Engineering Department, School of Engineering, Kyushu University, 2.Exploration Sector, Nuclear Materials Authority, 3.Center for Northeast Asian Studies, Tohoku University)

[STT53-P03] **Three Dimensional Geophysical Inversion of Airborne Magnetic Data from the Yellowstone National Park (YNP), Western North America**

*Mohammad Shehata[1,2], Hideki Mizunaga[2] (1.Department of Geology, Faculty of Science, Port Said University, Egypt, 2.Department of Earth Resources Engineering, Faculty of Engineering, Kyushu University, Japan)

[STT53-P04] Development of a multiband uncooled infrared cameras system for imaging volcanic sulfur dioxide (SO_2) gas

*Tetsuya Jitsufuchi[1] (1.National Research Institute for Earth Science and Disaster Resilience)

[STT53-P05] Topographic changes in Kirishima Iwo-yama volcanic area obtained by UAV photogrammetry

*Yuichi Iwasa[1], Takeshi Matsushima[2] (1.department of earth and planetary sciences, graduate school of sciences, Kyushu University, 2.Institute of Seismology and Volcanology, Faculty of Sciences, Kyushu University)

[E] Poster | S (Solid Earth Sciences)：S-TT Technology & Techniques

[S-TT54] Creating future of solid Earth science with high performance computing (HPC)

convener:Takane Hori(R&D Center for Earthquake and Tsunami, Japan Agency for Marine-Earth Science and Technology), Yuji Yagi(Graduate School of Life and Environmental Sciences, University of Tsukuba, Tsukuba), Katsuhiko Shiomi(National Research Institute for Earth Science and Disaster Resilience)

[STT54-P01] **Python based finite element code development for fluid geodynamics using JIT compiler and benchmark test**

*Sangjin Park[1] (1.Kangwon National University)

[STT54-P02] Hybrid parallelization of Discrete Element Method (DEM): Toward a large-scale geotechnical HPC applications

*Mikito Furuichi[1] (1.Japan Agency for Marine-Earth Science and Technology)

[STT54-P03] Elastic Green’s function library based on subduction zone models of high fidelity using the finite element method

*Takane Hori[1], Ryoichiro Agata[1], Tsuyoshi Ichimura[2], Kohei Fujita[2], Takuma Yamaguchi[2], Takeshi Iinuma[1] (1.Research Institute for Marine Geodynamics, Japan Agency for Marine-Earth Science and Technology, 2.ERI, The University of Tokyo)

[E] Poster | S (Solid Earth Sciences)：S-CG Complex & General

[S-CG55] Petrology, Mineralogy & Resource Geology

convener:Yu Nishihara(Geodynamics Research Center Ehime University), Koichi Momma(National Museum of Nature and Science), Tatsuo Nozaki(Submarine Resources Research Center, Research Institute for Marine Resources Utilization, Japan Agency for Marine-Earth Science and Technology), Nobutaka Tsuchiya(Department of Geology, Faculty of Education, Iwate University)

[SCG55-P01] Generation of mafic and felsic magmas of the Iwanoyama-Iyuzan volcanic chain in the Higashi-Izu Monogenetic Volcano Field, Izu-Bonin arc, Japan

*Yoji Arakawa[1], Hiromichi Kani[2], Soichiro Ueno[3], Taro Shinmura[4], Kei Ikehata[1] (1.Earth Evolution Sciences, Faculty of Life and Environmental Sciences, University of Tsukuba, 2.Sabo and Landslide Technical Center, 3.College of Geosciences, School of Life and Environmental Sciences, 4.Faculty of Economics, Kumomoto Gakuen University)

[SCG55-P02] Redox paths of granitic magma in Chiquicamata, northern Chile.

*Tetsuichi Takagi[1] (1.Research Institute for Geo-Resources and Environment, National Institute of Advanced Industrial Science and Technology)

[SCG55-P04] Anatomy of the Cretaceous Shaku-dake High-Mg diorite (HMD) intrusion, north Kyushu, SW Japan: Sheet on sheet model, and its genesis

*Keisuke Eshima[1], Masaaki Owada[1], Atsushi Kamei[2] (1.Yamaguchi University Graduate school of sciences and technology for innovation, 2.Shimane University Department of earth science, interdisciplinary faculty of science and engineering)

[SCG55-P05] Formation process of pegmatitic pyroxenite in the western limb of Bushveld Igneous Complex, South Africa

Shuhei Yoshida[1], *Takuya Echigo[1], Yasushi Watanabe[1] (1.Graduate School of International Resource Sciences, Akita University)

[SCG55-P06] **Ilmenite-series granitoids of the Peninsular Ranges batholith of southern and Baja California and the inner zone batholith of southwestern Japan**

*Mia Flores[1] (1.Stanford University)

[SCG55-P07] Whole-rock chemical composition analysis of granitic rocks in the Goto Islands, southwestern Japan

*Kazuhiro Koga[1], Motohiro Tsuboi[1], Ryunosuke Ikeda[1], Misaki Kubo[1] (1.Kwansei Gakuin University)

[SCG55-P08] Geochemical constraints on origin and formation of the Mikabu–Sorachi Plateau

*Naoto Kimura[1,2], Yuji Ichiyama[3], Takashi Miyazaki[2], Bogdan S. Vaglarov[2], Qing Chang[2], Takeshi Hanyu[2], Jun-Ichi Kimura[2] (1.Graduate School of Science and Engineering, Chiba University, 2.Japan Agency for Marine–Earth Science and Technology, 3.Graduate School of Science, Chiba University)

[SCG55-P09] Gesis of vesiculation in basalt sills of the Shimokawa ophiolite in the northern Hidaka belt, Hokkaido with influence on basalt sill of the Ab-Kfs vein

*Kato Satomi[1], Sumio Miyashita[2] (1.Graduate school of science and technology, Niigata university, 2.Hokkaido Research Center of Geology)

[SCG55-P10] Siliceous concretion in Miocene diatomaceous muddy rock, northeastern Noto Peninsula, central Japan

*Seika Oto[1], Kosei Komuro[1], Masaaki Shimizu[2], Hisatada Akahane (1.Toyama University, 2.Hokuriku Polytechnic College)

[SCG55-P11] Spectral Analysis of Cathodoluminescence of Barite

*Tomita Makiko[1], Shin Toyoda[1], Hirotsugu Nishido[1] (1.Okayama university of science)

[SCG55-P13] Mineralogical study on bur-shaped pyrite in SK050 volcanic ash in Uonuma Groupe, Niigata Prefecture

*Hiroaki Ohfuji[1], Akinori Matsuda[1], Takeshi Kakegawa[2] (1.Geodynamics Research Center, Ehime University, 2.Graduate School of Science, Tohoku University)

[SCG55-P14] Multi-photon luminescence measurement of natural and treated diamonds

*Shoko Odake[1], Hiroaki Ito[2], Hiroshi Takahashi[3], Shingo Ono[2] (1.GIA Tokyo Godokaisha, 2.Nagoya Institute of Technology, 3.Gemological Institute of America)

[SCG55-P15] Study for development of geothermal exploration technique using thermoluminescence of feldspar

*Takahiro Sato[1], Nobuo Hirano[1], Noriyoshi Tsuchiya[1], Atsushi Okamoto[1] (1.Tohoku University)

[SCG55-P16] Synthesis of highly dense and fine-grained crustal and mantle mineral aggregates by spark plasma sintering (SPS) technique

*Sanae Koizumi[1], Takehiko Hiraga[1] (1.Earthquake Research Institute,The University of Tokyo)

[SCG55-P17] Development of simultaneous measurement system of viscosity and permeability for highly accurate evaluation of groundwater under high pressure and high temperature condition

*Tomoya Muramoto[1] (1.National Institute of Advanced Industrial Science and Technology)

[SCG55-P18] **Evaluation of the influence of particle size on characteristics of particle shape using an automated particle image analysis**

*AIKO HAYAUCHI[1], Daisuke Sasakura[1] (1.Malvern Panalytical division of Spectris Co., Ltd)

[SCG55-P19] Genesis of the low-Sr Granitoid in the northern Kyushu

*Yayoi Muraoka[1], Masaaki Owada[2], Teruyoshi Imaoka[2], Atsushi Kamei[3], Kazuhiro Miyazaki[1] (1.Advanced Industrial Science and Technology, 2.Yamaguchi Univ., 3.Shimane Univ.)

[E] Poster | S (Solid Earth Sciences)：S-CG Complex & General

[S-CG56] ICDP Oman Drilling Project: Oman to Oceanic Lithosphere to Island Arc Formation and Beyond

convener:Eiichi TAKAZAWA(Department of Geology, Faculty of Science, Niigata University), Katsuyoshi Michibayashi(Department of Earth and Planetary Sciences, Nagoya University), Sayantani Chatterjee(Niigata University, Department of Geology, Faculty of Science)

[SCG56-P01] Numerical prediction of effect of olivine content for proceeding of serpentinization

*Kazuki Yoshida[1], Atsushi Okamoto[1], Ryosuke Oyanagi[2], Hiroyuki Shimizu[3], Noriyoshi Tsuchiya[1], Oman Drilling Project Phase 2 Science Party (1.Tohoku university, 2.Japan Agency for Marine-Earth Science and Technology, 3.Kajima Corporation)

[SCG56-P02] Variable occurrences of magnetite and iron mobility during serpentinization: insights from samples from CM1A of Oman Drilling Project

★Invited Papers

*Ryosuke Oyanagi[1], Kazuki Yoshida[2], Yasuhiro Niwa[3], Yasuo Takeichi[3], Masao Kimura[3], Kenta Yoshida[1], Atsushi Okamoto[2], Oman Drilling Project Phase 2 Science Party (1.Japan Agency for Marine-Earth Science and Technology (JAMSTEC), 2.Graduate school of environmental studies, Tohoku University, 3.High Energy Accelerator Research Organization (KEK))

[SCG56-P04] **Crack aspect ratio in the serpentinized peridotites inferred from onboard ultrasonic data by the Oman Drilling Projects**

★Invited Papers

*Ikuo Katayama[1], Natsue Abe[2], Keishi Okazaki[3], Kohei Hatakeyama[1], Yuya Akamatsu[1], Katsuyoshi Michibayashi[4], Marguerite Godard[5], Peter B Kelemen[6], Phase 2 Science Party The Oman Drilling Project (1.Department of Earth and Planetary Systems Science, Hiroshima University, 2.Mantle Drilling Promotion Office, MarE3, JAMSTEC, 3.Kochi Institute for Core Sample Research, JAMSTEC, 4.Department of Earth and Planetary Sciences, Nagoya University, 5.Géosciences Montpellier, CNRS, Université de Montpellier, 6.Lamont Doherty Earth Observatory, Columbia University)

[SCG56-P05] Pore geometry in diabase collected by the Oman DP inferred from elastic wave velocity

*KUMPEI NAGASE[1], Ikuo Katayama[1], Kohei Hatakeyama[1], Yuya Akamatsu[1], Keishi Okazaki[2], Natsue Abe[3], Katsuyoshi Michibayashi[4] (1.Department of Earth and Planetary Systems Science, Graduate School of Science, Hiroshima University, 2.Japan Agency for Marine-Earth Science Technology, 3.Mantle Drilling Promotion Office, MarE3, Japan Agency for Marine-Earth Science and Technology, 4.Department of Earth and Planetary Sciences, Graduate School of Environmental Studies, Nagoya University)

[SCG56-P06] Water Content in Nominally Anhydrous Mineral of Crust/Mantle Boundary Recovered by International Oman Drilling Project

*Muhamad Asyraf Aminuddin[1], Tomoaki Morishita[1,2], Juan Miguel Ramirez Guotana[1,2], Keita Itano[1], Kenji Shimizu[3], Takayuki Ushikubo[3] (1.Kanazawa University Graduate School Natural Science and Technology, 2.Oman Science Party, 3.Kochi Institute for Core Sample Research,JAMSTEC)

[SCG56-P08] Microstructures, bulk and mineral chemistry of the gabbro cores of Holes GT1A and GT2A drilled in the Oman Drilling Project – Melt distribution in the subaxial lower crust

★Invited Papers

*Susumu Umino[1,3], Takahiro Fudai[1], Osamu Ishizuka[2], Yuki Kusano[2] (1.Kanazawa University, 2.Geological Survey of Japan, 3.JAMSTEC)

[SCG56-P09] Trace element and Sr isotopic compositions of gabbros and peridotites at the CM1A drilling site of Wadi Tayin block in the Oman ophiolite

*Masako Yoshikawa[1], Tomoaki Morishita[2], Ryoko Senda[3], Tomoyuki Shibata[1] (1.Department of Earth and Planetary systems Science, Hiroshima University, 2.Faculty of Geosciences and Civil Engineering, Kanazawa University, 3.Faculty of Social and Cultural Studies, Kyushi University)

[SCG56-P10] **First geochemical and mineralogical results of Oman Crust-Mantle transition: holes CM1A and CM2B characterization aboard DV-Chikyu_ Oman Drilling Project, Phase 2 Leg3**

*Fatma Kourim[1], Mathieu Rospabé[2], Sayantani Chatterjee[3], Manolis Giampouras[4], Keisuke Ishii Ishii[3], Akihiro Tamura[5], Nick Dygert[6], Ryosuke Oyanagi[2], Kou-Lung Wang[1,7], Marguerite Godard [8], Mathieu Benoit[9], Damon A-H

Teagle[10], Eiichi Takazawa Takazawa[11,3], Peter Kelemen[11], Jude Coggon[10], Oman Drilling Project Phase 2 Science Party (1.Institute of Earth Sciences, Academia Sinica, 2.Research Institute for Marine Geodynamics, JAMSTEC, 3.Nigata University, 4.University of Granada, 5.Kanazawa University, 6.The university of Tennessee, 7.National Taiwan University, 8.University of Montpellier, 9.Toulouse university, 10. Southampton University, 11.Columbia University)

[SCG56-P11] Petrological study of the crust-mantle boundary using CM2B cores from the ICDP Oman Drilling Project.

*Natsuki Oyanagi[1], Eiichi TAKAZAWA[1,2], Sayantani Chatterjee[1], Oman Drilling Project Phase 2 Science Party (1.Faculty of Science, Niigata University, 2.VERC, IMG, JAMSTEC)

[SCG56-P12] Mantle-melt reaction recorded in the ICDP Oman Drilling Project Hole CM2B in Wadi Tayin massif of the Samail ophiolite

*Eiichi TAKAZAWA[1,2], Natsuki Oyanagi[1], Sayantani Chatterjee[1], Fatma Kourim[3], Katsuyoshi Michibayashi[4], Oman Drilling Project Phase 2 Science Party (1.Department of Geology, Faculty of Science, Niigata University, 2.VERC, IMG, JAMSTEC, 3.Institute of Earth Sciences, Academia Sinica, 4.Graduate School of Environmental Studies, Nagoya University)

[SCG56-P13] **High resolution X-ray computed tomography and scanning electron microscopy studies of inclusions in Oman podiform chromitite: implications for rapid cooling in Moho Transition Zone**

*Yuan YAO[1], Eiichi TAKAZAWA[2,3], Sayantani CHATTERJEE[2], Antonin RICHARD[4], Christophe MORLOT[4], Laura CRÉON[5], Salim AL-BUSAIDI[6], Katsuyoshi MICHIBAYASHI[7] (1.Graduate School of Sciences & Technology, Niigata University, 2.Department of Geology, Faculty of Science, Niigata University, 3.Volcanoes and Earth's Interior Research Center, Research Institute for Marine Geodynamics, Japan Agency for Marine-earth Science and Technology, 4.Université de Lorraine, CNRS, GeoRessources lab, France, 5.Sorbonne Université, nstitut de Minéralogie, de Physique des Matériaux et de Cosmochimie (IMPMC), France, 6.Maadin Enterprises LLC, Oman, 7.Department of Earth & Planetary Sciences, Graduate School of Environmental Studies, Nagoya University)

[SCG56-P14] **Silicate inclusions in dispersed chromites at the mantle-crust transition zone: the link between dunite and chromitite formations**

*Mathieu Rospabe[1], Georges Ceuleneer[2], Mathieu Benoit[2], Mary-Alix Kaczmarek[2] (1.Research Institute for Marine Geodynamics (IMG), Japan Agency for Marine-Earth Science and Technology, 2.Géosciences Environnement Toulouse (GET), Observatoire Midi-Pyrénées, Université de Toulouse, CNRS, IRD)

[SCG56-P15] **Mantle petrological mapping in the Oman ophiolite reveals large scale heterogeneities possibly in relation with mantle source variation**

Tomoya Suzuki[1], *Marie Python[1], Main Tokinaga[1], Masako Yoshikawa[2], Georges Marie Ceuleneer[3], Shoji Arai[4] (1.Hokkaido University Department of Natural History Science Division of Earth and Planetary Systems Sciences, 2.Department of Earth and Planetary systems Science, Hiroshima University, 3.Université Paul Sabatier, GET, OMP, Toulouse, 4.Department of Earth Sciences, Faculty of Science, Kanazawa University)

[SCG56-P16] Peridotites beneath the ophiolite: Petrology and chemistry of peridotite bodies located below the metamorphic sole of the Oman ophiolite
Main Tokinaga, Marie Python, Georges Ceuleneer, Tomoya Suzuki and Jean-Paul Breton

*Tokinaga Main[1] (1.Hokkaido University Department of Natural History Science Division of Earth and Planetary Systems Sciences)

[SCG56-P17] Evolution of Island Arc Volcanoes: Ankaramite-Andesite-Basalt (ANANBA) Model

*Yoshihiko Tamura[1], Tomoki Sato[1], Osamu Ishizuka[1], Yasuhiro Hirai[1], Takashi Miyazaki[1] (1.Research Institute for Marine Geodynamics, Japan Agency for Maine-Earth Science and Technology)

[E] Poster | S (Solid Earth Sciences)：S-CG Complex & General

[S-CG57] New perspectives of subduction zone earthquake dynamics through experiments across-scales

convener:Masataka Kinoshita(Earthquake Research Institute, University of Tokyo), Yoshio Kono(Geodynamics Research Center, Ehime University), Eiichiro Araki(Japan Agency for Marine-Earth Science and Technology), Hiroko Kitajima(Texas A&M University College Station)

[SCG57-P01] Spatiotemporal variation in frictional behavior within the Nankai accretionary prism

*Hanaya Okuda[1], Matt J Ikari[2], Alexander Roesner[2], Katja Stanislowski[2], Andre Hüpers[2], Asuka Yamaguchi[1], Achim J Kopf[2] (1.Atmosphere and Ocean Research Institute, University of Tokyo, 2.MARUM – Center for Marine Environmental Sciences, University of Bremen)

[SCG57-P02] Changes in frictional properties of mud gouge with depth in the Nankai Trough accretionary prism

*Kyuichi Kanagawa[1], Takuma Ogawa[2], Tomoya Funaki[2], Tomoya Nakanishi[3], Sayumi Sagano[3], Junya Fujimori[3], Michiyo Sawai[1] (1.School of Science, Chiba University, 2.Faculty of Science, Chiba University, 3.Graduate School of Science and Engineering, Chiba University)

[SCG57-P03] Frictional properties of greenstone: Effects of the seamount subduction on faulting at the subduction zone

*Michiyo Sawai[1], Junya Fukaumi[1], Miki Takahashi[2], Yasutaka Hayasaka[3], Kyuichi Kanagawa[1] (1.Chiba University, 2.Geological Survey of Japan, AIST, 3.Hiroshima University)

[SCG57-P04] Mechanical weakness of the Nankai accretionary prism: Insights from a correlation between Vp and strength of cuttings

*Manami Kitamura[1], Takehiro Hirose[2] (1.National Institute of Advanced Industrial Science and Technology , 2.Japan Agency for Marine-Earth Science and Technology, Kochi Instutute for Core Sample Research)

[SCG57-P05] Structural analyses of inner accretionary wedge in the Nankai trough based on borehole resistivity image

*Yohei Hamada[1], Takehiro Hirose[1], Yoshinori Sanada[2] (1.Japan Agency for Marine-Earth Science and Technology Kochi Institute for Core Sample Research, 2.Japan Agency for Marine-Earth Science and Technology Institute for Marine-Earth Expolaration and Engineering)

[SCG57-P06] Dynamic strain energy as new evaluation item of a seismogenic fault

*Arito Sakaguchi[1], Masato Ichiki[2], Kikka Takiguchi[1] (1.Yamaguchi Univ., 2.SANO TAISEIKISO ENGINEERING Co.Ltd)

[SCG57-P07] Depth dependent spatial variation of pore size distribution for sediments at Nankai accretionary prism

Kouku Inoue[2], *Wataru Tanikawa[1], Yoshitaka Hashimoto[2], Osamu Tadai[4], Manami Kitamura[5], Yohei Hamada[1], Takehiro Hirose[1], Weiren Lin[3] (1.Japan Agency for Marine-Earth Science and Technology, Kochi Instutute for Core Sample Research, 2.Kochi University, 3.Kyoto University, 4.Marine Works Japan LTD., 5.AIST)

[SCG57-P08] Reconstruction of splay fault activity based on integrated subsurface geological data of the slope basin on the Nankai accretionary prism off Muroto

*Yuichi Okuma[1,2], Asuka Yamaguchi[1], Rina Fukuchi[3], Hiroaki Koge[4], Juichiro Ashi[2,1] (1.Atmosphere and Ocean Research Institute, the University of Tokyo, 2.Department of Natural Environmental Studies, Graduate School of Frontier Science, the University of Tokyo, 3.DIA CONSALTANTS COMPANY LIMITED., 4.The National Institute of Advanced Industrial Science and Technology)

[SCG57-P10] Subduction of Kyushu-Palau Ridge can cause local thermal disturbance, as estimated from new heat flow data in the forearc in the eastern Kyushu, Japan

*Masataka Kinoshita[1], Rie Nakata[1], Yoshitaka Hashimoto[2] (1.Earthquake Research Institute, University of Tokyo, 2.Kochi University)

[E] Poster | S (Solid Earth Sciences)：S-CG Complex & General

[S-CG58] Science of slow earthquakes: Toward unified understandings of whole earthquake process

convener:Satoshi Ide(Department of Earth an Planetary Science, University of Tokyo), Hitoshi Hirose(Research Center for Urban Safety and Security, Kobe University), Kohtaro Ujiie(Graduate School of Life and Environmental Sciences, University of Tsukuba), Takahiro Hatano(Department of Earth and Space Science, Osaka University)

[SCG58-P01] CMT inversion of offshore earthquakes along the Nankai Trough: Separated distributions of slow and regular earthquakes on the plate boundary

*Shunsuke Takemura[1], Ryo Okuwaki[2], Tatsuya Kubota[3], Katsuhiko Shiomi[3], Takeshi Kimura[3], Akemi Noda[3] (1.Earthquake Research Institute, the University of Tokyo, 2.University of Tsukuba, 3.National Research Institute for Earth Science and Disaster Resilience)

[SCG58-P02] Understanding of temporal change in slow earthquake migration speed

*Keisuke Ariyoshi[1], Roland Burgmann[2], Jean-Paul Ampuero[3] (1.Japan Agency for Marine-Earth Science and Technology, 2.University of California, Berkeley, 3.Université Côte d'Azur)

[SCG58-P03] One-hour-duration SSEs found during a Short-term SSE in the Tokai region.

*Kazuki Miyaoka[1], Akio Katsumata[2], Satoshi Itaba[3] (1.Japan Meteorological Agency, 2.Meteorological Research Institute, 3.National Institute of Advanced Industrial Science and Technology)

[SCG58-P04] Activities of low frequency tremors in Sanriku-Oki before the 2011 Tohoku-Oki earthquake

*Hidenobu Takahashi[1], Ryota Hino[1], Naoki Uchida[1], Kazuaki Ohta[2], Masanao Shinohara[3], Ryosuke Azuma[1], Susumu Kawakubo[1] (1.Graduate school of Science Tohoku University , 2.National Research Institute for Earth Science and Disaster Resilience, 3.Earthquake Research Institute, the University of Tokyo)

[SCG58-P05] Detailed Spatial Slip Distribution for Short-term Slow Slip Events along the Nankai Subduction Zone, Southwest Japan

*Masayuki Kano[1], Aitaro Kato[2] (1.Graduate school of science, Tohoku University, 2.Earthquake research institute, The University of Tokyo)

[SCG58-P06] Fist detection of shallow tremor at the Guerrero gap, Mexico.

*Raymundo Omar Plata Martinez[5], Satoshi Ide[1], Naoto Mizuno[1], Masanao Shinohara[2], Tomoaki Yamada[3], Allen Husker[4], Jorge Real[4], Victor Cruz-Atienza[4], Yusuke Yamashita[5], Akiko Toh[1], Yoshihiro Ito[5] (1.Department of Earth an Planetary Science, University of Tokyo, 2.Earthquake Research Institute, University of Tokyo, 3.Japan Meteorological Agency, 4.Institute Geophysics, UNAM, 5.Disaster Prevention Research Institute, Kyoto University)

[SCG58-P07] Depth profile of frictional properties inferred from cuttings obtained at the Nankai trough C0002 drilling site

*Riho Fujioka[1], Ikuo Katayama[1], Takehiro Hirose[2], Manami Kitamura[3] (1.Hiroshima Univercity, 2.Kochi Institute for Core Sample Research, Japan Agency for Marine-Earth Science and Technology, 3.National Institute of Advanced Industrial Science and Technology)

[SCG58-P08] Slip rate dependence of dynamic water permeability for low permeable fault and the role of fluid

*Wataru Tanikawa[1] (1.Japan Agency for Marine-Earth Science and Technology, Kochi Instutute for Core Sample Research)

[SCG58-P09] Gouge friction on a meter-scale laboratory fault

*Futoshi Yamashita[1], Eiichi Fukuyama[2,1], Akihiro Shimoda[2], Shun Watanabe[3] (1.National Research Institute for Earth Science and Disaster Resilience, 2.Graduate School of Engineering, Kyoto University, 3.Faculty of Engineering, Kyoto University)

[SCG58-P10] Spatio-temporal correlations in tremor activity in south-west Japan

*Anca Opris[1], Takahiro Hatano[1] (1.Department of Science, Osaka University)

[SCG58-P11] On 3-D resistivity structure in the SW part of Shikoku-Island, SW Japan, and sensitivity of the Network-MT responses to the structure

*Makoto Uyeshima[1], Ryoukei Yoshimura[2], Maki Hata[1], Hiroshi Ichihara[3], Koki Aizawa[4] (1.Earthquake Research Institute, The University of Tokyo, 2.Disaster Prevention Research Institute, Kyoto University, 3.Graduate School of Environmental Studies, Nagoya University, 4.Graduate School of Science, Kyushu University)

[SCG58-P12] Variations of scaling relationships for shallow tremor; implications from the probabilistic cell automaton model

*Masaru Nakano[1], Suguru Yabe[2] (1.Japan Agency for Marine-Earth Science and Technology, 2.Geological Survey of Japan, AIST)

[SCG58-P13] High Fluid Pressure Patch beneath the Décollement as a Potential Source of Slow Earthquakes at the Nankai Trough

*Takehiro Hirose[1], Yohei Hamada[1], Wataru Tanikawa[1], Nana Kamiya[2], Yuzuru Yamamoto[3], Takeshi Tsuji[4], Masataka Kinoshita[5] (1.Kochi Institute for Core Sample Research, Japan Agency for Marine-Earth Science and Technology, 2.Graduate School of Engineering, Kyoto University , 3.Japan Agency for Marine-Earth Science and Technology, 4.Department of Earth Resources Engineering, Kyushu University, 5.Earthquake Research Institute, the University of Tokyo)

[SCG58-P14] The November 11, 2018 long-period-monotonic big earthquake occuring near Mayotte island off East Africa and seismic activity observed by the Iranian broadband seismic stations

*Sadaomi Suzuki[1], Hossein Sadeghi[2] (1.Tono Research Institute of Earthquake Science, Association for the Development of Earthquake Prediction, 2.Department of Geology, Faculty of Science, Ferdowsi University of Mashhad, Iran)

[SCG58-P15] Dense broadband seismic campaign for deep very low frequency earthquakes in Shikoku, Kii and Tokai regions in the Nankai subduction zone

*Akiko Takeo[1], Kazushige Obara[1] (1.Earthquake Research Institutute, the University of Tokyo)

[SCG58-P16] **Fluid flow patterns in fluid injection into swelling gel particles**

*Kojiro Otoguro[1], Yutaka Sumino[1] (1.Department of Applied Physics, Faculty of Science Division I, Tokyo University of Science)

[SCG58-P17] Seismic reflection profiling across deep low-frequency tremor zone in western Shikoku, southwestern Japan

*Eiji Kurashimo[1], Kimihiro Mochizuki[1], Takashi Iidaka[1], Kazushige Obara[1] (1.Earthquake Research Institute, the University of Tokyo)

[SCG58-P18] Long-term Viscoerastic Relaxation and Spatially Inhomogeneous Viscosity Structure

*Yusaku Tanaka[1] (1.Earthquake Research Institute, University of Tokyo)

[SCG58-P19] A physical model of tremor response to periodic external stresses in poroelastic medium

*Ryunosuke Sakamoto[1], Yoshiyuki Tanaka[1] (1.University of Tokyo Graduate School of Science)

[SCG58-P20] The radial pattern of brittle viscoelastic fluids between rotating parallel plates

*Tatsuya Nishikubo[1], Hiroki Ishikawa[1], Shoma Kato[1], Yutaka Sumino[1] (1.Department of Applied Physics, Faculty of Science Division I, Tokyo University of Science)

[SCG58-P21] Offshore surveys of seismic structures and seismicity of regular and low-frequency earthquakes around Amami islands

*Tsutomu Takahashi[1], Ayako Nakanishi[1], Yojiro Yamamoto[1], Yasushi Ishihara[1], Aki Ito[1], Ryuta Arai[1], Seiichi Miura[1], Shuichi Kodaira[1], Yoshiyuki Kaneda[2] (1. Japan Agency for Marine-Earth Science and Technology, 2.Kagawa Univ.)

[SCG58-P22] Slip distributions of short-term slow slip events in the northern Kii Peninsula based on NIED Hi-net tilt measurements

*Chujo Naoya[1], Hitoshi Hirose[2,1,3], Takeshi Kimura[3] (1.Department of Planetology, Graduate School of Science, Kobe University, 2.Research Center for Urban Safety and Security, Kobe University, 3.National Research Institute for Earth Science and Disaster Resilience)

[SCG58-P23] Trial detection of deep low frequency tremor using analog seismograms of Kanto-Tokai Observation Network in 1988-1990

*Takanori Matsuzawa[1], Tetsuya Takeda[1] (1.National Research Institute for Earth Science and Disaster Resilience)

[SCG58-P24] Estimation of the spatial distribution of Qs values beneath the Kii Peninsula, Japan by the twofold spectral ratio method

*Kodai Sagae[1], Hisashi Nakahara[1], Takeshi Nishimura[1], Kazutoshi Imanishi[2] (1.Solid Earth Physics Laboratory,Department of Geophysics,Graduate School of Science,Tohoku University, 2.National Institute of Advanced Industrial Science and Technology (AIST))

[SCG58-P25] 3-D thermal modeling of generation mechanisms for short-term slow slip events and low-frequency earthquakes along the Ryukyu trench

*Nobuaki Suenaga[1], Shoichi Yoshioka[1,2] (1. Research Center for Urban Safety and Security, Kobe University, 2.Department of Planetology, Graduate School of Science, Kobe University)

[SCG58-P26] Spatio-temporal evolution of long- and short-term slow slip events in the Tokai region, central Japan estimated from a very dense GNSS network, during 1997-2017

*Hiromu Sakaue[1], Takuya NISHIMURA[2], Jun'ichi Fukuda[3], Teruyuki Kato[4] (1.Graduate School of Science, Kyoto University, 2.Disaster Prevention Research Institute Kyoto University, 3.Earthquake Research Institute,The University of Tokyo, 4.Hot Springs Research Institute of Kanagawa Prefectural Government)

[SCG58-P27] Repeating activity of shallow low-frequency tremor in Hyuga-nada

*Yusuke Yamashita[1], Masanao Shinohara[2], Hiroko Sugioka[3], Aki Ito[4], Tsutomu Takahashi[4], Daisuke Suetsugu[4] (1.Disaster Prevention Research Institute, Kyoto University, 2.Earthquake Research Institute, the University of Tokyo, 3.Graduate School of Science, Kobe University, 4.Japan Agency for Marine-Earth Science and Technology)

[SCG58-P28] Shallow low-frequency tremor in the Japan Trench subduction zone

*Sachiko Tanaka[1], Takanori Matsuzawa[1], Youichi Asano[1] (1.National Research Institute for Earth Science and Disaster Resilience)

[SCG58-P29] Shallow low-frequency tremor activity off Erimo, Hokkaido from 2006 to 2007 revealed from pop-up type ocean bottom seismometers

*Susumu Kawakubo[1], Ryosuke Azuma[1], Ryota Hino[1], Hidenobu Takahashi[1], Kazuaki Ohta[2], Masanao Shinohara[3] (1.Graduate School of Science, Tohoku University, 2.National Research Institute for Earth Science and Disaster Resilience, 3.Earthquake Research Institute, University of Tokyo)

[SCG58-P30] High-velocity frictional behavior of fault gouges in the presence of pore fluid

*Akito Tsutsumi[1] (1.Graduate School of Science, Kyoto University)

[SCG58-P31] Detection of low-frequency aftershocks of the 2019 Ridgecrest earthquake sequence

*Ayako Tsuchiyama[1], Taka'aki Taira[2], Junichi Nakajima[1], Roland Bürgmann[3] (1.Earth and Planetary Sciences at Tokyo Institute of Technology, 2.Berkeley Seismological Laboratory, 3.Earth and Planetary Science, University of California, Berkeley)

[SCG58-P32] Structural characteristics of the Nankai trough subduction zone off Kii channel revealed from densely obtained seismic reflection profiles

*Yasuyuki Nakamura[1], Shuichi Kodaira[1], Tetsuo No[1], Yuka Kaiho[1], Kazuya Shiraishi[1], Gou Fujie[1], Seiichi Miura[1], Koichiro Obana[1] (1.Japan Agency for Marine Earth Science and Technology)

[SCG58-P34] Long-Term Activity Changes of Very Low Frequency Earthquakes in the Ryukyu Trench

*Mamoru Nakamura[1] (1.Faculty of Science, University of the Ryukyus)

[SCG58-P35] Seismic Velocity Mapping of the Plate Boundary Structures in the Slow Earthquake Gap Zone off Western Kii Peninsula, Nankai Trough

*Yanfang Qin[1], Gou Fujie[1], Shuichi Kodaira[1], Yasuyuki Nakamura[1], Yuka Kaiho[1], Tetsuo No[1], Koichiro Obana[1], Seiichi Miura[1] (1.JAMSTEC Japan Agency for Marine-Earth Science and Technology)

[SCG58-P36] Distribution of very low-frequency earthquakes in the Miyako Strait, central Ryukyu Trench

*Hiromu Furugen[1], Mamoru Nakamura[1] (1.Graduate School of Engineering and Sience, Univercity of the Ryukyus)

[SCG58-P38] Spatiotemporal evolution of interplate slip in the Hyuganada and the Bungo Channel from 1996 to 2000 based on GNSS data

*Sawako Teshiba[1], Hitoshi Hirose[1,2] (1.Department of Planetology, Graduate School of Science, Kobe university, 2.Research Center for Urban Safety and Security, Kobe University)

[SCG58-P39] An estimation of stress changes based on earthquake swarm seismicity accompanied by Boso slow slip events

*Tomoki Ukawa[1], Hitoshi Hirose[2,1] (1.Department of Planetology, Graduate School of Science, 2.Research Center for Urban Safety and Security, Kobe University)

[SCG58-P40] Spatial heterogeneity of shallow tremor activity near the Japan Trench

*Shukei Ohyanagi[1], Kazuaki Ohta[2], Yoshihiro Ito[3], Ryota Hino[4], Yusaku Ohta[4], Ryosuke Azuma[4], Masanao Shinohara[5], Kimihiro Mochizuki[5], Toshinori Sato[6], Yoshio Murai[7] (1.Kyoto University, Graduate School of Science, 2.National Research Institute for Earth Science and Disaster Resilience, 3.Kyoto University, Disaster Prevention Research Institute, 4.Tohoku University, 5.Tokyo University, Earthquake Research Institute, 6.Chiba University, 7.Hokkaido University)

[SCG58-P41] Can crack-seal veins record recurrence intervals of slow earthquakes?

*Naoki Nishiyama[1], Kohtaro Ujiie[1], Masayuki Kano[2] (1.University of Tsukuba, 2.Tohoku University)

[SCG58-P42] Complementary Distribution between Very Low Frequency Earthquakes and Interplatecoupling area in the southwestern Ryukyu Trench

*Ren Yakabu[1], Mamoru Nakamura[1] (1.University of the Ryukyus)

[SCG58-P43] Different deformation styles in the source regions of the 2019 Yamagata-oki earthquake and the 1964 Niigata earthquake

*Taku Ueda[1], Lina Yamaya[1], Yosihiko Ogata[2], Aitaro Kato[1] (1.Earthquake Research Institute, the University of Tokyo, 2.The Institute of Statistical Mathematics)

[SCG58-P44] Uncovering complex characteristics of earthquake time series using complex network analysis

*Sumanta Kundu[1], Anca Opris[1], Takahiro Hatano[1] (1.Department of Earth and Space Science, Osaka University.)

[SCG58-P45] Exploring slow slip events and their scaling in 3D simulations of fault slip

*Luca Dal Zilio[1], Nadia Lapusta[1], Jean-Philippe Avouac[1] (1.Seismological Laboratory, California Institute of Technology, Pasadena, CA)

[SCG58-P46] Nature of the Lithosphere in Alternating Regions of Slow Earthquakes in South America

*POUSALI MUKHERJEE[1], Yoshihiro Ito[1], Takuo Shibutani[1], Emmanuel Soliman M Garcia[1], Raymundo Omar Plata Martinez[1] (1.Disaster Prevention Research Institute, Kyoto University)

[E] Poster | S (Solid Earth Sciences)：S-CG Complex & General

[S-CG59] Evolution and movement of the crustal surface and application of geo- and thermochronology

convener:Noriko Hasebe(Institute of Nature and Environmental Technology, Kanazawa University), Shigeru Sueoka(Japan Atomic Energy Agency), Frederic Herman(University of Lausanne), Takahiro Tagami(Graduate School of Science, Kyoto University)

[SCG59-P01] Thermochronology on the fore-arc side of Northeast Japan Arc

*Yuya Kajita[1], Shigeru Sueoka[2], Shoma Fukuda[1], Noriko Hasebe[3], Akihiro Tamura[4], Tomoaki Morishita[4], Barry P. Kohn[5], Takahiro Tagami[1] (1.Graduate School of Science, Kyoto University, 2.Japan Atomic Energy Agency, 3.Institute of Nature and Environmental Technology, Kanazawa University, 4.Department of Sciences, Kanazawa University, 5.School of Earth Sciences, University of Melbourne)

[SCG59-P02] AFT thermochronology of Cretaceous granites from the northern part of the NE Japan Arc: estimating thermal/denudation histories based on thermal inverse modeling

*Shoma Fukuda[1,2], Shigeru Sueoka[2], Noriko Hasebe[3], Akihiro Tamura[4], Tomoaki Morishita[4], Takahiro Tagami[1] (1.Graduate School of Science, Kyoto University , 2.Japan Atomic Energy Agency, 3.Institute of Nature and Environmental Technology, Kanazawa University, 4.Department of Earth Sciences, Kanazawa University)

[SCG59-P03] Izu-Bonin arc collision and mountain formation of the South Fossa Magna region: New insights from low-temperature thermochronology

*Yumi Kobayashi[1], Shigeru Sueoka[2], Shoma Fukuda[1], Barry P. Kohn[3], Tatsunori Yokoyama[2], Noriko Hasebe[4], Akihiro Tamura[5], Tomoaki Morishita[5], Takahiro Tagami[1] (1.Division of Earth and Planetary Science, Graduate School of Science, Kyoto University, 2.Tono Geoscience Center, Japan Atomic Energy Agency, 3.School of Earth Sciences, University of Melbourne, 4.Institute of Nature of Environmental Technology, Kanazawa University, 5.Department of Earth Science, Faculty of Science, Kanazawa University)

[SCG59-P05] **Analyses of Sag Pond Stratigraphy to Assess the Disaster History along Lembang Fault, West Java, Indonesia**

Januar Ridwan[2], *Noriko Hasebe[1], Eko Yulianto[2], Nandang Supriatna[2], Amar Amar[2] (1.Institute of Nature and Environmental Technology, Kanazawa University, 2.Research Center for Geotechnology, Indonesian Institute of Science)

[SCG59-P06] Dating marine terraces by terrestrial cosmogenic nuclides: applicability and limitations

★Invited Papers

*Yuki Matsushi[1], Tetsuya Komatsu[2], Shigeru Sueoka[2], Yusuke Yonaga[2], Yumi Ogawa[2], Natsuko Fujita[2], Yoko Saito-Kokubu[2] (1.Disaster Prevention Research Institute, Kyoto University, 2.Japan Atomic Energy Agency)

[SCG59-P07] Constraining thermal/denudation histories in the last 0.1 Myr using multi-OSL-thermochronometry applied to samples from deep boreholes

*Manabu Ogata[1], Georgina King[2], Frédéric Herman[2], Shigeru Sueoka[1], Ryuji Yamada[3], Kentaro Omura[3] (1.Tono Geoscience Center, Japan Atomic Energy Agency, 2.Institute of Earth Surface Dynamics, University of Lausanne, 3.National Research Institute for Earth Science and Disaster Prevention)

[SCG59-P08] Thin section etching of zircon for micro thermochronology by fission track method: A trial

Hiroaki Koyama[2], *Noriko Hasebe[1] (1.Institute of Nature and Environmental Technology, Kanazawa University, 2.Department of Earth Sciences, Kanazawa University)

[E] Poster | S (Solid Earth Sciences)：S-CG Complex & General

[S-CG60] Toward Discoveries in Solid Earth Sciences by Machine Learning

convener:Takahiko Uchide(Research Institute of Earthquake and Volcano Geology, Geological Survey of Japan, National Institute of Advanced Industrial Science and Technology (AIST)), Yuki Kodera(Meteorological Research Institute, Japan Meteorological Agency), Hisahiko Kubo(National Research Institute for Earth Science and Disaster Resilience)

[SCG60-P02] Detection of seismic signals under low SNR condition using an artificial neural network: Toward development of dense low cost citizen seismic network in Yokohama

*Ahyi KIM[1], Hiroki UEMATSU[1], Gakuto NAKAO[1] (1.Yokohama City University)

[SCG60-P03] Earthquake detection based on deep learning

Junyu Yu[1,2], *Takahiko Uchide[2], Yuji Yagi[1] (1.Graduate School of Life and Environmental Sciences, University of Tsukuba, 2.Geological Survey of Japan, AIST)

[SCG60-P04] Large-scale matched-filter analysis with similarity search

*Naoto Mizuno[1], Satoshi Ide[1] (1.Department of Earth and Planetary Science, The University of Tokyo)

[E] Poster | S (Solid Earth Sciences)：S-CG Complex & General

[S-CG61] The Japan Trench: Learning from the 2011 M=9 Tohoku-Oki earthquake, a decade later

convener:Takeshi Iinuma(National Research and Development Agency Japan Agency for Marine-Earth Science and Technology), Asuka Yamaguchi(Atomosphere and Ocean Research Institute, The University of Tokyo), Aitaro Kato(Earthquake Research Institute, the University of Tokyo), Tianhaozhe Sun(Pacific Geoscience Centre, Geological Survey of Canada)

[SCG61-P01] Vertical deformation style along the Sanriku coast inferred from coastal geology examined after the Tohoku earthquake

*Yuichi Niwa[1], Toshihiko Sugai[2] (1.Faculty of Science and Engineering, Chuo University, 2.Department of Natural Environmental Studies, Graduate School of Frontier Sciences, The University of Tokyo)

[SCG61-P02] Trial of the crustal deformation detection accompanied with the tremor activities in Fukushima-Oki deduced from the ocean bottom pressure gauge data

*Hideto Otsuka[1], Yusaku Ohta[1], Ryota Hino[1], Kazuaki Ohta[2] (1.Research Center for Prediction Earthquakes and Volcanic Eruptions, Graduate School of Science, Tohoku University, 2.National Research Institute for Earth Science and Disaster Resilience)

[SCG61-P03] Seafloor Displacement along the Japan Trench Caused by the 2011 Tohoku-Oki Earthquake Examined by Repeated Bathymetric Surveys

★Invited Papers

*Toshiya Fujiwara[1,9], Shuichi Kodaira[1], Gou Fujie[1], Yuka Kaiho[1], Toshiya Kanamatsu[1], Takafumi Kasaya[2], Yasuyuki Nakamura[1], Tetsuo No[1], Tsutomu Takahashi[1], Takeshi Sato[3], Narumi Takahashi[4,1], Yoshiyuki Kaneda[5,1], Katharina Bachmann[6], Christian dos Santos Ferreira[6], Gerold Wefer[6], Michael Strasser[7], Tianhaozhe Sun[8] (1.Research Institute for Marine Geodynamics, Japan Agency for Marine-Earth Science and Technology, 2.Research Institute for Marine Resources Utilization, Japan Agency for Marine-Earth Science and Technology, 3.Sapporo Regional Headquarters, Japan Meteorological Agency, 4.National Research Institute for Earth Science and Disaster Resilience, 5.Kagawa University, 6.MARUM, University of Bremen, 7.Institute of Geology, University of Innsbruck, 8.Pacific Geoscience Centre, Geological Survey of Canada, 9.Kochi University)

[SCG61-P04] Modelling of spontaneous and periodic slow slip in the northern part of the Japan Trench

*Ryoko Nakata[1,2], Takane Hori[1], Ryota Hino[2] (1.Japan Agency for Marine-Earth Science and Technology, 2.Graduate School of Science, Tohoku University)

[SCG61-P05] Structural-morphological and sedimentary features of forearc slope off Miyagi, NE Japan: implications for development of forearc basins and plumbing systems

*Jih-Hsin Chang[1], Jin-Oh Park[2], Tzu-Ting Chen[3], Asuka Yamaguchi[2], Tetsuro Tsuru[4], Yuji Sano[2], Ho-Han Hsu[3], Kotaro Shirai[2], Takanori Kagoshima[2], Kentaro Tanaka[2], Chiori Tamura[2] (1.Geological Survey of Japan, National Institute of Advanced Industrial and Science Technology., 2.Atmosphere and Ocean Research Institute, The University of Tokyo., 3.Institute of Oceanography, National Taiwan University., 4.Tokyo University of Marine Science and Technology.)

[SCG61-P06] Structural variation in the shallowest part of the Japan Trench subduction zone and its correlation with shallow megathrust slip and tsunamigenesis

*Yasuyuki Nakamura[1], Toshiya Fujiwara[1], Shuichi Kodaira[1], Seiichi Miura[1], Koichiro Obana[1] (1.Japan Agency for Marine Earth Science and Technology)

[E] Poster | S (Solid Earth Sciences)：S-CG Complex & General

[S-CG62] Investigation of inputs to subduction zones: Influence of tectonic processes on the incoming plate

convener:Makoto Yamano(Earthquake Research Institute, the University of Tokyo), Tomoaki Morishita(School of Geoscience and Civil Engineering, College of Science and Technology, Kanazawa University), Gou Fujie(Japan Agency for Marine-Earth Science and Technology)

[SCG62-P01] Incoming Plate Faulting at the Outer Slope of the Middle America Trench offshore Mexico

*Emmanuel Soliman M Garcia[1], Yoshihiro Ito[1] (1.Disaster Prevention Research Institute, Kyoto University)

[SCG62-P02] Analysis of the variations in topographic features around the outer-rise of Japan trench

*Tomoko Hanyu[1], Jin-Oh Park[2], YUE SUN[2], Ehsan Jamali Hondori[2], Yukari Kido[3] (1.Kobe Ocean-Bottom Exploration Center, Kobe University, 2.Atmosphere and Ocean Research Institute, The University of Tokyo, 3.Japan Agency for Marine-Earth Science and Technology)

[SCG62-P03] Drift sediments recording bottom current history in NW Pacific

*Kiichiro Kawamura[1], Tomoka Adachi[1], Maki Suzukawa[1] (1.Yamaguchi University)

[SCG62-P04] Effects of lithology on the mechanical properties of the input materials at the Hikurangi margin

*Alexi Kristina Allen[1], Hiroko Kitajima[1] (1.Texas A and M University)

[SCG62-P05] Subduction initiation at active spreading mid-ocean ridge indicated by ultrahigh temperature slab melting

*Chiou-ting Lin[1], Kuei-Chih Feng[2], Masaki Enami[3], Hou-Chun Liu[4], Ji-Hao Zhu[6], Ron Harris[5], Wei-Dong Sun[1] (1.Center of Deep Sea Research, Institute of Oceanology, Chinese Academy of Sciences, 2.Department of Mechanical Engineering, Ming Chi University of Technology, 3.Institute for Space–Earth Environmental Research, Nagoya University, 4.Department of Earth Science, National Cheng Kung University, 5.Department of Geology, Brigham Young University, 6.State Oceanic Administration, Second Institute of Oceanography, Ministry of Natural Resources)

[E] Poster | S (Solid Earth Sciences)：S-CG Complex & General

[S-CG63] Dynamics in mobile belts

convener:Yukitoshi Fukahata(Disaster Prevention Research Institute, Kyoto University), Ray Y Chuang(Department of Geography, National Taiwan University), Toru Takeshita(Department of Natural History Sciences, Graduate School of Science, Hokkaido University), Hikaru Iwamori(Earthquake Research Institute, The University of Tokyo)

[SCG63-P01] Seismic potential along the Caribbean subduction zone northwestern Colombia revealed by GPS data

*Sindy Carolina Lizarazo[1], Takeshi Sagiya[2], Hector Mora-Paez[3] (1.Graduate School of Environmental Studies - Nagoya University, 2.Disaster Mitigation Research Center - Nagoya Univesity, 3.Geological Survey of Colombia - GeoRED Project)

[SCG63-P02] New Megathrust Locking Model for the Southern Kurile Subduction Zone Incorporating Viscoelastic Relaxation and Non-uniform Compliance of Upper Plate

*Yuji ITOH[1], Takuya NISHIMURA[2], Kelin WANG[3], Jiangheng HE[3] (1.Graduate School of Science, Kyoto University, 2.Disaster Prevention Research Institute, Kyoto University, 3.Pacific Geoscience Centre, Geological Survey of Canada)

[SCG63-P03] Occurrence of normal-type earthquakes and stress loading model under Boso Peninsula, Japan

*Akinori Hashima[1], Hiroshi Sato[1], Toshinori Sato[2] (1.Earthquake Research Institute, University of Tokyo, 2.Graduate School of Science, Chiba University)

[SCG63-P04] 3-D Numerical Simulation of Island Arc Deformation Due to Steady Plate Subduction

*Yutaro Mori[1], Yukitoshi Fukahata[2] (1.Graduate School of Science, Kyoto University, 2.Disaster Prevention Research Institute, Kyoto University)

[SCG63-P05] Cause of the horizontal deformation of the Philippine Sea plate subducting beneath southwestern Japan

*Kazuki Miyazaki[1], Junichi Nakajima[1] (1.Department of Earth and Planetary Sciences, Tokyo Institute of Technology)

[SCG63-P06] Modeling strain concentration zones in Kyushu Island considering heterogeneous rheological structure

*Bunichiro Shibazaki[1] (1.International Institute of Seismology and Earthquake Engineering, Building Research Institute)

[SCG63-P07] Estimation of inelastic strain rate in the lower crust based on GNSS and seismic data and its implication for dynamics in Kyushu, southwest Japan

*Yuhei Yuasa[1], Satoshi Matsumoto[2] (1.Department of Earth and Planetary Sciences, Graduate School of Science, Kyushu University, 2.Institute of Seismology and Volcanology, Faculty of Science, Kyushu University)

[SCG63-P08] Tectonic development along the Hinagu fault zone, Kumamoto Prefecture, Japan

*Kenta Kobayashi[1], Keiji Ogashiwa[1] (1.Department of Geology, Faculty of Science, Niigata University)

[SCG63-P09] Physical modeling of postseismic deformation following the 2008 Iwate-Miyagi Nairiku Earthquake

*Yoshiki Takei[1], Youichiro Takada[2], James Daniel Paul Moore[3], Mako Ohzono[4] (1.Department of Natural History Sciences, Hokkaido University, 2.Faculty of Science, Hokkaido University, 3.Earth Observatory of Singapore, Nanyang Technological University, 4.Institute of Seismology and Volcanology, Graduate School of Science, Hokkaido University)

[SCG63-P10] Spatial change of extension direction detected by paleostress analysis in the Miocene Tanabe Group, Southwest Japan

*Noriaki Abe[1], Katsushi Sato[1] (1.Division of Earth and Planetary Science, Graduate School of Science, Kyoto University)

[SCG63-P11] Non-double-couple earthquake in the focal area of the 2000 Western Tottori earthquake by “0.1 manten” hyperdense seismic observation and spatial distribution of non-double-couple components

*Yuto Hayashida[1], Takumi Motokoshi[1], Satoshi Matsumoto[2], Yoshihisa Iio[3], Shin'ichi Sakai[4], Aitaro Kato[4], Group for "0.1 manten" hyperdense seismic observation Group registration (1.Department of Earth and Planetary Sciences, Graduate School of Science, Kyushu University, 2.Institute of Seismology and Volcanology, Faculty of Sciences, Kyushu University , 3.Disaster Prevention Research Institute, Kyoto University, 4.Earthquake Research Institute, University of Tokyo)

[SCG63-P12] **Driving stress of the 2013 M_W5.8 Awaji Island earthquake, Japan, inferred from well-constrained focal mechanisms and its seismotectonic implication**

*Kazutoshi Imanishi[1], Makiko Ohtani[2], Takahiko Uchide[1] (1.Geological Survey of Japan, AIST, 2.Earthquake Research Institute, The University of Tokyo)

[SCG63-P13] A systematic investigation of rupture directivity, stress drop, fault geometry, and radiation efficiency of small inland earthquakes in Japan

*Keisuke Yoshida[1] (1.Tohoku University)

[SCG63-P14] Modeling Internal Deformation Due to Inelastic Sources Under Inhomogeneous Structures

*Daisuke Sato[1], James Daniel Paul Moore[2] (1.Disaster Prevention Research Institute, Kyoto University, 2.Earth Observatory of Singapore)

[SCG63-P15] Combined inversion technique to determine stress condition and friction coefficient from fault orientation

*Katsushi Sato[1] (1.Division of Earth and Planetary Sciences, Graduate School of Science, Kyoto University)

[SCG63-P16] **Correlation between physical and hydraulic properties of rock fractures constrained by surface geometry: Digital rock physics approach**

*Kazuki Sawayama[1], Takuya ISHIBASHI[2], Fei Jiang[3], Takeshi Tsuji[4], Yasuhiro Fujimitsu[4] (1.Graduate school of engineering, Department of Earth Resources Engineering, Kyushu University, 2.Fukushima Renewable Energy Institute, National Institute of Advanced Industrial Science and Technology, 3.Department of Mechanical Engineering, Faculty of Engineering, Yamaguchi University, 4.Department of Earth Resources Engineering, Faculty of engineering, Kyushu University)

[SCG63-P17] The evolution of cataclastic rocks and their implication on the development of the Median Tectonic Line fault architecture, Japan

*Thomas Jing Yi Yeo[1], Toru Takeshita [1], Wencheng Huang[1] (1.Department of Natural History Sciences, Graduate School of Science, Hokkaido University)

[SCG63-P18] Development history of the mylonite zone distributed along the Mie Prefecture Median Tectonic Line

*Huang Wencheng[1], toru Takeshita[1], Thomas Jing Yi Yeo [1], Jun-Ichi Ando[2] (1.Department of Natural History Sciences, Graduate School of Science, Hokkaido University, 2.Department of Earth and Planetary Systems Science, Graduate School of Science, Hiroshima University)

[SCG63-P19] **Extensional stress conditions determined from the orientations of Middle Miocene dikes in the Kumano area**

*Toshiki Haji[1,2], Atsushi Yamaji[1] (1.Graduate School of Science, Kyoto University, 2.Institute of Geology and Geoinformation, AIST)

[SCG63-P20] Syn-orogenic extrusion of HP-LT blueschists in the northern Tyrrhenian Sea (northern Apennines, Italy)

*Samuele Papeschi[1], Eric Ryan[2], Hans Joachim Massonne[3,4], Giovanni Musumeci[5,6], Francesco Mazzarini[6], Giulio Viola[7] (1.Japan Agency for Marine Earth-Science and Technology, Kochi, Japan, 2.Department of Geoscience and Petroleum, Norwegian University of Science and Technology, Trondheim, Norway, 3.School of Earth Sciences, China University of Geosciences, Wuhan, P.R. China, 4.Fakultät Chemie, Universität Stuttgart, Stuttgart, Germany, 5.Dipartimento di Scienze della Terra, Università di Pisa, Pisa, Italy, 6.Istituto Nazionale di Geofisica e Vulcanologia, Pisa, Italy, 7.Dipartimento di Scienze Biologiche, Geologiche e Ambientali, Università di Bologna, Bologna, Italy)

[SCG63-P21] **Elastic wave velocities and electrical conductivity in a brine-saturated granitic rock with single fracture**

*Tohru Watanabe[1], Arina Tomioka[1] (1.University of Toyama)

[SCG63-P22] Hydraulic monitoring results during SIMFIP injection experiments through Shionohira fault zones in Fukushima Prefecture, Japan

*Kazuhiro Aoki[1], Hiroshi Wakahama[2], Haruka Nojo[2], Etuo Iwasaki[2], Masao Kametaka[2], Yukumo Tanaka[1], Takumi Yoshida[1], Kazuyoshi Seshimo[1] (1.Japan Atomic Energy Agency, 2.Dia Consultants)

[SCG63-P23] Change in electrical conductivity in a brine-saturated granite under uni-axial compression

*Yui Aikawa[1], Tohru Watanabe[1] (1.University of Toyama)

[SCG63-P24] Grain shape and connevtivity of pores in granular materials

*Katazakai Haruka[1], Tohru Watanabe[1] (1.Toyama University)

[SCG63-P25] Grain shape and pressure sensitivity of transport properties in granular materials

*Maremichi Abe[1], Tohru Watanabe[1] (1.Toyama University)

[E] Poster | S (Solid Earth Sciences)：S-CG Complex & General

[S-CG64] Crust-mantle connections

convener:Yoshihiko Tamura(Research Institute for Marine Geodynamics, Japan Agency for Maine-Earth Science and Technology), Osamu Ishizuka(Geological Survey of Japan, AIST)

[SCG64-P01] Temporal evolution of proto-Izu-Bonin-Mariana arc volcanism over 10 Ma: Constraints from statistical analysis of melt inclusion compositions

★Invited Papers

*Morihisa Hamada[1], Hikaru Iwamori[1,2,3], Philipp A. Brandl[4], Takayuki Ushikubo[1], Kenji Shimizu[1], Motoo Ito[1], He Li[5], Ivan P. Savov[6] (1.Japan Agency for Marine-Earth Science and Technology, 2.Department of Earth and Planetary Sciences, Tokyo Institute of Technology, 3.Earthquake Research Institute, University of Tokyo, 4.GEOMAR Helmholtz Centre for Ocean Research Kiel, 5.Institute of Oceanology, Chinese Academy of Sciences, 6.School of Earth and Environment, University of Leeds)

[SCG64-P02] Evolution of Rear Arc Magmas following backarc basin formation behind the Izu arc: Site U1437, IODP Exp. 350

*Takashi Miyazaki[1], J B Gill[2], C Hamelin[3], S M DeBari[4], Tomoki Sato[1], Yoshihiko Tamura[1], Jun-Ichi Kimura[1], Bogdan Stefanov Vaglarov[1], Qing Chang[1], Ryoko Senda[5], Satoru Haraguchi[6] (1.Research Institute for Marine Geodynamics, Japan Agency for Marine-Earth Science and Technology, 2.University of California, Santa Cruz, 3.University of Bergen, 4.Western Washington University, 5.Kyushu University, 6.University of Tokyo)

[SCG64-P03] The earliest stage of Izu rear-arc volcanism revealed by drilling at Site U1437, IODP Expedition 350

Tomoki Sato[1], Takashi Miyazaki[1], *Yoshihiko Tamura[1], James B Gill[2], Martin Jutzeler[3], Ryoko Senda[4], Jun-Ichi Kimura[1] (1.Research Institute for Marine Geodynamics, Japan Agency for Maine-Earth Science and Technology, 2.Department of Earth and Planetary Science, University of California Santa Cruz, Santa Cruz, California, USA, 3.School of Natural Sciences and Centre for Ore Deposit and Earth Sciences, University of Tasmania, Tasmania, Australia, 4.Faculty of Social and Cultural Studies, Kyushu University, Fukuoka, Japan)

[SCG64-P04] The origin of fertile plagioclase lherzolite in the Upper Zone of the Horoman peridotite complex

★Invited Papers

*Yumeto KOGURE[1], Eiichi TAKAZAWA[1,2] (1.Department of Geology, Faculty of Science, Niigata University, 2.VERC, IMG, JAMSTEC)

[SCG64-P05] Water-saturated solidus and second critical endpoint of peridotite determined by textures and chemistry of the quenched liquid

*Jintuan Wang[1], Eiichi Takahashi[1] (1.Guangzhou Institute of Geochemistry, Chinese Academy of Sciences)

[E] Poster | B (Biogeosciences)：B-BC Biogeochemistry

[B-BC03] Earth and Planetary Science Frontiers for Life and Global Environment

convener:Yoshinori Takano(Japan Agency for Marine-Earth Science and Technology (JAMSTEC)), Yohey Suzuki(Graduate School of Science, The University of Tokyo), Shingo Kato(RIKEN), Keisuke Fukushi(Institute of Nature & Environmental Technology, Kanazawa University)

[BBC03-P01] **Radiocarbon and noble gas isotope study to constrain origin of methane in Hakuba Happo serpentinite-hosted hot spring**

*Konomi Suda[1], Takahiro AZE[2], Yosuke Miyairi[1], Yusuke Yokoyama[2], Yohei Matsui[2,3], Hisahiro Ueda[3], Takuya Saito[3], Tomohiko Sato[4], Yusuke Sawaki[2], Ryosuke Nakai[1], Hideyuki Tamaki[1], Hiroshi A Takahashi[1], Noritoshi Morikawa[1] (1.National Institute of Advanced Industrial Science and Technology, 2.The University of Tokyo, 3.Japan Agency for Marine-Earth Science and Technology, 4.Tokyo Institute of Technology)

[BBC03-P02] Deep Microbial Colonization in Saponite-Bearing Fractures in Aged Basaltic Crust: Implications for Subsurface Life on Mars

*Yuri Sueoka[1], Seiya Yamashita[1], Mariko Kouduka[1], Yohey Suzuki[1] (1.Graduate School of Science, The University of Tokyo)

[BBC03-P03] Trace element chemistry of deep-sea corals from different oceanic regions

*Kazuko Saruwatari[1], Makoto Miura[1], Nozomu Iwasaki[2] (1.GIA Tokyo Godo Kaisha, 2.Rissho University)

[BBC03-P04] Verification of ice-mineralization process: formation of authigenic carbonates in alkaline lakes during freezing condition in south Mongolia.

*TAKUMA KITAJIMA[1], Keisuke Fukushi[2,1], Baasansuren Gankhurel[1], Yasuhito Sekine[4], Masahiro Yoda[3,4], Davaadorj Davaasuren[5] (1.kanazawa university, 2.Institute of Nature and Environmental Technology Kanazawa University, 3.the university of Tokyo, 4.Earth-Life Science Institute, 5.National University of Mongolia)

[BBC03-P05] The rediscovery of diversity of archaeol derivative in halophilic archaea especially living in high salt concentration

*Noriaki YAMAUCHI[1] (1.Department of Earth and Planetary Sciences, Faculty of Sciences, Kyushu University)

[BBC03-P06] China’s terrestrial ecosystem carbon balance during the 20th century: An analysis with a process-based biogeochemistry model

*Yanyu Lu[1], Wei Sun[2], Dongyan He[1], Hanqing Deng[1], Hong Tian[1], Biwen Wu[1] (1.Anhui Climate Center, Anhui Meteorological Administration, 2.Anhui Public Meteorological Service Center, Anhui Meteorological Administration)

[BBC03-P07] Adsorption behavior of molybdenum on ferrihydrite :dynamics analysis of Mo in Erdenet river, Mongolia

*Akihiro Okuyama[1], Solongo Tsetsgee[1], Keisuke Fukushi[2] (1.Kanazawa University , 2.Institute of Nature and Environmental Technology)

[BBC03-P08] Genomic and geochemical characterization of antimony-reducing microbial consortium obtained from mine tailing soil

*Okubo Tomotaka[1], Daisuke Yamashita[1], Hiroyuki Kashima[2], Satoshi Mitsunobu[3], Natsuko Hamamura[1] (1.Kyushu University , 2.JAMSTEC, 3.Ehime University)

[E] Poster | B (Biogeosciences)：B-PT Paleontology

[B-PT04] Biomineralization and Geochemistry of Proxies

convener:Takashi Toyofuku(Japan Agency for Marine-Earth Science and Technology (JAMSTEC)), Jelle Bijma(Alfred-Wegener-Institut Helmholtz-Zentrum für Polar- und Meeresforschung), Hiroshi Kitazato(Tokyo University of Marine Science and Technology (TUMSAT)), Kotaro Hirose(Faculty of Science and Engineering, Waseda University)

[BPT04-P01] Variation of geochemistry in sea urchins cultured under the long-term acidification experiment

Riki Miyai[1], Hideki Takami[2], Daisuke Muraoka[2], Atsushi Suzuki[3], Yukihiro Nojiri[4], *Mayuri Inoue[1] (1.Department of Earth Sciences, Okayama University, 2.Tohoku National Fisheries Research Institute, 3.Geological Survey of Japan, AIST, 4.Faculty of Science and Technology, Hirosaki University)

[BPT04-P02] Relationship between anthropogenic pollution and spatiotemporal change in element composition contained in the bottom sediments from Tokyo Bay, Japan.

*Sumika Yoneto[1], Kotaro Hirose[1], Hideo Yamazaki[2], Kazuo Kamura[1] (1.Faculty of creative science and engineering of the department of resources and environmental engineering, Waseda University, 2.Department of Life Science, School of Science and Engineering, Kindai University)

[BPT04-P03] Morphologic changes of a calcareous nannofossil group, *Reticulofenestra* group, from Eocene to Miocene in the Atlantic Ocean

*Doi Nobuhiro[1], Koji Kameo[2] (1.Division of Earth and Environmental Sciences, School of Science and Engineering, Chiba University, 2.Department of Earth Sciences, Faculty of Sciences, Chiba University)

[BPT04-P04] The formation process of axial internode skeletons in deep-sea isidid octocorals inferred from crystal orientation

*Yukiko Kozaka[1], Katsuyoshi Michibayashi[2], Yui Kouketsu[2], Yuki Tokuda[3], Hiroshi Sato[4] (1.Institute for Space-Earth Environmental Research, Nagoya University, 2.Department of Earth & Planetary Sciences, Graduate School of Environmental Studies, Nagoya University, 3.Faculty of Environmental Studies, Tottori University of Environmental Studies, 4.School of Business Administration, Senshu University)

[BPT04-P05] A challenge to 3D morphological analysis of diatom cells

*Megumi Saito-Kato[1], Yukiko Nagai[1,2], Hayato Yokoyama[3] (1.Department of Geology and Paleontology, National Museum of Nature and Science, 2.Japan Agency for Marine-Earth Science and Technology, 3.RC Gear)

[BPT04-P06] The cell dynamics of sexual reproduction in foraminifera *Spirillina vivipara*

*Yukiko Nagai[1,2], Remi Tsubaki[3], Nanami Kishigami[2], Takashi Toyofuku[2,4] (1.National Museum of Nature and Science of Tokyo, 2.Japan Agency for Marine-earth Science and Technology , 3.The University Museum, The University of Tokyo, 4.Tokyo University of Marine Science and Technology)

[BPT04-P07] Foraminifera: either biological organs or chemical factories

*Hiroshi Kitazato[1] (1.Tokyo University of Marine Science and Technology (TUMSAT))

[BPT04-P08] Identification of factors affecting partitioning of rare arth elements between calcite and seawater

*Kana Fujimori[1], Hirotaka Nishino[1], Tasuku Akagi[1] (1.Department of Earth and Planetary Sciences, Faculty of Sciences, Kyushu University)

[E] Poster | B (Biogeosciences)：B-PT Paleontology

[B-PT05] Biotic History

convener:Isao Motoyama(Faculty of Science, Yamagata University), Takao Ubukata(Division of Geology & Mineralogy, Department of Earth & Planetary Sciences, Kyoto University), Kazuyoshi Moriya(Department of Earth Sciences, Faculty of Education and Integrated Arts and Sciences, Waseda University)

[BPT05-P01] **Chemostratigraphy and paleoenvironmental reconstruction of the Ediacaran-Cambrian section in Khubsugul Group, northern Mongolia**

*Hatena Osawa[1], Tatsuo Oji[1], Hideko Takayanagi[2], Pedro J. Marenco[3], Koichi Mimura[1], Sersmaa Gonchigdorj[4], Kano onodera[1] (1.Nagoya University, 2.Tohoku University, 3.Bryn Mawr College, 4.Mongolian University of Science and Technology)

[BPT05-P02] Planktic foraminiferal biostratigraphy across the mid-Cretaceous Oceanic Anoxic Events

Soichi Shirakawa[3], Ryo Nakanishi[2], *Kazuyoshi Moriya[1] (1.Department of Earth Sciences, Faculty of Education and Integrated Arts and Sciences, Waseda University, 2.Department of Earth Sciences, School of Education, Waseda University, 3.Department of Earth Sciences,Resources and Environmental Engineering, Graduate School of Creative Science and Engineering, Waseda University)

[BPT05-P03] Organic carbon isotope stratigraphy across the Cenomanian/Turonian boundary at northern Atlantic

Yasuko Miyakura[2], *Kazuyoshi Moriya[1], Akiko S. Goto[3], Takashi Hasegawa[3] (1.Department of Earth Sciences, Faculty of Education and Integrated Arts and Sciences, Waseda University, 2.Department of Earth Sciences,Resources and Environmental Engineering, Graduate School of Creative Science and Engineering, Waseda University, 3.Faculty of Earth Science and Civil Engineering, Institute of Science and Engineering, Kanazawa University)

[BPT05-P04] The analysis of periostracum on Ammonoid shells from Cretaceous Yezo Group

*Hideharu Kohno[1], Haruyoshi Maeda[1] (1.Kyushu University)

[BPT05-P05] A functional-morphospace analysis of allometrically growing ammonoids

*Takao Ubukata[1] (1.Department of Geology & Mineralogy, Kyoto University)

[BPT05-P06] Phylogenetic aspect of ontogenetic trajectory of whorl shape in ammonoids

*Takao Ubukata[1], Fumitaka Katsuno[1] (1.Department of Geology & Mineralogy, Kyoto University)

[BPT05-P07] Evaluation of the metabolic status in extant Amniota based on nasal structures

*Seishiro Tada[1], Takanobu Tsuihiji[1,2] (1.Department of Earth and Planetary Science, Graduate School of Science, The University of Tokyo, 2.Department of Geology and Paleontology, National Museum of Nature and Science)

[E] Poster | B (Biogeosciences)：B-CG Complex & General

[B-CG06] Decoding the history of Earth: From Hadean to the present

convener:Tsuyoshi Komiya(Department of Earth Science & Astronomy Graduate School of Arts and Sciences The University of Tokyo), Yasuhiro Kato(Department of Systems Innovation, Graduate School of Engineering, University of Tokyo), Katsuhiko Suzuki(Submarine Resources Research Center, Japan Agency for Marine-Earth Science and Technology), Kentaro Nakamura(Department of Systems Innovation, School of Engineering, University of Tokyo)

[BCG06-P01] Ocean oxidation and microbial activity just after the Marinoan Snowball Earth

*Tsuyoshi Komiya[1], Miyuki Anzai[1], Teruyuki Maruoka[2], Yohei Matsui[3], Manabu Nishizawa[3], Yusuke Sawaki[1] (1.Department of Earth Science & Astronomy Graduate School of Arts and Sciences The University of Tokyo, 2.Faculty of Life and Environmental Sciences, University of Tsukuba, 3.Japan Agency for Marine-Earth Science and Technology)

[BCG06-P02] Alkaline magmatism in a fore-arc region: igneous activity in relation to the Ashizuri igneous complex, SW Japan

Takumi Matsumoto[1], *Kazumasa Aoki[1] (1.Department of Applied Science Okayama University of Science)

[BCG06-P03] Feedback mechanism of solid earth system on glacial-interglacial climate cycles: Constraints from osmium isotopic mass-balance in the ocean

★Invited Papers

*Yusuke Kuwahara[1], Kazutaka Yasukawa[2,1,3], Koichiro Fujinaga[3,2], Tatsuo Nozaki[4,2,5,3], Junichiro Ohta[2,3,6], Honami Sato[3,4], Jun-Ichi Kimura[6], Kentaro Nakamura[1], Yasuhiro Kato[2,1,3,4] (1.Department of Systems Innovation, School of Engineering, The University of Tokyo, 2.Frontier Research Center for Energy and Resources, School of Engineering, The University of Tokyo, 3.Ocean Resources Research Center for Next Generation, Chiba Institute of Technology, 4.Submarine Resources Research Center, Japan Agency for Marine-Earth Science and Technology, 5.Department of Planetology, Graduate School of Science, Kobe University, 6.Volcanos and Earth's Interior Research Center, Research Institute for Marine Geodynamics, Japan Agency for Marine-Earth Science and Technology)

[BCG06-P04] Geochemical constraints on the Earth environment after the Lomagundi Event;The Cape Smith belt, Canada

★Invited Papers

*Kento Motomura[1], Shoichi Kiyokawa[1], Minoru Ikehara[2], Takashi Sano[3], Kentaro Tanaka[4], Tsubasa Miki[4], Yuji Sano[4] (1.Kyushu Univ., 2.Kochi Univ., 3.National Museum of Nature and Science, 4.Univ. of Tokyo)

[BCG06-P05] Occurrence, petrography and chemical compositions of black shale in the Isua supracrustal belt: A potential to decode surface environmental conditions on the early Earth

*Suzuki Akiko[1], Yusuke Sawaki[2], Tsuyoshi Komiya[2] (1.The University of Tokyo , Graduate School of Science, 2.Department of Earth Science & Astronomy Graduate School of Arts and Sciences The University of Tokyo)

[BCG06-P06] U-Pb chronology and geochemistry of detrital monazites from major North American rivers

*Kazumi Yoshiya[1], Keita Itano[2], Tsuyoshi Iizuka[1], Shigenori Maruyama[3] (1.The University of Tokyo, Department of Earth and Planetary Science, 2.Kanazawa University, 3.Tokyo Institute of Technology, Earth-Life Science Institute)

[BCG06-P07] Variations of burial rates of organic carbon in terrestrial and marine environments during the Phanerozoic

*Kazuhiro Aoyama[1], Eiichi Tajika[1], Kazumi Ozaki[2] (1.Department of Earth and Planetary Science, Graduate School of Science, The University of Tokyo, 2.Toho University)

[BCG06-P08] New morphotypes, cell-wall structures, and elemental distribution of the Gunflint microfossils

*Kouhei Sasaki[1], Akizumi Ishida[1], Naoto Takahata[2], Yuji Sano[2], Takeshi Kakegawa[1] (1.Department of Earth Science, Graduate school of Science, Tohoku University, 2.Atmosphere and Ocean Research Institute, The University of Tokyo)

[BCG06-P09] Modelling the behaviors of marine carbon isotopic composition after Neoproterozoic snowball Earth event

*Akari Miki[1], Eiichi Tajika[1], Kazumi Ozaki[2] (1.Department of Earth and Planetary Science, Graduate School of Science, The University of Tokyo, 2.Toho University)

[BCG06-P10] Paleoecological variations reconstructed by organic matter derived from lichens and fungi across the Cenomanian/Turonian boundary in the Tomamae area, northern Hokkaido, Japan

*Masashi A. Ikeda[1], Ken Sawada[2], Takuto Ando[3], Hideto Nakamura[4], Reishi Takashima[5], Hiroshi Nishi[5] (1.Graduate School of Science, Hokkaido University, 2.Department of Earth and Planetary Sciences, Faculty of Science, Hokkaido University, 3.Estuary Research Center, Shimane University, 4.Faculty of Science, Osaka City University, 5.The Center for Academic Resources and Archives, The Tohoku University Museum, Tohoku University)

[BCG06-P11] Petrography of magnesite-orthopyroxene-olivine veins in the Ujaragssuit Nunât layered ultramafic body terrane, southern West Greenland

*Toma Takahashi[1], Tomoaki Morishita[1], Tomoyuki Mizukami[1], Akihiro Tamura[1], Keita Itano[1], Juan Miguel Guotana[1], Ikuya Nishio[1], Kanta Takahashi[1], Kristoffer Szilas[2] (1.Kanazawa university, 2.University of Copenhagen)

[BCG06-P12] Palynomorph assemblage in sedimentary rocks of the Mesoproterozoic Qaanaaq Formation from northwestern Greenland.

*Yuki Hara[1], Takuto Ando[3], Ken Sawada[2] (1.Graduate School of Science, Hokkaido University, 2.Department of Earth and Planetary Science, Faculty of Science, Hokkaido University, 3.Estuary Research Center, Shimane University)

[BCG06-P13] Pb-Pb chronology of Fe-Ti oxides

*Ito Kengo[1], Tsuyoshi Iizuka[1] (1.The University of Tokyo)

[E] Poster | B (Biogeosciences)：B-CG Complex & General

[B-CG07] Phanerozoic biodiversity change: radiation and extinction

convener:Yukio Isozaki(Department of Earth Science and Astronomy, Multi-disciplinary Sciences - General Systems Studies, Graduate School of Arts and Sciences, The University of Tokyo), Yusuke Sawaki(The University of Tokyo)

[BCG07-P01] Investigation on the internal texture of demospongiae fossil in meta-tuff from the Cambrian Akazawa Formation, Hitachi district

*Michio Tagiri[1], Katsutoshi Hanawa[2], Akira Oikawa[2], Noriaki Watanabe[3] (1.Hitachi City Museum, 2.Geonet Hitachi, 3.Graduate School of Environmental Studies, Tohoku Univ.)

[BCG07-P02] **Re-evaluating acid digestion for the analysis of organic carbon and nitrogen contents and stable isotope ratios in geological reference materials**

*Wataru Fujisaki[1], Yohei Matui[1] (1.Japan Agency for Marine-Earth Science and Technology)

[BCG07-P03] Taxonomy of Silurian conodonts from the Yokokurayama Group, Kurosegawa tectonic zone, distributed in Kochi Prefecture

*Akifumi Ito[1], Sachiko Agematsu[1], Yuichi Fukushima[1] (1.University of Tsukuba)

[BCG07-P04] **Devonian ostracods from the Fukuji area, Takayama City, Gifu Prefecture, central Japan**

*Mai Harashima[1], Sachiko Agematsu[1] (1.University of Tsukuba)

[E] Poster | G (General)：General

[G-01] Amazing technologies and capabilities that contribute to STEAM

convener:Day Brian Hamilton(NASA Ames Research Center), Emily Law(Jet Propulsion Laboratory), Go Murakami(Institute of Space and Astronautical Science, Japan Aerospace Exploration Agency), Kristen J Erickson(NASA Headquarters)

[G01-P01] Dagik Earth: 3-D digital globe for STEAM education in schools and museums

*Akinori Saito[1], Takuya Tsugawa[2], Takahito Kazama[1], Noriyuki Nishi[3], Yoshisuke Kumano[4] (1.Department of Geophysics, Graduate School of Science, Kyoto University, 2.National Institute of Information and Communications Technology, 3.Faculty of Science, Fukuoka Universtiy, 4.Graduate School of Science and Technology, Graduate School of Education, Shizuoka University)

[G01-P02] Increasing the understanding of abstract chemical concepts using VR programming

Garrison Penzo[1], Dante H Delgado[1], *Colleen M Knight[1] (1.College of Coastal Georgia)

[G01-P03] **STEAM Engagement with NASA's Solar System Treks**

*Brian Hamilton Day[1], Emily Law[2], NASA Solar System Treks Team -[2] (1.NASA Ames Research Center, 2.NASA Jet Propulsion Laboratory)

[E] Poster | M (Multidisciplinary and Interdisciplinary)：M-IS Intersection

[M-IS01] Tsunami deposit

convener:Daisuke Ishimura(Department of Geography, Tokyo Metropolitan University), Takashi Chiba(Faculty of Bioresource Sciences, Akita Prefectural University), Masaki Yamada(Department of Geology, Faculty of Science, Shinshu University), Takashi Ishizawa(International Research Institute of Disaster Science, Tohoku University)

[MIS01-P01] Distribution of tephra and tsunami deposits in Shikotan Island: Outline of the Japan-Russia joint research in 2019

*Yuichi Nishimura[1], Alexander Shishkin[2], Yasuhiro Takashimizu[3], Daisuke Sugawara[4], Takashi Ishizawa[5], Koichiro Tanigawa[6] (1.Graduate School of Science, Hokkaido University, 2.Institute of Marine Geology and Geophysics, Russian Academy of Sciences, 3.Faculty of Education, Niigata University, 4.Museum of Natural and Environmental History, Shizuoka, 5.International Research Institute of Disaster Science, Tohoku University, 6.The National Institute of Advanced Industrial Science and Technology)

[MIS01-P02] Facies description of 15 valley-filled tsunami deposits observed in Lake Tokachi-Chobushi for the past 2500 years and evaluation of their recurrence intervals

*Kiyoyuki Shigeno[1], Futoshi Nanayama[2,5], Kazuaki Watanabe[2], Masayuki Ishii[3], Keita Fukatsu[4] (1.Meiji consultant co.,Ltd., 2. Geological Survey of Japan, AIST, 3.Ishii Professional Engineer Office, 4.Notsuke Peninsula Nature Center, 5.CWMD,Kumamoto Univ.)

[MIS01-P03] Relationship between facies of tsunami deposits and paleo sedimentary environment which were reconstructed from plant macro fossils in peat

*Takashi Ishizawa[1], Yuichi Nishimura[2] (1.International Research Institute of Disaster Science, Tohoku University, 2.Institute of Seismology and Volcanology, Hokkaido University)

[MIS01-P04] Ages and distribution of paleo-tsunami deposits since 6 ka at Koyadori, Yamada Town, Iwate Prefecture, northeast Japan

*Daisuke Ishimura[1], Keitaro Yamada[2] (1.Department of Geography, Tokyo Metropolitan University, 2.Research Organization of Science and Technology, Ritsumeikan University)

[MIS01-P05] Machine-learning for correlation of tsunami deposits using geochemical proxy

*Kamiya Tomohisa[1], Kazuhisa Goto[2], Takashi Ishizawa[1], Hiroshi Tetsuka[1], Erick Velasco R.[1], Daisuke Ishimura[3], Kenta Satoh[1] (1.Tohoku University, 2.University of Tokyo, 3.Tokyo Metropolitan University)

[MIS01-P08] Numerical study of the formation process of sandy deposit formed by the 2011 Tohoku-oki tsunami

*wataru nakamura[1], Kazuhisa Goto[2], MASASHI WATANABE[3] (1.Tohoku University, 2.The University of Tokyo, 3.Chuo University)

[MIS01-P09] Reduction Effect of Tsunami Sediment Transport by Coastal Forest: Numerical Simulation of the 2011 Tohoku Tsunami on Sendai Plain, Japan

*Satoshi Kusumoto[1], Kentaro Imai[1], Aditya Gusman[2], Kenji Satake[3] (1.JAMSTEC, 2.GNS Science, 3.ERI, The University of Tokyo)

[MIS01-P10] Temporal change in sedimentological and geochemical characteristics of the 2011 Tohoku-oki tsunami deposits in the northeastern region of Fukushima Prefecture

*Kentaro Izumi[1], Ikuro Narayama[1], Tomoya Abe[2] (1.Faculty & Graduate School of Education, Chiba University, 2.Geological Survey of Japan, National Institute of Advanced Industrial Science and Technology)

[MIS01-P11] Flow reflection of onshore tsunami and features of the deposits

*Yasuhiro Takashimizu[1], Hibiki Saito[1] (1.Niigata University)

[MIS01-P12] Numerical estimation of paleotsunami size at southern part of Japan Trench based on geological records

*Hokuto Higaki[1], Kazuhisa Goto[2], Hideaki Yanagisawa[3], Daisuke Sugawara[4] (1.Tohoku University, 2.Department of Earth and Planetary Science, The University of Tokyo, 3.Department of regional Management, Faculty of Liberal Arts, Tohoku Gakuin University, 4.Museum of Natural and Environmental History, Shizuoka)

[MIS01-P13] Detailed analysis of tsunami deposits made by large-scale laboratory experiments

*Takumi Yoshii[1], Shiro Tanaka[1], Masafumi Matsuyama[1] (1.Central Research Institute of Electric Power Industry)

[E] Poster | M (Multidisciplinary and Interdisciplinary)：M-IS Intersection

[M-IS02] Environmental, socio-economic and climatic changes in Northern Eurasia

convener:Pavel Groisman(NC State University Research Scholar at NOAA National Centers for Environmental Information, Asheville, North Carolina, USA), Shamil Maksyutov(National Institute for Environmental Studies), Evgeny P Gordov(Institute of Monitoring of Climatic and Ecological Systems SB RAS), Akiyo Yatagai(Hirosaki University)

[MIS02-P01] BIOAVAILABILITY OF METALS DEPENDING ON THEIR SPECIATION IN NORTHERN LOW-SALINE WATER

*Tatyana I Moiseenko[1], Marina I Dinu[1] (1.Russian)

[MIS02-P02] Divergent responses of ecosystem water-use efficiency to extreme droughts over Northern Eurasia

*Mengtian Huang[1], Panmao Zhai[1] (1.Chinese Academy of Meteorological Science)

[MIS02-P03] Homogeneity analysis of air temperature and wind speed records of the Azov-Black sea region

*Natalia Alexandrovna Lemeshko[1], Vladislav P. Evstigneev[2,3], Maxim P. Evstigneev[2], Pavel Ya. Groisman[4] (1.SPBU, 2.IPTS, 3.SevSU, 4.IORAS)

[MIS02-P04] Soil response to sub centennial climate change

*Natalia Alexandrovna Lemeshko[1], Vladislav P. Evstigneev[2,3], Alexey V. Rusakov[1], Pavel Groisman[4] (1. SPBU , 2.IPTS , 3.SevSU, 4.IORAS)

[MIS02-P05] Climate change impacts on seed quality and distribution of light-needled *Pinus sylvestris* and *Larix* spp. in Northern Eurasia in a warming climate

*Nadezhda Tchebakova[1], Elena I. Parfenova[1], Elena V. Bazhina[1], Nina A. Kuzmina[1], Pavel Y. Groisman[2] (1.Institute of Forests, Siberian Branch, Russian Academy of Sciences, 2.NC State University Research Scholar)

[MIS02-P06] Northern Eurasia Future Initiative (NEFI), Update

*Pavel Groisman[1,2,3] (1.NC State University Research Scholar at NOAA National Centers for Environmental Information, Asheville, North Carolina, USA, 2.Shirshov Institute of Oceanology, Russian Academy of Sciences, Moscow, Russia , 3.Hydrology Science and Services Corporation, Asheville, North Carolina, USA)

[E] Poster | M (Multidisciplinary and Interdisciplinary)：M-IS Intersection

[M-IS03] Structure and deformation in the overlying plate due to subduction and related feedbacks

convener:Hiroshi Sato(Earthquake Prediction Research Center, Earthquake Research Institute, The University of Tokyo), David A Okaya(University of Southern California), Eh Tan(Institute of Earth Sciences, Academia Sinica), Masahiro Ishikawa(Graduate School of Environment and Information Sciences Yokohama National University)

[MIS03-P01] Three-dimensional seismic velocity model of the Nankai Trough subduction zone considering marine seismic reflection and onshore seismic data

*Ayako Nakanishi[1], Minako Katsuyama[1], Narumi Takahashi[1,2], Hiromi Kamata[1], Katsuhiko Shiomi[2], Shuichi Kodaira[1], Yoshiyuki Kaneda[1,3] (1.Japan Agency for Marine-Earth Science and Technology, 2.National Research Institute for Earth Science and Disaster Resilience, 3.Kagawa University)

[MIS03-P02] Deformation of the seismogenic zone in the northeastern part of the Izu Peninsula, Japan, inferred from GNSS observations

*Ryosuke Doke[1], Ryou Honda[1], Masatake Harada[1], Kazuki Miyaoka[2], Teruyuki Kato[1], Mikio Satomura[3] (1.Hot Springs Research Institute of Kanagawa Prefecture, 2.Japan Meteorological Agency, 3.Shizuoka University)

[MIS03-P03] Shift in provenance composition of Cretaceous Japan arc: from Jurassic granitoids/accretionary complex to Cretaceous granitoids

*Ryo Hasegawa[1], Yukio Isozaki[1], Atsushi Yamamoto[3], Yukiyasu Tsutsumi[2] (1.The University of Tokyo, 2.National Museum of Nature and Science, 3.Kindai University)

[MIS03-P04] High-resolution seismic profiles in the Shonai plain and Yamagata basin, northern Honshu, Japan

*Naoko Kato[1], Tatsuya Ishiyama[1], Hiroshi Sato[1], Shin Koshiya[2], Taro Koike[3], Katsuya Noda[3] (1.Earthquake Research Institute,University of Tokyo, 2.Faculty of science and engineering, Iwate University, 3.Geosys, Inc.)

[MIS03-P05] Seismic transect across the central part of Northern Honshu, Japan

*Hiroshi Sato[1], Tatsuya Ishiyama[1], Hirokazu Ishige[2], Naoko Kato[1], Masanao Shinohara[1], Takaya Iwasaki[1,6], Eiji Kurashimo[1], Hidehiko Shimizu[2], Shinji Kawasaki[2], Susumu Abe[2], Makoto MATSUBARA[3], Shin Koshiya[4], Tetsuo No[5], Shuichi Kodaira[5], Naoshi Hirata[1] (1.Earthquake Prediction Research Center, Earthquake Research Institute, The University of Tokyo, 2.JGI, Inc., 3.National Research Institute for Earth Science and Disaster Resilience, 4.Iwate University, 5.Japan Agency for Marine-Earth Science and Technology, 6.Association for the Development of Earthquake Prediction)

[E] Poster | M (Multidisciplinary and Interdisciplinary)：M-IS Intersection

[M-IS04] An asteroid impact in SE Asia at 0.8 Ma and its effect on the environment and biota

convener:Ryuji Tada(Department of Earth and Planetary Science, Graduate School of Science, The Univeristy of Tokyo), Paul A Carling(University of Southampton), Wickanet Songtham(Nakhon Ratchasima Rajabhat University, Thailand), Kerry Sieh(Nanyang Technological University)

[MIS04-P01] Discovery of Australasian microtektites in the hemipelagic sediments of the Japan Sea: It's significance and implications

*Ryuji Tada[1,2,3], Toshihiro Tada[3], Jumpei Yoshioka[4] (1.Geo-Cosmology Center, Chiba Institute of Technology, 2.Research Center for Earth System Science, Yunnan University, 3.Department of Earth and Planetary Science, the Univeristy of Tokyo, 4.Atmospheric and Ocean Research Institute, the University of Tokyo)

[MIS04-P02] Ejection behavior after hypervelocity oblique impacts in an atmosphere

*Kosuke Kurosawa[1], Ryota Moriwaki[1], Kojiro Suzuki[2], Takafumi Matsui[1] (1.Planetary Exploration Research Center, Chiba Institute of Technology, 2.Department of Advanced Energy, Graduate School of Frontier Sciences, The University of Tokyo)

[MIS04-P03] Shock-induced vitrification affected on cathodoluminescence of quartz: possibility as a shock barometer and its potential application to natural impact samples

*Yu Chang[1], Masahiro KAYAMA[2], Eiichi Tajika[1], Yasuhito Sekine[3], Toshimori Sekine[4], Hirotsugu nishido[5], Takamichi Kobayashi[6] (1.Department of Earth and Planetary Science, Graduate School of Science, The University of Tokyo, 2.Department of General Systems Studies, Graduate School of Arts and Sciences, The University of Tokyo, 3.Earth-Life Science Insitute, Tokyo Institute of Technology, 4.Center for High Pressure Science and Technology Advanced Research, 5.Research Institute of Natural Science, Okayama University of Science, 6.National Institute for Materials Science)

[MIS04-P04] Evaluation of shock deformation of the basement sandstone around the probable impact site of Australasian Tektite Event using synchrotron X-ray diffraction analysis

★Invited Papers

*Toshihiro Tada[1], Masahiro KAYAMA[2], Yu Chang[1], Akira Miyake[3], Yohei Igami[4], Ryuji Tada[1,5,6], Paul A Carling[7], Wickanet Songtham[8], Eiichi Tajika[1] (1.Department of Earth and Planetary Science, The University of Tokyo , 2.Department of Multi-Disciplinary Sciences, The University of Tokyo , 3.Division of Earth and Planetary Sciences, Kyoto University , 4.Institute of Materials and Systems for Sustainability, Nagoya University, 5. Planetary Exploration Research Center, Chiba Institute of Technology, 6.Research Center for Earth System Science, Yunnan University, 7.Geography and Environmental Science, University of Southampton, 8. Northeastern Research Institute of Petrified Wood & Mineral Resources, Nakhon Ratchasima Rajabhat University)

[MIS04-P05] Quaternary stratigraphy and occurrence of the Australasian tektites in Thailand, Laos PDR, and Cambodia: implication of the impact location

*Wickanet Songtham[1], Ryuji Tada[2], Paul A Carling[3], Toshihiro Tada[2], Praphas Chansom[1] (1.Nakhon Ratchasima Rajabhat University, Thailand , 2.The University of Tokyo, Japan, 3.The University of Southampton, United Kingdom)

[MIS04-P06] Assessment for BPCA method as biomass burning proxies and their application to meteorite impact event

*Song Lu[1], Youhei Yamashita[2], Tomohisa Irino[2], Toshihiro Tada[3], Ryuji Tada[3] (1.Graduate School of Environmental Science, Hokkaido University , 2.Faculty of Environmental Earth Science, Hokkaido University, 3.Department of Earth and Planetary Science , Graduate School of Science, The University, of Tokyo)

[MIS04-P07] Converging lines of evidence for burial of the Australasian impact crater within the Bolaven volcanic field, Southern Laos

*Kerry Sieh[1], Jason Herrin[1], Dayana Schonwalder Angel[1], Vanpheng Sihavong[2], Brian Jicha[3], Brad Singer[3], Weerachat Wiwegwin[4], James Daniel Paul Moore[1], Paramesh Banerjee[1], Tawachai Chualaowanich[4], Punya Charusiri[5] (1.Earth Observatory of Singapore, Nanyang Technological University, 639798 Singapore, 2.Department of Geology and Mines, Ministry of Energy and Mines, Vientiane, Lao People's Democratic Republic, 3.Department of Geoscience, University of Wisconsin–Madison, Madison, WI 53706, 4.Department of Mineral Resources, Ministry of Natural Resources and Environment, Ratchatewi, 10400 Bangkok, Thailand, 5.Department of Geology, Chulalongkorn University, Khet Pathumwan, 10330 Bangkok, Thailand)

[E] Poster | M (Multidisciplinary and Interdisciplinary)：M-IS Intersection

[M-IS05] Cenozoic Evolution of the Asian Monsoon and the Indo-Pacific Paleoclimates

convener:Masanobu Yamamoto(Faculty of Environmental Earth Science, Hokkaido University), Steven C Clemens(Brown University), Hongbo Zheng(Research Center for Earth System Science, Yunnan University), Ryuji Tada(Department of Earth and Planetary Science, Graduate School of Science, The Univeristy of Tokyo)

[MIS05-P01] Isotope analysis of Neogene marine sediment from Maldives

*Yuka Tatera[1], Katsuyuki Yamashita[1], Tsuyoshi Ishikawa[2], Mayuri Inoue[1] (1.Okayama University, 2.Kochi Institute for Core Sample Research, JAMSTEC)

[MIS05-P02] Human activities during last 700 years as recorded in the concentrations of polycyclic aromatic hydrocarbons and pentacyclic triterpene methyl ethers in sediment cores from Lake Suigetsu

*Masaya Inagaki[1], Hideto Nakamura[2], Masanobu Yamamoto[1], Takeshi Nakagawa[3] (1.Graduate School of Environmental Science, Hokkaido University, 2.Faculty of Science, Osaka City University, 3.Research Center for Palaeoclimatorogy, Ritsumeikan University)

[MIS05-P03] Reconstruction of paleoclimate changes in the region where the Okhotsk culture flourished over the past 2,700 year

*Ryuichi Seto[1], Osamu Seki[2], Masanobu Yamamoto[3], Takuya Itaki[4] (1.Graduate School of Environmental Science, Hokkaido University, 2.Institute of Low Temperature Science, Hokkaido University, 3.Facility of Environmental Earth Science, Hokkaido University, 4.Geological Survey of Japan, AIST)

[MIS05-P04] Fluvio-sedimentary response to late Quaternary climate at the Himalayan frontal thrust, central Nepal

*Mari Hamahashi[1], Judith Hubbard[1], Samuel Haines[1], Rafael Almeida[2], Edgardo Latrubesse[1], Sanjita Mishra[3], Lewis Owen[4], Soma Nath Sapkota[3] (1.Earth Observatory of Singapore, Nanyang Technological University, 2.Yachay Technical University, Ecuador, 3.Department of Mines and Geology, National Seismological Center, Nepal, 4.North Carolina State University, USA)

[MIS05-P05] Tropical western Pacific hydrology during the last 6000 years based on charcoal records from Borneo

*Masanobu Yamamoto[1], Takafumi Kikuchi[1], Hiromichi Sakurai[1], Ryoma Hayashi[2], Osamu Seki[1], Takafumi Omori[3], Abdullah Sulaiman[4], Hasrizal Shaari[5], Lulie Melling[6] (1.Faculty of Environmental Earth Science, Hokkaido University, 2.Lake Biwa Museum, 3.The University of Tokyo, 4.Minerals and Geoscience Department Malaysia, 5.Universiti Malaysia Terengganu, 6.Tropical Peat Research Institute)

[E] Poster | M (Multidisciplinary and Interdisciplinary)：M-IS Intersection

[M-IS06] Dust

convener:Ishizuka Masahide(Kagawa University), Yasunori Kurosaki(Arid Land Research Center, Tottori University), Thomas Sekiyama(Meteorological Research Institute), Kana Nagashima(Japan Agency for Marine-Earth Science and Technology, Research and Development Center for Global Change)

[MIS06-P01] Detection of aeolian dust in a sedimentary sequence at Tsujita Site

*Haranosono Daichi[1], Shin Toyoda[1], Kenji Nagai[2], Toshirou Naruse (1.Okayama Univesity of Science, 2.Aichi Gakuin University)

[MIS06-P02] Effect of stone on threshold friction velocity in Tsogt-Ovoo, Mongolia: Observation and Model simulation

*Batjargal Buyantogtokh[1], Yasunori Kurosaki[1], Masahide Ishizuka[3], Tsuyoshi T Sekimaya[2], Taichu Y Tanaka[2], Atsushi Tsunekawa[1], Mitsuru Tsubo[1] (1.Arid Land Research Center, Tottori University, 2.Japan Meteorological Agency, Meteorological Research Institute, 3.Faculty of Engineering and Design, Kagawa University, Japan)

[MIS06-P03] Monitoring dry-season vegetation mass at a dust hotspot (Tsogt-Ovoo) in the northern Gobi Desert

*Jing Wu[1], Yasunori Kurosaki[1], Ganatsetseg Batdelger[2], Adrian Chappell[3], Ishizuka Masahide[4], Batjargal Buyantogtokh[1] (1. Arid Land Research Center, Tottori University, 2.Information and Research Institute of Meteorology, Hydrology and Environment, Mongolia, 3.School of Earth and Ocean Science, Cardiff University, UK, 4.Faculty of Engineering and Design, Kagawa University)

[MIS06-P04] Wind tunnel experiment on sand saltation splash by using a high-speed camera

*Ishizuka Masahide[1], Yasunori Kurosaki[2], Hiroaki Hagino[3], Kazuki Nanko[4], Gantsetseg Batdelger[5], Yukio Yasuda[4], Satoru Suzuki[6] (1.Kagawa University, Faculty of Engineering and Design, 2.Tottori University, Arid land research center, 3.Forestry and Forest Products Research Institute, Tohoku Research Center, 4.Forestry and Forest Products Research Institute, Department of Disaster Prevention, Meteorology and Hydrology, 5.Information and Research Institute of Meteorology Hydrology and Environment, Mongolia, 6.Forestry and Forest Products Research Institute, Center for Forest Damage and Risk Management)

[E] Poster | M (Multidisciplinary and Interdisciplinary)：M-IS Intersection

[M-IS07] Aqua planetology

convener:Yasuhito Sekine(Earth-Life Science Insitute, Tokyo Institute of Technology), Hidenori Genda(Earth-Life Science Institute, Tokyo Institute of Technology), Keisuke Fukushi(Institute of Nature & Environmental Technology, Kanazawa University), Tomohiro Usui(Japan Aerospace Exploration Agency)

[MIS07-P01] Isotopic fractionation of methane gas with clathrate hydrate formation under the condition of ice crust / internal ocean boundary in icy satellite

*Kushi Kudo[1], Atsushi Tani[1], Keita Yamada[2], Naohiro Yoshida[2,3] (1.Department of Human Environmental Science, Graduate School of Human Development and Environment, Kobe University, 2.Department of Chemical Science and Engineering, School of Materials and Chemical Technology, Tokyo Institute of Technology, 3.Earth–Life Science Institute, Tokyo Institute of Technology)

[MIS07-P02] Observation of the interface between ice and water under high pressure with gas as a simulation of the bottom of ice crust in icy bodies

*Kenshiro Moriyama[1], Atsushi Tani[1] (1.Department of Human Environmental Science, Graduate School of Human Development and Environment, Kobe University)

[MIS07-P03] H_2-rich hydrothermal environment in the Enceladus' subsurface ocean

*Takazo Shibuya[1], Sota Numaho[1,2], Hisahiro Ueda[1], Sakiko Kikuchi[1], Yutaro Takaya[3], Takuya Saito[1], Mariko Abe[1], Masaru Tomita[2], Ken Takai[1] (1.Japan Agency for Marine-Earth Science and Technology, 2.Keio University, 3.Waseda University)

[MIS07-P04] Abiotic nitrate reduction in hydrothermal environments and nitrogen cycle in early earth

*Manabu Nishizawa[1], Takuya Saito[1], Akiko Makabe[1], Takazo Shibuya[1], Ken Takai[1] (1.Japan Agency for Marine-Earth Science and Technology)

[MIS07-P05] Experimental study of phosphorus dissolution from hydroxyapatite in liquid CO_2

*Kaito Seo[1,2,3], Takazo Shibuya[3], Fujishima Kosuke[4], Ken Takai[3], Masaru Tomita[1,2] (1.Graduate School of Media & Governance, Keio Univ., 2.Inst. Adv. Biosci., Keio Univ., 3.X-Star, JAMSTEC, 4.ELSI, Tokyo Tech)

[MIS07-P06] Effects of minerals on the formose reaction: implication for the potential ribose formation on ancient Mars

*Chinatsu Ono[1], Takeshi Kakegawa[1], Yoshihiro Furukawa[1] (1.Graduate School of Science, Tohoku University)

[MIS07-P07] **Hydrogen generation by water-rock reactions on the early Mars**

*Hisahiro Ueda[1], Takazo Shibuya[1] (1.JAMSTEC)

[MIS07-P08] Impact-generated hydrothermal systems that can promote organic synthesis: Implications for the origin of life

*Kazumu Kaneko[1], Yasuhito Sekine[2], Takazo Shibuya[3], Hisahiro Ueda[3], Natsumi Noda[2,4] (1.Department of Earth and Planetary sciences, School of science, Tokyo Institute of Technology, 2.Earth-Life Science Institute, Tokyo Institute of Technology, 3.Japan Agency foe Marine-Earth Science and Technology, 4.Department of Earth and Planetary science, Graduate School of science, The University of Tokyo)

[MIS07-P09] Clumped isotope signatures of abiotic methane formed via Fischer-Tropsch catalysis and their implications

*ZHANG NAIZHONG[1], YASUHITO SEKINE[1], MAYUKO NAKAGAWA[1], NAOHIRO YOSHIDA[1] (1.Earth-Life Science Institute, Tokyo Institute of Technology)

[MIS07-P10] **Development of novel characterization method for extraterrestrial clay mineral**

*Kosuke Inoue[1], Keisuke Fukushi[2], Koki Morida[3], Hiroki Suga[4], Yoshio Takahashi[4] (1.Kanazawa University , 2.Institute of Nature and Environmental Technology, 3.Graduate School of Science, The University of Kanazawa, 4.Graduate School of Science, The University of Tokyo)

[MIS07-P11] Evolution of aqueous environment on Early Mars inferred from reconstructed water chemistry at Gale

*Keisuke Fukushi[1], Yasuhito Sekine[2,1] (1.Institute of Nature & Environmental Technology, Kanazawa University, 2.Earth-Life Science Institute, Tokyo Institute of Technology)

[MIS07-P12] Effective formation of Al-rich surface clays through acidic water activity on early Mars

*Mitsuteru Sugiuchi[1], Yasuhito Sekine[2], Shuya Tan[2,3], Natsumi Noda[2,3], Yoshio Takahashi[3], Ramses M Ramirez[2] (1.Department of Earth and Planetary Science, School of Science, Tokyo Institute of Technology, 2.Earth-Life Science Institute, Tokyo Institute of Technology, 3.Department of Earth and Planetary Science, Graduate School of Science, The University of Tokyo)

[MIS07-P13] **The Preparation for Return Sample from Asteroid Ryugu by STXM at KEK-PF**

*Hiroki Suga[1,2], Sakiko Kikuchi[3], Shuya Tan[1,4], Shohei Yamashita[2], Yasuo Takeichi[2], Daisuke Wakabayashi[2], Masao Kimura[2], Yoshio Takahashi[1,2], Yasuhito Sekine[4] (1.Graduate School of Science, The University of Tokyo., 2.Institute of Materials Structure Science, High Energy Accelerator Research Organization (KEK)., 3.Institute for Extra-cutting-edge Science and Technology Avant-garde Research (X-star), Japan Agency for Marine-Earth Science and Technology (JAMSTEC)., 4.Earth-Life Science Institute (ELSI), Tokyo Institute of Technology.)

[MIS07-P14] Clustering analysis of Ryugu spectral data obtained by NIRS3 infrared spectrometer onboard Hayabusa2 spacecraft

*Moe Matsuoka[1], Hikaru Iwamori[2], Deborah Lolin Domingue[3], Tomohiro Usui[1], Kohei Kitazato[4], Takahiro Iwata[1] (1.ISAS/JAXA, 2.Earthquake Research Institute, the University of Tokyo, 3.Planetary Science Institute, 4.University of Aizu)

[MIS07-P15] Recognition and classification of Martian chaos terrains using imagery machine learning

*Hiroki Shozaki[1], Yasuhito Sekine[2], Nicholas Guttenberg[2,3] (1.Tokyo Institute of Technology, School of Science, Dept. of Earth and Planetary Sciences, 2.Earth-Life Science Insitute, Tokyo Institute of Technology, 3.Cross Compass Ltd.)

[MIS07-P16] Reactive iron supply control dominant sulfur species in the limestones of Ediacaran Doushantuo and Dengying Formations

*Fumihiro Matsuura[1], Ryoichi Nakada[2], Yuichiro Ueno[3,2], Yusuke Sawaki[4], Masafumi Saitoh[5], Kajitani Iori[4], Tomohiro Usui[1] (1.JAXA, 2.JAMSTEC, 3.Tokyo Tech, 4.The University of Tokyo, 5.University of Lausanne)

[MIS07-P17] New sulfur isotopes 1-D photochemical model for revealing early earth's atmosphere

*Yoshiaki Endo[1,2], Mark W. Claire[2], Chester E. Harman[2,3], Laura Crick[2] (1.Tokyo Institute of Technology, 2.University of St Andrews, 3.NASA Ames Research Center)

[MIS07-P18] Retrieval of vertical structure in the Martian atmosphere during 2007 global dust storm by OMEGA/MEx limb observation

*Risei Kogure[1], Arnaud Mahieux[2,3], Hiromu Nakagawa[1], Shohei Aoki[2], Yasumasa Kasaba[1], Nao Yoshida[1] (1.TOHOKU University, 2.Belgian Institute for Space Aeronomy (BIRA-IASB), 3.University of Texas at Austin, USA)

[MIS07-P19] Numerical experiments of climate of early Mars by the use of DCPAM

*Masaki Ishiwatari[1], Yoshiyuki O. Takahashi[2], George L. Hashimoto[3], Kiyoshi Kuramoto[1], Yoshi-Yuki Hayashi[2] (1.Department of Cosmosciences, Graduate school of Science, Hokkaido University, 2.Department of Planetology, Graduate School of Science, Kobe University, 3.Department of Earth Sciences, Faculty of Science, Okayama University)

[MIS07-P20] Habitable zone for a planet with a small amount of water on its surface

*Takanori Kodama[1], Hidenori Genda[2], Ryouta O'ishi[3], Ayako Abe-Ouchi[3] (1.University of Bordeaux, 2.Earth-Life Science Institute, Tokyo Institute of Technology, 3.Atmosphere and Ocean Research Institute, University of Tokyo)

[MIS07-P21] Formation region of volatile-rich asteroids inferred from nucleosynthetic isotope variations in carbonaceous chondrites

*Ryota Fukai[1], Sota Arakawa[2] (1.Japan Aerospace Exploration Agency, 2.National Astronomical Observatory of Japan)

[E] Poster | M (Multidisciplinary and Interdisciplinary)：M-IS Intersection

[M-IS08] Paleoclimatology and paleoceanography

convener:Yusuke Okazaki(Department of Earth and Planetary Sciences, Graduate School of Science, Kyushu University), Benoit Thibodeau(University of Hong Kong), Akitomo Yamamoto(Japan Agency for Marine-Earth Science and TechnologyAtmosphere and Ocean Research Institute), Hitoshi Hasegawa(Faculty of Science and Technology, Kochi University)

[MIS08-P01] Reconstruction of the climate condition in the Carnian from bedded chert by using a new index of chemical weathering

*Tenichi Cho[1] (1.Waseda University)

[MIS08-P02] Response of Climate and Water Cycle to Atmospheric CO2; Cretaceous vs. Modern

*Taro Higuchi[1], Ayako Abe-Ouchi[1], Wing-Le Chan[1] (1.Atmospheric and Ocean Research Institute, the University of Tokyo)

[MIS08-P03] Enhanced dinoflagellate productivity by ocean stratification and eutrophication in the Anthropocene, Miocene, and Cretaceous

★Invited Papers

*Takuto Ando[1], Ken Sawada[2] (1.Estuary Research Center, Shimane University, 2.Faculty of Science, Hokkaido University)

[MIS08-P04] Study on productivity feedback during the recovery phases of early Eocene hyperthermals: Comparison between the central North Pacific Ocean and southern Indian Ocean

★Invited Papers

Koshiro Sato[1], *Kazutaka Yasukawa[1,2], Junichiro Ohta[1,2], Keishiro Azami[1], Kentaro Nakamura[1], Koichiro Fujinaga[2,1], Minoru Ikehara[3], Yasuhiro Kato[1,2] (1.School of Engineering, The University of Tokyo, 2.ORCeNG, Chiba Institute of Technology, 3.Center for Advanced Marine Core Research, Kochi University)

[MIS08-P05] Sulfur isotope ratios in co-occuring barite and carbonate from Eocene sediments: A comparison study

*Kotaro Toyama[1], Adina Paytan[2], Ken Sawada[3], Takashi Hasegawa[4] (1.The University of Tokyo, 2.UCSC, 3.Hokkaido Univ., 4.Kanazawa Univ.)

[MIS08-P06] Late Eocene travertine in the SE Tibet and cyclical change in its isotopic composition implying the monsoon climate

*Aki Sakuma[1], Hirokazu Kato[1], Yoshihiro Kakizaki[1], Akihiro Kano[1], Ryuji Tada[2,3], Hongbo Zheng[2] (1.Department of Earth and Planetary Science, School of Science, the University of Tokyo, 2.Yunnan University, 3.Chiba Institute of Technology)

[MIS08-P07] **Reconciling marine influences in the Eastern Siwaliks through the use of biomarkers and reconstructing the Miocene-Pliocene closure of Himalayan Foreland Basin**

*Biswajit Roy[1], Sohom Roy[1], Sambit Ghosh[1], Prasanta Sanyal[1] (1.Indian Institute of Science Education Research Kolkata)

[MIS08-P08] The paleo ocean temperature recorded in carbonate clumped isotope of early Pleistocene fish otolith fossils from the Dainichi Formation of the Kakegawa Group, Shizuoka

*Hirokazu Kato[1], Shota Amekawa[1], Akihiro Kano[1] (1.Department of Earth and Planetary Science, The University of Tokyo)

[MIS08-P09] **Orbital–scale paleoceanographic changes around the Pacific side of Japan in Early Pleistocene based on calcareous nannofossil records**

*Daisuke Kuwano[1], Koji Kameo[1], Yoshimi Kubota[2], Kanako Mantoku[2], Masayuki Utsunomiya[3], Makoto Okada[4] (1.Chiba University, 2.National Museum of Nature and Science, 3.Geological Survey of Japan, AIST, 4.Ibaraki Uviversity)

[MIS08-P10] Sea-ice history in the central Okhotsk Sea based on diatom assemblages during the Middle Pleistocene Transition

Araki Eisuke[1], *Yusuke Okazaki[1], Lo Li[2] (1.Department of Earth and Planetary Sciences, Graduate School of Science, Kyushu University, 2.Department of Geosciences, National Taiwan University)

[MIS08-P11] Millennial-scale hydrographic changes in the northwestern Pacific during marine isotope stage 19: Teleconnections with ice melt in the North Atlantic

★Invited Papers

*Yuki Haneda[1], Makoto Okada[2], Yoshimi Kubota[3], Yusuke Suganuma[1] (1.National Institute of Polar Research, 2.Department of Earth Science, College of Science, Ibaraki University, 3.National Museum of Nature and Science)

[MIS08-P12] Influence of Southern Ocean Intermediate water on the South Pacific's thermocline during the last ~500 Ka

*RAUL TAPIA[1,3], Sze Ling Ho[1], Nele Meckler[2], Dirk Nürnberg[3] (1. Institute of Oceanography, National Taiwan University, Taipei, Taiwan, 2.Bjerknes Centre for Climate Research and Department of Earth Science, University of Bergen, Norway, 3.GEOMAR – Helmholtz Centre for Ocean Research Kiel, Kiel, Germany)

[MIS08-P13] Simulating selected time intervals during the Quaternary using MIROC-ES2L earth system model in comparison with paleo-proxy data

★Invited Papers

*Rumi Ohgaito[1], Akitomo Yamamoto[1], Tomohiro Hajima[1], Manabu Abe[1], Hiroaki Tatebe[1], Michio Kawamiya[1], Ayako Abe-Ouchi[2,3,1] (1.Japan Agency for Marine-Earth Science and Technology, 2.U. Tokyo, AORI, 3.NIPR)

[MIS08-P14] Fossil diatom records from IODP Exp. 382 Sites U1536 and U1538 (preliminary results)

*Yuji Kato[1], Michael E. Weber[2], Maureen E. Raymo[3], Trevor Williams[4], - The IODP Expedition 382 Scientists (1.Center for Advanced Marine Core Research, Kochi University, 2.University of Bonn, Germany, 3.Lamont-Doherty Earth Observatory of Columbia University, USA, 4.International Ocean Discovery Program, Texas A&M University, College Station, USA)

[MIS08-P15] Variations of the North and South Pacific Subtropical Gyres over the past 400 kyrs

*Furukawa Keisuke[1], Osamu Seki[2] (1.Graduate School of Environmental Science, Hokkaido University, 2.Institute of Low Temperature Science, Hokkaido University)

[MIS08-P16] Paleovegetation and paleoenvironmental changes in the northern Mongolia since MIS 3 (preliminary results)

*Ryosuke Imaoka[1], Koji Shichi[2], Hitoshi Hasegawa[1], Niiden Ichinnorov[3], Nagayoshi Katsuta[4], Davaasuren Davaadorj[5], Masafumi Murayama[1], Miho Sasaoka[1], Masao Iwai[1] (1.Kochi University, 2.Forestry and Forest Products Research Institute, 3.Mongolian Academy of Sciences, 4.Gifu University, 5.National University of Mongolia)

[MIS08-P17] Constraining the magnitude and spatial pattern of low-to-mid latitudes western Pacific ocean temperature changes in the past 25 kyr

*Sze Ling Ho[1], Sicheng Le[1], Ren Yi Ooi[1], RAUL TAPIA[1], Da-Cheng Lin[2], Min-Te Chen[2], Yuan-Pin Chang[3], Masanobu Yamamoto[4], Liang-Jian Shiau[2,5], Chuan-Chou Shen[6], Pai-Sen Yu[7] (1.Institute of Oceanography, National Taiwan University, Taipei, Taiwan., 2.Institute of Applied Geosciences, National Taiwan Ocean University, Keelung, Taiwan, 3.Department of Oceanography, National Sun Yat-sen University, Kaohsiung, Taiwan, 4.Faculty of Environmental Earth Science, Hokkaido University, Sapporo, Japan, 5.Exploration and Development Research Institute, CPC Corporation, Miaoli, Taiwan, 6.High-Precision Mass Spectrometry and Environment Change Laboratory (HISPEC), Department of Geosciences, National Taiwan University, Taipei, Taiwan, 7.Taiwan Ocean Research Institute, NARLabs, Kaohsiung, Taiwan)

[MIS08-P18] Changes in oceanic carbon and oxygen cycle during Heinrich event

*Akitomo Yamamoto[1], Ayako Abe-Ouchi[2] (1.Japan Agency for Marine-Earth Science and TechnologyAtmosphere and Ocean Research Institute, 2.Atmosphere and Ocean Research Institute, The University of Tokyo)

[MIS08-P20] Stalagmite evidence for ^{18}O-depleted surface water of Japan Sea during the last glacial

*Shota Amekawa[1], Kenji Kashiwagi[2], Masako Hori[3], Tomomi Sone[4], Hirokazu Kato[1], Tomoyo Okumura[5], Tsai-Luen Yu[6], Chuan-Chou Shen[6,7,8], Akihiro Kano[1] (1.Graduate School of Science, The University of Tokyo, 2.Department of Environmental Biology and Chemistry, Faculty of Science, University of Toyama, 3.Division of Natural Sciences, Osaka Kyoiku University, 4.Marine Works Japan LTD., 5.Center for Advanced Marine Core Research, Kochi University, 6.High-precision Mass Spectrometry and Environment Change Laboratory (HISPEC), Department of Geosciences, National Taiwan University, 7.Global Change Research Center, National Taiwan University, 8.Research Center for Future Earth, National Taiwan University)

[MIS08-P21] Biogenic opal changes at the Kamchatka Strait in the Bering Sea since the last glaciation

*Koshiro Matsuo[1] (1.Department of Earth and Planetary Sciences, Graduate School of Science, Kyushu University)

[MIS08-P22] Intermediate water formation in the Bering Sea since the last glacial maximum based on *Cycladophora davisiana* abundances.

*Kento Ogata[1], Yusuke Okazaki[1] (1.Kyushu university Earth and Planetary sciences)

[MIS08-P23] Analysis from Benthic foraminifera populations of expansion and intensify of the northwestern Pacific oxygen minimum zone during the last deglaciation

*Keisuke Sakai[1], Ken'ichi Ohkushi[1], Akihiko Shibahara[2] (1.Graduate School of Human Development and Environment, Kobe University, 2.Fukui Prefectural University Institute of Dinosaur Research)

[MIS08-P24] Changes in carbon and oxygen isotopes of benthic foraminifera in the East China Sea since the last glacial maximum

*Miki Muranaka[1], Yusuke Okazaki[2], Yoshimi Kubota[3] (1.Department of Earth and Planetary Sciences, Kyushu University, 2.Department of Earth and Planetary Sciences, Graduate School of Science, Kyushu University, 3.National Museum of Nature and Science)

[MIS08-P26] **Southward Migration of Inter-Tropical Convergence Zone (ITCZ) during Mid-Late Holocene: New Evidence from Sri Lanka**

*Kasun Gayantha[1], Patrick Roberts[2], Joyanto Routh[3], Achim Brauer[4], Rohana Chandrajith[5], Oshan Wedage[2], Florian Ott[2], Gerd Gleixner[1] (1.Max Planck Institute for Biogeochemistry, Jena, Germany, 2.Max Planck Institute for the Science of Human History, Jena, Germany, 3.TEMA-M, Linköping University, Linköping, Sweden, 4.GFZ, Potsdam, Germany, 5.Department of Geology, University of Peradeniya, Sri Lanka)

[MIS08-P27] Diatom and Chrysophyceae Assemblages from the Holocene Alluvial Core Sediments at Southern and Western Coasts of Korea Peninsula

*Kaoru Kashima[1], Yu Fukumoto[3], Sangheon Yi[2], Dong-Yoon Yang[2], Min Han[2] (1.Department of Earth and Planetary Sciences, Kyushu University, 2.Korea Institute of Geoscience & Mineral Resources (KIGAM) , 3.Ritsumeikan University)

[MIS08-P28] Correlation between stable isotope ratio of pollen and climate, as well as its possible application for paleoclimatology

*Yamasaki Akiteru[1], Keitaro Yamada[2], Takayuki Omori[3], Ikuko Kitaba[2], Takeshi Nakagawa[2] (1.Fukui Prefectural Satoyama-Satoumi Reserch Institute, 2.Research Centre for Palaeoclimatology, Ritsumeikan University, 3.The University museum, The University of Tokyo)

[MIS08-P29] Uncertainty of tree-ring based temperature reconstruction: Effects of soil moisture environment and air pollution on reconstruction records

*Shunsuke Tei[1], Shinya Takano[1], Teppei J Yasunari[1] (1.Arctic Research Center, Hokkaido University)

[MIS08-P30] Horizontal distribution of diatoms in the western Bering Sea surface waters

*Aika Yamamoto[1], Yusuke Okazaki[2] (1.Department of Earth and Planetary Sciences, Kyushu University, 2.Department of Earth and Planetary Sciences, Graduate School of Science, Kyushu University)

[MIS08-P31] Spatio-temporal variations in fossil coral assemblages in late Middle Pleistocene limestones of the Minatogawa Formation, southern Okinawa-jima, Japan

*Riho Tomatsu[1], Marc Humblet[1], Kazuhiko Fujita[2], Yui Kouketsu[1], Yasufumi Iryu[3] (1.Graduate School of Environmental Studies, Nagoya University, 2.Department of Physics and Earth Sciences, University of the Ryukyus, 3.Institute of Geology and Paleontology Graduate School of Science Tohoku University)

[E] Poster | M (Multidisciplinary and Interdisciplinary)：M-IS Intersection

[M-IS09] Interdisciplinary studies on pre-earthquake processes

convener:Katsumi Hattori(Department of Earth Sciences, Graduate School of Science, Chiba University), Dimitar Ouzounov(Center of Excellence in Earth Systems Modeling & Observations (CEESMO) , Schmid College of Science & Technology Chapman University, Orange, California, USA), Jann-Yenq LIU(Department of Space Science and Engineering, National Central University, Taiwan), Qinghua Huang(Peking University)

[MIS09-P01] FORMOSAT-7/COSMIC-2 observing seismo-ionospheric precursors of the 14 November 2019 M7.1 Indonesia Earthquake

*JANN-YENQ Liu[1,2], CHIYEN LIN[1,2], FU-YUAN CHANG[1,2], Yuh-Ing Chen[3] (1.Center for Astronautical Physics and Engineering, National Central University, Taiwan, 2.Department of Space Science and Engineering, National Central University, Taiwan, 3.Graduate Institute of Statistics, National Central University, Taiwan)

[MIS09-P02] Statistical Analysis of Pre-Seismic Ionospheric Anomalies and their Characteristic

*Sanaka Saito[1], Chie Yoshino[1], Katsumi Hattori[1] (1.Chiba University)

[MIS09-P03] **Pre-earthquake early-warning signals of ULF geoelectric data and their earthquake forecasting probability: A case of Kakioka, Japan**

★Invited Papers

*Hong-Jia Chen[1], Katsumi Hattori[1], Ryo Takahira[1] (1.Chiba University)

[MIS09-P04] Numerical simulation of ULF electromagnetic wave propagation in the lithosphere associated with earthquakes by using the WLP-FDTD method

*Ryota Kimura[1], Yoshiaki Ando[1], Katsumi Hattori[2] (1. The University of Electro-Communications, 2.Chiba University)

[MIS09-P05] **Geomagnetic *Sq* equivalent currents variation characters in the 210°mm meridian region**

*Xiaocan Liu[1], Katsumi Hattori[2,3], Huaran Chen[1], Peng Han[4], Chie Yoshino[2], Xudong Zhao[1] (1.Institute of geophysics China Earthquake Administrition, 2.Graduate School of Science, Chiba University, Chiba, Japan, 3.Center for Environmental Remote Sensing, Chiba University, Chiba, Japan, 4.Department of Earth and Space Sciences, Southern University of Science and Technology, ShenZhen, China)

[MIS09-P06] Measurement of vertical distribution of environmental radiation using a drone at Choshi

*Tohru Okabayashi[1], Kiyotaka Ninagawa[2], Isao Yamamoto[2], Nobuhiro Maeda (1.Chiba Institute of Science, 2.Okayama University of Science)

[MIS09-P07] Ground Rn flux anomaly and crustal activity around Asahi station, Boso Peninsula, Japan

*Haruna Kojima[1], Chie Yoshino[1], Katsumi Hattori[1], Michikuni Shimo[2], Toshiharu Konishi[3], Ryuichi Furuya[4] (1.Chiba University, 2.Fujita Health University, 3.OHYO KOKEN KOGYO Co.,Ltd, 4.COM SYSTEM Inc.)

[MIS09-P08] **The Study of Sq Equivalent Current during the Solar Cycle**

*Xudong Zhao[1] (1.Institute of Geophysics, China Earthquake Administration)

[MIS09-P09] Development of 3D self-potential tomography and electro-kinetic effects

*ayaka ishikawa[1], Katsumi Hattori[1] (1.chiba university)

[MIS09-P10] Application of Multi-channel Spectrum Analysis (MSSA) in noise reduction to MT data observed at Boso Peninsula in Japan

*Shu Kaneko[1], Katsumi Hattori[2], Toru Mogi[2], Chie Yoshino[2] (1.Chiba University Graduate School of Science and Engineering, 2.Chiba University Graduate School of Science)

[MIS09-P11] Development of Ionospheric Electron density tomography using linear regularization.

*Sanaka Saito[1], Rui Song[1], Katsumi Hattori[1] (1.Chiba University)

[E] Poster | M (Multidisciplinary and Interdisciplinary)：M-IS Intersection

[M-IS10] Coupling between the atmosphere, ionosphere and magnetosphere above thunderstorms

convener:Pasko Victor P(Pennsylvania State University Main Campus), Yukihiro Takahashi(Department of Cosmosciences, Graduate School of Science, Hokkaido University), Mitsuteru Sato(Department of Cosmoscience, Hokkaido University), Teruaki Enoto(RIKEN)

[MIS10-P01] Thunder Cloud Project : Ground-based multipoint radiation measurement campaign of high-energy atmospheric phenomena

*Teruaki Enoto[1], Yuuki Wada[2,1], Takayuki Yuasa, Yuko Ikkatai[2], Kazuhiro Nakazawa[3], Shohei Hisadomi[3], Yuna Tsuji[3], Harufumi Tsuchiya[4,1], Takeshi Morimoto[5], Yoshitaka Nakamura[6], Masashi Kamogawa[7], Yousuke Sato[8] (1.RIKEN, 2.The University of Tokyo, 3.Nagoya University, 4.Japan Atomic Energy Agency, 5.KINDAI Univeristy , 6.Kobe City College of Technology , 7.University of Shizuoka, 8.Hokkaido University)

[MIS10-P02] The Contribution of Lightning and Precipitation Currents to the Global Atmospheric Electric Circuit

Bandholnopparat Kittanapat[1], *Mitsuteru Sato[1], Yukihiro Takahashi[1], Kamogawa Masashi[2] (1.Department of Cosmoscience, Hokkaido University, 2.Global Center for Asian and Regional Research, Univ. of Shizuoka)

[MIS10-P03] Photodetachment of electrons at sprite altitudes by molecular nitrogen emissions as a mechanism of initiation of sprite streamers

*Victor P Pasko[1], Reza Janalizadeh[1] (1.Pennsylvania State University Main Campus)

[E] Poster | M (Multidisciplinary and Interdisciplinary)：M-IS Intersection

[M-IS11] Expedition Earth: discovering our planet's past and future through scientific drilling

convener:Junichiro Kuroda(Department of Ocean Floor Geoscience, Atmosphere and Ocean Research Institute, the University of Tokyo), Katsuyoshi Michibayashi(Department of Earth and Planetary Sciences, Nagoya University), Kohtaro Ujiie(Graduate School of Life and Environmental Sciences, University of Tsukuba), Clive Robert Neal(University of Notre Dame)

[MIS11-P01] Monsoon-influenced variations in calcareous and siliceous plankton community structure and upper- water column stratificatio of the western Bay of Bengal during the past 80 kyr

★Invited Papers

*Yuki Ota[1], Hodaka Kawahata[2,3,1], Junichiro Kuroda[2,3], Atsushi Suzuki[1], Toyoho Ishimura[4] (1.National Institute of Advanced Industrial Science and Technology, 2.Atmosphere and Ocean Research Institute, The University of Tokyo, 3.Department of Earth and Planetary Science, The University of Tokyo, 4.National Institute of Technology, Ibaraki College)

[MIS11-P02] Preliminary results of IODP Exp. 382: Iceberg Alley and Subantarctic Ice and Ocean Dynamics

*Yuji Kato[1], Osamu Seki[2], Mutsumi Iizuka[2], Masanobu Yamamoto[3], Michael E. Weber[4], Maureen E. Raymo[5], Victoria L. Peck[6], Trevor Williams[7], - The IODP Expedition 382 Scientists (1.Center for Advanced Marine Core Research, Kochi University, 2.Institute of Low Temperature Science, Hokkaido University, 3.Faculty of Environmental Earth Science, Hokkaido University, 4.University of Bonn, Germany, 5.Lamont-Doherty Earth Observatory of Columbia University, USA, 6.British Antarctic Survey, UK, 7.International Ocean Discovery Program, Texas A&M University, College Station, USA)

[MIS11-P03] Osmium isotopic composition and platinum group element abundances of Cretaceous-Paleogene boundary section at Site U1514C on the Mentelle Basin, SW Australia

Hayu Ota[1], *Junichiro Kuroda[2,3], Maria Luisa Tejada[3], IOPD Exp 369 Shipboard Science Party (1.University of Tsukuba, 2.AORI, University of Tokyo, 3.JAMSTEC)

[MIS11-P04] Short-term environmental disturbance of early Turonian (Cretaceous) in southern high latitude : Insights from organic geochemistry

*Yusuke Takagi[1], Yukina Takeda, Kengo Sadami, Akiko S. Goto[2], Takashi Hasegawa[2] (1.Earth Science Course School of Natural System, College of Science and Engineering, Kanazawa University, 2.Faculty of Geoscience and Engineering, Institute of Science and Engineering, Kanazawa University)

[MIS11-P05] Neogene Kuroshio variability and evolution of the North Pacific subtropical gyre

*Yusuke Okazaki[1] (1.Department of Earth and Planetary Sciences, Graduate School of Science, Kyushu University)

[MIS11-P06] SCORE Drilling: Preliminary results of Expedition 912-Leg 1 at Tokai, Nankai Trough, southwest Japan

*KanHsi Hsiung[1], Toshiya Kanamatsu[1], Ken Ikehara[2], Io Miura[3], Juichiro Ashi[3], Shuichi Kodaira[1], Kohsaku Arai[2], Natsumi Okutsu[1], Kan Aoike[1] (1.Japan Agency for Marine-Earth Science and Technology, 2.Institute of Geology and Geoinformation, National Institute of Advanced Industrial Science and Technology, 3.The Atmosphere and Ocean Research Institute, The University of Tokyo)

[MIS11-P07] Analytical method of noble gases using cuttings to understand distribution and origin of noble gases in accretionary prism in precise -

*Tomohiro Toki[1], Shugo Kurahashi[1], Naoto Takahata[2], Yuji Sano[2,3] (1.Faculty of Science, University of the Ryukyus, 2.Atmosphere and Ocean Research Institute, The University of Tokyo, 3.Institute of Surface-Earth System Science, Tianjin University)

[MIS11-P08] Variation of pore water geochemistry across the mass transport deposits off Cape Erimo, Hokkaido, Japan

*Sara Fujiwara[1], Hitoshi Tomaru[1] (1.Chiba University)

[MIS11-P09] 3.1Ga Banded Iron Formation drilling: DXCL drilling project in the coastal Pilbara terrane in Australia

*Shoichi Kiyokawa[1], Takashi Ito[2], Minoru Ikehara[3], Kosei E. Yamaguchi[4], Kohei Ishikawa[1], Mami Takehara[5], Kenji Horie[5] (1.Department of Earth and Planetary Sciences Faculty of sciences, Kyuushu University, 2.Faculty of Education, Ibaraki University , 3.Center for Advanced Marine Core Research, Kochi University, 4. Toho University and NASA Astrobiology Institute, 5.National Institute of Polar Research)

[MIS11-P10] In-situ crustal stress measurement in inland Japan - Applications of DCDA method to rock core samples from NIED seismic observation wells -

*Kentaro Omura[1], Akio Funato[2], Takatoshi Ito[3] (1.National Research Institute for Earth Science and Disaster Resilience, 2.Fukada Geological Institute, 3.Institute of Fluid Science, Tohoku University)

[MIS11-P11] Rock magnetic properties, grain size, and layer thickness of turbidites at the northern Hikurangi margin, New Zealand: Results from IODP Exp. 375, Site U1520

*Atsushi Noda[1], Annika Greve[2] (1.National Institute of Advanced Industrial Science and Technology, 2.Department of Earth Sciences, Utrecht University, The Netherlands)

[MIS11-P13] An attempt to integrate 3D seismic and borehole datasets: construction of a 3D geomechanical model at the Nankai Trough, SW Japan.

*Yasuhiro Yamada[1,2,3], Adam Wspanialy[1], Kazuya Shiraishi[1] (1.Japan Agency for Marine-Earth Science and Technology (JAMSTEC), 2.Kochi University, 3.Royal Holloway University of London)

[MIS11-P14] A Perspective of the Mantle Drilling and Observatory Initiative

*Nan XIAO[1], Natsue Abe[1], Yasuhiro Yamada[1], Fumio Inagaki[1] (1.Japan Agency for Marine Earth Science and Technology)

[MIS11-P15] **Learning Lessons is Key to the Success in Future Scientific Ocean Drilling**

*KYAW MOE[1] (1.Japan Agency for Marine-Earth Science and Technology)

[MIS11-P16] **The upcoming IODP Japan Trench Paleoseismology Expedition: New perspectives from tracking past earthquakes in the sedimentary record**

*Michael Strasser[1], Ken Ikehara[2], Carol J. Cotterill[3], Lena Maeda[4] (1.University of Innsbruck, Austria, 2.Institute of Geology and Geoinformation, National Institute of Advanced Industrial Science and Technology, Japan, 3.British Geological Survey, U.K., 4.JAMSTEC Japan Agency for Marine-Earth Science and Technology)

[E] Poster | M (Multidisciplinary and Interdisciplinary)：M-IS Intersection

[M-IS12] Developments and applications of XRF-core scanning techniques in natural archives

convener:Huang Jyh-Jaan Steven(Institute of Geology, University of Innsbruck), Atsuko Amano(National institute of Advanced Industrial Science and Technology), Masafumi MURAYAMA(Faculty of Agriculture and Marine Science, Kochi University), Liang-Chi Wang(National Chung Cheng University)

[MIS12-P01] Reconstruction of variations in South Pacific westerly jet path during the last glacial

★Invited Papers

*Hitoshi Hasegawa[1], Fuyu Nagaya[1], Kana Nagashima[2], Nagayoshi Katsuta[3], Masafumi MURAYAMA[1], Naomi Harada[2] (1.Kochi University, 2.JAMSTEC, 3.Gifu University)

[MIS12-P03] The chemical composition and temporal change of varve-like sediment in Beppu Bay.

*Yoshiaki Suzuki[1], Michinobu Kuwae[2], Ken Ikehara[1], Kazuno Arai[3], Masafumi MURAYAMA[3] (1.National Institute of Advanced Industrial Science and Technology, 2.Ehime Univ., 3.Kochi Univ.)

[MIS12-P04] Change of depositional environment in Lake Tazawa estimated by X-ray fluorescence core scanner

*Yoko Ishiyama[1], Daizo Ishiyama[1], Kazuyoshi Yamada[2], Masafumi MURAYAMA[3], Takeshi Hayashi[4] (1.Graduate School of International Resource Sciences, Akita University, 2.Museum of Natural and Environmental History, Shizuoka, 3.Center for Advanced Marine Core Research, Kochi University, 4.Faculty of Education and Human Studies, Akita University)

[MIS12-P05] **Multiproxies applied on sediment core for revealing the environmental changes and natural disaster events in Lake Kitaura, central Japan**

Huei-Fen Chen[1], Jun-You Wu[1], *Liang-Chi Wang[2], Hao-Yang Lee[3], Jyh-Jaan Steven Huang[4], Nobuyoshi Yamashita[5], Tomonori Naya[6] (1.Institute of Earth Sciences, National Taiwan Ocean University, Taiwan, R.O.C, 2.Department of Earth and Environmental Sciences, National Chung Cheng University, Taiwan, R.O.C., 3.Institute of Earth Sciences, Acedemia Sinica, Taiwan, R.O.C., 4.Department of Geology, University of Innsbruck, Austria, 5.Research Institute for Environmental Management, AIST, Japan, 6.Institute of Geology and Geoinformation, Geological Survey of Japan, AIST, Japan)

[MIS12-P06] Detecting the seismo-turbidites of off Kumano, the Nankai Trough using ITRAX profile

*Natsumi Okutsu[1], Juichiro Ashi[2], Rina Fukuchi[3], Asuka Yamaguchi[2] (1.Japan Agency for Marine-Earth Science and Technology, 2.Atmosphere and Ocean Research Institute, The University of Tokyo, 3.Dia consultants Ltd.)

[MIS12-P07] **Multivariate statistical and multi-proxy constraints on earthquake-triggered sediment remobilization processes in the central Japan Trench**

Tobias Schwestermann[1], *Jyh-Jaan Steven Huang[1,5], J. Konzett[2], A. Kioka[3], G. Wefer[4], Ken Ikehara[5], J. Moernaut[1], T.I. Eglinton[6], M. Strasser[1,4] (1.Institute of Geology, University of Innsbruck, 2.Institute of Mineralogy and Petrography, University of Innsbruck, 3.Department of Earth Resources Engineering, Kyushu University, 4.MARUM – Center for Marine Environmental Sciences, University of Bremen, 5.Geological Survey of Japan, National Institute of Advanced Industrial Science and Technology (AIST), 6.Geological Institute, ETH Zürich)

[MIS12-P09] Comparison of element profiles obtained from Itrax-XRF core scanner in evaluating data quality among laboratories used by geological reference material.

*Atsuko Amano[1], Jyh-Jaan Steven Huang[2], Ken Ikehara[1], Masafumi MURAYAMA[3], Takuya Matsuzaki[3] (1.National institute of Advanced Industrial Science and Technology, 2.University of Innsbruck, 3.Kochi University)

[E] Poster | M (Multidisciplinary and Interdisciplinary)：M-IS Intersection

[M-IS13] Integrated Analysis of Geoscience Observations from the Floor to Surface of the Ocean

convener:Keisuke Ariyoshi(Japan Agency for Marine-Earth Science and Technology), Joan S Gomberg(USGS Earthquake Science Center), Narumi Takahashi(National Research Institute for Earth Science and Disaster Resilience), Motoyuki Kido(International Research Institute for Disaster Science, Tohoku University)

[MIS13-P01] Launch of GNSS-Acoustic observation for horizontal and vertical movements off Nemuro using a triangular PXP array with an optional centered-PXP.

*Yukiho Kimura[1], Motoyuki Kido[2], Yusaku Ohta[1], Chie Honsho[1], Fumiaki Tomita[3] (1.Graduate School of Science, Tohoku University , 2.International Research Institute of Disaster Science, Tohoku University, 3.JAMSTEC)

[MIS13-P02] A study on the effects of sea surface height and density of sea water on bottom pressure off the southeastern coast of Hokkaido, Japan after El Nino events using a high-spatial-resolution ocean assimilation data

*Takuya Hasegawa[1,2], Akira Nagano[1], Keisuke Ariyoshi[1], Toru Miyama[1], Hiroyuki Matsumoto[1], Masahide Wakita[1] (1.JAMSTEC, 2.Tohoku University)

[MIS13-P03] Bottom Pressure Variation in Association with the 2017-Present Large-meander of the Kuroshio South of Japan

*Akira Nagano[1], Yusuke Yamashita[2], Keisuke Ariyoshi[1], Takuya Hasegawa[1,4], Hiroyuki Matsumoto[1], Masanao Shinohara[3] (1.JAMSTEC Japan Agency for Marine-Earth Science and Technology, 2.Kyoto University, 3.The University of Tokyo, 4.Tohoku University)

[E] Poster | M (Multidisciplinary and Interdisciplinary)：M-IS Intersection

[M-IS14] Evolution of Pelagic Realm

convener:Atsushi Matsuoka(Department of Geology, Faculty of Science, Niigata University), Toshiyuki Kurihara(Graduate School of Science and Technology, Niigata University), Tetsuji Onoue(Department of Earth and Planetary Sciences, Faculty of Science, Kyushu University), XIN LI(State Key Laboratory of Palaeobiology and Stratigraphy, Nanjing Institute of Geology and Palaeontology, Chinese Academy of Sciences)

[MIS14-P01] **Preservation of Permian–Triassic boundary section in the Jurassic accretionary complex of the Lake Hamana, Central Japan**

*Wang Ding[1], Kohtaro Ujiie[1], Katsuo Sashida[1] (1.University of Tsukuba)

[MIS14-P02] Outreach activities for radiolarian science since the InterRad 15 in Niigata, 2017

*Atsushi Matsuoka[1] (1.Department of Geology, Faculty of Science, Niigata University)

[MIS14-P03] **Phyletic evolution and paleogeographic distribution of the Early Cretaceous radiolarian *Turbocapsula***

*XIN LI[1], Matsuoka Atsushi[2] (1.State Key Laboratory of Palaeobiology and Stratigraphy, Nanjing Institute of Geology and Palaeontology, Chinese Academy of Sciences, 2. Department of Geology, Faculty of Science, Niigata University)

[MIS14-P04] New tectonostratigraphic unit of the Ashio terrane in the Ashio Mountains, central Japan

*Tsuyoshi Ito[1] (1.Geological Survey of Japan, National Institute of Advanced Industrial Science and Technology)

[E] Poster | M (Multidisciplinary and Interdisciplinary)：M-IS Intersection

[M-IS15] Global climate change driven by the Southern Ocean and the Antarctic Ice Sheet

convener:Osamu Seki(Institute of Low Temperature Science, Hokkaido University), Akira Oka(Atmosphere and Ocean Research Institute, The University of Tokyo), Yoshifumi Nogi(National Institute of Polar Research), Robin Elizabeth Bell(Lamont Doherty Earth Observatory)

[MIS15-P02] Inflows of offshore-origin warm water toward Totten Ice Shelf region, East Antarctica

*Daisuke Hirano[1], Kohei Mizobata[2], Takeshi Tamura[3], Masato Ito[1], Kaihe Yamazaki[1], Yoichiro Koh[1], Masaaki Kiuchi[4], Hiroto Murase[2], Hiroko Sasaki[5], Shigeru Aoki[1] (1.Institute of Low Temperature Science, Hokkaido University, 2.Tokyo University of Marine Science and Technology, 3.National Institute of Polar Research, 4.Fisheries Sciences, Hokkaido University, 5.National Research Institute of Far Seas Fisheries)

[MIS15-P03] Changes of Antarctic Bottom Water off the Wilks Land coast of the Australia-Antarctic Basin

*Taiyo Kobayashi[1] (1.Japan Agency for Marine-Earth Science and Technology)

[MIS15-P04] Preliminarily results from numerical modeling of chlorofluorocarbons (CFCs) and sulfur hexafluoride (SF_6) in the Southern Ocean

*Yoshihiko Ohashi[1], Michiyo Yamamoto-Kawai[1], Kazuya Kusahara[2] (1.Tokyo University of Marine Science and Technology, 2.Japan Agency for Marine Earth Science and Technology)

[MIS15-P05] Dense water production and downslope flow off Cape Darnley reproduced by a realistic numerical model

*Vigan Mensah[1], Yoshihiro Nakayama[1], Masakazu Fujii[2], Yoshifumi Nogi[2], Kay I. Ohshima[1] (1.Institute of Low Temperature Science, 2.National Institute of Polar Research)

[MIS15-P06] Modeling Ice-shelf ocean interactions of West Antarctic and East Antarctic ice shelves

*Yoshihiro Nakayama[1], Hong Zhang[2], Vigan Mensah[1], Shigeru Aoki[1], Dimitris Menemenlis[2] (1.Institute of Low Temperature Science, Hokkaido University, 2.NASA Jet Propulsion Laboratory, California Institute of Technology)

[MIS15-P08] **Geological evidences for Cape Darnley Bottom Water in the Wild Canyon, Antarctica: Preliminary results of R/V Hakuho-maru KH-20-1 cruise**

*Minoru Ikehara[1], Hiroshi Sato[2], Masakazu Fujii[3], Keiko Takehara[4] (1.Center for Advanced Marine Core Research, Kochi University, 2.Senshu University, 3.National Institute of Polar Research, 4.Soka University)

[MIS15-P09] Boulder, cobble, pebble, and granule of continental crust rocksfrom the Wild Canyon, off Cape Darnley, East Antarctica: Preliminary results of dredged samples during KH-20-1 cruise, R/V Hakuho-maru

*Hiroshi Sato[1], Masakazu Fujii[2], Minoru Ikehara[3], Keiko Takehara[4] (1.School of Business Administration, Senshu University, 2.National Institute of Polar Research and SOKENDAI, 3.Center for Advanced Marine Core Research, Kochi University, 4.SOKA University)

[MIS15-P11] **Revising the Dome Fuji ice core chronology**

*Ikumi Oyabu[1], Kenji Kawamura[1,2,3], Kyotaro Kitamura[1], Frédéric Parrenin[4], Anais Orsi[5], Christo Buizert[6] (1.National Institute of Polar Research, Research Organization of Information and Systems, 2.The Graduate University of Advanced Studies (SOKENDAI), 3.Japan Agency for Marine Science and Technology (JAMSTEC), 4.Institut des Géosciences de l'Environnement, 5.Laboratoire des sciences du climat et de l'environnement, 6.Oregon State University)

[MIS15-P12] Carbonaceous aerosol records in Domu Fuji ice core over the past 160 kyrs

Haruki Honda[2], *Osamu Seki[1], Kaori Ono[1], Yoshinori Iizuka[1] (1.Institute of Low Temperature Science, Hokkaido University, 2.Graduate School of Environmental Science, Hokkaido University)

[MIS15-P13] **CO_2 sensitivity experiments to study the climate of the mid-Pliocene Warm Period: results from Antarctica and the Southern Ocean**

*Wing-Le Chan[1], Ayako Abe-Ouchi[1,2] (1.Atmosphere and Ocean Research Institute, The University of Tokyo, 2.National Institute for Polar Research)

[MIS15-P14] Glacial ocean carbon cycle changes caused by enhanced stratification in the Southern Ocean and iron fertilization from glaciogenic dust

*Hidetaka Kobayashi[1], Akira Oka[1], Akitomo Yamamoto[2], Ayako Abe-Ouchi[1] (1.Atmosphere and Ocean Research Institute, The University of Tokyo, 2.Japan Agency for Marine-Earth Science and Technology)

[MIS15-P15] **Incorporation of grounding line parameterizations in the three-dimensional ice sheet model SICOPOLIS**

*Takashi Obase[1], Ayako Abe-Ouchi[1,2], Fuyuki SAITO[3], Ralf Greve[4] (1.Atmosphere and Ocean Research Institute, the University of Tokyo, 2.National Institute of Polar Research, 3.Japan Agency for Marine-Earth Science and Technology, 4.Institute of Low Temperature Science, Hokkaido University)

[MIS15-P16] Modeling the evolution of the Antarctic ice sheet driven by basal melting using the three-dimensional ice sheet model SICOPOLIS

*Kaho Harada[1], Ayako Abe-Ouchi[1,2], Takashi Obase[1], Fuyuki SAITO[3], Ralf Greve[4] (1.Atmosphere and Ocean Research Institute, The University of Tokyo, 2.National Institute of Polar Research, 3.Japan Agency for Marine-Earth Science and Technology, 4.Institute of Low Temperature Science, Hokkaido University)

[MIS15-P17] **Antarctic ozone and precipitation variability in the Southern Hemisphere**

*Alessandro Damiani[1], Raul Cordero[2], Pedro Llanillo[3], Sarah Feron[4], Hitoshi Irie[1], Shingo Watanabe[5] (1.Chiba University, Japan, 2.Santiago University, Chile, 3.AWI, Germany, 4.Stanford University, USA, 5.JAMSTEC, Japan)

[MIS15-P18] Position of grounding line at outlet glacier.

*Chiyuki Narama[1], Tsutomu Yamanokuchi[2], Shin Sugiyama[3] (1.Program of Field Research in the Environmental Sciences, Niigata University, , 2.RESTEC, 3.Institute of Low Temperature Science, Hokkaido University)

[MIS15-P19] Acceleration and retreat of Langhovde Glacier, East Antarctica, after the breakup of land-fast sea ice in 2016

*Ken Kondo[1,2], Shin Sugiyama[2] (1.Graduate School of Environmental Science, Hokkaido University, 2.Institute of Low Temperature Science, Hokkaido University)

[MIS15-P20] **Flow velocity and ice sheet elevation of Shirase Glacier and Totten Glacier from SAR and Laser altimetry**

*Shotaro Ohkawa[1], Koichiro Doi[2], Kazuki Nakamura[3], Hiroto Nagai[1] (1.WASEDA University, 2.National Institute of Polar Research, 3.Nihon University)

[MIS15-P21] Summary of the 3rd Year Activities of the Project on the Interaction of the solid Earth and the
Antarctic Ice Sheet

*Yoichi Fukuda[1], Jun Nishijima[2], Takahito Kazama[1], Kazuki Nakamura[3], Koichiro Doi[4], Yusuke Suganuma[4], Jun'ichi Okuno[4], Akito Araya[5], Heitaro Kaneda[6], Yuichi Aoyama[4], Hideki Miura[4] (1.Department of Geophysics, Graduate School of Science, Kyoto University, 2.Graduate School of Engineering, Kyushu University, 3.Faculty of Engineering, Nihon University, 4.National Institute of Polar Research, 5.ERI, University of Tokyo, 6.Graduate School of Science, Chiba University)

[MIS15-P22] **Dependences of GIA model parameters on the geodetic data in East Antarctica**

*Jun'ichi Okuno[1,2], Koichiro Doi[1,2], Akihisa Hattori[2], Yoichi Fukuda[3] (1.National Institute of Polar Research, 2.The Graduate University for Advanced Studies, 3.Kyoto Univ.)

[MIS15-P23] Antarctic ice sheet dynamics during the Last Interglacial

*Mutsumi Iizuka[1], Osamu Seki[1], Keiji Horikawa[3], Tina van de Flierdt[2], Tomohisa Irino[1], Masanobu Yamamoto[1], Takuya Itaki[4], Saiko Sugisaki[4], Minoru Ikehara[5], Yusuke Suganuma[6] (1.Hokkaido university, 2.Imperial College London, 3.University of Toyama, 4.Geological Survey of Japan, 5.Center for Advanced Marine Core Research, Kochi University, 6.National Institute of Polar Research)

[MIS15-P24] **East Antarctic meltwater influx from the Wilkes Subglacial Basin since the Last Glacial Maximum as determined by beryllium isotopes**

*Bethany Behrens[1,2], Yosuke Miyairi[1], Adam David Sproson[1], Masako Yamane[3], Yusuke Yokoyama[1,2,4] (1.Atmosphere and Ocean Research Institute, University of Tokyo, 5-1-5 Kashiwanoha, Kashiwa, Chiba 277-8564, Japan, 2.Graduate Program on Environmental Science, University of Tokyo, Komaba, Meguro, Tokyo 153-0041, Japan, 3.Institute for Space-Earth Environmental Research, Nagoya University, Furocho, Chikusa, Nagoya, Aichi, 464-8601, Japan, 4.Department of Earth and Planetary Science, Graduate School of Science, University of Tokyo, Hongo, Bunkyo, Tokyo 113-8654, Japan)

[MIS15-P25] Geophysical and geological signatures of submarine canyons off Cape Darnley, Antarctica

*Masakazu Fujii[1,2], Minoru Ikehara[3], Hiroshi Sato[4], Keiko Takehara[5], Takuya Itaki[6], Yoshifumi Nogi[1,2], Yasuyuki Nakamura[7] (1.National Institute of Polar Research, 2.The Graduate University for Advanced Studies, SOKENDAI , 3.Center for Advanced Marine Core Research, Kochi University, 4.Senshu University, 5.SOKA University, 6.Geological Survey of Japan, AIST, 7.Japan Agency for Marine Earth Science and Technology)

[MIS15-P26] Structure across the South Shetland Trench from the incoming plate to the back-arc basin

*Hiroaki Koge[1], Masakazu Fujii[2], Jinyu ZHOU[3], Kyoko Okino[3], Minoru Ikehara[4], Asuka Yamaguchi[3], Taichi Sato[1] (1.GSJ, AIST, 2.NIPR, 3.AORI, UTokyo, 4.Kochi University)

[MIS15-P27] Preliminary results of the JARE 61 geomorphological survey at Langhovde in Lutzow Holm Bay, East Antarctica

*Takeshige Ishiwa[1], Yuki Tokuda[2], Takuya Itaki[3], Satoshi Sasaki[4], Yusuke Suganuma[1], Shintaro Yamasaki[5] (1.National Institute of Polar Research, 2.Tottori University of Environmental Studies, 3.National Institute of Advanced Industrial Science and Technology, 4.Shimane University, 5.Disaster Prevention Research Institute, Kyoto University)

[MIS15-P28] Changes in oxygen and CFC concentrations in AABW along 115°E from 1990s to 2010s

*Michiyo Yamamoto-Kawai[1], Narimi Baba[1], Yoshihiko Ohashi[1] (1.Graduate School of Marine Science and Technology, Tokyo University of Marine Science and Technology)

[E] Poster | M (Multidisciplinary and Interdisciplinary)：M-IS Intersection

[M-IS16] Rift-related tectonics, magmatism, mineralization, and paleoceanographic effects

convener:Luisa Tejada Maria(Volcano and Earth Interior Research Center, Institute for Marine Geodynamics, Japan Agency for Marine-Earth Science and Technology), Eun Young Lee(Chonnam National University), Erik Wolfgring

[MIS16-P01] Rift-related volcanism at Naturaliste Plateau, Indian Ocean

*Maria Luisa Tejada[1], Eun Young Lee[2], Hans-Jurgen Brumsack[3], Bernhard Schnetger[3], Dennis Harry[4], Seong Soo Chun[2], Jun-Ichi Kimura[1] (1.Volcano and Earth Interior Research Center, Institute for Marine Geodynamics, Japan Agency for Marine-Earth Science and Technology, 2.Faculty of Earth System and Environmental Sciences, Chonnam National University, Gwangju, Republic of Korea, 3.Institut für Chemie und Biologie des Meeres (ICBM), Carl von Ossietzky Universität Oldenburg, Oldenburg, Germany, 4.Department of Geosciences, Colorado State University, Fort Collins, CO, USA)

[MIS16-P02] Qualitative Assessment of the Transition and Noble Metal Enrichment in Hydrothermally Altered Volcanic Sequence Using a Portable X-ray Fluorescence Spectrometer

*Xandr Neal Borja Uboan[1], Maria Luisa Tejada[2], Eun Young Lee[3], Wataru Tanikawa[4] (1.National Institute of Geological Sciences, University of the Philippines Diliman, Philippines, 2.Institute for Marine Geodynamics (IMG), Japan Agency for Marine-Earth Science and Technology, Yokosuka, Kanagawa 237-0061 Japan, 3.Faculty of Earth and Environmental Science, Chonnam National University, Gwangju, Republic of Korea, 4.Kochi Institute for Core Sample Research, Japan Agency for Marine-Earth Science and Technology, Nankoku 783-8502 Japan)

[MIS16-P03] Petrophysical characteristics of the volcanic succession at IODP Site U1513: Implications for stratigraphy and alteration

*Eun Young Lee[1], Maria Luisa Tejada[2], Seung Soo Chun[1], Insun Song[3], Erik Wolfgring [4] (1.Faculty of Earth Systems and Environmental Sciences, Chonnam National University, Gwangju, Rep. Korea, 2.Institute for Marine Geodynamics (IMG), Japan Agency for Marine-Earth Science and Technology, Yokosuka, Kanagawa, Japan, 3.Korea Institute of Geoscience and Mineral resources, Daejeon, Rep. Korea, 4.Department of Geodynamics and Sedimentology, University of Vienna, Vienna, Austria)

[MIS16-P04] Paleoenvironments of a Cretaceous marginal ocean basin - the Turonian to Santonian of the Australo-Antarctic Gulf, IODP Site U1512

*Erik Wolfgring [1], Michael Anthony Kaminski[2], Anna Waśkowska[3] (1.University of Vienna, Geodynamics and Sedimentology, Althanstrasse 9, 1090 Vienna, Austria, 2.King Fahd University of Petroleum and Minerals (KFUPM), Earth Sciences Department, Geosciences, Dhahran, SaudiArabia, 3.Faculty of Geology, Geophysics and Environmental Protection, AGH University of Science and Technology, Mickiewicza St. 50, Cracow, Poland)

[MIS16-P06] The facies architecture of felsic subaqueous volcanoes in “Green Tuff” Formation in the Katakai field, Niigata, Japan

*Miyuki Nonaka[1,2], Masahiko Yagi[1], Yasuo Yamada[1], Susumu Umino[3] (1. Japan Petroleum Exploration Co.,Ltd., 2.Graduate School of Natural Science & Technology, Kanazawa University, 3.Department of Earth Sciences, Kanazawa University)

[E] Poster | M (Multidisciplinary and Interdisciplinary)：M-IS Intersection

[M-IS17] Astrobiology

convener:Hikaru Yabuta(Hiroshima University, Department of Earth and Planetary Systems Science), Seiji Sugita(Department of Earth and Planetary Science, Graduate School of Science Sciece, The University of Tokyo), Misato Fukagawa(National Astronomical Observatory of Japan), Fujishima Kosuke(Tokyo Institute of Technology, Earth-Life Science Institute)

[MIS17-P01] Stability of Amino Acids and Amino Acid Precursors in Space: Approaches Through Space Experiments (Tanpopo and Tanpopo 2) and Ground Simulation Experiments

*Kensei Kobayashi[1], Tomohito Sato[1], Takuya Yokoo[1], Itsuki Sakon[2], Kazumichi Nakagawa[3], Hajime Yano[4], Miki Nakayama[5], Hajime Mita[5], Hirofumi Hashimoto[4], Shin-ichi Yokobori[6], Akihiko Yamagishi[4,6], Satoshi Yoshida[7], Isao Yoda[8], Hitoshi Fukuda[8], Yoshiyuki Oguri[8], Kazuhiro Kanda[9], Hiromi Shibata[3], Jun-ichi Takahashi[1], Yoko Kebukawa[1] (1.Yokohama National Univ., 2.Univ. Tokyo, 3.Osaka Univ., 4.JAXA/ISAS, 5.Fukuoka Inst. Tech., 6.Tokyo Univ. Pharm. Life Sci., 7.QST, 8.Tokyo Inst. Tech., 9.Univ. Hyogo)

[MIS17-P02] Radiation transfer simulation of circular polarization at the NIR/UV wavelengths

*Hajime Fukushima[1], Hidenobu Yajima[1], Masayuki Umemura[1] (1.Center for Computer Sciences, University of Tsukuba)

[MIS17-P03] Analysis of nucleic acid bases formed from simulated interstellar media

*Kotomi Sugaya[1], Kensei Kobayashi[1], Yoko Kebukawa[1], Yoshiyuki Oguri[2], Hitoshi Fukuda[2] (1.Yokohama National University, 2.Tokyo Institute of Technology)

[MIS17-P04] Astronomical detections of prebiotic molecules with the next generation Very Large Array

*Misato Fukagawa[1], Daisuke Iono[1], Munetake Momose[2] (1.National Astronomical Observatory of Japan, 2.Ibaraki University)

[MIS17-P05] Evaluation of the aldononitrile acetate ester derivatization method for aldose analysis in products from chemical evolution experiments

*Shunpei Abe[1], Yoko Kebukawa[1], Kensei Kobayashi[1] (1.Yokohama National University)

[MIS17-P06] **Polycyclic aromatic hydrocarbons in Jbilet Winselwan carbonaceous CM chondrite: Novel molecular proxies for thermal metamorphism of asteroids**

Hiroki Kato[1], *Hikaru Yabuta[1] (1.Hiroshima University, Department of Earth and Planetary Systems Science)

[MIS17-P07] Relationship between visible reflectance at 550 nm and carbon contents in carbonaceous chondrites: At-tempt to estimate the bulk carbon contents of asteroid Ryugu's surface

*Hikaru Yabuta[1] (1.Hiroshima University, Department of Earth and Planetary Systems Science)

[MIS17-P08] Minerals and their catalytic effects on amino acid formations in environments simulating asteroids

*Walaa Elmasry[1], Yoko Kebukawa[1], Kensei Kobayashi[1] (1.Yokohama national university, graduate school of Engineering Science)

[MIS17-P09] The Surviving Rate of Organic Materials after the Cometary Impacts

*Taiki Suzuki[1,2], Takashi Shibata[2], Natsuki Hosono[3] (1.Astrobiology Center, 2.National Astronomical Observatory of Japan, 3.Japan Agency for Marine-Earth Science and Technology)

[MIS17-P10] **Supercritical fluids in the search for origins-of-life in Earth and beyond**

*CANER AKIL[1], Kosuke Fujishima[1] (1.Earth-Life Science Institute)

[MIS17-P11] Estimation of the fraction of life-bearing planets that evolve intelligence f_i in the Drake equation by the terrestrial extinction history

*KOHJI TSUMURA[1] (1.Department of Natural Science, Faculty of Science and Engineering, Tokyo City University)

[MIS17-P12] The safety assessments of reaction vessels used for the space exposure experiments in order to synthesize nucleotide by UV irradiation

*Madoka Shiromizu[1], Kazumichi Nakagawa[2], Yoshitaka Bessho[3], Hajime Mita[1] (1.Fukuoka Institute of Technology, 2.Osaka University, 3.Academia Sinica, Institute of Biological Chemistry)

[E] Poster | M (Multidisciplinary and Interdisciplinary)：M-IS Intersection

[M-IS19] Conservation of geoparks, natural geosites, and cultural heritage: weathering and damage assessment

convener:Luigi Germinario(Saitama University), Celine Schneider(University of Reims-Champagne-Ardenne), Chiaki T. Oguchi(Institute for Environmental Science and Technology, Graduate School of Science and Engineering, Saitama University), Tetsuya Waragai(Graduate School of Science and Engineering, Nihon University), Miguel Gomez-Heras(Universidad Autonoma de Madrid), Patricia Vazquez(GEGENAA EA 3795 University of Reims Champagne-Ardenne), Magdalini Theodoridou(Cardiff University), Wonsuh Song(Waseda University)

[MIS19-P01] Development of magnetic resonance surface scanners for the nondestructive in-situ measurement of water fractions in cultural heritages

*Yoshito Nakashima[1] (1.National Institute of Advanced Industrial Science and Technology)

[MIS19-P02] Effect of temperature and humidity changes on salt weathering: Verification by rock surface moisture content and color measurements

Masaki Oi[1], *Masato Sato[2], Tsuyoshi Hattanji[3] (1.Graduate School of Life and environmental Sciences, University of Tsukuba, 2.National Research Institute for Earth Science and Disaster Resilience, 3.Faculty of Life and Environmental Sciences, University of Tsukuba)

[MIS19-P03] Study on relationship between water content, NIR absorbance and colour values of various stones and cement mortars

*Chiaki T. Oguchi[1], Keni'chiro Tanaka[2] (1.Institute for Environmental Science and Technology, Graduate School of Science and Engineering, Saitama University, 2.Department of Engineering, Saitama University)

[MIS19-P04] Surface morphology representations at different scales for rock art characterisationSurface morphology representations at different scales for rock art characterisation

Mohammad Hafez Seada[1,3], *Miguel Gomez-Heras[1], Laura Lopez-Gonzalez[2], Ayman Hamed[3] (1.Universidad Autonoma de Madrid, 2.Art Fabrik, 3.Suez University)

[MIS19-P05] THERMOGRAPHIC ANALYSIS AS AN NON DESTRUCTIVE TECHNIQUE FOR AN EARLY DETECTION OF BIOCOLONISATION ON BUILDING STONE

*Stephanie Eyssautier Eyssautier[1], Kamel Mouhoubi Mouhoubi[2], Fany Reffuveille Reffuveille[3], jean-luc Bodnar Bodnar[2] (1.GEGENAA EA 3795 UFR Sciences Exactes et Naturelles – 2, Esplanade Roland Garros, France, University of Reims Champagne-Ardenne (URCA), 51100 cedex, Reims, France, 2.ITHEMM, UFR Sciences Exactes et Naturelles, BP 1039, Reims Cedex 02, 51687, France, University of Reims Champagne-Ardenne (URCA), Moulin de la Housse BP 1039, 51687 Reims, France, 3.BIOS EA 4691, U.F.R. Pharmacie, 51, rue Cognacq Jay, University of Reims Champagne-Ardenne (URCA), 51095 Reims Cedex, France)

[MIS19-P06] Effectiveness of waterproofing protection coating on salt weathering experiment using building stones

*Chiaki T. Oguchi[1], Akimune Sasaki[2] (1.Institute for Environmental Science and Technology, Graduate School of Science and Engineering, Saitama University, 2.Department of Engineering, Saitama University)

[MIS19-P07] Integration of durability parameters of cultural heritage building stones using by integrated geomatic methodologies

*Sebastien LARATTE[1], Céline THOMACHOT-SCHNEIDER[1], Gilles FRONTEAU[1], Alexandra GUILLANEUF [1], Patricia VAZQUEZ[1] (1.University of Reims-Champagne-Ardenne)

[E] Poster | M (Multidisciplinary and Interdisciplinary)：M-GI General Geosciences, Information Geosciences & Simulations

[M-GI33] Data assimilation: A fundamental approach in geosciences

convener:Shin ya Nakano(The Institute of Statistical Mathematics), Yosuke Fujii(Meteorological Research Institute, Japan Meteorological Agency), Takemasa Miyoshi(RIKEN), SHINICHI MIYAZAKI(Graduate School of Science, Kyoto University)

[MGI33-P01] Oceanic iron distribution of the global ocean estimated by data assimilation approach

★Invited Papers

*Toshimasa Doi[1], Satoshi Osafune[1], Shuhei Masuda[1], Hajime Obata[4], Kazuhiro Misumi[3], Jun Nishioka[2] (1.Japan Agency for Marine-Earth Science and Technology, 2.Hokkaido University, 3.Central Research Institute of Electric Power Industry, 4. The University of Tokyo)

[MGI33-P02] Enhanced correlations between SST and precipitation in the weather time scale represented by a coupled atmosphere-ocean data assimilation system

*Yosuke Fujii[1], Chiaki Kobayashi[1], Ichiro Ishikawa[1], Takaya Yuhei[1] (1.Meteorological Research Institute, Japan Meteorological Agency)

[MGI33-P03] Non-Gaussian statistics in global atmospheric dynamics with a 10240-member ensemble Kalman filter experiment using an intermediate AGCM

★Invited Papers

*Keiichi Kondo[1,2], Takemasa Miyoshi[2] (1.Meteorological Research Institute, 2.RIKEN Center for Computational Science)

[MGI33-P04] Data assimilation of lightning observation data for global numerical weather prediction

*Toshiyuki Ishibashi[1] (1.Meteorological Research Institute/Japan Meteorological Agency)

[MGI33-P05] Development of a "multilingual" data assimilation library

*Shin ya Nakano[1], Genta Ueno[1], Shunichi Nomura[1], Daisuke Murakami[1] (1.The Institute of Statistical Mathematics)

[MGI33-P06] Observation impact study in global numerical weather prediction

*Toshiyuki Ishibashi[1] (1.Meteorological Research Institute/Japan Meteorological Agency)

[E] Poster | M (Multidisciplinary and Interdisciplinary)：M-GI General Geosciences, Information Geosciences & Simulations

[M-GI34] Near Surface Investigation and Modeling for Groundwater Resources Assessment and Conservation

convener:Jui-Pin Tsai(National Taiwan University, Taiwan), Hwa-Lung Yu(National Taiwan University), Makoto Taniguchi(Research Institute for Humanity and Nature), Ping-Yu Chang(National Central University)

[MGI34-P01] **Digital water level analysis based on well tide and air pressure effect**

*feng he ding[1] (1.Earthquake Administration of Ningxia Hui Autonomous Region)

[MGI34-P02] **Applying Independent Component Analysis and Wavelets Analysis to Explore the Response of Groundwater Level to Surface Hydrology**

*Chin Wei Huang[1], Liang Cheng Chang[1], Chin Tsai Hsiao[2], Wan Chung Lu[3], Tzu Hua Lai[3] (1.Department of Civil Engineering, National Chiao-Tung University, Hsinchu, Taiwan 30010, R.O.C., 2.Department of Landscape Architecture, Chung Chou University of Science and Technology, Changhua County, Taiwan, 510, R.O.C, 3.Central Geological Survey, MOEA, Taiwan 235, R.O.C)

[MGI34-P03] **Optimal Artificial-Recharge Planning to Raise the Groundwater Level of Land Subsidence Area**

*Ming-Sheng Wang[1], Liang Cheng Chang[1], Wan Chun Lu[2], Yun Shuen Wang[2] (1.Department of Civil Engineering, National Chiao-Tung University, Hsinchu, Taiwan, 30010, R.O.C, 2.Central Geological Survey, MOEA, Taiwan 235, R.O.C)

[E] Poster | M (Multidisciplinary and Interdisciplinary)：M-GI General Geosciences, Information Geosciences & Simulations

[M-GI36] Open Science in Progress: Data Sharing, e-Infrastructure, and Transparency in International Contexts

convener:Yasuhisa Kondo(Research Institute for Humanity and Nature), Baptiste Cecconi(LESIA, Observatoire de Paris, CNRS, PSL Research University), Yasuhiro Murayama(Strategic Program Produce Office, National Institute of Information and Communications Technology), Shelley Stall(American Geophysical Union)

[MGI36-P01] Research Data: Emerging Challenges and Opportunities in International Research Collaborations

★Invited Papers

*Kamata Takehito[1] (1.Sophia University)

[MGI36-P02] Data Management and Computing Services for the NenuFAR Telescope

*Baptiste Cecconi[1,2], Loh Alan[1,2], Evangelia Tremou[1], Julien N Girard[3], Brice Lamire[4], Philippe Hamy[4], Albert Shih[4], Pierre Le Sidaner[4], Cédric Viou[2], Emmanuel Thétas[2], Philippe Zarka[1,2], Laurent Denis[2] (1.LESIA, Observatoire de Paris, CNRS, PSL Research University, France, 2.Station de radioastronomie de Nançay, CNRS/Observatoire de Paris - PSL - Université d'Orléans/OSUC, France, 3.AIM/CEA Paris-Saclay, Université de Paris, CNRS, Gif-sur-Yvette, France, 4.DIO, Observatoire de Paris, CNRS, PSL Research University, France)

[MGI36-P03] Open data action to publish the GNSS-A seafloor geodetic data

*Tadashi Ishikawa[1], Yusuke Yokota[2], Shun-ichi Watanabe[1] (1.Hydrographic and Oceanographic Department, Japan Coast Guard, 2.Institute of Industrial Science, the University of Tokyo)

[MGI36-P04] Sample management in JAMSTEC: Cooperation-based management of diverse samples

★Invited Papers

*Takayuki Tomiyama[1], Tohru Iseto[1], Yasumi Toyoda[1], Miki Morioka[1], Makoto Ito[1] (1.Japan Agency for Marine-Earth Science and Technology)

[MGI36-P05] Improving the Reusability of Data and Sample Obtained JAMSTEC's Research Vessels and Submersibles

*Kazuyo Fukuda[1], Hajime Kawakami[1], Hiroki Horikawa[1], Tomoki Sasaki[1], Takako Sato[1], Takayuki Tomiyama[1], Makoto Ito[1], Yasumi Toyoda[1], Hideaki Saito[1], Chizuru Saito[1] (1.Japan Agency for Marine-Earth Science and Technology)

[MGI36-P06] Activities toward research data management at NIES/CGER

*Yoko Fukuda[1], Chisato Wada[1], Yasuhiro Tsukada[1], Jiye Zeng[1], Tomoko Shirai[1] (1.National Institute for Environmental Studies)

[E] Poster | M (Multidisciplinary and Interdisciplinary)：M-GI General Geosciences, Information Geosciences & Simulations

[M-GI37] Integration of Earth Observations and Multiple Use for Earth Science and Benefits to Societies - GEO

convener:Hiroyuki Muraoka(River Basin Research Center), Kentaro Ando(Japan Agency for Marine and Earth Science and Technology), Osamu Ochiai(Japan Aerospace Exploration Agency), Shinichi Sobue(Japan Aerospace Exploration Agency)

[MGI37-P01] Biodiversity and ecosystem observations by Asia Pacific Biodiversity Observation Network (APBON)

*Hiroyuki Muraoka[1], Yayoi Takeuchi[2], Takehisa Yamakita[3], Yuichi Kano[4], Shin Nagai[3], Sheila Vergara[5], Eun-Shik Kim[6], Tetsukazu Yahara[4,7] (1.Gifu University, 2.National Institute for Environmental Studies, 3.Japan Agency for Marin-Earth Science and Technology, 4.Kyusyu University, 5.ASEAN Centre for Biodiversity, 6.Kookmin University, 7.Kyusyu Open University)

[MGI37-P02] Ocean data networks and its utilization in Asia-Oceania region - challenges in AOGEO

*Kentaro Ando[1], Andy Steven[2], Aidy Mohamed Shawal M Muslim[3], Danling Tang[4], Fumihiko Akazawa[1] (1.Japan Agency for Marine and Earth Science and Technology, 2.Commonwealth Scientific and Industrial Research Organisation, 3.University Malaysian Terenganu, 4.South China Sea Institute of Oceanography)

[MGI37-P03] Multidisciplinary efforts towards regional to global scale CO_2 budget estimation

*Kazuhito Ichii[1], Masayuki Kondo[1], Prabir Patra[2], Nobuko Saigusa[3], Josep Canadell[4] (1.Chiba University, 2.Japan Agency for Marine-Earth Science and Technology, 3.National Institute for Environmental Studies, 4.Commonwealth Scientific and Industrial Research Organisation)

[E] Poster | M (Multidisciplinary and Interdisciplinary)：M-AG Applied Geosciences

[M-AG42] CTBT IMS Technologies for Detecting Nuclear Explosion and Their Applications to Earth Science

convener:Ozel Nurcan Meral(Comprehensive Nuclear-Test-Ban Treaty Organization), Hiroyuki Matsumoto(Japan Agency for Marine-Earth Science and Technology), Noriko Kamaya(Earthquake Research Institute, The University of Tokyo), Yosuke Naoi(Japan Atomic Energy Agency)

[MAG42-P01] Overview of Integrated Operational Exercise conducted under CTBT national operational system in Japan.

*RYOHEI EMURA[1], Takayuki Otsu[1], Masashi Motohashi[1], Toyomi Sakamoto[1], Soshi Iwata[1], Takanari Fujii[1], Mami Nogami[1], Makiko Iwakuni[1] (1.Japan Weather Association)

[MAG42-P02] Contribution of the hydroacoustic hydrophone stations of the International Monitoring System to natural disaster mitigation

*Hiroyuki Matsumoto[1], Mario Zampolli[2], Georgios Haralabus[2], Jerry Stanley[2], Nurcan Meral Özel[2] (1.Japan Agency for Marine-Earth Science and Technology (JAMSTEC), 2.Comprehensive Nuclear-Test-Ban Treaty Organization (CTBTO))

[MAG42-P03] Detection of hydroacoustic signals associated with the 2015 Torishima volcanic tsunami earthquake

*Hiroko Sugioka[1], Natsuo Nemoto[1] (1.Kobe University)

[MAG42-P04] **Noble Gas Joint Measurement Project regarding CTBT**

*Yuichi Kijima[1], Yoichi Yamamoto[1], Yutaka Tomita[1] (1.Japan Atomic Energy Agency)

[E] Poster | M (Multidisciplinary and Interdisciplinary)：M-AG Applied Geosciences

[M-AG43] The Application Usability Level (AUL): A Standard Measure of Progress to Benefit Space Research

convener:Jeffrey Klenzing(NASA Goddard Space Flight Center), Adam C Kellerman(University of California Los Angeles), Brett A Carter(RMIT University), Tam Dao(Geospatial Center, RMIT University)

[MAG43-P01] HF-START web tool

★Invited Papers

*Kornyanat Hozumi[1], Ryo Nakao[2], Hiroyuki Nakata[2], Susumu Saito[3], Takuya Tsugawa[1], Chihiro Tao[1], Hidekatsu Jin[1], Masato Nagahara[1], Mamoru Ishii[1] (1.National Institute of Information and Communications Technology (NICT), Tokyo, Japan, 2.Graduate School of Engineering, Chiba University, Chiba, Japan, 3.National Institute of Maritime, Port and Aviation Technology, Electronic Navigation Research Institute (ENRI), Tokyo, Japan)

[MAG43-P02] On the assessment of daily Equatorial Plasma Bubble occurrence modeling and forecasting

*Brett A Carter[1], Julie Currie[1], Tam Dao[1], Endawoke Yizengaw[2], John Retterer[3], Michael Terkildsen[4], Keith Groves[3], Ronald Caton[5] (1.RMIT University, 2.Aerospace, 3.Boston College, 4.Bureau of Meteorology, 5.Air Force Research Laboratory)

[MAG43-P03] The sami2py ionospheric model: a Phase 1 AUL project

*Jeffrey Klenzing[1], Jonathon Smith[1,2], Alexa Jean Halford[1], Michael Hirsch[3], Joe Huba[1,4] (1.NASA Goddard Space Flight Center, 2.Catholic University of America, 3.Boston University, 4.Symtek)

[E] Poster | M (Multidisciplinary and Interdisciplinary)：M-AG Applied Geosciences

[M-AG45] Satellite Land Physical Processes Monitoring at Medium/High/Very High Resolution

convener:Jean-Claude Roger(University of Maryland College Park), Shinichi Sobue(Japan Aerospace Exploration Agency), Eric Vermote(NASA Goddard Space Flight Center), Ferran Gascon(European Space Agency)

[MAG45-P01] **Toward a Consistent Data Records from Coarse, Medium and High Spatial Resolution Earth Observation Satellites**

*Eric Vermote[1], Sergii Skakun[1,2], Jean-Claude Roger[1,2] (1.NASA Goddard Space Flight Center, 2.University of Maryland, Dept. of Geographical Sciences)

[MAG45-P02] Mapping and analysis of irrigation water quality index of Hisar district Haryana, India by using Surfer Software

*shilpa singh[1], Amit Kumar[1], Yogesh Pandey[1], JAHANGEER -[2] (1.SKUAST- Kashmir, 2.University of Nebraska)

[MAG45-P03] **Aerosol models for satellite atmospheric corrections.**

*Jean-Claude Roger[1,2], Eric Vermote[2], Sergii Skakun[1,2], William Rountree[1,2], Andres Santamaria Artigas[1,2], Natacha Kalecinski[1,2], Oleg Dubovik[4], Brent Holben[3] (1.University of Maryland College Park, Departement of Geographysical Sciences, College Park, MD 20742, USA, 2.Nasa Goddard Space Flight Center, Code 619, Greenbelt, MD 20771, USA, 3.Nasa Goddard Space Flight Center, Code 618, Greenbelt, MD 20771, USA, 4.Laboratoire d'Optique Atmospherique, University of Lille, Villeneuve d'Ascq, 59655, France)

[MAG45-P04] **AVHRR LTDR product cloud and snow mask using Support Vector Machines**

*Jose Luis Villaescusa[1,2], Eric Vermote[2], Jean-Claude Roger[1,2], Belen Franch[3,1], Sergii Skakun[1,2] (1.University of Maryland College Park, 2.NASA Goddard Space Flight Center, 3.Universitat de Valencia)

[MAG45-P05] **Winter wheat yield assessment from Landsat 8 and Sentinel-2 data**

*Sergii Skakun[1,2], Eric Vermote[2], Belen Franch[1,3], Jean-Claude Roger[1,2] (1.University of Maryland College Park, 2.NASA Goddard Space Flight Center, 3.University of Valencia)

[MAG45-P06] **INDICATORS OF HIGH VARIABILITY COVER LAND with Landsat-8 and Sentinel-2**

*Natacha kalecinski[1,2], Sergii Skakun[1,2], Jean-Claude Roger[1,2], Eric Vermote[2] (1.Department of Geographical Sciences, University of Maryland College Park, USA, 2.NASA Goddard Space Flight Center, Greenbelt, USA)

[MAG45-P07] CAMSIS: An Automated System for the Validation of Surface Reflectance from High Spatial Resolution Sensors

Eric Vermote[2], Joel McCorkel[3], *Andrés Eduardo Santamaría-Artigas[1,2], William Henry Rountree[1,2], Sergii Skakun[1,2], Belen Franch[4,1], Jean-Claude Roger[1,2] (1.University of Maryland, College Park, 2.NASA Goddard Space Flight Center Code 619, 3.NASA Goddard Space Flight Center Code 618, 4.Universitat de Valencia, Spain)

[E] Poster | M (Multidisciplinary and Interdisciplinary)：M-SD Space Development & Earth Observation from Space

[M-SD46] Effects of lightning, severe weather and tropical storms

convener:Mitsuteru Sato(Department of Cosmoscience, Hokkaido University), Yoav Yair(Interdisciplinary Center Herzliya), Xiushu Qie(Institute of Atmospheric Physics, Chinese Academy of Sciences), Yukihiro Takahashi(Department of Cosmosciences, Graduate School of Science, Hokkaido University)

[MSD46-P01] Modelling of streamer ignition and propagation in the system of two approaching hydrometeors

★Invited Papers

*Victor P Pasko[1], Jaroslav Jansky[2] (1.Pennsylvania State University Main Campus, 2.Department of Mathematics and Physics, University of Defense, Brno, Czechia)

[MSD46-P02] Estimation of cloud base altitude using cloud images captured by all-sky camera

*Atsuya Nemoto[1], Hiroyo Ohya[2], Alessandro Damiani[3], Tamio Takamura[3], Toshiaki Takano[2], Hiroyuki Nakata[2] (1.Graduate School of Science and Engineering, Chiba University, 2.Graduate School of Engineering, Chiba University, 3.Center for Environmental Remote Sensing, Chiba University)

[MSD46-P03] Variation of Phase Relation Between OLR in Western Pacific Warm Pool and the Equator

*Kambiz Torabi[1], Yukihiro Takahashi (1.Department of Cosmosciences, Hokkaido University)

[MSD46-P04] An observational study on thunder cloud activities over Tama, Tokyo based on atmospheric electrostatic field measurements - Case study for the hail storm event in May 4, 2019 -

★Invited Papers

*Jun-Ichi Hamada[1], Jun Matsumoto[1], Tomoshige Inoue[1], Masashi Kamogawa[2], Yukihiro Takahashi[3] (1.Faculty of Urban Environmental Sciences, Tokyo Metropolitan University, 2.Global Center for Asian and Regional Study, University of Shizuoka, 3.Department of Cosmosciences, Graduate School of Science, Hokkaido University)

[MSD46-P05] Relation between Lightning Activities Measured by the V-POTEKA Network and Intensity Development of Western North Pacific Typhoons

*Mitsuteru Sato[1], Loren Joy Estrebillo[1], Yukihiro Takahashi[1], Hisayuki Kubota[1], Shunsuke Niwa[1], Glenn Vincent Lopez[2], Joel Marciano[2] (1.Department of Cosmoscience, Hokkaido University, 2.ASTI, DOST)

[E] Poster | M (Multidisciplinary and Interdisciplinary)：M-TT Technology & Techniques

[M-TT48] Cryoseismology - A new proxy for detecting surface environmental variations of the Earth -

convener:Masaki Kanao(National Institute of Polar Research), Seiji Tsuboi(JAMSTEC, Center for Earth Information Science and Technology), Genti Toyokuni(Research Center for Prediction of Earthquakes and Volcanic Eruptions, Graduate School of Science, Tohoku University), Yoshihiro Hiramatsu(School of Geosciences and Civil Engineering, College of Science and Engineering, Kanazawa University)

[MTT48-P01] Seismic observations in Greenland by a joint USA and Japanese GLISN team (2011–2019)

*Genti Toyokuni[1], Masaki Kanao[2], Seiji Tsuboi[3] (1.Research Center for Prediction of Earthquakes and Volcanic Eruptions, Graduate School of Science, Tohoku University, 2.NIPR, 3.JAMSTEC)

[MTT48-P02] Estimation of seismic source location around East Ongul Island, East Antarctica, by using two seismic arrays

*Manami Nakamoto[1], Masaki Kanao[2] (1.Association for the Development of Earthquake Prediction, 2.National Institute of Polar Research)

[MTT48-P03] Progress in Cryoseismology – A review of Japanese contribution -

*Masaki Kanao[1] (1.National Institute of Polar Research)

[MTT48-P04] Characteristic multi-sphere interaction in the coastal and marine environment inferred from infrasound observation at Terra Nova Bay, Antarctica

*Takahiko Murayama[1], Masaki Kanao[2] (1.Japan Weather Association, 2.National Institute of Polar Research)

[E] Poster | M (Multidisciplinary and Interdisciplinary)：M-TT Technology & Techniques

[M-TT49] GEOSCIENTIFIC APPLICATIONS OF HIGH-DEFINITION TOPOGRAPHY AND GEOPHYSICAL DATA IN THE ANTHROPOCENE

convener:Yuichi S. Hayakawa(Faculty of Environmental Earth Science, Hokkaido University), Shigekazu Kusumoto(Graduate School of Science and Engineering for Research, University of Toyama), Christopher A Gomez(Kobe University Faculty of Maritime Sciences Volcanic Risk at Sea Research Group)

[MTT49-P01] **A Study of Slope Displacement Monitoring with PSInSAR Technique**

*Chin-jen Lin[1], Shen Yu Hsiao[1] (1.National Chung Hsing University)

[MTT49-P02] Monitoring Soil Erosion Changes by SBAS-InSAR Technology

*Yu-Chi Hsieh[1], Shen Yu Hsiao[1] (1.National Chung Hsing University)

[MTT49-P03] Spatiotemporal analysis of topography and vegetation in check dams using RTK-UAV and SfM-MVS photogrammetry

*Masato Hayamizu[1], Yasutaka Nakata[1], Satoshi Hasui[1], Hajime Sato[1], Yu Nagasaka[1], Akiko Nagasaka[1] (1.Hokkaido Research Organization Forestry Research Institute)

[MTT49-P04] A new method to measure in situ soil density using SfM-MVS photogrammetry

*Christopher A Gomez[1] (1.Kobe University Faculty of Maritime Sciences Volcanic Risk at Sea Research Group)

[MTT49-P05] **Comparison of wide-range topographic data derived from UAV-SfM and airborne lidar: a case study at Taal Volcano, the Philippines**

*Yuichi S. Hayakawa[1], Shigekazu Kusumoto[2], Takuro Ogura[3,5], Toshiyasu Nagao[4], Paul Karson B. Alanis[6] (1.Faculty of Environmental Earth Science, Hokkaido University, Japan, 2.Graduate School of Science and Engineering for Research, University of Toyama, Japan, 3.Graduate School of Frontier Science, The University of Tokyo, Japan, 4.Institute of Oceanic Research and Development, Tokai University, Japan, 5.Graduate School of Environmental Science, Hokkaido University, Japan, 6.Philippine Institute of Volcanology and Seismology (PHIVOLCS), Department of Science and Technology, The Philippines)

[E] Poster | M (Multidisciplinary and Interdisciplinary)：M-TT Technology & Techniques

[M-TT50] Distributed Fiber Optic Sensing for Geophysical Applications

convener:Matthew Becker(California State University Long Beach), Xiangfang Zeng(Institute of Geodesy and Geophysics, Chinese Academy of Sciences), Ziqiu Xue(Research Institute of Innovative Tech for the Earth), Herbert F Wang(University of Wisconsin Madison)

[MTT50-P01] Advances in Distributed Acoustic Sensing for Applications in the Earth Sciences

*Thomas Coleman[1], Tom Parker[1], Sergey Shatalin[1], Jack Maxwell[1], Mahmoud Farhadiroushan[1], Michael Mondanos[1] (1.Silixa Ltd.)

[MTT50-P02] Lessons learned from dark fiber distributed arrays in a large urban campus

*Dante Fratta[1], Herbert F Wang[1], Neal Lord[1], Shreeshrita Patnaik[1], Agatha Podrasky[2], Alexander Malamet[1], Paul Barford[1] (1.University of Wisconsin Madison, 2.Silixa Ltd.)

[MTT50-P03] Combining DAS and air-gun: a cost-effective medium change monitoring system

*Xiangfang Zeng[1], Baoshan Wang[2], Jun Yang[3], Yuansheng Zhang[4], Zhenghong Song[2,1], Xiaobin Li[4], Rongbin Lin[1], Manzhong Qin[4], Congxin Wei[4] (1.State Key Laboratory of Geodesy and Earth's Dynamics, Innovation Academy for Precision Measurement Science and Technology, Chinese Academy of Sciences, 2.School of Earth and Space Sciences, University of Science and Technology of China, 3.Earthquake Agency of Yunnan Province, 4.Earthquake Agency of Gansu Province)

[MTT50-P04] DAS Research Coordination Network in Geosciences and Engineering

*Herbert F Wang[1], Robert Woodward[3], Robert Detrich[3], Scott Tyler[2] (1.University of Wisconsin Madison, 2.University of Nevada, Reno, 3.Incorporated Research Inst Seismology)

[MTT50-P05] **Distributed Acoustic Sensing (DAS) as a Distributed Hydraulic Sensor**

*Matthew Becker[1], Thomas I Coleman[2], Christopher Ciervo[1] (1.California State University Long Beach, Long Beach California, 2.Silixa LLC, Houston, USA)

[E] Poster | M (Multidisciplinary and Interdisciplinary)：M-ZZ Others

[M-ZZ53] Availability of earth science data in renewable energy field

convener:Hideaki Ohtake(National Institute of Advanced Industrial Science and Technology), Fumichika Uno(Nihon University, College of Humanities and Sciences), Teruhisa Shimada(Graduate School of Science and Technology, Hirosaki University), Daisuke Nohara(Central Research Institute of Electric Power Industry)

[MZZ53-P01] Geothermal exploration of the Iwaki Volcano using the Br/Cl ratio in river, spring, and hot spring waterGeothermal exploration of the Iwaki Volcano using the Br/Cl ratio in river, spring, and hot spring water

*Seiichiro Ioka[1], Kazuyoshi Asai[2], Kazumi Asai[2], Ayako Mikami[3], Sachi Wakasa[1] (1.Institute of Regional Innovation, Hirosaki University, 2.Geo Science Laboratory, 3.Aomori Prefectural Kizukuri Senior High School)

[MZZ53-P02] **Machine learning based prediction of solar power generation by utilizing all-sky camera**

*Masataka Imai[1], Toru Kouyama[1], Hideaki Ohtake[1], Takashi Oozeki[1], Mitsuteru Sato[2] (1.National Institute of Advanced Industrial Science and Technology, 2.Hokkaido University)

[MZZ53-P03] Probabilistic Wind Power Prediction Based on Ensemble Weather Forecasting

*Daisuke Nohara[1], Masamichi Ohba[1], Takeshi Watanabe[1], Shinji Kadokura[1] (1.Central Research Institute of Electric Power Industry)

[MZZ53-P04] Improvement of prediction of wind power generation output for an area and its sub-area by using monitoring data

*Shinji Kadokura[1], Daisuke Nohara[1], Masamichi Ohba[1], Atsushi Hashimoto[1], Hiromaru Hirakuchi[1] (1.Central Research Institute of Electric Power Industry)

[MZZ53-P05] Detectability of large forecast error on surface solar radiation using grand ensemble method considering atmospheric circulation patterns

*Fumichika Uno[1,4], Mio Matsueda[2], Takashi Oozeki[3], Hideaki Ohtake[3,4], Yoshinori Yamada[4] (1.Atmoshere and Ocean Research Institute, The University of Tokyo, 2.University of Tsukuba, 3.National Institute of Advanced Industrial Science and Technology, 4.Japan Meteorological Agency, Meteorological Research Institute)

[E] Poster | M (Multidisciplinary and Interdisciplinary)：M-ZZ Others

[M-ZZ54] Communicating Hazard and Risk: What do we know about how to make this information understandable?

convener:Danijel Schorlemmer(GFZ German Research Centre for Geosciences), Alexandra Freeman(Winton Centre for Risk and Evidence Communication, University of Cambridge), Sarah Dryhurst(University of Cambridge), Naoshi Hirata(National Research Institute for Earth Science and Disaster Resilience)

[MZZ54-P01] **An Integrated GIS and Big Data Platform for Meteorological Disaster Risk Management and its Application**

*YING LI[1] (1.Beijing Climate Center)

[MZZ54-P02] Emergency flood detection using multiple information: Integrated analysis of natural hazard monitoring and social media data

*Kikuko Shoyama[1] (1.National Research Institute for Earth Science and Disaster Resilience)

[MZZ54-P03] Global Dynamic Exposure and the OpenBuildingMap - Communicating Risk and Involving Communities

*Danijel Schorlemmer[1], Naoshi Hirata[2], Kuo-Fong Ma[3], Karsten Prehn[1], Cecilia Nievas[1], Thomas Beutin[1], Fabrice Cotton[1], Max Wyss[4] (1.GFZ German Research Centre for Geosciences, Potsdam, Germany, 2.National Research Institute for Earth Science and Disaster Resilience, Tsukuba. Japan, 3.Earthquake-Disaster & Risk Evaluation and Management (E-DREaM) Center, National Central University, Taiwan, 4.International Centre for Earth Simulation Foundation, Geneva, Switzerland)

[MZZ54-P04] Tokyo Metropolitan Resilience Project, from CSR to CSV

*Takashi Furuya[1], Keiko Tamura[2], Danijel Schorlemmer[3], Naoshi Hirata[1] (1.National Research Institute for Earth Science and Disaster Resilience, Tsukuba, Japan, 2.Niigata University, Risk Management Office, Niigata, Japan, 3.GFZ German Research Center for Geosciences)

[E] Poster | U (Union)：Union

[U-02] Assessment and Accountability of Scientific Knowledge Creation

convener:Michiyo SHIMAMURA(Japan Agency for Marine-Earth Science and Technology), Yasuhiro Yamanaka(Faculty of Environmental Earth Science, Hokkaido University), Kiyoshi Suyehiro(Japan Agency for Marine-Earth Science and Technology), Brooks Hanson(American Geophysical Union)

Scientific indices such as the number of citations or impact factor have been widely adopted in Japan and elsewhere to gauge scientific outputs without sufficient deliberations on their relationships to the true value of science and researchers' efforts or the harm and perverse incentives that result. If such disconnect exists, overreliance to these indices may lead to biases in research including in aiming for shorter-term goals. They are often requested by the solution-seeking stakeholders as well.

In the field of geoscience, a wide latitude of research styles exists and forms our community, from a focus on urgent societal needs to intellectual curiosity about our Earth. Such characteristics vary among fields making general comparisons across fields not straightforward. The adoption of simple evaluation indices as above may hinder the truly useful assessment of research. This trend influences gravely the research environment and thus the behavior of early-career researchers. What is the right direction for science and how should science be assessed?

In this session, we invite the members of the geoscience research community to discuss "ideal" science, recognize its diversity and identify the needs for changes. We welcome reports from different parts of the world and novel ideas to evaluate our own research activities that may lead to creating a culture that fulfills accountability to society. We envision this session to have infuse lively discussion and invite the audience to interactive exchanges.

[U02-P01] Let's start the discussion of the international tuning of research assessment in earth science to create a culture and indicators of “creation of knowledge”

*Yasuhiro Yamanaka[1], Michiyo SHIMAMURA[2], Kiyoshi Suyehiro[2] (1.Faculty of Environmental Earth Science, Hokkaido University, 2. Japan Agency for Marine-Earth Science and Technology)

Let's start the discussion of the international tuning of research assessment in earth science to create a culture and indicators of “creation of knowledge”

*Yasuhiro Yamanaka[1], Michiyo SHIMAMURA[2], Kiyoshi Suyehiro[2]

1. Faculty of Environmental Earth Science, Hokkaido University, 2. Japan Agency for Marine-Earth Science and Technology

We propose to the members of international Earth science communities a challenging attempt to create a culture in which the research community self-evaluates its research activities and fulfill its accountability to the public.

The Science Council of Japan amended the “Code of Conduct for Scientists-Revised Edition-” (2013), to include in “Research activities” that “Scientists should publish their research results in papers, etc.” and in “Dialogue with the public” that “Scientists will strive to provide scientific advice”. A proposal on open science recognizes that “data users can make research achievements with papers and patents, but data producers and data distributors cannot make research achievements with individual names”(Science Council of Japan, 2016). That is, the responsibilities of researchers (scientists) to entrustments by the society are becoming clearer.

However, the research community still implicitly believes that “research achievements = papers”. We think that this has led to the misuses of indicators such as citation counts and impact factors (IFs), to “*the worship of papers*” in organizations and researchers' performance evaluations, and the over-emphasis on research fields, such as science and technology, which excel at directly solving problems. These are distortions caused by easily adopting quantifiable items as evaluation indices without the ideals of science and researchers contributing to “creation of knowledge,” and it is strongly desired to review them from the ground up. Also, as the medieval university has died due to the spread of typographic printing (Yoshimi, 2011), the explosive development of the information infrastructure using the Internet with artificial intelligence has fundamentally shaken not only the presence of the university but also the value for “creation of knowledge”. Meanwhile, the society strongly expects the academia to contribute to the realization of a sustainable society, and the “Scientific and Technological Community” was designated as one of the nine “Major Groups” in the formulation of “2030 Agenda” well known as SDGs (United Nations, 2015).

We propose to get started with the following steps:

(A) as a grasp of research activities (Institutional Research, IR), we will clarify researchers’ perception of “creation of knowledge” and their actual state of research activities. We respect that the researchers have their own philosophies and values for "creation of knowledge," which may likely derived from their disciplinary roots. To clarify these, we aim to conduct interviews and questionnaires for JpGU ID holders (members and meeting participants).

(B) We would like to survey the recognition of “creation of knowledge” of the overseas researcher communities and stakeholders and the actual state of their research activities. To this end, we ask AGU, EGU, national science policy officials, funding agencies for information on advanced initiatives and the

©2020. Japan Geoscience Union. All Right Reserved.

code of conduct of researchers etc. in each country. We intend to make an international comparison of the value measures related to “creation of knowledge”.

(C) As we will hold this session at JpGU on the visualization of “creation of knowledge” and proposal of its indicators according to the progress of (A, B) surveys and syntheses, and will also start dialogues with the public as well as discussions in the researcher community. To this end, the emphasis is on the process of discussion and dialogue based on the concept of “tuning”, and mutual understanding and respect of individual "research style" is to be achieved in a multicultural symbiosis of the research community (securing academic diversity).

Keywords: Institutional Research, the worship of papers, creation of knowledge, tuning, impact factors, ideals of science and researchers

©2020. Japan Geoscience Union. All Right Reserved.

[E] Poster | U (Union)：Union

[U-03] Sustainable global groundwater management for human security

convener:Yoshihide Wada(International Institute for Applied Systems Analysis), Makoto Taniguchi(Research Institute for Humanity and Nature)

Sustainable management of water resources is an overwhelming task, when faced with a growing population that is increasing its demand for food, energy and water. Except frozen ice, groundwater is world's largest fresh water resource, but increasing over-exploitation of groundwater resources has been reported over intensely irrigated regions. Groundwater is the prime source for drinking water supply and irrigation, hence critical to global water, food and energy security contributing to human security. But also for sustaining low flow requirements and ecological values of groundwater dependent ecosystems, the contribution by groundwater flow is essential. Groundwater therefore needs to be managed wisely, protected and especially sustainably used. In itself this is a challenge, however under a changing environment including climate, land use, population growth, this task becomes a challenge especially in the light of limited data availability and consequential uncertainties. From arid over humid to arctic regions, in every type of climate changing environmental conditions become apparent and have very different effects. In this session we invite contributions, which report on research on the consequences of a changing environment for future management, protection, and sustainable use of groundwater. Methodologies, strategies, case studies as well as quantitative techniques for dealing with uncertainty and limited data availability are of interest for this session. We welcome studies describing how groundwater resources benefit from an Integrated Water Resources Management approach. Furthermore, contributions describing case studies and new techniques for active management and protection of groundwater resources such as artificial recharge and conjunctive use are welcome.

[U03-P01] **Estimating yield is key to obtaining global material flux via the submarine groundwater discharge**

*Chen-Tung Arthur Chen[1,2], Ting-Hsuan Huang[1], Hon-Kit Lui[1], JING ZHANG[3] (1.National Sun Yat Sen University, 2.Zhejiang University, 3.University of Toyama)

[U03-P02] Quantitative assessment of the impacts of sustainable irrigation on global bioenergy production

*Zhipin Ai[1], Naota Hanasaki[1] (1.National Institute for Environmental Studies, Japan)

[U03-P03] Integrated structural, geophysical and hydrogeological approaches for sustainable groundwater resources in Precambrian basement rock terranes, India

*Rudra Mohan Pradhan[1], Tapas Kumar Biswal[1] (1.Department of Earth Sciences, Indian Institute of Technology Bombay, India)

Estimating yield is key to obtaining global material flux via the submarine groundwater discharge

*Chen-Tung Arthur Chen[1,2], Ting-Hsuan Huang[1], Hon-Kit Lui[1], JING ZHANG[3]

1. National Sun Yat Sen University, 2. Zhejiang University, 3. University of Toyama

Excess nutrients have been discharged into the oceans by rivers, making many coastal regions hypoxic or even anoxic. Most people do not realize that a substantial fraction of the freshwater on land also enters the oceans directly from the seabed, unseen by human eyes. This process is called submarine groundwater discharge (SGD) and it amounts to 0.2-10% of global river discharge. The SGD releases nutrients, alkalinity (TA), and dissolved inorganic carbon (DIC) into the oceans while reducing their dissolved oxygen (DO) content and pH but the results are largely unknown quantitatively. A case study indicates that the freshwater component of the SGD equals around 5.2% of the annual river discharge in Taiwan, where the over-pumping of groundwater has been a serious problem. Further, the SGD exports N, P, Si, TA, and DIC in amounts equivalent to 12.7, 0.9, 9.3, 21.1 and 19.6%, respectively, of those in riverine fluxes. Unfortunately, such results cannot be generalized to a region - let along to all coastal seas around the world - because the total area of Taiwan is too small. Whereas rivers have been extensively studied, only a handful of reports concerning nutrients, TA and DIC fluxes have focused on SGD. Worse, the relevant literature is mainly concerned with the flux per unit area of SGD discharge into oceans. Such data cannot be extrapolated to the global oceans as the discharge area is unknown. On the other hand, the yield, which is the flux per unit area of the river basin, can be extrapolated from readily available river basin data but to the best of our knowledge the yield has been reported for only three river basins. An accurate estimate of the SGD flux is essential to predicting coastal environments in an era of rapid global change but most - if not all - coastal biogeochemical models have no SGD component. Substantial errors may arise if SGD is ignored, especially in estuaries, bays, inland seas, deltas and salt marshes. Since the areas of thousands of river basins worldwide are known, with a knowledge of even a limited number of data on the yield the global amount of material flux by SGD may be reasonably estimated and its effect on the coastal biogeochemistry better evaluated.

Keywords: Submarine Groundwater Discharge, nutrients, carbon cycle

©2020. Japan Geoscience Union. All Right Reserved.

Quantitative assessment of the impacts of sustainable irrigation on global bioenergy production

*Zhipin Ai[1], Naota Hanasaki[1]

1. National Institute for Environmental Studies, Japan

Bioenergy production plays a critical role in many stringent climate scenarios to achieve the 2-degree target at the end of this century. Earlier reports showed that unconstrained irrigation can substantially increase the global bioenergy production and therefore reduce land requirement for bioenergy production. However, the extent and consequences of water-resources-constrained irrigation has been poorly explored. We first developed a future bioenergy land use scenario with strict natural and food protection considerations. Next, we quantitatively investigated the effects of a new sustainable irrigation scheme on the global bioenergy production in 2090 under representative concentration pathway (RCP) 2.6 based on an enhanced global hydrological model. Finally, we investigated the possible uncertainties from different irrigation schemes, general circulation models, and social economic pathways and made explicit comparisons with previous studies. Under our scenario, although we can stay within the planetary boundary for freshwater, the global bioenergy production falls short of the requirement prescribed in IPCC-RCP2.6.

Keywords: Bioenergy potential, Sustainable irrigation, IPCC-RCP2.6

©2020. Japan Geoscience Union. All Right Reserved.

Integrated structural, geophysical and hydrogeological approaches for sustainable groundwater resources in Precambrian basement rock terranes, India

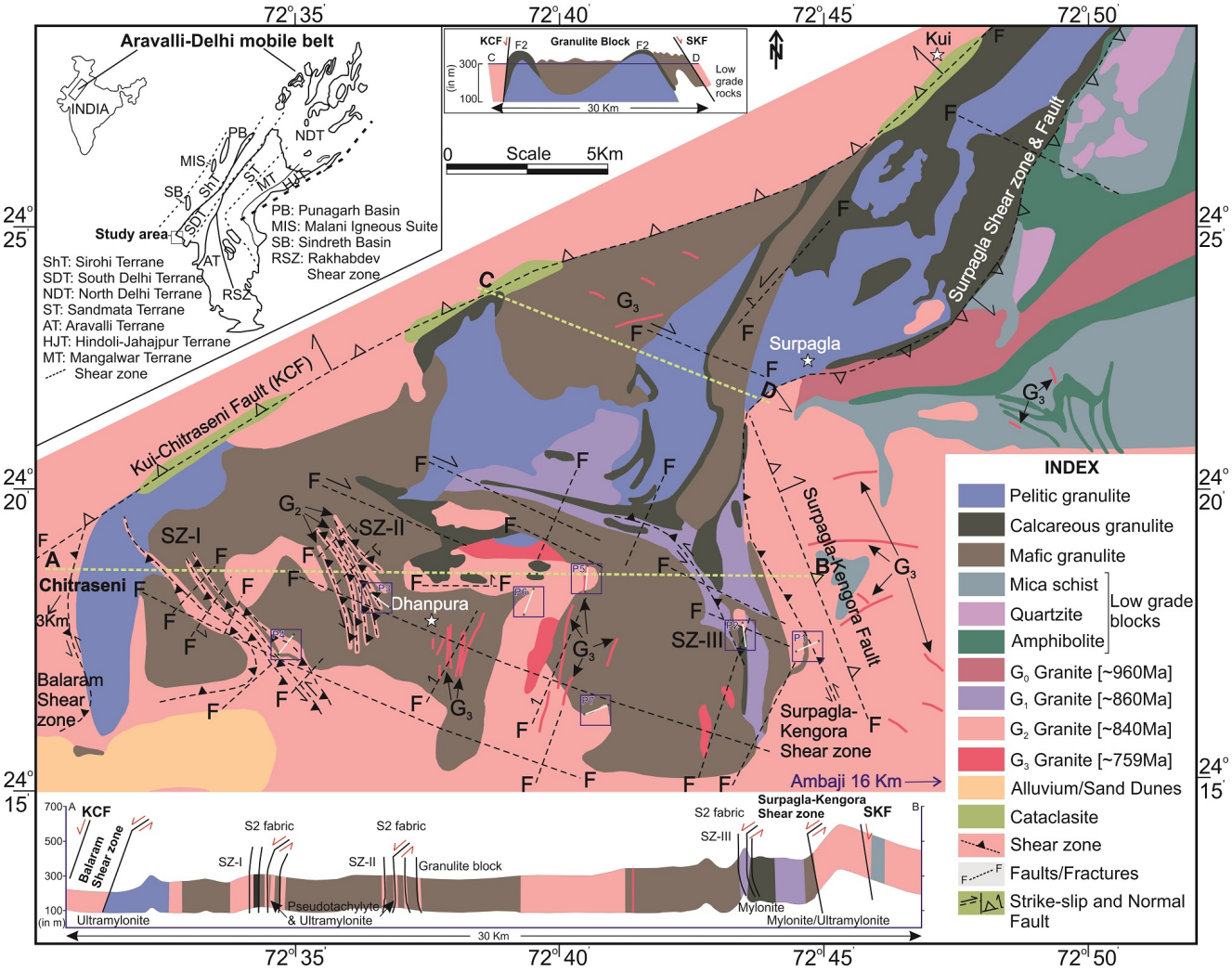
*Rudra Mohan Pradhan[1], Tapas Kumar Biswal[1]

1. Department of Earth Sciences, Indian Institute of Technology Bombay, India

The flow and occurrence of groundwater in Precambrian basement rock aquifers are mainly governed by various factors such as geologic structures, lithology, fault and fracture densities, and topography. The study attempts to investigate sustainable groundwater resources to meet the demand in semi-arid Precambrian basement terrane using integrated field-based structural, geophysical, and hydrogeological approaches. The study area is a part of the Aravalli Delhi Mobile Belt (ADMB) that comprises low to high-grade rocks. Structural features such as brittle and ductile shear zones have mapped in detail followed by subsurface resistivity tomography for mapping deep-seated aquifers. The paleostress results from the fault slip data show two prominent stress regimes i.e. NE-SW and NW-SE extensional regimes in the study area. Further, resistivity imaging data have been collected based on the structural features in 07 different locations and interpreted to obtain the resistivity parameters and to locate high yielding groundwater bearing zones. For a pilot study, a total of 06 boreholes (150 m depth) were drilled for pumping test analysis based on the acquired structural and geophysical data. The study reveals that the high yielding aquifers (Q=180-220 lpm) are confined to ductile shear zones than brittle shear zones. Thus, the hydrogeological importance of various factors related to movement and occurrence of groundwater presented here will provide a basis for future water supply development programs to meet the groundwater needs.

Keywords: Brittle and Ductile Shear zones, Precambrian terranes, Sustainable groundwater resources

©2020. Japan Geoscience Union. All Right Reserved.



©2020. Japan Geoscience Union. All Right Reserved.

[E] Poster | U (Union)：Union

[U-04] International Efforts Supporting Global Navigation Satellite System-Enhanced Tsunami Early Warning

convener:Rundle John B(University of California Davis), Kazuyoshi Nanjo(University of Shizuoka), Eiichi Fukuyama(Kyoto University / National Research Institute for Earth Science and Disaster Resilience)

With little to no warning more than 230,000 lives were lost to the Great Indian Ocean Tsunami of December 26, 2004. This devastating loss of life focused the efforts of scientists, engineers and politicians to strengthen tsunami early warning systems beginning with an accurate and rapid estimate of tsunami potential. A combined network of seismic and geodetic sensors quickly emerged as an accurate, efficient, and cost effective enhancement to tsunami early warning systems for those at risk communities nearest the earthquake epicenter. In the months following the Great Indian Ocean Tsunami, geophysicists demonstrated that analysis the GPS network of the Global Geodetic Observing System could have provided warning within 15 minutes after the Sumatran earthquake if the network data were available in real time. On March 11, 2011, the Tohoku-oki earthquake and tsunami unleashed another terrible tragedy upon the Japanese people and posed great challenges to the Japanese government. The Tohoku-oki earthquake occurred off shore from the world's most advanced GPS network, the GEONET, designed and operated by The Geospatial Information Authority of Japan (GSI). The Tohoku-oki earthquake did underscore the potential and extraordinary societal value of Global Navigation Satellite Systems (GNSS) to tsunami warning systems. Several retrospective studies of the Tohoku-oki earthquake deformation captured by the GEONET demonstrated that accurate tsunami inundation predictions could be provided within 5 minutes of the earthquake occurrence.

In this session, we solicit papers on topics related to the realization of such a system, including instrumentation, data collection and availability, modeling, forecasting/nowcasting, and software development, as well as capacity building and linkages to international organizations, the Sendai Framework for Disaster Risk Reduction, and UN Sustainable Development Goals.

[U04-P01] GNSS total electron content for ionospheric tsunami early warning

Tien-Chi Liu[1], Katsumi Hattori[2], *JANN-YENQ Liu[3,4,5], CHIYEN LIN[3,4], Yu-Lin Tsai[1], Tso-Ren Wu[1]
(1.Graduate Institute of Hydrological and Oceanic Sciences, National Central University, Taiwan, 2.Graduate School of Science, Chiba University, Japan, 3.Center for Astronautical Physics and Engineering, National Central University, Taiwan, 4.Department of Space Science and Engineering, National Central University, Taiwan, 5.Center for Space and Remote Sensing Research, National Central University, Taiwan)

GNSS total electron content for ionospheric tsunami early warning

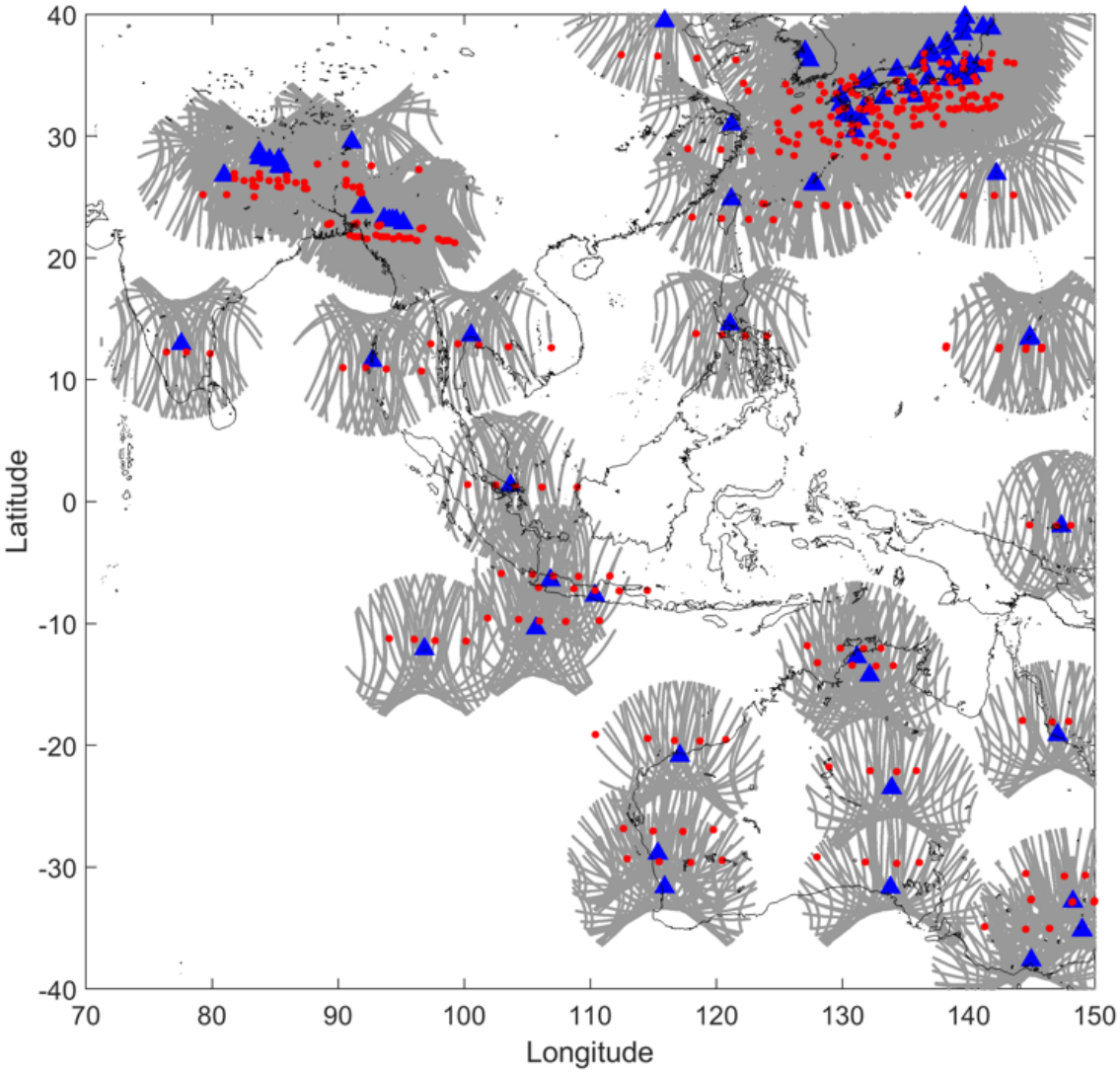
Tien-Chi Liu[1], Katsumi Hattori[2], *JANN-YENQ Liu[3,4,5], CHIYEN LIN[3,4], Yu-Lin Tsai[1], Tso-Ren Wu[1]

1. Graduate Institute of Hydrological and Oceanic Sciences, National Central University, Taiwan, 2. Graduate School of Science, Chiba University, Japan, 3. Center for Astronautical Physics and Engineering, National Central University, Taiwan, 4. Department of Space Science and Engineering, National Central University, Taiwan, 5. Center for Space and Remote Sensing Research, National Central University, Taiwan

Tsunami waves can induce Tsunami Traveling Ionospheric Disturbances (TTIDs) of the total electron content (TEC). In this study, we examine the TEC derived by ground-based receivers of the global positioning system (GPS) and identify TTIDs induced by 2004 Indian Ocean tsunami. Simulations of the COMCOT (Cornell Multi-grid Coupled Tsunami) model and analyses of the circle method, the ray-tracing technique, and the beam-forming technique are used to show that TTIDs can be quickly detected and confirmed after the tsunami occurrence. Finally, the ionospheric TEC derived by existing ground-based GNSS (global navigation satellite systems) receiving stations is demonstrated to be useful to support the tsunami early warning system.

Keywords: ionospheric total electron content, tsunami early warning, global navigation satellite system

©2020. Japan Geoscience Union. All Right Reserved.



©2020. Japan Geoscience Union. All Right Reserved.

[E] Poster | U (Union)：Union

[U-05] Advanced understanding of Quaternary and Anthropocene hydroclimate changes in East Asia

convener:Chuan-Chou Shen(High-Precision Mass Spectrometry and Environment Change Laboratory, Department of Geosciences, National Taiwan University), Yusuke Yokoyama(Atmosphere and Ocean Research Institute, University of Tokyo), Kaoru Kubota(Graduate School of Human Development and Environment, Kobe University), Li Lo(Department of Geosciences, National Taiwan University)

For the sustainability of biosphere and human society, it is crucial to in-depth understand Earth climate system changes on different timescales in Quaternary. Anthropogenic forcing is also strongly affecting different aspects of human living environments, natural ecological through physical and chemical climatic perturbations, especially in East Asia with swift economic takeoff in the recent decades. We welcome climate and environmental reconstructions based on natural archives, proxy data, numerical simulations especially on the topics of monsoon, precipitation belt shifting, typhoon, and drought histories in Quaternary and Anthropocene. Atmospheric and oceanic interactions, greenhouse gases radiative forcing and anthropogenic forcing impact from regional to global scale are also welcomed.

[U05-P01] Precessionally Paced Foraminifera-bound Nitrogen Isotope Variations in the Solomon Sea Influenced by Eastern Equatorial Pacific Upwelling Intensity

★Invited Papers

*Haojia Abby Ren[1], Wei-Ning Fang[1], Yi-Chi Chen[1], Kuo-Yen Wei[1], Chuan-Chou Shen[1] (1.National Taiwan University)

[U05-P02] Annual record of boron isotopes of massive *Porites* coral skeleton from Chichijima Island in the western North Pacific

*Kaoru Kubota[1], Ryo Nakano[2], Masafumi MURAYAMA[2], Tsuyoshi Ishikawa[1], Yusuke Yokoyama[3], Atsushi Suzuki[4] (1.Kochi Institute for Core Sample Research, JAMSTEC, 2.Faculty of Agriculture and Marine Science, Graduate School of Integrated Arts and Sciences, Kochi University, 3.Atmosphere and Ocean Research Institute, The University of Tokyo, 4.Geological Survey of Japan, National Institute of Advanced Industrial Science and Technology)

[U05-P03] Gauging Quaternary Sea Level Changes using various sea level indicators and GIA model

*Yusuke Yokoyama[1], Anthony Purcell[2], Takeshige Ishiwa[3] (1.Atmosphere and Ocean Research Institute, University of Tokyo, 2.Research School of Earth Sciences, The Australian National University, 3.National Institute of Polar Research)

[U05-P04] Sea-level change in Tongatapu, the Kingdom of Tonga for the last 3000 years based on local marine reservoir effect and geophysical modeling

*Naoto Fukuyo[1,2], Anthony Purcell[3], Geoffrey Clark[4], Phillip Parton[4], Yusuke Yokoyama[1,2] (1.Atmosphere and Ocean Research Institute, The University of Tokyo, 2.Department of Earth and Planetary Sciences, Faculty of Science, The University of Tokyo, 3.Research School of Earth Sciences, The Australian National University, 4.College of Asia and the Pacific, Australian National University)

[U05-P05] High-resolution Holocene records of a stalagmite from maritime Japan

*Shota Amekawa[1], Akihiro Kano[1], Kenji Kashiwagi[2], Taiki Mori[3], Fumito Shiraishi[4], Chuan-Chou Shen[5,6,7] (1.Graduate School of Science, The University of Tokyo, 2.Department of Environmental Biology and Chemistry, Faculty of Science, University of Toyama, 3.Graduate School of Integrated Sciences for Global Society, Kyushu University, 4.Department of Earth and Planetary Systems Science, Graduate School of Science, Hiroshima University, 5.High-precision Mass Spectrometry and Environment Change Laboratory (HISPEC), Department of Geosciences, National Taiwan University, 6.Global Change Research Center, National Taiwan University, 7.Research Center for Future Earth, National Taiwan University)

[U05-P06] Mg/Ca and stable oxygen isotopes of individual foraminifera in the tropics: Climate variability or ecology?

★Invited Papers

*Sze Ling Ho[1], Jeroen Groeneveld[2,3], Andreas Mackensen[4], Mahyar Mohtadi[3], Thomas Laepple[2] (1.Institute of Oceanography, National Taiwan University, 10617 Taipei, Taiwan, 2.Alfred Wegener Institute, Helmholtz Center for Polar and Marine Research, Telegrafenberg A45, D-14473 Potsdam, Germany, 3.MARUM-Center for Marine Environmental Sciences, University of Bremen, Klagenfurter Strasse 2-4, D-28359 Bremen, Germany, 4.Alfred Wegener Institute, Helmholtz Center for Polar and Marine Research, Am Alten Hafen 26, D-27568 Bremerhaven, Germany)

[U05-P07] Insight to Western Pacific circulation from coral skeletal radiocarbon

*Shoko Hirabayashi[1,2,3], Yusuke Yokoyama[2,3], Atsushi Suzuki[4], Tezer Esat[5], Yosuke Miyairi[2], Takahiro Aze[2], Fernando Siringan[6], Yasuo Maeda[7], Hironobu Kan[1] (1.Faculty of Social and Cultural Studies, Kyushu University, 2.Atmosphere and Ocean Research Institute, The University of Tokyo, 3.Department of Earth and Planetary Science, Graduate School of Science, The University of Tokyo, 4.Geological Survey of Japan, National Institute of Advanced Industrial Science and Technology (AIST), 5.Research School of Earth Sciences, The Australian National University, 6.Marine Science Institute, University of the Philippines, 7.Institute of Natural and Environmental Sciences, University of Hyogo)

[U05-P08] Surface productivity and potential terrestrial ecology system in the central Okhotsk Sea during the middle-early Pleistocene

*Li Lo[1], Lukas Smik[2], Simon T. Belt[2] (1.Department of Geosciences, National Taiwan University, 2.School of Geography, Earth and Environmental Sciences, University of Plymouth)

[U05-P09] **Lake water distribution derived from surface water oxygen and hydrogen isotopes around Fuji Five Lakes**

*Ota Kosuke[1,2], Yusuke Yokoyama[1,2], Yosuke Miyairi[2], Shinya Yamamoto[3], Toshihiro Miyajima[2] (1.University of Tokyo, 2.Atmosphere and Ocean Research Institute, The University of Tokyo, 3.Mount Fuji Research Institute, Yamanashi Prefectural Government,)

[U05-P10] Carbon and oxygen isotopes and ^{14}C age of travertine and spring water in NW Iran

*Yubo Zhang[1], Yoshihiro Asahara[1], Masayo Minami[2], Masaki kaneko[1], Hadi Amin-Rasouli[3], Hossein Azizi[3] (1.Graduate School of Environmental Studies, Nagoya Univercity , 2.Institute for Space Earth Environmental Research, Nagoya University, 3.University of Kurdistan)

Precessionally Paced Foraminifera-bound Nitrogen Isotope Variations in the Solomon Sea Influenced by Eastern Equatorial Pacific Upwelling Intensity

*Haojia Abby Ren[1], Wei-Ning Fang[1], Yi-Chi Chen[1], Kuo-Yen Wei[1], Chuan-Chou Shen[1]

1. National Taiwan University

The surface water in the Western Equatorial Pacific (WEP), although is depleted with nitrate and other major nutrients, bears isotopic signature of partial nitrate assimilation in the nutrient-rich Eastern Equatorial Pacific (EEP). Driven by the easterlies, Equatorial Under Current upwells to the surface of the EEP, where biological uptake only partially consumes nitrate and leaves the remaining nitrate enriched in its nitrogen isotopic composition. Through multiple cycles of uptake and remineralization, the elevated nitrogen isotopic composition is recorded by organic matter and is spread out to regions away from the EEP, partly causing the WEP thermocline nitrate $\delta^{15}N$ to be much more elevated than the global mean. We then expect the $\delta^{15}N$ in the WEP to be sensitive to the expansion and shrinking of the EEP high nutrient region during past climatic cycles.

This study reports foraminifera-bound $\delta^{15}N$ (FB-$\delta^{15}N$) of two planktonic species –*Globigerinoides sacculifer* and *Globigerinoides ruber* –from a sediment core in the Solomon Sea over the last 158 ka. The FB-$\delta^{15}N$ values, similar between the two species, fall between 7‰ to 13‰. The core-top FB-$\delta^{15}N$ (9.2‰) is approximately equal to the modern subsurface nitrate $\delta^{15}N$ (9.4‰), the dominate nitrate source to the Solomon Sea surface. The FB-$\delta^{15}N$ values are significantly elevated during periods with high local summer/fall insolation with a strong precessional pacing. While without a clear glacial/interglacial difference, at both terminations, the FB-$\delta^{15}N$ hits lowest values (~8.3‰) before an abrupt increase.

The lack of clear glacial/interglacial change, yet a strong precessional pacing in the Solomon Sea FB-$\delta^{15}N$ record, implies a low latitude control and an insignificant influence from oxygen minimum zones in the eastern tropical Pacific. Supported by modern hydrologic data and modeling exercises, we argue that the variations in our FB-$\delta^{15}N$ record reflects changes in the EEP surface nutrient status, such that expansions of the high nitrate pool cause the observed high FB-$\delta^{15}N$ values. Together with reconstruction in the EEP paleoproductivity, our record strongly indicates enhanced EEP upwelling during periods with local insolation maximum, consistent with previous modelling studies showing a strong precessional control on ENSO evolution.

Keywords: Equatorial Pacific, Foraminifera-bound nitrogen isotopes, Precessional

©2020. Japan Geoscience Union. All Right Reserved.

Annual record of boron isotopes of massive *Porites* coral skeleton from Chichijima Island in the western North Pacific

*Kaoru Kubota[1], Ryo Nakano[2], Masafumi MURAYAMA[2], Tsuyoshi Ishikawa[1], Yusuke Yokoyama[3], Atsushi Suzuki[4]

1. Kochi Institute for Core Sample Research, JAMSTEC, 2. Faculty of Agriculture and Marine Science, Graduate School of Integrated Arts and Sciences, Kochi University, 3. Atmosphere and Ocean Research Institute, The University of Tokyo, 4. Geological Survey of Japan, National Institute of Advanced Industrial Science and Technology

Long-term pH record in the surface ocean is limited to the very recent period, for the last three decade, hampering our understanding of natural variability of surface seawater pH and recent anthropogenic decline due to surface ocean carbon dioxide concentration increase (ocean acidification). Boron isotope composition of skeleton of long-living massive Porites coral, a known seawater pH proxy, can potentially provide continuous, long-term record. Here we present result of boron isotope measurement for the century-long living massive *Porites* coral from Chichijima Island in the western North Pacific in annual time resolution. Boron isotope ratio was measured by using multi-collector ICPMS, Thermo Scientific *Neptune* installed at Kochi Core Center, in a precision of ±0.1 permil (2 standard deviation). A method of boron isotope measurement for the coral sample was modified from the previous application, namely anion exchange column was skipped to make the measurement simple and enhance the sample throughput. The new annually resolved boron isotope record shows good agreement with previously reported one from Guam Island, at least in decadal timescales.

Keywords: boron isotope, multi-collector ICPMS, ocean acidification

©2020. Japan Geoscience Union. All Right Reserved.

Gauging Quaternary Sea Level Changes using various sea level indicators and GIA model

*Yusuke Yokoyama[1], Anthony Purcell[2], Takeshige Ishiwa[3]

1. Atmosphere and Ocean Research Institute, University of Tokyo, 2. Research School of Earth Sciences, The Australian National University, 3. National Institute of Polar Research

Past sea level indicators play a key role in tracking the history of global climate. Variations in global sea level are controlled mainly by growth and decay of continental glaciers and temperatures that are closely correlated with the mean global climate state (glacial and interglacial cycles). Our understanding of global climate and sea level has benefited significantly from improvements in ocean floor sampling as well as from the application of new analytical techniques and isotope mass spectrometry. This presentatin will overview of recent advances in paleo-sea level studies based on analysis of samples and data from deep-sea sediment cores and drowned coral reefs.

Keywords: Sea level, glacier, Paleoclimate

©2020. Japan Geoscience Union. All Right Reserved.

Sea-level change in Tongatapu, the Kingdom of Tonga for the last 3000 years based on local marine reservoir effect and geophysical modeling

*Naoto Fukuyo[1,2], Anthony Purcell[3], Geoffrey Clark[4], Phillip Parton[4], Yusuke Yokoyama[1,2]

1. Atmosphere and Ocean Research Institute, The University of Tokyo, 2. Department of Earth and Planetary Sciences, Faculty of Science, The University of Tokyo, 3. Research School of Earth Sciences, The Australian National University, 4. College of Asia and the Pacific, Australian National University

Reconstructing the history of Holocene relative sea levels around Tonga provides essential constraints on the recent geological evolution of this region and paleoenvironmental context for archaeological studies. However, there are few sea-level records currently available from the region, and no quantitative paleoenvironmental studies using geochemical/physical methods have been reported. In this study, we reconstruct sea-level histories for Tongatapu island using radiocarbon measurements and glacio-hydro-isostatic adjustment (GIA). Our analyses suggest that changes in the average size of bivalves (Gafrarium tumidum) are synchronous with corresponding changes in the paleoenvironment. These changes also correspond to the timing of the increase of local marine reservoir effects (ΔR) from 219±78 to 376±69. Sea surface salinity (SSS) changes within Fanga ' Uta lagoon were also synchronous with these changes caused by a gradual decrease in the exchange of water in and out of the lagoon. Salinity seems to have been higher than present at approximately 2.6 cal kyr BP, suggesting an embayment that was relatively open to the ocean. Predicted mid-Holocene sea level height using GIA modeling indicates less than 1 m above sea level in Tongatapu, suggesting that previously reported observations of mid-Holocene high stand require additional factors other than GIA. Furthermore, present-day satellite-based observed (i.e., GPS) vertical uplift rate in Tongatapu is ten orders of magnitude higher than the long-term uplift rate obtained from Holocene sea-level data.

Keywords: Holocene, Southern Pacific, Local marine reservoir effect, GIA modeling, Bivalves

©2020. Japan Geoscience Union. All Right Reserved.

High-resolution Holocene records of a stalagmite from maritime Japan

*Shota Amekawa[1], Akihiro Kano[1], Kenji Kashiwagi[2], Taiki Mori[3], Fumito Shiraishi[4], Chuan-Chou Shen[5,6,7]

1. Graduate School of Science, The University of Tokyo, 2. Department of Environmental Biology and Chemistry, Faculty of Science, University of Toyama, 3. Graduate School of Integrated Sciences for Global Society, Kyushu University, 4. Department of Earth and Planetary Systems Science, Graduate School of Science, Hiroshima University, 5. High-precision Mass Spectrometry and Environment Change Laboratory (HISPEC), Department of Geosciences, National Taiwan University, 6. Global Change Research Center, National Taiwan University, 7. Research Center for Future Earth, National Taiwan University

In East Asia, the climatic factor for the lowered meteoric water $\delta^{18}O$ during mid-Holocene than the last glacial period is still controversial. Previous interpretations on stalagmite $\delta^{18}O$ were recently re-examined with new records from the maritime Japan, in eastern part of the Asian monsoon region beyond the influence from Indian summer monsoon (Mori et al. 2018). However, their stalagmite presented limited records in the Holocene section because of low growth rate. Here, we report another stalagmite from the same cave (Kiriana cave in Mie Prefecture), which provides high-resolution records of stable isotopes and trace element during Holocene.

The ages of the 34-cm-long stalagmite were determined at 17 horizons through Uranium-Thorium dating method at the National Taiwan University. Stable isotopes were measured at 0.2-mm intervals using an isotope ratio mass spectrometer (Thermo Finnigan DeltaPlus) connected with an on-line gas separation and introduction system (GASBENCH II) at the Kyushu University. Trace element analysis was performed with inductivity coupled plasma optical emission spectrometer (iCAP7200, Thermo Fisher Scientific) at the Hiroshima University.

The stalagmite $\delta^{18}O$ displays similar temporal patterns with the Chinese records but exhibits much smaller amplitude of $\delta^{18}O$ than the Chinese records. This result supports the idea of Mori et al. (2018) that the stalagmite $\delta^{18}O$ record from this cave is a superimposed signal of variations in air temperature and seawater $\delta^{18}O$, rather than the hydroclimatic control on meteoric water $\delta^{18}O$. On the other hand, $\delta^{13}C$ of the stalagmite has more than 2‰ shift from mid- to late-Holocene with ~1‰ excursions in millennial timescale. The variation synchronized with Mg/Ca suggests that the $\delta^{13}C$ change is largely affected by prior calcite precipitation (PCP) from the infiltrating water in the karst bedrock, which generally increases under a dry condition. Supposing that $\delta^{13}C$ record of this stalagmite reflects PCP induced by precipitation change, we propose that precipitation or EASM variability is recorded more clearly in $\delta^{13}C$ rather than $\delta^{18}O$ of stalagmite in maritime Japan.

Keywords: Stalagmite, Stable isotope, Trace element, East Asian summer monsoon, Holocene

©2020. Japan Geoscience Union. All Right Reserved.

Mg/Ca and stable oxygen isotopes of individual foraminifera in the tropics: Climate variability or ecology?

*Sze Ling Ho[1], Jeroen Groeneveld[2,3], Andreas Mackensen[4], Mahyar Mohtadi[3], Thomas Laepple[2]

1. Institute of Oceanography, National Taiwan University, 10617 Taipei, Taiwan, 2. Alfred Wegener Institute, Helmholtz Center for Polar and Marine Research, Telegrafenberg A45, D-14473 Potsdam, Germany, 3. MARUM-Center for Marine Environmental Sciences, University of Bremen, Klagenfurter Strasse 2-4, D-28359 Bremen, Germany, 4. Alfred Wegener Institute, Helmholtz Center for Polar and Marine Research, Am Alten Hafen 26, D-27568 Bremerhaven, Germany

Foraminifera are commonly used in paleoclimate reconstructions as they occur throughout the world's oceans and are often abundantly preserved in the sediments. Traditionally, foraminifera-based proxies like $d^{18}O$ and Mg/Ca are analyzed on pooled specimens of a single species. Analysis of single specimens of foraminifera allows reconstructing climate variability on timescales related to El Niño-Southern Oscillation (ENSO) or seasonality, thus has the potential to shed more light on the hydroclimate changes in regions such as East Asia. However, quantitative calibrations between the statistics of individual foraminiferal analyses (IFA) and climate variability are still missing. We performed Mg/Ca and $d^{18}O$ measurements on single specimens from surface sediments (modern to 300 years old) from different settings to better understand the signal recorded by individual foraminifera. We used three species of planktic foraminifera (*G. ruber* (s.s.), *T. sacculifer*, and *N. dutertrei*) from the Indo-Pacific Warm Pool (IPWP) and one species (*G. ruber* (pink)) from the Gulf of Mexico (GoM). The Mg/Ca-$d^{18}O$ relationships for different species agree well with published calibrations. IFA statistics (both mean and standard deviation) of Mg/Ca and $d^{18}O$ between the different sites show a strong relationship indicating that both proxies are influenced by a common factor, most likely temperature variations during calcification. This strongly supports the use of IFA to reconstruct climate variability. However, our combined IFA data for the different species only show a weak relationship to seasonal and interannual temperature changes, especially when seasonal variability increases at a location. This suggests that the season and depth habitat of the foraminifera strongly affect IFA variability, such that ecology needs to be considered when reconstructing past climate variability. Further studies on surface sediments and depth-stratified plankton tows would allow better characterization of IFA signal, and ultimately improve the robustness of IFA-based climate variability reconstructions.

Keywords: Climate variability, Individual foraminifer analyses, Planktic foraminifera, Mg/Ca, d18O

©2020. Japan Geoscience Union. All Right Reserved.

Insight to Western Pacific circulation from coral skeletal radiocarbon

*Shoko Hirabayashi[1,2,3], Yusuke Yokoyama[2,3], Atsushi Suzuki[4], Tezer Esat[5], Yosuke Miyairi[2], Takahiro Aze[2], Fernando Siringan[6], Yasuo Maeda[7], Hironobu Kan[1]

1. Faculty of Social and Cultural Studies, Kyushu University, 2. Atmosphere and Ocean Research Institute, The University of Tokyo, 3. Department of Earth and Planetary Science, Graduate School of Science, The University of Tokyo, 4. Geological Survey of Japan, National Institute of Advanced Industrial Science and Technology (AIST), 5. Research School of Earth Sciences, The Australian National University, 6. Marine Science Institute, University of the Philippines, 7. Institute of Natural and Environmental Sciences, University of Hyogo

Radiocarbon ($\Delta^{14}C$) in seawater is used as a reliable tracer of water mass advection and mixing in water bodies. The calcium carbonate (aragonite) skeletons of reef-building corals contain annual density bands that records the $\Delta^{14}C$ values of surface water at the time at which the coral skeletons took up dissolved inorganic carbon from ambient seawater. Thus, coral skeletal $\Delta^{14}C$ records can also be used as a sensitive proxy of water mass mixing. $\Delta^{14}C$ values for the pre-bomb period can be also used for estimation of local marine reservoir age (R) and their regional offset (ΔR), which varies not only spatially, but also temporally because of changes in ocean circulation associated with climatic changes. Compiling coral skeletal $\Delta^{14}C$ datasets in the western Pacific will contribute to our understanding of the oceanography of the region and can be used for discussion of its relationship to climate change such as El Nino-Southern Oscillation.

In this study, high-resolution coral skeletal $\Delta^{14}C$ dataset during the Anthropocene and Holocene are reported from the western Pacific. Our $\Delta^{14}C$ data indicates a significant increase in $\Delta^{14}C$ from 1946 to 1994 related to atmospheric nuclear bomb testing, with more rapid increase in the South China Sea (SCS) than in the Pacific. The unusual, rapid $\Delta^{14}C$ increase (early bomb-^{14}C spikes) in the 1950s related to the “close-in fallout” found in our SCS and Ryukyu corals. Although three early bomb-^{14}C spikes have been reported from Guam and from Ishigaki, only one such spike was clearly detected in the SCS. The amplitude of the bomb-^{14}C spike in the SCS was less than half that in Ishigaki, likely due to upwelling around Luzon Island and the Kuroshio intrusion into the SCS. We also calculated ΔR during the Holocene using paired analyses of $\Delta^{14}C$ and ^{230}Th on pristine corals. An abrupt ΔR shift occurred between 5.5 ka BP and 4.0 ka BP in the northwest Pacific. Compared with the previously reported data from the Tropical East Pacific and Great Barrier reef, the timing of the shift was different because the ^{14}C content of the northwestern Pacific was affected by not only the intensity of upwelling at the Peru-Chile coast, but also by the East Asian monsoon.

Keywords: Coral, Western Pacific, Radiocarbon, East Asian monsoon, Kuroshio

©2020. Japan Geoscience Union. All Right Reserved.

Surface productivity and potential terrestrial ecology system in the central Okhotsk Sea during the middle-early Pleistocene

*Li Lo[1], Lukas Smik[2], Simon T. Belt[2]

1. Department of Geosciences, National Taiwan University, 2. School of Geography, Earth and Environmental Sciences, University of Plymouth

Here we present the first multi sterol biomarkers results from the central Okhotsk Sea using Site MD01-2414 (53°11.77’ N, 149°34.80’ E, water depth 1123 m) during the past 1.2-1.5 million years ago (Ma). We measured brassicalsterol, campesterol, and beta-sitosterol. Results show that the brassicalsterol, campesterol and beta-sitosterol varied from 0-1200, 0-12 and 10-40 ng g^{-1} dried sediment, respectively. The brassicalsterol shows both significant 23- and 41-kyr cycles, where the campesterol and beta-sitosterol show only precession cycle. This is the first report of sterols variations in the central Okhosk Sea during the 41-kyr world. Brassicalsterol variations may be mixed with surface productivity changes and terrestrial organic matter input, meanwhile the potential use of campesterol and beta-sitosterol as regional terrestrial plant biota changes may need further geographical verification in the future.

Keywords: Okhotsk Sea, Pleistocene, Surface productivity, Terrestrial biota

©2020. Japan Geoscience Union. All Right Reserved.

Lake water distribution derived from surface water oxygen and hydrogen isotopes around Fuji Five Lakes

*Ota Kosuke[1,2], Yusuke Yokoyama[1,2], Yosuke Miyairi[2], Shinya Yamamoto[3], Toshihiro Miyajima[2]

1. University of Tokyo, 2. Atmosphere and Ocean Research Institute, The University of Tokyo, 3. Mount Fuji Research Institute, Yamanashi Prefectural Government,

The process of water flowing into lakes through precipitation, groundwater, and river water varies depending on the region and season, and it is important to clarify the details in order to know the state of the lake in the future. In previous studies, oxygen and hydrogen isotope ratios have been widely used as effective tools for estimating the origin of precipitation and groundwater.
The results of oxygen and hydrogen isotope ratios in precipitation and groundwater have been reported around Mt. Fuji. However, it is difficult to estimate the groundwater catchment area in the northern part of Mt. Fuji where Fuji Five Lakes are located due to the lack of oxygen and hydrogen isotope data compared to the southern and eastern parts.Results of oxygen and hydrogen isotope ratios in precipitation and groundwater have been reported around Mt. Fuji. However, it is only reported that the oxygen isotope / hydrogen isotope ratio is lighter in the northern ridge of Mt. Fuji, where Fuji Five Lakes are located, than in the southern and eastern ridges.
For example, in Lake Motosu, continuous surveys of surface water vanadium concentration, water temperature and water quality surveys in summer and winter, and vertical surveys of water temperature and water quality throughout the year, show that precipitation accounts for a large part of the water balance. However, since the northern foot of Mt. Fuji was formed by a lava flow, it is difficult to identify the catchment area and was necessary to consider the groundwater flow between Lakes Motosu, Shoji, and Sai.
In the hydrological survey and lake bottom survey of Lake Kawaguchi, at the observation point about 100 m east of Unoshima located in the center of the lake, disturbances in the stratified structure of water temperature and electrical conductivity were observed, and from the bottom of the lake at a depth of about 8 m, the outflow of water with different water quality was newly confirmed.
As described above, continuous accumulation of data is small in the Fuji Five Lakes area, and since the surroundings of Fuji Five Lakes are complex topography with lava, estimation of the groundwater catchment area only from the results of oxygen and hydrogen isotope ratios was difficult.
In this study, the oxygen and hydrogen isotopes of the lake water of Fuji Five Lakes are continuously measured at monthly intervals. Therefore, the surface water of Fuji Five Lakes was collected periodically at monthly intervals from June 2018, and the oxygen and hydrogen isotope ratios of the lake water were measured. A wavelength scan cavity ring-down spectrometer of the Institute of Atmosphere and Ocean Research, The University of Tokyo was used for the measurement. In addition, the results of the groundwater measurement and the water balance study were combined to give a comprehensive discussion, and seasonal changes in the oxygen isotope ratio of Fuji Five Lakes and the groundwater catchment area of Fuji Five Lakes were estimated.
Lakes Kawaguchi, Sai and Yamanaka tended to have higher isotopic ratios during the summer. This result is consistent with the strong effect of evaporation in summer. On the other hand, isotope ratio in Lake Motosu became lighter in summer. Since Lake Motosu is located near the Pacific Ocean, there is a possibility that precipitation with different travel routes is supplied in summer.
In addition to the above results, the groundwater catchment area of Fuji Five Lakes is estimated by comprehensively considering the measurement results of groundwater around the lake and the results of water balance studies.

©2020. Japan Geoscience Union. All Right Reserved.

Keywords: Oxgen and hydrogen isotopes, Fuji Five Lakes

©2020. Japan Geoscience Union. All Right Reserved.

Carbon and oxygen isotopes and ^{14}C age of travertine and spring water in NW Iran

*Yubo Zhang[1], Yoshihiro Asahara[1], Masayo Minami[2], Masaki kaneko[1], Hadi Amin-Rasouli[3], Hossein Azizi[3]

1. Graduate School of Environmental Studies, Nagoya Univercity , 2. Institute for Space Earth Environmental Research, Nagoya University, 3. University of Kurdistan

Travertine is calcium carbonate precipitated from spring water, groundwater and so on and is widely distributed in northwest Iran. It is one of suitable samples which can reconstruct paleoenvironment on land with a high resolution because of its high deposition rate (1 –20 mm/yr) (Henning et al., 1983; Liu et al., 2003). In this study, we focus on one of the travertine hills in northwest Iran, and discuss the formation age and source of the travertine based on a series of data for ^{14}C, $\delta^{13}C$, $\delta^{18}O$ and major and trace elements.

More than 20 travertine rock samples were collected from the base to the top of a travertine hill in the Takab area, NW Iran. The elevation of the travertine hill is about 60 m. A fault is found near the base of the hill. Several water samples from springs of various sizes (10 cm to 100 m) were collected near the hill in October 2018 and May 2019 to compare the isotope and chemical compositions between the travertine and spring water.

Firstly, ^{14}C concentrations were measured for the travertine rocks and dissolved inorganic carbon (DIC) in the spring water samples by AMS, and $\delta^{13}C$ and $\delta^{18}O$ were determined by IR-MS. Then, major (Ca, Mg) and trace elements (As, Sr, REE, etc.) were analyzed by ICP-MS.

The ^{14}C ages for the travertines range from 42 kBP to 22 kBP. Above the fault, as the elevation increases, the ^{14}C age tends to get younger, but not monotonically. The ^{14}C age of the hill top is 25 kBP. DIC of large spring water has a younger ^{14}C age (18 kBP) than that of small spring water (31 kBP). When we assume that the travertine was precipitated from the small spring like water (31 kBP), we cannot calculate formation age ofn the hill top travertine. Therefore, the large spring water is assumed as the source spring water for the hilltop travertine at the hill top. Based on this assumption and the ^{14}C data, the formation age at the hill top can be estimated as 8–5 ka. In addition, one of the estimation on the growth rate is approximately 5 mm/yr.

The carbon stable isotope compositions ($\delta^{13}C$) is +7 to +12‰, indicating that the travertine is thermogene. Above the fault, the $\delta^{13}C$ value gradually decreases from the base to the top. The $\delta^{13}C$ value at the base (~+10‰) is higher than that at the hill top (~+7‰). So it is assumed that, during the formation of travertine, the travertine spring water type changed from the small spring type water to the large spring type water. In the presentation, we will also discuss data for $\delta^{18}O$ values and major and trace element compositions, possibly indicating paleoclimate and paleotemperature.

Keywords: Travertine, Spring water, 14C age, Oxygen isotope, Carbon isotope

©2020. Japan Geoscience Union. All Right Reserved.

[E] Poster | U (Union)：Union

[U-10] Linking Education and Research Communities in Geosciences: Engaging the Public and Local Communities

convener:Vincent Tong(University College London), Takashi Oguchi(Center for Spatial Information Science, The University of Tokyo), Renee M Clary(Mississippi State University), Keiko Kuge(Department of Geophysics, Graduate School of Science, Kyoto University)

Developing links between research and education is important for maximizing the impact of Earth and Space Sciences and for nurturing a global geoliterate community. Initiatives involving research, education and public engagement abound, building communities that bring educators, researchers and those with dual interests together is, however, not always straightforward. While many researchers are engaged in activities at national and international levels, educators may focus on projects primarily shaped by institutional and national priorities. In this session, we investigate the challenges and opportunities of advancing research-education synergies in Earth and Space Sciences through engaging the general public and local communities. We focus on success stories showcasing educational and outreach initiatives that aim to bring researchers and educators together. Ways of fostering collaborations, evidencing impact and developing leadership will be highlighted. Projects that address the UN Sustainable Development Goals (SDGs) are particularly welcomed.

[U10-P01] Activities of the Committee for School Education, Seismological Society of Japan: Communicating with educators

*Makoto Yamano[1], Ken'ichi Arai[2], Akihiko Ito[3], Yasuyuki Kano[1], Osamu Kuwano[4], Masashige Minamishima[5], Ayako Misawa[6], Eiichi Misawa[7], Hiroo Nemoto[8], Akiko Sato[9], Nobuyuki Yamada[10] (1.The University of Tokyo, 2.Sakae Higashi High School, 3.Utsunomiya University, 4.JAMSTEC, 5.Tokyo Metropolitan High School of Ryogoku, 6.Shizuoka Prefectural Shizuoka Senior High School, 7.Chiba Prefectural Keiyo Senior High School, 8.Ritsumeikan University, 9.Hiratsuka City Nakahara Junior High School, 10.Kochi University)

[U10-P02] Activities of Education and Outreach by the Seismological Society of Japan

*Keiko Kuge[1], Takashi Furumura[2], Mitsuyuki Hoshiba[3], Naoji Koizumi[4], Kazuyuki Nakagawa[5], Masayuki Obayashi[6], Shin'ichi Sakai[2], Katsuhiko Shiomi[7], Keiichi Tadokoro[8], Satoru Tanaka[6], Hiroshi Tsuruoka[2], Takahiko Uchide[9], Makoto Yamano[2] (1.Department of Geophysics, Graduate School of Science, Kyoto University, 2.Earthquake Research Institute, The University of Tokyo, 3.Meterological Research Institute, 4.School of Environmental Science, The University of Shiga Prefecture, 5.Jiji Press, 6.Japan Agency for Marine-Earth Science and Technology, 7.National Research Institute for Earth Science and Disaster Resilience, 8.Earthquake and Volcano Research Center, Nagoya University, 9.Geological Survey of Japan, National Institute of Advanced Industrial Science and Technology)

[U10-P03] 20th Children's Summer School on Seismology and Volcanology in the Tango Peninsula, Japan

*Yasuyuki Kano[1], 20th School Children's Summer Course on Seismology and Volcanology (1.Earthquake Research Institute, The University of Tokyo)

[U10-P04] Development of e-learning materials for GIS exercises in Japan and their outcomes

*Hiroyuki Yamauchi[1], Takashi Oguchi[2], Yuichi S. Hayakawa[3,2], Toshikazu Seto[2] (1.Department of Natural Environmental Studies, Graduate School of Frontier Sciences, The University of Tokyo, 2.Center for Spatial Information Science, The University of Tokyo, 3.Environmental Geography, Faculty of Environmental Earth Science, Hokkaido University)

[U10-P06] Enhancing the impact of sustainability research and education: Distributed leadership as a guiding model

*Vincent Tong[1] (1.University College London)

Activities of the Committee for School Education, Seismological Society of Japan: Communicating with educators

*Makoto Yamano[1], Ken'ichi Arai[2], Akihiko Ito[3], Yasuyuki Kano[1], Osamu Kuwano[4], Masashige Minamishima[5], Ayako Misawa[6], Eiichi Misawa[7], Hiroo Nemoto[8], Akiko Sato[9], Nobuyuki Yamada[10]

1. The University of Tokyo, 2. Sakae Higashi High School, 3. Utsunomiya University, 4. JAMSTEC, 5. Tokyo Metropolitan High School of Ryogoku, 6. Shizuoka Prefectural Shizuoka Senior High School, 7. Chiba Prefectural Keiyo Senior High School, 8. Ritsumeikan University, 9. Hiratsuka City Nakahara Junior High School, 10. Kochi University

The Seismological Society of Japan (SSJ) started various outreaching activities following the 1995 Kobe earthquake. As a component of the activities, the Committee for School Education was formed aiming to communicate with educators for delivering updated knowledge in seismology and solid earth science through school education. The committee members consist of both researchers and school teachers.

The committee has been trying to build communication networks among researchers and school teachers so that they can provide and exchange information on earth science and science education. One of major activities is annual summer school for teachers and university students, which has been held since 1996 at various places visiting sites of geophysical/geological interest. In 2009, the committee also started to conduct teaching certificate renewal courses, lectures and practices which school teachers must take in order to renew their certificates every ten years. Courses are held at about ten sites in cooperation with SSJ members. In conjunction with the SSJ Fall Meeting, two kinds of classes on earthquakes have been given since 2014. One is for children to make simplified seismometers and the other is for school teachers to learn about teaching materials related to earthquakes.

Keywords: Seismological Society of Japan, school education, educator, outreach, earthquake

©2020. Japan Geoscience Union. All Right Reserved.

Activities of Education and Outreach by the Seismological Society of Japan

*Keiko Kuge[1], Takashi Furumura[2], Mitsuyuki Hoshiba[3], Naoji Koizumi[4], Kazuyuki Nakagawa[5], Masayuki Obayashi[6], Shin'ichi Sakai[2], Katsuhiko Shiomi[7], Keiichi Tadokoro[8], Satoru Tanaka[6], Hiroshi Tsuruoka[2], Takahiko Uchide[9], Makoto Yamano[2]

1. Department of Geophysics, Graduate School of Science, Kyoto University, 2. Earthquake Research Institute, The University of Tokyo, 3. Meterological Research Institute, 4. School of Environmental Science, The University of Shiga Prefecture, 5. Jiji Press, 6. Japan Agency for Marine-Earth Science and Technology, 7. National Research Institute for Earth Science and Disaster Resilience, 8. Earthquake and Volcano Research Center, Nagoya University, 9. Geological Survey of Japan, National Institute of Advanced Industrial Science and Technology

Since the occurrence of the 1995 Kobe earthquake, the Seismological Society of Japan (SSJ) has made significant efforts on education and outreach (EO) by setting several committees effective. Development of each committee, which has been supported by the participation of teachers and journalists, has made a wide range of contributions on EO. After the 2011 Tohoku earthquake, the SSJ decided to act in a more comprehensive way in order to promote the EO activities by starting a special committee in 2013 to exchange information of all EO activities in the associated committees and construct comprehensive plans as SSJ. This presentation shows the ongoing EO activities by the SSJ, which are listed below.

- Short courses for the renewal of teaching licenses (every year)
- Annual summer school for teachers
- Annual summer school for kids
- Short class of earthquakes for kids and teachers before/after the SSJ fall meeting
- Activities to support Geoparks (for example, tours in geoparks)
- Training courses concerning the prediction of strong ground motions
- Essays associated with strong ground motions
- Open seminars associated with strong ground motions
- Seminars in earthquake affected areas
- Quarterly magazines ‘Naifuru’ of earthquake topics for the public
- FAQs on earthquakes for the public on the SSJ website
- Mailing list linking between researchers and public
- Press conferences during the SSJ fall meeting and JpGU meeting every year

©2020. Japan Geoscience Union. All Right Reserved.

20th Children's Summer School on Seismology and Volcanology in the Tango Peninsula, Japan

*Yasuyuki Kano[1], Executive Committee for 20th School Children's Summer Course on Seismology and Volcanology

1. Earthquake Research Institute, The University of Tokyo

The 20th Children's Summer School on Seismology and Volcanology was held in the Tango peninsula, part of which is covered by the San’in Kaigan UNESCO Global Geopark, Japan. The main subject of the summer school is the shape of the tango peninsula and the 1927 Kita tango earthquake. The summer school was held on August 10 and 11. The students enjoyed a variety of lectures, experiments, and fieldworks. They also made discussion in small groups to present their summary of the summer school. The stops for the field trip and outdoor experiments includes: Miyazu History Hall, Amanohashidate Sightseeing Boat, Niizaki shrine, Tango Eco-Future Park, Amino station of Hi-net operated by NIED, Amino train station, two outcrops of Goumura fault which appeared at the time of the 1927 earthquake, and Kyotango City Local Museum.

The summer school is organized by the executive committee consists of members from the Seismological Society of Japan (SSJ), the Volcanological Society of Japan (VSJ), the Geological Society of Japan (JGS), and Earth Design School as local organization. The preparation begins in December 2017 by calling for venue of the summer school. The venue, Tango area, is officially announced in March 2018. The executive committee is organized in October 2018. Thirty members of the executive committee share the role of lecturer, facilitator for the entire school or separate group, public relation, logistics, safety officer and so on. The continuous effort to provide the summer school yields the rich knowledge of organizing summer school for school children.

The 21th Children's Summer School on Seismology and Volcanology will be held on August 18 and 19, 2020 at the area of Mt. Asama North Geopark, Japan.

Keywords: Children's Summer School, Tango Peninsula, 1927 Kita Tango earthquake

©2020. Japan Geoscience Union. All Right Reserved.

Development of e-learning materials for GIS exercises in Japan and their outcomes

*Hiroyuki Yamauchi[1], Takashi Oguchi[2], Yuichi S. Hayakawa[3,2], Toshikazu Seto[2]

1. Department of Natural Environmental Studies, Graduate School of Frontier Sciences, The University of Tokyo, 2. Center for Spatial Information Science, The University of Tokyo, 3. Environmental Geography, Faculty of Environmental Earth Science, Hokkaido University

We have been conducting a project to develop GIS exercise materials for Japanese university students. In this project, we distribute the materials on the Internet via GitHub. The learning contents in the materials are divided into four sections according to the target of learning: 1) basic operations of GIS software, 2) equipment usage for field data collection, 3) utilization of Web GIS, and 4) GIS programming with Python. Explanation of GIS analyses in the materials consists of short text descriptions and screen-captured images showing data processing using free GIS software packages such as QGIS. We also provided sample data compiled from open data for the exercises. Users can learn GIS using the materials with free of charge. The online materials have been utilized in not only universities but also industries, governments, and groups of citizens in Japan. In this presentation, we introduce the construction and operation of the materials, and demonstrate how they worked in the community.

Keywords: GIS education, Exercise, E-learning

©2020. Japan Geoscience Union. All Right Reserved.

Enhancing the impact of sustainability research and education: Distributed leadership as a guiding model

*Vincent Tong[1]

1. University College London

United Nations Sustainable Development Goals (SDGs), which are presented as a set of highly connected objectives, provide a comprehensive framework for addressing a wide range of global challenges. Higher education institutions play a special role in advancing the SDGs. Here I present some key findings from case studies of Japanese academics working on sustainability research and education, ranging from natural sciences to social science and policy. The academics in this study are at different career stages and are from both research-intensive and teaching-focused institutions in Japan. Qualitative research methods including questionnaires, semi-structured interviews, document analysis were used. I discuss the significance of the research findings through the lens of leadership models and approaches to data in academic work. In particular, I will highlight the transformational potential of distributed leadership in research and education. Distributed leadership requires not only building new institutional structures but also questioning established academic identities and cultures. Informed by findings from this study, I will also argue that distributed leadership may serve as an effective guiding model for enhancing the impact of SDG research and education. In addition, I will also discuss how distributed leadership is implemented in other cultural contexts, including the new American Geophysical Union's Education Section and a UK consortium that aimed to bring research and education closer together.

Keywords: SDGs, American Geophysical Union Education Section, Working with students as partners

©2020. Japan Geoscience Union. All Right Reserved.

[E] Poster | U (Union)：Union

[U-20] "Open Colloquium" Exploring the Earth's interior using cutting edge science and technology

convener:Hiroko Watanabe(Research Center for Neutrino Science, Tohoku University), William F McDonough(Department of Earth Science and Research Center for Neutrino Science, Tohoku University, Sendai, Miyagi 980-8578, Japan), Kenta Ueki(Japan Agency for Marine-Earth Science and Technology), Eiichiro Araki(Japan Agency for Marine-Earth Science and Technology)

New advances in technology are being used to explore the Earth. These include, but are not restricted to, neutrino geophysics, drilling the deep oceanic biosphere, and drilling to the Moho. Application of these new technologies to studies of the Earth provide critical new constraints and hopefully, new and unimagined insights. Recent technological advances, as well as advances in experimental and theoretical studies are revealing clues of how the Earth operates at a wide range of scales (microns to mega-meters). We seek to understand links from the core to atmosphere that connects the biosphere and geosphere through time. Near-future exploration of the Earth's interior with these new technologies will provide much-needed data on the internal structure of our planet and potentially its habitability. We anticipate presentations on recent advances in science and technologies that provide insights into physical, chemical, and biological processes and structures on and in the Earth. We welcome contributions from science and engineering.

[U20-P01] Study of Ocean Bottom Detector for observation of geo-neutrinos from mantle

*Taichi Sakai[1], Kunio Inoue[1], Hiroko Watanabe[1], William F McDonough[2,3], Kenta Ueki[4], Natsue Abe[4], Noriaki Sakurai[4], Masanori Kyo[4], Eiichiro Araki[4], Takafumi Kasaya[4], Hiroshi Yoshida[4] (1.Tohoku university,Research Center for Neutrino Science, 2.Tohoku university, 3.University of Maryland, 4.JAMSTEC)

Study of Ocean Bottom Detector for observation of geo-neutrinos from mantle

*Taichi Sakai[1], Kunio Inoue[1], Hiroko Watanabe[1], William F McDonough[2,3], Kenta Ueki[4], Natsue Abe[4], Noriaki Sakurai[4], Masanori Kyo[4], Eiichiro Araki[4], Takafumi Kasaya[4], Hiroshi Yoshida[4]

1. Tohoku university,Research Center for Neutrino Science, 2. Tohoku university, 3. University of Maryland, 4. JAMSTEC

Observation of geo-neutrinos originating from radioactive isotopes in the Earth (238U,232Th, etc.) can be converted to the amount of radioactive isotopes and the heat generated by their decays which governs the Earth dynamics.
KamLAND experiment achieved world's first observation of geo-neutrinos in 2005. Improvement of observation accuracy allowed us to reach the level where we can obtain geoscientific knowledge. However, it is hard to obtain information on the mantle because 70% of neutrinos observed by detector currently operating or planned are derived from the crust (Figure 1).
Given that the oceanic crust is thinner than the continental crust and has lower densities of U and Th, Ocean Bottom Detector (OBD) makes it sensitive to geo-neutrinos originating from Earth's mantle. OBD is expected to provide transformative insights into the deep Earth.Unique feature of OBD is separation from the reactors which are the main background sources of continental detectors. In addition, this movable detector can observe at multiple points in the ocean.
Scientists at the University of Hawaii started to discuss the idea of observing the geo-neutrinos on the sea floor 15 years ago as the detector called "Hanohano"(Figure 2). Unfortunately, the idea has not been realized yet.
In 2019 joint research between Tohoku University and JAMSTEC was started to lead the comprehensive research relating to understanding the Earth's deep interior and realize OBD. We are currently working on the design of 10-ton prototype detector for the ultimate goal of a 10-50kt detector.
The prototype detector will demonstrate necessary technological developments and measure the environment which will be references for future detector design.
In this presentation, we will present results of detector design based on Monte Carlo simulation.

Keywords: Geo-neutrino, mantle, solid earth science

©2020. Japan Geoscience Union. All Right Reserved.

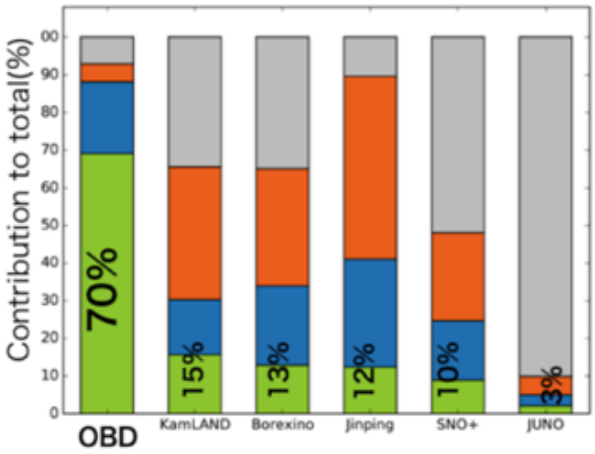


Figure 1: Percentage of each source
Gray: reactor neutrino
Orange: crust wihin 500km
Blue: other crust
Green: mantle-derived Geo-neutrino

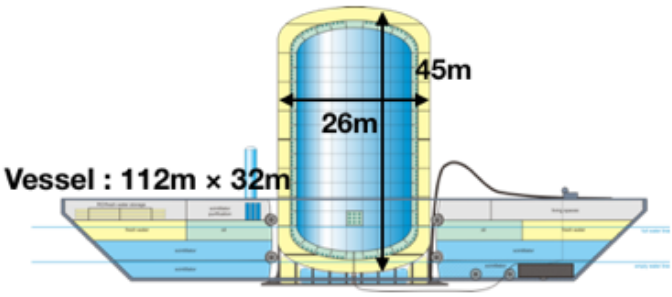


Figure 2:design of Hanohano

©2020. Japan Geoscience Union. All Right Reserved.

[E] Poster | U (Union)：Union

[U-22] Environmental drivers and impacts of the evolving COVID-19 pandemic

convener:Benjamin F Zaitchik(Johns Hopkins University), Teppei J Yasunari(Arctic Research Center, Hokkaido University)

[U22-P01] Learning from the war against the Corona epidemic to ensure the availability of drinking water

*SHUBHAM TIWARI[1] (1.Indian Institute of Technology Roorkee)

[U22-P02] Integrate NASA Remote Sensing Data into your COVID-19 Research with our new Data Pathfinder

*Cynthia Hall[1], Kevin Ward[2] (1.NASA Goddard Space Flight Center, 2.NASA Earth Science Data Systems)

[U22-P03] Is the impact of COVID-19 modulated by well-water arsenic in rural Bangladesh? Setting a baseline.

*Alexander van Geen[1], Prabhat Barnwal[2], Yiqian Wang[2], Nishat Jui[3], Shabib Raihan[3], Ashraful Haque[3] (1.Columbia University of New York, 2.Michigan State University, 3.Innovations for Poverty Action, Bangladesh)

[U22-P04] The Spatial Pattern of Coronavirus Disease 2019 in China over Four Periods

*ZILAI ZHENG[1] (1.Graduate School of Life and Environmental Sciences, University of Tsukuba)

[U22-P05] Consequences of modeling assumptions and scope of analysis on connections between meteorology and COVID-19

*Gaige Hunter Kerr[1], Hamada Badr[2], Lauren Gardner[3], Javier Perez-Saez[4], Benjamin F Zaitchik[2] (1.George Washington University, 2.Department of Earth and Planetary Sciences, Johns Hopkins University, 3.Department of Civil and Systems Engineering, Johns Hopkins University, 4.Department of Epidemiology, Johns Hopkins Bloomberg School of Public Health)

[U22-P06] Limited Regional Aerosol Changes Despite Unprecedented NO2 Decline During the February Coronavirus Shutdown in China

*Michael S S Diamond[1], Robert Wood[1] (1.University of Washington Seattle)

[U22-P07] Will the pandemic of COVID-19 change climate?: tests using MIROC-ES2L earth system model

*Rumi Ohgaito[1], Michio Kawamiya[1], Tomohiro Hajima[1], Ken'ichi Matsumoto[1,2] (1.Japan Agency for Marine-Earth Science and Technology, 2.Nagasaki University)

[U22-P08] Using mathematical models to assess the number of total deaths and deaths per 10000 people from the COVID-19 epidemic

*Qingqing Sun[1], Chunyi Wang[2] (1.Tianjin University, 2.Mathematics Faculty, University of Waterloo)

[U22-P09] Global early warning system by Complex-Envelope (CE) Processing of Seismic Waves

*Rudolf Unger[1] (1.Delft University of Technology)

[U22-P10] A possible role of environmental arsenic against COVID-19

*Satadal Das[1], Milan Sengupta[2], Rathin Chakraborty[3] (1.peerless hospital and b. k. roy research centre, kolkata, india, 2.D. N. De H. Medical College, Kolkata, India., 3.Dr.Bholanath Chakravarty Integrated Medical Research & Treatment Centre, Howrah,West Bengal, India.)

Learning from the war against the Corona epidemic to ensure the availability of drinking water

*SHUBHAM TIWARI[1]

1. Indian Institute of Technology Roorkee

The solidarity and morale with which the world is fighting the Corona epidemic encourages citizens as a society to reimburse various basic needs. Today, the developing countries are fast moving towards reimbursement of the basic needs of its citizens (such as food to eat, clothes to wear and house to stay, etc.). On the other hand, the availability of water for drinking and agriculture need to pay attention and launch a comprehensive campaign. Long-term water security and access to clean water are essential for public health. We have to stand as an organized society and fight together to ensure the availability of water by learning from the war of the Corona epidemic. When the world is in the grip of an epidemic, it is difficult to draw attention to the global water crisis, one of the greatest environmental risks to mankind. Nevertheless, the coronavirus threat reminds us how important water is to our lives. This study highlights the strategies learnt from Corona epidemic for management of water resources.

Keywords: Corona, Drinking Water

©2020. Japan Geoscience Union. All Right Reserved.

Integrate NASA Remote Sensing Data into your COVID-19 Research with our new Data Pathfinder

*Cynthia Hall[1], Kevin Ward[2]

1. NASA Goddard Space Flight Center, 2. NASA Earth Science Data Systems

NASA and other Earth-observing agencies are using satellite and airborne data to assess regional and global environmental, economic, and societal impacts of the COVID-19 pandemic. Whether the goal is to discover the forces behind the virus' spread or to look at effects on the environment due to changes in human behavior, NASA's remote sensing data can provide baselines for comparison and show new trends over time.

NASA's Earth science data collections provide a wealth of information to aid in our understanding of Earth processes and the data are all freely and openly available at earthdata.nasa.gov. Choosing the right datasets and tools to answer a scientific question often requires expert knowledge and guidance. To help novice users access, explore, and use NASA Earth science data, we have developed a series of data pathfinders.

Data pathfinders provide direct links to commonly used datasets and data products across NASA's Earth science data collections. Pathfinders supplement Earthdata search capabilities by providing access to datasets through commonly used tools, providing different ways of visualizing the data, options for subsetting the data, and options for saving the data in different file formats.

The COVID-19 pathfinder is for users who are studying the environmental signals surrounding the novel severe acute respiratory syndrome (SARS) coronavirus, SARS-CoV-2. It provides links to datasets that can be used to research changing environmental impacts on air quality, water quality, land cover changes, and more, that are the result of modified human behavior
patterns. This pathfinder provides links to measurements of temperature, humidity, and ultraviolet (UV) irradiance, which offer an opportunity to assess the possibility of seasonal trends in virus transmission. It also provides links to datasets related to water availability, such as the amount and rate of precipitation, soil moisture, and groundwater resources. Water availability and possible drought conditions need to be continuously monitored to ensure uninterrupted water services for hospitals and other critical services during the pandemic.

Come see how you can easily find NASA data to enhance your research.

Keywords: Remote sensing, Data access, COVID-19

©2020. Japan Geoscience Union. All Right Reserved.

Is the impact of COVID-19 modulated by well-water arsenic in rural Bangladesh? Setting a baseline.

*Alexander van Geen[1], Prabhat Barnwal[2], Yiqian Wang[2], Nishat Jui[3], Shabib Raihan[3], Ashraful Haque[3]

1. Columbia University of New York, 2. Michigan State University, 3. Innovations for Poverty Action, Bangladesh

The first three known COVID-19 cases were reported in Bangladesh on March 7, 2020. Almost two months later, the official count exceeded 50,000 cases while the number of deaths attributed to COVID-19 was still below 1000. Even these numbers, widely held to be underestimates, show no sign that a plateau has been reached as of June 4, 2020. This contribution describes the launch of a series of phone-based surveys to gauge the impact of COVID-19 in rural Bangladesh. The new monitoring builds on a recently launched randomized-controlled trial across 135 villages of Bangladesh to compare the effectiveness of different ways of delivering well-water tests for arsenic in terms of triggering household responses that reduce exposure to arsenic. To set the stage for the trial, our field team visited during the middle two weeks of January 2020 a total of 16,000 households in person to conduct a census. Two cell phone numbers were recorded for each household at the time and these made it possible to start calling them during the two middle weeks of May. All households were asked if anyone had died in 2019 to establish the pre-COVID-19 mortality for this population of 75,000.
Household were also asked if anyone had died since the beginning of 2020. As of May, 2020, the number of deaths reported for 2019, corresponding to a crude mortality rate of 7.7 per 1000, was if anything higher than in 2020 after correcting for the portion of the year covered. There was no difference between 2019 and 2020 as of May 2020 either in the distribution among different causes of death, self-reported in broad categories, the distribution of ages at death, or the location of death. This could well have change dramatically by the time our second round of phone surveys is completed later this summer. When field activities resume, hopefully in September 2020, all 12,000 wells in the study village will be tested for arsenic and are anticipated to span a wide range of concentrations. By combining phone and field surveys, we will be uniquely positioned to ascertain if the documented impact of arsenic exposure on the immune system translated also into differential responses to COVID-19.

Keywords: Groundwater, Arsenic, Health, COVID-19

©2020. Japan Geoscience Union. All Right Reserved.



©2020. Japan Geoscience Union. All Right Reserved.

The Spatial Pattern of Coronavirus Disease 2019 in China over Four Periods

*ZILAI ZHENG[1]

1. Graduate School of Life and Environmental Sciences, University of Tsukuba

Coronavirus disease (COVID-19) broke out in Wuhan city and expanded rapidly throughout China. The government has taken a series of tough unprecedented interventions to prevent the spread of the disease. Now, COVID-19 in China has passed the peak and entered the last stage of the pandemic. The aim of this study is to identify the spatial distribution pattern of new confirmed cases in China, in order to understand how interventions affected the COVID-19 spread. First, four-time periods were categorized according to the proportion of new confirmed cases in Hubei. Then, spatial autocorrelation analyses were employed to explore geographic patterns in these four periods. Finally, outliers were analyzed by calculating an Anselin local Moran's I statistic. The results show that the spatial patterns of the COVID-19 in the first three periods spread are the high cluster and random in the fourth period. As the proportion of new confirmed cases in Hubei has dropped significantly, the spatial pattern of the epidemic also has a major transformation. Many economic and culturally developed cities became the focus in addition to Wuhan city.

Keywords: Coronavirus disease (COVID-19), Spatial pattern, Moran's I, Spatial autocorrelation

©2020. Japan Geoscience Union. All Right Reserved.

Consequences of modeling assumptions and scope of analysis on connections between meteorology and COVID-19

*Gaige Hunter Kerr[1], Hamada Badr[2], Lauren Gardner[3], Javier Perez-Saez[4], Benjamin F Zaitchik[2]

1. George Washington University, 2. Department of Earth and Planetary Sciences, Johns Hopkins University, 3. Department of Civil and Systems Engineering, Johns Hopkins University, 4. Department of Epidemiology, Johns Hopkins Bloomberg School of Public Health

Research on past influenza and coronavirus outbreaks demonstrates that the spatiotemporal evolution of transmission exhibits pronounced associations with meteorological variables, such ambient temperature and humidity. There are many open questions regarding the causal pathways that connect the ambient meteorology to the transmission of the novel coronavirus (COVID-19), but evaluating the statistical associations between COVID-19 and meteorology represents an important first step and presents potential challenges and opportunities for controlling the future spread of the virus.
Many recent refereed and non-refereed studies have examined the connection between meteorological variables and COVID-19; however, the landscape of the literature is constantly changing, and it is important to provide a synthesis to evaluate gaps. These studies yield contrasting results linking COVID-19 with meteorology both within and across regions. Differences likely stem from different focus regions and measuring periods, different methodologies (i.e., statistical methods, dependent variable(s), controls, etc.), or a combination of these two factors. To understand how methodology impacts key findings, we discuss how studies draw statistical associations between meteorology and COVID-19 and their intrinsic limitations and suggest ways that future research could improve the detection of associations.

Keywords: COVID-19, temperature, humidity, transmission

©2020. Japan Geoscience Union. All Right Reserved.

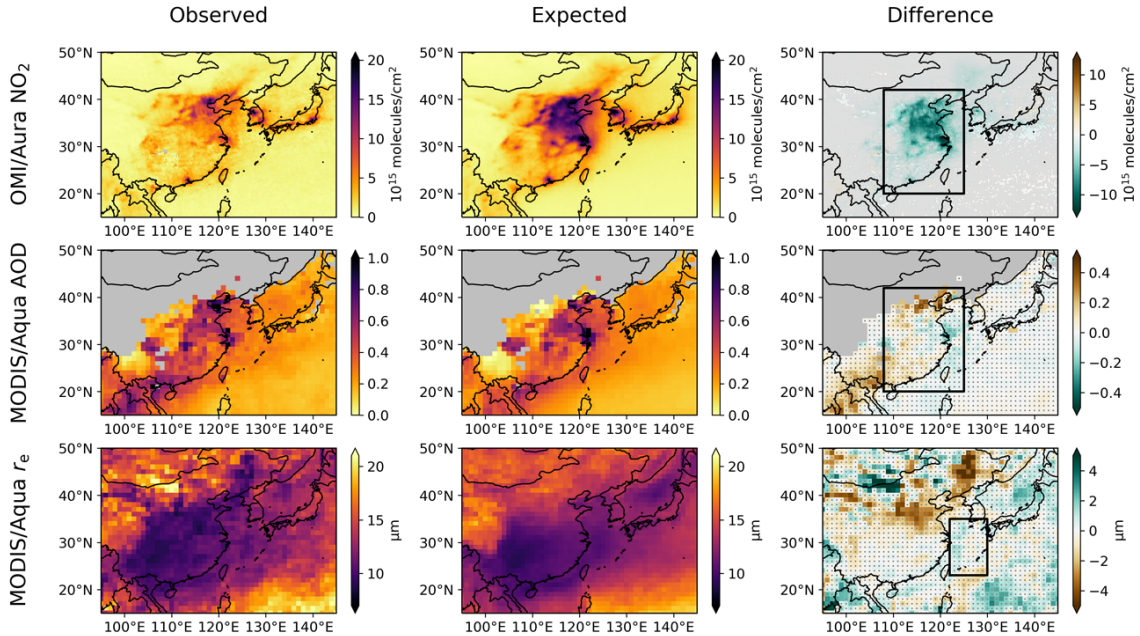
Limited Regional Aerosol Changes Despite Unprecedented NO2 Decline During the February Coronavirus Shutdown in China

*Michael S S Diamond[1], Robert Wood[1]

1. University of Washington Seattle

Following the emergence of a novel coronavirus in Wuhan, the People’ s Republic of China instituted a number of strict lockdown and more general socio-economic shutdown measures throughout the country starting in late January and continuing into February 2020 in order to arrest the spread of the disease. This resulted in a sharp economic contraction unparalleled in recent Chinese history. Satellite remote sensing shows that nitrogen oxide pollution declined by an unprecedented amount (~50% regionally) from its expected unperturbed value, but regional-scale column aerosol loadings and cloud microphysical properties were not detectably affected. The disparate impact may be tied to differential economic impacts of the shutdown, in which the transportation sector, a disproportionate source of nitrogen oxide emissions, underwent drastic declines (~90% reductions in passenger traffic), whereas industry and power generation, responsible for >90% of particulate emissions, were relatively less affected (~10% reductions in electricity and thermal power generation). Meteorology (particularly warm temperatures) and non-linear chemical reactions also likely played a role in driving the disparity.

Keywords: Aerosol, Cloud, NOx, COVID-19, Pollution, Remote sensing



©2020. Japan Geoscience Union. All Right Reserved.

Will the pandemic of COVID-19 change climate?: tests using MIROC-ES2L earth system model

*Rumi Ohgaito[1], Michio Kawamiya[1], Tomohiro Hajima[1], Ken'ichi Matsumoto[1,2]

1. Japan Agency for Marine-Earth Science and Technology, 2. Nagasaki University

The world is now being altered by the pandemic of COVID-19 that has limited economic activity in the first half of 2020 to protect human lives from the virus. This restriction on economic activity has resulted in lower emissions of anthropogenic greenhouse gases and aerosols (Le Quere et al. 2020). Will this reduction in emissions have an impact on the climate? Using an earth system model MIROC-ES2L (Hajima et al. 2020) used to project global warming in CMIP6, we conducted sensitivity experiments to reduce anthropogenic greenhouse gases, black carbon, and SO2 by 20% in 2020 and 2021, branching off from the global warming scenario experiments submitted to CMIP6 (the 20% reduction in greenhouse gas emissions is driven by an 18.6% reduction in per capita gross domestic product in 2020).

As a result, it was suggested that the Arctic region may have a warming effect. It is also suggested that this may modulate decade-scale climate change. Further analysis will be carried out and presented.

Keywords: COVID-19, climate, greenhouse gases, aerosol

©2020. Japan Geoscience Union. All Right Reserved.

Using mathematical models to assess the number of total deaths and deaths per 10000 people from the COVID-19 epidemic

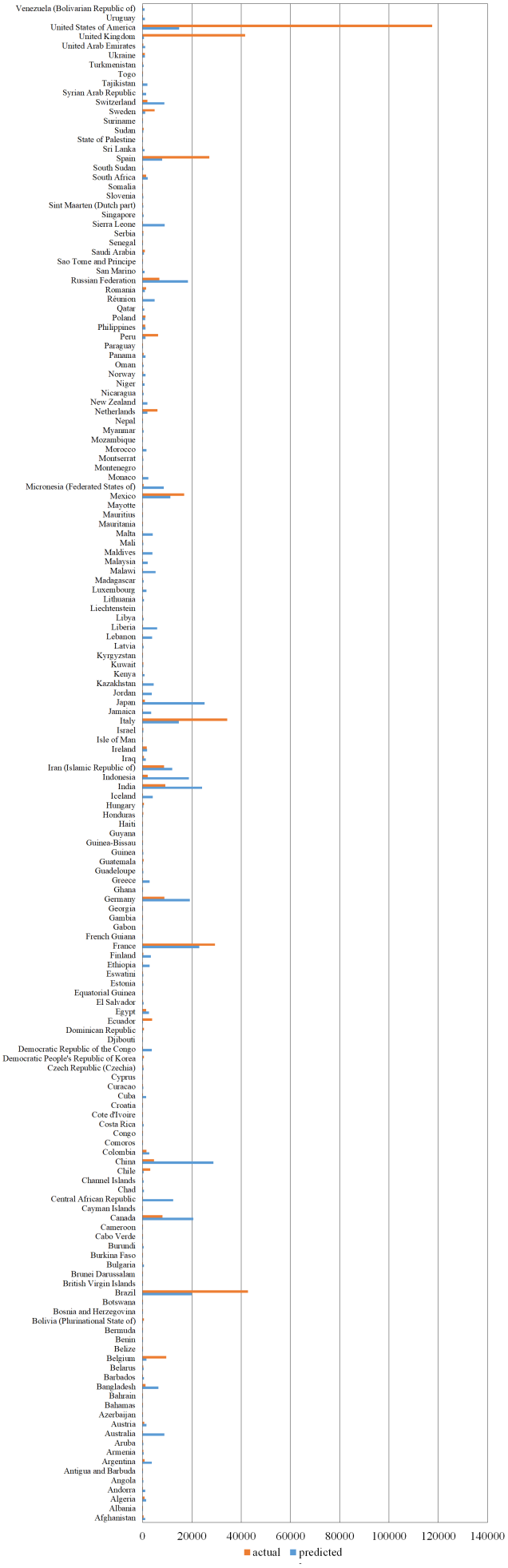
*Qingqing Sun[1], Chunyi Wang[2]

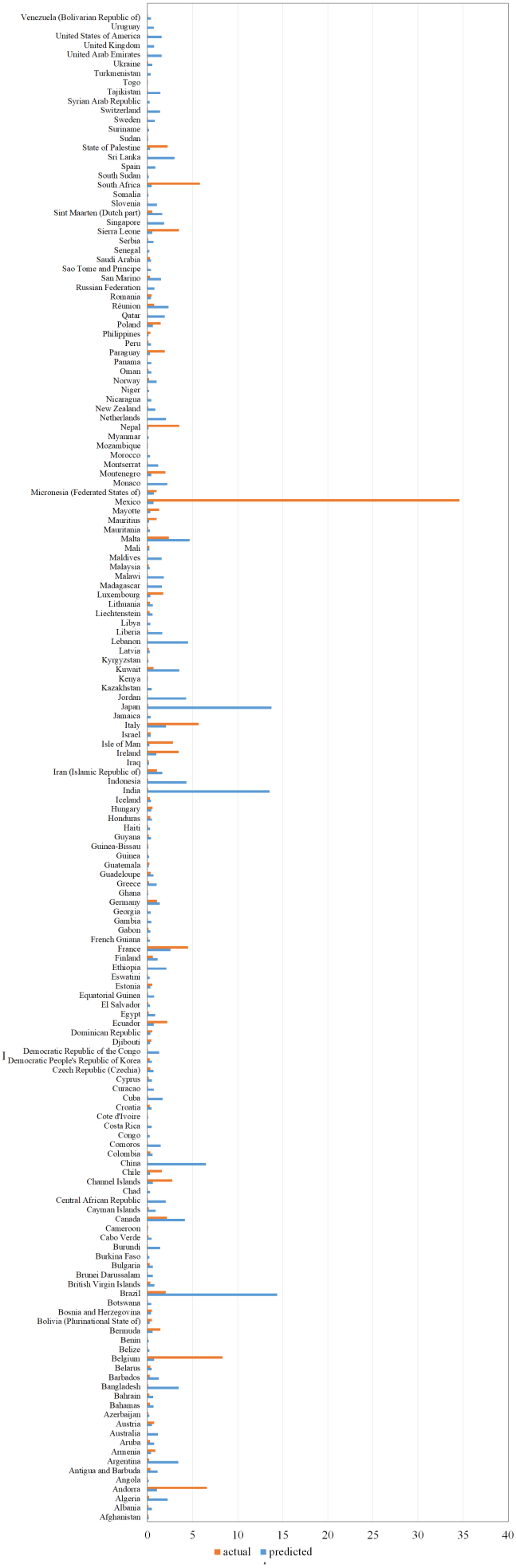
1. Tianjin University, 2. Mathematics Faculty, University of Waterloo

Death tolls and death tolls per 10000 people of 161 countries and regions as 13 June, 2020 were predicted by "random forest" (https://github.com/qingqingsun-code/covid-19-prediction). The reference indexes are (1) past and present flight routes, (2) change rate of population, world share, population density, net change population density, migrant density, land area, (3) fertility rate, density, median age, (4) urban population proportion, urban areas, urban population density, (5) 65+ older population density, proportion of 65+ older population, (6) numbers of hospital beds per 1,000 people, intensive care unit (ICU) beds per 10000 people, density of medical doctors (per 10000 population), density of nursing and midwifery personnel (per 10000 population), density of pharmacists (per 10000 population), (7) gross domestic product (GDP) Nominal ($) per people, GDP per chasing power parity (PPP) (Int. $) per people, (8) out of pocket expenditure as percentage of current health expenditure % (US$), direct financial plan on fighting COVID-19, current health expenditure (CHE) as percentage of gross domestic product (GDP)(%), CHE per capital (US$), domestic general government health expenditure (GGHED) as percentage of general government expenditure (GGE)(%), (9) average of international health regulation score capacity scores, universal health coverage (UHC) service coverage index. Based on the heatmap of correlations, the highest indexes were annual rate of population change, urban area, and GGHED as percentage of GGE. Predicted death tolls (441,692) were 4.64% high than the statistical death toll (422,090). Predicted mean death toll per 10,000 was 1.14, higher than the statistical one 0.78. Because patients with basic diseases are less resistant to COVID-19, there is a possible statistical bias in the number of deaths in some country and region. It is also not ruled out that some of the dead patients have not been diagnosed. Quarantine order is the main reason for the difference between simulated data and statistical data. As a global community, we need solidarity, disclosure information, cooperation in the development of vaccines, sound medical relief supplies to limit the spread of COVID-19.

Keywords: COVID-19, Random forest, Death toll

©2020. Japan Geoscience Union. All Right Reserved.





©2020. Japan Geoscience Union. All Right Reserved.

©2020. Japan Geoscience Union. All Right Reserved.

Global early warning system by Complex-Envelope (CE) Processing of Seismic Waves

*Rudolf Unger[1]

1. Delft University of Technology

Given a pandemic situation such as C-19 or any other potential mutation, and an earthquake striking at some point during its development, how could science aid to confront two simultaneous disasters?

We answer from a) an anthropological/psychological point of view and b) a seismic technology perspective.

A) Strict isolation and a disaster such as earthquake or volcanic eruption imply antagonist forces and strategies which require original and dynamic disaster preparedness. Michael Levitt (Nobel 2013) has alerted on the dangers of strict confinement and has compared SARS-Cov-2 and its predecessor SARS-Cov (2003) and its effects on the lives of the populations (suicides, domestic violence, etc.) including worries which lower the immune system. Enhancing the immune system and implementing hygiene are important steps as is social physical distancing. Cognitive approach strengthens the mind through statistics and understanding of the process.

B) As we are learning again from C-19 the importance of early warnings and open global data sharing, we need to enhance the search for medical and natural disaster precursors, and to develop efficient global Big Data (BD) communicating precursor systems. To achieve this objective, we elaborate on a system for continuous Active Geophysical Monitoring (AGM, controlled-source high-resolution 3D time-lapse monitoring of Earth physics parameters and potential earthquake precursors), Geophysical Exploration (GE) resolution optimization and multiple-signal analysis by Complex-Envelope (CE) Processing of Seismic Waves.

CE = dual time series of Instantaneous Amplitude (IA) and Instantaneous Phase (IP), obtained through quadrature processing of (seismic) wave time series. We show significant CE contributions in Nuclear Test Ban Treaty (NTBT) earthquake vs. underground explosion verification and monitoring (automatic detection and classification), in AGM, and in GE.

Should two disasters happen simultaneously, technology provides precise (seismic) methods to accurately contribute to a better preparedness and stronger psychological stamina to face reality.

©2020. Japan Geoscience Union. All Right Reserved.

A possible role of environmental arsenic against COVID-19

*Satadal Das[1], Milan Sengupta[2], Rathin Chakraborty[3]

1. peerless hospital and b. k. roy research centre, kolkata, india, 2. D. N. De H. Medical College, Kolkata, India., 3. Dr.Bholanath Chakravarty Integrated Medical Research & Treatment Centre, Howrah,West Bengal, India.

Before 20th Century arsenic compounds were the first drug of choice in most of the diseases, however, as it is a known poison, it lost its status with the development of modern science, and at present they are only used in four important diseases - acute promyelocytic leukaemia, hepatocellular carcinoma, autoimmune diseases, and in African trypanosomiasis. In this study we first observed much less COVID-19 cases in some arsenic rich groundwater areas of West Bengal. Then we aimed to find out whether negative correlate between groundwater arsenic levels and COVID-19 incidence is present in different parts of the world. We presumed that in developed countries it would be extremely difficult as groundwater arsenic, even if it is present in a much higher level in some areas; it will not influence human beings due to polished modern water supply system. Even then after analysis we became totally convinced that there is a definite relationship and in areas where groundwater arsenic levels are high COVID-19 incidence is much less, and in many countries it is lowest, compared to all other areas in those countries. This finding may be an incidental one, however, we must look details into it.

Keywords: COVID-19, arsenic, arsenic compounds

©2020. Japan Geoscience Union. All Right Reserved.

[E] Poster | U (Union)：Union

[U-23] New challenges to diversity, equality and inclusion under COVID-19

convener:Chiaki T. Oguchi(Institute for Environmental Science and Technology, Graduate School of Science and Engineering, Saitama University), Rie Hori, S.(Department of Earth Science, Faculty of Science, Ehime University), Claudia Jesus-Rydin(European Research Council), Hodaka Kawahata(Atmosphere Ocean Research Institute, the University of Tokyo)

[U23-P01] GEOLATINAS: embracing, empowering, and inspiring Latinas in Geoscience

*Angela Meneses-Gutierrez[1,2,3], Rocío Caballero-Gill[4,3], Adriana Crisóstomo-Figueroa[7,3], Clara Rodriguez[8,3], Carolina Villarraga Morales[3], Grisel Jiménez Soto[5,3], Natalia A. Cifuentes[6,3] (1.Institute for Advanced Research, Nagoya University, Japan, 2. Disaster Mitigation Research Center, Nagoya University, Japan, 3.GeoLatinas, 4.George Mason University, USA, 5.South East Asia Carbonate Research Laboratory, Universiti Teknologi PETRONAS, Malaysia , 6.Department of Geosciences and Environment, National University of Colombia (Medellin), Colombia, 7.University of Leeds, Leeds, UK, 8.Petronas, Mexico)

[U23-P02] How the COVID-19 Response Opens Broader Viewpoints for Promoting Inclusive Conferences in the Earth and Space Sciences

*Beverly Smith-Keiling[1], Andreas Keiking[2] (1.University of Minnesota Twin Cities, 2.University of California-Berkeley)

[U23-P03] How to empower diversity, equality and inclusion for risk management in the COVID-19 Era

*Megumi Sugimoto[1] (1.Kyushu University)

[U23-P04] The Effect of COVID-19 on AGU Journal Authors by Gender and Geographical Location

*Paige Rene Wooden[1], Brooks Hanson[1] (1.American Geophysical Union)

GEOLATINAS: embracing, empowering, and inspiring Latinas in Geoscience

*Angela Meneses-Gutierrez[1,2,3], Rocío Caballero-Gill[4,3], Adriana Crisóstomo-Figueroa[7,3], Clara Rodriguez[8,3], Carolina Villarraga Morales[3], Grisel Jiménez Soto[5,3], Natalia A. Cifuentes[6,3]

1. Institute for Advanced Research, Nagoya University, Japan, 2. Disaster Mitigation Research Center, Nagoya University, Japan, 3. GeoLatinas, 4. George Mason University, USA, 5. South East Asia Carbonate Research Laboratory, Universiti Teknologi PETRONAS, Malaysia , 6. Department of Geosciences and Environment, National University of Colombia (Medellin), Colombia, 7. University of Leeds, Leeds, UK, 8. Petronas, Mexico

The lack of representation of women in geoscience is a reality, and although recent efforts have been made towards closing the gender gap, we are far from achieving gender balance. Furthermore, this problem is amplified for women with mixed heredity or coming from developing countries, who rarely find themselves represented in leadership roles in academia and industry. To tackle this issue, GeoLatinas, an initiative to empower women of Latin-American ethnicity, started in 2018.

GeoLatinas is an inclusive, member-driven organization dedicated to promote, embrace and empower the work and research of Latinas, and inspire current and future generations of Latin Americans to pursue careers in Earth and Planetary Sciences. The organization relies on six interactive groups to increase its reach and potential: an Advisory Committee, a Board of Directors, Liaisons, Regional leaders (Ambassadors), a Leadership Council, and Local Teams. Aided by the development of remote communication and a strong Visibility and Social Media team, GeoLatinas has now more than 240 active members and volunteers across 27 countries.

In this presentation, we will discuss the GeoLatinas organization, its collective efforts, and use one of our initiatives as an example of how we catalyze inclusion, equity, and retention in Geoscience. We will specifically discuss the strategies undertaken by the Visibility and Social media committee that have helped increase the visibility of Latinas in Earth Sciences and the importance of social media as a tool for representation. Furthermore, we will share lessons learned from the GeoLatinas group journey towards diversity and gender equality, as well as future initiatives to continue supporting our community.

Keywords: Diversity, Earth and Planetary Sciences, Latinas

©2020. Japan Geoscience Union. All Right Reserved.

How the COVID-19 Response Opens Broader Viewpoints for Promoting Inclusive Conferences in the Earth and Space Sciences

*Beverly Smith-Keiling[1], Andreas Keiking[2]

1. University of Minnesota Twin Cities, 2. University of California-Berkeley

From the 1948 Universal Declaration of Human Rights to current diversity statements, science entities in the U.S. and globally promote and enhance diversity and equity. For example, AGU, EGU, and Europlanet aim to 'foster an inclusive environment where science and scientific careers can flourish,' 'improve equality of opportunity and diversity,' and 'build a diverse inclusive community,' 'respectively. Clarity from JpGU members' broader viewpoints on diversity and inclusion statements are needed for promoting inclusion. One area is in scientific conferences, not only in the participation in the conference but also engagement and representation at every level. With a goal to increase equitable participation in scientific conferences, engagement and representation at every level, we made initial observations and employed strategies while hosting (together with colleagues) four AGU Chapman conferences between 2011-2016. Within the Social Ecological Model Framework, individual and interpersonal inner-level determinants were our primary target leading us to seek broader viewpoints through an internationally distributed survey. Early observations from this survey and participation in a virtual EGU 2020 conference following the Covid-19 response highlighted the importance of two inclusive practices that were highly ranked in our survey by respondents prior to the outbreak: 1) Live streaming or conference chats for open access, and 2) Additional accommodations for disability (vision, hearing, etc.). These early survey results about what constitutes an inclusive conference apply to virtual delivery, and can help develop strategies to promote advocacy for policy changes and for additional measures that could be applied at conference initiation. This would target the outer level determinants at the policy level to promote inclusion. Yet, through an equity lens, virtual access does not solve all challenges.

Keywords: Diversity, Equity, Inclusion, Human Rights, Virtual, Accommodations

©2020. Japan Geoscience Union. All Right Reserved.

How to empower diversity, equality and inclusion for risk management in the COVID-19 Era

*Megumi Sugimoto[1]

1. Kyushu University

Natural disasters happen, so it has been a situation where vulnerabilities and minorities are historically liable to be sacrificed as secondary disaster. For example, the 1906 San Francisco earthquake caused a large number of immigrants from China, whose English and geography were unknown, due to fires. The Great Kanto Earthquake in 1923 spread social unrest among people and spread the hoax that Koreans attacked, killing Koreans by vigilante band.

In the COVID-19 Era, violence and repulsion of people from China and Asians, which seem to be the source, occurred. Even in Indonesia, which is famous as a pro-Japanese nation, rumors spread that the first person was infected by a Japanese person, several attacks on Japanese were reported, and Japanese people were alerted as Japan embassy information. Minorities are week in foreign countries. A black man was killed by a police in US and demonstrations are taking place all over the world. In some areas, looting has occurred and social unrest is easily amplified. These have been repeatedly historically. It is extremely difficult to see if this secondary damage can be stopped by ethics, understanding of people, and harmony of races.

UN Secretary-General alarmed COVID-19 risk to women could harm us all. Pandemics economic impact likely to fall hard on females already facing burdens. This situation means excellent young scientist, especially females from developing countries face more difficulties to study in developed countries than before.
What kind of countermeasures can humans take in this situation? This paper specifically explains that diversity, equality and inclusion function for risk management.

Keywords: Gender Equality, Risk management, Minorities, Diversity, Racism, History

©2020. Japan Geoscience Union. All Right Reserved.

The Effect of COVID-19 on AGU Journal Authors by Gender and Geographical Location

*Paige Rene Wooden[1], Brooks Hanson[1]

1. American Geophysical Union

AGU’ s commitment to building and supporting a diverse group of Earth and space scientists impels us to monitor the data we have on our constituents. When the COVID-19 pandemic forced institutions to close their physical spaces, many researchers and professors were forced to work from home. Media outlets and individuals wondered if women specifically would be shouldering the childcare and/or homeschooling responsibilities decreasing the time they had to for professional and research duties. AGU has been monitoring the effect that the stay-at-home orders have had on our journal authors by analyzing our monthly submission data. We focused specifically on gender, age, and geographical region of individuals submitting manuscripts (“corresponding author”). We found that there have been no statistically significant monthly fluctuations in the number of women across all age groups submitting articles in 2020 and compared to their monthly submissions of 2018 and 2019. We did see some decrease in submissions in February from certain countries but as of May 2020, most countries have returned to their normal submission rates. We do see that submissions of revised manuscripts, which may require access to physical spaces and/or equipment and collaboration with co-authors, decreased among both male and female corresponding authors from February through April. The relative stability of new submissions from various groups may indicate a few things: 1) that stay-at-home orders may afford some more time to submit an article while others less, 2) article submission itself is a relatively simple and straightforward task if the research, analysis, and writing is complete, and 3) we may see decreased submissions later in the year or next year if there is a sustained lack of access to research subjects/materials and analytical tools.

Keywords: COVID-19, Gender, Demographics, Articles, Journals, American Geophysical Union (AGU)

©2020. Japan Geoscience Union. All Right Reserved.

[E] Poster | P (Space and Planetary Sciences)：P-PS Planetary Sciences

[P-PS01] Outer Solar System Exploration Today, and Tomorrow

convener:Jun Kimura(Osaka University), Kunio M. Sayanagi(Hampton University), Fuminori Tsuchiya(Planetary Plasma and Atmospheric Research Center, Graduate School of Science, Tohoku University), Steven Douglas Vance(NASA Jet Propulsion Laboratory, California Institute of Technology)

The giant planets provide many keys to understanding planetary processes. They play an important role in shaping our solar system, and the physical and chemical processes they harbor also provide a unique opportunity to study the phenomena relevant for studying Earth and other planets, including exoplanetary systems. In this session, we discuss a wide range of topics encompassing the giant planets and their moons, including their origins, interiors, atmospheres, compositions, surface features, and electromagnetic fields. To advocate for current and future outer planets exploration (Juno, New Horizons, JUICE, Europa Clipper, Dragonfly and beyond), we also call for discussions on future missions to explore giant planet systems, including how to develop better international cooperation. Discussion in this latter category will include progress in developing a solar sail mission concept for observing the Jupiter system and its trojan asteroids.

[PPS01-P01] Pluto's surface albedo distribution and its evolution due to sublimation and condensation of ices

Hisashi Matsui[1], *Jun Kimura[1] (1.Osaka University)

[PPS01-P02] A low-energy energetic neutral atom analyzer (PEP/JNA) for JUICE mission

*Kazushi Asamura[1], Manabu Shimoyama[2], Yoshifumi Futaana[2], Yoshizumi Miyoshi[3], Takeshi Sakanoi[4], Yoshifumi Saito[1] (1.Institute of Space and Astronautical Science, Japan Aerospace Exploration Agency, 2.Swedish Institute of Space Physics, 3.Nagoya University, 4.Tohoku University)

[PPS01-P03] The Ganymede Laser Altimeter (GALA) for the JUICE mission – overview and current status

*Enya Keigo[1], Masanori Kobayashi[2], Jun Kimura[3], Noriyuki Namiki[4], Hiroshi Araki[4], Hirotomo Noda[4], Shoko Oshigami[1], Shingo Kashima[4], Shin Utsunomiya[4], Ko Ishibashi[2], Masanobu Ozaki[1], Takahide Mizuno[1], Yoshifumi Saito[1], Kazuyuki Touhara[1], Shunichi Kamata[5], Koji Matsumoto[4], Kiyoshi Kuramoto[5], Sho Sasaki[3], Satoru Iwamura[6], Yoshiaki Matsumoto[7], Masayuki Fujii[8], Naofumi Fujishiro[9], Yuki Sato[10], Takeshi Yokozawa[10], Tsutomu Numata[10], Satoko mizumoto[10], Hiroyuki Mizuno[10], Akihiko Sawamura[10], Kazuo Tanimoto[10], Hisato Imai[11], Hiroyuki Nakagawa[11], Okiharu Kirino[11], Hussmann Hauke[12], Kay Lingenauber[12], Reinald Kallenbach[12], Christian Althaus[12], Simone DelTogno[12], Thomas Behnke[12], Christian Huettig [12] (1.ISAS, 2.CIT, 3.Osaka Univ., 4.NAOJ, 5.Hokkaido Univ., 6.MRJ, 7.PTIJ, 8.FAM Science, 9.Astro-Opt, 10.Meisei Electric, 11.Cristal Optics, 12.DLR)

[PPS01-P04] Tidally heated convection and the occurrence of melting in icy satellites: application to Europa

*Kenny Vilella[1], Gael Choblet[2], Wei-En Tsao[3], Frederic Deschamps[3] (1.Hokkaido University, 2.LPG Nantes, 3.Institute of Earth Sciences, Academia Sinica)

[PPS01-P05] Measurements of Saturn's Zonal Wind from Voyager Images using Modern Cloud-Tracking Method

*Justin Garland[1], Kunio M. Sayanagi[1], Jacob L. Gunnarson[1], John J. Blalock[2,1] (1.Hampton University, 2.USGS Astrogeology Science Center)

[PPS01-P06] Inhibition of moist convection in the atmospheres of Jovian planets: the case of NH4SH formation by chemical reaction of NH3 and H2S

*Ko-ichiro SUGIYAMA[1], Kensuke Nakajima[2], Kiyoshi Kuramoto[3], Yoshi-Yuki Hayashi[4] (1.National Institute of Technology, Matsue College, 2.Kyushu University, 3.Hokkaido University, 4.Kobe University)

[PPS01-P07] Detectability of water plumes on icy moons with Earth-orbiting UV telescope

*Ryoichi Koga[1], Fuminori Tsuchiya[1], Go Murakami[3], Kazuo Yoshioka[2], Masato Kagitani[1], Tomoki Kimura[1], Atsushi Yamazaki[3], Ichiro Yoshikawa[2], Hajime Kita[3], Masaki Kuwabara[3] (1.Tohoku University, 2.The University of Tokyo, 3.JAXA/ISAS)

[PPS01-P08] **Development of a radial diffusion model of Jovian inner magnetospheric plasma transportation for a comparison with HISAKI data**

*Kazuki Yamaguchi[1], Takeshi Sakanoi[1], Fuminori Tsuchiya[1], Masato Kagitani[1], Tomoki Kimura[2], Ryoichi Koga[1], Reina Hikida[3] (1.Tohoku university, 2.Frontier Research Institute for Interdisciplinary Sciences, Tohoku University, 3.Department of Earth and Planetary Science, Graduate School of Science, Tokyo University)

[PPS01-P09] Light Curve of Jupiter's UV Aurora and Io Plasma Torus after 2016 Obtained from Hisaki EXCEED

*Hajime Kita[1], Tomoki Kimura[2], Fuminori Tsuchiya[2], Go Murakami[1], Atsushi Yamazaki[1], Ryoichi Koga[2], Reina Hikida[3], Kazuo Yoshioka[3], Ichiro Yoshikawa[3] (1.Institute of Space and Astronautical Science, Japan Aerospace Exploration Agency , 2.Tohoku Univ., 3.The University of Tokyo)

[PPS01-P10] Laboratory demonstration of cryogenic-specific reddish coloration with cryoplasma

*Noritaka Sakakibara[1], Yu Yu Phua[1], Tsuyohito Ito[1], Kazuo Terashima[1] (1.The University of Tokyo)

Pluto's surface albedo distribution and its evolution due to sublimation and condensation of ices

Hisashi Matsui[1], *Jun Kimura[1]

1. Osaka University

Flyby Observations of NASA's New Horizons spacecraft of Pluto in 2015 revealed that H_2O, N_2, CH_4, CO ices coexist on the surface of Pluto and that the surface has a strong difference of reflectivity in lalitudes, middle and high latitudes are bright and low latitudes are dark, which strongly suggests a different amount of ice. However, an origin of such bright and dark color distribution on the surface is still unclear. In previous researches about a temporal changing of albedo on the Jovian and Saturnian moons, it has been shown that sublimation of H_2O ice due to an insolation affects albedo changing on their surfaces. On Pluto, condensation of ice in the atmosphere also should affect Pluto's surface albedo because Pluto has an atmosphere with surface pressure of approximately 1 Pa. In this study, we model relationship between ice behavior such as sublimation and condensation and change of albedo, and consider quantitatively about N_2 and CH_4 that is main components of atmosphere with a numerical simulation for the purpose of investigating the origin of the albedo variation on Pluto.
In our model, we assume an initial surface state that bright ice and dark non-ice material exist uniformly mixed in depth by micrometeorite bombardment and that surface has uniform albedo which can be modeled by the volume ratio between ice and non-ice materials. Subsequently, entire surface of Pluto is divided into 12 latitudinal bands by 15 degrees, and we calculate the surface temperature with thermal inertia according to a change of insolation on each latitude considering orbit, rotation cycle and precession. When the temperature exceeds the sublimation point which depends on the surface atmospheric pressure, the ice sublimes and the non-ice material remain on the surface. Sublimed ice exists as the atmospheric gas, and the gas can be condensed on the surface when the temperature of atmosphere falls below the condensation point. Moreover, we calculate a cycle that time variation of the volume ratio of ice and non-ice material due to sublimation and condensation changes albedo, and nally we examine temporal change of the Pluto's surface albedo over millions of years.
As a result, we nd that insolation varies greatly for each latitude and seasons because Pluto has the large inclination of the obliquity, and thus sublimation and condensation amount of ice change greatly for each latitude and seasons. Amount of N_2 atmosphere formed by sublimation is consistent with observation, and this suggests that Pluto has a large N_2 circulation between surface and atmosphere. In addition, we nd a possibility to reach the overall trend of the albedo on current Pluto from initial globally uniform surface albedo through this process. Also, because the changes of albedo distribution depending on the thermal inertia and initial albedo, there is a possibility that thermal inertia depending on porosity and initial albedo affects albedo distribution on current Pluto.

©2020. Japan Geoscience Union. All Right Reserved.

A low-energy energetic neutral atom analyzer (PEP/JNA) for JUICE mission

*Kazushi Asamura[1], Manabu Shimoyama[2], Yoshifumi Futaana[2], Yoshizumi Miyoshi[3], Takeshi Sakanoi[4], Yoshifumi Saito[1]

1. Institute of Space and Astronautical Science, Japan Aerospace Exploration Agency, 2. Swedish Institute of Space Physics, 3. Nagoya University, 4. Tohoku University

We are developping a low-energy (10eV-3keV) energetic neutral atom analyser (PEP/JNA) which is to be onboard European JUICE spacecraft. Ganymede has its own intrinsic magnetic moment. There is considered to be a magnetosphere around Ganymede because of interactions between plasma in the Jovian magnetosphere and Ganmede's magnetic field. However, its characteristics is different from the terrstrical one, since Alfven mach number of upstream plasma flow (corotational plasma flow around Jupiter) is less than 1 (sub-sonic). JNA (Jovian Neutral Analyzer) will reveal characteristics of the Ganymede's magnetosphere by measurement of scattered and sputtered particles generated by precipitation of plasma particles onto Ganymede's surface. Measurement of these particles will provide spatial distribution of plasmas in remote sense, since electric/magnetic field do not affect trajectories of neutral particles. For the instrument development, the flight model is under development. We will discuss current status of JNA.

Keywords: Jupiter, Energetic neutral atoms, JUICE

©2020. Japan Geoscience Union. All Right Reserved.

The Ganymede Laser Altimeter (GALA) for the JUICE mission –overview and current status

*Enya Keigo[1], Masanori Kobayashi[2], Jun Kimura[3], Noriyuki Namiki[4], Hiroshi Araki[4], Hirotomo Noda[4], Shoko Oshigami[1], Shingo Kashima[4], Shin Utsunomiya[4], Ko Ishibashi[2], Masanobu Ozaki[1], Takahide Mizuno[1], Yoshifumi Saito[1], Kazuyuki Touhara[1], Shunichi Kamata[5], Koji Matsumoto[4], Kiyoshi Kuramoto[5], Sho Sasaki[3], Satoru Iwamura[6], Yoshiaki Matsumoto[7], Masayuki Fujii[8], Naofumi Fujishiro[9], Yuki Sato[10], Takeshi Yokozawa[10], Tsutomu Numata[10], Satoko mizumoto[10], Hiroyuki Mizuno[10], Akihiko Sawamura[10], Kazuo Tanimoto[10], Hisato Imai[11], Hiroyuki Nakagawa[11], Okiharu Kirino[11], Hussmann Hauke[12], Kay Lingenauber[12], Reinald Kallenbach[12], Christian Althaus[12], Simone DelTogno[12], Thomas Behnke[12], Christian Huettig [12]

1. ISAS, 2. CIT, 3. Osaka Univ., 4. NAOJ, 5. Hokkaido Univ., 6. MRJ, 7. PTIJ, 8. FAM Science, 9. Astro-Opt, 10. Meisei Electric, 11. Cristal Optics, 12. DLR

We present an introduction, current status, and role of the Japan team for the Ganymede Laser Altimeter (GALA) for the Jupiter Icy Moon Explorer (JUICE) mission. JUICE is a mission of ESA to be launched in 2022, and GALA is one of the payloads of JUICE.

Major objectives of GALA are to provide topographic data of Ganymede, the largest satellite of Jupiter, and to measure its tidal amplitudes. The latter is crucially important to detect and to characterize an underground ocean on Ganymede. Furthermore, GALA supports geological studies, e.g., identification of characterization of tectonic and cryo-volcanic regions, impact basins, and craters. GALA also provides information on surface roughness and the albedo.

For the laser altimetry, GALA emits and receives laser pulses at about 500 km altitude above Ganymede. Wavelength, energy, and repetition frequency of the laser plus are 1064 nm, 17 mJ, and 30 Hz, respectively. Reflected beam from the Ganymede surface is received by the receiver telescope with 25 cm diameter aperture, re-focused by the BEO including a narrow band-pass filter, and then detected by the APD detector.

Development of GALA is carried out in international collaboration by Germany, Japan, Switzerland, and Spain. GALA-Japan will develop the Backend Optics (BEO), the Focal Plane assembly (FPA) including an avalanche photo-diode (APD) detector, and the Analog Electronics module (AEM) in the receiver chain.

Keywords: GALA, JUICE, Jupiter, Ganymede, Laster altimeter

©2020. Japan Geoscience Union. All Right Reserved.

Tidally heated convection and the occurrence of melting in icy satellites: application to Europa

*Kenny Vilella[1], Gael Choblet[2], Wei-En Tsao[3], Frederic Deschamps[3]

1. Hokkaido University, 2. LPG Nantes, 3. Institute of Earth Sciences, Academia Sinica

Observations of icy satellites have revealed widespread marks of cryovolcanism. Because aqueous cryomagmas are negatively buoyant, two processes are required to explain these observations: one mechanism to generate melt close enough to the surface, and another one to transport this melt to the surface. Here, we investigate the generation of melting in a systematic way, using a set of 85 numerical simulations where we vary the viscosity contrast, Rayleigh number, and tidal heating rate. Applied to Europa, and considering a hydrosphere composed of pure water, our simulations suggest that isolated melt pockets can be generated close to the surface (≈5 km) as long as the ice layer thickness (d*) remains modest (15<d*<35 km). However, the generation of melting becomes increasingly difficult as the amount of anti-freeze compounds in the subsurface ocean increases. Furthermore, the proportion of melting increases very sharply with increasing tidal heating rate. In particular, when the tidal heating rate exceeds a threshold, an asymptotic regime is reached where the surface heat flux remains constant, i.e., the tidal heat generated above this threshold is only used for melting the ice shell. In that regime, we found a direct relationship between the surface heat flux and d*. Finally, we provide a new assessment of Europa's thermal state. Using available constraints, we propose that the ice shell thickness should exceed 25 km. However, d*≈25-35 km implies a tidal power (>3 TW) much larger than expected. An extrapolation of the trends suggested by our results indicates that a more reasonable tidal power (<1 TW) would involve d*≈ 80-100 km.

Keywords: Europa, Icy Satellites, Thermal convection, Melting, Cryovolcanism, Tidal Heating

©2020. Japan Geoscience Union. All Right Reserved.

Measurements of Saturn's Zonal Wind from Voyager Images using Modern Cloud-Tracking Method

*Justin Garland[1], Kunio M. Sayanagi[1], Jacob L. Gunnarson[1], John J. Blalock[2,1]

1. Hampton University, 2. USGS Astrogeology Science Center

We present preliminary analysis of Saturn images captured by the Voyager mission investigating how the planet’s zonal wind speeds have evolved in time between 1980 and the Cassini era. Global zonal wind as a function of latitude during the Voyager flybys have been retrieved by previous studies; notably Sanchez-Lavega et al. 2000's measurements have been treated as the standard wind profile of Saturn. However, they employed manual tracking methods that returned only 2075 wind vectors, while newer analyses of Cassini data employ automated digital tracking algorithms. No study has systematically analyzed the wind speeds during the Voyager flybys and the Cassini era using a consistent method. We aim to make new wind measurements by first improving the navigation of the images of Saturn captured by the Voyager spacecraft’s Imaging Science Subsystem (ISS) camera, and then applying an automated 2D Correlation Imaging Velocimetry (CIV) technique. We also analyze Cassini Imaging Science Subsystem (Cassini ISS) images using the same methodology. This provides a long-baseline (more than a Saturnian year) analysis of global zonal winds over time for the planet. I hypothesize that new measurements of Saturn’s equatorial wind will address the longstanding discrepancy between results from Voyager and those from later observations. Sanchez-Lavega et al. 2000 reports a wind speed of approximately double that found by later studies using Hubble and Cassini. I expect that analyzing the Voyager datasets with modern, automated methods will help us better constrain previously published trends in wind profiles retrieved for the planet. I also aim to provide a stronger baseline Voyager wind profile for future studies than what is currently available in the literature.

Keywords: Saturn, Atmospheric Dynamics, Giant-planet Atmospheres, Voyager, Cassini

©2020. Japan Geoscience Union. All Right Reserved.

Inhibition of moist convection in the atmospheres of Jovian planets: the case of NH4SH formation by chemical reaction of NH3 and H2S

*Ko-ichiro SUGIYAMA[1], Kensuke Nakajima[2], Kiyoshi Kuramoto[3], Yoshi-Yuki Hayashi[4]

1. National Institute of Technology, Matsue College, 2. Kyushu University, 3. Hokkaido University, 4. Kobe University

In the atmospheres of Jovian planets, condensation of heavy components, such as H2O, NH3, CH4, is thought to suppress vertical convection (Guillot, 1995). In addition to these clouds resulting from condensation of the above components, the formation of NH4SH by chemical reaction of NH3 and H2S is predicted as the important cloud formation processes. Because the chemical process consumes the components heavier than the lighter major components as condensation process does, it can be anticipated that the formation of NH4SH can also suppress convection. However, the degree of possible suppression, or whether it can inhibit convection, have not investigated yet.

Here we investigate the criterion of convection inhibition associated with the formation of NH4SH in thermochemical equilibrium framework. With the convection inhibition criteria obtained in the investigation, we also examine the structure of convection in parameters where convection inhibition by NH4SH formation is thought to emerge using cloud convection model (Sugiyama et al 2009; 2011; 2014).

Keywords: atmosphere of Jovian planet, cloud convection, numerical calculation

©2020. Japan Geoscience Union. All Right Reserved.

Detectability of water plumes on icy moons with Earth-orbiting UV telescope

*Ryoichi Koga[1], Fuminori Tsuchiya[1], Go Murakami[3], Kazuo Yoshioka[2], Masato Kagitani[1], Tomoki Kimura[1], Atsushi Yamazaki[3], Ichiro Yoshikawa[2], Hajime Kita[3], Masaki Kuwabara[3]

1. Tohoku University, 2. The University of Tokyo, 3. JAXA/ISAS

In this study, we consider the mirror size of UV space telescope, which can detect OI and HI emissions emitted from plumes on icy moons. Hubble Space Telescope (HST) observed the enhancement of HI 121.6 nm and OI 130.4 nm emissions near the Europa South Pole (Roth et al., 2014). They considered the electron impact of H_2O in the plume yields HI and OI emissions. However, geological conditions of emitting gasses form Europa plumes are not known.

The EXCEED (Extreme Ultraviolet Spectroscope for Exospheric Dynamics) spectrometer onboard the Hisaki satellite has conducted long term monitoring of ultraviolet emissions (52.0-148.0 nm) from the Io plasma torus and Jupiter’s aurora since 2013. We also observed OI 130.4 nm around Jupiter moon Io’s orbit, and analyzed spatial distribution and temporal variations of oxygen atoms in Io torus. However, the spatial resolution of Hisaki/EXCEED is too rough (~17”) to resolve Io and Icy moon’s disk (for example, Europa’s diameter is ~1.0”). One of the main goal of post Hisaki UV satellite is to observe icy moon’s atmosphere continuously with high resolution and confine conditions under which plume eruptions occur.

We calculated the OI 130.4 nm and HI 121.6 nm counts of Europa plume (signal) and atmosphere, solar reflection, geocorona and interplanetary medium (noise), and estimated the mirror diameters, which can meet the demand that the signal to noise ratio is over 3 with integration time of 10 hours and spatial resolution of ~0.2 arcsec. Requested mirror diameters are ~140 cm when the altitude of the satellite is 1000 km, and ~100 cm when the altitude is 30,000 km.

©2020. Japan Geoscience Union. All Right Reserved.

Development of a radial diffusion model of Jovian inner magnetospheric plasma transportation for a comparison with HISAKI data

*Kazuki Yamaguchi[1], Takeshi Sakanoi[1], Fuminori Tsuchiya[1], Masato Kagitani[1], Tomoki Kimura[2], Ryoichi Koga[1], Reina Hikida[3]

1. Tohoku university, 2. Frontier Research Institute for Interdisciplinary Sciences, Tohoku University, 3. Department of Earth and Planetary Science, Graduate School of Science, Tokyo University

We developed a time-dependent radial diffusion model to calculate chemical reactions and radial transport of ions and electron in the Jovian inner magnetosphere. We compared the model results with HISAKI observation, and found that the neutral source rate from Io to the magnetosphere is 5.0×10^{-4} ($/m^3/s$), the oxygen-sulfur ratio is 2.0, and the radial diffusion coefficient is 4.2×10^{-8} ($/R_J^2/s$) near Io.
Jovian first satellite Io has active volcanoes and releases the plasma of the volcanic gas origin to the magnetosphere. The 90% of total mass of the plasma is mainly supplied from Io (Hill, Dessler, and Goertz, 1983). The plasmas co-rotate with Jupiter and distribute in a donut shape called Io Plasma Torus (IPT). The plasma diffuses outward on the time scale of several tens of days while obtaining the rotation angular momentum of Jupiter. Revealing the mass and energy balance of plasmas is an important subject to understand the macroscopic physical phenomena in the Jovian inner magnetosphere. The radial distribution of Jovian magnetospheric plasma has been examined based on steady state models and observations of Voyage 1, 2 and Cassini spacecraft. However, the time dependent model and comparison of the model with continuous observations have not been reported yet.
The purpose of this study is to develop a model that has a capability to track the time variation of the radial plasma distribution and compare it with HISAKI observation.
In the model, we track mass and energy balances of major heavy ions of Io origin (O^+-O^{3+} and S^+-S^{4+}). The equation system is based on the mass and energy transport model of steady state magnetospheric plasma developed by Delamere et al. (2005). The time evolution of radial transport was solved with the Fokker-Planck equation and we used FTCS method for numerical computation. The radial diffusion coefficient is expressed as $D_{LL}=D_0(L/L_0)^m$, where L is the L-value, $L_0=5.9$, and D_0 is a free parameter of the model. We set a radial grid size (dL) as a function of exponentials of the radial distance so that radial dependence of the Courant number ($2D_{LL}dt/dL^2$, dt is a time step) becomes weak. For the inner and outer boundary conditions, we set the radial gradient of the density and temperature to 0 at the Io's orbit (5.9 R_J), and fixed them with extrapolated values of HISAKI observation at 30 R_J. We considered several chemical interactions: charge exchange, electron impact ionization, electron recombination, Coulomb interaction and radiation due to electron collision excitation based on Delamere & Bagenal (2003). Radiative and recombination rates are calculated from the CHIANTI atomic database. The initial values of temperature and density of each ions and thermal electrons were given from the HISAKI observations in November 2013 when Io's volcanic activity was quiet (Yoshioka et al. 2018). The density of neutral atoms (O, S) were also given by HISAKI observation (Koga et al. 2018b) as initial values, and their total source rates and the source composition ratio (O/S) are free parameters.
In order to verify the validity of the model, the steady state temperature and density of ions and electrons in the region of 6-10 R_J were compared with the HISAKI observation. We found that highly ionized ions have low density, and temperature of ions is almost stable around 100 eV except S^+ which has 200 eV. We obtained the parameters that best matched with HISAKI observation. As a result, the O/S is 2.0, the neutral source rate is 5.0×10^{-4} ($/m^3/s$), and D_{LL} is estimated to be 4.2×10^{-8} ($/R_J^2/s$) near Io. The source

©2020. Japan Geoscience Union. All Right Reserved.

characteristic is consistent with the main atmospheric composition of Io (SO_2) and DLL is found within a range of previous estimations. As a future work, we aim at quantitative verification by comparing with D_{LL} based on a numerical analysis.
In this presentation, we'll show the correspondence between the quantitative inspection results of each parameter and the observation results of HISAKI.

Keywords: Jovian magnetosphere, HISAKI satellite, Io plasma torus

©2020. Japan Geoscience Union. All Right Reserved.

Light Curve of Jupiter's UV Aurora and Io Plasma Torus after 2016 Obtained from Hisaki EXCEED

*Hajime Kita[1], Tomoki Kimura[2], Fuminori Tsuchiya[2], Go Murakami[1], Atsushi Yamazaki[1], Ryoichi Koga[2], Reina Hikida[3], Kazuo Yoshioka[3], Ichiro Yoshikawa[3]

1. Institute of Space and Astronautical Science, Japan Aerospace Exploration Agency , 2. Tohoku Univ., 3. The University of Tokyo

Hisaki is an Earth-orbiting satellite launched in 2013. The purpose of this mission is to observe UV emission from planetary atmospheres and magnetospheres by the spectrometer EXCEED (Extreme Ultraviolet Spectroscope for Exospheric Dynamics). Hisaki EXCEED began its monitoring of the Jovian system in December 2013 with a 140 arcsec −20 arcsec dumbbell slit which is designed to observe the Io plasma torus and Jovian aurora simultaneously. Hisaki EXCEED can continuously observe the Jovian system along the 106 min orbit for several months, which is a feature never available for large facilities such as Hubble Space Telescope.

The guide camera of Hisaki broke down around mid-2016. From 2016 to 2017, we tried to observe the aurora and torus simultaneously without the guide camera. The location of Jupiter was set to in the narrow slit region, however, sometimes aurora moved away from the narrow slit region. Therefore, we use two observing modes, “torus mode” and “aurora mode” since 2017. The Jovian disk is located in the wide-slit region for the aurora mode. Both north and south auroras are observed, and only one side of the torus can be seen. For the torus mode, we set the location of Jupiter to the narrow slit region, and the torus fit within the wide-slit region. We made a light curve of the aurora and torus over 900-1480A and 650-780A, respectively.
Although the light curves obtained after 2016 are missing some parts, we compare the light curves with HST and ground-based observation. A large HST campaign has been made since the arrival of Juno, and aurora brightenings were observed by both Hisaki and HST. The torus light curve shows minor enhancement of volcanic activity around the end of 2017, which is roughly consistent with the sodium observation. Therefore, we successfully corrected Jupiter’s position and the obtained aurora and torus light curve are consistent with other observations.

Keywords: Jupiter, Aurora, Io Plasma Torus

©2020. Japan Geoscience Union. All Right Reserved.

Laboratory demonstration of cryogenic-specific reddish coloration with cryoplasma

*Noritaka Sakakibara[1], Yu Yu Phua[1], Tsuyohito Ito[1], Kazuo Terashima[1]

1. The University of Tokyo

Reddish coloration and color diversity among icy bodies in the outer solar system are one of the important characteristics for understanding the environment and history of the solar system. Ultra-red objects only occur far from the Sun such as some Trans-Neptunian objects and Centaurs, whereas the reddish coloration is absent among cometary nuclei and dead comets closer to the Sun lack (Luu & Jewitt 1996; Sheppard 2010). The reddish color has been attributed to refractory tholin-type materials (Cruikshank et al. 2005). However, because the tholin-type materials are very stable even when warmed to room temperature, the origin of color distribution in the cryogenic world remains debatable (Dalle Ore et al. 2011). In this presentation, we will provide experimental demonstration of reddish coloration that is stable only at cryogenic temperatures.

The reddish coloration was produced on methanol- and water-containing ice irradiated with 3% nitrogen-containing helium cryoplasma at 85 K. Cryoplasma is non-equilibrium plasma source whose gas temperature can be controlled continuously at wide range of cryogenic temperatures below room temperature (Stauss et al. 2018), which enables coexistence of plasma with ice without melting (Sakakirbara & Terashima 2017; Sakakibara et al. 2019). The reddish color faded and disappeared at 120–150 K as the ice was heated. This behavior is distinct from well-known refractory organic tholins that are stable even when heated to room temperature. By temperature programmed desorption analysis and LC-MS/MS analysis of the residue at room temperature, the reddish material was suggested to be nitrogen-containing organic compounds.

The temperature dependence of reddish coloration under cryogenic conditions could add on a new explanation for the absence of ultra-red coloration closer to the Sun in the outer solar system; the cryogenic-specific reddish materials sublimate or convert to other colorless compounds at higher cryogenic temperatures, as an icy body travels from the Trans-Neptunian region to the inner solar system. Our result implies that a reddish material specific to cryogenic environments might be a promising clue for the investigation of color diversity and formation mechanism of the outer solar system. Moreover, cryoplasma was expected as a novel modern technology for accelerating the investigation of chemistry and materials science in cryogenic space environments including the outer solar system.

Luu J., & Jewitt D. 1996, *AJ*, **112**, 2310; Sheppard S. S. 2010, *AJ*, **139**, 1394; Cruikshank D. P., Imasaka H., Dalle Ore C. M. 2005 *AdSpR*, **36**, 178; Dalle Ore C. M., Fulchignoni M., Cruikshank D. P., et al. 2011 *A&A*, **533**, A98; Stauss S., Muneoka H., Terashima K. 2018 *PSST*, **27**, 023003; Sakakibara N., Ito T., Terashima K. 2019 *Langm*, **35**, 3013; Sakakibara N., & Terashima K. 2017 *JPhD*, **50**, 22LT01

Keywords: cryoplasma, reddish coloration, outer solar system, ice, color diversity, astrochemistry

©2020. Japan Geoscience Union. All Right Reserved.

[E] Poster | P (Space and Planetary Sciences)：P-PS Planetary Sciences

[P-PS02] Lunar Science and Exploration

convener:Masaki N Nishino(Japan Aerospace Exploration Agency, Institute of Space and Astronautical Science), Masahiro KAYAMA(Department of General Systems Studies, Graduate School of Arts and Sciences, The University of Tokyo), Hiroshi Nagaoka(Japan Aerospace Exploration Agency), Yusuke Nakauchi(Japan Aerospace Exploration Agency)

Scientific data sets acquired by Japanese lunar mission SELENE (Kaguya) have become the standard of the lunar sciences. Other missions such as Chandrayaan-1, LRO, GRAIL, LCROSS, LADEE, Artemis, and Chang'e series as well as ground observations are also providing new knowledges of the Moon. Apollo/Luna samples and lunar meteorite analyses are also being advanced. In concurrence with these studies, some countries including Japan are planning near-future lunar missions. In this session, we will discuss scientific results based on newly acquired lunar data, strategies for future missions, lunar sample analyses, and theoretical and experimental studies of lunar sciences.

[PPS02-P01] Cause of boulder falls near a lobate scarp on the Moon: source estimate based on the attenuation relation of peak ground accelerations

*Ayame Ikeda[1], Hiroyuki Kumagai[1], Tomokatsu Morota[2] (1.Graduate School of Environmental Studies, Nagoya University, 2.Department of Earth and Planetary Science, The University of Tokyo)

[PPS02-P02] The lunar tidal dissipation energy by the Earth-moon tide

*Ryuichiro Tanaka[1], Satoshi Kaneshima[2] (1.Department of Earth and Planetary Sciences, Graduate School of Science, Kyushu University, 2.Department of Earth and Planetary Sciences, Faculty of Science, Kyushu University)

[PPS02-P03] The heterogeneity of lunar plasma environment and its influences on lunar surface hydration

*Huizi Wang[1], Jiang Zhang[1], Quanqi Shi[1,2], Yoshifumi Saito[3], Ying Ye[1] (1.Shandong Key Laboratory of Optical Astronomy and Solar-Terrestrial Environment, School of Space Science and Physics, Institute of Space Sciences, Shandong University, Weihai, Shandong, China., 2.State Key Laboratory of Space Weather, National Space Science Center (NSSC), Chinese Academy of Sciences, Beijing, China, 3.Institute of Space and Astronautical Science, Japan Aerospace Exploration Agency, Sagamihara, Japan.)

[PPS02-P04] **Phase boundary and kinetics of moganite-coesite phase transition at high-pressure and high-temperature: implications for an impact event and trace of water on the Moon**

*Shin Ozawa[1], Masahiro KAYAMA[1,2], Tatsuya Sakamaki[1], Tomonori Ohashi[1], Akio Suzuki[1] (1.Department of Earth Science, Graduate School of Science, Tohoku University, 2.Department of General Systems Studies, Graduate School of Arts and Sciences, The University of Tokyo)

[PPS02-P05] Evaluating the thickness and stratigraphy of ejecta materials at the Chang'e-4 landing site

*Luyuan Xu[1], Xunyu Zhang[1], Le Qiao[2] (1.State Key Laboratory of Lunar and Planetary Sciences, Macau University of Science and Technology, 2.Shandong Provincial Key Laboratory of Optical Astronomy and Solar-Terrestrial Environment, Shandong University, Weihai)

[PPS02-P06] An explaination of the origin of Davy Crater Chain on the Moon other than impacts of fragments comprising a comet

Akiya Saito[1,2], *Junichi Haruyama[1], Wataru Miyake[2] (1.Japan Aerospace Exploration Agency, 2.Tokay University)

[PPS02-P07] UZUME: A Lunar Lava Tube Exploration of Japan

*Junichi Haruyama[1] (1.Japan Aerospace Exploration Agency)

[PPS02-P08] On magnetic field observation in and near a lunar pit for understanding magnetic history of the Moon

*Hisayoshi Shimizu[1] (1.Earthquake Research Institute, University of Tokyo)

[PPS02-P09] Radiation dose and protection by a lunar hole and lava tube

*Masayuki Naito[1], Nobuyuki Hasebe[2], Satoshi Kodaira[1], Yoshiharu Amano[2], Junichi Haruyama[3] (1.National Institutes for Quantum and Radiological Scinence and Technology, 2.Waseda University, 3.JAXA)

[PPS02-P10] Breadboard Model of Bionic Legged Robot for Lunar Lava Cave Exploration

*LIANG CHEN[1] (1.Ashikaga University)

[PPS02-P11] Study of lunar 3-D terrain mapping using both the camera and the LIDAR loaded on the rover

*Ryuhei Yamada[1], Yuichi Yaguch[1], Keitaro Naruse[1] (1.The University of Aizu, Department of Computer Science and Engineering)

[PPS02-P12] **Characterizing Sites for Landed Lunar Missions with NASA's Moon Trek Portal**

*Emily Law[1], Brian Hamilton Day[2] (1.Jet Propulsion Laboratory, 2.Ames Research Center)

[PPS02-P13] Development of a compact LIBS instrument for future lunar explorations: a feasibility study using lunar meteorites

*Akinojo Ogura[1], Yuichiro Cho[2], Naoki Yamamoto[1], Koki Yumoto[2], Takafumi Niihara[3], Shingo Kameda[4], Seiji Sugita[2], Takahide Mizuno[5] (1.Department of Earth and Planetary Physics, University of Tokyo, 2.Department of Earth and Planetary Science, University of Tokyo, 3.Department of Systems Innovation, University of Tokyo, 4.School of Science, Rikkyo University, 5.Institute of Space and Astronautical Science, Japan Aerospace Exploration Agency)

[PPS02-P14] **Preparation status of Multi-Band Camera onboard SLIM lander**

*Kazuto Saiki[1], Makiko Ohtake[2], Yusuke Nakauchi[2], Hiroaki Shiraishi[2], Chikatoshi Honda[3], Hiroyuki Sato[2], Yoshiaki Ishihara[4], Takao Maeda[5], Chihiro Yamanaka[1], Hiroshi Nagaoka[2] (1.Graduate School of Science, Osaka University, 2.Japan Aerospace Exploration Agency, 3.University of Aizu, 4.National Institute for Environmental Studies, 5.Chuo University)

[PPS02-P15] The search for whistler-mode chorus emissions related to the Moon using ARTEMIS

*Wataru Sawaguchi[1], Yuki Harada[1], Satoshi Kurita[2] (1.Graduate School of Science, Kyoto University, 2.RISH, Kyoto University)

Cause of boulder falls near a lobate scarp on the Moon: source estimate based on the attenuation relation of peak ground accelerations

*Ayame Ikeda[1], Hiroyuki Kumagai[1], Tomokatsu Morota[2]

1. Graduate School of Environmental Studies, Nagoya University, 2. Department of Earth and Planetary Science, The University of Tokyo

High-resolution images obtained by the Lunar Reconnaissance Orbiter Camera (LROC) show that lobate scarps were widely distributed on the whole Moon [Watters et al., 2010; 2015]. Kumar et al. [2016] suggested that boulder falls, that produced boulder trails on crater wall, might be triggered by moonquakes in the lobate scarps. However, they did not quantitatively estimate the magnitude of the moonquake and the relationship with landslide areas. In this study, to examine whether or not boulders falls were triggered by moonquakes in nearby lobate scarps, we evaluated the moonquake magnitude required for boulder falls on inner ring the Schrödinger Basin. We identified boulder trails using LROC images and measured the entire area of source region of boulder falls. The empirical relationship between the landslide area and the maximum acceleration of large-scale earthquakes ($M > 5$) on the Earth is approximated by a power-law [Tiwari and Ajmera, 2017]. We derived the relationship between the landslide area and the maximum acceleration under the lunar gravitational acceleration from the relationship for earthquakes. Based on the relationship, the maximum acceleration for moonquake was calculated from the surface area of source region of boulder falls. We used the attenuation equation for seismic wave [Kanno et al., 2006] to estimate the magnitude of the moonquake from the maximum acceleration. Since estimated land slide area was small, we extrapolated both the landslide relationship and the attenuation equation to apply to the Moon. Based on an assumption of the epicenter on the lobate scarp, the magnitude of the moonquake generating the boulder falls was estimated to be about 2, comparable to that for shallow moonquakes observed by Apollo’s seismometer. This result is compatible to the interpretation that the boulders falls were due to the moonquake along the lobate scarp.

Keywords: boulder falls, lobate scarp

©2020. Japan Geoscience Union. All Right Reserved.

The lunar tidal dissipation energy by the Earth-moon tide

*Ryuichiro Tanaka[1], Satoshi Kaneshima[2]

1. Department of Earth and Planetary Sciences, Graduate School of Science, Kyushu University, 2. Department of Earth and Planetary Sciences, Faculty of Science, Kyushu University

It is assumed that the magnetic field with the dynamo existed about 4 billion years ago in the moon. It seems that the tidal power is related to this. The moon is being distorted into an oval form by the tidal power, and besides, heating occurs in the lunar inside. The tidal power becomes strong so that the distance from the Earth to the moon is near. Because the distance was nearer than the present in the past, it is assumed that the tidal power is related to the lunar dynamo. In addition, it seems that there is a low viscosity layer in the mantle bottom of the moon from seismic wave observation. Heating by the tidal power grows big in such a layer and may affect the lunar core. In this study, I calculated the lunar tidal dissipation energy and examined the influence that the low viscosity layer gives around.

When the lunar tidal quality factor is 100, I calculated the tidal dissipation energy. I could get the result that the dissipation in the low viscosity layer accounted for 99% of the whole.

Keywords: moon, tide

©2020. Japan Geoscience Union. All Right Reserved.

The heterogeneity of lunar plasma environment and its influences on lunar surface hydration

*Huizi Wang[1], Jiang Zhang[1], Quanqi Shi[1,2], Yoshifumi Saito[3], Ying Ye[1]

1. Shandong Key Laboratory of Optical Astronomy and Solar-Terrestrial Environment, School of Space Science and Physics, Institute of Space Sciences, Shandong University, Weihai, Shandong, China., 2. State Key Laboratory of Space Weather, National Space Science Center (NSSC), Chinese Academy of Sciences, Beijing, China, 3. Institute of Space and Astronautical Science, Japan Aerospace Exploration Agency, Sagamihara, Japan.

The evidences for lunar water (e.g., polar ice and OH^-/H_2O) have been discovered in recent lunar missions. The dynamic lunar hydration/dehydration cycle over a lunar day and the suppression of lunar water within lunar magnetic anomalies indicated that solar wind proton should be an important source of lunar surface water. However, the Moon passes through its surrounding plasma environment comprised of solar wind, magnetosheath, and magnetotail. Therefore, the dependence of lunar water content on plasma parameter remains further deep investigations. In this study, we try to find the relevance between the variability of lunar water and lunar plasma environment based on the observations from the Kaguya MAP-PACE and Chandrayaan-1 M^3 spectrometer. We first study lunar hydration inside/outside the magnetosphere using the M^3 spectral data, from which it is unexpectedly found that the polar surficial OH/H_2O abundance remains the same level when in the solar wind and in the magnetosphere. We suggest that the particles from the magnetosphere (Earth wind, naturally different from solar wind) contribute to lunar hydration. And then we studied lunar hydration inside/outside the plasma sheet, in which the proton has a broad velocity distribution with a wide thermal spread. A case study shows that the water content at the same region on the Moon is different when in the plasma sheet and in the lobe of Earth’s magnetotail. Nevertheless, more work is needed to understand the physical mechanism.

Keywords: Earth wind, Lunar water, Solar wind

©2020. Japan Geoscience Union. All Right Reserved.

Phase boundary and kinetics of moganite-coesite phase transition at high-pressure and high-temperature: implications for an impact event and trace of water on the Moon

*Shin Ozawa[1], Masahiro KAYAMA[1,2], Tatsuya Sakamaki[1], Tomonori Ohashi[1], Akio Suzuki[1]

1. Department of Earth Science, Graduate School of Science, Tohoku University, 2. Department of General Systems Studies, Graduate School of Arts and Sciences, The University of Tokyo

Moganite is a monoclinic SiO_2 mineral that forms by precipitation from alkaline fluid under high-pressure condition. Recently, moganite was first discovered in a lunar meteorite NWA 2727, supporting water activity on the surface of the Moon (Kayama et al., 2018). Moganite in NWA 2727 always coexists with coesite, a high-pressure polymorph of SiO_2. This fact suggests that a heavy impact event occurred on the host site of NWA 2727 on the Moon, resulting in high-pressure phase transition of moganite to coesite. On the other hand, other silica polymorphs such as quartz, tridymite and cristobalite in NWA 2727 have not been transformed into coesite. Although moganite seems to change into coesite more easily than other silica polymorphs, the phase boundary and kinetics of the moganite-coesite phase transition remain unknown. In this study, we performed high-pressure and high-temperature experiments on terrestrial moganite up to 8 GPa and 500 ˚C to determine the phase boundary and kinetics of the moganite-coesite phase transition.

In all experiments, natural terrestrial moganite (Gran Canaria, Spain) and synthetic quartz powders were loaded separately in two different sample rooms in a high-pressure cell and kept at the same pressure and temperature conditions. The samples were first compressed to the target press load at ambient temperature and then heated to the target temperature. The high-pressure and -temperature experiments and X-ray diffraction (XRD) measurements were conducted at the beamline AR-NE5C of the Photon Factory at the High Energy Accelerator Research Organization (KEK).

As a result of time-resolved XRD analysis, it was revealed that moganite transformed into coesite more rapidly than quartz under the conditions of ~5 GPa and 425 ˚C and ~8 GPa and 250 ˚C. The different kinetics between moganite and quartz would be due to a similar crystal structure between moganite and coesite with a common four-membered rings structure (Murashov and Svishchev 1998) and/or relatively high water content of moganite (1-5 wt% in general) compared with quartz, both of which reduce the activation energy of the phase transition from moganite into coesite. Our result demonstrated that the different phase transition kinetics of silica polymorphs to coesite can explain the contrasting coexistence relationship of silica minerals in NWA 2727: in a short duration of an impact event, only moganite was able to transform into coesite with a relatively high phase transition speed. In addition, this fact revealed here supports the possibility that moganite in NWA 2727 is indigenous to the Moon.

Keywords: moganite, coesite, phase boundary, kinetics, high-pressure, lunar meteorite

©2020. Japan Geoscience Union. All Right Reserved.

Evaluating the thickness and stratigraphy of ejecta materials at the Chang'e-4 landing site

*Luyuan Xu[1], Xunyu Zhang[1], Le Qiao[2]

1. State Key Laboratory of Lunar and Planetary Sciences, Macau University of Science and Technology, 2. Shandong Provincial Key Laboratory of Optical Astronomy and Solar-Terrestrial Environment, Shandong University, Weihai

On 3rd January 2019, China's Chang'e-4 (CE-4) lunar probe successfully landed on the Von Kármán crater on lunar far-side and deployed Yutu-2 rover. The Von Kármán crater is located in the highly-cratered terrain within the South Pole-Aitken (SPA), indicating the CE-4 landing site has experienced complex emplacement sequences of both near and distant ejecta materials. This complicates the interpretation of CE-4 surface *in-situ* measurements of the Visible and Near Infrared Spectrometer (VNIS) and Lunar Penetrating Radar (LPR) onboard Yutu-2 rover. In order to evaluate the sources and amounts of all considerable (> 10 cm in thickness) ejecta materials on the landing site of Chang'e-4, we thoroughly examine the ejecta delivered by all crater-forming events possibly occurred later than the formation of mare unit within Von Kármán crater in this study. We find a total of 20 craters throughout the Moon may deliver unneglectable ejecta (> 10 cm in thickness) superposed on the mare units of the landing site of Chang'e-4 and confirm that the ejecta from Finsen crater is the most dominant foreign materials, followed by the ejecta of Von Kármán L.

Keywords: Moon, Chang'e-4, impact ejecta

©2020. Japan Geoscience Union. All Right Reserved.

An explaination of the origin of Davy Crater Chain on the Moon other than impacts of fragments comprising a comet

Akiya Saito[1,2], *Junichi Haruyama[1], Wataru Miyake[2]

1. Japan Aerospace Exploration Agency, 2. Tokay University

The Lunar Davy crater chain (located at 11.0 ˚S , 6.3 ˚W on the Moon) is a line of about 20 craters, the averaged diameter of which is about a few km, and extends over a length of 45 km.
The origin of the formation of the Davy crater chain have not been clarified. One explanation is the collision of ejectors from a primary crater that should exist in the direction of the chain, Another one is those of the split nuclei of a comet. In both cases,however,difficulties have been pointed out.
We have studied it with high resolution ortho-image data and elevation data (Digital terrain model, DTM) obtained by the Terrain Camera onboard Japanese lunar orbiter SELENE and large area image data from LRO WAC, and found that the Davy crater chain is a group of young craters and forms an arc. We, furthermore,investigated the central direction of the arc of the Davy crater chain, and identified a young crater Lalande (4.4 ˚S, 8.6 ˚W) with about 22 km in diameter at 210 km north-northwest from the Davy crater chain.
We deduced relations for the physical parameters between a primary crater and its secondary craters and applied it to Crater Lalande and Davy crater chain for (1) the ratio of total mass released from the primary crater to mass per an ejector vs. the primary crater diameter, (2) the average of secondary crater diameters and the distance between the primary crater and (3) the secondary craters.between a primary crater and its secondary crater. The results were harmonious with the relations between other previously identified primary-secondary craters on the Moon.
We conclude that the Davy crater chain is a group of secondary craters forming an arc shape prospective from the Crater Lalande.
Furthermore, we found that Catena Aburfeda, also forming an arc, is a group of secondary craters from Crater Tycho, too.

Keywords: moon, crater chain, catena, cometary impact, secondary craters

©2020. Japan Geoscience Union. All Right Reserved.

UZUME: A Lunar Lava Tube Exploration of Japan

*Junichi Haruyama[1]

1. Japan Aerospace Exploration Agency

In this century, huge vertical holes with a diameter and depth of several tens of meters have been discovered on the Moon by the Japanese lunar explorer SELENE (Kaguya). From the US Lunar Reconnaissance Orbiter (LRO) high-resolution images revealed that the floors of the holes are not bowl-shaped like a normal craters.
It is reasonable to think that such a vertical hole formed when a meteorite collided with an underground space such as a lava tube. In fact, data from oblique observations by LRO showed that there are deep spaces at the bottom of the vertical holes. In addition, in the US gravity field observation satellite GRAIL data, large mass deficits were found along a rille (lava river) in the Marius Hills, at the middle of which a vertical hole exists. In addition, along the rille, specific underground echoes implying the existence of a lava tube were also identified in SELENE Lunar Radar Sounder data. The existence of lava tubes on the Moon becomes more certain.
Lava tubes will be effective shelters from meteorites and radiation on the Moon, making them the best lunar base construction sites. Exploration of lava tubes is therefore the most important topic of international space exploration programs. In the third edition of the Global Exploration Roadmap (GER) submitted by the International Space Exploration Coordination Group (ISECG), which aims to create an international space exploration framework led by national space agencies.
On the other hand, exploration of the lava tube on the moon provides various scientifically important information. We are examining a plan to explore lunar vertical holes and associated lava tubes, with naming it as "UZUME"(Unprecedented Zipangu Underworld of the Moon Exploration).
In this presentation, we will explain how the UZUME will contribute on planetary science, the main purposes of it are
(1) Increasing knowledge about how habitable regions that nurtured life formed, evolved and maintained and then life was born in the past,
(2) Increasing knowledge of the universe which is necessary for us humans to expand our habitable regions from the Earth to the space.

Keywords: Moon, Exploration, lava tube, SELENE, Hole

©2020. Japan Geoscience Union. All Right Reserved.

On magnetic field observation in and near a lunar pit for understanding magnetic history of the Moon

*Hisayoshi Shimizu[1]

1. Earthquake Research Institute, University of Tokyo

History of the Moon and lunar dynamo can be discussed using quantities related with magnetization near the lunar surface. For example, paleointensity studies of lunar rock samples showed that the Moon likely possessed strong intrinsic magnetic field until 3.56 Ga, and probably had weaker magnetic field up to around 1 Ga. Also, directions of isolated magnetizations estimated from magnetic field observations by Lunar Prospector and SELENE-Kaguya show possibility of reorientation of lunar pole in the past. However, it is not well understood what was the energy source to drive the lunar dynamo during the period, and also when the dynamo stopped generating the magnetic field.

Magnetic field observation at the lunar surface by Apollo project revealed existence of local-scale magnetic anomalies which cannot be detected by satellite magnetic field observations. The local-scale magnetic anomalies are likely due to the magnetization close to the surface of the Moon. Since this magnetization also contain information of the magnetic field at the time when the part of the crust was magnetized, it is worth pursuing further information of the magnetization by in-situ magnetic field observations.

A lunar pit can be a suitable place for magnetic field observation to estimate magnetization very close to the lunar surface. A reason is that a pit is a place where large magnetic field signal due to magnetization is expected, because it introduces inhomogeneity to the crustal magnetization. In addition, layered magnetization, which is caused by variation of lunar magnetic field, may be obtained by magnetic field observations along the pit wall.
A feasibility study on the use of magnetic field observation in and around a lunar pit to estimate local crustal magnetization was conducted. In this presentation, requirement to prove the magnetization and favorable configuration of observation are discussed by supposing location and size of the lunar pit.

Keywords: lunar magnetic field, lunar pit, magnatization

©2020. Japan Geoscience Union. All Right Reserved.

Radiation dose and protection by a lunar hole and lava tube

*Masayuki Naito[1], Nobuyuki Hasebe[2], Satoshi Kodaira[1], Yoshiharu Amano[2], Junichi Haruyama[3]

1. National Institutes for Quantum and Radiological Scinence and Technology, 2. Waseda University, 3. JAXA

The lunar surface is directly exposed to high energetic particles such as Galactic Cosmic Ray (GCR) particles and Solar Energetic Particles (SEPs), which are shielded by thick atmosphere and geomagnetic field on the Earth. Long term manned missions to the Moon, Mars or deep space will occur more severe radiation exposure than that we have experienced, which may result serious health hazards of space crews. Then, strategic radiation protection is mandatory to guarantee health of crews by relieving radiation dose.

The Moon is the closest celestial body to the Earth and expected as a next body developed by humans in near future. Recently, cameras on SELENE have discovered vertical holes on the lunar surface, at Marius Hills, Mare Tranquillitatis and Mare Ingenii. It is considered that such lunar vertical holes are formed by meteorite impacts collapsing the roof on lava tubes. Therefore, entrances of lava tubes may open at the bottom of the vertical holes. Radar observation suggests a possible lava tube exists about 100m in depth at a subsurface near a vertical hole at Marius Hills. Vertical holes associating lava tubes reduce radiation dose of cosmic ray particles coming from the zenith. In this work, the radiation dose at the lunar surface was numerically evaluated, and its reduction in the lunar vertical hole was estimated. The GCR particles in solar minimum and maximum phases and large SEP events, called ground level enhancement (GLE) events observed on the Earth, are assumed as primary events.

The effective dose equivalent due to GCR particles reached up to 267.8 mSv/y in solar minimum phase, and that due to a GLE event observed at Jul. 2000 was 509 mSv/event at the lunar surface. It was found that the contribution of secondary particles to the total radiation dose was ~8% at most. This fact implies that the elemental composition of lunar surface, whether mare region or highland region for example, does not make any considerable difference in the total radiation dose. On the other hand, the radiation dose become ~10% at the center bottom of vertical hole expecting Marius Hills, 50 m in diameter and 43 m in depth. The radiation dose reduction is mainly due to the solid angle of primary particle. However, the contribution of secondary particles increased to ~20% at the bottom. This is also due to the solid angle subtended by the secondary particle sources, the wall and bottom of the hole. The effective dose equivalent reduced to 20 mSv/y at the edge bottom of the vertical hole. This value corresponds to the reference value of occupational exposure determined by ICRP. If there is over 25 m space, 50 m from the hole center, the effective dose equivalent becomes less than 1.0 mSv/y, the reference value of public exposure. Our results show that the vertical hole and lava tubes are promising sites for human long stay in future from the aspect of radiation protection. The detail results of numerical experiments and evaluation of space radiation protection will be presented and discussed.

Keywords: Radiation dose, Lunar holes, Radiation protection

©2020. Japan Geoscience Union. All Right Reserved.

Breadboard Model of Bionic Legged Robot for Lunar Lava Cave Exploration

*LIANG CHEN[1]

1. Ashikaga University

C. Liang and T. Arai

Ashikaga University, Tochigi, Japan (liangchen960809@gmail.com)

Recently, some large, deep vertical holes were discovered at Marius Hills, *Mare Tranquillitatis*, and *Mare Ingenii* on the lunar surface by Japanese spacecraft SELENE (Kaguya) using lunar surface image data acquired by the Terrain Camera (TC) (Haruyama et al., 2009; Robinson et al., 2012; Kaku et al., 2017). Lunar lava tubes can play an important role in both science and human exploration. They might be ideal sites for future lunar bases, because of their stable thermal conditions and potential to protect people and instruments from micrometeorites and cosmic ray radiation. Their stable and protected environment also makes them an enticing research target: original lava compositions, textures, and even magmatic volatiles are expected to be preserved in pristine condition within these lava tubes (Haruyama et al., 2012; Haruyama et al., 2016). Examining their interiors could provide unique insights concerning the evolutionary history of Moon. In the future, we will expand our search to other regions on Moon where additional subsurface lava tubes may be discovered. In this study, we have been developing the lunar exploration robot. We believe using a bionic mechanism with intelligence will be more stable for complex rocks than a wheel mechanism in the lunar environment. Our robot has individual motors for every single joint compared with other legged robots, hence it has higher flexibility. However, for the prototype to safely and efficiently explore lunar caves, certain conditions are required: 1. Stability of the survey instrument in space and cave environment 2. the optimum size of robot and onboard instruments, 3: Autonomous control under lunar cave. Currently, we have developed a reinforcement learning method for the robot. This presentation will introduce the current status and highlights of our bionic legged robot, including mobility, flexibility and agility. To test the function of the survey instrument, we are creating a simulated environment of lunar caves. We will also improve the balance system of the robot by testing it in the simulated environment, and ensure its functionality during a real exploration on the moon. The results of these experiments will be published at JpGU-AGU joint meeting 2020.

Keywords: Lunar Exploration

©2020. Japan Geoscience Union. All Right Reserved.

Study of lunar 3-D terrain mapping using both the camera and the LIDAR loaded on the rover

*Ryuhei Yamada[1], Yuichi Yaguch[1], Keitaro Naruse[1]

1. The University of Aizu, Department of Computer Science and Engineering

The lunar landing mission is next main topic for survey and utilization of the Moon. Many remote sensing observations by Kaguya, LRO, GRAIL, LADEE and Chang’ e programs have almost completed comprehensive knowledge of the lunar surface in recent 15 years. The landing exploration can provide details of local terrain, geology and chemical composition on a selected area. Then, deployment of the geophysical sensors such as seismometer, thermometer and magnetometer using a lunar lander and/or a rover should provide the new chances to investigate the lunar interior structure since Apollo-era. In this study, we target to construct the accurate 3-D terrain map around the landing site in range from several hundreds of m to a few km using both the camera and the 3-D LIDAR loaded on the lunar rover.

The accurate 3-D terrain map can provide the detailed frequency distribution of size of the boulder and its shape, geometries of the craters and relief of the surface around the site. This information helps us to investigate the formation process and age of the area. Then, we can utilize the map to select the scientific target with other sensor data and design the route of the rover to the target.

We have studied the method to construct the 3-D terrain map using the 3-D LIDAR point cloud data by the SLAM (Simultaneous Localization and Mapping) algorithm, and we can construct the 3-D map with accuracy of a few –about 10 cm [Yamada et al., 2019]. On the other hand, the 3-D map consisting of only the LIDAR data is usually sparse especially in far range. The camera image can be used to complement the space and provide color information in the map. We have also studied the calibration method to match the camera image and the LIDAR point cloud data to construct the accurate 3-D map with high resolution [Yamada et al., 2020]. In this presentation, we will introduce the methods of 3-D map construction and calibration. Then, we will perform the mapping test using the both the camera and the LIDAR loaded on the wagon and/or the small rover in outside area and indicate the result of the 3-D map. Finally, we will also discuss the application of the method to the lunar science and exploration, operation of the rover and the future vision using the lunar rover.

Keywords: Lunar terrain, 3-D mapping, LIDAR, camera, rover

©2020. Japan Geoscience Union. All Right Reserved.

Characterizing Sites for Landed Lunar Missions with NASA's Moon Trek Portal

*Emily Law[1], Brian Hamilton Day[2]

1. Jet Propulsion Laboratory, 2. Ames Research Center

NASA's Moon Trek (https://trek.nasa.gov/moon/) is one of a growing number of interactive, browser-based, online portals for planetary data visualization and analysis produced by NASA's Solar System Treks Project (SSTP). Moon Trek continues to be enhanced with new data and new capabilities enabling it to facilitate the planning and conducting of upcoming lunar missions by NASA, its commercial partners, and its international partners.

Moon Trek is being used for growing number of mission planning, specifically for site characterization. Its baseline visualization and analysis tools allow users to measure the diameters, heights and depths of surface features. Users can plot Sun angles altitude and azimuth. More advanced account-level tools allow users to perform computationally-intensive analyses. These include ray-traced lighting analysis for user-specified areas over user-specified time/date ranges and time intervals. Lighting analyses also produce maps of watts per square meter for the area specified. Electric surface potential analyses can also be generated for user-specified areas and intervals. Machine learning-based hazard analyses include boulder detection and distribution, crater detection and distribution, and slope analysis. Large data products can be subsetted, allowing users to download regions of specific interest. The LRR/LLR Geometry Calculator allows researchers to find, visualize, and analyze images taken by the Lunar Reconnaissance Orbiter (LRO) that are applicable to Lunar Laser Retro-Reflector (LRR) and Lunar Laser Ranging (LLR) studies and planning.

Using an in-house stereo workflow, SSTP is able to produce new NAC-based high-resolution mosaics and DEMs. These are particularly useful in our work with Commercial Lunar Payload Services (CLPS) providers using Moon Trek in site characterization for landing and surface operations.

Important new tools are currently being integrated into Moon Trek. A Convolutional Neural Network (CNN) is being implemented, trained to automatically detect rockfalls in LRO NAC imagery, and integrated into Moon Trek. Such rockfalls are interesting because they enable remote analysis of tectonic activity, surface evolution, and mechanical surface properties. A new line-of-sight tool will support detailed studies of solar illumination, line-of-sight communications with the Earth, and communications with assets in lunar orbit.

This presentation for JpGU will highlight Moon Trek's tools that are useful in facilitating site characterization for future Lunar missions.

Keywords: Lunar site characterization, Analysis, Visualization

©2020. Japan Geoscience Union. All Right Reserved.

Development of a compact LIBS instrument for future lunar explorations: a feasibility study using lunar meteorites

*Akinojo Ogura[1], Yuichiro Cho[2], Naoki Yamamoto[1], Koki Yumoto[2], Takafumi Niihara[3], Shingo Kameda[4], Seiji Sugita[2], Takahide Mizuno[5]

1. Department of Earth and Planetary Physics, University of Tokyo, 2. Department of Earth and Planetary Science, University of Tokyo, 3. Department of Systems Innovation, University of Tokyo, 4. School of Science, Rikkyo University, 5. Institute of Space and Astronautical Science, Japan Aerospace Exploration Agency

The composition of lunar surface is a fundamental observable for understanding the geology of the Moon. For example, in situ measurements of Mg# on a mineral-by-mineral basis help us understand the differentiation process of the lunar magma ocean, adding information to the Mg# map obtained from the orbit [Ohtake et al., 2012]. Elemental analysis is also important for the future lunar polar missions because it provides possible water detection with its geologic context.

Laser-induced breakdown spectroscopy (LIBS) is a method that enables such spot-by-spot analyses. LIBS analyzes the emission spectra from laser-induced plasma that exhibits a number of emission lines characteristic to individual elements. The laser beam is focused on a sample to ~100 microns, allowing the analysis of individual minerals. In addition, LIBS analysis can be conducted from several meters away in a few minutes and the laser pulses can excavate the surface of a sample up to several millimeters. In fact, LIBS was/will be used on Mars for NASA’ s Curiosity and Mars 2020 rovers [Reess et al., 2018]. In contrast, no actual measurements have been made on the Moon yet. A previous study for a lunar LIBS revealed that major elements can be measured with the accuracy of several wt% [Lasue et al., 2012]. However, their laboratory study did not focus on the miniaturization of the instrument: they switched three spectrometers with different wavelength ranges; the laser in their research was about 1 m long.

In our study, the entire LIBS components were assembled in a package to be portable. Our LIBS instrument is 35 cm×30 cm×20 cm and ~8 kg including a laser, spectrometer, CCD camera, optics with an automatic focusing function, controllers, breadboard, and enclosure. The instrument has a simple electrical interface, namely 12, 15, and 24-28 VDC power lines and one USB hub for communication.

Using the LIBS package, we constructed a quantitative analysis model for major elements with a goal to achieve the precision sufficient to classify lunar crusts. We conducted a series of experiments as follows: 20 geological standard samples from National Institute of Advanced Industrial Science and Technology (AIST) and United States Geological Survey (USGS) were pressed and located in the vacuum chamber under 3×10-2 Pa, 1 m away from the LIBS components. Laser pulses from a Nd:YAG laser (~30 mJ at 1064 nm) were applied 100 times at 5 spots. Ninety spectra were averaged after correcting dark, continuum emission, and relative sensitivity of the optical system. The corrected data were used to build the models with univariate analysis (UVA) (i.e., calibration curves) and multivariate analysis (Partial Least Squares, PLS). The precision of the model was acquired by the leave-one-out cross validation. Then, the concentrations of major elements (Si, Fe, Al, Mg, Na, Ca, Ti, K) in the lunar mare meteorite NWA479 were predicted (phenocryst and groundmass separately) using the models.

Our quantitative analyses yielded the model prediction precisions better than 1 wt% (Na2O and TiO_2), 2 (CaO and K2O), 3 (FeO), and 8 wt% (SiO_2). We also found that elements with strong emission lines were better predicted by UVA than by PLS: as 6.29 wt% (PLS) vs 3.90 (UVA) wt% for MgO, 1.04 wt% (PLS) vs

©2020. Japan Geoscience Union. All Right Reserved.

0.69 wt% (UVA) for Na_2O. Also, the predicted concentrations of Mg, Al, and Ca in phenocryst (olivine) and groundmass (plagioclase and pyroxene) of the lunar meteorite were distinguished against each other, indicating the possibility of mineral-to-mineral measurements on the Moon. From the calibration activity, we also found that the geological samples with Fe_2O_3> 20 wt% and CaO > 16 wt% are necessary to improve the accuracy of Mg# and An# predictions, because lunar meteorites contain higher $Fe2O_3$ and CaO than typical igneous rocks on the Earth. In addition, we conducted a separate LIBS experiment with the engineering model of the Nd:YAG laser used for Hayabusa-2's LIDAR instrument. The obtained LIBS spectra exhibited a number of emission lines, indicating the feasibility of LIBS measurements with the flight-proven laser. The preliminary results from the lunar meteorite experiment using the compact LIBS instrument suggest the possibility to analyze the composition of minerals quantitatively on the lunar surface.

References

Dyar, M. D. et al. (2012), *Spectrochim. Acta B,* **70**, 51–67.

Lasue, J. et al. (2012), *Journal of Geophysical Research*, **117**, E01002.

Li, S. et al. (2018), *PNAS*, **115** (36) , 8907-8912.

Ohtake, M. et al. (2012), *Nat. Geosci.*, **5**, 384-388.

Reess, J. -M et al. (2018), *ICSO*.

Keywords: Moon, LIBS, space chemistry, lunar exploration

©2020. Japan Geoscience Union. All Right Reserved.

Preparation status of Multi-Band Camera onboard SLIM lander

*Kazuto Saiki[1], Makiko Ohtake[2], Yusuke Nakauchi[2], Hiroaki Shiraishi[2], Chikatoshi Honda[3], Hiroyuki Sato[2], Yoshiaki Ishihara[4], Takao Maeda[5], Chihiro Yamanaka[1], Hiroshi Nagaoka[2]

1. Graduate School of Science, Osaka University, 2. Japan Aerospace Exploration Agency, 3. University of Aizu, 4. National Institute for Environmental Studies, 5. Chuo University

Smart Lander for Investigating Moon (SLIM) project is on going at JAXA. It will be launched in fiscal year 2021 as Japan’ s lunar-landing mission. The main purpose of this project is to demonstrate various techniques for pinpoint landing within a hundred meters in radius on the moon. Demonstration of the SLIM landing technology will cause a paradigm shift from "exploring where it is easy to land" to "exploring where we want to land." After landing, the SLIM project plans to operate Multi-Band Camera (MBC) to observe around the landing site. We are now testing an engineering model of MBC.

As a landing site for SLIM mission, one of the small fresh craters just outside of the Theophilus crater is selected. This crater (diameter ~200 m) locates 13.3º S, 25.2º E outside the southwest rim of Theophilus and named “Shioli”. There is olivine-rich lithology, which is probably mantle (or the lower part of the crustal) origin excavated by the Nectaris basin forming impact as suggested by the global distribution of the olivine-rich sites (Yamamoto et al. , 2010) , well before the formation of the Theophlius. In order to identify this unknown lithology and estimate its origin, MBC has a spatial resolution (1.3 mm/pixel at 10 m) that distinguishes plutonic rock texture and a band combination (10 bands; 750, 920, 950, 970, 1000, 1050, 1100, 1250, 1550, 1650 (nm)) that identifies mineral species. And most importantly, MBC has plan to estimate Mg # (=Mg/(Mg+Fe) atomic ratio) of olivine.

In order to advance basic research on spectroscopic observation of lunar rocks, we have developed a line spectrometer using the same image sensor (Xenics, FPA0.9-1.7_640_4_TE1) as MBC. The range of observable wavelength is 850 - 1700 nm (can be expand to 750 - 1700 nm in the future) . Line Spectrometer can observe continuous spectra and also have one-dimensional spatial information. By observing various rock samples with this spectrometer, we would like to succeed in deriving the detailed mineralogy of the olivine-rich exposure in the lunar spectroscopic observation at the SLIM project. Preliminary observations show that olivine grains in rocks are more difficult to observe than powdered olivine, and the locations where absorption peaks can be observed are biased toward mineral grain boundaries.

This study is supported in part by JSPS Grants-in-Aid for Scientific Research: Grant Number 19H01953.

Keywords: the moon, lander, near infrared spetrometry

©2020. Japan Geoscience Union. All Right Reserved.

The search for whistler-mode chorus emissions related to the Moon using ARTEMIS

*Wataru Sawaguchi[1], Yuki Harada[1], Satoshi Kurita[2]

1. Graduate School of Science, Kyoto University, 2. RISH, Kyoto University

Whistler-mode chorus emissions are narrow band emissions observed mostly on the dawn and day side in the Earth’s inner magnetosphere [Burtis and Helliwell, 1969; Burtis and Helliwell, 1976]. Their frequency band is typically from 0.2 f_{ce} to 0.8 f_{ce}, where f_{ce} is the electron cyclotron frequency at the magnetic equator. They are also found in the magnetospheres of Jupiter [Coroniti et al, 1980], Saturn [Hospodarski et al, 2008] and Mars [Harada et al, 2016], but their presence has not been confirmed near unmagnetized bodies without dense atmospheres.

The generation of whistler-mode waves is based on the linear theory in which the free energy source of waves is provided by the temperature anisotropy of electrons with respect to the background magnetic field [e.g., Tsurutani et al., 1979]. However, it does not explain the characteristic chirping of chorus. Therefore, nonlinear theories were proposed and it was shown that whistler-mode waves in an inhomogeneous medium could effectively trap cyclotron-resonant electrons [Dysthe, 1971] and then resonant current could strongly amplify waves [Nunn, 1974; Omura et al,1991]. The incoherent waves occur first based on the linear theory, then the wave field traps cyclotron-resonant electrons, and eventually the amplitudes of the waves increase nonlinearly.

The Moon is an unmagnetized and airless body. Various kinds of plasma phenomena occur as a result of the interaction of solar wind and magnetospheric plasmas with the Moon’s exosphere, surface, and crustal magnetic field [Halekas et al,. 2012]. For example, electron anisotropy caused by the absorption on the lunar surface drives cyclotron resonance of waves traveling toward the Moon with electrons reflected from the lunar surface by magnetic mirroring, leading to generation of whistler-mode waves [Harada et al., 2014]. As the amplitudes of the whistler-mode waves are comparable to those of chorus emissions in the Earth’s inner magnetosphere, it may be expected that chorus-like waves are possibly present in the vicinity of the Moon.

We searched for and identified chorus-like events with discrete rising tone elements from the magnetic field data obtained by the ARTEMIS mission, and tested whether they are consistent with the nonlinear model by Omura et al. (2008) and whether they are Moon-related waves by two point measurements.

Keywords: Moon, chorus, wave-particle interaction, ARTEMIS, whistler mode

©2020. Japan Geoscience Union. All Right Reserved.

[E] Poster | P (Space and Planetary Sciences)：P-PS Planetary Sciences

[P-PS03] High-pressure phases in shocked meteorites: key to understanding impact events on parent asteroids

convener:Kishan Tiwari(Indian Institute of Technology Kharagpur)

Shocked meteorites, which are the products of collisions in between their parent asteroids, contain shock melt veins, which are pervasive localized zones of very high pressure, temperature, and frictional melting. Minerals entrained in and around such SMVs being subjected to such extreme conditions are transformed to high-pressure polymorphs and thus such shocked meteorites serve as unique natural samples to study the mechanism of such polymorphic transformations. Based on shock metamorphic features observed in olivine and plagioclase, produced at different P-T conditions, a shock stage classification system has been developed with highest shock stage, S6 corresponds to 75-90 GPa. But the pressure stability range established by static high-pressure experiments for the high-pressure polymorphs reported in shocked meteorites is much lower than that indicated by their corresponding shock stage. Such a large difference is mainly because such polymorphic transformations depend on kinetics of the reaction and the actual P-T-t path experienced by the mineral grains during the shock. Computational modeling and microscopic studies of shock front behavior and shocked samples indicate that interaction of shock waves with mineral grain of different shock impedance may result in pressure heterogeneity and localized spikes in temperature. Compositional and textural analyses of matrix portions in shocked meteorites have revealed that they have crystallized directly from the chondritic melt at high pressure. Thus, phase relations and mineral stability at different P-T conditions derived from static high-pressure experiments can be used to infer the crystallization pressure and shock pressure. Estimated shock pressure can be used to calculate shock velocity, impact velocity, and parent body size by using the Rankine-Hugoniot equation. So apart from transformation mechanisms, shocked meteorites can provide us with information about collision dynamics on their parent asteroids.

[PPS03-P01] Thermal infrared measurement of impact in laboratory experiment

*Tetsuya Fukuhara[1], Shinsuke Abe[2], Masahisa Yanagisawa, Ryota Fuse[2], Naoya Sakatani[3] (1.Rikkyo University, 2.Nihon University, 3.JAXA/ISAS)

Thermal infrared measurement of impact in laboratory experiment

*Tetsuya Fukuhara[1], Shinsuke Abe[2], Masahisa Yanagisawa, Ryota Fuse[2], Naoya Sakatani[3]

1. Rikkyo University, 2. Nihon University, 3. JAXA/ISAS

Ground based observations of Lunar impact flash with visible wavelength contributes progress of the impact physics. Meanwhile, the visible observations are restricted to the direct flash at the night side. When the thermal infrared emission from an impact is observed, coverage can be expanded not only to the nightside but also to the dayside. The thermal infrared observation also would detect residual hot spot after the impact event. When the temperature variation is derived from the continuous observation of the residual hot spot, thermal inertia, from which an energy budget correlated with size of the crater, would be obtained. Epoch of the impact and the temperature at that time may be estimated from the thermal relaxation profile even if the impact could not be directly detected. As a first step, we have measured artificial impact flashes using a thermal infrared camera in a laboratory experiment.

The impact experiment with 15 shots has been carried out in a vacuum chamber. SiO_2 sand with ~345 μm diameter was set inside, and an uncooled microbolometer array (UMBA) camera detecting the thermal infrared wavelengths at 10 μm (8 -14 μm) was configured outside of the chamber. Thermal infrared images were continuously obtained with 10 Hz via a thermal transmission window. When a polycarbonate impactor with a size of 2 mm struck the sand with a speed of 6.6 km/s, the temperature distribution and profile of the crater created on the sand surface was obtained from brightness temperature distribution in the UMBA images.
The temperature profile of the sand surface after the impact has been estimated in each pixel using images continuously obtained. The maximum temperatures were estimated to 1700-2600 K at the time of impacts. Notably, the result showed unexpected horizontal temperature distributions; the temperature of the crater limb was higher than that of the crater center at the time of impact. However, the limb temperature drastically decreased less than 1000 K, and the limb temperature became lower than center temperature after 0.5 seconds.

Keywords: Moon, Meteoroid, impact

©2020. Japan Geoscience Union. All Right Reserved.

[E] Poster | P (Space and Planetary Sciences)：P-PS Planetary Sciences

[P-PS04] Regolith Science

convener:Koji Wada(Planetary Exploration Research Center, Chiba Institute of Technology), Akiko Nakamura(Graduate School of Science, Kobe University), Patrick Michel(Universite Cote D Azur Observatoire De La Cote D Azur CNRS Laboratoire Lagrange), Kevin John Walsh(Southwest Research Institute Boulder)

Recent planetary explorations have revealed that almost all solid bodies in the solar system are covered with small particles, called regolith. The surface geology, especially regolith behavior on the surfaces of solid bodies, becomes increasingly more important as represented by Hayabusa mission and other on-going and planned sample-return missions such as Hayabusa2, OSIRIS-REx, and MMX.
For fully understanding the regolith science, it is required to know and compare the regolith conditions on various celestial bodies, from asteroids to planets, with various methods.
Therefore, this session welcomes broad topics related to regolith on various celestial bodies, such as asteroids, comets, the Moon, the martian moons, Mars, etc. Papers on the formation, evolution, and alteration processes of regolith particles and regolith systems on the surface of planetary bodies, remote and in-situ observational results and techniques, analyses and results of returned samples, and laboratory, numerical, and theoretical studies on the fundamental physical and chemical processes are all welcome.
Note that what we call regolith is not just fine grains: all kinds of materials (more or less loose) that lie on the surface, from cobbles to finer grains, are our targets.

[PPS04-P01] Laboratory penetration experiments conducted at low effective gravity II

*Akiko Nakamura[1], Junpei Nakahata[2], Yuuya Nagaashi[1] (1.Graduate School of Science, Kobe University, 2.Faculty of Science, Kobe University)

[PPS04-P02] Experimental study of high-velocity impacts into granular material in reduced gravity

*Masato Kiuchi[1], Takaya Okamoto[1], Sunao Hasegawa[1], Akiko Nakamura[2] (1.Japan aerospace exploration agency, Institute of space and astronautical science, 2.Graduate School of Science, Kobe University)

[PPS04-P03] A Tentative Numerical Study on the Effect of Aspect Ratio of Cylindrical Projectile on Crater Morphology using iSALE code

*Yuri Shimaki[1] (1.Institute of Space and Astronautical Science, Japan Aerospace Exploration Agency)

[PPS04-P05] Automated Identification of Particles in Rock Gravel of Small Bodies

*Yuta Shimizu[1], Hideaki Miyamoto[1] (1.University of Tokyo)

[PPS04-P06] Development of lunar regolith simulants based on previous lunar explorations

*Takemura Tomohiro[1], Takafumi Niihara[1], Hideaki Miyamoto[1] (1.The University of Tokyo)

[PPS04-P07] **Estimation of abrasion rates of regolith particles on Itokawa and the Moon based on abration experiments.**

*Akira Tsuchiyama[1], Hirotaka Yamaguchi[2], Akiko Nakamura[3] (1.Research Organization of Science and Technology, Ritsumeikan University, 2.Graduate School of Science, Kyoto University, 3.Graduate School of Science, Kobe University)

Laboratory penetration experiments conducted at low effective gravity II

*Akiko Nakamura[1], Junpei Nakahata[2], Yuuya Nagaashi[1]

1. Graduate School of Science, Kobe University, 2. Faculty of Science, Kobe University

Laboratory measurements of the penetration depth of an impactor with a velocity of m/s in a granular layer under Earth’ s gravity were compiled to give an empirical relationship between drop height and penetration depth that is applicable for various granular materials (Uehara et al., 2013). There are limited data on the penetration depth under low gravity. In low-velocity (2–40 cm/s) impact experiments with a quartz sand target under low effective gravities (~0.2–1 m/s^2), the penetration depth was independent of the effective gravity (Murdoch et al., 2016).

To investigate the penetration of an impactor into granular material as an analogue of planetary regolith, we examined the low-velocity impact of a sphere into a granular layer at low effective gravity in the laboratory experiments. The target granular material was packed in a bucket. The bucket was fixed with two electromagnets; when the electromagnets were switched off, it dropped vertically downward, reducing the effective gravity, which was monitored by an accelerometer. In our previous set-up we used constant-force springs to hang the bucket and the effective gravity averaged 2.5 m/s^2 (Nakamura et al., 2019JpGU). In our new study, we used two linear shafts to guide the bucket. The impactor was a 16. 7-mm-diameter glass sphere. A plastic straw with horizontal lines drawn on it was glued to the glass sphere. The penetration process of the glass sphere with the straw was imaged at 960 fps by a camera attached to the bucket. We used 1-mm-diameter glass spheres and 0.7-1 mm peach seed fragments as targets.

In this study, the effective gravity was lower than 0.09 m/s^2. The glass sphere collided with the granular target at a relative velocity of between 3 and 4.5 m/s. The final depth of the impactor roughly matched the expected value given by an analytic penetration model (Katsuragi and Durian, 2013).

Keywords: Regolith, Impact, Penetration

©2020. Japan Geoscience Union. All Right Reserved.

Experimental study of high-velocity impacts into granular material in reduced gravity

*Masato Kiuchi[1], Takaya Okamoto[1], Sunao Hasegawa[1], Akiko Nakamura[2]

1. Japan aerospace exploration agency, Institute of space and astronautical science, 2. Graduate School of Science, Kobe University

The surfaces of small bodies are in a microgravity environment. Therefore, it is important to understand how gravity affects crater size to estimate physical properties of the surface. Several studies have investigated the effect of gravity on crater size for low-velocity to high-velocity (1 m s^{-1} to 6.6 km s^{-1}) impacts: the gravitational dependence of crater size was obtained in the low- and high-gravity range (Gault & Wedekind, 1977; Schmidt & Housen, 1987; Cintala et al., 1989; Takagi et al., 2007; Kiuchi et al., 2019). It was shown that the crater diameter was proportional to -0.165 ~ -0.19 power of the gravitational acceleration except for the one conducted using drop tower and showed that the crater diameter formed under microgravity was not different from the one formed under 1 G (Takagi et al., 2007) . The difference in the results of previous studies is not understood because the number of available laboratory data is limited. On the other hand, collisions between planetary bodies generally occur at high-velocities ranging from several kilometers per second to several tens of kilometers per second. However, there are few experimental examples in high-velocity regions over several kilometers per second in reduced gravities. A drop tower or a parabolic flight are generally used for microgravity experiments, however, it is difficult to conduct impact experiments at a velocity of several kilometers per second in these experimental facility.
In this study, we developed a drop system to conduct high-velocity impact experiments in reduced gravity. By assembling a simple drop tower in the vacuum chamber of a two-stage light-gas gun at the Japan Aerospace Exploration Agency (JAXA), low gravity experiments at the impact velocity of several kilometers per second can be realized. The drop system is consists of ball bearings and two rails for dropping a target container smoothly. The top of the container was fixed near the ceiling of a chamber with a height of 2 m by electromagnets, and the container is dropped by turning off electromagnets. The acceleration values are measured by an accelerometer placed at the bottom of the container. When the container filled with 12 kg of sand was dropped under vacuum condition, simulated gravity on the container was obtained in the range of 0.06 - 0.07 G. The falling time of the container was about 0.4 s in these condition.
In addition, we conducted high-velocity impact experiments. The ambient pressure was 100 Pa. While the container was falling, a projectile was fired by the two-stage light-gas gun. The crater formation process was observed with a high-speed video camera installed outside the vacuum chamber. We used quarts sand of representative diameter 425 μm as the target material, and used a polycarbonate sphere of diameter 4.76 mm as the projectile. A polycarbonate sphere is 1.2 g cm^{-3} in density. The target material was loosely filled in a stainless steel container with a diameter of 30 cm and a height of 10 cm. A projectile was impacted at a velocity of 1.2 km s^{-1}. As a result, the diameters of craters formed at 0.06± 0.03 G was about 1.8 times larger than the one formed at 1 G. Gravitational dependence of the crater diameter was clearly observed. We organized the results using pi-scaling (e.g., Holsapple, 1994) and found that our results in reduced gravity agreed well with the crater size scaling law for the sand targets (Housen and Holsapple, 2011). Note that diameters of craters formed in reduced gravity shows the lower limit of the final crater diameter because the crater formation may not have been completed before the container dropped. In the presentation, we will discuss the crater formation time and introduce the additional impact experimental results.

©2020. Japan Geoscience Union. All Right Reserved.

Keywords: Impact ctater, High-velocity impact experiments, Low gravity

©2020. Japan Geoscience Union. All Right Reserved.

A Tentative Numerical Study on the Effect of Aspect Ratio of Cylindrical Projectile on Crater Morphology using iSALE code

*Yuri Shimaki[1]

1. Institute of Space and Astronautical Science, Japan Aerospace Exploration Agency

The small carry-on impactor (SCI) onboard the Hayabusa2 spacecraft successfully detonated on April 5, 2019, and created an artificial crater on the surface of asteroid Ryugu. Besides the main copper liner, the SCI produces irregular-shaped forward debris composed of copper or SUS that form concentric features on the target surface. These concentric features, including sub-crater candidates, were also observed on the surface of Ryugu. However, it is not obvious whether irregular-shaped debris produces typical bowl-shaped craters, although the effect of SCI-like hollow-shaped projectile has been investigated numerically (Kurosawa et al., 2015). In this study, I report a tentative numerical study on the effect of the aspect ratio of a cylindrical projectile on the crater morphology.

In this work, I use the iSALE shock physics code (Amsden et al., 1980; Collins et al., 2004; Wünnemann et al., 2006). A cylinder with an aspect ratio (height/width) and a uniform sand layer was used as the projectile and the target. The impact velocity was set to 2 km/s. The Tillotson EOS for iron and quartz were used. The aspect ratio was varied from 0.36 (disk) to 8.0 (rod), while the volume was almost constant. A gravity of 9.8 m/s^2 was included in the calculation. After the calculations, the depth and diameter of the crater were measured.

With the increase of the aspect ratio of the projectile, the depth of the crater increased, while its diameter was almost unchanged. In this poster, the detailed analysis of the crater morphologies will be described.

Acknowledgments: I appreciate the developers of iSALE, including G. Collins, K. W ünnemann, B. Ivanov, J. Melosh, and D. Elbeshausen. Numerical computations were carried out on PC cluster at Center for Computational Astrophysics (CfCA), National Astronomical Observatory of Japan. I am grateful for the iSALE users group in Japan, including K. Kurosawa, Y. Kanada, R. Suetsugu, and S. Wakita, and the LOC of iSALE workshop 2019 at CfCA.

Keywords: Asteroid, iSALE, Impact

©2020. Japan Geoscience Union. All Right Reserved.

Automated Identification of Particles in Rock Gravel of Small Bodies

*Yuta Shimizu[1], Hideaki Miyamoto[1]

1. University of Tokyo

Numerous boulders and fine particles are commonly distributed over the surface of small bodies, as revealed by the recent space exploration missions [e.g. 1]. Their mechanical properties, such as the shape and size distribution, are considered to be critical for the understanding of the geological surface processes [2], and for the landing safety of the landing/touchdown missions [3]. However, precise identification of the outlines of such particles is challenging due to irregular particle shapes, overlapping particles, image resolution limits. Here, we present a computational approach for the automated identification of particles based on the image feature extraction algorithm utilizing the convolutional neural networks (CNNs). We prepare images of the imitated surface of small bodies by using simulated material (simulant) of the regolith of small bodies [4], and then carefully identified thousands of particles manually. With the data of profiles, the model is trained, enabling nearly 80 % of profiles of particles of simulant to be correctly traced without the aid of manual analysis. Moreover, particles on the global surface of asteroid Itokawa are automatically identified by using tens of images taken in the Hayabusa mission, and identified profiles are mapped on the shape model. We measure the sizes of particles, revealing the cumulative size-frequency distribution (CSFD) of particles on the global surface of Itokawa to have the power-law index of -3.48±0.08, which is consistent with the CSFD calculated in the previous research [5]. The approach of this study can rapidly identify numerous particles, which can be a promising tool for analyzing countless images of the surface of small bodies taken in current and near future space exploration missions.

References

[1] Fujiwara A. et al. (2006), *Science*, 312, 5778 [2] Michikami T. et al. (2019), *Icarus*, 331 [3] Yamaguchi T. et al. (2018), *Acta Astron.*, 151 [4] Miyamoto H. et al. (2018), *LPSC*, 1882 [5] Mazrouei S. et al. (2014), *Icarus*, 229

Keywords: Small bodies, Automated identification, Particles in rock gravels, Boulders

©2020. Japan Geoscience Union. All Right Reserved.

Development of lunar regolith simulants based on previous lunar explorations

*Takemura Tomohiro[1], Takafumi Niihara[1], Hideaki Miyamoto[1]

1. The University of Tokyo

Several countries and agencies plan lunar missions to lunar polar regions in the 2020s (e.g., NASA's Lunar Flashlight, Chinese Chang'E 6, NASA's VIPER, Japanese SELENE-R) to investigate the existence (abundance) of water ice, with the aim to establish lunar bases as gateways to deep space explorations including a manned mission. For the assessment of lunar surface environment (e.g., surface temperatures, regolith properties) and its interaction to lunar lander/rover, as well as the planning of observations and in-situ analyses on surface compositions, subsurface structures, and water ice, a vast amount of lunar regolith simulants, which should be as realistic as possible, are necessary to produce. Previous lunar regolith simulants were developed based on Apollo samples, so that they approximate compositions of materials on the lunar nearside only, which is insufficient for the modeling of the surface of lunar farside and polar regions. Therefore, the objective of this study is to compile remote-sensing data (several chemical composition maps) (Elphic et al., 1998; Lawrence et al., 1998; Lawrence et al., 2007; Lucey et al., 2000; Lucey et al., 1995; Ohtake et al., 2009) and Apollo sample data, and to establish a procedure of the development of simulants of the far-side and polar region as well as the nearside.

In this study, we collected several types of igneous rock and test the accuracy of rock type and texture to use for simulants. Then we revisited Apollo sample data and decided the most favorable ranges of particle size distribution, chemical composition, mineral assemblage, particle shape and texture of our simulant, and established manufacturing procedure.

We finally developed four different types of lunar simulants: mare simulant of the lunar near side, highland simulant of the lunar near side, the South Pole Aitken (SPA) basin simulant, and highland simulants of lunar far-side were prepared by the above procedure using an analysis technique such as XRF. Unlike the existing simulants (e.g., JSC-1), the simulant produced in this study are within the constraints of elemental/chemical compositions of Apollo samples and remote-sensing data, and they show a wide range of validity for modeling the surface of each site, in terms of particle size-frequency distribution, mineral abundance and the chemical composition, which would lead to precise estimates of the surface conditions of future landing sites.

References:

Elphic R. C. et al., (1998) *Science* **281**(5382), 1493-6.

Lawrence D. J. et al., (1998) *Science* **281**(5382), 1484-9.

Lawrence D. J. et al., (2007) *Geophysical Research Letters* **34**(3).

Lucey P. G. et al., (2000) *Journal of Geophysical Research: Planets* **105**(E8), 20297-20305.

Lucey P. G. et al., (1995) *Science* **268**(5214), 1150-3.

©2020. Japan Geoscience Union. All Right Reserved.

Ohtake M. et al., (2009) *Nature* **461**(7261), 236-40.

Keywords: lunar simulant, regolith material, In-Situ Resource Utilization, Apollo Programs

©2020. Japan Geoscience Union. All Right Reserved.

Estimation of abrasion rates of regolith particles on Itokawa and the Moon based on abration experiments.

*Akira Tsuchiyama[1], Hirotaka Yamaguchi[2], Akiko Nakamura[3]

1. Research Organization of Science and Technology, Ritsumeikan University, 2. Graduate School of Science, Kyoto University, 3. Graduate School of Science, Kobe University

External 3D shapes and surface morphologies of Itokawa and lunar regolith particles examined by X-ray nanotomography and SEM showed that some particles have rounded edges, which should be formed by mechanical abrasion [1-3]. Seismic shaking by micrometeoroid impacts on the Itokawa surface was proposed for the abrasion [1]. In order to understand abrasion processes and evolution of regolith particles on the airless bodies, abrasion experiments have been made [4,5]. In this study, we have performed additional abrasion experiments together with SEM observation of abraded grains in order to examine abrasion process and obtaine a general equation for the abrasion rate and the results were applied to abrasion of Itokawa and lunar particles.

The samples used were quartz, olivine ($Fo_{\sim 90}$) and basalt. They were crushed and grains 1~2 mm in size were selected except for some to examine grain size effect (0.5~1 mm and 2~4 mm). These grains (~6.5g) were put into a vessel (10 mL) of agate, dunnite or basalt with ~50% fraction. Then the vessel was shaken with vertically-vibrational motion in a mill (Multi-beads-shocker: YASUIKIKAI Co.). Powder with the size less than 1/6 of the grain size (e.g., <250 mm for 1~2 mm grains) produced by abrasion was removed by sieving. The amount of abrasion, P, was defined as the difference between the grain masses before and after the abrasion, which was normalized by the initial grain mass.

For quartz grains, P increases with abrasion duration, t, (20 sec to 360 min) with the power of ~0.25 irrespective of vibration rate, Ω(100 to 2500 rpm). The amount of abrasion in the first 1 min, P_1, increases with Ω(100 to 3000 rpm) for quartz, olivine and basalt. The powers of P_1 - Ωrelation, m_i, at Ω< ~700 rpm (m = 0.1~0.4) are smaller than those at Ω> ~700 rpm (m_i = 1.2~2). P_1 increases with the grain size, d, at Ω = 2000 rpm for quartz and the power value is temporally ~1.6. If we assume that the power relation between P and t is applicable to different sample materials and that between P_1 and d to different sample materials and Ω, we can obtain the following equation; $P = A_i \times \Omega^{mi} \times d^{1.6} \times t^{0.25}$ (Eq.1), where A_i is the proportionality and the suffix i denote the sample materials. SEM observation together with the P–t relation showed that the abrasion advances by chipping grain corners (chipping) for P < ~1% while grain corners and edges become rounded (wearing) for P > ~1%.

The maximum accelerations by impact on Itokawa and the Moon can be estimated to be ~1 and ~100 m/s^2 based on the impact experiments [6], which correspond to $\Omega$of ~100 and ~700 rpm, respectively. This gives A_i' s in Eq.1 with d = 1.5 mm and t = 1 min are ~0.2 % (olivine) on Itokawa and ~0.5 % (basalt) on the Moon. If typical grain convection time by impact of ~180 s on Itokawa [7] is adopted as the maximum value of t, P is estimated to be ~0.003 and ~0.1 % for d = 100 μm and 1 mm, respectively. As the Itokawa grains have rounded edges (wearing), >~4×10^9 and >~3000 times of impact are required, respectively, for P > 1 %. If the impact frequency on Itokawa [7] is considered, these numbers of impact required for wearing are too large, suggesting that grain abrasion on Itokawa is not expected and impact on the larger parent body (>~20 km) [8] should be necessary. In contrast, on the Moon, A_i ~ 0.5% suggests possible abrasion because of longer residence time in a regolith layer than Itokawa.

References:[1] Tsuchiyama et al. (2011) *Science*, 333: 1121. [2] Matsumoto et al. (2016) *GCA*, 187: 195. [3] Tsuchiyama et al. (2016) 4th *Symp. Solar System Materials*. [4] Tsuchiyama et al. (2018) *Abstr.*49th *LPSC*, 1844.pdf. [5] Yamaguchi et al. (2019) Abstr. *JpGU*, PPS02-P01. [6] Yasui et al. (2015) *Icarus*, 260: 320. [7] Yamada et al. (23016)Icarus, 272: 165. [8] Nakamura et al. (2011) *Science*, 333: 1113.

©2020. Japan Geoscience Union. All Right Reserved.

Keywords: Abrasion, Hayabusa mission, Impact

©2020. Japan Geoscience Union. All Right Reserved.

[E] Poster | P (Space and Planetary Sciences)：P-PS Planetary Sciences

[P-PS05] Planetary Seismic Exploration-From InSight and Apollo to Future Missions-

convener:Taichi Kawamura(Institut de Physique du Globe de Paris), Takeshi Tsuji(Department of Earth Resources Engineering, Kyushu University), Ralph Lorenz(Johns Hopkins University Applied Physics Laboratory), William Bruce Banerdt(Jet Propulsion Laboratory)

Given that seismic exploration is one of the most successful approach to study the internal structure of planetary bodies, it has been proposed to various planetary missions. Starting from Passive Seismic Experiment on Apollo missions, various seismic experiments were proposed over the next 50 years. Recently, several such proposals have been approved and thus we are entering a new active era of planetary seismology. In early 2019, the NASA InSight Lander successfully deployed the first seismometer on the surface of Mars and detected the first Marsquakes. In addition, recent global interest in lunar exploration has rekindled interest in a new seismic network on the Moon. In-situ resource utilization is being intensively discussed and seismic exploration has been investigated as an approach to search for subsurface water/ice. Finally, the Dragonfly mission was selected as NASA's next New Frontiers mission and a set of short period seismometers is being considered for its payload. With such a diversity of on-going and future missions, the next decade should see significant advances planetary seismology. The aim of this session will be to discuss the latest planetary seismology discoveries and possible future exploration and developments in this field. In terms of recent discoveries, the focus will be on analyses of InSight seismic data from Mars as well as results from other missions. The session will also include discussion on future missions, both selected and proposed. These include the active seismic experiment on the Japanese Lunar Resource Prospector mission and the seismic experiment on NASA's Dragonfly. Though planetary seismology has a long history dating back to the Apollo era, the associated research community is relatively immature due to the nearly 50-years gap in new data. We propose this session to provide opportunity to bring together scientist working on related topics and encourage discussion and collaboration for future development of this theme.

[PPS05-P01] Estimation of the lunar near-surface effects on Moonquake waves amplification.

*Mohamed Amrouche[1], Renee Weber[2] (1.Schlumberger., 2.NASA Marshall Space Flight Center.)

[PPS05-P02] Scattering properties near Apollo 12 landing site inferred from numerical simulation of seismic wave propagation

*Keisuke Onodera[1,2], Taichi Kawamura[1], Satoshi Tanaka[3], Yoshiaki Ishihara[4], Takuto Maeda[5] (1.University of Paris/Institut de Physique du Globe de Paris, 2.The Graduate University for Advanced Studies (SOKENDAI), 3.Institute of Space and Astronautical Science/Japan Aerospace Exploration Agency, 4.National Institute for Environmental Studies, 5.Hirosaki University)

[PPS05-P03] **INSIGHT SEIS data and dataless dynamic production.**

*Taoufik GABSI[1], Philippe Lognonne[1], Constanza Pardo[1], Charles Yana[2], Eric Beucler[3], John Clinton[4], Vincent Conejero[1], Taïchi Kawamura[1], Gregory Sainton[1], Tanguy Nebut[1], Clément Perrin[1], Matthieu Plasman[1], Simon Stähler[4], Renee Weber[5], Bruce W Banerdt[7], Nobuaki Fuji[1], Sébastien de Raucourt[1], Eléonore Stutzmann[1], Rudolf Widmer-Schnidrig[6] (1.Institut de Physique du Globe de Paris , France, 2.Centre National des Etudes Spatialles, France, 3.Laboratoire de planétologie et géodynamique Nantes Université, France, 4.ETH, Zürich, Switzerland, 5.NASA Marshall Space Flight Center, USA, 6.Universität Stuttgart, Stuttgart, Germany, 7. Jet Propulsion Laboratory, NASA, USA)

[PPS05-P05] **Comparison of attenuation and scattering of Lunar and Martian structures**

*Sabrina Menina[1], Taichi Kawamura[1], Ludovic Margerin[2], Mélanie Drilleau[1], Philippe Henri Lognonné[1], Marie Calvet[2], Marc Monnereau[2] (1.Institut de Physique du Globe de Paris, 2.Institut de Recherche en Astrophysique et Planétologie (IRAP), Toulouse, France)

[PPS05-P06] Orbital Remote sensing seismology on Venus: the VAMOS concept.

*Philippe Henri Lognonné[1], Attila Komjathy[2], Siddharth Krishnamoorthy[2], Raphael F. Garcia[3], Balthasar Kenda[1], Brian M. Sutin[2] (1.Université de Paris, Institut de physique du globe de Paris, CNRS, 2.Jet Propulsion Laboratory, California Institute of Technology, Pasadena, CA 91109, USA, 3.Institut Supérieur de l'Aéronautique et de l'Espace SUPAERO, 10 Avenue Edouard Belin, 31400 Toulouse, France)

Estimation of the lunar near-surface effects on Moonquake waves amplification.

*Mohamed Amrouche[1], Renee Weber[2]

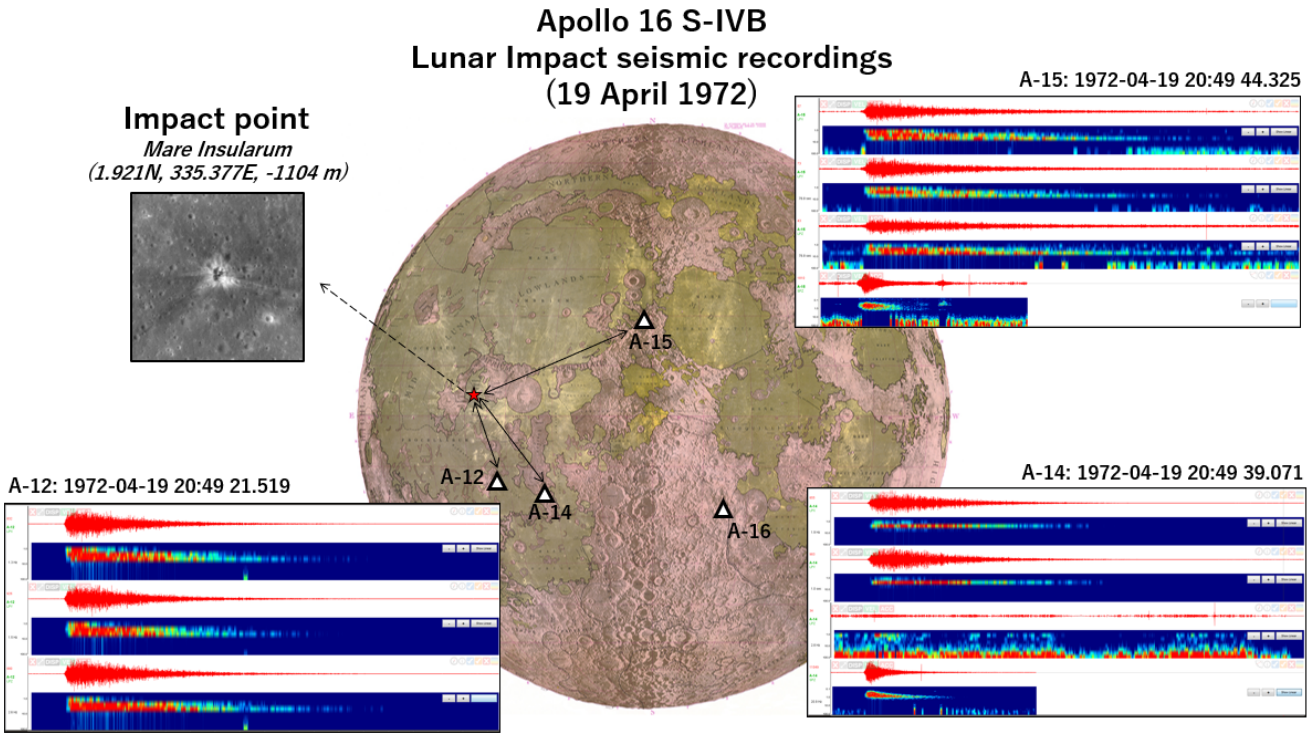
1. Schlumberger., 2. NASA Marshall Space Flight Center.

Ever since the Apollo days, pioneering works on lunar seismology have mainly focused on understanding the deep structure of the Moon. Over the last decades we have witnessed a significant leap in high-resolution mapping of the surface of the Moon and lunar surface geology and topography became well known. However, the effects of the lunar surface geological features on moonquakes amplification remain poorly described in the lunar seismology literature. Meanwhile, studies of the terrestrial near-surface geology and topography effects on earthquake wave-amplification evolved and led to the establishment of a whole new branch of seismology, referred to as ‘Near-surface seismology’. It became a scientific fact today that the near-surface geology and the complexity of the topography play significant roles as far as earthquake wave amplification is concerned.

The aim of this study is to attempt an initial near-surface seismology analysis of the lunar seismic data recorded at the different Apollo Lunar Surface Experiments Packages (ALSEP) sites deployed by NASA during the different Apollo missions. We propose to adapt and apply modern seismic site effect estimation techniques, such as the seismic spectral ratio and the reference site response to the surface lunar meteorite and artificial impacts, as well as the shallow moonquakes cataloged by ALSEP. Results from this study will provide a new perception of the near-surface wave behavior in a lunar environment, and help the estimation of the lunar regolith effects on moonquake wave amplification. The understanding of the lunar near-surface geological and topographical effects on the moonquakes behavior will provides key elements for the future Lunar Geophysical Network deployment site selection, by avoiding the potentially high amplification sites based on the surrounding topography and local geology.

Keywords: Lunar seismology, Site effect estimation, Near-surface geology amplification

©2020. Japan Geoscience Union. All Right Reserved.



©2020. Japan Geoscience Union. All Right Reserved.

Scattering properties near Apollo 12 landing site inferred from numerical simulation of seismic wave propagation

*Keisuke Onodera[1,2], Taichi Kawamura[1], Satoshi Tanaka[3], Yoshiaki Ishihara[4], Takuto Maeda[5]

1. University of Paris/Institut de Physique du Globe de Paris, 2. The Graduate University for Advanced Studies (SOKENDAI), 3. Institute of Space and Astronautical Science/Japan Aerospace Exploration Agency, 4. National Institute for Environmental Studies, 5. Hirosaki University

Abstract

As demonstrated on the Earth, seismological investigation is a well-established way to constrain the planetary interior, and it has been applied to extraterrestrial bodies, such as the Moon [1] and Mars [2]. Basically, the uncertainty of an inner structure model highly depend on how precisely seismic phases can be read. However, in the case of the Moon, the scattering coda in the data is so intense that it is difficult to determine the phase arrivals, resulting in a large uncertainty in the resulting structure model.

This intense scattering is considered to be caused by the subsurface fractured layers called regolith or megaregolith and local topographies. The previous studies mainly investigated the scattering properties of regolith and megaregolith (e.g. quality factor Q, thickness of the layer) by analyzing the Apollo seismic data (e.g. [3][4][5][6]). Yet, there are several different models, and the lunar scattering property is still under discussion [7]. As for the scattering effect by the lunar topography, few studies looked into this although its influence on scattering-coda development has been discussed [5].

This study conducted numerical simulations of seismic wave propagation in order to constrain the scattering properties around the Apollo 12 and 14 landing sites. Because we introduced both scattering media and topographical models (surface and Moho), the output waveforms include both scattering effects. As reference seismic events, the Apollo artificial impacts were selected because their origin times, impact locations and impact parameters are well-constrained (e.g. [8][9]). The velocity structure consists of 4 layers (scattering layer 1, scattering layer 2, crust, mantle) whose parameters were referred from VPREMOON [10]. In the top 2 layers, 2 different random media based on the results by Blanchette-Guertin et al. [5] and Onodera et al. [11] were inserted. As for the source condition, we assumed isotropic radiation of P-wave as an analogue of an impact [12] and Kupper wavelet as source time function with excitation time of 0.65 s. In the simulations, we performed parameter studies on V_p/V_s ratio and thickness for the top 2 scattering layers. By comparing each simulated wave with the Apollo data in terms of rise time and seismic energy, we evaluated what kind of model is preferable to explain the data.

As a result, one of the coda envelopes for the Apollo S-IVB impact events was well reproduced from the simulations, leading to the constraint on the scattering properties of Mare Cognitum region. Our results indicate that the scattering layer in this region can be modeled with 2 different scattering layers. The first 7.5 km layer consists of 200 m scale heterogeneity with 28% velocity fluctuation while the second layer exists up to 10 km depth including 600 m scale scatterers with 14% fluctuation. As for velocity structure, we obtained the smaller V_p/V_s ratio (1.2-1.4) compared to the previous studies (> 1.7 [13]). Since the P and S-wave velocity ratio becomes smaller as the sample gets drier, our results are consistent with our understandings that the Moon has much drier environment than the Earth.

References

©2020. Japan Geoscience Union. All Right Reserved.

[1]Latham et al. (1970), *Science*, 167, 3918, 455-457.
[2]Lognonné et al. (2020), *Nature Geoscience* (in press).
[3]Cooper et al. (1974), *Rev. Geophys. Space Phys.*, 12, 3.
[4]Dainty et al. (1974), *Earth, Moon, Planets*, 9, 11-29.
[5]Blanchette-Guertin et al. (2012), *JGR Planets*, 117, E06003.
[6]Gillet et al. (2017), *Phys. Earth Planet. Inter.*, 262, 28-40.
[7]Jaumann et al. (2012), *Planet. Space Sci.*, 74, 15-41.
[8]Toksoz et al. (1974), *Rev. Geophys. Space Phys.*, 12, 4, 539-567.
[9]Wagner et al (2017), *Icarus*, 283, 92-103.
[10]Garcia et al. (2011), *Phys. Earth Planet. Inter.*, 188, 96-113.
[11]Onodera et al. (2020), *LPSC 51*th, #1277.
[12]Blanchette-Guertin et al. (2015), *JGR Planets*, 120, E004654.
[13]Nakamura et al. (1982), *LPSC 13*th, part 1, 87, A117-A123.

Keywords: Moon, Moonquake, Planetary Seismology

©2020. Japan Geoscience Union. All Right Reserved.

INSIGHT SEIS data and dataless dynamic production.

*Taoufik GABSI[1], Philippe Lognonne[1], Constanza Pardo[1], Charles Yana[2], Eric Beucler[3], John Clinton[4], Vincent Conejero[1], Taïchi Kawamura[1], Gregory Sainton[1], Tanguy Nebut[1], Clément Perrin[1], Matthieu Plasman[1], Simon Stähler[4], Renee Weber[5], Bruce W Banerdt[7], Nobuaki Fuji[1], Sé bastien de Raucourt[1], Eléonore Stutzmann[1], Rudolf Widmer-Schnidrig[6]

1. Institut de Physique du Globe de Paris , France, 2. Centre National des Etudes Spatialles, France, 3. Laboratoire de planétologie et géodynamique Nantes Université, France, 4. ETH, Zürich, Switzerland, 5. NASA Marshall Space Flight Center, USA, 6. Universität Stuttgart, Stuttgart, Germany, 7. Jet Propulsion Laboratory, NASA, USA

Seismologist are used to handle seismometer dataless in addition to the raw data generated by the instruments, and for classical seismometer, the dataless is fixed and provided with the instrument. No change in the sampling rate is also made.

As Insight Seismometer evolve in a very demanding environment, both the sampling rate and instrument configuration might change, especially due to possible limitation in the transmission bandwidth. The instrument configuration varies also on several level. Primary acquisition may vary, according to the operational needs of scientist or the engineering team. According to the external environment used fir filters may be changed, especially during HP3 hammering sessions and calibrations. Each time, we need the to set a specific FIR filter on the acquisition electronics and return back to a classical one just after the hammering or calibration session ends. The datalogger processing varies depending on the way some channels combination has to be made. Insight dataless provides also the possibility to detect a variation of the instrument transfer function during the mission and set it on a established date and time.

Insight dataless has to take into account all the configuration changes and report it into the dataless which may required to be updated for every telemetry.

Data processing is based on flight software configuration files which describes the data flow from the acquisition electronics to the continuous telemetry waveform, including used FIR filters or channels combination if needed. This also determines the continuous data sampling rate.

The link between the channel and its environment is described in CFCT files containing the channel starting and ending date and the used software configuration file during this period. This period determines the fir filters used by the acquisition electronics, or transfer function if they change.

All these needs have been satisfied using a python based program which fetches in arborescent directories whom names are related to the utilisation date and time and contain the needed information and its expiration date for the acquisition electronics part for the first part of the channels dataless. This program also reads the flight software configuration files to provide the second part of the dataless until the continuous or the event waveform.

All the above process is checked every week by the team, which also check for gaps and any off-nominal operations. Gaps, mostly due to transmission issues, can be later filled by specific event request, in addition to those associated to Mars Quake Service detected events At the end, all SEIS data, including their datales, are available through requests made to the Mars SEIS data service (https://www.seis-insight.eu/en/science/science-summary), IRIS-DMC and PDS.

©2020. Japan Geoscience Union. All Right Reserved.

Keywords: Insight, Dataless, Software

©2020. Japan Geoscience Union. All Right Reserved.

Comparison of attenuation and scattering of Lunar and Martian structures

*Sabrina Menina[1], Taichi Kawamura[1], Ludovic Margerin[2], Mélanie Drilleau[1], Philippe Henri Lognonné[1], Marie Calvet[2], Marc Monnereau[2]

1. Institut de Physique du Globe de Paris, 2. Institut de Recherche en Astrophysique et Planétologie (IRAP), Toulouse, France

A limited number of seismic investigations have been performed on other planets and satellites. The only extraterrestrial seismic data available were those collected by the Apollo missions on the Moon and the InSight mission (Interior exploration using Seismic Investigations, Geodesy and Heat Transport) on Mars. Lunar and Martian seismograms appear to be extremely different from terrestrial ones. The seismic signals are characterized by a gradual beginning, a broad maximum and a very long decay lasting up to 20 minutes and 1 hour for Mars and the Moon respectively, compared to a few minutes on Earth. This unexpected long coda results from the low attenuation and intense scattering of highly porous and fractured regolith and megaregolith layers. This intense multiple scattering generates long ringing coda waves and makes difficult to identify direct arrivals of seismic waves such as P and S-waves. However, radiative transfer is well suited to model this process, and it can be approximated by the diffusion equation. Based on the envelope records of Mars and Moon events, the coda has been quantified by two parameters: the time arrival of the maximum of energy (t_{max}) and the decay rate of the energy, named the coda quality factor (Q_c). t_{max} quantifies the diffusion and Q_c is sensitive to attenuation. The data analysis of event 128a revealed that t_{max} and Q_c of Mars differ from those of Moon or Earth. In fact, Q_c of Mars is significantly smaller than that of the Moon and closer to the value of the Earth. This first result may imply that Mars contains more volatiles than the Moon and less than the Earth. To confirm this hypothesis, we need to separate the attenuation from the scattering by using more data which is in process.

Keywords: Attenuation and Scattering, Extraterrestrial seismology, InSight SEIS data, Apollo seismic data

©2020. Japan Geoscience Union. All Right Reserved.

Orbital Remote sensing seismology on Venus: the VAMOS concept.

*Philippe Henri Lognonné[1], Attila Komjathy[2], Siddharth Krishnamoorthy[2], Raphael F. Garcia[3], Balthasar Kenda[1], Brian M. Sutin[2]

1. Université de Paris, Institut de physique du globe de Paris, CNRS, 2. Jet Propulsion Laboratory, California Institute of Technology, Pasadena, CA 91109, USA, 3. Institut Supérieur de l'Aéronautique et de l'Espace SUPAERO, 10 Avenue Edouard Belin, 31400 Toulouse, France

Due to the adverse surface conditions on Venus with its extremely high temperature and pressure, it is infeasible, even using flagship mission resources, to place seismometers on the surface for an extended period of time. Performing remote atmospheric seismic monitoring from an orbiting platform could provide a breakthrough in the detection of seismicity on Venus and the monitoring of seismic wave propagation in the Venus ionosphere.

Venus is surrounded by the brightest naturally occurring airglow layer known in the Solar System. Airglow is a result of various atoms, molecules, and ions that get photoionized by ultraviolet radiation from the Sun and then release energy as visible and infrared light when they recombine and return to their normal state. Perturbations in the neutral atmosphere caused by seismicity on Venus leave an imprint in this airglow layer, spanning altitudes from 90-110 km.

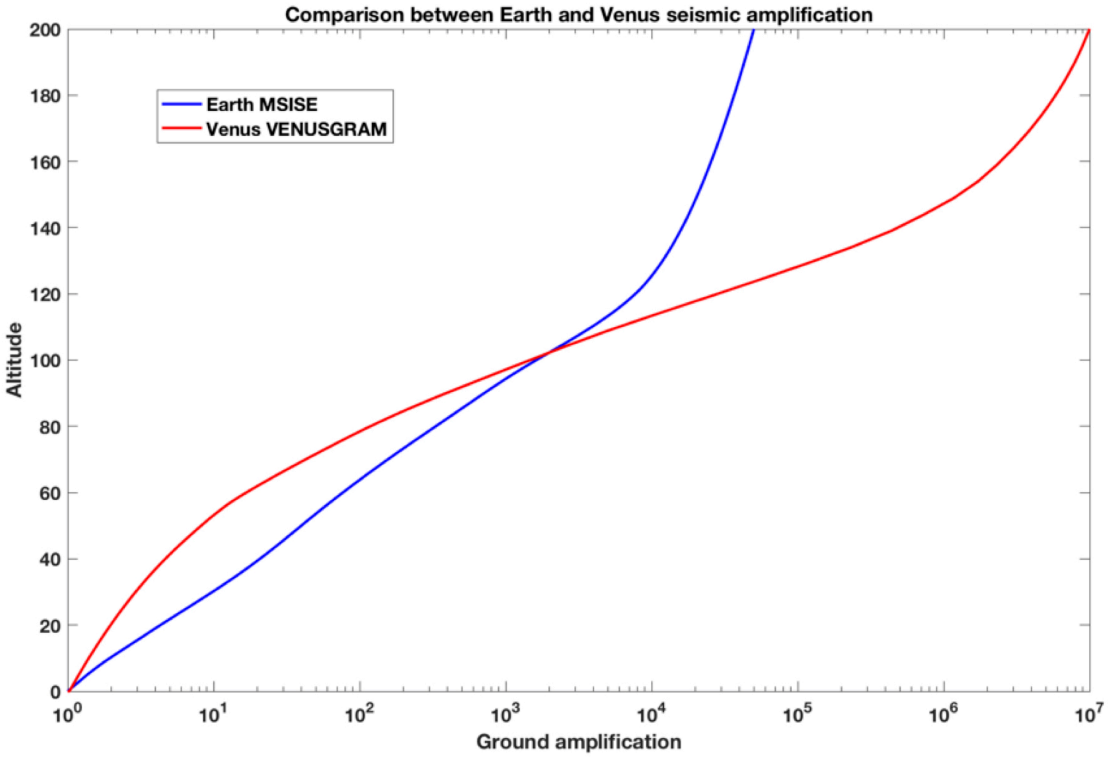
We propose to use remote optical observations of this layer to study these perturbations, allowing us to infer the currently unknown seismicity of the solid planet below. Two specific airglow emissions are investigated, one occurring at 1.27 μm (visible on the night-side) and the other at 4.3 μm (visible on the day-side).

The seismic signal in the Venus atmosphere will be related to the amplification generated by the decay of the density with altitude. This is provided on Figure 1 and compared to Earth. An amplification comparable to Earth is obtained at 100 km, the height of the 1.27 microns on Venus. We get a factor 30 of additional amplification at the height of the 4.3 micron emission (135 km) and even more at higher altitude/
We will summarize here the principal findings of the VAMOS concept study, for which we performed an in-depth analysis and modeling both for the 1.27 μm nightglow and the dayside 4.28 μm non-local thermodynamics equilibrium (non-LTE) signals associated with the waves. The results show that the detection threshold for the proposed imager is expected to be Ms=6 for 1.27 μm and Ms=5 for 4.28 μm.

Figure1: Comparison of the amplification of surface waves for Earth and Venus. Earth model is MSISE while Venus model is VENUSGRAM. See Lognonné et al (*J. Acoust. Soc. Am.*, doi: 10.1121/1.4960788, 2016) for models properties and references.

Keywords: Venus, seismology, airglow

©2020. Japan Geoscience Union. All Right Reserved.



©2020. Japan Geoscience Union. All Right Reserved.

[E] Poster | P (Space and Planetary Sciences)：P-PS Planetary Sciences

[P-PS06] Science of Venus: Venus Express, Akatsuki, and beyond

convener:Takehiko Satoh(Institute of Space and Astronautical Science, Japan Aerospace Exploration Agency), Kevin McGouldrick(University of Colorado Boulder), Hideo Sagawa(Kyoto Sangyo University), Thomas Widemann(Observatoire De Paris)

In this century, our knowledge about the earth's twin sister, Venus, has greatly been advanced through two latest missions, ESA's Venus Express and JAXA's Akatsuki. The latter, in Venus orbit since December 2015, is providing high-quality data that allow studies of atmospheric dynamics in particular. Successful missions are the trigger of ideas of new missions (Russian Venera-D and Indian Shukrayaan-1 under development, European EnVision, and some US proposals). This session invites papers of the new results from data (spacecraft and ground-based), latest results of theoretical and numerical works, and descriptions of new missions as well.

[PPS06-P01] Polarimetry of Venus upper atmosphere with a new single-shot type polarimeter

*Takehiko Satoh[1,2], Masato Kagitani[3], Takeshi Sakanoi[3], Takao M. Sato[4], James O'Donoghue[1] (1.Institute of Space and Astronautical Science, Japan Aerospace Exploration Agency, 2.Department of Space and Astronautical Science, The Graduate University for Advanced Studies, SOKENDAI, 3.Faculty of Science, Tohoku University, 4.Space Information Center, Hokkaido Information University)

[PPS06-P02] Venus's Atmospheric Features in UV as Viewed from Ground-Based Observations

*Ryan M. McCabe[1], Kunio M. Sayanagi[1], John J. Blalock[1], Jacob L. Gunnarson[1], Javier Peralta[2], Candace L. Gray[4], Kevin McGouldrick[5], Takeshi Imamura[2], Shigeto Watanabe[3], Yeon Joo Lee[6] (1.Hampton University, 2.Institute of Space and Astronautical Sciences, JAXA, 3.Department of Earth and Planetary Sciences, Hokkaido Univ., Japan, 4.Apache Point Observatory , Sunspot, NM, 5.LASP, Univ. of Colorado Boulder, 6.Technical University of Berlin, Germany)

[PPS06-P03] 3-D Thermal Structure of the Venus Atmosphere Obtained by Akatsuki/LIR

*Masahiro Akiba[1], Makoto Taguchi[2], Tetsuya Fukuhara[2], Takeshi Imamura[3], Toru Kouyama[4], Takao M. Sato[5] (1.Rikkyo graduate School, 2.Rikkyo University, 3.The University of Tokyo, 4.National Institute of Advanced Industrial Science and Technology, 5.Hokkaido Information University)

[PPS06-P04] An uppermost haze layer above 100 km found over Venus by the SOIR onboard Venus Express

*Seiko Takagi[1], Arnaud Mahieux[2], Valérie Wilquet[2], Séverine Robert[2], Ann Carine Vandaele[2], Naomoto Iwagami (1.Hokkaido University, Graduate School of Science, 2.Belgian Institute for Space Aeronomy)

[PPS06-P05] **Variations in the activities of planetary-scale waves at the Venusian cloud top observed by Akatsuki UVI**

★Invited Papers

*Masataka Imai[1], Toru Kouyama[1], Atsushi Yamazaki[2], Shigeto Watanabe[3], Manabu Yamada[4], Shin-ya Murakami[2], Takeshi Imamura[5], Takehiko Satoh[2], Masato Nakamura[2], Kazunori Ogohara[6], Takeshi Horinouchi[7] (1.Advanced Industrial Science and Technology, 2.Institute of Space and Astronautical Science, 3.Hokkaido Information University, 4.Chiba Institute of Technology, 5.The University of Tokyo, 6.The University of Shiga Prefecture, 7.Hokkaido University)

[PPS06-P06] The global variation of Venus cloud investigated from AKATSUKI 1-μm camera

*Seiko Takagi[1], Naomoto Iwagami (1.Hokkaido University, Graduate School of Science)

[PPS06-P07] **Cosmic rays and high energetic particles at Venus: Analysis of triggered pulse events detected by Akatsuki/LAC**

*Masataka Imai[1], Yukihiro Takahashi[2], Ralph Lorenz[3], Mitsuteru Sato[2] (1.National Institute of Advanced Industrial Science and Technology, 2.Hokkaido University, 3.Johns Hopkins University Applied Physics

Laboratory)

[PPS06-P08] Ground-based Observation of planetary lightning flashes by using Photomultiplier tube

*Tatsuharu Ono[1], Yukihiro Takahashi[1], Mitsuteru Sato[1], Shigeto Watanabe[1], Seiko Takagi[1], Masataka Imai[2] (1.Department of Cosmosciences, Graduate School of Science, Hokkaido University, 2.National Institute of Advanced Industrial Science and Technology)

[PPS06-P09] Observation of the Venusian Lower Atmosphere in the 1.7 μm Band by Near-infrared Echelle Spectrometer onboard PIRKA Telescope in Nayoro Observatory

Daiki Tsukiyama[1], *Hiroyuki Maezawa[1], Atsushi Nishimura[1], Masataka Imai[4], Hidenori Takahashi[2], Masuo Tanaka[2], Yukihiro Takahashi[3], Mitsuteru Sato[3], Seiko Takagi[3], Shin-ichiro Okumura[5], Yeon Joo Lee[6] (1.Department of Physical Science Osaka Prefecture University, 2.Institute of Astronomy, School of Science, The University of Tokyo, 3.Hokkaido University, Graduate School of Science, 4.The National Institute of Advanced Industrial Science and Technology, 5.Japan Spaceguard Association, 6.Technical University of Berlin)

[PPS06-P10] A sensitivity study of the radiative-convective equilibrium temperature profile in Venus atmosphere

★Invited Papers

*Miho Sekiguchi[1], Masahiro Takagi[2], Hideo Sagawa[2], Yoshihisa Matsuda[3] (1.Tokyo University of Marine Science and Technology, 2.Kyoto Sangyo University, 3.Tokyo Gakugei University)

[PPS06-P11] Meridional distribution of CO on Venus

*Shinya Kuwayama[1], George HASHIMOTO[1] (1.Okayama University)

[PPS06-P12] Trials toward first Venus analysis product by data assimilation of Akatsuki observation

★Invited Papers

*Yukiko Fujisawa[1], Shin-ya Murakami[2], Norihiko Sugimoto[1], Masahiro Takagi[3], Takeshi Imamura[4], Takeshi Horinouchi[5], George HASHIMOTO[6], Masaki Ishiwatari[5], Takeshi Enomoto[7], Takemasa Miyoshi[8], Yoshi-Yuki Hayashi[9] (1.Keio University, 2.JAXA, 3.Kyoto Sangyo University, 4.Tokyo University, 5.Hokkaido University, 6.Okayama University, 7.Disaster prevention Research Institute, Kyoto University, 8.RIKEN, 9.Kobe University)

[PPS06-P13] Dynamics of Decadal Sulfur Dioxide Variability in Venus' Atmosphere with a Simple Model

*Pushkar Kopparla[1], Ashwin Seshadri[2], Takeshi Imamura[1], Yeon Joo Lee[3], Javier Peralta[4] (1.University of Tokyo, 2.Indian Institute of Science, 3.Technical University of Berlin, 4.ISAS JAXA)

Polarimetry of Venus upper atmosphere with a new single-shot type polarimeter

*Takehiko Satoh[1,2], Masato Kagitani[3], Takeshi Sakanoi[3], Takao M. Sato[4], James O'Donoghue[1]

1. Institute of Space and Astronautical Science, Japan Aerospace Exploration Agency, 2. Department of Space and Astronautical Science, The Graduate University for Advanced Studies, SOKENDAI, 3. Faculty of Science, Tohoku University, 4. Space Information Center, Hokkaido Information University

Polarimetry is a powerful mean of sensing aerosol properties in the upper atmosphere of Venus as demonstrated by Hansen and Hovenier (1974). They analyzed the ground-based linear polarization data of Venus (disk integrated) and found that the data were consistent with a uniform cover of sulfuric acid droplets of which effective radius and variance are 1.05 um and 0.07, respectively. In 1980’s, OCPP onboard Pioneer Venus Orbiter performed spatially-resolved imaging polarimetry, and studied in detail characteristics of aerosols and their variability (Kawabata et al. 1980; Knibbe et al. 1998; Braak et al. 2002).

Our team carried out polarimetric observations of Venus in 2012, 2014, and 2015 at Kyoto University’s Hida Observatory, by attaching HOPS (Hida Optical Polarimetry System) to the 65-cm refracting telescope. The 930-nm data revealed rapid decrease of the polar haze from 2012 to 2014, while 435-nm data indicated change in cloud-top altitude in polar regions (Enomoto et al., in revision). HOPS is a traditional two-beam type polarimeter and thus requires a set of 4 images with the half-wave retarder plate rotated every 22.5 degrees to obtain the linear polarization vectors. From the ground, variable seeing condition during these 4 exposures is unavoidable and is major source of error when obtaining linear polarization.

A single-shot type polarimeter should therefore be advantageous for observations of planets as required exposure time is usually short and small spatial scale (~arcsecond order) matters. We are developing such a polarimeter by utilizing a “Wedged Double Wollastone (WeDoWo)” (Oliva, 1997) device as an analyzer. The device is composed of 6 precision-shaped calcite blocks: the first two (wedges) separate the incident light into two beams, and beams are subsequently separated to four beams of different polarization state ($I \pm Q$, and $I \pm U$). This allows us to obtain linear polarization vectors just in one shot. We plan to use this instrument during BepiColombo’s flyby to Venus (closest approach on 15 October 2020). There will be 4 instruments (UVI and LIR onboard Akatsuki, plus PHEBUS and MERTIS onboard BepiColombo/MPO) to observe the upper atmosphere of Venus but none has the polarimetric capability. Therefore, our observations with a new single-shot type polarimeter will complement observations from the space.

Keywords: shingle-shot polarimetry, Venus cloud, BepiColombo flyby

©2020. Japan Geoscience Union. All Right Reserved.

Venus's Atmospheric Features in UV as Viewed from Ground-Based Observations

*Ryan M. McCabe[1], Kunio M. Sayanagi[1], John J. Blalock[1], Jacob L. Gunnarson[1], Javier Peralta[2], Candace L. Gray[4], Kevin McGouldrick[5], Takeshi Imamura[2], Shigeto Watanabe[3], Yeon Joo Lee[6]

1. Hampton University, 2. Institute of Space and Astronautical Sciences, JAXA, 3. Department of Earth and Planetary Sciences, Hokkaido Univ., Japan, 4. Apache Point Observatory , Sunspot, NM, 5. LASP, Univ. of Colorado Boulder, 6. Technical University of Berlin, Germany

We are currently investigating the dynamics of Venus's atmosphere to understand the link between variability of atmospheric superrotation to the existence and occurrences of the Y-feature. The atmospheric superrotation, in which the equatorial atmosphere rotates with a period of approximately 4-5 days (~60 times faster than the solid planet), has forcing and maintenance mechanisms that remain to be explained. Temporal evolution of the zonal wind could reveal the transport of energy and momentum in or out of the equatorial region, and eventually shed light on mechanisms that maintain the Venusian superrotation. We postulate that the Y-feature is a manifestation of equatorial waves (either Kelvin, Rossby, or a combination of the two in nature) that may play a role in such energy transport that could affect Venus's superrotation. To understand the connection between the Y-feature and the superrotation, we must determine the frequency of the Y-feature's existence, the variability of the atmospheric wind field, and analyze the connection between the two to determine to what extent the Y-feature plays a role in Venus's superrotation.

We characterize the existence of the Y-feature's occurrence and phase speed between 2006 and 2017. It is observed in ultraviolet images captured by the Venus Monitoring Camera on board the ESA Venus Express (VEX) spacecraft which observed Venus's southern hemisphere as well as the Ultraviolet Imager on the Akatsuki spacecraft which viewed pole to pole latitudes. We also extend our analysis to ground-based observations between 2016 and 2019. This includes data captured with the 3.5 m Astrophysical Research Consortium telescope at the Apache Point Observatory (APO) in Sunspot, NM and small 10-inch scale telescopes at Hampton University in Hampton, VA. Images we have captured demonstrate that, even under unfavorable illumination, it is possible to see large features that could be used to supplement gaps in dayside UV data during Akatsuki.

The method for observing and analysis of atmospheric features seen in UV from ground-based observations is discussed. Preliminary Akasuki wind measurements made using a 2D Correlation Image Velocimetry method developed at Hampton University are also presented.

Our work has been supported by NASA MUREP NNX15AQ03A and NASA PATM NNX14AK07G.

Keywords: Venus, Atmosphere, Superrotation, Y-feature, Ground-based observing, Cloud top UV absorber

©2020. Japan Geoscience Union. All Right Reserved.

3-D Thermal Structure of the Venus Atmosphere Obtained by Akatsuki/LIR

*Masahiro Akiba[1], Makoto Taguchi[2], Tetsuya Fukuhara[2], Takeshi Imamura[3], Toru Kouyama[4], Takao M. Sato[5]

1. Rikkyo graduate School, 2. Rikkyo University, 3. The University of Tokyo, 4. National Institute of Advanced Industrial Science and Technology, 5. Hokkaido Information University

To maintain the fast circulation of the Venus atmosphere, thermal tides have been considered a very important candidate of a driving engine, because they can transfer eastward momentum from the accelerating region of the upper atmosphere to the ground [Kouyama et al., 2019]. We investigated the vertical structure of brightness temperature distribution above the cloud-tops based on the emission angle dependence of the sensing altitude of LIR onboard Akatsuki. We used LIR data obtained when Akatsuki was in the altitude range from 60,000 to 100,000 km during the period from October 19, 2016 to October 2, 2018. Each brightness temperature image with 328x248 pixels was divided into 3280x2480 sub-pixels, and 32 successive images were accumulated after precise adjustment of the Venus disk position. Emission angles are converted to sensing altitudes by a radiative transfer calculation with nominal temperature and cloud particle distributions [Sato et al., 2014]. Thus, we derived a local time-altitude cross section of the brightness temperature deviation above the cloud-tops in the latitude ranges of 0-30, 40-50, 55-65, 70-80, and 80-90. Sensing altitudes change slightly with latitude but range vertically about 7 km depending on the emission angles. A Fourier analysis shows the vertical distribution of temperature in the equator region is dominated by a semidiurnal tide with a tilt of the phase with increasing altitude. The maximum positive temperature deviation appears around 10 and 21 LT at the bottom of the sensing altitudes. It is suggested that the thermal tide is generated deep in the cloud deck by solar heating and propagates upward. On the other hand, a diurnal tide dominates in the higher latitudes. Latitudinal dependence of the observed amplitudes, phases and their tilt angles of diurnal and semidiurnal tides will be discussed by comparing with those from a numerical simulation.

Keywords: dynamics, atmosphere

©2020. Japan Geoscience Union. All Right Reserved.

An uppermost haze layer above 100 km found over Venus by the SOIR onboard Venus Express

*Seiko Takagi[1], Arnaud Mahieux[2], Valérie Wilquet[2], Séverine Robert[2], Ann Carine Vandaele[2], Naomoto Iwagami

1. Hokkaido University, Graduate School of Science, 2. Belgian Institute for Space Aeronomy

The Venus cloud consists of a main cloud deck at 47 –70 km, with thinner hazes above and below.The upper haze on Venus lies above the main cloud surrounding the planet, ranging from the cloud top (70 km) up to as high as 90 km.
The Solar Occultation in the InfraRed (SOIR) instrument onboard Venus Express (ESA) was designed to measure the Venusian atmospheric transmission at high altitudes (65 –220 km) in the infrared wavelength range (2.2 –4.3 μm) with a high spectral resolution. We investigate the optical properties of Venus’ s haze layer above 90 km using SOIR observations. Vertical and latitudinal profiles of the extinction coefficient, optical thickness, and mixing ratio of aerosols are retrieved. One of the most remarkable results is that the aerosol mixing ratio tends to increase with altitude above 90 km at both high and low latitude. It is speculated that sources of haze are transported upward from under altitude 90 km and haze is produced at high altitude. In this presentation, we will report the results and speculate how aerosols could be produced at such high altitudes.

Keywords: Venus, Venus Express, SOIR

©2020. Japan Geoscience Union. All Right Reserved.

Variations in the activities of planetary-scale waves at the Venusian cloud top observed by Akatsuki UVI

*Masataka Imai[1], Toru Kouyama[1], Atsushi Yamazaki[2], Shigeto Watanabe[3], Manabu Yamada[4], Shin-ya Murakami[2], Takeshi Imamura[5], Takehiko Satoh[2], Masato Nakamura[2], Kazunori Ogohara[6], Takeshi Horinouchi[7]

1. Advanced Industrial Science and Technology, 2. Institute of Space and Astronautical Science, 3. Hokkaido Information University, 4. Chiba Institute of Technology, 5. The University of Tokyo, 6. The University of Shiga Prefecture, 7. Hokkaido University

Planetary-scale waves at the Venusian cloud-top cause periodic variations in both ultraviolet (UV) albedo patterns and winds. Since planetary-scale waves are considered to play crucial roles in the momentum and material transports in the Venusian atmosphere, investigating these periodicities and its temporal change could provide a better picture of how these waves get involved in the atmospheric dynamics on Venus. In this study, we analyzed the periodicities in the UV albedo and the cloud-tracking wind variations (Horinouchi et al., 2017) derived from both 283-nm and 365-nm UVI channels observed in the OP2016 (October 2016 -- April 2017), OP2017 (June -- October 2017), OP2018A (January -- June 2018), and OP2018B (August -- December 2018). We used the successive time blocks having a time range of ±15 days extracted from the original time series and conducted Time-Shifting Lomb-Scargle (TSLS) periodogram analysis [Imai et al., 2019].

Our previous study revealed the temporal evolution of prominent 5-day waves in OP2017 for the first time, and we could find corresponding temporal changes in planetary-scale UV features. Since the reconstructed horizontal wind field had planetary-scale vortices, which was nearly equatorially symmetric and centered at ~35° latitude in both hemispheres, the observed 5-day wave can be interpreted as the equatorial symmetric Rossby wave. The amplitude of wind variation associated with the observed Rossby wave was amplified gradually over ~20 days and attenuated over ~50 days. An ~3.8-day periodic signals were observed in the zonal wind and brightness variations in the equatorial region before the Rossby wave amplification. Although the amplitude and significance of the 3.8-day mode were relatively low in the observation season, this feature is consistent with a Kelvin wave. In this observation season, there was only a small difference in the periodicities and wind field between 283-nm and 365-nm channels.

In OP2018B, we also found ~4-day and ~5-day periodicity in winds. However, the reconstructed horizontal wind field showed southwest and northeast elongated oscitation in the southern hemisphere rather than the vortices, and latitudinal asymmetry in the amplitude of wind variation was prominent. In contrast to the OP2017, ~4-day wave had relatively large amplitude to the ~5-day wave, and ~4-day wave seems gradually degraded through the observation season. While the difference in the sensing altitude of both 283-nm and 365-nm still unclear, wave signals were much clear in 283-nm channel, and these findings might indicate OP2018 was the active season for the wave excitation and the wave source was closer to the 283-nm observation altitude. In the Akatsuki observation era since the end of 2015, OP2017 and OP2018B are the representative season for investigating the evolution of planetary-scale waves. In this presentation, we will show the summary of how these two observation seasons are different and what kind of mechanisms are related to the prominence of ~4-day wave and ~5-day wave.

Keywords: Venus, Akatsuki, Planetary-scale waves

©2020. Japan Geoscience Union. All Right Reserved.

©2020. Japan Geoscience Union. All Right Reserved.

The global variation of Venus cloud investigated from AKATSUKI 1-μm camera

*Seiko Takagi[1], Naomoto Iwagami

1. Hokkaido University, Graduate School of Science

Venus is our nearest neighbor, and has a size very similar to the Earth’ s. However, previous observations discovered an extremely dense (90 bar at the surface) and CO_2-rich atmosphere, with H_2SO_4 thick clouds. The Venus cloud consists of H_2SO_4 main cloud deck at 40 −70 km, with thinner hazes above and below.The upper haze on Venus lies above the main cloud surrounding the planet, ranging from the top of the cloud (70 km) up to as high as 90 km.
Near infrared (0.986 μm) dayside image of Venus has taken by solid state imaging (SSI) of the Galileo spacecraft (NASA). It appears almost flat, there are some small scale features with a contrast of 3 % [Belton et al., 1991]. In Takagi and Iwagami. (2011), it may be calculated that the source of the contrast of the order of 3 % in near infrared Venus dayside image is due to variation in the cloud optical thickness.
On December 7, 2015, AKATSUKI (JAXA) approached Venus and the Venus orbit insertion was successful. After the Venus orbit insertion, many 0.90 μm Venus dayside images were taken by the 1 μm near infrared camera (IR1) onboard AKATSUKI.
In this study, Venus cloud variations are investigated from 0.90 μm Venus dayside images taken by IR1 cameraglobally. Further, meteorological some changes that contribute to cloud variation are examined with radiative transfer calculation including high-altitude cloud model [Takagi et al., 2019]. Furthermore, I will introduce Venus observation plan using the 1.6 m Pirka telescope and Multi-Spectral Imager (MSI) [Watanabe et al., 2012] mounted on the Cassegrain focus of the telescope at the Nayoro Observatory of Hokkaido University.

Keywords: AKATSUKI, IR1, cloud

©2020. Japan Geoscience Union. All Right Reserved.

Cosmic rays and high energetic particles at Venus: Analysis of triggered pulse events detected by Akatsuki/LAC

*Masataka Imai[1], Yukihiro Takahashi[2], Ralph Lorenz[3], Mitsuteru Sato[2]

1. National Institute of Advanced Industrial Science and Technology, 2. Hokkaido University, 3. Johns Hopkins University Applied Physics Laboratory

Cosmic rays and high energetic particles from astrophysical sources outside the solar system are an important contributor to planetary radiation environments. On Venus, cosmic rays cause ionization in the atmosphere, and this effect is considered as a dominant ionization source. We have known that some bodies within the solar system shine to X-rays, and in the case of Venus, charge exchange interactions between highly charged ions in the solar wind and the Venusian atmosphere would be one of the X-ray sources. However, our understanding of the environment of the high energetic particles around the Venus orbit is quite limited. Therefore, the detection of cosmic rays by the instrument onboard Venus orbiter provides us precious information.

Lightning and Airglow Camera (LAC), which is one of the onboard instruments of Akatsuki, is a new type of lightning detector equipping 8×8 pixels (16×16 mm) APD (avalanche photodiode) detector and enables detecting optical lightning flash with 30 kHz sampling rate. LAC adopts the pre-trigger sampling method to record pulsed signals by using half of 64 pixels. Despite no detection of flashes attributable to lightning, LAC recorded over 500 cosmic ray events during the 49 observation sessions of LAC from August 2016 to January 2020. The estimated average event rate of LAC was 0.44 events min^{-1}. Considering the director size, the previous detection report of Pioneer Venus star sensor [Burucki et al., 1981; 1991] was 38 (or 12 during quiet sun) events min^{-1}, and this low event rate might be caused by the LAC shielding is less susceptible to cosmic ray triggers. The output peak values of the pulsed signals have covered almost from 6 digits to 80 digits, and intense events having large peak value (>80 digits) seem to be randomly recorded. Since the energy of cosmic rays is high enough to excite photoelectron inside the detector, this wide range of the peak values can be caused by the incidence angle of cosmic rays to the face of the APD detector. Under this assumption, the possibility of the incidence angle (θi) is proportional to sin2 θi when we expect the isotropic cosmic ray incidence, where θi is the angle measured from the normal vector of the sensor plane. We conducted a statistical analysis with 501 recorded cosmic ray events and found that detected events roughly follow the assumed isotropic incidence relation. However, there was minor disagreement, and one of the possible explanations is that we should consider the energy distribution of cosmic rays and/or the complex structure of LAC shielding. On the other hand, we could find the event rate has some dependence on Venus–Spacecraft distance, and our result indicates a slightly higher rate of around 6000 km and almost monotonical increase of event rate from 9000 to 12000 km from the Venus surface. If they are some high energetic particles from the sun, then these observation distances correspond to the refraction angle of ~30° and 24°–19°. Hoever, we currently do not have any plausible explanation for this.

Keywords: Venus, Cosmic rays, Akatsuki, LAC

©2020. Japan Geoscience Union. All Right Reserved.

Ground-based Observation of planetary lightning flashes by using Photomultiplier tube

*Tatsuharu Ono[1], Yukihiro Takahashi[1], Mitsuteru Sato[1], Shigeto Watanabe[1], Seiko Takagi[1], Masataka Imai[2]

1. Department of Cosmosciences, Graduate School of Science, Hokkaido University, 2. National Institute of Advanced Industrial Science and Technology

The lightning flashes observation is useful as a way to understand the atmospheric large structure and the chemical reaction constituting the atmosphere. The lightning flashes have been observed in the Earth and Jupiter. It is suggested that there is a relationship between the zonal jet and the cumulonimbus with lightning in Jupiter (Gierasch et al.,2000, Ingersol et al., 2000). It is difficult to know the vertical convection covered by the dense clouds by using multi-wavelength observation. However, the lightning flashes observation can use for monitoring the atmosphere dynamics like the vertical convection covered by dense clouds. And one hypothesis suggests that some components of the Jovian atmosphere are created by lightning flashes. It is important to know the lightning to understand the formation mechanism of the atmosphere. In Venus, it is considered that there are lightning generated by the charge separation by the ice particle like the Earth or cloud particles of sulfuric acid. The existence of Venusian lightning is controversial for over 20 years. In the previous study, there are radio wave observations and optical observations by CCD. There is no robust evidence of existence the lightning because it is difficult to distinguish between the lightning signal and the electrical noise or other plasma waves, the observation area is limited, and the CCD's sensitivity is not enough for lightning flashes. If we can confirm the existence of Venusian lightning like the Jovian, it leads to an understanding of the Venusian atmosphere dynamics and atmospheric components.

Our study’s purpose is to reveal the relationship between lightning and atmospheric dynamics. For this purpose, we develop the instrument to equip for the Pirka telescope. By using it, we observe Venus more than tens of hours to obtain the lightning’s light curve, occurrence frequency, and distribution. We reveal the relationship between lightning and atmosphere dynamics by comparing the lightning data and wind velocity and cloud distribution.

The Planetary Lightning Detector (PLD) we developed is designed for Venusian and Jovian lightning flashes' observation. From the previous study, the dominant wavelength of the lightning flashes could be 777 nm in Venus (Borucki et al.,1996). PLD equips narrowband filter (FWHM = 1nm) of 777 nm. PLD observes the light by using a Photomultiplier tube. The minimum exposure time is 50 microseconds. The maximum time resolution is about $2x10^4$ points/s. PLD’s FOV can be changed to 5”, 10”, 30”, 60” pinhole and 2”x11” slit by using field stops. Slit and Pinhole are used for Venus’s night-side observation. To obtain the lightning’s light curve, we operate the bandpass filter to remove noise and large time scale variation by the atmosphere. And then, we search the large count value over 3-sigma. We have observed Venus by using PLD. For Venus’s data, we have obtained a few events whose count value is over the 3-sigma. These energies are estimated. The energy is about 10^9 to 10^{10} J. However, the light curves are too short less than 2 milliseconds and similar to the cosmic ray’s light curves obtained on different days. From this result, it’s considered we only observed the cosmic ray in this observation time. The observation time is not enough to reveal the lightning occurrence frequency for Venus. In the future, we increase the total observation time by using shorter exposure time.

©2020. Japan Geoscience Union. All Right Reserved.

In this presentation, we introduce the PLD and discuss the result observed from Jan 2020. And we report the plan of the cooperative observation with LAC (Lightning and Airglow Camera) onboard the AKATSUKI.

Keywords: Venus, Lightning, Ground-based telescope, Photomultiplier tube, LAC

©2020. Japan Geoscience Union. All Right Reserved.

Observation of the Venusian Lower Atmosphere in the 1.7 μm Band by Near-infrared Echelle Spectrometer onboard PIRKA Telescope in Nayoro Observatory

Daiki Tsukiyama[1], *Hiroyuki Maezawa[1], Atsushi Nishimura[1], Masataka Imai[4], Hidenori Takahashi[2], Masuo Tanaka[2], Yukihiro Takahashi[3], Mitsuteru Sato[3], Seiko Takagi[3], Shin-ichiro Okumura[5], Yeon Joo Lee[6]

1. Department of Physical Science Osaka Prefecture University, 2. Institute of Astronomy, School of Science, The University of Tokyo, 3. Hokkaido University, Graduate School of Science, 4. The National Institute of Advanced Industrial Science and Technology, 5. Japan Spaceguard Association, 6. Technical University of Berlin

Over the past 20 years, various exoplanets have been discovered, and observations of habitable Earth-like planets have been actively promoted. Venus, which is surrounded by the CO2 atmosphere, is one of the important observation targets for understanding the fundamental atmospheric properties of planets. The surface of Venus has the higher atmospheric temperature and pressure than those of the Earth. However, the temperature and pressure in the cloud region of Vebus are similar to those at the Earth’ s troposphere. Recently based on the ultraviolet band absorption features toward the cloud region of Venus, the possibility that microbes such as bacteria may remain in this region has been discussed. Therefore, a more detailed understanding of how the lower and upper layers of the atmosphere circulate through these cloud regions, and how the physical and chemical environments of the atmosphere are balanced between them is expected.

The 10 m radio telescope at the Nobeyama Radio Observatory (Nagano Prefecture) of the National Astronomical Observatory of Japan has been monitoring of the millimeter-wave band spectral lines of carbon monoxide in the Venusian middle atmosphere since 2011. CO at an altitude of around 80 km shows long-term changes in the time-scale of the solar activity cycle and shorter-term ones. For a detailed understanding of these changes, it is important to promote systematic simultaneous observations of trace molecular species toward the upper and lower atmospheres by the milli/submillimeter-wave band and the near-infrared band spectroscopies, respectively.

In August 2018, a test observation of the Venusian lower atmosphere was performed at Nayoro Observatory using a near-infrared echelle spectrometer (NICE) (University of Tokyo) mounted on the PIRKA telescope (Hokkaido University). Although there were many days when the atmospheric condition was unstable due to the influence of typhoons, on 8/22, we succeeded in detecting the spectrum from the night side lower atmosphere of Venus in the 1.7 μm band. The resolution of the spectrometer was $\lambda / \delta \lambda = 5600$, the slit size was 1 "×6.7", and HIP 69701 was observed as the standard star for the intensity calibration. The seeing (1 sigma) was 2.5”. The profile of the obtained spectrum was well consistent with the atmospheric radiative transfer model (Y.-J, Lee et al.) of Venus using the HITEMP database.

The University of Tokyo Atacama Observatory (TAO) Project is promoted by Institute of Astronomy (IoA), the University of Tokyo with many collaborators. In 2021, NICE is scheduled to be installed on the infrared band TAO telescope with a 6.5m diameter aperture on the summit of Cerro Chajnantor at Atacama in Cile (alt. 5640 m). Near the TAO site, Atacama large millimeter-wave submillimeter-wave interferometers are operated. Therefore, it is expected that simultaneous observations toward the Venusian upper and lower atmospheres on the same day will be possible. We will report the results of the

©2020. Japan Geoscience Union. All Right Reserved.

observation with NICE and the installation plan of NICE onto TAO.

Keywords: Venus, Near Infrared , Radio Telescope, Planetary Atmosphere, TAO

©2020. Japan Geoscience Union. All Right Reserved.

A sensitivity study of the radiative-convective equilibrium temperature profile in Venus atmosphere

*Miho Sekiguchi[1], Masahiro Takagi[2], Hideo Sagawa[2], Yoshihisa Matsuda[3]

1. Tokyo University of Marine Science and Technology, 2. Kyoto Sangyo University, 3. Tokyo Gakugei University

Venus has a dense atmosphere entirely covered by a thick cloud layer (ranging over 50 –70 km altitude). Due to the high opacity of the atmosphere, there is almost no remote-observational access to the lower atmosphere below the cloud. Past (only a few, though) in-situ measurements suggest that the atmosphere is stable below the cloud down to 32 km, and then a convective layer appears down to 18 km. The lower atmosphere below 18 km seems to be stable again. The nature of such a thermal structure is still not understood clearly.

To better knowledge on the thermal structure (radiative transfer of the thermal flux), we calculated the radiative-convective equilibrium temperature profile of Venus atmosphere using a newly developed 1-D radiative transfer model “MSTRN-Venus”. The absorption coefficients of the molecular gases in the Venus atmosphere (CO_2, H_2O, CO, SO_2, HF, HCl, and OCS) are calculated in each 0.025cm^{-1} wavenumber and correlated k-distribution are calculated and applied. The spectroscopic parameters such as the transition position and line strength are taken from the recent compilations of HITRAN, HITEMP, and UCL08 catalogs. In addition, the collision-induced absorption of CO_2 is also included. We prepared the absorption coefficients under several pressure and temperature conditions within the ranges of 0.01 - 100 bar and 100 - 800 K, respectively. The results are kept in a look-up table of (p, T) domain so that we can interpolate the absorption coefficient for any pressure and temperature condition without repeating a burden computation. The upward and downward flux density is calculated for a given atmospheric profile using the MSTRN code. This code has been successfully applied in several studies of our terrestrial atmosphere, and also adopted as the radiation calculation module of several general atmospheric circulation models.

The presentation will discuss the sensitivity of the radiative-convective temperature profile concerning the abundance of minor species, incoming solar heating, and cloud opacities.

Keywords: Venus, Radiative transfer model, Radiative-convective equilibrium

©2020. Japan Geoscience Union. All Right Reserved.

Meridional distribution of CO on Venus

*Shinya Kuwayama[1], George HASHIMOTO[1]

1. Okayama University

We constructed a model which calculates the meridional distribution of some minor chemical species such as CO, H_2O, and H_2SO_4 in the Venus' atmosphere. Our model consists of chemical reactions, advection, diffusion, condensation/evaporation, and sedimentation of cloud particles. The atmospheric temperature and density profiles are fixed, and a steady one-cell structure of the meridional circulation in each hemisphere is assumed. A steady state distribution is numerically solved by using time-marching.

Keywords: Venus, carbon monoxide, meridional circulation

©2020. Japan Geoscience Union. All Right Reserved.

Trials toward first Venus analysis product by data assimilation of Akatsuki observation

*Yukiko Fujisawa[1], Shin-ya Murakami[2], Norihiko Sugimoto[1], Masahiro Takagi[3], Takeshi Imamura[4], Takeshi Horinouchi[5], George HASHIMOTO[6], Masaki Ishiwatari[5], Takeshi Enomoto[7], Takemasa Miyoshi[8], Yoshi-Yuki Hayashi[9]

1. Keio University, 2. JAXA, 3. Kyoto Sangyo University, 4. Tokyo University, 5. Hokkaido University, 6. Okayama University, 7. Disaster prevention Research Institute, Kyoto University, 8. RIKEN, 9. Kobe University

Observations of the Venus Orbiter "Akatsuki" provide us horizontal distributions of the horizontal wind derived from cloud tracking of the UVI camera images and of temperature observed by the LIR camera. However, these observations are very limited with respect to altitude, local time (day or night side), and frequency. It is difficult to elucidate general circulation including with various temporal and spatial scales only from observations. In this study, we aim to produce a Venus objective analysis that has high temporal and spatial resolutions by assimilating the Akatsuki observations into a general circulation model.

The model used in this study is a Venusian GCM (AFES-Venus) and the Venus AFES LETKF Data Assimilation System (ALEDAS-V) based on the Local Ensemble Transform Kalman Filter (LETKF) that has been developed for the first time[1]. Using ALEDAS-V, we have examined impact of data assimilation on thermal tides for the Venus Express wind observations[2]. In addition, we have examined the reproducibility of a unique atmospheric structure so-called “cold collar”, a cold latitudinal band encircling the warm polar vortex at about 60–70 km altitudes, in order to elucidate the effects of fixed temperature observations by multiple small satellites[3].

In this presentation, we will introduce results obtained for idealized data assimilation. One is for vertical profiles of temperature assuming radio occultation observation with realistic trajectory (Related to Hosono et al.[4]). The other is for distributions of horizontal wind assuming camera observation (Related to Fujisawa et al.[5]). These are necessary attempts before assimilating actual observation data. Furthermore, we will also introduce the results of assimilating actual Akatsuki observation data.

[1] Development of an ensemble Kalman filter data assimilation system for the Venusian atmosphere, N. Sugimoto, A. Yamazaki, T. Kouyama, H. Kashimura, T. Enomoto, and M. Takagi, Scientific Reports, Vol. 7, (2017), 9321, 9pp.
[2] Impact of data assimilation on thermal tides in the case of Venus Express wind observation, N. Sugimoto, T. Kouyama, and M. Takagi, Geophys. Res., Lett., Vol. 46, (2019), pp. 4573–4580.
[3] Observing system simulation experiment for radio occultation measurements of the Venus atmosphere among small satellites, N. Sugimoto, M. Abe, Y. Kikuchi, A. Hosono, H. Ando, M. Takagi, I. Garate-Lopez, S. Lebonnois and C. Ao, Journal of Japan Society of Civil Engineers A2: Applied Mechanics, Vol. 75, No.2, (2019), pp. I_477-I_486.
[4] The study for designing the future Venus atmosphere observing mission of radio occultation measurement among small satellites using data assimilation, A. Hosono, Y. Fujisawa, N. Sugimoto, M. Abe, Y. Kikuchi, T. Yamamoto, Y. Kawabata, S. Ikari, H. Ando, M. Takagi, I. G. Lopez, S. Lebonnois, C. Ao, JpGU, (2020), A-OS21.
[5] Data Assimilation of the Venus Atmosphere to Reproduce Planetary-scale Wave, Y. Fujisawa, M. Shirasaka, N. Sugimoto, A. Hosono, M. Abe, H. Ando, M. Takagi, and M. Yamamoto, JpGU, (2020), A-OS21.

©2020. Japan Geoscience Union. All Right Reserved.

Keywords: Akatsuki, Venus atmosphere, Data assimilation

©2020. Japan Geoscience Union. All Right Reserved.

Dynamics of Decadal Sulfur Dioxide Variability in Venus' Atmosphere with a Simple Model

*Pushkar Kopparla[1], Ashwin Seshadri[2], Takeshi Imamura[1], Yeon Joo Lee[3], Javier Peralta[4]

1. University of Tokyo, 2. Indian Institute of Science, 3. Technical University of Berlin, 4. ISAS JAXA

Water and sulfur dioxide are important trace gases in the atmosphere of Venus. The photolysis of sulfur dioxide in the upper clouds produces sulfuric acid, which forms the thick cloud decks characteristic of the planet's atmosphere. Sulfur dioxide concentrations at the cloud top of Venus have been observed to oscillate on decadal timescales, characterized by sharp spikes and gradual declines. The variation is suspected to occur due to dynamical variability in the deep atmosphere of Venus but the exact mechanism has remained a mystery. Using a simple one dimensional box model where water and sulfur dioxide are cycled between the cloud tops and the deep atmosphere, we explore the dynamics of the sulfur dioxide oscillations. We find that the periodicity of the oscillation is dependent on vertical transport and thermal decomposition timescales in the deep atmosphere, while the shape of the oscillation depends on the transport timescale in the cloud layer.

Keywords: Venus, Venus atmosphere, oscillations, atmospheric variability

©2020. Japan Geoscience Union. All Right Reserved.

[E] Poster | P (Space and Planetary Sciences)：P-PS Planetary Sciences

[P-PS07] Solar System Small Bodies: Explorations of Ryugu, Bennu, and the Solar System at Large

convener:Taishi Nakamoto(Tokyo Institute of Technology), Tatsuaki Okada(Institute of Space and Astronautical Science, Japan Aerospace Exploration Agency), Dante S Lauretta(University of Arizona), Masateru Ishiguro(Department of Physics and Astronomy, Seoul National University)

Small Solar System bodies, including asteroids, comets, satellites, and inter-planetary dust particles, are interesting and provide lots of information on the origin and evolution of our Solar System. They can be remotely sensed by telescopes, be visited by spacecraft and studied at high resolution in a variety of wavelengths from IR to visible, UV, X-rays, and gamma rays, and even with neutrons. In addition, recently spacecrafts have been sent to return samples. In this session, all the contributions on the small solar system bodies are welcome. But this year, we especially welcome contributions on recent advances on the study of Ryugu and Bennu whether obtained by rendezvous spacecraft, remote sensing, or other methods.

[PPS07-P01] Tests and rehearsals for curation of samples returned from asteroid Ryugu by Hayabusa2 spacecraft

*Toru Yada[1], Masanao Abe[1], Aiko Nakato[1], Kasumi Yogata[1], Akiko Miyazaki[1], Tatsuaki Okada[1], Masahiro Nishimura[1], Kazuya Kumagai[2], Miwa Yoshitake[1], Shizuho Furuya[1], Ayako Iwamae[2], Tasuku Hayashi[1], Daiki Yamamoto[1], Shogo Tachibana[1,3], Tomohiro Usui[1], Hisayoshi Yurimoto[1,4] (1.Japan Aerospace Exploration Agency, 2.Marine Works Japan, 3.University of Tokyo, 4.Hokkaido University)

[PPS07-P02] Soluble organic matter in Ryugu: The first rehearsal analysis

*Hiroshi Naraoka[1], Yoshinori Takano[2], Nanako O. Ogawa[2], Minako Hashiguchi[1], Hannah L. McLain[3], Eric T. Parker[3], Kenji Hamase[1], Francois-Régis Orthous-Daunay[4], Junko Isa[4], Dan Aoki[5], Kazuhiko Fukushima[5], Philip Schmitt-Kopplin[6], Jason P. Dworkin[3], SOM Analysis Team (1.Kyushu University, Japan, 2.Japan Agency for Marine-Earth Science Technology, Japan, 3.NASA Goddard Space Flight Center, USA, 4.Université Grenoble Alpes, France, 5.Nagoya University, Japan, 6.Helmholtz Zentrum Muenchen, Germany)

[PPS07-P03] Visible Wavelength Normal Albedo Map of Ryugu Derived by Hayabusa2 Optical Navigation Camera

*Yasuhiro Yokota[1,2], Rie Honda[2], Eri Tatsumi[3,4,5], Deborah Domingue[6], Stefanus E. Schröder[7], Moe Matsuoka[1], Seiji Sugita[5], Tomokatsu Morota[5,8], Shingo Kameda[9], Toru Kouyama[10], Hidehiko Suzuki[11], Manabu Yamada[12], Naoya Sakatani[1], Chikatoshi Honda[13], Masahiko Hayakawa[1], Kazuo Yoshioka[5], Yuichiro Cho[5], Hirotaka Sawada[1], Kazunori Ogawa[1,14] (1.ISAS/JAXA, 2.Kochi Univ., Japan, 3.Instituto de Astrofisica de Canarias, Spain, 4.Univ. of La Laguna, Spain, 5.Univ. of Tokyo, Japan, 6.Planetary Science Institute, USA, 7.DLR, Germany, 8.Nagoya Univ., Japan, 9.Rikkyo Univ., Japan, 10.AIST, Japan, 11.Meiji Univ., Japan, 12.Chiba Inst. Tech, Japan, 13.Univ. of Aizu, Japan, 14.Kobe Univ., Japan)

[PPS07-P04] Change in boulder surface spectra on asteroid Ryugu induced by touchdown operations of Hayabusa2

*Yudai Takai[1], Seiji Sugita[1], Rie Honda[2], Tomokatsu Morota[1], Shingo Kameda[3], ERI TATSUMI[4], Yuichiro Cho[1], Kazuo Yoshioka[1], Hirotaka Sawada[5], yokota yasuhiro[5], Naoya Sakatani[5], Masahiko Hayakawa[5], Moe Matsuoka[5], Manabu Yamada[6], Toru Kouyama[7], Hidehiko Suzuki[8], Chikatoshi Honda[9], Kazunori Ogawa[5] (1.University of Tokyo, 2.Kochi University, 3.Rikkyo University, 4.University of La Laguna, 5.JAXA, 6.Chiba Institute of Technology, 7.National Institute of Advanced Industrial Science and Technology, 8.Meiji University, 9.The University of Aizu)

[PPS07-P05] The Surface Roughness of (162173) Ryugu based on the Topography from HAYABUSA2 Laser Altimeter (LIDAR)

*Shinsuke Abe[1], Noriyuki Namiki[2], Koji Matsumoto[2], Hirotomo Noda[2], Hiroki Senshu[3], Naru Hirata[4], Hirohide Demura[4] (1.Department of Aerospace Engineering, College of Science and Technology, Nihon University, 2.National Astronomical Observatory of Japan, 3.Planetary Exploration Research Center, Chiba Institute of Technology, 4.The University of Aizu)

[PPS07-P06] Estimation based on analysis of boulder motion of bulk density of the boulders on the surface of Ryugu at touchdown operation

*Kousuke Kitsunai[1], Shingo Kameda[1], ERI TATSUMI[2], Naoya Sakatani[3], Shogo Tachibana[4], Osamu Mori[3], Seiji Sugita[4], Rie Honda[5], Tomokatsu Morota[4], yokota yasuhiro[3], Toru Kouyama[6], Hidehiko Suzuki[7], Manabu Yamada[8], Chikatoshi Honda[9], Masahiko Hayakawa[3], Kazuo Yoshioka[4], Yuichiro Cho[4] (1.Rikkyo University, 2.IAC, 3.JAXA/ISAS, 4.University of Tokyo, 5.Kochi University, 6.AIST, 7.Meiji University, 8.Chiba Inst. Tech, 9.University of Aizu)

[PPS07-P07] **East-west asymmetric crater ejecta on Ryugu**

*Naoyuki Hirata[1], Noriyuki Namiki[2] (1.Kobe University, 2.National Astronomical Observatory of Japan)

[PPS07-P08] Crack orientation of surface boulders on Ryugu

*Sho Sasaki[1], Shiho Kanda[1], Hiroshi Kikuchi[2], Tatsuhiro Michikami[3], Tomokatsu Morota[4], Chikatoshi Honda[5], Hideaki Miyamoto[6,7], Ryodo Hemmi[7], Seiji Sugita[4], Eri Tatsumi[8], Masanori Kanamaru[1], Naoya Sakatani[2], Sei-ichiro Watanabe[9], Noriyuki Namiki[10], Terunori Irie[9], Patrick Michel[11], Masatoshi Hirabayashi[12], Naru Hirata[5], Tomoki Nakamura[13], Takaaki Noguchi[14], Takahiro Hiroi[15], Koji Matsumoto[10], Hirotomo Noda[10], Shingo Kameda[16], Toru Kouyama[17], Hidehiko Suzuki[18], Manabu Yamada[19], Rie Honda[20], Yuichiro Cho[4], Kazuo Yoshioka[4], Masahiko Hayakawa[2], Moe Matsuoka[2], Hirotaka Sawada[2], Yokota Yasuhiro[20], Makoto Yoshikawa[2] (1.Department of Earth and Space Sciences, School of Science, Osaka University, 2.ISAS/JAXA, 3.Faculty of Engineering, Kindai University, 4.Department of Earth and Planetary Science, The University of Tokyo, 5.The University of Aizu, 6.School of Engineering, The University of Tokyo, 7.The University Museum, The University of Tokyo, 8.Instituto de Astrofisica de Canarias, 9.Division of Earth and Planetary Sciences, Nagoya University, 10.RISE Project, National Astronomical Observatory of Japan, 11.Observatoire De La Cote D'Azur, 12.Auburn University, 13.Department of Earth and Planetary Materials Sciences, Tohoku University, 14.Department of Arts and Science, Kyushu University, 15.Brown University, 16.Department of Physics, Rikkyo University, 17.National Institute of Advanced Industrial Science and Technology, 18.Department of Physics, Meiji University, 19.Planetary Exploration Research Center, Chiba Institute of Technology, 20.Department of Science and Technology, Kochi University)

[PPS07-P09] Temperature variations of boulders on Ryugu observed in Hayabusa2 decent operations

*Ayumu Ohsugi[1], Naoya Sakatani[2], Yuri Shimaki[2], Hiroki Senshu[3], Takehiko Arai[4], Hirohide Demura[5], Satoshi Tanaka[2], Tetsuya Fukuhara[6], Tatsuaki Okada[1,2] (1.The University of Tokyo, 2.Institute of Space and Astronautical Science, Japan Aerospace Exploration Agency, 3.Planetary Exploration Research Center, Chiba Institute of Technology, 4.Faculty of Engineering, Department of Innovative Engineering, Division of Systems and Information Engineering, Ashikaga University, 5.Department of Computer Science and Engineering, University of Aizu, 6.Department of Physics, College of Science, Rikkyo University)

[PPS07-P10] **Evaluation of Surface Temperature Variation on Asteroid Ryugu caused by Space Weathering**

*Takehiko Arai[1], Tatsuaki Okada[2], Satoshi Tanaka[2], Tetsuya Fukuhara[3], Hirohide Demura[4], Naoya Sakatani[2], Toru Kouyama[5], Yuri Shimaki[2], Hiroki Senshu[6], Tomohiko Sekiguchi[7], Jun Takita[8] (1.Ashikaga University, 2.Japan Aerospace Exploration Agency, 3.Rikkyo University, 4.The University of Aizu, 5.National Institute of Advanced Industrial Science and Technology, 6.Chiba Institute of Technology, 7.Hokkaido University of Education, 8.Hokkaido Kitami Hokuto High School)

[PPS07-P11] The effects of porosity of surface materials on the reflectance spectra of C-type asteroids

*Eiichi Kagawa[1], Tomoki Nakamura[1], Kana Amano[1], Lucie Riu[2], Moe Matauoka[2], Osamu Sasaki[3] (1.Department of Earth and Planetary Materials Sciences, Faculty of Science, Tohoku University, 2.Institute of Space and Astronautial Siences/Japan Aerospace Exploration Agency, 3.The Tohoku University Museum)

[PPS07-P12] Evidence of Boulder Mass Movement in the Northern Latitudes of Asteroid Bennu and Implications for its Surface Evolution

*Yuhui Tang[1], Dante S Lauretta[1], Ronald Ballouz[1], Daniella DellaGiustina[1], Carina Bennet[1] (1.University of Arizona)

[PPS07-P13] Q-type asteroids: possibility of having non-fresh weathered surfaces without fine particles

*Sunao Hasegawa[1], Takahiro Hiroi[2], Katsuhito Ohtsuka[3], Masateru Ishiguro[4], Daisuke Kuroda[5], Takashi Ito[6], Sho Sasaki[7] (1.Japan Aerospace Exploration Agency, 2.Brown University, 3.Tokyo Meteor Network, 4.Seoul National University, 5.Kyoto University, 6.National Astronomical Observatory of Japan, 7.Osaka University)

[PPS07-P14] Three-dimensional tracking of various sized glass beads ejected from crater formed by high-velocity impact

*Hatsune Okawa[1], Minami Yasui[1], Masahiko Arakawa[1], Sunao Hasegawa[2], Yusaku Yokota[1], Yuya Yamamoto[1] (1.Graduate School of Science, Kobe University, 2.Japan Aerospase Exploration Agency, Institute of Space and Astronautical Science)

[PPS07-P15] Effects of surface topography on ejecta growth and crater formation process

*Yusaku Yokota[1], Masahiko Arakawa[1], Minami Yasui[1], Yuya Yamamoto[1], Hatsune Okawa[1], Sunao Hasegawa[2] (1.Graduate School of Science, Kobe University, 2.Japan Aerospace Exploration Agency)

[PPS07-P16] Heating effects on the structures and elemental ratios of IOM in Jbilet Winselwan and Y 793321 CM chondrites

*Ryota Ichimura[1], Yoshihiro Furukawa[1], Tomoki Nakamura[1], Megumi Matsumoto[1], Mariko Ando (1.Department of Earth and Planetary Materials Sciences, Faculty of Science, Tohoku University)

[PPS07-P17] Survival of organic materials during atmospheric entry of micrometeorites

*Masayuki Uesugi[1], Motoo Ito[2], Naotaka Tomioka[2], Yu Kodama[3], Takuji Ohigashi[4], Hayato Yuzawa[4], Kentaro Uesugi[1], Akira Yamaguchi[5], Naoya Imae[5], Naoki Shirai[6], Yuzuru Karouji[7], Aiko Nakato[7], Kasumi Yogata[7], Kaori Hirahara[8], Ikuya Sakurai[9], Toru Yada[7], Masanao Abe[7] (1.Japan synchrotron radiation research institute, 2.Kochi institute for Core Sample Research JAMSTEC, 3.Marine Works Japan Ltd., 4.UVSOR Institute for Molecular Science, 5.National institute of Polar Research, 6.Tokyo metropolitan university, 7.Japan aerospace exploration agency, 8.Osaka University, 9.Nagoya University)

[PPS07-P18] Near-Earth Asteroid Survey with Tomo-e Gozen

*Ryou Ohsawa[1], Jin Beniyama[1], Shigeyuki Sako[1], Seitaro Urakawa[2], Shin-ichiro Okumura[2], Jun-ichi Watanabe[3], Makoto Yoshikawa[4], Tomoki Morokuma[1], Tomo-e Gozen collaboration (1.Institute of Astronomy, Graduate School of Science, The University of Tokyo, 2.Japan Spaceguard Association, 3.National Astronomical Observatory of Japan, 4.JAXA Institute of Space and Astronautical Science)

[PPS07-P19] Phase curves of >20,000 small solar system bodies obtained by the Tomo-e Gozen transient survey

*Fumi Yoshida[1], Takashi Ito[2], Seitaro Urakawa[3], Tsuyoshi Terai[4], Nozomu Tominaga[5], Tomoki Morokuma[6], Shigeyuki Sako[6], Ryou Ohsawa[6], Masaomi Tanaka[7], Ryo Hamasaki[5], Tomo-e Gozen

collaboration (1.Planetary Exploration Research Center, Chiba Institute of Technology, 2.National Astronomical Observatory of Japan, Center for Computational Astrophysics, 3.Japan Spaceguard Assosication, Bisei Spaceguard Center, 4.National Astronomical Observatory of Japan, Subaru Telescope, 5.Konan University, 6.University of Tokyo, 7.Tohoku University)

[PPS07-P20] Size distribution of Jupiter's Trojan asteroids in the L5 swarm obtained by the Subaru/Hyper Suprime-Cam

Kotomi Uehata[1], *Tsuyoshi Terai[2], Keiji Ohtsuki[1], Fumi Yoshida[3] (1.Graduate School of Science, Kobe University, 2.Subaru Telescope, National Astronomical Observatory of Japan, National Institutes of Natural Sciences, 3.Planetary Exploration Research Center, Chiba Institute of Technology)

[PPS07-P21] Measurement of Size Distribution of Cold Classical Trans-Neptunian Objects

*Tsuyoshi Terai[1], Fumi Yoshida[2], Keiji Ohtsuki[3] (1.Subaru Telescope, National Astronomical Observatory of Japan, National Institutes of Natural Sciences, 2.Planetary Exploration Research Center, Chiba Institute of Technology, 3.Graduate School of Science, Kobe University)

[PPS07-P22] Comparison of original orbits of Oort Cloud new comets given in various catalogues

*Takashi Ito[1], Arika Higuchi[1] (1.National Astronomical Observatory of Japan, National Institutes of Natural Science)

[PPS07-P23] Observational campaigns of (3200) Phaethon in 2017-2019

*Fumi Yoshida[1], Tomoko Arai[1], Ko Ishibashi[1], Peng Hong[1], Ryo Ishimaru[1], Takaya Okamoto[2], Jun-ichi Watanabe[3], DESTINY+ collaborators (1.Planetary Exploration Research Center, Chiba Institute of Technology, 2.Institute of Space and Astronautical Science, 3.National Astronomical Observatory of Japan)

[PPS07-P24] Flyby Observation of Asteroid (3200) Phaethon to Be Conducted by Cameras onboard DESTINY$^+$ Spacecraft

*Ko Ishibashi[1], Peng Hong[1], Takaya Okamoto[2], Takahiro Ishimaru[2], Shunsuke Sato[2], Manabu Yamada[1], Osamu Okudaira[1], Tomoko Arai[1], Fumi Yoshida[1], Shingo Kameda[3], Masato Kagitani[4], Takahiro Iwata[2], Tatsuaki Okada[2], Takeshi Takashima[2] (1.Chiba Institute of Technology, 2.Japan Aerospace Exploration Agency, 3.Rikkyo University, 4.Tohoku Universtiy)

[PPS07-P25] Imaging experiment simulating DESTINY$^+$ flyby exploration

*Peng Hong[1], Ko Ishibashi[1], Takaya Okamoto[2], Osamu Okudaira[1] (1.Planetary Exploration Research Center, Chiba Institute of Technology, 2.Institute of Space and Astronautical Science, Japan Aerospace Exploration Agency)

[PPS07-P26] Modeling of an Ejecta Cloud in the Vicinity of Asteroid (3200) Phaethon: A Predicton for the Detection of Ejecta Dust by the DESTINY+ Dust Analyzer (DDA)

*Hiroshi Kimura[1], Masanori Kobayashi[1], Koji Wada[1], Tomoko Arai[1], Hiroki Senshu[1], Ko Ishibashi[1], Takayuki Hirai[1], Fumi Yoshida[1], Peng Hong[1] (1.PERC/Chitec)

[PPS07-P27] Development and ground calibration strategy of DESTINY$^+$ Dust Analyzer

*Takayuki Hirai[1], Masanori Kobayashi[1], Tomoko Arai[1], Hiroshi Kimura[1], Ralf Srama[2], Harald Krueger[3], Hikaru Yabuta[5], Motoo Ito[6], Mario Trieloff[4], Sho Sasaki[7], Tomoki Nakamura[8], Hajime Yano[9] (1.Chiba Institute of Technology, Planetary Exploration Research Center, 2.University of Stuttgart, 3.Max Planck Institute for Solar System Research, 4.Heidelberg University, 5.Hiroshima University, 6.Japan Agency for Marine-Earth Science and Technology, 7.Osaka University, 8.Tohoku University, 9.Japan Aerospace Exploration Agency)

[PPS07-P28] **Visualization and Analysis of Data from Small-Body Missions with NASA's Solar System Treks Portals**

*Brian Hamilton Day[1], Emily Law[2], NASA Solar System Treks Team -[2] (1.NASA Ames Research Center, 2.NASA Jet Propulsion Laboratory)

[PPS07-P29] Comet Interceptor mission: an overview and an expected contribution from Japan

*Satoshi Kasahara[1], Shingo Kameda[2], Kazuo Yoshioka[1], Ayako Matsuoka[3], Hideyo Kawakita[4], Shinnaka Yoshiharu[4], Jun-ichi Watanabe[5], Yoshifumi Saito[6], Ryu Funase[1,6], Ozaki Naoya[6] (1.The university of Tokyo, 2.Rikkyo University, 3.Kyoto University, 4.Kyoto Sangyo University, 5.National Astronomical Observatory of Japan, 6.Institute of Space and Astronautical Science)

[PPS07-P30] **Thermal Infrared Multi-band Imager for the Hera Mission**

*Tatsuaki Okada[1,2], Tetsuya Fukuhara[3], Satoshi Tanaka[1], Takehiko Arai[4], Naoya Sakatani[1], Yuri Shimaki[1], Hiroki Senshu[5], Hirohide Demura[6], Toru Kouyama[7], Tomohiko Sekiguchi[8], Sunao Hasegawa[1], Makoto Yoshikawa[1] (1.Institute of Space and Astronautical Science, Japan Aerospace Exploration Agency, 2.University of Tokyo, 3.Rikkyo University, 4.Ashikaga University, 5.Chiba Institute of Technology, 6.University of Aizu, 7.National Institute of Advanced Industrial Science and Technology, 8.Hokkaido University of Education)

[PPS07-P31] **Janus: A NASA SIMPLEx mission to explore two NEO Binary Asteroids**

*Daniel Jay Scheeres[1], J W McMahon[1], E B Bierhaus[2], J Wood[2], L A.M. Benner[3], C Hartzell[4], P Hayne[1], R Jedicke[5], J Hopkins[2], L Le Corre[6], S Naidu[3], P Pravec[7], M Ravine[8] (1.University of Colorado Boulder, 2.Lockheed Martin, 3.JPL, 4.University of Maryland, 5.University of Hawaii, 6.Planetary Science Institute, 7.Astronomical Institute of the Academy of Sciences, Czech Republic, 8.Malin Space Science Systems)

[PPS07-P32] Time evolution of the Jacobi integral of the elliptic restricted three-body problem

*Arika Higuchi[1] (1.National Astronomical Observatory in Japan)

[PPS07-P33] Planetesimal Formation by Collisional Growth of Dust Aggregates in Disk Formation Phase

Ryohei Ozaki[1], *Taishi Nakamoto[1] (1.Tokyo Institute of Technology)

Tests and rehearsals for curation of samples returned from asteroid Ryugu by Hayabusa2 spacecraft

*Toru Yada[1], Masanao Abe[1], Aiko Nakato[1], Kasumi Yogata[1], Akiko Miyazaki[1], Tatsuaki Okada[1], Masahiro Nishimura[1], Kazuya Kumagai[2], Miwa Yoshitake[1], Shizuho Furuya[1], Ayako Iwamae[2], Tasuku Hayashi[1], Daiki Yamamoto[1], Shogo Tachibana[1,3], Tomohiro Usui[1], Hisayoshi Yurimoto[1,4]

1. Japan Aerospace Exploration Agency, 2. Marine Works Japan, 3. University of Tokyo, 4. Hokkaido University

Hayabusa2 spacecraft had accomplished the 1st and 2nd touchdown sampling onto C-type near-Earth asteroid Ryugu in Feb. and Jul. 2019 [1]. The spacecraft left the asteroid in last Nov. to return its reentry capsule including recovered asteroidal samples in this Dec. We have been preparing for receiving the samples and performing their initial description at the Extraterrestrial Sample Curation Center (ESCuC) of Japan Aerospace Exploration Agency (JAXA). The recovered samples will be the first C-type asteroid samples never experienced terrestrial atmosphere. Thus we have developed clean chambers for handling the Hayabusa2-returned samples without exposing to terrestrial air and installed them into the newly developed clean room in the ESCuC [2]. The clean chambers consist of five components; CC3-1 and CC3-2 for vacuum procedures, CC3-3 for changing environment from vacuum to nitrogen condition, CC4-1 and CC4-2 for procedures in nitrogen condition.

The procedures after the recovery of reentry capsule at the landing site will be mainly done by Hayabusa2 Sampler developing team, securing the capsule, removing support frame to extract the sample container, cleaning its surface and setting it into the gas sampling system to recover gaseous sample inside the sample container. Then the condition inside the container will be kept in vacuum to be enclosed into its transportation box in which will be sealed in nitrogen condition and sent back to Japan by air. After it will arrive to Japan, it will be instantly transported to ESCuC in the JAXA Sagamihara campus, to be introduced into the class 10,000 clean room for further procedures. Subsequently, procedures for the sample container after then are planned as follows; (1) opening the transportation box to extract the container, (2) removing the heat shield using the milling machine, (3) cleaning the outer surface of the container and checking its cleanliness, (4) fixing the container into the container opening system and removing parts of container which must not be introduced to the clean chamber, (5) introducing the container to the CC3-1, (6) evacuating the CC3-1 to reach high vacuum condition, (7) opening the container, (8) extracting a sample catcher from the container, (9) transferring the catcher to the CC3-2, (10) removing the cover of the chamber A of the catcher, (11) recovering small amount of samples from the chamber A under the vacuum condition, (12) setting a temporal cover to the chamber A of the catcher, (13) transferring the catcher to the CC3-3, (14) changing the environment of the CC3-3 from vacuum to purified nitrogen condition, (15) setting the handling jig to the catcher, (16) transferring the catcher to CC4-2 via CC4-1, (17) measuring bulk weight of the samples including the catcher and the jigs and observing the interior of the chamber A of the catcher, (18) transferring the catcher to CC4-1, (19) dismantling the catcher, (20) recovering samples inside each of the chambers of the catcher, (21) transferring the samples to CC4-2, (22) measuring the weight of the samples from of the chambers of the catcher and observing them with the optical microscope, (23) picking up individual samples, (24) performing their weight measurements, optical observations, FT-IR analyses and MicrOmega analyses, and (25) enclosing them into their containers for transportation or preservation.

So far, we have done rehearsals for the procedures (4) and (9) to (14) two times for each, and will continue tests and rehearsals for each of the procedures as those necessary for them will be ready to use

©2020. Japan Geoscience Union. All Right Reserved.

until this Sep. Then we will refresh the clean chambers, instruments, jigs and tools for the procedures to be ready for receiving samples returned by Hayabusa2 in this Dec.

References:

[1] Tachibana S. et al. (2020) LPS XXXXXI, abstract #2027.

[2] Yada T. et al. (2019) LPS XXXXX, abstract #1795.

Keywords: Hayabusa2, Ryugu, sample return, asteroid, curation

©2020. Japan Geoscience Union. All Right Reserved.

Soluble organic matter in Ryugu: The first rehearsal analysis

*Hiroshi Naraoka[1], Yoshinori Takano[2], Nanako O. Ogawa[2], Minako Hashiguchi[1], Hannah L. McLain[3], Eric T. Parker[3], Kenji Hamase[1], Francois-Régis Orthous-Daunay[4], Junko Isa[4], Dan Aoki[5], Kazuhiko Fukushima[5], Philip Schmitt-Kopplin[6], Jason P. Dworkin[3], SOM Analysis Team

1. Kyushu University, Japan, 2. Japan Agency for Marine-Earth Science Technology, Japan, 3. NASA Goddard Space Flight Center, USA, 4. Université Grenoble Alpes, France, 5. Nagoya University, Japan, 6. Helmholtz Zentrum Muenchen, Germany

Introduction: Ryugu is a C-type asteroid possessing a low-albedo surface with low abundance hydrous minerals [1], which is similar characteristics observed for carbonaceous meteorites. Therefore, the asteroid material is expected to contain many types of organic matters including amino acids. The occurrence of organic compounds in Ryugu will provide clues to the evolution of prebiotic molecules, redox and thermal condition as well as aqueous alteration of the asteroids in the solar system. We have organized an international analytical team for the soluble organic matter (SOM) of the Hayabusa2-returned samples. Because the total sampling amount is expected to be small (~100 mg) [2], and because meteoritic SOM usually occurs as a complex mixture consisting of various types of organic compounds with very small concentrations at each compound, we have been developing high-sensitive and high-resolution analytical techniques [3]. The first rehearsal analysis is conducted using small amounts of carbonaceous chondrites.

Samples and Methods: The powdered samples (~50 mg) of CM carbonaceous chondrites and baked serpentine (as a blank) were extracted sequentially with non-polar to polar solvents in a clean room. The solvent extracts were analyzed using: 1) High-resolution mass spectroscopy (HRMS) using Fourier Transform-Ion Cyclotron Resonance/Mass Spectrometry (FT-ICR/MS) [4], 2) HRMS with nano-liquid chromatography (nanoLC) with Orbitrap MS [5],3) Chiral amino acid analysis using multi-dimensional (2D or 3D) high-performance liquid chromatography (HPLC) with high-sensitive fluorescence detection (FD) coupled with HRMS [6, 7]. 4) Compound-specific isotope analysis using gas chromatography (GC)/Orbitrap MS and GC/combustion/isotope ratio mass spectrometry (GC/C/IRMS), 5) *In situ*organic compound analysis and molecular imaging using desorption electrospray ionization (DESI) equipped with Orbitrap MS [8, 9]. 6) Spatial resolution imaging of organic compounds using time of flight-secondary ion mass spectrometry (ToF-SIMS) [10], and 7) Bulk chemical and isotopic compositions of organic matter (C and N) using nanoEA-IRMS [11].

Results and Discussion: The 3D-HPLC/FD analysis clarified some chiral amino acid distribution using ~mg of the Murchison meteorite, in which non-proteinogenic amino acids were present as racemic mixtures. The FT-ICR/MSanalysis of Murchison revealed significantly diverse molecular compositions with the homologous series using both positive and negative ions, being consistent with the previous studies [4]. The various structural isomers (the same molecular composition but different chemical structures) were identified using nanoLC/nanoESI/Orbitrap MS. The nanoLC coupled with nanoESI could enhance the sensitivity of detection by three magnitudes compared to that of conventional HPLC with ESI. The chromatographic HRMS data was deconvoluted by a hand-made software, in which the CHN compounds were predominant, being similar results as the previous study [5]. The heterogeneous distribution of the CHN compounds was revealed usingDESI/HRMS. These results indicate that the current analytical methods can be available to reveal organic molecular characteristics of the Ryugu samples, if the returned samples contain SOM similar to the Murchison SOM. We further plan to conduct the second rehearsal

©2020. Japan Geoscience Union. All Right Reserved.

analysis using less samples (~10 mg) of various carbonaceous meteorites.

References: [1] Kitazato K. et al. (2019) *Science* **364**, 272. [2] Tachibana S. (2014) *Geochem. J.* **48**, 571. [3] Naraoka H. et al. (2019) *Life* **9**, 62. [4] Schmitt-Kopplin P. et al. (2010) *PNAS USA* **107**, 2763. [5] Naraoka H. et al. (2017) *ACS Earth & Space Chem.* **1**, 540. [6] Glavin D. P. et al. (2011) *MAPS* **45**, 1848. [7] Hamase K. et al. (2014) *Chromatography* **35**, 103. [8] Naraoka H. & Hashiguchi M. (2018) *Rapid Commun. Mass Spectrom.* **32**, 959. [9] Hashiguchi M. & Naraoka H. (2019) *MAPS,* **54**, 452. [10] Naraoka H. et al. (2015) *EPS* **67**, 67. [11] Ogawa N. O. et al. (2019) *82th METSOC Meeting*, Abstract #6208.

Keywords: Hayabusa2, Ryugu, Soluble organic matter, High resolution

©2020. Japan Geoscience Union. All Right Reserved.

Visible Wavelength Normal Albedo Map of Ryugu Derived by Hayabusa2 Optical Navigation Camera

*Yasuhiro Yokota[1,2], Rie Honda[2], Eri Tatsumi[3,4,5], Deborah Domingue[6], Stefanus E. Schröder[7], Moe Matsuoka[1], Seiji Sugita[5], Tomokatsu Morota[5,8], Shingo Kameda[9], Toru Kouyama[10], Hidehiko Suzuki[11], Manabu Yamada[12], Naoya Sakatani[1], Chikatoshi Honda[13], Masahiko Hayakawa[1], Kazuo Yoshioka[5], Yuichiro Cho[5], Hirotaka Sawada[1], Kazunori Ogawa[1,14]

1. ISAS/JAXA, 2. Kochi Univ., Japan, 3. Instituto de Astrofisica de Canarias, Spain, 4. Univ. of La Laguna, Spain, 5. Univ. of Tokyo, Japan, 6. Planetary Science Institute, USA, 7. DLR, Germany, 8. Nagoya Univ., Japan, 9. Rikkyo Univ., Japan, 10. AIST, Japan, 11. Meiji Univ., Japan, 12. Chiba Inst. Tech, Japan, 13. Univ. of Aizu, Japan, 14. Kobe Univ., Japan

Asteroid explorer Hayabusa2 observed Cb-type asteroid 162173 Ryugu between June 2018 and November 2019 at a distance below 20km. The Telescopic Optical Navigation Camera (ONC-T) [1–4] onboard Hayabusa2 observed Ryugu with 7 broadband filters ranging in wavelength from 0.40–0.95 μm. On 8 January 2019, ONC-T observed the asteroid in the opposition geometry from ~20 km distance, through one rotation period (7.6 hr) in 7-band. The local solar phase angle of each pixel ranges from 0.0° to ~1.7°. This data set is well suited to derive the normal albedo, defined as the radiance factor (I/F) at phase angle 0° [5]. We present the normal albedo map from this observation.

The data number of the raw image pixels are converted [4] to I/F. The observation geometry of each pixel is calculated using the Ryugu shape model [6] produced by the Hayabusa2 shape model team. We fit a linear function to the phase function plot within the phase angle range 0.2–1.7°. Using this phase function, each pixel's I/F was extrapolated to normal albedo. Finally, we create a mosaic map of normal albedo for each band.

Since the observed brightness at the opposition condition is less affected by shadows or topographic undulation than other geometries, the derived map successfully shows the albedo distribution under minimal noise conditions. The color study [e.g. 1, 6, 7, 8] of Ryugu reported that the spectral slope from b-band (0.48 μm) to x-band (0.86 μm) exhibits the greatest regional variation on Ryugu. We found that the normal albedo is well correlated with the b-x spectral slope. Further study is necessary to interpret this relationship.

Acknowledgment: We thank the entire Hayabusa2 team to achieve the observation and analysis. This study was supported by Japan Society for the Promotion of Science (JSPS) Core-to-Core Program "International Network of Planetary Sciences", NASA's Hayabusa2 participating scientist program (grant number NNX16AL34G), and NASA's Solar System Exploration Research Virtual Institute 2016 (SSERVI16) Cooperative Agreement (NNH16ZDA001N) for TREX (Toolbox for Research and Exploration).

References: [1] Sugita S. et al. (2019) Science 10.1126/science.aaw0422. [2] Kameda S. et al. (2017) SSR 208, 17–31. [3] Suzuki H. et al. (2018) Icarus 300, 341–359. [4] Tatsumi E. et al. (2019) Icarus 325, 153–195. [5] Li J.-Y., et al. (2015) Asteroids IV, University of Arizona Press, 129–150. [6] Watanabe S. et al. (2019) Science 364, 268-272. [7] Morota T. et al. (2020) (submitted). [8] Tatsumi E. et al. (2020) (in preparation).

Keywords: Hayabusa2, Asteroid, Ryugu, Photometry, Albedo

©2020. Japan Geoscience Union. All Right Reserved.

©2020. Japan Geoscience Union. All Right Reserved.

Change in boulder surface spectra on asteroid Ryugu induced by touchdown operations of Hayabusa2

*Yudai Takai[1], Seiji Sugita[1], Rie Honda[2], Tomokatsu Morota[1], Shingo Kameda[3], ERI TATSUMI[4], Yuichiro Cho[1], Kazuo Yoshioka[1], Hirotaka Sawada[5], yokota yasuhiro[5], Naoya Sakatani[5], Masahiko Hayakawa[5], Moe Matsuoka[5], Manabu Yamada[6], Toru Kouyama[7], Hidehiko Suzuki[8], Chikatoshi Honda[9], Kazunori Ogawa[5]

1. University of Tokyo, 2. Kochi University, 3. Rikkyo University, 4. University of La Laguna, 5. JAXA, 6. Chiba Institute of Technology, 7. National Institute of Advanced Industrial Science and Technology, 8. Meiji University, 9. The University of Aizu

The Hayabusa2 spacecraft arrived at the asteroid Ryugu in June 2018, and various static observations have revealed a large number of boulders on Ryugu's surface and its low bulk density of 1190 kg/m^3, suggesting its "rubble-pile" structure (Watanabe et al., 2019). Sugita et al. (2019) reported two main types of boulders on Ryugu: a type 1 boulder is dark and rugged and a type 2 boulder is brighter and has smooth surfaces. The variety of boulders might be the results of sampling from different lithologies in its parent body.
On 21 February 2019, Hayabusa2 successfully touched down for the first time. During the touchdown operation, the optical navigation cameras (ONCs) onboard Hayabusa2 obtained high-resolution images. These imagesshow that boulder's surfaces swept by the sampling projectile impact and thruster gas jets apparently changed in brightness. In this study, using the high-resolution image data we investigated quantitatively the brightness and spectra of the boulders before and after the touchdown to understand the intrinsic optical characteristics of the boulders.
We analyzed 43 continuous images taken by ONCs when the spacecraft gradually descended from an altitude of 10 meters and touched down on Ryugu's surface and then the thruster made it lifted up. Multiple images show that the existence of a variety of boulders even in a few cm scale. The thruster gas jets during the touchdown produced a large amount of debris from Ryugu's surface, and the entire field of view was darkened. Finally, the surface of area near the touchdown site was covered by the dark debris.
We focused on a boulder nicknamed "Turtle Rock", which is classified as type 1. The boulder seems to become brighter immediately after the touchdown. We measured its relative brightness to a boulder that was defined as a reference of brightness because it wasn't covered by the debris through the touchdown. The result shows that the relative brightness of "Turtle Rock" increased by 5~20% compared with before the touchdown and became as bright as type 2 boulders. In addition, a comparison of its spectra before and after touchdown shows that the boulder became bluer after the touchdown. The results are summarized as follows. "Turtle Rock", which is dark and redder and is classified as type1, became brighter and bluer after the touchdown. These results suggest that spectral characteristics of the boulders changed from "type1" to "type2" by sweeping of the dark debris from the boulder surface, suggesting that the variations in boulder surface spectra might be caused by geologic processes on Ryugu such as space weathering and thermal metamorphism not by processes on the parent body.

Keywords: Ryugu, Hayabusa2, touchdown, boulder

©2020. Japan Geoscience Union. All Right Reserved.

The Surface Roughness of (162173) Ryugu based on the Topography from HAYABUSA2 Laser Altimeter (LIDAR)

*Shinsuke Abe[1], Noriyuki Namiki[2], Koji Matsumoto[2], Hirotomo Noda[2], Hiroki Senshu[3], Naru Hirata[4], Hirohide Demura[4]

1. Department of Aerospace Engineering, College of Science and Technology, Nihon University, 2. National Astronomical Observatory of Japan, 3. Planetary Exploration Research Center, Chiba Institute of Technology, 4. The University of Aizu

Introduction: The Japanese asteroid explorer Hayabusa2 spacecraft explored the near-Earth asteroid (162173) Ryugu between June 2018 and November 2019. During this period, the laser altimeter (LIght Detection And Ranging, LIDAR) onboard Hayabusa2 collected over 7 million measurements of the spacecraft range to the asteroid surface [8]. The surface roughness and global surface roughness maps for Ryugu were carried out using the LIDAR topography data. The surface roughness which is defined as RMS deviation over different horizontal scales enables to give a new insight into an origin and geologic processes of a small body. The roughness is also related to the self-affine nature of planetary surfaces through a value called the Hurst exponent, H (0 In this study, we investigated the correlations between the surface roughness and the geological features on Ryugu compared with those on Itokawa and Eros. Comparing Hurst exponent of Ryugu with other bodies, the surface evolution of rubble-pile small bodies will be discussed.

Results and Discussion: Deviograms provide a quantitative way to compare the surfaces of different bodies to one another [2-7]. The deviogram of Ryugu appears to have shallower slopes over all baselines than Eros and Moon. On the other hand, comparing the deviogram with Itokawa, it looks like a straight line that increases with increasing baseline. The Hurst exponent of Ryugu is 0.69 at L=8~60m (0.74, L=8~30m). The deviograms of Eros and Moon showed self-affine (straight-line in the deviogram) nature [4], and have a similar Hurst exponent (0.97, L=4~200m) compared to Mercury [3]. On the other hand, the Hurst exponent of Itokawa is 0.51 (L=8~32m). According to [4], Higher Hurst exponent (~1) might be indicative of the surfaces dominated by impact cratering. Several craters on Ryugu have topographically distinctive raised rims while those on Itokawa do not. Unlike Eros (which is believed to be a Fractured Monolith), Ryugu is thought to have a rubble-pile structure [9]. Therefore, due to lack of the ability to support large-scale topography, it is assumed that the Hurst exponent of Ryugu is higher than Itokawa but lower than Eros, Moon and Mercury. It is indicated that the Hurst exponent of Ryugu showed well-correlation to the surfaces topography which is dominated by impact cratering [3-5]. The surface roughness change by a collision will be examined by using the SCI (Small Carry-on Impactor) event.

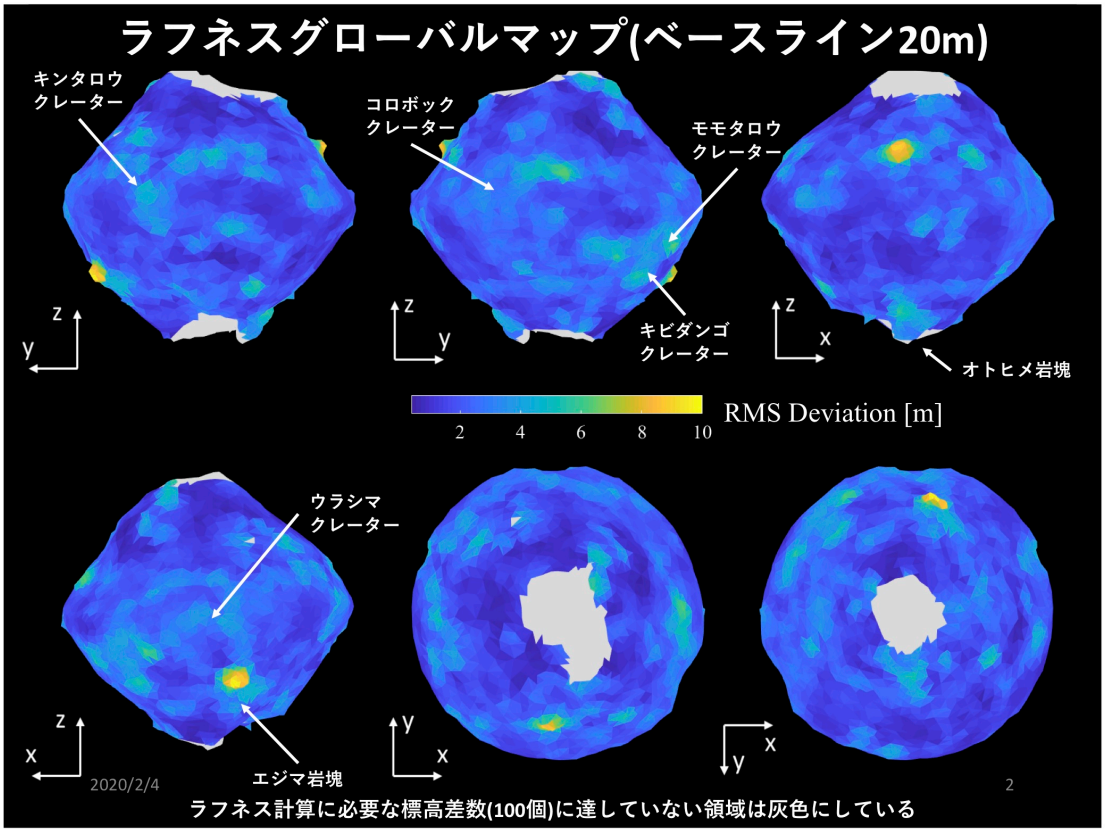
Acknowledgement: This research have been summarized by Mr. Yosuke Masuda (Nihon University) as his master thesis. This work was carried out by the joint usage / research program at the Research Center for Space Informatics, University of Aizu.

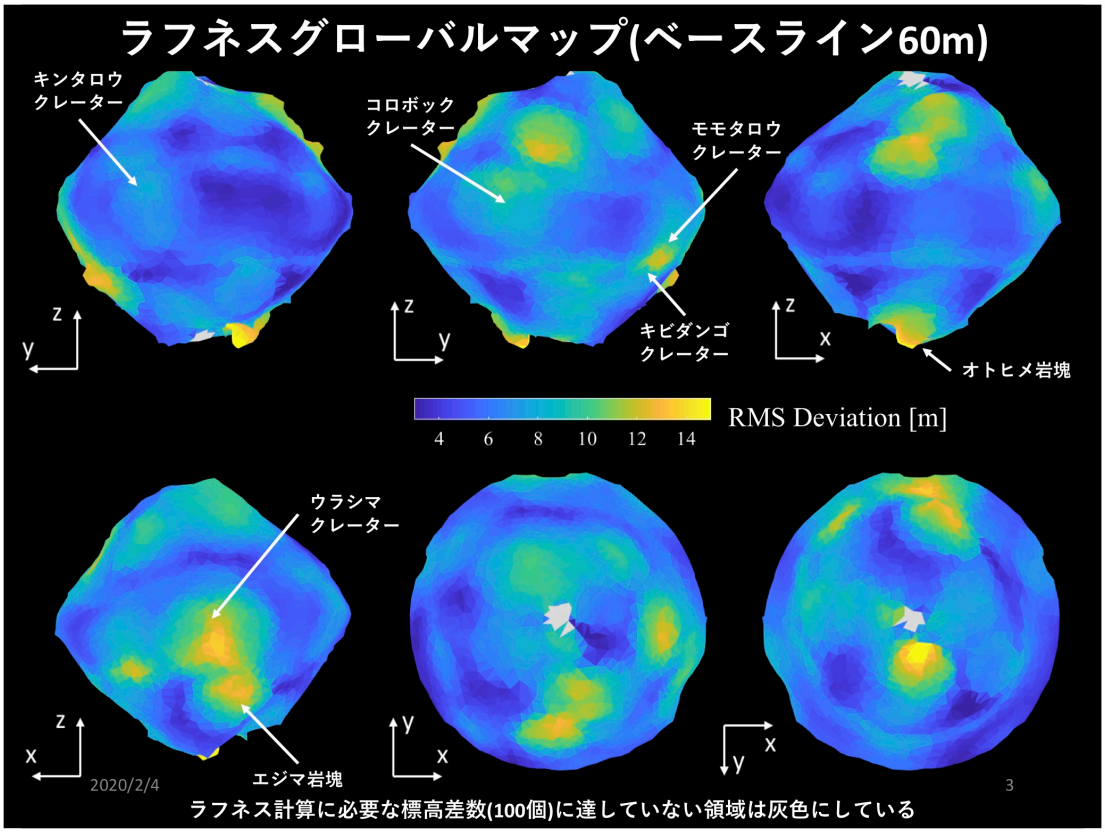
References: [1] Abe S. et al. (2006) Science, 312, 1344-1347. [2] Barnouin-Jha O. S. et al. (2008) Icarus,198,108-124. [3] Susorney H. C. M. (2017) J.Geophys.Res.,122, 1372-1390. [4] Susorney H. C. M. (2018) Icarus, 314, 299-310. [5] Susorney H. C. M. et al. (2019) Icarus, 325, 141-152. [6] Susorney H. C. M. et al. (2019) LPSC XXXIX, Abstract #2083 [7] Shepard M.K. et al. (2001) J. Geophys. Res., 106, 32777-32796. [8] Matsumoto K. et al. (2020) Icarus,338,113574. [9] Watanabe S. et al. (2019) Science, 364, 268-272.

©2020. Japan Geoscience Union. All Right Reserved.

Keywords: Asteroids, Ryugu, Roughness, Craters, Boulders

©2020. Japan Geoscience Union. All Right Reserved.





©2020. Japan Geoscience Union. All Right Reserved.

Estimation based on analysis of boulder motion of bulk density of the boulders on the surface of Ryugu at touchdown operation

*Kousuke Kitsunai[1], Shingo Kameda[1], ERI TATSUMI[2], Naoya Sakatani[3], Shogo Tachibana[4], Osamu Mori[3], Seiji Sugita[4], Rie Honda[5], Tomokatsu Morota[4], yokota yasuhiro[3], Toru Kouyama[6], Hidehiko Suzuki[7], Manabu Yamada[8], Chikatoshi Honda[9], Masahiko Hayakawa[3], Kazuo Yoshioka[4], Yuichiro Cho[4]

1. Rikkyo University, 2. IAC, 3. JAXA/ISAS, 4. University of Tokyo, 5. Kochi University, 6. AIST, 7. Meiji University, 8. Chiba Inst. Tech, 9. University of Aizu

The Hayabusa2 project is a sample return mission that aims to bring back samples from the C-type asteroid "Ryugu".The Hayabusa2 spacecraft successfully touched down on Ryugu on February 22, 2019. Previous observations suggest thatRyugu has a relatively high porosity of >50% and many largesurface boulders.These characteristics indicate that Ryugu has a rubble pile structure. Estimation of the macroporosity requires the bulk density of the constituent blocks of Ryugu, which is currently unknown. At present, the estimated porosity is calculated using the grain density values of two carbonaceous meteorites withsimilar spectrato Ryugu. The grain densities are 2.42±0.06 g/cc(CI) and 2.74-3.26 g/cc(CM)respectively. The total porosity is estimated using these values of 51±1% and 57-63%, respectively.On February 22, when the Hayabusa2 spacecraft touched down, the optical navigation camera, ONC-W1, observed the state of the landing. In this study, we analyzed the images from ONC-W1 and estimated the bulk density of the boulders on Ryugu's surface.

Keywords: Rubblepile

©2020. Japan Geoscience Union. All Right Reserved.

East-west asymmetric crater ejecta on Ryugu

*Naoyuki Hirata[1], Noriyuki Namiki[2]

1. Kobe University, 2. National Astronomical Observatory of Japan

Asteroid 162173 Ryugu is a top-shaped body formed by a prior period of rapid spin. Major craters on Ryugu appears an east–west asymmetric profile of crater rims; their western crater rims are sharp and tall, while their eastern crater rims are rounded and low. Although there are various possible explanations, we theoretically assess the effect of rotation as a possible origin of this east-west asymmetry. It is known that the trajectories and fates of ejecta are affected by the effect of rotation, especially the Coriolis force and the inertial speed of the rotating surface. As a result, we found that east-west asymmetric crater rim can be explained by the effect of a rotation, only if the inertial speed of the rotating surface is nearly equal to the first cosmic velocity of the body. In particular, Urashima, Cendrillon, and Kolobok craters might be formed, when Ryugu was fast rotator with a rotation period of ~3.6 hours. Brabo crater may be relatively younger.

Keywords: Ryugu, impact crater, Hayabusa 2

©2020. Japan Geoscience Union. All Right Reserved.

Crack orientation of surface boulders on Ryugu

*Sho Sasaki[1], Shiho Kanda[1], Hiroshi Kikuchi[2], Tatsuhiro Michikami[3], Tomokatsu Morota[4], Chikatoshi Honda[5], Hideaki Miyamoto[6,7], Ryodo Hemmi[7], Seiji Sugita[4], Eri Tatsumi[8], Masanori Kanamaru[1], Naoya Sakatani[2], Sei-ichiro Watanabe[9], Noriyuki Namiki[10], Terunori Irie[9], Patrick Michel[11], Masatoshi Hirabayashi[12], Naru Hirata[5], Tomoki Nakamura[13], Takaaki Noguchi[14], Takahiro Hiroi[15], Koji Matsumoto[10], Hirotomo Noda[10], Shingo Kameda[16], Toru Kouyama[17], Hidehiko Suzuki[18], Manabu Yamada[19], Rie Honda[20], Yuichiro Cho[4], Kazuo Yoshioka[4], Masahiko Hayakawa[2], Moe Matsuoka[2], Hirotaka Sawada[2], Yokota Yasuhiro[20], Makoto Yoshikawa[2]

1. Department of Earth and Space Sciences, School of Science, Osaka University, 2. ISAS/JAXA, 3. Faculty of Engineering, Kindai University, 4. Department of Earth and Planetary Science, The University of Tokyo, 5. The University of Aizu, 6. School of Engineering, The University of Tokyo, 7. The University Museum, The University of Tokyo, 8. Instituto de Astrofisica de Canarias, 9. Division of Earth and Planetary Sciences, Nagoya University, 10. RISE Project, National Astronomical Observatory of Japan, 11. Observatoire De La Cote D'Azur, 12. Auburn University, 13. Department of Earth and Planetary Materials Sciences, Tohoku University, 14. Department of Arts and Science, Kyushu University, 15. Brown University, 16. Department of Physics, Rikkyo University, 17. National Institute of Advanced Industrial Science and Technology, 18. Department of Physics, Meiji University, 19. Planetary Exploration Research Center, Chiba Institute of Technology, 20. Department of Science and Technology, Kochi University

Hayabusa 2 spacecraft revealed that a small carbonaceous asteroid (162173) Ryugu is a rubble pile with overall density 1.19 x 10^3kg/m^3 [1].
The surface of Ryugu is covered with various sizes of boulders. On Ryugu, the relative abundance of large boulders (>20m) is about twice as that of Itokawa or Bennu [2,3]. On the surface of Itokawa, several cracked boulders are observed and compared with cracked fragments from impact experiments [4]; impacts on Itokawa or its parent body would form boulder cracks.

Thermal fatigue is advocated for the disintegration process of surface rocks [5], where diurnal / annual thermal cycle may promote crack growth in the rocks on regolith over various spatial and temporal scales [6]. Growth of crack is rapid enough to fracture a few 10 cm size rock [7].

In preliminary analysis, we noticed that cracks on Ryugu boulders have preferred meridional orientation [8]. Desert rocks of the Earth and Mars have preferred orientation of cracks [9,10]. Here in this study, we analyzed more than 500 cracks on Ryugu boulders and checked their orientations. We analyzed 101 images (taken from 29-4083m height at proximity operation phase by Hayabusa-2 ONC-T. Image resolution is 3mm/pixel at best. We confirm the image position and resolution from shape model matching (SPC) and/or altimetry data by LIDAR. Hayabusa 2 usually observes the surface from the direction of the sun, which provide low phase angle data with short shadow width. We carefully check images so that we do not pick up the shadowed surface structure as a crack. Some cracks are confirmed using the image with different (larger) solar phase angle.

To check if a rock has a crack or not, 15-20 pixels are necessary. At the highest resolution, we may check a rock as small as 20cm. Assuming the same range size, about 2-5% of boulders have cracks. So far, we do not observe changes of the abundance ratio of cracked rocks on the Ryugu surface.

We classified cracks into four styles (as shown in the Figure):

(a) Straight cracks: Some cracks are running linearly without bending or kinking. (b) Sinuous cracks: Some

©2020. Japan Geoscience Union. All Right Reserved.

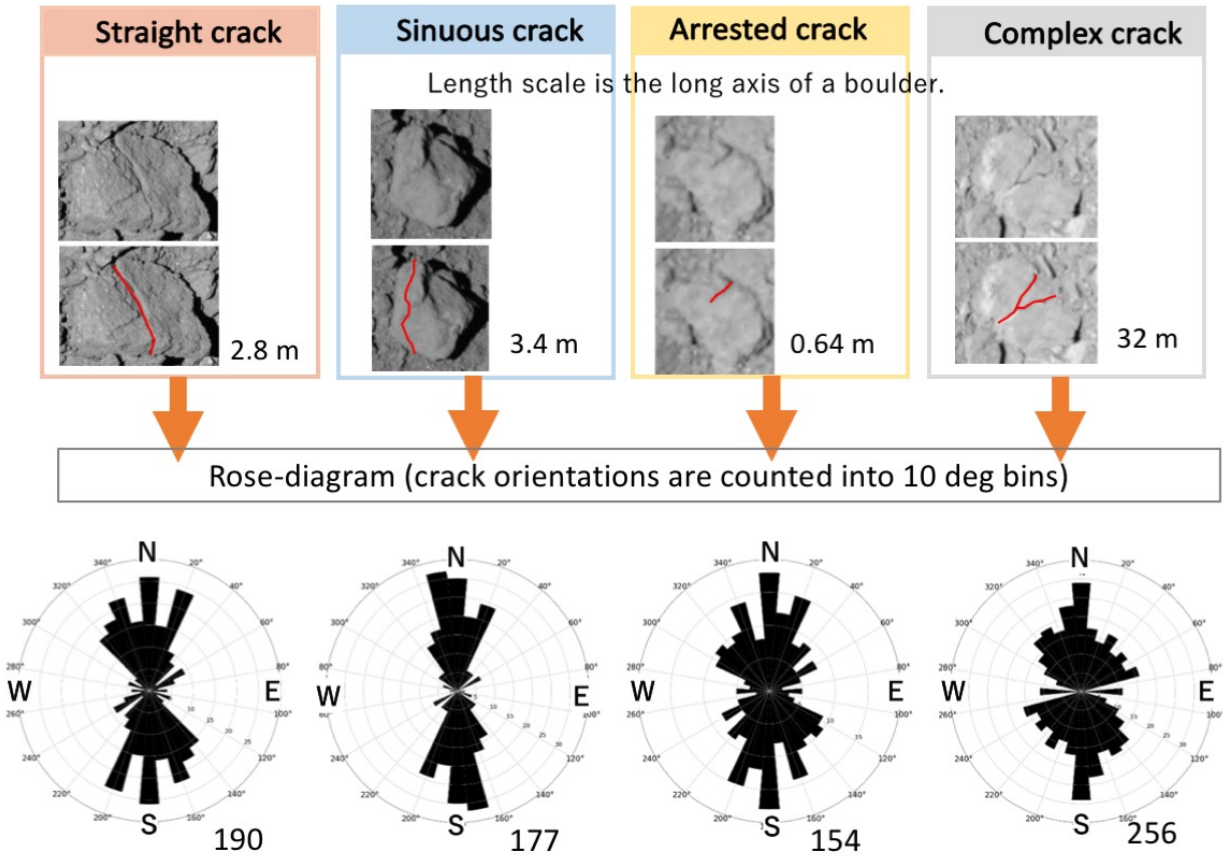
cracks have bowing, bending, and wavy structure. (c) Arrested cracks: We observed many rocks have a crack which does not go through. (d) Complex (typically branched) cracks.

We separated the strike of cracks into 18 directions with 10deg bin. We analyzed 538 boulders and found 60% of their cracks have the meridional direction (+-15deg from N-S) except complex type. This trend is common among crack types as well as rock size.

If boulder cracks on Ryugu are formed by impact processes, whether impacts occur before or after Ryugu formation, the direction of cracks should distribute more randomly. So far, solar-induced thermal stress on a surface boulder by diurnal rotation and annual revolution of Ryugu might be a possible process for the growth of boulder cracks in the meridional direction.

Ref: [1] Watanabe, S. et al (2019) Science 364. [2] Sugita, S. et al (2019) Science 364. [3] Michikami, T. et al (2019) Icarus, 331, 179-191 [4] Nakamura et al. (2008) EPS 60, 7-12. [5] Delbo M. et al. (2014) Nature 508, 233–236. [6] Molaro, J. L. et al. (2017) Icarus 294, 247-261. [7] El Mir, C., et al. (2019) Icarus, [8] Sasaki, S. et al. (2019) LPSC L, #1368. [9] MacFadden et al., (2005) Geol. Soc. Am. Bull. 117, 161-173. [10] Eppes, M. C. et al. (2015) Nature Comm., 6, 6712, [11] Delbo, M. et al (2019) EPSC-DPS-176-2.

Keywords: Hayabusa-2, Ryugu, thermal fatigue, crack orientation



©2020. Japan Geoscience Union. All Right Reserved.

Temperature variations of boulders on Ryugu observed in Hayabusa2 decent operations

*Ayumu Ohsugi[1], Naoya Sakatani[2], Yuri Shimaki[2], Hiroki Senshu[3], Takehiko Arai[4], Hirohide Demura[5], Satoshi Tanaka[2], Tetsuya Fukuhara[6], Tatsuaki Okada[1,2]

1. The University of Tokyo, 2. Institute of Space and Astronautical Science, Japan Aerospace Exploration Agency, 3. Planetary Exploration Research Center, Chiba Institute of Technology, 4. Faculty of Engineering, Department of Innovative Engineering, Division of Systems and Information Engineering, Ashikaga University, 5. Department of Computer Science and Engineering, University of Aizu, 6. Department of Physics, College of Science, Rikkyo University

C-type asteroids are considered to be parent bodies of carbonaceous chondrites and formed from fragments of undifferentiated celestial bodies. The carbonaceous chondrites are enriched in volatile species such as carbon, organics, and water thus thought to be the most primitive chondrites. The elemental abundance of the carbonaceous chondrites is consistent with that of the sun. The asteroid explorer Hayabusa2 has been accomplished its asteroid proximity phase operations, unraveling poorly known connections between the C-type asteroids and the carbonaceous chondrites.

The purpose of the Hayabusa2 mission is not only to obtain samples of the C-type asteroid 162173 Ryugu but also to acquire lots of information about Ryugu [1]. After arrival at Ryugu, the Hayabusa2 has performed a variety of science observations using remote sensing instruments such as Optical Navigation Camera (ONC), Near-Infrared Spectrometer (NIRS3), and Light Detection and Ranging (LIDAR) to characterize Ryugu. The observations by the Thermal Infrared Imager (TIR) [2], a mid-infrared thermographic camera mounted on Hayabusa2, allow us to analyze the digital thermal images which indicate the thermal radiation from Ryugu in order to determine the physical state of the asteroid surface.

TIR has a field of view (FOV) of 16.7˚×12.7˚ and the effective pixels of the detector of 328×248, resulting in the spatial resolution about 0.051˚ per pixel [2]. A temperature range that TIR can cover is 150 to 460 K and the well-calibrated temperature range is 230 to 420 K.

Global thermal images of Ryugu indicate low thermal inertia, suggesting a highly porous physical state of the surface relative to typical carbonaceous chondrites, even for large boulders [3]. Close-up thermal images taken during the descent operations show that most of the surface is also covered with highly porous boulders, but some boulders are obviously more consolidated like typical carbonaceous chondrites.

In this study, we investigated temperature variations of boulders and their physical state in the specific regions. We used the high-resolution thermal images taken below the altitude of 500 m during the descent operations for the release of MINERVA rovers on 21st September 2018, the release of MASCOT lander on 3rd October 2018, the touchdown rehearsals (TD1-R1A on 15th October 2018 and TD1-R3 on 25th October 2018), the first touchdown (TD1) on 21st February 2019, and the close-up observations around the second touchdown candidate region (DO-S01) on 8th March 2019. We measured the temperatures of individual boulders on these areas using the TIR images. We will report and discuss the details of the results of the temperature variations of surface boulders of these above regions on asteroid Ryugu.

©2020. Japan Geoscience Union. All Right Reserved.

Acknowledgments: The authors appreciate Dr. Koji Matsumoto and Kyoko Yamamoto at the National Astronomical Observatory of Japan for the use of the LIDAR corrected trajectory of the Hayabusa2 spacecraft. This study is partly supported by the JSPS Kakenhi No. JP17H06459 (Aqua Planetology) and the JSPS Core-to-Core Program “International Network of Planetary Sciences”.

References: [1] Watanabe S. *et al.,* Science 464, 268-272 (2019), [2] Okada, T. *et al.,* Space Sci. Rev., 208, 255-286 (2017), [3] Okada, T. *et al.,* Nature (accepted).

Keywords: Hayabusa2, Ryugu, C-type asteroid , The thermal infrared imager, Temperature variations, Boulder

©2020. Japan Geoscience Union. All Right Reserved.

Evaluation of Surface Temperature Variation on Asteroid Ryugu caused by Space Weathering

*Takehiko Arai[1], Tatsuaki Okada[2], Satoshi Tanaka[2], Tetsuya Fukuhara[3], Hirohide Demura[4], Naoya Sakatani[2], Toru Kouyama[5], Yuri Shimaki[2], Hiroki Senshu[6], Tomohiko Sekiguchi[7], Jun Takita[8]

1. Ashikaga University, 2. Japan Aerospace Exploration Agency, 3. Rikkyo University, 4. The University of Aizu, 5. National Institute of Advanced Industrial Science and Technology, 6. Chiba Institute of Technology, 7. Hokkaido University of Education, 8. Hokkaido Kitami Hokuto High School

Recently, space weathering is known as the phenomenon that causes spectral differences between meteorites and asteroids by ground observations (Clark et al., 2002). A result of analysis for a returned sample of Hayabusa spacecraft revealed surface modification on the asteroid Itokawa occurred due to space weathering (Noguchi et al., 2011). An inverse correlation was found in the observed parameters of the surface albedo and the characteristic peak of infrared spectra, known as the Christiansen feature, on the lunar surface (Lucey et al., 2017). These results imply that spectral shape in the thermal infrared range of asteroids may be changed due to space weathering. This study evaluates the effect of space weathering that occurred on the surface of the asteroid 162173 Ryugu by numerical calculation and compares that with the observed temperature by the Thermal Infrared Imager (TIR) onboard Hayabusa2 observation (Okada et al., 2017). TIR observed surface temperature of Ryugu with a spatial resolution of 0.051 degrees from June 27, 2018, to November 13, 2019 (Watanabe et al., 2019). TIR reveals the evolutional history of Ryugu, such as the physical properties of the coalesced bodies, and the thermal changes of the surface and inner materials. Thermal inertia is the main target, and surface roughness (Groussin et al., 2013) is also an important parameter that caused by surface shadows of light, and multiple radiations apparently change the local temperature of the surface. Both thermal inertia and surface roughness affects the peak shift of diurnal time on the surface temperature of Ryugu and probably cause the orbital changes as studied as the Yarkovsky effect (Bottke et al., 2002). The space weathering will be minor effects for the temperature change of Ryugu. In this study, we compare the anticipated temperature on Ryugu due to space weathering and the observed temperature with TIR. We assumed the solar spectral irradiance at the orbit of Ryugu and the surface composition of carbonaceous chondrites similar to the asteroid Ryugu. The amount of space weathering is assumed in dissociation energy as energetic erosion due to ion radiation of <10^6 years (Kracher and Sears, 2005). The result of the spectral change in an anticipated flux was a few W/m^2 in the spectral range of 8-12 micrometers. Therefore, TIR is not able to resolve such a faint difference in radiation. However, space weathering also changes in the whole range of spectra, and that will cause the darkening and reddening on the surface material (Thompson et al., 2019). These effects will decrease the bond albedo and increase the surface emissivity. The space weathering may cause an increase in temperature of the inner material, as well as the uppermost surface. Thus, the observed brightness temperature may be increased. We calculated the variation of radiation temperature with the reflection of solar flux, which is depended on the value of the bond albedo using the thermal model code of TIR (Takita et al., 2017). The result of this calculation indicated that variation of the surface temperature due to space weathering is a few Kelvin. Therefore, TIR is potentially able to detect the temperature variation due to space weathering, as well as surface thermal properties, depended on the thermal inertia and the surface roughness.

Keywords: Hayabusa2, Space weathering, Thermal Infrared Imager

©2020. Japan Geoscience Union. All Right Reserved.

The effects of porosity of surface materials on the reflectance spectra of C-type asteroids

*Eiichi Kagawa[1], Tomoki Nakamura[1], Kana Amano[1], Lucie Riu[2], Moe Matauoka[2], Osamu Sasaki[3]

1. Department of Earth and Planetary Materials Sciences, Faculty of Science, Tohoku University, 2. Institute of Space and Astronautial Siences/Japan Aerospace Exploration Agency, 3. The Tohoku University Museum

C-type asteroids are classified into several subtypes based on their reflectance spectra. Compositional and physical properties (e.g., mineral composition, surface roughness, and alteration and weathering degrees) are responsible for the diversity of the reflectance spectra of C-type asteroids. Some previous studies (e.g., Cloutis et al. 2018) have investigated how these properties impact the reflectance spectra of carbonaceous chondrites (CCs) whose parent bodies are C-type asteroids. In this study, we have carried out compaction experiments of Murchison CM chondrite powder ($< 155\ \mu$m) in order to understand quantitively the porosity dependence on the reflectance spectra.

The Murchison powder sample was put in a sample holder, compacted by manual tapping of the holder, and further compressed by a SUS plate to make six different porosity levels of the sample. The initial, uncompacted sample was prepared by leveling the surface (and designated as tap-0 sample). To reduce the surface porosity, the sample holder was tapped 10 times (tap-10 sample), 20 times (tap-20 sample) and 40 times (tap-40 sample). After the sample holder were tapped 40 times, the sample holder was pressed with the SUS plate by hand (hand-press sample) and by 500 kg (500kg-press sample). The reflectance spectra and the porosity of all samples were then measured by FT-IR and micro-tomography CT, respectively, at Tohoku University.

The porosity of the sample powder decreases as the sample were compacted from the tap-0 to 500kg-press sample. In addition, we found that the porosity decreases from the surface to the bottom of the sample powder and thus it is essential to obtain the surface porosity (not bulk porosity) to understand the porosity dependence on the spectra. We define the surface porosity as the porosity between the surface to the depth to which light comes in from vertical direction: light can penetrate through spaces between small grains and stop at a depth at which it is absorbed.

The measurement of the reflectance spectra showed that decreasing the surface porosity of the powder sample with tapping 0 to 40 times results in an increase in reflectance at 550nm wavelength with a small change of the slope of spectra. On the other hand, decreasing the surface porosity by pressing (hand-press and 500kg-press samples) results in brightening at shorter wavelengths and bluer-sloped spectra. The bluing of the spectra is probably due to an increase of the surface flatness by pressing using the flat surface of the SUS plate.

Our results indicate that the surface porosity and the spectral features are correlated: as the surface porosity decreases, the reflectance increases with a slight reddening of the slope of spectra. Small changes of the slope indicate small changes of the roughness of the surface by tapping. On the other hand, pressing with the flat SUS plate changed the roughness of the surface making it flatter surface, which results in bluing of the spectra. Therefore, the changes of spectral properties of the hand-press and 500kg-press samples are resulting from mixed effects of decreasing surface porosity and flattening of the surface. Our results provide a quantitative relationship between grain-size, porosity, and spectral features of C-type asteroids. Further studies with the same experimental procedures using different grain size of

©2020. Japan Geoscience Union. All Right Reserved.

the powder sample are required to distinguish between porosity and grain-size effects and to isolate only porosity effect on the spectra of C-type asteroids.

Keywords: C-type asteroids, carbonaceous chondrites, reflectance spectra, porosity

©2020. Japan Geoscience Union. All Right Reserved.

Evidence of Boulder Mass Movement in the Northern Latitudes of Asteroid Bennu and Implications for its Surface Evolution

*Yuhui Tang[1], Dante S Lauretta[1], Ronald Ballouz[1], Daniella DellaGiustina[1], Carina Bennet[1]

1. University of Arizona

The OSIRIS-REx spacecraft has returned data from the mission's Detailed Survey of the boulder-dominated surface of asteroid (101955) Bennu, which has allowed the creation of a global basemap at a pixel scale of 5 cm (Bennett et al. 2020). With only small (<20-m diameter) patches of smooth regolith, Bennu's surface evolution is likely dominated by boulder mobility. Here, we perform a focused investigation of a region between 295° and 340° longitude, and 15° and 80° N latitude, where a large concentration of boulders is distributed in a pattern indicating a possible mass flow.

We used the Small Body Mapping Tool (SBMT; Ernst et al. 2018) to measure and count boulders, utilizing the 5-cm global basemap projected on the Bennu shape model (Barnouin et al. 2019), with additional images supplemented to view shadowed areas. Using this mosaic, we delineated the hypothesized mass flow region. Within the resulting boundary, there is a large elevation change (50 m), relative to the geoid, in the north-south direction and a minimal elevation change (5 m) in the east-west direction. Within this region, we characterized boulders larger than 1.5 m, using an ellipse to capture their overall shape, size, and orientation in order to provide quantitative information regarding their spatial distribution and physical properties.

The results of the boulder count are combined with gravitational and elevation data from the 80-cm (facet size) shape model. Our preliminary results reveal a relationship between the elevation of the site and the density of boulders present, where a higher density of larger boulders sit at lower elevation in the east-west direction. This implies that mass movement in the east-west direction resulted in the migration of these boulders into their current lower-elevation position. Analysis of boulder orientations, however, shows a preferential alignment with the north-south direction, hinting at sliding movement in that direction. The nature of the flow, such as its origins and history, therefore, are still being investigated.

The method developed here will be further used to model similar flow features that may be present in other regions of Bennu. Such studies could help elucidate the processes that formed the Bennu surface that we see today, both globally and locally (for example, changes following cratering events).

References:
Bennett, C., et al. 2020. Icarus, In Review.
Ernst, C.M., et al., 2018, The Small Body Mapping Tool (SBMT) for Accessing, Visualizing, and Analyzing Spacecraft Data in Three Dimensions, LPSC 49, abstract no. 1043.
Barnouin, O.S., et al. 2019. Nature Geoscience 12, 247.

Keywords: Bennu, Surface Evolution, Asteroid

©2020. Japan Geoscience Union. All Right Reserved.

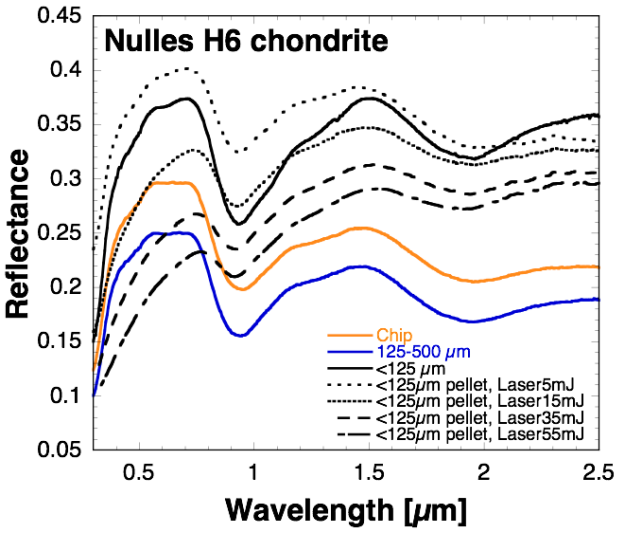
Q-type asteroids: possibility of having non-fresh weathered surfaces without fine particles

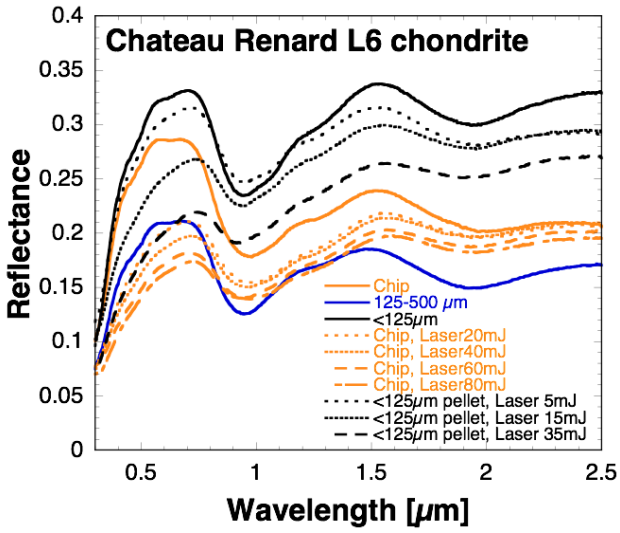
*Sunao Hasegawa[1], Takahiro Hiroi[2], Katsuhito Ohtsuka[3], Masateru Ishiguro[4], Daisuke Kuroda[5], Takashi Ito[6], Sho Sasaki[7]

1. Japan Aerospace Exploration Agency, 2. Brown University, 3. Tokyo Meteor Network, 4. Seoul National University, 5. Kyoto University, 6. National Astronomical Observatory of Japan, 7. Osaka University

Itokawa particles not only put an end to the S-complex asteroid problem, but also brought the new mystery that space weathering time scale three orders of magnitude shorter than previously thought mechanisms.
The orbital evolution caluculation in this study (Hasegawa *et al.* 2019, *PASJ* **71**, 103) reveals that the mechanism of refreshing the surface by the close encounter of the planet can be applied to maximally about halves of currently known Q-type asteroids, but not to the remaining about halves.
The results of laboratory experiments on space weathering show that the spectrum of Q-type asteroids in the case of asteroid surface without less than 100 micron particles even when space weathered can be explained.
Solar radiation pressure and electrostatic force can be considered as a mechanism to release particles smaller than 100 micron and it has been found that they can be applied to Q-type asteroids less than 0.5 km in diameter with very small perihelion or less than 0.3 km in diameter.

Keywords: asteroid, space weathering





©2020. Japan Geoscience Union. All Right Reserved.

Three-dimensional tracking of various sized glass beads ejected from crater formed by high-velocity impact

*Hatsune Okawa[1], Minami Yasui[1], Masahiko Arakawa[1], Sunao Hasegawa[2], Yusaku Yokota[1], Yuya Yamamoto[1]

1. Graduate School of Science, Kobe University, 2. Japan Aerospase Exploration Agency, Institute of Space and Astronautical Science

Impact cratering has been recognized to be a general phenomenon occurring during the formation and evolution of solar system bodies. During crater formation, impact ejecta deposits on the surface around the crater, so it is important to consider the resurfacing process of solid bodies. Many researchers studied the velocity distribution of impact ejecta and the velocity distribution is well described by the π-scaling theory [1]. We can apply this scaling law for homogeneous targets, but recent asteroid explorations revealed that the boulders on the asteroid surface had a wide size frequency distribution [2][3], so this size frequency distribution might affect the scaling laws. Previous cratering experiments using a uniform-sized granular targets showed that an axisymmetric cone-like ejecta curtains were observed. On the other hand, Kadono et al. [4] observed non-axisymmetric and non-uniform ejecta curtain for targets with non-uniform particle sizes. They proposed that the formation mechanism of a non-uniform ejecta curtain might be related to the ejecta velocity distribution depending on the particle size. In this study, we carried out impact cratering experiments using granular targets with a particle size distribution, and established a three-dimensional particle tracking method for various sized ejected particles in order to examine the effects of the particle size on the ejecta velocity distribution.

Impact experiments were conducted by using a one-stage vertical gas gun at Kobe Univ., and a two-stage vertical gas gun at ISAS. Targets were glass beads with the size of 0.1, 1, 3, and 10 mm; they mixed evenly with an equal mass. We used 3-mm-sized spherical projectiles made of nylon, glass, alumina, titanium, zirconia, and iron at Kobe. The impact velocity ranged from 129 to 208 m/s. At ISAS, we used 1-mm-sized spherical projectiles made of aluminum, titanium, iron, and copper. The impact velocity ranged from 1.2 to 4.4 km/s. We used two synchronized high-speed cameras with a framing rate of 2000 to 10000 fps in order to obtain the three-dimensional trajectory of ejected beads.

The observational procedure is described as follows. First, we recorded a rectangular parallelepiped reference (30 cm ×30 cm ×40 cm) by two cameras to determine the spatial coordinate of the bead in the chamber. Next, we conducted impact experiment without a reference and recorded the ejecta curtain by synchronized two cameras. In order to identify each bead on their images, 6-8 colored glass beads (3, 5, 10, 18mm in the diameter) were set on the target surface near an impact point before the shot. Finally, we tracked the colored beads on each image, then obtained each bead position in the three-dimensional coordinate system based on the reference.

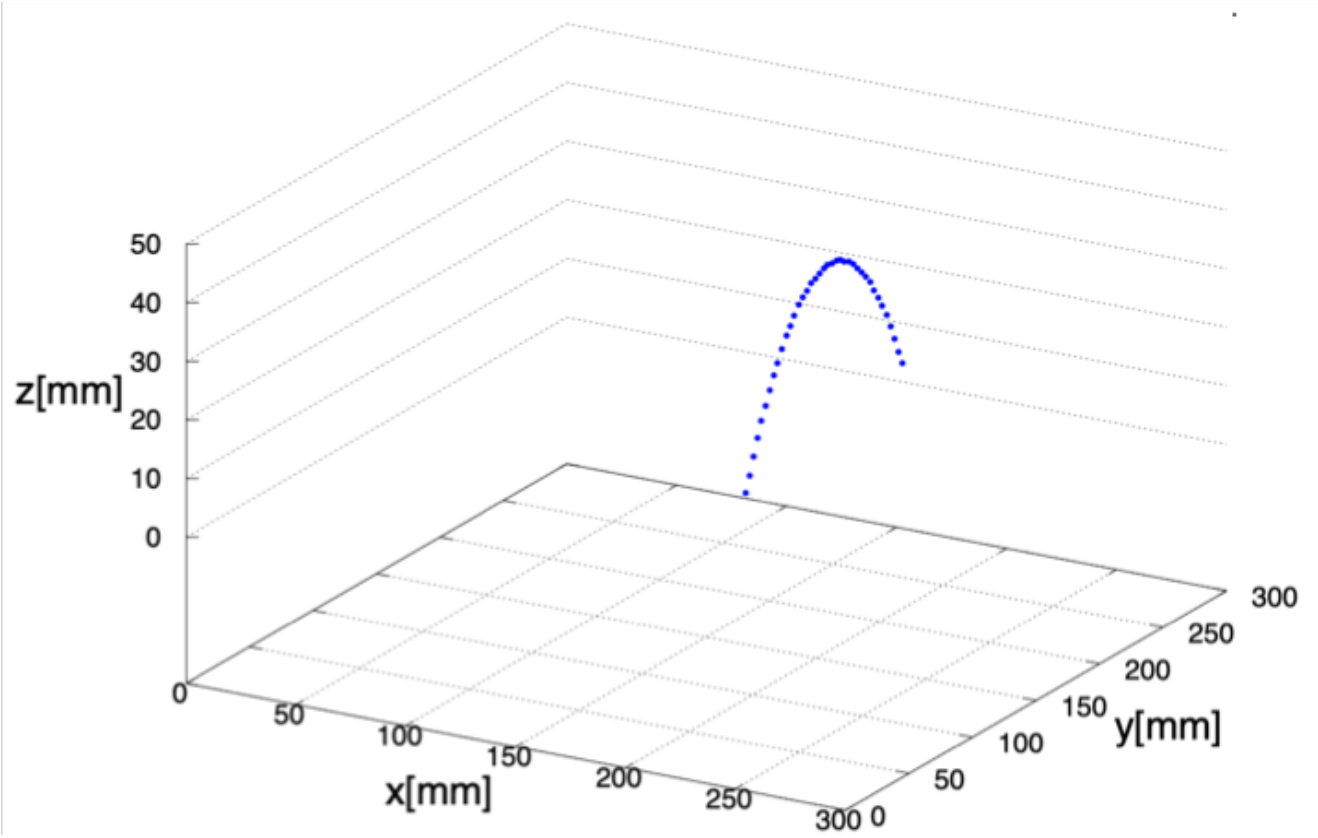
In this study, non-axisymmetric and non-uniform ejecta curtain was observed for all shots. And we succeeded to obtain three-dimensional trajectories of ejected beads by using the above method. The analyzed beads moved at a constant velocity in the horizontal direction, while they were accelerated in a vertical direction by the earth's gravity (~10 m/s^2), showing a parabola trajectory. Our data was scattered slightly, but they could be approximate by the π-scaling theory. The ejection velocity distributions were divided into two trends which the one was twice larger than the other at same initial position. We should clarify this cause in the future. Besides, we did not observe the effects of bead size on the velocity

©2020. Japan Geoscience Union. All Right Reserved.

distribution. Most beads were ejected radially from the impact point regardless of bead size while a part of them were ejected in different directions. This large angle deviation might be caused by the collision with larger beads before or after being ejected from the target surface.

[1] Housen & Holsapple, 2011, Icarus 211, p. 856. [2] Sugita et al., 2019, Science 364, aaw0422. [3] Michikami et al., 2019, Icarus 331, p.179. [4] Kadono et al., 2019, ApJL, 880, L30.

Keywords: Ejecta curtain, Impact crater, π-scaling theory, Three-dimensional particle tracking



©2020. Japan Geoscience Union. All Right Reserved.

Effects of surface topography on ejecta growth and crater formation process

*Yusaku Yokota[1], Masahiko Arakawa[1], Minami Yasui[1], Yuya Yamamoto[1], Hatsune Okawa[1], Sunao Hasegawa[2]

1. Graduate School of Science, Kobe University, 2. Japan Aerospace Exploration Agency

Impact craters are a typical geological feature found on solid bodies such as asteroids and satellites. The crater shape was observed to change depending on an impact angle and surface topographies. The crater formed on a plane surface usually looks like a circle except for craters formed by an oblique impact. Then, most impact craters are observed to be circular, but the crater found on a slope is usually elliptical. In addition, recent spacecrafts such as Hayabusa2 and OSIRIS-REx have revealed that Ryugu and Bennu have a bulge terrain at the equatorial region and large impact craters with a unique shape are found on the bulge. However, the effects of the bulge topography on the crater formation process have not been well understood. In this study, we performed crater formation experiments on targets simulating a bulge and a ridge made of regolith and investigated the effects of the topography on crater shape, ejecta growth and its sedimentation process.

We have prepared a mountain range and a cone shape target in order to simulate a bulge and a ridge. The target is composed of quartz sand with a diameter of 100 mm and the angle of repose for quartz sand is about 30 degrees. The slope was controlled to be 20 degrees and 30 degrees for the mountain range type and 30 degrees for the cone shape type. The impact experiments were conducted by using a vertical gas gun, and the mountain range target was set in a glass container to observe the crater formation from the side. The cone type target was set in a stainless container, and was placed in a vacuum chamber. The chamber was evacuated below 1000 Pa or less. The projectile was an alumina sphere with the diameter of 3 mm and an aluminum sphere with the dimeter of 2 mm, and it was impacted on the target surface vertically at the speed from 69 m/s to 202 m/s for the mountain range type target and from 1.19 km/s to 4.19 km/s for the cone type target. For the mountain range type target, the horizontal distance from the summit to the impact point, d, was changed from 1 mm to 19 mm, and for the cone type target, the width of the cone shape was changed from 85 mm to 280 mm.

As a result, the crater shape was found to strongly depend on d in the mountain range type target, and the craters formed near the summit were observed to be elliptical. The major axis of the ellipse appeared to be along the ridge direction, and the minor axis appeared to be along the slope direction. The aspect ratio of the major axis to the minor axis decreased with the increase of d, and at the same d, it increased with increasing the impact velocity. In the cone type target, the depth-to-diameter ratio was always smaller than that of the crater formed on the plane surface, and it was found that the ratio became smaller as the impact velocity increased. Furthermore, the smaller the width of the cone shape is, the greater the excavation efficiency is. In addition, it was found that the ejecta curtain formed on the slope had a smaller curtain angle on the side of the impact point, and that the asymmetry of the ejecta curtain increased when the d was smaller (figure).

©2020. Japan Geoscience Union. All Right Reserved.

Keywords: impact cratering experiment, ejecta



©2020. Japan Geoscience Union. All Right Reserved.

Heating effects on the structures and elemental ratios of IOM in Jbilet Winselwan and Y 793321 CM chondrites

*Ryota Ichimura[1], Yoshihiro Furukawa[1], Tomoki Nakamura[1], Megumi Matsumoto[1], Mariko Ando

1. Department of Earth and Planetary Materials Sciences, Faculty of Science, Tohoku University

Organic compounds in carbonaceous chondrites record heating and mechanical modifications induced by parent-body and nebular processes. In particular, insoluble Organic Matter (IOM) has been modified by thermal and aqueous processes and its irreversible carbonization has proceeded during alteration. Using solid-state ^{13}C nuclear magnetic resonance (NMR) spectroscopy, Raman spectroscopy, light elemental composition analyses, and electron microscopy, we investigated chemical structure of carbon, C, H, N elemental abundance, and morphology of IOM. The IOM extracted from two CM2 chondrites, Jbilet Winselwan and Y 793321, which may be a good analog for C-type asteroid Ryugu of the Hayabusa2 sample-return mission. These meteorites are classified to heating stage- II in the mineralogical classification scheme based on Nakamura (2005) and experienced a similar degree of aqueous alteration. However, it was suggested that they might have undergone a different thermal history: Jbilet Winselwan was subjected to long-term internal heating by short-lived radionuclide ^{26}Al (Fujiya et al., 2019), while Y 793321 was subjected to short-term impact-induced heating (Nakamura, 2006).

The results of Raman analysis of both IOMs show negligible difference from IOMs in other unheated and heated CM chondrites. The solid-state ^{13}C NMR spectra indicate that low molar ratios of aliphatic carbon to aromatic carbon (~0.14) for both IOM. These ratios are clearly lower than that ratio of lower heating stage-I samples (~0.5) (Yabuta et al. 2005). This indicates that the loss of aliphatic component or the increase of aromatic component of IOMs during heating of the meteorites in asteroids. Elemental analysis shows low H/C ratios (~0.40) in the two meteorites. These ratios are lower compared with stage-I samples (~0.70) (Yabuta et al. 2005). Therefore, the structural and elemental properties of IOMs in both two CM chondrites are similar and consistent with heating stage-II samples.

The results of Raman analysis of IOMs in the two meteorites show no difference from heating stage-I samples in contrast to the NMR and elemental analysis results. The difference suggest that the stage II heating transformed most organic carbon into aromatic but did not transform the carbon to graphitic. The results suggest that incipient structural changes by low-temperature heating of IOMs can be better characterized by NMR and elemental analysis, and further graphitization at high temperature can be well detected by Raman spectroscopy (e.g., Busemann et al. 2007).

Keywords: CM chondrite, C-type asteroid, Insoluble Organic Matter

©2020. Japan Geoscience Union. All Right Reserved.

Survival of organic materials during atmospheric entry of micrometeorites

*Masayuki Uesugi[1], Motoo Ito[2], Naotaka Tomioka[2], Yu Kodama[3], Takuji Ohigashi[4], Hayato Yuzawa[4], Kentaro Uesugi[1], Akira Yamaguchi[5], Naoya Imae[5], Naoki Shirai[6], Yuzuru Karouji[7], Aiko Nakato[7], Kasumi Yogata[7], Kaori Hirahara[8], Ikuya Sakurai[9], Toru Yada[7], Masanao Abe[7]

1. Japan synchrotron radiation research institute, 2. Kochi institute for Core Sample Research JAMSTEC, 3. Marine Works Japan Ltd., 4. UVSOR Institute for Molecular Science, 5. National institute of Polar Research, 6. Tokyo metropolitan university, 7. Japan aerospace exploration agency, 8. Osaka University, 9. Nagoya University

Organic compounds in extraterrestrial materials are thought to be one of the important components for the building block of Earth, especially for the origin of life. It is considered that those organic materials would be transported to the Earth by micrometeorites, because previous studies suggested that the flux of micrometeorite to the Earth is much larger than that of meteorites (5.38 x 10^4 kg/y for meteorites and 4 x 10^7 kg/yr for micrometeorites) [1-2]. In addition, micrometeorites show distinct feature that their composition is rather similar to carbonaceous chondrites than ordinary chondrites [3]. Thus, micrometeorites should be an important carrier for the organic materials from interplanetary space to the earth. It is well known that the micrometeorites heated up to 2000 degree Celsius during the atmospheric entry, due to frictional heating. During such intense heating under the oxidized condition, organic compound would be modified and/or destructed. It is important to evaluate the effect of heating of organic compounds during the atmospheric entry, to investigate origin and evolution of terrestrial organics.

In April of 2019, the Hayabusa2 spacecraft succeeded in the sampling of regolith materials from surface of the asteroid Ryugu, which is classified to C type asteroid and considered to be a parent body of carbonaceous chondrites. The sample would contain organic materials those free from the effect of heating during atmospheric entry and even free from terrestrial contamination or weathering. The Phase2 curation team Kochi started the rehearsal analysis of the Hayabusa2 returned samples, using Antarctic micrometeorites (AMMs)[4-5], and found that amount of organic nano-globules survived in the AMMs larger than 150 μm, those would have experienced intense heating during atmospheric entry due to large moment of inertia. Numerical calculations showed that such AMMs would have heated higher than 1000 degree Celsius, and also showed that ram pressure during the heating is almost equivalent to 1 atm.

In order to investigate the possibility of survival of organic matters in intense heating, we conducted heating experiment of carbonaceous meteorites at 1 atm, and evaluate the effect on the organic materials using scanning transmission x-ray microscopy and near edge x-ray absorption fine structure (STXM-NEXAFS) analysis. Results of the experiments show that organic materials are easily destructed in oxidized condition even by short-term heating, and are robust against heating for reduced environment.

We can examine the conditions of atmospheric entry of the micrometeorites by comparing the structural features of organic materials in extraterrestrial materials (e.g. the Hayabusa2 returned samples and AMMs), with experimental products, and would give important constraints on the evolution of organic matters in early Earth or primitive terrestrial environment.

References:

©2020. Japan Geoscience Union. All Right Reserved.

[1] Yada T. et al. (2004) The global accretion rate of extraterrestrial materials in the last glacial period estimated from the abundance of micrometeorites in Antarctic glacier ice, Earth. Planet. Space, 56:67-79.

[2] Zolensky M. et al. (2006) Flux of extraterrestrial materials, in Meteorites and the early solar system II, pp. 869-888.

[3] Imae N. et al. (2013) Micrometeorite precursors: Clues from the mineralogy and petrology of their relict minerals, Geochim. Cosmochim. Acta, 100:116-157.

[4] Ito M. et al. (2020) The Ryugu Grain Analysis: Approach by the Phase 2 Curation "Team Kochi", 82nd Annual Meeting of The Meteoritical Society, held 7-12 July, 2019 in Sapporo, Japan. LPI Contribution No. 2157, 2019, id.6082

[5] Uesugi M. et al. (2020) Preparation for the analysis of Hayabusa2 returned samples, 82nd Annual Meeting of The Meteoritical Society, held 7-12 July, 2019 in Sapporo, Japan. LPI Contribution No. 2157, 2019, id.6269

Keywords: micrometeorite, organic materials, atmospheric entry

©2020. Japan Geoscience Union. All Right Reserved.

Near-Earth Asteroid Survey with Tomo-e Gozen

*Ryou Ohsawa[1], Jin Beniyama[1], Shigeyuki Sako[1], Seitaro Urakawa[2], Shin-ichiro Okumura[2], Jun-ichi Watanabe[3], Makoto Yoshikawa[4], Tomoki Morokuma[1], Tomo-e Gozen collaboration

1. Institute of Astronomy, Graduate School of Science, The University of Tokyo, 2. Japan Spaceguard Association, 3. National Astronomical Observatory of Japan, 4. JAXA Institute of Space and Astronautical Science

Advances in astronomical observation has rapidly increased the number of solar system small bodies. Up to now, more than 930,000 objects have been discovered. Large part of newly discovered objects are near-earth asteroids, whose perihelion distances are less than 1.3 au. About 2,000 near-earth asteroids are newly discovered annually. Only a small fraction of near-earth asteroids smaller than about 140 m have, however, been discovered so far. Surveys of such small near-earth asteroids are important in the contexts of the evolution of solar system small bodies as well as the planetary defense. Small asteroids become sufficiently bright to be detected only when they are in the vicinity of the Earth. The closer asteroids are, the faster their apparent motion become. Such a fast apparent motion causes significant sensitivity loss by trailing in observations with standard observation systems with CCD cameras.

We have developed a wide-field mosaic CMOS camera, Tomo-e Gozen, mounted on the 105-cm Schmidt Telescope in Kiso Observatory, the University of Tokyo. Tomo-e Gozen is equipped with 84 CMOS sensors and monitors the sky of about 20 sq-degrees at 2 Hz. The total amount of the data obtained in a night is as much as 20 TB. An unique feature of Tomo-e Gozen is a continuous, video-like observation. Tomo-e Gozen is designed to detect every transient phenomena with timescale of about 1 second. The specifications of Tomoe Gozen, a high sensitivity, large field-of-view, and high frame rate, are ideal to detect fast moving objects, such as near-earth asteroids close to the Earth.

A wide-field survey with Tomo-e Gozen have started in October, 2019. A number of transient phenomena, near-earth asteroids, and space debris have been detected by dedicated data reduction pipelines. A near-earth asteroid pipeline detects every linear motion in the video data. Objects moving at 1–50"/s are successfully extracted even in crowded fields. In the operation in 2019, 6 near-earth asteroids are newly discovered. All the absolute magnitudes of the detected asteroids are fainter than 25 mag, corresponding to about 40 m in diameter assuming that the geometric albedo is 0.1. The survey with Tomo-e Gozen successfully detected small near-earth asteroids. In this presentation, the specifications of Tomo-e Gozen and the survey design are presented, as well as the algorithm to detect moving object in huge data, as much as 20 TB per day. Then, future prospects of the Tomo-e Gozen survey are discussed

Keywords: solar system small bodies, near earth asteroids, surveys, CMOS camera

©2020. Japan Geoscience Union. All Right Reserved.

Phase curves of >20,000 small solar system bodies obtained by the Tomo-e Gozen transient survey

*Fumi Yoshida[1], Takashi Ito[2], Seitaro Urakawa[3], Tsuyoshi Terai[4], Nozomu Tominaga[5], Tomoki Morokuma[6], Shigeyuki Sako[6], Ryou Ohsawa[6], Masaomi Tanaka[7], Ryo Hamasaki[5], Tomo-e Gozen collaboration

1. Planetary Exploration Research Center, Chiba Institute of Technology, 2. National Astronomical Observatory of Japan, Center for Computational Astrophysics, 3. Japan Spaceguard Assosication, Bisei Spaceguard Center, 4. National Astronomical Observatory of Japan, Subaru Telescope, 5. Konan University, 6. University of Tokyo, 7. Tohoku University

The Tomo-e Gozen project conducts optical wide-field survey programs with a wide-field CMOS camera, Tomo-e Gozen, attached on the 105-cm Schmidt telescope at the Kiso Observatory, the University of Tokyo. Tomo-e Gozen is the world's first wide-field CMOS camera which covers 20 square degrees with 84 chips of 35 mm full HD CMOS image sensors. A wide-field and high-cadence survey in the optical wavelengths began in 2018 with the Tomo-e Gozen (hereafter referred to as the Tomo-e Gozen transient survey). The main purpose of this survey is to detect young supernovae. However, the survey simultaneously detects a large number of moving objects in their images. As one of the by-products of the survey, here we show our preliminary result about production of phase curves (solar phase angles versus absolute magnitude) of more than 20,000 small solar system bodies including main-belt asteroids, near-Earth asteroids, Jupiter Trojans, Centaurs, and Transneptunian objects. Combining the moving object catalogue derived from the survey and the output ephemeris that the Horizons/JPL system provides, we are now able to obtain phase curves of these objects almost automatically. As the Kiso moving object catalogue is updated and being expanded on a daily basis, the number of the objects (small bodies) that we deal with goes up as well. Our result, when completed, will make a fair complement as well as a significant keystone to what is already published such as from the Pan-STARRS systematic survey on the knowledge of the surface characteristics of the small solar system bodies.

Keywords: Asteroids, Survey, Phase curve

©2020. Japan Geoscience Union. All Right Reserved.

Size distribution of Jupiter's Trojan asteroids in the L5 swarm obtained by the Subaru/Hyper Suprime-Cam

Kotomi Uehata[1], *Tsuyoshi Terai[2], Keiji Ohtsuki[1], Fumi Yoshida[3]

1. Graduate School of Science, Kobe University, 2. Subaru Telescope, National Astronomical Observatory of Japan, National Institutes of Natural Sciences, 3. Planetary Exploration Research Center, Chiba Institute of Technology

We obtained the size distribution of asteroids in Jupiter's L5 Trojan swarm using the Hyper Suprime-Cam (HSC) attached to the Subaru Telescope. Observation was carried out on January 9, 2016 (UT). The survey covered about 18 square degrees of sky area near the opposition and around the ecliptic plane with 240-sec exposure with the *r*-band filter. We detected 189 L5 Jupiter Trojans (JTs) with the detection limit of $m_r = 25.6$ mag. Out of these detected objects, 90 objects with absolute magnitude $H_r < 17.08$ mag and heliocentric distance $R < 5.5$ au were selected as our unbiased sample to derive the size distribution. Assuming a geometric albedo of 0.07, which is a mean albedo of JTs, the size range of our unbiased sample corresponds to 2–20 km in diameter. We fit a single-slope power law to the cumulative distribution for the absolute magnitude H (i.e., $dN/dH \propto 10^{\alpha H}$) and found the best-fit index α to be 0.37 ± 0.01. This value agrees well with the one for L4 JTs obtained by Yoshida & Terai (2017) also through a survey with the Subaru/HSC. Combining the cataloged magnitude distribution for larger objects, we obtained a magnitude distribution of L5 JTs for $8 < H_V < 17$, and found that the obtained broken power-law distribution agrees well with the one obtained by Yoshida & Terai for the L4 swarm in the same size range. This suggests that the L4 and L5 populations have the same origin. On the other hand, according to Fraser et al. (2014), comparison of the size distributions of still larger objects (diameter larger than about 100 km) showed that the distributions of JTs and hot TNOs are indistinguishable, which supports the model that JTs were captured from scattered TNOs. Our results are consistent with the model that both L4 and L5 JTs were originated from the scattered TNOs.

Keywords: Jupiter Trojans, size distribution, Subaru Telescope

©2020. Japan Geoscience Union. All Right Reserved.

Measurement of Size Distribution of Cold Classical Trans-Neptunian Objects

*Tsuyoshi Terai[1], Fumi Yoshida[2], Keiji Ohtsuki[3]

1. Subaru Telescope, National Astronomical Observatory of Japan, National Institutes of Natural Sciences, 2. Planetary Exploration Research Center, Chiba Institute of Technology, 3. Graduate School of Science, Kobe University

Trans-Neptunian objects (TNOs), a small-body population beyond Neptune's orbit, are generally divided into several dynamical subpopulations. One of them, so-called "cold classical" (CC) population, consists of non-resonant objects with dynamically cold orbits, i.e., low inclinations and eccentricities. Since they have been free from significant gravitational perturbation from Neptune and thus are likely to maintain the primordial orbits since the formation, the CC population is a key for understanding the formation and evolution of the planetesimal disk in the outer solar system. In particular, the size distribution of CC population provides essential clues to unveil their nature and history of the primordial planetesimal disk. The shape of its size distribution reflects the results from the planetesimal accretion and mutual collision processes, which is useful information to explore the environment of planetesimal disk and the dynamical/collisional evolutions.

Our study is to measure the luminosity function (corresponding to the size distribution) of CCs down to a diameter of 100 km or less. Since TNOs are so far/faint, their sky number density with the same detection limit is very low compared with other small-body populations. Therefore, a combination of a large aperture telescope and a wide-field imaging instrument is required to obtain sufficient data for deriving the luminosity function with high accuracy. We performed an optical survey observation for TNOs using the 8.2-m Subaru Telescope and Hyper Suprime-Cam, a gigantic mosaic CCD camera with a wide field-of-view of 1.5 deg in diameter, around the ecliptic sky area of 14 deg^2 with two (*g*- and *r*-band) filters on January 26, 2015 UT. Few have ever reported the absolute magnitude distribution of the CC population around 100 km in diameter from a single survey. Our homogeneous survey data acquired with the same instrument, at the same field, and by the same technique allows us to obtain a precise statistical sample.

We detected 173 TNOs from our survey data. The 50%-completeness detection limit is 25.0 mag in *r* band, corresponding to 80 km in diameter at heliocentric distance of 45 au assuming a geometric albedo of 0.1. We extracted a debiased sample containing 47 of the CC candidates based on their sky motion, brightness, and color. The absolute magnitude distribution derived from our CC sample are well fitted by a broken power law as pointed out by previous studies, but the bright-end slope looks shallower than those of the previous studies. We will discuss the similarity and difference between the obtained size distribution and that of other small-body populations such as Jupiter Trojans and Neptune Trojans.

Keywords: Trans-Neptunian objects, size distribution, Subaru Telescope

©2020. Japan Geoscience Union. All Right Reserved.

Comparison of original orbits of Oort Cloud new comets given in various catalogues

*Takashi Ito[1], Arika Higuchi[1]

1. National Astronomical Observatory of Japan, National Institutes of Natural Science

Nearly isotropic comets with very long orbital period are supposed to come from the Oort Cloud. Recent observational and theoretical studies have greatly revealed the dynamical nature of this cloud and its evolutionary history. However, many issues are yet to be known. Our goal is to understand current structure of this cloud as well as its dynamical origin. For estimating the current structure of the Oort Cloud, key information lies in the original orbit of the Oort Cloud new comets (OCNCs) that are defined at a distance where these objects do not receive gravitational perturbation from major planets (such as at rg = 250 au from the Sun before comets enter into the planetary region). There have been several attempts to obtain OCNC's original orbits, but it never has been an easy task. This requires numerical orbit propagation of the observed comets with high accuracy including perturbation from major disturbing bodies. In addition, non-gravitational forces often play significant roles here. First and foremost, the orbit determination of OCNC includes substantially large uncertainty because of limited number of observational arcs and very large eccentricity of the comets (~1). Here we show our preliminary result of comparison of various catalogues of OCNCs' original orbital elements at rg = 250 au: So-called the Warsaw catalogues by Krolikowska, the ephemeris given by MPC (Minor Planet Center), that given by Horizons/JPL, and others calculated by a few individuals (Marsden, Kinoshita, and Nakano). The resulting orbits that these catalogues yield are overall similar, but sometimes they are starkly different by reasons yet to be known. Through a series of plots with a help of our own orbit propagation using numerical and analytic methods, we give considerations on which catalogue yields the information that is the most significant (or the most fundamental) for understanding structure, origin, and evolution of the Oort Cloud.

Keywords: comet, Oort Cloud, dynamics

©2020. Japan Geoscience Union. All Right Reserved.

Observational campaigns of (3200) Phaethon in 2017-2019

*Fumi Yoshida[1], Tomoko Arai[1], Ko Ishibashi[1], Peng Hong[1], Ryo Ishimaru[1], Takaya Okamoto[2], Jun-ichi Watanabe[3], DESTINY+ collaborators

1. Planetary Exploration Research Center, Chiba Institute of Technology, 2. Institute of Space and Astronautical Science, 3. National Astronomical Observatory of Japan

The asteroid (3200) Phaethon is the flyby target of the DESTINY+ mission. Generally flyby missions requires a detail investigation of the flyby targets for the mission planning and instrument design. Thus, ground-based observations for the flyby targets have important roles for leading the mission success.

We have investigated (3200) Phaethon and related objects by ground based observations from 2017 to 2019. We organized observation campaigns every year : for Phaethon in 2017, for (155140) 2005UD, which is a possible fragment from Phaethon, in 2018, and again for Phaethon to determine the size by occultation observations in 2019.
Our presentation will show the observational results of Phaethon and 2005UD, which were updated every year, and also the observation plan next several years.

Keywords: Asteroids, (3200) Phaethon, (155140) 2005UD

©2020. Japan Geoscience Union. All Right Reserved.

Flyby Observation of Asteroid (3200) Phaethon to Be Conducted by Cameras onboard DESTINY$^+$ Spacecraft

*Ko Ishibashi[1], Peng Hong[1], Takaya Okamoto[2], Takahiro Ishimaru[2], Shunsuke Sato[2], Manabu Yamada[1], Osamu Okudaira[1], Tomoko Arai[1], Fumi Yoshida[1], Shingo Kameda[3], Masato Kagitani[4], Takahiro Iwata[2], Tatsuaki Okada[2], Takeshi Takashima[2]

1. Chiba Institute of Technology, 2. Japan Aerospace Exploration Agency, 3. Rikkyo University, 4. Tohoku Universtiy

DESTINY$^+$ (Demonstration and Experiment of Space Technology for INterplanetary voYage, Phaethon fLy-by and dUst Science) is a mission proposed for JAXA/ISAS Epsilon class small program, currently in the pre-project phase (Phase-A). DESTINY$^+$ is a joint mission of technology demonstration and scientific observation. The near-Earth asteroid (3200) Phaethon, the flyby target, is known as a parent body of the Geminid meteor shower, the size of which is approximately 5 to 6 km in diameter.

In this mission, spatially resolved images of Phaethon will be taken by two onboard cameras, the Telescopic CAmera for Phaethon (TCAP) and the Multiband CAmera for Phaethon (MCAP) during the flyby, in order to understand the nature of a meteor shower's parent body, which is one of the sources of interplanetary dust particles that are thought to be an important transport medium of organic matter to the Earth. The spacecraft flybys Phaethon with relative speeds of 30 to 40 km/s. Despite such a high flyby speed, the cameras are required to take unblurred images of Phaethon.

The main purposes of the DESTINY$^+$ flyby observation of Phaethon is to understand the geology of a parent body of a meteor shower, and in particular constrain the dust ejection mechanisms from active (i.e., dust-ejecting) asteroids. The specific objectives of the camera observation are taking images for (1) obtaining the global shape of Phaethon, (2) obtaining the semi-global features of Phaethon such as large impact craters and an evidence of surface disruption, (3) observing the local features of Phaethon such as topography related to dust ejection, and (4) observing the material distribution on Phaethon. The observations (1) to (3) will be conducted by TCAP, and (4) by MCAP.

TCAP is a telescopic panchromatic camera for high spatial resolution imaging of the surface of Phaethon and have a rotational mirror for automatic asteroid tracking during flyby. The rotational mirror can change the direction of the boresight from 0 to 180 deg. This enables to observe Phaethon throughout the flyby with wide solar phase angles, which is extremely important to image and understand the surfaces of planetary bodies because the solar phase angle affects significantly the appearance of geological features in taken images.

MCAP is a multiband camera, the wavelengths of which are 400, 480, 550, 700, 850, and 950 nm (700 and 950 nm are optional bands) and has multiple optical systems and sensors in order to take all band images simultaneously. This is because there is not enough time to take each band image in turn with changing bandpass filters using such as a filter wheel in this high-speed flyby mission. MCAP does not have a tracking mirror due to the weight limitation. Instead, the boresight of MCAP is fixed to the spacecraft with 40 deg off the relative velocity vector of the spacecraft and, Phaethon will be imaged while it is in the relatively wide field of view of MCAP.

We will explain the flyby imaging sequence of DESTINY$^+$, and show the conceptual designs of TCAP and MCAP.

©2020. Japan Geoscience Union. All Right Reserved.

Keywords: Phaethon, DESTINY+, Flyby, Camera

©2020. Japan Geoscience Union. All Right Reserved.

Imaging experiment simulating DESTINY$^+$ flyby exploration

*Peng Hong[1], Ko Ishibashi[1], Takaya Okamoto[2], Osamu Okudaira[1]

1. Planetary Exploration Research Center, Chiba Institute of Technology, 2. Institute of Space and Astronautical Science, Japan Aerospace Exploration Agency

DESTINY$^+$ (Demonstration and Experiment of Space Technology for INterplanetary voYage, Phaethon fLyby and dUst Science) mission plans to conduct high-resolution imaging during close flyby of asteroid (3200) Phaethon, which is considered as a parent body of Geminid meteor shower. During the high-speed flyby, the asteroid tracking mirror of Telescopic Camera for Phaethon (TCAP) will rotate to obtain unblurred high-resolution images with a spatial resolution up to 3.5 m/pixel at closes approach. Because of the nature of flyby mission which has limited duration of spatially-resolved imaging by TCAP, it is very important to design imaging sequence in order to maximize scientific achievements. Currently TCAP plans to observe the surface of Phaethon with a spatial resolution less than 120 m/pixel for about 9 minutes with an imaging rate of about 1 frame per second, which results in about 50 images with spatial resolutions less than 10 m/pixel. We have conducted ground-based experiment simulating the imaging sequence of TCAP during the flyby to understand how much scientific achievements, especially for creating 3D shape models, would be obtained with the current mission design. Also, the optimization of the imaging conditions during the flyby would be possible based on the results of the experiment, We used a CMOS camera using a candidate sensor for TCAP and a downscaled telescopic lens in order to realize the actual TCAP imaging sequence in a 20m-wide dark room. Asteroid models made by a 3D printer were irradiated with a collimated light source simulating the sunlight. We slid the camera mounted on an optical rail and took images of the asteroid models simulating the observation sequence of TCAP from 151 seconds to 0 seconds before the closest approach. We will report 3D shape models produced from the obtained images and discuss potential scientific results achieved by the current mission design and implication for optimizing the TCAP imaging conditions during the flyby.

Keywords: DESTINY+, imaging observation, camera, 3D shape model

©2020. Japan Geoscience Union. All Right Reserved.

Modeling of an Ejecta Cloud in the Vicinity of Asteroid (3200) Phaethon: A Predicton for the Detection of Ejecta Dust by the DESTINY+ Dust Analyzer (DDA)

*Hiroshi Kimura[1], Masanori Kobayashi[1], Koji Wada[1], Tomoko Arai[1], Hiroki Senshu[1], Ko Ishibashi[1], Takayuki Hirai[1], Fumi Yoshida[1], Peng Hong[1]

1. PERC/Chitec

We report on the detectability of an ejecta cloud around Asteroid (3200) Phaethon by the DESTINY+ Dust Analyzer (DDA), based on a model of dust dynamics in the cloud for a collection of spherical dust particles of blackbody with a power-law mass distribution. We demonstrate that solar radiation pressure plays a vital role in shaping the spatial distribution of dust particles in the ejecta cloud of Phaethon by expelling small particles from the sunward direction. We find that the DDA onboard the DESTINY+ spacecraft will have an opportunity of detecting dust particles in the ejecta cloud of Phaethon if the closest approach to the asteroid is confined within 500 km at 1 au from the Sun. Increased opportunities are seen if the Phaethon flyby takes place at a closer distance of 250 km and a smaller heliocentric distance of 0.8 au, and if the surface of Phaethon is porous and the initial velocity of ejecta exceeds 20 m/s. It turns out that impacts of 100 μm-sized ejecta particles scarcely happen to make tiny holes on the surface of the spacecraft during a flyby and that the spacecraft does not seem to suffer a serious damage nor encounter a centimeter-sized particle that causes catastrophic destruction of the spacecraft.

Keywords: Phaethon, dust, ejecta cloud, DESTINY+, in situ measurements, regolith

©2020. Japan Geoscience Union. All Right Reserved.

Development and ground calibration strategy of DESTINY$^+$ Dust Analyzer

*Takayuki Hirai[1], Masanori Kobayashi[1], Tomoko Arai[1], Hiroshi Kimura[1], Ralf Srama[2], Harald Krueger[3], Hikaru Yabuta[5], Motoo Ito[6], Mario Trieloff[4], Sho Sasaki[7], Tomoki Nakamura[8], Hajime Yano[9]

1. Chiba Institute of Technology, Planetary Exploration Research Center, 2. University of Stuttgart, 3. Max Planck Institute for Solar System Research, 4. Heidelberg University, 5. Hiroshima University, 6. Japan Agency for Marine-Earth Science and Technology, 7. Osaka University, 8. Tohoku University, 9. Japan Aerospace Exploration Agency

DESTINY$^+$ mission aims to perform fast flyby observation of an active asteroid, 3200 Phaethon, dust observation during the interplanetary cruising and Phaethon flyby phases. DESTINY$^+$ Dust Analyzer (DDA) for the dust observation is the successor to the Cosmic Dust Analyser (CDA) onboard the Cassini spaceprobe, using impact ionization time-of-flight mass spectrometry. The develpment of DDA has been led by University of Stuttgart, Germany, while the interface adjustment between the spacecraft and DDA, the ground calibration, and so on are conducted in coordination between Japanese and German research team. In this presentation, the latest instrument design reflected the restriction of mass resource and the strategy of ground calibration utilizing secondary ion mass spectrometry (SIMS) will be reported.

Keywords: Cosmic dust, 3200 Phaethon, Dust mass analyzer, SIMS

©2020. Japan Geoscience Union. All Right Reserved.

Visualization and Analysis of Data from Small-Body Missions with NASA's Solar System Treks Portals

*Brian Hamilton Day[1], Emily Law[2], NASA Solar System Treks Team -[2]

1. NASA Ames Research Center, 2. NASA Jet Propulsion Laboratory

This presentation provides an overview of portals within NASA's Solar System Treks Project (SSTP) that specifically target small bodies within our Solar System.

These portals each allow for visualization of different data products in 2D maps with various projections. They also allow users to conduct interactive 3D flyovers. The VR tool allows users to generate their own virtual reality flyovers for any user-defined paths along the bodies' surfaces. Other tools let users measure distances, generate elevation plots, and create 3D print files for user-defined regions or the entire body.

JAXA's Hayabusa 2 mission recently completed a campaign of reconnaissance, sample collection, and rover deployment at the near-Earth asteroid (162173) Ryugu. JAXA is providing mission data to SSTP, which is incorporating it into the new Ryugu Trek portal (https://trek.nasa.gov/ryugu). The internationalized user interface features controls in both English and Japanese. The portal's bookmarks feature takes users to particular areas of interest for more detailed looks at specific landforms and sites. On Ryugu, we focus on the surface sample site, impactor and sub-surface sample site, as well as landing sites and traverse paths for the HIBOU, OWL, and MASCOT rovers.

While Hayabusa2 was exploring Ryugu, NASA's OSIRIS-REx mission began conducting a detailed examination of the asteroid (101955) Bennu, another near-Earth object. At the request of NASA's Planetary Science Division and the OSIRIS-REx mission, SSTP began implementation a new portal for the asteroid Bennu, featuring data that is being returned from OSIRIS-REx. The Bennu Trek portal (https://trek.nasa.gov/bennu) reveals Bennu's top-like shape, a fascinating commonality with Ryugu. It also reveals details of Bennu's intensely boulder covered terrain. Bookmarked features include Nightingale, Sandpiper, Osprey, and Kingfisher, the top four candidates for sample collection.

In its investigations of Vesta and Ceres, NASA's Dawn mission has returned spectacular data of the surfaces of these two prominent small bodies within the asteroid belt. This presentation will showcase the use of the Ceres Trek (https://trek.nasa.gov/ceres) and Vesta Trek (https://trek.nasa.gov/vesta) portals and demonstrate how they can be used to visualize and analyze particularly interesting landforms such as the pitted terrain on Vesta and relic cryovolcanoes on Ceres.

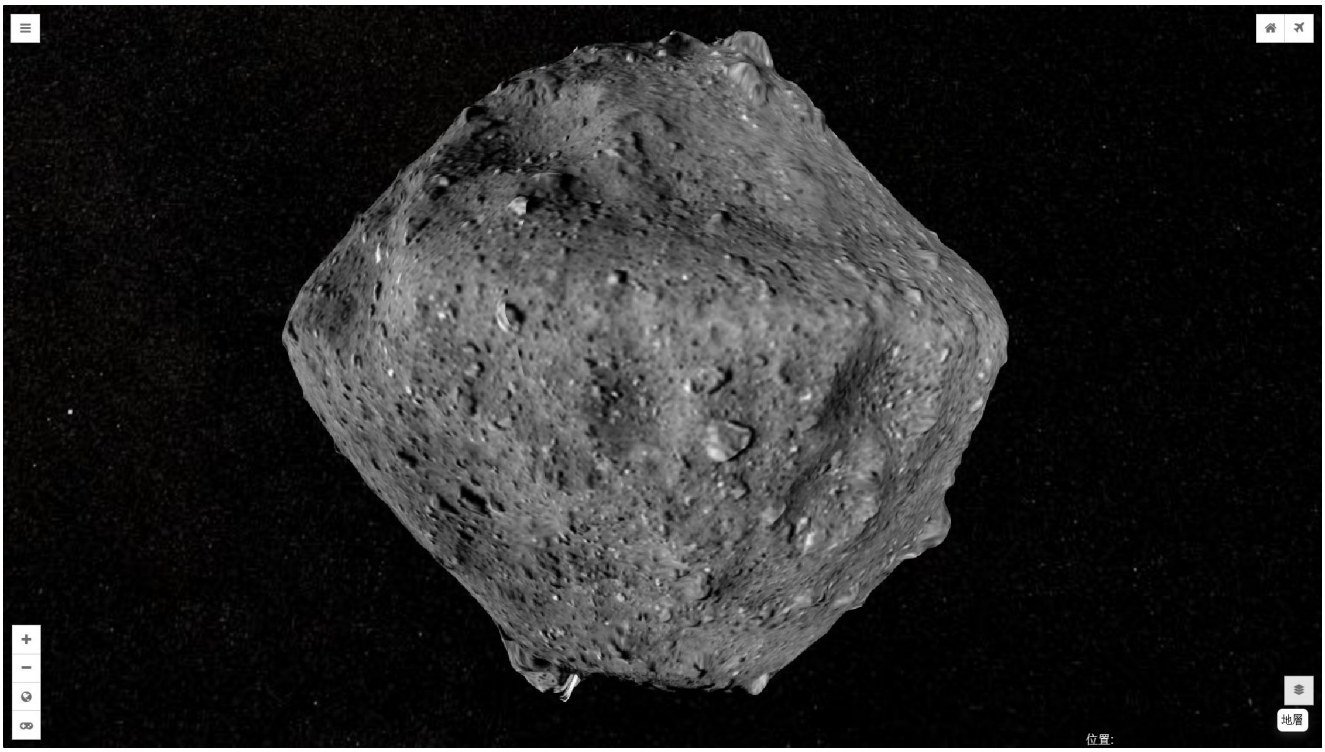
Under development at this time is a new portal for Mars' larger Moon, Phobos. This portal will make extensive use of data from ESA's Mars Express. It is being designed in collaboration with JAXA to support Japan's upcoming Martian Moons eXploration (MMX) mission. This presentation will provide a preview of a prototype for Phobos Trek.

Other Near-Earth asteroids being considered as candidates for future portals include (433) Eros utilizing data gathered by the NEAR Shoemaker mission, and (25143) Itokawa using data from JAXA's Hayabusa mission. Together, a growing collection of small body Trek portals would enhance capabilities for comparative planetology among this fascinating class of objects.

©2020. Japan Geoscience Union. All Right Reserved.

All of these products are efforts in the NASA Solar System Treks Project, available at https://trek.nasa.gov. NASA's Solar System Trek online portals provide web-based suites of interactive data visualization and analysis tools to enable mission planners, planetary scientists, students, and the general public to access mapped data products from past and current missions for a growing number of planetary bodies. These portals are being used for site selection and analysis by NASA and its international partners, supporting upcoming missions. In addition to demonstrating the capabilities of selected portals in this presentation, we will solicit input from the community for ideas for future enhancements to the portals.

Keywords: Ryugu, Hayabusa2, Bennu, Asteroids, Phobos, Data Visualization



©2020. Japan Geoscience Union. All Right Reserved.

Comet Interceptor mission: an overview and an expected contribution from Japan

*Satoshi Kasahara[1], Shingo Kameda[2], Kazuo Yoshioka[1], Ayako Matsuoka[3], Hideyo Kawakita[4], Shinnaka Yoshiharu[4], Jun-ichi Watanabe[5], Yoshifumi Saito[6], Ryu Funase[1,6], Ozaki Naoya[6]

1. The university of Tokyo, 2. Rikkyo University, 3. Kyoto University, 4. Kyoto Sangyo University, 5. National Astronomical Observatory of Japan, 6. Institute of Space and Astronautical Science

Comets are pristine small bodies and thus provide key information about the solar system evolution. Remote observations by ground observatories have characterized various comets, while in-situ observations by spacecraft have brought much more detailed information on several comets. However, the direct observations by spacecraft fly-by or rendezvous have been limited to the short-period comets, which neared the sun many times in the past and thus lost some of primitive characteristics. The Comet Interceptor mission, led by ESA, aims at a long period comet or an interstellar object. We, Japanese team, will provide an ultra-small daughter spacecraft, whose closest approach will be less than 1,000 km, allowing the first-ever multi-spacecraft fly-by observations of a comet.

©2020. Japan Geoscience Union. All Right Reserved.

Thermal Infrared Multi-band Imager for the Hera Mission

*Tatsuaki Okada[1,2], Tetsuya Fukuhara[3], Satoshi Tanaka[1], Takehiko Arai[4], Naoya Sakatani[1], Yuri Shimaki[1], Hiroki Senshu[5], Hirohide Demura[6], Toru Kouyama[7], Tomohiko Sekiguchi[8], Sunao Hasegawa[1], Makoto Yoshikawa[1]

1. Institute of Space and Astronautical Science, Japan Aerospace Exploration Agency, 2. University of Tokyo, 3. Rikkyo University, 4. Ashikaga University, 5. Chiba Institute of Technology, 6. University of Aizu, 7. National Institute of Advanced Industrial Science and Technology, 8. Hokkaido University of Education

Introduction: Thermal infrared multi-band imager TIRI is now under study to investigate thermophysical properties and materials of the surface of S-type binary asteroid Didymos in the ESA Hera mission.

Hera Mission: Hera is the ESA's asteroid mission to explore the S-type binary asteroids Didymos (780 m in diameter, 2.26 hours in rotation, 2.1 kg m^{-3}) and its moon (160 m in diameter, 11.9 hours in 1.2 km orbit), and a part of the first international planetary defense mission AIDA (Asteroid Impact and Deflection Assessment) with the NASA DART (Double-Asteroid Redirection Test) mission [2]. DART will be launched in 2021 and perform an impact to Didymoon in 2022. Impact phenomena like impact flash and the moon's orbit change will be observed by ground observations, but the dimension of impact crater, the possible alteration of materials, and the detailed orbit and nutation will be observed by Hera. Hera will be launched in 2024 and arrive at the binary asteroid in 2027.

Hera Operations: Early Phase will start at 30 to 20 km altitude, followed by observations at the altitude of 20 to 10 km. CubeSats will be deployed, followed by observations at 20 to 10 km, then at 10 to 5 km. Finally, Extended Phase will start for closer flyby or orbiting the Didymos.

TIRI Instrument: TIRI is a one-box instrument, consisting of the sensor unit BOL and the electronics unit SHU, with the targeted specification of the total mass < 5 kg, the power < 30 W, and the envelope area < 300 x 150 x 200 mm. Power of unregulated 28 V and 2 channel survival heaters are supplied from the Hera spacecraft. A basic design is from UNIFORM2 [3].

BOL: BOL is based on an uncooled micro-bolometer array of 1024 x 768 pixels, reads at 60 Hz, covers 8 to 14 μm wavelength, and has the FOV of 10° x 7.5°. The detector is pre-calibrated before launch to convert to brightness temperatures. Detector temperature should be controlled using a Peltier during operation. BOL has a capability of multi-band thermal imaging using an 8-point filter wheel, 3 narrow bands for Christensen Features (CF) at 8-10 μm, the other 3 bands for Reststrahlen Features (RF) around 11-13 μm, another one wide band for 8 to 14 μm or no filter for thermal imaging, and the rest for blank as a shutter. BOL possibly has a mechanical shutter outside of the 100 mm-diameter aperture, for on-board temperature calibration and direct insolation avoidance.

SHU: SHU has the functions of data readout from BOL, an on-board data processing, a HK collection, a packet production, a command and telemetry control via Spacewire, a power supply control, a filter wheel control, and a shutter control. SHU captures the raw thermal images of 1024 x 768 pixels at 14 bit depth at 30 or 60 Hz. Image integration and bit-shifts are performed to produce high-S/N 15-bit images. Dark frame subtraction is performed with shutter-close or deep sky images before lossless image compression and CCS-DS packetization. The packets are stored into telemetry queue buffers, to be sent to the spacecraft OBC via Spacewire. The concept is inherited from TIR [4].

©2020. Japan Geoscience Union. All Right Reserved.

Contribution to Hera by Japan: In addition to remote sensing of surface physical state of the binary asteroid by TIRI, just lilke the TIR on Hayabusa2 [5], Japanese contribution to Hera is strongly desired for its advanced experiences in Hayabusa2 mission: impact experiment and simulations, shape modeling, thermal mapping, operations at asteroid approach and proximity, and ground observations.

Acknowledgments: This work is partly supported by ISAS/JAXA Research Fund for International Collaborative Missions in FY2019.

References: [1] Carnelli I. et al. (2019) *ISTS2019*, Fukui, 16-21 June 2019, 2019-o3-04. [2] Cheng A.F. et al. (2018) *PSS* 157, 104-115. [3] Fukuhara T. et al. (2017) *IEEE Trans. Geosci. Rem. Sens.* 55, 4314-4324. [4] Okada T. et al. (2017) *SSR.* 208, 255-286. [5] Okada T. et al. (2020) *Nature*, in print.

Keywords: Hera, Planetary Defense, Thermal Imaging

©2020. Japan Geoscience Union. All Right Reserved.

Janus: A NASA SIMPLEx mission to explore two NEO Binary Asteroids

*Daniel Jay Scheeres[1], J W McMahon[1], E B Bierhaus[2], J Wood[2], L A.M. Benner[3], C Hartzell[4], P Hayne[1], R Jedicke[5], J Hopkins[2], L Le Corre[6], S Naidu[3], P Pravec[7], M Ravine[8]

1. University of Colorado Boulder, 2. Lockheed Martin, 3. JPL, 4. University of Maryland, 5. University of Hawaii, 6. Planetary Science Institute, 7. Astronomical Institute of the Academy of Sciences, Czech Republic, 8. Malin Space Science Systems

Janus is a NASA SIMPLEx mission currently in Phase B. The SIMPLEx program is designed around the idea of using secondary launch opportunities to explore interplanetary destinations. The Janus mission concept plans to take advantage of the NASA Psyche launch to send two spacecraft to fly by Near Earth Objects of interest. A specific point design has been developed that sends two spacecraft to two binary asteroid systems, (175706) 1996 FG3 and (35107) 1991 VH, both of which have been observed repeatedly with photometry, spectrometry and radar (see Figure 1).

The Janus mission sends light-weight, low-cost spacecraft built by Lockheed Martin to encounter these high-science value small body targets. The science instruments are a visible and IR imager, from Malin Space Science Systems. The spacecraft will perform a rigorous remote sensing campaign when the object is a point source, and when resolved. The spacecraft will track the binary asteroid systems through closest approach, allowing for a combination of absolute surface resolution, relative resolution across the target asteroids and phase angle coverage unparalleled in previous asteroid flyby missions.

Janus science will combine flyby observations of the target binary asteroids with ground-based observations, enabling the high resolution imaging and thermal data to be placed into a global context and leveraging all available data to construct an accurate topographical and morphological model of these bodies. Based on these measurements, the formation and evolutionary implications for small rubble pile asteroids will be studied.

The science team members all have experience on asteroid missions or have made extensive ground based observations of NEAs. The industry team has extensive experience in the design, fabrication and operation of interplanetary spacecraft and instrumentation.

Acknowledgements: The Janus mission is supported by NASA under a contract from the SIMPLEx Program Office. Part of this research was conducted at the Jet Propulsion Laboratory, California Institute of Technology, under a contract with NASA.

Keywords: Binary Asteroids, NASA SIMPLEx Mission, Flyby Asteroid Science

©2020. Japan Geoscience Union. All Right Reserved.

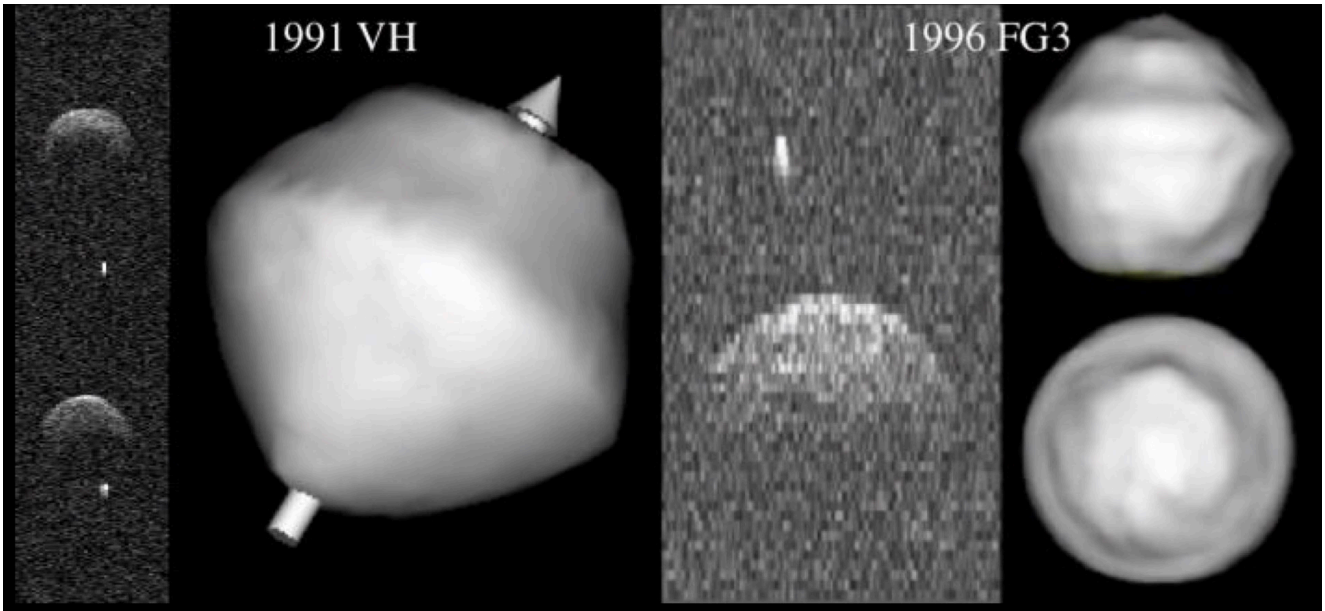


Figure 1: The binary asteroid systems to be targeted have extensive ground-based observations, enabling the high resolution observations taken during flyby to be placed into a global context, and related to many other observed single asteroid systems.

©2020. Japan Geoscience Union. All Right Reserved.

Time evolution of the Jacobi integral of the elliptic restricted three-body problem

*Arika Higuchi[1]

1. National Astronomical Observatory in Japan

In our previous studies, we investigated the conditions for the temporary capture of asteroids around a planet. For permanent capture of asteroids as stable satellites, so-called irregular satellites, energy dissipation is required. Interactions of temporarily captured asteroids with a hypothetical gas disk or atmosphere around Mars, the tidal force from the host planet, and the split-up of binary asteroids have been considered as the mechanism of energy dissipation. For all these mechanisms require fine-tuning of parameters for reasonable results. As new research, I investigate the effect of the eccentricity of the host planet on energy dissipation in the framework of the elliptic restricted three-body problem. Jacobi integral, which is a well-known conservational quantity in the circular restricted three-body problem, is no longer conserved in the elliptic restricted three-body problem. However, the behavior of the non-conserved part could tell us the behavior of the asteroids temporarily captured. In the presentation, I will analiticaly and numericaly show if the region on the orbital parameter space exists, where the Jacobi integral keeps changing toward a value that is suitable for satellites.

Keywords: elliptic restricted three-body problem, irregular satellites, celestial mechanism

©2020. Japan Geoscience Union. All Right Reserved.

Planetesimal Formation by Collisional Growth of Dust Aggregates in Disk Formation Phase

Ryohei Ozaki[1], *Taishi Nakamoto[1]

1. Tokyo Institute of Technology

Introduction: Planets are thought to be formed from planetesimals, though the formation process of planetesmals has not been understood well. Some proposed mechanisms include the gravitational instability of the dust layer, the streaming instability, and the successive collisional growth of dust aggregates. It is not clear if required conditions for these mechanisms are met in real protoplanetary disks or in the early solar nebula.

Recent astronomical observations of protoplanetary disks suggest that planets start to form in the class 0 phase, i.e., the disk formation phase, in which the mass accretion from a parental molecular cloud core to the disk continues [1]. If this is the case, planetesimals should be formed in the disk formation phase, too. Theoretically, however, it was suggested that the planetesimal formation seems difficult in the disk formation phase [2], mainly because the disk temperature in the class 0 phase is so high that dust aggregates are likely to drift into the central star due to the gas drag.

In the previous study [2], the disk was assumed to be a viscous accretion disk in which turbulence and viscous energy dissipation are present in the whole disk. This disk tends to have a higher temperature structure. On the other hand, it is known that when the ionization degree of the disk is low enough, the region becomes “dead” and neither turbulence nor dissipation takes place. In the disk with the dead zone, the temperature becomes lower than that of the “active” disk. Then, it is expected that the radial drift of dust aggregates is suppressed. In this study, we examine the temperature structure of the disk in the class 0 phase with the dead zone, and see if dust aggregates can grow to planetesimals or not.

Dust Growth in Dead Zone: We theoretically modeled and obtained the temperature structure of the disk with the dead zone and examined if the dust aggregates can grow to planetesimals with some physical parameters such as the mass accretion rate in the disk and the distance from the central star. We found that with a typical parameter range, it is hard for dust aggregates to grow to planetesimals. However, when the mass accretion rate in the disk is as low as 10^{-7} M_{sun} yr^{-1} or lower, planetesimal may be formed through collisional growth. Those parameter sets may be realized in a quiescent phase of the FU Ori phenomenon.

References:

[1] e.g., Ansdell, M. *et al.* (2016) *Astrophysical Journal* **828**, 46.

[2] Homma, K. and Nakamoto, T. (2018) *Astrophysical Journal* **868**, 118.

Keywords: planetesimal, Protoplanetary Disk, dust growth

©2020. Japan Geoscience Union. All Right Reserved.

[E] Poster | P (Space and Planetary Sciences)：P-PS Planetary Sciences

[P-PS08] Mars and Mars system: results from a broad spectrum of Mars studies and aspects for future missions

convener:Hideaki Miyamoto(University of Tokyo), Tomohiro Usui(Japan Aerospace Exploration Agency), Yuki Harada(Kyoto University), Sushil K Atreya(University of Michigan Ann Arbor)

A wealth of new data from the US, European, Russian, and the Asian exploration missions are contributing to improved understanding of geologic and climate evolution and the habitability of Mars. Eight spacecraft are currently operating at Mars, with six in orbit (Odyssey, MRO, MAVEN, Mars Express, Mangalyaan and TGO) and two on the surface (MSL-Curiosity and InSight), the largest number ever at any given time. In addition, Mars 2020, ExoMars and the Emirates Mars Mission are all scheduled to be launched in 2020. JAXA's MMX mission to explore Phobos, Deimos, and Mars is scheduled for a 2024 launch. This shows that the scientific community, international space agencies and the general public are committed to the exploration of the fascinating world of Mars. Synergistic investigations of ongoing or already completed missions together with modeling studies and earth-based observations are gradually revealing the nature of Earth's most closely resembling planet, which took a different evolutionary track than the other terrestrial planets. Seasonally, temporally and episodically variable phenomena seen on the surface and the atmosphere indicate that Mars is presently active. Thus, this session is planned to discuss recent results from a broad spectrum of Mars studies encompassing the interior, surface, atmosphere, plasma environment, and the Mars system including its two satellites. Abstracts on instrumentation and future mission plans are also encouraged for this session, as both the presenters and the audience would greatly benefit from ensuing discussions and feedbacks.

[PPS08-P01] Experimental study on thermal properties of high porosity particles for understanding physical properties of Phobos surface

*Amiko Takano[1], Naoya Sakatani[1], Hideaki Miyamoto[2], Tomohiro Usui[1], Takafumi Niihara[2], Bernadett Pál[3], Takahiro Iwata[1] (1.Japan Aerospace Exploration Agency, 2.University of Tokyo, 3.Hungarian Academy of Sciences)

[PPS08-P02] Near-infrared Hyperspectral Imager MacrOmega on MMX to Observe Martian System: Its Observation Plans and Development

*Takahiro Iwata[1], Hiromu Nakagawa[2], Tomoki Nakamura[2], Jean-Pierre Bibring [3], Cedric Pilorget [3], Vincent Hamm[3], Fuminori Tsuchiya[2], Lucie Riu[1], Moe Matsuoka[1], Hiroyuki Kurokawa[4] (1.Institute of Space and Astronautical Science, Japan Aerospace Exploration Agency, 2.Tohoku University, 3.Institut d'Astrophysique Spatiale, Université Paris-Sud, 4.Tokyo Institute of Technology)

[PPS08-P03] Shape modeling strategy for MMX

*Koji Matsumoto[1], Toru Kouyama[2], Naru Hirata[3], Hitoshi Ikeda[4], Hiroki Senshu[5] (1.RISE Project, National Astronomical Observatory of Japan, 2.National Institute of Advanced Industrial Science and Technology, 3.University of Aizu, 4.Japan Aerospace Exploration Agency, 5.Chiba Institute of Technology)

[PPS08-P04] Restoration of highest-resolution images of Phobos observed by the High-Resolution Stereo Camera (HRSC) onboard Mars Express

*Ryodo Hemmi[1], Hiroshi Kikuchi[2] (1.The Universit Museum, The University of Tokyo, 2.Institute of Space and Astronautical Science, Japan Aerospace Exploration Agency)

[PPS08-P05] Re-impacts from the craters residing at the deepest location generating the blue units on Phobos

*Hiroshi Kikuchi[1] (1.Japan Aerospace Exploration Agency)

[PPS08-P06] Mars and Earth - distinct inner Solar System products

*Takashi Yoshizaki[1], William F McDonough[1,2] (1.Tohoku University, 2.University of Maryland, College Park)

[PPS08-P07] Examination of the similarity between crack patterns due to dry fracture on the ground and heat-shrink polygons on Mars

*Chihiro Uemura[1], Takahiro Iwata[1,2], Akio Nakahara[3], Tomohiro Usui[2], Yosuke Matsuo[3], Rina Noguchi[2] (1.SOKENDAI, 2.ISAS/JAXA, 3.Nihion Univ.)

[PPS08-P08] Search of shallow subsurface reflectors in Chryse and Acidalia Planitiae on Mars

*Aina Oura[1], Yasumasa Kasaba[1], Atsushi Kumamoto[1], Rina Noguchi[2], Ken Ishiyama[3], Fuminori Tsuchiya[1], Tomohiro Usui[2], Chihiro Uemura[4] (1.Tohoku University, 2.ISAS/JAXA, 3.National Institute of Technology, Tsuruoka College, 4.Sokendai)

[PPS08-P09] Development of subsurface radar for future Mars, the Moon, and asteroid explorations

*Atsushi Kumamoto[1], Hideaki Miyamoto[2], Toshiyuki Nishibori[3], Fuminori Tsuchiya[1], Ken Ishiyama[4] (1.Department of Geophysics, Graduate School of Science, Tohoku University, 2.University of Tokyo, 3.JAXA, 4.Tsuruoka College, National Institute of Technology)

[PPS08-P10] Increase in trivalent iron elution amount and iron compounds from fayalite by ultraviolet C

*Nobuo Komori[1] (1.The United Graduate School of Education Tokyo Gakugei University)

[PPS08-P11] Introduction of the highest resolution image to the Mars Web-GIS “RedAce ” to study the local and detailed surface environment

*Hiroshi Sakai[1], Hayashi Yohei[2], Hironori Fukuchi[1], Yuya Matsubara[3], Yoshiko Ogawa[1] (1.The University of Aizu, 2.National Observatory of Japan, 3.The University of Aizu(Now NTTDocomo Inc.))

[PPS08-P12] **Estimation of dust optical depth observed by MGS/TES from visible images observed by MGS/MOC using a convolutional neural network**

*Karin miyabe[1], Kazunori Ogohara[1] (1.Graduate school of the University of Shiga Prefecture)

[PPS08-P13] Survey of dayside reconnection signatures at Mars with MAVEN

*Yuki Harada[1], Jasper S. Halekas[2], Gina A. DiBraccio[3], Shaosui Xu[4], Suranga Ruhunusiri[2], Takuya Hara[4], Jared Espley[3], James P McFadden[4], David L Mitchell[4], Christian Mazelle[5] (1.Graduate School of Science, Kyoto University, 2.Department of Physics and Astronomy, University of Iowa, 3.NASA Goddard Space Flight Center, 4.Space Sciences Laboratory, University of California, Berkeley, 5.IRAP, University of Toulouse, CNRS, UPS, CNES)

[PPS08-P14] **Seasonal variation of neutral and ion compositions in the Martian upper atmosphere observed by MAVEN/NGIMS**

*Nao Yoshida[1], Naoki Terada[1], Hiromu Nakagawa[1], Dave A Brain[2] (1.Dep. Geophysics Graduate School of Science Tohoku University, 2.LASP, University of Colorado)

Experimental study on thermal properties of high porosity particles for understanding physical properties of Phobos surface

*Amiko Takano[1], Naoya Sakatani[1], Hideaki Miyamoto[2], Tomohiro Usui[1], Takafumi Niihara[2], Bernadett Pál[3], Takahiro Iwata[1]

1. Japan Aerospace Exploration Agency, 2. University of Tokyo, 3. Hungarian Academy of Sciences

Origin of Martian satellites; Phobos and Deimos is important in clarify the history of Mars system. Martian Moons eXploration (MMX) has been selected for JAXA's next sample return mission. Observation of the physical properties of the target bodies' surfaces are expected to lead to obtaining geological information on the surface, which could constraint their origin and evolution. It is also important for developing technology for the sample return mission.

In this study, we focus on thermal inertia which is the main factor that determines the surface temperature and one of the important parameters for understanding the surface properties (ex. density and particle size) of planetary surface. The average thermal inertia of Phobos was estimated at ~70 J $m^{-2}K^{-1}s^{-½}$ from infrared observations by Mars Global Surveyor (MGS) [1].

Spectral observation data suggests that Phobos may be a primitive D-type asteroid [2]. Thermal infrared observation of a primitive C-type asteroid Ryugu by Hayabusa2 spacecraft and a primitive B-type asteroid Bennu by OSIRIS-REx spacecraft revealed that the surface of these primitive asteroids are covered with high porosity boulders and pebbles [3, 4, 5]. These observation results suggest that the materials on primitive body are highly porous. Therefore, the particles themselves on Phobos also may have a high porosity. However, experimental research on thermophysical properties for such materials is lacked. Thus, it is essential to understand the thermal properties of the high porosity particles of the Phobos surface layer.

In this study, we will conduct an experimental study on the thermal conductivity of the high porosity particles, understand the heat transport mechanism of porous particle system, and constrain the surface physical properties of primitive small bodies from thermal inertia data. This study will not only deepen the understanding of the geological background of the Phobos surface, but also provide future exploration methods such as MMX landing site selection.

In this presentation, we report the results of thermal conductivity measurements in vacuum using Phobos regolith simulant (UTPS, [6, 7]) and glass beads. UTPS is an artificially generated sample that has been used as a reference simulant of the Phobos surface for the MMX mission, and has many voids inside the grains. Therefore, UTPS was used to understand the surface condition of Phobos, which may have high voids. Based on the experimental results on the thermal conductivity of UTPS and glass beads, we will discuss about the effect of micro-porosity within grains on thermal conductivity.

Referrences

[1] Smith, N. M. et al. (2018) *LPSC XLIX,* abst#2083. [2] Murchie, S. et al. (1999) *Jour. Geophys. Res.: Planets*, 104(E4), 9069-9079. [3] Grott, M. et al. (2019) *Nat. Astron.*, 3, 971-976. [4] Okada, T. et al., (2020) *Nature*(in print). [5] DellaGiustina, D. et al. (2019) *Nat. Astron.*, 3, 341–351. [6] Miyamoto, H. et al. (2018) *LPSC XLIX,* abst#2083. [7] Miyamoto, H. & Niihara, T. (2020) *Nat. Resour. Res.*, 1-10.

©2020. Japan Geoscience Union. All Right Reserved.

Keywords: Martian satellites; Phobos, surface physical property, experimental study on the thermal conductivity, high porosity particles, thermal inertia

©2020. Japan Geoscience Union. All Right Reserved.

Near-infrared Hyperspectral Imager MacrOmega on MMX to Observe Martian System: Its Observation Plans and Development

*Takahiro Iwata[1], Hiromu Nakagawa[2], Tomoki Nakamura[2], Jean-Pierre Bibring [3], Cedric Pilorget [3], Vincent Hamm[3], Fuminori Tsuchiya[2], Lucie Riu[1], Moe Matsuoka[1], Hiroyuki Kurokawa[4]

1. Institute of Space and Astronautical Science, Japan Aerospace Exploration Agency, 2. Tohoku University, 3. Institut d'Astrophysique Spatiale, Université Paris-Sud, 4. Tokyo Institute of Technology

The Martian Moons Exploration (MMX) is a probe which will be launched by the Japanese launch vehicle H-III and will navigate the quasi satellite orbit of Phobos and will make a fly-by of Deimos. MacrOmega is a hyperspectral imager in the wavelength range of 0.9 to 3.6 micrometers which is under development to be installed on the MMX spacecraft. It is based on MicrOmega on the ExoMars Rover and Hayabusa2 MASCOT and modified as a hyper-spectral imager with spectroscopic function provided by an Acousto-Optic Tunable Filter (AOTF).

MMX aims to elucidate the evolution of our solar system by investigating the migration process of primitive materials in the early stage. NIRS4/MacrOmega will observe hydroxide or hydrated mineral absorptions on Phobos and Deimos in the wavelength of 2.7-3.2 micrometers. By analyzing the shape of the spectra, we will distinguish between water in hydrous silicate minerals, water molecules, and water ice particles. MacrOmega will also try to detect the absorption by organic matter in the wavelength range of 3.3-3.5 micrometers. These results will support efforts to answer the question of the origin of the Martian satellites and identify whether they are satellites formed by a giant impact or asteroids captured by Mars. MacrOmega will observe Phobos to survey the sampling site before sampling, to investigate the sampling site precisely at the touch-down mode, and to make global mapping. Global mapping of Phobos to select prior areas and landing sites will be performed on the quasi satellite orbit. Precise mapping for candidate landing sites will be followed on the lower altitude. In the touch down phase, we will observe toward sampling site at full wavelength in the descending and landing processes. Observations for Deimos will be basically executed from the fly-by orbit, and they are examined to be made at the near circular orbit. It will also monitor the global distributions and dynamics of the Martian atmosphere. We will report and discuss on the observation plans and the development status of the instruments.

Keywords: MMX, Phobos, Deimos, Mars, near infrared, hydrated mineral

©2020. Japan Geoscience Union. All Right Reserved.

Shape modeling strategy for MMX

*Koji Matsumoto[1], Toru Kouyama[2], Naru Hirata[3], Hitoshi Ikeda[4], Hiroki Senshu[5]

1. RISE Project, National Astronomical Observatory of Japan, 2. National Institute of Advanced Industrial Science and Technology, 3. University of Aizu, 4. Japan Aerospace Exploration Agency, 5. Chiba Institute of Technology

The JAXA-led Martian Moons Exploration (MMX) mission is scheduled for launch in 2024 to reveal the origin of two moons: Phobos and Deimos. MMX spacecraft will be inserted into quasi-satellite orbit (QSO) to observe Phobos, which will contribute to improving our geodetic knowledge such as shape, rotation, and gravity field of the satellite. Although it is not straightforward to relate internal properties to the origin, these geodetic observations are precious to infer internal structure (Le Maistre et al., 2019). A shape model, one of the geodetic products, is also of importance for interpreting remote sensing observation as well as selecting landing site to sample surface materials. This paper describes current strategy for MMX shape modeling.

In contrast to the current situation of limited number of Phobos images with inhomogeneous spatial resolution (Karachevtseva et al., 2014), MMX will provide number of images with more homogenous quality and resolution. The initial base shape model will be constructed from telescopic camera images to be acquired during terminal rendezvous phase from a few thousand kilometers distance, with Phobos being framed within the field of view of the camera. More detailed topography will be reconstructed from images taken from QSO with higher spatial resolution. The size of QSO are roughly divided into three levels, i.e., high (QSO-H, 100x200 km), mid (QSO-M, 50x100 km), and low (QSO-L < 50 km). For QSO-H configuration, the apparent orbital period in Phobos-centered inertial frame is about 35 days and we will be able to observe dayside of Phobos for about two weeks. In order to provide a shape model in early stage of investigation, we will make use of the first QSO-H period with spatial resolution better than 2 m and with scan observation covering at least ±30 deg latitudinal band.

Stereophotoclinometry (SPC), the same technique as used for Hayabusa2 (Watanabe et al., 2019), is also one of the candidates to be applied to MMX. In order to make the shape modeling effective, based on a planned QSO-H trajectory, we investigated the optimal timings of observations with illumination conditions that are preferable for SPC. The LIDAR data, that will be available at least around regions with the lowest altitude, give the scale of the shape model. Preliminary study shows that the necessary observations will be completed within the first dayside observation chance, even if we consider realistic bus operation time during which Phobos cannot be observed, when certain speed of spacecraft attitude scan is realized.

References

Karachevtseva et al., Planet.SpaceSci., 102, 74-85, 2014; Le Maistre et al., Icarus, 321, 272-290, 2019; Watanabe et al., Science, 364, 268-272, 2019.

Keywords: MMX, Phobos, shape modeling

©2020. Japan Geoscience Union. All Right Reserved.

Restoration of highest-resolution images of Phobos observed by the High-Resolution Stereo Camera (HRSC) onboard Mars Express

*Ryodo Hemmi[1], Hiroshi Kikuchi[2]

1. The Universit Museum, The University of Tokyo, 2. Institute of Space and Astronautical Science, Japan Aerospace Exploration Agency

Spacecraft camera images generally contain imaging artifacts (e.g., distortions, blurs, and noises) which can substantially affect the accuracy of image-based measurements (e.g., crater counting) and their higher-level products (e.g., a global image mosaic). On 23 July 2008 (orbit 5851) and 9 January 2011 (orbit 8974), the Mars Express spacecraft acquired highest-resolution (~0.9 m/pixel) images of Phobos surface by the Super Resolution Channel (SRC [1]) of the High-Resolution Stereo Camera (HRSC [2]). Despite their high spatial resolution, previous studies have not investigated these SRC images because they contain severe pepper noises (“blemish” pixels [1]) and motion smears. However, the surface of Phobos is covered by a number of small craters, roughly circular or oval in outline, which enables us to estimate a point spread function (PSF). Thus, the objective of this study is to characterize and reduce these artifacts with the estimated PSF and to restore high-quality SRC images.
We selected ten raw datasets of highest-resolution SRC images, removed pepper noises from them by using a boxcar filter, and tested several deconvolution techniques (e.g., blind deconvolution, Wiener filter, iterative Lucy-Richardson method) assuming a linear PSF, which we found by try-and-error. Here, we report the results from the deconvolution of the SRC images and discuss the advantages of our method.

References

1. Oberst, J.; Schwarz, G.; Behnke, T.; Hoffmann, H.; Matz, K.D.; Flohrer, J.; Hirsch, H.; Roatsch, T.; Scholten, F.; Hauber, E., et al. The imaging performance of the SRC on Mars Express. Planetary and Space Science 2008, 56, 473-491, doi:10.1016/j.pss.2007.09.009.
2. Neukum, G.; Jaumann, R. HRSC: The High Resolution Stereo Camera of Mars Express. In Mars Express: The Scientific Payload, ESA: 2004; Vol. SP-1240, pp. 17-35.

Keywords: Phobos, Mars Express, Image restoration

©2020. Japan Geoscience Union. All Right Reserved.

Re-impacts from the craters residing at the deepest location generating the blue units on Phobos

*Hiroshi Kikuchi[1]

1. Japan Aerospace Exploration Agency

Re-impact sites from the deepest crater on a body in space preserve much of original information. The surface of the Martian satellite Phobos is spectrally divided into red and blue units [1]. The former are globally distributed, while the blue units have been observed inside and outside the Stickney crater—the largest and deepest crater on Phobos. Outside the crater, the blue units are concentrated in the region from the south to the west (south-west blue units) and in the region east of the crater (east blue units). Several models can explain the east blue units [e.g., 2, 3]. However, the mode of formation of the south-west blue units is still unknown, despite its vast area. We propose that the combination of ejecta from Stickney and Limtoc (a crater located on the floor of Stickney) contributes to the formation of the blue units. We test the model using ballistic simulations incorporating an updated shape model with randomly generated ejecta velocities, different values of orbital radii to Mars, and various launching velocities to track the emplacements of the ejecta particles. The results show the distribution of global blue units are recreated when the combined re-impact sites of ejecta from Stickney and Limtoc have orbital radius (X_{Ph}) values of $X_{Ph} > 3.34\ R_M$ and $X_{Ph} < 3.04\ R_M$, respectively. This suggests that the blue material is concentrated deep underneath the surface, and the age of Stickney crater may be sufficiently old to be estimated from the crater densities [4].

References

1. Murchie, S.L., et al., *COLOR HETEROGENEITY OF THE SURFACE OF PHOBOS - RELATIONSHIPS TO GEOLOGIC FEATURES AND COMPARISON TO METEORITE ANALOGS.* Journal of Geophysical Research-Solid Earth and Planets, 1991. **96**(B4): p. 5925-5945.
2. Shingareva, T.V. and R.O. Kuzmin, *Mass-wasting processes on the surface of Phobos.* Solar System Research, 2001. **35**(6): p. 431-443.
3. Thomas, P.C., *Ejecta emplacement on the Martian satellites.* Icarus, 1998. **131**(1): p. 78-106.
4. Schmedemann, N., et al., *The age of Phobos and its largest crater, Stickney.* Planetary and Space Science, 2014. **102**: p. 152-163.

Keywords: Impact processes, Mars satellites, Cratering

©2020. Japan Geoscience Union. All Right Reserved.

Mars and Earth - distinct inner Solar System products

*Takashi Yoshizaki[1], William F McDonough[1,2]

1. Tohoku University, 2. University of Maryland, College Park

Terrestrial planets provide Solar System insights into the evolution of accretion, core-mantle and crust-mantle differentiation, and surface processes. Similarities and differences between the Earth and Mars made the former habitable and the other inhospitable to uninhabitable. Here we com-pare compositional models for Mars and the Earth to reveal their shared and distinctive properties. Terrestrial planets accreted more high-temperature materials and are depleted in the moderately volatile elements as compared to chondritic asteroids, with the Earth being more depleted than Mars. These compositional properties resulted from nebular chemical fractionation processes, not post-accretionary losses of moderately volatile elements. In agreement with Wänke and Dreibus (1988), Mars' accretion occurred under nearly uniform oxidizing conditions in the presence of a nebular disk, whereas Earth's accretion likely initially occurred under reducing conditions followed by additions of more oxidizing materials. Growth of the Earth occurred during and post-nebular disk's lifetime. Mars' lower Mg# in the mantle reflects a more oxidizing core formation condition than that of the Earth's, leading to Mars' smaller core size and an absence of nominally lithophile elements (e.g., V, Cr and Mn) in its core. Early loss of its dynamo is consistent with Mars having quickly spent its primordial heat (i.e., heat of accretion and core formation), leading to a low sur-face heat flow and a planetary engine driven by its radioactive elements (planetary Urey number ~0.9). These observations may also explains the absence of plate tectonics on Mars even in the presence of surface water early in its history.

Keywords: Mars, Terrestrial planets, Mantle, Core, Cosmochemistry

©2020. Japan Geoscience Union. All Right Reserved.

Examination of the similarity between crack patterns due to dry fracture on the ground and heat-shrink polygons on Mars

*Chihiro Uemura[1], Takahiro Iwata[1,2], Akio Nakahara[3], Tomohiro Usui[2], Yosuke Matsuo[3], Rina Noguchi[2]

1. SOKENDAI, 2. ISAS/JAXA, 3. Nihion Univ.

Polygons of several tens of meters formed by thermal contraction have been found in the middle and high latitudes of Mars. These polygons may limit the past and present Mars environmental conditions, and research is ongoing. (e.g., Levy et al., J. Geophys. Res. (2009))
Shape, size, and direction of the polygon are determined by various environmental conditions around the polygons. In particular, the shape of polygons found in the crater tends to have anisotropy according to the angle of the slope. It is reported that the shape is close to a rectangle parallel to the slope direction in the steep region, but it becomes random in the gentle slope region at the bottom of the crater bottom(e.g., Ulrich et al., Geomorphology (2011)). A conventional theory suggested that the anisotropy of the shape depends on the slope angle.
On the other hand, it was reported that a similar anisotropic crack pattern appeared in an analog experiment on the ground. When the shear stress induced by vibration exceeds the yield stress of the paste, it can remember the memory of vibration and, when it dries, the direction of crack propagation depends on the memory of such motion(memory effect of paste; Nakahara and Matsuo, PRE (2006)). The dry crack pattern usually takes a random shape. Since the paste is easily broken in the flowing direction, when the paste is flowed along the slope, a dry crack pattern close to a rectangle parallel to the slope is formed. This phenomenon is attributable to that a cluster structure of particles extending parallel to the flowing direction is formed microscopically, and this structure is maintained because of its plasticity. The point is that not only the external force but also the rheology (plasticity, etc.) of the fluid affects the shape of the dry crack pattern. This phenomenon is close to the thermal contraction polygon on Mars, and anisotropic shapes may be formed due to factors other than the slope angle. In that case, it is expected that not only the slope angle but also the properties of the soil in the past are factors that determine the anisotropy of the polygon shape. By testing this hypothesis, it may be possible to constrain the properties of the soil in the past (such as plasticity, rheology and then water content).
In this study, we used the image data of HiRISE, a high resolution camera mounted on MRO(NASA). We quantify the anisotropy by measuring the angle of the polygon shape and find the threshold of the slope angle where the anisotropy appears. We further check a range of the threshold values in different types of polygons and evaluate the validity of slope angle as a controlling factor of the polygon anisotropy.

Keywords: Mars, Polygons, rheology

©2020. Japan Geoscience Union. All Right Reserved.

Search of shallow subsurface reflectors in Chryse and Acidalia Planitiae on Mars

*Aina Oura[1], Yasumasa Kasaba[1], Atsushi Kumamoto[1], Rina Noguchi[2], Ken Ishiyama[3], Fuminori Tsuchiya[1], Tomohiro Usui[2], Chihiro Uemura[4]

1. Tohoku University, 2. ISAS/JAXA, 3. National Institute of Technology, Tsuruoka College, 4. Sokendai

Recurring slope lineae (RSL), one of recent major discoveries on Mars, are surface features which may be linked to current icy processes. These are characterized by narrow dark features which incrementally lengthen down steep slopes, fade in colder seasons, and recur annually. Candidate and confirmed RSL sites are mainly distributed in four regions, (1) southern mid-latitudes (SML), (2) Valles Marineris (VM), (3) equatorial highlands, and (4) northern Chryse Planitia and southwestern Acidalia Planitia (CAP). The RSLs in (2) VM and (4) CAP are more densely located than others, and it may indicate the existence of cryosphere in both regions. For the VM area, Noguchi et al. (submitted) investigated from this point of view. In this paper, we investigated subsurface structures of the other region, CAP, by the subsurface radar data taken by Mars SHAllow RADar sounder (SHARAD) onboard the Mars Reconnaissance Orbiter (MRO). For the geological information, we also used the Java Mission-planning and Analysis for Remote Sensing (JMARS, https://jmars.asu.edu/).

The RADAR frequency of SHARAD is 15-25 MHz with the bandwidth of 10 MHz which corresponds to the depth resolution of 15 m in vacuum. The spatial resolution is 0.3 to 1 km along the track direction and 3 to 7 km along cross-track direction. For the comparison with the SHARAD radargrams, we created virtual radargrams emulating the surface and clutter echoes by the Kirchhoff approximation with the topographic altitude maps from MGS/MOLA data. These emulated radargrams were used for the identification of nadir signals not from subsurface reflectors. We also investigated digital terrain models (DTMs) created on MarsSI (https://marssi.univ-lyon1.fr/MarsSI/) to sample the elevation (or thickness) of crater walls close to the candidates of subsurface reflectors. We produced the stratigraphic columns which were divided into fine, coarse and very coarse layers from each DTM, and then identified their depth in the plane around craters. Those procedures are common with the ones which were adopted in Noguchi et al.

We surveyed over 200 orbits in the CAP region. The confirmed detection of subsurface reflectors were in 10 orbits, and the candidates were in more than 50 orbits. Using geologic map, we try to discuss the subsurface structure and identify what kind of layers they are. For example, one radargram (data ID: 03814501) showed a subsurface reflector at mean depth of 125 m in vacuum (2-way delay time: 831 ns). Another radargram (data ID: 04923501) showed a different reflector at mean depth of 55 m in vacuum (2-way delay time: 367 ns). On the other hand, 2 DTMs near these orbits indicated that the boundary of fine and coarse layers was at the depth of about 50 m. We have not precisely calculated the plausible dielectric constant yet, but it ranges from almost 1 to nearly 8 if the reflection happens at that boundary (e.g. pure water ice: 3.15 [Matsuoka et al., 1997], basalt with no voids: 14.9 [Rust et al., 1999]). It will be tough and difficult to conclude the permittivity in the lack of DTMs.

Our statistical result suggested that the distribution of subsurface reflectors was not correlated with RSL sites, but those reflectors were distributed in close to the boundary of geological unit. Furthermore, these subsurface reflectors located shallower than previous study in other regions (e.g. Arcadia Planitia [Bramson et al., 2015]). Although we do not expect that there is abundant subsurface ice, the characteristics of these reflectors should be deeply studied.

Keywords: Mars, RSL, SHARAD, radar sounding

©2020. Japan Geoscience Union. All Right Reserved.

©2020. Japan Geoscience Union. All Right Reserved.

Development of subsurface radar for future Mars, the Moon, and asteroid explorations

*Atsushi Kumamoto[1], Hideaki Miyamoto[2], Toshiyuki Nishibori[3], Fuminori Tsuchiya[1], Ken Ishiyama[4]

1. Department of Geophysics, Graduate School of Science, Tohoku University, 2. University of Tokyo, 3. JAXA, 4. Tsuruoka College, National Institute of Technology

Specification and design of radar for subsurface structure measurements in future Mars, the Moon, and asteroid exploration missions have been investigated. In Mars Aqueous-environment and space Climate Orbiter (MACO), measurements of mars subsurface ices in mars low and mid-latitude region (suggested by recurring slope lineae (RSL)) by subsurface radar sounder are planned in order to clarify the contribution of subsurface water cycle to mars climate. This observation also enables us to select out candidate sites for future landing explorations. In JAXA's lunar ice prospector mission by an international collaboration between Japan and India in early 2020s, measurements of three-dimensional distribution of ice below the lunar surface by ground penetrating radar (GPR) installed on the rover are proposed. Design of this GPR could be a baseline of designs of future space-born GPR. Based on the observations of bulk density and boulder size on the surface by Hayabusa, 25143 Itokawa is suggested to be a rubble-pile asteroid. If the size and shape of the rocks inside the asteroid are determined by radar sounder, we can discuss the formation process of the asteroid based on them.

For MACO mission, we are proposing a radar sounder installed on the orbiter transmitting chirp pulse in a frequency range of 50-150 MHz with a peak power of 10 W in order to detect ice within a depth of several 100 meters at a vertical resolution of 1.5 m. For JAXA's lunar ice prospector mission, we are proposing a ground penetrating radar installed on the rover transmitting chirp pulse in a frequency range of 0.5-3 GHz with a peak power of 15 dBm in order to detect ice within a depth of several meters at a vertical resolution of 6 cm. For exploration of asteroid internal structures, the radar sounder for MACO will be applicable also. If we can plan bistatic radar sounding by using radar, transponder, and reflector installed on another orbiter or lander in addition, we can determine not only the subsurface structure of permittivity contrast but also the absolute value of permittivity for discussion of porosity and composition of the internal rock lumps.

In design of the radars for space missions, we can not select parts freely. We have to use limited rad-hard semiconductor parts. In 50-150 MHz, there are selectable D/A converter (DAC) and A/D converter (ADC). So we can select the method using DAC and ADC: Transmitting and reference signals are generated by DAC, and receiver output is sampled by ADC. On the other hand, in 0.5-3 GHz, there are not selectable DAC and ADC. So, we are planning to use VCO for generation of transmitting and reference signals. We are now developing BBM of transmitter and receiver considering parts selection and design for space-born instruments. In late 2020, we are planning performance tests with BBM by measuring soil simulant.

Acknowledgment: This study was supported by JSPS KAKENHI Grant Number 19K21891.

Keywords: Ground penetrating radar (GPR) installed on the rover, Subsurface radar sounder installed on the orbiter, Lunar polar ice exploration, Mars Aqueous-environment and space Climate Orbiter (MACO)

©2020. Japan Geoscience Union. All Right Reserved.

Increase in trivalent iron elution amount and iron compounds from fayalite by ultraviolet C

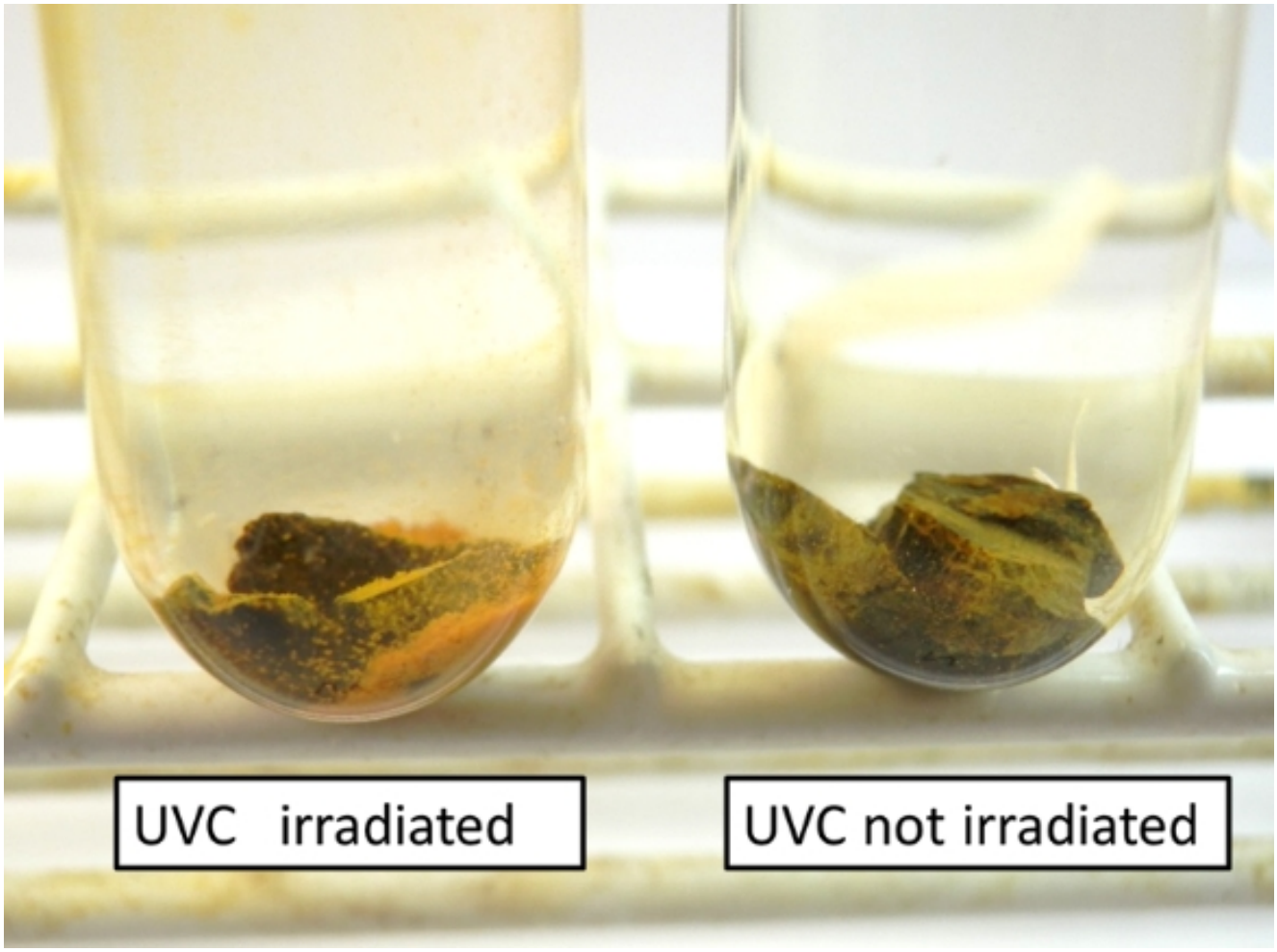
*Nobuo Komori[1]

1. The United Graduate School of Education Tokyo Gakugei University

In order to explain one of the causes of the large amount of iron oxide on the surface of Mars, the following experiment was conducted by a science club at my junior high school.Ultraviolet rays C was applied to fayalite in hydrochloric acid and sulfuric acid which had been degassed to pH2 as much as possible. Fayalite we used is from Kawamata-machi, Fukushima Prefecture. We selected similarly shaped fayalite and weighted ones at a weight of 1g.These fayalite samples were immersed in acidic aqueous solution in test tubes.Then, ultraviolet rays were irradiated for 200 hours or longer. Every few days, the concentration of total iron ions and trivalent iron ions in the aqueous solution were measured using a digital pack test.Ultraviolet rays C are generated by a germicidal lamp.This peak wavelength is 245 nm and the ultraviolet intensity is about 20 W / m^2.
The results of the this experiment showed that , the concentration of trivalent iron ions in the acidic aqueous solution was significantly increased more than the ones that were not irradiated by ultraviolet rays. Also, the ratio of the trivalent iron ion concentration to the total iron ion concentration was larger when it was radiated by ultraviolet rays.We conducted this experiment three times and the results came to be the same for all three experimet. Also,after the experiment, more brown fine powder was generated in the test tube irradiated with ultraviolet rays than not irradiated. According to the result of X-rays diffraction,,this brown powder seemed to be mostly made from non-crystallized in brown fine powder. Furthermore in the case of hydrochloric acid, it turned out that this brown powder contained Lawrenceite and goethite. Similarly , in the case of sulfuric acid, we found out that metahohmannite and alum were contained.
For the results mentioned above, we can say that ultraviolet rays C increases the concentration of trivalent iron ions eluted from rocks immersed in an aqueous solution and increases the amount of iron compounds.Iron oxide and sulfate minerals have been found on Mars. It is presumed that ultraviolet rays C from the sun promoted the production of these minerals in the past when the Martian sea dried up.

Keywords: ultraviolet C, acidic aqueous solution , trivalent iron, mars, goethite, metahohmannite

©2020. Japan Geoscience Union. All Right Reserved.



©2020. Japan Geoscience Union. All Right Reserved.

Introduction of the highest resolution image to the Mars Web-GIS “RedAce” to study the local and detailed surface environment

*Hiroshi Sakai[1], Hayashi Yohei[2], Hironori Fukuchi[1], Yuya Matsubara[3], Yoshiko Ogawa[1]

1. The University of Aizu, 2. National Observatory of Japan, 3. The University of Aizu(Now NTTDocomo Inc.)

Water is thought to be an important element in terraforming. There is certain evidence of water on Mars. Therefore, many probes have been launched to Mars. A lot of observation data have been accumulated about Mars. To understand the surface environment of Mars consistently, it is essential to examine these diverse and large amounts of observational data. In such a situation, Geographic Information System (GIS) is very useful. GIS is good at visualizing, integrating and analyzing multiple kinds of information. Web-GIS is a tool which can handle a wide variety of observational data on the web. Among the various kinds of Mars observation data, spectral data are important to identify the types and distributions of hydrous minerals on Mars. Hydrous minerals are important keys to understand the water on Mars.

We have developed a Web-GIS “Red Ace” [1] focusing on the visualization of spectral data from multiple instruments: THEMIS data and CRISM data.

The Web-GIS "RedAce" shows some kinds of image data, too: DEM data from MOLA, band ratio images from THEMIS data, and thumbnail images of CRISM. Those image data are all installed in the system and displayed to the users. However, these images are viewed from a wide angle and it is difficult to perform local analysis.

In this study, we introduce high quality image to the Web-GIS “Red Ace”. The objective is to extend the system so that user can visually and intuitively grasp the features of the Mars surface topography in detail and conduct integrated analysis combining image data and spectral data.
Image data of Mars have been collected from many cameras. We select HiRISE to install in the system. HiRISE is one of the six devices in the Mars Reconnaissance Orbiter (MRO) that can capture the highest quality images (up to 25cm/pix). About 1.8 million pieces of data exist. There are mainly Experimental Data Record (EDR), Reduced Data Record (RDR), and Digital Terrain Model (DTM) types of data. RDR is processed from the EDR and is provided and published in the format of JP 2000. We use RDR data which are calibrated image data. Currently, image data installed in Web-GIS "RedAce" are formatted as CUB data.

[1] Matsubara, Y. et al., A Mars Web-GIS “Red Ace” for viewing reflectance spectral data, American Geophys. Union, Fall Meeting 2018, abst. #IN33E-0896.

Keywords: Mars, Web-GIS, Spectral data, Minerals

©2020. Japan Geoscience Union. All Right Reserved.

Estimation of dust optical depth observed by MGS/TES from visible images observed by MGS/MOC using a convolutional neural network

*Karin miyabe[1], Kazunori Ogohara[1]

1. Graduate school of the University of Shiga Prefecture

For understanding cause and movement of dust haze, we need the atmospheric dust distribution ranging from O(10) to O(100) km in order to understand the initiation and development of dust haze. Although visible image data have been observed by several orbiters, dust optical depth (DOD) cannot be derived from them. And we cannot distinguish thin dust haze from water ice clouds. Therefore, DOD measured by a infrared spectrometer is useful. However, FOV of the spectrometer is generally so narrow that it cannot resolve the development of fine structures of dust haze.

For that reason, we develop a method for estimating DOD of each pixel in images observed by MGS/MOC from the local patterns of the visible images themselves by using the Convolutional Neural Network (CNN), where the ground truth is given by DOD observed by MGS/TES.

Because most of DOD data was much smaller than 1. Such imbalance in the data volume between large and small DODs tends to results in poor estimation of DOD. Therefore, we extracted the same number of DOD data from each regularly divided bin. And trained the CNN model using the data. Validation loss was 0.148. However, it was turned out that predicted DOD highly depended on local brightness in MGS/MOC images. Hence we tried to improve CNN model by normalizing the input data. Consequently, the validation loss increased from 0.148 to 0.181, which means degradation of the model. This degradation is not a serious problem but pave the way to improve the performance of the estimation because dependency of the DOD estimation on local brightness has been reduced.

At my presentation, we will report results of improvement of the CNN model by data augmentation or complication of the model structure.

Keywords: Mars, CNN, deep learning, MGS/MOC, MGS/TES

©2020. Japan Geoscience Union. All Right Reserved.

Survey of dayside reconnection signatures at Mars with MAVEN

*Yuki Harada[1], Jasper S. Halekas[2], Gina A. DiBraccio[3], Shaosui Xu[4], Suranga Ruhunusiri[2], Takuya Hara[4], Jared Espley[3], James P McFadden[4], David L Mitchell[4], Christian Mazelle[5]

1. Graduate School of Science, Kyoto University, 2. Department of Physics and Astronomy, University of Iowa, 3. NASA Goddard Space Flight Center, 4. Space Sciences Laboratory, University of California, Berkeley, 5. IRAP, University of Toulouse, CNRS, UPS, CNES

We present a preliminary survey of magnetic reconnection signatures observed in the upper ionosphere of Mars. A variety of recent measurements from MAVEN suggested that magnetic reconnection likely takes place on both dayside and nightside of Mars. For nightside reconnection signatures in the Mars' magnetotail, a statistical analysis revealed notable asymmetry in their spatial distributions with respect to the motional electric field in the upstream solar wind (Harada et al., 2017), demonstrating that these statistical properties could provide valuable information on the driving mechanisms of magnetic reconnection processes at Mars. In contrast to the relatively well-studied nightside counterpart, the dayside reconnection at Mars has been examined only for very limited cases (Halekas et al., 2009; Harada et al., 2018), and its statistical properties remain unclear. Such information would have important implications for global dynamics of the Martian magnetosphere because it is proposed that the dayside reconnection plays a major role in changing magnetic topology and morphology not only in the dayside upper ionosphere but also in the nightside magnetotail, thereby globally modifying pathways of escaping ionospheric ions. Here we conduct a systematic survey of dayside current sheet crossings and reconnection signatures embedded therein in a similar manner to the previous nightside survey. We will discuss the occurrence rate, spatial distributions, and upstream driver control of the reconnection signatures detected in the dayside upper ionosphere of Mars.

Keywords: Mars, magnetic reconnection

©2020. Japan Geoscience Union. All Right Reserved.

Seasonal variation of neutral and ion compositions in the Martian upper atmosphere observed by MAVEN/NGIMS

*Nao Yoshida[1], Naoki Terada[1], Hiromu Nakagawa[1], Dave A Brain[2]

1. Dep. Geophysics Graduate School of Science Tohoku University, 2. LASP, University of Colorado

The Martian thermosphere, exosphere, and ionosphere are intermediate atmospheric regions strongly impacted by coupling from below with the lower-middle atmosphere and coupling from above with external forces, such as solar EUV and solar wind. Atmospheric reservoir in these regions is believed to determine the composition of species that escape to space. Jakosky et al. (2017) and Slipski et al. (2018) recently showed substantial variations in the altitude of a compositional boundary, called the homopause, below which gases are well-mixed by eddy diffusion (homosphere) and above which gases are diffusively separated according to their own scale heights by molecular diffusion (heterosphere). Yoshida et al. (submitted) showed that N_2/CO_2ratio in the lower thermosphere varies seasonally and latitudinally owing to the variation of the homopause altitude. However, the variation of the ionospheric composition, which can escape to space, responding to the lower thermospheric variation has not been well understood.

The variation of the ionospheric composition is observed by Neutral Gas and Ion Mass Spectrometer (NGIMS) aboard Mars Atmosphere and Volatile EvolutioN (MAVEN). The variation of CO_2^+density at 200 km altitude in the ionosphere resembles that of CO_2density at 140 km altitude at the top of the lower thermosphere. Higher CO_2^+density appears near perihelion and lower CO_2^+density near aphelion. Additionally, the observed sinusoidal trend of CO_2^+density suggests that ionospheric density is relatively controlled by the seasonal variation of the neutral upper atmosphere than the long-term variation of solar EUV flux. On the other hand, N^+density shows the opposite trend with CO_2^+density, which could be explained by the fact that the photochemical loss of $N^+$is caused by the reaction with CO_2. We also have investigated the vertical structures of CO_2^+, O_2^+. $O^+$and N^+densities between 150 and 400 km altitude. The closer relationship between the neutral upper atmosphere and ionosphere is also confirmed below 250 km altitude. The scale height of the major ion species is almost two times larger than that of neutral species. We find that CO_2^+density has a largest variation, by a factor of ~7 at 200 km altitude. Meanwhile, the slopes of ion densities in the photodynamical region between 300 and 380 km altitudes increase compared with those in the diffusion region between 180 and 230 km altitudes in MY34 L_s= 59˚ - 63˚, MY33 L_s= 70˚ - 73˚, and MY33 L_s= 148˚ -154˚, except for in MY33 L_s= 342˚- 346˚. This fact implies that effects from external forces, such as upward flow and local heating induced by the solar wind interaction, may change the slopes of ion densities in the photodynamical region. Additionally, mixing ratio of CO_2^+/O_2^+can vary along the season in the range of ~0.017 to ~0.097, by a factor of ~6, around 370 km altitude. However, mixing ratios of $O^+/O_2^+$and $N^+/O_2^+$are almost constant and their seasonal variations are unclear. The larger variation of the observed CO_2^+/O_2^+than that of O^+/O_2^+might suggest that CO_2^+escape rate can change by up to a factor of ~6 due to the ionospheric composition, however, the observed CO_2^+/O_2^+ cannot fully explain the reported ratio of heavy ion escape rates (e.g., Lundin et al., 2009; Carlsson et al., 2006). It may imply that additional mechanisms to change CO_2^+/O_2^+might exist above our observation range.

In this study, we will classify the NGIMS dataset in terms of (1) the intensity of solar wind pressure and (2) the intensity and direction of interplanetary magnetic field to understand the increase of the slopes of ion densities observed in the photodynamical region. Additionally, we will discuss the possibility of local heating by low-frequency waves (e.g., Fowler et al., 2018; Harada et al., 2019). Thus, we can evaluate the connection between the lower thermospheric composition and the ionospheric composition that can

©2020. Japan Geoscience Union. All Right Reserved.

escape to space.

Keywords: Mars, Thermosphere, Ionosphere, Atmospheric composition

©2020. Japan Geoscience Union. All Right Reserved.

[E] Poster | P (Space and Planetary Sciences)：P-EM Solar-Terrestrial Sciences, Space Electromagnetism & Space Environment

[P-EM11] Heliosphere and Interplanetary Space

convener:Kazumasa Iwai(Institute for Space–Earth Environmental Research (ISEE), Nagoya University), Yasuhiro Nariyuki(Faculty of Education, University of Toyama), Ken Tsubouchi(University of Electro-Communications), Masaki N(Japan Aerospace Exploration Agency, Institute of Space and Astronautical Science)

This session aims to secure comprehensive insights into physical processes of plasmas and fields in the heliosphere. Presentations of the recent studies from any approaches (integrated observation/theoretical modeling/massive numerical simulation) are welcomed. Topics are not restricted to any specific issues: phenomenological studies on solar flares/CME/solar wind, and related fundamental physics problems such as shocks/waves/turbulence/particle transport and acceleration can be the main target, including heliospheric high-energy phenomena and their impact on the Earth's environment.

[PEM11-P01] Measurement of solar wind density distribution using dispersion measures of Crab pulsar

*Maeda Ryuya[1], Munetoshi Tokumaru[1], Kaito Tawara[1], Toshio Terasawa[2], Kazuhiro Takafuji[3] (1.Institute for Space-Earth Environmental Research, Nagoya University, 2.Inter-University Research Institute Corporation, National Institutes of Natural Sciences, National Astronomical Observatory of Japan, 3.Japan Aerospace Exploration Agency)

[PEM11-P02] Occurrence dependence on solar activity cycle for type III radio bursts based on the automatic detection analyses

*Yuichiro Seki[1], Hiroaki Misawa[1], Fuminori Tsuchiya[1], Takahiro Obara[1], Tatsuya Fujimoto[1] (1.Tohoku University)

[PEM11-P03] The characteristics of type III solar radio bursts in ^{3}He-rich impulsive solar energetic particle phenomena

*Tatsuya Fujimoto[1], Hiroaki Misawa[1], Fuminori Tsuchiya[1], Takahiro Obara[1] (1.Tohoku University)

[PEM11-P04] Relationship between solar energetic particles and spectral fine structures of metric type II radio bursts

*Hiroaki Misawa[1], Fuminori Tsuchiya[1], Takahiro Obara[1], Tatsuya Fujimoto[1] (1.Planetary Plasma and Atmospheric Research Center, Graduate School of Science, Tohoku University)

[PEM11-P05] Spectral Structures of Type II Solar Radio Bursts and Solar Energetic Particles

*Kazumasa Iwai[1], Seiji Yashiro[2], Nariaki Nitta[3], Yuki Kubo[4] (1.Institute for Space–Earth Environmental Research (ISEE), Nagoya University, 2.The Catholic University of America/NASA GSFC, 3.Lockheed Martin Advanced Technology Center, 4.National Institute of Information and Communications Technology)

[PEM11-P06] Stellar flare of a close binary system during the NICER-Hisaki Observing Campaign 2018-2019

*Tomoki Kimura[1], Wataru Iwakiri[2], Atsushi Yamazaki[3], Go Murakami[3], Fuminori Tsuchiya[4], Kazuo Yoshioka[5], Hajime Kita[3], Masaki Kuwabara[3], Shin Toriumi[3] (1.Frontier Research Institute for Interdisciplinary Sciences, Tohoku University, Sendai, Japan, 2.Faculty of Science and Engineering, Chuo University, Tokyo, Japan, 3.Institute of Space and Astronautical Science, Japan Aerospace Exploration Agency, Sagamihara, Japan, 4.Planetary Plasma and Atmospheric Research Center, Tohoku University, Sendai, Japan, 5.Department of Complexity Science and Engineering, University of Tokyo, Kashiwa, Japan)

[PEM11-P07] 5-season's optical observations of neutral helium distribution in interplanetary space by Hisaki

*Atsushi Yamazaki[1], Go Murakami[1], Kazuo Yoshioka[2], Tomoki Kimura[3], Fuminori Tsuchiya[4], Masato Kagitani[4], Takeshi Sakanoi[4], Naoki Terada[5], Yasumasa Kasaba[6], Ichiro Yoshikawa[7] (1.Institute of Space and Astronautical Science / Japan Aerospace Exploration Agency, 2.Graduate School of frontier Science, The University of Tokyo, 3.Tohoku University, 4.Planetary Plasma and Atmospheric Research Center, Graduate School of Science, Tohoku University, 5.Graduate School of Science, Tohoku University, 6.Planetary Plasma and Atmospheric Research Center, Tohoku University, 7.The University of Tokyo)

[PEM11-P08] **Group movement by magnetic coupling of high-speed protons running side by side in the chromosphere of the Sun**

*Shinji Karasawa[1] (1.Miyagi National College of Technology Professor emeritus)

Measurement of solar wind density distribution using dispersion measures of Crab pulsar

*Maeda Ryuya[1], Munetoshi Tokumaru[1], Kaito Tawara[1], Toshio Terasawa[2], Kazuhiro Takafuji[3]

1. Institute for Space-Earth Environmental Research, Nagoya University, 2. Inter-University Research Institute Corporation, National Institutes of Natural Sciences, National Astronomical Observatory of Japan, 3. Japan Aerospace Exploration Agency

Dispersion measures(DMs) derived from pulsar observations provide an integral of the plasma density on the line-of-sight (LOS) from the pulsar to the observer. The purpose of this research is to estimate the solar wind (SW) plasma density in this cycle from the rise in DM value when the LOS of pulsar approaches the sun. The solar activity of this cycle is very low and the SW plasma density decreases. Pulsar observation is useful for examining this change because they cover a wide range of distances and latitude. We used the Crab pulsar in this research. Crab pulsar is a neutron star that emits pulsed radiation over a wide frequency range, and radiation is observed at intervals of about 33 milliseconds. This radiation is affected by plasma, such as interstellar medium (ISM) and SW, causing signal propagation delays. This delay depends on frequency; i.e. DM. The LOS of Crab pulsar approaches a distance of ~$5R_s$(R_s: solar radius) in mid-June every year. Previous observations showed an excessive rise in DM when the LOS of Crab pulsar approached the sun. We observed the Crab pulsar for the period from September 2018 to June 2019 using a 327MHz radio telescope (SWIFT) for IPS observation in Toyokawa. The observation time for a given day was 6 minutes, and 8 minutes for June 2019. Focusing on strong pulses (SNR > 15) during observation, we determine the optimal DM so that the pulses have the highest intensity. Observations from January to March 2018, relatively many pulses were observed. DM data with little influence of SW is obtained from this observation data and this DM data represents the effect of ISM. We analyze the DM value of June 2019 to investigate the SW plasma density at ~$5R_s$. We will present the results of this analysis at the JpGU 2020.

Keywords: solar wind, plasma density, pulsar

©2020. Japan Geoscience Union. All Right Reserved.

Occurrence dependence on solar activity cycle for type III radio bursts based on the automatic detection analyses

*Yuichiro Seki[1], Hiroaki Misawa[1], Fuminori Tsuchiya[1], Takahiro Obara[1], Tatsuya Fujimoto[1]

1. Tohoku University

Type III solar radio bursts are one of intense radio wave emissions that appear with the solar flares. They appear in the wide frequency range from the GHz to kHz band, and show a large negative frequency drift. A generation process of type III bursts is thought that high energy electrons originally generated with magnetic reconnections during a flare event excite Langmuir waves in the solar corona and/or interplanetary space, then the Langmuir waves are converted into electromagnetic waves observed as type III bursts. It is therefore generally assumed that the frequency of type III bursts reflects the plasma density in the solar corona and/or interplanetary space where the radio waves are generated, and their frequency drift reflect the plasma density distribution and the velocity of high-energy electrons.

It is well known that density distributions of the solar plasma differ depending on the activity of solar surface area (ex. Aschwanden and Acton, 2000). This implies that the plasma density distribution roughly varies with the solar activity cycle and therefore the frequency drift rates of type III bursts might show solar cycle dependence since the drift rate should reflect plasma density distributions along the paths of high energy electrons and also their energies. Although the occurrence rates of type III bursts are known to show a positive correlation with solar activity, our knowledge for solar cycle dependence of the drift rates has been still limited (ex. Zhang et al., 2018).

In this study, we have investigated statistical occurrence features of type III bursts, especially drift rate, flux density and their mutual relations, to clarify their solar cycle dependence. For this purpose, we have tried to make statistical analyses of type III bursts using a database of solar radio spectra observed with the Nancay Decameter Array (NDA) in France since 1977. We have analyzed the low-resolution data (175 kHz frequency resolution, 1 second time resolution) of the Nancay Decameter Array (NDA) in Paris, France. Although the observation frequency range of NDA is 10MHz-80MHz, we have used the spectra for 30-80MHz to avoid hard artificial radio noises below 30MHz.

In this analysis, an automatic burst detection system was newly developed to make the statistical analyses. At first, the spectrum data were divided every few minutes and reduced the thermal radiation level of the sun which temporally changes with the altitude of the sun due to atmospheric extinctions. Next, candidates of solar radio bursts were picked up as the ones whose radio flux exceeded some threshold level. Then, more plausible candidates as type III bursts were sorted out automatically as the bursts appearing continuity in the frequency and time domains at some extents and also with the negative frequency drift. Finally, we identified type III bursts through a visual check.

Using the developed automatic detection system, analyses for the NDA data observed in the solar cycle 24 have been performed. A preliminary result shows that the number of detected type III bursts in 2018 (near the solar minimum) was reduced to about 1/55 compared to that in 2013 (around the solar maximum). In the presentation, we will introduce the automatic type III bursts detection system and show solar cycle dependence for the occurrence characteristics of type III bursts with the discussion of their background processes.

©2020. Japan Geoscience Union. All Right Reserved.

Acknowledgments: The solar radio spectrum data was provided by the Nancay Observatory, Observatoire de Paris, France. We would appreciate Dr. L. Lamy and the NDA operation group.

Keywords: radio emission, corona, particle acceleration, ground-based observation, Type III burst, Nancay decameter array

©2020. Japan Geoscience Union. All Right Reserved.

The characteristics of type III solar radio bursts in ^{3}He-rich impulsive solar energetic particle phenomena

*Tatsuya Fujimoto[1], Hiroaki Misawa[1], Fuminori Tsuchiya[1], Takahiro Obara[1]

1. Tohoku University

Solar Energetic Particles (SEPs) are protons, electrons, and heavy ions of 10 keV to several tens GeV generated with flares and coronal mass emissions (CMEs), which are explosive phenomena near the solar surface. SEPs are classified into two types; i.e., impulsive and gradual types, based on the elemental abundances and the time profile of ion flux variations. Also, it has been reported that a phenomenon called type III radio bursts, which are suddenly appearing emissions caused by flares, are often observed in the tens to hundreds of MHz band when impulsive SEPs occur [Cane et al., 1986; McDowell, 2003]. Type III bursts are thought to be generated by energetic electrons accelerated by magnetic reconnections during flares, which propagate along the open magnetic field lines. That is, an injection of the energetic electrons into the solar corona leads to the generation of Langmuir plasma waves, and the waves are converted into radio waves as Type III bursts where the radio wave frequency is as same as the local plasma frequency. Type III bursts appear in the frequency range from GHz to kHz, and show rapid negative frequency drifts. The spectral structure is considered to reflect the motion of accelerated electron beams.
Impulsive SEPs, also known as electron-based events, show higher ratios of ^{3}He/^{4}He and Fe/O than general composition of the solar corona. Temerin and Roth [1992] proposed that the electromagnetic ion cyclotron (EMIC) waves would exist in the accelerating region of the electron beams that generate type III bursts in the solar corona by a similar physical process of the electron beam generation to that in the Earth’ s auroral region. In this idea, EMIC waves are thought to play a resonator which selectively increases flux of ions, such as ^{3}He and Fe. According to this idea, it is expected that both the flux of impulsive SEPs and the spectral structure of type III bursts include some features related to particle accelerations. However, there are few reports comparing characteristics of SEPs and spectrum structures of type III bursts from such a viewpoint, and the relationship between both of them has not been clarified. In this study, we have tried to make a detailed comparative analysis for impulsive SEP phenomena and type III bursts to elucidate relationship between both of them. We have analyzed energy and flux time profiles of SEPs using solar particle data observed with the ACE, WIND, and SOHO satellites staying around the L1 point. On the other hand, we have analyzed spectra of type III bursts such as frequency drift rates and micro structures using solar radio wave data observed with the WIND satellite, and ground-based solar radio telescopes AMATERAS of Tohoku University and the other domestic and overseas radio telescopes. In the presentation, we will report the results of the comparison studies for the characteristics of ion and electron fluxes of impulsive SEPs and those of the spectra of the type III bursts, and discuss the relationship both of them including generation processes of impulsive SEPs.

Acknowledgments: Solar energetic particle data are provided by the ACE Science Center, NASA, and the Turku University Space Research Laboratory. We thank the operation groups of the ACE, WIND, and SOHO projects.

Keywords: the Sun, solar energetic particles, radio burst, particle acceleration

©2020. Japan Geoscience Union. All Right Reserved.

Relationship between solar energetic particles and spectral fine structures of metric type II radio bursts

*Hiroaki Misawa[1], Fuminori Tsuchiya[1], Takahiro Obara[1], Tatsuya Fujimoto[1]

1. Planetary Plasma and Atmospheric Research Center, Graduate School of Science, Tohoku University

It is well known that a type II burst is one of sporadic and intense solar non-thermal radio phenomena, which shows gradual negative frequency drift in the metric to kilometric wavelength ranges and is generated with a coronal mass ejection (CME) event. As a plausible generation process of type II bursts, it is proposed that electro-static plasma waves originated from energetic electrons are effectively converted to electro-magnetic waves (type II bursts) at the region where the local plasma frequency is equal to wave frequency. A type II burst often occurs with energetic protons and ions with the energy of more than the MeV grade, and such an energetic phenomena is called a solar energetic particle (SEP) event. The coincident occurrence of type II bursts and SEPs strongly suggests that both energetic electrons and protons/ions would be the same origin initiated by a CME event. The occurrence characteristics of type II radio bursts and also SEPs have important information on the origins and generation processes of energetic particles and have been of course investigated well individually, however their relationships have been not well known except a recent research for the kilometric to hectometric type II bursts (Iwai et al., 2020).

We have investigated the relationship between SPEs and metric type II bursts from a view point of the clarification of characteristics of SEPs from the occurrence characteristics of type II bursts. We have especially paid attention to spectral fine structures of type II bursts identified in the metric wavelength by our group (Kashiwagi et al., 2016). At the first stage of this study, we have reanalyzed drift rates of fundamental elements of type II bursts using the radio data observed with the AMATERAS system, Tohoku University for three type II burst events observed in 2011 –2013 with weak to extinct SEP natures. In our presentation, we will introduce purpose of this study including a viewpoint of space-weather and preliminary results of the relationship between SEPs and spectral fine structures of type II bursts.

Keywords: sun, energetic particle event, type II radio bursts, fine spectral structure

©2020. Japan Geoscience Union. All Right Reserved.

Spectral Structures of Type II Solar Radio Bursts and Solar Energetic Particles

*Kazumasa Iwai[1], Seiji Yashiro[2], Nariaki Nitta[3], Yuki Kubo[4]

1. Institute for Space–Earth Environmental Research (ISEE), Nagoya University, 2. The Catholic University of America/NASA GSFC, 3. Lockheed Martin Advanced Technology Center, 4. National Institute of Information and Communications Technology

We investigated the relationship between the spectral structures of type II solar radio bursts in the hectometric and kilometric wavelength ranges and solar energetic particles (SEPs). To examine the statistical relationship between type II bursts and SEPs, we selected 26 coronal mass ejection (CME) events with similar characteristics (e.g., initial speed, angular width, and location) observed by the Large Angle and Spectrometric Coronagraph (LASCO), regardless of the characteristics of the corresponding type II bursts and the SEP flux. Then, we compared associated type II bursts observed by the Radio and Plasma Wave Experiment (WAVES) onboard the Wind spacecraft and the SEP flux observed by the Geostationary Operational Environmental Satellite (GOES) orbiting around the Earth. We found that the bandwidth of the hectometric type II bursts and the peak flux of the SEPs has a positive correlation (with a correlation coefficient of 0.64). This result supports the idea that the nonthermal electrons of type II bursts and the nonthermal ions of SEPs are generated by the same shock and suggests that more SEPs may be generated for a wider or stronger CME shock with a longer duration. Our result also suggests that considering the spectral structures of type II bursts can improve the forecasting accuracy for the peak flux of gradual SEPs. This study is based on the results obtained from the Coordinated Data Analysis Workshop for SEPs organized by PSTEP on 2017 (PSTEP-SEP-CDAW).

Keywords: Solar Energetic Particles (SEPs), solar radio burst, coronal mass ejection (CME)

©2020. Japan Geoscience Union. All Right Reserved.

Stellar flare of a close binary system during the NICER-Hisaki Observing Campaign 2018-2019

*Tomoki Kimura[1], Wataru Iwakiri[2], Atsushi Yamazaki[3], Go Murakami[3], Fuminori Tsuchiya[4], Kazuo Yoshioka[5], Hajime Kita[3], Masaki Kuwabara[3], Shin Toriumi[3]

1. Frontier Research Institute for Interdisciplinary Sciences, Tohoku University, Sendai, Japan, 2. Faculty of Science and Engineering, Chuo University, Tokyo, Japan, 3. Institute of Space and Astronautical Science, Japan Aerospace Exploration Agency, Sagamihara, Japan, 4. Planetary Plasma and Atmospheric Research Center, Tohoku University, Sendai, Japan, 5. Department of Complexity Science and Engineering, University of Tokyo, Kashiwa, Japan

Dynamics of stellar flare is still not well understood compared to the sun because of lack of continuous monitoring of distant stars at multiple wavelengths. Here we present a flare event at a close binary system, UX Arietis, monitored with the planetary extreme ultraviolet (EUV) space telescope Hisaki and the NICER X-ray Telescope from late 2018 to early 2019. Time variabilities in the EUV and X-ray spectra of the binary were successfully monitored from the beginning to the end of flare. Emission power at the Hisaki EUV wavelengths peaked at 6e+24 W, which is comparable with that measured in the NICER X-ray wavelength at 0.4-8 keV. The EUV spectrum was indicative of carbon, nitrogen, oxygen, and silicon ion emission lines. Electron temperature and density, emission measure, and ion balance were reduced from the emission lines by the spectral diagnostics. The spectral diagnostic indicates that EUV emission region with density and temperature comparable to the solar chromosphere expanded to spatial scale of a stellar radius (1-4e+6 km) during the flare. We interpret the EUV emission region is a flare ribbon expanding in the chromosphere. The X-ray spectrum was also diagnosed in a similar manner with the EUV spectrum with a collisional plasma emission model implemented in the XSPEC tool. Derived parameters are indicative of a compact flare loop on a spatial scale of stellar radius heated up simultaneously with the flare ribbon expansion. The derived flare spatial scale clearly contradicts the previous implication that the flare loop bridges between the two stars of binary system separated by 1.6 AU (2.4e+8 km) (Simon et al., 1980). At the flare rising time, the total mass of flare loop 3e+18 kg was significantly supplied from the chromosphere by the evaporation upflow with a speed of ~500km/s. The total energy of 1e+30 W was dissipated in the flare, which leads the magnetic flux of the flare loop to be more than 55G. These results are the first ever constraints on the mass and energy transfer processes between the flare loop and chromosphere at the stars.

Keywords: star, flare, Hisaki satellite

©2020. Japan Geoscience Union. All Right Reserved.

5-season's optical observations of neutral helium distribution in interplanetary space by Hisaki

*Atsushi Yamazaki[1], Go Murakami[1], Kazuo Yoshioka[2], Tomoki Kimura[3], Fuminori Tsuchiya[4], Masato Kagitani[4], Takeshi Sakanoi[4], Naoki Terada[5], Yasumasa Kasaba[6], Ichiro Yoshikawa[7]

1. Institute of Space and Astronautical Science / Japan Aerospace Exploration Agency, 2. Graduate School of frontier Science, The University of Tokyo, 3. Tohoku University, 4. Planetary Plasma and Atmospheric Research Center, Graduate School of Science, Tohoku University, 5. Graduate School of Science, Tohoku University, 6. Planetary Plasma and Atmospheric Research Center, Tohoku University, 7. The University of Tokyo

The Hisaki (SPRINT-A) satellite has main scientific objectives of the planetary magnetospheric physics and atmospheric evolution by long-term observations, but also carried out an observation of helium atom resonance scattering in interplanetary space. A material in the interstellar medium (ISM) travels into the heliosphere over the heliopause due to the relative velocity between the heliosphere and interstellar gases. The helium atoms move into the neighboring from the sun without ionizing because of its high ionization energy. The helium atoms are bent by sun gravity along the Keplerian orbit and forms a high density region on the down wind side, which is called helium cone. The distribution of helium atoms in the helium cone can estimate the speed and direction of the interstellar wind, and the density and the temperature of the helium atom in interstellar gases. This study has been carried out from the 1970s, but the interplanetary helium atoms observation is one of powerful tools to recognize the interstellar medium from inside the heliosphere. The Hisaki satellite carried out the observation of the resonance scattering in the helium cone during November and December from 2015 to 2019 five times. The interstellar wind direction derived from the comparison between the observation and the model simulation coincide the results of the other satellite observation. It means that the interstellar wind is stable in these years.

Keywords: EUV spectral observation, Interstellar wind and gas, Interplanetary neutral helium, HISAKI stellite

©2020. Japan Geoscience Union. All Right Reserved.

Group movement by magnetic coupling of high-speed protons running side by side in the chromosphere of the Sun

*Shinji Karasawa[1]

1. Miyagi National College of Technology Professor emeritus

There are a lot of spicules in the chromosphere at the surface of the Sun. The proton (H^+) rises at high speed from the bottom of the chromosphere to the top increasing the speed by the magnetic effect. When H^+ reaches the corona region, the mean free path becomes longer and does not occur the ionization. In the surface layer of the Sun, the movement of electrons is changed by the motion of H^+, but the movement of H^+ does not change by electromagnetic waves and the momentum of electrons.
The magnetic field that moves with H^+ generates an electric field vertically, and electrons accompany with the field. The high-speed H^+ that runs side by side is magnetically coupled, and the electron rarely re-combine with H^+ by the repulsive magnetic force. The distance d_{eq} that brings the force of magnetic equal to the force of the coulomb is obtained by using the relationship $\mu_0(qv)^2/(2\pi d_{eq}) = (q)^2/(d_{eq})^2$. In case that the speed of H^+ is 100km/sec, d_{eq} is 0.5 mm.
There is a cusp structure at the top of the plasma loop. There is an Electromagnetic Fluid Dynamic theory that the soft X-rays are generated by magnetic reconnection. However, when H^+ is bundled together by magnetic effects, a cross point becomes a cusp structure and it releases soft X-rays. When the subsequent plasma develops larger than the preceding plasma, it becomes faster and flare is generated.
The momentum of H^+ groups causes the superrotation of west side wider on the mid-day hemisphere on Venus by accelerating the west side and slowing down the east side. The solar wind has significant effects on the solar system [1].
[1] S. Karasawa, " Effects of high-speed protons of solar wind on the ionosphere of the Earth", Technical Report, IEICE Vol. 119, No. 203, AP2019-70, pp. 1-6.
http://www7b.biglobe.ne.jp/~shinji-k/Eg2019IEICE%20A-P.pdf

Keywords: Chromosphere, Corona, Spicule, Flare, Cusp Structure, Electromagnetic Fluid Dynamics

©2020. Japan Geoscience Union. All Right Reserved.

[E] Poster | P (Space and Planetary Sciences)：P-EM Solar-Terrestrial Sciences, Space Electromagnetism & Space Environment

[P-EM12] Coupling Processes in the Atmosphere-Ionosphere System

convener:Huixin Liu(Earth and Planetary Science Division, Kyushu University SERC, Kyushu University), Yuichi Otsuka(Institute for Space-Earth Environmental Research, Nagoya University), Yue Deng(University of Texas at Arlington), Loren Chang(Institute of Space Science, National Central University)

The Atmosphere-Ionosphere (A-I) system forms the so-called near-Earth space. Recent rapidly expanding use of satellite constellations in Low-Earth Orbit (LEO) drives a high demand for better understanding and accurate forecast of the global A-I system for scientific and operational purposes. This session aims to provide a forum for research advances and frontiers related to these aspects, and we invite presentations on global A-I coupling at all temporal and spatial scales. This includes but is not limited to: A-I coupling via atmospheric waves (tides, gravity waves, planetary waves) and trace gases (CO2, O3, H2O), A-I response to Space Weather events (solar flares, CMEs, CIRs), polar-equatorial or inter-hemispheric coupling via TADs/TIDs/disturbance dynamo/penetration electric field, ionospheric plasma irregularities, ionospheric currents, etc. Observations, theoretical studies, model simulations, data assimilation, instruments development are all highly welcome.

[PEM12-P01] LOW IONOSPHERE AS A SOURCE OF REMOTE SENSING

*ALEXEI DMITRIEV[1,2], S.O. Adamson[3], A.A. Berlin[4], Y.A. Dyakov[5], L.V. Eppelbaum[6], G.V. Golubkov[3,5], A.A. Lushnikov[6], M.I. Manzhelii[7], M.G. Golubkov[3] (1.Institute of Space Science and Engineering, National Central University, Jungli City, Taiwan, 2.Skobeltsyn Institute of Nuclear Physics, Lomonosov Moscow State University, Moscow, Russia, 3.Semenov Federal Research Center for Chemical Physics, Russian Academy of Sciences, Moscow 119991, Russian Federation , 4.Department of Earth Sciences, Tel Aviv University, Tel Aviv 69978, Israel, 5.National Research Center “Kurchatov Institute”, Moscow 123182, Russian Federation, 6.Geophysical Center, Russian Academy of Sciences, Moscow 119296, Russian Federation, 7.Center for Chemical Physics of Atmosphere, Moscow 119991, Russian Federation)

[PEM12-P02] Relationship between Na layer and CNA variations observed over Syowa, Antarctic

*Takuo T. Tsuda[1], Ryo Tozu[1], Kyogo Takizawa[1], Yoshimasa Tanaka[2], Takuya Kawahara[3], Mitsumu K. Ejiri[2], Takanori Nishiyama[2], Takuji Nakamura[2] (1.University of Electro-Communications, 2.National Institute of Polar Research, 3.Shinshu University)

[PEM12-P03] Occurrence feature of plasma bubble observed in mid-latitudes during geomagnetic storms using GNSS-TEC data

*Sori Takuya[1], Yuichi Otsuka[1], Atsuki Shinbori[1], Takuya Tsugawa[2], Michi Nishioka[2] (1.Institute for Space-Earth Environmental Research, Nagoya University, 2.National Institute of Information and Communications Technology)

[PEM12-P04] Three-dimensional ionospheric simulation of the Es layer: Physical mechanism of the sporadic appearance

*Satoshi Andoh[1], Akinori Saito[1], Hiroyuki Shinagawa[2], Mitsumu K. Ejiri[3], Shinichi Miyazaki[1] (1.Graduate School of Science, Kyoto University, 2.National Institute of Information and Communications Technology, 3.National Institute of Polar Research)

[PEM12-P05] Time and height variability of Fe-layer in the Mesosphere and the Lower Thermosphere region at Syowa Station, Antarctica (69.0°S, 39.6°E) based on a resonance scattering lidar measurements in two winter seasons

*Takanori Nishiyama[1,2], Mitsumu K. Ejiri[1,2], Takuo T. Tsuda[3], Katsuhiko Tsuno[4], Toru Takahashi[5], Makoto Abo[6], Takuya Kawahara[7], Takayo Ogawa[4], Satoshi Wada[4], Takuji Nakamura[1,2] (1.National Institute of Polar Research, 2.The Graduate University for Advanced Studies, SOKENDAI, 3.The University of Electro-Communications, 4.RIKEN, 5.University of Oslo, 6.Tokyo Metropolitan University, 7.Shinshu University)

[PEM12-P06] **Analysis of VLF Band Waves near the Sq Current System observed by S-310-44 Sounding Rocket**

*Taketoshi Miyake[1], Ryuichiro Nakamura[1], Keigo Ishisaka[1], Takumi Abe[2], Atsushi Kumamoto[3], Makoto Tanaka[4] (1.Department of Electrical and Computer Engineering, Faculty of Engineering, Toyama Prefectural University, 2.Japan Aerospace Exploration Agency Institute of Space and Astronautical Science Department of Solar System Sciences, 3.Department of Geophysics, Graduate School of Science, Tohoku University, 4.Tokai University, ICT Education Center)

[PEM12-P07] Monte Carlo simulation of solar EUV scattering by oxygen ions

*Shin ya Nakano[1], Yuta Hozumi[2], Akinori Saito[3] (1.The Institute of Statistical Mathematics, 2.University of Electro-Communications, 3.Department of Geophysics, Graduate School of Science, Kyoto University)

[PEM12-P08] Automatic detection of Spread-F on ionogram using Machine Learning

*Shimizu Junji[1], Hiroyuki Nakata[1], Hiroyo Ohya[1], Toshiaki Takano (1.Graduate School of Engineering, Chiba University)

[PEM12-P09] Examination of the ionospheric perturbations propagation associated with H-IIA rocket launchings

*Junpei Yamazaki[1], Hiroyuki Nakata[2], Hiroyo Ohya[2], Toshiaki Takano[2], Keisuke Hosokawa[3] (1.Graduate School of Science and Engineering, Chiba University, 2.Graduate School of Engineering, Chiba University, 3.Department of Communication Engineering and Information, University of Electro-Communications)

[PEM12-P10] Spatial and temporal distributions of atmospheric gravity wave potential energy evaluated using ERA-5 temperature data over the equatorial latitudes

*Shih-Sian Yang[1], Chen-Jeih Pan[1], Uma Das[2], Chian-Chiau Lin[3] (1.National Central University, Jhongli, Taoyuan 32001, Taiwan, 2.Department of Physics, Indian Institute of Information Technology, India, 3.Environmental Research and Information Center, Chang Jung Christian University, Taiwan)

[PEM12-P11] Atmospheric wave propagation observed by GNSS-TEC: Fireball explosion and atmospheric mode

*Ai Matsushita[1], Kosuke Heki[1] (1.Hokkaido University Graduate School of Science)

[PEM12-P12] Investigation of the climatology and long-term variations of the stratospheric Kelvin waves using ERA-Interim

*Chen-Jeih Pan[1], Shih-Sian Yang[1], Uma Das[2], Wei-Sheng Chen[1] (1.Institute of Space Science, National Central University, Taiwan, 2.Department of Physics, Indian Institute of Information Technology, India)

[PEM12-P13] **Statistical study of seasonal dependence of MSTID occurrence and propagation velocity using the SuperDARN Hokkaido East HF radar**

*Wataru Hazeyama[1], Nozomu Nishitani[1], Tomoaki Hori[1] (1.Institute for Space-Earth Environmental Reseach)

[PEM12-P14] First simultaneous observation of nighttime medium-scale traveling ionospheric disturbance (MSTID) by a ground airglow imager and the Arase satellite in the inner magnetosphere

*Kouki Kawai[1], Kazuo Shiokawa[1], Yuichi Otsuka[1], Yoshiya Kasahara[2], Fuminori Tsuchiya[3], Ayako Matsuoka[4], Yasumasa Kasaba[3], Kazushi Asamura[4], Satoshi Kasahara[6], Yoshizumi Miyoshi[1], Shin-ichiro Oyama[1,7,8], Yoichi Kazama[5] (1.Institute for Space-Earth Environmental Research, Nagoya Univ, Japan, 2.Kanazawa Univ, Japan, 3.Tohoku Univ, Japan, 4.Japan Aerospace Exploration Agency, 5.Academia Sinica, 6.Tokyo Univ, Japan, 7.Oulu Univ, Finland, 8.National Institute od polar Research)

[PEM12-P15] Study of variations in the D-region ionosphere after the 2016 Kumamoto earthquakes using VLF/LF transmitter signals

*Tekkan Akashi[1], Hiroyo Ohya[2], Hiroyuki Nakata[2], Fuminori Tsuchiya[3] (1.Graduate School of Science and Engineering, Chiba University, 2.Graduate School of Engineering, Chiba University, 3.Graduate School of Science, Tohoku University)

[PEM12-P16] Analysis of source and generation mechanism of atmospheric gravity waves and MSITDs observed in airglow images in Hawaii

*Hideto Naito[1], Kazuo Shiokawa[1], Yuichi Otsuka[1], Takeshi Sakanoi[2], Akinori Saito[3], Takuji Nakamura[4] (1.Nagoya University, 2.Tohoku University, 3.Kyoto University, 4.National Institute of Polar Research)

[PEM12-P17] Solar flare effects of the D-region ionosphere using daytime tweek atmospherics and VLF/LF standard radio waves

*Kodai Yamanobe[1], Hiroyo Ohya[1], Hiroyuki Nakata[1], Kazuo Shiokawa[2], Fuminori Tsuchiya[3], Kozo Yamashita[4], Yukihiro Takahashi[5] (1.Chiba Univ., 2.Nagoya Univ., 3.Tohoku Univ., 4.Ashikaga Univ., 5.Hokkaido Univ.)

[PEM12-P18] **The spatial structures and seasonal variations of the polar mesospheric clouds seen from the meteorological satellite Himawari-8**

*Yuta Hozumi[1], Takuo T. Tsuda[1], Kento Kawaura[1], Yoshiaki Ando[1], Keisuke Hosokawa[1], Hidehiko Suzuki[2], Takuji Nakamura[3], Ken T. Murata[4] (1.University of Electro-Communications, 2.Meiji University, 3.National Institute of Polar Research, 4.National Institute of Information and Communications Technology)

[PEM12-P19] Fireball-associated variations in the D-region ionosphere observed using VLF/LF transmitter signals

*Takeru Suzuki[1], Hiroyo Ohya[2], Fuminori Tsuchiya[3], Kazuo Shiokawa[4], Hiroyuki Nakata[2] (1.Graduate School of Science and Engineering, Chiba University, 2.Graduate School of Engineering, Chiba University, 3.Graduate School of Science, Tohoku University, 4.Institute for Space-Earth Environmental Research, Nagoya University)

[PEM12-P20] Calcium ion layer observed with resonance scattering lidar at Syowa Station

*Mitsumu K. Ejiri[1,2], Takanori Nishiyama[1,2], Takuo T. Tsuda[3], Makoto Abo[4], Katsuhiko Tsuno[5], Takuya Kawahara[6], Takayo Ogawa[5], Satoshi Wada[5], Takuji Nakamura[1,2] (1.National Institute of Polar Research, 2.The Graduate University for Advanced Studies, SOKENDAI, 3.The University of Electro-Communications, 4.Tokyo Metropolitan University, 5.RIKEN, RAP, 6.Shinshu University Faculty of Engineering)

[PEM12-P21] **Generation and movement of equatorial plasma bubbles: Roles of vertical plasma drifts, seeding perturbations, and geomagnetic storms**

*Chaosong Huang[1] (1.Air Force Research Laboratory Albuquerque)

[PEM12-P22] Variations of the Earth's magnetic field during fall of the Tunguska and Chelyabinsk bolides: analogies and differences

*Ravil Rakhmatulin[1] (1.Institute of Solar-Terrestrial Physics, SB RAS)

[PEM12-P23] Atmospheric-ionospheric vertical coupling study focusing on the quasi-6-day oscillation in Sq-EEJ current system

*Takayama Kumi[1], Yasunobu Miyoshi[1], Akimasa Yoshikawa[1] (1.Kyushu University)

[PEM12-P24] Investigating of cusp heating process by using chemical releases of Ba/Sr: Initial result of CHI rocket experiment

*Taro Watanabe[1], Yoshihiro Kakinami[2], Masa-yuki Yamamoto[1], Miguel Larsen[3], Mark Conde[4], Takao M. Sato[2], Yuuichi Kaga[2], Takako Kaga[2] (1.Kochi University of Technology, 2.Hokkaido Information University, 3.Clemson University, 4.University of Alaska Fairbanks)

[PEM12-P25] Characterization of counter electrojet current according to specific time frame in Southeast Asian sector

*Nur Izzati Mohd Rosli[1], Nurul Shazana Abdul Hamid[1], Mardina Abdullah[1], Akimasa Yoshikawa[2], Teiji Uozumi[2] (1.Universiti Kebangsaan Malaysia, 2.Kyushu University)

[PEM12-P26] Characterizing ionospheric irregularities with GEONET

*Guanyi Ma[1], Qi Li[1], Takashi Maruyama[2,1], Jinghua Li[1], Qingtao Wan[1], Xiaolan Wang[1], Jiangtao Fan[1], Jie Zhang[1] (1.National Astronomical Observatories, Chinese Academy of Sciences, 2.National Institute of Information and Communications Technology)

[PEM12-P27] Imaging observation of Ionospheric Field Aligned Irregularities by the PANSY radar at Antarctic Syowa Station

*Daisuke Kagawa[1], Taishi Hashimoto[2], Akinori Saito[1], Koji Nishimura[2], Masaki Tsutsumi[2], Toru Sato[3], Kaoru Sato[4] (1.Graduate School of Science, Kyoto University, 2.National Institute of Polar Research, 3.Graduate School of Informatics, Kyoto University, 4.Graduate School of Science, Tokyo University)

[PEM12-P28] Vertical profile of ionospheric disturbances associated with Tohoku Earthquake using GPS occultation observation

*Hiroyuki Nakata[1], Yuto Imae[2], Toshiaki Takano[1], Hiroyo Ohya[1] (1.Graduate School of Engineering, Chiba University, 2.Department of Electrical and Electronics Engineering, Faculty of Engineering, Chiba University)

[PEM12-P29] **Statistical study of the growth rates of medium-scale traveling ionospheric disturbances observed with GNSS-TEC**

*Takafumi Ikeda[1], Akinori Saito[1], Takuya Tsugawa[2] (1.Department of Geophysics, Graduate School of Science, Kyoto University, 2.National Institute of Information and Communications Technology)

[PEM12-P30] Retrieval of the Mesosphere and Lower Thermosphere (MLT) physical and chemical properties with the proposed Superconducting Submillimeter-Wave Limb-Emission Sounder 2 (SMILES-2)

*Philippe Baron[1], Satoshi Ochiai[1], Hideo Sagawa[2], Akinori Saito[3], Takatoshi Sakazaki[3], Masato Shiotani[3], Makoto Suzuki[4] (1.National Institute of Information and Communications Technology, 2.Kyoto Sangyo University, 3.Kyoto University, 4.Japan Aerospace Exploration Agency)

[PEM12-P31] Formation of a Ring-Like Region of Increased Electron Temperature in the Subauroral Ionosphere in Winter

Innokentiy Alexeevich Golikov[1], Artem Yurevich Gololobov[2], *Ilia Ilyich Varlamov[1,2] (1.Yu.G.Shafer Institute of Cosmophysical Research and Aeronomy (IKFIA), Siberian Branch of the Russian Academy of Sciences, 2.M. K. Ammosov Northeastern Federal University (NEFU),)

[PEM12-P32] Magnetic Field Measurement in the Ionosphere by using 2U-size CubeSat

*Kentarou Kitamura[1], Kazumasa Imai[2], Taku Takada[2], Manabu Shinohara[3], Makoto Wakabayashi[4], Masahiro Tokumitsu[5] (1.NIT, Tokuyama College, 2.NIT, Kochi College, 3.NIT, Kagoshima College, 4.NIT, Niihama College, 5.NIT, Yonago College)

[PEM12-P33] Observations of night time Sporadic-E layer by HF Doppler sounder network: association with Medium-Scale Traveling Ionospheric Disturbance (MSTID)

*Ryo Matsushima [1], Keisuke Hosokawa[1], Jun Sakai[1], Mitsumu K Ejiri[2], Michi Nishioka[3], Takuya Tsugawa[3] (1.The University of Electro-Communications, 2.National Institute of Polar Research, 3.National Institute of Information and Communications Technology)

[PEM12-P34] SMILES-2, satellite mission for observation of the stratosphere, mesosphere, and lower thermosphere with THz receivers

*Satoshi Ochiai[1], Philippe Baron[1], Yoshihisa Irimajiri[1], Akira Kawakami[1], Toshiyuki Nishibori[2], Makoto Suzuki[2], Yoshinori Uzawa[3], Yasunori Fujii[3], Hiroyuki Maezawa[4], Akinori Saito[5], Takatoshi Sakazaki[5], Masato Shiotani[5] (1.National Institute of Information and Communications Technology, 2.Japan Aerospace Exploration Agency, 3.National Astronomical Observatory of Japan, 4.Osaka Prefecture University, 5.Kyoto University)

[PEM12-P37] Numerical study of the internal mesh structure for ion drift velocity analyzer on sounding rocket

*Ryuto Hashiba[1], Takumi Abe[2] (1.Graduate School of Science, Hokkaido University, 2.Institute of Space and Astronautical Science, Japan Aerospace Exploration Agency)

[PEM12-P38] **Using a Software Defined Radio to Receive the FORMOSAT-7 RF Beacon and Derive the Total Electron Content**

*Tsai-Ju Yu[1], Loren C. Chang[1], Jann-Yenq Liu[1], Tung-Yuan Hsiao[2] (1.Graduate Institute of Space Science and Engineering, National Central University, Taoyuan City, Taiwan, 2.Accelerator Laboratory, Nuclear Science and Technology Development Center, National Tsing Hua University, Hsinchu, Taiwan)

[PEM12-P39] Neutral and ion dynamics seen in GAIA with variable high-latitude input

*Chihiro Tao[1], Hidekatsu Jin[1], Hiroyuki Shinagawa[1], Yasunobu Miyoshi[2], Hitoshi Fujiwara[3] (1.National Institute of Information and Communications Technology, 2.Department of Earth and Planetary Sciences, Kyushu University, 3.Faculty of Science and Technology, Seikei University)

[PEM12-P41] Time-dependent responses of the neutral mass density to magnetospheric energy inputs into the cusp region in the thermosphere

*Tomokazu Oigawa[1], Hiroyuki Shinagawa[2], Satoshi Taguchi[1] (1.Department of Geophysics, Graduate School of Science, Kyoto University, 2.National Institute of Information and Communications Technology)

[PEM12-P42] 2-dimentional FDTD simulation about spatial structure change of sporadic E layer

*takuto tawaki[1], Taketoshi Miyake[1] (1.Toyama prefectural university)

[PEM12-P43] **Atmospheric density variations observed by GOCE**

*Nakayama Sayuka [1], Liu Huixin[1] (1.Earth and planetary science division,Kyushu university,Japan)

[PEM12-P44] revision and data assimilation of a whole atmosphere-ionoshere model GAIA

*Hidekatsu Jin[1], Yasunobu Miyoshi[2], Chihiro Tao[1], Hiroyuki Shinagawa[1], Hitoshi Fujiwara[3] (1.National Institude of Information and Communications Technology, 2.Kyushu university, 3.Seikei university)

[PEM12-P45] Overview of Vertical Incidence Pulsed Ionospheric Radar 2 (VIPIR2) observation in Japan

*Michi Nishioka[1], Hideo MAENO[1], Hiroyuki YAMAKAWA[1], Takumi Kondo[1], Takuya Tsugawa[1], Mamoru Ishii[1] (1.National Institute of Information and Communications Technology)

LOW IONOSPHERE AS A SOURCE OF REMOTE SENSING

*ALEXEI DMITRIEV[1,2], S.O. Adamson[3], A.A. Berlin[4], Y.A. Dyakov[5], L.V. Eppelbaum[6], G.V. Golubkov[3,5], A.A. Lushnikov[6], M.I. Manzhelii[7], M.G. Golubkov[3]

1. Institute of Space Science and Engineering, National Central University, Jungli City, Taiwan, 2. Skobeltsyn Institute of Nuclear Physics, Lomonosov Moscow State University, Moscow, Russia, 3. Semenov Federal Research Center for Chemical Physics, Russian Academy of Sciences, Moscow 119991, Russian Federation , 4. Department of Earth Sciences, Tel Aviv University, Tel Aviv 69978, Israel, 5. National Research Center “Kurchatov Institute”, Moscow 123182, Russian Federation, 6. Geophysical Center, Russian Academy of Sciences, Moscow 119296, Russian Federation, 7. Center for Chemical Physics of Atmosphere, Moscow 119991, Russian Federation

One of the fundamental problems of remote sensing is to establish the nature of the source of decimeter microwave radiation, taking into account the dependence of its intensity on the current state of the atmosphere and to determine the interfering factors of radiation propagation (charged aerosol layers, their hydration, etc.). This leads to uncontrolled behavior of the measured intensity and to difficulties in calibrating the receiving equipment.

It was previously assumed that this source has a cosmic origin and corresponds to the radiation of a hydrogen radio line observed at radio telescopes with a wavelength of 21 cm and a transition frequency of 1.4204 GHz. The estimates show that the power of the flux of cosmic radiation arriving at the radiometer is several orders of magnitude lower than the flux density of its own incoherent microwave radiation D and E of the layers of the ionosphere in the decimeter range. Therefore, incoherent super background decimeter radiation, which is formed at an altitude of 80–110 km due to the population of Rydberg states, is the main source.
Since the source is located below the orbiting satellites, a fundamentally new method for making the necessary measurements is proposed.

Keywords: bottomside ionosphere, remote sensing

©2020. Japan Geoscience Union. All Right Reserved.

Relationship between Na layer and CNA variations observed over Syowa, Antarctic

*Takuo T. Tsuda[1], Ryo Tozu[1], Kyogo Takizawa[1], Yoshimasa Tanaka[2], Takuya Kawahara[3], Mitsumu K. Ejiri[2], Takanori Nishiyama[2], Takuji Nakamura[2]

1. University of Electro-Communications, 2. National Institute of Polar Research, 3. Shinshu University

Metallic layers, such as Na, Fe, Mg, K, and Ca layers, exist in the mesosphere and lower thermosphere, that correspond to the height range of the ionospheric D and E regions. In the polar region, energetic particles precipitating from the magnetosphere can often penetrate into the E region and even into the D region. Therefore, the influence of energetic particles on the metallic layers is of interest regarding changes in atmospheric composition accompanied by auroral activity or geomagnetic activity.

In this study, we have performed a statistical data analysis on Na layer responses to geomagnetic activity using Na density data, together with simultaneous cosmic noise absorption (CNA) data, obtained at Syowa, Antarctic (69.0ºS, 39.6ºE) in 2000-2002. It is found that the Na densities around the topside of Na layers tended to decrease during geomagnetic active days, but in contrast the CNA tended to increase. The amounts of Na density responses, i.e., Na density decrease or Na loss, were increasing with magnetic local time (MLT) from dusk hours to dawn hours, and those of CNA responses, i.e., CNA increase, were also increasing with MLT. Thus, there were clear negative correlations between the Na density and the CNA variations. These results indicate that the the Na loss around the topside of Na layer was induced by the energetic particle precipitation during geomagnetic active days.

Keywords: Na layer, CNA, Lidar

©2020. Japan Geoscience Union. All Right Reserved.

Occurrence feature of plasma bubble observed in mid-latitudes during geomagnetic storms using GNSS-TEC data

*Sori Takuya[1], Yuichi Otsuka[1], Atsuki Shinbori[1], Takuya Tsugawa[2], Michi Nishioka[2]

1. Institute for Space-Earth Environmental Research, Nagoya University, 2. National Institute of Information and Communications Technology

Plasma bubbles, which have a significantly sharp depletion of plasma density, are one of the ionospheric irregularities in the low-latitude and equatorial regions. Within the plasma bubbles, plasma density irregularities with different spatial scales exist. They are generated in the bottomside F region of the nighttime equatorial ionosphere after sunset by Rayleigh-Taylor instability (RTI) mechanism [e.g., Farley et al., 1970; Kelley, 2009]. The growth rate of RTI increases with increasing eastward electric fields and increasing ionospheric altitude. During large geomagnetic storms, plasma bubbles are sometimes observed at mid-latitudes because they extend to higher altitudes and latitudes by larger upward $\mathbf{E} \times \mathbf{B}$ drifts [e.g., Ma and Maruyama, 2006; Aa et al., 2018]. In this study, we analyzed total electron content (TEC) and rate of TEC index (ROTI) [Pi et al., 1997] data obtained from global navigation satellite system (GNSS) receivers over the world after 2000 to clarify causes of storm-time plasma bubbles which reach mid-latitudes. We regard plasma bubbles extending the mid-latitude of more than 30° during geomagnetic storms as mid-latitude plasma bubbles. Two-dimensional GNSS-TEC and ROTI data with spatial and temporal resolutions of 0.5°×0.5° in longitude and latitude and 5 minutes, respectively are used. In order to find storm-time mid-latitude plasma bubble events, we create geomagnetic latitude-time plots of ROTI at 20 h (local time) for 1 year. We defined the SYM-H variations with the minimum value of less than -40 nT as geomagnetic storm events, and identified 49 events during 2000. For each storm event, we investigated the relationship between temporal and spatial variations of ROTI and other parameters (solar wind and geomagnetic indexes) in these events. As a result, we have found that the plasma bubbles in 6 of 49 storm events extended to mid-latitudes associated with geomagnetic storms. These plasma bubbles are caused during the main phase of large geomagnetic storms having the minimum SYM-H values of less than -150 nT and the steep gradient of SYM-H values (more than -40 nT/h). The dawn-to-dusk (Ey) component of interplanetary electric field, derived from solar wind speed (Vx) and the north-south (Bz) component of interplanetary magnetic field (IMF) ($Ey = -(Vx \times Bz)$), shows larger value, compared with other geomagnetic storms. This suggests that the dawn-to-dusk convection electric field in the polar ionosphere is significantly enhanced by solar wind-magnetosphere interaction under the southward IMF condition. The electric field imposed on the polar ionosphere propagates instantaneously to the equatorial ionosphere [Kikuchi et al., 1996]. The eastward electric field induced by the southward-turning of IMF Bz could enhance of the eastward electric field at the dusk sector, causing the mid-latitude plasma bubbles by RTI. In the presentation, we will show statistical characteristics of storm-time mid-latitude plasma bubbles by analyzing ROTI data in other storm events after 2001.

Keywords: plasma bubble, geomagnetic storms, mid-latitude, electric field

©2020. Japan Geoscience Union. All Right Reserved.

Three-dimensional ionospheric simulation of the Es layer: Physical mechanism of the sporadic appearance

*Satoshi Andoh[1], Akinori Saito[1], Hiroyuki Shinagawa[2], Mitsumu K. Ejiri[3], Shinichi Miyazaki[1]

1. Graduate School of Science, Kyoto University, 2. National Institute of Information and Communications Technology, 3. National Institute of Polar Research

Physical mechanism of sporadic appearance of the mid-latitude sporadic E layer (Es layer) was studied by using a three-dimensional high precision numerical model. Es layer is a thin layer of metallic ion plasma appearing in the ionospheric E region. When the layer is observed from a point, it shows sporadic appearances. While it is widely accepted that the vertical wind-shear of the diurnal/semi-diurnal tide is responsible for the generation of the Es layer, the sporadic appearance of the Es layer cannot be explained by this tide-windshear theory. Recently, the self-consistent atmosphere-ionosphere model GAIA (Ground-to-topside model of Atmosphere and Ionosphere for Aeronomy) has reproduced three-dimensional neutral wind fields containing both tidal and gravity waves. Consequently, it has become that the effect of tidal and gravity waves on structures of Es layer can be investigated at the same time.

We have developed a three-dimensional ionospheric numerical model. Three-dimensional neutral winds of the GAIA were used as an input in every 10 minutes for given day. The ionospheric model successfully reproduced the day-to-day variability of the Es layers that was observed by a Ca-ion lidar. Structures of Es layer reproduced in the neutral winds containing both tidal and gravity waves were circular or belt-like, and their scales were about 100-1000 km. As a result, we found that the structure of the Es layer was horizontally transported by the neutral wind, causing sporadic appearance of the Es layer.

Keywords: sporadic E layer, numerical simulation, ionosphere

©2020. Japan Geoscience Union. All Right Reserved.

Time and height variability of Fe-layer in the Mesosphere and the Lower Thermosphere region at Syowa Station, Antarctica (69.0˚S, 39.6˚E) based on a resonance scattering lidar measurements in two winter seasons

*Takanori Nishiyama[1,2], Mitsumu K. Ejiri[1,2], Takuo T. Tsuda[3], Katsuhiko Tsuno[4], Toru Takahashi[5], Makoto Abo[6], Takuya Kawahara[7], Takayo Ogawa[4], Satoshi Wada[4], Takuji Nakamura[1,2]

1. National Institute of Polar Research, 2. The Graduate University for Advanced Studies, SOKENDAI, 3. The University of Electro- Communications, 4. RIKEN, 5. University of Oslo, 6. Tokyo Metropolitan University, 7. Shinshu University

The National Institute of Polar Research (NIPR) is leading a prioritized project of the Antarctic research observations. One of the sub-projects is entitled the global environmental change revealed through the Antarctic middle and upper atmosphere. Profiling dynamical parameters such as temperature and wind, as well as minor constituents is the key component of observations in this project, together with a long-term observation using existent various instruments at Syowa, Antarctica (69.0˚S, 39.6˚E). As a part of the sub-project, we developed a new resonance lidar system with multiple wavelengths. The lidar transmitter is based on injection-seeded, pulsed alexandrite laser for 768-788 nm (fundamental wavelengths) and a second- harmonic generation (SHG) unit for 384-394 nm (second harmonic wavelengths). The laser wavelengths can be tuned into the resonance wavelengths by a wavemeter that is calibrated and validated using a wavelength- stabilized He-Ne laser and a potassium vapor cell for doppler-free spectroscopy.

This lidar has capabilities to measure density variations of minor constituents such as atomic iron (Fe, 386 nm), atomic potassium (K, 770 nm), calcium ion (Ca^+, 393 nm), and nitrogen molecular ion (N_2^+, 390, 391 nm) and temperature profiles in the mesosphere and lower thermosphere (MLT) region. It can also estimate temperature profiles from the upper Stratosphere to the lower mesosphere using signals of Rayleigh scattering. The lidar system installed at the Syowa Station by the 58th Japan Antarctic Research Expedition (JARE 58) in January 2017, and then its observation has been continued by October 2018.

In this presentation, we are going to report initial results focusing on Fe atom and temperature variability in MLT region. In the two seasons, Fe measurements have been carried out for a total of 59 nights (653 hours). Preliminary analysis demonstrated that the seasonal variability of Fe atom abundance from February to October, which has a peak and a secondary peak at May and September respectively, is well agreed to those in preceding studies. In addition to seasonal variations, Fe atom response to energetic particles forcing due to magnetic storms and substorms will be analyzed in detail and discussed. Since Syowa station is located under aurora oval in the southern hemisphere, chemical reactions and electromagnetic dynamics are important for understanding of short-term variations on Fe density as well as wave forcing driven by atmospheric gravity waves.

Keywords: Mesosphere and Lower Themosphere, Metallic atom layer, Energetic particle forcing , Resonance scattering lidar

©2020. Japan Geoscience Union. All Right Reserved.

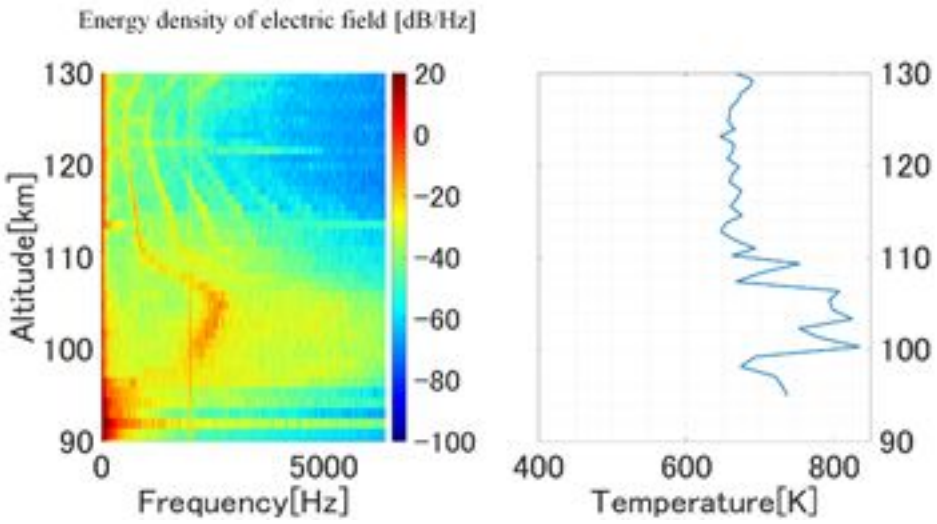
Analysis of VLF Band Waves near the Sq Current System observed by S-310-44 Sounding Rocket

*Taketoshi Miyake[1], Ryuichiro Nakamura[1], Keigo Ishisaka[1], Takumi Abe[2], Atsushi Kumamoto[3], Makoto Tanaka[4]

1. Department of Electrical and Computer Engineering, Faculty of Engineering, Toyama Prefectural University, 2. Japan Aerospace Exploration Agency Institute of Space and Astronautical Science Department of Solar System Sciences, 3. Department of Geophysics, Graduate School of Science, Tohoku University, 4. Tokai University, ICT Education Center

The Sq current system is one of the ring current which occurs in the lower ionosphere in the winter daytime. It is caused the specific plasma phenomena such as electron heating and strong electron density disturbance. S-310-44 sounding rocket experiment was carried out to investigate the special phenomena near the Sq current focus, at 12:00 JST on January 15th, 2016. The rocket passed through the Sq current focus, and all the scientific instruments onboard the rocket worked successfully. In this experiment, the Electric Field Detector (EFD) observed the VLF band AC electric fields up to 6.4kHz in the altitude from 100km to 160km. We made the altitude profile of the electric field spectra, and found clear VLF band waves with the frequencies from 2kHz to 3kHz at the altitude about 100km. These VLF band waves are observed during only the rocket ascent. The Fast Langmuir Probe (FLP) observed that the electron temperature increase about 150K larger than the background in this region, and the frequency variation of the VLF band waves shows good correlation with the electron temperature as shown in Figure 1. According to the polarization analyses, the electric fields of the VLF band waves are oblique, not parallel to the magnetic field. The frequency range of this VLF band waves is consistent with the ion cyclotron frequency. These results suggest that the VLF band waves observed in this experiment are one of the ion cyclotron harmonic waves whose frequencies vary with the temperature ratio of the electron and the ion (Te/Ti). We are going to investigate further the VLF waves observed by the rocket experiment, and clarify the heating mechanism of the electrons near the Sq current focus.

Keywords: Electric field, Sq current system, Sounding rocket mesurement, Ionosphere



©2020. Japan Geoscience Union. All Right Reserved.

Monte Carlo simulation of solar EUV scattering by oxygen ions

*Shin ya Nakano[1], Yuta Hozumi[2], Akinori Saito[3]

1. The Institute of Statistical Mathematics, 2. University of Electro-Communications, 3. Department of Geophysics, Graduate School of Science, Kyoto University

It has been reported that the Extreme ultraviolet (EUV) at 83.4 nm, which is scattered by oxygen ions (O+), was observed by an imager of ISS-IMAP in the umbra of the Earth. However, the single scattering of solar radiation in the upper atmosphere would not well explain the observation. This study modeled the EUV scattering by a Monte Carlo method. This method allows us to consider multiple scattering. The result suggests the EUV at 83.4 nm is observable even in the umbra. However, the feature of the observation by ISS-IMAP is not necessarily reproduced. Possible reasons of the discrepancy between the simulation and the observation will be discussed.

Keywords: Oxygen ion, Extreme Ultraviolet

©2020. Japan Geoscience Union. All Right Reserved.

Automatic detection of Spread-F on ionogram using Machine Learning

*Shimizu Junji[1], Hiroyuki Nakata[1], Hiroyo Ohya[1], Toshiaki Takano

1. Graduate School of Engineering, Chiba University

Ionospheric irregularities referred to as equatorial spread-F are very important phenomena in terms of radio wave propagation because their spatial scales are from centimeters to tens of kilometer and they affect wide-band radio waves. Therefore, they interfere the reliability of satellite-ground communications, navigation systems and so on. The ionozonde is one of the useful observation systems of spread-F. If spread-F in the ionogram, which shows the reflection height of HF radio waves versus carrier frequency, is detected automatically by a machine learning system, real time detection of spread-F could be replaced by the automatic detection system using the machine learning system. In this study, therefore, we have developed an automatic detection of spread-F in the ionogram using machine learning.

In order to construct the classifer, the ionograms observed at 4 observatories (Wakkanai, Kokubunji, Yamagawa, Okinawa) utilized by National Institute of Information and Communications Technology were prepared. As for learning data, we used 400 ionograms with spread-F observed at each stations in 2018. HOG (Histogram of Oriented Gradients) feature extraction is used in obtaining the feature quantity.

Using the classifier to detect spread-F in the ionograms observed at Okinawa in May 2019, a detection rate reached about 90%. This classifier is also enable to detect the spread-F in the ionograms obtained at Kokubunji and Yamagawa with the detection rate of 90%. However, the detection rate of the spread-F in the ionograms observed at Wakkannai is very low (about 60%). In the presentation, we will present the comparison with another observation point at the same period.

Keywords: Ionosphere, spread-F, plasma bubble

©2020. Japan Geoscience Union. All Right Reserved.

Examination of the ionospheric perturbations propagation associated with H-IIA rocket launchings

*Junpei Yamazaki[1], Hiroyuki Nakata[2], Hiroyo Ohya[2], Toshiaki Takano[2], Keisuke Hosokawa[3]

1. Graduate School of Science and Engineering, Chiba University, 2. Graduate School of Engineering, Chiba University, 3. Department of Communication Engineering and Information, University of Electro-Communications

It is reported that passage and exhaust plumes associated with rocket launches generate TEC perturbations observed by GEONET data (e.g. Furuya and Heki, 2008; Lin et al, 2014, 2017). On the other hand, there are few studies about ionospheric perturbations associated with rocket launches away from rockets' trajectories. Becouse the disturbances due to exhaust plumes do not apper in the distance from the trajectories, we can extract the disturbances only affected by the atmospheric wave. Using HF Doppler sounding, therefore, we analyzed ionospheric perturbations associated with H-IIA (Flight.25 and 26) whose trajectories are relatively far from the Japanese Islands. The Doppler sounding system is utilized by the University of Electro-Communications. In this system, the radio waves of 5.006 MHz and 8.006 MHz are transmitted from Chofu campus of University of Electro-Communications and those of 6.055 MHz and 9.595 MHz are from Nagara transmitter Radio NIKKEI. In this study, the Doppler shifts data observed at Sugadaira, Oarai, Kakioka, and Fujisawa were used. In those data, the perturbations of Doppler frequency associated with H-IIA (Flight.25 and 26) were observed about 35 minutes after the launches. It is confirmed that this delay corresponds to the propagation time of the infrasound wave from the rocket to observation points once reflected on the ground. In both events, the periods of the disturbance of Doppler shift were 100~200 s (5~10 mHz). The Doppler frequency perturbations appered when the infrasound wave reached the obserbations point after reflection on the ground as compared to the case where the infrasound wave reached the observation point directly. The Doppler frequency perturbation consist of two packets, the first half (packet A) and the second half (packet B). In case of packet A, the arrival time of the perturbations at high altitude were faster than that of at low altitude. Therefore, it denoted that infrasound wave propagated from high altitude to low altitude. In case packet of B, the arrival time of the perturbations at both high and low altitude were simultaneously observed. This result indicates that the infrasound wave propagate almost horizontally.

Keywords: Ionospheric, rocket, HF Doppler Sounding

©2020. Japan Geoscience Union. All Right Reserved.

Spatial and temporal distributions of atmospheric gravity wave potential energy evaluated using ERA-5 temperature data over the equatorial latitudes

*Shih-Sian Yang[1], Chen-Jeih Pan[1], Uma Das[2], Chian-Chiau Lin[3]

1. National Central University, Jhongli, Taoyuan 32001, Taiwan, 2. Department of Physics, Indian Institute of Information Technology, India, 3. Environmental Research and Information Center, Chang Jung Christian University, Taiwan

In this study, we used the temperature profiles retrieved from ERA5, the newest atmospheric reanalysis dataset issued by the European Centre for Medium-Range Weather Forecasts (ECMWF), to evaluate the potential energy (E_P) in the atmosphere from the near ground surface to ~80 km altitude over the equatorial latitudes of ±10°. E_P is calculated from the fluctuation of temperature, which is considered to be generated by atmospheric gravity waves (AGWs), and we have constructed the spatial and temporal distributions of E_P over the equatorial latitudes using the high-resolution data from ERA5. In this study, we will present the variations of E_P in time, altitude, and longitude. Overall, E_P is controlled by the zonal flow of the background atmosphere. Especially the time-varied descending structures of high E_P value coincide with the westerly shear of zero-wind in the stratosphere, which implies the Kelvin wave-mean flow interactions in the stratospheric altitudes. Besides, the longitudinal analysis shows that E_P is higher in the eastern Pacific at all altitudes except around the tropopause. In addition, we checked the E_P values during different atmospheric and oceanic conditions, to examine the possible relationship between El Niño/La Niña and atmospheric gravity waves. With regards to the E_P distribution caused by Kelvin waves in the stratosphere, we will also compare the results with the Kelvin wave amplitudes obtained by the two-dimensional fast Fourier transform (2D-FFT) method in this presentation.

Keywords: Atmospheric gravity waves, Potential energy, Zonal wind, Wave-mean flow interactions, ERA-5

©2020. Japan Geoscience Union. All Right Reserved.

Atmospheric wave propagation observed by GNSS-TEC: Fireball explosion and atmospheric mode

*Ai Matsushita[1], Kosuke Heki[1]

1. Hokkaido University Graduate School of Science

The electron distribution in the ionosphere is often disturbed by various phenomena in the atmosphere. They are observed as changes in TEC (Total Electron Content) along line-of-sight connecting GNSS (Global Navigation Satellite System) satellites and receivers. For example, large meteorites entering the Earth’ s atmosphere often explode and are recognized as fireballs. Sound waves and internal gravity waves excited by them propagate through the atmosphere, reach the ionospheric F region, and change TEC. A fireball appeared near Chelyabinsk, Russia, on February 15, 2013, one of the largest fireball events in the observation history, made significant disturbance signals in TEC observed with multiple GPS satellites and ground receivers. In our study, we first confirm the TEC signals in the 2013 Chelyabinsk event, and then look for the TEC disturbance signals following the emergence of a large-scale fireball over the Bering Sea in December 2018 using data from nearby GNSS stations. We found temporary positive TEC changes and continuous TEC fluctuations shortly after the fireball event. Although the numbers of satellites and stations were not sufficient, these signals are considered to have originated from this fireball event.

Next we obtained continuous TEC records in 2019 using the QZSS (Quasi-Zenith Satellite System) geostationary satellite (PRN07), which enables long-term stable TEC observations in and around Japan. We performed preliminary investigations to detect various kinds of TEC disturbances. First, we conducted spectral analysis of the QZSS-TEC time series with various time windows. As a result, we identified peaks such as the diurnal changes and its harmonics, and the rotation period of the sun. Ground observations of gravimeters and broadband seismometers revealed incessant excitation of the Earth's free oscillations. It was also found that the two components having periods close to the atmospheric modes with periods of 3- 4 minutes have significantly larger amplitudes than other components. This suggests the coupling between the solid earth and the atmosphere. It is possible that there are same frequency components in TEC variations, but it has not yet been confirmed. In this study, we examine if we can detect weak atmospheric modes by using continuous QZSS-TEC data.

Keywords: TEC, GPS, QZSS

©2020. Japan Geoscience Union. All Right Reserved.

Investigation of the climatology and long-term variations of the stratospheric Kelvin waves using ERA-Interim

*Chen-Jeih Pan[1], Shih-Sian Yang[1], Uma Das[2], Wei-Sheng Chen[1]

1. Institute of Space Science, National Central University, Taiwan, 2. Department of Physics, Indian Institute of Information Technology, India

In this study, we proposed a new aspect, based on the temporal evolution of the stratospheric zonal wind, investigating the properties of Kelvin waves during different temporal stages of quasi-biennial oscillation (QBO) in the stratosphere. 16 cycles of the stratospheric QBO were found during the period of 1979–2018 using the zonal wind profiles over the equatorial region (±10˚), which was retrieved from ERA-Interim, a long-term reanalysis dataset produced by the European Centre for Medium-Range Weather Forecasts (ECMWF). The duration of each QBO cycle varies from 23 to 42 months among the 16 cycles, and this variability causing the investigations regarding Kelvin waves and QBO are unexpectedly arduous. Therefore, we tried to standardize the elapsed time during each QBO cycle to 0–1, to study the climatological connections between the QBO phase and the amplitudes of wavenumber 1 as well as wavenumber 2 Kelvin waves. Another reanalyzed atmospheric parameter of temperature were retrieved from the same ERA-Interim dataset, and the Kelvin wave amplitudes at 6–24 days periods were analyzed using the method of two-dimensional fast Fourier transform (2D-FFT). The results of the present study show the dominant wave period varies from shorter to longer periods as the time elapses in a QBO cycle. Fast Kelvin waves are more evident in the upper stratosphere, but slow Kelvin waves are further apparent in the lower stratosphere. Besides, we also found the Kelvin wave activities have significantly increased in the 21st century. The present study is the first attempt to investigate the long-term (40 years) morphology of Kelvin waves using the ERA-Interim reanalysis dataset. Conclusions regarding the climatological variations of Kelvin waves lend us further understanding of the Wave-mean flow interactions in the stratosphere over the equatorial region.

Keywords: Atmospheric Kelvin waves, Quasi-biennial oscillation, Wave-mean flow interactions, ERA-Interim

©2020. Japan Geoscience Union. All Right Reserved.

Statistical study of seasonal dependence of MSTID occurrence and propagation velocity using the SuperDARN Hokkaido East HF radar

*Wataru Hazeyama[1], Nozomu Nishitani[1], Tomoaki Hori[1]

1. Institute for Space-Earth Environmental Reseach

We present the results of the statistical study of medium-scale traveling ionospheric disturbances (MSTIDs) using the SuperDARN Hokkaido East (43.53˚N, 143.61˚E) high-frequency (HF) radar data from 2009 to 2018. We applied a three-dimensional fast Fourier transform method developed by Matsuda et al. (2014) to the dataset and analyzed the diurnal and seasonal dependences of the propagation direction and horizontal phase velocity of MSTIDs. Southwestward propagating MSTIDs are common during winter in the nighttime and southward propagating MSTIDs are common during winter and equinoxes in the daytime. Although rare in comparison with the southwestward propagating MSTIDs, certain number of northward propagating MSTID events are found. We also found a clear negative correlation between the yearly power spectral density of nighttime MSTIDs and F10.7 solar flux index. This negative correlation can be explained in terms of the linear growth rate of the Perkins instability.

Keywords: MSTID, SuperDARN radar

©2020. Japan Geoscience Union. All Right Reserved.

First simultaneous observation of nighttime medium-scale traveling ionospheric disturbance (MSTID) by a ground airglow imager and the Arase satellite in the inner magnetosphere

*Kouki Kawai[1], Kazuo Shiokawa[1], Yuichi Otsuka[1], Yoshiya Kasahara[2], Fuminori Tsuchiya[3], Ayako Matsuoka[4], Yasumasa Kasaba[3], Kazushi Asamura[4], Satoshi Kasahara[6], Yoshizumi Miyoshi[1], Shin-ichiro Oyama[1,7,8], Yoichi Kazama[5]

1. Institute for Space-Earth Environmental Research, Nagoya Univ, Japan, 2. Kanazawa Univ, Japan, 3. Tohoku Univ, Japan, 4. Japan Aerospace Exploration Agency, 5. Academia Sinica, 6. Tokyo Univ, Japan, 7. Oulu Univ, Finland, 8. National Institute od polar Research

Medium Scale Traveling Ionospheric Disturbance (MSTID) is the propagation of the electron density fluctuation in the ionospheric F-layer. The mechanism of MSTID generation is based on the theories of atmospheric gravity waves from the ground and ionospheric E-F coupling and Perkins instability. It is known by simultaneous observation of airglow imagers in both hemispheres that the MSTID has a mirror image structure at the magnetic conjugate hemisphere. If the MSTID is generated by the E-F coupling and Perkins instabilities and grow up with **E**×**B** drift, the polarization electric field associated with the growth of the MSTID should propagate along the magnetic field lines. So, we are expected to observe the electric field variations by the Arase satellite flying in the inner magnetosphere. This observation has never been reported. Therefore, in this study, we have analyzed the MSTID observed at 06:00:00-06:30:00 UT on November 3, 2018, in detail by the airglow camera at Gakona (62.39 N, 214.78 E), Alaska, and the Arase satellite in the inner magnetosphere. The purpose of this study is to understand the correspondence between the MSTID structure in the ionosphere and the electromagnetic field and plasma in the conjugate inner magnetosphere. The electric field observed by the electric field detector (EFD) and the electron density observed by the high frequency analyzer (HFA) of plasma wave experiment (PWE) on board the Arase satellite fluctuated associated with the structure of the MSTID, when the satellite footprint in the ionosphere crossed almost perpendicularly to the phase surface of the MSTID. We projected the electric field variations observed by the satellite onto the ionosphere. We found that the electric field variations were nearly perpendicular to the phase surface of the MSTID. This variation indicates the polarization field that causes the MSTID through **E**×**B** drift. We also inferred the direction of the possible Pedersen current and the background electric field from the observed direction of the propagation and the electric field variations in the ionosphere, though we could not obtain direct evidences of these current and electric field from the current observation. We discuss these observation results in relation to the generation and growth mechanisms of MSTIDs.

Keywords: Medium-Scale Traveling Ionospheric disturbance (MSTID), Arase satellite, Optical Mesosphere thermosphere Imagers (OMTIs), Plasma Wave Experiment (PWE), Electric Field Detector (EFD), high Frequency Analyzer

©2020. Japan Geoscience Union. All Right Reserved.

Study of variations in the D-region ionosphere after the 2016 Kumamoto earthquakes using VLF/LF transmitter signals

*Tekkan Akashi[1], Hiroyo Ohya[2], Hiroyuki Nakata[2], Fuminori Tsuchiya[3]

1. Graduate School of Science and Engineering, Chiba University, 2. Graduate School of Engineering, Chiba University, 3. Graduate School of Science, Tohoku University

There have been many reports for the variations in the F-region ionosphere associated with earthquakes based on GPS-TEC (total electron content), ionosondes, SuperDARN(Super Dual Auroral Radar Network) Hokkaido HF (high frequency, 3-30 MHz) radars, and HF Doppler observations [e.g., Tsugawa et al., 2011].In the D-region ionosphere, oscillations of LF (low frequency, 30-300 kHz) transmitter signals with a period of 100 s were reported about five minutes after mainshock of the 2011 Tohoku Earthquakes [Ohya et al., JGR, 2018]. The reflection height of the LF waves was 67 km, and the LF oscillations were caused by acoustic waves excited by seismic Rayleigh waves based on simulation of neutral atmosphere. However, the D-region response after earthquakes was reported only in above case study, and more investigation is required. In this study, we investigate the lower ionospheric variations associated with the 2016 Kumamoto earthquake using VLF(very low frequency, 3-30 kHz)/LF transmitter signals. The foreshock (Mw 6.2) and mainshock (Mw 7.0) of the 2016 Kumamoto earthquakes occurred at 12:26:34 UT on April 14, and at 16:25:05 UT on April 15, 2016, respectively. The propagation paths were BPC(68.5 kHz, China)-SGR (Sasaguri, Japan), JJY60kHz(Saga, Japan)-SGR, and JJY40kHz(Fukushima, Japan)-SGR, and JJI(22.2 kHz, Miyazaki, Japan). In addition, we used vertical velocity data of seismometers of the F-net (Full range ,,,network) provided by the Data and Disaster Prevention Research Institute, Japan. As for the mainshock, variations in the LF intensity had a period of 100 s about five minutes after the maishock based on wavelet analysis. The duration of the LF variations was about six minutes. The onset of the LF variations was agreement with arrival time of acoustic waves excited by the Rayleigh waves below the LF path. The coherence between the JJY40kHz-SGR intensity and seismic velocity at SBR (Seburi, Japan) close to the JJY40kHz-SGR path (the distance: 35 km) was high to be 0.73 for the period of 128 s. It suggests that acoustic waves that propagated vertically from the location of the LF path caused the LF variations. In the session, we will also show the results of the foreshock, and discuss the cause of the VLF/LF variations in addition with the mainshock.

©2020. Japan Geoscience Union. All Right Reserved.

Analysis of source and generation mechanism of atmospheric gravity waves and MSITDs observed in airglow images in Hawaii

*Hideto Naito[1], Kazuo Shiokawa[1], Yuichi Otsuka[1], Takeshi Sakanoi[2], Akinori Saito[3], Takuji Nakamura[4]

1. Nagoya University, 2. Tohoku University, 3. Kyoto University, 4. National Institute of Polar Research

Atmospheric gravity waves (AGWs) and medium-scale traveling ionospheric disturbances (MSTIDs) are important wave phenomena in the upper atmosphere, since they can control global dynamics of the atmosphere and affect GNSS positioning. Matsuda et al. [JGR, 2014] proposed a method of deriving the horizontal phase velocity and propagation direction of the power spectral density of waves found in images using three-dimensional Fast Fourier transform. However, there has been few report to apply this method to airglow images obtained near the equator except for Perwitasari et al. (AnnGeo, 2018) in Indonesia. In this study, we applied the analysis method of Matsuda et al. [2014] to airglow images obtained at wavelengths of 557.7 nm and 630.0 nm during the three years from 2013 to 2016 at Haleakala (20.7°N, 203.7°E) in Hawaii. We clarified the statistical features of AGWs and MSTIDs over Hawaii, and compared them with features seen in Japan reported by Takeo et al. [JGR, 2017] and Tsuchiya et al. [JGR, 2018], where the latitude, longitude and orography are greatly different those of Hawaii.

The three-year averages of the phase velocity spectra of AGWs observed in airglow images at a wavelength of 557.7 nm show that there was no difference in the zonal propagation between summer and winter. In Japan, however, it is known that the propagation direction is eastward in summer and westward in winter. We reported this result in JpGU2019 and discussed this difference due to latitudinal variation of mesospheric jet wind which controls AGW propagation through wind filtering effect. In the presentation we will discuss the source of atmospheric gravity waves from the tropospheric upward flow and jet using reanalysis data in the troposphere. As a result, the upward flow in the troposphere was not strongly observed in the area where the wave source was expected. This is probably due to the averaging, so we will analyze each observation day.

The MSTIDs observed in airglow images at a wavelength of 630.0 nm show that the power spectral density (PSD) was strongest and the waves propagate mainly in the east-west direction in winter. We reported this result in SGEPSS2019 and discussed a mechanism for generating MSTIDs due to atmospheric gravity waves. We will discuss the source of atmospheric gravity waves related to this mechanism from the tropospheric upward flow and jet using reanalysis data. As a result, the upward flow in the troposphere was not strongly observed in the east-west direction where the wave source is expected. This is probably due to the averaging, so we will analyze each observation day. Regarding the east-west propagation of MSTIDs in winter, we made detailed event study using zonal keogram and wave number spectrum, and compared with MSTIDs observed in Japan.

Keywords: Airglow, MSTIDs, Hawaii, AGWs

©2020. Japan Geoscience Union. All Right Reserved.

©2020. Japan Geoscience Union. All Right Reserved.

Solar flare effects of the D-region ionosphere using daytime tweek atmospherics and VLF/LF standard radio waves

*Kodai Yamanobe[1], Hiroyo Ohya[1], Hiroyuki Nakata[1], Kazuo Shiokawa[2], Fuminori Tsuchiya[3], Kozo Yamashita[4], Yukihiro Takahashi[5]

1. Chiba Univ., 2. Nagoya Univ., 3. Tohoku Univ., 4. Ashikaga Univ., 5. Hokkaido Univ.

It has been known that intensity and phase of very low frequency (VLF, 3-30 kHz)/low frequency (LF, 30-300 kHz) transmitter signals significantly change due to intense ionization by solar flares [e.g., Mitra, 1974; Thomson et al., 2005]. The duration of the D-region enhancements due to X-ray is easier to be estimated using the VLF/LF waves, because the relaxation time for recombination in the D-region ionosphere is short to be within ~100 s [e.g., Ohya et al., 2015]. Santolik and Kolmasova [2017] showed daytime tweek atmospherics (1.5-10.0 kHz) did not become observable for two hours at least just after a solar flare of M2.2 class, which suggests large absorption due to the solar flare. In this study, we investigate solar flare effects on the D-region ionosphere using tweek atmospherics and VLF/LF transmitter signals. We analyzed the daytime tweek atmospherics observed at Moshiri (44.37N, 142.27E), Japan, during several M-class flares occurred in 2015. The sampling frequency was 20 kHz, and the wideband VLF data were recorded for each two minute at 20-22 and 50-52 minutes every hour. The transmitters used in this study were NWC (21.817S, 114.167E, 19.8 kHz), JJI (32.05N, 130.82E, 22.2 kHz), JJY40kHz (37.37N, 140.85E), JJY60kHz (33.47N, 130.18E), and BPC (34.63N, 115.83E, 68.5 kHz).The receivers were PTK (Pontianak, Indonesia, 0.003N, 109.367E), and SGR (Sasaguri, Japan, 33.632N, 130.505E). The occurrence rate of the tweeks after the M-class solar flares was smaller than that before the flares except for a M2.0-class flare. When the distance between the sub-solar point and the middle point of the VLF/LF paths decreased, amplitude of the variations in the VLF/LF phase and time difference between onsets of variations in X-ray flux and the VLF/LF intensity increased for a few M-class solar flares. It suggests that the D-region ionization near the sub-solar point was more intense than that located away from the sub-solar point. In the session, we will show the results in detail and discuss the solar flare effects on the D-region ionosphere.

©2020. Japan Geoscience Union. All Right Reserved.

The spatial structures and seasonal variations of the polar mesospheric clouds seen from the meteorological satellite Himawari-8

*Yuta Hozumi[1], Takuo T. Tsuda[1], Kento Kawaura[1], Yoshiaki Ando[1], Keisuke Hosokawa[1], Hidehiko Suzuki[2], Takuji Nakamura[3], Ken T. Murata[4]

1. University of Electro-Communications, 2. Meiji University, 3. National Institute of Polar Research, 4. National Institute of Information and Communications Technology

Polar mesospheric clouds (PMCs) consist of water-ice particles, and have been observed near the summer polar mesopause region. Production and disruption of PMC are sensitive to the background mesospheric state, such as the temperature and water vapor conditions. Its distribution is strongly affected by the background wind. Hence, PMC is a good proxy for the thermal structure and dynamics in the high latitude summer mesosphere.

Observations of PMC have been widely performed by various methods from the ground as well as from Low-Earth-Orbit (Leo) satellites. However, these methods have some limitations, especially in local time coverage or observational continuity to monitor the long-term PMC activity. While a large number of studies have been done with the LEO satellites data, there are only a few studies of PMC observations from Geostationary Earth Orbit (GEO) satellites, which include Meteosat First Generation (MFG) and Meteosat Second Generation (MSG). The GEO satellites provide full-disk images of the Earth including the polar mesosphere on the Earth's limb, which would give valuable opportunities for PMC observations.

Recently, our group found that the PMC signal can be observed by the Advanced Himawari Imager (AHI) onboard Himawari-8, the Japanese Geostationary-Earth-Orbit meteorological satellite (Tsuda et al., 2018). In the presentation, we will show the PMC detection method for application to Himawari-8 AHI images. To evaluate the PMC signal correctly, the background emissions from atmospheric scattering (i.e., Rayleigh scattering) should be removed. We present how we remove the background emissions and evaluate the PMC signal. The detection capability, especially the limit of sensitivity, of AHI on the PMC observations will be discussed. Based on the detection method, The PMC spatial structures and its temporal variations will be presented.

©2020. Japan Geoscience Union. All Right Reserved.

Fireball-associated variations in the D-region ionosphere observed using VLF/LF transmitter signals

*Takeru Suzuki[1], Hiroyo Ohya[2], Fuminori Tsuchiya[3], Kazuo Shiokawa[4], Hiroyuki Nakata[2]

1. Graduate School of Science and Engineering, Chiba University, 2. Graduate School of Engineering, Chiba University, 3. Graduate School of Science, Tohoku University, 4. Institute for Space-Earth Environmental Research, Nagoya University

Meteors and fireballs are known to ionize the D-region and lower E-region ionospheres at 80-120 km heights [Davies, 1966]. The fireballs are meteors that the magnitude of brightness is larger than -4 based on the IAU (International Astronomy Union) definition. TID (traveling ionospheric disturbance) associated with the Chelyabinsk meteoroid in Russia was reported based on GPS-TEC (total electron content) observations [Perevalova et al., 2015]. The amplitude of the TEC variations was 0.07-0.5 TECU, and the period was 10 minutes. The epicenter of the TID was airburst point at 20-30 km heights of the meteoroid, and the velocities were 250-660 m/s. However, few quantitative studies for the lower ionosphere associated with meteors and fireballs have been reported. In this study, we investigate the variation in the lower ionosphere during a fireball occurred in Hokkaido, using VLF (very low frequency, 3-30 kHz) / LF (low frequency, 30-300 kHz) transmitter signals. The VLF/LF transmitter signals are reflected in the lower ionosphere and are sensitive for variations in electron density in the lower ionosphere. The transmitters used in this study were JJY40kHz (Fukushima, Japan, 37.37˚N, 140.85˚E), JJY60kHz (Saga, Japan, 33.47˚N, 130.18˚E), and JJI (Miyazaki, Japan, 22.2 kHz, 32.05˚N, 130.82˚E). The receiver was located at RKB (Rikubetsu, Japan, 43.45˚N, 143.77˚E). Periodic variations of 100-200 s were identified by a wavelet transformation of the signal intensities for the JJY40kHz-RKB, JJY60kHz-RKB, and JJI-RKB paths at about five minutes (12:01 UT) after the fireball. The phases of the JJY40kHz-RKB and JJY60kHz-RKB paths had similar periods of 100-200 s at that time. We consider that these variations of intensity and phase are caused by the D-region variations due to acoustic waves in the atmosphere excited by the fireball. If the acoustic waves were excited at the luminous point (118 km altitude), the VLF/LF reflection point (90 km altitude) or vanishing point (25 km altitude) of the fireball, the propagation times of the acoustic waves from the exited point to the LF reflection point at 90 km height over RKB were calculated to be 138 s, 126 s, or 311 s, respectively. The arrival time (311 s) of the acoustic waves excited from the vanishing point at the 25-km altitude agrees with the onset timing of the VLF/LF variations (~5 minutes), suggesting that the acoustic waves excited from the fireball caused the variations in electron density in the D-region ionosphere. We will also show results with another fireball event over Nagano, Japan, at 13:00 UT on 12 November, 2019, and discuss the fireball effects on the lower ionosphere.

©2020. Japan Geoscience Union. All Right Reserved.

Calcium ion layer observed with resonance scattering lidar at Syowa Station

*Mitsumu K. Ejiri[1,2], Takanori Nishiyama[1,2], Takuo T. Tsuda[3], Makoto Abo[4], Katsuhiko Tsuno[5], Takuya Kawahara[6], Takayo Ogawa[5], Satoshi Wada[5], Takuji Nakamura[1,2]

1. National Institute of Polar Research, 2. The Graduate University for Advanced Studies, SOKENDAI, 3. The University of Electro-Communications, 4. Tokyo Metropolitan University, 5. RIKEN, RAP, 6. Shinshu University Faculty of Engineering

Layers of metal ions in the mesosphere and lower-thermosphere (MLT) are produced by meteoric ablation. The meteoric metal ions have relatively long chemical life time in the MLT region and behave as plasma affected by neutral atmosphere dynamics. In the mid-latitude, the meteoric metal ions in the MLT region are generally accepted as key species for generation of sporadic E (E_s) layer in the wind shear theory. The close link between the E_s layer and metal ion layer has been also clearly by radar and lidar observations [Raizada et al., 2012; Ejiri et al., 2019]. On the other hand, the latitudinal differences in behaviors of the metal ion are still unknown. Recently, the Whole Atmosphere Community Climate Model incorporated a large database of neutral and ion–molecule reaction kinetics of calcium (Ca) species (WACCM-Ca) simulated the seasonal Ca^+ layer globally [Plane et al., 2018]. However, the results cannot be vilified well because observation lacks except at the mid-latitude in the northern hemisphere.

A new resonance scattering lidar system with frequency-tunable alexandrite laser was developed by the National Institute of Polar Research (NIPR) and installed at Syowa Station (69˚S, 40˚E) by the 58th Japan Antarctic Research Expedition (JARE 58). Density profiles of Ca^+ in the MLT region over Antarctic were successfully observed 6 nights in total in 2017 and 2018. In this presentation, we will show temporal variation of the Ca^+ layer in Antarctic for all events and discuss its characteristics.

Keywords: mesospheric Ca+ layer, Antarctic, Lidar observation

©2020. Japan Geoscience Union. All Right Reserved.

Generation and movement of equatorial plasma bubbles: Roles of vertical plasma drifts, seeding perturbations, and geomagnetic storms

*Chaosong Huang[1]

1. Air Force Research Laboratory Albuquerque

We study the characteristics and generation mechanism of equatorial plasma bubbles measured with the Communication/Navigation Outage Forecasting System satellite. It is found that the global distribution of the prereversal enhancement (PRE) of the postsunset equatorial vertical ion drift is very similar to that of the bubble occurrence. Ion density perturbations in different local time sectors are analyzed, and there is no obvious correlation between the afternoon ion density disturbances and the evening bubble occurrence. The results indicate that the PRE is the primary factor that controls the generation of plasma bubbles and that seeding perturbations may always exist in the equatorial region. Effects of geomagnetic storms on the PRE are examined. Penetration electric fields during the storm main phase cause enhancements of the PRE, increasing the occurrence of plasma bubbles, and disturbance dynamo electric fields during the storm recovery phase cause the PRE to decrease, suppressing the occurrence of plasma bubbles. Furthermore, geomagnetic storms cause strong westward plasma drifts in the nighttime equatorial ionosphere, which can reverse the normal eastward drifts of plasma bubbles to westward. The relationship among plasma bubble occurrence, postsunset vertical plasma drift, seeding perturbations, and geomagnetic storms will be addressed.

Keywords: Equatorial plasma bubble, Prereversal enhancement, Seeding perturbation, Vertical plasma drift, Geomagnetic storm

©2020. Japan Geoscience Union. All Right Reserved.

Variations of the Earth's magnetic field during fall of the Tunguska and Chelyabinsk bolides: analogies and differences

*Ravil Rakhmatulin[1]

1. Institute of Solar-Terrestrial Physics, SB RAS

A superbolide with an estimated mass of 13,000 tonnes exploded at an altitude of 22 km over the city of Chelyabinsk (Russia) at 03 hours 20 min. 33 sec. UTC on February 15, 2013. It is now known as the Chelyabinsk meteorite. Over the past 100 years after the fall of the Tunguska meteorite on June 30, 1908, this event was an entry of the second largest object from outer space into the Earth’s atmosphere. In the literature describing the occurrence of magnetic effects during the fall and explosion of the Tunguska meteorite in the magnetosphere and atmosphere of the Earth on June 30, 1908, some researchers mentioned a change in variations in the Earth's magnetic field 80 minutes before the explosion itself [Kucherov, 2008]. Similar features of the magnetic field components observed by the Irkutsk Magnetic Observatory are identified by the comparative analysis of the magnetic field variations during the falls of the Tunguska and Chelyabinsk space bodies through the magnetosphere.

Acknowledgments

The reported study was funded by RFBR, Russian-Taiwanese joint research project number 18-55-52006 MHT_a. Experimental data recorded by the magnetometric complex of Center for Common Use «Angara» (http://ckp-rf.ru/ckp/3056/) obtained with budgetary funding of Basic Research program II.16 were used.

References

Kucherov V.I. About the explosion of the Tunguska cosmic body in the Earth’s atmosphere // Bulletin of Moscow State University, 2008, No. 4, p. 32-47

Keywords: meteorite; magnetosphere; magnetic field; magnetic variations; geomagnetic pulsations

©2020. Japan Geoscience Union. All Right Reserved.

Atmospheric-ionospheric vertical coupling study focusing on the quasi-6-day oscillation in Sq-EEJ current system

*Takayama Kumi[1], Yasunobu Miyoshi[1], Akimasa Yoshikawa[1]

1. Kyushu University

Atmospheric oscillations in the Sq-EEJ current system using MAGDAS (Global Geomagnetic Observation Network) magnetic field data were analyzed for a comprehensive understanding of the three-dimensional coupled atmosphere-ionosphere-magnetosphere system. In this study, we focus on the 6-day oscillation phenomenon (Q6DO) excited in the troposphere and report its globality, its seasonal dependence of its excitation characteristics, and its solar activity dependence respectively.

It is known that, the quasi-6-day wave (Q6DW), one of the atmospheric waves, is caused by atmospheric heating by moist air in the tropical troposphere [Miyoshi and Hirooka1999] and has a seasonal dependence that strongly develops in the spring and autumn equinoxes [H.-L. Liu et al. 2004]. It has been suggested that the equatorial electrojet (EEJ) has a very high "variability" that fluctuates under the influence of various forcing mechanisms including atmospheric waves from the lower layer. Q6DO in Sq-EEJ current system was verified with CHAMP satellite, Swarm satellite, EEJ intensity data and EEJM (EEJ empirical model) and geopotential height of MLS measurement [Yamazaki et al., 2018]. In addition, the distribution of it near the equator was clarified using the total electron content (TEC) from GPS data and the geopotential height of Aura satellite / MLS measurements. A nearly one-to-one correspondence is found between Q6DW activities in the ionosphere and lower thermosphere [Yamazaki et al., 2019]. However, understanding of wave components in the atmosphere, which is expected to appear in the ground magnetic field fluctuation data excited by the Sq-EEJ current system, is not advanced.

In this study, we analyzed the globality of the 6-day oscillation phenomena in EEJ, the seasonal dependence of its excitation characteristics, and solar activity dependence using magnetic field data of MAGDAS.

For the analysis, we use EE-index, a proprietary index developed by Kyushu University to capture in real time the EEJ, a phenomenon of the ionosphere on the magnetic equator [T. Uozumi et al. 2008] and [T. Ueno et al. 2008]. EE-index is composed of three elements: EDst, EU and EL. EDst represents the global symmetric variation of the magnetic field above the magnetic equator, and EU ·EL represents the variation component of the magnetic field due to EEJ and CEJ, respectively. In this study, we extracted Q6DO in EEJ using the EUEL data from January 1, 2005 to February 25, 2019. The main analysis procedure is as follows.

(1) For the daytime peak of EUEL data (1h value) of each observation point, the quasi-6-day fluctuation component was extracted by a bandpass filter for 5-7 days.

(2) Compare the results of three observation points with more than 60% of the annual data and verify if it is a global phenomenon.

(3) Verification of solar activity dependence by comparison with solar activity index F10.7.

(4) Verification of seasonal dependence.

©2020. Japan Geoscience Union. All Right Reserved.

As a result, it was revealed that Q6DO in the Sq-EEJ current system is a global phenomenon that develops at about the same time regardless of magnetic longitude and latitude and is dependent on solar activity. It was also found that Q6DO has similar seasonal dependence to Q6DW in the atmosphere. Details of the analysis will be introduced in the lecture.

As a future work, it is necessary to look at mid-latitude observation points in order to see a wider range of global distribution. Also, between stations with similar magnetic latitudes such as ANC and DAV, there is a difference in the amplitude of Q6DO, therefore it is necessary to grasp and verify the annual fluctuation trends of each station.

Henveforth, how Q6DO originating from thermal convection in the atmosphere will be affected before reaching the ionosphere and excite EEJ fluctuations

That will be displayed using the GAIA model (the numerical model integrated with the atmospheric model that covers the whole atmospheric region and the ionospheric model) This study will be carried out as a part of the joint research of the Kyushu University-GFZ group.

Keywords: Quasi-6-day wave, Equatorial electrojet, Ionosphere, vertical coupling

©2020. Japan Geoscience Union. All Right Reserved.

Investigating of cusp heating process by using chemical releases of Ba/Sr: Initial result of CHI rocket experiment

*Taro Watanabe[1], Yoshihiro Kakinami[2], Masa-yuki Yamamoto[1], Miguel Larsen[3], Mark Conde[4], Takao M. Sato[2], Yuuichi Kaga[2], Takako Kaga[2]

1. Kochi University of Technology, 2. Hokkaido Information University, 3. Clemson University, 4. University of Alaska Fairbanks

In the thermosphere of the cusp region, there are atmospheric heating phenomena that mechanisms are unexplained so far. Lühr et al. [2004] showed atmospheric density enhancements accompanied by the very intense small-scale field-aligned currents (FAC) filaments in the cusp region observed by the CHAMP satellite. They concluded that the Joule heating in the E region of ionosphere caused an up-welling of neutral atmosphere and it led to a density enhancement at 400 km and above. And they also concluded that the small-scale electric field associated with the closure currents of small-scale FACs causing Joule heating may play an important role in the enhancement. In order to obtain the evidence of the Joule heating, more quantitative measurements, especially electric field measurements with high-resolution are required. We observed neutral wind and ion drift with chemical release experiments of Ba/Sr. In November 2014, the sounding rocket experiment named the Cusp Region Experiment 1 (C-REX-1) was launched from Andøya Space Center. C-REX-1 was aimed at measuring the up-welling in the cusp region causing the neutral density enhancements. However, no signatures of the up-welling and small-scale electric field were observed.
We newly developed band-pass filters for ionized Ba (Ba^+, 614.2 nm) and Sr (460.7 nm) with 6 nm bandwidth. The wavelengths of 614.2 nm / 460.7 nm corresponding to the resonance scattering emission of Ba^+/Sr, respectively. We calibrated absolute sensitivity of our system with the filters to determine exposure and ISO speed for Ba/Sr chemical release experiment.
In December 2019, two rocket experiments named C-REX-2 and the Cusp Heating Investigation (CHI) were planned. CHI was launched, but C-REX-2 was postponed due to the low magnetospheric activity and weather conditions. CHI was launched from Svalbard Rocket Range at 09:30 UT, 10 December 2019. And Ba/Sr gases successfully released between the altitude of about 350 km and 180 km (planned nominal) from all of 8 canisters. The resonance scattering emission of Ba^+/Sr gases was optically observed from two ground observation sites of Longyearbyen and Ny-Ålesund in Svalbard, where are about 120 km apart from each other, to determine the velocity of ion drift and neutral wind by triangulation. At each site, we installed two cameras with the filters for Ba^+/Sr. And we successfully obtained the image of Ba^+/Sr drifting. In this paper, we report the initial results of CHI.

References:
Lühr, H., M. Rother, W. Köhler, P. Ritter, L. Grunwaldt, Thermospheric up-welling in the cusp region: Evidence from CHAMP observations, *Geophys. Res. Lett.*, **Vol. 31**, L06805, 2004.

Keywords: Ionosphere, Thermosphere, Cusp Region, Chemical Release, Sounding Rocket

©2020. Japan Geoscience Union. All Right Reserved.

Characterization of counter electrojet current according to specific time frame in Southeast Asian sector

*Nur Izzati Mohd Rosli[1], Nurul Shazana Abdul Hamid[1], Mardina Abdullah[1], Akimasa Yoshikawa[2], Teiji Uozumi[2]

1. Universiti Kebangsaan Malaysia, 2. Kyushu University

Counter electrojet, CEJ current refers to the sudden reversal of equatorial electrojet, EEJ current towards the opposite direction (westward) that is usually happen at dip-equatorial region. In this study, the CEJ occurrence at Southeast Asia region is identified using EUEL index during solar cycle 24. The EUEL index is selected as it is a local index that define EEJ at particular location without global magnetospheric disturbance. The CEJ current can be categorized into a few types depending on its occurrence: morning CEJ (0500-1100), afternoon CEJ (1300-1700), evening CEJ (1800-2200) and night CEJ (2300-0400). The continuous 1-minute data has been utilized to describe CEJ behaviour in each time frame. This behaviour is including the amplitude and duration of the current itself, as well as its dependence toward local time and seasons.

©2020. Japan Geoscience Union. All Right Reserved.

Characterizing ionospheric irregularities with GEONET

*Guanyi Ma[1], Qi Li[1], Takashi Maruyama[2,1], Jinghua Li[1], Qingtao Wan[1], Xiaolan Wang[1], Jiangtao Fan[1], Jie Zhang[1]

1. National Astronomical Observatories, Chinese Academy of Sciences, 2. National Institute of Information and Communications Technology

Ionospheric irregularities disrupt the propagation of radio waves in the frequency range below a few GHz, a band used by navigation and communication systems such as Global Navigation Satellite System (GNSS). Detailed understanding of the irregularity characteristics is helpful to estimate potential degradation of the performance of radio systems. Dense GNSS network can work as two-dimensional array to provide the spatial structure of the irregularities. With high spatial resolution vertical total electron content (VTEC), we propose a spatial fluctuation of total electron content (TEC), SFT parameter, to identify and analyze ionospheric irregularities by using the world’s densest GNSS Earth Observation Network (GEONET) of Japan. The data used in this study are carrier phase of the dual frequency GNSS signals from more than 1300 GNSS receivers of GEONET. VTEC is derived by assuming that it is identical in a grid of 0.1˚× 0.1˚ in longitude and latitude, and removing a quantity of inter-frequency hardware bias mixed with integer ambiguity. SFT is defined as the spatial dispersion of TEC within a specific area at a given time. The size of the specific area for SFT calculation is chosen as 0.8˚× 0.8˚ in longitude and latitude, which corresponds to approximately 77 km×95 km at 400 km height 35˚N of Japan. An SFT map is generated by sliding window to show the spatial variation of the ionospheric irregularities in two dimensions. The map can be used to obtain the size, shape, orientation and intensity distribution of the irregularity structures. Case studies are carried out for three strong irregularity events on 12 February 2000, 20 March 2001 and 10 November 2004. The irregularities are found to be anisotropic branching structures, which elongate in north-south direction when first seen at lower latitudes. The structures can move and deviate from their previous orientations, and eventually drift perpendicular to their orientations. Such analyses of SFT maps with GEONET observation successfully provide a new perspective of irregularity morphology and evolution.

Keywords: Ionospheric irregularity, TEC, SFT

©2020. Japan Geoscience Union. All Right Reserved.

Imaging observation of Ionospheric Field Aligned Irregularities by the PANSY radar at Antarctic Syowa Station

*Daisuke Kagawa[1], Taishi Hashimoto[2], Akinori Saito[1], Koji Nishimura[2], Masaki Tsutsumi[2], Toru Sato[3], Kaoru Sato[4]

1. Graduate School of Science, Kyoto University, 2. National Institute of Polar Research, 3. Graduate School of Informatics, Kyoto University, 4. Graduate School of Science, Tokyo University

Program of the Antarctic Syowa MST/IS Radar (PANSY radar) is a large atmospheric and VHF-band radar located at the Antarctic Syowa Station. This radar has the capability of a MST radar which observes mesosphere, stratosphere, and troposphere, furthermore it is capable of observing plasma quantities in an altitudinal range from 100km to 500km using the ionospheric incoherent scatter (IS). In 2015, the PANSY radar performed the first ionospheric IS observation in the Antarctica. PANSY radar has a frequency of 47MHz, so it is capable of observing the echoes of field aligned irregularities (FAI) in E region. If FAI has a space scale of half wavelength of radio waves they are coherently backscattered, so PANSY radar observes the coherent echoes from 3-m-scale FAI. Signal processing using adaptive beamforming has been developed, because IS observation of PANSY radar is affected by the FAI echoes. PANSY radar has the FAI array of 24 antennas in addition to the main array of 1045 antennas. FAI array comprises of a pair of peripheral linear arrays of 12 antennas, and it can separate the signal from various angles using the directionally-constrained minimization of power (DCMP) algorithm. In fact, by this algorithm, we can observe not only electron density in the background but also FAI and its motion. In the presentation, we will show the temporal variation of FAI by the imaging observation using the PANSY radar, and figure out a physical process of FAI generation, development, and vanish, by comparing with the data of geomagnetic field or aurora at Antarctic Syowa Station.

Keywords: PANSY, Antarctic Syowa Station, Ionospheric Field Aligned Irregularities, adaptive signal processing

©2020. Japan Geoscience Union. All Right Reserved.

Vertical profile of ionospheric disturbances associated with Tohoku Earthquake using GPS occultation observation

*Hiroyuki Nakata[1], Yuto Imae[2], Toshiaki Takano[1], Hiroyo Ohya[1]

1. Graduate School of Engineering, Chiba University, 2. Department of Electrical and Electronics Engineering, Faculty of Engineering, Chiba University

Many studies have reported that ionospheric disturbances occur after giant earthquakes. One of the causes is the infrasound wave excited by ground motions and/or tsunami. The horizontal propagation of the ionospheric disturbances after large earthquake have been examined in detail by using a network of ground-based GPS receivers. On the other hand, the vertical propagation of coseismic ionospheric disturbances especially is rarely reported. In this study, to examine the vertical propagation of the ionospheric disturbances excited by tsunami, we have examined electron density profiles observed by GPS radio occultation measurements of FORMOSAT-3/COSMIC satellites. We analyzed the ionospheric disturbances caused by Tohoku Earthquake (M9.0) occurred at 5:46:18UT on 11 March 2011. Density profiles observed within 3 hours after the passage of tsunami were analyzed. In extracting disturbed components from observed density profiles using Chapman model, short wavelength fluctuations were recognized over altitude 300~500 km. Wavelength spectrums of these fluctuations were calculated using wavelet transform. It is confirmed that the spectrum intensity for the wavelength of 10~64 km were enhanced. Maruyama and Shinagawa (2014) showed that acoustic waves generated by ground motions of seismic wave excite ionospheric disturbances with the wavelength of several tens kilometers. The present results is consistent with these previous studies.

Keywords: Acoustic Wave, Vertical Propagation, Occultation, Tsunami, Tohoku Earthquake

©2020. Japan Geoscience Union. All Right Reserved.

Statistical study of the growth rates of medium-scale traveling ionospheric disturbances observed with GNSS-TEC

*Takafumi Ikeda[1], Akinori Saito[1], Takuya Tsugawa[2]

1. Department of Geophysics, Graduate School of Science, Kyoto University, 2. National Institute of Information and Communications Technology

Medium scale traveling ionospheric disturbance is one of phenomenon in ionosphere and has been studied after 1960th [Hines, 1960].We think two mechanisms, E-F coupling and Perkins Instability, will relate to growth for MSTID at night in mid-latitude [Tsunoda and Cosgrove, 2001 ; Perkins, 1973].Perkins instability can explain propagating direction,but not for generation. Maximum linear growth rate of perturbation intensity of Pedersen conductivity expected from E-F coupling is less than 5 minutes [Yokoyama et al., 2009], which is far shorter than one expected from Perkins Instability [Fukao and Kelley, 1991 ; Miller et al., 1997 ; Shiokawa et al., 2003]. However, Es layer's spatial and temporal scale is less than 100km and 15min [Maeda et al., 2013 ; S.Saito et al., 2007],which is different from E-F coupling model's ones [Yokoyama, 2009]. And also they are different from MSTID’s ones, which are 200-400 km and around 2hours [Otsuka et al., 2011].
So we can't explain MSTID's saturating process only by E-F coupling and we have not observed the rletaion between that process and two mechanisms about growth rate. Therefore, to decide which instability is responsible for growth of nighttime MSTID after generating frontal structure, the growth rate of MSTID was observationally determined with ground-based GNSS network data.
We statistically investigated the growth rate of nighttime-MSTID in Japan in 2014 observed with GNSS-TEC. We applied twospace and time spectral analysis to calculate MSTID’s growth rates. We compared growth rate observed with linear growth rate of Perkins Instability for two method. We calculated latter using by ion temperature, neutral wind velocity, electric field and O mass density of GAIA model [Jin et al., 2008] and magnetic field of IGRF model.
The growth rate of nighttime -MSTID observed was 1.0 - 6.0 ×10-4 s-1 during 1800LT-2400LT in summer.Linear growth rate of Perkins instability in summer was 1.0 - 6.0 ×10-4 s-1 during 1800LT - 2400LT, so they were less than one of the E-F coupling instability.And we observed Es layer by Ionozonde at Kokubunji in 2014 and compared with LT distribution of growth rates in summer. At the result, the peak time of Es layer after midnight was consistent with that of growth rates.However, seasonal distribution of linear growth rates was different from observed growth rates, because we didn't considered about the effect about southern hemisphere for linear growth rates.
In presentation, we talk the detail about the relation between growth rates and two mechanisms, also relation between north and sourthern hemishphere about
nighttime MSTID's generation.

Keywords: Ionosphere, E-F coupling, GNSS

©2020. Japan Geoscience Union. All Right Reserved.

Retrieval of the Mesosphere and Lower Thermosphere (MLT) physical and chemical properties with the proposed Superconducting Submillimeter-Wave Limb-Emission Sounder 2 (SMILES-2)

*Philippe Baron[1], Satoshi Ochiai[1], Hideo Sagawa[2], Akinori Saito[3], Takatoshi Sakazaki[3], Masato Shiotani[3], Makoto Suzuki[4]

1. National Institute of Information and Communications Technology, 2. Kyoto Sangyo University, 3. Kyoto University, 4. Japan Aerospace Exploration Agency

Submillimeter-Wave Limb-Emission Sounder 2 (SMILES-2) is a satellite mission proposed in Japan to probe the middle and upper atmosphere (20–160 km) [1,2]. The main instrument is composed of 4K cooled radiometers operating near 0.7 and 2 THz. The geophysical information would be retrieved from the molecular lines contained in the spectral bands. The diurnal changes of the horizontal wind above 30 km, temperature above 20 km, ground-state atomic oxygen above 90 km, as well as abundance of about 15 chemical species, could be retrieved. In this study we discuss the sounding of the mesosphere and lower thermosphere (60–160 km). Unlike [3] that only considered the radiometer at 763 GHz, a special focus will be put on the complementarity of the 3 spectral bands for retrieving the physical parameters (wind, temperature and density) as well as the composition (O, O_3, H_2O, NO, CO, HO_2 and OH). The presentation will also include a discussion on the retrieval of the 3 components of the geomagnetic fields using the Zeeman effect on the molecular and atomic oxygen lines at 773 GHz and 2.05 THz. The measurement performance will be discribed as the retrieval precision assessed with simulations.

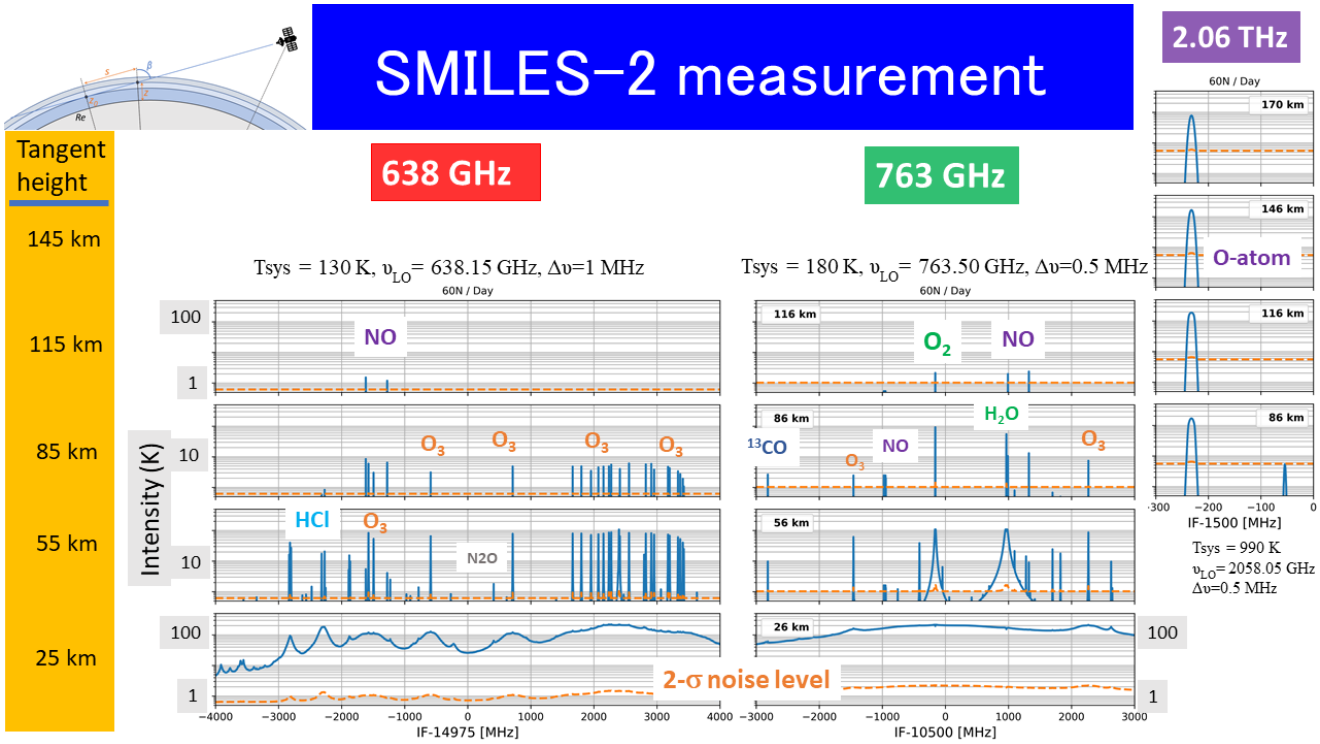
[1] Ochiai, S., Baron, P., Nishibori, T., Irimajiri, Y., Uzawa, Y., Manabe, T., Maezawa, H., Mizuno, A., Nagahama, T., Sagawa, H., Suzuki, M.., and Shiotani, M.: SMILES-2 mission for temperature, wind, and composition in the whole atmosphere, SOLA, 13A, 13–18, https://doi.org/10.2151/sola.13A-003, 2017.

[2] Shiotani, M., Saito, A., Sakazaki, T., Ochiai, S., Baron, P., Nishibori, T., Suzuki, M., Abe, T., Maezawa, H., and Oyama, S.: A proposal for satellite observation of the whole atmosphere –Superconducting Submillimeter-Wave Limb-Emission Sounder-2 (SMILES-2), IGARSS 2019–2019, IEEE T. Geosci. Remote, 8788–8791, https://doi.org/10.1109/IGARSS.2019.8898423, 2019.

[3] Baron, P., Ochiai, S., Dupuy, E., Larsson, R., Liu, H., Manago,N., Murtagh, D., Oyama, S., Sagawa, H., Saito, A., Sakazaki, T., Shiotani, M. and Suzuki, M., Potential for the measurement of mesosphere and lower thermosphere (MLT) wind, temperature, density and geomagnetic field with Superconducting Submillimeter-Wave Limb-Emission Sounder 2 (SMILES-2), Atmos. Meas. Tech., 13, 219–237, 2020, https://doi.org/10.5194/amt-13-219-2020.

Keywords: Mesosphere and lower thermosphere, wind, temperature, composition, SMILES-2

©2020. Japan Geoscience Union. All Right Reserved.



©2020. Japan Geoscience Union. All Right Reserved.

Formation of a Ring-Like Region of Increased Electron Temperature in the Subauroral Ionosphere in Winter

Innokentiy Alexeevich Golikov[1], Artem Yurevich Gololobov[2], *Ilia Ilyich Varlamov[1,2]

1. Yu.G.Shafer Institute of Cosmophysical Research and Aeronomy (IKFIA), Siberian Branch of the Russian Academy of Sciences, 2. M. K. Ammosov Northeastern Federal University (NEFU),

The results of numerical simulations of the electron temperature (Te) are compared with measurement data provided by the CHAMP satellite to show the possibility of the formation of a ring-like region of temperature increase in the subauroral ionosphere surrounding the auroral oval in the range of 04–07 h (UT) when the high-latitude ionosphere is on the night (shaded) side.
Brace et al. (1982) and Kofman (1984) used experimental data to reveal the effects of an increase in the electron temperature in the subauroral ionosphere— “hot spots.” Numerical modeling of the thermal regime of the high-latitude ionosphere was addressed in a number of studies (Schunk et al., 1986; Klimenko et al., 1991; Mingalev and Mingaleva, 2002; Prölss, 2006; David et al., 2011) analyzing the sources of hot spots. The hot spots were shown to be associated with descending heat fluxes, electric fields, and decreased electron densities ne in the region of the main ionospheric trough (MIT). These results were obtained mainly for equinox conditions, and they allow a good description of the spots as structural features of the spatial distribution of Te. We compare the results of numerical simulations and measurements obtained by the CHAMP satellite to study specific features of the spatial distribution of the electron temperature in the F region of the high-latitude ionosphere for winter conditions

Keywords: subauroral ionosphere, electron temperature, heat flux, ring current

©2020. Japan Geoscience Union. All Right Reserved.

Magnetic Field Measurement in the Ionosphere by using 2U-size CubeSat

*Kentarou Kitamura[1], Kazumasa Imai[2], Taku Takada[2], Manabu Shinohara[3], Makoto Wakabayashi[4], Masahiro Tokumitsu[5]

1. NIT, Tokuyama College, 2. NIT, Kochi College, 3. NIT, Kagoshima College, 4. NIT, Niihama College, 5. NIT, Yonago College

We started a development of CubeSat with the dimension of 20*10*10 cm under collaboration with 10 colleges to observe the small perturbation of the geomagnetic field at the LEO. Focus of the observation is to understand the global distribution of the Sq (Solar quiet) currents flowing in the dayside ionosphere, and to try an in-situ observation of the InterHemispheric Field Aligned Current (IHFAC). In particular, the IHFAC was theoretically predicted by Maeda [1974] and Fukushima [1979, 1991] to interpret the north-south asymmetry in the potential pattern. However, the fine structures and natures of IHFAC have not been well understood, although there are several observations of IHFAC from the ground magnetic observation and satellite observations (e.g. Yamashita and Iyemori, 2002, and Park et al., 2002).

In this study, the fluxgate magnetometer is installed in the CubeSat to observe the 3D fine structures of Sq current system. The thermal vacuum test was conducted for the fluxgate magnetometer to confirm the temperature drift of the sensor. As a result, the temperature drift of the magnetic sensor is less than 1nT/degree which is satisfy the requirement of the specification for observations of the Sq current. In addition, the fundamental feasibility studies depending on the electric power budget, orbital life time, the communication capacity, and specification of the magnetometer show that the observation of the Sq current by CubeSat is well feasible with a short duration of the development and quite low-cost.

Keywords: CubeSat, Sq current system, Fluxgate magnetometer

©2020. Japan Geoscience Union. All Right Reserved.

Observations of night time Sporadic-E layer by HF Doppler sounder network: association with Medium-Scale Traveling Ionospheric Disturbance (MSTID)

*Ryo Matsushima [1], Keisuke Hosokawa[1], Jun Sakai[1], Mitsumu K Ejiri[2], Michi Nishioka[3], Takuya Tsugawa[3]

1. The University of Electro-Communications, 2. National Institute of Polar Research, 3. National Institute of Information and Communications Technology

Sporadic-E (Es) is a thin layer in the E-region ionosphere (~100 km) composed of dense metallic ions and electrons. Es is known to appear in the mid-latitude region during summer months. Extremely high electron density within Es sometimes reflects radio waves in VHF frequency range, especially above 100 MHz. Such a Es-related reflection of radio waves causes anomalous long- distance propagation of waves leading to radio interferences of commercial/navigation signals. Thus, Es is one of the important ionospheric phenomena which should be studied in the framework of space weather applications. Recent theoretical studies and numerical simulations have suggested that Es plays an important role in generating wave-like structures at F-region altitudes in summer nighttime, which are known as Medium-Scale Traveling Ionospheric Disturbances (MSTIDs). However, there have been only a few studies investigating the simultaneous observations Es and MSTIDs appearing in the E and F regions, respectively. Such a situation is primarily due to the lack of instruments that can directly observe Es in summer night time. To overcome this limitation, we employed data from HF Doppler (HFD) sounder network in Japan to detect Es in summer night time and tried to evaluate the E-F coupling, i.e., Es in the E-region and MSTIDs in the F-region. The HFD system is composed of a transmitting station in Chofu, Tokyo (35.7˚N, 139.5˚E) and receiving stations at ~10 places in Japan. Based on such multi-point observations, we can derive the dynamical characteristics of Es layer, for example, its moving speed and direction.
In this paper, we show an Es event on August 22, 2014 (00:00 to 02:00 JST). This Es event was analyzed in detail by Ejiri et al. (2019) who used a Lidar system to detect Es above Tokyo. The HFD system also detected the same Es feature near the Tokyo area. We made use of Es reflection data from the HFD receivers in Sugito, Saitama (36.0˚N, 139.7˚E), Fujisawa, Kanagawa (35.3˚N, 139.5˚E) and Sugadaira, Nagano (36.4˚N, 138.3˚E). By using this triangle observation, we succeeded in deriving the horizontal speed and direction of the motion of Es. In addition, we estimated the phase velocity of MSTIDs seen in the maps of Total Electron Content (TEC) from GPS receivers of GEONET. The Es layer propagated with a horizontal speed of 68.9 m/s in the azimuthal direction of - 113.0˚ from the geographic pole (approximately SWW). The phase speed of the simultaneously observed MSTIDs was estimated to be 68.1 m/s and the propagation direction was -110.1˚. This striking correspondence of the dynamical characteristics of Es and MSTIDs implies that the E-F coupling is actually working in the generation process of summer night time MSTIDs and MSTIDs are moving in tandem with Es.

Keywords: Sporadic-E (Es), MSTIDs

©2020. Japan Geoscience Union. All Right Reserved.

SMILES-2, satellite mission for observation of the stratosphere, mesosphere, and lower thermosphere with THz receivers

*Satoshi Ochiai[1], Philippe Baron[1], Yoshihisa Irimajiri[1], Akira Kawakami[1], Toshiyuki Nishibori[2], Makoto Suzuki[2], Yoshinori Uzawa[3], Yasunori Fujii[3], Hiroyuki Maezawa[4], Akinori Saito[5], Takatoshi Sakazaki[5], Masato Shiotani[5]

1. National Institute of Information and Communications Technology, 2. Japan Aerospace Exploration Agency, 3. National Astronomical Observatory of Japan, 4. Osaka Prefecture University, 5. Kyoto University

The Satellite Observation of the Whole Atmosphere - Superconducting Submillimeter-Wave Limb-Emission Sounder (SMILES-2) is a satellite mission for observation of the stratosphere, mesosphere, and lower stratosphere with submillimeter-wave receivers at frequencies of 638 GHz, 763 GHz, and 2 THz. SMILES-2 will measure submillimeter-wave limb emission spectra from atmospheric molecules and atom, that is molecular oxygen, atomic oxygen, water vapor, ozone, and many chemical species. Atmospheric temperature and horizontal wind can be retrieved from the limb spectra as well as the concentrations of those species. The SMILES-2 satellite is planned to have an orbit at an altitude of 550 km and an inclination of 66 degree. with which the latitude coverage of limb observation reaches 80 degree. Since the non-sunsynchronous orbit precesses at a rate of one round per 119 days, SMILES-2 can observe diurnal cycles in 1.5 or 3 month. Height profiles will be measured with a horizontal interval of 690 km along the satellite subtrack. By measuring the same atmosphere two times at an interval of 8 min., horizontal wind vector can be retrieved from two measurements in different looking directions. Superconducting heterodyne receivers will be used to receive the submillimeter-wave limb emission. Receiver configuration is basically same with that of JEM/SMILES, which is a predecessor of SMILES-2 and was operated on the International Space Station in 2009. Unlike JEM/SMILES, SMILES-2 has three frequencies, two antennas, and digital spectrometers. The precision and altitude range for temperature and wind are improved in SMILES-2 comparing with JEM/SMILES. The estimated precisions of temperature and wind measurements would be 0.2 K and 3 m/s in the stratosphere, and 40 K and 20 m/s in the lower thermosphere, respectively, when the vertical resolution is 2.5 km. Those measurement precisions can be achieved only with superconducting receivers. If we use Schottky mixers for submillimeter-wave receivers, we will get 10 times worse noise level and cannot get enough data for latitude-altitude section even with 1 day mean.

Mission part of SMILES-2 is being designed to have 3 year lifetime, using a mechanical 4-K cryocooler that is demonstrated 4 year life in a ground test. The design of the cryostat, which contains superconducting mixers to be cooled, follows that of JEM/SMILES, so that a risk of the development is largely mitigated. Superconducting mixer (HEB mixer) for the 2 THz receiver us developed at NICT and also at Osaka Prefecture University.

We estimated the resource requirement of the SMILES-2 mission to study feasibility of SMILES-2 on a JAXA M-class mission. The power resource is very limited in an M-class satellite comparing with the case of JEM/SMILES. The power consumption of the cryocooler, which is the largest power consuming component, is estimated to be about 159 W after three year operation on orbit. The estimation is made on the assumption that the cooling power required receiver components is less than that of JEM/SMILES and that a recent efficient compressors are used. The total power consumption of the mission system can be balanced with the satellite bus power provision, which will be 323 W for the mission system when the satellite is at the status of a maximum sun-shade ratio of 37 % for the SMILES-2 orbit. Another issue is to keep the development cost low. We studied measures to reduce the cost on the condition that we use superconducting receivers for the mission and that the satellite takes non-sunsynchronous orbit. The cost

©2020. Japan Geoscience Union. All Right Reserved.

estimated is within the scale of M-class mission if we suppose that some receiver components are developed in collaboration with outside-funded partners.
The SMILES-2 proposal was submitted to the competitive M-class missions announced by JAXA/ISAS.

Keywords: microwave observation, limb sounding, wind measurement, temperature measurement, atomic oxygen, cryocooler

©2020. Japan Geoscience Union. All Right Reserved.

Numerical study of the internal mesh structure for ion drift velocity analyzer on sounding rocket

*Ryuto Hashiba[1], Takumi Abe[2]

1. Graduate School of Science, Hokkaido University, 2. Institute of Space and Astronautical Science, Japan Aerospace Exploration Agency

In the upper atmosphere (above 80 km), the neutral atmosphere and plasma coexist. The momentum transfer between the neutral atmosphere and plasma is the important process in elucidating phenomena such as ionospheric dynamo and ionospheric plasma density disturbance. However, there are very few reports on simultaneous and in-situ observation of the key parameters. Especially in the lower ionosphere where this process plays an important role, observation data is limited because satellites cannot fly for long periods of time. Therefore, in order to understand the interaction between the neutral atmosphere and plasma in the ionosphere, it is necessary to develop an analyzer that can observe the ion drift velocity.

To measure the ionospheric plasma, we are developing the ion drift velocity analyzer for sounding rocket. The analyzer is composed of a combination of RPA (Retarding Potential Analyzer) and IDM (Ion Drift Meter), which have been used for ionospheric ion observation. RPA enables ion energy analysis by applying voltage to metal mesh. In addition, the normal component of the drift velocity and the ion density and temperature can be estimated.

In the analyzer under development, the RPA section is composed of six mesh grids. The ions are accelerated or decelerated by the voltage applied to the mesh grid. Inside the RPA, it is desirable that the potential distribution between the meshes is uniform in the tangential direction. However, it is expected that this condition is not satisfied. In the case of non-uniform potential distribution, the magnitude of acceleration or deceleration differs depending on the ion trajectory, which may affect the velocity estimation error. Further, the mesh spacing and the wire diameter are directly connected to the transmittance, and the potential distribution may be non-uniform in the plane if the mesh is too coarse.

In this study, the potential distribution near the mesh grid was examined using SIMION, a software that calculates the trajectory of charged particles in the space where electromagnetic fields exist. By estimating the potential distribution, problems relating to the design of the mesh configuration can be sorted out, and the type and structure of the metal mesh suitable for the measurement can be determined. In this presentation, we will present the simulation results, the current status of mesh grid electrode design, and future work.

©2020. Japan Geoscience Union. All Right Reserved.

Using a Software Defined Radio to Receive the FORMOSAT-7 RF Beacon and Derive the Total Electron Content

*Tsai-Ju Yu[1], Loren C. Chang[1], Jann-Yenq Liu[1], Tung-Yuan Hsiao[2]

1. Graduate Institute of Space Science and Engineering, National Central University, Taoyuan City, Taiwan, 2. Accelerator Laboratory, Nuclear Science and Technology Development Center, National Tsing Hua University, Hsinchu, Taiwan

FORMOSAT-7/COSMIC-2 is a joint US-Taiwan six satellite constellation launched in 2019 focused on atmospheric and space weather. One of the payloads is a radio frequency (RF) beacon that transmits at 400 MHz, 965 MHz and 2200 MHz. By receiving two of these frequencies and calculating the phase difference, the ionospheric total electron content (TEC) can be derived. For this purpose, a simple RF beacon receiver was set up using the GNU Radio, a free and open-source signal processing software, and a Universal Software Radio Peripheral (USRP) software defined radio (SDR). We compare the results with the data obtained by existing ground based GNSS receivers to determine if the results are consistent.

Keywords: GNU Radio, FORMOSAT-7, USRP, beacon, total electron content (TEC)

©2020. Japan Geoscience Union. All Right Reserved.

Neutral and ion dynamics seen in GAIA with variable high-latitude input

*Chihiro Tao[1], Hidekatsu Jin[1], Hiroyuki Shinagawa[1], Yasunobu Miyoshi[2], Hitoshi Fujiwara[3]

1. National Institute of Information and Communications Technology, 2. Department of Earth and Planetary Sciences, Kyushu University, 3. Faculty of Science and Technology, Seikei University

Upper atmosphere shows variations reflecting complex interactions under inputs from lower and upper regions. These interactions have been an important target of the upper atmosphere physics and space weather purpose. GAIA, Ground-to-Topside Model of Atmosphere and Ionosphere for Aeronomy, is the whole atmosphere model including interaction with ionized plasma under solar EUV variation and a various waves input using a meteorological reanalysis data. We input magnetospheric variation into GAIA via electric field deposition at polar region and auroral electron precipitation using empirical models. We input polar electric potential map based on Weimer model driven by solar wind and interplanetary magnetic field with saturation effect of cross-polar-cap potential for large potential case. Variable auroral precipitation driven by Kp index is considered. Enhancement of total electron content upto mid-to-low latitude during the magnetospheric storm event is produced due to the consideration of penetration electric field. We will discuss application to neutral density variation and ionospheric storms in this presentation.

Keywords: GAIA, atmosphere-ionosphere coupling, high latitude variation

©2020. Japan Geoscience Union. All Right Reserved.

Time-dependent responses of the neutral mass density to magnetospheric energy inputs into the cusp region in the thermosphere

*Tomokazu Oigawa[1], Hiroyuki Shinagawa[2], Satoshi Taguchi[1]

1. Department of Geophysics, Graduate School of Science, Kyoto University, 2. National Institute of Information and Communications Technology

Recent satellite observations have shown that the neutral mass density around 400 km altitude in the cusp is significantly larger than that of ambient regions. The mass density enhancement is 33 % on average, and can be over 100 % during geomagnetic storms. It is considered that soft electron precipitation and local heating in the F region play significant roles in generating the mass density anomaly. However, we still have not understood how such processes contribute to the mass density anomaly in detail. Previous modeling studies are partially successful in reproducing the mass density anomaly under geomagnetically disturbed conditions, whereas previous studies have difficulties reproducing sufficient mass density enhancements under quiet conditions. In the cusp ionosphere-thermosphere system, various processes, such as ion-neutral drag, Joule heating, heating and ionization by particle precipitation, chemical processes, and diffusion, are strongly coupled. Furthermore, the mass density anomaly has small scale features, such as kilometer-scale field-aligned currents and strong vertical dependence of heating. In order to study the mesoscale density anomaly in the cusp, we employ a new high-resolution numerical model including various physical and chemical processes. In the high-latitude ionosphere, the ion density, temperature and velocity are highly variable and affect to the neutral dynamics significantly. Thus, precise calculations of spatially-dependent and time-dependent profiles of ions are crucial to study such ionosphere-thermosphere dynamics. Therefore, we also include time-dependent processes of ions in our model. At first, Joule heating rate is maximized immediately by ionization. However, ion-neutral drag, chemical processes, and diffusion all act to decrease the Joule heating rate significantly. Modeled mass density enhancements are smaller than the observations, indicating that additional energy sources, such as Alfvén waves propagating from the magnetosphere, are needed.

Keywords: cusp, mass density anomaly, Joule heating, numerical model

©2020. Japan Geoscience Union. All Right Reserved.

2-dimentional FDTD simulation about spatial structure change of sporadic E layer

*takuto tawaki[1], Taketoshi Miyake[1]

1. Toyama prefectural university

Sporadic E layer occurred in the E region of the ionosphere at the altitude of 90km to 140km causes unexpected propagation characteristics of the MF radio waves. Es layers with spatial structure are found in recent observations. In order to confirm the influence of spatial structures of the sporadic E layer on the MF radio waves propagation, we performed a series of 2-dimensional FDTD simulations using different Es layer models. In these simulations, we observed the spatial profiles of the magnetic field and the altitude profiles of the magnetic field along the assumed trajectory of the sounding rocket.

Simulation results indicate that spatial structure of Es layer affect the propagation characteristics of MF radio waves. These influences are shown especially on propagation characteristics of MF radio waves above the altitude of the Es layer. Therefore, spatial structure of Es layer can be estimated by analyzing the altitude profile of the magnetic field.

Keywords: sporadic E layer, ionosphere

©2020. Japan Geoscience Union. All Right Reserved.

Atmospheric density variations observed by GOCE

*Nakayama Sayuka [1], Liu Huixin[1]

1. Earth and planetary science division,Kyushu university,Japan

Using observations from the GOCE satellite, we examined the dependence of the thermospheric density with solar flux level at different local times. The results show that at dawn there is positive correlation. The coefficient of correlation is 0.6279. At dusk positive correlation can be found. The coefficient of correlation is 0.5390. Seasonal variation of density shows maximum in spring and fall, and it shows minimum in summer. We further examined the ratio between dawn and dusk. The results show an increasing in the ratio from 2010 to 2013, however, there is only a very weak dependence on solar flux is found. We further compare these results with those obtained by CHAMP, and found the ratio between dawn-dusk, day-night thermospheric densities is a relatively stable value than is not much influentially by solar flux levels. This feature can serve as a constrain parameter for thermosphere models.

Keywords: thermospheric density, ratio

©2020. Japan Geoscience Union. All Right Reserved.

revision and data assimilation of a whole atmosphere-ionoshere model GAIA

*Hidekatsu Jin[1], Yasunobu Miyoshi[2], Chihiro Tao[1], Hiroyuki Shinagawa[1], Hitoshi Fujiwara[3]

1. National Institude of Information and Communications Technology, 2. Kyushu university, 3. Seikei university

Temporal and spatial variations in the ionospheric electron density and thermospheric mass density can have significant impacts
on radio communications between ground and space, GNSS navigations, satellites' orbit and attitude and so on. In order to nowcast
and forecast upper atmospheric variations and disturbances, a whole atmospheric model, GAIA, has been developed, Since 2011, when the initial version of GAIA was developed, we have revised it several times so that it can better reproduce upper atmospheric states. Recent updates include more rigorous treatments of ion and electron energetics, ion compositions and chemical reactions, solar radiation effects, and so on. Those updates lead to smaller RMSEs by up to several tens of percents for climatological ionospheric parameters. Data assimilation technique is also being implemented into the model using global ionospheric observations. We will show results from these revisions and assimilation of GAIA, and discuss future directions.

Keywords: ionosphere, thermosphere, space weather, assimilation, simulation, model

©2020. Japan Geoscience Union. All Right Reserved.

Overview of Vertical Incidence Pulsed Ionospheric Radar 2 (VIPIR2) observation in Japan

*Michi Nishioka[1], Hideo MAENO[1], Hiroyuki YAMAKAWA[1], Takumi Kondo[1], Takuya Tsugawa[1], Mamoru Ishii[1]

1. National Institute of Information and Communications Technology

National Institute of Information and Communications Technology (NICT) has been observing ionosphere by ionosondes for over 70 years in Japan. In 2017, we replaced the previous ionosondes with Vertical Incidence Pulsed Ionospheric Radar 2 (VIPIR2) ionosondes, which is mainly developed in NOAA. VIPIR2s are automatically operated at four stations at Wakkanai (Sarobetsu), Kokubunji, Yamagawa, Okinawa (Ogimi). In the presentation, we give an overview of our system and introduce some recent topics on our observation: 1. Estimation of arrival directions of received echo, and 2. Improvement of automatic scaling method. For estimation of arrival directions, two methods of Fourie imaging and Capon method are tried. These methods are confirmed by using data of oblique sounding. For the improvement of automatic scaling, we apply one of machine learning techniques and construct a model for scaling. The accuracy of some parameters is improved.

Keywords: VIPIR2, ionosonde, ionosphere, arraival angle, manual scaling, machine learning

©2020. Japan Geoscience Union. All Right Reserved.

[E] Poster | P (Space and Planetary Sciences)：P-EM Solar-Terrestrial Sciences, Space Electromagnetism & Space Environment

[P-EM13] Dynamics of Magnetosphere and Ionosphere

convener:Aoi Nakamizo(Applied Electromagnetic Research Institute, National Institute of Information and Communications Technology), Mitsunori Ozaki(Faculty of Electrical and Computer Engineering, Institute of Science and Engineering, Kanazawa University), Akiko Fujimoto(Kyushu Institute of Technology), Yuka Sato(Nippon Institute of Technology)

This session provides an opportunity to present recent results from satellite and ground-based observations and theoretical and simulation studies on the magnetosphere, ionosphere, and their coupling processes. We invite talks and posters discussing various phenomena related to the magnetosphere-ionosphere system: solar wind-magnetosphere interaction, magnetosphere-ionosphere convection, field-aligned current, magnetic storms/substorms, neutral-plasma interaction, ionospheric ion inflow and outflow, aurora phenomena, and so forth. Discussions on planetary and satellite ionospheres and magnetospheres, future missions and instrument developments are also welcome.

[PEM13-P01] Overview of electron number density and plasma wave observations by SS-520-3 NEI/PWM

*Atsushi Kumamoto[1], Yuto Katoh[1], Hirotsugu Kojima[2], Keigo Ishisaka[3] (1.Department of Geophysics, Graduate School of Science, Tohoku University, 2.Research Institute for Sustainable Humanosphere, Kyoto University, 3.Toyama Prefectural University)

[PEM13-P02] Geomagnetic N+/O+ variation in the Ring Current Observed by the Arase (ERG) Satellite

*Koichiro Tsuda[1], Shoichiro Yokota[1], Satoshi Kasahara[2], Kunihiro Keika[3], Tomoaki Hori[4], Yoshizumi Miyoshi[4], Iku Shinohara[5], Kentaro Terada[1] (1.Department of Earth and Space Science, Graduate School of Science, Osaka University, 2.The University of Tokyo, 3.Department of Earth and Planetary science, Guraduate School of Science, The University of Tokyo, 4.Institute for Space-Earth Environment Research, Nagoya University, 5.Japan Aerospace Exploration Agency/Institute of Space and Astronautical Science)

[PEM13-P03] Precipitation Loss of Radiation Belt Electrons by Two-band Plasmaspheric Hiss Waves

*Zhaoguo He[1] (1.Sun Yat-sen University)

[PEM13-P04] On the possible scenario of MeV electrons at the plasma sheet boundary

*Iku Shinohara[1], Nagai Tsugunobu[1], Takefumi Mitani[1], Nana Higashio[2], Satoshi Kasahara[3], Yoichi Kazama[4], Shiang-Yu Wang[4], Sunny Tam[5], Ayako Matsuoka[1], Kazushi Asamura[1], Shoichiro Yokota[6], Takeshi Takashima[1], Yoshizumi Miyoshi[7] (1.Japan Aerospace Exploration Agency/Institute of Space and Astronautical Science, 2.Japan Aerospace Exploration Agency, 3.University of Tokyo, 4.ASIAA, 5.NCKU, 6.Osaka University, 7.Nagoya University/Institute for Space-Earth Environmental Research)

[PEM13-P05] PARM-HEP Observation of Microburst Precipitation over Pulsating Aurora

*Taku Namekawa[1,2], Takefumi Mitani[1], Kazushi Asamura[1], Yoshizumi Miyoshi[3], Keisuke Hosokawa[4], Yasunobu Ogawa[5], Shinji Saito[6], Yoshifumi Saito[1] (1.Japan Aerospace Exploration Agency, 2.The University of Tokyo, 3.Nagoya University, 4.The University of Electro-Communications, 5.National Institute of Polar Research, 6.National Institute of Information and Communications Technology)

[PEM13-P06] Plasma waves causing 20 Hz intensity modulation of pulsating aurora

*Herbert Akihito Uchida[1], Ryuho Kataoka[2,1], Kiyoka Murase[1], Shoya Matsuda[3], Yoshiya Kasahara[4], Masafumi Shoji[5], Yoshizumi Miyoshi[5], Iku Shinohara[3], Ayako Matsuoka[3], Satoshi Kurita[5], Keisuke Hosokawa[6] (1.The Graduate University for Advanced Studies, 2.National Institute of Polar Research,

3.Institute of Space and Astronautical Science, 4.Kanazawa University, 5.Institute for Space–Earth Environmental Research, 6.The University of Electro-Communications)

[PEM13-P07] Relationship between ECH waves, ionospheric F-region ionization and pulsating aurora based on ground-based optical, EISCAT and Arase satellite observations

*Mizuki Fukizawa[1], Takeshi Sakanoi[1], Yasunobu Ogawa[2], Keisuke Hosokawa[3], Yoshiya Kasahara[4], Shoya Matsuda[5], Ayako Matsuoka[6] (1.Planetary Plasma and Atmospheric Research Center, Graduate School of Science, Tohoku University, 2.National Institute of Polar Research, 3.Department of Communication Engineering and Informatics, University of Electro-Communications, 4.Information Media Center, Kanazawa University, 5.Institute of Space and Astronautical Science/Japan Aerospace Exploration Agency, 6.Research Division for Space Plasma, Institute of Space and Astronautical Science, Japan Aerospace Exploration Agency)

[PEM13-P09] Simultaneous ground-satellite observation of dayside pulsating aurora

*Shumpei Abe[1], Keisuke Hosokawa[1], Yasunobu Ogawa[2] (1.The University of Electro-Communications, 2.National Institute of Polar Research)

[PEM13-P10] Characteristics of periodicity of the dayside pulsating aurora and its response to solar wind obtained by multi-wavelength all-sky cameras at South Pole Station

*Miki Kawamura[1], Takeshi Sakanoi[1], Mizuki Fukizawa[1], Naoshi Yagi[1], Yusuke Ebihara[2], Tetsuo Motoba[3], Akira Kadokura[4], Yasunobu Ogawa[4] (1.Tohoku University, 2.Research Institute for Sustainable Humanosphere, Kyouto University, 3.Nagoya University, 4.National Institute of Polar Research)

[PEM13-P11] Latitudinal distributions of magnetic variations in the near-earth magnetosphere during substorm

*Shun Imajo[1], Masahito Nose[1], Mari Aida[2], Nana Higashio[2], Haruhisa Matsumoto[2], Kiyokazu Koga[2], Akimasa Yoshikawa[3], Yoshizumi Miyoshi[1] (1.Institute for Space-Earth Environmental Research, Nagoya University, 2.Japan Aerospace eXploration Agency, 3.ICSWSE, Kyushu University)

[PEM13-P12] If Pi2 is onset indicator of substorms, what triggers Pi2s?

*Osuke Saka[1] (1.Office Geophysik)

[PEM13-P13] Time evolution of aurora structures associated with inverted-V electron distributions

*Morio Tanaka[1], Satoshi Taguchi[1], Keisuke Hosokawa[2] (1.Department of Geophysics, Graduate school of science, Kyoto University, 2.Department of Communication Engineering and Informatics, University of Electro-Communications)

[PEM13-P14] Automatic Classification of Auroral videos based on 3D-CNN

*Toru Mikuriya[1], Akiko Fujimoto[1], Yoshizumi Miyoshi[2], Yasunobu Ogawa[3], Keisuke Hosokawa[4] (1.Kyushu Institute of Technology, 2.Nagoya University, 3.National Institute of Polar Research, 4.The University of Electro-Communications)

[PEM13-P15] Spectral investigations on short-wavelength infrared aurora and airglow (0.9-1.6 μm): Ground-based observations in the both polar regions and developments of 2-D imaging spectrograph with high resolutions

*Takanori Nishiyama[1,2], Makoto Taguchi[3], Masato Kagitani[4], Yasunobu Ogawa[1,2], Hidehiko Suzuki[5], Takeshi Sakanoi[4], Fuminori Tsuchiya[4], Peter Dalin[6], Urban Brändström[6] (1.National Institute of Polar Research, 2.The Graduate University for Advanced Studies, SOKENDAI, 3.Rikkyo University, 4.Tohoku University, 5.Meiji University, 6.Swedish Institute of Space Physics)

[PEM13-P16] “Great Wall” seen in the omega band: full-color digital camera observation from the International Space Station

*Sota Nanjo[1], Natsuo Sato[2], Yuta Hozumi[1], Keisuke Hosokawa[1], Ryuho Kataoka[2,3], Yoshizumi Miyoshi[4], Shin-ichiro Oyama[2,4,5], Mitsunori Ozaki[6], Kazuo Shiokawa[4], Satoshi Kurita[4] (1.The University of Electro-Communications, 2.National Institute of Polar Research, 3.Department of Polar Science, School of Multidisciplinary Sciences, SOKENDAI, The Graduate University for Advanced Studies, 4.Institute for Space-Earth Environmental Research, Nagoya University, 5.Ionospheric Physics Research Unit, University of Oulu, 6.Graduate School of Natural Science and Technology, Kanazawa University)

[PEM13-P17] A tool to diagnose magnetosphere under northward IMF conditions: Simultaneous detections of TPA and omega-band aurora

*Motoharu Nowada[1] (1.Shandong Provincial Key Laboratory of Optical Astronomy and Solar-Terrestrial Environment, Institute of Space Sciences, Shandong University, Weihai)

[PEM13-P18] Transient and localized field-aligned current in the cusp region associated with the Sudden Commencement

*Shigeru Fujita[1] (1.Meteorological College, Japan Meteorological Agency/ Nationa Institute of Polar Research)

[PEM13-P19] Existence of the Region1 field-aligned current system for zero interplanetary magnetic field

*Tsubasa Hashimoto[1], Masakazu Watanabe[2], Ryuho Kataoka[3], Shigeru Fujita[4], Takashi Tanaka[5] (1.Department of Earth and Planetary Sciences, Graduate School of Science, Kyushu University, 2.Department of Earth and Planetary Sciences, Faculty of Science, Kyushu University, 3.National Institute of Polar Research, 4.Meteorological College, Japan Meteorological Agency/ National Institute of Polar Research, 5.International Center for Space Weather Science and Education)

[PEM13-P20] A Modified Magnetosphere-Ionosphere Coupling Model by Including the Hall Effects due to Thinning of the Near-Earth Plasma Sheet

*Pai-Sheng Wang[1], Ling-Hsiao Lyu[1] (1.Institute of Space Science and Engineering, National Central University, Taoyuan, Taiwan)

[PEM13-P21] **Alfvénic disturbances generated by the ionospheric polarization and the convection reversal in the magnetosphere**

*Aoi Nakamizo[1], Akimasa Yoshikawa[2], Shinichi Ohtani[3], Takashi Tanaka[2] (1.Applied Electromagnetic Research Institute, National Institute of Information and Communications Technology, 2.Faculty of Science, Kyushu University, 3.The Johns Hopkins University Applied Physics Laboratory)

[PEM13-P22] **Near-earth plasma environment and injection simulated by global magnetosphere model with precession of magnetic axis**

*Aoi Nakamizo[1], Yasubumi Kubota[1], Tsutomu Nagatsuma[1], Takashi Tanaka[2] (1.Applied Electromagnetic Research Institute, National Institute of Information and Communications Technology, 2.Faculty of Science, Kyushu University)

[PEM13-P23] Automatic identification of FLR events in VLOS data of multiple SuperDARN radars

*Hideaki Kawano[1,2], Akira Sessai Yukimatu[3,4], Nozomu Nishitani[5], Yoshimasa Tanaka[3,4], Satoko Saita[6], Tomoaki Hori[5] (1.Department of Earth and Planetary Sciences, Kyushu University, 2.ICSWSE, Kyushu University, 3.National Institute of Polar Research, 4.SOKENDAI, 5.ISEE, Nagoya University, 6.Kitakyushu College)

[PEM13-P24] Statistical study of SAPS occurrence characteristics using the SuperDARN HOkkaido Pair of (HOP) HF Radars

*Kento Oya[1], Nozomu Nishitani[1], Tomoaki Hori[1] (1.Institute for Space-Earth Environmental Research, Nagoya University)

[PEM13-P25] Ion precipitation in the cusp for stably northward IMF: Seasonal dependence

*Haruto Koike[1], Satoshi Taguchi[1] (1.Department of Geophysics, Graduate School of Science, Kyoto University)

[PEM13-P26] Hemispheric Asymmetry of the Vertical Ion Drifts at Dawn Observed by DMSP

*Mohan Liu[1], Xiao-Xin Zhang[1], Fei He[2], Wenbin Wang[3] (1.National Satellite Meteorological Center, 2.Institute of Geology and Geophysics, Chinese Academy of Sciences, 3.High Altitude Observatory, National Center for Atmospheric Research)

[PEM13-P28] Ground-based observations of MF/HF auroral radio emissions at three stations

*Yuka Sato[1,2], Atsushi Kumamoto[2], Yuto Katoh[2], Yasunobu Ogawa[3], Akira Kadokura[3], Atsuki Shinbori[4] (1.Nippon Institute of Technology, 2.Graduate school of Science, Tohoku University, 3.National Institute of Polar Research, 4.Institute for Space-Earth Environmental Research, Nagoya University)

[PEM13-P29] Application of Magneto-Impedance Sensor to Geomagnetic Field Measurements for Constructing Distributed Arrays of Small Instruments (DASI)

*Nomura Hiroshi[1], Masahito Nosé[1], Hitoshi Aoyama[2], Takeshi Kawano[2], Masafumi Hirahara[1] (1.Institute for Space-Earth Environmental Research, Nagoya University, 2.Aichi Steel Corporation)

Overview of electron number density and plasma wave observations by SS-520-3 NEI/PWM

*Atsushi Kumamoto[1], Yuto Katoh[1], Hirotsugu Kojima[2], Keigo Ishisaka[3]

1. Department of Geophysics, Graduate School of Science, Tohoku University, 2. Research Institute for Sustainable Humanosphere, Kyoto University, 3. Toyama Prefectural University

Preparations and preparative studies for electron number density and plasma wave observations in the earth' cusp region by impedance probe and plasma wave monitor (NEI/PWM) onboard the SS-520-3 sounding rocket are overviewed. The main objective of SS-520-3 is to observe acceleration processes of escaping ions from ionosphere in the cusp region. It was originally scheduled to launch from Svalbard in 2017. However, due to failure of the rocket avionics found in the integration test in Japan, the launch was postponed. The development and unit test of SS-520-3 NEI/PWM were already finished before the integration test in 2017. So, we were performing some preparative studies.

The observations of accurate electron number density in a range from 10^3 to 5 x 10^6 /cc and plasma wave spectrum in a wide frequency range from 300 Hz to 20 MHz will be performed by SS-520-3 NEI/PWM. The electron number density is determined from measured capacitance of impedance probe (NEI-S) extended into the ionospheric plasma. Plasma waves are detected by antenna and preamplifier of Low Frequency Analyzer System (LFAS). NEI/PWM obtains plasma wave spectrum from the signal from LFAS. Electron number density is an essential parameter to discuss resonance conditions between plasma waves and particles in their interactions. SS-520-3 NEI/PWM is designed to perform monopole measurements of plasma waves in order to clarify the distribution of the wake-induced plasma waves around the rocket [Endo et al., 2015]. Detection of lower hybrid resonance (LHR) by wideband impedance probe operated in a frequency range from 1 to 10 kHz will be tried first in the ionosphere by SS-520-3 NEI/PWM. It provides information of ion density including cold components and ion composition. The wideband impedance probe is planned to be used also in S-520 sounding rocket experiment in 2022.

We performed preparative analyses on relations between broadband extremely low frequency waves (BBELF) and ion heating by using Akebono data. The results suggest that not only the Alfvenic component of plasma waves around O+ cyclotron frequency but also electrostatic component around lower hybrid resonance (LHR) frequency contribute to the ion heating [Ishigaya, 2019].

Acknowledgement: The SS-520-3 rocket observation will be conducted by the Institute of Space and Astronautical Science, Japan Aerospace Exploration Agency (ISAS/JAXA). NEI/PWM was manufactured by System Keisoku Co.Ltd. Antenna and preamplifier of LFAS, which provides signals to PWM, was developed by H. Kojima of Kyoto University, and manufactured by Sakase Adtech Co.,Ltd., and Meiwa System Co. Ltd., respectively. Preflight environmental tests of NEI/PWM were performed using the facilities of the Industrial Technology Institute of the Miyagi Prefectural Government (ITIM), and Space Chamber Laboratory, ISAS/JAXA.

Keywords: Ionospheric ion outflow, Electron number density measurements, Plasma waves, SS-520-3

©2020. Japan Geoscience Union. All Right Reserved.

Geomagnetic N+/O+ variation in the Ring Current Observed by the Arase (ERG) Satellite

*Koichiro Tsuda[1], Shoichiro Yokota[1], Satoshi Kasahara[2], Kunihiro Keika[3], Tomoaki Hori[4], Yoshizumi Miyoshi[4], Iku Shinohara[5], Kentaro Terada[1]

1. Department of Earth and Space Science, Graduate School of Science, Osaka University, 2. The University of Tokyo, 3. Department of Earth and Planetary science, Guraduate School of Science, The University of Tokyo, 4. Institute for Space-Earth Environment Research, Nagoya University, 5. Japan Aerospace Exploration Agency/Institute of Space and Astronautical Science

O+ and N+ are important ring current ions in magnetic storms and they can be a tracers of ion outflows from the deep ionosphere. Much Many researches haves been devoted to the escape of O+, but N+ has not been studied much, possibly because its mass per charge ratio is similar to that of O+ and separating the two is difficult.
We investigated the statistical properties of O+ and N+ in the ring current based on ion composition measurements (~10-180keV/q) by medium-energy particle experiments-ion mass analyzer (MEP-i) on board the Arase (Exploration of energization and Radiation in Geospace, ERG) satellite. By applying a fitting function to the TOF spectrum, we can separated N+ and O+ in the data obtained during geomagnetic storm on 16 July 2017. From the results of fitting we obtained the ratio of N+/O+. As a result the ratio of N+/O+ during geomagnetic storm and during geomagnetic quiet times is found to be about 0.2~0.4 and <0.2 respectively. In this presentation we will discuss ion outflow from the deep ionosphere.

Keywords: Arase (ERG) satellite, Ion outflow, Ionosphere, Nitrogen ion

©2020. Japan Geoscience Union. All Right Reserved.

Precipitation Loss of Radiation Belt Electrons by Two-band Plasmaspheric Hiss Waves

*Zhaoguo He[1]

1. Sun Yat-sen University

A two-band plasmaspheric hiss consisting of an upper band (frequency up to 10 kHz) and a lower band (frequency below 1 kHz) was observed by the Van Allen Probes. The electron scattering effect driven by this two-band plasmaspheric hiss is evaluated by the quasilinear diffusion theory for the first time. The calculated pitch angle diffusion rates of the lower-band hiss exist a "gap" with minimum magnitude at around α=70deg, a condition not conductive to the transport of large pitch angle electrons toward the loss cone. However, the diffusion rates of the upper-band hiss have peak values at ~ α=70deg, making up for the "gap" of the lower-band hiss diffusion rates. The wave data-driven quasilinear diffusion simulations demonstrate that the collaborated effect of the lower and upper band hiss can cause significant precipitation loss of energetic electrons of tens to several hundred keV within 1 day.

Keywords: Radiation belt, Two-band hiss, Precipitation Loss

©2020. Japan Geoscience Union. All Right Reserved.

On the possible scenario of MeV electrons at the plasma sheet boundary

*Iku Shinohara[1], Nagai Tsugunobu[1], Takefumi Mitani[1], Nana Higashio[2], Satoshi Kasahara[3], Yoichi Kazama[4], Shiang-Yu Wang[4], Sunny Tam[5], Ayako Matsuoka[1], Kazushi Asamura[1], Shoichiro Yokota[6], Takeshi Takashima[1], Yoshizumi Miyoshi[7]

1. Japan Aerospace Exploration Agency/Institute of Space and Astronautical Science, 2. Japan Aerospace Exploration Agency, 3. University of Tokyo, 4. ASIAA, 5. NCKU, 6. Osaka University, 7. Nagoya University/Institute for Space-Earth Environmental Research

We have found that energetic electron bursts up to (sometimes, up to 1 MeV) 300 keV appear at the plasma sheet boundary at substorm onsets. The purpose of this study is to address where do the energetic electron bursts at higher latitude come from and what is the contribution of magnetotail reconnection and its associated acceleration process to the generation of the energetic electron bursts. The electron bursts show uni- and bi-directional components (possibly generated by near-Earth reconnection) in the lower energy part (E < 200 keV), while lack of parallel and anti-parallel components are observed in the higher energy part. The magnetic field line model indicates that the Arase satellite was located in the transition region between dipole-like and tail-like fields. Interestingly, the higher energy component of bursts shows signatures of the drift echo. In order to explain these observational features of the electron bursts at the plasma sheet boundary, we have performed test particle simulations traced from magnetotail. At this moment, a possible interpretation of the higher energy electron burst is a signature of substorm injections in the high latitude. We will discuss the origin of MeV electrons at the plasma sheet boundary based on the particle dynamics as well as comparing the distribution functions with those observed in the magnetotail.

Keywords: high-energy electrons, magnetotail, substorm

©2020. Japan Geoscience Union. All Right Reserved.

PARM-HEP Observation of Microburst Precipitation over Pulsating Aurora

*Taku Namekawa[1,2], Takefumi Mitani[1], Kazushi Asamura[1], Yoshizumi Miyoshi[3], Keisuke Hosokawa[4], Yasunobu Ogawa[5], Shinji Saito[6], Yoshifumi Saito[1]

1. Japan Aerospace Exploration Agency, 2. The University of Tokyo, 3. Nagoya University, 4. The University of Electro-Communications, 5. National Institute of Polar Research, 6. National Institute of Information and Communications Technology

The phenomenon called microburst that radiation belt particles precipitate to the Earth’s atmosphere is thought to be largely related to the dissipation of high energy electrons in radiation belt. It is suggested that this phenomenon is caused by pitch angle scattering of the magnetospheric particles by plasma waves, which is a mechanism similar to the cause of the pulsating aurora observed in the Earth’s polar region. There is a possibility that the origin of microburst can be clarified by proving simultaneous occurrence of microburst and pulsating aurora, but observational verification has not been made yet. For that purpose, we have developed a high-energy electron detector (HEP) for the observation of sub-relativistic - relativistic energy electrons that make up the microburst. This instrument is installed as one of the core instruments of the PARM instrument package developed for the simultaneous observation of the pulsating aurora and microburst by the international student sounding rocket experiment RockSat-XN and LAMP (Loss through Auroral Microburst Pulsation) sounding rocket experiment. We have succeeded in obtaining the flight data on 13 January 2019 from RockSat-XN sounding rocket experiment. Since the rocket was unfortunately launched on the dayside under quiet condition, simultaneous observation with pulsating aurora was impossible and the significant microbursts cannot be detected, but we detect quasi-relativistic energy electrons that can be explained by pitch angle scattering by weak chorus waves in the quiet dayside magnetosphere. On the other hand, LAMP rocket experiments are prepared for launch in winter 2020. We load an anti-coincidence counter on HEP mounted on LAMP to eliminate the effects of penetrating particles such as galactic cosmic rays. In this presentation, we will show the outline and observation results of HEP as well as the current status of the preparation for the launch of LAMP.

Keywords: microburst, sounding rocket, PARM, pitch angle scattering, pulsating aurora

©2020. Japan Geoscience Union. All Right Reserved.

Plasma waves causing 20 Hz intensity modulation of pulsating aurora

*Herbert Akihito Uchida[1], Ryuho Kataoka[2,1], Kiyoka Murase[1], Shoya Matsuda[3], Yoshiya Kasahara[4], Masafumi Shoji[5], Yoshizumi Miyoshi[5], Iku Shinohara[3], Ayako Matsuoka[3], Satoshi Kurita[5], Keisuke Hosokawa[6]

1. The Graduate University for Advanced Studies, 2. National Institute of Polar Research, 3. Institute of Space and Astronautical Science, 4. Kanazawa University, 5. Institute for Space–Earth Environmental Research, 6. The University of Electro-Communications

We observed ~20 Hz intensity modulation of pulsating aurora at Syowa Station by high-speed camera pointing at magnetic zenith for a few min time interval, 30 min after the aurora breakup occurred on September 22, 2018. The footprints of the Arase satellite was located within the all-sky field of view at that time, and ~20 Hz intensity modulation was observed in the intensity of the lower band chorus waves. We present the possible correlations between the plasma waves and pulsating aurora in more detail, and examine the resonant energy quantitatively.

Keywords: Pulsating aurora, Chorus waves, Fast modulation

©2020. Japan Geoscience Union. All Right Reserved.

Relationship between ECH waves, ionospheric F-region ionization and pulsating aurora based on ground-based optical, EISCAT and Arase satellite observations

*Mizuki Fukizawa[1], Takeshi Sakanoi[1], Yasunobu Ogawa[2], Keisuke Hosokawa[3], Yoshiya Kasahara[4], Shoya Matsuda[5], Ayako Matsuoka[6]

1. Planetary Plasma and Atmospheric Research Center, Graduate School of Science, Tohoku University, 2. National Institute of Polar Research, 3. Department of Communication Engineering and Informatics, University of Electro-Communications, 4. Information Media Center, Kanazawa University, 5. Institute of Space and Astronautical Science/Japan Aerospace Exploration Agency, 6. Research Division for Space Plasma, Institute of Space and Astronautical Science, Japan Aerospace Exploration Agency

When a substorm occurs, various plasma waves are excited near the magnetic equator of the inner magnetosphere. In particular, there are chorus waves and electrostatic electron cyclotron harmonic (ECH) waves from midnight to morning. These waves can scatter a pitch angle of electrons by cyclotron resonance and the electrons scattered in a loss cone precipitate into the Earth’s atmosphere, causing diffuse auroral emission. Since the resonance energy of chorus waves is a few keV to tens of keV and that of ECH waves is a few hundred eV to a few keV, chorus waves contribute to the auroral emission in the ionospheric D–E region and ECH waves contribute to that in the ionospheric F region (Fukizawa et al., 2018, GRL). The relationship between chorus waves and pulsating aurora and ionization in the D–E region has been clarified by previous studies (e.g., Kasahara et al., 2018, Nature; Miyoshi et al., 2015, JGR: Space Phys.; Nishimura et al., 2010, Science). However, the relationship between ECH waves and pulsating aurora and ionization in the F region is not well understood. In this study, based on ground-based optical, incoherent scatter radar, and satellite-based observations, we investigated the relationship between ECH waves, pulsating aurora and ionization in the F region.

First, we analyzed the observation data of an all-sky imager and European Incoherent Scatter (EISCAT) radar from September 2016 to December 2019. The proportion of events where ionization was observed in the F region by EISCAT radar was 50 % of the events where pulsating aurora was observed at the magnetic zenith by the all-sky imager (filter transmission wavelength: 560 nm ±5 nm) installed in Tromsø (69˚35’ N, 19˚14’ E, invariant latitude: 66˚12’ N), Norway. When a pulsating aurora with a wavelength of 557.7 nm is generated, there are chorus waves as a driving source near the magnetic equator. It has been confirmed by statistical analysis of satellite observation data that the probability that ECH waves are also excited in the magnetic equator when chorus waves are excited is high (Meredith et al., 2009, JGR: Space Phys.). Therefore, ECH waves may be the driving source of the F-region ionization detected by our analysis.

Secondaly, we investigated a simultaneous EISCAT-Arase event obtained from 01:40 to 03:00 UT on September 26, 2019. Although the ionospheric footprint of the Arase satellite was located within the filed of view of the all-sky imager, the weather in Tromsø was cloudy and no pulsating aurora was detected by the all-sky imager. However, chorus and ECH waves were observed by the Arase satellite and ionization in the D–E and F regions was observed by EISCAT radar. The chorus wave and ECH wave observed by the Arase satellite are partially observed exclusively, and the D–E region ionization and the F region ionization observed by the EISCAT radar show similar characteristics. Although the footprint of the Arase satellite at an altitude of 110 km derived from the IGRF magnetic field model was located about 170 km south of the EISCAT radar observation point, these results suggest that there is a relationship between chorus wave

©2020. Japan Geoscience Union. All Right Reserved.

and ionization in the D–E region and that between ECH wave and ionization in the F region.

In the future works, we will analyze spectroscopic data with a wavelength of 427.8 nm that emits in the D–E region and those with a wavelength of 844.6 nm that mainly emits in the F region to investigate whether the time change of each emission has characteristics similar to that of chorus waves or ECH waves.

Keywords: Electrostatic wave, Pulsating aurora, EISCAT radar, ERG (Arase) satellite

©2020. Japan Geoscience Union. All Right Reserved.

Simultaneous ground-satellite observation of dayside pulsating aurora

*Shumpei Abe[1], Keisuke Hosokawa[1], Yasunobu Ogawa[2]

1. The University of Electro-Communications, 2. National Institute of Polar Research

Pulsating aurora (PsA) is a type of diffuse aurora which shows quasi-periodic modulation of luminosity. It has been known that PsA is usually observed during the late recovery phase of substorms in a magnetic local time (MLT) sector extending from the post-midnight to dawn. Previous studies indicated that PsA originates from quasi-periodic precipitation of electrons, which are scattered by whistler mode chorus waves near the equatorial plane of the magnetosphere. Most of the previous studies of PsA are focused on observations on the nightside and dawnside. However, recent studies, for example Han et al. (2015), indicated that PsA is observed even on the dayside (from the morning to the noon sector) at high-latitudes slightly below the cusp region. Those studies presented the MLT distributions of such Dayside-PsA (D-PsA) events, but detailed characteristics of D-PsA, such as its pulsating period and the origin of its temporal variation, have not yet been clarified. To reveal such properties of D-PsA, we have used optical data obtained from the all-sky WATEC imagers (AWIs, Ogawa et al., 2019) in Longyearbyen, Norway (78.1N˚,16.04˚E), whose temporal resolution is 1 Hz for the green-line (557.7 nm) observations. In addition, to observe chorus waves in the magnetospheric counter part of the DPsA region, we made use of wave data from the THEMIS satellite located near the equatorial plane of the magnetosphere. To verify the association between chorus wave and D-PsA, we investigated a D-PsA event in 25 minutes from 0720 to 0745 UT on December 10, 2018. This D-PsA event was observed by AWI and THEMIS simultaneously. Through direct comparison of the auroral luminosity from AWI with the chorus intensity from THEMIS, and additional cross-correlation analyses, we confirmed that there is a one-to-one correspondence between the brightness variation of D-PsA and the intensity modulation of chorus wave, which is very similar to the situation of PsA on the nightside and dawnside. To highlight the difference between PsAs on the nightside and dayside, we derived the distribution of pulsating period of D-PsA by applying the Stockwell transform to 6 events of D-PsA seen in Longyearbyen. From this statistical analysis, we found that the typical period of D-PsA is relatively longer (the peak was located at 35 sec) than that of nightside PsA. According to these results, we suggest that the driver of electron precipitation causing D-PsA is again whistler mode chorus waves in magnetosphere; thus, the mechanisms is similar to that of the nightside PsA. However, the prominent difference in the pulsating period of D-PsA means that the property of dayside chorus wave differs from that on the nightside to dawn side.

Keywords: Pulsating aurora, Chorus wave, Dayside aurora

©2020. Japan Geoscience Union. All Right Reserved.

Characteristics of periodicity of the dayside pulsating aurora and its response to solar wind obtained by multi-wavelength all-sky cameras at South Pole Station

*Miki Kawamura[1], Takeshi Sakanoi[1], Mizuki Fukizawa[1], Naoshi Yagi[1], Yusuke Ebihara[2], Tetsuo Motoba[3], Akira Kadokura[4], Yasunobu Ogawa[4]

1. Tohoku University, 2. Research Institute for Sustainable Humanosphere, Kyouto University, 3. Nagoya University, 4. National Institute of Polar Research

We report the event analysis on the characteristics of dayside pulsating aurora obtained with ground-based imagers, and its solar wind response. Pulsating aurora is a diffuse aurora that shows time variation with a period from a few to several tens s. It l usually seen from the midnight to the morning sectors (0-6MLT).Recent studies showed that pulsating aurora is caused cyclotron resonance between chorus waves and electrons near the magnetospheric equator [e.g., Kasahara et al., 2018]. Electrostatic electron cyclotron harmonics (ECH) play additional role to cause the pulsating aurora. Considering the dayside pulsating aurora, changes of solar wind dynamic pressure would affect the resonance conditions in the dayside magnetosphere [Engebretson et al., 1994, Vorobjev et al., 1999, Motoba et al., 2017]. However, it is difficult to observe dayside pulsating aurora because of sunlit conditions, and detailed characteristics, and generation mechanisms of pulsating aurora are not understood well.
It is important to examine the similarity and discrepancy between dayside pulsating aurora and morning side pulsating aurora, and its solar wind response to understand these issues,We examined the multi-spectral all-sky image data taken at the South Pole Station (geomagnetic latitude 74.4 ˚) to clarify the characteristics of the dayside pulsating aurora. The South Pole Station is a suitable for dayside auroral observations which provide continuous auroral images for 24 hours from May to August. From the data obtained with a panchromatic Watec all-sky camera (time resolution 0.5 s) and ASI-1 (time resolution 64 s, wavelength 557.7 nm and 630 nm) , we found dayside pulsating auroral events in the two nights of June 24 and 25, 2014. The main pulsation period was in the range of 10-50 s on the both cases on June 24 and 25, which is consistent with previous studies of dayside pulsating aurora, and similar to that seen in the morning-side pulsating aurora. We also found that the pulsating aurora on June 25 moved toward the higher magnetic latitudes greater than 74.5 deg. Compared the pulsating aurora with geomagnetic activity, solar wind dynamic pressure, and auroral intensity ration of 630nm and 557.7 nm emission, we see that the magnetic activities were quiet (AE˜50-100, IMPBz˜0-+6[nT]) on the both cases of June 24 and 25, 557.7 nm aurora was more intense than 630 nm aurora which indicates that the source region is the magnetospheric plasma sheet. Interestingly, the solar wind dynamic pressure increased from P = 1.0 [nPa] (8MLT) to P = 5.5 [nPa] (11MLT) only for the case on June 25. These results suggest that the source region of pulsating aurora in the dayside magnetosphere expanded toward higher latitudes caused by significant enhancement of solar wind dynamic pressure. The expansion of the source region of pulsating aurora is probably related with the minimum B pockets [Tsurutani and Edward, 1977] which is a weak magnetic field region at high-latitudes distorted by strong solar wind dynamic pressure. The increase of chorus wave growth rate may contribute to electron pitch angle scattering in this region.

Keywords: pulsating aurora, dayside, South Pole Station

©2020. Japan Geoscience Union. All Right Reserved.

Latitudinal distributions of magnetic variations in the near-earth magnetosphere during substorm

*Shun Imajo[1], Masahito Nose[1], Mari Aida[2], Nana Higashio[2], Haruhisa Matsumoto[2], Kiyokazu Koga[2], Akimasa Yoshikawa[3], Yoshizumi Miyoshi[1]

1. Institute for Space-Earth Environmental Research, Nagoya University, 2. Japan Aerospace eXploration Agency, 3. ICSWSE, Kyushu University

We examine the latitudinal distributions of magnetic variations in the near-earth magnetosphere during substorms by simultaneous magnetic observations of the first Quasi-Zenith Satellite (QZS-1) and the Engineering Test Satellite VIII (ETS-VIII). QZS-1, which has a unique orbit of quasi-zenith orbit with an inclination of 41º, an apogee of 7.1 Re radial distance, and an orbital period of 24 h, can stay for a long time in the near-earth magnetosphere away from the magnetic equator. ETS-VIII is a geosynchronous satellite located at the E146º longitude, which is within the QZS-1 longitude range. We selected 356 dipolarization events at ETS-VIII when the difference of magnetic local time between QZS-1 and ETS-VIII was less than 1 h.
Typical magnetic variations are classified into 5 types roughly depending on the magnetic latitude of QZS-1 (MLAT) as below:
(Type 1) In |MLAT|<~ 20º, QZS-1 naturally observed magnetic variations similar to those at ETS-VIII with a small delay (1–2 minutes).
(Type 2) In ~20º<|MLAT|<~30º, the onset of large magnetic excursions at QZS-1 was several tens of minutes delayed by the dipolarization onset at ETS-VIII. The excursions were not similar to those at ETS-VIII and were polarized in the azimuthal direction with large-amplitude oscillations.
(Type 3) In ~30º<|MLAT|<~50º, QZS-1 observed small magnetic excursions without oscillations. Surprisingly, the time delay between QZS-1 and ETS-VIII was only within 1–2 minutes.
(Type 4) In ~40º<|MLAT|<~50º, QZS-1 sometimes did not observe any variations.
(Type 2+3) Some events had both features of Type 2 and Type 3.

The large-magnetic excursion of type 2 events can be considered to be a direct crossing of the field-aligned currents (FACs). The large delay time corresponds to the poleward expanding time of the substorm currents system. The oscillations with the excursion may be caused by a small-scale structure of FACs. On the other hand, the small magnetic excursion of type 3 events can be considered to be a magnetic effect outside (polar side) the FACs. This is similar to the magnetic bay on the low-latitude ground, which is the magnetic effect inside (equator side) the FACs. We call the magnetic variation that we found “magnetospheric polar side bay”. If the intensity of the FAC is small or QZS-1 is far away from the FACs, any magnetic variations may not be observed at QZS-1, so the event was classified into type 4. The latitudinal distribution of polarization, amplitude, and delay time will be quantitively examined. Also, we will further investigate the relation among the magnetic variation away from the magnetic equator, plasma particles, and aurora, using the Arase satellite, which has a large inclination of 32º.

Keywords: substorm, geosynchonous alititude, quasi-zenith orbit, field-aligned current

©2020. Japan Geoscience Union. All Right Reserved.

If Pi2 is onset indicator of substorms, what triggers Pi2s?

*Osuke Saka[1]

1. Office Geophysik

Close analyses of substorm onset using data from all-sky imagers, ground magnetometers, and plasma and magnetic field measurements at geosynchronous orbit obtained in the Global Aurora Dynamics Campaign (1985-1995) revealed that equatorial Pi2s can pick up in statistical base as well as for case studies the onset of individual field line dipolarization of substorms [Saka et al., 2010; Saka and Hayashi, 2017]. The analyses also show that field-aligned flows towards the equatorial plane (inflow) intensified radial inhomogeneity of plasma pressure in the pre-onset intervals, which initiated slow magnetoacoustic wave through Ballooning instability. The excited slow magnetoacoustic wave would smooth out the radial inhomogeneity by the associated azimuthal expansion of the flux tubes. The smoothing of the radial inhomogeneity is consisted of oscillating transition of flux tubes (at Pi2 periodicity) from one stable geometry with smaller curvature radius to the other of larger curvature radius of geomagnetic field lines, which will be referred to as field line dipolarization [Saka, 2019b].
The analyses also showed that flux tubes linked to negative and positive bays at higher and lower latitudes, respectively, oscillated coherently at Pi2 periods [Saka et al., 2012; Saka, 2019b]. Oscillating flux tubes associated with positive bay may trigger cavity/waveguide mode in low latitudes [Allan et al., 1996; Li et al., 1998], while flux tubes for negative bay yields convection surge in the midnight magnetosphere [Saka, 2019b]. Electromotive force generated in the auroral ionosphere by the convection surge produced field-aligned currents in it [Saka, 2019a].

In the dip-equator, a singular latitude of the cavity/waveguide mode [Allan et al., 1996], only isotropic mode can be excited. This leads us to suppose that a very large propagation velocity (or large wavelength exceeding whole circle of the Earth) of Pi2s in the nightside sector [Kitamura et al., 1988] would be caused by the dawn-dusk asymmetry of non-propagating compressions. This contrasts with the high-latitude Pi2s that propagated typically at 20km/s eastward and westward in the sector east and west of the substorm center, respectively [Samson and Harrold, 1985].

Keywords: Pi2 pulsation, Slow magnetoacoustic wave, Ballooning instability, Field line Dipolarization

©2020. Japan Geoscience Union. All Right Reserved.

Time evolution of aurora structures associated with inverted-V electron distributions

*Morio Tanaka[1], Satoshi Taguchi[1], Keisuke Hosokawa[2]

1. Department of Geophysics, Graduate school of science, Kyoto University, 2. Department of Communication Engineering and Informatics, University of Electro-Communications

The inverted-V is an energetic electron precipitation event, which can be seen as a V-shape structure in electron flux spectrograms, and causes intense auroral arcs. Previous satellite observations have suggested that the inverted-V structure would be stable for 5 min at least, but the detailed characteristics of its time evolution are still unclear. Aurora image data (557.7 nm and 630 nm) from an all-sky imager at Longyearbyen, Svalbard, and precipitating electron and magnetic field data from the DMSP spacecraft (F16, F17, F18, F19) are used to identify the aurora structures associated with inverted-V, and track their time evolution. The result of the analysis indicates that the auroral structures associated with inverted-V electron distributions tend to have longer durations than previously reported from the satellite observations. Some periodic features of the auroral structures are also seen. Key parameters for the stability of the inverted-V, i.e., parallel electric field are discussed in terms of phases of a substorm.

Keywords: field-aligned current, aurora, electron precipitation , inverted-V

©2020. Japan Geoscience Union. All Right Reserved.

Automatic Classification of Auroral videos based on 3D-CNN

*Toru Mikuriya[1], Akiko Fujimoto[1], Yoshizumi Miyoshi[2], Yasunobu Ogawa[3], Keisuke Hosokawa[4]

1. Kyushu Institute of Technology, 2. Nagoya University, 3. National Institute of Polar Research, 4. The University of Electro-Communications

There are several approaches for classifying all-sky images of aurora with handcrafted methods. The recent enhanced on the fields of computer vison and machine learning research resulted from growing the environment of information processing allows to easily develop the automatic classification of aurora images into some labeled groups. The previous researchers have proposed handcrafted classification models of snapshot aurora images with aurora shapes, color features and aurora velocity (motional differences between two aurora images), etc. They work well for the type of discrete aurora, since they have fine structure of aurora shape. Now we attempt the non-handcrafted and automatic distinction of diffuse aurora such as pulsating aurora with the supervised 3D-Convolutional Neural Network (3D-CNN) technique. We use 605 aurora all-sky imager videos (each movie has 60 frames with 1 second time resolution) to extract the feature of quasi-periodic pulsation aurora motion which is the main characteristic of pulsating aurora. The supervised learning data has two categories, 1) pulsating aurora and 2) no pulsating aurora, and we divide all videos into 8:2 for learning /evaluation processes and test process, respectively. The k-Cross Validation (k=5) resulted in higher accuracy of our model (larger than 90 %). We found the classification accuracy depends on the number of 3D-CNN filter in time direction, and our model works well on the lower number than the typical frequency of pulsating aurora.

Keywords: Machine Learning, 3D-CNN, auroral movies

©2020. Japan Geoscience Union. All Right Reserved.

Spectral investigations on short-wavelength infrared aurora and airglow (0.9-1.6 μm): Ground-based observations in the both polar regions and developments of 2-D imaging spectrograph with high resolutions

*Takanori Nishiyama[1,2], Makoto Taguchi[3], Masato Kagitani[4], Yasunobu Ogawa[1,2], Hidehiko Suzuki[5], Takeshi Sakanoi[4], Fuminori Tsuchiya[4], Peter Dalin[6], Urban Brändström[6]

1. National Institute of Polar Research, 2. The Graduate University for Advanced Studies, SOKENDAI, 3. Rikkyo University, 4. Tohoku University, 5. Meiji University, 6. Swedish Institute of Space Physics

Dayside aurora, polar patch, and airglow are the key phenomena for the understanding of the dayside magnetosphere, ionosphere, and neutral atmosphere coupling process. Those phenomena have been mainly monitored by active/passive radio remote sensing such as HF/VHF/UHF radar, GPS/GNSS and LF wave receiver, and riometer, but spatial and temporal resolutions by those measurements are basically not so good in comparison to optical measurements. Short-wavelength infrared (SWIR) wavelength is crucially important because lower sky irradiation by Rayleigh scattering may allow us to conduct ground-based optical observations even on the dayside. In order to make spectral investigations on the dayside and a feasibility study for the future dayside optical measurements, we operated a Czerny-Turner type 1-D imaging spectrograph at Syowa station (69.0˚S, 39.6˚E, from March to October in 2018) and Kiruna (67.8˚N, 20.4˚E, from late August in 2019).

The spectrograph with two selectable gratings (150 lpmm and 600 lpmm), whose spectral ranges and those per pixel are 510 nm and 119 nm, and 0.50 nm/pixel and 0.11 nm/pixel, respectively, focuses on continuous measurements of SWIR aurora (N_2 1st Positive band and N_2^+ Meinel band) and SWIR airglow (mainly, OH 3-1 band). We presented two events on 6 and 8 May 2018 in which strong intensifications of SWIR aurora emissions are found synchronized with auroral breakup at Syowa station. This is the first study that show absolute intensity of N_2^+ Meinel band (1-0 and 0-0) and N_2 1st Positive band (0-0, 1-2, and 0-1) in the unit of Rayleigh and temporal evolutions of the emissions with high temporal and wavelength resolutions less than 30 seconds and 1.0 nm respectively so far. With regard to airglow, $P_1(2)$ and $P_1(4)$ emissions in OH 3-1 band allow us to estimate OH rotational temperature near the mesopause with errors less than 8 K for data of signal-to-noise (S/N) ratio greater than 2, which show good correlations to neutral temperature measured simultaneously by co-located Fe resonance scattering lidar. The continuous measurements of OH rotational temperature make it possible to study a variability of atmospheric waves and temperature changes due to energetic particle forcing in polar regions.

In addition, we are currently developing a 2-D imaging spectrograph with a fast optical system and a wide field-of-view (FOV). This spectrograph is designed for SWIR wavelength ranging from 1.09 to 1.25 microns that covers strong auroral emissions in N_2^+ Meinel band (0-0) and N_2 1st Positive band (1-2, and 0-1). FOV and angular resolution are 55 degrees and 0.11 degrees per pixel, respectively. If a 30-microns slit is used, wavelength resolutions are 2230 and 5070, with two different gratings (950 lpmm and 1500 lpmm). The S/N ratio for 1 kR emissions can be expected to be larger than 1.0 in a few seconds exposure time. Therefore, we can investigate temporal variability of dayside reconnection and pulsating auroras with sufficient sampling rates of a few seconds. This spectrograph will be installed at The Kjell Henriksen Observatory/The University Centre in Svalbard, Longyearbyen (78.2˚N, 15.6˚E). Taking advantage of its location, 24-hours continuous observations can be expected (solar zenith angle larger than 96 degrees)

©2020. Japan Geoscience Union. All Right Reserved.

near the winter solstice. Additionally, collaborative studies with active/passive radio remote sensing such as EISCAT Svalbard radar and LF radio receiver will be done in the near future to evaluate spatial and temporal characteristics of dayside aurora.

Keywords: Aurora, Airglow, M-I coupling, Mesosphere and Lower Thermosphere , Short-wavelength infrared, Imaging spectrograph

©2020. Japan Geoscience Union. All Right Reserved.

“Great Wall” seen in the omega band: full-color digital camera observation from the International Space Station

*Sota Nanjo[1], Natsuo Sato[2], Yuta Hozumi[1], Keisuke Hosokawa[1], Ryuho Kataoka[2,3], Yoshizumi Miyoshi[4], Shin-ichiro Oyama[2,4,5], Mitsunori Ozaki[6], Kazuo Shiokawa[4], Satoshi Kurita[4]

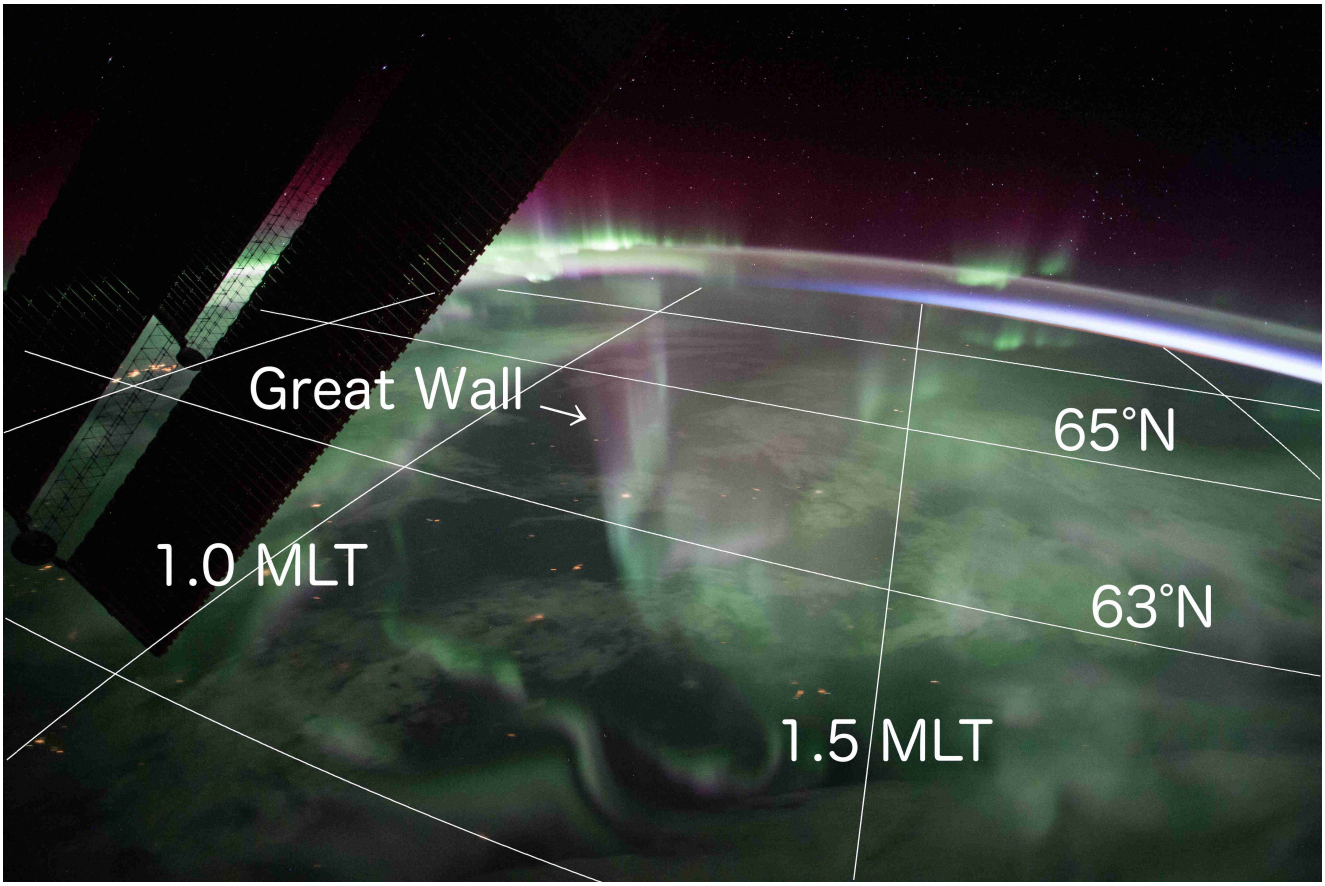
1. The University of Electro-Communications, 2. National Institute of Polar Research, 3. Department of Polar Science, School of Multidisciplinary Sciences, SOKENDAI, The Graduate University for Advanced Studies, 4. Institute for Space-Earth Environmental Research, Nagoya University, 5. Ionospheric Physics Research Unit, University of Oulu, 6. Graduate School of Natural Science and Technology, Kanazawa University

Astronauts have been taking a large number of sequential auroral photographs from the International Space Station (ISS) using digital single lens reflex cameras. These images have been published online (Gateway to Astronaut Photography of Earth). We have introduced that a method for projecting such images on the horizontal surface at the altitude of aurora by using city lights as markers [Nanjo et al., 2020, submitted]. This method could also be used for estimating the height structure of aurora. Since ISS orbits the Earth with a period of about 90 min, it is possible to observe large-scale structures of aurora in the MLT direction of 4-5 hours as a snapshot. As one example of such large-scale structures, we investigate omega bands which are wave-like structures in the morning sector. Various terrestrial/satellite observations of aurora from below/above have indicated that the western (night) side of the omega structure tend to be brighter than the eastern (morning) side [e.g. Opgenoorth et al., 1994; Amm et al., 2005]. However, since these observations have captured the omega structure as a two-dimensional image, the vertical structure of omega bands has not yet been revealed. The rim direction observations from ISS enable us to see the aurora obliquely; thus, its vertical structure (i.e., height profile) can be captured.

During several cases of omega bands, we found that there are thin wall-like discrete auroras (“Great Wall”) showing a few hundreds of km height. Great Walls are observed in the borderlines of the western flank of the torch structures and the dark part, and extends in 300-600 km mainly in the north-south direction. As shown in the figure, Great Wall is greenish at the bottom and reddish at the topside. It is also confirmed that the existence of Great Wall in the western side of torch is common in both the hemispheres. The simultaneous appearance of reddish and greenish lights extending in the magnetic field direction infers precipitation of electrons in a broadband energy range. This result is somewhat different from the earlier UV observation by Amm et al (2005) who reported the energy of precipitating electrons in a range of 2-5 keV in the omega structures. This could be because the spatio-temporal resolution of the UVI imager was insufficient and the Great Wall could not be extracted. In addition, active pulsating aurora are seen inside the omega structure. Owing to simultaneous observation of chorus waves at the conjugate area in the magnetosphere with the THEMIS satellite, they are typical pulsating aurora caused by the wave particle interaction. In the presentation, we will show the energy range of electron precipitation in the region of Great Wall estimated from the ISS measurement and discuss the origin of the Wall in the context of current closure in the magnetosphere-ionosphere coupling system.

Keywords: omega band, Magnetosphere-Ionosphere Coupling, pulsating aurora, International Space Station, Digital Single Lens Reflex camera, Field-Aligned Current

©2020. Japan Geoscience Union. All Right Reserved.



©2020. Japan Geoscience Union. All Right Reserved.

A tool to diagnose magnetosphere under northward IMF conditions: Simultaneous detections of TPA and omega-band aurora

*Motoharu Nowada[1]

1. Shandong Provincial Key Laboratory of Optical Astronomy and Solar-Terrestrial Environment, Institute of Space Sciences, Shandong University, Weihai

In this study, we try to explore the feasibility on whether or not the magnetospheric processes under northward Interplanetary Magnetic Field (IMF) conditions can be diagnosed using two different auroral phenomena; transpolar arc (TPA) and omega-band aurora. Both TPA and omega-band aurora can occur during the northward IMF intervals, and their appearances are closely related with the nightside magnetospheric processes. TPA can be formed and grown by the field-aligned currents induced by the plasma flow shear or the plasm vortex structures between the fast plasma flows generated by magnetotail magnetic reconnection and slower background magnetospheric flows, and the convection of the reconnection-formed closed magnetic fluxes, which cause in the nightside plasma sheet. On the other hand, the omega-band aurora can be attributed to the Kelvin-Helmholtz instabilities triggered by the flow shear between the plasma flows of the nightside magnetospheric boundary layer such as low-latitude boundary layer (LLBL) and background magnetospheric (plasma sheet) flows. If both auroral phenomena can simultaneously be observed, we might remotely investigate (diagnose) how the plasma and its energy are transported in the nightside magnetosphere and at the magnetospheric boundary region under northward IMF conditions. We will discuss the feasibility of this magnetospheric diagnosis, giving the observational example(s) of simultaneous observations of two different auroral phenomena, that is, TPA and omega-band aurora, and in-situ magnetospheric observation(s).

Keywords: Transpolar arc and omega band aurora, Solar wind-magnetotail-ionosphere coupling , Magnetospheric diagnosis, Magnetospheric dynamics under northward IMF conditions

©2020. Japan Geoscience Union. All Right Reserved.

Transient and localized field-aligned current in the cusp region associated with the Sudden Commencement

*Shigeru Fujita[1]

1. Meteorological College, Japan Meteorological Agency/ Nationa Institute of Polar Research

The Preliminary Impulse (PI) and the Main Impulse (MI) are the characteristic geomagnetic variations in the high-latitude region associated with the Sudden Commencement (SC) [Araki, 1994]. These geomagnetic variations appear mainly in the region below the auroral latitudes. This is because the field-aligned currents (FACs) causing these variations appear there [Fujita et al., 2003a,b]. Thus, many studies have been treating the behavior of SC in the region below the auroral latitudes. However, there are few studies about the SC-associated plasma and geomagnetic variations in the cusp region and the polar cap region.

We will report the transient and localized FAC in the cusp region associated with the SC. This FAC is found in the numerical results by REPPU (the global MHD simulation). This current appears in the northward IMF condition with a non-zero IMFBy component. The transient FAC in the cusp region is upward for the positive SC in the pre-noon sector when IMFBy is eastward. The upward FAC in the afternoon sector appears in the negative SI case under the same IMF condition. This transient FAC does not seem to appear in the southward IMF condition. We note that the FAC is too small to make a significant ground magnetic signature.

We will explain the mechanism of the transient FAC associated with the SC. Before the SC, there exists the magnetospheric convection corresponding to the round cell convection in the ionosphere for the north IMF condition. The simulation reveals that the sudden compression of the magnetosphere deforms the pattern of this magnetospheric convection to create a small-scale clockwise vortex transiently in the pre-noon sector. Deformation of the magnetospheric convection and formation of the vortex causes the transient FAC from the NBz current system. In the negative SI case, the clockwise vortex appears in the afternoon sector. When the IMF is southward, such transient vortex does not seem to appear in the two-cell pattern of the magnetospheric convection.

Araki, T., A physical model of the geomagnetic sudden commencement. In *Solar Wind Sources of Magnetospheric Ultra-Low-Frequency Waves*, ed. by M. J. Engebretson, K. Takahashi, and M. Scholer, American Geophysical Union, Washington, D.C., 183-200, 1994.

Fujita, S., T. Tanaka, T. Kikuchi, K. Fujimoto, K. Hosokawa, and M. Itonaga (2003a), A numerical simulation of the geomagnetic sudden commencement: 1. Generation of the field-aligned current associated with the preliminary impulse, *J. Geophys. Res.*, **108**(A12), 1416, doi:10.1029/2002JA009407.

Fujita, S., T. Tanaka, T. Kikuchi, K. Fujimoto, and M. Itonaga (2003b), A numerical simulation of the geomagnetic sudden commencement: 2. Plasma processes in the main impulse, *J. Geophys. Res.*, **108** (A12), 1417, doi:10.1029/2002JA009763.

Keywords: cusp , global MHD simulation

©2020. Japan Geoscience Union. All Right Reserved.

Existence of the Region1 field-aligned current system for zero interplanetary magnetic field

*Tsubasa Hashimoto[1], Masakazu Watanabe[2], Ryuho Kataoka[3], Shigeru Fujita[4], Takashi Tanaka[5]

1. Department of Earth and Planetary Sciences, Graduate School of Science, Kyushu University, 2. Department of Earth and Planetary Sciences, Faculty of Science, Kyushu University, 3. National Institute of Polar Research, 4. Meteorological College, Japan Meteorological Agency/ National Institute of Polar Research, 5. International Center for Space Weather Science and Education

The interaction between the solar wind and the magnetosphere for southward interplanetary magnetic field (IMF) is manifested in the development of the region 1 field-aligned current system and equivalently in the formation of ionospheric two-cell convection. Recent research indicates that the energy source of the region 1 current system is the high-pressure plasma in the magnetospheric cusp. Thus, understanding the cusp formation process is one critical issue in magnetospheric physics. On the other hand, solar activity has been modulating anomalously since solar cycle 23. In particular, a prolongation of the minimum period and a decrease of the maximum have been reported. If this trend continues, the IMF intensity is expected to become very small in the future. Therefore, investigating the cusp for infinitesimal IMF (for which reconnection effects are minimal) in comparison with the ‘normal’ cusp for southward IMF, contributes significantly not only to better understanding of the solar wind-magnetosphere interaction but also to future prediction of the global environment. For this purpose, we reproduced the magnetosphere under very small IMF using the Reproduce Plasma Universe (REPPU) code [Tanaka, 2015]. In the simulation, a quasi-steady state magnetosphere was produced under the solar wind and IMF conditions of density = 5cm^{-3}, Vx = -370km/s, Bx = 0.0nT, By = -0.05nT, Bz = 0.086nT (total intensity B = 0.1nT and clock angle $\theta = 30^{\circ}$), and temperature = 340,000K. The simulation reproduced the observed field-aligned current system for small IMF(-0.5nT < Bz < 1.5nT,|By| < 1.5nT) [Watanabe et al,1998]. There exists a clear difference between the cusp for infinitesimal IMF and the cusp for southward IMF. Normally, the cusp consists of the equatorward “load” in which electromagnetic energy is converted to thermal energy and the poleward "dynamo" in which thermal energy is converted to electromagnetic energy. The dynamo on the high latitude side is the energy source for the region 1 current system. Although this structure does not change even for infinitesimal IMF, a salient feature for infinitesimal IMF is the imbalance between the load and the dynamo. In the normal cusp, the load and the dynamo are almost balanced. However, in the cusp for infinitesimal IMF, the load is much smaller than the dynamo. This imbalance implies the existence of more than one energy supply route to the cusp dynamo, with one of them emerging solely for infinitesimal IMF. In the presentation, we report the detailed analysis of the simulation data and discuss the role of the cusp from the point of view of the functional aspect in the solar wind-magnetosphere interaction.

Keywords: field-aligned current, cusp

©2020. Japan Geoscience Union. All Right Reserved.

A Modified Magnetosphere-Ionosphere Coupling Model by Including the Hall Effects due to Thinning of the Near-Earth Plasma Sheet

*Pai-Sheng Wang[1], Ling-Hsiao Lyu[1]

1. Institute of Space Science and Engineering, National Central University, Taoyuan, Taiwan

Thinning of the near-Earth plasma sheet is commonly observed during the growth phase of a substorm. If the thickness of the near-Earth plasma sheet is between the ion’ s gyro radius and the electron’ s gyro radius, the unmagnetized ions and the magnetized electrons will move in different directions and result in a Hall effect in the near-Earth plasma sheet. This situation is similar to the collisional ions and the collisionless electrons in the E-region ionosphere. Kan et al. (1988) have proposed a Magnetosphere-Ionosphere coupling model to simulate the field-aligned current distributions in the ionosphere before the onset of a substorm. We modify the 1988 M-I coupling model by adding the Hall effect in the near-Earth plasma sheet during the growth phase of a substorm. We find that the Hall effect in the tail can enhance the field-aligned current and change the spatial distribution of the field-aligned current. As a result, both the intensity of the field-aligned currents and the spatial distribution of the upward field-aligned currents obtained in our simulations are in good agreement with the observed field-aligned currents at the onset of a substorm.

Keywords: Substrom, Field-aligned current, Magnetosphere-Ionosphere coupling

©2020. Japan Geoscience Union. All Right Reserved.

Alfvénic disturbances generated by the ionospheric polarization and the convection reversal in the magnetosphere

*Aoi Nakamizo[1], Akimasa Yoshikawa[2], Shinichi Ohtani[3], Takashi Tanaka[2]

1. Applied Electromagnetic Research Institute, National Institute of Information and Communications Technology, 2. Faculty of Science, Kyushu University, 3. The Johns Hopkins University Applied Physics Laboratory

The ionospheric polarization due to conductance non-uniformities largely deforms the global ionospheric convection pattern [*Nakamizo and Yoshikawa*, 2019]. Then it is supposed that the ionospheric polarization should act as the internal driver of the magnetosphere and our succeeding study using global MHD model shows that the ionospheric polarization actually and largely affects the magnetosphere; When the ionospheric Hall conductance is distributed non-uniformly, regardless of IMF-By=0 condition, the whole magnetosphere shows dawn-dusk asymmetry and a kink-type structure appears in the near-earth convection field. The structure resembles the magnetospheric Harang Reversal reported by preceding model studies. It is also confirmed that the magnetosphere remains symmetric between the dawn and dusk sides and the near-earth convection field shows no kink-type structure for the uniform ionospheric Hall conductance (no Hall polarization field). The result for the near-earth region suggests that the Hall polarization is necessary not only for the ionospheric Harang Reversal but also for the magnetospheric one.

The process by which the ionospheric polarization affects the magnetosphere in the simulation space should be as follows: The ionospheric potential deformed by the ionospheric polarization is mapped back to the inner boundary (I.B) of simulation space. The bulk velocity is updated there, and the perturbation propagates in the magnetosphere, modifying the momentum and energy balance. The FAC is determined in the magnetosphere updated in this way and is inputted to the ionospheric solver, where the ionospheric potential mapped back again to the magnetosphere is calculated. The M-I system develops with the succession of this cycle [*Yoshikawa et al.*, 2010], in which the ionospheric polarization effect is accumulatively included.

In order to confirm[visualize] this process and understand how the ionospheric driven component modifies the magnetosphere, we implemented the parallel/anti-parallel Alfvén mode separation method proposed by *Yoshikawa et al.* [2011] in the global simulation. When this method is applied to satellite observational data, it enables us to separate Alfvénic disturbances into components propagating parallel and anti-parallel to the ambient magnetic field, that is, components propagating from/to the ionosphere to/from the magnetosphere. We apply the separation to the 3-D simulation data.

In this study, we focus on the Harang Reversal and corresponding region in the magnetosphere. In the case of the uniform Hall conductance distribution, the Alfvénic disturbance from the I.B. propagates to the magnetosphere symmetrically between the dawn and dusk sides with opposite signs, corresponding to the dawn-dusk symmetric 2-cell ionospheric convection pattern. Both the ionospheric and magnetospheric convection pattern stay symmetric, never showing reversal structures no matter how the M-I system is activated by the external driver (solar wind and IMF). In the case of the non-uniform Hall conductance distribution, the Alfvénic disturbances from the I.B. propagates to the magnetosphere asymmetrically between the dawn and dusk sides because of the ionospheric potential deformed by Hall polarization. The magnetospheric convection gradually shows a meandering. As the time proceed, the kink-type structure is formed corresponding to the Harang Reversal in the ionosphere. The result indicates

©2020. Japan Geoscience Union. All Right Reserved.

that the cause of magnetospheric Harang structure is, at least in the global model, the ionospheric Hall polarization.

References:
Nakamizo, A., & Yoshikawa, A. (2019). Deformation of ionospheric potential pattern by ionospheric Hall polarization. Journal of Geophysical Research: Space Physics, 124, 7553–7580. https://doi.org/10.1029/2018JA026013

Keywords: M-I coupling, Alfvén mode separation, Global magnetosphere simulation, Harang Reversal

©2020. Japan Geoscience Union. All Right Reserved.

Near-earth plasma environment and injection simulated by global magnetosphere model with precession of magnetic axis

*Aoi Nakamizo[1], Yasubumi Kubota[1], Tsutomu Nagatsuma[1], Takashi Tanaka[2]

1. Applied Electromagnetic Research Institute, National Institute of Information and Communications Technology, 2. Faculty of Science, Kyushu University

The plasma distribution from the inner plasma sheet to the geosynchronous orbit is the important information not only as the plasma supply for the inner magnetosphere but also as the environment for artificial satellites. Besides, disturbances such as the plasma bubble intrusion and/or plasma injection associated with tail dynamics and substorms are superposed on the background population in that region.

Global MHD simulation is one of the powerful ways to complement observations and to know deductively what is going on in that region. However, there has been much room for improvement in our model toward the realistic simulation. In this paper, we report our recent model improvements and the performances. The improvement targeting on the magnetosphere-ionosphere coupling process is reported separately.

In order to accurately calculate the magnetic field configuration, we introduced the inclination of the magnetic axis (tilt). Besides, we introduce the precession between the magnetic axis and the rotation axis. Although the precession may appear to be less effective, it is considered to be effective because it alters the ionospheric conductance distribution, which largely modify the magnetospheric convection and dynamics (and therefore the plasma environment in the near-earth region) through the M-I coupling processes as shown by *Nakamizo and Yoshikawa* [2019]. Actually, background plasma distribution and intrusion from the plasma sheet are quite different between simulations with and without precession. We will show the results for equinoxes and solstices.

References:
Nakamizo, A., & Yoshikawa, A. (2019). Deformation of ionospheric potential pattern by ionospheric Hall polarization. *Journal of Geophysical Research: Space Physics*, 124, 7553– 7580. https://doi.org/10.1029/2018JA026013

Keywords: Ionospheric conductance effect, Plasma injection, Global magnetosphere simulation

©2020. Japan Geoscience Union. All Right Reserved.

Automatic identification of FLR events in VLOS data of multiple SuperDARN radars

*Hideaki Kawano[1,2], Akira Sessai Yukimatu[3,4], Nozomu Nishitani[5], Yoshimasa Tanaka[3,4], Satoko Saita[6], Tomoaki Hori[5]

1. Department of Earth and Planetary Sciences, Kyushu University, 2. ICSWSE, Kyushu University, 3. National Institute of Polar Research, 4. SOKENDAI, 5. ISEE, Nagoya University, 6. Kitakyushu College

The FLR (field-line resonance) can take place where the frequency of waves coming into the magnetosphere matches the eigenfrequency of a geomagnetic field line, which runs through the ground, the ionosphere, and the magnetosphere. The FLR causes field-line eigen-oscillations having the maximum in power and the largest changing rate in phase (as functions of L or the latitude) at the resonance point. From the FLR frequency one can estimate the density along the corresponding magnetic field line, because, in a simplified expression, 'heavier' field line oscillates more slowly.
Since the FLR oscillates the ionospheric plasma, too, the SuperDARN radars could monitor the two-dimensional (2D) instantaneous distribution of the FLR frequency, from which one could estimate the 2D plasma-density distribution on the magnetospheric equatorial plane, including the location of the plasmapause. However, visual identification of the FLR in the SuperDARN VLOS (Velocity along the Line of Sight) data is time-consuming, and the visual identification could miss FLR events superposed by non-FLR oscillations of VLOS (which could be called 'hidden' FLR events). In addition, there are lots of VLOS data to be analyzed.
Thus, we have been developing a computer code to automatically identify the FLR by using the Gradient method (a general name referring to both the amplitude-ratio and the cross-phase methods). This method cancels out the superposed perturbations by dividing the data from a Range Gate (RG) by the data from a nearby RG along the same beam, since the FLR frequency tends to depend on the latitude more strongly than the superposed perturbations. Another advantage of applying the Gradient method to the SuperDARN VLOS data is that we can choose any pair of RGs (along the same beam) with different distances, and thus can identify what distance is the best to identify the FLR. This distance reflects the resonance width, which is an important quantity reflecting the diffusion and dissipation of the FLR energy.
We have been developing a computer code to do the above. So far we have developed a subroutine to be applied to one beam, and tested it: We have applied the subroutine to the VLOS data of a few tens of beams of a few radars, and compared the results with the results of visual identifications we had independently made by examining the raw amplitude and phase distribution along the beams.
As a result, the subroutine has identified all the visually identified FLR events at the right location. The subroutine has also identified FLR events which were missed by the visual identification. In addition, the subroutine has identified possible 'hidden' FLR events.
We are now developing a code to automatically apply the subroutine to all the beam-aligned RG pairs (with all the RG-RG distances) of all the beams of a SuperDARN radar. By using the code we expect to identify much more FLR events than by visual identification; the automatically identified FLR events would include events simultaneously observed at several locations by several radars, enabling to monitor the 2D distributions of the plasma density.

©2020. Japan Geoscience Union. All Right Reserved.

Statistical study of SAPS occurrence characteristics using the SuperDARN HOkkaido Pair of (HOP) HF Radars

*Kento Oya[1], Nozomu Nishitani[1], Tomoaki Hori[1]

1. Institute for Space-Earth Environmental Research, Nagoya University

We investigate the occurrence characteristics of Sub-Auroral Polarization Streams (SAPS), using the Super Dual Auroral Radar Network (SuperDARN) Hokkaido pair of (HOP) radars. The goal is to clarify the longitudinal dependence of SAPS occurrence characteristics. In this study, we studied the occurrence rate of the flow that can be considered as SAPS, vs MLT and MLAT by using the beam swinging technique (*Ruohoniemi et al.,* 1989) and ovation technique (*Kunduri et al.,* 2017). Finally, we could catch the true occurrence characteristics of SAPS. We set criteria for the SAPS event, i.e., the flow speed should exceed 150 m/s and should have mainly westward component. We obtained the overall characteristics of SAPS, i.e., equatorward shift of high occurrence rate region with increasing MLT and geomagnetic activity. Some of the characteristics are different from previous studies (e.g., Kunduri et al., 2017). The SAPS regions seem to be located at higher latitudes than the previous studies and the SAPS occurrence peak regions are located at later MLT. These differences might be due to the difference in geographic longitude, as well as the relative values between geographic and geomagnetic latitudes (Far-East Siberia to Pacific vs North American region). We also found new feature, i.e, westward flows from midnight to morning at relatively low geomagnetic latitudes, that could not be caught in the previous studies probably due to the limitation of radars fields of view, especially lower latitude boundary.

Keywords: SAPS, SuperDARN, magnetosphere-ionosphere coupling, geomagnetic activity

©2020. Japan Geoscience Union. All Right Reserved.

Ion precipitation in the cusp for stably northward IMF: Seasonal dependence

*Haruto Koike[1], Satoshi Taguchi[1]

1. Department of Geophysics, Graduate School of Science, Kyoto University

Plasmas are injected into the cusp through lobe reconnection when IMF is northward. Previous studies have shown that the flux of the cusp ion precipitation at the ionospheric heights tends to increase as the solar wind dynamic pressure increases. In order to quantify the solar wind control of the flux of the cusp ion precipitation and understand other key parameters for the ion precipitation for northward IMF, we examined ion precipitation data obtained by DMSP F16, F17, and F18 during three years. Our automated detection of the cusp ion precipitation took more than 500 events that occurred at higher latitudes than 78 MLAT during stably northward IMF. The result of the statistical analysis shows that the seasonal dependence of the cusp ion flux exists in addition to the solar wind parameter dependence. We discuss the result in terms of the dipole tilt angle effect and/or the effect of the solar illumination of the ionosphere.

Keywords: Cusp, ion precipitaion, solar wind, northward IMF

©2020. Japan Geoscience Union. All Right Reserved.

Hemispheric Asymmetry of the Vertical Ion Drifts at Dawn Observed by DMSP

*Mohan Liu[1], Xiao-Xin Zhang[1], Fei He[2], Wenbin Wang[3]

1. National Satellite Meteorological Center, 2. Institute of Geology and Geophysics, Chinese Academy of Sciences, 3. High Altitude Observatory, National Center for Atmospheric Research

Based on the measurements from Defense Meteorological Satellite Program (DMSP) F12, F13, and F15 satellites in 1995–2014, we report significant hemispheric asymmetries in vertical ion drift velocity (Vz) at dawn (0500–0700 solar local time) in geomagnetic and geographic coordinates. Vz is distributed in 0300–0900 magnetic local time sector in both the northern (NH) and southern (SH) hemispheres. The north-south asymmetries are persistent no matter under what kind of seasonal, solar activity, and IMF conditions. In the polar cap, downward Vz is stronger in the SH. Such difference shows clear IMF BY dependence and is more significant in the local winter and/or under low solar activity conditions. In the geomagnetic coordinates, the auroral zone is dominated by upward Vz in the NH but by downward Vz in the SH statistically. In the geographic coordinates, the geographic longitudinal variation of Vz is more pronounced in the SH. The seasonal variations of high-latitude Vz are different in the NH and SH. The average asymmetric feature of Vz largely depends on the occurrence and magnitude of ion upflow/outflow, which are modulated by the combined effects of the asymmetric magnetic field configuration between the two hemispheres, and the dynamic processes in the tightly coupled ionosphere-thermosphere system, and their (probably nonlinear) interactions with each other.

Keywords: the topside ionosphere, vertical ion velocity, hemispheric asymmetry

©2020. Japan Geoscience Union. All Right Reserved.

Ground-based observations of MF/HF auroral radio emissions at three stations

*Yuka Sato[1,2], Atsushi Kumamoto[2], Yuto Katoh[2], Yasunobu Ogawa[3], Akira Kadokura[3], Atsuki Shinbori[4]

1. Nippon Institute of Technology, 2. Graduate school of Science, Tohoku University, 3. National Institute of Polar Research, 4. Institute for Space-Earth Environmental Research, Nagoya University

We launched ground-based observations of MF/HF auroral radio emissions more than a decade ago at two stations (The Husafell Station, Iceland, September 2005; The Kjell Henriksen Observatory, Svalbard, September 2008) and found multiple unknown properties of MF/HF auroral radio emissions, e.g. polarization features [*Sato et al.*, 2008, 2015] and existence of a higher frequency component [*Sato et al.*, 2012]. To make a next siginificant step for a futher understanding of MF/HF auroral radio emissions, we installed a new dedicated instrumentation at the KAIRA (Kilpisjärvi Atmospheric Imaging Receiver Array) site in Kilpisjärvi, Finland (Latitude: 60.07 N, Longitude: 20.76 E) in the summer of 2018. It is a passive receiving system designed to realize a high-resolution spectral, interferometric and polarization measurements using 4 loop antennas and a software-defined radio (SDR) receiver. This SDR receiver can implement high-speed, flexible digital signal processing of RF signals and obtain high-resolution spectra pauselessly throughout the night in a wide frequency range up to 6 MHz. In addition, we plan to upgrade the receiving system in Iceland to utilize a similar SDR receiver this summer. One of the main research subjects of this project is radio emission spontaneously emitted from aurora. There are long-known three types of MF/HF auroral radio emissions identified at ground level: auroral hiss, medium frequency burst (MFB), and auroral roar. Investigation into the generation of these emissions not only offers a tool of great promise for remote sensing of ionospheric plasma processes and parameters but also gives the foundation for understanding various radiation mechanisms that occur in planetary magnetospheres and plasma in space. In combination with the long-term continuous observations in Iceland and Svalbard and future EISCAT_3D experiments, observation with this new instrumentation will provide a first-time opportunity to reveal spatiotemporal variations of macro and fine structures of MF/HF auroral radio emissions associated with substorm evolution. In this presentation, we show detailed specification of the new instrumentations and some initial results.

Keywords: radio emissions, auroral phenomena, wave-particle interactions

©2020. Japan Geoscience Union. All Right Reserved.

Application of Magneto-Impedance Sensor to Geomagnetic Field Measurements for Constructing Distributed Arrays of Small Instruments (DASI)

*Nomura Hiroshi[1], Masahito Nosé[1], Hitoshi Aoyama[2], Takeshi Kawano[2], Masafumi Hirahara[1]

1. Institute for Space-Earth Environmental Research, Nagoya University, 2. Aichi Steel Corporation

Magneto-impedance (MI) effect was discovered about 25 years ago and micro-size magnetic sensors that utilizes this effect become commercially available. We made some modifications to the commercially available MI sensors as they can cover the range of the geomagnetic field. For the period of March 30 to April 27, 2018, we conducted experimental observations of geomagnetic field variations with the MI sensors at Mineyama observation site, which is located about 100 km north-west of Kyoto. Data obtained with the MI sensors were compared with those from the fluxgate magnetometer that has been working at the site. Results showed that the MI sensor recorded geomagnetic variations with amplitudes of ~1 nT that were also detected with the fluxgate magnetometer. This suggests that MI sensors are useful for researches in geomagnetism or space physics. Furthermore, MI sensors are much less expensive than fluxgate magnetometers.
We are developing a low-cost system to measure the geomagnetic field using the MI sensor. This system includes a Raspberry Pi, a commercially available AD converter, and power supply circuits for generating a stable power supply voltage. In presentation, we will show observation data from this system and discuss the possibility of using this system in Distributed Arrays of Small Instrument (DASI).

Keywords: Geomagnetic Field Measurements, Magneto-Impedance Sensor, Raspberry Pi, Distributed Arrays of Small Instruments (DASI)

©2020. Japan Geoscience Union. All Right Reserved.

[E] Poster | P (Space and Planetary Sciences)：P-EM Solar-Terrestrial Sciences, Space Electromagnetism & Space Environment

[P-EM14] Frontiers in solar physics

convener:Shinsuke Imada(Institute for Space-Earth Environmental Research, Nagoya University), Alphonse Sterling(NASA/MSFC), Takaaki Yokoyama(School of Science, University of Tokyo), Toshifumi Shimizu(Institute of Space and Astronautical Science, JAXA)

Over recent decades, Sun-observing satellite missions have told us much about the dynamic solar atmosphere. These satellites can observe magnetic activity in the solar corona at wavelengths inaccessible from ground-based telescopes, such as X-rays and EUV. Additionally, the seeing-free conditions of space allow for consistent, high-spatial resolution at visible wavelengths; e.g. the HInode satellite can observe solar surface magnetic field elements down to ~0.2 arcsec. From observations such as these, we have identified three important points regarding what is required form future space-based solar missions to solve fundamental solar problems, such as how the corona is heated and what drives solar eruptions: (1) seamless observation over all temperature regimes of the solar atmosphere, from the chromosphere to the corona, at the same time; (2) high spatial and temporal resolution to resolve elemental structures of the solar atmosphere, and to track their evolution; and (3) plasma diagnostic capability to quantify the dynamics of elementary process taking place in the solar atmosphere. To meet these requirements, recently the solar physics community in Japan proposed the Solar-C_EUVST mission, which will be launched in the mid-2020s. Furthermore, additional top-rate solar observatories, such as the Parker Solar Probe (PSP), Solar Orbiter, and the Daniel K. Inouye Solar Telescope (DKIST), will be operating in the years leading up to Solar-C_EUVST. In this session we will discuss what solar physics observational and numerical-simulation studies are required prior to the mid-2020s, to prepare most efficiently for the new observational era. We welcome contributions dealing with remote-sensing space-based observations (e.g. from Hinode and SDO), in-situ observations from near- and deep-space (e.g., PSP, Pioneer), ground-based observations, and numerical studies.

[PEM14-P01] Prediction of sunspot number and latitude distribution using machine learning

*Kento Michiwaki[1], Shinsuke Imada[1], Yoshizumi Miyoshi[1] (1.Institute for Space-Earth Environmental Research, Nagoya University)

[PEM14-P02] Image analysis of sunspot drawings in Dalton minimum(the early 1800s) and reproduction of magnetograms from sunspot drawings by using machine learning.

*SHOMA UNEME[1], Shinsuke Imada[1], Hisashi hayakawa[2], Lee Harim[3], Moon Yongjae[3], Park Eunsu[3], Yoshizumi Miyoshi[1] (1.nagoya university institutive for Space Earth for enviornmental research, 2.Osaka University School of Letters , 3.School of Space Research, Kyung Hee University)

[PEM14-P03] Solar surface flow around the cycle 24 minimum

*Kengo Matoba[1], Shinsuke Imada[1] (1.Institute for Space-Earth Environmental Research, Nagoya University)

[PEM14-P04] Impact of morphological asymmetry in a sunspot group on the solar cycle prediction

★Invited Papers

*Haruhisa Iijima[1], Hideyuki Hotta[2], Shinsuke Imada[1] (1.Institute for Space-Earth Environmental Research, Nagoya University, 2.Faculty of Science, Chiba University)

[PEM14-P05] Thermal non-equilibrium plasma during a solar flare

*Shinsuke Imada[1] (1.Institute for Space-Earth Environmental Research, Nagoya University)

[PEM14-P06] Hall MHD calculation of magnetic reconnection assuming coronal heating

*Kyohei Murakami[1], Shinsuke Imada[1], Haruhisa Iijima[1], Yoshizumi Miyoshi[1] (1.Nagoya University Institute for Space-Earth Environmental)

[PEM14-P07] Statistical investigation of magnetic and temperature properties of white-light flares

*Kyoko Watanabe[1], Kosuke Tsuruda[1], Satoshi Masuda[2], Sam Krucker[2,3,4] (1.National Defense Academy of Japan, 2.Institute for Space-Earth Environmental Research, Nagoya University, 3.University of Applied Sciences Northwestern Switzerland, 4.UC Berkeley)

[PEM14-P08] Validation of EUV dynamic spectra and their impact on the ionosphere

★Invited Papers

*Shohei Nishimoto[1], Kyoko Watanabe[1], Shinsuke Imada[2], Toshiki Kawai[2], Tomoko Kawate[3], Hidekatsu Jin[5], Kyoung-Sun Lee[4] (1.National Defense Academy, 2.Institune for Space-Earth Environmental Research, Nagoya University, 3.Institute of Space and Astronautical Science, Japan Aerospace Exploration Agency, 4.Center for Space Plasma and Aeronomic Research, University of Alabama in Huntsville, 5.National Institute of Information and Communications Technology)

[PEM14-P09] Recent and Upcoming Studies of Solar Coronal Jets

*Alphonse Sterling[1], Ronald Moore[2,1], Navdeep Panesar[3,4] (1.NASA/MSFC, 2.U of Alabama Huntsville, 3.LMSAL, 4.Baeri)

[PEM14-P11] Perspective of simulation studies for the Solar-C_EUVST science

*Takaaki Yokoyama[1], Shinsuke Imada[2], Haruhisa Iijima[2], Shin Toriumi[3] (1.School of Science, The University of Tokyo, 2.Institute for Space-Earth Environmental Research, Nagoya University, 3.Institute of Space and Aeronautical Science, JAXA)

Prediction of sunspot number and latitude distribution using machine learning

*Kento Michiwaki[1], Shinsuke Imada[1], Yoshizumi Miyoshi[1]

1. Institute for Space-Earth Environmental Research, Nagoya University

For space weather study, it is important to estimate the solar activity in near future. Recently, it is believed that the polar magnetic field at the solar minimum is one of the indicators for the next solar activity. Therefore, many studies try to estimate the solar polar magnetic field for the cycle prediction. The temporal variation of the polar magnetic field can be reproduced by using the surface magnetic flux transport calculation model (SFT model). The SFT model consists of advection term due to differential rotation and meridional circulation, magnetic diffusion term, and flux emergence term. The advection and the diffusion coefficients are estimated by modern observations. On the other hand, estimation of future flux emergence is still very difficult. Therefore, estimating when and where the sunspots will be emerge is crucial for cycle prediction study.
In this study, we predicted the sunspot number using RNN (Recurrent Neural Network), which is one of the machine learning technique. Also, the latitude distribution (batterfly diagram) was predicted using CNN (Convolutional Neural Network). As a result, for the prediction of the number of sunspots, by using the sunspot number of former half of the cycle as the input data, we succeeded to predict the sunspot number of latter half of the cycle. For the prediction of the appearance latitude, the transition and the periodicity of the appearance of the sunspot from the middle latitude to the low latitude were able to be reproduced.

Keywords: sun, prediction, machine learning

©2020. Japan Geoscience Union. All Right Reserved.

Image analysis of sunspot drawings in Dalton minimum(the early 1800s) and reproduction of magnetograms from sunspot drawings by using machine learning.

*SHOMA UNEME[1], Shinsuke Imada[1], Hisashi hayakawa[2], Lee Harim[3], Moon Yongjae[3], Park Eunsu[3], Yoshizumi Miyoshi[1]

1. nagoya university institutive for Space Earth for enviornmental research, 2. Osaka University School of Letters , 3. School of Space Research, Kyung Hee University

Solar activity varies periodically in 11 years. Because the solar activity is one of the main origins of the variability of the solar-terrestrial environment, it is important to predict the solar activity especially in the category of space weather study. It is known that the polar magnetic field at the solar minimum is closely correlated with the solar activity at the next solar activity. This correlation was confirmed by observing the current sun precisely. On the other hand, it is not clear whether there was a similar correlation in the past sun. Therefore, the aim of this study is to analyze the past sunspot drawing images to verify whether the polar field value at the solar minimum is also good correlation with the next solar activity. Especially, we focused on the Dalton minimum when sunspots were little in the early 1800s. We extracted latitude and longitude of sunspot from drawings in the early 1800 's. Furthermore, we generated magnetograms from sunspot drawings by using cGAN(Conditional Generative Adversarial Nets), one of the popular machine learning methods, and will discuss the validity of these magnetograms. In future, we will calculate the polar magnetic field in the Dalton minimum from these generated magnetograms by surface magnetic flux transport model and compare it with the correlation.

Keywords: Solar activity, Dalton minimum, machine learning, Sunspot drawings

©2020. Japan Geoscience Union. All Right Reserved.

Solar surface flow around the cycle 24 minimum

*Kengo Matoba[1], Shinsuke Imada[1]

1. Institute for Space-Earth Environmental Research, Nagoya University

Solar flares have significant impacts on the Earth’s environment. Flares are now believed to be associated with sunspot’s activities. Therefore the 11-year variability in sunspot numbers is one of the major origins of the decadal variability in the solar environment. Predicting sunspot number in next solar cycle is very important for space weather. Building the next solar cycle prediction scheme is the key to long-term space weather research. Recently, it is believed that the polar magnetic field during the minimum period is one of the good indicator for the next solar cycle activity. Surface flux transport (SFT) models are often used to estimate polar magnetic fields. On the other hand, the SFT model requires several parameters, such as meridional circulation, rotational difference, and turbulent diffusion. These parameters are not fully understood, and especially their temporal variation is still unclear.

In this study, we focused on two typical solar surface flows, differential rotation and meridional circulation. We apply a magnetic element tracking (MET) module to SDO/HMI magnetic field data to obtain solar surface velocities. Because HMI has been available since 2010, we calculated solar surface flow using ten years data. We can capture more than 5,000,000 elements and average for each latitude. As a result, we obtain the latitudinal profile of the meridional flow and differential rotation speed. We also studied the temporal variations of the meridional flow and differential rotation speed in cycle 24. We find that the differential rotation/meridional flow speed is faster/slower at the latitude where the sunspots frequently emerge, respectively.

Keywords: Sun, Sunspot, Magnetic field

©2020. Japan Geoscience Union. All Right Reserved.

Impact of morphological asymmetry in a sunspot group on the solar cycle prediction

*Haruhisa Iijima[1], Hideyuki Hotta[2], Shinsuke Imada[1]

1. Institute for Space-Earth Environmental Research, Nagoya University, 2. Faculty of Science, Chiba University

The spatial structure of leading sunspots is more coherent than that of following sunspots. This well-known characteristic of sunspots produces significant impact on the formation of polar magnetic field and cycle prediction. Using the surface flux transport model, we quantified the effect of this morphological asymmetry of sunspots on the polar field formation for the first time. We find that (1) the morphological asymmetry prevents the build-up of the polar magnetic field by orders of magnitude and (2) the model with the asymmetry shows better agreement in the temporal profile of the observed axial dipole strength. Considering the clear relation between the polar magnetic field and the cycle amplitude, our results suggest a strong impact of the morphological asymmetry on the solar cycle prediction.

Keywords: Sunspot, Solar Cycle Activity, Magnetic field

©2020. Japan Geoscience Union. All Right Reserved.

Thermal non-equilibrium plasma during a solar flare

*Shinsuke Imada[1]

1. Institute for Space-Earth Environmental Research, Nagoya University

Plasma in the solar corona is believed to be in thermal equilibrium because of the occurrence of weak Coulomb collisions. To date, many studies have discussed the plasma dynamics in the solar corona assuming thermal equilibrium. Most phenomena observed in the solar corona can be explained under this assumption because the available temporal resolution is not sufficient to resolve non-equilibrium conditions. After Hinode was launched, a very high temporal resolution became available, especially for spectroscopic observation. Now, we can discuss plasma heating or acceleration in the solar corona using extreme-ultraviolet (EUV) spectroscopic observations with high time resolution. Further, we can also observe the solar corona at multiple wavelengths with high spectral resolution. Owing to Hinode observations, we can now discuss plasma dynamics under thermal non-equilibrium conditions, such as non-equilibrium ionization. In this talk we will discuss Thermal non-equilibrium plasma during a solar flare oberved by Hinode.

Keywords: Sun, Corona, Flare

©2020. Japan Geoscience Union. All Right Reserved.

Hall MHD calculation of magnetic reconnection assuming coronal heating

*Kyohei Murakami[1], Shinsuke Imada[1], Haruhisa Iijima[1], Yoshizumi Miyoshi[1]

1. Nagoya University Institute for Space-Earth Environmental

The solar corona is hotter than the solar surface, and its heating mechanism is not clear. Coronal heating can be explained by dissipating even 1% of the convective energy on the solar surface. One of the models that explain coronal heating is energy dissipation by nanoflares, which are thought to be small magnetic reconnections. Fast magnetic reconnection can occur by the Hall effect when the current layer scale is comparable to the ion inertia length. If the magnetic field lines twisted inside the sun rise to the corona, the density around the current layer will decrease sharply, and the ion inertia length will increase. This plasma condition might cause Hall reconnection during flux emergence. The purpose of this study is to create a model for magnetic reconnection when flux emergence occurs using Hall MHD. Gravity was added horizontally along the current sheet to simulate flux emergence. This gravity represents the gravity along the loop when the magnetic field emerges. Simulating gravitational stratification in the direction along the loop reproduced the situation where the density in the emerging magnetic field decreases in the corona. No reconnection occurs in the ideal MHD, but reconnection occurs when gravity is applied. This is because the density of the current layer was reduced by gravity, and the current layer was thinned and numerically dissipated. We added the Hall effect to the simulation and discuss the effect in the current sheet considering the gravitational stratification.

Keywords: coronal heating, nano flares, Hall MHD

©2020. Japan Geoscience Union. All Right Reserved.

Statistical investigation of magnetic and temperature properties of white-light flares

*Kyoko Watanabe[1], Kosuke Tsuruda[1], Satoshi Masuda[2], Sam Krucker[2,3,4]

1. National Defense Academy of Japan, 2. Institute for Space-Earth Environmental Research, Nagoya University, 3. University of Applied Sciences Northwestern Switzerland, 4. UC Berkeley

White-light flare is a phenomenon in which has enhancement of visible continuum in a solar flare, and is mainly associated with a large flare. Although the emission mechanism of white-light flares has not been well understood yet, previous studies have suggested that their origin is accelerated non-thermal electrons and that a relatively strong magnetic field exists in the acceleration site (e.g. Watanabe et al., 2017).

So, we tried to estimate the coronal magnetic field strength by using the turn-over frequency of gyro-synchrotron emission in microwaves (Dulk 1985). We used the Nobeyama Radio Polarimeters (NoRP) for >M3 class flares during the period from January 2011 to December 2017. We found 29 events which were simultaneously observed with white-light (SDO/HMI continuum) and microwave (NoRP) which had loop-top microwave source in the image observed with Nobeyama Radioheliograph. However, we couldn't find any difference in turn-over frequencies with or without white-light emission. In order to investigate the relationship between white-light emission and coronal magnetic field, this method might be too simple because the turn-over frequency is determined by not only the magnetic field strength but also the electron density and so on (Dulk 1985).

To overcome this problem, next, we tried to compare field strength and temperature of white-light emission region. The former/latter can be derived from SDO/HMI magnetogram/three continuum bands of Hinode/SOT. We performed a statistical analysis for 35 Hinode white-light events and then found the field strength of white-light emission region were correlated with the maximum brightness of the white-light emission. Assuming that the magnetic field strength at the acceleration site in the corona is somehow proportional to the photospheric magnetic field strength at the white-light emitting region, this result suggested the strong acceleration process which produces WLFs takes place at the strong magnetic field region in the corona. Moreover, we also found that the amount of the white-light enhancement was approximately proportional to the fourth power of the radiation temperature. From this result, it is considered that the white-light enhancement is black body radiation. From the above results, it is considered that in the white-light flare, large number of electrons accelerated by strong magnetic fields penetrate to the foot-points near the photosphere, and as a result, black body radiation emits as white-light emission at the heated region.

Keywords: Sun: flares, Sun: radio radiation, Sun: magnetic fields

©2020. Japan Geoscience Union. All Right Reserved.

Validation of EUV dynamic spectra and their impact on the ionosphere

*Shohei Nishimoto[1], Kyoko Watanabe[1], Shinsuke Imada[2], Toshiki Kawai[2], Tomoko Kawate[3], Hidekatsu Jin[5], Kyoung-Sun Lee[4]

1. National Defense Academy, 2. Institune for Space-Earth Environmental Research, Nagoya University, 3. Institute of Space and Astronautical Science, Japan Aerospace Exploration Agency, 4. Center for Space Plasma and Aeronomic Research, University of Alabama in Huntsville, 5. National Institute of Information and Communications Technology

Solar flares suddenly emit strong multi-wavelength electromagnetic emissions. Among these emissions, soft X-ray and extreme ultraviolet (EUV) emissions cause the sudden ionospheric disturbance (SID) and effect on radio communication (Dellinger 1937). We need soft X-ray and EUV flare spectra for predicting SID, however, EUV flare spectra observation with high spectral and temporal resolution are very limited, the numerical model for predicting EUV emissions is needed. One of them is the Flare Irradiance Spectral Model (FISM; Chamberlin et al., 2008). Although FISM is the most widely used model now, this model has some problems such as uncertain physical processes due to empirical model.

Hence, we are trying to construct new prediction model of flare EUV dynamic spectra which can explain simple physical models in flare loop (Imada et al., 2015; Kawai et al., under review). In this model, we use the hydrodynamic simulation of the solar flare model given in the CANS (Coordinated Astronomical Numerical Software) 1D package and the CHIANTI atomic database (Del Zanna et al., 2015). First, by using CANS1D, we calculate the time evolution of density and temperature of a single flare loop whose loop length is estimated from observed flare ribbon distance. Then we obtain the flare (X-ray and EUV) spectra of the simulated coronal loop by using the CHIANTI atomic database. Using this model, we reproduced EUV dynamic spectra for some flare events, and compared with observed EUV spectra by SDO/EVE. As a result, we found that our calculation results clearly reproduced most of the EUV lines on short wavelength during flare. Moreover, we found that our model well reproduce the total EUV flare energy especially at wavelengths shorter than 14 nm.

Furthermore, in order to examine the effect of flare EUV emission on the Earth’ s ionosphere, we input our calculated flare EUV spectra to the Earth's atmospheric model GAIA (Ground-to-Topside Model of Atmosphere and Ionosphere for Aeronomy; Jin et al., 2011), and reproduced the ionospheric response.

In this presentation, we will discuss the physical parameters that affect flare EUV spectra and the effects of flare emissions on the Earth’ s ionosphere.

Keywords: Solar Flare, UV emission, X-ray emission

©2020. Japan Geoscience Union. All Right Reserved.

Recent and Upcoming Studies of Solar Coronal Jets

*Alphonse Sterling[1], Ronald Moore[2,1], Navdeep Panesar[3,4]

1. NASA/MSFC, 2. U of Alabama Huntsville, 3. LMSAL, 4. Baeri

Solar jets occur throughout the solar atmosphere, including in coronal holes, quiet regions, and active regions. Observations at X-ray and EUV wavelengths show that frequently jets are made by eruptions of small-scale filaments, called “minifilaments.” Recent studies indicate that many of, or even the majority of, these jet-producing minifilament eruptions occur at locations where opposite-polarity photosphere magnetic fluxes merge and cancel. These observations support the idea that flux cancelation builds a magnetic flux rope along which cool minifilament material gathers, and that the flux rope subsequently erupts to form the jet through a sequence of magnetic reconnections. In this presentation we will update our recent investigations into jets, and discuss expectations and needs for jet studies with new Sun-observing instruments.

Keywords: Sun, Solar Coronal Jets, Solar Coronal Activity

©2020. Japan Geoscience Union. All Right Reserved.

Perspective of simulation studies for the Solar-C_EUVST science

*Takaaki Yokoyama[1], Shinsuke Imada[2], Haruhisa Iijima[2], Shin Toriumi[3]

1. School of Science, The University of Tokyo, 2. Institute for Space-Earth Environmental Research, Nagoya University, 3. Institute of Space and Aeronautical Science, JAXA

The proposed science objectives of the Solar-C_EUVST are I. formation of the solar atmosphere and the solar wind and II. driving mechanisms of solar flares and eruptions. For the understanding of the complicated observational data, the complementary supports of the numerical MHD simulations are absolutely essential. In this presentation, we are going to summarise the current status of the simulation studies in the viewpoint as supporting tools for the Solar-C_EUVST data interpretations, and attempt to make a prospect for further development.

Keywords: Sun, simulations, magnetohydrodynamics

©2020. Japan Geoscience Union. All Right Reserved.

[E] Poster | P (Space and Planetary Sciences)：P-EM Solar-Terrestrial Sciences, Space Electromagnetism & Space Environment

[P-EM15] Plasma Theory and Simulation

convener:Seiji Zenitani(Kobe University), Fan Guo(Los Alamos National Laboratory), Takayuki Umeda(Institute for Space-Earth Environmental Research, Nagoya University), Takanobu Amano(Department of Earth and Planetary Science, University of Tokyo), Yasuhiro Nariyuki(Faculty of Education, University of Toyama)

This session invites contributions in plasma theories and simulations. Theoretical and/or numerical results on plasma processes (magnetic reconnection, collisionless shocks, wave-particle interactions, and boundary problems) and their applications in space, solar, astrophysical, and laboratory environments are welcome. Results in computational techniques for simulations and for data analysis are also welcome, including applications of Machine Learning. The session will be held in English.

[PEM15-P01] Full particle-in-cell simulation of the interaction between two plasmas for laboratory experiments on the generation of magnetized collisionless shocks with high-power lasers

*Takayuki Umeda[1], Ryo Yamazaki[2], Yutaka Ohira[3] (1.Institute for Space-Earth Environmental Research, Nagoya University, 2.Aoyama Gakuin University, 3.The University of Tokyo)

[PEM15-P02] PIC simulation on non-linear development of lower hybrid waves instabilities driven by energetic ions with a ring-like velocity distribution: the comparison of initial value problems and energetic-ion injection models.

*Tsubasa Kotani[1], Mieko Toida[2], Toseo Moritaka[2], Satoshi Taguchi[1] (1.Department of Geophysics, Graduate School of Science, Kyoto University, 2.National Institute for Fusion Science)

[PEM15-P03] A comparison of relativistic particle integrators in a fast magnetized flow (2)

*Seiji Zenitani[1], Tsunehiko Kato[2] (1.Kobe University, 2.National Astronomical Observatory of Japan)

[PEM15-P04] Particle Simulation of Triggered Emissions from Large Amplitude Whistler-mode Waves

*Takeshi Nogi[1], Satoko Nakamura[1,2], Yoshiharu Omura[1] (1.Reserch Institute for Sustainable Humanosphere, Kyoto University, 2.Institute for Space-Earth Environmental Research, Nagoya University)

[PEM15-P05] Electromagnetic particle simulation of whistler mode triggered emissions in the equatorial magnetosphere

*Yuya Fujiwara[1], Yoshiharu Omura[1], Takeshi Nogi[1], Yikai Hsieh[1], Satoko Nakamura[1,2] (1.Research Institute for Sustainable Humanosphere, Kyoto University, 2.Institute for Space-Earth Environmental Research, Nagoya University)

[PEM15-P06] Study of the Pitch Angle Scattering of Small Pitch Angle Electrons by Coherent Whistler-Mode Waves

*Genki Ishizawa[1], Yuto Katoh[1], Masahiro Kitahara[1], Atsushi Kumamoto[1], Tomoki Kimura[1,2], Yohei Kawazura[1,2] (1. Department of Geophysics Graduated School of Science Tohoku university , 2.Frontier Research Institute for Interdisciplinary Sciences Tohoku University)

[PEM15-P07] Development of numerical code of the electron transport equation with spectral method

*Takuma Katou[1], Takanobu Amano[1] (1.The University of Tokyo)

[PEM15-P08] Vlasov solver using rational Chebyshev function

*Taiki Jikei[1], Takanobu Amano[1] (1.The University of Tokyo)

[PEM15-P09] A Multistate Low-dissipation Advection Upstream Splitting Method for Ideal Magnetohydrodynamics

*Takashi Minoshima[1], Keiichi Kitamura[2], Takahiro Miyoshi[3] (1.Center for Mathematical Science and Advanced Technology, Japan Agency for Marine-Earth Science and Technology, 2.Yokohama National University, 3.Hiroshima University)

[PEM15-P10] On the rate of electron injection at collisionless shocks

*Takanobu Amano[1] (1.Department of Earth and Planetary Science, University of Tokyo)

[PEM15-P11] A Study of Evolutions of Growth Rates and the Most Unstable Modes in the Events of Sub-magnetosonic Kelvin-Helmholtz Instabilities in an MHD plasma

*Chun-Yen Hsu[1], Ling-Hsiao Lyu[1] (1.Institute of Space Science and Engineering, National Central University, Taoyuan, Taiwan)

[PEM15-P12] Structure formation in chiral magnetohydrodynamics: Effect of background magnetic field

*Takahiro Miyoshi[1] (1.Hiroshima University)

[PEM15-P13] Synchrotron maser emission and associated particle acceleration in relativistic shocks

*Masanori Iwamoto[1], Takanobu Amano[2], Masahiro Hoshino[2], Yosuke Matsumoto[3] (1.Interdisciplinary Graduate School of Engineering Sciences, Kyushu University, 2.Graduate School of Science, The University of Tokyo, 3.Graduate School of Science, Chiba University)

Full particle-in-cell simulation of the interaction between two plasmas for laboratory experiments on the generation of magnetized collisionless shocks with high-power lasers

*Takayuki Umeda[1], Ryo Yamazaki[2], Yutaka Ohira[3]

1. Institute for Space-Earth Environmental Research, Nagoya University, 2. Aoyama Gakuin University, 3. The University of Tokyo

A preliminary numerical experiment is conducted for laboratory experiments on the generation of magnetized collisionless shocks with high-power lasers by using one-dimensional particle-in-cell simulation. The present study deals with the interaction between a moving aluminum plasma and a nitrogen plasma at rest. In the numerical experiment, the nitrogen plasma is unmagnetized or magnetized by a weak external magnetic field. Since the previous study suggested the generation of a spontaneous magnetic field in the piston (aluminum) plasma due to the Biermann battery, the effect of the magnetic field is of interest. Sharp jumps of the electron density and magnetic field are observed around the interface between the two plasmas as long as one of the two plasmas is magnetized, which indicates the formation of tangential electron-magneto-hydro-dynamic discontinuity. When the aluminum plasma is magnetized, strong compression of both the density and the magnetic field takes place in the pure aluminum plasma during the gyration of nitrogen ions in the aluminum plasma region. The formation of a shock downstream is obtained from the shock jump condition. The results suggest that the spontaneous magnetic field in the piston (aluminum) plasma plays an essential role in the formation of a perpendicular collisionless shock.

Keywords: plasma, shock waves, PIC simulation, laboratory astrophysics

©2020. Japan Geoscience Union. All Right Reserved.

PIC simulation on non-linear development of lower hybrid waves instabilities driven by energetic ions with a ring-like velocity distribution: the comparison of initial value problems and energetic-ion injection models.

*Tsubasa Kotani[1], Mieko Toida[2], Toseo Moritaka[2], Satoshi Taguchi[1]

1. Department of Geophysics, Graduate School of Science, Kyoto University, 2. National Institute for Fusion Science

Instabilities driven by energetic ions are important issues both for space plasma and magnetically confined plasma aimed for fusion energy. In the auroral region of the Earth’ s magnetosphere, waves near the lower hybrid resonance frequency, ω_{LH}, driven by energetic ions can contribute ion energization. Here, ω_{LH} is estimated as $\omega_{LH} \sim \sqrt{\Omega_i \Omega_e}$ where Ω_i is the ion cyclotron frequency and Ω_e is the electron cyclotron frequency. These waves, namely lower hybrid waves (LHWs) driven by energetic ions are also observed in the Large Helical Device (LHD) for fusion plasma. In the LHD, energetic ions are generated by the perpendicular neutral beam injection (NBI) for plasma heating.

One-dimensional, electromagnetic, particle-in-cell (PIC) simulations are used to investigate the non-linear evolution of lower hybrid waves instabilities driven by energetic ions with a non-Maxwell velocity distribution. These instabilities can excite LHWs. Energetic ions have a ring-like velocity distribution perpendicular to the magnetic field. Here two models with and without the continuous injection of energetic ions into plasma are examined in detail. The speed of the energetic ions is smaller than the Alfvé n speed, and the density ratio of the energetic ions to the bulk ions is several percent. The following results are obtained in the injection model. LHWs keep the larger amplitudes after the saturation. The clear wavenumber shift is found due to the change of the velocity distribution function. Furthermore, the electric field resulting from the instabilities gives energy to the bulk ions. On the other hand, in the value problem, LHWs get damped immediately after the saturation and the clear wavenumber shift is not observed. Other simulations varying the width of the ring-like velocity distribution are also performed.

Keywords: lower hybrid wave, energetic ion, PIC simulation

©2020. Japan Geoscience Union. All Right Reserved.

A comparison of relativistic particle integrators in a fast magnetized flow (2)

*Seiji Zenitani[1], Tsunehiko Kato[2]

1. Kobe University, 2. National Astronomical Observatory of Japan

The particle-in-cell (PIC) method is one of the most important tools to study kinetic processes in space and in astrophysical sites. Basic frameworks and numerical schemes for PIC simulation have long been established. For example, the Boris (1970) integrator to advance particles has long been used in PIC simulation, as it is introduced by several textbooks. Recently, there is a renewed attention to numerical schemes for PIC simulation, in particular in particle integrators, because the classical schemes are incapable of the situations in astrophysics. For example, Vay (2008) and Higuera & Cary (2017) have proposed numerical schemes to preserve the force-free condition, E + V x B = 0, which is ideal to study a magnetized relativistic flow.
In this contribution, we will present a comparison of various particle integrators for PIC simulation in a relativistic plasma flow. Carrying out 80,000 long-term test-particle simulations, we have evaluated particle motions in the electromagnetic field. It is found that many numerical schemes fail to advance particles at the correct speed, because they are unable to satisfy the force-free condition. As a consequence, we observe numerical acceleration/deceleration of particles, whose amplitude is proportional to (delta t)**2. We have developed a second-order theory to predict the numerical acceleration/deceleration. We extend our earlier results in the SGEPSS 2019 meeting, and then we will present a general theory to deal with non-zero parallel velocity.

Keywords: Particle-In-Cell simulation, Numerical scheme, Relativistic motion

©2020. Japan Geoscience Union. All Right Reserved.

Particle Simulation of Triggered Emissions from Large Amplitude Whistler-mode Waves

*Takeshi Nogi[1], Satoko Nakamura[1,2], Yoshiharu Omura[1]

1. Reserch Institute for Sustainable Humanosphere, Kyoto University, 2. Institute for Space-Earth Environmental Research, Nagoya University

We perform one-dimensional electromagnetic particle simulations to study basic processes of whistler-mode wave radiation from an antenna locatd at the magnetic equator and its nonlinear interaction with energetic electrons. Approximating the dipole magnetic field by a parabolic magnetic field, we assume a cylindrical geometry for particle dynamics with a parabolic magnetic field taken along the axis of the cylinder, while we solve Maxwell's equations including Poisson's equation on the axis by the FDTD method. We put an antenna perpendicular to the background magnetic field, and oscillate the antenna current at fixed frequencies with different durations to change the length of the triggering pulse. We observe falling-tone emissions triggered from a short pulse at a frequency close to half the electron cyclotron frequency. Through the process of falling tone emissions, we find trapped particles generates the resonant current parallel to the wave magnetic field, which decreases the frequency of the seed waves near the equator. By changing the wave frequency and the length of the triggering wave packet, we can control the occurrence of rising and falling tone emissions.

©2020. Japan Geoscience Union. All Right Reserved.

Electromagnetic particle simulation of whistler mode triggered emissions in the equatorial magnetosphere

*Yuya Fujiwara[1], Yoshiharu Omura[1], Takeshi Nogi[1], Yikai Hsieh[1], Satoko Nakamura[1,2]

1. Research Institute for Sustainable Humanosphere, Kyoto University, 2. Institute for Space-Earth Environmental Research, Nagoya University

We performed a one-dimensional electromagnetic particle simulation with a uniform magnetic field. We studied electromagnetic waves radiating from two orthogonally aligned antennas in a transverse plane. To find generation of whistler mode waves, we drove anntenas by currents oscillating with frequencies below the electron cyclotron frequency. We confirmed the mode of radiated waves in 3 cases: right-hand polarized external currents, left-hand polarized external currents, and the linearly polarized external current. We found that we can generate propagating waves without evanescent waves by right-hand polarized external currents and we applied this setting of external currents in the simulation. We injected energetic electrons during the propagation of the triggering wave and found some triggered emissions after electrons injection. We analyzed the dependency of the triggering wave amplitude and the number of injected energetic electrons in the simulation. By changing the frequency of the driving currents temporally, we simulated propogation of rising or falling tone emissions and analyzed interactions between triggering waves and injected energetic electrons on the basis of the nonlinear wave growth theory [1].

Reference:

[1] Omura, Yoshiharu, Yuto Katoh, and Danny Summers. ” Theory and simulation of the generation of whistler-mode chorus.” Journal of Geophysical Research: Space Physics 113.A4 (2008).

Keywords: whistler mode wave, triggered emission, particle simulation

©2020. Japan Geoscience Union. All Right Reserved.

Study of the Pitch Angle Scattering of Small Pitch Angle Electrons by Coherent Whistler-Mode Waves

*Genki Ishizawa[1], Yuto Katoh[1], Masahiro Kitahara[1], Atsushi Kumamoto[1], Tomoki Kimura[1,2], Yohei Kawazura[1,2]

1. Department of Geophysics Graduated School of Science Tohoku university , 2. Frontier Research Institute for Interdisciplinary Sciences Tohoku University

Previous studies indicated that whistler mode chorus emissions scatter the pitch angle of energetic electrons, contributing diffuse and pulsating aurora, and reported a high correlation of observed wave amplitude to both auroral luminosity [Nishimura et al, 2010] and electron flux in loss-cone [Kasahara et al, 2018]. However, detailed processes scattering electrons into the loss cone are still unclear. Conventionally, the pitch angle scattering of energetic electrons has been considered as a diffusion process based on the quasi-linear theory. On the other hand, recently Kitahara and Katoh (2019) theoretically and numerically revealed that coherent whistler-mode waves effectively trap small pitch angle electrons and change their pitch angle away from the loss cone. Further investigation for the detailed process of the pitch angle scattering by chorus emissions has been required.

In the present study, we have updated the test particle code of Kitahara and Katoh (2019) in order to treat a large number of electrons at a massively parallelized supercomputer system. By using the developed code, we compute the motion of energetic electrons moving along a field line under the presence of a packet of monochromatic whistler-mode waves generated at the magnetic equator. We assume both the wave amplitude and frequency of whistler-mode waves by referring to the typical parameters observed in the magnetosphere; we assume the wave frequency 0.3 times of the electron gyrofrequency at the magnetic equator, and change the wave amplitude from 0.01 to 0.1% of the background magnetic field intensity at the equator. We also change the duration of the wave packet as well as the amplitude modulation in time, corresponding to the sub-packet structure of the waveform of chorus elements; the duration time of main wave packet and sub-packet at the magnetic equator are assumed to be 97.2 ms and 14.6 ms, respectively. Our simulation results show that most of resonant electrons are trapped by the waves and scattered in the pitch angle range away from the loss cone in the case of waves without amplitude modulation, as reported by Kitahara and Katoh (2019). When the amplitude modulation is present, we find electrons scattered into the loss cone and evaluate the ratio of the number of electrons inside/outside the loss cone quantitatively.

Furthermore, since previous studies revealed that whistler mode waves propagating toward the equator also contribute nonlinear trapping of resonant electrons (e.g., Omura and Summers, 2006), we consider the effects of the location of whistler-mode wave's source region by changing the wave generation region in the simulation system from the magnetic equator to the off-equatorial region. Simulations with initial conditions based on the observed pitch angle distribution in the inner magnetosphere are also performed to compare with the Arase satellite observation. Based on the simulation results, we discuss the favorable condition and roles of nonlinear trapping in the pitch angle scattering of energetic electrons.

©2020. Japan Geoscience Union. All Right Reserved.

Keywords: Pitch angle scattering, whistler-mode wave, pulsating aurora

©2020. Japan Geoscience Union. All Right Reserved.

Development of numerical code of the electron transport equation with spectral method

*Takuma Katou[1], Takanobu Amano[1]

1. The University of Tokyo

An acceleration process of non-thermal particles is one of the fundamental subjects of space physics. The standard theory of cosmic ray electrons is the diffusive shock acceleration (DSA). However, DSA cannot explain an acceleration of non-relativistic electrons. Although the alternative acceleration process is needed to generate higher energy electrons, it has still been unclear.

We proposed the stochastic shock drift acceleration model (SSDA, Katou and Amano 2019) as this acceleration process. In the previous study, we calculated the energy dependence of electron function under the assumption of the spatial dependence and isotropic pitch-angle distribution. The result is consistent with observations of Earth's bow shock by the MMS spacecraft (Amano et al. submitted). Comparing with observations more precisely, we need to solve the electron transport equation, and derive both the spatial and pitch-angle dependence of distribution function. However, it is not easy to calculate analytically, then we must calculate numerically.

We developed the numerical code to derive spatial, energy, and pitch-angle dependence of the electron distribution function by solving the electron transport equation. We used a 5th order finite-difference method with MP5 for spatial and energy dependence, and 3rd order Runge-Kutta method for calculating time dependence. On the other hand, we used the pseud-spectral method for determining pitch-angle dependence by expanding into Legendre polynomials. It makes the calculation of the pitch-angle scattering process simpler. We calculated the energy and spatial distribution of electrons under DSA by our code and compared with analytical solutions. In this presentation, we report the result of this test.

Keywords: Acceleration of particles, Earth, Shock wave

©2020. Japan Geoscience Union. All Right Reserved.

Vlasov solver using rational Chebyshev function

*Taiki Jikei[1], Takanobu Amano[1]

1. The University of Tokyo

Vlasov simulation solves the Vlasov equation using a mesh in phase space. Compared to popular Particle-In-Cell method, it gives higher accuracy in general because of the noiseless property. However, it requires a lot more computational resource because of the use of additional mesh in velocity space. Velocity space essentially has an infinite interval, so the procedure of discretizing it is not obvious. A solver which is both accurate and efficient at the same time is needed.

In this study, a new Vlasov-Poisson solver using spectral method has been developed. The Vlasov equation is splitted into advection in x and v directions, both are calculated by a semi-Lagrangian method. Interpolation is done by approximating the distribution function by Fourier series expansion in x direction and rational Chebyshev series, which is Chebyshev polynomial transformed to cover infinite interval, expansion in v direction. One has to choose a "map parameter" which determines how far the grid points are spread out. This expansion should have the accuracy advantage of spectral method as well as being able to treat the distribution function as a truly unbounded function in v direction. Expansion of both x and v directions can be done using FFT.

Comparison against other methods for application to standard test problems in 1D such as linear and nonlinear Landau dampings and two stream instability will be presented. The optimum choice of “map parameter” L will also be discussed.

Keywords: Vlasov simulation

©2020. Japan Geoscience Union. All Right Reserved.

A Multistate Low-dissipation Advection Upstream Splitting Method for Ideal Magnetohydrodynamics

*Takashi Minoshima[1], Keiichi Kitamura[2], Takahiro Miyoshi[3]

1. Center for Mathematical Science and Advanced Technology, Japan Agency for Marine-Earth Science and Technology, 2. Yokohama National University, 3. Hiroshima University

The magnetohydrodynamic (MHD) simulation is an indispensable way to study nonlinear dynamics in space and astrophysical plasmas. To capture high speed flows, discontinuities, and shocks that are frequently observed in these environments, many modern MHD simulation codes are built based on upwind schemes such as the Flux Vector Splitting method and the Flux Difference Splitting method. In particular, the HLLD approximate Riemann solver developed by Miyoshi and Kusano (2005) has an advantage of shock capturing capability with sufficient accuracy and robustness, and thus it becomes a de fact standard method for computational plasma physics.

The upwind schemes sometimes encounter severe numerical difficulties in stringent condition. The scheme tends to suffer from the numerical shock instability when a high Mach number multidimensional shock is well aligned to the grid spacing, and it causes a catastrophic solution such as the odd-even decoupling and “Carbuncle” phenomena. The mechanism of the instability has not been fully understood yet. On the other hand, the scheme is inherently hard to obtain a correct solution of very low Mach number (~0.01) flows, owing to excessive numerical diffusion. We need a novel numerical scheme to tackle a situation including both incompressible and hypersonic flows.

The Advection Upstream Splitting Method (AUSM; Liou et al.1993) and its variants (e.g., Liou 1996) have been widely adopted in computational aerodynamics. The AUSM-family schemes are alternative to other upwind schemes (FVS, FDS, HLL-type) in order to improve accuracy, robustness, and computational efficiency, and some of them are known to be robust against the numerical shock instability. Furthermore, recent AUSM-family schemes are extended to “all-speed” regime, in which a compressible simulation can get accurate solutions in low Mach number limit (Liou 2006, Shima and Kitamura 2011, Kitamura and Shima 2013). Although these advantages are quite attractive to MHD simulations as well, the extension of the scheme has been quite limited thus far (Han+09, Shen+12, Xisto+14, Kitamura+18).

Consequently, we propose a new AUSM-family scheme for MHD simulations. Following the AUSM methodology, we split the flux in MHD equations into the mass flux, pressure flux, and magnetic tension flux. The mass and pressure fluxes are designed to improve the robustness against the numerical shock instability and the accuracy of low Mach number MHD flows. The magnetic tension flux is built to be consistent with the HLLD solver so as to capture MHD discontinuities. The resulting scheme, terms Multistate Low-dissipation AUSM, is expected to overcome numerical difficulties inherent in familiar upwind schemes. We present several benchmark tests including typical shock tube problems, nearly incompressible Kelvin-Helmholtz instability, and Richtmyer-Meshkov instability to verify the expected capability. Hence, the scheme must be a promising tool to tackle the solar-terrestrial system that includes low speed flows (e.g., solar interior and surface) as well as high speed flows (e.g., solar wind and CMEs).

Keywords: magnetohydrodynamics, shocks, shear flow, magnetic fields, all-speed scheme

©2020. Japan Geoscience Union. All Right Reserved.

On the rate of electron injection at collisionless shocks

*Takanobu Amano[1]

1. Department of Earth and Planetary Science, University of Tokyo

The acceleration of charged particles at a collisionless shock is conventionally understood in terms of the first-order Fermi acceleration, also known as the diffusive shock acceleration (DSA) mechanism. The nonthermal emission spectrum from relativistic electrons accelerated at strong astrophysical shocks is roughly consistent with the standard mechanism. However, it is well known that the DSA can not efficiently accelerate non-relativistic electrons because of the lack of scattering agents. There must be a mechanism that extracts a fraction of particles in the thermal pool and inject them into the relativistic energy range. Such a mechanism appears to be inactive at shocks of modest strength in the heliosphere, where relativistic electrons are usually not observed. The observations imply that the injection process must operate efficiently at strong astrophysical shocks, which should, however, be suppressed at weak and moderate shock strength.

Recent theoretical development and observational verification of the stochastic shock drift acceleration (SSDA) model [Katou & Amano 2019, Amano et al. 2020] have cast light on the electron injection problem. The model predicts that the injection into the relativistic energy range is possible only at high-speed and highly-oblique shocks. Therefore, it discriminates fast astrophysical shocks (such as young supernova remnant shocks with > a few thousand km/s) from heliospheric shocks (with typical speeds of a few to several hundred km/s). Such a success in explaining existing observations naturally raises the question of how many particles are then finally injected into the population of cosmic-ray electrons. We here make an attempt at a quantitative estimation of the electron injection rate within the framework of the SSDA model.

The SSDA theory at this moment is not sophisticated enough to predict the amount of the injected electrons by itself. We thus take a phenomenological approach using the information available from in-situ observations of the Earth's bow shocks reported in the past. The electron velocity distribution function (VDF) measured at the bow shock often exhibits the so-called flat-top VDF, which is nearly constant at low velocities up to some threshold and then decreases in a power-law from beyond that. There have been observational indications that the threshold velocity corresponds to the energy of the quasi-static cross-shock electrostatic potential in the de Hoffmann-Teller frame. Since the potential may be estimated from the flow kinetic energy of the shock, we can estimate the transition velocity between the flat and power-law parts. We adopt the flat-top VDF and assume that the power-law index is given by the SSDA theory. Under these assumptions, we have constructed a model that can estimate the injection rate as a function of macroscopic parameters of the shock (such as the shock speed).

The model shows that the electron injection rate naturally possesses a strong dependence on the shock speed, a tend independent of the shock obliquity. The higher shock speeds lead to much more efficient rates of electron injection. The shock obliquity may potentially strengthen the shock speed dependence even more. We find that a reasonable amount of electron injection rate may be reached with parameters relevant for young supernova remnant shocks. The validity of the model may, in principle, be tested using available in-situ spacecraft observations at planetary bow shocks.

©2020. Japan Geoscience Union. All Right Reserved.

Keywords: shock wave, plasma, particle acceleration

©2020. Japan Geoscience Union. All Right Reserved.

A Study of Evolutions of Growth Rates and the Most Unstable Modes in the Events of Sub-magnetosonic Kelvin-Helmholtz Instabilities in an MHD plasma

*Chun-Yen Hsu[1], Ling-Hsiao Lyu[1]

1. Institute of Space Science and Engineering, National Central University, Taoyuan, Taiwan

The growth rates of the sub-magnetosonic Kelvin-Helmholtz (K-H) instability in an unbounded magnetohydrodynamic (MHD) plasma are studied theoretically based on the new shooting method we proposed in Refs. [1] and [2]. Traditionally, the eigenfunction of the unstable mode in the K-H instability is obtained by integrating the governing equations from a given perturbation boundary. In the new shooting method, the eigenfunction of the unstable mode in the K-H instability is obtained by integrating the governing equations from the center of the velocity shear layer. We found that the location of the perturbation boundary varies with tangential wavelength, the growth rate, and the Mach numbers of the surface waves. To verify our theoretical results, we have carried out a higher-order MHD simulation. Our simulation results indicate that when the locations of the perturbation boundaries expand away from the center of the velocity shear layer, the growth rate decreases, and the tangential wavelength of the most unstable mode increases. Both the amplitude distributions and the phase distributions of the eigenfunctions obtained in our simulations are in good agreement with those obtained in our theoretical studies.

References

[1] Chang, Y. W., and L. H. Lyu (2015), A new analysis of the vortex-size dependent growth rate of Kelvin-Helmholtz instability. 2015 AGU Fall Meeting, San Francisco, California, U.S.A.

[2] Lyu, L. H., and Y. W. Chang (2016), Stability analysis of the sub-magnetosonic Kelvin-Helmholtz instability in an unbounded magnetohydrodynamic plasma. 2016 AGU Fall Meeting, San Francisco, California, U.S.A.

Keywords: Kelvin-Helmholtz (K-H) instability, magnetohydrodynamic (MHD) plasma

©2020. Japan Geoscience Union. All Right Reserved.

Structure formation in chiral magnetohydrodynamics: Effect of background magnetic field

*Takahiro Miyoshi[1]

1. Hiroshima University

Anomalous transports due to quantum anomalies have been theoretically predicted. In a system with a chirally imbalanced medium and a magnetic field, the so-called chiral magnetic effect (CME) that induces a current along the magnetic field is expected to appear, such as in electroweak plasmas in the early Universe and in quark-gluon plasmas in heavy-ion collisions. The macroscopic dynamics of a charged medium, on the other hand, is controlled by magnetohydrodynamics (MHD). In order to investigate the linkage between microscopic CME and macroscopic motion of the charged and chirally imbalanced medium, chiral MHD has recently been proposed [Yamamoto, 2016; Rogachevskii, et al., 2017]. Its properties, however, are not fully clarified though several theoretical and simulation studies have been carried out so far. In this study, we investigate the effect of the background magnetic field on the chiral plasma instability (CPI) driven by the chiral term in the induction equation using two-dimensional chiral MHD simulations. The results show that finer magnetic structures than those in CPI without the background magnetic field are formed.

N. Yamamoto, Phys. Rev. D, 93, 125016 (2016)
I. Rogachevskii, et al., Astrophys. J., 846, 153 (2017)

Keywords: Chiral magnetic effect, Magnetohydrodynamics, simulation

©2020. Japan Geoscience Union. All Right Reserved.

Synchrotron maser emission and associated particle acceleration in relativistic shocks

*Masanori Iwamoto[1], Takanobu Amano[2], Masahiro Hoshino[2], Yosuke Matsumoto[3]

1. Interdisciplinary Graduate School of Engineering Sciences, Kyushu University, 2. Graduate School of Science, The University of Tokyo, 3. Graduate School of Science, Chiba University

Relativistic shocks are ubiquitous in the universe, in which synchrotron maser instability produces intense electromagnetic precursor waves. Recent one-dimensional simulations show that longitudinal electrostatic waves, which are called wakefields, are induced in the wake of the large-amplitude electromagnetic waves and that nonthermal particles are generated during the nonlinear collapse of the wakefields (Lyubarsky 2006; Hoshino 2008). This particle acceleration may explain the origin of ultra-high-energy cosmic rays (Chen et al. 2002).
Although the synchrotron maser instability in the context of relativistic shocks are important for the cosmic ray acceleration, it has so far been discussed solely with one-dimensional simulations (e.g., Langdon et al. 1988) and it is not well known whether the same mechanism can operate in more realistic multidimensional systems. However, our high-resolution two-dimensional (2D) PIC simulations (Iwamoto et al. 2017, 2018) showed that the wave emission continues with substantial amplitude for the first time. We confirmed that the large-amplitude electromagnetic precursor waves continue to persist and that the wakefields are indeed excited by the intense electromagnetic waves (Iwamoto et al. 2019). The wakefields collapse during the nonlinear process of the parametric decay instability in the near-upstream region, where both ions and electrons are accelerated by the motional electric field in the upstream and produce clear nonthermal tails in the particle energy spectra measured in the upstream rest frame. In this talk, we discuss this particle acceleration and wave-plasma interaction for more details.

Keywords: acceleration of particles, cosmic rays, shock waves

©2020. Japan Geoscience Union. All Right Reserved.

[E] Poster | P (Space and Planetary Sciences)：P-EM Solar-Terrestrial Sciences, Space Electromagnetism & Space Environment

[P-EM16] Magnetospheric Multi Scale (MMS) mission: Accomplishments and Future Plans

convener:Yoshifumi Saito(Solar System Science Division, Institute of Space and Astronautical Science, Japan Aerospace Exploration Agency), James L Burch(Southwest Research Institute), Barbara L Giles(NASA Goddard Space Flight Center), Hiroshi Hasegawa(Institute of Space and Astronautical Science, Japan Aerospace Exploration Agency)

NASA's Magnetospheric Multiscale (MMS) formation flying satellites have been making unprecedentedly high time resolution measurements of collisionless plasmas in and around Earth's magnetosphere since it was launched in 2015. After completing its nominal mission in 2018, MMS has continued its observations including targeting the magnetic reconnection in the Earth's magnetotail.
The major purpose of this session is to summarize the new world of electron physics that MMS has so far revealed and also to consider a future observation plan recently submitted by the mission team for the extended mission of MMS especially during the coming several years.
The collaboration with multiple missions including Geotail, Cluster II, THEMIS, Arase and other solar terrestrial probes while MMS focuses into electron scale is the key to understanding multiscale phenomena in the Earth's magnetosphere.
We solicit contributions from satellite observations, numerical simulations, laboratory observations, and theories that relate MMS observations. Contributions to the possible future observation plans are especially welcome.
This is a joint session with American Geophysical Union (AGU).
We hope this session will promote further international collaboration among Japan, United States and space physicists all over the world.

[PEM16-P01] Magnetic island formation in reconnecting electron-scale current sheet: MMS observations in the magnetotail

*Hiroshi Hasegawa[1], Richard E. Denton[2], Rumi Nakamura[3], Kevin J. Genestreti[4], Takuma Nakamura[3], Kyoung Joo Hwang[5], Narges Ahmadi[6], Tai D. Phan[7], Roy B. Torbert[4], Jim L. Burch[5], Barbara L. Giles[8], Dan J. Gershman[8], Christopher T. Russell[9], Robert J. Strangeway[9], Per Arne Lindqvist[10], Yuri V. Khotyaintsev[11], Robert E. Ergun[6], Yoshifumi Saito[1] (1.Institute of Space and Astronautical Science, Japan Aerospace Exploration Agency, 2.Dartmouth College, 3.Space Research Institute, Austrian Academy of Science, 4.University of New Hampshire, 5.Southwest Research Institute, 6.University of Colorado, 7.Space Sciences Laboratory, University of California Berkeley, 8.NASA Goddard Space Flight Ceter, 9.University of California Los Angeles, 10.Royal Institute of Technology, 11.Swedish Institute of Space Physics)

[PEM16-P02] Multi-spacecraft observations of cold-dense plasma sheet under northward IMF

*Masaki N Nishino[1], Yoshifumi Saito[1], Iku Shinohara[1], Tsugunobu Nagai[1], Kazushi Asamura[1], Yoichi Kazama[2], Shiang-Yu Wang[2], Sunny Wing-Yee Tam[3], Ayako Matsuoka[1], Yoshizumi Miyoshi[4], Barbara L Giles[5], Christopher T Russell[6], Daniel J Gershman[7], Benoit Lavraud[8], Yukinaga Miyashita[9] (1.Japan Aerospace Exploration Agency, Institute of Space and Astronautical Science, 2.Institute of Astronomy and Astrophysics, Academia Sinica, Taiwan, 3.Institute of Space and Plasma Sciences, National Cheng Kung University, Taiwan, 4.Institute for Space-Earth Environmental Research, Nagoya University, 5.NASA, Goddard Space Flight Center, 6.University of California, Los Angeles, 7.University of Maryland, College Park, 8.Institut de Recherche en Astrophysique et Planétologie, 9.Korean Astronomy and Space Science Institute)

[PEM16-P03] Uncertainties on Fields Gradients and Propagation Velocities Estimated From Multi-Spacecraft Missions

*Gerard Marcel CHANTEUR[1] (1.CNRS & Sorbonne Université, Laboratoire de Physique des Plasma)

[PEM16-P04] PIC simulation of electron acceleration at quasi-perpendicular collisionless shock: Application to Earth's bow shock

*Fumiko Otsuka[1], Shuichi Matsukiyo[2], Mitsuo Oka[3] (1.NIT, Kurume College, 2.ESST, Kyushu Univ., 3.UC Berkeley)

Magnetic island formation in reconnecting electron-scale current sheet: MMS observations in the magnetotail

*Hiroshi Hasegawa[1], Richard E. Denton[2], Rumi Nakamura[3], Kevin J. Genestreti[4], Takuma Nakamura[3], Kyoung Joo Hwang[5], Narges Ahmadi[6], Tai D. Phan[7], Roy B. Torbert[4], Jim L. Burch[5], Barbara L. Giles[8], Dan J. Gershman[8], Christopher T. Russell[9], Robert J. Strangeway[9], Per Arne Lindqvist[10], Yuri V. Khotyaintsev[11], Robert E. Ergun[6], Yoshifumi Saito[1]

1. Institute of Space and Astronautical Science, Japan Aerospace Exploration Agency, 2. Dartmouth College, 3. Space Research Institute, Austrian Academy of Science, 4. University of New Hampshire, 5. Southwest Research Institute, 6. University of Colorado, 7. Space Sciences Laboratory, University of California Berkeley, 8. NASA Goddard Space Flight Ceter, 9. University of California Los Angeles, 10. Royal Institute of Technology, 11. Swedish Institute of Space Physics

Magnetic reconnection controls the transport of solar wind mass and energy into Earth's magnetosphere and is the key to explosive energy release in the magnetotail during magnetospheric substorms. A simplest form of magnetic reconnection in space occurs in the magnetotail where the magnetic fields are nearly antiparallel, no significant jumps in plasma parameters exist across the current sheet, and no significant turbulence is seen in the inflow (lobe) regions. The Magnetospheric Multiscale (MMS) spacecraft, however, have revealed complex features such as a displacement of the stagnation point relative to the X point in the outflow jet direction even for magnetotail reconnection. Here, using in situ observations from MMS in the magnetotail, we present evidence of secondary magnetic island formation in a reconnecting electron-scale current sheet in the magnetotail detected by MMS. The electron diffusion region (EDR) of the event, first reported by Zhou et al. (ApJ, 2019), was recovered by two reconstruction techniques. One is based on electron magnetohydrodynamics equations (Sonnerup et al., JGR, 2016), and the other on polynomial expansion of the magnetic field using instantaneous measurements by the four spacecraft of the magnetic field and particle current density (Denton et al., JGR, 2020). The results from both reconstructions show that a small-scale magnetic island was growing in a reconnecting current sheet with a thickness of about one electron inertial length, consistent with fully kinetic simulations of antiparallel reconnection (Daughton et al., PoP, 2006). It suggests that secondary island formation is an intrinsic process in the EDR of antiparallel reconnection, and reconnection may drive turbulence energy cascade at sub-ion scales by creating sub-ion-scale islands in electron-scale current sheets.

References:
Daughton, W., J. Scudder, and H. Karimabadi, Fully kinetic simulations of undriven magnetic reconnection with open boundary conditions, Phys. Plasmas, 13, 072101, https://doi.org/10.1063/1.2218817, 2006.
Denton, R. E., R. B. Torbert, H. Hasegawa, et al., Polynomial reconstruction of the reconnection magnetic field observed by multiple spacecraft, Journal of Geophysical Research: Space Physics, 125, https://doi.org/10.1029/2019JA027481, 2020.
Sonnerup, B. U. O., H. Hasegawa, R. E. Denton, and T. K. M. Nakamura, Reconstruction of the electron diffusion region, J. Geophys. Res. Space Physics, 121, 4279-4290, doi:10.1002/2016JA022430, 2016.
Zhou, M., X. H. Deng, Z. H. Zhong, et al., Observations of an electron diffusion region in symmetric reconnection with weak guide field, Astrophys. J., 870, 34, https://doi.org/10.3847/1538-4357/aaf16f, 2019.

Keywords: magnetic reconnection, electron magnetohydrodynamics, magnetotail, magnetic island, Earth's magnetosphere

©2020. Japan Geoscience Union. All Right Reserved.

©2020. Japan Geoscience Union. All Right Reserved.

Multi-spacecraft observations of cold-dense plasma sheet under northward IMF

*Masaki N Nishino[1], Yoshifumi Saito[1], Iku Shinohara[1], Tsugunobu Nagai[1], Kazushi Asamura[1], Yoichi Kazama[2], Shiang-Yu Wang[2], Sunny Wing-Yee Tam[3], Ayako Matsuoka[1], Yoshizumi Miyoshi[4], Barbara L Giles[5], Christopher T Russell[6], Daniel J Gershman[7], Benoit Lavraud[8], Yukinaga Miyashita[9]

1. Japan Aerospace Exploration Agency, Institute of Space and Astronautical Science, 2. Institute of Astronomy and Astrophysics, Academia Sinica, Taiwan, 3. Institute of Space and Plasma Sciences, National Cheng Kung University, Taiwan, 4. Institute for Space-Earth Environmental Research, Nagoya University, 5. NASA, Goddard Space Flight Center, 6. University of California, Los Angeles, 7. University of Maryland, College Park, 8. Institut de Recherche en Astrophysique et Planétologie, 9. Korean Astronomy and Space Science Institute

The near-Earth plasma sheet becomes cold and dense under northward interplanetary magnetic field (IMF) condition, which suggests entry of solar wind plasma into the magnetosphere across the magnetopause. The cold and dense trend of the plasma sheet is more apparent in the magnetotail flank regions that are interface between cold solar wind plasma and hot magnetospheric plasma. Several physical mechanisms have been proposed to explain the solar wind plasma entry across the magnetopause and resultant formation of the cold-dense plasma sheet in the tail flank regions. However, cold-dense plasma is occasionally found in the midnight magnetotail as well, and plasma transport from the magnetopause deeper into the magnetosphere has not been understood yet. Here we report that cold-dense plasma is simultaneously detected in a wide region of the near-Earth plasma sheet, including the inner magnetosphere, under the prolonged northward IMF and relatively high dynamic pressure conditions, by using data from Geotail, MMS, ERG, and Cluster. In one event, the ion distribution functions on the duskside both in the outer magnetosphere and in the inner magnetosphere show two distinct populations in low- and high-energy ranges, which implies that the low-energy (cold) population of solar wind origin may enter the magnetosphere by a common process. On the other hand, energies of the cold component and the magnetic field strengths suggest that the cold component in the inner magnetosphere may not have its origin in the magnetotail. We also note that no southward turning of the IMF took place for the period of our interest and thus no injection from the magnetotail into the inner magnetosphere was expected. The entry location(s) of the cold-dense plasma found deep inside the magnetosphere and its transport mechanism remain to be studied.

Keywords: Magnetospheric plasma transport, Cold dense plasma, Northward IMF, Multi-spacecraft observation (MMS, Geotail, Arase, etc.)

©2020. Japan Geoscience Union. All Right Reserved.

Uncertainties on Fields Gradients and Propagation Velocities Estimated From Multi-Spacecraft Missions

*Gerard Marcel CHANTEUR[1]

1. CNRS & Sorbonne Université, Laboratoire de Physique des Plasma

Multi-spacecraft missions involving at least four spacecraft with identical instruments allow to estimate :
i/ three-dimensional spatial gradients of fields simultaneously measured by the different spacecraft
The estimation of the spatial gradient of a physical field relies generally upon the hypothesis of linear spatial variations of this field throughout the volume of the cluster of measurement points. Within this approximation the estimated gradient is unique whatever is the weighting of the different points of the cluster. However uncertainties affecting the estimated gradient depend upon the adopted weighting. Case studies will be discussed and simulated uncertainties will be compared with respect to weighting.
ii/ three-dimensional propagation velocities of waves or discontinuities
Propagation velocities of waves or discontinuities can be estimated by timing methods. Usually a reference spacecraft is chosen and only three pairs of non coplanar spacecraft are used, nevertheless results can be improved by considering all pairs of spacecraft and looking for the optimal weighting of all time delays. The optimal approach will be presented and applied to reanalyze some Bow-Shock crossings by CLUSTER.

Keywords: Multi-spacecraft data analysis, spatial gradients of fields, velocities of waves and discontinuities, uncertainties

©2020. Japan Geoscience Union. All Right Reserved.

PIC simulation of electron acceleration at quasi-perpendicular collisionless shock: Application to Earth's bow shock

*Fumiko Otsuka[1], Shuichi Matsukiyo[2], Mitsuo Oka[3]

1. NIT, Kurume College, 2. ESST, Kyushu Univ., 3. UC Berkeley

At Earth's quasi-perpendicular bow shock, non-thermal electrons are observed in-situ measurements. The electrons are thought to be accelerated at the shock through the scatterings by electromagnetic waves upstream and downstream of the shock. Oka et al. (2017, 2019) reported in situ evidences of pitch-angle scattering of non-thermal electrons by whistler waves at the Earth's bow shock, by using data provided by the Magnetospheric Multiscale (MMS) mission. However, the detail electron acceleration process remains unclear.

In this study we perform a self-consistent one-dimensional full particle-in-cell (PIC) simulation of a quasi-perpendicular shock to model the Earth's bow shock. The simulation parameters are the Alfven Mach number 7.1, the shock angle 70 degree, plasma beta 0.3, the ion to electron mass ratio 625, and the ratio of electron plasma to cyclotron frequency 10. In the simulation power-law energy distribution of the electron is formed at the shock transition region, and the anisotropic pitch-angle distribution is found in the upstream region of the shock. We investigate the upstream wave properties and the non-thermal electron trajectories to reveal the electron acceleration and scattering processes in detail. The result will be compared with the MMS data at the Earth's quasi-perpendicular bow shock.

Keywords: quasi-perpendicular collisionless shock, electron acceleration, PIC simulation

©2020. Japan Geoscience Union. All Right Reserved.

[E] Poster | P (Space and Planetary Sciences)：P-EM Solar-Terrestrial Sciences, Space Electromagnetism & Space Environment

[P-EM17] Space Weather and Space Climate

convener:Ryuho Kataoka(National Institute of Polar Research), Antti A Pulkkinen(NASA Goddard Space Flight Center), Kanya Kusano(Institute for Space-Earth Environmental Research, Nagoya University), Kaori Sakaguchi(National Institute of Information and Communications Technology)

We share the latest scientific papers to understand how the space environment changes in various time scales, and to discuss how we will react via international and interdisciplinary collaborations. More specifically, welcomed papers include space climate studies to reconstruct the long-term variations from radio isotopes; cutting-edge observational and modeling studies of the ionosphere, geospace, heliosphere and the sun; simulation and statistical studies to predict the future space weather and space climate; applied science such as operational space weather forecast and mitigation of the social impact due to extreme space hazards. Specific topics in 2020 will be extreme events, theoretical maxima and benchmarks for hazard assessments, and space weather and deep space human spaceflight activities at Moon and at Mars.

[PEM17-P01] Preparedness for extreme space weather events

*Mamoru Ishii[1], Daikou Shiota[1], Chihiro Tao[1] (1.National Institute of Information and Communications Technology)

[PEM17-P02] Value of forecast: forecast verification in user's perspective

*Yuki Kubo[1] (1.National Institute of Information and Communications Technology)

[PEM17-P03] Statistical analysis of short-wave fadeout toward extreme event estimation for space weather hazardous map of Japan

*Chihiro Tao[1], Michi Nishioka[1], Takuya Tsugawa[1], Daikou Shiota[1], Susumu Saito[2], Kyoko Watanabe[3], Mamoru Ishii[1] (1.National Institute of Information and Communications Technology, 2.Electronic Navigation Research Institute, 3.National Defense Academy)

[PEM17-P04] Effect of equatorial plasma bubbles on midlatitude region

*Tatsuhiro Yokoyama[1], Hiroyuki Shinagawa[2], Yuichi Otsuka[3] (1.Research Institute for Sustainable Humanosphere, Kyoto University, 2.National Institute of Information and Communications Technology, 3.Institute for Space-Earth Environmental Research, Nagoya University)

[PEM17-P05] Calculation of the ray paths and propagation times of HF radio waves in the simulator of HF-START project.

*Ryo Nakao[1], Hiroyuki Nakata[2], Kornyanat Hozumi[3], Takuya Tsugawa[3], Susumu Saito[4], Hiroyo Ohya[2], Toshiaki Takano[2], Mamoru Ishii[3] (1.Graduate School of Engineerings, Chiba University, 2.Graduate School of Engineering, Chiba University, 3.National Institute of Information and Communications Technology, 4.Electronic Navigation Research Institute)

[PEM17-P06] Characteristics of F-region irregularities near a northern anomaly crest during the rising half of solar cycle 23

Hsin-Hua Wu[1], Pei-Yu Chen[1], *Chien-Chih Lee[1] (1.Department of Applied Geomatics, Chien Hsin University of Science and Technology)

[PEM17-P07] Variations of thermospheric mass density probed from satellite orbit change

*Wataru Miyake[1] (1.Tokai University)

[PEM17-P09] Influence of the solar wind on El Nino

*Kazuyoshi Yamashita[1] (1.Yokohama National University, Graduate School of Env. & Inf. Sciences)

[PEM17-P10] Development of Space Environment Customized Risk Estimation for Satellite (SECURES)

*Tsutomu Nagatsuma[1], Haruhisa Matsumoto[2], Kiyokazu Koga[2], Masao Nakamura[3], Aoi Nakamizo[1], Yasubumi Kubota[1], Yoshizumi Miyoshi[4] (1.National Institute of Information and Communications Technology, 2.Japan Aerospace Exploration Agency, 3.Osaka Prefecture University, 4.Nagoya Unibersity)

[PEM17-P11] Spacecraft surface charging and discharging risk estimation method around geosynchronous altitude

*Masao Nakamura[1], Hirotaka Maeda[1], Tsutomu Nagatsuma[2], Mamoru Ishii[2] (1.Osaka Prefecture University, 2.NICT)

[PEM17-P12] Study of IMF By dependence of plasma injection position using real-time magnetosphere simulation data

*Yasubumi Kubota[1], Aoi Nakamizo[1], Kaori Sakaguchi[1], Tsutomu Nagatsuma[1], Mitsue Den[1], Yuki Kubo[1], Takashi Tanaka[1,2] (1.National Institute of Information and Communications Technology, 2.Kyushu University)

[PEM17-P14] Multi point measurements of geomagnetically induced currents in the Chugoku region

*Kumiko K. Hashimoto[1], Kentarou Kitamura[2], Takashi Kikuchi[3], Yusuke Ebihara[4] (1.Kibi International University, 2.National Institute of Technology, Tokuyama College, 3.Nagoya University, 4.Kyoto University)

[PEM17-P15] SuperDARN future plan in terms of Planning of phase X 6-year project of Japanese Antarctic Research Expedition and beyond

*Akira Sessai Yukimatu[1,2] (1.National Institute of Polar Research, 2.SOKENDAI)

[PEM17-P16] Study of dependence of solar flare induced SuperDARN Doppler velocity on X-ray intensity, SZA and season

*Tomoya Takada[1], Nozomu Nishitani[1], Tomoaki Hori[1] (1.Institute for Space-Earth Environmental Research)

[PEM17-P17] Summary of the five-year extended observations of Nobeyama Radioheliograph

*Satoshi Masuda[1] (1.Institute for Space-Earth Environmental Research, Nagoya University)

[PEM17-P18] Phesant tail aurora: The oldest record of astronomical phenomenon in Japan

*Ryuho Kataoka[1], Kazuaki Yamamoto[2], Yasunori Fujiwara[1], Kozue Shiomi[1], Nobuo Kokubun[1] (1.National Institute of Polar Research, 2.National Institute of Japanese Literature)

[PEM17-P19] Plasma waves causing relativistic electron precipitation events at International Space Station

*Ryuho Kataoka[1], CALET Collaboration, Arase Collaboration (1.National Institute of Polar Research)

[PEM17-P20] Investigation of the Relation Between Magnetospheric Activity and Solar Wind Parameters Based on Potential Learning

*Ryozo Kitajima[1], Motoharu Nowada[2], Ryotaro Kamimura[3] (1.Dept. Engineering, Tokyo Polytechnic University, Kanagawa, Japan, 2.Shandong Provincial Key Laboratory of Optical Astronomy and Solar-Terrestrial Environment, Institute of Space Sciences, Shandong University, Weihai, P. R. China, 3.IT Education Center, Tokai University, Kanagawa, Japan)

[PEM17-P21] Cosmic Ray Intensity Increase Associated with Slow Coronal Mass Ejection

*Wataru Kihara[1], Chihiro Kato[1], Kazuoki Munakata[1], Yukino Ko[1], Ryuho Kataoka[2], Akira Kadokura[2], the GMDN collaborations - (1.Department of Physics, Shinshu University, 2.National Institute of Polar Research)

[PEM17-P22] Study on the global occurrence characteristics of Pc2 pulsation with the 10Hz data of the MAGDAS9 system

*Taisei Kabasawa[1], Akimasa Yoshikawa[2], Teiji Uozumi[3], Akiko Fujimoto[4], Shuji Abe[3] (1.Kyushu University, 2.Department of Earth and Planetary Science, Kyushu University, 3.International center for space weather science and education, Kyushu university, 4.Department of information technology, Kyushu Institute of Technology)

[PEM17-P23] Data assimilation of radiation belt electrons using the DREAM code and multiple spacecraft data of Arase, Himawari, and GPS

*Kaori Sakaguchi[1], Andrew Walker[2], Sophie Graf[2], Reinhard Friedel[2], Takefumi Mitani[3], Nana Higashio[3], Takeshi Takashima[3], Tsutomu Nagatsuma[1], Mamoru Ishii[1] (1.National Institute of Information and Communications Technology, 2.Los Alamos National Laboratory, 3.Japan Aerospace Exploration Agency)

Preparedness for extreme space weather events

*Mamoru Ishii[1], Daikou Shiota[1], Chihiro Tao[1]

1. National Institute of Information and Communications Technology

Space weather is phenomenon in near-Earth space which can impact on human society. It is important to estimate the quantitative influence of space weather for social activities, however, it has not been discussed the relation between the space weather activity and it's impact on each social utility. One of the reasons is discommunications between space weather researchers and users in the society. We have been discussing with space weather information users to make clear the quantitative impact of space weather on the social activity, in addition to discuss plausible maximum level of space weather event in Japan. This study has been executed in the framework of PSTEP since 2015, and we prepare a document to show our results. In this presentation, we show the present results of our discussion.

Keywords: space weather, satellite positioning, geomagnetically induced current

©2020. Japan Geoscience Union. All Right Reserved.

Value of forecast: forecast verification in user's perspective

*Yuki Kubo[1]

1. National Institute of Information and Communications Technology

Recently, forecast verification and model validation have become popular topic in space weather research, especially, in operational space weather forecast. These verification studies focus on assessing a forecast skill in viewpoint of forecast providers. These are useful for forecasters or model developers to improve the forecast systems or models. On the other hand, the optimal forecast for a forecast provider is not always the optimal forecast for forecast users. Also, the forecast which is the optimal for certain user is not always the optimal for all users, that is, value of forecast depends on each user. Therefore, an assessment of value of forecast is important for forecast users.

In this study, we perform forecast verification in user's perspective. The decision-theoretic approach is employed to evaluate value of forecast. This method is not new, and already well-known in terrestrial weather forecasting community. However, it is not widely used in space weather forecasting community. We show some examples of value of forecast for a deterministic and probabilistic forecast. We will discuss the strength point of probabilistic forecast.

Keywords: Forecast verification, User's perspective, Deterministic forecast, Probabilistic forecast

©2020. Japan Geoscience Union. All Right Reserved.

Statistical analysis of short-wave fadeout toward extreme event estimation for space weather hazardous map of Japan

*Chihiro Tao[1], Michi Nishioka[1], Takuya Tsugawa[1], Daikou Shiota[1], Susumu Saito[2], Kyoko Watanabe[3], Mamoru Ishii[1]

1. National Institute of Information and Communications Technology, 2. Electronic Navigation Research Institute, 3. National Defense Academy

Solar flares trigger enhancements of ionospheric plasma density including D-region which causes absorption of radio waves especially at high-frequency (HF) ranges. This phenomena is called short wave fadeout (SWF) or Dellinger effect. This SWF interrupts trans-ionospheric radio communication system including ground-to-ground radio communications, satellite communication system, and disaster prevention radio system. SWF is one of important topics of space-weather hazardous-map for Japan society. In order to understand SWF statistical characteristics and behaviour, we analyse long-term (~20 years) ionosonde data observed by NICT and estimate extreme case based on the results.

We analyse manually scaled parameters with 15 min. resolution from ionosonde observation in Tokyo over 1997 to 2016. We use minimum reflection frequency, fmin, for detection of Dellinger effect. Since fmin varies with local time (LT) and season, we refer to dfmin, fmin subtracted by its 27-day running average at the same LT. SWF is detected by (i) dfmin>2.5 MHz, (ii) dfmin>3.5 MHz, and (iii) blackout criteria, occurred daytime associated with any flare(s) greater than C-class in this study. We refer to GOES flare list for the flare size.

As a result, SWF occurrence maximizes at local noon and decreases with the solar zenith angle. We confirm that the dfmin value and SWF duration increase with the flare size. We estimate the absorption strength and compare it with an empirical relationship derived from long-distance circuits by Maeda and Inuki [1972]. The absorption strength of ionosonde is almost ~1/3 of that of the long-distance circuits, which would be affected by elongation of ionospheric pass due to oblique propagation. From our analysis and extension of the empirical relationship, we estimate the duration of extreme events, i.e., once per 10-year, 100-year, and 1000-year occurrence events, to be 1-2.2 hour, 2.3-5 hour, and 4.6-11 hour, respectively. We also discuss probable longest duration of originating solar flare.

Keywords: short-wave fadeout, space weather hazardous map, ionosphere, solar flare

©2020. Japan Geoscience Union. All Right Reserved.

Effect of equatorial plasma bubbles on midlatitude region

*Tatsuhiro Yokoyama[1], Hiroyuki Shinagawa[2], Yuichi Otsuka[3]

1. Research Institute for Sustainable Humanosphere, Kyoto University, 2. National Institute of Information and Communications Technology, 3. Institute for Space-Earth Environmental Research, Nagoya University

Equatorial plasma bubble (EPB) is a well-known phenomenon in the equatorial ionospheric F region. As it causes severe scintillation in the amplitude and phase of radio signals, it is important to understand and forecast the occurrence of EPB from a space weather point of view. In order to simulate the instability in the equatorial ionosphere, a 3D High-Resolution Bubble (HIRB) model has been developed. It provides a unique opportunity to study the development of EPBs under various conditions. During a severe space weather event, intense penetration electric fields are expected even in the equatorial ionosphere. If the penetration electric fields enhance the pre-reversal enhancement of the eastward electric field in the dusk sector, the growth rate of the Rayleigh--Taylor instability is greatly intensified to force EPBs to reach very high apex altitude. Such EPBs can reach midlatitude regions along the flux tubes with very high apex altitude and cause communicaton/navigation outage in midlatitude. We will expand the simulation domain of the HIRB model to cover the midlatitude region, for example the latitude of Tokyo area, and estimate the background conditions under which EPBs can reach and affect the midlatitude ionosphere. Previous observations of such extreme events will be compared with the simulation results.

Keywords: Equatorial plasma bubble, Ionosphere, Scintillation

©2020. Japan Geoscience Union. All Right Reserved.

Calculation of the ray paths and propagation times of HF radio waves in the simulator of HF-START project.

*Ryo Nakao[1], Hiroyuki Nakata[2], Kornyanat Hozumi[3], Takuya Tsugawa[3], Susumu Saito[4], Hiroyo Ohya[2], Toshiaki Takano[2], Mamoru Ishii[3]

1. Graduate School of Engineerings, Chiba University, 2. Graduate School of Engineering, Chiba University, 3. National Institute of Information and Communications Technology, 4. Electronic Navigation Research Institute

HF simulator Targeting for All user's Regional Telecommunications (HF-STRAT) is a collaborative project with NICT, ENRI and Chiba University to provide the information of nowcast of radio propagation. In this project, propagation of HF radio waves is calculated by ray-tracing. Using the results of ray-tracing, we have determined whether HF radio wave travels between any two points. To verify the results of ray-tracing, we have compared the differences of the propagation time determined by the ray-tracing with the observation of the HF radio waves transmitted from Nagara transmitter, RadioNIKKEI (35.46˚N, 140.20˚E). HF receivers are located at Chiba University (Chiba, 35.62˚N, 140.10˚E), Sarobetu (Hokkaido, 45.16˚N, 141.74˚E), Yamagawa (Kagoshima, 31.20˚N, 130.61˚E), Ogimi (Okinawa, 26.68˚N, 128.15˚E). In comparing the propagation time between Chiba and the other receivers, it is found that there was a difference of the propagation time between the ray-tracing results and the observations. This is because it is assumed that ground waves are propagated from Nagara to Chiba. By calculating the loss of electric field strength between Nagara and Chiba, we found that the loss of sky wave that is reflected by ionosphere was almost comparable to that of ground wave. Thus, it is possible that the radio wave propagation between Nagara and Chiba is not ground wave but sky wave that is reflected by ionosphere or both ground wave and sky wave signals are received simultaneously by receiver at Chiba. In addition, the comparison between observation of propagation time differences using distant receivers except Chiba and propagation times derived from ray-tracing calculation is in progress to validate results of simulator. In the simulator, we also plan to provide users with options to choose three types of electron density models (IRI, GNSS tomography, GAIA). For these options, we will use the electron density distributions determined by each model in the ray-tracing calculation and analyze the differences between the ray-tracing results statistically.

©2020. Japan Geoscience Union. All Right Reserved.

Characteristics of F-region irregularities near a northern anomaly crest during the rising half of solar cycle 23

Hsin-Hua Wu[1], Pei-Yu Chen[1], *Chien-Chih Lee[1]

1. Department of Applied Geomatics, Chien Hsin University of Science and Technology

In this work, we study the F-region irregularities near the northern crest of equatorial ionization anomaly (EIA) in the west Pacific sector. During 1996-2000, the F-region irregularities are observed by the Chungli ionosonde (24.9˚N, 121.2˚E), YMSM GPS receiver (25˚N, 121.6˚E), and DMSP satellites. It is noted that the 23rd solar cycle began in 1996 and had a maximum in 2000. The data of F-region irregularities are spread F of ionosonde, GPS phase fluctuations of GPS, and plasma bubbles of DMSP satellites. The seasonal and nighttime variations in occurrence probabilities for spread-F, GPS phase fluctuations, and plasma bubbles are calculated. In general, the seasonal variations in occurrence probabilities are different each year. In any year, the seasonal variations of three instruments are different from one another. In the nighttime variations in occurrence probabilities, the variations of spread-F are not the same as that of GPS phase fluctuations. And, the effects of solar activity on the nighttime variations are different each season. These results indicate that the characteristics and mechanisms of F-region irregularities would vary with seasons and/or solar activities.

Keywords: F-region irregularities, spread F, GPS phase fluctuations , plasma bubbles

©2020. Japan Geoscience Union. All Right Reserved.

Variations of thermospheric mass density probed from satellite orbit change

*Wataru Miyake[1]

1. Tokai University

The kinetic energy of LEO satellites is generally decreased by atmospheric drag in the thermosphere. The drag is dependent on atmospheric mass density especially near the perigee. The mass density has been investigated through the decrease of kinetic energy of LEO satellites. The mass density in the thermosphere is controlled by the temperature, and solar EUV radiation and geomagnetic activity cause large variation of the temperature. This leads to variation of satellite drag with progress of 11 year cycle of sun spots. In the last solar minimum, record-low thermospheric density was reported, which may not be simply attributted to low solar activity. Increased concentration of CO2 in the lower thermosphere is expected to produce a cooler, more contracted thermosphere. It is, therefore, of interest how low the thermospheric density is in the current solar minimum. The Geospace Exploration Satellite Arase launched on December 20, 2016. The initial apogee and perigee are 32,000 km and 440 km, respectively. Its low perigee enables us to investigate the mass density in the thermosphere. We have so far found long-term decrease of the kinetic energy of the satellite, which can be interpreted in terms of the atmospheric drag. From the change in the satellite orbit, we will discuss how the atmospheric density of the thermosphere changes in the current solar minimum.

Keywords: satellite drag, mass density

©2020. Japan Geoscience Union. All Right Reserved.

Influence of the solar wind on El Nino

*Kazuyoshi Yamashita[1]

1. Yokohama National University, Graduate School of Env. & Inf. Sciences

Although it is certain that the sun magnetic activity affects the global environment, the details are not clear.In this presentation, we analyze the influence of the solar wind on global environment on the basis of our previous studies [1, 2].The AE index and total ozone data were used to detect the influence of the solar wind on El Nino.In the analysis, we considered that the influence of the energetic particle fluxes(EPP)-NOx on ozone at low latitudes may be comparable to the effects of solar UV radiation [Callis et al., 2000, 2001; Langematz et al., 2005; Rozanov et al., 2005].
We found that the change of the total amount of ozone in the region at low latitudes affects atmospheric stability and a monsoon, and thus, it may become the harbinger of the El Nino.

[1]K.Itoh, JpGU 2008-2013
[2]K.Yamashita, JpGU 2014-2016

Keywords: AE index, El Nino, ozone, solar wind

©2020. Japan Geoscience Union. All Right Reserved.

Development of Space Environment Customized Risk Estimation for Satellite (SECURES)

*Tsutomu Nagatsuma[1], Haruhisa Matsumoto[2], Kiyokazu Koga[2], Masao Nakamura[3], Aoi Nakamizo[1], Yasubumi Kubota[1], Yoshizumi Miyoshi[4]

1. National Institute of Information and Communications Technology, 2. Japan Aerospace Exploration Agency, 3. Osaka Prefecture University, 4. Nagoya Unibersity

Variations of space environment in geospace driven by the solar activity is one of the factors that cause satellite anomaly. When a failure occurs in a satellite, it is important to understand the current condition of the space environment around the satellite in order to identify the cause and take proper action quickly.
However, risk of satellite anomaly due to space environment is not the same as each satellite, because the risk depends not only on the space environment but also on the design and materials of individual satellite.
Based on this idea, we have developed SECURES (Space Environment Customized Risk Estimation for Satellite) by combining space environment models and spacecraft charging models. In SECURES, we are focusing on the risk of spacecraft charging (surface/internal) for geosynchronous satellites. For estimating surface charging, we have combined the global MHD simulation model with the satellite surface charging models. And for internal charging, we have combined the radiation belt models with the satellite internal charging models. We have also developed the test product based on the SECURES. The current status and future directions of SECURES will be reported in this presentation.

Keywords: Tailor-made type space weather forecast, Spacecraft Charging, The Earth's magnetosphere

©2020. Japan Geoscience Union. All Right Reserved.

Spacecraft surface charging and discharging risk estimation method around geosynchronous altitude

*Masao Nakamura[1], Hirotaka Maeda[1], Tsutomu Nagatsuma[2], Mamoru Ishii[2]

1. Osaka Prefecture University, 2. NICT

Spacecraft surface charging often induces spacecraft anomalies by electrostatic discharging (ESD) around the geosynchronous altitude. We are developing a real-time spacecraft surface charging risk estimation system for the Space Environment Customized Risk Estimation for Spacecraft (SECURES) of the space weather forecast Project for Solar-Terrestrial Environment Prediction (PSTEP). For the surface charging analysis, we make charging analysis models of target satellites and simulate their surface charging potentials by using the Spacecraft Plasma Interaction Software (SPIS). Since it takes hours or days to calculate the surface potentials for a given plasma environment, we develop a real-time estimation method using empirical functions based on the pre-calculated results. The method can quickly estimate the equilibrium floating potentials of the spacecraft surfaces for the predicted on-orbit plasma environments, e.g., by a global MHD simulation. The differential potentials between the spacecraft surfaces are important to evaluate the ESD risk assessment. We study the time scale of the differential potential development to evaluate the frequency of recurrent ESD for severe plasma environments.

Keywords: Spacecraft surface charging, Space weather, Spacecraft risk assessment

©2020. Japan Geoscience Union. All Right Reserved.

Study of IMF By dependence of plasma injection position using real-time magnetosphere simulation data

*Yasubumi Kubota[1], Aoi Nakamizo[1], Kaori Sakaguchi[1], Tsutomu Nagatsuma[1], Mitsue Den[1], Yuki Kubo[1], Takashi Tanaka[1,2]

1. National Institute of Information and Communications Technology, 2. Kyushu University

Surface charging of artificial satellite is one of the risks caused by dynamical variations of space environment. It often occurs when a satellite is exposed by electrons of ~10 keV injected from the tail plasma sheet during substorms. Magnetosphere-ionosphere coupling global MHD simulation is one of the powerful ways to predict the timing and location of plasma injection.
Now we are developing a real-time numerical simulator for space weather forecast using magnetosphere-ionosphere coupling global MHD simulation called REPPU (REProduce Plasma Universe) code. The feature of the simulation code is high robustness for extreme solar wind parameters; the unstructured grid system enables us to calculate the whole region with the uniform accuracy. The spatial resolution is 30722 grids in the spherical planes and 240 grids in the radial direction. The simulator is driven by the real-time solar wind data obtained by the DSCOVR spacecraft.
We investigate the IMF By dependence of plasma injection position using real-time simulation data. We found that injection position tends to distribute in the dusk side (dawn side) when the IMF By is positive (negative). Comparison of the simulation results with the CPCP, AE index, and plasma variations observed by geostationary orbiting satellites will also be reported.

©2020. Japan Geoscience Union. All Right Reserved.

Multi point measurements of geomagnetically induced currents in the Chugoku region

*Kumiko K. Hashimoto[1], Kentarou Kitamura[2], Takashi Kikuchi[3], Yusuke Ebihara[4]

1. Kibi International University, 2. National Institute of Technology, Tokuyama College, 3. Nagoya University, 4. Kyoto University

With cooperation from Yamaguchi power management office of the Chugoku Power Electric Co., we installed instruments of the geomagnetically induced current (GIC) measurement in Higashi-Yamaguchi and Shin-Yamaguchi electric power substations on March 2018 and March 2019, respectively. We analyzed correlations between the GIC from the two substations and magnetometer data for Space weather events, such as magnetic sudden commencements, magnetic pulsations, substorm positive bay etc. Our results show that the GIC at Higashi-Yamaguchi and Shin-Yamaguchi substations mainly correlates with east-west component of magnetic field or north-south component of the induced electric field. On the other hands, intensities of the GIC at Shin-Yamaguchi substation are 2-4 times larger than that at Higashi-Yamaguchi. The Chugoku region is characterized by power lines parallel to coasts extending east and west. Shin-Yamaguchi substation is located at the west end of the two trunk power lines from the Sanyo- and Sanin-region, whereas Higashi-Yamaguchi substation is in the middle of the power line network. The geometric feature may be a main cause to amplify the GIC at Shin-Yamaguchi.

Keywords: geomagnetically induced current, low latitude, induced electric field, Substorm, magnetic sudden commencement

©2020. Japan Geoscience Union. All Right Reserved.

SuperDARN future plan in terms of Planning of phase X 6-year project of Japanese Antarctic Research Expedition and beyond

*Akira Sessai Yukimatu[1,2]

1. National Institute of Polar Research, 2. SOKENDAI

Planning of phase X 6-year project of Japanese Antarctic Research Expedition (JARE 64-69, 2022-2028) has been actively discused. We here try to discuss and summarise SuperDARN future plan at Antarctic Syowa station in terms of Phase X JARE project and beyond.
NIPR in Japan has joined the SuperDARN (Super Dual Auroral Radar Network) project since its establishment in 1995 and run 2 SENSU SuperDARN radars, Syowa South and Syowa East radars (SENSU stands for “Syowa South & East HF Radars of NIPR for SuperDARN”) in Japanese Antarctic Syowa station (69.00 S, 39.58 E) in polar auroral zone. Both radars have substantially contributed to the SuperDARN project and scientific researches, for example, studies on various types of auroral phenomena, geomagnetic pulsations, substorms, reconnection, precise neutral wind observation around mesopause region using meteor echoes, studies on polar mesospheric summer echoes (PMSEs), magnetosphere-ionosphere-neutral atmosphere vertical coupling, studies on influence of low solar activity or grand minimum on geospace space weather. We here summarise our important achievements so far including during current phase IX JARE project period and will discuss on issues remaining unresolved and ways forward and the future perspective of the scientific direction of our SENSU SuperDARN research towards phase X JARE period and beyond as one of the comprehensive observations at Syowa station and as one of the most important basic, long-term and cutting-edge geospace scientific tools especially in terms of space weather and space climate.

References
1. SuperDARN Japan web site: http://polaris.nipr.ac.jp/~SD/sdjapan/
2. Greenwald, R. A., et al., “DARN/SuperDARN A global view of the dynamics of high-latitude convection,” Space, Sci., Rev., 71, 761-796, doi:10.1007/BF00751350, 1995.
3. Chisham, G., et al., “A decade of the Super Dual Auroral Radar Network (SuperDARN): scientific achievements, new techniques and future directions,” Surv. Geophys., 28(1), 33-109, doi:10.1007/s10712-007-9017-8, 2007.
4. Nishitani, N., et al., “Review of the accomplishments of mid-latitude Super Dual Auroral Radar Network (SuperDARN) HF radars,” Earth and Planetary Sci., 6, 27, doi:10.1186/s40645-019-0270-5, 2019.

Keywords: SuperDARN, JARE Phase X, space weather

©2020. Japan Geoscience Union. All Right Reserved.

Study of dependence of solar flare induced SuperDARN Doppler velocity on X-ray intensity, SZA and season

*Tomoya Takada[1], Nozomu Nishitani[1], Tomoaki Hori[1]

1. Institute for Space-Earth Environmental Research

Solar flares cause various ionospheric disturbances. Short wave fadeout (SWF) is one typical example, and has been studied for several years using several kinds of instruments. Doppler flash, which is a sudden increase in Doppler speed of ground scatter echoes observed by SuperDARN radars, has been recently reported, but has not been studied comprehensively yet. Watanabe and Nishitani (2013) investigated the dependence of Doppler speed on radar slant range and elevation angle, and they found that the effect of the D-region ionosphere change plays a dominant role in generating Doppler flash effect. In this study, we examined the dependence of X-ray flux, Solar Zenith Angle (SZA) and season. We analyzed 70 solar flare events from Feb 2011 to Sep 2017. Doppler speed is positively correlation with instantaneous X-ray flux. On the contrary, we cannot find the clear relationship between the Doppler speed and SZA / season. Possible reasons for such poor correlation will be discussed..

Keywords: SuperDARN, Solar flare, Doppler flash

©2020. Japan Geoscience Union. All Right Reserved.

Summary of the five-year extended observations of Nobeyama Radioheliograph

*Satoshi Masuda[1]

1. Institute for Space-Earth Environmental Research, Nagoya University

Nobeyama Radioheliograph (NoRH) had been operated by the International Consortium for the Continued Operation of Nobeyama Radioheliograph (ICCON) since April 2015. However, the operation of NoRH finished at the end of March in 2020. Nagoya University collected the operational costs from international/domestic partners was unique and operated NoRH as a representative of ICCON. This style was very unique in the Japanese solar telescopes. The daily check of the instruments/computers/data were done by international/domestic collaborators. Finally, for five years, 33 researchers in nine countries (Belgium, China, Germany, Japan, South Korea, Russia, Switzerland, U.K., U.S.A.) did this task as a chief observer. Thanks to their contributions, scientific data were taken for almost the whole period except the following two periods, from late January 2018 to early April 2018, and from early May 2019 to early June 2019.

The original scientific targets were ‘particle acceleration in solar flares’ and ‘long-term solar activity variation’ for this extension. Unfortunately, since the solar flare activity was very low since April 2015, only 38 solar flares (max ~ M6.7 class) were detected during this extension period. Before the extension, about 900 flares were observed. So the increment of solar flare data was not so large. As for the latter topic, we could derive the data of the polar brightening in this solar cycle in addition to the previous two cycles. Then, Gopalswamy et al. (2018) predicted the peak sunspot number of the next solar cycle from the polar brightness at 17 GHz and Fujiki et al. (2019) found the very good correlation between the solar wind speed and the polar brightness at 17 GHz.

One of the most outstanding outcomes is the growth of the international collaboration in this field. Based on this activity, now we are considering the next framework of the international collaboration with the Chinese new solar radio telescope, so-called MUSER.

Keywords: solar radio, solar flare, solar activity

©2020. Japan Geoscience Union. All Right Reserved.

Phesant tail aurora: The oldest record of astronomical phenomenon in Japan

*Ryuho Kataoka[1], Kazuaki Yamamoto[2], Yasunori Fujiwara[1], Kozue Shiomi[1], Nobuo Kokubun[1]

1. National Institute of Polar Research, 2. National Institute of Japanese Literature

The oldest record of an astronomical phenomenon in Japan was recorded in the Nihon-shoki as follows: "On December 30 in 620, a red sign appeared in heaven. The length was more than 1 jo (10 degrees). The shape was similar to a pheasant tail (Suiko-Tennou, 28)". The appearance of a red sign has been recognized as an expression of a bad omen in literature, while it has been interpreted as the northern lights in geophysics. We introduce the latest scientific findings that the northern lights show a fan-shaped appearance with a red background when appearing over Japan (Kataoka et al., 2019). After showing that the fan-shape is similar to a pheasant tail, also pointing out the low possibility of comets, we conclude that the oldest record of the red sign is consistent with the appearance of the northern lights over Japan.

Reference:
Kataoka, R., S. Uchino, Y. Fujiwara, S. Fujita, and K. Yamamoto (2019), Fan-shaped aurora as seen from Japan during a great magnetic storm on 11 February 1958, 9, A16, https://doi.org/10.1051/swsc/2019013.

©2020. Japan Geoscience Union. All Right Reserved.

Plasma waves causing relativistic electron precipitation events at International Space Station

*Ryuho Kataoka[1], CALET Collaboration, Arase Collaboration

1. National Institute of Polar Research

We introduce the latest paper (Kataoka et al., 2020) showing three different types of relativistic electron precipitation (REP) events observed at International Space Station (ISS), associated with electromagnetic ion cyclotron (EMIC) waves or whistler mode waves as observed by the Arase satellite at conjugate locations near the magnetic equator. Three different detectors installed on the ISS were complementarily used; CALET/CHD as the detector of precipitating MeV electrons, MAXI/RBM as the detector of sub-MeV electrons from horizontal and vertical directions, and SEDA-AP/SDOM to quantitatively measure the energy spectrum. The REP event on Aug 21, 2017 shows a quasi-periodic intensity variation at ~1 Hz which corresponds to variations of the EMIC waves at the Arase altitudes. The REP event on April 24, 2017 shows rapid and irregular intensity variation which corresponds to the amplitude variation of chorus waves, while the REP events on October 26, 2017 shows a smooth quasi-periodic time variation at ~0.2 Hz which corresponds to the amplitude variation of “electrostatic” whistler mode waves. This study clearly demonstrates that the time variation of REP events at ISS are caused by various types of plasma waves near the magnetic equator.

Reference: Kataoka et al. (2020), Plasma waves causing relativistic electron precipitation events at International Space Station: Lessons from conjunction observations with Arase satellite, submitted to JGR Space Physcs.

©2020. Japan Geoscience Union. All Right Reserved.

Investigation of the Relation Between Magnetospheric Activity and Solar Wind Parameters Based on Potential Learning

*Ryozo Kitajima[1], Motoharu Nowada[2], Ryotaro Kamimura[3]

1. Dept. Engineering, Tokyo Polytechnic University, Kanagawa, Japan, 2. Shandong Provincial Key Laboratory of Optical Astronomy and Solar-Terrestrial Environment, Institute of Space Sciences, Shandong University, Weihai, P. R. China, 3. IT Education Center, Tokai University, Kanagawa, Japan

Nowadays, it is so important in saving our economic activity and evading the disasters caused by terrestrial electromagnetic effects to predict both temporal and spatial scales of the geomagnetic disturbances based on in-situ solar wind observations. Recently, Neural Network (NN) is one of the notable techniques for the predictions of the magnetospheric activities. However, NN has a problem referred to as ‘black box’, which is difficult to extract which solar wind parameters are the most important for prediction. In this study, we examine a significant relationship between K_p index, which represents the magnetospheric activity, and the solar wind conditions based on an interpretable neural network: ‘Potential Learning (PL)’. A feature of the PL is to make a network that can understand the input variables by learning the “input potentialities”, which are indices calculated using the variances of the solar wind parameters as input variables.
In this study, we investigate the magnetospheric activity profile when the Interplanetary Magnetic Field (IMF) oriented southward ($B_z < 0$). As the input solar wind data, we utilize the two components of the magnetic field (B_x, B_y) in GSE, and solar wind flow speed, and number density during 20 years between 1999 and 2018. Furthermore, we divide the associated values of K_p into two groups (targets): ‘K_p = 6- to 9 (positive target)’ and ‘K_p = 0 to 1+ (negative target)’. Because the data number of positive target was smaller than that of negative target, the negative target samples are randomly selected so that the data numbers of both targets become equal. Based on the PL neural network, we obtain two important results; 1) the solar wind plasma flow speed might have the most influential in the increase of the K_p index, and 2) as the secondary influential parameter for the K_p increase, the solar wind proton density is considered. In the presentation, we will discuss feasibility of the application to the prediction of the magnetospheric activity based on the solar wind parameters.

Keywords: Space Weather Modeling, Magnetospheric Activity and Solar Wind, Neural Network (Potential Learning)

©2020. Japan Geoscience Union. All Right Reserved.

Cosmic Ray Intensity Increase Associated with Slow Coronal Mass Ejection

*Wataru Kihara[1], Chihiro Kato[1], Kazuoki Munakata[1], Yukino Ko[1], Ryuho Kataoka[2], Akira Kadokura[2], the GMDN collaborations -

1. Department of Physics, Shinshu University, 2. National Institute of Polar Research

Shinshu University installed a cosmic ray detectors at Syowa Station in the Antarctic, in cooperation with the National Institute of Polar Research, and started muon and neutron observations at the same point in February 2018. As a result we observed cosmic ray fluctuations due to coronal mass ejection on 2018 August 25. This event caused a large geomagnetic storm with a Dst index of -174nT despite of a miner coronal mass ejection that occurred during the solar minimum. Furthermore, satellite observations showed that the coronal mass ejection was slow and the high-speed solar wind from the corona hole was catching up. From these perspectives, this event is a very interesting. In this study, we analyzed this coronal mass ejection event by using the global muon detector network and neutron monitors installed around the world and Syowa Station in the Antarctic. As a result, it was found that the cosmic ray density increased in the latter half of the period when this coronal mass ejection event was observed. We discuss the cause of the increase in cosmic ray intensity.

Keywords: Space Weather, Coronal Mass Ejection, Cosmic Ray

©2020. Japan Geoscience Union. All Right Reserved.

Study on the global occurrence characteristics of Pc2 pulsation with the 10Hz data of the MAGDAS9 system

*Taisei Kabasawa[1], Akimasa Yoshikawa[2], Teiji Uozumi[3], Akiko Fujimoto[4], Shuji Abe[3]

1. Kyushu University, 2. Department of Earth and Planetary Science, Kyushu University, 3. International center for space weather science and education, Kyushu university, 4. Department of information technology, Kyushu Institute of Technology

Geomagnetic field disturbance observed on the ground is affected by the space weather phenomena such as magnetic storms and auroral substorms. Recent research shows that the Pc2 pulsation of which frequency range 5-10 seconds is observed at the inner magnetosphere as EMIC wave that is associated with the high-energy process activated O^+ during magnetic disturbance.
By using 10Hz sampling MAGDAS data, we found that the Pc2 type pulsation are simultaneously observed from high to middle-and-low latitudinal region during a magnetic storm time substorm. Also, we found that such global Pc2 pulsations have the local time distribution peaked at 6LT and during 11-15LT local noon time and the mainly enhanced at March-July. This occurrence characteristics is different from that of Pc1 pulsation that previous research reports.
In this presentation, we will report the preliminary results of observational analysis of Pc2 pulsation by using MAGDAS network. We also discuss the comprehensive approach for understanding global coupling process among inner magnetosphere and high-middle-low latitude to the equatorial region by using FM-CW radar data, PWING induction magnetometer data, and the geo-space environment data from the ERG satellite.

Keywords: Pc2 pulsation, EMIC waves, global coupling

©2020. Japan Geoscience Union. All Right Reserved.

Data assimilation of radiation belt electrons using the DREAM code and multiple spacecraft data of Arase, Himawari, and GPS

*Kaori Sakaguchi[1], Andrew Walker[2], Sophie Graf[2], Reinhard Friedel[2], Takefumi Mitani[3], Nana Higashio[3], Takeshi Takashima[3], Tsutomu Nagatsuma[1], Mamoru Ishii[1]

1. National Institute of Information and Communications Technology, 2. Los Alamos National Laboratory, 3. Japan Aerospace Exploration Agency

We report data assimilation results of multi radiation belt electron data into Dynamic Radiation Environment Assimilation Model (DREAM). DREAM is a data assimilation software that can calculate radiation belt electron flux for arbitrary spacecraft positions using 1-D radial diffusion equation based on the ensemble Kalman filtering method. In this study, observation data from three spacecrafts with different orbits; Arase (high elliptical orbit with inclination 31 degrees), Himawari-8 (geosynchronous), and seven GPS (semi-geosynchronous) were fed into DREAM, and energetic electron fluxes along Van Allen Probe in the high elliptical orbit with inclination 10 degrees were sampled for the evaluation. Data assimilation were performed for one month of August 2018 which includes a geomagnetic storm event of Dst=-188 nT on 26 Aug. The observed flux variations of ~700 keV and ~1 MeV electrons were almost perfectly reproduced by DREAM both for quiet and storm times along the orbit of Van Allen Probe A. We found that the performance of prediction highly depended on energy range, L shell, and quality fed data set. The results suggest that DREAM can be a powerful tool for prediction of radiation belt electron flux along arbitrary orbits with high accuracy if it is fed appropriate data set.

Keywords: radiation belt, data assimilation

©2020. Japan Geoscience Union. All Right Reserved.

[E] Poster | P (Space and Planetary Sciences)：P-EM Solar-Terrestrial Sciences, Space Electromagnetism & Space Environment

[P-EM18] Study of coupling processes in solar-terrestrial system

convener:Mamoru Yamamoto(Research Institute for Sustainable Humanosphere, Kyoto University), Yasunobu Ogawa(National Institute of Polar Research), Satonori Nozawa(Institute for Space-Earth Environmental Research, Nagoya University), Akimasa Yoshikawa(Department of Earth and Planetary Sciences, Kyushu University)

The Earth accepts vast input of energy and material from the Sun. The Earth's environment is maintained by the balance between their inputs and outputs. It is therefore important to study energy and mass transport on the Earth. This is an international session that discusses studies of the coupling processes in the Sun-Earth system based on the project "Study of coupling processes in solar-terrestrial system" that was approved by the Master Plan 2014/2017 of Science Council of Japan. We continue proposing the project to the Master Plan 2020. The facilities and networks included are Equatorial MU Radar (EMU) in Indonesia to study the whole equatorial atmosphere, the EISCAT_3D radar system in northern Scandinavia to study detailed structures and elementary processes of the magnetosphere-ionosphere coupling in the polar region, and global networks of various ground-based instruments and observation data. We will show the current status of the project and discuss sciences by soliciting variety papers. This session is open to the world, and we strongly encourage submission of papers related to other facilities and projects, i.e., atmospheric or incoherent scatter radars, observation networks, satellites, and simulation or theoretical studies, etc.

[PEM18-P01] Development of Software-Defined Multichannel Receiver for Equatorial Atmosphere Radar (EAR)

*Hiroyuki Hashiguchi[1], Nor Azlan Bin Mohd Aris -[1], Mamoru Yamamoto[1] (1.Research Institute for Sustainable Humanosphere, Kyoto University)

[PEM18-P02] Observation of ozone vertical mixing due to KH instability in tropical tropopause layer

*Momoko Hashino[1], Hiroyuki Hashiguchi[1], Richard Wilson[2], Shin-Ya Ogino[3], Junko Suzuki[3] (1.Research Institute for Sustainable Humanosphere, Kyoto University, 2.LATMOS/IPSL, Sorbonne Université, 3.Japan Agency for Marine-Earth Science and Technology)

[PEM18-P03] Study of daily and seasonal variation of the equatorial ionization anomaly in Asia based on satellite-ground beacon experiment

*Mamoru Yamamoto[1], Yuki Sakamoto[1], Kornyanat Hozumi[2] (1.Research Institute for Sustainable Humanosphere, Kyoto University, 2.National Institute of Information and Communications Technology)

[PEM18-P04] Development of transmitter and antenna on board of sounding rocket for the TEC measurement

*Koki Kurokawa[1], Mamoru Yamamoto[1] (1.Research Institute for Sustainable Humanosphere, Kyoto University)

[PEM18-P05] Ionospheric observations by Equatorial Atmosphere Radar during annular eclipse in December 2019

*Rieko Takagi[1], Tatsuhiro Yokoyama[1], Mamoru Yamamoto[1], Kornyanat Hozumi[2] (1.Research Institute for Sustainable Humanosphere, Kyoto University, 2.National Institute of Information and Communications Technology)

[PEM18-P06] Upgrade of equatorial plasma bubble simulation toward coupling with GAIA model

*Taichi Komoto[1], Tatsuhiro Yokoyama[1], Hiroyuki Shinagawa[2] (1.Research Institute for Sustainable Humanosphere, 2.National Institute of Information and Communications Technology)

[PEM18-P07] Long-term statistical analysis of the ionospheric observation with the MU radar

*Tatsuhiro Yokoyama[1], Masanori Ueno[1], Mamoru Yamamoto[1] (1.Research Institute for Sustainable Humanosphere, Kyoto University)

[PEM18-P08] **Space weather modelling of the dayside polar ionosphere and thermosphere**

*Hitoshi Fujiwara[1], Yasunobu Miyoshi[2], Satonori Nozawa[3], Yasunobu Ogawa[4], Hidekatsu Jin[5], Chihiro Tao[5], Hiroyuki Shinagawa[5] (1.Faculty of Science and Technology, Seikei University, 2.Department of Earth and Planetary Sciences, Kyushu University, Japan, 3.Institute for Space-Earth Environmental Research, Nagoya University, Japan, 4.National Institute of Polar Research, Japan, 5.National Institute of Communication Technology, Japan)

[PEM18-P09] Network observations of aurora and airglow with low-cost multi-wavelength imager system

*Yasunobu Ogawa[1], Akira Kadokura[1], Yoshimasa Tanaka[1] (1.National Institute of Polar Research)

[PEM18-P10] A pulsating aurora event observed by an optical spectrograph at Tromsø, Norway

*Takuo T. Tsuda[1], Chengyu Li[1], Keisuke Hosokawa[1], Satonori Nozawa[2], Tetsuya Kawabata[2], Akira Mizuno[2], Shin-ichiro Oyama[2], Junichi Kurihara[3] (1.University of Electro-Communications, 2.Nagoya University, 3.Hokkaido University)

[PEM18-P11] Study of atmospheric stability in the polar upper mesosphere and lower thermosphere above Tromsø by using sodium LIDAR data

*Sakiho Maeda[1], Satonori Nozawa[1], Takuya Kawahara[2], Norihito Saito[3], Takuo T. Tsuda[4], Satoshi Wada[3], Toru Takahashi[5], Tetsuya Kawabata[1], Chris Hall[6] (1.Institute for Space-Earth Environmental Research, Nagoya University, 2.Faculty of Engineering, Shinshu University, 3.RIKEN Center for Advanced Photonics, RIKEN, 4.The University of Electro-Communications, 5.Department of Physics, University of Olso, 6.UiT The Arctic University of Norway)

[PEM18-P12] Observational evaluation of temperature/wind perturbations associated with small-scale AGWs : Parameterisation and validation of wave structures

*Shin Suzuki[1], Satonori Nozawa[2] (1.Faculty of Regional Policy, Aichi University, 2.ISEE, Nagoya University)

[PEM18-P13] Development of SDR-based scintillation detector system integrated with MAGDAS project

*Akiko Fujimoto[1], Shuji Abe[2], Akimasa Yoshikawa[2] (1.Kyushu Institute of Technology, 2.Kyushu University)

[PEM18-P14] Recent and future activities of ICSWSE and MAGDAS project

*Shuji Abe[1], Akiko Fujimoto[2], Teiji Uozumi[1], Akimasa Yoshikawa[1,3] (1.International Center for Space Weather Science and Education, Japan, 2.Kyushu Institute of Technology, Japan, 3.Department of Earth and Planetary Sciences, Kyushu University, Japan)

[PEM18-P16] Day-to-day Variability of Field-Aligned Irregularities Occurrence in Nighttime F-region Ionosphere over Equatorial Atmosphere Radar : A Combinatorics Analysis

*Dyah Rahayu Martiningrum[1], Mamoru Yamamoto[2], Rezy Pradipta[3] (1.National Institute of Aeronautics and Space - LAPAN, Indonesia, 2.Research Institute for Sustainable Humanosphere (RISH), Kyoto University, Japan, 3.Institute for Scientific Research, Boston College, Chestnut Hill, MA, United States)

Development of Software-Defined Multichannel Receiver for Equatorial Atmosphere Radar (EAR)

*Hiroyuki Hashiguchi[1], Nor Azlan Bin Mohd Aris -[1], Mamoru Yamamoto[1]

1. Research Institute for Sustainable Humanosphere, Kyoto University

Equatorial Atmosphere Radar (EAR) is a very high frequency (VHF) Doppler radar operated with an active phased-array antenna system at 47 MHz. It had originally been equipped with a single receiving channel system since its establishment in 2001 at the equator in Kototabang, West Sumatra, Indonesia (0.20S, 100.32E). We have developed a multichannel receiver system for the EAR using a combination of the Universal Software Radio Peripheral X300 (USRP X300) and GNU Radio software. There are a number of advantages to have multichannel receiver systems such as to enable spaced-antenna method and spatial domain interferometry.

Two USRP X300 devices, corresponding to four receiving channels, were synchronized using 10 MHz reference clock and a pulse per second (1 PPS) signal. The standard observation system of the EAR is retained by splitting the received echo signals through directional couplers which enabled simultaneous observation of the two different techniques, spaced-antenna and Doppler beam swinging. The signal <gwmw class="ginger-module-highlighter-mistake-type-3" id="gwmw-15814652745326432130038">for</gwmw> spaced-antenna application is fed to the USRP X300s for digital conversion, and then stored on a Hard Disk Drive (HDD). The <gwmw class="ginger-module-highlighter-mistake-type-2" id="gwmw-15814652881083188773963">ranging</gwmw> of the data is carried out by taking advantage of the leaked transmitted pulse, before demodulated and coherently integrated.

Performance analysis using multiple receiving <gwmw class="ginger-module-highlighter-mistake-type-3" id="gwmw-15814652985556454852304">antennas</gwmw> orientation for the application of spaced-antenna methods on the EAR has been carried out through multiple experiments over the duration between April 2019 and September 2019. Phase correction is applied to all channels for a single spectrum in the real time signal processing for improving the phase synchronization. The initial results show the existence of noticeable fluctuations in the estimated horizontal wind. Then, a comparison of the EAR spaced-antenna (SA) performance with five different orientations taking into consideration the size of receiving antenna and its separation distance has been presented, where the horizontal wind profiles using Full Correlation Analysis (FCA) were estimated and compared with the standard EAR data. Based on the results, the configuration with the largest aperture shows slight advantages over the other four configurations but with limited improvement.

We can apply the achievement of this study to the Equatorial MU radar (EMU), which is proposed to be constructed at West Sumatera, Indonesia. The EMU system is the similar to the MU radar, but its antenna consists of 1045 Yagi antennas with 55 groups and it has 64 receiver channels.

Keywords: Software Defined Radio, Equatorial Atmosphere Radar, Multi-Channel Receiver

©2020. Japan Geoscience Union. All Right Reserved.

Observation of ozone vertical mixing due to KH instability in tropical tropopause layer

*Momoko Hashino[1], Hiroyuki Hashiguchi[1], Richard Wilson[2], Shin-Ya Ogino[3], Junko Suzuki[3]

1. Research Institute for Sustainable Humanosphere, Kyoto University, 2. LATMOS/IPSL, Sorbonne Université, 3. Japan Agency for Marine-Earth Science and Technology

The tropical tropopause layer (TTL) is a transition region between the troposphere and the stratosphere peculiar to the tropical zone. Physical and chemical processes in the TTL are important because they affect Stratosphere-Troposphere Exchange (STE). However, there have been few direct observations of TTL, and most previous researches have focused on large-scale waves, so the details of smaller processes related to TTL and STE are still unknown. In this study, we analyzed small-scale turbulence near the TTL region and the associated transport using the data of observation campaign conducted in collaboration with STRATEOLE-2 (TTL / lower stratospheric observation project using super pressure long duration balloons). In particular, we investigated whether the Kelvin-Helmholtz instability, which was shown to occur in TTL in previous studies, affects the vertical distribution of ozone.

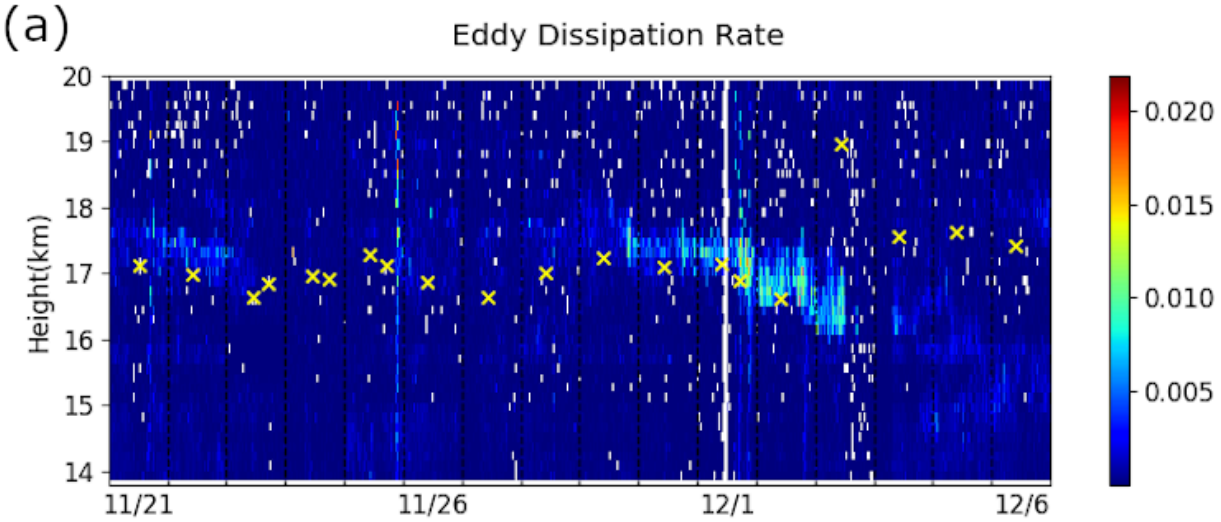
We use the data obtained by ozone and GPS sondes released from the Equatorial Atmospheric Observatory in West Sumatra, Indonesia from November 21 to December 6, 2019, and the data observed with the Equatorial Atmospheric Radar (EAR) during the same period.

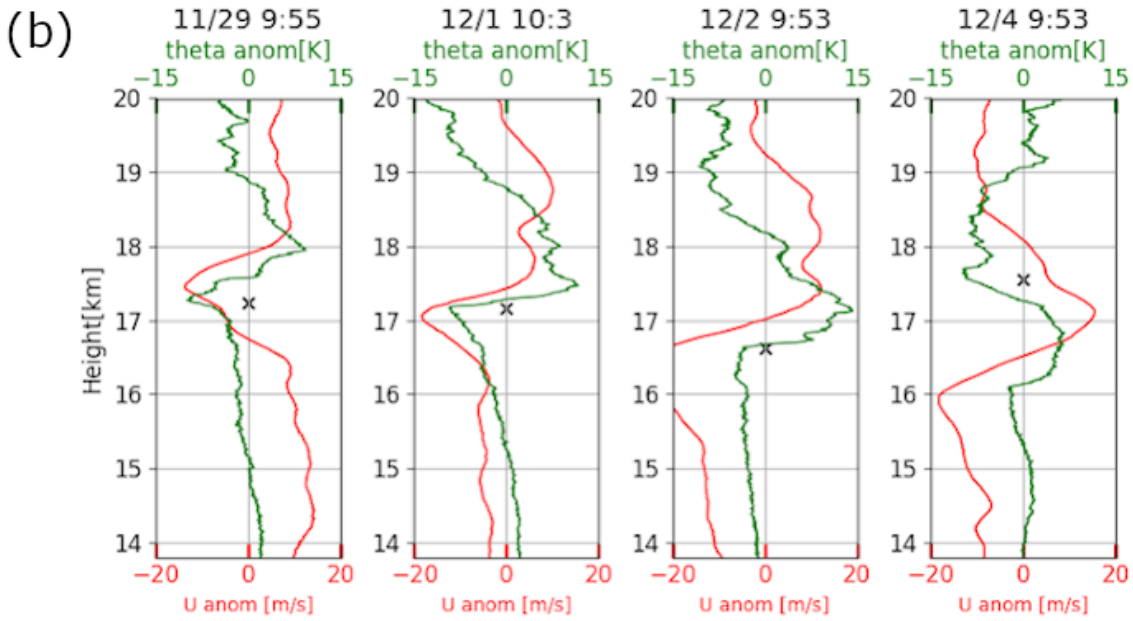
Figure (a) shows the turbulence intensity calculated from the EAR spectral width data, and the crosses indicate the tropopause defined as the lowest temperature (Cold Point Tropopause; CPT). The feature of CPT jump and strong turbulence observed on December 2-3 is similar to previous observations, suggesting the breaking of equatorial Kelvin waves. Figures (b) and (c) are the profiles of four sonde observations before and after the CPT jump. Figure (b) shows the deviation from the mean of the zonal wind (red) and the potential temperature (green), and (c) shows the vertical wind shear (red), deviation of ozone mixing ratio (green), and Richardson number (blue) (blue vertical line indicates Ri = 0.25). The phase shift between the zonal wind field and the temperature field shown in (b) is similar to that of the equatorial Kelvin wave, and propagates downward with increasing amplitude. The vertical wind shear shown in (c) is large in the altitude regions where the zonal wind anomaly shown in (b) suddenly changes from negative to positive and the amplitude is large (17.5-18 km altitude on November 29, moving downward with time). In this altitude regions, although the Richardson number does not always satisfy the condition in which KH instability occurs (Ri <0.25), the features of wind shear and Brunt-Väisälä frequency (not shown) are consistent with previous studies, suggesting the existence of KH billows. In the same altitude regions, the amount of ozone increases with altitude.

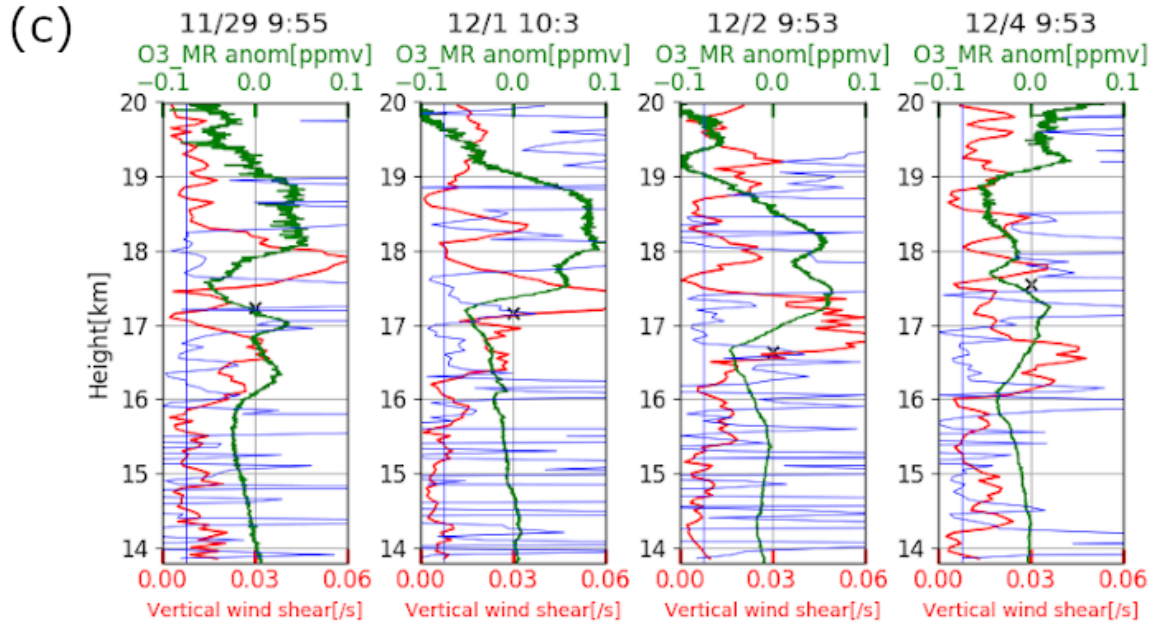
We have conducted direct observations of TTL and have shown that KH billows caused by strong vertical shear due to the increase in the amplitude of the zonal wind before and after the equatorial Kelvin wave breaking may cause vertical mixing of ozone. As a future work, we will investigate whether other factors than atmospheric mixing are related to the fluctuation of ozone amount.

Keywords: Tropical tropopause layer, Stratosphere-Troposphere Exchange, Kelvin-Helmholtz instability

©2020. Japan Geoscience Union. All Right Reserved.







©2020. Japan Geoscience Union. All Right Reserved.

©2020. Japan Geoscience Union. All Right Reserved.

Study of daily and seasonal variation of the equatorial ionization anomaly in Asia based on satellite-ground beacon experiment

*Mamoru Yamamoto[1], Yuki Sakamoto[1], Kornyanat Hozumi[2]

1. Research Institute for Sustainable Humanosphere, Kyoto University, 2. National Institute of Information and Communications Technology

Studies of ionospheric structures by the satellite-ground beacon experiment have been conducted in Southeast Asia. We have deployed a meridional chain of five beacon receivers from 0.2S to 18.2N along 100E meridian and investigated the meridional distribution of total electron content (TEC) of the ionosphere. Although there were preceding studies of time and spatial variabilities of the equatorial ionization anomaly (EIA), the data analysis was limited in the short period. It was because the estimation of bias values was not easy and time-consuming. In this study, we developed a method to automate the bias estimation. As a result, we obtained absolute TEC distribution from a large amount of data and created the TEC database. Using this database, we analyzed latitudinal TEC distribution in a wide area, from Thailand to Indonesia in 2012-2015.
EIA is characterized by two crests in latitudinal TEC distribution that are generated by the plasma fountain effect. We defined EIA by representing the TEC latitudinal structure by a fourth-order polynomial function. By investigating the occurrence ratio of EIA at each hour, we found that EIA grows in the period from 9 to 12 LT, showed its maximum at around 13 LT, and decays in the period after 13 until 23 LT. We further investigated the EIA hemispheric asymmetry at different local timings. In the period from 13 to 23 LT, while EIA is already generated and gradually decays in time, the northern crest tends to exceed the southern crest in summer. In winter, the hemispheric asymmetry is reversed. By comparing this result with the wind model, we found that the hemispheric asymmetry in the period is affected by the meridional winds. In the period from 9 to 12 LT, while EIA is growing, the trend of hemispheric asymmetry was opposite; the southern crest is larger in summer, and the northern crest is larger in winter. By comparing this result with O/N2 distribution model, we found the possibility that, during the growing phase of EIA, the hemispheric asymmetry is affected by the composition of atoms and molecules in the atmosphere.

Keywords: Ionospheric Total Electron Content, Equatorial Anomaly, Satellite-ground beacon experiment

©2020. Japan Geoscience Union. All Right Reserved.

Development of transmitter and antenna on board of sounding rocket for the TEC measurement

*Koki Kurokawa[1], Mamoru Yamamoto[1]

1. Research Institute for Sustainable Humanosphere, Kyoto University

A sounding rocket experiment is planned by JAXA in 2021/2022 period for the study of medium-scale traveling ionospheric disturbance (MS-TID). By transmitting two radio beacon with a frequency ratio of 3 : 8 from the rocket and measuring the phase difference between the two signals on the ground, the total electron content (TEC) on the radio wave path from the rocket to the ground can be measured. To realize this observation, we are now developing the observation equipment onboard of this rocket. The instruments are a dual-band beacon transmitter of 150MHz and 400MHz and a set of antennas that are installed on the rocket skin. The transmitter needs to output two phase-coherent radio waves at the same time. As the signal source, we selected Si5338 which is a high-performance, low-jitter clock generator capable of synthesizing at most four signals with different frequencies. The antenna system consists of four elements that can transmit both frequencies. The elements must fit the harsh environment (high temperature, intense vibration, etc.) that is expected at the outside of the sounding rocket at launch. As we transmit a relatively low frequency of 150 MHz / 400 MHz signals, we selected the dual-band Planar Inverted-F Antenna (PIFA) that is useful to reduce the size of the antenna. Selection of high dielectric-constant material is another important issue for antenna-size reduction. This antenna is designed by using electromagnetic-field simulation software called CST. This software can be linked with other antenna design software. With this software, we tried to find the optimized antenna shape by simulating electromagnetic response of the antenna with variety of parameter settings.In the presentation, we report the current status of the transmitter and antenna for the sounding rocket experiment.

©2020. Japan Geoscience Union. All Right Reserved.

Ionospheric observations by Equatorial Atmosphere Radar during annular eclipse in December 2019

*Rieko Takagi[1], Tatsuhiro Yokoyama[1], Mamoru Yamamoto[1], Kornyanat Hozumi[2]

1. Research Institute for Sustainable Humanosphere, Kyoto University, 2. National Institute of Information and Communications Technology

The area of the Earth's atmosphere above an altitude of about 80 km is called the ionosphere, where molecules and atoms are partially ionized. Since the electron density varies depending on altitude, time, and location, radio waves passing through the ionosphere are delayed or refracted, which cause satellite communication failures and decrease GPS positioning accuracy. There is a need to accurately measure and predict the electron density distribution. It is known that a solar eclipse reduces the amount of sunlight when the moon passes in front of the sun in the daytime and affects the electron density distribution. In this study, during the annular solar eclipse near Southeast Asia on December 26, 2019, we observed the ionospheric E region with the Equatorial Atmosphere Radar (EAR) near the equator in West Sumatra, Indonesia, and analyzed the observation data. We also compared the results with ionosonde observations in Southeast Asia. Although clear 150-km echoes were observed with the EAR in the days before and after the eclipse, the 150-km echoes were not detected on the eclipse day. On the other hand, the E-region echoes showed significant variation in the distribution of echo power and Doppler velocity, which is thought to be affected by the solar eclipse.

Keywords: Ionosphere, Equatorial Atmosphere Radar, solar eclipse

©2020. Japan Geoscience Union. All Right Reserved.

Upgrade of equatorial plasma bubble simulation toward coupling with GAIA model

*Taichi Komoto[1], Tatsuhiro Yokoyama[1], Hiroyuki Shinagawa[2]

1. Research Institute for Sustainable Humanosphere, 2. National Institute of Information and Communications Technology

As space development progresses rapidly, stable use of satellite communication and navigation is strongly demanded, and a highly accurate and reliable positioning system using GPS is required. One of the causes of the GPS error is a physical phenomenon that occurs in the equatorial ionosphere called plasma bubble. A plasma bubble is a phenomenon in which the density stratification in the lower ionosphere becomes unstable and the low-density region rises like a bubble, and the inside of the bubble has a very unstable and irregular structure. Therefore, it has a great influence on radio wave propagation, but it is almost impossible at present to predict the occurrence of plasma bubbles. The purpose of this study is to develop a numerical model that combines a global ionospheric numerical model and a local ionospheric numerical model to predict the occurrence of plasma bubbles self-consistently, and to clarify the conditions of their generation. The global atmosphere-ionosphere coupled model GAIA has a grid spacing of about several hundred kilometers and cannot reproduce local structures such as plasma bubbles. On the other hand, the local ionosphere model can represent the fine internal structure of plasma bubbles because the grid spacing is less than 1 km, but it is limited to a narrow simulation domain and also applies periodic boundary conditions. Therefore, it is not possible to simply expand the simulation domain. Thus, by combining the global model and the local model hierarchically, we aim to develop a model that can reproduce the generation of plasma bubbles consistently with retaining their original advantages. Toward the coupling of the two models, we expand the simulation domain of the local model to cover the whole longitude under natural boundary conditions including diurnal plasma density variations. We will report the current status and initial results of the model development.

Keywords: equatorial plasma bubble, simulation, ionosphere

©2020. Japan Geoscience Union. All Right Reserved.

Long-term statistical analysis of the ionospheric observation with the MU radar

*Tatsuhiro Yokoyama[1], Masanori Ueno[1], Mamoru Yamamoto[1]

1. Research Institute for Sustainable Humanosphere, Kyoto University

An incoherent scatter radar (ISR) is a powerful tool to observe various ionospheric parameters. The ISR enables us to estimate various physical quantities in the ionosphere from the spectrum of the radar backscatters. The MU radar located in Shigaraki, Japan has regularly been operated as the ISR since the beginning of the MU radar operation in 1986. Electron and ion temperatures, ion drift, and echo power are observed and released in a public database. We have conducted a long-term statistical analysis of the IS observation with the MU radar from 1986 to 2019. The results are mostly consistent with the past results and IRI model outputs. The results during the deep solar minimum in the previous solar cycle show a large discrepancy between the observation and IRI model.

Keywords: MU radar, Ionosphere, Incoherent scatter observation

©2020. Japan Geoscience Union. All Right Reserved.

Space weather modelling of the dayside polar ionosphere and thermosphere

*Hitoshi Fujiwara[1], Yasunobu Miyoshi[2], Satonori Nozawa[3], Yasunobu Ogawa[4], Hidekatsu Jin[5], Chihiro Tao[5], Hiroyuki Shinagawa[5]

1. Faculty of Science and Technology, Seikei University, 2. Department of Earth and Planetary Sciences, Kyushu University, Japan, 3. Institute for Space-Earth Environmental Research, Nagoya University, Japan, 4. National Institute of Polar Research, Japan, 5. National Institute of Communication Technology, Japan

From the European Incoherent Scatter (EISCAT) radar observations, we have shown some features of the ionospheric disturbances in the dayside polar cap region where ionospheric and thermospheric observations are not enough to understand the space weather effects. For example, some ionospheric disturbances have been observed in the northward of Longyearbyen (> 80° latitude) even during geomagnetically quiet periods, while disturbances are generated in the auroral region (at Tromsø) during the geomagnetically disturbed periods. CME-induced disturbances and ionization due to high energy particle precipitation have been also observed in the dayside polar ionosphere.
In order to understand and predict the phenomena in the dayside polar ionosphere and thermosphere, we have also made modelling/simulation studies. In particular, we focus on modelling the effects of precipitating particles on the dayside polar ionosphere and thermosphere in the context of the Japanese Space Weather projects. In the present study, we will show some observational and simulation results: for example, the dayside ionospheric disturbances observed with the EISCAT radar system and simulations with a GCM. In addition, we will introduce our attempt to estimate productions of ions, NOx, and HOx in the altitude of 50-500 km due to precipitating particles.

Keywords: Polar ionosphere and thermosphere, Space Weather, Modelling

©2020. Japan Geoscience Union. All Right Reserved.

Network observations of aurora and airglow with low-cost multi-wavelength imager system

*Yasunobu Ogawa[1], Akira Kadokura[1], Yoshimasa Tanaka[1]

1. National Institute of Polar Research

This paper introduces a new system that can monitor aurora and atmospheric airglow using a low-cost Watec monochromatic imager (WMI) equipped with a sensitive camera, a filter with high transmittance, and the non-telecentric optics. It is demonstrated that the WMI system is capable of detecting 428-nm, 486-nm, 558-nm, and 630-nm auroral intensities properly, through comparison with those measured with a collocated imager system with narrower band-pass filter. Since 2013 a set of multi-wavelength WMIs has been operating in northern Scandinavia, Svalbard, and Antarctica. The WMI system is currently used to obtain (1) 428-nm auroral data at multipoint sites (located in the horizontal range of about 50-100 km) for research on three-dimensional structure of aurora using the auroral tomography method, and (2) multipoint data with a wavelength of 630-nm (in the horizontal range of about a few 1000 km) for study of large scale phenomena such as dynamic variation of the auroral oval and drift motion of polar patches. Most of the current WMI databases are open to the public via the web page (http://pc115.seg20.nipr.ac.jp/www/opt/index.html). Future development of the low-cost WMI system is expected to provide a great opportunity for constructing a global network for multi-wavelength aurora and airglow monitoring.

Reference:
Ogawa, Y., Y. Tanaka, A. Kadokura, K. Hosokawa, Y. Ebihara, T. Motoba, B. Gustavsson, U. Brandstrom, Y. Sato, S. Oyama, M. Ozaki, T. Raita, F. Sigernes, S. Nozawa, K. Shiokawa, M. Kosch, K. Kauristie, C. Hall, S. Suzuki, Y. Miyoshi, A. Gerrard, H. Miyaoka, and R. Fujii, Development of low-cost multi-wavelength imager system for studies of aurora and airglow, Polar Science, doi:10.1016/j.polar.2019.100501, 2019.

Keywords: polar region, aurora, airglow

©2020. Japan Geoscience Union. All Right Reserved.

A pulsating aurora event observed by an optical spectrograph at Tromsø, Norway

*Takuo T. Tsuda[1], Chengyu Li[1], Keisuke Hosokawa[1], Satonori Nozawa[2], Tetsuya Kawabata[2], Akira Mizuno[2], Shin-ichiro Oyama[2], Junichi Kurihara[3]

1. University of Electro-Communications, 2. Nagoya University, 3. Hokkaido University

Pulsating auroras are a diffuse-type aurora, and are characterized by a repetition of brighter (on-phase) and darker (off-phase) auroral emissions with periods of a few to a few tens of seconds. Optical observations for pulsating auroras have been widely performed for many years. Recent major activities in the optical imaging observation would be, for example, high-speed observations for faster modulations (3-Hz or higher) in the emission intensity during on-phases of pulsating auroras, and ground network observations in association with satellites in the magnetosphere for source regions of pulsating auroras. While such imaging observations equipped with bandpass or cutoff filters are useful for observing several auroral emission lines and bands of specific atoms and molecules, there is relatively less information on optical spectra of pulsating auroras.

We have been investigating optical spectra of pulsating auroras observed by an optical spectrograph at Tromsø, Norway (69.6ºN, 19.2ºE). Our spectrograph is capable of measuring optical emission intensity in mainly visible range from 480 to 880 nm with a resolution of 1.6 nm. The aperture, i.e. F-number, is 4. The field-of-view (FOV) is 0.03ºx2º, which is pointed at magnetic field-aligned direction. The time resolution is 1 second, and thus it can observe pulsating auroras, which have periods from a few to a few tens of seconds.

In this presentation, we show a pulsating aurora event occurred in morning hours on 6 March 2017. The event was a relatively long-lasting event over the FOV of spectrograph, and it allowed us to make more data integrations to enhance signal-to-noise ratios. According to a time-series of observed auroral emission data, we integrated spectral data for on- and off-phases separately. After such data integrations, auroral emission lines, such as OI 557.7 nm, OI 630.0 nm, and OI 844.6 nm, as well as emission bands, such as N2 1PG, were clearly found in both integrated-optical spectra of on- and off-phases. Then, we calculated a difference spectrum between the optical spectra of on- and off-phases. In the difference spectrum, clear line-like shapes were found for the emission lines of OI 557.7 nm and OI 844.6 nm. On the other hand, a shape of the difference spectrum around 630 nm does not seem to be a line-like shape due to OI 630.0 nm, and it seems to be a part of band-like shape of the emission band of N2 1PG. These results would suggest an importance of spectral observations of pulsating auroras, in addition to imaging observations.

Keywords: Pulsating aurora, Optical spectrograph, Tromsø

©2020. Japan Geoscience Union. All Right Reserved.

Study of atmospheric stability in the polar upper mesosphere and lower thermosphere above Tromsø by using sodium LIDAR data

*Sakiho Maeda[1], Satonori Nozawa[1], Takuya Kawahara[2], Norihito Saito[3], Takuo T. Tsuda[4], Satoshi Wada[3], Toru Takahashi[5], Tetsuya Kawabata[1], Chris Hall[6]

1. Institute for Space-Earth Environmental Research, Nagoya University, 2. Faculty of Engineering, Shinshu University, 3. RIKEN Center for Advanced Photonics, RIKEN, 4. The University of Electro-Communications, 5. Department of Physics, University of Olso, 6. UiT The Arctic University of Norway

We will report atmospheric stability in the polar upper Mesosphere and Lower Thermosphere (MLT) region (80-105 km) above Tromsø, Norway (69.6˚N, 19.2˚E) based on 2500 hours of sodium LIDAR data.

We have analyzed temperature and velocity data (6 min and 0.5 km resolutions) obtained over 8 seasons from October 2012 to March 2019 (about 2500 hour measurements of 237 nights). We have evaluated both static (convective) instability and dynamic (shear) instability using the square of Brunt–Väisälä frequency (N^2) and Richardson number (R_i), respectively. Furthermore, we have calculated the instability probability defined as the percentage of an occurrence rate of unstable regions over the time interval. The probabilities of static instability and dynamic instability are shown as P($N^2 < 0$) and P($0 < R_i < 1/4$), respectively. The temperature data and wind data are used to calculate N and wind shear (dv/dz), respectively.

We have found that P($N^2 < 0$) varies from a maximum of 20.6 % to a minimum of 0.5 %, and P($0 < R_i < 1/4$) varies from a maximum of 14 % to a minimum of 1.6% in the altitude region between 85 km to 95 km. P($N^2 < 0$) tends to be larger than P($0 < R_i < 1/4$). These probabilities do not show any obvious monthly variations from October to March, rather day-to-day variabilities are prominent. As shown in Figure 1, over the entire period, P($N^2 < 0$) at around 90 km altitude tends to be lower than those at around 80 km and 100 km: the static instability was less likely to occur at around 90 km. There is a weak correlation between P($0 < R_i < 1/4$) and the semidiurnal tidal amplitude, but no correlation between P($N^2 < 0$) and the semidiurnal tidal amplitude is found.

Based on these observational results, we will present the characteristics of the atmospheric stabilities in the polar winter MLT region above Tromsø. Furthermore, the results will be compared with those in mid-latitude.

©2020. Japan Geoscience Union. All Right Reserved.

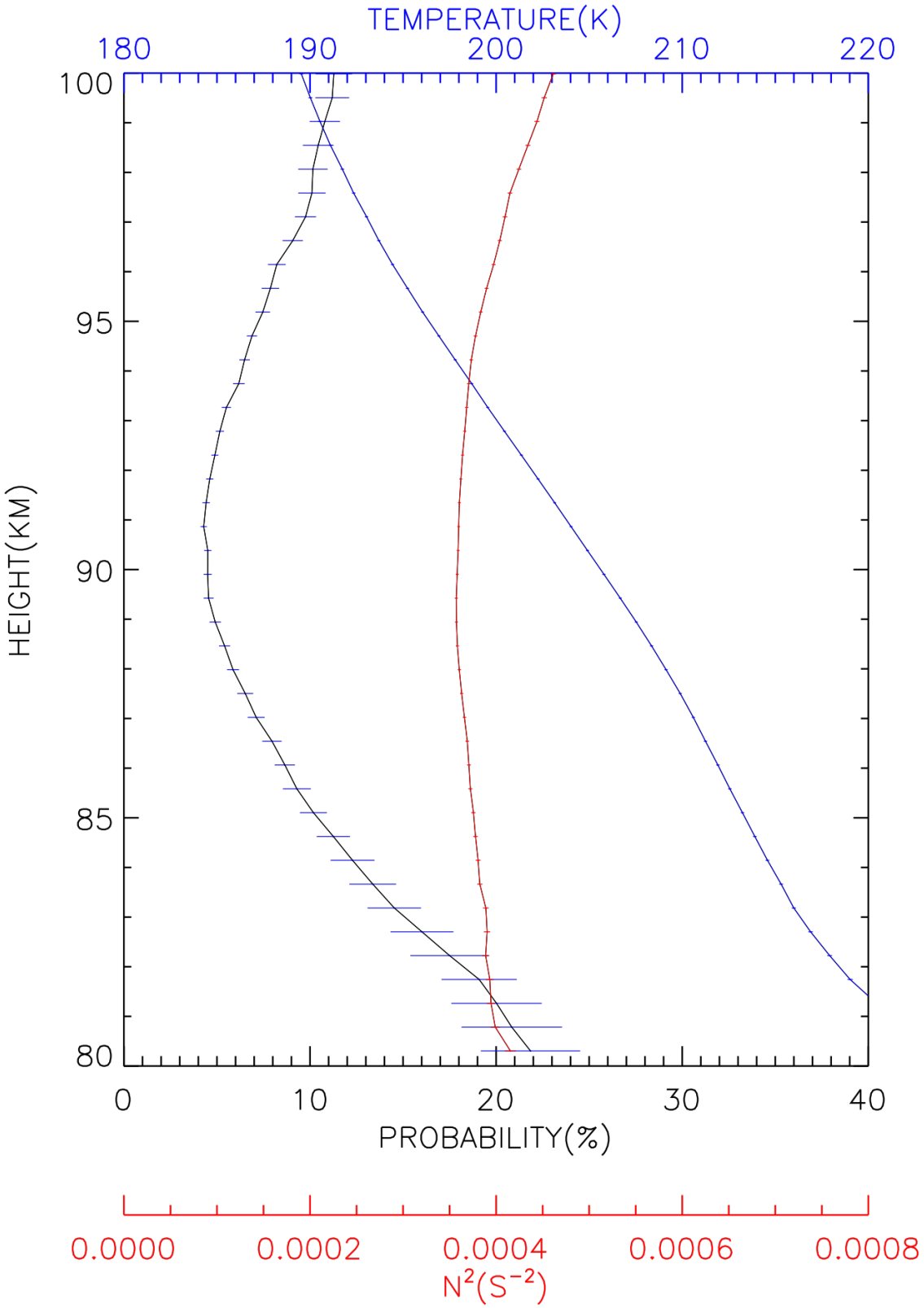


Figure 1. Height profiles of P($N^2 < 0$) (black line), averaged temperature (blue line) and N^2 (red line) associated with error bars (horizontal lines at each data point) from 80 to 100 km.

©2020. Japan Geoscience Union. All Right Reserved.

Observational evaluation of temperature/wind perturbations associated with small-scale AGWs : Parameterisation and validation of wave structures

*Shin Suzuki[1], Satonori Nozawa[2]

1. Faculty of Regional Policy, Aichi University, 2. ISEE, Nagoya University

The Tromsoe Na lidar operated by the Institute for Space-Earth Environmental Research, Nagoya University has monitored wind and temperature structures associated with auroral activity in the high latitude upper atmosphere since 2010. Although the observations are limited during the winter night, the lidar detected atmospheric wave signatures with period of a few hours and temperature change related to the wave propagation with high precision (less than 1K). Furthermore, this lidar started five-direction observation from 2012: horizontal distance between the beam positions are 58 km or 22 km at a height of 100 km and the observational setup can detect smaller-scale perturbations.

In this study, we tried to identify small-scale (less than 100 km) and short-period (less than 1 h) gravity waves by using the Tromsoe Na lidar. Gravity waves contribute significantly to the wind field and thermal balance in the mesosphere and lower thermosphere (MLT) region because they vertically transport horizontal momentum from the lower atmosphere. It is also pointed that, in particular, smaller-scale and shorter-period waves tend to transport larger momentum. Small-scale gravity waves in the MLT region are mainly studied with airglow imaging measurements. The airglow measurements, however, cannot observe temperature and wind perturbations directly, which are necessary for the estimation of wave’s momentum flux. Based on temperature and wind perturbations with the five-direction lidar, we evaluate dynamical effect of small-scale gravity waves propagating in the upper atmosphere quantitatively.

In this presentation, we will report some initial results derived from simultaneous measurements of the lidar and airglow imaging in 2013-2016.

Keywords: atmospheric gravity waves, lidar observation

©2020. Japan Geoscience Union. All Right Reserved.

Development of SDR-based scintillation detector system integrated with MAGDAS project

*Akiko Fujimoto[1], Shuji Abe[2], Akimasa Yoshikawa[2]

1. Kyushu Institute of Technology, 2. Kyushu University

Radio communications and radio navigation (GPS: global positioning system, GNSS: Global Navigation Satellite System) are used in worldwide and widely deployed in a variety of fields, for example, tracking, automated vehicle, clock synchronization or sport analysis. The ionosphere, where is a part of Earth's upper atmosphere between 80 and about 600 km in altitude, plays an important role in the radio/telecommunication and navigation. The ionosphere is characterized by the high density of free electrons produced by the energetic photo-ionization of ultraviolet (UV) and X-rays from the Sun. The structure of ionosphere is not stable and variable in the time of day, season, latitude and solar activity, because of the differences of the energetic photo-ionization process. The irregularities and disturbances in the ionosphere cause various severe problems, for example, lower accuracy of the radio navigation due to GPS/GNSS scintillation, disruption in High Frequency (HF) radio wave bands or interference due to anomalous propagation, etc. Especially, more robust correction models for ionospheric GPS/GNSS delay errors are required to enhance the utility value of GPS/GNSS clock synchronization for the fifth generation (5G) wireless technology. Also, the real-time alert for interference on HF radio waves is necessary for the safety navigation.
We have developed the SDR (Software-Defined Radio) -based scintillation detector system integrated with MAGDAS (http://data.icswse.kyushu-u.ac.jp) project. This system will be installed at the observatory where operates the FMCW radar to measure ionograms. Thus, our new system allows to investigate and monitor simultaneously the magnetic field variation recorded by MAGDAS magnetometer, the ionosphere plasma density profile in altitude with high time resolution and GPS scintillation level. We will present our initial development status.

©2020. Japan Geoscience Union. All Right Reserved.

Recent and future activities of ICSWSE and MAGDAS project

*Shuji Abe[1], Akiko Fujimoto[2], Teiji Uozumi[1], Akimasa Yoshikawa[1,3]

1. International Center for Space Weather Science and Education, Japan, 2. Kyushu Institute of Technology, Japan, 3. Department of Earth and Planetary Sciences, Kyushu University, Japan

International Center for Space Weather Science and Education (ICSWSE), Kyushu University is the research institute for conducting research and education in space weather. We are operating world-wide magnetometer array named as "MAGDAS/CPMN (MAGnetic Data Acquisition System/Circum-pan Pacific Magnetometer Network)" (Principal Investigator: Dr. A. Yoshikawa) for these. It consists of over seventy fluxgate magnetometers, one induction magnetometer, and four FM-CW (Frequency Modulated Continuous Wave) radars. One of our recent research topics is Equatorial Electrojet (EEJ). To accelerate the understanding of EEJ structure, we are constructing dense instrument array across the magnetic equator at Peru and Malaysia in recent year. The latest magnetometer is installed at Penang, Malaysia last September. On last March, we maintained the latest FM-CW radar at Sicaya, Peru. We calculate EE-index (Uozumi et al, 2008; Fujimoto et al., 2016) for space weather nowcast/forecast using realtime magnetometer data along the magnetic equator, and publish it at each hour on the web. We provide our observational information and data including old project via our website, and via IUGONET (Inter-university Upper Atmosphere Observation NETwork) web service and data analysis software. We believe MAGDAS data will help any researchers for their research under proper rule.

©2020. Japan Geoscience Union. All Right Reserved.

Day-to-day Variability of Field-Aligned Irregularities Occurrence in Nighttime F-region Ionosphere over Equatorial Atmosphere Radar : A Combinatorics Analysis

*Dyah Rahayu Martiningrum[1], Mamoru Yamamoto[2], Rezy Pradipta[3]

1. National Institute of Aeronautics and Space - LAPAN, Indonesia, 2. Research Institute for Sustainable Humanosphere (RISH), Kyoto University, Japan, 3. Institute for Scientific Research, Boston College, Chestnut Hill, MA, United States

This paper presents a statistical analysis to investigate day to day variability of field-aligned irregularities (FAI) occurrence in nighttime F-region ionosphere over the Equatorial Atmosphere Radar (EAR), West Sumatra, Indonesia. FAI echoes were identified based on signal intensity of backscatter radar observations. We analyzed nighttime F-region FAI during 3 years starting in January 2011 to December 2013. For the first time, a combinatoric analysis was applied to examined the statistical likehood of various day-to-day FAI occurrence patterns. The empirical day-to-day combinatorics analysis was performed based on binary classification of EAR observation data into either FAI occurrence (+) or FAI absence (-) for each calendar data. We gathered all possible permutations of various day-to-day FAI occurrence patterns, from 1-day to 6-day patterns, and compile them into histogram. The combinatorics analysis was performed in 4 separate time interval to account for seasonal variation : two equinoxes (March and September) and two solstices (June and December). EAR data show that FAI occurrence probability is maximum for the two equinoxes, and that it is minimum for the two solstices. The combinatorics analysis shows that certain day-to-day patterns are more likely to occur than others, and such “combinatorics fingerprints” also depend on season. During the solstices, persistent absence of FAI over several consecutive days far outweighed persistent FAI occurrence over an equivalent grouping of days with the same length. Meanwhile, during equinoxes, we found a generally more equitable distributions between persistent day-to-day FAI occurrence and persistent day-to-day FAI absence. This findings may open new ways to help forecast FAI occurrence on a regional basis.

Keywords: Combinatorics analysis, Ionosphere irregularities, Day to day variability

©2020. Japan Geoscience Union. All Right Reserved.

[E] Poster | P (Space and Planetary Sciences)：P-EM Solar-Terrestrial Sciences, Space Electromagnetism & Space Environment

[P-EM19] Dynamics of the Inner Magnetospheric System

convener:Kunihiro Keika(Department of Earth and Planetary Science, Graduate School of Science, The University of Tokyo), Aleksandr Y Ukhorskiy(Johns Hopkins University Applied Physics Laboratory), Yoshizumi Miyoshi(Institute for Space-Earth Environmental Research, Nagoya University), Lynn M Kistler(University of New Hampshire Main Campus)

The inner magnetosphere is highly variable because dynamical
variations of incoming energy from the solar wind, magnetospheric tail,
and the ionosphere. Cross-regional/cross-scale/cross-energy couplings
are key processes to understand this dynamical system, and coordinated
observations by multi-satellites and ground-based observations are
very essential to reveal these processes. In the 24th solar cycle,
a number of satellites such as Van Allen Probes, MMS, THEMIS, DSX and
Arase, coordinated ground-based observations (THEMIS-GBO, SuperDARN,
EISCAT, magnetometers, riometer, etc), and numerical simulations
(global kinetic model, MHD model, micro PIC, hybrid simulations) have
successfully investigated the inner magnetosphere system. Papers on recent results
on the inner magnetosphere and/or its coupling with the other regions,
including the ionosphere and the outer magnetosphere are invited. And
presentations on new projects for the inner magnetosphere are also
welcome.

[PEM19-P01] Numerical simulation on energetic electron precipitations by chorus waves

*Yoshiki Ito[1], Shinji Saito[2], Yoshizumi Miyoshi[1] (1.Nagoya University, ISEE, 2.National Institute of Information ans Communications Technology)

[PEM19-P02] A pipeline for comprehensive tracking of pulsating patches in All-Sky Imager data

*Riku Nomiyama[1], Yoshizumi Miyoshi[2], Kohei Toyama[2], Yasunobu Ogawa[3], Keisuke Hosokawa[4], Terumasa Tokunaga[1] (1.Kyushu Institute of Technology, 2.Institute for Space-Earth Environmental Research, Nagoya University, 3.National Institute of Polar Research, 4.Department of Communication Engineering and Informatics, University of Electro-Communications)

[PEM19-P03] Estimation of precipitating electron energy of pulsating aurora by multiwavelength aurora optical observation

*Kohei Toyama[1], Yoshizumi Miyoshi[1], Satoshi Kurita[1], Keisuke Hosokawa[2], Yasunobu Ogawa[3], Shin-ichiro Oyama[1], Satonori Nozawa[1] (1.Institute for Space-Earth Environmental Research, Nagoya University, 2.Department of Communication Engineering Informatics,Univarsity Electro-Communications, 3.National Institute of Polar Research)

[PEM19-P04] Observation plan of pulsating aurora by the multi-spectral auroral camera on the LAMP rocket

Naoshi Yagi[1], *Takeshi Sakanoi[1], Miki Kawamura[1], Kazushi Asamura[2], Yoshizumi Miyoshi[3], Keisuke Hosokawa[4], Sarah L Jones[5], Marc Lessard[6] (1.Planetary Plasma and Atmospheric Research Center, Graduate School of Science, Tohoku University, 2.ISAS/JAXA, 3.ISEE, Nagoya University, 4.Graduate School of Informatics and Engineering, The University of Electro-Communications, 5.Goddard Space Flight Center, NASA, 6.University of New Hampshire)

[PEM19-P05] Statistical study of EMIC waves and energetic electron precipitation: ground-based magnetometer and subionospheric VLF/LF radio measurements at subauroral latitude

*Asuka Hirai[1], Fuminori Tsuchiya[1], Takahiro Obara[1], Yasumasa Kasaba[1], Yuto Katoh[2], Hiroaki Misawa[1], Kazuo Shiokawa[3], Yoshizumi Miyoshi[3], Satoshi Kurita[3], Chae-Woo Jun[3], Martin G Connors[4] (1.Planetary Plasma and Atmospheric Research Center, Graduate School of Science, Tohoku Univ. , 2.Department of Geophysics, Graduate School of Science, Tohoku University, 3.Institute for Space-Earth Environmental Research, Nagoya University, 4.Athabasca University)

[PEM19-P06] First simultaneous observation of the isolated proton aurora at subauroral latitudes by a highly sensitive all-sky camera and the Van Allen Probes satellite

*Kohki Nakamura[1], Kazuo Shiokawa[1], Yuichi Otsuka[1], Atsuki Shinbori[1], Martin G Connors[2], Geoff Reeves[4], Charles Smith[3] (1.Institute for Space-Earth Environmental Research, 2.Athabasca Univ., 3.New Hampshire Univ., 4.Los Alamos National Laboratory)

[PEM19-P07] Modulation of Pc1 wave ducting by equatorial plasma bubbles

*Hyangpyo Kim[1], Kazuo Shiokawa[1], Jaeheung Park[2,3], Yoshizumi Miyoshi[1], Junga Hwang[2,3], Akira Kadokura[4] (1.Institute for Space-Earth Environmental Research, Nagoya University, Nagoya, Japan, 2.Korea Astronomy and Space science Institute, Daejeon, South Korea, 3.Korea University of Science and Technology, Daejeon, South Korea, 4.Space and Upper Atmospheric Sciences, National Institute of Polar Research, Tokyo, Japan)

[PEM19-P08] Modulation of energetic electron distribution caused by toroidal mode ULF waves in association with periodic enhancement of chorus emissions

Atsuhiro Ono[1], *Yuto Katoh[1], Mariko Teramoto[2], Atsushi Kumamoto[1], Fuminori Tsuchiya[1], Yoshiya Kasahara[3], Shoya Matsuda[4], Ayako Matsuoka[4], Satoshi Kasahara[5], Shoichiro Yokota[7], Kunihiro Keika[5], Takefumi Mitani[4], Tomoaki Hori[6], Yoshizumi Miyoshi[6], Iku Shinohara[4] (1.Department of Geophysics, Graduate School of Science, Tohoku University, 2.Kyutech, 3.Kanazawa University, 4.ISAS/JAXA, 5.The University of Tokyo, 6.Nagoya University, 7.Osaka Univ.)

[PEM19-P10] **Comparative study of magnetic field and ion flux variations in inner magnetosphere during magnetic storms using Arase observations and RAM-SCB simulations**

*Sandeep Kumar[1], Yoshizumi Miyoshi[1], Vania Jordanova[2], Ayako Matsuoka[3], Kazushi Asamura[3], Shoichiro Yokota[4], Satoshi Kasahara[5], Kunihiro Keika[5], Tomoaki Hori[1], Iku Shinohara[3] (1.ISEE, Nagoya University, Japan, 2.Los Alamos National Laboratory, USA, 3.ISAS/JAXA, Japan, 4.Osaka University, Japan, 5.University of Tokyo, Japan)

[PEM19-P11] **Observational study on mass and charge dependence of plasma energization in the inner magnetosphere and near-Earth magnetotail**

*Kunihiro Keika[1], Satoshi Kasahara[1], Shoichiro Yokota[2], Masahiro Hoshino[1], Kanako Seki[1], Takanobu Amano[1], Lynn M Kistler[3], Masahito Nose[4], Yoshizumi Miyoshi[4], Tomoaki Hori[4], Iku Shinohara[5] (1.Graduate School of Science, The University of Tokyo , 2.Graduate School of Science, Osaka University, 3.University of New Hampshire, 4.Institute for Space-Earth Environmental Research, Nagoya University, 5.Institute of Space and Astronautical Science, Japan Aerospace Exploration Agency)

[PEM19-P12] Improvement of detector response matrices of the high-energy electron experiments (HEP) onboard the Arase satellite

*Takefumi Mitani[1], PARK INCHUN[2], Tomoaki Hori[2], Takeshi Takashima[1], Satoshi Kasahara[3], Satoshi Kurita[2], Mariko Teramoto[4], Nana Higashio[1], Yoshizumi Miyoshi[2], Iku Shinohara[1] (1.Japan Aerospace Exploration Agency, 2.Nagoya University, 3.The University of Tokyo, 4.Kyushu Institute of Technology)

[PEM19-P13] Inter-channel normalization and energy spectrum correction of the high-energy electron experiments (HEP) onboard the Arase satellite

*Tomoaki Hori[1], Takefumi Mitani[2], Takeshi Takashima[2], InChun Park[1], Satoshi Kurita[1], Mariko Teramoto[3], Nana Higashio[4], Satoshi Kasahara[5], Shoichiro Yokota[6], Yoshizumi Miyoshi[1], Iku Shinohara[2] (1.Institute for Space-Earth Environmental Research, Nagoya University, 2.JAXA/ISAS, 3.Kyushu Inst. of Tech., 4.JAXA, 5.The Univ. of Tokyo, 6.Osaka Univ.)

[PEM19-P14] Evaluation of response characteristics of the XEP onboard the Arase spacecraft

*Kohei Ueda[1], Takefumi Mitani[2], Nana Higashio[3], Shoichiro Yokota[1], Takeshi Takashima[2], Yoshizumi Miyoshi[4], Iku Shinohara[2], Kentaro Terada[1] (1.Osaka University, 2.Japan Aerospace Exploration

Agency/Institute of Space and Astronautical Science, 3. Japan Aerospace Exploration Agency, 4.Nagoya University/Institute for Space-Earth Environment Research)

[PEM19-P15] The observational study for high energy particles below L=2.1 using Hisaki

*Kazuo Yoshioka[1], Ichiro Yoshikawa[1], Atsushi Yamazaki[2], Go Murakami[2], Hajime Kita[2], Fuminori Tsuchiya[3], Tomoki Kimura[4], Yoshizumi Miyoshi[5], Satoshi Kurita[5], Mariko Teramoto[6] (1.Graduate School of frontier Science, The University of Tokyo, 2.Institute of Space and Astronautical Science / Japan Aerospace Exploration Agency, 3.Planetary Plasma and Atmospheric Research Center, Graduate School of Science, Tohoku University, 4.Tohoku University, 5.Institute for Space-Earth Environmental Research, Nagoya University, 6.Kyushu Institute of Technology)

[PEM19-P16] Calibration of waveform data measured by the electric sensors on board the Arase satellite

*Yoshiya Kasahara[1], Hiroyuki Nishizawa[1], Shoya Matsuda[2], Hirotsugu Kojima[3], Fuminori Tsuchiya[4], Atsushi Kumamoto[4], Yasumasa Kasaba[4], Ayako Matsuoka[2] (1.Kanazawa University, 2.ISAS/JAXA, 3.Kyoto University, 4.Tohoku University)

[PEM19-P17] Machine learning classification of low frequency waves observed by Arase satellite

*Shun Amano[1], Taketoshi Miyake[1], Yoshiya Kasahara[2] (1.Toyama prefectural university , 2.Kanazawa university)

[PEM19-P18] Evaluation of Automatic Determined UHR Frequencies by a Convolutional Neural Network

*Shoya Matsuda[1], Tatsuhito Hasegawa[2], Atsushi Kumamoto[3], Fuminori Tsuchiya[3], Yoshiya Kasahara[4], Yoshizumi Miyoshi[5], Yasumasa Kasaba[3], Ayako Matsuoka[1], Iku Shinohara[1] (1.Institute of Space and Astronautical Science/Japan Aerospace Exploration Agency, 2.University of Fukui, 3.Tohoku University, 4.Kanazawa University, 5.Nagoya University)

Numerical simulation on energetic electron precipitations by chorus waves

*Yoshiki Ito[1], Shinji Saito[2], Yoshizumi Miyoshi[1]

1. Nagoya University, ISEE, 2. National Institute of Information ans Communications Technology

Whistler mode chorus waves cause scattering and acceleration of energetic electrons in the inner magnetosphere. The interaction processes have been modeled as a diffusive process. The pitch angle diffusion coefficients of the pitch angle scattering depend on the power of chorus waves so that the scattering rate also depends on the wave amplitude. On the other hand, several previous studies indicated that the Lorentz force by the wave magnetic field is larger than the mirror force if the wave amplitudes increase and the electron trajectories in the velocity space are different from the diffusive distributions. In this study, we investigate the chorus wave amplitude dependence of electron scattering using the GEMSIS-RBW simulation code. The RBW simulation demonstrates the generation of periodical rising-tone chorus waves propagating along a magnetic field line to higher latitudes and local pitch angle scattering by the imposed waves on the field line.
As the wave amplitude increases, the pitch angle of the electrons is scattered by the non-resonant interaction due to the influence of the wave magnetic field. We discriminate of resonant and non-resonant electron population, and investigate the amplitude dependence of precipitating electron counts for two populations. A positive correlation was found between the wave intensity and precipitating counts of resonant electron when the wave amplitudes are smaller than 10^-4 of the ambient magnetic fields..
When the wave intensity becomes large, precipitating counts of resonant electrons decrease. The parameter ρ (e.g., Saito et al., 2016) has used as a proxy to discriminate different interaction processes among diffusion, phase trapping and dislocation. Note that a positive correlation between the wave intensity and precipitating counts of resonant electrons are violated despite of small ρ (<1), i.e., diffusive interactions. Simultaneously, precipitating counts of non-resonant electrons increases, indicating that non-resonant interactions contribute to precipitation of electrons.

©2020. Japan Geoscience Union. All Right Reserved.

A pipeline for comprehensive tracking of pulsating patches in All-Sky Imager data

*Riku Nomiyama[1], Yoshizumi Miyoshi[2], Kohei Toyama[2], Yasunobu Ogawa[3], Keisuke Hosokawa[4], Terumasa Tokunaga[1]

1. Kyushu Institute of Technology, 2. Institute for Space-Earth Environmental Research, Nagoya University, 3. National Institute of Polar Research, 4. Department of Communication Engineering and Informatics, University of Electro-Communications

Pulsating aurora is a type of diffuse aurora with quasi-periodic variations in intensity. It is characterized as multiple on-off switching patches with a typical horizontal size from 10 to 200 km. The pulsating aurora is caused by intermittent precipitations of a few –tens keV electrons. With the development of auroral optical observations based on All-Sky Imager (ASI) system, it is expected to elucidate long-term variations, detailed spatiotemporal properties of pulsating aurora, including size evolutions, dominant frequencies, drift velocities, life times.

However, quantifications of comprehensive spatiotemporal properties of pulsating aurora are formidable task due to increasing amount of ASI data. In addition, an existence of non-pulsating background diffuse auroras often makes it difficult to identify individual patches. Hence, it is important to establish a fundamental technique for tracking multiple pulsating patches in ASI data undisturbed background arcs.

In this study, we built a new pipeline for comprehensive tracking of multiple pulsating patches over video sequences of the ASI. The process consists of three distinct steps: (i) extraction of pulsating patches to distinguish them from non-pulsating background arcs, (ii) segmentation individual patches over spatiotemporal domain and (iii) linking segmented regions lined up in time direction. The extraction step is carried out by a spatiotemporal filtering called Eulerian Video Magnification. This technique amplifies periodic color variations in a given temporal frequency band of interest. Since pulsating patches periodically switches in a characteristic frequency, we can successfully amplify them by selecting an appropriate frequency band. In the segmentation step, we apply a simple thresholding image binarization technique for each sequence over time. Then, we link identical patches by applying Hough transformation for identifying lines from a 3D point-cloud which describes centroid positions of segments in a spatiotemporal domain. This step is done under the assumption that an identical pulsating patch drifts roughly in a same direction affected by the global magnetospheric convection.

We examined the performances of our tracking pipeline using the WATEC ASI data obtained at Tromso, Norway. The exposure time of the WATEC ASI is second. In a visual inspection, our method successfully tracked noticeable pulsating patches in spite of the existence of background arcs. In the presentation, we demonstrate the tracking results showing trajectories of pulsating patches. Further, we will discuss some technical issues to be overcome for comprehensive tracking of pulsating patches. Moreover, we will discuss the MLT and geomagnetic activity dependence of the derived patch motions of the pulsating aurora.

Keywords: pulsating aurora, aurora all-sky imager, automatic tracking, Video Magnification

©2020. Japan Geoscience Union. All Right Reserved.

Estimation of precipitating electron energy of pulsating aurora by multiwavelength aurora optical observation

*Kohei Toyama[1], Yoshizumi Miyoshi[1], Satoshi Kurita[1], Keisuke Hosokawa[2], Yasunobu Ogawa[3], Shin-ichiro Oyama[1], Satonori Nozawa[1]

1. Institute for Space-Earth Environmental Research, Nagoya University, 2. Department of Communication Engineering Informatics,Univarsity Electro-Communications, 3. National Institute of Polar Research

Pulsating aurora (PsA) is a type of diffuse aurora that is mainly observed from post-midnight to the morning sectors during the recovery phase of substorms. PsA is characterized by quasi-periodic intensity modulation with ~2 -20 s intervals as a main modulation. The main modulation includes an internal modulation of about 1.5 to 3 Hz called an internal modulation.Mainly Electrostatic Cyclotron Harmonic (ECH) waves and whistler-mode waves cause the pitch angle scattering of energetic electrons in the magnetosphere, and PsA is generated by the precipitating electrons with high energy of several to 100 keV. In particular, the whistler-mode chorus waves play the role. The lower-band chorus (LBC) causes an electron precipitation of more than several keV, and the upper-band chorus causes steady precipitation of less than 1 keV. Estimations of the precipitating electron energy of the pulsating aurora from the ground-based observations have been performed. Ono et al.[1993] observed the emission intensities of a nitrogen molecule ion at 427.8 nm emission line and an oxygen atom at 844.6 nm emission line using a photometer, and estimated the energy of the precipitating electron by combining the ratio of the two emission intensities and the model calculation. However, Ono et al.[1993] conducted observations using narrow-field instrument, and the energy estimation by observation using an all-sky camera has not been performed. In Tromso, Norway, several high-sensitivity EMCCD cameras have been installed, which have been simultaneously observing the all-sky image of the emission intensity of sky image of the emission intensity of the 427.8 nm emission line and the 844.6 nm emission line at a sampling frequency of 10 Hz. In addition, a five-wavelength photometer that can observe the emission intensity of the emission lines at 427.8 nm and 844.6 nm in the magnetic zenith direction is also operated. In this study, we compared the data of the photometer and the EMCCD cameras installed in Tromso, and evaluated the sensitivity of the cameras. In addition, we estimated the precipitating electron energy of the pulsating aurora by compering emission intensity ratio of the two emission lines using the all-sky image reflecting the sensitivity evaluation results and the emission intensity calculation results obtained by the GLOW model[Solomon, 2017]. In this presentation, we report the results of the two-dimensional spatial distribution of the estimated precipitating electron energy. Moreover, we discuss the possible errors of the estimated energy.

Keywords: pulsating aurora, precipitating electron energy

©2020. Japan Geoscience Union. All Right Reserved.

Observation plan of pulsating aurora by the multi-spectral auroral camera on the LAMP rocket

Naoshi Yagi[1], *Takeshi Sakanoi[1], Miki Kawamura[1], Kazushi Asamura[2], Yoshizumi Miyoshi[3], Keisuke Hosokawa[4], Sarah L Jones[5], Marc Lessard[6]

1. Planetary Plasma and Atmospheric Research Center, Graduate School of Science, Tohoku University, 2. ISAS/JAXA, 3. ISEE, Nagoya University, 4. Graduate School of Informatics and Engineering, The University of Electro-Communications, 5. Goddard Space Flight Center, NASA, 6. University of New Hampshire

We are developing the multi-spectral auroral imager (AIC2) installed on the LAMP rocket. We report the current status of development and future plan of AIC2. Chorus waves generated in the magnetospheric equatorial region are thought to cause the pitch angle scattering of electrons in a wide energy range (several keV –1 MeV or more). Therefore, a correlation between pulsating aurora and microbursts is expected. However, there is no simultaneous observation between them. The LAMP rocket aims to carry out simultaneous observation of pulsating aurora and microbursts with comprehensive instrument of plasma particles, magnetic fields, and optical imaging to reveal the mechanism. This rocket is scheduled to be launched at Poker Flat Research Range in December 2020. The project PI is Dr. Sarah L, Jones of NASA/GSFC, and instruments measuring thermal electrons, low energy electrons, intermediate energy electrons and magnetic field are provided from institutes in US, and the instrumental package called PARM2 (Pulsating AuRora and Microburst 2) is proved by the Japanese team.
AIC2 consists of two CMOS detectors AIC-S1 and S2 and an electrics AIC-E, and will perform simultaneous auroral imaging at two wavelengths. We adopted the consumer CMOS camera ZWO ASI183MM for detector. Compared with the detector of AIC on the Rocksat-XN rocket launched last year, we improved 5 times lower noise (3.6 e-RMS) and 16 times wider dynamic range (12 bit A/D) in sampling at the detector. AIC-S1 targets the E region N2 aurora with an interference filter (Andover, CW 670 nm, FWHM 20 nm) and an objective lens (SpaceCom JF17095M, f = 17 mm, F/0.95, field of view 29 deg x 29 deg). AIC-S2 is designed for F-regin O 844.6 nm aurora with an interference filter (Andover, CW 846.1 nm, FWHM 4.4 nm) and an objective lens (SpaceCom HF3.5M-2, f = 3.5mm, F/1.6, field of view 106 deg x 106 deg). To gain S/N and reduce data size, binning is performed for original 3660 pix x 3600 pix image, and a 60 bin x 60 bin image is produced for each frame. AIC2 is mounted on a despun platform to cancel a rocket spin. Combining the despun platform with rocket attitude control, AIC-S1 will point to the magnetic footprint to perform simultaneous observation between fine structure of pulsating aurora and precipitating electrons. AIC-S2 will point west and cover the wide area from the rim of the earth to nadir, and obtain the height profile of O 844.6 nm emission as well as the pulsating auroral distribution in the wide range. The time resolution is 10 frame/s. At the apex altitude (~ 450km), the spatial resolution at nadir is 3.0 km x 3.0 km for AIC-S1 (E-region), and 6.3 km x 6.3 km for AIC-S2 (F-region). The AIC-E consists of two NanoPi M4 board computers, custom FPGA, power supply, and signal processing electronics to handle a large amount of image data generated from two cameras. We also newly developed a heat pipe to cool the heat generated at two CPUs of NanoPi M4.
On the development of AIC2, we carried out the electrical interface test between AIC-S1, S2 and AIC-E from September 2019 to this February, and confirmed the data acquisition with 10 frame/s, image binning and data communication. We also made the calibration test with the integrated sphere in NIPR in June and August 2019, and estimated the dynamic ranges of AIC-S1 and S2 to be 0.27-3100 kR and 2.2-27000 kR, with the resolutions of 48 R/bit and 410 R/bit, respectively, in the case with a gain of 450. In addition, we conducted a data communication test using a despun table with slip ling connector that is almost similar to the flight model in March 2019. We confirmed that that the data communication via the

©2020. Japan Geoscience Union. All Right Reserved.

slip ring works as expected if we use a differential signal interface, and shielded and twist-pair cables. By July 2020, we will perform environmental tests, such as vacuum, temperature and vibration tests, in Japan, and interface test with the flight model despun table is planned at the University of New Hampshire.

Keywords: pulsating aurora, development, rocket, microburst, optics

©2020. Japan Geoscience Union. All Right Reserved.

Statistical study of EMIC waves and energetic electron precipitation: ground-based magnetometer and subionospheric VLF/LF radio measurements at subauroral latitude

*Asuka Hirai[1], Fuminori Tsuchiya[1], Takahiro Obara[1], Yasumasa Kasaba[1], Yuto Katoh[2], Hiroaki Misawa[1], Kazuo Shiokawa[3], Yoshizumi Miyoshi[3], Satoshi Kurita[3], Chae-Woo Jun[3], Martin G Connors[4]

1. Planetary Plasma and Atmospheric Research Center, Graduate School of Science, Tohoku Univ. , 2. Department of Geophysics, Graduate School of Science, Tohoku University, 3. Institute for Space-Earth Environmental Research, Nagoya University, 4. Athabasca University

Electromagnetic ion cyclotron (EMIC) waves are observed as Pc1-2 pulsations in the Earth’s magnetosphere. These waves are excited due to the temperature anisotropy of ring current ions near the magnetic equator, and scatter the pitch angle of relativistic electrons through cyclotron resonance. This process causes the precipitation of high-energy electrons into the atmosphere, and is considered as one of the mechanisms to cause the loss of the outer radiation belt. There are two major questions left in this scenario. One is the amount of the contribution from the EMIC waves to the overall loss of radiation belt electrons. Another one is the conditions favorable to pitch angle scattering.
We performed a statistical study of EMIC waves associated with electron precipitations from November 2016 to December 2018. EMIC waves were observed by ground-based magnetometers installed at Athabasca, Canada (54.6˚N, 246.7˚E, L=4.3), which are operated by the PWING (‘study of dynamical variation of Particles and Waves in the INner magnetosphere using Ground-based network observations’) project. We used an automatic detection algorithm based on Bortnik et al. (2007) to identify EMIC wave events. Electron precipitation events were identified from the VLF radio waves propagating from transmitters at NDK, US (25.2kHz, 46.37˚N, 261.47˚E) and NLK (24.8kHz, 48.20˚N, 238.08˚E) to the receiver installed at Athabasca. Since these transmitted VLF waves are sensitive to ionization changes in the lower ionosphere, they are modulated when electrons with energies of > 100 keV precipitate above the propagation paths of VLF radio waves. In order to detect the electron precipitation events caused by EMIC waves, we identified the decreases in the amplitude of VLF signals temporally corresponding with the appearance of EMIC waves by visual inspection. In the period of analysis, we identified 999 EMIC wave events, and found 23 events clearly associated with electron precipitations. While total EMIC waves had higher occurrence rates in the dawn sector than in the dusk sector, most of the EMIC waves accompanied by electron precipitation occurred in the dusk sector during substorms. Theoretical study suggests that resonance energies of electrons interacting with EMIC waves decrease in the region of high plasma density (e.g. Summers and Thorne, 2003). Inside the plasmasphere, the resonant energy becomes down to several hundred keV. From statistical analysis and theoretical considerations, we suggestthat the ring current protons are injected inside the duskside plasmapause during substorms and excite EMIC waves in the high plasma density regions. These EMIC waves are likely to scatter relativistic electrons with energies from several hundred keV to a few MeV.

Keywords: EMIC waves, electron precipitation

©2020. Japan Geoscience Union. All Right Reserved.

First simultaneous observation of the isolated proton aurora at subauroral latitudes by a highly sensitive all-sky camera and the Van Allen Probes satellite

*Kohki Nakamura[1], Kazuo Shiokawa[1], Yuichi Otsuka[1], Atsuki Shinbori[1], Martin G Connors[2], Geoff Reeves[4], Charles Smith[3]

1. Institute for Space-Earth Environmental Research, 2. Athabasca Univ., 3. New Hampshire Univ., 4. Los Alamos National Laboratory

Isolated Proton Aurora (IPA) is the spotted aurora extending east and west at subauroral latitudes produced by energetic proton precipitation. Proton auroras are produced by energetic protons precipitating from the magnetosphere through charge-exchange collisions with atmospheric particles in the ionosphere. From previous studies, IPA has been considered to be generated by electromagnetic ion cyclotron (EMIC) waves which can scatter the pitch angle of energetic protons into the loss cone. However, simultaneous observation of IPA and its source plasma and electromagnetic fields in the magnetosphere has never been done before. Because EMIC waves are a key component contributing to the rapid loss of radiation-belt particles into the atmosphere, it is important to understand the mechanisms of EMIC wave-particle interaction. In the present study, we studied simultaneous observation events of EMIC-associated IPAs by ground all-sky camera at Athabasca and plasma and electromagnetic fields in the magnetosphere by the Van Allen Probes satellite. The EMIC waves were observed by the Van Allen Probes satellite at ~5:30 UT when the footprint of the satellite passed over an IPA on March 16, 2015. Proton flux from 5 eV to 20 keV observed by HOPE onboard the satellite increased rapidly at the time when satellite crossed the IPA. Electron flux at energies of ~500 eV also increased. The proton temperature anisotropy was 1.5-2.5 during the arc crossing. In addition, electron density observed by EMFISIS decreased from 4:20 UT to 6:20 UT, indicating that the IPA crossing was near the plasmapause. Electric field observed by EFW had no characteristic fluctuation associated with the IPA crossing. We will discuss these observations in relation to the possible IPA generation mechanisms.

Keywords: Isolated Proton Aurora, Electromagnetic Ion Cyclotron Wave, Inner Magnetosphere, Van Allen Probes Satellite

©2020. Japan Geoscience Union. All Right Reserved.

Modulation of Pc1 wave ducting by equatorial plasma bubbles

*Hyangpyo Kim[1], Kazuo Shiokawa[1], Jaeheung Park[2,3], Yoshizumi Miyoshi[1], Junga Hwang[2,3], Akira Kadokura[4]

1. Institute for Space-Earth Environmental Research, Nagoya University, Nagoya, Japan, 2. Korea Astronomy and Space science Institute, Daejeon, South Korea, 3. Korea University of Science and Technology, Daejeon, South Korea, 4. Space and Upper Atmospheric Sciences, National Institute of Polar Research, Tokyo, Japan

Pc1 waves generally propagate along the ambient magnetic field in the magnetosphere, but turn to oblique or perpendicular directions when they reach the ionosphere. If the waves are continuously observed over a wide latitudinal range, they can be considered as ducting waves. Ducting Pc1 waves can be attenuated by various physical processes such as absorption, scattering, and leakage as they propagate away from the injection region, and the sustainability of wave ducting depends on the ionospheric condition such as conductivity and plasma density. An earlier study from Kim et al. (2018) from the Swarm observations suggested that plasma density variations can affect Pc1 wave propagation within the ionosphere, i.e., wave attenuation can be controlled by electron density structure of the ionosphere. This finding, however, is not yet sufficient to fully elucidate density dependence of wave propagation, because they did not consider wave source variations, and did not discuss in detail possible inter-satellite differences of the wave intensity and electron density observed by the Swarm-A and Swarm-C, which fly in a tight formation.

In this study, we present remarkable relationship between ducting Pc1 wave and electron density based on the Swarm satellites. We show two ducting Pc1 events propagating across equatorial plasma bubbles (EPBs) that occurred on 7 April 2016 and on 27 September 2017. From the observations, we found that the EPBs modulate the Pc1 wave propagation by setting up boundaries and holes in the ionospheric waveguide, which can cause wave reflection and leakage. We also found that changes of Pc1 wave intensities generally follow the electron density variation, and that the intensity is stronger at high-density region than relatively low-density region. From the comparison between Swarm-A and Swarm-C observations, we conclude that ionospheric plasma plays a vital role in Pc1 waveguide even though their density becomes significantly low in EPBs.

Keywords: Pc1 wave, ducting, equatorial plasma bubble, Swarm, Ionospheric Alfven Resonator

©2020. Japan Geoscience Union. All Right Reserved.

Modulation of energetic electron distribution caused by toroidal mode ULF waves in association with periodic enhancement of chorus emissions

Atsuhiro Ono[1], *Yuto Katoh[1], Mariko Teramoto[2], Atsushi Kumamoto[1], Fuminori Tsuchiya[1], Yoshiya Kasahara[3], Shoya Matsuda[4], Ayako Matsuoka[4], Satoshi Kasahara[5], Shoichiro Yokota[7], Kunihiro Keika[5], Takefumi Mitani[4], Tomoaki Hori[6], Yoshizumi Miyoshi[6], Iku Shinohara[4]

1. Department of Geophysics, Graduate School of Science, Tohoku University, 2. Kyutech, 3. Kanazawa University, 4. ISAS/JAXA, 5. The University of Tokyo, 6. Nagoya University, 7. Osaka Univ.

Whistler-mode chorus emissions play significant roles in the acceleration and the loss of energetic electrons in the terrestrial magnetosphere. Previous studies revealed that chorus emissions satisfy the cyclotron resonance condition with electrons in the wide ranges of the kinetic energy and pitch angle and cause the periodic precipitations of energetic electrons into the atmosphere through wave-particle interactions, contributing to diffuse and pulsating auroras [e.g. Nishimura et al., 2010, S. Kasahara et al., 2018a]. While the mechanism controlling the periodicity of the chorus wave generation is one of essential problems unsolved in the magnetospheric physics, the roles of ULF waves have been discussed in several decades. In the present study, we analyze substorm-related toroidal mode ULF waves, chorus emissions, and energetic electrons simultaneously observed by the ERG satellite, and propose a model explaining how toroidal mode waves modulate energetic electrons. We focus on the event observed from 21:30 UT to 22:00 UT on March 27, 2017, the recovery phase of the CIR-driven storm. The ERG satellite traversed in the dawn sector of the ring current region, where the range of L-value was from 6.3 to 5.9, the magnetic local time from 04:00 to 04:12, and the magnetic latitude from -12.7 to -7.4 degrees during the analyzed event. From the observations of the Onboard Frequency Analyzer (OFA) of the Plasma Wave Experiment (PWE), the Magnetic Field Experiment (MGF), the Medium-energy particle experiments - electron analyzer (MEP-e) and the High-energy electron experiments (HEP), we find one-to-one correspondence among chorus emissions, toroidal mode ULF waves, and energetic electrons in the energy range 35-60 keV. We estimate the resonant energy to be about 30-300 keV, considering the first-order cyclotron resonance condition under the parameters determined based on the observations of the High Frequency Analyzer (HFA) and the OFA of the PWE and the MGF. Based on the results of analysis, we suggest that the intensity variations of chorus emissions are caused by the modulations of energetic electrons. The intensity of chorus emissions enhances at the timings when the toroidal component of the wave magnetic field has a peak in the westward direction as well as the enhancement of the flux and the temperature anisotropy of energetic electrons. From the observed phase relationship between the wave magnetic field of the ULF waves and the modulations of energetic electrons, it is expected that the locations corresponding to the wave phases when the flux enhancement (depletion) are expected to be the dense (sparse) region due to the concentration (divergence) of the E×B drift velocity between the wave electric field of the ULF waves and the ambient magnetic field. The azimuthal wave number and the wavelength of the observed ULF waves are estimated to be about 49-120 and 2000-4900 km, respectively, assuming that modulated energetic electrons satisfy the drift resonance condition with the ULF waves. The estimated m-numbers correspond to those reported as Transient Toroidal Waves [e.g. Takahashi et al., 1996], rather than the typical values of externally generated toroidal mode ULF waves observed in the inner magnetosphere.

Keywords: ULF waves, whistler-mode chorus, energetic electrons, inner magnetosphere

©2020. Japan Geoscience Union. All Right Reserved.

©2020. Japan Geoscience Union. All Right Reserved.

Comparative study of magnetic field and ion flux variations in inner magnetosphere during magnetic storms using Arase observations and RAM-SCB simulations

*Sandeep Kumar[1], Yoshizumi Miyoshi[1], Vania Jordanova[2], Ayako Matsuoka[3], Kazushi Asamura[3], Shoichiro Yokota[4], Satoshi Kasahara[5], Kunihiro Keika[5], Tomoaki Hori[1], Iku Shinohara[3]

1. ISEE, Nagoya University, Japan, 2. Los Alamos National Laboratory, USA, 3. ISAS/JAXA, Japan, 4. Osaka University, Japan, 5. University of Tokyo, Japan

Understanding the physical processes that control the dynamics of energetic particles in the inner magnetosphere is important for both space-borne and ground-based assets essential to the modern society. The storm time distribution of ring current ions in the inner magnetosphere depend strongly on their transport in evolutions of electric and magnetic fields along with acceleration and loss. In this study, we compare the magnetic field and ion flux (H^+, He^+, and O^+) variations during geomagnetic storms using Arase observations with the self-consistent inner magnetosphere model: **R**ing current **A**tmosphere interactions **M**odel with **S**elf **C**onsistent magnetic field (RAM-SCB). We investigate evolutions of ambient magnetic field taken from Arase MGF observations and RAM-SCB simulation during different phases of geomagnetic storms. Moreover, we compare pressure distributions of H^+, He^+ and O^+ from both the Arase LEPi/MEPi measurements and the RAM-SCB simulation to investigate which ions contribute the magnetic field deformation.

©2020. Japan Geoscience Union. All Right Reserved.

Observational study on mass and charge dependence of plasma energization in the inner magnetosphere and near-Earth magnetotail

*Kunihiro Keika[1], Satoshi Kasahara[1], Shoichiro Yokota[2], Masahiro Hoshino[1], Kanako Seki[1], Takanobu Amano[1], Lynn M Kistler[3], Masahito Nose[4], Yoshizumi Miyoshi[4], Tomoaki Hori[4], Iku Shinohara[5]

1. Graduate School of Science, The University of Tokyo , 2. Graduate School of Science, Osaka University, 3. University of New Hampshire, 4. Institute for Space-Earth Environmental Research, Nagoya University, 5. Institute of Space and Astronautical Science, Japan Aerospace Exploration Agency

The ion pressure in the Earth's inner magnetosphere is generally dominated by a few to a few 100s keV protons. Oxygen ions of ionospheric origin, O^+, can make a significant contribution to the ion pressure during geomagnetically active periods. Our previous study showedclear oxygen-proton differences in energy spectra in the outer part (L>5) of the ring current region. The results indicate the occurrence of mass-dependent or selective acceleration in the inner magnetosphere and/or near-Earth magnetotail. The present study extends analysis toward ions with different mass and/or charge states. We primarily use data from the MEP-i (Medium-Energy Particle experiments - ion mass analyzer) on board the Arase spacecraft, particularly when the Arase apogee was positioned on the night side during magnetic storms. MEP-i measures ions with energies of ~10 to 180 keV/q and distinguishes between different ion species.

Energy spectra of singly-charged ions (H^+, He^+, O^+) show mass dependence, with He^+ and O^+ having harder spectra than H^+. The spectral slope of doubly-charged ions (He^{++}, O^{++}) is steeper for H^{++} than O^{++}. For ions with the same mass, singly-charged ions show harder spectra than doubly-charged ones. The results indicate that energization processes in the near-Earth magnetotail are more dependent on mass than charge. This suggests that the ion energy gain in the magnetotail is not determined by a complete displacement across the global electric field potential only. An important factor is likely the limited spatial scale of the electric field associated with narrow flow channels during magnetic field reconfiguration (dipolarization), which has been reported comparable to gyro-radii of heavy ions.

Keywords: Ring current, Magnetic storms, Substorms and dipolarization, Ion composition, Arase

©2020. Japan Geoscience Union. All Right Reserved.

Improvement of detector response matrices of the high-energy electron experiments (HEP) onboard the Arase satellite

*Takefumi Mitani[1], PARK INCHUN[2], Tomoaki Hori[2], Takeshi Takashima[1], Satoshi Kasahara[3], Satoshi Kurita[2], Mariko Teramoto[4], Nana Higashio[1], Yoshizumi Miyoshi[2], Iku Shinohara[1]

1. Japan Aerospace Exploration Agency, 2. Nagoya University, 3. The University of Tokyo, 4. Kyushu Institute of Technology

The high-energy electron experiments (HEP) onboard the Arase satellite detects 70 keV-2 MeV electrons and generates three-dimensional velocity distribution data for these electrons in every period of the satellite's rotation. Electrons are detected by two instruments, HEP-L and HEP-H, which differ in their geometric factor (G-factor) and energy range they cover. HEP-L detects 70 keV–1 MeV electrons with the G-factor of 9.3 $\times 10^{-4}$ cm^2 sr at maximum, while HEP-H observes 0.7 MeV–2 MeV electrons with the G-factor of 9.3 $\times 10^{-3}$ cm^2 sr at maximum. The instruments utilize silicon strip detectors and application-specific integrated circuits to read out incident charge signals from each strip.

In order to deduce the distribution of incident electrons from the direction and energy detections in orbit, we have developed a detector simulator using the Geant4 toolkit. Using the simulator, we calculate response matrices of the detectors and derive incident fluxes from the detected counts. The derived fluxes of electrons at around 100 keV are consistent with those observed by the medium-energy particle experiments - electron analyzer (MEP-e), which utilizes an electrostatic analyzer.

Recently, we have evaluated effects on detection efficiency caused by on-board signal processing. We found that the detection efficiency for higher energy electrons affected by parameters such as an energy threshold and readout noise, which are used to determine whether to read out the signal from the detector. We have updated the response matrices taking those parameters into account. In this presentation, we will present our calibration methods and their evaluation status. Especially, we will show a comparison before and after updating the matrices.

Keywords: Arase, high-energy electron

©2020. Japan Geoscience Union. All Right Reserved.

Inter-channel normalization and energy spectrum correction of the high-energy electron experiments (HEP) onboard the Arase satellite

*Tomoaki Hori[1], Takefumi Mitani[2], Takeshi Takashima[2], InChun Park[1], Satoshi Kurita[1], Mariko Teramoto[3], Nana Higashio[4], Satoshi Kasahara[5], Shoichiro Yokota[6], Yoshizumi Miyoshi[1], Iku Shinohara[2]

1. Institute for Space-Earth Environmental Research, Nagoya University, 2. JAXA/ISAS, 3. Kyushu Inst. of Tech., 4. JAXA, 5. The Univ. of Tokyo, 6. Osaka Univ.

Detailed evaluation of the relative efficiency of azimuthal channels and their dependence on the energy of incident electrons has been conducted for the high-energy electron experiments (HEP) onboard the Arase satellite since the start of the satellite operation. Recently the simulation model of the instrument response has been improved to consider a realistic threshold and noise level of the onboard electronics for triggering an event of electron incidence in the detector system. The updated simulation model brings out new response properties of the instrument which could significantly modify the incident energy dependence as well as the relative efficiency among azimuthal channels, particularly at high energy. Accordingly, science data products such as Level-2 electron differential flux data are also to be updated on the basis of newly deduced calibration parameters. We show how the new electron flux data and their angular distribution are compared to the previous versions. Comparison with flux data of the other electron instruments onboard shows the same level of consistency in flux value for the lower energy part, while there still remains some discrepancy in the MeV range.

©2020. Japan Geoscience Union. All Right Reserved.

Evaluation of response characteristics of the XEP onboard the Arase spacecraft

*Kohei Ueda[1], Takefumi Mitani[2], Nana Higashio[3], Shoichiro Yokota[1], Takeshi Takashima[2], Yoshizumi Miyoshi[4], Iku Shinohara[2], Kentaro Terada[1]

1. Osaka University, 2. Japan Aerospace Exploration Agency/Institute of Space and Astronautical Science, 3. Japan Aerospace Exploration Agency, 4. Nagoya University/Institute for Space-Earth Environment Research

The extremely high-energy experiment (XEP) onboard the Arase spacecraft was designed to measure 0.4-20MeV electrons. Electrons are detected by five solid-state silicon detectors (SSDs) and a single-crystal inorganic scintillator of cerium-doped gadolinium orthosilicate (GSO). The SSDs detect 0.4-5.4MeV electrons and the GSO detects 6-20MeV electrons. While the XEP plays an important role in observing the main components of the radiation belt, its energy response has not been fully examined. In this study, we reproduced XEP geometry which is almost the same as the flight model and conducted an irradiation test using the Geant4 toolkit to examine its energy response in detail. The simulation results show how high energy electrons affect low energy bins. We have found that when high-energy electrons (about 5 MeV or more) are incident, the SSD detection area detects most of them as about 1.8-2.8 MeV. We have also performed a more accurate calibration of the observed data using the response function matrix obtained from the simulation. We will present pre- and post- calibration comparisons of observed data.

Keywords: Asase, XEP, Geant4

©2020. Japan Geoscience Union. All Right Reserved.

The observational study for high energy particles below L=2.1 using Hisaki

*Kazuo Yoshioka[1], Ichiro Yoshikawa[1], Atsushi Yamazaki[2], Go Murakami[2], Hajime Kita[2], Fuminori Tsuchiya[3], Tomoki Kimura[4], Yoshizumi Miyoshi[5], Satoshi Kurita[5], Mariko Teramoto[6]

1. Graduate School of frontier Science, The University of Tokyo, 2. Institute of Space and Astronautical Science / Japan Aerospace Exploration Agency, 3. Planetary Plasma and Atmospheric Research Center, Graduate School of Science, Tohoku University, 4. Tohoku University, 5. Institute for Space-Earth Environmental Research, Nagoya University, 6. Kyushu Institute of Technology

Hisaki is a low-altitude satellite with an orbital altitude of about 1000 km and an inclination of 30 degrees which is equivalent to 1.2-2.1 in L-value. Hisaki has been designed as an EUV spectroscope for observing Jupiter and other planets, but its photon-detector is also sensitive to radiation such as protons and electrons. In particular, electrons of more than 5 MeV and protons of more than 50 MeV can penetrate the shield of the instrument and reach the detector. Therefore, Hisaki can be used as a radiation monitor in the low altitude area (low L-value).

The Hisaki launched in November 2013 has been observing planets for more than 6 years. We have summarized the count rates caused by radiation and clarified that the trend is dependent on solar activity in orbital regions with L-values greater than 1.8. In addition, it was confirmed that the count increased several times with a timescale of several hours in response to solar activity like SEP. These phenomena were also captured by radiation monitors onboard the ISS in the orbital region of higher L-values (L>3) and were recognized as SEP particle injection. However, no clear observational evidence has been obtained for the behavior near L-value 2.

In this presentation, we will discuss the behavior of high-energy particle at various time constants in the low-altitude region around Earth.

Keywords: High energy particle, Hisaki, Low altitude

©2020. Japan Geoscience Union. All Right Reserved.

Calibration of waveform data measured by the electric sensors on board the Arase satellite

*Yoshiya Kasahara[1], Hiroyuki Nishizawa[1], Shoya Matsuda[2], Hirotsugu Kojima[3], Fuminori Tsuchiya[4], Atsushi Kumamoto[4], Yasumasa Kasaba[4], Ayako Matsuoka[2]

1. Kanazawa University, 2. ISAS/JAXA, 3. Kyoto University, 4. Tohoku University

The Plasma Wave Experiment (PWE) on board the Arase satellite measures electric field from DC to 10 MHz, and magnetic field from a few Hz to 100 kHz. The waveform capture (WFC) is one of subsystems of the PWE and is dedicated to measuring waveform for the two electric components and three magnetic field components. The WFC aims at detailed measurements of plasma waves in the VLF range such as chorus, hiss and lightning whistler, but it is necessary to be corrected for gain and phase according to the frequency responses of sensors and receivers. In particular, the electric field data needs to be corrected in consideration of the antenna impedance of the electric field sensor. The characteristics of the impedance strongly depend on the electron density and temperature at the observation point. We have been operating the onboard calibration system regularly, and the frequency response is statistically derived as a function of electron density. In the present study, we evaluated the frequency response by deriving the refractive indices of lightning whistlers or chorus emissions in two different ways; one from E/B ratio of the waveform data measured by the WFC and the other from dispersion relation of whistler mode wave.
First, we select the events when wave normal directions of chorus or lightning whistlers were almost parallel (< 30 degrees) against the ambient magnetic field. Second, we derive refractive indices by calculating the E/B ratio from the waveform data. On the other hand, we also derive the refractive indices theoretically by the dispersion relation of whistler mode wave using in situ cyclotron frequency, plasma frequency and wave normal direction. These refractive indices shall essentially match when the electric field is appropriately calibrated. In other words, we estimate the quantitative error of frequency response of electric sensor comparing the difference between them. In the present study, we report the current status of the calibration process and show the reliability of the waveform data in electric field after calibration.

Keywords: Arase, Whistler mode wave, electric field sensor, calibration

©2020. Japan Geoscience Union. All Right Reserved.

Machine learning classification of low frequency waves observed by Arase satellite

*Shun Amano[1], Taketoshi Miyake[1], Yoshiya Kasahara[2]

1. Toyama prefectural university , 2. Kanazawa university

Various types of low frequency waves are observed by Electric Field Detector (EFD) onboard Arase satellite. In this study, we are going to detect these low frequency waves from EFD data, and classify these waves into several types by using machine learning.Various types of low frequency waves are observed by Electric Field Detector (EFD) onboard Arase satellite. In this study, we are going to detect these low frequency waves from EFD data, and classify these waves into several types by using machine learning.
At first, we use SVM method to detect low frequency waves from 24 hour plots of EFD spectrum data. We tested several parameters of SVM, and detected low frequency waves with more than 96% accuracy ratio. We applied this SVM method to EFD spectrum data from 2017 to 2019, and succeeded in detecting 806 low frequency waves.
Next, we try to classify these detected low frequency waves into several types by clustering. We apply K-means method and hierarchical clustering method to the image data of EFD spectrum plot and the numerical data which are the duration time and the center frequency of the low frequency waves, respectively. Therefore, we found 5 types of low frequency waves with different characteristics.

Keywords: Magnetosphere, Arase science satellite, Machine learning

©2020. Japan Geoscience Union. All Right Reserved.

Evaluation of Automatic Determined UHR Frequencies by a Convolutional Neural Network

*Shoya Matsuda[1], Tatsuhito Hasegawa[2], Atsushi Kumamoto[3], Fuminori Tsuchiya[3], Yoshiya Kasahara[4], Yoshizumi Miyoshi[5], Yasumasa Kasaba[3], Ayako Matsuoka[1], Iku Shinohara[1]

1. Institute of Space and Astronautical Science/Japan Aerospace Exploration Agency, 2. University of Fukui, 3. Tohoku University, 4. Kanazawa University, 5. Nagoya University

The ambient electron density is one of the important properties of space plasma. Typical regions in the geospace is characterized by the different electron density profile (e.g., plasmasphere, plasma trough and plasma plume.) The most popular way to determine the quantitative electron density is observing the upper hybrid resonance (UHR) emission. The High Frequency Analyzer (HFA) and the Onboard Frequency Analyzer (OFA) is subsystems of Plasma Wave Experiment (PWE) aboard Arase [Miyoshi et al. (2018), Kasahara et al. (2018), Kumamoto et al. (2018), Matsuda et al. (2018)]. The HFA measures wide frequency range (0.1-10 MHz) electric power spectra with a time resolution of 1, 8 or 60 s. This covers a typical frequency range of UHR frequency in the inner magnetosphere. The OFA measures the electric field from DC to 20 kHz with a time resolution of 1 s and a good frequency resolution compared with the HFA.

A neural-network-based approach for the automatic detection of UHR frequencies is proposed by Zhelavskaya et al. (2016), using the local electron cyclotron frequency f_{ce}, orbital parameters (L and MLT), geomagnetic index (Kp), and observed electric field spectra. Recently, Hasegawa et al. (2019) proposed a technique for the automatic UHR frequency determination using convolutional neural network (CNN). They reported that the mean absolute error of the predicted UHR frequencies by the ResNet model was 3.664 bins when excluding additional inputs except for the observed electric field spectra observed by the Arase/PWE and labeled UHR frequency data. They also pointed out that additional features (orbital parameters and geomagnetic index) had almost no impact for the accuracy on the UHR frequency determined by CNN. In this study, we perform the further evaluations of the CNN-based UHR frequency determination from the point of view of science. We found that the error rate of the predicted UHR frequencies from the HFA spectra is less than 0.07 (7% of wave frequency) above 30 kHz. However, the error rate derived from the HFA spectra becomes worse when the wave frequency is below 10 kHz. We considered that this worsening shows a detection limit of UHR emissions due to the increasing of the noise level of the HFA receiver. On the other hand, the noise level in the overlapped frequency range (1-20 kHz) is smaller than the noise level of the HFA. We found that the error rate derived by the OFA spectra is better than the error rate derived from the HFA spectra in this frequency range. The best error rate was 0.07 at 8.41 kHz, while the error rate from HFA spectra was 27.7%.

Keywords: Convolutional Neural Network, Arase satellite, UHR frequency

©2020. Japan Geoscience Union. All Right Reserved.

[E] Poster | P (Space and Planetary Sciences)：P-EM Solar-Terrestrial Sciences, Space Electromagnetism & Space Environment

[P-EM20] Recent Advances in Ionosphere Observation and Modeling through New Observation Opportunities

convener:CHIYEN LIN(Center for Astronautical Physics and Engineering, National Central University, TAIWAN), Yen-Jung Wu(Space Sciences Laboratory, University of California, Berkeley), Yang-Yi Sun(China University of Geosciences), Charles Lin(Department of Earth Sciences, National Cheng Kung University)

Rapid developments in space technology are advancing our understanding of ionospheric space weather by increasing a great number of ground- and space-based observations over the recent decades. In the ground segment, the dense ground-based GNSS networks, radars, and airglow instruments have greatly extended the observational coverages. In the space segment, the extraordinary satellite missions, such as FORMOSAT-7/COSMIC-2, ESA-SWARM NASA-ICON and -GOLD, providing a variety of observations all over the world such as airglow, temperature, neutral winds, current, ion drifts, plasma density that contribute to the understanding of middle and upper atmospheric dynamics. Increasing ground based observations are also important for coordinations with these satellite missions.
With the large amount and diversity of datasets, theoretical and empirical models can be validated, and implemented for inclusion of new thermosphere and ionosphere phenomena. Furthermore, remarkable breakthrough of data assimilation techniques advances the ionosphere monitoring and forecast.
The purpose of this session is to solicit studies providing observations, theoretical and empirical modeling and data assimilation on the multiple scales of ionospheric phenomena, from global morphology to small-scale irregularities and traveling ionospheric disturbances. Studies from magnetically quiescent to storm conditions as well as influences from lower atmosphere will also be solicited.

[PEM20-P01] Compact Ionospheric Probe for CubeSat-based Science Missions

*Chi-Kuang Chao[1,2] (1.Graduate Institute of Space Science, National Central University, 2.Center for Astronautical Physics and Engineering, National Central University)

[PEM20-P02] Global Ion Density Distributions Observed by Advanced Ionospheric Probe Onboard FORMOSAT-5 Satellite

Pei-Cii Hong[1], *Chi-Kuang Chao[1,2] (1.Graduate Institute of Space Science and Engineering, National Central University, 2.Center for Astronautical Physics and Engineering, National Central University)

[PEM20-P03] Ionospheric responses on the 21 August 2017 solar eclipse by using three-dimensional GNSS tomography

*Chia-Hung Chen[1], Charles Lin[1], Akinori Saito[2], Mamoru Yamamoto[3], Susumu Saito[4] (1.Department of Earth Sciences, National Cheng Kung University, 2.Department of Geophysics, Graduate School of Science, Kyoto University, 3.Research Institute for Sustainable Humanosphere, Kyoto University, 4.Electronic Navigation Research Institute, National Institute of Maritime, Port, and Aviation Technology)

[PEM20-P04] Traveling Ionospheric Disturbances Triggered by Typhoon Hagibis (2019)

*Yu-Chen Cheng[1], Charles Lin[1], Shih-Ping Chen[1], Min-Yang Chou[2] (1.Department of Earth Science, National Cheng Kung University, Tainan, Taiwan, 2.COSMIC Program Office, University Corporation for Atmospheric Research Boulder, CO, USA)

[PEM20-P05] Study of Medium-Scale Traveling Ionospheric Disturbances in Low-Latitude Ionosphere Using an Automatic Algorithm

*Pin-Hsuan Cheng[1], Charles Lin[1], Hanli Liu[2] (1.Department of Earth Sciences, National Cheng Kung University, 2.University Corporation For Atmospheric Research)

[PEM20-P06] Short-term Variabilities of Wave-3 and 4 Structures in the Low-latitude Ionosphere

*Jia-Ting Lin[1], Charles Lin[1], CHIYEN LIN[2,3], P. K. Pedatella[1], Nicholas M Pedatella[4,5] (1.Department of Earth Sciences, National Cheng Kung University, Taiwan, 2.Center for Astronautical Physics and Engineering, National Central University, Taoyuan, Taiwan, 3.Graduate Institute of Space Science, National Central University, Taoyuan, Taiwan, 4.High Altitude Observatory, National Center for Atmospheric Research, Boulder, CO, USA, 5.COSMIC Program Office, University Corporation for Atmospheric Research, Boulder, CO, USA)

[PEM20-P07] Taiwan Radio Occultation Process System (TROPS) : Preliminary results of ionospheric products

*Wen-Hao Yeh[1], Cheng-Yung Huang[1], Kun-Lin Chen[1], Tzu-Pang Tseng[2], Hsu-Hui Ho[3], Jing-Mei Wu[4], Jyun-Ying Huang[3], Hsiu-Wen Li[4], Ching-Chieh Lin[3] (1.National Space Organization, National Applied Research Laboratories, Taiwan, 2.Geoscience Australia, Australia, 3.Taiwan Analysis Center for COSMIC, Central Weather Bureau, Taiwan, 4.GPS Science and Application Research Center, National Central University, Taiwan)

[PEM20-P08] GNSS observation of ionospheric variation due to perturbations near the Earth's surface

*Yang-Yi Sun[1] (1.China University of Geosciences (Wuhan))

[PEM20-P09] A multi-directional particle detector on HXMT

*Hong Guo Shen

[PEM20-P10] New observations of the total electron content over Ho Chi Minh City

*Tam Dao[1,2], Minh Huy Le[3], Brett A Carter[1], Que Le[2] (1.SPACE Research Centre, School of Science, RMIT University, Australia, 2.Department of Physics, International University, Vietnam, 3.Institute of Geophysics, Vietnam Academy of Science and Technology (VAST), Vietnam)

Compact Ionospheric Probe for CubeSat-based Science Missions

*Chi-Kuang Chao[1,2]

1. Graduate Institute of Space Science, National Central University, 2. Center for Astronautical Physics and Engineering, National Central University

Compact Ionospheric Probe (CIP) is an all-in-one ion sensor that can measure ion concentrations, velocity, or temperature in a time-sharing way. It is also capable of in-situ measuring ionospheric plasma density irregularities up to 1,024 Hz over a wide range of spatial scales. CIP is developed by National Central University (NCU) to occupy in a 0.7U form factor for CubeSat science missions. Currently NCU has completed all CIP design reviews and started production for sounding rocket and CubeSat missions. It is expected to be placed on a hybrid sounding rocket for a preliminary flight test at the middle of 2020 and then will be installed on INSPIRESat-1 and IDEASSat CubeSats for launch at the end of 2020. In this poster, CIP specifications will be outlined and some observations done by its predecessor, Advanced Ionospheric Probe onboard FORMOSAT-5 satellite, will also be presented.

Keywords: INSPIRESat-1, IDEASSat, CIP

©2020. Japan Geoscience Union. All Right Reserved.

Global Ion Density Distributions Observed by Advanced Ionospheric Probe Onboard FORMOSAT-5 Satellite

Pei-Cii Hong[1], *Chi-Kuang Chao[1,2]

1. Graduate Institute of Space Science and Engineering, National Central University, 2. Center for Astronautical Physics and Engineering, National Central University

A FORMOSAT-5 satellite has been launched on 25 August 2017 CST into a 98.28° inclination sun-synchronous circular orbit at 720 km altitude along the 1030/2230 local time sectors. The orbital coverage provides a great opportunity to survey terrestrial ionosphere from equatorial to polar region every two days. Advanced Ionospheric Probe (AIP) is a piggyback science payload developed by National Central University for the FORMOSAT-5 satellite to measure ionospheric plasma concentrations, velocities, and temperatures. It is also capable of measuring ionospheric plasma density irregularities at a sample rate up to 8,192 Hz over a wide range of spatial scales. In this poster, global ion density distributions observed by FORMOSAT-5/AIP in the pre-midnight sector can be averaged monthly and seasonally from in-situ measurement since November 2017. Wave-3 and wave-4 patterns are clearly detected from the distributions and varied with season and solar cycle. It is adversely indicated that FORMOSAT-5/AIP can provide high quality data to identify long-term ionospheric ion density variations.

Keywords: FORMOSAT-5, AIP

©2020. Japan Geoscience Union. All Right Reserved.

Ionospheric responses on the 21 August 2017 solar eclipse by using three-dimensional GNSS tomography

*Chia-Hung Chen[1], Charles Lin[1], Akinori Saito[2], Mamoru Yamamoto[3], Susumu Saito[4]

1. Department of Earth Sciences, National Cheng Kung University, 2. Department of Geophysics, Graduate School of Science, Kyoto University, 3. Research Institute for Sustainable Humanosphere, Kyoto University, 4. Electronic Navigation Research Institute, National Institute of Maritime, Port, and Aviation Technology

In this study, we study the ionospheric responses on the August 2017 solar eclipse event by using a three-dimensional tomography algorithm with the ground-based GNSS (global navigation satellite system) total electron content observations around the Northern America. This three-dimensional ionospheric electron density structure from the tomography can provide us more information regarding to how the density variations and propagations are. Results show that the ionospheric electron density depletion triggered by the solar eclipse is distributed to all the altitudes. The most electron density depletion is around 40% compared with the previous day of solar eclipse. We further conduct a procedure of Fourier analyses to derive the vertical phase and group velocities of the electron density propagations. Results show that the opposite directions of the vertical phase and group velocities around 300 km altitude imply the energy source by the solar eclipse.

Keywords: ionospheric GNSS tomography, August 2017 solar eclipse

©2020. Japan Geoscience Union. All Right Reserved.

Traveling Ionospheric Disturbances Triggered by Typhoon Hagibis (2019)

*Yu-Chen Cheng[1], Charles Lin[1], Shih-Ping Chen[1], Min-Yang Chou[2]

1. Department of Earth Science, National Cheng Kung University, Tainan, Taiwan, 2. COSMIC Program Office, University Corporation for Atmospheric Research Boulder, CO, USA

The tropospheric severe weather system could affect the ionospheric plasma structure through triggering vertical propagating gravity wave disturbances. By analyzing receiving signals from Global Position System (GPS), we calculate the total electron content (TEC) to observe the corresponding ionosphere variations triggered by the severe weather events. On 11 October 2019, a series of traveling ionospheric disturbances (TIDs) generated by a strong typhoon Hagibis was observed in the ionosphere over Japan region. Over the central Japan, concentric TIDs (CTIDs) signature with periods 10-25 min, phase velocity 277.8m/s characters were observed. Over the Hokkaido area, north of the typhoon, another TIDs with the south-westward propagation was also observed. It has the concentric gravity wave characteristics of 10-25 min period and 500 km radius at 200 km altitude traveling for 103 minutes. Although the TIDs at the north has the characteristics of concentric gravity wave, it also has the property of medium scale TIDs (MSTIDs).

Keywords: ionosphere, gravity wave, MSTID, typhoon

©2020. Japan Geoscience Union. All Right Reserved.

Study of Medium-Scale Traveling Ionospheric Disturbances in Low-Latitude Ionosphere Using an Automatic Algorithm

*Pin-Hsuan Cheng[1], Charles Lin[1], Hanli Liu[2]

1. Department of Earth Sciences, National Cheng Kung University, 2. University Corporation For Atmospheric Research

This study investigates the medium–scale traveling ionospheric disturbances (MSTIDs) and plasma bubbles statistically at the low–latitude equatorial ionization anomaly (EIA) region. To distinguish and categorize the MSTID and plasma bubble features, we apply both the three–dimensional fast Fourier transform (3D–FFT) and support vector machine. Statistical results together with COSMIC–1 RO data and the high–resolution Whole Atmosphere Community Climate Model (WACCM) indicate the following characteristics. First, the southward (equatorward) MSTIDs are observed almost every evening and morning during spring and winter. On the contrary, southward MSTIDs are more discernible at midnight in summer, majorly propagate from Japan, but least observed in autumn. Second, northward (poleward) MSTIDs are detected more frequently from noon to midnight in spring and summer with secondary occurrence rate peak in spring likely caused by atmospheric gravity waves (AGWs). Third, the occurrence rates of equatorial plasma bubbles in descending order are Spring, Fall, Summer, and Winter.

Keywords: Poleward MSTID, Plasma Bubble, Machine Learning, Atmospheric Gravity Waves

©2020. Japan Geoscience Union. All Right Reserved.

Short-term Variabilities of Wave-3 and 4 Structures in the Low-latitude Ionosphere

*Jia-Ting Lin[1], Charles Lin[1], CHIYEN LIN[2,3], P. K. Pedatella[1], Nicholas M Pedatella[4,5]

1. Department of Earth Sciences, National Cheng Kung University, Taiwan, 2. Center for Astronautical Physics and Engineering, National Central University, Taoyuan, Taiwan, 3. Graduate Institute of Space Science, National Central University, Taoyuan, Taiwan, 4. High Altitude Observatory, National Center for Atmospheric Research, Boulder, CO, USA, 5. COSMIC Program Office, University Corporation for Atmospheric Research, Boulder, CO, USA

In this study, the day-to-day variabilities of wavenumber-3 and 4 longitudinal structures in the ionosphere after the launch of FORMOSAT-7/COSMIC-2 (F7/C2) in July 2019 is investigated using the Global Ionosphere Specification (GIS). The GIS is based on implementation of assimilating 1500-1800 F7/C2 radio occultations (ROs) per day, in conjunction with ground-based global positioning system (GPS) TEC measurements with international reference ionosphere providing background electron density information. The most prominent components of wavenumber-3 and 4, the eastward propagating nonmigrating diurnal tide with zonal wavenumber 3 (DE3), diurnal eastward propagating nonmigrating tide with zonal wavenumber 2 (DE2), and stationary planetary wave 3 and 4 are examined. The results reveal that wave-3 and 4 tidal amplitudes change of 2-4 TECu (represent ~15-25% in background TEC value) regularly occur on very short timescales (~1–2 days) at the equatorial ionosphere anomaly (EIA) crests, it could be considered as the modulation of the E region dynamo. The strong asymmetries of wavenumber 4 occur around the maxium amplitude of the whole period in October, which implies the in-situ effects due largely to meridional neutral winds. Further, to investigate their relationship to the tidal wind field of this hypothesis, these results are compared to the Whole Atmosphere Community Climate Model (WACCM) using the Data Assimilation Research Testbed (DART).

Keywords: longitudinal structure in ionosphere, wavenumber-3 and 4, short-term variabilities of tides

©2020. Japan Geoscience Union. All Right Reserved.

Taiwan Radio Occultation Process System (TROPS) : Preliminary results of ionospheric products

*Wen-Hao Yeh[1], Cheng-Yung Huang[1], Kun-Lin Chen[1], Tzu-Pang Tseng[2], Hsu-Hui Ho[3], Jing-Mei Wu[4], Jyun-Ying Huang[3], Hsiu-Wen Li[4], Ching-Chieh Lin[3]

1. National Space Organization, National Applied Research Laboratories, Taiwan, 2. Geoscience Australia, Australia, 3. Taiwan Analysis Center for COSMIC, Central Weather Bureau, Taiwan, 4. GPS Science and Application Research Center, National Central University, Taiwan

Taiwan Radio Occultation Process System (TROPS) is a Taiwan-built data process system has developed by National Space Organization (NSPO), Taiwan Analysis Center for COSMIC (TACC), and GPS Science and Application Research Center (GPSARC). Presently, TROPS is used for data processing of FORMOSAT-7/COSMIC-2 (F-7/C-2) mission, which contains six low Earth orbit (LEO) satellites and launched in late June, 2019. F-7/C-2 is the follow on mission of FORMOSAT-3/COSMIC (F-3/C) mission, which also contains six LEO satellites to receive GPS signal for RO observation. F-3/C mission can provide around 1000 electron density profiles of ionosphere. F-7/C-2 mission can provide around 2000 electron density profiles of ionosphere due to F-7/C-2 satellites not only receive GPS signal but also GLONASS signal. In this study, the data performance and the validation results of preliminary ionospheric retrieve results of TROPS for F-7/C-2 will be presented.

Keywords: Radio Occtultation, FORMOSAT-7/COSMIC-2, Taiwan Radio Occultation Process System

©2020. Japan Geoscience Union. All Right Reserved.

GNSS observation of ionospheric variation due to perturbations near the Earth’s surface

*Yang-Yi Sun[1]

1. China University of Geosciences (Wuhan)

Both solar activity (e.g. solar flare, coronal mass ejection, and moon shadow) and perturbations from the lower atmosphere (e.g. cyclone, walker circulation, and El Niño - Southern Oscillation) and ground (e.g. earthquake, tsunami, and volcanic eruption) change the ionospheric structure. The ground- and space-based Global Navigation Satellite System (GNSS) is a powerful technique for capturing atmospheric variabilities in both horizontal and vertical directions at various altitudes, that help us to seek a deeper understanding of the solar-terrestrial environment. Other than the impact of solar activities, numerous ionospheric phenomena that result from perturbations from lower atmosphere and ground remain unexplained. This study first shows the effect of longitudinal distribution of convection, such as El Niño - Southern Oscillation (ENSO), on the quasi-biennial oscillation (QBO) from the stratosphere (U30 index) to ionosphere at low latitude. The ENSO signals in the QBOs at various altitudes are observed by the FORMOSAT-3/COSMIC radio occultation (RO) sounding profiles of temperature and electron density. The RO technique records ENSO signals which are pertinent to the ongoing study attempting to establish the long-term change in the troposphere connection to the upper atmosphere. Moreover, surface perturbations due to a large earthquake and tsunami can also significantly perturb the ionosphere. The horizontal movement of seismo-traveling atmospheric disturbance (STAD) in the ionosphere have been comprehensively observed by dense ground-based GNSS networks. However, evidence for the vertical component of STAD is rare. This study shows that the 2010 Mw8.8 Chile, 2011 Mw9.0 Tohoku, and 2015 Mw7.8 Nepal earthquake/tsunami can perturb the vertical structure of not only the ionosphere but also the stratosphere. The detection of STAD in the lower atmosphere and a more comprehensive understanding of STAD propagation in the whole atmosphere benefit to earthquake/tsunami early warning system.

Keywords: GNSS, ionospheric weather, surface perturbation

©2020. Japan Geoscience Union. All Right Reserved.

A multi-directional particle detector on HXMT

*Hong Guo Shen

The hard X-ray Modulation Telescope(HXMT) lunched on June 15, 2017 is the first special space science experiment project in China. HXMT operates in a low earth orbit with an altitude of 550km and an inclination of 43 degrees. The radiation of high-energy charged particles is an important environmental factor threatening the satellite and on-board payloads. Among them the background of the main detector (high energy detector which energy spectrum is 20~250keV) that the high-energy proton interacts with its material and the satellite material may affect the observation sensitivity of the telescope, and a large number of electrons and the secondary effects of electrons can also affect the working state of the main detector. The complex spatial distribution and dynamic changes of high energy charged particles are revealed by the results of the radiation environment detection of space charged particles carried out by low orbit satellites such as SAMPEX, NOAA and FY-1 in China. As the first orbit to carry out scientific exploration, HXMT satellite has not yet measured charged particle observation data.
As one of the payloads of the satellite, the newly developed multi-directional particle detector carries out the wide energy spectrum detection of high-energy electrons(0.2MeV~1.5MeV) and protons(3MeV~150MeV) in orbit space and the particle flux measurement from 16 directions covering 180 degrees. These observation data will provide more accurate dynamic data of orbital space particle radiation environment for the safe operation of HXMT satellite in orbit and the realization of scientific objectives, and also provide detailed data for future space environment modeling and in-depth space environment research.

Keywords: HXMT, Particle detector , Multi-directional detector

©2020. Japan Geoscience Union. All Right Reserved.

New observations of the total electron content over Ho Chi Minh City

*Tam Dao[1,2], Minh Huy Le[3], Brett A Carter[1], Que Le[2]

1. SPACE Research Centre, School of Science, RMIT University, Australia, 2. Department of Physics, International University, Vietnam, 3. Institute of Geophysics, Vietnam Academy of Science and Technology (VAST), Vietnam

In January 2018, a Trimble NetR9 GNSS receiver was installed at Ho Chi Minh City International University (HCMIU), Vietnam National University, which is located at 10˚52' N, 106˚48' E in the geomagnetic equatorial region. This GNSS receiver continuously records data every 1s and 30 s every day over Ho Chi Minh City. From the obtained data, we estimated the total electron content (TEC) using the carrier-phase method which is a combination of code and phase measurements. The results present some features for the diurnal and seasonal TEC variations using this GNSS receiver during 2018 - 2019. The changes of TEC observed at HCMIU as well as other nearby stations and the same longitude region in the latest moderate geomagnetic storm G3 on August 2018 were investigated. Furthermore, we calculate the rate of change TEC index (ROTI) concerning time from the satellite signal phases. The distributions of ROTI over these two years of solar minimum show significant occurrences of scintillation, which are caused by small-scale ionospheric irregularities in the equatorial region during equinox months after sunset. The results presented indicate that the GNSS data recorded at HCMIU is a worthy reference dataset near the geomagnetic equator for further research about ionospheric monitoring.

Keywords: GNSS receivers, Total Electron Content (TEC), The rate of change of TEC index (ROTI), Geomagnetic storms, Scintillation

©2020. Japan Geoscience Union. All Right Reserved.

[E] Poster | P (Space and Planetary Sciences)：P-EM Solar-Terrestrial Sciences, Space Electromagnetism & Space Environment

[P-EM21] Surprises from the Subauroral Zone: Synthesizing Ground and Space-Based Observations and Theory

convener:Connors Martin G(Athabasca University), Kazuo Shiokawa(Institute for Space-Earth Environmental Research, Nagoya University)

Recent studies, including some facilitated by citizen science, have shown the subauroral ionosphere to be more active than previously suspected. Unusual emissions, from SAR arcs to STEVE, indicate previously little studied physical processes in this region. Some arise from conjugacy to the radiation belts, while others have origins which remain unclear. This session attempts to stimulate synthesis of observations from different domains to address phenomena which appear difficult to explain when examined from only one of the many new sources of information about the subauroral zone. Optical observations have expanded to include those with the very high resolution of amateur DSLR cameras, yet this sporadic source is well complemented by continuous observation from the few comprehensive subauroral observatories. As ever, conjugacy with spacecraft plays an important role in assessing possible sources of precipitation or waves that may stimulate the subauroral ionosphere, and there are indeed now many space assets (RBSP, Arase, THEMIS, MMS) with footprints at least sometimes in that region. Various polar-orbiting low-altitude satellites traverse it regularly. The installation of low-latitude poleward-looking incoherent scatter radars, with large fields of view in the subauroral zone, also provides context and the ability to extract physical parameters continuously. The sometimes-extreme conditions now known to exist in the subauroral region have stimulated theory to expand the parameter range needed to explain ionospheric phenomena. We welcome contributions integrating multiple sources of observation and theoretical approaches to hopefully transform what is initially surprising into a new view of an unsuspectedly active region.

[PEM21-P01] Subauroral-zone surprises obtained from the PWING project

*Kazuo Shiokawa[1], Martin G Connors[2] (1.Institute for Space-Earth Environmental Research, Nagoya University, 2.Athabasca University)

[PEM21-P02] The pulsating aurora of January 27, 2017 as observed by e-POP, NOAA spacecraft, and ground assets

*Martin G Connors[1], Andrew W Yau[2], Kazuo Shiokawa[3], Claudia Martinez Calderon[3], Xinlin Li[4] (1.Athabasca University, 2.University of Calgary, 3.Nagoya University, 4.University of Colorado)

[PEM21-P03] SAR arc at 68^{o} geomagnetic (71^{o} geographic) North for Kp = 0+

*Shin-ichiro Oyama[1,2,3], Atsuki Shinbori[1], Anita Aikio[2], Heikki Vanhamaki[2], Yasunobu Ogawa[3], Mirjam Kellinsalmi[4], Tero Raita[2], Mike Rietveld[5], Kazuo Shiokawa[1], Ilkka Virtanen[2], Lei Cai[6], Abiyot Workayehu[2], Marcus Pedersen[2], Kirsti Kauristie[4], Boris Kozelov[7], Andrei Demekhov[7] (1.Institute for Space-Earth Environmental Research, Nagoya University, Japan, 2.Space Physics and Astronomy Research Unit, University of Oulu, Finland, 3.National Institute of Polar Research, Japan, 4.Finnish Meteorological Institute, Finland, 5.EISCAT, Norway, 6.KTH Royal Institute of Technology, Sweden, 7.Polar Geophysical Institute, Russia)

[PEM21-P04] Simultaneous observation of detachment of a bright Stable Auroral Red (SAR) arc by a ground-based camera and the Arase satellite on 4 November 2019

*Yudai Inaba[1], Kazuo Shiokawa[1], Shin-ichiro Oyama[1,9,10], Yuichi Otsuka[1], Atsuki Shinbori[1], Yoshizumi Miyoshi[1], Yoichi Kazama[2], Shiang-Yu Wang[2], Sunny W.T. Tam[3], Tzu-Fang Chang[3], Bo-Jhou Wang[2], Kazushi Asamura[4], Shoichiro Yokota[5], Satoshi Kasahara[6], Kunihiro Keika[6], Tomoaki Hori[1], Ayako Matsuoka[4], Yoshiya Kasahara[7], Atsushi Kumamoto[8], Shoya Matsuda[4], Yasumasa Kasaba[8], Masafumi Shoji[1], Iku Shinohara[4] (1.Institute for Space-Earth Environmental Research, 2.Academia Sinica Institute of Astronomy and Astrophysics, Taipei, Taiwan, 3. Institute of Space and Plasma Sciences, National Cheng Kung University, Tainan, Taiwan, 4.JAXA, 5.Osaka Univ., 6.Univ. Tokyo, 7.Kanazawa Univ., 8.Tohoku Univ., 9.Univ. of Oulu, Finland, 10.National Institute of Polar Research)

[PEM21-P05] Spatial-temporal variations of the SAPS structure with recurrent period of a few minutes observed by the SuperDARN HOP radars

*Nozomu Nishitani[1], Tomoaki Hori[1], Mariko Teramoto[2] (1.Institute for Space-Earth Environmental Research, Nagoya University, 2.Kyushu Institute of Technology)

[PEM21-P06] New curiosities observed from ground-based data: KHF-VLF Emissions

*Claudia Martinez Calderon[1], Jyrki Manninen[2], Tauno Turunen[2] (1.Institute for Space-Earth Environmental Research, Nagoya University, 2.Sodankylä Geophysical Observatory, University of Oulu, Sodankylä)

Subauroral-zone surprises obtained from the PWING project

*Kazuo Shiokawa[1], Martin G Connors[2]

1. Institute for Space-Earth Environmental Research, Nagoya University, 2. Athabasca University

Additional Coauthor: PWING Team (http://www.isee.nagoya-u.ac.jp/dimr/PWING/en/)

The PWING stands for “study of dynamical variation of Particles and Waves in the INner magnetosphere using Ground-based network observations”. This project is a 5-year project (2016-2020) by the Grant-in-Aid for Specially Promoted Research of the Japan Society for the Promotion of Science (JSPS) (16H06286). This project deploys all-sky imagers, induction magnetometers, VLF receivers, and broad-beam riometers at 8 stations at subauroral latitudes around the north-pole to cover longitudinal variation of aurora and electromagnetic disturbances in the inner magnetosphere. Details of the PWING project can be seen at http://www.isee.nagoya-u.ac.jp/dimr/PWING/PWING_web_e.htm. In this presentation, we review recent new results obtained by the PWING project at subauroral latitudes, particularly at Athabasca (ATH), Canada, (55°N, 247°E, magnetic latitude: 61.7N).

Keywords: PWING Project, SAR arc, ELF/VLF wave

©2020. Japan Geoscience Union. All Right Reserved.

The pulsating aurora of January 27, 2017 as observed by e-POP, NOAA spacecraft, and ground assets

*Martin G Connors[1], Andrew W Yau[2], Kazuo Shiokawa[3], Claudia Martinez Calderon[3], Xinlin Li[4]

1. Athabasca University, 2. University of Calgary, 3. Nagoya University, 4. University of Colorado

The Cassiope/e-POP (now also known as Swarm-E) Canadian scientific satellite`s Fast Auroral Imager observed pulsating aurora with its infrared camera in two passes over North America on January 27, 2017. On one of these passes the Radio Receiver Instrument was also operating. The ground path of NOAA-19 was nearly coincident geographically with that of e-POP, although offset slightly in time. The most relevant ground instrumentation was the THEMIS ASI array which showed the pulsating aurora with 3 second cadence, and VLF receivers at Athabasca and Kapuskasing of the PWING project led by Nagoya University, and University of Calgary`s ABOVE VLF array. Both FAI and ground cameras show a distinct poleward border to the pulsating aurora, which lay between magnetic latitudes of approximately 64º and 68º. The MEPED instrument on NOAA-19 showed broad maxima in electron precipitation in the 40 and 130 keV channels, with distinct peaks in the loss cone electrons at several latitudes within the pulsating aurora zone. Chorus emissions were also observed in the VLF during the event. The footpoints of THEMIS A,D, and E were slightly poleward of the pulsating aurora when it was most active. A lack of wave activity there suggests that the mechanisms generating pulsating aurora were tightly confined to the region within about 10 Re of the Earth, which is consistent with where filled loss cones were observed by NOAA-19.

Keywords: pulsating aurora, electron precipitation, satellite imaging, chorus waves

©2020. Japan Geoscience Union. All Right Reserved.

SAR arc at 68° geomagnetic (71° geographic) North for Kp = 0+

*Shin-ichiro Oyama[1,2,3], Atsuki Shinbori[1], Anita Aikio[2], Heikki Vanhamaki[2], Yasunobu Ogawa[3], Mirjam Kellinsalmi[4], Tero Raita[2], Mike Rietveld[5], Kazuo Shiokawa[1], Ilkka Virtanen[2], Lei Cai[6], Abiyot Workayehu[2], Marcus Pedersen[2], Kirsti Kauristie[4], Boris Kozelov[7], Andrei Demekhov[7]

1. Institute for Space-Earth Environmental Research, Nagoya University, Japan, 2. Space Physics and Astronomy Research Unit, University of Oulu, Finland, 3. National Institute of Polar Research, Japan, 4. Finnish Meteorological Institute, Finland, 5. EISCAT, Norway, 6. KTH Royal Institute of Technology, Sweden, 7. Polar Geophysical Institute, Russia

Stable Auroral Red (SAR) arc has been studied for more than half century since its academic discovery in Southern France in 1958 as one of the typical optical features occasionally seen at subauroral latitudes. Generation mechanism of the SAR arc is related to storm-time interactions at the overlapped region between the plasmasphere and the ring current. Thus most events have been found out of the auroral oval such as ~60 deg in geomagnetic latitude. In this study, however, we will present a SAR arc event at 68 deg geomagnetic (71 deg geographic) north in the Scandinavian sector during period of geomagnetically quiet condition of Kp = 0+. The SAR arc, which was captured with cameras (630 nm) at Abisko and Kirpisjärvi, appeared coinciding with a pseudo substorm onset at 71-72 deg geomag. N and rapid equatorward expansion of the polar cap potential estimated with the SuperDARN. However, the SAR arc disappeared in about 7 minutes along with a sudden shrinking of the polar cap potential. Conjunction measurement with the Swarm A/C suggests that the SAR arc was located at poleward slope of the ionospheric trough or slightly its outside. These experimental evidences suggest that, in the early stage of this SAR arc generation, the magnetosphere compressed the ring current region inward, resulting in a contact of the ring current region to the plasmasphere but expansion of the polar cap potential was too short to coalescent the ring-current hot ions and plasmaspheric electrons at the plasmapause, which corresponds to the trough minimum in the ionosphere.

Keywords: SAR arc, geomagnetically quiet period, Ionosphere

©2020. Japan Geoscience Union. All Right Reserved.

Simultaneous observation of detachment of a bright Stable Auroral Red (SAR) arc by a ground-based camera and the Arase satellite on 4 November 2019

*Yudai Inaba[1], Kazuo Shiokawa[1], Shin-ichiro Oyama[1,9,10], Yuichi Otsuka[1], Atsuki Shinbori[1], Yoshizumi Miyoshi[1], Yoichi Kazama[2], Shiang-Yu Wang[2], Sunny W.T. Tam[3], Tzu-Fang Chang[3], Bo-Jhou Wang[2], Kazushi Asamura[4], Shoichiro Yokota[5], Satoshi Kasahara[6], Kunihiro Keika[6], Tomoaki Hori[1], Ayako Matsuoka[4], Yoshiya Kasahara[7], Atsushi Kumamoto[8], Shoya Matsuda[4], Yasumasa Kasaba[8], Masafumi Shoji[1], Iku Shinohara[4]

1. Institute for Space-Earth Environmental Research, 2. Academia Sinica Institute of Astronomy and Astrophysics, Taipei, Taiwan, 3. Institute of Space and Plasma Sciences, National Cheng Kung University, Tainan, Taiwan, 4. JAXA, 5. Osaka Univ., 6. Univ. Tokyo, 7. Kanazawa Univ., 8. Tohoku Univ., 9. Univ. of Oulu, Finland, 10. National Institute of Polar Research

Stable auroral red (SAR) arc is an aurora with dominant 630.0-nm emission of oxygen atoms generated at subauroral latitudes slightly lower than the aurora oval. SAR arcs were first reported in southern France [Barbier, 1958] and have long been investigated since then. Precipitating electrons (or heat flux) of ~several electronvolts (eV) have been considered as the source of SAR-arc emissions. Kozyra et al. [1997] noted that there were three possible mechanisms to generate these low energy electrons. The first hypothesis is the Coulomb collision between plasmaspheric electrons (energies less than 1 eV) and ring current ions (several tens of keV) [e.g., Rees and Roble, 1975; Kozyra et al., 1987]. The energy is transported into the ionosphere via heat conduction or as a low energy electron flux [e.g., Cole, 1965; Prolss, 2006]. The second hypothesis is that the Landau damping of electromagnetic ion cyclotron (EMIC) waves causes heated electrons and their pitch angle scattering and precipitation into the ionosphere [Cornwall et al., 1971]. The third is that the kinetic Alfven wave with the parallel electric field to the magnetic field accelerates plasmaspheric electrons to the ionosphere. In our previous study, we reported the first conjugate observation of a SAR arc on March 28, 2017 using an all-sky imager and the Arase satellite [Inaba et al., JpGU (PEM13-P14), 2019; Inaba et al., SGEPSS (R006-27), 2019]. We confirmed that EMIC or kinetic Alfven waves associated with the SAR arc were not observed by the Arase satellite and concluded that Coulomb collisions between ring-currrent protons and plasmaspheric electrons are the main cause of SAR arc generation. In this presentation, we show a new conjunction event of a bright Stable Auroral Red (SAR) arc observed by a ground-based camera and the Arase satellite on 4 November 2019. The conjunction was obtained at the time when the arc was detached equatorward from the main auroral oval. Similar to the previous event, the Arase satellite was near the plasmapause and in ring current at the crossing of the detaching SAR arc. However, Arase observed both electron and proton flux enhancements at energies below 1 keV near the magnetic equator over the bright detaching SAR arc (~1 kR). On the basis of these facts, we discuss the difference of particle and field characteristics between the newly-detached, bright arc on 4 November 2019 and the somewhat stable, faint arc on 28 March 2017.

Keywords: SAR arc, Arase satellite, All-sky camera

©2020. Japan Geoscience Union. All Right Reserved.

Spatial-temporal variations of the SAPS structure with recurrent period of a few minutes observed by the SuperDARN HOP radars

*Nozomu Nishitani[1], Tomoaki Hori[1], Mariko Teramoto[2]

1. Institute for Space-Earth Environmental Research, Nagoya University, 2. Kyushu Institute of Technology

Super Dual Auroral Radar Network (SuperDARN) is a powerful tool for monitoring ionospheric plasma convection not only at high latitudes, but also at sub-auroral and mid- latitudes. The SuperDARN Hokkaido Pair (HOP) of radars are 2 mid-latitude SuperDARN radars, located at the lowest geomagnetic latitude (36.9 degrees) at present. In this paper, the SuperDARN Hokkaido Pair (HOP) of radars data with special operation modes are used to study the spatial-temporal structure of the wavy variations of plasma flow with recurrent period of a few minutes embedded in larger-scale, fast flow structures at subauroral latitudes (SAPS). We focus mainly on the events on Sep 08, 2017 and Aug. 26, 2018, both of which occurred near the peak of large geomagnetic storm (minimum Dst: -124 nT and -174 nT). These events were recorded by the SuperDARN radars with higher temporal resolution (3 and 12 seconds respectively) camping beams. Using both camping beam data and 2-dimensional data (with 1 to 2 min temporal resolution) enable us to examine the period, wavelength and propagation speed of these wave structures. In addition, using the data with the new fitting algorithm (fitacf Ver. 3) we have more extended coverage of the echo regions. The wave structures have limited spatial extent in magnetic local time. On the other hand, there are several differences between these events such as period, propagation speed and geomagnetic latitude. Their possible generation mechanisms will be discussed.

Keywords: SuperDARN, SAPS, wave variations

©2020. Japan Geoscience Union. All Right Reserved.

New curiosities observed from ground-based data: KHF-VLF Emissions

*Claudia Martinez Calderon[1], Jyrki Manninen[2], Tauno Turunen[2]

1. Institute for Space-Earth Environmental Research, Nagoya University, 2. Sodankylä Geophysical Observatory, University of Oulu, Sodankylä

Thanks to the implementation of sferics filtering above f = 4 kHz, a previously unknown strange spectral world of differently structured high-frequency waves has been observed on the ground station of Kannuslehto (KAN, MLAT=64.4˚N, L=5.46). These type of signals were first reported reported by Manninen et al. 2016 using using 1-hour spectrogram, where they often resembled 'sticks' or 'wands'. However, looking more closely they seem to be mostly composed of hiss bursts with durations of a few seconds. An example of two observations made by KAN is shown in Figure 1. These high frequency VLF emissions have been named KHF-VLF, standing for Kannuslehto High-Frequency VLF.

During campaigns where KAN was active between 2006 and 2015, they KHF-VLFs were observed during 60 to 90% of all campaign days. KHF-VLFs were often detected during the winter campaigns in the period between 2016 and 2019. We noted that when solar activity was high KHF-VLFs were observed very regularly. For example, during the winter 2014-2015 campaign, they were observed on 52 days out of 59, and in winter 2015-2016 on 75 days out of 91.

While these type of emissions are clearly observed quite often, currently there are no statistical studies on the occurrence and properties of these waves. Here, we will present the main characteristics of KHF-VLF emissions, their latest observational results from KAN data, as well as discussing observations at other VLF ground-stations and/or satellites in the inner magnetosphere.

Keywords: ELF/VLF, plasma waves, ground-based observations, subauroral latitudes

©2020. Japan Geoscience Union. All Right Reserved.

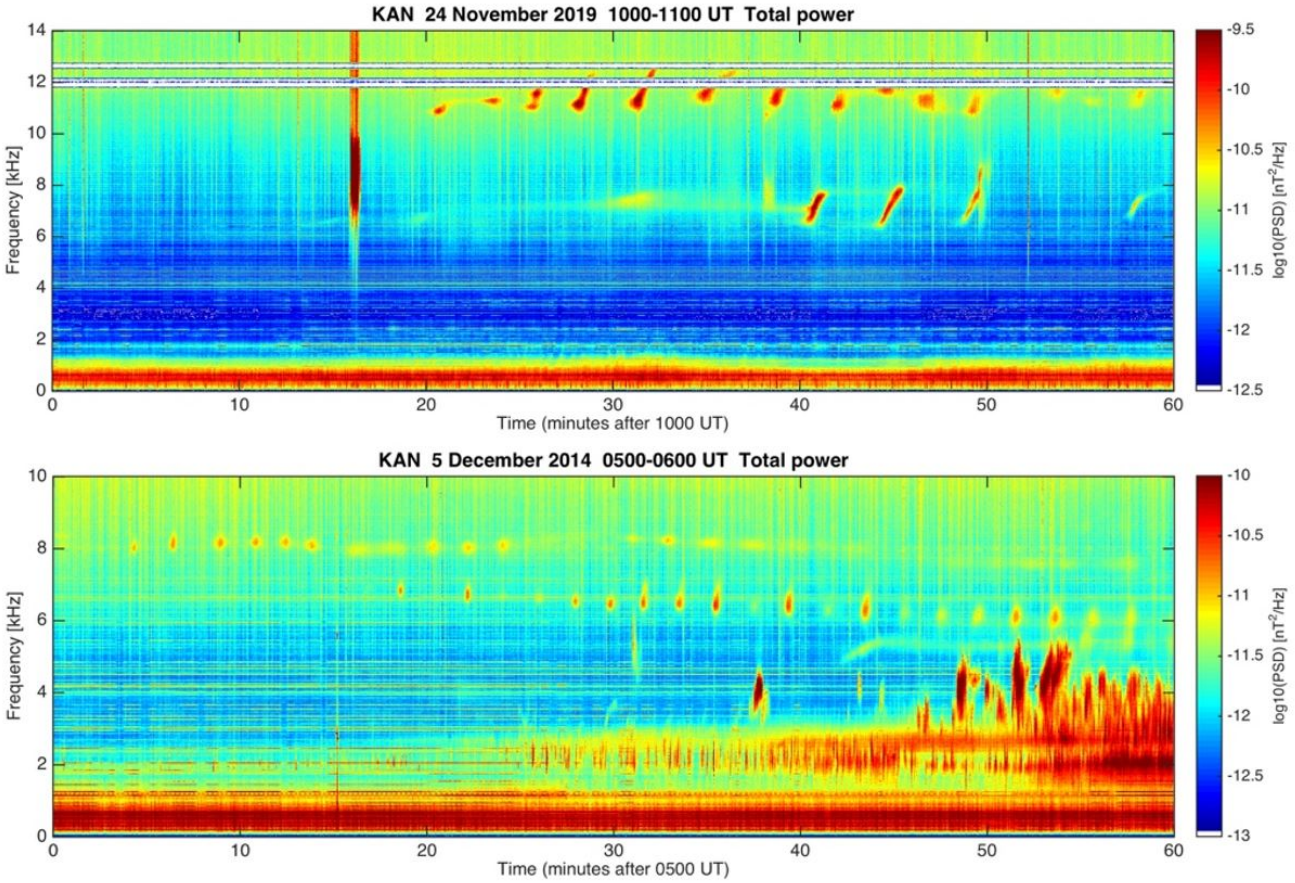


Figure 1. Two examples of KHF-VLF events. Non-typical emissions are seen above 6 kHz.

©2020. Japan Geoscience Union. All Right Reserved.

[E] Poster | P (Space and Planetary Sciences)：P-AE Astronomy & Extrasolar Bodies

[P-AE22] Exoplanets

convener:Masahiro Ikoma(Department of Earth and Planetary Science, The University of Tokyo), Norio Narita(The University of Tokyo), Yuka Fujii(National Astronomical Observatory of Japan)

Exoplanetary science, which began with the discovery of a hot Jupiter in 1995, reached a significant turning point by the detection of countless super-Earths by the Kepler space telescope. In 2018, the new space telescope TESS was launched to conduct an extensive survey of exoplanets orbiting nearby bright stars, opening a new era of characterization of exoplanet atmospheres. Moreover, recent observations have identified a growing number of terrestrial planets in the so-called habitable zone. While exoplanets have been targeted mainly for astronomy until recently, it would be fair to say that Earth and planetary science is finally becoming a research field to make a central contribution. This session aims at allowing participants to share their research results and new ideas regarding exoplanets and also inform the current status of their projects. Exoplanet science is a growing, interdisciplinary research field. We welcome participants from various fields.

[PAE22-P01] Climate for land planets

*Takanori Kodama[1] (1.University of Bordeaux)

[PAE22-P02] The Numerical Simulation for Detecting Atmospheric Oxygen on Exoplanets Around M and K Stars.

*Toru Muraoka[1], Osada Naoya[1], Shingo Kameda[1], Go Murakami[2], Norio Narita[3], Masahiro Ikoma[4], Hitoshi Fujiwara[5] (1.Rikkyo University, 2.Institute of Astronomical Science, Japan Aeronomy Exploration Agency, 3.National Astronomical Observatory of Japan, 4.Tokyo University, 5.Seikei University)

[PAE22-P03] Prevalence and extent of magma oceans in rocky bodies

Diogo Lourenço[1,2], *Matthieu Laneuville[1] (1.Earth-Life Science Institute, Tokyo Institute of Technology, 2.University of Califorinia, Berkeley)

[PAE22-P04] Exploring Super-Earth Surfaces: Albedo of Near-Airless Magma Ocean Planets and Topography

*Yuichi Ito[1], Darius Modirrousta-Galian[2,3], Giuseppina Micela[2] (1. University College London, 2.INAF - Osservatorio Astronomico di Palermo, 3.University of Palermo)

[PAE22-P06] How does the nodal precession affect observations of hot Jupiters around A-type stars?

*Noriharu Watanabe[1], Norio Narita[2] (1.The Graduate University for Advanced Studies, SOKENDAI, 2.Astrobiology Center)

[PAE22-P07] WASP-76 b: A Tale of Two Spectra

*Billy Nelson Edwards[1], Quentin Changeat[1], Robin Baeyens[2], Angelos Tsiaras[1], Ingo Waldmann[1] (1.University College London , 2.Instituut voor Sterrenkunde, KU-Leuven)

[PAE22-P08] A feasibility study on the detection of molecular species in exoplanet atmospheres by high-resolution transmission spectroscopy with SPICA/SMI

*Kawauchi Kiyoe[1], Yui Kawashima[2], Teruyuki Hirano[3], Yuka Fujii[4], Taro Matsuo[5], Kazumasa Ohno[3], Ayaka Okuya[3] (1.University of Tokyo, 2.SRON - Netherlands Institute for Space Research, 3.Tokyo Institute of technology, 4.Earth-Life Science Institute, Tokyo Institute of technology, 5.Nagoya University)

[PAE22-P09] Characterizing exoplanets with low-frequency radio observations

*Yuka Fujii[1], Keitaro Takahashi[2], Tomoki Kimura[3], Jun Hashimoto[4], Yuhiko Aoyama[5], Yuta Shiohira[2], Yuka Terada[6], Hajime Kita[7], Fuminori Tsuchiya[3], SKA-JP planet team (1.Earth-Life Science Institute, Tokyo Institute of Technology, 2.Kumamoto University, 3.Tohoku University, 4.National Astronomical

Observatory of Japan, 5.Tsinghua University, 6.University of Tokyo, 7.Institute of Space and Astronautical Science, Japan Aerospace Exploration Agency)

[PAE22-P10] The evolution outcome of the planetary systems predicted from the observed protoplanetary disk of HL Tau

*Shijie Wang[1], Kazuhiro Kanagawa[1], Toshinori Hayashi[1], Yasushi Suto[1] (1.University of Tokyo)

[PAE22-P11] Stability of resonant trapping of planetesimals during the migration of a giant planet

*Sho Shibata[1], Masahiro Ikoma[1] (1.Graduate School of Science, The University of Tokyo)

[PAE22-P12] **Variety of Planets from the Outer Edge of the Inner Hole**

*Masahiro Morikawa[1], Suzuka Amaya[1] (1.Department of Physics, Ochanomizu University)

[PAE22-P13] Orbital evolution of close-in super-Earths via atmospheric escape

*Naho Fujita[1], Yasunori Hori[2], Takanori Sasaki[1] (1.Department of Astronomy, Kyoto University, 2.Astrobiology Center, National Institutes of Natural Sciences)

[PAE22-P14] Bayesian inference of occurrence rates of super-Earths in systems with cold-Jupiters around low-mass stars

*Masahiro Ogihara[1], Hiroki Harakawa[2] (1.National Astronomical Observatory of Japan, 2.Subaru Telescope)

[PAE22-P15] Filling in the gaps: imputing the missing properties of exoplanets with machine learning

*Elizabeth Tasker[1], Matthieu Laneuville[2], Nicholas Guttenberg[2] (1.Institute of Space and Astronautical Science (ISAS), JAXA, 2.Earth-Life Science Institute (ELSI), Tokyo Institute of Technology)

Climate for land planets

*Takanori Kodama[1]

1. University of Bordeaux

Most of the studies for habitable planets focus on the boundary of the habitable zone in which a planet can maintain liquid water on its surface for a long term. Previous studies assumed a planet with a large amount of water on its surface. However, exoplanets should have various amounts of water on their surface.

Kodama et al. (2019) showed the relationship between the insolation at the inner edge of the habitable zone and the water distribution on a planetary surface. A land planet that has a small amount of water on its surface can maintain liquid water when it receives stronger insolation than that at the inner edge of the habitable zone for a planet with a large amount of water.

In this presentation, we summarize the climate for a land planet and show the results for TRAPPIST-1 d as a land planet.

Keywords: Habitable Planet, Climate

©2020. Japan Geoscience Union. All Right Reserved.

The Numerical Simulation for Detecting Atmospheric Oxygen on Exoplanets Around M and K Stars.

*Toru Muraoka[1], Osada Naoya[1], Shingo Kameda[1], Go Murakami[2], Norio Narita[3], Masahiro Ikoma[4], Hitoshi Fujiwara[5]

1. Rikkyo University, 2. Institute of Astronomical Science, Japan Aeronomy Exploration Agency, 3. National Astronomical Observatory of Japan, 4. Tokyo University, 5. Seikei University

To date, more than 4000 exoplanets have been detected. In recent years, thanks to the activities of probes such as Kepler and TESS, study on terrestrial planets in the habitable zone (HZ) around M-type and K-type low-mass, low-temperature stars has been advanced. Characterization of such a habitable exoplanet requires Transit spectroscopy and the detection of a planet's atmospheric elements. However, in general, the detection of planetary atmospheric elements other than hydrogen is difficult owing to their small distribution compared to the size of the planet. M and K stars are relatively active and emit strong UV radiation. An oxygen-rich, carbon dioxide-poor (i.e., Earth-like) atmosphere of a planet located in such a star's HZ would get heated by ionization and dissociation and expand to significant size compared to the planetary radius [Kulikov et al., 2007, Tian et al., 2008b]. The World Space Observatory-UV (WSO-UV) is a multi-national space telescope project, led by Russia, to be launched in 2025. The key scientific objective would involve studying extrasolar planetary atmospheres in the presence of strong UV radiation fields. In this study, we simulated Earth’ s atmosphere by considering that the Earth was placed in the HZ of M and K stars. Furthermore, we estimated the possibility of detecting oxygen by means of simulated transit spectroscopic observations.

Keywords: exoplanetaly atmosphere, transit spectroscopy

©2020. Japan Geoscience Union. All Right Reserved.

Prevalence and extent of magma oceans in rocky bodies

Diogo Lourenço[1,2], *Matthieu Laneuville[1]

1. Earth-Life Science Institute, Tokyo Institute of Technology, 2. University of Califorinia, Berkeley

It is well accepted that the Earth and most rocky bodies in the Solar System went over a magma ocean stage during and immediately after their accretion (e.g., Tonks and Melosh, JGR 1993; Elkins-Tanton, Annu. Rev. Earth Planet. Sci. 2012). Based on this, it is generally assumed that magma oceans are common and widespread throughout the Universe, and that they exist throughout all the accretion stage of different bodies. Another common assumption made is that magma oceans extend deep inside the bodies and cover their entire surface. However, how frequent magma oceans are, and how deep do they extend, is not well constrained. In this work, we aim to understand the factors that control the formation duration of magma oceans, and the conditions that lead to deep ones. Understanding these questions is of extreme importance, as a magma ocean sets up the conditions for future mantle dynamics and tectonic activity, the composition of the atmosphere, and the possibility for the existence of oceans, and life.

We present a model that computes the extent of melting in a planet by taking into account the input of energy from impacts during accretion, and output of energy from radiative cooling of a magma ocean. We test two ways of taking into account the energy input due to impacts: (1) a parameterized distribution of impactors' distribution and energy, following Shibaike et al., (Icarus, 2016) and (2) using frequency and intensity of impacts extracted from N-body simulations (e.g., de Vries et al., PEPS 2016). Furthermore, we will show how the results are affected by: (1) how opaque the atmosphere is, (2) different impacts histories and accretion times, and (3) how the energy of a single impact is distributed in the interior of the body, i.e, does the melt generated spread out evenly across the globe as assumed by, for example, de Vries et al. (PEPS 2016), or the magma ocean generated has different depths at different locations around the planet as predicted by Reese and Solomatov (Icarus, 2006) for higher solid mantle viscosities.

Keywords: magma ocean, accretion, planetary formation, planetary diversity

©2020. Japan Geoscience Union. All Right Reserved.

Exploring Super-Earth Surfaces: Albedo of Near-Airless Magma Ocean Planets and Topography

*Yuichi Ito[1], Darius Modirrousta-Galian[2,3], Giuseppina Micela[2]

1. University College London, 2. INAF - Osservatorio Astronomico di Palermo, 3. University of Palermo

We propose an analytic function for the bond albedo of an airless or near-airless magma ocean planet (AMOP). We generated multiple 1D fractal surfaces with varying compositions unto which we individually bombarded 10,000 light rays. Using an approximate form of the Fresnel equations we measured how much of the incident light was reflected. Having repeated this algorithm on varying surface roughnesses we find the albedo as a function of the Hurst exponent, the geochemical composition of the magma, and the wavelength. As a proof of concept, we used our model on Kepler-10 b to demonstrate the applicability of our approach. We present the albedos of different lava compositions and multiple tests that can be applied to observational data in order to determine their characteristics. Currently, there is a strong degeneracy in the surface composition of AMOPS due to the large uncertainties in their measured albedos. In spite of this, when applied to Kepler-10 b we show that the high albedo could be caused by a moderately wavy ocean that is rich in oxidised metallic species such as FeO, Fe2O3, Fe3O4. This would imply that Kepler-10 b is a coreless or near-coreless body.

Keywords: Exoplanet , Rocky planet, Magma ocean

©2020. Japan Geoscience Union. All Right Reserved.

How does the nodal precession affect observations of hot Jupiters around A-type stars?

*Noriharu Watanabe[1], Norio Narita[2]

1. The Graduate University for Advanced Studies, SOKENDAI, 2. Astrobiology Center

More than 4,000 exoplanets have been found. Even though most of these discovered exoplanets are orbiting around Solar-type (F/G/K type) stars, there are also a small number (~20) of exoplanets, most of them are hot Jupiters, around hot (B/A type) stars. Despite the small number, we have known that they tend to have a wide range of projected spin-orbit obliquities, the apparent angle between the stellar spin axis and the planetary orbital axis. Because hot stars are rapidly rotating in general, they make themselves more oblate. When a planetary system satisfied these two conditions, the misaligned orbit and the flatten host star, its orbital nodal precession occurs. The nodal precessions of two planets have been reported so far: Kepler-13Ab (Szabó et al. 2012) and WASP-33b (Johnson et al. 2015), both of which are orbiting around A-type stars. Especially, Watanabe et al. (2020) found that the nodal precession period of WASP-33b is ~840 years and this hot Jupiter transits in front of the host star for only ~20% of the whole precession period. In this research, we focused that how the nodal precession affects observations of hot Jupiters around A-type stars by theoretical models.

Zhou et al. (2019) estimated the occurrence rate of hot Jupiters around A-type stars 0.26±0.11% from the TESS sample, which is a little lower than rates of F/G type stars (F-type star: 0.43±0.15%, G-type star 0.71±0.31%). However, this previous study did not consider orbital nodal precession around A-type stars. Thus, we have calculated how the occurrence rate of hot Jupiters around A-type stars changes when the precession is applied. First, we formulated the ratio between the period for transiting in front of a host star and the orbital nodal precession period (ε). Then, we simulated 100,000 models of planetary systems of a hot Jupiter and an A-type star. In this simulation, we set values of essential parameters randomly based on the detected values of hot Jupiters around A-type stars. In general, the possibility of planetary transit almost equals to the ratio of the sum of the ratio of the stellar radius to the semi-major axis to the number of samples, but the possibility should be calculated by the sum of ε when the orbits are precessing. However, we derived that the possibility of planetary transit of hot Jupiters is 17.8% whether we consider the nodal precession or not. Therefore, the nodal precession does not affect the occurrence rate of hot Jupiters around A-type stars.

We also calculated how many orbits of hot Jupiters enter and leave in front of hot stars for ten years. First, we derive we computed the precession speeds of 100,000 models using equations from Barners et al. (2013) and Iorio (2010). Then, we simulated the ten-year-changes of impact parameters of all simulated models. As a result, ~2,500 models begin to transit their host stars as viewed from the Earth, other ~2,500 models finish transiting, and ~120 planetary orbits pass through their stellar disks for ten years. We have also found that there are a few hot Jupiters whose trajectories will depart from their stellar disks even though their impact parameters are almost zero. This simulation shows that the transit possibility is stable but perhaps a part of detected hot Jupiters will be disappeared after ten years later. Consequently, we should observe a hot Jupiter around a hot star continuous by Doppler tomography, a method to measure projected spin-orbit obliquity and impact parameter, and estimate how its transit trajectory is shifting and when it will end to transit.

©2020. Japan Geoscience Union. All Right Reserved.

Keywords: Exoplanets, Planet–star Interactions, Hot Stars, Hot Jupiters

©2020. Japan Geoscience Union. All Right Reserved.

WASP-76 b: A Tale of Two Spectra

*Billy Nelson Edwards[1], Quentin Changeat[1], Robin Baeyens[2], Angelos Tsiaras[1], Ingo Waldmann[1]

1. University College London , 2. Instituut voor Sterrenkunde, KU-Leuven

The Hubble Space Telescope’ s Wide Field Camera 3 (WFC3) has been widely used for transmission and emission spectroscopy of exoplanet atmospheres, identifying the main molecular constituents, detecting the presence of clouds and probing their thermal structure. Hubble observations of the emission spectra of a number of ultra-hot Jupiters have led to somewhat surprising results. Initially, these very hot planets were predicted to have inverted temperature pressure profiles due to strong optical absorption by TiO/VO in the upper atmospheres. However, observations of their emission spectra have been inconclusive on their thermal structure and composition. While some datasets show rich spectral features, others can be fit with simple blackbody models.

I will present the analysis of the Hubble transmission and emission spectra of WASP-76 b, an ultra-hot Jupiter with a day-side temperature of ~2500 K. The data was reduced and fitted using the open-source codes Iraclis and TauREx3. Previous studies of the WFC3 transmission spectra of WASP-76 b found hints of TiO and VO or non-grey clouds. Accounting for a fainter stellar companion to WASP-76, we reanalyse this data and show that removing the effects of this background star changes the slope of the spectrum, resulting in these visible absorbers no longer being detected, removing the need for a non-grey cloud model to adequately fit the data but maintaining the strong water feature previously seen. However, our analysis of the emission spectrum suggests the presence of vanadium oxide (VO) and an atmospheric thermal inversion, with tentative evidence for titanium oxide (TiO) and a muted water (H_2O) feature.

Keywords: Transmission and emission spectroscopy, Ultra-hot Jupiters, Hubble Space Telescope

©2020. Japan Geoscience Union. All Right Reserved.

A feasibility study on the detection of molecular species in exoplanet atmospheres by high-resolution transmission spectroscopy with SPICA/SMI

*Kawauchi Kiyoe[1], Yui Kawashima[2], Teruyuki Hirano[3], Yuka Fujii[4], Taro Matsuo[5], Kazumasa Ohno[3], Ayaka Okuya[3]

1. University of Tokyo, 2. SRON - Netherlands Institute for Space Research, 3. Tokyo Institute of technology, 4. Earth-Life Science Institute, Tokyo Institute of technology, 5. Nagoya University

Spectroscopic observations during planetary transits allow us to probe atmospheres of exoplanets (so-called "transmission spectroscopy").
In particular, high-resolution spectroscopy (R>20,000) has been proved to be one of the most powerful tools to directly investigate specific atoms/molecules in exoplanet atmospheres.
At optical wavelengths, alkali metals (i.e., Na and K) and Hα lines have been traditionally studied by ground-based telescopes (e.g., Casasayas-Barris et al. 2018, Gibson et al. 2018). In more recent studies, atoms and molecules, such as He and CO, were also detected by near-infrared high-resolution spectroscopy (e.g., Salz et al. 2018, Brogi et al. 2016), but more molecules in exoplanet atmospheres are still awaiting detections by current and future instruments.
Rich features and absorption bands of many molecules, which are important to understand the planet formation and evolution, are also located in the mid-infrared region (>5 micron); for instance, disequilibrium species such as HCN and C2H2 are crucial in the context of testing scenarios of UV irradiation and atmospheric mixing on exoplanets. However, detections of those molecules in the mid-infrared are unfeasible with observations from the ground, due to strong background emissions. Those molecules are expected to be detected by future observations from the space, such as by the JWST and SPICA missions.
In order to conduct a feasibility study on the detections of those molecules by future space missions, we performed a series of numerical simulations for high-resolution spectroscopy in the mid-infrared, taking into account the expected instrumental properties and background noises.
We specifically focused on SPICA/SMI observations, which provide us a unique opportunity to perform mid-infrared high-resolution spectroscopy. In this presentation, we will report on the results of our simulations and discuss the prospect to study exoplanet atmospheres using mid-infrared spectroscopy.

Keywords: Exoplanet Atmosphere, Transmission spectroscopy, Space telescope

©2020. Japan Geoscience Union. All Right Reserved.

Characterizing exoplanets with low-frequency radio observations

*Yuka Fujii[1], Keitaro Takahashi[2], Tomoki Kimura[3], Jun Hashimoto[4], Yuhiko Aoyama[5], Yuta Shiohira[2], Yuka Terada[6], Hajime Kita[7], Fuminori Tsuchiya[3], SKA-JP planet team

1. Earth-Life Science Institute, Tokyo Institute of Technology, 2. Kumamoto University, 3. Tohoku University, 4. National Astronomical Observatory of Japan, 5. Tsinghua University, 6. University of Tokyo, 7. Institute of Space and Astronautical Science, Japan Aerospace Exploration Agency

While characterization of individual exoplanets is often performed in the ultraviolet, optical, and infrared domains where the main observables are the atmospheric properties, low-frequency radio observations would serve as a complementary approach to characterize certain aspects of planets, mainly associated with the magnetospheric and ionospheric properties. With the Square Meter Array (SKA; around 0.1-10 GHz) being built, we explore the potential of SKA observations for characterizing various types of exoplanets as a part of SKA-JP science working group.

One of the recognized scientific goals of SKA is to search for the auroral emissions from exoplanets, which can constrain the planetary magnetic field strengths (e.g., Zarka 1997). A number of observations have been conducted so far, but no clear evidence has been obtained yet (e.g., Grießmeier et al., 2017 and references therein). We discuss the synergies with transit observations (due to the anisotropy of emission), direct imaging observations of young massive planets (for constraining the internal structure or the magnetic scaling laws by, e.g., Christensen et al., 2009), and gravitational microlensing observations (with the characteristic magnification curves; Shiohira et al., submitted). We also discuss the auroral radio generation by the pair of a close-in rocky planet and the host star via a mechanism similar to Io-Jupiter system as a probe of the planetary ionospheres.

A radio source observed through an exoplanet atmosphere (i.e., transmission observations in the radio domain) would be another opportunity to study the planetary magnetic fields as well as the surrounding plasmas, through the Faraday rotation and the time delay (Withers & Vogt 2017). This can be tested with Jovian magnetosphere passing in front of distant pulsars. We find that such events occur about 0.5 times/year on average, and SKA will have a sufficient sensitivity to detect the effects of Jovian magnetosphere.

Lastly, we argue that the gas-accreting proto-planets being formed in the protoplanetary disks emit the radio recombination lines (RRL) that are detectable with SKA, as estimated based on Aoyama et al., (2018). Compared with the tracers of the accretion processes at the shorter wavelengths (e.g., Hα; Haffert et al. 2019), RRL will be more sensitive to the (proto-)planets in young, optically thick disks, due to the reduced extinction efficiency. Detecting RRL would be critical to identify the very birthplace of the gaseous planets as well as to constrain the geometry and the rate of the planetary gas accretion at the early phase.

Keywords: Exoplanets, Auroral radio emission, Planet formation, Gravitational microlensing, Planetary transit

©2020. Japan Geoscience Union. All Right Reserved.

The evolution outcome of the planetary systems predicted from the observed protoplanetary disk of HL Tau

*Shijie Wang[1], Kazuhiro Kanagawa[1], Toshinori Hayashi[1], Yasushi Suto[1]

1. University of Tokyo

The ring/gap substructure of HL Tau has been intensively studied. Conventionally, it is interpreted as a result of unseen massive planets located inside the gaps. Motivated by this interpretation, we carried out N-body simulations to evolve the HL Tau planetary system from the current configuration to eventually 10 Gyrs after the disk dispersal. At the disk phase, we implement both planetary migration and mass growth effects coupled with the evolution of the disk profile. By varying the disk parameters, we produced a variety of widely-separated planetary systems consisting of three super-Jupiters at the end of the disk dispersal. We showed how the final configuration and planetary mass depend on disk parameters. We found no planet-pair has a period ratio less than 2.1 due to convergent migration. We continue integrating the orbits up to 10 Gyrs after the disk dispersal using pure gravitational N-body simulations. Most of the systems are found to be stable for at least 10 Gyr in only marginal resonance state. We discuss implications of our results in terms of the observed widely-separated planetary systems HR 8799 and PDS 70.

Keywords: Protoplanetary Disk, Planetary system evolution

©2020. Japan Geoscience Union. All Right Reserved.

Stability of resonant trapping of planetesimals during the migration of a giant planet

*Sho Shibata[1], Masahiro Ikoma[1]

1. Graduate School of Science, The University of Tokyo

Recently revealed close-in exo-gas-giants contain much heavy elements. Standard planetary formation theory cannot explain the origin of their heavy elements, however, the capture of planetesimals via planetary migration might be a source of those heavy elements. We focus on the resonant trapping, which has an important role for the accretion of planetesimals. The stability of resonant trapping, which means how strongly the resonance keep trapping planetesimals under perturbations, like collisions and gravitational interactions between planetesimals, is still not clear. In this study, we investigate the stability of resonant trapping using numerical integration of planetesimals. We expands an analytical equations for resonant trapping obtained by Malhotra 1993. We discuss the relation between the stability of resonant trapping and heavy elements contained in close-in gas giants. Our results would be important for discussing other problems related with resonances, like satellite formation or asteroid distribution in our solar system.

Keywords: exoplanet, heavy element, mean motion resonance

©2020. Japan Geoscience Union. All Right Reserved.

Variety of Planets from the Outer Edge of the Inner Hole

*Masahiro Morikawa[1], Suzuka Amaya[1]

1. Department of Physics, Ochanomizu University

Planets are very common objects in the Universe. This is already evident from recent discoveries of thousands of exoplanets. However, the standard theory of their formation encounters many notorious difficulties, such as the dust/planet fall and the disk lifetime problems. We do not try to avoid each problem but accept and use all of them positively to find a natural scenario that all these problems indicate.

All the falling problems indicate that dust falls, by the dissipation with gas, toward the central star. All the time scale problems indicate that the relevant processes of planet formation should be rapid. Therefore, **there must be a void of gas very inside**, say at radius 0.04 AU, and the falling dust must stop there at the outer edge of this inner hole. This is our first assumption, without specifying any Physical processes such as MRI, co-rotation instability, photoevaporation, or whatever. Then the following processes, 1 to 5, take place in the sequence, which naturally yields the variety of planets we observe today(Fig.1).

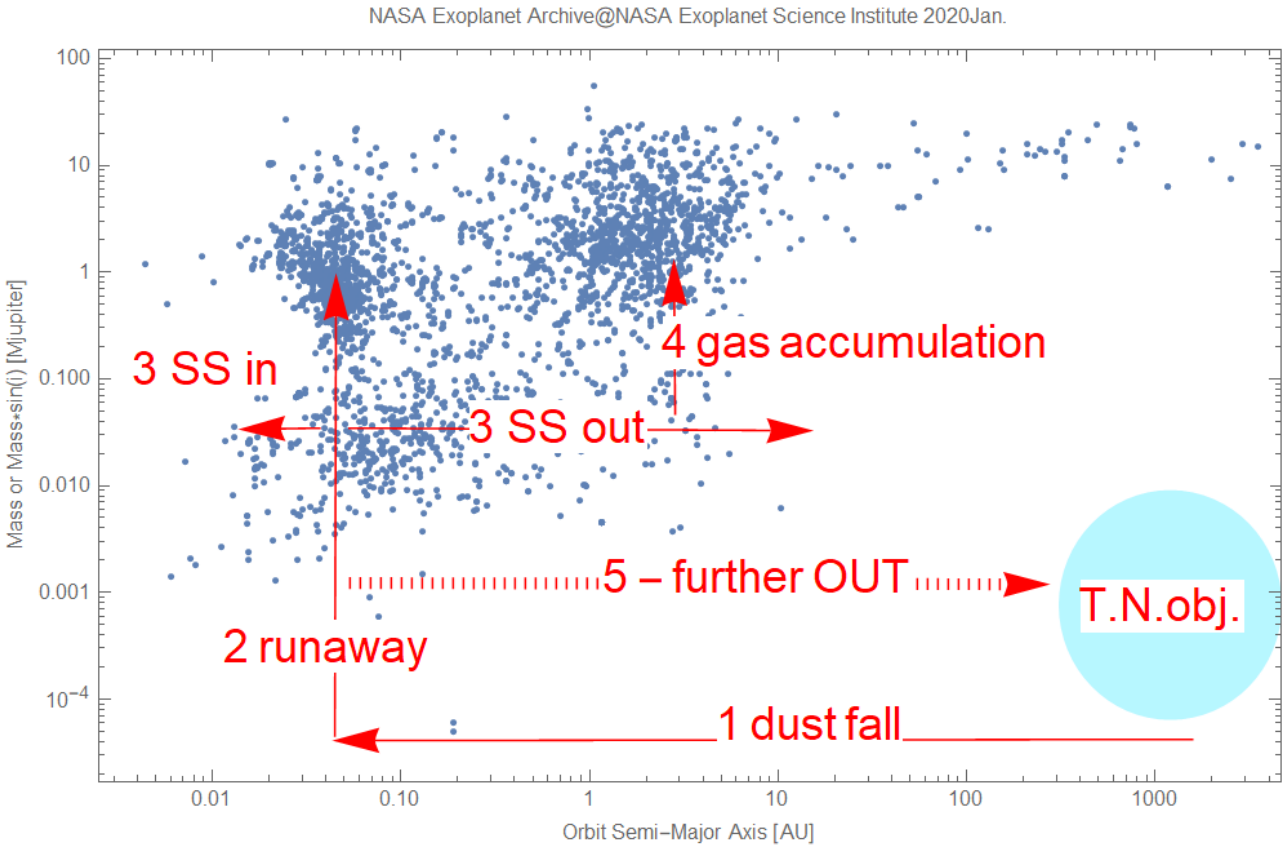
Dust and dust clusters fall toward the center but stops at the edge of the inner hole and accumulate there. We analytically estimate the size-dependent falling time scales. They may be very short such as several hundred years. Turbulence and frequent destructive collision, with dissipation, on the common Kepler orbit, promote their coalescence. **The dense and coherent motion of dust at the edge of the inner hole induces the runaway growth of several huge planets of size Jupiter.** This species is the Hot-Jupiters. This orbit is too close to the center and Hot-Jupiters may not be stable. However, this runaway time scale is short and several hundred years based on the standard disk model parameters. **These massive planets at the outer edge slingshot dust clusters inward and outward.** This stage of evolution is essential to yield a variety of planet species. Small dust clusters of size less than 10 Earth-mass are shot in and out, but cannot effectively accrete gas, and the size of them cannot grow. This species is the Rockey-Planets. They can be shot widely to 0.01AU to 1000 AU. On the other hand, dust clusters of size more than 10 Earth-mass can be shot up to 0.4AU by one Jupiter (pure three-body system) and 1 to 100 AU by two Jupiters (pure four-body system). These shot planets would migrate toward the center but shot again outward; the migration problem does not arise since the planets are always dynamical objects regulated by the outer edge of the inner hole. **Large dust clusters of size more than 10 Earth-mass shut outside can effectively accrete gas**, and the size of them can grow while the gas exists there. In this process, their initially large eccentricity dramatically reduces by acquiring the angular momentum of the gas. This species is the Cold-Gas-Giants or Ice-Giants, depending on the distance blown. They form gap and spiral structures on the planetary disk. **Much smaller dust clusters can be shot very far and become the seeds of `Trans-Neptunian Objects`,** including `Kuiper Best` of exoplanet systems. The dust cluster of 10^{12}Kg, for example, can be shot 100 to 1000AU within a time scale of 5000 years. Their orbital inclination can easily exceed 30 degrees. Furthermore, the eccentricity of them sometimes exceeds one. Therefore, a vast number of stray objects in the interstellar space can be produced.

We verify our model based on the basic predictions of the model.
a) All the cores of the planets, as well as small diffuse objects, are made from a common ratio of materials. This is because all the planet cores are formed at the outer edge of the inner hole as a mixture of falling

©2020. Japan Geoscience Union. All Right Reserved.

dust.
b) These core materials had experienced a thermal metamorphosis in the past. This is because all the planet cores are formed at the outer edge of the inner hole near to the central star. The temperature can easily rise to 2000 K there, which is enough to yield thermal metamorphosis.
These properties also apply to the `Trans-Neptunian Objects`. The study on comets and meteorites of our solar system may provide some information for our model.

Keywords: Planet formation, Slingshot, gas accretion, Planetary species, Trans-Neptunian Objects



©2020. Japan Geoscience Union. All Right Reserved.

Orbital evolution of close-in super-Earths via atmospheric escape

*Naho Fujita[1], Yasunori Hori[2], Takanori Sasaki[1]

1. Department of Astronomy, Kyoto University, 2. Astrobiology Center, National Institutes of Natural Sciences

Recently, a lot of super-Earths close to their host stars have been discovered especially around M dwarfs. Orbital distributions of planets in multiple close-in super-Earth systems are different each other. The mass-radius relationship of the super-Earths indicates that some of them have a substantial atmosphere, while others have almost no atmosphere. The origin of these differences remains unclear.

Close-in super-Earths would undergo atmospheric escape via the energy-limited hydrodynamic escape driven by stellar X-ray and UV irradiations. Considering the angular momentum exchange of a system, the super-Earths those experience atmospheric escape and lose their mass must move outward. However, little attention has been given to the orbital evolution of the planets due to the mass loss by hydrodynamic escape of their atmosphere.

In this study, we aim to gain a better understanding of the origin of multiple close-in super-Earth systems by calculating the atmospheric mass loss and the orbital evolution of the planets. We also aim to make theoretical predictions for the future observations of super-Earths around M dwarfs.

Keywords: super-Earth, atmospheric escape, orbital evolution

©2020. Japan Geoscience Union. All Right Reserved.

Bayesian inference of occurrence rates of super-Earths in systems with cold-Jupiters around low-mass stars

*Masahiro Ogihara[1], Hiroki Harakawa[2]

1. National Astronomical Observatory of Japan, 2. Subaru Telescope

Transit observations of exoplanets with space telescopes (e.g., Kepler) have revealed an abundant class of close-in super-Earths (SEs). The occurrence rate of giant planets in wide orbits (also known as cold Jupiters or CJs) can be studied using the data obtained via radial velocity (RV) observations, which have been conducted for more than 20 years. As the occurrence rates of SEs and CJs are estimated, the correlation between SEs and CJs can also be discussed. According previous studies, it is likely that CJs coexist with SEs, and this is expressed by a high conditional probability P(SE|CJ) of about 90%.

Recently, observations of super-Earths around low-mass stars have attracted increasing attention. In fact, several new RV surveys of M dwarfs have been initiated; these operations include IRD-SSP with the Subaru telescope and CARMENES. We are interested in whether the conditional probability of P(SE|CJ) is also high around M dwarfs.

In this study, we present an estimate of the conditional probability of P(SE|CJ) around M dwarfs using Bayes' inference. We find that the conditional probability of the existing SEs under the existence of CJs is quite high even around M dwarfs. We also discuss whether the existence of CJs enhances the growth of SEs. It is likely that the high conditional probability of P(SE|CJ) is simply a reflection of the high amount of solids available for planet formation. For a more robust discussion, more RV observation data are needed. In addition, dynamical simulations that include the effects of CJs on SEs are also required.

Keywords: Super-Earth, Cold-Jupiter, low-mass star

©2020. Japan Geoscience Union. All Right Reserved.

Filling in the gaps: imputing the missing properties of exoplanets with machine learning

*Elizabeth Tasker[1], Matthieu Laneuville[2], Nicholas Guttenberg[2]

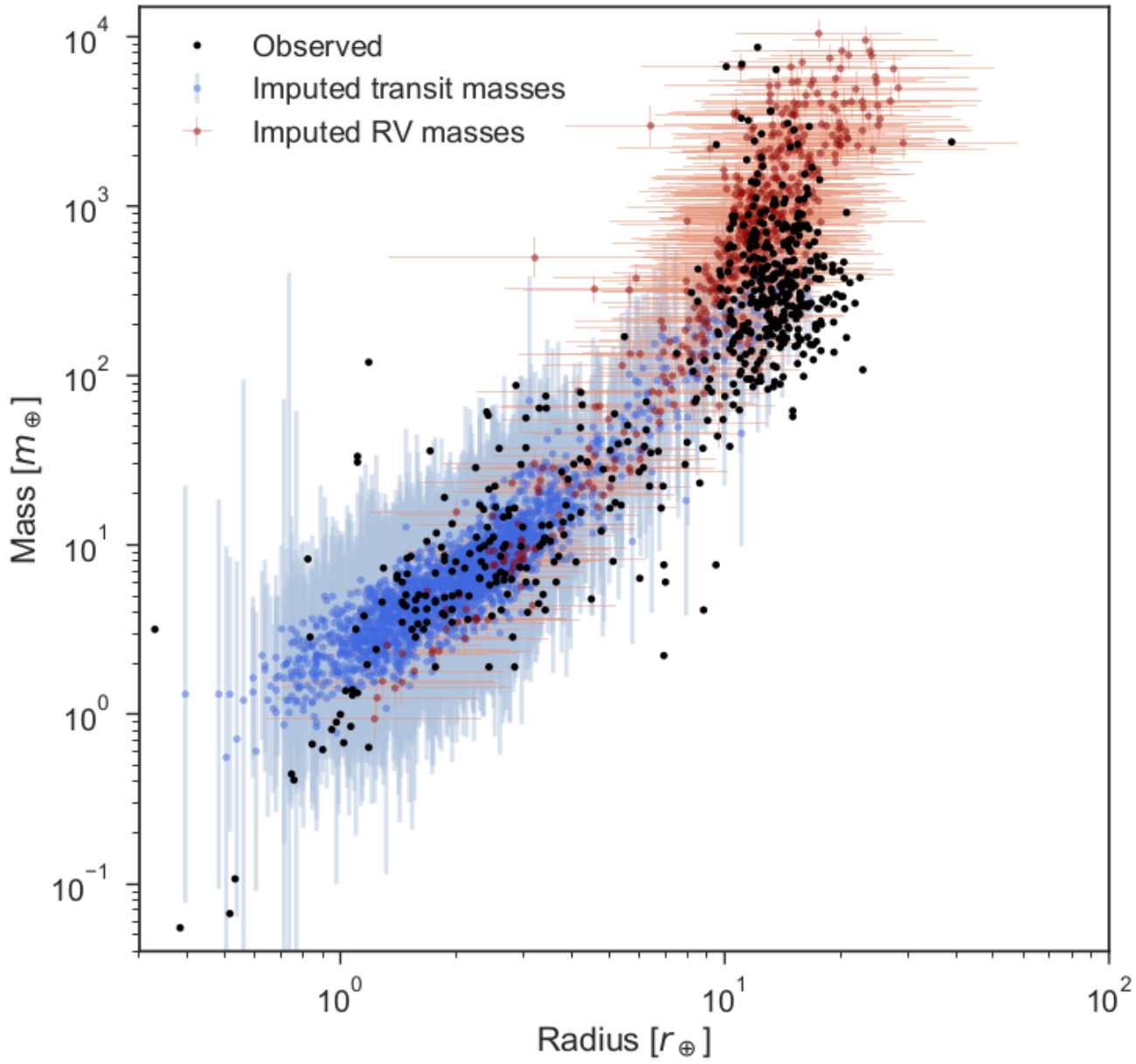
1. Institute of Space and Astronautical Science (ISAS), JAXA, 2. Earth-Life Science Institute (ELSI), Tokyo Institute of Technology

Understanding planet formation requires a large statistical sample. However, while the total number of extrasolar planets discovered is large, the known properties of individual worlds remains sparse. This issue cannot be resolved by more observations alone. Measurable planet properties depend on detection technique, but multiple detections are frequently impossible: a situation likely to degrade still further as we probe smaller worlds on longer orbits. One solution is to impute missing properties based on the current known distribution. In this talk, I will present one method for such an interpolation using a neural network.

Neural networks are strong at identifying complex trends within data that has a high number of dimensions, making this technique well suited to mining the maximum information from the exoplanet archive. The results focus on imputing planetary mass; a particularly tricky measurement as neither of the two main techniques for exoplanet detection --radial velocity and transit methods-- can estimate this value alone. However, the principal could be applied to other planetary properties and used to explore both formation theories or target selection schemes for future instruments.

Keywords: exoplanets, machine learning, catalogues

©2020. Japan Geoscience Union. All Right Reserved.



©2020. Japan Geoscience Union. All Right Reserved.

[E] Poster | P (Space and Planetary Sciences)：P-CG Complex & General

[P-CG23] Shock responses of planetary materials elucidated from meteorites and laboratory experiments

convener:Takuo Okuchi(Institute for Planetary Materials, Okayama University), Toshimori Sekine(Center for High Pressure Science and Technology Advanced Research), Naotaka Tomioka(Kochi Institute for Core Sample Research, Japan Agency for Marine-Earth Science and Technology)

Impact phenomena have been recognized to play essential roles in the processes of planetary evolution. Recent progresses in nanoscale analysis of meteorites, asteroid explorations, as well as laboratory experiments for simulating shock dynamics on planetary materials are collaboratively revealing complex effects of shock-induced processes in planetary evolution. Recently, several new metastable high-pressure phases have been identified in strongly shocked meteorites. Their occurrences indicate that the shock-induced physical states are far from thermodynamic equilibrium and contain very complicated processes. On the other hand, laboratory experiments including laser-driven shock techniques have recently been making remarkable progresses. They successfully simulate a variety of fast non-equilibrium processes at transient high-pressure conditions reaching tens to a few hundreds of gigapascals, that uniquely affect the physical and chemical properties of planetary materials upon impacts. Here we discuss how planetary materials are compressed, fractured, transformed, melted, and quenched during impact events by referring these recent studies. We welcome presentations from interdisciplinary research fields related to shock responses of planetary materials.

[PCG23-P01] Nanofragmentation as potential marks of multiple low-velocity impacts in carbonaceous chondrites

*Balazs Bradak[1], Yusuke Seto[2], Akos Kereszturi[3,4], Martin Chadima[5], Masayuki Hyodo[6] (1.Department of Physics, University of Burgos, Burgos, Spain, 2.Department of Planetology, Kobe University, Kobe, Japan, 3.Konkoly Thege Miklos Astronomical Institute, Research Centre for Astronomy and Earth Sciences, MTA Centre for Excellence, Budapest, Hungary, 4.European Astrobiology Institute, virtual institute hosted by the European Science Foundation, Strasbourg, France, 5.AGICO Inc., Brno, Czech Republic, , 6.Research Center for Inland Seas, Kobe University, Kobe, Japan)

[PCG23-P02] *In-situ* observations of shock-induced dehydration of goethite

*Tsubasa Tobase[1], Huijeong Hwang[2], Yongjae Lee[2], Takuo Okuchi[3], Toshimori Sekine[1,4] (1.Center for High Pressure Science and Technology Advanced Research, 2.Department of Earth System Sciences, Yonsei University, 3.Institute of Planetary Materials, Okayama University, 4.Graduate School of Engineering, Osaka University)

[PCG23-P03] Gekko XII experiment on magnetized collisionless shock

*Shuichi Matsukiyo[1], Takumi Higuchi[2], Hiroo Murakami[2], Youichi Sakawa[3], Taichi Morita[1], Kentaro Tomita[1], Ryo Yamazaki[4], Takayoshi Sano[3], Yasuhiro Kuramitsu[5], Shuta J Tanaka[4], Natsuki Ishizaka[4], Shin Kakuchi[4], Shuto Sei[4], Kei Sugiyama[4], Masato Ota[3], Shunsuke Egashira[3], Tomohiro Izumi[3], Kentaro Sakai[5], Takumi Minami[5], Hiroki Nishioka[2], Mariko Takagi[2], Takuto Kojima[2], Kento Aihara[4], Shota Kanbayashi[4], Sara Tomita[4], Yoshiharu Nakagawa[3], Takahiro Nishimoto[5], Masaki Takano[5] (1.Faculty of Engineering Sciences, Kyushu University, 2.Interdisciplinary Graduate School of Engineering Sciences, Kyushu University, 3.Institute of Laser Engineering, Osaka University, 4.Department of Physics and Mathematics, Aoyama Gakuin University, 5.Graduate School of Engineering, Osaka University)

[PCG23-P04] Laser-driven shock compression experiments of synthetic wadsleyite and ringwoodite crystals

*Takuo Okuchi[1], Narangoo Purevjav[1], Norimasa Ozaki[2], Takayoshi Sano[3], Yuhei Umeda[2], Ryosuke Kodama[2,3] (1.Institute for Planetary Materials, Okayama University, 2.Graduate School of Engineering, Osaka University, 3.Institute of Laser Engineering, Osaka University)

[PCG23-P05] *In situ* observation of phase transition behavior of shocked baddeleyite

*Sota Takagi[1,2], Atsushi Kyono[1], Shunsuke Nozawa[2], Nobuaki Kawai[3], Koji Inukai[4], Ryo Fukaya[2], Nobumasa Funamori[2], Shin-ichi Adachi[2], Kouhei Ichiyanagi[2] (1.University of Tsukuba, 2.KEK, 3.Kumamoto University, 4.Noritake Co., Limited)

[PCG23-P06] Dynamic behavior of calcite under planetary impact condition

★Invited Papers

*Yuhei Umeda[1,2], Keiya Fukui[1], Toshimori Sekine[3,1], Marco Guaruaglini[4], Alessandra Benuzzi-Mounaix[4], Nobuki Kamimura[1], Kento Katagiri[1], Ryosuke Kodama[1,2], Takeshi Matsuoka[1], Kohei Miyanishi[5], Alessandra Ravasio[4], Takayoshi Sano[2], Norimasa Ozaki[1,2] (1.Graduate School of Engineering, Osaka University, 2.Institute of Laser Engineering, Osaka University, 3.Center for High Pressure Science & Technology Advanced Research, 4.Ecole Polytechnique, 5.Riken, Spring-8, SACLA)

Nanofragmentation as potential marks of multiple low-velocity impacts in carbonaceous chondrites

*Balazs Bradak[1], Yusuke Seto[2], Akos Kereszturi[3,4], Martin Chadima[5], Masayuki Hyodo[6]

1. Department of Physics, University of Burgos, Burgos, Spain, 2. Department of Planetology, Kobe University, Kobe, Japan, 3. Konkoly Thege Miklos Astronomical Institute, Research Centre for Astronomy and Earth Sciences, MTA Centre for Excellence, Budapest, Hungary, 4. European Astrobiology Institute, virtual institute hosted by the European Science Foundation, Strasbourg, France, 5. AGICO Inc., Brno, Czech Republic, , 6. Research Center for Inland Seas, Kobe University, Kobe, Japan

The research focuses on the paradox between the low shock stage of carbonaceous chondrites and the marks of hypervelocity impacts, indicated by magnetic parameters which shows the mark of significant alteration triggered by impact induced shock.

Solving the paradox above a theory about the role of multiple impact produced structures instead of one energetic hypervelocity impact has been already introduced. Based on this theory, we propose a hypothesis and test of nanoscale fragmentation as evidence for multiple low-intensity impacts by nanoscale mineral components. Nano-scale minerals may be created and re-aligned by the physical weathering of coarser grains triggered by the shock of multiple impacts. Our goal is to support or decline the hypothesis by performing magnetic fabric studies, which are capable of separating the ultra-fine grain components, i.e., the possible indicator of nanofragments and their character.

Scanning electron microscope, rock magnetic and magnetic fabric studies were conducted on three carbonaceous chondrites: Allende, Jbilet Winselwan (Jbilet) and Murchison. FeNi alloys, iron sulphides (pyrrhotite) and magnetite were the main magnetic minerals contributing to the magnetic fabric. The fabric was foliated, and the susceptibility ellipsoid was oblate, thus indicating that impacts are an important process in the development of the fabric; this finding is consistent with previous studies. Significant differences were revealed between the studied meteorites by comparison of the anisotropy of the magnetic susceptibility and the frequency dependence of the anisotropy of magnetic susceptibility parameters (a sensitive indicator of the alignment of nano-size magnetic grains).

Comparison of the three studied meteorites suggested a complex ‘impact history’. The foliated well-aligned directions in the fabric of the studied meteorites and homogenized (non-scattering fabric parameters) may suggest the influence of a hypervelocity impact, which probably influenced the fabric of the (parent body of the) meteorite at the regional level. In contrast to the influence of the hypervelocity impact, which caused the fracturing and dislocation of the grains in the entire fabric, the repeating low-velocity impact potentially induced 1.) the weakening of the foliation (e.g., Allende, Murchison) in general and 2.) the formation and dispersed distribution of nanofragments (e.g. Allende and Jbilet) by e.g. physical erosion of the coarser grains or their re-alignment (e.g., Murchison). This phenomenon might appear differently in various parts of the meteorite, in which heterogeneity (in the magnetic parameters –scattering data) might indicate the limitation in spreading of the effect of multiple low-intensity impacts.

Keywords: multiple low velocity impacts, magnetic fabric alteration, nanofragmentation

©2020. Japan Geoscience Union. All Right Reserved.

In-situ observations of shock-induced dehydration of goethite

*Tsubasa Tobase[1], Huijeong Hwang[2], Yongjae Lee[2], Takuo Okuchi[3], Toshimori Sekine[1,4]

1. Center for High Pressure Science and Technology Advanced Research, 2. Department of Earth System Sciences, Yonsei University, 3. Institute of Planetary Materials, Okayama University, 4. Graduate School of Engineering, Osaka University

Hydrous minerals play a role as water carrier because of their high temperature stabilities and shock resistance. Water is present as a major component of the atmospheres, surfaces, and interiors of planets, and it is important to investigate the dehydration reactions in hydrous minerals by impact processes to understand the formation and evolution of planets and the origin of life. We presented the shock recovery experimental results on goethite last year. At that time, powdered samples were capsuled in steel containers although the containers were not completely closed and there was a small gap space for dehydrated water to escape freely. The results indicated partial dehydration and produced hematite. However, it remains an open question when the dehydration occurred and what effects are expected at the partial water pressure. This time we carry out direct observation of the dehydration reaction by *in-situ* x-ray diffraction using an x-ray free electron laser (XFEL) to confirm the dehydration of goethite.

We tried to prepared sintered bodies of goethite at high pressures but failed to have thin plates. Instead we prepared thin films of goethite powders glued by manicure (~200 mm thick). We used XFEL at Pohang with a flat panel x-ray detector to observe the diffractions and an optical laser to drive shock wave. The XFEL beam is 25 fs at 12 keV and focused ~20 mm diameter and optical laser beam with 150 ps FWHM, 800 nm wavelength, and ~1 mJ energy focused ~40 mm diameter. The samples were free standing and subject to vertical XFEL beam and 5 degree off optical laser beam from the normal.

We obtained a series of diffraction images as a function of delay time for optical laser irradiation. All the diffractions consisted of those from the starting goethite without manicure, detailed analyses for the strong peaks of hematite as the dehydration product revealed that the shoulders of goethite peaks contains part of hematite peaks at late delay times. This can confirm *in-situ* formation of hematite by the shock-induced dehydration of goethite. The nucleation and growth of hematite during shock compression are extreme fast, and can be explained to be quenchable from the previous shock recovery experiments. We did not measure the pressure directly, and we can evaluate the threshold pressure from the diffraction peak shit of the hematite. These results suggest dehydration of goethite at relatively low shock pressures. The usage of manicure glue will help powdered sample preparation for XFEL that requires thin enough samples and we will develop further to apply not only hydrous minerals but also silicates by the help of manicure for XFEL experiments.

We thank the PAL-XFEL team for their help. This research was partially supported by the National Natural Science Foundation of China (NSFC No. 41974099).

Keywords: Goethite, Dehydration, Laser shock compression, XFEL

©2020. Japan Geoscience Union. All Right Reserved.

Gekko XII experiment on magnetized collisionless shock

*Shuichi Matsukiyo[1], Takumi Higuchi[2], Hiroo Murakami[2], Youichi Sakawa[3], Taichi Morita[1], Kentaro Tomita[1], Ryo Yamazaki[4], Takayoshi Sano[3], Yasuhiro Kuramitsu[5], Shuta J Tanaka[4], Natsuki Ishizaka[4], Shin Kakuchi[4], Shuto Sei[4], Kei Sugiyama[4], Masato Ota[3], Shunsuke Egashira[3], Tomohiro Izumi[3], Kentaro Sakai[5], Takumi Minami[5], Hiroki Nishioka[2], Mariko Takagi[2], Takuto Kojima[2], Kento Aihara[4], Shota Kanbayashi[4], Sara Tomita[4], Yoshiharu Nakagawa[3], Takahiro Nishimoto[5], Masaki Takano[5]

1. Faculty of Engineering Sciences, Kyushu University, 2. Interdisciplinary Graduate School of Engineering Sciences, Kyushu University, 3. Institute of Laser Engineering, Osaka University, 4. Department of Physics and Mathematics, Aoyama Gakuin University, 5. Graduate School of Engineering, Osaka University

Collisionless shocks often play important roles in various high energy phenomena in space. Shock reformation is a periodic collapse and formation process of the shock front occurring even when the upstream plasma is completely uniform and steady, and contributes to the generation of large amplitude waves and to particle acceleration. It is a phenomenon unique to a collisionless system. The structure called a foot, ramp, and overshoot repeats formation and collapse with gyro motion of the ions reflected at a shock. It was theoretically predicted in the 1980s by using computer simulation, but has not been proven yet. In this research we aim at the demonstration of shock reformation, which is not realized by the in-situ observation in space, by using the Gekko XII high power laser experiment at Institute of Laser Engineering (ILE), Osaka University. An aluminum plate target surrounded by nitrogen gas, to which an external magnetic field is applied, is irradiated by the Gekko XII laser (700 J * 4 beam, a wavelength of 1053 nm, a Gaussian long pulse (1.3 ns)). The target plasma sweeps the magnetized gas plasma which is produced by the strong radiation due to laser-target interaction. As a result, a shock wave is generated in the magnetized gas plasma. In the experiment in 2019 we could successfully apply 3.8T ambient magnetic field in the experimental system for the first time. The observed shock clearly contains inner structures not seen in our previous experiments without ambient magnetic field. We identified the so-called overshoot and foot in the shock transition region. In addition, a precursor of a shock modified by the ambient magnetic field is also identified in the early stage after the main laser shot.

Keywords: high power laser experiment, collisionless shock, magnetic field

©2020. Japan Geoscience Union. All Right Reserved.

Laser-driven shock compression experiments of synthetic wadsleyite and ringwoodite crystals

*Takuo Okuchi[1], Narangoo Purevjav[1], Norimasa Ozaki[2], Takayoshi Sano[3], Yuhei Umeda[2], Ryosuke Kodama[2,3]

1. Institute for Planetary Materials, Okayama University, 2. Graduate School of Engineering, Osaka University, 3. Institute of Laser Engineering, Osaka University

Dense mineral polymorphs of Mg_2SiO_4 (β-phase as wadsleyite, γ-phase as ringwoodite, and ε-phase as poirierite [1,2]) are possible major constituents of mantles of terrestrial planets, as well as of extrasolar super-Earths. Physical properties of these polymorphs at high pressure and temperature conditions are essential for understanding the past evolution history and current status of these rocky planets. Laser-shock Hugoniot measurements of α-Mg_2SiO_4 forsterite with the lowest initial denstiy, previously conducted at GEKKO-XII high-power laser system at Osaka University, had provided significant evidences on its incongruent melting and crystallization phenomena at ~ 300 GPa and ~ 10^4 K [3], which has stimulated discussion on physical and chemical processes of Mg_2SiO_4 system during the growth histories of the large-sized rocky planets. On the other hand, Hugoniot equation of states of the other polymorphs of Mg_2SiO_4, as represented by those of wadsleyite with ~ 8 % larger density and of ringwoodite with ~14 % larger density than forsterite, were not yet systematically studied; these will provide independent evidences on the relevant properties of Mg_2SiO_4, such as the existences of inhomogenious liquids generated by incongruent melting at wide pressure and temperature regimes.

We are therefore conducting systematic measurements on the Hugoniot states of these polymorphs by using GEKKO-XII laser system [5], which includes the regimes of their melting. The target sample crystals of dense minerals were synthesized using our pre-established slow-cooling method at static high pressure and temperature conditions [4]. These sample crystals are physically homogeneous and optically perfectly transparent, which give very high quality datasets of velocity interferometer system coupled with the high-power laser. The current results and technical developments will be presented and discussed.

References

[1] Tomioka, N. and Okuchi, T. (2017) Sci. Rep. 7, 17351.
[2] Tomioka, N. et al. submitted.
[3] Sekine, T. et al. (2016) Sci. Adv. 2, e1600157.
[4] Okuchi, T. et al. (2015) Am. Mineral. 100, 1483.
[5] Purevjav et al. (2019) JpGU abstract PCG22-P04.

Keywords: dense polymorphs of Mg2SiO4, shock compression, Hugoniot, melting

©2020. Japan Geoscience Union. All Right Reserved.

In situ observation of phase transition behavior of shocked baddeleyite

*Sota Takagi[1,2], Atsushi Kyono[1], Shunsuke Nozawa[2], Nobuaki Kawai[3], Koji Inukai[4], Ryo Fukaya[2], Nobumasa Funamori[2], Shin-ichi Adachi[2], Kouhei Ichiyanagi[2]

1. University of Tsukuba, 2. KEK, 3. Kumamoto University, 4. Noritake Co., Limited

1. Introduction

Baddeleyite (ZrO_2), commonly found in mafic igneous rock, can be applied as a shock pressure barometer and a geochronometer in meteorites. It can offer essential information on the timing and intensity of a meteorites impact, which help us to understand the planetary formation and evolution. Previous researches on natural shocked-baddeleyite in the earth’s rock and meteorites have observed grain refinement and the orthogonally related crystallographic orientations of the baddeleyite grains, which may infer the occurrence of phase transition. Although the phase transition behavior of baddeleyite at high pressures has been intensively investigated under hydrostatic conditions, there is little information on dynamic response of the phase transition under shock loading conditions. Therefore, it is required to clarify the phase transition behavior of baddeleyite under shock compression in order to utilized as a shock barometer.

Here, we performed *in situ* X-ray diffraction measurements on shock-loaded baddeleyite on nanosecond time scale using shock-driving laser and synchrotron X-ray.

2. Methods

We performed the experiments at NW14A beamline at PF-AR (Photon Factory Advanced Ring), High Energy Accelerator Research Organization (KEK), Japan. Baddeleyite samples were in form of square-shaped plates with dimensions 5 ×5 and a thickness of 0.06 mm. A 25 μm PET film ablator with Al coating was attached on the sample surface. The crystal structure of the sample was determined by XRD to be monoclinic (space group $P2_1/c$) with lattice parameter of a = 5.156(2) Å, b = 5.199(2) Å, c = 5.310(2) Å, β = 99.23(3)°, and V = 140.54(6) Å^3. Nd:glass laser with the wavelength of 1064 nm, pulse energy of 16 J, pulse width of 12 ns at the beamline was used for shock-driving source. The laser beam was focused by optical lens to a diameter of 500 μm on the sample surface. The velocity data was obtained by VISAR (velocity interferometer system for any reflector) measurement. For TR-XRD experiments, the synchrotron X-ray pulse of PF-AR was used as a probe source. The energy, the pulse width, and the size on the sample surface were 15.57 keV, about 100 ps, and 450 μm (H) ×250 μm (W), respectively. The XRD data at the timing within 40 ns after shock compression and that beyond 1000 ns were collected. For each XRD data, lattice parameters were refined by Rietveld method.

3. Results

The free surface velocity reached 0.914 km/s. From the velocity, the peak shock pressure determined by the U_s–u_p Hugoniots (U_s = 4.38 + 1.37 u_p km/s) (Mashimo et al., 1983) was 13.4 GPa.

The phase transition from monoclinic phase to orthorhombic-I ZrO_2 phase (the first high-pressure phase) was observed at 6.5 ns (compression state). The phase transition boundary under shock compression was determined to be 3.3 GPa, which is slightly lower than that observed in the previous static compression experiments. The compression of orthorhombic-I ZrO_2 reached to V/V_0 = 0.956, corresponding to the pressure of 14.0 GPa. Although the peak pressure in the study was beyond the phase transition boundary between orthorhombic-I and orthorhombic-II ZrO_2 (the second high-pressure phase) in phase diagram, orthorhombic-II ZrO_2 did not appear. During release state, orthorhombic-I ZrO_2 returned to monoclinic

©2020. Japan Geoscience Union. All Right Reserved.

phase, and finally orthorhombic-I ZrO_2 disappeared completely. Our direct observation revealed that the displacive-type phase transition between monoclinic and orthorhombic-I ZrO_2 can occur regardless of strain rate, but the reconstructive-type phase transition between orthorhombic-I and orthorhombic-II ZrO_2 depends on the time scale of compression.

Keywords: baddeleyite, laser shock, synchrotron time-resolved XRD

©2020. Japan Geoscience Union. All Right Reserved.

Dynamic behavior of calcite under planetary impact condition

*Yuhei Umeda[1,2], Keiya Fukui[1], Toshimori Sekine[3,1], Marco Guaruaglini[4], Alessandra Benuzzi-Mounaix[4], Nobuki Kamimura[1], Kento Katagiri[1], Ryosuke Kodama[1,2], Takeshi Matsuoka[1], Kohei Miyanishi[5], Alessandra Ravasio[4], Takayoshi Sano[2], Norimasa Ozaki[1,2]

1. Graduate School of Engineering, Osaka University, 2. Institute of Laser Engineering, Osaka University, 3. Center for High Pressure Science & Technology Advanced Research, 4. Ecole Polytechnique, 5. Riken, Spring-8, SACLA

No EOS models over 100 GPa, which corresponds to planetary impacts conditions, has been investigated by the experimental approach although calcite is a common mineral in chodritic meteorites and surface materials of rocky planets. In this study, calcite single crystals were shock compressed to pressures between 200 and 1000 GPa using the laser driven decaying shock method. Our temperature profiles by decaying shock experiments indicated the large difference from the theoretical model (SESAME 7331) with increasing pressure, and a melting of shocked calcite occurred between 140 and 270 GPa along the Hugoniot. The residual temperature of released calcite was estimated to be approximately 3300 K at the shock pressure of 200 GPa (at shock temperature of 6000 K).

Keywords: Laser shock compression, Planetary impact, Calcite, Shock-induced gas

©2020. Japan Geoscience Union. All Right Reserved.

[E] Poster | P (Space and Planetary Sciences)：P-CG Complex & General

[P-CG24] Future missions and instrumentation for space and planetary science

convener:Kazuo Yoshioka(Graduate School of frontier Science, The University of Tokyo), Satoshi Kasahara(The university of Tokyo), Kazunori Ogawa(Japan Aerospace Exploration Agency), Mitsunori Ozaki(Faculty of Electrical and Computer Engineering, Institute of Science and Engineering, Kanazawa University)

Not only national space agencies but some universities and even companies in the world are now leading a number of space science and exploration missions and also energetically initiating new research activities for satellite and rocket developments and international collaborations in these days because the Earth observations from the space and the space explorations could be achieved much easier than a few decades ago (e.g. ultra-small satellite). The deployment to the space, which itself is not purely a scientific purpose but one of methods for better sciences, is vigorously motivating the technical innovation and the educational development. For successful space missions, it is also crucial to research and develop aim-oriented on-board instruments, and the fundamental research and development of observational instrumentation with future perspectives could totally lead space missions in some case. Detailed investigation and evaluation on various on-board instruments are needed during their proposals, selections, and fabrications in order to promote the missions, and inevitably we have to make multi-sided arrangements and evolution at every process and aspect of any type of space missions, independently of their mission sizes. In this session, we focus on these comprehensive research activities in the space and astronomy missions, including the mission integrations and the individual instrumental developments, and we also call many presentations showing the uniqueness and renovation regarding the mission strategy and methodology, and the status and latest results in the related state-of-the-art researches and developments, which would provide all of researchers and developers with invaluable opportunities for active discussion, information sharing, and collaboration toward the realization of more missions for more fruitful space sciences and explorations in nearer future.

[PCG24-P01] Stray-Light Analysis and Improvement Method of Wide-Angle Multiband Camera OROCHI onboard MMX

*Ryota Fuse[1], Keigo Enya[2], Shingo Kameda[3], Hiroki Kato[3], Masanobu Ozaki[2], Ko Ishibashi[4], Toru Kouyama[5], Shinsuke Abe[1] (1.Nihon University, 2.Japan Aerospace Exploration Agency, 3.Rikkyo University, 4.Chiba Institute of Technology, 5.National Institute of Advanced Industrial Science and Technology)

[PCG24-P02] Organizational framework for scientific studies and instruments in Martian Moons Exploration (MMX) mission

*Kazunori Ogawa[1], Koji Wada[2], Tomohiro Usui[1], Shingo Kameda[3], Tomoki Nakamura[4], Kiyoshi Kuramoto[5], Jean-Pierre Bibring[6], Masaki Fujimoto[1], Hidenori Genda[7], Jörn Helbert[8], Naru Hirata[9], Takeshi Imamura[10], Yasuhiro Kawakatsu[1], Masanori Kobayashi[2], Hiroki Kusano[11], David Lawrence[12], Koji Matsumoto[13], Patrick Michel[14], Hideaki Miyamoto[10], Hiromu Nakagawa[4], Hisashi Otake[1], Sara Russell[15], Sho Sasaki[16], Hirotaka Sawada[1], Hiroki Senshu[2], Naoki Terada[4], Stephan Ulamec[8], Sei-ichiro WATANABE[17], Shoichiro Yokota[16] (1.Japan Aerospace Exploration Agency, 2.Chiba Institute of Technology, 3.Rikkyo University, 4.Tohoku University, 5.Hokkaido University, 6.Université de Paris-Sud, 7.Tokyo Institute of Technology, 8.Deutsches Zentrums für Luft- und Raumfahrt, 9.Aizu University, 10.The University of Tokyo, 11.National Institutes for Quantum and Radiological Science and Technology, 12.The Johns Hopkins University, 13.National Astronomical Observatory of Japan, 14.Observatoire de la Côte d'Azur, 15.Natural History Museum, 16.Osaka University, 17.Nagoya University)

[PCG24-P03] Design of Small Ion Mass Spectorometer for Comet Interceptor Mission

*Rurie Mizuno[1], Satoshi Kasahara[1] (1.The university of Tokyo)

[PCG24-P04] An international multi-point space exploration mission for intergrated observations in the space-Earth coupling system

*Masafumi Hirahara[1], Masatoshi Yamauchi[2], Yoshifumi Saito[3], Hirotsugu Kojima[4], Kazushi Asamura[3], Takeshi Sakanoi[6], Yoshizumi Miyoshi[1], Naritoshi Kitamura[5] (1.Institute of Space-Earth Environmental Research, Nagoya University, 2.Swedish Institute of Space Physics, 3.Institute of Space and Astronautical Science, Japan Aerospace Exploration Agency, 4.Research Institute for Sustainable Humanosphere, Kyoto University, 5.Graduate School of Science, The University of Tokyo, 6.Graduate School of Science, Tohoku University)

[PCG24-P05] Auroral imaging at visible and far-ultra-violet wavelengths for the future polar orbiting satellite mission FACTORS

*Takeshi Sakanoi[1], Masafumi Hirahara[2], Yoshizumi Miyoshi[2], Kazushi Asamura[3], Keisuke Hosokawa[4], Yoshifumi Saito[3], Hirotsugu Kojima[5], Naritoshi Kitamura[7], Mizuki Fukizawa[1], Shin-ichiro Oyama[2], Takuo T. Tsuda[4], Akinori Saito[6], Harald Frey[8], Nick Shneider[9] (1.Planetary Plasma and Atmospheric Research Center, Graduate School of Science, Tohoku University, 2.ISEE, Nagoya University, 3.ISAS/JAXA, 4.School of Informatics and Engineering, The University of Electro-Communications, 5.RISH, Kyoto University, 6.Graduate Shool of Science, Kyoto University, 7.Graduate Shool of Science, The University of Tokyo, 8.SSL, University of California, Berkeley, 9.LASP, University of Colorado Boulder)

[PCG24-P06] Design of electric field measurements in the future mission FACTORS targeting transverse ion acceleration in the terrestrial polar magnetosphere

*Hirotsugu Kojima[1], Naritoshi Kitamura[2], Koji Shibuya[1], Ibuki Fukasawa[1], Yasumasa Kasaba[3], Masafumi Hirahara[4], Yoshiya Kasahara[5], Yohei Miyake[8], Hideyuki Usui[6], Kazushi Asamura[7], Yoshifumi Saito[7] (1.Research institute for sustainable humanosphere, Kyoto University, 2.Graduate School of Science, University of Tokyo, 3.Planetary Plasma and Atmospheric Research Center, Graduate School of Science, Tohoku University, 4.Institute for Space–Earth Environmental Research, Nagoya University, 5.Advanced Research Center for Space Science and Technology, Kanazawa University, 6.Graduate School of System Informatics, Kobe University, 7.Institute of Space and Astronautical Science, Japan Aerospace Exploration Agency, 8.Education Center on Computational Science and Engineering, Kobe University)

[PCG24-P07] Investigation of requirements for regolith thrusters

*Noruji MUTO[1], Necmi Cihan ORGER[1], Jose Rodrigo CORDOVA-ALARCON[1], Kazuhiro Toyoda[1], Mengu Cho[1] (1.Kyushu Institute of Technology)

[PCG24-P08] Attitude Control System for Kanazawa-SAT3 Microsatellite

*Yuki Yasuda[1], Kohei Fujiki[1], Takuya Nakashima[1], Tomohiko Imachi[1], Satoshi Yagitani[1], Yoshiya Kasahara[1], Daisuke Yonetoku[1], Tatsuya Sawano[1], Makoto Arimoto[1] (1.Kanazawa University)

[PCG24-P09] Microsatellite Development and Education of Space Science and Technology at Kanazawa University

*Tomohiko Imachi[1], Satoshi Yagitani[1], Daisuke Yonetoku[1], Yoshiya Kasahara[1], Tatsuya Sawano[1], Makoto Arimoto[1], Kei Sano[1], Yoshitaka Goto[1], Mitsunori Ozaki[1], Ryuichi Fujimoto[1] (1.Kanazawa University)

[PCG24-P10] S Band and UHF Band Communication Systems for Kanazawa-SAT3 Microsatellite

*Koyo Ina[1], Mayuko Tachiya[1], Teruya Minamoto[1], Tomohiko Imachi[1], Satoshi Yagitani[1], Yoshitaka Goto[1], Daisuke Yonetoku[1], Yoshiya Kasahara[1], Tatsuya Sawano[1], Makoto Arimoto[1] (1.Kanazawa University)

[PCG24-P11] Development of ASIC for energetic electron detector for future planetary explorations

*Shin Sugo[1], Satoshi Kasahara[1], Hirokazu Ikeda[2], Hirotsugu Kojima[3], Takahiro Zushi[4], Motoyuki Kikukawa[3], Kazushi Asamura[2] (1.The University of Tokyo, 2.Institute of Space and Astronautical Science, 3.Research institute for sustainable humanosphere, Kyoto University, 4.National Institute of Technology, Nara College)

[PCG24-P12] Development and Integration of the High-Speed Current Detection Circuits in Particle Sensors Dedicated to Wave-Particle Interaction Analyzer

*Motoyuki Kikukawa[1], Hirotsugu Kojima[1], Kazushi Asamura[2], Yoshifumi Saito[2] (1.Research Institute for Sustainable Humanosphere, Kyoto University, 2.Institute of Space and Astronautical Science)

[PCG24-P13] Development of the wideband analog integrated circuit for plasma wave receivers

*Shoya Nakao[1], Takahiro Zushi[1], Hirotsugu Kojima[2] (1.National Institute of Technology, Nara College, 2.Kyoto University)

[PCG24-P14] Basic study on search coil magnetometer for improving magnetic sensitivity

*Yohei Yamaka[1], Yuya Tokunaga[1], Mitsunori Ozaki[1], Satoshi Yagitani[1] (1.Kanazawa University)

[PCG24-P15] Development of an instrument to measure ion drift velocity and density in the ionosphere

*Takumi Abe[1], Shigeto Watanabe[2], Akinori Saito[3], Ryuto Hashiba[4] (1.Japan Aerospace Exploration Agency, Institute of Space and Astronautical Science Department of Solar System Sciences, 2.Hokkaido Information University, 3.Kyoto University, Graduate School of Science, 4.Hokkaido Universiity)

[PCG24-P16] Satellite-to-satellite radio occultation for the exploration of planetary atmospheres

*Takeshi Imamura[1], Hiroki Ando[2], Norihiko Sugimoto[4], Hideo Sagawa[2], Masahiro Takagi[2], Katsuyuki Noguchi[8], Kazunori Ogohara[7], Atsushi Yamazaki[9], Takahiro Iwata[9], Tomotaka Yamamoto[3], Satoshi Ikari[3], Yosuke Kawabata[3], Shoko Sano[3], Yukiko Fujisawa[4], Ryu Funase[3], Mutsuko Morimoto[4], Mirai Abe[6], Asako Hosono[5] (1.Graduate School of Frontier Sciences, The University of Tokyo, 2.Faculty of Science, Kyoto Sangyo University, 3.Department of Aeronautics and Astronautics, The University of Tokyo, 4.Department of Physics, Keio University, 5.Toshimagaoka Women High School, 6.Faculty of Law, Keio University, 7.School of Engineering, The University of Shiga Prefecture, 8.Department of Information and Computer Sciences, Nara Women's University, 9.Institute of Space and Astronautical Science, Japan Aerospace Exploration Agency)

[PCG24-P17] Life-signature Detection fluorescence Microscope (LDM)

*Enya Keigo[1], Yoshitaka - Yoshimura[2], Satoshi - Sasaki[3], Akihiko - Yamagishi[1,4], Atsuo - Miyakawa[4], Eiichi - Imai[5], Hajime - Mita[7], Takehiko Satoh[1], Kensei - Kobayashi[6], Yoko - Kebukawa[6], Tomoka - Okada[6], Hikaru - Yabuta[8], Takeshi - Naganuma[8], Tomoiro - Usui[1], Kazuhisa - Fujita[1] (1.Institute of Space and Astronautical Science, 2.Tamagawa University, 3.Tokyo University of Technology, 4.Tokyo University of Pharmacy and Life Science, 5.Nagaoka University of Technology, 6.Yokohama National University, 7.Fukuoka Institute of Technology, 8.Hiroshima University)

[PCG24-P18] Development of a near-infrared high-resolution Echelle spectrograph ESPRIT for planetary atmospheric observations

*Ayumu Kambara[1], Takeshi Sakanoi[1], Masato Kagitani[1], Yasumasa Kasaba[1], Aya Otomo[1], Yasuhiro Hirahara[2] (1.Planetary Plasma and Atmospheric Research Center, Graduate School of Science, Tohoku University, 2.Graduate School of Environmental Studies, Nagoya University)

[PCG24-P19] Development of the absorption cell filters for remote D/H observation

*Masaki Kuwabara[1], Kazuo Yoshioka[2], Makoto Taguchi[3], Takuya Kawahara[4], Shingo Kameda[3] (1.JAXA, 2.The Univ. of Tokyo, 3.Rikkyo Univ., 4.Shinshu Univ.)

Stray-Light Analysis and Improvement Method of Wide-Angle Multiband Camera OROCHI onboard MMX

*Ryota Fuse[1], Keigo Enya[2], Shingo Kameda[3], Hiroki Kato[3], Masanobu Ozaki[2], Ko Ishibashi[4], Toru Kouyama[5], Shinsuke Abe[1]

1. Nihon University, 2. Japan Aerospace Exploration Agency, 3. Rikkyo University, 4. Chiba Institute of Technology, 5. National Institute of Advanced Industrial Science and Technology

The Martian Moons eXploration (MMX) is planned to survey two Martian moons, Phobos and Deimos, and return samples from Phobos. MMX will be launched in 2024 and carries several scientific instruments. The OROCHI (Optical RadiOmeter composed of Chromatic Imagers) is wide-angle multiband camera which consists of 7 cameras with bandpass filter in specific visible wavelength (e.g., 730nm; Phyllosilicate feature). The specification is 12.22 mm/F4, 3296(H) x 2472(V) pix, 73(H) x 58(V) deg, 20 m/pix@20km, MTF@Nyquist>0.3. The OROCHI is aimed to constrain the global surface composition and physical structure of Phobos. In our scientific goals, Signal-to-Noise ratio of the OROCHI needs to be S/N > 100 in order to detect faint absorption clearly. Origins of the noise are mainly electrical noise from a CCD sensor and stray light from a optical system, and we focused on the latter. Stray light is generated by reflected lights at sensor, filter, and lens surfaces, therefore, the S/N ratio depends on these reflectance. We designed a similar optical system of the OROCHI in software and performed stray light analysis by measuring the reflectance of a sensor candidate and assuming that of filter and lens. Then, we estimated the S/N ratio. Although the S/N did not reach 100 at the beginning of analysis, we could achieve finally over 100 by following approaches; decreasing the reflectance of the filter and lens, keeping the filter away from the sensor, and reducing the number of lenses. In this study, we propose the OROCHI’s optical design, results of stray light analysis, and the improvement method.

Keywords: MMX, camera, stray light

©2020. Japan Geoscience Union. All Right Reserved.

Organizational framework for scientific studies and instruments in Martian Moons Exploration (MMX) mission

*Kazunori Ogawa[1], Koji Wada[2], Tomohiro Usui[1], Shingo Kameda[3], Tomoki Nakamura[4], Kiyoshi Kuramoto[5], Jean-Pierre Bibring[6], Masaki Fujimoto[1], Hidenori Genda[7], Jörn Helbert[8], Naru Hirata[9], Takeshi Imamura[10], Yasuhiro Kawakatsu[1], Masanori Kobayashi[2], Hiroki Kusano[11], David Lawrence[12], Koji Matsumoto[13], Patrick Michel[14], Hideaki Miyamoto[10], Hiromu Nakagawa[4], Hisashi Otake[1], Sara Russell[15], Sho Sasaki[16], Hirotaka Sawada[1], Hiroki Senshu[2], Naoki Terada[4], Stephan Ulamec[8], Sei-ichiro WATANABE[17], Shoichiro Yokota[16]

1. Japan Aerospace Exploration Agency, 2. Chiba Institute of Technology, 3. Rikkyo University, 4. Tohoku University, 5. Hokkaido University, 6. Université de Paris-Sud, 7. Tokyo Institute of Technology, 8. Deutsches Zentrums für Luft- und Raumfahrt, 9. Aizu University, 10. The University of Tokyo, 11. National Institutes for Quantum and Radiological Science and Technology, 12. The Johns Hopkins University, 13. National Astronomical Observatory of Japan, 14. Observatoire de la Côte d'Azur, 15. Natural History Museum, 16. Osaka University, 17. Nagoya University

The Martian Moons Exploration (MMX) mission has been planned to launch a Martian moons probe in 2024 as one of next planetary exploration missions in Japan. In this mission, the spacecraft reaches on quasi-satellite orbits around Phobos and makes remote-sensing observations. The spacecraft then carries out two times of landing and samples material of the Phobos surface. The spacecraft finally comes back to the Earth to bring the collected samples back. The MMX program shifted to the Phase-B in the beginning of February 2020 and basic design of the spacecraft and instruments have been started. In this presentation, we introduce the science-side organizational framework of MMX including science teams and scientific instrument teams we have constructed so far in the entire organization of MMX.

MMX has a new concept of organized science teams and this concept is a new attempt in the Japanese planetary exploration missions to enhance scientific results. As the largest science team Science Working Team (SWT) is defined to have all scientific researchers in MMX and achieve the science objectives of MMX. The SWT consists of Science Board (SB), Sub-Science Teams (SSTs), and a part of Instrument Teams (ITs) and Working Teams (WTs). SB is in charge of making decisions as recommendation to the project from scientific point of view, and manages and controls all teams in SWT. The SSTs are organized to fulfill the MMX's science objectives by using all available observation and analysis data taken from remote sensing observation, rover observation, and return sample analysis. For this purpose, the SSTs are responsible to making science and data analysis strategy, consider requirements for the instruments, check instrument performances, and actually analyze observation data to make science results. MMX has currently the following five SSTs: Origin of Phobos and Deimos, Early Solar System Evolution, Surface Science and Geology, Mars Science, and Geodesy. Most science objectives of MMX require multi-instrument data analyses and they will be effectively conducted in these SSTs.

MMX has a large number of instruments for observations and sampling, including non-scientific instruments which are possibly used also for science studies. These are: Circum-Martian Dust Monitor (CMDM), Light Detection and Ranging (LIDAR), Macroscopique Observatoire pour la Minéralogie, l'Eau, le Glaces et l'Activité (Near-Infrared Spectrometer, MacrOmega), Mars-Moon Exploration with Gamma-Rays and Neutrons (MEGANE), Mass Spectrum Analyzer (MSA), Rover developed by CNES-DLR, Telescopic Nadir Imager for Geomorphology (TENGOO), Optical Radiometer Composed of Chromatic Imagers (OROCHI), Interplanetary Radiation Environment Monitor (IREM), Super High Vision Camera (SHV), Coring Sampler (CSMP), Pneumatic Sampler (PSMP), Sample Return Capsule (SRC), etc. The ITs develop these

©2020. Japan Geoscience Union. All Right Reserved.

instruments and will conduct single-instrument data analysis mainly.

Keywords: MMX, Martian Moons Exploration, Phobos

©2020. Japan Geoscience Union. All Right Reserved.

Design of Small Ion Mass Spectorometer for Comet Interceptor Mission

*Rurie Mizuno[1], Satoshi Kasahara[1]

1. The university of Tokyo

Time-of-flight mass spectrometers have measured dynamics and compositions of space plasmas. In particular, linear-electric-field time-of-flight analyzers have high mass resolution and are useful for in-situ measurement. Comet interceptor mission which is planned by ESA and JAXA will also use this type of mass spectrometer.

Comet interceptorInterceptor, currently studied in ESA and JAXA, is a mission to observe a dynamically new comet by flyby multi-spacecraft flyby. The mission goal is to characterize a dynamically new comet, which is relatively pristine compared to returning comets explored so far, to obtain a unique view along the evolutionary path of comets from their formation to migration into the inner solar system. One of the key measurements to achieve this goal is the ion measurement, which provides information on nucleus/coma composition as well as the solar wind-coma plasma interaction. Major molecules in a cometary coma, such as H_2O, CO_2, CO, NH_3, and hydrocarbons, consist of volatiles H, C, N, and O. Therefore, in this mission we have to divide the component of coma: C^+, N^+, O^+. To distinguish these atomic ions, the ion mass spectrometer needs relatively high to meet the constraint of the mass resolution, $m/\Delta m > 50$. There is also a constraint of on the size: volume (< 4U), to be accommodated on a relatively small (~24U) Japanese sub-spacecraft for this mission.

However, there has been no ion mass spectrometers meeting satisfying this resolution and size constraint simultaneously. Here we designed a small and high mass resolution ion mass spectrometer for the Comet Interceptor mission. For the high mass resolution, we adopt a linear-electric-field time-of-flight technique. To reduce the size of linear-electric-field time-of-flight the analyzer, we optimized the sensor optics by using a software keeping their high mass resolution. We simulated the design with through SIMION 3D calculation.
Changing the electrode’ s forms and voltages, we obtained a high mass resolution $m/\Delta m$>50~130 at full width at half maximum, with under the following condition: the sensor radius was 50 mm and height was 70mm.

Keywords: Comet Interceptor Mission, Mass Spectrometer

©2020. Japan Geoscience Union. All Right Reserved.

An international multi-point space exploration mission for intergrated observations in the space-Earth coupling system

*Masafumi Hirahara[1], Masatoshi Yamauchi[2], Yoshifumi Saito[3], Hirotsugu Kojima[4], Kazushi Asamura[3], Takeshi Sakanoi[6], Yoshizumi Miyoshi[1], Naritoshi Kitamura[5]

1. Institute of Space-Earth Environmental Research, Nagoya University, 2. Swedish Institute of Space Physics, 3. Institute of Space and Astronautical Science, Japan Aerospace Exploration Agency, 4. Research Institute for Sustainable Humanosphere, Kyoto University, 5. Graduate School of Science, The University of Tokyo, 6. Graduate School of Science, Tohoku University

We report the current status and plan of a multi-point space plasma exploration mission for intergrated in-situ and remote-sensing satellite observations in the space-Earth coupling system. This mission is based on the international collaboration by Japanese FACTORS mission consisting of two identical compact satellites and the Swedisn InnoSat program of a micro satellite in order to realize the first Japanese formation flight configuration in the space and upper atmosphere, whose scientific goal of the most significance is the demonstrative and quantitative investigations on the plasma acceleration/transport mechanisms and the electromagnetic coupling processes emerging in the terrestrial polar magnetosphere and ionosphere. Beyond any previous space plasma exploration in our Japanese research community and the other overseas, we are proposing serveral cutting-edge measurement methodologies using high-time/spatial resolution techniques and direct evaluations for the energy transports between the plasma waves and particles as well as the simultaneous multi-point observations by the adjacent satellites with their controllable separation distances of 1-50 km. In this presentation, we focus particularly on the importance and strategy of the multi-point simultaneous observations carried out by these three compact/micro satellites of FACTORS and InnoSat.

Keywords: multi-point simultaneous satellite observation, integrated satellite observation, formation flight observation, international space exploration mission, space-Earth coupling system, space plasma

©2020. Japan Geoscience Union. All Right Reserved.

Auroral imaging at visible and far-ultra-violet wavelengths for the future polar orbiting satellite mission FACTORS

*Takeshi Sakanoi[1], Masafumi Hirahara[2], Yoshizumi Miyoshi[2], Kazushi Asamura[3], Keisuke Hosokawa[4], Yoshifumi Saito[3], Hirotsugu Kojima[5], Naritoshi Kitamura[7], Mizuki Fukizawa[1], Shin-ichiro Oyama[2], Takuo T. Tsuda[4], Akinori Saito[6], Harald Frey[8], Nick Shneider[9]

1. Planetary Plasma and Atmospheric Research Center, Graduate School of Science, Tohoku University, 2. ISEE, Nagoya University, 3. ISAS/JAXA, 4. School of Informatics and Engineering, The University of Electro-Communications, 5. RISH, Kyoto University, 6. Graduate Shool of Science, Kyoto University, 7. Graduate Shool of Science, The University of Tokyo, 8. SSL, University of California, Berkeley, 9. LASP, University of Colorado Boulder

We report the science objectives, feasible design of instruments, and current status of the future polar orbiting satellite mission FACTORS, mainly focusing on the auroral imaging. FACTORS stands for Frontiers of Formation, Acceleration, Coupling, and Transport Mechanisms Observed by the Outer Space Research System, which is going to be proposed as a next-generation multi-satellite formation flight mission. Major scientific targets are: 1) energy transport in the magnetosphere-ionosphere (MI) coupling system and their relationship to small-scale auroral phenomena, 2) particle transport in the MI system by ion outflow, and 3) neutral-ion coupling in the auroral thermosphere. Observation of small-scale plasma parameters and simultaneous auroral imaging data obtained with multi-satellite measurements in the altitude range from ~300 km to 4000 km enable us to understand dynamical spatial and time variations in the MI coupling system, such as an Alfvenic wave acceleration and small-scale discrete aurora. Field-aligned current, particle distribution function, and Poynting flux obtained with FACTORS are the key parameters to reveal small-scale aurora.

We are making the design and development of visible and far-ultra-violet (FUV) imagers for this mission. To observe dynamical morphology of small-scale aurora, both visible and FUV images are required to have high-spatial and high-time resolution capability. Therefore, we set the instrumental requirement for visible imager to measure small-scale faint aurora with a spatial resolution of ~1km x 1km at apogee (~4000km altitude), a time resolution of ~10 frame/sec and sufficient sensitivity for auroral intensity of ~1 kR. Target auroral emission should be permitted lines, and N2+ 1NG (391 or 428nm) or N2 1PG (670nm) are candidates. We have established high-spatial and high-time resolution auroral imaging measurement with Reimei/MAC, and the similar objective lens (F/1.6, f =50 mm) made of fused silica, which has radiation hard capability, can be used. For the visible detector, we are discussing CCD or space-qualified sCMOS which has low-noise and radiation-hard performances.

Concerning the FUV imager, it was originally designed to measure a wide area (a few thousand km range) to monitor medium scale auroral phenomena, such as westward travelling surge and omega band. However, from recent discussion, the satellite will not be in the noon-midnight meridian sun-synchronous orbit, but in an orbit with a lower inclination angle. In this case, the period of satellite sunlit conditions increases where the visible camera cannot operate due to the scattering of sunlight and earth’ s dayside reflection. On the other hand, the intensity of sunlight is relatively lower in the FUV range, and we can obtain auroral FUV images during sunlit conditions. Thus, the FUV imager now plays a more important role to achieve the scientific objectives of FACTORS. Here, we require the high-time and high-spatial resolution capabilities with a few km x a few km, several frame/sec, and sufficient sensitivity for auroral emission at ~1 kR. We examined the FUV detector and objective system so far. Recent progress in FUV detector technology enables us to use a space-qualified FUV 2D array detector without high-voltage image intensifier. We investigated the performance of CCD and sCMOS detectors for the FUV imager. We set the field-of-view (FOV) of the FUV imager to be ~10 deg x 10 deg. According to this relatively narrow

©2020. Japan Geoscience Union. All Right Reserved.

FOV requirement, and thanks to the latest lens polishing technology, we designed the objective system made of CaF2 aspherical lenses with a F-number of 2.5 and focal length of 50 mm. The candidate auroral emission is OI 135.6 nm, and/or N2 LBH band (140-180 nm), and the wavelength is selected by a space-qualified FUV bandpass interference filter. We present estimations of counts detected by the preliminary designed FUV imager.

Keywords: aurora, airglow, imager

©2020. Japan Geoscience Union. All Right Reserved.

Design of electric field measurements in the future mission FACTORS targeting transverse ion acceleration in the terrestrial polar magnetosphere

*Hirotsugu Kojima[1], Naritoshi Kitamura[2], Koji Shibuya[1], Ibuki Fukasawa[1], Yasumasa Kasaba[3], Masafumi Hirahara[4], Yoshiya Kasahara[5], Yohei Miyake[8], Hideyuki Usui[6], Kazushi Asamura[7], Yoshifumi Saito[7]

1. Research institute for sustainable humanosphere, Kyoto University, 2. Graduate School of Science, University of Tokyo, 3. Planetary Plasma and Atmospheric Research Center, Graduate School of Science, Tohoku University, 4. Institute for Space–Earth Environmental Research, Nagoya University, 5. Advanced Research Center for Space Science and Technology, Kanazawa University, 6. Graduate School of System Informatics, Kobe University, 7. Institute of Space and Astronautical Science, Japan Aerospace Exploration Agency, 8. Education Center on Computational Science and Engineering, Kobe University

Transverse ion acceleration (TIA) in the terrestrial polar magnetosphere is one of science targets in the future mission FACTORS. Although plausible mechanisms of the TIA have been discussed in a lot of studies, they are still unclear. Since the TIA is believed to be a source for escaping ions in the polar region, understanding the TIA process is crucial in studying scenarios of time evolution in the earth’s atmosphere. There is a strong view that the energy source for the TIA is plasma waves. Since there are various plasma waves as candidates for the energy source including both of electrostatic and electromagnetic modes, measurements of electric field components of plasma waves are significant in the FACTORS mission. However, there are some issues to be fixed for precisely measuring electric fields by the satellites. For example, three axial measurements of electric fields are essential even though we don’t have experiences installing three axial electric field sensors on former satellites. To meet the scientific objectives of the FACTORS mission, we design a new measurement system of electric field components of plasma waves considering the following points: (1) development of three axial electric field sensors, (2) implementation of an interferometry mode for identifying phase velocities of observed plasma waves with short wavelengths, and (3) computer simulations for precise calibrations of electric fields. The development of three axial electric field sensors is very new because we have been using long wire antennas that are deployed using satellite spins. We need to develop new antennas deployed by their own mechanisms for the FACTORS mission. Since 6 units of electric field sensors in number are installed on the satellite, their mass resource should be reduced drastically. As for the interferometry mode, knowing phase velocities of observed plasma waves allows us to interpret plasma wave modes consulting plasma wave dispersions. Since the interferometry mode uses electric field sensors as monopoles, it requires a lot of resources in receivers and telemetries. The design considering the use of the interferometry mode is inevitable. Three axial electric field sensors and the interferometry mode provide us with unique observation data of electric field components. To achieve quantitative and precise observations, precise calibrations of electric fields picked up by sensors are crucial. Electric field sensors on board satellites show complicated characteristics in space plasmas. In particular, their characteristics for plasma waves with short wavelengths are more complicated. We evaluate the characteristics of electric field sensors in space plasmas with help from computer simulations. In the present paper, we introduce the current design of the electric field measurement system in the FACTORS mission and discuss crucial aspects to be considered for measuring electric fields in the FACTORS mission.

Keywords: Plasma waves, FACTORS, Transverse ion acceleration

©2020. Japan Geoscience Union. All Right Reserved.

©2020. Japan Geoscience Union. All Right Reserved.

Investigation of requirements for regolith thrusters

*Noruji MUTO[1], Necmi Cihan ORGER[1], Jose Rodrigo CORDOVA-ALARCON[1], Kazuhiro Toyoda[1], Mengu Cho[1]

1. Kyushu Institute of Technology

A problem in lunar-orbit missions is the short orbital life of low-orbit spacecraft due to the moon's irregular gravity field. To sustain the orbit, much propellant is required to be loaded, whereby the mission would be costly. In recent years, electric propulsion devises have been applied to small satellites, which are growing in demand because of their short time required for development and the low risk of mission failure. We here suggest the "Regolith thruster", a new electric propulsion system which collects propellant material during the lunar-orbit flight. The Moon surface is covered with clastic materials derived from the weathered surface rocks called regolith, and its dust particles are of micro-meters in diameter. The dust particles are suspended above the moon surface, as observed by American lunar explorers.

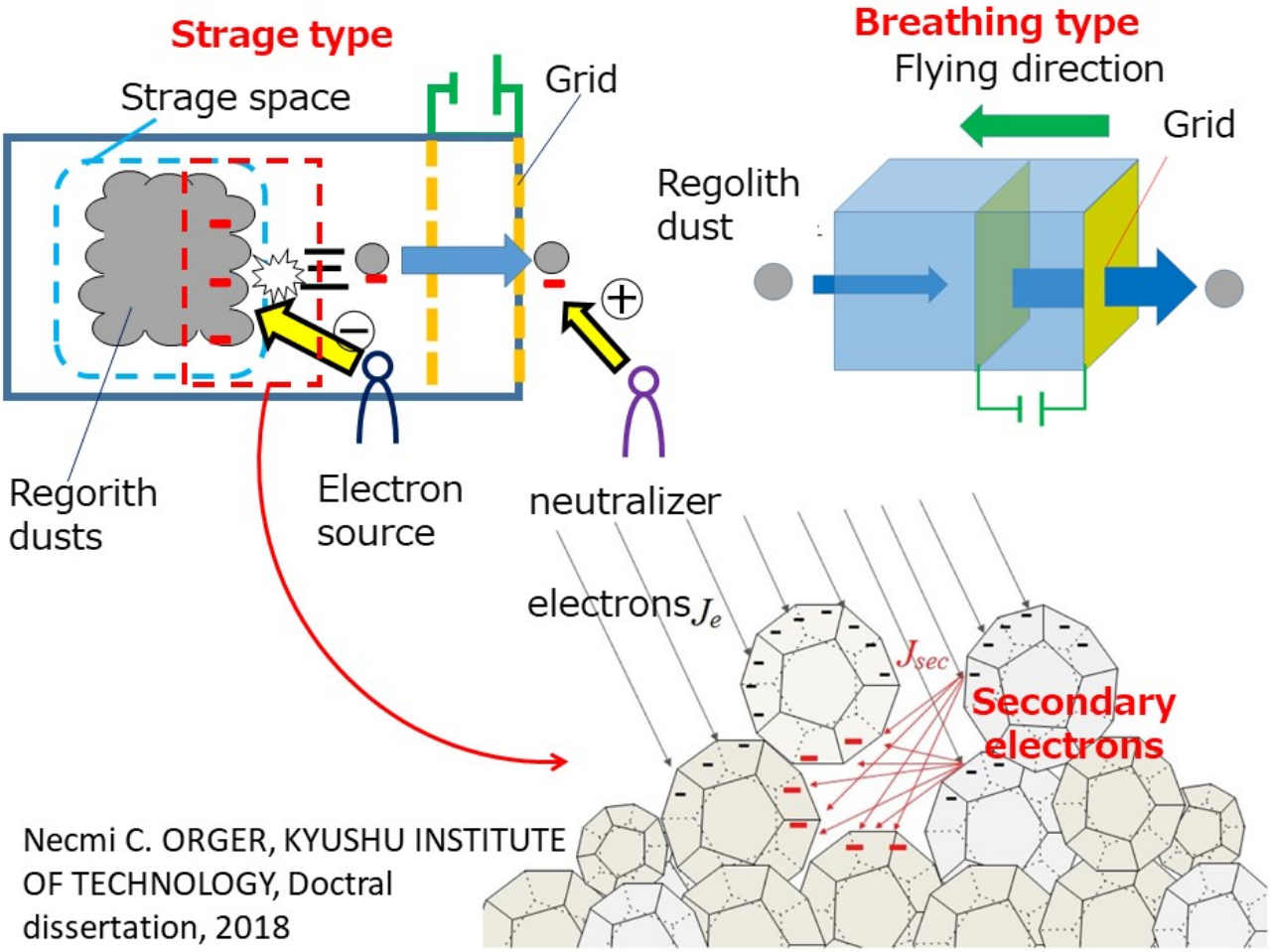
Two types of regolith thruster have been considered. The "breathing type" captures lofted dust particles in orbit and accelerates them directly with a voltage applied grid. Our theoretical studies suggest that a grid of several-tens-of-square-meters class will be necessary to obtain sufficient thrust with this type. The “storage type” thruster uses electron source to generate secondary electrons to release the dust particles by micro-cavity charging. Dust particles are released by electrification in micro cavities (microcavities) formed by each other. This is due to the very small size of the microcavities on the lunar surface, so that the patched surface charge causes a strong repulsion against adjacent dust particles, which moves to the grid and is accelerated. When using a regolith simulant with a particle radius of 45 μm or less, only a small thrust of about 10^{-9} N can be obtained with the storage type. The volume required for the “particle storage space” of a storage-type regolith propulsion system, assuming that particles of each size fill the storage space, exponentially increases as the particle radius increases. If the particle radius is 5μm or less, each side can be made to fit into a cube of 10×10×10 cm (= 1U size small satellite).

Assuming that the regolith thruster obtains the velocity increment ΔV used in the previous studies, the required propulsion and satellite specifications can be investigated: the weight ratio of propellant and regolith thruster increases as the particle radius increases. This tendency is significant with a large value of ΔV. The propulsion device gains thrust because it shoots mass from the fuselage and propels by reaction. Once the weight ratio required to obtain the ΔV of the launched object (and propellant) and the spacecraft is obtained, the weight ratio will increase as the particle radius increases. The particles are desired to be of 1.0μm or less in radius so that the weight ratio can be easily achieved for a small satellite.

The minimum required number of orbits per month to obtain a specific ΔV is 10^8, and it has been found that filling the particle storage in orbit takes a considerable amount of time. If a method other than loading regolith dust directly on lunar surface is wanted, it is necessary to consider collecting particles using tethers, etc. While regolith dust is being used in the lunar orbiter, it continues to fill the storage units with new regolith dust.

©2020. Japan Geoscience Union. All Right Reserved.

Keywords: Moon, Regolith, Lunar exploration, Electric propulsion



©2020. Japan Geoscience Union. All Right Reserved.

Attitude Control System for Kanazawa-SAT3 Microsatellite

*Yuki Yasuda[1], Kohei Fujiki[1], Takuya Nakashima[1], Tomohiko Imachi[1], Satoshi Yagitani[1], Yoshiya Kasahara[1], Daisuke Yonetoku[1], Tatsuya Sawano[1], Makoto Arimoto[1]

1. Kanazawa University

Kanazawa University has been developing a micro satellite, Kanazawa-SAT^3. This satellite is equipped with a device to observe celestial bodies emitting gravitational waves with X rays, and aims to elucidate the mechanism of black hole formation by estimating the time of arrival and direction of arrival of gravitational waves.

In this research, we studied algorithm for attitude control of the satellite. We plan to spread SAP (Solar Panel) after the satellite is separated from the rocket, and stop rotation of the satellite by attitude control called de-tumbling. After that, we plan to judge if the current location sunshine or shady by using STT (Star Tracker) and solar sensors. If it is sunshine, we plan to capture the sun. If it is shady, we plan to decide attitude of the satellite by using STT, and wait until it is sunshine. We plan to turn SAP to the sun and turn mission devices to the deep space direction.

We studied attitude control used GAS (Geomagnetic Aspect Sensor) and MTQ (Magnetic Torque), and implemented the control system. We constructed the environment for unit test of RW (Reaction Wheel) used for attitude control of the satellite. We measured errors of GYR (Gyro Sensor) used for detecting angular velocity of the satellite, and corrected the errors.

MTQ is a device that controls the attitude of the satellite by generating torque by interference with the geomagnetism by applying a voltage to flow an electric current to the magnetic coil. GAS is a device for detecting the direction of the geomagnetic vector. MTQ and GAS are controlled by OBC (On Board Computer) and MC (Media Convertor). We can get maximum torque when MTQ generates torque is orthogonal to the geomagnetism. Because the torque generated by MTQ influence on the detection value of GAS, we have to wait after stopping to input voltage to MTQ to be stabilize output voltage of GAS. This waiting time is revealed to be more than 200 msec by our measurement. And we implemented de-tumbling-mode used to stop rotation of the satellite, unloading-mode used to unload when the rotation per minutes of RW is saturated, and manual-mode used to assign directly the effective voltage to input MTQ as attitude control using MTQ.

RW is a device to generate a control torque from the reaction of a rotor which is accelerated by a motor and is controlled by transmitting commands from the OBC by serial communication under RS-422 standard. The unit test has already been carried out by substituting OBC for PC, however the cable has a bad influence on the operation because RW is a rotating object. Therefore, we studied and constructed a system for wirelessly connecting the RW and PC by making the RS-422 communication wireless. Specifically, commands from the PC are wirelessly transmitted to Arduino by XBee, and the RW is controlled via the RS-422 transceiver. We use air-bearing for the operation test to reduce friction.

GYR have characteristics that fluctuate the bias voltage is fluctuated in a stationary state and it is also changed by temperature change. To reduce the fluctuation, we multiply the bias voltage by the average used the program implemented on microcomputer in a stationary state. We calculated the correction function basis on the measurement result of the GYR’ s bias voltage by temperature change.

©2020. Japan Geoscience Union. All Right Reserved.

In the future, we plan to evaluate de-tumbling-mode and unloading-mode implemented to MC, evaluate RW by performing the operation test using the wireless RS-422 communication system, make circuit board for satellite to mount GYR.

Keywords: Microsatellite, ACS, Kanazawa SAT3

©2020. Japan Geoscience Union. All Right Reserved.

Microsatellite Development and Education of Space Science and Technology at Kanazawa University

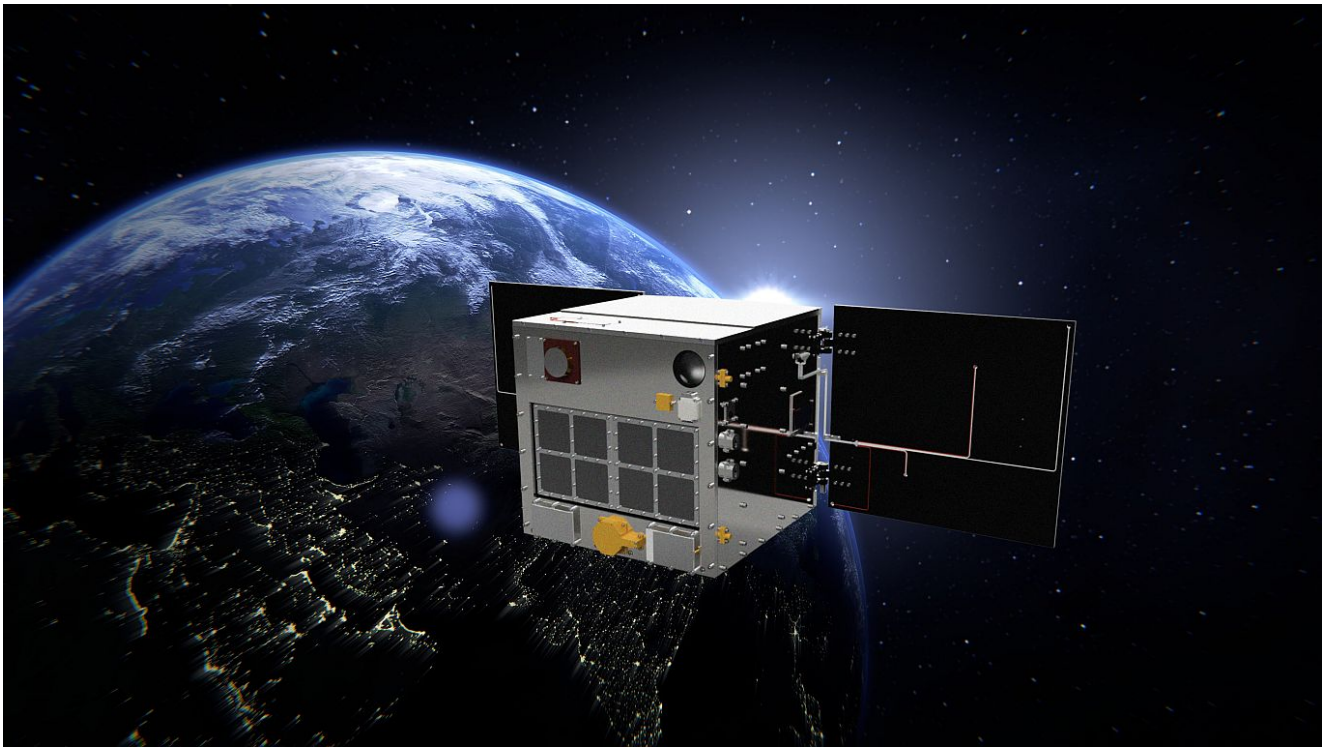
*Tomohiko Imachi[1], Satoshi Yagitani[1], Daisuke Yonetoku[1], Yoshiya Kasahara[1], Tatsuya Sawano[1], Makoto Arimoto[1], Kei Sano[1], Yoshitaka Goto[1], Mitsunori Ozaki[1], Ryuichi Fujimoto[1]

1. Kanazawa University

At Kanazawa University, Advanced Research Center for Space Science and Technology (ARC-SAT) has been established on July 1, 2019. ARC-SAT has 3 research divisions: Satellite Development Division, Astronomy & Astrophysics Division and Solar-Terrestrial Science Division. ARC-SAT is concluding “Kanazawa University Satellite Project (Kanazawa-SAT^3: Study and Training in Space Science and Technology for Kanazawa Cube-Satellites)”. In this project, a space science and engineering course has been established in the Graduate School of Natural Sciences in April 2018. This course is based on the 'satellite development by students', and students are actually involved in the design, fabrication, ground tests, and operation of scientific satellites, aiming to train personnel who are familiar with space science and space engineering, with satellite-development skills.
As an activity of ARC-SAT and Kanazawa-SAT^3 project, a microsatellite is being developed by staff and students of Kanazawa University. It is a scientific satellite which will contribute to the elucidation of the mechanism of gravitational wave generation by identifying the source of gravitational wave by detecting the arrival direction of gamma rays and X rays radiated at the same time when a gravitational waves are generated by collision of astronomical objects. It is a microsatellite with a total weight of 50 kg or less, and its size is cubic with a side of 50 cm, and will be inserted into a solar synchronous orbit at about 660 km altitude. The satellite is on the stage of flight model assembly. And for the ground station, we have installed a paraboric antenna (2.4 m is diamiter) and a crossed Yagi antenna (14 elements) in Kanazawa university.
In the presentation, we will report the details of ARC-SAT and Kanazawa-SAT^3 project, and the development status of our satellite.

Keywords: Microsatellite, Gravitational wave, Kanazawa SAT3

©2020. Japan Geoscience Union. All Right Reserved.



©2020. Japan Geoscience Union. All Right Reserved.

S Band and UHF Band Communication Systems for Kanazawa-SAT3 Microsatellite

*Koyo Ina[1], Mayuko Tachiya[1], Teruya Minamoto[1], Tomohiko Imachi[1], Satoshi Yagitani[1], Yoshitaka Goto[1], Daisuke Yonetoku[1], Yoshiya Kasahara[1], Tatsuya Sawano[1], Makoto Arimoto[1]

1. Kanazawa University

Kanazawa University is developing the first Kanazawa University's microsatellite, named as Kanazawa-SAT3(Study and Training in Space and Technology for Kanazawa Cube-Satellite). Kanazawa University satellite's mission object is to identify the source of gravitational waves by detecting the occurrence time and arrival direction of X-rays and gamma rays observed simultaneously with gravitational waves.

In this research, we are developing communication system for Kanazawa University satellite. Kanazawa University satellite has three communication systems, S band communication, UHF band communication and Iridium communication. There systems is composed of each antennas and transceivers. We summarize S band communication system and UHF communication system in detail as the following.

About the S band communication system, Kanazawa University satellite are equipped with two types of antennas: S band patch antennas and S beacon antennas. On the satellite side, the S band patch antennas for both transmission and reception are mounted on the front panel and the rear panel of the satellite. The S beacon antennas are also mounted on the front panel and the rear panel of the satellite. On the ground station side, we use a parabolic antenna of 2.4 m in diameter at Kanazawa University. S band system is a main communication system between the satellite and the ground station, and plays a role of high speed data communication and beacon transmission. We tested transceivers to be mounted on the satellite and communicator for the ground station by wired connection. And we developed satellite tracking system for the S band antenna. We evaluated the tracking system by performing tracking experiments for a satellite which passes over Kanazawa and receiving the S band signal. As a result of tracking experiments using the satellite tracking system, we confirmed that we could continuously receive signals from the satellite. As future work, we have to test communication system using the S band antenna. And also, it is necessary to develop the communication software for transceiver.

About the UHF communication system, Kanazawa University satellite are equipped with antennas we are developing. On the satellite side, the antennas are mounted for receiving and transmitting independently on the front panel and the rear panel of the satellite. On the ground station side, we use the Yagi antenna with 14 crossed elements at Kanazawa University. This system plays a role of transmitting commands from the ground station to the satellite and transmitting telemetry information from the satellite to the ground station. We adopt PIFA(planar inverted-F antenna) as UHF band antennas on the satellite. In this antenna, a dielectric is inserted into the gap between the patch plane and the ground plane to shorten the wavelength and miniaturization. This antenna body is made of aluminum, and the dielectric is made of polycarbonate. We measured the developed antenna and compared it with the simulation results to evaluate the characteristics. Also, like S band communication system, we developed satellite tracking system for the UHF band. As future work, we have to test transceiver to be mounted on the satellite and communicator for the ground station by wired connection. After that, we test communication system using the PIFA. Also, it is necessary to develop the communication software for transceiver.

©2020. Japan Geoscience Union. All Right Reserved.

Keywords: Microsatellite, Communications system, Kanazawa SAT3

©2020. Japan Geoscience Union. All Right Reserved.

Development of ASIC for energetic electron detector for future planetary explorations

*Shin Sugo[1], Satoshi Kasahara[1], Hirokazu Ikeda[2], Hirotsugu Kojima[3], Takahiro Zushi[4], Motoyuki Kikukawa[3], Kazushi Asamura[2]

1. The University of Tokyo, 2. Institute of Space and Astronautical Science, 3. Research institute for sustainable humanosphere, Kyoto University, 4. National Institute of Technology, Nara College

The origins of electrons in our solar system are the solar wind and the ionized atmosphere of planets and satellites, and their energy is typically less than 1 eV, at most 1 keV. Nevertheless, energetic electrons of more than tens of keV have been observed in all planetary magnetospheres. Some fraction of these electrons precipitate into the atmosphere and deposit their energy. However, it is difficult to quantitatively evaluate the effects of energetic electrons on the atmospheric dynamics and chemistry of outer planets and their satellites, due to the lack of detailed measurements. For such future observations, it is important to cover the large solid angle, since the energetic electron flux is not necessarily isotropic. Keeping this in mind, we develop an energetic (10 - 100 keV) electron detector which has hemispherical field of view without the spacecraft spin. For planetary explorations, which place stringent limitation on payload mass, we aim to miniaturize the sensor by applying the ASIC (Application Specific Integrated Circuit) technology to analog signal processing circuits. It is composed of preamplifiers, shaping amplifiers, peak holders, comparators, and Analog-to-digital converters. We designed an ASIC so that its dynamic range and the wave form peaking time to be 10^6 e^- and ~1 us, respectively, in consideration of the gain and the high capacitance of the assumed detector (Avalanche Photodiode, APD). The performance was confirmed in the simulation. Furthermore, we designed the layout of the ASIC circuit optimized for APD and estimated that it could be mounted on a 5 mm square chip. This size is about 100 times smaller than the size of the analog circuit board (70 mm x 30 mm) before applying ASIC technology and it is estimated to reduce the weight of the energetic electron detector by half (about 1.5 kg).

Keywords: ASIC, Energetic electron, Instrument

©2020. Japan Geoscience Union. All Right Reserved.

Development and Integration of the High-Speed Current Detection Circuits in Particle Sensors Dedicated to Wave-Particle Interaction Analyzer

*Motoyuki Kikukawa[1], Hirotsugu Kojima[1], Kazushi Asamura[2], Yoshifumi Saito[2]

1. Research Institute for Sustainable Humanosphere, Kyoto University, 2. Institute of Space and Astronautical Science

In the terrestrial inner magnetosphere, there is a population of particles whose energies are in ~MeV range and much higher than those of the solar wind. The magnetosphere is so tenuous that particle to particle binary collisions rarely occur. Therefore, particles exchange their energies through plasma waves. However, especially for high-frequency waves, it is not easy to observe a direct clue of the energy transfer from the particles to waves and vice versa.

A conventional observation method of wave-particle interaction has a problem that phase difference information of the plasma wave vector and the particle velocity vector is lost. For this reason, it is difficult to calculate the amount of energy transfer quantitatively. However, WPIA (Wave-Particle Interaction Analyzer) is recently introduced for observation of the wave-particle energy transfer [1]. It calculates inner product of plasma wave vectors and particle velocity vectors for each particle detection event on a satellite and determines the amount of energy conversion directly. The high relative time precision for detecting vectors of plasma waves and particles is essential in WPIA. This requires a synchronous measurement of plasma wave receivers and particle detectors. We introduce a system that feeds feeble current pulses generated by particle detectors into plasma wave receivers to achieve the synchronization. The developing system is a chip consists of two stages based on an ASIC (application specific integration circuit) technology. The first stage is the current-voltage conversion circuit. It picks up a current pulse and converts into a voltage signal with enough amplitude to drive the second stage. The second stage contains a comparator and a peak-hold circuit. They ensure picking up the real signals with availability of threshold settings. Because of the ASIC technology, our system is highly compact in size and weight compared to conventional circuits which are made of discrete electronic components. When our system is onboard micro-satellites, simultaneous multipoint observation of wave-particle interactions can be realized at low cost.
In this study, we develop the circuit which can output detection signals within 30ns after the arrival of particles. These signals can be reset within 12ns from the reset command. The size of one channel of the developed circuit is 210μm×570μm. Since the conventional circuit was several centimeters in size, we have reduced the area of this circuit by more than one tenth.

In this session, we show the details of the chip designed for the particle detection circuits including experimental results.

[1] H. Fukuhara, H. Kojima, Y. Ueda, Y. Omura, Y. Kato, and H. Yamakawa. ” A new instrument for the study of wave-particle interactions in space: One-chip Wave-Particle Interaction Analyzer.” Earth Planets Space 61 (2009) : 765-778.

Keywords: Wave-Particle Interaction, WPIA, ASIC, Particle Detection Circuits

©2020. Japan Geoscience Union. All Right Reserved.

Development of the wideband analog integrated circuit for plasma wave receivers

*Shoya Nakao[1], Takahiro Zushi[1], Hirotsugu Kojima[2]

1. National Institute of Technology, Nara College, 2. Kyoto University

Plasma waves are the important observation target for scientific missions investigating space plasma phenomena, and many scientific satellites observe plasma waves using onboard plasma wave instruments. Plasma wave receivers are composed of electromagnetic sensors and a plasma wave receiver which processes signals picked up by sensors. The plasma wave receiver requires high-performance electronic circuits, and it causes an increase in mass and volume. On the other hand, the miniaturization of observation instruments is highly demanded. Part of its reasons is the expanding usage of microsatellites and the increasing onboard instruments of satellites. To resolve this problem, we use the Application-Specific Integrated Circuits (ASIC) technology which enables to miniaturize electronic circuits. We already realized miniaturized waveform and spectrum types of plasma wave receiver by developing ASIC; however, frequency coverages of the developed receivers are up to 100 kHz, and wideband receiver is required.

In this study, we improve analog ASIC to become wideband. In previous analog ASIC, upper limit of the frequency coverage is determined by the frequency coverage of the anti-aliasing filter. The anti-aliasing filter is realized by using switched capacitor filter, and it requires high frequency clock signal. Thus, the operational amplifiers which compose switched capacitor filter requires wider frequency coverage then the receiver’ s frequency coverage, and it is the biggest issue in broadening the previous ASIC. In this study, we develop the operational amplifier specialized for switched capacitor filter. In the presentation, we describe detailed design of the developed operational amplifier and switched capacitor filter.

Keywords: Instruments, Plasma wave

©2020. Japan Geoscience Union. All Right Reserved.

Basic study on search coil magnetometer for improving magnetic sensitivity

*Yohei Yamaka[1], Yuya Tokunaga[1], Mitsunori Ozaki[1], Satoshi Yagitani[1]

1. Kanazawa University

In order to safely operate satellite services, we have been investigating the plasma waves from 1 Hz to 10 kHz. To probe the magnetic field vectors of plasma waves, we use search coil magnetometers along with preamplifiers. The magnetic sensitivity are important profiles to determine the electrical performance of search coil. The lower value of magnetic sensitivity is better for probing the weaker plasma waves. In this study, we propose two methods for improving the magnetic sensitivity of previous search coils. The noise components characterized by the search coil impedance are dominant of the magnetic sensitivity in the frequency range from 100 Hz to 10 kHz, so decreasing the inductance values of search coils is necessary to achieve the better magnetic sensitivity. By using two search coils connected in parallel, the first method decreases a total inductance. The decreased inductance improves the magnetic sensitivity from 100 Hz to 10 kHz. In the second method, we use an adder circuit to synthesize the outputs of three search coils each having preamplifiers. The magnetic sensitivity from 1 to 10 kHz is better than the previous search coil because of decreasing the inductance of each search coil. We evaluated the magnetic sensitivity for two methods of the search coils. From the measurement results, the magnetic sensitivities at 2.5 kHz of first and second methods improve by 5.37 dB and 4.19 dB compared with that of the previous search coil, respectively. The magnetic sensitivity of first method is better than that of the second one, but the first method is impractical for scientific satellites due to having the mass and volume with 2 times larger than those of the previous search coil. On the other hand, the search coil by the second method increases the total power consumption depending on the number of preamplifiers, but it can be practical because of suppressing power consumption using application specific integrated circuit technology.
In this presentation, we will present the basic study on the search coil magnetometers for improving the magnetic sensitivity in detail.

Keywords: Plasma wave observation, Magnetic field measurement, Search coil magnetometer

©2020. Japan Geoscience Union. All Right Reserved.

Development of an instrument to measure ion drift velocity and density in the ionosphere

*Takumi Abe[1], Shigeto Watanabe[2], Akinori Saito[3], Ryuto Hashiba[4]

1. Japan Aerospace Exploration Agency, Institute of Space and Astronautical Science Department of Solar System Sciences, 2. Hokkaido Information University, 3. Kyoto University, Graduate School of Science, 4. Hokkaido Universiity

The lower ionosphere is known as a unique region where charged particles and neutral particles co-exist. The charged particles tend to move in a direction different from neutral particles, because of a difference in those behaviors against the electromagnetic force. Characteristic phenomena such as dynamo current and polarization electric field existing in this region are attributed to such peculiarity in this region. The momentum transfer between the charged and neutral particles plays an important role in generating these phenomena. It is desirable to make a direct measurement of charged and neutral particles by using instrument on the sounding rocket to further understand such unresolved phenomena.

In 2018, we started developing an ion drift velocity analyzer which enables us to estimate the ion drift velocity and density in the lower ionosphere. It is well known that Ion Drift Meter (IDM) and Retarding Potential Analyzer (RPA) had been installed on low-altitude satellite, such as Dynamic Explorer-2 and Atmospheric Explorer series. Our instrument will be required to have the functions that these two have.

As the first step of the instrument development, a numerical simulation was carried out to design the internal structure, and thereby we determined a basic structure of the instrument which consists of RPA section in the front and multiple sector anodes of IDM section in the end. In the first half of 2019, the prototype model was developed after we obtained the design outlook that the instrument provides the ion density and velocity in a good accuracy. The IDM section has a total of 72 small sector electrodes so that an estimation of the drift velocity vector can be made with enough accuracy. The electrodes are arranged in the hemispheric inner surface which receives the incident ions passing through the RPA section.

Then, we put the prototype instrument in the vacuum chamber to evaluate its performance on the ionospheric plasma condition. The main results from our evaluation are summarized as follows:
1) Individual electrode in the IDM section can measure significant level of current due to thermal ions which pass through the RPA section.
2) The electrode can independently detect incident current even though the space between adjacent electrodes is small.
3) The ion current distribution represented by the 72 electrodes seems reasonable as expected from a velocity of the incident ions.
4) The current collected by the electrodes has a decreasing trend as expected as an RPA function, and it significantly changes depending on the DC bias applied to the RPA voltage.

In the next step, we are going to develop a low-energy ion source which can generate drifting ions whose energy is several eV. Through the experiment using the ion source, a function to estimate the bulk energy of the ions will be evaluated. The latest status of our instrument development will be explained in the presentation.

Keywords: Ionosphere, Ion drift, Instrument development

©2020. Japan Geoscience Union. All Right Reserved.

©2020. Japan Geoscience Union. All Right Reserved.

Satellite-to-satellite radio occultation for the exploration of planetary atmospheres

*Takeshi Imamura[1], Hiroki Ando[2], Norihiko Sugimoto[4], Hideo Sagawa[2], Masahiro Takagi[2], Katsuyuki Noguchi[8], Kazunori Ogohara[7], Atsushi Yamazaki[9], Takahiro Iwata[9], Tomotaka Yamamoto[3], Satoshi Ikari[3], Yosuke Kawabata[3], Shoko Sano[3], Yukiko Fujisawa[4], Ryu Funase[3], Mutsuko Morimoto[4], Mirai Abe[6], Asako Hosono[5]

1. Graduate School of Frontier Sciences, The University of Tokyo, 2. Faculty of Science, Kyoto Sangyo University, 3. Department of Aeronautics and Astronautics, The University of Tokyo, 4. Department of Physics, Keio University, 5. Toshimagaoka Women High School, 6. Faculty of Law, Keio University, 7. School of Engineering, The University of Shiga Prefecture, 8. Department of Information and Computer Sciences, Nara Women's University, 9. Institute of Space and Astronautical Science, Japan Aerospace Exploration Agency

In order to understand the climate system of planets, it is necessary to reveal the three-dimensional circulation of energy and atmospheric compounds. Methods of observing planetary atmospheres that have made significant achievements to date can be broadly classified into direct measurements by landers and optical remote sensing by orbiters and ground telescopes. Although the former can accurately measure various physical quantities, it cannot capture physical and/or chemical processes involving large spatial changes. The latter enables global observations; however, the vertical resolution is typically limited to a scale height (several kilometers), and thus layered structures characteristic of planetary atmospheres cannot be well resolved. Moreover, the pressure field, which is critical for understanding atmospheric dynamics, cannot be measured. Because of these limitations, for example, the three-dimensional structures of water and dust transport on Mars have not yet been identified, and the three-dimensional structure of the angular momentum transport in Venus’ s atmosphere that sustains the high-speed atmospheric circulation has not yet been identified.

We consider satellite-to-satellite radio occultation can make a breakthrough in the sciences of planetary atmospheres. In conventional radio occultation observations, the planetary atmosphere is observed by using radio waves transmitted from the spacecraft and received at a ground station when the spacecraft is hidden behind the planet as seen from the ground station. This method can measure the temperature, the pressure and absorbing materials at high vertical resolutions of several hundred meters; however, it has a disadvantage that it cannot capture the spatial structure because the observation points are limited by the positional relationship among the spacecraft, the planet and the earth. Based on this recognition, we are studying the possibility of radio occultation observation between a mother spacecraft and small satellites from the viewpoint of both science and engineering. By this method, the altitude distributions of physical quantities can be acquired with high vertical resolution globally at dozens of observation points every day. Such a method has already been used for the earth’ s atmosphere.

Satellite-to-satellite radio occultation, when applied to Mars, would enable to (1) derive the three-dimensional wind structure from the temperature and pressure distributions using data assimilation, (2) understand the atmosphere-crustal water exchange and water transport using three-dimensional data of water vapor and atmospheric dynamics including the boundary layer, and (3) expand the observation points, which have been limited to the morning and evening regions in the conventional radio occultation, to all local time to understand the diurnal cycle. Such measurements also serve as basic information for the analysis of observational data taken by other methods in the same period. For Venus, satellite-to-satellite occultation can retrieve three-dimensional atmospheric motions in broad altitude

©2020. Japan Geoscience Union. All Right Reserved.

regions including inside and below the sulfuric acid cloud that is difficult to observe optically. It will also reveal the three-dimensional circulation of sulfuric acid, which is the cloud forming material, leading to the understanding of climate control by cloud processes. In addition to the observations of the neutral atmospheres, three-dimensional tomography of the ionospheres by electron density measurements is also possible. In this presentation we will discuss scientific values of the measurements and introduce preliminary results of engineering studies.

Keywords: radio occultation, planetary atmospheres

©2020. Japan Geoscience Union. All Right Reserved.

Life-signature Detection fluorescence Microscope (LDM)

*Enya Keigo[1], Yoshitaka - Yoshimura[2], Satoshi - Sasaki[3], Akihiko - Yamagishi[1,4], Atsuo - Miyakawa [4], Eiichi - Imai[5], Hajime - Mita[7], Takehiko Satoh[1], Kensei - Kobayashi[6], Yoko - Kebukawa[6], Tomoka - Okada[6], Hikaru - Yabuta[8], Takeshi - Naganuma[8], Tomoiro - Usui[1], Kazuhisa - Fujita[1]

1. Institute of Space and Astronautical Science, 2. Tamagawa University, 3. Tokyo University of Technology, 4. Tokyo University of Pharmacy and Life Science, 5. Nagaoka University of Technology, 6. Yokohama National University, 7. Fukuoka Institute of Technology, 8. Hiroshima University

Though surface of Mars is cold and dry, Mars had harboured a large amount of liquid water on the surface in early stage of the history. Several billion years ago, Mars was similar to the early Earth from which life arose, and life would have also emerged on Mars. Although the Viking mission in 1976, which explored life on Mars, did not find evidence for life [1], many findings supporting the habitability on Mars have been discovered since the Viking mission: past and present aqueous environments, organic compounds, methane and reduced compounds supporting microorganism as energy sources, and so on [2] [3]. These findings tend to suggest that microorganisms might still exist on Mars surface.

For searching extant microorganisms, a microscopic instrument is a powerful tool, which directly images life forms and identify their shapes, sizes, and other morphological and biochemical characteristics. However, it has not been used in space missions yet. For *in situ* imaging of particles and microbial cells, we have proposed the Life-signature Detection fluorescence Microscope (LDM) which visualizes organic compounds by staining the samples with fluorescent pigments [4]. The LDM scans a volume of 1 mm^3 and detects organic compounds including cells and other biological materials in high sensitivity ($<10^4$ cells per gram clay). The fluorescent pigments have been selected to identify the fundamental features of cells by differentiating organic compounds surrounded by membranes or those show enzyme activity. The LDM is also equipped with a high-resolution imaging system (1 μm/pixel) which visualizes detailed life forms as well as regolith and dust particles [5]. Our investigation goals are the followings. 1) High-resolution characterization of regolith and dust particles. 2) Search for organic compounds in Mars surface samples. The compounds include cells, other biological materials, and abiotic polycyclic aromatic hydrocarbon (PAH). 3) Identify cell-like structure in which organic compounds are enveloped by membrane, which may represent Martian life.

In this presentation we will report the current status of the development of LDM and potential application to planetary explorations.

References

[1] Margulis, L. et al. *J. Mol. Evol.* 14 (1979)
[2] Eigenbrode, J.L. et al. *Science*, 360 (2018)
[3] Webster, C.R. et al. *Science.* 360 (2018)
[4] Yamagishi, A. et al. *Biol. Sci. Space*, 24 (2010)
[5] Yamagishi, A. et al. *Trans. JSASS Aerospace Tech. Japan*, 16 (2018)

Keywords: Life sigunature, fluorecence microscope

©2020. Japan Geoscience Union. All Right Reserved.

Development of a near-infrared high-resolution Echelle spectrograph ESPRIT for planetary atmospheric observations

*Ayumu Kambara[1], Takeshi Sakanoi[1], Masato Kagitani[1], Yasumasa Kasaba[1], Aya Otomo[1], Yasuhiro Hirahara[2]

1. Planetary Plasma and Atmospheric Research Center, Graduate School of Science, Tohoku University, 2. Graduate School of Environmental Studies, Nagoya University

We report the latest status of development of near-infrared spectrograph, ESPRIT (Echelle Spectrograph for Planetary Research In Tohoku university). This spectrograph is designed to be optimized for observations of near-infrared emission and absorption from planetary atmospheres and satellites. The emission and absorption in the infrared wavelength range have information of physical phenomena, such as the composition and density of the molecular species of the atmosphere, temperature and wind speed. Because of the high-resolution spectroscopic capability of ESPRIT, we can obtain the atmospheric velocity from the Doppler shift of the emission lines and the temperature from the intensity ratio of multiple emission lines. To understand the time and spatial variations in the various ranges, it is necessary to carry out long-term and flexible observations of planetary atmosphere with ground-based telescopes and planetary probes. Since an infrared high-resolution spectrograph is big and heavy, in most cases they are installed on medium- and large-class ground telescopes, and opportunities were limited with proposal-based operations. We will install ESPRIT on our 60 cm telescope (T60) at the summit of Haleakala (3040m), and achieve the monitoring measurement. Our main observation target is the infrared emissions in Jovian thermospheric H_3^+/H_2 aurora and airglow, and ESPRIT will be provided to wider users in observations of various targets including the lower cloud layer (around 2.3 um) and airglow (1.27 um) in Venus and H_2O and CO_2 atmosphere in Mars. We plan to install ESPRIT on T60 first, and in the future, we will install it on the 1.8 m off-axis telescope PLANETS.

ESPRIT can change an imaging mode and spectral mode with a long slit (length 50 arcsec). A slit viewer will be installed to monitor the position of slit on a planetary disk. We adopt the Raytheon InSb 256x256 array of which wavelength range is in the range of 1-4 um. The plate scale at the detector is 0.3 arcsec/pixel (field of view 76 arcsec) in the case of F12 incident light. The whole optical system is cooled down to 90 K with the radiation shield by using the He refrigerator, and the detector unit is cooled down to 35 K. For the spectral mode, the echelle grating (31.6 gr/mm, blaze angle 71 degrees, 29mmW x 136mmL x 20mmT) is used. This was selected so that the diffraction efficiency is greater than 0.8 at the wavelengths of Jovian H_3^+ emission (3.95 um), and H_2 emission (2.12 and 2.30 um). The resolution of spectrograph is R~20,000. The mechanism is used to change the grating angle from 62 to 80 degrees, and we can observe the 1.27, 2.12, 2.30, 3.41, and 3.95 um wavelength bands (wavelength coverage $1.0\times10^{-3}\lambda$) by this mechanism. with an angle stability of 1 arcsec/5min (corresponding to a Doppler velocity of 0.5 km/s in Jovian auroral emission). This stability was verified by previous tests. When ESPRIT is installed to T60 and we set the slit the polar aurora emissions in the east-west direction, we estimate that this data can be obtained for every 3 min (SNR~15), and the intensity distribution in Jovian polar region with 5-10 frames can be acquired in about 1 hour. This time resolution would be sufficient to clarify the time variations of disturbances in the magnetosphere and ionosphere, as well as the coupling processes between ions and neutral winds in Jovian thermosphere.

In the present situation, we almost completed the fabrication of mechanical and optical systems, such as the echelle grating mechanism, filter turret, slit-imaging change mechanism, collimating and camera mirrors, grating and other components. We will manufacture the heat path and the cooling box for the detector. Further, we will perform the electrical tests of the detector using the driving and read-out

©2020. Japan Geoscience Union. All Right Reserved.

electronics and software under vacuum and cooling conditions. We plan to install the detector unit to ESPRIT by this June, and start the integration test of ESPRIT from July.

Keywords: near-infrared spectrograph, planet, high-resolution spectrograph

©2020. Japan Geoscience Union. All Right Reserved.

Development of the absorption cell filters for remote D/H observation

*Masaki Kuwabara[1], Kazuo Yoshioka[2], Makoto Taguchi[3], Takuya Kawahara[4], Shingo Kameda[3]

1. JAXA, 2. The Univ. of Tokyo, 3. Rikkyo Univ., 4. Shinshu Univ.

The hydrogen atoms in the planetary exosphere scatter the solar Lyman-alpha radiation and produce a faint glow surrounding the planet. The brightest emission among the planetary coronas is hydrogen Lyman-alpha. Absorption cell technique is an efficient tool for remote sensing of the planetary coronas and allows us to measure not only an intensity distribution of the Lyman-alpha emission but also a temperature distribution in the planetary exosphere. These distributions are quite important to quantitatively estimate of the escape rate of the present planetary atmosphere. Since the absorption cell technique can be used as a light-weight ultra-high resolution filter, it will be crucial for realizing an imaging instrument for observation of planetary coronas with small spacecraft. Absorption performance of the cell strongly depends on parameters such as filament shape, filament temperature, applied power to the filament, filled gas pressure, optical path length, and position of the beam path. The hydrogen absorption cells have been developed to optimize the above parameters and evaluated using an ultra-high spectral resolution Fourier transform spectrometer installed at the DESIRS beamline of Synchrotron SOLEIL in France. In this presentation, the summary of the development and the remaining issues are presented. The basic design of an absorption cell imager and the application of it for future space missions are also presented.

Keywords: Lyman-alpha, Hydrogen corona, D/H ratio

©2020. Japan Geoscience Union. All Right Reserved.

[E] Poster | P (Space and Planetary Sciences)：P-CG Complex & General

[P-CG25] Planetary Magnetosphere, Ionosphere, and Atmosphere

convener:Kanako Seki(Graduate School of Science, University of Tokyo), Takeshi Imamura(Graduate School of Frontier Sciences, The University of Tokyo), Hiroyuki Maezawa(Department of Physical Science Osaka Prefecture University), Naoki Terada(Graduate School of Science, Tohoku University)

Exploration of Moon, Venus, Mars, Mercury, Jupiter, Saturn, and beyond together with rapid developments of numerical simulations provides us new view of planetary environment. This session collects general contributions of new findings about planetary magnetosphere, ionosphere, and atmosphere. New methodology and technology development studies for future explorations are also welcome. In order to put the common knowledge at different planets into perspective, this session aims to facilitate discussions on comparative planetary environments.

[PCG25-P01] Estimation of the drift rate and intensity of Neptune’s storm by Pirika telescope

*Yuuki Sato[1], Yukihiro Takahashi[1], Mitsuteru Sato[1], Seiko Takagi[1], Masataka Imai[2], Tatsuharu Ono[1] (1.Graduate School of Science, Hokkaido University, 2.National Institute of Advanced Industrial Science and Technology)

[PCG25-P02] Multi spectral observation of changes in Uranus' cloud obtained by Pirka telescope

*Haruki Sugiyama[1], Yukihiro Takahashi[1], Mitsuteru Sato[1], Seiko Takagi[1], Yuuki Sato[1], Tatsuharu Ono[1], Shuntaro Yokota[1] (1.Hokkaido University)

[PCG25-P03] Parameter experiments of climates of various planets by the use of a general circulation model

*Yoshi-Yuki Hayashi[1], Yoshiyuki O. Takahashi[1], Masaki Ishiwatari[2], Kensuke Nakajima[3], George HASHIMOTO[4] (1.Department of Planetology/CPS, Graduate School of Science, Kobe University, 2.Department of Cosmosciences, Graduate school of Science, Hokkaido University, 3.Department of Earth and Planetary Sciences,Flculty of Sciences,Kyushu University, 4.Department of Earth Sciences, Faculty of Science, Okayama University)

[PCG25-P04] The influence of carbon escape on the evolution of the Martian atmosphere

Ryosuke Yagi[1], *Naoki Terada[1], Shungo Koyama[1], Takeshi Kuroda[1], Hiromu Nakagawa[1], Isao Murata[1], Yasumasa Kasaba[1] (1.Graduate School of Science, Tohoku University)

[PCG25-P05] Radiative Transport Simulations for 0.4 - 1.9 THz Band Heterodyne Spectroscopy of Martian Atmospheric Trace Gases

*Yuki Hamaguchi[1], Hiroyuki Maezawa[1], Hideo Sagawa[2] (1.Osaka Prefecture University, 2.Kyoto Sangyo University)

Estimation of the drift rate and intensity of Neptune’s storm by Pirika telescope

*Yuuki Sato[1], Yukihiro Takahashi[1], Mitsuteru Sato[1], Seiko Takagi[1], Masataka Imai[2], Tatsuharu Ono[1]

1. Graduate School of Science, Hokkaido University, 2. National Institute of Advanced Industrial Science and Technology

A storm more than 4,000 km in diameter occurs occasionally in Neptune. In previous study, Voyager 2 observed Neptune on May 24, 1989 and discovered a storm of 13,000 km in diameter called Great Dark Spot (GDS). GDS was located in southern hemisphere like Great Red Spot of Jupiter. But GDS became extinct when Hubble Space Telescope observed it in 1994. It is unknown whether it is a sudden thing or storms such as GDS always occur in Neptune. In addition, a huge storm of 9,000 km was observed on July 2 and June 26, 2017 by Keck observatory. It’s considered that storms of Neptune occurs at mid latitude in the north and south that an ascending air occurs. However, this huge storm occurred near the equator. A rotation axis of Neptune is 29.6 degrees, and the storm possibly occurred near the equator because of seasonal change. Neptune is observed by large telescopes such as Keck observatory and the Hubble Space Telescope, but it is difficult to always use those telescopes for Neptune observation. Therefore Neptune is not observed for long term on a short time scale. We developed the technique to estimate the drift rate and intensity of storms by observing a whole spectrum of Neptune in this study. When seeing is bad, it’s possible to observe and acquire the observation data of Neptune for a long term on a short time scale. The purpose is to deepen the understanding of the atmosphere convection structure of Neptune by chasing the detailed change of storms. In this study, we observed Neptune by using 1.6 m Pirka telescope that Hokkaido University owned. The observation time is from August 7, 2017 to January 17, 2018 and from October 22, 2018 to November 26 2018. The wavelength is 650-1050 nm in 2017, and 890, 855 nm in 2018. In this study, we used methane absorption 890 nm. Storms look brighter at 890 nm because the altitude of storms is higher than that of other areas. In addition, the appearance size of storms from the observation point changes by the rotation of Neptune, so an 890 nm flux changes by the rotation. We took the ratio of an 890 nm flux and an 855 nm flux to correct the effect of the earth atmosphere and calculated the theoretical values of the relative intensity by the rotation. We assumed storm's area and fit the observed values with the theoretical values in the least squares method to estimate the drift rate and 890 nm reflectance of the storms. We estimated that the drift rate and the 890 nm reflectance are 47.5˚/day, 0.252 in 2017, 24.9˚/day, 0.054 in 2018, respectively. In 2019, we assumed that there are three storms and estimated that the drift rate and 890 nm reflectance of the first storm are 22.8˚/day, 0.128, those of the second one are 39.6˚/day, 0.081, those of the third one are 51.9˚/day, 0.149, respectively. Molter et al., (2019) study shows that 2017 storm is located at 2˚N and the drift rate is 237.4±0.2 m/s or 47.78±0.04˚/day. This drift rate is consistent with the drift rate estimated in my study. We will compare the results of 2018 and 2019 with observations of other reseacher and amateur, and then discuss in the future.

Keywords: Neptune, Ground-based telescope

©2020. Japan Geoscience Union. All Right Reserved.

Multi spectral observation of changes in Uranus' cloud obtained by Pirka telescope

*Haruki Sugiyama[1], Yukihiro Takahashi[1], Mitsuteru Sato[1], Seiko Takagi[1], Yuuki Sato[1], Tatsuharu Ono[1], Shuntaro Yokota[1]

1. Hokkaido University

Uranus was first observed to be free of severe weather changes like Jupiter. However, recent observations (Voyager 2, Hubble Space Telescope, Keck telescope) have revealed that Uranus has a long-time scale phenomenon of several decades and a short-time scale phenomenon of several days or weeks. Hammel and Lockwood (2007) reported a change in brightness on a time scale of about 20 years, which is half the orbital period of Uranus. Irwin et al. (2010) and Peter et al. (2015) showed that some bright clouds fluctuate in a few days. However, there are few observations of short-time scale cloud changes, and the time scale of these cloud phenomena is uncleared. Most observations have been performed once or twice a year, often for several days. This is because it is difficult to have observation time for large telescopes and space telescopes with high spatial resolution. The purpose of this study is to elucidate the time scale of cloud changes. In this study, we used a 1.6 m Pirka telescope and Multi Spectral Imager (MSI)(Watanabe et al., 2012) mounted at Cassegrain focus of Pirka telescope. This is a ground telescope located at Nayoro observatory of Hokkaido University, Japan, and mainly used for planetary observation. MSI enables to take images that cover a 3.3'x3.3' field of view with 0.389" pixel resolution at several visible to near infrared wavelength in a short time. Because this instrument has a liquid crystal tunable filters (LCTFs) that can change the transmission wavelength from 400 nm to 1100 nm, in about 150 ms. We made imaging observations at several wavelengthes from 650 nm to 900 nm for a total of 6 months from September 2019 to February 2020. However, the seeing of Nayoro is about 3 arcsec, which is almost the same size of Uranus. Therefore, in order to confirm the existence of clouds, I use a method of comparing the reflection flux at a methane absorption wavelength ($F_{methane}$) and the reflection flux at a non-absorption wavelength (F_{normal}). If there is a cloud, the incident light will be reflected by the cloud, so the absorption by methane will be weaker than without the cloud, and $F_{methane}$ / F_{normal} will be larger than without the cloud. Using this, it is possible to estimate the change in clouds by comparing the theoretical value of changes in $F_{methane}$ / F_{normal} due to the presence of clouds with actual observations. In this presentation, we will introduce the initial results of the data acquired from September to November 2019.

Keywords: Uranus, multi spectral imaging, planetary atmosphere

©2020. Japan Geoscience Union. All Right Reserved.

Parameter experiments of climates of various planets by the use of a general circulation model

*Yoshi-Yuki Hayashi[1], Yoshiyuki O. Takahashi[1], Masaki Ishiwatari[2], Kensuke Nakajima[3], George HASHIMOTO[4]

1. Department of Planetology/CPS, Graduate School of Science, Kobe University, 2. Department of Cosmosciences, Graduate school of Science, Hokkaido University, 3. Department of Earth and Planetary Sciences,Flculty of Sciences,Kyushu University, 4. Department of Earth Sciences, Faculty of Science, Okayama University

One of the interesting quests on exoplanets is to investigate the variety of thier possible surface environments and circulation structures of their atmospheres. For the propose of accumulating knowledge on those questions, we have been developing a general circulation model and have been performing parameter experiments on possible climates of exoplanets by the use of a general circulation model.

The model used in this study is DCPAM (http://www.gfd-dennou.org/library/dcpam/), which has been developed in our group. The model is composed of a dynamics of the primitive equation system and a number of parameterizations, such as radiation, turbulent mixing, and so on. In this study, we focus on the atmospheres whose composition is the same as that of the Earth. The parameters on which we consider dependence of the atmospheres are obliquity, rotation period, and radius of the planets. The values of obliquity we adopt for our parameter experiments are 0, 23.4, 60, 90 degrees, those of rotation periods are 1, 3, 10, 30 Earth days, and those of radius are 6371, 4247, 3186 km. We have to note we have not completed all of the sets given by the arbitrary combinations of them; the values of the parameters are extended from those of the present Earth's parameters.

A several interesting features are observed in the results of those experiments. One of those is the morphological change of mean meridional circulation. The latitudinal width of Hadley cell becomes larger with the increase of rotational period. As a result, Ferrel cells disappear in the experiments with rotation periods of 10 and 30 Earth days. In the presentation, additional features of parameter dependence will be also presented.

Keywords: exoplanets, climate, obliquity, rotational period, planetary radius

©2020. Japan Geoscience Union. All Right Reserved.

The influence of carbon escape on the evolution of the Martian atmosphere

Ryosuke Yagi[1], *Naoki Terada[1], Shungo Koyama[1], Takeshi Kuroda[1], Hiromu Nakagawa[1], Isao Murata[1], Yasumasa Kasaba[1]

1. Graduate School of Science, Tohoku University

The purpose of this study is to investigate the evolution of atmospheric composition in the early Martian atmosphere. Not only hydrogen and oxygen escapes but also carbon escape to space is considered in this study for two reasons. The first reason is that thermal escape of atomic carbon could be stronger than atomic oxygen on early Mars. The early Martian atmosphere was exposed to stronger Sun’s EUV and FUV radiations than today. The escape parameter, defined as the ratio of the gravitational potential to kinetic energy at the exobase level, could have been small enough to allow massive escapes of these species under such strong radiations. For example, the escape parameter of atomic carbon in the Martian atmosphere was estimated 0.75 times smaller than that of atomic oxygen, and because of an efficient dissociation of CO_2 the densities of these species at the exobase level were comparable at 4.1 billion years ago [Tian et al., 2009]. Hence, we consider that on early Mars, thermal escape of atomic carbon could have been stronger than atomic oxygen. The second reason is the discovery of the concentration of Mn in Gale Crater by Curiosity, which suggests that the early Martian atmosphere could have several mbar or more of O_2 partial pressure in the Hesperian [Noda et al., 2019]. Previous 1-dimensional photochemical models that considered hydrogen and oxygen escapes on current Mars suggested that the O_2 partial pressure could increase only up to 10^{-5} bar [e.g., Chaffin et al., 2017]. This is because the atmosphere self-regulates the loss of hydrogen and oxygen to 2:1 [McElroy and Donahue, 1972], which limits the imbalance between the hydrogen and oxygen escapes and hence prevents a massive oxygen buildup in the atmosphere. In this study, we consider atomic carbon escape as an agent to accumulate O_2 in the atmosphere.

We investigated the effect of carbon escape on the accumulation of O_2 in the atmosphere using two models. The first is a 1-box model that considers only the supply and loss of atmosphere from the atmospheric boundaries. This model was used to get an overview of the atmospheric evolution. The second is a 1-dimensional photochemical model. This model investigated the evolution of atmospheric composition taking into account atmospheric photochemistry in addition to the supply and loss from the atmospheric boundaries. This model was applied during periods when the atmosphere was expected to regenerate to be an O_2-dominated atmosphere after a massive loss of the atmosphere. The results of our 1-box model suggested that an O_2-dominated atmosphere was formed during times when oxygen thermal escape was diminished and carbon thermal escape was still strong. Applying the 1-dimensional photochemical model in the same period, i.e., early in Noachian, ~1 mbar of O_2-dominated atmosphere was formed in about 10^4 years. However, the period of the O_2-dominated atmosphere formation is inconsistent with the Curiosity measurement.

Therefore, we invoked the uncertainly in the evolution of stellar EUV flux due to the difference in the initial rotational speed of the star. When the star's initial rotation speed is fast, the period when the stellar EUV is strong lasts longer. Hence, the period during which the atmosphere cannot be maintained due to massive escape would be longer. This effect shifts the period when the O_2-dominated atmosphere is formed, so that it is in the Hesperian period. Our study suggests that ~1 mbar O_2-dominated atmosphere may be formed during the Hesperian period by taking into account carbon escape, if the stellar evolution

©2020. Japan Geoscience Union. All Right Reserved.

is the type of the fast rotator. This is consistent with the results of the Curiosity measurement.

Keywords: Mars, Atmospheric escape, Atmospheric evolution

©2020. Japan Geoscience Union. All Right Reserved.

Radiative Transport Simulations for 0.4 - 1.9 THz Band Heterodyne Spectroscopy of Martian Atmospheric Trace Gases

*Yuki Hamaguchi[1], Hiroyuki Maezawa[1], Hideo Sagawa[2]

1. Osaka Prefecture University, 2. Kyoto Sangyo University

Radiative transport simulations and line surveys for 0.4 -1.9 THz band heterodyne spectroscopy of the Martian atmospheric trace gases were performed assuming nadir and limb-sounding observations with an orbiter. Heterodyne spectroscopy with frequency high resolution is a useful tool to observe the vertical distributions of the temperature, trace molecules (CO, ^{13}CO, C^{18}O, C^{17}O, H_2O, HDO, $H_2{}^{18}O$, $H_2{}^{17}O$, ^{18}OCO, H_2O_2, HO_2, O_3, O_2, etc.), and their isotopes from the surface layer of the Martian atmosphere to an altitude of approximately 100 km. In particular, since a background emission source such as the sun is not required, observations can be carried out at any local time such as day/night, morning/evening, etc. In addition, this wavelength range is less affected by dust absorption and scattering so that this tool allows us to observe the lower atmosphere near the surface of Mars even during dust storms. It is also possible to measure the velocity fields of the atmosphere by utilizing the Doppler shift effect. These strengths will provide us the important information for understanding of the atmospheric oxidation processes and photochemical reaction networks in the Martian atmosphere, the three-dimensional information of the material and water circulations driven by seasonal and diurnal changes from the surface layer to the upper layer, the dissipation history of water vapor into space, the resources for terraforming and future manned Mars missions, and so on.

At present, a working group on the Mars Aqueous Environment and Space Climate Orbiter (MACO) project, with an eye to a future small or medium size Mars orbiter satellite, has been formed in Japan. In this study, we also investigated the optimum frequency bands for the THz-band heterodyne spectrometer, which is an optional instrument in this mission plan. The diameter of the antenna is assumed to be 35 cm. The heterodyne detector and spectrometer are assumed to be a Schottky barrier diode (SBD) mixer operated at room temperature and an autocorrelation type digital spectrometer with a bandwidth of 8 GHz and a resolution of 1 MHz, respectively. The shot noise of the SBD mixer detector was taken into account for the spectrum calculations. For example, in 0.9 THz band the emission lines of ^{13}CO, C^{18}O, C^{17}O, H_2O, HDO, ^{18}OCO, H_2O_2, HO_2, and O_3 can be observed simultaneously by optimizing the frequency setting in double-sideband mode. An altitudinal resolution of better than 6 km will be achieved. When observing high-rise H_2O up to around 100 km, it is possible to respond by switching to a dedicated frequency. How limb-sounding data is processed and compressed on board and downlinked is an important future issue.

In this conference, we will present the results of these simulations.

Keywords: Mars, Planetary Atmosphere, Heterodyne Spectroscpy, Terahertz Remote Sensing

©2020. Japan Geoscience Union. All Right Reserved.

[E] Poster | A (Atmospheric and Hydrospheric Sciences)：A-AS Atmospheric Sciences, Meteorology & Atmospheric Environment

[A-AS01] High performance computing for next generation weather, climate, and environmental sciences

convener:Hiromu Seko(Meteorological Research Institute), Takemasa Miyoshi(RIKEN), Chihiro Kodama(Japan Agency for Marine-Earth Science and Technology), Masayuki Takigawa(Japan Agency for Marine-Earth Science and Technology)

A lot of advanced simulation studies are being conducted by high performance supercomputers, such as K computer and Earth Simulator, in various fields including meteorology. The high performance supercomputers enable us to conduct numerical simulations and data assimilation of observation big-data (huge high-density and high-frequency data) with a few orders of magnitude higher resolutions and ensemble numbers than those with the previous supercomputers. In addition, the post-K computer, Fugaku will be available as a successor of K, and studies for the Fugaku computer are in progress. At this session, we comprehensively pick up the topics in the Atmospheric and Hydrospheric Sciences Sessions of the 2020 Union Meeting that comprise the atmospheric, oceanic and land sciences. This session aims to promote recent studies related to the issues on high performance computing in weather, climate, and environmental studies using the K computer and other supercomputers, study plans using the Fugaku computer, and to enhance discussions on future directions of numerical simulations in meteorology.

[AAS01-P01] Ultra-high Resolution Numerical Weather Simulation and Dependency of Simulated Convective Cells on Model Resolutions

*Tsutao OIZUMI[1,2], Kazuo Saito[1,3,2], Duc Le[1,2], Junshi Ito[3,2] (1.The Japan Meteorological Business Support Center, 2.Meteorological Research Institute, 3.The Atmosphere and Ocean Research Institute)

[AAS01-P02] The Assimilation of Dual Phased Array Weather Radar Observations to Short-range Convective Forecasts

*James David Taylor[1], Guo-Yuan Lien[3], Shinsuke Satoh[2], Takemasa Miyoshi[1] (1.RIKEN Research center for computational science, 2.NICT National Institute of Information and Communications Technology, 3.Central Weather Bureau)

[AAS01-P03] Toward assimilation of dense and frequent 3-D lightning location data on a severe local rainfall forecast

★Invited Papers

*Yasumitsu Maejima[1], Tomoo Ushio[2], Takemasa Miyoshi[1] (1.RIKEN Center for Computational Science, 2.Graduate School of Engineering, Osaka University)

[AAS01-P04] Simulation of fog in Tokyo Bay: the role of atmosphere-ocean-river interaction

★Invited Papers

*Kohei Takatama[1], Takemasa Miyoshi[1] (1.RIKEN)

[AAS01-P05] **The ensemble Kalman inversion and its application into estimating parameters of a distributed rainfall-runoff model**

*Le Duc[1,2] (1.JMBSC, 2.MRI)

[AAS01-P06] **Retrieval of hygroscopic growth factor of uniformly mixed aerosol particles based on immune evolution algorithm**

*Zhicha Zhang[1,2], Changjian Ni[1,2] (1.Chengdu University of Information Technology, 2.Plateau Atmospheres and Environment Key Laboratory of Sichuan Province)

[AAS01-P07] A scale-aware PBL scheme: for the unified simulation in mesoscale and global circulation models

*Wei Wei[1] (1.Chinese Academy of Meteorological Sciences)

[AAS01-P08] The resent progress of the weather forecast system based on the NICAM-LETKF assimilation system

★Invited Papers

*Ying-Wen Chen[1], Koji Terasaki[2], Shunji Kotsuki[3], Kaya Kanemaru[4], Masaki Satoh[1], Takemasa Miyoshi[2], Takuji Kubota[5] (1.Atmospheric and Ocean Research Institute, The University of Tokyo , 2.Center for Computational Science, RIKEN, 3.Chiba University, 4.National Institute of Information and Communications Technology, 5.Japan Aerospace Exploration Agency)

超高解像度数値気象シミュレーションと対流コアのモデル解像度依存性
Ultra-high Resolution Numerical Weather Simulation and Dependency of Simulated Convective Cells on Model Resolutions

*大泉 伝[1,2]、斉藤 和雄[1,3,2]、Le Duc[1,2]、伊藤 純至[3,2]
*Tsutao OIZUMI[1,2], Kazuo Saito[1,3,2], Duc Le[1,2], Junshi Ito[3,2]

1. 気象業務支援センター、2. 気象研究所、3. 東京大学大気海洋研究所
1. The Japan Meteorological Business Support Center, 2. Meteorological Research Institute, 3. The Atmosphere and Ocean Research Institute

本研究は数値気象モデルの要素（解像度と境界層スキーム（PBL））が豪雨のシミュレーションに与える影響を調べた。対象事例は2014年8月広島での豪雨である。モデルの解像度は5km, 2 km,と500m, 250 mであり、PBLスキームには、Mellor-Yamada-Nakanishi-Niino level3とDeardorffを用いた。

高解像度モデル（500mと250m解像度）は、低解像度モデル（5kmと2km解像度）よりも降水帯の位置や強度を正確に再現した。本事例ではPBLスキームの影響は小さかった。本研究では対流コア（CC s）のモデル解像度依存性についても調査を行った。モデルの解像度に対する対流コアの数の変化率は解像度500ｍで低くなる事がわかった。この結果は対流コアの数は解像度500mより高くすると収束する可能性を示した。これらの結果より本研究では高い解像度のモデル（解像度500m以下）の有用性について示した。

キーワード：豪雨シミュレーション、高解像度モデル、京コンピューター
Keywords: heavy rainfall simulation, high-resolution model, K computer

©2020. Japan Geoscience Union. All Right Reserved.

The Assimilation of Dual Phased Array Weather Radar Observations to Short-range Convective Forecasts

*James David Taylor[1], Guo-Yuan Lien[3], Shinsuke Satoh[2], Takemasa Miyoshi[1]

1. RIKEN Research center for computational science, 2. NICT National Institute of Information and Communications Technology, 3. Central Weather Bureau

The assimilation of Doppler velocity and reflectivity observations from phased array weather radar (PAWR) has been widely studied for the use of short-range numerical weather prediction (NWP) and have been found to have positive impact on analyses and forecasts of convective scale weather systems (Maejima et al 2017). However, these studies only assimilated observations from a single PAWR and the use of multiple PAWR observations for NWP has not yet been explored. With the recent development of PAWR located at sites in Osaka University and Kobe a common observation region has been established providing dual radar observations over a large area of the Kobe region, where sudden convective storms can develop and bring intense rain, causing hazardous conditions.

In this study we investigate the impact of utilizing dual PAWR observations for the prediction of a localized convective weather system. We employ the use of the SCALE-LETKF system (Lien et al, 2017), which couples the Local Ensemble Transform Kalman Filter (LETKF) with the Scalable Computing for Advanced Library and Environment (SCALE)-Regional Model (RM), to perform data assimilation experiments with 30-second-update of PAWR observations within a high-1km resolution mesh in order to capture the rapid development of convective activity. The dual reflectivity observations are initially used to identify and remove remaining false echoes from observations, including range sidelobes which are a common radar artifact, thereby improving upon existing quality control measures. Next, we introduce a process of combining reflectivity observations from both radars to reduce the loss of information from rain attenuation, which is a major problem for X-band radars. The results show that implementing these new data assimilation methods lead to improvements in both rainfall intensity and distribution in short range forecasts.

Keywords: convection, LETKF, assimilation, radar

©2020. Japan Geoscience Union. All Right Reserved.

Toward assimilation of dense and frequent 3-D lightning location data on a severe local rainfall forecast

*前島 康光[1]、牛尾 知雄[2]、三好 建正[1]
*Yasumitsu Maejima[1], Tomoo Ushio[2], Takemasa Miyoshi[1]

1. 理化学研究所　計算科学研究センター、2. 大阪大学大学院　工学研究科
1. RIKEN Center for Computational Science, 2. Graduate School of Engineering, Osaka University

In recent years, a dense and frequent lightning observation system named “BOLT” was developed (e.g. Yoshida et al. 2014), observing every 10^{-6} seconds 3-dimensional lightning locations at 100-m resolution. The original data has a 70-km range in the horizontal and a 20-km range in the vertical. To assimilate the lightning location data with a regional numerical weather prediction model “SCALE” (Nishizawa et al. 2015), an observation operator to convert the model variables to lightning data is needed. In general, lightning is triggered by large electric charge originated from graupel collisions with strong updraft. Therefore, we investigated a relationship between the lightning observation data and the model graupel data. First, we performed a 30-seceond-update, 100-m-mesh SCALE-LETKF (Miyoshi et al. 2016, Lien et al. 2017) experiment with every 30-second Phased Array Weather Radar at Osaka University (Ushio et al. 2014), and we created every 30-second model data. For the lightning data, we calculated every 30-second lightning frequency per model grid. We investigated a scatter plot of the lightning frequency and the model graupel mixing ratio.

Using all lightning and graupel data, we could not find a clear relationship. However, by applying a criterion on lightning generation (Takahashi 1978), we found a high correlation between the lightning frequency and the graupel mixing ratio. Based on the result, we will develop an observation operator and try to contribute to a severe local rainfall forecast.

キーワード：データ同化、数値天気予報、メソ気象学
Keywords: Data assimilation, Numerical weather forecast, Meso-scale meteorology

©2020. Japan Geoscience Union. All Right Reserved.

東京湾の霧のシミュレーション：大気海洋河川相互作用の役割
Simulation of fog in Tokyo Bay: the role of atmosphere-ocean-river interaction

*高玉 孝平[1]、三好 建正[1]
*Kohei Takatama[1], Takemasa Miyoshi[1]

1. 理化学研究所
1. RIKEN

River water often plays an important role in fog formation in the coastal ocean. Fresh and light water input from rivers makes a thin layer over the ocean around the river mouth. Even if the thin layer is cooled in a cold season, water column can keep stratification. As a result, near surface atmosphere becomes colder than the surrounding area, and an inversion layer tends to occur in the lower atmosphere. This condition leads to generate and maintain fog near the river mouth.

It is important to predict the occurrence and duration of fog for air- and sea-port operations near the coast. For example, Haneda Airport is closed about once a year due to heavy fog events. In particular, a heavy fog event on March 8, 2016 would be related to the river inflow.

This study aims to simulate the coastal fog using a coupled atmosphere-ocean-river model and to enhance our forecasting capabilities. We conducted offline coupled experiments with atmospheric and ocean models for the heavy fog event on March 8, 2016. To generate the bottom boundary condition with fine resolution for the atmospheric model over Tokyo Bay, we used the Regional Ocean Modeling System (ROMS). We performed two experiments: the RIV/CTL experiments with/without the effect of the river input, respectively. The grid spacing was chosen to be 500 m, and the atmospheric forcing was taken from the operational numerical weather prediction data of the Japan Meteorological Agency (JMA) Meso-scale Model (MSM). The obtained sea-surface temperatures (SSTs) were merged with those of the National Centers for Environmental Prediction-Final Operational Global Analysis data (NCEP FNL). By using the merged data as the lateral and bottom boundary conditions, we calculated the atmospheric states by a regional atmospheric model SCALE with three nested domains: the grid spacing in the innermost domain was chosen to be 500 m.

The results showed that relative humidity north of the Haneda Airport in the RIV experiment was larger by 2-3% than that in the CTL experiment from the night of March 7 to the morning of March 8. This feature was found over a cold SST region in the RIV experiment extended from the mouths of the Arakawa-river and the Sumida-river. The cold SST was generated by an above-normal fresh water inputs from both rivers due to precipitation in the morning of March 7. Over the cold SST region, the atmospheric inversion layer was maintained for a longer time than the surrounding regions. South-westward near-surface wind at that time potentially contributed to generate the fog over the airport by bringing the humid air.

キーワード：霧、大気海洋河川相互作用、東京湾
Keywords: Fog, Atmosphere-ocean-river interaction, Tokyo Bay

©2020. Japan Geoscience Union. All Right Reserved.

The ensemble Kalman inversion and its application into estimating parameters of a distributed rainfall-runoff model

*Le Duc[1,2]

1. JMBSC, 2. MRI

In data assimilation, the ensemble Kalman filter (EnKF) is a technique that based on sampling in estimating any system states given observations. Thus, uncertainties of the system state are represented by an ensemble of points which is propagated through time by a model and adjusted whenever observations are available. Compared with the variational methods, EnKF has two advantages: (1) the computation of EnKF is inherently parallel, and (2) the tangent linear model and its adjoint are not needed.

If we run a data assimilation scheme many times for the same observations, the system state would tend to overfit the observations. This simple fact shows that we can turn any data assimilation method to an optimization method. Now it becomes clear that for nonlinear optimization problems which have complicated nonlinear operators as complex models, EnKF suggests a viable derivative-free optimization method since we do not need to compute the derivatives of such nonlinear operators. The EnKF when applied in such problems is called the ensemble Kalman inversion (EKI) which inherits the two aforementioned advantages of EnKF. In this study we introduce and demonstrate the work of EKI by applying it into estimating parameters for a distributed rainfall-runoff model.

Keywords: Parameter estimation, Ensemble Kalman inversion

©2020. Japan Geoscience Union. All Right Reserved.

Retrieval of hygroscopic growth factor of uniformly mixed aerosol particles based on immune evolution algorithm

*Zhicha Zhang[1,2], Changjian Ni[1,2]

1. Chengdu University of Information Technology, 2. Plateau Atmospheres and Environment Key Laboratory of Sichuan Province

Based on decomposition of atmospheric extinction coefficient and Mie scattering theory, the objective function, which has the sole variable of the hygroscopic growth factor of uniformly mixed aerosol particles, was established. Furthermore, immune evolution algorithm was further used to optimize the objective function, and a feasible method was proposed to retrieve hygroscopic growth factor of uniformly mixed aerosol particles. The performance of the method was evaluated by utilizing the hourly ground observation data from nephelometer, aethalometer and GRIMM180 environment particle monitor in Chengdu from October 2017 to December 2017, as well as the coincidental environmental and meteorological data, which includes atmospheric visibility, relative humidity (RH) and NO_2 mass concentration. The results suggest that the retrieval algorithm is characterized by fast convergence, robustness and precision for all tested samples. hygroscopic growth model of uniformly mixed aerosol particles was established during autumn and winter in Chengdu. Note that this model could significantly improve the simulation accuracy of aerosol scattering coefficient in ambient conditions. The advantage of this model is that the average relative error between the simulated and the measured is only 12.7%. The universal algorithm is beneficial for subsequent study on the aerosol hygroscopic properties and its radiative forcing impacts.

Keywords: aerosol, Mie scattering theory, hygroscopic growth factor, retrieval, immune evolution algorithm

©2020. Japan Geoscience Union. All Right Reserved.

A scale-aware PBL scheme: for the unified simulation in mesoscale and global circulation models

*Wei Wei[1]

1. Chinese Academy of Meteorological Sciences

With the development of high performance supercomputers, kilometer- or sub-kilometer-scale numerical simulations have been realized. In the past, turbulence is well resolved by three-dimensional (3D) large-eddy simulation (LES) at very fine grid sizes (10~100 m) and for grid sizes greater than 2 km, one-dimensional (1D) planetary boundary layer (PBL) parameterizations represent sub-grid turbulence in the PBL. When it comes to kilometer- to sub-kilometer-scale grid sizes, neither 3D LES nor 1D PBL parameterization perform appropriately, called the “Gray zone”. This study readapted the turbulence mixing length in the UW PBL parameterization by adding a partition function which is related to the horizontal resolution and PBL height. The developed UW parameterization (UWnew) and several other 1D PBL schemes were applied to the simulation of an ideal convective boundary layer at “Gray zone” scales using WRF model.

The results show that, in terms of the profiles of the area mean values and sub-grid heat/momentum flux, scale-aware UWnew and ShinHong schemes perform the best at “Gray zone” scales among all the schemes (including UWnew, UW, ShinHong, MYNN2.5, YSU, BouLac). And UWnew scheme shows more rational results in the PBL simulation compared with UW scheme. To specify the performance of UWnew scheme in the simulation at “Gray zone” scales, four simulations with different horizontal resolutions were launched using UWnew and UW schemes. In the case of “Gray zone” scales, the profiles of sub-grid heat/momentum flux from the UWnew simulation is smaller than that of the UW scheme. This is mainly resulted from the reduced turbulent heat/momentum exchange coefficient values in the PBL. The weakened vertical flux confirms that the UWnew scheme improves the simulation of the physical process at “Gray zone” scales in which the process is partly resolved and partly parameterized.

Keywords: scale-aware , PBL scheme, high resolution simulation

©2020. Japan Geoscience Union. All Right Reserved.

The resent progress of the weather forecast system based on the NICAM-LETKF assimilation system

*Chen Ying-Wen[1]、寺崎 康児[2]、小槻 峻司[3]、金丸 佳矢[4]、佐藤 正樹[1]、三好 建正[2]、久保田 拓志[5]
*Ying-Wen Chen[1], Koji Terasaki[2], Shunji Kotsuki[3], Kaya Kanemaru[4], Masaki Satoh[1], Takemasa Miyoshi[2], Takuji Kubota[5]

1. 東京大学 大気海洋研究所、2. 理化学研究所 計算科学研究センター、3. 千葉大学、4. 情報通信研究機構、5. 宇宙航空研究開発機構
1. Atmospheric and Ocean Research Institute, The University of Tokyo , 2. Center for Computational Science, RIKEN, 3. Chiba University, 4. National Institute of Information and Communications Technology, 5. Japan Aerospace Exploration Agency

A near-real time weather forecast system based on a data assimilation system of Local Ensemble Transform Kalman Filter for the Nonhydrostatic ICosahedral Atmospheric Model (NICAM-LETKF Terasaki and Miyoshi 2017, Kotsuki et al., 2017) called NEXRA (NICAM-LETKF JAXA Research Analysis) has been developed by the collaboration of JAXA, RIKEN, and the University of Tokyo. The operational system, which is operated at JAXA’ s super computer (JSS2), provides 5-day weather forecast every 6-hour initialized by the ensemble mean of 100 members of the NICAM-LETKF data assimilation system. The assimilated observations are GSMaP (precipitation), AMSU-A (temperature), and PREPBUFR. At current stage, the 5-day forecast data with horizontal resolution at 112 km are available on the website (https://www.eorc.jaxa.jp/theme/NEXRA/index_j.htm). We introduce two resent progress toward the next generation NEXRA in this presentation. One is the development of the 5-day forecast system with finer horizontal resolution at 28/14 km, and the other one is a new NICAM-LETKF system assimilated observation data obtained from mhs (humidity) and atms (temperature and humidity), in addition with GSMaP, AMSU-A, and PREPBUFR. The new forecast system is initialized with 28/14 km data linear interpolated from 112 km initial states obtained from the current NICAM-LETKF system and the cloud microphysics scheme NSW6 (Tomita 2008) is used. To validate the new forecast system, we show the forecast experiment for the typhoon KROSA in August 2019 which hit SHIKOKU Island of Japan. Results show that the forecasted typhoon structure and the rain pattern of KROSA showing good agreements with observations. To validate the new system, we compare assimilation performance between the current and new NICAM-LETKF system.

キーワード：気象予測システム、データ同化
Keywords: weather forecast system, data assimilation

©2020. Japan Geoscience Union. All Right Reserved.

[E] Poster | A (Atmospheric and Hydrospheric Sciences)：A-AS Atmospheric Sciences, Meteorology & Atmospheric Environment

[A-AS02] Abnormal weathers and disasters in urban environments in East Asia related to climate change

convener:Masaru Inatsu(Faculty of Science, Hokkaido University), Yukari Takayabu(Atmosphere and Ocean Research Institute, the University of Tokyo)

Global climate change possibly increases weather disasters such as heatwave, gale, torrential rain, and heavy snowfall. Abnormal global-to-synoptic scale phenomena at least lay behind the frequent occurrence of local-scale extremes. The relation between large-scale pattern and local-scale abnormal weathers has recently been scrutinized by statistical analysis of high-resolution data derived from artificial-satellite observation and numerical simulations. Moreover, impact assessment of climate change to various sectors like water resource management, agriculture, energy control should be reduced to adaptation policies for industries and local governments including urban areas. This reduction generally requires close communication between scientists and stakeholders, with an aid of storyline approach to represent uncertain information on climate change. Therefore, studies on climate change, if limited to East Asia, range from global to urban scales and are interdisciplinary from fundamental to applications. This session calls for research topics in a various related field, and the participants can share possible future extensions of climate change studies.

[AAS02-P01] Drawing Storylines of Extraordinary Weather Phenomena around Japan in Changing Climate

*Yukari Takayabu[1], Hisashi Nakamura[2], Takeshi Horinouchi[3], Tosiyuki Nakaegawa[4], Seita Emori[5] (1.Atmosphere and Ocean Research Institute, the University of Tokyo, 2.Research Center for Advanced Science and Technology, the University of Tokyo, 3.Hokkaido University, 4.Meteorological Research Institute, JMA, 5.National Institute for Environmental Studies)

[AAS02-P02] Climate change adaptation to disaster in urban areas

*Masaru Inatsu[1], Kusaka Hiroyuki[2], Takemi Tetsuya[3] (1.Faculty of Science, Hokkaido University, 2.Center for Computer Sciences, Tsukuba University, 3.Disaster Prevention Center, Kyoto University)

[AAS02-P03] Assessing the impacts of typhoons on extreme winds in densely-built urban districts

*Tetsuya Takemi[1], Guangdong Duan[1], Kumi Nakamae[1] (1.Disaster Prevention Research Institute, Kyoto University)

[AAS02-P04] A strategy towards the Japan regional reanalysis to protect our lives, properties and the social infra-structure under the changing climate

*Kenichi Kuma[1], Toshiki Iwasaki[2], Hisashi Nakamura[1] (1.Research Center for Advanced Science and Technology, The University of Tokyo, 2.Department of Geophysics. Graduate School of Science. Tohoku University)

[AAS02-P05] Impacts of climate change on heavy wet snowfall in Japan: differences among wether patterns

*Masamichi Ohba[1], Soichiro Sugimoto[1] (1.Central Research Institute of Electric Power Industry)

[AAS02-P06] An application of the detection method for atmospheric fronts to a large ensemble climate data

*Maki Miyamoto[1], Tomohito Tomohito[1] (1.Hokkaido University)

[AAS02-P07] Diurnal Variability of Urban Heat Island Intensity in Metro Manila, Philippines: An Initial Investigation

*John Asaula Manalo[1,2], Jun Matsumoto[1,3] (1.Department of Geography, Graduate School of Urban Environmental Sciences, Tokyo Metropolitan University, 2.Climatology and Agrometeorology Division, Philippine Atmospheric Geophysical and Astronomical Services Administration, Quezon City, Philippines, 3.Department of Coupled Ocean-Atmosphere-Land Processes Research, JAMSTEC, Yokosuka, Japan)

[AAS02-P08] **Land suitability evaluation for agricultural cropland in the Dornod province, Mongolia using Remote Sensing and GIS tools**

*Tsolmon Renchin[1], Bayanjargal Darkhijav[1], Davaajargal Jargalsaikhan[2], Enkhjargal Natsagdorj[3], Batbayar Ganchudur[1] (1.National University of Mongolia, Mongolia, 2.Institute of Mathematics and Digital technology Mongolian Academy of Sciences, Mongolia , 3.Dept. of Geography, Ghent University, Ghent, Belgium)

Drawing Storylines of Extraordinary Weather Phenomena around Japan in Changing Climate

*高薮 縁[1]、中村 尚[2]、堀之内 武[3]、仲江川 敏之[4]、江守 正多[5]
*Yukari Takayabu[1], Hisashi Nakamura[2], Takeshi Horinouchi[3], Tosiyuki Nakaegawa[4], Seita Emori[5]

1. 東京大学 大気海洋研究所、2. 東京大学先端技術研究センター、3. 北海道大学、4. 気象庁気象研究所、5. 国立環境研究所
1. Atmosphere and Ocean Research Institute, the University of Tokyo, 2. Research Center for Advanced Science and Technology, the University of Tokyo, 3. Hokkaido University, 4. Meteorological Research Institute, JMA, 5. National Institute for Environmental Studies

Frequent occurrences of extraordinary weather events in recent years have disclosed the vulnerability of our society to unexperienced kinds of extreme events. Increase of such extreme weather events are attributed to the global warming. Since we expect to face even further increases of extreme events in future, it is necessary to help policy makers for making adequate adaptation plans. To this end, an essential point is to estimate the range of uncertainty for future changes of phenomena, and to adequately convey such information to the policy makers.

In this talk, we will introduce our project supported by the Environment Research and Technology Development Fund (2-1904). In this research, we employ the Storyline method, which is introduced to make physical explanations why and how extraordinary weather phenomena are affected by the global climate change. We especially focus on local phenomena around Japan, such as extreme rainfall, extreme droughts, heat waves, etc.

In our project, we study how extraordinary weather phenomena are linked to large-scale dynamics. We also discuss how to choose climate models from the CMIP5 and CMIP6 model ensembles, in order to represent a wide range of uncertainty in future change. Finally, we aim to extract small numbers of climate storylines which represent the possible range in future changes of extreme weather phenomena around Japan and their connections to changes in large-scale atmospheric condition.

キーワード：ストーリーライン、気候変動、異常天候、CMIP6
Keywords: storyline, climate change, extraordinary weather, CMIP6

©2020. Japan Geoscience Union. All Right Reserved.

気候変動に伴う都市災害への適応
Climate change adaptation to disaster in urban areas

*稲津 將[1]、日下 博幸[2]、竹見 哲也[3]
*Masaru Inatsu[1], Kusaka Hiroyuki[2], Takemi Tetsuya[3]

1. 北海道大学大学院理学研究院、2. 筑波大学計算科学研究センター、3. 京都大学防災研究所
1. Faculty of Science, Hokkaido University, 2. Center for Computer Sciences, Tsukuba University, 3. Disaster Prevention Center, Kyoto University

本研究プロジェクト（環境再生保全機構環境研究総合推進費2-1905）では、暑熱による都市災害（熱中症）、強風による都市災害（建築物被害）、豪雨豪雪による都市災害（浸水氾濫や交通障害）といった近未来の気候変動に伴うリスクを評価する。暑熱は熊谷市・新潟市、強風は大阪市・京都市、豪雨豪雪は札幌市を対象とする。まず、近未来の気候変動影響を暑熱・強風・豪雨豪雪に着目して明らかにするため、d4PDF データベース(*)から気温傾向、極端事象、気圧配置の変化を抽出し、都市に対しとくに甚大な影響を及ぼす暑熱、強風、豪雨豪雪といったハザードと、近未来に都市災害をもたらす気象の典型事例を同定する。都市災害をもたらす気象は都市スケールから総観スケールに及ぶ多様な要素を含んでいる。そこで、各サブテーマが分担して、暑熱・強風・豪雨豪雪と関係する都市スケール、メソスケール、総観スケールの気象を分析する。次に、同定した事例に基づき都市特有の災害リスクを評価する。ここではスケールに応じて、汎用の領域気象モデルによる空間解像度数キロメートル程度の計算または最先端の都市街区気象ラージエディーシミュレーション(LES)による空間解像度数メートル程度の計算を実施する。この際、これまでの気候変動適応研究で培ったサンプリングや擬似温暖化技法を駆使して、評価を効率的に行う。以上により得た各サブテーマ（各対象都市）の暑熱、強風、豪雨豪雪に対する都市災害リスク評価結果を総合して、対象都市における適応策を地方自治体の実務者と協議する。本研究課題により国内都市における気象・気候に係るハザードとそれに適応するための方策の方向性が提示され、効率的なリスク評価の実施とともに気候変動の適応策に係る研究・技術開発を進める点において、環境政策への貢献となる。

キーワード：気候変動適応
Keywords: Climate change adaptation

©2020. Japan Geoscience Union. All Right Reserved.

都市域での暴風の発現に及ぼす台風の影響評価
Assessing the impacts of typhoons on extreme winds in densely-built urban districts

*竹見 哲也[1]、Duan Guangdog[1]、中前 久美[1]
*Tetsuya Takemi[1], Guangdong Duan[1], Kumi Nakamae[1]

1. 京都大学防災研究所
1. Disaster Prevention Research Institute, Kyoto University

A gusty wind by typhoons is one of the major natural hazards and has been the most threatening windstorm in urban districts. In Osaka City, the recorded highest instantaneous wind speed reached up to 60 m/s. The recent intense tropical cyclone, Typhoon Jebi, which landed the central part of Japan in September 2018 with the lifetime minimum central pressure of 915 hPa and the maximum wind speed of 48 m/s, exhibited a similar track compared to past disastrous typhoons: Typhoon Nancy (1961) and Muroto Typhoon (1934). Urban surface roughnesses, e.g. building obstacles, exert significant influences on the magnitude of wind gustiness. With the growing urbanization globally, quantification of turbulent winds in densely-built, urban districts is important to the assessment and prediction of risks of wind damages and the understanding of the underlying physical mechanisms. The influlences of densely built urban environments on the occurrence of wind gusts in urban districts of Osaka and Kyoto City during the landfall of Typhoon Jebi are studied by merging mesoscale meteorological and building-resolving large-eddy simulations (LES), which allows an explicit representation of the complicated building structures while retaining the strong mesoscale perturbations from the typhoon. With the successful reproduction of the track and intensity of the typhoon in meteorological simulations, the simulated winds at the boundary-layer top of the LES model are used to quantify the wind gusts in the urban district. The maximum wind gust in the analysis area of Osaka is around 60-70 m/s, which is comparable to the wind speed at the height of about 300 m. Such wind gusts are generated by the instantaneous downward momentum transfer in areas, where buildings with a high variability in the height are clustered. The instantaneous wind gusts are found to be the strongest when the building packing density is moderate. The results suggest that the risks of wind damages are mostly likely to be maximized in urban districts where the building height is highly variable and the packing density is moderate.

キーワード：暴風、都市災害、都市気象、乱流、気候変動影響、台風
Keywords: extreme wind, urban disaster, urban meteorology, turbulent flow, climate change impact, typhoon

©2020. Japan Geoscience Union. All Right Reserved.

変動する気候において生命、財産、社会インフラを守るための日本域気象再解析の戦略について

A strategy towards the Japan regional reanalysis to protect our lives, properties and the social infra-structure under the changing climate

*隈 健一[1]、岩崎 俊樹[2]、中村 尚[1]
*Kenichi Kuma[1], Toshiki Iwasaki[2], Hisashi Nakamura[1]

1. 東京大学先端科学技術研究センター、2. 東北大学大学院理学研究科
1. Research Center for Advanced Science and Technology, The University of Tokyo, 2. Department of Geophysics. Graduate School of Science. Tohoku University

近年の相次ぐ極端な気象を経験することで、変動する気候に備えていくことの重要性が社会により理解されるようになってきた。この備えにはハード対策とソフト対策があり、その双方に領域再解析が重要な役割を果たすことができる。

領域再解析は全球再解析の枠組みのもとで、過去の観測データを用いて領域の４次元データ同化システムを回すことで実行することができる。この領域再解析にはかなりの計算資源や人的資源が必要であり、領域再解析が私たちの社会にどの程度のベネフィットをもたらすのかを考えることが必要である。

すでに気候モデルの専門家たちはd4PDF (Mizuta et al. 2017)など巨大アンサンブルによる将来予測実験を通じて、河川堤防や防潮堤などのハード対策の計画に貢献しつつある。気候変動への適応策が進められる中、d4PDFの結果は農業、水文、リスク管理など、様々な分野にも使われている。気候モデルの利用者たちは、シミュレーション結果を将来計画の意思決定に活用しつつある。ハード対策では、予算規模の大きさや長期間にわたる整備が必要であることから、情報の信頼度をしっかり確認しつつ進めていく必要がある。気候シミュレーションの信頼性を確認する一つの選択肢は、シミュレーション結果と自然変動の観測結果を比較することである。地域での適応策に肝要な地域の気候変動においては、全球の再解析よりも領域の再解析がこの比較において重要な役割を果たす。

領域再解析は気候変動の把握だけでなく、リスク管理やレジリエンスの強化にも重要な役割を持つ。領域再解析は、過去の顕著な現象について事実に基づいたシナリオを提供する。また、再解析は領域モデルによる予報の初期条件も提供し、これによる過去の予報は再予報と呼ばれる。特定の地域から見ると、気象による災害の頻度は一般に稀である。例えば、市町村単位で極端な現象への備えをするためには、長期間の再解析や再予報を用いて過去の極端現象から学ぶ必要がある。過去現象の再現に最新の数値予報システムを用いると、過去の事例を通じて得られた知見が今後の極端現象について数値予報で予測された時の行動判断に生かされることになる。というのは、極端現象に対する予報の信頼性についての知見を利用者が持つことができるからである。気象予測には大なり小なり誤差が必ず伴うことから、気象分野以外の様々な分野の専門家や利用者が意思決定をする際に、予報の信頼性を彼らが理解していることが極めて重要である。

このように、領域再解析には２つの重要な役割があることがわかる。一つは実際に起きている気候変動を把握し、確認すること、もう一つは過去の極端現象の知見を今後の極端現象への対応に活かすことである。前者の役割では、Fukui et al. (2018)のような手法を選択することが良いだろうし、後者については現業で使われている数値予報システムに近いもので衛星観測などの観測データも活用したものを使う手法を選択したい。防災対応分野や再生可能エネルギー分野が領域再解析・再予報の主要な利用者になるものと考える。

領域再解析の社会へのベネフィットをさらに高めるためには、海洋学、水文学・雪氷学、エネルギー部門、大気化学など様々な分野の専門家やデータ利用者たちとの連携の活性化が重要である。そのためには、d4PDFの活動を通じて発展してきた関係分野、利用者との連携を活用することが鍵となる。

最後に、国際連携の重要性も指摘しておきたい。第一段階としては、過去の観測データを近隣国で交換、共有化することが、各国での領域再解析の活動に貢献することになる。さらには再解析結果を共通する領域で比較することがこれらの国々にとって有益であろう。

©2020. Japan Geoscience Union. All Right Reserved.

Reference

Fukui, S, T. Iwasaki, K. Saito, H. Seko and M. Kunii 2018: A feasibility study of the high-resolution regional reanalysis over Japan assimilating only conventional observations as an alternative to the dynamical downscaling. J. Meteor. Soc. Japan 2018, 565-585

Mizuta, R et al., 2017: Over 5000 years of ensemble future climate simulations by 60 km global and 20 km regional atmospheric models. Bull. Amer. Meteor. Soc. July 2017, 1383-1398

キーワード：領域再解析、数値予報、レジリエンス、変動する気候
Keywords: regional reanalysis, NWP, resilience, changing climate

©2020. Japan Geoscience Union. All Right Reserved.

Impacts of climate change on heavy wet snowfall in Japan: differences among wether patterns

*大庭 雅道[1]、杉本 聡一郎[1]
*Masamichi Ohba[1], Soichiro Sugimoto[1]

1. 電力中央研究所
1. Central Research Institute of Electric Power Industry

Wet snow is a primary cause of atmospheric icing, which can lead to severe damage to power towers and lines, resulting in electrical breakdowns and blackouts. This study investigated the influence of climate change on heavy wet snowfall events during the winter season in Japan. Self-organizing maps (SOMs) were used to explore the weather patterns (WPs) associated with changes in heavy wet snowfall. This study used climate projections obtained from the database for Policy Decision-making for Future climate change (d4PDF) to investigate the impacts of climate change on wet snowfall in Japan. The SOM technique was applied using the surface atmospheric circulation to determine the dominant heavy wet snowfall WP. The SOMs showed that some WPs had a significant effect on the magnitude, frequency, and location of heavy wet snowfall in Japan. The projected changes in the amount of heavy wet snowfall showed a nonuniform spatial distribution. Additionally, the impact of climate forcing on WPs associated with heavy wet snowfall was evaluated to understand the spatially heterogeneous changes in wet snowfall. The SOM analysis results suggest that the future changes in spatially heterogeneous extreme wet snowfall can be attributed to differences in WP responses to climate change. These differences can be attributed to the future variations in the region of the atmospheric layer at temperatures near 0 ˚C (rain-snow transition layer) among WPs, which can alter the spatial distribution and frequency of heavy wet snowfall. The findings can help inform structural design requirements to withstand regional climate change.

キーワード：大気着氷雪、気候変動、豪湿雪、自己組織化マップ、気象パターン、湿着雪
Keywords: Atmospheric icing, Climate change, Heavy wet snowfall, Self-organizing map, Weather patterns, Wet snow accretion

©2020. Japan Geoscience Union. All Right Reserved.

An application of the detection method for atmospheric fronts to a large ensemble climate data

*宮本 真希[1]、山田 朋人[1]
*Maki Miyamoto[1], Tomohito Tomohito[1]

1. 北海道大学
1. Hokkaido University

In recent years, heavy rainfall disasters attributed to atmospheric fronts often occur in Japan, such as the heavy rain event of July 2018 in western Japan and 2017 in northern Kyushu. A forecasting of the fronts as well as rainfall associated with them make impacts on society in disaster prevention such as risk avoidance due to heavy rainfall. To give an example, a weather forecast for short-term within 1 week, is useful to take refuge and for yearly long term is helpful to determine an evacuation plan.

A previous study made normalized parameter of thermal and dynamical variables, horizontal temperature gradient and isobaric relative vorticity. There is an atmospheric front at isobaric surface of 900hPa where the parameter is over threshold value. Around an atmospheric front, horizontal temperature gradient is larger than other regions. The wind converges in the boundary between warm air mass and cold air mass with rotation. Therefore, horizontal wind fields of the fronts have positive relative vorticity compared to others. This diagnostic detected the front accompanying passing of extratropical cyclone across the North Atlantic.

In this study, a thermal variable of the parameter used by the diagnostic is equivalent potential temperature and the objective diagnostic is specialized for the climate of north-western Pacific Ocean region around Japan. The equivalent potential temperature means the temperature and quantity of water vapor. Thus, the new diagnostic would detect the boundary between air masses which has the difference in quantity of water vapor as fronts. It called as water vapor front. It appears on East China Sea at south side of Baiu front. In the case of the heavy rain from June 28th to July 8th, 2018, nine o’ clock (Japan standard time) each day, the diagnostic detected a part of Baiu front in four days and all part of it in seven days. In addition, it detected water vapor fronts in the term of heavy rain in 2018. In other cases, it detected cold fronts, warm fronts, occluded fronts embedded with an extratropical depression. The parameter value increases with improvement of the depression.

This diagnostic would be used to detect the fronts in future climate. The used data is d4PDF, a database composed of the results from model experiments for 3,000 years in past climate and 5,400 years in future climate. We apply the method to the data for climate of the past and future. These application results would be compared and used to examine the variation of the frontal distribution with climate change.

キーワード：前線の抽出、大量アンサンブル、無次元パラメータ、豪雨災害
Keywords: detection of atmospheric fronts, large ensemble climate, non-dimensional parameter, heavy rainfall disaster

©2020. Japan Geoscience Union. All Right Reserved.

Diurnal Variability of Urban Heat Island Intensity in Metro Manila, Philippines: An Initial Investigation

*John Asaula Manalo[1,2], Jun Matsumoto[1,3]

1. Department of Geography, Graduate School of Urban Environmental Sciences, Tokyo Metropolitan University, 2. Climatology and Agrometeorology Division, Philippine Atmospheric Geophysical and Astronomical Services Administration, Quezon City, Philippines, 3. Department of Coupled Ocean-Atmosphere-Land Processes Research, JAMSTEC, Yokosuka, Japan

Studies have shown that the Urban Heat Island (UHI) Effect driven by urbanization and industrialization is one of the major problems in the 21st century. In this study, the diurnal variability of urban heat island (UHI) intensity in the four stations located in populated cities in Metro Manila was investigated using the AWS measurements retrieved from the Philippine Atmospheric Geophysical and Astronomical Services Administration (PAGASA) of the Department of Science and Technology (DOST) from 2014 to 2018. Highest UHI intensity occurred at 20:00 PST was observed in the City of Manila (Port Area station, 4.03˚ C), at 21:00 PST in Pasig City (Pasig City Hall station, 2.95˚C), and at 19:00 PST and 21:00 PST in Quezon city (Science Garden station, 3.02˚C; La Mesa station, 4.28˚C, respectively). The maximum UHI intensity was observed generally during night time and lowest UHI intensity was observed during day time for all the stations. The results of this study will enable further research to better understand and mitigate the challenges brought by urbanization.

Keywords: Urban Heat Island (UHI), Temperature, Urbanization, Philippines

©2020. Japan Geoscience Union. All Right Reserved.

Land suitability evaluation for agricultural cropland in the Dornod province, Mongolia using Remote Sensing and GIS tools

*Tsolmon Renchin[1], Bayanjargal Darkhijav[1], Davaajargal Jargalsaikhan[2], Enkhjargal Natsagdorj[3], Batbayar Ganchudur[1]

1. National University of Mongolia, Mongolia, 2. Institute of Mathematics and Digital technology Mongolian Academy of Sciences, Mongolia , 3. Dept. of Geography, Ghent University, Ghent, Belgium

The purpose of this study is to create an estimation of cropland suitability map in the study area Dornod province, which belong to the Gobi and steppe region of Mongolia. The soil of the study area is suitable for agriculture, which is one of the main sectors of our economy. However, the pasturing livestock and the crop production are very vulnerable to climate change in the study area. Dry land expansion and pasture land degradation cause to agriculture land vulnerability. It is important to evaluate the impacts of climate change affecting to effectiveness of agriculture and implement the adaptation methods.

We used MODIS data over 2003-2018 to study how the soil moisture content and long term data have changed in the past and what trend is in the future. Multivariable regression analysis using satellite images for Normalized Vegetation Index (NDVI) and Land surface Temperature (LST) from MODIS and DEM Elevation soil and climate data were applied for the potential for crop production in the study area. Multivariable regression analysis provides an opportunity for understanding and analyzing the nature of other factors affecting the factors. In particular, we would propose some models for cropland suitability, which depends on many factors such as surface temperature, elevation, slope, orientation and other soil parameters in the Gobi and steppe regions of Mongolia. The result shows that output map created accurate result and reasonable for cropland suitability. The approach can be an advantageous indicator for carrying out agricultural management decisions and advise for decision-makers in the Gobi and steppe regions of Mongolia.

Keywords: Cropland suitability, soil properties, GIS, Mongolia

©2020. Japan Geoscience Union. All Right Reserved.

[E] Poster | A (Atmospheric and Hydrospheric Sciences)：A-AS Atmospheric Sciences, Meteorology & Atmospheric Environment

[A-AS03] Atmospheric Chemistry in Highly Polluted Environments

convener:Hongliang Zhang(Fudan University), Jianlin Hu(NUIST Nanjing University of Information Science and Technology), Jia Xing(Tsinghua University), Siyu Chen(Lanzhou University)

Due to the rapid growth of economy and fossil fuel consumption and lack of emission controls, Many Asian regions have experienced substantially elevated concentrations of air pollutants, such as China, India, and Southeast Asia. High concentrations of air pollutants have significant impacts on public health and also play an important role in the climate system. Understanding the emissions, fate, and impact of high air pollution in these regions is essential for designing effective control strategies.
In the many highly polluted regions, large amount of anthropogenic emissions from industrial and/or residential activities are mixed with biogenic emissions, wind-blown dust, and biomass burning, then undergo complex atmospheric chemistry processes and form secondary pollutants such as ozone and particulate matter. Many studies suggested that high pollution formation is much faster in these regions and cannot be completely explained by knowing atmospheric chemistry, indicating additional chemistry processes in highly polluted environments, which are likely associated with the complex emission sources, unique climate and topography. Progress has been made in several aspects, such as additional sources and formation pathways of atmospheric radicals, heterogeneous reactions on particle surface for sulfate and organic aerosol formation.
Studying atmospheric chemistry in highly polluted environments involves field measurements, lab experiments, and numeric modeling. It will advance our scientific understanding of the formation processes, improve our knowledge in sources of air pollutants, help develop air pollution control strategies for protecting public health and climate in these regions.

[AAS03-P01] Significant contributions of upwind sources to ground-level ozone in the North China Plain

*Hongliang Zhang[1,2], Kaiyu Chen[2], Pengfei Wang[2], Siyu Wang[1], Peng Wang[3], Qi Ying[4], Jianlin Hu[5] (1.Fudan Univ., 2.LSU, 3.HKPU, 4.TAMU, 5.NUIST)

[AAS03-P02] **How much do emissions from China affect Northeast Asia?**

*Hongliang Zhang[1,2], Pengfei Wang[2], Chun Cheng[3], Yele Sun[3] (1.Fudan Univ., 2.LSU, 3.IAP, CAS)

[AAS03-P03] **Modeling analysis of the spatiotemporal distribution characteristics of the atmospheric ultrafine particle in North China Plain and Yangtze River Delta of China in 2016**

Yanhong Zhu[1], *Jianlin Hu[1] (1.NUIST Nanjing University of Information Science and Technology)

[AAS03-P04] **Impact of land-use changes on biogenic emissions and formation of ozone and secondary organic aerosols in China from 2013 to 2017**

*JinLong Ma[1], Yu Wang[1], Peng Wang[2], hongliang Zhang[1] (1.Fudan University, 2.The Hong Kong Polytechnic University)

[AAS03-P05] Long term trends in air pollution in China

*Shengqiang Zhu[1], Siyu Wang[1], Zhihao Shi[2], Fei Ye[2], Jianlin Hu[2], Hongliang Zhang[1] (1.Fudan University, 2.Nanjing University of Information Science & Technology)

[AAS03-P06] **Improving ozone simulation and understanding its adverse effects in India**

*Mengyuan Zhang[1], Siyu Wang[1], Kaiyu Chen, Xue Qiao, Sri Harsha Kota, Hongliang Zhang[1] (1.Fudan University)

[AAS03-P07] **Comparison of the SAPRC18 and SAPRC11 photochemical mechanisms for ozone simulation in China**

*Yu Wang[1], JinLong Ma[1], Peng Wang[2], Hongliang Zhang[1] (1.Fudan University, 2.The Hong Kong Polytechnic University)

[AAS03-P08] **Contribution of biogenic sources to secondary organic aerosol in summertime in Shaanxi, China**

*Yong Xu[1], Hongliang Zhang[2], Dexiang Wang[3] (1. Yangzhou University, 2.Fudan University, 3.Northwest A&F University)

[AAS03-P09] **Preliminary study on physical and chemical properties of dust**

*Yuan Luo[1], Siyu Chen[1] (1.Lanzhou university)

[AAS03-P10] Associations of fine particulate matter and health burdens in Handan city

*aifang gao[1,2,3,4,5,6], junyi wang[1], jianfei luo[1], aiguo li[1], jingyi li[4,5,6], Hongliang Zhang (1.School of Water Resources and Environment, Hebei GEO University, 2.Hebei Province Collaborative Innovation Center for Sustainable Utilization of Water Resources and Optimization of Industrial Structure , 3.Hebei Province Key Laboratory of Sustained Utilization and Development of Water Resources, 4.Jiangsu Key Laboratory of Atmospheric Environment Monitoring and Pollution Control, 5.Collaborative Innovation Center of Atmospheric Environment and Equipment Technology, 6.Nanjing University of Information Science & Technology)

[AAS03-P11] Data assimilation of lidar-derived aerosol extinction coefficients and its application in China

*Zengliang Zang[1], Xiaobin Pan[1], Yanfei Liang[1], Wei You[1], Yiwen Hu[1] (1.National University of Defense Technology)

[AAS03-P12] The effectiveness of the Air Pollution Prevention and Control Action Plan on the air quality and human health during 2013-2017 in China

Dian Ding[1], *Jia Xing[1], Shuxiao Wang[1] (1.Tsinghua University)

[AAS03-P13] Modeling the source-receptor relationships in highly polluted regions

*Jia Xing[1], Dian Ding[1], Shuxiao Wang[1], Jim Kelly[2], Carey Jang[2], Yun Zhu[3] (1.Tsinghua University, 2.U.S. Environmental Protection Agency, 3.South China University of Technology)

[AAS03-P14] **Opposite Role of H_2SO_4 Formation Pathway on Secondary Organic Aerosol Formation Derived from Ethyl Ethacrylate Ozonolysis**

*Peng Zhang[1] (1.Rcees)

[AAS03-P15] **Investigating the performance of satellite-based models in estimating the surface $PM_{2.5}$ over China**

*Siwei Li[1], Lechao Dong[1], Jie Yang[1], Wenxuan Shi[1] (1.Wuhan University)

[AAS03-P16] Tiramisu snow and the weakening of surface albedo

Siyu Chen[1], *Hongru Bi[1] (1.Lanzhou University)

[AAS03-P17] Diurnal variations and source apportionment of ozone at the summit of Mount Huang, a rural site in Eastern China

*Jinhui Gao[1] (1.Southern university for science and technology)

[AAS03-P18] **Optical Properties and Molecular Compositions of Atmospheric Brown Carbon in Nanjing, East China**

*Junjun Deng[1], Xinfeng Wang[2], Wei Hu[1], Libin Wu[1], Pingqing Fu[1] (1.Institute of Surface-Earth System Science, Tianjin University, 2.Environment Research Institute, Shandong University, Jinan 250100, China)

[AAS03-P19] **Quantification of household emissions in non-attainment cities of Punjab, India**

Arpit Katiyar[1], Jagriti Suneja[1], Mukesh Khare[1], Arvind K Nema[1], *Sri Harsha Kota[1] (1.Indian Institute of Technology Delhi)

[AAS03-P20] Regional Source Apportionment of Summertime Ozone and Its Precursors in the Megacities of Beijing and Shanghai using a Source-Oriented Chemical Transport Model

*Peng Wang[1], Tao Wang[1], Qi Ying[2] (1.the Hong Kong Polytechnic University, 2.Texas A&M University)

Significant contributions of upwind sources to ground-level ozone in the North China Plain

*Hongliang Zhang[1,2], Kaiyu Chen[2], Pengfei Wang[2], Siyu Wang[1], Peng Wang[3], Qi Ying[4], Jianlin Hu[5]

1. Fudan Univ., 2. LSU, 3. HKPU, 4. TAMU, 5. NUIST

With its adverse impacts on air quality, human health and ecosystem and increasing concentrations, ground-level ozone (O_3) is receiving increasing attention in China. Emissions of O_3 precursors, nitrogen oxides (NOx) and volatile organic compounds (VOCs), vary significantly spatiotemporally. Background and long transport of O_3 and its precursors have been shown to be important for O3 concentrations in the North China Plain (NCP). However, there is no study quantifying the contributions for designing effective controlling measures. This study uses a source-oriented version of the Community Multi-scale Air Quality (CMAQ) model with updated mechanisms to estimating contributions of different source regions to O3 in the NCP in summer 2017. Anthropogenic emissions are generated by an improved Emissions Database for Global Atmospheric Research (EDGAR+) and biogenic emissions are from the Model for Emission of Gas and Nature (MEGAN). Emissions from open burning are based on the Fire Inventory from NCAR (FINN). This study provides evidences the importance of considering regional transport to understanding O_3 formation, O_3-related human health risk and economic loss and helps policy makers in making control strategies.

Keywords: ozone, upwind, North China Plain

©2020. Japan Geoscience Union. All Right Reserved.

How much do emissions from China affect Northeast Asia?

*Hongliang Zhang[1,2], Pengfei Wang[2], Chun Cheng[3], Yele Sun[3]

1. Fudan Univ., 2. LSU, 3. IAP, CAS

Air pollution in Asian countries is attracting local and international concerns and a common debate is that emissions from larger countries like China are likely to affect surrounding areas. Although this case is true at special meteorological conditions from observation analysis, it is very important to quantify the transport of pollution among different countries over long period. In this study, a source-oriented version of Community Multi-scale Air Quality (CMAQ) model was applied to quantify the contributions of nine source regions (North Korea, South Korea, Japan, Northeast China, Jing-Jin-Ji area, Shandong, Jiangsu and Shanghai (YRD) 1, Anhui and Zhejing and rest areas in China) to $PM_{2.5}$ and its primary PM (PPM) and secondary inorganic aerosol (SIA) in East Asia in 2019. Anthropogenic emissions were generated from a combination of the Multi-resolution Emission Inventory (MEIC) (for China area) and the MIX Asian emission inventory (for all other areas).

Keywords: Transport, Northeast Asia, PM2.5

©2020. Japan Geoscience Union. All Right Reserved.

Modeling analysis of the spatiotemporal distribution characteristics of the atmospheric ultrafine particle in North China Plain and Yangtze River Delta of China in 2016

Yanhong Zhu[1], *Jianlin Hu[1]

1. NUIST Nanjing University of Information Science and Technology

Epidemiological studies identify the strongest health associations with particles that have diameters <2.5 μm ($PM_{2.5}$) but toxicology studies suggest that particle with diameters <0.1 μm ($PM_{0.1}$) maybe even more dangerous. And $PM_{0.1}$ can be used as cloud condensation nuclei (CCN) to influence cloud processes. At present, there is no conventional observation of $PM_{0.1}$ in China, so its spatiotemporal distribution characteristics are not clear.

Model simulation is another effective method for the study of air pollution. Chemical transport model (CTM) is often used to reproduce the past pollution event, test the new air pollution mechanism, predict future air quality and provide high time-and-space resolution data for the epidemiological study. Until now there have been many CTMs analyzing the air pollution events in China, and the Community Multiscale Air Quality model (CMAQ) is one of the most commonly used CTM in China. In the numerical simulation of particulate matter by the CMAQ model, except for one level of nanometer of nucleation, simulation of particulate matter less than 2.5 μm is often used without smaller particle size bins. Therefore, the domestic model simulation study of $PM_{0.1}$ is rare.

The University of California, Davis/California Institute of Technology (UCD/CIT) regional reactive chemical transport model is a third-generation air quality model developed by the UC Davis team based on the 1980s California Institute of Technology (CIT). The composition, mass and number concentrations of the particle with the diameter between 0.01 and 10 μm are showed in 15 size bins. The first 5 size bins of the UCD/CIT model are for $PM_{0.1}$, so it can simulate $PM_{0.1}$. At present, the UCD/CIT model has been applied in the simulation of $PM_{0.1}$ in America. In this paper, for the first time, we use the UCD/CIT model to simulate the pollution of gas and particulate matter in China, compare the model performance of UCD/CIT with CMAQ and analyze the spatiotemporal distribution characteristics of $PM_{0.1}$ in China.

Keywords: ultrafine particle, spatiotemporal distribution, China, modeling

©2020. Japan Geoscience Union. All Right Reserved.

Impact of land-use changes on biogenic emissions and formation of ozone and secondary organic aerosols in China from 2013 to 2017

*JinLong Ma[1], Yu Wang[1], Peng Wang[2], hongliang Zhang[1]

1. Fudan University, 2. The Hong Kong Polytechnic University

Biogenic volatile organic compounds (BVOCs) emissions are the major source of secondary organic aerosol (SOA) and ground-level ozone (O_3), and are harmful to human health, especially in urban areas. However, with the rapid growth of urbanizations, changes in land-use in China will result in inaccuracies in the understanding of regional BVOCs emissions. In this study, the Model of Emissions of Gases and Aerosols from Nature version 2.1 (MEGAN2.1) module embedded within the Community Multi-scale Air Quality (CMAQ), coupled with the land-use dataset derived from Moderate Resolution Imaging Spectroradiometer (MODIS), was used to estimate the changes in emissions of BVOCs and their impacts on O_3 and SOA in China from 2013 to 2017. The results would highlight the importance of considering land-use changes due to urbanization in predicting O_3 and SOA.

Keywords: biogenic emissions, land-use, ground-level ozone, secondary organic aerosol, MEGAN2.1

©2020. Japan Geoscience Union. All Right Reserved.

Long term trends in air pollution in China

*Shengqiang Zhu[1], Siyu Wang[1], Zhihao Shi[2], Fei Ye[2], Jianlin Hu[2], Hongliang Zhang[1]

1. Fudan University, 2. Nanjing University of Information Science & Technology

With the rapid growth of industries and population in China over the past 30 years, the air pollutants emissions have increased and resulted in high pollution levels than past. This study predicts ozone and particulate matter (PM) in China over the past 30 years from 1990 to 2019 using the Community Multi-scale Air Quality (CMAQ) model. The meteorology in China over the past 30 years has been acquired by using Weather Research and Forecasting (WRF) model version 4.1.2. The past 30 years' anthropogenic emissions were generated based on the Emissions Database for Global Atmospheric Research (EDGAR). The emissions after 2012 were adjusted based on factors reflecting control measures. And the biogenic emission was from the Model for Emissions of Gases and Aerosols from Nature (MEGAN) version 2.1. The open burning emissions was from National Center for Atmospheric Research (NCAR) while the dust and sea salt emissions were generated in line CMAQ. The long term trends of emissions and ambient concentrations with spatial and temporal variations of air pollutants from 1990 to 2019 will be investigated after model validation against available measurements in China and around countries/regions.

Keywords: WRF, CMAQ, Chinese Air Pollution Trend

©2020. Japan Geoscience Union. All Right Reserved.

Improving ozone simulation and understanding its adverse effects in India

*Mengyuan Zhang[1], Siyu Wang[1], Kaiyu Chen, Xue Qiao, Sri Harsha Kota, Hongliang Zhang[1]

1. Fudan University

In India, large anthropogenic emissions and relatively high solar intensity provide the most favorable conditions for the formation of ozone (O_3), which has significant adverse effects to human health and ecosystems. However, there are very limited sites with O_3, and assessments of O_3 effects are hindered. This study aims to simulate regional O_3 concentrations in India from 2012 to 2015 using the Community Multi-scale Air Quality (CMAQ) model at the resolution of 36 ×36 km^2. The meteorological fields are generated by the Weather Research and Forecasting (WRF) model. The anthropogenic emissions are generated from Emissions Database for Global Atmospheric Research (EDGAR) and the MIX Asian emission inventory. Emissions are adjusted to simulation years with different adjustment coefficients for different sectors and states. Biogenic and wildfire emissions are also provided to CMAQ. After the model results are validation, the levels, health and ecosystem effects are analyzed. The study reveals the importance of controlling O_3 in India and indicates more studies are needed for designing effective control strategies.

Keywords: ozone, simulation, adverse effects

©2020. Japan Geoscience Union. All Right Reserved.

Comparison of the SAPRC18 and SAPRC11 photochemical mechanisms for ozone simulation in China

*Yu Wang[1], JinLong Ma[1], Peng Wang[2], Hongliang Zhang[1]

1. Fudan University, 2. The Hong Kong Polytechnic University

The latest SAPRC photochemical mechanism SAPRC18 (S18), an update from SAPRC11 (S11), is implemented into the Community Multi-scale Air Quality (CMAQ) model and applied to simulate ozone formation during the China Air Quality Study 2017. Compared to S11, S18 can better simulate NO_x recycling processes and formation of SOA precursors. The results from the S11 mechanism are compared with those from the S18 mechanism. The photolysis rates of new model species added to the mechanism by S11 are much lower than those of S18.

Keywords: S18, S11, CMAQ, photolysis rates

©2020. Japan Geoscience Union. All Right Reserved.

Contribution of biogenic sources to secondary organic aerosol in summertime in Shaanxi, China

*Yong Xu[1], Hongliang Zhang[2], Dexiang Wang[3]

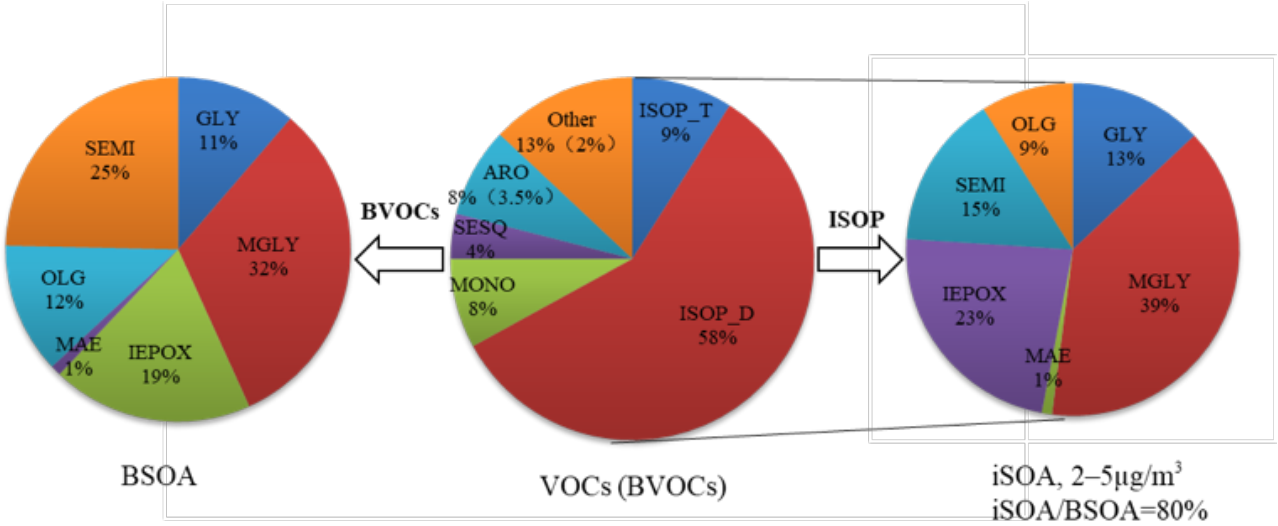
1. Yangzhou University, 2. Fudan University, 3. Northwest A&F University

Abstract:A revised Community Multi-scale Air Quality (CMAQ) model with updated secondary organic aerosol (SOA) yields and a more detailed description of SOA formation from isoprene (ISOP) oxidation was applied to study the spatial distribution of SOA, its components and precursors in Shaanxi in July of 2013.

The emissions of biogenic volatile organic compounds (BVOCs) as the CMAQ input were generated using Model of Emissions of Gases and Aerosols from Nature (MEGAN). Emissions of ISOP and monoterpene (MONO) mostly were the highest with 1.73×10^{9}mol and 1.82×10^{8}mol in July in total, respectively. The spatial distribution of BVOCs emission was significantly correlated with the vegetation coverage distribution in Shaanxi. ISOP and its intermediate semi–volatile gases were the highest among BVOCs in the ambient with highest concentrations of about 7.0 and 1.4 ppb, respectively, and formaldehyde from biogenic sources was up to ~3 ppb in South Shaanxi.

Predicted SOA was generally 2–6 $\mu g/m^3$, of which biogenic SOA (BSOA) from biogenic source in the study region accounted for as high as 84% in average in Shaanxi. Three main BVOCs Precursors included ISOP (58%) and MONO (8%) emit in the studied domain, and ISOP transported from south China (9%). The Guanzhong Plain had the highest BSOA concentrations of 3–5 $\mu g/m^3$, and the North Shaanxi had the lowest of 2–3 $\mu g/m^3$. More than half of BSOA was due to reactive surface uptake of ISOP epoxide (IEPOX) (0.2–0.7 $\mu g/m^3$, ~19%), glyoxal (GLY) (0.2–0.5 $\mu g/m^3$, ~11%) and methylglyoxal (MGLY) (0.4–1.4 $\mu g/m^3$, ~32%), while the remaining was due to the traditional equilibrium partitioning of semi-volatile components (SEMI) (0.1–1.2 $\mu g/m^3$, ~25%) and oligomerization (0.2–0.4 $\mu g/m^3$, ~12%). Overall, SOA formed from ISOP (iSOA) contributed 1–3 $\mu g/m^3$ (~80%) to BSOA, of which GLY and MGLY accounted for 13% and 39%, respectively.

Keywords: CMAQ, MEGAN, precursors, isoprene, BSOA



©2020. Japan Geoscience Union. All Right Reserved.

Preliminary study on physical and chemical properties of dust

*Yuan Luo[1], Siyu Chen[1]

1. Lanzhou university

Dust aerosol is an important part of atmospheric aerosol, which affects the climate system through direct, indirect and semi-direct effects. The aerosol of dust can be divided into natural dust and man-made dust according to the source. Natural dust mainly comes from the desert, gobi desert and other bare surface. Anthropogenic dust is the part of dust that is directly or indirectly brought into the atmosphere by human activities.

The size of dust particles is an important factor that determines the suspension, transfer, deposition and life of particles. At the same time, the dust particles are easy to absorb bacteria, heavy metal pollutants, sulfate and organic pollutants during the transmission process, which are harmful to human health. In this study, we collected 400 samples from a variety of surfaces to further study the effects of different land cover and human activities on the properties of sand dust, and to provide a research basis for the differences between man-made sand dust and natural sand dust and the impact of such differences on man-made sand dust.

Particle size analysis the Malvern Mastersizer 2000 laser particle size analyzer was used for experimental related operations. The measuring range of the machine is 0.02~2000 μm, and the related operations such as testing, basic analysis, cleaning and so on can be well completed by using the Mastersizer 2000 software accompanying the machine. Element and mineral analysis was performed using an X-ray fluorescence spectrometer, Magic PW2403, and sample preprocessing was performed using a grinder and press.

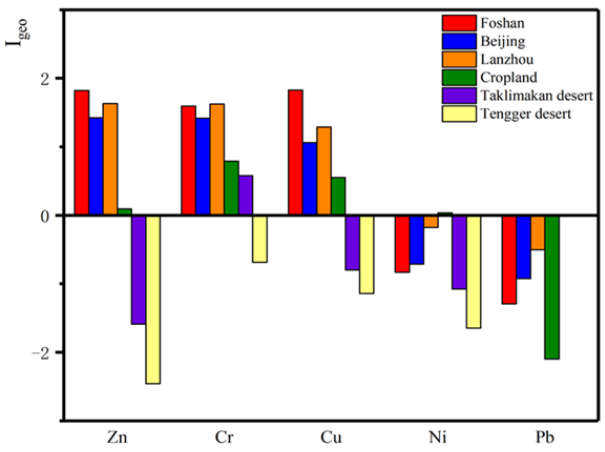
The mean value of median particle size was shown as urban (151.25 μm) > desert (121.91 μm) > farmland (21.07 μm). The peak of grain size distribution curve is also shown as urban > desert > farmland, among which the bimodal distribution of urban road dust reflects the multi-source of road dust. On the one hand, human activities such as industry, transportation and agriculture produce large amounts of man-made dust. On the other hand, natural dust is transported over long distances to densely populated urban areas with high anthropogenic pollution emissions, and new anthropogenic dust is generated by mixing with local materials. According to the movement characteristics of different particle sizes of surface particles under the action of wind and their influence on human health, road dust particle sizes were classified according to the classification standards of atmospheric particles. The most concerned inhalable particles with particle size less than 10 m had the highest content in the farmland samples (31%), followed by the urban road samples (9%) and the desert samples (3%).

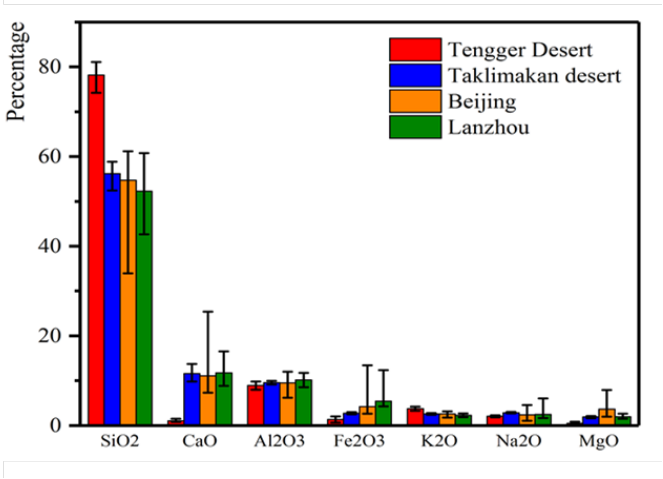
The study on the mineral composition of dust shows that natural dust is more different from manmade dust in SiO_2, CaO and Fe_2O_3. Compared with Taklimakan desert, Beijing and Lanzhou, the content of SiO_2 and CaO in Tengger desert is higher and CaO content is lower. The content of SiO_2 in natural dust is higher, while the content of Fe_2O_3 in man-made dust is higher. In terms of heavy metal analysis, Lanzhou is more polluted than Beijing, and Zn, Cr and Cu are more polluted.

In conclusion, particle size is shown as urban > desert > farmland. The content of SiO2 in natural dust is high, and the pollution of manmade dust by heavy metal is obvious.

©2020. Japan Geoscience Union. All Right Reserved.

Keywords: anthropogenic dust, particle size distribution, heavy metal





©2020. Japan Geoscience Union. All Right Reserved.

Associations of fine particulate matter and health burdens in Handan city

*aifang gao[1,2,3,4,5,6], junyi wang[1], jianfei luo[1], aiguo li[1], jingyi li[4,5,6], Hongliang Zhang

1. School of Water Resources and Environment, Hebei GEO University, 2. Hebei Province Collaborative Innovation Center for Sustainable Utilization of Water Resources and Optimization of Industrial Structure , 3. Hebei Province Key Laboratory of Sustained Utilization and Development of Water Resources, 4. Jiangsu Key Laboratory of Atmospheric Environment Monitoring and Pollution Control, 5. Collaborative Innovation Center of Atmospheric Environment and Equipment Technology, 6. Nanjing University of Information Science & Technology

The North China Plain (NCP) has been experiencing severe air pollution in recent decades and high levels of fine particulate matter ($PM_{2.5}$) are related to different diseases. However, it is not clear the relationship between very high $PM_{2.5}$ and human health outcomes as most studies are conducted in developed countries with lower concentrations. At the present study, the integrated exposure-response (IER) model was applied to estimate the health effects of exposure to fine particulate matter ($PM_{2.5}$) in Handan city, China. The premature mortality(ΔMort), years of life lost (YLL), and mortality benefits due to $PM_{2.5}$ reductions were quantified in 2015-2017. According to YLL per 1000 person, the males had higher health risks than females. Decreasing $PM_{2.5}$ concentrations would lead to a significant reduction of premature mortality and YLL. This indicates that a more stringent measure adopted by Handan government would be needed to reduce fine particulate matter pollution and enhance the health benefits.

Keywords: PM2.5 , ΔMort, YLL, integrated exposure-response model

©2020. Japan Geoscience Union. All Right Reserved.

Data assimilation of lidar-derived aerosol extinction coefficients and its application in China

*Zengliang Zang[1], Xiaobin Pan[1], Yanfei Liang[1], Wei You[1], Yiwen Hu[1]

1. National University of Defense Technology

A three-dimensional variational (3DVAR) assimilation system for lidar-derived aerosol extinction coefficient profiles is developed, with the observational operator for aerosol extinction coefficients based on IMPROVE (The Interagency Monitoring of Protected Visual Environments) equation. Using the 3DVAR system, three experiments are performed by assimilating hourly lidar-derived aerosol extinction coefficient profiles and hourly mass concentrations of PM2.5 of air quality monitoring stations over China. Then, the subsequent 24h forecasts are carried out by using WRF-Chem (Weather Research and Forecasting model coupled to Chemistry) model. The results show that the data assimilation of lidar profiles can improve the skill score of aerosol following forecast with higher correlation coefficient and lower RMSE.

Keywords: data assimilation, lidar, aerosol extinction coefficients, WRF-Chem

©2020. Japan Geoscience Union. All Right Reserved.

The effectiveness of the Air Pollution Prevention and Control Action Plan on the air quality and human health during 2013-2017 in China

Dian Ding[1], *Jia Xing[1], Shuxiao Wang[1]

1. Tsinghua University

In 2013, China released the “Air Pollution Prevention and Control Action Plan”, which set the roadmap for national air pollution control actions for the period of 2013-2017. A decrease in the PM2.5 concentration may lead to a substantial benefit for human health. This study aims to quantify the relative contributions four factors: emission reductions, changed meteorology, population growth, and a change in baseline mortality rates to the reduced PM2.5-related mortality (PM2.5-mortality) during the 2013-2017 period and evaluate the importance of emission controls for human health protection in China. We used the chemical transport model (i.e., WRF-CMAQ) as well as an integrated scientific assessment system (i.e., ABaCAS) in this study. The estimated total PM2.5-mortality in China was 1,389,000 (95% CI, 1,005,000-1,631,000) in 2013 but was substantially reduced to 1,102,000 (95% CI, 755,000-1,337,000) in 2017. Emission controls contributed 88.7% to this reduction in PM2.5-mortality, while changed meteorology, the change in baseline mortality rates, and population growth during 2013-2017 contributed 9.6%, 3.8% and -2.2%, respectively. The implementation of the Action Plan has significantly reduced the PM2.5 concentration in regions of China where population density is high, dominating the decline in PM2.5-mortality during 2013-2017. However, the health burden of PM2.5 pollution in China is still extremely high compared to that in other developed countries. An aggressive air pollution control strategy should be implemented in densely populated areas to further reduce the health burden.

Keywords: air pollution, PM2.5-mortality, control action plan

©2020. Japan Geoscience Union. All Right Reserved.

Modeling the source-receptor relationships in highly polluted regions

*Jia Xing[1], Dian Ding[1], Shuxiao Wang[1], Jim Kelly[2], Carey Jang[2], Yun Zhu[3]

1. Tsinghua University, 2. U.S. Environmental Protection Agency, 3. South China University of Technology

Efficient prediction of air pollution responses to precursor emissions is a prerequisite for an integrated assessment system in developing effective control policies. Representing the nonlinear response of air pollutants to emissions control with accuracy remains a major challenge for policymakers and modelers. Here, we propose a novel method by applying the deep-learning approach in atmospheric chemical transport model (CTM), and employ the Extended Response Surface Modeling (ERSM) technique to develop response surfaces of PM2.5 and O3 concentrations as a function of pollutant emissions. The proposed method significantly enhances the computational efficiency and practicality by requiring CTM simulations with mean and 95th maximal normalized errors within 5% and 10% across all grid cells. With the newly developed method, we systematically investigate the nonlinear response of PM2.5 and O3 to emissions of multiple pollutants from different sources in three highly polluted regions in China including the Northern China Plain (NCP), Fen-Wei Plain (FWP), and Chuan Yu region (CYR). We found that the effectiveness of NO*x* controls for reducing $PM_{2.5}$ and O_3 are largely influenced by the ambient levels of NH_3 and VOC, exhibiting strong nonlinearities characterized as NH_3-limited/-poor and NO*x*-/VOC-limited conditions, respectively. The contribution from regional sources becomes larger during more polluted episodes, suggesting the importance of joint controls on regional sources for reducing the heavy air pollution.

Keywords: air pollution, source-receptor , emission

©2020. Japan Geoscience Union. All Right Reserved.

Opposite Role of H_2SO_4 Formation Pathway on Secondary Organic Aerosol Formation Derived from Ethyl Ethacrylate Ozonolysis

*Peng Zhang[1]

1. Rcees

Stressed plants and polymer production can emit many unsaturated volatile organic esters (UVOEs). However, few studies attempt to explore secondary organic aerosol (SOA) formation of unsaturated esters under complex ambient conditions. In this study, we employed ethyl methacrylate (EM) as a UVOEs proxy to investigate SOA formation resulting from EM ozonolysis with or without seed particles in the presence of SO_2. Results showed that, in the absence of seed particles, a substantial increase in homogeneous formation of H_2SO_4 particles and enhanced acid-catalyzed oligomerization of carbonyl species promoted the increase of SOA with increasing SO_2. In contrast, increased particle acidity enhanced EM uptake and the chemical conversion of SOA but reduced SOA formation in the presence of seed particles. This was mainly ascribed to the fact that the ozonolysis of more adsorbed EM was hampered due to the formation of surface H_2SO_4 with increasing particle acidity. This study demonstrated that the opposite roles of SO_2 and seed particle addition on SOA formation and composition were closely related to the H_2SO_4 formation pathway. This research will not only help to advance our understanding of the complex chemical processes involved in UVOE-derived SOA but also of the complicated role of H_2SO_4 in SOA formation.

Keywords: SOA , Ethyl Ethacrylate Ozonolysis, H2SO4 paritcles

©2020. Japan Geoscience Union. All Right Reserved.

Investigating the performance of satellite-based models in estimating the surface $PM_{2.5}$ over China

*Siwei Li[1], Lechao Dong[1], Jie Yang[1], Wenxuan Shi[1]

1. Wuhan University

Accurate estimation of atmospheric particulate matter with particle diameter less than 2.5 μm ($PM_{2.5}$) concentration is important because of its adverse impacts on public health. Due to the limited spatial coverage of ground monitoring stations, satellite products are often used to estimate surface $PM_{2.5}$ concentration by constructing a comprehensive relationship between satellite-retrieved aerosol optical depth (AOD) and ground-based in-situ measured $PM_{2.5}$ concentration. The accuracy of the satellite-based models in estimating $PM_{2.5}$ concentration is critical for its usage in health assessment, however, the performance of satellite-based models has not been well evaluated yet. In this study, we propose a new method to validate and evaluate the accuracy and performance of two popular machine learning models Random Forest (RF) and the BP Neural Network (BPNN) in estimating $PM_{2.5}$ concentration over China. The two models were trained and tested based on a whole year of satellite-retrieved hourly AOD from HIMAWARI, ground-based in-situ measured $PM_{2.5}$ from China National Environmental Monitoring Center, ERA5 meteorological conditions and other auxiliary variables in 2017. It is found that the traditional validation method may overestimate the performance of the models in estimating the $PM_{2.5}$ at the area with sparse in-situ measurements. Moreover, the spatial distribution of the training data will largely affect the performance of the models. A variable parameter retrieval algorithm based on RF model shows a better overall performance than the fixed parameter RF model. The R^2 is greater than 0.83 when the distance of the test station to the nearest training station is smaller than 100 km, but reduces to 0.51 when the distance is larger than 500 km . Such results suggest that the performance of satellite-based model in estimating the surface $PM_{2.5}$ need carefully examined, and still exhibits considerable uncertainties to be further improved.

Keywords: PM2.5, remote sensing, HIMAWARI-8, AOD, machine learning

©2020. Japan Geoscience Union. All Right Reserved.

Tiramisu snow and the weakening of surface albedo

Siyu Chen[1], *Hongru Bi[1]

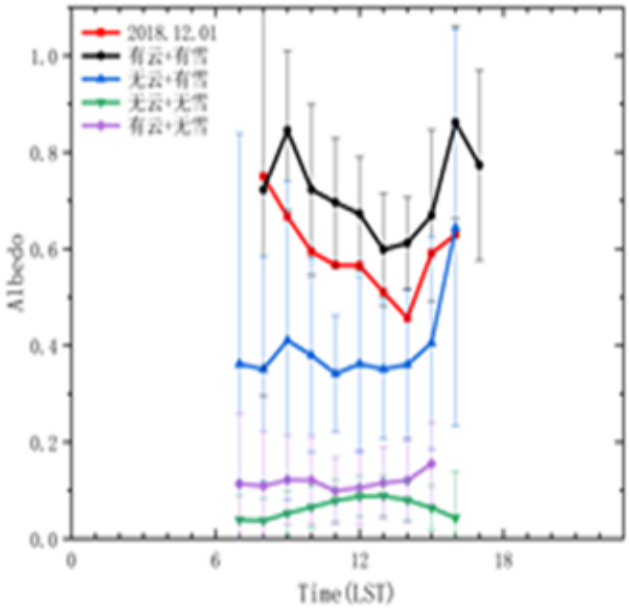
1. Lanzhou University

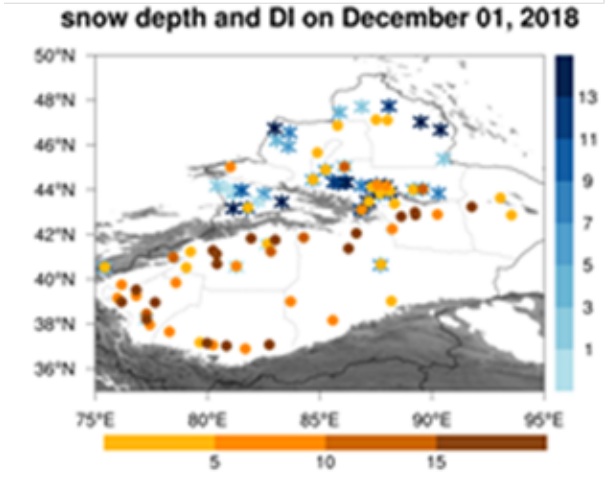
Since 1850, Earth's cryosphere has shown a global shrinking trend. The retreat of snow and ice had strongly impact on the hydrological cycle and the energy balance of the Earth system. And the melting of snow and ice attributed to the variation in snow albedo caused by LAIs deposited on the snow surface. These LAIs absorbed solar radiation, accelerated snow aging process, reduced albedo of the snow surface, and enhanced the melting of snow. However, the uncertainty of the emission of LAIs and the differences in research methods and regions, as well as the lack of observation data, resulted in the surface radiation forcing caused by LAIs, especially dust, still very uncertain. Dust is as a key factor in controlling albedo and subsequent glacier melting within the global warming perspective. Thus, quantitative studies on reduction of dust on snow surface albedo from synoptic scale are very important. On December 1, 2018, a rare weather event occurred in Urumqi, China, where snow accumulating on the land surface was covered with a layer of yellow dust. This rare weather event provided an excellent natural experiment for quantifying the effect of dust in snow on surface albedo. Based on ground observation data and reanalysis data such as MERRA-2 and ERA5, it was found that the dust snow was mainly caused by the large-scale strong cold caused by the Siberian trough and the southeast transport of dust-storms particles under the influence of the westerly jet. The generation dust particles reduced reflected radiation 20 W m^{-2} approximately. Compared with the changes of solar radiation under similar historical conditions, it was found that the cloud cover resulted in the surface albedo increase by about 0.23, when snow lead to counterpart increase about 0.28. But dust particles in the snow significantly reduced the surface albedo. Compared to historical conditions with the same snow depth and cloud cover, snow albedo caused by dust in snow decreased by approximately 28% and up to 34%.

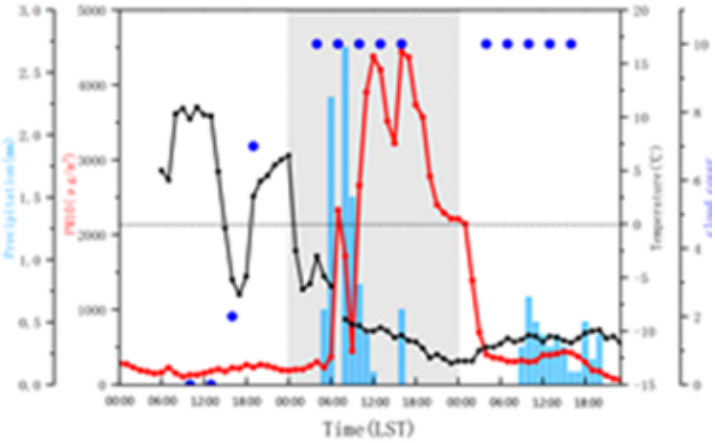
Keywords: surface albedo, solar radiation, dust snow

©2020. Japan Geoscience Union. All Right Reserved.









©2020. Japan Geoscience Union. All Right Reserved.

Diurnal variations and source apportionment of ozone at the summit of Mount Huang, a rural site in Eastern China

*Jinhui Gao[1]

1. Southern university for science and technology

Comprehensive measurements were conducted at the summit of Mount (Mt.) Huang, a rural site located in eastern China during the summer of 2011. They observed that ozone showed pronounced diurnal variations with high concentrations at night and low values during daytime. The Weather Research and Forecasting with Chemistry (WRF-Chem) model was applied to simulate the ozone concentrations at Mt. Huang in June 2011. With processes analysis and online ozone tagging method we coupled into the model system, the causes of this diurnal pattern and the contributions from different source regions were investigated. Our results showed that boundary layer diurnal cycle played an important role in driving the ozone diurnal variation. Further analysis showed that the negative contribution of vertical mixing was significant, resulting in the ozone decrease during the daytime. In contrast, ozone increased at night owing to the significant positive contribution of advection. This shifting of major factor between vertical mixing and advection formed this diurnal variation. Ozone source apportionment results indicated that approximately half was provided by inflow effect of ozone from outside the model domain ($O_{3\text{-}INFLOW}$) and the other half was formed by ozone precursors ($O_{3\text{-}PBL}$) emitted in eastern, central, and southern China. In the $O_{3\text{-}PBL}$, 3.0% of the ozone was from Mt. Huang reflecting the small local contribution ($O_{3\text{-}LOC}$) and the non-local contributions ($O_{3\text{-}NLOC}$) accounted for 41.6%, in which ozone from the southerly regions contributed significantly, for example, 9.9% of the ozone originating from Jiangxi, representing the highest geographical contributor. Because the origin and variation of $O_{3\text{-}NLOC}$ was highly related to the diurnal movements in boundary layer, the similar diurnal patterns between $O_{3\text{-}NLOC}$ and total ozone both indicated the direct influence of $O_{3\text{-}NLOC}$ and the importance of boundary layer diurnal variations in the formation of such distinct diurnal ozone variations at Mt. Huang.

Keywords: ozone, source apportionment, wrf-chem

©2020. Japan Geoscience Union. All Right Reserved.

Optical Properties and Molecular Compositions of Atmospheric Brown Carbon in Nanjing, East China

*Junjun Deng[1], Xinfeng Wang[2], Wei Hu[1], Libin Wu[1], Pingqing Fu[1]

1. Institute of Surface-Earth System Science, Tianjin University, 2. Environment Research Institute, Shandong University, Jinan 250100, China

Brown Carbon (BrC) shows solar absorption behavior in ultraviolet and near-infrared region, and plays a significant role in atmospheric radiative forcing and regional/global climate. In present study, light absorption properties of water- and methanol-soluble BrC in ambient $PM_{2.5}$ in Nanjing in Western Yangtze River Delta in China during 2014-2015 were investigated. Besides, typical molecular compositions of BrC (nitrophenol compounds) with their light absorption contributions to BrC were also identified with ultra-performance liquid chromatography-triple quadrupole tandem mass spectrometry. The average concentration of water-soluble organic carbon (WSOC) was 6.1±3.0 $\mu g/m^3$, contributing to 61% of total organic carbon (OC). Larger WSOC concentrations in autumn and winter were related to the intense emissions from biomass burning. Light absorption coefficient (Abs), mass absorption efficiency (MAE) and absorption Angstrom exponent (AAE) of WSOC (methanol-soluble OC (MSOC)) were 5.8 Mm^{-1} (11.9 Mm^{-1}), 0.92 m^2g^{-1} (1.15 m^2g^{-1}) and 5.36 (4.97), respectively. Strong positive correlation (R^2=0.93) was found between light absorption of WSOC and MSOC. Both light absorption of WSOC and MSOC showed distinct seasonal variations, with larger Abs values in winter and autumn. The average concentration of the detected nitrophenol compounds was 9.1±7.9 ng m^{-3}. Among the detected nitrophenol compounds, nitrocatechols (NCs), which can be used as tracers of biomass burning, increased significantly in winter (8.6 ng m^{-3}) and autumn (5.6 ng m^{-3}). While nitrosalicylic acids (NSAs), which were mainly generated by secondary reactions, accounted for larger proportions in summer (52.4%) and spring (40.9%). Nitrophenols contributed 0.32±0.13% to total light absorption of MSOC. Light absorption contributions of nitrophenol varied in different seasons in the order of winter (0.43%) > autumn (0.32%) > spring (0.27%) > summer (0.21%). NCs are the most important light-absorbing components among all the nitrophenol compounds, with the light absorption contribution of 64.7%. These findings will help to better understand optical properties and climatic effects of light-absorbing organic aerosols.

Keywords: brown carbon, light absorption, water-soluble organic carbon, methanol-soluble organic carbon, nitrophenol

©2020. Japan Geoscience Union. All Right Reserved.

Quantification of household emissions in non-attainment cities of Punjab, India

Arpit Katiyar[1], Jagriti Suneja[1], Mukesh Khare[1], Arvind K Nema[1], *Sri Harsha Kota[1]

1. Indian Institute of Technology Delhi

Air pollution has become a grave problem in recent times throughout the world, especially in north India. Studies have shown that household emissions is one of the major contributors to $PM_{2.5}$ in north India. In this study, a bottom-up emission inventory for household emissions from non-attainment cities in Punjab is developed. Emissions from household fuels such as wood, brushwood, straw, grass, coal, coal briquette, charcoal, dung, natural gas, LPG (Liquified Petroleum Gas), biogas and electricity have been quantified. The conclusions from this emission inventory is used to modify the European Union's EDGAR emission inventory. With this modified emission inventory, the contribution of $PM_{2.5}$ due to household emissions in Punjab is predicted using Weather Research and Forecasting model coupled with Chemistry (WRF-Chem). Results indicate significant contribution from household emissions calling for an urgent action to control $PM_{2.5}$ in this region.

Keywords: PM2.5, Biomass burning, India

©2020. Japan Geoscience Union. All Right Reserved.

Regional Source Apportionment of Summertime Ozone and Its Precursors in the Megacities of Beijing and Shanghai using a Source-Oriented Chemical Transport Model

*Peng Wang[1], Tao Wang[1], Qi Ying[2]

1. the Hong Kong Polytechnic University, 2. Texas A&M University

The Community Multiscale Air Quality (CMAQ) model with a source-oriented SAPRC-11 photochemical mechanism is developed in this study to quantify the source region contributions to surface O_3 in Beijing and Shanghai in August 2013. Non-background O_3 attributed to NO_x (O_3_NO_x) and VOCs (O_3_VOC) emitted from different source regions are determined using a three-regime approach that correctly attributes O_3 to NO_x and VOC precursors throughout the entire range of NOx-VOC-O_3 formation sensitivity. Averaged over the entire month and all grid cells, local emissions (51%) and emissions from Hebei (31%) are the two major contributors to non-background daily maximum 8-hour (DM8H) O_3 in Beijing. In Shanghai, local, Zhejiang and Jiangsu emissions account for 53%, 19% and 14% of the non-background DM8H O_3. Significant variations in local emission contributions are predicted among different model grid cells for both cities (Beijing, 6-80%; Shanghai, 3-76%). On high O_3 days in Beijing, the wind is persistently from the south with high wind speed (~5 m s^{-1}) in the evening and night. This leads to significant regional contributions of O_3 from Hebei, along with regional transport of VOCs and NO_x. In Shanghai, high O_3 days are associated with southwesterly/westerly wind in the morning, rotating to southeast in the early afternoon in a counter-clockwise direction. The surface wind then gradually turns back to southwest in the afternoon until the next morning, along with reduced wind speed. In Shanghai, daytime O_3 at the urban center is almost entirely due to local emissions. Low wind speed in the evening and night time allows local NO_x emissions to efficiently titrate regional O_3. In both cities, NO_x emissions are not transported regionally as efficiently as VOCs. Source region contribution analysis of the concentration weighted maximum incremental reactivity (CWMIR) shows that VOCs from other regions are less reactive than locally emitted VOCs. HCHO and acetaldehyde (CCHO) generated from the oxidation of other VOCs are important contributors to regionally transported reactive VOCs. In both regions, the overall CWMIR in both cities is quite similar (~4 moles O_3 per mole of VOC^{-1}).

Keywords: photochemical model, regional transport, nitrogen oxides, volatile organic compounds, emission

©2020. Japan Geoscience Union. All Right Reserved.

[E] Poster | A (Atmospheric and Hydrospheric Sciences)：A-AS Atmospheric Sciences, Meteorology & Atmospheric Environment

[A-AS04] Formation of Air Pollution and Its Interactions with Weather/Climate

convener:Yang Yang(Nanjing University of Information Science & Technology), Meng Gao(State Key Laboratory of Environmental and Biological Analysis), Guangxing Lin(Pacific Northwest National Laboratory)

Air pollutants, such as aerosols and ozone, have significantly affected environment, human health, ecosystem, and climate. Anthropogenic emissions of air pollutants in major economic regions of the world, which have changed rapidly over the past few decades owing to economic development and environmental measures, will continue to change in the near future. Air pollution from the changing sources not only degrades local and remote air quality, but also modifies energy balance, cloud, precipitation and circulation patterns, leading to regional and global environmental and weather/climate change. Climate change and variabilities in the changing world can in turn affect the emission, chemistry, transport and removal of air pollutants at different scales. To better understand the formation of air pollution, and air pollution-weather/climate interactions, advances are needed in theoretical, observational and modeling studies.
Relevant topics include but are not limited to:
(1) formation mechanism of air pollution, both physical and chemical;
(2) source attribution of air pollutants in the past and future;
(3) impact of air pollution on weather (boundary layer, cloud, precipitation, etc.), modes of variability and climate change;
(4) influence of historical climate variability on air pollution (ENSO, PDO, AO, etc.);
(5) predictability of future climate change associated with projected emission changes and feedback on air pollution.

[AAS04-P01] **Seasonal distribution and vertical structure of different types of aerosols in southwest China observed from CALIPSO**

*Tingting Liao[1], Zhengwu Ouyang[1], Bihan Wang[1], Ke Gui[2] (1.Chengdu University of Information Technology, 2.Key Laboratory of Atmospheric Chemistry (LAC), Chinese Academy of Meteorological Sciences)

[AAS04-P02] Estimation of biogenic VOC emissions and their corresponding impact on ozone and secondary organic aerosol formation in China

*Xianyu Yang[1] (1.Chengdu university of information technology)

[AAS04-P03] Characteristics of Severe Air Pollution in Jiangsu Province and its Relationship with Meteorological Conditions under Cold Air

*Lu Cao[1,2], Duanyang Liu[1,2], Peng Zhou[3], Wenlian Yan[2], Chen Hao[2] (1.Key Laboratory of Transportation Meteorology, 2.Jiangsu Meteorological Observatory, 3.Nanjing Meteorological Bureau)

[AAS04-P04] **Spatiotemporal variations of recent NO_2 concentrations and anthropogenic and meteorological drivers over typical urban agglomerations in China**

*Yang Shen[1], Fei Jiang[1] (1.Nanjing University)

[AAS04-P05] Sub-seasonal seesaw of PM2.5 over the North China Plain in autumn and early winter

*Lian Xue[1] (1.Nanjing University)

[AAS04-P06] Transport of Ozone Pollution Over the East China Sea and the Yellow Sea: a Case Study in Coastal Cities in Eastern China

*Yanhua Zheng[1], Fei Jiang[1], Shuzhuang Feng[1], Zhe Cai[2] (1.Nanjing Univ., 2.Nanjing CLIMBLUE Technology co.LTD)

Seasonal distribution and vertical structure of different types of aerosols in southwest China observed from CALIPSO

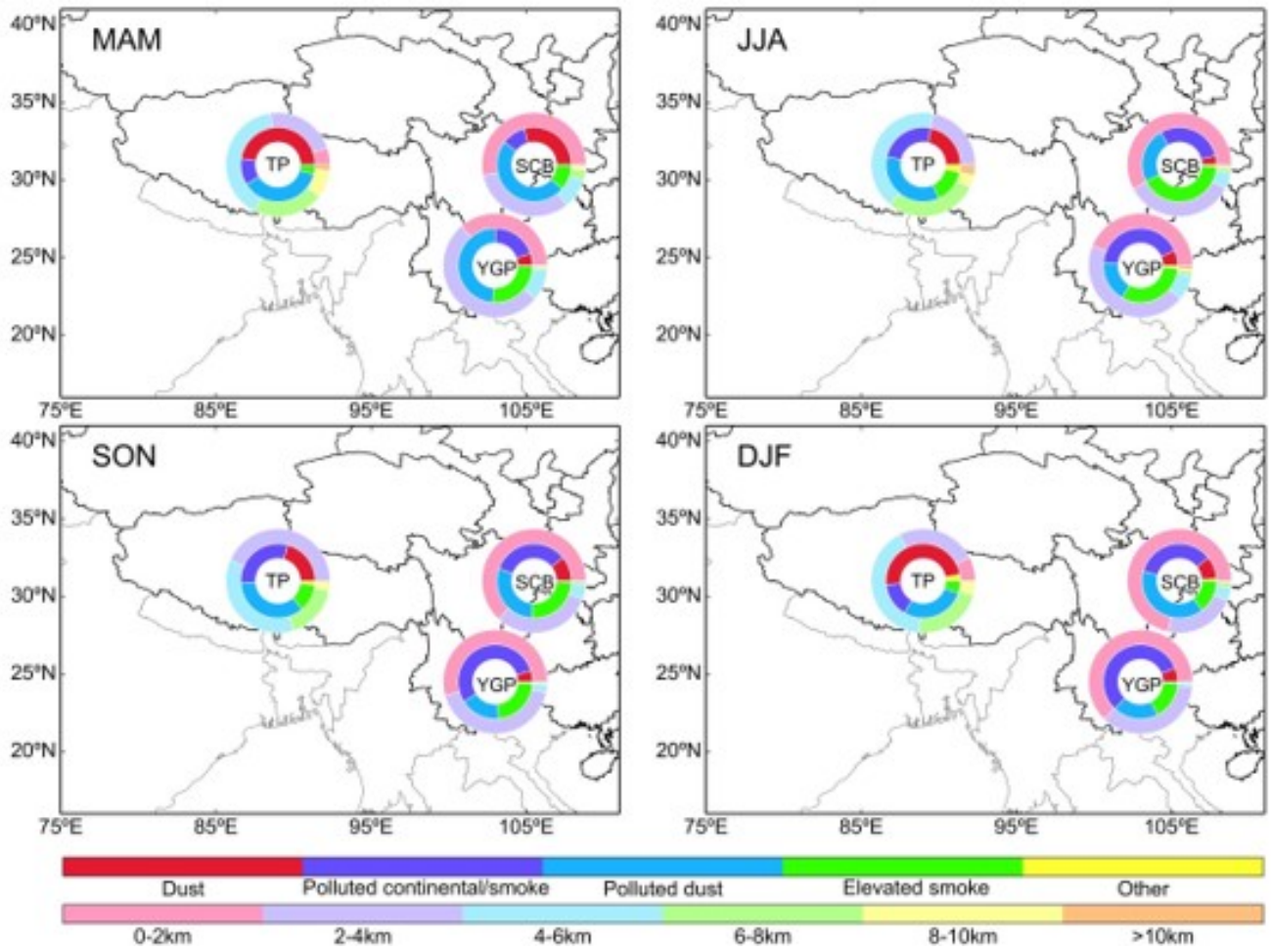
*Tingting Liao[1], Zhengwu Ouyang[1], Bihan Wang[1], Ke Gui[2]

1. Chengdu University of Information Technology, 2. Key Laboratory of Atmospheric Chemistry (LAC), Chinese Academy of Meteorological Sciences

Aerosols significantly influence global and regional atmospheric systems. Different types of aerosols play different roles in atmosphere according to their radiation characteristics and existing height. Southwest China is recognized as a region with very complex terrain, consisted of three absolutely different geomorphic units (Sichuan Basin (SCB), Yungui Plateau (YGP) and Tibetan Plateau (TP)) with distinct characteristic in air quality and climate. However, a comprehensive understanding of the regions and three-dimensional (3D) characteristics of aerosol distribution and evolutions over Southwest China is yet to be achieved. Here, the seasonal distribution and vertical structure four types of aerosols including dust, polluted continental/smoke, polluted dust and elevated smoke was studied by using CALIPSO Level 2 nighttime aerosol profile product from 2007 to 2016. It is observed that the extinction coefficient of total aerosols over SCB is highest, among which, the type of polluted continental/smoke and polluted dust, related to anthropogenic sources, made the most contributions. Whereas we can also find these two types of aerosols declined since 2013, which might due to the strict supervision measures on industry emissions and biomass burning in agriculture in recent years. The elevated smoke aerosols over YGP in the altitude of 3km in spring were significantly higher than other seasons which might related to the biomass burning transported from South Asia, while the polluted continental/smoke aerosols in the altitude of 1-2 km were higher in autumn and winter, which is considered to be contributed by local biomass burning. The aerosol extinction coefficient over TP is nearly one magnitude lower than other two regions. However, either the dust and polluted continental/smoke from the Qaidam Basin, or smoke elevated from the Indo-Gangetic Basin, could be transported to the layer as high as 6km over TP, which might make profound impact on the climate system in Southwest China, event in Asia. The vertical structure and evolution of aerosols of different radiation properties over the complex terrain is supposed to provide reliable research foundation to the further study on the aerosols transport and the bifunctional feedback between aerosols, especial the absorptive aerosols, and the climate change.

Keywords: CALIOPSO, Southwest China, Vertical structure, Smoke

©2020. Japan Geoscience Union. All Right Reserved.



©2020. Japan Geoscience Union. All Right Reserved.

Estimation of biogenic VOC emissions and their corresponding impact on ozone and secondary organic aerosol formation in China

*Xianyu Yang[1]

1. Chengdu university of information technology

Biogenic volatile organic compounds (BVOC) play an important role in global environmental chemistry and climate. In the present work, biogenic emissions from China in 2017 were estimated based on the Model of Emissions of Gases and Aerosols from Nature (MEGAN). The effects of BVOC emissions on ozone and secondary organic aerosol (SOA) formation were investigated using the WRF-CMAQ modeling system. Three parallel scenarios were developed to assess the impact of BVOC emissions on China's ozone and SOA formation in July 2017. Biogenic emissions were estimated at 23.54 Tg/yr, with a peak in the summer and decreasing from southern to northern China. The high BVOC emissions across eastern and southwestern China increased the surface ozone levels, particularly in the BTH (Beijing-Tianjin-Hebei), SCB (Sichuan Basin), YRD (Yangtze River Delta) and central PRD (Pearl River Delta) regions, with increases of up to 47 μgm−3 due to the sensitivity of VOC-limited urban areas. In summer, most SOA concentrations formed over China are from biogenic sources (national average of 70%). And SOA concentrations in YRD and SCB regions are generally higher than other regions. Excluding anthropogenic emissions while keeping biogenic emissions unchanged results that SOA concentrations reduce by 60% over China, which indicates that anthropogenic emissions can interact with biogenic emissions then facilitate biogenic SOA formation. It is suggested that controlling anthropogenic emissions would result in reduction of both anthropogenic and biogenic SOA.

Keywords: BVOC, Ozone, Modeling, MEGAN, SOA

©2020. Japan Geoscience Union. All Right Reserved.

Characteristics of Severe Air Pollution in Jiangsu Province and its Relationship with Meteorological Conditions under Cold Air

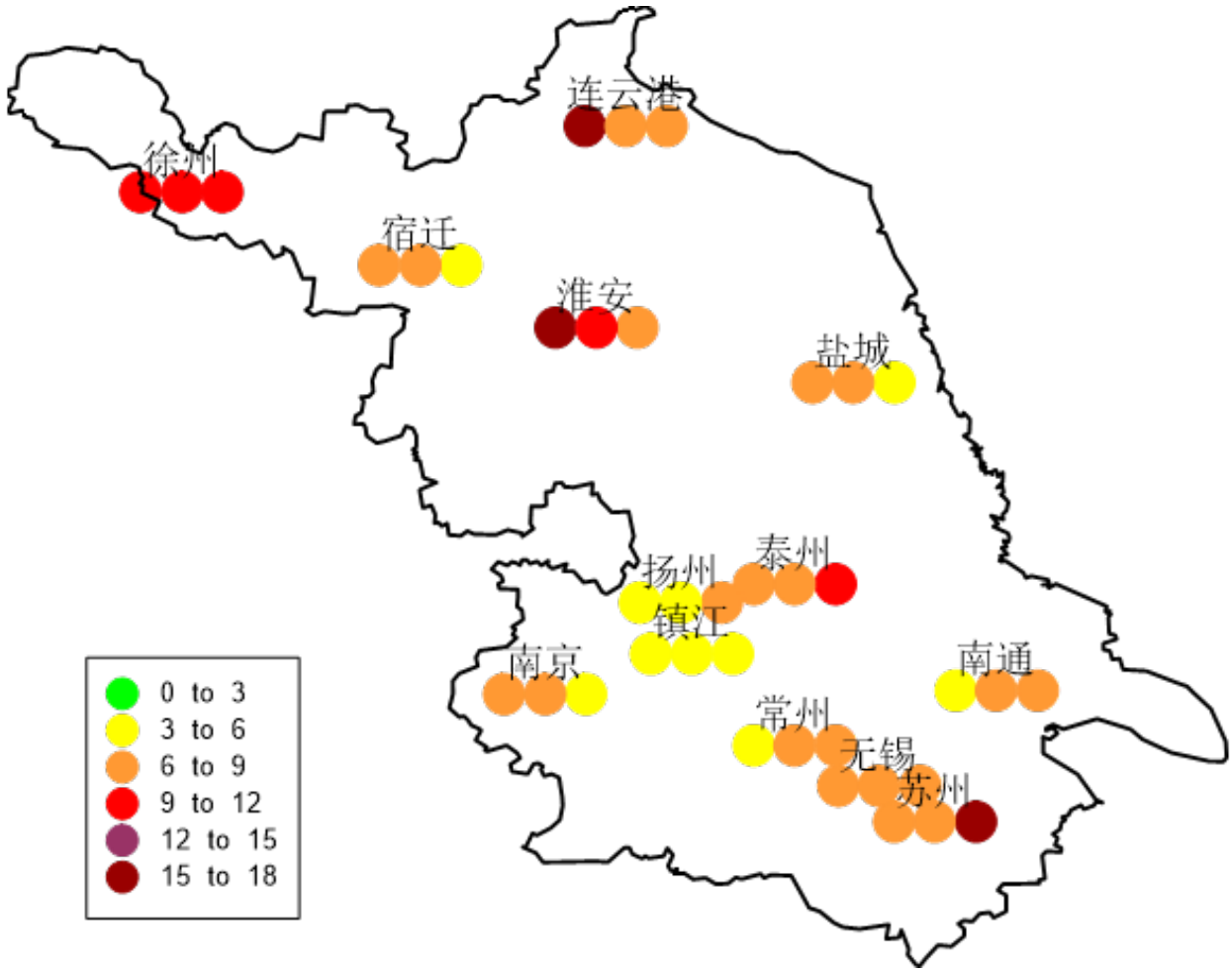
*Lu Cao[1,2], Duanyang Liu[1,2], Peng Zhou[3], Wenlian Yan[2], Chen Hao[2]

1. Key Laboratory of Transportation Meteorology, 2. Jiangsu Meteorological Observatory, 3. Nanjing Meteorological Bureau

By analyzing the severe air pollution cases in Jiangsu Province during 2013-2018, we investigated the characteristics of meteorological conditions during those polluted episodes in this study. The results showed that in Jiangsu Province, the level of air pollution happened under cold air was mostly in Level 5. There were only 14% of all events in Level 6, which mostly took place when the cold air was from central pathway, and rarely cases were from easterly pathway. Generally, the air pollution episodes under central and western pathway were regional and continuous, with primary pollutant of $PM_{2.5}$, followed by O_3; while those under eastern pathway were local and short, frequently with primary pollutant of O_3. During severe pollution episodes, at high altitude, the cold air was mainly at north side of Jiangsu Province; at mid and low altitude, there was northwest airflow in front of ridge or weak shear; on the surface, Jiangsu was in the front of cold air. The stratification was stable with the mixing layer height less than 1.2 km, and there were vertical temperature inverse happened of more than 50% events. At the day and the day before the severe pollution episode, the wind speed was generally less than 4 m/s, and there was no or weak precipitation (<1.0mm/day). Compared to the easterly pathways, more air pollutants were transported from central or westerly pathway. The heavy pollution might be intensified under stable weather conditions with negative transportation upstream, very strong inverse and weak wind. In the circulation beneficial to the severe pollution, the maximum elevate of the 24-h mean concentration in Nanjing was less than 150 $\mu g/m^3$ from central-pathway cold air and less than 100 $\mu g/m^3$ from westerly and easterly pathway cold air. Overall, the severe air pollution in Jiangsu province was attributed to the combined contributions from local emission, regional transportation and unfavorable weather conditions.

Keywords: Pathway of cold air, characteristics of heavy air pollution, meteorological conditions

©2020. Japan Geoscience Union. All Right Reserved.



©2020. Japan Geoscience Union. All Right Reserved.

Spatiotemporal variations of recent NO_2 concentrations and anthropogenic and meteorological drivers over typical urban agglomerations in China

*Yang Shen[1], Fei Jiang[1]

1. Nanjing University

Nitrogen dioxide (NO_2) is an important pollution gas that can affect air quality and human health. In this study, spatiotemporal distribution of NO_2 concentrations throughout China, and specifically in twelve typical urban agglomerations, were statistically analyzed with ground−based NO_2 observations from June 2014 to May 2019. The WRF−CMAQ model were also applied to separate and quantify the emission−related and meteorology−related NO_2 variations. NO_2 concentration in Beijing−Tianjin−Hebei (BTH) urban agglomeration showed an upward trend in 2014−2015, and a downward trend after 2016, while NO_2 in Yangtze River Delta (YRD), Yangtze River Middle−Reach (YRMR) and Cheng−Yu (CY) urban agglomerations continued to decline until 2017. High NO_2 values were predominantly concentrated in urban agglomerations with high NOx emissions like BTH, Shandong Peninsula (SP), Central Plain (CP), Central Shaanxi (CS) and YRD urban agglomeration. The number of sites with NO_2 decreasing in 2018 accounts for 67.37% compared to 2015, especially in BTH and CP, with the decrease of more than 20 $\mu g \cdot m^{-3}$. High−high concentration centers of NO_2 pollution were observed in high NO_2 areas, while low−low aggregations were observed in the South and southwest of China. In general, anthropogenic emissions contributed dominantly to NO_2 variations, and the contribution in winter was greater than in summer. The reduction of emissions in the winter of 2018 led to emission−related NO_2 variations in YRD, YRMR, CY, and Pearl River Delta (PRD) urban agglomeration reaching −7.41, −9.15, −9.57, and −15.09 $\mu g \cdot m^{-3}$, respectively. While in the winter of BTH, meteorological influence on NO_2 was more obvious than that of other regions, leading variations of 4.42, 4.09, −9.77, and 5.99 $\mu g \cdot m^{-3}$, respectively between 2014 and 2018 in adjacent years. This study makes it possible to look into the differences in NO_2 concentrations among typical urban agglomerations and provide a more complete understanding of NO_2 exposures in China.

Keywords: NO2, urban agglomeration, spatiotemporal pattern, WRF−CMAQ, quantitative impact

©2020. Japan Geoscience Union. All Right Reserved.

Sub-seasonal seesaw of PM2.5 over the North China Plain in autumn and early winter

*Lian Xue[1]

1. Nanjing University

Severe PM2.5 pollution often strikes the North China Plain in autumn and winter in recent years. Due to its high impacts on society and human health, the prediction of pollution level at the end of the year is crucial to policymakers. Despite emission control policies, natural climatic variability is remarkably important in air quality prediction by modulating circulation and chemical production. Traditional analyses are mostly based on the seasonal averaged. While recent studies revealed a significant sub-seasonal variation of circulation which could mediate the air quality over the NCP on a higher frequency. In this study, a seesaw phenomenon on sub-seasonal timescale is reported, providing a new aspect to conduct sub-seasonal air quality prediction. Possible links to sub-seasonal atmospheric oscillation are also discussed.

Keywords: Sub-seasonal, PM2.5, NCP

©2020. Japan Geoscience Union. All Right Reserved.

Transport of Ozone Pollution Over the East China Sea and the Yellow Sea: a Case Study in Coastal Cities in Eastern China

*Yanhua Zheng[1], Fei Jiang[1], Shuzhuang Feng[1], Zhe Cai[2]

1. Nanjing Univ., 2. Nanjing CLIMBLUE Technology co.LTD

During August 28 and September 5, 2017, a large-scale ozone pollution occurred in the eastern coastal of China.According to the characteristics of the observed ozone, there are three different pollution stages(with slight differences among cities). In the Stage 1, there were significant overall pattern of diurnal high and nocturnal low in O_3 named "single peak pattern". In the Stage 2, the diurnal ozone decreased slightly compared with the Stage 1 while the nighttime ozone increased. The daily minimum O_3 was basically above 20ppb, and the diurnal variation was weakened. In the Stage 3, the nighttime ozone decreased significantly, which restored the "single peak pattern". Using WRF-CMAQ model to simulate the contamination and combining the ozone distribution with weather situation,results are as follows.In the Stage 2,compared with other stages,the eastern coastal regions are controlled by high pressure, lower temperature made the daytime photochemical reaction abate, the bigger northeaster made the air mass above the yellow sea and East China Sea carrying high ozone to coastal regions, so ozone was lower in the day but higher at night.Analyzing the ozone contribution of the main physicochemical processes, it was found that the contribution of horizontal transport in the Stage 2 was significantly higher than that in other stages especially at night.Based on the above analysis, the contribution of transport over the yellow sea and East China Sea to ozone pollution is confirmed.The particle diffusion analysis showed that the air mass had passed over the Beijing-Tianjin-Hebei, the three northeast provinces, Japan-Korea and sea before affecting China's eastern coastal.Using the ISAM source apportionment to further determine the pollutant source, the results showed that pollutant emissions of Japan-Korea and the Beijing-Tianjin-Hebei had obvious contribution to eastern coastal ozone and the contribution of the former than the latter, larger scope and more widely.

Keywords: Ozone pollution, Coastal eastern China, Maritime transport

©2020. Japan Geoscience Union. All Right Reserved.

[E] Poster | A (Atmospheric and Hydrospheric Sciences)：A-AS Atmospheric Sciences, Meteorology & Atmospheric Environment

[A-AS05] Large-scale moisture and organized cloud systems

convener:Hiroaki Miura(The University of Tokyo), Atsushi Hamada(University of Toyama), Satoru Yokoi(Japan Agency for Marine-Earth Science and Technology), Masaki Satoh(Atmosphere and Ocean Research Institute, The University of Tokyo)

Water vapor plays a significant role in regulating the global atmospheric circulation, especially in the troposphere. The overturning circulation is directly driven by the longwave radiative cooling of water vapor and the latent heating/cooling through microphysical processes to balance it. This global circulation is composed of diverse atmospheric phenomena with various spatial and temporal scales. Developments of some significant turbulent motions such as 3D isotropic turbulence in clouds, stratocumulus and cumulus convection, squall lines and tropical cyclones, and the Madden-Julian oscillation, are essentially associated with moisture anomaly in each scale. Moisture is accumulated relatively slowly in larger horizontal scales, but is consumed relatively quickly in smaller ones. This significant scale gaps between the accumulation and consumption may be one of the causes of the long-lasting difficulty in developing the theory of the moist atmosphere. The aim of this session is to share the recent researches about the relationships between moisture and organized cloud systems in wider spatial and temporal scales to enhance collaborations between modeling, observational, and theoretical approaches in tackling this challenging task. Research results relating to the Years of the Maritime Continent (YMC), Radiative-Convective Equilibrium Model Intercomparison Project (RCEMIP), and mesoscale simulations of severe weather are welcome.

[AAS05-P01] Inversion and Preliminary Validation for Global Cloud Classification and Cloud Phase Products of Fengyun-3D in CMA-NSMC

★Invited Papers

*Bo Li[1,2], Ruixia Liu[1,2] (1.China Meteorological Administration, 2.National Satellite Meteorological Center)

[AAS05-P02] An Initiation Process of TD-type Disturbances under an Influence of Upper-Level Troughs

*Yuya Hamaguchi[1,2], Yukari Takayabu[1] (1.Atmosphere and Ocean Research Institute, The University of Tokyo, 2.Department of Earth and Planetary Science, The University of Tokyo)

[AAS05-P03] Numerical Study on the Diurnal Cycle of Precipitation Observed near the West Coast of Sumatra Island

*Mamiko Terada[1], Hiroaki Miura[1] (1. The University of Tokyo)

[AAS05-P04] A statistical study on precipitation characteristics coupled with equatorial Kelvin waves and equatorial Rossby waves.

*Yuhi Nakamura[1], Yukari Takayabu[1] (1.Department of Earth and Planetary Science, School of Science / Division of Climate System Research, Atmosphere and Ocean Research Institute, The University of Tokyo)

[AAS05-P05] **Gravity wave response to convective heating and its importance to understanding the weak temperature gradient approximation and its limitation**

★Invited Papers

*Ching-Shu Hung[1], Hiroaki Miura[1] (1.The University of Tokyo)

Inversion and Preliminary Validation for Global Cloud Classification and Cloud Phase Products of Fengyun-3D in CMA-NSMC

*Bo Li[1,2], Ruixia Liu[1,2]

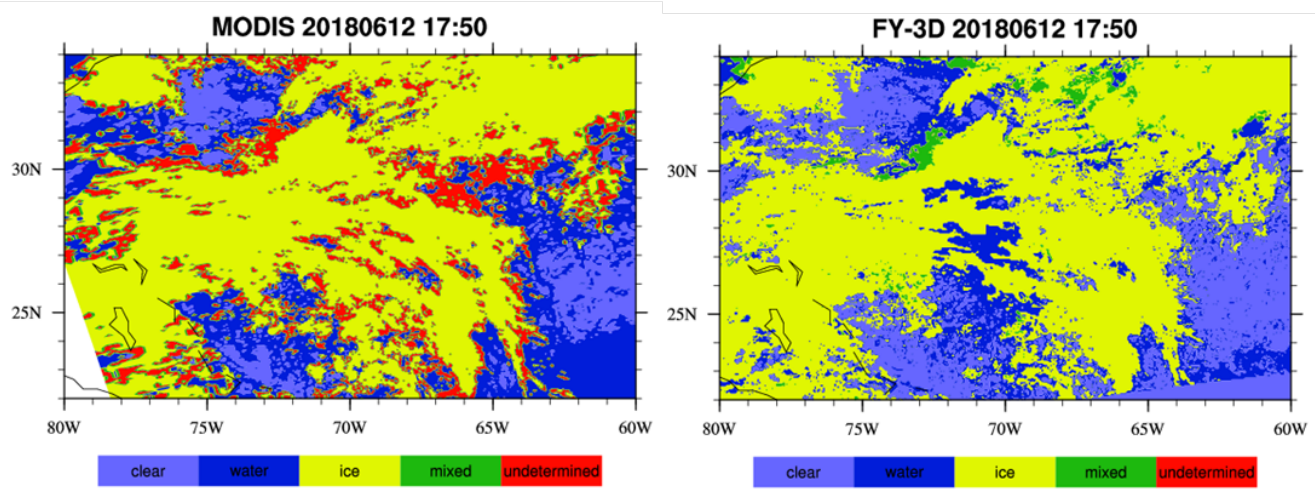
1. China Meteorological Administration, 2. National Satellite Meteorological Center

FY-3 is the second generation polar orbiting meteorological satellite in China. The visible (0.58-0.68 μm), near infrared (1.55-1.64, 3.55-3.93 μm) and two long-wave infrared channels (10.3-11.3 μm and 11.5-12.5 μm) of the FY-3D MERSI (Medium Resolution Spectral Imager) instrument can be used to retrieve cloud classification and cloud phase (hereinafter referred to as CTY and CPH) products.

CPH and CTY products of FY-3D are retrieved based on the MERIS L1 data and cloud mask product. By using the spectral and texture characteristics of visible, infrared and near infrared channels data of L1 as well as the surface type classification data, threshold method is used to identify cloud phases of cloudy pixels, and 1 km resolution CPH is obtained. Then, combined with the results of thin cirrus cloud and broken cloud identification results, high, medium and low cloudy pixels are identified by threshold method, and a CTY product with 1 km resolution is obtained.

The precision of CPH is higher for simple-structured clouds, and POD (probability of detection) as well as CR (Consistency rate) is slightly lower for complex clouds. In general, FY-3D has a better performance on identification of water clouds and a slightly lower accuracy for the identification of ice phase. Compared with MODIS, the algorithm of FY-3D MERSI can recognize more than 90% CPH of the total cloud pixels. It should be noted that due to the different algorithm, the methods and criteria for identifying mixed and uncertain phases are different, which results in some differences between FY -3D and MODIS CPH outputs.

Keywords: FY-3D/MERSI, Cloud Classification, Cloud Phase



©2020. Japan Geoscience Union. All Right Reserved.

An Initiation Process of TD-type Disturbances under an Influence of Upper-Level Troughs

*Yuya Hamaguchi[1,2], Yukari Takayabu[1]

1. Atmosphere and Ocean Research Institute, The University of Tokyo, 2. Department of Earth and Planetary Science, The University of Tokyo

In this study, the initiation process of the summertime tropical depression-type disturbances (hereafter, TDDs) in the western and central Pacific is investigated. TDDs are widely known as westward-travelling synoptic-scale disturbances over the western Pacific (Takayabu and Nitta 1993). As Ritchie and Holland (1999) reported, roughly 50% of western Pacific tropical cyclones form in association with TDDs. In spite of their social importance in terms of tropical cyclogeneses over the western Pacific, their initiation process has not been fully understood.
At the same time, though TDDs are thought to be originated from lower-tropospheric eddies in association with convection in principle, several studies have indicated that some of TDDs are initiated by upper-tropospheric forcing (*e.g.* Tam and Li, 2006; Heta, 1991). Despite the plausibility of the upper-level contribution on the initiation of TDDs, little research has been conducted on the statistical properties of TDDs induced by upper-level activities.
From these perspectives, using CLAUS brightness temperature and JRA-55 products, we statistically analyzed the relationship between TDDs' occurrences and the upper-level perturbations to understand the mechanism of the initiation process of TDDs.
As a result, it is revealed that about 30% of TDDs are generated under an influence of upper-level troughs (so called Mid-Pacific Trough), especially in the off-equatorial region near the date line. The initiation of such trough-related TDDs is associated with a preceding dynamical updraft at the back of the upper-level troughs. It enables convections to become deeper, which results in the development of low-level disturbances via the moisture-convection feedback. Furthermore, according to the composite figures on the trough-related TDDs, it is shown that their environments are much drier than those of other TDDs, which indicates that the upper-level troughs play important roles at the initial stage of their occurrence, especially in relatively drier conditions.

Keywords: TD-type disturbance, Upper-tropospheric trough , Extratropical forcing

©2020. Japan Geoscience Union. All Right Reserved.

Numerical Study on the Diurnal Cycle of Precipitation Observed near the West Coast of Sumatra Island

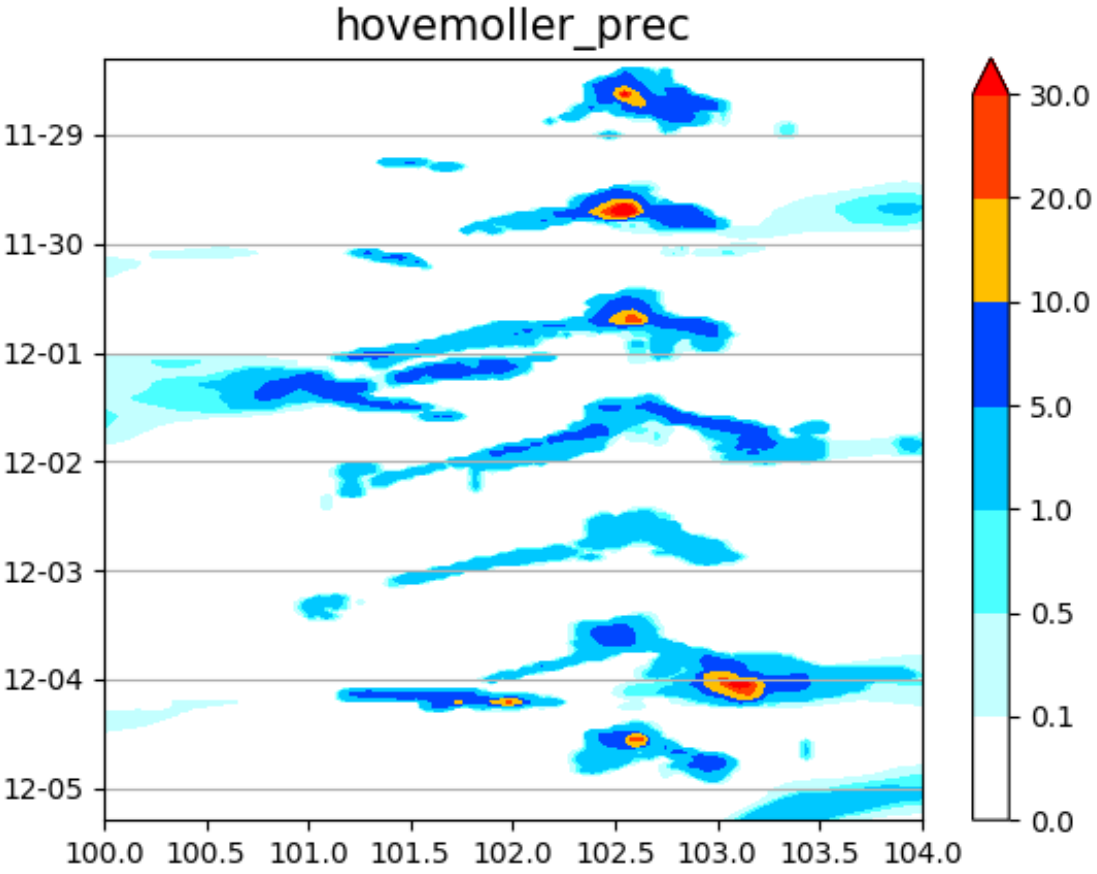
*Mamiko Terada[1], Hiroaki Miura[1]

1. The University of Tokyo

Diurnal cycles of precipitation events are often observed around the Indonesian maritime continents region. Around the western coast of Sumatra, a diurnal cycle has a feature that a precipitation system develops over land in the afternoon, and then, moves offshore from evening through nighttime. Several mechanisms has been proposed about this precipitation movement but has not been sufficiently evaluated yet. Recently, two intensive observation campaigns named as the Pre Years of the Maritime Continent (Pre-YMC) and the Years of the Maritime Continent (YMC) have been operated near the west coast of Sumatra by the Japan Agency for Marine-Earth Science and Technology (JAMSTEC) to observe diurnal cycles and their interactions with larger-scale features. In this study, we simulate atmospheric phenomena in the Pre-YMC period using the Scalable Computing for Advanced Library and Environment –Regional model (SCALE-RM) and examine the mechanism of the precipitation migration.
At first, we perfomed a one week simulation initialized at 00 UTC on November 28, 2015 with a cumulus parameterization. In this simulation, the movements of the precipitation systems were reproduced every day at least marginally. Comparisons of the SCALE-RM simulation with the Pre-YMC radiosonde data confirms that the zonal wind and the specific humidity were quite similar. Then, another simulation was performed by setting the initial time at 00 UTC on November 23, 2015. This calculation was performed without any cumulus parameterization. Precipitation was reproduced everyday over land but its migration toward offshore did not happen except for one day. We are planning to examine the reason for this difference possibly due to with or without the cumulus parameterization.

Keywords: Diurnal Cycle of Precipitation, Simulation, Pre-YMC Observation Campaign

©2020. Japan Geoscience Union. All Right Reserved.



©2020. Japan Geoscience Union. All Right Reserved.

A statistical study on precipitation characteristics coupled with equatorial Kelvin waves and equatorial Rossby waves.

*Yuhi Nakamura[1], Yukari Takayabu[1]

1. Department of Earth and Planetary Science, School of Science / Division of Climate System Research, Atmosphere and Ocean Research Institute, The University of Tokyo

Coupling structures between convection and equatorial waves are investigated using space-borne precipitation radar observation. Recent theoretical studies suggest that different equatorial wave modes can have different coupling mechanisms. However, observational studies on their precipitation characteristics are yet not enough. In order to tackle this issue, we quantitatively characterize precipitation coupled with equatorial Rossby waves (ERW) and equatorial Kelvin waves (EKW).
Based on wave phases determined with brightness temperature observed from the Geostationary Meteorological Satellites, composite analyses are conducted. TRMM 2A25 and 2H25 products are used to analyze precipitation characteristics. We prepare rainfall-area dataset by identifying areas of consecutive precipitating pixels. ERA-interim is used to obtain synoptic scale wave structures.
In the ERW, organized convective systems dominate directly following a shallow convection stage, without a developed convection stage. On the other hand, in the EKW, precipitation shows a tri-modal evolution: shallow convection, developed convection and organized convection stages. We also find a contrast in column water vapor (CWV) anomaly structures. With ERW, positive and negative CWV anomalies have similar amplitudes, while negative CWV anomaly in EKW is not clear.
As for the vertical structures, ERW has an upright structure, while EKW has a vertical tilt. The evolution of moisture field driven by wave disturbances may cause the contrast of the CWV anomaly.
These contrasts of convective evolution and moisture field suggest that these two equatorial waves have different unstable modes. ERW well correspond to ‘moisture mode’, which is driven by CWV anomaly. On the other hand, EKW well correspond to ‘gravity mode’, which is driven by buoyancy perturbation.
In order to clarify interaction between precipitation and wave disturbances in details, we further investigate energy and moisture budget.

Acknowledgment: This research was supported by the Environment Research and Technology Development Fund (2-1904) of the Environmental Restoration and Conservation Agency of Japan.

Keywords: Equatorial Waves, Moist Convection

©2020. Japan Geoscience Union. All Right Reserved.

Gravity wave response to convective heating and its importance to understanding the weak temperature gradient approximation and its limitation

*Ching-Shu Hung[1], Hiroaki Miura[1]

1. The University of Tokyo

Convection is a key process in tropical weather and climate. Its buoyant energy generation and turbulent mixing directly change the temperature and moisture distribution in the small area around clouds, while the secondary compensative circulations driven by its strong latent heating indirectly modulate the environment outside convective regions. Internal gravity waves generated by convection are considered as the key mechanism that communicates the imposed localized perturbation to the surrounding atmosphere. As these gravity waves propagating outward from heating centers, compensating subsidence is induced to balance the strong upward mass fluxes within clouds. The resulting adiabatic warming spreads the localized latent heating over a much wider domain that didn't experience convection. Through its propagation, convective-generated gravity wave quickly homogenizes the buoyancy perturbation, leading to the weak temperature gradient (WTG) feature widely observed in the tropic.

The analytical solutions of the gravity wave response to an isolated heat source were first derived in a two-dimensional hydrostatic Boussinesq fluid by Bretherton and Smolarkiewicz (1989). Their solution suggests that the adjustment time scale and range of gravity wave on temperature field depend on its propagation speed, which is simply controlled by background stratification and vertical structure of imposed heating. Dissipation, rotation, stratosphere, and cylindrically symmetry was further added into this highly idealized model. The modified solutions showed that both the extension to full dimensions and the inclusion of the stratosphere damped the wave signals in the troposphere as they propagated away from the heating source, trapping the response within a confined distance like dissipation and rotation. The combination of these damping scales could help identify the suitable time and space scales for the WTG approximation.

A regional model named SCALE-RM (Scalable Computing for Advanced Library and Environment) is utilized to justify the behavior of gravity wave response predicted by theoretical solutions and to further identify the damping scales in our cloud-resolving model. Several idealized experiments were carried out in a high-resolution configuration that is capable to resolve convective-generated gravity waves. The features in the numerical simulation are generally consistent with that in theory; however, for real convection, the situation becomes much more complicated as the strength and heating structure change along with the cloud's life cycle. Non-linear interaction might be another reason that deviates simulation from the linearized solution.

Keywords: gravity wave, weak temperature gradient approximation

©2020. Japan Geoscience Union. All Right Reserved.

[E] Poster | A (Atmospheric and Hydrospheric Sciences)：A-AS Atmospheric Sciences, Meteorology & Atmospheric Environment

[A-AS06] Advances in Tropical Cyclone Research: Past, Present, and Future

convener:Yoshiaki Miyamoto(Faculty of Environment and Information Studies, Keio University), Sachie Kanada(Nagoya University), Akiyoshi Wada(Department of Typhoon and Severe Weather Research, Meteorological Research Institute), Kosuke Ito(University of the Ryukyus)

Tropical cyclones (TC) cause severe disasters in many countries by torrential rainfall and destructive winds. Strong TCs caused severe damages in many areas of Japan in this couple years; a record-breaking heavy rainfall occurred in western Japan due partly to Typhoon Prapirooon (2018), Kansai airport was forced to be closed by Typhoon Trami (2018), and Typhoon Faxai (2019) caused a long-term shut-down in Chiba prefecture. As the surface temperature of ocean, - the energy source of TC -, increases with global warming, TCs are expected to intensify in the future. Therefore, it is an urgent problem to obtain deeper understanding of mechanisms on TC intensity, structure, and motion, more accurate mid- to long-term projections of the TC parameters, and better forecast of TC. The TC researches are important for disaster prevention as well as the academic development, and hence do contribute to the future progress of earth and planetary science. In this session, we welcome papers on various aspects of TC studies. We hope that the session will provide a new direction for future TC researches.

[AAS06-P01] Increased severe landfall typhoons in China since 2004

*Cai Yao[1,2], zhixiang Xiao[1], Song Yang[2,3], Xiaoli Luo[4] (1.Guangxi Institute of Meteorological Sciences, Nanning , China, 2.Southern Marine Science and Engineering Guangdong Laboratory (Zhuhai), Zhuhai , China, 3.School of Atmospheric Sciences, and Guangdong Province Key Laboratory for Climate Change and Natural Disaster Studies, Sun Yat-sen University, Guangzhou, China, 4.Guangxi Weather Service Center, Nanning, China)

[AAS06-P02] Perspective on Landfalling Frequency and Genesis Location Variations of Southern China Typhoon During Peak Summer

*Chengyang Zhang[1], Chundi Hu[2,3,4], Gang Huang[4], Cai Yao[1], Zhihai Zheng[5], Song Yang[2,3,6], Dake Chen[3,7] (1.Climate Center & Guangxi Institute of Meteorological Sciences, Guangxi Meteorological Bureau, Nanning, China, 2.School of Atmospheric Sciences & Guangdong Province Key Laboratory for Climate Change and Natural Disaster Studies, Sun Yat-sen University, Zhuhai, China, 3.Southern Marine Science and Engineering Guangdong Laboratory (Zhuhai), Zhuhai, China, 4.State Key Laboratory of Numerical Modeling for Atmospheric Sciences and Geophysical Fluid Dynamics, Institute of Atmospheric Physics, Chinese Academy of Sciences, Beijing, China, 5.Laboratory for Climate Studies, National Climate Center, China Meteorological Administration, Beijing, China, 6.Institute of Earth Climate and Environment System, Sun Yat-sen University, Guangzhou, China, 7.State Key Laboratory of Satellite Ocean Environment Dynamics, Second Institute of Oceanography, Ministry of Natural Resources, Hangzhou, China)

[AAS06-P04] **Analysis of Multi-scale Circulation Characteristics Affecting the Multiple Tropical Cyclogenesis in Midsummer of 2018**

*JIANYUN GAO[1], LIJUN YOU[2] (1.Fujian Institute of Meteorological Sciences, 2.Fujian Climate center)

[AAS06-P05] **Improvement of Prediction Accuracy of 3-second gust caused by Typhoon – FDDA and High Resolution SST -**

*Woosik Jung[1] (1.INJE University, Department of Atmospheric Environment Information Engineering, Gimhae, Republic of Korea)

[AAS06-P06] **Improvement of Prediction Accuracy of 3-second gust caused by Typhoon – Meteorological Input Data : GDAPS, RDAPS, GFS -**

*Woosik Jung[1] (1.INJE University, Department of Atmospheric Environment Information Engineering, Gimhae, Republic of Korea)

[AAS06-P07] **Improvement of Prediction Accuracy of 3-second gust caused by Typhoon – Soil Data : GDAPS SOIL, GFS SOIL -**

*Woosik Jung[1] (1.INJE University, Department of Atmospheric Environment Information Engineering, Gimhae, Republic of Korea)

[AAS06-P08] **Autumn Typhoon on the Korean Peninsula - Comparison of Past and Present**

*Woosik Jung[1], Hana Na[1] (1.INJE University, Department of Atmospheric Environment Information Engineering, Gimhae, Republic of Korea)

[AAS06-P09] **Water vapor transport associated with remote precipitation caused by typhoon in autumn season**

*Shinichi Kodama[1], Masaki Satoh[1] (1.Atmosphere and Ocean Research Institute, Univ. of Tokyo)

[AAS06-P10] The impact of lower stratospheric temperature change on Typhoon

*Kenta Kobayashi[1], Nawo Eguchi[1], Kosuke Ito[2] (1.Interdisciplinary Graduate School of Engineering Science, Kyushu University , 2.Faculty of Science, University of the Ryukyus)

[AAS06-P13] Sensitivity Experiments of Relative Humidity Assimilation on Typhoon Lan (2017)

Jaedeok Lee[1], *Kosuke Ito[1], Chun-Chieh Wu[2] (1.University of the Ryukyus, 2.National Taiwan University)

[AAS06-P14] **Role of VHTs and Helical flow organization in the formation of Tropical Cyclogenesis over North Indian Ocean**

*EMMANUEL RONGMIE[1,4], Medha Deshpande[2], Mano Kranthi Ganadhi[1], Sopan Tukaram Ingle[3], Phani Murali krishna[2] (1.Research Scholar in Indian Institute of Tropical Meteorology Pune, 2.Scientist D in Indian Institute of Tropical Meteorology Pune, 3.Professor and Director in K.B.C. North Maharashtra University, Jalgaon, 4.North Maharashtra University, Jalgaon)

[AAS06-P15] **Monthly Variation and Spatial Distribution of Quadrant Tropical Cyclone Size in the Western North Pacific**

*Tonghua Su[4], Wei Hong[1], Yulan Zheng[2], Bin Chen[3], Xiaoqing Ke[5] (1.Fujian Meteorological Observatory of of China Meteorological Administration, 2.Fujian Meteorological Information Center of China Meteorological Administration, 3.Electric Power Research Institute of State Grid Fujian Electric Power Company, 4.Fujian Climate Center of China Meteorological Administration, 5.Fujian Meteorological Service Center of China Meteorological Administration)

Increased severe landfall typhoons in China since 2004

*Cai Yao[1,2], zhixiang Xiao[1], Song Yang[2,3], Xiaoli Luo[4]

1. Guangxi Institute of Meteorological Sciences, Nanning , China, 2. Southern Marine Science and Engineering Guangdong Laboratory (Zhuhai), Zhuhai , China, 3. School of Atmospheric Sciences, and Guangdong Province Key Laboratory for Climate Change and Natural Disaster Studies, Sun Yat-sen University, Guangzhou, China, 4. Guangxi Weather Service Center, Nanning, China

ABSTRACT: Severe landfall typhoons (SLTYs) are defined as those with maximum sustained wind speed ≧ 41.5 m s^{-1} at landfalls, which strongly affect the coastal regions of China and cause grave losses of life and property. In this study, we analyze the SLTYs in China in peak summer (July-September) during the period 1973-2017, which are separated into three periods: period-I (1973–1987), period-II (1988–2003), and period-III (2004–2017). Results show that the SLTYs in China have abruptly increased since 2004, characterized by the count of about 65.9% (72.7%) of the SLTYs in China (South China) in period-III only. This phenomenon is partly attributed to the significantly-increased severe typhoon frequency and the longer duration of severe typhoon stage over the western North Pacific. The most potential factors can be summarized as follows. First, the abnormal easterly steering flow over the western North Pacific in period-III is beneficial for typhoons to march westward. Second, typhoons continue to strengthen before landfall in South China, which may be attributed to warming in the northern South China Sea and enhanced warm moist southerly monsoon flow. About 9.7% of typhoons with landfall in South China experienced a rapid intensification process in 24 h before landfalls in period-III. However, the percentage is only 1.6% and 3.1% for period-I and period-II, respectively. Third, intensified typhoons have been attracted to the warming land surface over South China since 2004, which is generally a result of air-land-sea interaction, and the conditions of air, land and sea are increasingly beneficial for SLTYs in China.

Keywords: Severe landfall typhoons (SLTYs), air-land-sea interaction

©2020. Japan Geoscience Union. All Right Reserved.

Perspective on Landfalling Frequency and Genesis Location Variations of Southern China Typhoon During Peak Summer

*Chengyang Zhang[1], Chundi Hu[2,3,4], Gang Huang[4], Cai Yao[1], Zhihai Zheng[5], Song Yang[2,3,6], Dake Chen[3,7]

1. Climate Center & Guangxi Institute of Meteorological Sciences, Guangxi Meteorological Bureau, Nanning, China, 2. School of Atmospheric Sciences & Guangdong Province Key Laboratory for Climate Change and Natural Disaster Studies, Sun Yat-sen University, Zhuhai, China, 3. Southern Marine Science and Engineering Guangdong Laboratory (Zhuhai), Zhuhai, China, 4. State Key Laboratory of Numerical Modeling for Atmospheric Sciences and Geophysical Fluid Dynamics, Institute of Atmospheric Physics, Chinese Academy of Sciences, Beijing, China, 5. Laboratory for Climate Studies, National Climate Center, China Meteorological Administration, Beijing, China, 6. Institute of Earth Climate and Environment System, Sun Yat-sen University, Guangzhou, China, 7. State Key Laboratory of Satellite Ocean Environment Dynamics, Second Institute of Oceanography, Ministry of Natural Resources, Hangzhou, China

Abstract: Increasing intense landfalling typhoons (LFTYs) are of great coastal threatens to southern China. However, changes in genesis location and landfalling frequency of western North Pacific (WNP) LFTY dedicated to southern China remain unclear. Here we identified such LFTYs during peak summer and found that most LFTYs formed south of 20˚N and the LFTY genesis locations over southern WNP have also experienced a sharp interdecadal shift since 1998, which are mainly attributed to the large-scale environment changes induced by the Mega-La Niña-like climate shift. However, LFTY frequency (= “landfalling frequency of southern China typhoon”) shows a slight increasing trend but without significant interdecadal variation. Variations of LFTY frequency are mainly affected by the easterly steering flows near 20˚N over the South China Sea and the Philippine Sea, which are closely linked to the WNP subtropical high activity. Our results provide a new perspective on the LFTY activities dedicated to southern China.

Keywords: landfalling typhoon, steering flows

©2020. Japan Geoscience Union. All Right Reserved.

Analysis of Multi-scale Circulation Characteristics Affecting the Multiple Tropical Cyclogenesis in Midsummer of 2018

*JIANYUN GAO[1], LIJUN YOU[2]

1. Fujian Institute of Meteorological Sciences, 2. Fujian Climate center

This study investigates the impact of multi-scale circulations (including large-scale circulation, intra-seasonal oscillation (ISO) and tropical waves) on the multiple tropical cyclogenesis (MTC) and discusses the deviation of vertical disturbance field of the whole atmosphere in the MTC active and inactive phases by taking a typical MTC in midsummer of 2018 as an example. The results are as follows. (1) The Western North Pacific (WNP) undergoes a 16-days MTC active phase with eight tropical cyclones (TCs) generated in sequence and a 19-days MTC inactive phase with only one TC generated in midsummer of 2018. (2) During the MTC active phase, the cross-equatorial airflow strengthens and monsoon trough extends eastward. The atmospheric circulation configuration of the low-level convergence and the upper level divergence in South China Sea (SCS) and WNP is conducive to TC formation. (3) The northward propagation of Eastern Asia and WNP ISO in summer has a significant modulation effect on the MTC sub-seasonal changes. The SCS and WNP are just in a northward wet (dry) phase of a strong ISO during the MTC active (inactive) phase. (4) The generation of the eight TCs in the MTC active phase is all related to tropical fluctuation, five of which are affected by two kinds of tropical waves at the same time. Tropical fluctuation provides the trigger conditions for the TC generation by changing local thermal and dynamic conditions. (5) The common influence of multi-scale circulation eventually leads to significant differences in the vertical structure characteristics of temperature-pressure disturbance field configuration, vertical motion disturbance and specific humidity disturbance in the MTC active and inactive phase. The application of the disturbance analysis method provides a new idea for the extended range forecast.

Keywords: multiple tropical cyclogenesis, multi-scale oscillation, tropical waves, perturbation analysis

©2020. Japan Geoscience Union. All Right Reserved.

Improvement of Prediction Accuracy of 3-second gust caused by Typhoon –FDDA and High Resolution SST -

*Woosik Jung[1]

1. INJE University, Department of Atmospheric Environment Information Engineering, Gimhae, Republic of Korea

As industrialization has progressed rapidly since the 1980s, global warming is steadily going on. According to a study by the IPCC(2015), as global warming progresses, SST increases, the number of typhoons occurs decreases and intensity becomes stronger. In fact, SST around the western Pacific and the Korean Peninsula have recently increased at a faster rate than the average global increase in SST, and the intensity of typhoons affecting the Korean Peninsula has become stronger. In order to reduce the damage caused by typhoons in Korea, Typhoon Pre-prevention Disaster Model is developed and operated to calculate 3-second gust(maximum instantaneous wind speed) and damage cost that could occur during the typhoon’ s effect. In studies related to Typhoon Pre-prevention Disaster Model, studies on the development process and the characteristics of the Korean Peninsula impact typhoon applied to Typhoon Pre-prevention Disaster Model were preceded mainly by studies that conducted basic analysis to develop Typhoon Pre-prevention Disaster Model. However, studies to improve the accuracy of the 3-second gust, the result of the Typhoon Pre-prevention Disaster Model, were not preceded. Therefore, in this study, we apply the High resolution SST and FDDA to the WRF model used to derive input informations from the typhoon pre-prevention model, and then analyse the improvement of predictive accuracy of 3-second gust calculated from the Typhoon Pre-prevention Disaster Model. A total of four experiments were performed with the default experiment(EXP1) with no application, the experiment with adding high resolution SST(EXP2), the experiment with adding FDDA(EXP3) and the experiment with applying high resolution SST and FDDA simultaneously(EXP4). As a result, 3-second gust was best simulated when the results of the experiment using both high resolution SST and meteorological data FDDA were used as input data for the Typhoon Pre-prevention Disaster Model.

This research was supported by Basic Science Research Program through the National Research Foundation of Korea(NRF) funded by the Ministry of Education(2017R1D1A3B03036152)

Keywords: Typhoon Pre-prevention Disaster Model, UM, GDAPS SOIL, GFS SOIL

©2020. Japan Geoscience Union. All Right Reserved.

Improvement of Prediction Accuracy of 3-second gust caused by Typhoon - FDDA and High Resolution SST -

Woo-Sik Jung

INJE University, Department of Atmospheric Environment Information Engineering, Gimhae, Republic of Korea

As industrialization has progressed rapidly since the 1980s, global warming is steadily going on. According to a study by the IPCC(2015), as global warming progresses, SST increases, the number of typhoons occurs decreases and intensity becomes stronger. In fact, SST around the western Pacific and the Korean Peninsula have recently increased at a faster rate than the average global increase in SST, and the intensity of typhoons affecting the Korean Peninsula has become stronger. In order to reduce the damage caused by typhoons in Korea, Typhoon Pre-prevention Disaster Model is developed and operated to calculate 3-second gust(maximum instantaneous wind speed) and damage cost that could occur during the typhoon's effect. In studies related to Typhoon Pre-prevention Disaster Model, studies on the development process and the characteristics of the Korean Peninsula impact typhoon applied to Typhoon Pre-prevention Disaster Model were preceded mainly by studies that conducted basic analysis to develop Typhoon Pre-prevention Disaster Model. However, studies to improve the accuracy of the 3-second gust, the result of the Typhoon Pre-prevention Disaster Model, were not preceded. Therefore, in this study, we apply the High resolution SST and FDDA to the WRF model used to derive input informations from the typhoon pre-prevention model, and then analyse the improvement of predictive accuracy of 3-second gust calculated from the Typhoon Pre-prevention Disaster Model. A total of four experiments were performed with the default experiment(EXP1) with no application, the experiment with adding high resolution SST(EXP2), the experiment with adding FDDA(EXP3) and the experiment with applying high resolution SST and FDDA simultaneously(EXP4). As a result, 3-second gust was best simulated when the results of the experiment using both high resolution SST and meteorological data FDDA were used as input data for the Typhoon Pre-prevention Disaster Model.

This research was supported by Basic Science Research Program through the National Research Foundation of Korea(NRF) funded by the Ministry of Education(2017R1D1A3B03036152)

Key words: Typhoon Pre-prevention Disaster Model, UM, GDAPS SOIL, GFS SOIL

©2020. Japan Geoscience Union. All Right Reserved.

Improvement of Prediction Accuracy of 3-second gust caused by Typhoon –Meteorological Input Data : GDAPS, RDAPS, GFS -

*Woosik Jung[1]

1. INJE University, Department of Atmospheric Environment Information Engineering, Gimhae, Republic of Korea

The damage caused by recent typhoons affecting the Korean Peninsula has been increasing rapidly. The top 10 records of maximum instantaneous wind speed caused by typhoons has shown by typhoons since the 2000s. Compared to the past, the frequency of typhoons is decreasing and the intensity of typhoons is getting stronger. In order to reduce damage from typhoons, a Typhoon Pre-prevention Disaster Model developed and operated to predict 3-second gust(maximum instantaneous wind speed) caused by typhoons and to calculate the possible damage. In order to improve the accuracy of Typhoon Pre-prevention Disaster Model, meteorological input data such as GDAPS(Global Data Assimilation Prediction System), RDAPS(Regional Data Assimilation System), and GFS(Global Forecast System) were applied to the Model. 3-second gust calculated using GDAPS as the meteorological input data showed the most similar results to the observed values for the RMSE, MB, and IOA values used as statistical indicators, followed by RDAPS and GFS.

This research was supported by Basic Science Research Program through the National Research Foundation of Korea(NRF) funded by the Ministry of Education(2017R1D1A3B03036152).

Keywords: Typhoon Pre-prevention Disaster Model, 3-second gust, GDAPS, RDAPS, GFS

©2020. Japan Geoscience Union. All Right Reserved.

Improvement of Prediction Accuracy of 3-second gust caused by Typhoon - Meteorological Input Data : GDAPS, RDAPS, GFS -

Woo-Sik Jung

INJE University, Department of Atmospheric Environment Information Engineering, Gimhae, Republic of Korea

The damage caused by recent typhoons affecting the Korean Peninsula has been increasing rapidly. The top 10 records of maximum instantaneous wind speed caused by typhoons has shown by typhoons since the 2000s. Compared to the past, the frequency of typhoons is decreasing and the intensity of typhoons is getting stronger. In order to reduce damage from typhoons, a Typhoon Pre-prevention Disaster Model developed and operated to predict 3-second gust(maximum instantaneous wind speed) caused by typhoons and to calculate the possible damage. In order to improve the accuracy of Typhoon Pre-prevention Disaster Model, meteorological input data such as GDAPS(Global Data Assimilation Prediction System), RDAPS(Regional Data Assimilation System), and GFS(Global Forecast System) were applied to the Model. 3-second gust calculated using GDAPS as the meteorological input data showed the most similar results to the observed values for the RMSE, MB, and IOA values used as statistical indicators, followed by RDAPS and GFS.

This research was supported by Basic Science Research Program through the National Research Foundation of Korea(NRF) funded by the Ministry of Education(2017R1D1A3B03036152).

Key words: Typhoon Pre-prevention Disaster Model, 3-second gust, GDAPS, RDAPS, GFS,

©2020. Japan Geoscience Union. All Right Reserved.

Improvement of Prediction Accuracy of 3-second gust caused by Typhoon –Soil Data : GDAPS SOIL, GFS SOIL -

*Woosik Jung[1]

1. INJE University, Department of Atmospheric Environment Information Engineering, Gimhae, Republic of Korea

In order to reduce the damage caused by the typhoon, 3-second gust, which is the maximum wind speed that can occur during the typhoon, is a very important factor in terms of disaster prevention. Therefore, this study conduct to improve the prediction accuracy of Typhoon Pre-prevention Disaster Model that calculates the 3-second gust. UM(Unified Model) data has a problem in being used as input data because the initial soil moisture and the soil temperature unit and depth are different. Therefore, soil data from GFS(Global Forecast System) and FNL(NCEP final analysis) are mainly used as a substitute. In this study, soil moisture and soil temperature of UM data were adjusted to Typhoon Pre-prevention Disaster Model, and experiments were conduct to use the GDAPS(Global Data Assimilation Prediction System) as meteorological input data, and soil data as the existing method. At the same time, a single model using GDAPS as the meteorological input data and GDAPS SOIL as the soil data is also conduct. The results of 3-second gust calculated using Typhoon Pre-prevention Disaster Model were compared with 'GUST wind speed' in the buoy and 'Maximum instantaneous wind speed' on the beacon. The results of the analysis showed that the experiments using the results of a model using a GDAPS SOIL (Single Model) as input data for Typhoon Pre-prevention Disaster Model was more similar to the observed values and more consistent with the trend than the experiment applying soil data to GDAPS meteorological input data using GFS SOIL. In conclusion, if a single model is used as WRF soil data, which is input data, it is deemed possible to determine the optimal results when performing Typhoon Pre-prevention Disaster Model.

This research was supported by Basic Science Research Program through the National Research Foundation of Korea(NRF) funded by the Ministry of Education(2017R1D1A3B03036152)

Keywords: Typhoon Pre-prevention Disaster Model, 3-second gust, soil moisture, soil layer

©2020. Japan Geoscience Union. All Right Reserved.

Improvement of Prediction Accuracy of 3-second gust caused by Typhoon -Soil Data : GDAPS SOIL, GFS SOIL -

Woo-Sik Jung

INJE University, Department of Atmospheric Environment Information Engineering, Gimhae, Republic of Korea

In order to reduce the damage caused by the typhoon, 3-second gust, which is the maximum wind speed that can occur during the typhoon, is a very important factor in terms of disaster prevention. Therefore, this study conduct to improve the prediction accuracy of Typhoon Pre-prevention Disaster Model that calculates the 3-second gust. UM(Unified Model) data has a problem in being used as input data because the initial soil moisture and the soil temperature unit and depth are different. Therefore, soil data from GFS(Global Forecast System) and FNL(NCEP final analysis) are mainly used as a substitute. In this study, soil moisture and soil temperature of UM data were adjusted to Typhoon Pre-prevention Disaster Model, and experiments were conduct to use the GDAPS(Global Data Assimilation Prediction System) as meteorological input data, and soil data as the existing method. At the same time, a single model using GDAPS as the meteorological input data and GDAPS SOIL as the soil data is also conduct. The results of 3-second gust calculated using Typhoon Pre-prevention Disaster Model were compared with 'GUST wind speed' in the buoy and 'Maximum instantaneous wind speed' on the beacon. The results of the analysis showed that the experiments using the results of a model using a GDAPS SOIL (Single Model) as input data for Typhoon Pre-prevention Disaster Model was more similar to the observed values and more consistent with the trend than the experiment applying soil data to GDAPS meteorological input data using GFS SOIL. In conclusion, if a single model is used as WRF soil data, which is input data, it is deemed possible to determine the optimal results when performing Typhoon Pre-prevention Disaster Model.

This research was supported by Basic Science Research Program through the National Research Foundation of Korea(NRF) funded by the Ministry of Education(2017R1D1A3B03036152)

Key words: Typhoon Pre-prevention Disaster Model, 3-second gust, soil moisture, soil layer

©2020. Japan Geoscience Union. All Right Reserved.

Autumn Typhoon on the Korean Peninsula - Comparison of Past and Present

*Woosik Jung[1], Hana Na[1]

1. INJE University, Department of Atmospheric Environment Information Engineering, Gimhae, Republic of Korea

Recently, the characteristics of typhoons affecting the Korean Peninsula are rapidly changing. As the typhoon affects the Korean Peninsula, and the SST in the Northwest Pacific, including the growing Korean Peninsula, increases at a faster rate than the global average SST, the intensity of the typhoon affecting the Korean Peninsula is increasing. In particular, the frequency and intensity of typhoons affecting the Korean Peninsula in September and October, called “Autumn Typhoon,” are increasing. In 2019, there were seven typhoons in the Korean Peninsula, of which three typhoons occurred in September, causing significant damage to the Korean Peninsula. Although the frequency and intensity of autumn typhoons are increasing, but previous studies on autumn typhoons are very insufficient. Therefore, this study compared and analyzed the change in overall characteristics including frequency, intensity, maximum instantaneous wind speed, and track for autumn typhoon. The analysis of maximum instantaneous wind speed and distribution during the typhoon period was carried out using the Typhoon Pre-prevention Disaster Model. The analysis showed that the proportion of autumn typhoons affecting the Korean Peninsula was increasing sharply in the 2011-2019 period compared to 2002-2010, and that the maximum instantaneous wind speed that occurs during the period of the fall typhoon was also increasing. In recent years, as the frequency and intensity of autumn typhoons increase simultaneously, the damage caused by autumn typhoons is gradually increasing. Therefore, in terms of disaster prevention, further research on autumn typhoon should be conducted later.

This research was supported by Basic Science Research Program through the National Research Foundation of Korea(NRF) funded by the Ministry of Education(2017R1D1A3B03036152).

Keywords: Autumn, Typhoon, 3-second gust

©2020. Japan Geoscience Union. All Right Reserved.

Autumn Typhoon on the Korean Peninsula – Comparison of Past and Present

Woo-Sik Jung, Hana Na

INJE University, Department of Atmospheric Environment Information Engineering, Gimhae, Republic of Korea

Recently, the characteristics of typhoons affecting the Korean Peninsula are rapidly changing. As the typhoon affects the Korean Peninsula, and the SST in the Northwest Pacific, including the growing Korean Peninsula, increases at a faster rate than the global average SST, the intensity of the typhoon affecting the Korean Peninsula is increasing. In particular, the frequency and intensity of typhoons affecting the Korean Peninsula in September and October, called "Autumn Typhoon," are increasing. In 2019, there were seven typhoons in the Korean Peninsula, of which three typhoons occurred in September, causing significant damage to the Korean Peninsula. Although the frequency and intensity of autumn typhoons are increasing, but previous studies on autumn typhoons are very insufficient. Therefore, this study compared and analyzed the change in overall characteristics including frequency, intensity, maximum instantaneous wind speed, and track for autumn typhoon. The analysis of maximum instantaneous wind speed and distribution during the typhoon period was carried out using the Typhoon Pre-prevention Disaster Model. The analysis showed that the proportion of autumn typhoons affecting the Korean Peninsula was increasing sharply in the 2011-2019 period compared to 2002-2010, and that the maximum instantaneous wind speed that occurs during the period of the fall typhoon was also increasing. In recent years, as the frequency and intensity of autumn typhoons increase simultaneously, the damage caused by autumn typhoons is gradually increasing. Therefore, in terms of disaster prevention, further research on autumn typhoon should be conducted later.

This research was supported by Basic Science Research Program through the National Research Foundation of Korea(NRF) funded by the Ministry of Education(2017R1D1A3B03036152).

Key words: Autumn, WRF, Typhoon Pre-prevention Disaster Model, 3-second gust

©2020. Japan Geoscience Union. All Right Reserved.

Water vapor transport associated with remote precipitation caused by typhoon in autumn season

*Shinichi Kodama[1], Masaki Satoh[1]

1. Atmosphere and Ocean Research Institute, Univ. of Tokyo

In the autumn season of Japan, typhoon located far away from Japan increases the supply of water vapor to the rain front and causes significant precipitation. This phenomenon is called remote precipitation due to the indirect effects of typhoon, and in Japan there are only a few case studies. On the other hand, precipitation by the indirect effects of tropical cyclone on the North American continent is called the predecessor rain event (PRE), and many cases or statistical studies have been conducted. In this study, in order to clarify the mechanism of remote precipitation in Japan, I focused on the water vapor transport associated with remote precipitation caused by typhoon in autumn season and analyzed it.

The analysis period is from September 2004 to 2018 for 15 years, covering strong typhoons that developed below 950 hPa. When I checked the course of typhoons obtained, it was found that they were roughly classified into two courses: a course approaching while recurving to Japan and a course proceeding westward. Moreover, when I checked the water vapor transport by course, it was confirmed that a course approaching while recurving to Japan had large impact on Japan. Therefore, the analysis was limited to only typhoons on course that approaching while recurving to Japan.

In order to classify all 12 recurving typhoons into those with and without remote precipitation, I determined the definition of remote precipitation in Japan. As a result, 5 cases were judged as Japanese version of PRE and 7 cases as Not PRE (N-PRE). Moreover, as a result of a composite analysis of PRE cases with the typhoon center aligned with latitude lines, it was confirmed that PRE occurs around Japan on the day the typhoon center is located at 22.5 degrees north latitude. Furthermore, I defined the day as the reference day of day0 and compared the environmental fields before remote precipitation occurred from the composite analysis of PRE cases and N-PRE cases for 1 day before (day-1) and 2 days before (day-2). When I compared the extending changes of the subtropical high, PRE cases showed a weakening tendency from day-2 to day0, and N-PRE cases showed an increasing tendency. As a result, in PRE cases, the water vapor carried by the typhoon is blocked by the downward flow of the subtropical high in front, and there is no route to escape to the north or west, and the high water vapor situation is maintained mainly on the east side of the typhoon. Subsequently, the extending of the subtropical high will weaken, causing water vapor transport northward to Japan, which will lead to the occurring of PRE.

Keywords: Typhoon, Remote precipitation

©2020. Japan Geoscience Union. All Right Reserved.

The impact of lower stratospheric temperature change on Typhoon

*Kenta Kobayashi[1], Nawo Eguchi[1], Kosuke Ito[2]

1. Interdisciplinary Graduate School of Engineering Science, Kyushu University , 2. Faculty of Science, University of the Ryukyus

In recent years, it is statistically clarified that the stratospheric dynamical change, such as sudden stratospheric warming (SSW) and quasi-biennial oscillation (QBC), affects on the cumulus convective activity in tropical zone. For example, the study examining the effect of stratospheric conditions during SSW has found that the activity of cumulus convection becomes deeper due to descending the unstable region from the lower stratosphere [e.g., Eguchi et al., 2015; Kodera et al., 2015]. For this reason, the importance of a quantitative understand of stratospheric effects on the troposphere has been recognized internationally [e.g., SATIO-TCS (Stratospheric And Tropospheric Influences On Tropical Convective Systems) on SPARC]. Although there are a few previous studies, it is not clear the relationship between the stratosphere and typhoons, yet. Therefore, we researched the effects of temperature changes at the lower stratosphere on typhoons by using the two-dimensional axial symmetry model (Rouunno and Emanuel, 1987). We changed temperature profile at the lower stratosphere and checked the changes in typhoon’s wind speed, height, etc. As a result, it was found that the upper troposphere becomes unstable, and the upper, lower, radial, tangential wind velocity increases due to deep convection when the temperature in the stratosphere is lower than the control simulation. At the presentation, we will show the effect of temperature change at the lower stratosphere on the typhoon activity in detail.

Keywords: Typhoon, Stratosphere, Temperature

©2020. Japan Geoscience Union. All Right Reserved.

Sensitivity Experiments of Relative Humidity Assimilation on Typhoon Lan (2017)

Jaedeok Lee[1], *Kosuke Ito[1], Chun-Chieh Wu[2]

1. University of the Ryukyus, 2. National Taiwan University

Typhoon Lan (2017) caused tremendous flooding while passing through mainland Japan. A day before making landfall, Lan had robust eyewall and eye structures. During this period, valuable in-situ data were obtained through the Observing System Research and Predictability Experiment Pacific Asian Regional Campaign Ⅱ (T-PARC Ⅱ). The present study has constructed the three-dimensional relative humidity of Lan by performing statistical analyses between in-situ data obtained by T-PARC Ⅱ and the IRWVln produced by the Himawari-based technique. To assimilate this three-dimensional relative humidity, the initial conditions of Lan have been improved by using the dynamical initialization. The results of the sensitivity experiments show that as the magnitude of the innovation scale increases, the simulated precipitation structures seen by the outgoing longwave radiation or radar fields tend to well account for actual characteristics compared to satellite images or radar images. However, the influence of relative humidity correction appears to have little impact on track and intensity forecasts.

©2020. Japan Geoscience Union. All Right Reserved.

Role of VHTs and Helical flow organization in the formation of Tropical Cyclogenesis over North Indian Ocean

*EMMANUEL RONGMIE[1,4], Medha Deshpande[2], Mano Kranthi Ganadhi[1], Sopan Tukaram Ingle[3], Phani Murali krishna[2]

1. Research Scholar in Indian Institute of Tropical Meteorology Pune, 2. Scientist D in Indian Institute of Tropical Meteorology Pune, 3. Professor and Director in K.B.C. North Maharashtra University, Jalgaon, 4. North Maharashtra University, Jalgaon

Tropical Cyclogenesis (TCs) remains one of the most complex enigmas of dynamic meteorology. Many environmental factors contribute to the genesis of TCs. The main objective of this study is to understand ‘why’ and ‘how’ Mesoscale convective vortices (MCVs) cluster and the role of Vortical Hot towers (VHTs) in the Tropical Cyclones (TC). Reanalysis and satellite data for various cases of TC shows that the Mesoscale convective system (MCS) interaction in the presence of a large Scale. Multiple waves interact and modulate different requisite parameters compared to the presence of individual waves. To understand the interaction of MCVs and VHTs in the Pregenesis period, a numerical simulation experiment is carried out using ‘Model for Prediction across Scales (MPAS)’ focused over the Indian. Linkage of the primary and secondary circulation in the developing and non-developing TCs, the total kinetic terms and scalar quantity, total helicity are examined. Role of different component of horizontal and vertical helicity is examined. The importance of the study is to investigate the validity of helicity as an indication of large scale vortex instability.

Keywords: helicity, Tropical Waves, Mesoscale Convective Systems

©2020. Japan Geoscience Union. All Right Reserved.

Role of VHTs and Helical flow organization in the formation of Tropical Cyclogenesis over North Indian Ocean

Emmanuel Rongmie[1,2] Medha Deshpande[1], Mano Kranthi Ganadhi[1], R Phani Murali Krishna[1],
S. T. Ingle[2]
1. Indian Institute of Tropical Meteorology, Pune, Pashan, 411008
2. Kavayitri Bahinibai Chaudhari North Maharashtra University, Jalgaon, Maharashtra, 425001

Tropical Cyclogenesis (TCs) remains one of the most complex enigmas of dynamic meteorology. Many environmental factors contribute to the genesis of TCs. The main objective of this study is to understand 'why' and 'how' Mesoscale convective vortices (MCVs) cluster and the role of Vortical Hot towers (VHTs) in the Tropical Cyclones (TC). Reanalysis and satellite data for various cases of TC shows that the Mesoscale convective system (MCS) interaction in the presence of a large Scale. Multiple waves interact and modulate different requisite parameters compared to the presence of individual waves. To understand the interaction of MCVs and VHTs in the Pregenesis period, a numerical simulation experiment is carried out using 'Model for Prediction across Scales (MPAS)' focused over the Indian. Linkage of the primary and secondary circulation in the developing and non-developing TCs, the total kinetic terms and scalar quantity, total helicity are examined. Role of different component of horizontal and vertical helicity is examined. The importance of the study is to investigate the validity of helicity as an indication of large scale vortex instability.

©2020. Japan Geoscience Union. All Right Reserved.

Monthly Variation and Spatial Distribution of Quadrant Tropical Cyclone Size in the Western North Pacific

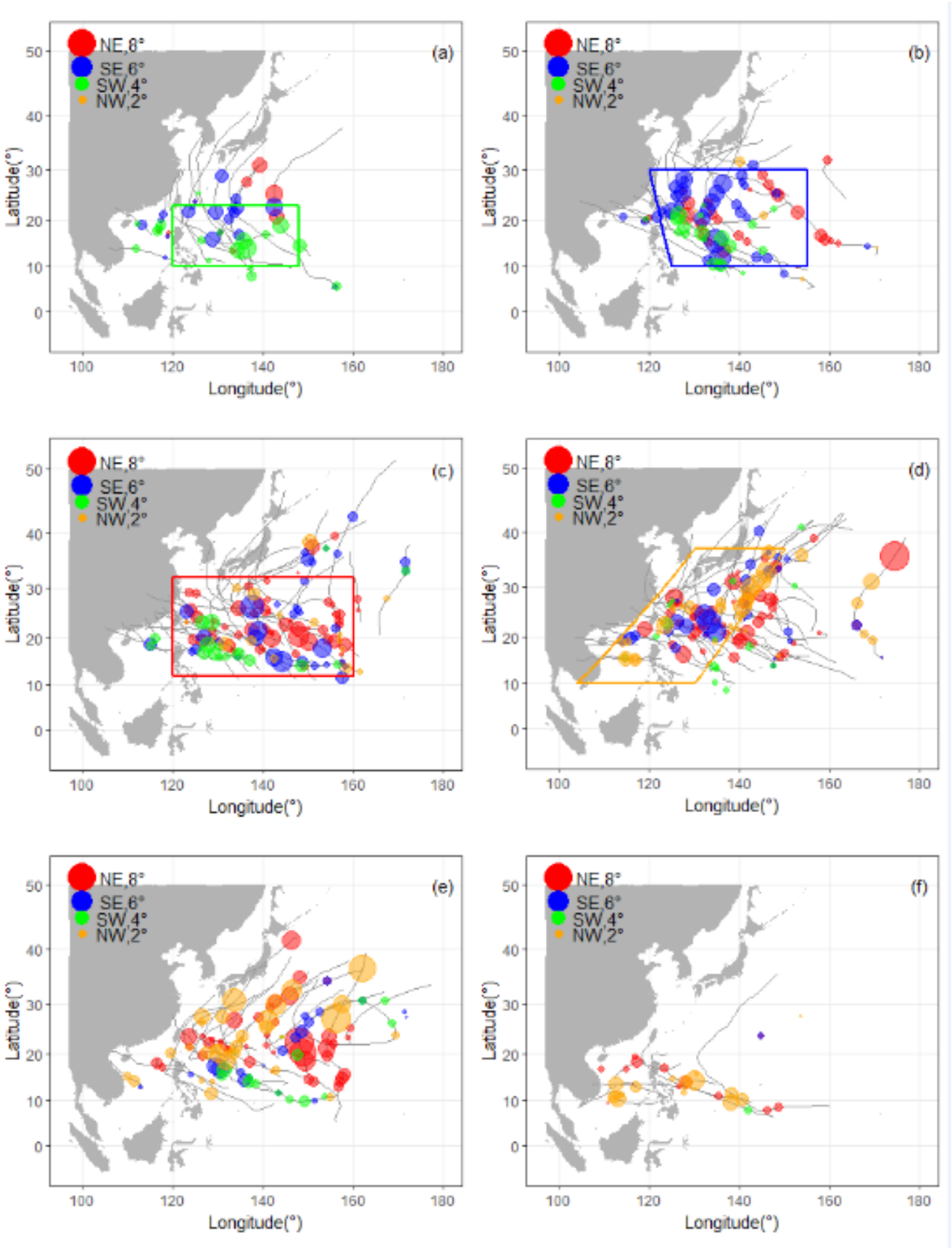
*Tonghua Su[4], Wei Hong[1], Yulan Zheng[2], Bin Chen[3], Xiaoqing Ke[5]

1. Fujian Meteorological Observatory of of China Meteorological Administration, 2. Fujian Meteorological Information Center of China Meteorological Administration, 3. Electric Power Research Institute of State Grid Fujian Electric Power Company, 4. Fujian Climate Center of China Meteorological Administration, 5. Fujian Meteorological Service Center of China Meteorological Administration

With the tropical cyclone (TC) size parameter defined as the radius of 17-m·s^{-1} oceanic surface wind, 225 TC cases were recorded in the western North Pacific during 2000–2009 based on the QuikSCAT near-surface wind vector database and the best-track dataset. In accordance with the symmetry index (the ratio of minimum and maximum quadrant sizes), the TCs were classified into symmetric and asymmetric structures. The asymmetric TCs were divided into four types: the northeast, southeast, southwest, and northwest. The spatio-temporal characteristics of these TC types were further investigated. The monthly variation and the spatial distribution of maximum quadrant TC size exhibited significant differences among the four types. By contrast, the quadrant size of the symmetric TCs from June to November showed few changes (2.6˚–2.7˚ latitude). It was found that the TC lifetime is an important factor affecting the quadrant TC size because of its close relationship with the activities of the western Pacific subtropical high. In addition, the climatological mean circulation also has a notable influence on the quadrant TC size through superposition of prominent background wind. Symmetric TCs are more likely to occur in the oceanic region where the background low-level wind is the weakest.

Keywords: tropical cyclone, size, quadrant, lifetime, circulation, symmetry

©2020. Japan Geoscience Union. All Right Reserved.



©2020. Japan Geoscience Union. All Right Reserved.

[E] Poster | A (Atmospheric and Hydrospheric Sciences)：A-AS Atmospheric Sciences, Meteorology & Atmospheric Environment

[A-AS07] Atmospheric Chemistry

convener:Naoko Saitoh(Center for Environmental Remote Sensing), Tomoki Nakayama(Graduate School of Fisheries and Environmental Sciences, Nagasaki University), Sakae Toyoda(Department of Chemical Science and Engineering, Tokyo Institute of Technology), Risa Uchida(Japan Automobile Research Institute)

This session provides a forum for the presentation of the broad spectrum of tropospheric and stratospheric chemistry, including various research topics (e.g., dynamical processes, air quality and climate), approaches (modeling, field measurements, remote sensing, and laboratory studies), and species (gas and aerosol). This session also provides an opportunity for discussing possible future collaboration with other research fields relevant to atmospheric chemistry.

[AAS07-P01] Top-down estimation of terrestrial CO_2 flux in Northern Eurasia

*Tomoko Shirai[1], Misa Ishizawa[2], Motoki Sasakawa[1], Akihiko Ito[1], Toshinobu Machida[1], Shamil Maksyutov[1] (1.National Institute for Environmental Studies, 2.Environment and Climate Change Canada)

[AAS07-P02] Recent stagnation of CH_4 emission growth from East Asia based on the analysis of synoptic variations of atmospheric CH_4 and CO_2 observed at Hateruma Island

*Yasunori Tohjima[1], Jiye Zeng[1], Akihiko Ito[1], Naveen Chandra[2], Yosuke Niwa[1], Hitoshi Mukai[1], Tomoko Shirai[1], Motoki Sasakawa[1], Prabir Patra[2], Toshinobu Machida[1] (1.National Institute for Environmental Studies, 2.Japan Agency for Marine-Earth Science and Technology)

[AAS07-P03] Spatio-temporal variations of atmospheric methane concentrations over Japan: Data analysis of governmental monitoring and TROPOMI satellite from air pollution research viewpoint

*Yugo Kanaya[1] (1.Research Institute for Global Change, Japan Agency for Marine-Earth Science and Technology)

[AAS07-P04] Variations of surface ocean pCO_2 and air-sea CO_2 fluxes in the Western Pacific Ocean

*Wataru Konarita[1], Shinji Morimoto[1], Shuji Aoki[1] (1.Center for Atmospheric and Oceanic Studies, Graduate School of Science, Tohoku University)

[AAS07-P05] In-situ and continuous observation of atmospheric N_2O and CO concentrations at Syowa Station, Antarctica.

*Shogo Akai[1], Shinji Morimoto[1], Wei Li[1], Daisuke Goto[2], Shuji Aoki[1] (1.Graduate School of Science, Tohoku University, 2.National Institute of Polar Research)

[AAS07-P06] Seasonal variations in the atmospheric Ar/N_2 ratio observed at ground-based stations in Japan and Antarctica and its application to an evaluation of the air-sea heat flux

*Shigeyuki Ishidoya[1], Kentaro Ishijima[2], Satoshi Sugawara[3], Yosuke Niwa[4], Yasunori Tohjima[4], Daisuke Goto[5], Kazuhiro Tsuboi[2], Shohei Murayama[1], Nobuyuki Aoki[1], Takashi Maki[2], Taichu Y Tanaka[2], Takashi Nakamura[6] (1.National Instutite of Advanced Industrial Science and Technology (AIST), 2.Meteorological Research Institute, 3.Miyagi University of Education, 4.National Institute for Environmental Studies, 5.National Institute of Polar Research, 6.Japan Meteorological Agency)

[AAS07-P07] Development of a new ISEE Chemical Lagrangian Model to elucidate the atmospheric composition changes in the mesosphere

*Tomoo Nagahama[1], Shingo Nakanishi[2], Fujita Ken[2], Tac Nakajima[1], Akira Mizuno[1] (1.Institute for Space-Earth Environmental Research, Nagoya University, 2.Graduate School of Science, Nagoya University)

[AAS07-P08] Analysis of the mesospheric ozone enhancement event in the Arctic winter with a new ISEE Chemical Lagrangian Model

*Fujita Ken[1], Tomoo Nagahama[2], Shingo Nakanishi[1] (1.Graduate School of Science, Nagoya University, 2.Institute for Space-Earth Environmental Research, Nagoya University)

[AAS07-P09] Short-term variations of HCl and HF trends observed with FTIR at Tsukuba

*Isao Murata[1], Yoshihiro Tomikawa[2,3], Isamu Morino[4], Hideaki Nakajima[4], Hideharu Akiyoshi[4] (1.Graduate School of Environmental Studies, Tohoku University, 2.National Institute of Polar Research, 3.The Graduate University for Advanced Studies, SOKENDAI , 4.National Institute for Environmental Studies)

[AAS07-P11] **Impact of HFCs on stratospheric ozone and temperature as simulated by chemistry-climate models**

*Hideharu Akiyoshi[1], Eric Dupuy[1], Yousuke Yamashita[2,1] (1.National Institute for Environmental Studies, 2.Japan Agency for Marine-Earth Science and Technology)

[AAS07-P12] ODS and GHG dependence of total ozone at mid- and high latitudes indicated by multi-ensemble simulations using MIROC3.2 and MIROC5 chemistry-climate models

*Hideharu Akiyoshi[1], Masanao Kadowaki[2], Yousuke Yamashita[3,1], Eric Dupuy[1], Toshiharu Nagatomo[1] (1.National Institute for Environmental Studies, 2.Japan Atomic Energy Agency, 3.Japan Agency for Marine-Earth Science and Technology)

[AAS07-P13] A modeling study on the roles of cloud distribution in global tropospheric chemistry: detailed evaluation of clouds in a chemistry climate model (MIROC-CHASER)

*Ryoki Matsuda[1], Kengo Sudo[1,2] (1.Graduate School of Environmental Studies, Nagoya University , 2.Japan Marine-Earth Science and Technology)

[AAS07-P14] Impacts of tropospheric bromine and iodine on global tropospheric ozone: a modeling study using CHASER

*Takashi Sekiya[1], Yugo Kanaya[1], Kengo Sudo[2,1], Fumikazu Taketani[1], Maki Noguchi Aita[1], Akitomo Yamamoto[1], Yoko Iwamoto[3], Katsuhiro Kawamoto[4] (1.Japan Agency for Marine-Earth Science and Technology, 2.Graduate School of Environmental Studies, Nagoya University, 3.Graduate School of Integrated Sciences for Life, Hiroshima University, 4.Graduate School of Maritime Sciences, Kobe University)

[AAS07-P15] **The weekday/weekend ozone differences induced by the emissions change in Guangzhou megacity of China**

*Yu Zou[1] (1.Institute of Tropical and Marine Meteorology, CMA,Guangzhou,China)

[AAS07-P16] **A Study on the Optimization of 3D Expressions for the Analysis of Local Scale Meteorological and Air Quality Information**

*Woosik Jung[1], Gunwoo Kim[1] (1.INJE University, Department of Atmospheric Environment Information Engineering, Gimhae, Republic of Korea)

[AAS07-P17] Validation of tropospheric NO_2 column density data observed by TROPOMI: Comparison with 4AZ-MAXDOAS

*Hikaru Saito[1], Hitoshi Irie[1] (1.University of Chiba)

[AAS07-P18] **Chemical composition of atmospheric aerosols over Jakarta megacity**

*Masahide Nishihashi[1], Hitoshi Mukai[1], Yukio Terao[1], Shigeru Hashimoto[1], Rizaldi Boer[2], Muhammad Ardiansyah[2], Bregas Budianto[2], Adi Rakhman[2], Gito Sugih Immanuel[2], Rudi Nugroho[3], Nawa Suwedi[3], Anies Marufatin[3], Muhammad Agus Salim[3], Dodo Gunawan[4], Eka Suharguniyawan[4], Asep Firman Ilahi[4], Muharam Syam Nugraha[4], Ronald Christian Wattimena[4], Bayu Feriaji[4], Qoriana Maulani[4] (1.National Institute for Environmental Studies, 2.IPB University, Indonesia, 3.Agency for the Assessment and Application of Technology (BPPT), Indonesia, 4.Meteorological, Climatological, and Geophysical Agency (BMKG), Indonesia)

[AAS07-P19] Seasonal Variation of Wet Deposition of Black Carbon in Arctic Alaska

*Tatsuhiro Mori[1], Yutaka Kondo[2], Sho Ohata[3,4], Yongjing Zhao[5], Puna Ram Sinha[6], Naga Oshima[7], Hitoshi MATSUI[8], Nobuhiro Moteki[9], Makoto Koike[9] (1.Tokyo University of Science, 2.National Institute of Polar Research, 3.Institute for Space–Earth Environmental Research, Nagoya University, 4.Institute for Advanced Research, Nagoya University, 5.Air Quality Research Center, University of California-Davis, 6.Department of Earth and Space Sciences, Indian Institute of Space Science and Technology, 7.Meteorological Research Institute, 8.Graduate School of Environmental Studies, Nagoya University, 9.Graduate School of Science, The University of Tokyo)

[AAS07-P20] Investigation of wet removal rate of black carbon in East Asia: A perspective from airmass pathways

*Yongjoo Choi[1], Yugo Kanaya[1], Masayuki Takigawa[1], Chunmao Zhu[1], Seung-Myung Park[2], Atsushi Matsuki[3], Yasuhiro Sadanaga[4], Sang-Woo Kim[5], Xiaole PAN[6] (1.Japan Agency for Marine-Earth Science and Technology, Japan, 2.National Institute of Environmental Research, Korea, 3.Kanazawa University, Japan, 4.Osaka Prefecture University, Japan, 5.Seoul National University, Korea, 6.Chinese Academy of Sciences, China)

[AAS07-P21] Light absorption properties of organic aerosols at Fukue Island in 2018 spring

*Chunmao Zhu[1], Takuma Miyakawa[1], Hitoshi Irie[2], Fumikazu Taketani[1], Yugo Kanaya[1] (1.Japan Agency for Marine-Earth Science and Technology, 2.Chiba University)

[AAS07-P22] **Can a global chemistry climate model reproduce interannual variabilities and trends of depositions of sulfate, nitrate, and ammonium preserved in the Southeastern Greenland Dome ice core?**

*Kengo Sudo[1,2], Hinako Shiratsuchi[1], Yoshinori Iizuka[3] (1.Graduate School of Environmental Studies, Nagoya University, 2.Japan Agency for Marine-Earth Science and Technology (JAMSTEC), 3.Institute of Low Temperature Science, Hokaido University)

[AAS07-P23] **Evaluation of GCOM-C aerosol products using ground-based sky radiometer observations**

*Hossain Mohammed Syedul Hoque[1], Hitoshi Irie[1], Alessandro Damiani[1], Mashiro Momoi[1] (1.Center for Environmental Remote Sensing (CEReS), Chiba University)

[AAS07-P24] Atmospheric sulfate formation pathways over the past 60 years constrained by a global chemical transport model

*Shohei Hattori[1], Becky Alexander[2], Sakiko Ishino[3], Shuting Zhai[2] (1.Department of Chemical Science and Engineering, School of Materials and Chemical Technology, Tokyo Institute of Technology, 2.Department of Atmospheric Sciences, University of Washington, Seattle WA 98195-1640, USA, 3.National Institute of Polar Research, Research Organization of Information and Systems, Tokyo 190-8518, Japan)

[AAS07-P25] High-temporal-resolution elemental characterization of fine-mode aerosols in springtime Asian outflow: Emission and removal characteristics, and comparison with model simulation

*Takuma Miyakawa[1], Akinori Ito[1], Chunmao Zhu[1], Yugo Kanaya[1] (1.Japan Agency for Marine-Earth Science and Technology)

[AAS07-P26] **Comparison of compositional characteristics of aerosol and rainwater samples collected in Nagoya**

*Wei Chenran[1], Sonia Afsana[1], Qingcai Chen[2], Dhananjay Kumar Deshmukh[3], Kimitaka Kawamura[3], Michihiro Mochida[1,4] (1.Graduate School of Environmental Studies, Nagoya University, Nagoya, Japan, 2.School of Environmental Science and Engineering, Shaanxi University of Science and Technology, Xi'an, China, 3.Chubu Institute for Advanced Studies, Chubu University, Kasugai, Japan, 4.Institute for Space-Earth Environmental Research, Nagoya University, Nagoya, Japan)

[AAS07-P27] Formation processes of dimers measured in α-pinene secondary organic aerosol particles

*Kei Sato[1], Sathiyamurthi Ramasamy[1], Satoshi Inomata[1], Shinichi Enami[1], Yu Morino[1] (1.National Institute for Environmental Studies)

[AAS07-P28] Nitric acid gas captured in quasi-liquid layers on ice surfaces

*Ken Nagashima[1], Josée Maurais[2], Ken-ichiro Murata[1], Yoshinori Furukawa[1], Patrick Ayotte[2], Gen Sazaki[1] (1.The Institute of Low Temperature Science, Hokkaido University, 2.Université de Sherbrooke, Québec, Canada)

[AAS07-P29] Five-years seasonal variations of nitrogen and triple oxygen isotopic compositions of atmospheric nitrate at Noto Peninsula, Japan

*Kazuki Kamezaki[1], Shohei Hattori[1], Atsushi Matsuki[2], Naohiro Yoshida[1,3] (1.Department of Chemical Science and Engineering, School of Materials and Chemical Technology, Tokyo Institute of Technology, 2.Institute of Nature and Environmental Technology, Kanazawa University, 3.Earth-Life Science Institute)

[AAS07-P30] **Impacts of ship emissions on atmospheric particulate matter and gaseous components over the Seto Inland Sea areas**

*Moe Tauchi[1], Katsuhiro Kawamoto[2], Kazuyo Yamaji[1], Ryohei Nakatsubo[3], Yoshie Oshita[3], Yasuyuki Itano[4] (1.Kobe University, 2.Takamatsu Local Meteorological office, 3.Hyogo Prefectural Institute of Environmental Sciences, 4.Osaka City Research Center of Environmental Science)

[AAS07-P31] Spatiotemporal variations of NO_2 over Fukuoka Japan, observed by multiple MAX-DOAS and 3-D coherent Doppler lidar

*Hironobu Ueki[1], Hisahiro Takashima[2], Martina Michaela Friedrich[3] (1.Fukuoka university graduate school, 2.Fukuoka university, 3.Belgian Institute for Space Aeronomy)

Top-down estimation of terrestrial CO_2 flux in Northern Eurasia

*Tomoko Shirai[1], Misa Ishizawa[2], Motoki Sasakawa[1], Akihiko Ito[1], Toshinobu Machida[1], Shamil Maksyutov[1]

1. National Institute for Environmental Studies, 2. Environment and Climate Change Canada

We present a multi-year trend of terrestrial CO_2 flux from northern Eurasia, estimated by atmospheric inversion using a coupled model GELCA (Global Eulerian-Lagrangian Coupled Atmospheric model). Global monthly CO_2 flux distributions were estimated for the period 2002-2015 for 42 land and 22 ocean regions using the Observation Package data products (ObsPack GLOBALVIEWplus) which includes data from various types of atmospheric CO_2 direct measurements provided by large numbers of laboratories in the world. In this study, we added 9 tower observations from JR-STATION (Japan-Russia Siberian Tall Tower Inland Observation Network) to better constrain the area of interest.

In order to examine the impact of additional observational constraints in Siberia, we compared the inversion results with and without JR-STATION data. For the entire period, estimated global land fluxes agreed well with each other regardless of JR-STATION data. At regional scales, estimated fluxes showed significant difference mostly in Siberia and northeastern Europe. When focusing on the mean seasonal variations, summer uptake increased in western Siberia and northeastern Europe whereas it decreased in northeastern Siberia by adding JR-STATION data.

In terms of the long-term trend, the terrestrial sink was increasing both in Siberia and in Europe. Terrestrial CO_2 fluxes estimated for Siberia using JR-STATION data is -0.88 ±0.55 $GtCyr^{-1}$ and -1.36 ±0.42 $GtCyr^{-1}$ over the period 2002-2009 and 2010-2015, respectively. Those for Europe is -0.19 ±0.43 $GtCyr^{-1}$ and -0.42 ±0.30 $GtCyr^{-1}$, respectively. The increasing trend of the carbon sink in northern boreal areas can be explained by the combination of warming climate and the fertilization effect . Time series of these fluxes also reflect the effect of ENSO and extreme weather conditions. The interpretation of the multi-year variation of estimated fluxes in northern Eurasia will be presented.

Keywords: CO2, carbon flux, inverse modeling, greenhouse gas, Siberia, climate change

©2020. Japan Geoscience Union. All Right Reserved.

Recent stagnation of CH_4 emission growth from East Asia based on the analysis of synoptic variations of atmospheric CH_4 and CO_2 observed at Hateruma Island

*Yasunori Tohjima[1], Jiye Zeng[1], Akihiko Ito[1], Naveen Chandra[2], Yosuke Niwa[1], Hitoshi Mukai[1], Tomoko Shirai[1], Motoki Sasakawa[1], Prabir Patra[2], Toshinobu Machida[1]

1. National Institute for Environmental Studies, 2. Japan Agency for Marine-Earth Science and Technology

Atmospheric mixing ratios of greenhouse gases including CO_2 and CH_4 have been monitored at Hateruma Island, Japan (HAT; lat. 24.1˚N, long. 123.8˚E) for more than 20 years by the National Institute of Environmental Studies (NIES). The observed CO_2 and CH_4 show secular increasing trends and seasonal variations, typical of a regional background sites, and consist of synoptic variations (ΔCO_2 and ΔCH_4) with duration ranging from several hours to several days. These synoptic variations were contain signals arising from the regional emissions from the continental East Asia, especially China, and were observed more often during late fall to early spring because of the suppression of the continental emissions signal during the East Asian monsoon in summer. Since the observed ΔCO_2 and ΔCH_4 in wintertime generally showed fairly good correlations, the variation ratio ($\Delta CH_4/\Delta CO_2$ ratio) can be used to constrain the regional emission ratio. In previous study (Tohjima et al., 2014), based on the fact that the fossil fuel CO_2 emissions were relatively well determined, we obtained the increasing rate of the CH_4 emission from China (about 1 Tg-CH_4 yr^{-2}) in 2000s from the comparison of the $\Delta CH_4/\Delta CO_2$ ratios between the observation and simulation. In this study, we revisited the temporal change in $\Delta CH_4/\Delta CO_2$ ratio at HAT and investigate the recent change in the CH_4 emissions from China. The observed $\Delta CH_4/\Delta CO_2$ ratio showed decrease for the entire period (1997-2019) from about 13 ppb/ppm to 8 ppb/ppm while its decreasing rate showed a gradual slowdown and appeared to reach bottom after 2010. Such change in the decreasing rate is mostly attributed to the slowdown of the increase in the fossil fuel CO_2 emissions from China. We calculated ΔCO_2 and ΔCH_4 by using a Lagrangian Particle Dispersion Model (LPDM) and several CH_4 and CO_2 flux maps based on bottom-up and top-down approaches. Then we scaled the CH_4 emissions from China so as to match the calculated $\Delta CH_4/\Delta CO_2$ ratio with the observation. The results suggested that the linear increasing trend of the CH_4 emissions from China for 2010s is significantly reduced in comparison with that for the 2000s.

Keywords: atmospheric CH4, atmoshperic CO2, synoptic variation

©2020. Japan Geoscience Union. All Right Reserved.

Spatio-temporal variations of atmospheric methane concentrations over Japan: Data analysis of governmental monitoring and TROPOMI satellite from air pollution research viewpoint

*Yugo Kanaya[1]

1. Research Institute for Global Change, Japan Agency for Marine-Earth Science and Technology

As being an important greenhouse gas as well as a short-lived climate forcer, sources of atmospheric methane need to be understood well toward effective mitigation of climate change. Our best practice is to build bottom-up emission inventories by compiling available socio-economic data and emission-relevant information to optimize control measures; however, the uncertainty in the inventories is large and thus independent information is required for their evaluation and improvement. Ground-based and satellite observations will serve for the purpose. In this study, we analyzed long-term methane measurement data contained in the governmental monitoring to elucidate features of spatio-temporal variations. Here, the measured methane concentration levels are generally only used to be subtracted from the total hydrocarbon concentrations to yield non-methane hydrocarbon levels, important to ozone chemistry - and thus the data set has seldom been analyzed. Among the available data at several hundreds of sites during FY2009-2016, data at 39 non-roadside sites were selected, where annual average concentrations ranked within top 20 at least once. The data during 6-9 LT were monthly averaged and their normalized seasonal patterns were analyzed. From cluster analysis, three distinct patterns were found: First pattern was with large increases in summer/autumn. Two sites (Toasa in Hokkaido and Narashino-Saginuma in Chiba) with very high monthly-averaged concentrations (>2.5 ppm) were categorized to this cluster, where very strong local emissions were suspected. Second pattern was with wintertime increases, to which 20 sites normally within Tokyo/Osaka metropolitan areas were categorized. The pattern was understood as general air pollution behavior in terms of dilution/diffusion, suggesting influence from urban sources. The third pattern was with summertime increases, particularly during June-August. The categorized 17 sites are mostly from rural regions and emissions from rice paddy fields were implied. We will show more results on correlations with wind and other pollutants (e.g., NOx, CO). Features from TROPOMI satellite observations of methane over Japan are also to be discussed together with the analysis of the ground-based observations.

Keywords: Atmospheric environment, climate change, methane, cluster analysis, seasonal patterns, source analysis

©2020. Japan Geoscience Union. All Right Reserved.

Variations of surface ocean pCO_2 and air-sea CO_2 fluxes in the Western Pacific Ocean

*Wataru Konarita[1], Shinji Morimoto[1], Shuji Aoki[1]

1. Center for Atmospheric and Oceanic Studies, Graduate School of Science, Tohoku University

Temporal and spatial variations of CO_2 partial pressure in surface sea water ($pCO_{2,sea}$) observed in the western Pacific were analyzed in terms of physics and chemistry of the ocean and the CO_2 fluxes between the atmosphere and ocean were also evaluatedand the CO_2 flux between the atmosphere and ocean . The $pCO_{2,sea}$ has been observed continuously on-board a cargo ship “Trans Future 5” on her round-trip between Japan and Australia. Systematic observations for the atmospheric pCO_2 ($pCO_{2,air}$) were have been also conducted in the western Pacific by a grab-sampling method using container ships sailing almost similar route.

In the equatorial region, interannual variabilities of $pCO_{2,sea}$ were clearly observed, and were highly correlated with the El Niño Southern Ocsillation (ENSO). Higher $pCO_{2,sea}$ observed in 2008 and 2012, coincident with La Nina, could be caused by transport of high salinity, low temperature and high dissolved inorganic carbon water upwelled off the coast of Peru to the observation line at the western Pacific Ocean. When large and strong El Nino occurred from 2015 to 2016, significant increase of $pCO_{2,sea}$ was observed between 25˚N and 25˚S. The $pCO_{2,sea}$ increase could be associated with remarkable decrease of the precipitation observed in the western Pacific region.

The CO_2 flux between the atmosphere and the ocean was calculated by using the air-sea pCO_2 difference in pCO_2 ($DpCO_2$) between the atmosphere and the surface ocean, sea surface temperature and wind speed at 10m height. In the western Pacific Ocean, the largest CO_2 absorption was found at 20˚S (−13.0 gC m^{-2} yr^{-1}), and the net CO_2 outgassing at equatorial area (1.2 gC m^{-2} yr^{-1}) were found.

The increase in $pCO_{2,sea}$ associated with the strong El Niño event in 2015 and 2016 may have caused a decrease in the oceanic CO_2 absorption throughout the western Pacific.

Keywords: co2 partial pressure, Pacific, ENSO

©2020. Japan Geoscience Union. All Right Reserved.

In-situ and continuous observation of atmospheric N_2O and CO concentrations at Syowa Station, Antarctica.

*Shogo Akai[1], Shinji Morimoto[1], Wei Li[1], Daisuke Goto[2], Shuji Aoki[1]

1. Graduate School of Science, Tohoku University, 2. National Institute of Polar Research

Nitrous oxide (N_2O) is one of the most important anthropogenic greenhouse gases and its infrared absorption efficiency is 200 times more than that of carbon dioxide (CO_2). In addition, since N_2O catalytically decomposes stratospheric ozone (O_3), N_2O is concerned to be a major factor for the destruction of the stratospheric ozone after the concentrations of atmospheric chlorofluorocarbons decreases in near future. Carbon monoxide (CO) is not considered as greenhouse gas generally, but atmospheric CO is closely related to the atmospheric CH_4 concentration through OH radicals, which are important reactant both with CH_4 and CO. Furthermore, CO is also a useful tracer for biomass burning and has an important role in the atmospheric chemistry. Therefore, it is important to reveal the temporal and spatial variations the atmospheric N_2O and CO concentration and to understand the cause of their variations quantitatively.

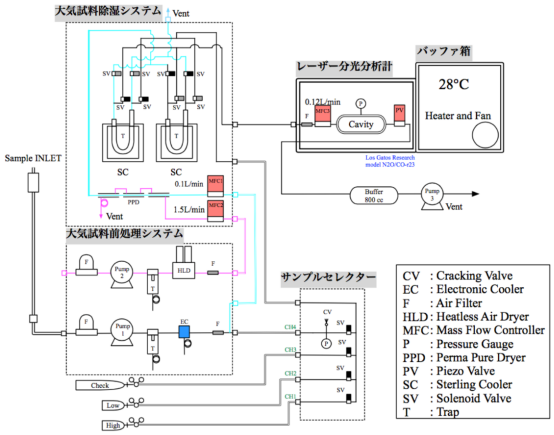
In this study, we developed a new continuous observation system for atmospheric N_2O and CO concentrations based on an OA-ICOS (Off-Axis Integrated Cavity Output Spectroscopy) laser spectrometer (Los Gatos Research, model N2O/CO r23) (Fig.1). Repeatability for the analysis of N_2O and CO concentrations by the system is estimated to be 0.14 ppb and 0.09 ppb (one standard deviation), respectively. The system was installed at Syowa Station, Antarctica, and continuous observation started in January 2019.

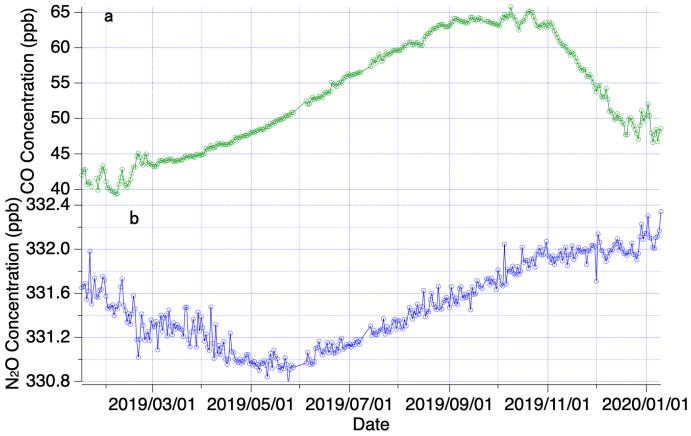
Figure 2 shows the temporal variations of the N_2O and CO concentrations observed by our system at Syowa Station since January, 2019. As shown in the figure, characteristic variations of N_2O and CO are found in each season. In the austral summer, in-phase and out-of-phase fluctuations of N_2O and CO were observed several times. These fluctuations could be caused by the transport of high N_2O and CO air mass affected by outgassing from the Southern Ocean and downward transport of stratospheric air into Syowa Station. In austoral spring, high CO event was captured at Syowa Station. It had been affected by serious biomass burning in Amazon and Australia.

In this presentation, we will introduce the observation system, thus developed, and show the temporal variations in the N_2O and CO concentration observed at Syowa Station in more detail.

Keywords: Global Warming, Atmosphere, Antarctica, Syowa, N2O, CO

©2020. Japan Geoscience Union. All Right Reserved.





©2020. Japan Geoscience Union. All Right Reserved.

Seasonal variations in the atmospheric Ar/N_2 ratio observed at ground-based stations in Japan and Antarctica and its application to an evaluation of the air-sea heat flux

*Shigeyuki Ishidoya[1], Kentaro Ishijima[2], Satoshi Sugawara[3], Yosuke Niwa[4], Yasunori Tohjima[4], Daisuke Goto[5], Kazuhiro Tsuboi[2], Shohei Murayama[1], Nobuyuki Aoki[1], Takashi Maki[2], Taichu Y Tanaka[2], Takashi Nakamura[6]

1. National Instutite of Advanced Industrial Science and Technology (AIST), 2. Meteorological Research Institute, 3. Miyagi University of Education, 4. National Institute for Environmental Studies, 5. National Institute of Polar Research, 6. Japan Meteorological Agency

Variations of the atmospheric Ar/N_2 ratio at the ground surface are driven principally by air-sea Ar and N_2 fluxes due to changes in solubility in seawater (e.g. Keeling et al., 2004). Recently, we expanded our model study for the gravitational separation to Ar/N_2 ratio, and found that temporal variations of gravitational separation in the middle atmosphere could also modify the long-term trend of the surface Ar/N_2 ratio (Ishidoya et al., in preparation). Therefore, the surface Ar/N_2 ratio is a unique tracer of the spatiotemporally-integrated air-sea heat flux and the circulation in the middle atmosphere. We have continued systematic observations of the Ar/N_2 ratio by using a mass spectrometer at Cape Ochiishi (43˚N, 146˚E), Tsukuba (36˚N, 140˚E), Takayama (36˚N, 137˚E), Hateruma Island (24˚N, 124˚E) and Minamitorishima (24˚N, 154˚E), Japan and Syowa station (69˚S, 40˚E), Antarctica since 2012. Clear seasonal Ar/N_2 ratio cycles with summertime maxima have been observed at the middle to high latitudinal stations, and the peak-to-peak amplitudes of the average seasonal cycles at Ochiishi, Tsukuba, Hateruma and Syowa were found to be 21, 11, 5 and 32 per meg, respectively. To evaluate the seasonal air-sea heat flux based on seasonal cycles of Ar/N_2 ratio in the atmosphere, we carried out simulations of the Ar/N_2 ratio using an atmospheric transport model (GSAM-TM) that incorporated the Ar (N_2) flux derived from an equation of the relationship between the air-sea Ar (N_2) flux and the air-sea heat flux (Keeling et al., 1993; Weiss, 1970). We use the air-sea heat flux components, which mainly drive spatiotemporal variations of the air-sea Ar (N_2) fluxes, and sea surface temperature (SST) from the ERA5 (Hersbach et al., 2019). Thus simulated seasonal cycles of Ar/N_2 ratio agreed well with those observed. On the other hand, the amplitudes of the seasonal cycles of Ar/N_2 ratio simulated by using the TransCom seasonal air-sea N_2 flux (Garcia and Keeling, 2001), widely used in the simulation of the atmospheric O_2/N_2 ratio and based on the past ECMWF seasonal air-sea heat flux, underestimate the observed seasonal cycles significantly. These facts suggest that the air-sea heat fluxes and SST from the ERA5 is reasonable to reproduce the atmospheric Ar/N_2 variations on the seasonal time scale.

Acknowledgements

We thank staff of Global Environmental Forum (GEF), the Science Program of the Japan Antarctic Research Expedition (JARE) and Japan Meteorological Agency (JMA) for their works to collect the air samples at Hateruma and Ochiishi stations (GEF), Syowa station (JARE) and Minamitorishima (JMA), respectively. This study was partly supported by the JSPS KAKENHI Grant Number 15H02814 and 18K01129, and the Global Environment Research Coordination System from the Ministry of the Environment.

References

©2020. Japan Geoscience Union. All Right Reserved.

Garcia, H. & Keeling, R.: On the global oxygen anomaly and air-sea flux. J. Geophys. Res. 106 (C12), 31155-31166, 2001.
Hersbach et al., Global reanalysis: goodbye ERA-Interim, hello ERA5, ECMWF Newsletter No. 159-Spring 2019, 17-24, 2019.
Ishidoya et al., Secular change of the atmospheric Ar/N_2 ratio and its implications for ocean heat uptake and Brewer-Dobson circulation, in preparation.
Keeling, R. F. et al., What atmospheric oxygen measurements can tell us about the global carbon cycle, Global Biogeochem. Cycles, 7, 37-67, 1993.
Keeling, R. F. et al., Measurement of changes in atmospheric Ar/N_2 ratio using a rapid-switching, single-capillary mass spectrometer system, Tellus B, 56, 322–338, 2004.
Weiss, R. F., The solubility of nitrogen, oxygen and argon in water and seawater, Deep-Sea Res., 17, 721-735, 1970.

Keywords: Atmospheric Ar/N2 ratio, air-sea heat flux, seasonal cycle, atmospheric transport model

©2020. Japan Geoscience Union. All Right Reserved.

Development of a new ISEE Chemical Lagrangian Model to elucidate the atmospheric composition changes in the mesosphere

*Tomoo Nagahama[1], Shingo Nakanishi[2], Fujita Ken[2], Tac Nakajima[1], Akira Mizuno[1]

1. Institute for Space-Earth Environmental Research, Nagoya University, 2. Graduate School of Science, Nagoya University

Chemical composition in the mesosphere fluctuates significantly due to factors such as temperature, solar UV radiation and energetic particle precipitation from the space. In order to elucidate these mechanisms and evaluate their impacts, we have newly developed a chemical Lagrangian model that can handle from the troposphere to the mesosphere (e.g. Nakanishi et al., JpGU meeting, 2019). In the model, the trajectory of the particle box is calculated by a Lagrangian particle dispersion model which works with meteorological input data, and the chemical reactions in the particle box are also calculated by using a box model simultaneously. As the Lagrangian particle dispersion model, we used the FLEXible PARTicle (FLEXPART) model, which is extended so that the MERRA-2 reanalysis data can be used as input. As a result, we can calculate the trajectory up to an altitude of about 80 km from the surface. The position of the particle box is calculated every 15 minutes. As a box chemistry model, neutral molecule reactions consisting of 156 chemical reactions involving 58 chemical species and ion reactions of 263 reactions involving 77 species are calculated, respectively, using chemical reaction calculation software Kinetic Preprocessor (KPP). The concentration of each molecule in the box is calculated every 10 and 0.1 seconds, respectively. To validate the model calculations, 324 airmass boxes were released from the point at the altitude of 70 km in the polar and mid-latitude regions, and the two-day change in the concentration of ozone and ozone related substances was calculated. As a result, the diurnal variation of mesospheric ozone was qualitatively reproduced, although the value was about half of the value observed with Aura/MLS. In addition, we find that the difference in the ozone concentration in the Arctic region depends on the temperature on the transport route of the airmass. In the presentation, we will report on the details of the developed model, the characteristics of the time variation of the substances in the mesosphere as well as the results of comparison with observations.

Keywords: Chemical Lagrangian model, Mesospheric composition, Trajectory analysis

©2020. Japan Geoscience Union. All Right Reserved.

Analysis of the mesospheric ozone enhancement event in the Arctic winter with a new ISEE Chemical Lagrangian Model

*Fujita Ken[1], Tomoo Nagahama[2], Shingo Nakanishi[1]

1. Graduate School of Science, Nagoya University, 2. Institute for Space-Earth Environmental Research, Nagoya University

Mesospheric chemical composition largely varies caused by environmental changes from the earth inside and outside. Environmental changes are, for example, temperature changes, solar UV, a large event of energetic particle precipitation. To understand the atmospheric composition changes caused by natural phenomena, we have installed millimeter-wave spectrometers in Rikubetsu (Japan), Syowastation (Antarctic), Atacama (Chile), Rio Gallegos (Argentine), and Tromso (Norway), and have been observing atmospheric minor molecules such as ozone, NO_x, HO_x, and ozone-depleting substances in the stratosphere and mesosphere. In addition to these observations, we need to analyze model simulation results to understand the impact of these changes on the global. For this purpose, ISEE has developed a new chemical transport model which is a combination of two models, FLEXPART and KPP. FLEXPART is a Lagrangian transport and dispersion model that is extended so that the MERRA2 reanalysis data can be used as input. Also, a chemical reaction software KPP (Kinetic Preprocessor) can calculate chemical changes simultaneously with the transport model. In order to validate the model calculation results, we compared the model output with mesospheric ozone dataset measured with JEM-SMILES from December 2009 to January 2010. During this period, a sudden increase in the ozone concentration (1 to 5 ppmv) in the Arctic mesosphere occurred. The analysis of the trajectories and ozone distribution in the mesosphere revealed that the ozone increase over Alaska region was caused by the effect of the air mass passing through the low temperature region. On other hand, the air mass passing through a region where the temperature was high contains with low ozone concentration. Therefore, it was found that the ozone concentration in the mesosphere depends on the temperature on the transport route. In this presentation, we will present the results of the comparison between the simulation and the JEM-SMILES dataset as well as the analysis results of the event which mesospheric ozone suddenly increases in the Arctic winter in 2009/2010 season.

Keywords: Chemical Lagrangian model, Mesosphere, Composition change

©2020. Japan Geoscience Union. All Right Reserved.

Short-term variations of HCl and HF trends observed with FTIR at Tsukuba

*Isao Murata[1], Yoshihiro Tomikawa[2,3], Isamu Morino[4], Hideaki Nakajima[4], Hideharu Akiyoshi[4]

1. Graduate School of Environmental Studies, Tohoku University, 2. National Institute of Polar Research, 3. The Graduate University for Advanced Studies, SOKENDAI , 4. National Institute for Environmental Studies

HCl is a main chlorine reservoir species in the stratosphere. The amount of HCl is a good indicator of the potential for ozone depletion. Observed total column of HCl was decreasing in the 2000s after CFC regulations were introduced but showed increase from 2007 to 2011. Mahieu et al. [2014] investigated that this increase is due to interannual dynamical variability in the northern stratosphere from Fourier Transform Infrared spectrometer (FTIR) observations at 8 sites including Tsukuba and 3D-chemical transport model simulations.
In this study we extended the analysis of HCl total column observed with FTIR at Tsukuba to 2018 and HF total column was also anlyzed. HF is a good tracer of atmospheric transport. The temporal variation of HCl and HF total columns showed decrease again from 2011 to 2014 then increase from 2015 to 2018. Mass stream function was calculated from ERA-Interim meteorological data to confirm that these temporal variations are also due to stratospheric circulation change. The difference of the mass stream function between the average of 2003 - 2006 and the average of 2007 - 2010 shows negative values in the northern lower stratosphere. This means the deceleration of circulation and it is consistent with the result of Mahieu et al. [2014]. The difference between the average of 2007 - 2010 and the average of 2011 - 2014 shows positive values in the northern lower stratosphere that means the acceleration of circulation. These changes correspond to the HCl and HF temporal variation. Thus we confirm that the temporal variation of HCl and HF is basically due to stratospheric circulation change.
The situation is somewhat different for the period after 2015. The difference of mass stream function between the average of 2011 - 2014 and the average of 2015 - 2018 shows negative values in the northern lower stratosphere again and this is also consistent with the increase of HCl and HF total columns after 2015. However, MIROC3.2 Chemistry-Climate Model (CCM) results show that the decrease rates of HCl and HF became lower but continue to decrease after 2015. This means that the circulation change after 2015 isn't enough to explain the trend reversal and there are some possibility that the emission change in CFC-11 affects the increase of HCl and HF after 2015.

Keywords: FTIR, Ozone depletion, Chlorine compounds

©2020. Japan Geoscience Union. All Right Reserved.

Impact of HFCs on stratospheric ozone and temperature as simulated by chemistry-climate models

*Hideharu Akiyoshi[1], Eric Dupuy[1], Yousuke Yamashita[2,1]

1. National Institute for Environmental Studies, 2. Japan Agency for Marine-Earth Science and Technology

Hydrofluorocarbons (HFCs) are anthropogenic compounds used as substitutes for ozone-depleting substances (ODSs). While they do not chemically interact with ozone (O_3), as greenhouse gases (GHGs) they substantially affect stratospheric temperature and circulation patterns, thus indirectly influencing O_3 concentrations. Steps have been taken to curb production of HFCs (Kigali Amendment to the Montreal Protocol, 2016). Assuming global compliance, HFC emissions should, therefore, reach their peak around 2040. Until then, however, their atmospheric abundance will keep increasing [1]. We present ensemble model simulations designed to assess the response of O_3, temperature and atmospheric circulation to increasing levels of HFCs. We analyze this response for climate conditions of 2095, following the Representative Concentration Pathway (RCP) 2.6 [2]. In this scenario, uncontrolled HFC emissions would induce a radiative forcing comparable to that of carbon dioxide, methane and nitrous oxide combined.

We simulate the effect of varying HFC concentrations in a 2095 climate, using the CCSRNIES-MIROC3.2 and CCSRNIES-MIROC5.0 three-dimensional (3D) chemistry-climate models [3,4]. These models use the same chemical module, but their physical modules are partly different. For each model, three ensemble simulations (“experiments”) are performed with different amounts of HFCs: no HFCs (control run), and two or three times (“2xHFC”, “3xHFC”) the HFC concentrations of Hurwitz et al. (2015) [5]. These correspond to abundance estimates for 2050, in the case of unregulated HFC emissions. Each experiment is an ensemble of 100 independent, year-long simulations. Background atmospheric levels of GHGs follow the RCP2.6 scenario for 2095. Estimated abundances of ODSs assume full compliance with the Montreal Protocol.

For each model version, results for the “2xHFC” and “3xHFC” cases are qualitatively similar. Therefore, we focus our analysis on the “3xHFC” experiment and illustrate ensemble-mean results for total column O_3, as well as for latitude/pressure cross-sections of O_3, temperature and zonal mean zonal wind.

At tropical and subtropical latitudes, we obtain ozone responses to increasing HFC concentrations which are roughly consistent with those from the zonal-mean two-dimensional (2D) model of Hurwitz et al. (2015) [5]. In addition, at these latitudes, the O_3 responses of the MIROC3.2 and MIROC5.0 models are consistent. For O_3, this robust response is a decrease around 50 hPa and an increase above and below. The temperature response to HFC increases is a warming of the stratosphere below 20 hPa. The resulting total ozone response is very small, because the positive and negative O_3 anomalies cancel each other vertically. When considering the high latitudes, however, the calculated O_3 responses are quite different, not only between the 2D model and both 3D MIROC models, but also between MIROC3.2 and MIROC5.0.

©2020. Japan Geoscience Union. All Right Reserved.

Such discrepancies in the high-latitude responses may be due to differences of planetary wave activity in the models, and of their interaction with stratospheric HFCs and O_3.

References

[1] WMO, 2018, Project Report No.58.

[2] IPCC, 2014, Climate Change 2014: Synthesis Report.

[3] Morgenstern, O., 2017, Geosci. Model Dev., 10, 639-671.

[4] Akiyoshi, H., 2016, J. Geophys. Res., 121, 1361-1380.

[5] Hurwitz, M., 2015, Geophys. Res. Lett., 42, 8686-8692.

Keywords: HFC, ozone, chemistry-climate model, stratosphere, temperature

©2020. Japan Geoscience Union. All Right Reserved.

ODS and GHG dependence of total ozone at mid- and high latitudes indicated by multi-ensemble simulations using MIROC3.2 and MIROC5 chemistry-climate models

*Hideharu Akiyoshi[1], Masanao Kadowaki[2], Yousuke Yamashita[3,1], Eric Dupuy[1], Toshiharu Nagatomo[1]

1. National Institute for Environmental Studies, 2. Japan Atomic Energy Agency, 3. Japan Agency for Marine-Earth Science and Technology

Total ozone in the Arctic shows large interannual variations. The total ozone amount during Arctic spring is larger when the meridional circulation in the wintertime is stronger, thus when the Arctic polar vortex is weaker, and vice-versa. These variations mask the dependence of ozone concentration on ozone depleting substances (ODSs) and greenhouse gases (GHGs). Therefore, it is difficult to evaluate and isolate the effects of ODS regulations and GHG emissions from natural atmospheric variability, although ODSs and GHGs may influence the interannual variation of the atmosphere.

We conducted multi-ensemble simulations using two chemistry-climate models (CCMs). We considered the variability of interannual ozone variations to be a statistical variance. We investigated the ODS and GHG dependence of total ozone for extreme values of the variance, as well as for the mean of all ensemble members. In these simulations, the ODS and GHG concentrations were fixed at observed or projected values for specific years in the past and future (e.g., for the years 1960, 2000, 2050). Each simulation or experiment is uniquely defined by ODS and GHG levels corresponding to a specific year (for example, observed ODS levels of 1980 and projected GHG levels for 2050). For one experiment, the ozone variability among the ensemble members is then considered to be the interannual variation. We examined the ODS and GHG dependence of total ozone (i.e., as a function of the experiment), based on the minimum value found for each ensemble member at latitudes 45-90˚N (‘polar cap’) during Northern spring (March –May). From the single-member minimum values, we then calculated the multi-ensemble mean, the mean for the 5 ensemble members with largest minimum value (hereafter “highest 5 members”), and for the 5 ensemble members with the smallest minima (hereafter “lowest 5 members”). The results show that the ODS and GHG dependence is large for the lowest 5 ensemble members and small for the highest 5 ensemble members. For the lowest 5 members, ozone levels should be smaller in a high-ODS atmosphere and larger in a high-GHG atmosphere. Furthermore, the zonal-mean zonal wind is stronger than for the multi-ensemble mean, while the corresponding polar cap temperature in the lower stratosphere is lower than the mean. This indicates that the Arctic polar vortex is comparatively stronger in the lowest 5 members.

The dependence of total ozone between 45-90˚S in September –November (Southern spring) was also investigated. We found much smaller GHG dependence and much larger ODS dependence than for the Northern Hemisphere. The differences in the ODS and GHG dependence were much smaller among the multi-ensemble mean, the highest 5 members, and the lowest 5 members. This is consistent with much smaller interannual variations in the Southern Hemisphere and, hence, more influence of atmospheric chemistry on the ozone variations.

We conducted these analyses for MIROC3.2-CCM and MIROC5-CCM and compared the results of the two models. The difference in the ODS and GHG dependence of total ozone between these two models is

©2020. Japan Geoscience Union. All Right Reserved.

consistent with their transport properties.

Keywords: ozone, ODS, GHG, chemistry-climate model, multi-ensemble simulation, polar regions

©2020. Japan Geoscience Union. All Right Reserved.

A modeling study on the roles of cloud distribution in global tropospheric chemistry: detailed evaluation of clouds in a chemistry climate model (MIROC-CHASER)

*Ryoki Matsuda[1], Kengo Sudo[1,2]

1. Graduate School of Environmental Studies, Nagoya University , 2. Japan Marine-Earth Science and Technology

Chemical reactions in the atmosphere directly affect the formation and loss of ozone, methane, nitrogen oxides, sulfur oxides, and aerosols, and have a great influence on the atmospheric environment and climate change. Since these reactions are driven by photodissociation of ozone and related species caused by ultraviolet radiation, they can be largely modulated by the distribution of clouds. This study quantitatively investigates the photolytic impacts of clouds on atmospheric chemistry by using a global chemical transport model (chemical climate model, CHASER), observational (satellite and aircraft) data, and reanalysis data.
For cloud fields, CHASER reproduced generally well the global distribution of total cloud amount as observed in the satellite (ISCCP D2) and reanalysis data (JRA-55). This model, however, tends to underestimate low-level clouds in the tropics with an overestimate in the high latitudes. Further verification for the other cloud parameters like optical thickness and radiative forcing is now in progress and will be discussed in the presentation.
Our sensitivity experiments with respect to the impacts of clouds on photolytic processes show that clouds reduce OH radical concentrations by 10-20% near the surface and increase by 10-20% in the upper troposphere, basically as a result of scattering and reflection of UV radiation by low-middle level clouds. Our simulations also suggest that the global mean OH concentration, proxy of the oxidizing capacity of the atmosphere, increases by about 14% due to clouds. Also, tropospheric ozone (O_3) concentrations decreaced by about 3% near the surface and increased by about 4% in the upper troposphere reflecting changes in NO_x concentration. These clouds' impacts on the atmospheric chemistry were verified by using aircraft observation data (NASA ATom-1, 2, 3). The result shows that the observed OH and O_3 concentrations are reproduced more accurately when clouds are properly considered in the model.
These results indicate that clouds have significant influences on the global atmospheric chemistry (especially on the OH concentration field). Since OH determines the concentrations of chemical species such as methane, carbon monoxide (CO), fluorocarbons (CFCs), etc. which are important for climate and stratospheric ozone, this study suggests that the variation and trends in the clouds can largely affect the chemical species, which may give an additional influence on climate and atmospheric environment.

Keywords: Cloud, Chemistry-transport model, Ozone, OH radical

©2020. Japan Geoscience Union. All Right Reserved.

Impacts of tropospheric bromine and iodine on global tropospheric ozone: a modeling study using CHASER

*Takashi Sekiya[1], Yugo Kanaya[1], Kengo Sudo[2,1], Fumikazu Taketani[1], Maki Noguchi Aita[1], Akitomo Yamamoto[1], Yoko Iwamoto[3], Katsuhiro Kawamoto[4]

1. Japan Agency for Marine-Earth Science and Technology, 2. Graduate School of Environmental Studies, Nagoya University, 3. Graduate School of Integrated Sciences for Life, Hiroshima University, 4. Graduate School of Maritime Sciences, Kobe University

Bromine and iodine catalytic cycles are recognized as additional and important sinks of tropospheric ozone, though most of global climate transport models do not consider processes relevant to tropospheric bromine and iodine compounds (Young et al., 2018). A few global models have been used to evaluate impacts of tropospheric bromine and iodine on global tropospheric ozone (e.g., Saiz-Lopez et al., 2014; Sherwen et al., 2016), while large uncertainties in emission model process representation and emission estimation still remain. We newly implement iodine chemistry process, short-lived halocarbon emission, and ozone-mediated inorganic iodine release from the ocean (Chang et al., 2004; Carpenter et al., 2013) in the CHASER chemical transport model (Sudo et al., 2002; Sekiya et al., 2018) and evaluated impacts of tropospheric bromine and iodine on global tropospheric ozone. Incorporating these processes reduced surface ozone concentration by 20% on the annual and global average over the ocean. The model which incorporates these processes showed better agreements with ship-borne in-situ observations on the R/V Mirai and Hakuho-maru (Kanaya et al., 2019) during 2014-2018 (mean bias = 0.04 ppbv, $r = 0.82$) than the standard model (mean bias = 2.36 ppbv, $r = 0.73$). We evaluated impacts of tropospheric bromine on global tropospheric ozone loss using different three oceanic emission estimates of short-lived brominated halocarbons ($CHBr_3$, CH_2Br_2, CH_2BrCl, $CHBr_2Cl$, and $CHBrCl_2$): a bottom-up estimate based on SeaWIFS satellite observations of chlorophyll-a (Ordóñez et al., 2012), a bottom-up estimate for $CHBr_3$ and CH_2Br_2 using ship-borne observations (Ziska et al., 2013), and a top-down estimate for $CHBr_3$, CH_2Br_2, $CHBr_2Cl$, and $CHBrCl_2$ derived from the ATOM aircraft-campaign observations (Wofsy et al., 2018) using the Bayesian inversion technique. When using these three emissions, the global tropospheric ozone loss owing to bromine were estimated to be 284, 72, and 211 Tg O_3/yr, respectively, which suggested that bromine-catalyzed loss highly depends on short-lived halocarbon emissions. For tropospheric iodine sources, oceanic iodine release (as HOI and I_2) triggered by heterogeneous ozone loss at the sea surface was dominant over iodinated halocarbons (CH_3I, CH_2ICl, CH_2IBr, and CH_2I_2). The global tropospheric ozone loss owing to atmospheric iodine chemistry was estimated to be 643 Tg O_3/yr, which was comparable to the values reported by previous studies. Furthermore, model results suggested that the initial heterogeneous ozone loss at the sea surface (192 Tg O_3/yr) was an important sink of global tropospheric ozone which has not been evaluated explicitly in the previous studies. These results demonstrated the importance of the processes related to tropospheric bromine and iodine on global tropospheric ozone. In future studies, it is necessary to get a better understanding of tropospheric bromine and iodine compounds' emission processes and to reduce their uncertainties.

Keywords: Tropospheric ozone, Halogen, Chemical transport model

©2020. Japan Geoscience Union. All Right Reserved.

The weekday/weekend ozone differences induced by the emissions change in Guangzhou megacity of China

*Yu Zou[1]

1. Institute of Tropical and Marine Meteorology, CMA,Guangzhou,China

Guangzhou, one of China’ s megacities, is beset with frequent occurrence of atmospheric photochemistry events in summer and autumn. In this study, weekday/weekend mixing ratios of ozone (O_3) and the O_3 precursors of non-methane hydrocarbons (NMHCs) and nitrogen oxides (NOx) were recorded at Guangzhou Panyu Atmospheric Composition (GPACS), a comprehensive site in Guangzhou, during the summer (June, July, and August) and autumn (September, October and November) of 2011. In both summer and autumn, weekday/weekend O_3 differences in the morning and at midday largely depend on how much the O_3 precursors are affected by anthropogenic emissions. In the mornings (6:00–9:00 LT), pollutants (i.e. NOx and NMHCs) were more strongly influenced by vehicular emissions in autumn than in summer. In autumn, O_3 titration and lower NOx on weekends in NMHCs-limited regimes lead to more rapid O_3 production, which resulted in the O_3 weekend effect during autumn morning. No O_3 weekend effect occurred on summer mornings because O_3 formation was in a NOx-limited regime, although O_3 titration still existed. At midday (10:00–16:00 LT), the increase of biogenic NMHCs emissions reversed the sensitivity of O_3 production from NMHCs-to NOx-sensitive. The weekday/weekend diurnal pattern of vehicular sources was the same at midday, more intense other human industrial activities in autumn not only gave rise to the higher mixing ratios of high-reactive anthropogenic NMHCs (e.g. aromatics) on weekdays, but also could affected the temperature in the city, leading to higher isoprene mixing ratio on weekdays. All these factors are likely to contribute to the O_3 weekday effect in autumn. Meanwhile no weekday O_3 effect occurred in summer due to the low-intensity industrial anthropogenic activities. Our results show that high-reactive NMHCs and NOx control can be effective for reducing peak O_3 mixing ratios in Guangzhou. Further investigation based on numerical models is required to reach more robust conclusions.

Keywords: Emissions change, Weekday/ weekend ozone, Guangzhou

©2020. Japan Geoscience Union. All Right Reserved.

A Study on the Optimization of 3D Expressions for the Analysis of Local Scale Meteorological and Air Quality Information

*Woosik Jung[1], Gunwoo Kim[1]

1. INJE University, Department of Atmospheric Environment Information Engineering, Gimhae, Republic of Korea

In the last 10 years (2007 ~ 2016), 162 people have been killed and about 6.3 trillion won in property damage in Korea alone, the report showed. This is due to the increase of severe weather on the local scale as climate change progresses due to global warming. This study developed the 3D expression system specialized for the local scale. We used one of the commercial engines, Unreal Engine 4 and C++ language, to express meteorological and air quality information in 3D. As input data, the result of WRF and CMAQ modeling were used. Using high-resolution DEM data, 3D terrain was created, and wind vector field was implemented to indicate wind. And we have implemented isolines that indicate temperature and precipitation. In addition, by studying a new expression method to represent the wind, we implemented a stream vector and stream line, which is a vector and streamline moving along the wind flow. And the 3D volume rendering method using Raymarching algorithm is applied to express 3D data, cloud and air pollutant density.

For the analysis of local scale 3D expression cases, the day when the land and sea breeze was blown off the west coast including Seoul and Incheon was selected. And we analyzed a typhoon case of mesoscale. To show that air quality information can also be analyzed, the density of air pollutants such as fine dust and carbon monoxide was expressed and analyzed in 3D volume rendering. As a result of the case analysis, the modeling results were well reflected and the changes in meteorological and air quality information over time were easily identified. And the 3D volume rendering expression allowed us to analyze the vertical structure and distribution of clouds and air pollutants density in a new perspective.

This research was supported by Basic Science Research Program through the National Research Foundation of Korea(NRF) funded by the Ministry of Education(2017R1D1A3B03036152)

Keywords: Air Quality information, 3D expression, Local scale

©2020. Japan Geoscience Union. All Right Reserved.

A Study on the Optimization of 3D Expressions for the Analysis of Local Scale Meteorological and Air Quality Information

Woo-Sik Jung, Gun-Woo Kim

INJE University, Department of Atmospheric Environment Information Engineering, Gimhae, Republic of Korea

In the last 10 years (2007 ~ 2016), 162 people have been killed and about 6.3 trillion won in property damage in Korea alone, the report showed. This is due to the increase of severe weather on the local scale as climate change progresses due to global warming. This study developed the 3D expression system specialized for the local scale. We used one of the commercial engines, Unreal Engine 4 and C++ language, to express meteorological and air quality information in 3D. As input data, the result of WRF and CMAQ modeling were used. Using high-resolution DEM data, 3D terrain was created, and wind vector field was implemented to indicate wind. And we have implemented isolines that indicate temperature and precipitation. In addition, by studying a new expression method to represent the wind, we implemented a stream vector and stream line, which is a vector and streamline moving along the wind flow. And the 3D volume rendering method using Raymarching algorithm is applied to express 3D data, cloud and air pollutant density.

For the analysis of local scale 3D expression cases, the day when the land and sea breeze was blown off the west coast including Seoul and Incheon was selected. And we analyzed a typhoon case of mesoscale. To show that air quality information can also be analyzed, the density of air pollutants such as fine dust and carbon monoxide was expressed and analyzed in 3D volume rendering. As a result of the case analysis, the modeling results were well reflected and the changes in meteorological and air quality information over time were easily identified. And the 3D volume rendering expression allowed us to analyze the vertical structure and distribution of clouds and air pollutants density in a new perspective.

This research was supported by Basic Science Research Program through the National Research Foundation of Korea(NRF) funded by the Ministry of Education(2017R1D1A3B03036152).

Key Words : Meteorological and Air Quality information, Local scale, 3D expression, Volume Rendering

©2020. Japan Geoscience Union. All Right Reserved.

Validation of tropospheric NO_2 column density data observed by TROPOMI: Comparison with 4AZ-MAXDOAS

*Hikaru Saito[1], Hitoshi Irie[1]

1. University of Chiba

TROPOspheric Monitoring Instrument (TROPOMI) aboard the Sentinel-5 Precursor satellite has an unprecedented fine horizontal resolution of 7 km×3.5 km (at nadir) for tropospheric nitrogen dioxide (NO_2) column observations and is expected to improve estimation of emissions, including localized kilometer-scale emissions. However, previous studies reported that underestimation could occur in tropospheric NO_2 column data from satellite observations, although its causes are still under discussion. The present study attempts to validate TROPOMI tropospheric NO_2 column data to confirm that the underestimate occurs and clarify the causes. For this purpose, we used ground-based 4-different-azimuth-viewing Multi-Axis Differential Optical Absorption Spectroscopy (4AZ-MAXDOAS) installed at Chiba, Japan (35.63ºN, 140.10ºE, 21 m asl). The 4AZ-MAXDOAS observed tropospheric NO_2 simultaneously in 4 different azimuth directions, enabling the evaluation of spatial inhomogeneity of NO_2, which has been considered to be the major cause of the underestimate. From 4AZ-MAXDOAS data, we found that differences in tropospheric NO_2 column data among 4 different azimuth directions reached up to 40%, indicating the existence of significant horizontal spatial inhomogeneity in NO_2 around the observation site. Then, we compared 4AZ-MAXDOAS data with coincident TROPOMI data. TROPOMI data showed an underestimation by up to about 50% compared to 4AZ-MAXDOAS data, confirming the underestimate in TROPOMI data. However, the correlation was not clear between the magnitude of the underestimate and the coefficient of variance in 4-azimuth data from 4AZ-MAXDOAS observations. This suggests that the observed underestimate cannot be explained only by the effect of the NO_2 spatial inhomogeneity. Instead, the underestimate should be attributed more significantly to the assumption made in the air mass factor calculation.

Keywords: Atmosphere, Satellite observation, Nitrogen dioxide

©2020. Japan Geoscience Union. All Right Reserved.

Chemical composition of atmospheric aerosols over Jakarta megacity

*Masahide Nishihashi[1], Hitoshi Mukai[1], Yukio Terao[1], Shigeru Hashimoto[1], Rizaldi Boer[2], Muhammad Ardiansyah[2], Bregas Budianto[2], Adi Rakhman[2], Gito Sugih Immanuel[2], Rudi Nugroho [3], Nawa Suwedi[3], Anies Marufatin[3], Muhammad Agus Salim[3], Dodo Gunawan[4], Eka Suharguniyawan[4], Asep Firman Ilahi[4], Muharam Syam Nugraha[4], Ronald Christian Wattimena[4], Bayu Feriaji[4], Qoriana Maulani[4]

1. National Institute for Environmental Studies, 2. IPB University, Indonesia, 3. Agency for the Assessment and Application of Technology (BPPT), Indonesia, 4. Meteorological, Climatological, and Geophysical Agency (BMKG), Indonesia

We have implemented a comprehensive observation of air pollutants and greenhouse gases around Jakarta megacity in Indonesia since 2016 to quantify anthropogenic emissions from the city and characterize them in terms of socioeconomic activities in the city.

In addition to the continuous monitoring systems of NO_x, SO_2, O_3, CO, CO_2, CH_4, and meteorological parameters, we installed three continuous dichotomous aerosol chemical speciation analyzers (ACSA-14, Kimoto) at Bogor (center of Bogor city) in 2016, Cibeureum (mountainous area, background-like site) in 2017, and Serpong (Jakarta suburb) in 2019. The ACSA-14 can automatically measure not only the mass concentrations of $PM_{2.5}$ and $PM_{10-2.5}$ and optically measured black carbon (OBC), but also the chemical composition of $PM_{2.5}$ and $PM_{10-2.5}$ (nitrate ion (NO_3^-), sulfate ion (SO_4^{2-}), water soluble organic compounds (WSOC), ammonium ion (NH_4^+)), simultaneously. The measurement interval is 3 hours to extend the replacement interval of filter tapes and chemical reagents for the chemical composition analysis of $PM_{2.5}$ and $PM_{10-2.5}$.

The averages of $PM_{2.5}$ from November 2017 to October 2019 are 23.9 $\mu g/m^3$ at Bogor and 18.3 $\mu g/m^3$ at Cibeureum. The seasonal averages of $PM_{2.5}$ observed at Bogor and Cibeureum in the dry season (May to October in 2018/2019) are 34.2 and 28.0 $\mu g/m^3$, which are 2.4 and 3.2 times higher than those of rainy season (November 2017/2018 to April 2018/2019), respectively. While the long-term trends of $PM_{2.5}$ observed at Bogor are similar to Cibeureum, the averaged $PM_{2.5}$ concentrations at Bogor in the dry and rainy seasons are 1.2 and 1.6 times larger than Cibeureum, respectively.

We compared the chemical composition of $PM_{2.5}$ observed at three sites in February 2020. The amount of SO_4^{2-} (20.9%) is almost same as WSOC (20.8%) at Bogor. The dominant components at Cibeureum are SO_4^{2-} (27.4%) and WSOC (13.4%). While the most dominant component at Serpong is WSOC (22%), the percentage of NO_3^- (13.2%) at Serpong is larger than Bogor (11.8%) and Cibeureum (8.7%). The NO_3^-/SO_4^{2-} ratio at Serpong (1.76) is higher than Bogor (0.82) and Cibeureum (0.43). These results suggest that the urban pollution caused by NO_x in automobile exhausts is significant at Serpong compared to Bogor and Cibeureum.
In our presentation, we will also present the result of $PM_{10-2.5}$, OBC, and the other species.

Keywords: atmospheric aerosols, PM2.5, chemical composition, urban monitoring, Indonesia

©2020. Japan Geoscience Union. All Right Reserved.

Seasonal Variation of Wet Deposition of Black Carbon in Arctic Alaska

*Tatsuhiro Mori[1], Yutaka Kondo[2], Sho Ohata[3,4], Yongjing Zhao[5], Puna Ram Sinha[6], Naga Oshima[7], Hitoshi MATSUI[8], Nobuhiro Moteki[9], Makoto Koike[9]

1. Tokyo University of Science, 2. National Institute of Polar Research, 3. Institute for Space–Earth Environmental Research, Nagoya University, 4. Institute for Advanced Research, Nagoya University, 5. Air Quality Research Center, University of California-Davis, 6. Department of Earth and Space Sciences, Indian Institute of Space Science and Technology, 7. Meteorological Research Institute, 8. Graduate School of Environmental Studies, Nagoya University, 9. Graduate School of Science, The University of Tokyo

Black carbon (BC) aerosol deposited in and onto Arctic snow increases the snow's absorption of sunlight and accelerates snowmelt. Wet removal of BC from the atmosphere plays a key role in determining its abundance in the Arctic atmosphere and in Arctic snow. However, this process is poorly understood, mainly due to the scarcity of relevant measurements. To reveal characteristic features of the wet deposition of BC, we made highly accurate measurements of mass concentrations of BC in snow and rain (C_{MBC}) and mass concentrations of BC in surface air (M_{BC}) at the Barrow Atmospheric Baseline Observatory, Alaska, from July 2013 to August 2017 and analyzed them along with routinely measured meteorological parameters from Barrow. Monthly mean M_{BC} and C_{MBC} were poorly correlated from midwinter to early spring, when C_{MBC} was close to the annual median while M_{BC} was at its annual peak. Seasonal variations in the altitude distribution of ambient BC concentration may lead to these differences in seasonal variation of M_{BC} and C_{MBC}, as may microphysical processes in mixed phase clouds. About 50% of the annual wet deposition of BC occurred in the three months of summer, associated with high values of total precipitation and BC originating from biomass burning. Size distributions of BC in snow and rain were stable throughout the year, suggesting that the size distribution of BC in the lower troposphere is similarly stable. These observations improve our understanding of the loss processes and hence the BC budget in the Arctic.

Keywords: Black carbon, Wet deposition, Arctic, single-particle soot photometer, seasonal variation

©2020. Japan Geoscience Union. All Right Reserved.

Investigation of wet removal rate of black carbon in East Asia: A perspective from airmass pathways

*Yongjoo Choi[1], Yugo Kanaya[1], Masayuki Takigawa[1], Chunmao Zhu[1], Seung-Myung Park[2], Atsushi Matsuki[3], Yasuhiro Sadanaga[4], Sang-Woo Kim[5], Xiaole PAN[6]

1. Japan Agency for Marine-Earth Science and Technology, Japan, 2. National Institute of Environmental Research, Korea, 3. Kanazawa University, Japan, 4. Osaka Prefecture University, Japan, 5. Seoul National University, Korea, 6. Chinese Academy of Sciences, China

Using long-term and harmonized measurements of black carbon (BC) and carbon monoxide (CO) from three representative background sites in East Asia (Baengnyeong and Gosan in South Korea, and Noto in Japan), the regional and seasonal differences in wet removal rates were investigated according to airmass transport pathways and meteorological conditions. To identify the airmass origin and accumulated precipitation along with trajectories (APT), backward trajectories at 500 m during 72 hours were calculated by the Hybrid Single Particle Lagrangian Integrated Trajectory 4 model. The European Center for Medium-Range Weather Forecasts (ECMWF) ERA5 hourly pressure and surface level meteorological data (0.25˚ ×0.25˚) were used as input data to obtain accurate and detailed information of each endpoint of trajectories. The wet removal rates were more efficient in South Korea and Japan among the region and in fall and winter among the season. These differences depending on the regional and seasonal division could be partially explained by the inherent difference in the coating thickness of BC particles, according to the dominant emission sectors. Because the industrial sector (thin coated) is dominant in East and North China, in contrast, the transportation sector (thick coated), mainly emitted from diesel vehicles, has a high portion in South Korea and Japan. By the same token, wet removal rates in winter and summer showed the highest and lowest depending on the dominant emission sectors, such as house heating (thick coated) and industry, respectively. Next, we calculated transport efficiency (TE) from FLEXible PARTicle (FLEXPART) Lagrangian transport model (version 10.4) to investigate the representativeness of wet removal rate of model. Overall median TE from FLEXPART was overestimated compared to measurement, implying underestimation of wet scavenging coefficients. The median of estimated below cloud scavenging coefficients showed slightly overestimation than that calculated from FLEXPART as a factor by 1.7. On the other hand, the median of calculated in-cloud removal coefficients including sub-grid effect was highly underestimated than that of estimation by a factor of 5.1. From the analysis of artificial neuron networks, the convective available potential energy (CAPE), which is well known as an indicator of vertical instability, should be considered in in-cloud scavenging process to improve the better representative regional difference in BC wet scavenging over East Asia.

Keywords: Black carbon, Wet scavenging coefficients, FLEXPART, Long-term measurements

©2020. Japan Geoscience Union. All Right Reserved.

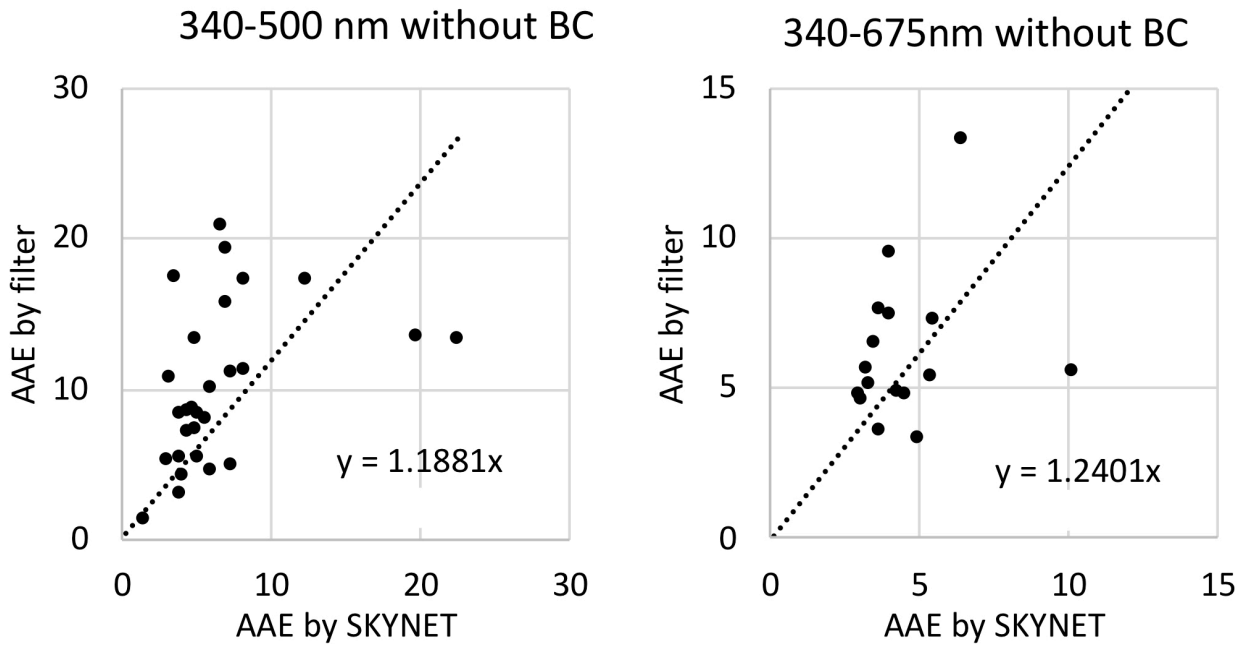
Light absorption properties of organic aerosols at Fukue Island in 2018 spring

*Chunmao Zhu[1], Takuma Miyakawa[1], Hitoshi Irie[2], Fumikazu Taketani[1], Yugo Kanaya[1]

1. Japan Agency for Marine-Earth Science and Technology, 2. Chiba University

Light-absorbing organic aerosol, also termed as brown carbon (BrC) aerosol, is one of the most understudied aerosol components for its sources and effects on climate change. For a long time, organic aerosols had been deemed to cause cooling on the earth’ s surface. Recently model studies indicated that BrC is accounting for ~1/4 of warming effect by carbonaceous aerosols at the tropopause globally. However, observation about the light absorption properties of BrC aerosols, which are fundamental for climate change prediction, is very limited, especially in East Asia. The SKYNET observational data at Fukue Island were used to derive the Absorption Aerosol Optical Depth (AAOD) based on the aerosol optical depth and single scattering albedo. AAOD of BrC and AAE_{SKYNET}were then derived based on the light absorption characteristic differences among BrC, BC and dust. Teflon (PTFE) filter samples were also collected using the Continuous Particulate Monitor with X-ray Fluorescence (PX375, Horiba Inc.). BrC in the filters were extracted using methanol followed by syringe-filtration to remove black carbon and mineral particles. The light absorption coefficient and Absorption Angstrom Exponent (AAE_{filter}) of BrC were quantified based on measurement of light absorption spectra in the UV-visible light (300–800 nm). The extracts were filtered to remove dusts and black carbon and analyzed for light absorption. We found that AAE_{filter}were generally higher than AAE_{SKYNET}. Vertical profile of aerosol light absorption properties needs to be further studied in the future.

Keywords: Brown Carbon Aerosol, Light Absorption, Skyradiometer, Filter Observation



©2020. Japan Geoscience Union. All Right Reserved.

Can a global chemistry climate model reproduce interannual variabilities and trends of depositions of sulfate, nitrate, and ammonium preserved in the Southeastern Greenland Dome ice core?

*Kengo Sudo[1,2], Hinako Shiratsuchi[1], Yoshinori Iizuka[3]

1. Graduate School of Environmental Studies, Nagoya University, 2. Japan Agency for Marine-Earth Science and Technology (JAMSTEC), 3. Institute of Low Temperature Science, Hokaido University

Inorganic compounds like sulfur and nitrogen oxides (SOx/NOx) are mainly emitted from fossil fuel combustion or high-temperature air combustion associated with anthropogenic activities. Those components are chemically oxidized in the atmosphere to form sulfate and nitrate which cause air pollution and acid rain. Aerosols like sulfate and nitrate are also involved in the global climate change, inducing negative radiative forcing by scattering solar incident and changing clouds. For accurate evaluation and future projection of global changes in atmospheric environment and climate, it is vital to quantitatively validate a chemistry climate model that simulates global distributions of aerosols including sulfate and nitrate making maximal use of available observations. In this study, we evaluate global simulation by a chemistry climate model (CHASER) using a long-term (60 years) record of aerosol depositions preserved in the High-Accumulation Dome ice core in Southeast Greenland (SE-Dome) and investigate controlling factors of interannual variation and trends in inorganic ions of sulfate (SO_4^{2-}), nitrate (NO_3^-), and ammonium (NH_4^+).

It is found that our model simulation basically well captures both seasonal cycles and interannual variabilities in the flux of each component as seen in the ice core record for 1970s to 2010. The model calculations suggest that the long-term SO_4^{2-} trend seen in the ice core (-0.15 μmol L^{-1} d^{-1}) is mostly from SO_2 emission changes in the source areas like Europe, U.S. , and Asia over the decades. In contrast, long-term trends for NO_3^- and NH_4^+ (-0.06 and 0.01 μmol L^{-1} d^{-1}, respectively) appear to be affected largely by changes in natural sources and meteorological conditions in addition to the anthropogenic emissions of NOx and NH_3.

Interestingly the model simulation replicates the spiky peaks (positive anomalies) in concentrations (particularly for SO_4^{2-}) recorded in May 1992. The peaks were tentatively attributed to the 1991 eruption of Mt. Pinatubo in the previous studies. Our model simulation, however, nicely reproduces the concentration peaks even without any direct injection from the Mt. Pinatubo to the atmosphere, implying that anomalous changes in meteorological fields (most probably for transport and precipitation) are the dominant factors of the peaks in May 1992. Actually, the model simulation suggests that there were anomalously enhanced transport pathways from Europe and North America toward Greenland and the SE-Dome site for both of SOx, NOx, and NHx.

Keywords: chemistry climate model, ice core, Arctic, Aerosol deposition, Greenland, Sulfate/Nitrate/Ammonium

©2020. Japan Geoscience Union. All Right Reserved.

Evaluation of GCOM-C aerosol products using ground-based sky radiometer observations

*Hossain Mohammed Syedul Hoque[1], Hitoshi Irie[1], Alessandro Damiani[1], Mashiro Momoi[1]

1. Center for Environmental Remote Sensing (CEReS), Chiba University

Aerosol optical thickness (AOT) at 380 and 670 nm retrieved from the Global Change Observation Mission-Climate (GCOM-C) observations from January to September 2019 was evaluated using the ground-based SKYNET sky radiometer measurements at Chiba (35.62˚ N, 140.10˚ E), Japan and Phimai (15.18˚ N, 102.56˚ E), central Thailand. Chiba and Phimai are urban and rural sites, respectively. AOT retrieved from the sky radiometer observations from were compared with the coincident multi-axis differential optical absorption spectroscopy (MAX-DOAS) AOT values. Under clear sky conditions, both the datasets show excellent agreement. The sky radiometer and GCOM-C AOT values show a good positive correlation (*R*) ~ 0.90 at 380 nm in both sites. At 670 nm, the *R*-values were 0.67 and 0.87 for Chiba and Phimai, respectively. Despite the low *R*-value at 670 nm over Chiba, the temporal variation of AOT was well reproduced by the satellite observations. Over both sites, the agreement between the datasets was mostly within ±0.2. Over Chiba, the higher differences in the AOT values were mostly related to cloud screening in the datasets. The mean bias error (MBE) (GCOM-C –Sky radiometer) for the Chiba site was ~ -0.08 and ~ -0.02 at 380 and 670 nm, respectively, for the coincidence criterion of 0.1˚ x 0.1˚. For the similar coincidence criterion, the MBE values were higher for the observations over the Phimai site. The potential reason was the influence of biomass burning in addition to the cloud influence. The spatial resolution of the satellite coincidence data had a significant impact on the MBE at 380 nm over the Chiba site. Overall, the retrieved AOT values of both datasets were generally consistent indicating the excellent potential of the GCOM-C observations of aerosol properties, especially in the ultra-violet region.

©2020. Japan Geoscience Union. All Right Reserved.

Atmospheric sulfate formation pathways over the past 60 years constrained by a global chemical transport model

*Shohei Hattori[1], Becky Alexander[2], Sakiko Ishino[3], Shuting Zhai[2]

1. Department of Chemical Science and Engineering, School of Materials and Chemical Technology, Tokyo Institute of Technology, 2. Department of Atmospheric Sciences, University of Washington, Seattle WA 98195-1640, USA, 3. National Institute of Polar Research, Research Organization of Information and Systems, Tokyo 190-8518, Japan

Since the industrial revolution, the increase of sulfur dioxide (SO_2) had increased the SO_4^{2-} load. The period including the 1950s to 1970s had significant SO_2 emissions, but these emissions decreased after the 1980s across North America (NA) and Western Europe (WE), reducing atmospheric SO_4^{2-} burden. However, SO_4^{2-} aerosols decreased less rapidly than SO_2 reduction, suggesting the existence of chemical feedback processes.
In the atmosphere, SO_4^{2-} is produced from gas-phase SO_2 oxidation by hydroxyl radicals (•OH) and oxidation in aqueous-phase (i.e., in clouds). SO_2, dissolved in an aqueous-phase, forms S(IV) species (i.e., $SO_2{\cdot}H_2O$, HSO_3^-, and SO_3^{2-}) that react with hydrogen peroxide (H_2O_2), ozone (O_3), and molecular oxygen (O_2) to form SO_4^{2-}. Among these chemical processes, several studies have proposed several mechanisms causing the weakened response of SO_4^{2-} to SO_2 decreases.
To obtain quantitative information in sulfate formation pathways, we simulate global tropospheric sulfate chemistry using the version 12.5.0 of the GEOS-Chem chemical transport model. We performed the model simulations with anthropogenic emissions corresponding to the years 1960, 1973, 1986, 1999, and 2013, to investigate the past changes in atmospheric sulfate formation and its efficiency in response to the changes in anthropogenic emission.
Relative contributions of S(IV)+ O_3 and H_2O_2 were increased between 1973 and 2013 over the Eastern NA (ENA) and WE, and the proportional increases of S(IV) + O_3 pathway are consistent with our previous observation of triple oxygen isotopic composition of SO_4^{2-} in a Greenland ice core. The increase of S(IV) + O_3 pathway is best explained by an increase in the cloud water pH over the period, and not by O_3 concentration increase.
The promotion of S(IV) + O_3 pathway over the period caused higher SO_2 conversion efficiency for both summertime and wintertime in ENA and WE. On the basis of the GEOS-Chem model outputs, we found two regional characteristics: (i) gradual increase of SO_2 conversion efficiency in WE over the period, and (ii) a small increase of SO_2 conversion efficiency in ENA between 1960 and 1999 and an abrupt increase between 1999 and 2013.
In the presentation, we will discuss several implications including perspective for future sulfate formation by the worldwide reduction of SO_2 and the important role of acidity (defined as cloud pH) in the atmospheric chemistry.

Keywords: Global chemical transport model, Sulfate, Triple oxygen isotopes, Aerosol, Anthropogenic activity

©2020. Japan Geoscience Union. All Right Reserved.

High-temporal-resolution elemental characterization of fine-mode aerosols in springtime Asian outflow: Emission and removal characteristics, and comparison with model simulation

*Takuma Miyakawa[1], Akinori Ito[1], Chunmao Zhu[1], Yugo Kanaya[1]

1. Japan Agency for Marine-Earth Science and Technology

Trace metals in aerosol particles exhibit the various impacts on the ocean biogeochemistry (Mahowald et al., 2018). We conducted the semi-continuous measurements of elemental composition of fine mode ($PM_{2.5}$) aerosols using an automated X-ray fluorescence analyzer (PX-375, Horiba, Ltd., Asano et al., 2017) in a remote island, Fukue (32.75ºN, 128.68ºE), in Japan in the spring of 2018. Here we report the temporal variations of mass concentrations of geochemically important elements for this period, namely sulfur (S), lead (Pb), copper (Cu), manganese (Mn) and iron (Fe), and their relationships with some tracers, carbon monoxide (CO), black carbon (BC), and calcium (Ca). Positive correlation of Pb and Cu with CO and BC were found during the observation period, indicating the emission sources of these metals share the region where the large CO (and BC) emission sources are located. Further analyses of concentration-weighted trajectories also suggested the similar geographical characteristics of these elements and combustion tracers. We extracted the continental outflow air masses with minimized impacts of the (especially wet) removal during the transport to elucidate the emission ratio of Pb and Cu to CO, which were evaluated, for the first time in Asian outflow, to be 97.8 and 37.4 μg/g, respectively. The wet removal of Pb together with BC was also investigated based on the precipitation along the air mass transport. Impacts of Asian dust and anthropogenic (i.e., combustion) sources on Fe in $PM_{2.5}$ aerosols were diagnosed by using the measured BC concentration with the emission ratio of iron oxides to BC, and by comparing those simulated by the IMPACT model (Ito et al., 2019). Fraction of combustion-derived Fe for fine mode aerosols was evaluated to be less than 20% on average during the observation period.

References

Asano et al. (2017), Highly Time-Resolved Atmospheric Observations Using a Continuous Fine Particulate Matter and Element Monitor, *Earth Space Chem.*, 1, 9, 580-590.
Ito A., et al. (2019), Pyrogenic iron: The missing link to high iron solubility in aerosols, *Sci. Adv.*, 5, eaau7671.
Mahowald N. M., et al. (2018), Aerosol trace metal leaching and impacts on marine microorganisms, *Nat. Comm.*, 9:2614.

Keywords: Elemental composition, Aerosol, PM2.5, Iron

©2020. Japan Geoscience Union. All Right Reserved.

Comparison of compositional characteristics of aerosol and rainwater samples collected in Nagoya

*Wei Chenran[1], Sonia Afsana[1], Qingcai Chen[2], Dhananjay Kumar Deshmukh[3], Kimitaka Kawamura[3], Michihiro Mochida[1,4]

1. Graduate School of Environmental Studies, Nagoya University, Nagoya, Japan, 2. School of Environmental Science and Engineering, Shaanxi University of Science and Technology, Xi' an, China, 3. Chubu Institute for Advanced Studies, Chubu University, Kasugai, Japan, 4. Institute for Space-Earth Environmental Research, Nagoya University, Nagoya, Japan

Organic aerosol is one of major components of atmospheric aerosol particles. Some volatile organic compounds (VOCs) react in the aqueous-phase of cloud droplets, and after the evaporation of liquid water, they form aerosol, which is called aqueous secondary organic aerosol (aqSOA). Further, organic aerosols may also change to aqSOA through aging in the aqueous phase. Although a number of laboratory experiments and model simulations have explored the mechanism of aqSOA formation, the mechanism in real atmospheric environments is still unclear. To find a clue to understand how aqSOA is formed in could droplets through aqueous-phase reactions, this study compares compositional characteristics of water-soluble components in aerosol and rainwater samples, as a means to compare the components of aerosols before and after the reactions in the real atmosphere.

Aerosol and rainwater samples were collected on campus of Nagoya University in Nagoya, Japan. The organics therein were fractionated into humic-like substances with a neutral nature (HULIS-n), humic-like substances with an acid nature (HULIS-a) and high-polar water-soluble organic matter (HP-WSOM). The optical properties of the samples were measured using a fluorescence spectrophotometer and an ultraviolet-visible spectrophotometer. Fourier transform infrared spectroscopy (FT-IR) was used to compare the chemical structural characteristics of aerosol and rainwater samples.

The analysis of the 3D fluorescence spectra shows that the HULIS-n-to-HULIS-a ratios based on the fluorescence intensity of two spectra regions (excitation wavelength from 240 to 260 nm and emission wavelength from 400 to 460 nm , and excitation wavelength from 320 to 360 nm and emission wavelength from 420 to 460 nm) from aerosol samples were in most cases larger than those of rainwater. A possible explanation is that some of the low-polar fluorescent substances (fluorescent substances in HULIS-n) were decomposed to non-fluorescent substances and that more-polar fluorescent substances (fluorescent substances in HULIS-a) were formed by aqueous-phase reactions. The FT-IR results present that HULIS-n and HULIS-a in aerosol samples show a smaller fraction of carboxyl group but a larger fraction of carbonyl group than those in rainwater samples, implying that the oxidation of carbonyl groups to carboxyl groups occured for HULIS-n and HULIS-a, and/or that aqSOA containing carboxyl group was formed from VOCs. Because the presence of water in the samples for the FT-IR analysis may have influenced on the quantification of functional groups, compositional characteristics of aerosol and rainwater samples should be further compared using other instruments such as an aerosol mass spectrometer.

©2020. Japan Geoscience Union. All Right Reserved.

Formation processes of dimers measured in α-pinene secondary organic aerosol particles

*Kei Sato[1], Sathiyamurthi Ramasamy[1], Satoshi Inomata[1], Shinichi Enami[1], Yu Morino[1]

1. National Institute for Environmental Studies

Formation of low-volatility compounds such as dimers detected in atmospheric aerosol particles will affect atmospheric organic aerosol level due to the influence from these dimers on volatility and viscosity of particles. In order to study formation mechanisms of dimers detected in forest particles,[1)] we used liquid chromatograph-mass spectrometry (LCMS) to analyze filter extracts of secondary organic aerosol (SOA) particles generated by chamber experiments on the oxidation of α-pinene. We determined the ratios of dimer to SOA mass for those with molecular weights (MWs) of 344, 358, and 368 as a function of experimental conditions including the oxidant of VOC, initial VOC concentration, the acidity of seed particles, and the temperature of chamber. We used 6 m^3 NIES smog chamber and temperature-controllable 0.7 m^3 Teflon bag chamber for generation of SOA particles. The dimer/SOA ratios measured for the reactions of O_3 with α-pinene were higher than those measured for the reactions of OH and NO_3 radicals with α-pinene. Formation of dimers barely occurred during reactions with OH and NO_3 radicals although the reactions of OH and NO_3 radicals with α-pinene forms carbonyl compounds, which could form dimers through acid catalyzed heterogeneous reactions, and organic peroxy radicals, which could form dimers through gas-phase association reactions. Furthermore, the concentrations of dimers with MWs of 344 and 358 in sample solutions showed linear correlations with the product from multiplication of the concentrations of corresponding monomers. Dimers with MW 358 could be successfully separated with a LC column from the chromatographic peaks of presumed monomers, pinic acid and terpenylic acid; suggesting that signals of dimers with MW 358 are not instrument artifacts and result from stable dimers existing in solution or particle phases. Dimers with MW 358 are likely to be formed through the reactions of Criegee intermediates; however, as formation process for dimer with MW 358 we cannot exclude hydrogen bonding formation[2)] from monomers formed from the gas-phase reaction with O_3. This research has been supported by the Environmental Research and Technology Development Fund from Environmental Restoration and Conservation Agency (grant no.5-1801) and NIES Research Founding Type A.

Reference:
1) Sato et al., LC/MS analysis of molecular markers present in biogenic secondary organic aerosols collected during year-round observations at a cool-temperature forest, Japan Geoscience Union Meeting 2019, AASO4-22, Chiba, Japan (2019).
2) DePalma et al., Thermodynamics of oligomer formation: implications for secondary organic aerosol formation and reactivity, Phys. Chem. Chem. Phys., 15, 6935-6944 (2013).

Keywords: Biogenic volatile organic compound, Secondary organic aerosol, Chemical mechanism, Low-volatility organic compound, Smog chamber

©2020. Japan Geoscience Union. All Right Reserved.

Nitric acid gas captured in quasi-liquid layers on ice surfaces

*Ken Nagashima[1], Josée Maurais[2], Ken-ichiro Murata[1], Yoshinori Furukawa[1], Patrick Ayotte[2], Gen Sazaki[1]

1. The Institute of Low Temperature Science, Hokkaido University, 2. Université de Sherbrooke, Québec, Canada

Ice crystal surfaces act as “reaction fields” for heterogeneous chemical reactions that involve atmospheric acidic gases, thereby causing serious environmental issues such as the catalytic ozone depletion by hydrogen chloride gas and the generation of nitrogen oxide gases (NOx) from the photolysis of nitric acid/nitrates. These chemical reactions cannot be explained solely by homogeneous processes. In addition, the surfaces of ice crystals near the melting point are covered with thin liquid water layers, called quasi-liquid layers (QLLs), which may play crucial roles in various chemical reactions. In this study, we chose HNO_3 as a model atmospheric gas, and directly observed the QLLs on ice basal faces by advanced optical microscopy [1]. Because P_{HNO3} in the troposphere shows considerable variations (e.g., ranging from ~10^{-6} Pa in clean air to ~10^{-2} Pa in polluted urban air [2,3]), the observations in this study were performed under some P_{HNO3} conditions (0, 10^{-4} and 10−2 Pa).

Irrespective of the presence/absence of the HNO_3 gas, the pure-QLLs and HNO_3-QLLs appeared with increasing temperature and disappeared with decreasing temperature. The shape of pure-/HNO_3-QLLs showed spherical dome and the contact angle of them on the ice basal face was ~1˚. The appearance temperatures of the pure-/HNO_3-QLLs were not so different (-1.9 and -0.5 to -1.8 ˚C, respectively). Although the disappearance temperature of pure-QLLs (-2.2 ˚C) was almost same as the appearance temperature, the disappearance temperature of the HNO_3-QLLs (-6.4 ˚C) was significantly lower than the appearance temperature of them under high-P_{HNO3} condition (10^{-2} Pa). The large thermal hysteresis between the appearance and disappearance temperatures suggests that the disappearance mechanisms of the pure-/HNO_3-QLLs were different. We found that the HNO_3-QLLs are not composed of pure water, but rather of aqueous HNO_3 solutions, and also that the HNO_3-QLL and the ice crystal were in equilibrium. The evidence and the disappearance mechanism are showed as follows.

The size of the HNO_3-QLLs decreased immediately after we started reducing the temperature. We could not observe such changes in the sizes of pure-QLL with temperature in the absence of the HNO_3 gas. When we assumed that the mass of HNO_3 in the HNO_3-QLL was constant during the relatively short observation time period, the volume reduction of the HNO_3-QLLs with decreasing temperature meant increasing of HNO_3 concentration of the HNO_3-QLL. We calculated the volume reductions as a function of temperature by using the HNO_3-H2O phase diagram. The calculated volume reductions were in good agreement with the volume reductions determined experimentally.

One of the plausible causes for the disappearance of HNO_3-QLLs could be the evaporation of HNO_3 from the HNO_3-QLLs. We calculated the equilibrium HNO_3 partial vapor pressure, Pe(HNO_3), of the HNO_3 -QLLs. As temperature decreases, Pe(HNO_3) increases. It is very reasonable to expect that when Pe(HNO_3) exceeds P_{HNO3} in the observation chamber with decreasing temperature, HNO_3 evaporates from the HNO_3-QLLs, resulting in the disappearance of the HNO_3-QLLs.

Recently, we studied the effects of hydrogen chloride gas on the behavior of QLLs (HCl-QLLs) on ice basal faces [4,5]. We found that the HCl-QLLs were also aqueous hydrochloric acid solution, and that the temperature and HCl concentration of the HCl-QLLs were also very close to those of a liquidus line: these

©2020. Japan Geoscience Union. All Right Reserved.

results were similar to those found in this study. Therefore, ice crystal surfaces would capture large amount of acidic gas components in the acidic-QLLs.

[1] Nagashima et al. (2020) Crystals 10, 72.

[2] Goldan et al. (1983) Atmos. Environ. 17, 1355.

[3] Hanke et al. (2003) Atmos. Chem. Phys. 3, 417.

[4] Nagashima et al. (2016) Cryst. Growth Des. 16, 2225.

[5] Nagashima et al. (2018) Cryst. Growth Des. 18, 4117.

The details of this study are shown in our paper [1]. We will present this study from other viewpoints in “A-CC39 Glaciology” and "M-IS23: Growth and dissolution of crystal" sessions.

Keywords: Ice, quasi-liquid layer, nitric acid gas, optical microscopy

©2020. Japan Geoscience Union. All Right Reserved.

Five-years seasonal variations of nitrogen and triple oxygen isotopic compositions of atmospheric nitrate at Noto Peninsula, Japan

*Kazuki Kamezaki[1], Shohei Hattori[1], Atsushi Matsuki[2], Naohiro Yoshida[1,3]

1. Department of Chemical Science and Engineering, School of Materials and Chemical Technology, Tokyo Institute of Technology, 2. Institute of Nature and Environmental Technology, Kanazawa University, 3. Earth-Life Science Institute

Anthropogenic nitrogen oxides (NO_x) emission from land to the atmosphere have been accelerated in East Asia. By increase of the anthropogenic pollutants in the atmosphere, atmospheric oxidizing capacity can be changed in East Asia. Moreover, the biological cycle can be changed because the atmospheric nitrate deposition is a source of nitrogen. Thus, the understanding of sources and formation pathways of atmospheric nitrate is important.

The nitrogen and triple oxygen isotopic compositions ($\delta^{15}N$ and $\Delta^{17}O = \delta^{17}O - 0.52 \times \delta^{18}O$) of atmospheric nitrate can be a tracer of the sources and formation pathways of atmospheric nitrate. The $\delta^{15}N$ of atmospheric nitrate can be used to estimate the sources and sinks of atmospheric nitrate. The $\Delta^{17}O$ of atmospheric nitrate can be a tracer of the relative importance of mass-independent oxygen-bearing species (e.g. O_3, BrO; $\Delta^{17}O \neq 0$ ‰) and mass-dependent oxygen-bearing species (e.g. OH radical; $\Delta^{17}O \approx 0$ ‰) during the conversion of NO_x to atmospheric HNO_3. In this study, we present five-years data of $\delta^{15}N$ and $\Delta^{17}O$ values in atmospheric nitrate collected at NOTO Ground-based Research Observatory (NOTOGRO) (37.5˚N, 137.4˚E) located at the north coast of Noto Peninsula, Japan.

The atmospheric nitrate concentrations did not show a clear trend, while the $\delta^{15}N$ and $\Delta^{17}O$ showed a clear seasonal variation with summer minimum and winter maximum. The trend of $\Delta^{17}O$ is caused by the seasonal changes in the O_3 / HO_x ratios decreasing in summer by ozone destruction and HO_X production (e.g. OH, HO_2 radicals) via UV irradiance. Although the correlation between $\delta^{18}O$ and $\Delta^{17}O$ values was observed throughout the year, the slope between $\delta^{18}O$ and $\Delta^{17}O$ values for coarse particles for the winter-spring period is only different from other seasons and fine particles. We will discuss possible explanations of this different isotope pattern for the winter and spring periods.

Keywords: Nitrate, Aerosol, Triple oxygen isotopes, Nitrogen isotope ratio

©2020. Japan Geoscience Union. All Right Reserved.

Impacts of ship emissions on atmospheric particulate matter and gaseous components over the Seto Inland Sea areas

*Moe Tauchi[1], Katsuhiro Kawamoto[2], Kazuyo Yamaji[1], Ryohei Nakatsubo[3], Yoshie Oshita[3], Yasuyuki Itano[4]

1. Kobe University, 2. Takamatsu Local Meteorological office, 3. Hyogo Prefectural Institute of Environmental Sciences, 4. Osaka City Research Center of Environmental Science

Our interest issue is to be clear control factors of elevated atmospheric pollutants over the Seto Inland Sea (SIS) and surroundings, where $PM_{2.5}$ levels are still higher than the other regions in Japan (Nakatsubo et al., 2020). The SIS area is closed and congested with many people live along its coastal zones. Even now, it has been concerned that high sulfur emissions from vessels using heavy fuel oil with relatively high sulfur content effect on air quality.

From 1 January 2020, in such a situation, the sulfur contents in fuel oil used on board ships operating outside emission control areas have been reduced from 3.50% to 0.50% (the sulfur limits). The global sulfur limits will make significantly reductions of sulfur oxides emissions from ships, and that should have major health and environmental benefits for the world, especially for populations living close to ports and coasts. The reduced ship sulfur emissions are expected to affect not only ambient sulfur-containing substance concentrations but also the other atmospheric pollutant components.

To assess the impacts of the fuel sulfur changes on air quality of the SIS areas, we investigated concentrations of SO_2 and $PM_{2.5}$ substances in the atmosphere over both land and sea from March 2017 to March 2020 only for the duration of the research voyage. Automatic sampling data at ambient air pollution monitoring stations facing to SIS were used for analyzing the coastal-landmass pollutants. As regards the marine air mass, SO_2 and $PM_{2.5}$ were sampled over the SIS area on board Training-ship Fukaemaru owned by Kobe University.

From January 1 to March 31 in 2018, percentage of sulfate ion in $PM_{2.5}$ along the SIS area is about 24.1%. We are carefully watching the atmospheric particulate matter and gaseous components around the SIS after starting the sulfur limits. Continued observation research should contribute for improvement of air quality and formulating environmental policy in the future.

Keywords: Global Sulphur Cap, Maritime vessel emissions, gaseous pollutants, particulate pollutants, Inland Sea

©2020. Japan Geoscience Union. All Right Reserved.

Spatiotemporal variations of NO_2 over Fukuoka Japan, observed by multiple MAX-DOAS and 3-D coherent Doppler lidar

*Hironobu Ueki[1], Hisahiro Takashima[2], Martina Michaela Friedrich[3]

1. Fukuoka university graduate school, 2. Fukuoka university, 3. Belgian Institute for Space Aeronomy

To clarify spatiotemporal variations and transport processes in nitrogen dioxide (NO_2) over Fukuoka, an urban area in Japan, continuous NO_2 profile observations using Multi Axis Differential Optical Absorption Spectroscopy (MAX-DOAS) with high temporal resolution of four minutes have been conducted since October 2018 at three observatories: Yakuin (33.580˚N, 130.396˚E), Sohara (33.580˚N, 130.356˚E) and Fukuoka University (33.550˚N, 130.364˚E).

We first performed case studies at particular days and observed enhanced NO_2 contents above the city center on some days. In the case of 29 November 2018, high NO_2 concentrations were observed near the ground in the morning (around 7:00–10:30 am). Higher contents of NO_2 appeared gradually at higher altitudes over the urban area, and disappeared at around 13:00–14:00 pm. We investigated a three-dimensional (3-D) wind field observed using a 3-D coherent Doppler lidar installed at Fukuoka University. The NO_2 variations were consistent with the wind variation: the airmass with high NO_2 concentration was transported upward from near the ground over an urban area; it advected southward (landward) because of a sea breeze in the afternoon.

We also validated the tropospheric NO_2 vertical column density (VCD) using the Sentinal-5P/TROPospheric Ozone Monitoring Instrument (TROPOMI) satellite with MAX-DOAS observations. Results showed that the satellite data are underestimates, as shown in earlier studies (e.g., Kanaya et al., 2014), but large variations exist from 34% to 154%. These results suggest that underestimation can be attributable not only to the shield effect by aerosols near the ground but also to inhomogeneity and transport processes of the NO_2 airmass over urban areas.

Keywords: NO2, MAX-DOAS, TROPOMI, doppler lidar

©2020. Japan Geoscience Union. All Right Reserved.

[E] Poster | A (Atmospheric and Hydrospheric Sciences)：A-AS Atmospheric Sciences, Meteorology & Atmospheric Environment

[A-AS08] Stratosphere-troposphere interaction

convener:Takatoshi Sakazaki(Graduate School of Science, Kyoto University), Takenari Kinoshita(Japan Agency for Marine-Earth Science and Technology), Pu Lin(Princeton University/NOAA Geophysical Fluid Dynamics Laboratory), Peter Hitchcock(Cornell University)

The dynamical, radiative, and chemical processes involved in the interactions between the stratosphere and troposphere are essential for understanding the present and future climate. Both observed data and high-resolution models have now clearly demonstrated that stratospheric processes can affect various tropospheric phenomena. Recently, processes coupling the troposphere and stratosphere in the tropical region have become a new focus.
 It has also been shown that the accuracy of tropospheric sub-seasonal and seasonal scale forecasts can be improved by more accurate representations of the stratosphere. As a result, interest is increasing in the predictability and reproducibility of specific stratospheric phenomena, including the Quasi-Biennial Oscillation (QBO) and its recent disruption as well as Stratospheric Sudden Warmings (SSW).
 This session will highlight recent progress in our understanding of stratosphere-troposphere interaction. We welcome studies of these and related phenomena in the troposphere and stratosphere (and mesosphere) based on observation, models and theory. Further, this session builds upon the middle atmosphere session traditionally held at the JpGU annual meetings and aims to provide a platform for sharing recent findings and promoting international collaborations on this topic.

[AAS08-P01] **Representation of the Equatorial Stratopause Semiannual Oscillation in Global Atmospheric Reanalyses**

*Yoshio Kawatani[1], Toshihiko Hirooka[2], Kevin Hamilton[3], Anne K. Smith[4], Masatomo Fujiwara[5] (1.Japan Agency for Marine-Earth Science and Technology, 2.Faculty of Science, Kyushu University, 3.International Pacific Research Center, University of Hawaii, 4.National Center for Atmospheric Research, 5.Faculty of Environmental Earth Science, Hokkaido University)

[AAS08-P02] Laplace's Atmosphere: An Array of Ringing Modes Discovered in Global Reanalysis Data

*Takatoshi Sakazaki[1], Kevin Hamilton[2] (1.Graduate School of Science, Kyoto University, 2.International Pacific Research Center and Department of Atmospheric Sciences, University of Hawai'i at Manoa)

[AAS08-P03] Bias correction of satellite multi-sensor total column ozone datasets and their merged ozone dataset

*Hiroaki Naoe[1], Takanori Matsumoto[2], Keisuke Ueno[3], Takashi Maki[1], Makoto Deushi[1], Ayako Takeuchi[2,4] (1.Meteorological Research Institute, 2.Japan Meteorological Agency, 3.Japan Meteorological Agency, Aerological Observatory, 4.Ministry of Land, Infrastructure, Transport and Tourism)

[AAS08-P04] **Relationship between the Boreal Summer Intra-seasonal Oscillation and the Stratospheric Quasi-Biennial Oscillation**

*Yayoi Harada[1] (1.Meteorological Research Institute)

[AAS08-P05] A statistical analysis of the turbulent kinetic energy dissipation rate estimated from the PMWE spectral width in the Antarctic

*Masashi Kohma[1], Kaoru Sato[1], Koji Nishimura[2], Masaki Tsutsumi[2], Toru Sato[3] (1.Department of Earth and Planet Science, Graduate School of Science, The University of Tokyo, 2.National Institute of Polar Research and The Graduate University for Advanced Studies (SOKENDAI), Tokyo, Japan, 3.Institute for Liberal Arts and Sciences, Kyoto University, Kyoto, Japan)

[AAS08-P06] Influence of stratospheric dynamics on tropical convection and equatorial waves

*Nawo Eguchi[1], Tomoe Nasuno[2], Kunihiko Kodera[3] (1.Kyushu University, 2.Japan Agency for Marine-Earth Science and Technology, 3.Meteorological Research Institute)

[AAS08-P07] The impact of stratosphere to troposphere: raising model top from 5hPa to 0.1hPa of GRAPES_GFS (weather model)

*Yong Su[1] (1.Yong Su)

[AAS08-P08] **Parametrization of tropical coastal nonstationary gravity waves robustizing QBO**

*Manabu D. Yamanaka[1] (1.Research Institute for Humanity and Nature / Professor Emeritus of Kobe University)

[AAS08-P10] Height-dependent expression for the energy flux of equatorial waves: exact and approximate versions for unified model diagnosis

*Hidenori AIKI[1,2], Fukutomi Yoshiki[1], Yuki Kanno[2], Tomomichi Ogata[2], Takahiro Toyoda[3], Hideyuki Nakano[3] (1.Nagoya University, 2.Japan Agency for Marine-Earth Science and Technology, 3.Meteorological Research Institute)

[AAS08-P11] CCMI stratospheric trends in relation to the stratospheric shrinkage

*Michal Zak[1], Petr Pisoft[1], Petr Sacha[1,2] (1.Dept. of Atmospheric Physics, Faculty of Mathematics and Physics, Charles University, Prague, Czech Republic, 2.Inst. of Meteorology, University of Natural Resources and Life Sciences, Vienna, Austria)

[AAS08-P12] A study of wave activities and ozone fluctuations around the Maritime Continent during YMC-BSM 2018

*Takenari Kinoshita[1], Junko Suzuki[1], Shin-Ya Ogino[1], Ryuichi Shirooka[1] (1.Japan Agency for Marine-Earth Science and Technology)

[AAS08-P13] **Traveling Planetary Waves in the Northern Hemisphere Winter Middle Atmosphere**

*Koki Iwao[1], Toshihiko Hirooka[2] (1.National Institute of Technology, Kumamoto College, 2.Kyushu University)

[AAS08-P14] Impact of Satellite Observations on Forecasting Sudden Stratospheric Warmings

*Shunsuke Noguchi[1,2], Yuhji Kuroda[2,3], Hitoshi Mukougawa[4], Ryo Mizuta[2], Chiaki Kobayashi[2] (1.Japan Agency for Marine-Earth Science and Technology, 2.Meteorological Research Institute, 3.Meteorological College, 4.Kyoto University)

Representation of the Equatorial Stratopause Semiannual Oscillation in Global Atmospheric Reanalyses

*Yoshio Kawatani[1], Toshihiko Hirooka[2], Kevin Hamilton[3], Anne K. Smith[4], Masatomo Fujiwara[5]

1. Japan Agency for Marine-Earth Science and Technology, 2. Faculty of Science, Kyushu University, 3. International Pacific Research Center, University of Hawaii, 4. National Center for Atmospheric Research, 5. Faculty of Environmental Earth Science, Hokkaido University

This paper reports on a project to compare the representation of the semiannual oscillation (SAO) in the equatorial stratosphere and lower mesosphere among six major global atmospheric reanalysis datasets and with recent satellite SABER and MLS observations. All reanalyses have a good representation of the quasi-biennial oscillation (QBO) in the equatorial lower and middle stratosphere and each displays a clear SAO centered near the stratopause. However, the differences among reanalyses are much more substantial in the SAO region than in the QBO dominated region. The degree of disagreement among the reanalyses is characterized by the standard deviation (SD) of the monthly-mean zonal wind and temperature; this depends on latitude, longitude, height, and time. The zonal wind SD displays a prominent equatorial maximum that increases with height, while the temperature SD is minimum near the equator and largest in the polar regions. Along the equator the zonal wind SD is smallest around the longitude of Singapore where consistently high-quality near-equatorial radiosonde observations are available. Interestingly the near-Singapore minimum in SD is evident to at least ~3 hPa, i.e. considerably higher than the usual ~10 hPa ceiling for *in situ* radiosonde observations. Our measurement of the agreement among the reanalyses shows systematic improvement over the period considered (1980–2016), up to near the stratopause. Characteristics of the SAO at 1 hPa, such as its detailed time variation and the displacement off the equator of the zonal wind SAO amplitude maximum, differ significantly among the reanalyses. Disagreement among the reanalyses becomes still greater above 1 hPa. One of the reanalyses in our study also has a version produced without assimilating satellite observations and a comparison of the SAO in these two versions demonstrates the very great importance of satellite derived temperatures in the realistic analysis of the tropical upper stratospheric circulation.

Keywords: middle atmosphere

©2020. Japan Geoscience Union. All Right Reserved.

Laplace's Atmosphere: An Array of Ringing Modes Discovered in Global Reanalysis Data

*Takatoshi Sakazaki[1], Kevin Hamilton[2]

1. Graduate School of Science, Kyoto University, 2. International Pacific Research Center and Department of Atmospheric Sciences, University of Hawai’ i at Manoa

We used newly-available ERA-5 hourly global reanalyses to examine the variations of atmospheric circulation on global scales and high frequencies. The space-time spectra of surface pressure displays a typical red background spectrum but also a striking number of isolated peaks. Some peaks represent astronomically forced tides but we show that most peaks are manifestations of the ringing of randomly excited global scale resonant modes. A few such modes have been tentatively identified in earlier observational investigations, but we demonstrate the existence of the full array of normal mode oscillations with periods as short as 2 hours. This is a powerful and uniquely detailed confirmation of the predictions of the theory of global oscillations that has its roots in the work of Laplace two centuries ago.

Keywords: Normal mode, Free oscillation, Surface pressure, Reanalysis

©2020. Japan Geoscience Union. All Right Reserved.

Bias correction of satellite multi-sensor total column ozone datasets and their merged ozone dataset

*Hiroaki Naoe[1], Takanori Matsumoto[2], Keisuke Ueno[3], Takashi Maki[1], Makoto Deushi[1], Ayako Takeuchi[2,4]

1. Meteorological Research Institute, 2. Japan Meteorological Agency, 3. Japan Meteorological Agency, Aerological Observatory, 4. Ministry of Land, Infrastructure, Transport and Tourism

This study evaluates 20 level 2 total column ozone (TCO) datasets acquired covering the 40 years from 1978 to 2017, by comparing satellite overpass data coincident with ground-based Dobson and Brewer spectrophotometer measurements. These 20 individual TCO datasets and a merged TCO datasets are corrected for systematic mean biases and drift. Two bias correction methods are used: simple linear regression (SLR) fitting of the data as a function of time and multiple linear regression (MLR) fitting of the data as a function of time, solar zenith angle, and effective ozone temperature. All of the satellite datasets agree well, within ±1-2%, with the ground-based measurements, except for some degraded data from the Total Ozone Mapping Spectrometer (TOMS)/Earth Probe during a terminated period and from the Ozone Mapping and profiling Suite (OMPS) provided from NOAA at an early stage of measurements. The OMPS data provided from NASA do not show any significant bias or trend relative to the ground-based data. The Global Ozone Monitoring Experiment/MetOp-A and -B datasets show abrupt changes of up to 7-8 DU coincident with the introduction of a new retrieval algorithm. The root mean square error of uncorrected merged datasets, 8.6 DU, is reduced to 8.4 DU after correction by multiple linear regression. Further, the negative trend is seen in 1979-1996 in the uncorrected merged dataset is reduced by 2 DU per decade in the corrected dataset. The TCO trend during 2000-2017 does not differ between the uncorrected and corrected merged datasets.

Reference

Naoe, H., T. Matsumoto, K. Ueno, T. Maki, M. Deushi, and A. Takeuchi, 2020: Bias correction of multi-sensor total column ozone satellite data for 1978-2017. J. Meteor. Soc. Japan, 98, https://doi.org/10.2151/jmsj.2020-019.

Acknowledgments

This research was supported by the Environment Research and Technology Development Fund (S-12) of the Environmental Restoration and Conservation Agency of Japan and by Grant-in-Aid (JP18K03748) for Science Research (KAKENHI) from the Ministry of Education, Culture, Sports, Science, and Technology of Japan.

Keywords: total column ozone, bias correction, satellite level 2, merged total ozone

©2020. Japan Geoscience Union. All Right Reserved.

Relationship between the Boreal Summer Intra-seasonal Oscillation and the Stratospheric Quasi-Biennial Oscillation

*Yayoi Harada[1]

1. Meteorological Research Institute

In the equatorial stratosphere, quasi-biennial oscillation (QBO) is the dominant mode. The previous studies have shown the influence of QBO on Madden Julian Oscillation (MJO) during the austral summer (Nshimoto and Yoden 2017; Son et al. 2017). On the other hand, Kikuchi et al. (2012) pointed out that boreal summer intra-seasonal oscillation (BSISO), in which active convective region migrate northward in the Indian Ocean and the western Pacific with a period of 30 –90 days, is the dominant mode compared to MJO during the boreal summer. In this study, statistical relationships between stratospheric BSISO and QBO are examined. BSISO index based on Kikuchi et al. (2012), the Japanese 55-year Reanalysis (JRA-55, Kobayashi et al. 2015), ERA-Interim (Dee et al. 2011), and cloud top pressure (Rossw and Schiffer 1999) provided by International Satellite Cloud Climatology Project (ISCCP, Schiffer and Rossw 1983) are used for composite analysis.

The results reveal that the amplitudes of BSISO tend to be extraordinarily large during the strong low-frequency easterly anomalies at around the 20-hPa level associated with QBO. we also found that the frequency of lower cloud top pressures (higher cloud top heights) tend to increase during the strong easterly phase of QBO in the BSISO region. Moreover, we analyze the vertical profile of the static stability around the tropopause. The results obtained from the two reanalyses show more unstable (stable) condition in the lower stratosphere in BSISO region during the strong and weak easterly phases (westerly phase) of QBO, although the vertical profiles of the static stability in the upper troposphere are different from each other.

References

Dee, D. P., and coauthers, 2011: *Quart. J. Roy. Meteor. Soc.*, 137, 553–597.

Kikuchi, K., B. Wang, and Y. Kajikawa 2012: *Clim. Dyn.*, 38, 1989–2000.

Kobayashi, S., and Coauthors, 2015: *Journal of the Meteorological Society of Japan*, 93(1), 5–48.

Nishimoto, E., and S. Yoden 2017: *J. Atmos. Sci.*, 74, 1105–1124.

Rossow, W.B., and R.A. Schiffer, 1999: *Bull. Amer. Meteorol. Soc.*, 80, 2261-2288.

Schiffer, R.A., and W.B. Rossow, 1983: *Bull. Amer. Meteorol. Soc.*, 64, 779-784.

Son, S.-W., Y. Lim, C. Yoo, H. H. Hendon, and J. Kim, 2017: *J. Climate*, 30, 1909–1922.

Keywords: Boreal Summer Intra-seasonal Oscillation , Stratospheric Quasi-Biennial Oscillation, cloud top height, static stability

©2020. Japan Geoscience Union. All Right Reserved.

©2020. Japan Geoscience Union. All Right Reserved.

A statistical analysis of the turbulent kinetic energy dissipation rate estimated from the PMWE spectral width in the Antarctic

*Masashi Kohma[1], Kaoru Sato[1], Koji Nishimura[2], Masaki Tsutsumi[2], Toru Sato[3]

1. Department of Earth and Planet Science, Graduate School of Science, The University of Tokyo, 2. National Institute of Polar Research and The Graduate University for Advanced Studies (SOKENDAI), Tokyo, Japan, 3. Institute for Liberal Arts and Sciences, Kyoto University, Kyoto, Japan

The radar volume reflectivity and turbulent kinetic energy dissipation rate in the Antarctic mesosphere have been estimated from the polar mesosphere winter echoes (PMWE) using a vertical beam of the PANSY radar, which is a Mesosphere-Stratosphere-Troposphere radar, at Syowa Station (69˚S, 40˚E) over four years. The radar volume reflectivity exhibits a lognormal distribution in the range of 2×10^{-18}–5×10^{-15} m^{-1} for a height region of 55–82 km. The turbulent energy dissipation rate estimated from the spectral width of the PMWE ranges from 3×10^{-5}–3×10^{-1} m^2s^{-3}. From monthly histograms of the turbulent energy dissipation rate for a fixed solar zenith angle and altitude, it is revealed that the summer-to-winter transition of the turbulent energy dissipation rate occurs in March, while the winter-to-summer transition occurs in September. This seasonal variation accords well with that of gravity wave activity, suggesting that the turbulence in the mesosphere is likely caused by the gravity wave breaking.

Keywords: Mesosphere, Turbulent energy dissipation rate, Polar Mesosphere Winter Echoes, MST radar

©2020. Japan Geoscience Union. All Right Reserved.

Influence of stratospheric dynamics on tropical convection and equatorial waves

*Nawo Eguchi[1], Tomoe Nasuno[2], Kunihiko Kodera[3]

1. Kyushu University, 2. Japan Agency for Marine-Earth Science and Technology, 3. Meteorological Research Institute

Previous studies based on satellite observational data and model simulation found an enhancement of tropical convection in association with an abrupt change in tropical circulation during a Stratospheric Sudden Warming (SSW) event. The principal process of the stratospheric impact on the tropospheric variability could be a decrease of the static stability in the Tropical Tropopause Layer (TTL) by intensified upwelling in ascending branch of the Brewer-Dobson circulation [Eguchi and Kodera, 2007; 2010; Kodera et al., 2011, 2015; Eguchi et al., 2015]. The present study focused on enhanced deep convection and tropical cyclones over the southwestern Indian Ocean and the southwestern Pacific Ocean during the SSW event in January 2010 simulated in a global nonhydrostatic model, NICAM (Nonhydrostatic ICosahedral Atmospheric Model) [Satoh, et al., 2014] which explicitly calculates moist physics at a cloud-system-resolving resolution.
The upwelling in the lower stratosphere associated with the SSW event started around 5 January 2010, and the deep convection was formed from 8 to 14 January along 10 south degree latitude in the whole tropics (except for South American sector in the simulation) due to the negative static stability at the upper layers at TTL. In particular, the precipitation was extended longitudinally over the Indian Ocean after 8 January, which developed over high SST region across the Indian Ocean. A tropical cyclone developed within this region on 11 January. It is noted that deep convection was enhanced over the equatorial Africa on 8 and 9 January before enhancement of the longitudinally extended precipitation over the Indian Ocean. Eastward propagation of a convective coupled Kelvin waves from the Africa to the Maritime continent, might excite the longitudinally extended precipitation through a reduction of the static stability in the TTL. The convection over the Maritime continent was enhanced around 15 January when the Kelvin wave arrived there. Difference in responses of convective activity over the equatorial Africa and that over the Maritime Continent could be arose from a difference in convective characteristic in two regions such as higher cloud top altitude over Africa than that over the Maritime Continent.

Keywords: Stratosphere-Troposphere Interaction, Tropical meteorology

©2020. Japan Geoscience Union. All Right Reserved.

The impact of stratosphere to troposphere: raising model top from 5hPa to 0.1hPa of GRAPES_GFS (weather model)

*Yong Su[1]

1. Yong Su

Over the past 15 or so years, there has been an increasing recognition of the role of the stratosphere in modulating tropospheric processes, especially for the winter hemisphere. Forecast centers such as ECMWF, Met Office have moved their model tops to the middle mesosphere, 80km or 0.01hPa, the GEM of ECCC also move their model top to 0.1hPa.

The Global Regional Assimilation and PrEdiction System, Global Forecast System, GRAPES_GFS, independently developed by the Numerical Weather Prediction Center of China Meteorological Administration, main task is the operational application of 0 to 10 day weather forecast. At present, the horizontal resolution is 0.25 degree, in vertical direction, height based terrain following coordinate is adopted, 60 layers, the model top is about 5hpa, located in the middle of stratosphere.

For the GRAPES_GFS, the model top is to low compare to other centers. The problem is that, on the one hand, the weather model generally adopts rigid boundary conditions, the distribution of the real atmosphere cannot be correctly simulated near the model top, so the low model top will cause the prediction deviation of the troposphere to increase gradually in the long-term cycle integration; On the other hand, raising the model top can make more satellite data into the data assimilation system, and this can directly improve the prediction effect of the stratosphere.

Based on the experience of IFS and GEM, we increase the vertical level of GRAPES_GFS from 60 to 87, and the model top is increased from 5hpa to 0.1hpa. We redesigned the sponge layer of the model, mainly including the Rayleigh Friction scheme which is close to the monthly average state, the W implicit damping scheme which changes with the altitude and latitude; In the physical process, we introduced the New non orographic gravity wave scheme, debugged the orographic gravity wave drag scheme, and adjusted the equation of saturation specific humidity at low temperatures.

Through the 4Dvar cycle forecast, we tested the prediction ability of the new high top system, with more reasonable simulation of the stratosphere and mesosphere, the prediction ability in troposphere is improved.

Keywords: GRAPES GFS, Stratosphere, Troposphere, Model top, Sponge layer

©2020. Japan Geoscience Union. All Right Reserved.

Parametrization of tropical coastal nonstationary gravity waves robustizing QBO

*Manabu D. Yamanaka[1]

1. Research Institute for Humanity and Nature / Professor Emeritus of Kobe University

The most dominant mode of cloud-rainfall generation in the equatorial troposphere is the diurnal cycle, which is seen typically in the world's longest coastlines surrounding major islands of the Indonesian maritime continent (IMC). Under the linear theory the coastal diurnal-cycle (so-called sea-land breeze) circulation is given by a sum of wave solutions, of which the dispersion relation is a cubic equation for vertical wavenumber squared m^2. Near the surface with large eddy viscosity/diffusivity (m^6 term) balancing the buoyancy (m^0 term), the velocity field is almost similar to a steady horizontal-convection cell, of which the intensity and horizontal scale (inverse horizontal wavenumber k^{-1}) are governed by the land-sea temperature contrast $k\Delta T$. Above this cell, with decreasing the viscosity/diffusivity, the acceleration (m^2 term) balances the buoyancy, which gives a combination of up/down-ward propagating gravity waves. Because $k\Delta T$ is reversed between day and night (with frequency $\omega = 2\pi/1$ day), the horizontal phase velocity $c = \omega/k$ directs land- and sea-ward, respectively. They are observed actually along the coastline of a major island larger than k^{-1} of a few hundreds of kilometers. They are longer and slower ($c \simeq 1\text{–}3\times10^2$ km/10 h $\simeq$ 3–7 m/s) than waves excited with an individual cloud convection, but shorter than intraseasonal scales (Kelvin or mixed Rossby-gravity waves).

With increasing altitude, the upward-propagating component of gravity waves is amplified to compensate the density decrease. Because the coastline is a closed curve, there are waves with c of all directions. However, waves with c of meridional directions may be filtered out by the Hadley meridional circulation, except for a calm zone along the equator (the ITCZ). The intraseasonal variations (Madden-Julian oscillations) with zonal (Walker-like) circulations pare down usually before landing the IMC (and the two true continents of Africa and South America). Therefore, waves with c of zonal (both east- and west-ward) directions are transmitted upward beyond the tropopause along the equator, which resembles Plumb's (1977) model considering waves with two discrete (equal but opposite) zonal c. If the velocity amplitude $|u|$ (with c of either east- or west-ward) reaches the magnitude of intrinsic phase velocity $|c - U|$ in a mean wind U, the wave breaks and U is accelerated (east- or west-ward, dependent on c), as parameterized for the middle atmospheric circulation since Lindzen (1981). Both east- and west-ward gravity waves are emitted upward from the tropical coasts every day, and their interactions with the middle-atmospheric circulation may induce the robust features of the stratospheric QBO. The wave amplitude $|u|$ and resulting acceleration (periodicity and amplitude of the QBO) are dependent on $k\Delta T$, which may be varied also with interannual variations of sea-surface temperature and much longer time-scale variations of the land distribution.

Keywords: diurnal-cycle sea-land breeze circulations, internal gravity waves, wave-mean flow interaction, quasi-biennial oscillation

©2020. Japan Geoscience Union. All Right Reserved.

Height-dependent expression for the energy flux of equatorial waves: exact and approximate versions for unified model diagnosis

*Hidenori AIKI[1,2], Fukutomi Yoshiki[1], Yuki Kanno[2], Tomomichi Ogata[2], Takahiro Toyoda[3], Hideyuki Nakano[3]

1. Nagoya University, 2. Japan Agency for Marine-Earth Science and Technology, 3. Meteorological Research Institute

Synoptic scale waves in the atmosphere and ocean play an important role in the teleconnection of tropical and subtropical regions. For mid-latitude Rossby waves in the atmosphere, the expression for the energy flux for use in a model diagnosis, and without relying on a Fourier analysis or a ray theory, has previously been derived using quasi-geostrophic equations and is singular at the equator. A recent analytical study has derived an exact universal expression for the energy flux which can indicate the direction of the group velocity at latitudes for linear shallow water waves (Aiki et al., 2017 PEPS, doi:10.1186/s40645-017-0121-1). This analytical result is extended in the present study to a height-dependent framework for zonally and vertically propagating equatorial waves in the atmosphere. This is achieved by investigating the classical analytical solution of equatorial inertia-gravity waves, Rossby waves, mixed Rossby-gravity waves, and Kelvin waves. Expressions for the horizontal component of the energy flux are similar to each other between the height-dependent framework given by the present study and the height-independent framework given by Aiki et al. (2017), both of which are linked to a scalar quantity associated with the inversion of Ertel’ s potential vorticity (EPV). This EPV- inverted scalar quantity reduces to geostrophic streamfunction for mid-latitude Rossby waves and vanishes for gravity waves, a novel aspect for considering the energy flux. The expression of the vertical component of the energy flux, as given by the present study, requires computation of another scalar quantity based on a three-dimensional Fourier analysis in the combination of a zonal-vertical section and time space. For ease of diagnosis from a model, an approximate version of the universal expression is explored and illustrated for the development of tropical synoptic-scale waves observed in the Indian Ocean–Maritime Continent region during Austral summer.

Keywords: group velocity, tropical-extratropical interaction

©2020. Japan Geoscience Union. All Right Reserved.

CCMI stratospheric trends in relation to the stratospheric shrinkage

*Michal Zak[1], Petr Pisoft[1], Petr Sacha[1,2]

1. Dept. of Atmospheric Physics, Faculty of Mathematics and Physics, Charles University, Prague, Czech Republic, 2. Inst. of Meteorology, University of Natural Resources and Life Sciences, Vienna, Austria

Warming of the troposphere is directly connected with a positive trend of geopotential heights of pressure levels. This trend reaches its maximum around the tropopause and results also in the tropopause upward shift. In the stratosphere, the geopotential height trends are affected by the stratospheric cooling –there is a gradual reduction of the upward shift and even its reversal at about 10 hPa. That leads to a decreasing trend of the stratospheric thickness - a so-called stratospheric shrinkage. In this study, we calculate CCMI inter-model correlations of shrinkage with trends of various variables to separate the possible shrinkage effect and to analyze influence of the shrinkage on other middle atmospheric trends detected in the CCMI simulations.

Keywords: stratospheric shrinkage, CCMI, stratospheric trends

©2020. Japan Geoscience Union. All Right Reserved.

A study of wave activities and ozone fluctuations around the Maritime Continent during YMC-BSM 2018

*Takenari Kinoshita[1], Junko Suzuki[1], Shin-Ya Ogino[1], Ryuichi Shirooka[1]

1. Japan Agency for Marine-Earth Science and Technology

The Transformed-Eulerian Mean (TEM) equations proposed by Andrews and McIntyre are useful tools for diagnosing the relationship between wave activities and the mean state. The three-dimensional (3D) extension of TEM equations has been conducted since 1980s and the recent study uses the 3D wave activity flux for the analysis of special structure of Rossby wave activities during Stratospheric Sudden Warming. On the other hand, to investigate the material transport associated with wave activities, it is necessary to consider the mean geostrophic flow (balanced flow) and the phase structure of stationary waves, which are included in the horizontal component of the 3D residual flow. Then, a unified analysis method using the 3D residual flow has not been established.
Based on the above, the purpose of this study is to establish a method for diagnosing the 3D structure of material transport associated with wave activities. We report the results of investigation on wave activities and ozone fluctuation around the Maritime Continent during the YMC-BSM 2018 campaign.

Keywords: meridional circulation, wave activities

©2020. Japan Geoscience Union. All Right Reserved.

Traveling Planetary Waves in the Northern Hemisphere Winter Middle Atmosphere

*Koki Iwao[1], Toshihiko Hirooka[2]

1. National Institute of Technology, Kumamoto College, 2. Kyushu University

It is a well-established overview that quasi-stationary planetary waves propagating upward from the troposphere dissipate in the stratosphere to drive the meridional circulation in the winter hemisphere, while the meridional circulation in the mesosphere is driven mainly by gravity waves. On the other hand, the importance of traveling planetary waves in the stratosphere and mesosphere has been underscored in recent studies to bring about significant impacts on mean flows through their generation and dissipation. However, observational studies are insufficient for this region, so that detailed features are still unclear. Hence, this study investigates contributions of planetary waves (PWs) to the mean flow in the stratosphere and mesosphere during the Northern Hemisphere winter when PW activities are strong, by analyzing satellite data from Sounding of the Atmosphere using Broadband Emission Radiometry (SABER). Our analyses suggest that there would be a cancellation mechanism between easterly acceleration by monthly mean stationary planetary waves (STPWs) and westerly acceleration by remaining travelling planetary waves (TRPWs) in the polar lower mesosphere. When easterly winds appear in the mesosphere, STPWs propagating from the troposphere would dissipate in the lower mesosphere to accelerate easterly winds because STPWs could not propagate in easterly regions, but TRPWs would be generated there due to barotropic and/or baroclinic instability caused by the easterly winds in the mesosphere and accelerate westerly winds. This cancellation would contribute to maintain the easterly wind in the mesosphere for more than 10 days in some cases. Further analyses reveal that the wave generated in the polar lower mesosphere would be a downward propagating TRPW with a zonal wave number 1 traveling eastward with a period ~20 days. Moreover, the easterly wind in the mesosphere is frequently triggered by the dissipation of TRPWs developed in the stratosphere in the recovery phase of sudden stratospheric warmings, in addition to the dissipation of STPW propagating from lower layers.

Keywords: Planetary wave, Stratospheric sudden warming, Stratosphere, Mesosphere

©2020. Japan Geoscience Union. All Right Reserved.

Impact of Satellite Observations on Forecasting Sudden Stratospheric Warmings

*Shunsuke Noguchi[1,2], Yuhji Kuroda[2,3], Hitoshi Mukougawa[4], Ryo Mizuta[2], Chiaki Kobayashi[2]

1. Japan Agency for Marine-Earth Science and Technology, 2. Meteorological Research Institute, 3. Meteorological College, 4. Kyoto University

The observational impacts of satellite data assimilation on extended-range forecasts of sudden stratospheric warmings (SSWs) are investigated by conducting ensemble forecast experiments. We use two Japanese novel reanalysis products: the Japanese 55-year reanalysis (JRA-55) and its subset that assimilates conventional observations only (JRA-55C). A comparative examination on the reproducibility for SSWs between the two ensemble forecasts reveals that the impact of satellite observations is significant for forecasts starting 5 days before the SSW onset, with 20% less accuracy in the JRA-55C forecasts. Moreover, some of forecasts of vortex-splitting SSWs show a sudden appearance of deep difference, which lasts over a few months in the lower stratosphere and significantly affects the surface climate. These results highlight an important role of mesospheric and upper stratospheric circulations on the onset and development of SSWs.

Reference: https://doi.org/10.1029/2019GL086233

Keywords: sudden stratospheric warming, stratosphere-troposhere coupling, satellite data assimilation, predictability, sub-seasonal to seasonal prediction, reanalysis

©2020. Japan Geoscience Union. All Right Reserved.

[E] Poster | A (Atmospheric and Hydrospheric Sciences)：A-AS Atmospheric Sciences, Meteorology & Atmospheric Environment

[A-AS09] Cloud-Resolving Model Simulations for Climate and Weather Studies

convener:Toshihisa Matsui(NASA Goddard Space Flight Center), Masaki Satoh(Atmosphere and Ocean Research Institute, The University of Tokyo), Wei-Kuo Tao(NASA Goddard Space Flight Center)

Cloud-resolving models (CRMs) employs nonhydrostatic dynamic core, explicit microphysics and radiation processes to provide physically-realistic simulations of cloud structures, optical properties, and latent heat release, without parameterizing deep convection in coarse-resolution weather and climate models. CRMs can be run at a few km down to sub-km of horizontal grid spacing depending on science application and focused cloud systems. Over the past few decades, CRMs have been utilized in a variety of weather and climate studies; such as 1) understanding cloud-precipitation processes and interactions with aerosols, surface, radiation, and lightning processes, 2) evaluating and developing microphysics and convection with various in-situ and remote sensing observations, and 3) addressing climate issues to develop or replace convective-cloud parametrizations for global or regional atmospheric models. The goal of this session is to showcase the current efforts for these studies in the atmospheric community.

[AAS09-P01] Polarimetric Radar Characteristics of Simulated and Observed Intense Convective Cores for a Midlatitude Continental and Tropical Maritime Environment

*Toshihisa Matsui[1,2], Brenda Dolan[3], Takamichi Iguchi[1,2], Steven A. Rutledge[3], Wei-Kuo Tao[1], Stephen Lang[1,4] (1.NASA Goddard Space Flight Center, 2.ESSIC University of Maryland, 3.Colorado State University, 4.Science Systems and Applications, Inc)

[AAS09-P03] Videosonde and HYVIS cloud particle imaging radiosondes: Carrier frequency migration from 1680 to 400 MHz

*Norio Nagahama[1], Kensaku Shimizu[1], Takuji Sugidachi[1], Kenji Yamaguchi[1], Kenji Suzuki[2], Fujiwara Masatomo[3] (1.meisei electric co.,ltd., 2.Graduate School of Sciences and Technology for Innovation, Yamaguchi University, 3.Faculty of Environmental Earth Science, Hokkaido University)

Polarimetric Radar Characteristics of Simulated and Observed Intense Convective Cores for a Midlatitude Continental and Tropical Maritime Environment

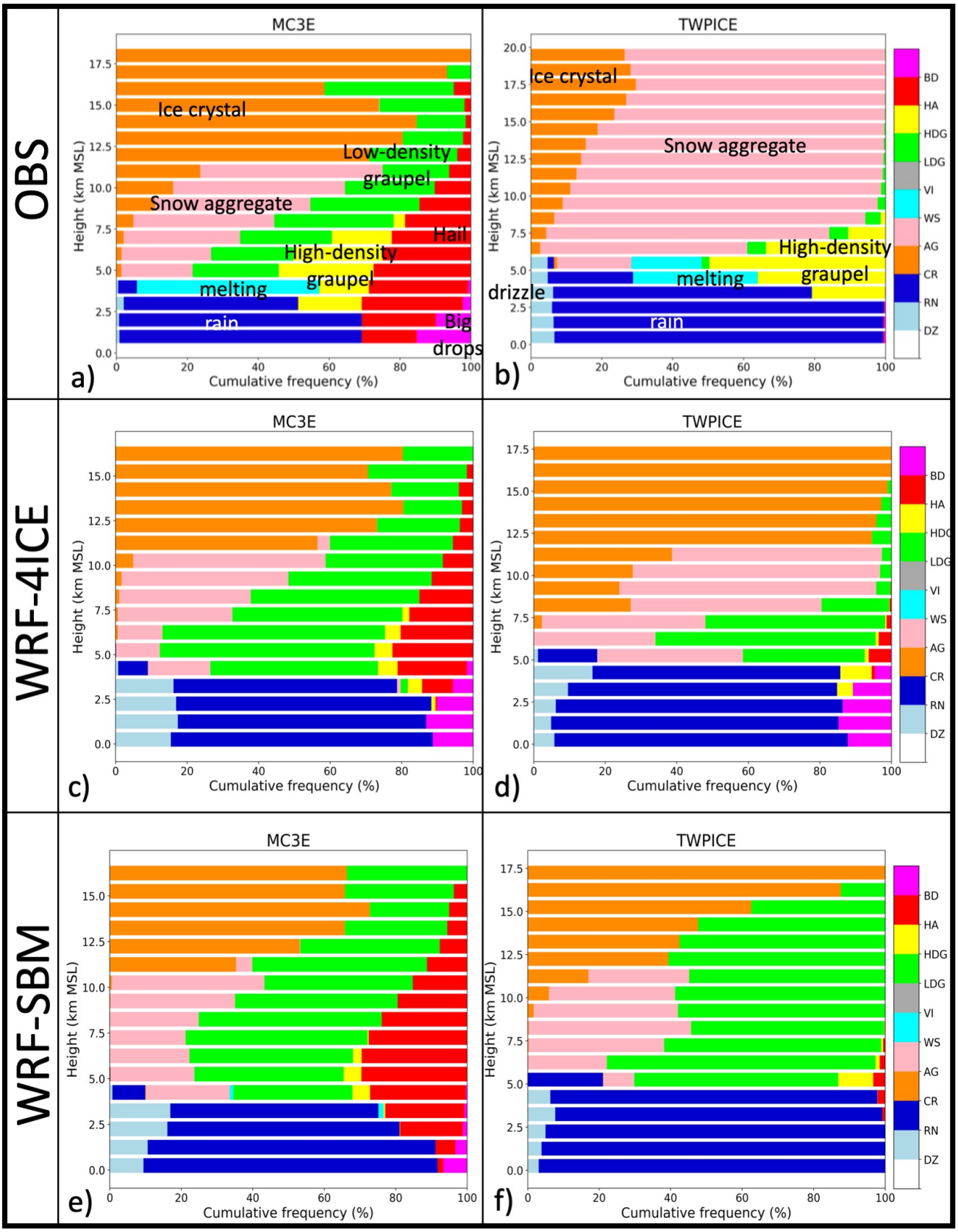
*Toshihisa Matsui[1,2], Brenda Dolan[3], Takamichi Iguchi[1,2], Steven A. Rutledge[3], Wei-Kuo Tao[1], Stephen Lang[1,4]

1. NASA Goddard Space Flight Center, 2. ESSIC University of Maryland, 3. Colorado State University, 4. Science Systems and Applications, Inc

This study contrasts midlatitude continental and tropical maritime deep convective cores using polarimetric radar observables and retrievals from selected deep convection episodes during the MC3E and TWPICE field campaigns. The continental convective cores produce stronger radar reflectivities throughout the profiles, while maritime convective cores produce more positive differential reflectivity (Z_{dr}) and larger specific differential phase (K_{dp}) above the melting level. Hydrometeor identification retrievals revealed the presence of large fractions of rimed ice particles (snow aggregates) in the continental (maritime) convective cores, consistent with the Z_{dr} and K_{dp} observations. The regional cloud-resolving model simulations with bulk and size-resolved bin microphysics are conducted for the selected cases, and the simulation outputs are converted into polarimetric radar signals and retrievals identical to the observational composites. Both the bulk and the bin microphysics reproduce realistic land and ocean (L-O) contrasts in reflectivity, polarimetric variables of rain drops, and hydrometeor profiles, but there are still large uncertainties in describing Z_{dr} and K_{dp} of ice crystals associated with the ice particle shapes/orientation assumptions. Sensitivity experiments are conducted by swapping background aerosols between the continental and maritime environments, revealing that background aerosols play a role in shaping the distinct L-O contrasts in radar reflectivity associated with raindrop sizes, in addition to the dominant role of background thermodynamics.

Keywords: Polarimetric radar, continental and maritime deep convection, cloud-resolving model

©2020. Japan Geoscience Union. All Right Reserved.



©2020. Japan Geoscience Union. All Right Reserved.

Videosonde and HYVIS cloud particle imaging radiosondes: Carrier frequency migration from 1680 to 400 MHz

*Norio Nagahama[1], Kensaku Shimizu[1], Takuji Sugidachi[1], Kenji Yamaguchi[1], Kenji Suzuki[2], Fujiwara Masatomo[3]

1. meisei electric co.,ltd., 2. Graduate School of Sciences and Technology for Innovation, Yamaguchi University, 3. Faculty of Environmental Earth Science, Hokkaido University

The Videosonde and HYVIS (Hydrometer Videosonde), which are weather-balloon-borne special instruments for observing cloud/precipitation particles, have been developed since the late 1980s to understand cloud microphysics. They are able to downlink images of cloud/precipitation particles to the ground station by using 1680 MHz band radiowaves. The Videosonde captures video images of precipitation particles in the air without contact to those particles. It sends those images to the ground station in real time and can provide information on the size and shape of those particles such as raindrops, snowflakes and graupel. It also has an induction ring to measure the electric charge of the particles. On the other hand, the HYVIS focuses on cloud particles, utilizing a method in which the images of cloud particles deposited on a clear filmstrip are taken with a microscope and sent to the ground station in real time.

The Videosonde and HYVIS have been used as a strong tool for understanding cloud microphysics. In the 2000s, with the progress of remote sensing technology such as cloud radars, and with the progress of cloud-resolving models, these instruments were started to be used also as a reference instrument.

Although the 1680 MHz carrier radiowaves used in the Videosonde and HYVIS systems have been designated as a meteorological band until now, the band is being considered worldwide to be open for other uses in the future. Therefore, the migration of the frequency to 400 MHz also needs to be considered for Videosonde and HYVIS. In the current Vidoesonde and HYVIS, the NTSC video signals of 30 fps outputted from the cameras are connected directly to the transmitter and are downlinked to the ground receiving system with 1680 MHz radiowaves. Because these video signals are analog, the received images become lower in quality as the balloon goes higher and farther. As a result, there is larger uncertainty when analyzing cloud/precipitation particles taken at a longer distance from the ground receiving system. In addition, it is not easy to utilize automatic image processing softwares to analyze the particle images because the quality of the images is unstable. To solve these issues, a digital transmission that does not cause image degradation within the data receivable range needs to be considered.

The bandwidth allowed for the 400 MHz band is 60 KHz. Experiments were conducted with various communication rates, modulation depths, and modulation methods. It was found that baudrate of 56 Kbps, deviation of 14 KHz, and modulation index of 0.5 are the upper limits that conform to the radiowave standard. Assuming that the transmission rate is 50 Kbps, 6 KBytes of data can be sent per second. A black-and-white image of 640 x 480 pixels is 50 to 100 KBytes per image, depending on complexity of the image. Considering the balance between the image quality and the image size, the optimal setting may be to compress the image to 10 KByte or less and to transmit one image every 2 seconds. Unlike analog images, digital images do not deteriorate with the transmission distance. Thus, stable image quality can be expected.

*This research and development work was supported by the MIC/SCOPE #195003007 in Japan.

©2020. Japan Geoscience Union. All Right Reserved.

Keywords: radiosonde, cloud/precipitation particle image

©2020. Japan Geoscience Union. All Right Reserved.

[E] Poster | A (Atmospheric and Hydrospheric Sciences)：A-AS Atmospheric Sciences, Meteorology & Atmospheric Environment

[A-AS10] Land-Atmosphere interactions and precipitation variations over the Asian monsoon region.

convener:Hiroshi G. Takahashi(Department of Geography, Tokyo Metropolitan University), Hirokazu Endo(Meteorological Research Institute, Japan Meteorological Agency), Shiori Sugimoto(JAMSTEC Japan Agency for Marine-Earth Science and Technology), Hatsuki Fujinami(Nagoya University)

This session aims to discuss land-atmosphere interaction over the Asian monsoon region because this interaction is one of the essential components of the Asian monsoon system. Precipitation characteristics and cloud-precipitation processes are closely tied with land-atmosphere interactions, which are also a key target. Over Asia, climate are various, which produces various land-atmosphere-precipitation interactions. Influences of complex topography on precipitation characteristics are also considered. It may be interesting that the interactions can vary with scales in space and in time.
In addition, monsoon precipitation variability is a target of this session, which can be also associated with land surface conditions. We would like to approach the mechanism behind the precipitation/precipitation characteristics variability. In addition, to understand past and future precipitation variability, impacts of land-use changes and/or global warming should be considered. A large variety of observation, numerical modeling and their combined analyses are encouraged.

[AAS10-P01] **Spatial differences of the Tibetan Plateau monsoon and its application**

*Shaobo Zhang[1], Xianyu Yang[1], Yong Zhao[1] (1.Chengdu University of Information Technology)

[AAS10-P02] The concurrent effects of the South Asian monsoon and Tibetan plateau monsoon on summer rainfall in Tarim Basin of China

*YONG ZHAO[1], XIAOJING YU[2] (1.Chengdu University of Information Technology, 2.Institute of Desert Meteorology, CMA)

[AAS10-P03] Numerical simulations of precipitation in high altitude Himalaya mountainous area by using JMA-NHM

*Akihiro Hashimoto[1], Masashi Niwano[1], Hatsuki Fujinami[2], Akiko Sakai[3], Koji Fujita[3] (1.Meteorological Research Institute, Japan Meteorological Agency, 2.Institute for Space-Earth Environmental Research, Nagoya University, 3.Graduate School of Environmental studies, Nagoya University)

[AAS10-P04] Moisture sources of summer precipitation over eastern China during 1979–2009: A Lagrangian transient simulation

*QIN HU[1] (1.Chengdu University of Information Technology)

[AAS10-P05] **Study on the severe weather caused by mesoscale convective system on the Meiyu front in northwestern Taiwan**

*LI-ZHEN SU[1], Jou-Ping Hou[1], Ba-Xiu Wei[2] (1.Chung Cheng Institute of Technology National Defense University, 2.Air Force Weather Wing)

[AAS10-P06] **Long-term trends and interannual variability in precipitation over Vietnam during 1984-2016**

*Hoa Thi Thanh Pham[1], Hiroshi G. Takahashi[1] (1.Department of Geography, Tokyo Metropolitan University)

[AAS10-P07] Recent increase of rain-on-snow events and rain proportion in north-eastern Japan

*Alexander Brandt[1,2], Maximo Larry Lopez Caceres[1] (1.Yamagata University, 2.United Graduate School of Agricultural Scienes (UGAS))

[AAS10-P08] Regional snowfall and precipitation distributions in a Japan-Sea side of central Japan associated with low-frequency variabilities in the Eurasian and East Asian regions

*Akira Yamazaki[1], Meiji Honda[2], Hiroaki Kawase[3] (1.Application Laboratory, Japan Agency for Marine-Earth Science and Technology, 2.Niigata University, 3.Meteorological Research Institute, Japan Mereorological Agency)

[AAS10-P09] Quantitative identification of moisture sources over the Tibetan Plateau and the relationship between thermal forcing and moisture transport

*Chen Pan[1,2,3,4], Bin Zhu[3,4], Zhiming Kang[1,2] (1.Jiangsu Meteorological Observatory, Nanjing, China, 2.Key Laboratory of Transportation Meteorology, China Meteorological Administration, Nanjing, China, 3.Key Laboratory for Aerosol-Cloud-Precipitation of China Meteorological Administration, Nanjing University of Information Science & Technology, Nanjing, China, 4.Collaborative Innovation Center on Forecast and Evaluation of Meteorological Disasters, Nanjing University of Information Science & Technology, Nanjing, China)

[AAS10-P10] **Multi-scale convection system simulation during Meiyu season in Taiwan**

*Yi Hao Liao[1], Jou-Ping Hou[1], Yu-De Wu[2] (1.Department of Environmental Information and Engineering, CCIT, National Defense University, 2.Air Force Weather Wing)

[AAS10-P11] Responses of rainfall characteristics to the land surface conditions over the wet Asian monsoon region

*Hiroshi G. Takahashi[1] (1.Department of Geography, Tokyo Metropolitan University)

[AAS10-P12] Analysis of Characteristics and Causes of Meiyu over the Yangtze–Huai River Basin in 2019

*Ruoyun Niu[1] (1.National Meteorological Center, China Meteorological Administration)

[AAS10-P13] Similarities and differences of summer persistent heavy rainfall and atmospheric circulation characteristics in the middle and lower reaches of the Yangtze River between 2016 and 1998

*Xiaolin ZHAO[1] (1.National Meteorological Centre, China Meteorological Administration)

[AAS10-P14] **Characteristics of the Precipitation Diurnal Variation over Jiangsu, Eastern China during Warm Season**

*Xiyu Mu[1], Qi Xu[2], Yang Wu[3], Anning Huang[3] (1.Key Laboratory of Transportation Meteorology of CMA; Jiangsu Institute of Meteorological Sciences; Nanjing Joint Institute for Atmospheric Sciences, 2.Jiangsu Air Traffic Management Branch Bureau of CAAC, 3.School of Atmospheric Sciences, Nanjing University)

[AAS10-P15] Frequency of noon/afternoon convective precipitation dominates on wet surface conditions over Indian summer monsoon region

*Rakesh Teja Konduru[1], Hiroshi G. Takahashi[1] (1.Department of Geography, Tokyo Metropolitan University)

[AAS10-P17] Modification of near-surface temperature over East Asia associated with local-scale paddy irrigation

*Shiori Sugimoto[1], Hiroshi G. Takahashi[2], Sekiyama Hirosato[2,3] (1.JAMSTEC Japan Agency for Marine-Earth Science and Technology, 2.Tokyo Metropolitan University, 3.Japan Meteorological Agency)

[AAS10-P18] **The freeze-thaw cycle and key parameters in a Tibetan Plateau lake using LAKE2.0 model and field observation**

*Zhaoguo Li[1], Shihua Lyu[2], Lijuan Wen[1], Lin Zhao[1], Xianhong Meng[1], Yinhuan Ao[1] (1.Northwest Institute of Eco-Environment and Resources, Chinese Academy of Sciences, 2.School of Atmospheric Sciences,

Chengdu University of Information Technology)

[AAS10-P19] **Numerical simulation of the climate effect of high-altitude lakes on the Tibetan Plateau**

*Yinhuan Ao[1], Shihua Lyu[2], Zhaoguo Li[1] (1.Northwest Institute of Eco-Environment and Resources, Chinese Academy of Sciences, 2.School of Atmospheric Sciences, Chengdu University of Information Technology)

[AAS10-P20] Impacts of four land-use products on the simulation of land surface temperature in East China

*Yongjie Pan[1] (1.Northwest Institute of Eco-Environment and Resources, Chinese Academy of Sciences)

[AAS10-P21] **Topographic and resolution impact on the monsoon rainfall in dynamical downscaling simulation**

*Yoshiyuki Kajikawa[1,2], Tsuyoshi Yamaura[1,2] (1.Research Center for Urban Safety and Security, Kobe University, 2.RIKEN Center for Computational Science)

Spatial differences of the Tibetan Plateau monsoon and its application

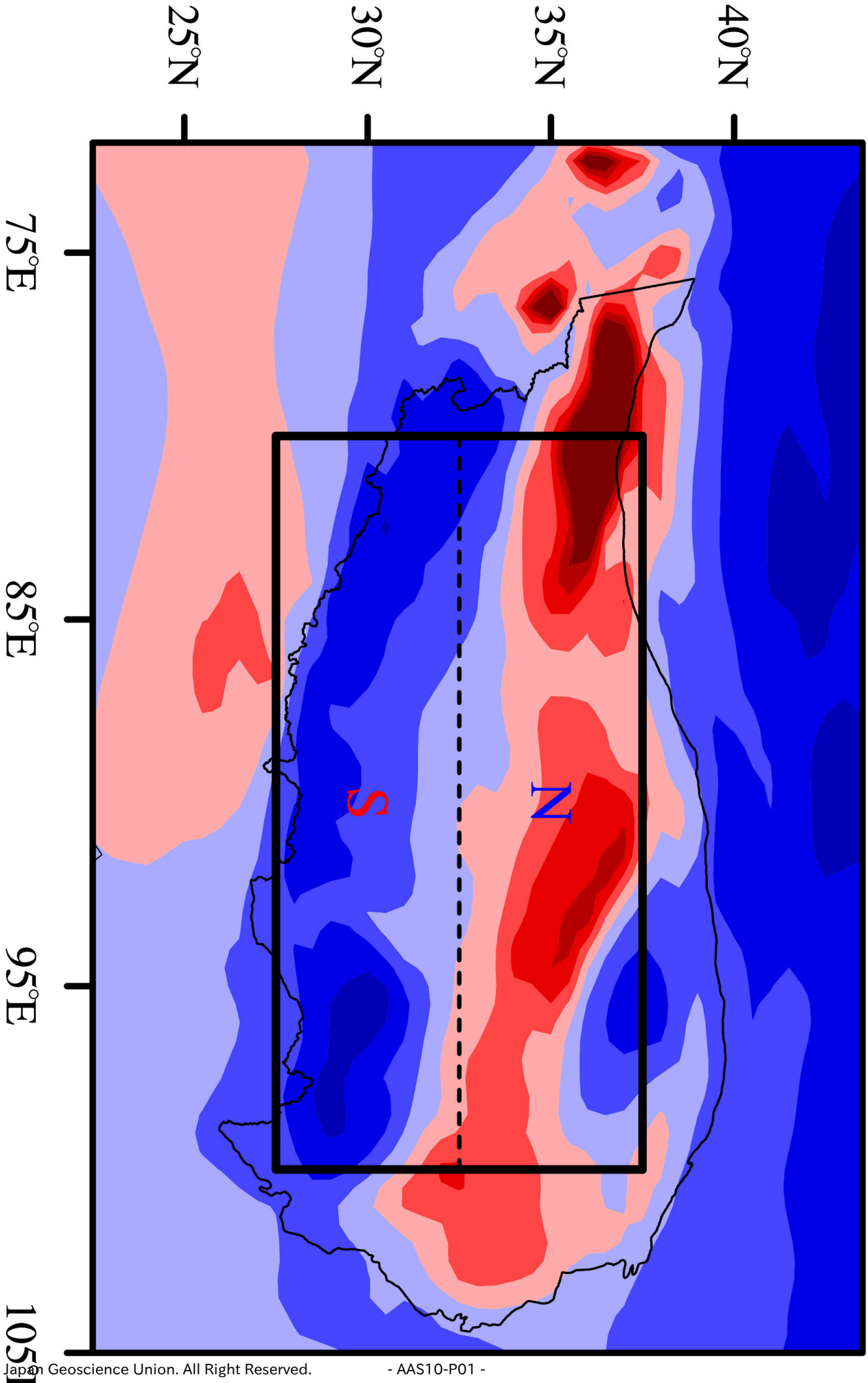
*Shaobo Zhang[1], Xianyu Yang[1], Yong Zhao[1]

1. Chengdu University of Information Technology

As a unique climate phenomenon forced by the Tibetan Plateau (TP) heat flux, the TP monsoon is closely connected with the global climate, especially the East Asian climate. The TP monsoon index, which reflects the TP monsoon extent, has been treated as a useful tool for studying the TP monsoon. In this work, a new TP monsoon index (PMI_{zhang}) was used to analyze the spatial differences among different parts of the TP, explore the relationship between the TP monsoon index and precipitation, and discuss its prediction value. The following conclusions were obtained: PMI_{zhang} had a reversed correlation coefficient with precipitation between the eastern and western parts of the TP, which reflected the first mode of summer precipitation in the TP and showed high consistency with the TP precipitation in terms of interannual and annual variation. When considering the correlation coefficient between the TP monsoon index and precipitation, the result of PMI_{zhang} was a combination of the results of the monsoon index in the northern part of the TP (PMI_{zhangN}) and the southern part of the TP (PMI_{zhangS}). Compared with the southern part of the TP, the northern part of the TP had a stronger surface sensible heat flux, which made the thermal wind characteristics in the region more apparent. As a result, the variation and intensity of PMI_{zhangN} were more evident than that of PMI_{zhangS}. When the PMI_{zhangN} in May positively anomalous, cyclonic circulation anomalies and anticyclonic circulation anomalies could be found in the western part and eastern part of the TP, respectively, leading to positive anomalies and negative anomalies of precipitation in the western part and eastern part of the TP, respectively. Therefore, the interannual variation in the PMI_{zhangN} in May had a proper correlation with the TP summer precipitation, showing its potential application value.

Keywords: Tibetan Plateau, sub-area monsoon index, spatial difference, precipitation

©2020. Japan Geoscience Union. All Right Reserved.



©2020. Japan Geoscience Union. All Right Reserved.

©2020. Japan Geoscience Union. All Right Reserved.

The concurrent effects of the South Asian monsoon and Tibetan plateau monsoon on summer rainfall in Tarim Basin of China

*YONG ZHAO[1], XIAOJING YU[2]

1. Chengdu University of Information Technology, 2. Institute of Desert Meteorology, CMA

Based on the observed rainfall data at 34 stations over the Tarim Basin (TB) and the NCEP–NCAR reanalysis data during 1961–2012, the concurrent effects of the plateau monsoon (PM) over the Tibetan Plateau and the South Asian monsoon (SAM) on summer rainfall over the TB are investigated. Mid-upper tropospheric temperature (500-200 hPa) (MUTT) plays an important role in linking the PM and the SAM with summer rainfall over the TB. The concurrent influential mechanisms of the PM and the SAM on summer rainfall over the TB can be summarized as follows. The strengthened (weakened) PM and the weakened (strengthened) SAM causes mid-upper tropospheric cooling (warming), which tends to result in the migration of the subtropical westerly jet further southward (northward). Then an anomalous southerly (northerly) flow prevails over the TB, and more (less) water vapor is transported into the TB by a two-step process. All above contribute significantly to an increase (decrease) in the occurrence of summer rainfall over the TB. In addition, we also discuss the relative contribution of the PM and the SAM to summer rainfall over the TB. Partial correlations show that the PM and the SAM can both individually influence summer rainfall over the TB. The PM has a direct effect on summer rainfall over the TB, for its considerable relations not only with MUTT but also with atmospheric circulation. But the SAM has an indirect effect, because it can influence only MUTT, which then gives rise to an anomalous circulation related to summer rainfall over the TB.

Keywords: South Asian monsoon, Plateau monsoon, Concurrent effects, Summer rainfall, Tarim Basin

©2020. Japan Geoscience Union. All Right Reserved.

Numerical simulations of precipitation in high altitude Himalaya mountainous area by using JMA-NHM

*Akihiro Hashimoto[1], Masashi Niwano[1], Hatsuki Fujinami[2], Akiko Sakai[3], Koji Fujita[3]

1. Meteorological Research Institute, Japan Meteorological Agency, 2. Institute for Space-Earth Environmental Research, Nagoya University, 3. Graduate School of Environmental studies, Nagoya University

Precipitation over high altitude Himalaya mountain area has a large influence to the mass balance of glaciers and the water discharge of rivers originating from there, which is an important factor not only in the water resource management but also the disaster mitigation for the countries in the watersheds. Although efforts have been made to reveal the temporal and spatial change of precipitation, its hydrological impacts, and related processes, they are not yet fully understood.

The authors have performed simulations to estimate annual precipitation amount in Himalaya's high altitude and the surrounding areas by using Japan Meteorological Agency Non-Hydrostatic Model (JMA-NHM), and additional simulations to examine the sensitivity to a topography smoothing technique, horizontal resolution and turbulence parameterization scheme. At first, we tested to relax the limitation of land surface slope angle to allow it to be up to 30 %, while the original threshold is 10 %, which is one of topography smoothing techniques for numerical stability of simulation. This did not much affect the simulation results. The simulations with the 5 km horizontal resolution tended to displace the major precipitation area toward the mountainside and to underestimate the precipitation on the plane in the summer season, compared with the observed precipitation amount provided by the Global Satellite Mapping of Precipitation (GSMaP), while the simulations with the 1 km horizontal resolution showed better agreement with the observation. Regarding the turbulence parameterization, Deardorff's scheme produced more precipitation on the plane than Mellor-Yamada's scheme in the summer season. In the presentation, we will also show the simulation results on annual and seasonal precipitation amounts in the several glacier catchments.

Acknowledgements
This study is partly supported by the Joint Research Program with Swiss National Science Foundation “High elevation precipitation in High Mountain Asia” of Japan Society for the Promotion of Science (JPSP). The computation was performed in part on the FX100 supercomputer system at the Information Technology Center, Nagoya University.

Keywords: Cloud resolving model, Himalaya, Seasonal simulation

©2020. Japan Geoscience Union. All Right Reserved.

Moisture sources of summer precipitation over eastern China during 1979–2009: A Lagrangian transient simulation

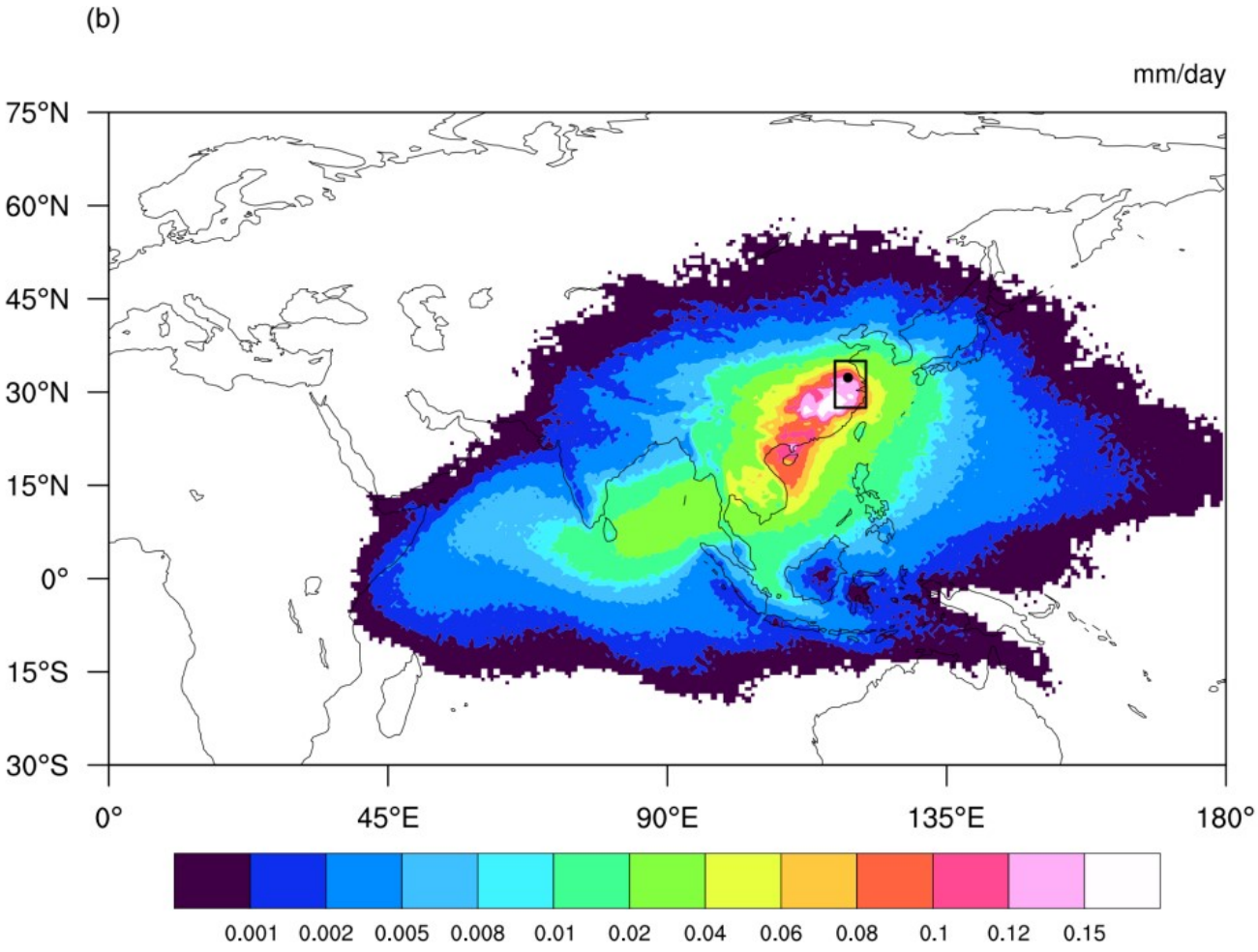
*QIN HU[1]

1. Chengdu University of Information Technology

In this study, moisture sources for summer (June–July–August) precipitation over eastern China are investigated by performing a transient simulation for the period 1979–2009 using the Lagrangian particle dispersion model FLEXPART. The results show that the Indochinese Peninsula plus southern China, the South China Sea, the northwestern Pacific Ocean, the Asian continent, and the Bay of Bengal are major moisture source regions for summer precipitation over eastern China and that the moisture originated from eastern China, the Arabian Sea, and the Indian subcontinent has minor contributions. The contribution of the oceanic sources significantly surpasses that of the continental sources. The contributions of the various moisture source regions exhibited significant interannual variations during 1979–2009, especially the Indochinese Peninsula plus southern China, the South China Sea, the northwestern Pacific Ocean, the Asian continent, and the Bay of Bengal. Moreover, moisture sources have obvious monthly variations and seasonal cycle features, which are responsible for providing moisture for precipitation in the different stages of the monsoon over eastern China. In addition, it is revealed that a great amount of moisture for the slight precipitation over eastern China originates from the local and northwestern continental regions and eastern oceanic regions adjacent to eastern China, while more moisture comes from southwestern oceanic source regions and their adjacent continental regions for heavy precipitation.

Keywords: moisture source, precipitation, eastern China, FLEXPART

©2020. Japan Geoscience Union. All Right Reserved.



©2020. Japan Geoscience Union. All Right Reserved.

Study on the severe weather caused by mesoscale convective system on the Meiyu front in northwestern Taiwan

*LI-ZHEN SU[1], Jou-Ping Hou[1], Ba-Xiu Wei[2]

1. Chung Cheng Institute of Technology National Defense University, 2. Air Force Weather Wing

Along the coast of northwestern Taiwan, when the Meiyu front passed, there were occasional rapids caused by the terrain, and after convergence with the prevailing wind field, it caused severe precipitation. In 1987, some studies conducted by Taiwan mesoscale experiment (TAMEX) found that low-level jet (about 1 km high) under certain conditions, known as barrier jet, strongly affected the heavy rainfall in northern Taiwan. On the morning of June 2, according to the results of the study in the meiyu frontal contact north Taiwan, in just 12 hours later to Keelung and north coast down to the super heavy rain of reason, may be related to frontal subject in northern Taiwan snowy mountains, the enhancement of barrier jets occurring near the surface height is related to the increase in barrier jets during the movement of the frontal body, which leads to cyclonic circulation around the jet zone, accompanied by the instability of temperature gradients and the enhancement of positive vortex anomalies, which indicates the cause of the strong water in this case. Based on the observation data and model simulation results, this study analyzed the main causes and physical mechanisms of the severe precipitation in northwest Taiwan, and then speculated on the dynamic and thermodynamic processes of such weather phenomena over time.

Keywords: Meiyu front, Severe precipitation, Low-level jet, Barrier jet

©2020. Japan Geoscience Union. All Right Reserved.

Long-term trends and interannual variability in precipitation over Vietnam during 1984-2016

*Hoa Thi Thanh Pham[1], Hiroshi G. Takahashi[1]

1. Department of Geography, Tokyo Metropolitan University

The precipitation variability in Vietnam is unique because different types of precipitation are dominant during the boreal summer and winter. During the late summer, tropical disturbances are associated with the precipitation variation in Vietnam. On the other hand, cold or northerly surges of the winter Asian monsoon play important role during winter. Thus, long-term variations in precipitation should be investigated with consideration of the seasonal march, including sub-seasonal time-scale. This study investigated the long-term variations in precipitation over Vietnam for the period from 1984 to 2016, which was corresponded to the economical exaggeration era of the country. The results showed that the long-term trends in precipitation over Vietnam greatly differed from region to region on decadal timescale. To understand the long-term changes associated with climatological precipitation characteristics, we analyzed the long-term changes on a monthly basis. Focusing on long-term changes in precipitation of decadal timescale from September to February, in October and February the decreasing trend was witnessed across mostly overall the country while in September, November and December, precipitation generally increased. In term of sub-climatological regions, North Central Area and Highland tended to be less rainy than South Central Area and Southern Vietnam. In addition, we also analyzed wind fields at 850hPa and water vapor fluxes. The decadal changes in atmospheric circulations are basically consistent with that of precipitation. Moreover, we will discussed the cause of the long-term changes in terms of the climatological seasonal march, including sub-seasonal time-scale, in precipitation and atmospheric circulation.

Keywords: rainfall trend, precipitation variations, vietnam, northeast monsoon

©2020. Japan Geoscience Union. All Right Reserved.

Recent increase of rain-on-snow events and rain proportion in north-eastern Japan

*Alexander Brandt[1,2], Maximo Larry Lopez Caceres[1]

1. Yamagata University, 2. United Graduate School of Agricultural Scienes (UGAS)

Winter precipitation along the Japan Sea depends on cold winter monsoons from Siberia. These winds bring cold air and heavy snowfall to north-eastern Japan and Hokkaido. With more than 1000 mm of precipitation within the winter period deep snow covers are the result. Snow cover is not only important for tourism (Toyama snow corridor, e.g.) but even more important for forest ecosystems and agriculture, since snowmelt is the main supply for plants in the relatively dry spring. However, recently snow cover decreases due to less snowfall and more rainfall during winter. Rain-to-snow proportion changed from 1:2 to almost 1:1 within the last decade in the Shonai plains in Yamagata prefecture. As consequence, snow cover (in a mild winter 2019/2020) was in January 80% smaller than in the years before. Results of the last decade show that the total amount of precipitation, especially between December and March does not significantly change. In contrast, because of significantly more rain, Snow Water Equivalent (SWE) will decrease.

Comparing different meteorological stations and the shifting snow-to-rain transition more recurrent mild and rainy winters can be expected for future. Those winters may result in water shortage in April and May, because snowmelt finishes early and precipitation is low in these months. Simultaneously forest plants start transpiration and agricultural lands are prepared, a significant decrease in snow due to climate change could therefore have negative impact on forest and agriculture. Climate change models already predicted weakening of Siberian winter monsoons, which will result in warmer winters with less snow. In order to characterize changes along the Japan sea we compared precipitation data of different meteorological stations and analyzed the change of rain proportion within the last decade.

Keywords: rain-to-snow proportion, Winter monsoon, SWE

©2020. Japan Geoscience Union. All Right Reserved.

Regional snowfall and precipitation distributions in a Japan-Sea side of central Japan associated with low-frequency variabilities in the Eurasian and East Asian regions

*Akira Yamazaki[1], Meiji Honda[2], Hiroaki Kawase[3]

1. Application Laboratory, Japan Agency for Marine-Earth Science and Technology, 2. Niigata University, 3. Meteorological Research Institute, Japan Mereorological Agency

This study found that regional snowfall distributions in a Japan-Sea side area of Japan are controlled by intraseasonal jet variability, particularly the 10-day-timescale quasi-stationary Rossby waves across the Eurasian continent and the atmospheric blocking over the East Asian region. Our results revealed that distribution types in which heavy snowfall events occurred over the area were related to the southward shift of the westerly jet over Japan associated with an intensified trough, i.e., cyclonic anomalies, originating from quasi-stationary Rossby waves along westerly jets over Eurasia (Eurasian jets). The cyclonic anomalies were found to be also related to blocking cyclones because the frequency of blocking events considerably increased in the East Siberian region.
Similar data analyses were conducted for regional precipitation distributions in the same area. Climatological features of the precipitation, such as seasonal marches and interannual frequencies were different from those for the snowfall events. However, composite fields for heavy precipitation events rather show similar features near Japan Island, such as the cyclonic anomalies, with those for the snowfall events. Those results imply that underlying mechanisms and/or boundary conditions which connect the global with the local atmospheric circulations can be different between the heavy snowfall and precipitation events.

©2020. Japan Geoscience Union. All Right Reserved.

Quantitative identification of moisture sources over the Tibetan Plateau and the relationship between thermal forcing and moisture transport

*Chen Pan[1,2,3,4], Bin Zhu[3,4], Zhiming Kang[1,2]

1. Jiangsu Meteorological Observatory, Nanjing, China, 2. Key Laboratory of Transportation Meteorology, China Meteorological Administration, Nanjing, China, 3. Key Laboratory for Aerosol-Cloud-Precipitation of China Meteorological Administration, Nanjing University of Information Science & Technology, Nanjing, China, 4. Collaborative Innovation Center on Forecast and Evaluation of Meteorological Disasters, Nanjing University of Information Science & Technology, Nanjing, China

Despite the importance of the Tibetan Plateau (TP) to the surrounding water cycle, the moisture sources of the TP remain uncertain. In this study, the moisture sources of the TP are quantitatively identified based on a 33-year simulation with a horizontal resolution of 1.9°×2.5° using the Community Atmosphere Model version 5.1 (CAM5.1), in which atmospheric water tracer technology is incorporated. Results demonstrate that the major moisture sources differ over the southern TP (STP) and northern TP (NTP). During the winter, Africa, the TP, and India are the dominant source regions, contributing nearly half of the water vapour over the STP. During the summer, the tropical Indian Ocean (TIO) supplies 28.5±3.6 % of the water vapour over the STP and becomes the dominant source region. The dominant moisture source regions of the water vapour over the NTP are Africa (19.0±2.8 %) during the winter and the TP (25.8±2.4 %) during the summer. The overall relative contribution of each source region to the precipitation is similar to the contribution to the water vapour over the TP. Like most models, CAM5.1 generally overestimates the precipitation over the TP, yielding uncertainty in the absolute contributions to the precipitation. Composite analyses exhibit significant variations in the TIO-supplied moisture transport and precipitation over the STP during the summer alongside anomalous TP heating. This relationship between moisture transport from the TIO and the TP heating primarily involves the dynamic change in the TIO-supplied moisture flux, which further controls the variation in the TIO-contributed precipitation over the STP.

Keywords: Tibetan Plateau, Heat source, Moisture source apportionment, Moisture transport

©2020. Japan Geoscience Union. All Right Reserved.

Multi-scale convection system simulation during Meiyu season in Taiwan

*Yi Hao Liao[1], Jou-Ping Hou[1], Yu-De Wu[2]

1. Department of Environmental Information and Engineering, CCIT, National Defense University, 2. Air Force Weather Wing

The first front of Mei-yu rainy season passed through Taiwan area on May 1, 2019. Although the front did not reach rainfall intensity of the typical Mei-yu front, but the multi-scale convective system triggered by it revealed important clues that caused the Meiyu front to produce severe precipitation. Diagnostic analysis of this case, we found that the position of overseas development of convective clouds were closed to the 700hPa convergence zone position. The analysis of 850hPa and 700hPa shows that there are obvious low-level jets that continuously supply vapor, so that 850hPa has a significant vapor flux, which improves the mixing ratio, resulting in low-level convergence and sufficient vapor. It is easy to make convection develop local rainfall. At the same time, during the rapid movement of the frontal system to the southeast, the frontal system was damaged by the terrain. Although this case has a large-scale linear convection system in northern Taiwan, there is no severe precipitation. In the small-scale convection system in central and southern Taiwan,, precipitation is more obvious. In addition, we use WRF V3.9.1.1 version, two nesting domain design to simulate the frontal system on May 1, 2019, where the horizontal spatial resolution of the outer grid and the inner grid is 3 km and 1 km. The simulation experiments found that the number of grid points in the outer grid will affect the radar echo and precipitation intensity simulated by the inner domain. At the same time, the sensitivity of different microphysical parameters and boundary layer parameters will be tested to simulate the intensity of precipitation. Significant differences also occur in the rainfall intensity simulations.

Keywords: Mei-yu front, Low Level Jet, Severe Precipitation, sensitivity test

©2020. Japan Geoscience Union. All Right Reserved.

Responses of rainfall characteristics to the land surface conditions over the wet Asian monsoon region

*Hiroshi G. Takahashi[1]

1. Department of Geography, Tokyo Metropolitan University

This study estimated the sensitivity of rainfall characteristics to land-surface conditions over Southeast Asia, which has a wet land surface during the rainy season. To obtain the regional difference in sensitivity and simulate basic cloud-precipitation systems, we used a high-resolution regional climate model. The sensitivity of rainfall amount to an increase in soil moisture was dependent on the location. This implies that the response of rainfall characteristics to soil moisture is not simple, suggesting that changes in rainfall characteristics are not solely determined by evapotranspiration. In addition, the sensitivity of rainfall characteristics displayed remarkable regional characteristics. The coupling of an increase in water vapor in the planetary boundary layer and a decrease of sensible heat flux can explain the response. The increase in water vapor in the planetary boundary layer was associated with a reduction of the development of deep convections and an increase of boundary layer clouds.

Keywords: rainfall characteristics, Asian monsoon

©2020. Japan Geoscience Union. All Right Reserved.

Analysis of Characteristics and Causes of Meiyu over the Yangtze–Huai River Basin in 2019

*Ruoyun Niu[1]

1. National Meteorological Center, China Meteorological Administration

Using the daily NCEP reanalysis dataset and the observations data of precipitation in China the characteristics of Meiyu over the Yangtze–Huai River Basin and its atmosphere circulation causes in 2019 are analyzed. The results show that: (1) In 2019, the onset date of Meiyu (June 16th) over the Yangtze–Huai River Basin was later than nomal, the outset date (July 17th) was close to normal, and the duration was shorter. The Meiyu precipitation (intensity) was more (stronger) than normal in the south of the Yangtze river and less (weaker) than normal in the north of the Yangtze river. (2) Between June 8 to 15 the cold air activities were intensified. In correspondingly, the Northwest Pacific Subtropical High (NWPSH) was phased southward, the fore boundary of East Asia summer monsoon (EASM) lied south of normal with the northward march delated. The above caused the onset date later. (3) During the Meiyu season (especially in July 1 to 15),the coast trough of East Asia was deeper and the western ridge of NWPSH was further south and the water vapor transport and its convergence at low level was is more southward. Meanwhile the eastern ridge of the South Asia High and upper-level westerly jet was southward, the upper-level divergence was also southward. The above all caused the Meiyu intensity with the southern stronger and the northern weaker.

Keywords: Meiyu, Analysis of Characteristics and Causes

©2020. Japan Geoscience Union. All Right Reserved.

Similarities and differences of summer persistent heavy rainfall and atmospheric circulation characteristics in the middle and lower reaches of the Yangtze River between 2016 and 1998

*Xiaolin ZHAO[1]

1. National Meteorological Centre, China Meteorological Administration

During the summer of 2016 and 1998 in the context of the decaying phase of the super El Niño event, the three persistent heavy rainfall events occurred in the middle and lower reaches of the Yangtze River from June 19 to July 7 in 2016 (hereinafter referred to as during the period of 2016), from June 12 to 27 (hereinafter referred to as during the period I of 1998) in 1998, and from July 17 to August 2 (hereinafter referred to as during the period II of 1998) in 1998, which brought great challenges to the national flood control business. Based on daily precipitation at 2407 meteorological observation stations in mainland China, daily reanalysis atmospheric data from NCEP/NCAR and other data, we have conducted a comparative analysis of the similarities and differences of summer persistent heavy rainfall and associated atmospheric circulation characteristics in the middle and lower reaches of the Yangtze River between 2016 and 1998. Results are as follows. (1) The persistent heavy rainfall belt is the northernmost during the period of 2016 and the southernmost during the period I of 1998 among the three events, while the rainfall intensity during the period of 2016 is roughly the same as that during the period I of 1998, and it for both periods is stronger than that for the period II of 1998. (2) There are many similarities in the atmospheric circulation characteristics during the three periods of persistent heavy rainfall. For example, there exist low troughs near the eastern coast of China, the Northwest Pacific Subtropical High (NWPSH) and South Asia High (SAH) are larger in range and stronger in intensity than normal, and the intensity of the upper westerly jet (UWJ) and low southwest jet and the easterly water vapor transport along the south side of the NWPSH are also stronger than normal. (3) The significant differences in the atmospheric circulation during the three periods of persistent heavy rainfall events are that the low trough near the coastal of eastern China during the persistent heavy rainfall of 2006 (1998) is shallow (deep). When upper-level divergence zone between the north sides of NWPSH and SAH ridge lines and the south sides of westerly jet belt, low-level jet belt and shear line with convergence, and Australian High in the southern hemisphere are northerly (southerly) in position, the persistent heavy rainfall zones are also northerly (southerly). NWPSH, SAH, and upper-level westerly jet during the period of 2016 and the period I of 1998 are significantly stronger than those during the period II of 1998. The rainfall intensity in the former two periods is also greater than that in the later period.

Keywords: persistent heavy rainfall, atmospheric circulation, El Niño, the middle and lower reaches of the Yangtze River

©2020. Japan Geoscience Union. All Right Reserved.

During the summer of 2016 and 1998 in the context of the decaying phase of the super El Niño event, the three persistent heavy rainfall events occurred in the middle and lower reaches of the Yangtze River from June 19 to July 7 in 2016 (hereinafter referred to as during the period of 2016), from June 12 to 27 (hereinafter referred to as during the period I of 1998) in 1998, and from July 17 to August 2 (hereinafter referred to as during the period II of 1998) in 1998, which brought great challenges to the national flood control business. Based on daily precipitation at 2407 meteorological observation stations in mainland China, daily reanalysis atmospheric data from NCEP/NCAR and other data, we have conducted a comparative analysis of the similarities and differences of summer persistent heavy rainfall and associated atmospheric circulation characteristics in the middle and lower reaches of the Yangtze River between 2016 and 1998. Results are as follows. (1) The persistent heavy rainfall belt is the northernmost during the period of 2016 and the southernmost during the period I of 1998 among the three events, while the rainfall intensity during the period of 2016 is roughly the same as that during the period I of 1998, and it for both periods is stronger than that for the period II of 1998. (2) There are many similarities in the atmospheric circulation characteristics during the three periods of persistent heavy rainfall. For example, there exist low troughs near the eastern coast of China, the Northwest Pacific Subtropical High (NWPSH) and South Asia High (SAH) are larger in range and stronger in intensity than normal, and the intensity of the upper westerly jet (UWJ) and low southwest jet and the easterly water vapor transport along the south side of the NWPSH are also stronger than normal. (3) The significant differences in the atmospheric circulation during the three periods of persistent heavy rainfall events are that the low trough near the coastal of eastern China during the persistent heavy rainfall of 2006 (1998) is shallow (deep). When upper-level divergence zone between the north sides of NWPSH and SAH ridge lines and the south sides of westerly jet belt, low-level jet belt and shear line with convergence, and Australian High in the southern hemisphere are northerly (southerly) in position, the persistent heavy rainfall zones are also northerly (southerly). NWPSH, SAH, and upper-level westerly jet during the period of 2016 and the period I of 1998 are significantly stronger than those during the period II of 1998. The rainfall intensity in the former two periods is also greater than that in the later period.

©2020. Japan Geoscience Union. All Right Reserved.

Characteristics of the Precipitation Diurnal Variation over Jiangsu, Eastern China during Warm Season

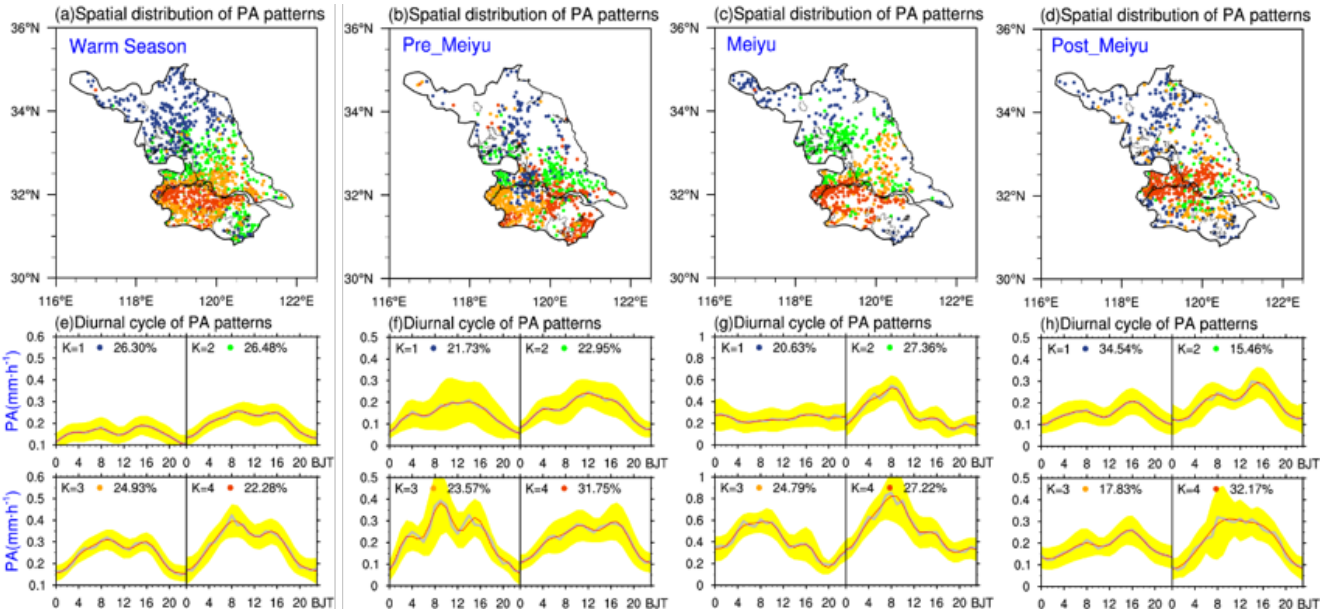
*Xiyu Mu[1], Qi Xu[2], Yang Wu[3], Anning Huang[3]

1. Key Laboratory of Transportation Meteorology of CMA; Jiangsu Institute of Meteorological Sciences; Nanjing Joint Institute for Atmospheric Sciences, 2. Jiangsu Air Traffic Management Branch Bureau of CAAC, 3. School of Atmospheric Sciences, Nanjing University

Based on the hourly precipitation data observed from ~1800 gauge stations during 2013-2017, the characteristics of precipitation diurnal variation over Jiangsu Province in Eastern China during warm season (May to September) have been revealed in this study. Results show that the precipitation amount (PA), frequency (PF) and intensity (PI) are zonally distributed over Jiangsu. The large PA center is located over the south side of the west end of Jiangsu Section of Yangtze River (JSYR). The PA shows distinct diurnal cycles. From midnight to noon, the PA center expands westwards and northwards from east JSYR to west JSYR with the PA increased. Hereafter the PA center shrinks eastwards and southwards with the PA decreased from noon to midnight. The strongest diurnal Peak of PA (PPA) is located over the south side of the west end of JSYR and the diurnal PPA gradually decreases northwards and eastwards from morning to midnight. The PA is larger in the daytime than in the nighttime over most Jiangsu. The PA shows two diurnal peaks with one in the early morning and the other in the afternoon contributed by the long duration rainfall and the short duration rainfall, respectively. The total rainfall is largely contributed by the long duration rainfall, which is determined by the summer monsoon circulation. The short duration rainfall is mainly affected by the local thermal conditions resulted from the underlying surface. The contribution of the rainfall with long (short) duration to the total rainfall over most areas shows very distinct sub-seasonal variations with a clear decreasing (increasing) trend from pre-Meiyu through Meiyu to post Meiyu. Among the three sub-periods, the PA and diurnal cycle of the total rainfall are mostly contributed by those during Meiyu period. The results of the cluster analysis show that the representative patterns of precipitation diurnal variation and their spatial distributions are closely connected with the underlying surface, such as the Yangtze River, big cities, Lake Taihu, Lake Hongze and coastal. The diurnal variation of the rainfall influenced by different underlying surface shows respective features.

Keywords: precipitation diurnal cycle, underlying surface, different duration rainfall, warm season

©2020. Japan Geoscience Union. All Right Reserved.



©2020. Japan Geoscience Union. All Right Reserved.

Frequency of noon/afternoon convective precipitation dominates on wet surface conditions over Indian summer monsoon region

*Rakesh Teja Konduru[1], Hiroshi G. Takahashi[1]

1. Department of Geography, Tokyo Metropolitan University

Soil moisture can play an important role for determining precipitation characteristics over the tropical Asian region. In this study with the help of convection-permitting regional climate model (RCM), impacts of soil moisture on precipitation characteristics are investigated on different temporal scales over the Indian monsoon region. A set of wet and dry soil moisture surface conditions were forced to the Weather Research and Forecasting model WRFv3.9.1.1 as the RCM during the summer monsoon season. The contrasting soil moisture conditions found to affect the timing, frequency, intensity, and duration of precipitation during the peak monsoon over central India, along the mountains of foothills of Himalayas and over the Bay of Bengal. To understand diurnal contribution to daily accumulated rainfall, we also analyzed diurnal variations of precipitation characteristics. The changes in precipitation characteristics due to the surface conditions are basically regional characteristics. During noon/afternoon, a greater frequency of convective precipitation over the Indian land region, along the mountains of western Ghats and foothills of Himalayas was simulated under the wet surface condition, compared with the dry surface condition. Weakening of convective precipitation was found associated with the wetter surface conditions over the Indian land region. The frequency of short duration (3-6 hours) rainfall events were found to increase over Indian land region under the wet surface conditions than dry. In addition, the frequency of mesoscale convective systems propagating from land to the offshore Bay of Bengal found to decrease during the early morning over the wet land surface condition, compared with the dry condition. Moreover, we will discuss the mechanisms why these changes are simulated.

Keywords: Convection-permitting simulation, impact of land surface condition, Indian summer monsoon, precipitation characteristics

©2020. Japan Geoscience Union. All Right Reserved.

Modification of near-surface temperature over East Asia associated with local-scale paddy irrigation

*Shiori Sugimoto[1], Hiroshi G. Takahashi[2], Sekiyama Hirosato[2,3]

1. JAMSTEC Japan Agency for Marine-Earth Science and Technology, 2. Tokyo Metropolitan University, 3. Japan Meteorological Agency

The Sichuan Basin is a major region for paddy irrigation in China. We conducted two kinds of numerical experiment using the Weather Research and Forecasting (WRF) model to assess the impact of paddy irrigation in the Sichuan Basin on the regional climate over East Asia. In the control experiment (CTL run), which was used to calculate soil moisture using the unmodified Noah land-surface scheme, near surface temperature was higher than in the observation. The sensitivity experiment (SEN run), which incorporated an increase in soil moisture over the basin at the beginning of the rice-growing season, improved the simulated near surface temperature because of the change in the Bowen ratio associated with the increase in soil moisture. The modification of the land surface wetness in the Sichuan Basin also decreased the near surface temperature over northeastern China and increased it over southern China comparing with the CTL run, which are caused by the changes in the cloud convection and the solar & net radiation at the surface as well as the partitioning into the sensible and latent heat fluxes. The greenhouse effect associated with an increase in precipitable water in the SEN run also influences near-surface warming over southeastern China and the ocean north of southwestern Japan, where the impacts of radiation processes and surface heat fluxes on the near-surface temperature are small. The local-scale modifications to soil moisture in the Sichuan Basin results in changes in the larger-scale spatial distribution of near surface temperature over East Asia.

Keywords: Paddy irrigation, Land-atmosphere coupling, East Asia

©2020. Japan Geoscience Union. All Right Reserved.

The freeze-thaw cycle and key parameters in a Tibetan Plateau lake using LAKE2.0 model and field observation

*Zhaoguo Li[1], Shihua Lyu[2], Lijuan Wen[1], Lin Zhao[1], Xianhong Meng[1], Yinhuan Ao[1]

1. Northwest Institute of Eco-Environment and Resources, Chinese Academy of Sciences, 2. School of Atmospheric Sciences, Chengdu University of Information Technology

Few studies have paid attention to the freeze-thaw process of Tibetan Plateau (TP) lakes and key control parameters. By combining 216 simulation experiments using a LAKE2.0 model with the observation, we evaluated the effects of ice and snow albedo, ice and water extinction coefficients on the lake ice phenology, water temperature, sensible and latent heat fluxes in Ngoring Lake. The increase of ice albedo, snow albedo and the ice extinction coefficient (K_{di}) induce significant decrease in water temperature. Compared with the latent heat, the sensible heat flux is more sensitive to these three parameters. With the decrease in high K_{di}, the ice thickness, water temperature and frozen days present an extensive increase. If K_{di} less than 2.5 m^{-1}, the increase of ice thickness is no longer obvious. In the frozen period with little snow, the K_{di} exhibit little influence on frozen days. The frozen days is significantly affected by the snow albedo and changes fastest in the snow albedo from 0.5 to 0.75.

Keywords: lake ice, snow, albedo, extinction coefficient

©2020. Japan Geoscience Union. All Right Reserved.

Numerical simulation of the climate effect of high-altitude lakes on the Tibetan Plateau

*Yinhuan Ao[1], Shihua Lyu[2], Zhaoguo Li[1]

1. Northwest Institute of Eco-Environment and Resources, Chinese Academy of Sciences, 2. School of Atmospheric Sciences, Chengdu University of Information Technology

In this study, the Weather Research and Forecasting Model (WRF v. 3.6.1) is employed to conduct three numerical experiments in the Ngoring Lake Basin (the original experiment, an experiment with a tuned model, and a no-lake experiment) to investigate the influences of parameter optimization on the lake simulation and of the high-altitude lake on the regional climate. After the lake depth, the roughness lengths, and initial surface temperature are corrected in the model, the simulation of the air temperature is distinctly improved. In the experiment using a tuned model, the simulated sensible-heat flux (H) is clearly improved, especially during periods of ice melting (from late spring to early summer) and freezing (late fall). The improvement of latent-heat flux (LE) is mainly manifested by the sharp increase in the correlation coefficient between simulation and observation, whereas the improvement in the average value is small.After the lakes are removed, the air temperature increases significantly from June to September over the area corresponding to the two lakes, and an abnormal convergence field appears; at the same time, the precipitation clearly increases over the two lakes and surrounding areas.

Keywords: Lake-surface temperature, roughness length, turbulent flux

©2020. Japan Geoscience Union. All Right Reserved.

Impacts of four land-use products on the simulation of land surface temperature in East China

*Yongjie Pan[1]

1. Northwest Institute of Eco-Environment and Resources, Chinese Academy of Sciences

Land surface temperature (LST) plays a crucial role in earth system for its uneven spatial distributions could trigger local circulations through land surface –atmosphere interactions. However, the accuracy of modelled LST depends on land surface characteristics, such as land use/cover types. In this study, the Community Land Model (CLM4.5) and four land-use products were employed to investigate the effect of underlying vegetation characters on LST simulation in East China. Moderate Resolution Imaging Spectroradiometer (MODIS) land surface temperature products (MOIDIS_LST) and observations from nine sites were used to evaluate the simulated LST. Compared with ground temperature from site observations, the CLM model could properly simulate ground temperature in urban area. However the differences between the MODIS_LST and simulated LST shown that the model overestimated LST in East China. Over the forest areas, the distributions of LST differences between model and remote sensing from four simulated cases are dissimilar because the different identifications of plant types in four land-use product. We also found a large deviation of leaf area index (LAI) between CLM prescribed value and remote sensing observation. The replacement of LAI in model surface data with MODIS LAI brings the modeled LST closer to MODIS LST. Besides the LAI, other factors contributing to the differences of LST between model and MODIS are also identified, including uncertainties in atmospheric forcing data, MODIS LST product, and land surface plant types identification. These findings could have implications for improving the simulation of land surface energy balance in regional weather models or global climate models.

Keywords: land surface temperautre, land use, CLM4.5

©2020. Japan Geoscience Union. All Right Reserved.

Topographic and resolution impact on the monsoon rainfall in dynamical downscaling simulation

*Yoshiyuki Kajikawa[1,2], Tsuyoshi Yamaura[1,2]

1. Research Center for Urban Safety and Security, Kobe University, 2. RIKEN Center for Computational Science

It is worthwhile to understand the monsoonal rainfall system comprehensively based on the boundary problem; e.g. surface condition, orographic effect or resolution of the climate model, for the future climate prediction. We first ever conducted the downscaling monsoon experiment for the broad scale computational domain (30E-160E, 20S-45N) by using regional climate model; SCALE-RM (http://r-ccs-climate.riken.jp/scale/index.html) to examine the impact of (1) horizontal resolution (45km and 15km) and (2) topography (steep terrain) on the climatological monsoonal rainfall. We also specifically examined the topographic effect over the monsoonal rainband area (0-20N, 60E-150E). The results show that Increase of horizontal resolution (45km to 15km) provides more rainfall over the Indochina Peninsula and the entire western Pacific (WP). In contrast, the rainfall over the Indian subcontinent and Arabian Sea (AS) is decreased. Increase of acceptable slope of the topography in the model enhances the rainfall along the Himalayan foothill and southwesterly wind toward to Himalayan foothill both in 45km and 15km experiment, while it suppresses the rainfall along the broad monsoonal rain area (0-20N). Topography along the monsoonal rain area (0-20N) clearly confine the monsoonal rainfall area along the steep terrain. We discuss the impact of continuous integration on the reproducibility of the monsoonal rainfall in the model as well in the presentation.

Keywords: monsoon, rainfall, topography

©2020. Japan Geoscience Union. All Right Reserved.

[E] Poster | A (Atmospheric and Hydrospheric Sciences)：A-AS Atmospheric Sciences, Meteorology & Atmospheric Environment

[A-AS11] Aerosol impacts on air quality, climate system, and our society

convener:Teppei J Yasunari(Arctic Research Center, Hokkaido University), Kyu-Myong Kim(NASA Goddard Space Flight Center), Hongbin Yu(NASA Goddard Space Flight Center), Toshihiko Takemura(Research Institute for Applied Mechanics, Kyushu University)

Aerosol particles degrade air quality, modulate the radiation budget, influence the formation and evolution of clouds and precipitation, affect the ecosystems and biogeochemical cycles. These impacts have important implications for global sustainability and societal benefits. This session invites papers reporting latest advances in understanding lifecycles of aerosol and assessing aerosol impacts on air quality, the climate system from regional to global scales using in situ observation, remote sensing, and numerical modeling techniques. We also welcome papers on how the important roles of aerosol in air quality and climate system have influenced our society such as economic and educational activities. The topics of interest include but are not limited to: (1) physical processes on aerosol emission, transport and deposition, (2) trends of regional aerosol and their controls by emissions and meteorology, (3) aerosol influences on radiation through scattering, absorption, as well as albedo changing, (4) aerosol impacts on monsoon hydrological cycle and extreme weather events such as drought, flood, wildfire, typhoon, as well as the influences of the extreme weather events on aerosol emissions and transport, (5) the role of aerosol in global biogeochemical cycles, (6) aerosol impact on our society and economy, (7) new analytical methods for assessment and prediction such as machine learning, and (8) aerosol related education and outreach.

[AAS11-P01] The impact of urbanization and consumption patterns on China's Black Carbon emissions — Based on SDA and IO Analysis

*Zhongci Deng[1], Xiaoling Zhang[1], Ping Kang[1] (1.School of Atmospheric Sciences, Chengdu University of Information Technology, China)

[AAS11-P02] **Size-resolved hygroscopic behaviour of submicron aerosols in a megacity of Sichuan Basin**

*Liang Yuan[1] (1.Chengdu University of Information Technology)

[AAS11-P04] Comparison of absorption coefficient and black carbon concentration at Byeongcheon, South Korea using Tricolor absorption photometer (TAP) and Multiangle absorption photometer (MAAP)

*Jeonghoon Lee[1] (1.KOREATECH)

[AAS11-P05] $PM_{2.5}$ vertical concentration observations using a drone based on comparison of $PM_{2.5}$ concentration data with small sensor and atmospheric environment measurement station data

*Takashi Chiba[1], Masatsugu Kodate[1], Osamu Kiguchi[1], Makoto Inoue[1], Hirokazu Madokoro[2], Takeshi Nagayosi[1] (1.Faculty of Bioresource Sciences, Akita Prefectural University, 2.Faculty of Systems Science and Technology, Akita Prefectural University)

[AAS11-P06] **Long-term measurements of aerosol physical properties in the Noto Peninsula**

*Seiji Kubota[1], Alessia Nicosia[2], Yoko Iwamoto[3], Naoki Kaneyasu[4], Ayumi Iwata[5], Hiroshi Tsurumaru[6], Atsushi Matsuki[2] (1.Graduate School of Natural Science and Technology, Kanazawa University, 2.Institute of Nature and Environment Technology, Kanazawa University, 3.Graduate School of Biosphere Science, Hiroshima University, 4.Atmospheric Environment Research Group, National Institute of Advanced Industrial Science and Technology, 5.Department of Applied Chemistry, Faculty of Science and Technology, Keio University, 6.Tokyo Metropolitan Research Institute for Environmental Protection)

[AAS11-P07] Recurrent Neural Network (RNN), Long short-term memory (LSTM) for Aerosol Optical Depth (AOD) using NASA's MERRA-2 Reanalysis

*Mohammed Ezzat Magooda[1], Muhammed Eltahan[2], Karim Moharm[3] (1.Aerospace Engineering Dept, Cairo Univ., Cairo, Egypt, 2.Institute of Bio-Geosciences (IBG-3, Agrosphere), Forschungszentrum Jülich, Jülich, Germany, 3.Electrical Engineering Dept., Alexandria University, Alexandria, Egypt)

[AAS11-P08] Development of SCALE-Chem and its application for regional simulation targeting on urban area and mountain area of Japan

*Makiko Nakata[1], Mizuo Kajino[2], Yousuke Sato[3,4], Hisashi Yashiro[5,4], Itaru Sano[1], Sonoyo Mukai[6] (1.Kindai University, 2.Meteorological Research Institute, 3.Faculty of Science, Department of Earth and Planetary Sciences, Hokkaido University, 4.RIKEN Center for Computational Science, 5.National Center for Environmental Studies, 6.The Kyoto College of Graduate Studies for Informatics)

[AAS11-P09] Regional trends of combustion aerosol and dust in recent decades: a satellite-model integrated analysis

*Hongbin Yu[1], Yang Yang[2], Hailong Wang[1], Qian Tan[3,4], Mian Chin[1], Robert Levy[1], Lorraine Remer[5], Steven Smith[2], Tianle Yuan[1,5], Yingxi Shi[1,5], Zhibo Zhang[5], Qianqian Song[5], Paul Ginoux[6] (1.NASA Goddard Space Flight Center, 2.Pacific Northwest National Laboratory, 3.Bay Area Environmental Research Institute, 4.NASA Ames Research Center, 5.University oof Maryland Baltimore County, 6.NOAA GFDL)

[AAS11-P10] Development of a regime-dependent autoconversion parameterization using satellite observations

*Tomoki Hirata[1], Takuro Michibata[2], Toshihiko Takemura[2] (1.Interdisciplinary Graduate School of Engineering Sciences, Kyushu University, 2.RIAM Research Institute for Applied Mechanics)

[AAS11-P11] Aerosol data assimilation experiment using GCOM-C SGLI aerosol product

*Taichu Y Tanaka[1], Keiya Yumimoto[3,1], Mayumi Yoshida[2], Hiroshi Murakami[2], Takashi M. Nagao[4], Megumi Okata[2] (1.Meteorological Research Institute, Japan Meteorological Agency, 2.Earth Observation Research Center, Japan Aerospace Exploration Agency, 3.Research Institute for Applied Mechanics, Kyushu University, 4.Atmosphere and Ocean Research Institute, The University of Tokyo)

[AAS11-P12] A study on the effects of sulfate aerosols on ocean circulation and the consequent atmospheric feedback

*Yuki Kusakabe[1], Toshihiko Takemura[2] (1.Interdisciplinary Graduate School of Engineering Sciences, Kyushu University, 2.Research Institute for Applied Mechanics, Kyushu University)

[AAS11-P13] Surface air temperature response to large-scale volcanic eruptions and its relationship with ENSO

*Sho Kitabayashi[1], Hiroshi G. Takahashi[1] (1.Tokyo Metropolitan University)

The impact of urbanization and consumption patterns on China's Black Carbon emissions —Based on SDA and IO Analysis

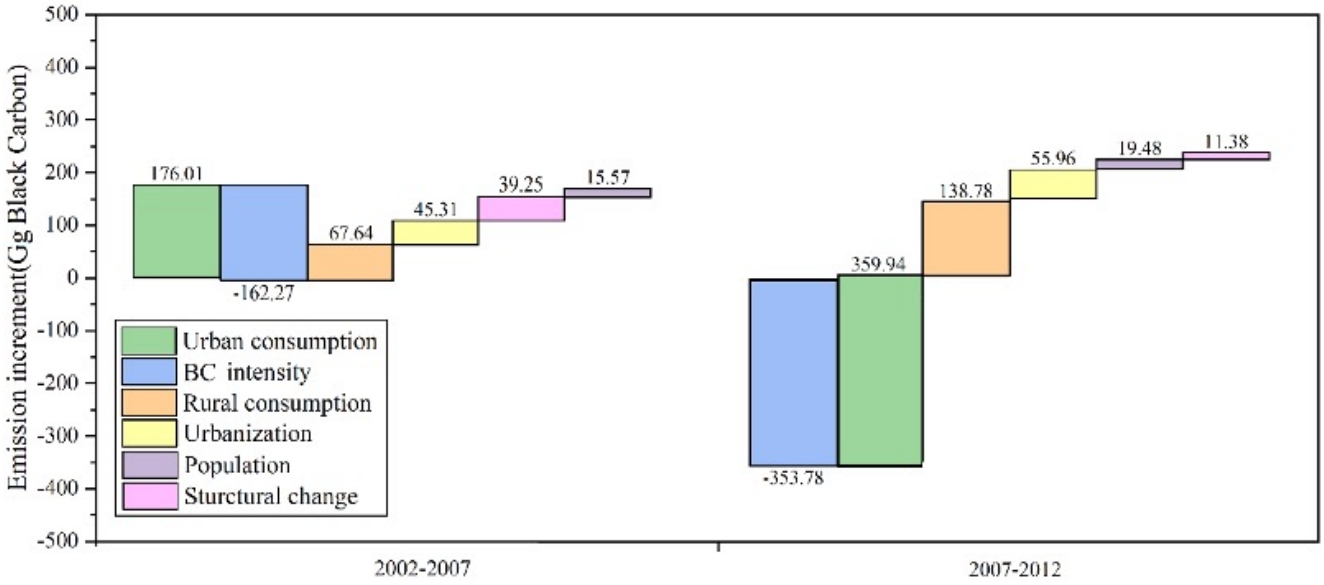
*Zhongci Deng[1], Xiaoling Zhang[1], Ping Kang[1]

1. School of Atmospheric Sciences, Chengdu University of Information Technology, China

With the gradual improvement of China's urbanization level and corresponding household consumption changes, emissions increase with time. However, little is known about black carbon (BC), not to mention their quantitative description of BC emissions. Therefore, we first collect the BC emission factor of various sectors to calculate the consumption-based BC emissions in China, and use the structural decomposition analysis (SDA) and input-output analysis (IOA) to explore the impact of urbanization and changes in consumption patterns on BC emissions from 2002 to 2012, focusing on sectoral BC emissions. The results showed that: the total BC emissions of various sectors in China increased from 1083Gg in 2002 to 1942Gg in 2007, and to 2551Gg in 2012. Meanwhile, with the deepening of urbanization (from 39.1% in 2002 to 45.9% in 2007, and to 52.6% in 2012), household consumption BC emissions increased from 446.2Gg in 2002 to 627.7 Gg in 2007, and to 895.5Gg in 2012. Focused on sectoral emissions, we found that urban consumption and BC intensity were the main contributing factors to the household BC emissions change. From 2002 to 2007, Urban consumption (positively) contributed 176.01 Gg of the incremental in household BC emissions, while 162.27 Gg were offset by BC intensity (negatively). From 2007 to 2012, due to per capita consumption or changes in consumption amount, urban consumption has increased. Consumption resulted in increased household emissions from 176.01 Gg to 359.94 Gg. However, due to the offset by BC intensity, we found that the total BC emissions increment from 2007 to 2012 was lower than that from 2002 to 2007(total BC emissions increment was 6.16Gg and 13.74Gg respectively). During the decade from 2002 to 2012, population-related factors contributed positively to total household BC emissions. The BC emissions increment impacted by urbanization was 45.31 Gg from 2002 to 2007 and 55.96 Gg from 2007 to 2012. Focused on the incremental BC emissions of each sector, transport, farming and residential contributed the most BC emissions. In particular, the transportation sector has the most significant impact on BC emissions. Urbanization affects BC emissions through its complex relationship with various sectors. So, it is necessary to formulate mitigation policies for the transportation sector.

Keywords: Black Carbon (BC) Emissions, Input-output (IO) Analysis, Structural Decomposition Analysis (SDA), Urbanization, Consumption Patterns

©2020. Japan Geoscience Union. All Right Reserved.



©2020. Japan Geoscience Union. All Right Reserved.

Size-resolved hygroscopic behaviour of submicron aerosols in a megacity of Sichuan Basin

*Liang Yuan[1]

1. Chengdu University of Information Technology

In situ measurements are performed to study the size-resolved hygroscopic behaviour of submicron aerosols during pollution and fireworks episodes in winter from late January to February 2019 in Chengdu, a megacity in Sichuan Basin, using a humidity tandem differential mobility analyser (H-TDMA). The H-TDMA is operated at a relative humidity of 90% with dry aerosol diameters between 40 and 200 nm. Three modes of aerosol particles, including nearly hydrophobic mode (NH), less hygroscopic mode (LH), and more hygroscopic mode (MH), are found in the probability distributions of the growth factor (*GF*-PDF) during the campaign. The *GF*-PDF shows that aerosol particles are usually externally mixed. The average ensemble mean hygroscopicity parameter values (κ_{Mean}) over the entire sampling period are 0.16, 0.19, 0.21, 0.23, and 0.26 for aerosols with diameters of 40, 80, 110, 150, and 200 nm, respectively. These averages are lower than those in Shanghai and Nanjing. κ_{Mean} for aerosols larger than 110 nm, however, are higher than those in Beijing and Guangzhou during winter. Distinct diurnal patterns for all measured sizes are observed for the number fractions of the NH (NF_{NH}) and MH (NF_{MH}) modes as well as κ-PDF and κ_{Mean}. The NF_{NH} values are lower, but κ_{Mean} exhibits peak values during daytime. More aerosols are internally mixed because of photochemical ageing during daytime. The number fraction of LH (NF_{LH}) for the 40-nm diameter aerosols in clean periods (CPs) is larger than that in the pollution episode (PEs) because of the increasing amount of SOA formation. More aerosols of diameters larger than 80 nm are internally mixed during CPs and stage of contaminant accumulation, resulting in higher κ_{Mean} values compared to those in PEs. The aerosol emissions of fireworks that accumulate during the Chinese New Year's Eve contribute to the slow and continuous increasing trend in κ_{Mean} with average values of 0.19, 0.19, 0.21,0.23, and 0.27 for the 40, 80, 110, 150, and 200-nm diameter aerosols, respectively. These values are higher than those during the pre- and post-fireworks days. The hygroscopic properties of submicron aerosols in Chengdu are essential for understanding the formation and evolution of severe haze events in Sichuan Basin.

Keywords: aerosols, hygroscopicity, H-TDMA, Chengdu

©2020. Japan Geoscience Union. All Right Reserved.

Comparison of absorption coefficient and black carbon concentration at Byeongcheon, South Korea using Tricolor absorption photometer (TAP) and Multiangle absorption photometer (MAAP)

*Jeonghoon Lee[1]

1. KOREATECH

We evaluate the tricolor absorption photometer (TAP) and the multiangle absorption photometer (MAAP) with respect to their response to black carbon concentration ranging 0-7 mg/m^3 at KOREATECH located in Byeongcheon, South Korea. While the MAAP employs basically similar principle to the TAP, that is, light extinction through an aerosol particle-deposited filter, it has a unique scheme to get rid of artifacts originating from the scattering effect of the aerosols deposited on the filter. In addition to comparing the absorption coefficients acquired by TAP at three different wavelengths, we also compare the absorption coefficients to the mass concentration of black carbon measured by the MAAP. We also derived absorption Ångström exponents (AAE) and mass absorption cross sections (MACs) by using the absorption coefficients reported by the TAP and the mass concentration reported by the MAAP without performing correction process. We observed that absorption coefficients showed similar trend to the mass concentration of black carbon. Our study finds that using the constant MAC value recommended by manufacturer at the wavelength used in MAAP results in aerosol light absorption coefficients that are different from those reported by the TAP. We also find that black carbon concentration at KOREATECH is as high as urban area although the campus is located in countryside. A discussion on high concentration, along with the results of an inter-comparison between TAP and MAAP will be presented.

Keywords: TAP, MAAP, Black carbon

©2020. Japan Geoscience Union. All Right Reserved.

$PM_{2.5}$ vertical concentration observations using a drone based on comparison of $PM_{2.5}$ concentration data with small sensor and atmospheric environment measurement station data

*Takashi Chiba[1], Masatsugu Kodate[1], Osamu Kiguchi[1], Makoto Inoue[1], Hirokazu Madokoro[2], Takeshi Nagayosi[1]

1. Faculty of Bioresource Sciences, Akita Prefectural University, 2. Faculty of Systems Science and Technology, Akita Prefectural University

Atmospheric particulate matter of size of 2.5 μm or less are denoted as $PM_{2.5}$. The generation of $PM_{2.5}$ encompasses primary processes on the ground surface and complicated secondary processes in the atmosphere. In the year 2009, an environmental standard value was set for $PM_{2.5}$ because of its health effects. Since then, their negative impacts on health have been reduced through continuous observations and warnings issued by measuring stations around Japan. Although component analysis is effective in identifying $PM_{2.5}$ sources, setup and operating costs for observation facilities are high, and high-frequency observation results cannot be obtained. In addition, there are automatic measuring machines (measuring at hourly intervals), which follow official methods, but the number of installations are low due to cost issues and difficulty in identification of $PM_{2.5}$ sources. On the other hand, in recent years, small particle sensors that are capable of measuring with high temporal resolution have become widespread. These sensors are based on light scattering methods; they can obtain observations at 1-second intervals and can be mounted on drones. Therefore, these sensors are expected to contribute to the diffusion process of $PM_{2.5}$ and identification of the source. However, since the mass concentration value obtained by the light scattering method is indirectly calculated from the particle number concentration, the accuracy of the obtained hourly values is not known. In this study, we compared the two data types by performing simultaneous observations with a sensor based on the laser light scattering method and an atmospheric environment measurement station that uses the official measurement method. We also compared these results with the $PM_{2.5}$ concentration obtained by the small sensor to estimate the accuracy of the obtained data Furthermore, based on the results, we attempted to correct the obtained observation values onboard the drone.The $PM_{2.5}$ concentration was measured using a Pocket $PM_{2.5}$ Sensor manufactured by Yaguchi Denshi Kogyo. To conduct simultaneous observations with the measurement station data, an observation station was constructed independently at the Shogunno General Atmospheric Environment Measurement Station in the East Third Block of Tsuchizaki Station on November 13, 2019, with the permission of Akita City. The height of the observation pole was 3.1 m, and $PM_{2.5}$ concentration data was acquired at 1-second intervals. For comparison with the measurement station, the 1-hour average values and standard deviation of the data were obtained from the small sensors. The 1-hour values, published as preliminary values by the Ministry of the Environment Air Pollutant Wide Area Monitoring System Soramame-kun (http://soramame.taiki.go.jp/Index.php), were used for the data from the measurement station. During the observation period from November 2019 to January 2020, 502 1-hour average values were obtained from sensor observations. The difference between the $PM_{2.5}$ concentrations measured by the sensor and the measurement station data, as well as the correlation coefficient between them are -1.7 ±4.7 μg/m³ and r = 0.48, respectively. A negative observation error of approximately 2 μg/m³ was observed. Based on these observations, corrections were made for the observed data up to an altitude of 500 m while using a drone from June 2018 to February 2019. The results of this study suggest that the $PM_{2.5}$ observations using a drone can be used to determine high and low concentrations, as defined by environmental standards, despite the observed errors. In this

©2020. Japan Geoscience Union. All Right Reserved.

presentation, we report the results obtained by extending the observation period.

Keywords: PM2.5, Laser light scattering, drone

©2020. Japan Geoscience Union. All Right Reserved.

Long-term measurements of aerosol physical properties in the Noto Peninsula

*Seiji Kubota[1], Alessia Nicosia[2], Yoko Iwamoto[3], Naoki Kaneyasu[4], Ayumi Iwata[5], Hiroshi Tsurumaru[6], Atsushi Matsuki[2]

1. Graduate School of Natural Science and Technology, Kanazawa University, 2. Institute of Nature and Environment Technology, Kanazawa University, 3. Graduate School of Biosphere Science, Hiroshima University, 4. Atmospheric Environment Research Group, National Institute of Advanced Industrial Science and Technology, 5. Department of Applied Chemistry, Faculty of Science and Technology, Keio University, 6. Tokyo Metropolitan Research Institute for Environmental Protection

According to Zeng et al. (2019) [1] the concentration of particulate matter (PM) have decreased significantly in China since 2013. Whether this decrease can be detected eastward, remains to be validated. In particular, the 2013-2017 summary report of the Long-range Transboundary Air Pollutants project [2] has estimated that China's contributions to PM2.5 concentration affecting Japan is 24.6 percent, while South Korea's contributions are 8.2 percent, based on source-receptor relationship simulations. Then, it is expected that a decrease of Long-range Transboundary Air Pollutants (LTP) will have a positive feedback in the air quality of many cities of Japan. To validate these assumptions and improve our understanding on LTP, it is necessary to perform continuous monitoring of air quality, especially in remote sites, scarcely affected by local emissions.

In this study we report a comprehensive survey on the trend of PM2.5 measured from 2013 to 2019 at NOTOGRO (acronym for NOTO Ground-based Research Observatory). Due to its special location, the site (37.45˚N, 137.36˚E) is well suited to assess the influence of transboundary air pollutants with respect to the background. Through the analysis of 7 years' worth of measurement data, we have investigated the seasonal and the long-term trend of the aerosol mass and size distributions.

Figure 1 shows the boxplot of the PM 2.5 mass concentration measured by a tapered element oscillating microbalance (TEOMseries1400). The blue fitting highlights the seasonal trend, while the red fitting traces the long-term trend based on Theil-Sen analysis. Monthly average concentrations are high in spring, and low in late autumn and winter. These variations are largely associated to the occurrence of long–range transport in spring, and increased amount of precipitation characteristically seen along the western coast of Japan in winter. Furthermore, PM2.5 concentrations are higher in summer, than in autumn, due to the influence of secondary formation that are driven by photochemical reactions.

In addition to these seasonal variations, a consistent decrease in the annual mean mass concentration can be observed. Considering that the analyzed period overlaps the ‘Chinese Action Plan on Prevention and Control of Air Pollution’, we suggest that LTP arriving in NOTOGRO are changing, as response to the decrease scenario of the Asian continent emissions. To further understand these modifications, our analysis has considered also the number and size distribution of the dried atmospheric aerosols for the same period 2013-2019.

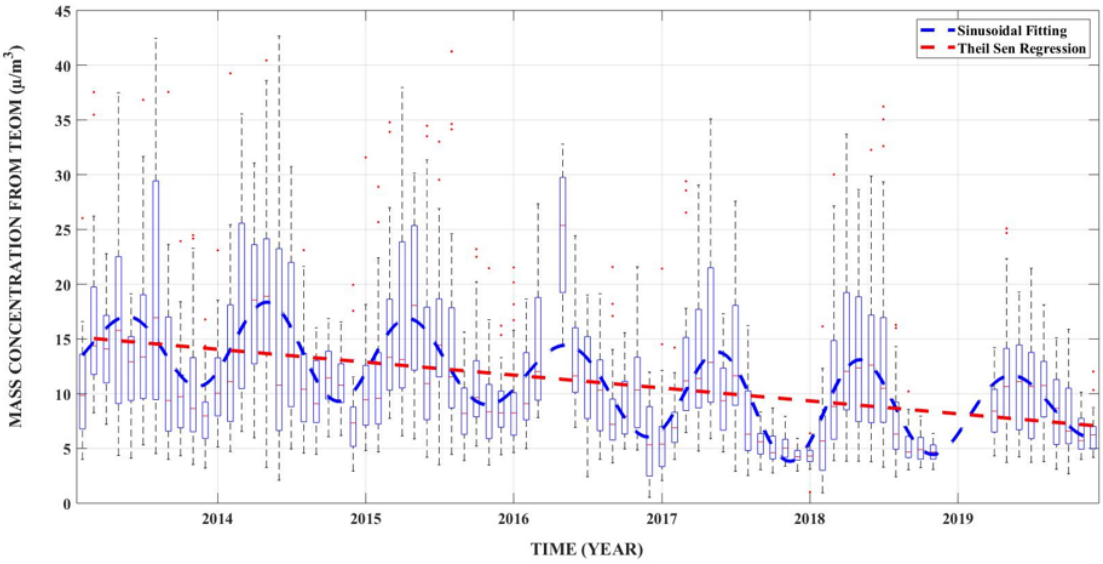
The analysis of the aerosol number concentration, for Dp>0.3 μm, measured by an optical particle counter (OPC from RION model KC-01E) shows a decrease of the total number concentration below 2 μ

©2020. Japan Geoscience Union. All Right Reserved.

m and mainly in the accumulation particles mode. The analysis of the particle size distributions measured in the range 0.01-0.3 μm, by a scanning mobility particle sizer (SMPS, from TSI DMA model 3081+CPC model 3776) is also considered. From the peak analysis of SMPS data, we observe that there was no significant change in the median seasonal distributions. However, the size segregated total aerosol number concentration indicates distinct behaviors in the long-term trends of different particles modes. Furthermore, SMPS data confirms a decrease only for the range 0.2-0.3 μm.

These findings support that a preferential particle size range (0.2-2 μm) is responding mostly to the decreases of LTP, and the decreased emissions doesn't affect equally all particle sizes. Our results are worthwhile for the validation of emission inventory and simulation models.

Keywords: Long-range Transboundary Air Pollutants, Monitoring, Atmospheric Aerosols, PM2.5



©2020. Japan Geoscience Union. All Right Reserved.

Recurrent Neural Network (RNN), Long short-term memory (LSTM) for Aerosol Optical Depth (AOD) using NASA's MERRA-2 Reanalysis

*Mohammed Ezzat Magooda[1], Muhammed Eltahan[2], Karim Moharm[3]

1. Aerospace Engineering Dept, Cairo Univ., Cairo, Egypt, 2. Institute of Bio-Geosciences (IBG-3, Agrosphere), Forschungszentrum Jülich, Jülich, Germany, 3. Electrical Engineering Dept., Alexandria University, Alexandria, Egypt

Predication of temporal trends of aerosol optical depth (AOD) within the numerical climate models with enabled chemistry module is very challenging and computationally expensive. In this work, new predication model is introduced based on artificial neural networks (ANN) in order to estimate average AOD over Egypt. Long short-term memory (LSTM) algorithm which is artificial recurrent neural network (RNN) architecture, is selected to construct the predication model. Seven input datasets for LSTM algorithm are from NASA's Modern-Era Retrospective analysis for Research and Applications, Version 2 (MERRA-2) reanalysis within period (1980-2017). The seven variables are pressure (PR), temperature (T), wind speed (W), dust surface particulate matter (PM2.5), surface (SO2) and (SO4) concentrations and (CO) concentration. AOD is the output of the trained and validated model. Effects of changing the number of both hidden layers and number of neurons per layers were evaluated.

The results of increasing the number of neurons per one hidden layer revealed that increasing the number of neurons leads to three main finding (a) leads to faster convergence of loss function. (b) Produces more realistic AOD estimation (c) RMSE is reduced by increasing number of neurons. It was also found that, the model with one hidden layer and 50 neurons is the best model setup with RMSE (0.06).

However, our studies showed also that increasing the number of hidden layers has no dominant effect on model RNN performance. The proposed LSTM model showed a very high level of accuracy with percentage 99.94 %. Future work can include more variables that has direct effect on AOD calculations. Both ensemble algorithms and different datasets can have more positive impact on the current proposed model.

Keywords: AOD, LSTM, MERRA-2

©2020. Japan Geoscience Union. All Right Reserved.

Development of SCALE-Chem and its application for regional simulation targeting on urban area and mountain area of Japan

*Makiko Nakata[1], Mizuo Kajino[2], Yousuke Sato[3,4], Hisashi Yashiro[5,4], Itaru Sano[1], Sonoyo Mukai[6]

1. Kindai University, 2. Meteorological Research Institute, 3. Faculty of Science, Department of Earth and Planetary Sciences, Hokkaido University, 4. RIKEN Center for Computational Science, 5. National Center for Environmental Studies, 6. The Kyoto College of Graduate Studies for Informatics

A chemical transport model (CTM) (Kajino et al., 2019) was implemented into a meteorological model; Scalable Computing for Advanced Library and Environment (SCALE; Nishizawa et al., 2015; Sato et al., 2015) for investigating the local scale transport of aerosol. The CTM coupled with SCALE (SCALE-Chem) enabled us to conduct numerical simulations with fine grid spacing (O(10 ~ 100 m)) enough to resolve the local scale phenomena contributing to the local scale transport of aerosols and chemical tracer. Using SCALE-Chem, we conducted the numerical simulation targeting on urban area of Osaka, Japan, and the validity of the SCALE-Chem was confirmed through the comparison between the aerosol optical thickness (AOT) and particulate matter measured by the observation campaign of Distributed Regional Aerosol Gridded Observation Networks (DRAGON) Osaka (Holben et al., 2018; Sano et al., 2016) and those simulated by SCALE-Chem. Figure 1 shows the DRAGON-Osaka site distribution. Our analyses indicated that SCALE-Chem successfully simulated the observed aerosol properties. As well as the simulation for the urban area of Osaka, we will conduct numerical simulations targeting on mountain area of Nagano Prefecture, Japan to investigate the contribution of the local aerosol and aerosols transported from continent to aerosols measured by the observational campaign of Joint work to the Aerosol Properties and process Simulations (J-ALPS).

Figure 1. These black circles indicate AERONET (Aerosol Robotic Network) station and these open circles indicate sites that sun photometers are put into place during a period of DRAGON field campaign. The extended figure shows DRAGON-Osaka site distribution. Osaka, Kobe, Kyoto, and Nara are located in very close each other.

Reference

Kajino, M., Deushi, M., Sekiyama, TT., Oshima, N., Yumimoto, K., Tanaka, TY., et al., NHM-Chem, the Japan meteorological agency’ s regional meteorology –chemistry model: Model evaluations toward the consistent predictions of the chemical, physical, and optical properties of aerosols. J. Meteorol. Soc. Japan. 2019;97(2):337–374.

Nishizawa, S., Yashiro, H., Sato, Y., Miyamoto, Y., Tomita, H., Influence of grid aspect ratio on planetary boundary layer turbulence in large-eddy simulations. Geosci. Model Dev. 2015; 28;8(10):3393–341.

Sato, Y., Nishizawa, S., Yashiro, H., Miyamoto, Y., Kajikawa, Y., Tomita, H., Impacts of cloud microphysics on trade wind cumulus: which cloud microphysics processes contribute to the diversity in a large eddy simulation? Prog. Earth Planet. Sci. 2015;2(1):23. doi:10.1186/s40645-015-0053-6

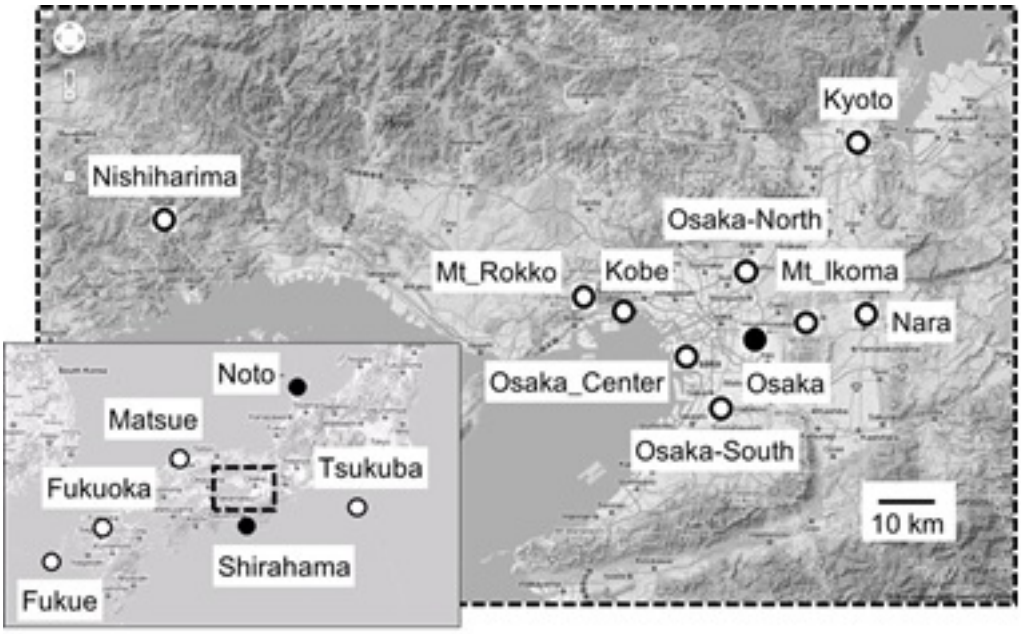
Holben, B. N., Kim, J., Sano, I., Mukai, S., Eck, T. F., Giles, D. M., Schafer, J. S., Sinyuk, A., Slutsker, I., Smirnov, A., Sorokin, M., Anderson, B. E., Che, H., Choi, M., Crawford, J. E., Ferrare, R. A., Garay, M. J., Jeong, U., Kim, M., Kim, W., Knox, N., Li, Z., Lim, H. S., Liu, Y., Maring, H., Nakata, M., Pickering, K. E.,

©2020. Japan Geoscience Union. All Right Reserved.

Piketh, S., Redemenn, J., Reid, J. S., Salinas, S., Seo, S., Tan, F., Tripathi, S. N., Toon, O. B., and Xiao, Q, An overview of meso-scale aerosol processes, comparison and validation studies from DRAGON networks, Atmos. Chem. Phys. 2018;18 (2): 655-671

Sano, I., Mukai, S., Nakata, M., Holben, B. N., Regional and local variations in atmospheric aerosols using ground-based sun photometry during distributed regional aerosol gridded observation networks (DRAGON) in 2012, Atmos. Chem. Phys. 2016; 16, 14795-14803, doi:10.5194/acp-16-14795-2016

Keywords: aerosol, ground observation, regional weather model



©2020. Japan Geoscience Union. All Right Reserved.

Regional trends of combustion aerosol and dust in recent decades: a satellite-model integrated analysis

*Hongbin Yu[1], Yang Yang[2], Hailong Wang[1], Qian Tan[3,4], Mian Chin[1], Robert Levy[1], Lorraine Remer[5], Steven Smith[2], Tianle Yuan[1,5], Yingxi Shi[1,5], Zhibo Zhang[5], Qianqian Song[5], Paul Ginoux[6]

1. NASA Goddard Space Flight Center, 2. Pacific Northwest National Laboratory, 3. Bay Area Environmental Research Institute, 4. NASA Ames Research Center, 5. University oof Maryland Baltimore County, 6. NOAA GFDL

Emissions and long-range transport of mineral dust and combustion-related aerosol from burning fossil fuels and biomass vary from year to year, driven by the evolution of the economy and changes in meteorological conditions and environmental regulations. This study offers both satellite and model perspectives of interannual variability and possible trends of combustion aerosol and dust in major continental outflow regions over the past 15 years (2003-2017). The decade-long record of aerosol optical depth (AOD, denoted as t), separately for combustion aerosol (t_c) and dust (t_d), is derived from the aerosol products of the Moderate Resolution Imaging Spectroradiometer (MODIS) onboard both Terra and Aqua. The MODIS datasets, complemented by aerosol source-tagged simulations using the Community Atmospheric Model Version 5 (CAM5), are then analyzed to understand the interannual variability and potential trend of t_c and t_d in the major continental outflows. Both MODIS and CAM5 consistently yield a similar decreasing trend of -0.017 to -0.020 per decade for t_c over the North Atlantic Ocean and the Mediterranean Sea that is attributable to reduced emissions from North America and Europe, respectively. On the contrary, both MODIS and CAM5 display an increasing trend of +0.017 to +0.036 per decade for t_c over the tropical Indian Ocean, the Bay of Bengal, and the Arabian Sea, which reflects the influence of increased anthropogenic emissions from South Asia and the Middle East in the last 2 decades. Over the northwestern Pacific Ocean that is often affected by East Asian emissions of pollution and dust, the MODIS retrievals show non-monotonic but overall decreasing trend of -0.021 per decade for t_c and -0.012 per decade for t_d, which is however not reproduced by the CAM5 model. In other outflow regions strongly influenced by biomass burning smoke or dust, both MODIS retrievals and CAM5 simulations show no statistically significant trends; and the MODIS observed interannual variability is usually larger than that of the CAM5 simulation. Seasonal variations of regional trends will also be discussed.

Keywords: pollution, dust, satellite, model, trend

©2020. Japan Geoscience Union. All Right Reserved.

Development of a regime-dependent autoconversion parameterization using satellite observations

*Tomoki Hirata[1], Takuro Michibata[2], Toshihiko Takemura[2]

1. Interdisciplinary Graduate School of Engineering Sciences, Kyushu University, 2. RIAM Research Institute for Applied Mechanics

Aerosol-cloud interactions (ACI) are major sources of uncertainty in climate modeling due to their complex dependences on cloud regimes, which are less understood. Most of the climate models tend to overestimate the magnitude of ACI compared with satellite observations partly because of an autoconversion parameterization in which the magnitude of warm rain modulation depending on aerosol perturbations is prescribed regardless of cloud regimes. Here we develop a new autoconversion parameterization which includes the regime-dependence of ACI inferred from satellite observations. The new scheme represents the magnitude of ACI as a function of the precipitation efficiency characterized by the ratio of rainwater to total liquid water. The proposed scheme is designed to reproduce a lower cloud susceptibility to aerosols in a more efficient precipitating regime according to the satellite-derived relationship, which allows to simulate nonmonotonic cloud responses to aerosol perturbations with spatial dependence in terms of cloud regimes. This is supported by the satellite statistics that show an inverse correlation between the cloud susceptibility and precipitation efficiency, and is also in good agreement with a steady-state model in a past study. Our results that are expected to fix the magnitude of ACI and hence ignore the regime dependence are more realistic than previous autoconversion schemes. The new scheme will reconcile some of the common biases in particular the excessive ACI in current global climate models. We show an impact of the new scheme on the simulated precipitation characteristics and aerosol effective radiative forcing using a single-column model and a global aerosol-climate model.

Keywords: Aerosol-cloud interaction, autoconversion, cloud regime, precipitation efficiency, cloud susceptibility

©2020. Japan Geoscience Union. All Right Reserved.

Aerosol data assimilation experiment using GCOM-C SGLI aerosol product

*Taichu Y Tanaka[1], Keiya Yumimoto[3,1], Mayumi Yoshida[2], Hiroshi Murakami[2], Takashi M. Nagao[4], Megumi Okata[2]

1. Meteorological Research Institute, Japan Meteorological Agency, 2. Earth Observation Research Center, Japan Aerospace Exploration Agency, 3. Research Institute for Applied Mechanics, Kyushu University, 4. Atmosphere and Ocean Research Institute, The University of Tokyo

The Global Change Observation Mission - Climate (GCOM-C) satellite was launched on 23 December 2017, for long-term environmental monitoring of the Earth. The GCOM-C satellite carries the second-generation global imager (SGLI), which is a multi-wavelength optical radiometer that has 19 observation wavelength bands from near-ultraviolet to thermal infrared and has characteristic functions such as polarization, multi-directional, and near-ultraviolet observation. SGLI observation data contributes to the improvement of the accuracy of the processes in climate models such as clouds, aerosols, sea colors, vegetation, and snow ice, and to be applied in various applications such as predictions of sand and dust storms, fishing ground, and understanding of red tide occurrence. JAXA Earth Observation Research Center (EORC) retrieves and provides quantitative information on atmospheric aerosols from SGLI data. The SGLI standard non-polarized aerosol product includes aerosol optical thickness (AOT), Angstrom exponent, and single scattered albedo on land are derived. JAXA EORC, Meteorological Research Institute of Japan Meteorological Agency (MRI/JMA), and Research Institute for Applied Mechanics (RIAM) of Kyushu University have been carrying joint research to utilize the geostationary and low-orbit satellites to monitor and predict the atmospheric aerosols, and to create an integrated aerosol product. MRI/JMA is currently developing a global aerosol prediction system that assimilates SGLI aerosol products using the global aerosol model MASINGAR. We will show the initial results of data assimilation experiments using two-dimensional variation (2D-Var) for the global aerosol model, and discuss the data verification, quality control, and the effects of the data assimilation.

Keywords: Aerosol, Satellite observation, Data assimilation

©2020. Japan Geoscience Union. All Right Reserved.

A study on the effects of sulfate aerosols on ocean circulation and the consequent atmospheric feedback

*Yuki Kusakabe[1], Toshihiko Takemura[2]

1. Interdisciplinary Graduate School of Engineering Sciences, Kyushu University, 2. Research Institute for Applied Mechanics, Kyushu University

Sulfate aerosols are generally known to have negative radiative forcing and then cool the earth. The effects on the atmosphere are not uniform globally, and regional variations have been simulated by atmosphere-ocean coupled global climate models. Although Collier et al. (2013) showed that anthropogenic aerosols can alter the ocean circulation, on the other hand, there are no detailed analysis of it due to specific anthropogenic aerosol components in past studies. Then, in this study, using sensitivity experiment data from MIROC-SPRINTARS it is examined how sulfate aerosols affect ocean circulation and atmospheric feedback. In the sensitivity experiment, the anthropogenic emissions of SO_2, a precursor of sulfate aerosol, are perturbed to be 0, 0.3, 0.5, 0.8, 1.5, 2, 5 and 10 times from the current emissions. The calculations were performed for 100 years in the equilibrium experiments, and the data in the last 50 years were used for analysis. The results show that spatial distributions of changes in sea surface temperature (SST) are similar to those of surface air temperature. A peculiar perturbation of SST is shown in the mid-latitude of the North Atlantic, which the SST increases (decreases) due to an increase (decrease) in SO_2 emission. Analysis of ocean currents and wind fields suggests that strengthening or weakening of westerly winds by sulfate aerosols perturbation may change a flow path of the Gulf Stream, causing the characteristic change in SST.

Reference

Collier, M.A., Rotstayn, L.D., Kim, K.Y., Hirst, A.C., and Jeffrey, S.J. 2013. Ocean circulation response to anthropogenic-aerosol and greenhouse gas forcing in the CSIRO-Mk3.6 coupled climate model, doi: 10.22499/2.6301.003.

Keywords: Sulfate aerosols, Galf stream, Ocean circulation, Atmospheric feedback

©2020. Japan Geoscience Union. All Right Reserved.

Surface air temperature response to large-scale volcanic eruptions and its relationship with ENSO

*Sho Kitabayashi[1], Hiroshi G. Takahashi[1]

1. Tokyo Metropolitan University

A volcanic eruption injects sulfate aerosols into the atmosphere, which decrease the surface air temperature (SAT). When the aerosols expand in the stratosphere, a decrease in SAT can be maintained globally during a few years, although it is generally difficult to estimate the effects of a volcanic eruption because of the existence of internal variations in the climate system. This study estimated the SAT change after large low-latitude volcanic eruptions focusing on the phase of El Niño-Southern Oscillation (ENSO) by analyzing CMIP5 historical experiments. Volcanic eruptions, as an external forcing of climate system, are prescribed based on the observational datasets. However, internal variabilities like ENSO are different in each ensemble. Thus, it is possible to analyze SAT changes in the same eruption that are different in the phase of ENSO. Results showed that global SAT changes after volcanic eruptions contain a difference in the phase of ENSO. In addition, the “combined” effect of ENSO and volcanic eruptions still was found after the eruptions globally. The contribution of the ENSO to SAT was estimated approximately 1/10 to 1/5 of the whole decrease in SAT. Furthermore, the SAT changes were different in the both hemispheres. In the northern (southern) hemisphere, the decrease in SAT was larger (smaller), and the SAT changes continued shorter (longer) periods.

©2020. Japan Geoscience Union. All Right Reserved.

[E] Poster | A (Atmospheric and Hydrospheric Sciences)：A-AS Atmospheric Sciences, Meteorology & Atmospheric Environment

[A-AS12] Weather and climate extremes in East Asian monsoon system: mechanism, predictability, and projection

convener:JinHo Yoon(GIST Gwangju Institute of Science and Technology), Shih-Yu (Simon) Wang(Utah State University), Hyungjun Kim(The Univ. of Tokyo)

Weather and climate extremes have happened in sequence with similar characteristics, such as long-lasting drought and severe forest fire. Recently, the succession of two extreme yet opposite characteristics occurring in close proximity, such as the 2018 Japan severe flood followed by record-breaking heat wave, calls for a closer look at the synoptic-climate, which is largely linked to the East Asian Summer Monsoon system. From Europe to Asia, heat waves and severe thunderstorms can happen in rapid succession as well, modulated by a quick phase change of the meandering yet semi-stationary short waves. The changing climate may or may not affect all those circulation ingredients, making extreme-event attribution analysis difficult. However, in-depth understanding of the mechanism and its lifecycle is critically important to disaster mitigation and water security in warming climate. This session calls for recent advancement in combining the mesoscale, synoptic-scale, and large-scale diagnostics and modeling towards understanding mechanism, prediction and its future with a focus on weather and climate extremes particularly in East Asian monsoon system.

[AAS12-P01] **The study on the dynamic influence factors of the interdecadal variability of the subtropical high in the Western Pacific Ocean based on the information flow method**

*Mei Hong[1], Ren Zhang[1], Kefeng Liu[1], Liang Zhao[1], Jingjing Ge[2] (1. National University of Defence Technology, 2.The 31110 troop of PLA)

[AAS12-P03] **Characteristics and Formation of a Synoptic Situation Causing Sudden Turning of Mesoscale Convective Systems over South China**

*Zhaoming Liang[1], Ying Liu[1], Jinfang Yin[1] (1.Chinese Academy of Meteorological Sciences)

[AAS12-P04] Large-Scale Circulation Anomalies Associated with Extreme Heat in South Korea and Southern–Central Japan

*Ke Xu[1] (1. Institute of Atmospheric Physics, Chinese Academy of Sciences)

[AAS12-P05] A Synoptic Assessment of Climate Models' Representation of Summer Precipitation Extremes over East China

*Yi Deng[1], Yang Hu[2], Zhimin Zhou[2] (1.Georgia Institute of Technology, Atlanta, Georgia, United States, 2.Institute of Heavy Rain, China Meteorological Administration, Wuhan, China)

[AAS12-P06] Comparison of the East Asian Summer Monsoon Activities Represented by Clouds and Precipitation

*Yunying Li[1], Yun Jia[1] (1.College of Meteorology and Oceanography, National University of Defense Technology, China)

[AAS12-P07] **Impact of the recant warming of the surrounding ocean on the heavy rain event of July 2018 in Japan**

*ATSUYOSHI MANDA[1], Satoshi Iizuka[2], Hisashi Nakamura[3], Takafumi Miyasaka[4,5,3] (1.Mie University, 2.National Research Institute for Earth Science and Disaster Resilience, 3.The University of Tokyo, 4.Japan Meteorological Business Support Center, 5.Meteorological Research Institute)

[AAS12-P08] The effects of boundary layer processes on snowfall in Yanqing Zone of 2022 Winter Olympic Games

*BO YU[1], Jia DU[1], Ruixin LIU[1], Yujue LIU[2], Ziming LI[3], Luyang XU[1] (1.Beijing Municipal Weather Forecast Center, 2.Institute of Urban Meteorology, China Meteorology Administration, 3.Environmental

Meteorology Forecast Center of Beijing-Tianjin-Hebei)

[AAS12-P09] MJO Effects on the Formation and Subseasonal Predictability of Record-breaking Northeast Asian Heatwave in the Summer of 2018

*Pang-Chi Hsu[1], Yitian Qian[1], Hiroyuki Murakami[2] (1.Nanjing University of Information Science & Technology, 2.NOAA/GFDL)

[AAS12-P10] Causes of Inter-decadal Increase in Intraseasonal Rainfall Variability over Southern China around Early 1990s

*Lu Wang[1], Tim Li[2,1], Yifeng Cheng[1] (1.Nanjing University of Information Science and Technology, Nanjing, 210044, China, 2.University of Hawaii, Honolulu, HI 96822, USA)

[AAS12-P11] Consecutive extreme flooding and heat wave in Japan: Are they becoming a norm?

*JinHo Yoon[1], Shih-Yu (Simon) Wang[2], Hyungjun Kim[3], Jeehoon Jeong[1] (1.GIST Gwangju Institute of Science and Technology, 2.Utah State University, 3.University of Tokyo)

[AAS12-P12] Consecutive compound extremes of flood and heatwave within East Asia Summer Monsoon Lifecycle

*Hyungjun Kim[1], Gavin Madakumbura[2], Shih-Yu (Simon) Wang[3], JinHo Yoon[4] (1.The Univ. of Tokyo, 2.University of California, Los Angeles, 3.Utah State University, 4.Gwangju Institute of Science and Technology)

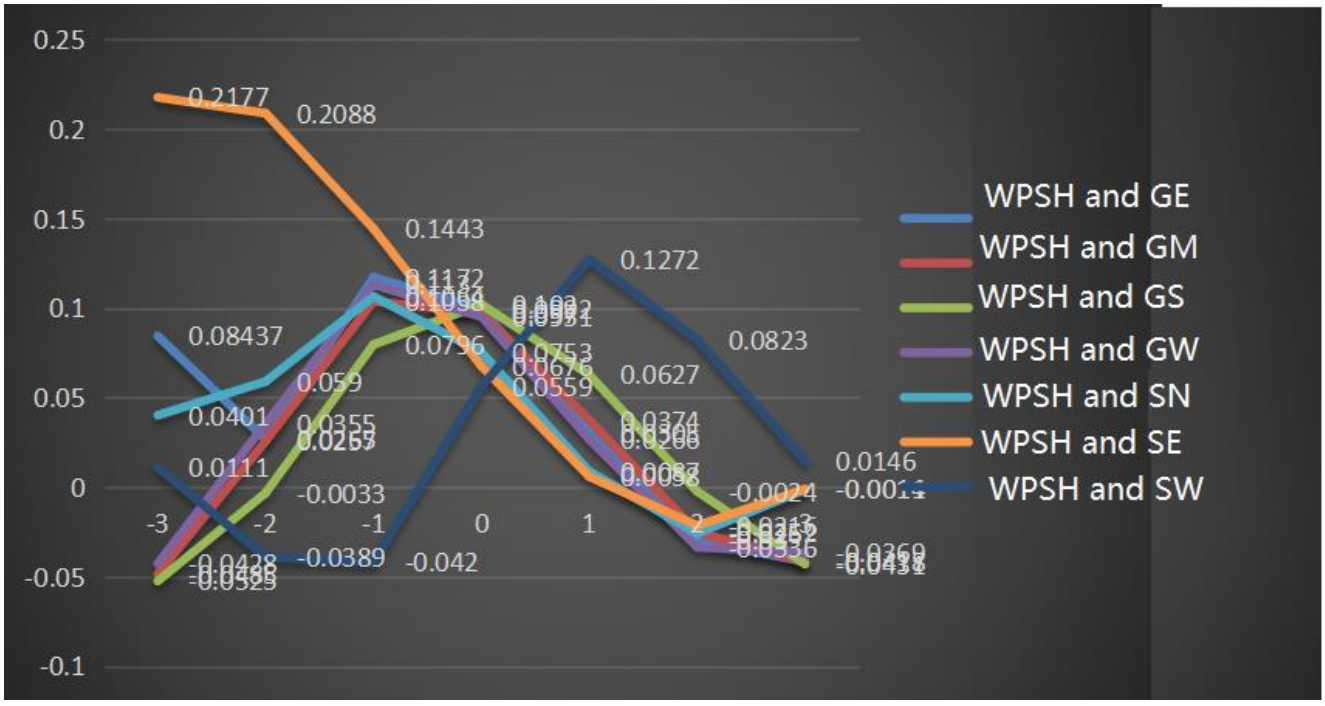
The study on the dynamic influence factors of the interdecadal variability of the subtropical high in the Western Pacific Ocean based on the information flow method

*Mei Hong[1], Ren Zhang[1], Kefeng Liu[1], Liang Zhao[1], Jingjing Ge[2]

1. National University of Defence Technology, 2. The 31110 troop of PLA

The subtropical high in the Western Pacific (WPSH)is one of the most important weather systems. It is the most important large-scale circulation system in low latitude. Its location and intensity directly affect the weather system in East Asia. Its abnormal activities often lead to disastrous weather in East Asia. Our paper deals with the complexity and uncertainty of the decadal variations of WPSH based on the information flow method. The eastern equatorial Pacific SST, the equatorial western Pacific SST, the equatorial Indian Ocean SST, eastern qinghai-tibet plateau geothermal flux of qinghai-tibet plateau, the main body of regional geothermal flux, geothermal flux in southern qinghai-tibet plateau region, the qinghai-tibet plateau in the western region of geothermal flux can be chosen as influence factors.By using the information flow method, the causal relationship between each factor and the interdecadal variability of the index of WPSH is calculated. On this basis, more important factors are screened out, and the interaction facts and mechanism between them and the interdecadal variability of WPSH are analyzed.

Keywords: western Pacific subtropical high, dynamic influence factors, information flow, SST near the equator



©2020. Japan Geoscience Union. All Right Reserved.

Characteristics and Formation of a Synoptic Situation Causing Sudden Turning of Mesoscale Convective Systems over South China

*Zhaoming Liang[1], Ying Liu[1], Jinfang Yin[1]

1. Chinese Academy of Meteorological Sciences

The rainfall of the pre-flood rainy season (April–June) contributes more than 40% of the annual rainfall for South China, and warm-sector mesoscale convective systems (MCSs) have been indicated as the principal systems causing heavy or extreme rainstorms in this rainy season [1–4]. Compared to frontal rainfall systems, warm-sector MCSs are harder to predict [5], owing to difficulties in accurately capturing their initiation, development and motion. In contrast to the initiation and development, the motion of MCSs over South China has seldom been investigated, especially for those with complex motion.
In the present study, the characteristics and formation of a synoptic situation that causes a sudden turning motion of warm-sector mesoscale convective systems (MCSs) over South China are described, based on the collection and investigation of associated cases during April–June 2011–2017 using high-resolution observational data and ERA (ECMWF Re-Analysis)-Interim data. The results show that the blocking of a marked low-level high over eastern China (eastern high) on a strengthening low-level trough over southwestern China (southwestern trough) results in significant enhancement of southerly winds ahead of the trough, which produces a strong southeastward vertical wind shear at low levels near western Guangdong province. This low-level vertical wind shear results in sudden southeastward turning motion for the warm-sector MCSs entering into Guangdong province from Guangxi province. The formation of the eastern high is mainly attributable to the strong cyclonic wind anomaly over the northwestern Pacific Ocean, which continuously brings cold air from higher latitudes to eastern China, where high synoptic-scale transient anomaly of geopotential height (SSTA-GH) forms. This cyclonic wind anomaly is induced by a low SSTA-GH, which travels from the north and south sides of the Tibetan Plateau to the northwestern Pacific Ocean and develops significantly as a result of a strong upper-level low SSTA-GH coupling with it or approaching it. On the other hand, the high SSTA-GH over eastern China blocks the eastward extension of the low SSTA-GH originating from the Tibetan Plateau. Consequently, this low SSTA-GH turns to extend or move southeastward/southward to southwestern China, leading to intensification of the southwestern trough.

References:

1. Tao, S.Y.; et al. Rainstorms in China; Science Press: Beijing, China, 1980. (In Chinese)

2. Huang, S.S.; et al. Rain Storm in South China in Early Summer; Guangdong Science and Technology Press: Guangzhou, China, 1986. (In Chinese)

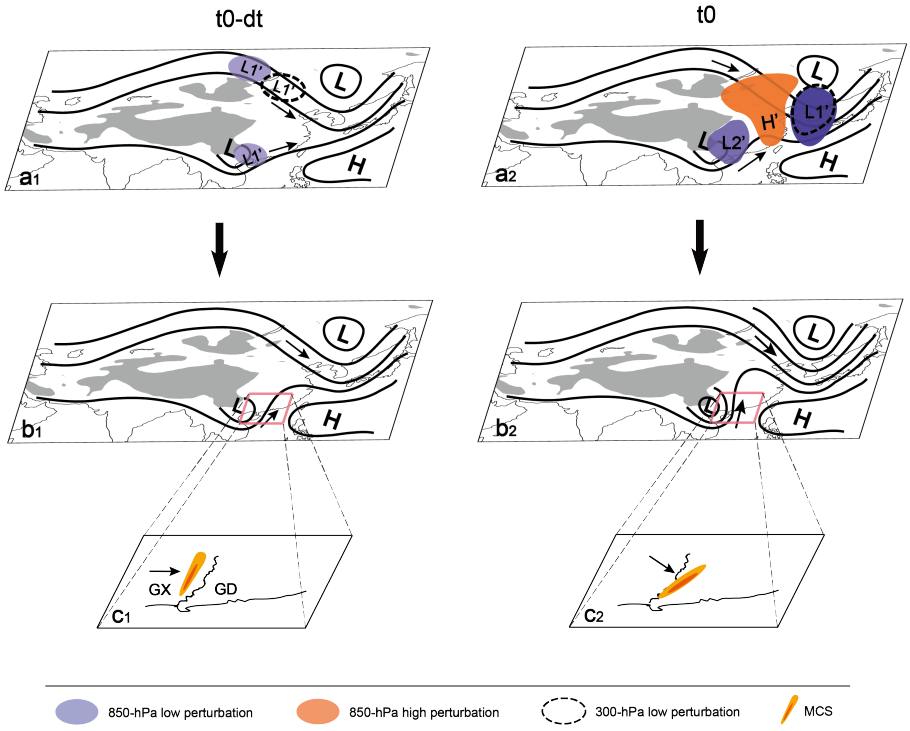
3. Zhou, X.J.; Xue, J.S.; Tao, Z.Y.; et al. Scientific Test Study of Rainstorm in Huanan in 1998; China Meteorological Press: Beijing, China, 2003.

4. Ni, Y.Q.; Zhang, R.H.; Liu, L.P.; et al. Rainstorms in South China Field Science Experiment (SCHeREX); China Meteorological Press: Beijing, China, 2013. (In Chinese)

5. He, L.F.; Chen, T.; Kong, Q. A review of studies on prefrontal torrential rain in South China. J. Appl. Meteorol. Sci. **2016**, 27, 559–569. (In Chinese)

©2020. Japan Geoscience Union. All Right Reserved.

Keywords: synoptic situation, sudden turning motion, warm-sector mesoscale convective system, South China



Schematic illustration of how (a1 − a2) the evolution of SSTA (color-shaded) and climatic average (contours) of geopotential height impact (b1 − b2) that of the complete geopotential height field (contours) at low levels, which promoted warm-sector MCSs to move suddenly from (c1) eastward/northeastward to (c2) southeastward when they entered Guangdong (GD) province from Guangxi (GX) province. “L” and “H” indicate the low and high value centers of geopotential height, respectively, while “L1’/L2’” and “H’” indicate the low and high SSTA-GH, respectively. The arrows indicate the (a1 − a2 and b1 − b2) flows or (c1 − c2) MCS motion directions.

©2020. Japan Geoscience Union. All Right Reserved.

Large-Scale Circulation Anomalies Associated with Extreme Heat in South Korea and Southern–Central Japan

*Ke Xu[1]

1. Institute of Atmospheric Physics, Chinese Academy of Sciences

The large-scale circulation anomalies associated with extreme heat (EH) in South Korea and southern–central Japan are examined using data during the time period 1979–2016. Statistical analysis indicates that EH days in these two regions are concentrated in July and August and tend to occur simultaneously. These EH days are therefore combined to explore the physical mechanisms leading to their occurrence. The composite results indicate that the anomalous atmospheric warming during EH days is dominantly caused by a significant subsidence anomaly, which is associated with a deep anomalous anticyclone over East Asia. Further investigation of the evolution of circulation anomalies suggests that the anomalous anticyclone over East Asia related to EH is primarily initiated by wave trains originating from upstream regions, which propagate eastward along the Asian westerly jet in the upper troposphere. These wave trains can be categorized into two types that are characterized by the precursor anticyclonic and cyclonic anomalies, respectively, over central Asia. The distinction between these two types of wave train can be explained by the wavenumbers of the Rossby waves, which are modulated by both the intensity and the shape of the Asian westerly jet as the background basic flow.

Keywords: extreme heat, large-scale circulation

©2020. Japan Geoscience Union. All Right Reserved.

A Synoptic Assessment of Climate Models' Representation of Summer Precipitation Extremes over East China

*Yi Deng[1], Yang Hu[2], Zhimin Zhou[2]

1. Georgia Institute of Technology, Atlanta, Georgia, United States, 2. Institute of Heavy Rain, China Meteorological Administration, Wuhan, China

The large-scale circulation anomalies associated with extreme precipitation events over the middle reaches of Yangtze River (MRYR) in early summer (June and July) are classified into three canonical synoptic patterns via hierarchical clustering. All clusters indicate a distinct connection between the MRYR extreme precipitation and anomalous moisture convergence driven by 1) low-level anomalous southwesterlies associated with the expansion of the Western Pacific Subtropical High, and 2) the anomalous northerlies tied to three distinct extratropical circulation anomalies ranging from zonally-elongated barotropic to developing baroclinic disturbances. The reproduction of these canonical patterns and their ties to extreme precipitation are found only in a subset CMIP5 models, where underestimates of the occurrence frequency of these patterns are largely responsible for underestimates of the occurrence frequency of extreme precipitation over East China in boreal summer. Our analysis also reveals that a few CMIP5 models simulate a reasonable rain rate spectrum in this region through a series of synoptic patterns that are not seen in observations. The differences in the potential responses among various synoptic patterns to greenhouse-gas forcing suggest the need of validating and better constraining climate model simulations of extreme events from a synoptic and weather perspective in order to achieve a more realistic projection of the near term changes in these events of tremendous societal impacts.

Keywords: extreme precipitation, synoptic assessment, CMIP models

©2020. Japan Geoscience Union. All Right Reserved.

Comparison of the East Asian Summer Monsoon Activities Represented by Clouds and Precipitation

*Yunying Li[1], Yun Jia[1]

1. College of Meteorology and Oceanography, National University of Defense Technology, China

Based on the pentad average ISCCP (International Satellite Cloud Climatology Project) D1 cloud data and a merged station and satellite precipitation data from 1998 to 2007, two types of cloud index and precipitation index are defined, which respectively reflect changes in clouds and precipitation locations and precipitation intensity associated with the East Asian summer monsoon (EASM) activities. The cloud and precipitation indices are used to study the advancing process of the EASM in mainland China. It is found that both indices can well represent the quasi-stationary stage and the north jump of the EASM, and they are consistent spatially and temporally. Based on changes in the cloud indices, active, transitional and interruptive monsoon periods in three regions of South China, East China and North China are defined. Differences in the cloud indices as well as differences in the circulation and water vapor fields at 500 hPa between the active and interruptive periods are examined, and the reasonability of the cloud indices is proved. Comparison of monsoon activity periods defined by the cloud indices and precipitation index shows that the monsoon active (interruptive) days are basically the same. However, the difference between the cloud and precipitation indices is that the precipitation index emphasizes the change in precipitation, while the cloud indices emphasize the change in cloudiness. The difference between monsoon active (interruptive) days respectively defined by cloud and precipitation indices could also reflect differences in the feature and type of precipitation.

Keywords: Cloud indices, East Asian summer monsoon, Active period

©2020. Japan Geoscience Union. All Right Reserved.

Impact of the recant warming of the surrounding ocean on the heavy rain event of July 2018 in Japan

*ATSUYOSHI MANDA[1], Satoshi Iizuka[2], Hisashi Nakamura[3], Takafumi Miyasaka[4,5,3]

1. Mie University, 2. National Research Institute for Earth Science and Disaster Resilience, 3. The University of Tokyo, 4. Japan Meteorological Business Support Center, 5. Meteorological Research Institute

The western North Pacific and the Asian marginal seas exhibit a rapid warming trend compared to the global average during the past century, and this trend is projected to continue toward the end of this century. Some recent studies suggest that the warming marginal seas in mid-latitudes plays a vital role in torrential rainfall events during a warm season, but the impact of the maritime warming is still debatable and thus under active research. A torrential rainfall that occurred from 28 June to 8 July 2018 caused widespread and devastating floods, landslides, and mudflows and they led to severe damages over wide areas in Japan, especially in its western part. We examine the impact of the recent warming of the surrounding ocean, including the marginal seas, on the torrential rainfall event, through the numerical simulations with a high-resolution regional atmospheric model. A fractional change of 3-day accumulated rainfall over land from 5 to 8 July, during which the most intensive rainfall was observed, is approximately 10%/K, which is consistent with a previous modelling study. This change cannot be explained quantitatively by the well-known theoretical argument based on the Clausius-Clapeyron relationship, i.e., change in precipitable water solely due to the atmospheric warming. Rather, our experiment suggests that the change in sea surface temperature can account for the rainfall change via the modification of convectively unstable air from the tropics. The specific mechanisms for the rainfall changes will be discussed in this presentation.

Keywords: torrential rain, ocean warming, event attribution

©2020. Japan Geoscience Union. All Right Reserved.

The effects of boundary layer processes on snowfall in Yanqing Zone of 2022 Winter Olympic Games

*BO YU[1], Jia DU[1], Ruixin LIU[1], Yujue LIU[2], Ziming LI[3], Luyang XU[1]

1. Beijing Municipal Weather Forecast Center, 2. Institute of Urban Meteorology, China Meteorology Administration, 3. Environmental Meteorology Forecast Center of Beijing-Tianjin-Hebei

Yanqing Zone of Beijing, as the venues for alpine skiing, sleigh and sled in 2022 Winter Olympic Games, the characteristics of snowfall have attracted much attention. According to the difficulty of snowfall forecast, the snowfall processes in Yanqing Zone during 2008 to 2018 was divided into two categories, synoptic scale system dominance and boundary layer process dominance (without obvious influence of synoptic scale system). In view of the snowfall dominated by the boundary layer processes, which was relatively difficult to predict, the analysis showed that one day of snowfall per year was caused by boundary layer processes. The snowfall dominated by boundary layer processes was divided into two types, northerly flow and westerly flow, and on the ground, it was usually a weak pressure field or an easterly flow. The northerly flow pattern accounted for a higher proportion of boundary layer process dominance, when the ground was easterly wind, if the saturated air and the terrain were forced to rise together, it could produce snowfall; when the lower layer was northerly wind, and it would produce local snowfall in high altitude area. The westerly flow pattern usually caused snowfall with large range and long duration, when the wind direction in boundary layer changed from easterly to southeasterly and the wind speed increased, it corresponded to the strongest period of precipitation; when the easterly wind speed decreased, the snowfall intensity also decreased.

Keywords: Boundary layer processes, Snowfall in Yanqing Zone, Classification analysis

©2020. Japan Geoscience Union. All Right Reserved.

The effects of boundary layer processes on snowfall in Yanqing Zone of 2022 Winter Olympic Games

Bo YU[1], Jia DU [1], Ruixin LIU[1], Yujue LIU[2], Ziming LI[3], Luyang XU[1]

(1. Beijing Municipal Weather Forecast Center, Beijing 100089,China;
2. Institute of Urban Meteorology, China Meteorology Administration, Beijing 100089,China;
3. Environmental Meteorology Forecast Center of Beijing-Tianjin-Hebei, Beijing 100089,China)

Keywords: Boundary layer processes, Snowfall in Yanqing Zone, Classification analysis

Abstract: Yanqing Zone of Beijing, as the venues for alpine skiing, sleigh and sled in 2022 Winter Olympic Games, the characteristics of snowfall have attracted much attention. According to the difficulty of snowfall forecast, the snowfall processes in Yanqing Zone during 2008 to 2018 was divided into two categories, synoptic scale system dominance and boundary layer process dominance (without obvious influence of synoptic scale system). In view of the snowfall dominated by the boundary layer processes, which was relatively difficult to predict, the analysis showed that one day of snowfall per year was caused by boundary layer processes. The snowfall dominated by boundary layer processes was divided into two types, northerly flow and westerly flow, and on the ground, it was usually a weak pressure field or an easterly flow. The northerly flow pattern accounted for a higher proportion of boundary layer process dominance, when the ground was easterly wind, if the saturated air and the terrain were forced to rise together, it could produce snowfall; when the lower layer was northerly wind, and it would produce local snowfall in high altitude area. The westerly flow pattern usually caused snowfall with large range and long duration, when the wind direction in boundary layer changed from easterly to southeasterly and the wind speed increased, it corresponded to the strongest period of precipitation; when the easterly wind speed decreased, the snowfall intensity also decreased.

©2020. Japan Geoscience Union. All Right Reserved.

MJO Effects on the Formation and Subseasonal Predictability of Record-breaking Northeast Asian Heatwave in the Summer of 2018

*Pang-Chi Hsu[1], Yitian Qian[1], Hiroyuki Murakami[2]

1. Nanjing University of Information Science & Technology, 2. NOAA/GFDL

In the summer of 2018, Northeast Asia experienced a heatwave event that broke the existing high-temperature records in several locations in Japan, the Korean Peninsula and northeastern China. At the same time, an unusually strong Madden–Julian Oscillation (MJO) was observed to stay over the western Pacific warm pool. Based on reanalysis diagnosis, numerical experiments and assessments of real-time forecast data from two subseasonal-to-seasonal (S2S) models, we discovered the importance of the western Pacific MJO in the generation of this heatwave event, as well as its predictability at the subseasonal timescale.

During the prolonged heat extreme period (11 July to 14 August), a high pressure anomaly with variability at the intraseasonal (30–90 days) timescale appeared over Northeast Asia, causing persistent adiabatic heating and clear skies in this region. As shown in the composites of MJO-related convection and circulation anomalies, the occurrence of this 30–90-day high anomaly over Northeast Asia was linked with an anomalous wave train induced by tropical heating associated with the western tropical Pacific MJO. The impact of the MJO on the heatwave was further confirmed by sensitivity experiments with a coupled GCM. As the western Pacific MJO-related components were removed by nudging prognostic variables over the tropics towards their annual cycle and longer timescales (>90 days) in the coupled GCM, the anomalous wave train along the East Asian coast disappeared and the surface air temperature in Northeast Asia reduced. The MJO over the western Pacific warm pool also influenced the predictability of the extratropical heatwave. Our assessments of two S2S models' real-time forecasts suggest that the extremity of this Northeast Asian heatwave can be better predicted 1–4 weeks in advance if the enhancement of MJO convections over the western Pacific warm pool is predicted well.

Keywords: Madden-Julian Oscillation, Heatwave, Mechanism, Predictability

©2020. Japan Geoscience Union. All Right Reserved.

Causes of Inter-decadal Increase in Intraseasonal Rainfall Variability over Southern China around Early 1990s

*Lu Wang[1], Tim Li[2,1], Yifeng Cheng[1]

1. Nanjing University of Information Science and Technology, Nanjing, 210044, China, 2. University of Hawaii, Honolulu, HI 96822, USA

The summer intraseasonal rainfall variability in Southern China (SC) shows a significant increase around 1992/1993, which coincides with the inter-decadal increase in summer mean rainfall. This study explores the causes of the inter-decadal change of 10-30-day rainfall variability over SC from 1979-1993 (P1) to 1994-2008 (P2). The SC intraseasonal rainfall events during 1979-2008 are objectively decomposed into three groups using K-means cluster analysis: southward propagating (SP) type, northwestward propagating (NWP) type and northward propagating (NP) type. A further analysis shows that it is the increase in the occurrence frequency of NP type that results in the enhancement of intraseasonal rainfall variability from P1 to P2, while the intensity of each type doesn't change significantly. Vorticity budget analysis suggests that the northward propagation results from the advection of intraseasonal vorticity anomaly by summer mean southerly wind in the middle-to-lower troposphere. A marked increase in the summer mean southerly wind in P2 relative to P1 causes more frequent occurrence of NP type and thus stronger intraseasonal rainfall variability over SC. No significant inter-decadal increase is found in the atmospheric instability over the south China Sea, suggesting that this factor doesn't contribute to more frequent NP type of rainfall in P2 than P1.

Keywords: Extreme Precipitation over Southern China, Decadal Change, Intraseasonal Rainfall Variability, Cluster Analysis

©2020. Japan Geoscience Union. All Right Reserved.

Consecutive extreme flooding and heat wave in Japan: Are they becoming a norm?

*JinHo Yoon[1], Shih-Yu (Simon) Wang[2], Hyungjun Kim[3], Jeehoon Jeong[1]

1. GIST Gwangju Institute of Science and Technology, 2. Utah State University, 3. University of Tokyo

In July 2018, Japan experienced two contrasting, yet consecutive, extreme events: a devastating flood in early July followed by unprecedented heat waves a week later. Death tolls from these two extreme events combined exceeded 300, accompanying tremendous economic losses (BBC: July 24, 2018; AP: July 30, 2018). Meteorological analysis on these 2018 events quickly emerged (JMA-TCC, 2018; Kotsuki et al., 2019; Tsuguti et al., 2019), highlighting several compound factors: a strengthened subtropical anticyclone, a deepened synoptic trough, and Typhoon Prapiroon that collectively enhanced the Baiu rainband (the Japanese summer monsoon), fostering heavy precipitation. The comprehensive study of these events, conducted within a month and released by the Japan Meteorological Agency (JMA) (JMA-TCC, 2018), reflected decades of knowledge of the Baiu rainband and new understanding of recent heat waves in southern Japan and Korea (Xu et al., 2019). Regardless, an extended forecast of this record-breaking precipitation remains challenging, with a skillful prediction of no more than 3 days (Kotsuki et al., 2019). Given the impending Baiu season of 2019, it is prudent to reflect upon these successive 2018 events by parsing out the critical components while discussing the potential of future compound extremes.

©2020. Japan Geoscience Union. All Right Reserved.

Consecutive compound extremes of flood and heatwave within East Asia Summer Monsoon Lifecycle

*Hyungjun Kim[1], Gavin Madakumbura[2], Shih-Yu (Simon) Wang[3], JinHo Yoon[4]

1. The Univ. of Tokyo, 2. University of California, Los Angeles, 3. Utah State University, 4. Gwangju Institute of Science and Technology

In recent years, East Asian countries have faced to wet and dry extremes frequently. For example, Japan experienced a catastrophic flood, and it was followed by a record-breaking heatwave in July 2018. The flood caused about 10 billion USD of economic damage which was a record breaking. The casualties by flood and drought exceeded 200 and 1000, respectively. In this study, we suggest that the timing of the consecutive flood and drought would not be coincident, but they are tightly connected with the active, break and revival phases of East Asia Summer Monsoon Lifecycle. Also, we examine the extend to which these back-to-back extreme events changes under the global warming and to which the human-induced warming is attributed to the intensification of the wet and dry swing. Multi-model large-ensemble simulations based on historical (naturalized and all-forcing) and future (+1.5 and +2.0 degree warming above preindustrial period) were adopted from Half a degree Additional warming, Prognosis and Projected Impacts project.

Keywords: Consecutive compound extremes, Flood, Drought, EASM, HAPPI, Compound event

©2020. Japan Geoscience Union. All Right Reserved.

[E] Poster | A (Atmospheric and Hydrospheric Sciences)：A-AS Atmospheric Sciences, Meteorology & Atmospheric Environment

[A-AS13] New particle formation and its impacts on atmospheric chemistry

convener:Jun Zheng(Nanjing University of Information Science and Technology), Lin Wang(Fudan University)

Despite of the fact that new particle formation (NPF) contributes about half of the aerosol population globally, the underlying mechanisms governing the NPF remain poorly understood. Current NPF models often lead to conflicting results with respect to real-time in-situ observations. Consequently, NPF process is seldomly incorporated into atmospheric models, causing great hindrance to accurately assess aerosol atmospheric impacts on air pollution formation and climate change on both regional and global scales. Although H2SO4, basic gases, and HOMs have been proposed to be responsible for NPF, searching for potential NPF precursors are still an active subject of research. Many recent studies strongly indicate that NPF mechanism may differ from place to place and the newly formed particles may also possess distinct properties (e.g., CCN activity). Nevertheless, there is a great demand to reconcile the conflicting results and to improve our understanding of the mechanisms for NPF. This session solicits contributions that describe research progresses on any aspects of NPF, including laboratory studies, theoretical calculation and modeling, and field measurements.

[AAS13-P01] **Formation of sulfuric acid clusters governed by a combined effect of dimethylamine and condensation sink in polluted northern China**

Yiqun Lu[1], Gan Yang[1], Yiliang Liu[1], Yuwei Wang[1], *Lin Wang[1] (1.Fudan University)

[AAS13-P02] Role of water molecule in aerosol nucleation and air-water interface reaction: quantum chemical and molecular dynamic simulation

*Fei Xu[1] (1.Shandong University)

[AAS13-P03] The Cloud Condensation Nuclei (CCN) activity during the New Particle Formation (NPF) events in the mountain region of China inland

*Mingfu Cai[1,2], Baoling Liang[1], Qibin Sun[1], Bin Yuan[2], Min Shao[2], Haobo Tan[3], Lihong Ren[4], Jun Zhao[1,5] (1.Institue for Environmental and Climate Research, Jinan University, 2.School of Atmospheric Sciences, Sun Yat-sen University, 3.Institute of Tropical and Marine Meteorology/Guangdong Provincial Key Laboratory of Regional Numerical Weather Prediction, CMA, 4.Atmospheric Chemistry and Aerosol Research Division, Chinese Research Academy of Environmental Science, 5.Southern Laboratory of Ocean Science and Engineering (Guangdong, Zhuhai), Zhuhai)

[AAS13-P04] **Nucleation events within an industrial zone in the YRD region of China**

*Jun Zheng[1], Yan Ma[1], Dongsen Yang[1] (1.Nanjing University of Information Science and Technology)

[AAS13-P05] Effects of SO2 on secondary organic aerosol generated from photooxidation of toluene

*Weigang Wang[1] (1.Institute of Chemistry,Chinese Academy of Sciences)

Formation of sulfuric acid clusters governed by a combined effect of dimethylamine and condensation sink in polluted northern China

Yiqun Lu[1], Gan Yang[1], Yiliang Liu[1], Yuwei Wang[1], *Lin Wang[1]

1. Fudan University

Formation of sulfuric acid (H_2SO_4, SA) clusters is considered to be responsible for atmospheric sulfuric acid - dimethylamine (C_2H_7N, DMA) nucleation in atmospheric new particle formation (NPF) processes, where the critical roles of both amines and condensation sink (CS) have been demonstrated. However, their combined effect is still not quantitively discussed in ambient observation. In this study, a comprehensive field campaign of NPF was carried out in Wangdu, Hebei province, which represents a typical polluted site in northern China. A number of key precursors and atmospheric parameters were recorded concurrently including the concentrations of sulfuric acid monomers and dimers, DMA, and aerosol particle number size distributions. H_2SO_4-DMA-H_2O ternary nucleation mechanism was responsible for the observed NPF events through the correlation analysis of sulfuric acid monomers, sulfuric acid dimers, CSs, and nucleation rates, and the comparisons with the results from atmospheric cluster dynamics code (ACDC) and CLOUD experiments. The CS and [DMA] varied significantly on NPF event days: CS ranged from 0.01 to 0.04 whereas the 25-75% percentiles of [DMA] covered 1.1-8.2 pptv (part per trillion by volume), which indicates that the formation of clusters should be govern by the two factors. Based on the well-accepted formation pathway of sulfuric acid dimers in the literature, we quantitatively described the combined effect of [DMA] and CS in the formation of sulfuric acid dimers. The ratio of sulfuric acid dimer to the square of sulfuric monomer, a parameter that describes the likelihood of NPF events, could be written as a function of [DMA] and CS. Our ambient observation in four strong NPF events validates this combined effect.

Keywords: new particle formation, sulfuric acid, dimethylamine

©2020. Japan Geoscience Union. All Right Reserved.

Role of water molecule in aerosol nucleation and air-water interface reaction: quantum chemical and molecular dynamic simulation

*Fei Xu[1]

1. Shandong University

Recently, quantum chemical calculation and molecular dynamic simulation methods have important theoretical significance and practical application value to study the formation and degradation of atmospheric pollutants, especially the micro-mechanism of atmospheric photodegradation, aerosol nucleation and heterogeneous reaction, and to identify structural information and energy information of the intermediates and products in the reaction process.
Water is the third most abundant species in the atmosphere after N2 and O2, corresponding to 50% of relative humidity at 298 K. Water plays an important role in several gas-phase chemical processes occurring in the atmosphere. For example, we carried out quantum calculation to study the interactions between benzoic acid (BA) and sulfuric acid (SA)/ammonia (NH3)/dimethylamine (DMA) with hydration by 1 to 6 water molecules, and found water molecules have different effect on BA-SA/NH3/DMA nucleation (Figure 1). For BA-DMA-(0-6)H2O, increasing water molecules can inhibit nucleation. For BA-NH3-(0-6)H2O, the most negative Gibbs free energy occur when NH3 are hydrated with 2/6 water molecules and BA is unhydrated. For BA-SA-(0-6)H2O, the most negative Gibbs free energy occur when SA is unhydrated and BA are hydrated with 6 water molecules. Moreover, the Born-Oppenheimer molecular dynamics (BOMD) was used to simulate ammonium bisulfate formation from a series of amines, SO3, and H2O molecules at the air-water interface. The results show that reactions between amines and SO3 involve multiple water molecules at the air-water interface. The reaction center’ s ring structure (amine-SO3-nH2O) promotes the transfer of protons in the water molecules (Figure 2). The formed ammonium cation (-RNH3+) and the bisulfate anion (HSO4-) are present and stable by means of hydrogen bond interaction.

Keywords: nucleation, interface, quantum simulation

©2020. Japan Geoscience Union. All Right Reserved.

The Cloud Condensation Nuclei (CCN) activity during the New Particle Formation (NPF) events in the mountain region of China inland

*Mingfu Cai[1,2], Baoling Liang[1], Qibin Sun[1], Bin Yuan[2], Min Shao[2], Haobo Tan[3], Lihong Ren[4], Jun Zhao[1,5]

1. Institue for Environmental and Climate Research, Jinan University, 2. School of Atmospheric Sciences, Sun Yat-sen University, 3. Institute of Tropical and Marine Meteorology/Guangdong Provincial Key Laboratory of Regional Numerical Weather Prediction, CMA, 4. Atmospheric Chemistry and Aerosol Research Division, Chinese Research Academy of Environmental Science, 5. Southern Laboratory of Ocean Science and Engineering (Guangdong, Zhuhai), Zhuhai

A one-month field measurement was conducted at a mountain site (32˚23′ N, 111˚02′ E, with an attitude of 862 m) on the Wudang Mountain, Hubei Province, China from 22nd May to 29th June 2018. The particle size number distribution (PNSD, with a size range of 3-400 nm), size-resolved cloud condensation nuclei (CCN, SS=0.2%, 0.4%, 0.6% and 0.8%) and non-refectory PM1 (NR-PM1) chemical composition was measured by a home-made Regular & Nano Scanning Mobility Particle Sizer System (R & N-SMPS), a Cloud Condensation Nuclei Counter (CCNc) and a Time-of-Flight Aerosol Chemical Speciation Monitor (ToF-ACSM). The new particle formation (NPF) events were observed on 4th, 7th and 11th June during the measurement. These events generally started at around 9:00-10:00 Local Time (LT) with a significant distribution mode of particles with a size range of 3-10 nm. During the events, the wind direction was south west or west and the wind speed was about 3-4 m s-1, which might be favor to the occurrence of NPF event, while the mechanism was unclear. The nucleated particles grew to about 40-50 nm at different time, owing to different growth rate (2.963, 7.573 and 11.383 nm h-1 on 4th, 7th and 11th June, respectively). Probably owing to different atmospheric environment, such as gaseous precursors, oxidant and particle concentration, the formation rate (J3) was different during three events varied from 0.59 to 5.05 cm-3 s-1. The contribution of newly formed particles to the CCN number (NCCN) was mainly depend on their final grown size and the time when they affect the NCCN was decided by the GR. Two types of NPF event enhanced by sulfuric acid or organic vapors was found out during the measurement. Therefore, the hygroscopicity of newly formed particles could varied from a large range (0.25-0.8) and exert a large uncertainty on the NCCN prediction. It found out that the deviation of the NCCN prediction at 0.8% SS could vary from -10% to 38%.

Keywords: New Particle Formation, Cloud Condensation Nuclei activity, Hygroscopicity

©2020. Japan Geoscience Union. All Right Reserved.

Nucleation events within an industrial zone in the YRD region of China

*Jun Zheng[1], Yan Ma[1], Dongsen Yang[1]

1. Nanjing University of Information Science and Technology

Nucleation processes contribute substantial secondary aerosols in the atmosphere, which often lead to severe air pollution episodes in China, especially in heavily populated urban area. In this work, we conducted field observations of nucleation events in Nanjing, China. The field observations were conducted during the Fall of 2015. Both gaseous sulfuric acid (H_2SO_4) and sub-3 nm particles were simultaneously detected. H_2SO_4 and sub-3 nm aerosols showed excellent correlations during the nucleation events. Multivariate analysis indicated that two or three molecules of H_2SO_4 might be present in the critical nuclei. Several nocturnal nucleation events with concurring H_2SO_4 peaks were also observed while the site was within the industrial plumes. High level of alkenes and relative high concentration of O_3 (~30 ppbv) indicated that alkene ozonolysis might be responsible for the nighttime production of H_2SO_4. The impacts of the nocturnal nucleation processes on the local air quality need to be further investigated.

Keywords: Nucleation, Criegee radicals, Sulfuric acid

©2020. Japan Geoscience Union. All Right Reserved.

Effects of SO2 on secondary organic aerosol generated from photooxidation of toluene

*Weigang Wang[1]

1. Institute of Chemistry,Chinese Academy of Sciences

Atmospheric aerosol plays an important role in air quality and climate change, in which secondary organic aerosol (SOA) is one of the most important aerosol species. Size distribution, chemical composition, and optical property of secondary organic aerosol (SOA) derived under various atmospheric conditions differ greatly. In this study, we investigated the effect of SO2 under different humidity on optical properties of toluene-derived SOA under four conditions with cavity ring-down spectrometer and photoacoustic extinctiometer at 532 and 375 nm, respectively. Our results showed that SO2 under different humidity can change the refractive complex index (RI, m = n + ki) of toluene SOA by influencing the multiphase processes and altering the aerosol chemical compositions. High relative humidity caused the scattering and absorption properties of SOAs increased greatly, similar to m-xylene and 1,3,5-trimethylbenzene, as previous studies proved. Adding SO2 under dry condition would reduce the refractory index of RI (n) but increase the imaginary index of RI (k), which might be a result of the partitioning of low oxidation state products and enhancement of charge transfer complexes. The extinction properties of condition high humidity with SO2 were 30% higher than condition dry, and mass cross section was about 0.2131 g/m2. Our study demonstrated that different atmospheric conditions could affect the properties of toluene SOA, as well as air quality and the global radiative balance.

Keywords: SO2, SOA, VOC, Photochemistry

©2020. Japan Geoscience Union. All Right Reserved.

[E] Poster | A (Atmospheric and Hydrospheric Sciences)：A-AS Atmospheric Sciences, Meteorology & Atmospheric Environment

[A-AS14] Extreme Events: Observations and Modeling

convener:Sridhara Nayak(Disaster Prevention Research Institute, Kyoto University), JAGABANDHU PANDA(National Institute of Technology Rourkela)

The frequencies and intensities of extreme events such as heavy rainfall, flash floods, droughts, heat waves, tropical cyclones etc. have increased in many regions across the globe and are of serious concern due to their socio-economic and climate change connections. Thus, understanding of the patterns of such events and particularly their characteristics have been the focus of many recent studies. This session invites abstracts on observational and numerical modeling studies to enhance the understanding of the spatial and temporal characteristics and predictability of the extreme events. In particular, abstracts are encouraged on regional analysis of the extreme events in past years and in near or far future (30-100 years), which would assist the policy makers to build potentially more resilient societies to face the extreme event related disasters. This session also welcomes the submissions on model simulations and evaluations to advance the understanding of the physics and dynamics associated with the extreme events.

[AAS14-P01] Heat Wave Identification Using an Operational Weather Model and Analog Ensemble

*Alon Sidel[1], Weiming Hu[1], Martina Calovi[1], Guido Cervone[1,2] (1.The Pennsylvania State University, 2.National Center for Atmospheric Research)

[AAS14-P02] **Assimilation radar reflectivity to improve the simulation of a squall line case**

*Linlin Zheng[1,2], Xuexing Qiu[1] (1.Anhui Meteorological Observatory, 2.Anhui Institute of Meteorological Sciences)

[AAS14-P03] Characteristics of **Low-level Jets** in *Tianjin* with a Wind Profile Radar during 2015-2016

*Bingui Wu[1,2], Zongfei Li[1,2], Tingting Ju[3] (1.Tianjin Key Labarotory of Marine Meteorology, China, 2.Tianjin Meteorological Bureau, China, 3.Institute of Navigation College, Dalian Maritime University, China)

[AAS14-P04] Climate change impacts on extreme rainfall and their differences between weather patterns

*Masamichi Ohba[1], Soichiro Sugimoto[1] (1.Central Research Institute of Electric Power Industry)

[AAS14-P05] **Spatial and Temporal Variation of Thermodynamic Indices in Relation to Pre-Monsoon Thunderstorms over Tripura, India**

*Rajesh Kumar Sahu[1], Bhishma Tyagi[1] (1.National Institute of Technology Rourkela, Odisha, India)

[AAS14-P06] **Probabilistic Forecast of Extreme High Temperature in Extended Period with the Bayesian Model Averaging**

*Wei Zhang[1], Jianyun Gao[1], Qiaozhen Lai[2], Yanzhen Chi[3], Tonghua Su[4] (1.Fujian Institute of Meteorological Sciences, Fuzhou, China, 2.Longyan Meteorological Bureau, Longyan, China, 3.Xiamen Meteorological Bureau, Xiamen, China, 4.Fujian Climate Center, Fuzhou, China)

[AAS14-P07] **Introduction of CLoud Analysis and Ingestion System(CLAIS)**

*Ruixia Liu[1], Bingyun Yang[1], Wen Hui[1] (1.China Meteorological Administration)

[AAS14-P08] **Verification of multiple-Doppler-radar derived vertical velocity using profiler data**

*Yi-An CHEN[1,2] (1.Yu-Chieng LIOU , 2.Jou-Ping Hou)

[AAS14-P09] Characteristics of the diurnal variations flood period precipitation in Anhui during the last 30
years

*chun liu[1] (1.ANHUI METEOROLOGY SERVICE)

[AAS14-P10] **Understanding the impact of soil moisture variations on temperature extremes over the Indian region**

*Naresh Govind Ganeshi[1,2], Milind Mujumdar[1], R Krishnan[1], Mangesh Goswami[1,3], Yuhei Takaya[4], Toru Terao[5] (1.Centre for Climate Change Research, Indian Institute of Tropical Meteorology, Pune, India, 2.Department of Atmospheric and Space Sciences, Savitribai Phule Pune University, Pune, India, 3.Kavayitri Bahinabai Chaudhari North Maharashtra University, Pune, India, 4.Meteorological Research Institute, Climate Research Department, Ibaraki, Japan, 5.Faculty of Education, Kagawa University, Kagawa, Japan)

[AAS14-P11] Diurnal Variations of Low-Level Winds and Precipitation Response to Large-Scale Circulations during a Heavy Rainfall Event

*Wenxin Zeng[1], Guixing Chen[1], Yu Du[1], Zhiping Wen[2] (1.School of Atmospheric Sciences, Sun Yat-sen University, 2.Department of Atmospheric and Oceanic Sciences, and Institute of Atmospheric Sciences, Fudan University)

[AAS14-P12] **Extreme weather in the context of solar wind coupling to the magnetosphere-ionosphere-atmosphere system**

*Paul Prikryl[1,2], Vojto Rušin[3], Pavel Šťastný[4], Maroš Turňa[4], Martina Zeleňáková[5] (1.Physics Department University of New Brunswick, Canada, 2.Geomagnetic Laboratory Natural Resources Canada, 3.Astronomical Institute, Slovak Academy of Sciences, Slovakia, 4.Slovak Hydrometeorological Institute, Slovakia, 5.Technical University of Košice, Slovakia)

[AAS14-P13] Increasing strength of typhoons in the Northwest Pacific Ocean in the recent years and their influencing seasonal factors

*Ravi Shankar Pandey[1], Yuei-An Liou[1] (1.National Central University)

[AAS14-P14] **High space resolution atmospheric simulation of severe regional precipitation and vehicle strain mode**

*Jou Ping Hou[1], Zan-Han Huang[1], Qun-Yu Fan[1] (1.Chung Cheng Institute of Technology)

[AAS14-P15] Variations of Daily Precipitation Extremes over Xinjiang Province, China

*MINGGANG LI[1], YONG ZHAO[1] (1.Chengdu University of Information Technology)

[AAS14-P16] Relevance of Background Error Statistics for Variational Radar Assimilation System

*THIRUVENGADAM PADMANABHAN[1], INDU J[1,2], SUBIMAL GHOSH[1,2] (1.Department of Civil Engineering, Indian Institute of Technology Bombay, Mumbai 400076, India., 2.Interdisciplinary Centre for Climate Studies, Indian Institute of Technology Bombay, Mumbai 400076, India.)

[AAS14-P19] Analysis of Hydroclimatic Extremes over Narmada Basin under Climate Change

*SABYASACHI SWAIN[1], SURENDRA KUMAR MISHRA[1], ASHISH PANDEY[1] (1.Indian Institute of Technology Roorkee)

[AAS14-P21] **Flashfloods and landslides along the foothills of the Himalayas: their precursors, dynamics and thermodynamics**

*Anu Gupta[1], Jun Matsumoto[1] (1.Tokyo Metropolitan University, Tokyo)

[AAS14-P22] Standardized Variability Index (SVI) : A multiscale index to assess the variability of precipitation

*Ravi kumar Guntu[1], Ankit Agarwal[1] (1.Department of Hydrology, Indian Institute of Technology Roorkee, 247667, India)

Heat Wave Identification Using an Operational Weather Model and Analog Ensemble

*Alon Sidel[1], Weiming Hu[1], Martina Calovi[1], Guido Cervone[1,2]

1. The Pennsylvania State University, 2. National Center for Atmospheric Research

Heat waves are notoriously difficult to forecast due to their highly localized variables, yet remain one of the world's deadliest natural disasters. This project uses the Analog Ensemble technique (AnEn), which generates probability information from a deterministic predictive model, to identify heat waves across the continental United States with further accuracy. Heat index was calculated to assess the intensity of heat waves and forecast ensembles for heat index were generated using weather analogs. AnEn was shown to outperform the baseline weather prediction model when a quantile was used to summarize the ensemble.

Keywords: heat waves, analog, ensembles

©2020. Japan Geoscience Union. All Right Reserved.

Assimilation radar reflectivity to improve the simulation of a squall line case

*Linlin Zheng[1,2], Xuexing Qiu[1]

1. Anhui Meteorological Observatory, 2. Anhui Institute of Meteorological Sciences

Based on assimilation of radar radial wind, radar retrieval wind and GPS water vapor data using Ensemble Kalman Filtering (EnKF) method, the initial water vapor field of a squall line occurred on July 30, 2014 in of East Central Anhui was adjusted according to radar reflectivity data. Compared with the simulation results of EnKF, this method has improved the intensity, location, duration, precipitation and surface wind of the squall line. Simulation performance of ground convergence zone near front the squall line is improved after adjusting humidity field, leading to better simulation results of the intensity and location of the squall line. In addition, the squall line maintained for a short time without humidity adjustment. This can be explained by that mid-level dry air entrainment is weak at the rear of the squall line, and the cold pool is quickly propagate away from the squall line, which is unfavorable for maintenance of squall line. In contrast, when the humidity field is adjusted, dry air entrainment at the rear of the squall line is strong, and the resultant downdraft generate the cold pool, which is located in the rear of the squall line, favorable for the squall line maintenance. The possible reason of dry air entrainment strengthening is: atmospheric instability is increased as the moisturizing of middle-low level (600 - 900 hPa) after the humidity field adjustment, and result in the enhancement of the convection and the meso-low system. The westerly in the south of meso-low intensifies, and strengths the rear dry cold air entrainment. This experiment reveals that the adjustment of the humidity leads to the adjustment of the dynamic field, and play an important role in the development and organization of the convection system.

Keywords: squall line, data assimilation, Ensemble Kalman Filtering, radar reflectivity data

©2020. Japan Geoscience Union. All Right Reserved.

Characteristics of **Low-level Jets** in *Tianjin* with a Wind Profile Radar during 2015-2016

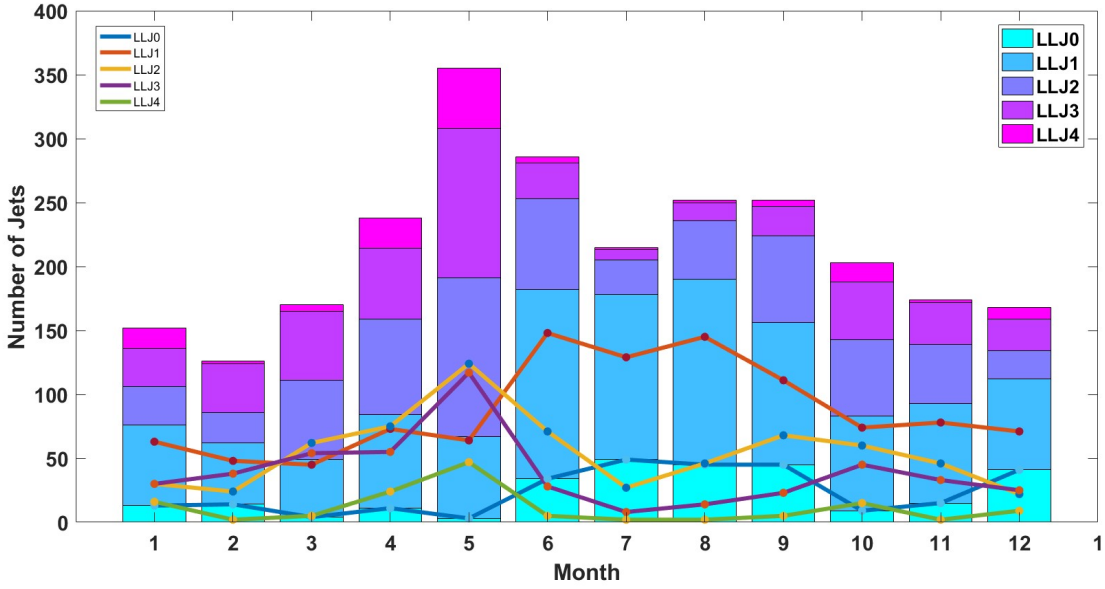
*Bingui Wu[1,2], Zongfei Li[1,2], Tingting Ju[3]

1. Tianjin Key Labarotory of Marine Meteorology, China, 2. Tianjin Meteorological Bureau, China, 3. Institute of Navigation College, Dalian Maritime University, China

Low-level jets (LLJ) are important mesoscale weather system. In this study, the characteristics of the LLJs are studied. The data are collected at a standard weather station Xiqing (54527) operated by the China Meteorological Administration from 2015 to 2016. Based on previous criteria for LLJs given by Bonner (1968) and Wei et al. (2013), a new set of criteria suitable for LLJs over NCP is defined in this study. LLJs were classified into five categories based on two criteria of the Vmax threshold value and difference value (ΔV) from Vmax upward to the adjacent Vmin. The definition are as follows. The criteria of LLJ0 are 6 m/s > Vmax ≧ 4 m/s and ΔV ≧ 2 m/s , and those of LLJ1, LLJ2, LLJ3, and LLJ4 are 10 m/s > Vmax ≧ 6 m/s and ΔV ≧ 3 m/s, 14 m/s > Vmax ≧ 10 m/s and ΔV ≧ 5 m/s, 20 m/s > Vmax ≧ 14 m/s and ΔV ≧ 7 m/s, and Vmax ≧ 20 m/s and ΔV ≧ 10 m/s , respectively. Based on the above criteria, LLJs observed at Xiqing were identified, and the number of 1-h LLJ periods was counted regardless of whether they were continuous or intermittent in the time series. Statistics showed that the most frequently directions of LLJs are 180˚–270˚, which accounted for nearly 47 %. The results of four seasons also verify the same conclusion, except the distribution of occurrence direction in winter. Moreover, compared with the relatively uniform distributions of wind directions of weak LLJs (LL0, LL1, and LL2), the distributions of wind directions of strong LLJs (LL3 and LL4) concentrate in a narrow range between 210˚ and 250˚, which suggests that southwesterly winds contribute to the formation of strong LLJs. The wind speeds of most of LLJs are less than 14 m/s, and the occurrence proportion of LLJ4 is only 5.1 %, which indicates that the super-strong LLJs is rare. The occurrence height distribution of LLJs that most LLJs occur below 2000 m, and the height distribution of LLJs is relatively uniform except the peak at lower levels (500-600 m), which can also be observed in different seasons. Moreover, compared with strong LLJs (LL3 and LL4), LL0 tended to occur at a higher level, however, the height distribution of different strength LLJs are different in four seasons. The result of monthly distribution of the frequency of LLJ occurrence shows that LLJs occur more frequently during warm season than cold season, which maybe because of the increasing amplitude of inertial oscillations in the boundary layer during the warm seasons. In addition, distribution of the frequency of LLJ occurrence display a unimodal distribution, with strong LLJs occur more frequently in spring (March to May), and the occurrence of weak LLJs concentrated in summer (June to August). In addition, it is worthwhile that moderate LLJs (LLJ1 and LLJ2) are contributories to the total LLJs through the whole year. The occurrence number of LLJs has an obvious diurnal variation, with the peak of occurrence number around midnight (2300–1400 CST). Unimodal curves are commonly observed for all categories of LLJs except the super-strong LLJ4, whose distribution can be separated into two parts, a relatively high occurrence number from 1400 CST to 2200 CST and extremely low occurrence number from 0000 CST to 1300 CST. The duration of the LLJs events is usually less than 6h and the most frequent duration is 1–2h (47 %) which suggests that the LLJs are gusty events. However, it is worthwhile the duration of weak LLJs is smaller that of relatively strong LLJs, which indicates that the stronger of the strength of LLJ, the longer duration it will last.

Keywords: low level jet, wind profile radar, tianjin

©2020. Japan Geoscience Union. All Right Reserved.



©2020. Japan Geoscience Union. All Right Reserved.

Climate change impacts on extreme rainfall and their differences between weather patterns

*Masamichi Ohba[1], Soichiro Sugimoto[1]

1. Central Research Institute of Electric Power Industry

The impacts of global warming/climate change on extreme rainfall events during the Baiu period in Japan and their dependency on weather patterns (WPs) were examined using the self-organizing map (SOM) method. To investigate the differences in climate change impacts on daily rainfall among the WPs, a SOM was applied to surface atmospheric circulation data from the Database for Policy Decision Making for Future Climate Change (d4PDF) to determine the dominant heavy rainfall WPs. The obtained SOM shows that different WPs are associated with regional variations in extreme rainfall events. Projected future changes in the occurrence of heavy rainfall displayed a non-uniform spatial distribution. To understand the spatial heterogeneous rainfall changes, the sensitivity of heavy rainfall WPs to climate forcing was evaluated. Results of the SOM analysis suggest that this regional variation in the future changes in extreme rainfall events could be attributed to sensitivity differences between WPs to the climate changes. These sensitivity differences can be attributed to the non-uniform spatial changes in the large-scale climatological background state in East Asia via modulations in the moist air intrusion into Japan.

Keywords: Climate change , Self-organizing map, d4PDF , Extreme rainfall , Weather pattern, Baiu

©2020. Japan Geoscience Union. All Right Reserved.

Spatial and Temporal Variation of Thermodynamic Indices in Relation to Pre-Monsoon Thunderstorms over Tripura, India

*Rajesh Kumar Sahu[1], Bhishma Tyagi[1]

1. National Institute of Technology Rourkela, Odisha, India

Thunderstorms are frequent in Eastern and Northeastern Indian region and are the primary source of precipitation and extreme events during Pre-monsoon season. The intensity and frequency of these storms are higher, which leads to impact the climate over these regions. Thermodynamic indices variations are globally accepted to see the variation of a thunderstorm (TD) and non-thunderstorm days (NTD) spatially and temporally, and are helpful in nowcasting of thunderstorm event. In this study, we have analysed both spatial and temporal variation of thermodynamic indices for a northeastern state Tripura, India, to study the prevalence of thunderstorm. Radiosonde observation data are used for the thirty years (1987-2016) to understand the temporal vaiation of thermodynamic indices over Agartala. The thermodynamic indices analysis has been divided in equal interval of five years to see the trend variation of the thermodynamic indices. For spatial variation of thermodynamic indices, we utilities ERA-5 reanalysis dataset with 0.25˚ X 0.25˚ (31 km) resolution over Tripura throughout TD and NTD days. The information of thunderstorm occurrence is obtained from the India Meteorological Department (IMD) for Agartala and over several other locations over Tripura. The results shows a shift in threshold values of some index which mark the impact of climate change by temporal variation of these indices. At the same time, some other indices are unable to show any change in the pattern over this area. For the spatial pattern, some indices (convective and potential) shows better results for categorising the thunderstorm days over Tripura and in contrast conditional instability indices unable to distinguish thunderstorm days spatially. We correlated the changes in the threshold value of the thermodynamic indices by using Man-Kendall trend test to analyse the spatial variation of thermodynamic indices.

Keywords: Radiosonde, Thunderstorm, Climate change, Thermodynamic indices

©2020. Japan Geoscience Union. All Right Reserved.

Probabilistic Forecast of Extreme High Temperature in Extended Period with the Bayesian Model Averaging

*Wei Zhang[1], Jianyun Gao[1], Qiaozhen Lai[2], Yanzhen Chi[3], Tonghua Su[4]

1. Fujian Institute of Meteorological Sciences, Fuzhou, China, 2. Longyan Meteorological Bureau, Longyan, China, 3. Xiamen Meteorological Bureau, Xiamen, China, 4. Fujian Climate Center, Fuzhou, China

The method of the Bayesian model averaging (BMA) is employed to improve extended probabilistic forecast of extreme high temperature based on the ensemble prediction system (EPS) outputs of ECMWF, NCEP, and UKMO from the sub-seasonal to seasonal (S2S) prediction project database in this study. The outcomes of BMA, single-model EPS and multi-model EPSs are verified with mean absolute error (MAE), correlation coefficient (ACC), brier score (BS), and continuous ranked probability score (CRPS). On the basis of comparison between the verifications, it is suggested that the BMA performs better than single-model EPS and multi-model EPS in all leading times for all verification method. Although the BMA has improved the raw probabilistic forecast substantially, the lead time can only reach up to 9 days in terms of positive skill of BMA Bier skill score for extreme high temperature (≧ 35˚C). To extend valid lead time, the raw outputs of single-model EPS are preprocessed with the running mean method for training before BMA. It turns out that the running-mean BMA is able to extend the lead time of positive skill to 11 days.

Keywords: Probabilistic Forecast , S2S, Bayesian Model Averaging

©2020. Japan Geoscience Union. All Right Reserved.

Introduction of CLoud Analysis and Ingestion System(CLAIS)

*Ruixia Liu[1], Bingyun Yang[1], Wen Hui[1]

1. China Meteorological Administration

1.Introduction of CLoud Analysis and Ingestion System(CLAIS)

In recent years, there is a growing demand for high spatial-temporal resolution, high-precision and three-dimensional cloud elements in the fields of numerical prediction, weather analysis, aviation meteorology, etc. Although there are more and more ways of meteorological observation and detection, such as surface observations, radar observations and satellite detection, etc. But any single observation of them still can not meet this demand. How to integrate multiple sources of ground, satellite, radar and other kinds of observation data to obtain spatiotemporal continuous, high efficiency, high-resolution cloud products has become one of the trends of technology development.

Through many years of study, National Satellite Meteorological Center of CMA has established the three-dimensional Cloud Analysis and Ingestion system (CLAIS) which can combine FY series meteorological satellite data with ground, sounding, radar and other observations to get 3D cloud parameters.The prototype of the three-dimensional Cloud Analysis and Ingestion system (CLAIS) comes from NOAA LAPS/ STMAS. It is a three-dimensional fusion analysis system that integrates the advantages of a variety of observation data. The accuracy of three-dimensional cloud construction was improved greatly after a series of algorithm updates and improvements including cloud top construction, cloud base constraints, multi-source data collaborative fusion algorithm etc. At present, it can integrate background field of numerical prediction (GRAPES of CMA, NCEP, ECMWF), conventional observation and sounding (MICAPS, CIMISS interface), satellite data (FY-2 VISSR, FY-4 AGRI, FY-4 LMI,FY3 MWHS,H8), radar (Reflectivity), GPS and other data. These observation data is comprehensively analyzed and fused to obtain three-dimensional cloud structure information, three-dimensional Microphysical parameters, and other atmospheric and surface parameters.Study shows that the distributions of the analyzed cloud structure is consistent with the CloudSat observations.Post-processing software was developed to display three-dimensional cloud structure and draw two-dimensional cross section of cloud, and has overlay display function, providing user a convenient tool for accomplishment display and scientific research.

2.The application of CLAIS system

First of all, cloud is one of the important uncertainties of the numerical prediction model. The lack of cloud information in the initial field of the model will lead to the phenomenon of significant delay in the development of cloud and precipitation at the early stage of a model forecast, that is, the problem of spin-up model. Therefore, how to obtain the accurate three-dimensional and space-time continue cloud field and provide the initial field of the model has always been the way of data assimilation efforts. Using 3D cloud analysis data of CLAIS as initial fields of GRAPES and WRF forecasting model, and through case and batch tests, the prediction performance is evaluated. The research shows that the application of CLAIS 3D cloud analysis system can improve the cloud process of NWP model and has a positive effect on the precipitation area and intensity forecast.The system has a very important application potential in convection analysis, artificial weather, aviation meteorology, military application and other fields.

Keywords: CLAIS, Three-dimensional cloud, multi-source data

©2020. Japan Geoscience Union. All Right Reserved.

Verification of multiple-Doppler-radar derived vertical velocity using profiler data

*Yi-An CHEN[1,2]

1. Yu-Chieng LIOU , 2. Jou-Ping Hou

The retrieval of vertical velocity using Doppler radar data always contains large uncertainty. In this study the quality of the vertical velocity retrieved by a 3DVar-based multiple-Doppler wind analysis system named WISSDOM (WInd Synthesis System using DOppler Measurement) is investigated. Data from one S-band (RCWF) radar and two C-band radars (RCTP and NCU) in northern Taiwan are utilized.

The accuracy of the vertical velocity from WISSDOM is examined using two profilers (L-band and UHF) observations. The inter-comparison shows that WISSDOM-derived vertical velocity agrees reasonably well with the profiler data. The highest correlation and the smallest RMSD (Root-Mean-Square Deviation) take place when comparing against the L-band profiler data obtained under vertical beam scanning mode. The WISSDOM-derived results are generally better than those reported in a previous study using ARM scanning radar network in Oklahoma.

The winds from the L-band profiler are also merged into WISSDOM, resulting in an overall improvement of the three-dimension wind field at low levels. UHF and RCTP are applied to verify the accuracy of the method. It is shown that WISSDOM assimilating the L-band can reduce RMSD and enhance correlation with UHF and RCTP. The result suggests that the method can get better three-dimension wind field.

Keywords: profiler, WISSDOM

©2020. Japan Geoscience Union. All Right Reserved.

Characteristics of the diurnal variations flood period precipitation in Anhui during the last 30 years

*chun liu[1]

1. ANHUI METEOROLOGY SERVICE

The characteristics of flood season daily precipitation were analyzed in the term of rainfall amount, frequency and intensity using the hourly data in Anhui during 1981-2010. The main results are as follows. (1) The daily rainfall amount and frequency have two diurnal peak, one in the early morning and the other in the late afternoon, while the rainfall intensity does not reflect an obvious peak. The peaks of light and moderate rain days lie in afternoon, and there are two peaks in heavy rain days. However, the peak of torrential rain days lies in morning. These differences are due to the different lasting rainfall events. (2) The spatial distributions of rainfall have large diurnal variation with considerable regional features. As amount of daily rainfall increasing, the spatial distribution of peak time performs less consistent. (3) In the 30 years, the annual change of afternoon-peak in rain amount and intensity is almost the same, reflecting an increase between 1993 and 2010. There are more stations of morning peak time in weak monsoon years than strong monsoon years.

Keywords: rainfall diurnal variation, feature of rainfall peak, monsoon

©2020. Japan Geoscience Union. All Right Reserved.

Understanding the impact of soil moisture variations on temperature extremes over the Indian region

*Naresh Govind Ganeshi[1,2], Milind Mujumdar[1], R Krishnan[1], Mangesh Goswami[1,3], Yuhei Takaya[4], Toru Terao[5]

1. Centre for Climate Change Research, Indian Institute of Tropical Meteorology, Pune, India, 2. Department of Atmospheric and Space Sciences, Savitribai Phule Pune University, Pune, India, 3. Kavayitri Bahinabai Chaudhari North Maharashtra University, Pune, India, 4. Meteorological Research Institute, Climate Research Department, Ibaraki, Japan, 5. Faculty of Education, Kagawa University, Kagawa, Japan

Soil moisture (SM) and its long-term memory are known to be linked to near-surface temperature variations through land-atmosphere interactions. While previous studies have reported the association between temperature extremes over India and large-scale atmospheric circulation, the role of land-atmosphere coupling on temperature extremes over the monsoon-dominated Indian region is not well understood. In the present study, we have analysed multiple hydro-meteorological datasets and climate model outputs to understand the impact of SM variations on the occurrence of temperature extremes in a changing climate. Long-term climate observations reveal that the surface temperature over India increased by 0.7^{o}C during 1901-2018, whereas the regional summer monsoon rains have decreased by about 7% since 1950. Our analysis shows that the decrease of SM over north-central India (NCI), in association with the declining monsoon precipitation, has altered the characteristics of temperature extremes in the region through strong land-atmosphere coupling. It is found that the frequency, duration and variability of temperature extremes over NCI have significantly risen during the post-1980, in association with the depletion of soil moisture in the region. Our analysis indicates that the drying trend of SM over the NCI in the recent decades has favoured a significant increase in the occurrence of temperature extremes through enhancement of sensible heat flux and reduction of latent heat flux. In addition, it is noted that the loss of soil moisture memory has led to an increase in the variability of temperature extremes over the region.

Keywords: Temperature extremes, soil moisture, soil moisture memory, soil moisture-temperature coupling, north-central India, surface energy partitioning

©2020. Japan Geoscience Union. All Right Reserved.

Diurnal Variations of Low-Level Winds and Precipitation Response to Large-Scale Circulations during a Heavy Rainfall Event

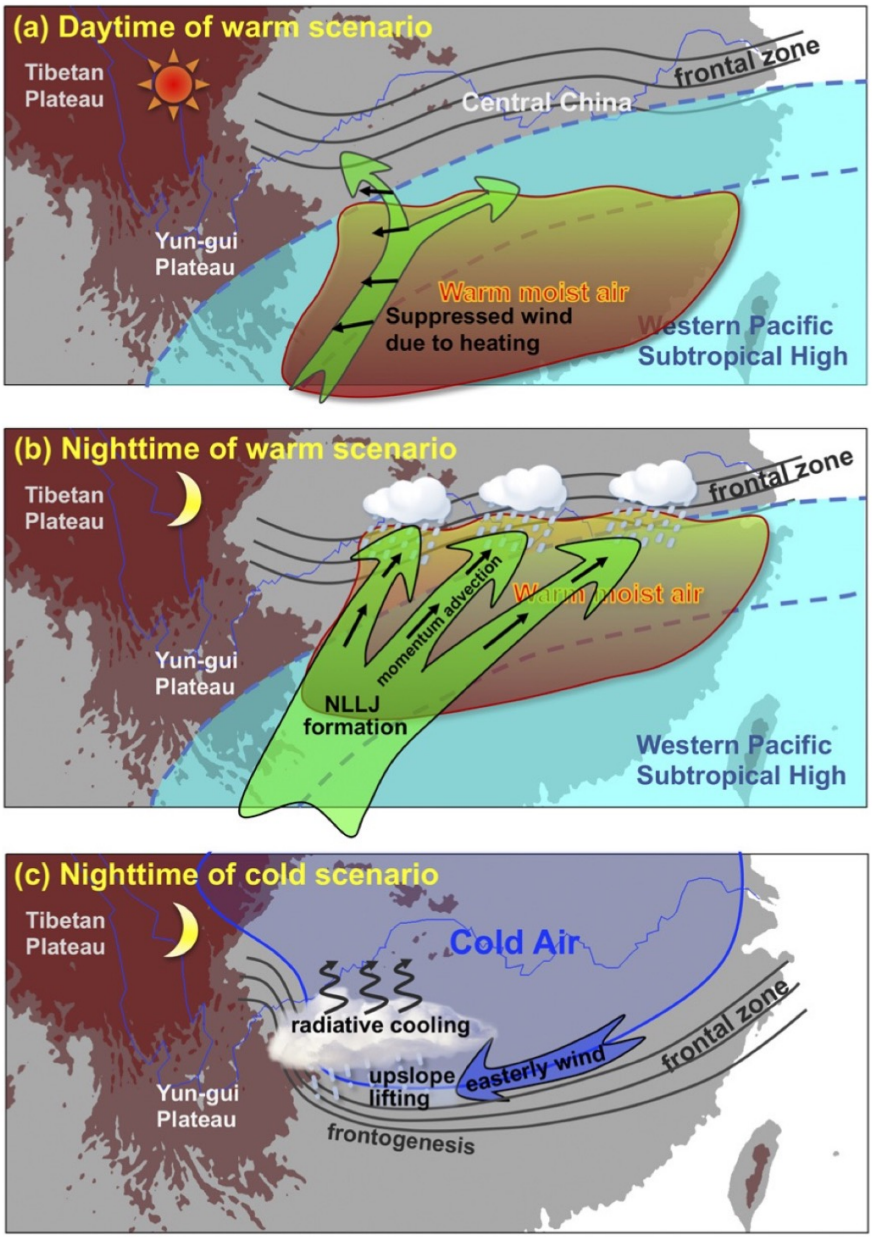
*Wenxin Zeng[1], Guixing Chen[1], Yu Du[1], Zhiping Wen[2]

1. School of Atmospheric Sciences, Sun Yat-sen University, 2. Department of Atmospheric and Oceanic Sciences, and Institute of Atmospheric Sciences, Fudan University

A succession of MCSs developed during the last week of October 2016 and produced extreme heavy rainfall in central China. The event underwent an evident shift from a mei-yu-like warm scenario to an autumn cold scenario. Diurnal cycles of rainfall and low-level winds may be modulated by the shifting of large-scale at- mospheric conditions. We conducted observational analyses and numerical experiments to examine how large-scale circulations influenced rainfall systems through diurnally varying processes. The results show that, in the first half (warm) period of the event, intense rainfall mostly occurred in eastern-central China with an early morning peak. It was closely related to a nocturnal southwesterly low-level jet (NLLJ) on the flank of the western Pacific subtropical high. The NLLJ formed near midnight in southern China where ageostrophic wind rotated clockwise due to Blackadar’ s inertial oscillation. The NLLJ extended downstream to central China during the predawn hours due to the horizontal advection of momentum. Both the formation and extension of the NLLJ were supported by an enhanced subtropical high that provided relatively warm conditions with surface heating for boundary layer inertial oscillation and strong background southwesterly winds for mo- mentum transport. The NLLJ induced MCSs at its northern terminus where the low-level ascent, moisture flux convergence, and convective instability were enhanced during the predawn hours. In the second half period with an intrusion of cold air, the diurnal amplitude of low-level winds became small under relatively cold and cloudy conditions. Moderate rainfall tended to occur in western-central China with a peak after midnight, most likely due to frontogenetic processes, upslope lifting, and nighttime cloud-top cooling.

Keywords: Diurnal cycle, Nocturnal low-level jet, Subtropical high, Rainfall systems

©2020. Japan Geoscience Union. All Right Reserved.



Conceptual model of the rainfall-producing processes in (a) daytime and (b) nighttime of the warm period and (c) nighttime of the cold period. The light blue area denotes the WPSH in (a),(b). The bold arrows denote the low-level winds with the black vectors denoting their diurnal deviations. The red area in (a),(b) denotes the warm and moist air mass, while the dark blue area in (c) denotes the cold air with high pressure. The nocturnal MCSs in the frontal zone are marked in (b). The clouds and rainfall are marked in (c).

©2020. Japan Geoscience Union. All Right Reserved.

Extreme weather in the context of solar wind coupling to the magnetosphere-ionosphere-atmosphere system

*Paul Prikryl[1,2], Vojto Rušin[3], Pavel Šťastný[4], Maroš Turňa[4], Martina Zeleňáková[5]

1. Physics Department University of New Brunswick, Canada, 2. Geomagnetic Laboratory Natural Resources Canada, 3. Astronomical Institute, Slovak Academy of Sciences, Slovakia, 4. Slovak Hydrometeorological Institute, Slovakia, 5. Technical University of Košice, Slovakia

Tropical and extratropical cyclones can intensify into the most destructive weather systems that have significant societal and economic impacts. Rapid intensification of such weather systems has been examined in the context of solar wind coupling to the magnetosphere-ionosphere-atmosphere (MIA) system. It has been shown [1,2] that explosive extratropical cyclones and rapid intensification of tropical cyclones tend to follow arrivals of high-speed solar wind when the MIA coupling is strongest. The coupling generates atmospheric gravity waves (AGWs) that propagate from the high-latitude lower thermosphere both upward and downward [3,4]. In the upper atmosphere, AGWs are observed as traveling ionospheric disturbances. In the lower atmosphere, they can reach the troposphere and be ducted [4] to low latitudes. Despite significantly reduced wave amplitude, but subject to amplification upon over-reflection in the upper troposphere, these AGWs can trigger/release moist instabilities leading to convection and latent heat release, which is the energy driving the storms. The release of conditional symmetric instability is known to initiate slantwise convection producing rain/snow bands in extratropical cyclones. Severe weather, including severe winter storms, heavy snowfall and rainfall events, have been examined in the context of MIA coupling [5]. The results indicate a tendency of significant weather events, particularly if caused by low pressure systems in winter, to follow arrivals of solar wind high-speed streams from coronal holes. In the present paper we review the published results and provide further evidence to support them. This includes the occurrence of heavy rainfall events and flash floods, as well as the rapid intensification of recent hurricanes and typhoons, with the goal to identify sources of AGWs at high latitudes that may play a role in triggering convective bursts potentially leading to such events.

[1] Prikryl P., et al., J. Atmos. Sol.-Terr. Phys., 149, 219–231, 2016.
[2] Prikryl P., et al., J. Atmos. Sol.-Terr. Phys., 183, 36–60, 2019.
[3] Prikryl P., et al., Ann. Geophys., 23, 401–417, 2005.
[4] Mayr H.G., et al., J. Geophys. Res., 89, 10929–10959, 1984.
[5] Prikryl P., et al., J. Atmos. Sol.-Terr. Phys., 171, 94–110, 2018.

Keywords: Extreme weather, Extratropical and tropical cyclones, Solar wind-magnetosphere-ionosphere-atmosphere coupling

©2020. Japan Geoscience Union. All Right Reserved.

Increasing strength of typhoons in the Northwest Pacific Ocean in the recent years and their influencing seasonal factors

*Ravi Shankar Pandey[1], Yuei-An Liou[1]

1. National Central University

The threat of stronger typhoons is getting bigger in the Northwest Pacific (NWP) ocean basin as the average number of Super-Typhoons (STYs) reached its maximum of 6 per year during the recent five years (2013-2017) in the recorded history. This study analyzes the favorable seasonal environmental factors for the STYs during the recent years by incorporating the remote sensing imagery and wind vector images created using U and V wind component data. The study successfully detects a crucial role of southwest air flow and northwest cold air mass in partially strengthening the STYs of the summer and winter seasons, respectively. In addition, it finds that most of winter STYs are also partially assisted by southwest air flows and, thus, exhibit higher intensities than summer STYs. The season-wise track angle analysis reveals that winter STYs' genesis positions lie more south in latitude, causing bigger genesis and turning angles, than summer STYs. The study uncovers that all summer STYs merely take recurvature once they finish their individual maximum intensity stage. The regions in the NWP basin, supporting the conversion of typical typhoons' evolution into STYs and consequent recurvature, are also detected. The findings of the current study are important for mitigating the risk related to increasing strength of typhoons in the NWP region by identifying their favorable seasonal environmental factors.

Keywords: Northwest Pacific, Super-Typhoon, Southwest Air Flow, Cold Air Mass

©2020. Japan Geoscience Union. All Right Reserved.

High space resolution atmospheric simulation of severe regional precipitation and vehicle strain mode

*Jou Ping Hou[1], Zan-Han Huang[1], Qun-Yu Fan[1]

1. Chung Cheng Institute of Technology

Under the weakly synoptic scale weather conditions, local thunder showers often occur in the afternoon in Taiwan during summer. Due to the characteristics of small range and heavy rainfall intensity (often exceeding 130 mm hr-1) during precipitation, flooding disasters are often caused and severe precipitation will make vehicles unable to drive on the roads normally, and traffic will be greatly affected. This study uses the WRF 3.9.1 model to simulate a severe precipitation potential area under the design of a two nesting domain with a horizontal spatial resolution of 1 km. We hope that by knowing the possible areas of precipitation, we will study the feasibility of reminding drivers of the degree of flooding after installing water level sensors and buzzers on cars from the perspective of disaster reduction. Airbags are added to the chassis of the vehicle to allow the vehicle to float on the water and reach the car body balance by itself. In addition, the paddles that can be automatically ejected on the wheels are used to enable the driver to control the direction of the water and allow the driver to safely cross the flooded area. This research is not only used for ordinary people's livelihood, it gives ordinary people more chances of survival and prolongs rescue time. In addition, it can also be applied to national defense technology.

Keywords: Severe precipitation, Water level sensor

©2020. Japan Geoscience Union. All Right Reserved.

Variations of Daily Precipitation Extremes over Xinjiang Province, China

*MINGGANG LI[1], YONG ZHAO[1]

1. Chengdu University of Information Technology

Based on observational daily rainfall data from China meteorological data service center from 1963 to 2017, the temporal and spatial variations of daily precipitation extremes (DPE) over Xinjiang province (the west part of northwest arid zone of China) were investigated. In this work, the statistical characteristics, the concentration degree (CD) and concentration period (CP), along with the persistence and regionality of DPE were discussed for understanding the change features of DPE from different aspects. During recent 55 years, the precipitation in Xinjiang province is becoming more extreme, which is reflected in the significant decrease of low-intensity rainfall but the significant increase of DPE. Both the frequency and intensity of DPE show positive trends at most sites in Xinjiang province, and the increase in DPE frequency is more significant than the increase in DPE intensity. The characteristics of DPE CD and CP in different regions of Xinjiang province vary a lot. The annual DPE CD values of stations over Southern Xinjiang is very large because of the annual occurrences of DPE is very few, which in most years the DPE occurs less than 2 days, therefore the DPE concentration in these stations is high. While the conditions differ in stations over Northern Xinjiang, the average annual DPE of these sites usually more than 3 days, and the annual DPE CD values is relatively low, indicate the occurrence time of DPE is more dispersed in Northern Xinjiang. The annual DPE CP values reflect that DPE occurs most intensively in boreal summer, both in Northern Xinjiang and Southern Xinjiang, but in stations over Northern Xinjiang, there exists a certain number of years that DPE occurs more frequently in spring or autumn, indicate a relatively long season of DPE occurrence. Results of trend analysis show that accompanying with the notable increasing of DPE frequency, this relatively dispersed occurrence time and longer occurrence season over Northern Xinjiang is intensified in the past few decades. Few indices are also calculated for investigate the persistence and regionality of DPE at each station in Xinjiang province, although there are some disparities in different regions, the DPE duration and regionality in Xinjiang stations is generally poor. These results are help for our better understanding the features and changes of climate extremes over arid region under a warming background.

Keywords: Daily precipitation extremes, Concentration degree , Concentration period

©2020. Japan Geoscience Union. All Right Reserved.

Relevance of Background Error Statistics for Variational Radar Assimilation System

*THIRUVENGADAM PADMANABHAN[1], INDU J[1,2], SUBIMAL GHOSH[1,2]

1. Department of Civil Engineering, Indian Institute of Technology Bombay, Mumbai 400076, India., 2. Interdisciplinary Centre for Climate Studies, Indian Institute of Technology Bombay, Mumbai 400076, India.

Skillful prediction of extreme convective weather events remains a challenge in regional Numerical Weather Prediction (NWP) models. Reduced forecast skill in regional NWP models is often attributed to improper representation of convective storm structure in the initial condition. Assimilation of high-resolution Doppler Weather Radar (DWR) observations through variational systems provide critical information about the pattern and evolution of convective systems in the initial conditions. However, the quality of variational radar assimilation hinges on the Background Error statistics (BES) which is a statistical measure of the error in model forecasts. The BES is generally modeled using control variables through either the National Meteorological Centre (NMC) or the ensemble method. Hence the choice of control variable and modeling method have a significant influence on the skill of analysis from the variational systems [Thiruvengadam et al., 2019]. In this study, we investigate the control variable (CV) properties of both NMC and ensemble-based BES and their impact on the skill of the three-dimensional variational radar assimilation system. Results demonstrate that the use of zonal and meridional momentum CV in both the NMC and ensemble method improves the moisture and dynamics forecast state variables when compared to the use of stream function and velocity potential CV. Best precipitation forecast results are obtained when ensemble-based BES modeled using zonal and meridional momentum CV are used for assimilating DWR observations.

Reference:

Thiruvengadam, P., J. Indu, and S. Ghosh (2019), Assimilation of Doppler Weather Radar data with a regional WRF-3DVAR system: Impact of control variables on forecasts of a heavy rainfall case, Adv. Water Resour., 126, doi:10.1016/j.advwatres.2019.02.004.

Keywords: Doppler Weather Radar, Data Assimilation, Background Error statistics

©2020. Japan Geoscience Union. All Right Reserved.

Analysis of Hydroclimatic Extremes over Narmada Basin under Climate Change

*SABYASACHI SWAIN[1], SURENDRA KUMAR MISHRA[1], ASHISH PANDEY[1]

1. Indian Institute of Technology Roorkee

A robust characterization and risk assessment of hydroclimatic extremes is essential considering their pervasiveness and consequences; however, their precise physical quantification is a difficult geophysical endeavor. This is becoming a serious issue for India, having 18% of the world’ s population and 4% of global freshwater, out of which 83% is used in agriculture. In this study, a detailed spatiotemporal assessment of the meteorological droughts (using Standardized Precipitation Index) and extreme rainfall events is carried out over the Narmada Basin for 1951- 2016, using the high-resolution (0.25˚ x 0.25˚, daily) gridded rainfall data. The non-parametric Mann-Kendall (MK) test is applied to investigate the trend of droughts and the 1-day maximum rainfall series. The entire duration is divided into two epochs i.e. 1951-1981 and 1982-2012, for a comparative assessment of hydrological extreme characteristics. Further, the frequency of these extremes are determined for 2020-2050 under RCP 4.5 and RCP 8.5 scenarios to assess the impacts of climate change. The results reveal that the Narmada basin is prone to droughts with a frequency of once in 3 to 6 years. The frequency and severity of droughts have significantly increased in 1982-2012 as compared to 1951-1981. The MK test results indicate a significant increase in the trend of droughts and 1-day maximum rainfall over most parts of the basin. The frequency, severity, persistence and areal extent of droughts are found to be increasing for both the RCP scenarios. The heavy rainfall events are also showing widespread prominence over the basin with a remarkable increase in frequency and intensity. This study suggests that appropriate measures must be taken for better management of the water resources in the basin, and also for mitigation of floods and droughts, considering the increased risk of the high-intensity storms as well as the severe drought occurrences under climate change.

Keywords: Narmada Basin, Droughts, Heavy rainfall events, Mann-Kendall test, Climate change

©2020. Japan Geoscience Union. All Right Reserved.

Flashfloods and landslides along the foothills of the Himalayas: their precursors, dynamics and thermodynamics

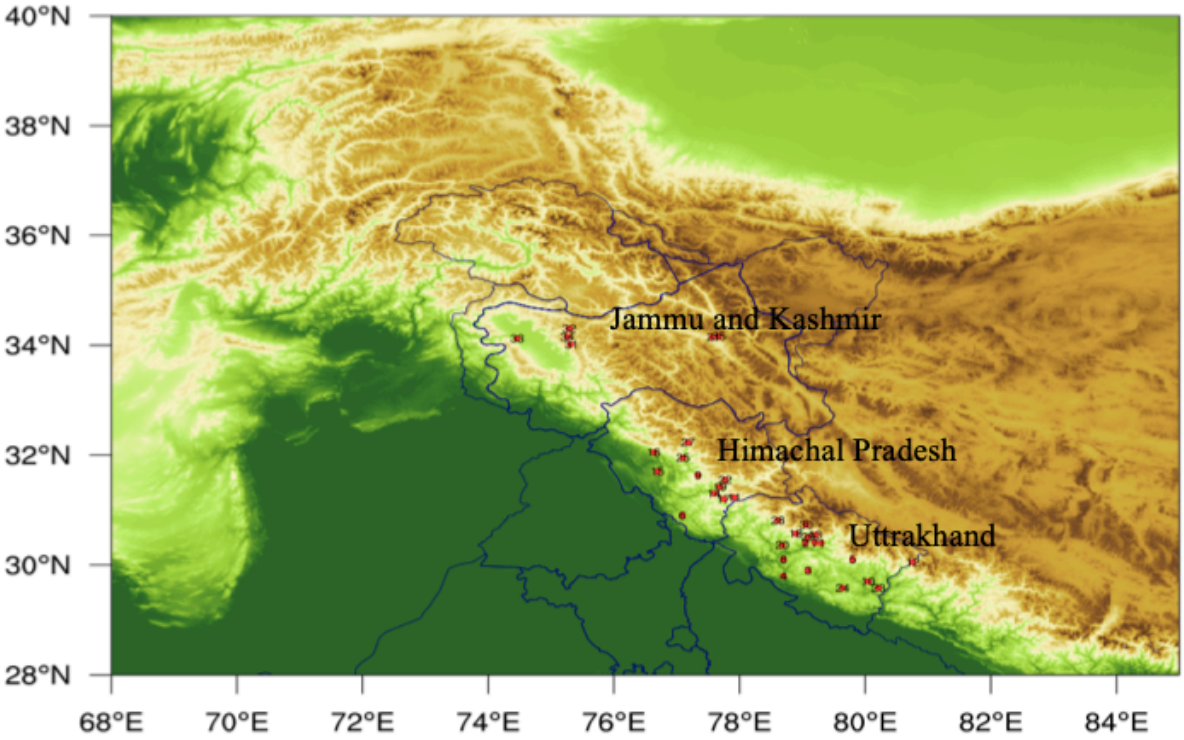
*Anu Gupta[1], Jun Matsumoto[1]

1. Tokyo Metropolitan University, Tokyo

In the past three decades, the total number of extreme precipitation events during summer monsoon season over north India has increased, which majorly caused flooding and landslides over the Himalayan foothills and north Indian region. Among those extreme precipitation events, some are reported as cloudburst events. In this article, those extreme precipitation events over north India are studied by employing satellite and gauge merged high-resolution precipitation CHIRPS (Climate Hazards Group InfraRed Precipitation with Station data) dataset for the period 1981-2015. Using ERA-Interim reanalysis dataset, cloudburst (CB) events are classified into five major classes C1, C2, C3, C4 and C5 based on the large-scale weather systems observed in the lower, middle and upper troposphere. Analysis shows that cloudburst events of classes C1, C2, and C3 occurs during active monsoon season, whereas, class C4 and C5 cloudburst events develop in the monsoon hiatus/break period. Classes C1, C2 and C3 cloudburst events associated with lower atmosphere cyclonic circulation over the head Bay of Bengal, cyclonic circulation centered over Central India, and East-West oriented low-pressure conveyor system over central India respectively. Further, thermodynamic analysis of each class revealed that class C1, C2, and C3 cloudbursts are associated with the moist instability of the local atmosphere during the cloudburst events, where orographic forcing created potential instability and made them intense and overwhelming. A detailed schematic of each class is presented to understand the overall processes during the cloudburst. This kind of careful knowledge about schematics of extreme precipitation events is very useful in comparing process-based model simulations and monitoring.

Keywords: Cloudburst events, Orographic forcing

©2020. Japan Geoscience Union. All Right Reserved.



In figure brown color represents the high mountains of the Himalayas in the northern part of India which includes Jammu and Kashmir, Himachal Pradesh and Uttrakhand states, and red dots represents the location of cloudburst events.

©2020. Japan Geoscience Union. All Right Reserved.

Standardized Variability Index (SVI) : A multiscale index to assess the variability of precipitation

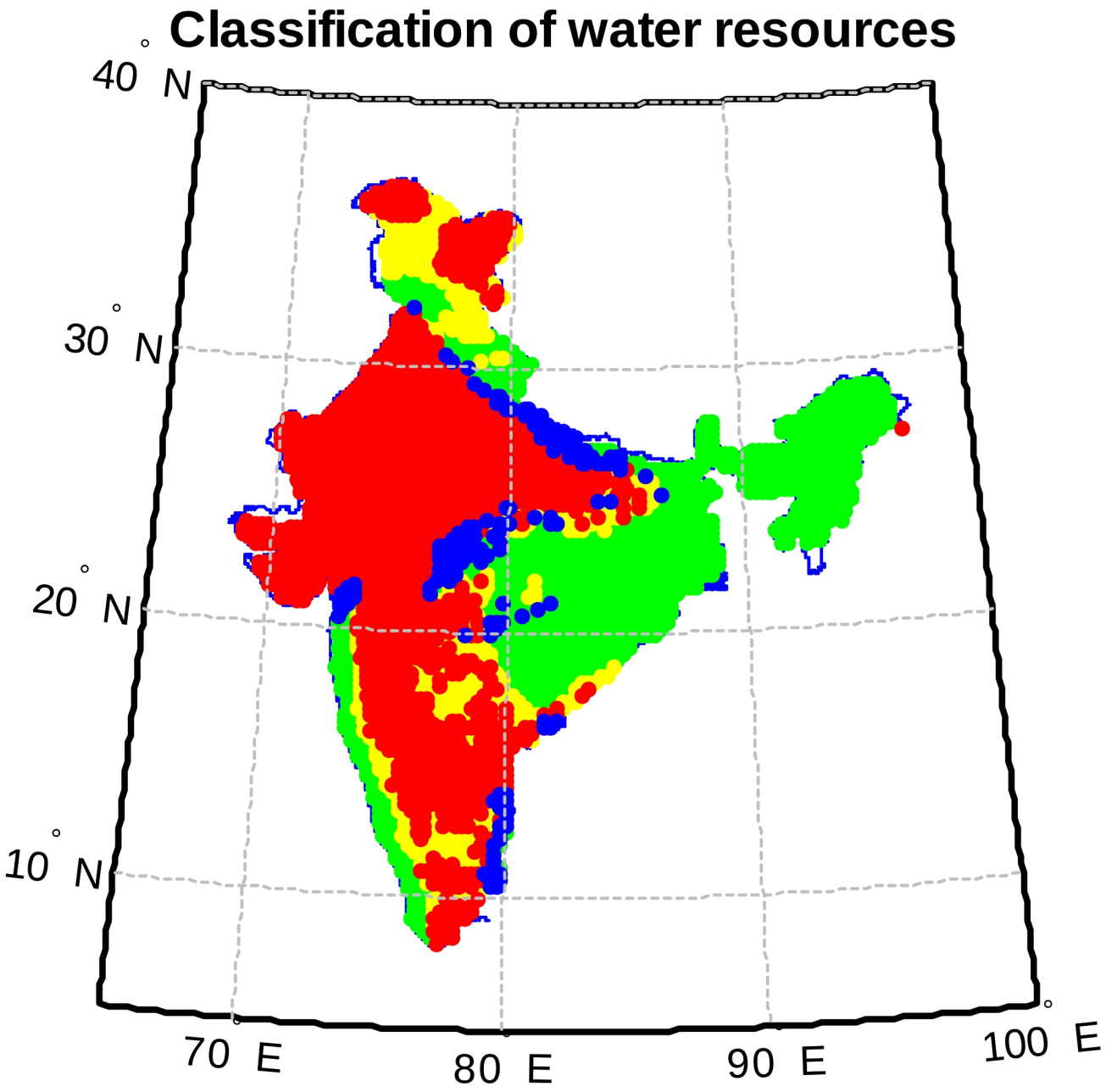
*Ravi kumar Guntu[1], Ankit Agarwal[1]

1. Department of Hydrology, Indian Institute of Technology Roorkee, 247667, India

Quantifying the spatiotemporal variability of precipitation is the principal component for the assessment of the impact of climate change on the hydrological cycle. A better understanding of the quantification of variability and its trend is vital for water resources planning and management. Therefore, a multitude of studies has been dedicated to quantify the precipitation variability over the years. Despite their importance for modeling precipitation variability, the studies mainly focused on the amount of precipitation and its spatial patterns. The studies investigating the spatial and temporal variability of precipitation across the Indian subcontinent, in general, and at multiscale, in particular, are limited. In this study, we introduce a novel measure, Standardized Variability Index (SVI), based on information entropy to investigate the spatiotemporal variability of precipitation. The proposed measure is independent of the temporal scale, the length of the data and can compare the precipitation variability at multiple timescales. Distinct spatial patterns were observed for information entropies at the monthly and seasonal scale. Stations with statistically significant trends were observed and vary from monthly to seasonal scale. There is an increase in the variability of precipitation amount across Central India. Trend analysis revealed there is changing behavior in the precipitation amount as well as rainy days, showing an increase in the probability of occurrence of extreme events in the near future.In addition, coupling the mean annual rainfall with SVI enables a relative assessment of the water resources availability.

Keywords: Precipitation variability, Apportionment entropy, Intensity entropy, Standardized variability index, Mann-Kendall test, Indian Subcontinent

©2020. Japan Geoscience Union. All Right Reserved.



©2020. Japan Geoscience Union. All Right Reserved.

[E] Poster | A (Atmospheric and Hydrospheric Sciences)：A-OS Ocean Sciences & Ocean Environment

[A-OS16] Ocean renewable energy: resource, impacts and technologies

convener:Bahareh Kamranzad(The Hakubi Center for Advanced Research/Graduate School of Advanced Integrated Studies in Human Survivability, Kyoto University), Simon P Neill(Bangor University), Zhaoqing Yang(Pacific Northwest National Laboratory)

The development of renewable energy technologies is a vital part of mitigating the negative impacts related to the combustion of fossil fuels, such as global warming and climate change. More than 70% of the surface of the Earth is covered by water, and the oceans hold more than 96% of all water on the Earth. In addition, two-thirds of the population of the world live within 100 km of the coast. Hence, ocean renewable energies (such as wave, tidal, current and offshore wind) present a sustainable solution to address current and future demand for electricity, particularly in areas that are adjacent to coastal zones. However, the ocean renewable energy resource is not only affected by intra-annual variability, but also longer-term variability due to changes in the climate. Accordingly, as well as quantifying the available resources, it is also important to assess variability over various time scales such as inter- and intra-annual, decadal, etc. Moreover, development of advanced wave and current energy converters that operate efficiently under various ocean conditions and minimizing the potential environmental impacts is crucial to the success of harvesting ocean renewable energy. The levelized cost of energy (LCOE) of ocean renewable energy has been gradually decreasing due to technology advancement. However, much more effort is required to reduce it more compared to other renewable energy resources. In this session, we welcome presentations across a wide-range of themes related to ocean renewable energy, including resource, impacts and technologies.

[AOS16-P01] On the coastal ocean modelling assessment of tidal stream and range energy resources

★Invited Papers

*Athanasios Angeloudis[1], Lucas Mackie[2], Daniel Stephen Coles[2], Anastasia Fragkou[1], Stephan C Kramer[2], Matthew D Piggott[2] (1.School of Engineering, Institute for Infrastructure and the Environment, University of Edinburgh, 2.Department of Earth Science and Engineering, Imperial College London)

[AOS16-P02] Feedbacks between tidal energy extraction and physical processes

★Invited Papers

*Simon P Neill[1], Peter Robins[1], Matthew Lewis[1] (1.Bangor Univ.)

[AOS16-P03] Climate Change Impact on Offshore Wind Energy Resources in Japan

*Masamichi Ohba[1] (1.Central Research Institute of Electric Power Industry)

[AOS16-P04] Sustainability of wave energy potential in Japan

*Bahareh Kamranzad[1] (1.The Hakubi Center for Advanced Research/Graduate School of Advanced Integrated Studies in Human Survivability, Kyoto University)

[AOS16-P05] The effect of future climate-related variabilities of tropical monsoons in the Indian Ocean on wave energy resource around Sri Lanka

*Bahareh Kamranzad[1], Pravin Maduwantha[3], Harsha Rathnasooriya[3], Kasun De Silva[3], Harshinie Karunarathna[2] (1.The Hakubi Center for Advanced Research/Graduate School of Advanced Integrated Studies in Human Survivability, Kyoto University, 2.Zienkiewicz Centre for Computational Engineering, College of Engineering, Bay Campus, Swansea University, 3.Department of Civil Engineering, University of Moratuwa)

On the coastal ocean modelling assessment of tidal stream and range energy resources

*Athanasios Angeloudis[1], Lucas Mackie[2], Daniel Stephen Coles[2], Anastasia Fragkou[1], Stephan C Kramer[2], Matthew D Piggott[2]

1. School of Engineering, Institute for Infrastructure and the Environment, University of Edinburgh, 2. Department of Earth Science and Engineering, Imperial College London

Tidal energy can be practically exploited from sites with either high velocity currents or high elevation range. This is accomplished through the deployment of technologies that harness the available kinetic (i.e. tidal stream turbine arrays) or potential (i.e. tidal barrages or lagoons) energy respectively. In particular, the UK features several amplifying coastal characteristics that present viable opportunities for both forms of energy. Even though the rationale for harnessing the energy is fundamentally different, progress has been made on the assessment of prospective schemes using coastal ocean modelling and optimisation methods. As part of the methods developed, we discuss the representation of each of these technologies in the coastal ocean model *Thetis* for several UK-based applications. *Thetis* is an unstructured-mesh, finite-element model that solves both the depth-averaged, as well as the three-dimensional equations with primary applications aimed at the coastal and estuarine zones. It is based on *Firedrake* which is a finite element framework, that automatically derives highly optimised code from a high-level-abstraction description of the finite element equations. Through several UK-based case studies, we present the insight and limitations of the coastal ocean modelling approaches, and highlight specific considerations of the hydrodynamics developed at tidal stream and range sites respectively.

Keywords: tidal energy, coastal modelling, marine renewable energy

©2020. Japan Geoscience Union. All Right Reserved.

Feedbacks between tidal energy extraction and physical processes

*Simon P Neill[1], Peter Robins[1], Matthew Lewis[1]

1. Bangor Univ.

It is agreed that exploitation of the tidal (stream) energy resource, particularly at significant scales of electricity generation, will impact the marine environment. Although significant levels of extraction will alter the resource itself, particularly in narrow channels, there is one physical process that can indirectly impact the tidal energy resource: sediment dynamics and associated morphodynamics. Here I review the physical mechanisms of how tidal energy conversion influences sediment dynamics, both at device and array scale. I review local and regional impacts, and examine methods of simulating and validating the impact, based on idealized numerical experiments, and case studies including the Alderney Race and the Pentland Firth.

Keywords: Tidal energy, Sediment dynamics, Numerical model, Pentland Firth, Alderney Race

©2020. Japan Geoscience Union. All Right Reserved.

Climate Change Impact on Offshore Wind Energy Resources in Japan

*Masamichi Ohba[1]

1. Central Research Institute of Electric Power Industry

This study investigated the impact of global warming on Japanese wind energy resources and their short-term variations using the large ensemble d4PDF dataset, which consists of dynamically downscaled historical and +4K future climate projections. The capacity factor under the future and present climate was estimated from an idealized power curve based on hourly near-surface wind speeds. The +4K warming future climate projections showed significant changes in wind energy resources that varied both regionally and seasonally. The wind energy potential was projected to slightly increase (decrease) from winter to spring over northern (southern) Japan and decrease from summer to autumn over most of Japan. The projected annual production decreased by about ~5% over Japan in response to climate change. The frequency of wind ramp events also decreased in the latter seasons. The relationship to synoptic weather was investigated using self-organizing maps, whereby weather patterns (WPs) over the region in the present and future +4K climate were classified for a two-dimensional lattice. Future probabilistic projections of WPs under the global warming scenario showed both increases and decreases in the frequency of dierent WPs, with corresponding advantages and disadvantages for wind power generation with regard to future changes in capacity factors in Japan. The importance of these frequency changes on the total change was further assessed by separating the dynamical and thermodynamic contributions.

Keywords: Wind energy, Wind ramp events, Climate change, Global warming, d4PDF , Weather pattern

©2020. Japan Geoscience Union. All Right Reserved.

Sustainability of wave energy potential in Japan

*Bahareh Kamranzad[1]

1. The Hakubi Center for Advanced Research/Graduate School of Advanced Integrated Studies in Human Survivability, Kyoto University

Marine renewable energies and especially the wave energy, as an alternative to fossil fuels, are sensitive to changing climate. In addition, considering both short-term variations and long-term changes in the available resources is necessary for sustainable development. Wave energy potential has been less investigated in Northeast Asia and Japan in long-term and the previous works are limited to three decades at the most and mainly in limited locations and based on wave records or satellite measurements [e.g., 1-5]. This study focuses on the estimation of wave energy resources in Japan using five decades of modeled wave characteristics. For this purpose, SWAN Cycle III version 41.31 (by the Delft University of Technology) [6] was utilized in order to model the wave characteristics in Northeast Asia. The input wind was JRA-55 re-analysis developed by the Japan Meteorological Agency (JMA) [7]. The spatial and temporal resolutions of the wind field are 60 km and 6 hrs, respectively and it is available for the period of 1958-2012. The boundary condition for the model was also obtained from a global performance. The model was validated against satellite measurements and the bias was calculated on a monthly scale showing the similarity between the monthly mean values in the domain. The validated model was performed to generate the wave climate for five decades. The decadal change of wave climate was assessed in 10-yearly periods, i.e., 1961-1970, 1971-1980, 1981-1990, 1991-2000, 2001-2010. The analysis was performed for wind and wave characteristics as well as wave power parameter and the relationship between their change was discussed. The results indicate the difference between the changing pattern in various decades. However, in general, wave height and wave power have been decreased in the Pacific side of Japan during the two latter decades, while the parameters did not change considerably in the Sea of Japan. In addition, the share of swells in the whole wave energy potential has been discussed and the results indicate that almost fifty percent of the total wave power is provided by swells in the Pacific side of Japan while this value reaches around 40 percent in the Ryukyu Islands. In the Sea of Japan side of Japan, the percentage of wave power obtained from swells varied between 15 and 25 percent of the total wave power. Further analysis will be discussed regarding the sustainability of wave energy resources in different time scales.

References:

[1] Tabata T, Yagyu T, Fukuda I. Wave energy on Japanese coast [in Japanese with English abstract]. 1980.
[2] Sasaki W. Changes in wave energy resources around Japan. Geophys Res Lett 2012;39.
[3] Saruwatari A, Maruyama T. Resource assessment of wave energy around Hokkaido in winter. Proceeding Japan Soc Civ Eng B3 2013;69:I_91-I_96. https://doi.org/https://doi.org/10.2208/jscejoe.69.I_91.
[4] Hirakawa T. Wave energy resource assessment around Kyushu based on numerical hindcast. J Renew Sustain Energy 2018;10:24501. https://doi.org/10.1063/1.5011431.
[5] Sasmal K, Webb A, Waseda T, Miyajima S. Wave energy resource asessment: A comparative study for two coastal areas in Japan. Adv. Renew. Energies Offshore Proc. 3rd Int. Conf. Renew. Energies Offshore (RENEW 2018), CRC Press; 2018, p. 67–71.
[6] Booij N, Ris RC, Holthuijsen LH. A third-generation wave model for coastal regions: 1. Model description and validation. J Geophys Res Ocean 1999;104:7649–66.

©2020. Japan Geoscience Union. All Right Reserved.

https://doi.org/10.1029/98JC02622.
[7] KOBAYASHI S, OTA Y, HARADA Y, EBITA A, MORIYA M, ONODA H, et al. The JRA-55 Reanalysis: General Specifications and Basic Characteristics. J Meteorol Soc Japan Ser II 2015;93:5–48. https://doi.org/10.2151/jmsj.2015-001.

Keywords: wave enegry, sustainability, decadal change

©2020. Japan Geoscience Union. All Right Reserved.

The effect of future climate-related variabilities of tropical monsoons in the Indian Ocean on wave energy resource around Sri Lanka

*Bahareh Kamranzad[1], Pravin Maduwantha[3], Harsha Rathnasooriya[3], Kasun De Silva[3], Harshinie Karunarathna[2]

1. The Hakubi Center for Advanced Research/Graduate School of Advanced Integrated Studies in Human Survivability, Kyoto University, 2. Zienkiewicz Centre for Computational Engineering, College of Engineering, Bay Campus, Swansea University, 3. Department of Civil Engineering, University of Moratuwa

The direct swell wave approach and relatively narrow continental shelf make more favorable conditions for wave energy harvesting in Sri Lankan coastal region. West and south coasts consist of relatively strong waves comparing to the north and east coasts providing the potential for wave energy harvesting. However, the wave climate in the south and west coasts is highly modulated by the tropical monsoon systems in the Indian Ocean. Southwest monsoon season normally occurs from June to September when winds blow from the southwest, the Indian Ocean and the Arabian Sea, and generate energetic waves in the west and south coasts of Sri Lanka. The northeast monsoon, which falls between December and February, generates high sea waves in the north and east coasts. Although, climate change may alter the regular seasonal cycle. Therefore, it is essential to examine the climate change impacts on available wave energy resource in long term aspects.

Present and future ocean wave climate around Sri Lanka was simulated using numerical wave modeling. The waves have been simulated using wind outputs from the super high-resolution Atmospheric Global Climate Model of the Japan Meteorological Agency, MRI-AGCM3.2S. The future climate scenario of Representative Concentration Pathway (RCP 8.5), as defined by representing trajectories of increasing global radiative forcing reaching + 8.5 W m^{-2}, by the year 2100 compared to pre-industrial conditions, was used. These outputs were first used to develop an Indian Ocean wave model (KU_IO) using SWAN spectral wave model and downscaled up to Sri Lankan Regional model (KU_SLK) (5˚-11˚N, 79.5˚-83.5˚E). Based on the generated wave characteristics, the total average wave power distribution under the present climate (total average power from 1979 to 2003) and future climate (total average power from 2075 to 2099) for the Sri Lankan domain were calculated. The results indicate that even though the west and south coasts of Sri Lanka have the highest available wave power, under the future wave climate, 2 to 3 kW/m wave power reduction can be observed in these regions. In addition, no noticeable change can be seen in the north and east coasts. Future reduction in the available wave power around Sri Lanka can be either due to change in swell conditions of the southern Indian Ocean or due to potential changes to the south-west tropical monsoon. However, these changes may be attributed to wave climate variations in southwest monsoon season since it highly modulates the wave conditions in the south and the west coasts. Therefore, the distribution of total average wave power reduction (total average wave power in the future –total average wave power in the present) was separated into two time periods as southwest monsoon and non-south-west monsoon period. Even in the southwest monsoon season, the highest wave power reduction (2-2.5 kW/m) can be observed along the west to the south coast of Sri Lanka. In this region, the wave power reduction in the future during the non-monsoon period is relatively low (0.4 - 0.6 kW/m). The wave power reduction may cause by the variations of either wave height or wave period. However, the results reveal that according to the model simulations, the future reduction of wave power may be attributed to the change in the southwest tropical monsoon generated wave heights as a result of global climate change.

©2020. Japan Geoscience Union. All Right Reserved.

Acknowledgement:

Financial support provided by Swansea University through the Global Challenge Research Fund project ‘Wave energy resource characterisation for Sri Lanka in a changing ocean climate’ to conduct the research presented in this paper is greatly acknowledged. Japan Meteorological Agency is acknowledged for sharing atmospheric model data. Bahareh Kamranzad is supported by the Hakubi Center for Advanced Research at Kyoto University and JSPS Grants-in-Aid for Scientific Research (KAKENHI), the Ministry of Education, Culture, Sports, Science, and Technology-Japan (MEXT).

Keywords: Climate change, Wave power, Wave projections, Sri Lanka

©2020. Japan Geoscience Union. All Right Reserved.

[E] Poster | A (Atmospheric and Hydrospheric Sciences)：A-OS Ocean Sciences & Ocean Environment

[A-OS17] Climate variability and predictability on subseasonal to decadal timescales

convener:Takashi Mochizuki(Department of Earth and Planetary Sciences, Kyushu University), V Ramaswamy(NOAA GFDL), Yushi Morioka(Japan Agency for Marine-Earth Science and Technology)

Many efforts have been made to understand and predict climate on subseasonal to decadal timescales (e.g. MJO, IOD, ENSO, PDV, AMV), while our knowledge still remains at an insufficient level to fully resolve socioeconomic challenges arising from climate variations and change. Model simulations and predictions usually present large uncertainties, particularly due to lack of understanding of weather and climate interactions across different spatial and temporal timescales (e.g. tropical cyclones and ENSO), as well as due to multiple physical processes underlying climate variations (e.g. troposphere-stratosphere coupling, air-sea-ice interactions; atmosphere-ocean-land interactions). Recently, datasets from Coupled Model Intercomparison Project Phase 6 (CMIP6) have been opened to the public, and understanding and predicting the changing climate together with its impacts on frequency and intensity of abnormal weather (e.g. cold/heat waves, tropical storms, and floods/droughts) should also be a timely topic in the areas of earth science and socioeconomics. This session aims to share current knowledge of subseasonal to decadal climate variability and predictability in order to identify the unresolved issues and aim at a better understanding and accurate prediction. This session invites all abstracts related to the observational, theoretical, process-level and modelling research on subseasonal to decadal variability and predictability of climate.

[AOS17-P01] Predictability of two flavors of El Nino and statistical downscaling by SVD analysis using the MIROC5 seasonal prediction system

★Invited Papers

*Yukiko Imada[1], Hiroaki Tatebe[2], Masayoshi Ishii[1], Yoshimitsu Chikamoto[6], Masato Mori[4], Miki Arai[2], Shinjiro Kanae[5], Masahiro Watanabe[3], Masahide Kimoto[3] (1.Meteorological Research Institute, Japan Meteorological Agency, 2.Japan Agency for Marine-Earth Science and Technology, 3.Atmosphere and Ocean Research Institute, the University of Tokyo, 4.Research Center for Advanced Science and Technology, the University of Tokyo, 5.Tokyo Institute of Technology, 6.University of Utah)

[AOS17-P02] Parameter sensitivity analysis for predicting two types of El Niño with an intermediate coupled model

*Haibo Chen[1,2,3] (1.CAS Key Laboratory of Ocean Circulation and Waves, Institute of Oceanology, Chinese Academy of Sciences, 2.Pilot National Laboratory for Marine Science and Technology, 3.Center for Ocean Mega-Science, Chinese Academy of Sciences)

[AOS17-P03] Interannual Salinity Variability Associated with the Central Pacific and Eastern Pacific El Niños in the Tropical Pacific

*Hai Zhi[1] (1. Nanjing University of Information Science and Technology, Nanjing, China)

[AOS17-P04] Forecast of summer precipitation in the Yangtze River Valley based on South China Sea springtime sea surface salinity

*LILI ZENG[1], Raymond W. Schmitt[2], Laifang Li[3], Qiang Wang[1] (1.State Key Laboratory of Tropical Oceanography (LTO), South China Sea Institute of Oceanology, Chinese Academy of Sciences, 2.Physical Oceanography Department, Woods Hole Oceanographic Instituti, 3.Earth and Ocean Sciences, Nicholas School of the Environment, Duke University)

[AOS17-P05] Scale-dependent effects on ENSO induced by ocean chlorophyll due to interannual variability and tropical instability waves

*Rong-Hua Zhang[1] (1.Institute of Oceanology, Chinese Academy of Sciences)

[AOS17-P06] Responses of the subseasonal to seasonal atmospheric variability to the recent Pacific SST anomaly

*Tomoe Nasuno[1], Masuo Nakano[1], Hiroyuki Murakami[2], Kazuyoshi Kikuchi[3] (1.Japan Agency for Marine-Earth Science and Technology, 2.Geophysical Fluid Dynamics Laboratory , 3.International Pacific Research Center)

[AOS17-P07] **Intraseasonal Variability over the Arabian Sea and Its Impact on the Indian Summer Monsoon Onset**

*Jing Cha[1], Yun Qiu[1], Xinyu Lin[1], Fuwen Qiu[1] (1.TIO, MNR)

[AOS17-P08] Zonal Displacement of the Western North Pacific Subtropical High from Early to Late Summer

*Xiao Dong[1], Chao He[2], Renping Lin[1] (1.Institute of Atmospheric Physics, Chinese Academy of Sciences, 2.Institute for Environmental and Climate Research, Jinan University, Guangzhou, China)

[AOS17-P09] Impacts of the Indian Ocean Dipole on Sea Level and Gyre Circulation of the Western Tropical Pacific Ocean

*Jing Duan[1,2,3], Yuanlong Li[1,2,3], Lei Zhang[4], Fan Wang[1,2,3] (1.Institute of Oceanology, Chinese Academy of Sciences, 2.Function Laboratory for Ocean Dynamics and Climate, Qingdao National Laboratory for Marine Science and Technology, 3.Center for Ocean Mega-Science, Chinese Academy of Sciences, 4.Department of Atmospheric and Oceanic Sciences, University of Colorado)

[AOS17-P10] Predictability study on the seasonal reduction of the upstream Kuroshio transport and related targeted observation application.

*Kun Zhang[1,2] (1.Institute of Oceanology, Chinese Academy of Sciences, 2.Center for Ocean Mega-Science, Chinese Academy of Sciences)

[AOS17-P11] Remote and local processes controlling decadal sea-ice variability in the Weddell Sea

*Yushi Morioka[1], Swadhin Behera[1] (1.Japan Agency for Marine-Earth Science and Technology)

[AOS17-P12] **Can tropical Pacific winds enhance the footprint of the Interdecadal Pacific Oscillation on the upper-ocean heat content in the South China Sea?**

*Fuan Xiao[1], Dongxiao Wang[2] (1.Guangzhou Univ., 2.Sun Yat-sen Univ.)

[AOS17-P13] The Atlantic SST influences on the Pacific subdecadal variability

*Takashi Mochizuki[1,2], Masahiro Watanabe[3], Masahide Kimoto[3] (1.Department of Earth and Planetary Sciences, Kyushu University, 2.Japan Agency for Marine-Earth Science and Technology, 3.Atmosphere and Ocean Research Institute, The University of Tokyo)

[AOS17-P14] **An evaluation of the Decadal Climate Prediction Experiments by the BCC_CSM Model**

*Yongjie Fang[1], Tongwen Wu[1], Xiaoge Xin[1] (1.National Climate Center, Chinese Meteorological Administration)

Predictability of two flavors of El Nino and statistical downscaling by SVD analysis using the MIROC5 seasonal prediction system

*Yukiko Imada[1], Hiroaki Tatebe[2], Masayoshi Ishii[1], Yoshimitsu Chikamoto[6], Masato Mori[4], Miki Arai[2], Shinjiro Kanae[5], Masahiro Watanabe[3], Masahide Kimoto[3]

1. Meteorological Research Institute, Japan Meteorological Agency, 2. Japan Agency for Marine-Earth Science and Technology, 3. Atmosphere and Ocean Research Institute, the University of Tokyo, 4. Research Center for Advanced Science and Technology, the University of Tokyo, 5. Tokyo Institute of Technology, 6. University of Utah

It is known that there are two flavors of ENSO events in the tropical Pacific Ocean: traditional eastern Pacific (EP) events and central Pacific (CP) events. Several studies indicated that the CP event is more difficult to predict than the EP event. Here, we assessed the difference of the seasonal predictability for two prominent types of El Nino using the coupled atmosphere-ocean general circulation model (AOGCM) MIROC5 co-developed by Atmosphere and Ocean Research Institute (AORI), National Institute for Environmental Studies (NIES), and Japan Agency for Marine-Earth Science and Technology (JAMSTEC). The spatial resolution is a horizontal triangular spectral truncation at total wave number 85 (T85) with 40 vertical layers, and eight ensemble forecast members are generated according to the protocol of the WCRP Climate-system Historical Forecast Project (CHFP). Hindcast products showed high predictability of tropical climate signals with the significant anomaly correlation coefficient skill scores, even though the ocean anomaly data assimilation is applied to the initialization process.
Overall, the predictable months of CP events are shorter than EP events because CP events are sensitive to atmospheric noises. Characteristics of each error growing process were also investigated.
We also developed a statistical downscaling technique using SVD analysis which is effective for rainfall prediction over the Indochina Peninsula and Australian continent.

Keywords: Seasonal prediction, ENSO, CGCM

©2020. Japan Geoscience Union. All Right Reserved.

Parameter sensitivity analysis for predicting two types of El Niño with an intermediate coupled model

*Haibo Chen[1,2,3]

1. CAS Key Laboratory of Ocean Circulation and Waves, Institute of Oceanology, Chinese Academy of Sciences, 2. Pilot National Laboratory for Marine Science and Technology, 3. Center for Ocean Mega-Science, Chinese Academy of Sciences

Sensitivity of El Niño simulation to model parameters is analyzed using the OPSA method, based on four El Niño events (two EP events and two CP events) simulated by an intermediate coupled model. Results show that the coefficient of entraining anomalous subsurface temperature and the ocean-atmosphere coupling coefficient are two important parameters, while the coefficient of anomalous heat flux is another important parameter for CP events. Observation system simulation experiments shows that El Niño predictions of can be effectively improved if the identified sensitive parameters are more accurately estimated, whereas the improvement is very low or even negative if the estimation of only the insensitive parameters is improved, indicating the significance of the sensitivity analysis result for El Niño prediction.

Keywords: Parameter sensitivity, OPSA, Predictability, El Niño diversity, Intermediate coupled model

©2020. Japan Geoscience Union. All Right Reserved.

Interannual Salinity Variability Associated with the Central Pacific and Eastern Pacific El Niños in the Tropical Pacific

*Hai Zhi[1]

1. Nanjing University of Information Science and Technology, Nanjing, China

El Niño exhibits diversity and modulation as indicated by the central Pacific (CP) El Niño and the eastern Pacific (EP) El Niño. Previously, sea surface temperature (SST) has been commonly used to characterize the differences in the two types of El Niño. But, physical processes responsible for the occurrence of the two types of El Niño are still not understood well. Here, ocean reanalysis products and observations are used to analyze the relationships between the two types of El Niño and interannual salinity variability; a budget analysis for mixed-layer salinity (MLS) is performed in the tropical Pacific. The center of negative MLS anomalies in winter tend to move further westward with the CP El Niño, compared with the EP El Niño. The oscillation period with the EP El Niño is found to be approximately 10 years, longer than that with the CP El Niño (approximately 6-8 years). Our results reveal that surface advection, surface forcing and subsurface effect are the three main contributors to mixed layer (ML) tendency of interannual salinity variability, which are regionally dependent. In the eastern edge of the warm pool (WP), surface advection makes a larger contribution (about 40-60 %) to the MLS budget, and subsurface effect (about 20%) and surface forcing (about 20-40%) are relatively smaller; in contrast, in the South Pacific Convergence Zone (SPCZ), the latter two processes make a larger contribution (about 60%). The subsurface effects on the MLS tendency tend to compensate for the imbalance induced by surface forcing and advection: a weakened MLS tendency occurs with the CP El Niño, whereas an enhanced MLS tendency occurs with the EP El Niño, respectively. The MLS tendency leads Niño3.4 by 12 months for the EP El Niño, whereas there is no such significant lead/lag relationship for the CP El Niño. It is demonstrated that the relationships between the interannual SST variability and MLS budget terms can be a clear indicator to distinguish the two types of El Niño.

Keywords: eastern and central Pacific El Nino, mixed layer salinity variability, salinity budget

©2020. Japan Geoscience Union. All Right Reserved.

Forecast of summer precipitation in the Yangtze River Valley based on South China Sea springtime sea surface salinity

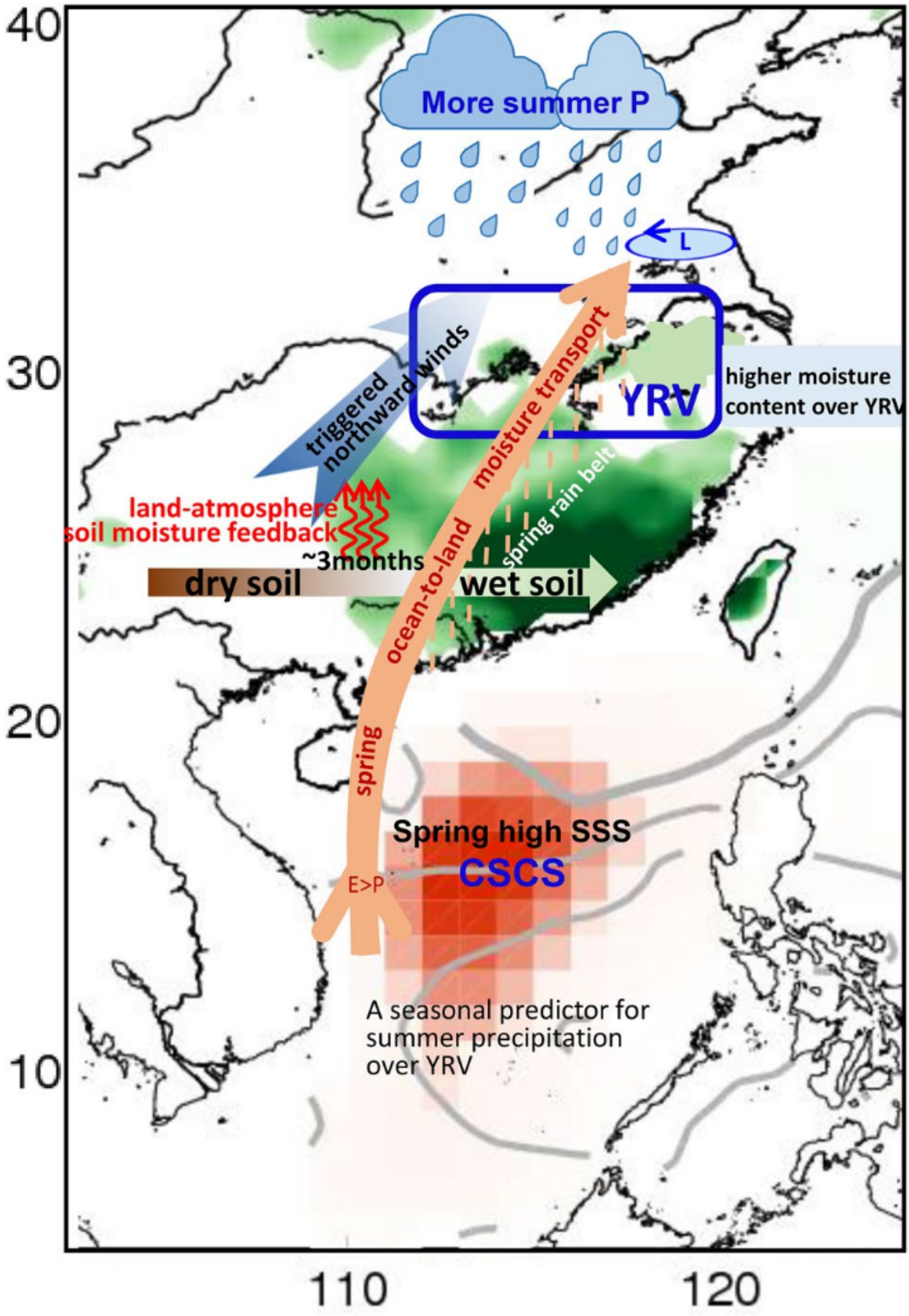
*LILI ZENG[1], Raymond W. Schmitt[2], Laifang Li[3], Qiang Wang[1]

1. State Key Laboratory of Tropical Oceanography (LTO), South China Sea Institute of Oceanology, Chinese Academy of Sciences, 2. Physical Oceanography Department, Woods Hole Oceanographic Instituti, 3. Earth and Ocean Sciences, Nicholas School of the Environment, Duke University

As a major moisture source, the South China Sea (SCS) has a significant impact on the summer precipitation over China. The ocean-to-land moisture transport generates sea surface salinity (SSS) anomalies that can be used to predict summer precipitation on land. This study illustrates a high correlation between springtime SSS in the central SCS and summer precipitation over the middle and lower Yangtze River Valley (the YRV region). The linkage between spring SSS in the central SCS and summer YRV precipitation is established by ocean-to-land moisture transport by atmospheric processes and land–atmosphere soil moisture feedback. In spring, oceanic moisture evaporated from the sea surface generates high SSS in the central SCS and directly feeds the precipitation over southern China and the YRV region. The resulting soil moisture anomalies last for about 3 months triggering land–atmosphere soil moisture feedback and modulating the tropospheric moisture content and circulation in the subsequent summer. Evaluation of the atmospheric moisture balance suggests both a dynamic contribution (stronger northward meridional winds) and a local thermodynamic contribution (higher tropospheric moisture content) enhance the summer moisture supply over the YRV, generating excessive summer precipitation. Thus, spring SSS in the SCS can be utilized as an indicator of subsequent summer precipitation over the YRV region, providing value for operational climate prediction and disaster early warning systems in China.

Keywords: Yangtze River Valley, South China Sea, sea surface salinity, summer precipitation

©2020. Japan Geoscience Union. All Right Reserved.



©2020. Japan Geoscience Union. All Right Reserved.

Scale-dependent effects on ENSO induced by ocean chlorophyll due to interannual variability and tropical instability waves

*Rong-Hua Zhang[1]

1. Institute of Oceanology, Chinese Academy of Sciences

Large perturbations in chlorophyll (Chl) are observed to coexist at interannual and tropical instability wave (TIW) scales in the tropical Pacific; their combined net effects on ENSO through ocean biology-induced heating (OBH) feedbacks are not known. Here, a new hybrid coupled model for atmosphere and ocean physics-biology (HCM AOPB) is used to quantify ways ENSO can be modulated, individually or collectively, by Chl perturbations at interannual and TIW scales, respectively. HCM-based sensitivity experiments demonstrate a counteracting effect on ENSO: the bio-feedback due to interannual Chl variability tends to damp ENSO via its influence on the stratification and vertical mixing in the upper ocean, whereas that due to TIW-scale Chl perturbations tends to amplify ENSO. A bias source for ENSO simulation is illustrated that is related with Chl effect in the tropical Pacific, adding in a new insight into interactions between the climate system and ocean ecosystem on different scales in the tropical acific. Because ENSO simulations are sensitively dependent on the way Chl effects are represented at different scales, it is necessary to adequately include the related Chl effects in climate modeling. These results reveal a level of complexity of ENSO modulations resulting from TIW-scale Chl effects associated with ocean biogeochemical processes and their interactions with physical processes in the tropical Pacific.

Keywords: Ocean chlorophyll, Interannual variability and Tropical instability waves, Compensated feedback effects , A coupled ocean-atmosphere model

©2020. Japan Geoscience Union. All Right Reserved.

Responses of the subseasonal to seasonal atmospheric variability to the recent Pacific SST anomaly

*Tomoe Nasuno[1], Masuo Nakano[1], Hiroyuki Murakami[2], Kazuyoshi Kikuchi[3]

1. Japan Agency for Marine-Earth Science and Technology, 2. Geophysical Fluid Dynamics Laboratory , 3. International Pacific Research Center

Warm sea surface temperature anomalies (SSTA) is pronounced in the Pacific in recent years. Sensitivity simulations revealed that the warm SST anomaly (SSTA), especially in the subtropics, is responsible for the abnormally active tropical cyclones (TCs) in the Pacific during boreal summer 2018 (Qian et al. 2019). We further examine the SSTA impacts on the TC precursors (e.g., easterly waves) and intraseasonal oscillation (ISO), which are closely related to the TC activity in the western North Pacific (WNP). Simulation dataset using 14-km mesh Nonhydrostatic Icosahedral Atmospheric Model (NICAM) is analyzed. The dataset consists of control experiments (i.e., forced by full SSTA in 2018) and sensitivity experiments without SSTA in a local domain (e.g., tropical Pacific, subtropical Pacific, etc.), and those forced by reginal SSTA in 2018 with other areas restored to the climatological SST. The simulations were forced by the 12 member SST time series for each setup, which were calculated using a coupled general circulation model, the GFDL Low Ocean Resolution (FLOR) model.

The seasonal mean large-scale atmospheric responses and lower tropospheric high-frequency kinetic energy (KE), as a proxy of TC precursor activity, are compared. In the control simulations (with full SSTA in 2018), eastward extension of westerly anomalies in the tropics manifest as the enhanced Asian summer monsoon, which is consistent with the observations. A marked zonal convergence and cross-equatorial flow collocate with high KE anomalies, suggesting the enhancement of the TC precursor activity by accumulation of moisture and large-scale upward motion in the central tropical Pacific. In the WNP, large-scale cyclonic circulation reaches mid-latitude, with positive KE anomalies there. This indicates that the atmospheric response to the SSTA in 2018 provide favorable conditions for the development of TC precursors, leading to the abnormal TC activity in the Pacific (Qian et al. 2019). In the simulations without the SSTA in the subtropics, tropical westerly anomalies in the tropical Pacific and cyclonic circulation in the WNP disappear, with negative KE anomalies over the broad Pacific domain. In the case without the SSTA in the tropics, dominant impacts appear in the WNP with negative KE anomalies and weakening of lower tropospheric westerly anomalies, despite the secondary importance in the central to eastern Pacific. These are closely associated with the different responses of local Hadley and Walker circulations to the regional SSTA, and possibly responsible for complicated responses of ISO in the WNP.

Keywords: Pacific SST anomaly, intraseasonal oscillation, TC precursor, global nonhydrostatic model

©2020. Japan Geoscience Union. All Right Reserved.

Intraseasonal Variability over the Arabian Sea and Its Impact on the Indian Summer Monsoon Onset

*Jing Cha[1], Yun Qiu[1], Xinyu Lin[1], Fuwen Qiu[1]

1. TIO, MNR

Based on the NCEP/NCAR and ERA-Interim reanalysis data, the processes associated with intraseasonal convection over the Arabian Sea (AS) are investigated during the Indian Summer Monsoon (ISM) onset. Onsets of the years 1980-2016 are sorted into early and late onset categories. Composites reveal that warm SST over the northern AS plays an active role in triggering anomalous convection and the reversal of prevailing winds through regional air-sea interaction before early onset of ISM. Increased latent heat release favors static instability and enhances convergence in lower troposphere which develops into Monsoon onset vortex (MOV). This convergent flow is well coupled with strong divergence pumping in upper troposphere, leading to appreciable growth of intraseasonal convection in early onset years.

On the other hand, the regional air-sea interaction contributes to intraseasonal convection after the late onset of ISM. The static instability plays a small role in the convection development which decays after onset due to anomalous diabatic heating in upper troposphere. Along with the decay of static instability, the de-coupled 3-dimentional circulation also results in the weak convection in late onset years.

Keywords: Indian Summer Monsoon, intraseasonal variability, air-sea interaction

©2020. Japan Geoscience Union. All Right Reserved.

Zonal Displacement of the Western North Pacific Subtropical High from Early to Late Summer

*Xiao Dong[1], Chao He[2], Renping Lin[1]

1. Institute of Atmospheric Physics, Chinese Academy of Sciences, 2. Institute for Environmental and Climate Research, Jinan University, Guangzhou, China

The zonal shift in the western North Pacific subtropical high (WNPSH) is closely associated with moisture transport in East Asia and is thus an important factor that determines the amount of summer precipitation in the region. Climatologically, the WNPSH retreats eastward from early to late summer. However, there is high variability in the early to late summer shift in the WNPSH from year to year. Thus, the interannual variability in the intraseasonal zonal displacement of WNPSH from early to late summer was examined in this study. The results showed that the El Niño or La Niña years were not predictive of how the WNPSH would shift zonally from early to late summer. Otherwise, the zonal displacements of the WNPSH were more of mid-latitude origin. In the strongly retreating years (SRY), the mid-latitude wave train was much more significant than that in the weakly retreating years (WRY). The mid-latitude wave train was reminiscent of the Silk Road teleconnection pattern (SRP). In the SRY, the centres of the wave trains had opposite signs in early and late summer, which resulted in the opposite features of the WNPSH between early and late summer. The consistency of the three reanalysis datasets confirmed the robustness of our results.

Keywords: Western North Pacific subtropical high, strongly/weakly retreating years, Silk Road pattern, interannual variation, wave activity flux

©2020. Japan Geoscience Union. All Right Reserved.

Impacts of the Indian Ocean Dipole on Sea Level and Gyre Circulation of the Western Tropical Pacific Ocean

*Jing Duan[1,2,3], Yuanlong Li[1,2,3], Lei Zhang[4], Fan Wang[1,2,3]

1. Institute of Oceanology, Chinese Academy of Sciences, 2. Function Laboratory for Ocean Dynamics and Climate, Qingdao National Laboratory for Marine Science and Technology, 3. Center for Ocean Mega-Science, Chinese Academy of Sciences, 4. Department of Atmospheric and Oceanic Sciences, University of Colorado

Interannual variabilities of sea level and upper-ocean gyre circulation of the western tropical Pacific Ocean (WTPO) were predominantly attributed to El Niño-Southern Oscillation (ENSO). Results of the present study put forward important modulation effects by the Indian Ocean Dipole (IOD) mode. The observed sea level in the WTPO shows significant instantaneous and lagged correlations (around -0.60 and 0.40, respectively) with the IOD mode index (DMI). Composite of 14 'independent' IOD events for 1958-2017 shows negative sea level anomalies (SLAs) of 4~7 cm in the WTPO during positive IOD events and positive SLAs of 6~8 cm in the following year that are opposite in sign to the El Niño effect. The IOD impacts are reproduced by large-ensemble simulations of a climate model which generate respectively 430 and 519 positive and negative independent IOD events. A positive IOD induces westerly winds over the western and central tropical Pacific and causes negative SLAs through Ekman upwelling, and it facilitates the establishment of a La Niña condition in the following year that involves enhanced Pacific trade winds and causes positive SLAs in the WTPO. Ocean model experiments confirm that the IOD affects the WTPO sea level mainly through modulating the tropical Pacific winds. Variability of the Indonesian Throughflow (ITF) induced by IOD winds has relatively weak effect on the WTPO. The IOD's impacts on the major upper-ocean currents are also considerable, causing anomalies of 1~4 Sv in the South Equatorial Current (SEC) and North Equatorial Countercurrent (NECC) volume transports.

Keywords: Sea level, Indian Dipole mode, western tropical Pacific Ocean, El Niño-Southern Oscillation

©2020. Japan Geoscience Union. All Right Reserved.

Predictability study on the seasonal reduction of the upstream Kuroshio transport and related targeted observation application.

*Kun Zhang[1,2]

1. Institute of Oceanology, Chinese Academy of Sciences, 2. Center for Ocean Mega-Science, Chinese Academy of Sciences

With the Regional Ocean Modeling System (ROMS), we realistically simulated the upstream Kuroshio transport (UKT) variations, especially for the transport reduction in autumn. Then the effects of the optimal initial errors estimated by the conditional nonlinear optimal perturbation (CNOP) approach on predicting one seasonal UKT reduction event were investigated. The CNOP-type initial errors are located around (128°E, 17°N) horizontally and in the upper 1000 m vertically. The CNOP greatly affects the UKT by developing into a westward eddy-like structure. Eddy-energetic analysis indicates that the errors obtain energy from the background state through both barotropic and baroclinic instabilities and that the latter plays a more important role. Based on the spatial distribution of the CNOP, the sensitive area for improving the prediction of the UKT reduction event was subsequently identified. Within this sensitive area, we further explored the CNOP-based adaptive observation system design by considering the impacts of two factors: the number of observation sites and observation distance. Observing system simulation experiments (OSSEs) indicate that improving the initial conditions can effectively improve the UKT prediction. Compared to the random or conventional observation system, the CNOP-based observation system always exhibits better performance. Optimal CNOP-based observation networks are established using six or eight observation sites and observation distances of 140 or 165 km, which produce a mean prediction improvement of 43.1%. This preliminary work is expected to provide guidance on future observations in the upstream Kuroshio region and to help realistic UKT predictions.

Keywords: the Kuroshio, predictability, targeted observation, the CNOP appraoch

©2020. Japan Geoscience Union. All Right Reserved.

Remote and local processes controlling decadal sea-ice variability in the Weddell Sea

*Yushi Morioka[1], Swadhin Behera[1]

1. Japan Agency for Marine-Earth Science and Technology

Physical mechanisms underlying decadal sea-ice variability over the Weddell Sea are investigated using a state-of-the-art coupled general circulation model (CGCM). Observational analysis during the satellite period (1982-2018) shows that decadal increase in sea-ice concentration (SIC) over the Weddell Sea is preceded by easterly wind anomalies. A 300-yr simulation of the CGCM confirms the observed relationship and demonstrates that the easterly wind anomalies act to weaken upwelling of warm water from the subsurface ocean and the associated ocean mixing/diffusion, and lower the near-surface ocean temperature thereby inducing the SIC increase. The zonal wind variability exhibits a close link to atmospheric intrinsic variability in the mid-high latitudes, called the Southern Annular Mode. Another sensitivity experiment with 300-yr simulation, in which interannual sea-surface temperature (SST) variations are suppressed outside the South Atlantic and the Weddell Sea, reveals that anomalous cooling of near-surface ocean temperature is induced by anomalous northward outflow of warm water from the northern Weddell Sea linked with the zonal wind variability and anomalous westward inflow of cold water from the eastern Weddell Sea accompanied by strengthening of the Weddell Gyre. The strengthening of the Weddell Gyre is associated with an increase in ocean density, which is mostly due to an increase in salinity induced by enhanced surface evaporation during the transition period of low to high sea-ice. These results indicate that remote atmospheric forcing together with the local ice-ocean interaction is greatly important for generation of decadal sea-ice variability over the Weddell Sea.

Keywords: Decadal variability, Sea ice, Weddell Sea

©2020. Japan Geoscience Union. All Right Reserved.

Can tropical Pacific winds enhance the footprint of the Interdecadal Pacific Oscillation on the upper-ocean heat content in the South China Sea?

*Fuan Xiao[1], Dongxiao Wang[2]

1. Guangzhou Univ., 2. Sun Yat-sen Univ.

In this study, an enhanced footprint of the Interdecadal Pacific Oscillation (IPO) on the upper-ocean heat content (OHC) in the South China Sea (SCS) since the 1990s was revealed. The negative OHC-IPO correlation is significant (r = -0.71) during 1990-2010 (P2), while it is statistically insignificant during 1960-1980 (P1). Analyses show that the scope of the equatorial Pacific wind anomalies is wider during P2 compared with that during P1 due to a larger east-west SST gradient and enhanced tropical warming in the Indian Ocean. When the IPO is negative during P2, a wider scope of the wind stress anomalies associated with the IPO could lead to 1) the southward migration of the North Equatorial Current bifurcation latitude (NECBL) by affecting the wind stress curl over the key region where it is near the climatological NECBL; 2) the interbasin pressure gradient (Sea Surface Height difference) between the western Pacific and the SCS increase; these two processes strengthen the Kuroshio Current and weaken the Luzon Strait transport (LST) or SCS throughflow into the SCS; and 3) the width of equatorial Pacific wind anomalies are wide enough to directly weaken the LST in the SCS through the Island Rule. These three pathways finally change the oceanic gyre in the SCS and increase the OHC. Our results suggest that the scope of the tropical wind stress is the crucial factor when we consider the relationship between the upper ocean thermal conditions in the SCS and the Pacific variability.

Keywords: Interdecadal Pacific Oscillation, Ocean heat content, South China Sea, Scope of trade wind

©2020. Japan Geoscience Union. All Right Reserved.

The Atlantic SST influences on the Pacific subdecadal variability

*Takashi Mochizuki[1,2], Masahiro Watanabe[3], Masahide Kimoto[3]

1. Department of Earth and Planetary Sciences, Kyushu University, 2. Japan Agency for Marine-Earth Science and Technology, 3. Atmosphere and Ocean Research Institute, The University of Tokyo

By performing two sets of partial data assimilation experiments using global climate model, we have demonstrated that sea surface temperature (SST) anomalies in the tropical and subtropical Atlantic Ocean contribute to forming high ocean temperature anomalies of the tropical Pacific in the early-2000s. Low SST over the tropical Atlantic changes the Walker circulation and the associated weakening of the Pacific trade wind raises the equatorial SST on the subdecadal timescales. At the same time, high SST anomaly is generated also in the off-equatorial North Pacific through deepening of the upper ocean thermocline due to an accompanying anti-cyclonic surface wind anomaly aloft. While the subtropical north Atlantic SST may help the subdecadal SST rising in the equatorial Pacific, the resultant SST anomalies show 1-year delay in phase transition and are hardly accompanied by the ocean thermocline deepening.

©2020. Japan Geoscience Union. All Right Reserved.

An evaluation of the Decadal Climate Prediction Experiments by the BCC_CSM Model

*Yongjie Fang[1], Tongwen Wu[1], Xiaoge Xin[1]

1. National Climate Center, Chinese Meteorological Administration

Retrospective decadal hindcasts were undertaken using the Beijing Climate System Model (BCC_CSM) as part of Coupled Model Intercomparison Project 6. The hindcasts were anomaly initialized by nudging the oceanic temperature and salinity from the monthly Simple Ocean Data Assimilation (SODA). Each forecast consists of an 8-member ensemble integrated over a 10-year period. Ensemble forecasts were evaluated using observations, and compared to an ensemble of uninitialized simulations (NoINT) which are subject to identical twentieth century historical radiative forcings. The results show that the warming trend of global mean SST simulated by the Decadal forecast is closer to the observation than that in the NoINT runs. The Decadal forecasts show high SST prediction skills over broad regions of Atlantic, western tropical Pacific and tropical Indian Oceans. The initialization increases the skill in forecasting the Pacific Decadal Oscillation (PDO) index for almost a decade compared to the NoINT runs, while reduces the skill in predicting the Atlantic Multidecadal Oscillation (AMO) index. Some features of the ocean state estimates used for initialization and their impact on the forecasts are discussed.

Keywords: Decadal prediction, BCC_CSM model, Anomaly initialization

©2020. Japan Geoscience Union. All Right Reserved.

[E] Poster | A (Atmospheric and Hydrospheric Sciences)：A-OS Ocean Sciences & Ocean Environment

[A-OS19] Marine ecosystems and biogeochemical cycles: theory, observation and modeling

convener:Takafumi Hirata(Arctic Research Center, Hokkaido University), Shin-ichi Ito(Atmosphere and Ocean Research Institute, The University of Tokyo), Enrique N Curchitser(Rutgers University New Brunswick), Eileen E Hofmann(Old Dominion University)

The ocean accounts for about 50% of global net primary production. This production is significant for carbon cycling and ecosystem functioning, and is related directly or indirectly to a variety of climatic and ecological phenomena. The responses to natural and anthropogenic environmental stressors that influence marine production and diversity can cause perturbations to marine ecosystems that alter trophic dependencies and interactions among organisms at a range of space and time scales. Quantification of the principal mechanisms driving spatio-temporal variability of marine ecosystem remains to be done, especially in terms of evaluation of uncertainty in responses. As a result, evaluating vulnerability of marine ecosystems to environmental change requires systematic and holistic approaches that integrate physics to ecology and are based in observations and modelling. In addition, expectations to deliver these science to public society is raising. This session aims to provide a venue for not only discussing recent advances in understanding marine biogeochemical cycles, ecosystems and their interactions, but also networking with a variety of people to seed new ideas in marine ecological research. Observational, modeling and conceptual studies, including technological development and operational applications, that consider linkages among biogeochemical and ecosystem processes, biodiversity, and the effects of multiple stressors from molecular to planetary scales are encouraged.

[AOS19-P01] A modeling study of early diagenesis using an ocean sediment model

*Hidetaka Kobayashi[1], Akira Oka[1] (1.Atmosphere and Ocean Research Institute, The University of Tokyo)

[AOS19-P02] **A simulation on seasonal variation of bottom oxygen in the Bohai Sea**

*Haiyan Zhang[1], Hao Wei[1], Liang Zhao[2] (1.Tianjing University, 2.Tianjin University of Science & Technology)

[AOS19-P03] Particulate organic carbon fluxes of the upper ocean response to typhoons in the northern South China Sea

*CHUNG-YU CHIANG[1], Yun Hsuan Lu[1], Yung-Yen Shih[1] (1.R.O.C NAVAL ACADEMY Dept. of Applied Science)

[AOS19-P04] **Mid-latitude Winter Carbon Export Is Missed Using Prescribed BCG-Argo Sampling ProtocolsAbstract**

*Xiaogang Xing[1], Mark Wells[2], Shuangling Chen[1], Yunwei Yan[1], Fei Chai[1,2] (1.Second Institute of Oceanography, MNR, China, 2.University of Maine, US)

[AOS19-P05] **Effects on ocean biology induced by El Niño-accompanied positive freshwater flux anomalies in the tropical Pacific**

*Feng Tian[1,2,3,4], Rong-Hua Zhang[1,2,3,4], Xiujun Wang[5] (1.Institute of Oceanology, Chinese Academy of Sciences, 2.Pilot National Laboratory for Marine Science and Technology, Qingdao, 3.Center for Ocean Mega-Science, Chinese Academy of Sciences, 4.University of Chinese Academy of Sciences, Beijing , 5.College of Global Change and Earth System Science, Beijing Normal University, and Joint Center for Global Change Studies, Beijing)

[AOS19-P06] Spatial and temporal variability of biological carbon pump in the northern South China Sea

*Jia-Jang Hung[1], Zong-Ying Lin, Ching-Han Tung, Shao-Hung Peng, Yen-Hui Lin (1.Department of Oceanography, National Sun Yat Sen University, Kaohsiung, Taiwan)

[AOS19-P07] Seasonal and Inter-annual variability of chlorophyll-*a* in the Gulf of Thailand

*Dudsadee Leenawarat[1], Anukul Buranapratheprat[2], Joji Ishizaka[3] (1.Graduate School of Environmental Studies, Nagoya University, 2.Department of Aquatic Science, Faculty of Science, Burapha University, Thailand , 3.Institute for Space-Earth Environmental Research, Nagoya University, Japan)

[AOS19-P08] **Comparison of spatiotemporal variety between *in-situ* and remote surface chlorophyll in the northern South China Sea**

*Yun Hsuan Lu[1], Ko Mei Lin[1], Yung Yen Shin[1] (1.Department of Applied Science, R.O.C Naval Academy)

[AOS19-P09] Effects of the Kuroshio meander on phytoplankton in Japanese waters as observed by satellite remote sensing

Satoshi Kitaoka[2], *Takafumi Hirata[1], Keiko Sato[1] (1.Arctic Research Center, Hokkaido University, 2.Faculty of Environmental Earth Science)

[AOS19-P10] Declining catch of Japanese sandeels

*Shin-ichi Ito[1] (1.Atmosphere and Ocean Research Institute, The University of Tokyo)

[AOS19-P11] Comparative study on respiration of Japanese anchovy (*Engraulis japonicus*) around Japan

*Shin-ichi Ito[1], Chenying Guo[1], Megumi Enomoto[1], Tomoya Aono[1], Michio Yoneda[2], Michiya Matsuyama[3], Takashi Kitagawa[1], Motomitsu Takahashi[2] (1.Atmosphere and Ocean Research Institute, The University of Tokyo, 2.Fisheries Research and Education Agency Japan, 3.Kyushu University)

[AOS19-P12] Estimation of migratory routes of Japanese sardine in the Tsushima Warm Current area by combining the microscale stable isotopic analysis of otoliths and a data assimilation mode

*Tomoya Aono[1,2], Tatsuya Sakamoto[2,3], Tohya Yasuda[4,3], Motomitsu Takahashi[3], Toyoho Ishimura[1] (1.National Institute of Technology, Ibaraki College, 2.Atmosphere and Ocean Research Institute, The University of Tokyo, 3.Seikai Nat. Fish. Res. Inst., 4.Nat. Res. Inst. Fish. Sci.)

[AOS19-P13] The transition of the experienced environment of jack mackerel in the East China Sea

*Tomihiko Higuchi[1], Motomitsu Takahashi[2], Kotaro Shirai[1], Shin-ichi Ito[1] (1.Atmosphere and Ocean Research Institute, The University of Tokyo, 2.Seikai National Fisheries Research Institute, FRA)

[AOS19-P14] Discussion on future collaboration

*Shin-ichi Ito[1], Takafumi Hirata[2] (1.Atmosphere and Ocean Research Institute, The University of Tokyo, 2.Hokkaido University)

[AOS19-P15] **Interannual salinity variability in the Western Tropical Pacific and along the Kuroshio**

*Chevarria Saravia Ricardo[1], Daniel Andres Lizarbe[1], Takeyoshi Nagai[2] (1.National Agrarian University La Molina, 2.Tokyo University of Marine Science and Technology)

[AOS19-P16] Phytoplankton blooms along the Kuroshio due to the Large Meander

*Lizarbe Andres Daniel[1], Ricardo Saravia Chevarria[1], Takeyoshi Nagai[2], Takafumi Hirata[3] (1.National Agrarian University La Molina, 2.Tokyo University of Marine Science and Technology, 3.Hokkaido University)

A modeling study of early diagenesis using an ocean sediment model

*Hidetaka Kobayashi[1], Akira Oka[1]

1. Atmosphere and Ocean Research Institute, The University of Tokyo

In the ocean upper sediments, the concentration of dissolved materials in pore water changes due to the decomposition or dissolution of biogenic solid particles that have settled down the water column. Because the condition of ocean sediments affects the long-term global ocean biogeochemical cycle through the interaction of dissolved materials at the sediment-water interface, it is necessary to properly simulate the early diagenesis. It is confirmed that the sediment model, which is created based on the formulation presented in previous studies, reproduces the burial and the distribution of biogenic solid particles by giving boundary conditions based on observational data at the sediment-water interface (the sedimentation flux of solid particles and the concentration of dissolved materials) and appropriate parameter settings. We quantitatively evaluate the impacts of the sedimentation flux of biogenic solid particles reaching the seafloor, dust deposition, the coefficient of dissolution rate, and the concentration of dissolved materials above the seafloor on the distribution of solid particles.

Keywords: ocean sediment model, ocean biogeochemical cycle, early diagenesis

©2020. Japan Geoscience Union. All Right Reserved.

A simulation on seasonal variation of bottom oxygen in the Bohai Sea

*Haiyan Zhang[1], Hao Wei[1], Liang Zhao[2]

1. Tianjing University, 2. Tianjin University of Science & Technology

In recent forty years, bottom low dissolved oxygen (DO) conditions (< 3 mg/L) in summer have indicated an intensifying trend in the Bohai Sea (BS). Recent observations reveal that oxygen deficit is a seasonal phenomenon occurring in the bottom water in the depressions northwest and southwest of the Liaodong Bank. In addition, low DO conditions in the BS are accompanied by low pH, suggesting a close coupling between oxygen deficit and acidification, which imposes great stress on marine ecosystems and implies the need for effective management to improve eco-environments. To explore oxygen dynamics and low-oxygen formation mechanisms, a coupled physical-biological model (ROMS-CoSiNE) covering the BS and the Yellow Sea (YS) is established. The model reproduces seasonal evolution of low-oxygen conditions in the BS, and capture the two observed low DO centers, near Qinhuangdao (QHD) and the Yellow River estuary (YRE) respectively. DO becomes unsaturated in June, and reaches a minimum in August. Relatively strong remineralization but weak stratification result in relatively higher DO near YRE compared to QHD. Low DO off QHD could extend northeastward to the northern depression where the DO is relatively high due to weak remineralization. Oxygen budget is evaluated to quantify the contribution of physical and biological processes. Oxygen diffusion across the thermocline is prohibited which favors oxygen deficit in the bottom waters. Water column respiration (WR) is a major oxygen sink for simulated low DO conditions, while more observations are required to figure out the relative importance of WR and sediment oxygen consumption (SOC) and improve models.

Keywords: Oxygen deficit; , Low oxygen conditions; , Bohai Sea;

©2020. Japan Geoscience Union. All Right Reserved.

Particulate organic carbon fluxes of the upper ocean response to typhoons in the northern South China Sea

*CHUNG-YU CHIANG[1], Yun Hsuan Lu[1], Yung-Yen Shih[1]

1. R.O.C NAVAL ACADEMY Dept. of Applied Science

Remote sensing of chlorophyll *a* (Chl) has revealed evidence of phytoplankton blooms evoked by typhoons in the tropical and subtropical ocean but it is difficult to assess if the particulate organic carbon (POC) fixed by marine phytoplankton can be downward exported into deep waters. Recent sea-going observations have shown increment in primary production, Chl and POC flux associated with the post-typhoons over the shallow waters (< 200 m) of the continental shelf. However, it is still unclear whether typhoons, which originate beyond the continental margin, can transfer the newly fixed carbon to deeper waters. Here we report POC fluxes and other biogeochemical data in the northern South China Sea (NSCS) before and shortly after the passage of typhoons, between September 2012 and June 2014. POC fluxes after the passage of typhoons *Tembin* and *Soulik* were 78 ±12 and 115 ±16 mg-C m^{-2} d^{-1} (average ±1 standard deviation), i.e. 1.6 and 2.4 times higher than those obtained before the typhoon (42~73 mg-C m^{-2} d^{-1}). In addition, variations in both surface and depth-integrated Chl were decoupled from POC fluxes. This decoupling may be resulted from a change in the plankton community composition due to water column instability or to lateral inputs of particulate matter released from shelf or slope sediments. Overall, our analysis of this two-year dataset highlights the spatial and temporal variability of the factors controlling POC exports to the deep NSCS.

Keywords: typhoon, carbon flux, northern South China Sea

©2020. Japan Geoscience Union. All Right Reserved.

Mid-latitude Winter Carbon Export Is Missed Using Prescribed BCG-Argo Sampling ProtocolsAbstract

*Xiaogang Xing[1], Mark Wells[2], Shuangling Chen[1], Yunwei Yan[1], Fei Chai[1,2]

1. Second Institute of Oceanography, MNR, China, 2. University of Maine, US

The mixed-layer pump (MLP) significantly augments the global carbon transport from the surface mixed layer to deeper waters when ephemeral springtime surface blooms are repeatedly mixed to depth by storms. Exploiting an unusual 8-month BGC-Argo dataset of daily profiles in the mid-latitude (31° N) northwestern Pacific, here we show repetitive mid-winter MLP episodes that generated a seasonally-averaged particulate organic carbon (POC) export of ~130 mg C m^{-2} day^{-1}; roughly 25% of the export from the North Atlantic spring bloom. But subsampling this dataset on a 5 or 10-day cycle, as planned in the BGC-Argo program, generated an order of magnitude less export (5-day & 10-day), or even totally missed all MLP events (10-day). These findings demonstrate that more frequent profiling data are needed in at least mid-latitude regions, but such daily cycling would shorten float lifetimes and thereby threaten BGC-Argo program sustainability. We propose that a small number of targeted floats be tasked with daily profiling, and that machine learning strategies be used to link these data with satellite-derived physical and biological parameters to estimate POC export; an approach that did show promise here with our limited dataset. The unexpected large magnitude of the mid-winter POC export suggests that this or other new strategies are essential if the BGC-Argo program is to adequately estimate global carbon export from MLP processes.

Keywords: Ocean carbon cycle, BGC-Argo, Mixed-layer pump, POC, Chlorophyll-a, Carbon export

©2020. Japan Geoscience Union. All Right Reserved.

Effects on ocean biology induced by El Niño-accompanied positive freshwater flux anomalies in the tropical Pacific

*Feng Tian[1,2,3,4], Rong-Hua Zhang[1,2,3,4], Xiujun Wang[5]

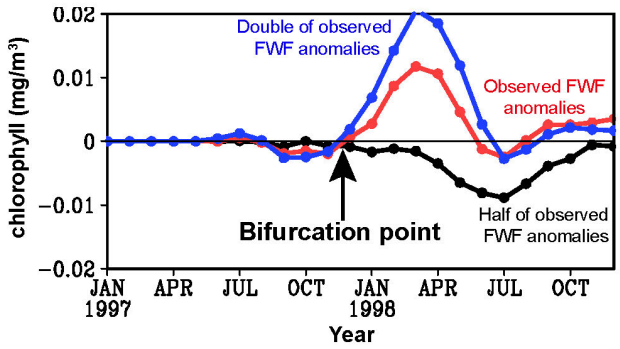
1. Institute of Oceanology, Chinese Academy of Sciences, 2. Pilot National Laboratory for Marine Science and Technology, Qingdao, 3. Center for Ocean Mega-Science, Chinese Academy of Sciences, 4. University of Chinese Academy of Sciences, Beijing , 5. College of Global Change and Earth System Science, Beijing Normal University, and Joint Center for Global Change Studies, Beijing

The El Niño and Southern Oscillation (ENSO) can induce large perturbations in freshwater flux (FWF, defined as precipitation minus evaporation) and ocean ecosystem in the tropical Pacific. However, how El Niño-induced FWF can affect the tropical Pacific ecosystem (e.g., chlorophyll) is still unknown. Here, a series of ocean-only experiments are performed using a coupled ocean-physical biogeochemistry model forced by prescribed climatological wind stress. Interannual FWF anomalies observed during the 1997-1998 El Niño event are imposed onto the ocean model and the related positive FWF anomalies are specified to be varying in the tropical Pacific, and the corresponding sensitivity experiments are performed to examine the ocean ecosystem response. In general, chlorophyll increases with the intensities of the El Niño-induced positive FWF anomalies at a certain strength, but decreases when the positive FWF forcing is under-represented (e.g., specified to be its half intensity). Additionally, chlorophyll in the eastern tropical Pacific keeps almost steady during the increasing stage of the El Niño-induced interannual FWF forcing, and then rapidly increases after the peak stage of the FWF forcing. The phytoplankton budget and diagnostic analyses are conducted to understand the behavior of chlorophyll in response to varying intensities of FWF forcing. Chlorophyll response to varying intensities of FWF forcing depends on the iron concentration in the mixed layer, suggesting that the ocean ecosystem response may be shifted from one regime to another when FWF forcing reaches a certain intensity. These results offer insights into biophysical interactions and chlorophyll-induced feedback effects on ENSO.

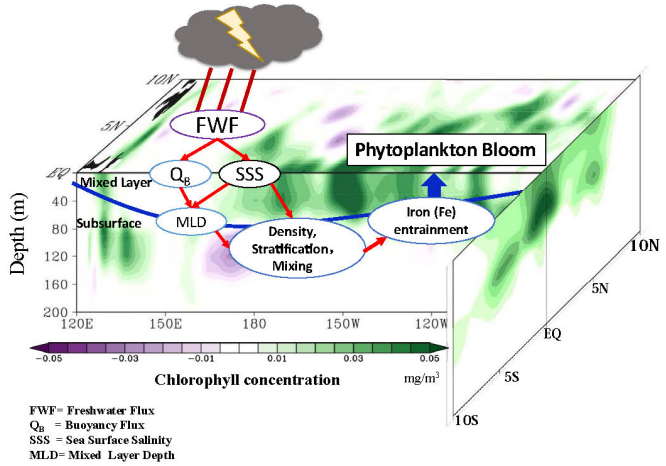
Keywords: El Niño, freshwater flux, ocean biology, chlorophyll, threshold, response

©2020. Japan Geoscience Union. All Right Reserved.

(a) Chlorophyll response to varying freshwater flux forcing



(b) Processes involved in chlorophyll response to FWF anomalies



©2020. Japan Geoscience Union. All Right Reserved.

Spatial and temporal variability of biological carbon pump in the northern South China Sea

*Jia-Jang Hung[1], Zong-Ying Lin, Ching-Han Tung, Shao-Hung Peng, Yen-Hui Lin

1. Department of Oceanography, National Sun Yat Sen University, Kaohsiung, Taiwan

The marine biological carbon pump (BCP) consists mainly of active and passive fluxes, which transfers organic carbon produced in the euphotic zone to the deep ocean, may be critical in controlling the air-sea flux of atmospheric CO_2. Here we report the spatial and temporal variability of BCP in the northern South China Sea (NSCS) through a moderately long period of investigation including an observation in the time-series station (SEATS). The spatial variability of BCP was large in the NSCS, ranging from 25.6 mg C m^{-2} d^{-1} to 93.4 mg C m^{-2} d^{-1} for active fluxes and from 66.8 mg C m^{-2} d^{-1} to 155 mg C m^{-2} d^{-1} for passive fluxes. Vertical diffusion flux of DOC was very small compared to both active and passive fluxes. The magnitude of flux was generally lower in the central basin with a calm weather condition and higher in the Dongsha shelf influenced by the shoaling processes of internal waves. Both active and passive fluxes were apparently determined by the inventories of nutrients and chlorophyll *a* in the euphotic zone. In terms of temporal variability of BCP in the SEATS Station, the difference of BCP magnitude was significant between summer and winter seasons but less in inter-annual variability. The internal forcing and climatic conditions are likely critical factors in driving the spatial and temporal variability of BCP in the NSCS.

Keywords: Biological carbon pump, Spatial and temporal variability, Northern South China Sea

©2020. Japan Geoscience Union. All Right Reserved.

Seasonal and Inter-annual variability of chlorophyll-*a* in the Gulf of Thailand

*Dudsadee Leenawarat[1], Anukul Buranapratheprat[2], Joji Ishizaka[3]

1. Graduate School of Environmental Studies, Nagoya University, 2. Department of Aquatic Science, Faculty of Science, Burapha University, Thailand , 3. Institute for Space-Earth Environmental Research, Nagoya University, Japan

The Gulf of Thailand (GoT) is a semi-enclosed shallow sea located in the southwest of the South China Sea. This area is important for fisheries and aquacultures for many countries. The seasonal variations of the GoT aredetermined by monsoon systems, while the large inter-annual variability GoT is affected by El Niño Southern Oscillation (ENSO). The ecosystems and abundance of fishery resources may be altered due to ENSO from the results of dry and wet weather during El Niño and La Niña, respectively. However, there are little information to assess how lower-trophic level ecosystem responds to ENSO. In this study, monthly satellite ocean color data from July 2002 to December 2018 was analyzed to compare with sea surface temperature, wind magnitude and direction, and river discharge data to understand the variability. The results showed that chl-a was positively and negatively correlate with wind magnitude and SST, respectively, in the GoT. However, chl-a near coastal area, including the upper GoT, responded to the increase of river discharge. To investigate the interannual variations, the Empirical Orthogonal Function (EOF) analysis have performed to evaluate the spatial and temporal variations of chl-a in the GoT.

Keywords: Gulf of Thailand, Chlorophyll-a, Variability

©2020. Japan Geoscience Union. All Right Reserved.

Comparison of spatiotemporal variety between *in-situ* and remote surface chlorophyll in the northern South China Sea

*Yun Hsuan Lu[1], Ko Mei Lin[1], Yung Yen Shin[1]

1. Department of Applied Science, R.O.C Naval Academy

The chlorophyll *a* (Chl) plays an important role as an indicator to assess phytoplankton biomass in the ocean. Many studies determine the amount of biomass and the level of primary production based on Chl concentrations. However, the difference between *in-situ* and remote Chl values may be influenced by specific factors of time and space. There will be cause an ambiguity in depicting of the marine biogeochemical cycle, if only a remote Chl is used to explore the marine biogeochemistry. Therefore, we conducted 10 cruise from February 2013 to November 2019 at the northern South China Sea (NSCS), collected and analyzed wide covers of surface Chl to assess diversities of *in-situ* and remote Chl. The measured/remote values of Chl in spring, summer, autumn and winter were 0.12±0.09/0.18±0.01, 0.22±0.02/0.14±0.24, 0.12±0.01/0.11±0.02 and 0.28±0.23/0.38±0.32 mg m^{-3}. The measured surface Chl in summer and winter are higher than the seasons of spring and autumn; the remote Chl is higher in spring and winter than in the seasons of summer and autumn. We can infer that the prevalence of the northeast monsoon and extreme weather events (e.g. typhoons, internal waves) may be main reasons to cause the elevated Chl in winter and summer, respectively. It implies that the satellite data cannot fully reflect the real natures. The measured/remote values in the shelf, slope and basin were 0.26±0.18/0.22±0.08, 0.23±0.15/0.20±0.06 and 0.18±0.09/0.18±0.05 mg m^{-3}. Although, the trend of Chl derived from field-measured and remote-sensed are quite similar, the difference of Chl from *in-situ* and remote in the region of shelf is more apparent than in other areas. It may result from the influence of topography. Our preliminary research shows that the spatiotemporal variety between *in-situ* and remote surface Chl is quite significant and the further utilization of remote Chl needs to be calibrated in the NSCS.

Keywords: chlorophyll, satellite, northern South China Sea

©2020. Japan Geoscience Union. All Right Reserved.

Effects of the Kuroshio meander on phytoplankton in Japanese waters as observed by satellite remote sensing

Satoshi Kitaoka[2], *Takafumi Hirata[1], Keiko Sato[1]

1. Arctic Research Center, Hokkaido University, 2. Faculty of Environmental Earth Science

The Kuroshio current is one of the western boundary currents and known as a thermal energy transporter from low latitudes to to mid-latitudes in the Western Pacific. On the other hand, the Kuroshio is also a unique western boundary current in that it causes a large meander. Indeed, the meander has occurred in 2017 and is still continuing (at the time of writing). In ecological perspective, the Kuroshio is characterized as a carrier of oligotrophic seawater. In spite of the oligotrophy, the Kuroshio water is known for spawning and feeding grounds of commercial/non-commercial fish larvae, explaining a higher fisheries production in the region. Thus, it currently puzzles an ecological representation of the Kuroshio water in that a relationship among nutrient fields, standing stock and productivity of organisms are not well understood. In order to better understand the Kuroshio ecosystems, phytoplankton dynamics, a lower-trophic organism, is investigated using remote sensing data of phytoplankton chlorophyll-a pigment and of phytoplankton community structure inferred from the pigment. Especially time series analysis was conducted to identify temporal scales of their variability from daily scale to decadal scale, thanks to the high-frequency observation by the Advanced Himawari Imager, AHI, and to the long-term observation by the Moderate Resolution Imaging Spectroradiometer, MODIS. In this presentation, we discuss how the temporal variability of different phytoplankton groups (as well as the total phytoplankton community) in the Kuroshio and adjacent waters are affected by the large meander of the Kuroshio occurring since 2017.

Keywords: Kuroshio, phytoplankton, meander, remote sensing

©2020. Japan Geoscience Union. All Right Reserved.

Declining catch of Japanese sandeels

*Shin-ichi Ito[1]

1. Atmosphere and Ocean Research Institute, The University of Tokyo

Sandeels are important fisheries target species in Japan. In addition, sandeels are important forage species for many piscivorous predators and key species in the coastal marine food web. Sandeels habitat on/in gravelly sand sediments and therefore their distribution shift is limited by the distribution of sandy sea floor. That unique characteristic might make sandeels vulnerable to climate variability and climate change. Recently, the catch of sandeels in Japan has decreased. To detect the geographical characteristics of sandeel catch decline, prefectural catch data from Statistics of Agriculture, Forestry and Fisheries was analyzed. Sandeel catches in 38 ocean-facing prefectures from 1956 to 2015 were used. The catch data was firstly log plus one transformed and then anomaly normalized by standard deviation was calculated in each prefecture to avoid the influence of fishery effort differences between prefectures. Since Kochi prefecture has no catch during the analyzed period, we applied principal component analysis to the normalized anomaly data of 37 prefectures. The contribution of the first principal component (PC1) was 28.6% and its score showed a decreasing trend since 1975. The contribution of the second principal component (PC2) was 12.2% and its score showed an increasing trend during 1956-1980 and a decreasing trend during 1995-2015. There are 12 prefectures (e.g. Okayama) which showed positive sing for PC1 and negative sing for PC2, hence sandeel catch drastically declined after 1975. There are 10 prefectures (e.g. Hyogo) which showed positive sings both for PC1 and PC2, hence sandeel catch gradually declined after 1975. Recently, it was reported three species of *Ammodytes* (*A. japonicus, A. heian and A. hexapterus*) distributed around Japan. It was impossible to divide the three species in the historical fisheries catch data, however it is an urgent task to elucidate life histories and distributions of each *Ammodytes* species to develop sustainable management of sandeels in Japan.

Keywords: sandeel, global climate change, fishery catch

©2020. Japan Geoscience Union. All Right Reserved.

Comparative study on respiration of Japanese anchovy (*Engraulis japonicus*) around Japan

*Shin-ichi Ito[1], Chenying Guo[1], Megumi Enomoto[1], Tomoya Aono[1], Michio Yoneda[2], Michiya Matsuyama[3], Takashi Kitagawa[1], Motomitsu Takahashi[2]

1. Atmosphere and Ocean Research Institute, The University of Tokyo, 2. Fisheries Research and Education Agency Japan, 3. Kyushu University

Japanese anchovy (*Engraulis japonicus*) is an important species not only as an exploited species but also as prey for variety of predators including marine mammals, tunas, mackerels, flounders, etc. However, the biomass of Japanese anchovy has shown large fluctuation and is one of the main actors of the fish species alternation responding to basin scale climate variabilities. From the stock management views, three sub-populations are defined in Japan: Pacific stock, Tsushima stock (also called the East China Sea stock), and Seto-inland Sea stock. The three sub-population shows difference in weights-at-age and longevity. While the three sub-populations of anchovy share their spawning grounds, the migration route and nursery grounds are divided. In addition, while Seto-inland Sea sub-populations do not show a large migration, Pacific and Tsushima sub-populations make long distance ontogenetic migrations.

All anchovy sub-populations are plankton feeders and mainly conduct filter feeding. Therefore, we hypothesized that different respiration characteristics induce different behaviors and hence growth and migration routes between the anchovy sub-populations. To test the hypothesis, we conducted laboratory respiration experiments using a 5L swimming tunnel. Since anchovy is sensitive and difficult to stabilize by individual, two anchovies were putted in the sealed tank and were measured oxygen consumption rate with various temperatures and velocities. Based on the experiment data, oxygen consumption rate dependencies on temperature, swimming speed, and body weight were determined. In addition, basic oxygen consumption rate at 0 degC temperature without swimming was estimated. Those derived oxygen consumption characteristics were different between the Pacific-stock and Seto-inland Sea stock, while the parameters of the Pacific-stock were similar to Peruvian anchoveta (*Engraulis ringens*) and South African anchovy (*Engraulis capensis*).

Keywords: respiration, migration, Japanese anchovy

©2020. Japan Geoscience Union. All Right Reserved.

Estimation of migratory routes of Japanese sardine in the Tsushima Warm Current area by combining the microscale stable isotopic analysis of otoliths and a data assimilation mode

*Tomoya Aono[1,2], Tatsuya Sakamoto[2,3], Tohya Yasuda[4,3], Motomitsu Takahashi[3], Toyoho Ishimura[1]

1. National Institute of Technology, Ibaraki College, 2. Atmosphere and Ocean Research Institute, The University of Tokyo, 3. Seikai Nat. Fish. Res. Inst., 4. Nat. Res. Inst. Fish. Sci.

Japanese sardine (*Sardinops melanostictus*) has been reported its abundance periodically fluctuates during last 3000 years (Kuwae *et al.*, 2017). More recently the catch of Japanese sardine declined to about 1/150 in 20 years (Fisheries Agency, 2011), but the mechanism of this phenomenon is still undetermined. In order to understand the mechanism of those fluctuations and hence enable future sustainable fishery, it is necessary to elucidate basic ecological information of sardine, such as their spawning place and migration pathway. In that situation, recent progress of analytical technique has allowed us utilize chemical compositions in fish otolith, which is formed in inner ear, to detect the life history of individual fishes. Otolith is a hard tissue composed of calcium carbonate ($CaCO_3$: aragonite), the concentric growth rings are formed from the center of otolith. The stable oxygen isotope ratio ($\delta^{18}O$) of $CaCO_3$ depend on (1) $\delta^{18}O$ of sea water and (2) ambient water temperature. Accordingly, the history of ambient water temperature through the life history of individual fish can be estimated by $\delta^{18}O$ record in the otoliths. Besides, by combining the otoliths $\delta^{18}O$ analysis and an individual-based model, recent study successfully clarified the migration pathway of Japanese sardine in the western North Pacific (Sakamoto *et al.*, 2019).

The purpose of this study is (1) to estimate the migration pathway of Japanese sardine in the Tsushima Warm Current area by combining methods of the high-resolution $\delta^{18}O$ analysis and the data assimilation model, and (2) to extract the biological information of Japanese sardine in the Tsushima Warm Current area.

In this study, we collected the otoliths of Japanese sardine caught in three sampling areas in the Sea of Japan: off Toyama (25/Aug./2016), Tsushima Strait (5/Sep./2016) and off Goto Islands (13/Sep./2016), and analyzed the otoliths in three individuals from each sampling area. The otoliths were continuously milled along the growth ring at every 10days (except near the core) by high-precision micro-milling system (GEOMILL326). After the milling, the stable carbon and oxygen isotopic compositions of otoliths powder were determined by microvolume isotope ratio mass spectrometry system (MICAL3c with IsoPrime100), then the migration pathway of each individuals were estimated based on high-resolution $\delta^{18}O$ analysis of otoliths and the data assimilation model.

As a result, there was no significant difference in the otolith $\delta^{18}O$ histories between the three individuals collected in each sampling area, and also we found similar trend in isotopic shift (experienced temperature) among sampling areas. The estimated location at the time of the hatching and sampling corresponded to the actual observed spawning grounds and the actual sampling area, respectively, which confirmed the consistency of the estimated migration pathways. In addition, it was suggested that all individuals grew in the same place (offshore west of Kyushu) after hatching and migrated to their caught area by different migration pattern from late June to early July. Our experimental study has successfully

©2020. Japan Geoscience Union. All Right Reserved.

drawn the variations of migration pathways of Japanese sardine in the Tsushima Warm Current area.

Keywords: otolith, stable oxgen isotope, sardine

©2020. Japan Geoscience Union. All Right Reserved.

The transition of the experienced environment of jack mackerel in the East China Sea

*Tomihiko Higuchi[1], Motomitsu Takahashi[2], Kotaro Shirai[1], Shin-ichi Ito[1]

1. Atmosphere and Ocean Research Institute, The University of Tokyo, 2. Seikai National Fisheries Research Institute, FRA

Jack mackerel *Trachurus japonicus* is distributed on the continental shelf waters along the subtropical Kuroshio Current and the Tsushima Warm Current in the western North Pacific. The East China Sea (ECS) is one of major spawning and nursery grounds for jack mackerel and understanding the recruitment processes of jack mackerel into the fishing grounds in the ECS is important. However, information of how jack mackerel respond to decadal temperature change is limited. Aim of this study is to know the transition of experienced environment of jack mackerel in the ECS from 1960s to 2000s. To estimate the experienced environment, oxygen ($\delta^{18}O$) and carbon ($\delta^{13}C$) stable isotope of jack mackerel otolith were analyzed. Fish samples were taken at ECS in 1960-70s and 2000-2010s (15 individuals, each period). The high-precision micromilling system GEOMILL 326 was used for otolith samples. At every 10 daily rings (20-30 daily rings in section including core), a ring was tracked and used as the boundary of the micromilling area. $\delta^{18}O$ and $\delta^{13}C$ were determined using isotope ratio mass spectrometer (Delta V plus). As a result, there was no significant differences between the two survey periods in the larval-juvenile experienced temperature which is estimated from $\delta^{18}O$. It was considered that both jack mackerel from different periods utilized a similar environment under a changing environment. There was a significant positive relationship between experienced temperature and growth rates based on otolith increment width in the juvenile stage. This suggested that the effect of water temperature on the growth of jack mackerel in early life stage. Thus, there is a possibility that jack mackerel in ECS may adapt environmental changes and select the preferred environment.

Keywords: jack mackerel, oxygen isotope, otolith

©2020. Japan Geoscience Union. All Right Reserved.

Discussion on future collaboration

*Shin-ichi Ito[1], Takafumi Hirata[2]

1. Atmosphere and Ocean Research Institute, The University of Tokyo, 2. Hokkaido University

Discuss on future collaboration potential relating to marine ecosystems and biogeochemical cycles.

Keywords: marine ecosystems, biogeochemical cycles, future collaboration potential

©2020. Japan Geoscience Union. All Right Reserved.

Interannual salinity variability in the Western Tropical Pacific and along the Kuroshio

*Chevarria Saravia Ricardo[1], Daniel Andres Lizarbe[1], Takeyoshi Nagai[2]

1. National Agrarian University La Molina, 2. Tokyo University of Marine Science and Technology

A previous study using hydrographic data in the North Pacific shows an interannual variability of salinity, including a basin wide freshening during the period from 2009 through 2017. However, how the basin wide freshening occurs and its influences along the Kuroshio have been still unclear. In this study, daily reanalysis salinity dataset from 2003 through 2018 are analyzed using temporal filters to separate the interannual variability and decadal changes with special emphasize on the salinity anomaly from the western tropical North Pacific (WTNP) to the downstream. The decadal variabilities are obtained by 6-year moving average of the daily data. The interannual variabilities is then obtained by subtracting this averaged decadal data from the daily salinity. Our analysis using maps of lagged correlation coefficients for the interannual variations of salinity along the density surface between σ_θ=25-26 shows relatively high correlation coefficients between WTNP , i.e., the Kuroshio origin and the downstream along the Kuroshio. The advection of the salinity anomaly from the WTNP to the coast of Japan along the Kuroshio takes approximately 3 months. It is found that the variations of the wind stress curl over the WTNP drive the interannual salinity variability with a negative correlation.

©2020. Japan Geoscience Union. All Right Reserved.

Phytoplankton blooms along the Kuroshio due to the Large Meander

*Lizarbe Andres Daniel[1], Ricardo Saravia Chevarria[1], Takeyoshi Nagai[2], Takafumi Hirata[3]

1. National Agrarian University La Molina, 2. Tokyo University of Marine Science and Technology, 3. Hokkaido University

The Kuroshio Large Meander (LM) is known to be highly aperiodic and can last from 1 to 10 years. The stationary cold core formed between the Kuroshio and the southern coast of Japan off Enshunada and approaching warm saltier water on the eastern side of the LM changes the local environment drastically, many commercially valuable fish species distribute differently from the no-LM period, impacting local fisheries. Despite this importance of the LM, the influences of the LM for low trophic levels such as phytoplankton and zooplankton have been still unclear. In this study, satellite daily sea surface chlorophyll data are analyzed in relation to the LM. The results show blooming (positive anomaly of the chlorophyll a concentration) along the Kuroshio path during LM periods, 2004-2005 and 2017-2019, from upstream (Shikoku) to downstream (140ºE). These blooms are started by the triggering meander in both LM periods. Even though the blooming pattern along the Kuroshio region in both LM periods was different, similar positive anomaly patterns emerge inside the meander' s trough, suggesting that submesoscale eddy' s restratification of MLD helps the primary production with upwelled nutrients along the Kuroshio. It turns out that there was no relation between the MLD and the wind stress over the large meander regions. Furthermore, we found a strong relationship between the minimum distance of the Kuroshio axis on a designated station located in Cape Shiono Misaki (St-A) and mean chlorophyll-a anomaly, indicating that every time Kuroshio axis detaches from the shore, mean chlorophyll-a anomaly rises. Also, this tendency seems depending on the Kuroshio recirculation strength off Shikoku.

©2020. Japan Geoscience Union. All Right Reserved.

[E] Poster | A (Atmospheric and Hydrospheric Sciences)：A-OS Ocean Sciences & Ocean Environment

[A-OS20] Coastal physical processes associated with mixing, eddies, and internal waves

convener:Taira Nagai(Graduate School of Science, The University of Tokyo), Eisuke Tsutsumi(Atmosphere and Ocean Research Institute, The University of Tokyo), Eiji Masunaga(Ibaraki University)

Recently developed observational and numerical approaches have revealed details of physical processes in coastal regions, which can affect large-scale oceanic/atmospheric circulations and ecosystems. This session aims to provide a platform to discuss mixing, eddies, and internal waves in coastal/marginal oceans including estuaries and lakes. This session also covers topics that consider linkages between coastal phenomena and large scale processes in the open ocean (e.g., the Kuroshio Current).

[AOS20-P01] Water exchange between the Bohai and Yellow Seas in response to high winds in winter

*Chao Ma[1,3], Xia Ju[2,3], Xiuquan Wan[1,3] (1.Ocean Univ. China, 2.Inst. Oceanog. 1, MNR, 3.Pilot Natl. Lab. Marine Sci. & Technol.)

[AOS20-P02] Eddy Induced Transport of Saline Kuroshio Water Into the Northern South China Sea

*Tao Xing[1,2], Yikai Yang[2] (1.MLR Key Laboratory of Marine Mineral Resources, Guangzhou Marine Geological Survey, 2.South China Sea Institute of Oceanology, Chinese Academy of Sciences)

[AOS20-P03] A temperature description of vortex street around the Green Island off the eastern coast of Taiwan

*Chia-Ying Ho[1], Hung-Jen Lee[1] (1.National Taiwan Ocean University)

[AOS20-P04] Summertime Upwelling in the Central South China Sea: Interannual Variability and Associated Dynamics

*Yi-Chia Hsin[1], Mai-Han Ngo[1] (1.Academia Sinica)

Water exchange between the Bohai and Yellow Seas in response to high winds in winter

*Chao Ma[1,3], Xia Ju[2,3], Xiuquan Wan[1,3]

1. Ocean Univ. China, 2. Inst. Oceanog. 1, MNR, 3. Pilot Natl. Lab. Marine Sci. & Technol.

Based on the observed data as well as Regional Ocean Modeling Systems (ROMS) diagnostic numerical model, we studied the influence of high wind processes on the circulation and water exchange between the Bohai and Yellow Seas (BYS) in winter. The results show that the vertical structure of the Yellow Sea Warm Current (YSWC) is relatively uniform under condition of high winds, showing obvious barotropic features. However, this flow is not a stable mean flow, showing strong paroxysmal and reciprocating characteristics. A comparison of the changes in sea level suggests that the intensity of the northwards upwind flow is consistent with the abnormal fluctuations in the sea level. It indicates that the upwind flow is closely related to the water exchange between the BYS. The impact of high wind processes on the water exchange between the BYS is enormous. It can make the flux through the Bohai Strait, as well as that through the mouth of each constituent bay (i.e., Liaodong Bay, Bohai Bay, and Laizhou Bay) far greater than usual, resulting in a significant increase in the water exchange rate. The exchange capacity, which is about 8% of the total volume of the Bohai Sea, can be completed in a few days. Therefore, the water exchange of the Bohai Sea may be completed by only a few occasional high wind processes in winter.

©2020. Japan Geoscience Union. All Right Reserved.

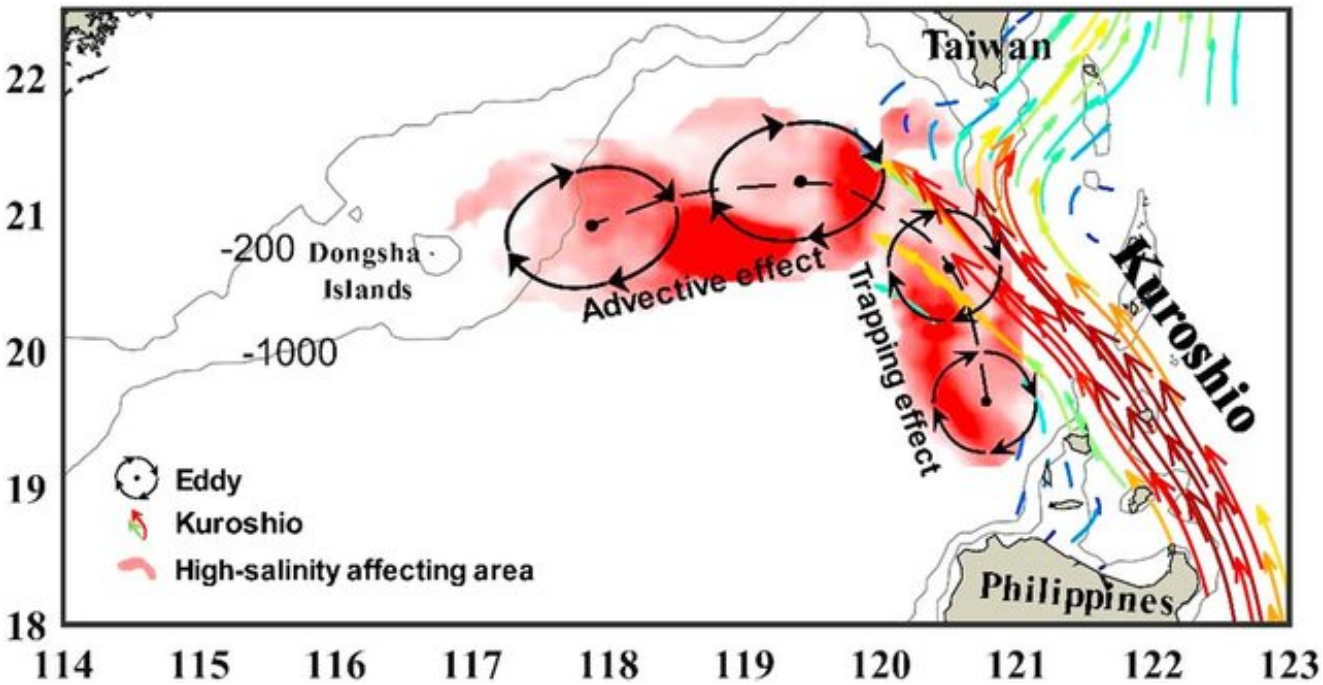
Eddy Induced Transport of Saline Kuroshio Water Into the Northern South China Sea

*Tao Xing[1,2], Yikai Yang[2]

1. MLR Key Laboratory of Marine Mineral Resources, Guangzhou Marine Geological Survey, 2. South China Sea Institute of Oceanology, Chinese Academy of Sciences

To better understand eddy induced heat and salt transport, a targeted joint hydrographic investigation focusing on an anticyclonic eddy was carried out in July 2017 in the northern South China Sea. In situ and satellite observations together with Hybrid Coordinate Ocean Model output show the transport of subsurface saline Kuroshio water into the northern South China Sea by an anticyclonic eddy. Subsurface high salinity cores are consistent with the anticyclonic eddy centers. The transport of saline Kuroshio water occurs in two stages accompanied by eddy shedding. First, saline Kuroshio water is trapped within the anticyclonic eddy at its generation location. Then, although the salinity within the eddy gradually weakens as the eddy carries the saline water westward, the quantity of saline water shows a sharp increase, dominated by eddy induced salinity advection. A diagnosis of the salinity budget further confirms that the contribution of eddy flow advection is greater than that of mean flow advection. The saline Kuroshio water is trapped and conveyed in this anticyclonic eddy, providing vital evidence and important implications for eddy induced salt transport and water exchange.

Keywords: mesoscale eddy, Kuroshio, Northern South China Sea, salt transport



©2020. Japan Geoscience Union. All Right Reserved.

A temperature description of vortex street around the Green Island off the eastern coast of Taiwan

*Chia-Ying Ho[1], Hung-Jen Lee[1]

1. National Taiwan Ocean University

For providing essential information for Kuroshio current passing Green Island off the eastern coast of Taiwan, a three-dimensional general circulation model (MITgcm) is used to study the vortex street issue. Real topography derived from the Ministry of Science and Technology Ocean Data Bank and some Hycom hydrographic data are imposed for the model. In the light of different conditions, such as changing the magnitude of the Kuroshio fluxes in summer and winter, two interesting features are worth noting. The model results show that the mixing-layer effects on the vortex streets are more closely associated with the strength of the vortex street upwelling. In the summer case, a low-temperature water mass is usually generated behind the Green-Island when the Kuroshio Current impacts on it. The temperature drop degree resulted from the upwelling water in the wake is over 1°C, which is similar to the von Kármán vortex street. However, the temperature drop degree is moderate when the initial temperature of the model is changed to the winter conditions. While the model boundary fluxes are increased, the temperature drop region is expanded. On the other hand, the low-temperature region is narrowed when the boundary fluxes are reduced.

Keywords: Green-Island, Kuroshio, vortex

©2020. Japan Geoscience Union. All Right Reserved.

Summertime Upwelling in the Central South China Sea: Interannual Variability and Associated Dynamics

*Yi-Chia Hsin[1], Mai-Han Ngo[1]

1. Academia Sinica

Based on the 30-year sea surface temperature images, we classify the locations of Vietnamese upwelling centers into three sub-regions: the Northern Coastal Upwelling region (*NCU*; north of 12.5˚N), the Southern Coastal Upwelling region (*SCU*; south of 12.5˚N), and the Offshore Upwelling region (*OU*; east of 110˚E). Variations of upwelling intensities in the three sub-regions are further quantified via the SST-based upwelling index, and possible processes relevant to wind field (including wind stress and its curl) and currents off southern Vietnam are, respectviely, proposed. The outcomes show that as the summer monsoon enhance, the alongshore wind stress strengthens offshore Ekman transport along the coast in the *SCU*, intensifying the coastal upwelling there. At the same time, the enhanced wind stress curl (WSC) dipole off the southern Vietnam strengthens the underlying oceanic gyre dipole, further leading to an intensification of the eastward-flowing jet in-between and southward-movement of the jet. As a result, the scaled up cyclonic gyre north of the jet helps the upwelling occurring in the *OU* region. Besides, accompanying the cyclonic gyre north of the jet, a southward counter-current develops along the eastern Vietnamese coast; further, it restricts upwelling in the *NCU* region but intensifies upwelling in the *SCU* region.

©2020. Japan Geoscience Union. All Right Reserved.

[E] Poster | A (Atmospheric and Hydrospheric Sciences)：A-OS Ocean Sciences & Ocean Environment

[A-OS21] Dynamics of oceanic and atmospheric waves, vortices, and circulations

convener:Yuki Tanaka(Fukui Prefectural University), Ryo Furue(APL/JAMSTEC), Yukiharu Hisaki(University of the Ryukyus), Norihiko Sugimoto(Keio University, Department of Physics)

Oceanic and atmospheric dynamics aims at abstracting general principles from observed phenomena and constructing a system of mathematical models, thereby leading to the understanding, prediction, and parameterization of those phenomena. It provides perspectives for the advancement of sciences in various areas such as wind waves, swells, internal waves, Rossby waves, equatorial waves, tides, eddies, meandering of jets and fronts, general circulation, boundary layers, and ocean-atmosphere coupled modes. It has also been and will continue to be benefited by new uses of ideas and methods from such theories as resonance, nonlinear interaction, spectral analysis, probability, statistics, and dynamical systems. In this session, we solicit presentations on observational, experimental, numerical, and theoretical studies of oceanic and atmospheric dynamics and on exploratory use of new ideas and methods. We also welcome presentations on interdisciplinary studies in fields such as ecosystems, climate, and environment.

[AOS21-P01] Data Assimilation of the Venus Atmosphere to Reproduce Planetary-scale Wave

*Yukiko Fujisawa[1], Mimo Shirasaka[2], Norihiko Sugimoto[1], Asako Hosono[3], Mirai Abe[1], Hiroki Ando[4], Masahiro Takagi[4], Masaru Yamamoto[5] (1.Keio University, 2.Seisen Senior High School, 3.Toshimagaoka Women High School, 4.Kyoto Sangyo University, 5.Research Institute for Applied Mechanics, Kyushu University)

[AOS21-P02] The study for designing the future Venus atmosphere observing mission of radio occultation measurement among small satellites using data assimilation

*Asako Hosono[1], Yukiko Fujisawa[2], Norihiko Sugimoto[2], Mirai Abe[2], Yukako Kikuchi[3], Tomotaka Yamamoto[4], Yosuke Kawabata[4], Satoshi Ikari[4], Hiroki Ando[5], Masahiro Takagi[5], Itziar Garate Lopez[6], Sebastien Lebonnois[7], Chi Ao[8] (1.Toshimagaoka Women High School, 2.Keio University, 3.Yokohama Futaba High School, 4.Tokyo University, 5.Kyoto Sangyo University, 6.Euskal Herriko Unibertsitatea, 7.Sorbonne Universite, 8.Jet Propulsion Laboratory)

[AOS21-P03] Verification of wave prediction model by drifting buoy observations

*Yukiharu Hisaki[1] (1.University of the Ryukyus)

[AOS21-P04] Size distribution of marine microplastics: A statistical mechanics approach

*Kunihiro Aoki[1], Ryo Furue[1] (1.Japan Agency for Marine Earth Science and Technology)

[AOS21-P05] Interannual modulation of intraseasonal wave activity over the equatorial Indian Ocean

*Tomomichi Ogata[1] (1.JAMSTEC Application Lab)

[AOS21-P06] On the statistics of deep zonal jets in the eastern North Pacific in an ensemble of eddy-resolving ocean general circulation model runs

*Ryo Furue[1], Masami Nonaka[1], Hideharu Sasaki[1] (1.APL/JAMSTEC)

[AOS21-P07] Predictability of interannual-to-decadal variability in eddy activity in the Kuroshio Extension

★Invited Papers

*Masami Nonaka[1], Hideharu Sasaki[1], Bunmei Taguchi[2], Niklas Schneider[3] (1.Application Laboratory, Japan Agency for Marine-Earth Science and Technology, 2.University of Toyama, 3.IPRC, University of Toyama)

[AOS21-P08] Surface water pathways in the subtropical-subarctic intergyre frontal zone of the western North Pacific

*Hatsumi Nishikawa[1], Humio Mitsudera[1], Takeshi Okunishi[2], Shin-ichi Ito[3], Taku Wagawa[4], Daisuke Hasegawa[2], Toru Miyama[5], Hitoshi Kaneko[3] (1.Institute of Low Temperature Science, Hokkaido University, 2.Tohoku National Fisheries Research Institute, 3.Atmosphere and Ocean Research Institute, The University of Tokyo, 4.Japan Sea National Fisheries Research Institute, 5.Japan Agency for Marine-Earth Science and Technology)

[AOS21-P09] Genesis of Spiciness Anomaly in the Northeast Pacific

*Yongqing Guo[1], Meng Wei[2] (1.Zhejiang Ocean University, 2.First Institute of Oceanography, Ministry of Natural Resources of the People's Republic of China)

[AOS21-P10] **Intensified Deep Ocean Variability Induced by Topographic Rossby Waves at the Pacific Yap-Mariana Junction**

*Qiang Ma[1], Jianing Wang[1], Fan Wang[1], Yilong Lyu[1] (1.Institute of Oceanology, Chinese Academy of Sciences)

[AOS21-P11] Direct measurements of near-surface upwelling and vertical heat flux in marginal ice zone of the Canada Basin, Arctic Ocean

*EunYae Son[1], Yusuke Kawaguchi[2] (1.Graduate School of Frontier Sciences, University of Tokyo, 2.Atmosphere and Ocean Research Institute, The University of Tokyo)

[AOS21-P12] Symmetric and Mixed Layer Instability at a Sharp Ocean Front

*Yuki Tanaka[1] (1.Graduate School of Science, The University of Tokyo)

[AOS21-P14] Reconstruct the 1970 Bhola Cyclone and Analysis the Effects of Cyclone Track and Tide to the Flooding Area

*Po-Sen Tseng[1], Tso-Ren Wu[1], CHIA-CHUN HSU[1], Chun-Wei Lin[1], Shun-Chun Chunag[1], Mei-Hui Chunag[1] (1.Graduate Institute of Hydrological and Oceanic Sciences, Nation Central University)

[AOS21-P15] Reconstruct the 1845 Kouhu Storm Surge Event with Ensemble Method

*CHIA-CHUN HSU[1], Tso-Ren Wu[1], Po-Sen Tseng[1], Shu-Chun Chuang[1], Chun-Wei Lin[1], Mei-Hui Chuang[1] (1.Graduate Institute of Hydrological and Oceanic Sciences, National Central University)

[AOS21-P16] Coastal Geographic Surveying Result on Gyoam beach in South Korea by Integrated Coastal Zone Management

*DongSeob Song[1] (1.Kangwon National University)

Data Assimilation of the Venus Atmosphere to Reproduce Planetary-scale Wave

*Yukiko Fujisawa[1], Mimo Shirasaka[2], Norihiko Sugimoto[1], Asako Hosono[3], Mirai Abe[1], Hiroki Ando[4], Masahiro Takagi[4], Masaru Yamamoto[5]

1. Keio University, 2. Seisen Senior High School, 3. Toshimagaoka Women High School, 4. Kyoto Sangyo University, 5. Research Institute for Applied Mechanics, Kyushu University

Planetary scale waves with about a 4-day period, which are considered to be “Kelvin waves”, have been observed in the equatorial region at the cloud top of the Venus atmosphere[1,2]. It is pointed out that these Kelvin waves could contribute to generate and maintain the atmospheric “super rotation”: the zonal wind circulating Venus 60 times faster than the solid part of Venus[3]. However, the Kelvin waves have not been simulated so far in any Venusian Atmospheric General Circulation Model (AGCM) in the world.

We have developed a Venusian GCM (AFES-Venus), and the Venus AFES LETKF Data Assimilation System (VALEDAS) based on the Local Ensemble Transform Kalman Filter (LETKF) for the first time[4,5]. Using VALEDAS, we have examined the reproducibility of a unique atmospheric structure so-called “cold collar”, a cold latitudinal band encircling the warm polar vortex at about 60–70 km altitudes, in order to elucidate the effects of temperature observations by multiple small satellites[6].

In this study, we prepared an idealized horizontal wind observation that was expected to be obtained from cameras with various wavelengths, and examined the reproducibility of Kelvin wave by varying conditions such as observation altitude, observation area, and time interval. The idealized observation data are created from CCSR/NIES Venus AGCM[7], in which the Kelvin wave was reproduced by forcing it at a lower level.

Fig (a) shows result of a free run forecast (without observation), and (b) shows assimilated result of horizontal wind observation at the altitude of 30 km with 24 hourly. By the data assimilation, the upper propagation of waves with a period of about 5 days at the equator was reproduced. We will also discuss how the observation and this kind of study would be helpful to design the future mission for understanding of Venus.

[1] Temporal variability of ultraviolet cloud features in the Venus stratosphere, A. D. Del Genio and W. B. Rossow, Icarus Vol. 51, (1982), p391–415.
[2] Planetary-scale wave and the cyclic nature of cloud top dynamics on Venus. A. D. Del Genio and W. B. Rossow, J. Atmos. Sci. 47, (1990), p293–318.
[3] Formation and maintenance of the 4-day circulation in the Venus middle atmosphere, M. Yamamoto and H. Tanaka, J. Atmos. Sci., 54, (1997), p1472-1489.
[4] Baroclinic modes in the Venus atmosphere simulated by GCM, N. Sugimoto, M. Takagi, and Y. Matsuda, Journal of Geophysical Research: Planets, Vol. 119, (2014), p1950–1968, doi:10.1002/2014JE004624.
[5] Development of an ensemble Kalman filter data assimilation system for the Venusian atmosphere, N. Sugimoto, A. Yamazaki, T. Kouyama, H. Kashimura, T. Enomoto, and M. Takagi, Scientific Reports, Vol. 7, (2017), 9321, 9pp.
[6] Observing system simulation experiment for radio occultation measurements of the Venus atmosphere

©2020. Japan Geoscience Union. All Right Reserved.

among small satellites, N. Sugimoto, M. Abe, Y. Kikuchi, A. Hosono, H. Ando, M. Takagi, I. Garate-Lopez, S. Lebonnois and C. Ao, Journal of Japan Society of Civil Engineers A2: Applied Mechanics, (2019).
[7] Venusian middle-atmospheric dynamics in the presence of a strong planetary-scale 5.5-day wave, M. Yamamoto and M. Takahashi, Icarus, (2012), 217, p702-713.

Keywords: Data assimilation, Venus atmosphere, Planetary-scale Wave

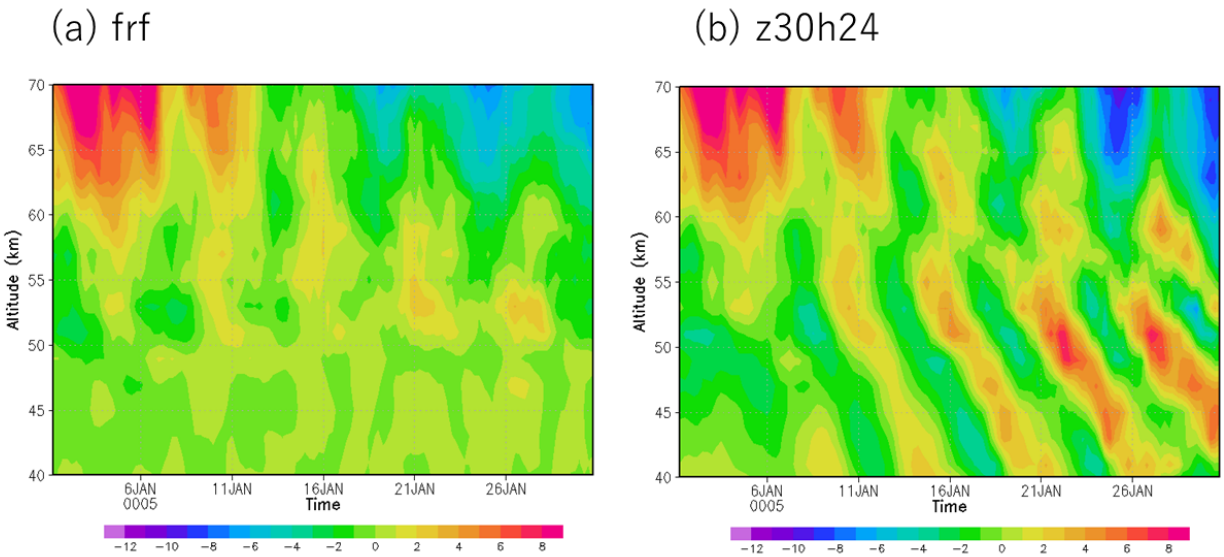


Fig: Time-height cross sections of the zonal wind at the equator.

©2020. Japan Geoscience Union. All Right Reserved.

The study for designing the future Venus atmosphere observing mission of radio occultation measurement among small satellites using data assimilation

*Asako Hosono[1], Yukiko Fujisawa[2], Norihiko Sugimoto[2], Mirai Abe[2], Yukako Kikuchi[3], Tomotaka Yamamoto[4], Yosuke Kawabata[4], Satoshi Ikari[4], Hiroki Ando[5], Masahiro Takagi[5], Itziar Garate Lopez[6], Sebastien Lebonnois[7], Chi Ao[8]

1. Toshimagaoka Women High School, 2. Keio University, 3. Yokohama Futaba High School, 4. Tokyo University, 5. Kyoto Sangyo University, 6. Euskal Herriko Unibertsitatea, 7. Sorbonne Universite, 8. Jet Propulsion Laboratory

In the Venus atmosphere, there is a unique phenomenon called “cold collar”, where the temperature at 60-80˚ latitude is lower than that of polar region at the altitude of about 65 km. So far, we developed the Venusian atmospheric GCM (AFES-Venus)[1] based on AFES (Atmospheric GCM For the Earth Simulator) and AFES-Venus succeeded in reproducing the cold collar for the first time. However, the temperature difference between the pole and the surroundings is smaller than that of the observations. Recently, introducing the Local Ensemble Transform Kalman Filter (LETKF), we have developed the Venus AFES LETKF Data Assimilation System (VALEDAS)[2]. In this study, we prepare idealized observations assuming radio occultation measurement among small satellites and assimilate them by VALEDAS. The idealized observations are provided from French Venus atmospheric GCM (IPSL VGCM)[3], in which the cold collar is realistically reproduced, and their conditions such as time interval, places and numbers are changed. We investigate the effectiveness of radio occultation measurement among small satellites by the reproducibility of the cold collar. As a result, the cold collar is reproduced if the observations are 2-3 vertical profiles 4-6 hourly, and it is expected that radio occultation measurement among small satellites will be promising to reproduce the polar atmospheric structures by 3 small satellites[4]. However, the cold collar is destroyed in the case which has a lot of observation points and high frequency, because there is a temperature bias between AFES-Venus and IPSL VGCM. In this study, correction of temperature bias between models is conducted. Bellow figures are temperature distribution at 30-90˚N at the altitude about 66 km in the cases which are 72 vertical profiles at temperature observations at 60-85˚N with every Earth hour; (a) is before the bias correction, and (b) is after. It is suggested that the bias correction enables us to correct temperature bias between models. In the poster presentation, in addition to these results, we will show the results considering real orbits.

[1] The puzzling Venusian polar atmospheric structure reproduced by a general circulation model, H. Ando et al., Nature Communications (2016).

[2] Development of an ensemble Kalman filter data assimilation system for the Venusian atmosphere, N. Sugimoto et al., Scientific Reports (2017).

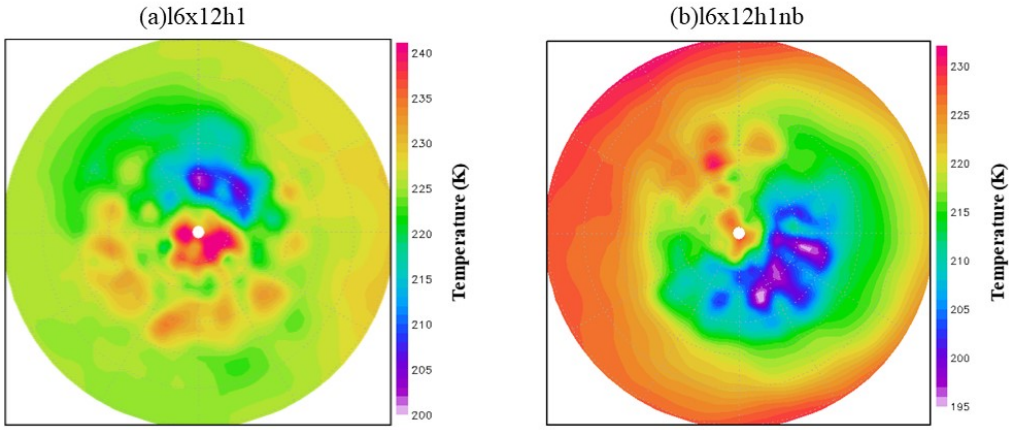
[3] Latitudinal variation of clouds’ structure responsible for Venus’ cold collar, I. Garate-Lopez and S. Lebonnois, Icarus, (2018).

[4] Observing system simulation experiment for radio occultation measurements of the

©2020. Japan Geoscience Union. All Right Reserved.

Venus atmosphere among small satellites, Norihiko Sugimoto., Journal of Japan Society of Civil Engineers A2: Applied Mechanics, (2019).

Keywords: Data assimilation, Venusian atmosphere, Radio occultation



©2020. Japan Geoscience Union. All Right Reserved.

Verification of wave prediction model by drifting buoy observations

*Yukiharu Hisaki[1]

1. University of the Ryukyus

It is necessary for verification of wave prediction model to compare predicted wave data with in-situ observation data such as buoy data. However, the verification by in-situ observation is limited to coastal wave sensors or moored wave buoys. It is impossible to conduct the verification by the moored wave buoy in the open sea far from the land or in the area with strong current. Therefore, the wave prediction model was verified by drifting buoys of the Japan Meteorological Agency(JMA). The predicted wave data is forced by the ERA interim wind data, and the spatial resolution is 0.75 degrees. We calculated wave parameters from 2017 to 2018. The correlation between wave heights by the JMA drifting buoys and predicted wave heights was about 0.9. The predicted wave heights agree well with observation in both the Pacific and the Sea of Japan. On the other hand, the wave period did not agree well especially in the Sea of Japan. The reason is that wave spectra could not be accurately reproduced by the low spatial resolution wave model due to the short fetch. Next, we compared the predicted wave data considering the current with observed wave data. It is shown that the accuracy of wave prediction improves. The effects of horizontal shear and relative wind on the accuracy of wave prediction were investigated. The relative wind effect the largest.

Keywords: wave height, drifting buoy, wave model

©2020. Japan Geoscience Union. All Right Reserved.

Size distribution of marine microplastics: A statistical mechanics approach

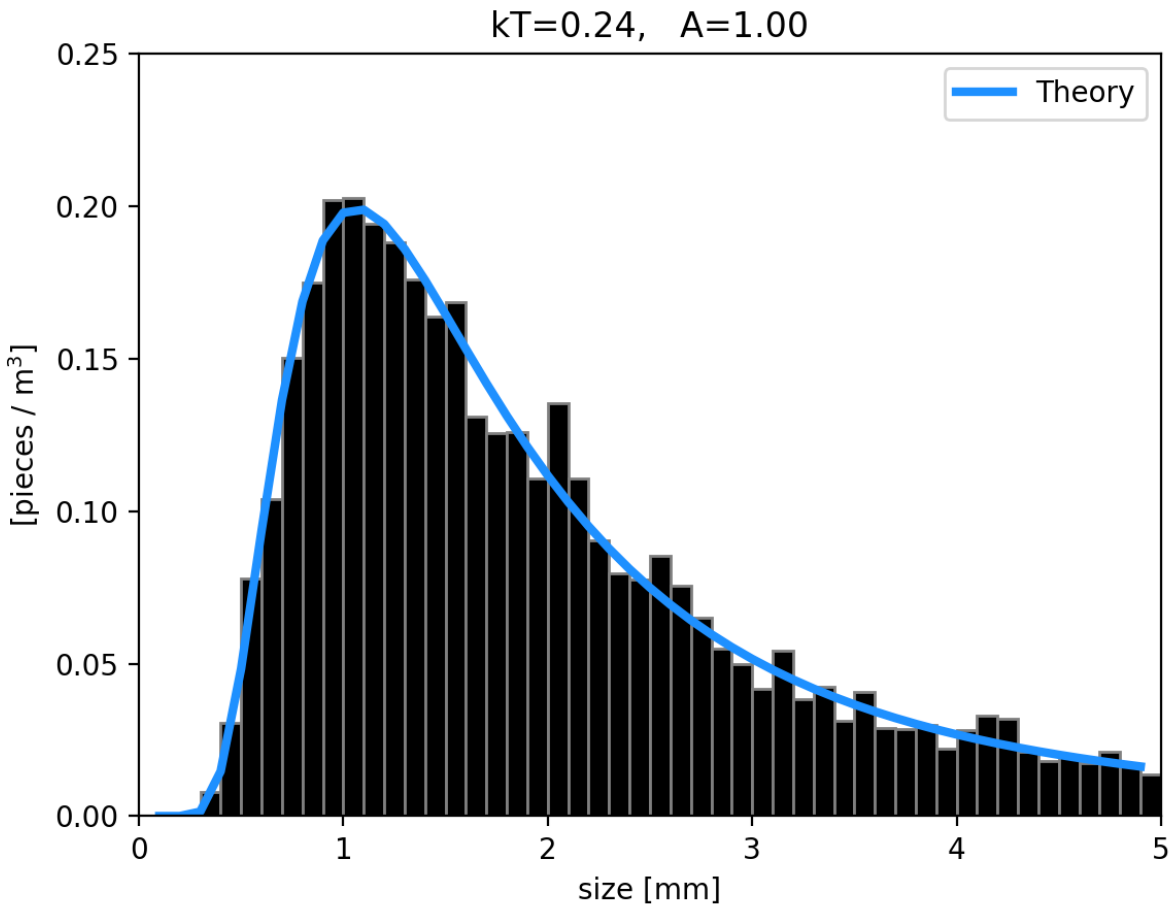
*Kunihiro Aoki[1], Ryo Furue[1]

1. Japan Agency for Marine Earth Science and Technology

The observed size distribution of marine microplastics generally shows, from large to small sizes, a gradual increase followed by a rapid, but smooth decrease (Figure). This decrease is puzzling because breaking up a plastic piece into smaller fragments naturally increases the number of fragments. This apparent discrepancy has led to a speculation that smaller plastic fragments somehow disappear ("missing plastics" problem). The present study aims to provide an alternative explanation for this size distribution, borrowing ideas from statistical mechanics. In our model, we assume that a flat plastic piece is fragmented into n x n equal cells that have a uniform size in a crush event. We further assume that the fragmentation of each piece is caused by “crush energy”, whose magnitude is assumed to be inversely proportional to the size of the cell, and whose occurrence probability follows the Boltzmann distribution. Under these assumptions and the constraint of the volume conservation of the plastics, we finally obtain the size distribution of the fragments, which follows Planck's formula for black body radiation. In our model, the total available "crash energy" is an unknown parameter. After adjusting it for the curve to fit the data, the Planck distribution agrees well with the observed distribution (Figure). In our model, smaller fragments beyond the peak of the distribution are fewer because the probability of getting "crash energy" large enough to produce such small fragments is low. Our formula predicts that the peak of the size distribution shifts to a smaller size and the total amount of the microplastics becomes larger with increasing crush energy. As a future extension, sink of plastic fragments may be included by the inclusion of an analogue of chemical potential.

Keywords: Marine microplastics, Size distribution, Statistical mechanics

©2020. Japan Geoscience Union. All Right Reserved.



©2020. Japan Geoscience Union. All Right Reserved.

Interannual modulation of intraseasonal wave activity over the equatorial Indian Ocean

*Tomomichi Ogata[1]

1. JAMSTEC Application Lab

In this study, interannual modulation of intraseasonal wave activity over the equatorial Indian Ocean was investigated using 1.5-layer reduced gravity model. Simulated interannual modulation of 30-day intraseasonal wave activity shows significant reduction of the wave activity during positive Indian Ocean Dipole (pIOD) mode events. Such inactive intraseasonal wave activity suggests that eastward warm water transport by the equatorial/coastal Kelvin wave is reduced. It seems favorable to maintain cold phase of SST in the eastern pole. In presentation, other dominant intraseasonal variability (60-day, 90-day) will be investigated.

©2020. Japan Geoscience Union. All Right Reserved.

On the statistics of deep zonal jets in the eastern North Pacific in an ensemble of eddy-resolving ocean general circulation model runs

*Ryo Furue[1], Masami Nonaka[1], Hideharu Sasaki[1]

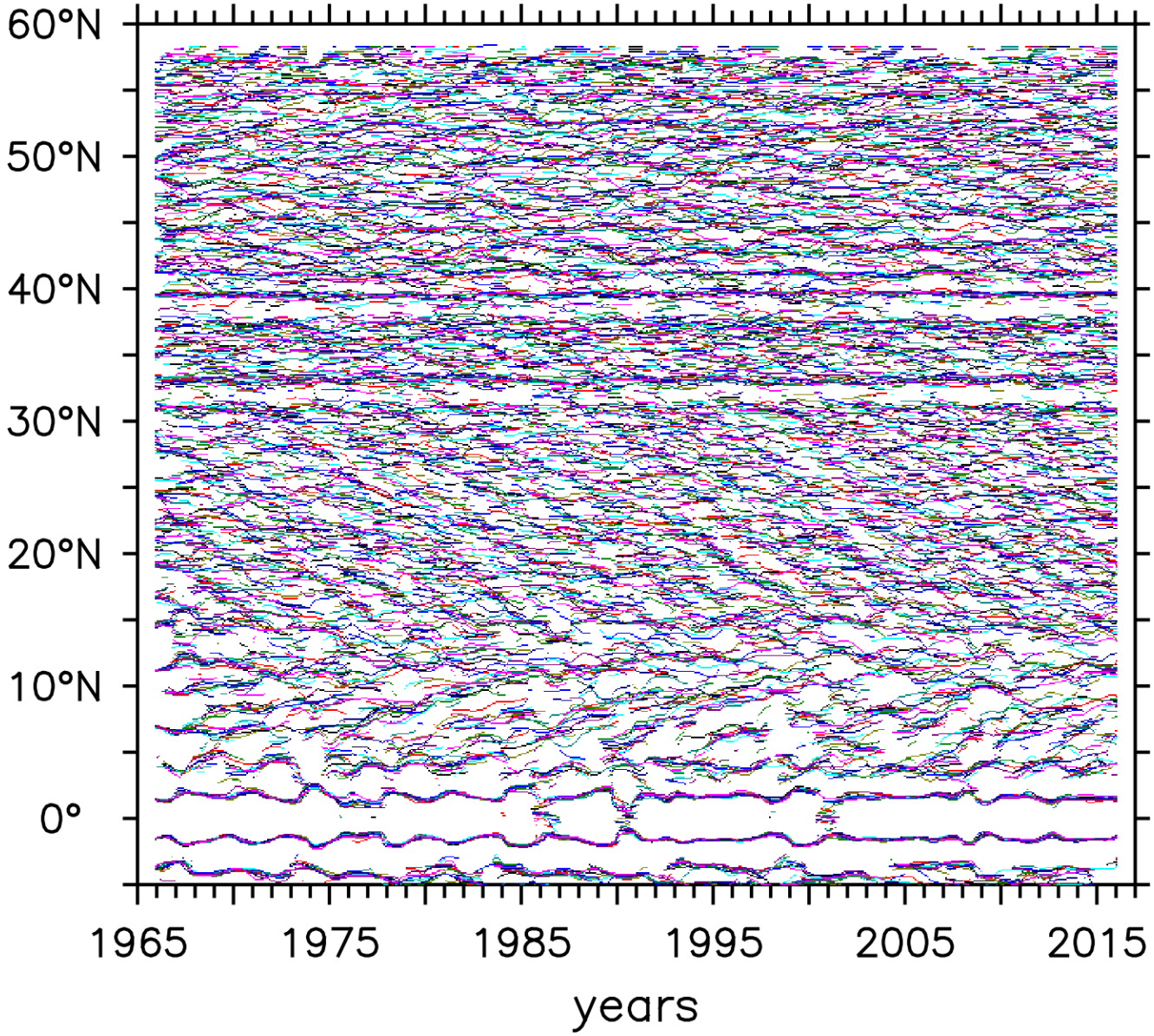
1. APL/JAMSTEC

It has been known for some time that the ocean basins are populated by "deep zonal jets" or "striations". A number of theories have been proposed to explain them, some of them predicting zonal jets at fixed latitudes and others implying that the positions of the jets are random. To investigate how deterministic the zonal jets are in the eastern North Pacific, a ten-member ensemble of long-term integrations of a semi-global, eddy-resolving ocean general circulation model is analyzed.

The figure shows the positions of the axes of eastward zonal jets at 500 m along 140W for all the ensemble members with different colors for different members. The equatorial jets, even their variability, seem to obey deterministic dynamics and some of the tropical jets migrate poleward coherently (similarly between ensemble members), whereas jets further poleward are more or less stochastic. The subtropical jets migrate equatorward and their positions are not very coherent; the subpolar jets are random and without systematic migration. Jets near the coast of North and South America tend to have shorter meridional wavelengths than interior ones. There are a few quasi-barotropic jets which are anchored to steep bottom topographic features and which also appear to trap shallower counter-flows on their poleward and equatorward flanks.

Keywords: deep zonal jets, eddy-resolving ocean general circulation model, ensemble, chaos

©2020. Japan Geoscience Union. All Right Reserved.



©2020. Japan Geoscience Union. All Right Reserved.

Predictability of interannual-to-decadal variability in eddy activity in the Kuroshio Extension

*Masami Nonaka[1], Hideharu Sasaki[1], Bunmei Taguchi[2], Niklas Schneider[3]

1. Application Laboratory, Japan Agency for Marine-Earth Science and Technology, 2. University of Toyama, 3. IPRC, University of Toyama

Eddies in the Kuroshio Extension have been shown to affect sea surface temperature, the atmosphere aloft, subsurface ocean, and also marine ecosystem. It is therefore important to explore variability and also predictability of the eddy activity in the region to improve our understanding of ocean-atmosphere variability over the North Pacific region. While interannual-to-decadal variability in the eddy activity in the Kuroshio Extension could be partly driven by atmospheric variability over the central/eastern North Pacific, it has also intrinsic variability that is independent from the atmospheric forcing and thus unpredictable. To examine predictability of the variability in eddy activities under realistic conditions, we analyze a ten-member ensemble, of fifty-year integration of an eddy-resolving OGCM driven by time-varying JRA55 reanalysis data. Focusing on interannual-to-decadal variability by the 13-month running mean, eddy activity in the downstream Kuroshio Extension region (32-38N, 153-165E) shows rather limited ensemble spread and uncertainty, and ensemble mean has significant correlation with the observation (correlation coefficient r=0.58). Also, the eddy activity variability highly correlates with the local current speed variability that propagates westward from the central North Pacific. With the propagation, the time series of area averaged current speed in the central North Pacific correlates with the eddy activities in the KE downstream region in four years later (r = 0.59), indicating predictability of the eddy activities. The four-year lagged correlation is also found in the observation. In contrast, in the upstream Kuroshio Extension region (32-38N, 141-153E), the ensemble spread is large and the ensemble mean does not correlate to the observation at all. While possibly model dependent, the result implies that the observed eddy activity in the upstream Kuroshio Extension may have a significant intrinsic component on the interannual time scale.

Keywords: eddy activity, predictability, Kuroshio Extension

©2020. Japan Geoscience Union. All Right Reserved.

Surface water pathways in the subtropical-subarctic intergyre frontal zone of the western North Pacific

*Hatsumi Nishikawa[1], Humio Mitsudera[1], Takeshi Okunishi[2], Shin-ichi Ito[3], Taku Wagawa[4], Daisuke Hasegawa[2], Toru Miyama[5], Hitoshi Kaneko[3]

1. Institute of Low Temperature Science, Hokkaido University, 2. Tohoku National Fisheries Research Institute, 3. Atmosphere and Ocean Research Institute, The University of Tokyo, 4. Japan Sea National Fisheries Research Institute, 5. Japan Agency for Marine-Earth Science and Technology

The Transition Domain in the western North Pacific, extending zonally at approximately 40˚N, is a boundary region between the subtropical and subarctic gyres, where a peculiar water mass forms as a result of mixing between the waters of the Kuroshio origin and the Oyashio origin. The Transition Domain is a very important area not only for oceanographic processes such as the inter-gyre exchange of the water masses, but also for mid-latitude climate and biological processes. It is not known, however, how the Kuroshio and Oyashio waters are transported to the Transition Domain and mix. This paper clarifies pathways of the Kuroshio water and the Oyashio water from a Lagrangian point of view, by conducting drifting buoy observations in 2015 and 2017, as well as by particle tracking using a geostrophic surface flow field derived from an absolute sea surface height product. Here we show that the Kuroshio water is carried to the Transition Domain through a narrow path with a width of ~ 50 km via a quasi-stationary jet in the western North Pacific (so called the J1). Time variations likely have important role in supplying the Kuroshio water to the Transition Domain; if a steady climatological flow field were used, the Transition Domain would be occupied by the Oyashio water. Much of the Kuroshio water is supplied at the Oyashio Second Branch and a large-scale meander of the J1, where the eddy strength shows local maxima.Eddy formation mechanisms are also discussed in relationship with the low bottom topographic features.

Keywords: the Transition Domain, Subtropical-Subarctic water exchange, bottom topography

©2020. Japan Geoscience Union. All Right Reserved.

Genesis of Spiciness Anomaly in the Northeast Pacific

*Yongqing Guo[1], Meng Wei[2]

1. Zhejiang Ocean University, 2. First Institute of Oceanography, Ministry of Natural Resources of the People's Republic of China

Spiciness anomaly is defined as salinity anomaly on certain isopycnal layer. Based on Argo observations, the most significant spiciness anomaly variations in the upper North Pacific are seen in the Northeast Pacific (145°-125°W, 25°-36°N; the study region) within $\sigma\theta$ = 25.0 - 25.4 kg m^{-3} isopycnal layer (the study isopycnal layer). The study region sits exactly at the formation region of the North Pacific Eastern Subtropical Mode Water (NPESTMW). Besides, the region is located at the subpolar front, with cold and fresh water mass in the northeast, and warm and salty water mass in the southwest. This leads a density-compensating feature of NPESTMW, which favours spiciness anomaly process. The genesis of spiciness anomaly on the study isopycnal layer is controlled by subduction of NPESTMW and spiciness anomaly injection processes during late winter. The spiciness anomaly on the ligher $\sigma\theta$ = 25.0 –25.2 kg m^{-3} isopycnal layer is decided by the subducted NPESTMW. The denser $\sigma\theta$ = 25.2 –25.4 kg m^{-3} isopycnal layer does not ventilate. The positive spiciness anomaly on this particular layer is caused by diapycnal mixing across the subduced isopycnal (i.e. spiciness anomaly injecion), while the negative spiciness anomaly is driven by southward advection of subpolar water.

Keywords: Spiciness anomaly genesis, Subduction, Spiciness anomaly injecion

©2020. Japan Geoscience Union. All Right Reserved.

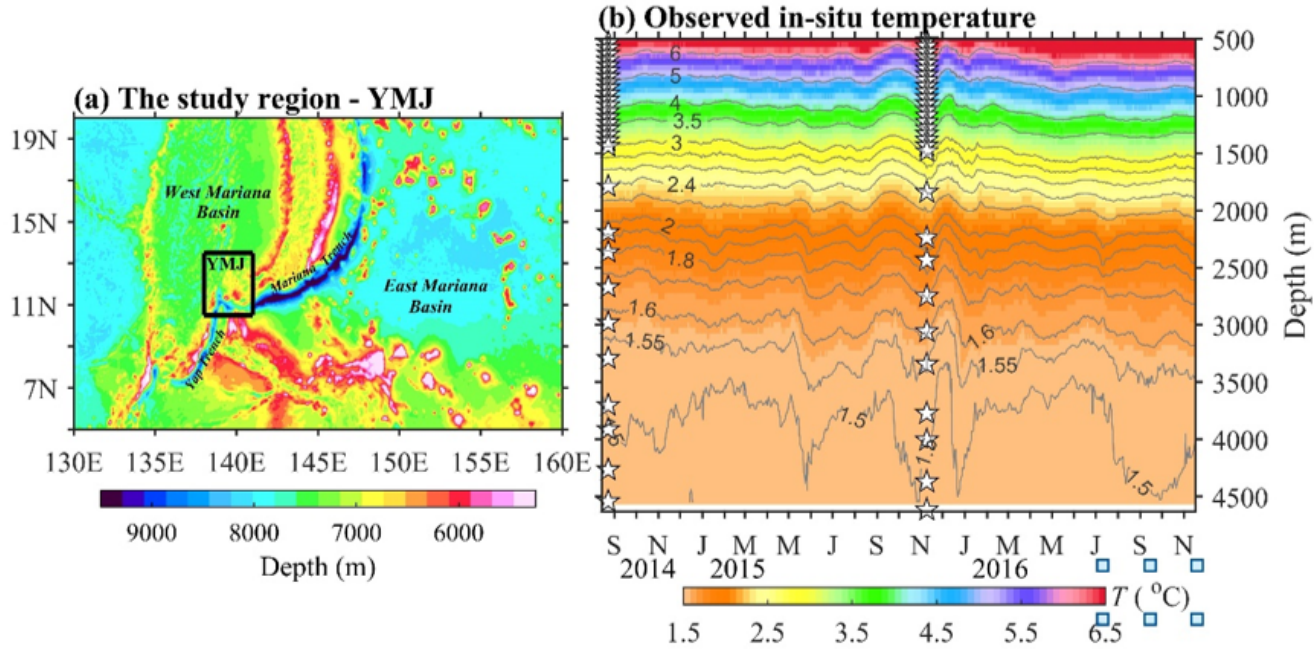
Intensified Deep Ocean Variability Induced by Topographic Rossby Waves at the Pacific Yap-Mariana Junction

*Qiang Ma[1], Jianing Wang[1], Fan Wang[1], Yilong Lyu[1]

1. Institute of Oceanology, Chinese Academy of Sciences

In a deep channel at the Pacific Yap-Mariana Junction, intensified variability of flow and isotherm displacement over 3000-4600 m is revealed by two separate observations: the recent one during 2014-2016, and the two 20 years ago during 1996-1998. Observed velocity and isotherm displacement can reach 45 cm s^{-1} and ~600 m at 4200 m, respectively. Such intensified variability is demonstrated to arise from topographic Rossby waves (TRWs), since vertical profiles of observed currents reasonably conform to TRW features of hyperbolic intensification with depth and highly vertical coherence in phase. Mercator Ocean model outputs reproduce observed TRWs and are used to discuss their energy sources. Both the energetic surface eddy moving across rough topography and mixed barotropic-baroclinic instability of the background flow appear to be the candidates to generate TRWs.

Keywords: deep ocean current, intraseasonal variability, Pacific Ocean, mooring observation



©2020. Japan Geoscience Union. All Right Reserved.

Direct measurements of near-surface upwelling and vertical heat flux in marginal ice zone of the Canada Basin, Arctic Ocean

*EunYae Son[1], Yusuke Kawaguchi[2]

1. Graduate School of Frontier Sciences, University of Tokyo, 2. Atmosphere and Ocean Research Institute, The University of Tokyo

The western Arctic Ocean observation was conducted using R/V "*Mirai*" from October to November 2019. We aim to figure out the oceanic contributions on the delayed onset of seasonal sea ice formation. The 2019 was the remarkable year that hit the lowest and the second lowest records of November and annual sea ice extent, respectively, which are sign of delayed sea ice recovery. The R/V Mirai expedition covers the Beaufort Sea in the western Arctic to conduct hydro-dynamic observations including conventional CTDs, direct microstructure measurement with TurboMap, and upper-water monitoring of temperature with an autonomous instrument, IceBTC60/40 (IceBTC). The IceBTC is a buoy with a 60-m long tether, consisting of 17 thermistors and 3 pressure sensors. The IceBTC was deployed in a marginal ice zone (MIZ) in the Canada Basin where was covered with grease ice. During that, the TurboMap and XCTDs were accompanied in the proximity. The IceBTC observation detected a strong signal of upwelling from the warm Pacific Summer Water (PSW) layer, which locates beneath the cold surface mixed layer. Upward heat flux has changed with the wind regime influencing marginal ice zone. The flux rapidly increased by wind blowing towards open ocean from pack ice, at the same time ice drift speed showed nearly 40 cm s^{-1}. On the other hand, it was stalled down under other wind directions. Surprisingly, a bulk estimate of vertical heat flux towards the ice bottom instantaneously reached 600 W m^{-2}.Our study suggests that the upward heat flux due to PSW might be traditionally underestimated and wind-ice-ocean coupled system can enhance it breaking through strong pycnocline in the marginal ice zone where covered with fragile ice.

Keywords: western Arctic, upwelling, vertical heat flux, sea ice

©2020. Japan Geoscience Union. All Right Reserved.

Symmetric and Mixed Layer Instability at a Sharp Ocean Front

*Yuki Tanaka[1]

1. Graduate School of Science, The University of Tokyo

Submesoscale processes at ocean fronts play a crucial role in transferring buoyancy, momentum, and tracers in both the horizontal and vertical directions, as well as in cascading energy from large to small scales. Although symmetric instability and mixed layer instability are believed to be two major types of submesoscale instability, clear evidence of them has not yet been obtained in the real ocean. This is partly because theoretical prediction of the dispersion and polarization relations of these submesoscale instability processes in the real ocean is still incomplete; most of the theoretical studies have assumed an infinite ocean with homogeneous negative potential vorticity sustaining the existence of symmetric instability. This idealized situation is quite different from the actual one where negative potential vorticity is confined within a narrow region centered at a front.

Here, we examine symmetric and mixed layer instability created at a realistic front in the surface mixed layer. For this purpose, we performe a linear stability analysis on a meridional–vertical plane with a zonally uniform background field characterized by a sharp front with a narrow region of negative potential vorticity. The analysis shows that symmetric instability is the most unstable mode when the zonal wavenumber of the disturbance is small enough. The symmetric instability is characterized by wave patterns mostly confined within the negative potential vorticity region and nearly aligned with the background isopycnals. As the zonal wavenumber of the disturbance becomes large, the dominant unstable mode is replaced by mixed layer instability. The meridional scale of the mixed layer instability is much larger than that of the symmetric instability, even larger than the width of the front. Furthermore, the zonal phase speed of the mixed layer instability is much smaller than that of the symmetric instability. These clear differences enable us to easily distinguish between the two types of instability even though they are continuous in the dispersion diagram. The results will be useful for identifying the symmetric and mixed layer instability in the real ocean.

Keywords: Submesoscale Processes, Symmetric Instability, Mixed Layer Instability, Ocean Fronts, Linear Stability Analysis

©2020. Japan Geoscience Union. All Right Reserved.

Reconstruct the 1970 Bhola Cyclone and Analysis the Effects of Cyclone Track and Tide to the Flooding Area

*Po-Sen Tseng[1], Tso-Ren Wu[1], CHIA-CHUN HSU[1], Chun-Wei Lin[1], Shun-Chun Chunag[1], Mei-Hui Chunag[1]

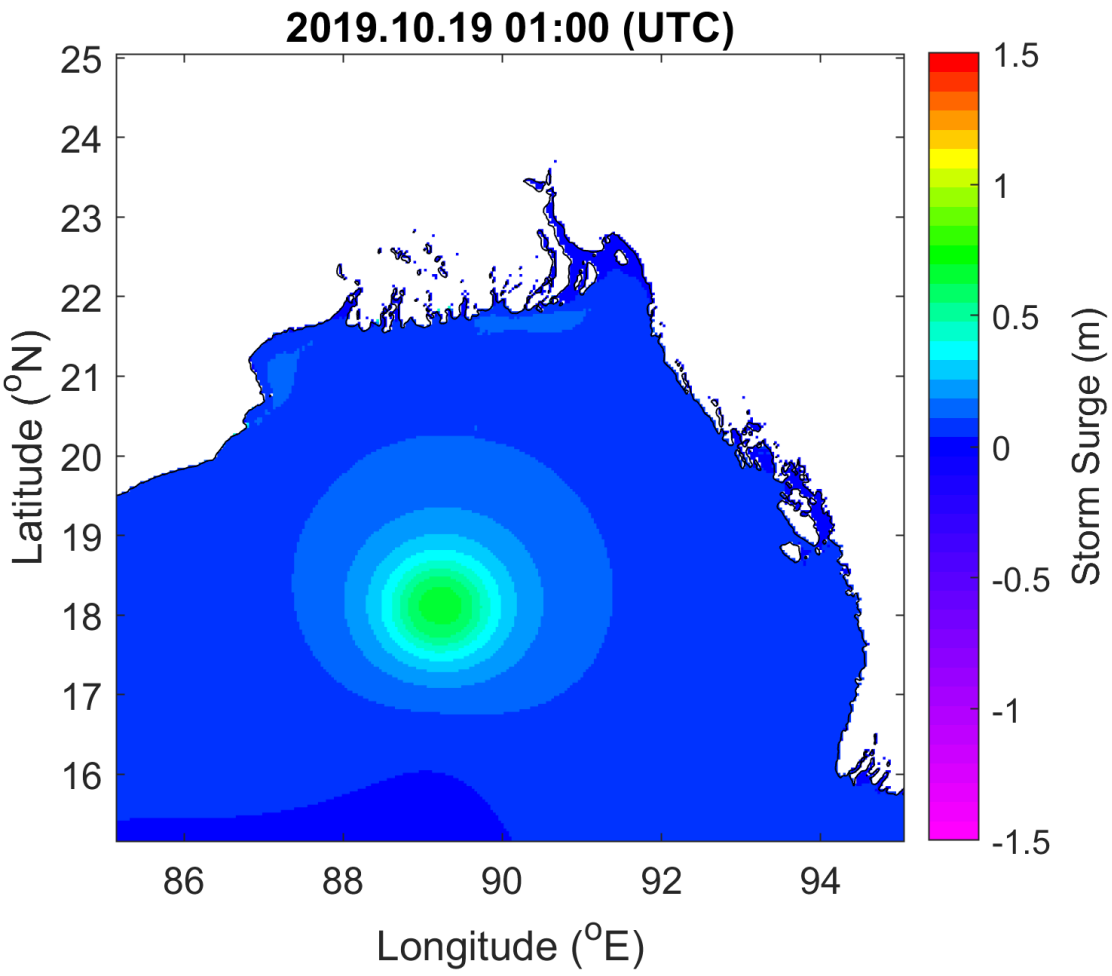
1. Graduate Institute of Hydrological and Oceanic Sciences, Nation Central University

Bhola Cyclone caused nearly half a million casualties in the Bay of Bengal in 1970 This research aims to reconstruct the storm surge event and understand the effects of tides and cyclone track on the flooding area. In this study, the numerical simulations were performed with COMCOT storm surge model. The nonlinear shallow-water wave equation was solved on spherical coordinates, and physical terms such as pressure gradient force, wind shear force, bed friction force and Coriolis force were added to the momentum equation. To reconstruct the storm surge event, the tide component was considered by importing tidal boundary forcing from TPXO Global Tidal Solutions. The scenarios take a variety of cyclone track, cyclone moving speed, and cyclone intensity. Sensitivity tests are further introduced to see the storm coincides with high tide.

The results can help to understand the influence of tides and other cyclone parameters on flooding, also provide a practical contribution to the quick alert and disaster control of the storm surge in the Bay of Bengal in the future.

Keywords: Cyclones in the Bay of Bengal, COMCOT Model, Storm Surge, Tide and Path, Overflow

©2020. Japan Geoscience Union. All Right Reserved.



©2020. Japan Geoscience Union. All Right Reserved.

Reconstruct the 1845 Kouhu Storm Surge Event with Ensemble Method

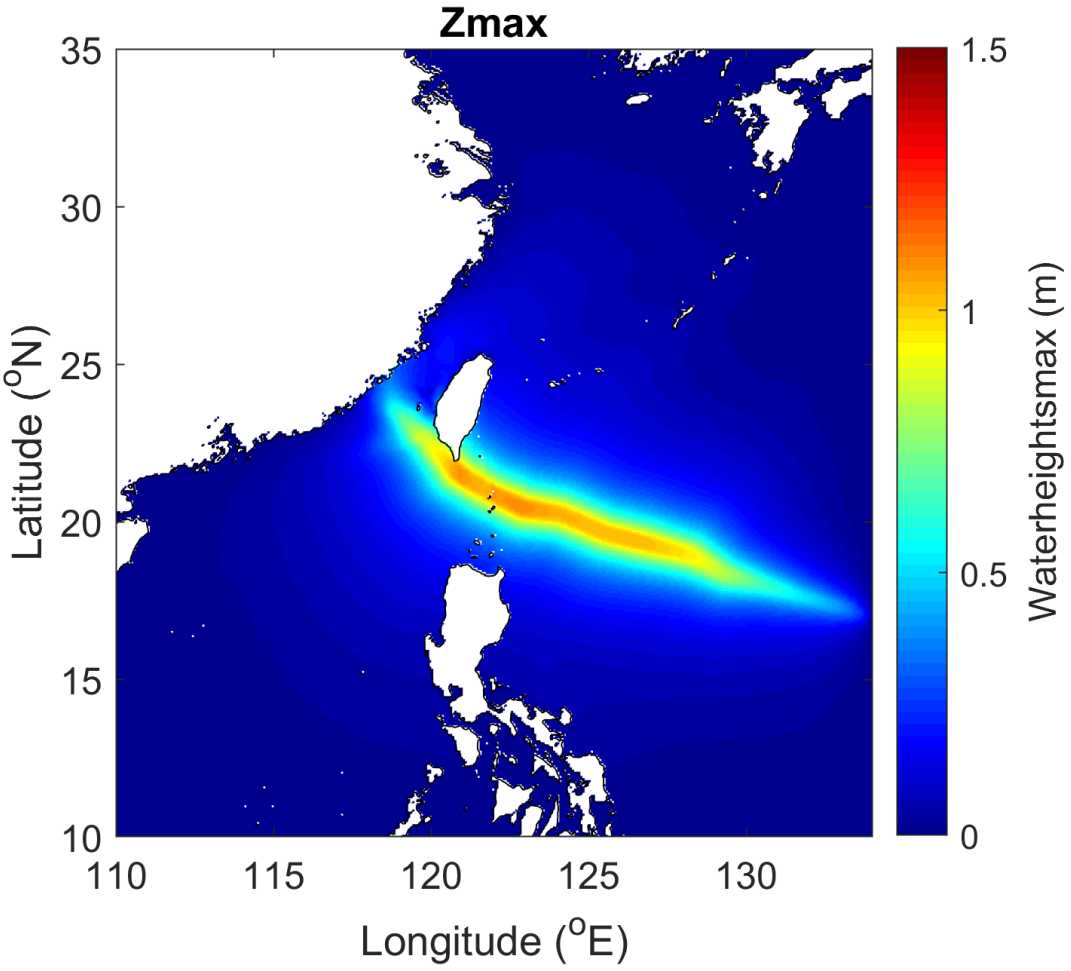
*CHIA-CHUN HSU[1], Tso-Ren Wu[1], Po-Sen Tseng[1], Shu-Chun Chuang[1], Chun-Wei Lin[1], Mei-Hui Chuang[1]

1. Graduate Institute of Hydrological and Oceanic Sciences, National Central University

In 1845, a severe storm surge event occurred in Kouhu, a township in southern western Taiwan. In this event, the storm surge caused more than 10,000 casualties which makes it the most serious storm surge event in the history of Taiwan. However, limited by the technology, no description of the typhoon track in the literature. Considering the dense population on the west coast of Taiwan in recent years, and also a large substation which transports the electric from a large number of offshore wind turbines to the cities in Taiwan. A deep understanding of the storm surge event is important. A non-linear multi-grid COMCOT storm surge model in conjunction with the ensemble method is applied to reconstruct the event and assessing future risks on the western coast of Taiwan. To reconstruct the storm surge event in 1845, cases are chosen from the modern typhoon database as a reference to build test scenarios. Then varying the typhoon track, typhoon moving speed, and typhoon intensity to find the most reasonable one which has the best agreement with the description in the historical documents. Besides, the effect of the tidal component is also considered on the storm surge height and inundation. Further discussion about the coastal hazard assessment is provided.

Keywords: Typhoon Track, COMCOT Model, Ensemble Method, Storm Surge, Inundation

©2020. Japan Geoscience Union. All Right Reserved.



©2020. Japan Geoscience Union. All Right Reserved.

Coastal Geographic Surveying Result on Gyoam beach in South Korea by Integrated Coastal Zone Management

*DongSeob Song[1]

1. Kangwon National University

Coastal erosion is generated by complex interrelationships of causes, influencing factors, and elements and appear by repetitive cycles of erosion and deposit over a long time. An increasing need exists for regional-scale measurements of shoreline change to aid in management and planning decisions over a broad portion of the coast and to inform assessments of coastal vulnerabilities and hazards. In order to prevent coastal erosion, the beach nourishment and the man-made construction, like a submerged breakwater, are widely used, it is desirable to monitor the post nourishment shoreline to evaluate the projects' success.

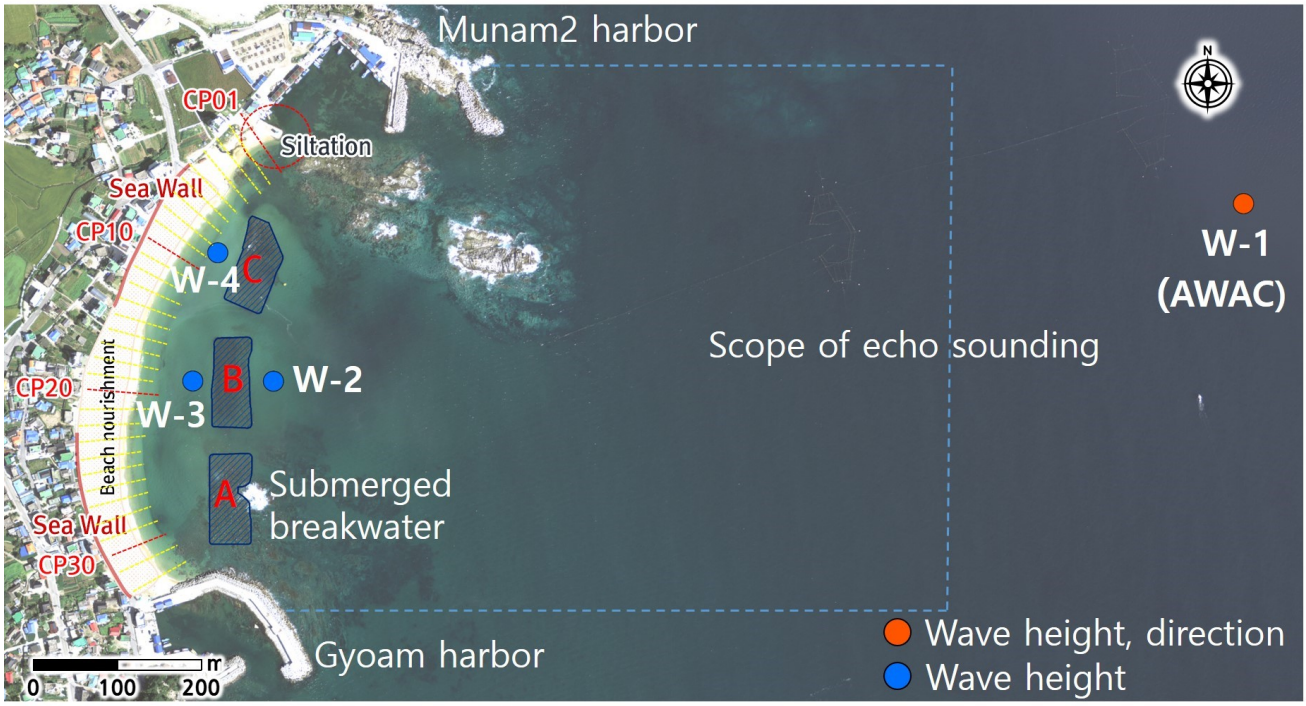
The Gyoam beach has the typical shape of a pocket beach. The river mouth of the Munam stream had been a sediment source in the littoral cell in the past. However, as the location of the river mouth changed from the Gyoam beach to the Backdo beach, the Gyoam beach was eroded by the blocking of the sediment source, as well as the construction of the coastal road. It is supposed that the coastal erosion was aggravated as the seasonal equilibrium collapsed after the construction of the Munam-2 Harbor. As the CIP progressed, the beach changes were analyzed by season through continuous monitoring in each construction phase. During the construction of submerged breakwaters from the first half of 2014 to the second half of 2016, the south of Gyoam beach was eroded and the northern beach received deposits in the summer, whereas the northern beach was eroded, and the southern areas were deposited during the winter season owing to the seasonal movement of sediments. After the completion of the submerged breakwaters in the second half of 2016 and the beach nourishments from 2016 to 2018, the shoreline is maintaining seasonal equilibrium as of February 2019. According to the stable shoreline analysis, a stable shoreline was not reached near the Gyoam beach on the south of the littoral cell due to the lack of sand volume in the littoral cell; however, as of August 2018, it seems that the total sand volume has been adjusted to some degree. After the implementation of submerged breakwaters, the results show that the fully submerged breakwaters produce more stable and balanced sediment loss/gain in the protected area, and yield more desirable formation of salient behind the breakwaters.

Acknowledgement

This work was supported by the National Research Foundation of Korea (NRF) grant funded by the Korea government (MSIP)(No.NRF-2017R1A2B2012392).

Keywords: Submerged breakwater, Coastal improvement project, Coastal erosion

©2020. Japan Geoscience Union. All Right Reserved.



©2020. Japan Geoscience Union. All Right Reserved.

[E] Poster | A (Atmospheric and Hydrospheric Sciences)：A-OS Ocean Sciences & Ocean Environment

[A-OS22] Physical, chemical and biological processes and variability in the Indian Ocean

convener:Yukio Masumoto(Graduate School of Science, The University of Tokyo), Hiroaki Saito(Atmosphere and Ocean Research Institute, The University of Tokyo)

The Indian Ocean has been recognized to play important roles in regional and global climate systems, material circulations, ecosystems, and their variability, with linked biophysical phenomena that span a wide range of spatial and temporal scales. These phenomena include, for example, diurnal cycling, intraseasonal disturbances, seasonal variations, Indian Ocean dipole events, and decadal to multi-decadal variations as well as secular trends under the global warming stress. In situ and remotely-sensed physical and biogeochemical observations using the Indian Ocean Observing System (IndOOS) and other means are now accumulating high quality data, and research efforts with numerical models and analyses of comprehensive datasets are also being conducted under International Indian Ocean Expedition-2 (IIOE-2) and the Eastern/Western Indian Ocean Upwelling Research Initiative (EIOURI/WIOURI). To advance our understanding of such Indian Ocean phenomena, disciplinary studies are essential, as are interdisciplinary investigations that elucidate the linkages between the physical and biogeochemical/ecological researches realms.
The objective of this session is to share our knowledge on, and to advance our understanding of, all facets of Indian Ocean variability. We invite papers on physical, biogeochemical and ecological aspects of the variability, as well as those related to atmosphere-ocean interactions, over the full spectrum of temporal and spatial scales. Discussions to facilitate mutual interactions among different research communities would also be expected and encouraged.

[AOS22-P01] IndOOS-2: A Roadmap to Better Observations of the Rapidly Warming Indian Ocean

Lisa M Beal[1], Jérôme Vialard[2], Matthew K Roxy[3], *Motoki Nagura[4] (1.Rosenstiel School of Marine and Atmospheric Science, University of Miami, 2.Institut de Recherche pour le Développement (IRD)/LOCEAN, 3.Indian Institute of Tropical Meteorology (IITM), 4.Japan Agency for Marine-Earth Science and Technology)

[AOS22-P02] The imprint of climate variability on the Maritime Continent surface ocean biology

*Eko Siswanto[1], Takanori Horii[1], Iskhaq Iskandar[2], Jonson Lumban Gaol[3], Riza Yuliratno Setiawan[4] (1.Japan Agency for Marine-Earth Science and Technology, 2.Sriwijaya University, 3.IPB University, 4.Gadjah Mada University)

[AOS22-P03] Particulate organic carbon distribution and primary production of Java-Sumatra upwelling system of Eastern Indian Ocean

*Edwards Taufiqurrahman[1], A'an Johan Wahyudi[1] (1.Research Center for Oceanography - Indonesian Institute of Sciences)

[AOS22-P04] The Pathways and Timescales of Indonesian Throughflow

*ISKANDAR MOCHAMAD RIZA[1], Toshio Suga[1], Kelvin John Richards[2], Hideharu Sasaki[3] (1.Graduate School of Sciences, Tohoku University, 2.International Pacific Research Center, University of Hawaii, 3.Application Laboratory, Japan Agency for Marine-Earth Science and Technology)

[AOS22-P05] Observation in the Java-Sumatra upwelling region during positive IOD in 2019

*Iwao Ueki[1] (1.JAMSTEC Japan Agency for Marine-Earth Science and Technology)

[AOS22-P06] A role of eastward-propagating intraseasonal oscillation in controlling coastal upwelling southwest of Sumatra

*Takanori Horii[1], Iwao Ueki[1] (1.Global Ocean Observation Research Center, Japan Agency for Marine-Earth Science and Technology (JAMSTEC))

[AOS22-P07] Distribution and isotopic composition of N_2O in the eastern Indian Ocean

*Sakae Toyoda[1], Kotaro Terajima[1], Naohiro Yoshida[2], Chisato Yoshikawa[3], Akiko Makabe[4], Fuminori Hashihama[5], Hiroshi Ogawa[6] (1.School of Materials and Chemical Technology, Tokyo Institute of Technology, 2.Earth-Life Science Institute, Tokyo Institute of Technology, 3.Research Institute for Marine Resources Utilization, Japan Agency for Marine-Earth Science and Technology, 4.Institute for Extra-cutting-edge Science and Technology Avant-garde Research (X-star), Japan Agency for Marine-Earth Science and Technology, 5.Department of Ocean Sciences, Tokyo University of Marine Science and Technology, 6.Atmosphere and Ocean Research Institute, The University of Tokyo)

[AOS22-P08] Nitrate isotopes in the Bay of Bengal

*Chisato Yoshikawa[1], Akiko Makabe[1], Yohei Matsui[1], Sakae Toyoda[2], Makio Honda[1], Naohiko Ohkouchi[1] (1.Japan Agency for Marine-Earth Science and Technology, 2.Tokyo Institute of Technology)

IndOOS-2: A Roadmap to Better Observations of the Rapidly Warming Indian Ocean

Lisa M Beal[1], Jérôme Vialard[2], Matthew K Roxy[3], *Motoki Nagura[4]

1. Rosenstiel School of Marine and Atmospheric Science, University of Miami, 2. Institut de Recherche pour le Développement (IRD)/LOCEAN, 3. Indian Institute of Tropical Meteorology (IITM), 4. Japan Agency for Marine-Earth Science and Technology

Over the last decade the Indian Ocean has absorbed 30% of the global oceanic heat uptake and the fate of this heat and its impact on future change is unknown. Projections foresee accelerating sea level rise, more frequent extremes in monsoon rainfall, and decreasing oceanic productivity. Almost two-thirds of humanity live around the Indian Ocean, many in countries dependent on fisheries and rain-fed agriculture. Coastal population growth is conflating with climate change to further increase exposure and vulnerability of these populations. The Indian Ocean observing system (IndOOS), established in 2006, is a multi-national network of sustained oceanic measurements that underpin understanding and forecasting of weather and climate for the Indian Ocean region and beyond. However, gaps in the IndOOS have so far limited forecasting efforts, left large discrepancies in the basin energy budget, and kept us in the dark about ecosystem stressors. A three-year, international review of the IndOOS by more than 60 scientific experts provides a roadmap to an improved observing network —IndOOS-2 —that can better meet future scientific and societal challenges. Core findings include the need for 1) chemical, biological, and ecosystem measurements alongside physical parameters; 2) better resolved upper-ocean processes to yield improved sub-seasonal to seasonal forecasts; 3) expansion into the western Arabian Sea; and 4) expansion into key coastal regions and the deep ocean to better constrain heat and freshwater changes. IndOOS-2 will require new resources and partnerships, creating opportunities for Indian Ocean rim countries to enhance their monitoring and forecasting capacity as part of a growing Global Ocean Observing System community.

Keywords: Indian Ocean, Observation system

©2020. Japan Geoscience Union. All Right Reserved.

The imprint of climate variability on the Maritime Continent surface ocean biology

*Eko Siswanto[1], Takanori Horii[1], Iskhaq Iskandar[2], Jonson Lumban Gaol[3], Riza Yuliratno Setiawan[4]

1. Japan Agency for Marine-Earth Science and Technology, 2. Sriwijaya University, 3. IPB University, 4. Gadjah Mada University

Understanding how the ocean surface biology will respond to climate variability is one of the important factors of climate change impact assessment, particularly the change in ocean biology represented by phytoplankton biomass or chlorophyll-a concentration (Chl-a). This is because phytoplankton are the base of the ocean food web from which carbon biomass and energy will be transferred to higher trophic level organism production (e.g., fish catch) hence affecting human life. Situated between Indian and Pacific Oceans, the Indonesian Maritime Continent (IMC) biophysical properties are greatly affected by both the Indian Ocean Dipole (IOD) and the El Nino-Southern Oscillation (ENSO) climate variations. All papers assessing the impacts of climate variability on Chl-a in the IMC were based on the datasets including the periods of concurrent IOD and ENSO events and mainly focused on the eastern Indian Ocean. The fingerprints of single IOD (positive or negative IOD) and single ENSO (El Nino or La Nina) events on surface ocean Chl-a have not been separately identified. Utilizing more than two-decade ocean color data we identified the fingerprint of climate modes, both during concurrent and single events. During concurrent positive IOD (+IOD) and El Nino years Chl-a mainly in the eastern Indian Ocean (west of Sumatra and south of Java), the Banda Sea, and the Arafura Sea tended to increase which was associated with upwelling as can be indicated by low sea surface height anomaly (SSHA). On the other hand, in the coastal areas surrounding Borneo, New Guinea, and the eastern coast of Sumatra, Chl-a tended to decline which was attributed to low rainfall. In contrast, during concurrent negative IOD (–IOD) and La Nina Chl-a in the eastern Indian Ocean, the Banda Sea, and the Arafura Sea tended to decline which was associated with downwelling indicated by high SSHA. On the other hand, in the coastal areas especially surrounding the Borneo, and the eastern coast of Sumatra, Chl-a tended to increase which can be attributed to high rainfall. The imprint of single +IOD (–IOD) on Chl-a resembled that of concurrent +IOD and El Nino (concurrent –IOD and La Nina) but with lower magnitudes of Chl-a changes. There was almost no distinct imprint on Chl-a associated with single El Nino and single La Nina events. The imprint of IOD on the IMC’ s Chl-a was obviously stronger than that of ENSO, even in the western Pacific Ocean where strong correlations between biophysical variables and Nino3.4 index were observed.

Keywords: Indonesian Maritime Continent, Climate variability, Ocean color, Phytoplankton

©2020. Japan Geoscience Union. All Right Reserved.

Particulate organic carbon distribution and primary production of Java-Sumatra upwelling system of Eastern Indian Ocean

*Edwards Taufiqurrahman[1], A'an Johan Wahyudi[1]

1. Research Center for Oceanography - Indonesian Institute of Sciences

The Eastern Indian Ocean region, particularly in south of Java and west of Sumatra, has been known for its periodical upwelling. The upwelling occurs during southeast monsoon period from June to October. During that time the upwelling center moves westward alongside the southern Java coast and then northward to the equator alongside western Sumatra waters. Upwelling will trigger the enhancement of primary productivity and then followed by changes on the organic carbon fixation in the ocean. Although the upwelling system in this area and its effect on the primary productivity are widely known, but a systematic study on its impact on the organic carbon variability is rarely conducted. We plan this research to find how the distribution of the particulate organic carbon related to the primary productivity and upwelling variability. It will be conducted in August –September (following the upwelling period) as part of the RV Hakuho-maru research cruise. The area observed is Java-Sumatra upwelling area. Seawaters will be sampled for the chlorophyll and particulate organic carbon content. With added satellite data, the upwelling strength can be determined and then correlated with the primary productivity and vertical-horizontal distribution of the particulate organic carbon.

Keywords: upwelling, particulate organic carbon, indian ocean

©2020. Japan Geoscience Union. All Right Reserved.

The Pathways and Timescales of Indonesian Throughflow

*ISKANDAR MOCHAMAD RIZA[1], Toshio Suga[1], Kelvin John Richards[2], Hideharu Sasaki[3]

1. Graduate School of Sciences, Tohoku University, 2. International Pacific Research Center, University of Hawaii, 3. Application Laboratory, Japan Agency for Marine-Earth Science and Technology

The major of Indonesian Throughflow (ITF) pathways are divided into two main routes, they are the western and eastern pathways. The properties differences of ocean circulation from these two pathways were examined by using Lagrangian particles in the high-resolution ocean model. The daily and monthly data fields also applied in the Lagrangian framework to see the discrepancies of the flows and crossing time. The particles originating from Mindanao need less than ~3 months to reach Makassar Strait and the same time needed to leave this strait to the southern end of Makassar Strait. The particles mostly flow out to the Indian Ocean via Timor Passages, Ombai Strait and Lombok Strait and associated with the upper ocean pathways. The eastern path originated from the north and south equator. The particles leaving the Lifamatola Strait to reach the Banda Sea and coming from the inflow both have broad of crossing time from ~3 months to ~1 year. The eastern path is concentrated in the 500-1000m depth range. Timor passages show as the strongest currents in the outflow channel in the eastern path. The application of the monthly fields in the Lagrangian framework shows the larger number of particles crossing the threshold section associated with the Lagrangian transport and faster crossing time

Keywords: Indonesian Throughflow, Lagrangian framework, OFES2

©2020. Japan Geoscience Union. All Right Reserved.

Observation in the Java-Sumatra upwelling region during positive IOD in 2019

*Iwao Ueki[1]

1. JAMSTEC Japan Agency for Marine-Earth Science and Technology

The positive dipole event in 2019 is one of the stronger events in the record and produced extreme forest fire in Australia and deadly flooding in Africa. The event started in May, took the peak in October and terminated in January 2020. Under the eastern Indian Ocean upwelling research initiative (EIOURI), JAMSTEC installed a surface mooring at 5S 100E from December 2018 for capturing upper ocean and meteorological variables associated with upwelling and IOD. Also we conducted research cruise in the Java-Sumatra upwelling region by Barunajaya I in cooperation with Badan Pengkajian dan Penerapan Teknologi (BPPT). Acquired data by CTD and LADCP observation indicate strong upwelling feature in the Java-Sumatra upwelling region. The details will be shown in the presentation.

Keywords: IOD, upwelling, EIOURI, IIOE2

©2020. Japan Geoscience Union. All Right Reserved.

A role of eastward-propagating intraseasonal oscillation in controlling coastal upwelling southwest of Sumatra

*Takanori Horii[1], Iwao Ueki[1]

1. Global Ocean Observation Research Center, Japan Agency for Marine-Earth Science and Technology (JAMSTEC)

Coastal upwelling along the southwestern coast of Sumatra and Java is closely associated with El Niñ o/Southern Oscillation and occurrence of the Indian Ocean Dipole (IOD). In this study, we used a combination of observational data and satellite-based datasets, and investigated the role of eastward-propagating atmospheric intraseasonal oscillation (MJO/ISO) in controlling the coastal upwelling system. Intraseasonal coastal upwelling events frequently occurs in June-September, in response to anomalous southeasterly alongshore winds, with weak (strong) amplitude along the coast of Sumatra (Java). Observational data reveal that due to salinity stratification and thick barrier layer southwest of Sumatra, subsurface cold-water upwelling signal tends not to reach to mixed layer. We also found that the coastal upwelling signal tends to be suppressed by eastward-propagated downwelling Kelvin waves which was driven by anomalous equatorial westerly winds 15-30 days ago. Implications of these observational results for understanding the IOD will be discussed.

Keywords: Coastal upwelling, Sumatra and Java, Eastern Indian Ocean, Atmospheric intraseasonal oscillation

©2020. Japan Geoscience Union. All Right Reserved.

Distribution and isotopic composition of N_2O in the eastern Indian Ocean

*Sakae Toyoda[1], Kotaro Terajima[1], Naohiro Yoshida[2], Chisato Yoshikawa[3], Akiko Makabe[4], Fuminori Hashihama[5], Hiroshi Ogawa[6]

1. School of Materials and Chemical Technology, Tokyo Institute of Technology, 2. Earth-Life Science Institute, Tokyo Institute of Technology, 3. Research Institute for Marine Resources Utilization, Japan Agency for Marine-Earth Science and Technology, 4. Institute for Extra-cutting-edge Science and Technology Avant-garde Research (X-star), Japan Agency for Marine-Earth Science and Technology, 5. Department of Ocean Sciences, Tokyo University of Marine Science and Technology, 6. Atmosphere and Ocean Research Institute, The University of Tokyo

Nitrous oxide (N_2O) is a trace gas that contributes to both global warming and stratospheric ozone depletion. Its major sources are nitrification and denitrification by microorganisms in soils and waters. Emission of N_2O from the ocean to the atmosphere is estimated to take account for 20% of global N_2O sources. It has been known that production of N_2O is enhanced in the oxygen minimum zone (OMZ) and regions such as Arabian Sea and Eastern tropical Pacific act as strong N_2O source to the atmosphere because of turbulent fluxes from the thermocline. Although OMZ is also found in the northern part of eastern Indian Ocean, Bay of Bengal, N_2O saturation in the surface water and calculated flux to the atmosphere have been reported to be substantially lower than those in the western counterpart, Arabian Sea. Moreover, vertical N_2O profiles obtained in the western and central Bay of Bengal by the previous studies were significantly different, the latter showing only a small increase of N_2O in OMZ. In this study, we aimed at revealing vertical and meridional profile of N_2O and its production/consumption processes in the eastern Indian Ocean by concentration and isotopic analyses of N_2O and related species.

Seawater samples were collected at 9 stations along 88˚E meridian (16˚N–20˚S) from 8 to 27 November, 2018 during the KH18-6 cruise of R/V *Hakuho-maru*. At each station, samples taken at 14–15 depths in the range of 0–5000 m were subsampled into 230 mL glass vials followed by addition by 1 mL saturated $HgCl_2$ solution for sterilization and by sealing with butyl rubber stoppers. Each was then preserved at 4–6˚C in the dark. Concentration and isotope ratios of N_2O ($\delta^{15}N$, $\delta^{18}O$, and SP, ^{15}N-site preference in NNO molecule) were measured using a gas chromatograph-isotope ratio mass spectrometer (GC-IRMS) equipped with a gas extraction and cryogenic concentration unit.

Concentrations of N_2O in the surface water were 6–7 nmol kg^{-1} which corresponds to saturation of 99–115% with respect to the atmosphere. The values obtained at four stations in the Bay of Bengal (5–16˚N, 88˚E) were lower than those observed in the western Bay of Bengal (10–20˚N, 80–88˚E) in March–April 1991 and were similar to those obtained in the central Bay of Bengal (7–15˚N, 85–89˚E) in February 1995 and 1996. At each station, the concentration increased with depth and showed a maximum around the bottom of thermocline (150–300 m in the Bay of Bengal and 300–1000 m at southern stations). The subsurface N_2O maxima in the Bay of Bengal were coincided with the core of OMZ, and the highest concentration of 136 nmol kg^{-1} was observed at the northern most station. The highest value observed in this study is larger than that reported in the west and central Bay by a factor of two and ten, respectively. Isotope ratios of N_2O showed a linear relation with inverse concentration, but the relationship was different between surface layer (0–40 m), thermocline or upper OMZ (100–250 m), lower OMZ (250–1000 m), and deep layer (> 2000m).
The enhanced accumulation of N_2O in OMZ in the Bay of Bengal compared to past studies suggests two possibilities: (1) there is a large seasonal variability in the vertical diffusion of N_2O in this region because

©2020. Japan Geoscience Union. All Right Reserved.

mixed layer depth is largely affected by wind and rainfall driven by monsoon, flow rate of fresh water from the rivers, and so on, (2) N_2O production rate has been increased during the past 20 years due to change in local oxygen or nutrient concentrations. If (1) is the case, the accumulated N_2O might be emitted to the atmosphere in a month scale and the Bay of Bengal would act as a significant source. Isotopic signatures of N_2O source (end member value) were estimated using the relationship between isotope ratios and concentration for each layer in the Bay of Bengal for the first time. By comparing the end member values with the isotopic ranges of known N_2O production and consumption processes, which was deduced from isotope fractionation factors in the literature and isotopic signature of N_2O precursors obtained by this study or deduced from the literature, we estimate that N_2O is produced by both archaeal nitrification and denitrification in the upper OMZ whereas it is produced mainly by denitrification in the lower OMZ.

Keywords: greenhouse gas, ozone depleting gas, stable isotopes, Bay of Bengal, nitrification, denitrification

©2020. Japan Geoscience Union. All Right Reserved.

Nitrate isotopes in the Bay of Bengal

*Chisato Yoshikawa[1], Akiko Makabe[1], Yohei Matsui[1], Sakae Toyoda[2], Makio Honda[1], Naohiko Ohkouchi[1]

1. Japan Agency for Marine-Earth Science and Technology, 2. Tokyo Institute of Technology

Nitrogen isotopic composition of nitrate ($\delta^{15}N_{Nitrate}$) is widely used as a tracer of ocean-internal nitrogen cycling (consumption and regeneration) and ocean-external nitrogen inputs and losses (N_2-fixation and denitrification). A $\delta^{15}N_{Nitrate}$ value increases, in conjunction with nitrate depletion, due to an isotopic effect during nitrate assimilation by phytoplankton. When denitrification occurs in the water column, a $\delta^{15}N_{Nitrate}$ value extremely increases due to a strong isotopic effect. N_2-fixation produces fixed nitrogen with a $\delta^{15}N$ value of ~0‰, as nitrogen fixers take up N_2 gas with little isotopic effect. Here we determined $\delta^{15}N_{Nitrate}$ and $\delta^{18}O_{Nitrate}$ along 88°E in the Bay of Bengal during the cruise KH-18-6-leg2 of R/V *Hakuho-Maru*. The nitrate concentrations were below 1 μM in the surface water of the whole area. Especially, the nitrate depleted water spreads out below the depth of 400 m at the station near 20°S. The $\delta^{15}N_{Nitrate}$ values were expected to increase toward the surface in conjunction with nitrate depletion unless ^{15}N depletion by N_2-fixation and ^{15}N enrichment by denitrification are dominant. The $\delta^{15}N_{Nitrate}$ showed 5‰ in the bottom and deep waters and increased to 7‰ in the intermediate water. The horizontal maximum of the $\delta^{15}N_{Nitrate}$ in the intermediate water was found at the northern edge site where the oxygen concentration dropped below 1 μM. The ^{15}N enrichment in the intermediate water suggests the nitrate in the Indian Central Water is affected by benthic or water-column denitrification. The $\delta^{15}N_{Nitrate}$ once decreased to 6‰ in the subsurface water and then increased to the surface. The horizontal minimum of the $\delta^{15}N_{Nitrate}$ in the subsurface water was found in the nitrate depleted water near 20°S. The ^{15}N depletion in the subsurface water suggests one of the sources of surface nitrogen is the remineralized nitrogen originated from N_2-fixation. In the presentation, we will discuss the nitrogen cycle of the Bay of Bengal in more detail by using the $\delta^{18}O_{Nitrate}$ values.

Keywords: Marine Nitrogen Cycle, Nitrogen Isotopes, Indian Ocean

©2020. Japan Geoscience Union. All Right Reserved.

[E] Poster | A (Atmospheric and Hydrospheric Sciences)：A-OS Ocean Sciences & Ocean Environment

[A-OS23] Atlantic climate variability, and its global impacts and predictability

convener:Ingo Richter(JAMSTEC Japan Agency for Marine-Earth Science and Technology), Hiroki Tokinaga(Research Institute for Applied Mechanics, Kyushu University), Andrea Taschetto(University of New South Wales), Noel S Keenlyside(Geophysical Institute Bergen)

The Atlantic Ocean is subject to pronounced climate variations that occur on a wide range of time scales, including interannual variability in the equatorial and subtropical regions, and Atlantic multi-decadal variability (AMV), which has been linked with the Atlantic meridional overturning circulation (AMOC). These are connected to other climate variations across the globe. The AMV, e.g., has long been known to have global impacts, such as changes in the Indian, Asian and South American summer monsoons, and changes in the Pacific associated with the "global hiatus". Interannual variability in the equatorial and subtropical Atlantic has also been shown to influence global climate, including over Asia, while the freshening of the North Atlantic by melting of the Greenland ice cap is expected to influence all ocean basins via atmospheric bridges. Likewise, misrepresentation of the Atlantic can have global ramifications in climate models. Misrepresentation of the AMOC, e.g., has been associated with model biases in the entire Northern Hemisphere.

This session seeks observational, modeling, and theoretical studies on the mechanisms that determine the Atlantic mean climate and variability, as well as the predictability and global impacts of such variability. We also seek studies that evaluate climate model performance in the region. Topics include atmosphere-ocean-cloud interactions in the tropical Atlantic; two-way interaction with other ocean basins; relationships between tropical and mid/high latitude variability; air-sea interaction along the Gulf Stream and its influence on cyclones and storm track evolution; variability in the Benguela upwelling region; influence of Agulhas leakage on the South Atlantic; coupled climate model biases in the region and their impacts; AMOC and long-term climate change.

[AOS23-P01] **An evaluation of the performance of CMIP6 models in the tropical Atlantic: mean state, variability, and remote impacts**

*Ingo Richter[1], Hiroki Tokinaga[2] (1.JAMSTEC Japan Agency for Marine-Earth Science and Technology, 2.Kyushu University, Kasuga, Fukuoka, Japan)

[AOS23-P02] Decadal variability of the Benguela Niño/Niña

*Hiroki Tokinaga[1] (1.Research Institute for Applied Mechanics, Kyushu University)

[AOS23-P03] Climate change in the tropical Atlantic

*Noel S Keenlyside[1], Lander Crespo[1], Shunya Koseki[1], Ingo Richter[2], Lea Svendsen[1] (1.Geophysical Institute, University of Bergen and Bjerknes Centre for Climate Research, Norway, 2.JAMSTEC, Japan)

[AOS23-P04] The extraordinary Atlantic Nino of 2019/2020

*Ingo Richter[1] (1.JAMSTEC Japan Agency for Marine-Earth Science and Technology)

[AOS23-P05] Impact of springtime cross-equatorial SST gradient on the Atlantic Niño/Niña

Takaaki Yokoi[1], *Hiroki Tokinaga[1] (1.Research Institute for Applied Mechanics, Kyushu University)

[AOS23-P06] Investigating South American monsoon during mid-Pliocene

*Andrea Taschetto[1], Gabriel Pontes[2], Ilana Wainer[2], Alex Sen Gupta[1] (1.Climate Change Research Centre and ARC Centre for Excellence in Climate Extremes, University of New South Wales, Australia, 2.Department of Physical Oceanography, University of São Paulo, Brazil)

An evaluation of the performance of CMIP6 models in the tropical Atlantic: mean state, variability, and remote impacts

*Ingo Richter[1], Hiroki Tokinaga[2]

1. JAMSTEC Japan Agency for Marine-Earth Science and Technology, 2. Kyushu University, Kasuga, Fukuoka, Japan

General circulation models of the Coupled Model Intercomparison Project Phase 6 (CMIP6) are examined with respect to their ability to simulate the mean state and variability of the tropical Atlantic, as well as its linkage to the tropical Pacific. While, on average, mean state biases have improved little relative to the previous intercomparison (CMIP5), there are now a few models with very small biases. In particular the equatorial Atlantic warm SST and westerly wind biases are mostly eliminated in these models. Furthermore, interannual variability in the equatorial and subtropical Atlantic is quite realistic in a number of CMIP6 models, which suggests that they should be useful tools for understanding and predicting variability patterns. The evolution of equatorial Atlantic biases follows the same pattern as in previous model generations, with westerly wind biases during boreal spring preceding warm sea-surface temperature (SST) biases in the east during boreal summer. A substantial portion of the westerly wind bias exists already in atmosphere-only simulations forced with observed SST, suggesting an atmospheric origin. While variability is relatively realistic in many models, SSTs seem less responsive to wind forcing than observed, both on the equator and in the subtropics, possibly due to an excessively deep mixed layer originating in the oceanic component. Thus models with realistic SST amplitude tend to have excessive wind amplitude. The models with the smallest mean state biases all have relatively high resolution but there are also a few low-resolution models that perform similarly well, indicating that resolution is not the only way toward reducing tropical Atlantic biases. The results also show a relatively weak link between mean state biases and the quality of the simulated variability. The linkage to the tropical Pacific shows a wide range of behaviors across models, indicating the need for further model improvement.

Keywords: CMIP6, tropical Atlantic, interannual variability

©2020. Japan Geoscience Union. All Right Reserved.

Decadal variability of the Benguela Niño/Niña

*Hiroki Tokinaga[1]

1. Research Institute for Applied Mechanics, Kyushu University

The Benguela Niño/Niña is a dominant mode of sea surface temperature (SST) variability along the southwest African coast, with large amplitudes in austral fall. While interannual characteristics and mechanisms of this event have been extensively investigated by previous studies, its decadal fluctuation remains unclear. By synthesizing historical climate observations, we show that decadal SST variability in the Angola-Benguela area (ABA) is affected not only by local air-sea feedback but also by remote forcing from the North Atlantic and Pacific. On decadal time scales, the Benguela Niños (Niñas) tend to co-occur with negative (positive) SST anomalies in the tropical North Atlantic. This SST pattern is not confined in the tropical Atlantic but characterized by SST tripole in the whole North Atlantic, with a negative (positive) North Atlantic Oscillation-like SLP anomaly pattern. The strengthening (weakening) of the Azores high cools (warms) the tropical North Atlantic and weakens (strengthens) cross-equatorial trade winds, making favorable conditions for development of the Benguela Niño (Niña). The Pacific Decadal Oscillation also contributes to decadal SST anomalies in the tropical North Atlantic through atmospheric teleconnection. We will discuss how these remote forcings affect the decadal fluctuation of the Benguela Niño/Niña events.

Keywords: Benguela Nino/Nina, Decadal variability, Ocean-atmosphere interaction

©2020. Japan Geoscience Union. All Right Reserved.

Climate change in the tropical Atlantic

*Noel S Keenlyside[1], Lander Crespo[1], Shunya Koseki[1], Ingo Richter[2], Lea Svendsen[1]

1. Geophysical Institute, University of Bergen and Bjerknes Centre for Climate Research, Norway, 2. JAMSTEC, Japan

The tropical Atlantic SST have warmed by about 1 degree over the historical period, with greatest warming in the east, along the African coast and in the Gulf of Guinea. Experiments performed from the Coupled Model Intercomparison Projects (CMIP) indicate that models fail to reproduce this warming pattern, instead showing a rather uniform warming. Future projections with these models also tend to show rather uniform warming. In constrast. results from anomaly coupled models indicate that model biases impact the ability of climate models to simulate warming patterns in the tropical Atlantic. Here we investigate the role of model biases on climate change in the tropical Atlantic in the CMIP experiments. In addition, we have analyzed impacts of global warming on tropical Atlantic climate variability, and we assess the sensitive of the results are to model biases.

Keywords: Climate Change, Tropical Atlantic, Climate modelling

©2020. Japan Geoscience Union. All Right Reserved.

The extraordinary Atlantic Nino of 2019/2020

*Ingo Richter[1]

1. JAMSTEC Japan Agency for Marine-Earth Science and Technology

From December 2019 onward there was an increase in equatorial Atlantic sea-surface temperatures (SST), with anomalous warming in the eastern part of the basin. While such interannual warm events (also known as Atlantic Ninos) are a common occurrence in the region, the 2019/2020 event stands out for two reasons: 1) It is the warmest event to occur in at least two decades, thereby punctuating a period of relatively low variability in the equatorial Atlantic. 2) Its timing was unusual, as Atlantic Niños almost exclusively develop in boreal spring and peak in summer.
Here we analyze SST, surface winds, surface heat fluxes, and sea-surface height to explain the unusual development of the 2019/2020 event. Preliminary results suggest that it was primarily driven by surface heat fluxes rather than by ocean dynamics. We further attempt to put this event into the context of previous studies that have argued for a decrease of equatorial Atlantic variability in recent decades.

Keywords: equatorial Atlantic, Atlantic Nino, global warming

©2020. Japan Geoscience Union. All Right Reserved.

Impact of springtime cross-equatorial SST gradient on the Atlantic Niño/Niña

Takaaki Yokoi[1], *Hiroki Tokinaga[1]

1. Research Institute for Applied Mechanics, Kyushu University

A strong linkage between the Benguela Niño/Niña and Atlantic Niño/Niña events suggests that the same forcing may trigger the two phenomena in different seasons. On the other hand, several Atlantic Niño/Niña events have occurred without strong Benguela Niño/Niña events. When the Atlantic Nino (Nina) occurs following the Benguela Niño (Niña), springtime sea surface temperature (SST) anomalies in the tropical North Atlantic tend to be negative, acting to weaken the cross-equatorial SST gradient and southeasterly trade winds. On the other hand, when the Atlantic Nino (Nina) occurs without the Benguela Niño (Niña), SST anomalies in the tropical North Atlantic tend to be positive, consistent with non-canonical Atlantic Nino events suggested by previous studies. We will show a heat budget analysis for these Atlantic Nino/Nina events.

Keywords: Atlantic, Atlantic Nino, Benguela Nino

©2020. Japan Geoscience Union. All Right Reserved.

Investigating South American monsoon during mid-Pliocene

*Andrea Taschetto[1], Gabriel Pontes[2], Ilana Wainer[2], Alex Sen Gupta[1]

1. Climate Change Research Centre and ARC Centre for Excellence in Climate Extremes, University of New South Wales, Australia, 2. Department of Physical Oceanography, University of São Paulo, Brazil

South America receives more than 50% of its total annual rainfall from November to March, when convection increases over the Amazon Basin and the South Atlantic Convergence Zone (SACZ) strengthens, forming the South American Monsoon System (SAMS). Extreme SAMS events have great economical and societal impacts (e.g. agriculture, housing subject to flooding, water supply). Evaluation of possible changes in South America rainfall associated with warmer scenarios is of urgent demand. Here we investigate how Southern Hemisphere rainfall may had been different during the mid-Pliocene Warm Period (~3Ma), a time of mean global warming between 2-3ºC that share characteristics of the currently CO2-induced warming. We examine simulations undertaken as part of the Pliocene Model Intercomparison Project and performed climate model experiments using the atmospheric component of the NCAR Community Earth System Model (CESM) to understand the mid-Pliocene climate as well as to provide insights on possible rainfall changes in a warmer world. We show that higher rates of warming in the North Atlantic compared to the South Atlantic generated an interhemispheric temperature gradient that in turn enhanced the southward cross-equatorial energy flux by up to 48%. The enhanced energy flux equator resulted in a strengthening of the Southern Hemisphere Hadley circulation, that in turn intensified the South Atlantic Subtropical High. These atmospheric changes weakened and displaced the SACZ poleward. In addition, the intensified energy flux equator shifted the Atlantic Inter-Tropical Convergence Zone northward, weakening the contribution of oceanic moisture advection to the Amazon Basin and the SACZ. Curiously those changes in the mid-Pliocene relative to present day climate are not accompanied by significant variations in the Atlantic Meridional Overturning Circulation. The evaluation of the mid-Pliocene adds a constraint associated with differing rates of warming between hemispheres.

Keywords: mid-Pliocene, South America, precipitation, South Atlantic Convergence Zone, Atlantic ITCZ

©2020. Japan Geoscience Union. All Right Reserved.

[E] Poster | A (Atmospheric and Hydrospheric Sciences)：A-OS Ocean Sciences & Ocean Environment

[A-OS24] Exploring new frontiers of oceanic mixing research in the next decade

convener:Toshiyuki Hibiya(Department of Earth and Planetary Science, Graduate School of Science, University of Tokyo), Ichiro Yasuda(Atmosphere and Ocean Research Institute, The University of Tokyo), Lakshmi Kantha(Aerospace Engineering Sciences, University of Colorado, Boulder, Colorado, USA)

Mixing plays many important roles in the global ocean through a variety of different processes. In the upper ocean, mixing affects the sea surface temperature and hence air-sea interactions, which in turn influence the state of the atmosphere on a variety of time scales. Mixing in the deep ocean maintains the abyssal stratification of the world's oceans and influences the global overturning circulation, which in turn affects long-term climate. Ocean mixing modulates the transport and dispersal of dissolved and suspended materials, including pollutants, plankton and fish larvae. It also plays an important role in the oceanic food chain in so far as primary productivity, which occurs predominantly in the euphotic zone, is affected by nutrient uptake from the deep associated with ocean mixing.

 Microstructure profilers are being increasingly and routinely used to measure turbulence in the oceans, including the deep. Mixing models with more inclusive physics are being developed. Increasing computer power is making it possible to include sophisticated mixing models in global circulation models. As such, it is time to take stock of where we stand at present and explore the frontiers of mixing research over the next decade to advance our knowledge and utilize it for societal benefit.

 This session encompasses a wide variety of aspects of mixing within the water column from the surface to the seabed, as well as the impact of mixing on key physical, biological, and chemical processes, such as those mentioned above, with special attention to new findings obtained through improvements in oceanographic instrumentation, mixing models and the use of supercomputers. Observational, theoretical, experimental, and numerical approaches are all welcome. In this session, we particularly encourage discussion that can confirm how far our understanding of related topics has advanced and help define the new frontiers of ocean mixing research to be tackled in the next decade.

[AOS24-P01] Synchronized interdecadal periodic variations behind regime shifts in Pacific Decadal Oscillation

*Masaki Hamamoto[1], Ichiro Yasuda[1] (1.Atmosphere and Ocean Research Institute, The University of Tokyo)

[AOS24-P02] Role of the vertical mixing in the bottom water warming in a new ocean state estimate using tidally induced mixing parameterization

*Satoshi Osafune[1], Shuhei Masuda[1], Nozomi Sugiura[1], Toshimasa Doi[1], Tadashi Hemmi[1] (1.Japan Agency for Marine-Earth Science and Technology)

[AOS24-P03] Global distribution of the ocean vertical diffusivity derived from an ocean tracer inverse model approach

*Akira Oka[1] (1.Atmosphere and Ocean Research Institute, The University of Tokyo)

[AOS24-P05] A theoretical and observational study of the vertical decay scale of tidal mixing over rough seafloor topography

Takahiro Yanagimachi[1], *Toshiyuki Hibiya[1] (1.Department of Earth and Planetary Science, Graduate School of Science, University of Tokyo)

[AOS24-P07] Estimation of energy source of near-inertial oscillations observed at abyssal depths in Main Gap of the Emperor Seamount Chain

*Daigo Yanagimoto[1] (1.Atmosphere and Ocean Research Institute University of Tokyo)

[AOS24-P08] Characteristics of Vertically Propagating Near-inertial Internal Waves in the Japan Sea Excited in Northern Area

*Akie Sakai[1], Tomoharu Senjyu[2], Kosuke Mori[3], Takahiro Endo[2] (1.Department of Earth System Science and Technology, Interdisciplinary Graduate School of Engineering Sciences, Kyushu University, 2.Research Institute for Applied Mechanics, Kyushu University, 3.Okinawa Marine Science Support Section, Okinawa Institute of Science and Technology Graduate University)

[AOS24-P09] Near-inertial shear and widespread intensified thermocline mixing in a seasonally stratified shelf sea

*Wei Yang[1] (1.Tianjin University)

[AOS24-P10] The estimation of the vertical mixing in double diffusive favorable regions of the Indian Ocean by CTD-attached microstructure measurement

*Yusuke Sasaki[1], Ichiro Yasuda[1], Katsuro Katsumata[2], Shinya Kouketsu[2], Hiroshi Uchida[2] (1.Atmosphere and Ocean Research Institute, The University of Tokyo, 2. Japan Agency of Marine-Earth Science and Technology)

[AOS24-P11] Turbulence, internal waves, and associated nutrient supply caused by the Kuroshio southeast of Kyushu

*Duran Gomez Silvana Gloria[1], Takeyoshi Nagai[2] (1.Graduate School of Tokyo University of Marine Science and Technology, 2.Tokyo University of Marine Science and Technology)

[AOS24-P12] Revisit of typhoon's effect on biogeochemistry in the western Pacific subtropical-oligotrophic region

*Makio Honda[1], Yutaka Yoshikawa[2] (1.Japan Agency for Marine-Earth Science and Technology, 2.Kyoto University)

[AOS24-P13] Study on the vertical mixing and nutrient supply off the east coast of the Kamchatka

*kimura shino[1] (1.The Univercity of Tokyo)

[AOS24-P14] Reproduction of Iron-rich Intermediate Water in the Subarctic North Pacific by High-resolution Biogeochemical Model

*Hatsumi Nishikawa[1], Humio Mitsudera[1] (1.Institute of Low Temperature Science, Hokkaido University)

[AOS24-P15] Role of tidal mixing on biogeochemical cycling in the northwestern North Pacific

*Kazuhiro Misumi[1], Tsubono Takaki[2], Daisuke Tsumune[2] (1.Planning Group, Central Research Institute of Electric Power Industry, 2.Environmental Science Research Laboratory, Central Research Institute of Electric Power Industry)

[AOS24-P16] Interannual variations in primary productivity in the North Pacific western subarctic gyre (WSG), assessed by using settling particle delta N-15

*Yoshihisa Mino[1], Makio Honda[2], Fujiki Tetsuichi[2], Minoru Kitamura[2], Naomi Harada[2] (1.Nagoya University, 2.Japan Agency for Marine-Earth Science and Technology)

[AOS24-P17] Seasonal dynamics of zooplankton at station K2, NW Pacific, reconstructed from archived ADCP data

*Minoru Kitamura[1], Motoyo Itho[1] (1.Japan Agency for Marine-Earth Science and Technology)

[AOS24-P18] Variations in egg production rates of *Calanus sinicus* (Copepoda: Calanoida) estimated by gonad morphology

*Kiyotaka Hidaka[1], Shinji Shimode[2], Takashi Fushima[2] (1.Japan Fisheries Research and Education Agency, 2.Yokohama National University)

Synchronized interdecadal periodic variations behind regime shifts in Pacific Decadal Oscillation

*Masaki Hamamoto[1], Ichiro Yasuda[1]

1. Atmosphere and Ocean Research Institute, The University of Tokyo

Interdecadal climate variability over the North Pacific is examined using a 298-yr (1700-1997) Pacific Decadal Oscillation (PDO) index reconstructed from tree-ring records. Three statistically significant variations including the bi-decadal (~20yr), the tri-decadal (~30yr), and the multi-decadal (>50yr) variations are identified. The latter two variations exhibit 'phase-lock' features respectively with the bi-decadal variation: zero-crossings of the tri-decadal (multi-decadal) variation and the bi-decadal variation take place within significantly short duration. Above-mentioned characteristics imply that the two variations with longer timescale receive notable influence from the bi-decadal variation. These three variations together explain phase reversals identified using an instrumental 119-yr PDO index (1900-2018) including the period after 1997, where only the observed PDO index covers. Besides, these variations provide a viewpoint which integrates two contrary perspectives on the climatic regime shifts presented by previous studies. We further discuss possible linkages between these variations and the 18.6-yr lunar nodal cycle, as well as a phenomenon known as subharmonic resonances, which involves excitements of longer variations in nonlinear systems.

Keywords: regime shift, Pacific Decadal Oscillation, phase-lock, 18.6-yr lunar nodal cycle

©2020. Japan Geoscience Union. All Right Reserved.

Role of the vertical mixing in the bottom water warming in a new ocean state estimate using tidally induced mixing parameterization

*Satoshi Osafune[1], Shuhei Masuda[1], Nozomi Sugiura[1], Toshimasa Doi[1], Tadashi Hemmi[1]

1. Japan Agency for Marine-Earth Science and Technology

Decadal repeat of modern, high-quality, full-depth, hydrographic section observation has revealed the basin-wide warming of the bottom water in the Pacific Ocean, which cannot be neglected for precise estimation of the global heat balance. An ocean state estimate has shown that surface warming around Antarctica can remotely induce bottom water warming in the northern North Pacific through the propagation of internal Kelvin and Rossby waves more quickly than expected from the thermohaline circulation timescale. However, this wave response must depend on the background structures of density and temperature, which are determined by a balance between advection and diffusion. We investigated the bottom water warming in our new ocean state estimate that uses vertical mixing schemes based on well-known tidal energy distribution and discuss the mechanism especially focusing on the role of the vertical mixing.

Keywords: vertical mixing, data assimilation, bottom water warming

©2020. Japan Geoscience Union. All Right Reserved.

Global distribution of the ocean vertical diffusivity derived from an ocean tracer inverse model approach

*Akira Oka[1]

1. Atmosphere and Ocean Research Institute, The University of Tokyo

The ocean vertical diffusivity is important for controlling the distribution of various ocean tracer including the temperature and salinity. Recent studies clarified that its spatial distribution is very inhomogeneous but the global coverage of its direct measurements from turbulent mixing observations are not enough and its quantification is still difficult. On the other hand, recent observational data about the ocean tracer including temperature and salinity are increasing significantly and dataset covering the global ocean is available. The inversion of ocean velocity distribution from ocean tracer has been reported in the previous studies (e.g. Wunsch, 1996). In the same way as this velocity inversion, some studies tried the inversion of the ocean vertical diffusivity (e.g. Ganachaud and Wunsch, 2000) but there are few studies which discuss its detail 3-dimmensional distribution. By using an ocean tracer inverse model and an ocean general circulation model, I have tried the inversion of the ocean vertical diffusivity from the ocean tracer observations. In this presentation, I will report my attempt and discuss how observed temperature/salinity distribution is useful for obtaining the 3-dimmensional distribution of the ocean vertical diffusivity.

Keywords: ocean vertical diffusivity, ocean tracer, inverse model, adjoint method

©2020. Japan Geoscience Union. All Right Reserved.

A theoretical and observational study of the vertical decay scale of tidal mixing over rough seafloor topography

Takahiro Yanagimachi[1], *Toshiyuki Hibiya[1]

1. Department of Earth and Planetary Science, Graduate School of Science, University of Tokyo

There are much limited studies for tidal mixing enhanced over abyssal rough seafloor, compared with that in the surface mixed layer and/or in the interior ocean. Part of the reason is that direct observation of abyssal turbulent mixing requires special instrument as well as enormous time and cost, leaving the most universal method to estimate abyssal turbulent mixing in terms of finescale parameters. The most widely used parameterization for tidal mixing over abyssal seafloor is the one proposed by Jayne and St. Laurent (2001). However, this parameterization contains several ambiguities; in particular, although the vertical decay scale of tidal mixing over rough seafloor topography is usually assumed to be constant at 500 meters, recent field observations show that it varies depending on the roughness of the seafloor topography and the amplitude of tidal flow.

In the present study, using a microstructure profiler called VMP-X, we conducted detailed field observations at two locations (Station 1 and Station 2) with different seafloor topography of the Izu-Ogasawara Ridge to examine the spatial and temporal variations of the vertical profile of turbulent dissipation rates off the seafloor. At the same time, we carried out numerical simulations using high-resolution vertical two-dimensional numerical model incorporating the realistic seafloor topography and the spatial and temporal variations of tidal velocity to clarify the physical mechanism behind the observed results.

The vertical decay scales of turbulent dissipation rates off the seafloor at both stations were observed to vary with the amplitude of tidal flow. The decay scale of turbulent dissipation rates at Station 1 was observed to increase with the increase of the tidal flow amplitude, whereas the decay scale of turbulent dissipation rates at Station 2 was observed to decrease with the increase of the tidal flow amplitude.

We next investigate the generation of internal waves at each station using the results of the numerical simulations. At Station 1, the vertical decay scale extending higher up off the seafloor is attributed to the continuous generation of upward propagating internal lee waves with harmonic frequencies of M_2 tidal forcing, consistent with the theoretical prediction by Bell (1975). At Station 2, on the other hand, the dominant process of turbulent mixing is density overturning just over the steep sloping bottom that occurs as the amplitude of tidal flow increases, so that the vertical decay scale of turbulent mixing shows the dependence on the amplitude of tidal flow, quite contrary to that at Station 1.

These results indicate that microstructure observations combined with the information of roughness of the seafloor topography and the amplitude of tidal flow are absolutely necessary to improve the parameterization of tidal mixing over rough seafloor topography.

Keywords: Parameterization, Energy dissipation rates, Vertical decay scale, Tidal flow, Abyssal rough seafloor, Internal lee waves

©2020. Japan Geoscience Union. All Right Reserved.

Estimation of energy source of near-inertial oscillations observed at abyssal depths in Main Gap of the Emperor Seamount Chain

*Daigo Yanagimoto[1]

1. Atmosphere and Ocean Research Institute University of Tokyo

Prominent peaks near the inertial frequency (local f is 9.24×10^{-5} rad s^{-1} and actual peak frequency is 1.05 f) in clockwise rotary spectra were found at 5445-meter and 5855-meter depths in the deepest, widest gap in the Emperor Seamount Chain, called “Main Gap”, with mooring observation at 39° 20′ N, 169° 56′E (5895-m bottom depth) from 10 June 2016 to 25 June 2017. Band-passed current speed focused to the near-inertial frequency has a tendency of seasonal change; it was the lowest during the period from July to October 2016, the highest during the period from November 2016 to January 2017, and decreased toward June 2017. This temporal variation coincides roughly with the time series of 10-m wind speed above the mooring site according to the ERA5 dataset. The actual peak frequency (1.05 f) which is slightly higher than the local f indicates the southward energy propagation of the inertial oscillation from the northern surface according to Garrett (2001). Estimation of its ray shows that it would be generated at the surface by wind around 42°30'N (depending on the assumption of spatial distribution of buoyancy frequency) and its energy would propagate southward beyond Nintoku Guyot.

Keywords: abyssal ocean current, near-inertial oscillation, direct current measurement, Main Gap of Emperor Seamount Chain

©2020. Japan Geoscience Union. All Right Reserved.

Characteristics of Vertically Propagating Near-inertial Internal Waves in the Japan Sea Excited in Northern Area

*Akie Sakai[1], Tomoharu Senjyu[2], Kosuke Mori[3], Takahiro Endo[2]

1. Department of Earth System Science and Technology, Interdisciplinary Graduate School of Engineering Sciences, Kyushu University, 2. Research Institute for Applied Mechanics, Kyushu University, 3. Okinawa Marine Science Support Section, Okinawa Institute of Science and Technology Graduate University

Near-inertial internal waves (NIWs) have been considered to be an important agent for mixing. Near-inertial oscillations had been observed in the deep sea of the Japan Sea, and they are suggested to be the effect of NIWs induced by wind. However, the propagation processes of NIWs are unclear. In this study, velocities from current meters in the deep sea were calculated to estimate the generation regions of NIWs in the deep sea. The frequency of near-inertial oscillations observed in the current meters at Stn. PM5 (134º41' E, 37º42' N) from Oct 12, 2017 to Oct 14, 2018 had lower than the local inertial frequency at Stn. PM5. The current at the deeper depth was more blueshifted than shallower one. This result suggests that the NIWs observed in different depth in the same station were excited in different regions. The characteristics of NIWs based on the climatological density also suggested the NIWs reaching the deep sea are generally excited in the northern area in few degree lower latitude.

Keywords: the Japan Sea, internal waves

©2020. Japan Geoscience Union. All Right Reserved.

Near-inertial shear and widespread intensified thermocline mixing in a seasonally stratified shelf sea

*Wei Yang[1]

1. Tianjin University

Mixing within and across the thermocline in seasonally stratified shelf seas controls nutrients supply from depth, laying the foundation for the growth and distribution of primary producers. Thermocline mixing is nevertheless suppressed by the strong stratification, as a result of which nutrients are usually depleted in the euphotic zone, substantially limiting new productivity. Here we show for the first time that there is widespread intensified thermocline mixing in the summer stratified Yellow Sea with the average thermocline dissipation rate and vertical eddy diffusivity to be 2.2×10^{-7}W $kg^{-1}$and $4.4\times10^{-5}m^2s^{-1}$, respectively. Analysis of mooring and shipboard velocity measurements reveals the presence of energetic downward-propagating near-inertial waves. These waves appeared to have induced strong velocity shear across the thermocline, which generated the observed intensified thermocline turbulence. These results have important implications for nutrients cycling and the maintenance of primary productivity in seasonally stratified shelf seas.

©2020. Japan Geoscience Union. All Right Reserved.

The estimation of the vertical mixing in double diffusive favorable regions of the Indian Ocean by CTD-attached microstructure measurement

*Yusuke Sasaki[1], Ichiro Yasuda[1], Katsuro Katsumata[2], Shinya Kouketsu[2], Hiroshi Uchida[2]

1. Atmosphere and Ocean Research Institute, The University of Tokyo, 2. Japan Agency of Marine-Earth Science and Technology

Although it is suggested in several previous studies that double diffusion is a potentially effective contributor to vertical mixing, it is still challenging for estimating how double diffusion vertically transports heat and salt quantitatively. During the cruise of R/V Mirai along the I08N and I07S sections (MR19-04), microstructure measurements were carried out by fast response thermistors FP07, which were mounted on the CTD rosette. We obtained micro-temperature profiles in salt finger (diffusive convection) favorable regions such as tropical and subtropical zones (Antarctic zones) of the Indian Ocean. The high value of thermal variance dissipation (χ) in these double diffusion favorable regions potentially indicates the enhanced thermal vertical diffusivity, although we should also consider the contribution from the horizontal thermal diffusion. In addition, we discuss the difference of thermal variance spectral shape between double diffusion and turbulence.

Keywords: double diffusion, turbulence, microstructure measurement

©2020. Japan Geoscience Union. All Right Reserved.

Turbulence, internal waves, and associated nutrient supply caused by the Kuroshio southeast of Kyushu

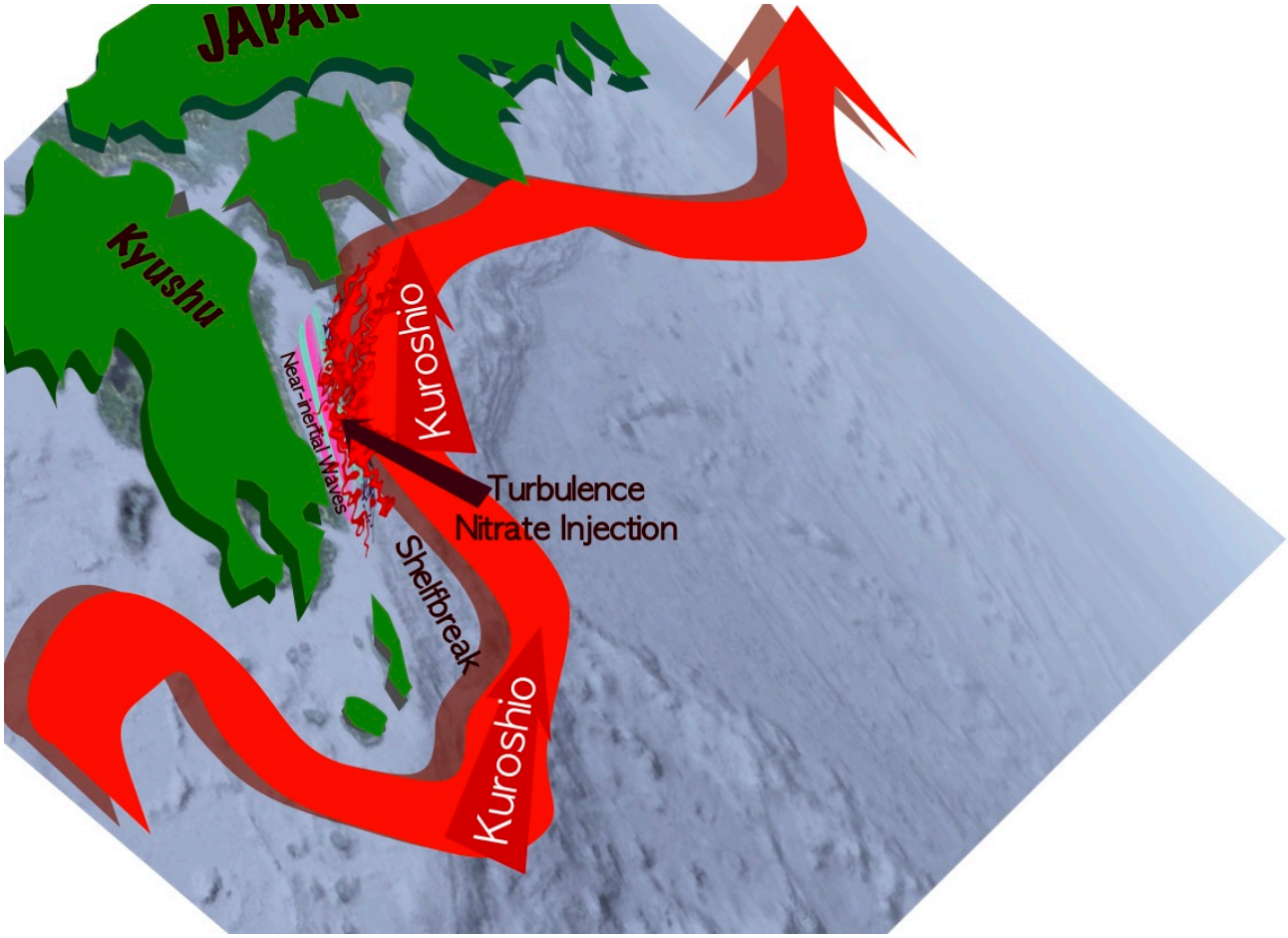
*Duran Gomez Silvana Gloria[1], Takeyoshi Nagai[2]

1. Graduate School of Tokyo University of Marine Science and Technology, 2. Tokyo University of Marine Science and Technology

While surface layers of the Kuroshio Current have been known for being nutrient poor, previous studies reported that the Kuroshio carries a large amount of nutrients in dark subsurface layer. Despite of this, it has been unclear whether these subsurface nutrients can be supplied to the upper layers on the continental shelf in the south of Japan. Results published recently, by the author, showed that the Kuroshio flowing on the shelfbreak induces very strong turbulent dissipation rates O(10^{-7} W kg^{-1}) associated with bands of large amplitude near-inertial internal wave shear, leading to a large diffusive nitrate flux to euphotic zone of >O(1 mmol N m^{-2} day^{-1}). However, questions remain of how these near-inertial internal waves are generated, trapped and induce mixing, and how much contributions to the phytoplankton increase arise. In this study, using a nested high-resolution numerical model, we successfully reproduced these observed features, described above, including banded shear near the Kuroshio. In the presentation, more detailed results will be shown for the lower trophic responses using a coupled ecosystem model.

Keywords: Turbulence, Negative PV, Nitrate flux

©2020. Japan Geoscience Union. All Right Reserved.



©2020. Japan Geoscience Union. All Right Reserved.

Revisit of typhoon's effect on biogeochemistry in the western Pacific subtropical-oligotrophic region

*Makio Honda[1], Yutaka Yoshikawa[2]

1. Japan Agency for Marine-Earth Science and Technology, 2. Kyoto University

Comparative study for biogeochemistry between the western North Pacific subarctic eutrophic region (SAER) and subtropical oligotrophic region (STOR) (K2S1project, Honda et al. JO 2017) revealed that primary productivity in STOR is comparable to or higher than that in SAER. In their study, it was proposed that mesoscale cyclonic eddies contribute to nutrient supply to support primary productivity. On the other hand, it was evaluated that, based on the observation and vertical one-dimensional model (1D model), typhoon passing over the buoy site (KEO) plays minor role in the nutrient supply. However, many previous studies have reported typhoons effects on biogeochemical environments through intense turbulent mixing and upwelling. In addition, it was criticized that the numerical simulation by using the 1D model is less precise in evaluating the typhoon’s effect. Thus, we initiated the revisit of typhoon’s effect on the physical and biogeochemical environments using three-dimensional model (3D model). As preliminary experiment, we performed experiments with axis-symmetric wind stress of virtual typhoon with parameters (e.g., radius and transition speed) similar to observed ones in the STOR, and compared the typhoon effects simulated in the 1D and the 3D models. It was found that, after the virtual typhoon passed, the Ekman upwelling and the near inertial internal wave as observed at the ocean buoy in 2014 at subtropical time-series station KEO appeared in 3D model simulation. It was also found that, in addition to the 1D effect (wind-induced turbulent mixing effect), these 3D effects make the simulated nutrient (N) supply to upper 50 m larger. In future, numerical simulation with actual parameters of observed typhoon data and the associated meteorological / physical oceanographic / chemical oceanographic data will be conducted in order to evaluate typhoon effect on biogeochemistry. In addition, variable case studies will be conducted and it will be discussed what kind of typhoon impact on the subtropical-oligotrophic biogeochemistry significantly.

Keywords: typhoon, subtropical-oligotrophic region, biogeochemistry, 3 dimensional model simulation, Ekman upwelling, near inertial internal wave

©2020. Japan Geoscience Union. All Right Reserved.

Study on the vertical mixing and nutrient supply off the east coast of the Kamchatka

*kimura shino[1]

1. The Univercity of Tokyo

The western subarctic North Pacific and the marginal seas of the Bering Sea and the Okhotsk Sea are known as the areas of world-highest biological CO_2absorption, where the nutrients and carbon significantly decrease from spring to autumn by biological production. This nutrient loss must be compensated by vertical turbulent nutrient transport across the clines of nutrients and density, however diapycnal nutrient supply has not been observed because no turbulence observation has been performed in this area. In the present study, by using the simultaneous observations of turbulence and nutrients performed in the joint Russia and Japan expedition from July 23 to September 14 in 2018, turbulence structure and turbulent nutrient transportwere examined for the first time in the area off the Kamchatka Peninsula. Near at the pycnocline between 150m to 200m depth (potential density 26.5-26.6) corresponding to the maximum density stratification and buoyancy frequency N,′not only turbulent energy dissipation rate ε but also turbulent diffusivity)took the maxima, even though could be decreased for large N. Since the verticalnutrient gradients were also the maxima at pycnocline, vertical turbulent nutrient transporttended to take the maxima, indicating the enhanced turbulence processes of efficient upward nutrient transport. Since these maxima were located just below the dichothermal (temperature minimum) layer representing the base of the previous winter surface mixed layer,it is suggested that the enhanced turbulence plays a role in upward transport of salt and nutrients and in supplying nutrients to the surface mixed layer exposed to surface in winter.Time-series observations of moored multilayer current measurements in the Kamchatka Strait revealed the continuous maxima of vertical shear of horizontal velocity from broad frequency bands from semi-diurnal, near-inertial, diurnal and low-frequency waves at the maxima of turbulent mixing and vertical gradients of density and nutrients. Since the amplitude of downward energy propagating near-inertial wave was attenuated below the pycnocline,breaking of the wind-generated near-inertial waves could contribute to strengthening turbulence and mixing. The observed turbulent vertical nutrient transport across the pycnocline in the offshore of the Kamchatka Peninsula accounts for 20-30% (20% nitrate, 30% silicate, 26% phosphate) of the biological drawdown of nutrients from March to August with the data of Yasunaka et al. (2014).

Keywords: The western subarctic North Pacific, Bering Sea, turbulence, nutrient

©2020. Japan Geoscience Union. All Right Reserved.

Reproduction of Iron-rich Intermediate Water in the Subarctic North Pacific by High-resolution Biogeochemical Model

*Hatsumi Nishikawa[1], Humio Mitsudera[1]

1. Institute of Low Temperature Science, Hokkaido University

Recent observation studies suggest that iron supply from sediment on the northwest continental shelf of the Okhotsk Sea plays an important role in the subarctic primary production (e.g. Nishioka et al., 2013). Dense shelf water (DSW) takes up iron from sediment, thereby transporting iron into the Okhotsk Sea intermediate water. However, observational data is still limited. In this study, we aim to reproduce the iron-rich intermediate water and the iron circulation, using a high-resolution iron circulation model. Our first version model did not reproduce iron-rich intermediate water. Biogeochemical model developed by Parekh et al. (2005) set total ligand concentration to be constant in all places. Recent observations, however, suggest that ligand concentration varies with sea area and water depth. Therefore, we conducted a new experiment with the ligand concentration changed in the vertical direction. The iron concentration of the intermediate water became higher in the new experiment than in the first experiment. Our model also reproduced high biological production, which utilizes the iron-rich intermediate water. In addition, we investigated effect of the tide and the18.6-year cycle.

Keywords: Iron-rich intermediate water, High-resolution model, Tide

©2020. Japan Geoscience Union. All Right Reserved.

Role of tidal mixing on biogeochemical cycling in the northwestern North Pacific

*Kazuhiro Misumi[1], Tsubono Takaki[2], Daisuke Tsumune[2]

1. Planning Group, Central Research Institute of Electric Power Industry, 2. Environmental Science Research Laboratory, Central Research Institute of Electric Power Industry

The northwestern North Pacific is one of the regions with the highest net primary production and the largest seasonal variation in pCO_2 due to carbon uptake by marine phytoplankton. The northwestern North Pacific is adjacent to marginal seas such as the Sea of Okhotsk and the Bering Sea, where strong vertical mixing is caused by breaking internal waves generated by tidal currents and rough submarine topography. It is speculated that the vertical mixing in the straits drives the large pCO_2 variation in the northwestern North Pacific by pumping up nutrients abundant below the surface water, but the quantitative relationship between the tidal mixing and pCO_2 variation is still unclear.

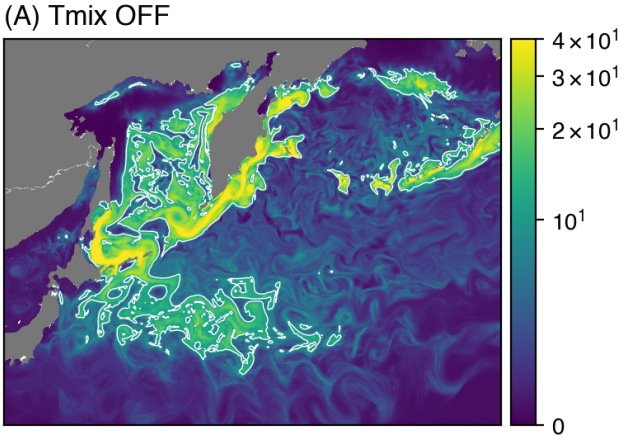
In this study, a marine ecosystem-biogeochemical cycle model was developed targeting on the northwestern North Pacific to investigate the effects of tidal mixing on the primary production in the northwestern North Pacific. ROMS (Regional Ocean Modeling System) was used for the ocean model, and BEC (Biogeochemical Elemental Cycling) model was used for the ecosystem-biogeochemical cycle model. The resolution of the physical model was set to 1/12˚ to realistically reproduce the marine physical characteristics of the northwestern North Pacific: the subtropical and subarctic circulations, the Kuroshio-Oyashio confluence zone and the formation of the North Pacific Intermediate Water. The BEC model incorporates the five nutrient cycling (nitrate, ammonia, phosphate, silicate, iron) and carbonate system geochemistry, and can simulate the dynamics of large and small phytoplankton. The vertical mixing due to tide was calculated by converting the energy conversion rates calculated by a tide model into vertical diffusion coefficients by a parameterization.

The results of the cases where the vertical mixing due to tide was not considered (Tmix OFF) and considered (Tmix ON) showed a clear difference in the concentrations of phytoplankton biomass in the northwestern North Pacific (Figure: monthly mean phytoplankton biomass concentrations on April, units are in $mmolC/m^3$, the while line represents 10 $mmolC/m^3$ and colors above it are filled in log scale). The increase in phytoplankton biomass was remarkable in the straits, suggesting that vertical mixing due to tides increased the net primary production locally by pumping nutrients up. In addition, the increase in the biomass was also observed periphery of the straits and the Kuroshio-Oyashio confluence zone. The increase in the periphery of the straits is likely attributed to horizontal transport of biomass and/or nutrients by eddies, while the increase in the confluence zone is likely because tidal mixing changed a large-scale vertical structure of nutrient, which increased nutrient entrainment by the surface boundary layer mixing.

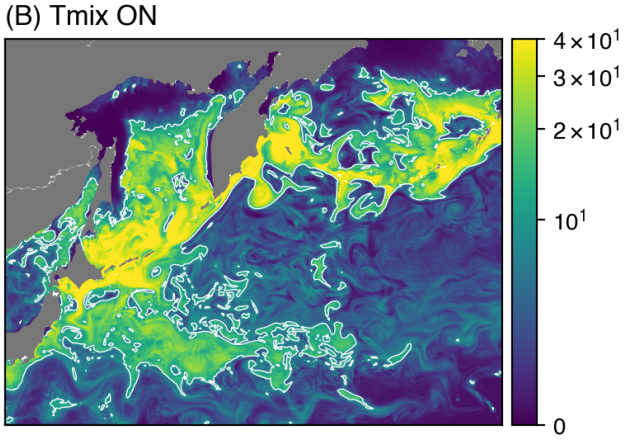
Keywords: Diapycnal mixing, Net primary productivity, Nutrients, Iron

©2020. Japan Geoscience Union. All Right Reserved.

(A) Tmix OFF



(B) Tmix ON



©2020. Japan Geoscience Union. All Right Reserved.

Interannual variations in primary productivity in the North Pacific western subarctic gyre (WSG), assessed by using settling particle delta N-15

*Yoshihisa Mino[1], Makio Honda[2], Fujiki Tetsuichi[2], Minoru Kitamura[2], Naomi Harada[2]

1. Nagoya University, 2. Japan Agency for Marine-Earth Science and Technology

Stable delta N-15 of particles trapped at 500 m of station K2 showed higher values in winter and lower in summer. This pattern would reflect mainly seasonal change in surface layer ammonium delta N-15 due to isotopic fractionation by light-controlled nitrification and the subsequent ammonium assimilation by phytoplankton. As a result, particle delta N-15 variations at K2 were significantly correlated with primary productivity (PP) (R^2= 0.94), which is attributable to their respective dependencies on light condition in the upper mixed layer. By applying this relationship to the time-series particle delta N-15, we here constructed monthly mean PP at K2 during 2010–14. The estimated PP ranged from 89 to 790 mg m^{-2} d^{-1} (in carbon equivalents) with the annual maximums appeared in Jun to Aug. As for the seasonal means in each year, we found an increasing trend of spring PP (Apr–Jun) while summer PP (Jul–Sep) decreased with time. If this indicates that the initiation timing of phytoplankton bloom became earlier during 2010–14, it would result from less light limitation in spring 2013–14 than before due to a reducing upper ocean mixing. With data in 2015–2019, interannual variations in the WSG productivity are addressed further.

Keywords: North Pacific western subarctic gyre, Primary productivity, Sediment trap, Stable nitrogen isotope

©2020. Japan Geoscience Union. All Right Reserved.

Seasonal dynamics of zooplankton at station K2, NW Pacific, reconstructed from archived ADCP data

*Minoru Kitamura[1], Motoyo Itho[1]

1. Japan Agency for Marine-Earth Science and Technology

By using the archived mooring ADCP data, we obtained time-series of acoustic backscattering strength at station K2 (47ºN, 160ºE), the western subarctic North Pacific. In the pelagic water column, main acoustic scatterers are thought to be zooplankton. Actually, many researches showed that the acoustic backscattering strengths have good correlation with zooplankton biomasses in many area of the oceans. In this study, we reconstructed zooplankton dynamics using the acoustic backscattering strength as proxy of zooplankton biomass. ADCPs were moored at 370-400 m in depths at the K2 from 2015 summer to 2018 summer. The echo intensities recorded by ADCPs were converted to acoustic backscattering strength (Sv) in dB according to the following equation (Deines, 1999);

$$Sv = C + 10\log_{10}((T_x + 273.16) \times R^2) - L_{DBM} - P_{DBM} + 2\alpha R + K_c(E - E_r)$$

where C is an empirical constant, T_x is the temperature of the transducer, R is the range along the beam to the scatterers, L_{DBM} is the transmit pulse length, P_{DBM} is the transmit power, α is the absorption coefficient, K_c is a conversion factor for eco intensity from counts to dB, E is the echo intensity in counts, and E_r is the reference echo intensity which was taken as the instrument-specific lowest measured value over the mooring period. Although we could not obtain the acoustic data between sea surface and ca 30 m in depth due to side lobe effect of sound, four years time-series of backscattering strengths between 30 and 350 m was successfully collected. In the poster, we will describe seasonal variability and diel change of acoustic backscattering strength at K2. During the summer of 2016, strong current velocity was observed and the moored ADCP sank down to 660 m in depth. We will also discuss zooplankton dynamics during the event.

Keywords: zooplankton, acoustic backscattering , western subarctic North Pacific

©2020. Japan Geoscience Union. All Right Reserved.

Variations in egg production rates of *Calanus sinicus* (Copepoda: Calanoida) estimated by gonad morphology

*Kiyotaka Hidaka[1], Shinji Shimode[2], Takashi Fushima[2]

1. Japan Fisheries Research and Education Agency, 2. Yokohama National University

Ocean mixing brings nutrients to surface layer, which in turn enhance phytoplankton production. Phytoplankton can increase in number and biomass in a short time by cell division, hence increase of cell abundance or chlorophyll concentration can be seen nearby the area of nutrient supply. In contrast, multicellular zooplankton, e.g. copepods, takes time to increase in number, as improvement of food condition brings increase in egg production first. It takes several days to weeks for the development of the eggs to the adults and thus biomass increase in multicellular zooplankton would occur away from the area of nutrient supply, which makes it difficult to be distinguished. Here, we developed a method to estimate egg production rate (EPR) of *Calanus sinicus*, one of the dominant copepods around Japan, based on the observation of gonad morphology. Niehoff and Runge (2003) first established the method for *C. finmarchicus* and EPR can be estimated without culture experiment. The method was applied to the time series sample collected around the Tosa Bay and we found the long-term fluctuation of the EPR of *C. sinicus,* which was different to its abundance fluctuation.

Keywords: ocean mixing, copepoda, egg production, Calanus sinicus

©2020. Japan Geoscience Union. All Right Reserved.

[E] Poster | A (Atmospheric and Hydrospheric Sciences)：A-OS Ocean Sciences & Ocean Environment

[A-OS25] Continental-Oceanic Mutual Interaction: Planetary scale Material Circulation

convener:Yosuke Alexandre Yamashiki(Earth & Planetary Water Resources Assessment Laboratory Graduate School of Advanced Integrated Studies in Human Survivability Kyoto University), Yukio Masumoto(Graduate School of Science, The University of Tokyo), Swadhin Behera(Climate Variation Predictability and Applicability Research Group, Application Laboratory, JAMSTEC, 3173-25 Showa-machi, Yokohama 236-0001), Takanori Sasaki(Department of Astronomy, Kyoto University)

The main purpose of this session is to promote discussion on mutual interaction between Continental zone and Oceanic zone. The global-scale material circulation induced by River runoff through oceanic general circulation as major topic on Continental-Oceanic Interaction, where the ENSO / IOD influence into continental climate as major topics on Oceanic-Continental Interaction. Numerical simulation and field observation of radionuclide transport from continental zone into ocean and its potential impact is also important topics of this session. The session also extend discussion on planetary hydrology and oceanography focusing on subsurface ocean in Jupiter's moon & Ancient Martian Oceanography & Hydrology by possible application of terrestrial GCM into Ancient Mars. In addition, impact of planetary radiation environment induced by Solar Energetic Particles on the transition of surface hydrological environment will be focused.

[AOS25-P01] Ionizing Radiation at the Martian Surface during Young and Current Sun

*Yosuke Alexandre Yamashiki[1], Hiroyuki Maehara[2], Vladimir Airapetian[3], Yuta Notsu[4], Tatsuhiko Sato[5] (1.Earth & Planetary Water Resources Assessment Laboratory Graduate School of Advanced Integrated Studies in Human Survivability Kyoto University, 2.Okayama Branch Office, Subaru Telescope, National Astronomical Observatory of Japan, 3.NASA/GSFC, 4.Laboratory for Atmospheric and Space Physics, University of Colorado Boulder, 5.Nuclear Science and Engineering Center, Japan Atomic Energy Agency (JAEA),)

[AOS25-P02] The internal ocean in a closure environment

*Hiroaki Sato[1], Tomomi Kubo[1], Ami Hashimoto[1], Hayate Hirai[1], Yusaku Miyashita[1], Yosuke Alexandre Yamashiki[3], Katie Morgan[2] (1.Kyoto University, 2.University of Arizona, 3.Graduate School of Advanced Integrated Studies in Human Survivability Kyoto University)

[AOS25-P03] Japanese small water supply facility and depopulation

*Sayaka Hori[1] (1.Kyoto University)

[AOS25-P04] A Method to Forecast Extreme River Discharges from Typhoon Hagibis 2019 and Western Japan Floods 2018

*Josko Troselj[1], Han Soo Lee[1] (1.Graduate School for International Development and Cooperation, Hiroshima University)

[AOS25-P05] Scientific illustration and Computer Graphics of exoplanets in *Exo* Kyoto's extrasolar planet catalog

*Nami Kimura[1], Yosuke Alexandre Yamashiki[1], Hiroaki Sato[1] (1.Kyoto University)

[AOS25-P06] Methodology for Recognizing Marine Creature by Using Neural Network Based Image Recognition in Shirahama Area: Example of *Dendronephthya gigantea*

*Okamura Shin[1], Yamashiki Yosuke[1] (1.Graduate School of Advanced Integrated Studies in Human Survivability Kyoto University)

[AOS25-P07] Continental-Oceanic Material and Non-Material Interaction: Investigating Methodologies for Heterogenous Dataset Integration

*Andrea Yuri Flores Urushima[1], Yosuke Alexandre Yamashiki[1], Takeshi Ise[1], Yoh Yamashita[1] (1.Kyoto University)

[AOS25-P08] Toward a global SPH simulation of an icy moon with internal ocean

*keiya murashima[1], Takanori Sasaki[1], Natsuki Hosono[2], Yosuke Alexandre Yamashiki[1] (1.Kyoto University, 2.Japan Agency for Marine-Earth Science and Technology)

Ionizing Radiation at the Martian Surface during Young and Current Sun

*Yosuke Alexandre Yamashiki[1], Hiroyuki Maehara[2], Vladimir Airapetian[3], Yuta Notsu[4], Tatsuhiko Sato[5]

1. Earth & Planetary Water Resources Assessment Laboratory Graduate School of Advanced Integrated Studies in Human Survivability Kyoto University, 2. Okayama Branch Office, Subaru Telescope, National Astronomical Observatory of Japan, 3. NASA/GSFC, 4. Laboratory for Atmospheric and Space Physics, University of Colorado Boulder, 5. Nuclear Science and Engineering Center, Japan Atomic Energy Agency (JAEA),

The enhanced magnetic activity of the young sun was an important in the atmospheric evolution and dynamics of the early solar system. Lower solar luminosity associated provided planets a cooler atmospheric and surface environment on the early Earth and Martian surfaces and required production of potent greenhouse gasses in their atmospheres. Within these environments, the dose of ionizing radiation from solar energetic particles (SEPs) from the young Sun could have played an important role in the early phases of planetary habitability. Here, we present a theoretical model of the exposure of the early Mars to high fluence and hard spectra SEPs from the young sun by evaluating the possible magnitude and frequency of solar flares by using possible star spot area, derived from their rotational period. We evaluated annual and maximum flare energy in different cases of sunspot areas for 3%, 5% and 10% of their surfaces. The maximum dose at the Martian top of the atmosphere reaches 5.86 x 10^3Gy (2.65 x 10^2 Sv) at the time when the sunspot area is ~10% of the solar surface. Early atmospheric condition and possible hydrological cycles could have been affected by this strong ionizing radiation.

Keywords: Mars, Ionizing Radiation, Solar Flare

©2020. Japan Geoscience Union. All Right Reserved.

The internal ocean in a closure environment

*Hiroaki Sato[1], Tomomi Kubo[1], Ami Hashimoto[1], Hayate Hirai[1], Yusaku Miyashita[1], Yosuke Alexandre Yamashiki[3], Katie Morgan[2]

1. Kyoto University, 2. University of Arizona, 3. Graduate School of Advanced Integrated Studies in Human Survivability Kyoto University

The inner ocean created in Biosphere 2 was a unique structure, imitating the major components of the surface of the Earth inside of a closed environment. During SCB2 (Space Camp at Biosphere 2) all participants joining the camp evaluated the vertical structure of the internal artificial ocean and its basic physical parameters. We found that the all parameters are quite uniform due to the continuous mixing process in the facility. There were some regions where not enough mixing was found with characteristic local ecosystems cultivated inside of the artificial ocean. In this survey we discuss the ideal form of a space colony on the surface of other terrestrial planets and advantages and disadvantages of creating an “artificial ocean” inside of the structure. A certain atmospheric pressure is needed to maintain water in liquid form on the surface of those structures. On a smaller scale, the hydrological cycle may not be able to maintain certain salinity level in the ocean components, at the same time, freshwater should be used for drinking water and irrigation. The ocean, as the dominant component of the Earth, has a certain difficulty in maintaining in a different environment, and it may have specific characteristics for providing new earth-like environments essential for human life.

Keywords: Ocean, closure environment

©2020. Japan Geoscience Union. All Right Reserved.

Japanese small water supply facility and depopulation

*Sayaka Hori[1]

1. Kyoto University

The population decline in Japan is expected to change the function of its local small water supplies. Those water supplies would no longer be able to independently maintain their public function such as services that have formerly taken for granted. The population is decreasing in 40 prefectures among all 47 in 2018. Only seven prefectures are increasing populations. In the depopulated area, shortage of human resources and lack of financial sources are a situation without waiting, and without the aid of the national government, the future will be challenging to maintain the small village any longer. The youth was leaving their hometown, and the old residents take care of its local small water supply's utilities. What kind of immediate action can be taken becomes a bottleneck. The progress of depopulation is inevitable, and many of the problems that are occurring in rural areas are the area where community power is gone.

Not more than 100 population served by piped water is not governed by Water Law. National Water Law does not have a broader application range for small water supplies. It is difficult to extend an application range, that considered in a limited way. Rural residents who live in the region unruled by Water Law, they operate and maintain drinking water by themselves to live.

The Waterworks Law was newly revised to show measures to compensate for the limitations of the water supply projects and strengthen them. Usually, the ordinance still plays a role to compensate for deficiencies in the law. Regarding the management of small-scale water supply, the management situation for each area is also different, so detailed arrangements are in place according to the ordinance. It is very common to enact a local law supplementary against an opaque legal system on the national level. For example, there is no law so-called Groundwater Law, and many local municipalities make an original ordinance supplementary to manage local groundwater resources as the common property. Enacting an ordinance can be said to be the law to complement loopholes of Water Law.

In this research, we conducted interviews and literature surveys on the small scale water supply present problem and situation, and also, we explore the new future image of Japan's small scale water supply project after the revision law enforcement exploratory. As a result, the current small water supply facility situation is not enough to make complementary or alternative solutions to support rural water supply issues. We still need to discuss how to promote the new revision concept in practice.

Keywords: small water supply, population decline, water law, ordinance

©2020. Japan Geoscience Union. All Right Reserved.

A Method to Forecast Extreme River Discharges from Typhoon Hagibis 2019 and Western Japan Floods 2018

*Josko Troselj[1], Han Soo Lee[1]

1. Graduate School for International Development and Cooperation, Hiroshima University

Introduction and Objective

As a result of climate change impact, record breaking disasters are occurring every year with unprecedented amounts of heavy rainfalls, typhoon intensities and associated coastal sea disasters which bring huge amounts of river water and associated nutrients pollution towards river mouths and into coastal sea zones, where they greatly decrease sea water quality and can negatively impact marine environment for several days or weeks. To mitigate negative impact of such disasters, it is important to develop forecasting or nowcasting of extreme river water levels during flood events, but it is still not well developed due to high uncertainty of its occurrence and absence of available historical data for unprecedented rainfall events.

Troselj et al. (2017) quantitatively evaluated the impact of extreme freshwater outflow to the coastal ocean due to typhoon passage by combining river and ocean models using hourly time step data and remote-sensing technology. With the advance of weather forecasting systems and specific availability of forecasting typhoon trajectory and intensity, we aim to be able to apprehend freshwater impacts on the coastal marine environment in advance of typhoon events.

Objective of the study is to show how to utilize methodology developed in the previous study to forecast the most recent extreme flood events occurred in Kanto region of Japan due to passage of Typhoon Hagibis in October 2019 and in Hiroshima region of Japan due to an unprecedented rainfall induced disaster in July 2018.

Methods

We continued the study from Troselj et al. (2017) by testing how river mouth discharges for 9 first class rivers calibrated in the previous study on Typhoons Chataan 2002 and Roke 2011 could have been nowcasted during the passage of Typhoon Hagibis in 2019. We assumed that we had available input meteorologically forecasted data which corresponds to MLIT observed data after the event. Furthermore, the same methodology was applied for heavy rainfall events of 2005 and 2018 for Ota River basin in Hiroshima, Japan, because these events had similar rainfall patterns.

Discussions

We showed that the model used in the study has the capability of simulating extreme discharge events by calibration using previous extreme Typhoon case events with similar trajectory. When using calibrated river basins parameters from Typhoons Chataan and Roke for projection of the Typhoon Hagibis, the

©2020. Japan Geoscience Union. All Right Reserved.

calculated Nash-Sutcliffe efficiency values (NSE) have mostly been bigger than 0.8 and 0.9, respectively. Exceptions are the most northern rivers Mabechi and Takase which did not show a significant fit due to being located too far away from the trajectory of the Typhoon Hagibis. These results suggest that our models calibrated on Typhoons Roke or Chataan cases can be successfully applied to forecast river runoff values from other similar extreme precipitation events, and furthermore newly calibrated parameters from Typhoon Hagibis can be used as an additional forecasting tool.

Results for cross-calibration and cross-validation of the heavy rainfall events of 2005 and 2018 for Ota River basin in Hiroshima will be finalized and similarly discussed before the JpGU conference, when MLIT releases Ota River discharge data for 2018.

Summary

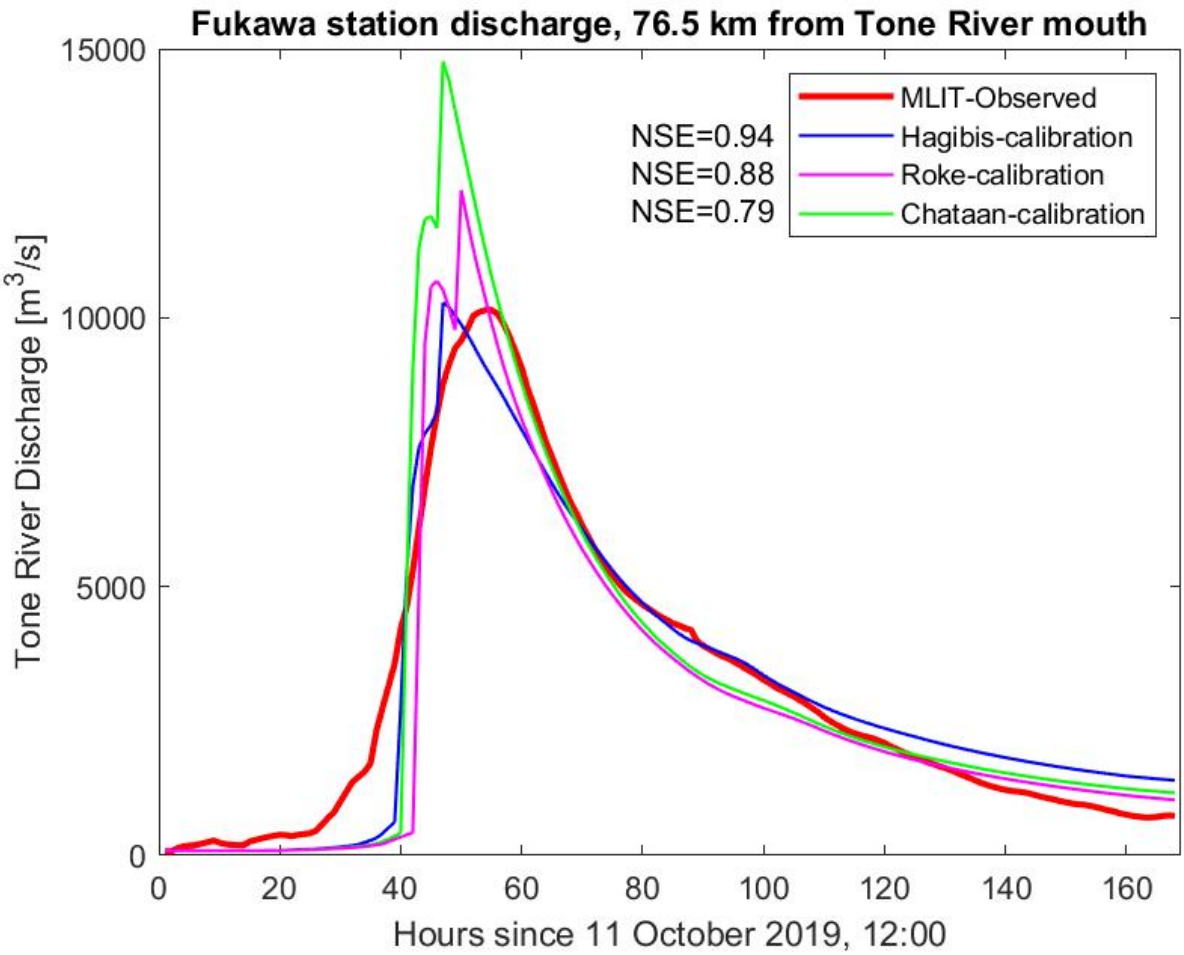
The extreme discharge events have a lot of uncertainties and differences among their physical processes. However, we emphasize their similarities by calibrating river basin response to particular rainfall and afterwards using the calibrated parameters of the basin to forecast the river discharge from a future event with similar forecasted rainfall pattern.

Reference

Troselj J, Sayama T, Varlamov SM, Sasaki T, Racault M-F, Takara K, Miyazawa Y, Kuroki R, Yamagata T, Yamashiki Y (2017). Modeling of extreme freshwater outflow from the north-eastern Japanese river basins to western Pacific Ocean, Journal of Hydrology, Vol. 555, pp. 956-970, doi:10.1016/j.jhydrol.2017.10.042.

Keywords: extreme river discharge, Typhoon Hagibis 2019, western Japan floods 2018, CDRM hydrological model, SCE-UA optimization method, nowcasting

©2020. Japan Geoscience Union. All Right Reserved.



©2020. Japan Geoscience Union. All Right Reserved.

Scientific illustration and Computer Graphics of exoplanets in *Exo* Kyoto’ s extrasolar planet catalog

*Nami Kimura[1], Yosuke Alexandre Yamashiki[1], Hiroaki Sato[1]

1. Kyoto University

The Exoplanetary database ExoKyoto possesses several different components concerning the habitability, together with the illustration of newly discovered planets. In this platform we generate texture of ocean planets for most of the cases, assuming that the surface of those planets are covered with the similar type of terrestrial ocean. The texture are selected based on the estimated physical characteristics of discovered exoplanets. In addition to these scientific images, we make 3D animation with the adobe After effects plugin,OPB which supports physical base shading and implements bump mapping and environmental reflection. The adjustable parameters are 3D objects, Radius, Position, Rotation XYZ, Material, Maps, UV, Render etc. Users can create realistic planets by adjusting these parameters. In this study we’ ll discuss the motivation and scientific validity in using such imaginary ocean planet for the scientific outreach purpose.

Keywords: exoplanet, scientific illustration , outreach

©2020. Japan Geoscience Union. All Right Reserved.

Methodology for Recognizing Marine Creature by Using Neural Network Based Image Recognition in Shirahama Area: Example of *Dendronephthya gigantea*

*Okamura Shin[1], Yamashiki Yosuke[1]

1. Graduate School of Advanced Integrated Studies in Human Survivability Kyoto University

At the 10th Conference for the Convention on Biological Diversity (CBD / COP10) that was held in Nagoya, Aichi Prefecture in October 2010, some global goals were set that form the core of the Strategic Plan for Conserving Biodiversity 2011-2020. The meeting agreed to take urgent and effective action to halt the loss of biodiversity by 2020. One of the goals of Aichi is that by 2020, at least 17% of terrestrial and inland waters, and 10% of coastal and marine waters, especially those that are particularly important to biodiversity and ecosystem services. However, to achieve this goal, several problems need to be overcome. For example, it is unclear where to set up new protected areas and how to expand existing ones. When considering the spatial design of a protected area, it should be considered that protected areas should be located in areas where many species live or areas where valuable organisms are distributed. Therefore, it can be said that spatial distribution information of various species that constitute biodiversity is indispensable for the spatial design of protected areas. From the above background, it can be said that it is necessary to accumulate information on the spatial distribution of various species that constitute biodiversity from the viewpoint of ecosystem protection. It is especially required to collect and accumulate information on seawater environment from the viewpoint of ecosystem protection. Currently, the International Oceanographic Data and Information Exchange (IODE) is known as an international oceanographic data and information exchange system, and the Ocean Biographic Information System (OBIS) is responsible for the database part. OBIS is a database that holds records of the appearance of marine life, and data is collected from various parts of the world. However, OBIS has a problem which is the quantity of data is not enough. Specifically, of the 250,000 species of marine life that have been discovered, only about 120,000 species exist in this database, and only about 56,000 species out of about 33,000 species in the Sea of Japan. In addition, OBIS has spatial data bias because these data are difficult to obtain underwater position information. It has also been found that maintaining these databases requires a great deal of effort. Confirmation work by specialists is required to specify the species, and it is considered that the more data the data amount, the more difficult it becomes. Given this background, I would like to propose a method for identifying species using image recognition. Specifically, we hope to use machine learning to create a comprehensive species-specific model. Such a model reduces the time and effort required to maintain for specialists, and enables species to be confirmed in various regions. We believe that this will affect various areas such as strengthening the marine database, concomitant ecosystem maintenance, and fisheries. In this paper, a classification model of *Dendronephthya gigantea* was created by using underwater image data acquired in the Shirahama area and convolutional neural network. As a result, we observed 83% of accuracy for gray scaled image classification task for *Dendronephthya gigantea.* From our results, it was confirmed that the accuracy did not get better for 60 iterations. This behavior seems to have caused over-learning was confirmed. In particular, the reason why there is no change in accuracy in train step and accuracy in test is considered to be that certain image data is extremely difficult to recognize. Therefore, it is considered necessary to select the data to be used in order to achieve high accuracy.

©2020. Japan Geoscience Union. All Right Reserved.

Keywords: Ocean biology, Image recognition, Neural Network

©2020. Japan Geoscience Union. All Right Reserved.

Continental-Oceanic Material and Non-Material Interaction: Investigating Methodologies for Heterogenous Dataset Integration

*Andrea Yuri Flores Urushima[1], Yosuke Alexandre Yamashiki[1], Takeshi Ise[1], Yoh Yamashita[1]

1. Kyoto University

This research aims to develop a methodology that allows to correlate the human perception of watersheds' change with oceanic water quality change due to run off from a hydrographic system. This will be done through correlating heterogenous datasets from natural and social sciences between 2003-2019 with a focus on the case study of Yuragawa watershed. This investigation will discuss research pathways that potentially allow to relate Chlorophyll-a variation at river mouth with the results from the text mining analysis of articles which mention the Yuragawa River from newspapers' database. This research responds to recent trends addressing complex systems, such as the European FuturICT Project, that emphasizes the relevance of combining heterogenous datasets, of both quantitative and qualitative data, from natural and social sciences. This is a preliminary study that aims at investigating the possible threads of correlation between two types of datasets that are rarely analysed together. While text mining has been increasingly used to investigate social behavior prediction, chlorophyll-a data has been mainly used in natural sciences as a bio-chemical description of water nutrients. The relevance of using newspaper text mining data to analyze environmental change is that this type of data allows to combine cognitive and emotional perception of human everyday life needs to the analysis of natural changes.

Keywords: Yuragawa Watershed, Continental-Oceanic Interaction, Heterogenous Data

©2020. Japan Geoscience Union. All Right Reserved.

Toward a global SPH simulation of an icy moon with internal ocean

*keiya murashima[1], Takanori Sasaki[1], Natsuki Hosono[2], Yosuke Alexandre Yamashiki[1]

1. Kyoto University, 2. Japan Agency for Marine-Earth Science and Technology

There are some traces of existence of internal ocean in some icy moons, such as a plumes of vapor of Europa and Enceladus. Since liquid water would be essential for the origin of life, it is important to understand the development of inner sea, especially the temperature distribution/evolution inside the icy moons. Thus, we aim to simulating the development of an internal ocean of an icy moon by 3-dimensional numerical fluid calculations using Smoothed Particle Hydrodynamics (SPH) method.

It is considered that the balance between the tidal heating caused by tidal acceleration and radiative cooling sustains liquid water beneath the surface of an icy moon. So, we added viscosity, conductive heat transfer and radiative cooling terms into the governing equations of SPH method. In addition, we take latent heat of phase transition into consideration. We will report the progress of our project toward a global SPH simulation of the internal ocean.

Keywords: inner ocean, SPH

©2020. Japan Geoscience Union. All Right Reserved.

[E] Poster | A (Atmospheric and Hydrospheric Sciences)：A-HW Hydrology & Water Environment

[A-HW30] Hydrology & Water Environment

convener:Ayumi Kotani(Graduate School of Bioagricultural Sciences, Nagoya University), Takeshi Hayashi(Faculty of Education and Human Studies, Akita University), Keisuke Fukushi(Institute of Nature & Environmental Technology, Kanazawa University), Masahiro Tanoue(School of Engineering, The University of Tokyo)

We focus on various issues of water cycle and environment and aim to answer questions of hydrological and earth system sciences; 1) surface, subsurface and evapotranspiration processes of water cycle, 2) natural and anthropogenic hydrothermal systems, 3) environments issues and studies on a watershed or global scale, 4) water-related issues with ecological, environmental, and geochemical aspects, and 5) other issues in hydrological sciences. We welcomes presentations regarding various kinds of approaches and techniques such as field survey, remote sensing, isotope tracers, numerical simulation, and theoretical analysis. This session is jointly hosed by societies of water-related geoscience (Geochemical Society of Japan, Japanese Association of Groundwater Hydrology, Japanese Association of Hydrological Sciences, and Japan Society of Hydrology and Water Resources), and accepts wide-range research topics related to water cycle and environment described above.

[AHW30-P01] Impact of climate change on the surface water balance and groundwater level in the Kurobe River basin, Japan

*Takuya Matsuura[1], TEBAKARI TAICHI[1] (1.Toyama prefectural University)

[AHW30-P02] Assessment of the precipitation characteristics and identification of urban flooding hotspots for an Indian satellite town

*Osheen Mehta[1], Mitthan Lal Kansal[1] (1.Indian Institute of Technology Roorkee)

[AHW30-P03] Dynamics of terrestrial water storage in three major river basins over Peninsular India

*Abhishek .[1], Tsuyoshi Kinouchi[2] (1.Indian Institute of Technology Roorkee, 2.Tokyo Institute of Technology)

[AHW30-P04] Comparing constant dispersivity with scale-dependent one: for heated water injection case

*Ye-Chen Lin[1], Hund-Der Yeh[1] (1.National Chiao Tung University)

[AHW30-P05] Similarities and differences among ten global water models in modelling water use

*Camelia Eliza Telteu[1], Hannes Müller Schmied [1,2], Wim Thiery [3], Guoyong Leng [4], Peter Burek [5], Xingcai Liu [4], Julien Eric Stanislas Boulange [6], Lauren Paige Seaby[7], Manolis Grillakis[8], Yusuke Satoh [6], Oldrich Rakovec[9], Tobias Stacke[10], Jinfeng Chang[11,5], Niko Wanders[12], Harsh Lovekumar Shah [13], Ganquan Mao[14], Aristeidis Koutroulis [8], Yadu Pokhrel [15], Luis Samaniego [9], Yoshihide Wada [5], Vimal Mishra [13], Junguo Liu [14], Petra Döll [1,2], Simon Newland Gosling [16], Jacob Schewe [7], Fang Zhao [17] (1.Institute of Physical Geography, Goethe University Frankfurt, Frankfurt am Main, Germany, 2.Senckenberg Leibniz Biodiversity and Climate Research Center, Frankfurt am Main, Germany, 3.Department of Hydrology and Hydraulic Engineering, Vrije Universiteit Brussel, Brussels, Belgium, 4.Key Laboratory of Water Cycle and Related Land Surface Processes, Institute of Geographic Sciences and Natural Resources Research, Chinese Academy of Sciences, Beijing, China, 5.International Institute for Applied Systems Analysis, Laxenburg, Austria , 6.National Institute for Environmental Studies, Tsukuba, Japan , 7.Potsdam Institute for Climate Impact Research, Potsdam, Germany , 8.School of Environmental Engineering, Technical University of Crete, Chania, Greece , 9.Helmholtz Centre for Environmental Research, Leipzig, Germany , 10.Institute of Coastal Research, Helmholtz-Zentrum Geesthacht, Geesthacht, Germany, 11.Laboratoire des Sciences du Climat et de l'Environnement, Gif-sur-Yvette, France, 12.Department of Physical Geography, Utrecht University, Utrecht, the Netherlands, 13.Indian Institute of Technology Gandhinagar,

Palaj, Gandhinagar, India, 14.School of Environmental Science and Engineering, Southern University of Science and Technology, Shenzhen, China , 15.Department of Civil and Environmental Engineering, Michigan State University, East Lansing, Michigan, United States of America , 16.School of Geography, University of Nottingham, Nottingham, United Kingdom of Great Britain and Northern Ireland, 17.School of Geographic Sciences, East China Normal University, Shanghai, China)

[AHW30-P06] Discussion on the correlation between professional characteristics and willingness to pay for ecosystem services

*Li-chun Peng[1], Yu-pin Lin[1], Wan-yu Lien[1] (1.National Taiwan University)

[AHW30-P07] Seasonal variability of stable isotopes in precipitation over Indonesia observed for 2010-2018

*Kimpei Ichiyanagi[1], Takayuki Uesugi[1], Rusmawan Suwarman[2], Halda Aditya Belgaman[3], Masahiro TANOUE[4] (1.Kumamoto University, 2.Bandung Institute of Technology, 3.Badan Pengkajian dan Penerapan Teknologi, 4.Shibaura Institute of Technology)

[AHW30-P08] Finding the optimal time for the integration in Lagrangian analysis for the best estimation of moisture sources.

*Raquel Nieto[1], Luis Gimeno[1] (1.University of Vigo)

[AHW30-P09] ATMOSPHERIC MOISTURE SOURCES ASSOCIATED WITH EXTREME PRECIPITATION DURING THE PEAK PRECIPITATION MONTH

*Luis Gimeno[1], Marta Vazquez[1,2,3], Raquel NIETO [1], Margarida Liberato[2,3] (1.Environmental Physics Laboratory (EPhysLab), CIM-UVigo, Universidade de Vigo, Ourense, Spain, 2.Instituto Dom Luiz (IDL), Faculdade de Ciências, Universidade de Lisboa, 1749-016 Lisboa, Portugal, 3.Escola de Ciências e Tecnologia, Universidade de Trás-os-Montes e Alto Douro, Vila Real, Portugal)

[AHW30-P10] SEASONAL VARIATION OF DISSOLVED TRACE ELEMNTS IN LAKE KIBA-GATA

*Ariunsanaa BATERDENE[1], Seiya NAGAO[2], Keisuke Fukushi[2], Kohei Sakaguchi[1], Tetsuya Matsunaka[2] (1.Graduate School of Natural Science and Technology Kanazawa University, 2.Institute of Nature and Environmental Technology, Kanazawa University)

[AHW30-P12] Study on the origin of hot spring water using the deep part of Inubohsaki Onsen’s core.

*Satoko Tezuka[1], Mana Kamata[1] (1.Chiba Institute of science)

[AHW30-P13] *Lysimeter experiments to assess the influence of afforested vegetation on effective infiltration and recharge in a semi- arid area*

*Zaiyong Zhang[1], Wenke Wang[1], Chengcheng Gong[1], Harrie-Jan Hendricks Franssen[2], Philip Brunner[3] (1.Chang'an University, 2.Agrosphere (IBG-3), Forschungszentrum Jülich GmbH, Jülich, Germany, 3.Center for Hydrogeology and Geothermics, (CHYN), University of Neuchatel, Switzerland)

[AHW30-P14] Development of a Multi-function Water Depth Sensor in the Irrigated Paddy Fields for Water Resource Management and Precision Agriculture

*Chun-Yen KUO[1] (1.National United University)

[AHW30-P15] Dynamic calibration of tipping-bucket rain gauges and flow meters for precise measurements of rainfall partitioning

*Shin'ichi Iida[1], Takanori Shimizu[1], Yoshinori Shinohara[2], Tomo'omi Kumagai[3], Darryl E. Carlyle-Moses[4], Delphis F. Levia[5] (1.Forestry and Forest Products Research Institute, 2.University of Miyazaki, 3.University of Tokyo, 4.Thompson Rivers University, 5.University of Delaware)

[AHW30-P16] Understory biomass measurement based on SfM data by a manual low-flying drone under the canopy

*Yupan Zhang[1], Yuichi Onda[1], Xinchao Sun[2], Takashi Gomi[3] (1.Center for Research on Isotopes and Environmental Dynamics, University of Tsukuba, Ibaraki, Japan, 2.Institute of Surface-Earth System Science, Tianjin University, Tianjin , PR China, 3.Department of International Environmental and Agricultural Science, Tokyo University of Agriculture and Technology, Tokyo , Japan)

[AHW30-P17] Seasonal changes in the canopy water balance of Japanese plantation forest

*Linh Thuy Pham[1], Yuichi Onda[1], Xinchao Sun[2], Sean Andrew Hudson[1], Janice Elaine Hudson[1], Yupan Zhang[1], Chiu Wei Chen[3] (1.University of Tsukuba, 2.Tianjin University, 3.Tokyo University of Agriculture and Technology)

Impact of climate change on the surface water balance and groundwater level in the Kurobe River basin, Japan

*Takuya Matsuura[1], TEBAKARI TAICHI[1]

1. Toyama prefectural University

The purpose of this study is to clarify the impact of climate change on the surface water balance of the Kurobe River basin using distributed water balance model. The impact of climate change on the groundwater level of the Kurobe River alluvial fan was clarified by using the infiltration estimated water balance analysis as the boundary condition of the three-dimensional groundwater model.

It has been pointed out that the late 21st century of temperature under RCP 8.5 scenario increase by 2.6-4.8 ℃ anomaly relative to 1986-2005. In the future, climate change is projected to raise the temperatures and reduce both snowfall and snowmelt, which is projected to alter snow melting and thus affect water resources and groundwater environment in the Kurobe River catchment. There are many studies on climate change impact on river flow and surface runoff. The impact of climate change on groundwater environment is predicted to change the groundwater level and the recharge area, but there is no quantitative impact assessment study just yet.

In this study, we assessed the impact of climate change on water resources and groundwater levels using the results of several future prediction models. We used two future scenarios (Representative Concentration Pathways RCP2.6 and RCP8.5). This study use the 2014 land use data from the Ministry of Land, Infrastructure, Transport and Tourism, Japan. The layer structure of the groundwater model was created using 731 columnar data. The calculation time interval is daily for water balance analysis and monthly for groundwater analysis.

As a result of comparing the present climate (1981-2000) and future climate (2081-2100) under RCP2.6 and RCP8.5, it was clarified that the daily mean precipitation and solar radiation in the Kurobe River basin are not changing. In the case of RCP2.6 scenario, the daily mean temperature did not change between the present climate and the future climate. On the other hand, the RCP8.5 scenario, estimated that the daily mean temperature in the Kurobe River basin rise by 3.6 degrees in the future. As a result of the rise in temperature, the annual snow water equivalent in the Kurobe River basin decrease by 298 cm (50%), the peak of snow water equivalent is 8 days earlier than the current climate and the time of snow melts is the 22 days shifts earlier. In Kurobe River basin, the surface runoff and infiltration the peak timing shifts earlier (25 days) because of an earlier snow melt caused by global warming. As a result of estimating the water resources in the Kurobe River basin, the water cycle in the Kurobe River basin changed significantly in the futur. The main source of groundwater recharge in the Kurobe River alluvial fan is the Kurobe River, and changes in the water cycle of the Kurobe River are projected to have a significant impact on groundwater. As a result of three-dimensional groundwater analysis, it was clarified that the groundwater level of the alluvial fan increased from February to March and decreased from May to June in future.

©2020. Japan Geoscience Union. All Right Reserved.

Assessment of the precipitation characteristics and identification of urban flooding hotspots for an Indian satellite town

*Osheen Mehta[1], Mitthan Lal Kansal[1]

1. Indian Institute of Technology Roorkee

The rapid urbanization and population explosion have become major issues all around the world. Several satellite towns are developed to accommodate the ever-increasing population of metropolitan cities around the world. Gurugram, a prominent satellite city in the national capital region (NCR) of India, has faced frequent urban floods in recent years. Urbanization, besides having adverse impacts on hydro-climatic conditions, has led to a rapid increase in the impervious area. This seals the upper soil layers and thus generates excessive surface runoff causing urban floods. The problem of flooding has impacted public health and society as well as resulted in economic losses. Keeping this in mind, the present study makes an attempt to assess the extreme precipitation characteristics and identify the hotspots in Gurugram from the urban flooding point of view. The trend analysis of 1-day maximum rainfall series has been carried out for a period of 63 years (1951-2013) using the non-parametric Mann-Kendall (MK) test. The hotspots are identified through the rainfall-runoff modelling using the storm water management model (SWMM) developed by the Environmental Protection Agency (EPA), considering the criteria of the discharge rate, flooding hours and volume of flood. In order to initiate actions for its management, the prioritization of the potential hotspots is suggested through the multiple criteria decision analysis (MCDA) technique of choosing by disadvantage (CBD). The MK test results indicate an increase in the high-intensity rainstorms in recent years, leading to frequent urban floods. Further, it has been noticed that the urban drainage problem gets aggravated due to silting and choking of the Najafgarh and Badshahpur drains which ultimately joins the river Yamuna in the northern part of Delhi. This study will be helpful to devise effective planning and management strategies for the Gurugram town under the rapid urbanizing scenario.

Keywords: urbanization, precipitation, urban flooding, hotspots

©2020. Japan Geoscience Union. All Right Reserved.

Dynamics of terrestrial water storage in three major river basins over Peninsular India

*Abhishek .[1], Tsuyoshi Kinouchi[2]

1. Indian Institute of Technology Roorkee, 2. Tokyo Institute of Technology

Synergic impacts of natural and anthropogenic factors such as climate variability and excessive water consumption have led an unprecedented stress on the global water resources with higher concern for the developing nations. Peninsular Indian region has been highlighted as highly non-resilient to hydrological extremes such as droughts. Three major river basins namely, Mahanadi, Krishna, and Godavari having a combined geographical area share of 22 % of the total geographical area of India, and almost similar hydrogeological conditions were selected for the long term assessment of the terrestrial water storage (TWS) dynamics. Five gravity anomaly solutions (two mascon based products and three spherical harmonic based products) from different data processing centers were accessed and processed to get equivalent water thickness and subsequently utilized for understanding the TWS dynamics in terms of the relative anomaly. Generalized three-cornered hat (GTCH) method was employed to get the combined TWS data series corresponding to the minimum uncertainties. The resulting anomaly series showed a piecewise TWS trend of -1.21mm yr^{-1} and -18.81 mm yr^{-1} from April 2002 to June 2010 and July 2010 to May 2017 respectively in Mahanadi basin. The piecewise TWS trends in Krishna and Godavari basins are -12.55 and -4.45 from April 2002 to June 2010, and -30.95 and -10.41 mm yr^{-1} from July 2010 to May 2017, respectively. Despite the different patterns of trends until June 2010, all three basins are showed a high rate of decline in TWS (volume equivalent of 18.17, 54.53, 21.75 km^3, respectively) thereafter. These declining trends of TWS highlight the need of the conjunctive water management strategies, and policymaking in the region for achieving a sustainable and efficient water use at the basin scales.

Keywords: GRACE, Terrestrial Water Storage, Peninsular India

©2020. Japan Geoscience Union. All Right Reserved.

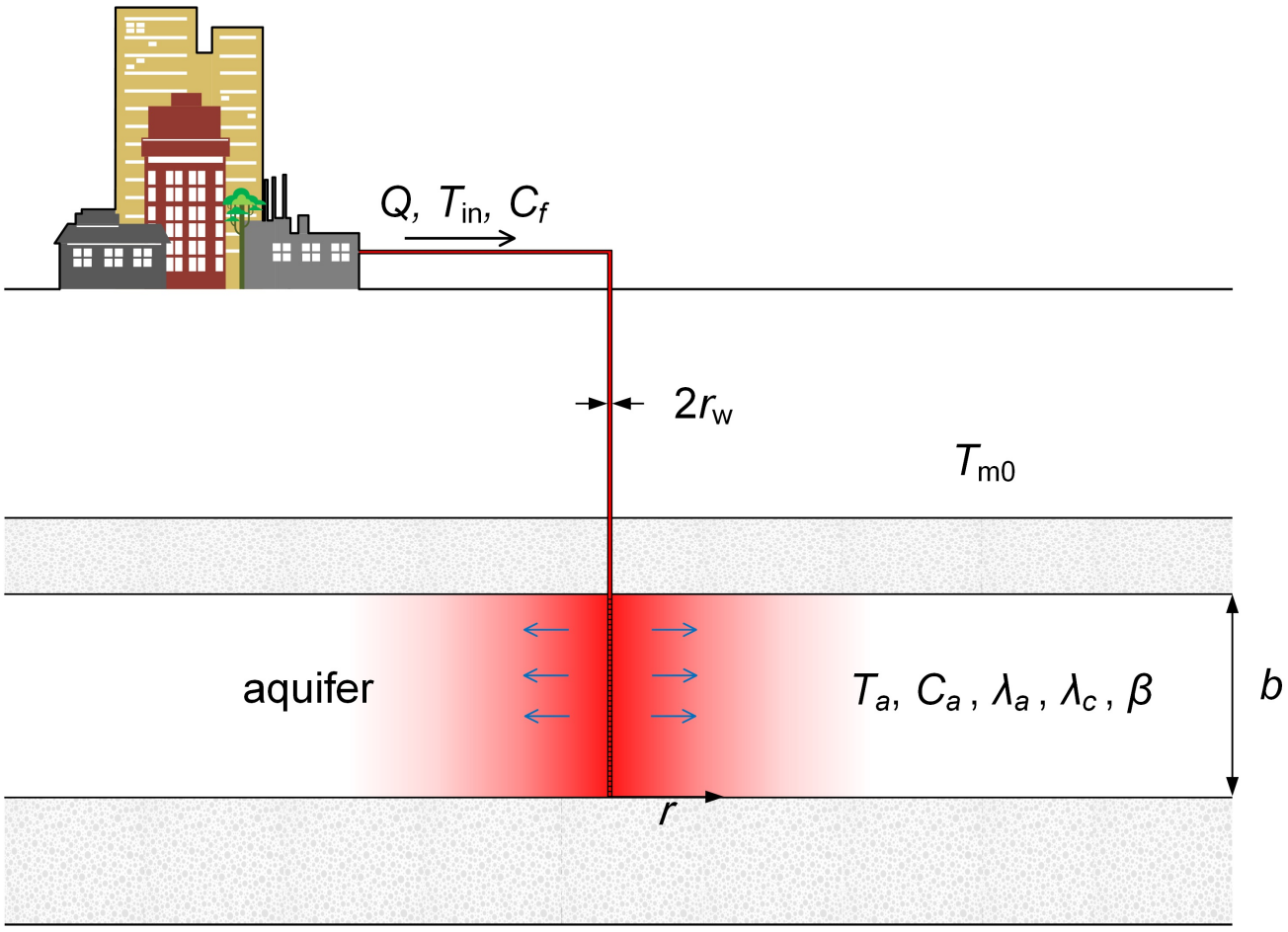
Comparing constant dispersivity with scale-dependent one: for heated water injection case

*Ye-Chen Lin[1], Hund-Der Yeh[1]

1. National Chiao Tung University

Prior studies indicated that the thermal dispersivity generally nonlinearly increases with the distance from a heat flow source in a porous medium. Such dispersivity is termed as scale-dependent dispersivity (SD). However, the existing analytical models for injecting heated water into an aquifer, e.g., aquifer thermal energy storage system, usually assume the dispersivity as a constant to obtain analytical solutions. A question arises here: Is it possible to use a fixed value of constant dispersivity (CD) to represent SD one? To address the question, this study first develops a finite-element model adopting a SD formula to describe the dispersion process due to heated water injection in a confined aquifer. Then, an analytical model considering the CD is used to compare with the aforementioned SD model. The results from this study show that a CD can be found by using an average value of the thermal frontal position over the entire operating period to approximate SD one.

Keywords: aquifer, thermal dispersivity, scale dependence, analytical model, finite-element model



©2020. Japan Geoscience Union. All Right Reserved.

Similarities and differences among ten global water models in modelling water use

*Camelia Eliza Telteu[1], Hannes Müller Schmied [1,2], Wim Thiery [3], Guoyong Leng [4], Peter Burek [5], Xingcai Liu [4], Julien Eric Stanislas Boulange [6], Lauren Paige Seaby[7], Manolis Grillakis[8], Yusuke Satoh [6], Oldrich Rakovec[9], Tobias Stacke[10], Jinfeng Chang[11,5], Niko Wanders[12], Harsh Lovekumar Shah [13], Ganquan Mao[14], Aristeidis Koutroulis [8], Yadu Pokhrel [15], Luis Samaniego [9], Yoshihide Wada [5], Vimal Mishra [13], Junguo Liu [14], Petra Döll [1,2], Simon Newland Gosling [16], Jacob Schewe [7], Fang Zhao [17]

1. Institute of Physical Geography, Goethe University Frankfurt, Frankfurt am Main, Germany, 2. Senckenberg Leibniz Biodiversity and Climate Research Center, Frankfurt am Main, Germany, 3. Department of Hydrology and Hydraulic Engineering, Vrije Universiteit Brussel, Brussels, Belgium, 4. Key Laboratory of Water Cycle and Related Land Surface Processes, Institute of Geographic Sciences and Natural Resources Research, Chinese Academy of Sciences, Beijing, China, 5. International Institute for Applied Systems Analysis, Laxenburg, Austria , 6. National Institute for Environmental Studies, Tsukuba, Japan , 7. Potsdam Institute for Climate Impact Research, Potsdam, Germany , 8. School of Environmental Engineering, Technical University of Crete, Chania, Greece , 9. Helmholtz Centre for Environmental Research, Leipzig, Germany , 10. Institute of Coastal Research, Helmholtz-Zentrum Geesthacht, Geesthacht, Germany, 11. Laboratoire des Sciences du Climat et de l'Environnement, Gif-sur-Yvette, France, 12. Department of Physical Geography, Utrecht University, Utrecht, the Netherlands, 13. Indian Institute of Technology Gandhinagar, Palaj, Gandhinagar, India, 14. School of Environmental Science and Engineering, Southern University of Science and Technology, Shenzhen, China , 15. Department of Civil and Environmental Engineering, Michigan State University, East Lansing, Michigan, United States of America , 16. School of Geography, University of Nottingham, Nottingham, United Kingdom of Great Britain and Northern Ireland, 17. School of Geographic Sciences, East China Normal University, Shanghai, China

Human activity affects river flows and water-related hazards (Veldkamp et al., 2018). Global water models are indispensable tools for the assessment and prediction of water availability and demand under climate change. Through analysis of historical simulations and future projections, we can gain insights about past and current trends, and plan for efficient future water use. This study evaluates ten models that follow a common protocol and contribute with simulations for the global water sector of the Inter-Sectoral Impact Model Intercomparison Project phase 2b (ISIMIP2b). We analyze the equations used by the models to model the water use. We identify and present similarities and differences among them regarding: (1) how human activity is parameterized by global water models; (2) what are the water withdrawal sources, (3) what are the sinks of the return flows, (4) how many reservoirs are included in the models; (5) what type of reservoirs are included; (6) if and how the reservoir operations are included; (7) how land use, land management and land cover change are represented in the models.

Reference:

Veldkamp, T. I. E., Zhao, F., Ward, P. J., de Moel, H., Aerts, J. C. J. H., Müller Schmied, H., Portmann, F. T., Masaki, Y., Pokhrel, Y., Liu, X., Satoh, Y., Gerten, D., Gosling, S. N., Zaherpour, J., and Wada, Y.: Human impact parameterizations in global hydrological models improve estimates of monthly discharges and hydrological extremes: a multi-model validation study, Environ. Res. Lett., 13, 1–16, https://doi.org/10.1088/1748-9326/aab96f, 2018.

Keywords: global water models, modelling water use, parameterization , Inter-Sectoral Impact Model Intercomparison Project phase 2b

©2020. Japan Geoscience Union. All Right Reserved.

©2020. Japan Geoscience Union. All Right Reserved.

Discussion on the correlation between professional characteristics and willingness to pay for ecosystem services

*Li-chun Peng[1], Yu-pin Lin[1], Wan-yu Lien[1]

1. National Taiwan University

Abstract

Most decision-making processes would take the economic practice as the core component. To recent years, more and more decision-making processes have centered the environmental consideration as one of the major components because of raising awareness and concern of climate change. This study continues the previous published results to simulate the effects of ecosystem services by climate change, and further to conduct a trial to quantify the change. Based on provided new information, we use the Contingent Valuation Method to explore the non-market value of ecosystem service functions.

Through a questionnaire survey to collect expert opinions in the fields of water resources, ecological engineering, and social sciences, we aim to understand the willingness of experts to pay for maintaining ecosystem service functions and the due level they are willing to pay. The correlation between personal experience and professional fields as well as their willingness are statistically analyzed. Our result shows that income and willingness to pay are positively correlated. In addition, the average willingness to pay for experts who have experienced the participation in ecosystem service related research projects is higher than those who have no experience in related research projects. This result allows us be more thoughtful in planning the integration of climate-change related ecosystem services into our decision-making process.

Keywords: Ecosystem services, willingness to pay

©2020. Japan Geoscience Union. All Right Reserved.

Seasonal variability of stable isotopes in precipitation over Indonesia observed for 2010-2018

*Kimpei Ichiyanagi[1], Takayuki Uesugi[1], Rusmawan Suwarman[2], Halda Aditya Belgaman[3], Masahiro TANOUE[4]

1. Kumamoto University, 2. Bandung Institute of Technology, 3. Badan Pengkajian dan Penerapan Teknologi, 4. Shibaura Institute of Technology

This study reveals the seasonal variability of stable isotopes in precipitation over Indonesia based on weekly rainfall sampling from 2010 to 2018 at 63 stations belong to Indonesia Agency for Meteorological, Climatological and Geophysical (BMKG). More than 4,300 samples were collected and analyzed stable water isotopes ($\delta^{18}O$ and δD) by using the Cavity Ring-Down Spectroscopy (Picarro, L2120i) in the Hydrology Laboratory of Kumamoto University, Japan. Daily rainfall amount data was used from the Global Satellite Mapping of Precipitation (GSMaP) by JAXA/EORC. Monthly mean $\delta^{18}O$, δD, and d-excess values weighted by the rainfall amount was calculated from the dataset.
The Cluster analysis was used to distinguish the spatial grouping of seasonal variability of monthly rainfall. As a result, there are three clusters in this region. Clusters 1 has clear seasonal patterns with the highest in the dry season and lowest in the wet season which stations are located in central Indonesia around Java Sea. Cluster 2 shows opposite patterns of the Cluster 1 located in east Indonesia. There is not significant seasonal variation in Cluster 3, which stations are located in the Java Island near the Equator.
From monthly mean $\delta^{18}O$ data at 40 observation sites, multiple regression analysis was performed using latitude, longitude, and rainfall amount as explanatory variables. A significant correlation was observed from May to December, while not significant in other months. Especially from January to March, monthly mean $\delta^{18}O$ in rainfall has not any significant correlations with these three variables because the $\delta^{18}O$ values are spatially uniform over this area.

Keywords: Indonesia, stable isotopes in precipitation, seasonal variability

©2020. Japan Geoscience Union. All Right Reserved.

Finding the optimal time for the integration in Lagrangian analysis for the best estimation of moisture sources.

*Raquel Nieto[1], Luis Gimeno[1]

1. University of Vigo

Moisture transport from their sources (continents/oceans) towards their sinks establishes the connection between evaporation and continental precipitation (or the available moisture). Different methods have been used to establish source-sink relationships for the atmospheric water vapour. The major part of the studies has used Lagrangian approaches to investigate the changes in the net water vapour along a large number of back trajectories to infer the moisture sources for precipitation falling in a target region. However, the results derived from these approaches are very sensitive to the integration time of the trajectories used in the analyses. The use of different time periods to find sources and sinks of moisture could alter the initial results, the subsequent analyses, and the interpretations.

We present here the annual and monthly optimal integration time for Lagrangian methods for the best estimation of sources of moisture. To do that we have implemented a Lagrangian moisture transport approach using the FLEXPART model with data from the European Centre for Medium-Range Weather Forecasts (ECMWF) Interim Re-Analysis (ERA-Interim) (Dee et al., 2011). This reanalysis (the most appropriate for representing the hydrological cycle), covers the period from January 1979 to the present, and contains data at 6-h intervals with a spatial resolution of 1°x1º in latitude and longitude for 61 vertical levels (1000 to 0.1 hPa).

To achieve the optimal integration time we have compared the monthly precipitation estimated by the Lagrangian approach to gridded data such as ERA-Interim, GPCP and/or MSWEP precipitation. All the data was downscaled to 0.25 degrees using linear interpolations and aggregated over monthly intervals for the common period 1980 - 2015.

Keywords: Lagrangian models, Moisture transport, Optimal integration time, Sources and sinks of moisture

©2020. Japan Geoscience Union. All Right Reserved.

ATMOSPHERIC MOISTURE SOURCES ASSOCIATED WITH EXTREME PRECIPITATION DURING THE PEAK PRECIPITATION MONTH

*Luis Gimeno[1], Marta Vazquez[1,2,3], Raquel NIETO [1], Margarida Liberato[2,3]

1. Environmental Physics Laboratory (EPhysLab), CIM-UVigo, Universidade de Vigo, Ourense, Spain, 2. Instituto Dom Luiz (IDL), Faculdade de Ciências, Universidade de Lisboa, 1749-016 Lisboa, Portugal, 3. Escola de Ciências e Tecnologia, Universidade de Trás-os-Montes e Alto Douro, Vila Real, Portugal

The moisture transport is a crucial element in the understanding of the continental precipitation and its extremes. In this work, a Lagrangian approach was used to investigate the contribution of the main oceanic and continental global moisture sources to extreme precipitation during the peak precipitation month (month showing higher climatological precipitation). This was done for every grid point using four different precipitation thresholds to define precipitation extremes. Compared with the climatological sources, it is remarkable the increase of the contribution for extreme precipitation of the North Atlantic and the Mediterranean Sea sources over Eurasia, the Indian Ocean over Australia, the North and South Pacific sources over North and South America respectively and the South Atlantic source over Africa

Keywords: hydrological cycle, atmospheric moisture sources, extreme precipitation

©2020. Japan Geoscience Union. All Right Reserved.

SEASONAL VARIATION OF DISSOLVED TRACE ELEMNTS IN LAKE KIBA-GATA

*Ariunsanaa BATERDENE[1], Seiya NAGAO[2], Keisuke Fukushi[2], Kohei Sakaguchi[1], Tetsuya Matsunaka[2]

1. Graduate School of Natural Science and Technology Kanazawa University, 2. Institute of Nature and Environmental Technology, Kanazawa University

This study addresses the changes in dissolved trace element concentrations of the Lake Kiba-gata, which is located at Komatsu City, Ishikawa Prefecture, Japan and is a small, shallow and semi-closed environment. The water chemistry of trace elements is an important issue since it is a micronutrient for the growth of a phytoplankton and involves many environmental problems in water quality.

Surface water samples were taken from 6 points that evenly scattered across the lake territory and one inflow river during April 2017-January 2020 in monthly intervals for understanding spatio-temporal distribution of the main and trace elements. The water samples were vertically collected at KBG3, central part of the lake, with 0.5 m depth interval from surface to 2.0 m depth.

The seasonal variation of trace elements as Fe and Mn are observed significantly in horizontal and vertical distribution. The higher concentration of Fe and Mn in surface water was detected in the station near the river mouth in December to February and the lower concentration was observed in summer season. The dissolved iron concentration decreased with increasing depth in winter season at the central part of the lake but shows increasing trend with water depth. There is positive linear correlations between concentration of trace elements (Fe and Mn) and NH_4^+ and a negative correlation with lake water pH. The results indicate that the redox condition maybe related to the spatial and temporal variation of Fe and Mn in Lake Kiba-gata.

This research was supported by Functional materials based on Mongolian natural minerals for environmental engineering, cementitious and flotation processes (No. J11A15) sub-project under the Mongolian –Japanese Engineering Education Development Project.

Keywords: trace elements, redox transformation, surface water quality

©2020. Japan Geoscience Union. All Right Reserved.

Study on the origin of hot spring water using the deep part of Inubohsaki Onsen’ s core.

*Satoko Tezuka[1], Mana Kamata[1]

1. Chiba Institute of science

Inubohsaki Onsen in Choshi, Chiba is a Na-Cl type hot spring sourced from groundwater at a depth of 1000 m or more. In previous studies, we have reported that Inubohsaki Onsen is derived from 10,000 to 20,000 years old seawater, and has a different chemical composition from current seawater due to geological effects. In this report, the purpose of this study is to obtain information on the origin of the source of Inubozaki Onsen from the relation between the composition of rocks in the Atagoyama Group, which is considered to be the core of the source well and the hot spring water dissolved components. Hot spring water was collected from the source well of Inubosaki Onsen “Kuroshio-no-yu” and the amount of ions was determined by ion chromatography. The components and crystal phases of a 1280-1290 m deep drilling core and Atagoyama rock were measured by X-ray fluorescence and X-ray diffraction measurements, respectively. The component concentrations of hot spring water tended to be higher for Cl^- and Ca^{2+} and lower for Na^+, K^+ and Mg^{2+} than current seawater. The contents of core and rock main components were in the order of Si >> F > Al > Ca > K. These contained quartz, Mg-calcite, albite and chlorite. These results indicate that the presence of the calcite that elutes Ca^{2+} and the ion-exchangeable silicate minerals that take up Na^+, K^+ and Mg^{2+} in seawater and release Cl^- and Ca^{2+} to hot spring water relate to the origin of the source.

Keywords: Hot spring, Clay, Coae, Chemical composition

©2020. Japan Geoscience Union. All Right Reserved.

Lysimeter experiments to assess the influence of afforested vegetation on effective infiltration and recharge in a semi- arid area

*Zaiyong Zhang[1], Wenke Wang[1], Chengcheng Gong[1], Harrie-Jan Hendricks Franssen[2], Philip Brunner[3]

1. Chang'an University, 2. Agrosphere (IBG-3), Forschungszentrum Jülich GmbH, Jülich, Germany, 3. Center for Hydrogeology and Geothermics, (CHYN), University of Neuchatel, Switzerland

The Mu Us desert is located in the semi-arid area of Northwestern China. The major environmental problem is desertification. To effectively control and prevent desertification, a policy called “Returning Farmland to Forest and Grassland” has been implemented since 2000 which resulted in large afforested areas. Groundwater is an important source of water for the local people and ecosystems. The influence of these trees on the hydrological cycle and groundwater resources has not been studied in detail and accurate experimental data are needed to quantify how trees affect effective infiltration, groundwater recharge and water table dynamics. We designed four lysimeters: two with different depths to groundwater and bare soil as well as two additional lysimeters again with two different depths to groundwater and each with a planted tree (Salix Psammophila). In all the lysimeters, we monitored profiles of soil water content and the groundwater dynamics. The data suggest that the presense of tree increases the minimal amount of rainfall to trigger infiltration. Moreover, no groundwater recharge was observed for the vegetated lysimeters. The trees triggered a significant drop of the water table. These data have important implications for future water resources management.

Keywords: The Mu Us desert, lysimeters, Salix Psammophila

©2020. Japan Geoscience Union. All Right Reserved.

Development of a Multi-function Water Depth Sensor in the Irrigated Paddy Fields for Water Resource Management and Precision Agriculture

*Chun-Yen KUO[1]

1. National United University

Water resource management is one of the most critical issues in the worldwide area. Taiwan area is lack of water resources due to that the main rainfall is concentrated in summer seasons and the water storages in rivers and dams are also difficult. In Taiwan, the water consumptions for agricultural purposes are around 71% of the total water use, and the water use for irrigated paddy fields is close 72% of the agricultural water use. Therefore, the water use for irrigated paddy fields is around 50% of the total water use in Taiwan. Similar water consumptions situations were also found in Japan and some southeast Asian countries. A systematic, real-time and optimal management for the water use in irrigated paddy fields is the most critical issue in the water resource management in Taiwan. The Internet of Things (IoT) connects the physical devices, software, appliances and sensors, which is able to inter-operate within the existing internal infrastructure, which provides the opportunities for more effective, precise and economic benefit of water resource management. Moreover, the Precision Agriculture is a farming management concept based on observing, measuring and responding to inter and intra-field variability in crops to optimize the yields while preserving resources, which was considered as one of the key components of the third wave of modern agricultural revolutions. Indeed, the Precision Agriculture is one of the implementations of the IoT. However, one the most critical points for these applications of IoT is to develop a useable and multi-function sensor.

This research focuses on the development of a multi-function water depth sensor for the irrigated paddy fields based on the concept of continuous conductivity measurements in different depths of the water in the irrigated paddy fields. According to the experimental results, the conductivity profiles can precisely indicate the depths of water level in the irrigated paddy fields. Moreover, a wireless sensor network system (WNS) will also be constructed to detect and collect the conductivity data from different sensors located in different fields and water channels. This information can be used to optimize the water use for the irrigated paddy fields by cooperating a water gate to control the water flow into the field, resulting the saving of water resource for paddy fields. Then a systematic and real-time using the concepts of IoT for the optimal management of the water use of irrigated paddy fields can be constructed.

Additionally, the fertilizer substances (for example the nitrogen, phosphate, potash) drawn in the paddy fields will alter the measured conductivities in the fields. This proposed multi-function water depth sensor based on the continuous conductivity measurements can indicate the approximate concentrations of the fertilizer substances in the fields. A series of tests were also conducted using the proposed water depth sensor to measure the conductivities of the samples which were added different concentrations of chemical fertilizers into the collected water from the real paddy field. A linear relationship was found between the measured conductivities and the concentrations fertilizer (presented by ammonia nitrogen) added in the samples. This finding indicates that this proposed depth sensor can also measure the approximate concentrations of the fertilizer substances in the fields, and provides the multiple information in the paddy field. On the other hand, this proposed sensor can be used as an early warning when the irrigation water was polluted by the discharged wastewater, especially form the industrial

©2020. Japan Geoscience Union. All Right Reserved.

wastewater.

Both of the peasants and the governor of the water use of irrigation system can connect to the on-line sensor system. The governor can use this information from the system to optimal the water use for paddy fields even for the other agricultural purposes, and also provide a basis for the development of the Precision Agriculture. The peasants can also more effectively manger the water depth in their paddy fields by using a cell phone to connect to this on-line sensor system.

Keywords: Conductivity, Internet of Things, on-line sensor, water resources, water use of irrigated paddy

Keywords: Conductivity, Internet of Things, on-line sensor, water resources, water use of irrigated paddy

©2020. Japan Geoscience Union. All Right Reserved.

Dynamic calibration of tipping-bucket rain gauges and flow meters for precise measurements of rainfall partitioning

*Shin'ichi Iida[1], Takanori Shimizu[1], Yoshinori Shinohara[2], Tomo'omi Kumagai[3], Darryl E. Carlyle-Moses[4], Delphis F. Levia[5]

1. Forestry and Forest Products Research Institute, 2. University of Miyazaki, 3. University of Tokyo, 4. Thompson Rivers University, 5. University of Delaware

Tipping-bucket rain gauges (TBRGs) and flow meters (TBFMs) are widely applied to measure gross rainfall (*GR*), throughfall (*TF*), stemflow (*SF*) and other water fluxes, including outflow from trenches (e.g., Freer et al., 2002; Liang et al., 2011; Iida et al., 2017). However, it is well known that TBRGs and TBFMs commonly underestimate the inflow of water (e.g., Edwards et al., 1974). Basically, these instruments measure the inflow of water by counting tips of buckets. Thus, if water flow continues during bucket tipping, a certain amount of water is not captured by the bucket, and finally is underestimated (e.g., Iida et al., 2020). To evaluate the inflow of water precisely, calibration of TBRGs and TBFMs is required. We recently tested eleven types of TBRG and TBFM based on the dynamic calibration procedures (Shiraki and Yamato, 2004; Iida et al., 2012), and obtained the calibration curves (Iida et al., 2012; 2018; 2020; Shimizu et al., 2018). In this presentation, we show the simple and handmade equipment necessary to generate constant inflow of water, and the difference in calibration results among various TBRGs and TBFMs. Finally, the effects of applying dynamic calibrations on measurements of rainfall partitioning into interception loss ($I = GR - TF - SF$) are investigated.

We calibrated three TBRGs (0.2 mm tip, type RG-3M [Onset Computer Corp.] and type Rain Collector II [Davis Instruments]; 0.5 mm tip, type OW-34-BP [Ota keiki seisakusho Co., Ltd.]), and eight TBFMs (50 mL tip, type UIZ-TB-50; 100mL tip, type UIZ-TB-100; 200 mL tip, type UIZ-TB-200; 500 mL tip, type UIZ-TB-500 [Uizin Co., Ltd, Tokyo.], 200 mL tip, type TXQ-200; 400mL tip, type TXQ-400 [Ikeda keiki seisakusho Co., Ltd.], and 500 mL tip [Yokogawa Electric Corp.]) (Iida et al., 2012; 2018; 2020; Shimizu et al., 2018). At first, the static amount of one tip (c) was determined. We dripped water into the bucket with an injector until it tips. Then, c was calculated as the difference in mass of injector between initial and final conditions. Constant inflows of water (q) with different intensities were generated by the handmade equipment and applied to various TBRGs and TBFMs. We measured the time interval between tips (t), and obtained the actual amount of one tip (v) as the product of q and t. We derived the scaled amount of tip ($V = v/c$) and inflow ($Q = q/c$) as dividing them by the static amount of tip (c) (e.g., Shiraki and Yamato, 2004).

The relationships between Q and V were fitted reasonably by quadratic equations for all TBRGs and TBFGs (Iida et al., 2012; 2018; 2020; Shimizu et al., 2018). Rain Collector II and UIZ-TB-100 showed the largest underestimation among TBRGs and TBFMs, respectively, and 10% underestimation was detected when $Q > 0.14$ (s^{-1}) and $Q > 0.12$ (s^{-1}), respectively. The calibration curves for 7 of 8 TBFM lay within ±2% of that of TXQ-400 when $Q < 0.2$ (s^{-1}) (e.g., Shimizu et al., 2018; Iida et al., 2020). Thus, there are some possibilities that most types of TBFMs have similar calibration curves with TXQ-400 (Shimizu et al., 2018). By applying the calibrations, effects on the interception loss (I) ranged from -20% to +4% (Iida et al.,

©2020. Japan Geoscience Union. All Right Reserved.

2018). Therefore, to evaluate *I* precisely, the application of dynamic calibrations on *GR*, *TF* and *SF* measured by TBRG and TBFM are highly recommended.

Cited papers

Edwards et al. (1974) Agric. Meteorol., 13, 189–201.

Freer et al. (2002) Water Resour. Res., 38, 1269.

Liang et al. (2011) Water Resour. Res., 47, W02541.

Iida et al. (2012) Hydrol. Proc., 26, 2445–2454.

Iida et al. (2017) J. Hydrol., 548, 770–783.

Iida et al. (2018) J. Hydrometeorol., 19, 547–553.

Iida et al. (2020) in Levia et al. (eds.) Forest-Water Interactions, Ecological Studies Series, No.240, 29-54.

Shimizu et al. (2018) J. Hydrol., 563, 1051–1056.

Shiraki and Yamato (2005) J. Jpn. Soc. Hydrol. Water Resour., 17, 159–162 (in Japanese with English summary).

Keywords: Dynamic calibration, Tipping-bucket rain gauge, Tipping-bucket flow meter, Underestimation

©2020. Japan Geoscience Union. All Right Reserved.

Understory biomass measurement based on SfM data by a manual low-flying drone under the canopy

*Yupan Zhang[1], Yuichi Onda[1], Xinchao Sun[2], Takashi Gomi[3]

1. Center for Research on Isotopes and Environmental Dynamics, University of Tsukuba, Ibaraki, Japan, 2. Institute of Surface-Earth System Science, Tianjin University, Tianjin , PR China, 3. Department of International Environmental and Agricultural Science, Tokyo University of Agriculture and Technology, Tokyo , Japan

Understory vegetation has the important effect that cannot be ignored on Evapotranspiration. In this study, Structure from Motion (SfM) was used to reconstruct understory vegetation structure by a manual low-flying drone under the canopy with radial paths in a line thinning plantation and a spot thinning plantation made by Japanese cedar and cypress. By generating Orthomosaic image and dense point cloud data, we then extracted Excess Green Index (ExG) and Canopy Height Model (CHM), combining with understory biomass data from field harvesting to establish a quantitative relationship between the CHM and biomass, which was then used to map biomass and vegetation coverage in the study area. The results indicated that (1) a flight height of 7-10 meters is more conducive to understory vegetation reconstruction, with a photo quality greater than 0.8 and a point cloud density of more than 20 points/cm ^{2} . (2) a regression cubic model based on the CHM has acceptable accuracy and biomass estimate capability ($P<0.01$), with a coefficient of determination of 0.75. (3) compared with the spot thinning, the understory biomass under the line thinning scenario was higher(average biomass 3.03kg/m^2). (4) vegetation coverage based on the ExG index of visible light analysis was affected by ambient light(strong sunlight on a sunny day), and it cannot reflect the seasonal changes of understory vegetation biomass. These results disclosed the potential of the dense point cloud from drone SfM for estimating understory biomass. With this method, we will measure more than 5000m^2 of headwater catchment in the future.

Keywords: Drone, Understory biomass, Evapotranspiration, Structure-from-Motion Multi-View Stereo Photogrammetry

©2020. Japan Geoscience Union. All Right Reserved.



©2020. Japan Geoscience Union. All Right Reserved.

Seasonal changes in the canopy water balance of Japanese plantation forest

*Linh Thuy Pham[1], Yuichi Onda[1], Xinchao Sun[2], Sean Andrew Hudson[1], Janice Elaine Hudson[1], Yupan Zhang[1], Chiu Wei Chen[3]

1. University of Tsukuba, 2. Tianjin University, 3. Tokyo University of Agriculture and Technology

Stemflow, throughfall, and canopy interception are some of the most critical parameters for hydrologic behavior and watershed management. When rainfall occurs within a forest ecosystem, small amounts of rainfall will be trapped by the tree canopy (Canopy interception –Ic) until it becomes saturated and canopy storage is exceeded, throughfall (TF) –precipitation which reaches the forest floor by passing through or dripping from the canopy, will occur. When the trunk storage capacity is exceeded, water will flow down the tree trunk and reach the ground as stemflow (SF). Among the factors that can affect canopy water balance, seasonal change is one that requires further investigation (because of the differences in meteorological parameters). Previous research on canopy water balance and interception loss has mostly focused on the growing season - when plants have a greater demand for water (Ahmadi et al, 2009). However, it is also critically important to know the amount of water that will be in the water budget of the catchment delivered via stemflow and throughfall because it helps to better regulate streamflow between seasons, especially in the dry season. (Hewlett, 1982). In Japan, 60% of coverage is the forest with 44% being plantation forests. However, the plantation forests are not well managed with a very high density of trees, leading to undeveloped understory vegetation cover which causes low soil infiltration, low groundwater levels, high soil runoff, and soil erosion. To combat these negative processes silvicultural activities such as thinning, especially strip thinning - in which plantations are thinned parallel to the direction of the slope - have been widely adopted in Japan. The research site was in mountain Karasawa - covered by dense cypress plantation forest, located in the northeast of Sano city, Tochigi prefecture of Japan, where strip thinning was implemented on November of 2011. During thinning, 50% of trees were cut, stand density was lowered from 2198 to 1099 trees/ha, and the basal area was reduced from 50.4 to 26.2 m^2/ha. Canopy water balance parameters were recorded from November of 2010 (1 year before thinning) until November of 2012 (1 year after thinning). Throughfall was measured by 20 tipping rain gauges distributed in 2x2 m grid under the canopy, stemflow was collected with a polyvinyl tube around the trunk, connected with a draining hole to a bucket equipped with an Odyssey water level probe. Meteorological factors such as rainfall, temperature, humidity, wind speed were recorded by the weather station. After analysis, the data showed some changes in the canopy water balance before and after thinning, and also some differences between seasons. Within the partitioning of Pg, TF has the largest proportion (64.2%), followed by Ic (25.2%) and SF (10.6%). After thinning, the TF rate increased to 12%, the SF rate decreased to 4%, and the Ic rate decreased to 8%. With the decrease in Ic, there will be more water in the soil matrix during the dry season. TF, SF, and Ic amounts tend to be higher in summer and autumn but lower in winter and spring. TF and SF also tended to be higher during summer and autumn, but Ic rate is higher during winter and spring.

Keywords: seasonal changes, stemflow, throughfall, canopy interception loss, thinning

©2020. Japan Geoscience Union. All Right Reserved.

[E] Poster | A (Atmospheric and Hydrospheric Sciences)：A-HW Hydrology & Water Environment

[A-HW31] Surface and subsurface hydrologic models: From uncertainty analysis to water management

convener:Tomochika Tokunaga(Department of Environment Systems, University of Tokyo), Rene Therrien(Laval University), Philip Brunner(Center for Hydrogeology and Geothermics, University of Neuchatel), Jiaqi Liu(The University of Tokyo)

Surface and subsurface hydrologic models (SSHM) simulate the relevant components of the water cycle that affect surface water and groundwater. Such models thus constitute important tools to support water resources management. For example, model predictions are used to manage increased water use, water pollution, droughts and floods.

Nevertheless, significant challenges are inherent to the development and application of SSHMs. One critical issue is the limited amount of data to inform model parameters. Moreover, automated calibration and a comprehensive uncertainty analysis of large-scale SSHMs are rarely carried out because of their high computational cost. In addition, there is a large uncertainty associated with the conceptualization of the relevant processes and the parametrization of subsurface heterogeneity, which can undermine the reliability of the predictions made.

For this session we seek presentations that focus on numerical simulations tools for water resources management and present solutions for pressing scientific challenges such as model calibration, uncertainty analysis or the conceptualization of the surface and subsurface and the relevant processes. Presentations that showcase examples where numerical modelling tools are employed for water resource management at emergency situations (e.g. earthquakes, tsunamis, droughts or stormfloods) are also encouraged.

[AHW31-P01] A method for estimating large scale groundwater recharge depending on forest management practice.

*Sean Hudson[1], Yuichi Onda[2], Takashi Gomi[3], Chen-wei Chiu[3], Yosuke Adachi[1] (1.University of Tsukuba, Faculty of Life and Environmental Sciences, 2.University of Tsukuba, Center for Research in Isotopes and Environmental Dynamics, 3.Tokyo University of Agriculture and Technology, Graduate School of Agriculture, Department of International Environmental and Agricultural Sciences)

[AHW31-P02] Developing a new data assimilation technique based on polynomial chaos expansion theory for hydrologic prediction

*Jongho Kim[1], Vinh Ngoc Tran[1] (1.University of Ulsan)

[AHW31-P03] Junction angles of river channels in uplifted basins and the effect of contributing area: Model experiments and comparison with natural cases

*Ryosei Hirosaki[1] (1.Graduate school of science and technology, Kanazawa University)

[AHW31-P04] **Quantifying uncertainty in soil hydraulic parameters for the dual porosity model using null-space Monte Carlo method - implications for uncertainty in potential groundwater recharge estimation**

*Sakambari Padhi[1], R Rangarajan[2], Tomochika Tokunaga[1], Philip Brunner[3] (1.The University of Tokyo, Japan, 2.CSIR-NGRI, India, 3.University of Neuchatel, Switzerland)

[AHW31-P05] Impacts of earthquake-induced surface elevation changes on flooding: a case example from Mobara area, Japan

*Mao Ouyang[1], Ito Yuka[1], Tomochika Tokunaga[1] (1.The University of Tokyo)

[AHW31-P06] Modeling of tsunami-induced seawater intrusion into unconfined coastal aquifers: uncertainties analysis and water management

*Jiaqi Liu[1], Tomochika Tokunaga[1] (1.The University of Tokyo)

[AHW31-P07] **Groundwater level fluctuations and land use changes in the basaltic aquifer of Narmada basin (Central India)**

*Sakshi Ramesh Shiradhonkar[1], Tomochika Tokunaga[1] (1.Department of Environment Systems, University of Tokyo)

[AHW31-P08] Estimation of stemflow using forest inventory data and funneling ratio for Japanese cedar and Japanese cypress plantations

*Seonghun Jeong[1], Kyoichi Otsuki[2], Yoshinori Shinohara[3], Akio Inoue[4], Ryuji Ichihashi[5] (1.Graduate School of Bioresources and Bioenvironmental Sciences, Kyushu University, 2.Kasuya Research Forest, Kyushu University, 3.Faculty of Agriculture, University of Miyazaki, 4.Faculty of Agriculture, Kindai University, 5.Shiiba Research Forest, Kyushu University)

A method for estimating large scale groundwater recharge depending on forest management practice.

*Sean Hudson[1], Yuichi Onda[2], Takashi Gomi[3], Chen-wei Chiu[3], Yosuke Adachi[1]

1. University of Tsukuba, Faculty of Life and Environmental Sciences, 2. University of Tsukuba, Center for Research in Isotopes and Environmental Dynamics, 3. Tokyo University of Agriculture and Technology, Graduate School of Agriculture, Department of International Environmental and Agricultural Sciences

The management of abandoned forest plantations in Japan has received significant attention in the past decade, specifically relating to increasing discharge from headwaters catchments through the reduction of evapotranspiration loss (Komatsu et al 2019). While the surface water balance and its associated processes are understood in these catchments, the responses to thinning, especially the response of groundwater recharge has not received enough attention. Additionally, the difficulty and cost in acquiring field measurements of evapotranspiration and runoff makes large spatial-scale forecasts of groundwater availability and recharge difficult. Further, where individual catchments are monitored, the spatial scale is often too small for water resource managers to effectively use in groundwater storage and recharge estimates. Here, we present a model that describes the effects of forest thinning on groundwater recharge rates calculated from stand density and accepted empirically derived models of evapotranspiration components and climate data. Data used in the model include forest inventory data and Japan meteorological agency climate station data. Model inputs are tree height and age, precipitation, and daily received solar radiation. The model output is mapped as a 250m^2 grid cell to make a GIS database of potential groundwater recharge rates. A simple model using widely available data and able to resolve a large spatial scale models such as this is of great importance to water resource managers especially in areas dependent on surface water who are looking to ground water as stream discharges vary due to climate change. The development of this model represents an interdisciplinary approach to problem solving as forest hydrologists and geomorphologist can share discipline specific knowledge of forest hydrologic processes to engineers, water resource managers and other stakeholders allowing them to make sustainable management decisions of plantation lands and water resources.

Keywords: Groundwater recharge, evapotranspiration, forest management

©2020. Japan Geoscience Union. All Right Reserved.

Developing a new data assimilation technique based on polynomial chaos expansion theory for hydrologic prediction

*Jongho Kim[1], Vinh Ngoc Tran[1]

1. University of Ulsan

Data assimilation (DA) has become popular in the hydrologic prediction, focusing on the improvement of accuracy and efficiency. In this study, we proposed a new surrogate filter using polynomial chaos expansion (PCE), which aims not only to ensure accuracy in streamflow forecasting by updating the model states and parameters but also to significantly improve the computational efficiency. We presented here eight different approaches which can be classified into two main categories: either time-invariant filters (surrogate filters needed to be built once and can be applied to multiple forecast periods) or time-variant filters (surrogate filters needed to be rebuilt at each forecasting time). Besides, an optimal framework that is necessary during the construction of surrogate filters was proposed to optimize the hyper-parameters of PCE with appropriate criteria, thereby increasing the efficiency in building a surrogate filter and avoiding the over-fitting phenomenon of PCE. These approaches proposed were verified with both single and dual ensemble Kalman filters (EnKFs). Applicable results of surrogate filters with both synthetic and real data experiments illustrate that (1) most of these surrogate filters can account for different sources of uncertainty like original EnKF; (2) All surrogate filters provide relatively good forecasting results with small lead times. However, time-variant filters are capable of providing predictive results as well as providing more appropriate posterior parameters than time-invariant filters; therefore, with long lead times, the forecast of time-invariant filters is less accurate than other filters; (3) surrogate filters have significantly increased performance compared to original filters at a faster rate of up to 500 times, significant in forecasting, mainly when it is applied to large domain or complex models. Generally, results from both real and synthetic studies suggest that the proposed filter guarantees the effectiveness and usefulness with a significant improvement in the computational performance for hydrologic prediction.

Acknowledgment:
This research was supported by the Water Management Research Program funded by Ministry of Environment of Korean government (127554) and by the National Research Foundation of Korea (NRF) grant funded by the Korea government (MSIT) (NRF-2019R1C1C1004833).

Keywords: Data assimilation, Ensemble Kalman filter, Polynomial chaos expansion, Flood forecasting

©2020. Japan Geoscience Union. All Right Reserved.

Junction angles of river channels in uplifted basins and the effect of contributing area: Model experiments and comparison with natural cases

*Ryosei Hirosaki[1]

1. Graduate school of science and technology, Kanazawa University

The previous study pointed out that the most likely junction angle of river channels are roughly affected by the climate of the basin and/or the closeness between surface processes and a groundwater aquifer (Devauchelle et al., 2012; Seybold et al., 2013; Kirchner et al., 2017). However, the previous statistics did not take accounts into the scale of converging rivers. In this study, we discuss the relationship between the difference in contributing areas of merging channels and the junction angles, based on physical model experiments simulating uplifted river basins that drain artificial rainwater, along with the comparison to natural cases. The experimental results showed that the junction angle tended to be large as time passed during which the uplift continued, although further investigation is needed because the number of junctions in the experimental basins were small. Despite of such tendency, the angle of each junction seemed to fluctuate with time randomly, so we combine the data of different time as different basins to enlarge the population for statistics. After such treatment, there was a tendency that the larger the difference in contributing area was, the more restrictive around 90˚the junction angle was. Besides, analysis of two natural river basins, Yakushima and Mt. Aso, showed a similar relationship between the river scale and the range of junction angle. These are thought to be caused by the effect of the valley slope formed by the larger river.

Keywords: Confluence angle, uplift, Contributing area

©2020. Japan Geoscience Union. All Right Reserved.

Quantifying uncertainty in soil hydraulic parameters for the dual porosity model using null-space Monte Carlo method - implications for uncertainty in potential groundwater recharge estimation

*Sakambari Padhi[1], R Rangarajan[2], Tomochika Tokunaga[1], Philip Brunner[3]

1. The University of Tokyo, Japan, 2. CSIR-NGRI, India, 3. University of Neuchatel, Switzerland

Estimating groundwater recharge is important to sustainably manage water resources and assess their vulnerability to pollution. Numerical water flow and tracer transport models of the vadose zone have been widely used to estimate potential groundwater recharge under different soil surface and climate conditions. Nevertheless, these parameter-based models require a large number of model parameters and input data. Uncertainty in these model parameters thus can result a large uncertainty in groundwater recharge estimation.

Inverse modeling is conventionally used to estimate model parameters, which could often lead to non-unique solutions. Monte-Carlo (MC) methods generate many different parameter sets which can be used by the model to match the observed data with some acceptable level of mismatch instead of a single ‘‘best’’ estimated parameter set.

This study was carried out in the over-exploited Indo-Gangetic alluvial plains of Punjab, India under grass cover to understand natural recharge, where its high water demand is causing a significant drawdown of the groundwater in the alluvium aquifer.

Time series soil moisture content (SMC) data and tritium tracer profile data have been used to estimate soil hydraulic parameters and solute transport parameters in order to predict potential groundwater recharge. Single and dual-porosity models of water flow and solute transport, implemented in HYDRUS 1D computer program, were used to calculate potential recharge from SMC and tracer profile data, both sequentially and simultaneously. Potential recharge was predicted for 1000 randomly generated parameter sets using a null-space Monte-Carlo method (NSMC) proposed by Tonkin and Doherty (2009) and implemented in the parameter estimation software PEST. NSMC is calibration constrained and significantly reduces computational cost as compared to other MC methods.

Results indicate that when soil hydraulic parameters were estimated from SMC alone, the parameter set could not predict tracer transport behavior, though a better fit to SMC was obtained, calling for a cautioned approach to estimate recharge from SMC alone.

Histograms for certain soil hydraulic parameters obtained from non-linear uncertainty analysis display bi-modal characteristics for the dual porosity model implying that the data are from different sets of population representing different retention and hydraulic conductivity functions. Majority of predicted recharge (50%) on the other hand showed a narrow range of 0.002 cm to 0.2 cm in contrast to previously reported recharge prediction of 4.1cm to 16.1 cm as calculated from tritium mass balance approach for Punjab, India (Datta and Goel, 1977). This shows that recharge calculated from vadose zone tritium profile assuming piston flow is significantly overestimated. Hence, quantifying uncertainty in predicted recharge could help in proper management of groundwater resources.

©2020. Japan Geoscience Union. All Right Reserved.

References
Tonkin, M., and Doherty, J.(2009), Wat.Res.Res.,45,W00B10. Datta, P.S., and Goel, P.S.(1977), Nordic.Hydrol.,8, 225-236.

Keywords: Groundwater, Recharge estimation, Uncertainty, Null-space Monte-Carlo method

©2020. Japan Geoscience Union. All Right Reserved.

Impacts of earthquake-induced surface elevation changes on flooding: a case example from Mobara area, Japan

*Mao Ouyang[1], Ito Yuka[1], Tomochika Tokunaga[1]

1. The University of Tokyo

Earthquake-induced surface elevation changes may affect the extent of flood inundation. We have studied the possible effect of earthquake-induced elevation changes in the Mobara area, Japan, as a case example. Based on our dynamic flood modelling results, around 10 % additional inundation areas were calculated to be exacerbated by the ground elevation changes in the flood event of the year 2004. However, variety of uncertain variables were included in the modelling approach. Here, we present some important issues associated with the uncertainty in flood inundation impacts of earthquake-induced surface elevation changes. We selected topographic representation, saturated hydraulic conductivity, and the inundation projection technique for this discussion as uncertain variables/methodology. Results revealed that the choice of the resolution of DEM and the threshold water depth to discuss the extent of floods greatly affected the appearance of the inundation areas. In this presentation, we summarize the influence of these uncertainties on flood modelling and discuss the effective ways in balancing the efficiency and reliability of the approach and results.

Keywords: Flood modeling, Uncertainty, Earthquake-induced elevation change, Inundation projection

©2020. Japan Geoscience Union. All Right Reserved.

Modeling of tsunami-induced seawater intrusion into unconfined coastal aquifers: uncertainties analysis and water management

*Jiaqi Liu[1], Tomochika Tokunaga[1]

1. The University of Tokyo

Tsunami-induced seawater inundation causes vertical seawater intrusion into coastal aquifers. Assessing future risks of seawater intrusion in tsunami-prone zones can provide essential information supporting disaster preparedness and water management. We investigated seawater intrusion and aquifer recovery processes under the future Nankai earthquake and tsunami scenarios at Niijima Island, Japan. Both 2D and 3D numerical groundwater models were developed to solve variable-density flow and mass transport in unsaturated-saturated porous media using the code, FEFLOW. Our analysis suggests that the tsunami inundation height, the rainfall recharge rate, hydraulic conductivity, and bedrock structures are the primary sources of uncertainties in the simulation results. The simulations indicated that the maximum amount of seawater intrusion during the tsunami was controlled by the total unsaturated void space of the soil beneath the inundation area. After the tsunami, directions of seawater movement and flushing time depended on the pre-tsunami groundwater flow conditions and bedrock structures. Some groundwater was found to be survived from seawater intrusion, and showed the potential to provide water supply in an equivalent amount of the pre-tsunami level without worsening the recovery process. The simulated attempt to remove the intruded seawater from a polluted well could accelerate aquifer recovery but might not be practical due to the cost of maintaining intensive pumping over years.

©2020. Japan Geoscience Union. All Right Reserved.

Groundwater level fluctuations and land use changes in the basaltic aquifer of Narmada basin (Central India)

*Sakshi Ramesh Shiradhonkar[1], Tomochika Tokunaga[1]

1. Department of Environment Systems, University of Tokyo

In an extremely populated country like India, with agriculture as its economic backbone and nearly 90% of water has been utilized for agriculture and related activities, a strategic water management approach is necessary to avoid unsustainable exploitation of fresh water resources. Understanding the drivers behind the changing trends and their magnitude with respect to the water resources can provide information to support managing and developing water resources in a better way. During 2003-2016, an apparent increase of TWS (terrestrial water storage) was evident from GRACE (Gravity Recovery and Climate Experiment) satellite data in the central west of India where the Narmada river basin is situated whereas TWS trends were declining in north and south of India. In this study, the part of the Narmada river basin was chosen as the study site to discuss the possible reasons for the observed increase of TWS in the area. In this area, between 2003 and 2016, two major dams (Indira Sagar dam (2005) and Omkareshwar dam (2008)) were constructed, and the canal systems were developed in the area. Moreover, several water bodies were developed in the non-canal command areas (non-CCA). The objectives of this study were set to (1) understand the possible effects of the canal system on groundwater level behaviour in the Indira Sagar canal command area (CCA) and in the non-CCA within the basaltic aquifer domain, and (2) analyse the land use change, especially the surface water bodies. The groundwater levels were analysed based on two timelines, i.e., before and after canal construction in dry pre-monsoon and rainy monsoon seasons. The canal construction began by around 2007, from Indira Sagar dam towards the west until 2012-2013. The area to the south of the Narmada river is divided as CCA and Non-CCA based on the canal irrigation scheme. After the canal construction, on an average, about 2 m rise was observed in the well water levels during pre-monsoon while 1.1 m in monsoon seasons. Mann-Kendall’ s statistic test was performed on the groundwater well levels situated in non-CCA during dry pre-monsoon, rainy monsoon seasons and annually. Out of the 20 studied wells, only the ones situated near local water bodies showed significant/insignificant increasing trends while all the others which were spatially located far from any surface water body indicated declining trends. The changes in land use land cover (LULC) pattern were studied using Landsat 5, Landsat 7 ETM+, and Landsat 8 OLI/TIRS imageries in the region. The area used for surface water storage increased from about 1% to about 12% in between 2003 and 2013. The water from rainfall and Narmada river are perhaps the major sources for developing these water bodies, since both the major dams are built across the Narmada river. Based on the statistics and the interpretations, groundwater storage has been increased after the canal operation than before, likewise the area of surface water body expanded during 2003-2016, this may at least partly explain the reason why GRACE demonstrates increasing TWS trends in central west region of India.

Keywords: Groundwater, TWS (Terrestrial Water Storage)

©2020. Japan Geoscience Union. All Right Reserved.

Estimation of stemflow using forest inventory data and funneling ratio for Japanese cedar and Japanese cypress plantations

*Seonghun Jeong[1], Kyoichi Otsuki[2], Yoshinori Shinohara[3], Akio Inoue[4], Ryuji Ichihashi[5]

1. Graduate School of Bioresources and Bioenvironmental Sciences, Kyushu University, 2. Kasuya Research Forest, Kyushu University, 3. Faculty of Agriculture, University of Miyazaki, 4. Faculty of Agriculture, Kindai University, 5. Shiiba Research Forest, Kyushu University

Even though the previous studies of stemflow (*SF*) had considered the portion of *SF* of gross rainfall (*GR*) minimal, the latest researches have demonstrated that the forest stand structure for specific species largely determines the stemflow ratio (*SF*/*GR*). This study develops two estimation models of *SF*/*GR* with commonly-available forest inventory data. A set of 25 *SF*/*GR*s and the forest inventory data (stand density (*SD*), total basal area (*BA*), mean diameter at breast height (*DBH*), and mean tree height) were collected from the previous studies of Japanese coniferous plantations (Japanese cedar and Japanese cypress). To further investigate the relation between *SF*/*GR* and forest stand structures, extra stand-structural variables (mean basal area, mean stem surface area, and total stem surface area) were derived from the inventory data, and the stand-scale funneling ratio (FR_{stand}) assessing the efficiency of funneling rainwater was examined. Of all the standard variables, *SD* solely determined the *SF*/*GR*, providing the best-fitting positive single linear regression equation as a density-based *SF*/*GR* model with a root mean square error (RMSE) of 2.4%. This model has a weak point for sustainable forest water management because the effect of tree growth over time on *SF*/*GR* cannot be reflected, but is a useful tool with the most commonly available forest inventory data for practical forest water management. On the basis of the strong correlation of the FR_{stand} with *DBH*, a size-based *SF*/*GR* model was developed with an RMSE of 2.0%. This model is adequate for sustainable forest water management because the effects of not only the *SD* but also tree growth on *SF*/*GR* can be reflected as the *SF*/*GR* approximately increases as a root of *DBH*. These models exploited from the common forest inventory data have potential implications in evaluating and controlling *SF* by forest water management and in developing similar models in other species and regions.

Keywords: Coniferous plantation, Diameter at breast height, Forest structure, Model, Stand density, Stand-scale funneling ratio

©2020. Japan Geoscience Union. All Right Reserved.

[E] Poster | A (Atmospheric and Hydrospheric Sciences)：A-HW Hydrology & Water Environment

[A-HW32] Material transportation and cycling in aquatic ecosystems; from headwaters to coastal areas

convener:Syuhei Ban(The University of Shiga Prefecture), Adina Paytan(University of California Santa Cruz), Takahiro Hosono(Faculty of Advanced Science and Technology, Kumamoto University), Morihiro Maeda(Okayama University)

This session aims to synthetize watershed sciences in order to understand dynamic processes in transportation and cycling of materials and nutrients in aquatic environments from headwaters to coastal areas. The session will integrate various inter-disciplinary researches including limnology, ground water hydrology, coastal oceanography, meteorology, pedology, sedimentology, forestry, agriculture, fishery, ecology, social science and so on. This session calls for ideas on new methods for understanding the watershed sciences, such as tracer and molecular techniques, hydrological modeling, paleontological approaches, and chemical analyses, in order to elucidate physical, chemical and biological mechanisms for shedding light on natural phenomena and their spatio-temporal variations in complex and dynamic aquatic systems under human and climate impacts. Both laboratory and field studies, social-scientific evaluation of ecosystem services and social-ecological systems will be also welcomed. Through this session, we would like to facilitate interdisciplinary collaboration among participants to create new knowledge on watershed sciences.

[AHW32-P01] Estimates of hydrological, thermal and chemical budgets of Okama Crater Lake, Zao Volcano, Japan: A preliminary study

*Kazuhisa A. Chikita[1], Akio Goto[2], Jun Okada[3], Satoshi Miura[4], Mare Yamamoto[4] (1.Arctic Research Center, Hokkaido University, 2.Center for Northeast Asian Studies, Tohoku University, 3.Volcanology Research Department, Meteorological Research Institute, , 4.Research Center for Prediction of Earthquakes and Volcanic Eruptions, Faculty of Science, Tohoku University)

[AHW32-P02] How the precipitation to the catchment effect on the lake water level using depth meter moored in north Lake Biwa

*Maho Iwaki[1], Kazuhide Hayakawa[2], Naoshige Goto[3] (1.Lake Biwa Museum, 2.Lake Biwa Environmental Research Institute, 3.The University of Shiga Prefecture)

[AHW32-P03] Observation for the spatial variation of lacustrine groundwater discharge (LGD) in the northern basin of Lake Biwa by multi-layer measurement of radon (^{222}Rn)

*Mitsuyo Saito[1], Shin-ichi Onodera[2], Yusuke Tomozawa[2], Kunyang Wang[2], Syuhei Ban[3], Noboru Okuda[4] (1.Graduate School of Environmental and Life Science, Okayama University, 2.Graduate School of Integrated Arts and Sciences, Hiroshima University, 3.School of Environmental Sciences, The University of Shiga Prefecture, 4.Research Institute for Humanity and Nature)

[AHW32-P04] Effects of disturbance events on primary production in the northern basin of Lake Biwa

*Naoshige Goto[1], Maho Iwaki[2], Shuhei Ban[1], Kazuhide Hayakawa[3] (1.The University of Shiga Prefecture, 2.Lake Biwa Museum, 3.Lake Biwa Environmental Research Institute)

[AHW32-P05] Estimation of lake water circulation mechanism in Lake Tazawa based on Physico-chemical characteristics

*Arata Katamura[1], Takeshi Hayashi[2], Daizo Ishiyama[1], Yasumasa Ogawa[1] (1.Graduate School of International Resource Sciences, Akita University, 2.Faculty of Education and Human Studies, Akita University)

[AHW32-P06] Impact of Nishi-Nihon Big Storm in 2018 on nutrient discharge in a Seto Inland Sea Catchment: example in Takahashi River

*Shin-ichi Onodera[1], Mitsuyo Saito[2], Yusuke Tomozawa[1], Toru Takeuchi[3] (1.Graduate School of Integrated and Arts Sciences, Hiroshima University, 2.Okayama University, 3.Fujita Geology Co.)

[AHW32-P07] **Ammonium sources in rural coastal aquifer using integrated water quality parameters: chemical, biological, and environmental isotopes**

*Anna Fadliah Rusydi[1,5], Mitsuyo Saito[2], Seiichiro Ioka[3], Morihiro Maeda[2], Fujio Hyodo[4], Rizka Maria[5], Shin-ichi Onodera[1] (1.Graduate School of Integrated Arts and Sciences, Hiroshima University, Japan, 2.Graduate School of Environmental and Life Sciences, Okayama University, Japan, 3.Institute of Regional Innovation, Hirosaki University, Japan, 4.Research Core for Interdisciplinary Sciences, Okayama University, 5.Research Center for Geotechnology, Indonesian Institute of Sciences, Indonesia)

[AHW32-P08] **Long-term Estimation on Nitrogen flux in the Yamato River Basin Influenced by the Construction of Sewerage Treatment Systems**

*Kunyang Wang[1], Shin-ichi Onodera[1], Mitsuyo Saito[2], Yuta Shimizu[3] (1.Graduate School of Integrated Arts and Science, Hiroshima University, 2.Faculty of Environmental Science and Technology, Okayama University, 3.National Agriculture and Food Research Organization)

[AHW32-P09] Characteristic of spatial distribution on nitrate shallow aquifer in a citrus watershed

*Yuta Shimizu[1], Kenji Matsumori[1] (1.Western Region Agricultural Research Center, National Agriculture and Food Research Organization)

[AHW32-P10] **Nitrate and Phosphate Contamination of Groundwater in Small and Steep Sedimentary Rock Island**

*Sharon Bih Kimbi[1], Shingo Nozaki[1], Shin-ichi Onodera[1], Kunyang Wang[1], Yusuke Tomozawa[1] (1.Graduate School of Integrate Arts and Sciences, Hiroshima University)

[AHW32-P11] Phosphorus in groundwater in the coastal area of Mataram, Lombok Island, Indonesia

*Seiichiro Ioka[1], Shin-ichi Onodera[2], Mitsuyo Saito[3], Anna Fadliah Rusydi[2,4], Sachi Wakasa[1] (1.Institute of Regional Innovation, Hirosaki University, Japan, 2.Graduate School of Integrated Arts and Sciences, Hiroshima University, Japan, 3.Graduate School of Environmental and Life Sciences, Okayama University, Japan, 4.Research Center for Geotechnology, Indonesian Institute of Sciences, Indonesia)

[AHW32-P12] Distribution of phosphate oxygen isotope in boring core samples for evaluation of phosphorus cycling in groundwater

*Takuya Ishida[1], Yusuke Tomozawa[2], Xin Liu[3], Jun Qian[3], Mitsuyo Saito[4], Shin-ichi Onodera[2], Noboru Okuda[1], Syuhei Ban[3] (1.Research Institute for Humanity and Nature, 2.Hiroshima Univ., 3.The Univ. of Shiga Pref., 4.Okayama Univ.)

[AHW32-P13] Bulk precipitation and throughfall depositions of atmospheric nitrogen and sulfur in forests surrounding the Tokyo metropolitan area

*Yuko Itoh[1], Masahiro Kobayashi[1], Toru Okamoto[1], Akihiro Imaya[2] (1.Forestry and Forest Products Research Institute, Japan, 2.Japan International Research Center for Agricultural Sciences)

[AHW32-P14] Numerical modeling of nutrient transport in the Ise Bay basin

*Taichi Matsuura[1], Yasuhiro Tawara[1], Susumu Saita[1], Takafumi Yoshida[1], Tetsunori Inoue[2] (1.Geosphere Environmental Technology Corp., 2.Port and Airport Research Institute)

[AHW32-P16] Influence of Material Supply and Human Intervention from Mt. Kusatsu-Shirane Volcano on the Surrounding Water Environment

*Yoshihiro Igari[1], Koji Kodera[2], Kazuki Asami[1] (1.Hosei University Graduate School, 2.Hosei University)

[AHW32-P17] Spatial distributions in groundwater (SGD) and nutrient discharge on tidal flat with the area of around 100m square in a small and steep island, western Japan

*Shingo Nozaki[1], Shin-ichi Onodera[2], Yusuke Tomozawa[2], Mitsuyo Saito[3] (1. Graduate school of integrate arts and sciences,Hiroshima University, 2.Graduate school of integrate arts and sciences,Hiroshima University, 3.Graduate school of Environmental and Life science, Okayama University)

[AHW32-P18] Estimation of unsteady confined groundwater flow with river water intrusion in coastal alluvial plain during a large flood.

*Yusuke Tomozawa[1], Shin-ichi Onodera[1], Mitsuyo Saito[2], Tohru TAKEUCHI[3], Yutaka MARUYAMA, Koichi Kitaoka[4] (1.Graduate School of Integrated Arts and Sciences Hiroshima University, 2.Graduate School of Environmental and Life Science, Okayama University, 3.Fujita Geology Co., Ltd., 4.Okayama University of Scienece)

[AHW32-P19] Establishment and evaluation of a method to reconstruct the past snow fall and winter monsoon intensity based on the inter-annual variabilities of river discharges in Hokkaido, northern Japan

*Airi Maruyama[1], Tomohisa Irino[1] (1.Biogeochemistry Course, Earth System Science, Faculty of Environmental Earth Science, Hokkaido University)

[AHW32-P20] Classification analysis of coastal seaweed beds using UAV and Near-Infrared camera

*Akimitsu Shiraishi[1], Mitsuyo Saito[1], Akira Hama[2], Shin-ichi Onodera[3], Toru Iwata[1] (1.Graduate School of Environmental Science, Okayama University, 2.College of Education, Yokohama National University, 3.Graduate School of Integrated Arts and Sciences, Hiroshima University)

[AHW32-P21] Biogeochemical pathways of critical environmental contaminants (PTTE, POPs) in the rhizospheric soil-plant system

*Hideyuki Inui[1], Vladimir Beskoski[2], Mikael Motelica-Heino[3] (1.Kobe University, 2.University of Belgrade, 3.University of Orléans)

[AHW32-P22] Study on water quality composition and its change in Ishigaki Island

*Masato Oda[1], Koji Kodera[1], Atsuki Sato[1] (1.Hosei University, faculty of literature ,Geography)

[AHW32-P23] **Effects of sugarcane growth on hydrological elements and sediment yield**

*Yang Cao[1], Shin-ichi Onodera[2], Mitsuyo Saito[3], Hide Omae[4], Yoshiko Iizumi[5] (1.Nanjing Institute of Geography and Limnology, Chinese Academy of Sciences, 2.Hiroshima University, 3.Okayama University, 4.Tropical Agriculture Research Front (TARF), Japan International Research Center for Agricultural Sciences (JIRCAS), 5.Nihon University)

[AHW32-P24] Field measurement and numerical simulation of water flux in a forest soil

*Masahiro Kobayashi[1] (1.Forestry and Forest Products Research Institute)

[AHW32-P25] Hydrogen and oxygen stable isotopic mapping that allows us to investigate water cycle regimes over Japanese Island

*Shota Nakauchi[1], Takahiro Hosono[1], Kimpei Ichiyanagi[1] (1.Kumamoto University)

[AHW32-P26] Estimation of discharge at small forest watersheds in Ibaraki Prefecture by using the SWAT model

*Naohiro Imamura[1], Naoyuki Yamashita[1], Masahiro Kobayashi[1], Takanori Shimizu[1], Shinji Sawano[1], Koji Tamai[1], Shin'ichi Iida[1], Naoki Kabeya[1], Yoshio Tsuboyama[1] (1.Forestry and Forest Products Research Institute)

Estimates of hydrological, thermal and chemical budgets of Okama Crater Lake, Zao Volcano, Japan: A preliminary study

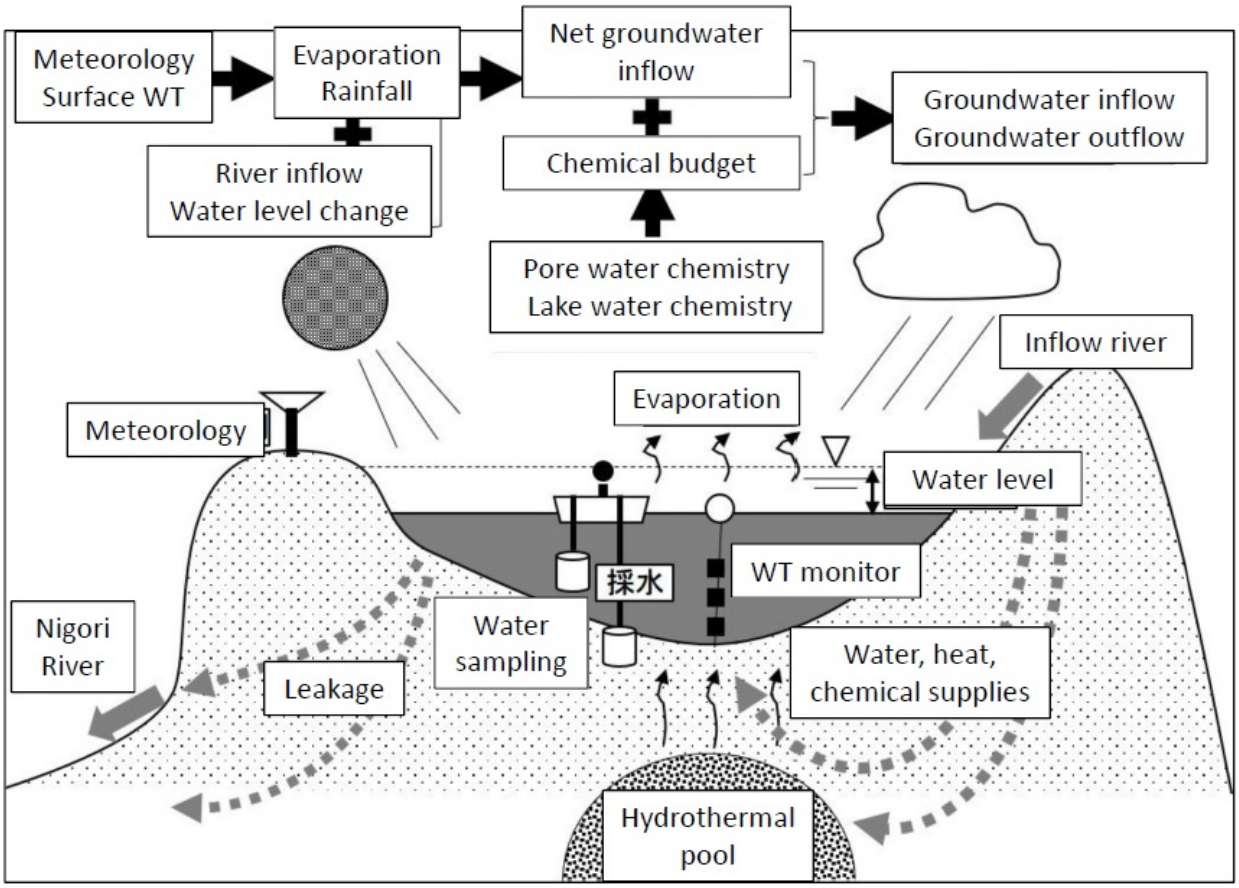
*Kazuhisa A. Chikita[1], Akio Goto[2], Jun Okada[3], Satoshi Miura[4], Mare Yamamoto[4]

1. Arctic Research Center, Hokkaido University, 2. Center for Northeast Asian Studies, Tohoku University, 3. Volcanology Research Department, Meteorological Research Institute, , 4. Research Center for Prediction of Earthquakes and Volcanic Eruptions, Faculty of Science, Tohoku University

In order to clarify a groundwater flow system below Zao Volcano, hydrologcal, thermal and chemical budgets of a crater lake, Okama, are estimated (see the schematic diagram). Since June 2019, profilings on a boat and meteorological observations at lake shore have been carried out. Also, using a mooring system, seven temperature loggers were vertically fixed at the deepest point to obtain thermal storage changes of Okama. This is a preliminary report about approaches for the estimates and some observational results in June - October 2019. Okama is at 1550 m asl with ca. 26 m at maximum depth and pH=3.2-3.7. The Okama water leakes into the Nigori River as groundwater, which could affect the ecosystem in the downstream region. In October 2019, Typhoon No. 19 attacked the lake with a rainfall of 396 mm per 15 hr. The heavy rainfall produced high sediment load into the lake, and formed the sedimentary delta at lake shore. Thereby, the infilling of the lake was probably proceeded.

Keywords: Okama Crater Lake, hydrological budget, chemical budget, thermal budget, groundwater flow system

©2020. Japan Geoscience Union. All Right Reserved.



Schematic of hydrological, thermal and chemical budgets in Okama Crater Lake.

©2020. Japan Geoscience Union. All Right Reserved.

How the precipitation to the catchment effect on the lake water level using depth meter moored in north Lake Biwa

*Maho Iwaki[1], Kazuhide Hayakawa[2], Naoshige Goto[3]

1. Lake Biwa Museum, 2. Lake Biwa Environmental Research Institute, 3. The University of Shiga Prefecture

Lake water levels are balanced by short-term events, such as direct rainfall, seiches, river inflow due to precipitation in the catchment land area and subsurface flow, evaporation (both at the lake surface and in its catchment area), and groundwater inflow and outflow. Each factor controlling the water level of a lake has a unique temporal and spatial scale. To understand complex lake level changes, it is better to have a spectral analysis that can separate the waves into several periods, and to determine on which time scale these processes are dominant. The shape of the response function reflects the lake system itself, such information will further be helpful to lake resource managers. If we could know the effect of rapid response of the water level, it makes possible to determine the precipitation retention time at the surface (above the impermeable layer) of a catchment area and how long it takes precipitation to reach the lake. By calculating the impulse response function using the data obtained by the depth meter installed in the mooring system in Lake Biwa from 2017 to 2018, we discussed how long it takes rainfall to reach the lake through the river. We observed water depth (10-min intervals) in the northern basin of Lake Biwa in August 2017 to October 2018, we calculate the response functions the rainfall to lake level during a severe heavy rainfall event. We could separate the delay time, direct rainfall into the lake and rapid river inflow. A response of 6-8 hours has been confirmed in analysis of water level by FFT (Fast Fourier Transform) (Iwaki et al. 2014), since the first mode of seiche is about 4 hours, then, the cause is hypothesized to be river inflow, however it was unclear why the response appeared clearly. Then we try to identify the delay time of rapid response (< 12 h) after rainfall. We could identify that the delay time of 6-8 hours may be due to the inflow by approximately 20-25 km rivers found in the North Lake Biwa. The proposed method can be used to evaluate the impacts of rivers on the lake, and the results can help to clarify the lake metabolism and lake managements.

Keywords: lake, lake level response, frequency response function

©2020. Japan Geoscience Union. All Right Reserved.

Observation for the spatial variation of lacustrine groundwater discharge (LGD) in the northern basin of Lake Biwa by multi-layer measurement of radon (^{222}Rn)

*Mitsuyo Saito[1], Shin-ichi Onodera[2], Yusuke Tomozawa[2], Kunyang Wang[2], Syuhei Ban[3], Noboru Okuda[4]

1. Graduate School of Environmental and Life Science, Okayama University, 2. Graduate School of Integrated Arts and Sciences, Hiroshima University, 3. School of Environmental Sciences, The University of Shiga Prefecture, 4. Research Institute for Humanity and Nature

Primary productivity in freshwater lakes and reservoirs are usually controlled by phosphorus (P). Lacustrine groundwater discharge (LGD), direct discharge of subsurface water to lake, is regarded as a potential nutrient paths, including phosphorus from a catchment to lake water environment. Some researchers have pointed out the presence of LGD into Lake Biwa, however, its spatial variation including deep groundwater discharge from offshore lake bed has not been well examined. In the present research, we aimed to observe the spatial variation in LGD to the northern basin of Lake Biwa by multi-layer measurement of radon (^{222}Rn).

The field campaigns were conducted several times from 2017 to 2019. ^{222}Rn is a radioactive element of uranium (^{238}U) series with 3.8 day of half-life. ^{222}Rn is a powerful tracer of groundwater discharge because it generally enriched in groundwater than surface water. To examine the spatial variation in LGD, ^{222}Rn concentration in lake water was measured in eastern and western transects with different depths (5m, 10m, 20m, and 60m). At each station, ^{222}Rn was measured in different depths (surface, intermediate, and bottom) to observe both of shallow and deep groundwater discharge.

^{222}Rn concentration was totally higher in the bottom than surface layer at each station. It suggests LGD from lake bed. The highest ^{222}Rn was observed in the bottom layer at 20m-deep station on the eastern transect in some periods. This result suggests LGD from offshore lake bed via deep groundwater discharge.

*This work is supported by JSPS Grant-in-Aid for Scientific Research (A) (18H03961, PI: Syuhei BAN) and RIHN research project (D-06 Biodiversity-driven Nutrient Cycling and Human Well-being in Social-Ecological Systems, PI: Noboru OKUDA).

Keywords: lacustrine groundwater discharge, Lake Biwa, Radon (222Rn)

©2020. Japan Geoscience Union. All Right Reserved.

Effects of disturbance events on primary production in the northern basin of Lake Biwa

*Naoshige Goto[1], Maho Iwaki[2], Shuhei Ban[1], Kazuhide Hayakawa[3]

1. The University of Shiga Prefecture, 2. Lake Biwa Museum, 3. Lake Biwa Environmental Research Institute

The effects of environmental factors on primary production by phytoplankton were elucidated at a site in the center of the northern basin of Lake Biwa, Japan. Chlorophyll *a* concentration, which is used as an index of phytoplankton biomass, and photosynthetic photon flux density (PPFD) were measured continuously at depths of 5, 10 and 15 m from August 2017 to February 2018. Monthly measurements of photosynthetic activity were performed using a pulse amplitude-modulated chlorophyll fluorometer, and photosynthesis-PPFD curves were produced throughout the observation period; these results were then used to calculate daily gross primary production per unit area. Primary production ranged from 0 to 3.92 g C m^{-2} d^{-1} (1.11±0.83, mean±SD) during the observation period, tending to be higher in spring (April-June) and summer (July-September), and lower in fall (October-December) and winter (January-March). In addition, primary production peaked in the late spring of 2018, with high production levels in this period attributed mainly to two large species in the Chlorophyceae (*Staurastrum dorsidentiferum* and *Micrasterias hardyi*). The meteorological events, such as typhoons and/or heavy rain, greatly affected the light and nutrient conditions in the water column and had a marked influence on primary production. In general, meteorological events increased the supply of nutrients and other essential material inputs from the terrestrial environment into the lake. However, such extreme weather events were also associated with increases in the supply of large amounts of sediment in runoff, greatly increasing the turbidity of the water column and decreasing primary production for a period of several weeks. These marked changes in environmental conditions were associated with the dominance of large-celled phytoplankton in blooms. Temporal variation in primary production was highly dependent on PPFD (R^2 = 0.46), although the contribution of biomass (chlorophyll *a*) to primary production also increased during the algal blooms (R^2 = 0.36).

Keywords: primary production, disturbance events, nutrients, Lake Biwa

©2020. Japan Geoscience Union. All Right Reserved.

Estimation of lake water circulation mechanism in Lake Tazawa based on Physico-chemical characteristics

*Arata Katamura[1], Takeshi Hayashi[2], Daizo Ishiyama[1], Yasumasa Ogawa[1]

1. Graduate School of International Resource Sciences, Akita University, 2. Faculty of Education and Human Studies, Akita University

Lake Tazawa, located in Akita Prefecture, is the deepest lake in Japan. The elevation of the lake surface is around 249 m and the maximum depth of the lake is 423.4 m. Acidic water of Tama-River has been introduced to the lake since 1940 for electricity development. As the result, the rapid acidification of the whole lake water had progressed and most kinds of fish had been killed by the acidification. After that, a neutralization treatment of acidic river water began in 1991 and the neutralized river water has been introduced to the lake. According to Akita Prefectural Government (2015), the water qualities of the shallower and deeper layers of the lake were different from 1991 to the beginning of 2000s, and they became almost uniform since around 2003. This fact suggests the possibility that the circulation mechanism of lake water has been changed and the turnover has occurred since around 2003 (Boehrer et al., 2008; Ishiyama et al., 2013). However, the circulation mechanism of the large amount of lake water in the lake has not been clarified. Considering the results of previous studies, the two possibilities of the circulation mechanism of lake water are considered. First possibility is an inflow of the river water having heavier density due to high concentration of dissolved components especially metals. If the river water has the heavier density than the lake water, the river water may affect the circulation of lake water by the heavier density flow. Second possibility is the circulation of the lake water by strong wind under the conditions of almost uniform temperature and density of lake water. Considering these points, we study on the circulation mechanism of the lake water based on the physico-chemical characteristics and water quality of the lake water. This study will contribute to predict the circulation variation in the future and the efficiency of the water quality improvement in the lake.
The water samples of Lake Tazawa were collected at five locations in the lake and at some depths at each point. The samplings were carried out between June and October in 2019. Water temperature, pH, EC, Eh, density, specific gravity, quantity of suspended solids, and major dissolved ions were analyzed.
Water temperature was different between shallower and deeper layers and the water temperature in deep layer was almost constant around 4℃ from June to October. So, the thermocline existed through this period. On the other hand, values of pH and concentrations of major dissolved elements of the lake water were similar between all the sampling points and the depths. This result showed the water quality as the whole lake was almost uniform. In addition, the specific gravity and the quantity of suspended solids of lake water and river water of Tama-River were similar. The existence of thermocline and the results of specific gravity and suspended solids of lake water and river water showed that the difference of water density based on the water temperature is much larger than that based on the water quality. Thus, the first possibility was denied. On the other hand, if the shallower water is sufficiently cooled and the water temperature from bottom to surface becomes around 4℃ in winter, the difference of the density of lake water between the shallower and deeper layer will become small. Then, strong winds in this season are considered to cause the turnover of the lake water. The results of this study suggest that the future environment change such as the global warming and climate change may affect the circulation of lake water and the ecosystem of the lake.

Keywords: Lake Tazawa, Water quality, Circulation, Turnover, Thermocline, Wind

©2020. Japan Geoscience Union. All Right Reserved.

©2020. Japan Geoscience Union. All Right Reserved.

Impact of Nishi-Nihon Big Storm in 2018 on nutrient discharge in a Seto Inland Sea Catchment: example in Takahashi River

*Shin-ichi Onodera[1], Mitsuyo Saito[2], Yusuke Tomozawa[1], Toru Takeuchi[3]

1. Graduate School of Integrated and Arts Sciences, Hiroshima University, 2. Okayama University, 3. Fujita Geology Co.

In July 5 to 7 in 2018, the serious disaster by the huge storm event more than 500mm occurred and more than 200 persons dead in a wide area of western Japan. In that time, high turbidity was observed in the wide area of Seto Inland Sea by the satellite image. However, these nutrient flux has not been monitored.

In this research, we aimed to confirm the real situation of high turbidity and nutrient concentration just after this event. We observed those from the river mouth area to 10km offshore of Takahashi River in Okayama Prefecture at three times of 7days, 14 days and 30 days after the disaster. In addition, we monitored groundwater and river water around river mouth area once a week since 2017.

The turbidity in river mouth area of Takahashi River normally was 5 to 8 FTU. On the other hand, it increased drastically more than 1000 FTU just 7 days after the disaster. Especially, high turbidity water of more than 500 FTU expanded to 10km offshore. Though the turbidity decreased on 30 days after, the high turbidity area with around 100 FTU appeared not only at the river mouth but at 8km offshore. These would be by the resuspension from the bottom. The nutrient also indicated same as these.

Keywords: turbidity, nutrient, big storm

©2020. Japan Geoscience Union. All Right Reserved.

Ammonium sources in rural coastal aquifer using integrated water quality parameters: chemical, biological, and environmental isotopes

*Anna Fadliah Rusydi[1,5], Mitsuyo Saito[2], Seiichiro Ioka[3], Morihiro Maeda[2], Fujio Hyodo[4], Rizka Maria[5], Shin-ichi Onodera[1]

1. Graduate School of Integrated Arts and Sciences, Hiroshima University, Japan, 2. Graduate School of Environmental and Life Sciences, Okayama University, Japan, 3. Institute of Regional Innovation, Hirosaki University, Japan, 4. Research Core for Interdisciplinary Sciences, Okayama University, 5. Research Center for Geotechnology, Indonesian Institute of Sciences, Indonesia

Ammonium, although, is not regulated in drinking water quality standards, its existence is undesirable because indicated an extinction of domestic waste pollution. In Indonesian coastal aquifer, the dominant presence of ammonium compared to other dissolved nitrogen parameters is not always found. In many cases, the dominant dissolved nitrogen parameter is a nitrate, while ammonium is usually detected in land-use that is heavily impacted by domestic waste, such as densely populated residential and land-fill. Interestingly, in our research area, we detected a dominant existence of ammonium in many types of land-uses, which is not only limited to the area that suspected polluted by domestic waste. Our preliminary results from 46 groundwater samples show ammonium is dominant compared to nitrate at almost samples. Meanwhile, samples from the river (4) and spring water (2), those are taken as a comparison, are dominated by nitrate. Through this research, we analyze the source of ammonium by analyzing major elements, coliform bacteria, and ammonium isotope in order to evaluate coastal aquifer vulnerability towards ammonium contamination.

Keywords: ammonium, coastal aquifer, chemical, coliform, isotope

©2020. Japan Geoscience Union. All Right Reserved.

Long-term Estimation on Nitrogen flux in the Yamato River Basin Influenced by the Construction of Sewerage Treatment Systems

*Kunyang Wang[1], Shin-ichi Onodera[1], Mitsuyo Saito[2], Yuta Shimizu[3]

1. Graduate School of Integrated Arts and Science, Hiroshima University, 2. Faculty of Environmental Science and Technology, Okayama University, 3. National Agriculture and Food Research Organization

The quantification of the nitrogen discharge in water were most important indicators of the water environment in coastal area because these processes are related to the transport of large nutrient loads. The nitrogen pollution sources of the surface water environment are divided into point source pollution and non-point source pollution according to the different spatial distribution (Niraula et al. 2013; Lee et al. 2010). Nonpoint source nitrogen pollution is a leading contributor to world water quality impairments. (Steffen et al 2015). Sewage treatment system can significantly reducing pollutant emissions by multiple methods.

The construction of sewage treatment systems does not happen overnight, it is divided into two parts: construction of sewage treatment plant and laying of underground pipelines into buildings. Especially for plumbing system, it is a long process. During this period, non-point source pollution from urban areas will be gradually transformed into point sources.

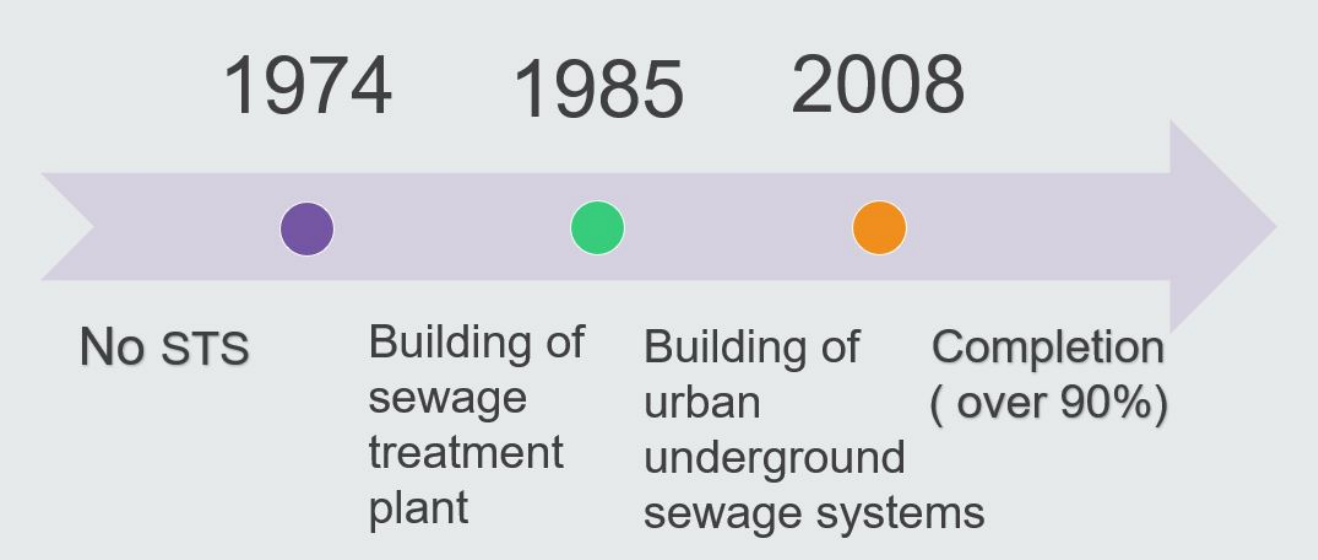
Yamato river is a very important river in west Japan. It has a watershed area of 1067 square kilometers, covering almost half area of Nara prefecture. These have 5 sewage treatment plant in the watershed, 3 of them are located in Osaka Prefecture and others are in Nara Prefecture. These sewage treatment plants were successively constructed and put into use between 1974 and 1985. The progress of pipeline laying varies widely in different cities. As of 2010s, the overall sewage treatment pipeline in the basin covers more than 90% of buildings.

SWAT model could meet this need and has proven to be an effective tool for assessing nonpoint source pollution for a wide range of scales and environmental conditions (Gassman et al. 2007), and it supports inputting point source data according to monthly data (Neitsch et al, 2005). This study used the SWAT model to simulate nitrogen fluxes in the Yamatogawa Basin for more than 50 years, divided into 4 period including 1) no sewage treatment system; 2) sewage treatment plant construction stage; 3) plant completion, pipeline laying stage and 4) full completion stage.

The results show that: 1) SWAT has a very good effect on the nitrogen simulation of mixed watershed with urban and agricultural area. 2) The construction of a sewage treatment plant has a very good effect on the improvement of the river basin environment. As of 2010s, total nitrogen emissions were 9.7 kg/ha, of which point source emissions accounted for 65%.

Keywords: Nitrogen discharge, sewerage treatment, point source, non-point source, urban BMP

©2020. Japan Geoscience Union. All Right Reserved.



©2020. Japan Geoscience Union. All Right Reserved.

Characteristic of spatial distribution on nitrate shallow aquifer in a citrus watershed

*Yuta Shimizu[1], Kenji Matsumori[1]

1. Western Region Agricultural Research Center, National Agriculture and Food Research Organization

As aspect of agriculture production, techniques of precise water and fertilizer controlling for individual citrus tree are required to improve quality and quantity of harvest. Citrus orchard dominated watersheds tend to contain abundant nitrate in the shallow aquifer. Using the nitrate-rich groundwater to irrigate and fertigate the tree is effective for both sides of agriculture and environment conservation. The objective of this study aimed to assess spatial distribution of nitrate concentration in a watershed for evaluation the possibility of the groundwater as fertilizer. The target watershed has an area of 0.75 km2 located on Ehime Prefecture. Steep mountains locate the upper stream and an alluvial fan lays between the mountains. The main citrus orchards are cultivated on the fan using groundwater irrigation. A field campaign was conducted on March 2017 to survey groundwater level and nitrate concentration at 91 wells. It was confirmed that shallow groundwater flows mountainous area towards to downstream along the topography based on measured groundwater potential. Mean nitrate concentration was 8.9 mg N/l (Maximum: 26.0 mg N/l, minimum: 0.0 mg N/l). High nitrate concentration was found in central part of the fan while low concentration was found in the area where converted from paddy field on downstream. Especially, very low concentration below detection limit was found near beach that was implies nitrate attenuation by denitrification. However, some hot spots contain high nitrate concentration are expected as fertilizer resource. Evaluation of total nitrate amount in the aquifer and its availability considering with flowing speed is necessary for future work.

Keywords: nitrate, groundwater, agriculture

©2020. Japan Geoscience Union. All Right Reserved.

Nitrate and Phosphate Contamination of Groundwater in Small and Steep Sedimentary Rock Island

*Sharon Bih Kimbi[1], Shingo Nozaki[1], Shin-ichi Onodera[1], Kunyang Wang[1], Yusuke Tomozawa[1]

1. Graduate School of Integrate Arts and Sciences, Hiroshima University

Over the past years, there has been a constant trend towards greater agricultural intensification and higher agricultural productivity which has been accompanied by a significant increase in the use of inorganic nitrogen and phosphorus in fertilizers. Nitrogen in particular the very soluble nitrate, is vital for life and is found naturally in soil and water however because many crop plants require large quantities of nitrogen to produce high yields, additional nitrogen in the form of fertilizer is applied to crops which easily dissolves into percolating water. Phosphorus on the other hand is less mobile and reaches surface water due to erosion with the bounded soil particles. These different pathways cause a problem with water protection, because elimination of one water pollution source may aggravate another. Phosphates are essential for growth of plants and animals but human activities have altered its natural cycle. Phosphate in excess causes nutrient boost which often equates to excessive algae growth. The present study was carried out in Osaki-Shimojima which is one of the island in the Seto island sea famous for citrus fruit cultivation. The aim of this study was to assess the impact of agriculture, with special attention on nitrate and phosphate contamination of the groundwater quality and to propose mitigative methods for implementing nitrogen-phosphate reduction measures. A total of 49 water samples were collected during the month of October, 2019 and subject to nutrient analysis using the Automatic Nutrient Analyzer. The startling results showed both high nitrate and phosphate concentrations in groundwater. Thus an unfavorable N: P ratio in supplied nutrients were detected. Severe shortage of phosphorus in applied fertilizers maybe one of the major factors causing leaching of nitrogen due to limited possibilities of its consumption by plants.

Keywords: nitrate contamination, phosphate, sedimentary rock, mountain catchment

©2020. Japan Geoscience Union. All Right Reserved.

Phosphorus in groundwater in the coastal area of Mataram, Lombok Island, Indonesia

*Seiichiro Ioka[1], Shin-ichi Onodera[2], Mitsuyo Saito[3], Anna Fadliah Rusydi[2,4], Sachi Wakasa[1]

1. Institute of Regional Innovation, Hirosaki University, Japan, 2. Graduate School of Integrated Arts and Sciences, Hiroshima University, Japan, 3. Graduate School of Environmental and Life Sciences, Okayama University, Japan, 4. Research Center for Geotechnology, Indonesian Institute of Sciences, Indonesia

Several previous studies of phosphorus in groundwater at highly contaminated sites exist. However, although studies on the behavior of phosphorus in pristine aquifers have been increasing, they are still limited. Urban development in Indonesia’ s coastal areas may lead to an increase in groundwater contamination. Mataram City on Lombok Island is a developing area in terms of tourism, and it is important to evaluate the phosphorus in the groundwater prior to the expansion of urban development. Mataram City was therefore selected as the study area for this work and groundwater was sampled at 26 sites.
Our results show that the concentrations of PO_4^{3-} in groundwater analyzed using ion chromatography range from approximately 0.1 to 8.5 mg/L. Fe concentrations in groundwater at 21 sites was lower than 0.1 mg/L. No correlation was found between the Fe and PO_4^{3-} concentrations. In addition, no correlation was found between the DOC (dissolved organic carbon) and PO_4^{3-} concentrations. These results indicate that the DOC and Fe-(hydr) oxides cannot represent the source of P. However, the values of the saturation index of hydroxyapatite for some groundwater samples were close to equilibrium; Therefore, hydroxyapatite may represent the source of P.

Keywords: Phosphorus, Groundwater, Mataram

©2020. Japan Geoscience Union. All Right Reserved.

Distribution of phosphate oxygen isotope in boring core samples for evaluation of phosphorus cycling in groundwater

*Takuya Ishida[1], Yusuke Tomozawa[2], Xin Liu[3], Jun Qian[3], Mitsuyo Saito[4], Shin-ichi Onodera[2], Noboru Okuda[1], Syuhei Ban[3]

1. Research Institute for Humanity and Nature, 2. Hiroshima Univ., 3. The Univ. of Shiga Pref., 4. Okayama Univ.

Phosphorus (P) input through groundwater discharge plays a significant role in nutrient cycling and primary productivity in the coastal area (Slomp & Cappellen., 2004). Therefore, its biogeochemical cycling in underground environment is important in proper land management and understanding of natural systems. Recently, phosphate oxygen isotope ratio ($\delta^{18}O_{PO4}$) has been used as a promising tool to elucidate the P cycling. Previous studies showed the possibility to evaluate P sources, metabolism by organism in some ecosystems (Paytan & McLaughlin 2011). However, it is not clear whether $\delta^{18}O_{PO4}$ is useful for evaluating the P cycling of in underground environment, because few researches have applied the $\delta^{18}O_{PO4}$ analysis for underground P cycling.
In the present study, we investigated the $\delta^{18}O_{PO4}$ values of boring core samples and groundwater to clarify P cycling in underground.
A boring core (28 m depth) and groundwater (5 m and 28 m depth) were collected at The University of Shiga Prefecture, which is located on coastal area of Lake Biwa, central Japan. Boring core was divided by 1 m and ground to powder using a multi-bead shocker (Yasui Kikai) with tungsten carbide beads. The powdered boring core samples were immersed in 1 M HCl for 16 h to extract the inorganic P. Groundwater samples were filtered through 0.45-μm membrane filters (Advantec). The SRP concentration of each samples was measured using the molybdenum-blue method on a microplate spectrophotometer (Multiskan GO; Thermo Fisher Scientific). For the $\delta^{18}O_{PO4}$ analysis, the extract and groundwater samples were converted to Ag_3PO_4 according to McLaughlin et al. (2004) or Tamburini et al. (2010). The $\delta^{18}O_{PO4}$ values reported relative to the Vienna Standard Mean Ocean Water (VSMOW) of the Ag_3PO_4 samples were measured using a TC/EA-IRMS (thermal conversion elemental analyzer connected to a Delta plus XP via ConFlo III, Thermo Fisher Scientific) at the Research Institute for Humanity and Nature (RIHN).
The soluble reactive P (SRP) concentrations in 5 m and 28 m depth of groundwater were 0.74 and 6.78 μ mol L^{-1}, respectively. Deeper groundwater has much higher SRP concentration than river and lake water (< 0.7 μmol L^{-1}) near The University of Shiga Prefecture. The $\delta^{18}O_{PO4}$ values in 5 m and 28 m depth of groundwater were 15.1 and 17.1‰, respectively. In our poster, we will show the result of distribution of $\delta^{18}O_{PO4}$ in boring core samples and discuss the P cycling in groundwater.

Reference

McLaughlin, K., Silva, S., Kendall, C., Stuart-Williams, H., and Paytan, A. (2004) A Precise Method for the Analysis of $\delta^{18}O$ of Dissolved Inorganic Phosphate in Seawater. Limnolgy and Oceanography: Methods, 2, pp. 202–212.

Paytan, A., and McLaughlin, K. (2011) Tracing the sources and biogeochemical cycling of phosphorus in aquatic systems using isotopes of oxygen in phosphate. In M. Baskaran, ed. *Handbook of Environmental Isotope Geochemistry*. Berlin: Springer-Verlag, pp. 419–436.

Slomp, CP., and Cappellen, PV. (2004) Nutrient inputs to the coastal ocean through submarine groundwater discharge: Controls and potential impact. *Journal of Hydrology*, 295, pp. 64-86.

©2020. Japan Geoscience Union. All Right Reserved.

Tamburini, F., Bernasconi, SM., Angert, A., Weiner, T., and Frossard, E. (2010) A Method for the Analysis of the $\delta^{18}O$ of Inorganic Phosphate Extracted from Soils with HCl. *European Journal of Soil Science,* 61, pp. 1025–1032.

©2020. Japan Geoscience Union. All Right Reserved.

Bulk precipitation and throughfall depositions of atmospheric nitrogen and sulfur in forests surrounding the Tokyo metropolitan area

*Yuko Itoh[1], Masahiro Kobayashi[1], Toru Okamoto[1], Akihiro Imaya[2]

1. Forestry and Forest Products Research Institute, Japan, 2. Japan International Research Center for Agricultural Sciences

Increased atmospheric deposition of nitrogen (N) and sulfur (S) compounds from anthropogenic sources remains a concern in some areas of the world. The impact of increased N emissions on a global scale extends to forest ecosystems as well. N influx into the forested areas distorts the N dynamics in the forest ecosystem. High nitrate concentrations in some stream water have been observed at forest watersheds on the surroundings of the Tokyo metropolitan area. Atmospheric N and S depositions by bulk precipitation (BP) and throughfall (TF) were investigated on 12 (BP) and 15 plots (TF) in forest stands located on the surroundings of the Kanto plain of Tokyo metropolitan area, with intense human activities. In this study, it was observed that throughfall contributes more to N and S influxes than BP. At the majority of the studied sites, nitrogen influx resulting from TF was 2 to 3 times the N influx resulting from BP. The increase in N outflow from watershed surrounding Tokyo metropolis can be attributed to the N influx induced by the forest canopy structure. In contrast, the S influx was higher at sites located far from the Tokyo metropolitan area, which resulted from high annual rainfall and particularly from the influence of seasonal wind, including sea-salt and air pollutants from Asian continent during the winter season. Furthermore, to determine the influences of atmospheric N and S influxes and N saturation, it pertinent to observe the cycling of elements within various forest watersheds, including snowy area.

©2020. Japan Geoscience Union. All Right Reserved.

Numerical modeling of nutrient transport in the Ise Bay basin

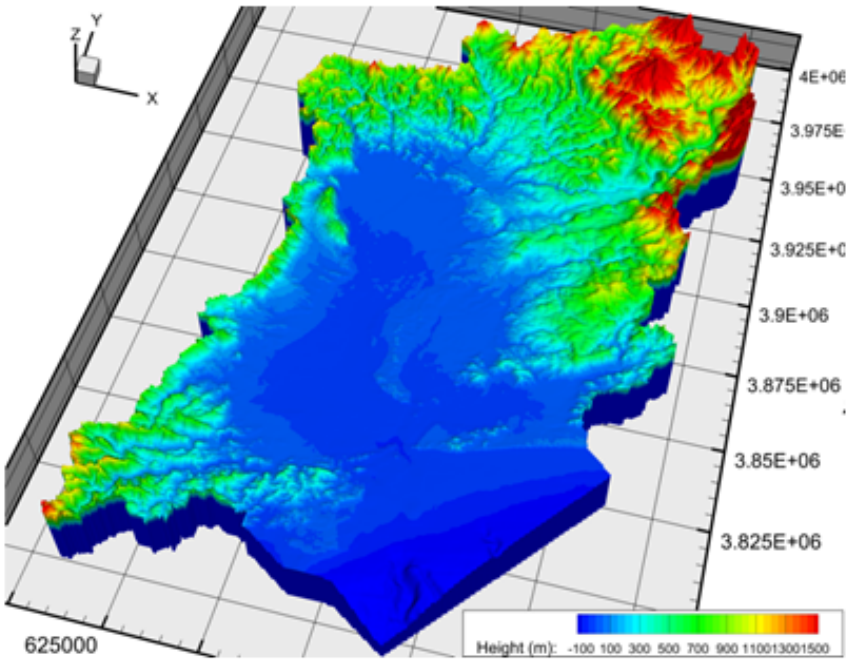
*Taichi Matsuura[1], Yasuhiro Tawara[1], Susumu Saita[1], Takafumi Yoshida[1], Tetsunori Inoue[2]

1. Geosphere Environmental Technology Corp., 2. Port and Airport Research Institute

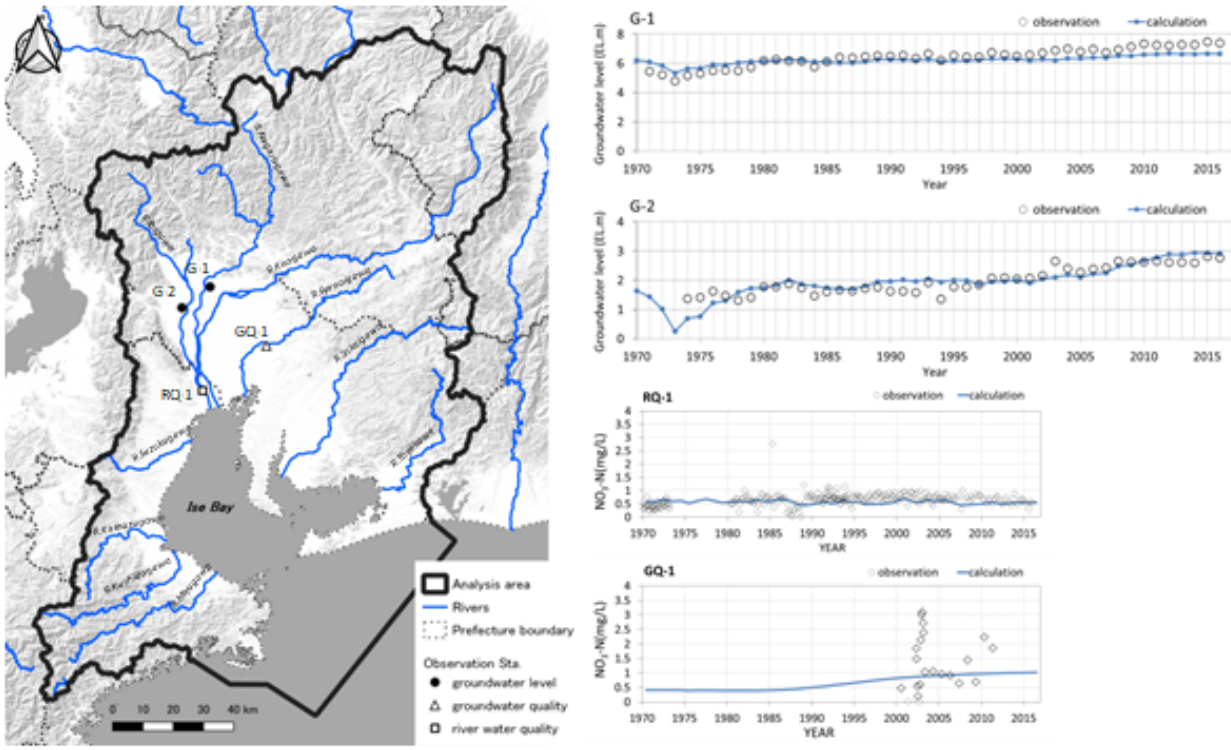
Eutrophication is the main cause of the occurrence of red tides in semi-enclosed coastal areas. Studies performing numerical simulations have reproduced the complicated phenomena that caused problems in bays including mid-layer oxygen depletion and the occurrence of discolored tides. The nutrient inflow conditions used in such simulations reflect measured values as closely as possible, however, they are often not temporally and spatially considered in detail. There are limitations on the available measurement data, making accurate simulations difficult to realize. Furthermore, nutrients are transported not only from the surface water but also from the groundwater, and the actual temporal and spatial transport mechanisms are not always understood. The inflow of nutrients in groundwater largely depends on factors such as the geological characteristics of the coastal area, groundwater utilization, and nutrient load in the basin. Models of nutrient transport at watershed scales can therefore be useful tools for elucidating complex mass-transfer phenomena in coastal areas. In this study, we developed a nutrient transport model for marine numerical simulations to track nutrient behavior in Ise Bay by focusing on the actual long-term circumstances of nutrient load and groundwater use in the basin, thereby enabling more accurate reproduction of nutrient load conditions in terrestrial areas.
To calculate the nutrient flow from land to sea in the Ise Bay basin, we constructed a basin model that reflects the hydrological processes and the water usage occurring on the land surfaces, including basin-scale hydrogeological structures. In particular, we incorporated groundwater pumping and nutrient loading processes into models to simulate changes in groundwater levels and nitrogen concentrations from the 1970s until present. During that time, the groundwater level showed a large temporary decrease, from which it gradually recovered, and the initially extremely low nitrogen concentration tended to gradually increase. The constructed model was validated via matching of multiple historical data, including measured river flow, groundwater levels, and water quality factors such as ammonia nitrogen and nitrate nitrogen. The simulation was conducted using the geofluid simulator of GETFLOWS.
The simulation of groundwater levels was successfully reproduced the trend of gradual groundwater level recovery from the 1970s to the 2010s. Furthermore, the simulated ammonium and nitrate nitrogen concentrations in rivers were well-reproduced when compared with measured data. Consequently, we considered that the estimated nutrient loads in the basin using statistical data are temporally and spatially consistent with the actual situation. Regarding observed groundwater concentrations, while responses to seasonal changes have not yet been verified, reproductions of change over time were generally consistent.
The results show that the fluctuation patterns of nitrate nitrogen inflowing from land to sea are highly affected by annual changes in precipitation and are particularly dependent on surface-ground water components. However, there are indications that while groundwater components show small year-round fluctuations, they comprise up to 10% of inflowing surface water. Therefore, we suggest that the nutrient influx should be considered not only from surface water but also from groundwater when evaluating nutrient behavior in semi-enclosed coastal areas. This will lead to a better understanding of marine nutrient transport and more accurate predictions of the effects of countermeasures.

Keywords: Ise Bay, Watershed water cycle, Basin-scale modeling, Nutrient transport, GETFLOWS

©2020. Japan Geoscience Union. All Right Reserved.



Constructed 3D model of Ise Bay basin



The reproduction state of simulation model with observation data

©2020. Japan Geoscience Union. All Right Reserved.

Influence of Material Supply and Human Intervention from Mt. Kusatsu-Shirane Volcano on the Surrounding Water Environment

*Yoshihiro Igari[1], Koji Kodera[2], Kazuki Asami[1]

1. Hosei University Graduate School, 2. Hosei University

I. Introduction

In Japan, a maritime nation, it is important to understand the material balance and water balance between upstream and coastal areas. In order to manage the impact of forests, agricultural land, cities, factories, and other terrestrial ecosystems on the coast within a river basin, it is necessary to understand the entire basin (Mukai 2012). Groundwater stored in volcanic bodies, especially in volcanic areas, has long been used as an important water resource (Yamamoto 1995). On the other hand, acidic rivers around volcanic bodies have a great impact on the ecosystem, water source development, and flood control of the basin. The purpose of this study is to clarify the influence of substances supplied mainly from volcanic bodies on the water quality of rivers, lakes, and precipitation around Mt. Kusatsu-Shirane.

II. Regional Summary

The Kusatsu Shirane Volcano area has a large amount of hot spring water, as typified by the Kusatsu Hot Spring, and hot springs with high temperature and strong acidity can be seen in various places. The acidic water seen in the Agatsuma River basin is caused by acidic hot spring water and acidic sulfur mine wastewater in the surrounding area, and a neutralization project has been carried out for the Yu River basin, where Kusatsu Hot Spring, one of the acidic sources, is the main stream (Oi et al. 1991).

III. Research methods

Field survey items (Temperature, water temperature, EC: conductivity, pH, RpH, flow rate) were measured and sampled at about 45 rivers around Mt. Kusatsu Shirane from May 23 2017 to October 2019. After filtration in the laboratory, some samples were analyzed for dissolved ingredients (TOC, Na^{+}, K^{+}, Ca^{2+}, Mg^{2+}, Cl^{-}, HCO_3^{-}, NO_3^{-}, SO_4^{2-}).

IV. Results and Discussion

In the basin of the Manza River, which is located at the western foot of the mountain, many rivers were affected by the inflow of groundwater with a high proportion of sulfuric acid, but in the mountain stream near the fumarole group, the water quality composition to which chloride was added was observed. Water composition affected by domestic wastewater is also observed.
In the small basins extending north and south at the southern foot of the mountain, the elevation of the headwaters and the distance from the crater are related to the concentration of calcium sulfate-type water quality. If the headwaters of the basin are close to the crater, the water quality of the river will contain many volcanic components, and if the headwaters of the basin are far from the crater, the volcanic components will weaken and the influence of the surrounding fields will appear.
The strongly acidic river (Yu River, Yazawa River, and Osawa River) in the Yu River basin to the east of the mountain is neutralized and flows down through aqueducts to the middle reaches of Shirasuna River and the junction of Shirasuna River and Agatsuma River, but the main stream of the Agatsuma River is strongly affected by this.

V. Conclusion

Research on volcanic bodies with well-developed hydrothermal systems has been taken up in Japan and

©2020. Japan Geoscience Union. All Right Reserved.

overseas, but many studies have focused on specific issues and targets, and few have discussed the water environment of the entire mountain body. By treating not only rivers affected by strong acid drainage but also mountain streams, lakes, and precipitation far from craters, we were able to evaluate natural and human impacts and discuss the target areas in a wide range of fields.

Keywords: Water Environment, Volcano, Mt.Kusatsu-Shirane, River, Hot Spring

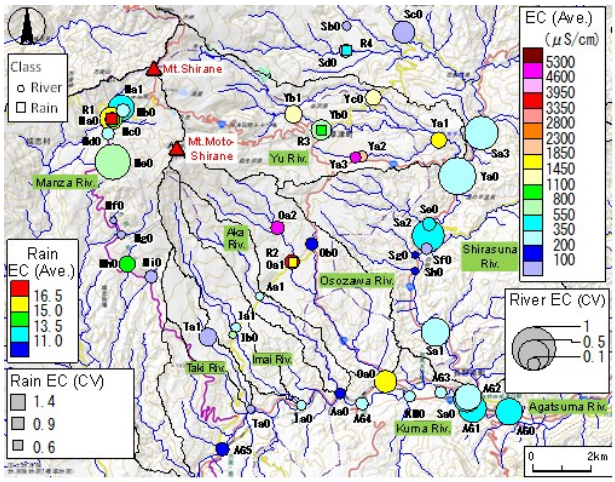


Fig.1 Spatial distribution of EC average

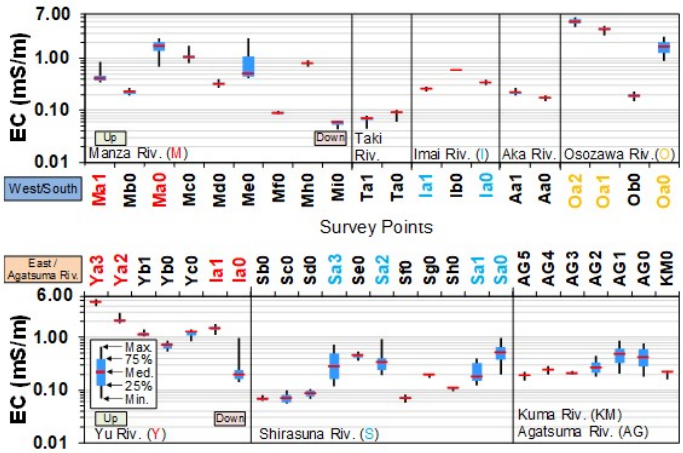


Fig.2 EC variation by basin (2017.05 – 2019.10)

©2020. Japan Geoscience Union. All Right Reserved.

Spatial distributions in groundwater (SGD) and nutrient discharge on tidal flat with the area of around 100m square in a small and steep island, western Japan

*Shingo Nozaki[1], Shin-ichi Onodera[2], Yusuke Tomozawa[2], Mitsuyo Saito[3]

1. Graduate school of integrate arts and sciences,Hiroshima University, 2. Graduate school of integrate arts and sciences,Hiroshima University, 3. Graduate school of Environmental and Life science, Okayama University

Abstract

The purpose of this study was to confirm spatial distribution in groundwater (SGD) and nutrient discharge on tidal flat with the area of around 100m square in a small and steep island. The experimental sites were located on Ikuchi Island in Onomichi City, Hiroshima Prefecture, western Japan. Pore water samples were collected and water levels were monitored at 10 and 17 piezometers on two experimental tidal flats, which is composed of E site (100m x 30m) at the alluvial fan edge of an experimental catchment and W sites at the steep mountain slop foot (300m x 30m), respectively. In addition, rain water samples were collected monthly at seven plots with different elevation from April 2019 in an experimental small and steep catchment with a maximum altitude of 400 meters The stable isotope ratio and nutrient concentration of water samples were analyzed by PICARO and SWAt of Beltech, respectively.

Various groundwater and nutrient discharges were observed at the W and E sites. E site on the catchment foot with a stream had smaller groundwater and nutrient discharge with the pore water of low nutrient concentration and flesh water content as compared at W site. Though experimental Ikuchi Island was small with the altitude of only 400m, we could confirm the elevation effects of stable isotopic ratios in rain waters. However, the rainfall volumes were not clarified to increase with the altitude. These results were only based on the observations for only about six months from April to September 2019, we will show more detail results for more than one year in the presentation, Based on the relationship between the altitude and stable isotopic ratios in rainwater, we could estimate groundwater recharge altitude at some pore waters at W site. It was estimated to be 50m to 300m in altitude. The lower area is covered by the citrus plantation, and high dissolved nitrogen and phosphorus was contained by leaching of fertilizer component. On the other hand, groundwater from the higher area flows longer and deeper path, and high silica was contained. We were able to confirm the difference between groundwater well-rising in tidal flats at low and high tides at the At W test site, the nutrient load was large in the west side.

©2020. Japan Geoscience Union. All Right Reserved.

Estimation of unsteady confined groundwater flow with river water intrusion in coastal alluvial plain during a large flood.

*Yusuke Tomozawa[1], Shin-ichi Onodera[1], Mitsuyo Saito[2], Tohru TAKEUCHI[3], Yutaka MARUYAMA, Koichi Kitaoka[4]

1. Graduate School of Integrated Arts and Sciences Hiroshima University, 2. Graduate School of Environmental and Life Science, Okayama University, 3. Fujita Geology Co., Ltd., 4. Okayama University of Scienece

Several aquifers underlie alluvial plains, and confined groundwater is mainly used intensively. The water potential depression and land subsidence have been caused in the coastal area. On the other hand, confined groundwater is generally recharged in the boundary area (ie. Alluvial fan) between the mountain foot and alluvial plain. The groundwater recharge in alluvial fan mainly and preferentially occurs in the high flow period. This type of groundwater flow is considered to be in the steady to semi-steady state.
In this research, we focused on a small alluvial plain with a little bit slope, we examined to confirm the recharge process and confined groundwater flow, using 10 years monitoring of groundwater level, water chemistry, and oxygen and hydrogen stable isotopic ratios. Our research area was in Okayama alluvial plain, western Japan, buried by the sediment transported from Asahi river, Yoshii river and Takahashi river. We monitored groundwater level and collected water samples at the 6 observation boreholes on the 4 experimental sites.
The component separation of groundwater by stable isotopes of water indicates that the major recharge source is river water in the upper stream section, whereas the contribution of rainwater increases in the lower stream section, and mixing of seawater in to the coastal groundwater with about 20m deep. In addition, large decline of isotopic ratios, chloride and sodium concentration were observed in the confined groundwater in the central part of the plain after an extreme flooding event. This suggests intensive recharge by river water with low isotopic ratios by volume and elevation effect of precipitation during this period.

Keywords: Coastal alluvial plain, groundwater flow, stable oxygen and hydrogen isotope

©2020. Japan Geoscience Union. All Right Reserved.

Establishment and evaluation of a method to reconstruct the past snow fall and winter monsoon intensity based on the inter-annual variabilities of river discharges in Hokkaido, northern Japan

*Airi Maruyama[1], Tomohisa Irino[1]

1. Biogeochemistry Course, Earth System Science, Faculty of Environmental Earth Science, Hokkaido University

Monsoon is the seasonally alternating wind due to heat contrast between continents and ocean by solar radiation (Tada, 2005), and the one of the most characteristic seasonal variation of climate in east Asia. Winter monsoon, which is characterised by cold and dry wind and blows from continents, promotes heavy snowfall along the Japan Sea side of Japanese Islands, while Baiu, where moist tongue characterised by wet wind turning around the north Pacific Ocean, brings seasonal rain front along the Japanese Islands in summer. Although past summer monsoon has been successfully reconstructed in many studies (Ikehara and Itaki, 2005), researches on winter paleoclimate including winter monsoon have not been developed well. In this study, we analyzed the inter-annual variability of river water discharge in Hokkaido, subarctic Japan, to examine how the seasonal precipitation affects the spatio-temporal variability of sediment and water discharge, and tried to utilize it to reconstruct the past variability of winter snowfall from sediment archives.

We collected 10-year water discharge data of 13 class A rivers between 2006-2016 in Hokkaido from Water Information System of Ministry of Land, Infrastructure, Transport and Tourism. Then, we conducted principal component analysis (PCA) using *R*. Missing data was interpolated by the mean values. Out of 13 principle components, we examined PC1, PC2, and PC3 which occupy a large proportion of total variance. Based on the spatial distribution of the principle component loadings and the timings of maximum and minimum of principle component scores, these PCs are characterised like below.

1. PC1 represents average temporal discharge variation in Hokkaido, where the discharge depends on precipitation during summer to autumn and melting of snow in spring

2. PC2 loadings are significantly positive in the Okhotsk Sea side and negative in the Japan Sea side, where timing of maximum score is associated by summer precipitation in the Okhotsk Sea side and minimum score is associated by spring snow melt in the Japan Sea side

3. PC3 loading shows significantly positive in the Okhotsk Sea side and negative in the Pacific side, where timing of maximum score is associated with spring snow melt and minimum score occurs at heavy precipitation in summer and autumn

Considering the timing of maxima and minima in PC2 score, we suggest that the comparison of sediment discharge between the Okhotsk Sea and the Japan Sea may enable us to extract the information of spring snow melt discharge in the Japan Side as well as winter snow fall. However, when magnitude of both PC2 and PC3 scores becomes large, melting snow also depends on temperature that depends on insolation intensity (Chikita. 1994). Therefore, we need to further examine not only precipitation and snowfall but also data of temperature and insolation.

©2020. Japan Geoscience Union. All Right Reserved.

©2020. Japan Geoscience Union. All Right Reserved.

Classification analysis of coastal seaweed beds using UAV and Near-Infrared camera

*Akimitsu Shiraishi[1], Mitsuyo Saito[1], Akira Hama[2], Shin-ichi Onodera[3], Toru Iwata[1]

1. Graduate School of Environmental Science, Okayama University, 2. College of Education, Yokohama National University, 3. Graduate School of Integrated Arts and Sciences, Hiroshima University

Seaweed beds play a role in the coastal sea keeping water quality better and maintain ecosystem itself in shallow waters. However, the coastal environment has been affected by economic development. In Seto Inland Sea separating Honshu from Shikoku and Kyushu of Japan, where water quality has been improved by environmental conservation efforts, and some area appeared to be locally oligotrophic.

Satellite data has been used for remote sensing of seaweed beds, so far, however, it is susceptible to weather and clouds. Furthermore, free satellite data could be used with some problem such as low spatial resolution. Other typical monitoring methods include airborne platforms, grand based surveys and snorkel / scuba surveys. These techniques can suffer from temporal and spatial inconsistency, or are very restricted making it hard to assess seagrass meadows in a structured manner.

This research aims to obtain distribution of shallow seaweed beds by analyzing the combined data of visible and near-infrared images acquired using UAV. The UAVs can reduce effects of clouds and atmosphere. In addition, by conducting surveys at the same location during the daytime in the intertidal zone, the conditions for on-site observations can be made the same. Furthermore use of commercially available UAVs and inexpensive near-infrared cameras also reduce cost of research compared to expensive satellite data and snorkel / scuba surveys. The distribution data of shallow seaweed beds is to be analyzed with ground survey samples and the factors affecting on changes in seagrass bed ecosystems will be revealed.

The study area is Gohonmatsu Beach, Ikuchijima, Onomichi City, Hiroshima Prefecture.

UAV cameras shot about 100 at coasts vertically downward. Next, an ortho mosaic image was created (3.6 cm pixel^{-1}) in Structure from Motion (SfM). The same procedure was used for images from Near-Infrared cameras. Although NDVI were used as first analysis index, NDVI showed negative values for seaweed on the intertidal beach and submerged seagrass. Newly proposed NSGI showed positive value for those ones. Furthermore, we propose SGI1 and SGI2 as a method of seaweed bed classification using the brightness intensity of each band. SGI1 and SGI2 determines the seaweed beds under sea surface and on sandy beach, respectively. By combining these, most seaweed beds in the coastal area could be determined.

Duffy, J.P., Pratt, L., Anderson, K., Land, P.E., Shutler, J.D., 2018. Spatial assessment of intertidal seagrass meadows using optical imaging systems and a lightweight drone. Estuarine, Coastal and Shelf Science. 200, 169-180. https://www.sciencedirect.com/science/article/pii/S0272771417302202

*This work is supported by JSPS Grant-in-Aid for Scientific Research (B) (18H03411, PI: Mitsuyo Saito).

©2020. Japan Geoscience Union. All Right Reserved.

Keywords: coastal seaweed beds, UAV, near-infrared camera

©2020. Japan Geoscience Union. All Right Reserved.

Biogeochemical pathways of critical environmental contaminants (PTTE, POPs) in the rhizospheric soil-plant system

*Hideyuki Inui[1], Vladimir Beskoski[2], Mikael Motelica-Heino[3]

1. Kobe University, 2. University of Belgrade, 3. University of Orléans

Plants have a significant role in the biogeochemical cycling in continental ecosystems namely in the transformation and chemical export of anthropogenic chemicals in the critical zone environments. In particular the rhizosphere soil, which is the few millimeters of soil covering the roots of plants and influenced by their biological activity, is a dynamic system characterized by feedback interactions between soils characteristics, roots processes and dynamics of the associated microbial communities. It is a geochemical micro-environment influenced by plants physiology (roots exudation of compounds such as organic acids etc., respiration, …), microorganism activity (mineralization of organic matter…) and soil characteristics (SOM, pH, texture, WHC, CEC etc). These dynamic small-scale biogeosystems are characterized by feedback interactions between soil characteristics, plant roots and dynamics of the associated microbial communities and play an essential role in the transformation of natural organic matter, nutrients and trace elements. They may also locally influence the ecodynamic of critical environmental contaminants such as potentially toxic trace elements (PTTE) and/or persistent organic contaminants (POPs), either directly (precipitation, complexation, adsorption, degradation, plant uptake) and indirectly (effects of the rhizosphere on pH and redox potential, dissolution of minerals…) in contaminated soils.
The study of rhizosphere-related processes on mobility, availability and toxicity of PTTE and POPs in rhizospheric soils, based, in particular, on the role of the root-mycorrhizae-bacteria associations in their transformation of, is thus a major challenge to understand the ecodynamics of these contaminants in natural or anthropogenic continental biogeosystems. Identifying these feedbacks, positive or negative, for the study of physical-chemical processes, biological and microbial requires to be done at different spatial scales, micro (eg. soil pore –organo/mineral aggregates–microorganism interface), local (biological community or soil unit) to regional (ecosystem in its watershed). This objective will be reached through characterization of rhizosphere microflora, identifying the role of roots exudates, evidencing the influence of these biogeochemical factors on the speciation, transformation, mobility and phytoavailability of PTTE and POPs in rhizospheric soil.
Generic issues to be addressed are:
1) What and how do the structure and dynamics of microbial soil populations control zoning of critical environmental contaminants?
2) Can the foreseen spatio-temporal changes in microbial communities and distribution of these contaminants at a small spatial scale solve their contributions in terms of source and sink on large biogeochemical cycles?
3) What is the role of the rhizosphere on their transformation, mobility and transfer?
4) How can local sources and sinks be upscaled at the watershed and global transfer level?
The specificity of our work is to bring together a diversity of approaches at different spatial scales and in different conditions (laboratory, mesocosm, land) with a holistic integration of components (mineral and organic fractions of soil) and different biological factors (micro-organisms, plants). Results illustrating root-bacteria associations in the mobility, availability and toxicity will be discussed to understand their ecodynamics in soils, study the contribution of rhizospheric microbial communities their (im)mobilization processes, elucidate their transfer from soil to vegetation compartments and more global pathways in the critical zone. Far from being isolated, the different compartments of the critical zone interact according to

©2020. Japan Geoscience Union. All Right Reserved.

and on very variable spatial and time scales still largely unknown.

Keywords: Persistent organic pollutants, Potentially toxic trace elements

©2020. Japan Geoscience Union. All Right Reserved.

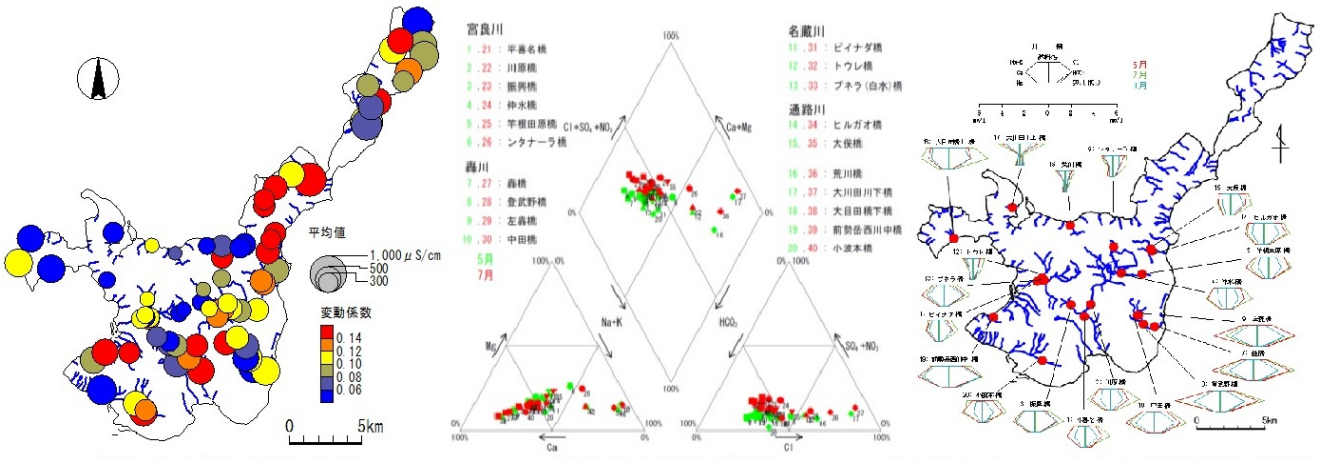
Study on water quality composition and its change in Ishigaki Island

*Masato Oda[1], Koji Kodera[1], Atsuki Sato[1]

1. Hosei University, faculty of literature ,Geography

In Ishigaki Island in the Yaeyama Islands, valuable coastal environments such as coral reefs exist, and the impact of land water flowing through the island on the coastal environment is very large. Research has been conducted on the formation of water quality composition by soil, soil and nutrient salts mainly in rivers such as the Nagura River and the Todorogawa River. Our laboratory has been conducting surveys on Ishigaki Island since 2006 –2011 and 2018, and we report a comparison between past research data and recent survey results.
The water quality composition of Ishigaki Island is classified as alkaline earth carbonate type because the dissolved components are overwhelmingly larger than the average river in Japan. In particular, the distribution of the Na-Cl and Ca-HCO3 forms is remarkable. This can be attributed to the geological condition of being a limestone area, sea salt, and agriculture. Nitrogen pollution was significant in upland farming areas and urban areas, and nitrite and ammonia components were detected in some urban areas. It seems that there are areas where wastewater treatment is insufficient.
In the future, it is necessary to collect more samples in cooperation with local citizens' groups, accumulate data through long-term surveys, clarify changes in water quality composition by comparing with past research data, and conduct research on the effects on the surrounding environment.

Keywords: Ishigaki Island, limestone, Nagra River, nitrogen pollution



a）ECと変動係数（0905-1012）　b）水質組成（0905/0907）　C）水質のバランスと変化（0905/0907/1001）

図１　石垣島の河川水質と変化

©2020. Japan Geoscience Union. All Right Reserved.

Effects of sugarcane growth on hydrological elements and sediment yield

*Yang Cao[1], Shin-ichi Onodera[2], Mitsuyo Saito[3], Hide Omae[4], Yoshiko Iizumi[5]

1. Nanjing Institute of Geography and Limnology, Chinese Academy of Sciences, 2. Hiroshima University, 3. Okayama University, 4. Tropical Agriculture Research Front (TARF), Japan International Research Center for Agricultural Sciences (JIRCAS), 5. Nihon University

In this work, the effects of sugarcane growth on main hydrological elements and sediment yield were investigated using SWAT model and monitoring data. The growth of sugarcane was controlled by setting tillage and fertilization information in the model. Calibration and validation of the model showed that the reasonable runoff and sediment simulation results were obtained. The results showed that with the growth of sugarcane, the dense roots and branches effectively regulated the runoff during the period of abundant precipitation. Compared with the year 2017 at the initial stage of sugarcane growth, evapotranspiration at the later stage of sugarcane growth in 2018 was lower because of low soil moisture. Reduced evapotranspiration has also led to a significant increase in water yield in the sugarcane region in 2018. In addition, the growth of sugarcane contributed to the reduction of sediment yield in the small basin, with the average sediment yield in sugarcane regions dropping by about 58% in 2018 compared with 2017. The research methods and results proposed in this paper can be used for reference for agricultural management in other small watersheds with abundant rainfall.

Keywords: SWAT model, small catchment, sugarcane, sediment, evapotranspiration

©2020. Japan Geoscience Union. All Right Reserved.

Field measurement and numerical simulation of water flux in a forest soil

*Masahiro Kobayashi[1]

1. Forestry and Forest Products Research Institute

To clarify the movement of dissolved substances, such as by nitrogen leaching in forest soil, it is necessary to quantify the water flux. However, measuring water flux in unsaturated soils is not easy. Porous plate tension lysimeters (PPTL), which automatically control the vacuum according to the wetness of the soil, are considered to be one of the suitable methods for this purpose. In this study, the PPTL method was applied to evaluate the seasonal change of water flux in a forest soil. Furthermore, we simulated the observed seasonal water flux by numerical calculation using the experimentally measured soil hydraulic characteristics. In a Japanese cypress forest, a ceramic porous plate was installed in the soil at a depth of 1 m and connected to the vacuum system, and the amount of water flux was measured continuously. Throughfall was measured using a tipping rain gauge and soil water storage was measured using time domain reflectometry sensors. Then, the water balance in the soil layer was determined. The observation period was divided into shorter periods so that the soil water storage at the beginning and end of the period was equal. The average daily water losses (transpiration) in each small period were calculated to be within the range of about 0.2 mm/d in winter to about 3 mm/d in summer. The observed water flux by PPTL was simulated by numerical calculation using water content–potential–hydraulic conductivity relationships determined by laboratory experiments. The numerical simulations were conducted using the HYDRUS1D program. Using the daily water loss by field observation as the value of root water uptake, the water flux for each period was simulated. The simulated temporal change of water flux was comparable to the observed value obtained by PPTL.

Keywords: water flux, forest soil

©2020. Japan Geoscience Union. All Right Reserved.

Hydrogen and oxygen stable isotopic mapping that allows us to investigate water cycle regimes over Japanese Island

*Shota Nakauchi[1], Takahiro Hosono[1], Kimpei Ichiyanagi[1]

1. Kumamoto University

In the earth surface water cycle, waters fall to the surface ground as precipitation, and then flow through ground and stream waters, and finally flow back to the sea. Oxygen and hydrogen isotopic ratios of water molecular reflect the source mixing and physical processes, i.e., evaporation, in such fluid dynamics. Many studies have applied these tools in revealing processes taken placed in regional watershed systems. Even enormous data have adequately been accumulated by the year 2020, only few researches have summarized and integrated these datasets in regional and continental scales. This study collected these data covering whole Japanese Islands from published literatures, domestic reports and internet websites, for all water regimes including precipitation, groundwater, spring water, and river water to discuss their overall flow systems. As a result, some major findings were obtained. First, it was confirmed that the waters at both higher latitude and the higher altitude showed lower isotopic ratios for precipitation, spring water and river water, that are latitude and altitude effects, except for groundwater which isotopic signatures are formed by involvement of other factors. Spatial distributions of surface and subsurface waters correspond well with that of precipitation. Second, water flow features were examined by characterizing the slope of regression lines on the delta diagram. It was suggested that precipitation fallen on the mountains percolates into ground and seeps mostly from mountain foots as springs that merge to become headwaters in the mountains. Most of downslope aquifer waters more resemble in isotopic compositions to these headwaters rather than mountain waters. The spring waters at lower altitude must be recharged in mountains with lower altitude where these headwaters present. The downslope groundwaters and, to more extent, rivers are most significantly affected by evaporation. Presence of NE-SW trending lower d-excess anomaly belt was suggested in the central part of Japanese Islands, which formation processes should be address in future work.

Keywords: stable isotopes, precipitation, groundwater, river water, spring water

©2020. Japan Geoscience Union. All Right Reserved.

Estimation of discharge at small forest watersheds in Ibaraki Prefecture by using the SWAT model

*Naohiro Imamura[1], Naoyuki Yamashita[1], Masahiro Kobayashi[1], Takanori Shimizu[1], Shinji Sawano[1], Koji Tamai[1], Shin' ichi Iida[1], Naoki Kabeya[1], Yoshio Tsuboyama[1]

1. Forestry and Forest Products Research Institute

Prediction and evaluation of the impact of forest operations on water and nutrient cycle in forest watershed are required recently. Whereas the SWAT model has been used for estimating discharge at large watersheds consisting of agricultural land, the application of the SWAT model to forest watersheds is expected due to the high versatility of the model. To evaluate the applicability of the SWAT model to small forest watershed, this research used the SWAT model to reproduce daily discharge at small forest watersheds in Ibaraki Prefecture from 2008 through 2011. The watersheds of the Tsukuba and Katsura research sites are 3.79 and 61.7 ha, respectively. In the model calculations, actual observed soil data (soil thickness, hydraulic conductivity, saturated hydraulic conductivity) were used. As a result, the parameters for curve number, canopy maximum water storage, and groundwater had to be calibrated to fit the observed discharge at both sites. In addition, at Tsukuba and Katsura research site, it was necessary to calibrate the average slope aspect and average slope length, respectively. These results indicated that adjusting the gradient parameters was important for applying the SWAT model to the forest watersheds with steep slopes which widely distribute in Japan.

Keywords: discharge, SWAT model, steep slope

©2020. Japan Geoscience Union. All Right Reserved.

[E] Poster | A (Atmospheric and Hydrospheric Sciences)：A-HW Hydrology & Water Environment

[A-HW33] Prediction of water and sediment dynamics from small to large scales

convener:Yoshiyuki Yokoo(Fukushima University), Yuko Asano(The University of Tokyo)

After the IAHS decade of PUB, challenges have been continued for understanding internal processes and developing models for elevating the predictability of hydrological response for watershed with multiple scales. Simultaneously, changes in the precipitation patterns and intensity as well as increases in associated sediment disasters due to global climate changes brought us challenges for developing tight linkages between water and sediment dynamics in the areas of observation and modeling approaches. For tacking the issues, we have conducted studies for comprehending scale dependency of processes for water and sediment movement from small to large watersheds and explored process representation of numerical models coupled to field-based evidences. Based on these studies, we proposed (1) classification for the behaviors of water and sediment movement from small and large watersheds depending on internal processes, (2) internal hydrologic and geomorphic processes can be included in models. Further discussion needs to be extended for applicability of the approaches.
This session aims to explore updated and current studies for scale dependencies and process representation of hydrologic and geomorphic processes in multiple watersheds. We welcome for topics related to hydrology, geomorphology, and biogeochemistry in small and large watersheds for both field and modeling approaches. Patterns and variability for water and sediment movements within watersheds are also included in the topics.
In this session, we will extend discussion for next step of field and modeling studies toward integrating hydrologic and geomorphologic processes in various landscapes and achieving prediction of ungauged basin in the areas of water and sediment dynamics. Finding through this session may advance our ability for hydrological predictions in any ungauged basins from small to large spatial scales toward sustainable water resources and sediment management.

[AHW33-P01] Quantitative evaluation of sediment dynamics caused by extreme rainfall events in August 2016 in the Pankenushi River, Hokkaido, northern Japan

*Hiromi Akita[1], Shigeru Mizugaki[1], Yasuhiro Murakami[1] (1.Civil Engineering Research Institute for Cold Region)

[AHW33-P02] Evaluation of suspended sediment sources at the basin scale: a case study of coastal basin, Hokkaido, northern Japan

*Shigeru Mizugaki[1], Junichi Ohtsuka[1], Yasuhiro Murakami[1], Hiromi Akita[1], Atsushi Tanise[1], Masa-aki Murayama[1] (1.Civil Engineering Research Institute for Cold Region, PWRI)

[AHW33-P03] Dependency of watershed-scale rainwater storage on watershed-area at the occurrence times of slope failures: a preliminary investigation in Japan

*Hikaru Satou[1], Yoshiyuki Yokoo[2], Chris Leong[2] (1.Graduate School of Symbiotic Systems Science, Fukushima University, 2.Faculty of Symbiotic Systems Science, Fukushima University)

[AHW33-P04] Sediment dynamics after the 1973 landslide event in mountain watersheds of Hokkaido, Japan

*Takashi Koi[1], Yasutaka Tanaka[1] (1.Center for Natural Hazards Research, Hokkaido University)

[AHW33-P05] Factors controlling concentration of dissolved ^{90}Sr and ^{137}Cs in river water in the Chernobyl exclusion zone.

*Matsushita Koki[1], Yasunori Igarashi[2], Yuichi Onda[1], Yoshifumi Wakiyama[2], Alexei Konoplev[2], Gennady Laptev[3], Sergii Obrizan[4], Volodymyr Demianovych[4], Mark Zheleznyak[2] (1.Tsukuba University, 2.Institute of Environmental Radioactivity at Fukushima University, 3.Ukrainian Hydrometeorological Institute, 4.Chernobyl Ecocentre, State Agency of Ukraine on Exclusion Zone Management)

[AHW33-P06] Explication the effect of thinning on suspended sediment runoff in a cypress and cedar plantation forest by end-member mixing analysis using Fukushima-derived Cs-137, Cs-

134 and Pb-210ex

*Motosuke Kinoshita[1], Yuichi Onda[2], Soo Youn Nam[3], Hiroaki Kato[2], Takashi Gomi[3], Chen-wei Chiu[3], Keisuke Taniguchi[4] (1.University of Tsukuba, 2.Center for Research in Isotopes and Environmental Dynamics, University of TSUKUBA, 3.Tokyo University of Agriculture and Technology Institute of Agriculture Division of International Environmental and Agricultural Science, 4.Fukushima Prefectural Centre for Environmental Creation)

Quantitative evaluation of sediment dynamics caused by extreme rainfall events in August 2016 in the Pankenushi River, Hokkaido, northern Japan

*Hiromi Akita[1], Shigeru Mizugaki[1], Yasuhiro Murakami[1]

1. Civil Engineering Research Institute for Cold Region

In this study, we conducted satellite image analysis and laser profiler (LP) measurements to clarify the sediment dynamics quantitatively in the Pankenushi River, a headwater catchment of the Saru River, where the landslides and river bank erosion occurred by the extreme rainfall events associated with four typhoons in August 2016. The disturbed areas caused by landslides and river bank erosion across the catchment were extracted using the normalized difference vegetation index (NDVI) calculated from satellite images before and after heavy rain. LP measurements were conducted along the main river channel from the mid- to down-stream areas where the disturbance of the river channel was remarkable, and the topographical changes after the rainfall events were evaluated. The 197 of fresh landslides were found across the catchment, of which 155 (79%) were distributed in the igneous rock area in the upstream area where rainfall of 300 mm or more over 24 hours was concentrated. The depth of landslide scar was estimated as 2 m or less for the 90% of the fresh landslides (N= 57) in the mid- to down-stream area, where the LP measurements was conducted. The volume of eroded and deposited sediment in the landslide scars across the catchment were estimated to be about 470,000 m^3 and 70,000 m^3, respectively, based on the power relationship between the sediment volume and landslide area. In result, about 400,000 m^3 of sediment was found to be supplied from the slope to the river channel by landslides. Along the channel from the mid- to down-stream areas, the sediment volume of erosion and deposition were estimated to be about 1,000,000 m^3 and 330,000 m^3, respectively. The erosion volume along the channel was about 2.0 times greater than that by landslides across the catchment suggesting that not only the landslides but also the bank erosion could play a significant role in sediment supply downstream during and after the extreme rainfall events.

Keywords: Landslides, Bank erosion, Satellite image analysis, Normalized difference vegetation index, Laser profiler measurements

©2020. Japan Geoscience Union. All Right Reserved.

Evaluation of suspended sediment sources at the basin scale: a case study of coastal basin, Hokkaido, northern Japan

*Shigeru Mizugaki[1], Junichi Ohtsuka[1], Yasuhiro Murakami[1], Hiromi Akita[1], Atsushi Tanise[1], Masa-aki Murayama[1]

1. Civil Engineering Research Institute for Cold Region, PWRI

In Japan, coastal erosion has been a problem throughout the country since the 1950s, and comprehensive sediment management of sediment transport through rivers from mountains to coasts is required. Understanding the source of sediment is an important and fundamental issue. In order to understand the connectivity of sediment from the mountainous area to the sea, this study conducted sediment hydrology observations on the Saru River basin in Hokkaido, and fingerprinting sources of suspended sediment using natural radionuclides as tracers. To evaluate the source of suspended sediment quantitatively, the rating curve for each lithological source group was developed. The annual amount of suspended sediment from the Saru River to the sea area was 150,000 t/yr on average from 2011 to 2014, but it was more than 17 times as large as 2.6 million ton in 2016 due to heavy rainfall. The main source areas of suspended sediment were found to be sedimentary rocks and metamorphic rocks, which widely distributed in the middle and lower reaches, during 2011-2014. This result seems to reflect the weathering characteristics of rocks. During the heavy rainfall events in August 2016, the main source areas were metamorphic rocks and sedimentary rocks in the first half, and the accretionary matrix and accretionary basalt blocks in the latter half, which were distributed in the upstream area. These results indicate that the sediment yield and major sediment production sources differ depending on the geological composition and rainfall distribution of the basin.

Keywords: source to sink, fingerprinting, radionuclide tracers, extreme rainfall events

©2020. Japan Geoscience Union. All Right Reserved.

Dependency of watershed-scale rainwater storage on watershed-area at the occurrence times of slope failures: a preliminary investigation in Japan

*Hikaru Satou[1], Yoshiyuki Yokoo[2], Chris Leong[2]

1. Graduate School of Symbiotic Systems Science, Fukushima University, 2. Faculty of Symbiotic Systems Science, Fukushima University

The authors investigated whether watershed-scale rainwater storage at the occurrence times of slope failures depended on watershed area. If slope failures can be regarded as near surface processes, then rainwater storage that causes slope failures would be independent of watershed area. However, if slope failures are not of near surface processes, slower hydrological processes would influence the slope failures and they would be dependent on watershed area. Towards the aim, we estimated watershed-scale rainwater storage at several watersheds with different watershed areas. We employed a methodology to estimate watershed-scale rainwater storage that was developed in our research group. The result showed that watershed-scale rainwater storage that caused slope failures increased with watershed area. This result suggest that slope failures are not just near surface processes but also slower processes deep in soil that would contribute to slope failures in relatively large watersheds.

Keywords: hydrograph separation, storage, hydrological processes

©2020. Japan Geoscience Union. All Right Reserved.

Sediment dynamics after the 1973 landslide event in mountain watersheds of Hokkaido, Japan

*Takashi Koi[1], Yasutaka Tanaka[1]

1. Center for Natural Hazards Research, Hokkaido University

When landslide or debris flow occurs due to heavy rainfall in a watershed, sediment movement becomes apparent instantaneously and locally in the form of a landslide disaster. On the other hand, not all of the produced sediment flows out at once, but part of the sediment is temporarily stored in the lower part of slopes or in river channels, and then moves and propagates downstream due to rainfall and other floods. These sediments stored in a watershed will be debris-flowed during the subsequent large-scale flooding, promoting sediment disasters again, and there is concern about effects of abnormal reservoir sedimentation at downstream storage dams. Therefore, to understand sediment dynamics after landslide event is important in terms of watershed management. In this study, we created a multi-period digital surface models (DSM) before and after the occurrence of a sediment production event, and clarified sediment dynamics on a scale of several decades from comparison with time-series hydrological data and vegetation invasion into river channels. Study sites are three mountain watersheds in Kotani’ ishi, Hokkaido, Japan, where multiple landslides occurred due to heavy rainfall event in 1973. The DSM was created by Structure-from-motion (SfM) using archive data of aerial photographs taken during nine periods from 1972 to 2008 and results of a field survey conducted in 2020. As a result of the investigation, although there was no noticeable movement of stored sediment for at least 35 years after the landslides, relatively large-scale sediment movement that caused riparian disturbance during flooding since 2009 has occurred. These results indicate that the constant sediment movement of the stored sediment is not remarkable, but that the sediment may cause large-scale sediment movement even after several decades since the occurrence of landslides.

Keywords: sediment movement, structure-from-motion (SfM), aerial photographs, decadal and longer time scales, landslide event, sediment disaster

©2020. Japan Geoscience Union. All Right Reserved.

Factors controlling concentration of dissolved ^{90}Sr and ^{137}Cs in river water in the Chernobyl exclusion zone.

*Matsushita Koki[1], Yasunori Igarashi[2], Yuichi Onda[1], Yoshifumi Wakiyama[2], Alexei Konoplev[2], Gennady Laptev[3], Sergii Obrizan[4], Volodymyr Demianovych[4], Mark Zheleznyak[2]

1. Tsukuba University, 2. Institute of Environmental Radioactivity at Fukushima University, 3. Ukrainian Hydrometeorological Institute, 4. Chernobyl Ecocentre, State Agency of Ukraine on Exclusion Zone Management

Dynamics of radionuclides, ^{90}Sr and ^{137}Cs, are still of great interest for mitigating radiological risks in the Chernobyl Exclusion Zone (CEZ) and its downstream area. Previous studies showed positive relationship between dissolved ^{90}Sr concentration and water discharge and it suggest that hydrological characteristics affects the ^{90}Sr transfer. However, in practice, the dynamics of radionuclides is closely related not only to hydrological characteristics but also to chemical characteristics and the surrounding environment. For understanding formation of solution concentration in the river water system, several studies attempted to evaluate spatial-temporal variations of factors of interest in a catchment and discussed relationship between catchment characteristics and the behavior of the factors. Such approaches can improve our understanding of radionuclides dynamics. The aim of this study is to clarify the factors controlling dynamics of radionuclides in the river water system in the CEZ and we evaluated spatial-temporal variations in dissolved ^{90}Sr and ^{137}Cs concentration in a small catchment. The study site was in the Sakhan catchment, locating at approximately 7 km northwest from the Chernobyl Nuclear Power Plant. Water samples were taken at main stream, tributaries and water spring points each season. The discharge rate was determined by cross-sectional survey of flow velocity and water level at the same time as water sampling. Each catchment area was made from digital elevation model (DEM) data and mean ^{90}Sr and ^{137}Cs inventory for each sub-catchment was determined by distribution maps of radionuclide. Moreover, the proportion of wetland in dry and wet season was calculated from satellite spectral images. In laboratory, samples were analyzed for dissolved ^{90}Sr and ^{137}Cs, dissolved anions and cations and Si concentration. Discharge rate at the main stream was the highest in snowmelt season and the lowest in summer. The concentration of dissolved ^{90}Sr and ^{137}Cs at the main stream was, as like discharge rate, high in snowmelt season and low in summer. However, the response of dissolved ^{90}Sr concentration to discharge rate was not clear at the spring points and river water in some headwater catchments. We also found that the positive relationship between the area of wetland and dissolved ^{90}Sr and ^{137}Cs concentration in the snowmelt season. Previous studies have showed that “wetlands” and “high water level in the floodplain” can affect high ^{90}Sr discharge. However, the relationship is not clear during the summer. From these results, the tight coupling between hydrological processes and the ^{90}Sr and ^{137}Cs concentration formation processes is suggested, and further study is necessary to elucidate the mechanisms that control the ^{90}Sr and ^{137}Cs concentration in the river water systems.

Keywords: Chernobyl catchment, Contaminant transport, Strontium-90 and Cesium-137, Wetland, Spatial-temporal variations

©2020. Japan Geoscience Union. All Right Reserved.

Explication the effect of thinning on suspended sediment runoff in a cypress and cedar plantation forest by end-member mixing analysis using Fukushima-derived Cs-137, Cs-134 and Pb-210ex

*Motosuke Kinoshita[1], Yuichi Onda[2], Soo Youn Nam[3], Hiroaki Kato[2], Takashi Gomi[3], Chen-wei Chiu[3], Keisuke Taniguchi[4]

1. University of Tsukuba, 2. Center for Research in Isotopes and Environmental Dynamics, University of TSUKUBA, 3. Tokyo University of Agriculture and Technology Institute of Agriculture Division of International Environmental and Agricultural Science, 4. Fukushima Prefectural Centre for Environmental Creation

Skid trail and heavy machinery for forest practice becoming more common for effective forest practices, but these causes soil disturbance in the forest, leading to a sudden increase in the amount of suspended sediment during and post thinning. The discharged sediment can flow into the river and may cause downstream water pollution. To evaluate the effect of thinning on sediment production, sediment fingerprinting techniques can be an effective tool for proper forest practices.

In Tochigi prefecture in Japan, in addition to the Cs-137 by global fallout and Pb-210ex, additional FRN, the Fukushima-derived Cs-137 and Cs-134 on March 2011 are available, but few studies area available for combining use of Fukushima-derived radiocesium and fallout Pb-210ex. Therefore, the objective of this study is to determine the transport of the fine sediment in the forest pre- and post- thinning with using fingerprinting techniques.

The study area is Mt. Karasawa, located 180 km southwest of the Fukushima nuclear power plant in Tochigi prefecture. The fallout inventory of Cs-137 and Cs-134 is 8 kBq/m2(Kato et al, 2012). The study site has two catchments which are called K2(17ha) and K3(9ha) respectively and the observation period was from August 2010 to August 2019. In K2, strip thinning was performed with heavy machines from June to October 2011 while randomly thinning without heavy machines was applied for K3 from January to March 2013.

Soil samples were collected from the slope surface, skid trail and stream bed, which are the possible sources of suspended sediment. The suspended sediment concentration was measured based on the data of the turbidity censor installed in the stream. The particle size distribution and radionuclide concentration of sediment collected from SS sampler and soil samples are also measured.

Hysteresis analysis based on suspended sediment concentration and flow rate and fingerprinting using Fukushima-derived Cs-137, Cs-134, and Pb-210ex, a natural radioactive isotope, was applied to determine the contribution of the slope surface layer and streambed to suspended sediment. By using the difference in the depth distribution of Cs-134 and Cs-137, the production source depth of suspended sediment was estimated.

In the K2 catchment where strip thinning was performed with heavy machinery, suspended sediment concentration during high flow period was rapidly increased up to 333 kg/day during thinning period. It is 30 times more than pre thinning. Then suspended sediment amount decreased down to 503 mg/L after

©2020. Japan Geoscience Union. All Right Reserved.

thinning. On the other hand, in the controlled catchment(K3), no increase in suspended sediment amount was observed during the same period.

By using hysteresis analysis, contribution from forest soil to suspended sediment increase from 0% to about 50% during thinning and that trend had continued by 3 years later of thinning. After that, contribution from stream bed increase and slope decreased.

By using End- Members Mixing analysis, contribution from streambed to suspended sediment are similar to the hysteresis analysis except for the period of midterm of thinning to immediately after thinning. In that period, contribution from the slope also decreased. It is considered to increase the sediment production from skid trails.

Then we focused on the characteristic of the soil from skid trail, which show low Pb-210ex content. In K2 catchment, Pb-210ex in suspended sediment quite decreased during thinning period to 1 month after of thinning. However, Pb-210ex in suspended sediment didn’t change during thinning. It is assumed that contribution from skid trails is very high during and soon after thinning.

Keywords: thinning, Cs-137, suspended sediment, finger printing

©2020. Japan Geoscience Union. All Right Reserved.

[E] Poster | A (Atmospheric and Hydrospheric Sciences)：A-HW Hydrology & Water Environment

[A-HW37] Interdisciplinary approach to support climate change adaptation measures in regional scale

convener:TEBAKARI TAICHI(Toyama Prefectural University), Yadu Pokhrel(Michigan State University), Masashi Kiguchi(University of Tokyo), Sompratana Ritphring(Kasetsart University)

In Japan, the impact of climate change has already become apparent and may become even more serious in the future. For example, there are the following specific damages; crop damage such as mandarin orange edema and white immature grains of rice, health hazards such as the northward distribution of Aedes albopictus and heat stroke patients, meteorological disasters such as increased torrential rain and increased number of strong typhoons, and coral bleaching Ecosystem.
The climate change adaptation law, which was enacted in 2018, clarified the legal position of adaptation measures in Japan, and is a legal for the national, local governments, businesses and citizens to cooperate and cooperate to promote adaptation measures. Based on this law, the Climate Change Adaptation Information Platform (A-PLAT) was established to develop and provide tools to support information provision and adaptation actions, and to collect, organize and provide best practices. AP-PLAT and T -Overseas development such as -PLAT is also progressing. Overseas expansion such as AP-PLAT and T-PLAT are also progressing.
In each research field, it is necessary to promote effective adaptation measures based on reliable and detailed information, and measures based on scientific knowledge of future impacts and strengthening of adaptation in the region are urgently needed.
This proposed session would like to invite presentations on the latest achievements in interdisciplinary fields such as hydrology, agriculture, forestry, weather, and climate that support specific climate change adaptation measures, as well as on the development of new research.

[AHW37-P01] **International Interdisciplinary Collaboration Essential to Linking the Changing Antarctic Ice Sheets with Global Coastlines**

*Robin Elizabeth Bell[1] (1.Lamont Doherty Earth Observatory of Columbia University)

[AHW37-P02] Development of climate change-related data accumulation system in Thailand

*Masashi Kiguchi[1], Chaiporn Jaikaeo[2], Eiji Ikoma[1] (1.The University of Tokyo, 2.Kasetsart University)

[AHW37-P03] Development of future climate scenario based on multi GCMs of CMIP5 and rain gridded data observed by multi-agencies in Thailand

*Masashi Kiguchi[1], Ruthaikarn BUAPHEAN[2], Aphantree YUTTAPHAN[2], Boonlert ARCHEVARAHUPROK[2], Eiji IKOMA[1], Taikan OKI[1,3] (1.The University of Tokyo, 2.Thai Meteorological Department, 3.United Nation University)

[AHW37-P04] Interannual variability of timing of monsoon-onset in South East Asia

*Ryosuke Kato[1], Tomohito Yamada[2] (1.Hokkaido university graduate school of engineering, 2.Hokkaido university faculty of engineering)

[AHW37-P05] Deep learning for seasonal to sub-seasonal rainfall prediction in Chaophraya river basin

*Kiyoharu Hasegawa[1], Shinjiro Kanae[1] (1.Toyko Institute of Technology)

[AHW37-P06] Seasonal precipitation forecast model in wet and dry seasons using global monthly surface temperature by deep learning

*Shingo Zenkoji[1], Taichi Tebakari[1], Kazutoshi Sakakibara[1] (1.Toyama Prefecural University)

[AHW37-P07] Using weather pattern recognition to classify and predict summertime heavy rainfall occurrence over the Upper Nan river basin, northwestern Thailand

*Ryosuke Kato[1], Dzung Nguyen-Le[2], Tomohito Yamada[2] (1.Hokkaido university graduate school of engineering, 2.Hokkaido university faculty of engineering)

[AHW37-P08] Impact of Rainfall on Urban Traffic Flow based on Probe Vehicle Data in Bangkok

*Tsuyoshi Takano[1], Hiroyoshi Morita[1], Shinichiro Nakamura[2], Miyazaki Hiroyuki[3], Wasan Pattara-atikom[4], Napaporn Piamsa-nga[5] (1.Nippon Engineering Consultants Co., Ltd, 2.Nagoya Univ., 3.Asian Institute of Technology, 4.National Electronics and Computer Technology Center, 5.Kasetsart Univ.)

[AHW37-P09] Investigation of Extreme Flood Changes in the Mekong River Basin Using +4K Climate Simulation

*Sophal Try[1], Shigenobu Tanaka[1], Kenji Tanaka[1], Takahiro Sayama[1], Chantha Oeurng[2] (1.Kyoto University, 2.Institute of Technology of Cambodia)

[AHW37-P10] Climate change and land use change impact assessment on flood and inundation in a river basin in Sumatra island in Indonesia

*Kodai Yamamoto[1], Takahiro Sayama[2], Apip Apip[3] (1.Graduate School of Engineering, Kyoto University, 2.Disaster Prevention Research Institute, 3.Research Center of Limnology, Indonesian Institute of Sciences)

[AHW37-P11] AN ASSESSMENT OF RESERVOIR OPERATION POTENTIAL FOR FLOW REGULATION IN THE CHAO PHRAYA RIVER BASIN

*SARITHA PADIYEDATH GOPALAN[1], Naota Hanasaki[1] (1.National Institute for Environmental Studies)

[AHW37-P12] Regional climate change impact on water quality in the lower Chao Phraya River, Thailand

Taichi Tebakari[1], Sanit Wongsa[2], *Horiuchi Yusuke[1] (1.Toyama Prefectural University, 2.King Mongkut's University)

[AHW37-P13] Research on the current thermal energy budget of land surface by continuous observation of near-surface ground temperature in Kanto Plain, Japan

*Osamu Matsubayashi[1], Hideki Hamamoto[2], Sachio Ehara[3] (1.National Institute of Advanced Industrial Science and Technology, 2.Center for Environmental Science in Saitama, 3.Institute for Geothermal Information)

[AHW37-P14] **Good Practices for Climate Change Adaptation in Agricultural Sector, Thailand**

*KOSHI YOSHIDA[1] (1.Ibaraki University)

[AHW37-P15] **Evaluation of salinity effects on rice production in farmers' fields in Ban Phai, Khon Kaen, Thailand**

*YI YANG[1], Rongling Ye[1], Thanyaluck Nontasri[2], Mallika Srisutham[2], Supranee Sritumboon[3], Masayasu Maki[4], KOSHI YOSHIDA[5], Kazuo Oki[6], Koki Homma[1] (1.tohoku university, 2.Khon Kaen Univ., Thailand, 3.LDD, Thailand, 4.Fukushima Univ., 5.Ibaraki Univ., 6.Univ. Tokyo)

[AHW37-P16] Calibration of cultivar parameters of SIMRIW-RS (rice simulation model for remote sensing) for the rice growth monitoring in Thailand

*Koki Homma[1], Mongkol Raksapatcharawong[2], Watcharee Veerakachen[2], Peerapon Prompitakporn[2], Masayasu Maki[3], Kazuo Oki[4] (1.Tohoku University, 2.Kasesart University, 3.Fukushima University, 4.The University of Tokyo)

[AHW37-P18] Farmers' perception of climate change induced drought in the Northeast Thailand

*Miki Nodera[1], Keigo Noda[1], Koshi Yoshida[2], Mallika Srisutham[3] (1.Gifu University, 2.Ibaraki University, 3.Khon Kaen University)

[AHW37-P19] **Research on farmers' awareness of adaptation to climate change and its information collection and sharing in rural area in Thailand**

*Kyoko Matsumoto[1], Mallika Srisutham[2], Supranee Sritumboon[3], Sompratana Ritphring[4], Masashi Kiguchi[1], Taikan Oki[5] (1.Institute of Industrial Science, The University of Tokyo, 2.Facutly of Agriculture, Khonkaen University, 3.Land Development Department, 4.Faculty of Engineering, Kasetsart University, 5.Institute for Future Initiatives, The University of Tokyo)

International Interdisciplinary Collaboration Essential to Linking the Changing Antarctic Ice Sheets with Global Coastlines

*Robin Elizabeth Bell[1]

1. Lamont Doherty Earth Observatory of Columbia University

International collaboration together with innovative technology have produced tremendous leaps in our understanding of the Antarctic Ice Sheet. Before the International Geophysical Year we did know how much water was locked in the Antarctic Ice Sheet. Before the launching of the modern suite of international satellites that measure the ice sheet elevation, velocity and mass we had no good constraints on how quickly the ice could change. Before we were collected and shared data on the structure of the ice sheet, the age of the ice and the temperature of the surrounding oceans we did not have good constraints on what might drive rapid change. Now we have the framework of warming oceans can trigger rapid change at grounding lines of marine ice sheets and warming atmospheres may lead to rapid collapse of buttressing ice shelves. Increasingly we are seeing the impact of the changing Antarctic ice along the coastlines around the globe. Our challenge has expanded from discovery of new frontiers to understanding how fast the ice will retreat and how fast the sea levels will rise. The ongoing work at US-UK effort at Thwaites Glacier is an example of internal collaboration targeting a vulnerable, rapidly changing marine outlet glacier. Looking as the Antarctic system as a whole, it is essential that we as the international community work collaboratively to understand the Antarctic ice-ocean-atmosphere-solid earth system. Our recent interdisciplinary work over the Ross Ice Shelf has built a framework for addressing ice sheet stability from a systems framework that enables new discoveries and eventually improved projections of how sea level will change at coastlines from Mumbai to Manhattan.

Keywords: Ice sheet, Coastlines, Sea level

©2020. Japan Geoscience Union. All Right Reserved.

Development of climate change-related data accumulation system in Thailand

*Masashi Kiguchi[1], Chaiporn Jaikaeo[2], Eiji Ikoma[1]

1. The University of Tokyo, 2. Kasetsart University

Although certain data may be available to researchers, accessing that data in a usable form is not always straightforward, especially for researchers without a programming background. Some data, such as weather observations, are accessible only for a short time. Historical datasets are usually not easy to download due to the large file sizes, which tend to consume an organization's network bandwidth. Although some organizations provide historical data, these are often in a form that is difficult to extract. For example, the Electricity Generating Authority of Thailand (EGAT) allows access to dam-operation data spanning many decades using an interactive web application. Researchers can view the data for a given date, and individual data points can then be copied into a spreadsheet. This procedure can be repeated as many times as needed; however, it is error-prone and time-consuming, especially when a large dataset is required. The Thai Meteorological Department (TMD) and Royal Irrigation Department (RID) use a different approach, by providing Application Programming Interfaces (APIs) that can specify data types and time periods of interest when downloading a dataset. This method saves considerable time and network bandwidth, but still requires a degree of programming knowledge.
To address these shortcomings and facilitate data access for researchers, our project (ADAP-T; Advancing Co-Design of Integrated Strategies with Adaptation to Climate Change in Thailand) has designed a data-sharing architecture. The main servers are responsible for downloading and archiving data in various forms from related organizations. At the time of writing, the ADAP-T project has been archiving weather observations and runoff data from the TMD and RID via their respective APIs. The TMD also publishes hourly QPE (Quantitative precipitation estimation) data, which can also be downloaded and archived. The EGAT, whose dam operation data are required by several groups, does not allow access to raw data, so a web scraping technique must be used. The archived data are then provided to ADAP-T researchers via a unified API, as well as simple comma-separated values (CSV) files. The results produced by different groups are also collated and can be accessed by researchers outside the ADAP-T project, if permitted. Unique results not found on other websites can be visualized in an interactive fashion and viewed by adaptation policymakers and the general public.

Keywords: climate change, open access, data-sharing

©2020. Japan Geoscience Union. All Right Reserved.

Development of future climate scenario based on multi GCMs of CMIP5 and rain gridded data observed by multi-agencies in Thailand

*Masashi Kiguchi[1], Ruthaikarn BUAPHEAN[2], Aphantree YUTTAPHAN[2], Boonlert ARCHEVARAHUPROK[2], Eiji IKOMA[1], Taikan OKI[1,3]

1. The University of Tokyo, 2. Thai Meteorological Department, 3. United Nation University

A bias-corrected future climate scenario is developed using multiple General Circulation Models (GCMs) outputs of CMIP5 (Coupled Model Intercomparison Project Phase 5) and rain gridded data observed by Thai Meteorological Department (TMD), Royal Irrigation Department (RID), and Department of National Parks, Wildlife and Plant Conservation (DNP) in Thailand during the period from 2080 to 2099. This dataset enabled us to conduct a projection considered spread in projections derived from multiple GCMs. Multiple performance-based projections were obtained using the correlation of monsoon rainfall between GCMs and several agencies observations. Because these three agencies (TMD, RID, and DNP) observation network covered mainly plain, area of along river, and mountainous region, respectively, it could avoid underestimating when we use only TMD and RID dataset as usual. Our results highlight the importance of appropriate evaluation for the performance of GCMs, and the impact assessment on climate change.

Keywords: climate change, general circulation model, driving dataset

©2020. Japan Geoscience Union. All Right Reserved.

Interannual variability of timing of monsoon-onset in South East Asia

*Ryosuke Kato[1], Tomohito Yamada[2]

1. Hokkaido university graduate school of engineering, 2. Hokkaido university faculty of engineering

There has been a lot of flooding in recent years in many places around the world because of climate change. In Thailand, in August 2011, there was a record-breaking heavy rainfall and the flood occurred on Chao Phraya river basin. About 800 people died in the flood and more than 9 million people suffered. In addition to human damages, the floods did much damage to agriculture area, industry area and urban area, and the total damage approximated to about 30 billion yen. The seasonal prediction of rainfall plays an important role in operating the dams for controlling the flood.
Especially, the onset of rainy season has an effect on agricultural fields. Rice production is one of the major agricultural practice in Thailand. It contributes 3600 which is about 12% of Thailand’ s GDP. In Thailand, Farmers usually raise two rice crops a year. The first seeding time and the second cultivating time is after the onset of rainy season. So, the onset of rainy season plays an important role in the rice agriculture. In the other agriculture fields, they also need to store adequate water in dams on rainy season to irrigate on dry season for cultivating rice whole year. For irrigating steadily in dry season, the seasonal prediction of rainfall is also utilized in operation of the large dams as dams can store more than 100 billion tons.
In this paper, we first examined the variation in onset of rainy season in Thailand by 37 years for the period 1981-2017. The definition of the monsoon onset date was the first Julian pentad in which monsoonal rainfall exceeds 5 mm/day following the method of Wang and Lin Ho [2002]. This variable is defined by the difference between the pentad mean and the January mean precipitation rates. The quantity is referred to as the relative pentad mean rainfall rate. Here, January mean rainfall represents the winter mean precipitation rate. Thus, the pentad essentially measures the contrast of the rainfall rates between a specific pentad and the corresponding winter.
We defined dates of monsoon onset by climatological pentad mean rainfall during 1981-2000 and compared the climatology with the pentad mean during 2001-2017. The monsoon onset dates in the western part of Thailand have shifted in advance of 10 days earlier. In the contrast, the onset dates in the eastern part of Thailand have shifted delay about 5 days.
To analyze possible factors causing the onset of rainy season, we applied probability density function to the onset dates and classified the earlier onset years and the later onset years. We examined the difference of the wind at 850hpa, 500hpa and 200hpa between earlier’ s year mean and climatology during 1981-2000. We followed the Welchi’ s t-test and took significant difference at 95 % level. On May, western wind from Indian ocean becomes larger at 850hpa and eastern wind along 15N becomes larger than climatology.

Keywords: Asia monsoon, rainy season, Thailand

©2020. Japan Geoscience Union. All Right Reserved.

Deep learning for seasonal to sub-seasonal rainfall prediction in Chaophraya river basin

*Kiyoharu Hasegawa[1], Shinjiro Kanae[1]

1. Toyko Institute of Technology

In Thailand 1-2 month ahead rainfall prediction is essential for flood mitigation of Chao Phraya river basin. Especially it is needed to decide dam operation for both purpose of preventing drought and flood. Such a seasonal to sub-seasonal scale prediction still remains as difficult problem since numerical prediction contains large uncertainty in this time scale. On the other hand, observed data has been collected for years and statistical analysis skill appeared as the possible solution. One of the most powerful statistical modeling methodology is deep leaning in terms of detecting hidden relationship beneath the complex combination of atmosphere, ocean and land conditions. In the field of rainfall prediction, however the number of observed data is still limited and not enough to train the deep learning model. It requires hundreds of data which enables us to use many variables. To overcome lacks of data, this research applied some data expanding methodology and verified its influence on modeling.

Keywords: deep learning, seasonal to sub-seasonal prediction, Chao Phraya river

©2020. Japan Geoscience Union. All Right Reserved.

Seasonal precipitation forecast model in wet and dry seasons using global monthly surface temperature by deep learning

*Shingo Zenkoji[1], Taichi Tebakari[1], Kazutoshi Sakakibara[1]

1. Toyama Prefecural University

In recent years, the number of extreme weather events has increased around the world, it has caused disasters such as drought and flood. Water management in Thailand has been very difficult because of conflicting extreme disasters such as drought and flood has occurred continuously in the same area. A typical method of predicting precipitation was a numerical prediction model based on physical equations. However, the accuracy of long-term precipitation prediction using numerical prediction model has not yet reached a level applicable to practical use. In this paper, seasonal forecast of monthly precipitation model in Bangkok, Thailand was made using deep learning and global surface temperature.

The used data were the global monthly surface temperature and monthly precipitation. The analysis period was from January 1958 to August 2017. The training phase was from January 1958 to December 2007, and the test period was from January 2008 to August 2017. Used data within training phase was divided into study data and validation data. Natural observation data had the characteristic that the number of occurrences decreased as the intensity increased. In order to eliminate the variation in precipitation intensity between the training data and the validation data, used data within training phase was rearranged them in the order of precipitation intensity and separated.

In this study, a seasonal precipitation forecast model was developed using convolutional neural network. Convolutional neural network algorithms excel in image processing. First, an ensemble forecast of precipitation was performed using random elements from machine learning. As a result, the forecasted precipitation was underestimated when the precipitation by JRA55 was large, and the forecasted precipitation was overestimated when the precipitation by JRA55 was small. It was difficult to predict monthly precipitation such as the past maximum. The range of predicted precipitation was different depending on whether or not the monthly precipitation by JRA55 exceeds 200 mm. As a cause of this, it was considered that the influence of the monthly surface temperature was different between the low intensity precipitation phenomenon and the high intensity precipitation phenomenon. For this reason, in this paper, as an initial study, the used data was divided into a dry season (November to April) and a rainy season (May to October). Precipitation forecast models in each period was developed.

Case 0 was a precipitation forecast model created using all the data of the training phase regardless of the season, and Case 1 was a precipitation forecast model created by dividing the used data into the dry season and the rainy season.

According to the validation data results, in Case0, the MAE was 55.3 mm and the RMSE was 74.2 mm. In Case 1, the MAE was 56.1 mm and the RMSE was 73.7 mm. Comparing the results of the dry season between Case0 and Case1, MAE was 2.7mm smaller and RMSE was 7mm smaller in Case1 value than in Case0 value. Comparing the results of the rainy season between Case0 and Case1, MAE was 4.5mm bigger and RMSE was 4.9mm bigger in Case1 value than in Case0 value.

According to the test data results, in Case0, the MAE was 49.1 mm and the RMSE was 66.2 mm. In Case 1, the MAE was 54.6 mm and the RMSE was 70.3 mm. Comparing the results of the dry season between

©2020. Japan Geoscience Union. All Right Reserved.

Case0 and Case1, MAE was 3.0mm smaller and RMSE was 3.8mm smaller in Case1 value than in Case0 value. Comparing the results of the rainy season between Case0 and Case1, MAE was 13.8mm bigger and RMSE was 9.1mm bigger in Case1 value than in Case0 value. The prediction accuracy of the dry season was higher, but the prediction accuracy of the rainy season was lower when the models were created for the two seasons-the dry season and the rainy season.

©2020. Japan Geoscience Union. All Right Reserved.

Using weather pattern recognition to classify and predict summertime heavy rainfall occurrence over the Upper Nan river basin, northwestern Thailand

*Ryosuke Kato[1], Dzung Nguyen-Le[2], Tomohito Yamada[2]

1. Hokkaido university graduate school of engineering, 2. Hokkaido university faculty of engineering

In Thailand and the Asian monsoon region in general, water-related disasters have taken many lives and devastated infrastructure such as bridges, roads, buildings, electrical grids and telecommunication. To mitigate damaging effects of such severe events, precise and timely rainfall prediction is crucial. In addition to dynamical approach, various statistical techniques have been proposed to improve the prediction of rainfall. Typically, in the case of statistical rainfall prediction, a perfect prognosis (PP) method in which a statistical relationship is established between a local-scale observed ‘predictand’ (i.e., rainfall) and simultaneously observed large-scale ‘predictors’ (e.g. temperature, humidity, wind or geopotential height) is taken and then applied to predicted ‘predictors’ derived from a global model to yield forecasts of the ‘predictand’. The weather pattern (WP) recognition such as the Self Organizing Map (SOM), developed by Kohonen (1982; 2001), is one of the widely used methods to determine this relationship. Nguyen-Le et al. (2017) recently uses SOM in combination with the K-means clustering to objectively classify the anomalous WPs causing heavy rainfall days over northern Kyushu, southwestern Japan, during the Baiu season. The classification results are then implemented with the PP and analogue method (Lorenz, 1969) to predict the occurrence (yes/no) of heavy rainfall days in the region. The forecast skill of this relative new method ASOM (combination of Analogue forecast and SOM) up to 7-days lead times is significantly improved than that from the traditional method using only the predicted rainfall intensity from an operational global model. Here, a work extending Nguyen-Le et al. (2017) to summertime (May–June, MJ, and July–August–September, JAS) heavy rainfall over the Upper Nan river basin (17.375° –19.375°N, 99.875° –101.125°E) in northwestern Thailand is conducted.
First, it shows that in MJ, intensive rainfall over the Upper Nan is mainly brought by the remarkable enhancement of westerly summer monsoon. Meanwhile, westward-propagating tropical disturbances including tropical cyclones are the primary factors reproduce heavy rainfall over the Upper Nan in JAS. It also suggests that the occurrence time of local heavy rainfall is strongly related to the seasonal transition of summer monsoon in the Indochina Peninsula.
These classification results are then used to predict the occurrence of heavy rainfall days in the studied basin in summer 2008–2017 using prognostic WPs from the operational Japan Meteorological Agency Global Spectral Model (GSM). In general, the forecast skills of ASOM up to 3-day lead times are significantly improved, in which it not only outperforms GSM with same forecast ranges but also its 3-day forecast is better than
1–2-day forecasts from GSM. However, the false alarms ratio is still high, particularly in JAS. In addition to overall results, the differences in the performance of ASOM between years and heavy rainfall-inducing WPs are evaluated. It is shown that it strongly depends on the WPs that bring heavy rainfall events. More specifically, the skill is higher if the WP is limited to one phenomenon such as intensified westerlies or tropical disturbances. In contrast, ASOM has more difficulties to capture the WP imposing the interaction between the monsoon westerlies and the trade easterlies or northeasterly winds. It is also suggested that the performance of ASOM (for the heavy rainfall occurrence) and GSM (for the prognostic WPs) is roughly in phase.

©2020. Japan Geoscience Union. All Right Reserved.

Keywords: heavy rainfall, forecast, Thailand

©2020. Japan Geoscience Union. All Right Reserved.

Impact of Rainfall on Urban Traffic Flow based on Probe Vehicle Data in Bangkok

*Tsuyoshi Takano[1], Hiroyoshi Morita[1], Shinichiro Nakamura[2], Miyazaki Hiroyuki[3], Wasan Pattara-atikom[4], Napaporn Piamsa-nga[5]

1. Nippon Engineering Consultants Co., Ltd, 2. Nagoya Univ., 3. Asian Institute of Technology, 4. National Electronics and Computer Technology Center, 5. Kasetsart Univ.

Adverse weather frequently affects the capacities and travel speeds on roadways, which result in worsened traffic congestion and incurred productivity loss. Further, with climate change predicted to increase rainfall in various cities in Southeast Asia, the risk of flood damage in this region is not only anticipated to increase and affect urban function but may also significantly aggravate daily traffic flow. This study highlighted an analysis of the effect of rainfall on urban traffic flow through the use of probe vehicle data and rainfall data in the center of Bangkok, which is known for problems with respect to maintenance of pumps and drainage channels and for many flooded roads after heavy rainfalls.

The probe vehicle data (observed in 2018) used in this study were obtained from open data (historical raw vehicles and mobile probe data in Thailand) provided by the Thai Intelligent Traffic Information Center Foundation. This data consists of Vehicle ID, GPS location collected every minute, time stamp, and speed. The rainfall data are a 5-minute unit data obtained (in 2018) from the Bangkok Metropolitan Flood Control Center.

To explain the relationship that exists between rainfall intensity and travel speed, regression models are developed.

The experimental results demonstrated that the average daily travel speed decreases by 0.02 km/h per 1 mm of daily rainfall. Especially during morning and evening peaks, the average travel speed greatly decreases due to 1-h rainfall (short-term impact) and 6-h rainfall (long-term impact) when compared to the case of no rain. As a result, loss time due to rainfall in 2018 was estimated to be about 4 million hour which is equivalent to 5% of the loss time due to much traffic demand.

Future rainfall forecast data makes it possible to assess the risk of climate change on urban traffic flow.

Keywords: Rainfall intensity, Climate change, Probe vehicle data, Urban traffic flow

©2020. Japan Geoscience Union. All Right Reserved.

Investigation of Extreme Flood Changes in the Mekong River Basin Using +4K Climate Simulation

*Sophal Try[1], Shigenobu Tanaka[1], Kenji Tanaka[1], Takahiro Sayama[1], Chantha Oeurng[2]

1. Kyoto University, 2. Institute of Technology of Cambodia

The future changes in frequency and intensity of precipitation will definitely affect the flooding due to climate change leading to the future direction for the development of social infrastructure. The study of flood was done by using the precipitation output from the climate model as input data to the hydrologic model. The uncertainty of climate simulation due to an insufficient number of ensemble members was inadequate to capture the change of the edge of the phenomenon. For this reason, the application of large ensemble data would reduce the uncertainty of climate simulation. This study aims to (1) define the effective duration of precipitation which has the highest correlation to the annual maximum flood in the Lower Mekong Basin (LMB); (2) assess the change of flood severity under climate change impacts using large ensemble dataset from Database for Policy Decision-Making for Future Climate Change (d4PDF). The data is available for 60-year (1950-2010) with 100 ensemble members for historical climate; the future climate simulation (2050-2110) consists of 90 ensemble members which were simulated under 4 K warmer experiment by 6 patterns of sea surface temperature (SST) from CMIP5 models. The flood inundation in the LMB was simulated using a coupling rainfall-runoff and inundation (RRI) model with 2-D diffusive wave approximation. The statistical Kolmogorov-Smirnov (K-S) test of two samples was used to determine the significant difference between the two cumulative distribution function (CDF) for each future SST pattern. The Generalized Extreme Value (GEV) was used for fitting the extreme flood. The results indicated that 90-day precipitation counting backward from the day of peak flooding has a high correlation to peak inundation volume and discharge (both R-sqr = 0.81). The historical simulation of d4PDF was able to catch up the past observed flood events in the LMB in 78 years of the data record (1934-2011) which had good agreement with the ensemble mean. The K-S test revealed the majority of significant difference of discharge simulation from each SST (i.e. 14 out of 15 cases) while the null hypothesis from only one case was accepted at a significant level of 5%. The relative changes of future and past experiments of 1:50, 1:100, and 1:1000 year flood events showed an increase by +25%, +33%, and +40% for peak discharge at Kratie and +19%, +29%, and +36% for inundation extent, respectively. In conclusion, the magnitude of extreme flood in the LMB in the future will definitely be severer than the historical experiment. To reduce its impacts and damages, we need to implement effective water resource management as well as flood mitigation and adaption countermeasures.

Keywords: flood frequency, climate change, d4PDF, Mekong River Basin

©2020. Japan Geoscience Union. All Right Reserved.

Climate change and land use change impact assessment on flood and inundation in a river basin in Sumatra island in Indonesia

*Kodai Yamamoto[1], Takahiro Sayama[2], Apip Apip[3]

1. Graduate School of Engineering, Kyoto University, 2. Disaster Prevention Research Institute, 3. Research Center of Limnology, Indonesian Institute of Sciences

Indonesia will face challenges on flood disaster management and environmental problems due to climate change. Previous IPCC AR5 describes that monsoon-related precipitation will increase in Southeast Asian countries. Combined with precipitation increase, larger urban area will be exposed to coastal floods and river floods in Indonesia (Muis et al. 2015). In addition, deforestation and land use change increase of flood hazards in a tropical catchment (Tarigan 2016). Moreover, tropical peatland area is more likely to have the significant impact due to flood hazards, where large area is developed for agriculture plantation.

One of the challenges of climate communities is to reproduce rainfall spatial and temporal patterns by GCM in many islands in oceans between the Indian and Pacific Oceans, which is known as Maritime Continent. This can attribute to coarse resolution of topography or imperfect representation of local weather in Maritime Continent. Regional Climate Models has high potential to represent the local weather at finer resolution. In addition, there are many studies on rainfall projections but their impact on river discharge is still limited in Indonesia (Ammar et al. 2016; Hero Marhaento et al. 2018). Moreover, very limited studies focus on the impact on inundation phenomena at catchment scale.

The primary objective of this research is to assess the possible climate change impact on flood and inundation in a catchment. This study uses Atmospheric General Circulation Model ver. 3.2 (hereafter AGCM) and Non-Hydrostatic Reginal Climate Model (hereafter NHRCM) developed by Japan Meteorological Research Institute (MRI). NHRCM is a regional climate model, which is dynamically downscaled at less than 5 km resolution with boundary condition of AGCM at 20 km resolution (Sasaki et al. 2008). Bias correction is applied to correct AGCM/NHRCM-simulated rainfall and evaluated based on annual maximum (1) daily and (2) 15 days rainfall. We discuss the impacts of the bias correction on hydrological projections using Rainfall-Runoff-Inundation (RRI) model (Sayama et al. 2010) applied to one of the largest river basin in Sumatra Island in Indonesia under current and future climate conditions. We assess the results according to (1) flow duration curve, (2) annual maximum daily discharge and (3) annual maximum inundation pattern/volume. Finally, future impact on flood is analyzed with the most reliable rainfall datasets of non-/bias corrected AGCM and NHRCM. RCP8.5 was used for the future scenario of climate change. Furthermore, future land use data (land use 2040) and climate change (RCP8.5) was applied to RRI model. The results of RRI model and was compared with the results of climate change ones with only RCP8.5 to clarify which impact is more significant.

Keywords: Climate Change, Humid Tropical River Basin, NHRCM, RRI Model, Tropical Peat Land

©2020. Japan Geoscience Union. All Right Reserved.

AN ASSESSMENT OF RESERVOIR OPERATION POTENTIAL FOR FLOW REGULATION IN THE CHAO PHRAYA RIVER BASIN

*SARITHA PADIYEDATH GOPALAN[1], Naota Hanasaki[1]

1. National Institute for Environmental Studies

The flow regulation of the Chao Phraya River is very crucial due to the frequent flood and drought occurrences. Therefore, it is essential to maintain a lower limit (to stabilize the flow) and an upper limit (for the flood control) of outflow, which can be achieved by building structures such as reservoirs. There are several large and small-sized reservoirs in the basin and many of them are multi-purpose that could be used to regulate the flow in the Chao Phraya River. Hence, this study examines the efficacy of the eight existing reservoirs for regulating the flow in the basin by quantifying the low as well as high flows for the baseline (1990-1999) as well as future (2090-2099) scenarios. The hydrological analysis was performed using the H08 global hydrological model with the reservoir operation module. The effect of the individual reservoir was analyzed at a point downstream to it, and the cumulative impact of all reservoirs was assessed at Nakhon Sawan and Bangkok, two major cities within the Chao Phraya River basin. It was clear from the baseline scenario simulation that the individual reservoir operation considerably reduced high flows with an exceedance probability of 10% (Q_{10}) and improved the low flows with an exceedance probability of 95% (Q_{95}). The Q_{10} was reduced to 1485 m^3/s from 1992 m^3/s, and the Q_{95} was increased to 233 m^3/s from 13 m^3/s at Nakhon Sawan after the cumulative reservoir operation. A similar pattern was observed for Bangkok City with a reduced Q_{10} value of 1837 m^3/s from 2366 m^3/s and an enhanced Q_{95} value of 265 m^3/s from 17 m^3/s. This further reveals that the reservoir operation can regulate the river flow by storing water in the wet season and releasing it in the dry season, and hence it benefits both flood and drought mitigation. Further, the simulated results for the future scenario exhibited an immense increase in the high flows compared with baseline scenario which can be attributed to (i) the climate change that increases precipitation/streamflow in the wet season, and (ii) the increased projection of precipitation by some general circulation models. The reservoir operation was able to reduce the downstream high flows to some extent, whereas as they well maintained the low flows. The results demonstrate that the Chao Phraya River basin is more likely susceptible to floods than the droughts in the near future which can be alleviated by combining structural as well as non-structural measures.

Keywords: CLIMATE CHANGE, RESERVOIR OPERATION , ADAPTATION

©2020. Japan Geoscience Union. All Right Reserved.

Regional climate change impact on water quality in the lower Chao Phraya River, Thailand

Taichi Tebakari[1], Sanit Wongsa[2], *Horiuchi Yusuke[1]

1. Toyama Prefectural University, 2. King Mongkut's University

River water quality requires a great deal of time, labor, and cost for measurement and analysis, but could be useful background information for returning to the present situation in the event of a quality problem. However, in developing countries and middle-developed countries, environmental water quality standards are still low, and many rivers do not satisfy even those standards. In Thailand, which has been middle-developing country in recent years, the environment of river water has not been significantly improved since 1996 due to socio-economic development, and it is the fact that major rivers are deteriorating. Also, in recent years, the change of river water quality is very complicated due to the construction and operation of many hydrological structures throughout the Chao Phraya River. Bangkok, is located on the coastal lowland, Thailand. At present, most of the tap water used in Bangkok is taken from the Chao Phraya River, which flows on the coastal lowland. This intake is located in the brackish water area of the lower Chao Phraya River. In the dry season, the rise in salinity of rivers and the rise in sea level caused by climate change may affect the intake. The Thai government has identified the Chao Phraya River as a priority area, where salinization is a problem in terms of water quality management.

Therefore, water quality observations were conducted in the lower Chao Phraya River November 2016, March 2017, August, November, April 2018, June and November, and using the results of the Thai government's automatic water quality observations from August 2016 to February 2020, By comparing these data (water level, discharge, air temperature, water temperature, pH, EC, salinity and dissolved oxygen) with each other, the secular variation of the water quality characteristic of saltwater run-up was clarified.

As a result, in the dry season, pH ranged from 7.2 to 8.2 along the river, from neutral to slightly alkaline. The water temperature was found to be between 28 ˚C and 34 ˚C along the river. The DO was very low, less than 3 mg / l from the estuary to 80 km from the estuary in the dry season from November to April. There was no seasonal change in pH, but the seasonal change in water temperature was about 4℃ between the dry season and the rainy season. The water quality along the Chao Phraya River was high salinity, low water temperature and low oxygen. In the rainy season, the water quality along the Chao Phraya River was low salinity, high water temperature and high oxygen state. the increase and decrease of EC were clearly divided according to the water level fluctuation during the rainy and dry seasons. It was found that the saltwater intrusion range was changed by the difference of discharge volume of Chao Phraya Dam during the rainy season and the dry season. During the rainy season, the salinity intrusion was suppressed by the natural discharge from the Chao Phraya Dam. In the dry season in February, the peak of EC increase was observed and the value was high from 80 to 100 km from the estuary. In the dry season of 2016 and 2020, the salinity of the intake water exceeded the standard of raw water in Thailand of 0.5 g / L. Thus, it is thought that the seasonal change is closely related to the inflow of saltwater due to the difference in discharge from the Chao Phraya Dam.

©2020. Japan Geoscience Union. All Right Reserved.

Research on the current thermal energy budget of land surface by continuous observation of near-surface ground temperature in Kanto Plain, Japan

*Osamu Matsubayashi[1], Hideki Hamamoto[2], Sachio Ehara[3]

1. National Institute of Advanced Industrial Science and Technology, 2. Center for Environmental Science in Saitama, 3. Institute for Geothermal Information

We are conducting a study on present-day changes of ground temperature at depths down to 1.0 m from the surface in order to know the physical processes currently occurring on the land surface. In the last few decades there have been many works to obtain by mathematical inversion the past climatic changes based on deep downhole temperature data, which are given as function of depth. But, we think that the relationship between such downhole temperature anomaly signals and the ongoing near-surface processes have not been fully clarified yet. For addressing such an issue we have started a campaign of long-term monitoring of near-surface ground temperature at some locations in the Kanto Plain area, Japan.

Three observation sites are selected in the Kanto Plain: Tsukuba in Ibaraki Prefecture, Toda and Sayama both in Saitama Prefecture. At these sites we have had good records of 1m depth ground temperature (denoted as GT1.0) for more than 4 years, and partly supplementary temperature records at shallower depths such as GT0.3 (those at 0.3 m depth). It is noted that one-year period ground temperature change is the most prominent component at all those sites, and we see longer phase delays and also larger amplitude attenuation of the sinusoidal variation at the deeper part of the same sites, where surface temperature is likely to be the primary driving force. Therefore, to compare with the change of ground temperature we have employed different information, which is time-series of satellite derived land surface temperature for each of the sites. In this study LST (Land Surface Temperature) data from MODIS sensor on Aqua and Terra satellites have been used. The observed LST seasonal change may be controlled by that of solar radiation from above to the particular sites. From the above-mentioned dataset, i.e., MODIS-LST, GT1.0, and GT0.3, we have attempted to estimate the effective thermal properties of the near-surface subsurface layers of the sites, with a result of fairly large variations of thermal properties among our study sites depending on the surface material characteristics.

Keywords: ground temperature, monitoring, thermal energy budget

©2020. Japan Geoscience Union. All Right Reserved.

Good Practices for Climate Change Adaptation in Agricultural Sector, Thailand

*KOSHI YOSHIDA[1]

1. Ibaraki University

Meteorological Uncertainty caused by Global Climate Change would have significant impact on agricultural sector, because agricultural systems are strongly affected by local climate condition. In Thailand, agriculture is major sector which producing 11% of GDP and 40% of employment. Ratio of irrigated agricultural land is 30% and other 70% is rain-fed so that climate change makes agriculture more unstable and also makes crucial damage to the societies and economics in local area. To mitigate these issues, it is desirable to develop and disseminate enhanced adaptation systems including impact assessment tool for drought problem by using water-soil-plant model, mapping technology of shallow ground water or soil salinity, and development of adaptive farming practice. Therefore, in this study, we introduce the good practices of following topics related to agricultural adaptation measures under CC condition in Thailand.

1.Enhancement of Production System Management in Orchid farming
Low water levels in the Chao Phraya River cause seawater intrusion. Salinity, in irrigation water, is one of the major environmental limiting factors for growth and productivity of orchids. Since orchid farmers do not know much about the effect of salinity, they are afraid of using saline water to irrigate mature plants, especially in the flowering stage. Therefore, the objective of this research was to determine the interaction between water salinity level and duration of growth, flower quality and photosynthesis parameters. And new growing material, the cement block and coconut shells were tested.
2.Development of Drought Monitoring Platform in whole Thailand
This research mainly develops drought monitoring model based on satellite data which can provide drought risk map country-wide on a weekly basis. In addition, an algorithm to combine phenological and demographic data will be pursued to generate a drought vulnerability map. Such results can be analyzed with other group’ s results (via Multi-Criteria Analysis) to provide useful information to the government for adaptation and mitigation to Climate Change.
3.Salt Affected Soil Mapping and Future Projection of Soil Salinity Level under Climate Change Condition
In North East Thailand, annual rainfall is about 1200mm and average rice yield is only 2.1 t/ha (rain-fed). In addition, 50% of total land area in this region are classified as salt affected area. Therefore, salt-affected soils are major environmental problems in NE Thailand. In future, climate change may cause negative impact on salt-affected soil problems. In this study, we investigate the climate change impact on salt affected soil, establish more useful salt affected soil maps to propose appropriate cropping system/crop calendar under CC condition.
4.Evaluation of Potential Yield of Shallow Ground Water for Countermeasure in Drought Problem
This research aimed to assess shallow ground water use for agricultural farming, as the countermeasure of severe drought problem. Firstly, we monitored the seasonal fluctuation of shallow ground water level in Dan Chang district, Suphanburi province, based on resistivity mapping data. Then, sugarcane yield estimation model was developed and applied. And numerical simulation was conducted to estimate the potential sugarcane yield by using shallow ground water.
5.Evaluation of Weather-Induced Economic Damage on Agricultural Production
In The Twelfth National Economic and Social Development Plan (2017), the Thai government advised farmers to cultivate cash crops rather than rice to increase farmer income. However, some upland crops

©2020. Japan Geoscience Union. All Right Reserved.

are more sensitive to climate condition than rice, so weather-induced economic damage should be previously evaluated for each crop. Therefore, in this study, weather-induced economic damages of rice and upland crops such as sugar cane and cassava were evaluated in Northeast Thailand.

Furthermore, it is necessary to conduct reliable research to find ways to achieve economic betterment through agriculture under CC condition. Therefore, cost-benefit analysis also should be applied to consider the possible and acceptable ways and planning.

Keywords: Agricultural Adaptation, Good Practices, Climate Change

©2020. Japan Geoscience Union. All Right Reserved.

Evaluation of salinity effects on rice production in farmers' fields in Ban Phai, Khon Kaen, Thailand

*YI YANG[1], Rongling Ye[1], Thanyaluck Nontasri[2], Mallika Srisutham[2], Supranee Sritumboon[3], Masayasu Maki[4], KOSHI YOSHIDA[5], Kazuo Oki[6], Koki Homma[1]

1. tohoku university, 2. Khon Kaen Univ., Thailand, 3. LDD, Thailand, 4. Fukushima Univ., 5. Ibaraki Univ., 6. Univ. Tokyo

Northeast Thailand is the major rice producing region in Thailand, but rice yield there is quite low. One of the major causes is salinity, which is derived from underground rock salt and anticipated to increase in the future under climatic change. Salinity lands in Thailand were classified into class 1 (severe) to class 4 (slight) depended on percentage of salt occupation on land surface, but the classification is not associated with crop productivity. Accordingly, field evaluation for assessment of rice production is recommended. This study evaluated salinity condition during rice cropping and its effect on rice growth and yield.

Field investigations were conducted at farmers' fields in Ban Phai district, Khon Kaen provice, Thailand, during September to November in 2017, 2018 and 2019. The fields were classified into class 2 to 4. Leaf area index (LAI) or leaf coverage (LC) was measured every week to evaluate rice growth and rice yield was determined by sampling. Soil EC and moisture were also measured every week and other soil properties suck as organic matter (OM) and exchangeable cations were determined occasionally. Drone images were also taken every week to evaluate spatial variation in rice growth.

Soil EC was significantly higher in severer class, but the clear thresholds between classes were not observed. Difference in precipitation among investigated years (the highest in 2017 and the lowest in 2018) also caused that in average soil EC (the highest in 2018 and lowest in 2017). Although the relation was not consistent, decrease in soil moisture content tended to increase soil EC.

Rice production was also affected by precipitation. The amount of precipitation seemed abundant in 2017, but scarce in 2018. The amount in 2019 was intermediate but some famers gave up planting because the precipitation in the first half of rainy season was quite limited.

The relation between rice yield and soil EC was not obvious, because the yield quite varied even though the EC level was similar. However, the classification of salinity level of USDA based on electrical conductivity of a saturated soil extract (ECe) clearly showed that rice yield was damaged by salinity level. The classification suggested that rice yield was damaged by slightly salinity level of ECe = 2~4 dS/m. The analysis of rice yield in 2018 showed that the primal factor of rice yield was drought and then salinity; that in 2019 showed rice yield was affected by interaction between salinity and OM.
Drone image analysis during dry season for salt occupation and rainy season for rice growth may contribute the evaluation of salinity level for rice production.

Keywords: rice, salinity, drough, electrical conductivity organic matter

©2020. Japan Geoscience Union. All Right Reserved.

Calibration of cultivar parameters of SIMRIW-RS (rice simulation model for remote sensing) for the rice growth monitoring in Thailand

*Koki Homma[1], Mongkol Raksapatcharawong[2], Watcharee Veerakachen[2], Peerapon Prompitakporn[2], Masayasu Maki[3], Kazuo Oki[4]

1. Tohoku University, 2. Kasesart University, 3. Fukushima University, 4. The University of Tokyo

Rice production is one of the most important agriculture in Thailand. Because the production variability caused large impact on the people living, the assessment of disaster impact before harvest is recommended. The authors have been developing a satellite based observation system for the purpose by employing SIMRIW-RS, a rice growth simulation model for remote sensing. SIMRIW-RS would be applied anywhere, but preparation of cultivar parameters is recommended before the application in order to adjust the relation between rice growth and production.

To obtain cultivar parameters, rice growth and production data obtained in a farmer’ s field in Nongchok districe in Bangkok was used. 50 sample points were selected from the field of 6.88-ha. The growth was evaluated in terms of LAI measured by LAI-2200 (Li-Cor Ltd), above ground biomass and grain yield was measured by 1-m^2 harvesting at the maturity.

The phenological parameters for the cultivar were substantially derived from the parameters that the authors previously obtained for a Thai rice cultivar, and adjusted for the growth duration provided as the cultivar information. The parameters for LAI growth was estimated on the basis of average LAI change for the 50 sample points with air temperature. The parameters for production against LAI growth was also estimated on the basis of average above ground biomass and grain yield for the 50 sample points.

LAI growth at each sample points can be calibrated by using the estimated cultivar parameters for the phenological development and LAI growth, and the calibration produces field parameters to explain locational variability for rice growth and production. The field parameters suggest the field has a large variability of soil fertility, most of which were caused by that of chemical fertilizer application. The estimated rice grain yield after the calibration showed a relative consistency with the measured yield, suggesting the estimated parameters would be reasonable.

Keywords: Rice, Leaf area index, Cultivar parameter, Field parameter

©2020. Japan Geoscience Union. All Right Reserved.

Farmers' perception of climate change induced drought in the Northeast Thailand

*Miki Nodera[1], Keigo Noda[1], Koshi Yoshida[2], Mallika Srisutham[3]

1. Gifu University, 2. Ibaraki University, 3. Khon Kaen University

Monsoon Asia has two distinct seasons; the rainy season and the dry season. This region has 52% of the total population of the world and future population is anticipated to increase. In this situation, climate change will greatly affect the social economy. There are two directions to control the progress of warming. One is emission reduction measures (mitigation measures) to suppress global warming, and the other is adaptation measures to the adverse effects of global warming. Northeast Thailand has an area and population approximately one-third of Thailand but Gross Regional Product (GRP) is the lowest in the country. In this region soil has low fertility and low water retention capacity and some areas have salt damage. The irrigation rate is the lowest in the country. So this region is vulnerable for climate change. So we have to promote adaptation measures.

We conducted a questionnaire survey in Khon Kaen province, Thailand in order to grasp farmers' condition of basic profile, agricultural management and perception of climate change. Three villages were selected to compare the different availability of agricultural resources in terms of salt damage and irrigation water. After that we analyzed objective data of rainfall monitoring and agricultural statistics in order to validate the results of questionnaire survey.

According to the 72 farmers' questionnaire result, the type of water used mainly differs by village. Many farmers recognized seasons from weather forecast and they decided to plant rice at the same time as last year or when they thought rainy season start. And they thought their farmland is not stable because of water shortage. About perception of climate change, many farmers thought rainfall had decreased and it caused low yield.

Crop calendar is more same in villages without water restrictions. According to the analysis of rainfall and agricultural statistical data, it's difficult to think that rainfall in cultivation period had decreased. In addition planting area, harvested area and production had also increased. So analysis result differed from farmers' perception.

According to the analysis of the relationship between rainfall and production, the timing of rainfall affecting production was different between the 1900s and 2000s. And dry spell which is the period of little rain in the rainy season appears in various timing. So we thought farmers thought rainfall had decreased and yield had decreased because rainfall patterns had changed compared to the past and they could not adapt that pattern. So if we could forecast the rainfall a few months ahead and propose a crop calendar suitable for the rainfall in the year, we thought it would be an adaptation measure.

Keywords: Climate change, Northeast Thailand, Rainfall

©2020. Japan Geoscience Union. All Right Reserved.

Research on farmers' awareness of adaptation to climate change and its information collection and sharing in rural area in Thailand

*Kyoko Matsumoto[1], Mallika Srisutham[2], Supranee Sritumboon[3], Sompratana Ritphring[4], Masashi Kiguchi[1], Taikan Oki[5]

1. Institute of Industrial Science, The University of Tokyo, 2. Facutly of Agriculture, Khonkaen University, 3. Land Development Department, 4. Faculty of Engineering, Kasetsart University, 5. Institute for Future Initiatives, The University of Tokyo

This research was conducted to clarify farmers' awareness of adaptation to climate change and its information collection and sharing in rural area in Thailand. Data were collected using face to face questionnaire survey from a total sample of 50 farmers in Khon Kaen province. The questionnaire was developed based on the semi-structured interview which was conducted in Songkhla province to extract components of questionnaire on perception, information collection and sharing of climate change and adaptation using previous studies. The data from questionnaires were collected in 2018. The attributes of respondents were fifties (34.0%) and sixties (30.0%), farmers (100%), Buddhism (100%) and natives of the study area (62.0%) have higher proportions.

It was found that 100% of respondents answered that they perceived local climate change, and 78.0% of respondents answered that their lifestyles were affected by climate change. Nevertheless, 92.0% of respondents answered that "I do not have willingness to adapt to climate change" and "I cannot decide whether I will take adaptation measures or not" from a long-term perspective. The proportion of respondents who perceive that lifestyles have been changed by climate change or natural disaster is high. However, even if the frequency of natural disaster increase, those who have willingness to do adaptation is less than half of respondents. Those who "undecided to take adaptation" have potential to take adaptation by providing appropriate information on adaptation.

Moreover, we found that 96.0% of respondents got climate information from TV. Next to TV, the percentage of respondents are high in the order of local wisdom based on their own experiences (58.0%), neighborhood (54.0%), radio (40.0%), SNS (Social Network Services) (24.0%), public speaker (18.0%) and TMD Smart Simulation (4.0%) which is weather forecast application at current location provided by Thai Meteorological Department (TMD). Regarding reliability of information resources, the highest percentage of "very reliable" and "reliable" information sources are TV (100%) (n=48), radio (100%) (n=20), public speakers (100%) (n=9) and TMD Smart Simulation (100%) (n=2). Next to neighborhood (96.3%) (n=27), SNS (91.7%) (n=12), local wisdom (82.8%) (n=29). Here it can be seen that it is necessary to make climate information spread from various sources.

Keywords: Adaptation to climate change, People's awareness, Collecting and sharing climate information, Thailand, Rural area

©2020. Japan Geoscience Union. All Right Reserved.

[E] Poster | A (Atmospheric and Hydrospheric Sciences)：A-CC Cryospheric Sciences & Cold District Environment

[A-CC38] Ice cores and paleoenvironmental modeling

convener:Ayako Abe-Ouchi(Atmosphere and Ocean Research Institute, The University of Tokyo), Ryu Uemura(Nagoya University), Kenji Kawamura(National Institute of Polar Research, Research Organization of Information and Systems), Nozomu Takeuchi(Chiba University)

Analyses of ice cores from polar and mountain regions have contributed to the reconstruction and understanding of the past environmental changes on timescales from years to several hundred thousand years. In this session, we welcome paleoenvironmental studies using ice cores and paleoclimatic modeling. Studies on reconstruction methods, recording processes and new paleoenvironmental proxies, technical aspects of paleo-modeling are also welcomed. Studies with marine sediment cores, terrestrial sediment cores and tree-rings on similar timescales are also important and welcomed, in order to discuss past environmental changes from multidisciplinary viewpoints.

[ACC38-P02] Compositions of dust and sea salts in the Dome C and Dome Fuji ice cores from Last Glacial Maximum to early Holocene based on ice-sublimation and single-particle measurements

*Ikumi Oyabu[1], Yoshinori Iizuka[2], Kenji Kawamura[1,3,4], Eric Wolff[5], Mirko Severi[6], Rumi Ohgaito[4], Ayako Abe-Ouchi[7,1,4], Margareta Hansson[8] (1.National Institute of Polar Research, Research Organization of Information and Systems, 2.Institute of Low Temperature Science, Hokkaido University, 3.Department of Polar Science, The Graduate University of Advanced Studies (SOKENDAI), 4.Japan Agency for Marine Science and Technology (JAMSTEC), 5.Department of Earth Sciences, University of Cambridge, 6.Department of Chemistry “Ugo Schiff”, University of Florence, 7.Atmosphere Ocean Research Institte, University of Tokyo, 8.Department of Physical Geography, Stockholm University)

[ACC38-P03] Evolution in geometry of firn in ice sheets detected by dielectric anisotropy

*Shuji Fujita[1,2], Kotaro FUKUI[3], Mikihiro Hirabayashi[1], Iizuka Yoshinori[4], Sumito Matoba[4], Atsushi Miyamoto[5], Takeshi Saito[4], Hideaki Motoyama[1,2], Toshitaka Suzuki[6] (1.National Institute of Polar Research, Research Organization of Information and Systems(ROIS), 2.SOKENDAI, Japan, 3.Tateyama Caldera Sabo Museum, Japan, 4.ILTS, Hokkaido Univ., Japan, 5.Hokkaido Univ., Japan, 6.Yamagata Univ., Japan)

[ACC38-P04] Dielectric anisotropy measurement of Dome Fuji ice core and implications for crystal orientation fabric development

*Tomotaka Saruya[1], Shuji Fujita[1,2] (1.National Institute of Polar Research, 2.The Graduate University for Advanced Studies)

[ACC38-P05] Development of a numerical ice-sheet model for simulation of summit dynamics

*Fuyuki SAITO[1], Ayako Abe-Ouchi[2,1], Takashi Obase[2] (1.Japan Agency for Marine-Earth Science and Technology, 2.Atmosphere Ocean Research Institute, Univ. of Tokyo)

[ACC38-P06] Layering, densification and bubble close-off of firn at a new site near Dome Fuji, East Antarctica

*Ryo Inoue[1], Shuji Fujita[2,1], Kenji Kawamura[2,1,3], Fumio Nakazawa[2,1], Ikumi Oyabu[2] (1.The Graduate University for Advanced Studies, SOKENDAI, 2.National Institute of Polar Research, 3.JAMSTEC)

[ACC38-P08] PMIP4/CMIP6 Last Interglacial simulations using different versions of MIROC, with and without vegetation feedback

*Ryouta O'ishi[1], Wing-Le Chan[1], Ayako Abe-Ouchi[1,2,3], Sam Sherriff-Tadano[1], Rumi Ohgaito[3] (1.Atmosphere and Ocean Research Institute, the Universitoy of Tokyo, 2.National Institute of Polar Research, 3.Japan Agency for Marine-Earth Science and Technology)

[ACC38-P09] Response of convective systems to changes in orbital forcing of the last interglacial

*Minoru Chikira[1], Yohei Yamada[2], Ayako Abe-Ouchi[1], Masaki Satoh[1] (1.The University of Tokyo, Atmosphere and Ocean Research Institute, 2.Japan Agency for Marine-Earth Science and Technology)

Compositions of dust and sea salts in the Dome C and Dome Fuji ice cores from Last Glacial Maximum to early Holocene based on ice-sublimation and single-particle measurements

*Ikumi Oyabu[1], Yoshinori Iizuka[2], Kenji Kawamura[1,3,4], Eric Wolff[5], Mirko Severi[6], Rumi Ohgaito[4], Ayako Abe-Ouchi[7,1,4], Margareta Hansson[8]

1. National Institute of Polar Research, Research Organization of Information and Systems, 2. Institute of Low Temperature Science, Hokkaido University, 3. Department of Polar Science, The Graduate University of Advanced Studies (SOKENDAI), 4. Japan Agency for Marine Science and Technology (JAMSTEC), 5. Department of Earth Sciences, University of Cambridge, 6. Department of Chemistry “Ugo Schiff”, University of Florence, 7. Atmosphere Ocean Research Institte, University of Tokyo, 8. Department of Physical Geography, Stockholm University

We analyzed the chemical compositions of dust and sea-salt particles in the EPICA Dome C (EDC) ice core during 26–7 kyr BP using an ice-sublimation technique, and compared the results with existing data of the Dome Fuji (DF) ice core. Combined with ion concentration data, our data suggested similar sea-salt fluxes in both cores and significantly lower dust flux in the EDC core. The differences in modal size and aspect ratio of dust particles between the two cores support the dominance of Patagonian source suggested by earlier works. The compositions of calcic dust showed major change at ~17 kyr BP, possibly reflecting a relative increase in dust transported via the upper troposphere. The calcium sulfate fraction was higher in the DF core than in the EDC core after ~17 kyr BP, suggesting that higher Patagonian dust contribution to the DF region. Abundant NaCl particles were found in the DF core in comparison with the EDC core from the LGM to early Holocene, possibly because of the high concentration of terrestrial dust in the DF core that reduced acid availability for sea-salt modification. During the Holocene, the lower NaCl fraction and Cl^-/Na^+ ratio in the EDC coresuggested that most Cl^- was lost to the atmosphere from snow at Dome C, while it was preserved at Dome Fuji as NaCl and solid solution.

Keywords: ice core, aerosol, dust, sea salt

©2020. Japan Geoscience Union. All Right Reserved.

Evolution in geometry of firn in ice sheets detected by dielectric anisotropy

*Shuji Fujita[1,2], Kotaro FUKUI[3], Mikihiro Hirabayashi[1], Iizuka Yoshinori[4], Sumito Matoba[4], Atsushi Miyamoto[5], Takeshi Saito[4], Hideaki Motoyama[1,2], Toshitaka Suzuki[6]

1. National Institute of Polar Research, Research Organization of Information and Systems(ROIS), 2. SOKENDAI, Japan, 3. Tateyama Caldera Sabo Museum, Japan, 4. ILTS, Hokkaido Univ., Japan, 5. Hokkaido Univ., Japan, 6. Yamagata Univ., Japan

Ice in polar ice sheets once experience a state of firn at near-surface depths. Therefore, it is important to understand physical processes of firn formation, metamorphism and deformation for ice core studies. We investigated firn through measurement of tensorial values of the dielectric permittivity at microwave and millimeter-wave frequencies. This method can detect presence and strength of anisotropic structure in the geometry of pore spaces and ice matrix. We applied the method to many firn cores drilled at both ice sheets. We find that firn that have shorter residence time at the near-surface depths does not form strong vertical anisotropy that is caused by vertical movement of moistures. In contrast, firn that have longer residence time at the near-surface depths tend to form vertical anisotropy. When density exceeds more than ~600 kg/m3, a common feature of firn at many polar sites is that there is evolution of vertically elongated features of pore spaces in firn despite growth of vertical compression. We hypothesize an explanation as follows. As firn becomes denser, air within firn escape to upward directions as compared to sinking firn. In firn, porous structure tends to have vertically elongated structure because of this vertical escape movement of air. The observed phenomena of the growth of the vertical dielectric anisotropy can be understood by this vertical movement of the air within firn.

Keywords: ice core, firn, metamorphism

©2020. Japan Geoscience Union. All Right Reserved.

Dielectric anisotropy measurement of Dome Fuji ice core and implications for crystal orientation fabric development

*Tomotaka Saruya[1], Shuji Fujita[1,2]

1. National Institute of Polar Research, 2. The Graduate University for Advanced Studies

Crystal orientation fabric (COF) is one of important factors in the physical properties of ice cores. Deformation and flow of ice-sheet ice are highly controlled by COF development. Generally, orientation of c-axes is measured using ice thin sections and crystal fabric analyzers. For the last decades, several systems of automatic fabric analyzers were invented. However, automatic methods still require making many thin sections of ice, which means that we need much effort and a long time. In addition, numbers of crystal grains within a thin section are of the order of several hundreds. To make bulk ice-core based measurements of the COF possible, we developed a new measurement method for COF of ice cores by measuring tensorial components of the dielectric permittivity of ice core using an open resonator.
Hexagonal ice crystal has physical properties with uniaxial symmetry around the c-axis. The dielectric property also has such a symmetry. High-frequency- limit permittivity in ice is approximately 3.15 under the temperature of Cryosphere of the earth. The difference in permittivity between parallel and perpendicular to the c-axis is approximately 0.037 (Fujita et al., 1993). Based on this anisotropic property of each crystal grain, polycrystalline ice has macroscopic anisotropy of permittivity caused by COF. By measuring the macroscopic dielectric property parallel and perpendicular to the ice core axis, we can estimate the degree of the c-axis cluster around the vertical.
We investigated Dome Fuji Station ice cores drilled at Dome Fuji, the second highest dome summit in East Antarctica. To better understand meaning of the COF with respect to glacial processes, successive measurement was performed with an interval of every 5 m. At each step, 1 m-long ice core was measured continuously with a resolution of about 30 mm. Measurements were done to a depth of 1800 m. We used an open resonator of microwave using frequencies between 15 and 20 GHz. All measurements were conducted under -30C in a cold temperature room. We used thick sections of slab-shaped ice core samples with thickness between 35 and 75 mm, which contains 1000 times volume of ice compared with thin section measurements.
As a result of the successive measurement down to 1800 m, we observed that the dielectric anisotropy increased with increasing depth. This trend is consistent with the c-axis clustering toward the core axis due to the uniaxial compression. In addition to the large-scale trend of increase, we found the small fluctuations of the degree of the c-axis cluster with scales of 10 –100 m. In this presentation, we discuss variations of the dielectric anisotropy along core depths in terms of (i) insolation at the timing of snow deposition and (ii) the other physical and chemical properties.

Keywords: dielectric anisotropy, crystal orientation fabric

©2020. Japan Geoscience Union. All Right Reserved.

Development of a numerical ice-sheet model for simulation of summit dynamics

*Fuyuki SAITO[1], Ayako Abe-Ouchi[2,1], Takashi Obase[2]

1. Japan Agency for Marine-Earth Science and Technology, 2. Atmosphere Ocean Research Institute, Univ. of Tokyo

Ice divides are important locations for deep drilling on ice-sheets. Precise computation around a divide requires spatially very high resolution due to the characteristics of ice-flow around the divide. In addition, ice flow pattern is significantly different between an ice divide and the other areas: the flow around the divide requires more stress terms to compute than the other area, which is still a challenging topic due to its heavy cost of computation.
This study presents a recent development of Ice sheet model for Integrated Earth system Studies (IcIES) in particular, for improvement and inclusion of higher-order mechanics.

Keywords: Numerical ice-sheet model

©2020. Japan Geoscience Union. All Right Reserved.

Layering, densification and bubble close-off of firn at a new site near Dome Fuji, East Antarctica

*Ryo Inoue[1], Shuji Fujita[2,1], Kenji Kawamura[2,1,3], Fumio Nakazawa[2,1], Ikumi Oyabu[2]

1. The Graduate University for Advanced Studies, SOKENDAI, 2. National Institute of Polar Research, 3. JAMSTEC

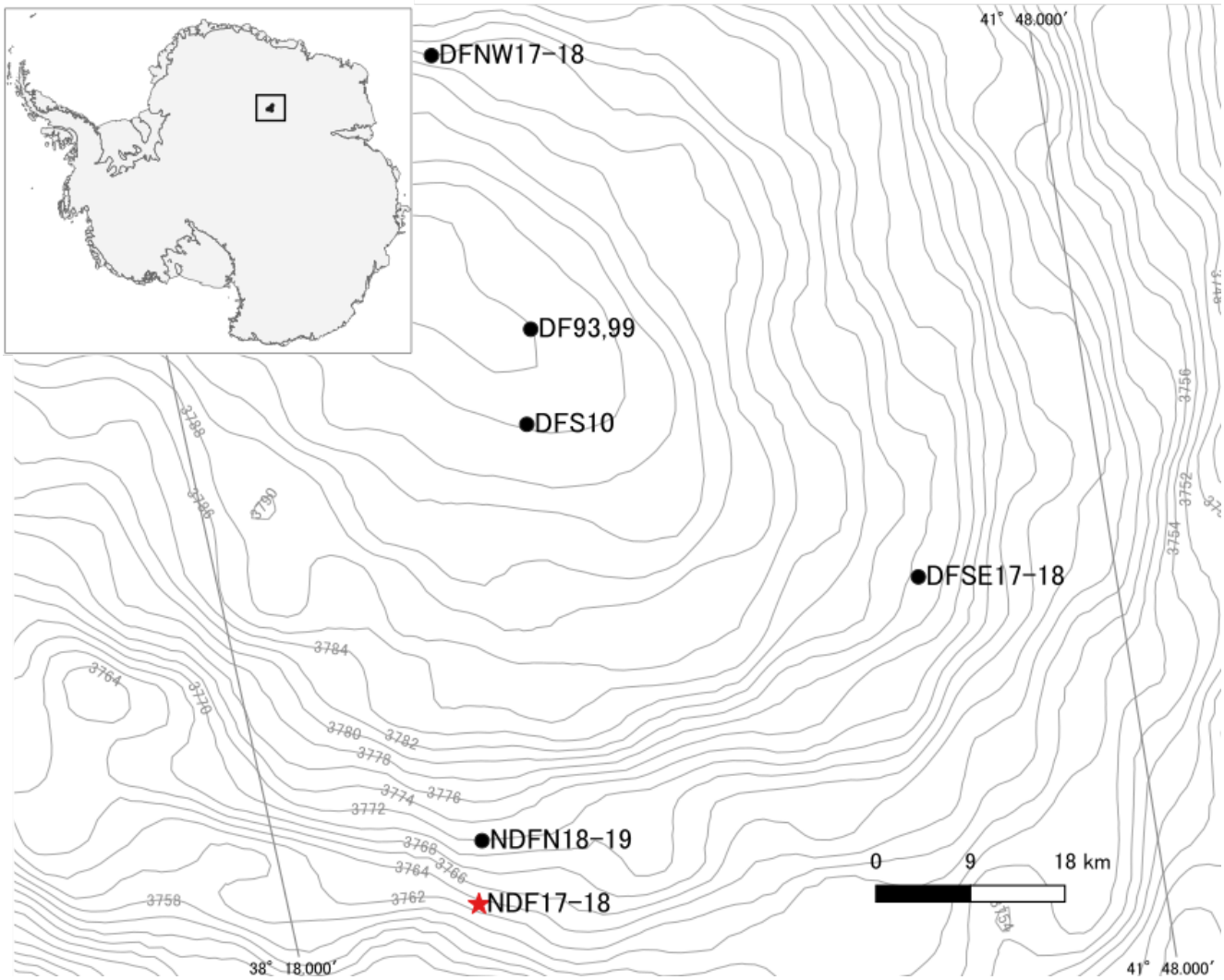
Ice cores provide proxies for chronology and past climatic changes from their ice and gas compositions, and the understanding of firn layering, densification and gas fractionation processes is crucial for better interpretation of the ice-core records. It has been hypothesized that metamorphism and geometric layer structure of firn determines the processes on gas trapping at deep firn, such as the depth range where bubbles are formed, close-off depth and the fractionation of gas components. Fujita et al. (2009; 2016) has reported in detail the layer structure of firn around Dome Fuji, East Antarctica. However, little is understood on the relationships between the geometric layer structure, bubble formation, and gas fractionation. For example, degree of growth of geometric anisotropy differ from one location to another (Fujita et al., 2016), but it is not known as to how such site-dependent difference influences gas trapping process. Another example is poor understanding of the effect of insolation on ice crystal fabric formation and/or water isotope composition. Therefore, it is important to clarify spatial variability of geometric properties of firn and gas trapping process to compare site-dependent variability of ice core signals, especially because a deep drilling of an oldest ice core is planned near Dome Fuji in the near future.

A new shallow ice core was drilled to ~152 m in December 2017 at a site about 54 km south of Dome Fuji station (named NDF, 77°47’ 18S, 39°3’ 15E, 3763 m a.s.l.). Up to now, we have measured multiple physical properties on this ice core; density and geometric anisotropy using a dielectric permittivity tensor measurement, near-infrared reflectance of firn (a proxy for specific surface area) using an optical method, and qualitative measure of permeability using an air-suction system. We also plan to analyze gas component of bubbles at high resolution to quantify gas fractionations in layer-by-layer scale. In the JpGU presentation, we will report the results of the physical properties on the NDF shallow core and compare them with those from the Dome Fuji and Dome Fuji South cores (Fujita et al., 2009; 2016).

Fig. Shallow core sites around Dome Fuji. Numbers after site names indicate the drilling season.

Keywords: firn, layering, densification, ice core

©2020. Japan Geoscience Union. All Right Reserved.



©2020. Japan Geoscience Union. All Right Reserved.

PMIP4/CMIP6 Last Interglacial simulations using different versions of MIROC, with and without vegetation feedback

*Ryouta O'ishi[1], Wing-Le Chan[1], Ayako Abe-Ouchi[1,2,3], Sam Sherriff-Tadano[1], Rumi Ohgaito[3]

1. Atmosphere and Ocean Research Institute, the Universitoy of Tokyo, 2. National Institute of Polar Research, 3. Japan Agency for Marine-Earth Science and Technology

We carry out a Last Interglacial (LIG) experiment, named lig127k and a Tier1 experiment of PMIP4/CMIP6, using three versions of the MIROC model, MIROC4m, MIROC4m-LPJ and MIROC-ES2L. The results are compared with reconstructions from climate proxy data. All models show summer warming over northern high latitude land, reflecting the differences between the distributions of the LIG and present-day solar irradiance. Only MIROC4m-LPJ, which includes dynamical vegetation feedback from the change in vegetation distribution, shows warming signals, even for the annual mean, at northern high latitudes, as shown by proxy data. However, the latest Earth System Model (ESM) of MIROC, MIROC-ES2L, in which there is only a partial vegetation effect through the leaf area index, shows no change or even annual cooling over large parts of the northern hemisphere. Results from the series of experiments show that the inclusion of vegetation feedback is necessary for the reproduction of the strong annual warming over land at northern high latitudes. The LIG experimental results show that the warming predicted by models is still underestimated, even with dynamical vegetation, compared to reconstructions from proxy data, suggesting that further investigation and improvement to the climate feedback mechanism are needed.

Keywords: paleoclimate, Last Interglacial, Atmosphere Ocean General Circulation Model

©2020. Japan Geoscience Union. All Right Reserved.

Response of convective systems to changes in orbital forcing of the last interglacial

*Minoru Chikira[1], Yohei Yamada[2], Ayako Abe-Ouchi[1], Masaki Satoh[1]

1. The University of Tokyo, Atmosphere and Ocean Research Institute, 2. Japan Agency for Marine-Earth Science and Technology

We ran a number of simulations using a global nonhydrostatic atmospheric model coupled with a slab ocean model for the orbital parameters of the last interglacial. The model used in this work is Nonhydrostatic ICosahedoral Atmospheric Model (NICAM): a framework to resolve cumulus convection when used with a proper resolution. Because of the limit of computational resources, we use NICAM with a horizontal resolution of 56km. The simulations were run with and without cumulus scheme to compare the performance. The integrations were continued for 5 years. The boreal summer climate of the last interglacial shows an enhancement of the monsoon activity. The spatial pattern of the mean-state precipitation is quite similar between the simulations with and without cumulus scheme, while the cumulus scheme tends to moderate the peak precipitation. Since the strength of NICAM is in its representation of variability associated with convective systems, we gave particular focuses on the behaviors of the equatorial waves and tropical cyclones represented by the model. We found that the Madden-Julian oscillation (MJO) is better represented in the present simulation when using the cumulus scheme. We also found that the signal of the MJO is stronger in the last interglacial, which was found both in the coherence-squared and lag-correlation regardless of the use of the cumulus scheme. Although the model does not represent the boreal summer intraseasonal oscillation (BSISO) very well, the lag-correlation shows its greater signal in the last interglacial. In particular, the lag correlation in the simulation of the last interglacial run with the cumulus scheme shows a very clear pattern of the BSISO, comparable to that of the present-day observation. The change in the global genesis frequency of the tropical cyclones was different depending on the use of the cumulus scheme. It decreases without the cumulus scheme, while it increases with the cumulus scheme.

Keywords: Paleoclimate, Last interglacial, Climate model

©2020. Japan Geoscience Union. All Right Reserved.

[E] Poster | A (Atmospheric and Hydrospheric Sciences)：A-GE Geological & Soil Environment

[A-GE40] Subsurface Mass Transport and Environmental Assessment

convener:Hirotaka Saito(Department of Ecoregion Science, Tokyo University of Agriculture and Technology), Shoichiro Hamamoto(Department of Biological and Environmental Engineering, The University of Tokyo), Yuki Kojima(Department of Civil Engineering, Gifu University), Yasushi Mori(Graduate School of Environmental and Life Science, Okayama University)

This session covers the topics on fluid flow and mass transport in geological media. Subjects related to laboratory testing, subsurface characterization, theoretical analysis and numerical modeling will be discussed. Presentations on geo-pollution, remediation, geological disposal of hazardous wastes, mass transport in vadose zone, and environmental assessment are especially encouraged.

[AGE40-P01] Environmental Impact Assessment of Open Loop Geothermal Heat Pump System in Gifu City, Central Japan

★Invited Papers

*Randa Permanda[1], Tomoyuki Ohtani[1] (1.Gifu University)

[AGE40-P02] Estimation of correlation between soil organic matter and soil components using neural network

*Masaki Kiyohiro[1], Yasushi Mori[1], Yutaro Yamamoto[1] (1.Okayama University Graduate school of Environmental and Life Science)

[AGE40-P03] Fracture domain of granite based on orientation analysis and its relation to water conducting fractures: an example from the “-500m access/research gallery-North” of the Mizunami Underground Research Laboratory

*Koji Shimada[1], Masakazu Niwa[1], Ryuji Takeuchi[1], Kenji Amano[1] (1.Japan Atomic Energy Agency)

[AGE40-P04] Effects of Moisture Content on Soil Water and Ion Movements in the Vicinity of Soybean Roots

*Rui Nakasone[1], Shoichiro Hamamoto[1], Naoto Nihei[2], Taku Nishimura[1] (1.Graduate School of Agricultural and Life Sciences, the University of Tokyo, 2.Fukusima University)

[AGE40-P05] The effect of gas emission from organic matter on the stability of rice terraces structure

*Yasushi Mori[1], Mayuka Kashi[1], Tomoyo Kurozumi[1], Hiroaki Somura[1], Milagros Ong How[2] (1.Graduate School of Environmental and Life Science, Okayama University, 2.Global Harvester)

[AGE40-P06] **Effects of Macropore Structures on Agricultural Soil’s Greenhouse Gases Emission**

*Thanh Long Bui[1], Yasushi Mori[1] (1.Graduate School of Environmental and Life Science, Okayama University)

[AGE40-P07] **Interaction between Nano-Bubbles and Colloidal Particles in Saturated Porous Media under Flowing Condition**

Takuya Sugimoto[1], *Shoichiro Hamamoto[1], Taku Nishimura[1] (1.Department of Biological and Environmental Engineering, The University of Tokyo)

[AGE40-P08] Numerical Analysis of the Effects of Capillary Barrier under Subsurface Drip Irrigation to Improve Water-use Efficiency

*Koichi Noguchi[1], Hirotaka Saito[1] (1.Tokyo University of Agriculture and Technology)

[AGE40-P09] Deformation analysis of fill dams due to level 2 earthquakes using PIV

*Mai Masutani[1], Tomotaka Sato[2], Hirotaka Saito[3], Yuji Kohgo[2] (1.Graduate School of Agriculture, Tokyo University of Agriculture and Technology, 2.United Graduate School of Agricultural Science, Tokyo

University of Agriculture and Technology, 3.Department of Ecoregion Science, Tokyo University of Agriculture and Technology)

[AGE40-P10] An observation of swelling behavior and microstructural change for granulated bentonite mixtures under controlled relative humidity

*Mazhar Nazir[1], Akihiro Matsuno[1], Takeshi Saito[1], Ken Kawamoto[1] (1.Graduate School of Science and Engineering, Saitama University)

Environmental Impact Assessment of Open Loop Geothermal Heat Pump System in Gifu City, Central Japan

*Randa Permanda[1], Tomoyuki Ohtani[1]

1. Gifu University

Geothermal heat pumps (GHPs) are most efficient and eco-friendly energy that used for heating and cooling system. In Japan, the number of shallow geothermal installations has increased by year. Open loop GHPs is a type of GHP system which use groundwater as heat source for heating and cooling of building. In fact, there are still no regulations related to thermal use of groundwater and the subsurface in Japan. The aim of this study is to simulate regional and local groundwater flow and heat transport in study area and to assess the environmental impact by extraction and injection of open loop system from the wells into subsurface.

The study area is an alluvial fan of the Nagara River, Gifu city central, Japan. It is bounded by mountain ranges from north to northeast side and plain area remains. The Nagara River flows in the center of the plain. The underground temperature in alluvial fan is influenced by rapid groundwater flow recharged from the river. Rapid groundwater flow has potentiality to spread the environmental impact of GHP system greater than slow groundwater flow. This alluvial fan is composed of sands and gravels and often intercalate thin fine sand and silt layers. Groundwater flow occur mainly in the Quaternary sediments. For assessment of potential energy of open loop GHP system, regional 3D model of groundwater flow with heat transport in study area was developed using FEFLOW program. Model area has size of 13 km (NS), 12 km (EW) and 300 m (depth). Model is constructed first by geological data. In addition, pre-existing hydrogeological data which consist of groundwater table, underground temperature, and temperature of river water data in study area are compiled to construct the simulation model. Boundary condition of groundwater flow system is defined by water table distribution. Bottom of the model is basement rock, treated as impermeable boundary and lateral sides are set as no flow boundaries. For boundary conditions of heat transport, top and bottom of the model are fixed by constant temperature boundaries. In order to study environmental impact of open loop system, local simulation of open loop system was operated. We built local simulation with more fine mesh to create detailed information with wide area 1.2 km (NS), 1 km (EW) and 100 m (depth). Open loop simulation model was consisting of one extraction and injection wells. Both the extraction and injection wells were screened in the first aquifer (gravel layer). The operation mode was applied for heating from January to March, and cooling from July to September. The operation mode of pumping/injection was obtained a time-varying rate with keeping the temperature difference at constant pumping rate 288 m^3/d. The temperature difference of the pumping and injection are contained 3 variant values: 3, 5, 10˚C for heating and cooling periods.

To confirm the results of regional groundwater flow and heat transport simulation, there were comparison groundwater temperature data between calculated results and measured ones at some points. Based on this result, there is reasonably good match between calculated and measured data at southern region of model. Furthermore, the local simulation of open loop GHP system was shown that the distance of thermal discharge from injection activities gets further as variation of temperature difference increase. When the temperature difference between the pumping and injection is 10˚C, temperature changes caused rising groundwater temperatures surrounding injection area up to 37 m in the beginning of winter season and 47 m in the beginning of summer season. Temperature change is defined by a change more than 0.1°C at groundwater temperatures around injection activities. However, variation of temperature changes have impact to rise groundwater temperature less than 300 m from injection well and it is still in allowable range of interference effect from another open loop GHP system according to regulation of

©2020. Japan Geoscience Union. All Right Reserved.

other countries (Haehnlein et al., 2010).

Keywords: Geothermal heat pump, Open loop system, Groundwater flow, Environmental impact

©2020. Japan Geoscience Union. All Right Reserved.

Estimation of correlation between soil organic matter and soil components using neural network

*Masaki Kiyohiro[1], Yasushi Mori[1], Yutaro Yamamoto[1]

1. Okayama University Graduate school of Environmental and Life Science

Soil is the terrestrial largest carbon storage, and, it is key to predict the carbon storage and loss. However, there are many estimation models, and we still cannot understand natural processes. Therefore, instead of predicting the organic matter from the conventional function system, we thought about letting the neural network learn anew and infer the feature value closely related to the soil organic matter.

Deep learning is a type of machine learning and it is also called a neural network. A neural network is composed of a unit called a node or a layer. The node receives a weighted input, outputs the weighted input to a next layer with a specific weight. After passing through all layers, output data can be obtained. The feature of deep learning is that the weight between each node can be selected other than 0 and 1, and other judgment criteria can be selected. Moreover, by preparing a plurality of hidden layers, it is possible to predict more complicated phenomena.

In this study, we conducted an experiment to predict the amount of organic matter in soil, and to estimate the correlation between organic matter and soil constituents using a neural network.

The surface soil data of HWSD (Harmonized World Soil Database) was used as data for learning. The target areas were Europe, Asia and Australia. The input items (features) are 17 items such as particle size distribution and cation exchange capacity.

In addition, feature selection was performed as data preprocessing. Feature selection is a method of automatically selecting important features to create a highly accurate model. In this experiment, the recursive feature elimination method (RFE) was used. Among the estimation models using the features, the one with the highest accuracy was obtained and its performance was evaluated. The model was used to estimate the effect of the selected feature on the amount of organic matter by changing each feature.

Among the features selected by the high-precision model created from the data of the target area, those that matched in three areas were silt content, dry density, cation exchange capacity of soil, and base saturation.

In addition, a model was created again using the features and parameters selected by the model with the highest accuracy, and the effect on organic matter by increasing or decreasing the value of a specific feature by 10% from the average value was determined. As a result, the impact was confirmed in Europe and Australia.

The experimental results suggest that the base model has a positive effect on the European model and a negative effect on the Australian model. In the Asian model, soil organic matter did not change significantly even when each feature was changed.

Prediction of soil organic matter and correlation estimation were performed using neural networks. Four common features were selected in the high-precision model generated from the data of three regions.

©2020. Japan Geoscience Union. All Right Reserved.

However, it was suggested that the effect of selected features on the amount of organic matter differed from region to region.

Keywords: Neural network , Soil organinc carbon, Correlation estimation

©2020. Japan Geoscience Union. All Right Reserved.

Fracture domain of granite based on orientation analysis and its relation to water conducting fractures: an example from the “-500m access/research gallery-North” of the Mizunami Underground Research Laboratory

*Koji Shimada[1], Masakazu Niwa[1], Ryuji Takeuchi[1], Kenji Amano[1]

1. Japan Atomic Energy Agency

Groundwater flow in the deep ground composed of crystalline rocks such as granite is largely controlled by the fracture system. Fracture intersections, steps and branches (spray structure) are potential and spatially linear main water conduits (Sugimura et al., 1997). So, it is important to confirm the applicability and sophistication of the geological technique to grasp the distribution of the fracture intersections. A homogenous region characterized by a predominant fracture direction is called a domain, and the domain boundary is a dense zone of the fracture intersections. To make clear spatial distribution of fracture domain, i.e. domain analysis is, therefore, a simple way to depict spatial distribution of fracture intersections. Sophistication of geological technique at the site-scale could be utilized to wide-scale advanced studies such as geological fracture mapping on the kilometer scale and groundwater discharge in relation to geological disposal of HLW.
Domain analysis of granite on the basis of fracture orientation in the 100 m scale by means of structural geologic techniques such as stereographic projection, Strike Versus Traverse Distance (SVTD) diagram (Marshak and Mitra, 1988) and Sequential Linked Median (SLIME) plot (Fisher, 1993) revealed relationship between distribution of water conducting fractures and fracture orientations. This attempt used fracture data taken from the “-500m access/research gallery-North” of the Mizunami Underground Research Laboratory (Kawamoto et al., 2014a, b). Improvement of the SLIME plot based on running median of span 3 shows domain boundary (large kink of fracture trend) and kink in domains of fracture trend (small kink), and their relation to positions of water conducting fractures (Ishibashi et al., 2016, Hayashida et al., 2018, JAEA, 2020), more clearly. Water conducting fractures are concentrated at these kinks of fracture trend. A location of one of the large kinks corresponds to a region of fractures with geochemically high connectivity from deeper parts. Methods to make SLIME plot would also be shown in our presentation.
References:Fisher, N. I., 1993, Statistical analysis of circular data. Cambridge, 277p. Hayashida, et al., 2018, Chikyukagaku (Geochemistry), 52, 55-71.* Ishibashi, et al., 2016, Engineering Geology, 208, 114-127. Kawamoto, et al., 2014a, JAEA-Research, 2014-021, 30p.* Kawamoto, et al., 2014b, JAEA-Data/Code, 2014-014, 27p.* Marshak, S. and Mitra, G., 1988, Basic methods of structural geology. Prentice Hall, 446p. Sugimura, et al., 1997, Journal of Japan Society of Civil Engineers, 582, 229-246.* [URL] JAEA, 2020, https://www.meti.go.jp/shingikai/energy_environment/chiso_shobun/pdf/005_03_03.pdf ** *(in Japanese with English abstract), **(in Japanese).

Keywords: water conducting fracture, domain analysis, Granite

©2020. Japan Geoscience Union. All Right Reserved.

Effects of Moisture Content on Soil Water and Ion Movements in the Vicinity of Soybean Roots

*Rui Nakasone[1], Shoichiro Hamamoto[1], Naoto Nihei[2], Taku Nishimura[1]

1. Graduate School of Agricultural and Life Sciences, the University of Tokyo, 2. Fukusima University

Radioactive cesium was emitted from the disabled Fukushima Dai-ichi Nuclear Power Plant on March, 2011, and diffused into the environment, including agricultural area in eastern Japan. As one of most effective countermeasure to reduce Cs uptake by crops, additional potassium (K) fertilization at applying basal fertilizer is recommended. It is generally known that with increasing exchangeable K in soils the soil-to-plant transfer factor (TF) of Cs decreases. However, it is also reported that the TF is variable under lower exchangeable K. Further understandings of Cs uptake by roots, governed by mass transport in the vicinity of roots, are required. Soil physical properties such as moisture content affect mass transport in soils, hereunder influencing water and ion uptake by roots.
In this study, using a rhizobox system, soil water and ion movements in the vicinity of soybean roots were investigated for soils with different moisture contents. Sandy soil taken from the agricultural field at Namie-town, Fukushima Prefecture, Japan was repacked to soil box compartment (width:14 cm x height:10 cm x thickness: 3 cm) in rhizobox system. The ^{137}Cs concentration of the soil was around 3000 Bq/kg. Mass water content (w) of the samples was adjusted to either 20% or 28%. The soybean roots which were pre-grown up to root length of around 6 cm were placed on the surface of soil box compartment. The soybean in the rhizobox was grown for around 7 days in the climate controlled room. After the growth, soil box compartment was removed from the rhizobox and sliced at 2.0 mm interval. Mass water content and ion concentration of each sliced sample were measured.
Results showed mass water content in the soil decreased due to root water uptake and more significant decrease was observed at the condition of w = 28%. In addition, mass of K uptake by the roots was higher at w = 28% as compared to the one at w = 20%. Those results indicate water stress at w = 20% reduced water and K uptake by the roots. Mass of ^{137}Cs uptake was higher at w = 20% as compared to w = 28%, likely suggesting the ^{137}Cs was more selectively absorbed due to reduced K uptake under lower moisture condition. The K and ^{133}Cs concentrations at w = 20% increased and decreased near roots (within 5 mm), respectively, while those concentrations at w = 28% maintained almost constant regardless of the distance from the roots in the soil box.

Keywords: rhizosphere, mass transport, Cesium

©2020. Japan Geoscience Union. All Right Reserved.

The effect of gas emission from organic matter on the stability of rice terraces structure

*Yasushi Mori[1], Mayuka Kashi[1], Tomoyo Kurozumi[1], Hiroaki Somura[1], Milagros Ong How[2]

1. Graduate School of Environmental and Life Science, Okayama University, 2. Global Harvester

The rice terraces are not only cultural heritage, but also playing a part of natural material circulation. They contributes to the water conservation and organic matter preservation, otherwise inclined slope causes surface flow and organic matter loss. However, in recent years, rice terraces have not been sufficiently preserved, leading to collapse. In the world heritage rice terraces in Banaue, Philippines, drainage channels are not well-organized, and some of the rice terraces are rich in organic matter in the situation where sewage is mixed. Although ponding water was maintained, this water has been kept by clogging of organic matter or small particles rather than hardpan formation.

In this research, we examined how gas emission prevented hard pan formation. Incubation tube experiment was conducted for gas emission and bulk density change, and also soil column experiment was conducted for water content and Eh measurement. Both experiments were conducted by changing organic matter content.

The results showed that methane gas emission was observed only with one week and the methane stayed in the column in bubble shape, not soluble condition. This was supported by the Eh reduction and volumetric water fluctuation. Bulk density of incubation tube decreased by 10-20%, which would result in unstable basement. Volumetric water fluctuation meant the frequent bubble formation and disappearance, causing fluctuation of basement. If this happens in rice terraces, saturated zone would be deeply developed, making unstable rice terraces which has a risk of collapsing. Therefore, we need to tell local people to check hardpan formation, sewage water control and appropriate organic matter application, rather than just confirming ponded water.

Keywords: rice terraces, methane gass, hardpan, organic matter

©2020. Japan Geoscience Union. All Right Reserved.

Effects of Macropore Structures on Agricultural Soil’s Greenhouse Gases Emission

*Thanh Long Bui[1], Yasushi Mori[1]

1. Graduate School of Environmental and Life Science, Okayama University

Agriculture is not only the important economic sector via production of crop and livestock but also a significant contributor of greenhouse gases emission. In 2010, it contributed slightly more than 10% to total anthropogenic emissions of greenhouse gases, which totaled some 49 billion tonCO_2eq *(Francesco Nicola Tubiello, 2019).* Increasing organic matter stocks in soils reduces atmospheric carbon dioxide *(Nadine Jäger et al, 2011)*, but they may promote emissions of nitrous oxide by providing substrates for nitrification and denitrification and by increasing microbial O_2 consumption or may boost methane emission in anaerobic condition.

Both natural and agricultural wetland contribute an estimated 40 to 50% of total methane emission each year *(G. J. Whiting & J. P. Chanton, 1993)*. According to modern agricultural practices in Southeast Asia’s countries and others such as Japan, Korea, etc., rice is grown in flooding paddy field which reliably generate the great deal of methane in anaerobic condition. To hold maximum water in the fields, hardpan was created under paddy field. This meant that the infiltration to deeper layer was decreased. Meanwhile, roots created macropores played pathways’ role to largely and quickly emit greenhouse gases in soil. It may highly emit greenhouse gases to atmosphere than natural wetland. Increasing greenhouse gases emission is in results of the global warming potential, therefore, study of effects of macropores on the generation process and reduction of soil’s greenhouse gases emission was conducted.

In this study, 1st column experiment was set up for granite decomposition soil (Masa soil) and paddy field soil. Furthermore, 2nd column experiment was conducted for paddy field soil in ponding condition to see the difference between with and without drainage (0.4mm-pinhole). Tubular macropore (1.5mm) and manure were applied to both soil texture in two experiments. Then, methane and carbon dioxide were measured by sensors once a week for 1st experiment and every water-adding time for 2nd experiment.

The 1st experiment results showed that high methane and carbon dioxide emission were observed in paddy field soil in ponding condition. In contrast, low concentration of the gases was observed in Masa soil. The methane and carbon dioxide emission of both soil textures increased in the 1st and 2nd week, then decreased in 3rd week. Both experiments indicated that column with manure showed gases emission much higher than without manure. Thus, organic matter is an important impact factor on the methane and carbon dioxide emission of paddy soil in ponding condition. In addition, macropores played as pathways to emit methane and carbon dioxide with higher concentration of the gases in the columns. This is in accordance with the explanation of K. Kusa et al. (2010). However, the 2nd experiment results also pointed that the methane and carbon dioxide gas emission observed at columns with drain were lower than ones without drain.

Keywords: Macropores, Greenhouse gas emission, Organic Matter, Manure, Drain

©2020. Japan Geoscience Union. All Right Reserved.

Interaction between Nano-Bubbles and Colloidal Particles in Saturated Porous Media under Flowing Condition

Takuya Sugimoto[1], *Shoichiro Hamamoto[1], Taku Nishimura[1]

1. Department of Biological and Environmental Engineering, The University of Tokyo

Nano-bubbles (NBs) have a considerable potential for the remediation of soil and groundwater contaminated by organic compounds, especially when used in conjunction with bioremediation technologies. Understanding the transport mechanisms of NBs in soils is essential to optimize NB-based remediation techniques. In natural soils, there are several types of colloids, which are particles with diameters of around 10 nm to 10 mm, in various organic and inorganic sources: silicate clays, iron and alumium oxides, or humic minerals. Deposited colloidal particles on the soil particles likely affect NBs transport. However, interaction between NBs and deposited colloidal particles in saturated porous media under flowing condition is not fully understood.

In this study, one-dimensional column transport experiments using glass beads with 0.1 mm size were conducted, where carboxyl latex (CL) with 500 nm and NBs created by oxygen gas were consecutively injected to the column at the constant flow rate. Effluents were collected at the same time interval. Bubble and particle concentrations in the effluents were measured by a resonant mass measurements. Results showed that NBs retention was enhanced at the condition where CLs were initially deposited in the porous media, suggesting deposited CLs worked as additional deposition sites for NBs. The obtained breakthrough curves of NBs were well simulated by one-dimensional advection-dispersion equation with first-order deposition kinetics.

Keywords: Nano-Bubble, Colloidal Particle, Porous Media

©2020. Japan Geoscience Union. All Right Reserved.

Numerical Analysis of the Effects of Capillary Barrier under Subsurface Drip Irrigation to Improve Water-use Efficiency

*Koichi Noguchi[1], Hirotaka Saito[1]

1. Tokyo University of Agriculture and Technology

In semi-arid and arid regions, efficient water-use in agriculture is crucial. The installation of the capillary barrier (CB) has been suggested as a promising approach for such a purpose. CB reduces deep drainage by suppressing the downward water movement. The downside of CB is that it may enhance surface evaporation by keeping irrigated water near the surface (Wongkaew *et al.*, 2018). One of the remedies to water loss by evaporation is to use subsurface drip irrigation (SDI) techniques. However, there are few studies on its feasibility in a system with CB. This study aims to evaluate the feasibility of CB under SDI numerically. The effects of the installation depths of the emitter and CB on water use efficiency were also investigated. In this study, the ring-shaped emitter was used because of its high performance and affordability (Saefuddin *et al.* 2019). HYDRUS (2D/3D) (Simunek *et al.*, 2016) was used to simulate water flow and root water uptake (RWU).

The emitter was installed at 10 different depths within the root zone. CB was installed at 5 different depths below the root. Strawberry and spinach were selected as model plants for the long-root and short-root plants because of their distinct root distributions. The installation depths for the emitter and the CB layer were defined relative to the root depth. The objective function (*OF*) was introduced to evaluate water-use efficiency. Uniform soil water pressure of -80 cm was applied to the Tottori Dune sand profile as the initial condition. The potential evaporation rate was set as 7.0 mm d^{-1}. The bottom boundary condition was set as gravity flow. Durner (1994) model was used to account for capillary flow and non-capillary type flow. RWU was simulated by the compensated model (Šimůnek and Hopmans, 2009).

For the long-root plant (strawberry), the peak of the *OF* value was obtained when the emitter was slightly above half the root depth and CB was inserted immediately below the root, which were found to be the optimal depths. This appears to be the result of the trade-off between active RWU near the surface and intense evaporation from the wetted ground surface. Smaller *OF* values were obtained for shallow-root plants when the emitter is near the surface. The water applied at a shallow depth might increase actual evaporation by wetting the upper layer. The best CB depth was found to be far below the root in this study. Installing CB shallowly may lead to an increase in evaporation and the breakage of CB due to the water accumulating upon CB.

References

Durner, W. 1994. Water Resources Research. 30(2): 211-223.
Šimůnek, J., J. W. Hopmans. 2009. Ecological Modeling. 220(4): 505-521.
Saefuddin, R., Saito, H., Šimůnek, J. 2019. Agricultural Water Management. 211: 111–122.
Šimůnek, J., van Genchten MTh, Sejna M. 2016. Vadose Zone Journal. 6: 1-25.
Wongkaew, A., Saito, H., Fujimaki, H., Šimůnek, J. 2018. Soil Use and Management. 34(2): 206–215.

©2020. Japan Geoscience Union. All Right Reserved.

Keywords: Subsurface irrigation, Ring-shaped emitters, Capillary barrier

©2020. Japan Geoscience Union. All Right Reserved.

Deformation analysis of fill dams due to level 2 earthquakes using PIV

*Mai Masutani[1], Tomotaka Sato[2], Hirotaka Saito[3], Yuji Kohgo[2]

1. Graduate School of Agriculture, Tokyo University of Agriculture and Technology, 2. United Graduate School of Agricultural Science, Tokyo University of Agriculture and Technology, 3. Department of Ecoregion Science, Tokyo University of Agriculture and Technology

A lot of civil engineering structures have been severely damaged by Level 2 earthquakes. An agricultural fill dam in Fukushima prefecture was failed and washed out due to the Great East Japan earthquake in 2011 and a few people were killed in the downstream region. In order to increase the level 2 earthquake resistances, understanding the failure mechanism of fill dams is necessary. The fill dams normally consist of unsaturated and saturated geomaterials. Namely the parts of fill dams above or below the seepage surfaces respectively remain under unsaturated or saturated conditions. Then we should understand the mechanical properties of both saturated and unsaturated geomaterials. Especially it is very important to consider the unsaturated mechanical properties to understand deeply the failure mechanism of fill dams. In unsaturated geomaterials, pore water pressures are normally negative (suction) and the suction effects play important roles. Kohgo et al. (1993) clarified that there were two suction effects: 1) an increase in suction increases effective stresses and 2) suction enhances the internal confinement and an increase in suction increases yield stresses.

In this research we try to investigate the suction effects in the model levels of fill dams. So, several centrifugal shaking model tests were conducted. Two types of model materials: sandy soil and the soil mixed with silty soil named DL clay and No. 6 Silica sand were used. The dimensions of models in prototype were 6 m in height, 31.5 m and 1.5 m in base and crest widths and 12 m in depth after 30g centrifuge acceleration applied. The inclines of both slopes were 1:2.5. Accelerometers, pore water pressure and pore air pressure sensors were installed inside the model. Laser displacement sensors were set above the models. Input sine waves were applied by increasing their acceleration step by step. Before and after each shaking, photographs were taken using a digital camera mounted in front of the embankment model. These photographs were used to calculate inner displacements by using particle image velocimetry (PIV) technology. The displacement data might be used to estimate volumetric and shear strains within the embankments.

It was found that in the sandy model, the crest deformed roundly and vertically. Moreover, slip failures occurred in both slopes. On the other hand, in the mixed soil model, the whole embankment deformed downward but no slide was observed. The displacement vectors obtained from PIV could well reflect the differences of these deformations. The shear strains in the sandy soil model developed near the slops and finally the volumetric strains changed to dilation there while in mixed soil model both shear and volumetric strains developed at the center of the bottom of the embankment.

Applying PIV to deformation analysis in the fill dam model, the strain distribution could be obtained in detail. As a next step, we will try to discuss totally including the behavior of pore water pressures.

Keywords: Fill dam, Suction, Centrifugal model test, PIV

©2020. Japan Geoscience Union. All Right Reserved.

An observation of swelling behavior and microstructural change for granulated bentonite mixtures under controlled relative humidity

*Mazhar Nazir[1], Akihiro Matsuno[1], Takeshi Saito[1], Ken Kawamoto[1]

1. Graduate School of Science and Engineering, Saitama University

The granulated bentonite mixtures (GBM) are considered as potential sealing materials in the radioactive waste disposal concepts due to their high swelling capacity, low permeability and good compaction properties. Therefore, it is necessary that the hydro-mechanical behavior of GBM should be thoroughly examined for an efficient design of the repository. This study investigated the swelling behavior and microstructural change of a GBM. OK Bentonite from Kunimine Industries, Japan, was used in this study. First, OK Bentonite grains were sieved and the particle size distribution was adjusted to follow a fuller curve (similar to FE-GBM used by NAGRA, Switzerland). Air-dried GBM samples (RH = 60%, T = 20º C) were packed at dry density 1.2 and 1.3 g/cm^3 in the apparatus and then stored at RH = 95% to observe the swelling behavior and microstructural changes with time (t = 0, 1, 2, 4, 8 weeks). A constant volume rigid cell was used to measure the swelling pressure. The microstructural changes were observed by Microfocus X-ray Computerized Tomography (MFXCT) system. The results provided a quantitative observation of microstructural changes in the GBM under the swelling process at a controlled relative humidity and a better insight to understand the complex hydro-mechanical behavior of the GBM.

©2020. Japan Geoscience Union. All Right Reserved.

[E] Poster | A (Atmospheric and Hydrospheric Sciences)：A-GE Geological & Soil Environment

[A-GE41] Energy-Environment-Water Nexus and Sustainable Development

convener:Ming Zhang(Institute for Geo-Resources and Environment, Geological Survey of Japan, AIST), Yonghong Hao(Tianjin Normal University), Jet-Chau Wen(National Yunlin University of Science and Technology), Ken Kawamoto(Graduate School of Science and Engineering, Saitama University)

This session provides a broad platform for discussion and presentation of fundamental and up-to-date scientific results related to clean energy production, environmental remediation and restoration, waste management, water cycle, monitoring of water quality, management of water resources and interconnections among them for sustainable development. Presentations on the topics associated with social science that enhance public awareness, stakeholder empowerment and involvement, and policy decisions regarding the management of water, energy and the environment are also encouraged.

[AGE41-P01] **Season Effect of the Operation of IPCC Reactor on Solar Photocatalysis of Phenol Wastewater**

*Wen-Shiuh Kuo[1], An-Chi Chen[1] (1.National United University, Taiwan)

[AGE41-P02] Solar photocatalysis of MeO wastewater with metal@TiO_2 film

*Ting-Yu Zeng[1], Ling-Syuan Tzeng[1], Wen-Shiuh Kuo[1] (1.National United University, Taiwan.)

[AGE41-P03] **Effects of fine content on mechanical properties of recycled concrete aggregates for unbound road base materials in Vietnam**

*Thai Hong Nam[1], Akira Kato[1], Takeshi Saito[1], Ken Kawamoto[1] (1.Graduate School of Science and Engineering, Saitama University)

[AGE41-P04] Development of filtering materials for removing heavy metals utilizing industrial by-products

*Akito Ujiie[1], Buddhika Bandara[1], Akihiro Matsuno[1], Takeshi Saitou[1], Ken Kawamoto[1] (1.Saitama university)

[AGE41-P05] Effects of Silicic Acid on Arsenite Leaching from Spent Calcium-Based Arsenic Adsorbents

*Hajime Sugita[1], Terumi Oguma[1], Ming Zhang[1], Junko Hara[1], Yoshishige Kawabe[1] (1.National Institute of Advanced Industrial Science and Technology)

Season Effect of the Operation of IPCC Reactor on Solar Photocatalysis of Phenol Wastewater

*Wen-Shiuh Kuo[1], An-Chi Chen[1]

1. National United University, Taiwan

Solar photocatalysis with partial shell-core Ag(0.1%)/P3HT(0.5%)@TiO_2 as catalyst was used to treat phenol wastewater (10 mg/L) in a pilot-scale inclined plate curvature channel (IPCC) reactor. Season effect on the performance of IPCC reactor was investigated. Results showed that the degradation efficiency of phenol in water (180 min) with Ag(0.1%)/P3HT(0.5%)@TiO_2 as photocatalyst were 98.35%, 95.06%, 98.92%, and 99.89% in autumn, winter, spring, and summer (in which UV_{a+b} intensity: 32.85, 27.80, 37.92, 45.86 W/m^2, respectively; VIS intensity: 743.91, 723.05, 822.72, 869.48 W/m^2, respectively), respectively. The degradation efficiency of phenol in water were increased 28.79%, 32.78%, 22.29%, and 5.19%, respectively and phenol degradation rate (k_{phenol}) were increased 2.94 times, 2.73 times, 2.66 times, and 1.98 times, respectively in four season as compared to using TiO_2 as photocatalyst. With the assistance of Fresnel lens (39.5 cm L*39.5 cm W*2 mm T, Fresnel circle width: 0.5 mm, Facet depth: 0.2 mm, Fresnel circles: 395), solar light intensity (UV_{a+b}) were increased approximately 1.86 to 2.34 times and the temperature of wastewater could be raised about 5 ˚C. Hence, the degradation efficiency of phenol wastewater were increased 12.4%, 6.29%, 19.18%, and 2.72% in autumn, winter, spring, and summer season, respectively as compared to that without Fresnel lens. Moreover, the molecules of phenol were more efficiently decomposed into hydroquinone, p-benzoquinone and low-molecular-weight organic acids which were further mineralized into CO_2 and H_2O. The mineralization efficiency of phenol wastewater could reach almost 60% in summer season. Accordingly, it was showed that the Fresnel lens enhanced IPCC reactor would be a promising operation system for solar photocatalysis not only in effectively dealing with a large amount of industrial organic wastewater such as phenols wastewater, but also in the sector of energy conservation in terms of efficient utilization of solar energy for practical application.

Keywords: solar photocatalysis, phenol wastewater, inclined plate curvature channel reactor (IPCC), Fresnel lens

©2020. Japan Geoscience Union. All Right Reserved.

Solar photocatalysis of MeO wastewater with metal@TiO_2 film

*Ting-Yu Zeng[1], Ling-Syuan Tzeng[1], Wen-Shiuh Kuo[1]

1. National United University, Taiwan.

One of advanced oxidation processes (AOPs) - solar photocatalysis with novel Ag@TiO_2 film as catalyst for the treatment of an azo dye (methyl orange (MeO)) wastewater was investigated in this study. Ag@TiO_2 films were prepared successfully by a Dip-coating method and following by a photoreduction method on glass plate. The results of SEM/EDS analysis illustrated that Ag nanoparticles were partially and indeed deposited on the surface of TiO_2 film. The UV-VIS/DRS spectra showed that Ag@TiO_2 film could extend the absorption of TiO_2 film in visible light band, which reduced the defect that TiO_2 film could only absorb ultraviolet light band (λ <387 nm) and made it more efficient to use solar energy. The diagram of XRD analysis showed that Ag@TiO_2 film would not change the basic crystal structure of TiO_2 and the characteristic peak of Ag (2θ : 44.27^0) was observed. Under solar light irradiation (UV_{a+b}: 54.2 W/m^2), the abs@λ_{max} reduction efficiency and MeO molecular degradation efficiency of MeO wastewater (10 mg/L) were more than 90%. Moreover, the results showed that the optimal addition ratio of Ag was 0.5%(w/w) on TiO_2 film and an increase of 1.39 times of the abs@λ 464 nm reduction rate and 1.36 times of MeO degradation rate were achieved for using Ag(0.5%)@TiO_2 film as compared to use TiO_2 film, respectively. Increasing the light irradiation was found to be beneficial to enhance the formation rate of hydroxyl radicals and then promoted the oxidation reaction rate. Increasing the temperature of wastewater from 15 ^{0}C to 25^{0}C could improve the degradation efficiency of MeO which was probably resulted from increasing the frequency of collision between hydroxyl radicals and MeO molecules. However, the enrich effect of wastewater temperature was limited as compared to that of light intensity. In addition, a little lower MeO degradation rate was observed with the reuse of Ag@TiO_2 film. Accordingly, the feasibility of solar photocatalsis using Ag@TiO_2 film for the treatment of dye wastewater was obvious.

Keywords: Solar Photocatalysis, MeO, Ag@TiO2 film

©2020. Japan Geoscience Union. All Right Reserved.

Effects of fine content on mechanical properties of recycled concrete aggregates for unbound road base materials in Vietnam

*Thai Hong Nam[1], Akira Kato[1], Takeshi Saito[1], Ken Kawamoto[1]

1. Graduate School of Science and Engineering, Saitama University

Unbound aggregates crushed from natural rock such as limestone, granite are the most popular materials used to construct the base of the pavements. However, nowadays the resources of natural materials have been increasingly exhausted while the demand for using aggregates in road construction has been increasing due to economic growth and rapid urbanization. Currently, construction and demolition waste (CDW) generated in urban areas in Vietnam is not fully recycled and is used on- and/or off-site for landfilling and ground leveling without the quality control of materials. Besides, some of CDW has been being dumped along a road or river, or in a pond for landing illegally. Therefore, the utilization of CDW for recycling is a crucial issue to reduce the generation amount of CDW and consumption of natural resources.
There were many studies on various factors that affect the mechanical properties of recycled concrete aggregates (RCA). Among of the factors, the fine content influences significantly on the mechanical properties of unbound aggregate road base and subbase. However, the effect of fine content (F in wt.%; typically, with particle size less than 0.075 mm) has not been fully evaluated quantitatively. This study focused on the effect of F on the compaction properties and California Bearing Ratio (CBR) of the RCA base. The samples with the maximum particle size of 25mm, and four different F values, i.e. 0, 5, 10, and 20 %, were prepared and their test results were compared to the current Vietnamese standard. The experimental results showed that the maximum dry density reached highest value with F of 5-10%. Except for the tested sample with F of 20%, the measured CBR values with F of 0, 5, and 10% satisfied the technical requirements of Vietnamese standards, i.e. CBR over 100.

Keywords: Base, Recycled Concrete Aggregate (RCA), fine content, compaction, California Bearing Ratio (CBR)

©2020. Japan Geoscience Union. All Right Reserved.

Development of filtering materials for removing heavy metals utilizing industrial by-products

*Akito Ujiie[1], Buddhika Bandara[1], Akihiro Matsuno[1], Takeshi Saitou[1], Ken Kawamoto[1]

1. Saitama university

In developing countries, waste materials including industrial by-products are often dumped directly without any segregation and treatment. The amount of discharge is significantly increasing and segregation and treatment of these materials are essentially needed. From waste materials, harmful substances such as heavy metals can leach, causing soil and groundwater pollutions. To solve these problems, cost effective filter materials for removing harmful heavy metals were developed utilizing industrial by-products. This study also contributes to increase additional values for waste materials. For development of filter materials, AAC (Autoclaved Aerated Concrete) and SS (Steel Slag) were selected and column tests using only AAC and mixture material of AAC and SS were carried out to evaluate their adsorption capacities for Pb^{2+} and Cd^{2+}. As a result, AAC adsorbed almost 100% of Pb^{2+} from the Pb^{2+} solution (100 ppm), but, it did not adsorb Cd^{2+} much from the Cd^{2+} solution (100 ppm). On the other hand, the mixture material of AAC and SS adsorbed almost 100% of each heavy metal (100 ppm). It also adsorbed almost 100% of both Pb^{2+} and Cd^{2+} simultaneously from their mixed solution (Cd: 50 ppm and Pb: 50 ppm). These results suggested that the mixture of AAC and SS can be applied as cost effective filter materials for removing heavy metals.

Keywords: heavy metals, filter materials, industrial by-products, adsorption, column test

©2020. Japan Geoscience Union. All Right Reserved.

Effects of Silicic Acid on Arsenite Leaching from Spent Calcium-Based Arsenic Adsorbents

*Hajime Sugita[1], Terumi Oguma[1], Ming Zhang[1], Junko Hara[1], Yoshishige Kawabe[1]

1. National Institute of Advanced Industrial Science and Technology

The spent adsorbents after arsenic removal in arsenic contaminated water itself contain a large amount of arsenic. If they are discarded without appropriate treatment, there is a concern that secondary arsenic pollution may occur due to arsenic leaching from them. In our previous studies, it was suggested silicic acid greatly affects leaching behavior of arsenate from the spent adsorbents. In this study, in order to examine the effects of silicic acid on arsenite leaching from the spent adsorbents, leaching tests with silicic acid solution and 2 kinds of spent calcium-based adsorbent (CaO and $Ca(OH)_2$) were carried out. This study revealed that when the initial silicic acid concentration in solution is high, the leaching of arsenite is also inhibited as in the case of arsenate. This was inferred that when the silicic acid component in the solution reacted with the calcium component eluted from the spent adsorbents to form the calcium silicate species, the arsenite component leached from the spent adsorbents was taken into the products.

Keywords: Arsenite Leaching, Spent Adsorbent, Calcium Oxide, Calcium Hydroxide, Silicic Acid

©2020. Japan Geoscience Union. All Right Reserved.

[E] Poster | A (Atmospheric and Hydrospheric Sciences)：A-GE Geological & Soil Environment

[A-GE42] Interactions between Earth Critical Zone Hydrogeological Processes and Ecosystem

convener:Wang Wenke(Chang'an University), Yaqian Zhao(Xian University of Technology), Jet-Chau Wen(National Yunlin University of Science and Technology), Ming Zhang(Institute for Geo-Resources and Environment, Geological Survey of Japan, AIST)

This session provides a broad platform for the discussion and presentation of fundamental and up-to-date scientific results related to near-surface, earth critical zone hydrogeological processes, ecological system, and interactions between them. Presentations on but not limited to the research topics targeted to arid and semiarid regions are especially welcome. In addition, presentations on related research areas, such as climate change, environmental conservation, ecological risk assessment, water resource management, sand control and desert greening are also encouraged.

[AGE42-P01] The Impact of LSTM Network Structure on Flood Process Simulation and Forecast Period: A Case Study of the Middle Yellow River

★Invited Papers

*Caihong Hu[1] (1.school of water conservancy science and engineering, zhengzhou university, Zhengzhou city, Henan Province, P.R.China, 450001)

[AGE42-P02] CHARACTERIZATION OF WATER RETENTION AND HYDRAULIC CONDUCTIVITY PROPERTIES FOR GRADED RECYCLED AGGREGATES BLENDED WITH AUTOCLAVED AERATED CONCRETE GRAINS IN VIETNAM

*Nam Pham Van[1], Akira KATO[1], Akihiro MATSUNO[1], Hoang Giang NGUYEN[2], Van Tuan NGUYEN[2], Takeshi SAITO[1], Ken KAWAMOTO[1,2] (1.Graduate School of Science and Engineering, Saitama University, Japan, 2.National University of Civil Engineering, Vietnam)

[AGE42-P03] UTILIZATION OF CONSTRUCTION aND DEMOLITION WASTE (CDW) AND INDUSTRIAL BY-PRODUCTS(IBPS) AS LOW-COST LIMING AGENTS FOR NEUTRALIZATION OF SOIL ACIDITY

*Isiri Upeksha Nagasinghe[1], Takeshi Saito[1], Akihiro Matsuno[1], Akira Kato[1], Ken Kawamoto[1] (1.Department of Civil and Environmental Engineering, Graduate School of Science and Engineering, Saitama University, Japan)

[AGE42-P04] Estimation of Coastal Aquifer Properties Using Multiple-Frequency Ocean Tides

*Ming Zhang[1], Ling Yang[2], Yonghong Hao[2], Zhixue Zhao[2], Tongke Wang[2] (1.Institute for Geo-Resources and Environment, Geological Survey of Japan, AIST, 2.Tianjin Normal University)

The Impact of LSTM Network Structure on Flood Process Simulation and Forecast Period: A Case Study of the Middle Yellow River

*Caihong Hu[1]

1. school of water conservancy science and engineering, zhengzhou university, Zhengzhou city, Henan Province, P.R.China, 450001

Flood forecasting is an important non-engineering measure for flood prevention and disaster reduction. Recently, owing to the breakthrough in the field of computational science, neural network technology based on deep learning have received a growing interest from scientists. The Long Short-Term Memory (LSTM) neural network, one of the most advanced applications of deep learning technology, is applied to rainfall runoff simulation in the hydrological field. Most previous studies focused on verifying the feasibility of LSTM in hydrological forecasting. This paper explores the effects of LSTM network structure on flood process simulation and forecast period by constructing LSTM models with different network structures. The hydrological situation in the middle reaches of the Yellow River has changed significantly in the past 50 years. Jingle station control basin in the upper reaches of the Fenhe River is selected as the case study, which including 98 flood events from 1956 to 2014. The datasets of 1954-2003 was selected as the training sets and the dataset of 2003-2014 was selected as the verified set. The results show that, on the one hand, the prediction effect decreases with the increase of the foresight period. The LSTM simulation effect is the best when the foresight period is 1h. The number of cells and the cycle index are 120 and 200 respectively. The Nash-Sutcliffe efficiency (NSE) coefficient reaches 0.9958, Root Mean Square Error (RMSE) reaches 10.1595, BIAS reaches 0.5575%, and the allowable errors of flood peak forecast and peak time forecast were within 5% and 1h, respectively. At this time, LSTM has a perfect performance in flood forecasting; when the forecast period is 1-6h, the number of cells and the cycle index are 140 and 300 respectively, NSE reaches 0.8857, RMSE reaches 39.0867, BIAS reaches 10.5886%, and the allowable errors of flood peak forecast and peak time forecast are within 10% and 6h, respectively, which meet the allowable errors of flood forecast. When the forecast period exceeds 6h, NSE is lower than 0.8, RMSE is higher than 50, BIAS is higher than 15%, and the forecast error of peak time exceeds the length of a calculation period, and it does not have the ability to forecast floods. On the other hand, as far as the forecast period is selected as 1h, both the number of cells and the cycle index in the network structure are positively correlated with simulation accuracy. At first, when the network structure is simple which has 20 cells and 50 cycles index, the NSE is not higher than 0.5. As the number of cells and cycle index increase at the same time, the simulation accuracy increases rapidly. The NSE stabilizes until the number of neurons and the number of iterations reach 120 and 200, respectively. The reason is that the more cells cause the model more complex which can learn more features of data. By increasing the cycle index, the more the model updates the parameters, the better the simulation effect. In summary, LSTM can be used for short-term flood forecasting in the middle reaches of the Yellow River. It is recommended to use LSTM for flood process simulation when the forecast period is selected as 1h. The effect is best when the number of cells and the cycle index are selected as 120 and 200, respectively.

Keywords: LSTM;, network structure; , rainfall-runoff simulation; , middle Yellow River

©2020. Japan Geoscience Union. All Right Reserved.

CHARACTERIZATION OF WATER RETENTION AND HYDRAULIC CONDUCTIVITY PROPERTIES FOR GRADED RECYCLED AGGREGATES BLENDED WITH AUTOCLAVED AERATED CONCRETE GRAINS IN VIETNAM

*Nam Pham Van[1], Akira KATO[1], Akihiro MATSUNO[1], Hoang Giang NGUYEN[2], Van Tuan NGUYEN[2], Takeshi SAITO[1], Ken KAWAMOTO[1,2]

1. Graduate School of Science and Engineering, Saitama University, Japan, 2. National University of Civil Engineering, Vietnam

Permeable pavement systems (PPS) play a crucial role in contribution for reducing surface runoff during heavy rainfall (flood control) and mitigating road surface temperature (reduction in urban heat island).The purpose of this study is to improve water retention capacity for recycled road-base materials blending with autoclave aerated concrete (AAC) grain and to evaluate the effect of mixing proportion of AAC grains on water retention and hydraulic conductivity properties. Graded recycled concrete aggregate (RCA; 0.075-37.5 mm) and fired-clay brick (RCB; 0.075-37.5 mm) made from construction and demolition waste (CDW) masonry which was taken from the CDW dumping site in Vietnam and the graded recycled aggregates were blended with AAC grains (0.106-2 mm) from Vietnam in this study. A comprehensive laboratory evaluation of water retention and hydraulic conductivity characteristics of recycled CDW materials was carried out. The results showed that the mixing of AAC grains contributed highly to increase water retention capacity and hydraulic conductivity for both graded RCA and RCB.

Keywords: Recycled construction and demolition waste, Masonry, Autoclaved aerated concrete, Water retention capacity, Hydraulic conductivity

©2020. Japan Geoscience Union. All Right Reserved.

UTILIZATION OF CONSTRUCTION aND DEMOLITION WASTE (CDW) AND INDUSTRIAL BY-PRODUCTS(IBPS) AS LOW-COST LIMING AGENTS FOR NEUTRALIZATION OF SOIL ACIDITY

*Isiri Upeksha Nagasinghe[1], Takeshi Saito[1], Akihiro Matsuno[1], Akira Kato[1], Ken Kawamoto[1]

1. Department of Civil and Environmental Engineering, Graduate School of Science and Engineering, Saitama University, Japan

There are acidic soils widespread all over the world. Soil acidity has a greater potential to adversely impact on soil microorganisms, plant growth, deteriorating soil structure, heavy metal leaching and degradation of infrastructure. Liming has long been identified as a promising method to address the soil acidity. The most common liming agent is $CaCO_3$, which is received from natural resources. If it is possible to use alternative materials having alkaline property, it would preserve natural reserves of $CaCO_3$. Construction and demolition waste (CDW) and industrial by-products (IBPs) show alkaline property. If CDW and IBPs could neutralize the soil acidity, it would be a sustainable solution for the waste to be dumped into landfills too. Therefore, this study was carried out to evaluate the applicability of CDWs and IBPs for neutralization of soil acidity. Volcanic ash soil (VAS), laterite (L) and marine sediment (MS) were used as acidic geomaterials for neutralization. Their pH was 5.5, 4.9 and 4.8, respectively. The selected CDW was recycled concrete (RC) and, autoclaved aerated concrete (AAC) and IBPs were steel slag (SS), and fly ash. Two particle sizes (less than 0.106 mm and 0.106 - 2.00 mm) were used for SS, RC, and AAC. To compare the neutralization capacities of alternatives, typical liming agents of $CaCO_3$, $Ca(OH)_2$, and CaO were also tested. Liming agent was gradually added to each geomaterials until they become neutralized. The best neutralization capacity was shown by finer fraction of SS. 1.8%, 0.4%, and 0.5% weight of the finer SS neutralized VAS, L, and MS, respectively. Neutralization capacity of $CaCO_3$ was very similar to the finer fraction of SS. Thus, it is revealed that there is a potential of applying of CDW and IBPs as alternative liming agents. Nonetheless, it is necessary to evaluate the leaching of harmful chemical components including heavy metals from neutralized soils to soil and groundwater.

Keywords: Acidic soil, neutralization, construction and demolition waste , industrial by-products (IBPs), liming agents

©2020. Japan Geoscience Union. All Right Reserved.

Estimation of Coastal Aquifer Properties Using Multiple-Frequency Ocean Tides

*Ming Zhang[1], Ling Yang[2], Yonghong Hao[2], Zhixue Zhao[2], Tongke Wang[2]

1. Institute for Geo-Resources and Environment, Geological Survey of Japan, AIST, 2. Tianjin Normal University

Determination of the hydraulic properties of coastal aquifer systems has important implications that cover a number of research topics, such as seawater intrusion, submarine groundwater discharge, migration of contaminants, assessment of water resources, and geotechnical engineering. Although many theoretical solutions have been developed over recent decades, most of them assume that an aquifer system extends inland and subjected a single-frequency tidal fluctuation on coastline boundary. In addition, only one hydraulic parameter, i.e., the hydraulic diffusivity, a ratio of transmissivity to storage coefficient, of an aquifer can be obtained in most cases.

Considering more realistic conditions, the solution of groundwater response in a leaky confined coastal aquifer to dual frequency tidal fluctuations has been developed as an example. The solutions for a perfectly confined aquifer and single-frequency tidal fluctuations can be considered as special cases of the newly developed, generalized solution. The transport of ocean tides through a leaky confined aquifer depends on both the hydraulic diffusivity of the aquifer and leakage of semi-impermeable aquitard overlapped on it. Ocean tides could only transport to a limited distance towards inland if the hydraulic diffusivity is low and/or the leakage is large. Cautions should be excised that both earth tides and changes in local atmospheric pressure may induce similar tidal fluctuations in hydraulic head within an inland monitoring well. Both the hydraulic diffusivity and leakage can be identified from the monitored, time-depended fluctuations of hydraulic head detected with reliable accuracies. By incorporating the use of aquifer thickness that can be determined independently from observation of core materials during drilling of a monitoring well, both the transmissivity and storage coefficient of a perfectly confined aquifer or a confined aquifer with small leakage can be simultaneously estimated. The findings obtained from this study may provide a better understanding of using ocean tides for determining the hydraulic properties of coastal aquifer systems and a practical example for examining the applicability and/or limitations of the tidal method.

Keywords: Coastal Aquifer , Hydraulic properties, Tidal method, Mutiple-frequency

©2020. Japan Geoscience Union. All Right Reserved.

[E] Poster | A (Atmospheric and Hydrospheric Sciences)：A-GE Geological & Soil Environment

[A-GE43] Extending Hydropedology- -in memory of Professor Henry Lin

convener:Kosuke Noborio(Meiji University), Yasushi Mori(Graduate School of Environmental and Life Science, Okayama University)

To commemorate Prof. Henry Lin of Pennsylvania State University who passed away at the age of 54 on September 26, 2019, we intend to extend interdisciplinary hydropedology with hydrology and pedology that he proposed in his life. We expect presentations from the interdisciplinary fields. Of course, presentations on water transfer in soil are also welcome.

[AGE43-P01] History of Hydropedology and perspectives

*Kosuke Noborio[1] (1.Meiji University)

[AGE43-P02] Simulation of Water Harvesting with a Sand Ditch using WASH_2D

*Haruyuki Fujimaki[1], Majed Abu-Zreig[1] (1.Arid Land Research Center, Tottori University)

[AGE43-P03] Hydraulic properties of clay loam paddy soils in Japan.

*Taku Nishimura[1], Shoichiro Hamamoto[1] (1.Deptartment of Biological and Environmental Engineering, Graduate School of Agricultural and Life Sciences, University of Tokyo)

[AGE43-P04] Cosmic-Ray Neutron Sensing for Measuring Soil Water Content at Area Wide Scale: Case Study at IAEA and Future Collaboration

★Invited Papers

*Ammar Wahbi[1], Trenton Franz[2], Hami Said Ahmed[3], Lee Kheng Heng[3], Peter Strauss[4], Hisashi Tsujimoto[1], Haruyuki Fujimaki[1] (1.Arid Land Research Center, Tottori Univeristy, Tottori, Japan, 2.School of Natural Resources, University of Nebraska-Lincoln, Nebraska, USA, 3.Soil and Water Management & Crop Nutrition Subprogramme, Joint FAO/IAEA Division of Nuclear Techniques in Food and Agriculture, International Atomic Energy Agency, Vienna, Austria, 4.Institute for Land and Water Management Research, Federal Agency for Water Management Austria, 3252 Petzenkirchen, Austria)

[AGE43-P05] Relationship between GPS signal and soil volume moisture content / electrical conductivity

*Natsumi Naganuma[1], Shinsuke Aoki[2], Tetsushi Ikegami[3], Kosuke Noborio[4] (1.Graduate School of Agriculture, Meiji University, 2.Institute of Soil, Water, and Environmental SciencesAgricultural Research, The Volcani Center, 3.School of Science and Technology, Meiji University, 4.School of Agriculture, Meiji University)

[AGE43-P06] Reviewing the EC Temperature Calibration Equations and Tracing Two Dimensional Distribution of Soil Nutrients.

*Yuki Sunakawa[1], Satoko Fujita[2], Yuki Ito[3], Shinsuke Aoki[4], Kosuke Noborio[2] (1.Graduate School of Agriculture, Meiji University , 2.School of Agriculture, Meiji University, 3.Gilat Research Center, Agricultural Research Organization, Israel, 4.Institute of Soil, Water, and Environmental Sciences Agricultural Research, The Volcani Center, Israel)

[AGE43-P07] Case study of current status and issues of new entrant apple farmers in Nagano Prefecture

*Takamitsu Kai[1] (1.Meiji University)

History of Hydropedology and perspectives

*Kosuke Noborio[1]

1. Meiji University

Hidropedology was first proposed by Professor Henry Lin in 2003. He defined Hidropedology as an intertwined branch of soil science and hydrology that embraces interdisciplinary and multiscale approaches for the study of interactive pedologic and hydrologic processes and properties in the earth’s critical zone. He hosted the First International Hydropedlopgy Conference in 2008 at Pennsylvania State University. In 2012 he edited a book entitled Hydropedology, which was published by Academic Press. He hosted two more International Hydropedology Conferences. The fourth is scheduled to be held in Australia in 2020, but he cannot make it. He passed away on September 26, 2019 at the age of 54. His idea of the interdisciplinarity should be inherited and extended into soil physics as well.

Keywords: soil, water, interdisciplinary

©2020. Japan Geoscience Union. All Right Reserved.



©2020. Japan Geoscience Union. All Right Reserved.

Simulation of Water Harvesting with a Sand Ditch using WASH_2D

*Haruyuki Fujimaki[1], Majed Abu-Zreig[1]

1. Arid Land Research Center, Tottori University

Capture of surface runoff by constructing ditches has been widely practiced. Filling the ditch with sands may be useful to conserve its shape and minimize area for ditch. Through a series of laboratory experiment, we have confirmed the effect of a sand ditch to enhance groundwater recharge. To optimize design such as width, depth, and spacing under various combinations of soil and climate, numerical model may be applied to save time and cost for experiments. The purpose of this study was to incorporate surface runoff process into a numerical model to solve two-dimensional water flow and solute movement, WASH_2D, and demonstrate its performance in a numerical experiment. We employed the Manning equation which presents overland flow velocity as square root of hydraulic gradient, caused by slope of ground surface and/or non-uniform depth of standing water. Results of the numerical experiments matched with experimental results: enhanced downward drainege, enhanced storage by surrounding soil and prevention of run off beyond the sand ditch. The modified WASH_2D is now ready to be applied to optimize design of sand ditches.

©2020. Japan Geoscience Union. All Right Reserved.

Hydraulic properties of clay loam paddy soils in Japan.

*Taku Nishimura[1], Shoichiro Hamamoto[1]

1. Deptartment of Biological and Environmental Engineering, Graduate School of Agricultural and Life Sciences, University of Tokyo

Introduction

Paddy rice is a typical agricultural practice in monsoon Asian countries such as Japan. Historically, paddy fields adopted to wet soil conditions such as low land and high precipitations. Since it was assumed paddy field is ponding during cropping season, unsaturated soil properties such as water retention and unsaturated hydraulic conductivity had not been a topic of science in paddy soils. However, recent agricultural practices i.e. direct seeding and winter sowing of rice may be affected by soil moisture condition of spring before surface water ponding.

Methods and Materials

We choose 11 experimental sites. Four of them are clay loam soil (CL) and rest of five soils were boundary of either clay loam-sandy clay loam (SCL) or clay loam-light clay (LiC). Rest of two soils were still CL but had distinctly more clayey. Soil moisture sensors were varied at a depth of 5 and 10 cm and soil temperature and moisture were monitored. Besides, undisturbed and disturbed soil samples were taken and texture, dry bulk and particle densities, and saturated hydraulic conductivity were measured. For soil water retention, sand box was employed for high matric potential range, 0 to -6 kPa. Evaporation method by Hyprop (Meter Environment, Inc.) was employed for middle range of matric potential such as higher than approximately -40 kPa. Also, water content at -101.3 kPa by pressure plate and at smaller than -200 kPa by psychrometer (WP4, Meter Environment, Inc.) were used as supplementary for low matric potential range. In addition to the measurement, water retention curve of each soil was predicted using soil texture and dry bulk density by Rosetta model (Schaap et al., 1998) and SolphyJ database combined with RETC (Kato and Nishimura, 2016).

Results and Discussion.

Water retention measured by sand box often showed smaller water contents. Still the reason is not clear however, in comparison with porosity it could be underestimation of water retention. Thus, we omitted the results of sand box for further discussion.

Even for the same texture water retention varied a lot. Within the one texture class, LiC and CL soils, water retention curves of soils in both texture class were very different. Natural factor such as soil type and mineralogy, and artificial effect such as tillage practice could affect the hydraulic property.

Distinctly low matric potential, i.e. smaller than -100 kPa, is important to discuss growth of plant. For this matric potential range, water retention predicted by Rosetta model agreed well with the measured water retention curves, even though there was large discrepancy in high matric potential range. SolphyJ combined with RETC could consider information of soil type more than Rosetta model, however, it could not evaluate water retention of the eleven experimental well. So only for assessing draught risk for spring germination, prediction of water retention from dry bulk density and soil texture may be usuful.

©2020. Japan Geoscience Union. All Right Reserved.

As mentioned above, soil texture of the nine experimental sites are very similar. However, small difference in texture could affect soil moisture conditions. According to the soil monitoring data, three experimental sites with soil texture of either SCL or SiCL were suffered from very low soil water matric potential during early spring. This could inhibit sprout of germinated seeds. This trend was rarely observed the other experimental sites with CL and LiC soils.

This study was supported by Research Program on Development of Innovative Technology, BRAIN, NARO (Leader: Hiroyuki, Shimono). We would send deep appreciation to project members who maintained this experiment at 11 study sites and Mr. Baba Toshiki and Ms. Isumi Kyoko of UTokyo.

Keywords: Pedo transfer function, water retention, clay loam, paddy field

©2020. Japan Geoscience Union. All Right Reserved.

Cosmic-Ray Neutron Sensing for Measuring Soil Water Content at Area Wide Scale: Case Study at IAEA and Future Collaboration

*Ammar Wahbi[1], Trenton Franz[2], Hami Said Ahmed[3], Lee Kheng Heng[3], Peter Strauss[4], Hisashi Tsujimoto[1], Haruyuki Fujimaki[1]

1. Arid Land Research Center, Tottori Univeristy, Tottori, Japan, 2. School of Natural Resources, University of Nebraska-Lincoln, Nebraska, USA, 3. Soil and Water Management & Crop Nutrition Subprogramme, Joint FAO/IAEA Division of Nuclear Techniques in Food and Agriculture, International Atomic Energy Agency, Vienna, Austria, 4. Institute for Land and Water Management Research, Federal Agency for Water Management Austria, 3252 Petzenkirchen, Austria

General circulation models predict that annual rainfall rates in many countries will decline by the end of the century. Coupled with population growth, there will be stiff competition for water resources. It is therefore important that new and advanced irrigation technology be developed to help mitigate this challenge. Currently, 40% of global food production comes from irrigated areas that account for only 20% of the cultivated land. Regrettably, water use efficiency in many irrigated systems around the globe is less than 50%, as most of the applied water does not go towards plant transpiration. Hence, there is an urgent need for improvement in the efficiency with which irrigation water is applied to secure sufficient water for both humans and the ecosystem. One critical gap is the disconnection between current techniques for measuring soil moisture at plot-scale with water (and fertilizer) decisions often for larger areas. This difference in scale creates uncertainty and thus inefficiency in water resource management. To overcome this pressing challenge, the Joint FAO/IAEA Division of Nuclear Techniques in Food and Agriculture, the University of Nebraska (USA) and the Federal Agency of Water Management (Austria) have helped advance the nuclear technique (Cosmic-Ray Neutron Sensor, CRNS) that measures soil moisture over large area scale, compared with point sensor, by counting naturally occurring low-energy neutrons in the air above the selected area. The neutrons are created by incoming cosmic rays, providing an average soil moisture measurement over a ~10 ha of circle area and a depth of ~30 cm. The CRNS technique is a nuclear technique that does not need a radioactive source, with low power consumption, allowing for either stationary or mobile measurements.

There are 3 types of the devices, stationary which stay in place and can provide reading every one hour, backpack which can move in areas difficult to access and read few minutes, while rovering which is carried by a vehicle at low speeds and measures every minute. The last two are used for two- or three-dimensional heterogeneity mapping to measure the soil water content within the footprint.

The data of CRNS are freely available with about 70 devices in USA, and over 200 in independent networks around the world (mainly in developed countries), with additional data sets from developing countries in recent years.

In this study, we highlighting the research investigated and carried out by the Joint FAO/IAEA Division of the International Atomic Energy Agency using CRNS.

The research conducted at several studied sites in Austria. The Petzenkirchen study which is within the Austrian Institute for Land and Water Management Research, with heterogeneity cropping, employing stationary CRNS, has been established in Dec.2013 and it provides major dataset for this study, although we also used the backpack for short times. It represents a small watershed in a hilly area of northern foot

©2020. Japan Geoscience Union. All Right Reserved.

slopes of the Alps. Also, we used the backpack in Grabenegg (which is 5 km away from Petzenkirchen, and has a homogeneity cropping pattern). Apart from that short-term measurement campaigns were carried out using backpack CRNS in alluvial plain east of Neusiedler See Lake and in mountainous areas of Rauris Municipality, at different heights, in the central part of Austrian Alps. This study describes the results and interpretation of about 7 years of soil moisture data set (2013-2020).

In this study, we will present the calibration and validation of CRNS and illustrate the future research and constraints using this technology. We will also highlight future collaboration possibilities with institutions in Japan.

Keywords: Cosmic-ray neutron sensor, Soil water content, Dry land, Irrigation, IAEA, Austria

©2020. Japan Geoscience Union. All Right Reserved.

Relationship between GPS signal and soil volume moisture content / electrical conductivity

*Natsumi Naganuma[1], Shinsuke Aoki[2], Tetsushi Ikegami[3], Kosuke Noborio[4]

1. Graduate School of Agriculture, Meiji University, 2. Institute of Soil, Water, and Environmental SciencesAgricultural Research, The Volcani Center, 3. School of Science and Technology, Meiji University, 4. School of Agriculture, Meiji University

In the field of agriculture, we focused on the development of measurement methods to determine the appropriate irrigation water and fertilizer rates. Since 1980, the TDR water sensor, TDT water sensor and capacitance water sensor have been the mainstream of measurement methods because they enable nondestructive and continuous measurement of soil moisture and electrical conductivity. However, these methods have poor spatial representation. Therefore, we tried to estimate the soil moisture content using electromagnetic waves from a GPS satellite in the same 1GHz frequency band as the TDR water sensor. The purpose of this study was to clarify the relationship between the reflected signal received by an inexpensive GPS receiver and the soil water content and soil electrical conductivity.
We experimented at Kurokawa Farm in Meiji University in Kawasaki City, Kanagawa Prefecture. The experimental period is from November 22, 2018 to December 31, 2019. We calculated amplitude B and the phase of the complex reflection coefficient from the reflected signal and compared with the volumetric water content and soil electrical conductivity.

Keywords: Satellite, Sigbal to Noise Ratio

©2020. Japan Geoscience Union. All Right Reserved.

Reviewing the EC Temperature Calibration Equations and Tracing Two Dimensional Distribution of Soil Nutrients.

*Yuki Sunakawa[1], Satoko Fujita[2], Yuki Ito[3], Shinsuke Aoki[4], Kosuke Noborio[2]

1. Graduate School of Agriculture, Meiji University , 2. School of Agriculture, Meiji University, 3. Gilat Research Center, Agricultural Research Organization, Israel, 4. Institute of Soil, Water, and Environmental Sciences Agricultural Research, The Volcani Center, Israel

It is essential to control soil nutrient balance to gain an identical yield of crops. As an indicator of the amounts of soil nutrients, electrical conductivity (EC) is commonly used. Since EC depends on solution temperature, ECw25, which is EC of the solution whose temperature is 25 ℃, is used as a comparison criterion. To correct EC to ECw25, some calibration equations were developed like USDA Salinity Laboratory’s equation or Heimovaara’s equation. However, less attention has been paid for the accuracy of these equations. Therefore, the first objective of this study was reviewing the accuracy of the USDA Salinity Laboratory’s equation or Heimovaara’s equation. Because there is a linear relationship between EC and each dissolved ion when the ion concentration is low, each ion’s distribution can be traced by estimating ion concentration from EC. The second objective of this study was to determine soil nutrient’s two-dimensional distribution under a drip irrigation system. TDR method was used to measure EC of soil columns, which were put in an incubator. High EC conditions (ECw25 was about 400 mS m-1), and low EC conditions (ECw25 was about 150 mS m-1) were tested. The temperature of the incubator was changed from 10 ℃ to 50 ℃. When EC was high, the two equations corrected the EC well. However, when EC was low, the correction of two equations was not accurate, especially at low temperatures. It might be necessary to use different EC calibration equation depends on EC value and temperature of the solution. We modified Heimovaara’s equation for low EC conditions. From June 8th, 2019 to July 31st, 2019, volumetric water content and EC were measured with the TDR method, and soil temperature was measured with thermocouples in bell pepper grown drip-irrigated field. Soil samples were collected to measure its EC and chemical concentration with EC meter and ion analyzer, respectively. We will report how EC changed and each nutrient transported during the measurement period.

Keywords: TDR method, Electrical Conductivity (EC), Nutrients Distribution

©2020. Japan Geoscience Union. All Right Reserved.

Case study of current status and issues of new entrant apple farmers in Nagano Prefecture

*Takamitsu Kai[1]

1. Meiji University

In Japan's agriculture, the retirement of elderly farmers is expected to increase in the future, so they will be able to use them effectively on degraded farmland and farmland of farmers without successors and become human resources who will support Japan's agriculture in the future The urgent task is to secure new youth farmers and promote their establishment. Under these circumstances, the number of new farmers from 2014 to 2017 was 57,650, 65,030, 60,150 and 55,670.If new farmers under the age of 49 were limited, 21,860, 23,030, 22,050, 20,760 and 20,000 It has been maintaining more than people. The main reasons for this are that the government is promoting a system to support new employment of young people, such as the “employment of farming” and that the number of family-owned (sales farmers) is decreasing, but the number of organization-based entities is increasing. It is also possible that the number of workplaces that can farm as salaried workers has increased. In this study, a new self-employed farmer in the apple orchard in Nagano City, Nagano Prefecture, and a sales farmer aiming for the organic apple JAS certification. The current situation and issues of new farmers will be introduced, based on interviews with selling farmers and analysis results of apple orchard soil.

Keywords: Organic farming, Soil fertility, Soil microorganisms

©2020. Japan Geoscience Union. All Right Reserved.

[E] Poster | A (Atmospheric and Hydrospheric Sciences)：A-CG Complex & General

[A-CG44] Extratropical oceans and atmosphere

convener:Youichi Kamae(Faculty of Life and Environmental Sciences, University of Tsukuba), Toyama Katsuya(Meteorological Research Institute), Hyodae Seo(Woods Hole Oceanographic Institution), Yoshi N(Hokkaido University)

The extratropical ocean had been considered passive to atmospheric variability. Recent studies, however, revealed active roles of the extratropical ocean in modulating the atmosphere. The goal of this session is to deepen our understanding of the air-sea interaction in the extratropics. A wide variety of researches whose topics range from meso-scale to basin-scale interactions, and from daily to global warming timescales are welcomed. Researches on topics related to extratropical air-sea interaction, including cloud, aerosol, and ecosystem, are also welcomed.

[ACG44-P01] Seasonality and Regional Characteristics of Sea-Surface Wind Responses to Mesoscale SST Features assessed by Transfer Functions

*Ryusuke Masunaga[1], Niklas Schneider[1] (1.International Pacific Research Center, University of Hawaii)

[ACG44-P02] Ocean warming patterns and heavy rainfall over East Asia associated with atmospheric rivers

*Youichi Kamae[1], Wei Mei[2] (1.Faculty of Life and Environmental Sciences, University of Tsukuba, 2.University of North Carolina at Chapel Hill)

[ACG44-P03] Predictability of 2019 stratospheric sudden warming in the Southern Hemisphere and its impact of surface weather

*Hiroaki Naoe[1], Chiaki Kobayashi[1], Yayoi Harada[1], Yukiko Imada[1], Shuhei Maeda[1], Toshihiko Hirooka[2] (1.Meteorological Research Institute, 2.Kyusyu University)

[ACG44-P04] Interaction between a typhoon moving westward in western Japan and a cold vortex

*Mine Taisei[1], Yoshihiro Tachibana[1] (1.Faculty of Bioresources, Mie University)

[ACG44-P05] On the maintenance mechanisms for the wintertime subtropical high over the South Indian Ocean

*Ayumu Miyamoto[1], Hisashi Nakamura[1], Takafumi Miyasaka[1,2], Yu Kosaka[1], Bunmei Taguchi[3], Kazuaki Nishii[4] (1.Research Center for Advanced Science and Technology, The University of Tokyo, 2.Japan Meteorological Business Support Center, 3.School of Sustainable Design, University of Toyama, 4.Graduate School of Bioresources, Mie University)

[ACG44-P06] Surface velocity variation of the Kuroshio-Kuroshio Extension system -its relations with local monsoon winds-

*YUXIANG QIAO[1], Hirohiko Nakamura[2], Kako Shinichiro[3], Ayako Nishina[2] (1.The United Graduate School of Agricultural Sciences, Kagoshima University, 2.Faculty of Fisheries, Kagoshima University, 3.Graduate School of Science and Engineering, Kagoshima University)

[ACG44-P07] The potential impact of the 2014-2016 marine heat wave over the North Pacific on the atmosphere

*Kazuaki Nishii[1], Bunmei Taguchi[2], Hisashi Nakamura[3] (1.Graduate School of Bioresources, Mie University, 2. Faculty of Sustainable Design, University of Toyama, 3.Research Center for Advanced Science and Technology, The University of Tokyo)

Seasonality and Regional Characteristics of Sea-Surface Wind Responses to Mesoscale SST Features assessed by Transfer Functions

*Ryusuke Masunaga[1], Niklas Schneider[1]

1. International Pacific Research Center, University of Hawaii

Satellite observations have revealed that sea-surface temperature (SST) anomalies on a scale of 50–500 km exert significant influence on sea-surface winds. Warm (cold) SST anomalies act to accelerate (decelerate) surface winds. Recently, spectral transfer function approach, where the surface wind response is evaluated using linear regression coefficients on the wavenumber space, has been proposed to investigate the mesoscale air-sea coupling. In the present study, seasonality and regional differences of the wind responses are investigated by adopting the transfer function approach to the Gulf Stream, Kuroshio Extension, Southern Ocean regions based on satellite observations. Although structures of the transfer functions in the wavenumber space exhibit consistent characteristics between the ocean regions, their magnitude is found to be dependent on regions and seasons. When background winds are strong (weak), the mesoscale wind responses tend to be stronger in winter (summer). Furthermore, observed mesoscale wind fields are reasonably reconstructed from the transfer functions and observed SST, especially over the Southern Ocean domain. These results further support the validity of using transfer functions, and suggest that underlying dominant dynamics are ubiquitous over the globe.

Keywords: air-sea interaction, mesoscale

©2020. Japan Geoscience Union. All Right Reserved.

Ocean warming patterns and heavy rainfall over East Asia associated with atmospheric rivers

*Youichi Kamae[1], Wei Mei[2]

1. Faculty of Life and Environmental Sciences, University of Tsukuba, 2. University of North Carolina at Chapel Hill

Atmospheric rivers (ARs), narrow moisture transport bands developed over the mid-latitude oceans, have attracted much attention because they often cause natural disasters (flash flood, extreme wind) when they make landfall. Over East Asia, ARs explains 20-90% of heavy rainfall events occurred during warm seasons. On an interannual timescale, substantial fraction of East Asian AR frequency is explained by the Pacific and Indian Ocean SST variability, suggesting the potential predictability of seasonal AR-disaster risk. Recent studies suggested that the global SST rise under the global warming results in more occurrence of ARs due to increased water vapor content. In addition to the thermodynamic effect, change in atmospheric circulation associated with SST warming patterns may also increase AR-disaster risk over specific regions. We examine spatial patterns of change in AR-disaster risk under global warming using ensemble simulations assuming different ocean warming patterns. When we assume warm Indian Ocean during summer, an anomalous subtropical anticyclone over the western North Pacific results in an enhanced moist southwesterly over East Asia and more occurrence of ARs. In addition to the dynamic effect, warm condition over the East China Sea and the western North Pacific are also related to the enhanced AR activity over the western North Pacific. We further evaluate AR-related heavy rainfall using hourly model outputs and effects of ocean warming patterns.

Keywords: Atmospheric river, Global warming, Heavy rainfall

©2020. Japan Geoscience Union. All Right Reserved.

Predictability of 2019 stratospheric sudden warming in the Southern Hemisphere and its impact of surface weather

*Hiroaki Naoe[1], Chiaki Kobayashi[1], Yayoi Harada[1], Yukiko Imada[1], Shuhei Maeda[1], Toshihiko Hirooka[2]

1. Meteorological Research Institute, 2. Kyusyu University

This study analyzes observational features of displacement-type of minor sudden stratospheric warming (SSW) event that occurred in the Southern Hemisphere (SH) in September 2019 (SSW2019-SH). The predictability of SSW is also investigated examining the Japan Meteorological Agency operational 1-month and 6-month ensemble prediction data in comparison with the Japanese 55-year Reanalysis data. SSW events are rare in SH, with only two in recorded times - one in 2002 that is the first major (split-type) event and the other in 1988 classed as a minor warming. SSW2019-SH occurred under El Nino Modoki, westerly quasi-biennial oscillation together with solar minimum, positive Indian Ocean dipole, and phases 3-6 of the Madden-Julian oscillation. This SSW is characterized by the strongest Antarctic warming on record with a temperature increase of 70 K within 2 weeks, the strongest accumulated upward wave activity flux with zonal wavenumber 1 in July-August-September. The vertical profile of geopotential height anomalies averaged over the polar cap region illustrates the downward propagation of SH circulation anomalies from the stratosphere in September to the troposphere in late October. Months of October-December 2019 (the month of September) are marked by anomalously negative values (a positive value) of the southern annular mode (SAM) index. The negative SAM index is characterized by warm polar temperatures, high geopotential height over the polar cap, and weak circumpolar flow along 60˚S. Predictability of sea-level pressure anomalies averaged over 60-90S is usually about 10 days. However, this predictability is a little longer just after signals of such geopotential height anomalies or SAM index descend down from stratosphere to troposphere. Root-mean-square error, anomaly/pattern correlation coefficient between forecast and the reanalysis for diagnostics are investigated to measure the predictability skill of the model.

Acknowledgments
This research was supported by Grant-in-Aid (JP18K03748) for Science Research (KAKENHI) from the Ministry of Education, Culture, Sports, Science, and Technology of Japan.

Keywords: troposphere-stratosphere coupling, impact of surface weather, predictability, stratospheric sudden warming

©2020. Japan Geoscience Union. All Right Reserved.

Interaction between a typhoon moving westward in western Japan and a cold vortex

*Mine Taisei[1], Yoshihiro Tachibana[1]

1. Faculty of Bioresources, Mie University

Typhoon Jongdari (2018) made landfall near Ise, Mie Prefecture and proceed west through Western Japan.
This course of the typhoon was first time ever since records began in 1951.
We hypothesize that the abnormal course was controlled by a cold vortex in the south of Japan.
In this study, we focus on the interaction between the typhoon and the cold vortex, and we investigated whether the cold vortex affected the abnormal course of the typhoon.

Keywords: Typhoon, cold low

©2020. Japan Geoscience Union. All Right Reserved.

On the maintenance mechanisms for the wintertime subtropical high over the South Indian Ocean

*Ayumu Miyamoto[1], Hisashi Nakamura[1], Takafumi Miyasaka[1,2], Yu Kosaka[1], Bunmei Taguchi[3], Kazuaki Nishii[4]

1. Research Center for Advanced Science and Technology, The University of Tokyo, 2. Japan Meteorological Business Support Center, 3. School of Sustainable Design, University of Toyama, 4. Graduate School of Bioresources, Mie University

Over the South Indian Ocean, the subtropical Mascarene high exhibits a distinct seasonality from the other basins. While the high resides over the eastern portion of the basin in summer, the high resides over the western portion of the basin and its strength as a planetary-wave component is maximized in winter. The present study investigates the maintenance mechanisms for the wintertime subtropical high by using an atmospheric dynamical model and an atmospheric general circulation model.

We find that enhanced storm-track activity maintained by the Agulhas sea surface temperature (SST) front is important for the maintenance of the poleward portion of the subtropical high through the convergences of eddy heat and vorticity fluxes and the resultant acceleration of the climatological-mean westerlies on the poleward side of the high, as shown by the dynamical model experiments. The atmospheric general circulation model experiments further indicate that the Agulhas SST front acts to reinforce the high by energizing the storm-track activity.

The dynamical model experiments also reveal the remote influence from the tropics, especially the Asian summer monsoon region. The enhanced deep convection over the Asian summer monsoon region as well as the equatorial eastern Indian Ocean and western Pacific acts not only to shift the subtropical high westward but also to enhance mid-tropospheric subsidence and equatorward surface winds over the central and western portions of the subtropical South Indian Ocean. The induced subsidence acts to stabilize and dry the free troposphere, and the equatorward surface winds yield near-surface cold advection, both of which are favorable for the low-level cloud formation but unfavorable for the development of deep precipitating clouds. The resultant enhanced radiative cooling and reduced deep condensation heating can reinforce the equatorward portion of the subtropical high.

Keywords: subtropical high, storm track, South Indian Ocean, Asian summer monsoon

©2020. Japan Geoscience Union. All Right Reserved.

Surface velocity variation of the Kuroshio-Kuroshio Extension system -its relations with local monsoon winds-

*YUXIANG QIAO[1], Hirohiko Nakamura[2], Kako Shinichiro[3], Ayako Nishina[2]

1. The United Graduate School of Agricultural Sciences, Kagoshima University, 2. Faculty of Fisheries, Kagoshima University, 3. Graduate School of Science and Engineering, Kagoshima University

Our previous study focused on the decadal surface velocity variation over the entire Kuroshio-Kuroshio Extension (KE) current system, and found that such a variation is out of phase between the Kuroshio and KE. In another word, Kuroshio is strengthened (weakened) while KE is weakened (strengthened) for a decadal time scale. From our results, the above-mentioned phenomenon is caused by the climate oscillation such as Pacific Decadal Oscillation (PDO) through a remote process. The Sea Surface Height (SSH) anomalies excited by the PDO over the northeastern North Pacific and the area east of Philippines propagate to the Kuroshio-KE area, and then generate an opposite intensity variation between the Kuroshio and KE because of different propagation times. Following the above results, our present study focuses on the interannual surface velocity variation of the Kuroshio-KE system, and its relation with local monsoon. In order to pay attention to interannual modulation of the seasonal change, we investigate the yearly time series of the monthly Kuroshio-KE system velocity. Our preliminary result suggests that the interannual winter velocity variation of the Kuroshio has a significant correlation with the local winter monsoon. However, the interannual time-scale relation between the summer Kuroshio velocity variation and local summer monsoon is unclear.

Keywords: Kuroshio-Kuroshio Extension system, Interannual velocity variation, Monsoon

©2020. Japan Geoscience Union. All Right Reserved.

The potential impact of the 2014-2016 marine heat wave over the North Pacific on the atmosphere

*Kazuaki Nishii[1], Bunmei Taguchi[2], Hisashi Nakamura[3]

1. Graduate School of Bioresources, Mie University, 2. Faculty of Sustainable Design, University of Toyama, 3. Research Center for Advanced Science and Technology, The University of Tokyo

Anomalously warm anomalies of sea surface temperatures (SSTs) had been observed over the North Pacific, which is called the marine heat wave or the “blob”. One of the causes of the blob was weaker than normal wind associated with the anticyclonic circulation anomaly over the eastern North Pacific. We have conducted a series of ensemble experiments by using an atmospheric general circulation model (AGCM) to assess impacts of the blob on the atmospheric circulation. In the AGCM experiments forced by observed SSTs only over the extratropical North Pacific, a tropospheric anticyclonic circulation response is observed in the winter 2013-2014 over the Bering Strait, where an anticyclonic anomaly was actually observed. In the winter 2014-2015, a tropospheric anticyclonic circulation response is observed over western Canada, which is also consistent with the observation.

Keywords: Marine heat wave, AGCM

©2020. Japan Geoscience Union. All Right Reserved.

[E] Poster | A (Atmospheric and Hydrospheric Sciences)：A-CG Complex & General

[A-CG45] Multi-scale ocean-atmosphere interaction in the tropical Indo-Pacific region

convener:Yu Kosaka(Research Center for Advanced Science and Technology, University of Tokyo), Sang-Wook Yeh(Hanyang University), Takanori Horii(Research and Development Center for Global Change (RCGC), Strategic Research and Development Area, Japan Agency for Marine-Earth Science and Technology (JAMSTEC)), Hiroki Tokinaga(Disaster Prevention Research Institute, Kyoto University)

Tropical Indo-Pacific Oceans are home to ocean-atmosphere interaction on a broad range of spatio-temporal scales. Teleconnections induced by the tropical Indo-Pacific variability exert a significant imprint on global climate. Since the 1980s, in-situ and satellite observations, reanalysis products, and advancements in climate modeling have led to depicting various aspects of intraseasonal (e.g., MJO), interannual (e.g., ENSO and IOD) and decadal (e.g., IPO) variability in the tropical Indo-Pacific Oceans and their impacts on tropical (e.g., monsoons) and extratropical (e.g., storm track) climate. Newer studies find an active role of salinity in ocean-atmosphere interaction in the tropical Indian Ocean. Other recent studies highlight the inter-basin coupling between the tropical Pacific and the Indian Ocean in seasonal prediction of the Asian summer monsoon and decadal redistribution of ocean heat content associated with the so-called "hiatus" of global warming. Long term change in the Pacific Walker circulation has been recapturing attention in terms of the pattern effect of warming on climate feedback and sensitivity against radiative forcing as well as ENSO modulations under a warmer climate. A variety of processes are mutually interrelated and shape the climate, its variability, and change. To examine these challenging issues from various perspectives and foster understanding of the role of tropical air-sea interaction in the climate system, this session offers a forum to discuss recent progress in observational, modeling and theoretical studies of multi-scale tropical ocean-atmosphere interaction in the tropical Indo-Pacific Oceans.

[ACG45-P01] Diurnal cycles of precipitation and lightning in the tropics observed by TRMM3G68, GSMaP, LIS, and WWLLN

★Invited Papers

*Shoshiro Minobe[1], Jun Hyock Park[1], Katrina S. Virts[2] (1.Graduate School of Science, Hokkaido University, 2.The University of Alabama in Huntsville)

[ACG45-P02] Intermodel diversity in the impact of tropical volcanic eruptions on ENSO

*Masamichi Ohba[1] (1.Central Research Institute of Electric Power Industry)

[ACG45-P03] Revisiting the ENSO impact on the Indian Ocean SST based on the combined linear regression

*Lianyi Zhang[1,2,3], Yan DU[1,2], Tomoki Tozuka[3], Shoichiro Kido[3] (1.South China Sea Institute of Oceanology, Chinese Academy of Sciences, 2.University of Chinese Academy of Sciences, Chinese Academy of Sciences, 3.The University of Tokyo)

[ACG45-P04] Assessments of salinity impacts on SST using a linear inverse model

★Invited Papers

*Shoichiro Kido[1], Tomoki Tozuka[1] (1.Graduate School of Science, The University of Tokyo)

[ACG45-P05] The relationship between the boreal summer intraseasonal oscillation and the Pacific-Japan pattern

*Ayako Seiki[1], Yu Kosaka[2], Satoru Yokoi[1] (1.Japan Agency for Marine-Earth Science and Technology, 2.Research Center for Advanced Science and Technology, The university of Tokyo)

[ACG45-P06] The Impact of IOD on rainfall over Spain

*Sourabh Shrivastava[1], Saji Hameed[1] (1.University of Aizu)

[ACG45-P07] How Large-Scale Circulations Integratedly Influence Precipitation in the Source Region of the Yangtze River,China

*Yiheng Du[1], Dong An[1], Ronny Berndtsson[1] (1.Lund University)

[ACG45-P08] Summertime climate anomalies in Asia and the Northwestern Pacific induced by ENSO: Dependence on ENSO's phase transition

*Yu Kosaka[1], Daiki Kado[1] (1.Research Center for Advanced Science and Technology, University of Tokyo)

Diurnal cycles of precipitation and lightning in the tropics observed by TRMM3G68, GSMaP, LIS, and WWLLN

*Shoshiro Minobe[1], Jun Hyock Park[1], Katrina S. Virts[2]

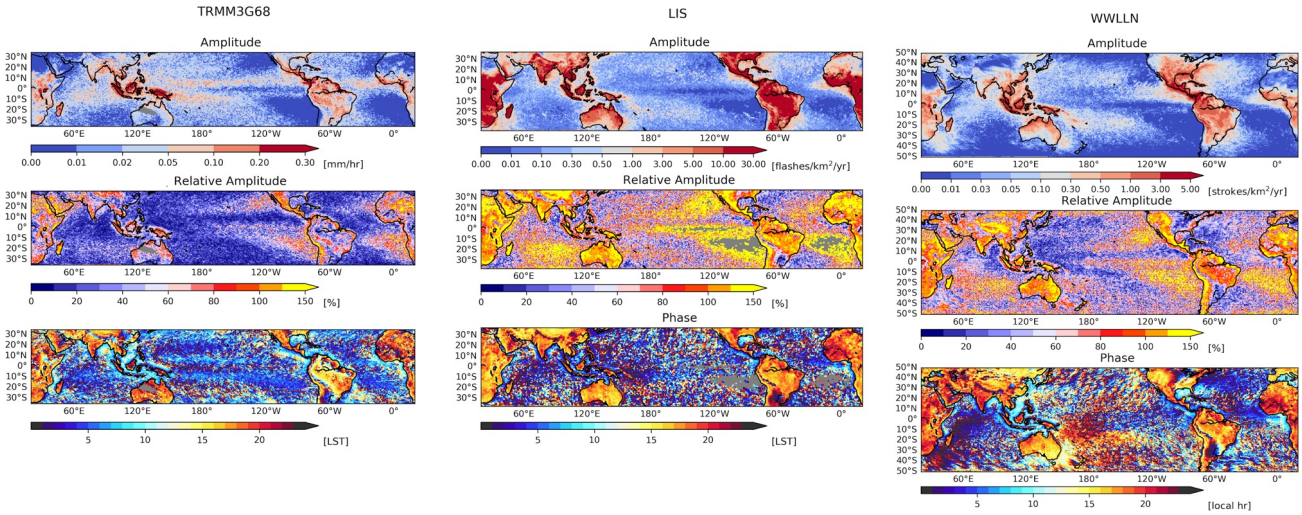
1. Graduate School of Science, Hokkaido University, 2. The University of Alabama in Huntsville

The diurnal cycle is a major atmospheric variation in conditions including temperature, wind, precipitation, and lightning. Diurnal precipitation and lightning are closely related because they are both associated with convection, and thus previous studies compared diurnal cycles of these two variables. However, previous diurnal cycle comparisons between precipitation and lightning are conducted as regional studies, and no global comparisons were made. Moreover, previous comparisons used precipitation data derived mainly from infra-red satellite observations, although it is known that IR-based precipitation observations have biases of about three-hour delay. Therefore, the purpose of the present study is to understand the difference and similarity of diurnal cycles of precipitation and lightning over the global tropics.

Diurnal cycles of precipitation and lightning are investigated by analyzing rain rate of TRMM3G68 dataset, consisting of precipitation radar and microwave imager data only, rain rates of Global Satellite Mapping of Precipitation (GSMaP), for which IR data are also used, lightning flash rates observed by TRMM Lightning Imaging Sensor (LIS), and lightning stroke rates of World Wide Lightning Location Network (WWLLN) over the tropics. Diurnal amplitudes relative to averages are generally larger for lightning than for precipitation. Over ocean, relative amplitudes are stronger in the stratocumulus deck region in the southeast Pacific than those over typical ocean regions. The phase of GSMaP is substantially delayed to TRMM3G68 due to the phase-delay problem of IR based estimation. The diurnal peaks tend to occur between 14:00 and 18:00 LST over the continent after spatial averaging with a phase leading order of TRMM3G68, LIS, and WWLLN, and between 0:00 and 7:00 LST over oceanic regions where diurnal cycles are prominent in all datasets. Off-equatorward phase propagations are found in the precipitation in the Pacific and Indian oceans. Over selected coastal regions, all data exhibit consistent oceanward phase propagation with the longest, medium, and shortest phase propagation distances for TRMM3G68 precipitation, WWLLN lightning, and LIS lightning, respectively, with a phase leading order of LIS, WWLLN, and TRMM3G68. The summertime diurnal cycle over the Gulf Stream also exhibits oceanward phase propagation, but with strong amplitude enhancement over the Gulf Stream. Diurnal cycle amplitude is also enhanced over the Kuroshio in the East China Sea in the Baiu-Meiyu rainy season.

Keywords: stratocumulus cloud deck, phase propagation

©2020. Japan Geoscience Union. All Right Reserved.



Amplitude (top), relative amplitude (middle), which is the amplitude divided by average, and phase (bottom) of diurnal cycle of annual climatology for rain rate of TRMM3G68 (left), lightning flash rate observed LIS (middle) and lightning stroke rate observed by WWLLN.

©2020. Japan Geoscience Union. All Right Reserved.

Intermodel diversity in the impact of tropical volcanic eruptions on ENSO

*Masamichi Ohba[1]

1. Central Research Institute of Electric Power Industry

Temporary negative radiative forcing caused by sudden super volcanic eruptions (SVEs) in the tropics reduces global surface temperatures and then weakens atmospheric and ocean circulations that can significantly affect interannual-to-interdecadal climate variations. Studies on the relationship between the El Nino-Southern Oscillation (ENSO) and SVEs had been discussed within limited data. However, the last 1000-years SST data reconstructed from the composited proxy suggested significant increase in the probability of the occurrence of El Niño one-year after the SVEs. Our SVE-forced experiment by using an air-sea coupled model (Ohba et al. 2013) also showed that El Niño is also tends to be excited in after the mature of SVEs as similar to findings from reconstructed SST. It is shown that the SVE-forcings can cause westerly wind anomalies in the western Pacific (i.e., weakened Walker circulation), and then El Niño can be excited one year after the SVEs. Similar results and mechanisms have been demonstrated from validation experiments on the other following studies. It is considered that the development of such westerly wind anomalies can be related to the decrease in precipitation on the Indian Ocean to the marine continent due to the SVE cooling that result in the basin-scale east-west gradient of surface temperature. In this study, we evaluate the effect of SVE-induced radiative forcing on ENSO in models using the results of the latest coupled model intercomparison data (CMIP5 and CMIP6) and verifiy the intermodel diversity of the SVE response among the models.

Keywords: ENSO, Volcanic eruption, CMIP6, Climate model

©2020. Japan Geoscience Union. All Right Reserved.

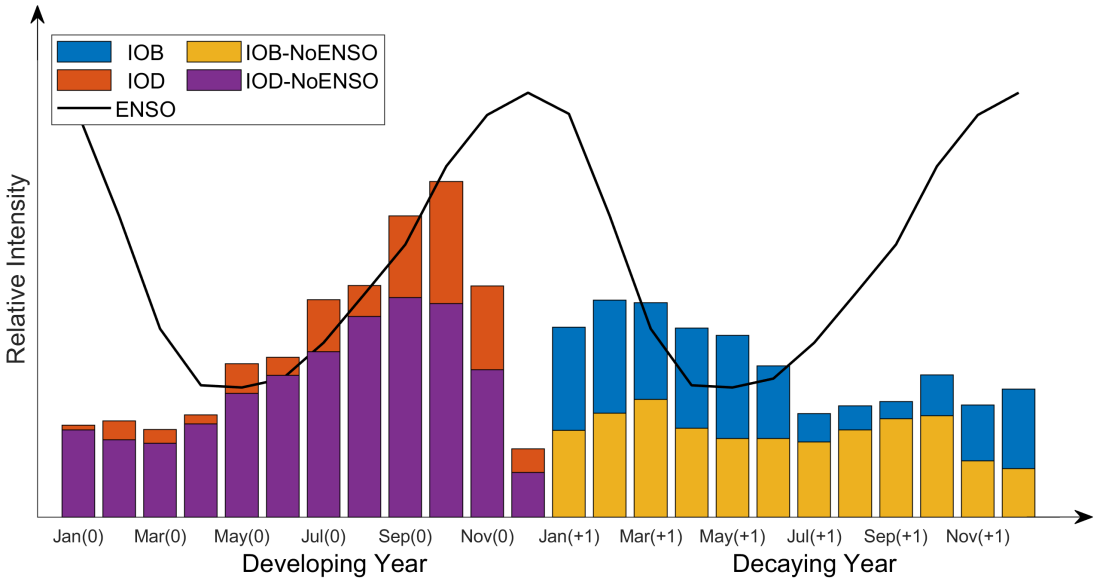
Revisiting the ENSO impact on the Indian Ocean SST based on the combined linear regression

*Lianyi Zhang[1,2,3], Yan DU[1,2], Tomoki Tozuka[3], Shoichiro Kido[3]

1. South China Sea Institute of Oceanology, Chinese Academy of Sciences, 2. University of Chinese Academy of Sciences, Chinese Academy of Sciences, 3. The University of Tokyo

El Niño-Southern Oscillation (ENSO) has great impacts on the Indian Ocean (IO) sea surface temperature (SST). In fact, two major climate modes of the IO that exert strong influences to the IO rim countries, namely the Indian Ocean Basin (IOB) and Indian Ocean Dipole (IOD) modes, are influenced by the ENSO. Based on the combined linear regression, this study quantifies ENSO impacts on these two modes in ENSO concurrent, developing and decaying phases. It is shown that the number of IOB and IOD events decreases by 83% and 25% after adequately removing ENSO influences, respectively. In terms of seasonal march, without ENSO signature, the spring peak of IOB disappears, while the autumn peak of IOD still exists with smaller amplitude. Also, the developing (decaying) phase of ENSO is more influential to the IOD (IOB) development. This implies that merely removing the concurrent ENSO impacts is not sufficient to study the intrinsic SST variability of the IO, and the present method may be useful to study the IO internal variability independent of ENSO.

Keywords: Indian Ocean, Sea Surface Temperature (SST), El Nino-Southern Oscillation (ENSO), Indian Ocean Dipole mode (IOD), Indian Ocean Basin mode (IOB), Combined Linear Regression



©2020. Japan Geoscience Union. All Right Reserved.

Assessments of salinity impacts on SST using a linear inverse model

*Shoichiro Kido[1], Tomoki Tozuka[1]

1. Graduate School of Science, The University of Tokyo

The upper ocean salinity undergoes significant variations associated with large-scale climate modes, such as the El-Niño and Southern Oscillation (ENSO) in the tropical Pacific and the Indian Ocean Dipole (IOD) in the tropical Indian Ocean. By changing the density of the seawater, these salinity variations alter the upper ocean stratification and circulation, and thus have the potential to feed back to the climate modes themselves. Indeed, by conducting a series of sensitivity experiments using a regional ocean model, our recent work has demonstrated that surface and subsurface salinity variations associated with the IOD act to damp sea surface temperature (SST) anomalies and serve as a negative feedback to the IOD. However, due to the complex nature of the coupling between temperature and salinity variability, it is not straightforward to clearly identify these salinity impacts only from observational datasets.

To address this issue, here we propose to apply a linear inverse model (LIM), which succinctly describes the evolution of tropical climate variations within a linear framework. We have first determined the linear operator of the LIM based on temperature and salinity anomalies in the tropical Indian Ocean derived from an ocean reanalysis product and carried out a long-term integration of the LIM as a reference experiment. It is found that our LIM reasonably reproduces the amplitude and spatial structure of the observed temperature and salinity anomalies associated with the IOD. Then, we have designed another LIM experiment *without* the coupling between temperature and salinity variations (referred as “T-S decoupled LIM”), by modifying the linear operator of the original LIM. A comparison of outputs from both LIM experiments reveals that the amplitude of the IOD in the T-S decoupled LIM is substantially stronger than that of the reference experiments. This suggests that the interactions between temperature and salinity act to reduce the amplitude of the IOD, consistent with our previous results based on dynamical approaches. Calculations of the growth rates of the IOD-related SST anomalies further confirmed the above idea. Our results imply that the LIM can be a powerful tool for understanding and diagnosing the salinity impacts on SST in a simple manner.

Keywords: Indian Ocean Dipole, Salinity variation, Linear inverse model

©2020. Japan Geoscience Union. All Right Reserved.

The relationship between the boreal summer intraseasonal oscillation and the Pacific-Japan pattern

*Ayako Seiki[1], Yu Kosaka[2], Satoru Yokoi[1]

1. Japan Agency for Marine-Earth Science and Technology, 2. Research Center for Advanced Science and Technology, The university of Tokyo

Convective activities over the Philippine Sea in boreal summer have been known to be associated with circulation anomalies over the midlatitude western north Pacific (WNP), called the Pacific-Japan (PJ) pattern. In this study, the relationship between the PJ pattern and tropical intraseasonal variability, called the boreal summer intraseasonal oscillation (BSISO), which influences the convective activities over the Philippine Sea is investigated. The monthly PJ indices are not correlated with the amplitude of the BSISO indices, but correlated with the phases of the BSISO indices. This result indicates that the negative (positive) PJ pattern, which is associated with warm (cold) anomalies over the midlatitude East Asia, tended to appear when the strong convective active (suppressed) signals of the BSISO are located over the tropical WNP. In the negative PJ years, convective activities over the tropical WNP drastically develop from the BSISO phase 6 simultaneous with significant increases of the eddy kinetic energy representing synoptic disturbances, compared to the positive PJ years and the other years. The development of the synoptic disturbances over the Philippine Sea might play a key role for exciting the PJ pattern.

Keywords: Pacific-Japan pattern, tropical intraseasonal oscillation, teleconnection

©2020. Japan Geoscience Union. All Right Reserved.

The Impact of IOD on rainfall over Spain

*Sourabh Shrivastava[1], Saji Hameed[1]

1. University of Aizu

Previous studies have shown that the Indian Ocean Dipole (IOD) has a significant impact on land temperatures over southern Europe. However, whether IOD influences rainfall over this region and how this impact compares to that of El Nino Southern Oscillation (ENSO) have not been established. Here using the E-OBS gridded rainfall datasets for the period 1958 to 2012, we have analyzed the influence of IOD and ENSO on European rainfall. We find that IOD impacts are predominantly felt over southwestern Europe in a region covering Spain and Portugal during the peak phase of the event. Correlations exceeding 0.4 are observed over the central regions of Spain. We find that ENSO impacts on European rainfall are substantially weaker compared to that of IOD, but occur with a pattern similar to the latter. Partial correlation analysis suggests that the marginal ENSO correlations are a statistical areifact arising from the co-occurrence of a fraction of the El Nino events with positive IOD events. Possible dynamical mechanisms by which IOD impacts rainfall over southwestern Europe will be discussed.

Keywords: IOD, ENSO, Rainfall

©2020. Japan Geoscience Union. All Right Reserved.

How Large-Scale Circulations Integratedly Influence Precipitation in the Source Region of the Yangtze River,China

*Yiheng Du[1], Dong An[1], Ronny Berndtsson[1]

1. Lund University

Precipitation patterns are highly sensitive to climate change. During recent years, researchers have made significant progress in the understanding of vapor transport by large-scale atmospheric circulation patterns (teleconnections). However, previous research has mainly focused on the influence of individual teleconnection patterns, regardless of joint impact. In our study, the combined influence from large scale circulations on precipitation are examined. Monthly precipitation data at regular grids of 0.5˚ ×0.5˚ derived from observations during June-August 1961-2016 were used to reveal characteristics of large-scale circulations associated with rainy season precipitation over the source region of the Yangtze River (SRYR). A comprehensive analysis of relationships between SST anomalies as well as large-scale circulation including ENSO and PDO and spatiotemporal patterns of rainy season precipitation in SRYR was presented. Our analysis indicated that the leading modes of rainy season precipitation variability can be explained by the variability of SST together with an integrated effect of ENSO and PDO with an explained variance of about 64.2%. It was shown that the influence of ENSO and PDO will enhance/decrease when they are in-/out-of-phase. Negative PDO induces more precipitation in La Niña years than in El Niño years for the SRYR, especially over central and eastern parts of the basin. Positive PDO induces precipitation decrease, and El Niño enhances the decrease. The mechanism behind this pattern is atmospheric circulation affecting the strength of westerlies that transport moisture to the inland areas and as well local convergence conditions. Our results have implications for predicting the rainy season precipitation for coming decades over the SRYR. If the current negative PDO phase continues together with more frequent extreme La Niña events, as suggested in previous research, more abnormal precipitation during rainy season is expected over the SRYR.

Keywords: PDO, ENSO, precipitation, moisture flux, SRYR

©2020. Japan Geoscience Union. All Right Reserved.

Summertime climate anomalies in Asia and the Northwestern Pacific induced by ENSO: Dependence on ENSO's phase transition

*Yu Kosaka[1], Daiki Kado[1]

1. Research Center for Advanced Science and Technology, University of Tokyo

Equatorial Pacific sea surface temperature (SST) anomalies associated with El Niño-Southern Oscillation (ENSO) typically peak in boreal winter and, when composited, dissipate by subsequent boreal summer (June-July-August; hereafter denoted as JJA(1)). Despite the lack of the equatorial Pacific signal, coherent climate anomalies emerge in Asia and the Indo-western Pacific in JJA(1). Studies have identified the so-called capacitor effect of the Indian Ocean for the ENSO's delayed, indirect influence. However, the lack of composited SST anomalies in the equatorial Pacific in JJA(1) does not always apply to individual ENSO events. Specifically, in some events the equatorial Pacific SST anomalies do not disappear in JJA(1) and redevelop toward the subsequent boreal winter (hereafter "multi-year ENSO events"), while in other cases the SST anomalies on average transition to the opposite polarity before JJA(1) ("single-year ENSO events"). We find in a reanalysis dataset and a coupled model pacemaker experiment that the single-year and multi-year ENSOs yield distinct climate anomalies in Asia and the Northwestern Pacific in JJA(1). Our bivariate linear regression analysis shows that the direct teleconnection from the equatorial Pacific interferes differently between single- and multi-year events with the delayed influence through the capacitor effect. The equatorial Pacific SST induces lower-tropospheric circulation anomalies that are spatially orthogonal to those induced by the Indian Ocean capacitor effect, and their different combination leads to the distinct climate anomalies. The distinct influence can explain asymmetry in JJA(1) climate anomalies between El Niño and La Niña. Namely, El Niño tends to decay rapidly while La Niña often persists for two years or more, and this persistence asymmetry is the key to asymmetric climate anomalies between El Niño and La Niña in JJA(1).

Keywords: Asian summer monsoon, ENSO, teleconnection

©2020. Japan Geoscience Union. All Right Reserved.

[E] Poster | A (Atmospheric and Hydrospheric Sciences)：A-CG Complex & General

[A-CG46] Atmospheric deposition impact on Terrestrial and marine Ecosystems

convener:Eyal Rahav(Israel Oceanographicand Limnological Research), Adina Paytan(University of California Santa Cruz)

Marine and terrestrial ecosystems are frequently subjected to high inputs of wet and dry atmospheric deposition. Aerosol deposition provide dissolved and particulate constituents such as inorganic nutrients and organic matter required for sustaining productivity, as well as toxic metals and other pollutants. In addition, dust also provide a wide array of viable airborne microorganisms such as bacteria, fungi and viruses that, in turn, can also affect productivity and impose strong constraints on global climate changes. These impacts may vary based on the aerosol load, source, trajectory, and its chemical and biological characteristics.

We welcome contributions studying the effects of aerosols on aquatic and terrestrial systems in particular the interactions between aerosols and organisms (i.e., biomass, activity, diversity). Approaches may include in situ observations, laboratory mesocosm/microcosm experiments and modeling.

[ACG46-P01] The hitchhike’s guide to bacterial transport: the role of viable dust-borne microbes deposition into marine environments

*Eyal Rahav[1], Barak Herut[1], Adina Paytan[2] (1.Israel Oceanographic and Limnological Research, Haifa 31080, Israel, 2.Institute of Marine Science, University of California, Santa Cruz, CA, 95064, USA)

The hitchhike’s guide to bacterial transport: the role of viable dust-borne microbes deposition into marine environments

*Eyal Rahav[1], Barak Herut[1], Adina Paytan[2]

1. Israel Oceanographic and Limnological Research, Haifa 31080, Israel, 2. Institute of Marine Science, University of California, Santa Cruz, CA, 95064, USA

Aerosols and dust are regularly transported across the oceans and seas supplying nutrients and trace metals to the surface water. In addition, aerosols may also contain a wide array of different airborne microorganisms (heterotrophic bacteria, virus, cyanobacteria and fungi), that can be easily transported for thousands of kilometers away from their place of origin within a few days. The southeastern Mediterranean Sea (SEMS) and the northern Red Sea (NRS) are ideal marine environments to study the role of aerosols and airborne microbes on surface microbial production for multiple reasons. First, both environments are subjected to relatively high aerosol deposition throughout the year. Secondly, they are oligotrophic environment with low inorganic nutrients and low autotrophic and heterotrophic activity for most months. Thus, any external input of micro/macronutrients, along with airborne microbes, can have a relatively substantial effect upon interaction with the ambient microbial populations; thereby having a potentially large effect on the system’s production and ecological function. Here, we will discuss who are the dominant airborne bacteria that are being transported to the SEMS/NRS during storm events. Further, we will present some of the ecological roles these microorganisms hold (carbon and nitrogen fixation) and how airborne microbes interact with ambient microbial populations. These results demonstrate that dust-borne microorganisms may play a significant role marine environments.

Keywords: Airborne microbes, Desert dust, Aerosols, Microbial interactions

©2020. Japan Geoscience Union. All Right Reserved.

[E] Poster | A (Atmospheric and Hydrospheric Sciences)：A-CG Complex & General

[A-CG47] Global Carbon Cycle Observation and Analysis

convener:Kazuhito Ichii(Chiba University), Prabir Patra(Research Institute for Global Change, JAMSTEC), Forrest M. Hoffman(Oak Ridge National Laboratory), Makoto Saito(National Institute of Environmental Studies)

The Paris Agreement under the United Nations Framework Convention on Climate Change (UNFCCC) is a landmark agreement, which aims at reduction of greenhouse gases (GHGs) emission to keep the global warming below 2 degC. The national commitments and progress should be carefully monitored and verified by international bodies using different but complementary methodologies.

In recent years, many observations and techniques to monitor GHGs budget have expanded. The improvements include observational platforms for monitoring atmospheric GHGs, national or regional emission inventories, top-down models (e.g. atmospheric inverse models), and bottom-up models (e.g. process-based models). However, due to uncertainties in modeling and sparse observation networks, large uncertainties exist in GHG sources/sinks estimations at global and regional scales. These uncertainties lead to large variations in future projections of GHG budgets and climate changes.

The purpose of the session is to discuss state-of-the-art techniques for estimation of GHG (e.g. CO2, CH4, N2O) budgets at global and regional scales. The topic includes natural and anthropogenic processes, various methodologies (e.g. in-situ observation, aircraft monitoring, remote sensing, modeling), and various targets (e.g. atmosphere, terrestrial, and ocean), various spatial and temporal coverage (e.g. regional to global scales and past-present-future). Improved estimates of emissions from land use change, forest fires, and other anthropogenic sources (urban developments and thermal power station etc.) are also of interest. We also welcome discussions for designs and plans for future studies targeting urban and rural scale emission estimations using sophisticated modeling tools and inventories.

[ACG47-P02] Preliminary results for GOSAT-2 Level 4 global surface fluxes

*Makoto Saito[1], Yosuke Niwa[1], Tazu Saeki[1], Kazutaka Murakami[1], Richao Cong[1], Tatsuya Miyauchi[1], Hisashi Yashiro[1], Tomohiro Shiraishi[1], Ryuichi Hirata[1], Yukio Yoshida[1], Isamu Morino[1], Hibiki M Noda[1], Hirofumi Ohyama[1], Akihide Kamei[1], Tsuneo Matsunaga[1] (1.National Institute of Environmental Studies)

[ACG47-P03] Toward a long-term global inversion of atmospheric CO_2 for elucidating seasonal and interannual variations of natural carbon fluxes

*Yosuke Niwa[1] (1.National Institute for Environmental Studies)

[ACG47-P04] INVERSION ESTIMATES OF METHANE EMISSION IN EAST, SOUTH AND SOUTHEAST ASIA IN 2010-2017 USING GOSAT AND GROUND-BASED OBSERVATIONS

*Fenjuan Wang[1,2], Shamil S Maksyutov[1], Rajesh Janardanan[1], Aki Tsuruta[3], Akihiko Ito[1], Isamu Morino[1], Yukio Yoshida[1], Johannes W. Kaiser[4], Greet Janssens Maenhout[5], Ed Dlugokencky[6], Ivan Mammarella[7], Jost V. Lavric[8], Tsuneo Matsunaga[1] (1.NIES National Institute of Environmental Studies, 2.Department of Climate Change, National Climate Center, 3.Finnish Meteorological Institute, 4.Deutscher Wetterdienst, 5.European Commission Joint Research Centre, 6.Earth System Research Laboratory, NOAA, 7.University of Helsinki, 8.Max Planck Institute for Biogeochemistry)

[ACG47-P05] Refinement of a diagnostic terrestrial ecosystem model using AsiaFlux network data toward GCOM-C SGLI GPP/NPP product

*LI JIAWEI[1], Kazuhito Ichii[1], Hideki Kobayashi[2], Wei Yang[1] (1.Chiba University, 2.Japan Agency for Marine-Earch Science and Technology)

[ACG47-P06] In-situ observation of greenhouse-gas flux at proglacial grounds of a glacier – preliminary result for Gulkana Glacier, Alaska-

*Keiko Konya[1], Go Iwahana[3,2], Tetsuo Sueyoshi[4], Tomoaki Morishita[5] (1.Japan Agency for Marine-Earth Science and Technology, 2.Universitry of Alaska, Fairbanks, 3.Hokkaido university, 4.Ninational Institute of Polar Research, 5.Forestry and Forest Products Research Institute)

[ACG47-P07] Testing machine-learning methods toward improvement of terrestrial CO2 flux estimations

*Zhiyan Liu[1], Kazuhito Ichii[1] (1.Center for Environmental Remote Sensing Chiba University, Chiba University)

Preliminary results for GOSAT-2 Level 4 global surface fluxes

*Makoto Saito[1], Yosuke Niwa[1], Tazu Saeki[1], Kazutaka Murakami[1], Richao Cong[1], Tatsuya Miyauchi[1], Hisashi Yashiro[1], Tomohiro Shiraishi[1], Ryuichi Hirata[1], Yukio Yoshida[1], Isamu Morino[1], Hibiki M Noda[1], Hirofumi Ohyama[1], Akihide Kamei[1], Tsuneo Matsunaga[1]

1. National Institute of Environmental Studies

The Greenhouse gases Observing SATellite 2 (GOSAT-2) was launched, as the successor of GOSAT, on 29th October 2018 into a sun-synchronous orbit at an altitude of 613 km with 6-day revisit cycle, then the satellite has been operated with normal mode since 1st February 2019. GOSAT-2 is designed to measure atmospheric carbon dioxide (CO_2), methane (CH_4) and carbon monoxide (CO) with two instruments: The Thermal And Near-infrared Sensor for carbon Observation Fourier Transform Spectrometer 2 (TANSO-FTS-2) and the Cloud and Aerosol Imager 2 (TANSO-CAI-2). The GOSAT-2 mission inherits the main objective of the GOSAT that improves our knowledge of spatiotemporal variations of CO_2 and CH_4 in the atmosphere and the process governing their exchange between the atmosphere and the Earth's surface and contributes climate change studies and related environmental policy making. The GOSAT-2 project provides Level 1 radiance spectral products of GOSAT-2 observations for general users and released FTS-2 shortwave infrared (SWIR) Level 2 atmospheric concetration products to the GOSAT series' Research Announcement users. The GOSAT-2 Level 4 products will provide estimates of global surface fluxes on CO_2 and CH_4 based on the FTS-2 SWIR Level 2 products and surface observations. This presentation will introduce detailed features for the GOSTA-2 Level 4 product including the prior information and preliminary results on multi-year global CO_2 flux estimates using GOSAT FTS SWIR Level 2 products, and additional information about the latest GOSAT-2 products.

Keywords: satellite observation, carbon cycle, inverse modeling

©2020. Japan Geoscience Union. All Right Reserved.

Toward a long-term global inversion of atmospheric CO_2 for elucidating seasonal and interannual variations of natural carbon fluxes

*Yosuke Niwa[1]

1. National Institute for Environmental Studies

A number of ground-based stations have been performing atmospheric measurements of CO_2 for several decades and have observed notable interannual variations of the growth rate of the atmospheric CO_2, which suggests that the natural CO_2 flux at the earth surface have been varying in conjunction with some climate key parameters (e.g., El Niño Southern Oscillation index). Furthermore, distinct seasonal variations of atmospheric CO_2 observed by those measurements give evidence of dynamic photosynthesis and respiration activities of terrestrial biospheres. However, the mechanisms underlying those natural CO_2 flux variations are not fully understood and that gives significant uncertainties in the global warming prediction by earth system models equipped with carbon cycle feedbacks. An atmospheric observation-based estimate of surface CO_2 fluxes, i.e., so-called top-down analysis, would improve our understanding of the surface CO_2 flux mechanisms. An atmospheric inverse analysis in which a transport model is used to connect surface fluxes with atmospheric mole fractions is a prominent method in that it gives spatiotemporal variations of surface fluxes. In order to give implications of surface flux mechanisms, we should conduct a long-term inverse analysis with a high spatial resolution. In this study, we first use a simple box model that emulates integration of the global atmospheric CO_2 and apply it to a long-term inverse analysis with a variational method. In that experiment, we investigate how surface flux estimation is optimized along iterative calculations. Furthermore, we extend the inverse analysis to a more realistic problem with a sophisticated inverse system name NICAM-TM 4D-Var (Niwa et al., 2017a,b), in which a global three-dimensional model is employed. By using synthetic data with a current observational network, we elucidate uncertainties behind coming inversion results from NICAM-TM 4D-Var with real observations.

Niwa, Y., H. Tomita, M. Satoh, R. Imasu, Y. Sawa, K. Tsuboi, H. Matsueda, T. Machida, M. Sasakawa, B. Belan, and N. Saigusa: A 4D-Var inversion system based on the icosahedral grid model (NICAM-TM 4D-Var v1.0) –Part 1: Offline forward and adjoint transport models, *Geosci. Model Dev.*, 10, 1157–1174, doi:10.5194/gmd-10-1157-2017, 2017a.

Niwa, Y., Y. Fujii, Y. Sawa, Y. Iida, A. Ito, M. Satoh, R. Imasu, K. Tsuboi, H. Matsueda, and N. Saigusa: A 4D-Var inversion system based on the icosahedral grid model (NICAM-TM 4D-Var v1.0) –Part 2: Optimization scheme and identical twin experiment of atmospheric CO_2 inversion, *Geosci. Model Dev.*, 10, 2201-2219, doi:10.5194/gmd-10-2201-2017, 2017b.

Keywords: carbon cycle, CO2, inverse analysis

©2020. Japan Geoscience Union. All Right Reserved.

INVERSION ESTIMATES OF METHANE EMISSION IN EAST, SOUTH AND SOUTHEAST ASIA IN 2010-2017 USING GOSAT AND GROUND-BASED OBSERVATIONS

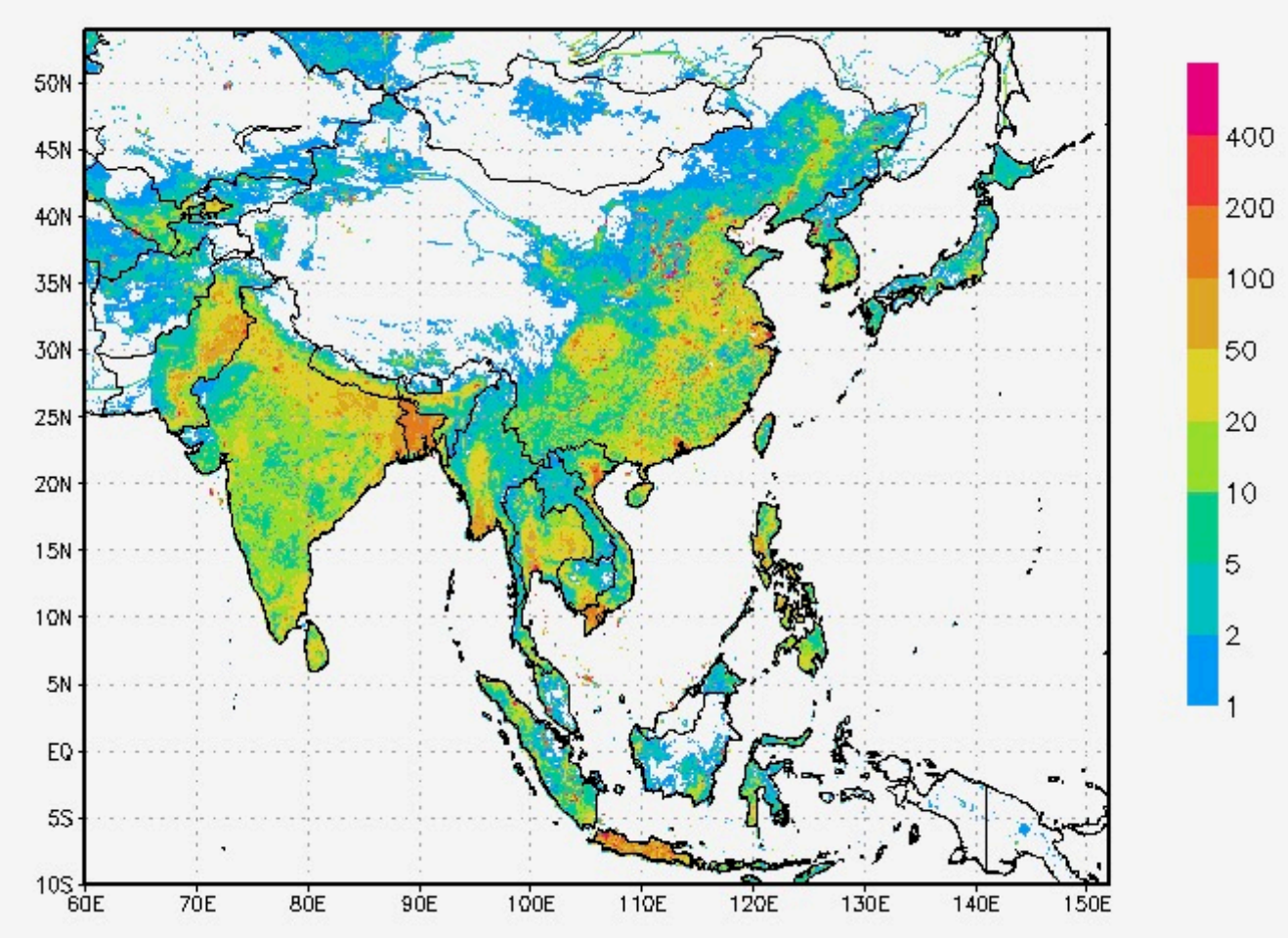
*Fenjuan Wang[1,2], Shamil S Maksyutov[1], Rajesh Janardanan[1], Aki Tsuruta[3], Akihiko Ito[1], Isamu Morino[1], Yukio Yoshida[1], Johannes W. Kaiser[4], Greet Janssens Maenhout[5], Ed Dlugokencky[6], Ivan Mammarella[7], Jost V. Lavric[8], Tsuneo Matsunaga[1]

1. NIES National Institute of Environmental Studies, 2. Department of Climate Change, National Climate Center, 3. Finnish Meteorological Institute, 4. Deutscher Wetterdienst, 5. European Commission Joint Research Centre, 6. Earth System Research Laboratory, NOAA, 7. University of Helsinki, 8. Max Planck Institute for Biogeochemistry

Greenhouse gas Observing SATellite (GOSAT) detected significant enhancements of column-averaged dry-air mole fraction of methane (XCH_4) in East, South and Southeast Asia in the course of its operation since 2009. The attribution and evaluation of these enhancements will benefit the national mitigation efforts for methane in this area. We compared national inventories submitted to the United Nations Framework Convention on Climate Change (UNFCCC) to top-down emissions estimated at country scale by the global high-resolution (0.1° ×0.1°) inverse model NIES-TM-FLEXPART-VAR (NTFVAR). Long-term GOSAT retrievals and ground-based observations were used in the inversion for the year 2010-2017. Prior fluxes contained adjusted EDGAR v4.3.2 emissions scaled to match the country totals by national reports to theUNFCCC, augmented by biomass burning emissions from the Global Fire Assimilation System (GFASv1.2) and wetland emissions from the Vegetation Integrative Simulator for Trace Gases (VISIT) model. The estimated regional total methane emissions is 163.5 Tg $CH_4\,yr^{-1}$(with an uncertainty of 24.3Tg $CH_4\,yr^{-1}$) from twenty-eight countries included in this study, and 94% are from the top ten emitting-countries China (52.2Tg $CH_4 yr^{-1}$), India (36.7Tg $CH_4\,yr^{-1}$), Indonesia (20.3Tg $CH_4\,yr^{-1}$), Bangladesh (11.3Tg $CH_4\,yr^{-1}$), Pakistan (7.9Tg $CH_4\,yr^{-1}$), Vietnam (6.9Tg $CH_4\,yr^{-1}$), Thailand (6.6Tg $CH_4\,yr^{-1}$), Burma (6.3Tg $CH_4\,yr^{-1}$), Philippines (2.9Tg $CH_4\,yr^{-1}$) and Cambodia (2.6Tg $CH_4\,yr^{-1}$). Among these ten countries, natural methane emissions are dominant in Bangladesh and Cambodia, and anthropogenic emissions are dominant in other counties. Statistically significant increasing trends in anthropogenic emissions are detected in China and Indonesia from 2010 to 2017. Optimized high-resolution anthropogenic fluxes show intensive anthropogenic fluxes in megacity clusters like in eastern China, northern India, western Pakistan and southern Indonesia (Figure 1.Posterior anthropogenic methane fluxes (2010–2017 average, unit: mg $CH_4 m^{-2} day^{-1}$)).

Keywords: GOSAT, anthropogenic and natural methane emissions, East, South and Southeast Asia

©2020. Japan Geoscience Union. All Right Reserved.



©2020. Japan Geoscience Union. All Right Reserved.

Refinement of a diagnostic terrestrial ecosystem model using AsiaFlux network data toward GCOM-C SGLI GPP/NPP product

*LI JIAWEI[1], Kazuhito Ichii[1], Hideki Kobayashi[2], Wei Yang[1]

1. Chiba University, 2. Japan Agency for Marine-Earch Science and Technology

GCOM-C satellite with SGLI sensor was launched in December 2017. Because of medium resolution(300m) of SGLI sensor, it’ s possible to get more accurate climate change prediction. Furthermore, terrestrial carbon cycle products are significant to create. This presentation will introduce our current work on GCOM-C SGLI terrestrial carbon flux products. We select BESS (Breathing Earth System Simulator) as basic mechanistic terrestrial biosphere model,with some GCOM-C satellite products as inputs and then get estimations of daily gross primary productivity (GPP), net primary productivity (NPP), and net ecosystem exchange (NEE).

For the original BESS model, here are some improvements, including (a) using eddy-covariance observation network data across Asia to optimize model parameters, (b) adding a practical ecosystem respiration module, (c) applying some GCOM-C SGLI land products as inputs. In the beginning, we check the BESS model performance by using existing Asia Flux observation sites (about 50 sites) and select several key parameters by using sensitive analysis. Then, for these parameters, we use a trust-region optimization algorithm to identify their optimized coefficient. Second, a classify method of different land cover is add to improve BESS model accuracy. We think areas with different land covers have their own mechanisms so that optimized coefficients should be different. According to this, we can get a new flux estimation on large scale. Third, we create a semi-empirical respiration model for the BESS model to do more further estimation. So far, we chose Terra and Aqua MODIS data all model inputs. Then, we choose some available input data, such as leaf area index (LAI) and land surface temperature (LST) and switched them from MODIS to SGLI.

In the furture, Our group will still improve the models and calculate GPP, NPP and NEE. Remote sensing data with high spatial resolution (e.g. 300m) and high temporal resolution (e.g. daily) will be helpful to understand terrestrial carbon cycle at global scales. These products will be available as an official SGLI research product soon and updated annually.

Keywords: terrestrial carbon cycle, vegetation, remote sensing

©2020. Japan Geoscience Union. All Right Reserved.

In-situ observation of greenhouse-gas flux at proglacial grounds of a glacier –preliminary result for Gulkana Glacier, Alaska-

*Keiko Konya[1], Go Iwahana[3,2], Tetsuo Sueyoshi[4], Tomoaki Morishita[5]

1. Japan Agency for Marine-Earth Science and Technology, 2. Universitry of Alaska, Fairbanks, 3. Hokkaido university, 4. Ninational Institute of Polar Research, 5. Forestry and Forest Products Research Institute

Methane is one of the major greenhouse gases (GHG), and the variation of its concentration in the atmosphere has the potential to bring a significant impact on the global climate and carbon cycle. The methane emission in the Arctic regions, which is largely attributed to the methane production in the seasonally freezing layer, has been considered to be enhanced by thawing of permafrost and to be one of the sources of uncertainty for future climate projection. On the other hand, a notable amount of methane emissions from the proglacial ground surfaces after retreats of glaciers in Greenland and Iceland have been reported (e.g. Lamarche-Gagnon et al., 2019; Burns et al., 2018). Those newly-recognized methane hotspots may exist in other proglacial areas, which could influence on estimation of global methane budget. However, field evidence for the large methane emission is still limited and there is a lack of information about other proglacial areas.
We carried out the field experiments in the Gulkana Glacier in the Alaska Range, United Status. The objective of our study is to measure methane fluxes at the proglacial area of a small mountain glacier to verify if the large emission can be observed as reported in Greenland and Iceland, and expanding the field data towards the evaluation of the generality of previously reported methane emissions. The observation was conducted on 15 and 16 July 2019, one month after the onset of melting of the glacier, at 18 locations in the terminus of the glacier. The in-situ observation was conducted with the chamber method (Morishita et al. 2019). The chambers were set on dry, wet, and inundated ground surfaces to capture differences in the surface conditions. Gas samples were also taken for the isotopic analysis. A small emission was observed at seven locations, most of which were wet surfaces. Stable isotopes in the emitted methane and carbon dioxide imply that the methane was generated by microbial process. Our observed methane emission was small in mid-July and previous studies detected high methane emission at the end of June starting with higher discharge. Therefore, it is plausible that larger methane emission occurs in earlier and warmer melting seasons.

Keywords: Methane, CO2, GHG, glacier, Alaska

©2020. Japan Geoscience Union. All Right Reserved.

Testing machine-learning methods toward improvement of terrestrial CO2 flux estimations

*Zhiyan Liu[1], Kazuhito Ichii[1]

1. Center for Environmental Remote Sensing Chiba University, Chiba University

Data-driven approach is effective for upscaling observation network data of terrestrial carbon fluxes. In this study, we estimated terrestrial gross primary productivity (GPP) and net ecosystem exchange (NEE) across the globe using machine learning methods –random forest regression (RF) with MODIS collection 6 datasets after previous studies used collection 5 [e.g. Ichii et al. 2017; Tramontana et al. 2016; Kondo et al. 2015]. Furthermore, we introduced lag effects of input parameters (simply input as a new column) on GPP and NEE in RF models and this lag effect include either historical or future (lag within a month) remote sensing based input parameters. Because the ecosystem is a dynamic system, which current status is affected by historical factors and meanwhile will be observed in the future as some other physics or biochemical quantities. Thus, both processes may include the lag effect which mechanism are also different. We also attempt to adopt a deep learning method called RNN (Recurrent Neural Network and its sub-types) in which data flows by each time step and make some comparision. Site-level RF experiments showed that the lagged parameter improved the accuracy of NEE estimation (R^2 0~0.06 increasing for total Koppen climate types). The lagged parameter worked well in site-level anomalies, particularly, lag effect by shortwave solar radiation or land surface temperature in the night. The estimated annual anomaly variations in GPP and NEE showed a good consistency with independent model-based estimations (TRENDY V6). In the future research, the lag-effected will be a more important factor for ecosystem’s prediction and estimation.

Keywords: Terrestrial GPP and NEE, MODIS Collection 6, Time Lag/Memory Effect, Data Driven

©2020. Japan Geoscience Union. All Right Reserved.

[E] Poster | A (Atmospheric and Hydrospheric Sciences)：A-CG Complex & General

[A-CG48] Projection and detection of global environmental change

convener:Michio Kawamiya(Japan Agency for Marine-Earth Science and Technology), Kaoru Tachiiri(Japan Agency for Marine-Earth Science and Technology), Hiroaki Tatebe(Japan Agency for Marine-Earth Science and Technology), V Ramaswamy(NOAA GFDL)

Anthropogenic forcings on global environment are expected to cause intensification of extreme events, sea level rise, ocean acidification and deoxygenation, as well as large-scale ecosystem changes. Earth System modeling groups across the world performed simulations and published projection data toward 6th IPCC assessment report due in 2021. Various new types of studies, such as event attribution and coupling of socio-economic processes and Earth system dynamics, are emerging in the field of global change projections. In addition, observational studies are becoming increasingly more important for grasping changes in the global environment and evaluating model projections. Interactions and collaborations beyond boundaries of conventional scientific disciplines are desired for dealing with the issue of global changes. This session thus aims to deepen our understanding on global change, from both disciplinary and interdisciplinary viewpoints.

[ACG48-P01] Methodology of probabilistic climate projections for the assessment of climate change mitigation pathways

*Junichi Tsutsui[1] (1.Central Research Institute of Electric Power Industry)

[ACG48-P02] Improvement in runoff reproducibility of a land surface model and its implications for the energy-water balances on land

*Kumiko TAKATA[1], Naota Hanasaki[1] (1.Center for Climate Change Adaptation, National Institute for Environmental Studies)

[ACG48-P03] **Impact of volcanic eruption on surface climate in VolMIP experiments by MIROC-ES2L**

*Manabu Abe[1], Tomohiro Hajima[1] (1.Japan Agency for Marine-Earth Science and Technology)

[ACG48-P04] Effect on the Earth system of realizing a 1.5 °C warming climate target after overshooting to the 2 °C level

*Kaoru Tachiiri[1], Diego Silva Herran[2], Xuanming Su[1], Michio Kawamiya[1] (1.Japan Agency for Marine-Earth Science and Technology, 2.National Institute for Environmental Studies)

Methodology of probabilistic climate projections for the assessment of climate change mitigation pathways

*Junichi Tsutsui[1]

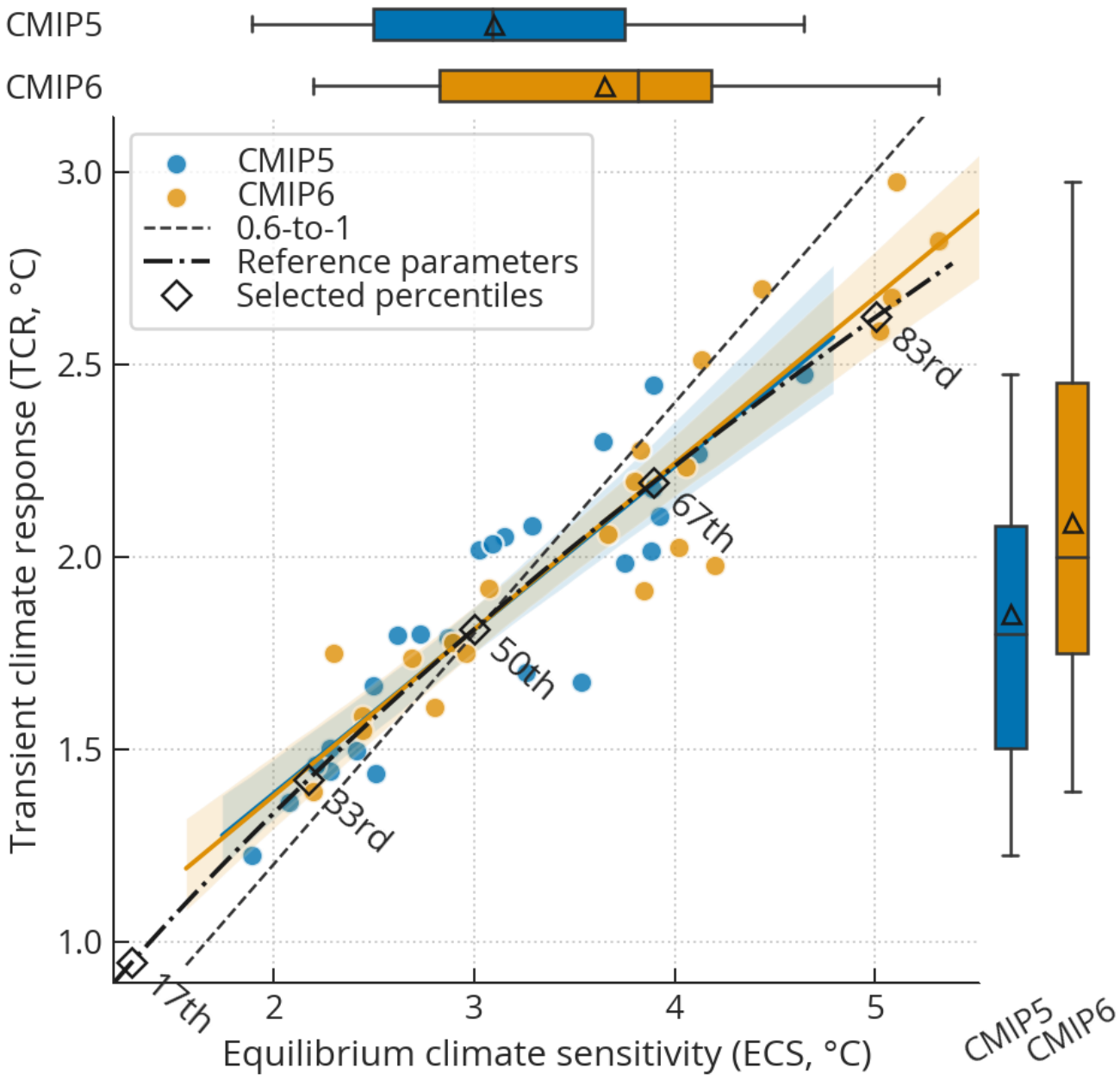
1. Central Research Institute of Electric Power Industry

Pathways of climate change mitigation are assessed for their consistency with a given temperature goal from probabilistic climate projections that reflect an ensemble of complex climate models and other lines of evidence. The author have been developing a climate model emulator for such probabilistic assessment and here describes and discusses its methodology.
The emulator consists of a thermal response module and a carbon cycle module. These are basically represented by impulse response functions to anthropogenic carbon input that alters the effective radiative forcing of the atmospheric CO_2 and natural processes in the ocean and terrestrial carbon cycle. The parameters of the thermal response module are calibrated for individual complex models from the latest and previous phases of Coupled Model Intercomparison Project (CMIP6 and CMIP5). The parameters of the carbon cycle module are currently fixed to their default values, which are calibrated to historical carbon balance assessed in the Fifth Assessment Report (AR5) of the Intergovernmental Panel on Climate Change and the mean properties of CO_2 increase experiments with CMIP5 Earth system models.
The thermal response parameters are characterized by the two climate sensitivity metrics, equilibrium climate sensitivity (ECS) and transient climate response (TCR). Figure 1 shows the relationship between the TCR and ECS for the individual CMIP models as well as the reference line representing the variation of the models. The reference line is built from principal component analysis for the variation, reflecting that the ratio of TCR to ECS generally decreases with increase in climate sensitivity. The probabilistic projection uses five parameter sets selected along the reference line so that resulting values of transient climate response to cumulative CO_2 emissions (TCRE) match nominal quantiles of 0.17, 0.33, 0.5, 0.67, and 0.83 based on the likely range of the TCRE assessed in the AR5.
Preliminary analysis of the current probabilistic projections compared with other approaches shows similar medians but large variation in ranges. It appears that the current method produces larger ranges than the others constrained by observed temperature changes. This difference implies that the assessed likely range is rather conservative and can be reduced with advanced constrain approaches and emerging observations. Figure 1 also shows that the 66% range of TCR diagnosed from the response parameters is comparable to the AR5-assessed likely range of 1 to 2.5 K despite the fixed carbon cycle parameters. This result implies that the AR5-assessed likely ranges are not necessarily consistent between TCR and TCRE, and that a consistent TCR range can be smaller by the contribution of the carbon-cycle uncertainties to the TCRE range.

Figure 1: Relationship between the TCR and the ECS from the CMIP5 and CMIP6 multi-model ensembles, as of October 2019. The dashed line is drawn to guide a proportional relation with a ratio of 0.6, representing an approximate multi-model mean. The color lines with plumes show regression estimates with a 95% confidence interval. The triangle markers in the marginal box plots indicates means. The dash-dotted line shows a reference line representing the variation of the models, and the five diamond markers along the reference line show reference parameters adjusted to nominal quantiles of 0.17, 0.33, 0.5, 0.67, and 0.83 in terms of the AR5-assessed TCRE range.

©2020. Japan Geoscience Union. All Right Reserved.

Keywords: transient climate response, climate model emulator, multi-model ensemble, cumulative CO2 emissions



©2020. Japan Geoscience Union. All Right Reserved.

Improvement in runoff reproducibility of a land surface model and its implications for the energy-water balances on land

*Kumiko TAKATA[1], Naota Hanasaki[1]

1. Center for Climate Change Adaptation, National Institute for Environmental Studies

Land surface hydrological processes are widely recognized as important elements in climate change studies, and land surface models have been developed by many research groups since the 1980s. MATSIRO (Takata et al., 2003; Nitta et al., 2014) is one of them; it calculates the surface and soil temperatures, evaporation, runoff, soil moisture, etc., based on the energy water balances, taking into account the effects of vegetation such as reflection and absorption of radiation, photosynthesis, transpiration, water uptake from roots, etc. The model has, however, had the strong bias of underestimation in runoff, for many years, compared to observed values. Until today, Hirabayashi et al. (2005) examined and revised the parameter for base runoff, and Yoshimura et al. (2006) improved the algorithms of groundwater level diagnosis. Nevertheless, MATSIRO is still one of the models producing least runoff among others (Haddeland et al., 2011).

We found that the diagnosed groundwater level that was used for calculation of surface runoff (Dunne flow) and base runoff tended to be too deep. Therefore, we tried a simple method to forcibly raise groundwater levels to examine its effect in this study. Specifically, we changed the condition for saturation judgment. In the base experiment (EP.0), a soil layer was judged saturated when soil moisture averaged over a grid cell was almost equal to saturation. In the sensitivity experiments, the condition was relaxed to about 75% (EP.1), 50% (EP.2), 25% (EP.3), and 0% (EP.4) of saturation. A series of numerical experiments was conducted in the Chao Phraya River basin (CP) in Thailand as a case study. The meteorological data from 1981 to 2004 at a horizontal resolution of 5 arc-minutes (i.e., approximately 9 km) (Kotsuki et al., 2013) was used.

The calculated monthly and daily river flow in EP.2 agree well with observation at the Bhumibol Dam (BB) on the Ping River in the northwestern part of CP. The groundwater level in the catchment of BB in EP.2 were much shallower (seasonal range was 1-3 m) than that in EP.0 and EP.1 (5-6 m). The seasonal changes in the vertical profiles of monthly mean soil moisture, and the monthly Bowen ratio were also improved.

The overall behavior of the model was dramatically improved by changing the condition of saturation judgment. The improvements in the Bowen ratio and soil moisture suggests that those impacts will be amplified when the land surface model is couled to the other components of climate models. In the results above, the streamflow and Bowen ratio agreed well with the measurements when the saturation threshold was at about 50% of saturation (EP.2). The good agreement in the experiment with the relaxed threshold implies that there are processes that yield large runoff at a sub-grid scale due to inhomogeneity of land surface, such as macro pore, landscape, land use, etc. An optimum saturation threshold is expected to exist, that simulates such local runoff.

Keywords: Runoff, Water table depth, Land surface model, land energy-water balances

©2020. Japan Geoscience Union. All Right Reserved.

Impact of volcanic eruption on surface climate in VolMIP experiments by MIROC-ES2L

*Manabu Abe[1], Tomohiro Hajima[1]

1. Japan Agency for Marine-Earth Science and Technology

Large-scale volcanic eruptions affect significantly surface climate. Also, uncertainties on the impact of volcanic eruption on the climate have remained. It is important to understand the volcanic impact on the past and future climate changes for improving basic knowledge of climate change. We have conducted the Tir1 experiments of VolMIP endorsed by CMIP6 with MIROC-ES2L. In this study, we summarize the results of VolMIP Tir1 experiments using MIROC-ES2L.

©2020. Japan Geoscience Union. All Right Reserved.

Effect on the Earth system of realizing a 1.5 ˚C warming climate target after overshooting to the 2 ˚C level

*Kaoru Tachiiri[1], Diego Silva Herran[2], Xuanming Su[1], Michio Kawamiya[1]

1. Japan Agency for Marine-Earth Science and Technology, 2. National Institute for Environmental Studies

An Earth system model (ESM) was used to investigate the effect of reaching the target of 1.5 ˚C warming (relative to preindustrial levels) after overshooting to the 2 ˚C level with respect to selected global environment indicators. Two scenarios were compared that diverged after reaching the 2 ˚C level: one stayed at the 2 ˚C level, and the other cooled to the 1.5 ˚C level. Unlike the internationally coordinated model intercomparison projects, the scenarios were developed for a specific climatic model with emissions and land use scenarios consistent with socioeconomic projections from an integrated assessment model. The ESM output resulted in delayed realization of the 1.5 ˚C and 2 ˚C targets expected for 2100. The cumulativeCO2 emissions for 2010–2100 (2300) were 358 (−53) GtCO2 in the 2 ˚C scenario and−337 (−936) GtCO2 in the 1.5 ˚C scenario. We examined the effect of overshooting on commonly used indicators related to surface air temperature, sea surface temperature and total ocean heat uptake. Global vegetation productivity at 2100 showed around a 5%increase in the 2 ˚C scenario without overshooting compared with the 1.5 ˚C scenario with overshooting, considered to be caused by more precipitation and strongerCO2 fertilization. A considerable difference was found between the two scenarios in terms of Arctic sea ice, whereas both scenarios indicated few corals would survive past the 21st century. The difference in steric sea level rise, reflecting total cumulative ocean heat uptake, between the two scenarios was <2 cm in 2100, and around 9 cm in 2300 in the Pacific Island region. A large overshoot may reduce the eventual difference between targets (i.e. 1.5 ˚C in contrast to 2 ˚C), particularly in terms of the indicators related to total ocean heat uptake, and to sensitive biological thresholds.

Keywords: Earth system model, 1.5℃ target, 2℃ target, overshoot

©2020. Japan Geoscience Union. All Right Reserved.

[E] Poster | A (Atmospheric and Hydrospheric Sciences)：A-CG Complex & General

[A-CG49] Greenhouse Gas Monitoring from Space: Current Capabilities, Challenges, and Future Needs

convener:kurosu thomas p(Jet Propulsion Laboratory, California Institute of Technology), Annmarie Eldering(Jet Propulsion Laboratory), Akihiko Kuze(Japan Aerospace Exploration Agency), Tsuneo Matsunaga(Center for Global Environmental Research and Satellite Observation Center, National Institute for Environmental Studies)

In a circulation letter of their Position Statement on Climate, the AGU writes

"Human-caused climate change is one of the most serious issues of our time. It will cause increasing health, economic, security, and ecological risks, from heat-related deaths and illnesses, hazards such as flooding, water scarcity, wildfire, and extreme weather and impacts to coastal infrastructure, agriculture, fisheries, and global migration."

With the constantly growing threat anthropogenically-induced climate change, global to local monitoring of atmospheric greenhouse gas (GHG) concentrations becomes increasingly important. Over the past decade, space-based GHG sensors have contributed substantially to our understanding of CO2 and CH4 emission sources and natural sinks on global and regional scales. Recent advances in these sensors have now extended these capabilities for studies of more compact sources, including large urban areas. NASAs OCO-3 on the ISS and Japans TANSO-FTS-2 on GOSAT-2 include target mapping modes that continue and extend the observation records of their precursors, and the Canadian commercial GHGSat provides high spatial resolution observations of CO2 and CH4 over selectable locations on the Earth. Sentinel 5P/TROPOMI measures CH4 with a wide swath instrument with daily near-global coverage. Future GHG observing systems are expected to further improve on the bridging of global and local scales, to provide optimized data records as basis for climate change mitigation policies.

We propose a session that focuses on the following aspects of space-based GHG monitoring: (1) capabilities of currently operating sensors measuring greenhouse gases on global to local scales, including OCO-2&3, TANSO-FTS/2, GHGsat, TROPOMI, and TANSAT; (2) identification and quantification of shortfalls in current data records, and requirements for future observation strategies; and (3) future observing systems and how these will address current gaps in GHG monitoring.

[ACG49-P01] A high-resolution CO_2 inverse modeling using observations from the global ground-based monitoring network and the GOSAT satellite

*Shamil Maksyutov[1], Rajesh Janardanan[1], Tomohiro Oda[2], Makoto Saito[1], Yukio Yoshida[1], Johannes W Kaiser[3], Vinu Valsala[4], Edward Dlugokencky[5], Tsuneo Matsunaga[1] (1.National Institute for Environmental Studies, Tsukuba, Japan, 2.USRA/NASA GSFC, Greenbelt, USA, 3.DWD, Offenbach, Germany, 4.Indian Institute for Tropical Meteorology, Pune, India, 5.Global Monitoring Division, NOAA, Boulder, USA)

[ACG49-P02] GOSAT series product validation with TCCON, Sky radiometer and lidar data

*TRIEU THI NGOC TRAN[1], Isamu Morino[1], Osamu Uchino[1], Yukitomo Tsutsumi[1], Tetsu Sakai[2], Tomohiro Nagai[2], Akihiro Yamazaki[2], Hiroshi Okumura[3], Kouhei Arai[3], Ben Liley[4] (1.National Institute for Environmental Studies (NIES), Tsukuba, Japan, 2.Meteorological Research Institute, Japan Meteorological Agency, Tsukuba, Japan, 3.Graduate school of Science and Engineering, Saga University, Saga, Japan, 4.National Institute of Water and Atmospheric Research, Lauder, New Zealand)

[ACG49-P03] Observations of the Tropical Land Biosphere response to the 2015-2016 El Niño with the Orbiting Carbon Observatory-2 (OCO-2) and Greenhouse gases Observing SATellite (GOSAT)

*David Crisp[1] (1.Jet Propulsion Laboratory, California Institute of Technology)

[ACG49-P04] Global and local flux estimation of carbon dioxide and methane by GOSAT satellites

*Akihiko Kuze[1], Nobuhiro Kikuchi[1], Hiroshi Suto[1], Kei Shiomi[1], Fumie Kataoka[2] (1.Japan Aerospace Exploration Agency, 2.Remote Sensing Technology Center of Japan)

A high-resolution CO_2 inverse modeling using observations from the global ground-based monitoring network and the GOSAT satellite

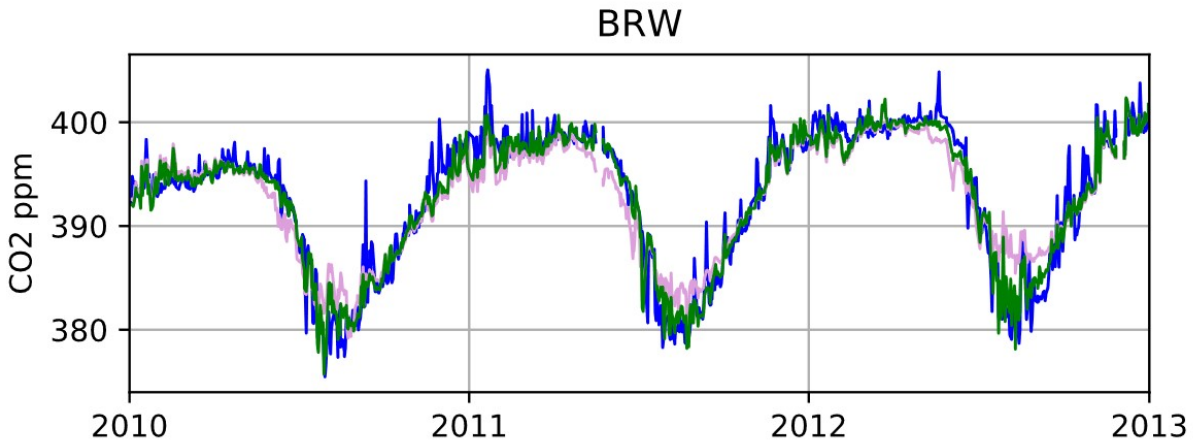
*Shamil Maksyutov[1], Rajesh Janardanan[1], Tomohiro Oda[2], Makoto Saito[1], Yukio Yoshida[1], Johannes W Kaiser[3], Vinu Valsala[4], Edward Dlugokencky[5], Tsuneo Matsunaga[1]

1. National Institute for Environmental Studies, Tsukuba, Japan, 2. USRA/NASA GSFC, Greenbelt, USA, 3. DWD, Offenbach, Germany, 4. Indian Institute for Tropical Meteorology, Pune, India, 5. Global Monitoring Division, NOAA, Boulder, USA

We present a high-resolution CO_2 flux inversion system designed to estimate surface fluxes from atmospheric CO_2 observational data collected by the GOSAT satellite as well as the global in-situ ground-based observation networks. Our inverse system NTFVAR is based on a coupled transport model combining the FLEXPART Lagrangian Particle Dispersion Model (LPDM) and the NIES-TM global Eulerian transport model. The system solves for flux corrections to the prior fluxes at a 0.1 x 0.1 degree spatial resolution via an iterative optimization procedure using the adjoint of the coupled transport model. We used high-resolution prior fluxes prepared from the ODIAC anthropogenic emissions data product, the GFAS global biomass burning dataset, the OTTM ocean model and the VISIT terrestrial biosphere model. The high-resolution version of VISIT biosphere flux was obtained using a separate VISIT CO_2 flux simulation implemented for each vegetation type identified by a vegetation mosaic map. The prior flux uncertainty for the land and ocean regions was scaled proportionally to monthly mean MODIS-GPP and the ocean flux variability. First, we estimated bi-weekly flux corrections over the period of 2010 to 2012 solely from in-situ CO_2 data by the ObsPack global observation network dataset. The application of the high-resolution atmospheric transport improved the representation of fine-scale anthropogenic CO_2 plumes. A comparison to NOAA’s CarbonTracker optimized simulations shows that our high-resolution model has some advantage at coastal and island observation sites, experiencing a mix of marine and continental air inflow. We also implemented an inversion using the ground-based data and the GOSAT satellite data. The GOSAT Level 2 data (NIES L2 v02.72) were corrected by estimating the deviation of GOSAT L2 data from an optimized simulation with the ObsPack for each latitude band and month. We confirmed the reduction of misfit between the GOSAT observations and the high-resolution model simulations after the inversion.

Keywords: inverse modeling, CO2, satellite observation, GOSAT

©2020. Japan Geoscience Union. All Right Reserved.



©2020. Japan Geoscience Union. All Right Reserved.

GOSAT series product validation with TCCON, Sky radiometer and lidar data

*TRIEU THI NGOC TRAN[1], Isamu Morino[1], Osamu Uchino[1], Yukitomo Tsutsumi[1], Tetsu Sakai[2], Tomohiro Nagai[2], Akihiro Yamazaki[2], Hiroshi Okumura[3], Kouhei Arai[3], Ben Liley[4]

1. National Institute for Environmental Studies (NIES), Tsukuba, Japan, 2. Meteorological Research Institute, Japan Meteorological Agency, Tsukuba, Japan, 3. Graduate school of Science and Engineering, Saga University, Saga, Japan, 4. National Institute of Water and Atmospheric Research, Lauder, New Zealand

Data from the Total Carbon Column Observing Network (TCCON) are the primary validation source for the column averaged dry air mole fraction XCO_2 and XCH_4 deduced from GOSAT. In addition, aerosol optical thickness, Angstrom exponent, and single scattering albedo, all obtained from sky radiometer measurements, and vertical profiles of aerosols and thin cirrus clouds from lidar observations are important for fully validating XCO_2 and XCH_4 retrievals.

In this presentation, we investigate influences of aerosols and clouds on GOSAT XCO_2 and XCH_4 data at three TCCON sites: Tsukuba, Saga, and Lauder. At these sites, both sky radiometer and lidar have been also operating. The match up was performed with a ±0.1˚ latitude/longitude rectangular area of each TCCON site and within 30 minutes of the GOSAT overpass time. The results showed that the bias and standard deviation were largest at Lauder (-0.99 ±1.91 [ppm] and -5.33 ±11.13 [ppb] for XCO_2 and XCH_4 , respectively). The bias and standard deviation at Tsukuba and Saga were 0.25 ±1.73 [ppm] and 0.24 ± 1.83 [ppm] for XCO_2 and -0.79 ±9.44 [ppb] and 7.19 ±8.17 [ppb] for XCH_4, respectively.

Both XCO_2 and XCH_4 differences between GOSAT and TCCON at Lauder were negatively correlated with AOT at 500 nm. In contrast, at Saga and Tsukuba the difference of XCO_2 only negatively correlated with AOT at 500 nm. AOT at 500 nm was largest especially in Spring at Saga (0.87) and Tsukuba (0.54). AOT at 500 nm of Lauder was smallest (0.15) among the three sites. The single scattering albedo at 500 nm at Tsukuba varied from 0.75 to 1.0 and from 0.67 to 1.0 at Saga and Lauder. The differences in XCO_2 and XCH_4 between GOSAT and TCCON had no relationship with the Angstrom exponents, which varied site by site. The causes for these findings will be discussed in the presentation. Preliminary results of vertical profiles of aerosols and/or clouds at Lauder will be also shown.

Keywords: GOSAT data, Validation, Sky radiometer

©2020. Japan Geoscience Union. All Right Reserved.

Observations of the Tropical Land Biosphere response to the 2015-2016 El Niño with the Orbiting Carbon Observatory-2 (OCO-2) and Greenhouse gases Observing SATellite (GOSAT)

*David Crisp[1]

1. Jet Propulsion Laboratory, California Institute of Technology

The first two years of the OCO-2 mission were dominated by the record-setting 2015–2016 El Niño. OCO-2 measurements were combined with GOSAT observations and analyzed to yield high spatial resolution estimates of the column-averaged dry air mole fraction, XCO_2, These products clearly resolved reductions in tropical ocean outgassing from net increases in CO_2 emissions from tropical forests. These XCO_2 estimates were combined with OCO-2 and GOSAT solar-induced chlorophyll fluorescence (SIF) measurements to trace the origin of the forest CO_2 emissions to the impacts of drought, temperature stress, and fires. Observations acquired between 2017-2019 documented the atmospheric CO_2 response following this El Niño when, unexpectedly, its XCO_2 and SIF measurements showed that the natural carbon cycle never fully recovered to the state anticipated by most earlier carbon cycle measurements and models. In particular, tropical forests, once thought to be significant CO_2 sinks, continued to be persistent net sources of CO_2 throughout this period. Understanding these results and their implications for the response of the natural carbon cycle to climate change requires longer continuous records of CO_2 and SIF.

Keywords: Orbiting Carbon Observatory-2, Greenhouse gases Observing SATellite, Carbon dioxide, Solar induced chlorophyll fluorescence

©2020. Japan Geoscience Union. All Right Reserved.

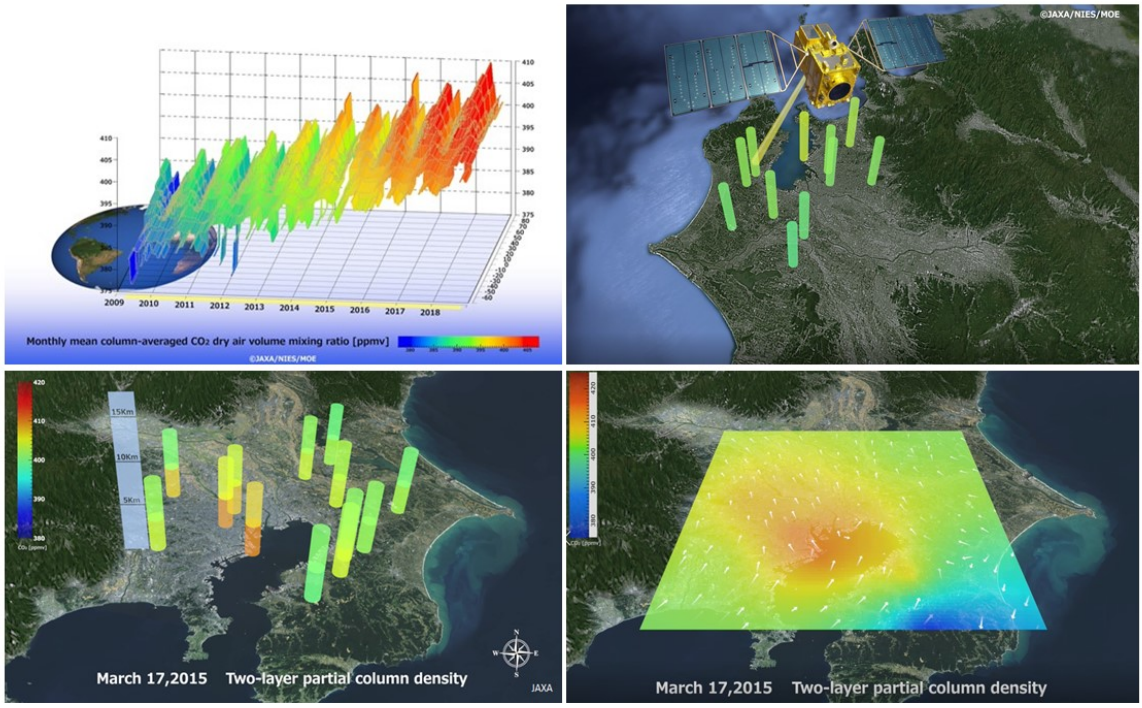
Global and local flux estimation of carbon dioxide and methane by GOSAT satellites

*Akihiko Kuze[1], Nobuhiro Kikuchi[1], Hiroshi Suto[1], Kei Shiomi[1], Fumie Kataoka[2]

1. Japan Aerospace Exploration Agency, 2. Remote Sensing Technology Center of Japan

GOSAT and GOSAT-2 have provided long-term radiance spectral data using Fourier transform spectrometer technology since 2009 and 2018, respectively. With the advantage of FTS multiplexing, they can simultaneously measure carbon dioxide (CO_2) and methane (CH_4) absorption bands of reflected solar light with two linear polarizations and thermal emission. Radiance spectra with two polarizations can distinguish between less-polarized reflections from the Earth’ s surface and highly polarized scattering by aerosols and thin clouds. The infrared band can add information to vertical profiles. By combining all these spectra data, partial column densities of the upper (4-12 km) and lower (0–4 km) troposphere can be retrieved, even under thick aerosol regions such as Africa, India, and South Africa. Two-layer vertical information enhances measurements of near-surface emission and uptake and reduces errors in transportation, therefore improving global flux estimation. With two-axis pointing systems, they can target large point sources and mega cities and have enhanced measurements of CO_2 and CH_4. However, local flux estimates by GOSAT may be problematic because of too large a footprint, a lack of proper upwind reference observations, and insufficient wind information. To contribute to the global stocktake of the Paris Agreement, we need a system to observe and estimate local flux from individual source sectors. We will present the status of flux estimation and discuss how to reduce such uncertainties.

Keywords: GOSAT, greenhouse gases, flux, carbon dioxide, methane



©2020. Japan Geoscience Union. All Right Reserved.

[E] Poster | A (Atmospheric and Hydrospheric Sciences)：A-CG Complex & General

[A-CG50] Earth & Environmental Sciences and Artificial Intelligence

convener:Tomohiko Tomita(Faculty of Advanced Science and Technology, Kumamoto University), Shigeki Hosoda(Japan Marine-Earth Science and Technology), Ken-ichi Fukui(Osaka University), Satoshi Ono(Kagoshima University)

In recent years, we have been required to explore various gigantic data leading earth and environmental sciences such as modern meteorology, oceanography, hydrology and so on, to accomplish Society 5.0 and Sustainable Development Goals (SDGs). To examine such environmental big data faithfully, it may be required to use the techniques of artificial intelligence (AI) including spatiotemporal data modeling of AI, prediction and detection by machine learning, techniques of automated data mining, and so forth. At the present, AI is also expected to lead the data-driven science as a bridge connecting science and big data. This session first calls for various studies applying the techniques of AI to global environmental issues and then will discuss them in both natural and information sciences.

[ACG50-P01] A precipitation prediction using an artificial neural network model based on observation time series data

He Zhang[1], Naoki Matsumoto[1], *Tomohiko Tomita[2] (1.Graduate School of Science and Technology, Kumamoto University, 2.Faculty of Advanced Science and Technology, Kumamoto University)

[ACG50-P02] Climate Prediction by Using Periodic Convolutional Recurrent Network

*Ekasit Phermphoonphiphat[1], Tomohiko Tomita[2], Masayuki Numao[1], Ken-ichi Fukui[1] (1.Osaka University, 2.Kumamoto University)

[ACG50-P03] K-means clustering of Argo profiles for identifying circulation patterns

*Nozomi Sugiura[1] (1.Japan Agency of Marine-Earth Science and Technology)

[ACG50-P04] A Preliminary Study on Algo Float Trajectory Prediction using Multimodal Convolutional LSTM

*Serina Higashi[1], Takahiro Kinoshita[1], Shigeki Hosoda[3], Ken-ichi Fukui[2], Satoshi Ono[1] (1.Kagoshima University, 2.Osaka University, 3.Japan Marine-Earth Science and Technology)

A precipitation prediction using an artificial neural network model based on observation time series data

He Zhang[1], Naoki Matsumoto[1], *Tomohiko Tomita[2]

1. Graduate School of Science and Technology, Kumamoto University, 2. Faculty of Advanced Science and Technology, Kumamoto University

In weather prediction, precipitation prediction is one of most difficult but strongly required for society. This work investigated performance of an artificial neural network (ANN) model for the precipitation prediction. In particular, this study examined how training of the ANN model improved the performance of precipitation prediction.

The datasets used in this study are observation time series data compiled by the Japan Meteorological Agency (JMA). The stations are five, i.e., Kumamoto, Fukuoka, Nagasaki, Kagoshima, and Oita located in Kyushu of Japan. The used observation variables are six, that is, hourly precipitation, temperature, pressure, vapor pressure, wind speed, and wind direction. Using these station data, this study diagnosed the performance of the ANN model's few-hour precipitation prediction at Kumamoto. In this study, the ANN prediction model was constructed by a multi-layer perceptron, in which the number of intermediate layers was set to be two for easy experiment and interpretation. Then, a variety of experiments were performed about training of the ANN prediction model. In particular, this work examined how stations and physical variables improved the precipitation prediction. As the evaluation of prediction outputs, this work diagnosed 1) the difference in maximum value, 2) the time lag of appearance of the maximum, and 3) the root mean squared error between and the prediction and real precipitation time series. In addition, a skill score, which was the ratio between the predicted precipitation and the real value larger than 10 mm/h, was used. This skill score has been designed to evaluate the performance of the JMA's physical prediction model for heavy precipitation events.

The results show that 1) Kumamoto's precipitation itself is most crucial for the prediction, 2) the data at western station effectively improve the prediction, and of course, 3) the most recent precipitation data is most valid. In order to improve the prediction at the maximum value in a precipitation event, this study removed the data with no precipitation from the training data as a preprocessing. It was found that this preprocessing effectively improved the maximum precipitation value from 30% to 80% of the real maximum value. The skill score of this ANN prediction model in precipitation, which was estimated for three-hour prediction, was that of JMA's physical prediction model in about 10 years ago. This study is still on going, and the further results will be shown at the conference, e.g., the results of the experiments increasing stations, improving the ANN structure, using other algorithms such as recurrent NN, and so on.

Keywords: Artificial Neural Network, precipitation prediction, observation time series data

©2020. Japan Geoscience Union. All Right Reserved.

Climate Prediction by Using Periodic Convolutional Recurrent Network

*Ekasit Phermphoonphiphat[1], Tomohiko Tomita[2], Masayuki Numao[1], Ken-ichi Fukui[1]

1. Osaka University, 2. Kumamoto University

Machine learning based prediction methods have been investigated to many climate predictions such as precipitation forecasting, and temperature prediction. However, most machine learning researches on this domain do not consider periodic patterns, which are important for climate data that has strong periodicity. For example, the positive and negative phases of North Atlantic Oscillation (NAO) are repeatedly every year that can indicate seasonal over the Northern Hemisphere. Features from such periodicity may improve prediction accuracy.
In order to consider periodicity, we adopt the periodic convolutional recurrent network (Periodic-CRN) to our research. The idea of this model is to store and load the hidden states that learned by convolutional recurrent network (CRN) as periodic representation. The stored periodic representation is loaded and combined with the current prediction output. The model also has the attention mechanism that is used to weigh multiple periodic representations (e.g., monthly and yearly representation). In this work, we extend the idea of the periodic attention mechanism component to includes nearby time interval (month) representation. The group of nearby periodic representation is considered instead of using only a single periodic time interval. Then we use convolutional long short-term memory (ConvLSTM) as CRN.
We applied the proposed method to upper tropospheric circulations over the Northern Hemisphere and the land surface variable, which are geopotential height at 300 hPa (Z300) and temperature at 2 meter height from the surface (T2M), respectively. These data have a dominant periodic pattern that repeats every year. The proposed method obtained the average root mean square error (RMSE) of Z300 short-term prediction from 2016 to 2018 of 62.48 meters (0.68% compared to average Z300 value). On the other hand, ConvLSTM, convolutional neural network (CNN), and linear regression (LR) obtained average RMSE of 79.24, 113.76, and 125.25 meters, respectively. The proposed method also outperforms in T2M prediction that obtained average RMSE of 1.79 degrees Celsius (˚C) while ConvLSTM, CNN, and LR obtained average RMSE of 2.54, 4.84, and 3.87 ˚C, respectively. The result has shown that the proposed method that considers data’s periodicity can improve prediction accuracy, which is a significant improvement from conventional methods.

Keywords: Climate prediction, Periodicity, Periodic-CRN, Convolutional recurrent network

©2020. Japan Geoscience Union. All Right Reserved.

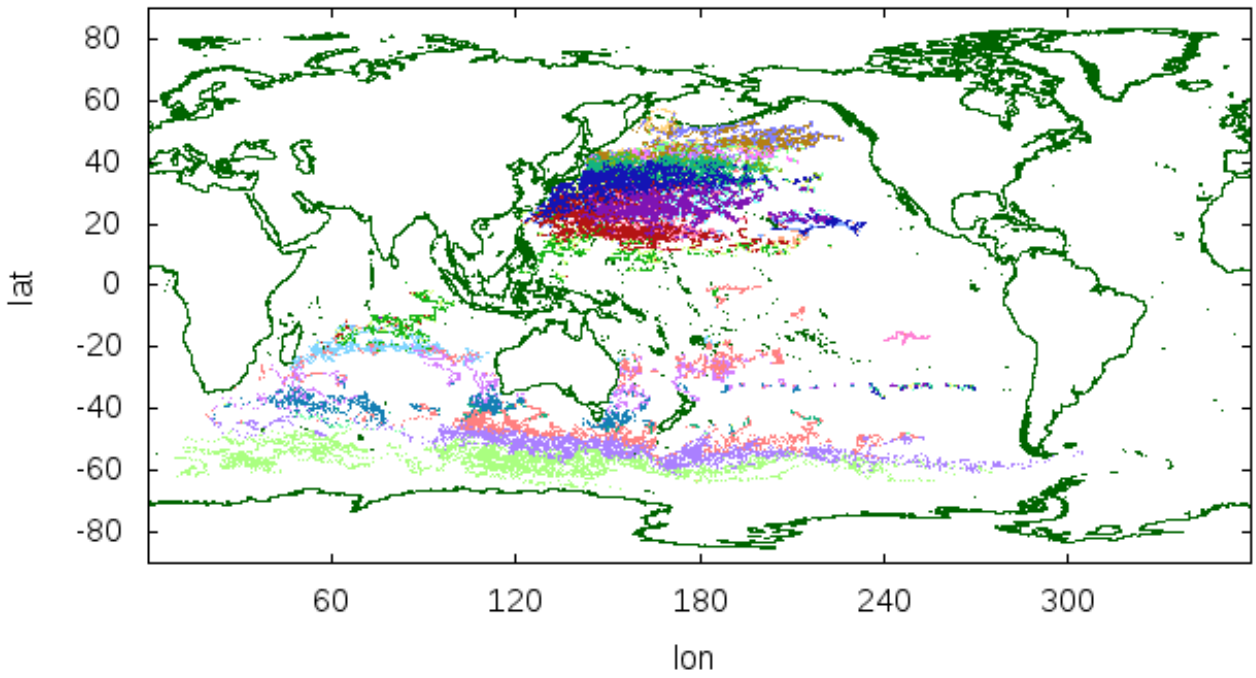
K-means clustering of Argo profiles for identifying circulation patterns

*Nozomi Sugiura[1]

1. Japan Agency of Marine-Earth Science and Technology

A k-means clustering of Argo profiles is performed. By using the signature of each data sequence as the coordinate system for feature space, major ocean ciculation patterns are better represented with distinct clusters, than by using conventional Temperature and Salinity coordinate. We will discuss why the signature, which is a key cencept in rough path theory, is relevant to representing a profile. Implications for its usage in data assimilation will also be discussed.

Keywords: k-means method, Argo, signature



©2020. Japan Geoscience Union. All Right Reserved.

A Preliminary Study on Algo Float Trajectory Prediction using Multimodal Convolutional LSTM

*Serina Higashi[1], Takahiro Kinoshita[1], Shigeki Hosoda[3], Ken-ichi Fukui[2], Satoshi Ono[1]

1. Kagoshima University, 2. Osaka University, 3. Japan Marine-Earth Science and Technology

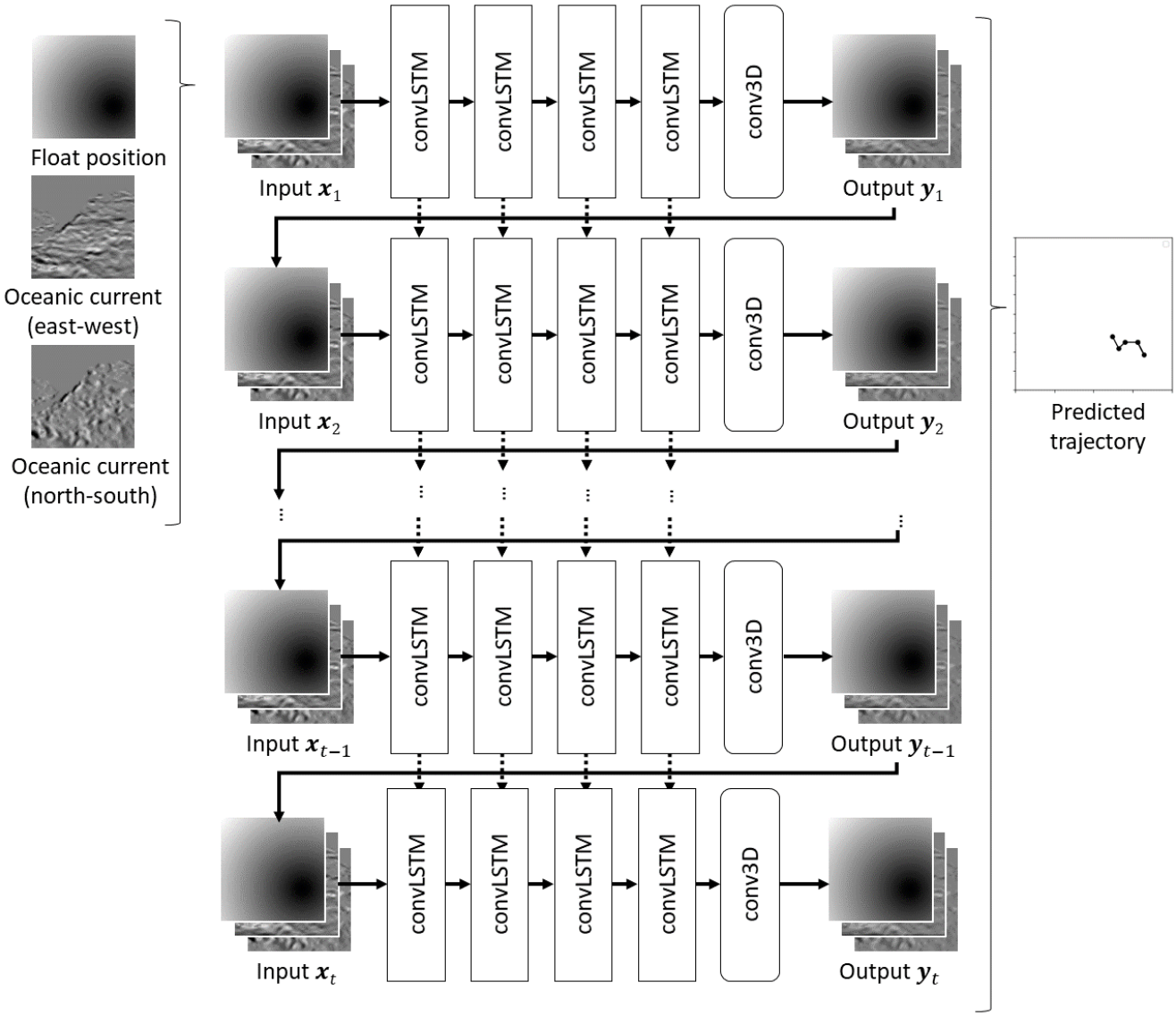
The ocean is recognized as a driving source of global warming and climate changes. This is because it occupies about 70% of the earth's surface and has a heat capacity more than 1000 times as much as of the atmosphere. The physical state observation inside the ocean is necessary to understand oceanic variability; however, it is difficult by research vessels to conduct long-term ocean monitoring. Therefore, the international Argo project has started since 2000 with the aim of long-term, real-time, and globally-covered ocean monitoring system.

In this program, more than 30 countries operate more than 3,800 Argo Floats, which are autonomous buoys and report observation data in real-time via satellites. A certain country manages each float, and it is necessary to obtain permission if there is a possibility of entering the economic zone of another country. Currently, numerical simulation is performed to predict float trajectory before deploying the float; however, the numerical simulation does not take into account the occurrence of vortices that may affect the movement of the float. Therefore, applications for permissions are being made to all possible countries of which the float may enter the economic zone.

Therefore, this study proposes a machine learning-based method for Argo float trajectory prediction, which allows reducing the number of countries that have to obtain permissions to enter the float. The proposed method adopts convolutional long short term memory (ConvLSTM), which is a recurrent neural network and also has the advantages of a convolutional neural network.

The advantages of the proposed methods are that it performs inductive learning based on past float trajectories, and allows adopting multiple observation data that have different properties such as float positions and ocean current data. The float data consists of the latitude and longitude position and the time when floating on the sea surface every ten days. The ocean current data is based on the monthly average flow velocity in each direction of east, west, north, and south in a range of 0.5 x 0.5 degrees square. To handle both data with different properties in a unified manner, all data is translated into a single image containing multiple channels. In addition, to unify the time resolution, images of ocean current are linearly interpolated.

©2020. Japan Geoscience Union. All Right Reserved.



©2020. Japan Geoscience Union. All Right Reserved.

[E] Poster | A (Atmospheric and Hydrospheric Sciences)：A-CG Complex & General

[A-CG51] Satellite Earth Environment Observation

convener:Riko Oki(Japan Aerospace Exploration Agency), Yoshiaki HONDA(Center for Environmental Remote Sensing, Chiba University), Yukari Takayabu(Atmosphere and Ocean Research Institute, the University of Tokyo), Tsuneo Matsunaga(Center for Global Environmental Research and Satellite Observation Center, National Institute for Environmental Studies)

In recent years, we cannot avoid facing issues on global environmental changes that occur in various spatiotemporal scales. The earth environmental observation data by satellites became the necessary basic data to tackle and solve those issues. Due to the recent advancement in the observation sensor technique and the data processing technique, the satellite observation has been showing rapid progress, and the time is changing from examining the accuracy of the observation sensor data to the advancement of the data application, leading to broaden potential users. In these days application became synergetic, so we comprehensively pick up this topic in the Atmospheric and Hydrospheric Sciences Session of this Union Meeting that enables to comprise the atmospheric, oceanic and land sciences; by combining the intelligence and the knowledge of the party, we propose a session that aims to prompt further studies towards the issues on earth environmental change, the advancement in the data application and future plans of Earth Observation missions.

[ACG51-P01] Australian bushfire captured by AHI/Himawari-8 and SGLI/GCOM-C

*Yukio Kurihara[1], Kazuhisa Tanada[1], Hiroshi Murakami[1], Misako Kachi[1] (1.Japan Aerospace Exploration Agency / Earth Observation Research Center)

[ACG51-P02] Detecting the Kuroshio-induced island vortices observed from GCOM-C and Himawari-8 data

*Po-Chun Hsu[1], Chung-Ru Ho[1] (1.Department of Marine Environmental Informatics , National Taiwan Ocean University)

[ACG51-P03] **Variability of groundwater storage in Northern India using the GRACE**

*Amit K Singh[1], M Saravanan[2], Swetabh Patel[3] (1.School of Environmental Sciences, Jawaharlal Nehru University,New Delhi, 2.College of Health Science,Mekelle University, Ethiopia, 3.Department of Agronomy,Iowa State University USA)

[ACG51-P04] The characteristics of precipitation and anvil cloud detected by GPM/DPR

*Koichi Toyoshima[1], Hitoshi Hirose[2], Atsushi Higuchi[1] (1.Center for Environmental Remote Sensing, Chiba University, 2.JAXA EORC)

[ACG51-P05] Improvement for infrared rainfall estimation algorithm of GSMaP using machine learning

*Hitoshi Hirose[1], Takuji Kubota[1], Atsushi Higuchi[2], Koichi Toyoshima[2], Shoichi Shige[3], Tomoo Ushio[4], Tomoaki Mega[4] (1.Japan Aerospace Exploration Agency, 2.Center for Environmental Remote Sensing, Chiba university, 3.Department of Science, Kyoto University, 4.Department of Engineering, Osaka University)

[ACG51-P06] Sensitivity experiment of aerosol models in aerosol retrieval algorithm and comparison with ground-based observation using GOSAT/CAI and GOSAT-2/CAI-2 data

*Makiko Hashimoto[1], Hideaki Takenaka[1], Chong Shi[1], Teruyuki Nakajima[1] (1.Japan Aerospace Explortion Agency)

[ACG51-P07] High resolution Motion Vector for the GSMaP MVK

*Tomoaki Mega[1], Tomoo Ushio[1] (1.Osaka Univ.)

[ACG51-P08] Validation of GSMaP toward practical hydrological use over Vietnam: basin-scale validation and estimation of accuracy with time lapse from microwave observation

*Masato I. Nodzu[1], Jun Matsumoto[1,2], Thanh Ngo-Duc[3], Long Trinh-Tuan[3], Tri Truong-Duc[4] (1.Tokyo Metropolitan University, 2.Japan Agency for Marine-Earth Science and Technology, 3.University of Science and Technology of Hanoi, Vietnam Academy of Science and Technology, 4.Ministry of Natural Resources and Environment, Vietnam)

[ACG51-P09] Cloud and aerosol discrimination algorithm for EarthCARE/ATLID lidar

*Eiji Oikawa[1], Hajime Okamoto[1], Tomoaki Nishizawa[2], Kaori Sato[1], Rei Kudo[3] (1.Research Institute for Applied Mechanics, Kyushu University, 2.National Institute for Environmental Studies, 3.Meteorological Research Institute, Japan Meteorological Agency)

[ACG51-P10] **Climate and air pollution impact on wheat crop over Eastern Indo Gangetic Plains of India**

*geetika sonkar[1] (1.Banaras Hindu University)

[ACG51-P11] Orverview of Earth Clouds, Aerosols and Radiation Explorer (EarthCARE) projects

*Takahashi Chikako[1], Riko Oki[1], Takuji Kubota[1], Maki Kikuchi[1], Yuichiro Hagihara[1], Mayumi YOSHIDA[1] (1.Japan Aerospace Exploration Agency)

[ACG51-P12] Sources of countercurrent in northeastern Taiwan

*Chen-Chen Ho[1], Po-Chun Hsu[1], Ching-Yuan Lu[1], Chung-Ru Ho[1] (1.Department of Marine Environmental Informatics, National Taiwan Ocean University)

[ACG51-P13] **An improved procedure for estimation of propagation distance of tweek atmospherics**

*Masafumi Kanno[1], Hiroyo Ohya[2], Kazuo Shiokawa[3], Hiroyuki Nakata[2], Toshiaki Takano[2] (1. Graduate School of Science and Engineering, Chiba University, 2.Graduate School of Engineering, Chiba University, 3.Institute for Space-Earth Environmental Research, Nagoya University)

[ACG51-P14] Current status of the calibration for the GPM DPR

*Takeshi Masaki[1], Toshio Iguchi[2], Kaya Kanemaru[3], Kinji Furukawa[4], Naofumi Yoshida[1], Takuji Kubota[5], Riko Oki[5] (1.Remote Sensing Technology Center of Japan , 2.Earth System Science Interdisciplinary Center, University of Maryland, 3.National Institute of Information and Communications Technology, 4.Satellite Applications and Operations Center, Japan Aerospace Exploration Agency, 5.Earth Observation Research Center, Japan Aerospace Exploration Agency)

[ACG51-P15] Observing Simulation System Experiment for Future Small Precipitation Radar Constellation: Impact on GSMaP Accuracy

*Yamaji Moeka[1], Takuji Kubota[1] (1.Japan Aerospace Exploration Agency (JAXA))

[ACG51-P17] **Calibration of INSAT-3D meteorological satellite imager visible channel using Moon**

*Shailesh Parihar[1], A.K. Mitra, R. Bhatla[1] (1.Banaras Hindu University, Varanasi, India)

Australian bushfire captured by AHI/Himawari-8 and SGLI/GCOM-C

*Yukio Kurihara[1], Kazuhisa Tanada[1], Hiroshi Murakami[1], Misako Kachi[1]

1. Japan Aerospace Exploration Agency / Earth Observation Research Center

JAXA in collaboration with JMA provides geophysical parameters retrieved from the data obtained with AHI/Himawari-8. The wildfire product is one of the Himawari-8 products by JAXA. We developed a new wildfire product in 2019, which provides the fire radiative power (FRP) determined by performing the bi-spectral method to 2.3- and 3.9-micron data. About 60 % of the preliminary detected wildfire has agreed with the MOD6 fire products, and the statistical comparison of FRP shows a good agreement between the new product and MOD6.

SGLI is the optical sensor onboard the GCOM-C satellite which JAXA launched in Dec. 2017. SGLI has 11 channels for visible to near-infrared wave range, 6 channels for short-wavelength to thermal infrared wave range, and two polarization channels for visible and near-infrared wavelength. The spatial resolution is switchable between 250 m and 1 km except for some channels which have the 1 km of the resolution. SGLI observes land and the seas near land with the 250 m resolution and open ocean with the 1 km resolution.

The newly developed Himawari-8 wildfire product and SGLI have captured the Australian bushfire from September 2019 to early 2020. The fire radiative energy (FRE) and the burned biomass emission have been calculated based on retrieved FRPs. And a cumulative total of the burned area has been calculated from the fire fractions determined for FRP and compared the area estimated based on NDVI calculated with the SGLI data obtained with the 250 m resolution.

Keywords: Wildfire, Himawari-8, GCOM-C

©2020. Japan Geoscience Union. All Right Reserved.

Detecting the Kuroshio-induced island vortices observed from GCOM-C and Himawari-8 data

*Po-Chun Hsu[1], Chung-Ru Ho[1]

1. Department of Marine Environmental Informatics , National Taiwan Ocean University

When the Kuroshio passes Green Island, a small island located southeast of Taiwan, well-organized vortices were formed by the interaction between the current and the island. Previous researches have used high-resolution satellite imagery, acoustic Doppler current profiler data, cruise observations, and numerical models to analyze the Green Island wakes, however, there are still many bottlenecks and questions to be resolved. To more understand the spatial structure of island wake and vortex trajectory, the sea surface temperature (SST) and chlorophyll-a (Chl-a) concentration derived from Himawari-8 and the second generation global imager (SGLI) of global change observation mission (GCOM-C) were used in this study. Based on the GCOM-C data, the horizontal SST and Chl-a variations in observed lines, the fronts of SST and Chl-a between the wake and the Kuroshio, the distance between two consecutive vortices, and different structures of SST and Chl-a in the same vortex have been investigated. Based on the Himawari-8 data, totals of 101 vortex cases from July 2015 to December 2019 have been calculated. The average vortex propagation speed was 0.95 m/s, and more than half of the vortices have propagation speed between 0.8-1.2 m/s. The average incoming surface current speed of Green Island was 1.15 m/s which was calculated by the maximum cross-correlation (MCC) method. In total of 38 cases of two continuous vortices, the average vortex shedding period was 14.8 hours, and the results agreed to the ideal Strouhal-Reynolds number fitting curve relation. Our results suggested that the size of Green island and the horizontal eddy viscosity are suitable selected 5 to 6 km and the 100 m^2s^{-1}, respectively.

Keywords: Island vortex, Kuroshio, Himawari-8, GCOM-C

©2020. Japan Geoscience Union. All Right Reserved.

Variability of groundwater storage in Northern India using the GRACE

*Amit K Singh[1], M Saravanan[2], Swetabh Patel[3]

1. School of Environmental Sciences, Jawaharlal Nehru University,New Delhi, 2. College of Health Science,Mekelle University, Ethiopia, 3. Department of Agronomy,Iowa State University USA

Groundwater is the vital and largest source of freshwater in India. Changing climate, anthropogenic activities and rising population have affected groundwater storage. Intensive exploitation of groundwater resources leads to depletion and scarcity of water which significantly affects the ecosystem and economic developments. In this work, we quantified the long-term spatiotemporal changes in the climate and groundwater storage in the northern region of India where significant depletion of the groundwater has been observed in recent years. For the monitoring and measuring groundwater changes in the region, observed well data and the satellite data from NASA’ s Gravity Recovery and Climate Experiment (GRACE) have been used for the period 2002 to 2016. The results were well-validated in correspondence with the observed and satellite data. The rainfall was highly variable during the study period and the satellite data reflects the occurrence of water loss in the region, The GRACE satellite showed a decline with the rate of 2.14 cm/year in the groundwater storage. This loss was influenced by the rise in temperatures and marked drought years which led to the anthropogenic withdrawals of groundwater for sustaining the agricultural crops. The information from the GRACE can be used for the various applications in groundwater studies which will be imperative to formulate the policies to achieve the goals of sustainable agricultural production and groundwater resources management.

Keywords: GRACE, Groundwater storage, , Climate

©2020. Japan Geoscience Union. All Right Reserved.

The characteristics of precipitation and anvil cloud detected by GPM/DPR

*Koichi Toyoshima[1], Hitoshi Hirose[2], Atsushi Higuchi[1]

1. Center for Environmental Remote Sensing, Chiba University, 2. JAXA EORC

The anvil cloud spreads thinly in the upper troposphere with deep convection. The upper clouds play an important role in the radiation budget of the earth, and in order to understand the characteristics of upper cloud using GPM. GPM dual frequency precipitation radar (DPR) is expected to detect a weak signal due to the anvil cloud because it has improved sensitivity compared to the PR of TRMM era. The purpose is to detect anvil clouds by GPM precipitation radar and clarify regional characteristics.
The data for this study is GPM/Ku and Ka band radar standard product version 6, the parameter is flag anvil, ZfactorCorrected, nearSurfaceRain. The study time period is March 2014 to December 2019.
From the results of the vertical structure using CFAD, signals (14 to 18 dBZ) weaker than 18 dBZ, which was the detection limit of TRMM/PR, were detected. In the central African continent where convection is active, the relative proportion of anvil clouds without rainfall is higher than that with anvil clouds with rainfall, suggesting that the anvil cloud is widespread. In the western Pacific Ocean, where the convective activity is high, the echo of mode is weaker and the altitude tends to be lower than that of the land in Africa. In the eastern Pacific Ocean where the short rainfall system is dominant, although the sample size was small, the echo intensity and mode were as high as the western Pacific Ocean. In the sea area, echoes are observed below 16 dBZ and below 5 km.
We also investigated the relationship between the echo top height and rainfall rate of adjacent rainfall samples and the anvil cloud profile. While there is a correspondence between the convection echo top height and the anvil cloud ice particle height, the anvil cloud profile does not depend on the intensity of adjacent rain samples.
In the presentation, we will introduce the evaluation of estimated precipitation products by Himawari-8 for precipitation that covered by anvil cloud.

Keywords: anvil cloud, precipitation, satellite, GPM/DPR

©2020. Japan Geoscience Union. All Right Reserved.

Improvement for infrared rainfall estimation algorithm of GSMaP using machine learning

*Hitoshi Hirose[1], Takuji Kubota[1], Atsushi Higuchi[2], Koichi Toyoshima[2], Shoichi Shige[3], Tomoo Ushio[4], Tomoaki Mega[4]

1. Japan Aerospace Exploration Agency, 2. Center for Environmental Remote Sensing, Chiba university, 3. Department of Science, Kyoto University, 4. Department of Engineering, Osaka University

The Global Satellite Mapping of Precipitation (GSMaP) produce global precipitation data with one hour temporal resolution by using microwave radiometer (MWR) on board low-Earth-orbit satellites and Infrared (IR) radiometer on board geostationary meteorological satellites (GEOs). In the GSMaP, the rainfall observed by a MWR is propagating along with the moving vector calculated by GEO IR observations for the interpolation of the gaps in MWR observation coverage. Since the GSMaP rainfall rate complemented with IR algorithms is based on the assumption that deeper clouds are more likely to produce heavy rainfall, conspicuous underestimation of rainfall occurred for heavy precipitation from low-level cloud. Observation bands available for GEO have dramatically increased from the conventional about 3 to 9 after latest GEO called Himawari-8 was launched in October 2014. By using the Himawari-8 IR multi-channel observations, we created high-frequency precipitation data, called Himawari Rainfall Estimation Algorithm (HRA; Hirose et al. 2019). We used Random Forest (RF) machine learning method to make the HRA and used Ku-band precipitation radar (KuPR) observation of the Global Precipitation Measurement Mission (GPM) core satellite as truth of rain.

Hirose et al. (2019) verified the accuracy of HRA in the mid-latitudes of the Northern Hemisphere using radar-AMeDAS rain rate and showed that HRA has higher estimation accuracy for heavy rainfall caused by clouds with relatively low cloud-top height than GSMaP with only single IR band. In particular, the three water vapor bands, which became available for the first time on Himawari-8, has greatly contributed to the improvement for the estimation accuracy of the heavy rain. In this presentation, we show the results of global accuracy verification using ground-based radar network in the tropics. The HRA showed the same estimation accuracy in the tropics as the GSMaP MWR observation. In addition, GSMaP tended to overestimate rainfall over sea where rainfall was complemented by using only a single IR band, but HRA did not show such overestimation with IR multiband. The effectiveness of IR multi-band observation was confirmed even in the tropical region. We will also present the results of an attempt to improve estimation accuracy of the GSMaP cloud movement vector with single IR band by using machine learning approach.

Keywords: machine learning, GSMaP, Himawari-8

©2020. Japan Geoscience Union. All Right Reserved.

Sensitivity experiment of aerosol models in aerosol retrieval algorithm and comparison with ground-based observation using GOSAT/CAI and GOSAT-2/CAI-2 data

*Makiko Hashimoto[1], Hideaki Takenaka[1], Chong Shi[1], Teruyuki Nakajima[1]

1. Japan Aerospace Explortion Agency

Aerosol particles in the atmosphere has an impact not only for the Earth’s radiation budget and changing the Earth’s climate, but also on human health. These aerosol particles are often generated by human activity and are transported to other regions. Satellite remote sensing is an effective way to monitor the atmospheric aerosols in wide area including a source region like an urban area.

Greenhouse gases Observing Satellite-2 (GOSAT-2) that is a successor of GOSAT was launched on October 29th, 2019. GOSAT- 2 has Cloud and Aerosol Imager called CAI-2. CAI-2 performs two-directional observation in forward and backward directions and makes an observation at ten bands composed of seven wavelengths at 340, 380, 443, 550, 674, 869 and 1630 nm. The spatial resolution (IFOV) is 920 m at a wavelength of 1630 nm and 460 m at the other wavelengths. CAI-2 is characterized by having two ultraviolet (UV) bands at 340 and 380 nm. UV band has sensitivity for light absorption of dust particles and light absorption particles such as BC and OC.

We have developed aerosol retrieval algorithm called MWPM (Multiple wavelengths and pixels method) (Hashimoto and Nakajima, 2017). The method simultaneously retrieves fine and coarse mode AOT and single scattering albedo by using several wavelengths and spatial difference of surface reflectance. The method is useful for aerosol retrieval over spatially inhomogeneous surface region like an urban area. The algorithm is applied to CAI-2 aerosol retrieval, and aerosol optical properties such as AOT of fine and coarse particles, Ångström exponent (AE), and BC volume fraction are derived.
In this algorithm, we assume aerosol models for fine and coarse mode aerosols. However, aerosol particle size and these light absorption properties are different in different regions. It is important to know a bias occurred by assumed aerosol models when we validate the aerosol products by ground-based observations and modify the algorithm, so we have investigated the impact on the products by assumed aerosol models, such as aerosol size distribution, complex refractive indices, aerosol height etc.. We show the result of the sensitivity test and discuss aerosol models in the algorithm using a comparison result between aerosol properties from GOSAT CAI/GOSAT-2 CAI-2 and that from ground- based observation such as AERONET and SKYNET.

Keywords: Aerosol, Remote sensing , Atmospheric radiative transfer

©2020. Japan Geoscience Union. All Right Reserved.

High resolution Motion Vector for the GSMaP MVK

*Tomoaki Mega[1], Tomoo Ushio[1]

1. Osaka Univ.

The Global Satellite Mapping of precipitation (GSMaP) is global precipitation map with 0.1 gridded every one hour. The GSMaP motion vector with Kalman filter (MVK) precipitation estimated by passive microwave radiometer on low-earth orbit. Although the observation area of the sensors does not cover all earth in an hour. Thus the GSMaP MVK fill the no observation area from previous and feature observation by the Kalman filter with cloud motion vector. The motion vector is estimated from brightness temperature of IR on geosynchronous observation satellites. We are developing high resolution technique for the GSMaP MVK. The observation area of radiometers becomes narrower in a shorter time interval. So the filling region of the high temporal and spatial resolution GSMaP MVK is wider than the current GSMaP MVK. The motion vector for the high-temporal-and-spatial resolution GSMaP MVK must be higher-spatial and temporal resolution by the current motion vector. The resent geosynchronous orbit weather satellite has a high spatial and temporal resolution microwave sounder. The atmospheric motion vector (AMV) is estimation from the sounder. The AMV is high resolution and include altitude information. We will apply the AMV for the high resolution GSMaP MVK. The AMV is, however, not gridded data. The GSMaP MVK algorithm requires motion vector as gridded data. Therefor we develop a technique to calculate motion vector for the high-resolution GSMaP MVK from the AMV. In my presentation, we introduce technique of high-resolution motion vector form the AMV.

Keywords: GSMaP, Precipitation, Atmospheric motion vector

©2020. Japan Geoscience Union. All Right Reserved.

Validation of GSMaP toward practical hydrological use over Vietnam: basin-scale validation and estimation of accuracy with time lapse from microwave observation

*Masato I. Nodzu[1], Jun Matsumoto[1,2], Thanh Ngo-Duc[3], Long Trinh-Tuan[3], Tri Truong-Duc[4]

1. Tokyo Metropolitan University, 2. Japan Agency for Marine-Earth Science and Technology, 3. University of Science and Technology of Hanoi, Vietnam Academy of Science and Technology, 4. Ministry of Natural Resources and Environment, Vietnam

1. Introduction

Satellite observation is a promising tool to grasp the horizontal distribution of precipitation intensity over mountainous regions where it is difficult to put gauge stations and surface weather radars are obstructed by orographic clutters. GSMaP has been developed based on passive microwave observation from the TRMM and GPM satellites with the aid of infrared observation and improved with some modification methods. However, the performance of GSMaP is still poor in one-to-one comparison in the scales of 0.1-degree-grid and one hour, i.e. at its highest resolution. Generally such precipitation data has tendency to perform better in lower resolution. It is useful to show a higher limit of resolution and expectant accuracy in a precipitation dataset. For example, in the use for flood warning, the highest resolution is not necessarily needed depending on features of a river basin like topography and expansion of the upstream region. In this study, we investigate the dependence of the GSMaP performance on scale of regional mean. We also examine the relationship between the performance of hourly precipitation and time lag from the microwave radiometer (MWR) observation.

2. Data and methods

The GSMaP version used in this analysis is the semi-standard product, RNL version 6 from 2006 to 2010.

The horizontal resolution dependency is assessed by daily regional mean precipitation in different regions within the Thu Bon River basin, compared with the VnGP data. The regions are A, B, C and D in order of areas. The parameters used for assessment are biases, root mean square difference (RMSD), probability of detection (POD) and false alarm ratio (FAR). The POD and FAR are determined for heavy precipitation over the 95th percentile of hourly precipitation in the VnGP. The analysis period is months from April to October in 5 years from 2006 to 2010.

We examine the relationship between the GSMaP performance and time lag from the MWR observation for hours with precipitation exceeding 1 mm/hour in gauge observation from April to September in 2010. The GSMaP data are compared with gauge precipitation data observed at 6 stations within northern Vietnam. Besides biases and RMSD, we also define GGR as the ratio of GSMaP precipitation to gauge observation. The GGR in the best skill is 1.0. The closer to 1.0 the GGR value is, the better performance we obtain. The performance is measured with the ratio of cases with GGR from 0.5 to 2.0 to all the cases.

3. Results and discussions

The daily regional mean of the GSMaP precipitation is compared with that of the VnGP over the upstream basin of the Thu Bon River in central Vietnam, over four different regions. Against our expectation, the GSMaP performance shows a small dependence on the difference of regions (Fig. 1). The RMSD normalized by the total precipitation shows smaller values for the regional mean over the larger areas, except the region A. The smallest bias is seen in the largest region D. However, it is difficult to be

©2020. Japan Geoscience Union. All Right Reserved.

convinced that GSMaP could reproduce the closer values to the VnGP in the larger-area region, because the biases are scattered in the positive and negative values over the smaller region. The POD and FAR show worse values in regional mean over the larger-area regions. In this analysis, only the larger-area regions (C, D) include highlands over 800 m above sea level. This variety of orographic features in the regions may affect impartiality in the comparison analysis.

The ratio of cases with GGR from 0.5 to 2.0 to all the cases is correlated with the time lag from the MWR observation (Fig. 2). At almost all the grids with gauge stations, the higher this ratio, the smaller time lag. A smaller RMSD between GSMaP and the gauge precipitation is roughly related with a smaller time lag from the MWR observation. However, exceptions to this tendency are not negligible. It is difficult to find correlation between the bias normalized by the total precipitation and the lag time. In the present study, we limited the analysis to time with precipitation exceeding 1 mm/hour. On the other hand, GSMaP sometimes shows zero precipitation under this limitation. Therefore, it is challenging for using a simple RMSD to sufficiently estimate the difference of the both data. This problem also applies to the bias analysis.

Keywords: satellite precipitation observation, GSMaP, validation

©2020. Japan Geoscience Union. All Right Reserved.

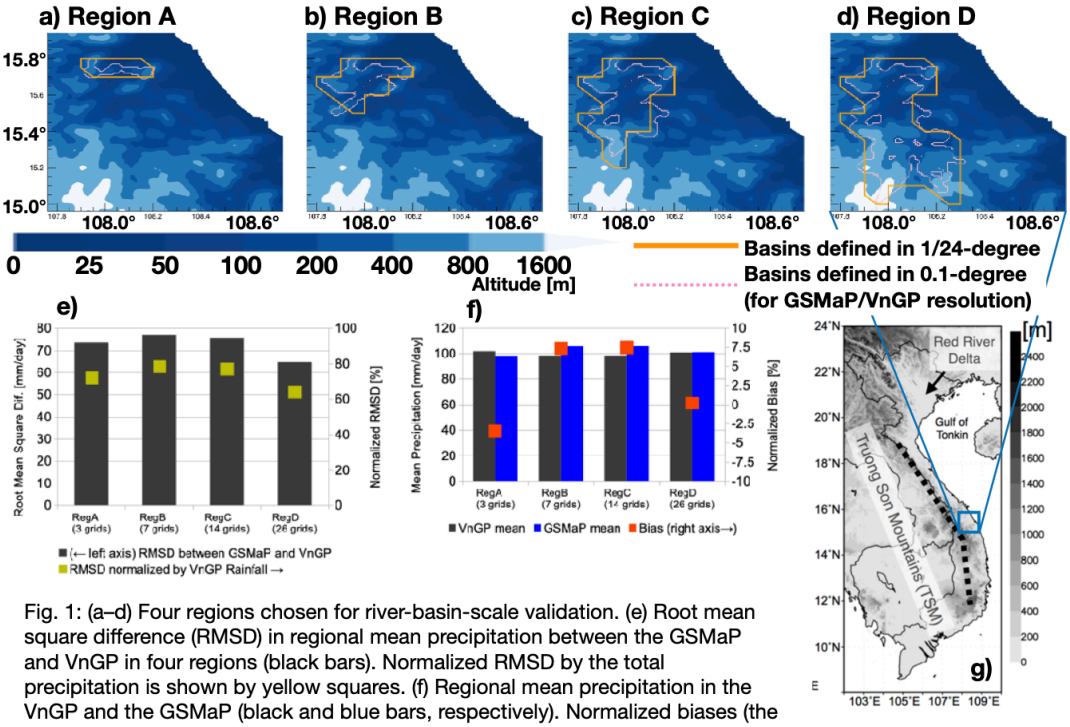


Fig. 1: (a–d) Four regions chosen for river-basin-scale validation. (e) Root mean square difference (RMSD) in regional mean precipitation between the GSMaP and VnGP in four regions (black bars). Normalized RMSD by the total precipitation is shown by yellow squares. (f) Regional mean precipitation in the VnGP and the GSMaP (black and blue bars, respectively). Normalized biases (the GSMaP minus the VnGP) are shown by red squares. (g) Countrywide map of Vietnam to show the location of the chosen area.

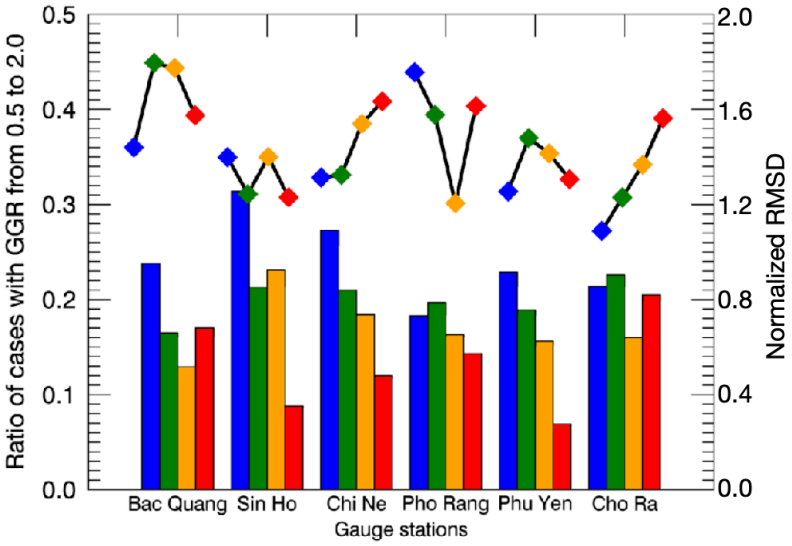


Fig. 2: Ratio of cases with GGR from 0.5 to 1.0, to all the cases (bars) and root mean square difference between the GSMaP and the VnGP normalized with the total precipitation (lines and diamonds). The green, orange and red bars and diamonds show the time lag from microwave observation with about one hour, from one to three hours and over three hours, respectively. The blue bars and diamonds show that the microwave radiometer observed almost over the gauge station.

©2020. Japan Geoscience Union. All Right Reserved.

Cloud and aerosol discrimination algorithm for EarthCARE/ATLID lidar

*Eiji Oikawa[1], Hajime Okamoto[1], Tomoaki Nishizawa[2], Kaori Sato[1], Rei Kudo[3]

1. Research Institute for Applied Mechanics, Kyushu University, 2. National Institute for Environmental Studies, 3. Meteorological Research Institute, Japan Meteorological Agency

The EarthCARE satellite with the high spectral resolution lidar (HSRL) at 355 nm will be launched in 2022. The cloud mask algorithm at 532 nm had been developed for the CALIPSO satellite retrieval (Hagihara et al., 2010). We have been working on development of the cloud mask algorithm for the EarthCARE lidar retrieval at 355 nm. In this study, we perform data analysis of the observation data of the NASA airborne HSRL (Burton et al., 2015; 2018) and AD-Net Raman lidar (Nishizawa et al., 2017) to determine the threshold values of attenuated and particle backscatter coefficients (β'_{th} and β_{th}) at 355 nm for the discrimination of clouds and aerosols. The color ratio (ratio of the backscatter coefficients between 2 wavelengths) at 355 and 532 nm, which is measured by the HSRL observations, is used to discriminate aerosols and clouds, because the wavelength dependence of backscatter coefficient for aerosols is larger than that for clouds. In the analysis of HSRL airborne observations, we defined the particles, which have attenuated and particle color ratios smaller than 1 below 6.5 km altitude, as aerosols. From these results, the threshold values of β at 355 nm for discrimination of clouds and aerosols are estimated as $\beta'_{th,355}$ = 4.5-5.7×10^{-6} [$m^{-1}sr^{-1}$] and $\beta_{th,355}$ = 2.2-5.7×10^{-6} [$m^{-1}sr^{-1}$]. In addition, we perform the test of EarthCARE lidar retrieval using these new threshold values and the simulated data of the global atmospheric model NICAM (Sato et al., 2014) and J-sim (Hashino et al., 2013).

Keywords: lidar, cloud, aerosol, EarthCARE, HSRL

©2020. Japan Geoscience Union. All Right Reserved.

Climate and air pollution impact on wheat crop over Eastern Indo Gangetic Plains of India

*geetika sonkar[1]

1. Banaras Hindu University

Rapid urbanization and economic development in India has led to an increase in the air pollution which in turn may affect the ecosystem such as crop production. The present study is aimed to analyze the long term variability of climate variables (Temperature maximum (TMAX), Temperature minimum (TMIN), Rainfall (RAIN) & Solar radiation (SRAD)) from 1986 to 2015 and satellite retrieved aerosol optical depths (AOD) from 2001 to 2015 during the wheat season over the Eastern Indo Gangetic plains of India. The study focuses on to examine the possible implications of aerosols loading on the wheat crop yield (rabi season). A decreasing trend in TMAX and TMIN was noted in the crop growing season. The long term variation in the SRAD had a significant influence in declining the solar radiation over the region. The statistical (regression) model suggests that there is an influence of aerosols on climatic parameters which indirectly had affected the wheat yield. For every unit increase in AOD, a decrease in TMAX, TMIN and SRAD was recorded. The influence of aerosols on wheat crop yield had declined the yield by 2%. The present analysis may be crucial in terms of establishing the potential impact of changing climate and air quality on regional food security and therefore, must need to be considered in policy decisions.

Keywords: IGP, Climate, AOD, Regression, Wheat

©2020. Japan Geoscience Union. All Right Reserved.

Climate and air pollution impact on wheat crop over Eastern Indo Gangetic Plains of India

Geetika Sonkar
DST-Mahamana Centre of Excellence in Climate Change Research
Institute of Environment and Sustainable Development
Banaras Hindu University, Varanasi-221005, India
Email: 17.geet@gmail.com; mall_raj@rediffmail.com

ABSTRACT

Rapid urbanization and economic development in India has led to an increase in the air pollution which in turn may affect the ecosystem such as crop production. The present study is aimed to analyze the long term variability of climate variables (Temperature maximum (TMAX), Temperature minimum (TMIN), Rainfall (RAIN) & Solar radiation (SRAD)) from 1986 to 2015 and satellite retrieved aerosol optical depths (AOD) from 2001 to 2015 during the wheat season over the Eastern Indo Gangetic plains of India. The study focuses on to examine the possible implications of aerosols loading on the wheat crop yield (rabi season). A decreasing trend in TMAX and TMIN was noted in the crop growing season. The long term variation in the SRAD had a significant influence in declining the solar radiation over the region. The statistical (regression) model suggests that there is an influence of aerosols on climatic parameters which indirectly had affected the wheat yield. For every unit increase in AOD, a decrease in TMAX, TMIN and SRAD was recorded. The influence of aerosols on wheat crop yield had declined the yield by 2%. The present analysis may be crucial in terms of establishing the potential impact of changing climate and air quality on regional food security and therefore, must need to be considered in policy decisions.

Keywords: IGP, Climate, AOD, Regression, Wheat

©2020. Japan Geoscience Union. All Right Reserved.

Orverview of Earth Clouds, Aerosols and Radiation Explorer (EarthCARE) projects

*Takahashi Chikako[1], Riko Oki[1], Takuji Kubota[1], Maki Kikuchi[1], Yuichiro Hagihara[1], Mayumi YOSHIDA[1]

1. Japan Aerospace Exploration Agency

Earth Clouds, Aerosols and Radiation Explorer (EarthCARE) have been developing in cooperation between Japan and Europe. The EarthCARE will be equipped with four sensors, which are the Cloud Profiling Radar (CPR), the Atmospheric Lidar (ATLID), the Multi-Spectral Imager (MSI), and the Broad-Band Radiometer (BBR). The EarthCARE is expected to contribute to improving the accuracy of climate change projections by continuously data collection for improving numerical climate models, such as cloud and aerosol distributions and radiation balance energy, through global observation using the four sensors.
The Japan Aerospace Exploration Agency (JAXA) have been developing the Cloud Profiling Radar (CPR) in cooperation with the National Institute of Information and Communications Technology (NICT). The CPR is the first satellite-borne Doppler radar on the W-band (94 GHz), and we can observe not only the vertical structure of clouds, but also the ascending and descending velocity of clouds.
In addition, the observation data product of each sensor mounted on EarthCARE is planned to be created and offered to the user, and the analysis of the observation data and the application research using the observation data are planned. In this poster session the current status of the EarthCARE mission will be introduced.

Keywords: EarthCARE, Cloud Profiling Radar, Clouds, Aerosols

©2020. Japan Geoscience Union. All Right Reserved.

Sources of countercurrent in northeastern Taiwan

*Chen-Chen Ho[1], Po-Chun Hsu[1], Ching-Yuan Lu[1], Chung-Ru Ho[1]

1. Department of Marine Environmental Informatics, National Taiwan Ocean University

A current along the coast of northeastern Taiwan has been reported by previous studies. Because it flows direction opposite to that of the Kuroshio, it is called a countercurrent. To know sources of the countercurrent, sea surface temperature data from Himawari-8, wind field data from WindSat, flow field data from The Copernicus Marine Environment Monitoring Service (CMEMS), outputs of the hybrid coordinate ocean model (HYCOM), cruise observations, and drifter data were analyzed. The field measurements by ship-board Acoustic Doppler Current Profiler (ADCP) during the cruise R/V Ocean Researcher II on November 13, 2019 showed that the countercurrent has an average speed of 0.18 m/s (ranges from 0.11 m/s to 0.25 m/s). This speed is consistent with the observation of drifters which originate from the Taiwan Strait Current. Satellite wind observations suggested that the countercurrent is forced by the summer monsoon from the Taiwan Strait. Satellite observations and model outputs also suggested that the cold dome near the northeast of Taiwan might be the other source of the countercurrent.

Keywords: Taiwan Strait Current, Kuroshio, Monsoon , Cold dome, Himawari-8, Drifter

©2020. Japan Geoscience Union. All Right Reserved.

An improved procedure for estimation of propagation distance of tweek atmospherics

*Masafumi Kanno[1], Hiroyo Ohya[2], Kazuo Shiokawa[3], Hiroyuki Nakata[2], Toshiaki Takano[2]

1. Graduate School of Science and Engineering, Chiba University, 2. Graduate School of Engineering, Chiba University, 3. Institute for Space-Earth Environmental Research, Nagoya University

Tweek atmospherics are very low frequency (VLF) / extremely low frequency (ELF) waves radiated from lightning discharge and propagate in the Earth-ionosphere waveguide for a long distance over 1000 - 12000 km. The tweeks have frequency dispersion that the frequency rapidly falls down from 10 kHz to 2 kHz during several tens of milliseconds. The occurrence rate of the tweeks are 50-60 per minute during nighttime in Japan [Ohya et al., JGR, 2015]. By analyzing tweeks, location of lightning in wide area and their reflection height in the D-region ionosphere can be estimated. However, it is difficult to estimate the horizontal propagation distance of tweeks with high accuracy, because of the rapid frequency variation of tweeks in frequency-time spectra and overlapping multiple tweeks. The accuracy of the lightning location estimated from tweek atmospherics has been estimated as less than 60 km in Europe [Santolik and Kolmasova, Sci. Rep, 2017]. The accuracy of lightning location for the lightning discharges of world-wide lightning location (WWLLN) data is less than 10 km [Rodger et al., 2004]. So far, the reflection height and the horizontal propagation distance of tweeks have been estimated by curve fitting on tweek dynamic spectra by the maximum entropy method (MEM). In this study, we improved our procedure to estimate the tweek propagation distances. The new procedure is based on conversion of non-linear dispersion equation to a linear equation. The linear equation would be more useful for estimating the propagation distance, even if attenuation around the cut-off frequency is significant. As a result of evaluation by pseudo-tweeks which have propagation distances in the range of 2000 –10000 km, the error of the propagation distance was estimated to be 6.7% by the new procedure and 13.8% by the previous method. In particular, the new procedure showed a great improvement for tweeks with propagation distances of less than 6000 km. In this presentation, we show the new procedure for tweek propagation distance in detail and discuss its accuracy.

©2020. Japan Geoscience Union. All Right Reserved.

Current status of the calibration for the GPM DPR

*Takeshi Masaki[1], Toshio Iguchi[2], Kaya Kanemaru[3], Kinji Furukawa[4], Naofumi Yoshida[1], Takuji Kubota[5], Riko Oki[5]

1. Remote Sensing Technology Center of Japan , 2. Earth System Science Interdisciplinary Center, University of Maryland, 3. National Institute of Information and Communications Technology, 4. Satellite Applications and Operations Center, Japan Aerospace Exploration Agency, 5. Earth Observation Research Center, Japan Aerospace Exploration Agency

The Global Precipitation Measurement (GPM) mission is an international collaboration mission between the United States and Japan to observe global precipitation using a GPM Core Observatory satellite and some collaborating satellites. The GPM Core Observatory, which was successfully launched in 2014, carries the Dual-frequency Precipitation Radar (DPR) and the GPM microwave imager (GMI).The mission requires that the DPR, which is composed of the Ku-band precipitation radar (KuPR) and the Ka-band precipitation radar (KaPR), be calibrated within ±1 dB because the estimation of precipitation rate depends significantly on the calibration. The calibration method basically follows the method that was used to calibrate the Precipitation Radar (PR) onboard the Tropical Rainfall Measuring Mission (TRMM) satellite. However, both the hardware and data processing method for calibration are improved by taking advantage of the lessons learned from the PR’s calibration. For instance, as to the estimation of radar’s antenna pattern, the effective beamwidths were determined by assuming an antenna pattern created by the Taylor distribution that was used to design the antennas instead of assuming a Gaussian antenna pattern. Four-year calibration including these improvements provides the new precise parameters of DPR’s calibration, and the analysis of calibration data shows that the DPR’s performance is very stable and that the error in the calibration accuracy is within ±1 dB. The new parameters increased the KuPR’s radar reflectivity factor (Z) by about 1.3 dB and that of the KaPR by about 1.2 dB from the pre-calibrated Z values, and the minimum detectable radar reflectivities were 16.41 dBZ, 20.12 dBZ, and 14.66 dBZ for KuPR, matched beam of KaPR and high-sensitivity beam of KaPR, respectively. The calibration methods were applied to the re-examination of the PR’s calibration. After applying the new calibration methods to both DPR and PR, normalized radar cross sections ($\sigma 0$) from the DPR and PR agree with each other.

©2020. Japan Geoscience Union. All Right Reserved.

Observing Simulation System Experiment for Future Small Precipitation Radar Constellation: Impact on GSMaP Accuracy

*Yamaji Moeka[1], Takuji Kubota[1]

1. Japan Aerospace Exploration Agency (JAXA)

Satellite observation is a unique and effective tool to cover a large area homogeneously in a short time. Its advantage is obvious when it observes geophysical parameters varying both in temporally and horizontally, like precipitation. One of the important global precipitation observation missions from space is the Global Precipitation Measurement (GPM) Mission, which is composed of the GPM core satellite and multi constellation satellites carrying passive microwave (PMW) instruments. GPM core satellite carries the Dual-frequency Precipitation Radar (DPR) and GPM Microwave Imager (GMI). DPR consists of the Ku-band Precipitation Radar (KuPR) and the Ka-band Precipitation Radar (KaPR), aiming to observe global precipitation with high accuracy under the GPM mission. GPM core satellite carries both active and passive sensors and is in non-sun-synchronous orbit, therefore, GPM core satellite can be a calibrator of PMW sensors onboard multi constellation satellites in sun-synchronous orbit. The constellation satellites can contribute to extending coverage and increasing frequency. Thus, GPM mission achieves high accurate and high frequent global precipitation measurement.

The Japan Aerospace Exploration Agency (JAXA) has developed the multi-satellite precipitation product called Global Satellite Mapping of Precipitation (GSMaP) with the GPM core and constellation satellites. GSMaP has been developed by using combined data from PMW sensors in low Earth orbit and infrared (IR) radiometers in geostationary Earth orbit, and provides hourly global (60˚S - 60˚N) precipitation map by 0.1 x 0.1 degrees latitude/longitude. As advanced knowledge given by previous studies have been implemented to the algorithms, the accuracy of GSMaP has been improved. Such kind of precipitation product with high spatiotemporal frequency leads to wider applications over societal benefit areas, such as weather forecasts, flood predictions, agricultural monitoring and so on. Especially over the tropical Asian countries, GSMaP has been used as an infrastructure in operational agencies for meteorology and disaster management. Hence, it is strongly desired to keep the GSMaP maintained and improved by updating the algorithms.

As one of the future precipitation observation missions discussed in JAXA, there is a concept of small spaceborne precipitation radar (PR) constellation in the Tropics. The PR can obtain quantitative precipitation measurements over the land as well as over the ocean. It is well-known that there are still large uncertainties of rainfall estimates over the land using the PMW because over-land PMW algorithms basically use only scattering signals due to high and variable emissivity of the land surface. Current GPM/DPR dataset is used as a database to calculate look-up tables for retrieving rainfall from PMW sensors, because the observation frequency is insufficient to retrieve rainfall directly from DPR. If the future PR constellation is realized, the frequency of the PR data with high accuracy can increase, which leads to improve the quality of the GSMaP.

The aim of this study is to quantify the contribution of the future PR constellation to the improvement of future GSMaP. We perform an Observing System Simulation Experiment (OSSE) for the future PR constellation. Also the pseudo PR data obtained from the experiment is input to the actual GSMaP processing system to evaluate the impact on the accuracy of GSMaP.

©2020. Japan Geoscience Union. All Right Reserved.

Keywords: GPM, GSMaP, Rainfall, Precipitation Radar, Future Mission

©2020. Japan Geoscience Union. All Right Reserved.

Calibration of INSAT-3D meteorological satellite imager visible channel using Moon

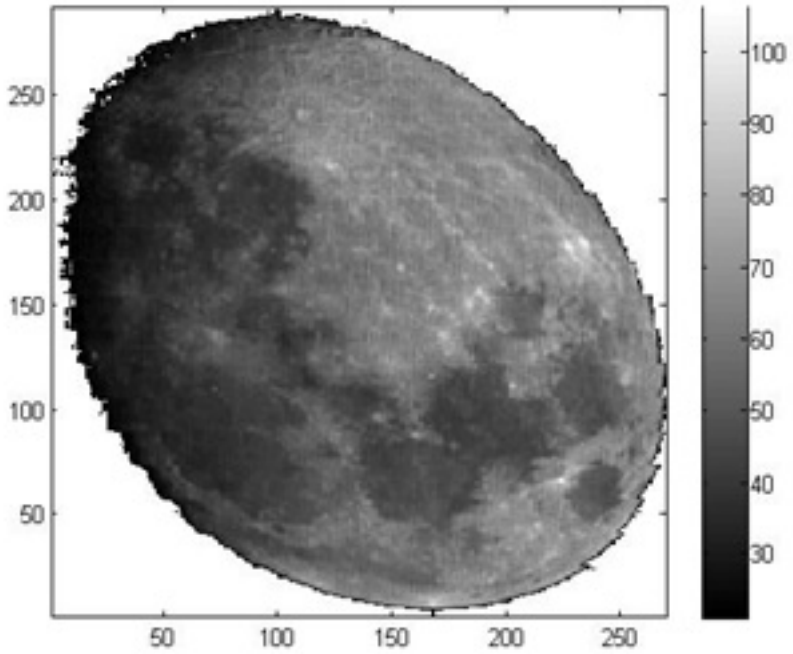
*Shailesh Parihar[1], A.K. Mitra, R. Bhatla[1]

1. Banaras Hindu University, Varanasi, India

INSAT-3D is India’s meteorological geostationary satellite an exclusive next generation mission designed for enhanced meteorological observations having 6 channel imager and 18 channel sounder. INSAT-3D Spacecraft was dedicated to Nation at National Satellite Meteorological Center (NSMC) indigenously designed developed INSAT-3D Meteorological Data Processing System (IMDPS), commissioned at India Meteorological Department (IMD) New Delhi on January 15, 2014. The Moon is being observed from INSAT-3D regularly in the of full-disk operational image of earth with rectangular field of regard in IMDPS New Delhi. INSAT-3D measurements of lunar surface observed in Visible (0.55 - 0.75 μm), Short Wave Infrared 1.55 - 1.70 μm, Mid Wave Infrared (3.80 - 4.00 μm), Water Vapor (WV) 6.50 - 7.10 μm, Thermal Infrared (TIR) 1 & 2, 10.3 - 11.3 μm & 11.5 - 12.5 μm wavelength regions. The visible and infrared wavelengths region provide a new and intriguing methodology of distinguish in sensitivities of Earth observing radiometers. The Moon has been widely used for calibration of earth-observation missions across international community due to its temporal stability absence of any intervening medium such as atmosphere and its spectral resemblance to ground targets. As a preliminary step, attempt has been made to calibrate the VIS channel of INSAT-3D imager using Moon as a calibration source. For the requirements, a GIRO (RObotic Lunar Observatory, ROLO) model has been installed in National Satellite Meteorological Centre, INSAT-3D Meteorological Data Processing System, India Meteorological Department and New Delhi for output irradiance of Moon. Further, this irradiance is compared with INSAT-3D-measured Moon irradiance during July 2015 to June 2016. The preliminarily result shows INSAT-3D is overestimating against the GIRO model output irradiance. However, the pattern found consistency during the period, and no degradation can be estimated with this short span of time and found useful to generate the coefficients.

Keywords: INSAT-3D, Lunar Calibration, GIRO Model

©2020. Japan Geoscience Union. All Right Reserved.



Moon is captured by INSAT-3D visible channel image acquired 2016 August 22, on 0858 UTC (right). (*Courtesy: GSICS Annual Meeting, Mitra A.K. and Parihar S., 2017).*

©2020. Japan Geoscience Union. All Right Reserved.

[E] Poster | A (Atmospheric and Hydrospheric Sciences)：A-CG Complex & General

[A-CG52] Large Ensemble Modeling Approaches as Tools for Climate and Impacts Research

convener:Rodgers Keith Bradley(IBS Center for Climate Physics), Shoshiro Minobe(Graduate School of Science, Hokkaido University), Hideo Shiogama(Center for Global Environmental Research, National Institute for Environmental Studies), Ryo Mizuta(Meteorological Research Institute)

Large ensemble model simulations are now integral tools for evaluating climate variability, climate change, and associated impacts. The range of tools applied encompasses Earth System Models (ESMs), Coupled General Circulation Models (CGCMs), Atmospheric General Circulation Models (AGCMs), Ocean General Circulation Models (OGCMs), and Regional Climate Models (RCMs), with the number of ensemble members typically spanning ten to several tens to one hundred. In addition to their utility in identifying emergent forced trends, they are also proving to be of great value in the study of extreme events and how extreme events evolve under anthropogenic perturbations. Furthermore, large ensembles of AGCMs nd OGCMs can prove invaluable as complements to fully coupled models in providing insights into scales and drivers of variability and trends, as well as climate feedbacks.
This session welcomes studies using the full range of large ensemble modeling tools. This includes studies of emergent trends and extreme events, and more generally studies that facilitate interpretation of observations as well as projections of future changes. Abstracts are particularly welcomed that address novel and emergent topics, including but not limited to compound events, biogeochemistry, and observing system design.

[ACG52-P01] Increase in Rain-on-Snow events in Japan as projected by large ensemble of regional climate simulations

*Masamichi Ohba[1], Hiroaki Kawase[2] (1.Central Research Institute of Electric Power Industry, 2.Meteorological Research Institute)

[ACG52-P02] Projected changes in extreme precipitation in a 60-km AGCM large ensemble and their dependence on return periods

*Ryo Mizuta[1], Hirokazu Endo[1] (1.Meteorological Research Institute)

[ACG52-P03] Detection and Analysis of Tropical Cyclones in the d4pdf Mega-ensemble Projection

*Adrean Webb[1], Tomoya Shimura[1], Nobuhito Mori[1] (1.Kyoto University, Disaster Prevention Research Institute, Coastal Disaster Research)

[ACG52-P04] ESM-projected global change in the indices of extreme weather using the TR3S method of bias-correction

*Martin Gomez-Garcia[1], Akiko Matsumura[1], Daikichi Ogawada[1] (1.Nippon Koei Co., Ltd. Research and Development Center)

[ACG52-P05] **Droughts, fires and fire emissions of CO_2 and $PM_{2.5}$ in equatorial Asia due to historical and future climate changes**

*Hideo Shiogama[1] (1.Center for Global Environmental Research, National Institute for Environmental Studies)

[ACG52-P06] Future change in phytoplankton phenology simulated by large ensemble experiment

*Ryohei Yamaguchi[1], Keith Rodgers[1,2], Karl J Stein[1,2], Axel Timmermann[1,2], John P Dunne[3], Richard D Slater[4], Sarah Schlunegger[4] (1.IBS Center for Climate Physics, 2.Pusan National University, 3.NOAA Geophysical Fluid Dynamics Laboratory, 4.Princeton University)

[ACG52-P07] Seasonality Constraints on the rate of Pteropod Habitat Compression under 21st Century Climate Change

*Keith Bradley Rodgers[1,2], Sarah Schlunegger[3], Richard Slater[3], Burke Hales[4] (1.IBS Center for Climate Physics, 2.Pusan National University, 3.AOS Program, Princeton University, 4.Oregon State University)

Increase in Rain-on-Snow events in Japan as projected by large ensemble of regional climate simulations

*Masamichi Ohba[1], Hiroaki Kawase[2]

1. Central Research Institute of Electric Power Industry, 2. Meteorological Research Institute

The phenomenon of rainfall on snow is called a rain-on-snow (ROS) event that can cause severe snowmelt hazards such as river flooding, snow avalanches, full-scale avalanches, slope failure, landslides that have significant impacts on various sectors (ecosystem, water resources, risk management and flood forecast). This study investigated the influence of climate change on the frequency of ROS events during the winter season in Japan. Climate projections obtained from the database for Policy Decision-making for Future climate change (d4PDF) is used to investigate the climate change impacts. The projected future climate in the regional model simulations showed increase in the ROS events over Japan Alps (mountainous regions in central Japan) and Hokkaido (northern part of Japan) where the region will record still large snow amount in the future.
Self-organizing maps (SOMs) was applied using the surface atmospheric circulation to determine the dominant snowmelt related weather patterns (WPs). The SOMs showed that some WPs had a significant effect on the cause of ROS events. Additionally, the difference in the impacts of climate change between WPs was evaluated to understand the future changes in runoff and snowmelt associated with ROS events. The SOM analysis results suggest that the increase of ROS events in the future climate is attributed to the changes in dominant ROS-related WP (from cyclonic-type to cold-surge-type) corresponding with the variations in the freezing point line (region of the atmospheric layer at temperatures near 0 ˚C i.e., rain-snow transition layer). These findings can help inform water hazard/resource-management requirements to withstand regional climate change.

Keywords: Rain-on-snow (ROS) events , Climate change, Regional climate modeling, Self-organizing map , Weather patterns, Flood

©2020. Japan Geoscience Union. All Right Reserved.

Projected changes in extreme precipitation in a 60-km AGCM large ensemble and their dependence on return periods

*Ryo Mizuta[1], Hirokazu Endo[1]

1. Meteorological Research Institute

The dependence of projected changes in extreme precipitation on the return period, as well as on the temporal and spatial scales, is investigated using a large ensemble climate simulation with a 60-km resolution global atmospheric model. The rate of increase is noticeably larger for longer return values in most parts of the world. While thermodynamic contribution to this increase generally follows the Clausius–Clapeyron relationship for all return periods, dynamic contribution determines the dependence on the return periods. While the dependence on the temporal scales of precipitation has similar characteristics, that on spatial scales is not large. Composites for days with the 100-year return value show that upward motion is enhanced in the middle and upper troposphere, and is accompanied by the enhanced horizontal water vapor convergence below, suggesting that an increase in latent heat release due to the water vapor increase plays a significant role in the dynamic contribution.

Keywords: extreme events, global warming

©2020. Japan Geoscience Union. All Right Reserved.

Detection and Analysis of Tropical Cyclones in the d4pdf Mega-ensemble Projection

*Adrean Webb[1], Tomoya Shimura[1], Nobuhito Mori[1]

1. Kyoto University, Disaster Prevention Research Institute, Coastal Disaster Research

Tropical cyclones (TCs) play an important role in the climate system and are a major source of natural hazards worldwide, such as those due to heavy precipitation, river flooding, and storm surges. TC-related hazards are sensitive to properties of the storm path and while climate models can provide data to accurately model these events, samples are inadequate for analysis of extreme events on climatological time scales. The climate dataset d4PDF, Database for Policy Decision Making for Future Climate Change, was created to overcome this low-occurrence frequency limitation and contains hundreds of thousands of simulated TCs under present and future +4 K warming conditions (11,400 years), making it possible to estimate 100 year or longer return values.

Here, a tropical cyclone track dataset has been created for the d4PDF dataset. The detection method uses pressure difference, wind speed, and SST threshold parameters and is tuned to optimize annual TC count and cyclogenesis locations. Tuning and validation of the method is conducted using 30-year IBTrACS observation and JRA-55 reanalysis data. We will present an overview of the detection method, validation, and performance, and analyze properties of the TC tracks, such as projected changes in occurrence frequency, and cyclogenesis and dissipation locations.

Keywords: tropical cyclone tracks, d4PDF, climate ensemble, IBTrACS, JRA-55

©2020. Japan Geoscience Union. All Right Reserved.

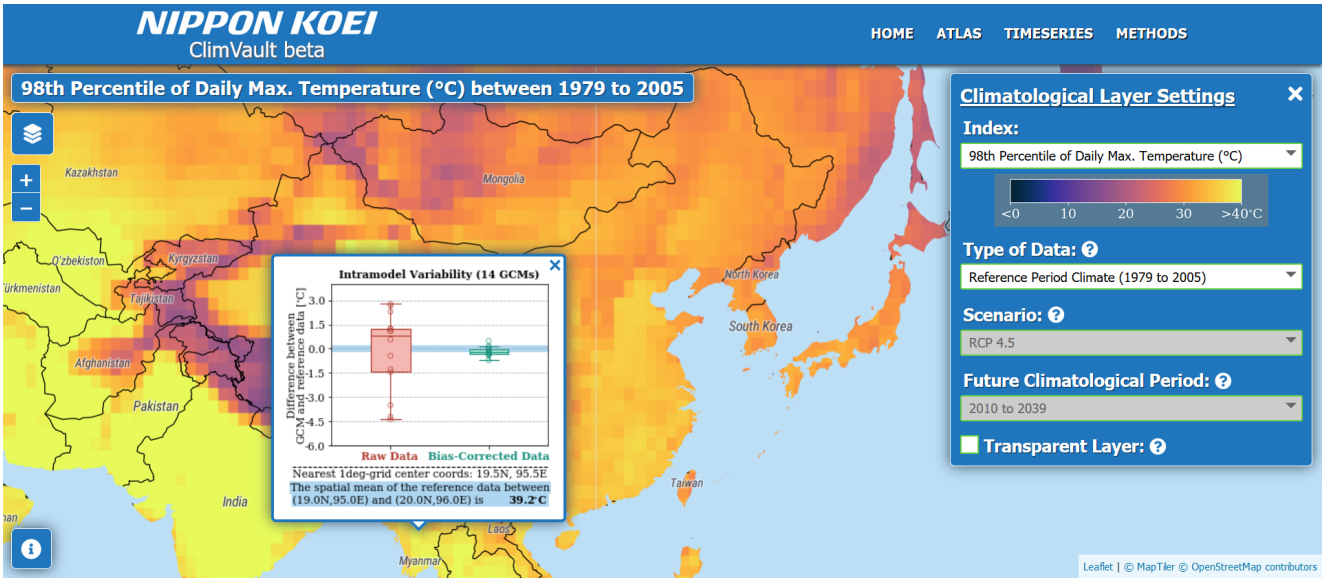
ESM-projected global change in the indices of extreme weather using the TR3S method of bias-correction

*Martin Gomez-Garcia[1], Akiko Matsumura[1], Daikichi Ogawada[1]

1. Nippon Koei Co., Ltd. Research and Development Center

To responsibly support the decision–making processes, the climate–modeling community has been discussing about the conceptual requirements that bias–correction methods should fulfill to avoid altering the relevant information of future climate that is provided by Earth System Models (ESM). Bearing in mind these discussions, a recently proposed method of bias–correction, based on TRend–preserving Synthetic Samples of Stable Distributions (TR3S), decomposes the atmospheric variables into three temporal elements that represent the climate mean state, the interannual variability, and the daily variability. This decomposition is aimed at correcting the biases at one time scale without affecting the projected climate trend or the distributional properties at other time scales. The novelty of this approach is, nevertheless, marked by the adjustment of interannual and daily variability that is made in a way that the ESM–projected changes in the scale, the symmetry, and the frequency of extremes can be measured and applied to the probability distribution of the observed data. The TR3S method differentiates from common quantile –mapping –type methods in that the quantiles (of variability) are corrected considering the change in several distributional properties instead of only the change in that particular quantile. In this work, we corrected the biases in the global surface temperature and precipitation generated by several ESMs using the TR3S method and present the projected changes of a few indices of extremes using an online Atlas of interactive maps. Furthermore, the TR3S method allowed us to document the spatial patterns of the biases in the distributional properties (i.e., scale, symmetry, and frequency of extremes) of daily and interannual variability of each ESM. We hope that this new analytical framework of model biases can be used by modelers to identify ways in which the ESM parameterizations could be improved and by end–users to support the climate change impact assessments.

Keywords: climate model, bias correction, climate Atlas, extreme weather indices



©2020. Japan Geoscience Union. All Right Reserved.

Droughts, fires and fire emissions of CO_2 and $PM_{2.5}$ in equatorial Asia due to historical and future climate changes

*Hideo Shiogama[1]

1. Center for Global Environmental Research, National Institute for Environmental Studies

In 2015, El Niño contributed to severe droughts in equatorial Asia (EA). The severe droughts enhanced fire activities in the dry season (June-November), leading to massive fire emissions of CO_2 and aerosols. Based on large event attribution ensembles of the MIROC5 atmospheric global climate model, we suggest that historical anthropogenic warming increased the chances of meteorological droughts exceeding the 2015 observations in the EA area. We also investigate changes in drought in future climate simulations, in which prescribed sea surface temperature data have the same spatial patterns as the 2015 El Niño with long-term warming trends. Large probability increases in stronger droughts than the 2015 event are projected when events like the 2015 El Niño occur in the 1.5˚C and 2.0˚C warmed climate ensembles according to the Paris Agreement goals. Further drying is projected in the 3.0˚C ensemble according to the current mitigation policies of nations.

We combine these experiments and empirical functions among precipitation, burned area, and fire emissions of CO_2 and fine (<2.5 micrometers) particulate matter ($PM_{2.5}$). Increases in the chances of burned areas and the emissions of CO_2 and $PM_{2.5}$ exceeding the 2015 observations due to past anthropogenic climate change are not significant. In contrast, there are significant increases in the burned area and CO_2 and $PM_{2.5}$ emissions even if the 1.5˚C and 2.0˚C goals are achieved. If global warming reaches 3.0˚C, as is expected from the current mitigation policies of nations, the chances of burned area, CO_2 and $PM_{2.5}$ emissions exceeding the 2015 observed values become approximately 100%, at least in the single model ensembles.

We also compare changes in fire CO_2 emissions due to climate changes and the land-use CO_2 emission scenarios of five shared socioeconomic pathways, where the effects of climate change on fire are not considered. There are two main implications. First, in a national policy context, future EA climate policy will need to consider these climate change effects regarding both mitigation and adaptation aspects. Second, the consideration of fire increases would change global CO_2 emissions and the mitigation strategy, which suggests that future climate change mitigation studies should consider these factors.

Keywords: Drought, Fire, Paris Agreement, Attribution, El Nino

©2020. Japan Geoscience Union. All Right Reserved.

Future change in phytoplankton phenology simulated by large ensemble experiment

*Ryohei Yamaguchi[1], Keith Rodgers[1,2], Karl J Stein[1,2], Axel Timmermann[1,2], John P Dunne[3], Richard D Slater[4], Sarah Schlunegger[4]

1. IBS Center for Climate Physics, 2. Pusan National University, 3. NOAA Geophysical Fluid Dynamics Laboratory, 4. Princeton University

While future changes in annual mean ocean biogeochemical properties (Net Primary Production, Export Production, Chlorophyll concentration etc.) has been studied, there are still only few descriptions and estimates of changes in the seasonal cycle itself. Changes in phytoplankton bloom phenology (initiation and peak timing) should have significant impacts on higher trophic levels, even on fisheries, and on the oceanic carbon cycle, since it is one of largest biogeochemical seasonal signal and could characterize the seasonal biological activity. However, it is challenging to estimate the forced long-term phenological changes as they are embedded in natural variability. In present study, we use a 30-member ensemble simulated by Geophysical Fluid Dynamics Laboratory Earth System Model 2 (GFDL-ESM2M) to deconvolve the forced signal from intrinsic variability in bloom phenology. Using daily mean surface chlorophyll concentrations, we detect the bloom timing shift precisely and estimate the emergence time-scale under a historical/RCP8.5 pathway over 1990-2100.
Over global scales, bloom initiation reveals large structured shifts over the 21st century, with large emergent shifts towards earlier blooms (~few days/decade) north of 30°N, and zonal heterogeneity of the sign of the shift over the Southern Ocean. On the other hand, bloom peak timing is expected to shift more than the initiation, indicating the bloom duration will also change significantly by the end of this century. As the results from budget analysis and the taylor decomposition, a range of variables are considered for attribution of the changes, including not only growth rate (that is, temperature, light, and nutrient) but also loss rate (grazing pressure as a function of temperature and biomass).

Keywords: Large ensemble, Phytoplankton bloom, phenology, future change

©2020. Japan Geoscience Union. All Right Reserved.

Seasonality Constraints on the rate of Pteropod Habitat Compression under 21st Century Climate Change

*Keith Bradley Rodgers[1,2], Sarah Schlunegger[3], Richard Slater[3], Burke Hales[4]

1. IBS Center for Climate Physics, 2. Pusan National University, 3. AOS Program, Princeton University, 4. Oregon State University

Under anthropogenic climate change, ocean acidificaiton is expected to pose mounting threats to ocean ecosystems. Here we consider habitat compression for the case of Pteropods over the North Pacific and Southern Ocean using a large ensemble suite with an Earth system model (GFDL's ESM2M considered for RCP8.5, RCP4.5, and RCP2.6 concentration pathways). Given that pteropods are vertically migrating and that their habitat is tied to the depth of the ocean's well-lit euphotic zone, our analysis of acidification is considered at both the surface and the euphotic zone depth. Our main finding is that the transition time between saturation and undersaturation is controlled by the ratio of the seasonal cycle amplitude to the rate of the secular trend of acidification. This is significanly more rapid at the euphotic zone base than at the sea surface, due to differenes in the amplitude of the seasonal cycle. The implications for adapataion will be considered.

Keywords: Acidification , Large Ensemble, Marine Ecosystems

©2020. Japan Geoscience Union. All Right Reserved.

[E] Poster | A (Atmospheric and Hydrospheric Sciences)：A-CG Complex & General

[A-CG53] Terrestrial monitoring using new-generation geostationary satellites

convener:Yuhei Yamamoto(Center for Environmental Remote Sensing, Chiba University), Yunyue Yu(NOAA National Environmental Satellite, Data, and Information Service), Tomoaki Miura(Univ Hawaii), Kazuhito Ichii(Chiba University)

The third-generation geostationary satellites, such as Himawari 8/9, GOES-16/17, Fengyun-4, and GeoKompsat-2A are recently launched, and earth observation is in a new phase. These sensors are equipped with new spectral bands suitable for terrestrial monitoring used in polar-orbiting satellite sensors, enabling detailed land observations such as land surface temperature, surface albedo, and land cover and vegetation dynamics. Furthermore, by utilizing the advantages of hypertemporal (e.g. 10 min) and moderate spatial resolution, various new land dynamics can be observable. By combining these satellites and polar-orbiting satellites/sensors such as Terra/MODIS and GCOM-C/SGLI, a new generation monitoring data covering Asia, Oceania and North and South America will become possible. This would allow for a consistent comparison of a variety of phenomena across continents. To this end, there are many issues to be discussed, such as the standardization of the estimation algorithms of physical quantities, calibration and verification using GEO-(LEO)-GEO satellites, and application of these new datasets to various phenomena.
In this session, we will discuss the retrieval algorithms of land surface parameters, inter-satellite calibration, validation efforts using in-situ data, and novel applications to various phenomena. Studies on atmospheric parameters in relation to land surface phenomena, such as cloud cover are aerosol, are highly welcomed.

[ACG53-P01] Evaluation of Estimated precipitation product by machine learning method using Himawari 8

*Koichi Toyoshima[1], Hitoshi Hirose[2], Atsushi Higuchi[1] (1.Center for Environmental Remote Sensing, Chiba University, 2.JAXA EORC)

[ACG53-P02] Development and application of land surface products using Himawari-8 AHI

*Kazuhito Ichii[1], Yuhei Yamamoto[1], Kodai Hayashi[1] (1.Chiba University)

[ACG53-P03] Monitoring seasonal variations in vegetation activities over Southeast Asia using Himawari-8

*Kodai Hayashi[1], Kazuhito Ichii[1], Yuhei Yamamoto[1] (1.Chiba University)

[ACG53-P04] Analysis of the spatial variations in the phenology of deciduous broadleaf forests in Japan with Himawari-8 NDVI hyper-temporal signatures

*Tomoaki Miura[1], Shin Nagai[2] (1.University of Hawaii at Manoa, 2.JAMSTEC)

Evaluation of Estimated precipitation product by machine learning method using Himawari 8

*Koichi Toyoshima[1], Hitoshi Hirose[2], Atsushi Higuchi[1]

1. Center for Environmental Remote Sensing, Chiba University, 2. JAXA EORC

GSMaP is a useful global precipitation product provided 1 hour resolution.
GSMaP estimates the precipitation by IR observation of the geostationary satellite to interpolate a gap of the microwave radiometer (MWR).
However, there is difference in the precision between MWR and IR data source.
This difference is due to the correction of rainfall intensity using only cloud top temperature (altitude) information. This difference is due to the fact that cirrus clouds without rainfall are detected as raining areas, and difficulty to detect and estimate warm rain.
In October 2014, the third generation Himawari-8 geostationary meteorological satellite was launched, and the infrared multi-band observations are available in the Asian monsoon region. Using Himawari-8 and GPM KuPR data as training data, we created a precipitation product estimated by Random Forest machine learning. The purpose of this study is to improve the accuracy of estimating heavy rainfall caused by warm clouds that are difficult to estimate with a single IR band observation.

Keywords: precipitation product, geostationary satellite

©2020. Japan Geoscience Union. All Right Reserved.

Development and application of land surface products using Himawari-8 AHI

*Kazuhito Ichii[1], Yuhei Yamamoto[1], Kodai Hayashi[1]

1. Chiba University

New generation geostationary satellites provide very high temporal earth observation with multiple visible, near-infrared, and shortwave-infrared wavelength regions. Thus, these datasets can provide us unexpectedly hyper-temporal resolution to monitor land surface. However, since geostationary satellite data are provided with top-of-atmosphere status, complex data pre-processing such as atmospheric correction, cloud masking are required.
Our group is trying to provide a new datasets for surface reflectance and surface temperatures based on Himawari-8 AHI. Our atmospheric corrected reflectance was calculated based on 6S code and we found that estimated reflectance were similar to those of polar orbiting satellites and sensors, such as Terra/MODIS and GCOM-C/SGLI. Cloud masks and land surface temperatures were generated by Yamamoto et al. (2018) algorithm. We will show our current status of data-processing and potential applications to understant land surface and vegetation dynamics.

Keywords: terrestrial monitoring, Himawari-8, vegetation

©2020. Japan Geoscience Union. All Right Reserved.

Monitoring seasonal variations in vegetation activities over Southeast Asia using Himawari-8

*Kodai Hayashi[1], Kazuhito Ichii[1], Yuhei Yamamoto[1]

1. Chiba University

Tropical forests distributed widely in Southeast Asia play an essential role in maintaining rich ecosystems, energy and water cycles, and flood control. In Southeast Asia, the spatial and temporal distributions of land cover, plant phenology, and biomass are changing rapidly due to human activities and climate change. For example, areas of tropical forests are still decreasing due to human activities. The resulting carbon emissions are one of the significant contributors to atmospheric CO2 increase and climate change. Besides, the magnitude and frequency of environmental fluctuation by anomalous climate are increasing. Especially in tropical regions, droughts occur due to prolonged periods without rainfall, and floods occur due to extreme increases in rainfall. As a result, large-scale forest fires and severe water stress occur, and forest degradation is progressing.

Therefore, monitoring changes in terrestrial ecosystems in Southeast Asia is indispensable and also provides useful information for the conservation of rich ecosystems and the capability of flood control. In particular, it is essential to conduct extensive and continuous monitoring without any defect using satellite data.

However, in Southeast Asia, severe cloud covers exist throughout the year. Moreover, in the rainy season, it is covered with clouds over a broader area and more continuously. Therefore, it is often impossible to obtain the cloud-free data even once a month when using sensor data mounted on medium spatial resolution polar-orbiting satellites such as MODIS, AVHRR, and SGLI.

New geostationary satellites, such as Himawari-8/AHI (H8-AHI), are expected to observe land surface better due to its high observation frequency (every 10 minutes). In this study, we quantified how much more cloud-free observations can be obtained, and how detailed can we understand rainforest phenology using H8-AHI data in Southeast Asia, compared to polar-orbiting satellite data, Terra and Aqua / MODIS. First, we confirmed that the cloud detection rate is similar between H8-AHI and MODIS cloud masks. Then, we found that H8-AHI observation substantially increased cloud-free observation compared with those of MODIS on a monthly scale. Finally, we compared resulting cloud-free vegetation index time-series between AHI and MODIS, and only H8-AHI successfully tracks seasonal plant phenology over tropical forests.

Keywords: Himawari-8, cloud mask, tropical forest, MODIS

©2020. Japan Geoscience Union. All Right Reserved.

Analysis of the spatial variations in the phenology of deciduous broadleaf forests in Japan with Himawari-8 NDVI hyper-temporal signatures

*Tomoaki Miura[1], Shin Nagai[2]

1. University of Hawaii at Manoa, 2. JAMSTEC

A new generation of geostationary satellite sensors, including Himawari-8 Advanced Himawari Imager (AHI), have been launched during the last decade. These sensors are equipped with a red and near-infrared bands and can image an Earth’ s hemisphere at 10 min intervals, providing the potential to generate high-temporal resolution vegetation index (VI) time series data even in cloud-prone areas and seasons. In this study, we assessed how AHI NDVI “hyper-temporal” signatures varied for deciduous broadleaf forests (DBFs) along a temperature, elevation, and latitudinal gradients in Japan. AHI 10-min data of Japan were obtained for a three-year period of 2016-2018 and reduced into daily NDVI time series. The warmth index (WI) and coldness index (CI), temperature-driven indices, were also obtained from mean monthly temperature. A land cover map derived from ALOS data was used to identify DBF areas along the transects. AHI NDVI hyper-temporal signatures, consisting of a large number of observations, had one growth cycle/season per year, but were different along temperature, elevation, and latitudinal gradients. The start of growth season (SGS) metric derived from AHI NDVI was positively, but weakly correlated with the latitude (r = .47) and elevation (r = .47). In contrast, the AHI NDVI-derived end of growth season (EGS) metric significantly correlated to the latitude (r = .73), but not to the elevation (r = .07). The highest correlations were obtained with the temperature-derived WI and CI for these metrices (r = .86 between the SGS and WI, and r = .75 between the EGS and CI). These results indicate that Himawari-8 hyper-temporal data were useful for regional-scale analysis of vegetation growing season.

Keywords: Himawari-8, NDVI, Phenology

©2020. Japan Geoscience Union. All Right Reserved.

[E] Poster | H (Human Geosciences)：H-GM Geomorphology

[H-GM02] Geomorphology

convener:Tsuyoshi Hattanji(Faculty of Life and Environmental Sciences, University of Tsukuba), Masayuki Seto(Fukushima Future Center for Regional Revitalization, Fukushima University)

The main subject of this session is interdisciplinary discussion on the whole range of themes relating to geomorphology, especially geomorphic processes, landform development and its relation to environmental changes, geomorphological hazards and their mitigation, relationships among geomorphic processes, other natural phenomena and human activities, and various techniques of geomorphological measurements and landform classification. All presentations and discussion of this session are made in English.

[HGM02-P01] Bank erosion owing to tidal currents and its impact on village distribution in the Sittaung River estuary, Myanmar

*Naoko Nagumo[1], Daisuke Harada[1], Tanjir Saif Ahmed[1,2], Shinji Egashira[1] (1.International Centre for Water Hazard and Risk Management, Public Works Research Institute, 2.National Graduate Institute for Policy Studies)

[HGM02-P02] Grain size and OSL dating of river bank dune deposits: an example from the Kiso River, central Japan

*Kazuaki Hori[1], Kohei Ohata[1], Yuji Ishii[2,3] (1.Nagoya Univ., 2.JSPS, 3.AIST)

[HGM02-P03] Topographic development process of bedrock river: model experiment

*Yuta Takase[1], Noritaka Endo[1] (1.Kanazawa University)

[HGM02-P04] Patterns of slopes and geological structure in the Atsuma River catchment, Hokkaido

*Takahisa Furuichi[1,2], Seiji Yanai[3], Tomoya Hayakawa[4] (1.Miyagi University of Education, 2.University of the Sunshine Coast, 3.Ishikawa Prefectural University, 4.Nippon Koei, Co. Ltd.)

[HGM02-P05] Radiocarbon-based Chronology of Valley Head Deposits: A Case Study of Landslide Scars in Hofu, Yamaguchi Prefecture

Takatoshi Kawano[1], *Tsuyoshi Hattanji[2], Takahisa Furuichi[3], Shoji Doshida[4], Yasushi Tanaka[5] (1.Graduate School of Life and Environmental Sciences, University of Tsukuba, 2.Faculty of Life and Environmental Sciences, University of Tsukuba, 3.Miyagi University of Education, 4.National Research Institute of Fire and Disaster, 5.Komazawa University)

[HGM02-P06] Impact of Understory Coverage and Tree Height on Sediment Transport Activity in Tenryu Artificial Forest, Japan

*Kautsar Qurratul Aini Binti Mahyudin[1], Fumitoshi Imaizumi[1] (1.Shizuoka University)

Bank erosion owing to tidal currents and its impact on village distribution in the Sittaung River estuary, Myanmar

*Naoko Nagumo[1], Daisuke Harada[1], Tanjir Saif Ahmed[1,2], Shinji Egashira[1]

1. International Centre for Water Hazard and Risk Management, Public Works Research Institute, 2. National Graduate Institute for Policy Studies

The Sittaung River is one of the large rivers in Myanmar, draining an area of about 36,000 km^2. It forms a tide-dominated estuary in its mouth, where dynamic river bank erosion and consequent bank-line changes occur under the influence of river flow and tidal currents enhanced by tidal bores. As the river line retreats inland, serious problems, such as the disappearance of settlements and farmland, have resulted; therefore, we have started research in collaboration with Directorate of Water Resources and Improvement of River Systems (DWIR) to understand the mechanism of the active river bank erosion and plan appropriate prevention measures. Our analyses have so far revealed that the main stream has been shifting its course at least since the 1920s, exhibiting a periodicity, which seems to be induced by meander deformation and channel bifurcation resulting from bank collapses and supplies of very fine sediment in the river reach and estuary areas. The interrelating phenomena among bank erosion, sediment transport, channel-bar formation and deformation, and associated cyclic mainstream shifts have threatened the livelihoods of local people along the bank line. However, our analyses on the historical distribution of local villages also found that the outer edge of the past bank lines indicates a boundary of the safety zone from active bank erosion. We employed a depth-averaged 2-D numerical model to evaluate the sediment transport and associated bed evolution by tidal currents, and the computed results well reproduced the channel bifurcation and channel closing that are responsible for channel bar development.

Keywords: bank erosion, tidal currents, fine sediments, channel shifts, estuary

©2020. Japan Geoscience Union. All Right Reserved.

Grain size and OSL dating of river bank dune deposits: an example from the Kiso River, central Japan

*Kazuaki Hori[1], Kohei Ohata[1], Yuji Ishii[2,3]

1. Nagoya Univ., 2. JSPS, 3. AIST

River bank dunes are common along the left side bank of the Kiso River. Existing studies have reported the distribution of dunes and the grain size of dune surface deposits. However, the vertical change of grain size of dune deposits is poorly known. Additionally, the age of dune formation is unknown because organic matter suitable for radiocarbon dating is uncommon in the dune sand. This study used a sand auger to dig the dunes up to a depth of 6 m, took the dune deposits, and performed the grain size analysis and optically stimulated luminescence (OSL) dating of the deposits. Grain size analysis of sand deposits shows that median grain size is 0.20–0.45 mm and vertical variation in grain size is relatively small. The size is similar to the present river bed sand. Ages from feldspar infrared-stimulated luminescence (IRSL) at 50˚C are 0.2–0.7 ka, and the youngest age of 0.2 ka indicate that residual doses are negligible. In contrast, post-IR IRSL measurements at 150˚C yielded 0.5–2.7 ka, which are significantly older than those from IRSL at 50˚C because of incomplete bleaching. IRSL ages suggest that the dunes have formed since approximately 600–700 years ago. The beginning of dune formation may be related to anthropogenic influence in the drainage basin.

Keywords: river bank dune, OSL dating, Holocene

©2020. Japan Geoscience Union. All Right Reserved.

Topographic development process of bedrock river: model experiment

*Yuta Takase[1], Noritaka Endo[1]

1. Kanazawa University

Understanding the evolution of channel topography helps to reproduce past landscape and predict future landscape. Since bedrock rivers are less well studied than alluvial rivers, further study of bedrock river topography is needed. Although the relationship between bedrock erodible and topographical features has been often discussed, both clear relationships are not understood in natural rivers, as various factors change irregularly.

In this study, we investigate the some relationships between complex and various factors through a single channel model experiment that can control the factors that affect the river topography. In addition, we observe the temporal change of the topography and aim to clarify the development process of river. The main controlling factors in this study are topographic uplift and bedrock erodible. The analysis targets are channel width, riverbed gradient, sinuosity, and erosion rate.

The experimental correlation diagram of each factor showed the same distribution as the natural river topography. High erosion rates are showed by steep river beds. The erosion rate tended to be low on the topography with high sinuosity. These distribution trends were showed during the uplift. In this experiment in which the uplift event lasted longer, the sinuosity tended to be lower than in the experiment in which the uplift event was short. On the other hand, the bed slope did not change significantly due to the uplift. Bed slope may not have a strong dependence on uplift event.

In the future, we will continue experiments that combined other bedrock and uplift patterns to study the effects of both.

Keywords: Bedrock, uplift, model experiment, topography

©2020. Japan Geoscience Union. All Right Reserved.

Patterns of slopes and geological structure in the Atsuma River catchment, Hokkaido

*Takahisa Furuichi[1,2], Seiji Yanai[3], Tomoya Hayakawa[4]

1. Miyagi University of Education, 2. University of the Sunshine Coast, 3. Ishikawa Prefectural University, 4. Nippon Koei, Co. Ltd.

The M6.7 Hokkaido Eastern Iburi Earthquake on 6 September 2018 induced numerous shallow landslides in the Atsuma River catchment and surrounding areas. The induced shallow landslides show several features in shape. One type has planar slipe-surfaces mostly on gentler slopes, while another has V-shaped slipe-surfaces generally on steeper slopes. It was anticipated that these slip features were fundamentally controlled by the geological structure because the Atsuma area lies in the E-W compressed geological setup. Folds, anticlines, synclines and domes have developed as the basement structure of the area, which may have formed gentle, planar slopes along the dip of the basement and steep, V-shaped slopes perpendicular to the dip angle, i.e. a cuesta landform.

However, field evidence indicates that V-shaped slip-surfaces formed along the dip of the basement and planar slip-surfaces developed on slopes perpendicular to the dip of the basement. This landform might be recognized as a ‘reverse cuesta’. We discuss possible mechanisms of the formation of this unanticipated, surprising feature developed in the Atsuma area.

Keywords: shape of slope, fold, dome, cuesta, sedimentary rock

©2020. Japan Geoscience Union. All Right Reserved.

Radiocarbon-based Chronology of Valley Head Deposits: A Case Study of Landslide Scars in Hofu, Yamaguchi Prefecture

Takatoshi Kawano[1], *Tsuyoshi Hattanji[2], Takahisa Furuichi[3], Shoji Doshida[4], Yasushi Tanaka[5]

1. Graduate School of Life and Environmental Sciences, University of Tsukuba, 2. Faculty of Life and Environmental Sciences, University of Tsukuba, 3. Miyagi University of Education, 4. National Research Institute of Fire and Disaster, 5. Komazawa University

Heavy rainfall on July 21, 2009 caused a lot of shallow landslides in Tsurugigawa river basin, Hofu, Yamaguchi prefecture. Most of the shallow landslides occurred around valley heads (hollows) in the basin. This paper discusses geomorphological history of hollows before the landslides based on radiocarbon dating. Samples were collected from buried layers of charcoal (hereinafter, referred to as charcoal layers) in two valley heads with shallow landslide scars. The calibrated radiocarbon years of the charcoal layers are about 1200-1300 cal AD and 1300-1400 cal AD. The development history of the valley heads is estimated as follows. First, wild fires occurred around the valley heads in 1200-1400 AD and then charcoals were produced on the land surface. Subsequently, sandy soil was transported from the upper slopes to the valley heads and a thick sand layer was deposited above the charcoal layers. In addition, the sedimentation rates for landslide scarps and valley heads were calculated based on the calibrated radiocarbon years and thickness of soil layers estimated by comparison of airborne LiDAR DEMs obtained before and after the shallow landslides. The sedimentation rates were 0.9-2.1 mm/year for the landslide scarps and 2.1-6.9 mm/year for the valley heads. Furthermore, these slopes were stable for 600-800 years and shallow landslides of similar magnitude to the event in 2009 probably occurred around or before 1230 AD.

Keywords: Charcoal, Radiocarbon dating, Shallow landslide

©2020. Japan Geoscience Union. All Right Reserved.

Impact of Understory Coverage and Tree Height on Sediment Transport Activity in Tenryu Artificial Forest, Japan

*Kautsar Qurratul Aini Binti Mahyudin[1], Fumitoshi Imaizumi[1]

1. Shizuoka University

Large-scale tree cutting that lead to deforestation could possibly lead to negative impact on ecosystem and the environment. Equivalent to the important factor of understory coverage in monitoring the overland flow and soil erosion, which include the soil particle detachment and transportation. In the interim, tree height could be considered as a parameter affecting energy of rain splash under canopy structure. In this study, we observed overland flow and soil erosion in 3 artificial forests with different tree height; tall tree, small tree and clearcutting sites. Within those sites, the effect of understory coverage on sediment transport activity was evaluated with different conditions of coverage: sparse grass understory grass, litter, fern densely understory, and without any understory coverage. We measured the soil type characteristic to figuring out the role of understory coverage and tree height in preventing soil erosion. We obtained the percentage of understory coverage (with understory) and monitored rainfall pattern overland flow and soil erosion annually in five replicated plots (approximately 1 X 2 m each) with and without understory. The highest overland flow occurred in the period with largest rainfall (total rainfall depth of 800 mm). In tall tree site (24 m), the prevention of overland flow and sediment transport activity by understory coverage were not essential due to capacity of overland flow was continuously high compared to without understory coverage. We found that the fern dense coverage at small tree sites (covered and uncovered understory) absorbed 95% of throughfall and stem fall, resulting in soil erosion activity compared to tall tree and small tree. Although the effect of tree cutting on amount of overland flow was clear, there was no relationship between understory coverage and amount of overland flow due to the crust formation induce in large amount of soil erosion activity. The tree height factor in small tree prevented 95% of high force of raindrop compared to tall tree that cause low dominant in soil detachment that lead to high sediment transport activity.

Keywords: Understory coverage, Tree height, Sediment transport activity, Overland flow

©2020. Japan Geoscience Union. All Right Reserved.

[E] Poster | H (Human Geosciences)：H-QR Quaternary research

[H-QR04] Innovative Applications of Trapped-Charge Dating to Quaternary Geochronology

convener:Toru Tamura(Institute of Geology and Geoinformation Geological Survey of Japan, AIST), Shin Toyoda(Department of Applied Physics, Faculty of Science, Okayama University of Science), Yuji Ishii(National Institute of Advanced Industrial Science and Technology), Sumiko Tsukamoto(Leibniz Institute for Applied Geophysics)

Trapped-Charge Dating (TCD) is a general term for absolute dating methods that use trapped electrons in crystal lattice, such as optically-stimulated luminescence (OSL) and electron spin resonance (ESR) dating. TCD presented one of the most successful progresses in geoscience and archaeology over the last 20 years, and still has a great potential in innovative applications. Technical progresses in optical dating of quartz and feldspar grains enables determination of depositional ages in a broad range from 10 to 500,000 years. Rock surface dating provides a way to determine surface exposure ages as well as burial ages of gravels. Thermochronometry with TCD is a state of the art method to determine the degradation and uplift rates on high temporal resolution. Further efforts have been made on TCD for extracting chronological information of past seismic activities. Innovative IRPL (infrared photoluminescence) method has also recently been invented. This session covers a wide range of TCD applications to problems in Quaternary geochronology as well as its technical advances. Comprehensive reviews on successful TCD applications and contributions of unestablished, challenging researches are also welcome.

[HQR04-P01] Optically stimulated luminescence (OSL) dating using quartz extracted from loess as archeo-sediments of Paleolithic site

*Yorinao Shitaoka[1] (1.Department of Environment System, Faculty of Geo-environmental Science, Rissho University)

[HQR04-P02] Luminescence dating and age correction of marine terrace deposits in Kamikita Coastal Plain and Shimokita Peninsula, northeastern Japan

*Kazumi Ito[1], Toru Tamura[1] (1.Geological Survey of Japan, AIST)

[HQR04-P03] Comparison of luminescence readers using post-Infrared Infrared stimulated luminescence of K-feldspar from last interglacial marine terrace deposits

*Hayashizaki Ryo[1], Eiji Nakata[1] (1.Central Research Institute of Electric Power Industry)

[HQR04-P04] **Late Quaternary loess accumulation at the Rudak section in Uzbekistan, central Asia: Chronology and palaeoclimate implications**

★Invited Papers

*Jingran Zhang[1], Xinying Zhou[2], Hao Long[3] (1.Nanjing Normal Univ., 2.IVPP, CAS, 3.NIGLAS)

[HQR04-P05] Dating of hydrothermal silicified sediments by thermoluminescence

*Naoya Obata[3,1], Takashi Goto[4,1], Chitaro Gouzu[1], Jun-ichiro Ishibashi[2], Shin Toyoda[3] (1.Hiruzen Institute for Geology and Chronology Co., Ltd., 2.Kyushu University, 3.Okayama University of Science, 4.Fuji Geological Institute)

[HQR04-P06] Applications of trapped-charge dating techniques to hydrothermal mineral deposits collected from active seafloor hydrothermal fields

*Jun-ichiro Ishibashi[1], Naru Tsukamoto[1], Yusuke Okazaki[1], Taisei Fujiwara[2], Naoya Obata[2], Takashi Goto[2], Chitaro Gouzu[2], Shin Toyoda[3] (1.Department of Earth and Planetary Sciences, Faculty of Science, Kyushu University, 2.Hiruzen Institute for Geology and Chronology, 3.Okayama University of Science)

[HQR04-P07] **Luminescence dating of the late Quaternary terrestrial-marine interaction sedimentary history of the north Jiangsu coastal plain and the Yangtze River delta in China**

*Lei Gao[1], Hao Long[1], Toru Tamura[2] (1.Nanjing Institute of Geography and Limnology, Chinese Academy of Sciences, 2.Geological Survey of Japan, National Institute of Advanced Industrial Science and Technology)

[HQR04-P08] Composite chronology of Paleolithic sites in Jebel Qalkha revealed by pIRIR dating

Risako Kida[1], *Toru Tamura[2], Seiji Kadowaki[1] (1.Nagoya University Museum, Nagoya University, 2.Institute of Geology and Geoinformation Geological Survey of Japan, AIST)

Optically stimulated luminescence (OSL) dating using quartz extracted from loess as archeo-sediments of Paleolithic site

*Yorinao Shitaoka[1]

1. Department of Environment System, Faculty of Geo-environmental Science, Rissho University

Datasets for a chronological framework of the Upper Paleolithic era in Nihewan Basin, northern China remain insufficient. Our team conducted optically stimulated luminescence (OSL) dating using fine quartz at Youfang site, and Loc. 73012 and Loc. 72117 of Hutouliang for additional dating studies. For this study, OSL dating was performed on loess as archeo-sediments from Erdaoliang site. Two samples were taken: one above the cultural layer (sample 1) and one below the cultural layer (sample 2).
Using the single aliquot regenerative-dose (SAR) protocol for course quartz (ca. 100 μm) extracted from loess of archeo-sediments, OSL dating was conducted. The OSL measurements were taken using an OSL reader (NRL-99-OSTL2-KU; Neoark Corp.). The value of paleodoses and their error were estimated using bootstrap method. Paleodoses of two samples were calculated using the central age model. The overdispersion (OD) values of sample 1 and sample 2 were, respectively, 24% and 12%. A sedimentary sample with OD of less than 20% was fully bleached as described by Olley *et al.* (2004). It is assumed that sample 1 was not well bleached. Therefore, the paleodose of sample 1 was obtained using the finite mixture age model. The main component contains a plurality (47%) of aliquots. OSL ages were found, respectively, as 19.0±0.98 ka for sample 1 and 23.9±1.2 ka for sample 2. The radiocarbon age obtained at this site was 18,085±235 yBP (no calibration). These OSL ages in this study are stratigraphically coherent.

Reference: Olley *et al.*, sedimentary Geology, 169: 175-189, 2004.

Keywords: OSL dating, archeo-sediment, Loess, quartz

©2020. Japan Geoscience Union. All Right Reserved.

Luminescence dating and age correction of marine terrace deposits in Kamikita Coastal Plain and Shimokita Peninsula, northeastern Japan

*Kazumi Ito[1], Toru Tamura[1]

1. Geological Survey of Japan, AIST

Middle and Late Pleistocene marine terraces formed during interglacial sea-level highstands are distributed across the coastal area in Japan. For Kamikita Coastal Plain and Shimokita Peninsula, northeastern Japan, the ages of marine terraces have been well defined by tephrochronology. Post-infrared infrared stimulated luminescence (pIRIR) dating of K-feldspar has been applied to date Pleistocene sediments since about 10 years ago. In this study, we applied pIRIR dating to date these marine terrace deposits and the age correction methods were discussed. The shallow marine deposits formed during interglacial highstands which are corresponding to Marine Isotope Stage (MIS) 5e, 7, 9, 11 (45 samples from 11 outcrops) were measured. We applied $pIRIR_{200/290}$ signal based on Ito *et al*. (2017) to D_e measurement and fading test. The fading-corrected ages based on Kars *et al*. (2008), except for 6 sample from 2 outcrops, are suitable to defined the stage of sea-level highstands, while all fading-corrected ages were overestimated compared with the expected ages. This age overestimation is corresponding with about 40~50 Gy. The dose recovery ratios of few samples were clearly high from unity, thus it was possible to the overestimation of D_e. On the other hand, $pIRIR_{200/290}$ signal is more difficult to bleach than the quartz OSL, K-feldspar $IRSL_{50}$ and $pIRIR_{50/290}$ signals, and this residual dose is about 10~20 Gy derived from the well-bleached modern beach sand. Additionally, in the previous study of Holocene marine sediments, the marine succession has formed by beach progradation since few thousand years (e.g., 6ka in Kujukuri strand plain, Tamura et al. 2008). This few Gy accumulated during beach progradation is added to residual dose of well-bleached modern beach sand, thus apparent residual dose of $pIRIR_{200/290}$ signals from whole shallow marine deposits may be >20 Gy. Considering this apparent residual dose, it may be possible to be concordant the fading- and residual dose-corrected ages with the expected ages. However, this apparent residual dose is corresponding with >10ka in study area, thus $pIRIR_{200/290}$ signal is useful to older samples, while it may be difficult to apply younger sample (e.g., MIS5a, 5c).

* This research project has been conducted as the regulatory supporting research funded by the Secretariat of Nuclear Regulation Authority (Secretariat of NRA), Japan.

Ito et al. (2017) Geochronometria 44, 352-365
Kars et al. (2008) Radiation Measurements 43, 786-790
Tamura et al. (2008) Marine Geology 248, 11-27

Keywords: Luminescence dating, Marine terrace, Kamikita Coastal Plain, Shimokita Peninsula, age correction

©2020. Japan Geoscience Union. All Right Reserved.

Comparison of luminescence readers using post-Infrared Infrared stimulated luminescence of K-feldspar from last interglacial marine terrace deposits

*Hayashizaki Ryo[1], Eiji Nakata[1]

1. Central Research Institute of Electric Power Industry

The two types of TL/OSL Readers, Risø TL/OSL Reader and Lexsyg series (Lexsyg Research and Lexsyg Smart), are widely used for luminescence dating. Some researches provide the same results of Quartz OSL dating using the two types of TL/OSL Readers (Lomax et al.2014), therefore it is thought that the two readers perform the same for OSL dating. However, few studies have compared with the two types of readers using K-feldspar OSL dating, especially where the samples are older than 100ka. This study examines post-infrared Infrared Stimulated Luminescence ($pIR_{50/200}IR_{290}$) dating from last interglacial marince terrace deposits using two types of TL/OSL readers (Risø TL/OSL-DA20 and Lexsyg Research). In addition to the results, we also discuss the differences between the readers, such as their analysis software for measuring fading rate and their differences in disc temperature during analysis.

References
Lomax, J., Kreutzer, S. and Fuchs, M. 2014. Performance tests using the Lexsyg luminescence reader. Geochronometria: 41, 327–333.

Keywords: pIRIR dating, last interglacial marince terrace, Risø OSL/TL Reader, Lexsyg Research

©2020. Japan Geoscience Union. All Right Reserved.

Late Quaternary loess accumulation at the Rudak section in Uzbekistan, central Asia: Chronology and palaeoclimate implications

*Jingran Zhang[1], Xinying Zhou[2], Hao Long[3]

1. Nanjing Normal Univ., 2. IVPP, CAS, 3. NIGLAS

Many studies have been carried out to understand the nature of the loess formation and its palaeoenvironmental significance in different parts of Eurasia, especially Europe and China. However, in spite of its key position, our knowledge about the loess deposits at the core of the Eurasian loess belt in central Asia is still limited, particularly in term of absolute dating. This study presents a new luminescence chronology of a loess-palaeosol sequence (Rudak section) in the vicinity of the Gissar Range, Uzbekistan, using both quartz optically stimulated luminescence dating and polymineral post-IR IRSL dating techniques. The dating results suggested a loess accumulation history over the past 180 kyr, but a great depositional hiatus during the entire last glacial period, likely owing to too harsh climate conditions for favouring dust deposition and loess preservation in the piedmont areas of central Asia. Hence, contrasting with the traditional concept of continuous (quasi-continuous) deposition of loess, the direct stratigraphical correlation might be problematic for climatic interpretation of loess-palaeosol sequence in this area. Furthermore, magnetic susceptibility of Rudak section demonstrated the moisture peaks in phase with ice-volume minima over the glacial and interglacial cycles, indicating moisture variation in the Westerlies dominated central Asia was broadly consistent with that in monsoonal Asia on orbital timescales, but nearly contrasting picture with each other on the suborbital timescales, at least through the Holocene. The Westerlies dominated central Asia has generally experienced a dry first-half and a wet second-half of the Holocene, which is likely triggered by solar insolation gradients between mid-latitudes and high-latitudes and meltwater flux.

Keywords: Loess-palaeosol sequence, Luminescence dating, sedimentary hiatus of loess, Moisture variations, Westerlies

©2020. Japan Geoscience Union. All Right Reserved.

Dating of hydrothermal silicified sediments by thermoluminescence

*Naoya Obata[3,1], Takashi Goto[4,1], Chitaro Gouzu[1], Jun-ichiro Ishibashi[2], Shin Toyoda[3]

1. Hiruzen Institute for Geology and Chronology Co., Ltd., 2. Kyushu University, 3. Okayama University of Science, 4. Fuji Geological Institute

The ages of hydrothermal activities are key issues in estimating the geothermal processes under the sea floor especially such as ore formation. Silicified sediments, widely distributed in hydrothermal fields of the sea floor, are potentially subject of trapped-charge dating, and their ages will contribute to the issues. Coarse and fine quartz grains were identified in the hydrothermal silicified sediments under a polarizing microscope. We tried thermoluminescence (TL) dating for each grain extracted from hydrothermal silicified sediments in the Okinawa Trough. We first checked the characteristics of silicified sedimentary quartz, such as TL peaks, wavelengths, and the dose response. The distribution of the radioactive elements was obtained by using imaging plates. As results of TL dating, coarse grains were found to be older than fine grains. Tentatively it is interpreted that coarse grains originated in volcaniclastic sediments have incompletely reset by hydrothermal activity, whereas fine grains precipitated from hydrothermal solutions, indicating the ages of the hydrothermal activities.

Keywords: thermoluminescence dating, quartz, hydrothermal silicified sediments

©2020. Japan Geoscience Union. All Right Reserved.

Applications of trapped-charge dating techniques to hydrothermal mineral deposits collected from active seafloor hydrothermal fields

*Jun-ichiro Ishibashi[1], Naru Tsukamoto[1], Yusuke Okazaki[1], Taisei Fujiwara[2], Naoya Obata[2], Takashi Goto[2], Chitaro Gouzu[2], Shin Toyoda[3]

1. Department of Earth and Planetary Sciences, Faculty of Science, Kyushu University, 2. Hiruzen Institute for Geology and Chronology, 3. Okayama University of Science

Chronological studies of hydrothermal mineral deposits are useful, because accumulation of metal elements to be resource requires duration and evolution of mineralization processes in a time scale of 10^3 to 10^5 years. However, conventional radiometric dating techniques are difficult to be applied for hydrothermal deposits, because they grow up by repeated mineralization. We tried to yield practical applications of trapped-charge dating techniques, expecting they provide appropriate averaged ages. We conducted electron spin resonance (ESR) dating of sulfate minerals (barite) in hydrothermal deposits, expecting they provide ages of hydrothermal mineralization. We also conducted thermoluminescence (TL) dating of quartz in volcaniclastic and siliceous sediment. Quartz of coarse grain in the volcaniclastic sediment is considered to provide igneous ages of original volcanic rocks, whereas quartz of fine grain in the siliceous sediment is expected to provide ages of intense hydrothermal alteration. Our test field is a hydrothermal field in the Okinawa Trough, where mineralization of hydrothermal deposits occurs not only on the seafloor but also within the subseafloor sediment layers. Radiocarbon (^{14}C) datings of planktic foraminifera in the uppermost unconsolidated sediment indicated monotonous sedimentation since ~30ka TL datings of thick volcaniclastic sediment provided ages between 20-50 ka, which are roughly in accordance with the radiocarbon ages. On the other hand, ESR datings of hydrothermal barite obtained from 10 and 20 mbsf (meters below the seafloor) provided rather young ages around 5-6 ka. These results suggest subseafloor mineralization of the barite after sedimentation of the volcaniclastic sediment.

Keywords: electron spin resonance dating, thermoluminescence dating, seafloor massive sulfide deposits, mineralization stage

©2020. Japan Geoscience Union. All Right Reserved.

Luminescence dating of the late Quaternary terrestrial-marine interaction sedimentary history of the north Jiangsu coastal plain and the Yangtze River delta in China

*Lei Gao[1], Hao Long[1], Toru Tamura[2]

1. Nanjing Institute of Geography and Limnology, Chinese Academy of Sciences, 2. Geological Survey of Japan, National Institute of Advanced Industrial Science and Technology

Abstract: Coastal deposits are ideal archives to decipher the history of interactions between the atmosphere, oceans and solid earth in view of exchanges of mass and energy, climate-induced sea-level changes and coastal sedimentary evolutions. Chronostratigraphy is one of the key clues to understand the links between them. However, robust age controls over glacial-interglacial timescales in Chinese coastal zones remain so scarse. Here, we apply luminescence dating methods, including single-aliquot-regenerative (SAR) quartz optically-stimulated luminescence (OSL) and feldspar/polymineral post-infrared infrared-stimulated (pIRIR) dating, to sediments from the north Jiangsu coastal plain (JSP) and the Yangtze River delta in China to ascertain their chronologies. In combination of sedimentology and microfossil analysis, the late Quaternary sedimentary environments are re-examined based on our newly refined chronostratigraphy. In the north JSP, the obtained chronostratigraphy of a invetigated core (EGWY02) revealed that terrestrial deposition occurred in marine isotope stage (MIS) 6, MIS 4-2 and the latest part of MIS 1, whereas marine-influenced sedimentation at MIS 5e, 5c, 5a and the majority of MIS 1. Specially, two sets of marine stratigraphic units (T1, T2) dated back to ~7 ka and 130-80 ka, respectively, were recognized, but no obvious MIS 3 transgression recorded in this core. In addition, the sedimentation rates (SR) resulted from Bayesian age-depth model show that two distinct high SR stages at 130-70 ka and 2-7 ka, corresponding to the global highstands of sea level and also strengthened East Asian summer monsoon (EASM); in contrast, much slower SR occurred through the last glacial as well as the late Holocene, when sea level was lower and the EASM intensity was weakened. However, in the Yangtze River delta, the chronostratigraphic comparison of our studying core (YZ07) with the adjacent cores along a south-north transection, suggested the tidal flat to delta deposits dated to the MIS3 at the basal part, which was erosionally overlain by terrigenous unconformity surface and fluvial deposit of the last glacial. This terrigenous unit is then overlain by the postglacial transgressive to regressive succession of tidal river, tidal sand bar, and delta front to tidal flat after ~13 ka. Both records in the north JSP and Yangtze River delta show strong links between the regional terrestrial-marine alternation sedimentary history and climate-induced global sea level changes, although the discrepancy in MIS 3 was existed between two regions, which might be due to the differences in distances of coring sites far from the offshore either or their paleotopographic relief.

Keywords: Luminescence dating, Late Quaternary, Coastal deposits, terrestrial-marine interaction sedimentary history

©2020. Japan Geoscience Union. All Right Reserved.

Composite chronology of Paleolithic sites in Jebel Qalkha revealed by pIRIR dating

Risako Kida[1], *Toru Tamura[2], Seiji Kadowaki[1]

1. Nagoya University Museum, Nagoya University, 2. Institute of Geology and Geoinformation Geological Survey of Japan, AIST

Several Paleolithic archaeological sites occur in the Jebel Qalkha area, southern Jordan, providing valuable records of the cultural dynamics and palaeoenvironment during the dispersal of *Homo sapiens* out of Africa. We attempted optically-stimulated luminescence (OSL) dating for sediment samples taken from Epipaleolithic to Middle Paleolithic layers at multiple sites, including Tor Hamar, Tor Fawaz, Wadi Aghar and Tor Faraj. Test measurements revealed that the OSL characteristics of quartz grains are not suitable for dating; quartz OSL leads to variable equivalent dose depending on preheat temperature and does not result in an appropriate dose recovery. In contrast, post-IR IRSL (pIRIR) is characterized by a good dose recovery and its equivalent dose does not highly depend on preheat and measurement temperatures. pIRIR also shows modest fading rates. While quartz OSL is usually the first choice for dating sediments younger than 50,000 years, in this site K-feldspar pIRIR protocol is considered more appropriate. Thus we attempted the $pIRIR_{50/150}$ protocol of K-feldspar grains of 62–90 μm diameter. We obtained dates of 11–46 ka at Tor Hamar, 14–45 ka at Tor Fawaz, 36–50 ka at Wadi Aghar, and 53–66 ka at Tor Faraj, being approximately concordant with ages inferred from stone tools. This indicates that further examination of the composite chronology of these sites may help clarify timings of lithic cultural changes and environmental background from the Middle Paleolithic to Epipaleolithic periods, corresponding to the human population change from *Neanderthals* to *Homo sapiens*.

Keywords: Archaeology, Late Pleistocene, Homo sapiens, Neanderthalensis, Climate change

©2020. Japan Geoscience Union. All Right Reserved.

[E] Poster | H (Human Geosciences)：H-DS Disaster geosciences

[H-DS08] Tsunami and tsunami forecast

convener:Hiroaki Tsushima(Meteorological Research Institute, Japan Meteorological Agency), Tatsuya Kubota(National Research Institute for Earth Science and Disaster Resilience)

This session discusses issues related to improving real-time and long-term prediction accuracy of tsunami from earthquakes, landslides, and volcanoes, which include such as a better understanding of tsunami dynamics, new real-time tsunami observing systems deployed in the open ocean and coastal waters, methodologies of more rapid and accurate prediction during tsunami emergencies, more extensive and accurate inundation maps, and long-term tsunami potential forecast.

[HDS08-P01] Probabilistic Hazard Assessment of Tsunami due to Large Earthquakes along the Nankai Trough

*Kazuhiro Ichijo[1], Yutaka Hayashi[1], Yasuyuki Kawazoe[2], Fumihiko Imamura[3], Hisashi Suito[1] (1.Ministry of Education, Culture, Sports, Science and Technology, 2.Japan Meteorological Agency, 3.International Research Institute of Disaster Science, Tohoku University)

[HDS08-P02] Characterized earthquake fault models along the Nankai Trough for probabilistic tsunami hazard assessment

*Kenji Hirata[1], Tadashi Kito[2], Nobuhiko Toyama[2], Hiroyuki Fujiwara[1], Hiromitsu Nakamura[1], Nobuyuki Morikawa[1], DOHI YUJI[1], Hisanori Matsuyama[2], Kenshi Ohshima[2], Yasuhiro Murata[3], Ryu Saito[3], Mariko Korenaga[4], Yuta Abe[4] (1.National Research Institue for Earth Science and Diaster Prevention, 2.OYO corporation, 3.KKC, 4.CTC)

[HDS08-P03] Tsunami simulations for probabilistic tsunami hazard assessment in the Nankai Trough

*Ryu Saito[1], Kenshi Ohshima[2], Tadashi Kito[2], Yasuhiro Murata[1], Tomoyuki Shibuki[1], Mariko Korenaga[3], Yuji Dohi[4], Hiromitsu Nakamura[4], Kenji Hirata[4], Hiroyuki Fujiwara[4] (1.KOKUSAI KOGYO CO., LTD, 2.OYO Corporation, 3.CTC (ITOCHU Techno-Solutions Corporation), 4.NIED (National Research Institute for Earth Science and Disaster Resilience))

[HDS08-P04] Probabilistic Tsunami Hazard Assessment for Nankai Trough:Weight Ratio and Results of PTHA

*Yuta Abe[1], Mariko Korenaga[1], Shinichi Akiyama[1], Teppei Ono[1], Hiroyuki Fujiwara[2], Kenji Hirata[2], Hiromitsu Nakamura[2], Tadashi Kito[3], Yasuhiro Murata[4] (1.ITOCHU Techno-Solutions Corporation, 2.National Research Institute for Earth Science and Disaster Resilience, 3.OYO Corporation, 4.Kokusai Kogyo Co., Ltd.)

[HDS08-P05] Consideration of tsunami source generated in the Hyuga-nada region in 1662

*Kei Ioki[1], Yusuke Yamashita[2], Yoshihiro Kase[3] (1.Geological Survey of Japan, National Institute of Advanced Industrial Science and Technology, 2.Disaster Prevention Research Institute, Kyoto University, 3.Geological Survey of Hokkaido, Hokkaido Research Organization)

[HDS08-P06] Source of the 1923 great Kanto earthquake explaining observed tsunami waveforms

*Yumi Nakadai[1], Yuichiro Tanioka[1] (1.Hokkaido University)

[HDS08-P07] Volcanic tsunami earthquakes repeating at submarine calderas (2): Kinematic source modeling of the 2015 Torishima earthquake

*Osamu Sandanbata[1], Shingo Watada[1], Kenji Satake[1], Hiroo Kanamori[2], Luis Rivera[3], Zhongwen Zhan[2] (1.Earthquake Research Institute, the University of Tokyo, 2.California Institute of Technology, 3.Université de Strasbourg, CNRS, IPGS UMR 7516, F-67000 Strasbourg)

[HDS08-P08] Sliding direction of the landslide that caused the 1998 Papua New Guinea tsunami

*Akio Katsumata[1], Yasuhiro Yoshida[2], Kenji Nakata[1], Kenichi Fujita[3], Masayuki Tanaka[1], Koji Tamaribuchi[1], Takahito Nishimiya[1], Akio Kobayashi[1] (1.Meteorological Research Institute, Japan Meteorological Agency, 2.Meteorological College, Japan Meteorological Agency, 3.Geospatial Information Authority of Japan)

[HDS08-P09] Simulation of reflected tsunami wave caused by the three cases of earthquake off Fukushima prefecture

*Kenji Nakata[1], Takeyasu Yamamoto[1] (1.Meteorological Research Institute, Japan Meteorological Agency)

[HDS08-P10] Real-Time Tsunami Detection Based on Ensemble Empirical Mode Decomposition

*Yuchen Wang[1], Kenji Satake[1], Takuto Maeda[2], Masanao Shinohara[1], Shin'ichi Sakai[1] (1.Earthquake Research Institute, University of Tokyo, 2.Graduate School of Science and Technology, Hirosaki University)

[HDS08-P11] Early estimation of tsunami height from near-fault ocean bottom pressure records: Comparison of DONET and S-net data

*Ayumu Mizutani[1], Kiyoshi Yomogida[1] (1.Graduate School of Science, Hokkaido University)

[HDS08-P13] Analytic solutions of seismic tsunamis' initial waveforms: a mathematical study

*Chi-Min Liu[1] (1.Department of Civil Engineering, Chienkuo Technology University)

[HDS08-P14] Predictions of tsunamis caused by possible outer-rise earthquakes in the Japan Trench

*Toshitaka Baba[1], Naotaka YAMAMOTO CHIKASADA[2], Yasuyuki Nakamura[3], Gou Fujie[3], Koichiro Obana[3], Seiichi Miura[3], Shuichi Kodaira[3] (1.Graduate School of Social Science and Technology, Tokushima University, 2.NIED, 3.JAMSTEC)

[HDS08-P15] Influence of coastal structures on probabilistic tsunami inundation assessments

*Toru Takeda[1], Toshitaka Baba[2], Tsuneo Ohsumi[3], Hiroyuki Fujiwara[4] (1.Graduate School of Advanced Science and Technology Education Department of Intelligent Mechanical Systems Engineering Construction Creative System Engineering Course, Tokushima University, 2.Graduate School of Science and Technology, Tokushima University, 3.National Research Institute for Earth Science and Disaster Prevention , 4.National Research Institute for Earth Science and Disaster Prevention)

[HDS08-P16] Simulations of sediment movement for tsunami deposits in Kamoda Pond along the Nankai Trough

*Takuya Saito[1], Toru Takeda[1], Kei Yamashita[2], Toshitaka Baba[3] (1.Graduate School of Advanced Science and Technology Education Department of Intelligent Mechanical Systems Engineering Construction Creative System Engineering Course, Tokushima University, 2.International Research Institute of Disaster Science, 3.Graduate School of Science and Technology, Tokushima University)

Probabilistic Hazard Assessment of Tsunami due to Large Earthquakes along the Nankai Trough

*Kazuhiro Ichijo[1], Yutaka Hayashi[1], Yasuyuki Kawazoe[2], Fumihiko Imamura[3], Hisashi Suito[1]

1. Ministry of Education, Culture, Sports, Science and Technology, 2. Japan Meteorological Agency, 3. International Research Institute of Disaster Science, Tohoku University

Earthquake Research Committee, the Headquarter of Earthquake Research Promotion (ERC/HERP) has released “*Probabilistic Hazard Assessment of Tsunami due to Large Earthquakes along the Nankai Trough*” (hereinafter-called PHAT) on 24 January 2020. This is the first report on hazard assessment of tsunami by ERC, and is based on "*Long-term evaluation of the Nankai Trough earthquake (Second edition)* " (ERC/HERP, 2013; hereinafter-called LTE2) and "*Tsunami prediction method for earthquakes with characterizing source faults (Tsunami Recipe)*" (ERC/HERP, 2017). PHAT evaluates the distribution of exceedance probabilities that will cause the tsunami height on the coast to be 3 m or more, 5 m or more, and 10 m or more due to various major earthquakes along the Nankai Trough within next 30 years. This abstract introduces the outline of PHAT.

The tsunamis targeted by PHAT are large repeating earthquakes along Nankai Trough whose seismic magnitudes and occurrence intervals has been evaluated by LTE2 as M8 to M9 class, and from 100 to 200 years, respectively. However, the so-called "largest-class earthquake" of Nankai Trough defined by the Cabinet Office is excluded from the target. The future possibility of occurrence of the largest-class earthquake cannot be denied logicaly because, very limited information of evidence on past occurrence of such huge earthquake is found from any written historical records or at least 2000 years-long sediment records.

PHAT assumed 176 patterns with different combinations of extent of epicenter area as next large earthquake cycle along the Nankai Trough by considering the diversity of it. In addition, according to the Tsunami Recipe, two or more cases having different large slip regions were prepared for each pattern in order to consider heterogeneity with respect to of the fault slip. As a result, source fault models of 348,345 cases were selected, and the distribution of tsunami height corresponding to each case were calculated.

Each case was weighted according to its similarity to past major earthquake along the Nankai Trough. Using these weights, the tsunami height computation results were superimposed at each evaluation point located at approximately 50-meter intervals along the coastline within potentially affected area due to the large earthquake along Nankai Trough. From the hazard curves obtained in this way, the exceedance probabilities of tsunami exceeding 3m, 5m or 10m within next 30 years was calculated. The upper limit of the excess probability is 0.743, which is the probability of occurrence probability of large earthquake occurring within the next 30 years from 2020 along the Nankai Trough.

The distribution of excess probability values has been compiled as maps for whole area and tables for each municipality. Each evaluation point or municipality is classified into 3 categories (less than 6%, from 6% to 26%, and 26% or more) according to its exceedance probability.

©2020. Japan Geoscience Union. All Right Reserved.

The characteristics of the map of "exceedance probability that a tsunami height on the coast will be 3m or more due to large earthquakes along the Nankai Trough within next 30 years" are as follows:

- Evaluation points classified into 26% or more are found in wide area.

- The Izu Islands and Kyushu, which are slightly away from the tsunami source, has locally large probability.

In the map of that of 5m or more, wide area centered on the Pacific side from the Kyushu region to the Tokai region indicate 6% or more, and some regions near the epicenter indicate 26% or more. The map of that of above 10m, some coastline near potential source area indicate from 6% to 26%.

According to three maps, the probability at inner bays in rias coast facing an open sea and the straight-shaped coast, which are in general sensitive to a tsunami source, and tends to be higher than surrounding area.

Keywords: Nankai trough, probabilistic tsunami hazard assessment, exceedance probability, long-term evaluation, large earthquake

©2020. Japan Geoscience Union. All Right Reserved.

Characterized earthquake fault models along the Nankai Trough for probabilistic tsunami hazard assessment

*Kenji Hirata[1], Tadashi Kito[2], Nobuhiko Toyama[2], Hiroyuki Fujiwara[1], Hiromitsu Nakamura[1], Nobuyuki Morikawa[1], DOHI YUJI[1], Hisanori Matsuyama[2], Kenshi Ohshima[2], Yasuhiro Murata[3], Ryu Saito[3], Mariko Korenaga[4], Yuta Abe[4]

1. National Research Institue for Earth Science and Diaster Prevention, 2. OYO corporation, 3. KKC, 4. CTC

The National Research Institute for Earth Science and Disaster Resilience (NIED) began a research project on a probabilistic tsunami hazard assessment (PTHA) for Japan in 2012 (Fujiwara et al., 2013, JpGU). After years of research on the PTHA, the “Probabilistic hazard assessment of tsunamis due to large earthquakes along the Nankai trough” was published by the Headquarters for Earthquake Research Promotion (HERP) in 2020. Although the largest-class earthquakes were not included in this assessment, this was for the first time that the probability of tsunami hazard information had become openly available to the general public in Japan.A PTHA consists primarily of three components: the construction of earthquake fault models, tsunami simulations, and the analysis of hazard curves. In this study, we focus on theconstruction of ‘characterized earthquake fault models’ (CEFMs) based on the long-term evaluation by the HERP (2013) to cover various types of possible earthquakes along the Nankai Trough.
We divided the entire source region on the upper boundary of the subducting Philippine Sea plateinto 18 sub-regionsas HERP(2013) did, and constructed total of 3480 CEFMs as various combinations of the 18 sub-regions.
Based on the CEFMs and tsunami simulations, we conducted two types of PTHAs for next Nankai earthquake sequence. One consists of 3480 CEFMs (83 source regions, Mw7.7-9.0), including CEFMs for the largest-class earthquakes as well as CEFMs with super-large slip areas. In this type of the PYHA, 180 combination patterns of source regions and the corresponding 916,669 combination patterns of CEFMs were incorporated into the PTHA. The other PTHA consists of 2720 CEFMs (79 source regions, Mw7.7-9.1), not including CEFMs for the largest-class earthquakes and CFMs with super-large slip areas. 176 combination patterns of source regions and the corresponding 348,345 combination patterns of CEFMs were incorporated into the PTHA, which is equivalent to the PTHA published by HERP (2020). The differences between these PTHAs will be presented by Saito et al. (JpGU, this meeting) and Abe et al. (JpGU, this meeting).
This study is conducted as a part of the research project “Research on the hazard and risk assessment” at NIED.

Keywords: Characterized earthquake fault model, Long-term evaluation, Nankai Trough, Probabilistic tsunami hazard assessment

©2020. Japan Geoscience Union. All Right Reserved.

Tsunami simulations for probabilistic tsunami hazard assessment in the Nankai Trough

*Ryu Saito[1], Kenshi Ohshima[2], Tadashi Kito[2], Yasuhiro Murata[1], Tomoyuki Shibuki[1], Mariko Korenaga[3], Yuji Dohi[4], Hiromitsu Nakamura[4], Kenji Hirata[4], Hiroyuki Fujiwara[4]

1. KOKUSAI KOGYO CO., LTD, 2. OYO Corporation, 3. CTC (ITOCHU Techno-Solutions Corporation), 4. NIED (National Research Institute for Earth Science and Disaster Resilience)

We have already reported the results of tsunami propagation simulations performed in each sea region along the Kuril Trench, the Japan Trench, the Sagami Trough, the Nankai Trough and the Ryukyu Trench (Takayama et al., 2016, JpGU; Saito et al., 2017, 2018, JpGU; Saito et al., 2016-2018, SSJ), along with a study on stochastic evaluation of tsunami hazards that would occur on coasts throughout Japan (Fujiwara et al., 2013, JpGU; Hirata et al., 2014-2018, JpGU; Hirata et al., 2018, SSJ). This time, we followed the method and concept of a probabilistic tsunami hazard assessment (PTHA) of earthquakes accompanying the interplate earthquakes excluding the largest class earthquake exceeding M9 announced by the government's Earthquake Research Committee (ERC) in January 2020. In addition, we calculated the tsunami propagation that would be caused by the Nankai Trough earthquake, taking into account the largest class of earthquakes excluded by ERC (see also Hirata et al., this meeting). Regarding whether to include the largest class earthquakes and others, in this presentation, we report the characteristics of tsunami heights simulated by the propagation calculation from the Kyushu to Kanto regions, that is, the Pacific coast, the Seto Inland Sea coast, and the Izu-Ogasawara Islands coast.

We describe the method of a tsunami propagation simulation. A tsunami propagation simulation used in this study estimated tsunami wave height along the coasts, solved by the non-linear shallow-water equation using a leap-frog scheme. These simulations were configured by a nested grid system consisting of four sub-regions from outer 1,350 meters to inner 50 m in a horizontal, landward inundation keeping, and transparent at the seaward edges. Initial wave height followed vertical displacement driven by seafloor deformation via Okada’ s equation (Okada, 1992). The sea surface deformation consisted of vertical and horizontal displacement of seabed deformation (Tanioka and Satake, 1996), and was filtered to remove high frequency components (Kajiura, 1963). The water level standard corresponded to mean sea level of Tokyo Bay (Tokyo Peil, T.P.). A seafloor and land topography model used was created using the topographic mesh data released by the “Nankai Trough Massive Earthquake Model Study Group” of the government's Cabinet Office. We converted the topographic mesh data with a minimum grid spacing of 10 m to 50 m, as in the nearshore tsunami calculation. In order to simulate the tsunami height from the epicenter to the coast, the calculation resolution was subdivided from offshore to shore at 1,350 m, 450 m, 150 m, and 50 m, and connected. PTHA in this study was conducted at approximately 420,000 points on a 50 m grid in the water area near the shoreline on the coast line.

The following is a brief description of a seismic source used in this study (for details, see Kito et al., this meeting). The seismic source used was a total of 2,720 characterized earthquake fault models (CEFMs) from Mw7.6 to Mw9.0 built based on 79 types of source regions diversified by combining 18 source regions shown in the long-term evaluation reports. In addition to these source regions and CEFMs, we adopted a total of 83 source regions, including the largest class of earthquakes excluded by ERC, and 3,480 types of CEFMs from Mw7.6 to Mw9.1. Therefore, the tsunami simulations were performed using 2,720 kinds of CEFMs that do not consider the largest class earthquake and 3,480 kinds of CEFMs that consider the largest class earthquake.

©2020. Japan Geoscience Union. All Right Reserved.

As a result of the tsunami simulation, the tsunami height was about 2 m at the maximum on the western coast of Kyushu and the Seto Inland Sea coast, which was lower than the other coasts. Conversely, along the Pacific coast, simulated tsunamis were relatively high around capes such as Ashizuri Cape, Muroto Cape, Shiono Cape, Daio-zaki, Irago Cape, and Iro-zaki. The tsunami height was less than 30 m for 2,720 CEFMs without considering the largest class earthquake, while the height was less than 50 m for 3,480 CEFMs considering them. The impact of including the largest earthquakes was remarkable around Ashizuri Cape, Muroto Cape, and Iro-zaki, and the tsunami rose about twice as much as without them.

The outputs form this study contributes to PTHA (Abe et al., this meeting) and stochastic research such as evaluation of coastal tsunami height including uncertainty. The use of the outputs is widely promoted by making them open access services (Dohi et al., this meeting).
This study was done as a part of the research project “Research on evaluation of hazard and risk” that is carried out by NIED.

Keywords: Nankai Trough, Tsunami simulation, Probabilistic tsunami hazard assessment

©2020. Japan Geoscience Union. All Right Reserved.

Probabilistic Tsunami Hazard Assessment for Nankai Trough:Weight Ratio and Results of PTHA

*Yuta Abe[1], Mariko Korenaga[1], Shinichi Akiyama[1], Teppei Ono[1], Hiroyuki Fujiwara[2], Kenji Hirata[2], Hiromitsu Nakamura[2], Tadashi Kito[3], Yasuhiro Murata[4]

1. ITOCHU Techno-Solutions Corporation, 2. National Research Institute for Earth Science and Disaster Resilience, 3. OYO Corporation, 4. Kokusai Kogyo Co., Ltd.

Earthquake Research Committee (ERC)/HERP (2020a) announced a probabilistic tsunami hazard assessment(PTHA) for the next Nankai earthquake based on the long-term evaluation reports for Nankai earthquake (ERC, 2013; ERC, 2020b). Although ERC (2020a) excluded possible maximum-sized ruptures over M9 on their PTHA, NIED conduct another PTHA for the next Nankai earthquake by adding earthquakes which have maximum-sized ruptures over M9 (Hirata et al., this meeting). In this presentation, we explain the setting of weight ratio on the two PTHAs and compare the results of the PTHAs.

ERC (2020a) constructed 79 earthquake source regions(ESR) by the combinations of 18 segments and a number of characterized earthquake fault models (CEFMs) for each ESR. As occurrence patterns for the next Nankai earthquake, they constructed 176 combos of ESRs and assigned weight ratio them. First, they divided the combos of ESRs into two groups; Group I had ESRs where the Tonankai and Nankai regions were ruptured individually (e.g.,1944 and 1946 sequence) and Group II had ESRs where both the Tonankai and Nankai regions were simultaneously ruptured (e.g.,1707 Hoei). The weight ratios for Group I vs Group II were assigned 2/3 vs 1/3 by taking account for occurrence pattern history. Next the combos of ESRs of Group I and II were addittionally devided into two groups; 2 segments of Tonankai region and 2 segments of Nankai regions ruptured simultaneously or individually where weight ratios were assigned 4/5 vs 1/5, respectively. The combos of ESRs were devided into two groups also about plate subduction direction; only ESRs with middle depth zone were ruptured or the others where weight ratios were assigned 4/5 vs 1/5, respectively.

The present study follows the methodology of ERC(2020a) principally, but newly adds (i) CEFMs in Group III that consists of maximum-sized ruptures over M9 and (ii) CEFMs with a super large slip(4 times amount of average slip) which is allowed to exist when earthquake ruptures reach the trough axis. Then we construct 83 ESRs and 180 combos of ESRs (Kito et al., this meeting) and conduct a PTHA with them. The weight ratios for Group III and GroupI&II are assigned 1/21 vs 20/21 based on the idea in “National Seismic Hazard Maps for Japan in 2014“(ERC,2014).

By adding earthquakes of maximum-sized ruptures and CEFMs with a super large slip, tsunami hazard curves exceed those of ERC(2020a) along coasts facing the Pacific between Kyushu and Boso Peninsula, especially for lower probability level. For example, the probabilistic coastal tsunami heights where exceedance probability in 30 years (P30) is equal to 3% are ~0.3m on average (~2.3m at maximum) larger than the PTHA of ERC(2020a), and those where P30 is equal to 0.3% are ~0.8m on average (~9.1m at maximum) larger. This suggests that when we want to know the tsunami risk of Nankai earthquake for frequency of once in a millennium or less, it is important to consider earthquakes of maximum-sized ruptures. However, the scientific evidence to the weight ratio to Group III vs Groups I &II is not so strong. We conduct a case study for weight ratio of Group III vs Groups I &II and show how the weight ratio affects PTHA largely.

©2020. Japan Geoscience Union. All Right Reserved.

Keywords: Tsunami, PTHA, Nankai Trough

©2020. Japan Geoscience Union. All Right Reserved.

Consideration of tsunami source generated in the Hyuga-nada region in 1662

*Kei Ioki[1], Yusuke Yamashita[2], Yoshihiro Kase[3]

1. Geological Survey of Japan, National Institute of Advanced Industrial Science and Technology, 2. Disaster Prevention Research Institute, Kyoto University, 3. Geological Survey of Hokkaido, Hokkaido Research Organization

Hyuga-nada region is located at the south-western part of Nankai Trough, in the Pacific Ocean. M7-class interplate earthquakes are repeatedly occurred by the subducting Philippine Sea plate beneath the Eurasian plate. The largest earthquake in this area was the 1662 Hyuga-nada earthquake (M=7.6) which occurred off Miyazaki Prefecture, south-eastern area of Kyushu region, Japan, and generated tsunami (after called the 1662 tsunami). The tsunami heights were estimated at least 4-5 m along the coast of Miyazaki city by historical records. The 1662 tsunami was much larger than tsunamis generated by usual M7-class interplate earthquakes. This region is also active area of the shallow slow earthquakes. It is known by the 2011 Tohoku earthquake that focal area of shallow slow earthquakes also become a tsunami source area. So, we hypothesized that the 1662 unusual large tsunami was caused by the coseismically slipping of focal area of shallow slow earthquakes. We firstly constructed the fault model of the 1662 earthquake based on the recent result of geophysical observation. To examine the tsunami source of the 1662 earthquake, we surveyed the 1662 tsunami deposits in the lowland along the coast of south-eastern Kyushu region. As a result, sandy event deposits interbedded with clay (organic clay) were recognized at several surveyed points. Based on facies features, these event deposits were possibly formed by the 1662 tsunami. Numerical simulation of the tsunami was carried out using the constructed fault model. Calculated tsunami inundation area can explain distribution of the likely tsunami event deposits at Komei, Miyazaki Prefecture. Furthermore, this study compares calculated tsunami inundation areas, distribution of other surveyed tsunami deposits and tsunami heights of historical records. Tsunami source of the 1662 earthquake proposed by our study could better explain geophysical, geological and historical records.

Keywords: tsunami, earthquake, tsunami deposit

©2020. Japan Geoscience Union. All Right Reserved.

Source of the 1923 great Kanto earthquake explaining observed tsunami waveforms

*Yumi Nakadai[1], Yuichiro Tanioka[1]

1. Hokkaido University

One of the most devastating natural disaster in Japan was caused by the 1923 great Kanto earthquake occurred just beneath the Tokyo Metropolitan area. The number of casualties by the earthquake was more than 100,000. The number of injured people was reached 2 million. In the southern Kanto region where the Philippine Sea plate is subducting along the Sagami trough, great underthrust earthquakes of M7-8 have repeatedly occurred. They also generated large tsunamis. It is, therefore, important to investigate the generation mechanism of large tsunamis that occur in such areas.

The 1923 Kanto earthquake is the most recent great earthquake along this plate interface. Source models for the 1923 event have been studied by many researchers using seismological and geodetical data. Aida (1993) proposed source models of the 1923 earthquake using regional tsunami heights from historical documents and experiences at the time of the earthquake. Namegaya et al. (2011) constructed a fault model consists of 34 subfaults and estimated the slip distribution by inversion of the co-seismic vertical deformation. Tsunami waveforms generated by the 1923 earthquake were also recorded by several tide gauges along the Pacific coast in Japan and reported by the Imperial Earthquake Investigation Committee (1926). However, those data have not been analyzed to estimate the source of the earthquake.

In this study, we used those variable tsunami waveforms to study the source of the earthquake. First, we digitized historical tsunami waveforms recorded at ten tide gauge stations, Ayukawa, Minatomachi, Choshi, Osaka, Owase, Kushimoto, Urado, Tokyo bay (Chiba, Shibaura, Fukagawa). Next, we needed to correct the bathymetry of Tokyo bay because the bay has been reclaimed significantly since the time of the earthquake. Finally, tsunami numerical simulation was conducted using previously proposed two source models (Aida,1993; Namagaya et al., 2011). Then, the computed tsunami waveforms at tide gauges were compared with the observed ones. The results of the comparison showed that computed tsunami waveforms from the source model estimated by Aida (1993) tended to overestimate the amplitude of observed waveforms. In Tokyo bay near the epicenter, computed waveform showed twice the amplitude of the observed waveform. On the other hand, the computed tsunami waveforms from source model estimated by Namegaya et al. (2011) well explained the observed tsunami waveforms. Especially at Tokyo bay, Minatomachi and Urado, the computed tsunami heights explained the observed heights much better than those computed from the Aida model.

This result indicates that the tsunami generation due to the 1923 great Kanto earthquake was a typical co-seismic vertical deformation caused by the earthquake.

Reference

Isamu Aida (1993): Historical Tsunamis and their Numerical Models which occurred in the North-Western Part of Sagami Bay, Journal of Geography 102(4) 427-436

Namegaya, Y., Satake, K. and Shishikura, M (2011): Fault models of the 1703 Genroku and 1923 Taisho Kanto earthquakes inferred from coastal movements in the southern Knato area, Annual Report on Active

©2020. Japan Geoscience Union. All Right Reserved.

Fault and Paleoearthquake Researches No. 11, 107-120

Imperial Earthquake Investigation Committee, (1925): Reports Imperial Earthquake Investigation Committee, No. 100, B 124p

Keywords: Tsunami numerical simulation, the 1923 Kanto earthquake

©2020. Japan Geoscience Union. All Right Reserved.

Volcanic tsunami earthquakes repeating at submarine calderas (2): Kinematic source modeling of the 2015 Torishima earthquake

*Osamu Sandanbata[1], Shingo Watada[1], Kenji Satake[1], Hiroo Kanamori[2], Luis Rivera[3], Zhongwen Zhan[2]

1. Earthquake Research Institute, the University of Tokyo, 2. California Institute of Technology, 3. Université de Strasbourg, CNRS, IPGS UMR 7516, F-67000 Strasbourg

1. Introduction

Almost every decade, v*olcanic tsunami earthquakes* occurred at a submarine volcano named Smith Caldera near Torishima Island in Japan (Torishima earthquakes). These earthquakes generated disproportionately large tsunamis for their seismic magnitudes (M_w 5-6) [e.g. *Fukao et al.*, 2018, Sci. Adv.]. In order to determine their physical mechanism, we constructed a kinematic source model based on analyses of tsunamis and long-period seismic waves. Here, we present the detail of kinematic source modeling of the 2015 Torishima earthquake. The overview of the project, including the physical mechanism, characteristic seismic properties, causes of tsunami earthquake nature and similarities of recurrent earthquakes, will be presented by *Sandanbata et al.* in "Active Volcanism (S-VC45)" session.

2. Hypothetical fault systems inferred from initial sea-surface displacement

We started the kinematic source modeling of the 2015 Torishima earthquake by estimating the initial sea-surface displacement around Smith Caldera by the tsunami waveform inversion. We used tsunami waveforms recorded at ocean-bottom pressure gauges deployed in the southern oceanic region of Japan, such as a temporary array [*Fukao et al.*, 2018], DONET, the Deep Sea Floor Observatory off Muroto Cape, and the DART system. We found (1) a large uplift concentrated just over the caldera floor, and (2) clear peripheral subsidence at least along the northern side of the rim structure.

Based on the results, we hypothesized a sub-caldera fault system composed of ring and horizontal faults (Fig.a). In the following sections, we examine whether the hypothetical fault system explains both tsunami and long-period seismic records. We also investigate the detailed fault geometries employing multiple fault models with variable fault parameters (i.e. depth of the horizontal fault, dip angle and length of the ring fault).

3. Inversion of tsunami waveforms for slip distributions of sub-caldera ring and horizontal faults

We determined slip distributions on the sub-caldera ring and horizontal faults from the tsunami records by applying a new efficient technique for computing tsunami Green's functions from subfault slips. In most cases, inverted slip distributions consist of *thrust slip on an inward-dipping ring fault* and *asymmetric opening and closing of a horizontal fault* (Fig.a).

The slip distributions on the multiple fault models accurately reproduce the tsunami records (Fig.b), indicating that these are plausible models for explaining tsunami excitation of the Torishima earthquake. However, if the ring fault extends to a horizontal fault lying at a depth of about 4 km below the caldera floor, slip direction of the ring fault becomes opposite between the upper and lower half portions, which we consider unrealistic. Hence, we believe that the horizontal fault lies at a shallower depth of approximately 2 km.

4. Forward modeling of long-period seismic waves from slip distributions

©2020. Japan Geoscience Union. All Right Reserved.

Finally, we investigated the plausibility of the slip models by comparing long-period seismic records at the F-net and GSN stations with their synthetic waveforms. Among the slip models, one with a ring fault with a 75° dip angle extending along an approximately three-quarter portion of the rim structure can best reproduce the observed long-period seismic waves (Fig.c). The waveforms of horizontal components and overall amplitude are sensitive to dip angle and length of the ring fault, respectively. This helps us to constrain the detailed fault parameters well.

5. Conclusion

We concluded that the slip model thus obtained can explain quantitatively both tsunami and long-period seismic records, and is a good kinematic source model of the 2015 Torishima volcanic tsunami earthquake. The source model consists of *thrust slip on inwardly down-dipping ring fault extending partially along the rim* and *asymmetric opening and closing of a sub-caldera horizontal fault* is attributed to the *trapdoor faulting* at the active submarine caldera.

Keywords: volcanic earthquake, tsunami, long-period seismic wave, tsunami waveform inversion, tsunami earthquake

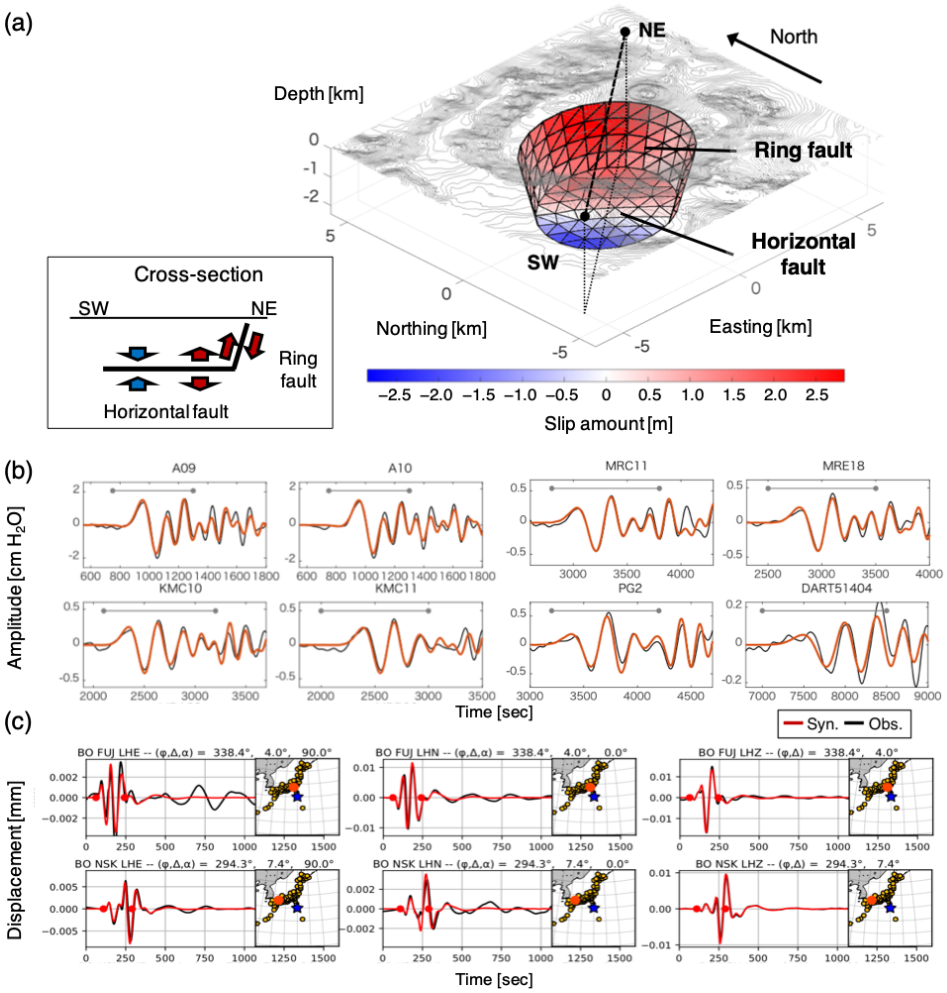


Fig. (a) Kinematic source model of the 2015 Torishima earthquake. Red color represents amount of thrust slips on the ring fault and opening of the horizontal fault. (b) Tsunami waveforms. (c) Long-period seismic waveforms.

©2020. Japan Geoscience Union. All Right Reserved.

Sliding direction of the landslide that caused the 1998 Papua New Guinea tsunami

*Akio Katsumata[1], Yasuhiro Yoshida[2], Kenji Nakata[1], Kenichi Fujita[3], Masayuki Tanaka[1], Koji Tamaribuchi[1], Takahito Nishimiya[1], Akio Kobayashi[1]

1. Meteorological Research Institute, Japan Meteorological Agency, 2. Meteorological College, Japan Meteorological Agency, 3. Geospatial Information Authority of Japan

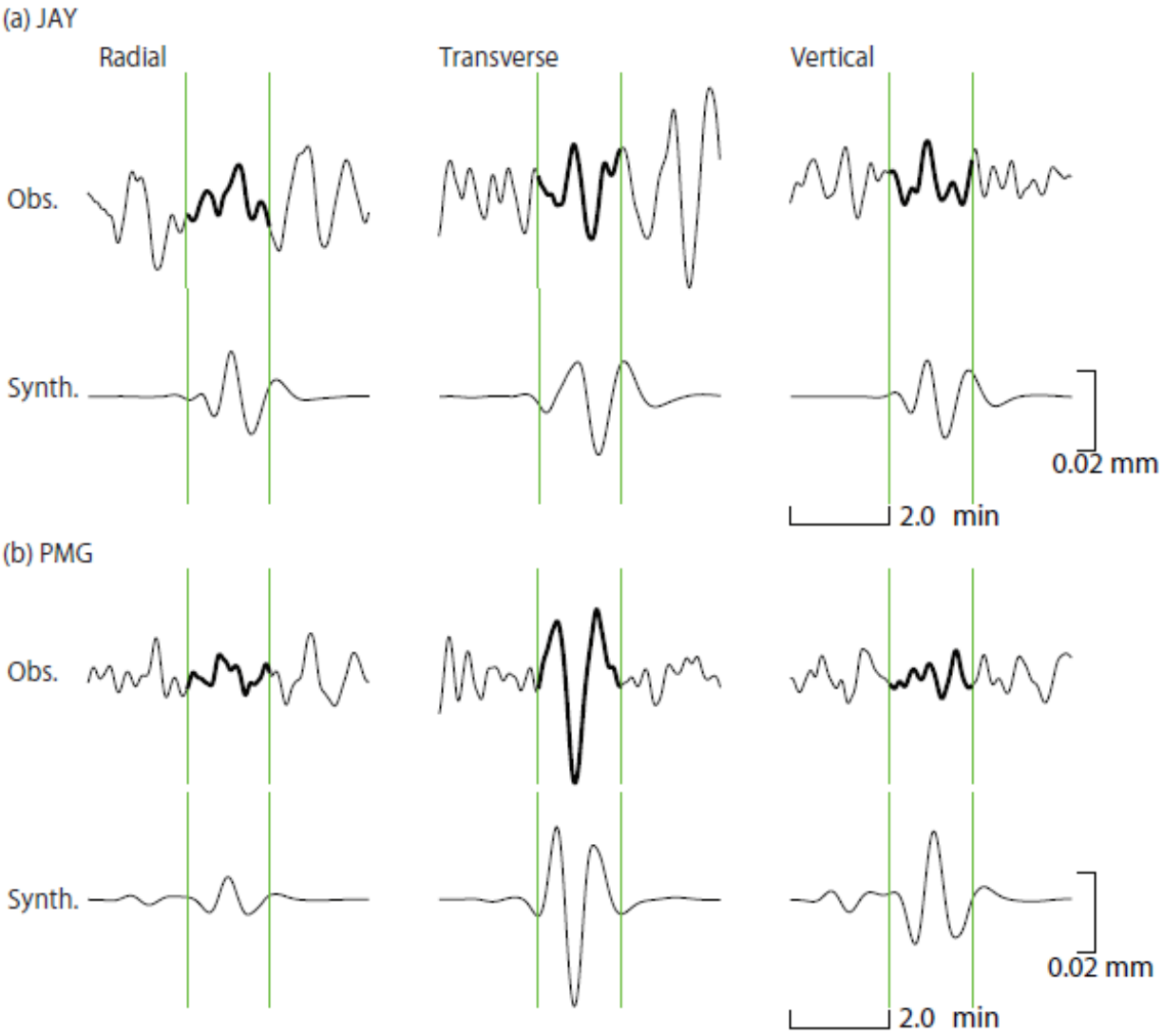
On 17 July 1998, a tsunami caused serious damage on the northern coast of Papua New Guinea about 20 min after an Mw 7.0 earthquake. The tsunami has been attributed to a submarine landslide that occurred about 13 min after the mainshock because its arrival at the coast was too late and its height too great to be the direct result of the fault slip of the earthquake. We found long-period (pass-band 50-100s) seismic phases possibly corresponding to the landslide event at JAY (about 150 km from the epicenter) and PMG (about 920 km from the epicenter). We investigated seismic records at nearby six stations. However, no possible phases were found expcept for JAY and PMG.

We tried to construct synthetic records for the observed records at JAY and PMG by the method of Takeo (1985) . To fit the synthetic records to the observed ones, various horizontal force directions were assumed, and checked cross-correlation functions between them. The landslide start time was adjusted to fit the synthetic waves to the waveform at JAY, and it was 12 min and 29 s after the mainshock origin time. The peak amplitudes of synthetic records were adjusted to the observed ones. The figure shows the comparison between the observed and synthetic records. The force size was estimated at 2-6 $X10^{12}$ N, and a landslide duration of 40 s showed the best fit. This force value was of the same order of magnitude estimated based on tsunami simulations in previous studies. The volume and the acceleration assumed for the tsunami simulations were confirmed with the observed seismic waves. The force of $6X10^{12}$ N is comparable to the force estimated by Kanamori and Given (1982) for the debris avalanche associated with the 1980 Mt St. Helens eruption (10^{13}N). The seismic waveform comparisons indicated that the force direction was oriented northeastward for both JAY (N72E) and PMG (N55E). A northward landslide was assumed in many previous tsunami simulations. There would be a possibility that the slump motion may have been oriented northeastward, which is along the downward direction of the topography.

Acknowledgements
We used seismic data archived at the Earthquake Research Institute (The University of Tokyo) and at the Incorporated Research Institutions for Seismology.

Keywords: The 1998 Papua New Guinea tsunami, submarine landslide tsunami, seismic waves from landslides

©2020. Japan Geoscience Union. All Right Reserved.



©2020. Japan Geoscience Union. All Right Reserved.

Simulation of reflected tsunami wave caused by the three cases of earthquake off Fukushima prefecture

*Kenji Nakata[1], Takeyasu Yamamoto[1]

1. Meteorological Research Institute, Japan Meteorological Agency

A tsunami, which was generated by the earthquake off Fukushima, was reflected on the coast of Fukushima Prefecture and propagated toward Sendai Bay, so 1.4 m height of tsunami was observed at the Sendai New Port on November 22, 2016.

In this study, we investigated similar phenomena that high reflected tsunamis were observed. We firstly searched the similar phenomena in tsunami cases occurred east off Tohoku and Kanto districts, the following three cases were detected:

July 19, 2008 (Mw 6.9),

July 12, 2014 (Mw 6.5),

December 20, 2008 (Mw 6.4).

Next, we executed tsunami simulations to reproduce these observed tsunami waveforms. For reproduction, we study accurate wave sources, propagation processes including dispersibility, and observation points including resolution of surrounding terrain.

The analysis showed that both the first wave and the reflected wave were reproduced for the cases of July 2008 and July 2014, whereas the calculated amplitude of the reflected wave was smaller than the observed one in the case of December 2008.

In the case of July 2008, shifting the horizontal position of the optimal fault by 0.2 degrees changes the amplitude ratio between the direct wave and the reflected wave, and changes the appearance of the predicted waveform.

Keywords: tsunami, reflected wave

©2020. Japan Geoscience Union. All Right Reserved.

Real-Time Tsunami Detection Based on Ensemble Empirical Mode Decomposition

*Yuchen Wang[1], Kenji Satake[1], Takuto Maeda[2], Masanao Shinohara[1], Shin'ichi Sakai[1]

1. Earthquake Research Institute, University of Tokyo, 2. Graduate School of Science and Technology, Hirosaki University

Offshore bottom pressure gauges (OBPGs) are useful in tsunami early warning because they are able to detect tsunami in real time. A reliable tsunami detection algorithm for OBPGs should be able to identify the tsunami signals and characterize the tsunami amplitude accurately, at a small computational cost. Traditional methods, like the DART algorithm adopted by the National Oceanic and Atmospheric Administration (NOAA), have to rely on the prediction of the tides and other lower frequency signals. These algorithms can detect a tsunami by subtracting predicted pressures from the observation, but they cannot properly identify its waveform. And they are unable to capture the feature of the background sea noise.
In our research, we propose a method of real-time tsunami detection based on Ensemble Empirical Mode Decomposition (EEMD). EEMD decomposes the time series into a set of intrinsic mode functions (IMFs) (Huang et al., 1998; Wu, 2005). Unlike Fast Fourier Transform or wavelet analysis, it does not need a priori basis. Instead, it adaptively determines the natural oscillatory modes embedded in the original signal. Therefore, it is applicable to nonlinear, non-stationary data like tsunami signals. In our practice, we use the series of the OBPG record of the past three hours, and then we conduct EEMD and obtain the IMFs. The tsunami signals can be separated from the tide signals, seismic signals, as well as background noise. By comparing the value with a threshold of 2 cm, we could decide whether the tsunami has arrived. We apply our method to the tsunami record of OBPGs of the 2016 Fukushima earthquake, Japan (M7.4; Gusman et al., 2017). Five OBPGs owned and operated by the Earthquake Research Institute recorded the tsunami generated by the earthquake. We retroactively conduct EEMD to the data. Our method automatically extracts tsunami-signals from the low-frequency components (e.g. tide) and the high-frequency components (e.g. seismic waves). The tsunami arrival is easily determined by setting the threshold. We compare our algorithm with STA/LTA (Short Time Average over Long Time Average) method (Allen, 1982). Our method is less influenced by the tide signals and is able to estimate the tsunami amplitude after detection. We also apply our method to the extremely large case of the 2011 Tohoku earthquake (M9.0), and the extremely small case of the 1998 off Sanriku earthquake (M6.1). The EEMD algorithm is able to detect and characterize the tsunami of the extremely large case, but it could not work for the extremely small case.

Keywords: Real-Time Tsunami Detection, Ensemble Empirical Mode Decomposition, Offshore Bottom Pressure Gauge

©2020. Japan Geoscience Union. All Right Reserved.

Early estimation of tsunami height from near-fault ocean bottom pressure records: Comparison of DONET and S-net data

*Ayumu Mizutani[1], Kiyoshi Yomogida[1]

1. Graduate School of Science, Hokkaido University

Ocean-bottom observation networks for earthquakes and tsunamis such as S-net and DONET have been deployed in the offshore Japan. These networks are designed to record tsunamis in terms of water pressure changes. During an earthquake, however, water pressure changes not only by tsunamis (i.e., sea surface heights) but also by water depth changes of instruments, vertical accelerations of a seafloor (i.e., reaction force from water column), and radiated P waves or ocean acoustic waves (e.g., Saito and Tsushima, 2016).

To extract only tsunami and sea bottom displacement components from coseismic ocean bottom pressure (OBP) records, we developed a new scheme based on the assumption that an OBP gauge records sea bottom acceleration at frequency range of 0.05–0.15 Hz (Mizutani and Yomogida, 2020, submitted). We applied it to DONET OBP records of the 2016 Off-Mie earthquake (M_w 6.0), and succeeded to extract tsunami and sea bottom displacement components (i.e., 100-s low pass filtered waveforms) only after 30 seconds of its origin time.

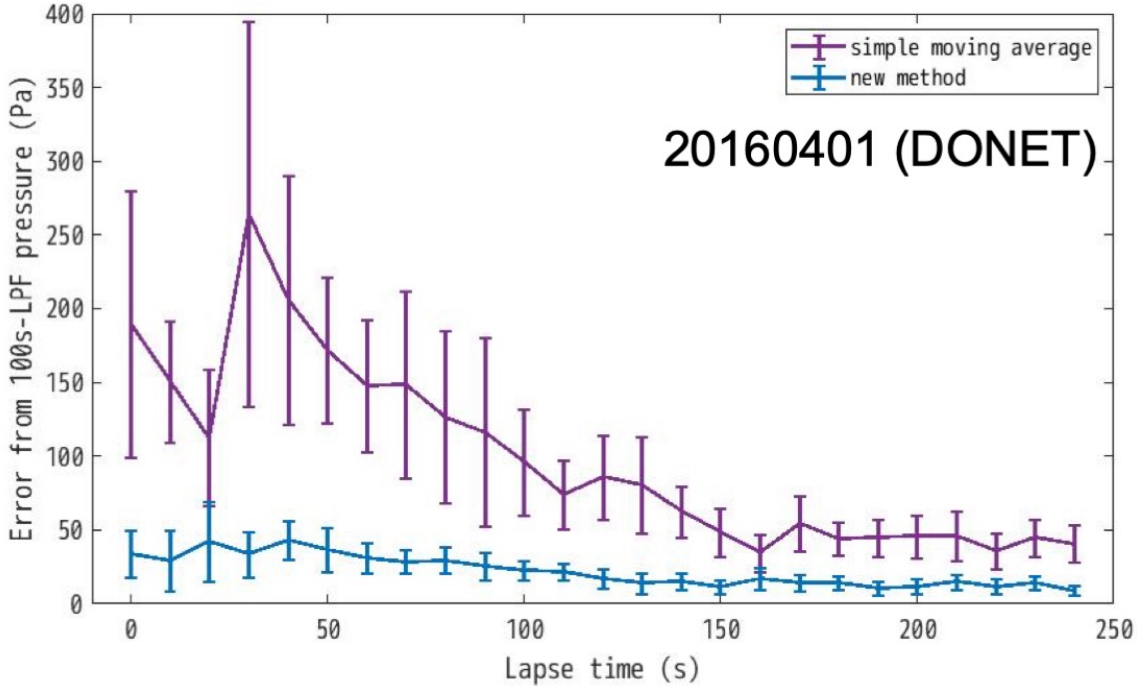
In this study, to confirm the validity of the above method, we applied it to the S-net OBP records associated with the 2016 and 2019 Off-Fukushima earthquakes of M_w 7.0 and 6.4, respectively. While relatively large tsunamis (~1 m) were observed for the 2016 event, no tsunamis for the 2019 event because of its depth was 45 km.

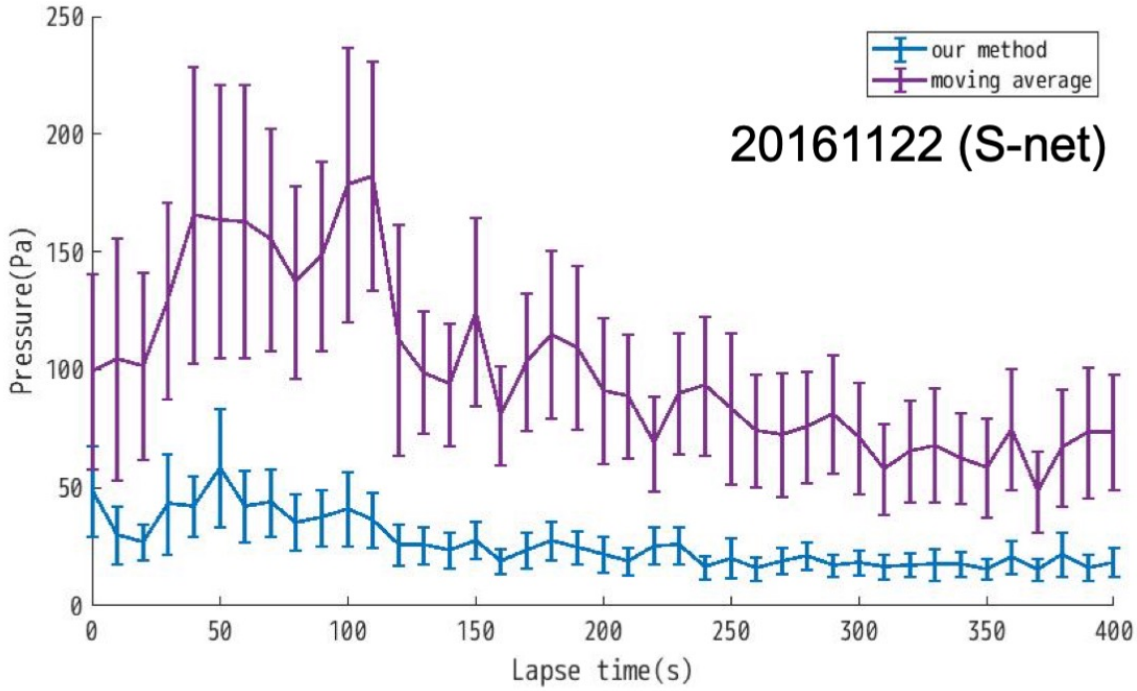
In both cases, the resulted waveforms show better agreement with 100-s low pass filtered waveforms than the ones that are applied simple moving average, similar to our previous result with their discrepancies reduced by half with our method. In other words, our method certainly removes the sea bottom acceleration components from the coseismic OBP records even with S-net data.

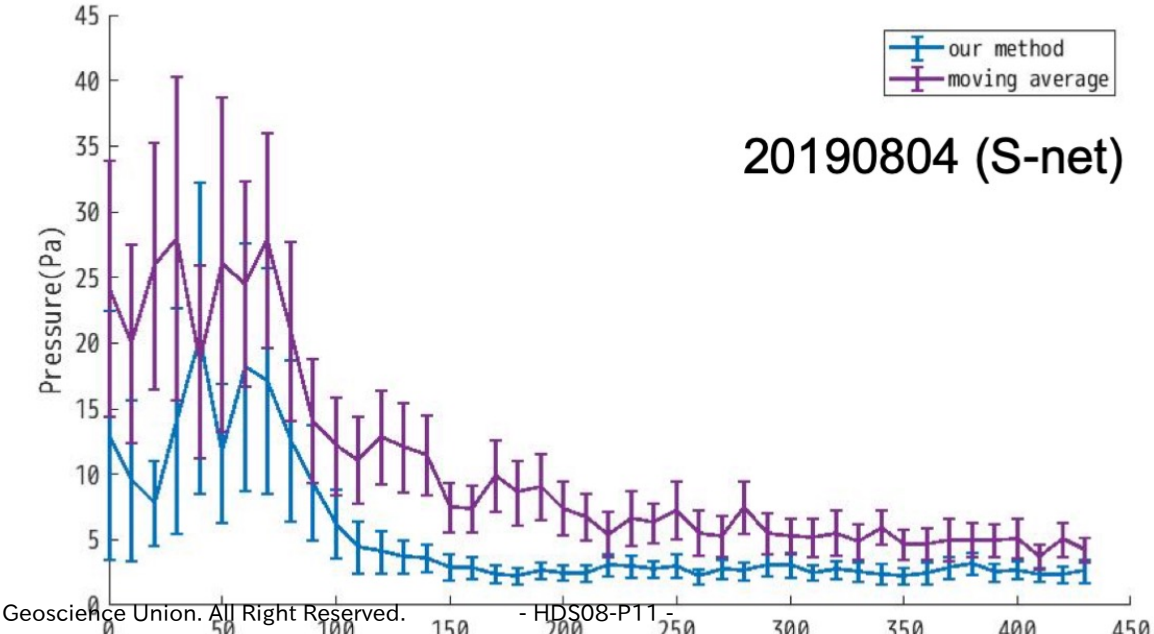
For the 2019 event, however, three stations (S2N02, S2N12, and S2N15) recorded the subsidences of about 30 cm. This may be caused by not the sea bottom displacement of each station but the rotation or tilt of OBP gauge, which were induced by strong ground motions. For more reliable tsunami early detection, we need to consider such unexpected signals.

Keywords: Tsunami, S-net, Early detection

©2020. Japan Geoscience Union. All Right Reserved.







©2020. Japan Geoscience Union. All Right Reserved.

©2020. Japan Geoscience Union. All Right Reserved.

Analytic solutions of seismic tsunamis' initial waveforms: a mathematical study

*Chi-Min Liu[1]

1. Department of Civil Engineering, Chienkuo Technology University

Analytical solutions of initial waveforms of seismic tsunamis are mathematically derived in this paper. Using the linear potential theory, solutions of integration forms for three fundamental seabed deformations, which include rectangular, sine and cosine liftings, are firstly solved with the help of integral transforms. Next, for the initial waveform that means the wave profile at the time when the seabed deformation stops, analytic (closed-form) solutions are derived by simplifying previous solutions with some mathematical techniques. These analytic solutions constitute an important basis which provides the accurate initial waveform and conditions for performing the subsequent numerical calculations.

Keywords: tsunami, initial waveforms, analytic solutions

©2020. Japan Geoscience Union. All Right Reserved.

Predictions of tsunamis caused by possible outer-rise earthquakes in the Japan Trench

*Toshitaka Baba[1], Naotaka YAMAMOTO CHIKASADA[2], Yasuyuki Nakamura[3], Gou Fujie[3], Koichiro Obana[3], Seiichi Miura[3], Shuichi Kodaira[3]

1. Graduate School of Social Science and Technology, Tokushima University, 2. NIED, 3. JAMSTEC

Great interplate earthquakes often induce outer-rise earthquakes in the subducting plate. An M8-class outer-rise earthquake which will be a pair of the 2011 Tohoku earthquake has not occurred yet, so it is anticipated to occur. We have conducted detailed seafloor topographic surveys, passive and active seismic observations to create possible 33 faults of outer-rise earthquakes near the Japan Trench axis in an area from 36.5 to 40.5 degrees north latitude. In this study, we predicted tsunamis caused by these outer-rise earthquakes using numerical simulations. Actual earthquakes do not exactly match the fault parameters of the assumed faults. Therefore, variations on the predictions due to the uncertainty of the assumed parameters were evaluated using the values of K and kappa of Aida (1978).
Each fault was modeled by one rectangular plane connecting endpoints of corresponding horst-and-graven structure on the seafloor. This defined fault length (L) and strike of the fault plane. The upper depth of the fault was set to be 0.1 km below the seafloor. Dip and rake angles were 60 and 270 degrees, respectively. An earthquake scaling law complied by outer-rise earthquakes around the world (Á lvarez-Gómez et al., 2012) determined earthquake magnitude from the fault length. The fault width was the same as the fault length (L=W). But when the lower edge of the fault was deeper than the bottom of the seismogenic zone (40 km), the width was shortened to match the depth of the bottom. The slip amount on the fault was determined by fault area (L x W) and magnitude assuming rigidity of $5x10^{10}N/m^2$.
In tsunami calculations, initial sea surface displacements were calculated assuming that the crust is a homogeneous elastic body in half-space (Okada, 1985). Additionally, horizontal movement effects (Tanioka and Satake, 1996) and a hydraulic filter based on the linear potential theory (Kajiura, 1963) were applied to the tsunami generation. The nonlinear long-wave equations were solved on a uniform finite-difference grid using JAGURS (Baba et al., 2015; 2017) for tsunami propagations. The interval of the grid points was 18 arc-sec. A nesting algorithm was not applied in this study. The large outer-rise fault model (No. 9, L=332 km, Mw=8.66) caused the maximum tsunami which reached 27 m at the coast in northeast Japan.
We repeated tsunami calculations using the fault parameters with variations. The marine seismic surveys showed that the dip angle of the outer-rise faults changed in a range from 45 to 75 degrees. Tsunamis from fault models with a dip of 45 and 75 degrees were calculated by the same method described above. Besides, a compound fault model consists of the upper half with 75 degrees and the lower half with 45 degrees was examined. Rake angle was changed in a range of ±15 degrees. We also performed calculations with models consisting of small subfaults with dimensions of about 60 km instead of a single large rectangular fault, other earthquake scaling laws and dispersive tsunami effects. The strike angle was unchanged because it can be determined from the seafloor topography. In results from the numerical tsunami simulations, using the difference earthquake scaling laws showed the most significant effect on the predicted tsunami heights which were changed by about 50 % on average of the 33 faults. The predicted tsunami heights were changed by a range from 5 to 10 % for changing the dip angle, about 5% for considering tsunami dispersion, about 2% for changing the rake angle, and about 1% for using the subfaults.
Acknowledgments: This work was supported by JSPS KAKENHI Grant Number 15H05718 and 19H02409.

©2020. Japan Geoscience Union. All Right Reserved.

Keywords: Tsunami, Outer-rise earthquakes, Japan Trench

©2020. Japan Geoscience Union. All Right Reserved.

Influence of coastal structures on probabilistic tsunami inundation assessments

*Toru Takeda[1], Toshitaka Baba[2], Tsuneo Ohsumi[3], Hiroyuki Fujiwara[4]

1. Graduate School of Advanced Science and Technology Education Department of Intelligent Mechanical Systems Engineering Construction Creative System Engineering Course, Tokushima University, 2. Graduate School of Science and Technology, Tokushima University, 3. National Research Institute for Earth Science and Disaster Prevention , 4. National Research Institute for Earth Science and Disaster Prevention

Studies on probabilistic hazard assessments are common in recent years to quantitatively understand the risks of disasters. For tsunami, probabilistic tsunami height assessments along the coast were conducted. But probabilistic tsunami inundation assessments are not shown yet because these need a huge number of tsunami calculations with highly resolved topographic data (~10m). However, recent developments of high-performance computers enable us to make a probabilistic tsunami inundation map if the study area narrowed down. We created a tsunami inundation database for Tokushima Prefecture along the Nankai Trough. Using the database, we estimated the probability of tsunami inundation on land by multiplying the occurrence probability based on the G-R law (Takeda et al., JpGU, 2019). Unlike the tsunami height on the coast, the inundations of the tsunami on land are greatly affected by the coastal structures. In this study, we created a new tsunami database without coastal structures to assess the contributions of coastal structures on the tsunami inundation probability.
Procedures for making the probability map without coastal structures were the same as that of the previous report except for non-considering coastal structures. We used Hirata et al. (2017)’ s 3967 faults models of the Nankai Trough earthquakes, and calculated tsunami propagations and inundations caused by the all fault models using the nonlinear shallow water equations. A nesting algorism was applied to improve the spatial resolution in the study area. Only the topographic data provided by the Cabinet Office was used. The coastal structure data was not involved in the calculations. We defined the relative weights among the earthquake fault models using the G-R law. The weights were used in superimposing all inundation maps to estimate the probabilities of tsunami inundation without the coastal structures. Comparing the probability maps with and without the coastal structures showed the great importance of the coastal structures reducing the tsunami impacts in the wide area. In particular, the probability of inundation was decreased very much in areas near the sea or river. The coastal structures reduced the probability by 60 % at the maximum near the estuary. However, it is surprising to us that, in some areas near the upstream, the probability of inundation was increased by about 30% with considering the coastal structures.
We will evaluate target earthquakes with a magnitude of 8.0 or more, evaluate tsunami arrival time, and analyze another area.
Acknowledgments: This work was supported by JSPS KAKENHI Grant Number 19H02409.

Keywords: probabilistic hazard assessments, Nankai Trough, G-R law

©2020. Japan Geoscience Union. All Right Reserved.

Simulations of sediment movement for tsunami deposits in Kamoda Pond along the Nankai Trough

*Takuya Saito[1], Toru Takeda[1], Kei Yamashita[2], Toshitaka Baba[3]

1. Graduate School of Advanced Science and Technology Education Department of Intelligent Mechanical Systems Engineering Construction Creative System Engineering Course, Tokushima University, 2. International Research Institute of Disaster Science, 3. Graduate School of Science and Technology, Tokushima University

One of the lessons learned from the 2011 off the Pacific coast of Tohoku Earthquake occurred in 2011 is a necessity to investigate the history of the occurrence of past earthquakes and tsunamis as old as possible. In this survey of past earthquakes, tsunami deposits give important information as physical evidence. After the 2011 off the Pacific coast of Tohoku Earthquake, tsunami sediment surveys have been vigorously conducted. Also, sediment movement simulation models for predicting tsunami deposits have been developed by Takahashi et al. (1999, 2000, 2011) and Fujii et al. (1998). However, comparisons between the survey results and the simulation results have been insufficient yet. The authors have compared tsunami deposits in coastal lakes along the Nankai Trough (Okamura et al., 2012) using the sediment transport model (STM) of Takahashi et al. For the source models, we used the largest class Nankai Trough earthquake assumed by the Cabinet Office and the 1707 Hoei earthquake (Furumura et al., 2011). But the difference from the survey results was observed at Kamoda Pond, one of the survey points by Okamura et al. They confirmed tsunami deposits at the sediment layer at two thousand years ago, but the all source models in the simulations didn’t cause any sediment movement in the pond. In this study, therefore, we focused on Kamoda Pond and examined whether tsunami inflow and sediment migration could occur in Kamoda Pond from three viewpoints: a submarine active fault, splay fault, and tsunami database.

The submarine active fault is the Kitan-Naruto strait section of the Median Tectonic Line fault zone, and the splay fault branches from the plate interface near Cape Muroto (Okamura, 1990). We examined whether each fault brings tsunami sediments in Kamoda Pond using STM. Also, from a tsunami database constructed by performing a large-scale tsunami calculation using 3967 earthquake scenarios of Hirata et al. (2017) and high-precision terrain data in the Nankai Trough. Scenarios that bring tsunami to Kamoda Point were searched from the tsunami database.

As a result of the investigation, Kamoda Pond was inundated in the case of considering the splay fault and in 13 scenarios of the tsunami database, in which a large slip area and a very large slip area were located in the area between the Kii Peninsula and Cape Muroto. The Cabinet Office's source model considered as "the largest class earthquake considering all possibilities" may not be the largest in some coast along the Nankai trough. However, we need more investigations to make sure that the Cabinet Office's source models do not inundate to Kamoda Pond by varying calculation conditions such as topography and tide level.

Acknowledgments: In this study, we used the sediment transport model developed by Takahashi et al. (1999, 2000, 2011). This work was supported by JSPS KAKENHI Grant Number 19H02409.

©2020. Japan Geoscience Union. All Right Reserved.

Keywords: Nankai Trough Earthquake, Sediment Transport software, Tsunami deposits

©2020. Japan Geoscience Union. All Right Reserved.

[E] Poster | H (Human Geosciences)：H-DS Disaster geosciences

[H-DS09] Landslides and related phenomena

convener:Masahiro Chigira(Disaster Prevention Research Institute, Kyoto University), Fumitoshi Imaizumi(Faculty of Agriculture, Shizuoka University), Gonghui Wang(Disaster Prevention Research Institute, Kyoto University)

Mass movements, such as landslides, rockfalls, and debris flows, have been occurring extensively in a large number of countries, causing heavy damage. In order to understand them and mitigate induced disasters, we invite contributions that report and discuss on mass movements and related phenomena, focusing on improved understanding of their characteristics; new insights into landslide mechanisms; the development of new approaches to monitoring; novel approaches to behavior forecasting and prediction; studies of successful landslide management; and the development of methods for hazard and risk evaluation. In particular, papers about recent landslide hazards, such as those induced by 2015 Kundasang earthquake in Malaysia, 2018 western Japan rainstorm, and 2018 Hokkaido earthquake are welcome.

[HDS09-P01] A new method for landslide extraction using optical and SAR images

*Yuga Kumagai[1], Masaru Fujita[2], Yasukuni Okubo[2], Kiichiro Kawamura[1] (1.Yamaguchi University, 2.Japan Space Systems)

[HDS09-P02] Landslides caused by the 2018 Hokkaido Iburi-tobu earthquake - Shallow slides of tephra deposits and deep-sheeted bedrock slides -

*Makoto Kaneko[1], Norio Oyagi[1], Hiroshi, P. Sato[2], Yusuke Muramiya[1] (1.Fukada Geological Institute, 2.College of Humanities and Sciences, Nihon University)

[HDS09-P03] **The geomorphic characteristics of landslides induced by The 2018 Eastern Iburi earthquake, Hokkaido**

★Invited Papers

*Rasis Putra Ritonga[1], Takashi Gomi[2,4], Hefryan Sukma Kharismalatri[2], Rozaqqa Noviandi[3], Yoshiharu Ishikawa[4] (1.United Graduate School of Agricultural Science, Tokyo University of Agriculture and Technology, 2.Institute of Global Innovation Research, Tokyo University of Agriculture and Technology, 3.International Environmental and Agricultural Science, Tokyo University of Agriculture and Technology, 4.Graduate School of Agriculture, Tokyo University of Agriculture and Technology)

[HDS09-P04] Relationship between the subsurface structure and the deformation area accompanied with the 2018 Hokkaido Eastern Iburi earthquake in a fill in Atsuma town, Hokkaido

*Issei Doi[1], Ryokei Azuma[2], Yuki Maenaka[2], Toshitaka Kamai[1] (1.Disaster Prevention Research Institute, 2.Faculty of Technology, Osaka Institute of Technology)

[HDS09-P05] Seismic site response of tephra slope: a case study for the landslides triggered by the 2018 Hokkaido Eastern Iburi Earthquake

*Gonghui Wang[1], Ning Ma[2], Issei Doi[1], Gen Furuya[3], Naoki Watanabe[4], Satoshi Ishimaru[5], Hiromichi Koyasu[5] (1.Kyoto University, 2.Southwest Jiaotong University, 3.Toyama Prefectural University, 4.Niigata University, 5.Hokkaido Research Organization)

[HDS09-P06] Microtremor Survey and Spectrum Analysis of a Coseismic Landslide: a Case Study in Subao Village, Ningxia, China

*Xiaobo LI[1,2], Jingshan BO[1], Issei DOI[2], Gonghui WANG[2], Toshitaka KAMAI[2] (1.Institute of Disaster Prevention, China Earthquake Adiministration, 2.Disaster Prevention Research Institute, Kyoto Unviersity)

[HDS09-P07] **Pore structure characteristics of wide-grading loose soils in the Wenchuan earthquake area**

*Yifei Cui[1], Chaoxu Guo[2] (1.State Key Laboratory of Hydroscience and Engineering, Tsinghua University, 2.Fujian Academy of Building Research, Co.LTD., Fujian Key Laboratory of Green Building Technology)

[HDS09-P08] Seismic Response of Rock Wedges under Dynamic Loading Revealed by Shaking Table Test

*Hung-Hui Li[1], Chi-Chieh Chen[1], Chang-Liang Chun[1], Ming-Han Lin[1], Chen-Shi Ping[1] (1.Chung-Cheng Institute of Technology, National Defense University of Taiwan)

[HDS09-P09] Seismic Response of Dip-Slope with Various Roughness of Weakness Revealed by Shaking Table Test

Wen-Zhang Chen [1], Ming-Han Lin[1], KAI-YANG LIN [1], *Hung-Hui Li[1] (1.Chung-Cheng Institute of Technology, National Defense University of Taiwan)

[HDS09-P10] Analytical solutions for submarine avalanche entraining/detraining process

*Yi Ping Lu[1], Chi-Yao Hung[1] (1.National Chung Hsing University)

[HDS09-P11] Slope failure - debris flow events in rhyolitic and granitic areas in Hiroshima triggered by 2018 torrential rainfall and its implications for disaster risk reduction – a quantitative approach by photogrammetry and field survey

*Toshihiko Sugai[1], Kunnga Mergen[1], Natsuki Sasaki[1], Sako Hasegawa[1], Shoichiro Uchiyama[2] (1.Department of Natural Environmental Studies, Institute of Environmental Studies, Graduate School of Frontier Science, The University of Tokyo, 2. National Research Institute for Earth Science and Disaster Resilience)

[HDS09-P12] **The effect of rainfall event characteristics on event-based landslide susceptibility map**

*Chun-Yi Wu[1], Chiao-Ling Hsueh[1], Sheng-Yu Lin[1] (1.Department of Soil and Water Conservation, National Chung Hsing University)

[HDS09-P13] Non-plastic fines content effect on the initiation and movement of rainfall-induced landslides in small flume tests

*Chao HUANG[1], Gonghui Wang[2] (1.Division of Earth and Planetary Sciences, Graduate School of Science, Kyoto University, 2.Disaster Prevention Research Institute, Kyoto University, Kyoto, Japan)

[HDS09-P14] **The influence of the orientation of weak planes on slope deformation**

*Chao-Yu Wang[1], Kuang-Tsung Chang[1] (1.National Chung Hsing University)

[HDS09-P15] Can we detect the acceleration of long-term gravitational deformation on steep slopes before catastrophic events? -A case study on two large-scale rapid landslides in Kii peninsular, Japan-

*Teruyuki Kikuchi[1], Norio Oyagi[2], Makoto Kaneko[2], Koki Sakita[3], Teruyoshi Hatano[4] (1.JP-Design. co. ltd., 2.Fukada Geological Institute, 3.Okayama University, 4.Electric Power Development Co., Ltd)

[HDS09-P16] Long-term distribution and evolution of landslide in the landslide-prone watershed: A case study in the Chishan river upstream watershed in Taiwan

*Chengyi Lin[1], Chunuhung WU[1] (1.Feng Chia University)

[HDS09-P17] A decade analysis of landslide distribution in the dense-landslide watersheds in Taiwan

*Chengyi Lin[1], Chunuhng WU[1] (1.Feng Chia University)

[HDS09-P18] **Study of Seeding Amount of Vegetation Pellets**

*Hung-Yen Hu[1], Guo-Zhang Michael Song[1], Shin-Hwei Lin[1], Kai-Chi Hsu[1] (1.National Chung-Hsing university, department of soil and water conservation)

A new method for landslide extraction using optical and SAR images

*Yuga Kumagai[1], Masaru Fujita[2], Yasukuni Okubo[2], Kiichiro Kawamura[1]

1. Yamaguchi University, 2. Japan Space Systems

Number of hazards dramatically increases in the world with global warming effects. For a decade from 1993 to 2002, 17% of fatality with various hazards is caused by landslides.
In recent years, some space agencies have released satellite data through their web pages in order to promote private use. With these datasets, we could understand surveillance of land surface motion risks. These supplies associated with satellite technology can open to study various hazards in any regions as developing countries, mountain regions, deserts and so on without a bunch of infrastructures.
Two acquisition systems by satellite technology can be used for the land surface motion analyses. One has an optical sensor detecting the sun light reflected from a ground surface. A NDVI value is one of the most useful tools that using optical satellite data to survey roughly a landslide activity. It is calculated with near infrared and visible red-light bands, and it can find vegetation area. If landslides occur in a research area, NDVI will decrease. Thus, we can see landslide activities using the NDVI values.
The other is a Synthetic Aperture Radar (SAR) system using a microwave. The microwave is transmitted from the satellite and the reflected wave from a ground surface is detected. SAR images are not affected by clouds because microwave passes through them.

In this paper, we discuss a new method to extract landslides efficiently using a combination of two acquisition systems; optical and SAR systems. Because of heavy rains and mountain region, there are many rain hazards and flush floods, and landslides in this district. We can use optical datasets at there, but most of them are widely covered with clouds, so that we need to confirm a new methodology.

We selected fifteen optical datasets without cloud covers from November 2016 to November 2019.
First, we examined the analyzed conditions using the optical datasets. The optical datasets should be generally controlled with shooting conditions as a sunlight direction, a sunlight intensity, a satellite direction and so on, so we chose three different conditions in the optical datasets. Therefore, we analyzed a small area being 2 km^2 or smaller in optical studies.
Second, we collected the SAR datasets in August 1^{st}, 4^{th}, 13^{th} and 16^{th} 2017 on the ESA website. We analyzed surface characteristics and topographical change using these datasets. Datasets of Augusts 1^{st} –13^{th} and August 4^{th} –16^{th} have descending and ascending orbit data, respectively. Land Cover Change Detection method and interferometric analysis were used to reveal the surface characteristics and topographical change, respectively.

As a result of calculation with the NDVI value (Expression; (NIR-R)/(NIR+R)), a vegetation field has higher number. With this value, we confirmed landslides that occurred in August 2017 using drone system from ground survey. As we follow the transition, we found a tendency of vegetation field/bare field percentage transition in the research area through years. The percentage rises in February to May, then it gradually decreases until next February. However, there are some rapid increases in the gradual decreasing period (from May to February). It might be affected by acquisition conditions because there is no apparent sign in an actual image. As a conclusion, it is hard to extract the change based on the effect of landslides.
As a result of SAR data analyzing, we found some surface characteristics and topography changes that occurred in the period. Some of them are on slopes and the others are between mountains. We can detect landslides within approximately 300 m diameter when they are assembled in a small region, but a

©2020. Japan Geoscience Union. All Right Reserved.

single landslide is not detected with the method. Most of landslides on slopes show both topography and surface characteristics changes but some of them demonstrate only topography change. There is an area that shows topography and surface characteristics changes even though it has no apparent change in the optical images through the period. These results need to be confirmed with ground survey. The result of Land Cover Change Detection shows the changes of landslides and artificial activities as same results. It is also necessary to confirm this result with ground survey or optical images.

Keywords: Remote Sensing, Landslide, SAR

©2020. Japan Geoscience Union. All Right Reserved.

Landslides caused by the 2018 Hokkaido Iburi-tobu earthquake - Shallow slides of tephra deposits and deep-sheeted bedrock slides -

*Makoto Kaneko[1], Norio Oyagi[1], Hiroshi, P. Sato[2], Yusuke Muramiya[1]

1. Fukada Geological Institute, 2. College of Humanities and Sciences, Nihon University

The 2018 Hokkaido Iburi-tobu earthquake (M 6.7) caused several thousands of the shallow slides and more than two hundreds of the deep-seated landslides. The shallow slides are attributed to the surface tephra, which was deposited in the late Pleistocene and Holocene, on the hilly slopes in the low-relief mountainous area. In the area there are several damaged locations, especially the residential site of Yoshino where is located on debris and/or alluvial cones in front of the undercut slopes. One of the largest deep-sheeted landslides lying on the Karumai Formation of Miocene deposits showed a spread-type movement and made the landslide dam blocking the Hidakahoronai River. So many landslides of spread-type were reported as earthquake induced ones in recent and ancient times in Japanese Islands that we consider those landslides of this type to be useful for the archive bodies of the old earthquakes.

Keywords: earthquake-induced-landslide,, tephra, undercut slope, housing location, spread, earthquake-archive body

©2020. Japan Geoscience Union. All Right Reserved.

The geomorphic characteristics of landslides induced by The 2018 Eastern Iburi earthquake, Hokkaido

*Rasis Putra Ritonga[1], Takashi Gomi[2,4], Hefryan Sukma Kharismalatri[2], Rozaqqa Noviandi[3], Yoshiharu Ishikawa[4]

1. United Graduate School of Agricultural Science, Tokyo University of Agriculture and Technology, 2. Institute of Global Innovation Research, Tokyo University of Agriculture and Technology, 3. International Environmental and Agricultural Science, Tokyo University of Agriculture and Technology, 4. Graduate School of Agriculture, Tokyo University of Agriculture and Technology

Up to 6000 landslides over 400 km^2 in Iburi Sub-prefecture, Hokkaido were induced by the Eastern Iburi Earthquake (EIE) on 6th September 2018. These landslides are unique because of their unusual topography, shape, and location where landslides occurred on hillslope. First, the landslides occurred on rather gentle and hilly topography (<500 m) with several landslides collapsed on entire hillslope and reaching valley while the others stopped on the middle part of hillslope. Moreover, those landslides formed into various shapes. Such unusual characteristics may affect sediment movement and production. We identified 1440 landslide scars in 18.87 km^2. Among them, 84% of landslides has area <3×10^3 m^2 while the greatest landslides area was 18×10^3 m^2. Landslide topography characteristic was examined based on frequency distribution of elevation, slope gradient, etc. Eastern Iburi area has elevation of 20-300 m with 75% of landslides were occurred on elevation of 100-200 m. Regarding slope gradient, landslides occurred over the whole range of gradients with 60% of them was occurred on the slope ranging from 25-35˚. Landslides tend to occur gradually until topography slope of 25˚, and increase rapidly as the topography slope increase until 35˚, then decrease after. However, Eastern Iburi topography range of >35˚ tends to collapse. Based on landslide shape characteristics of the ratio of length and width (L/W ratio), 92% of landslides had 1 to 3 of L/W ratio with 2 of mean value. Relationship between normalized distance to stream and ridge line indicates the locations of landslide occurrence on the hillslope. We found 56.4% of the landslide clustered near the stream and ridge, followed by near the ridge of upper quart of the slopes (11.5%), and near the stream lower quart of the slopes (3.8%). Meanwhile, the largest landslide area was found in those occurred near ridge and stream, followed by near the ridge, and near the stream for 2459 m^2, 797 m^2, and 236 m^2 respectively. Our study showed that those unique landslide characteristics may very advantageous for understanding the possible subsequent sediment transferred to channel in sediment management practice after earthquake.

Keywords: Earthquake-induced landslide, topography characteristics, landslide shape characteristics, landslide position

©2020. Japan Geoscience Union. All Right Reserved.

Relationship between the subsurface structure and the deformation area accompanied with the 2018 Hokkaido Eastern Iburi earthquake in a fill in Atsuma town, Hokkaido

*Issei Doi[1], Ryokei Azuma[2], Yuki Maenaka[2], Toshitaka Kamai[1]

1. Disaster Prevention Research Institute, 2. Faculty of Technology, Osaka Institute of Technology

Accompanied with the 2018 Hokkaido Eastern Iburi earthquake, some residential area suffered from landslides in Atsuma town, Hokkaido. The geology there was artificial fill on the tephra layer which overlay the sedimentary rock. It is important to know how the landslides were generated from the prospective of the subsurface structure for the mitigation of the residential areas with similar geological settings.

We conducted the surface wave exploration in and around the fill. As a result, low velocity zones were estimated, whose bottom shape was parallel to the old terrain. The thickness of the low velocity zones was larger than that of the fill. Kurosawa et al. (2019) showed that the slip surface was situated in the layer of Ta-d for our studied landslide. Comparing with the drill hole information, the low velocity zones that we estimated were corresponding to the moving body of the landslide which included the tephra layer as well as the fill.

©2020. Japan Geoscience Union. All Right Reserved.

Seismic site response of tephra slope: a case study for the landslides triggered by the 2018 Hokkaido Eastern Iburi Earthquake

*Gonghui Wang[1], Ning Ma[2], Issei Doi[1], Gen Furuya[3], Naoki Watanabe[4], Satoshi Ishimaru[5], Hiromichi Koyasu[5]

1. Kyoto University, 2. Southwest Jiaotong University, 3. Toyama Prefectural University, 4. Niigata University, 5. Hokkaido Research Organization

During the 2018 Hokkaido Eastern Iburi Earthquake, a huge number of landslides were triggered on the tephra slopes, resulting in great damage to local properties and 36 casualties. Although one large landslide was initiated with its sliding surface being in the bedrock of sandstone and siltstone, most of them occurred on the tephra slope. To understand the initiation and movement mechanisms of these landslides occurring on tephra slopes, understanding the coseismic response of the slopes during the earthquake is of great importance. To achieve this, we conducted microtremor observation on the tephra slopes on Yoshino and Tomisato areas, Atsuma immediately after the earthquake. We also installed seismometers on the tephra slope near the Yoshino area and performed continuous earthquake observation. Through analyzing the observed results and comparing them with those recorded in some earthquake observation stations during the mainshock, we examined the site response features of these tephra slopes and then the possible initiation mechanism of these tephra landslides during the earthquake.

Keywords: 2018 Hokkaido Eastern Iburi Earthquake, Seismic site response, Tephra slope, landslide

©2020. Japan Geoscience Union. All Right Reserved.

Microtremor Survey and Spectrum Analysis of a Coseismic Landslide: a Case Study in Subao Village, Ningxia, China

*Xiaobo LI[1,2], Jingshan BO[1], Issei DOI[2], Gonghui WANG[2], Toshitaka KAMAI[2]

1. Institute of Disaster Prevention, China Earthquake Adiministration, 2. Disaster Prevention Research Institute, Kyoto Unviersity

Coseismic landslides usually cause severe casualties and economic losses. The study of the spectrum characteristics of coseismic landslide sites is crucial to better understanding the possible site response during an earthquake, and then evaluate the risk of landslides. Therefore, we chose the Subao landslide to carry out microtremor survey and spectrum analysis. Subao landslide located in Subao village, Xiji County, Ningxia Hui autonomous region, China, which was a giant coseismic loess landslide induced by 1920 Haiyuan great earthquake. The plan of the landslide was irregular, with a length of nearly 1435 m, a width of almost 400 m, a height of nearly 172 m, and a mean thickness of almost 30 m, which indicated it was a typical low-angle and long-runout landslide.

To study the spectrum characteristics of the Subao landslide site. We applied a digital accelerograph to measure the microtremor on the displaced material, the outcropped surface of rupture, and also the slope outside of the landslide area. Based on the microtremor data, we used the open-source software Geopsy (http://www.geopsy.org/) to calculate and analyze the H/V value for all the measured data. Combined with three boreholes data, we can draw the following conclusions. (1) Most H/V curves of soil mass of the slope around the landslide had a clear peak, the range of the predominant frequency is 2.2 ~ 2.9 Hz, the peak amplification factor is 2.3 ~ 4.0, which reflected the magnification effect of ground motion about the soil mass and terrain. (2) H/V curves of the displaced material were relatively gentle, multi-peak type, and no significant predominant range. The peak amplification factor is 1.9 ~ 2.2, reflecting the complex interface of the soil after sliding and without amplification effect of the ground motion. (3) H/V curves at the outcropped surface of rupture had a narrow and steep predominant frequency band. The range of the predominant frequency is 2.4 ~ 2.6 Hz, and the peak amplification factor is 4.6 ~ 4.8, which was showing a significant topographic effect. (4) Compared with the stable soil mass of slopes around the landslide, the landslide deposits were of complicated soil structure, and the spectral characteristics were not distinct, therefore unable to well reflect the spectral features of the landslide site.

Accordingly, we found that the spectral characteristics of the slope around the landslide area are the reliable parameters for studying the dynamic stability and disaster mechanism of the landslide. The results would not only provide a criterion for the reasonable establish of geomechanical models of slopes but also provide the vital calculation parameter for the inversion of ground motion based on the coseismic landslide.

Keywords: Coseismic landslide, Microtremor, H/V method, Spectrum characteristics, Dynamic stability

©2020. Japan Geoscience Union. All Right Reserved.

Pore structure characteristics of wide-grading loose soils in the Wenchuan earthquake area

*Yifei Cui[1], Chaoxu Guo[2]

1. State Key Laboratory of Hydroscience and Engineering, Tsinghua University, 2. Fujian Academy of Building Research, Co.LTD., Fujian Key Laboratory of Green Building Technology

The 2008 Mw 7.9 Sichuan earthquake in China triggered nearly 200,000 landslides. Field observations show that wide-grading loose soils (WGLS) are a special slope deposit after earthquake that often serve as a source for debris flows in the western mountainous area of China. Previous research indicated that rainfall infiltration induced the migration of fine particles within soil slopes and lead to the initiation of shallow failure and subsequent debris flows. Clearly, soil pore structure exerts a profound influence on seepage during rainfall infiltration, which is closely related to soil permeability and corresponding internal erosion. The scientific challenge lies in how to systematically characterize WGLS pore structure so that it provides a foundation for future numerical simulations of fine particle migration-induced debris flows. In this study, the characteristics of WGLS pore structure were analyzed quantitatively using scanning electron microscopy. The results revealed that the pore size distribution of WGLS exhibited a bimodal nature separately occurring at 12 μm and 72 μm, and the pore radius of WGLS can be well-characterized using Rayleigh distribution with modified scale parameters. The pore complexity of all samples exceeded 0.75, which indicates a low aspect ratio for each pore. Meanwhile, it is verified that a lower Euler number (pore topology characterizes index) has high pore connectivity and high macro porosity in WGLS. The average diameter of the fine particles that migrated was then determined with a laboratory seepage test. Through a preliminary jamming probability analysis, both average pore complexity and 3D Euler number are significant contributors to the jamming probability of a soil sample during rainfall-induced fine particle migration, and jamming is most prevalent along the WGLS slope.

Keywords: Wide-grading loose soil, Micropore structure, Serial tomography, Fine particle migration, Shallow failure

©2020. Japan Geoscience Union. All Right Reserved.

Seismic Response of Rock Wedges under Dynamic Loading Revealed by Shaking Table Test

*Hung-Hui Li[1], Chi-Chieh Chen[1], Chang-Liang Chun[1], Ming-Han Lin[1], Chen-Shi Ping[1]

1. Chung-Cheng Institute of Technology, National Defense University of Taiwan

Rock slope failures are one of the most common natural disasters in Taiwan, and its stability depends upon the slope geometry, geological discontinuity, and mechanical properties of the rock mass, and greatly affected by earthquakes and rainfall as well. In northern Taiwan, the rock wedge exists frequently on the slope of the coastal road, and the rock slope failure is a potential threat to transportation safety.

To investigate the stability and seismic response of rock wedge under dynamic loading such as earthquake, this study adopts the physical model experiment and numerical analysis simultaneously to explore the seismic response of the single wedge block. The geometric factors, including the slope and wedge angles, and dynamic loading with different acceleration are considered. The results of the seismic response are discussed, and the critical acceleration which induces wedge block sliding are compared with the analytical results proposed by Kumsar et al. (2000).

In the physical model experiment, it shows that the smaller slope angle is, the sliding faster wedge block is. In the shaking table test, under the constant interaction angle 27˚, the smaller critical acceleration of the wedge block was observed when the slope angle is smaller and the wedge angle is larger, and the numerical analysis consequence presents identical results. Besides, when the slope angle is steeper and the wedge angle is lower, the sliding friction threshold is lower. In other words, when the friction of a fresh joint surface is continuously reduced due to weathering or water seepage, a wedge block with steep slope angle and small wedge angle have less tendency to slide result from lower friction angle.

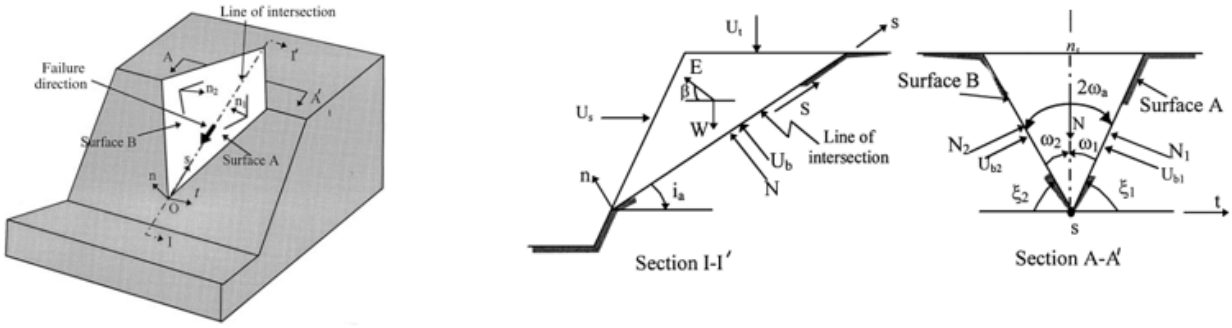
Keywords: rock wedge, shaking table test, numerical simulation

©2020. Japan Geoscience Union. All Right Reserved.

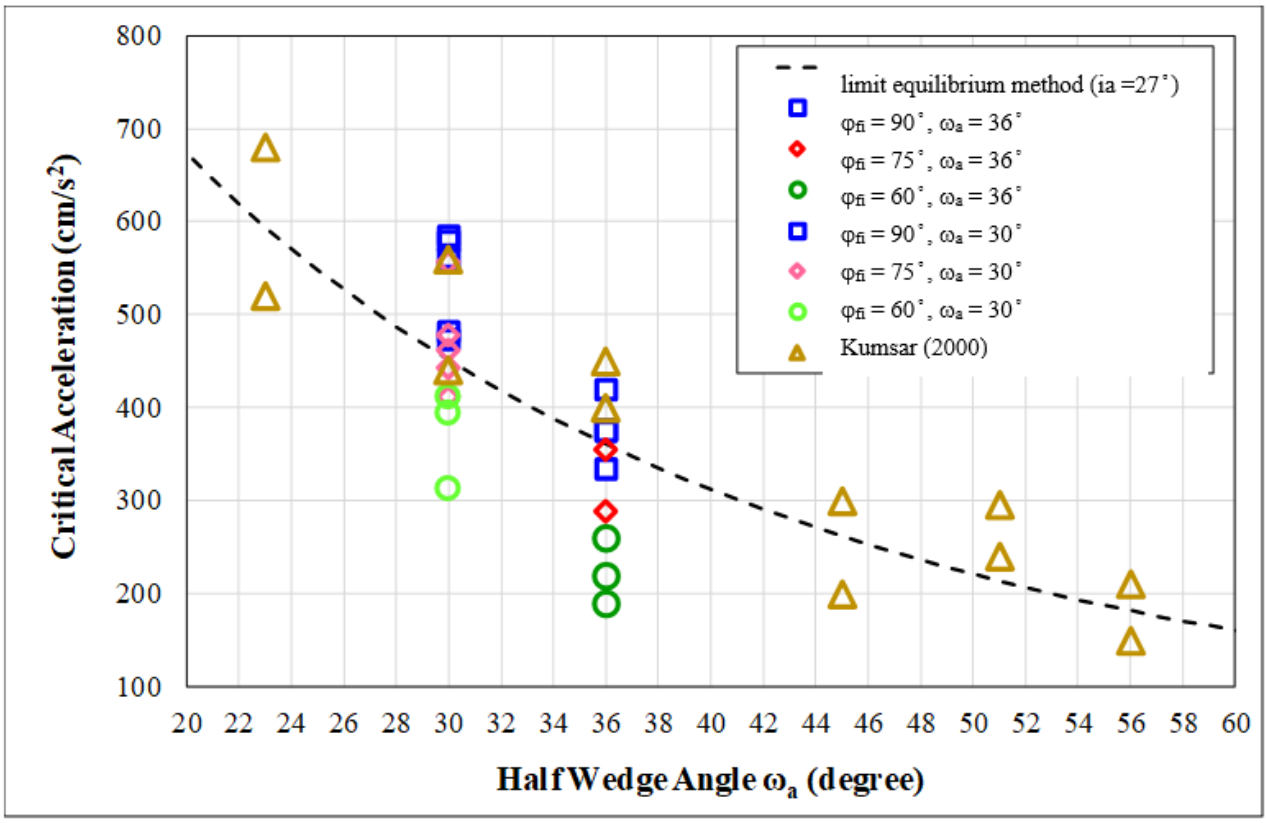
ϕ : the friction angle of the discontinuity surfaces

i_a : intersection angle

ω_a : half wedge angle



The considered single wedge block model proposed by Kumsar et al. (2000)



©2020. Japan Geoscience Union. All Right Reserved.

Seismic Response of Dip-Slope with Various Roughness of Weakness Revealed by Shaking Table Test

Wen-Zhang Chen [1], Ming-Han Lin[1], KAI-YANG LIN[1], *Hung-Hui Li[1]

1. Chung-Cheng Institute of Technology, National Defense University of Taiwan

The long-term interaction between the Eurasian Plate and the Philippine sea plate has caused frequent earthquakes and slope disasters in Taiwan. There are approximately 18,500 earthquakes in Taiwan per year which is alleged by Central Weather Bureau. It is obvious that slope disasters seriously threaten the safety of transportation facilities and residents. In the research of seismic-induced landslides, dip slope failure has always been an important issue in Taiwan. This study aims to investigate the seismic response of dip-slope with various joint roughness coefficient (JRC) of weakness and consider the influence of dynamic loading with various combinations of frequency and amplitude of cyclic motions
The preliminary results of this study are as follows: (1) As JRC increases, the critical acceleration that causes the block sliding increases; (2) when the inclination angle of joints increases, the critical acceleration decreases; (3) When the number of model layers increases, the acceleration at the top of the model is amplified.

Keywords: dip-slope, joint roughness coefficient, shaking table test

©2020. Japan Geoscience Union. All Right Reserved.

Analytical solutions for submarine avalanche entraining/detraining process

*Yi Ping Lu[1], Chi-Yao Hung[1]

1. National Chung Hsing University

Landslides, debris flows, and submarine avalanches are the geophysical examples that alter their volume and travel distance by entraining or detraining granular material at the base. Here, we focus on the entraining/detraining process of submarine landslides. We propose a depth-averaged model using conservation equations for mass, momentum, and kinetic energy. We assume a linearized mu(I) rheology and Coulomb friction law along the side boundary. To obtain the analytical solution, we simplify the model to become a simple nonlinear diffusion equation. Also, a scaling analysis is applied to derive the validity of our simplified model. To check the simplification, we use the HLL scheme and finite volume numerical method to solve the full equation. To verify the model, we propose a new submarine dam break experiment. The experiment is conducted with a new Refractive-Index-Matching (RIM) material. The motion of the granular is monitored with a high-speed camera, and the velocity field can be obtained with Particle Tracking Velocimetry (PTV) method. In the end, we compare the numerical simulation, the analytical solution, and the experimental measurement.

©2020. Japan Geoscience Union. All Right Reserved.

Slope failure - debris flow events in rhyolitic and granitic areas in Hiroshima triggered by 2018 torrential rainfall and its implications for disaster risk reduction –a quantitative approach by photogrammetry and field survey

*Toshihiko Sugai[1], Kunnga Mergen[1], Natsuki Sasaki[1], Sako Hasegawa[1], Shoichiro Uchiyama[2]

1. Department of Natural Environmental Studies, Institute of Environmental Studies, Graduate School of Frontier Science, The University of Tokyo, 2. National Research Institute for Earth Science and Disaster Resilience

Introduction
2018 torrential rainfall hit western Japan and large areas were covered in debris and mud. This study focused on several slope failure –debris flow depositional events occurred in both rhyolitic and granitic mountainous areas in Hiroshima Prefecture and estimated geomorphological changes quantitatively through the events by field survey coupled with photogrammetry. Furthermore, geomorphological land classification and river segmentation based on reach type classification was carried out to discuss the relationships between 2018 geomorphic changes and the surrounding geomorphic development history.

Case study in rhyolite mountain area
Two contrasting slope failure events named as case E and case W occurred on rhyolitic mountain slopes were picked up in the Kurose, Higashihiroshima city. In the case of E, the failure sediments became debris flow and went down through dissected river valley, destroying several Sabo dams alternately from side to side. At the mountain foot, the debris flow slightly denuded peaty silt at the bottom and eroded previous debris flow sediment laterally, and then deposited with the thickness of around 2 m, accompanying gigantic gravels including huge blocks of the destroyed Sabo dam on the depositional surface with upward coarsening structure. Lots of driftwood jammed behind the gigantic gravels with its long axis perpendicular to the flow direction. The debris lastly broadened the depositional area up to 100m.
In the case of W, failure sediments went down along the shallow unclear valley slightly denuding the surface soils keeping the width of the fluid area about 50 m. Reddish colored strongly weathered crust can be observed below the debris and the transportation area gradually changed into deposition area. The debris of the case W was much finer and slightly thinner than that of case E, with lots of driftwoods whose long axis parallel the flow direction.
To summarize in rhyolitic mountains partly covered with reddish weathering crust, even slightly dissected slopes (case W) may failure triggered by unprecedented heavy rainfall, while already dissected slopes (case E) may failure much more frequently to produce debris flows with huge gravels and continue to develop the dissected valleys progressively.

Case study in granitic mountain area
Concerning granitic mountain slopes, Kawasumi (KWS) in Kumano town, Yanohigashi (YNH) in Hiroshima city, and Koyaura (KYU) and Sakahigashi (SKH) in Saka town were picked up. KWS and YNH locate on artificially modified debris flow fan surfaces and/or mountain foot erosional gentle slopes, where plural small steep valleys met before the housing development. The distance between the present outlet of the valleys and valley heads are rather short, about 500m with steep slopes, and the 2^{nd} is the stream order of the valley defined as the Strahler system of stream ordering. Debris with huge core stones deposited below the outlet of the valley.
KYU and SKH locate on small alluvial lowlands produced by fluvial depositional processes by 5^{th} order

©2020. Japan Geoscience Union. All Right Reserved.

streams whose drainage basins have a dozen of slope failures occurred by the 2018 heavy rainfall. The river course can be divided into 3 segments of 1, 2a and 2b, based on the reach types consisting the segment. Segment 1 locates upstream of the fan apex characterized by marked lateral erosion by braided channel reaches. Segment 2a locates the upstream part of the alluvial lowland with the longitudinal slope of about 6 percent characterized as debris flow fan where braided channel potentially migrates laterally without artificial channel fixing. Segment 2b locates the downstream part of the lowland characterized by straight artificial channel on fan delta with the slope of less than 6 percent.
Because the drainage basins behind KYU and SKH may produce debris flows by valley-head failures frequently, the river side narrow plains in Segment 1 are not suitable for land use. Outside areas of the curved channels in Segment 2a are the same because debris flows directly hit the areas. Actuary crevasse spley was formed at the area by the 2018 event. Along Segment 2b sand and mud tend to flow over the bank and cover the lowland widely.

In conclusion, it is critical for mitigating flooding and debris flow disasters to evaluate the diversity of local geomorphic conditions quantitatively based on the regional geomorphological development history which has produced the conditions through time. Thus, nationwide-geomorphological classification mapping based on the local landform development history is crucial, and to do this we need to learn much more from the floods and landslides triggered by torrential rain in western Japan 2018.

Keywords: slope failure, crevasse spley, nationwide high-resolution landform classification map, river segment, photogrammertry

©2020. Japan Geoscience Union. All Right Reserved.

The effect of rainfall event characteristics on event-based landslide susceptibility map

*Chun-Yi Wu[1], Chiao-Ling Hsueh[1], Sheng-Yu Lin[1]

1. Department of Soil and Water Conservation, National Chung Hsing University

The landslide susceptibility models can be established based on either a long-term landslide inventory or a specified rainfall-induced landslide event. The susceptibility models established using different rainfall events may result in dissimilar susceptibility maps in the same area. The effect of rainfall event characteristics on event-based landslide susceptibility map needs to be discussed and as a reference for selection of a proper event to establish a susceptibility map. This study will be conducted in the Shihmen watershed, which has an area of 760 km^2 and is one of the main water sources for northern Taiwan. Landslide inventory caused by rainfall events in the Shihmen watershed will be collected during the period from 1996 to 2015. The intrinsic geomorphological and extrinsic rainfall factors of each individual slope unit will be derived, screened, and entered in the logistic regression to train the susceptibility model for each rainfall event. The prediction ability of the susceptibility model established based on one specified event will be compared according to the validation results of the others. The AUC values of the success rate curves (SRC) of the others will be calculated sequentially and then averaged to represent the ability of the model to predict landslide occurrence. This research is looking forward to understanding the relationship between the AUC values calculated for different rainfall events and the corresponding rainfall characteristics, and choosing the best susceptibility map to represent the characteristic of the Shihmen watershed.

Keywords: landslide susceptibility, event-based landslide model, rainfall characteristic, Shihmen watershed

©2020. Japan Geoscience Union. All Right Reserved.

Non-plastic fines content effect on the initiation and movement of rainfall-induced landslides in small flume tests

*Chao HUANG[1], Gonghui Wang[2]

1. Division of Earth and Planetary Sciences, Graduate School of Science, Kyoto University, 2. Disaster Prevention Research Institute, Kyoto University, Kyoto, Japan

Introduction

Landslides locally constitute an important natural hazard on Earth, causing great loss of properties and casualties. For original slope, some landslides with long traveling distances tend to occur on the material rich in fine soil particles like granitic soil generated by weathered coarse-grained granite, such as the 2014 Hiroshima landslides triggered by rainstorm. Debris avalanches are a kind of high-speed landslides. A hypothesis of dynamic fragmentation has been proposed as one of the reasons for their high mobility. Presence of fine-grained material may lower the shear resistance of the sliding debris. Some rock avalanche deposits show “inverse grading”. Wenchuan earthquake induced coseismic landslides and landslide dams, and some dams composed of unconsolidated fine debris. Recent study revealed that the secondary landsliding phenomena had been widely triggered on these landslide deposits, and the initiation and movement of these landslides are greatly related to the involvement of fine materials. Nevertheless, the detailed roles of fine materials had not been clarified. Therefore, study will focus on examining the effect of non-plastic fines content on the initiation and movement of rainfall-induced landslides through flume tests.

Material and Method

Samples for the tests are mixture of silica sand No. 7 with differing contents (0%, 10%, 20%, 30%, 40% and 50%) of silica powder by weight. Before setting, the mixtures were prepared to have an initial water content of 10%. During test, the flume was sloped to 20˚. Tilting transducers are installed at mid-depth within the soil model to monitor the possible inclination of the soil mass. Artificial rainfall (100 mm/h) was simulated by sprinklers mounted above the soil model to trigger landsliding.

Result

In general, the entire process required 30–45 min for slope wetting, and few minutes for failure. In the series tests on silica 7 and its mixtures with 10%, 40%, 50% silica powder, retrogressive sliding occurred in each test. However, in the series tests on the mixture of silica 7 and 20%, 30% silica powder, flowslides were initiated.

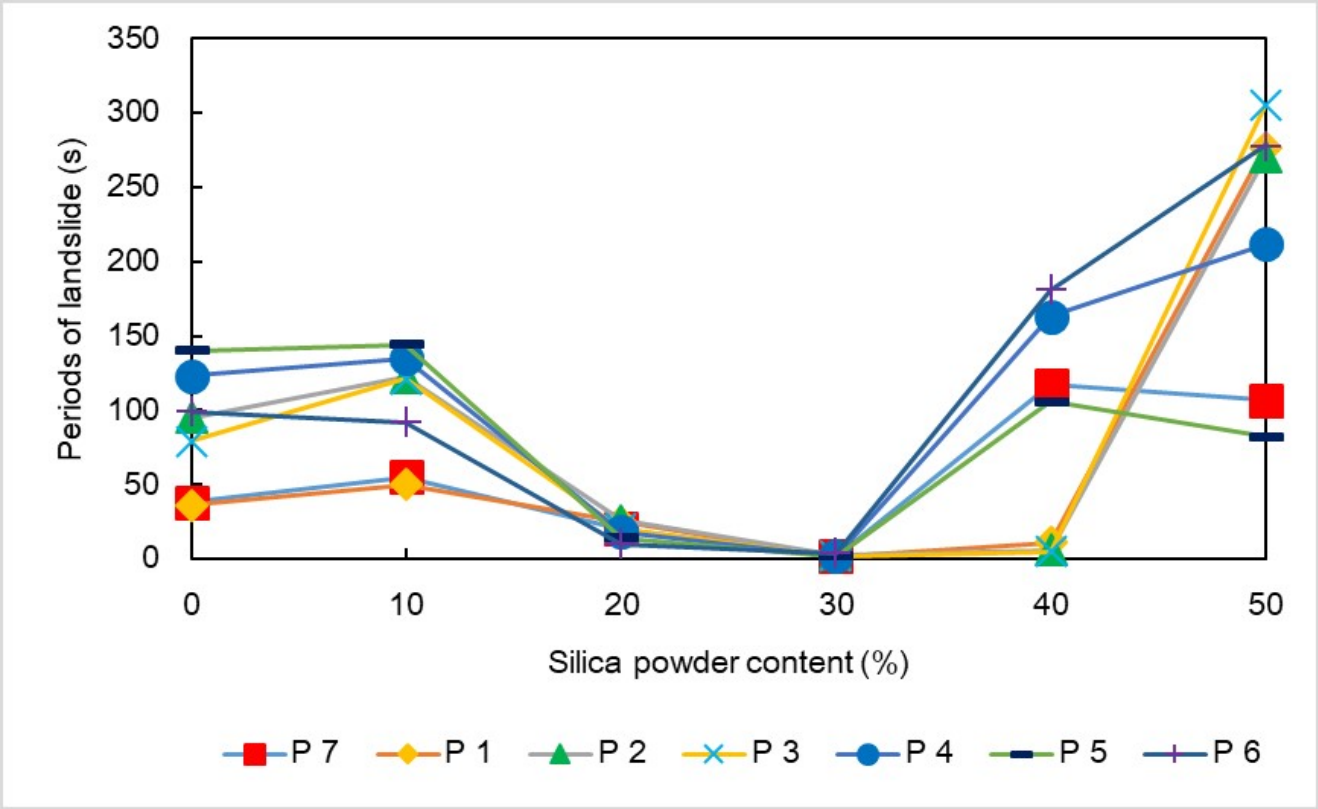
The figure shows the different periods of landslides in the flume tests. As shown in figure, the colorful point presents the results of each tilting transducers in the flume tests. It is noticed that the curve firstly decreases with increasing fine particles content until reaching 30%, then grows up with further increasing fine particles content. The period of landslide reaches to the lowest value when the silica powder content is at 30%. Videos recorded by cameras indicate that landsliding transforms from retrogressive one to fluidized landsliding with collapsed failure with the increasing of fines content, while the landslide type transforms from debris avalanche to retrogressive landslide with greater percentage (>30%) fines content.

Conclusion

Non-plastic fines content has an effect on the initiation and movement of rainfall-induced landslides in flume tests. With the increasing of fines content, the landslide type transforms from retrogressive landslide to flow sliding, while the landslide type transforms from flow sliding to retrogressive landslide with greater percentage (>30%) fines content. Periods of landslides and tilting rates of inner soil mass vary with increasing non-plastic fines content. Under the tested conditions, when the fines content reaches to 30%, the period of landslide is the shortest.

©2020. Japan Geoscience Union. All Right Reserved.

Keywords: Non-plastic fines content, Rainfall-induced landslides, Flume tests



©2020. Japan Geoscience Union. All Right Reserved.

The influence of the orientation of weak planes on slope deformation

*Chao-Yu Wang[1], Kuang-Tsung Chang[1]

1. National Chung Hsing University

With different orientations of weak planes, the accumulated displacement or deformation of slopes at failure are different. This study aims to examine how the orientation of weak planes influences the slope deformation behavior. A small-scale physical model is used for laboratory experiments. By using the PIV program, we analyze the deformation behavior of slopes with different orientations of weak planes under loading and rainfall conditions. The materials used in the slope model are small blocks made of quartz sand, clay, gypsum, cement, and water according to the mixing ratio. The 30 ˚slope models are composed of stacked blocks, and the dip angles of weak planes are 30 ˚or 60 ˚. The thicknesses of the blocks are 1 cm and 2 cm to simulate different spacings of weak planes. Two methods are used to make the slope models failure. One is a loading force on to the top of the slope models, and the other is rainfall to weaken the slope materials. We take pictures per minute in the experiments for the PIV program to analyze the displacement vectors of the sliding area. The relationships between the accumulated displacement of slopes at failure and the orientations of weak planes will be examined.

Keywords: weak planes, physical model, slope deformation

©2020. Japan Geoscience Union. All Right Reserved.

Can we detect the acceleration of long-term gravitational deformation on steep slopes before catastrophic events? -A case study on two large-scale rapid landslides in Kii peninsular, Japan-

*Teruyuki Kikuchi[1], Norio Oyagi[2], Makoto Kaneko[2], Koki Sakita[3], Teruyoshi Hatano[4]

1. JP-Design. co. ltd., 2. Fukada Geological Institute, 3. Okayama University, 4. Electric Power Development Co., Ltd

1. Introduction

Landslides are the combined effect of the risk and trigger mechanisms. To clarify the collapse process, collecting and analyzing multiple cases should be collected, analyzed, observed, and evaluated over a long period of time. The 2011 typhoon talus that hit the Kii Peninsula in Japan, along with the accompanying heavy rainfall, triggered several large and rapid landslides with volumes larger than 105 m^3 (Chigira, 2013).

2. Method

Table 1 shows the target sites, some of which had been observed several times from 1948 to May 2012, after the disaster. We recorded qualitatively the surface deformation on the high and steep slopes through field survey and “sequential-comparative air-photo analysis” using aerial photographs obtained during five seasons.

3. Result

3.1 Akatani

Figure 1 shows Area B already shows a clear decay surface in the 1948 aerial photograph. Aria B's moving bodies have been lost because of collapse. This area corresponds to the undercut slope of Akatani, and side erosion by rivers is considered to have caused past collapse.This Area received heavy rain together with the previous deformation from 1994 to April 2011.Consequently, the entire C became unstable and slid along with the upper Area A. This reasoning is clear in the following points of the 2011 aerial photograph. The collapse of Area C occurred, and the upper bare-land area increased.

3.2 Nagatono

This deep-sheeted landslide can be divided into nine areas (A to I). Each area is surrounded by a thick broken line inside the main scarp, which shows the sliding cliff that is the outermost part of the 2011 collapse. The deformation structure is a cliff-like steep slope with a small displacement at the head of Area A. The lower part of the slope was displaced downward using this steep cliff as a sliding cliff. Area C is a valley with a depth of 370 m, and its lower part reaches the riverbed of Nagatono Area D has repeated small-scale collapse.

4. Discussion and Conclusion

To predict the location of the deep-sheeted landslide, we performed a comparative interpretation using the aerial photographs taken during the five periods before the disaster. Therefore, we found some displacement and deformation in the microtopography that was a precursor to the heavy-rain disaster of September 2011.

In the future, we will expand the survey area both locally and temporally to clarify the development process and try to make it compatible using quantitative methods, such as the aviation laser measurement data method.

©2020. Japan Geoscience Union. All Right Reserved.

Reference
Chigira, M., Tsou, C.-Y., Matsushi, Y., Hiraishi, N., and Matsuzawa, M.(2013) Topographic precursors and geological structures of deep-seated catastrophic landslides caused by Typhoon Talas, Geomorphology vol.201, pp.479-493.

Keywords: Deep-seated landslide, Gravitational deformation , Aerial photograph, Deformation structure

©2020. Japan Geoscience Union. All Right Reserved.

Table 1 Using date of sequential-comparative air-photo analysis

No.	date	Planning organization	Photograph	Scale
①	Nov./1948	U.S. Army	monochrome	1/40,000
②	June/1976	Geographical Survey Institute	color	1/15,000
③	May/1994	Nara Prefecture	monochrome	1/16,000
④	May/2004	Nara Prefecture	monochrome	1/16,000
⑤	April/2011	NTT GEOSPACE CO.,LTD.	color	1/10,000
⑥	May/2012	NTT GEOSPACE CO. LTD.	color	1/5,000

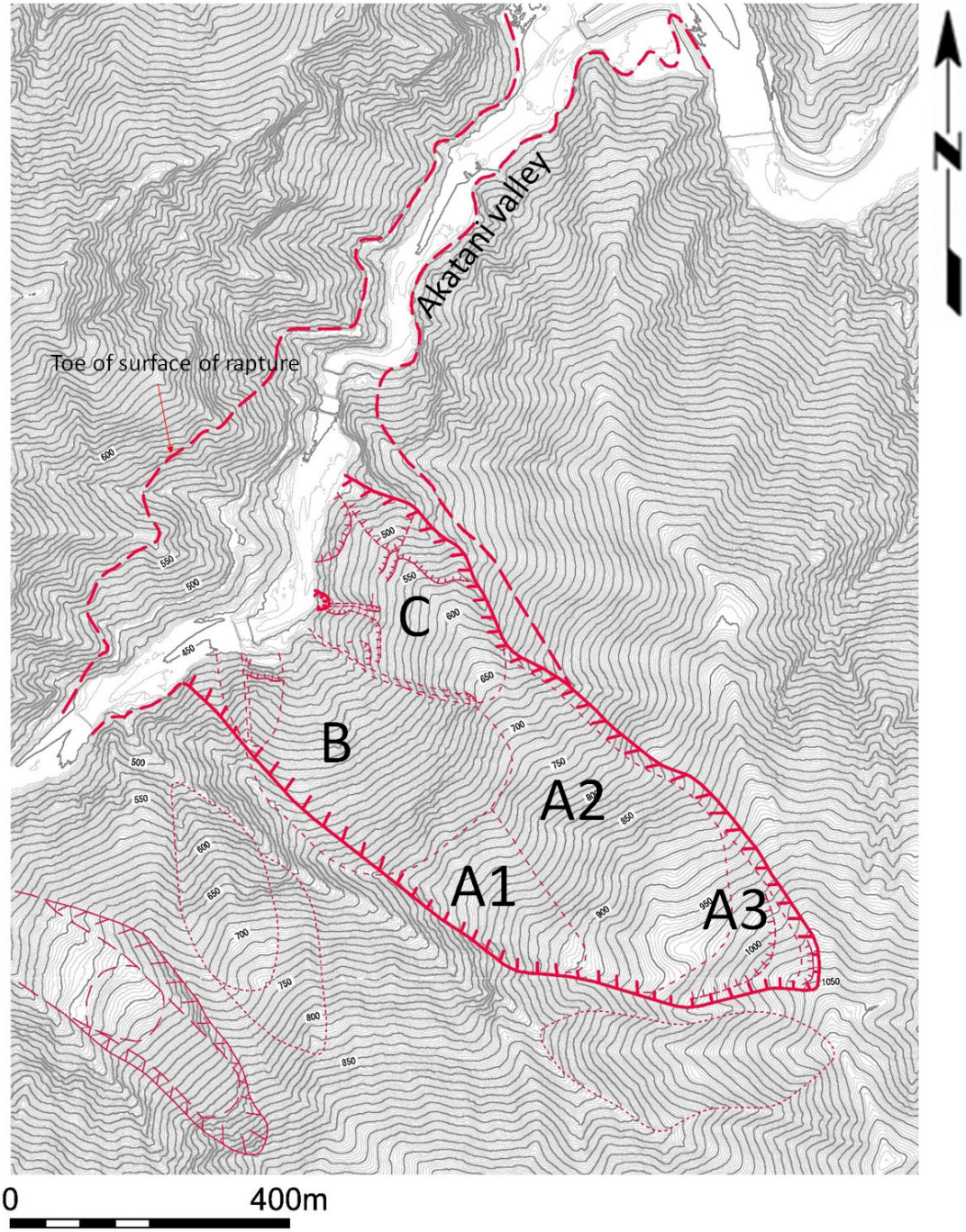


Fig-1 Distribution map of topographic features changes owing to the slope failure of Akatani.

©2020. Japan Geoscience Union. All Right Reserved.

©2020. Japan Geoscience Union. All Right Reserved.

Long-term distribution and evolution of landslide in the landslide-prone watershed: A case study in the Chishan river upstream watershed in Taiwan

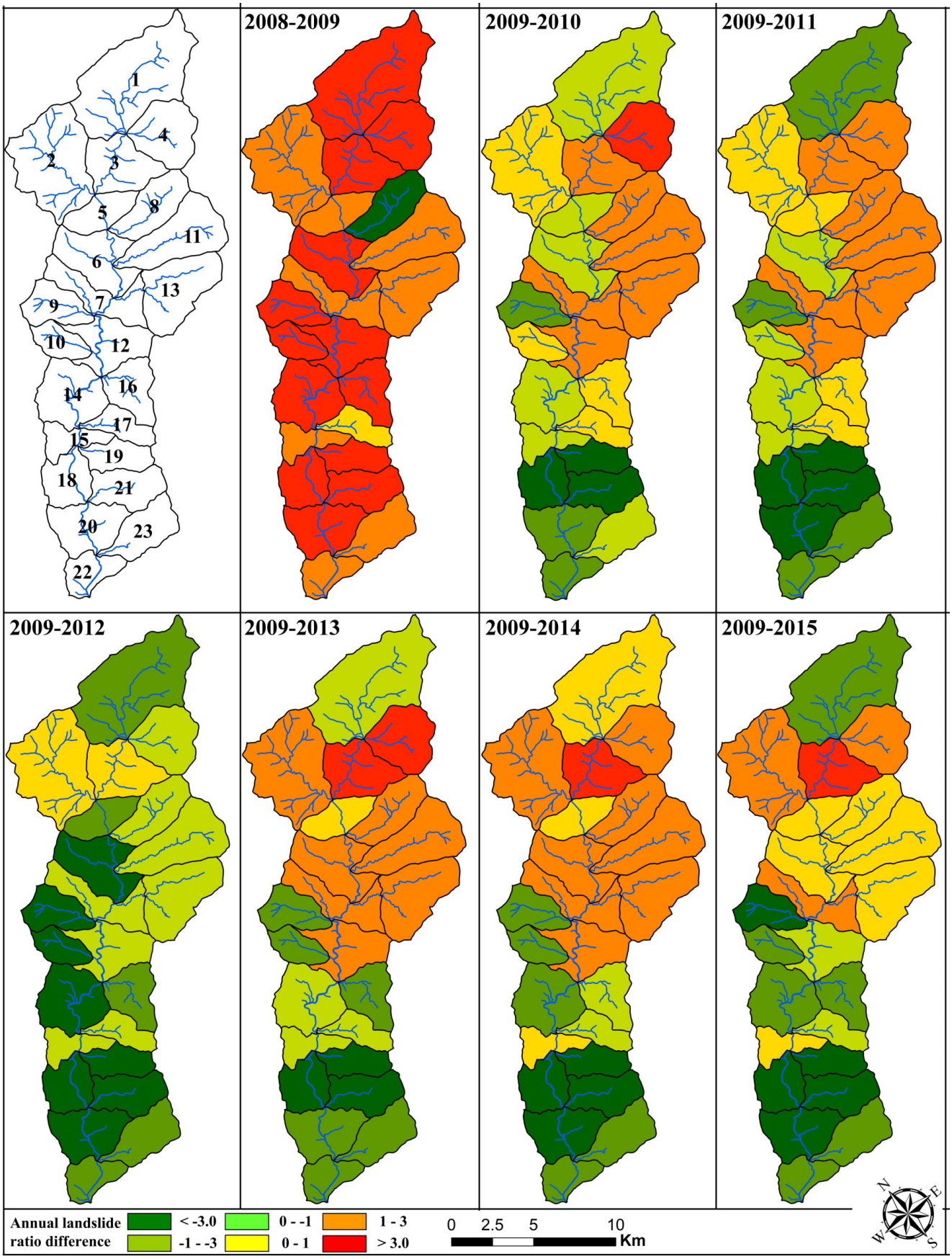
*Chengyi Lin[1], Chunuhung WU[1]

1. Feng Chia University

The research focuses on the long-term distribution and evolution of landslide in the Chishan river watershed in Taiwan. Numerous landslide had been induced by 2009 Typhoon Morakot in the Chishan river watershed, and the landslide ratio was 6.5%. It has been ten years from 2009 Typhoon Morakot to now, and this research uses annual landslide inventories from 2008 to 2015 to analyze the evolution of landslide induced by 2009 Typhoon Morakot. The Chishan river upstream watershed has been reported as the watershed in which the landslide was hard to recover by Wu (2017 and 2019). The landslide ratio in the upstream watershed in 2009 was 5.59%, and that in the following 6 years were larger than 3.87%. The count and area of landslide from 2009 to 2015 are the highest in 2010, not 2009. The research uses topographic position analysis of landslide to determine the characteristic of landslide location, and the topographic position analysis was to decide the main inducing factor for landsliding. The ratio of down-hillslope landslide area to the all landslide area has been gradually increased from 2009 to 2015. The ratio of down-hillslope landslide area to the all landslide area in 2009 was 67.6% and that increased to 75.3% in 2015. This data means that the riverbank erosion was a dominant factor for the landslide distribution and evolution from 2009 to 2015. We also estimate the new and old landslide percentage in the upstream watershed, and the mean old and new landslide percentage from 2009 to 2015 are 60.1% and 39.9%. This means that near or over 50% of landslide induced by 2009 Typhoon Morakot is still hard to recovery in 2015. The river intersection area and the river source area are the two main areas where the landslide is problematic to recover and easily induced from 2010 to 2015. The main strata in the upstream watershed includes the Nankang formation, Changchihkeng Formation, and Nanchuang formation. The accumulated occupied percentage of the three strata in the upstream is around 87.9%. The composition of the three strata is slate, sandstone and shale, i.e. three landslide-prone lithologies. The landslide occurred in the three strata in the upstream watershed in 2009 occupies 85.3% of the total landslide in the upstream, while that in 2014 still occupies 87.8 % of the total landslide in the upstream. The riverbank landslide area from 2012 to 2013 in the upstream and midstream watersheds are obvious comparisons for the difference in landslide recovery. The upstream watershed had suffered two heavy rainfall events on the same date, but the 3-day accumulated rainfall of Xingaokou station from August 21 to 23 and August 29 to 31 were only 449.5 mm and 353.5 mm, respectively. The riverbank landslide area in the upstream watershed in 2013 increased by 1.63 times of that in 2012, and the non riverbank landslide area also increased by 1.66 times.

Keywords: Loner-term landslide evolution, Taiwan, landslide distribution

©2020. Japan Geoscience Union. All Right Reserved.



©2020. Japan Geoscience Union. All Right Reserved.

A decade analysis of landslide distribution in the dense-landslide watersheds in Taiwan

*Chengyi Lin[1], Chunuhng WU[1]

1. Feng Chia University

The research focuses on using the multi-annual landslide inventories to observe the characteristic evolution of landslide after 2009 Typhoon Morkot in Taiwan. The research area includes Chengyulan river watershed (abbreviated as CRW) in the Central Taiwan, the Ailiao river watershed (abbreviated as ARW) in the South Taiwan and the Taimali river watershed (abbreviated as TRW) in the East Taiwan. Typhoon Morakot dumped more than 2000 mm rainfall during 2 days in southern Taiwan. After that, long-term evolution of landscape is developed from large area of landslides which are associated with specific typhoon events in landslide-prone sub-watersheds. The landslide ratio, i.e. the ratio of landslide area to the watershed area, in the three watersheds achieves the historical peak in 2009 or 2010, and that was 3.03% in CRW, 7.76% in ARW and 10.7% in TRW. This data means long-term evolution of landscape is related to the event-based large area landslide after few years, and the drop in three watersheds are determined to be that 1.87% to 3.03% higher than 1.21% to 1.73% in CRW, 3.27% to 7.76% higher than 1.41% to 2.23% in ARW and 3.96% to 10.7% higher than 1.98% to 2.73% in TRW. According to the above-mentioned data, the spatial and temporal characteristics of landscape is the point of the current study. Separate landslide ratio also appear in different sub-watersheds in the three watersheds, the landslide ratio are 11.16% to 24.17% of north-south flow direction sub-watersheds higher than the east-west flow direction sub-watersheds (2% to 5.24%) in ARW. The landslide ratio in some specific sub-watersheds has a dramatic increasing due to 2009 Typhoon Morakot. For example, the landslide ratio in the Heshe river watershed, i.e. a sub-watershed in CRW, after 2009 Typhoon Morakot was estimated as 2.76% to 6.53%, i.e. 3.6 to 4.3 times larger than that before 2009 Typhoon Morakot. Another obvious cases are the sub-watersheds in TRW, i.e. the Douli-douli river sub-watershed. The landslide ratio in the Douli-douli river sub-watershed after 2009 Typhoon Morakot was estimated as 7.3% to 24.5%, and that was around 2.9 to 6.3 times larger than that before 2009 Typhoon Morakot. The decade analysis from the landslide distribution data shows that the landslide ratio was hard to decrease as the landslide-prone sub-watersheds gather in the neighborhood.

Keywords: Taiwan, rainfall-induced landslide distribution , landslide characteristic

©2020. Japan Geoscience Union. All Right Reserved.

Study of Seeding Amount of Vegetation Pellets

*Hung-Yen Hu[1], Guo-Zhang Michael Song[1], Shin-Hwei Lin[1], Kai-Chi Hsu[1]

1. National Chung-Hsing university, department of soil and water conservation

Vegetation pellets are spheroids made of a mixture of seeds, soil, fertilizers and growth material, which can be dropped by unmanned aerial vehicles (UAV)into unreachable places where engineering machinery is difficult to reach. If a small vegetation pellet contains too many seeds, excessive seeding can cause high plant density, problems such as intraspecific competition or pests and diseases, which will reduce revegetation effects and increase cast costs. In contrast, a vegetation pellet contains too few seeds, the plant density on the slope will be too low to effectively protect the slope. To achieve the best revegetation effects, there must be an optimal seeding amount. Therefore, the present study aimed to identify the optimal seeding amount with which the germination and survival of seeds in vegetation pellets can be maximized. The seed materials were two common plants for vegetation engineering, including Tall Fescue (*Festuca arundinacea*Schreb.)and Taiwan Acacia(*Acacia confusa* Merr.). The seeding amount used for hydroseeding was set as 100%. The other five seeding amounts included120%, 100%, 80%, 60%, 40%, and 20%. For germination tests, these pellets were then placed on three kinds of soils (laterite, colluvial soil, and mudstone) commonly found in landslide areas of Taiwan. During the tests, the temperature inside the plant growth chamber was set to 25˚C, the humidity was 70%, and the sunshine duration was 12 hours. And provided a fixed amount of water to reduce environmental differences for a period of 50 days. For Taiwan Acacia, although the germination rate varied considerably seeding amounts and soil environments, less than 25% of seedlings survived at the end of tests due to high seedling mortality rates. Taiwan Acacia is not suitable for the revegetation of mudstone areas, because the survival rates of this tree species on mudstone were zero at the end of tests regardless of seeding amount. Regardless of soil types, it was found that the germination rate of Tall Fescue was highest if the seeding amount was 20%. When the seeding amount was controlled, the germination rate of Tall Fescue was the highest on laterite soil, followed by colluvial and mudstone. However, in terms of cost efficiency(to achieve the same plant stem density with the minimum material cost of pellets) for Tall Fescus, the seeding amount should be 100% or even more. Further studies should examine whether seeding mount higher than 120% can even increase cost efficiency.

Keywords: Seed ball, Aerial vegetation engineering, Seed treatment

©2020. Japan Geoscience Union. All Right Reserved.

[E] Poster | H (Human Geosciences)：H-DS Disaster geosciences

[H-DS10] Natural hazard impacts on human society, economics and technological systems

convener:ELENA PETROVA(Lomonosov Moscow State University, Faculty of Geography), Hajime Matsushima(Research Faculty of Agriculture, Hokkaido University)

The last decade set a record for the number and scale of natural disasters and demonstrates high vulnerability of human society, economics and ecosystems to their impacts. The most serious consequences have the so-called natural-technological disasters in which natural hazards trigger accidents at technology and infrastructure such as nuclear power and chemical plants, oil refineries and pipelines, power supply systems, buildings, roads, and railways. A distinctive feature of natural-technological events, such as of the 2011 Tohoku earthquake, is their multi-hazard and synergistic nature, which creates cascading impacts, resulting in simultaneous occurrences of myriad catastrophes. The main goal of this multidisciplinary session is to summarize case studies of relationships between natural hazards and technological disasters, their social and economic consequences; and to encourage a discussion about tools and methods to prevent disasters and to minimize their consequences, disaster reconstruction, and tourism for reconstruction, Eco-DRR, and green infrastructure.

[HDS10-P01] The 2019 Activity of Kamchatkan and Kurile Islands Volcanoes and Danger to Aviation

*Olga Girina[1], Dmitry Melnikov[1], Alexander Manevich[1], Anton Nuzhdaev[1], Elena Petrova[2] (1.Institute of Volcanology and Seismology, Far East Division, Russian Academy of Sciences, 2.Lomonosov Moscow State University, Geography Faculty, Russia)

[HDS10-P02] Annual and monthly risk assessment of typhoon disasters in China based on the information diffusion method.

*ge GAO[1], Dapeng Huang[1], Shanshan Zhao[1] (1.NCC, China)

[HDS10-P03] Study on the state of damage and the geographic distribution of flood damages in Japan from 2008 to 2017

*fumeng Zhang[1], Katsunori Furuya[1] (1.Chiba Univercity)

[HDS10-P04] A Research about the role of Eco-DRR: Ecosystem-based Disaster Risk Reduction in landscape design in Asian Cities

*Minghui Tang[1], Naoko Fujita[1] (1.University of Tsukuba)

[HDS10-P05] Impact of Climate Change on Socio-Economically Weaker Section in India

*Ruhma Khan[1], Jahangeer -[2] (1.Jamia Millia Islamia University, New Delhi , India, 2.University of Nebraska Lincoln USA)

[HDS10-P06] Cultural ecosystem services of green infrastructure: the comparison between Russia and Japan

*ELENA PETROVA[1], Hajime Matsushima[2], Anastasia Petrova[3], Yury Semenov[4] (1.Lomonosov Moscow State University, Faculty of Geography, 2.Hokkaido University, 3.Institute of Oriental Sudies of the Russian Academy of Sciences, 4.Sochava Institute of Geography, Siberian Branch of the Russian Academy of Sciences)

[HDS10-P07] The Reconstruction Assistance from Kumamoto Earthquake by the Grassland Conservation Volunteers in the Aso National Park

★Invited Papers

*REIKO MACHIDA[1] (1.TOKYO UNIVERSITY OF AGRICULTURE)

[HDS10-P08] Drought, War, and Cannibalism in Northern China in History

*Harry F Lee[1] (1.The Chinese University of Hong Kong)

[HDS10-P09] Design and evaluation of effective methods of green infrastructure for municipalities

*Shan Liu[1], Naoko Fujita[1] (1.University of Tsukuba)

The 2019 Activity of Kamchatkan and Kurile Islands Volcanoes and Danger to Aviation

*Olga Girina[1], Dmitry Melnikov[1], Alexander Manevich[1], Anton Nuzhdaev[1], Elena Petrova[2]

1. Institute of Volcanology and Seismology, Far East Division, Russian Academy of Sciences, 2. Lomonosov Moscow State University, Geography Faculty, Russia

Strong explosive eruptions of volcanoes are the most dangerous for aircraft because they can produce in a few hours or days to the atmosphere and the stratosphere till several cubic kilometers of volcanic ash and aerosols. Ash plumes and the clouds, depending on the power of the eruption, the strength and wind speed, can travel thousands of kilometers from the volcano for several days, remaining hazardous to aircraft, as the melting temperature of small particles of ash below the operating temperature of jet engines.
There are 68 active volcanoes in the Kamchatka and the Kurile Islands, and several of them are continuously active. Scientists of KVERT monitor Kamchatkan volcanoes since 1993, and Kurile Islands volcanoes since 2003. In 2019, six of the volcanoes (Sheveluch, Klyuchevskoy, Bezymianny, Karymsky, Ebeko, and Raikoke) had strong and moderate explosive eruptions.
The eruptive activity of Sheveluch volcano began since 1980 (growth of the lava dome) and it is continuing at present. In 2019, strong explosions sent ash up to 10-11.5 km a.s.l. on 09 March, 10 April, 29 August, 02 and 06 October, 03 and 11 November; and up to 6-8 km a.s.l. –in April, and August-November; ash plumes extended more 1300 km to different directions of the volcano. A resuspended ash was observed on April, May, September, and October: ash plumes extended for 250 km to the southeast of the volcano. Satellite data showed a thermal anomaly over the volcano all year. Activity of the volcano was dangerous to international and local aviation. The moderate explosive events (ash up to 5-6 km a.s.l.) of Klyuchevskoy volcano were observing on 21-22 April, 12 and 26 June, 01-02 July, 23-24 October, 29-30 December. Ash plumes extended for 200 km to different directions of the volcano. Explosive eruption of Strombolian type began on 01 November and continues in 2020. Satellite data sometimes showed a thermal anomaly over the volcano. Activity of the volcano was dangerous to local aviation. Two strong explosive eruptions occurred on Bezymianny volcano in 2019. 20 January explosions sent ash up to 10-12 km a.s.l., ash plumes extended for 900 km to the northwest of the volcano. 15 March explosions rose ash up to 15 km a.s.l., ash plumes extended for 1000 km to the east of the volcano. The eruption of 15 March was predicted by scientist of KVERT for 6.5 hours before this strong explosive event: www.kscnet.ru/ivs/kvert/ Activity of the volcano was dangerous to international and local aviation. The thermal anomaly over Karymsky volcano was noted on satellite images from time to time. According to visual and satellite data, explosions rose ash up to 6 km a.s.l. (21 August), ash plumes and clouds drifted for 500 km to the different directions from the volcano. The most intense eruptive activity of the volcano was observed in February, March, April, May, July, and August. Activity of the volcano was dangerous to local aviation. Moderate explosive eruption of Ebeko volcano began on October, 2016, and it is continuing at present. Daily occurred from one till eight-nine (27 April and 27 May) explosions, that raised ash up to 4.5 km a.s.l. Ash clouds drifted mainly to the eastern directions from the volcano. Ashfalls were noted at Severo-Kurilsk on January, February, and August-December. Activity of the volcano was dangerous to local aviation. The strong explosive eruption of Raikoke volcano occurred on 21-26 June. Paroxysmal phase of eruption continued for 15 hours. Explosions send ash up to 13.5 km a.s.l., a large ash cloud 750-800 km wide extended more 2500 km to the east from the volcano. Aerosol clouds were noting till 31 June from Baikal Lake till Arctic. A thermal anomaly was registered over the volcano from 21 June till end of year. Activity of the volcano was dangerous to international and local aviation.

©2020. Japan Geoscience Union. All Right Reserved.

Keywords: volcano, explosive eruption, Kamchatka, Kuriles, Aviation

©2020. Japan Geoscience Union. All Right Reserved.

Annual and monthly risk assessment of typhoon disasters in China based on the information diffusion method.

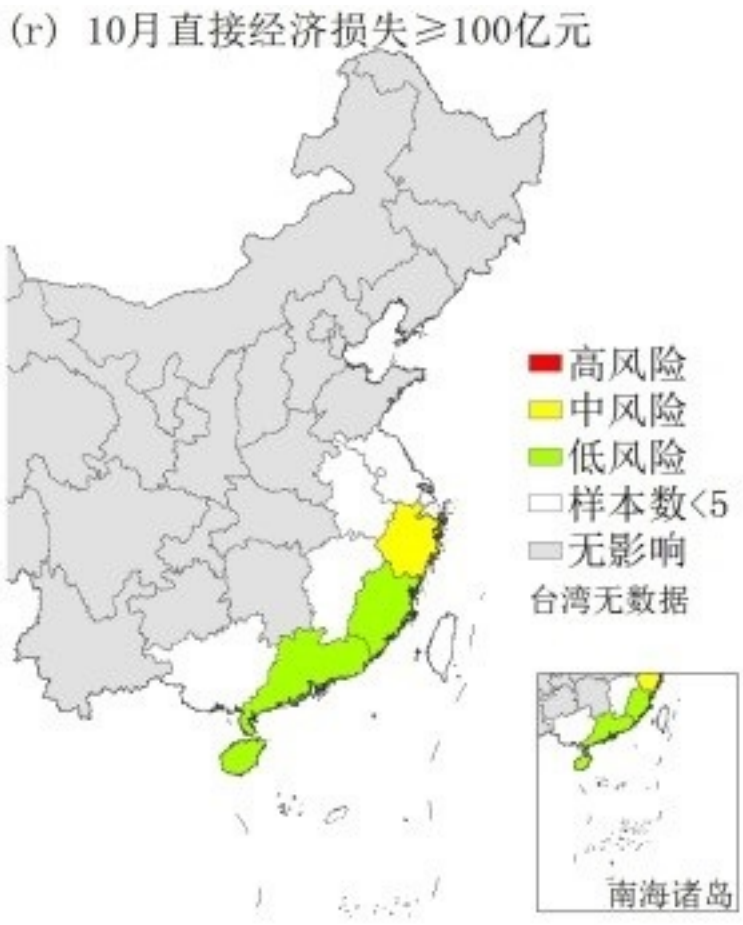
*ge GAO[1], Dapeng Huang[1], Shanshan Zhao[1]

1. NCC, China

In the context of typhoon disasters information, social and economic data of China during 1985 and 2014, temporal and spatial characteristics of annual and monthly typhoon direct economic losses are analyzed in China and on provincial scale. Risk assessments are carried out by the information diffusion method as the references for improving the capabilities of typhoon disaster risk management. The results are showed as following. Annual and monthly typhoon-caused direct economic losses from July to September of China show slightly increasing trends during 1985 and 2014.The monthly variation of direct economic losses are obvious, particularly in August, with the most number of disaster-caused typhoon and the most serious losses in a year. Comparing to the period during 1985-1994, the range of monthly variations became greater and total economic losses of September and October are greater than that of June and July in recent two ten-years periods: 1995-2004 and 2005-2014. Along with the increasing of direct economic losses levels, the numbers of province with middle and high risk level are all decreased gradually. Under the condition with annual direct economic losses greater than and equal to 5 or 10 billion RMB, the risk probability in Zhejiang is the most of China. Under the three risk levels(returning period=10,20,30years), annual direct economic losses of Zhejiang, Guangdong, Fujian and Guangxi kept in the special serious degree. Under the risk levels with 20, 30 years returning periods, annual and monthly direct economic losses of Shandong and Liaoning and annual losses of Hebei also reached the special serious degree, the defense response to typhoon should not be neglected in these areas.

Keywords: Thphoon, economic losses, risk assessment, information diffusion method

©2020. Japan Geoscience Union. All Right Reserved.



Distributions of risk grades evaluated by exceeding probability under conditions which typhoon-caused direct economic losses are equal or greater than 10 billion RMB for October in China.

©2020. Japan Geoscience Union. All Right Reserved.

Study on the state of damage and the geographic distribution of flood damages in Japan from 2008 to 2017

*fumeng Zhang[1], Katsunori Furuya[1]

1. Chiba Univercity

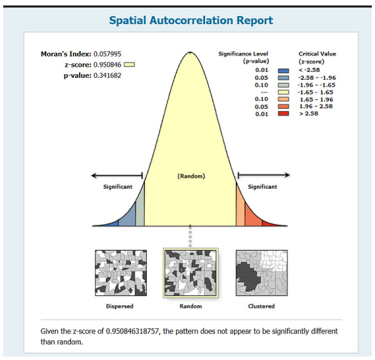
In recent years, under the influence of climate factors such as global warming, Japan has also suffered heavy rains year after year, causing serious losses.
Through the study of the flood disaster losses in the 10 years from 2008 to 2017, it was found that the severely affected areas tended to be concentrated in recent years. In addition, in the research, I divided the damaged assets into three types according to their ownership and use, and found that in the same disaster, the distribution patterns of these three types of asset losses are also different.

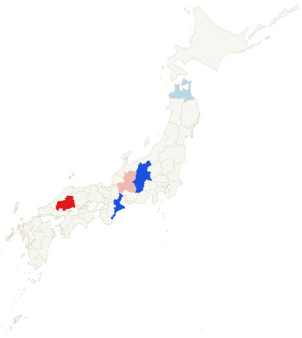
Keywords: Flood disasters, Clustering distribution, Spatially auto-correlated

©2020. Japan Geoscience Union. All Right Reserved.

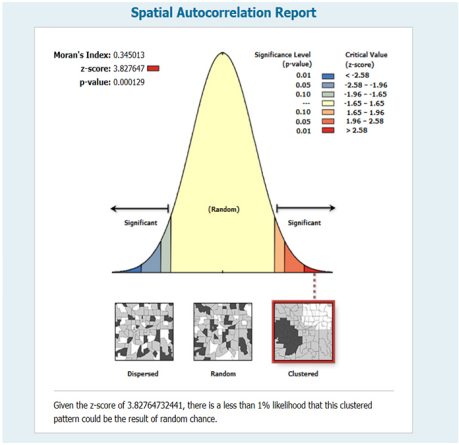
Spatial autocorrelation and clustering analysis of different asset types

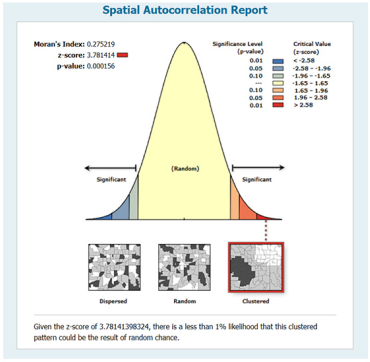
(Just shows the results of 2008 in this page)

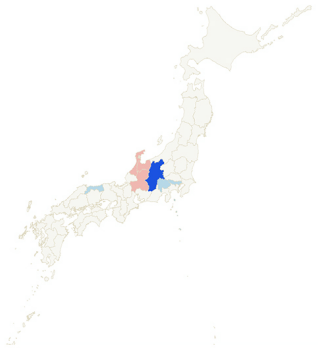




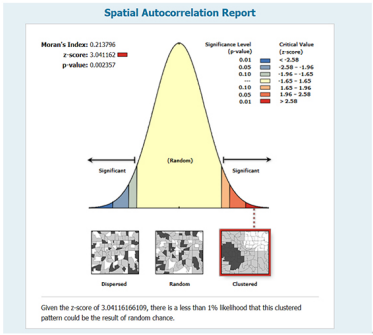
Moran Index Analysis of General Asset

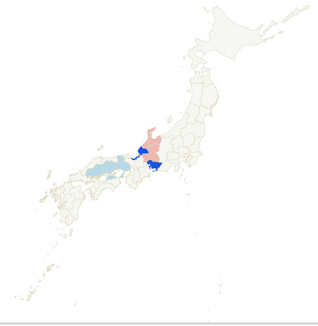




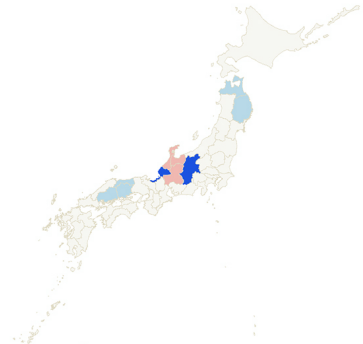


Moran Index Analysis of Public civil facility damage





Moran Index Analysis of Public utilities damage



Index Analysis of Moran Index Analysis of Total damage

©2020. Japan Geoscience Union. All Right Reserved.

A Research about the role of Eco-DRR: Ecosystem-based Disaster Risk Reduction in landscape design in Asian Cities

*Minghui Tang[1], Naoko Fujita[1]

1. University of Tsukuba

Introduction

When compared with other countries in a global point of view, Asia is a large area and the climate is diverse. In recent years, extreme natural phenomena affected by global warming have caused major natural disasters are frequent. There is a huge number of researches on the eco-application of proceeding in various countries and it is vitally important to verify their validity. There are some signs of adopting the Eco DRR concept in Asia. The scope and methods are limited, such as replacement and rainwater infiltration technology. Above all, the delay in research on planning and design is remarkable. Under these circumstances, landscapes are expected to be designed for gardens, parks, green spaces, etc. for simple beauty.

This research focuses on the analysis of the changes of the land cover on area-unit level with Mashiki-machi, the epicenter, as the target. By this research, the current disaster histories, disaster prevention policies, and urban plans of major Asian cities will be organized, analyzed, and evaluated. In addition, Asian economies expanding from the perspective of Eco DRR a new landscape design of the city will be presented, and it will show how a city coexists with frequent natural disasters.

Methods

In this study, to summarize the natural disasters and damage situation in Asian countries, and to identify the major cities most frequently affected in particular, organize the disaster prevention policies and city plans of each city and clarify the relationship with the disaster situation.Main research regarding the research method used in the above, evaluation of ecosystem services uses InVEST. Data will be collected using satellite data and UAV and organized as GIS data.

Results

After the earthquake, Mashiki town suffered 3278 completely destroyed houses and 926 partially destroyed houses. Residential areas in the reconstruction plan have increased the area of buildings in the city. Due to land cover change, collapsed residential land became a waste land among the building lands that caused environmental degradation in Mashiki town after the earthquake, and their environmental degradation sensitivity became more sensitive. The distribution of environmentally degraded areas in Mashiki Town after heavy rains remained the same mainly around urban building sites and road sites, and rice fields along the river changed to rough lands, but their sensitivity to environmental deterioration almost changed. The distribution of the environmentally degraded areas after the reconstruction project in Mashiki-cho the environmentally degraded area around the urban building site became wider. However, it was found that the high area became large. From the viewpoint of Eco-DRR, the change in

©2020. Japan Geoscience Union. All Right Reserved.

habitat quality was found to be large along the river because the habitat quality of some of the rice fields along the river was high. From the perspective of ecosystem disaster prevention, in the event of a heavy rain disaster after an earthquake, it is expected that designating green areas along the river, rice fields, and other agricultural lands as disaster prevention areas will have the effect of reducing disasters. In the Mashiki Reconstruction Plan, residential areas that contribute to reconstruction in response to the earthquake disaster have been set up, but the surrounding fields and other agricultural lands have been converted to building lands, and the surrounding habitat quality has deteriorated. From the perspective of ecosystem disaster prevention, it is desirable to formulate a reconstruction plan that does not cause a reduction in habitat quality in Mashiki town.

Keywords: Eco-DRR, landscape design, cities

©2020. Japan Geoscience Union. All Right Reserved.

Impact of Climate Change on Socio-Economically Weaker Section in India

*Ruhma Khan[1], Jahangeer -[2]

1. Jamia Millia Islamia University, New Delhi , India, 2. University of Nebraska Lincoln USA

The recent years have observed an increase in the temperatures globally which poses serious concern to the environment. India, being a developing country is already suffering from various chronic stresses like traffic congestion, pollution, poverty, improper sanitation facilities, non-renewable wastes and increasing informal settlements. Above all these pressures, extreme weather events like sea level rise, heat waves, flooding, cyclone etc occurring due to climate change only add to the miseries of urban problems and make development difficult to achieve. These disasters result in loss of infrastructure, lives, property, and livelihood and also leave a psychological impact on the survivors for a long period of time. The socio-economically weaker sections with lack of resources and skills are usually the ones severely affected due to the adverse affects of climate change. This paper intends to outline the impact of climate change on socio economic sector of the society in Indian cities and find out some mitigation measures at local level to reduce the impact of climate change.

Keywords: Climate change , Socio- Economically weaker section, Extreme weather events , Developing countries

©2020. Japan Geoscience Union. All Right Reserved.

Cultural ecosystem services of green infrastructure: the comparison between Russia and Japan

*ELENA PETROVA[1], Hajime Matsushima[2], Anastasia Petrova[3], Yury Semenov[4]

1. Lomonosov Moscow State University, Faculty of Geography, 2. Hokkaido University, 3. Institute of Oriental Sudies of the Russian Academy of Sciences, 4. Sochava Institute of Geography, Siberian Branch of the Russian Academy of Sciences

Over the past decades, ecosystems of the Earth at all levels from local to global have undergone significant changes due to the increasing in all types of anthropogenic pressure on the environment. The anthropogenic pressure has led to significant degradation of many ecosystem services. Ecosystem services are all those benefits that people receive from ecosystems. Four types of ecosystem services are distinguished: providing, such as the production of food and water; regulatory, such as the control of climate and natural disasters; cultural services, as well as supporting services that are necessary for the production of all other ecosystem services. Due to degradation of ecosystems, the task of protection and rational use of ecosystem services is particularly relevant. For the solution of this task, we propose to use the concept of "green infrastructure". The green infrastructure includes both natural areas (such as forests, grasslands, wetlands, sea costs, river banks, and others), as well as green spaces (parks, and other elements) that perform the functions of regulating runoff and protecting against floods and other natural disasters, purifying air and water, providing habitats for animals and birds, recreational use, and others. We apply an approach that takes into account the complex pattern of the green infrastructure. We pay special attention to the multifunctionality of the green infrastructure, its implementation of a whole complex of various ecosystem services, including regulating and cultural services. A comparative analysis of the usage and recognition of green infrastructure in Japan and Russia with varying economic, social and environmental conditions and with long-standing traditions of environmental management is carried out in this study. We take into consideration landscape differences and local cultural features of both countries. This ethno cultural cross-analysis is very important not only from a scientific, but also from a humanitarian point of view, since it contributes to a better understanding of each other by representatives of these territorially close, but simultaneously very different and for a long time isolated cultures.

Keywords: ecosystem services, green infrastructure, cultural ecosystem services, landscape and ethno cultural differences, natural disasters, multifunctionality

©2020. Japan Geoscience Union. All Right Reserved.

The Reconstruction Assistance from Kumamoto Earthquake by the Grassland Conservation Volunteers in the Aso National Park

*REIKO MACHIDA[1]

1. TOKYO UNIVERSITY OF AGRICULTURE

The Kumamoto Earthquake struck the Aso Area of Kumamoto Prefecture on April, 14 and April 16 in 2016, killing at least 24 people. The earthquake (The A magnitude-7.3) caused by the sediment disaster in the mountain slope. Regarding the damage to agriculture, the surface ruptures, landslides across the grasslands and damages to barns posed severe challenges to the continuation of the livestock industry. However, due to the assistance of volunteers such as Green Stock and the efforts of the Grassland Restoration Committee, local residents were able to overcome the destruction. This study analyzed the recovery efforts of the grassland conservation volunteers in a chronological order using the following time frames. The time to secure survival, the time to secure living conditions, the time to secure livelihood, and the time until the resumption of business activities. The study applied various research methods. Interviews were conducted with the members of Aso Green Stock and the Grassland Restoration Committee. The question topics were as follows: the reconstruction assistance and the implementation periods following the Kumamoto Earthquake, the support activities, and methods of information distribution. The interview surveys were conducted on May 4, 2017, September 12, and September 13, 2017, and September 8, 2018.Therefore, the Grassland Restoration Committee conducted an emergency questionnaire to the livestock farmers on the disaster support, immediately after the Kumamoto Earthquake. On June 15, about two months after the earthquake the Grassland Restoration Committee has restored a pasturage road, which was damaged by surface ruptures. On June 17 damaged water wells, feeders and farm fences were repaired or replaced. Three months after the Kumamoto Earthquake, on July 19 new water tanks were installed in the grasslands of Minami-Aso Village.Also, 11 months after the Kumamoto Earthquake, the Grassland Restoration Committee carried out supporting activities in order to restart the fire controlled burning for the livestock farmers on the grasslands where the land had been damaged by surface ruptures.3 days after the Kumamoto Earthquake, on April 19th, Aso Green Stock surveyed the area struck by the disaster and assessed the extent of damage to the grasslands. 11 days after Kumamoto Earthquake, the Aso Green Stock started raising funds for the affected livestock farmers. The donations have reached approximately 2.8 million yen in four months. So Green Stock implemented three projects as emergency support for the livestock farmers. Firstly, it supported the resumption of the fire controlled burning in the ruptured grassland areas. Secondly, it repaired the grassland roads that were damaged by the earthquake. Thirdly, it raised fences for preventing cattle and horses from slipping into the cracks across the grasslands. It also repaired the barns and cattle sheds damaged by the earthquake. Aso Green Stock organized sightseeing tours and exchange opportunities in order to facilitate constructive participation efforts. These tours included grassland management experiences, barbecues and visits to the local hot springs. The tours began in Oct, 2016; buses departed from the cities of Fukuoka and Kumamoto in Kyushu. In total, 119people have participated in these events. As a result of the aforementioned efforts, the partnerships with the volunteers of the grassland preservation before the Kumamoto Earthquake have led to the swift recovery of the livestock farmers following the earthquake. After 6 months, the disaster support activities of the grassland volunteers have successfully developed into various tourist and exchange projects.

Keywords: Kumamoto Earthquake, Aso, Reconstruction

©2020. Japan Geoscience Union. All Right Reserved.

©2020. Japan Geoscience Union. All Right Reserved.

Drought, War, and Cannibalism in Northern China in History

*Harry F Lee[1]

1. The Chinese University of Hong Kong

Despite the effort made by historians and archaeologists to investigate cannibalism in human societies, large-N statistical analysis of cannibalism and its triggering factors in pre-industrial societies is still missing in the literature. In this study, I base on 1194 cannibalism incidents in northern China in 1470–1911, together with other fine-grained paleo-climate and historical war datasets, to verify quantitatively the driving factors of cannibalism in pre-industrial societies. Granger causality, wavelet coherence, and phase analyses are employed. The key findings are that in historical northern China, cannibalism was primarily caused by drought and war, but their relationship is non-stationary and is mediated by environmental and socio-political contexts. The positive feedback between war and cannibalism is also revealed, indicating that they are mutually reinforced. The above findings supplement Malthusian theory with empirical evidence of the non-stationary influence of natural disasters on positive checks and how positive checks interact with and reinforce each other. The results also refine our knowledge about the regional environment-human nexus in northern China.

Keywords: Drought, War, Cannibalism, China

Table 1 Granger causality analysis (GCA) about the influence of climate and war in causing cannibalism in northern China

Null hypothesis	*F*	*P*
Drought does not *Granger-cause* cannibalism	2.640**	0.048
Flood does not *Granger-cause* cannibalism	2.072	0.101
Temperature does not *Granger-cause* cannibalism	0.827	0.479
Precipitation does not *Granger-cause* cannibalism	0.202	0.895
War does not *Granger-cause* cannibalism	10.245***	0.000
Cannibalism does not *Granger-cause* war	5.714***	0.000

All of the data are in annual units. $^{**}p < 0.05$; $^{***}p < 0.01$

©2020. Japan Geoscience Union. All Right Reserved.

Design and evaluation of effective methods of green infrastructure for municipalities

*Shan Liu[1], Naoko Fujita[1]

1. University of Tsukuba

The purpose of this study is to evaluate the effective method of green infrastructure in the level of municipalities. The research area is river basins and surrounding areas in Tsukuba, Ibaraki, Japan. According to analysis the data of local green areas, farmland, etc., and using PPGIS (Public participation geographic information system) and Hydrological modeling to select the locations of potent/effective functions of green infrastructure. Through the above analysis to clarify the ideal combination of river green infrastructure and regional landscape regeneration.
In 2013, the European Commission formulated a solution called "green infrastructure", and the concept of "Eco-Disaster Risk Reduction (Eco-DRR)" was submitted. In Japan, the introduction of "green infrastructure" was clearly stated in the national land formation plan decided by the Cabinet in August 2015 and the social capital development priority plan in December 2015, as an important direction in future infrastructure development.
Due to the heavy rains in the Kanto Tohoku region in September 2015 and the heavy rainfall from typhoon No. 19 in October 2019, flooding in areas such as Tsuchiura City and Tsukuba City in Ibaraki Prefecture, causing serious losses in residential areas and fields. Based on this situation, it is necessary to promote the rebuilding of a water disaster prevention awareness society. that works on disaster prevention and mitigation measures that integrate hardware and software throughout society.
During these five years from 2014 to 2018, The number of rivers that exceed the target discharge of the river improvement plan and the flood risk water level is increasing year by year. As a result, the countermeasures against urban floods such as external and inland water floods are required in each region.
Green infrastructure is not only a green and "green" infrastructure but also an infrastructure that intelligently uses the resources and mechanisms provided by the natural environment and various living things. It is a means to solve various environmental problems by making good use of the various functions of nature. Depending on the cases in Europe and the United States, green infrastructure is mainly of three types: basin size (river), site size (street), and neighborhood size (park). The scale of site size (street) and neighborhood size green infrastructure are mainly prevented for storing rainwater and mitigating flood risk by rain seepage. However, those types of green infrastructure are not limited, in some cases, there are also adopt a combination of parks and rivers to simultaneously prevent external and internal water inundation. The remaining four and five are acting on rainwater storage and flood mitigation.
By the above, not only the river scale but also the street and park scale green infrastructure is equally important. Therefore, the three elements of basin size (river), site size (street), and neighborhood size (park) are important in the formulation of a green infrastructure plan. Besides, as the population and land use rate is decreasing in Japan, there is a possibility that such green infrastructure means can be introduced by utilizing the open spaces, waste green spaces, and low unused land in urban areas.

Keywords: green infrastructure, municipality, region, landscape management

©2020. Japan Geoscience Union. All Right Reserved.

[E] Poster | H (Human Geosciences)：H-DS Disaster geosciences

[H-DS11] Subaqueous Landslides and Their Anthropogenic Impact for Coastal Regions

convener:Yujin Kitamura(Department of Earth and Environmental Sciences, Graduate School of Science and Engineering, Kagoshima University), Kiichiro Kawamura(Yamaguchi University)

A large number of people inhabit coastal areas around the world that are susceptible to natural catastrophes and subaqueous landslides are one of such hazards as demostrated recently. The risk associated with the occurrence of subaqueous landslides is not only constrained to passive margins or subduction zones but any of water areas is also susceptible to their occurrence since subaqueous failures can be triggered at very low slope angles. This realization poses a significant challenge that requires the collection of vast amounts of information and data to unravel the true nature of these events and their potential risk to coastal communities. Despite these challenges, recent technical and engineering advances in the acquisition and processing of sea floor and shallow subsurface data are encouraging. There has also been a concerted effort by scientists from different earth-science disciplines to increase interdisciplinary cooperation at an international level to advance our collective understanding of subaqueous landslides and their consequences.
This session calls for technical contributions covering all aspects of subaqueous landslide research including but not limited to: physical properties of deformed sediments (pre- and post- deformation), role of interstitial fluids in subaqueous landslide development, slope stability and risk assessments, geomorphological and sedimentological/stratigraphic descriptions, tsunamigenic risk and modeling, description of ancient subaqueous landslides, sand-box models and numerical simulations of subaqueous landslides. Case studies from lacustrine landslides and subaerial coastal landslides transitioning into the marine realm are also welcome. Case studies associated with the broader topic of subaqueous gravity-driven flows (e.g.: turbidites and transitional flows) and their relationship with seafloor faulting are also of interest to this session. Participants of IUGS project S4SLIDE IGCP-640 sponsor this session.

[HDS11-P01] Numerical Simulation of Submarine Landslide Tsunami due to the 1929 Grand Banks Earthquake

*Tatsuya Nakagaki[1], Yuichiro Tanioka[1] (1.Hokkaido University)

[HDS11-P02] Trial and error estimation of the initial sea surface deformation of the tsunami caused by the 2009 Suruga Bay earthquake

*Masahiro Kurozumi[1], Toshitaka Baba[2] (1.Tokushima University Graduate School of Frontier Sciences, 2.Tokushima University Graduate School of Industrial Science and Engineering)

[HDS11-P03] Effect of cohesion between sedimentary layers on water film formation in submarine landslides

*Shogo Kawakita[1], Daisuke Asahina[2], Takato Takemura[3], Hinako Hosono[3], Keiji Kitajima[4] (1.Graduate School of Science and Technology, Nihon Univ., 2.National Institute of Advanced Industrial Science and Technology, 3.College of Humanities and Sciences, Nihon Univ., 4.College of Science and Technology, Nihon Univ.)

Numerical Simulation of Submarine Landslide Tsunami due to the 1929 Grand Banks Earthquake

*Tatsuya Nakagaki[1], Yuichiro Tanioka[1]

1. Hokkaido University

On Nov 18th, 1929, The Grand Banks earthquake (Mw7.2) occurred off the southern coast of Burin Peninsula in Newfoundland, Canada. At the same time and few hours after, twelve Telegraph cables installed on the seafloor were cut, and several meter height tsunami hit the southern coast of Burin Peninsula and 28 people were killed. It is suggested that the earthquake generated the large submarine landslide and turbidity current (Doxsee, 1948; Heezen and Ewing, 1952) and this landslide cut the cables and generated this tsunami. The tsunami waveform was recorded at the tide gauge at Halifax, Canada. We numerically computed this submarine landslide using ‘Tsunami squares’ cord (Xiao et al., 2015; Yamanaka and Tanioka, 2017; Wang et al., 2019). This cord is a time-dependent landslide model. The area of the landslide is consistent with the previous study (Fine et al., 2005). Tsunami propagation was numerically calculated with JAGURS tsunami simulation code (Baba et al., 2017). As the ocean surface deformation input is calculated from the result of the time-dependent landslide simulation. Mass volume of the landslide is estimated by comparing the calculation result and observed tsunami waveform at Halifax. The result shows that, at least, in terms of arrival time and peak height, the first pulse of the observed tsunami is explained well by the computed one. The amount of landslide is estimated to be about 100 cubic km.

Reference

Baba, T., S. Allgeyer, J. Hossen, P.R. Cummins, H. Tsushima, K. Imai, K.Yamashita, and T. Kato (2017), Accurate numerical simulation of the far-field tsunami caused by the 2011 Tohoku earthquake, including the effects of Boussinesq dispersion, seawater density stratification, elastic loading, and gravitational potential change, Ocean Modelling, 111, 46-54, doi:10.1016/j.ocemod.2017.01.002

Brauce C. Heezen and Maurice Ewing (1958), Turbidity currents and submarine slumps, and the 1929 Grand Banks earthquake, American Journal of Science, 250, 849-873

I.V. Fine, A.B. Rabinovich, B.D. Bornhold, R.E. Thomson and E.A. Kulikov (2005), The Grand Banks landslide-generated tsunami of November 18, 1929: preliminary analysis and numerical modeling, Marine Geology, 215, 45-57

Jiajia Wang, Steven N. Ward and Lili Xiao (2019), Tsunami Squares modeling of landslide generated impulsive waves and its application to the 1792 Unzen-Mayuyama mega-slide in Japan, Engineering Geology, 256, 121-137

Lili Xiao, Steven N. Ward, and Jiajia Wang (2015), Tsunami Squares Approach to Landslide-Generated Waves: Application to Gongjiafang Landslide, Three Gorges Reservoir, China, Pure and Applied Geophysiics, 172, 3639-3654

©2020. Japan Geoscience Union. All Right Reserved.

Yusuke Yamanaka and Yuichiro Tanioka (2017), Estimating the Topography before Volcanic Sector Collapses Using tsunami Survey Data and Numerical Simulations, Pure and Applied Geophysics, 174, 3275-3291

Keywords: Submarine landslide tsunami, Tsunami numerical simulations, 1929 Grand Banks earthquake

©2020. Japan Geoscience Union. All Right Reserved.

Trial and error estimation of the initial sea surface deformation of the tsunami caused by the 2009 Suruga Bay earthquake

*Masahiro Kurozumi[1], Toshitaka Baba[2]

1. Tokushima University Graduate School of Frontier Sciences, 2. Tokushima University Graduate School of Industrial Science and Engineering

Tsunamis are caused by not only submarine earthquakes but also by submarine landslides. Because tsunami caused by earthquakes that simultaneously generate seismic waves can be expected due to precursory shaking. However, a submarine landslide would not generate strong seismic waves, so we would underestimate a coastal risk of submarine landslide tsunami. During the 2009 Suruga Bay earthquake, a tide gauge (Yaizu) recorded tsunami much larger than we expected from the magnitude of the earthquake. Bathymetric traces of submarine landslides were observed by post-event surveys (Matsumoto et al., 2012). A tsunami modeling based on the topographic change between before and after the event could not simulate the observed tsunami waveforms (Baba et al., 2012). In this study, the source of the tsunami was estimated by a trial and error method neglecting the topographic changes. For estimations of the initial sea surface deformation, we used a method proposed by Watts et al. (2005) and combination of multi Gaussian distributions. In tsunami propagations, the nonlinear long wave equations were solved by a finite difference method. Also, the volume and location of the submarine landslide body were estimated using a two-layer flow model.

In the model of Watts et al., the six parameters of landslide length, width, collapse depth, slope gradient, moving distance and thickness of sediment deposit, were changed in ranges between 130 to 1750 m, 115 to 660 m, 15 to 250 m, 2 to 10 ˚, 500 to 8000 m, 3 to 45 m, respectively, while parameters of landslide position, strike, depth, specific gravity, added mass coefficient, and shape were fixed. In the use of Gaussian distributions, three parameters of standard deviation, amplitude, and position were changed ranges between -15 to 6m, 8 to 19.2m, (x,y)=([BT1] 205 to 379, 81 to 183), respectively, where (x, y) is index number of 90m mesh grid of the calculated region. It is about 3 to 18km off Yaizu. For the two-layer flow model, the location of initial dirt mass was fixed at a position of about 5km off Yaizu. The dirt mass was given in a circular shape with radius, height, and seabed friction changing ranges between 2000 to 4000 m, 10 to 30 m, and 0 to 0.5 $sm^{-1/3}$, respectively. Tsunami calculations were repeated varying these models and parameters to find the best model that fits with the observed tsunami waveforms.

However, all examinations could not simulate the observations. In the Yaizu tide gauge record, the amplitude of the first drawn wave was observed by -0.62 m at about 720 seconds since the occurrence of the earthquake. The maximum wave of about 0.33 m appeared at about 1080 seconds. The best Watts model provided an amplitude of -0.63 m at 302 seconds for the first drawn wave, the amplitude of 0.55 m at 438 seconds for the maximum wave. In the best Gaussian model, these were -0.61 m at 427 seconds and 0.91 m at 709 seconds, respectively. In the two-layer flow model, these were -0.67 m at 350 seconds and 0.45 m at 504 seconds, respectively. To summarize, the amplitude of the maximum wave in the simulations was about 1.5 to 3 times larger than the observation even when the amplitude of the first drawn wave was close to the observation. The tsunamis in all simulations arrived at the Yaizu station earlier by 300-420 seconds.

©2020. Japan Geoscience Union. All Right Reserved.

Acknowledgments: This work was supported by JSPS KAKENHI Grant Number 19H02409.

Keywords: Trial and error estimation of the initial sea surface deformation, Submarine landslide

©2020. Japan Geoscience Union. All Right Reserved.

Effect of cohesion between sedimentary layers on water film formation in submarine landslides

*Shogo Kawakita[1], Daisuke Asahina[2], Takato Takemura[3], Hinako Hosono[3], Keiji Kitajima[4]

1. Graduate School of Science and Technology, Nihon Univ., 2. National Institute of Advanced Industrial Science and Technology, 3. College of Humanities and Sciences, Nihon Univ., 4. College of Science and Technology, Nihon Univ.

Over the past decades, submarine landslides have been reported in various sea areas. Submarine landslides can be larger in scale than landslides on land. Physical measurements of submarine landslides at the seafloor are not easy to conduct, largely because of the relevant scales and locations. This makes it difficult to understand the mechanism of seafloor destabilization. A possible triggering mechanism to destabilize the submarine sediments is the elevated pore-fluid pressure which is formed at sediment layer interfaces and can reduce their shear strength. Kokusho et al. (2000) proposed a water film effect and its mechanism on lateral flow with less frictional resistance to explain large-scale submarine landslides. Elger et al. (2018) discuss the relationship between submarine landslides due to the elevated pore pressure and gas hydrate system. Their study showed that the reduced permeability due to gas hydrate increases pore pressure, and it transfers to the shallower layer interface through the pipe structure. In both studies, elevated-pore pressure is formed at sedimentary interface where there is a permeability contrast. However, although the actual submarine ground may have been consolidated by compaction and diagenesis, limited studies have been conducted to investigate the effect of the degree of consolidation at the sediment layer interface on the formation of water films.

In this study, we conducted a series of experimental tests to observe the effect of a cohesion between layers on water film formation. Portland cement was used to change the cohesion of the sediment interface. We observed a clear relationship between the amount of Portland cement and pore pressure at which the water film was formed. This indicates that the degree of solidification (consolidation/ diagenesis) of sedimentary layers may have a significant effect on the occurrence of submarine landslides.

[Reference]
1. Kokusho, T.: Mechanism for water film generation and lateral flow in liquefied sand layer, Soils and Foundations, Vol.40, No.5, p99-111, 2000.
2. Elger, J., Berndt, C., Rupke, L., Krastel, S., Gross, F., and Geissler, W.H.: Submarine slope failures due to pipe structure formation, Nature communications, 9(715), 2018.

Keywords: Submarine landslides, Water film, Lateral Flow, cohesion

©2020. Japan Geoscience Union. All Right Reserved.

[E] Poster | H (Human Geosciences)：H-TT Technology & Techniques

[H-TT14] Geographic Information Systems and Cartography

convener:Takashi Oguchi(Center for Spatial Information Science, The University of Tokyo), Yoshiki Wakabayashi(Graduate School of Urban Environmental Sciences, Tokyo Metropolitan University), Yuei-An Liou(National Central University), Ronald C. Estoque(National Institute for Environmental Studies, Japan)

This session discusses various methods which acquire, store, analyze and visualize geospatial data, and presents the outcomes of empirical studies using GIS or mapping methods. The session also deals with applications of digital data, and GIS, and mapping to various fields of earth and planetary science and human society. All presentations and discussion of this session are made in English.

[HTT14-P01] Evaluation of seismic wave amplifications in the mountainous area with a temporary seismic network in Totsukawa Village

★Invited Papers

*Chi-Wen Chen[1,2], Masato Sato[1], Ryuji Yamada[1], Tomoyuki Iida[1,2] (1.National Research Institute for Earth Science and Disaster Resilience, 2.The University of Tokyo)

[HTT14-P02] **Landslide Detection from Remote Sensing Imagery Based on SPP-PCANet**

*Yimei Wei[1], Takashi Oguchi[2] (1.The University of Tokyo, 2.Center for Spatial Information Science, The University of Tokyo)

[HTT14-P03] **GIS-based frequency ratio, logistic regression and artificial neural network models for landslide susceptibility analysis in central Shenzhen, South China**

*DI LU[2], Takashi Oguchi[1] (1.Center for Spatial Information Science, The University of Tokyo, 2.The University of Tokyo)

[HTT14-P04] **Analysis of Morphometric Parameters and Precipitation Characteristics for Landslides Using GIS**

*Toshikazu Fukuba[1], Takashi Oguchi[2] (1.Department of Earth and Planetary Environmental Science, The University of Tokyo, 2.Center for Spatial Information Science)

[HTT14-P05] **GIS and remote sensing applied to topographic analyses of hilly and mountainous communities, Nishi-Awa, Japan**

★Invited Papers

*Roxanne Lai[1], Takashi Oguchi[1] (1.University of Tokyo)

[HTT14-P07] Development of e-learning materials for high school education on topography using GIS

*Hiroyuki Yamauchi[1], Takashi Oguchi[2] (1.Department of Natural Environmental Studies, Graduate School of Frontier Sciences, The University of Tokyo, 2.Center for Spatial information Science, The University of Tokyo)

[HTT14-P08] An Improved Mosaicking Algorithm for UAV Photographs of Vegetated Areas

*Zijin Wang[1], Takashi Oguchi[2] (1.Department of Natural Environmental Studies, Graduate School of Frontier Science, The University of Tokyo, 2.Center for Spatial Information Science, The University of Tokyo)

[HTT14-P09] Surge event of Alakesayi Glacier, West Kunlun Shan, based on remote sensing data

*Qiqi MA[1], Takashi OGUCHI[2,1] (1.Dept. of Natural Environmental Studies, Graduate School of Frontier Sciences, The University of Tokyo, 2.Center for Spatial Information Science, Division of Spatial Information Analysis, The University of Tokyo)

[HTT14-P10] Remote Sensing-Based Urban Heat Risk Assessment in Philippine Cities

★Invited Papers

*Ronald C. Estoque[1], Makoto Ooba[1], Xerxes T. Seposo[2], Takuya Togawa[1], Yasuaki Hijioka[1], Kiyoshi Takahashi[1], Shogo Nakamura[1] (1.National Institute for Environmental Studies, Japan, 2.Nagasaki University, Japan)

Evaluation of seismic wave amplifications in the mountainous area with a temporary seismic network in Totsukawa Village

*Chi-Wen Chen[1,2], Masato Sato[1], Ryuji Yamada[1], Tomoyuki Iida[1,2]

1. National Research Institute for Earth Science and Disaster Resilience, 2. The University of Tokyo

Seismic wave is one of the most important triggering factors of landslides. Amplification effect of seismic waves transmitted from bedrock to ground surface has been confirmed by many observations. However, very few seismic stations are located in mountain areas, so it is impossible to assess the amplification effect of seismic waves using pre-existing measured data. In addition, the fact that most earthquake-induced landslides initiate from the ridge indicates that the magnification of seismic waves may vary in different parts of a mountain. In this study, we installed a temporary seismic network in the mountainous area of the Totsukawa Village, Nara Prefecture, Japan, having four station sites at different parts of a mountain with an EW trending topography: a ridge, a valley, a north-south slope, and an east-west slope. The monitoring period of the temporary network is approximately two years from November 15, 2017 to December 10, 2019, and we selected 25 earthquakes that occurred during the period for further analyses of the seismic waves. The fast Fourier transform (FFT) was applied to each seismic wave with a duration of 81.92 s and a Parzen window of 0.2 Hz bandwidth. We obtained the EW and NS horizontal components and the UD vertical component of the observed Fourier spectrum for each earthquake at each site. The relative position of an earthquake epicenter was interpreted as the direction of the seismic wave transmitted to each station. It is found that the difference in magnitudes of seismic wave amplification seems to be related to the parts of a mountain and the seismic wave direction. This would be helpful to identify locations susceptible to earthquake-induced landslides.

Keywords: seismic wave, amplification, Fourier transform, earthquake, landslide, topography

©2020. Japan Geoscience Union. All Right Reserved.

Landslide Detection from Remote Sensing Imagery Based on SPP-PCANet

*Yimei Wei[1], Takashi Oguchi[2]

1. The University of Tokyo, 2. Center for Spatial Information Science, The University of Tokyo

Landslides are complex geological phenomena that can cause serious damage to the natural and social environments and may result in a significant loss of lives and properties. Therefore, it is crucial to conduct a timely post-disaster investigation. Landslide detection is an important step of landslide studies such as mapping, inventory preparation, and specific analyses for the coordination of practical actions including rapid disaster responses. Remote sensing images have been widely used in disaster research with the aid of image feature analysis based on computer vision. Traditional feature extraction methods depend on visual interpretation of feature characteristics such as color, gradient, and corners. However, such methods usually require a large amount of prior knowledge and tedious work. They also tend to be subjective and are only applicable to some specific environments, meaning that generalization ability is low. In recent years, the increasing maturity of machine learning, especially deep learning, enables features to be automatically detected from images, providing more robust analysis and interpretation of remote sensing images. This study explores a landslide detection method that uses a simple and effective image feature descriptor based on a highly simplified network designated as Spatial Pyramid Pooling Principal Component Analysis Network (SPP-PCANet) combined with the SVM classifier. We analyzed landslides due to the 2018 Hokkaido Eastern Iburi earthquake, using vertical aerial photographs and orthophotographs provided by the Geospatial Information Authority of Japan (GSI) for model training and hyperparameters optimization. Then we performed landslide detection using Google Earth imagery. Experimental results show that the proposed landslide detection method has promising performance and may contribute to future rapid responses to landslide hazards.

Keywords: Landslide detection, Image feature extraction, Spatial Pyramid Pooling Principal Component Analysis Network, Machine learning

©2020. Japan Geoscience Union. All Right Reserved.

GIS-based frequency ratio, logistic regression and artificial neural network models for landslide susceptibility analysis in central Shenzhen, South China

*DI LU[2], Takashi Oguchi[1]

1. Center for Spatial Information Science, The University of Tokyo, 2. The University of Tokyo

As major geological hazards, landslides account for a great number of human casualties and an enormous amount of property loss, and cause significant damage to natural ecosystems and human-built infrastructures, especially in urban areas. Landslide susceptibility analysis is regarded as a semi-quantitative risk assessment and has become an important part in landslide studies and risk management engineering. This study investigates landslide susceptibility in the new district of Shenzhen, South China. Shenzhen is a mountainous area, lying in the East Asia monsoon region, with a subtropical monsoon climate. The district has been rapidly developing so that there are broad construction areas and lots of living people. Some previous studies have shown the results of landslide susceptibility analyses for this area. This study aims to further develop such studies by analyzing landslide susceptibility using three different methods: frequency ratio, logistic regression, and artificial neural network (ANNs) models. The latter includes Back Propagation ANNs and Radial Basis Function ANNs. These models were established using elevation, slope, aspect, lithology, human activities, vegetation, and precipitation as independent variables. Land use data are utilized to represent human activities, and the Normalized Difference Vegetation Index (NDVI) is employed to indicate the level of vegetation coverage. Landslide susceptibility maps of the study area are created based on the three methods to show the relative risk of landslides. There are 429 landslide points and 400 points without landslides in the sample data. For the logistic regression model, the overall accuracy is 0.743, the recall is 0.799, and AUC (area under the receiver operating characteristic curve) is 0.790. For the BPANNs model, the overall accuracy is 0.724, the recall is 0.762, indicating that the two methods have similar high performances. The performance of the frequency ratio model is lower.

Keywords: Landslide susceptibility, GIS, Logistic regression, Artificial Neural Networks

©2020. Japan Geoscience Union. All Right Reserved.

Analysis of Morphometric Parameters and Precipitation Characteristics for Landslides Using GIS

*Toshikazu Fukuba[1], Takashi Oguchi[2]

1. Department of Earth and Planetary Environmental Science, The University of Tokyo, 2. Center for Spatial Information Science

Morphometric parameters calculated from DEMs have been used for producing landslide hazard maps. This study investigates morphometric parameters of areas affected by landslides due to the August 2014 heavy rain in Hiroshima and the July 2018 heavy rain in western Japan. Altitude, slope angle, slope aspect, slope curvature and geology are chosen for morphometric parameters to be investigated. In addition, precipitation distribution data are used for investigating the relationship among landslides, topography and rainfall amount.

Most landslides caused by the July 2018 heavy rain occurred on slopes gentler than 30 degrees with concave topography in plan curvature. In contrast, most landslides caused by the August 2014 heavy rain are located on slopes steeper than 30 degrees with convex topography in plan curvature. This result indicates locational differences in landslide distribution depending on precipitation characteristics.

Landslides caused by the July 2018 heavy rain in areas underlain by plutonic and volcanic rocks mostly occurred on slopes slightly steeper than 25 degrees, whereas landslides in areas with lithosol and regosol tended to take place on slopes slightly gentler than 25 degrees. This observation suggests that differences in surficial geology should be considered to estimate the threshold slope angle for landsliding.

Keywords: GIS, landslide, morphometric parameters

©2020. Japan Geoscience Union. All Right Reserved.

GIS and remote sensing applied to topographic analyses of hilly and mountainous communities, Nishi-Awa, Japan

*Roxanne Lai[1], Takashi Oguchi[1]

1. University of Tokyo

Quantifying topographic characteristics of hilly and mountainous settlements is important to fully understand the drivers of issues such as depopulation, as well as the implications of topographic characteristics in the face of future human development or climate change. These settlements are located on remote and difficult terrain such as steep slopes and thin soils. Consequently, these settlements are particularly vulnerable to environmental and social threats such as landslides from rainstorms, food insecurity, and political marginalization. Mountain topography plays a large role in defining multiple characteristics of hilly and mountainous settlements, and is also therefore important to understand within the context of the sustainability of these settlements.

While topographic studies have been conducted for individual settlements or on large country-scales, few regional studies have focused on the distribution of topographic characteristics across multiple settlements due to difficulties in obtaining multiple accurate settlement-level data. Regional or national-scale topographic studies in Japan tend to apply administrative boundary shapefile data freely offered by the government. However, these boundaries fail to distinguish the much smaller agriculture settlements.

To clarify the differences of using topographical characteristics at different scales (i.e., whether at settlement or at municipal scales) and better characterize hilly and mountainous settlements, this study applies medium-resolution topographic data and geospatial analysis. This study firstly identifies and quantifies the topographic characteristics (slope, profile curvature, elevation, and aspect) of agriculture settlements in the Nishi-Awa area, Shikoku, Japan, and secondly compares their topographical characteristics with the characteristics calculated from government-designated boundaries. Thereafter, correlation calculations are performed using the calculated topographical characteristics and other geographic variables to explore the relationship their relationship with depopulation.

The results show that aspects and profile curvatures of the settlements indicate directional tendencies most likely based on preferential agriculture conditions. Significant heterogeneity of topographical characteristics within the Nishi-Awa administrative area implies governance needs to account for the variety of environmental and social risks occurring. Furthermore, slope angle calculated from broader boundaries tends to overestimate actual mean slope angle of the settlements, resulting in exaggerated relationships between topography and depopulation. However, results also emphasize that even within mountainous settlements, slope remains a major driver of depopulation, compared to other topographical variables. This implies that other factors such as aging population may exacerbate slope influence on depopulation.

Keywords: Topography, GIS, Remote Sensing, Hilly and mountainous communities

©2020. Japan Geoscience Union. All Right Reserved.

©2020. Japan Geoscience Union. All Right Reserved.

Development of e-learning materials for high school education on topography using GIS

*Hiroyuki Yamauchi[1], Takashi Oguchi[2]

1. Department of Natural Environmental Studies, Graduate School of Frontier Sciences, The University of Tokyo, 2. Center for Spatial information Science, The University of Tokyo

Geomorphology education concerning characteristics of topography is important for learning the basic elements of natural environment and disaster prevention. However, geography education on topography in Japanese high schools faces difficulties in various aspects such as reading contour lines and understanding the development processes of landforms. A reason for this is that most high school teachers who teach topography did not learn a lot about geomorphology in universities. In Japanese high schools, a new geography course will become compulsory in 2022, and in the course GIS (Geographic Information Systems) have to be taught to all students. Therefore we started developing e-learning materials for geomorphology education in high schools using GIS. The materials under development consist of three components: 1) online text explaining geomorphology using digital maps, 2) utilization of 3D-printed topographic models and VR viewing, and 3) utilization of GIS software to analyze DEMs (Digital Elevation Models). In this presentation, we introduce the construction processes of the materials.

Keywords: Education, Topography, GIS, E-learning

©2020. Japan Geoscience Union. All Right Reserved.

An Improved Mosaicking Algorithm for UAV Photographs of Vegetated Areas

*Zijin Wang[1], Takashi Oguchi[2]

1. Department of Natural Environmental Studies, Graduate School of Frontier Science, The University of Tokyo, 2. Center for Spatial Information Science, The University of Tokyo

Unmanned Aerial Vehicle (UAV) photogrammetry is widely used for vegetation research because of its high resolution and superior cost efficiency. However, photographs taken by a UAV at one time are not consistent over the whole study area in terms of geometry, distortion, and color tone. In addition, high resolution aerial images of vegetation usually contain numerous similar features and illumination changes, which consequently brings a huge challenge to mosaicking and processing images using tie points efficiently and accurately. This study aims to propose an improved algorithm to mosaic aerial photographs of a vegetated area efficiently under various situations. The steps for mosaicking images include feature point extraction, point matching, elimination of mismatching points, fusion, and mosaicking. Among them, detecting and matching the feature points of images are the most important part for image mosaicking. In this research we analyzed traditional algorithms for feature point detection including the Scale Invariant Feature Transform (SIFT) and Speed up Robust Feature (SURF) algorithms, and found that both do not perform well. Then we adjusted parameters and used 128-element descriptors inside of 64-element descriptors without computing the orientation, to improve the SURF algorithm in terms of efficiency and accuracy. The improved mosaicking algorithm is expected to be applied in vegetation studies to provide better information with high efficiency.

Keywords: SURF, Image mosaicking, UAV image, Vegetation

©2020. Japan Geoscience Union. All Right Reserved.

Surge event of Alakesayi Glacier, West Kunlun Shan, based on remote sensing data

*Qiqi MA[1], Takashi OGUCHI[2,1]

1. Dept. of Natural Environmental Studies, Graduate School of Frontier Sciences, The University of Tokyo, 2. Center for Spatial Information Science, Division of Spatial Information Analysis, The University of Tokyo

Surging glaciers are glaciers that move periodically and rapidly. During a surge event, a glacier advances rapidly in a short time. The velocity is several times larger than usual, and glacier thickening at the terminus may be induced. After a surge, a compensatory glacier retreat may occur. These processes lead to potentially dangerous consequences, especially the outburst flood of a glacial lake. Although surging glaciers in Alaska and Svalbard Islands have been studied in detail, there are few studies on a large number of surging glaciers in the High Mountain Asia (HMA) including Kunlun. A better understanding of the dynamics of glacial surges in this region will help to predict future glacial behavior and assess potential disasters.
Alakesayi Glacier lies in West Kunlun Shan (WKS), northwestern Tibetan Plateau, China. A surge event was observed to have started in 2014. By utilizing more than 50 frames of Sentinel 1 and Landsat satellite images, we estimated the change in surface velocity (seasonal and inter-annul) and terminus morphology. Changes in surface elevation were also obtained using DEMs for different periods. The data analysis shows that, the surface velocity continued to increase during 2014-2015, reaching a maximum of more than 1,000 m/yr. Then the velocity gradually decreased but was still greater than other glaciers in the same region. During the surge, Alakesayi Glacier advanced by 1.3 km. Although the glacier continued to retreat during the 1980s and 1990s, the current terminus is close to that before the retreat because of the surge. Surge events similar to this time may have occurred also in the past. The elevation change of the glacial surface reflects the mass transport process during the surge, i.e., the mass lost in the midstream but increased in the downstream including the terminus. These results from remote sensing data provide an insight into the surge dynamics of Alakesayi Glacier and will be useful for understanding the glacier mass balance in this area.

Keywords: surging glacier, remote sensing, glacier change, surface velocity

©2020. Japan Geoscience Union. All Right Reserved.

Remote Sensing-Based Urban Heat Risk Assessment in Philippine Cities

*Ronald C. Estoque[1], Makoto Ooba[1], Xerxes T. Seposo[2], Takuya Togawa[1], Yasuaki Hijioka[1], Kiyoshi Takahashi[1], Shogo Nakamura[1]

1. National Institute for Environmental Studies, Japan, 2. Nagasaki University, Japan

More than half of the world’ s population today live in urban areas and are particularly at risk from the combined effects of the urban heat island phenomenon and heat increases due to climate change. Advances in remote sensing technology, including the increasing availability of remotely sensed thermal data, have been helpful in urban ecological studies, including the study of the urban heat island phenomenon. In this study, focusing on the dry season, we examined the potential of remotely sensed surface temperature as a proxy indicator for heat hazard as we assessed the current heat health risk in Philippine cities, whose population accounts for over 40% of the country’ s total population. The assessment was based on the risk framework of the Intergovernmental Panel on Climate Change, in which risk is expressed as a function of hazard, exposure and vulnerability. The assessment produced an overall heat health risk index which was validated by comparing it with heat-related mortality data. Results revealed that the overall heat health risk index had a positive and statistically significant relationship with heat-related mortality, indicative of the potential of remotely sensed surface temperature as a proxy indicator for heat hazard. This is important especially for the developing regions where data on air temperature is scarce. Empirically, the assessment revealed that the cities that were at high and very high risk were found in Metro Manila where levels of heat hazard and exposure were higher. The most vulnerable cities were, however, found mainly outside the national capital region where sensitivity was higher and capacity to cope and adapt was lower. The cities with high levels of vulnerability and exposure to heat need to be prioritized for adaptation. The results contribute to the risk profiling endeavor in the country and to the understanding of city-level heat health risks in the developing region of the Asia-Pacific.

Keywords: heat risk, land surface temperature, remote sensing, heat health risk index, urban heat island, adaptation

©2020. Japan Geoscience Union. All Right Reserved.

[E] Poster | H (Human Geosciences)：H-TT Technology & Techniques

[H-TT15] Environmental Remote Sensing

convener:Wei Yang(Chiba University), Akihiko Kondoh(Center for Environmental Remote Sensing, Chiba University), Carolynne Hultquist(Columbia University), Elena Sava(US Army Corps of Engineers Geospatial Research Laboratory), Guido Cervone(Pennsylvania State University Main Campus)

Our human beings are encountering various environmental issues on the Earth, and it is urgent to find out the solutions based on corresponding observations and models. Remote sensing is currently the only feasible means to observe the Earth environment at regional/continental /global scales over long periods, and consequently detects the environmental changes occurred all over the world. Although remote sensing has been extensively applied in numerous environmental studies, there are still many challenges for data analysis and applications. Consequently, this session invites presentations on theory, science, technology, and applications of remote sensing to study the Earth environment from local, regional to global scales. Both oral and poster presentations are sincerely welcome.(TBD)

[HTT15-P01] **Impacts of urbanization on the local thermal environment in Central America**

*Son Thanh Nguyen[1], Chi-Farn Chen[1], Cheng-Ru Chen[1] (1.Center for Space and Remote Sensing Research, National Central University, Zhongli District, Taoyuan City 32001, TAIWAN)

[HTT15-P03] Generation of the GCOM-C land surface phenology product: Algorithm development and performance evaluation

*MENGYU LI[1], Wei Yang[2], Akihiko Kondoh[2] (1.Graduate School of Science and Engineering, Chiba University, 2.Center for Environmental Remote Sensing, Chiba University)

[HTT15-P04] **Monitoring macrophyte phenology in Lake Inba-numa, Japan based on Sentinel-2 images**

*HU LIANG[1] (1.Chiba University, Graduate School of Science and Engineering, Center for Environmental Remote Sensing)

[HTT15-P06] **Detecting Urban Growth Using Remote Sensing and GIS Techniques in Taoyuan City, Taiwan**

*Cheng-Ru Chen[1,2], Chi-Farn Chen[1], Thanh-Son Nguyen[1] (1.CSRSR,NCU, 2.CLVSC)

[HTT15-P07] **Evaluation and comparison of *Karenia mikimotoi* detection in the Seto-Inland Sea by remote sensing**

*Zhenjia Zhou[1], Joji Ishizaka[2] (1.GSES, Nagoya Univ., 2.ISEE, Nagoya Univ.)

[HTT15-P08] Spectro-polarimetric BRF measurements of the desert sand with multispectral LCTF camera

*Begzsuren Tumendemberel[1], Yukihiro Takahashi[1], Junichi Kurihara[1], Tetsuro Ishida, Nobuyasu Naruse[2], Ahmad Shaqeer[1] (1.Hokkaido University, Department of Cosmosciences, Graduate School of Science, Kita 10-Nishi 8, Kita-ku, Sapporo, Hokkaido 060-0810, 2.Division of Physics Dept. of Fundamental Bioscience, Faculty of Medicine, Shiga University of Medical Science ZIP: 520-2192 Seta, Tsukinowa-cho, Otsu, Shiga, JAPAN)

[HTT15-P09] Mirror Reflection Measurement of Leaves from Different Environmental Stresses

*Garid Zorigoo[1], Begzsuren Tumendemberel[1], Yukihiro Takahashi[1] (1.Department of Cosmosciences, Graduate School of Science, Hokkaido University)

Impacts of urbanization on the local thermal environment in Central America

*Son Thanh Nguyen[1], Chi-Farn Chen[1], Cheng-Ru Chen[1]

1. Center for Space and Remote Sensing Research, National Central University, Zhongli District, Taoyuan City 32001, TAIWAN

Central America is recognized as the second-fastest urbanizing region in the world. Today, at least 60.5% of the region’ s population (30.7 million people) lives in urban areas, and is expected to double in size by 2050. The rapid urbanization has brought both employment opportunities and negative impacts, including heat island effect that is a phenomenon, where higher temperature is observed in urban areas due to changes in properties of land surface. Such effects coupled with congestion of population can trigger severe influences on the local thermal environment, consequently decreasing the health-related quality of life. Information on urbanization and its impacts on the local thermal environment is thus important for urban planning process. The objective of this study is to investigate impacts of urbanization on the local thermal environment in El Salvador, Central America using multi-temporal Landsat data. The data were processed for the period 1986–2016, following four main steps: (1) data pre-processing to account for atmospheric effects and geometric errors; (2) urban image classification using random forests; (3) retrieval of land surface temperature (LST); and (4) hotspot detection, and analysis of impacts of land-cover change on local surface temperature. The results of urban classification, verified with the ground reference data, revealed close agreement between these two datasets, with the overall accuracies and Kappa coefficients, achieved for 1986 and 2016, were respectively 89.8% and 0.8, and 91.4% and 0.84. From 1986 to 2016, the urban area had increased 2,654.7 ha, and the city had expanded into various directions, especially in the northern and eastern parts, owing to advantages of existing and newly developed infrastructures. Due to such a rapid urbanization, the proportion of hotspots (areas of elevated temperature) had also increased from 32% in 1986 to 39.9% in 2016, respectively. The results of decadal analysis of impacts of land-cover change on the local thermal environment also confirmed the significant association between the LST and Normalized Difference Vegetation Index (NDVI), and Normalized Difference Built-up Area Index (NDBI) ($R^2 > 0.72$). The research findings, achieved from this study, highlighted the importance of urban sprawls in conjunction with changes of vegetation cover and temperature. Such information would be valuable to urban planners to successfully devise strategies to regulate effects of urban heats on the city's liveability.

Keywords: Urbanization, Thermal environment, Remote sensing, San Salvador

©2020. Japan Geoscience Union. All Right Reserved.

Generation of the GCOM-C land surface phenology product: Algorithm development and performance evaluation

*MENGYU LI[1], Wei Yang[2], Akihiko Kondoh[2]

1. Graduate School of Science and Engineering, Chiba University, 2. Center for Environmental Remote Sensing, Chiba University

The satellite Global Change Observation Mission –Climate (GCOM-C) carrying the optical sensor, Second Generation Global Imager (SGLI) with 250 m spatial resolution, was launched on December 23, 2017. One of the major goals of the GCOM-C mission is to monitor global climate changes. Vegetation phenology not only describes the life cycle events of periodic plants in the growing season but also is an indicator of the sensitivity of the ecosystem to climate change. The long-term study of phenological records on the surface of vegetation is very important for exploring regional and global scale biological responses to environmental changes. Land surface phenology from satellite monitoring has been shown to capture the spatial patterns of vegetation dynamics at global scales. In this study, we will present a newly proposed algorithm to produce the Global Land Surface Phenology (GLSP) product based on the GCOM-C/SGLI data. The GCOM-C GLSP algorithm uses GCOM-C Atmospheric Corrected Reflectance (RSRF) data as the input to calculate the normalized difference greenness index (NDGI). The temporal NDGI trajectory is reconstructed using the iterative Savitzky-Golay filter and modeled using a hybrid piecewise logistic function to retrieve the state of seasonal vegetation development, detect phenological transition dates and characterize the confidence of phenology detections on an annual basis. The GCOM-C GLSP algorithm has been verified by the field phenology observations of specific species at multiple observation sites (i.e., Penological Eye Network, PhenoCam Network), and compared with the VIIRS and MODIS GLSP products to evaluate the resulting phenological metrics. The evaluations results demonstrated satisfactory agreements between the satellite-estimated and field-observed phenological metrics, indicating that the GCOM-C/SGLI data can be used to generate a new generation of the GLSP product at 250 m resolution.

Keywords: Land surface phenology product, Piecewise logistic, Evaluation

©2020. Japan Geoscience Union. All Right Reserved.

Monitoring macrophyte phenology in Lake Inba-numa, Japan based on Sentinel-2 images

*HU LIANG[1]

1. Chiba University, Graduate School of Science and Engineering, Center for Environmental Remote Sensing

Recently, the floating-leaved plants, especially Trapa spp., have been increased in eutrophic lake Inba-numa, Japan. The Trapa spp. can reduce phytoplankton blooms and stabilize a clear water state by storing nutrients. On the other hand, they can also block the water way and cause low dissolved oxygen concentration. In order to understand the processes of growth, senescence and reproduction of Trapa spp., it is necessary to monitor the phenology of Trapa spp. The improved spatial and temporal resolution of latest-generation Earth Observation missions, such as Sentinel-2, has provided new opportunity of remote sensing for mapping land surface phenology in small inland water systems like Lake Inba-numa, however the driving force for the spatial variation of Trapa spp. phenology is still unclear. The aim of this study was first to estimate the Trapa spp. phenology with sentinel-2A,B in years of 2018 and 2019, and then to analyze the mechanism for the spatial variation of Trapa spp. phenology. Phenology metrics including start and end of the growing season (SOS and EOS) were computed from NDVI time series using the software TIMESAT. The SOS in 2018 North Inba-numa and West Inba-numa was ranging from DOY110 to DOY130 and DOY100 to DOY120, the EOS of North Inba-numa and West Inba-numa was ranging from DOY265 to DOY275 and DOY250 to DOY300. Noticeable spatial variations of phenology were observed in Inba-numa. The relationship between the phenology variation, water depth and $K_{d(PAR)}$ (downwelling attenuation coefficient of photosynthetically active radiation) was also analyzed. The water depth data is provided by Geospatial Information Authority of Japan and the $K_{d(PAR)}$ was calculated from Sentinel-2A,B in years of 2018 and 2019 based on the semi-analytical approach for K_d retrieval which was presented by Lee et al. (2013). In general, for water depths up to 2 m, there is no obvious relationship between the phenology spatial variation and water depth, the phenology spatial variation was directly influenced by the $K_{d(PAR)}$. In conclusion, this study is helpful to improve our understanding of seasonal changes in macrophyte growth and help to manage the macrophyte to have a positive effect on water quality.

Keywords: Trapa spp., Lake Inba-numa, Phenology, Water depth, Kd(PAR)

©2020. Japan Geoscience Union. All Right Reserved.

Detecting Urban Growth Using Remote Sensing and GIS Techniques in Taoyuan City, Taiwan

*Cheng-Ru Chen[1,2], Chi-Farn Chen[1], Thanh-Son Nguyen[1]

1. CSRSR,NCU, 2. CLVSC

Understanding spatio-temporal dimensions of land-use changes that shape the urbanization is critical to the process of urban planning. In the recent years, remote sensing data and GIS techniques are widely being used for mapping the urban growth, land-use/land-cover, and sprawl. The aim of this study is to produce land use and cover map for the studied area at varied periods to monitor possible changes that may occurred, particularly in the urban areas and agriculture and subsequently predict likely changes. We explore the urban growth in Taoyuan city through remote sening data for each 10-year period form 1970 to 2019 using the ISODATA (Iterative Selforganizing Data Analysis Techniques Algorithm) classification to assess the changes of agricultural lands, urban encroachment and water areas during this period with integration by GIS. The data are processed through four steps: (1) data pre-processing, (2) image classification by regional ISODATA, (3) accuracy assessment of the classification results using field verification data, and (4) urban growth analysis to understand the spatial changes of land cover. The results achieved by comparisons between the classification results and ground reference data indicate that the overall accuracy and Kappa coefficient in five periods were all higher than 82.5% and 0.76, respectively. The results of urban growth analysis indicate that the growth rate of built-up areas has a highest value of 26% in 1980s, while the growth rate in other follwing periods are between 2.3% and 5.7%. Referancing to the development of public works in Taoyuan city, it reveals that urban growth of Taoyuan city was dominated initially by large-scale public work, such as the contruction of Taoyuan Airport and Industrial parks and then was subsequently affected by the demand of dwelling space of immgration from Taipei and its immediate vicinity.

Keywords: Remote sensing, GIS, Urban growth

©2020. Japan Geoscience Union. All Right Reserved.

Evaluation and comparison of *Karenia mikimotoi* detection in the Seto-Inland Sea by remote sensing

*Zhenjia Zhou[1], Joji Ishizaka[2]

1. GSES, Nagoya Univ., 2. ISEE, Nagoya Univ.

Harmful Algae Blooms (HABs) is a worldwide problem in coastal marine systems. Seto-Inland Sea is a semi-enclosed coastal area in Japan that suffered from HABs. Dinoflagellate *Karenia mikimotoi* is one of the most common species that form HABs in the Seto-Inland Sea. It could increase fish mortality, thereby causing economic losses for coastal aquaculture. A detection method based on the spectral difference in short wavelength was developed by limited field observation in the western part of the Seto-Inland Sea (Siswanto *et al.*, 2013). But the spectra in the short wavelength are always influenced by colored dissolved organic matters and non-algal particles as well as the error of atmospheric correction. Thus, it is necessary to evaluate the method with more filed observation data. Meanwhile, several methods for the detection of *Karenia brevis*, a HABs species belongs to the same genus and has similar optical properties with *Karenia mikimotoi*, were developed in the West Florida Shelf. These methods could be divided into chlorophyll-a based, apparent optical property based, inherent optical property based approach, etc. This research aims to compare results of different detection methods in the Seto-Inland Sea and evaluate them with the recent filed observation data.

Keywords: Seto-Inland Sea, Harmful Algae Blooms, Karenia mikimotoi, Remote Sensing

©2020. Japan Geoscience Union. All Right Reserved.

Spectro-polarimetric BRF measurements of the desert sand with multispectral LCTF camera

*Begzsuren Tumendemberel[1], Yukihiro Takahashi[1], Junichi Kurihara[1], Tetsuro Ishida, Nobuyasu Naruse[2], Ahmad Shaqeer[1]

1. Hokkaido University, Department of Cosmosciences, Graduate School of Science, Kita 10-Nishi 8, Kita-ku, Sapporo, Hokkaido 060-0810, 2. Division of Physics Dept. of Fundamental Bioscience, Faculty of Medicine, Shiga University of Medical Science ZIP: 520-2192 Seta, Tsukinowa-cho, Otsu, Shiga, JAPAN

Earth observation satellites have the ability to calibrate their radiometric characteristics of space-borne cameras and optical sensors on-orbit when traveling on Pseudo Invariant Calibration Sites (PICS). PICS are located mostly in deserts with high spatial homogeneity and high time-related stability of canopy optical properties. On the other hand, modern satellites are able to take images to alongside using attitude control. The light reflected from the sand is not only indicated by the intensity, but also by the phenomenon of polarization of light. The polarized light reflection of the earth’ s canopy begins to be a new strong method of earth observation. A polarization camera can be on flight devices or satellites to explore atmospheric chemistry or to detect hidden objects. If we study further efficiently the spectral signature of sand as well as the light reflection and polarization, we can do more precise calibration on polarization camera in space. This study aims to investigate the polarization properties and spectral relations of the sand Bidirectional Reflectance Distribution Function (BRDF) by separating specular and diffuse reflectance. For this purpose, the sands BRDF was measured in a laboratory by Liquid Crystal Tunable Filter (LCTF) camera in the wavelength range of 460-780 nm with a polarization intensity. The imaging with the multispectral LCTF camera has a great advantage that an arbitrary angle of the field of view can be selected in a specific area. Hundreds of combinations of light illumination and camera view direction are considered in this study, due for this reason we built a fully automatic goniometer with LCTF camera at Hokkaido University. The room window is closed by a dark curtain and the darkroom has built inside the room, which means it’ s ideal entirely dark. The laboratory and its equipment, including the automatic goniometer, control system, and sensor instruments covered with black absorbing materials for minimizing diffuse irradiance scattering. We have classified sand by grain size, and its properties are more accurate than in previous studies.

Keywords: BRDF, Sand, PICS

©2020. Japan Geoscience Union. All Right Reserved.

Mirror Reflection Measurement of Leaves from Different Environmental Stresses

*Garid Zorigoo[1], Begzsuren Tumendemberel[1], Yukihiro Takahashi[1]

1. Department of Cosmosciences, Graduate School of Science, Hokkaido University

Plants have a waxy-cuticle layer on their leaves to protect from dehydration. Different plant species have different waxy-cuticle layer thickness. The previous study suggests that one can estimate this waxy-cuticle layer thickness in the leaf with mirror reflection measurement with a polarizer.
In this work, some theoretical explanations are formulated for the previous study measurement. Yet, it did not match with new measurements. Theoretical explanations are still in development. Furthermore, we anticipate that within a single species, waxy-cuticle layers can be distinct depending on the environmental stresses. Especially by increasing its waxy-cuticle layer, plants may protect itself from losing more water in a dry environment. In this study, we investigated such occurrence of a change in thickness (or mirror reflection measurement output) of coffee-plants in 2-different environmental stresses: A healthy group (normal watered) and an Unhealthy group (dehydrated). This could lead to the possibility of detecting the leaf's health-status with a different approach. As a result of the measurement, a slight difference between the two groups is observed.

Keywords: Waxy cuticle layer, Plant leaf, Goniometer, Polarizer

©2020. Japan Geoscience Union. All Right Reserved.

[E] Poster | H (Human Geosciences)：H-CG Complex & General

[H-CG21] International Comparison of Landscape Appreciation

convener:yoji aoki(Open University of Japan)

Evaluation of landscape has been developed in a variety of fields, such as geography, landscape architecture, nature protection, and some others. Landscape appreciation is a complex and sophisticated psychological phenomenon. There is no consensus among researchers on what the phenomenon of "landscape" truly is, how people physiologically and mentally experience it, which human attributes affect the perception of it, and why it is apprehended the way it is. The concept of landscape appreciation has yet to be clearly defined and there is a lack of agreement on evaluation methods, the factors that determine landscape preferences, the steps in appreciation, and so forth. This session aims to discuss the research findings of landscape evaluation in various fields, including geography, geomorphology, landscape planning, architecture, engineering, social sciences, environmental psychology, meteorology, phenology, and so on.

[HCG21-P01] Sightseeing image of Asakusa based on Foreign Tourist Preference

*Xie Zijiao[1], saraswati Sisriany[1], Wang Huixin [1], Zhao Yuqing [1], Oka Masaya [1], Kobayashi Kumiko [1], Furuya Katsunori[1] (1.Chiba University)

[HCG21-P02] Study on the Influence of Japanese Traditional Garden and Culture on Japanese People’s Perception of Residential Garden

*Zhendong Liu[1], Tingyu Lu[1], Heyan Jiang[1], Junhei Watanabe[2], Fumeng Zhang[1], Zhi Li[1], Yingming Mao[1], Dibyanti Dibyanti Danniswari[1], Pratiwi Prita Indah[1], Katsunori Furuya[1] (1.Graduate School of Horticulture, Chiba University, 2.Faculty of Horticulture, Chiba University)

[HCG21-P04] **An attempt to manage both rural landscape conservation and tourism development**

*Kojima Shusaku[1], Megumi Aso[2] (1.Graduate School of Tokyo University of Agriculture, 2.Community-reactivating cooperator squard of Miyaki town)

[HCG21-P05] **Appreciations of Japanese landscapes by the western visitors arrived (1549-1858)**

*yoji aoki[1], Fumihiro Konta[2] (1.Open University of Japan, 2.National Science Museum)

[HCG21-P06] Trends of the methods of landscape presentation in the landscape appreciation test from 1967 to 1987

*yoji aoki[1] (1.Open University of Japan)

Sightseeing image of Asakusa based on Foreign Tourist Preference

*Xie Zijiao[1], saraswati Sisriany[1], Wang Huixin [1], Zhao Yuqing [1], Oka Masaya [1], Kobayashi Kumiko [1], Furuya Katsunori[1]

1. Chiba University

Upon the implementation of Japan's tourism policy, more and more foreigners are coming to Japan. According to data from the Japan National Tourism Organization, the number of foreigners visiting Japan in 2018 reached 31.19 million. Asakusais one of the tourist attractions in Tokyo, Japan.Despite the temple as the main attraction, tons of attractions are also available surrounding this Asakusa area, not only for the cultural and historical aspect. Foreign tourists often visit this area for the whole area, Asakusa, not only for Sensoji temple. In order to contribute and promote tourism growth in Japan, especially Asakusa,.This research uses the visitor-employed photography (VEP)method, which invites volunteers to photograph their liked scenes and then captures the visitors' landscape attitudes by deriving their intentions behind the photographs, was designed for capturing visitors' on-site and real-time perception while visiting (Cherem and Traweek 1977). The total participants in this research are 36 people, with 740 photographs that use as data. The photographs classify in Google Vision API to classify the attraction based on image character (information about entities in an image, across a broad group of categories) and landmark image (popular natural and man-made structures). The data later use for mapping the scenic attraction in the Asakusa area. The result shows that most attraction is still around the Sensoji Temple, but this research also identifies another potential sightseeing image. In conclusion, even if Sensoji temple is the main attraction, the other Asakusa area also have high potential to develop as a sightseeing attraction, not only perform as a tourism service area (souvenir shop and restaurant).

Keywords: tourist preferences, Google Vision API, visitor-employed photography, sightseeing image, preference mapping

©2020. Japan Geoscience Union. All Right Reserved.

Sightseeing image of Asakusa based on Foreign Tourist Preference

Xie Zijiao[1], Saraswati Sisriany[1], Zhao Yuqing[1], Wang Huixin[1], Tokiya Oka[1], Wu Yilin[1], Kumiko Kobayashi[1], Xiang Qiong Ying[1], and Katsunori Furuya[1]

[1] Department of Environment Science and Landscape Architecture, Graduate School of Horticulture, Chiba University, Chiba 271-8510, Japan;

Abstract

Upon the implementation of Japan's tourism policy, more and more foreigners are coming to Japan. According to data from the Japan National Tourism Organization, the number of foreigners visiting Japan in 2018 reached 31.19 million. Asakusa is one of the tourist attractions in Tokyo, Japan, with Sensoji Temple as one of its main attractions. It is a popular tourist destination that attracts people from all over the world. Based on its history, Sensoji is the oldest temple in Tokyo built in 628 AD.

Despite the temple as the main attraction, tons of attractions are also available surrounding this Asakusa area, not only for the cultural and historical aspect. Foreign tourists often visit this area for the whole area, Asakusa, not only for Sensoji temple. In order to contribute and promote tourism growth in Japan, especially Asakusa, research about foreign tourism is needed to understand the sightseeing image of Asakusa better based on their preferences. Tourist preference reflects the ability of different destinations to attract tourists and win the tourist market shares by utilizing tourism resources effectively.

This research uses the visitor-employed photography (VEP) method, which invites volunteers to photograph their liked scenes and then captures the visitors' landscape attitudes by deriving their intentions behind the photographs, was designed for capturing visitors' on-site and real-time perception while visiting (Cherem and Traweek 1977). The total participants in this research are 36 people, with 740 photographs that use as data. The photographs classify in Google Vision API to classify the attraction based on image character (information about entities in an image, across a broad group of categories) and landmark image (popular natural and man-made structures). The data later use for mapping the scenic attraction in the Asakusa area. The result shows that most attraction is still around the Sensoji Temple, but this research also identifies another potential sightseeing image. In conclusion, even if Sensoji temple is the main attraction, the other Asakusa area also have high potential to develop as a sightseeing attraction, not only perform as a tourism service area (souvenir shop and restaurant).

Keywords: tourist preferences, visitor-employed photography, Google Vision API, sightseeing image, preference mapping

©2020. Japan Geoscience Union. All Right Reserved.

Study on the Influence of Japanese Traditional Garden and Culture on Japanese People’s Perception of Residential Garden

*Zhendong Liu[1], Tingyu Lu[1], Heyan Jiang[1], Junhei Watanabe[2], Fumeng Zhang[1], Zhi Li[1], Yingming Mao[1], Dibyanti Dibyanti Danniswari[1], Pratiwi Prita Indah[1], Katsunori Furuya[1]

1. Graduate School of Horticulture, Chiba University, 2. Faculty of Horticulture, Chiba University

Background

Japan has a relatively small capita housing area, but many residents live in detached houses and have private gardens. For such choices, we believe that, besides economic considerations, we believe that Japanese are carrying on the tradition of their ethnic culture and customs.

A Japanese detached house has a total area of about 126 square meters per house. In addition, it is defined by the Urban Planning Act to protect the environment as a residential area and differs depending on the area. In the case of residential areas, the building coverage is about 60%, and 40% in the lower areas. A single-family house with a total area of 126 square meters stands on the second floor with a building coverage of 60% and has a garden of 42 square meters. Therefore, we think that houses with private gardens are not uncommon in Japan.

Japanese-style private gardens are handed down to the present age with the flow of history, but there are many private gardens such as Scandinavian, American and modern styles. Private gardens are usually designed in the style of a building but may be decided by the person. However, compared with other countries, we can feel small but Japanese design aesthetic in private gardens. We think this difference is related to Japanese culture.

So, our research purpose is to explore the influence of Japanese culture in private garden of Japanese residents and analyze the characteristics of landscape and culture in Japanese gardens under the background of global cultural blending.

Study Method

This research is a group cooperation study in method of questionnaire survey. Questionnaire includes three aspects, personal information, residential condition and landscape factors grading of residential garden. Fifty questionnaires were collected from volunteers of Japanese nationality.

In order to find out how much influence have Japanese traditional garden and culture put on modern residential garden, we selected eighteen landscape factors for volunteers to grade, six of them are typical elements in Japanese traditional garden. Each factor has five options of different degrees in importance, then we digitalized options into numbers from 1 to 5, 1 is negative elements, 2 is not important, 3 is normal, 4 is important and 5 is strongly important. The collected data was analyzed by software excel and SPSS.

Results

The results of questionnaire survey show that 54% of volunteers live or once lived in a house with garden

©2020. Japan Geoscience Union. All Right Reserved.

and Japanese style is most common, 33.3% of those gardens are Japanese style.

However, each factor with strong Japanese garden’ s characteristic gets an average point low than 3 except garden pine of 3.02. We also find that all six Japanese garden factors are highly associated, which means if one individual volunteer gives one factor a low point, it’ s more possible that he gives other five factors low points.

In result, although Japanese garden style is most common style now, volunteers didn’ t give positive assessment on traditional garden’ s elements. Some volunteers gave all six Japanese garden factors 1 or 2 point. Traditional garden doesn’ t meet people’ s demand in modern times.

©2020. Japan Geoscience Union. All Right Reserved.

Study on the Influence of Japanese Traditional Garden and Culture on Japanese People's Perception of Residential Garden

*Zhendong Liu[1], Tingyu Lu[1], Heyan Jiang[1], Junhei Watanabe[2], Fumeng Zhang[1], Zhi Li[1], Yingming Mao[1], Dibyanti Danniswari[1], Pratiwi Prita Indah[1], Katsunori Furuya[1]

1. Graduate School of Horticulture, Chiba University

2. Faculty of Horticulture, Chiba University

Background

Japan has a relatively small capita housing area, but many residents live in detached houses and have private gardens. For such choices, we believe that, besides economic considerations, we believe that Japanese are carrying on the tradition of their ethnic culture and customs.

A Japanese detached house has a total area of about 126 square meters per house. In addition, it is defined by the Urban Planning Act to protect the environment as a residential area and differs depending on the area. In the case of residential areas, the building coverage is about 60%, and 40% in the lower areas. A single-family house with a total area of 126 square meters stands on the second floor with a building coverage of 60% and has a garden of 42 square meters. Therefore, we think that houses with private gardens are not uncommon in Japan.

Japanese-style private gardens are handed down to the present age with the flow of history, but there are many private gardens such as Scandinavian, American and modern styles. Private gardens are usually designed in the style of a building but may be decided by the person. However, compared with other countries, we can feel small but Japanese design aesthetic in private gardens. We think this difference is related to Japanese culture.

So, our research purpose is to explore the influence of Japanese culture in private garden of Japanese residents and analyze the characteristics of landscape and culture in Japanese gardens under the background of global cultural blending.

Study Method

This research is a group cooperation study in method of questionnaire survey. Questionnaire includes three aspects, personal information, residential condition and landscape factors grading of residential garden. Fifty questionnaires were collected

©2020. Japan Geoscience Union. All Right Reserved.

©2020. Japan Geoscience Union. All Right Reserved.

An attempt to manage both rural landscape conservation and tourism development

*Kojima Shusaku[1], Megumi Aso[2]

1. Graduate School of Tokyo University of Agriculture, 2. Community-reactivating cooperator squard of Miyaki town

1. Introduction

As the number of farmers has been decreasing in the rural areas of Japan, the cultivation of some farmland and forest areas has been abandoned. Therefore, a recent trend involves developing tourism as one method for solving these problems. However, some practices have spoiled the rural landscape because of the promotion of tourism development. Hence, it is necessary to develop planning methods that manage both rural landscape conservation and tourism development sustainably. This study implemented and evaluated a new planning method to assess its future feasibility.

The Yamada area in Miyaki town was selected as a case study. Yamada Sunflower Farm (YSF), which has been managed by local farmers' union, is the main tourist attraction in Miyaki town. These days, over 20,000 tourists visit during the sunflowers' blooming season from October to November. Therefore, traffic jams sometimes happen and the local farmers have planned to develop new parking lots on other farmlands.

2. Methods

The fundamental policy for managing both rural landscape conservation and developing new parking lots as tourism infrastructure involved estimating the demand and the available supply of parking lots in Yamada area, then comparing the two data sets.

The demand for parking lots on YSF was estimated using data provided by a local farmer that indicated the number of visitors. Additionally, oral information about conditions when the maximum number of visitors arrived in the past was used to estimate the maximum demand.

When we tried to calculate the available supply of parking lots, our research team developed a footpath route with the cooperation of residents. The purpose was to invite visitors to look at the beautiful rural landscape. Second, we identified which farms were visible from the footpath route using a field survey. These farms were considered what most visitors would regard as a beautiful rural landscape that should not be developed. These farms were transformed into shapefiles for analysis by QGIS. Third, Warning Zone of Landside Disaster (WZLD) was added to QGIS because the development of parking lots on WZLD should be avoided. Fourth, the farms visible from the footpath and the WZLD were overlaid and we estimated the available supply of parking lots.

Finally, We held a workshop to explain the results to local residents and evaluated the proposed planning method by listening to their responses.

3. Results

At first, 452 cars per day was the estimated maximum figure according to the data on the number of visitors. Furthermore, the estimated maximum figure was 250 cars per hour according to residents' oral information. Therefore, 4508 m^2 would be needed to park 250 cars.

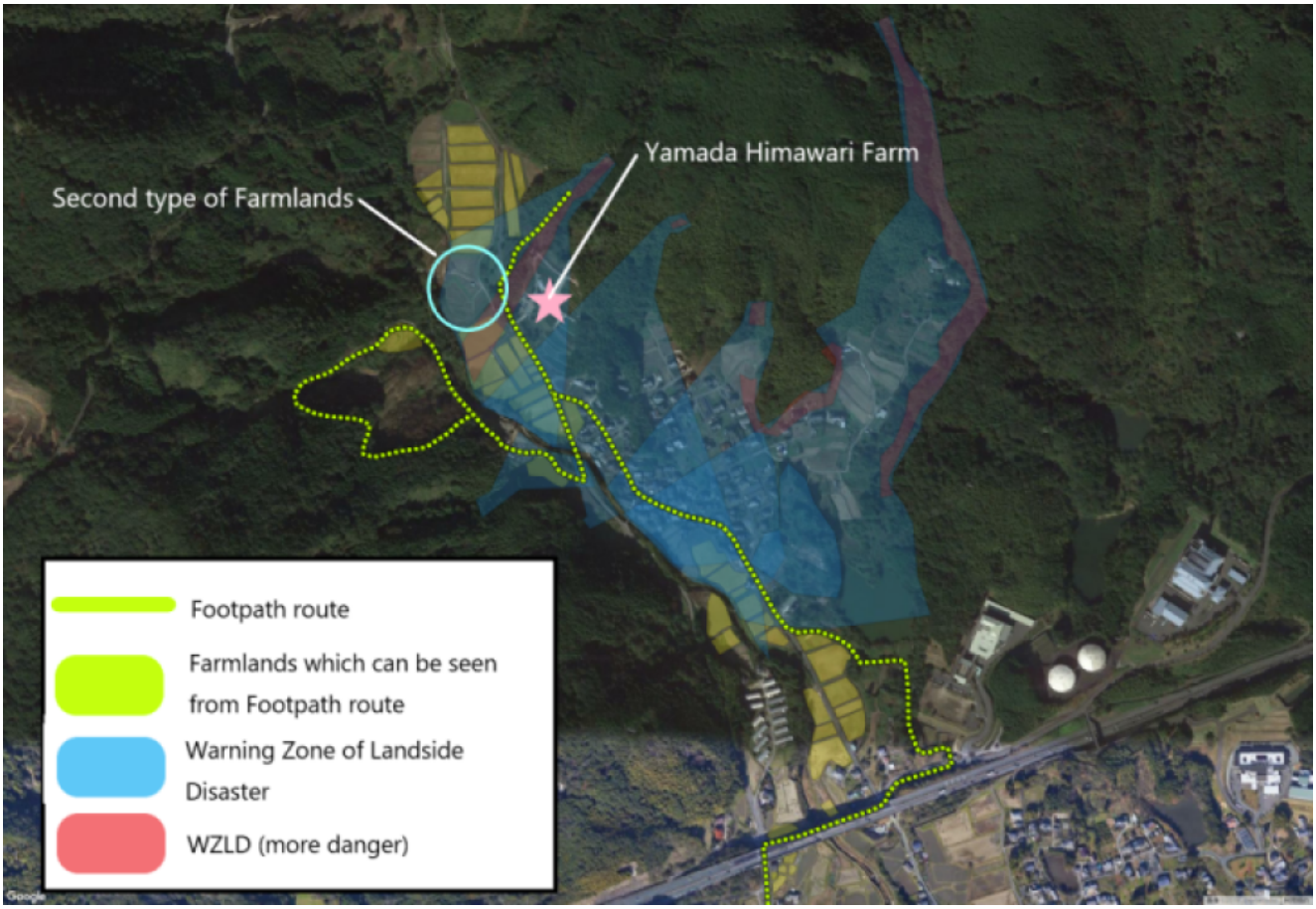
When both the farms visible from the footpath and WZLD was overlaid, four types of farmland were confirmed. The first type of farm was both visible from the footpath route and located on the WZLD. The second was only located on the WZLD. This type was located east of the YSF. The third was visible from the footpath route only. the fourth was not visible from the footpath route nor located on the WZLD.

Both the second and fourth types were suitable for parking lot development in rural landscape conservation terms and were bigger than 4508 m^2. However, the fourth, the most suited in terms of disaster prevention, was quite far from YSF so we decided that the new parking lots should be developed

©2020. Japan Geoscience Union. All Right Reserved.

on the second type of farm.
Finally, we explained the aforementioned results to local residents who provided the following responses. First, although residents understood that farmlands visible from the footpath route should be protected, they tended to hope that parking lots would be developed on farmlands near the YSF, or lands not suited for cultivation. Second, the ownership of farmlands in the Yamada area is finely differentiated so that there are various conflicting environment. This may make reaching agreement about parking lots among the people concerned difficult.

Keywords: rural landscape, land use, tourism development



©2020. Japan Geoscience Union. All Right Reserved.

Appreciations of Japanese landscapes by the western visitors arrived (1549-1858)

*yoji aoki[1], Fumihiro Konta[2]

1. Open University of Japan, 2. National Science Museum

Appreciations of Japanese landscapes by the western visitors arrived (1549-1858)

Introduction

This report listed and summarized the descriptions of Western visitors about "Fukei" of Japan since the first arrival on Tanegashima Island in 1549 (Table 1). We could define 'Fukei' as similar to the concept as the appreciation of landscape or the impression of scenery. Japanese appreciation of scenery had been affected by Chinese culture since ancient times. For example, the idea of "Eight Scenery", which evolved in the 10th century in old China, was introduced in the 14th century to Japan, has affected more than five centuries of the appreciation of Japanese landscape (Aoki, et al. 2003). Because Japan was closed to western foreigners until the end of the Edo era, i.e., the 19th century, those effects continued until the opening of the country. And the educated Japanese used the Chinese method for the sophisticated way of landscape observation as Chinese poetry. After the opening of the country, Japanese began to accept Western culture and its way of landscape appreciation. The educated Japanese began to understand the natural phenomena by the natural sciences developed in western countries. Although the western countries had experienced the period of Landscape Painting from the 16th to the 19th centuries and they sometimes described Japanese landscape to belong the similar kind of beauty, most Japanese never understand their appreciation. So by studying the descriptions of Western visitors to Japan, we find how they understood and appreciated Japanese landscapes and what the landscape beauty of Japan was existed in those times.

Summary of the focal objects appreciated were listed in table 2.
(1) Until open the country, 1853
The first period began with the arrival of the first Portuguese, Mendes Pinto, to Tanegashima Island in 1549 and ended at the time of opening the country by negotiation with Perry in 1853. During the period, Portuguese and Spaniards visited and mostly engaged in missionary work and obtained many believers in western Japan. Although the domestic warfare sometimes threatened not only Japanese lives but also Westerners' lives, they, established many churches as the result of their activities. But the Japanese government since the 17th century excluded them, because the government feared the country's stability. In that period, westerners were not yet accustomed to the plant taxonomy or landscape paintings. They never describe the natural landscape or vegetation in Japan, the outstanding features of Japanese landscape. During the closed country, i.e. the Edo era, the Dutch including German or Sweden visitors traveled from Nagasaki to Edo. Some of them knew plant taxonomy and found the features of Japanese landscape to be endowed with a diversity of plants. In this period, Russia also investigated Japanese landscape from the coasts and found pleasant impressions. Unfortunately, the Japanese government sometimes met them and arrested some Russians as prisoners unfortunately. They also reported the landscape beauty of Japan.

(2) Until diplomat residence, 1858

©2020. Japan Geoscience Union. All Right Reserved.

U. S. A. and Russia visited to negotiate the opening the country of Japan in 1853. Some members of the troop could understand Japanese and some had known plant taxonomy. They could describe the landscape and vegetation more precisely. Moreover the troops came accompanied with landscape painters, so they could report in detail the vegetation of Japan. Some enjoyed familiar vegetation at Hokkaido Island and some admired the beauty of topographic features of Japanese landscapes. Vysheslavtsov appreciated rice terraces at mountainside.

Acknowledgements

We express our gratitude's to Prof. Jay Appleton of Hull University for his kind explanation of the importance of "Experience of Landscape", and Prof. Takasuke Watanabe of Tokyokogyo University for his instruction of the description of western travelers. We thank Mr. Motoh Shoda and many other translators for their detailed information of travelers and hard efforts of their works.

Keywords: appreciation of landscape, 1549-1858, western visitor

©2020. Japan Geoscience Union. All Right Reserved.

Table 1 Chronogical table of western visitors to Japan translated into Japanese

Name of visitor	Period	Nationality	Literature	Published	Translator
Pinto, P. F. M.	1549-1556	Portugal	Pereginacao / Fernao Mendes Pinto, edicao popular com uma noticia, notas e glossario, J. I. de Brito Rebello, Ferreira, Lisboa, 1908-10, 4vols.	1980	Okamura, T.
Companhia de Iesus	1549-1590	Portugal	Cartas que os Padre e Irmaos da Companhia de Iesus, que andao nos Reynos de Iapao & China escreuerao aos da mesma Companihia da India & Europa, desdo anno de 1549 ate o de 1580., Manoel de Lyra, Erova, 1598.	1996	Murakami, N.
Frois, Luis	1562-1597	Portugal	Primeira Parte de Iapom, Biblioteca da Ajuda. Cod. 49-IV.54	1977	Matsuda, K. and Kawasaki, M.
Valignano, Alejandro	1579-1603	Italy	SUMARIO de las cosas de Japon 1583.	1996	Matsuda, K.
Giron, Bernardino Avila	1594-1616	Spain	Relacion del Reino de Nippon a que llaman corruptamente Jappon	1965	Aida, Y. and Iwao, S.
Vivero, D. R.	1609-1610	Spain	Relacion y noticas de el reino del Japon, C Otros abisos y proiects para el buen Gvereno de la Monarcia Espanola, quien la delica a la C. R. M. del Rei N. S. A. D 1609.	1929	Murakami, N.
Vizcaino, Sebastian	1611-1613	Spain	Coleccion de Documentos Ineditos relativos al descubrimiento, conquista y organization de las antioguas posesiones espanoles de America y Oceania, 8(2,3), biblioteca National, Madrid, 1867.	1929	Murakami, N.
Saris, John	1612-1613	U. K.	The voyage of Captain John Saris to Japan, 1613. ed. by Sir Ernest M. Satow, Printed for Hakluyt Society, London, 1900.	1986	Murakawa, K.
Cocks, Richard	1613-1624	U. K.	Diary keep by Head of the English factory in Japan: diary of Richard Cocks, June 1, 1615-March 24, 1622.	1979-82	Tokyo Uni.
Willman, O. E.	1651-1652	Sweden	Beskrifwes een ressa till Ost Indien, China och Japan, Johann Kankel, Wisingborgh, 1667.	1953	Ozaki, Y.
Kaempfer, Engelbert	1690-1692	Germany	Geschite und Beschreibung von Japan Aus den Originalhandschriften des Verfassers, Meyer, Lemgo, 1777-79.	1993	Saito, M.
Benyvzky, J. G.	1771	Hungery	Janko, Dr. Janos. Grof Benyovszky Moricz mint foeldrajzi Kutato, Kritikai mejegyzesek Kamcsatkatol Makaoig tett utjara, Budapest, 1890.	1994	Miziguchi, S. and Numata, J.
Thunberg, Carl Peter	1775-1776	Sweden	Resa uti Europa, Afrika, Asia, foerraettad aren 1770-1779, del 3-4, Upsala, 1791, 1793.	1996	Takahashi, F.
Tising, Issac	1779-1784	Holland	Illustration of Japan, London 1822.	1960	Numata, J.
Polonskii, A. S.	1792-1793	Russia	Terasawa Hajime, Chishimashi, Japanese translation, 1979.	1953	Hayashi, K.
Broughton, William Robert	1797	U. K.	Voyage of Discovery to the North Pacific Ocean, London 1804.	1974	Sudo, T.
Doeff, Hendrick	1798-1817	Holland	Herinneringen uti Japan, Haarlem, 1833.	1966	Saito, A.
Wardenaar, Willem	1800-1803	Holland	Nagasaki Oranda Shokan Nikki Vol. 1, Anno 1801-1803.	1989	Nitirangakkai
Krusenshtern, A. J.	1803-1804	Russia	Reise um die Welt in den Jahren 1803, 1804, 1805 und 1806, gedruckt in der Schnoorschen Buchdruckerey, St. Petersburg, 1810.	1931	Hani, G.
Rezanov, Nikolai Petrovich	1804-1805	Russia	Ohshima, M. Nihon Taizaiki, Japanese translation, Iwanami, Tokyo, 2000.	2000	Oshima, M.
Golovnin, W. M.	1811-1813	Russia	Zapiski Vasiliya Mikhailovicha Golounina plenuu yapontsev 1811, 1812 i 1813, godakh, i zhizneopisanie avtora, 1816.	1984	Tokuriki, S.
Hall, Basil	1816	U. K.	Account of voyage of discovery to the West Coast of Corea, and the Great Loo-choo Island, John Murray, London, 1818.	1986	Haruna, T.
M'Leod, John	1816	U. K.	Narrative of a Voyage, in His Majesty's Late Ship Alceste, to the Yellow Sea, along the Coast of Corea, and through tis Numerous Hitherto Undiscovered Islands to the Island of Lewchew; with an Account of Her Shipwreck in the Straits of Gaspar, John Murray	1999	Ohama, N.
Fisscher, J. F. O.	1820-1829	Holland	Bydrage tot de kennis van het Japansche Ryk, J. Muller, Amsterdam 1833.	1966	Saito, A.
Siebold, P. F.	1822-1829	Germany	NIPPON. Archivzur Beschreibung von Japan und dessen Neben und Schutzlaendern Jezo mit den suedlichen Kurilen, Sachalin, Korea und den Liukiu-Inseln. Herausgegeben von seinen Soenen. Zweite Auflage, K. U. K. Hofbuchhandlung von Leo Woerl, Wuerzburg und	1983	Saito, M.
Beechey, Frederick William	1827	U. K.	A narrative of the voyage and travel of Captain Beechey, London, 1836.	1979	Ohguma, R.
Peard, Georg	1827	U. K.	The journal of Lieutenant Georg Peard of H. M. S. Blossom', 1825-1828.	1979	Ohguma, R.
Meilan, G. F.	1827-1831	Holland	Japan, 1830.	2002	Shoji, M.
Adams, A. F. L. S.	1845	U. K.	Travel of a Naturalist in Japan and Manchuria, Hurst and Blackett, London, 1870.	1974	Sudo, T.
Levijssohn, Joseph Henry	1845-1850	Holland	Dag Register der door het Nederlandsh Opperhoofd, J. H. Levijssohn in het Jaar 1850 gedane Hofreize naar Jedo en terug naar Deshima.	2003	Katagiri, K.
MacDonald, Ranald	1848-1849	Canada	Japan, Story of Adventure of Ranald MacDonald, First Teacher of English in Japan, A. D. 1848-49.	1979	Tomita, T.
Goncharov, I. A.	1853-1854	Russia	Fregat "Pallada" ocherki po puteshestvii Inana Goncharova, C. Peterburg, 1857.	1988	Takano, A. and Shimada, Y.
Hawks, Francis L.	1853-1854	U. S. A.	Narrative of the expedition of an american squadron to the Cina Seas and Japan, The Congress of the United States, Washington, 1856, 2vols.	1997	Kanda, S.
Perry, Matthew	1853-1854	U. S. A.	The Japan Expedition, 1852-1854 The Personal Journal of Commodore Matthew C. Perry, Pineau, Roger, ed., Smithsonian Institution Press, Washington, 1968.	1989	Kanai, M.
Spalding, J. Willet	1853-1854	U. S. A.	The Japan Expedition, Japan and around the World,1855.	2002	Shimada, T.
Taylor, Bayard	1853-1854	U. S. A.	A vist to India, China, and Japan, in the year 1853, G. P. Puntum, New York 1855.	1979	Ohguma, R.
Williams, S. W.	1853-1854	U. S. A.	A Journal of the Perry Expedition to Japan (1853-1854), Transactions of the Asiatic Society of Japan 37(2), Maruya, Tokyo, 1910.	1993	Hora, T.
Heine, Wilhelm	1853-1855	Germany	Reise un die Erde nach Japan an Bord der Expeditions-Escadre unter Commodore M. C. Perry in den Jahren 1853, 1854 und 1855, unternommen im Auftrage der Regierung der Vereinigten der Staaten, Holzschnitt von Eduard Kretzschmar, Leipzig, Hermann Costnable u	1983	Nakai, A.
Morrow, James	1854	U. S. A.	A Scientist with Perry in Japan, the Journal of Dr. James Morrow, Edited by Allan B. Cole, The University of North Carolina press, 1947.	1974	Sudo, T.
Luehdorf, Fr. Aug.	1855-1856	Germany	Acht Monaten in Japan, nach Abschluss des Ver trags des von Kanagawa, H. Strack, Bremen, 1857.	1964	Nakamura, T.
Heusken, Henry	1856-1861	Holland	Diary of Henry Heusken 1855-1861 transrated and edited by Jeannette C. Van der Corput and Robert A. Wilson, Rutgers University Press, New Brunswick, 1964.	1989	Aoki, S.
Harris, Townsend	1856-1863	U. S. A.	The complete journal of Townsend Harris, Japan Society in New York, Garden City,1930.	1953	Sakata, S.
Kattendyke, W. J.	1857-1859	Holland	Uittreksel uit het dagboek van W. J. C. Ridder H. V. Kattendyke gedurende zijn verblijf in Japan in 1857, 1858 en 1859, W. P. van Stockum, 'sGravenhage, 1860.	1964	Mizuta, N.
Oliphant, Laurence	1857-1859	U. K.	Narrative of The Earl of Elgin's Mission to China and Japan in the years 1857, '58, '59, Willam Blackwood and son, Edinburgh and London, 1859, 2vols.	1995	Okada, A.
Osborn, Sherad	1857-1859	U. K.	A cruise in Japanese waters, William Blackwood and sons, Ediburgh and London, 1859.	2002	Simada, Y.
Meerdervoort, Ponpe	1857-1862	Belgium	Vijf Jaren in Japan (1857-1863): Bijdragen tot de kennis van het Japansche keizerrijk en zijne bevolking, 2 dls, Frima van den Heuvell & van Santen, Leiden, 1867.	1988	Numata, J.
Polsbroek, J. D. G.	1857-1870	Holland	Journaal van Jonkheer Dirk de Graeff van Polsbroek 1857-1870, Ingeleid en geannoteerd door Herman J. Moeshart, Van Gorcum, Assen, 1967.	1995	Ikuma, A.
Vysheslavtsov, A. V.	1858-1859	Russia	Ocherki perom i karandashom iz krugosvetnogo plavanija v 1857, 1858, 1859 i 1860 godakh, 1862.	1990	Nagashima, Y.

©2020. Japan Geoscience Union. All Right Reserved.

Trends of the methods of landscape presentation in the landscape appreciation test from 1967 to 1987

*yoji aoki[1]

1. Open University of Japan

Trends of landscape presentation method until 1987

Peterson (1967), who used psychometric measurements, evaluated 23 slides by projecting them onto a 50x50 cm screen. The slide evaluation method is an easy way to obtain data for many evaluators at once, and has since become widely used. Canter (1969) experimented with 20 black and white slides on a 2x2m screen. Carr and Schissler (1969) experimented with 10 scenes per second by video. Zube (1973) explored the effects of landscape changes using slides and line drawings. Law and Zube (1983) examined foreground effects in 19 pairs of slides. Hull, Buhyoff and Daniel (1984) conducted an evaluation experiment with a maximum of 134 slides.

Before using the slides, experts visited the site, scored it according to certain criteria, and decided on the quality of the landscape in the area (Fine1968). Although such a method is laborious and costly and there are not many studies have been carried out, but Penning-Rowsell (1977) reported two people evaluated 269 km2. Aoki (1981) conducted the field experiment at 21 sites with 40 subjects and Nasar et al. (1983) examined the effects of observations and widening and narrowing at four locations. Stewart et al. (1984) confirmed the association with 50 slides and field experiments. Nasar (1987) explored the observation directions at 20-point interview.

Carls (1974) began an experiment using photographs that were easier to experiment with than slides. He used 100 color photographs of 8x10 inches. Propst and Buhyoff (1980) performed 100 slide experiments. Schroeder (1982) rated the green on 35 5x7 inch photographs. Shuttleworth (1980) examined the differences between black-and-white and color photographs at six locations. Dearden (1984) conducted an evaluation experiment with 12x18 cm 30 color photographs. Benayas, Lucioto and Belnaldez (1987) gave an environmental assessment with 72 pairs of photographs.

However, it was immediately a matter of whether the photos matched the site evaluation. Dun (1974) examined the differences between the six-point rating and the photo rating. Although his experiments concluded that they were roughly the same, I examined the correlation analysis of the results and found no significant correlation. Dearinger (1979) examined the differences between the 20 slides and the field evaluation. Kane (1981) examined the difference between the site and the slide at 10 points and found a correlation of 0.96. However, Coeterier (1983) examined the five scenery sites and photographic evaluations and found a correlation of 0.39-0.68. Latimer et al. (1981) examined the effects of sky, morning, snow, and clouds. Malm et al. (1981) examined the effects of climatic conditions from 15-150km on 80 slides and on site. Kellomaki and Sabolainen (1984) conducted field and indoor evaluation

©2020. Japan Geoscience Union. All Right Reserved.

experiments at 34 locations. Shelby and Harris (1985) examined the relationship between a 5x7inch photograph and the description on the scene. Trent, Neumann and Kvashny (1987) examined differences between on-site and color photography at five locations.

Pogacnick (1976) experimented with a method of creating a montage photograph and evaluating the plan. He also used 20×30 cm black and white 36 photographs, and pointed out the project objects on the photographs (Pogacnick1979).

Myklestad and Wagar (1977) attempted to present landscapes with computer graphics. Killee and Buhyoff (1983) examined the difference between eight CP drawings and sketches with an 8-second presentation.

As for the panorama scenery, Banerjee (1977) tested a 360-degree coastal panoramic view on 16mm film. Clamp and Powell (1982) presented 40 panoramas with six slides. Nassauer (1983) examined the difference between a 140-degree panoramic view and a 65-degree wide-angle view on a 100 x147cm screen with 17 pairs of slides.

Ulrich (1984) examined the effect of the 182 x 122 cm window on postoperative recovery in a hospital.

Keywords: presentation of landscape, landscape appreciation, 1967-1987

©2020. Japan Geoscience Union. All Right Reserved.

Table1 List of interesting papers

Presentation tools	Name of authors	Year	Title of paper	Name of journal
50x50inches screen, 23 color slides	Peterson, G. L.,	1967	A predictive model of preference: Quantitative analysis of the perception of the visual appearance of residential neighborhoods,	J. of Regional Science, 7(1), 19-31.
on-site appreciation by responderits: 773 square miles, 90 days	Fine, K. D.,	1968	Landscape evaluation: a research project in East Sussex,	Regional Studies, 2, 41-55.
20 photos: 2x2m screen, b and w	Canter, D.	1969	An intergroup comparison of connotative dimensions in architecture,	Environment and Behavior, 1, 37-48.
observation by city trip: 10frames/s, 5 minutes, 40mph	Carr, S. and Schissler, D.	1969	The city as a trip: Perceptual Selection and Memory in the View from the Road,	Environment and Behavior, 1, 7-36.
landscape type: 15 slides, 3 min	Calvin, J.S., Dearinger, J.A. and Curtin, M.E.	1972	An attempt at assessing preferences for natural landscapes,	Environment and Behavior, 4(4), 447-470.
preference: 56 slides, 20seconds	Kaplan, S., Kaplan, R. and Wendt, J.S.	1972	Rated preference and complexity for natural and urban visual material,	Perception & Psychophysics 12(4), 354-356.
scaling: 15 slides, 50 slides	Acking, C.A. and Sorte, G.J.	1973	How do we verbalize what we see,	Landscape Architecture, 64, 470-475.
personality: 27 slides, 18 photo, 9 drawing	Zube, E.H.,	1973	Rating everyday rural landscapes of the Northeastern U. S.,	Landscape Architecture 63, 370-375.
predictive model: 100 color photos, 8x10inches	Carls, E.G.,	1974	The effects of people and Man-induced conditions on preferences for Outdoor recreation landscapes,	J. of Leisure Research, 6, 113-124.
comparison of on-site and photograph: 6 sites	Dunn, M.C.,	1974	Landscape evaluation: A further perspective,	The planner 60(10), 935-936.
personality: 2.25miles, 6 areas, car	Zube, E.H.,	1974	Cross-disciplinary and intermode agreement on the description and evaluation of landscape resources,	Environment and Behavior, 6(1), 69-89.
8 view on-site fields, 56 station photogrphed in color	Zube, E.H., Anderson, T. and Pitt, D.	1974	Measuring the landscape: Perceptual responses and physical dimensions	Landscape Research 1(6), no page
spatial sampling of landscape: survey line from avoiding major towns, 170 locations, 8 directions	Clamp P.,	1976	Evaluating English landscapes - some recent developments,	Environment and Planning A, 8, 79-92.
validation; b and w photos, 8 on-site	Dunn, M.C.,	1976	Landscape with photographs: Testing preference approach to landscape evaluation,	J. of Environmental Management 4, 15-26.
predictive model: 86 slides, label, imagery	Herzog, T.R., Kaplan, S. and Kaplan, R.	1976	The prediction preference for familiar urban places,	Environment and Behavior, 8(4), 627-645.
for planning; photo montage	Pogacnik, A.,	1976	Visual-aesthetic components in the cybernetics of urban planning,	Computer Aided Design, 8(1),41-48
video, 16mm sound film, 125 seconds, 360 panorama	Banerjee, T.	1977	Who Values What?, audience reaction to coastal scenery,	Landscape Architecture 67(3), 240-243.
presentation uses computer graphics	Mydestad, E. and Wagar, J.A.	1977	Preview: Computer assistance for visual management of forested landscapes,	Landscape Planning 4, 313-331.
predictive model: on-site evaluation, 8 man-days, 289km2, 2 people	Penning-Rowsell, E.C.,	1977	The 'Manchester' Landscape Evaluation Method: A Critical Appraisal,	Landscape Research 2(3), 6-11.
predictive model: b ad w photo, 8x10inch	Shafer Jr., E.L. and Brush, R.O.	1977	How to measure preferences for photographs of natural landscapes,	Landscape Planning 4, 237-256.
nationality: 53 photos, 30-40dgree alignment, b and w	Ulrich, R.S.,	1977	Visual landscape preference: A model and application,	Man-Environment Systems 7(5), 279-293.
effect of professional experience: 9 color slides, 36 pairs	Buhyoff, G.J., Wellman, J.D., Harvey, H. and Fraser, R.A.,	1978	Landscape architects' interpretations of people's landscape preference,	J. of Environmental Management 6, 255-262.
analysis: 20 slides, 5 sec	Ootendorp, A. and Berlyne, D.E.	1978	Dimensions in the perception of architecture: III. Multidimensional preference scaling,	Scandinavia Journal of Psychology 19, 145-
validation: 46 slides and color sketches, 0.74, 15 b and w sketches, color photo, 0.68	Schomaker, J.H.,	1979	Measurement of preferences for proposed landscape modifications,	Landscape Research 3(3), 5-9. College of Forestry, Idaho.
description: 8 photos	Byrne, S.M.	1979	Perception of the Landscape in the Lands End Peninsula	Landscape Research 5(1), 21-24.
difference between on-site and photograph: 20 slides, 2 min	Dearinger, J.A.,	1979	Measuring preferences for natural landscapes,	Journal of the Urban Planning and Development Division, ASCE, 63-80.
photointerpretation: 35 photos, 40x30cm, b and w	Pogacnik, A.,	1979	Environmental public preferences as obtained by the method of photointerpretation in the Ljubljana Region,	Urban Ecology 4, 45-51.
information: pre slide, after slide, 50slides	Ulrich, R.S.	1979	Visual Landscape and Psychological Well-Being	Landscape Research 4(1), 17-23.
information, label affected: 127x178mm photo, label 10x65mm	Hodgson, R.W. and Thayer Jr., R.L.	1980	Implied human influence reduces landscape beauty,	Landscape Planning 7, 171-179.
congestion: 360slides, 0.75x0.75m screen, 12sec, 1.15ha/boat	Pitt, D.G., et al.	1980	A Perceptually Based Definition of Valued Boating Environments on the Tributaries of Chesapeake Bay	Landscape Reseach 5(3), 19-21.
analysis: 100 color slides	Propst, D.B. and Buhyoff, G.J.	1980	Policy Capturing and Landscape Preference Quantification: A Methodological Study,	J. of Environmental Management, 11, 45-59
comparison of b-w and color photo: 6 sites	Shuttleworth, S.,	1980	The use of Photographs as an Environment Presentation Medium in Landscape Studies,	J. of Environmental Management 11, 61-76.
effects of regional familiarity: 11 slides, 5sec	Wellman, J.D. and Buhyoff, G.J.,	1980	Effects of regional familiarity on landscape preferences,	J. of Environmental Management 11, 105-110.
congruity: 48 slides, 90x75cm screen	Wohlwill, J.F. and Harris, G.	1980	Response to congruity or contrast for man-made features in natural-recreation setting,	Leisure Science 3(4), 349-365.
information: 90 color slides	Anderson, L.M.,	1981	Land Use Designations Affect Perception of Scenic Beauty in Forest Landscape,	Forest Science 27(2), 392-400.
on-site: 40 respondents, 21 sites	Aoki, Y.,	1981	A study of On-site Evaluation for Site Planning: Lake Kasumigaura,	Landscape Planning 8, 235-255.
SD method: 54 pairs b and w photo, 10sec	Bernaldez, F.G., Parra, F. and Garcia-Quintas, M.A.	1981	Environmental Preferences in Outdoor Recreation Area in Madrid(Spain),	J. of Environmental Management 13, 13-26.
on-site, 19 observers, minibus, 47 sites km2	Briggs, D.J. and France, J.	1981	Assessing Landscape Attractiveness: a South Yorkshire Study	Landscape Research 6(2), 2-5.
attributes: 19 pairs slides, pre and post, student, US Federal, BLM/Forest Service	Palmer, N.R. et al.	1981	Evaluating Effectiveness of Observer Based Visual Resurce and Impact Assessment Methods	Landscape Research 6(1), 12-16.
experienced: pre and post 30min hike; 24 photos, b and w	Hammitt, W.E.,	1981	The Familiarity-Preference Component of On-Site Recreation Experiences,	Leisure Science 4(2), 177-193.
Statistical test on-site to slide: 10 sites, 0.96 coefficient	Kaine, P.S.,	1981	Assessing landscape attractiveness: a comparative test of two new methods,	Applied Geography, 1, 77-98.
predictive model: percentage of sky, effect of morning, snow, clouds, 70 or 80 slides	Latimer, D.A., Hogo, H. and Daniel, T.C.	1981	The effects of atmospheric optical conditions on perceived scenic beauty,	Atmospheric Environment 15(10-11), 1885-1974.
meteorological; on-site and slides, 80 slides, 8 second, 15-150km	Malm, W., et al.	1981	Human Perception of Visual Air Quality (Uniform Haze),	Atmospheric Environment, 15(10/11), 1875-1890.
predictive model: sampling of photo points, 90 points	Schroeder, H. and Daniel, T.	1981	Progress in Predicting the Perceived Scenic Beauty of Forest Landscape,	Forest Science 27(1), 71-80.
other appraisals: 60 slides, 50x75cm screen	Ulrich, R.S.,	1981	Natural versus urban scenes, some Psychophysiological effects,	Environment and Behavior 13(5), 523-556.
effect of age: 20 slides	Balling, J.D. and Falk, J.H.,	1982	Development of visual preference for natural environments,	Environment and Behavior 14(1), 5-28.
on-site: twice, 37 sites	Beer, A.R.	1982	The Development Control Process and the Quality of the External Environment in Residential Areas	Landscape Research 7(3), 14-21.
40 color panoramic slide; 6 screens formed a circle, back-projected	Clamp, P. and Powell, M.	1982	Prospect-Refuge Theory under Test,	Landscape Research 7, 7-8.
information, 70 slides, 15s, 20ms, 10ms	Herzog, T.R., Kaplan, S. and Kaplan, R.	1982	The Prediction of preference for Unfamiliar Urban Places,	Population and Environment 5(1), 43-59.
greenery: 35photos, 5X7inch, slides	Schroeder, H.W.,	1982	Preferred features of urban parks and forests,	Journal of Arboriculture 8(12), 317-322.
difference of new residents and natives: 118x165mm photo	Aoki, Y.,	1983	An empirical study on the appraisals of landscape types by residential groups -Tsukuba Science City-,	Landscape Planning 10, 109-130.
validation: 5 scenes, field and photo, R=0.39-0.68	Coeterier, J.F.,	1983	A photo validity test,	Journal of Environmental Psychology 3, 315-323
distance: affect SBE: 38 slides, 4000-8000m	Hull IV, R.B. and Buhyoff, G.J.	1983	Distance and scenic beauty: A nonmonotonic Relationship,	Environment and Behavior 15(1), 77-91
other presentation: 8 slides, graphic, sketch, 8sec	Killeen, K. and Buhyoff, G.	1983	The relation of landscape preference and abstract topography,	J. of Environmental Management 17, 381-392
information: effect of foreground details: 19 pairs slides	Law, C.S. and Zube, E.H.	1983	Effects of photographic composition on landscape perception,	Landscape Research 8(1), 22-23.
evolutionary: openview 4 sites, 15 respondents, open or closed view, observation point	Nasar, J.L., et al.	1983	The emotional quality of scenes and observation points: A look at prospect and refuge,	Landscape Planning 10, 355-361.
information: 17 pairs, panorama(140), wide(65), 100x147cm screen	Nasssauer, J.I.,	1983	Framing the landscape in photographic simulation,	J. of Environmental Management 17, 1-16.
7 photos image: 128 color and 128 b and w sketches	Ross, M.G. and Kopka, S.J.	1983	An Elementary Linkage Analysis of Variables in the Communication of Landscape Simulations: Implications for Visual Resource Management	Landscape Research 8(1), 13-21.
greenery: 340 slides, tree shade management	Schroeder, H.W. and Cannon, Jr., W.N.	1983	The esthetic contribution of trees to residential streets in Ohio Town,	Journal of Arboriculture 9(9), 237-243.
personality: 56 color photos	Zube, E.H., Pitt, D.G. and Evans, G.W.	1983	A lifespan developmental study of landscape assessment,	Journal of Environmental Psychology 3, 115-128.
prediction model using silvicultural and photographic data: 30 sites	Buhyoff, GJ., Gauthier, L.J. and Wellman, J.D.	1984	Predicting Scenic Quality for Urban Forests Using Vegetation Measurements,	Forest Science 30(1), 71-82.
personality: 30 color photo, 12x16cm	Dearden, P.	1984	Factors influencing landscape preferences: An empirical investigation,	Landscape Planning 11, 293-306.
information: 100 slides, 15s, 200ms, 20ms	Herzog, T.R.,	1984	A cognitive analysis of preference for field-and-forest environments,	Landscape Research 9(1), 10-16.
scenic beauty: 134 slides	Hull IV, R.B., Buhyoff, G.J. and Daniel, T.C.	1984	Measurement of Scenic Beauty: The Law of Comparative Judgment and Scenic Beauty Estimation Procedures,	Forest Science 30(4), 1084-1096.
validation; field, laboratory; 34 sites	Kellomaki, S. and Savolainen, R.	1984	The scenic value of the forest landscape as assessed in the field and the laboratory,	Landscape Planning 11, 97-107.
validation: 10 photos, 10 variables, -0.02(middle ground)-0.86(variety)	Kopka, S. and Ross, M.	1984	A study of the reliability of the bureau of land management visual resource assessment scheme,	Landscape Planning 11, 161-166.
predictive model: 40 color slides	Miller, P. A.,	1984	A comparative study of the BLM scenic quality rating procedure and landscape preference dimensions,	Landscape Journal 3(2), 123-135.
predictive model using landform, color and uniqueness : 63 photos	Patsfall, M.R. et al.	1984	The prediction of scenic beauty from landscape content and composition,	Journal of Environmental Psychology 4, 7-26.
analysis; 16 color photos, 2x5inches	Russell, J.A. and Ulrich F.L.	1984	Adaptation level and the affective appraisal of environments,	Journal of Environmental Psychology 4, 119-135.
rank order and quality; 180photos	Shuttleworth, S.	1984	Consensus and the Perception of Landscape Quality	Landscape Research 9(1), 17-22.
validation: 50slides, on-site	Stewart, T.R., et al.	1984	Judgments of photographs vs. field observations in studies of perception and judgment of the visual environment,	Journal of Environmental Psychology 4, 283-302
needs and fears: 26 photos	Talbot, J.F. and Kaplan, R.	1984	Needs and fears: the response to trees and nature in the inner city,	Journal of Arboriculture 10(8), 222-228.
recovery from the surgery: 183x122cm window, 74cm height	Ulrich, R.S.,	1984	View Through a Window May Influence Recovery from Surgery,	Science 224, 420-421.
predictive model: 492 color slides, 319 color slides, 90 degree	Vining, J., Daniel, T.C. and Schroeder, H.W.	1984	Predicting Scenic Values in Forested Residential Landscape,	J. of Leisure Research 16(2), 124-136.
greenery: 82x112mm color	Aoki, Y., Yasuoka, Y. and Naito, M.	1985	Assessing the Impression of street-side Greenery,	Landscape Research 10(1), 9-13.
analysis: 18 color picture pairs	Barrios, J.C., Bernaldez, F.G. and Ruiz, J.P.	1985	Content analysis of landscape preferences: the environmental perception of Madrid livestock raisers,	Landscape Research 10(3), 2-8.
preference: 70color slides	Herzog, T.R.	1985	A cognitive analysis of preference for waterscapes,	Journal of Environmental Psychology 5, 225-241.
density of trees: 40 slides	Schroeder H.W. and Green, T.L.	1985	Public preference for tree density in municipal parks,	Journal of Arboriculture 11(9), 272-277.
validation: 28mm lens, 5x7inche print, on-site, photo, written	Selby, B. and Harris, R.	1985	Comparing methods for determining visitor evaluation of ecological impacts: site visits, photographs, and written description,	J. of Leisure Research 17(1), 57-67.
predictive model using dead-down wood and basal area: 5ft7 height, 3x90° additional shot	Vodak, M.C., et al.	1985	Scenic Impacts of Eastern Hardwood Management,	Forest Science 31(2), 289-301.
SD method: 60slides, b and w	Abello, R.P., Bernaldez, F.G. and Galiano, E.F.	1986	Consensus and contrast components in landscape preference,	Environment and Behavior, 18(2), 155-178.
predictive model pine tree, herbage and downed wood: 50 slides	Brown, T.C. and Daniel, T.C.	1986	Predicting Scenic Beauty of Timber Stands,	Forest Science 32(2), 471-487.
predictive model: 57 plots slides, tree density	Buhyoff, G.J. et al.	1986	Prediction of Scenic Quality for Southern Pine Stands,	Forest Science 32(3), 769-778.
predictive model using diameter, trees per acre and age: 30ft aside, 30ft focus, 24 degree sidelong, slides	Hull IV, R.B. and Buhyoff, G.J.	1986	The Scenic Beauty Temporal Distribution Method: An Attempt to Make Scenic Beauty Assessments Compatible with Forest Planning Efforts,	Forest Science 32(2), 271-286.
loggers, foresters, eagle club: 126 slides, 8sec	McCool, S.F., Benson, R.E. and Asor, J.L.	1986	How the public perceives the visual effects of timber harvesting: an evaluation of interest group preferences,	Environmental Management 10(3), 385-391.
planning: 40 slides, 10sec, distance 60 100 120ft	Schroeder, H.W.	1986	Estimating park tree densities to maximize landscape esthetics,	J. of Environmental Management 23, 325-333.
preference: photographs, 0.1-16 acres	Talbot, J.F. and Kaplan, R.	1986	Judging the Sites of Urban Open Areas: Is Bigger Always Better?,	Landscape Journal 5(2), 83-92.
difference between eastern nations and western tourist: 11 photos, 12x9cm	Tips, W.E.J. and Savasdisara, T.,	1988	Landscape preference evaluation and sociocultural background : a comparison among Asian countries,	J. of Environmental Management 22, 113-124.
personality: 11photos, b and w, 12x9cm	Tips, W.E.J. and Savasdisara, T.,	1988	The influence of the environmental background of subjects on their landscape preference evaluation,	Landscape and Urban Planning 13, 125-133.
on-site: 24 trails, scenic view	Westphal, J.M. and Lieber, S.R.	1986	Predicting the effect of alternative trail design on visitor satisfaction in park setting,	Landscape Journal 5(1), 39-44
for planning: 153x205mm, 61photos, photomontage	Yamada, H., et al.	1986	Visual vulnerability of streetscapes to elevated structures,	Environment and Behavior, 18(5), 733-754.
nature camp affect attitude: 72 pairs slides	Benayas, J., de Lucio J.V. and Bernaldez, F.G.	1987	Environmental Attitude Shifts as Revealed by Landscape Taste and Activity Preference,	The Environmentalist 7(1), 21-30.
personality: 6 photos, 50 pairs	Bernaldez, F.G., Gallardo, D. and Abello, R.P.	1987	Children's landscape preferences: from rejection to attraction,	Journal of Environmental Psychology 7, 169-176
information: 130 color slides	Brown, T.C. and Daniel, T.C.	1987	Context effects in perceived environmental quality assessment: scene selection and landscape quality rating,	Journal of Environmental Psychology 7, 233-250
other presentation: 15s, 200ms, 20ms, 70 color slides	Herzog, T. R.,	1987	A Cognitive Analysis of Preference for Natural Environments: Mountains, Canyons, and Deserts,	Landscape Journal 6, 140-152.
effect of wildflower society: 60color slides, 10sec	Kaplan, R. and Eugene J. Herbert,	1987	Cultural and sub-cultural comparisons in preferences for natural settings,	Landscape and Urban Planning 14, 281-293.
on-site: interview: 20sites, viewing direction	Nasar, J.L.,	1987	Environmental correlates of evaluative appraisals of central business district scenes,	Landscape and Urban Planning 14, 117-130.
analysis: 32 b & W photos, 2'x3'	Ruddell, E.J. and Hammitt, W.E.	1987	Prospect Refuge Theory: A psychological orientation for edge effect in recreation environment,	J. of Leisure Research 19(4), 249-260.
difference between on-site and color slide: 5 sites	Trent, R.B., Neumann, E. and Kvashny, A.	1987	Presentation mode and question format artifacts in visual assessment research,	Landscape and Urban Planning 14, 225-235.
survey paper; simulation techniques chronology, photo, drawing, computer, photomontage, three dimensional model, detailed model, dynamic model	Zube, E.H., Simcox, D.E. and Law, C.S.	1987	Perceptual landscape simulations: History and prospect,	Landscape Journal 6, 62-80.

©2020. Japan Geoscience Union. All Right Reserved.

[E] Poster | H (Human Geosciences)：H-CG Complex & General

[H-CG22] Deltas and estuaries: multidisciplinary analyses of complex river-mouth systems

convener:Yoshiki Saito(Estuary Research Center, Shimane University), David L Dettman(University of Arizona), Kazuaki Hori(Department of Geography, Graduate School of Environmental Studies, Nagoya University)

This session examines deltas and estuaries from multiple points of view: morphodynamics, hydrodynamics, material cycling, ecosystem, human impacts, and sustainability. We invite contributions that advance research on deltas and estuaries as complex river-mouth systems from both modern and ancient examples, and that develop integrated frameworks for modeling delta & estuary dynamics on a broad range of temporal and spatial scales: from studies of coastal evolution over the Quaternary to small-scale sediment/material transport processes. We also invite physical processes studies based on field observations, numerical simulation, and flume experiments. Finally, the conveners encourage contributions that promote data collection and sharing for both advancing science and local problem solving, that consider policy and governance issues linked to the sustainable development of deltas and estuaries, and that use in-situ and satellite data for modeling and risk assessment.

[HCG22-P01] Numerical estimation of Holocene paleowave changes in an estuarine environment: case of Tokyo Bay, central Japan

*Katsuto Uehara[1] (1.Kyushu University)

[HCG22-P02] **Channel deformation of the lower Mississippi and Yangtze Rivers – Implications for future backwater zone studies**

*Yi-Jun Xu[1], Maotian Li[2], Zhongyuan Chen[2], Bo Wang[1], Shuwei Zheng[3], Weiguo Zhang[2] (1.Louisiana State University, 2.East China Normal University, 3.Shandong Normal University)

[HCG22-P03] Offset in radiocarbon ages between marine bioclast and terrestrial plant pairs in the Holocene sediments along the Pacific coasts around Japan

*Nakanishi Toshimichi[1], Futoshi Nanayama[2], Kazuaki Hori[3], Yuichi Niwa[4], Junko Komatsubara[5], Akihisa Kitamura[6], Wan Hong[7] (1.Japan Atomic Energy Agency, 2.AIST/Kumamoto Univ., 3.Nagoya Univ., 4.Chuo Univ., 5.AIST, 6.Shizuoka Univ., 7.KIGAM)

Numerical estimation of Holocene paleowave changes in an estuarine environment: case of Tokyo Bay, central Japan

*Katsuto Uehara[1]

1. Kyushu University

During the Holocene, many estuaries and embayments has changed their shape due to shoreline transgressions caused by the sea-level rise and regressions due mainly to the sedimentation, which may have changed the condition of the wind-wave propagation and development within the area. In this study, a paleowave simulation of Tokyo Bay has been carried out by using SWAN model to estimate changes in the wave field and to evaluate the role of wind waves on the formation of the estuarine morphology taken place during the Holocene. Tokyo Bay was chosen as a study area due to the following three reasons: 1. paleoshorelines are well identified by a large number of geological and archeological proxies, 2. the head of the elongated bay has extended northward during the mid-Holocene transgression stage and the maximum length of the bay was estimated to be twice as large as that at present and the fetch within the area during the winter monsoon season and during typhoon events in summer are expected to have changed greatly, and 3. many erosive features are estimated to have formed by wave actions, such as erosive cliffs and underwater wave-cut platforms, indicating a strong relevance of waves on the formation of the present-day morphology.

Keywords: wind wave, Tokyo Bay, Holocene, numerical simulation, sea level change

©2020. Japan Geoscience Union. All Right Reserved.

Channel deformation of the lower Mississippi and Yangtze Rivers –Implications for future backwater zone studies

*Yi-Jun Xu[1], Maotian Li[2], Zhongyuan Chen[2], Bo Wang[1], Shuwei Zheng[3], Weiguo Zhang[2]

1. Louisiana State University, 2. East China Normal University, 3. Shandong Normal University

The lower reaches of many world’s large rivers serve as transportation hubs, commercial hotspots, and industry and population centers. This is especially the case of the Mississippi River in the United States and the Yangtze River in China. Draining a land surface of 3.2 and 1.8 million square kilometers, respectively, the lower Mississippi and lower Yangtze Rivers have become the world’s two most important shipping channels and their countries’ most vibrant economic corridors. However, as riverine sediment loads in the Mississippi and Yangtze have declined largely, these two alluvial rivers and their deltaic areas face challenges such as, among others, channel deformation, sediment transport, levee stability, and shipping safety. In this study, we analyzed channel changes in the final 500 kilometers of the Mississippi and the final 565 kilometers of the Yangtze in the past approximately 20 years, in order to identify common patterns with respect to where erosion and deposition occurred. For the lower Mississippi River, over 6,000 single-beam cross-sectional measurements surveyed in 1992, 2004, and 2013 were analyzed; For the Yangtze River, navigational charts surveyed in 1972, 2002, and 2013 were digitalized. These data were utilized to create channel bathymetric DEMs, which were used to quantify the changes in the riverbeds from bank to bank. Our study found that the two rivers showed similar fluvial patterns, specifically, 1) the average channel elevation lies below mean sea level; 2) there is a deep channel drawdown with a rapid elevation rise near the river mouth; and 3) widespread riverbed degradation in the recent decade. The lower Yangtze River experienced strong riverbed degradation since the completion of the Three Gorges Dam construction in 2003. Of the entire study river reach, 425 kilometers have undergone substantial erosion (i.e., 2.16 billion m^3 with an annual average channel incision rate between 0.01 and 0.19 m), while the other 140 kilometers have experienced marginal deposition (i.e., 0.31 billion m^3 with an annual average deposition rate ranging from 0 to 0.17 m). Changes in the riverbed of the lower Mississippi were more variable and can be classified into three geomorphic stages: aggradation, degradation, and dynamic equilibrium. While sediment loads in the lower Yangtze River sharply declined since 2003 (from ~270 MT yr^{-1} to ~140 MT yr^{-1}), sediment loads in the lower Mississippi River showed relatively small fluctuation in the past two decades (averaged 120 MT yr^{-1}). Large floods seemed to have a strong effect on riverbed erosion in the lower segment of the backwater zone owing to the drawdown effect. These findings suggest that the lower segments of large rivers are likely experiencing substantial channel erosion, and that the backwater zone of these rivers may shift upstream as global sea level rises. The consequence of these changes on sedimentation and geomorphic processes is unknown. Future studies are needed to determine the underlying mechanisms in these two and other rivers and to examine risk implications for channel stability and sediment transport in estuaries.

Keywords: Channel dynamics, Riverbed deformation, Backwater zone , Alluvial river, Lower Mississippi River, Lower Yangtze (Changjiang) River

©2020. Japan Geoscience Union. All Right Reserved.

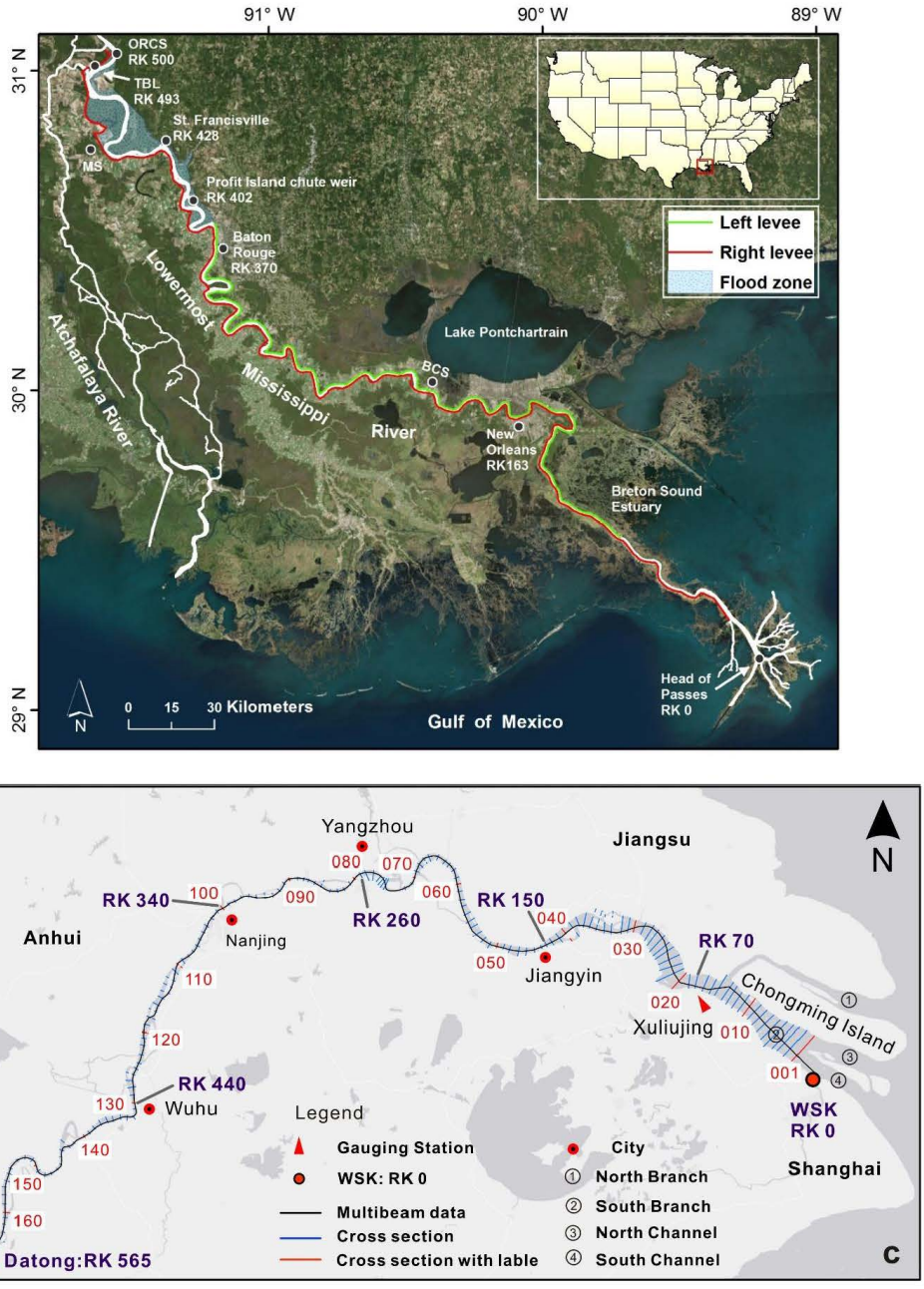


Figure: The last 500 kilometers of the Mississippi River before entering in the Gulf of Mexico (above), and the last 565 kilometers of the Yangtze River before emptying into the East China Sea (below).

©2020. Japan Geoscience Union. All Right Reserved.

Offset in radiocarbon ages between marine bioclast and terrestrial plant pairs in the Holocene sediments along the Pacific coasts around Japan

*Nakanishi Toshimichi[1], Futoshi Nanayama[2], Kazuaki Hori[3], Yuichi Niwa[4], Junko Komatsubara[5], Akihisa Kitamura[6], Wan Hong[7]

1. Japan Atomic Energy Agency, 2. AIST/Kumamoto Univ., 3. Nagoya Univ., 4. Chuo Univ., 5. AIST, 6. Shizuoka Univ., 7. KIGAM

To identify chronological and spatial changes in the radiocarbon (^{14}C) marine reservoir effects, the ^{14}C ages of eight pairs of marine shells and terrestrial plants were measured from the same horizons of one core of Holocene sediments around Japan. The reservoir ages ranged from 60 to 1100 years, scattered over the period 100-10,200 cal BP, which were significantly larger than the values from “prebomb” samples of known age, before AD 1955 in this area. These results indicate that the information on reservoir effects is indispensable for chronological control not only from prebomb samples but also from geological and archaeological samples. Moreover, the effects also reflects the influence of complex river-mouth systems such as deltas and estuaries. To determine the direct chronological changes of the marine reservoir effect between the Kuroshio and Oyashio Currents, radiocarbon ages were measured from the same stratigraphic horizons within Holocene sediment cores alomg the Pasific coast of Japan (eastern Hokkaido; Nanayama et al., 2003, Nanayama, 2020, Sanriku Coast; Niwa et al., 2017, 2019, Arakawa Lowland; Komatsubara et al., 2009, 2010, Shimizu Plain; Kitamura & Kobayashi, 2014; Nobi Plain) and Taiwan. Subsequently, the results were compared with values from the Oita Plain and Hakata Bay on the northern coast of Kyushu, as well as the Korean Peninsula. The study was partially funded by the Japan Society for the Promotion of Science Kakenhi grant number JP18H01310.

Reference:

Kitamura A, Kobayashi K. 2014. Geologic evidence for prehistoric tsunamis and coseismic uplift during the ad 1854 Ansei-Tokai earthquake in Holocene sediments on the Shimizu Plain, central Japan. *Holocene*, 24(7), 814–827.

Komatsubara J, Nakashima R, Kimura K. 2009. Sedimentary facies and physical properties of the latest Pleistocene to Holocene sediment core GS-TKT- in the Arakawa Lowland, Toda City, Saitama Prefecture, central Japan. Journal of Sedimentological Society of Japan, 68(1), 13-25 (Japanese with English abstract).

Komatsubara J, Nakashima R, Kimura K. 2009. Sedimentary facies and physical properties of the latest Pleistocene to Holocene sediment core (GS-KZK-1) in the Shibakawa Lowland, Kawaguchi City, central Japan. Journal of Sedimentological Society of Japan, 69(2), 73-84 (Japanese with English abstract).

Nanayama F. 2020. Evidence of giant earthquakes and tsunamis of the 17th-century type along the southern Kuril subduction zone, eastern Hokkaido, northern Japan: a review. Characterization of modern and historical seismic-tsunamic events, and their global-societal impacts, Geological Society, London, Special Publications, 501, DOI: 10.1144/SP501-2019-99.

Nanayama F, Sakake K, Furukawa R, Shimokawa K, Shigeno K, Atwater BF. 2003. Unusually large earthquakes inferred from tsunami deposits along the Kuril Trench. *Nature*, 424, 660–663.

©2020. Japan Geoscience Union. All Right Reserved.

Niwa Y, Sugai T, Matsushima Y, Toda S. 2017. Subsidence along the central to southern Sanriku coast, northeast Japan, near the source region of the 2011 Tohoku-oki earthquake, estimated from the Holocene sedimentary succession along a ria coast. *Quaternary International*, 456(15), 1-16.

Niwa Y, Sugai T, Matsushima Y, Toda S. 2019. Millennial-scale crustal movements inferred from Holocene sedimentary succession of the Omoto plain, northern Sanriku coast, Northeast Japan: Relevance for modeling megathrust earthquake cycles. *Quaternary International*, 519(10), 10-24.

Keywords: Radiocarbon dating, Marine reservoir, Sedimentary facies, Pacific coast

©2020. Japan Geoscience Union. All Right Reserved.

[E] Poster | H (Human Geosciences)：H-CG Complex & General

[H-CG23] Earth surface processes related to deposition, erosion and sediment transport

convener:Koji Seike(Geological Survey of Japan, AIST), Masayuki Ikeda(University of Tokyo), Hideko Takayanagi(Institute of Geology and Paleontology, Graduate School of Science, Tohoku University), Hajime Naruse(Department of Geology and Mineralogy, Graduate School of Science, Kyoto University)

To understand landscape evolution and dynamics of erosion, transport and sedimentation of earth-surface materials, the latest results of multiple research fields including engineering and earth sciences will be presented. As well as any researches of sedimentology and sedimentary petrology, interaction between fluid, sediments and geomorphology is focused. Interdisciplinary discussions of science, disaster prevention and resource exploration will be expected.

[HCG23-P01] Wind Dynamic Process and Ecological Effect in Sand Barrier Environment of Mu Us Sandy land

*Hongyue Li[1,2], Hasi -[1,2], Jie Yin[1,2] (1.School of Natural Resources,Beijing Normal Univ., 2.Faculty of Geographical Science,Beijing Normal Univ.)

[HCG23-P02] Comparison of Roughness-Cover Models for bedrock bed with Experimental Observations

*Jagriti Mishra[1], Takuya Inoue[1] (1.Civil Engineering Research Institute for Cold Region)

[HCG23-P03] Paleosols distributed in marine terraces in the Goshogawara area, Aomori Prefecture, Northeast Japan

*Aya Omata[1], Kohki Yoshida[2] (1.Division of Science and Technology, Graduate School of Shinshu University, 2.Department of Geology, Faculty of Science, Shinshu University)

[HCG23-P04] Effects of soil moisture variation on rainfall infiltration and erosion of the badland soil in Taiwan

*po yuan Chou[1], Yung-Chieh Wang[1] (1.National Chung Hsing University)

[HCG23-P05] Forced regression deposits during MIS 5c and 5a observed in the Iioka marine terrace (the Pleistocene Katori Formation, central Japan)

*Hiroko Okazaki[1], Hiroomi Nakazato[2], Toru Tamura[3], Kazumi Ito[3], Masakazu Nara[4] (1.Division of Earth Science, Natural History and Institute, Chiba, 2.Institute for Rural Engineering, NARO, 3.Institute of Geology and Geoinformation Geological Survey of Japan, AIST, 4.Sciences Unit, Natural Sciences Cluster, Research and Education Faculty, Kochi University)

Wind Dynamic Process and Ecological Effect in Sand Barrier Environment of Mu Us Sandy land

*Hongyue Li[1,2], Hasi -[1,2], Jie Yin[1,2]

1. School of Natural Resources,Beijing Normal Univ., 2. Faculty of Geographical Science,Beijing Normal Univ.

Abstract: Sand barriers are the main measures to control mobile dunes and promote vegetation restoration in sandy areas. In order to analyze the wind speed, wind direction and the characteristics of the structure of the wind-blown sand flow in the horizontal and vertical directions of the section, explore the degree of surface stability within the barrier, and determine the optimal configuration to promote vegetation restoration, we selected the barchan chain in the hinterland of Mu Us Sandy Land as the research object. Through field observations, we carried out quantitative research on the airflow field, wind-sand flow structure, micro surface morphology and erosion volume of different slopes with different materials (salix, PLA, straw rope), different specifications (1m ×1m, 2m ×2m, 3m ×3m) sand barrier measures. And furthermore,field investigation of vegetation restoration under the same conditions was carried out.The results show that: ①The wind speed at the top of dune is 1.3-1.7 times of the wind speed at the inlet due to the air compression and the effect of windbreak at the foot and middle of slope is better than on the slope.There are differences in the arrangement of sand barriers to achieve the best wind prevention effect at different slope positions: the 1m×1m PLA has the best protection effect at the foot of the slope, and the 2m×2m salix sand barrier in the middle and on the slope have the best performance in reducing wind speed.②The maximum difference of sand transport rate of different types of sand barriers appears in the slope of 2m ×2m: Salix is 24.25 times more than PLA material, and with the greatest sand blocking capacity, its effect is better than straw rope than PLA material.③The amount of surface erosion and accumulation in the sand barrier is significantly related to the years of sand barrier laying. With the increase of time, wind erosion gradually appears. And furthmore, the larger size of sand barrier is, the deeper central erosion depth is, and the more serious the erosion is. Besides, under the same specifications, the surface erosion amount of PLA sand barrier is much higher than that of other two materials. The 3m×3m PLA sand barrier reaches the maximum, and its surface inside the barrier is in a severely unstable state.④Among the three materials, salix sand barrier has the best material to promote the vegetation recovery ability, and straw rope sand barrier is the most beneficial to increase the vegetation diversity. In the lower part of the windward slope, the vegetation coverage under the three specifications of salix sand barriers is 2.67 times, 1.79 times, and 3.88 times than the slope, respectively, and the slope is better than the slope. Shrubs and herbaceous vegetation restoration are complementary. And the small size is more beneficial to herbaceous vegetation restoration. Based on comprehensive cost factors, it is considered that in Mu Us Sandy land, the most suitable sand barrier material is salix.As well as, laying 2m ×2m specifications at the foot and middle of the slope, 1m ×1m specification on the slope can exert the best sand control and ecological effect.

Keywords: Sand-barrier, Flow field, Structure of drifting sand flux, Erosion accumulation feature, Vegetation restoration

©2020. Japan Geoscience Union. All Right Reserved.

Comparison of Roughness-Cover Models for bedrock bed with Experimental Observations

*Jagriti Mishra[1], Takuya Inoue[1]

1. Civil Engineering Research Institute for Cold Region

Sediment availability and bedrock bed roughness are two important factors controlling the morphodynamics of a bedrock channel. Sediment availability can determine if the bedrock channel incises or adjusts its width and slope. In this study we compare various mathematical models and test their efficacy to reproduce laboratory scale experiments. Some mathematical models have suggested a linear relationship between sediment cover and ratio of sediment supply to sediment transport capacity of the channel.

Keywords: bed roughness, bed cover, bedrock channel

©2020. Japan Geoscience Union. All Right Reserved.

Paleosols distributed in marine terraces in the Goshogawara area, Aomori Prefecture, Northeast Japan

*Aya Omata[1], Kohki Yoshida[2]

1. Division of Science and Technology, Graduate School of Shinshu University, 2. Department of Geology, Faculty of Science, Shinshu University

The paleosol suggests the climatic conditions in the past because major soil groups are formed and affected by the normal soil forming action of climate. Already, Matsui and Kato (1962) reported the existence of red paleosols distributed in the wide area in Japanese Islands, from Kyushu to the northern end of Honshu, and discussed its implications. In particular, the existence of red paleosol in the Tsugaru Peninsula, located at the northern end of Honshu island, is important in discussing the spread of past warm climatic conditions during the last interglacial period.
At the foot of the Tsugaru Mountains, marine terraces formed during the last interglacial period widely developed (Azuma, 1995). In this study, we examined paleosol layers intercalated in the terrace located from Iizume, Goshogawara-city, to Nakasato, Nakadomari-machi, Aomori Prefecture. In the field, the soil color was described using the Munsell soil color chart, and sedimentary facies was described for reconstruction of sedimentary environments.
As a result, the sedimentary environments in the study area was divided into channel, river floodplain, and lake facies. It is conceivable that the lake facies was formed as a part of the river sedimentary facies since the lake facies is located at the top of the floodplain facies and the bottom of the river channel facies. In this study area, 7.5YR brown soil layer have the majority, and only 5YR red soil layer was found at one site. In the laboratory, thin sections of the samples collected from layers with different sedimentary facies and soil colors were observed under microscope to find the soil structure. The paleosol layers that have soil structures such as clay filling and clay coating were found at two sites. In addition, XRD analysis was conducted on the horizons where the development of the clay filling and clay coating were observed. As a result, the clay minerals such as halloysite, vermiculite and kaolinite were found in the sample where the accumulated clay minerals are contained, while the halloysite was almost the only clay mineral contained in the sample where the accumulated clay minerals were not observed. These layers, which were rich in clay minerals of the accumulated clay, correspond to horizon B of the general soil stratigraphy, suggesting the formation of a mature soil.
The paleosol color of B layer of the paleosol layer distributed in this study area is 5YR4 / 8 (red brown), 5YR5 / 8 (light red brown), 7.5YR4 / 6 (brown) and 7.5YR5 / 8 (light brown). The clay mineral composition of horizon B is mainly composed of halloysite and vermiculite and shows the similarity to typical red-yellow soil distributed around eastern Asia present days.
It is revealed that paleosol consisting of red-yellow soil developed on the terrace deposits formed during the last interglacial period in the Tsugaru Peninsula. The climate condition in the Tsugaru Peninsula at the last interglacial period is considered to have been very warm because the current red-yellow soils are formed around subtropical forests.

References

Azuma, T. (1995) Late Quaternary Terraces and Their Deformations on Tsugaru Peninsula, Northeastern Japan. *The Quaternary Research*, **34**, 75-89.
Matsui, T. and Kato, Y. (1962) Notes on Palaeopedology of Red Soils in Japan. *The Quaternary Research*, **2**, 161-179.

©2020. Japan Geoscience Union. All Right Reserved.

Keywords: Paleosols, Paleoclimate, Last interglacial, Marine terraces

©2020. Japan Geoscience Union. All Right Reserved.

Effects of soil moisture variation on rainfall infiltration and erosion of the badland soil in Taiwan

*po yuan Chou[1], Yung-Chieh Wang[1]

1. National Chung Hsing University

The mudstone area in southwestern Taiwan has poor geological conditions, severe erosion and poor vegetation. This area, recognized as the badland, is the most difficult area for remediation and revegetation after hillslope disasters. Widely distributed in southwestern Taiwan, the mudstone is known by its poor water permeability. The mudstone is softened with water, but hardens and cracks without water. In this study, we collected the mudstone deposits in the Agongdian Reservoir area, and used them as the soil specimens for investigating the soil erosion processes in the cases of different slope gradients and precipitations. Two major sets of experiments were carried out in this study. The first set of experiments aims to observe the characteristics of soil shrinkage and expansion under different soil moisture conditions. We measured the soil volume at different moisture contents, and estimated the porosity and infiltration rate, in order to obtain the soil characteristic curve values. In the second set of experiments, we applied the artificial rainfall experiments on the soil specimens, which was filled in a glass erosion planform with the dimension of 25 cm, 15 cm, and 75 cm, in width, depth, and length, respectively. Two rainfall intensities (75mm / hr, 100mm / hr) and seven slope gradients (0 ˚, 5 ˚, 10 ˚, 15 ˚, 20 ˚, 25 ˚, 30 ˚) were assigned in the 30-minute simulated rainfall events. During each trial of the simulated rainfall experiments, surface runoff, infiltration, and outflow sediments were collected for every five minutes. Meanwhile, the soil moisture content and erosion topography were monitored by using a soil hygrometer (TDT) and a digital camera. Results from the experiments are analyzed and discussed, in order to propose the inter-relationships among soil moisture content, porosity, infiltration, and runoff erosion. Consequently, the outcome of this study may provide references for the assessments of hillslope erosion and disaster evaluation of the badland in Taiwan.

Keywords: mudstone , rainfall erosion, artificial rainfall experiments, infiltration

©2020. Japan Geoscience Union. All Right Reserved.

Forced regression deposits during MIS 5c and 5a observed in the Iioka marine terrace (the Pleistocene Katori Formation, central Japan)

*Hiroko Okazaki[1], Hiroomi Nakazato[2], Toru Tamura[3], Kazumi Ito[3], Masakazu Nara[4]

1. Division of Earth Science, Natural History and Institute, Chiba, 2. Institute for Rural Engineering, NARO, 3. Institute of Geology and Geoinformation Geological Survey of Japan, AIST, 4. Sciences Unit, Natural Sciences Cluster, Research and Education Faculty, Kochi University

The Kanto Plain, eastern Japan, is known to be the largest Quaternary sedimentary basin characterized by the extensive presence of the raised Last Interglacial marine terrace. The Iioka marine terrace, which exposes a marginal terrace section at the eastern end of the Kanto Plain, consists of the Katori Formation. This report presents that the Katori Formation potentially contains the deposits formed during the MIS 5c and 5a with K-feldspar post-infrared infrared stimulated luminescence (pIRIR) dating, tephra correlation, etc. The depositional sequence of the Katori Formation consists of inner shelf, lower shoreface, upper shoreface, beach, and fluvial facies upward above the sequence boundary. The contact between the lower shoreface and the upper shoreface indicates a sharp erosional surface, and the upper shoreface is characterized by tabular-bed sets that may originate from alongshore or oblique shore dunes. The beach and fluvial facies level lower northeastwards (offshore) along with the marine terraces that descend stepwise, which is indicative of a forced regression succession.

Keywords: Forced regression, marine terrace, shallow marine

©2020. Japan Geoscience Union. All Right Reserved.

[E] Poster | H (Human Geosciences)：H-CG Complex & General

[H-CG24] Enhancing Integrated Research for Sustainable Future - a human geoscience perspective

convener:Yukio Himiyama(Emeritus Professor, Hokkaido University of Education), Takeshi Sakurai(Graduate School of Agricultural and Life Sciences, The University of Tokyo), Akihiko Kondoh(Center for Environmental Remote Sensing, Chiba University)

Global environmental programmes have been re-structured under the framework of Future Earth, and Future Earth is playing increasingly important role in guiding and coordinating research for the world sustainability, and in contributing to the United Nation's Sustainable Development Goals (SDGs), which has also been impressively successful in mobilizing and leading the society to the more sustainable paths at global, regional, national and local levels. Human geoscience, which has been built on geoscience which studies dynamic nature and phenomena of the Earth including lithosphere, hydrosphere, atmosphere and biosphere, is uniquely committed to human sphere, where human and its various activities, the environment, global environmental problems and disasters all exist and human dimensions of global change is of primary importance, and hence assumes important roles in Future Earth, SDGs, and other programmes for global sustainability or disaster risk reduction. This session relates to all these, and is intended to discuss crucial issues related with them and to seek right ways to implement needed integrated research for sustainable future in human geoscience perspective.

[HCG24-P01] Pattern of Electricity Consumption in Consecutive Hot Days with respect to Microclimate, a case study of Taipei city

*Po Yu Chen[1], Jehn-Yih Juang[1,2] (1.International Degree Program in Climate Change and Sustainable Development, National Taiwan University, Taiwan(R.O.C.), 2.Department of Geography, National Taiwan University, Taiwan(R.O.C.))

[HCG24-P02] Biodiversity and ecosystem functioning under different land management regimes -Case study in grazing lands in northern Ethiopia

*Keiichi Kimura[1], Akito Kono[1], Shigdaf Mekuriaw[2], Yeshambel Mekuriaw[3], Misganaw Wale[3], Asaminew Tassewe[3], Okuro Toshiya[1] (1.Graduate School of Agricultural and Life Sciences, The University of Tokyo, 2.Arid Land Research Center, Tottori University, 3.Bahir Dar University)

[HCG24-P03] Simulating the Spatial Flow of Carbon Sequestration Service: A Case Study of Tumen River Watershed

*Jian ZHANG[1], Shizuka HASHIMOTO[1], Weihong ZHU[2], Toshiya OKURO[1] (1. The University of Tokyo, 2.The Yanbian University)

[HCG24-P04] Measuring Urban Sustainability Using Spatial and Socio-Economic Factor and the Impact on Planning Policies in a Rapidly Urbanizing Area

*Anoraga Jatayu[1], Ernan Rustiadi[2,3], Didit Okta Pribadi[4,3] (1.Regional and Rural Development Planning Science Study Program, 2.IPB University, 3.Center for Regional Systems, Analysis, Planning and Development, 4.Research Center for Plant Conservation and Botanic Garden, Indonesian Institute of Science)

Pattern of Electricity Consumption in Consecutive Hot Days with respect to Microclimate, a case study of Taipei city

*Po Yu Chen[1], Jehn-Yih Juang[1,2]

1. International Degree Program in Climate Change and Sustainable Development, National Taiwan University, Taiwan(R.O.C.), 2. Department of Geography, National Taiwan University, Taiwan(R.O.C.)

Electricity consumption (EC) is highly related to the weather variation owing to utilization of air conditioner (AC) and its embedded design logic. As long as the relationship between electricity and microclimate or meteorological information could be examined and verified, the electricity saving potential could be found and responsive policy could be proposed to improve the situation and make contribution for reducing carbon emission. Cities with huge population and EC will become significant role on mitigating climate change. Taipei, a city with frequent commercial activities and basin-subtropical geographical features was set as the researching target because the ACEC here is considerable with its specific background. Weather data from observing station and electricity variation from electric substations were used in the analysis for examining the temporal and spatial pattern relationship. The variation of EC was compared with variation of temperature and apparent temperature (heat index), which integrated with humidity information, through a time series of consecutive hot days while discussed them by diurnal perspective respectively for precluding interference from the difference of human activities. Geographic information system (GIS) was applied for figuring out the spatial pattern and multilinear regression and geographically weighted regression (GWR) was conducted to quantify the result. Relationship was established through different location within the city area. It was found that both temperature and electricity varied significantly in the daytime and the influence from temperature dominant even though humidity influence apparent temperature which showed different spatial pattern from that of temperature. Outcome could be presented on Web-GIS for the access to the public for reference on the energy saving issue and the (apparent) temperature sensitive area could be improved by better heat insulation refurbishment or other electricity saving application.

Keywords: urban heat island, electricity consumption, microclimate, subtropical climate, air condition electricity consumption

©2020. Japan Geoscience Union. All Right Reserved.

Biodiversity and ecosystem functioning under different land management regimes -Case study in grazing lands in northern Ethiopia

*Keiichi Kimura[1], Akito Kono[1], Shigdaf Mekuriaw[2], Yeshambel Mekuriaw[3], Misganaw Wale[3], Asaminew Tassewe[3], Okuro Toshiya[1]

1. Graduate School of Agricultural and Life Sciences, The University of Tokyo, 2. Arid Land Research Center, Tottori University, 3. Bahir Dar University

Biodiversity improves ecosystem functions such as productivity and soil erosion resistance, while loss of biodiversity induces decrease of ecosystem functions through several pathways, depending on the state of functional diversity and process of species loss. However, no prior research conducted on application of positive relationship between biodiversity and ecosystem functioning to grazing land management under framework of sustainable land management (SLM). In northern Ethiopia, severe vegetation degradation and soil erosion have been induced by free grazing in communal lands, where pasture lands have been continuously grazed all year round. Recently seasonal grazing has been proposed as alternative grazing management system to mitigate grazing impact on lands. However, little is known about the effectiveness of seasonal grazing on land conservation through altering biodiversity and ecosystem functions.

Here we addressed the following research question; "how do the differences in grazing management regimes affect ecosystem functions through the changes of biodiversity?" and conducted a field investigation (1) to compare biodiversity (species and functional traits) between free grazing and seasonal grazing systems and explore non-random process of biodiversity loss, (2) to compare ecosystem functions between those systems and explore non-linear process of changes of ecosystem functions, (3) to analyze trade-off/synergy between ecosystem functions and identify key species/functional groups that play key roles in maximizing bundle of ecosystem services, and (4) to compare above results in grazing system with those in tree plantation system, which has been causing land use conflict in grazing land. This paper introduces the outline of the survey and preliminary results of comparison of species and functional diversity between two grazing management regimes.

Keywords: Biodiversity, Functional diversity, Ecosystem functioning, Sustainable land management, Free grazing, Seasonal grazing

©2020. Japan Geoscience Union. All Right Reserved.

Simulating the Spatial Flow of Carbon Sequestration Service: A Case Study of Tumen River Watershed

*Jian ZHANG[1], Shizuka HASHIMOTO[1], Weihong ZHU[2], Toshiya OKURO[1]

1. The University of Tokyo, 2. The Yanbian University

The awareness of the carbon sequestration service concept has gained prominence in the decision-making process towards climate change. The inclusion of this issue to date mostly depends on the distribution output of carbon sequestration service value on a static map, whereas its transmission over the spatial units is too often unexploited. On the basis of the cellular automata model and laws of thermodynamics, our research visualized the spatial flow of carbon sequestration service via a grid matching method with a focus on the Tumen river watershed. We simulated flow directions (N = 9) and potential fluxes (0 < F < 87.68 t) of carbon sequestration service flow in the Tumen river watershed, and presented it on a grid map with 1km resolution. Our results illustrated that 15.28% of the trans-boundary watershed was recognized as non-flow regions, which possessed 136.71 Tg of total carbon sequestration. We highlighted how, depending on the spatial flow being simulated, the landscape patterns impact the carbon sequestration service flow, thereby influencing the local value of actual carbon sequestration service supply.

Keywords: Carbon sequestration service, ecosystem service flow, grid-matching

©2020. Japan Geoscience Union. All Right Reserved.

Measuring Urban Sustainability Using Spatial and Socio-Economic Factor and the Impact on Planning Policies in a Rapidly Urbanizing Area

*Anoraga Jatayu[1], Ernan Rustiadi[2,3], Didit Okta Pribadi[4,3]

1. Regional and Rural Development Planning Science Study Program, 2. IPB University, 3. Center for Regional Systems, Analysis, Planning and Development, 4. Research Center for Plant Conservation and Botanic Garden, Indonesian Institute of Science

Regional growth and pattern in urban areas of Monsoon Asia have a relatively similar pattern, which is characterized by the expansion of core-urban areas to the surrounding areas. The growth of urban areas is also affecting its sustainability since spatial growth is followed by a transformation of economic and social activity. Cianjur Regency as one of the region that experiences the expansion process from Jakarta Metropolitan Area (JMA) is currently undergone major growth and transformation from the region with a mostly rural area to become “city-region”, characterized by its growth as a polycentric region with the emergence of newly established urban areas. Those growths are surely going to affect the region’s sustainability locally and regionally. The objective of this research is to measure Cianjur Regency urban areas sustainability (2000 and 2018), also its impact on future and current planning policies. Sustainability in those urban areas is measured using Local Sustainability Index (LSI) with spatial and socio-economic variables. The result shows that the new urban area (Puncak-Cipanas) is less sustainable than the majority of the existing urban area (Cianjur). The decline of urban sustainability on Puncak Cipanas is largely influenced by social and environmental sustainability, because of land-use change occurred in the area and the lack of social services/facilities. Meanwhile, Cianjur urban’s sustainability hardly experiencing any changes, mainly because regional development is currently focused on Puncak-Cipanas urban. Challenges on future and current planning policies are headed towards preserving the environment and providing better infrastructure coverage for all of the urban areas, as urban area tends to have a more complex needs of infrastructure. The integration of all planning policies also needed to achieve sustainable growth.

Keywords: Local sustainability, Urban Expansion, Sustainable Urban

©2020. Japan Geoscience Union. All Right Reserved.

[E] Poster | H (Human Geosciences)：H-CG Complex & General

[H-CG25] Turbidity current: generation, morphodynamics and deposits

convener:Hajime Naruse(Department of Geology and Mineralogy, Graduate School of Science, Kyoto University), Robert Michael Dorrell(University of Hull), Miwa Yokokawa(Osaka Institute of Technology)

We invite research based on all kinds of approaches to understand turbidity currents such as field observation, physical and numerical experiments, mathematical analysis, and studies from rock records. Recent progress in research methodologies has greatly changed our understanding of dynamics of turbidity currents and relevant submarine geomorphology and stratigraphy. The integration of such new knowledge on turbidity currents is important not only for scientific interests but also for practical application such as risk assessment of natural hazards, and exploration of resources. We anticipate interdisciplinary discussions about turbidity currents and related sediment gravity flows.

[HCG25-P01] Inverse Analysis of Experimental Scale Turbidity Currents by Deep Learning Neural Network

*Cai Zhirong[1], Hajime Naruse[1] (1.Kyoto University)

[HCG25-P02] Dynamic stratification enables auto-suspension and thus the ultra-long run-out of sediment-laden buoyancy driven flows

*Robert Michael Dorrell[1] (1.University of Hull)

[HCG25-P03] Dynamics of turbidity currents influenced by tidal flows

*Justine Poppeschi[1], Hajime Naruse[1], Robert Michael Dorrell[2] (1.Kyoto University, 2.University of Hull)

[HCG25-P04] Evaluation of plant-fragment concentration system in the turbiditic sequence by terrigenous biomarker analysis of sediments from the Kawabata Formation, Yubari area, central Hokkaido, Japan.

*Muhammad Adam Ismail[1], Hiroyasu Asahi[1], Satoshi Furota[3], Ken Sawada[2] (1.Graduate School of Science, Hokkaido University, 2.Department of Earth and Planetary Sciences, Faculty of Science, Hokkaido University, 3.Geological Survey of Japan, National Institute of Advanced Industrial Science and Technology)

[HCG25-P05] Grain fabric analysis of massive sandstone beds of the Upper Cretaceous Himenoura Group distributed in Amakusa-Kamishima Island, Kyushu, Southwestern Japan by Deep Learning Convolutional Neural Network

*Sayo Ishii[1], Hajime Naruse[1] (1.Department of Geology and Mineralogy, Graduate School of Science, Kyoto University)

[HCG25-P06] Revisiting the meandering channel developed in the Okinawa Trough

*Takeshi Matsumoto[1], Yasuhiro Morii[2], Nobuhiro Yamawaki[2], Itaru Aizawa[2], Sota Hoshina[2], Tsukasa Kinoshita[2] (1.Faculty of Science, University of the Ryukyus, 2.Faculty of Fisheries, Nagasaki University)

[HCG25-P07] Cyclic steps inside submarine canyon and in canyon-fan transition zone: Numerical experiments by 2D shallow-water model of turbidity currents

*Hajime Naruse[1] (1.Department of Geology and Mineralogy, Graduate School of Science, Kyoto University)

[HCG25-P08] Sedimentary facies related to supercritical-flow bedforms in foreset slopes of middle Pleistocene Gilbert-type delta, central Japan

*Hiroko Okazaki[1] (1.Division of Earth Science, Natural History and Institute, Chiba)

Inverse Analysis of Experimental Scale Turbidity Currents by Deep Learning Neural Network

*Cai Zhirong[1], Hajime Naruse[1]

1. Kyoto University

Turbidite deposits have been an active area of study due to its close association with petroleum resources and their role in the destruction of sea-floor equipment. Through studies of turbidity currents, the depositional process of turbidite, understanding of specific characteristics of turbidite deposits can be improved. However, knowledge in this area remains limited due to difficulties in the direct observation of turbidity currents. In order to better understand the structure of turbidity current, inverse analysis of turbidity current had been used to reconstruct the initial flow conditions from its turbidite deposits. However, past optimization methods had been computationally over expensive, making it impractical to be applied to actual turbidite deposits in nature. In order to resolve this issue, a new method for the inverse analysis of turbidity current using deep learning neural network (DNN) was proposed, and this research verified the method using artificial data and actual flume experiment data. In this study, DNN was applied to two different types of experiments. One using two different types of plastic particles and the other using a mixture of siliciclastic sand and plastic particles. Our results demonstrate that inverse analysis using DNN can reconstruct the hydraulic conditions and deposit profiles of both types of flume experiments with good accuracy. However, some variation in performance can be observed from the results of application for different types of experiments.

Keywords: Machine Learning, Turbidite, Flume Experiment

©2020. Japan Geoscience Union. All Right Reserved.

Dynamic stratification enables auto-suspension and thus the ultra-long run-out of sediment-laden buoyancy driven flows

*Robert Michael Dorrell[1]

1. University of Hull

Sediment-laden buoyancy driven flows, turbidity currents, are observed to traverse thousands of kilometers on the seafloor. Such behavior is predicated on auto-suspension, where sediment in suspension provides the motive force to drive the flow and the flow energy is expended keeping sediment in suspension. However, auto-suspension over such distances is enigmatic, as available flow energy is continuously dissipated through raising the centre of suspended mass of the flow. Thus, turbidity currents must ultimately stall and die. However, here a new model for turbidity current flow mechanics is proposed where the potential energy released in the deceleration of dynamically stratified turbidity currents provides sufficient energy to enable ultra-long flow run-out. The new model is validated against the first field-scale observations of a turbidity current traversing the entire length of a submarine canyon-channel system.

Here auto-suspension, and thus the ultra-long run-out of natural turbidity currents, is explained by depth-average dynamic weighting parameters, that appear in system scale shallow water models of turbidity current flow dynamics. In essence dynamic weighting is included to capture the fundamental process, that:

1) Whilst a flow decelerates, turbulent mixing decreases and thus stratification increases.

2) Whilst a flow accelerates, turbulent mixing increases and thus stratification decreases.

As stratification increases, with relative near-bed suspended sediment concentration increasing, the location of the velocity maximum becomes moves closer to the bed. As the velocity maximum is more closely aligned with the most concentrated region of the flow. Moreover, as the relative velocity is concentrated in a smaller region, closer to the bed. The paradoxical results of which is that with increasing stratification, downstream mass and momentum flux becomes more efficient.

As stratification increases the depth average hydrostatic pressure, decreases with the relative center of suspended mass being lowered towards the bed. The critical result is thus that whilst accelerating down steep slopes, where stratification increases, kinetic energy is transferred to, and stored as, potential energy. Yet whilst travelling over more gentle slopes, where the flow decelerates and stratification increases, the center of suspended mass is lowered releasing potential energy to drive the flow over long-distances.

Using dynamic models of flow stratification, turbidity currents traversing canyon-channel systems, over slopes down to 10^{-5} m/m may be predicted for the first time. Here temporally invariant flow, characteristic of the long-duration flows observed in real-world systems, is assumed. The model is applied to the Congo canyon-channel system. In both proximal and distal channel sections, modeled flow velocities match mean flow measurements of a 2004 turbidity current that traversed over 1000 kilometers of the canyon-channel seafloor system (Vangriesheim *et al.*, 2009). Sensitivity analysis shows weak dependence on initial flow conditions, if the flow has sufficient kinetic or potential energy to bypass the proximal

©2020. Japan Geoscience Union. All Right Reserved.

canyon, where it is fully confined. This suggests that flow tuning, through overspill, is a core control on the dynamics of partially confined flows within distal channel reaches.

Keywords: turbidity current, autosuspension, flow tuning

©2020. Japan Geoscience Union. All Right Reserved.

Dynamics of turbidity currents influenced by tidal flows

*Justine Poppeschi[1], Hajime Naruse[1], Robert Michael Dorrell[2]

1. Kyoto University, 2. University of Hull

Turbidity currents are flows lead by gravity and occur generally in the deep-sea floor in contrast to tidal flows that are known to be present in shallow marine regions. Thus, tidal influence on the dynamics of turbidity currents has been regarded as practically non-existent. However, cyclic oscillations in the grain-size distribution have been occasionally observed in turbidites, and in-situ measurements in turbidity currents have shown oscillations of flows velocity with periodicity of several hours. To understand these periodic oscillations in turbidity currents, we propose a hypothesis that the tidal flows in submarine canyon influence turbidity currents by causing the internal waves at the interface of the two flows. They could interacts each other by the mixing and entrainment processes inside submarine canyons. Firstly, this hypothesis will be tested by numerical experiments. Also, data analysis of in-situ measurements of turbidity currents will be conducted to search the presence of tidal influence. If this hypothesis is verified, that could shed light on the large disparity of the turbidity current presence in submarine canyon. In addition, due to the link between the global sea-level and the tide, the internal tides could be the bridge between global sea-level change and developments of submarine fans.

Keywords: Turbidity currents, Tidal flows, Turbidite

©2020. Japan Geoscience Union. All Right Reserved.

Evaluation of plant-fragment concentration system in the turbiditic sequence by terrigenous biomarker analysis of sediments from the Kawabata Formation, Yubari area, central Hokkaido, Japan.

*Muhammad Adam Ismail[1], Hiroyasu Asahi[1], Satoshi Furota[3], Ken Sawada[2]

1. Graduate School of Science, Hokkaido University, 2. Department of Earth and Planetary Sciences, Faculty of Science, Hokkaido University, 3. Geological Survey of Japan, National Institute of Advanced Industrial Science and Technology

Kawabata Formation distributed in Yubari area, central Hokkaido, is formed by basin-filled and slope-apron turbidite systems, and sandstone and mudstone are mainly predominated by turbiditic sequences. Distinctive plant-fragment (PF) concentrated sandstones were found in the Kawabata Formation, and their sedimentological and biomarker analyses suggests that these sediments were deposited by hyperpycnal flow (Furota et al., 2014). In the present study, we conducted biomarker analysis of sandstone and mudstone characterized as several turbidite type sequences from the Kawabata Formation to evaluate sedimentological processes and to compare with the plant-fragment concentrated sandstones in hyperpycnite.

The sandstones and mudstones analyzed were collected from the outcrops of the Takinoue Park, Yubari, central Hokkaido. For the biomarker analysis, lipids were extracted with dichloromethane/methanol, and separated to aliphatic, aromatic and polar fractions. These lipids were identified and quantified by GC-MS.

Three consecutive turbiditic sequences analyzed are two Bouma type sequences (ca. 60 cm and 25 cm thick) and a distinctive ‘PF-concentrated’ type sequence (ca. 34 cm thick), in which the sandstone layer is characterized by abundant plant fragments and particles as reported by Furota et al. (2014). Sedimentary layer in the Bouma type sequences equivalent to Ta units consists of medium - to fine sands with tiny black PFs. Tb unit consists of fine sands with parallel laminations containing the concentrated PFs. Tc unit also consists of fine sands about 1-2cm thick without cross laminations, and the concentrated PFs are observed as many black bands in this unit. Te unit is massive sediment that consists of very fine sands to silty muds without PFs. In the ‘PF-concentrated’ type sequence, a sandstone layer consists of medium to fine sands containing the large plant-derived blackish particles with diameters of ca. 5-10 cm, and many PF thin layers. The mudstone layer, corresponding to the Te unit, is a massive sediment that consists of very fine sands to silty muds without PFs as the Bouma type sequence.

The *n*-alkane concentrations in the turbiditic sequence are of minimal values in the Ta units. The concentrations increase in Tb and Tc, and then decrease in Te units. This trend is also shown in variations in the concentrations of plant-derived terpenoids. The *n*-alkane concentrations are lower than the turbiditic sandstone unit than the mudstone unit. Pristane / phytane ratio (Pr/Ph) of the mudstone unit is 2.12 while the lower and upper layer of the sandstone unit exhibits a strong oxic and terrigenous matter-abundant character at 5.18 and 9.98 respectively. In addition, a peak of higher branched isoprenoid (HBI) alkane, known to be derived from specific diatoms, was found in the mudstone sample. The C27/C29 sterane ratios, which are indicators of marine / terrigenous sources of organic matter, is 0.41 in the mudstone unit, and less than 0.21 in the sandstone units. These results suggest that the organic matter was mainly of terrestrial origin. Triterpenoid compositions are mostly dominated by lupane and oleanane (derived from angiosperms) in both the mudstone and sandstone layers. However, the

©2020. Japan Geoscience Union. All Right Reserved.

sandstone layers had a remarkably higher concentration of the triterpenoids, including A-ring degraded triterpenoid (*des*-A- triterpenoids) such as *des*-A-oleanane, *des*-A-lupane as well as monoaromatic and diaromatic *des*-A-triterpenoids. The *des*-A-triterpenoids are thought to be generated by microbial degradation during early diagenesis. The *des*-A- triterpenoid compositions are also nearly constant as the results of diterpenoids and non-degraded triterpenoids. However, the ratios of *des* -A-triterpenoid/pentacyclic (non-degraded) triterpenoid are higher throughout the turbiditic sequence, especially Tb and Tc units of the Bouma type sequences and sandstone units of the 'PF-concentrated' type sequence. Furota et al. (2014) reported that the *des*-A/pentacyclic triterpenoid ratios in sandstone units were clearly lower than mudstone units in the hyperpycnite, suggesting that more fresh terrigenous organic matter was rapidly transported by the hyperpycnal flow. Our results imply that the organic matter in the current study is mostly of terrestrial origin and rapidly transported by an efficient delivering system.

Keywords: Turbidite, Biomarker, Terpenoids, Hokkaido, Miocene

©2020. Japan Geoscience Union. All Right Reserved.

Grain fabric analysis of massive sandstone beds of the Upper Cretaceous Himenoura Group distributed in Amakusa-Kamishima Island, Kyushu, Southwestern Japan by Deep Learning Convolutional Neural Network

*Sayo Ishii[1], Hajime Naruse[1]

1. Department of Geology and Mineralogy, Graduate School of Science, Kyoto University

The purpose of this study is to clarify the grain fabric of massive sandstones deposited in submarine fans. It has been known that the massive structure is common in submarine sediment-gravity-flow deposits, their formation mechanisms have not been clarified. Rapid deposition from high concentration turbidity currents and en-masse deposition of sandy debris flows are candidates of processes to form massive structure, but it is difficult to distinguish the processes from visible sedimentary structures because they lack characteristic features in macroscopic observation of outcrops. To this end, this study investigated ancient massive deposits by means of the microscopic image analysis. We employed deep learning image analysis for identifying sand particles from rock sections in several tens cm scale. The study area is the Cretaceous Himenoura Group distributed in Amakusa-Kamishima Island, Kyushu, Southwestern Japan. Polished sections of sandstones were scanned by EPSON GT-970 to obtain images. Then the manually traced images were used as teacher images for deep learning. The developed model using Convolutional Neural Network(CNN) automatically distinguishes particles from fine-grained matrix. As a preliminary result, it was revealed that massive sandstones taken from submarine channel-fill deposits and lobe show different features in grain fabric observed at horizontal sections. Preferred orientation of grain long axes tends to vary vertically in channel-filling deposits, whereas those in lobe deposits show relatively stable trends. Future experimental studies may indicate origin of these difference in features of grain fabrics,

Keywords: Massive Sandstone, Turbidite, Grain Fabric

©2020. Japan Geoscience Union. All Right Reserved.

Revisiting the meandering channel developed in the Okinawa Trough

*Takeshi Matsumoto[1], Yasuhiro Morii[2], Nobuhiro Yamawaki[2], Itaru Aizawa[2], Sota Hoshina[2], Tsukasa Kinoshita[2]

1. Faculty of Science, University of the Ryukyus, 2. Faculty of Fisheries, Nagasaki University

In 1996, a French survey found that meandering channels existed on both north and south slopes of the trough north of Yonaguni Island, on the western edge of the Okinawa Trough, where active rifting in the north-south direction is taking place on the eastern margin of the Asian continent. Multibeam bathymetric survey during the ACT Cruise in the SPOT area east of Taiwan and the western end of the trough by the research vessel (R/V) 'l'Atalante' first revealed the channels (Sibuet et al., 1998). After that, LEQUIOS Cruise by R/V 'Yokosuka' and Submersible 'Shinkai6500' were conducted in 2000 (Matsumoto et al., 2001). The main purpose of the cruise was to study the formation and development of the central trough, hydrothermal activity in the trough, and wide-area tectonics and dynamics by use of the seafloor observation by the submersible. Marine geophysical observations including the detailed topographic survey in the eastern extension of the SPOT area was also carried out during the LEQUIOS Cruise. As a result, the entire meandering channel on both north and south slopes of the trough was revealed, and it was found that both channel complexes were almost the same size.

Kimura et al. (2001) pointed out that these channels were very similar to a fan formed on a flat land that transitions from a mountain to a plain, or a delta that can be formed at the mouth of a river, through an ROV (remotely operated vehicle) survey along these meandering channels. Then, the authors pointed out that it could have been formed in an environment such as the intertidal zone or the extremely shallow sea when part of the Okinawa Trough became land. However, considering that these meandering channels are developed on the elongated mounds of several kilometers wide in the east-west direction and are bordered by levees, these channels should be formed by turbidity currents from the continent of China. The channels should be in one stage of the process of forming a submarine fan. Larger ones can be found, for example, in the Amazon Fan drilled at ODP Leg155.

The University of the Ryukyus uses the Nagasaki Maru, a training ship of the Faculty of Fisheries of Nagasaki University, to offer undergraduate onboard training courses every year based on a credit exchange agreement with the Faculty of Fisheries. The ship is also used for research in the Ryukyu region. The old Nagasaki Maru was retired in 2017 and a new one entered service in 2018. The new ship is equipped with a multibeam echo sounder. Approximately 20 years have passed since the previous survey of the meandering channels on the Okinawa Trough, and during this time there might have been a supply of new turbidity currents from mainland China, and the shape of the existing meandering channel might have changed. Therefore, a re-survey of the precise bathymetry of these meandering channels was carried out during the one-week cruise of the training vessel 'Nagasakimaru' in May 2019. Due to rough sea conditions and time constraints, the authors focused on the channel on the northern slope of the trough during the cruise .

As a result, the position change of the flow path of the meandering channel developed on the mound for last 20 years were not detected. And also, no new mounds appeared. However, the water depth of the bottom of the meandering channel on the mound extending from 25° N, 122° 55’ E towards east-northeast is generally 5-15 m deeper than that of 20 years ago, while the levees on both sides of the channel is 15-20m shallower (higher). These suggest that the turbidity current supply from mainland

©2020. Japan Geoscience Union. All Right Reserved.

China has continued for last 20 years, and that the erosion of the bottom of the channel and the growth of the levees has been taking place. On the other hand, meandering channels located in the area near 25° 08’ N, 123° 25’ E, which is not on a mound, had no change in water depth.

Future monitoring of the channel topography regularly and conducting a topographic survey again on the southern slope of the Okinawa Trough will help clarify the turbidity current supply mechanism at the western end of the Okinawa Trough.

Keywords: Okinawa Trough, Meandering Channel, Turbidity Current

©2020. Japan Geoscience Union. All Right Reserved.

Cyclic steps inside submarine canyon and in canyon-fan transition zone: Numerical experiments by 2D shallow-water model of turbidity currents

*Hajime Naruse[1]

1. Department of Geology and Mineralogy, Graduate School of Science, Kyoto University

Cyclic steps are upstream-migrating bedforms accompanied with hydraulic jumps. Recent high-resolution geophysical surveys indicated that they are common topographic features especially in submarine canyons and fans where turbidity currents are dominant process of landform developments. Cyclic steps are common in submarine canyons or upstream regions of submarine fans (canyon-fan transition zone), but their morphological features are significantly different. Upstream bedforms inside submarine canyons are relatively small in wavelength and height, and generally show the crescent shaped or mound-like morphology. On the other hand, cyclic steps in less confined canyon-fan transition zone tend to be large in wavelength and height. The origin of these morphological features has not been clarified yet. Thus, we conducted numerical experiments to investigate the conditions for producing cyclic steps at the canyon-fan transition zone. The model is based on two dimensional shallow water equation of turbidity currents, and it was solved by CIP-CUP method that is the the third-order-accurate scheme. We set a submarine canyon and a flat basin plain in calculation domain, and the experimental turbidity currents is injected from the upstream end of the canyon. The canyon was 5% in slope, 2 m long and was 20 cm wide at the transition to the basin. The basin was 3 m in length and 2 m in width. The turbidity currents were 10 cm thick in maximum, 1vol.% in concentration. Grain size was set to be 30 micron meters. As a result of numerical experiments, upstream-migrating bedforms were formed both inside submarine canyon and on the canyon-fan transition zone. All bedforms are associate with hydraulic jumps, so that it can be classified to cyclic steps. However, bedforms inside the canyon show mound-like shape and have relatively short wavelength, whereas those developed on the canyon-fan transition zone were longer in wavelength and their crests were more continuous. The mound-like bedforms in canyons produced in this study resemble crescent bedforms observed in modern submarine canyons, and the laterally continuous cyclic steps are common features of lobate submarine fans at the upstream end. Judging from the observation of the velocity fields, it is inferred that difference of two bedforms was caused by diagonal cross waves that are steady three-dimensional surface waves of supercritical flows. It has been known that the steady surface waves interact with step and pool structures in mountain rivers. This study implies that the same mechanism may govern the supercritical bedforms in the natural submarine canyons systems.

Keywords: turbidity current, numerical model, bedform

©2020. Japan Geoscience Union. All Right Reserved.

Sedimentary facies related to supercritical-flow bedforms in foreset slopes of middle Pleistocene Gilbert-type delta, central Japan

*Hiroko Okazaki[1]

1. Division of Earth Science, Natural History and Institute, Chiba

This study examined sedimentary facies related to supercritical-flow bedforms in foreset slopes of a Gilbert-type delta in the middle Pleistocene Kamiizumi Formation, central Japan, paying particular attention to bed architectures and internal structures, grain-size distributions, and molluscan assemblages. Coarser grained chute-and-pool deposits laterally alternate with finer grained antidune to subcritical deposits on progradational steep delta slopes. The cyclicity of foresets is an intrinsic characteristic of supercritical flows on progradational steep delta slopes. Cyclic steps in the lower part of the delta foresets may reflect enhanced flood currents on the gentler parts of the delta slope. The vertical changes from cyclic steps to chutes-and-pools to antidunes represent decreasing flow velocity and are the result of autogenic flow transitions during rapid aggradation. Remarkable variations in the facies of delta foreset beds reflect the conditions of inflowing sediments as well as the intrinsic instability of supercritical flows on the foreset slope.

Keywords: supercritical-flow deposits, Gilbert-type delta, Pleistocene

©2020. Japan Geoscience Union. All Right Reserved.

[E] Poster | S (Solid Earth Sciences)：S-GD Geodesy

[S-GD01] Geodetic Infrastructure for Monitoring the Dynamic Earth: The Global Geodetic Observing System

convener:Basara Miyahara(GSI of Japan), Richard S Gross(NASA Jet Propulsion Laboratory)

The Global Geodetic Observing System (GGOS) measures the time-varying shape, rotation, and gravity field of the Earth, which provide accurate geodetic reference frames and enable us to understand various dynamic processes occurring on the Earth. The measurements are achieved with various geodetic techniques such as VLBI, SLR, GNSS, DORIS and gravity measurements. Many institutions in the world have developed their geodetic infrastructure to contribute to GGOS realization and devoted to research activities for Earth science. These activities are well coordinated and supported by the international scientific services of the International Association of Geodesy such as the International VLBI Service for Geodesy and Astrometry (IVS), the International Laser Ranging Service (ILRS), the International GNSS Service (IGS), the International DORIS Service (IDS), the International Gravity Field Service (IGFS), and so on. Through the coordination and support of these efforts, GGOS has fostered global collaboration and advocated stable production of geodetic products such as geodetic reference frames, earth rotation parameters and earth's gravity field models. This session will focus on reporting and discussing recent GGOS activities including geodetic data DOI working group, status of geodetic infrastructure and the results of data analysis for GGOS, and highlight the importance of geodetic observations to monitoring and understanding the dynamic Earth system for the benefit of science and society.

[SGD01-P01] The International VLBI Service and Its Role in GGOS

*Hiroshi Munekane[1], Dirk Behrend[2], Nancy Wolfe Kotary[3] (1.Geospatial Information Aurhotiry of Japan, 2.NVI, Inc., 3.MIT Haystack Observatory)

[SGD01-P03] DORIS: 30 years of success in precise orbit determination and ground station positioning

*Frank G Lemoine[1], Guilhem Moreaux[2], Jérôme Saunier[3], Pascale Ferrage[4], Laurent Soudarin[2], Koichiro Doi[5] (1.NASA Goddard Space Flight Center, Greenbelt, Maryland, U.S.A., 2.Collecte Localisation Satellites, Ramonville Saint-Agne, France, 3.Institut National de l'Information Géographique et Forestière, St-Mandé, France, 4.Centre National d'Etudes Spatiales, Toulouse, France, 5.National Institute of Polar Research, Tachikawa-City, Tokyo, Japan)

[SGD01-P04] The International Gravity Field Service (IGFS) and its contributions to the GGOS infrastructure

Riccardo Barzaghi[1], George S Vergos[2], *Basara Miyahara[3] (1.Politecnico di Milano, 2.Aristotle University of Thessaloniki, 3.GSI of Japan)

[SGD01-P05] Activities of the Ishioka VLBI Station as a VGOS station

*Haruka Ueshiba[1], Tomokazu Nakakuki[1], Saho Matsumoto[1], Nobuhiro Ishikura[1], Michiko Umei[1], Kyonosuke Hayashi[1], Toru Yutsudo[1], Tadao Kikkawa[1], Hiroshi Munekane[1] (1.GSI of Japan)

[SGD01-P06] Satellite Laser Ranging and GNSS observations in the Shimosato Hydrographic Observatory, Japan

*Shun-ichi Watanabe[1], Noritsune Seo[2], Yuto Nakamura[1], Yusuke Yokota[3], Hiroko Fukura[4] (1.Hydrographic and Oceanographic Department, Japan Coast Guard, 2.Shimosato Hydrographic Observatory, 5th Regional Coast Guard Headquarters, Japan Coast Guard, 3.Institute of Industrial Science, University of Tokyo, 4.8th Regional Coast Guard Headquarters, Japan Coast Guard)

[SGD01-P07] Current Status and Prospect of GEONET, Japanese dense GNSS network

*Takayuki Miyazaki[1], Koki Kumagai[1] (1.GSI of Japan)

[SGD01-P09] **Crustal Deformation Measurements in Himachal Himalaya: A New Evidence of Extensional Tectonics**

*Yogendra Sharma[1], Sumanta Pasari[1], Kuo En Ching[2], Onkar Dikshit[3], Javed N Malik[3] (1.Birla Institute of Technology and Science, Pilani, 2.National Cheng Kung University, Taiwan, 3.IIT Kanpur)

[SGD01-P10] Crustal deformation by the 2019 Typhoon Hagibis: High time-resolution study

*Wei Zhan[1], Kosuke Heki[2] (1.The First Monitoring and Application Center, China Earthquake Administration, 2.Department of Natural History Sciences, Hokkaido University)

[SGD01-P11] Analyzing the Tropospheric Delay Estimates on Global Navigation Satellite Systems (GNSS) with Precise Point Positioning (PPP) Services using the goGPS software.

*Syachrul Arief[1], Kosuke Heki[1], Andrea Gatti[2], Eugenio Realini[2] (1.Hokkaido University - Sapporo, Japan, 2.Geomatics Research and Development s.r.l. - Lomazzo, Italy)

[SGD01-P12] Development of novel ground-based microwave radiometer for earth science - results of the first measurements-

*Ryuichi Ichikawa[1], Hideki Ujihara[1], Shinsuke Satoh[1], Yusaku Ohta[2], Basara Miyahara[3], Hiroshi Munekane[3], Taketo Nagasaki[4], Osamu Tajima[5], Kentaro Araki[6], Takuya Tajiri[6], Hiroshi Takiguchi[7], Takeshi Matsushima[8], Nobuo Matsushima[9], Tatsuya Momotani[10], Kenji Utsunomiya[10] (1.National Institute of Information and Communications Technology, 2.Tohoku University, 3.Geospatial Information Authority of Japan, 4.RIKEN, 5.Kyoto University, 6.Meteorological Research Institute, JMA, 7.Japan Aerospace eXploration Agency, 8.Kyushu University, 9.National Institute of Advanced Industrial Science and Technology, 10.Japan Weather Association)

[SGD01-P13] Use Delay-Doppler Map Made by Oceanic Reflected GPS Signal to Evaluate Ocean Surface Wind

*Wen-Hao Yeh[1], Yung-Fu Tsai[1], Chen-Tsung Lin[1], Hwa Chien[2], Lin Zhang [2] (1.National Space Organization, National Applied Research Laboratories, Taiwan, 2.Institute of Hydrological & Oceanic Sciences, National Central University, Taiwan)

The International VLBI Service and Its Role in GGOS

*Hiroshi Munekane[1], Dirk Behrend[2], Nancy Wolfe Kotary[3]

1. Geospatial Information Aurhotiry of Japan, 2. NVI, Inc., 3. MIT Haystack Observatory

The International VLBI Service for Geodesy and Astrometry (IVS), inaugurated in 1999, is an international collaboration of organizations that operate or support very long baseline interferometry (VLBI) components. The IVS is a service of the International Association of Geodesy (IAG) and the International Astronomical Union (IAU) and comprises more than 80 permanent components in over 20 countries. IVS organizations are currently in the process of implementing the next-generation broadband VLBI component of GGOS. This broadband VLBI system, the VLBI Global Observing System (VGOS), will ultimately replace the legacy S/X-band systems worldwide. VGOS broadband observations are made by fast-slewing 12-meter antennas in four bands between 2.5 GHz and 14 GHz. Once fully realized, VGOS will provide positional accuracies of 1 mm on global scales and involve continuous observations. The IVS also provides highly accurate and unique products through VLBI for the realization and maintenance of the celestial and terrestrial reference frames, ICRF and ITRF, and the Earth Orientation Parameters (EOP). VLBI plays a unique and fundamental role in the realization and maintenance of the global reference frames and in the determination of the EOP, including observation of quasars (necessary to realize the ICRF), the complete set of EOP including UT1−UTC, and the most precise measurements of intercontinental baselines for the realization and maintenance of the ITRF.

Keywords: VLBI, VGOS, ITRF, ICRF, EOP

©2020. Japan Geoscience Union. All Right Reserved.

DORIS: 30 years of success in precise orbit determination and ground station positioning

*Frank G Lemoine[1], Guilhem Moreaux[2], Jérôme Saunier[3], Pascale Ferrage[4], Laurent Soudarin[2], Koichiro Doi[5]

1. NASA Goddard Space Flight Center, Greenbelt, Maryland, U.S.A., 2. Collecte Localisation Satellites, Ramonville Saint-Agne, France, 3. Institut National de l’ Information Géographique et Forestière, St-Mandé, France, 4. Centre National d’ Etudes Spatiales, Toulouse, France, 5. National Institute of Polar Research, Tachikawa-City, Tokyo, Japan

Doppler Orbitography and Radiopositioning Integrated by Satellite (DORIS) system is one of the four techniques that contributes to the International Terrestrial Reference Frame (ITRF). The technique was developed to support orbit determination on LEO satellites, most notably the suite of ocean radar altimeter satellites. The DORIS system consists of a global well-distributed set of ground beacons emitting on two frequencies (2 GHz and 401 MHz) and a satellite constellation consisting of an evolving suite of satellites that carry different generations of satellite receivers. Presently DORIS has colocations with other geodetic techniques at 47 out of 58 sites, many with GNSS. These include Badary, Greenbelt, Wettzell, and Yarragadee who host all four space geodesy techniques (DORIS, GNSS, SLR & VLBI), and Arequipa, Grasse, Kauai, Mt. Stromlo, Ny Alesund, Papeete, Jiufeng, and Syowa (Antarctica) who host three of the space geodetic techniques, including DORIS. The DORIS system became operational 30 years ago in February 1990, with its inauguration on the SPOT-2 satellite. Presently six satellites on-orbit carry a DORIS DGXX receiver (Cryosat-2, HY-2A, Jason-3, Saral, and Sentinel-3A and Sentinel-3B). A DGXX receiver can track up to seven ground beacons when they are in view of the orbiting satellite. This capability greatly increases the amount of data available for orbit determination and strengthens the DORIS contribution to the ITRF.

In this paper we provide a summary of the current status of the DORIS system, its science contributions, and its contributions to GGOS. We describe the evolution of the DORIS system including the improvements in the ground network, and summarize the products that are made possible by DORIS, including its contributions to the ITRF, and to the measurement of the change in Global Mean Sea Level.

In addition, we highlight the performance of select stations, such as the DORIS station in Syowa, Antarctica, including its contributions to science missions, and comparisons with other geophysical measurements.

Keywords: DORIS, Space geodesy, ITRF, colocation

©2020. Japan Geoscience Union. All Right Reserved.



©2020. Japan Geoscience Union. All Right Reserved.

The International Gravity Field Service (IGFS) and its contributions to the GGOS infrastructure

Riccardo Barzaghi[1], George S Vergos[2], *Basara Miyahara[3]

1. Politecnico di Milano, 2. Aristotle University of Thessaloniki, 3. GSI of Japan

The International Gravity Field Service (IGFS) promotes the interaction, cooperation and synergy between the Gravity Services, namely the Bureau Gravimétrique International (BGI), the International Service for the Geoid (ISG), the International Geodynamics and Earth Tides Service (IGETS), the International Center for Global Earth Models (ICGEM) and the International Digital Elevation Model Service (IDEMS). Furthermore, through its Product Center, namely the International Combination Service for Time-variable Gravity Fields (COST-G), IGFS provides consolidated monthly global gravity models in terms of spherical harmonic coefficients and thereof derived grids by combining solutions from individual Analysis Centers.

The IGFS Central Bureau is hosted at the Aristotle University of Thessaloniki (Greece) and, besides other activities, provides a link to the Global Geodetic Observing System (GGOS) Bureaus in order to communicate their requirements and recommendations to the IGFS-Centers. Moreover, IGFS provides a coordination host for the utilization of gravity-field related products and services towards their inclusion within a GGOS consistent frame.
In this work, an outline is given on the recent activities of IGFS, namely those related to the contributions to the implementation of the International Height Reference System/Frame; the Global Geodetic Reference System/Frame; the new Global Absolute Gravity Reference System/Frame and the combination of temporal monthly global gravity field models. Particularly, the impact that these activities have and will have in improving the estimation of the Earth’ s gravity field, either at global and local scale, is highlighted also in the framework of GGOS.

Keywords: gravity field, geoid, global geodtic observing system

©2020. Japan Geoscience Union. All Right Reserved.

Activities of the Ishioka VLBI Station as a VGOS station

*Haruka Ueshiba[1], Tomokazu Nakakuki[1], Saho Matsumoto[1], Nobuhiro Ishikura[1], Michiko Umei[1], Kyonosuke Hayashi[1], Toru Yutsudo[1], Tadao Kikkawa[1], Hiroshi Munekane[1]

1. GSI of Japan

The International VLBI Service for Geodesy and Astrometry (IVS) promotes the transition from the legacy VLBI system with S/X frequency bands to the next-generation VLBI system called VGOS (VLBI Global Observing System), which is part of Global Geodetic Observing System (GGOS). The goals of VGOS are to achieve: 1-mm position accuracy on global scales, continuous measurements for time series of station positions as well as Earth Orientation Parameters, and turnaround time to initial geodetic results of less than 24 hours. To achieve these goals, the VGOS stations should be equipped with antennas with high slewing rate, receivers for broadband observations (2-14 GHz) and high speed recording systems up to 32 Gbps. Currently, because the number of VGOS stations is not sufficient, legacy S/X observations are mainly conducted at IVS while VGOS observations are also regularly conducted.

The Geospatial Information Authority of Japan (GSI) constructed a new VLBI facility in Ishioka in 2014 which meets the VGOS requirements and began its operation in May 2016. The Ishioka Station uses two different types of receiver depending on a type of an observation: tri-band feed for S/X observations and QRFH for broadband observations, and it is necessary to replace receivers when switching types of observations, which takes about one week. Hence, the Ishioka Station mainly participates in legacy S/X international observation, and participates in broadband observation for several months every year. In the latest broadband observation term from December 2019 to February 2020, the Ishioka Station participated in VGOS Test observations organized by IVS (once every two weeks, 24 hours observation. Since January 2020, these have been operated as official observations.), and also participated in test observations organized by the European VLBI Group and VGOS-intensive test observations (once a week, 1 hour) for the first time. The Ishioka Station also participated in experiments for the inter-continental frequency comparison project conducted by National Institute of Information and Communications Technology (NICT).

To avoid the replacement of receivers when switching types of observations, we are promoting investigations and improvement for “Mixed Mode” observations in which S/X and broadband signals are received simultaneously without replacing receivers. In the Mixed Mode observations, S/X and broadband signals are received at the same time by QRFH. With the Mixed Mode Observations, the Ishioka Station may participate in broadband observations as one of VGOS stations while regularly participating in S/X observations for stable position products until IVS moves to full VGOS.

For achieving the Mixed Mode observations, it is necessary to mitigate the effect of strong RFI around S-band (2-3 GHz). Currently, a high pass filter which cuts off signals lower than 3GHz is inserted in the circuit of QRFH. To receive S-band signals by QRFH, it is necessary to design the band pass filter to allow the reception of S-band signal while avoiding signal saturation caused by RFI. The GSI is currently developing a superconductor band pass filter whose design reflects the investigation of RFI around the Ishioka Station (Hayashi et al., 2019), which will replace the current high pass filter.

This talk will summarize activities of the Ishioka station as one of VGOS stations and progress of improvement of QRFH for Mixed Mode observations.

©2020. Japan Geoscience Union. All Right Reserved.

Keywords: VLBI, VGOS, the Ishioka VLBI Station

©2020. Japan Geoscience Union. All Right Reserved.

Satellite Laser Ranging and GNSS observations in the Shimosato Hydrographic Observatory, Japan

*Shun-ichi Watanabe[1], Noritsune Seo[2], Yuto Nakamura[1], Yusuke Yokota[3], Hiroko Fukura[4]

1. Hydrographic and Oceanographic Department, Japan Coast Guard, 2. Shimosato Hydrographic Observatory, 5th Regional Coast Guard Headquarters, Japan Coast Guard, 3. Institute of Industrial Science, University of Tokyo, 4. 8th Regional Coast Guard Headquarters, Japan Coast Guard

The Shimosato Hydrographic Observatory (SHO) of Japan Coast Guard, located in the southernmost part of Wakayama Prefecture, operates Satellite Laser Ranging (SLR) observations since 1982 as well as continuous GNSS observation. Collected SLR and GNSS data are transferred to the International Laser Ranging Service (ILRS) and the International GNSS Service (IGS), respectively. The transferred data contribute to the construction and development of the International Terrestrial Reference Frame (ITRF). The SHO which operates two kinds of global geodetic techniques is now one of the Global Geodetic Observing System (GGOS) sites.

In order to enhance the usability of the SLR observation system, the SHO has updated its laser ranging equipment in 2018. We installed a laser oscillator with changeable pulse repetition rate up to 1 kHz (i.e., kilohertz laser), by which we can collect the ranging data at a higher rate than by the former one with a pulse repetition rate of 5 Hz. The relevant updates on the control devices contribute to the simplification of SLR operation.

In this presentation, we first describe the summary of our laser ranging system update in the SHO, and then show the geodetic results of SLR and GNSS positioning at the SHO. The SLR monthly positions were calculated using LAGEOS-1 and LAGEOS-2 ranging data with the analysis software C5++ (Otsubo et al., 2016, Earth Planets Space). The results clearly reproduced the coseismic displacements due to the 2004 southeastern off Kii Peninsula earthquakes (M7.4 and M6.9) and the 2011 Tohoku-oki earthquake (M9.0). In addition, significant postseismic displacements following the Tohoku-oki earthquake were also obtained.
Acknowledgments: Dr. Otsubo of the Hitotsubashi University provided us the analysis software “C5++” and the adjusted data/parameters for SHO’s data analysis.

Keywords: Satellite Laser Ranging, GNSS, LAGEOS, C5++ software, Co-location site

©2020. Japan Geoscience Union. All Right Reserved.

Current Status and Prospect of GEONET, Japanese dense GNSS network

*Takayuki Miyazaki[1], Koki Kumagai[1]

1. GSI of Japan

GSI of Japan has operated domestic dense GNSS network (GNSS Earth Observation NETwork system: GEONET), which consisted of over 1,300 observation stations covering most region of Japan and control center at GSI of Japan, Ibaraki prefecture. Observation data and daily coordinates of each GEONET station are provided for surveyors or earth scientists and so on. GEONET data and products are used as infrastructure regarding precise positioning.

For keeping GEONET being infrastructure of precise positioning, it is indispensable to devote considerable efforts to maintenance work. In 2019, two huge typhoons (typhoon 15 category 4 and typhoon 19 category 5) impacted Kanto and Tohoku region and these typhoons damaged many GEONET stations. In this presentation, we will introduce maintenance work of GEONET through response to these typhoons.

Introducing new techniques regarding GNSS observation to GEONET is also important. GSI conducts investigation for implementation of multi-GNSS and 5th generation mobile communication system. We will mention these topics.

©2020. Japan Geoscience Union. All Right Reserved.

Crustal Deformation Measurements in Himachal Himalaya: A New Evidence of Extensional Tectonics

*Yogendra Sharma[1], Sumanta Pasari[1], Kuo En Ching[2], Onkar Dikshit[3], Javed N Malik[3]

1. Birla Institute of Technology and Science, Pilani, 2. National Cheng Kung University, Taiwan, 3. IIT Kanpur

In this work, we have used five years of GPS data to understand the contemporary crustal deformation pattern in the Himachal region of the Northwest Himalaya. Surface velocities estimated in International Terrestrial Reference Frame 2008 (ITRF08) are observed to lie in the range of *42-48* mm/yr with an uncertainty level of *~1* mm/yr. To analyze the kinematics of major faults in the study region, horizontal and vertical GPS velocities are inverted for the fault slip rate and fault geometries using a 2-D dislocation model. The horizontal velocities are also decomposed into the fault-parallel and fault-normal components. We have then selected a velocity profile across two major faults, namely MFT (Main Frontal Thrust) and MBT (Main Boundary Thrust). To perform the 2-D fault modeling along the profile, we assume that the fault geometry comprises a décollement known as MHT (Main Himalayan Thrust). The considered fault parameters are dip angle, fault depth, locking depth, location of faults on the surface, slip rates and rake angle. We search for the optimized fault parameters using the Monte Carlo-Metropolis inversion method. In the velocity profile, no remarkable velocity gradient is observed across the fault lines. However, a small patch of extension with a rate of about 3.7 mm/yr between MFT and MBT can be seen in this profile. The slip rates of MFT and MBT are estimated as ~0.8 mm/yr and ~2.8 mm/yr, respectively. The low slip rate of MFT indicates a locking behavior of the thrust-fault. Nevertheless, the maximum vertical velocity between HFT and MBT reaches up to 17.5 mm/yr. Following the uplift and minor extension, this region appears to be rising upside or emerging as a new pop-up structure. However, spatial resolution of sparse GPS stations inhibits stringent conclusions on this localized deformation.

Keywords: GPS, 2-D Dislocation Model, Himalaya, Pop-Up structure

©2020. Japan Geoscience Union. All Right Reserved.



©2020. Japan Geoscience Union. All Right Reserved.

©2020. Japan Geoscience Union. All Right Reserved.

Crustal deformation by the 2019 Typhoon Hagibis: High time-resolution study

*Wei Zhan[1], Kosuke Heki[2]

1. The First Monitoring and Application Center, China Earthquake Administration, 2. Department of Natural History Sciences, Hokkaido University

Powerful typhoon Hagibis (2019 #19) which made landfall in Japan on 12 October 2019 was the one of the strongest typhoons to hit the country. In the Gulf Coast of southern USA, Milliner et al. (2018) analyzed crustal deformation using a dense network of continuous GNSS (Global Navigation Satellite System) receivers due to the stormwater load of the 2017 Hurricane Hurvey. They found ~1/3 of the total precipitation stayed on land for days and caused significant crustal subsidence. Here we study crustal deformation caused by the water load left by the 2019 Typhoon #19 Hagibis, based on the coordinate time series of the dense continuous GNSS network of Japan GEONET (GNSS Earth Observation Network) downloaded from the Univ. Nevada Reno (UNR) data base (Blewitt et al., 2018). Discussions using daily GSI F3 solution are given in another paper, Heki et al. (this session).

In this paper, we concentrate on high time resolution crustal deformation, and use the 5 min solution from the UNR data base to study sub-daily vertical coordinate changes in four regions, Izu (R1), Boso (R2), Fukushima (R3), and Jo’ etsu (R4) (Fig.1a). To reduce the noise, we calculated 1h-average and 6h-average coordinates and show their time series in Fig.lb. The station J620 (0620) in region R1 showed that the station started to subside by up to ~2 cm on 11 October, corresponding to the day of the year (DOY) 284, one day before the Typhoon Hagibis made landfall. It recovered to the original position on 12 October (DOY 285) (days and times are all in UT). Conversely, station I025 (3025) in region R2 did not show significant subsidence on 12 October. Station G176 (1176) in region R3 showed a large subsidence of 2-3 cm during 12 October. Station J820 (0820) showed a subsidence of ~2 cm over a longer duration, starting on 12 October and lasting until 13 October (DOY 286).

From these results, we can study distribution of stormwater load and its decay by draining to ocean as was done by Milliner et al. (2018) in USA. These results demonstrate that the dense GPS network is a useful sensor to understand water dynamics associated with extreme weather events with high spatial and temporal resolution.

Keywords: Crustal deformation, Typhoon Hagibis, GNSS

©2020. Japan Geoscience Union. All Right Reserved.

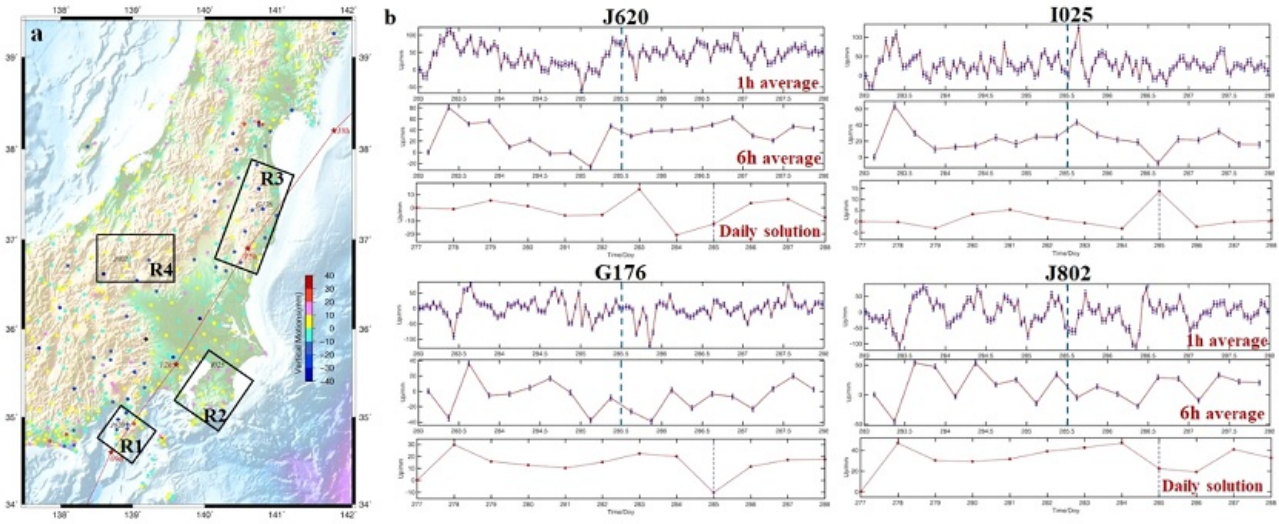


Figure 1. (a) Track of the 2019 Typhoon Hagibis on 12 October 2019 (red curve) and four studied regions R1-R4 shown in black rectangles. (b) Time series of the vertical coordinates of the GNSS stations J620, I025, G176 and J802 in the regions R1-R4 from DOY 277-289 (from 04 to 16 October 2019) in three different time resolution, hourly (top), every 6 hours (middle) and daily (bottom). Times and days are in UT. The dashed vertical lines indicate the beginning of 12 October (DOY 285).

©2020. Japan Geoscience Union. All Right Reserved.

Analyzing the Tropospheric Delay Estimates on Global Navigation Satellite Systems (GNSS) with Precise Point Positioning (PPP) Services using the goGPS software.

*Syachrul Arief[1], Kosuke Heki[1], Andrea Gatti[2], Eugenio Realini[2]

1. Hokkaido University - Sapporo, Japan, 2. Geomatics Research and Development s.r.l. - Lomazzo, Italy

The tropospheric delay is an essential source of error for positioning using the Global Navigation Satellite System (GNSS). Scientific applications of GNSS positioning such as the study of earth crust deformation and earthquake prediction require high accuracy in positioning, an analysis of tropospheric delay calculations is needed to improve the accuracy of GNSS positioning. One part of the tropospheric delay is Zenith tropospheric delays (ZTD), which are estimated using the Precise Point Positioning (PPP) method. ZTD estimates can be beneficial for meteorological applications, for example, is the estimation of water vapor levels in the atmosphere from the estimated ZTD. We use GNSS data from the BAKO station in Cibinong and JOG2 station located in Yogyakarta. The GNSS data format is an Independent Exchange Receiver (RINEX) which we extracted using the sophisticated open-source GNSS software, called goGPS version 1.0 Beta from Geomatics Research and Development s.r.l. - Lomazzo, Italy. We validate the results of the extraction process with two international tropospheric products from International GNSS Services (IGS) with commercial software Bernese version 5 and the University of Nevada Reno (UNR) with software from NASA Jet Propulsion Laboratory (JPL) namely GIPSY / OASIS II. Epoch in this study, we use days of the year (DOY) 022-025 / 22-25 January representing the rainy season and DOY 230-233 to coincide on August 17-20 representing the dry season 2018. Then we use DOY for a full month in January 2018 and August 2018 to determine the value of Zenith Wet Delay (ZWD). Our results obtained RMS values throughout DOY, both at BAKO and JOG2 stations showing small values < 2 mm. The RMS value is relatively minimal, meaning that the troposphere estimation process with goGPS shows good agreement because it is almost the same as the international troposphere product from UNR and IGS. Then the RMS values, both in January and August and the two BAKO and JOG2 stations, are relatively consistent and work well at different times and stations. ZWD values tend to be higher in the rainy season than in the dry season, which shows that ZWD can be useful for meteorological purposes.

Keywords: Tropospheric Delay , GNSS, PPP, goGPS

©2020. Japan Geoscience Union. All Right Reserved.

Development of novel ground-based microwave radiometer for earth science -results of the first measurements-

*Ryuichi Ichikawa[1], Hideki Ujihara[1], Shinsuke Satoh[1], Yusaku Ohta[2], Basara Miyahara[3], Hiroshi Munekane[3], Taketo Nagasaki[4], Osamu Tajima[5], Kentaro Araki[6], Takuya Tajiri[6], Hiroshi Takiguchi[7], Takeshi Matsushima[8], Nobuo Matsushima[9], Tatsuya Momotani[10], Kenji Utsunomiya[10]

1. National Institute of Information and Communications Technology, 2. Tohoku University, 3. Geospatial Information Authority of Japan, 4. RIKEN, 5. Kyoto University, 6. Meteorological Research Institute, JMA, 7. Japan Aerospace eXploration Agency, 8. Kyushu University, 9. National Institute of Advanced Industrial Science and Technology, 10. Japan Weather Association

We have started to develop a next-generation microwave radiometer to be used in millimeter-wave spectroscopy for the high-resolution and high-precision monitoring of water vapor behavior. The new radiometer will be suitable for not only space geodetic techniques such as VLBI and GNSS, but also field measurements to monitor, for example, volcanic activities and cumulonimbus cloud generation. The planned front-end system for our new microwave radiometer has a wide bandwidth feed of 20–60 GHz. A signal from the feed is separated into two linear orthogonal polarized signals using an orthomode transducer (OMT); one is in the 20–30 GHz feed and the other is in the 50–60 GHz feed. We are now planning to cool the wideband feed, OMT, and LNA for each signal at 77 K using a Stirling cryocooler to improve the signal-to-noise ratio. We assembled a room-temperature 20–30 GHz receiver without the cooling system until the middle of 2019 as a first step of our development. We implemented the new receiver into the 3.7 m dish at Okinawa Electromagnetic Technology Center, National Institute of Information and Communications Technology (NICT), and carried out the first measurements using this receiver for validation tests in October 2019. Quick-look data obtained by the new receiver shows good power signals for the expected receiving band of 18–28 GHz. We are now developing another receiver for a higher band of 50–60 GHz, and we are going to implement the second one into the new prototype radiometer by the end of this fiscal year.

©2020. Japan Geoscience Union. All Right Reserved.

Use Delay-Doppler Map Made by Oceanic Reflected GPS Signal to Evaluate Ocean Surface Wind

*Wen-Hao Yeh[1], Yung-Fu Tsai[1], Chen-Tsung Lin[1], Hwa Chien[2], Lin Zhang [2]

1. National Space Organization, National Applied Research Laboratories, Taiwan, 2. Institute of Hydrological & Oceanic Sciences, National Central University, Taiwan

The research of GNSS-Reflectometry (GNSS-R) begins at the end of 20 century. As the first GNSS-R satellite mission, UK-DMC satellite carries an experimental payload to receive the reflected GNSS signal from ocean surface. The output of UK-DMC GNSS-R payload is Delay-Doppler Map (DDM), which is the cross-correlation results of received ocean surface reflected GNSS signal in different delay and Doppler. After UK-DMC, the follow on GNSS-R mission are TDS-1 and CYGNSS, which are the mission from UK and USA. In the second half of the year in 2021, the Taiwan built satellite of GNSS-R mission, TRITON, will be launched. TRITON also carries the Taiwan built GNSS-R payload to receive ocean refelcted GNSS signal and produce DDM. In order to retrieve the ocean surface wind from DDM, the system for DDM retrieving will be developed. In this study, the retrieval method will be introduced.

Keywords: GNSS-Reflectometry, Delay-Doppler Map, TRITON

©2020. Japan Geoscience Union. All Right Reserved.

[E] Poster | S (Solid Earth Sciences)：S-SS Seismology

[S-SS03] Seismological advances in the ocean

convener:Takashi Tonegawa(Research and Development center for Earthquake and Tsunami, Japan Agency for Marine-Earth Science and Technology), Takeshi Akuhara(Earthquake Research Institute, University of Tokyo), Pascal Audet(University of Ottawa), Taka'aki Taira(Berkeley Seismological Laboratory, University of California, Berkeley)

Seismic observations in the oceans have been steadily increasing in the last two decades due to continued deployments and recent advances in temporary arrays and permanent (cabled) networks including seismometers, hydrophones, and pressure gauges. The use of ocean data on the seafloor and in the seawater has compelled the community to create/modify data processing techniques, with exciting new findings on, e.g., seismicity, wave phenomena, seismic structures from active and passive surveys, and underwater phenomena. Some of these studies may be related to environmental seismology in the ocean. The purpose of this session is to share recent advances in seismology from data obtained in the oceans, including new seismicity and seismic velocity, progress in instrumentation, data processing on active and passive seismic approaches, characterization of ambient noise, e.g., microseisms and infragravity waves, as well as challenges in suppressing contamination from ocean-related noise.

[SSS03-P02] Incoming directions of broadband infragravity waves observed at the central part of the Pacific Ocean

*Takashi Tonegawa[1], Kiwamu Nishida[2], Yoshio Fukao[1] (1.Research Institute for Marine Geodynamics, Japan Agency for Marine-Earth Science and Technology, 2.Earthquake Research Institute, The University of Tokyo)

[SSS03-P04] Structure of the northern Hikurangi margin from receiver functions using broadband OBS data from the HOBITSS experiment

*Pascal Audet[1], Martha K Savage[2], Anne Sheehan[3], Kimihiro Mochizuki[4] (1.University of Ottawa, 2.Victoria University of Wellington, 3.University of Colorado at Boulder, 4.University of Tokyo)

[SSS03-P05] Seismic interferometry analyses of teleseismic coda waves on a dense network of permanent ocean bottom seismometers (S-net) offshore Honshu, Japan

★Invited Papers

*Tomoya Takano[1,2], Florent Brenguier[1], Pierre Boue[1], Ryota Takagi[3], Kaoru Sawazaki[4], Tetsuya Takeda[4], Yosuke Aoki[2], Kiwamu Nishida[2] (1.Institut des Sciences de la Terre, Univ. Grenoble Alpes, 2.Earthquake Research Institute, The University of Tokyo, 3.Research Center for Prediction of Earthquakes and Volcanic Eruptions, Graduate School of Science, Tohoku University, 4.NIED)

[SSS03-P06] “N”-shaped Y/X coda spectral ratio observed for in-line type OBS of S-net and ETMC

*Kaoru Sawazaki[1], Takeshi Nakamura[1] (1.National Research Institute for Earth Science and Disaster Resilience)

[SSS03-P07] Spatiotemporal Variations of PM Excitation in the Northern Okinawa Trough Revealed by OBS Array

*Chih-Chieh Chien[6], Ying-Nien Chen[3], Yuancheng Gung[6], Ban-Yuan Kuo[1], Shu-Huei Hung[6], Eh Tan[1], Kate Huihsuan Chen[5], Shuichi Kodaira[2], Yasushi Ishihara[2], Mamoru Nakamura[8], Chau-Chang Wang[4,7], Ching-Ren Lin[1] (1.Academia Sinica, Taipei, Taiwan, 2.Japan Agency for Marine-Earth Science and Technology, Yokohama, Japan, 3.National Chung Cheng University, Chiayi, Taiwan, 4.National Sun Yat-sen University, Kaohsiung, Taiwan, 5.National Taiwan Normal University, Taipei, Taiwan, 6.National Taiwan University, Taipei, Taiwan, 7.Taiwan Ocean Research Institute, National Applied Research Laboratories, Kaohsiung, Taiwan, 8.University of the Ryukyus, Okinawa, Japan)

[SSS03-P08] Rayleigh wave ellipticity estimated from earthquake and noise cross-correlations of OBS data: Effect of ocean and sedimentary layers.

*Shun Fukushima[1], Kiyoshi Yomogida[2] (1.Hokkaido University,Graduate school of Science,Department of Natural History Sciences,Seismology Laboratory , 2.Department of Earth and Planetary Dynamics, Graduate School of Science, Hokkaido University)

[SSS03-P09] A Temporal Variation of Auto-correlation Function Calculated from Ocean Bottom Seismometers off Miyagi Prefecture

*Miyuu Uemura[1], Yoshihiro Ito[2], Kazuaki Ohta[3], Ryota Hino[4], Masanao Shinohara[5] (1.Graduate School of Science, Kyoto University, 2.Disaster Prevention Research Institute, Kyoto University, 3.National Research Institute for Earth Science and Disaster Resilience, 4.Graduate School of Science, Tohoku University, 5.Earthquake Research Institute, University of Tokyo)

[SSS03-P10] Similar earthquake activity in the northern part of the Ryukyu subduction zone observed by onshore and offshore seismic data

*Yukihiro Nakatani[1], Hiroshi Yakiwara[1], Shuichiro Hirano[2], Reiji Kobayashi[2], Hiroki Miyamachi[2], Shigeru Nakao[2], Yusuke Yamashita[3], Kazunari Uchida[4], Takeshi Matsushima[4], Hiroshi Shimizu[4], Kazuo Nakahigashi[5], Tomoaki Yamada[6], Hideji Abe[7], Masanao Shinohara[7] (1.Nansei-Toko Observatory for Earthquakes and Volcanoes, Kagoshima University, 2.Graduate School of Science and Engineering, Kagoshima University, 3.Disaster Prevention Research Institute, Kyoto University, 4.Institute of Seismology and Volcanology, Faculty of Science, Kyushu University, 5.Tokyo University of Marine Science and Technology, 6.Japan Meteorological Agency, 7.Earthquake Research Institute, the University of Tokyo)

[SSS03-P11] Spatiotemporal distribution of fin whale signals in northeast Japan

*Takeshi Nakamura[1], Ryoichi Iwase[2] (1.National Research Institute for Earth Science and Disaster Resilience, 2.Japan Agency for Marine-Earth Science and Technology)

Incoming directions of broadband infragravity waves observed at the central part of the Pacific Ocean

*Takashi Tonegawa[1], Kiwamu Nishida[2], Yoshio Fukao[1]

1. Research Institute for Marine Geodynamics, Japan Agency for Marine-Earth Science and Technology, 2. Earthquake Research Institute, The University of Tokyo

Infragravity waves (IGWs) are commonly observed at deep water, and their propagation characteristics have been investigated mainly by array analyses based on seafloor observations using seismometers and pressure gauges. Tonegawa et al (2018) revealed that IGWs at a frequency of 0.005-0.02 Hz observed at an absolute pressure gauge (APG) array with an aperture of 30 km off Aogashima Island, south of the Japanese Islands, are coming from South America in boreal summer and North and South America in boreal winter: the IGWs pass through the Pacific Ocean. To investigate the excitation and its seasonal variation of the IGWs in broadband frequency, arrays of seismometers or/and pressure gauges at the central part in the Pacific Ocean with wider apertures are useful. In this study, we used continuous records of differential pressure gauges (DPG) deployed around Hawaii islands by The Hawaiian PLUME Project to investigate IGW characteristics passing through the Pacific Ocean.

We used 22 DPGs with an array aperture of 600 km and station spacing of ~50 km. The observation periods were (1) from January 2005 to January 2006 and (2) from April 2006 to June 2007. In this study, we used the data from the first observation because the array aperture and station spacing in the first one was suitable for detecting IGWs. For continuous records, we applied a cross-correlation technique with one-bit normalization, and estimated incoming directions of IGWs using the calculated cross-correlation functions (CCFs) at frequency bands of 0.5 –1 mHz, 1–2 mHz, 2–10 mHz, and 10–20 mHz by assuming that IGWs wavefront is planar.

For the CCF, we changed the stacking time length of CCFs to detect IGW propagations. As a result, IGWs could not be retrieved in the 1-day averaged CCFs, but they emerged in the 30-day CCFs in the four frequency bands. Our results on the incoming IGW direction show that long-period IGWs (0.5–1 mHz) are coming from all directions in boreal winter and between east and south in boreal summer, while short-period IGWs (10–20 mHz) are coming between north and east in boreal winter and between east and south in boreal summer. This means that the IGW characteristics between long and short periods in boreal summer are consistent, but in boreal winter are significantly different. To investigate the excitation and seasonal variations of IGWs more details, the calculation of ray paths would be required.

Acknowledgement

The DPG data was acquired by The Hawaiian PLUME Project, and was downloaded by Incorporated Research Institutions for Seismology (IRIS) (https://www.iris.edu/hq/).

Keywords: Infragravity wave, Pacific Ocean, Incoming direction

©2020. Japan Geoscience Union. All Right Reserved.

Structure of the northern Hikurangi margin from receiver functions using broadband OBS data from the HOBITSS experiment

*Pascal Audet[1], Martha K Savage[2], Anne Sheehan[3], Kimihiro Mochizuki[4]

1. University of Ottawa, 2. Victoria University of Wellington, 3. University of Colorado at Boulder, 4. University of Tokyo

The HOBITSS (Hikurangi Ocean Bottom Investigation of Tremor and Slow Slip) experiment was designed to instrument the seafloor offshore northern New Zealand with absolute pressure gauges and ocean-bottom seismometers (OBS) to record an expected slow slip event on the Hikurangi subduction interface near Gisborne. The experiment was successful in recording the slow slip event, and the data yielded outstanding results showing slip to the trench (Wallace et al., 2016) as well as temporal changes in the seismic velocity structure of the overlying plate accompanying the SSE (Warren-Smith et al., 2019; Zal et al., 2020). In this work, we investigate the seismic velocity structure of the subduction zone using teleseismic receiver function data using the broadband OBS (BBOBS) stations deployed as part of HOBITSS. In total there are 10 BBOBS stations available; however, several instruments were found to have problems or did not record sufficient data for further processing (Zal et al., 2020). Here we re-examine this data set for its suitability to determine shallow crustal structure using receiver functions by first pre-processing the BBOBS data in two ways: 1) we re-orient the stations using a recently proposed method that minimizes the constant term in a harmonic expansion of tangential P-wave receiver functions near zero lag time (Lim et al., 2017). We find azimuths similar to those of Zal et al. (2020) and; 2) we remove compliance and tilt noise on the vertical component following the approach of Bell et al. (2015). Following pre-processing, we apply a standard receiver function method based on the multitaper deconvolution technique of Park and Levin (2000). We perform preliminary modeling of the receiver functions using stacks of horizontal layers (Audet, 2016; Audet et al., 2019), and find that the incoming Pacific plate can be modeled by a shallow, thin low-velocity sedimentary layer overlying a ~16 km thick crust.

References

Audet, P., 2016. Receiver functions using OBS data: promises and limitations from numerical modelling and examples from the Cascadia Initiative, *Geophys. J. Int.*, 205, 1740–1755.

Audet, P., Thomson, C.J., Bostock, M.G., Eulenfeld, T., 2019. Telewavesim: Python software for teleseismic body wave modeling. *Journal of Open Source Software*, 4(44), 1818.

Bell, S.W., Forsyth, D.W., Ruan, Y., 2015. Removing Noise from the Vertical Component Records of Ocean-BottomSeismometers: Results from Year One of the Cascadia Initiative, *Bull. Seism. Soc. Am.*, 105,

©2020. Japan Geoscience Union. All Right Reserved.

300–313.

Lim, H., Kim, Y., Song, T.-R.A., Shen, X., 2017. Measurement of seismometer orientation using the tangential P-wave receiver function based on harmonic decomposition, *Geophys. J. Int.*, 212, 1747-1765.

Park, J., Levin, V., 2000. Receiver Functions from Multiple-Taper Spectral Correlation Estimates, *Bull. Seism. Soc. Am.*, 90, 1507-1520.

Wallace, L.M., Webb, S.C., Ito, Y., Mochizuki, K., Hino, R., Henrys, S., Schwartz, S.Y., Sheehan, A.F., 2016. Slow slip near the trench at the Hikurangi subduction zone, New Zealand, *Science*, 352, 701–704

Warren-Smith, E., Fry, B., Wallace, L., Chon, E., Henrys, S.A., Sheehan, A.F., Mochizuki, K., Schwartz, S.Y., Lebedev, S., 2019. Episodic stress and fluid pressure cycling in subducting oceanic crust during slow slip, *Nat. Geosci.*, 12, 475–481

Zal, H.J., Jacobs, K., Savage, M.K., Yarce, J., Mroczek, S., Graham, K., Todd, E.K., Nakai, J., Iwasaki, Y., Sheehan, A., Mochizuki, K., Wallace, L., Schwartz, S., Webb, S., Henrys, S., 2020. Temporal and spatial variations in seismic anisotropy and VP/VS ratios in a region of slow slip, *Earth Planet. Sci. Lett.*, 532, 115970.

Keywords: HOBITSS experiment, Broadband ocean-bottom seismic data, Receiver functions

©2020. Japan Geoscience Union. All Right Reserved.

Seismic interferometry analyses of teleseismic coda waves on a dense network of permanent ocean bottom seismometers (S-net) offshore Honshu, Japan

*Tomoya Takano[1,2], Florent Brenguier[1], Pierre Boue[1], Ryota Takagi[3], Kaoru Sawazaki[4], Tetsuya Takeda[4], Yosuke Aoki[2], Kiwamu Nishida[2]

1. Institut des Sciences de la Terre, Univ. Grenoble Alpes, 2. Earthquake Research Institute, The University of Tokyo, 3. Research Center for Prediction of Earthquakes and Volcanic Eruptions, Graduate School of Science, Tohoku University, 4. NIED

Seismic imaging around the subducting slab where earthquakes nucleate is crucial. The S-net seismic network composed of 150 permanent ocean bottom seismometers offshore Honshu, Japan provides a unique opportunity to study the oceanic trench in one of the most active subductions. Ambient noise correlation analyses have been used to image the Earth’ s structure. However, since surface waves propagating in the thick sedimentary layer is dominant in ambient noise recorded at S-net, it is difficult to extract the waves propagating in a crustal scale structure. Here, we study the properties of cross-correlations of coda part of teleseismic earthquakes in the quest for reconstructing surface- and body-waves traveling across the network. We analyze 361 teleseismic earthquakes recorded at S-net from August 2016 to May 2019. The epicentral distances for the events range from 30 to 85 degrees. We compute cross correlations from 50 s to 300 s after the direct P arrival time. Peak arrival times of cross correlations for different station pairs depend on the source location. We therefore stack the correlations for station-pairs along a great circle path from the events to avoid the spurious phases. Stacked cross correlations show the wave packets traveling with about 8 km/s and 13 km/s, which seems to be corresponding to Pn velocity and apparent velocity of teleseismic phase, respectively. These observations might show the body waves propagating through ocean bottom stations are recovered from cross-correlation of the coda part of teleseismic events.

©2020. Japan Geoscience Union. All Right Reserved.

“N”-shaped Y/X coda spectral ratio observed for in-line type OBS of S-net and ETMC

*Kaoru Sawazaki[1], Takeshi Nakamura[1]

1. National Research Institute for Earth Science and Disaster Resilience

We detected anomalous peak and notch in spectral ratio of Y (perpendicular to cable axis) and X (along cable axis) components of coda wave in frequencies about 5 - 10 Hz and 10 - 20 Hz, respectively, for considerable number of S-net and ETMC (Earthquake and Tsunami Monitoring Cable deployed along the Sagami-Trough) OBS stations. The Y/X spectral ratio shows “N”-shape due to the peak and notch. This “N”-shape is not observed for S-net stations installed at water depths shallower than 1500 m, at which pressure vessels and cables are installed within groove in the seafloor. Seismograms of DONET are buried in the seafloor and do not show the “N”-shape, either. Considering these observations, we think the “N”-shaped Y/X spectral ratio is not caused by horizontal anisotropy below the subsurface medium, but is due to specificity of response functions of X and Y components.

We make a hypothesis that natural vibrations are excited in the pressure vessel due to insufficient coupling of cylindrical shaped pressure vessel placed on the seafloor. The natural vibrations are excited if longitudinal (X component) and transverse (Y component) guided waves incident from both ends of the pressure vessel via connected cables. Depending on the length L of the pressure vessel, these two types of natural vibrations have natural frequencies given by $f_X=V_P/2L$ and $f_Y=V_S/2L$, and relationship given by $f_X/f_Y=V_P/V_S$ is established. Considering that observed notch and peak frequencies correspond to f_X and f_Y, respectively, observed ratio of notch/peak frequencies are around 1.5 to 3 and the ratio seems to be reasonable for V_P/V_S of pressure vessel. Also, since the length L is 2.3 m and 1.6 m for S-net and ETMC, respectively, f_X and f_Y of ETMC are expected to be 1.4 times higher than that of S-net: it is actually found in the observed spectral ratio. Not only guided waves but also S-coda wave incidents from coupling zone and vibrates the pressure vessel. If coupling is sufficient, energy of S-coda wave will be much stronger than guided waves and natural vibrations of pressure vessel will become invisible. We think this is the reason why DONET and shallow S-net stations do not show “N”-shaped Y/X spectral ratio.

The “N”-shaped Y/X spectral ratio is likely to be specific to in-line type OBSs having cylindrical pressure vessel placed sideways. Enhancing coupling with seafloor by underwater technologies such as installation within groove and burial would be effective to suppress the emergence of natural vibrations in the pressure vessel. Users of in-line type OBS record without sufficient coupling are recommended to correct response functions of X and Y components if necessary, especially when using frequencies above about 3 Hz.

Keywords: S-net, ETMC, DONET, in-line type OBS, peak and notch in Y/X spectral ratio, natural vibration in pressure vessel, coupling with the seafloor

©2020. Japan Geoscience Union. All Right Reserved.

Spatiotemporal Variations of PM Excitation in the Northern Okinawa Trough Revealed by OBS Array

*Chih-Chieh Chien[6], Ying-Nien Chen[3], Yuancheng Gung[6], Ban-Yuan Kuo[1], Shu-Huei Hung[6], Eh Tan[1], Kate Huihsuan Chen[5], Shuichi Kodaira[2], Yasushi Ishihara[2], Mamoru Nakamura[8], Chau-Chang Wang[4,7], Ching-Ren Lin[1]

1. Academia Sinica, Taipei, Taiwan, 2. Japan Agency for Marine-Earth Science and Technology, Yokohama, Japan, 3. National Chung Cheng University, Chiayi, Taiwan, 4. National Sun Yat-sen University, Kaohsiung, Taiwan, 5. National Taiwan Normal University, Taipei, Taiwan, 6. National Taiwan University, Taipei, Taiwan, 7. Taiwan Ocean Research Institute, National Applied Research Laboratories, Kaohsiung, Taiwan, 8. University of the Ryukyus, Okinawa, Japan

The amplitude asymmetry between the causal and acausal signals of noise cross-correlation functions (NCFs) is closely related to the characteristics of the source excitations of ambient noises. In this study, we explore the spatiotemporal variations of the primary microseism (PM) excitations in the Northern Okinawa Trough using the data recorded by a newly deployed array in this area. The seismic array, composed by 32 ocean bottom seismometers (OBSs), was deployed from September, 2018 to June, 2019. With the recorded continuous data, we first compute NCFs of the Z-Z component for each station pair. During the calculation, the signal is whiten in frequency. The spectra of the resulting NCFs indicate that the major energy is dominated by PM (10 –20 s) energy, and the amplitude asymmetry in NCFs also suggests that there are strong spatial variations in its source excitations. We then apply the migration technique to image both the spatial and temporal distributions of the contributed PM sources. Such an approach is also applied to examine its temporal variations by taking a shorter term (monthly) stacking of NCFs. The results suggest that the strong PM sources are located around the offshore in Kyushu, and it is more energetic during the spring.

Keywords: ocean bottom seismometer, source excitation of ambient noise, Northern Okinawa Trough

©2020. Japan Geoscience Union. All Right Reserved.

Rayleigh wave ellipticity estimated from earthquake and noise cross-correlations of OBS data: Effect of ocean and sedimentary layers.

*Shun Fukushima[1], Kiyoshi Yomogida[2]

1. Hokkaido University,Graduate school of Science,Department of Natural History Sciences,Seismology Laboratory , 2. Department of Earth and Planetary Dynamics, Graduate School of Science, Hokkaido University

The ellipticity of Rayleigh waves can be used to infer shallow seismic structures.
Recent development of OBS stations such as S-net and DONET now enables us to measure the ellipticity of Rayleigh waves in detail. Boundary conditions of OBS are different from land observations, in addition to soft ocean bottom sedimentary layers, but their influence on the ellipticity has not been well studied yet. In this study, we numerically calculated the ellipticity on the seafloor with several models. We also measured V/H values of earthquake data recorded by DONET as well as ambient noise data recorded by S-net .
Phase velocity decreases with a period of about 20 seconds when there is a sedimentary layer, in the observation on land while their ellipticity is small, because the horizontal motions get large due to a low-velocity layer on the surface. In contrast, the ellipticity on sea bottom becomes large in a period range from 10 to 40 seconds, whose character gets stronger as the period shorter. Unlike the case of the sedimentary layer on land, only the vertical component selectively increases because there is a layer with only P wave above the observation point (i.e., sea water) . In the case of including a sedimentary layer on the ocean floor, the ellipticity is reduced as in the case of land, and the effect of the vertical enhancement is suppressed. As a result, there is some possibility of a large V/H observed on a seafloor, even with the existence of a soft sedimentary layer.
Next, we measured V/H values on the sea floor with two different approaches: ambient noise and signals from earthquakes. We processed the ambient noise recorded by S-net stations. We took cross-correlations of records at two selected stations: 1-day in each record length with 2-40 sec bandpass filtering and one-bit processing (e.g., Bensen et al., 2007). Cross-correlations among stations perpendicular to the trench axis clearly show surface wave signals with relatively good symmetry of causal and anti-causal waveforms in the period range from 4 to 8 sec. Their group velocity is very small, about 0.2-0.3 km/s. This signal probably correspond to Scholte waves. Scholte waves propagate parallel to the water-sediment interface, when the shear velocity of the solid is lower than the compressional velocity in the water (1.5 km/s). V/H spectral ratios observed by ambient noise data of S-net stations are dominant in the horizontal component, in the case that the P-waves velocity of the sedimentary layer is slower than that of the ocean, then P-wave in the ocean can't propagate in the vertical direction. In other words, V/H ratio of a too slow sedimentary layer is not affected by the existence of the ocean. In addition, we picked up Rayleigh-wave signals recorded at DONET stations for several earthquakes in the ocean with epicentral distance of 500 ~ 1300km. Their V/H ratios are relatively large, unlike the results of ambient noise, that is, the vertical component is dominant in period of 5 ~ 25 sec, as our calculations predict.
Since we have the precise information on the ocean depth (and P-wave velocity) at every point of the studied area, the recorded V/H ratios will help us to estimate S-wave velocity structure near the ocean bottom including a very soft sedimentary layer with the correction of the effect of the sea mater.

Keywords: Ellipticity of Rayleigh wave , Ambient noise, OBS

©2020. Japan Geoscience Union. All Right Reserved.

©2020. Japan Geoscience Union. All Right Reserved.

A Temporal Variation of Auto-correlation Function Calculated from Ocean Bottom Seismometers off Miyagi Prefecture

*Miyuu Uemura[1], Yoshihiro Ito[2], Kazuaki Ohta[3], Ryota Hino[4], Masanao Shinohara[5]

1. Graduate School of Science, Kyoto University, 2. Disaster Prevention Research Institute, Kyoto University, 3. National Research Institute for Earth Science and Disaster Resilience, 4. Graduate School of Science, Tohoku University, 5. Earthquake Research Institute, University of Tokyo

Seismic interferometry is one of the most effective techniques for detecting temporal variations in seismic velocity caused by a megathrust earthquake or a slow slip event (SSE). A lot of previous studies reported the temporal variations caused by megathrust earthquakes or SSEs (e.g. Wegler et al., 2009; Zhen and Song, 2009; Rivet et al., 2011; Sawazaki et al., 2016; Nimiya et al., 2017; Ikeda and Tsuji, 2018). We had evaluated temporal variations in seismic velocity with auto-correlation functions (ACFs) calculated from ambient noise recorded by ocean bottom seismometers (OBSs) installed near the Japan trench off Miyagi Prefecture (Uemura et al., 2018). As a result, we had pointed the velocity decrease caused by the 2011 Tohoku-oki earthquake (Mw. 9.0) and possible velocity fluctuation during SSE preceding the 2011 Tohoku-oki earthquake. However, because some of similar velocity fluctuations had been also detected without any megathrust earthquakes and SSEs, it was difficult to conclude that the fluctuation caused by the SSE.
To reveal causes of such temporal variations in ACF calculated during some of periods without any megathrust earthquakes and SSEs, we try to evaluate temporal variations in ACF calculated from 5-year data (from 2008 to 2012) in the same region. The result shows two interesting characteristics of some temporal variations in ACF. One is that ACFs have obviously annual variation which was detected only near the Japan trench. Another is that temporal variations in some specific phases on ACF are commonly detected in the whole study area. We will discuss what causes the annual variation on ACFs and their temporal variations in the specific phases.

Keywords: Seismic Interferometry, Ocean Bottom Seismometer, Auto-correlation Function

©2020. Japan Geoscience Union. All Right Reserved.

Similar earthquake activity in the northern part of the Ryukyu subduction zone observed by onshore and offshore seismic data

*Yukihiro Nakatani[1], Hiroshi Yakiwara[1], Shuichiro Hirano[2], Reiji Kobayashi[2], Hiroki Miyamachi[2], Shigeru Nakao[2], Yusuke Yamashita[3], Kazunari Uchida[4], Takeshi Matsushima[4], Hiroshi Shimizu[4], Kazuo Nakahigashi[5], Tomoaki Yamada[6], Hideji Abe[7], Masanao Shinohara[7]

1. Nansei-Toko Observatory for Earthquakes and Volcanoes, Kagoshima University, 2. Graduate School of Science and Engineering, Kagoshima University, 3. Disaster Prevention Research Institute, Kyoto University, 4. Institute of Seismology and Volcanology, Faculty of Science, Kyushu University, 5. Tokyo University of Marine Science and Technology, 6. Japan Meteorological Agency, 7. Earthquake Research Institute, the University of Tokyo

In the northern part of the Nansei Islands, regular and slow earthquake activities associated with subduction of the Philippine Sea plate have been observed by onshore seismic and geodetic network. By contrast, no earthquakes with magnitude 7 or more have occurred since the 1911 Kikaijima earthquake of magnitude 8.0. In comparison with other subduction zones around Japan, spatial patterns of regular and slow earthquakes and relationship between seismic gaps and past large earthquakes are less well understood in this region. The biggest reason is due to observational constraints; seismic stations are located only at the islands that are linearly arranged along the arc and far away from the Ryukyu Trench. We have conducted annual repeating long-term ocean bottom seismographic observation off the northern part of the Nansei Islands over the past five years. By integrating six ocean bottom seismometers data with station interval of 40-60 km, the accuracy of hypocenters, especially in focal depths, has been improved and geometry of the subducting plate interface is becoming clear. In addition, shallow low-frequency tremors have been also detected which may show a complementary spatial distribution to active seismic regions.
In this study, we investigate similar earthquakes which occur along the plate interface using both onshore and offshore seismic data. In order to obtain small-magnitude offshore earthquakes, we apply a matched-filter technique to continuous waveform data. As a result of the year 2017, we identify three types of similar earthquake families; repeating-type, burst-type, and mixed-type. These similar earthquake families occur at around 20 km depth of the plate interface. This result suggests the similar earthquake activity locates on the down-dip side of the observed tremor activity. In this presentation, we extend the analytical period and discuss the characteristics of the similar earthquake families.

Acknowledgements: This work is supported by Earthquake and Volcano Hazards Observation and Research Program, the MEXT of Japan and by ERI JURP.

Keywords: OBS observation, the Ryukyu subduction zone, similar earthquakes

©2020. Japan Geoscience Union. All Right Reserved.

Spatiotemporal distribution of fin whale signals in northeast Japan

*Takeshi Nakamura[1], Ryoichi Iwase[2]

1. National Research Institute for Earth Science and Disaster Resilience, 2. Japan Agency for Marine-Earth Science and Technology

We investigated spatiotemporal distributions of whale signals observed by ocean-bottom seismometers of S-net (Seafloor observation network for earthquakes and tsunamis along the Japan Trench) deployed in and around the source area of the 2011 Tohoku earthquake.

We used velocity waveform data from 2017 to 2019. We found characteristic signals with the spectral peak in narrow frequency bands of 14-25 Hz that are different with typical bands of seismic waves and T-phases. The signals have a short duration of about 1 second and are repeatedly found at regular intervals of several tens of seconds. These features are consistent with those of acoustic signals from fin whales as shown in hydroacoustic and seismic observation data by previous studies (e.g., Watkins et al., 1987; Sciacca et al., 2015). We thus assume that the characteristic signals observed at S-net stations are ones associated with fin whale activities.

We developed a detection system that automatically picks the signals of the activities from continuous seismic data. Most of the signals detected by this system are found at stations off Kushiro and Aomori areas from early fall to spring months. The signals are also detected at stations deployed in the outer rise area. In summer months, however, these are not clearly found at all stations. Our results also show that the migration of the signals among the stations from the northeast to southwest direction is found during winter. From analyzing the three-year data, these features are repeatedly seen every year. Considering whale sighting survey results that fin whales are abundant in high latitude areas during warm months and low latitude areas during cold months (e.g., Edwards et al., 2015), such spatial and seasonal variations of the detected signals shown in this study probably associate with the migratory behavior of fin whales. At some stations, we also find the rotation motion in horizontal components during several minutes or hours, which would be also caused by the migration around a station.

We suppose that integrated scientific studies across marine ecology to geophysics using S-net data could contribute to developing our understandings of various signal sources observed in ocean-bottom areas and of ecological behavior of marine mammals.

Keywords: ocean-bottom observation, S-net, fin whale

©2020. Japan Geoscience Union. All Right Reserved.

[E] Poster | S (Solid Earth Sciences)：S-SS Seismology

[S-SS04] Strong Ground Motion and Earthquake Disaster

convener:Kazuhiro Somei(Geo-Research Institute), Yasuhiro Matsumoto(Kozo Keikaku Engineering)

Strong ground motion has social impacts as it induces earthquake disasters. We solicit contribution on any seismological topics related to strong ground motion that includes, but are not limited to, source processes, wave propagation, and site effects. We also welcome contribution on earthquake related disaster mitigation.

[SSS04-P01] Toward to construction of strong-motion database for seismic hazard assessment in Japan

*Nobuyuki Morikawa[1], Hiroyuki Fujiwara[1], Asako Iwaki[1], Takahiro Maeda[1], Hisahiko Kubo[1], Shin Aoi[1], Kenichi Kato[2], Yusuke Tomozawa[2], Fumino Suzuki[2], Toshiaki Sato[3], Toru Ishii[3], Naomi Shimazu[3], Jun'ichi Miyakoshi[3], Atsuko Oana[3], Hongjun Si[4], Toshihiko Hayakawa[5], Takayuki Hayashi[6], Natsuki Kishida[6], Saburoh Midorikawa[7] (1.National Research Institute for Earth Science and Disaster Resilience, 2.Kobori Research Complex Inc., 3.Ohsaki Research Institute Inc., 4.Seismological Research Institute Inc., 5.Mitsubishi Space Software Co., Ltd., 6.Tokio Marine & Nichido Risk Consulting Co., Ltd., 7.Tokyo Institute of Technology)

[SSS04-P02] **Tilt and rotational motions during the strong shaking**

*Toshimi Satoh[1] (1.Shimizu Corporation)

[SSS04-P03] Analysis of pulse-like waves observed in the eastern part of Fukushima Prefecture during the 2011 Tohoku earthquake

*Tomiichi Uetake[1], Kazuhito Hikima[1], Akihito Shimmura[1], Masatoshi Fujioka[1], Ryosuke Sugimoto[1] (1.Tokyo Electric Power Company Holdings)

[SSS04-P04] **Ground Motion Estimation from the Initial P Wave of the Great Earthquake**

*Zijun WANG[1], Boming ZHAO[1], Takao KAGAWA[2], Masanori HORIKE[3] (1.Beijing Jiaotong University, 2.Tottori University , 3.Hanshin Consultants Co., Ltd.)

[SSS04-P05] **Damage Hazard Caused by the Great Earthquake Ground Motion**

*Boming ZHAO[1], Zijun WANG[1], Takao KAGAWA[2], Masanori HORIKE[3] (1.Beijing Jiaotong University, 2.Tottori University, 3.Hanshin Consultants Co., Ltd.)

[SSS04-P06] Disaster mainly of stone torii by the Yamagata Offshore Earthquake in 2019

*Takayuki Kawabe[1] (1.Ex. Faculty of Education, Arts and Sciences, Yamagata University)

[SSS04-P07] Source inversion using empirical Green's functions for the 2019 Off Yamagata earthquake (Mj 6.7)

*Yoshiaki Shiba[1] (1.Central Research Institute of Electric Power Industry)

[SSS04-P08] Source rupture process and strong motion generation areas for the 2018 Hokkaido Eastern Iburi earthquake

*Kazuhiro Somei[1], Ken Miyakoshi[1], Yujia Guo[1] (1.Geo-Research Institute)

[SSS04-P09] Conjugate fault model of the 2018 Anchorage, Alaska, intraplate earthquake (M_W 7.1) based on strong-motion waveform inversion

*Yujia Guo[1], Ken Miyakoshi[1], Masato Tsurugi[1] (1.Geo-Research Institute)

[SSS04-P11] An idea to extract effective fault size from a slip distribution estimated by inversion analysis

*Kazuhito Hikima[1], Akihiro Shimmura[1] (1.Tokyo Electric Power Company Holdings, Inc.)

[SSS04-P12] Estimation of subsurface structure based on microtremor and gravity observation in Shigaku area, Mt. Sanbe, Shimane Prefecture, Japan

*Tatsuya Noguchi[1], Yutaro Itohara[1], Mayuko Kuya[1], Isamu Nishimura[2], Takao Kagawa[1] (1.Faculty of Engineering, Tottori University, 2.Graduate School of Engineering, Tottori University)

[SSS04-P13] Estimation of Subsurface Structure and Ground Motion Characteristics in the Damaged Areas of the 2016 Central Tottori Prefecture Earthquake

*Isamu Nishimura[1], Tatsuya Noguchi[2], Takao Kagawa[2] (1.Tottori Univercity Graduate School of Engineering, Department of Management of Social Systems and Civil Engineering, Civil Engineering Course, 2.Tottori Univercity Graduate School of Engineering)

[SSS04-P14] CMP-SPAC and SPAC microtremor array surveys around Tegano active fault, Gifu, Japan

*Masayuki Yoshimi[1], Haruhiko Suzuki[2] (1.Geological Survey of Japan, AIST, 2.Oyo Corporation)

[SSS04-P15] Improvement of Accuracy to Estimate Phase Velocity using Arbitrary Shape Arrays with Extra Observation Sites

*Huan Zhang[1], Kahori Iiyama[1], Hitoshi Morikawa[1] (1.Tokyo Institute of Technology)

[SSS04-P16] Site Classification Method in Microtremor Array Exploration Using a Supervised Machine Learning

*Takumi Hayashida[1] (1.International Institute of Seismology and Earthquake Engineering, Building Research Institute)

[SSS04-P17] **Verification for the Deep Sedimentary Velocity Structure in the Kathmandu Valley using Receiver Function Analysis**

*Michiko Shigefuji[1], Nobuo Takai[2], Subeg Bijukchhen[3] (1.Kyushu University, 2.Hokkaido University, 3.Khwopa Engineering College, Nepal)

[SSS04-P18] Detect of Underground Velocity Discontinuity by Autocorrelation of Strong Motion Data in the Osaka and Kyoto Basins

*Shuta Fukutome[1], Kimiyuki Asano[1], Tomotaka Iwata[1] (1.Disaster Prevention Research Institute, Kyoto University)

[SSS04-P19] **CONSTRUCTION OF SHALLOW AND DEEP LAYERS COMBINED MODEL IN THE KANTO REGION, JAPAN**

*Hiroaki Yamanaka[1], Yoko Tono[2], Shigeki Senna[3], Masahiro Ohbuchi[4], Hiroyuki Fujiwara[3] (1.Interdisciplinary Graduate School of Science and Engineering,Tokyo institute of Technology, 2. Earthquake Research Institute, University of Tokyo, 3.National Research Institute for Earth Science and Disaster Resilience, 4.Ministry of Education, Culture, Sports, Science and Technology)

[SSS04-P20] Estimation of earthquake ground motions at MeSO-net stations

*Atsushi Wakai[1], Shigeki Senna[1], Atsushi Shimizu[1] (1.National Research Institute for Earth Science and Disaster Resilience)

[SSS04-P21] Modeling of subsurface velocity structure from seismic bedrock to ground surface based on array microtremor observation in Aso area

*Shigeki Senna[1], Atsushi Wakai[1], Atsushi Yatagai[2], Yoshiaki Inagaki[2], Hisanori Matsuyama[2], Hiroyuki Fujiwara[1] (1.National Research Institute for Earth Science and Disaster Resilience, 2.OYO Corp)

[SSS04-P22] The examination of liquafaction damage rate by recent earthquakes

*Shigeki Senna[1], Kyoko Ozawa[1] (1.National Research Institute for Earth Science and Disaster Resilience)

[SSS04-P23] **Ground Motion Estimation by using Microtremor H/V Spectral Ratio**

*Guan-Yu Chen[1], Che-Min Lin[2], Kuo-Liang Wen[1] (1.Department of Earth Science, National Central University, Taoyuan, Taiwan, 2.National Center for Research on Earthquake Engineering, Taipei, Taiwan)

[SSS04-P24] ISNL- - an new parameter of soil nonlinearity used for Taiwan and New Zealand earthquake

*Kao Ching[1], Huang Jyun-Yan[2], Wen Kuo-Liang [2] (1.National Central University, 2.National Center for Research on Earthquake Engineering)

[SSS04-P25] Assessment of the liquefaction risk at Re-liquefied site

*CHIH-SHENG KU[1], Yun-Ling Hsieh[1], Po-Wei Cheng[1] (1.I-SHOU University)

[SSS04-P26] Experimental Study on Dynamic Shear Modulus of Cohesive Soil in Beijing Plain

*Yi Fang, Guoxing Chen, Yanju Peng, Yuejun Lyu

Toward to construction of strong-motion database for seismic hazard assessment in Japan

*Nobuyuki Morikawa[1], Hiroyuki Fujiwara[1], Asako Iwaki[1], Takahiro Maeda[1], Hisahiko Kubo[1], Shin Aoi[1], Kenichi Kato[2], Yusuke Tomozawa[2], Fumino Suzuki[2], Toshiaki Sato[3], Toru Ishii[3], Naomi Shimazu[3], Jun'ichi Miyakoshi[3], Atsuko Oana[3], Hongjun Si[4], Toshihiko Hayakawa[5], Takayuki Hayashi[6], Natsuki Kishida[6], Saburoh Midorikawa[7]

1. National Research Institute for Earth Science and Disaster Resilience, 2. Kobori Research Complex Inc., 3. Ohsaki Research Institute Inc., 4. Seismological Research Institute Inc., 5. Mitsubishi Space Software Co., Ltd., 6. Tokio Marine & Nichido Risk Consulting Co., Ltd., 7. Tokyo Institute of Technology

After the 1995 Hyogoken-Nanbu (Kobe) earthquake, many records from nationwide strong-motion observation networks such as K-NET have been accumulated and released to the public, and have been widely used in the seismology and earthquake engineering. Under such circumstances, many research groups have proposed improved strong-motion prediction methods, such as ground-motion equations, based on the observed records. However, strong-motion databases have been constructed independently by individual research groups. As a result, the moment magnitude and the source fault model used are differ among research groups even if the same earthquake. For this reason, there is no strong-motion database in Japan at present to systematically develop a strong-motion prediction method and objectively verify the validity of the method.

To overcome this situation, we constructed a prototype strong-motion database consisting of K-NET and KiK-net records (about 1 million). As the source data (about 17,000 events), not only the hypocenter location and magnitude by Japan Meteorological Agency, but also the moment tensor parameters determined by F-net, NIED were registered. In addition, some source fault models by SRCMOD (Mai and Thingbaijam, 2014) were also registered. As the station data, site codes, location, and underground structure information were registered. We registered not only the average S-wave velocity up to 30m depth (Vs30) obtained from the PS logging data, the Vs30 from the engineering geomorphological classification and information on the deep sedimentary layers model by J-SHIS of NIED. Peak acceleration, peak velocity, instrumental seismic intensity, and 5% damped acceleration response spectrum (59 points with a period from 0.02 to 20 seconds) were registered as strong-motion data. For horizontal component, not only the amplitude of each of the two orthogonal components (NS, EW), but also RotD0, RotD25, RotD50, RotD75, and RotD100 were registered. We also registered vertical component.

In the future, we will add and expand data from other organizations such as Japan Meteorological Agency and overseas, and ground motion simulation data. Technical issues such as distinction of earthquake types (crustal, subduction inter-plate, and subduction intra-plate), selection of source fault models, and procedures to remove noise data remain. At the same time, efforts should be made to establish a framework for updating and maintaining the database.

Keywords: Strong-motion records, database, seismic hazard assessment, strong-motion prediction

©2020. Japan Geoscience Union. All Right Reserved.

Tilt and rotational motions during the strong shaking

*Toshimi Satoh[1]

1. Shimizu Corporation

Satoh (2019) showed that some velocity time histories by integrating acceleration records of vertical components have linear trends to the downward direction then become almost flat using mainly KiK-net records. Satoh (2019) defined the absolute flat value as Vnon. In this study we estimate Vnon from vertical components of K-NET, KiK-net, JMA and local government strong motion records with PGAs of larger than 300 cm/s^2. The velocity time histories of horizontal records with large Vnon have linear trends during the strong shaking except for records with the largest Vnon at Chokubetsu (HKD086) of the 2003 Tokachi-oki earthquake. In other words, acceleration records of horizontal components have step functions. Therefore, we also estimate the tilt angles and the rotational angles in the horizontal plane using the step values of horizontal components of records with Vnon greater than 1 cm/s.

NIED showed by the site investigation at HKD086 after the 2003 Tokachi-oki earthquake that the foundation of the seismometer had floated up accompanied with the tilt and rotation due to the liquefaction. Since the existence of Vnon suggests the settlement of the ground, the floating up occurred after the strong shaking, that it, post-liquefaction. The velocity time histories of horizontal components at HKD086 have curved trend. This result indicates that the tilt and rotation of the ground is changing during the strong shaking. For comparison, array records observed at Port Island during the 1995 Hyogo-ken Nanbu earthquake are analyzed. The velocity time history of the vertical component at the ground surface has no Vnon. Since the liquefaction intaneously occurred and excess pore water pressure ratio kept 100 % during the strong shaking (Kawase et al.,1998), it is thought that the consolidation settlement did not occur during the strong shaking. On the other hand, duration of records at HKD086 are long and so the dissipation of the excess pore water pressure is considered to occur during the strong shaking. The velocity time history of vertical component observed at the depth of 16 m at Port Island has the linear trend to the upward direction then becomes almost flat. This phenomenon may occur by the floating up due to upward seepage flow by liquefaction.

Many records with large Vnon are observed at special soil, such as volcanic clayey soil or high organic soil and the particle orbits on the horizontal-vertical plane show tilt or rotational motions. Some records with large Vnon have been pointed out the increase of the excess pore water pressure by previous studies. The record at Kushiro observed by JMA during the 1993 Kushiro-oki earthquake has large Vnon and the predominant frequency of vertical motion is twice of horizontal components. On the other hand, the record at Kushiro observed by BRI 50m away from the JMA Kushiro with smaller ground motions than JMA Kushiro has no Vnon and the vertical motion dose not dominant at twice of the peak frequency of horizontal components. The feature that vertical motions with very large Vnon are twice of predominant frequencies of horizontal motions has been pointed out as the negative dilatancy of dry soil by experimental and analytical studies. Therefore, the difference of strong motions at two statins can be interpreted by the difference of nonlinear site responses with and without the negative dilatancy.

The directions of tilt estimated from the linear trends of horizontal velocity time histories in the near-fault regions are almost radial and the tilt starts at S-wave potions. The tilt angles are much larger than tilt angles of the crustal deformation due to source processes. We interpret from these results that the tilt and rotational motions are caused by the increase and dissipation of excess pore water pressure or the

©2020. Japan Geoscience Union. All Right Reserved.

negative dilatancy.

Acknowledgements: We use NIED (K-NET, KiK-net), JMA, local government, BRI, and PARI strong motion records.

Keywords: tilt, rotation, nonliear site response, dilatancy, strong motion records, consolidation settlement

©2020. Japan Geoscience Union. All Right Reserved.

Analysis of pulse-like waves observed in the eastern part of Fukushima Prefecture during the 2011 Tohoku earthquake

*Tomiichi Uetake[1], Kazuhito Hikima[1], Akihito Shimmura[1], Masatoshi Fujioka[1], Ryosuke Sugimoto[1]

1. Tokyo Electric Power Company Holdings

1. Introduction

Strong motion records from the 2011 off the Pacific coast of Tohoku Earthquake (M9) were obtained over a wide area, and the waveform characteristics differed from region to region. In the records obtained in Fukushima Prefecture, several large pulse-like waves were observed. These pulses are considered to generated at the strong motion generation area (SMGA) existing on the fault plane, and source models considering multiple SMGAs has been proposed [e.g. Asano and Iwata (2012) , Kurahashi and Irikura (2013)]. There is also a study confirming the correspondence between pulse waves and high-frequency excitation sources on the fault plane by array analysis [Aoki et al. (2012)]. In this study, we focus on many strong motion records obtained in the eastern part of Fukushima prefecture, and examine the propagation and shape change of the pulse-like waves.

2. Records and target waves

In the eastern part of Fukushima Prefecture, many strong motion records have been obtained by K-NET, KiK-net and the seismic intensity meters. In this study, the velocity waveforms integrated from the acceleration records were used for the examination. A high-pass filter with a lower frequency limit of 0.05 Hz was applied during integration, but for records with poor signal to noise ratios in the lower frequency range, the lower limit frequency was raised to 0.1 Hz or 0.2 Hz. The figure shows the velocity waveform (EW component) of the stations along the coastline. In the velocity waveform, a plurality of pulse-like wave groups with different apparent periods are confirmed. In this study, the pulse-like wave that gave the maximum velocity at the FKSH20 was targeted.

3. Propagation characteristics of target waves

From the temporal continuity of the wave groups at adjacent observation stations, the target waves were detected along the coastline from north to south of Fukushima Prefecture. On the inland side, pulse waves can be recognized in a wide area of Abukuma Highland. The source of pulse-like waves estimated from the isochron using the JMA2001 travel-time table[Ueno et al. (2002)] was shown as the star mark (141.35 E, 37.10 N) in the figure. This position is close to the SMGA estimated by Kawabe and Kamae (2013).

4. Characteristics of target waves

Focusing on the shape of the pulse-like waves, it was a triangular shape at FKS010 and several stations close to SMGA, but a sine shape was clear at the stations a little away to the north along the coastline. The dominant frequency of the pulse wave part was about 0.5 Hz. On the south side of FKSH14 along the coast line, another wave group overlapped on the target waves. On inland side, the dominant frequency of the pulse shifted to higher frequencies and the amplitude of the pulse decreased. The largest amplitude of the target pulse wave was recorded at the station a little away from SMGA and the amplitude is different at the observation stations on the isochron. The amplitude variation of the pulse cannot be explained by a simple attenuation relation. It is considered that the site factors greatly influence the variation of wave characteristics including the amplitude.

©2020. Japan Geoscience Union. All Right Reserved.

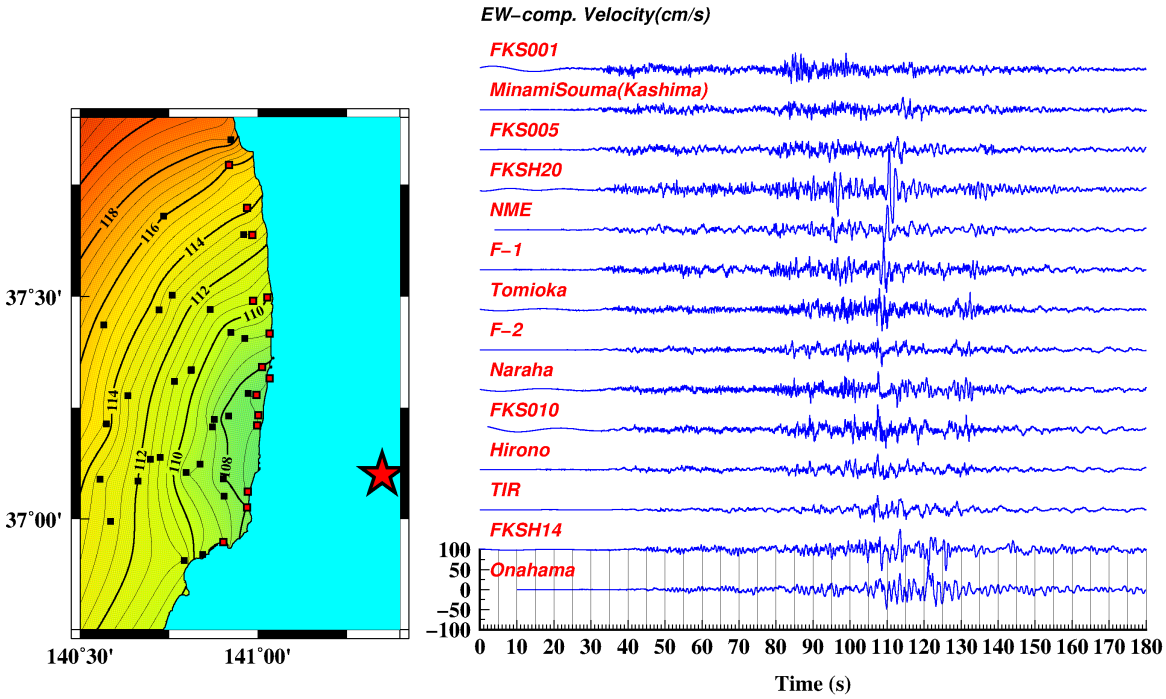
5. Conclusions

The propagation characteristics and shape variation of pulse-like waves observed in the eastern Fukushima Prefecture during the 2011 Tohoku Earthquake were investigated. Judging from the isochron of pulse-like waves, it was propagated from the SMGA off the east coast of Fukushima Prefecture. Also, considering the spatial change of the shape and amplitude, it is considered that site characteristics have a strong influence.

Acknowledgments

The strong motion records of the following organizations were used. Thank you for writing. National Institute for Earth Science and Disaster Resilience, Japan Meteorological Agency, Fukushima Prefecture, National Institute of Land and Infrastructure Management, Association for the Development of Earthquake Prediction and the Central Research Institute of Electric Power Industry.

Keywords: Velocity pulse, Travel time analysis, Site factor, Array analysis



©2020. Japan Geoscience Union. All Right Reserved.

Ground Motion Estimation from the Initial P Wave of the Great Earthquake

*Zijun WANG[1], Boming ZHAO[1], Takao KAGAWA[2], Masanori HORIKE[3]

1. Beijing Jiaotong University, 2. Tottori University , 3. Hanshin Consultants Co., Ltd.

We proposed a quick method to estimate the site ground motion using the initial P wave from a single station. First, the ground motion estimation technique from the first 3-second P wave spectral intensity ($SI_{(3s)}$) was presented; meanwhile the peak amplitude of displacement (P_d) and the integral of the squared velocity (IV2) were selected as comparisons. With the aftershocks of the 2008 Ms 8.0 Wenchuan earthquake, we investigated the regression relationships between these 3 parameters and ground motion parameters (the peak ground acceleration, peak ground velocity and spectral intensity), based on which the ground motion estimation formulas were derived accordingly. The results showed that the proposed $SI_{(3s)}$ was of the highest accuracy with regard to the PGA estimation. Aiming at large magnitude earthquakes i.e. the Wenchuan main-shock, we put forward to introduce an amplification coefficient to revise the characteristic parameters in advance to predict the ground motions, thus the underestimation of great earthquakes could be mitigated to a certain extent.

Keywords: ground motion estimation, Wenchuan earthquake, P wave, spectral intensity, single station

©2020. Japan Geoscience Union. All Right Reserved.

Damage Hazard Caused by the Great Earthquake Ground Motion

*Boming ZHAO[1], Zijun WANG[1], Takao KAGAWA[2], Masanori HORIKE[3]

1. Beijing Jiaotong University, 2. Tottori University, 3. Hanshin Consultants Co., Ltd.

Given the fact that the degree of structural damage caused by earthquakes depends both on the characteristics of strong ground motions and the anti-seismic performance of structures, we collected and processed the sufficient observation-based data of the Wenchuan earthquake, from which the corresponding ground motion parameters to the 10 targeted districts were derived by the methods of interpolation and attenuation curves. We then established the vulnerability curves between the damage ratios (DRs) and the peak accelerations, peak velocity, peak spectrum acceleration as well as spectrum intensity. In addtion, an effective method for estimating the structural damage levels by using the fragility curve between DR and PGA $/a_F$ was proposed to eliminate the deviation in the design forces for these structures, which can provide important benefits for the structural damage studies. We showed that the reasonable seismic fortification plays a decisive role in improving buildings' anti-seismic performance, that based on the improved "Code for Seismic Design of Buildings", the predicted DRs for the 10 targeted districts can be reduced significantly compared with the actual damage they were suffered.

Keywords: strong ground motion, Wenchuan earthquake, damage ratio, vulnerability

©2020. Japan Geoscience Union. All Right Reserved.

Disaster mainly of stone torii by the Yamagata Offshore Earthquake in 2019

*Takayuki Kawabe[1]

1. Ex. Faculty of Education, Arts and Sciences, Yamagata University

A large earthquake 6.7 Mj(according to JMA), called the Yamagata-ken Oki jishin (Yamagata Offshore Earthquake), occurred on 18th June 2019 at 22:22 JST, offshore of Yamagata Prefecture, northwest Japan. There is few human damage luckily, but damage of less than 800 houses occurred near the epicenter around the border of Yamagata and Niigata Prefectures.
Maximum seismic intensity is 6 upper in northern margin of Murakami City, Niigata Prefecture and the second largest seismic intensity if 6 lower in southern margin of Tsuruoka City, Yamagata Prefecture. According to JMA Estimated seismic intensity map. Seismic intensity decreases as moving farther away from the epicenter.
The Author made a survey of damage of stone toriis by the earthquake distributed in Tsuruoka City and northern part of Murakami City. According to prior research of Kawabe (2007) which surveyed damage of 250 stone toriis in Noto Peninsula, direction of strong seismic movement can be provided from the positions of damage of the stone torii as shown in Fig. 1, and converted seismic intensity can be converted from total damage points of individual point of individual place shown as Table 1 and 2.
According to the result of the survey of 135 stone toriis shown in Fig.2, distribution of converted seismic intensity is resembles generally JMA estimated seismic intensity map. but values of converted seismic intensity of several points in Murakami City are larger than JMA estimated seismic intensity. This may be caused by the difference of the calculation method of two seismic intensity. That is, converted seismic intensity depends on pulsed strong motion and JMA estimated seismic intensity depends on the amplitude and fr3equency of seismic wave.
Calculated directions of strong motion of stone toriis in northern Tsuruoka City show the direction to the epicenter, though the directions of strong motion in most of surveyed area direct diagonally to the epicenter. This difference may be caused by the geology of the Neogine non-concrete sediments in northern Tsuruoka City and of rigid granitic rocks in other area.
References:
JMA (2019) Monthly report of earthquake and volcanoes in Japan, June 2019.
Katabe Takayuki (2007) Strong quake motion estimated from the damage of Toriis by the 2007 Noto Peninsula Earthquake in the northwest part of the Noto Peninshurla, Hokuriku distict, Japan -method of examination-. Earth Science, 61, 379-387.

Keywords: Off-Yamagata earthquake in 2019, strong motion, stone toriis, earthquake disaster

©2020. Japan Geoscience Union. All Right Reserved.

表1 鳥居の部位毎の被害ポイント

部位	被害	点数
柱	倒壊	10
	破断	6
	貫部破断	3
	笠木部ヒビ	1
	貫部ヒビ	1
笠木	落下	4
	破断	3
	ズレ	2
	貫部ヒビ	1
貫	落下	3
	ヒビ	2
亀腹	割れ	3
	ヒビ	2
土台	ヒビ	1

表2 花崗岩鳥居の被害度と換算震度との関係

石造鳥居のおもな岩石の種類	被害度と計測震度の関係				
	被害度0	被害度1～3	被害度4～9	被害度10～12	被害度13～
花崗岩	震度4	震度5弱	震度5強	震度6弱	震度6強

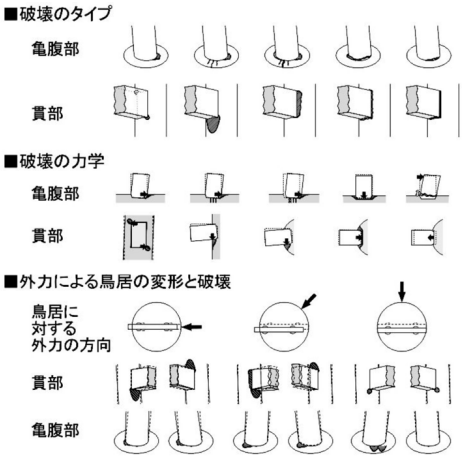


図1 石造鳥居の部位毎の損傷痕のタイプと損傷をもたらした損傷部位の力学，鳥居の変形

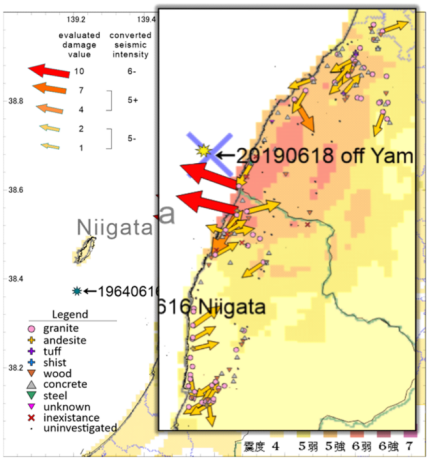


図2 鳥居の素材毎の分布と石造鳥居の被害度（換算震度）と地面の強震動の方向

©2020. Japan Geoscience Union. All Right Reserved.

Source inversion using empirical Green's functions for the 2019 Off Yamagata earthquake (Mj 6.7)

*Yoshiaki Shiba[1]

1. Central Research Institute of Electric Power Industry

During the 2019 Off Yamagata earthquake on June 18, JMA seismic intensity scale of 6 upper was recorded at maximum on Niigata Yamagata border region. Further even at the strong-motion station on the bedrock, seismic intensity of 5 lower was observed, which is located on the epicentral distance of 16 km. Aftershocks distribute on the area north of the 1964 Niigata earthquake (Mj 7.5) fault region, so that the relation of the slip area of both events should be focused. In this study the inversion method using empirical Green's functions is adopted for the source modeling of the 2019 Off Yamagata earthquake and estimated model is compared with the slips during the 1964 Niigata earthquake.
From the aftershock distribution and CMT solution of the main shock estimated by F-net, we assumed the reverse fault plane model with the strike in the N40E direction and the south-east dipping with 30 degrees. This fault plane model has the conjugate relation with that of the 1964 Niigata event adopted by Shiba and Uetake (2011). Observed records from the aftershock of Mj 4.0 occurring near the hypocenter of the main shock were used for the empirical Green's functions. Velocity motions of two horizontal components for KiK-net subsurface stations, K-NET stations and one bedrock station operated by CRIEPI (RK-net) are used for the source inversion in the frequency range up to 2 Hz. The spatial distribution of the seismic moment density, effective stress, rise time and rupture time on the fault plane are estimated simultaneously by using the simulated annealing, which is one of the heuristic search techniques.
The obtained source model indicates large slips mainly in the north east area apart from the hypocenter, which corresponds to the region just outside the fault plane of the 1964 Niigata earthquake. The distribution of the effective stress roughly coincides with the slip distribution. Peak slip and effective stress reach 1.0 m and 14.2 MPa respectively. On the other hand, the rise time distribution does now show obvious correlation to other source parameters, which might be due to the low resolution at the low frequency range. The rupture front propagates almost concentrically, but slightly accelerates on the high effective stress area. It suggests the increase of surface energy with high stress drop contributes the acceleration of rupture velocity on asperity or SMGA.

Keywords: 2019 Off Yamagata earthquake, Source process, Inversion analysis

©2020. Japan Geoscience Union. All Right Reserved.

Source rupture process and strong motion generation areas for the 2018 Hokkaido Eastern Iburi earthquake

*Kazuhiro Somei[1], Ken Miyakoshi[1], Yujia Guo[1]

1. Geo-Research Institute

The 2018 Hokkaido Eastern Iburi, Japan, earthquake (M_w 6.6) occurred at a depth of 37 km, which is provided by Japan Metrological Agency (JMA), in western part of the Hidaka arc-arc collision zone. This earthquake caused strong ground motions with a maximum seismic intensity of 7 in the JMA scale and a maximum peak ground acceleration of over 1000 cm/s^2. In order to understand the mechanisms of generating the broadband strong ground motions during this earthquake, we estimate the spatio-temporal source rupture process based on the waveform inversion using strong motion data, and also construct the characterized source model consisting of Strong Motion Generation Areas (SMGAs) through the broadband ground motion simulations around the source area. To reveal the rupture process, we employ the multi-time window linear waveform inversion by using the strong motion waveforms (0.05-0.5 Hz) recorded around the source area. A curved source fault with a variation in strike angle is assumed by referring the relocated aftershock distribution. The theoretical Green’s function is computed assuming a 1D velocity structure model for each station. The SMGAs are estimated on the basis of forward ground motion simulation in broadband frequency range from 0.2 to 10 Hz using the empirical Green’s function method.

From the results of these source models and ground motion simulation, our principal findings are following. 1) The main large ground motions observed at near-source stations were generated by the up-dip rupture in the large slip area (i.e., the asperity area) identified at the depth shallower than the hypocenter, which coincides with the position of the SMGA1. 2) The SMGA2 and 3 played a key role to generate the observed later phases, which are not explained enough only by the SMGA1 or asperity area. 3) The estimated stress drop or short-period level, which control the high-frequency ground motion radiations, were larger than the average value of past large crustal earthquakes usually occurring in Japan. These findings are important to understand the source characteristics of the earthquakes occurring at deep depth in arc-arc collision tectonic zone.

Acknowledgements: The strong motion data from K-NET, KiK-net, and F-net were provided by the National Research Institute for Earth Science and Disaster Resilience (NIED). We also used the strong motion data from the seismic intensity observation networks of the JMA, Moment tensor solutions were routinely determined by F-net. The JMA unified earthquake catalog was produced by the JMA in cooperation with the Ministry of Education, Culture, Sports, Science and Technology (MEXT). This study was based on the 2019 research project “Examination for uncertainty of strong ground motion prediction for inland crustal earthquakes” by The Secretariat of the Nuclear Regulation Authority (NRA), Japan.

Keywords: The 2018 Hokkaido Eastern Iburi earthquake, Rupture process, Strong motion generation area

©2020. Japan Geoscience Union. All Right Reserved.

Conjugate fault model of the 2018 Anchorage, Alaska, intraplate earthquake (M_W 7.1) based on strong-motion waveform inversion

*Yujia Guo[1], Ken Miyakoshi[1], Masato Tsurugi[1]

1. Geo-Research Institute

The Anchorage, Alaska, earthquake (M_W 7.1) on 30 November 2018 occurred in the upper part of the Pacific plate or Yakutat microplate subducting beneath the North American plate. A relocated aftershock distribution (Ruppert *et al.*, 2020) and moment tensor solutions (Richards, 2019; West *et al.*, 2020) suggested the possibility that this earthquake was a rare intraplate event with conjugate source faults. Based on this possibility, we performed a source inversion using strong-motion waveforms at periods of 2.5–20 s and investigated the source characteristics of this earthquake.

The source inversion was performed using the multi-time-window linear waveform inversion method (Hartzell and Heaton, 1983). The assumed conjugate faults consist of a gently east-dipping (strike = 5˚, dip = 30˚) fault and a steeply west-dipping (strike = 185˚, dip = 60˚) fault. The hypocenter was located on the former. The Green's functions were calculated by the discrete wavenumber method (Bouchon, 1981) and the reflection/transmission coefficient matrix method (Kennett and Kerry, 1979). For the calculations, 1D seismic velocity structure models (Dutta *et al.*, 2007; Eberhart-Phillips *et al.*, 2019) were adjusted using waveforms of an M_W 5.0 aftershock.

Our inversion estimated the seismic moment, average slip, and maximum slip to be 5.91×10^{19} Nm (M_W 7.11), 0.97 m, and 2.7 m, respectively. Two large slips were estimated on the steeply west-dipping fault and the deeper part of the gently east-dipping fault, respectively. Because the rupture initiated on the gently east-dipping fault, we also tested an inversion without assuming the steeply west-dipping fault. The test result showed that, compared with the inversion with assuming the steeply west-dipping fault (i.e., the large slip on the steeply west-dipping fault), the inversion without assuming could not sufficiently reproduce the waveforms observed at the stations on the northern and western sides of the source region. The necessity of the steeply west-dipping fault was also reported by the analyses of teleseismic body waves (Liu *et al.*, 2019) and GPS static displacements (West *et al.*, 2020).

Although this earthquake was a rare event with conjugate faults, the source scaling relationships of its source parameters (e.g., average slip, entire rupture area, and large slip area) to the seismic moment were consistent with the empirical relationships derived by Iwata and Asano (2011) and Allen and Hayes (2017). This consistency was found for the 2016 Iniskin, Alaska, intraplate earthquake (M_W 7.1), but not for the 2017 Puebla intraplate earthquake (M_W 7.1), which occurred in the Cocos plate beneath the central Mexico and severely damaged the Mexico City (Guo *et al.*, 2019). In spite of the same M_W of these recent earthquakes, the difference between Alaska and central Mexico implies that the source parameters of intraplate earthquakes have regional characteristics.

Acknowledgements: Strong-motion waveform data were downloaded from the data management center of the Incorporated Research Institutions for Seismology. This study was based on the 2019 research project "the methodology of ground motion prediction for megathrust earthquakes" by the Nuclear Regulation Authority, Japan.

©2020. Japan Geoscience Union. All Right Reserved.

Keywords: 2018 Anchorage earthquake, Intraplate earthquake, Conjugate fault, Source inversion, Source scaling relationship

©2020. Japan Geoscience Union. All Right Reserved.

An idea to extract effective fault size from a slip distribution estimated by inversion analysis

*Kazuhito Hikima[1], Akihiro Shimmura[1]

1. Tokyo Electric Power Company Holdings, Inc.

- Objective -

Fault length and width (also fault area of those multiplication) are the basic and important parameters for source information. In recent decades, these parameters are estimated by inversion analyses using observed data in most cases. When the source process inversions are performed using, for example, waveform or geodetic data, larger fault area than true area is set first. Therefore, we have to perform additional operations to extract real fault area from the derived slip distribution.

As such a method, Somerville *et al.* (1999) proposed a method in that marginal rows or columns having relatively small slips are trimmed from inverted slip distributions and rectangular main area is extracted. Mai and Beroza (2000) and Thingbaijam and Mai (2016) also proposed other methods which estimate effective source dimensions based on autocorrelation width of the spatially variable slip. Many authors have discussed source scaling relations using the parameters estimated in such a way. However, the roughness of estimated slip distributions (the amplitude of spatially variation) tends to differ depending on the analysis methods and analysts. Furthermore, it is some problem that the distinct and physically clear criteria are not determined to extract main slip area from those results.

Therefore, we considered a procedure to extract a rectangular effective fault area based on wavenumber spectra of slip distribution, considering more physical validity.

- Method -

Analyses considering wavenumber spectra of slip distributions have been already discussed by, for example, Somerville *et al.* (1999). We also calculate two-dimensional wavenumber spectrum of subject fault model as same as their procedure. The steps now adopted are follows.

First, a slip distribution at 1 km intervals for length (X-direction) and for width (Y-direction) is made from an original spatially variable slip. Then, zero values are added outside of the fault area to make 256 x 256 size data set. Amplitude wavenumber spectra of these data are calculated using two-dimensional FFT. For these spectra, we consider that the wavenumber spectrum at k_y=0 (k_y: wavenumber for Y-direction) is in length direction and the spectrum at k_x=0 (k_x: wavenumber for X-direction) is in width direction, respectively.

On the side, Fourier transform of a rectangular function having width as L is $f(\nu)=L\sin(\pi L \nu)/(\pi L \nu)$ [$\nu=1/\lambda$; λ: wavelength]. As well known, this sinc function crosses with zero line at n=n/L [n=1, 2, ⋯], and these correspond to trough of the spectrum in the case of amplitude spectrum.

To determine fault length, we basically fit this sinc function with the spectrum at k_y=0 in length direction previously obtained. However, the calculated spectrum becomes irregular curve actually due to its slip distribution. Therefore, only lower part than first trough (it corresponds to n=1) of sinc function is used for fitting operation. And we placed emphasis on lower wavenumber part especially. Additionally, we apply the same means to the spectrum at k_x=0 in width direction to determine fault width.

- Result -

We performed preliminary analyses using the fault models in the SRCMOD (Mai and Thingbaijam, 2014). Although goodness of fitting is evaluated visually, in the current procedures, the optimal dimensions can be determined with the error lower than a few km. Thingbaijam *et al.* (2017) estimated the fault length

©2020. Japan Geoscience Union. All Right Reserved.

and width by using their ways and have listed in the paper. The lengths determined by our methods were almost comparable with their values. However, we also recognized that some models show somewhat smaller length than published one. To pursue causes of these results, we performed a model calculation using synthetic fault model having asperity. As a result, the tendency that estimated area become smaller than whole fault area was found, depending on the conditions. It is thought because proposed method estimates an equivalent rectangular fault area with considering the slip distribution.
We would like to report on the features of the method after further considerations, also including comparison with other methods.

Keywords: Fault size, Rupture area, Trimming, Scaling of fault parameters, Slip distribution

©2020. Japan Geoscience Union. All Right Reserved.

Estimation of subsurface structure based on microtremor and gravity observation in Shigaku area, Mt. Sanbe, Shimane Prefecture, Japan

*Tatsuya Noguchi[1], Yutaro Itohara[1], Mayuko Kuya[1], Isamu Nishimura[2], Takao Kagawa[1]

1. Faculty of Engineering, Tottori University, 2. Graduate School of Engineering, Tottori University

An earthquake (Mj6.1) occurred in the vicinity Ohda city western Shimane Prefecture in Japan on April 9, 2018. Characteristics of site amplification effect of the temporary sites were understood from analysis of seismic data. We need to investigate the causes of the local site effects for the prevention or mitigation of earthquake disasters in the area. The purpose of our study was to estimate the subsuface structures of the target area by using microtremor and gravity survey. Therefore, densely microtremor and gravity observations were carried out to estimate the characteristic of ground motion in the damage area, Shigaku area, Mt. Sanbe, Shimane Prefecture. 3-compoent single-site observations at 80 points and array observations at 1 site were made to observe microtremor, and 51 points were made to observe gravity in the area.

There are two clear peaks in H/V spectrum in the short-period band (0.2 - 0.5 s) and the long-period band (1 - 3 s). The feature of the distribution of the predominant period is thought to be influenced by the ground structure of the sedimentary layer due to the volcanic deposits of Mt. Sanbe. From the estimation results of the S-wave velocity structure, the thickness of soft soil with S-wave velocity of 170m/s to 250m/s was about 40m. The S-wave velocities of 700m/s and 1300m/s corresponding to hard sedimentary rocks were about 200m and 500m, respectively.

Gravity anomalies were corresponded characteristic of the caldera topography of Mt. Sanbe, and there were low and high anomalies reflecting the complex structure near the summit. The basement altitude was obtained by performing a three-dimensional analysis using the gravity anomaly with a surface layer of 2.2g/m^3 and a base layer of 2.5g/m^3. As a result, the feature of the shape of the basin by the caldera topography were able to be grasped. It was found that the altitude of the basement surface was about -200m on a flat part (surface thickness of about 700 m) and about -1500m at the deepest part (surface thickness of about 1500m).

Keywords: microtremor observation, gravity observation, subsurface structure, Shigaku area, Mt. Sanbe, 2018 western Shimane Prefecture earthquake

©2020. Japan Geoscience Union. All Right Reserved.

Estimation of Subsurface Structure and Ground Motion Characteristics in the Damaged Areas of the 2016 Central Tottori Prefecture Earthquake

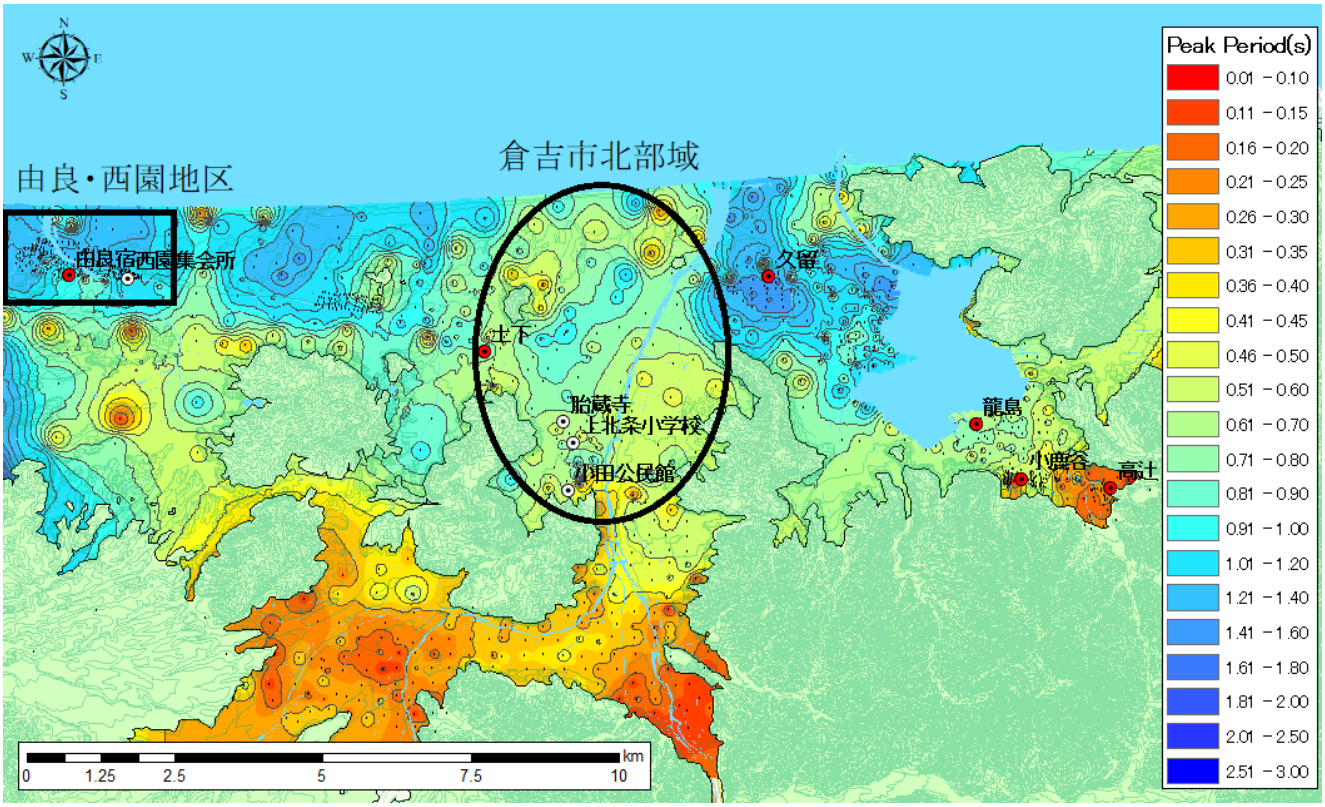
*Isamu Nishimura[1], Tatsuya Noguchi[2], Takao Kagawa[2]

1. Tottori Univercity Graduate School of Engineering, Department of Management of Social Systems and Civil Engineering, Civil Engineering Course, 2. Tottori Univercity Graduate School of Engineering

On October 21, 2016, an earthquake with MJMA 6.6 occurred in the central part of Tottori Prefecture in Japan. Observed JMA seismic intensity were 6 lower at Kurayoshi city, Yurihama town and Hokuei town. Housing damage due to the earthquake was concentrated in limited areas. In this study, we carried out microtremor observations around damaged area to estimate subsurface structure and ground motion characteristics with the data by previous studies. We consider that the damages are affected by ground motion characteristics.
Low-velocity layer with S-wave velocity 80-180 m/s were estimated at all observation sites and the layers tend to be thicker to coastal plain and thinner to inland areas. The thickness of deeper subsurface structure with S-wave velocity more than 700 m/s was found to be different between Yurihama town and Hokuei Town from diffuse wavefield approach to H/V spectrum estimated from earthquake ground motion data. Many microtremor H/V with multiple peaks were observed at limited regions Yura and Nishizono, and most H/V with a single peak were observed at northern Kurayoshi Plain. It is suspected to reflect the difference in velocity structures of surface layers. The predominant period at Yura and Nishizono regions were 1.0-1.6 seconds, and at northern Kurayoshi Plain was 0.4-1.0 seconds. Comparing with housing damage, the layer thickness estimated from the quarter wavelength low, it was found that the damage occurred at the part where the layer thickness changed steeply. Comparing the ground amplification index such as ARV with housing damage, the relevance was found to be weak. Therefore, it is suspected with 2-D or 3-D effects that the damage caused by irregular subsurface structures.

Keywords: microtremor observation, H/V spectra, the 2016 Central Tottori Prefecture Earthquake, subsurface structure

©2020. Japan Geoscience Union. All Right Reserved.



©2020. Japan Geoscience Union. All Right Reserved.

CMP-SPAC and SPAC microtremor array surveys around Tegano active fault, Gifu, Japan

*Masayuki Yoshimi[1], Haruhiko Suzuki[2]

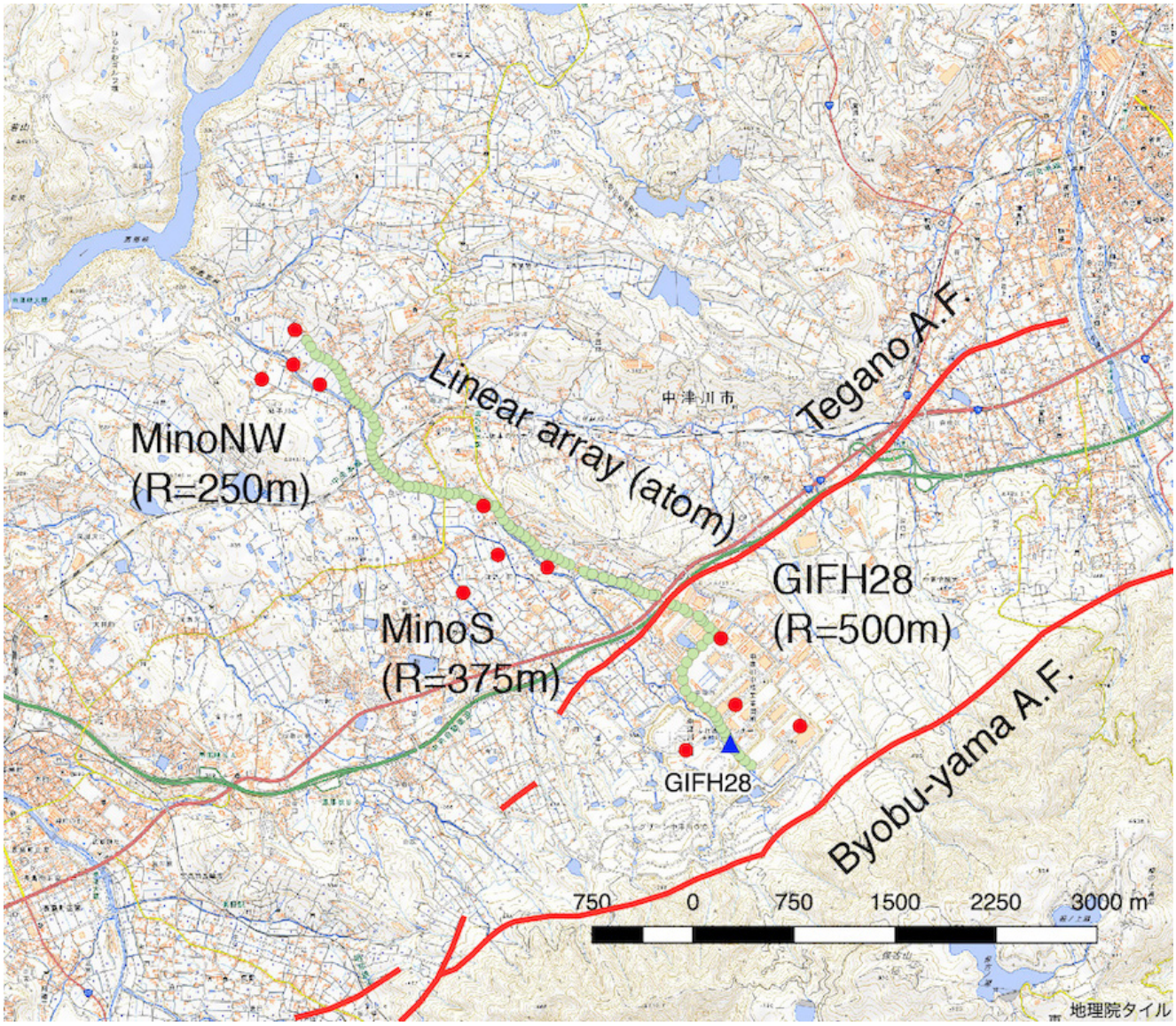
1. Geological Survey of Japan, AIST, 2. Oyo Corporation

We conducted microtremor array measurements for subsurface velocity structure around a reverse active fault, Tegano Active fault, Gifu prefecture, central Japan. We set about 5 km long NW-SE trending measurement line from the GIFH28 KiK-net station, where the bedrock depth is GL -360m, to the area where granite outcrop is seen.
Two types of microtremor observations were made on Dec. 2019. One is regular triangle array and the other is linear array. For the regular triangle array, we deployed eight 3-component velocimeters (Tokyo Sokushin Corp. SE-321, natural period 10 seconds), and for the linear array observation, we used 40 geological McSeis-AT systems (hereinafter Atom).
Regular triangle arrray observations were conducted at three locations: near GIFH28 (for one night), near the granite outcrop (MinoNW: for one hour), and at an intermediate point (MinoS: for one hour). The maximum array radius is 500 m for GIFH28, 375 m for MinoS, and 250 m for MinoNW. The SPAC method is used for analysis.
As for the linear array observation, we used a vertical motion velocimeter Sunful PS-2B with a natural frequency of 2 Hz (Suzuki et al., 2019). The seismometers were installed at intervals of about 50 m, and three sets of observations were made with a deployment of about 2 km and an overlap of 0.5 km, so the total line length was about 5 km . The measurement was performed at a sampling frequency of 250 Hz and about 40 minutes each time. Data are analyzed with a microtremor tomography CMP-SPAC method (Hayashi et al., 2018). The analysis section length is 65.536 seconds, and the bin size of CMP is 250m.
The observed phase velocities around GIFH28 showed good agreement with the theoretical phase velocities based on PS logging results. Furthermore, it was found that the phase velocity tended to increase from GIFH28 to the northwest, and especially at the Chuo rail way line, about 3 km NW from GIFH28) the phase velocity gets quite large.

Acknowledgement
We used PS logging data by the National Research Institute for Earth Science and Disaster Resilience.

Keywords: microtremor array survey, Linear array, Tegano fault

©2020. Japan Geoscience Union. All Right Reserved.



©2020. Japan Geoscience Union. All Right Reserved.

Improvement of Accuracy to Estimate Phase Velocity using Arbitrary Shape Arrays with Extra Observation Sites

*Huan Zhang[1], Kahori Iiyama[1], Hitoshi Morikawa[1]

1. Tokyo Institute of Technology

Based on the analytical solution of Lamb's problem for vertical components of Rayleigh wave, the relationship between two observation points, p and q for example, is given in a discrete representation with the Bessel function of the first kind and higher-order Bessel functions, which is called Complex Coherence Function (CCF) [4]. Zhang and Morikawa [5] extended the CCF to apply it to linear array situation. By adding an extra observation points, the relationship between p and s can be expressed [6]. At last, the CCF equations have only 5 unknowns left, including the phase velocity. Therefore, we proposed an algorithm [7] to estimate the phase velocity using Artificial Bee Colony (ABC) algorithm [8] under a constraint of $kr \in [0, 5]$. The numerical simulation results confirmed the availability of the proposed algorithm for array shapes that are not near linear-array situations [7]. And for near linear-array situations, relative accurate results might be get by increasing the observation time.

In theory, we can extend the CCFs to the array with 4 and more observation points [7]. Although the total number of CCFs increases with increasing observation points, the 5 unknowns remain the same. That is to say, with increased observation points, the number of CCFs will be greater than the unknowns' number 5. Then we think better results can be obtained due to the increased constraint conditions. Numerical simulations of a 4-site array, as shown in Figure 1, were conducted. It consists of one 3-site obtuse triangle and one 3-site near linear-array triangle. With same wave field consisting of 8 randomly generated wave sources, the results of shape 1 (obtuse triangle), shape 2 (near linear-array triangle), and 4-site array are shown in Figure 2. It can be seen that for shape 2, the near linear-array triangle, the results are not satisfactory and the constraint line $kr = 5$ can be obviously seen. And compared with shape 1's effective range [0.25Hz, 0.9Hz], the 4-site array's effective range can be seen as [0.25Hz, 1.25Hz], although still with fluctuations around 1.0Hz and the shape of the constraint line clearly seen after 1.0Hz. In conclusion, the 4-site array results are better than the more regular shape, as predicted before. But the computation time is longer than 3-site arrays since the total number of the equations increased from 3 to 6.

To confirm the availability of the proposed algorithm, a field test will be conducted.

[1] Capon, J. (1969). *Proceedings of the IEEE*, 57(8), 1408-1418.
[2] Aki, K. (1957). *Bull. Earthq. Res. Inst.*, 35, 415-456.
[3] Cho, I., Tada, T., & Shinozaki, Y. (2006). *Journal of Geophysical Research: Solid Earth*, 111(B9).
[4] Shiraishi, H. & Matsuoka, T. (2005). *BUTSURI-TANSA,* 58(2), 137-146.
[5] Zhang, X. & Morikawa, H. (2014). *British Journal of Applied Science & Technology*, 6(4), 350–363.
[6] Morikawa, H. & Iiyama, K. (2015). *Program and Abstracts, The Seismological Society of Japan, Fall Meeting.*
[7] Zhang, H., Iiyama, K. & Morikawa, H. (2020). *17th World Conference on Earthquake Engineering.*
[8] Karaboga, D. & Basturk, B. (2007). *Journal of global optimization*, 39(3), 459-471.

©2020. Japan Geoscience Union. All Right Reserved.

Keywords: CCF, SPAC method, CCA method, arbitrary-shape array, phase velocity, Artificial Bee Algorithm

©2020. Japan Geoscience Union. All Right Reserved.

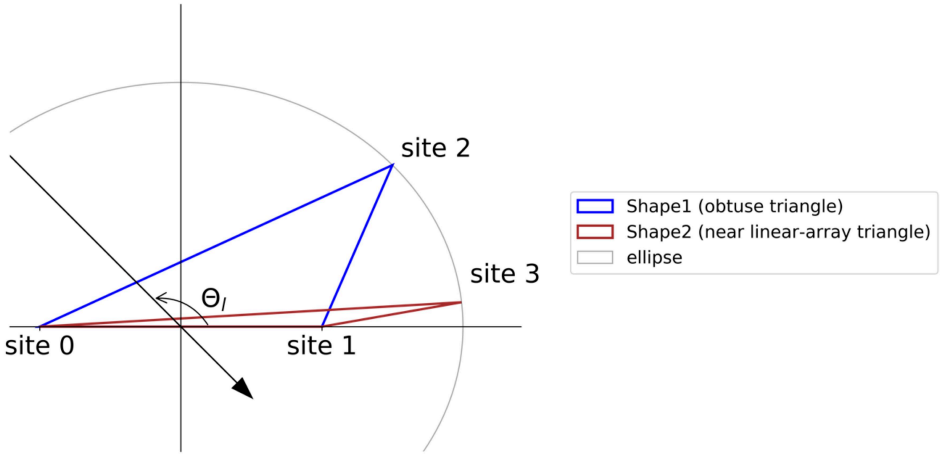


Figure 1: Array settings used for numerical simulations.

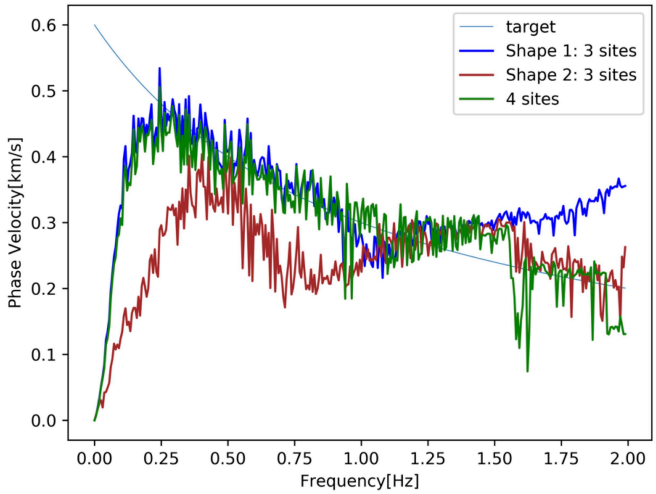


Figure 2: The average phase velocity results of 3 array shapes.

©2020. Japan Geoscience Union. All Right Reserved.

Site Classification Method in Microtremor Array Exploration Using a Supervised Machine Learning

*Takumi Hayashida[1]

1. International Institute of Seismology and Earthquake Engineering, Building Research Institute

Seismic wave is amplified in the subsurface soil layers and understanding of the amplification effect is important for the estimation of ground motion characteristics. The average S-wave velocity in the upper 30m (AVS30) has been widely used as a simplified indicator of site classification since the 1980s (e.g. NEHRP site classification). The microtremor array exploration, a method to estimate subsurface S-wave velocity structure using seismic noise recordings, has been used globally as a low-cost and practical tool for site classification. However, recent blind tests show the possibilities of different interpretation for the dataset among analysts (e.g. Yong et al., 2018; Ohori et al., 2018), which could be caused by different ways of preprocessing, parameter selection for data processing, initial model setting for phase-velocity inversion, or by differences of user’ s knowledge and experiences, as well as software for analysis. In this study we propose a way of dealing with the problem, using a machine learning method. Here we test the possibility of site classification with randomly constructed 720 subsurface soil structure models. Each model consists of three layers; the minimum S-wave velocity of the top layer is 100 m/s and the maximum value of the bottom layer is 1,700 m/s. Assuming array radii of 5, 10, 15, and 20 m we derive Bessel functions of the first kind of order zero (i.e. theoretical SPAC coefficients) and characterize each function by extracting frequencies at which the values become 0.5, 0.0, and the minimum value. We employ supervised machine learning methods to the extracted dataset and investigated the possibility of soil type classification. The results show that soil type could be classified well for soil classes B and E, but sometimes show the difficulties for soil classes C and D. On the other hand, when we assume that microtremor array surveys are conducted with two or more different size arrays, the performance has been substantially improved. Our results indicate that the machine learning methods effectively work for interpretation of microtremor exploration and variabilities attributable to analyzers and tools could be reduced.

Keywords: microtremor, SPAC method, supervised machine learning, site classification

©2020. Japan Geoscience Union. All Right Reserved.

Verification for the Deep Sedimentary Velocity Structure in the Kathmandu Valley using Receiver Function Analysis

*Michiko Shigefuji[1], Nobuo Takai[2], Subeg Bijukchhen[3]

1. Kyushu University, 2. Hokkaido University, 3. Khwopa Engineering College, Nepal

The Himalayan continental collision zone of the Indian plate and the Eurasian plate has experienced devastating earthquakes in the past. In addition, the future great earthquakes in Nepal Himalaya have the potential to occur in the Central Seismic Gap of the Main Frontal Thrust. The Kathmandu Valley in Nepal is filled with soft lake sediment of Plio-Pleistocene origin, more than 650 m thick in the central part of the valley. This soft lake sediment might be one of the causes of seismic heavy damage. Therefore, we must examine the amplification characteristics of the valley and grasp the susceptible to the risks of strong ground motion at the next great earthquake.

In order to understand the basement topography of the valley and depth of the sediment, Shigefuji *et al.* (WCEE2020) applied the receiver function analysis to strong-motion waveforms recorded at 17 stations in the Kathmandu Valley (Takai *et al.* EPS2016, Ichiyanagi *et al.* EPS2016; Takai *et al.* JpGU2018). We examined the relationships between the spatial variation of peak phase from the receiver functions and the basement topography of the valley. The peak times of the receiver functions almost correspond with the theoretical time differences between the direct P-wave and Ps-wave converted at the basement-sediment boundary calculated from the 1-D velocity structure (Bijukchhen 2018) under each station. The Ps-P times are large differences in the range of 0.28 to 1.06 second in the sedimentary sites, this feature shows the complex basement topography of the valley.

In this report, we verify the previous deep sedimentary velocity structure model in the Kathmandu Valley (Bijukchhen, 2018) by comparing the observed receiver function with the theoretical one. The theoretical receiver function was calculated in the previous model based on the P-SV propagator matrix method. The P-wave velocity and density were derived from S-wave velocity based on some empirical relationships. The observed receiver functions agreed with the theoretical ones in most stations except stations on the center and marginal part of the valley, which is not used by the construction of this velocity model. Additionary, We will examine the effect of the middle layer of the velocity structure, the direction of the epicenter and the Vp/Vs ratio, to the receiver functions.

This research was supported by Science and Technology Research Partnership for Sustainable Development (SATREPS), Japan Science and Technology Agency (JST) / Japan International Cooperation Agency (JICA) Grant Number JPMJSA1511.

Keywords: receiver function analysis, Kathmandu Valley, Nepal, deep sedimentary velocity structure

©2020. Japan Geoscience Union. All Right Reserved.

Detect of Underground Velocity Discontinuity by Autocorrelation of Strong Motion Data in the Osaka and Kyoto Basins

*Shuta Fukutome[1], Kimiyuki Asano[1], Tomotaka Iwata[1]

1. Disaster Prevention Research Institute, Kyoto University

The Osaka and Kyoto basins in southwest Japan are mainly composed of sedimentary layers called ”the Osaka Group”. Three-dimensional basin velocity models down to the basin basement have been constructed by using geophysical exploration results, such as reflection surveys, microtremor measurements, deep boring, etc. (e.g. Horikawa *et al.*, 2003; Kyoto prefecture, 2006; Iwata *et al.*, 2008; Sekiguchi *et al.*, 2016). It is important to validate those basin velocity models by using other methods or data set. The seismic interferometry technique is used to obtain a seismic response and it can be used to explore the underground structure. For example, Pham and Tkalcic (2017) demonstrated that the autocorrelation function of the seismic waveform observed at a station shows the response of the reflected waves from the velocity discontinuities (Moho discontinuity and ice-rock interface) and they wrote that this method can be applied to more shallow construction (e.g. sedimentary layer). We use autocorrelation functions of strong motion waveform data at some KiK-net strong motion stations in the Osaka plain and Kyoto basin. Since the strongest velocity discontinuity above the crust is the basin basement, dominant signals emerging in the autocorrelation functions would be the reflected S-waves propagating between the ground surface and the basin basement (e.g. Yoshimoto *et al.*, 2007; Watanabe *et al.*, 2011; Chimoto and Yamanaka, 2019). We use the spectral whitening that enlarge high frequency components to detect the response waves more clearly, then we stack the autocorrelation functions of records from local events using the phase weighted stack (PWS) to emphasize the response as with Pham and Tkalcic (2017), pick up the delay time of the reflected waves and estimate the depth of the underground velocity discontinuity surface of the Osaka and Kyoto basins. Acknowledgement: The observed waveform data from KiK-net were used in this study.

Keywords: autocorrelation function, strong motion, reflected wave, the Osaka Group

©2020. Japan Geoscience Union. All Right Reserved.

CONSTRUCTION OF SHALLOW AND DEEP LAYERS COMBINED MODEL IN THE KANTO REGION, JAPAN

*Hiroaki Yamanaka[1], Yoko Tono[2], Shigeki Senna[3], Masahiro Ohbuchi[4], Hiroyuki Fujiwara[3]

1. Interdisciplinary Graduate School of Science and Engineering,Tokyo institute of Technology, 2. Earthquake Research Institute, University of Tokyo, 3. National Research Institute for Earth Science and Disaster Resilience, 4. Ministry of Education, Culture, Sports, Science and Technology

The Earthquake Research Committee, the Headquarters for Earthquake Research Promotion (ERC/HERP) keeps updated "National Seismic Hazard Maps for Japan" consisting of two types of maps: probabilistic seismic hazard maps, and scenario-based ground motion maps. The latter requires a three-dimensional velocity structure model involving density, P- and S-wave velocities, Q-values, and the boundary shapes for each layer. Conventional nation-wide velocity models ERC used (e.g., Koketsu et al., 2008) have been only deep sedimentary layers by which accuracy of broadband ground motion is limited. For improving reliability of the seismic ground motion prediction, ERC newly applied the procedures to develop 3D models of shallow soil layers with S-wave velocity less than 350 m/s over engineering bedrock with S-wave velocities of 350-700 m/s and deep sedimentary layers having S-wave velocities from 350 to 3,000m/s over the seismic basement with an S-wave velocity of about 3 km/s for the shallow and deep layers combined model (SDLCM in the following). So far, ERC published “Procedures to establish a subsurface structure model” and established a new SDLCM for the Kanto region, Japan. This paper shows characteristics of the shallow and deep layers combined model constructed in the Kanto region.

One of advantages of application of SDLCM to seismic hazard maps is that amplification factors of ground motion on the surface to that in the seismic basement can directly be obtained at every grid point of the SDLCM. The new distribution of amplification factors by SDLCM shows a more complex spatial variation of the Vs30s than ones by geomorpholgical classification which was applied in the previous method. In particular much low Vs30s are identified in the new map along the major rivers. We furthermore calculate amplification factors of PGV between the surface and the top of the engineering bedrock using the two maps of the Vs30s. As comparing the amplification factors by SDLCM and by the previous method, it is noted that the amplification factors are calculated using the same empirical equation of a Vs30 from different Vs30s and the S-wave velocities of the engineering bedrock of the two models. The variation of the amplification factors for the new model is much wider than that of the previous one. In particular the amplification factors for the two types of the terraces are so large in the new model of SDLCM. Thus, it’s concluded that the new SDLCM for Kanto region, Japan can be used for a reliable seismic ground motion prediction for future large events.

Keywords: Shallow soil, Deep sediments, S-wave velocity, Ground motion prediction, 3D velocity structure, Average S-wave velocity

©2020. Japan Geoscience Union. All Right Reserved.

Estimation of earthquake ground motions at MeSO-net stations

*Atsushi Wakai[1], Shigeki Senna[1], Atsushi Shimizu[1]

1. National Research Institute for Earth Science and Disaster Resilience

In the past national project of Japan, “Metropolitan Seismic Observation network” (hereinafter, referred to as “MeSO-net”) was constructed for the investigation of the tectonic plate structures and earthquake ground motions in the Tokyo metropolitan area around ten years ago. The MeSO-net has about 300 stations with sensors installed around 20 meters underground in the area. Also, they are spatially distributed at intervals of 2 to 5 kilometers in the area.

In recent years, we have worked a subproject of “acquisition of spatially very-high-resolution earthquake observation data and development of the database by private-public partnerships” as a member in a national project or “Tokyo Metropolitan Resilience Project.” As one of the topics, we have tackled a challenge for estimation of seismic ground motions based on bore-hole seismic records observed at each MeSO-net station.

The point is as follows. First, a seismometer is installed on the ground surface at each station during two to three months and some earthquake observation records are obtained in addition to the bore-hole records at each station. And then, an observed frequency response function is obtained by calculating spectral ratios of the ground surface records to the bore-hole ones. Also, increment of seismic intensity is obtained by calculating that from the ground surface records and from the bore-hole records. At the same time, a miniature and centerless array microtremor measurement is performed at each station. This method of measurement can be adopted principally for estimation of an S-wave velocity structure in the surface ground. It consists of 4-point miniature array with a radius of 60 centi-meters and 3-point centerless array with around 10 meters on a side. An S-wave velocity structure is estimated based on a disperse curve of a phase velocity and an H/V spectrum calculated from microtremor data. And then it can be enhanced based on an observed frequency response function described above. Therefore, a transfer function can be obtained using 1-dimensional multiple reflection theory based on the S-wave velocity structure at a station.

In this project, we will develop the system for estimation of earthquake ground motions based on bore-hole seismic records by means of the a variety of amplification factors mentioned above. In this presentation, we will report on the results in the analyses of earthquake observation data and microtremor measurement ones at this moment.

Keywords: earthquake ground motion, MeSO-net, microtremor, S-wave veloctiy structure

©2020. Japan Geoscience Union. All Right Reserved.

Modeling of subsurface velocity structure from seismic bedrock to ground surface based on array microtremor observation in Aso area

*Shigeki Senna[1], Atsushi Wakai[1], Atsushi Yatagai[2], Yoshiaki Inagaki[2], Hisanori Matsuyama[2], Hiroyuki Fujiwara[1]

1. National Research Institute for Earth Science and Disaster Resilience, 2. OYO Corp

One of the important issues for improving the prediction of strong ground motion is to construct a ground model that can evaluate broadband ground motion characteristics. For that purpose, it is essential to integrate the shallow ground model and the deep ground model, which have been separately modeled, and to create a model that can reproduce the observation records. In this study, the K-NET, KiK We collected seismic records at seismic stations such as -net, the Japan Meteorological Agency, and local governments, as well as array surveys and records of single points (H / V spectral ratios) using many microtremors. In addition, the S-wave velocity structure model was examined from the analysis results as a basic study for constructing the ground model of the Aso area. In this report, we report the results of microtremor array observations and the results of the study on the construction of an integrated shallow and deep ground model.
In this study, an initial geological model was created, and the distribution of AVS30 (m/s) and an integrated shallow / deep ground model were constructed using microtremor array survey and microtremor measurement results. The distribution of the AVS30 and the engineering-based equivalent layer based on the ground model created in the Aso region this time is harmonious with the existing drilling data, similar to the results of research conducted in the Kanto and Tokai regions. ing. The theoretical H/V (periodic characteristics) and amplification characteristics calculated from the S-wave velocity structure model calculated in this study were also confirmed to be in harmony with the seismic records. The results show that the evaluation of phase velocities and periodic characteristics (H / V spectral ratios) per se by microtremor observations is very effective in improving the accuracy of the model, and is very effective for engineering platforms (for example, S-wave velocities such as Vs350). When it is difficult to set the depth of the upper surface of the structure, it is considered to be very useful as a method of correcting the engineering base depth based on geological and geological information using micro array microtremor observation. In the future, we plan to examine various amplification factor indices in comparison with the method using micro-topography and earthquake records, which are used as the ground amplification factor.

Keywords: Subsurface velocity structure, Microtremors, Strong Ground Motion, Array observation

©2020. Japan Geoscience Union. All Right Reserved.

The examination of liquafaction damage rate by recent earthquakes

*Shigeki Senna[1], Kyoko Ozawa[1]

1. National Research Institute for Earth Science and Disaster Resilience

The 2011 off the Pacific coast of Tohoku Earthquake caused liquefaction that caused large-scale and severe damage. The quake was severely shaken by a seismic intensity of less than 5 and liquefaction occurred in many areas. In this study, it was possible to determine liquefaction using detailed aerial photographs, and seismic intensity 6 or lower was observed. Based on information on liquefaction occurrence points of five earthquakes such as the 2018 Hokkaido Eastern Iburi Earthquake, estimate liquefaction occurrence rate based on 250m mesh unit and liquefaction area rate considering liquefaction area in each mesh, A formula for estimating liquefaction risk based on liquefaction occurrence rate and area ratio was proposed. We also examined the building damage rate from information on building damage caused by liquefaction.

Keywords: Liquefaction Occurrence Ratio, Strong Ground Motion, Fragility, Geomorphologic Classification, Building damage Ratio

©2020. Japan Geoscience Union. All Right Reserved.

Ground Motion Estimation by using Microtremor H/V Spectral Ratio

*Guan-Yu Chen[1], Che-Min Lin[2], Kuo-Liang Wen[1]

1. Department of Earth Science, National Central University, Taoyuan, Taiwan, 2. National Center for Research on Earthquake Engineering, Taipei, Taiwan

It has been proved that the H/V spectral ratio method, proposed by Nakamura (1989), is effective in estimating the site response of ground motion. Because the density of strong-motion stations is still insufficient to provide accurate ground motion distribution in a highly developed region. This study proposes a method by using microtremor H/V spectral ratio (HVSR) to correct the site effect and predict the ground motion of nearby sites. Considered two sites at a very close distance and assume that under the influence of the same earthquake, the source and path effect in observed seismic waves are almost the same, the difference ground motion between this two sites just control by their site characteristics, that is the different of their HVSR. So, the ratio of HVSR can be seen as a correction factor to estimate the ground motion of the sites around a strong-motion station. Here, we selected the Ilan plain of Taiwan as a test site, and the seismic records with PGA > 8 gal from 1993 to 2013 were collected to evaluate the error and stability of this method including the relative site distance, hypocenter distance, Vs30, and the spectral different. Finally, the scenarios of several historical events in the Ilan plain were simulated by using the site correction of microtremor HVSR. Consolidate the variations in ground motion for these events to evaluate the effect of site characteristics for ground motion distribution.

Keywords: H/V spectral ratio, site effect, correction factor, ground motion estimation, site characteristic

©2020. Japan Geoscience Union. All Right Reserved.

ISNL-- an new parameter of soil nonlinearity used for Taiwan and New Zealand earthquake

*Kao Ching[1], Huang Jyun-Yan[2], Wen Kuo-Liang [2]

1. National Central University, 2. National Center for Research on Earthquake Engineering

Previous studies indicated that nonlinear site response occurred when strong ground motion wave propagating through surface soft soil layers. This phenomenon can be identified from comparing site transfer functions (i.e. Horizontal to vertical spectral ratio method, HVSR, Wen et al., 2006) of strong ground motion against the reference weak motion.

Meanwhile, Noguchi and Sasatani (2008) constructed a quantitatively method to identify soil nonlinearity (Degree of nonlinearity, DNL) that was calculated from the summation of differences between HVSR of strong and weak motions. However, basic idea of DNL calculation might miss some hint from identification of de-amplification or amplification in high frequency band.

Therefore, this study attempts to build a new and improved nonlinearity method ISNL (Index of soil nonlinearity) to avoid the traditional DNL only considering the difference between HVSR of the strong and weak motions that it couldn’ t recognize dominant frequency drop and de-amplification of high frequency band correctly. Finally, in this study, comparison from traditional DNL and improved ISNL were checked with PGV/Vs30 (Strain proxy, Idriss, 2011) from 2016 Meinong, Taiwan; 2010 Jiaxian, Taiwan and 2018 Hwalien, Taiwan earthquakes.

Finally, higher correlation between both DNL, ISNL against PGV/Vs30 proxy was resulting in 2018 Hwalien earthquake comparing to 2016 Meinong as well as 2010 Jiaxian earthquakes. Moreover, ISNL behaved better linear correlations with PGV/Vs30 than DNL. Then, earthquake sequences in New Zealand will be also checked in this study to test the ability of newly constructed ISNL for application to worldwide regions.

Keywords: nonlinear site effect

©2020. Japan Geoscience Union. All Right Reserved.

Assessment of the liquefaction risk at Re-liquefied site

*CHIH-SHENG KU[1], Yun-Ling Hsieh[1], Po-Wei Cheng[1]

1. I-SHOU University

The Beishih village, Hsinhua Dist., Tainan City, Taiwan is the only confirmed location in Taiwan having soil liquefaction and sand boil for the Hsinhua earthquake on 1946, Taoyuan earthquake on 2010, and Meinong earthquake on 2016. The soil liquefaction and sand boil in Beishih Village were observed from Taoyuan earthquake on March 4, 2010 and Meinong earthquake on Feb. 6, 2016. The authors surveyed the two liquefaction sites and used GPS to obtain the coordinates of each crater of sand boil cone, the authors found that the locations of the liquefaction were highly overlapped for those two liquefaction cases.

The seismic stations at Koupi elementary school (CHY063) and Yongkang meteorological station (CHY078) are close to Beishih Village. The seismic peak ground accelerations in the vertical, N-S, and W-E motion measured at station CHY063 for the earthquakes of Taoyuan and Meinong were 71.24, 174.66, and 385.18gal, and 163.26, 238.64, and 416.92 gal, respectively. Moreover, the seismic peak ground accelerations in the vertical, N-S, and W-E motion measured at station CHY078 for the earthquakes of Taoyuan and Meinong were 25.3, 61.54, and 101.66gal, and 43.6, 101.86, and 143.86 gal, respectively. The monitor information of the groundwater level obtained from liquefaction site shows that the variations of the groundwater level were quite a lot in this area. The ground water levels were about 0.24 to 3.67m below the ground surface.

The re-liquefied site is an alluvium at the west edge of the Hsinhua Hill. The Hsinhua fault passes through the east of the site. Based on the site investigated results, four different sub-soil layers were categorized for the soil layer within the depth of 30m in the site studied. The first sub-soil layer was from ground surface to the depth about 3m below surface and was characterized as low resistances soft soil. The second layer was at 3-6m below the surface and was characterized as sandy soil; the third layer was at 6-11m below the surface and was characterized as clayey soil (clay or silt); the fourth layer was characterized as dense sandy soil. The average shear wave velocities (V_{s30}) obtained from 3 different sampling locations for soil layers 30m below ground surface were 215, 201, and 213m/sec, respectively.

In this study, the CPT-based, SPT-based and Vs-based methods were applied to the LPI for the evaluation of the liquefaction potential. The LPIs obtained from different evaluation method were varied. The smaller and the largest of the LPI were obtained from SPT-based method and CPT-based method, respectively. Based on the Iwasaki criteria the liquefaction risk potentials were classified as high to extremely high under attack of these two earthquakes. However, the real investigation report shows that the liquefaction hazards were classified as moderate in which was conservative comparing to the analyzed results.

Keywords: Liquefaction, Cone Penetration Test (CPT), Liquefaction Potential Index (LPI)

©2020. Japan Geoscience Union. All Right Reserved.

Experimental Study on Dynamic Shear Modulus of Cohesive Soil in Beijing Plain

*Yi Fang, Guoxing Chen, Yanju Peng, Yuejun Lyu

As an important parameter of soil dynamic characteristics, the dynamic shear modulus can better reflect the nonlinearity of the soil, but it is affected by the combination of factors such as the genesis, age, burial depth. A class needs specific analysis to determine its dynamic shear modulus characteristics. The seismic environment of the Beijing Plain area is complex, and the site soil is mainly cohesive soil. There is no systematic study on the dynamic shear modulus of cohesive soil. In this paper, 17 undisturbed soil samples from Beijing area were collected for laboratory test used resonance column and field shear wave velocity tests, the results show that: (1) The results of Gmax by filed test are greater than Gmax of laboratory tests, both of which have a linear relationship with depth, and also show good linear correlation between them; (2) There are many reasons which lead to the difference between the field test with the laboratory test, such as the mechanism of the tests, the conditions of tests ; (3)G/Gmax of regional clay soil is significantly affected by the groundwater level. Non-linearity of the soil above the groundwater level decreases with depth, and non-linearity of the soil below the groundwater level increases with depth. (4) The non-linearity of cohesive soils in Beijing Plain is significantly stronger than Fuzhou and other places within 0-20m, but slightly weaker than Suzhou, which is closely related to the genesis and sedimentary environment of each place.

Keywords: Dynamic Shear Modulus, Cohesive, Beijing Plain

©2020. Japan Geoscience Union. All Right Reserved.

[E] Poster | S (Solid Earth Sciences)：S-SS Seismology

[S-SS05] Innovative data analysis methods for characterization of seismicity

convener:Francesco Grigoli(ETH Zurich Swiss Federal Institute of Technology Zurich), Bogdan Enescu(Department of Geophysics, Kyoto University), Aitaro Kato(Earthquake Research Institute, the University of Tokyo), Yosuke Aoki(Earthquake Research Institute, University of Tokyo)

In the last two decades the number of high quality seismic instruments being installed around the world has grown exponentially and likely will continue to grow in the coming decades. This led to a dramatic increase in the volume of available seismic data and pointed out the limits of the current standard routine seismic analysis, often performed manually by seismologists. Exploiting this massive amount of data is a challenge that can be overcome by using new generation, fully automated and noise-robust seismic processing techniques. In the last years, waveform-based detection and location methods have grown in popularity and their application has dramatically improved seismic monitoring capability. Moreover, machine learning techniques, which are dedicated methods for data-intensive applications, are showing promising results in seismicity characterization applications, opening new horizons for the development of innovative, fully automated and noise-robust seismic analysis methods. Such techniques are particularly useful when working with data sets characterized by large numbers of weak events, with low signal-to-noise ratio, such as those collected in induced seismicity, seismic swarms and volcanic monitoring operations. This session aims to bring to light new methods that can be applied to large data sets, either retro-actively or in (near) real-time, to characterize seismicity (i.e., perform detection, location, magnitude and source mechanisms estimation) at different scales and in different environments. We thus encourage contributions that demonstrate how the proposed methods help improve our understanding of earthquake and/or volcanic processes.

[SSS05-P01] Erecting and Observation Data of Broadband Seismic Array in Haiyuan-Liupanshan Fault Zone, Ningxia, China

*Guofu luo[1], Heqin - Ma[1] (1.Earthquake Administration of Ningxia Hui Autonomous Region)

[SSS05-P02] Energy release patterns and shaking effects of earthquakes in the Japan Trench: A Hilbert-Huang Transform approach

*Swapnil Mache[1], Kusala Rajendran[1] (1.Indian Institute of Science, Bangalore)

[SSS05-P03] The 2019 September 15th Stigliano natural seismic sequence revealed by a local network designed for induced seismicity monitoring

*Chiara Cocorullo[1], Giancarlo Graci[2], Stefano Limonta[1], Alexander Garcia[3], Thomas Braun[3], Francesco Grigoli[4] (1.SolGeo srl, 2.TOTAL E&P ITALIA, 3.INGV, 4.ETH-Zurich, Swiss Seismological Service)

[SSS05-P04] The systematic spatial bias pattern of earthquakes related to tectonic heterogeneity

*Yijun Zhang[1] (1.Southwest JiaoTong University)

[SSS05-P05] Location of seismic events with a single station using Distance Geometry Solvers

*Francesco Grigoli[1], William L Ellsworth[2], Miao Zhang[3], Simone Cesca[4], Claudio Satriano[5], Mostafa Mousavi[2], Gregory C Beroza[2], Stefan Wiemer[1] (1.ETH-Zurich, Switzerland, 2.Stanford University, United States, 3.Dalhousie University, Halifax, Canada, 4.GFZ-Potsdam, Germany, 5.IPGP-Paris, France)

[SSS05-P06] Evaluation of deep-neural-network-based seismic arrival-time picking method for S-net data

*Rintaroh Suzuki[1], Naoki Uchida[1], Weiqiang Zhu[2], Gregory C Beroza[2] (1.Research Center for Prediction of Earthquakes and Volcanic Eruptions Graduate School of Science, Tohoku University, 2.Department of Geophysics, Stanford University)

Erecting and Observation Data of Broadband Seismic Array in Haiyuan- Liupanshan Fault Zone, Ningxia, China

*Guofu luo[1], Heqin - Ma[1]

1. Earthquake Administration of Ningxia Hui Autonomous Region

Ningxia Haiyuan –Liupanshan fault zone is located at the junction of southern Ningxia Hui Autonomous Region and eastern Gansu province. The seismogenesis and active structure of this fault zone are highly similar to the seismogenic structure Longmenshan fault of Wenchuan 8.0 earthquake in 2008. There is also a large thrust fault tectonic system, and there is no record of large earthquakes in history. Therefore set up broadband seismometers around Haiyuan-Liupanshan fault zone, seismic array, using seismic waves of the interior of the earth "projector", the fault zone around the earth's crust, mantle and core structures, deepen the flame breeds of deep structure in the region, environment, promote the development of earthquake prediction and earthquake prediction research, for Ningxia to make positive contribution to earthquake prevention and disaster relief cause.

Since Campillo and Paul established the relationship between the two points' wake wave cross-correlation function and green's function, and extracted the surface wave green's function, they pioneered the application of background noise in seismology. Then Shapiro and Campillo obtained California high-resolution surface wave tomography using the US array, and the background noise method has been widely used in high-resolution tomography at global scale, regional scale and small scale. The imaging of background noise combined with highly dense seismic array with uniform distribution greatly improves the horizontal and vertical resolution of imaging, and provides a possibility for the research of 3d high-resolution fine structure.

In this project, on the basis of observation data from regional fixed stations, a two-dimensional mobile seismic array consisting of 50 seismographs was scientifically and rationally arranged around the Haiyuan - Liupanshan fault zone in October 2018. Continuous seismic observations were carried out for a period of 2 years to obtain continuous waveform data (figure 1).Using the two-year data, three methods, such as the method of receiving function, the method of noise surface wave dispersion and the method of seismic surface wave dispersion joint inversion of three-dimensional s-wave velocity structure, were used to analyze the relationship between the velocity structure and the seismic mechanism and the dynamic mechanism of fault zone.

In this project, 50 sets of mobile and dense seismic array are arranged around the Haiyuan-Liupanshan fault zone in Ningxia, and the observation data are carried out for 2 years, so as to draw the following conclusions.

(1) More than 50 sets of wide-band seismographs were installed across the Haiyuan-Liupanshan fault zone for continuous observation of earthquakes over a period of 2 years, providing basic observation data for subsequent studies on fine structure of the crust.

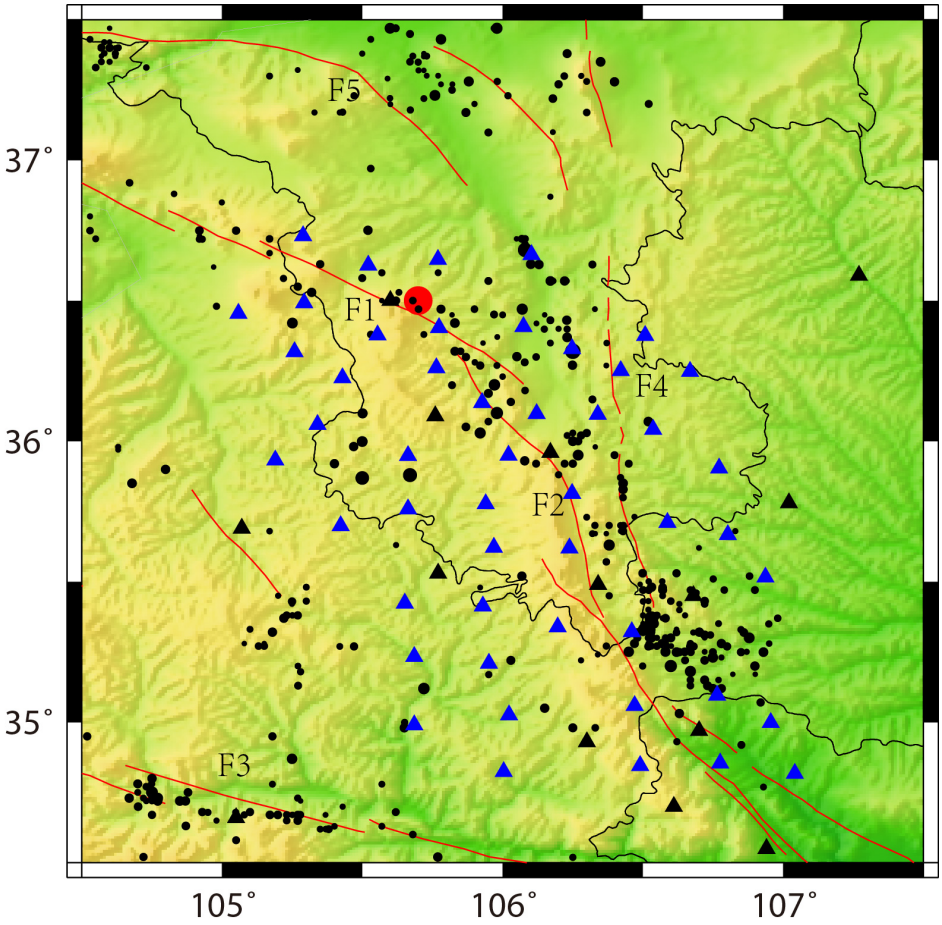
(2) Extracted from distant earthquake seismic waveform P wave and S wave function, the study area is obtained by receiver function inversion depth of Moho surface, and on this basis, the joint background noise and obtain Haiyuan seismic surface wave dispersion inversion - Liupanshan fine 3 d crustal velocity structure in the fault zone and its adjacent area, the study of seismic activity and the relationship between

©2020. Japan Geoscience Union. All Right Reserved.

velocity structure, explore the mechanism of earthquake gestation, the seismogenic mechanism, crustal dynamics and seismic risk.

(3) Collect seismic phase travel time data of near earthquake and artificial blasting, carry out tomography research of near earthquake travel time, and obtain 3d fine velocity model of the study area.

Keywords: Ningxia Haiyuan –Liupanshan fault zone, Seismic Array, Ningxia, Observation Data



©2020. Japan Geoscience Union. All Right Reserved.

Energy release patterns and shaking effects of earthquakes in the Japan Trench: A Hilbert-Huang Transform approach

*Swapnil Mache[1], Kusala Rajendran[1]

1. Indian Institute of Science, Bangalore

Subduction zones showcase the multiplicity of earthquakes—interplate, intraplate and intraslab—with shallow, intermediate, or deep focus, associated with different energy release patterns and frequency contents. An understanding of the duration and frequencies associated with various pulses of energy is useful for damage assessment. Empirical Mode Decomposition (EMD) of strong-motion records and the application of Hilbert transform have been suggested to overcome the limitations of the Fourier spectral analysis in dealing with highly non-linear strong-motion records (Huang et al., 1998, Zhang et al., 2003). Following the same approach, we have been trying various methods of analysis using the KiK-net strong-motion records to explore the efficacy of these techniques in representing the source of the rupture, in terms of energy release and frequency distribution. Our previous studies used EMD and time-frequency analysis tools such as spectrogram, scalogram, and Hilbert spectrum, using Intrinsic Mode Functions (IMFs) of the original signals as inputs. Nishant (2019) made random picks of IMFs to represent sources by correlating the sum of the selected IMFs with the original signal but found that the results were station dependent. We selected IMFs based on their frequency content (0.1 to 3 Hz) and used their linear combinations to develop the Energy Release Functions (ERF) for individual earthquakes (Mache et al., 2019). They reported that the ability to capture the signature of the original signal using the IMFs varied between earthquakes and stations. Next, we selected stations based on the direction of rupture inferred from teleseismic waveform models. The use of appropriate combinations of individual IMFs, chosen based on the direction of slip, resulted in ERFs whose shapes compared better with the Moment Rate Functions (MRFs) obtained from the teleseismic models. To further explore the station dependence on the resolution of ERFs viz-a-viz the MRFs, we used the instrumental seismic intensity distribution maps (JMA 1996, Shabestari and Yamazaki 2001) to select the stations. We analyzed five earthquakes; two interplate (Mw 7.2 2005 Miyagi, and Mw 6.9 2008/07/19), two intraplate (Mw 7.0 2003 Sendai, and Mw 7.2 2012 Kamaishi) and one intraslab (Mw 7.1 2011 Miyagi), following the above methodologies. This abstract presents the initial results of our study, which to our knowledge, is the first of its kind and holds significant potential in understanding the spatial and temporal patterns of energy release and their associated frequencies.

On the use of IMFs based on their frequencies, we find that a linear combination of appropriate signals can lead to ERFs that compare well with their respective MRFs. The selection of stations in the direction of rupture generates better-resolved spectra. While using the seismic intensities, we find that for values three and higher, stations located along the direction of rupture propagation produce ERFs that correlate better with their respective MRFs, as observed for the 2011 Miyagi earthquake. The use of stations located along the direction of the trench also shows a good correlation. For seismic intensities lower than 3, there is a decay in the energy release and hence a poor reproduction of the ERFs. For complex ruptures (2003 Sendai, 2005 Miyagi, and 2012 Kamaishi), the ERFs are not smooth, with their energy distributed in bands of varying frequencies. It could be due to changes in slip direction or generation of sub-events, but the fact that the shapes of both the MRF and ERF are comparable adds credence to our analysis. We find that the local geology also plays an essential role in limiting the energy distribution within a frequency range, an issue that needs further exploration using more examples.

©2020. Japan Geoscience Union. All Right Reserved.

Keywords: strong-motion, spectral analysis, Hibert-Huang transform, energy release, Japan Trench, intraslab, intraplate, and interplate earthquakes

©2020. Japan Geoscience Union. All Right Reserved.

The 2019 September 15th Stigliano natural seismic sequence revealed by a local network designed for induced seismicity monitoring

*Chiara Cocorullo[1], Giancarlo Graci[2], Stefano Limonta[1], Alexander Garcia[3], Thomas Braun[3], Francesco Grigoli[4]

1. SolGeo srl, 2. TOTAL E&P ITALIA, 3. INGV, 4. ETH-Zurich, Swiss Seismological Service

In 2014, after the public debate about the possibility that the industrial activities in the Emilia region (North Italy) could have triggered the Magnitude Mw 6.1 earthquake occurred on 20 May 2012, the Italian Oil & Gas Safety Authority (DGS-UNMIG, Ministry of Economic Development) published a set of guidelines that establish the need to monitor seismicity in areas subject to industrial activities such as hydrocarbon production, waste water injection and natural gas storage operations. In this framework, TOTAL E&P ITALIA, company owner of the Gorgoglione Concession for hydrocarbon production in the Basilicata region (Southern Italy), is monitoring the seismicity with a local microseismic network. The network, installed and managed by SOLGEO srl on behalf of TOTAL E&P ITALIA, consists of 12 seismic stations, each equipped with two sensors (surface seismometer (11 short period and 1 broadband) + accelerometer). In this work, we focus on the seismic sequence occurred on 2019 September 15th, near the Stigliano town, in the eastern edge of the local microseismic network. In order to demonstrate how the data integration of local and national networks can produce better results, both in terms of number of detected events and location quality, we show the comparison of the catalogues produced by analysing the data from the national seismic network, the local microseismic network and the combination of the two. While the INGV catalogue based on the national seismic network shows only 4 events associated with this sequence, by using the data of the local seismic network, we detected and located more than 25 events with local magnitude between 0.2 and 2.0. Since the smallest events are visible only at the closest station, we used a new single station location technique that allow to better constrain the location of clustered seismic sequences.

Keywords: earthquake location, single station location

©2020. Japan Geoscience Union. All Right Reserved.

The systematic spatial bias pattern of earthquakes related to tectonic heterogeneity

*Yijun Zhang[1]

1. Southwest JiaoTong University

Back-projection (BP) is a source imaging approach that combines both time-reversal and grid-search techniques. BP utilize coherent waveforms to image a finite source process without any prior parameterization of the source itself, and the recent development of large dense seismic array has triggered its severe growth. BP can also be used for earthquake detection and location. As aftershocks of one earthquake always occur in the neighboring area, their rays towards a specific teleseismic array will travel along similar paths as that of the mainshock. The travel time errors from the mainshock hypocenter can be derived by cross-correlating its P-arrival waveforms, and if applied right on the waveforms of aftershocks, one can obtain the aftershocks' BP-inferred locations. However, small-scale heterogeneity caused by the real Earth 3-D structure will result in the so called 'spatial bias', which is the spatial offset between the BP-inferred location and the true epicenter locations. Meng et al (2016) has proposed an aftershock-based method to calibrate the travel time errors due to the near source structural heterogeneity. In this study, we take the 2017 July Mw 7.8 Near-Islands Aleutian earthquake as an example to investigate the spatial bias artifact of the source region. We found that in the ~500 km long rupture area, three systematic patterns of spatial biases exist, which correlate to three different structure characteristics. The three segments are the northwestern termination of the Aleutian island (169°-170°E), southeast of Mednyi Island with the Shirshov Ridge in the arc (170°-171°E), and the western segment of the Aleutian arc around Attu Island and northwest of it (171°-172 °E). The spatial bias directions in the three areas can be observed to have a good consistence with the nodal planes of focal mechanisms in the three areas, separately. This phenomena can be attributed to the sudden change in this elongate area brought by the Shirshov Ridge in the arc (170°-171°E). Besides, the coincidence between fault-planes solutions for the earthquakes in this area and the systematic spatial bias patterns also demonstrate that the state of stress experiences a sudden change, which reflects the tectonic heterogeneity in the near-source area, validating the necessity of subarea slowness calibration for this earthquake and providing us insight into the tectonic structure characteristics of this area.

Keywords: BP-projection technique, aftershock-based calibration method, systematic patterns of spatial biases, near source structural heterogeneity

©2020. Japan Geoscience Union. All Right Reserved.

Location of seismic events with a single station using Distance Geometry Solvers

*Francesco Grigoli[1], William L Ellsworth[2], Miao Zhang[3], Simone Cesca[4], Claudio Satriano[5], Mostafa Mousavi[2], Gregory C Beroza[2], Stefan Wiemer[1]

1. ETH-Zurich, Switzerland, 2. Stanford University, United States, 3. Dalhousie University, Halifax, Canada, 4. GFZ-Potsdam, Germany, 5. IPGP-Paris, France

Earthquake location is one of the oldest problem in seismology. With the advent of modern seismic monitoring networks it is possible nowadays to obtain reliable locations also for tiny events. However, there are still many cases where the lack of a dense enough microseismic monitoring network affects the performance of the routine data analysis procedures, limiting the ability to obtain reliable results increasing the risk of wrong interpretations. In this work we propose a novel approach based on Distance Geometry Solvers (DGS) that allow to locate seismic events by using a single seismic station.
DGS are used to solve a Distance Geometry Problem (DGP), consisting in the characterization and study of sets of points based only on given values of the distances between member pairs. The DGP is the one of finding the coordinates of a set of points by using the distances between some pairs of such points. In this work we introduce a new method that allow locate earthquakes using only the inter-event distance between pair of seismic events using one or two seismic stations. This location method requires only four non-coplanar reference locations for which the absolute hypocentral coordinates are known (at least). In order to show the potential of this approach we firstly validated the method with synthetic datasets resembling different cluster geometries. We finally tested the methods with two seismic sequences occurred in California, 1) the Mw 6.0 Napa Earthquake occurred in August 2014 and 2) the Mw 7.1 Ridgecrest seismic sequence occurred in July 2019. We show that our approach provides better results than any other single station location method and when using the inter-event station estimated with two optimally oriented stations the results are comparable to high resolution Double Difference locations based on the use of multiple stations. This method is particularly useful in poorly monitored areas where only a limited number of stations is available.

Keywords: Single Station Location, Seismicity

©2020. Japan Geoscience Union. All Right Reserved.

Evaluation of deep-neural-network-based seismic arrival-time picking method for S-net data

*Rintaroh Suzuki[1], Naoki Uchida[1], Weiqiang Zhu[2], Gregory C Beroza[2]

1. Research Center for Prediction of Earthquakes and Volcanic Eruptions Graduate School of Science, Tohoku University, 2. Department of Geophysics, Stanford University

The number of detectable earthquakes is increasing rapidly as seismograph networks expand. Off the Pacific coast of Tohoku Japan, seismograms recorded by a 150 cabled ocean bottom seismic stations (S-net) available from 2016 enable much clearer characterization of offshore seismicity. Many approaches to automatic phase picking methods have been proposed to improve seismic monitoring. In this study, we evaluate an arrival-time picking method based on a deep neural network, PhaseNet (Zhu and Beroza, 2019), to detect and locate more earthquakes offshore Tohoku. PhaseNet estimates P and S arrivals as probability distributions using three-component seismic waveforms. PhaseNet has already achieved good performance for the Northern California Earthquake Data Center Catalog using the model trained by the seismograms of the region as input.

To evaluate the performance of the deep-neural-network-based seismic arrival-time picking model, we compared the output of PhaseNet with manual picks for S-net data. We used 512 offshore earthquakes listed in the Japan Metrological Agency (JMA)’s catalogue which are detected by land stations and the manual picks for S-net performed by the analysts in Graduate School of Science, Tohoku University. Please note that in this comparison we have not re-trained PhaseNet model with S-net arrival data for the evaluation of the model. According to the application for 22 stations belonging to the S-net S1 cable during 22 months, PhaseNet detected P-picks within 0.1 second from the manual picks (hereafter we call this good P or S-picks) for about the half of input, and good S-picks for 24.7% of input. We note that the data of S-net located at the ocean bottom tends to have weaker first arrivals for P and S waves than do on land stations on which the model was trained.

To evaluate the performance with existing method, we compared the result of PhaseNet with the ‘auto pick’ function of the WIN system (Urabe and Tsukada, 1991). We found that the ratio of good P-picks is larger for PhaseNet (53.2%) than that for the WIN system (21.4%). For S-wave, PhaseNet also achieves a higher ratio (24.7%) than that for the WIN system (10.0%). We also compared the results with the automatic earthquake location system in operation at Tohoku University (Horiuchi et al., 2014; Nakayama et al., 2014). Please note the system is working for land stations and the comparison does not contains S-net data as input. For 695 waveform data recorded in January 2017, PhaseNet was able to detect 99.9% of the P-picks with high precision (81.4%) and recall rate (81.3%) that are two standard performance measures for deep learning models (Zhu and Beroza, 2019). In addition, the performance for S-wave is much better than existing methods (the Tohoku University’s automatic earthquake location system and the WIN system could detect good S-picks for about 10 % of input, but the PhaseNet detected 54.8% of input).

These results suggest that even for S-net data, PhaseNet is an effective method to find accurate arrival times for both P and S waves, though the performance could be improved with a re-trained model. We expect that arrival-time picking methods based on deep neural networks will help reveal the distribution of small earthquakes in offshore Japan from continuous S-net waveform data.

©2020. Japan Geoscience Union. All Right Reserved.

Acknowledgements: We thank the staff of the National Research Institute for Earth Science and Disaster Resilience who deployed the S-net, maintained the network and opened the data to the public.

Keywords: S-net, Neural networks, Computational seismology, Seismic monitoring

©2020. Japan Geoscience Union. All Right Reserved.

[E] Poster | S (Solid Earth Sciences)：S-SS Seismology

[S-SS06] Active faults and Paleoseismology

convener:Hisao Kondo(Geological Survey of Japan, National Institute of Advanced Industrial Science and Technology), Mamoru Koarai(Earth Science course, College of Science, Ibaraki University), Takashi OGAMI(National Institute of Advanced Industrial Science and Technology), Yoshiki Sato(Advanced Industrial Science and Technology, Geological Survey of Japan)

Recurrence of past earthquakes through historic, geomorphic and geologic time provide us essential information on location, size and timing of future large earthquakes. The study of past faulting, source fault and seismicity has played important role for seismic hazard assessment and mitigation of the related hazards. Furthermore, active fault studies contribute to understanding active tectonics under the on-going tectonic stress field. In this session, we encourage submissions from scientists in relation with all aspects of active fault studies and paleoseismology, including interdisciplinary fields of geology, geomorphology, archaeology, historical earthquake, seismology, geodesy and numerical simulations.

[SSS06-P01] Active tectonics of the northern Banda Arc, eastern Indonesia: a preliminary geomorphic mapping

*Adi Patria[1,3], Hiroyuki Tsutsumi[2], Danny Hilman Natawidjaja[3] (1.Graduate School of Science and Engineering, Doshisha University, 2.Department of Environmental Systems Science, Doshisha University, 3.RC for Geotechnology, Indonesian Institute of Sciences (LIPI))

[SSS06-P02] Paleoseismological studies along the un-ruptured southern segment of Yokote Basin Fault Zone, northeast Japan

*SHREYA Arora[1], Hisao Kondo[1] (1.Geological Survey of Japan, National Institute of Advanced Industrial Science and Technology)

[SSS06-P03] Parametric study on ground surface deformation forming pull-apart basin

*Hidetaka Saomoto[1] (1.National Institute of Advanced Industrial Science and Technology)

[SSS06-P04] S wave seismic reflection survey on the Shikano fault appeared in the 1943 Tottori earthquake

*Takao Kagawa[1], Tatsuya Noguchi[1], Koji Yamada[2], Tetsuya Takemoto[2] (1.Tottori University Graduate School of Engineering, 2.Hanshin Consultants Co., Ltd.)

[SSS06-P05] Offset streams across active faults in Chugoku region in the southwestern Japan

*Takashi Azuma[1] (1.National Institute of Advanced Industrial Science and Technology)

[SSS06-P06] Change in stress with seismic cycles in coherent and mélange units in the Cretaceous Shimanto Belt, SW Japan

*Makoto Hashiguchi[1], Yoshitaka Hashimoto[1] (1.Kochi University)

Active tectonics of the northern Banda Arc, eastern Indonesia: a preliminary geomorphic mapping

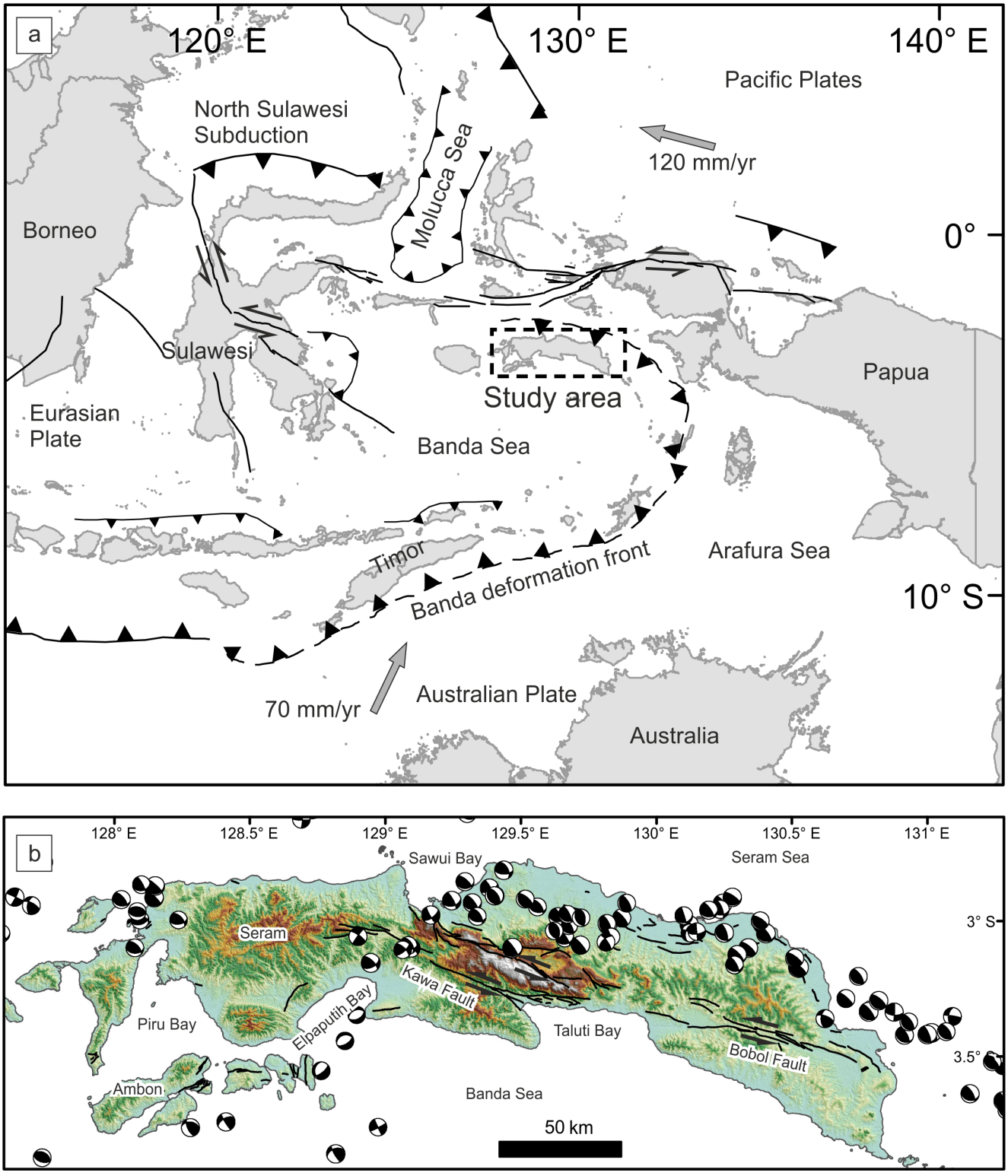
*Adi Patria[1,3], Hiroyuki Tsutsumi[2], Danny Hilman Natawidjaja[3]

1. Graduate School of Science and Engineering, Doshisha University, 2. Department of Environmental Systems Science, Doshisha University, 3. RC for Geotechnology, Indonesian Institute of Sciences (LIPI)

The 180°-curved Banda Arc is located in the tectonically complex region where the Eurasian, Indo-Australian, and Pacific plates converge. The northern Banda Arc, which includes Seram, Buru, Ambon, and surrounding islands, is a seismically active region. Seismicity is mainly observed around the northeast Seram with the domination of thrust faulting mechanisms, while strike-slip faulting activity is mainly located in the central Seram. Although the area is vulnerable to earthquakes, there has been limited effort to study the active tectonics of the area. This study investigates the tectonic geomorphology of the northern Banda Arc based on the Indonesian DEM (DEMNAS) to understand the active tectonics of the region and relates the interpreted structures to seismicity in the region. The Kawa and Bobol faults elongate across Seram and show a left-lateral movement. The faulting activity is recorded in geomorphic features such as triangular facet, beheaded river, pressure ridge, and river offset. The northeast Seram lacks geomorphic expression, but evidence such as uplifted marine terrace, deformed fluvial terrace, and water gap illustrate thrust faulting activity. Other faults with less than 20-km length are observed in Ambon, Haruku, and Saparua, majorly deforming uplifted marine terraces. The faulting activities in the region might be related to the oblique convergence between the northern Banda Arc and the West Papua.

Keywords: Active tectonics, Eastern Indonesia, Tectonic geomorphology

©2020. Japan Geoscience Union. All Right Reserved.



©2020. Japan Geoscience Union. All Right Reserved.

Paleoseismological studies along the un-ruptured southern segment of Yokote Basin Fault Zone, northeast Japan

*SHREYA Arora[1], Hisao Kondo[1]

1. Geological Survey of Japan, National Institute of Advanced Industrial Science and Technology

The mapping of active faults and how the associated earthquakes have repeated in space and time are the key to unraveling future seismic activity. With the advent of extensive paleoseismic and geodetic data, the more complex behavior of earthquake ruptures such as events incompletely rupturing or bleeding into adjacent segments is indicated (e.g. Zielke, et al., 2010; Bilham, et al., 2019; Katsube et al., 2017). The 1896 Rikuu earthquake, Mw 7.2, is one such example which ruptured 35 km of the northern section of the eastern margin of the Yokote Basin (EFZYB), which is one of the largest east-dipping fault system in northeast Japan (e.g. Matsuda, et al., 1980; Kagohara, et al., 2009) while leaving the southern section un-ruptured since at least 100 years. Since then tremendous efforts have been made along the ruptured section of EFZYB to determine slip rates and recurrence interval of the earthquakes (Kagohara, et al., 2006; 2009; Imaizumi et al.,1997; Research Group for the Senya Fault, 1986). However, the trace of the active faults, slip rates, past earthquake chronology and recurrence intervals along the un-ruptured southern section of EFZYB remained poorly understood. Therefore, through detailed aerial photo interpretation, airborne LiDAR DEM survey, and field investigation an attempt has been made to map the active faults in the un-ruptured southern section of EFZYB, which is integrated with seismic survey and borehole data to determine slip rates. Here we will present the preliminary results of the work which will help in the seismic hazard assessment of the Yokote Basin.

Keywords: Active Fault, Borehole Survey, Slip Rates, LiDAR DEM, 1896 Rikuu earthquake

©2020. Japan Geoscience Union. All Right Reserved.

Parametric study on ground surface deformation forming pull-apart basin

*Hidetaka Saomoto[1]

1. National Institute of Advanced Industrial Science and Technology

Understanding the forming process of pull-apart basin due to faulting is an important topic in the field of geomorphology and several types of studies on pull-apart structure have been widely conducted: field works (e.g., Aydin and Nur, 1982), theoretical studies (e.g., Du and Aydin, 1995), and numerical studies (e.g., Liu and Konietzky, 2018). As an example in Japan, the Suwa Basin along the Itoigawa-Shizuoka Tectonic Line is considered to be a pull-apart basin produced by two left-lateral strike-slip faults (e.g., Fujimori, 1991).

Since most of the previous studies were limited to individual case studies or a few simulation cases, a systematic parametric study is needed to methodically understand ground deformation patterns resulting in pull-apart basins. Here, I performed a series of three-dimensional finite element analyses to understand the deformation patterns of the ground surface by changing the parameters that control both the fault configuration and the stress field around the faults. In this study, all procedures for the finite element simulations were implemented in a multi-purpose finite element package (COMSOL Multiphysics).

On the basis of 715 simulations, the followings are obtained:

(1) When the step-over width equals to 3.0 km and the overlap equals to 2.0 km, strong basin subsidence is observed irrespective of the directions for principal stresses.

(2) An extremely large overlap cannot produce strong basin subsidence irrespective of the magnitudes of step-over widths.

(3) The direction of principal stress affects the magnitude of the basin subsidence, but it does not affect the displacement pattern of the ground surface.

(4) The sensitivity of overlap to the basin subsidence is larger than that of the step-over width to the basin subsidence.

Acknowledgments:

This study was supported by ``Research Project for Long-term Evaluation Methods of Active Faults related to Multi-segment Earthquakes" in the Ministry of Education, Culture, Sports, Science and Technology (MEXT).

References:

Aydin, A. and Nur, A. (1982) ‘Evolution of pull-apart basins and their scale independence’, *Tectonics*, 1(1), pp. 91–105.

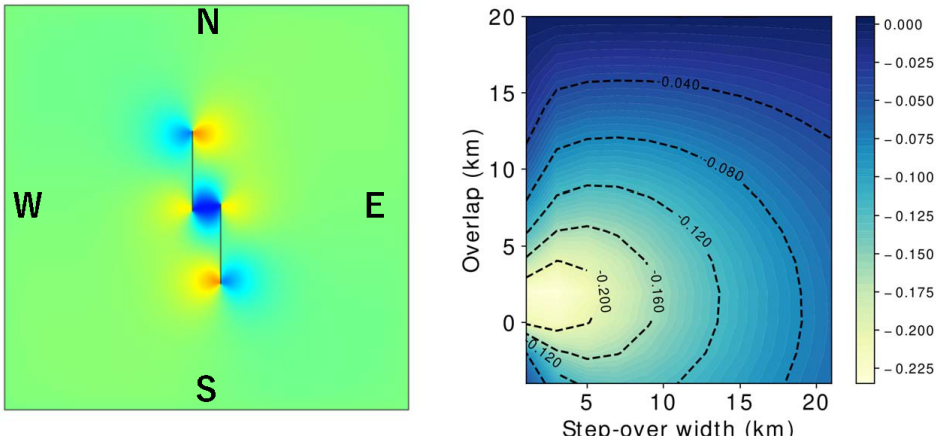
©2020. Japan Geoscience Union. All Right Reserved.

Du, Y. and Aydin, A. (1995) 'Shear fracture patterns and connectivity at geometric complexities along strike-slip faults', *Journal of geophysical research*. (Publ.), 100(B9), pp. 18093–18102.

Fujimori, T. (1991) 'Active Faults in the Suwa Basin, and Its Evolution as a Pull-Apart Basin on the Itoigawa-Shizuoka Tectonic Line, Central Japan', *Geographical review of Japan series A*, 64(10), pp. 665-696 (in Japanese).

Liu, Y. and Konietzky, H. (2018) 'Particle-Based Modeling of Pull-Apart Basin Development', *Tectonics*. (Geological Society, London, Special Publications), 37(1), pp. 343–358.

Keywords: Finite element method, pull-apart basin, simulation



(a) The up-down component of displacement (red: up, blue: down) with 7 km step-over and 2 km overlap.

(b) Relationship among step-over, overlap, and the basin subsidence at the center of the simulation model.

Figure 1: A part of parametric study in which step-over, overlap, and principal stress direction are selected as the parameters.

©2020. Japan Geoscience Union. All Right Reserved.

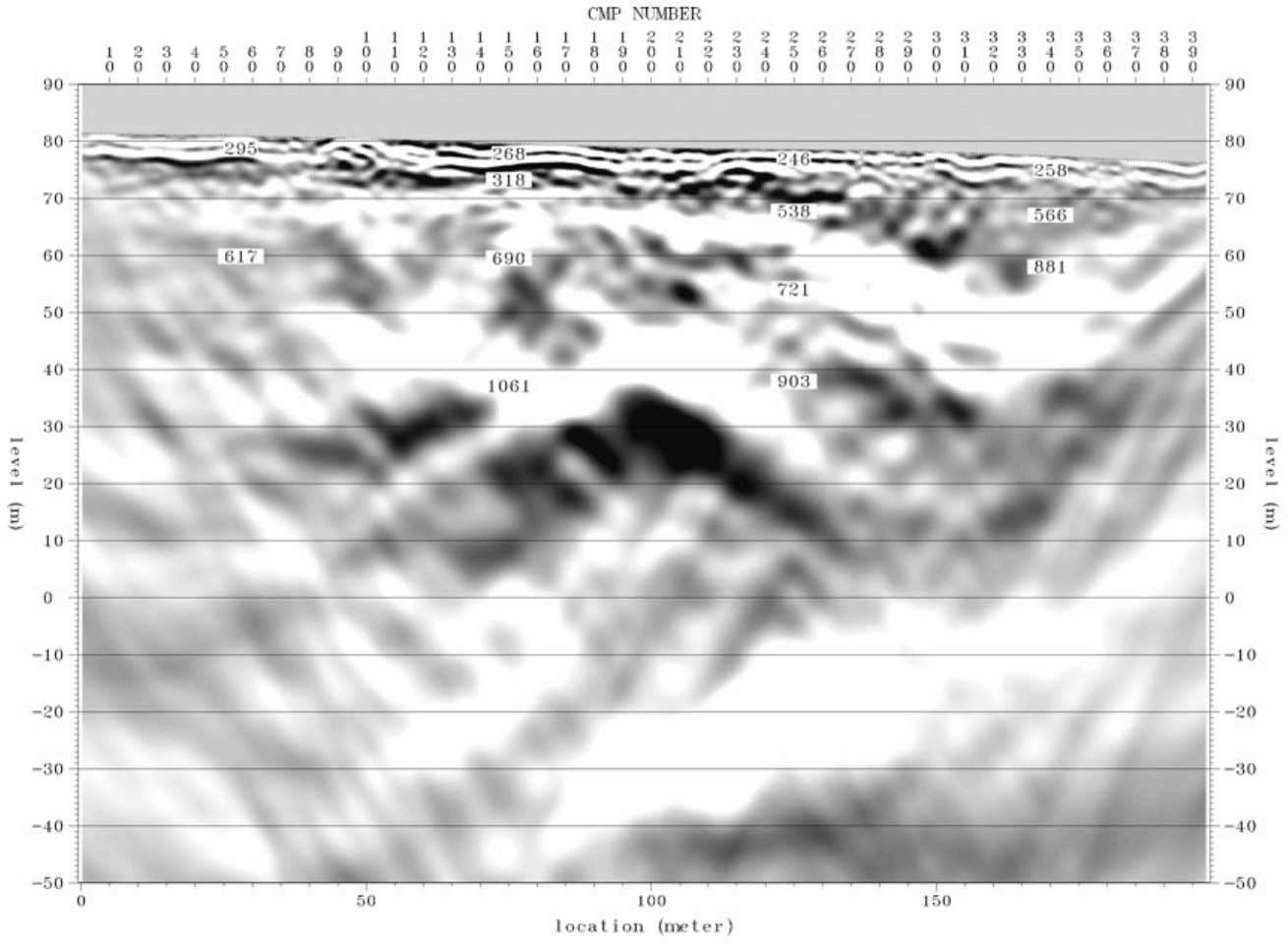
S wave seismic reflection survey on the Shikano fault appeared in the 1943 Tottori earthquake

*Takao Kagawa[1], Tatsuya Noguchi[1], Koji Yamada[2], Tetsuya Takemoto[2]

1. Tottori University Graduate School of Engineering, 2. Hanshin Consultants Co., Ltd.

A shear wave seismic reflection survey was conducted across the Shikano fault that appeared in the 1943 Tottori earthquake (M_J7.2) at Horakuji area in Shikano, Tottori city, Japan. The length of the survey line was 200 meters, shot and seismograph intervals were both set as 1 meter. The resulting interval of Common Mid Point (CMP) was 0.5 meters. Mechanical plate hitting machine by hydraulic pressure was used as seismic source. The figure shows the depth section along the survey line with evaluated shear velocities. The Shikano fault locates at CMP number 200. Disturbance is seen in shallow surface layers in around the point. Furthermore, rather strongreflection boundary is seen at depth about 45 meters. We will interpret the results together with the data of microtremor surveys conducted in the surrounding area.
Accnowledgement: This work was supported by JSPS KAKENHI Grant Number 19H02406.

Keywords: S wave seismic reflection survey, Shikano fault, the 1943 Tottori earthquake



©2020. Japan Geoscience Union. All Right Reserved.

Offset streams across active faults in Chugoku region in the southwestern Japan

*Takashi Azuma[1]

1. National Institute of Advanced Industrial Science and Technology

Evaluation of slip rate of strike slip fault is difficult caused by absence of age information for references, such as streams and mountain ridges. Relationships between amount of stream offset (D) and length of stream upper than fault (L) were used as one of the methods to estimate it. In this study, data of D and L were gather from four active faults (Itsukaichi, Tsutsuga, Jifuku, and Ooharako) in Chugoku region in the southwestern part of Japan. These faults are right-lateral strike-slip faults with direction of northeast-southwest. Length of faults are 27 km, 58 km, 27 km, 42 km, respectively. Digital elevation model was used to measure amount of stream offset and length of stream. Results will be used for studies of slip rate of strike-slip faults, together with data of erosion rate around this region.

Keywords: Active fault, Slip rate, Offset stream

©2020. Japan Geoscience Union. All Right Reserved.

Change in stress with seismic cycles in coherent and mélange units in the Cretaceous Shimanto Belt, SW Japan

*Makoto Hashiguchi[1], Yoshitaka Hashimoto[1]

1. Kochi University

Stress state in a subduction unit can be exchanged between reverse and normal fault regimes with earthquake cycles. A similar change in paleostresses has been also obtained in some exhumed accretionary complexes. However, the previous studies in exhumed accretionary complexes cover only mé lange units along the coastline.In this study, we spatially examined a regional paleostress change in a coherent unit as well as an adjacent mélange unit in a mountain area.

The study area is located in the Cretaceous northern Shimanto Belt. A coherent unit distributs in the north and a mélange unit is located at the south adjacently. Strike and dip of the bedding and foliations of mé lange are NE-SW and steeply to the north, respectively. Many micro-faults are observed in both areas with nicely visible slicken side and slicken steps. We have measured slip data from the micro-fault for the inversion analysis of paleostress. Among six stresses estimated, our stresses could be reasonable for each unit because many unique faults are found. In the coherent unit, the stress states include two reverse fault regimes, one strike-slip fault regime and one normal fault regime. In mélange unit, one reverse fault regime, one strike-slip fault regime and two normal fault regime were identified. The orientations of the principal stresses are mostly consistent in NW-SE, NE-SW and almost vertical directions. The results suggest that the stress exchange is commonly observed in both coherent and mélange units.

In order to constrain stress magnitude, stress polygon was employed. Effective vertical stress (Sv’) was assumed as 140 MPa corresponding to the depth about 5.5 km which came from the maximum paleo-temperature (165 ˚C) of vitrinite reflectance. The stress magnitude for the reverse fault regimes is larger than that for the normal fault regime normally in both areas. In addition, the difference of the maximum shear stress (stress drop) was examined. The maximum shear stresses for each stress regime were estimated by the half of the differential stress (SHmax-Shmin). The stress drops between reverse and normal stresses ranges 1.8-63 MPa in the coherent unit. The stress drops are consistent with the range of 0.01-100 MPa in trench type earthquakes. Therefore, it is possible for our results to be related to earthquake cycles at least for the coherent unit.

In the mélange unit, because reverse fault regime did not fit the stress polygon with 140 MPa of Sv’, the stress drop could not be estimated.

Fluid inclusion analysis was conducted in mélange unit to obtain pressure-temperature (P-T) conditions of mélange unit. Homogenization temperatures of methane inclusions give methane density and these of water-rich inclusions show the trap temperature because water was saturated with methane at the time. The trap pressure can be obtained from the combination between methane density and the trap temperature. Two samples were measured so far. One is a normal fault and the other is a reverse fault. The P-T conditions for the normal fault range 190–237˚C and 174.2–196.9 MPa, respectively. These for the reverse fault are 167–211˚C and 79.5–91.5 MPa, respectively. The pressure for the normal fault shows twice higher than that for the reverse fault. The P-T conditions are not consistent each other, suggesting that the timing of the micro-fault development in the units are different.

©2020. Japan Geoscience Union. All Right Reserved.

In conclusion, the exchange of stress accompanying earthquake cycles could occur both in the coherent and mélange units. The interpretation that the exchange of stress observed both in mélange and coherent units implies that the exchange in stress state could be recorded after mélange unit was located adjacent to coherent unit. It suggests that the micro-faults were activated within an accretionary wedge. However, the P-T condition of fluid in the both faults show inconsistent. To understand the effects of fluid, further fluid inclusion analyses in the mineral veins will be required.

Keywords: micro-faults analysis, fulid inclusion, accretionary complex

©2020. Japan Geoscience Union. All Right Reserved.

[E] Poster | S (Solid Earth Sciences)：S-SS Seismology

[S-SS07] Earthquake prediction and forecast+pre-earthquake geoscientific changes(TBD)

convener:Masayuki Obayashi(Japan Agency for Marine-Earth Science and Technology), Toshitaka Baba(Graduate School of Science and Technology, Tokushima University), Chi-Yu King(Retired)

This session provides the opportunity for contributions that fall within the scientific spectrum of earthquake prediction and forecasting. We welcome theoretical, observational or numerical papers that are either on long- or short-term predictions, and either based on deterministic or probabilistic approaches. (TBD)

[SSS07-P01] Long-term level and temperature changes in groundwater at the frontier land zone for impending great earthquakes at the Nankai trough, southwest Japan
- Recent anomalous changes, possible great earthquake precursors -

*Tameshige Tsukuda[1] (1.none)

[SSS07-P02] **Application of different statistical tools to investigate radon time-series data for earthquake precursory studies in Taiwan**

*Vivek Walia[1], Arvind Kumar[1], Ching-Chou Fu[2], Shih-Jung Lin[1], Cheng-Horng Lin[1,2] (1.National Center for Research on Earthquake Engineering, NARL, Taipei, Taiwan , 2.Institute of Earth Sciences, Academia Sinica, Taiwan)

[SSS07-P03] Correlations of earthquake properties with geomagnetic ULF precursor characteristics over multiple events

*Muhammad Khairul Adib Muhammad Yusof[1], Mardina Abdullah[1,2], Nurul Shazana Abdul Hamid[1,3], Suaidi Ahadi[4], Akimasa Yoshikawa[5] (1.Space Science Center, Institute of Climate Change, Universiti Kebangsaan Malaysia, Malaysia, 2.Department of Electrical, Electronic and Systems Engineering, Faculty of Engineering and Built Environment, Universiti Kebangsaan Malaysia, Malaysia, 3.Department of Applied Physics, Faculty of Science and Technology, Universiti Kebangsaan Malaysia, Malaysia, 4.Department of Geophysics, Indonesian Agency for Meteorology, Climatology and Geophysics, Jakarta, Indonesia, 5.International Center for Space Weather Science and Education, Kyushu University, Fukuoka 812-8581)

[SSS07-P04] Recent Advances in Earthquakes Relocation and Probabilistic Seismic Hazard Assessment for Risk Mitigation and Planning in West Africa

*Umar Afegbua Kadiri[1], Tahir Abubakar Yakubu[1], Friday Ezomo, Brassnavy Manzunzu (1.Centre for Geodesy and Geodynamics Toro)

[SSS07-P05] Ionosphere Magnetic Field Precursor Anomalies Extraction Associated with 2016 Ecuador Earthquake using NMF

*Mengxuan Fan[1], Kaiguang Zhu[1], Xiaodan He[1], Kaiyan Li[1], Dedalo Marchetti[2], Chengquan Chi[1], ZINING YU[1] (1.Jilin University, 2.National Institute of Geophysics and Volcanology)

Long-term level and temperature changes in groundwater at the frontier land zone for impending great earthquakes at the Nankai trough, southwest Japan
- Recent anomalous changes, possible great earthquake precursors -

*Tameshige Tsukuda[1]

1. none

For the purpose of monitoring the preparing process of the impending Nankai and Tonankai earthquakes, groundwater measurements are being conducted in the Nanki region,Wakayama Prefecture, southwest Japan. Semiconductor pressure sensors for water level and platinum resistance thermometers for water temperature are exploited.
We have 16 groundwater observation stations for temperature, and 3 stations for water level in the Tokai and Nanki regions, central and southwest Japan, respectively, where are close to the source regions of the great Nakai-trough earthquakes. This paper reports the seismological meaning of the data from Nanki region.
At stations HA and WA in Shionomisaki, Nanki region, Wakayama Prefecture, the long-term trend of the water level is rising with a rate of about 70mm/year, corresponding to the ground subsidence found by levelling and GNSS data (Kobayashi, 2013) till around 2015. The recent water level changes are nearly constant in time. Here, we deal with one-year moving average of levelling data. At the two stations, the trend of temperature is similarly rising with a rate of about 50 m degree/year, suggesting contraction of the rock medium under Shionomisaki, the southernmost end of Honshu.
At KZ(Kozagawa)about 15km northeast of HA or WA in the Nanki region, the temperature is monotonously falling since the observation started in 2002 with some precursory change for the 2004 Kii-Hanto-Oki earthquake(M7.4). However, the decreasing temperature changed to severely increase in the middle of 2015, and changed to decrease again in 2017.
The groundwater temperature changes are related to preparatory earthquake generations. In the preparing process of a large earthquake, the medium would be deformed generating regions of contraction and dilatation around the nucleus of the shearing stresses. According to a hydraulic model, pore fluid flow is driven upward to the ground surface through crack systems serving as flowing pipes by high pressure pumps at a deep spot. The change in the quantity of the upwelling hot water from deep underground causes a change of groundwater temperature(Tsukuda et al., 2005).
As mentioned above, the deformations of the rock medium are accelerated under the regions close to the source regions of the great erthquakes at the Nankai trough. For prediction studies for the impending great erthquakes, we should start to conduct detailed and multidisciplinary observations.
The observations are supported by the NPO, CADASU(Collaborators Association for Detecting Anomalous Signs from Underground).

Keywords: dilatation , contraction, water level, groundwater temperature, precursor

©2020. Japan Geoscience Union. All Right Reserved.

Application of different statistical tools to investigate radon time-series data for earthquake precursory studies in Taiwan

*Vivek Walia[1], Arvind Kumar[1], Ching-Chou Fu[2], Shih-Jung Lin[1], Cheng-Horng Lin[1,2]

1. National Center for Research on Earthquake Engineering, NARL, Taipei, Taiwan , 2. Institute of Earth Sciences, Academia Sinica, Taiwan

For past few decades, anomalous temporal changes in radon concentrations have been reported in relation to earthquake occurrences. However, radon anomalies in all cases are not only controlled by seismic activity but also by meteorological parameters which make isolation of earthquake precursory signals complicated. The present study is an attempt to assess and quantify the influence of the meteorological and hydrological parameters on the soil gas radon emission at monitoring stations established along different active faults of Taiwan. Characteristics of temporal variability of soil-gas radon concentrations for the monitoring stations have been examined by using statistical tools e.g.Singular Spectrum Analysis. In order to make continuity and regularity of the data before applying the analysis, the radon data were carefully edited for rare duplicate sampling, gaps and discontinuous jump following intervals of malfunctioning of equipments. Digital filter has been applied in eliminating the long term trend in the data and retains variations of less than 30 days. The radon variations exhibit dominant daily variations, which are controlled by atmospheric temperature inducted evaporation in surface water saturated soil (Capping Effect). The decay of radon after the recession of rainfall is approximated by double exponential decay terms, one corresponding to the natural decay of radon with half life of 3.84 days and second representing slow weakening of capping effect. The effect related to internal loading due to rise and fall of groundwater modulates the propagation of radon in overlying strata, accounting for the long term variations in radon. The rainfall inflicted changes in radon look strikingly similar to earthquake related precursory or co-seismic perturbations, inferred by long term synotopic observations. It is surmised that unless radon variations are corrected for meteorological/hydrological contamination, some precursory signals are masked on one hand while on the other hand some anomalies are falsely viewed as earthquake precursors.

Keywords: Earthquake Precursors, Radon, Stasticial Tools, Taiwan

©2020. Japan Geoscience Union. All Right Reserved.

Correlations of earthquake properties with geomagnetic ULF precursor characteristics over multiple events

*Muhammad Khairul Adib Muhammad Yusof[1], Mardina Abdullah[1,2], Nurul Shazana Abdul Hamid[1,3], Suaidi Ahadi[4], Akimasa Yoshikawa[5]

1. Space Science Center, Institute of Climate Change, Universiti Kebangsaan Malaysia, Malaysia, 2. Department of Electrical, Electronic and Systems Engineering, Faculty of Engineering and Built Environment, Universiti Kebangsaan Malaysia, Malaysia, 3. Department of Applied Physics, Faculty of Science and Technology, Universiti Kebangsaan Malaysia, Malaysia, 4. Department of Geophysics, Indonesian Agency for Meteorology, Climatology and Geophysics, Jakarta, Indonesia, 5. International Center for Space Weather Science and Education, Kyushu University, Fukuoka 812-8581

We investigated the correlations of earthquake properties with precursor characteristics over multiple events by analyzing geomagnetic field data from 10 observatory stations around the world. Earthquake precursory anomalies were detected by employing the polarization ratio analysis method to process the signal in ultra-low frequency (ULF) ranges (i.e., 0.01 –0.1 Hz), while the polarization ellipse method was utilized for direction estimation. Earthquakes (n = 34) were studied to characterize their precursors in terms of the frequency band, amplitude, error percentage of direction estimation and lead time. The correlations of these characteristics with earthquake properties (i.e., magnitude, epicentral distance, hypocentral depth and local seismicity index) were then determined. We found that 20 earthquakes were preceded by precursors. Weak correlations were identified when all found precursors were included, but stronger correlations were identified when the study was focused on precursors from a station in Japan. We concluded that some earthquake properties are correlated with several precursor characteristics when the study area is restricted to a specific location.

Keywords: Geomagnetic ULF, Earthquake precursor, Correlational study

©2020. Japan Geoscience Union. All Right Reserved.

Recent Advances in Earthquakes Relocation and Probabilistic Seismic Hazard Assessment for Risk Mitigation and Planning in West Africa

*Umar Afegbua Kadiri[1], Tahir Abubakar Yakubu[1], Friday Ezomo, Brassnavy Manzunzu

1. Centre for Geodesy and Geodynamics Toro

This work is aimed at utilizing modern techniques to improve earthquakes location and establish seismic hazard parameters for planning in West Africa. Over the years, dearth of data and well-defined velocity models have hindered robust seismological researches in the region. For the first time therefore, Regional Seismic Travel Times and iloc in Geotool software were used to relocate significant earthquakes; and Probabilistic Seismic Hazard Assessment was carried out using earthquake catalogue (1618-2018), with different levels of magnitude completeness determined for the sub-catalogues. The results showed enhanced events characterization and epicenters with attendant improved seismicity scenario. Maps of b-values, earthquakes density and that for updated seismicity have been produced for West Africa from this study. The regional maximum possible magnitude is estimated to fall in the range of [6.62; 7.17]. The b-value and activity rate were computed as 0.71±0.2 and 3.44±0.17 respectively. A forecast of future earthquakes occurrence shows that a magnitude 6.80 is likely to occur in West Africa approximately every 370 years. The Probabilities of the same event occurring annually and once in 50, 100 and 1000 years are 0.27%, 12.59%, 23.50% and 91.8% respectively. The annual probability of occurrence of small magnitude earthquakes (less than 5.0) is high. The 10% probability of exceedance of PGAs in 50 years ranged from 0.05 m/s² to 0.34 m/s². The significant hazard levels were observed in South Western Cameroon, South-Western Nigeria, Southern parts of Ghana, Eastern parts of Benin Republic, Guinea, Togo, Guinea Bissau, The Gambia, and Sierra Leone respectively.

Keywords: West Africa, Earthquakes relocation, Seismicity, PSHA, earthquakes forecast, planning,

©2020. Japan Geoscience Union. All Right Reserved.

Ionosphere Magnetic Field Precursor Anomalies Extraction Associated with 2016 Ecuador Earthquake using NMF

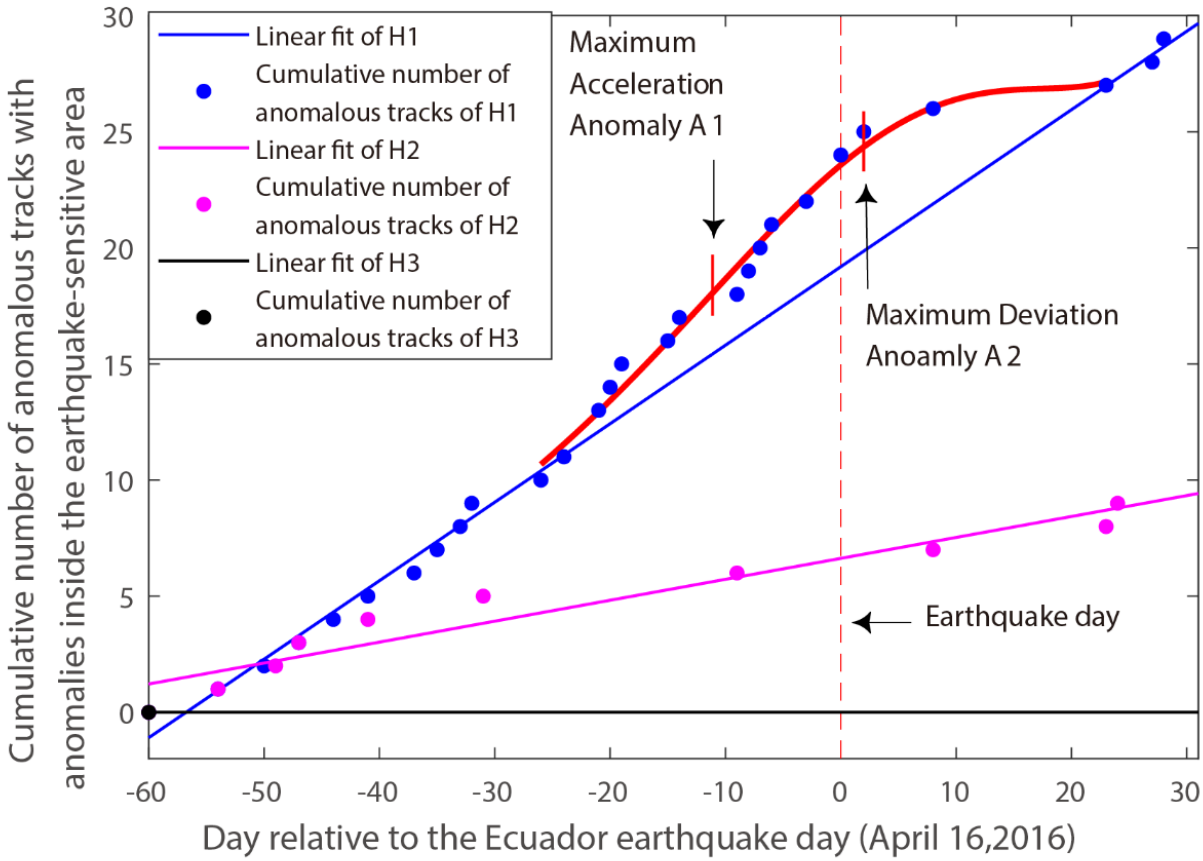
*Mengxuan Fan[1], Kaiguang Zhu[1], Xiaodan He[1], Kaiyan Li[1], Dedalo Marchetti[2], Chengquan Chi[1], ZINING YU[1]

1. Jilin University, 2. National Institute of Geophysics and Volcanology

Some ionosphere anomalies are found in satellite observations during the preparation phase of earthquakes. In previous earthquake studies, the magnetic field data under strong geomagnetic activity are usually deleted to avoid the influence of the geomagnetic activity, therefore the dataset are reduced. In this paper, we decompose the Swarm satellite time series magnetic field data under all geomagnetic conditions and all local time by Nonnegative Matrix Factorization to study the April 16, 2016 Mw7.8 Ecuador earthquake. The data are decomposed into basic vectors and their corresponding weights, and we find that the energy and entropy of component H1, one of the weight components, are more concentrated inside the earthquake sensitive area than other weight components. The cumulative number of anomalous tracks with anomalies inside the earthquake sensitive area evaluated by component H1 shows accelerated growth before the earthquake and recovers to linear growth after, which obey the power law behavior of a critical system, while for other components H2 and H3 show linear growth before and after the earthquake. Furthermore, the cumulative anomalies of component H1 also correspond to two previous studies which also use the magnetic field data of Swarm satellite, but removed the data or component influenced by the geomagnetic activity. And the test on the anomalous track percentages versus different geomagnetic levels indicates the cumulative anomalies of component H1 are hardly affected by geomagnetic activity. After a confutation analysis of four random low seismicity area cases and two 90 days low seismicity period cases, the cumulative anomalies of component H1 are also confirmed as not obtained by simple chance. Moreover, we find the cumulative result of component H1 has similar growth to the cumulative Benioff strain S around the Ecuador earthquake epicenter, that suggests that the ionosphere magnetic anomalies are associated with the lithosphere activities which are related to the Ecuador earthquake and agrees with the Lithosphere Atmosphere Ionosphere Coupling.

Keywords: Eearthquake, Satellites magnetic field, non-negative matrix factorization, lithosphere atmosphere ionosphere coupling

©2020. Japan Geoscience Union. All Right Reserved.



©2020. Japan Geoscience Union. All Right Reserved.

[E] Poster | S (Solid Earth Sciences)：S-SS Seismology

[S-SS08] Statistical seismology and underlying physical processes

convener:Yasuhiro Yoshida(Meteorological College, Japan Meteorological Agency)

This session aims to improve our understanding on seismicity and underlying physical processes. Any contribution on behavior of earthquakes as a cluster, such as regional seismicity and aftershocks, is welcomed. We also welcome contribution on temporal and spatial interactions that control seismicity, and tectonic processes, and geological and thermal structures that regulate seismicity.

[SSS08-P01] Stress induced from large earthquakes since 1900 and temporal b value change in Nankai trough

Junhyung Lee[1], Ilgoo Kim[1], *Tae-Kyung Hong[1] (1.Department of Earth System Sciences, Yonsei University)

[SSS08-P02] Microseismicity distribution and inferred fault geometry beneath the western Marmara Sea, Turkey, deduced from long-term ocean bottom seismographic observations

*Yojiro Yamamoto[1], Dogan Kalafat[2], Ali Pinar[2], Narumi Takahashi[3,1], Zeynep Coskun[2], Remzi Polat[2], Haluk Ozener[2], Yoshiyuki Kaneda[4,1] (1.Japan Agency for Marine-Earth Science and Technology, 2.KOERI, Bogaziti University, 3.National Research Institute for Earth Science and Disaster Resilience, 4.Kagawa University)

[SSS08-P03] Spatio-temporal characteristics of seismicity in the source region of the 2011 Tohoku earthquake

*MEITONG DUAN[1], Takuji Yamada[1], Jun Kawahara[1] (1.IBRAKI University)

Stress induced from large earthquakes since 1900 and temporal b value change in Nankai trough

Junhyung Lee[1], Ilgoo Kim[1], *Tae-Kyung Hong[1]

1. Department of Earth System Sciences, Yonsei University

The perception of impending great earthquakes may be useful for seismic hazard mitigation. The seismicity is dependent on the stress field as well as medium properties. The Nankai trough is recognized to have a high hazard potental. Large earthquakes occur periodically in the Nankai trough with recurrence intervals of 100-200 years. The influence of fractional stress changes by precedent earthquakes on the induction of forthcoming earthquakes is investigated. We assess the global stress perturbation induced by 1626 earthquakes with magnitudes greater than or equal to 7.0 since 1900. We stack the Coulomb stress changes. The cumulative Coulomb stress changes reach up to an order of tens to hundreds of bars at convergent plate boundaries. Descendant large earthquakes appeared to occur in the regions with large lateral gradients in cumulative Coulomb stress changes induced by precedent earthquakes. The cumulative Coulomb stress changes over a century are comparable among subduction zones. The instability and inhomogeneity in stress field may play an important role in nucleation of great earthquakes. We also determine the temporal variation of the Gutenberg-Richter b values in the slow slip region along the Nankai trough for 40 years. It is observed that the b values were generally bounded between 0.6 and 1.0. The slow slips and associated plate motions accompany micro and small earthquakes, inducing b value increase. The b values increase concurrently at the times of slow slips. The b decay rates after slow slips are observed constant. The consistent b-value decrease rate since 2014 may suggest temporal approaching to a large earthquake.

Keywords: induced stress, Nankai trough, b value

©2020. Japan Geoscience Union. All Right Reserved.

Microseismicity distribution and inferred fault geometry beneath the western Marmara Sea, Turkey, deduced from long-term ocean bottom seismographic observations

*Yojiro Yamamoto[1], Dogan Kalafat[2], Ali Pinar[2], Narumi Takahashi[3,1], Zeynep Coskun[2], Remzi Polat[2], Haluk Ozener[2], Yoshiyuki Kaneda[4,1]

1. Japan Agency for Marine-Earth Science and Technology, 2. KOERI, Bogaziti University, 3. National Research Institute for Earth Science and Disaster Resilience, 4. Kagawa University

The North Anatolian Fault (NAF) is the transform plate boundary between Eurasian and Anatolian plates. The reginal rate of its dextral strike-slip displacement is about 25 mm/yr. In particular, a part of NAF beneath the Marmara Sea is recognized as a seismic gap for M >7 earthquake during more than 100 years. Earthquake hazard and disaster mitigation studies in Marmara region are sensitive to detailed information on fault geometry and its coupling status beneath the Marmara Sea. However, it is difficult to obtain precise hypocenter location from only onshore permanent seismic stations. Thus, we have started a series of long-term ocean bottom seismographic (OBS) observations beneath the western and central Marmara Sea since 2014. First, we have installed 15 OBSs along the western part of Main Marmara Fault (MMF) from 2014 to 2015. Using these data, Yamamoto et al. (2017) identified a segment boundary of the MMF beneath the central basin of the Marmara Sea (28.05˚E). Besides, they proposed that the zones of no seismicity within the upper crust appear to indicate locked sections of the MMF. In this study, we analyze the second observation data (from 2015 to 2016). The OBS location for first and second observations were almost same. We have conducted the double-difference relocation by using 3-D velocity model obtained by Yamamoto et al. (2017), and obtained 818 relocation results.
The result shows that the feature of hypocenter distribution, including the location of no seismicity zones obtained by Yamamoto et al. (2017), is not changed, suggesting that the coupling status along the fault is almost same during at least two years. The largest no seismicity zone extended over the upper crust is located between 28.45˚E and 28.65˚E, where strong coupling is suggested from seafloor geodetic observation (Lange et al., 2019; Sakic et al., 2016). By combining the relocation result of first and second phases, the detailed fault geometries were clarified. Beneath the Western High and western Central Basin (27.75˜28.05˚E), we found two branch faults whose dip angles are gentler (30˜60) than that of MMF (almost vertical). The cross point of two branch faults and MMF locates about 15 km depth of MMF. Although these faults might relate to the pull-apart or negative flower structure around the Central Basin, we could not find similar structure in eastern Central Basin.

Keywords: The North Anatolian Fault, Marmara Sea, Seismicity, Fault geometry

©2020. Japan Geoscience Union. All Right Reserved.

Spatio-temporal characteristics of seismicity in the source region of the 2011 Tohoku earthquake

*MEITONG DUAN[1], Takuji Yamada[1], Jun Kawahara[1]

1. IBRAKI University

A major earthquake will be followed by many smaller earthquakes and tremors, which are called aftershocks, around its hypocenter in the source area. Omori (1894) discovered that the number of aftershocks generally decreased inversely proportional to the elapsed time from the origin time of the largest earthquake. Later, Utsu (1961) found a simple equation that describes the number of aftershocks n(t) as a function of the elapsed time t: n(t)=K(t+c)^(-p) where p indicates the decay rate of aftershocks and K represents the aftershock activity immediately after a major earthquake. The parameter c controls the retarded time of aftershock activity (Nanjo et al., 2007) and is usually a finite short time. Omi et al. (2015) reported that the parameter p is generally from 0.9 to 1.5 around Japan.

In this study, we focused on aftershock activity of The 2011 off the Pacific coast of Tohoku Earthquake (hereinafter, referred to as the 2011 Tohoku earthquake) and analyzed its p and K values. We then investigated their relationships in space and time with respect to the slip distribution of the 2011 Tohoku earthquake and the regular seismicity before the earthquake.

We analyzed the number of earthquakes on the subducting Pacific plate that occurred from 34.0N to 42.0N in latitude and from 141.0E to 145.0E in longitude during the 16 years from 2003 to 2018. Since it is important that all the earthquakes are detected, earthquakes with a magnitude (M) of 3.0 or larger were used for the analysis. As a result, 24,942 earthquakes were included in the analysis.

The number of daily earthquakes in each area of 0.5 degrees in latitude and longitude was counted and averaged over each month for the period from April 2011 to December 2018. We then deduced values of p and K in the equation of Utsu (1961) that explain the aftershock activity for individual areas, assuming that the parameter c is equal to zero. We obtained values of p and K in the range of 0.07-1.06 and 0.06-400, respectively. Estimated p values were smaller than those derived by Omi et al. (2015), suggesting that the aftershock activity of the 2011 Tohoku Earthquake has been decaying slower than those of other large earthquakes around Japan. We also found that values of p and K had positive correlation. Although these two parameters may not be always independent as suggested by the equation of Utsu (1961), the correlation was significant in taking the estimation error into account.

Focusing on their spatial pattern, values of p and K in the area around the source region of the 2005 Miyagi-oki earthquake were smaller than those in other areas. In addition, these parameters had also smaller values in areas with a large coseismic displacement during the 2011 Tohoku earthquake and in the northern border of its source region. It should be noted, however, that numbers of earthquakes in these areas were relatively small and they might be apparent.

In order to investigate the relationship between the seismicity before and after the 2011 Tohoku earthquake, we finally investigated the spatial pattern of the number of earthquakes N that occurred in 2003 through 2010 and its correlation to the values of p and K of the aftershock activity. We found that values of N and K had a positive correlation. It would be natural to assume that aftershocks take place as a result of the disturbance of shear stress and strength due to a large earthquake and some previous studies

©2020. Japan Geoscience Union. All Right Reserved.

reported a spatial correlation of aftershocks and the coseismic displacement and the change of shear stress associated with a large earthquake. Our results, however, suggests that the spatial pattern of the coseismic slip during the 2011 Tohoku earthquake and of the stress perturbation due to the earthquake may not control the aftershock activity in the study area.

Acknowledgments.

We used the hypocenter data determined by the Japan Meteorological Agency. We would like to express sincere thanks to Dr. Takeshi Iinuma for providing the result of the coseismic slip during the 2011 Tohoku earthquake estimated by Iinuma et al. (2012).

Keywords: 2011 Tohoku earthquake, Aftershock, Omori law

©2020. Japan Geoscience Union. All Right Reserved.

[E] Poster | S (Solid Earth Sciences)：S-SS Seismology

[S-SS09] INDUCED AND TRIGGERED SEISMICITY: CASE STUDIES, MONITORING AND MODELING TECHNIQUES

convener:Luca Urpi, Yusuke Mukuhira(Institute of Fluid Science, Tohoku University), Bogdan Enescu(Department of Geophysics, Kyoto University), Francesco Grigoli(ETH Zurich Swiss Federal Institute of Technology Zurich)

Induced and triggered seismicity occurs in conjunction with human activities such as reservoir impoundments, mining operations, conventional and non-conventional hydrocarbon production, geothermal energy exploitation, wastewater disposal, CO2 sequestration and gas storage operations as well as volcanic and hydrogeological processes. The stability of faults is affected by external solicitations such as pore-pressure diffusion, relaxation effects as well as perturbations related to mass, pressure, temperature and/or volume changes, dike intrusions and earthquake-earthquake interactions. A better understanding of the physical processes governing induced and triggered seismicity is important for the assess the risk of current and future industrial activities.

The study of induced and triggered seismicity is inherently an interdisciplinary problem, which requires the combination of seismological, hydrogeological, geodetic data and a wide range of modeling approaches. This session welcome contributions covering the analysis and modeling of induced and triggered seismicity at different spatial scales and environments.

Relevant topics to be presented include but are not limited to induced seismicity characterization, spatio-temporal variations of physical parameters (including stress, pressure and temperature changes), spatio-temporal patterns of seismicity, modeling strategies and case-studies.

The goal of the session is to cover both theoretical, numerical and experimental aspects of these topics.

[SSS09-P01] Investigation of the physical link between the injection induced seismicity and information from borehole logging

*Yusuke Mukuhira[1], Martin Ziegler[2], Takatoshi Ito[1], Hiroshi Asanuma[3], Markus O Häring[4] (1.Institute of Fluid Science, Tohoku University, 2.Department of Earth Sciences, Engineering Geology, ETH Zurich, 3.AIST, 4.Häring GeoProject)

[SSS09-P03] Estimation of focal mechanisms of large number of induced seismicity to understand fracture system in the geothermal reservoir

*Kangnan Yan[1,2], Yusuke Mukuhira[1], Takatoshi Ito[1], Yinhui Zuo[2], Hiroshi Asanuma[3], Markus O Häring[4] (1.Institute of Fluid Science, Tohoku University, 2.State Key Laboratory of Oil and Gas Geology and Exploitation, Chengdu University of Technology, 3.Fukushima Renewable Energy Institute (FREA), National Institute of Advanced Industrial Science and Technology (AIST), 4.Häring GeoProject)

[SSS09-P04] Source Mechanism and triggering process for the April 12th and 13th 2014 earthquake doublet in the Solomon Islands

*Calvin Luiramo Qwana[1], Masatoshi Miyazawa[1], James Mori[1] (1.Disaster Prevention Research Institute Kyoto University)

[SSS09-P05] Ultra-microearthquakes observed at Mizunami Underground Research Laboratory

*Osamu Murakami[1], Yasuhiro Asai[1], Hiroshi Ishii[1] (1.Tono Rearch Institute of Earthquake Science, Association for the Development of Earthquake Prediction)

[SSS09-P06] Seismoelectromagnetic conversions generated by a double-couple source in partially saturated media.

*Sheldon Dwight Warden[1], Pascal Sailhac[2], Stéphane Garambois[3] (1.Hyperion Geophysical Services, 7 rue de Châtenois, 67100, Strasbourg, France., 2.GEOPS (Geosciences Paris Sud), Université de Paris Saclay, 15 Rue Georges Clemenceau, 91400, Orsay, France., 3.ISTerre (Institut des Sciences de la Terre), Université de Grenoble Alpes, 1381 rue de la piscine, 38400, Saint Martin d'Heres, France.)

[SSS09-P07] Investigation of the pore pressure sensitivity toward ocean loading influence from seismic ambient noise monitoring

*Rezkia Dewi Andajani[1], Takeshi Tsuji[1,2] (1.Department of Earth Resources Engineering, Kyushu University, 2.International Institute for Carbon-Neutral Energy Research, Kyushu University)

[SSS09-P08] **The character of the Focal mechanisms with Kagan angles in Japan area for the extended 2-D ETAS model**

*Maita Eri[1], Jiancang Zhuang (1.SOKENDAI)

Investigation of the physical link between the injection induced seismicity and information from borehole logging

*Yusuke Mukuhira[1], Martin Ziegler[2], Takatoshi Ito[1], Hiroshi Asanuma[3], Markus O Häring[4]

1. Institute of Fluid Science, Tohoku University, 2. Department of Earth Sciences, Engineering Geology, ETH Zurich, 3. AIST, 4. Häring GeoProject

Understanding of the physics behind induced seismicity is an important research topic in seismology. Geoscientists have used seismological analyses, numerical simulations, and seismostatistical analyses to investigate the processes occurring in and the behavior of reservoir rock masses upon hydraulic stimulations that frequently led to substantial induced seismicity. Knowledge of the physics related to induced seismicity associated with fluid injections is key to seismic hazard mitigation. In this study, we approach this problem unconventionally, analyzing at high spatial resolution the natural fracture and in-situ stress information inferred from borehole logging, i.e. data available prior to stimulations, while conventional seismological approaches study the waveforms of induced seismicity, which are posterior phenomena. Injection-induced seismicity is primarily caused by an increase of fluid pressure in the existing fractures, which decreases the fracture’ s shear strengths. Using pre-stimulation information, we investigate the potential of induced seismicity by evaluating the state of stress of natural fractures. Then, we try to find the link to the tendency of observed induced seismicity where we got fault plane geometry information from waveform analysis.

In this study we investigate the natural fracture and in-situ stress data sets from the Basel EGS project in Switzerland. The data originates from the lowermost 2.4 km long borehole section through the basement consisting of granitic to monzonitic rocks. The natural fractures were inferred by careful analysis of acoustic borehole logging images (Ziegler et al. 2015), the in-situ stress data was derived from borehole breakout analysis and some well-test constraint (Valley and Evans, 2009; 2015). Ziegler and Evans, (2020) discovered that the orientation of the seismically inferred faults and natural fractures are similar. Based on these findings of the link between the fault to cause induced seismicity and natural fracture from borehole logging, we investigate the physical link between those beyond the geometrical consistency. We estimated various geomechanical parameters such as shear stress, normal stress, apparent shear strength, i.e., critical pore pressure, and slip tendency. We compared the distributions of those parameters estimated from induced seismicity and natural fractures. We try to find the link between those relationships and discuss the preliminary foundings. Then, we will extend our findings to the theory proposed by the conceptual theory of b-value reduction with increasing stress (Scholtz, 1968).

Keywords: induced seismicity, borehole logging, natural fracture

©2020. Japan Geoscience Union. All Right Reserved.

Estimation of focal mechanisms of large number of induced seismicity to understand fracture system in the geothermal reservoir

*Kangnan Yan[1,2], Yusuke Mukuhira[1], Takatoshi Ito[1], Yinhui Zuo[2], Hiroshi Asanuma[3], Markus O Häring[4]

1. Institute of Fluid Science, Tohoku University, 2. State Key Laboratory of Oil and Gas Geology and Exploitation, Chengdu University of Technology, 3. Fukushima Renewable Energy Institute (FREA), National Institute of Advanced Industrial Science and Technology (AIST), 4. Häring GeoProject

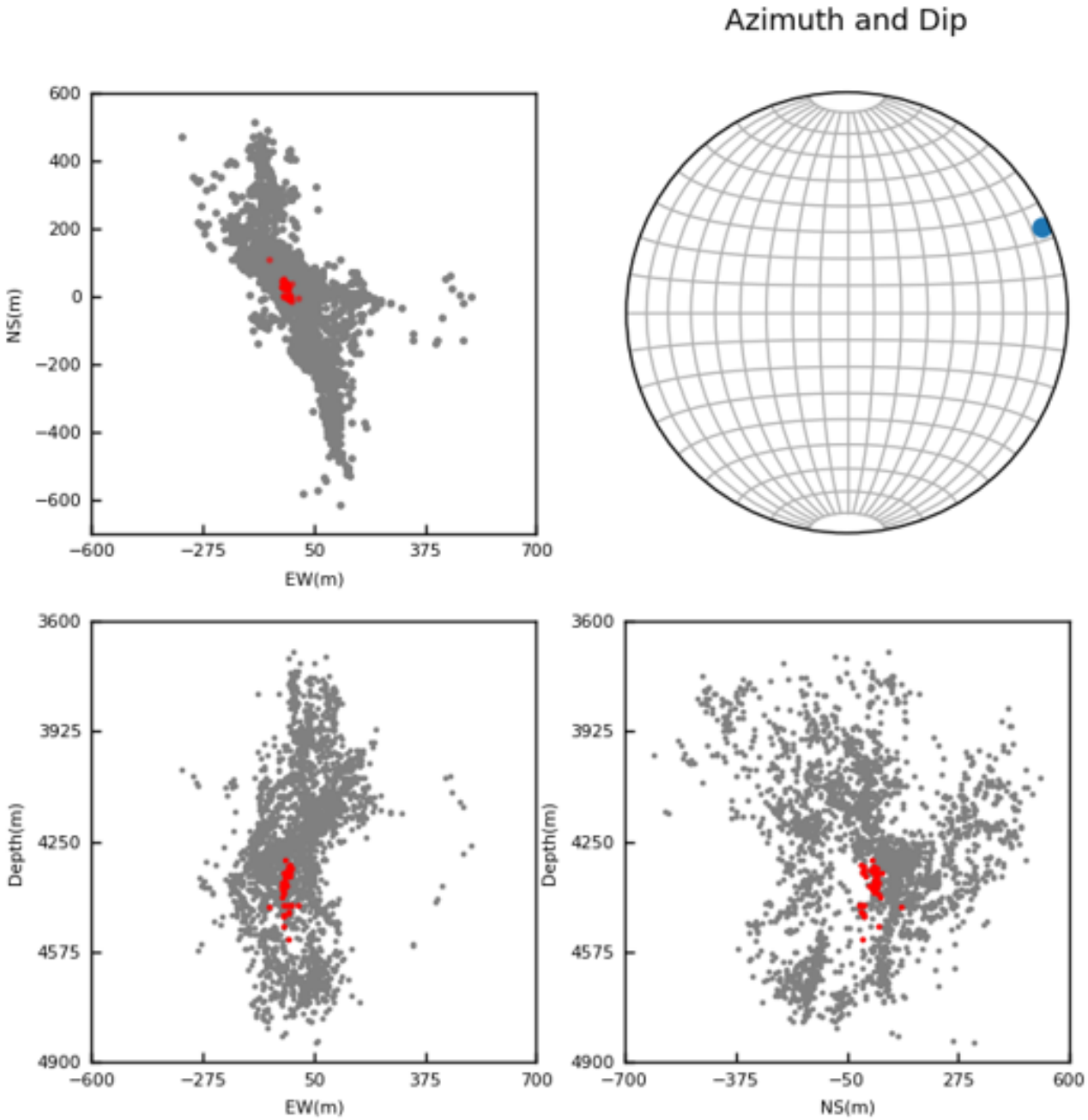
Induced microseismicity is a phenomenon often observed in hydrocarbon and geothermal reservoirs accompanying changes in pore pressure due to injection. Estimation of the focal mechanism of induced microseismicity is beneficial to characterize the distribution of the existing fractures in the reservoir. The focal mechanism of microseismicity is often constrained by the polarity information of first P-wave arrivals. However, it’ s difficult to obtain enough P-wave polarities from a limited number of stations due to cost consideration. The new method was proposed to better constrain the focal mechanism of injection induced microseismicity by introducing *in situ* stress magnitude/orientation information and the injection wellhead pressure (Mukuhira et al., 2018). The range of possible focal mechanism estimated by available polarization information was constrained by in situ stress data further.

We have applied this method to 47 microseismicity events with relatively larger magnitude during the hydraulic stimulation in Basel, Switzerland. In this study, we apply our method to more than 2,000 smaller magnitude events of which the orientations of fault are unknown. By estimating more fault orientation, we can understand the entire fracture system of the reservoir.

All the events are divided into 101 groups based on waveform similarity, and assume all group member occur from one single fracture. we choose one group (group 4) based on good linear shape, relatively larger magnitude of members, large number of events and occurrence time during the injection period. We estimate the fault orientation by principal component analysis (PCA) of hypocenter distribution of 54 events from group 4, and then regard this fault orientation as reference. Meanwhile, we also use the first P-wave arrivals polarities and *in situ* stress information to constrain the focal mechanism together. Then, we will compare the two estimates of fault orientation by PCA and our method, and discuss the validity of our method for smaller events. Then, we will apply our method and constrain the focal mechanisms of other groups. Consequently, we will estimate the focal mechanism of more than 2,000 events from Basel, Switzerland using this method. Our work will enhance the validity of our method further and also contribute to better understanding the fracture system in the reservoir in Basel, Switzerland.

Keywords: Induced seismicity, Fracture system, Basel, Switzerland, Focal mechanism

©2020. Japan Geoscience Union. All Right Reserved.



©2020. Japan Geoscience Union. All Right Reserved.

Source Mechanism and triggering process for the April 12th and 13th 2014 earthquake doublet in the Solomon Islands

*Calvin Luiramo Qwana[1], Masatoshi Miyazawa[1], James Mori[1]

1. Disaster Prevention Research Institute Kyoto University

On 12th and 13th April 2014, a pair of earthquakes with magnitudes Mw 7.6 and Mw7.4, respectively, occurred near Makira Island (San Cristobal) in the Solomon Islands. The depth of the main event (Mw 7.6) was 27 km and the depth of the second event (Mw 7.4) was 37 km respectively (USGS). The second event occurred 16 hours later after the Mw 7.6, approximately 20 km southwest of the location of the hypocenter of Mw 7.6. The study aims to analyze and evaluate the source mechanism for the two-doublet earthquake Mw 7.6 and Mw 7.4 and evaluates if any interrelation between the main event (Mw 7.6) and the second event (Mw 7.4). To understand “why the Solomon Islands has the highest rate of doublet earthquakes” (Lay and Kanamori, 1979; Schwartz et al., 1989; Felzer et al., 2004, Yamamoto et al., 2002 and Xu and Schwartz, 1993). We utilize the role of static Coulomb stress function to evaluate if the Mw 7.4 earthquake was triggered by the static Coulomb stress changes. Initially, the teleseismic P waveform data were retrieved from more than 20 stations for both events from the Global Seismographic Network from azimuthal coverage distances between 30˚ and 90˚. The retrieved P-waveform data were filtered to obtain the best-fit reduction variant between the observed waveform with the synthetic waveform. The retrieved P-wave form data were filtered separately for each event. The cutoff frequency for P –wave filtered separately between 0.04 Hz - 0.1 Hz. The Green’s function is utilized to determine the slip distribution on the fault planes where the observed seismogram inverted. Based on the presumption that a fault plane with fixed strike and dip angles placed in the region of the earthquake hypocenter and divided into sub faults, a constant rupture velocity of 2.5 km/s is assumed and the synthetic waveforms are calculated at the teleseismic stations according to the dislocations of each sub faults. We calculated the values for the Coulomb Failure Stress function at the hypocenter for the mechanism of the second event and obtained +48.59 kPa for the north dipping fault and south-dipping fault to be +18.24 kPa. Furthermore, the spatial distribution of aftershocks for 16 hours seems to agree with the northern dipping fault for the triggered event. Both cases, however, show an increase of stress changes which encourages the likelihood that the recipient's fault triggered by static Coulomb Stress Changes. We proposed a model that might support the complexity of the region to produce these doublet events.

Keywords: Earthquake doublet, Source Mechanism, Coulomb Stress, Solomon Islands

©2020. Japan Geoscience Union. All Right Reserved.

Ultra-microearthquakes observed at Mizunami Underground Research Laboratory

*Osamu Murakami[1], Yasuhiro Asai[1], Hiroshi Ishii[1]

1. Tono Rearch Institute of Earthquake Science, Association for the Development of Earthquake Prediction

Mizunami Underground Research Laboratory (MIU) was constructed by Japan Atomic Energy Agency (JAEA) in order to achieve these two main goals: establishing technology for investigation, analysis and assessment of the deep geological environment, and developing a range of engineering technology for deep underground application. MIU has two vertical shafts, and has the horizontal galleries and the sub stages at every 100 m depth from 100 m depth to 500 m depth.

We deployed the seismic observation network in MIU. We installed 3 components accelerometers (JEP-6A3-10, Mitutoyo co.) at each station, and continuously recorded the ground accelerations at 10 kHz sampling (SC-ADH10K, Scimolex co.). Because of the high frequency sampling, we succeeded to detect some ultra-microearthquakes occurred around MIU. An ultra-microearthquake occurred at 16:27 (JST) on January 17, 2019. This event was observed at one of the stations installed at 500m depth. Another station (400m depth) also showed the seismic waveform, although we could not find the clear P and S wave arrivals due to the bad signal-to-noise ratio. If we assume that S-P time is 0.05 s at this 500 m depth station, and that the velocity of S wave is 2200 m/s (Okubo et al., 2012) and Vp/Vs is 1.73, we obtain that the hypocentral distance is 150 m. Thus, the depth of this event is 650 m assuming this event occurred just beneath this station.

There is the almost vertical fault (Main Shaft Fault) in MIU (e.g., Tsuruta et al., 2013). The hypocenter of the event is likely to locate in this fault. However, we could not determine the location of the event, because we found the clear P or S wave arrivals at only one station. We will discuss some source parameters of the ultra-microearthquakes observed in MIU.

Acknowledgment: We would like to acknowledge the permission and cooperation to the Tono Geoscience Center, the Japan Atomic Energy Agency and the Mizunami City Office.

Keywords: microearthquake, Mizunami Underground Research Laboratory

©2020. Japan Geoscience Union. All Right Reserved.

Seismoelectromagnetic conversions generated by a double-couple source in
partially saturated media.

*Sheldon Dwight Warden[1], Pascal Sailhac[2], Stéphane Garambois[3]

1. Hyperion Geophysical Services, 7 rue de Châtenois, 67100, Strasbourg, France., 2. GEOPS (Geosciences Paris Sud), Université de Paris Saclay, 15 Rue Georges Clemenceau, 91400, Orsay, France., 3. ISTerre (Institut des Sciences de la Terre), Université de Grenoble Alpes, 1381 rue de la piscine, 38400, Saint Martin d'Heres, France.

Seismoelectromagnetic conversions of electrokinetic origin have triggered new interest since the theory for the coupled propagation of seismic and electromagnetic (EM) waves was reformulated by Pride (1994). Over the last couple of decades, several modelling programs were developed to simulate seismoelectromagnetic propagation. Most of these programs share in common that they only allow to model point sources, well suited to simulate seismic surveys, but inappropriate when attempting to simulate earthquakes, often described using a double-couple source.

In this work, we present a program allowing to model the seismoelectromagnetic waves triggered by a double-couple source, based on the Synthetic Kennett Bouchon Program (SKBP) developed by Garambois & Dietrich (2002); this program is modified to account for partial saturation conditions (Warden et al., 2013) and high salinities (Vinogradov et al., 2010). We implement both M13+M31 and M12+M21 geometries. We validate our program by comparing its results with those obtained by modelling a double-couple source through a numerical derivative and find excellent agreement between both approaches. We then study the symmetry properties of the waves generated by this new source type for a homogenous half-space.

We then perform a sensitivity study considering a simple tabular medium consisting of a homogeneous layer overlying a homogeneous half-space. When considering a source of frequency fpeak=40Hz of magnitude Mw=1, located 4km below the ground surface and 1.5km below the boundary between both media, we model coseismic electric field amplitudes of the order of several

©2020. Japan Geoscience Union. All Right Reserved.

hundreds of μV.m−1. Analyzing these amplitudes in the light of magnetotelluric measurements suggests that even a microearthquake could trigger a coseismic response large enough to be measured at the ground surface.

We also study the characteristics of the interface response (IR) generated at the boundary between the two homogenous media for a M13+M31 double-couple and show that this IR consists of a conversion between an incident S wave and a converted EM wave; its amplitude variations can be approximated by those of a horizontal dipole located at the boundary. We also quantify the contributions of the SH and SV polarizations to the total converted amplitude and find that although the SH waves are coupled to the Transverse Electric (TE) mode, they contribute to the Transverse Magnetic (TM) mode component of the electric field through the IR.

We conclude our study by considering a more realistic model, designed to approximate the context of a geothermal field. We also provide examples of possible coseismic signals observed in electric and magnetic data acquired during geothermal monitoring experiments.

Keywords: Electrokinetic conversions, Seismoelectric imaging, Induced seismicity monitoring

©2020. Japan Geoscience Union. All Right Reserved.

Investigation of the pore pressure sensitivity toward ocean loading influence from seismic ambient noise monitoring

*Rezkia Dewi Andajani[1], Takeshi Tsuji[1,2]

1. Department of Earth Resources Engineering, Kyushu University , 2. International Institute for Carbon-Neutral Energy Research, Kyushu University

Spatial mapping of pore pressure sensitivity toward surface perturbations can be useful to characterize crustal dynamic activities. This is due to pore pressure controls the activity of earthquakes and volcanic eruptions. Recent studies have discussed that the status of pore pressure can be evaluated from ambient noise seismic velocity change. Seismic velocity changes are known to exhibit variations induced by surface perturbations such as rainfall, snow, ocean loading, and atmospheric pressure change. Among these perturbations, the mechanism of the ocean loading influencing seismic velocity changes remain unclear. In regards to this, variations in ocean mass are known to cause inland deformation. We aim to investigate the response of the crustal pore pressure toward perturbations from the ocean by seismic velocity monitoring. We used the estimated seismic velocity in the Chugoku-Shikoku region, Japan. In this study, we used a statistical approach to draw a conclusion. To evaluate the influence of the ocean, we calculate the correlation coefficient between seismic velocity changes and sea-level. We assume a linear model between the absolute correlation and the station distance from the coast. The significance of the linear model is evaluated by considering the probability value. Our result suggests that for a specific period band, the absolute correlation between seismic velocity change and sea-level tends to decrease with the increasing distance from the coast. We conclude that ocean perturbations could spatially influence estimated seismic velocity changes, which might infer inland deformation due to ocean loading.

Keywords: seismic velocity change, ocean loading, surface perturbations, pore pressure

©2020. Japan Geoscience Union. All Right Reserved.

The character of the Focal mechanisms with Kagan angles in Japan area for the extended 2-D ETAS model

*Maita Eri[1], Jiancang Zhuang

1. SOKENDAI

The original epidemic-type aftershock sequence (ETAS) model which describes how each earthquake produces subsequent events considers only the locations, times, and magnitudes of each event. This time, we explore the possibility of combining the focal mechanisms into the model formulation to increase the estimation accuracy.

To find the suitable conditional intensity (time-varying seismicity rate) of the new form of the ETAS model, we use the F-net data from 1997 to 2017 and select focal mechanism of events with magnitudes . We use the Kagan angles (rotation angles) to transform each focal mechanism, a 3*3 matrix into a vector called a quaternion.

The data calculation leads to the model reconstruction to get the focal mechanism probability densities, under the assumption of a special symmetry, DC4 symmetry with the distribution of the Kagan angle. We also found that the rotation poles are uniformly distributed.

In the background events, the probability density of the focal mechanism or rotation angles, could be independent of any locations in the very small areas. We investigate the Japan area to find the character of .

Keywords: Focal mechanism, Kagan angle

©2020. Japan Geoscience Union. All Right Reserved.

[E] Poster | S (Solid Earth Sciences)：S-SS Seismology

[S-SS10] Rethinking PSHA

convener:Naoshi Hirata(National Research Institute for Earth Science and Disaster Resilience), Danijel Schorlemmer(GFZ German Research Centre for Geosciences), Matt Gerstenberger(GNS Science), Kuo-Fong Ma(Institute of Geophysics, National Central University, Taiwan, ROC)

The core methods behind probabilistic seismic hazard analysis (PSHA) were first formalized by Cornell in 1968. Since that time, the fundamental components have largely remained unchanged in most applications: 1) a source model, often made up of zones of expected activity, or an active fault model coupled with a smoothed seismicity model based on catalog data, and; 2) empirically based ground motion prediction equations (GMPE) that are based on several basic parameters, such as moment magnitude and distance. The development of the individual components has become increasingly complex in recent years, however the basic structure has largely remain unchanged.
We invite presentations that explore some of the key assumptions currently used in PSHA and their implications for hazard, or alternative PSHA methods that might provide different insight into the hazard. Some examples might be the improved quantification of uncertainty in the source modeling, and moving beyond the typical Poisson-based formulations. How are uncertainties propagated through the model and can they correctly reflect the knowledge. How can non-Poissonian dynamics be best built into time-independent PSHA? How to quantify and use uncertainties in fault and earthquake-catalog source models as well as those in ground-motion prediction? How can fault segmentation be overcome? New types of models (with increasing complexity) are being developed and they will be integrated into PSHA. How can hybrid models be used to improve the forecasting skill of PSHA? Can earthquake simulators contribute to PSHA? What are improvements in GMPEs but also their limits? Is their increasing complexity justified? Or are there viable modeling alternatives for PSHA that can improve current best practice?How can all these potential improvements being tested before they contribute to societal relevant decisions?

[E] Poster | S (Solid Earth Sciences)：S-EM Earth's Electromagnetism

[S-EM18] Paleomagnetism and rock magnetism applied to solving geological and geophysical problems

convener:Martin Chadima(Institute of Geology of the Czech Academy of Sciences), Balazs Bradak(University of Burgos, Spain), Daniel Pastor-Galan(Center for North East Asian Studies, Tohoku University), Myriam Annie Claire Kars(Center for Advanced Marine Core Research)

Paleomagnetic studies have provided much key information about the geomagnetic field and plate motions, and rock magnetic methods have considerable potential for detecting and monitoring signals from past and recent environments. Integrated paleomagnetic and magnetic fabric studies, together with structural geology and petrology, are effective tools for increasing our knowledge about sedimentological, tectonic or volcanic processes on various scales. Determining how the geomagnetic field changes (i.e., reversals and paleointensity variations) helps to understand the evolution of Earth's interior, plate kinematics, dynamics of the core and mantle, long-term climate change, and true polar wander. We welcome presentations of innovative studies that make use of paleo-, rock, and environmental magnetic data in relation to geological, geomagnetic, and environmental processes, especially contributions that combine rock magnetic methods or novel approaches to data evaluation. We also solicit contributions from both experimental and theoretical aspects of paleomagnetic reconstructions, acquisition of petrofabrics, characteristic remanences, remagnetizations, polarity reversal records, paleointensity, and environmental magnetic methods.

[SEM18-P01] Anisoft – Advanced Treatment Of Magnetic Anisotropy Data

*Martin Chadima[1,2] (1.Institute of Geology of the Czech Academy of Sciences, Prague, Czech Republic, 2.AGICO Ltd., Brno, Czech Republic, e-mail: chadima@agico.cz)

[SEM18-P02] Anisotropy of out-of-phase magnetic susceptibility as an alternative proxy for lattice preferred orientation of graphite

*Martin Chadima[1,2], Frantisek Hrouda[2,3], Josef Jezek[3], Štěpánka Mrázová[4], Michal Poňavič[4] (1.Institute of Geology of the Czech Academy of Sciences, Prague, Czech Republic, 2.AGICO, Brno, Czech Republic, 3.Faculty of Science, Charles University, Prague, Czech Republic, 4.Czech Geological Survey, Prague, Czech Republic)

[SEM18-P03] Magnetic fabric of anthropogenic ash horizons in cave sediment succession

*Balazs Bradak[1], Ángel Carrancho Alonso[1], Ángela Herrejon Lagunilla[1], Juan J. Villalain Santamaria[1], Carolina Mallol[2,3], Gilbert Tostevin[4], Gilliane F. Monnier[4], Goran Pajović[5], Mile Baković[6], Nikola Borovinić[6] (1.Paleomagnetic Laboratory, Department of Physics, Burgos University, Spain, 2.UDI de Prehistoria, Arqueología e Historia Antigua, Facultad de Geografía e Historia, Universidad de La Laguna, La Laguna, Spain. , 3.Archaeological Micromorphology and Biomarker Research Lab, University of La Laguna, La 10 Laguna, Spain., 4.Department of Anthropology, University of Minnesota Twin Cities, United States, 5.National Museum of Montenegro, Cetinje, Montenegro, 6.Center for Conservation and Archaeology of Montenegro)

[SEM18-P04] Bacterial magnetosome morphology in Hiroshima Bay sediments

*Noriko Kawamura[1], Kengo Hiyamizu[2], Toshitsugu Yamazaki[3] (1.Japan Coast Guard Academy, 2.Japan Coast Guard, 3. Atmosphere and Ocean Research Institute, The University of Tokyo)

[SEM18-P05] FORC-PCA analyses of red clay in the Pacific

*Toshitsugu Yamazaki[1], Wei Fu[1], Takaya Shimono[2], Yoichi Usui[3] (1.Atmosphere and Ocean Research Institute, The University of Tokyo, 2.Meiji University, 3.Japan Agency for Marine-Earth Science and Technology)

[SEM18-P06] A new $^{40}Ar/^{39}Ar$ age and magnetostratigraphy of the Afro-Arabian Large Igneous Province in the Lima-Limo section erupted in Oligocene

*Yutaka Yoshimura[1], Osamu Ishizuka[2], Toshitsugu Yamazaki[1], Yuhji Yamamoto[3], Hyeon-Seon Ahn[4], Tesfaye Kidane[5], Yo-ichiro Otofuji[6], Naoto Ishikawa[7] (1.Atmosphere and Ocean Research Institute, The University of Tokyo, 2.National Institute of Advanced Industrial Science and Technology, 3.Center for Advanced Marine Core Research , Kochi Univ., 4.Korea Institute of Geoscience & Mineral Resources, 5.School of Agricultural, Earth, and Environmental Sciences, University of KwaZulu Natal, 6.Institute of Geohistory, 7.School of Sustainable Design, University of Toyama)

[SEM18-P07] **PRELIMINARY ARCHAEOMAGNETIC STUDY IN THE ARCHAEOLOGICAL SITE OF GRAKLIANI (REPUBLIC OF GEORGIA)**

*Manuel Calvo-Rathert[1,5], Natalia Garcia-Redondo[1], Angel Carrancho[2], Avto Gogichaishvili[3], Vakhtang Licheli[4] (1.Departamento de Fisica, EPS, Universidad de Burgos, Burgos, Spain , 2.Departamento de Historia, Geografía y Comunicación, Universidad de Burgos, Burgos, Spain., 3.Servicio Arqueomagnetico Nacional – Instituto de Geofisica, Universidad Nacional Autonoma de Mexico, Morelia, Mexico, 4.Institute of Archaeology, Ivane Javakhishvili Tbilisi State University, Tbilisi, Georgia., 5.Hawaii Institute of Geophysics and Planetology, University of Hawaii at Manoa, Honolulu, Hawaii, United States)

[SEM18-P08] Paleomagnetism.org 2.0: an online multiplatform, open source and FAIR paleomagnetic data management software

Mathijs Koymans[2], *Daniel Pastor-Galan[1], Douwe van Hinsbergen[2], Bram Vaes[2], Cor Langereis[2] (1.Center for North East Asian Studies, Tohoku University, 2.Utrecht University)

[SEM18-P09] Brunhes and Matuyama Chron Paleosecular variation study from dated lava flows erupted from West Maui, Hawaii, USA.

*Emilio Herrero-Bervera[1] (1.University of Hawaii at Manoa)

[SEM18-P10] Centennial-resolution terrestrial climatostratigraphy and Matuyama-Brunhes transition from a loess sequence in China

*Masayuki Hyodo[1], Kenta Banjo[2], Tianshui Yang[3], Shigehiro Katoh[6], Shi Meinan[3], Yuki Yasuda[4], Jun-ichi Fukuda[1], Masako Miki[2], Balázs Bradák[5] (1.Research Center for Inland Seas, Kobe University, 2.Department of Planetology, Kobe University, 3.China University of Geosciences, 4.Institute of Seismology and Volcanology, Hokkaido University, 5.Department of Physics, EPS, University of Burgos, 6.Museum of Nature and Human Activities, Hyogo)

[SEM18-P12] **Paleomagnetism of sediment cores taken from the Ontong-Java plateau: for better understanding of the role of biogenic magnetite in geomagnetic paleointensity recording**

*Jiaxi Li [1] (1.Atmosphere and Ocean Research Institute, The University of Tokyo)

[SEM18-P13] **New paleomagnetic data from of Late Cretaceous volcanics of the northern part of the Okhotsk-Chukotka volcanic belt**

*Aleksandr Pasenko[1], Ivan Lebedev[1], Florian Lhuillier[2], Baha Eid[2], Vladimir Pavlov[1] (1.The Schmidt Institute of Physics of the Earth of the Russian Academy of Sciences, Moscow, Russia, 2.Department of Earth and Environmental Sciences, Ludwig Maximilians University, Munich, Germany)

Anisoft –Advanced Treatment Of Magnetic Anisotropy Data

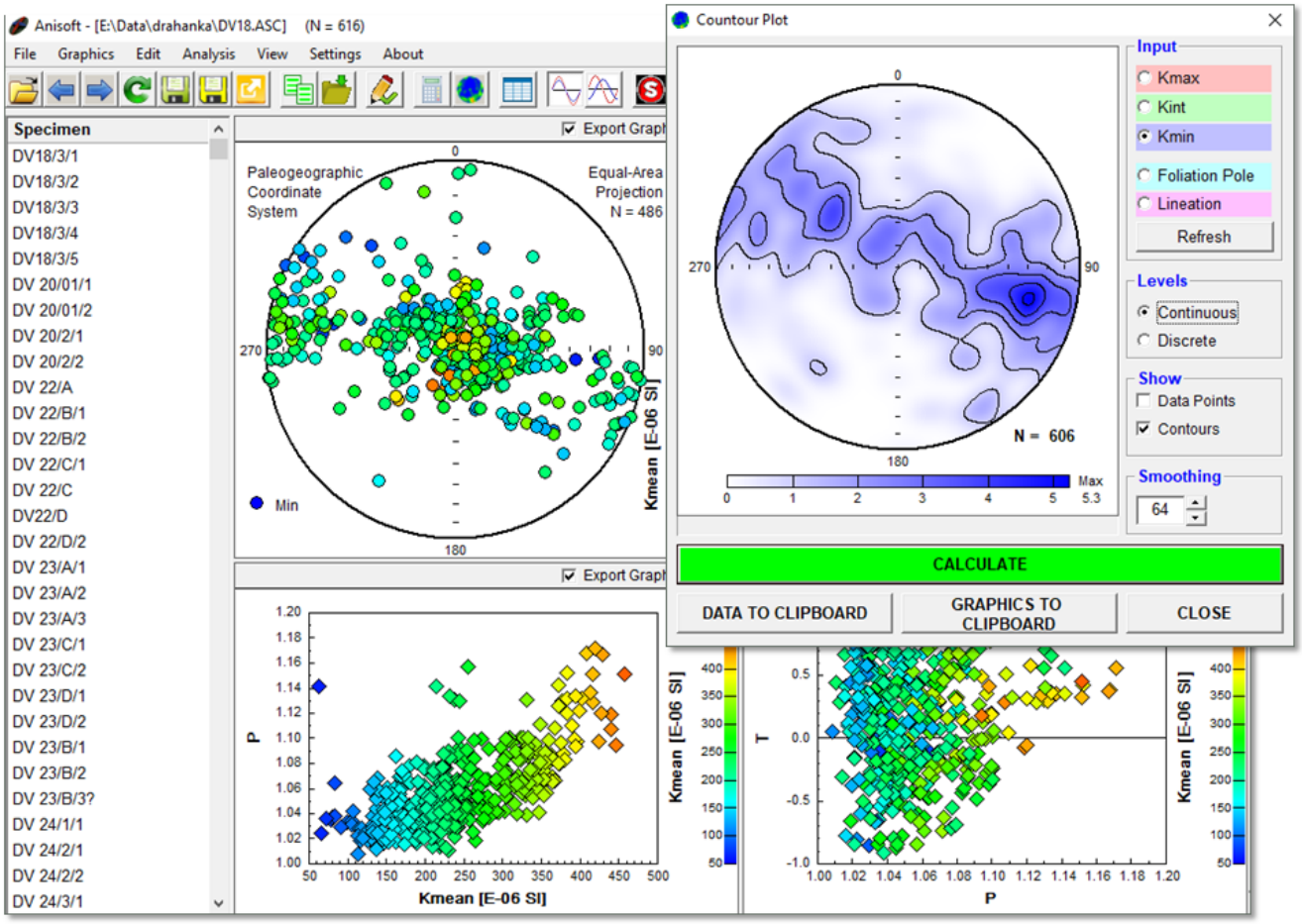
*Martin Chadima[1,2]

1. Institute of Geology of the Czech Academy of Sciences, Prague, Czech Republic, 2. AGICO Ltd., Brno, Czech Republic, e-mail: chadima@agico.cz

Since its first release, Anisoft (Anisotropy Data Browser) has been very well accepted by magnetic fabric community mainly due to its simple and user-friendly interface enabling convenient visualization of magnetic anisotropy data. Here, a major software update is presented transforming a rather simple data viewer into a platform offering an advanced data treatment. The update introduces new data format which stores both in-phase and out-of-phase (if measured) susceptibility tensors (AMS) or tensors of anisotropy of magnetic remanence (AMR) together with their confidence limits. In addition to the tensor data, specimen sampling angles are stored for each record enabling later editing or corrections. Each record also contains an array mesoscopic structural data enabling data transformation into various coordinate systems. Multiple anisotropy files can be combined together or split into several files by manual data selection or data filtering. Anisotropy tensors are conventionally visualized as principal directions (eigenvectors) in stereoplots together with a user’ s choice of quantitative anisotropy parameters presented in histograms or in color-coded scatter plots showing mutual relationship of three variables. For a group of specimens, principal anisotropy directions can be contoured, or a mean tensor and respective confidence ellipses can be calculated using either the Hext-Jelinek statistics or the Bootstrap method. To facilitate the AMR tensor calculation, a simple toolbox is available. The AMR tensors are fitted by a least-square algorithm using a set of pre-selected full-vectors (full-vector method) or their projections to the respective magnetizing directions (projection method). Each graphical output can be exported into several vector or raster graphical formats or, via clipboard, pasted directly into a presentation or publication manuscript. Calculated principal directions or anisotropy parameters can be exported into various types of text files ready to be visualized or processed by any software of user's choice. The software can be downloaded from this link: https://www.agico.com/text/software/anisoft/anisoft.php

Keywords: magnetic fabric, magnetic anisotropy, software

©2020. Japan Geoscience Union. All Right Reserved.



©2020. Japan Geoscience Union. All Right Reserved.

Anisotropy of out-of-phase magnetic susceptibility as an alternative proxy for lattice preferred orientation of graphite

*Martin Chadima[1,2], Frantisek Hrouda[2,3], Josef Jezek[3], Štěpánka Mrázová[4], Michal Poňavič[4]

1. Institute of Geology of the Czech Academy of Sciences, Prague, Czech Republic, 2. AGICO, Brno, Czech Republic, 3. Faculty of Science, Charles University, Prague, Czech Republic, 4. Czech Geological Survey, Prague, Czech Republic

Single crystals of graphite are known to exhibit high electrical conductivity and extremely strong conductivity anisotropy. Their AC magnetic susceptibility can be decomposed into a weak negative (diamagnetic) in-phase component and relatively strong out-of-phase component which is due to electrical eddy currents. Anisotropy of magnetic susceptibility (AMS) of graphite is known to be very strong and it is thus expected to be a good proxy for the lattice preferred orientation (LPO) of graphite in a graphite ore.

Here, we present the AMS results of natural graphite ores from the Moldanubian Unit (Bohemian Massif, Czech Republic), which were mined for the pencil industry in the past. The ores are metamorphic in origin and a strong graphite LPO is thus expected.

In-phase susceptibility is very low, in the order of 10^{-6} [SI units], being positive in some specimens and negative in the others. This indicates simultaneous control by graphite and paramagnetic and/or ferromagnetic minerals. On the other hand, the out-of-phase susceptibility is much higher, in the order of 10^{-4}, and no doubt indicates its graphite control. The degree of opAMS is truly high, $P = 2$ to 3, and the opAMS foliation is closely related to the metamorphic foliation created during the Variscan regional metamorphism and associated ductile deformation.

Our results show that the standard AMS, which is in fact the anisotropy of the in-phase component of susceptibility (ipAMS), reflects not only the LPO of graphite, but also the preferred orientation of paramagnetic and ferromagnetic admixtures. On the other hand, the anisotropy of out-of-phase susceptibility (opAMS) indicates LPO of graphite, free of the effects of non-conductive paramagnetic and ferromagnetic minerals and can be used as an alternative proxy for the lattice preferred orientation of graphite in a graphite ore.

Keywords: anisotropy of magnetic susceptibility, graphite, lattice preferred orientation

©2020. Japan Geoscience Union. All Right Reserved.

Magnetic fabric of anthropogenic ash horizons in cave sediment succession

*Balazs Bradak[1], Ángel Carrancho Alonso[1], Ángela Herrejon Lagunilla[1], Juan J. Villalain Santamaria[1], Carolina Mallol[2,3], Gilbert Tostevin[4], Gilliane F. Monnier[4], Goran Pajović[5], Mile Baković[6], Nikola Borovinić[6]

1. Paleomagnetic Laboratory, Department of Physics, Burgos University, Spain, 2. UDI de Prehistoria, Arqueología e Historia Antigua, Facultad de Geografía e Historia, Universidad de La Laguna, La Laguna, Spain. , 3. Archaeological Micromorphology and Biomarker Research Lab, University of La Laguna, La 10 Laguna, Spain., 4. Department of Anthropology, University of Minnesota Twin Cities, United States, 5. National Museum of Montenegro, Cetinje, Montenegro, 6. Center for Conservation and Archaeology of Montenegro

Rock magnetic and magnetic fabric study has been elaborated on the anthropogenic ash horizons in Crvena Stijena (‘Red Rock Cave’, Montenegro) sediment succession. The study has multiple goals including the identification of mineral forming during burning, alteration after the fire, revelation of the magnetic fabric and its significance in the characterization of cave facies.

Magnetite has been identified as a main ferromagnetic magnetic component of the ash. In addition, a ‘recently unknown’ contributor(s) was found by thermomagnetic experiments (Variable Field Translation Balance - VFTB, Mag Instruments UG, Germany). Various type of minerals are the candidates, such as SD magnetite, siderite and greigite. The forming of all candidates can be described by various processes in cave environment, including burning, post-burning alteration, precipitation from groundwater and so on. But no any theory is supported fully by the rock magnetic results.

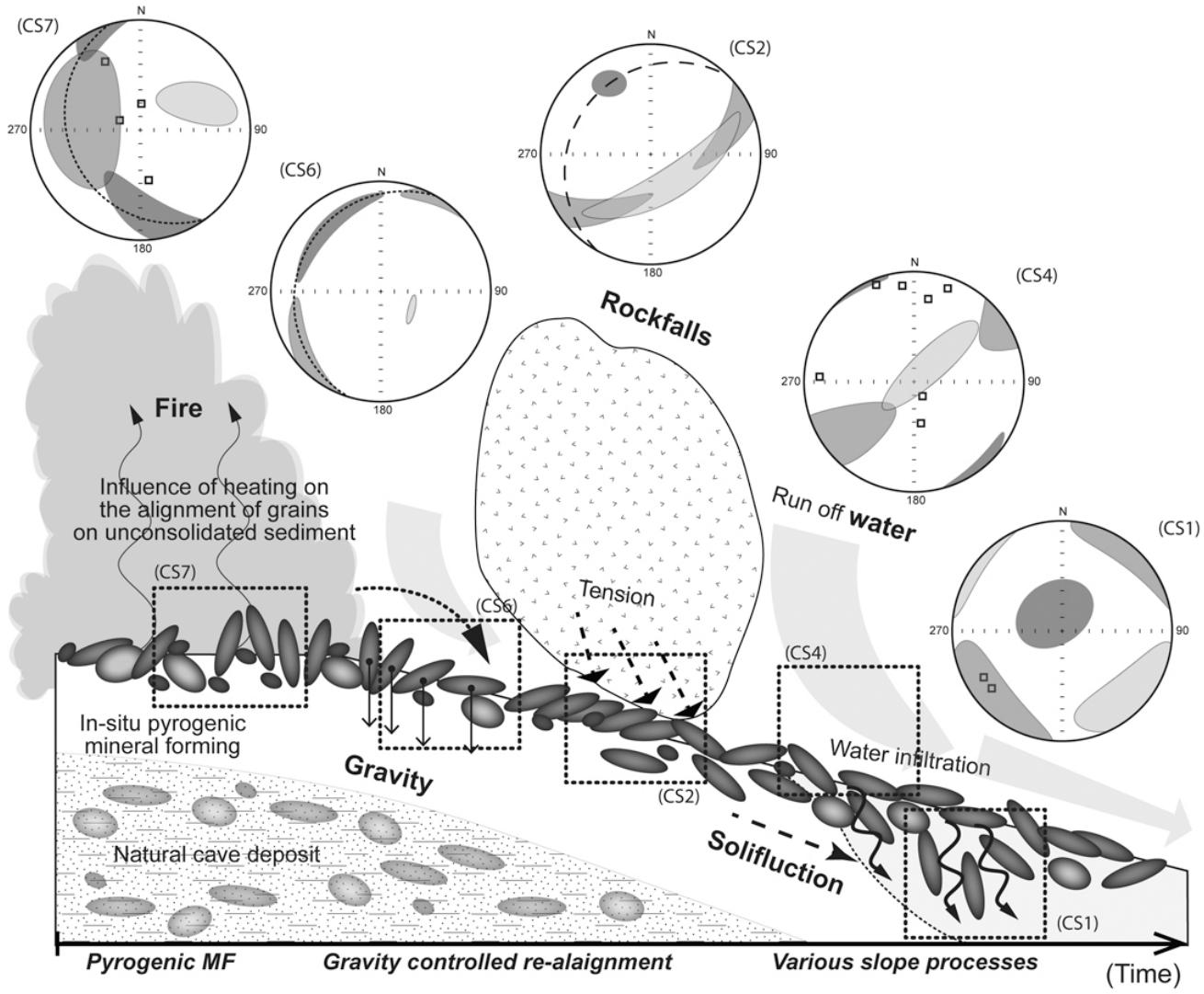
The magnetic fabric of the ash was characterized by low field anisotropy of magnetic susceptibility measurements (AMS; KLY-4S Kappabridge, AGICO, Czech Republic). The statistical analysis (Whisker’s box plot) of the basic anisotropy parameters, such as foliation, lineation, degree of anisotropy and the shape parameter, along with the alignment of the principal susceptibilities on stereoplots, revealed varied characteristics of the ash units. The diverse, oblate to prolate, lineated or strongly foliated, horizontally oriented and inverse fabrics of the units like the magnetic contribution. It may indicate multiple processes (on slope), such as orientation by gravity, solifluction, run off water, quasi-vertical migration of groundwater and post-burning/post-depositional alteration of the fabric by the impact of a rockfall (Figure 1).

Acknowledgements

B. Bradák acknowledges the financial support of project BU235P18 (Junta de Castilla y Leon, Spain) and the European Regional Development Fund (ERD).

Keywords: ash, magnetic fabric, cave sediments

©2020. Japan Geoscience Union. All Right Reserved.



©2020. Japan Geoscience Union. All Right Reserved.

Bacterial magnetosome morphology in Hiroshima Bay sediments

*Noriko Kawamura[1], Kengo Hiyamizu[2], Toshitsugu Yamazaki[3]

1. Japan Coast Guard Academy, 2. Japan Coast Guard, 3. Atmosphere and Ocean Research Institute, The University of Tokyo

Magnetotactic bacteria play an important role in remanent magnetization acquisition of sediments. Bacterial magnetosome morphology depends on chemical conditions with burial depth in deep-sea sediments, and can be classified into three different groups according to shape: teardrop, elongated, and equant (Yamazaki et al., 2019). In order to clarify reaction time of bacterial magnetosome morphology, the distribution of magnetotactic bacteria in surface sediments was investigated in Hiroshima bay as a reference area. Vertical stratification of the water column in the bay changes throughout the year, and magnetic hysteresis parameters and mineralogy in the bay sediments vary in response to changes in redox conditions of bottom waters (Kawamura et al., 2016). Surface sediments (0-1 cm) were taken using a hand sampler at three stations in February and July 2019. The remanent coercivity/coercivity ratio (Hcr/Hc) of the sediment samples also varies, both spatially and temporally, which reflects changes in magnetic mineralogy. Magnetic minerals were extracted from the dried sediment samples (10.0 g), and were counted using a transmission electron microscope (TEM). They were classified into the groups depended on temperature and nutrient in seawater. From magnetic minerals of February 2019 seen in TEM images, grains in 20~100 m size which seem to have formed by bacteria are rare. In contrast, the equant-shaped chained magnetic minerals are recognized in June 2019 samples at all stations. Seawater temperature and nutrients in July are higher than February. The results imply that magnetotactic bacteria increase in the bay within six months at least.

Keywords: Magnetotactic bacteria, Magnetosome morphology, Seasonal changes

©2020. Japan Geoscience Union. All Right Reserved.

FORC-PCA analyses of red clay in the Pacific

*Toshitsugu Yamazaki[1], Wei Fu[1], Takaya Shimono[2], Yoichi Usui[3]

1. Atmosphere and Ocean Research Institute, The University of Tokyo, 2. Meiji University, 3. Japan Agency for Marine-Earth Science and Technology

Red clay is widely distributed in deep-sea in mid-latitudes, and potentially preserves long-term paleoceanographic changes, although lack of calcareous and siliceous microfossils and extremely slow sedimentation with numerous hiatuses limit resolution. We conducted a rock magnetic study of some red clay cores in the North and South Pacific in order to identify magnetic mineral components and estimate paleoenvironmental changes. Three piston cores (MR13E02-PC1, KR1402-PC4, and KR1302-PC6) collected from near Minamitorishima Island in the northwestern Pacific and IODP Site U1365 cores in the South Pacific were used in this study. Principal component analyses of FORC diagrams (FORC-PCA) revealed that core KR1302-PC6 contains three main magnetic components (endmembers EM1 through EM3). Two of them, EM2 and EM3, show the features of non-interacting SD, which are interpreted to be biogenic magnetites with lower and higher coercivity, respectively. Combined with TEM observation, EM2 is dominated by magnetofossils of equant ochtahedral shape, while the proportion of bullet-shape magnetofossils is larger in EM3. The other endmenber EM1 showing interacting SD/PSD/MD is interpreted to be a terrigenous component. EM1 contribution suddenly increased upcore at about 3 m in depth, which suggests a significant increase of eolian dust input caused by a global cooling event. The age of this event can roughly be estimated as Oligocene to Eocene from lithostratigraphic correlation with a nearby core having age estimation based on Os isotope ratios (Nozaki et al., 2019; Tanaka et al., submitted). The results of cores MR13E02-PC1 and KR1402-PC4, whose ages are estimated to be Miocene and younger, suggest that eolian input has been kept enhanced since the event observed in PC6. An increase of bullet-shape magnetofossils at a certain depth interval of PC6 suggests that the core had the oxic-anoxic transition zone (OATZ) (Yamazaki et al., 2019), although the core is totally oxidized now and there is no OATZ. The less oxic environment might have been caused by higher biogenic productivity near the equator; the paleoposition of PC6 site calculated with GPlates software suggests that the site was within 5 degrees from the equator between about 70 and 85 Ma. FORC-PCA results of core U1365 show two endmembers, terrigenous (EM1) and biogenic (EM2), respectively. The coercivity distribution of EM2 of Site U1365 is similar to that of EM2 in the North Pacific, while EM1 of Site U1365 includes particles with finer SP grain. Site U1365 also shows a sudden upcore increase of the EM1 component, and its age was roughly estimated to be Oligocene (Shimono and Yamazaki, 2016). Although there are large uncertainties in age estimations, the eolian input increases in the both hemispheres might be a coeval global event. A possible candidate of such an event is the global cooling known to have occurred at the Eocene-Oligocene boundary.

Keywords: red clay, FORC, rock magnetism

©2020. Japan Geoscience Union. All Right Reserved.

A new $^{40}Ar/^{39}Ar$ age and magnetostratigraphy of the Afro-Arabian Large Igneous Province in the Lima-Limo section erupted in Oligocene

*Yutaka Yoshimura[1], Osamu Ishizuka[2], Toshitsugu Yamazaki[1], Yuhji Yamamoto[3], Hyeon-Seon Ahn[4], Tesfaye Kidane[5], Yo-ichiro Otofuji[6], Naoto Ishikawa[7]

1. Atmosphere and Ocean Research Institute, The University of Tokyo, 2. National Institute of Advanced Industrial Science and Technology, 3. Center for Advanced Marine Core Research , Kochi Univ., 4. Korea Institute of Geoscience & Mineral Resources, 5. School of Agricultural, Earth, and Environmental Sciences, University of KwaZulu Natal, 6. Institute of Geohistory, 7. School of Sustainable Design, University of Toyama

We report new $^{40}Ar/^{39}Ar$ ages on fresh groundmass grains from a 2 km-thick section in the Lima-Limo area of the NW Afro-Arabian Large Igneous Province (AALIP). A succession of seven magnetozones (R4-N3-R3-N2-R2-N1-R1, from top to base) were identified by Ahn et al. (submitted), which are tentatively correlated to Chron C11n.1r (29.477-29.527 Ma) (R4) - C11n.2n (29.527-29.970 Ma) (N3 to N2) - C11r (29.970-30.591 Ma) (R2 to R1) of the geomagnetic polarity time scale 2016 (GPTS 2016; Ogg et al., 2016). A new age was obtained from the R4 magnetozone agrees with the previously reported ages by Coulié et al. (2003) and Hofmann et al. (1997) but has higher precision. From our age and its uncertainty, the R4 magnetozone can be correlated to Chron C11n.1r of the radio-isotopic age model considered for constructing GPTS 2012 (Vandenberghe et al., 2012) rather than the astronomical age model adopted for GPTS 2012. Our correlation is consistent with the two previously proposed magnetostratigraphy (Rochette et al., 1998; Ahn et al., submitted). From the time-interval of 0.12 Myr of C11n.1r for the radio-isotopic age model and the area of ~600,000 km^2 (Mohr, 1983), the average eruption within the R4 magnetozone is estimated to be 5 km^3/yr, which is higher than that of the Siberian LIP.

Keywords: Afro-Arabian Large Igneous Province, magnetostratigraphy, 40Ar/39Ar dating

©2020. Japan Geoscience Union. All Right Reserved.

PRELIMINARY ARCHAEOMAGNETIC STUDY IN THE ARCHAEOLOGICAL SITE OF GRAKLIANI (REPUBLIC OF GEORGIA)

*Manuel Calvo-Rathert[1,5], Natalia Garcia-Redondo[1], Angel Carrancho[2], Avto Gogichaishvili[3], Vakhtang Licheli[4]

1. Departamento de Fisica, EPS, Universidad de Burgos, Burgos, Spain , 2. Departamento de Historia, Geografía y Comunicación, Universidad de Burgos, Burgos, Spain., 3. Servicio Arqueomagnetico Nacional –Instituto de Geofisica, Universidad Nacional Autonoma de Mexico, Morelia, Mexico, 4. Institute of Archaeology, Ivane Javakhishvili Tbilisi State University, Tbilisi, Georgia., 5. Hawaii Institute of Geophysics and Planetology, University of Hawaii at Manoa, Honolulu, Hawaii, United States

We present a preliminary archaeomagnetic study carried out in the archaeological site of Grakliani (Republic of Georgia). Samples were taken during two different samplings (2018 and 2019) from nine combustion structures (ovens and possibly altars) and from different pottery fragments with a good age control. The age of all these samples varies between the 12th century BC and the 1st century BC, a broad period with scarce reliable archaeomagnetic data in the region.

We have performed an archeomagnetic and archaeointensity study on these samples at the paleomagnetic laboratory of the University of Burgos (Spain) and at the paleomagnetic laboratory Fort Hoofddijk in Utrecht University (The Netherlands). We carried out directional studies including both thermal demagnetization and stepwise alternating field as well as rock magnetic analyses, consisting in the measurement of IRM acquisition curves, hysteresis loops, *backfield* curves and high temperature thermomagnetic curves. Archaeointensity determinations were carried out with the Thellier-IZZI and Thellier –Coe protocols. They included additional experiments for anisotropy correction of the archaeointensity results.

So far, we have obtained a mean direction for each combustion structure and archaeointensity results for five combustion structures and five pottery fragments of different ages in the studied time range, which provide new full vector and intensity data of the Earth’ s magnetic field variations in the Caucasus. Additional archaeointensity determinations in two other combustion structures are still in progress.

Keywords: archaeomagnetism, archaeointensity, magnetic properties , anisotropy of thermoremanence, geochronology

©2020. Japan Geoscience Union. All Right Reserved.

Paleomagnetism.org 2.0: an online multiplatform, open source and FAIR paleomagnetic data management software

Mathijs Koymans[2], *Daniel Pastor-Galan[1], Douwe van Hinsbergen[2], Bram Vaes[2], Cor Langereis[2]

1. Center for North East Asian Studies, Tohoku University, 2. Utrecht University

Scientific communities are placing an increasing emphasis on the implementation of data management protocols concerning data archiving and distribution. For instance, every proposal submitted to the European Horizon 2020 program, as well as to the National Science Foundation in the USA, requires a dedicated section that outlines project data management and accessibility. The widely adopted FAIR data guidelines identify four fundamental principles concerning the Findability, Accessibility, Interoperability and Reproducibility of data. They form a cornerstone of modern data infrastructures and are being increasingly adopted by scientific communities. FAIR data means that data sets are effortlessly searched and discovered, freely downloaded, shared, usable between multiple disciplines, and that derived results and the applied methodology are fully transparent. The wide variety of data formats, the low data volume, and the general lack of a culture of data sharing makes that the paleomagnetic community rarely follows any of the FAIR principles. Most institutions define their own data formats and use inhouse software to analyse their demagnetization data, which are critical to Paleomagnetic research. In this presentation we present the second iteration of Paleomagnetism.org, an online multiplatform open source environment for paleomagnetic data analysis. Paleomagnetism.org provides an interactive environment where paleomagnetic data can be interpreted, evaluated, visualized, and exported. The Paleomagnetism.org application is split in to an interpretation portal, statistics portal, geography portal, and a portal for miscellaneous paleomagnetic tools. In the interpretation portal, principle component analysis can be performed on visualized demagnetization diagrams. Interpreted directions and great circles can be combined to find great circle solutions. These directions can be used in the statistics portal, or exported as data and figures. The tools in the statistics portal cover standard Fisher statistics for directions and VGPs, including other statistical parameters used as reliability criteria, foldtest, bootstrapped common true direction test reversal and correction of inclination shallowing in sediments following TK03.GAD. The geography portal provides a module to visualize VGPs and expected paleolatitudes, declinations, and inclinations relative to widely used global apparent polar wander path models in coordinates of major continent bearing plates. The 2.0 update of Paleomagnetism.org comprises a full overhaul of the application to satisfy the increasingly demanding data management requirements. The application now facilitates a workflow that respects FAIR guidelines by documenting data provenance. All data analysed through the application are easily submitted to a public data library which distributes data and results through an HTTPS web service that lives up to modern data management standards.

Keywords: Paleomagnetism, FAIR data principles, Open Access, Data sharing, Software

©2020. Japan Geoscience Union. All Right Reserved.

Brunhes and Matuyama Chron Paleosecular variation study from dated lava flows erupted from West Maui, Hawaii, USA.

*Emilio Herrero-Bervera[1]

1. University of Hawaii at Manoa

Fifteen sites of oriented basaltic lava flows from the West Maui Volcano series (island of Maui, Hawaii) were selected to improve the determination of the Brunhes and Matuyama time-averaged geomagnetic field between >0.7 and 1.8 and 2.6 Ma respectively. We sampled five flows from the Wailuku Volcanics (ca. 1.97+/-0.96-1.58+/-0.13 Ma), five flows from the Honolua Volcanics (ca.1.50+/-0.13 Ma) and five flows were drilled from the rejuvenated-stage Lahaina Volcanics (ca. <0.610+/-0.012 Ma). Identical Characteristic Remanent Magnetization (ChRM) directions with reverse polarity carried by magnetite were isolated by stepwise alternating-field and thermal demagnetization in 12-15 specimens from each site. The final mean direction points south while the inclination is ~7 degrees lower than the inclination of the geocentric axial dipole (GAD). This offset is reduced after correcting the site latitude for the Pacific plate motion, which has been neglected so far in most studies. The mean corrected direction is almost perfectly antipodal to the Brunhes mean direction derived from the Lahaina Volcanics in the same island of Maui and for the Honolulu Volcanic series (HVS) which are part of the Koolau Volcano on the island of Oahu. After applying the tectonic correction, the inclination remains several degrees larger than the inclination of the axial dipole and cannot be accounted for by a small axial quadrupole which would reverse with the dipole. The mean inclinations of other Hawaiian records (mostly younger than 1 Ma) involving long sequences of lava flows exhibit similar deviations from the GAD which are too large to be accounted for by a small axial quadrupole. Tilting of all sections is difficult to defend for so many localities and persistent secondary components have not been detected. Thus these inclination anomalies would reflect the presence of a long-term standing component under Hawaii but crustal magnetization linked to the volcanic edifice cannot be completely ruled out.

Keywords: Paleosecular variation, West Maui Volcano, Brunhes, Matuyama

©2020. Japan Geoscience Union. All Right Reserved.

Centennial-resolution terrestrial climatostratigraphy and Matuyama-Brunhes transition from a loess sequence in China

*Masayuki Hyodo[1], Kenta Banjo[2], Tianshui Yang[3], Shigehiro Katoh[6], Shi Meinan[3], Yuki Yasuda[4], Jun-ichi Fukuda[1], Masako Miki[2], Balázs Bradák[5]

1. Research Center for Inland Seas, Kobe University, 2. Department of Planetology, Kobe University, 3. China University of Geosciences, 4. Institute of Seismology and Volcanology, Hokkaido University, 5. Department of Physics, EPS, University of Burgos, 6. Museum of Nature and Human Activities, Hyogo

Terrestrial records of the last geomagnetic reversal often have few age constraints. Chronostratigraphy using suborbital-scale paleoceanic events during marine isotope stage 19 may contribute to solving this problem. We applied the method to an 8-m-long, high-resolution paleomagnetic record from a loess sequence in China, and revealed millennial-to-sub-centennial scale features of the Matuyama-Brunhes (MB) transition. All samples were subjected to progressive thermal demagnetization with 14-15 steps up to 650-680˚C. As a result, 96 % of the samples yielded a high-quality remanent magnetization. The MB transition terminated with a 75-cm-thick zone with nine polarity flips. The polarity flip zone, dated at about 779-777 ka, began between the warm events “I” and “J” and terminated at the end of the cooling event coincident with the lowest axial-dipole strength interval. Most polarity flips occurred within 70 years. The virtual geomagnetic poles (VGPs) in the upper polarity flip zone clustered in the SW Pacific region, where the MB transitional VGPs from lavas of the Hawaiian and Canary Islands and lacustrine deposits of Java also clustered. These sites were probably dominated by dipolar fields. The absence of transitional fields across polarity flips implies a short time span for averaging fields due to a thin loess-magnetization lock-in zone. The reverse-to-normal polarity reversal dated at about 778 ka in Lingtai occurred at the end of the SW Pacific VGP zone, an important key bed for MB transition stratigraphy. The reversal is a good candidate for the main MB boundary. We found an excursion at about 766 ka spanning about 1 ka.

Keywords: geomagnetic reversal, Calabrian-Chibanian boundary, East Asian monsoon, loess magnetism

©2020. Japan Geoscience Union. All Right Reserved.

Paleomagnetism of sediment cores taken from the Ontong-Java plateau: for better understanding of the role of biogenic magnetite in geomagnetic paleointensity recording

*Jiaxi Li [1]

1. Atmosphere and Ocean Research Institute, The University of Tokyo

We studied sediment cores taken from the Ontong-Java plateau and managed to extract the geomagnetic paleointensity signal from them. Relative paleointensity (RPI) variations are widely used to understand geomagnetic field behavior and to develop age models for sedimentary sequences. Biogenic and detrital magnetic components are considered as the two major components, but for RPI estimations it is conventionally assumed that these two contribute to the remanent magnetization acquisition in an identical manner. However our RPI estimation shows some intriguing results. Normalizations of NRM with different artificial remanent magnetizations yielded inconsistent results; NRM-ARM demagnetization slope plots show curvature whereas NRM-IRM slope plots show a linear relation. It can be interpreted as the coercivity distributions of NRM and ARM are different. Moreover, relative paleointensity normalized by ARM shows artificial downcore decreases, and this may correlate with the variations of the ARM/SIRM ratio, which suggests the increasing proportion of biogenic to detrital magnetite. Then considering that biogenic magnetites have SD particle sizes with higher coercivity, the way biogenic magnetic components contribute to the remanent magnetization acquisition may be different from the way detrital components do. So the varying proportion of biogenic components may have considerable influence on the RPI signal recording in the sediments. The purpose of our research is trying to figure out the mechanism how magnetic minerals derived from different sources contribute to the remanent magnetizations of sediments. Then, it is expected that influences on the relative paleointensity records brought by different proportions between biogenic and detrital components in the sediments are able to be known.

Keywords: Geomagnetic paleointensity, Biogenic magnetite, Ontong-Java plateau

©2020. Japan Geoscience Union. All Right Reserved.

New paleomagnetic data from of Late Cretaceous volcanics of the northern part of the Okhotsk-Chukotka volcanic belt

*Aleksandr Pasenko[1], Ivan Lebedev[1], Florian Lhuillier[2], Baha Eid[2], Vladimir Pavlov[1]

1. The Schmidt Institute of Physics of the Earth of the Russian Academy of Sciences, Moscow, Russia, 2. Department of Earth and Environmental Sciences, Ludwig Maximilians University, Munich, Germany

At the moment, there is an increasing interest in the evolution of the Arctic Ocean and the tectonic history of North-Eastern Asia. The paleomagnetic method can be applied to solve the range of corresponding problems, in particular, to test the hypotheses of the formation and evolution of the eastern part of the Arctic

In the summer of 2019, we sampled an extensive collection of paleomagnetic samples (~ 2000 samples) from 9 remote Late Cretaceous volcanic sections of the central and eastern parts of the Okhotsk-Chukotka volcanic belt (OCVB). At each point, from 7 to 21 volcanic flows were sampled.

The majority of studied rocks contain clear paleomagnetic record, with characteristic remanent magnetization which can be isolated by both AF and thermal demagnetization. The preliminary results which we have obtained when laboratory paleomagnetic treatment of this collection allow to calculate the paleomagnetic pole which is in very good agreement with Late Cretaceous paleomagnetic poles obtained earlier by Stone et al., 2009 for near-located Elgygytgyn region (Chukotka) and by Otofuji et al., 2015 for Magadan region.

In our report we discuss the significance of obtained data for deciphering the history of the Amerasia basin and Arctic Alaska-Chukotka microcontinent.

This work is supported by the Russian Science Foundation under grant №19-47-04110.

Keywords: Paleomagnetism, OCVB, Chukotka, Late Cretaceous volcanism

©2020. Japan Geoscience Union. All Right Reserved.

[E] Poster | S (Solid Earth Sciences)：S-EM Earth's Electromagnetism

[S-EM19] Earth and planetary magnetism: Observations, modeling, and implications on dynamics and evolution

convener:Hirokuni Oda(Institute of Geology and Geoinformation, Geological Survey of Japan, AIST), Futoshi Takahashi(Faculty of Sciences, Kyushu University), Courtney Jean Sprain(University of Florida), Yoichi Usui(Japan Agency for Marine-Earth Science and Technology)

Paleomagnetism and paleointensity are essential tools that are useful in investigating the history of Earth's lithosphere, deep interior, and environment. Likewise, geomagnetic observations, modeling, and dynamo simulations are also important tools that help elucidate the dynamics of the Earth's magnetic field and the core. Beyond Earth, studies on extracting ancient magnetic fields recorded by extraterrestrial materials are increasing, which are improving our understanding of the evolution of other planetary bodies in addition to the solar system. Here, we invite contributions in the broad spectrum of paleomagnetic research with special emphasis on the "Study of the Earth's Deep Interior" (SEDI) that illustrate modern advances and highlight further work to better understand the dynamics and evolution of Earth and other planetary bodies. Topics of interest include (but are not limited to): geomagnetic jerks, secular variation, excursions and reversals, magnetic field modeling and dynamo simulations, geometry of the geomagnetic field, paleointensity and evolution of the core and core-mantle boundary, polarity reversal frequency through time, magnetic shielding and solar radiation effects, evolution of magnetotactic bacteria and magnetic field, in addition to planetary magnetic fields and evolution of solar system.

[SEM19-P01] Magnetic survey for buried old kilns with paleomagnetic and rock magnetic interpretation

*Tadahiro Hatakeyama[1,2], Yu Kitahara[3], Nobutatsu Mochizuki[4], Yorinao Shitaoka[5], Kenji Kanegae[6], Hirotsugu Matsusaki[7], Naoko Nakamura[8] (1.Information Processing Center, Okayama University of Science, 2.Graduate School of Biosphere-Geosphere Science, Okayama University of Science, 3.Graduate School of Social and Cultural Studies, Kyushu University, 4.Faculty of Advanced Science and Technology, Kumamoto University, 5.Faculty of Geo-Environmental Science, Rissho University, 6.Archaeological Museum, The International University of Kagoshima, 7.Education Board, Ibusuki City, 8.Research Center for Archaeology, Kagoshima University)

[SEM19-P02] Paleomagnetic study on the transitionally magnetized volcanic rocks from the Tahaa Island, French Polynesia

*Yuhji Yamamoto[1], Kenneth A Hoffman[2], Myriam Annie Claire Kars[1] (1.Center for Advanced Marine Core Research, Kochi University, 2.California Polytechnic State University)

[SEM19-P03] High resolution paleomagnetic secular variation records from Lake Biwa and its implications on core dynamics

*Hirokuni Oda[1], Yuhji Yamamoto[2], Yoshio Inouchi[3] (1.Institute of Geology and Geoinformation, Geological Survey of Japan, AIST, 2.Kochi University, 3.Waseda University)

[SEM19-P04] Paleomagnetism around the Cretaceous-Paleogene boundary in the Pacific red clay

*Yoichi Usui[1], Toshitsugu Yamazaki[2], Junichiro Ohta[3,4,1], Honami Sato[4], Akira Ishikawa[5] (1.Japan Agency for Marine-Earth Science and Technology, 2.Atmosphere and Ocean Research Institute, The University of Tokyo, 3.FRCER, The University of Tokyo, 4.ORCeNG, Chiba Institute of Technology, 5.Department of Earth and Planetary Sciences, Tokyo Institute of Technology)

[SEM19-P05] Avalonia, get bent! Paleomagnetism from SW Iberia confirms the Greater Cantabrian Orocline

Bruno Daniel Leite Mendes[2], *Daniel Pastor-Galan[1], Mark J. Dekkers[2], Wout Krijgsman[2] (1.Center for North East Asian Studies, Tohoku University, 2.Paleomagnetic Laboratory 'Fort Hoofddijk', Utrecht University)

[SEM19-P06] The Magnetics Information Consortium (MagIC) Data Repository: Status and Future Evolution

*Catherine Constable[1], Nicholas Jarboe[1], Rupert Minnett[2], Anthony A.P. Koppers[3], Lisa Tauxe[1], Lori Jonestrask[1] (1.Scripps Institution of Ocenaography, University of California San Diego, 2.Cogense Inc., 3.Oregon State University)

[SEM19-P08] **Assessing the robustness of long-term field variations in the palaeomagnetic record**

*Courtney Jean Sprain[1,2], Andrew J. Biggin[2], Richard K. Bono[2], Chris Davies[3], Greig Paterson[2], Louise Hawkins[2], Lauri J. Pesonen[4], Pavel Doubrovine[5], Toni Veikkolainen[6], Aleksey Smirnov[7], Elisa Piispa[8], Evgeniy Kulakov[5], Siim Ots[9], Luke Fairchild[10] (1.Department of Geological Sciences, University of Florida, Gainesville, FL, USA, 2.Department of Earth, Ocean and Ecological Sciences, University of Liverpool, UK, 3.School of Earth and Environment, University of Leeds, Leeds, UK, 4.Physics Department, University of Helsinki, Finland, FI-00014, Finland, 5.Centre for Earth Evolution and Dynamics, University of Oslo, Norway, 6.Department of Geosciences and Geography, University of Helsinki, Finland, 7.Department of Geological and Mining Engineering and Sciences and Department of Physics, Michigan Technological University, Houghton, MI, USA, 8.School of Earth Sciences, Energy and Environment, Yachay Tech, Ibarra, Ecuador, 9.Department of Geology, University of Tartu, Estonia, 10.Department of Earth and Planetary Sciences, University of California, Berkeley, CA, USA)

[SEM19-P09] Inferring geomagnetic secular variation using MHD/kinematic dynamo modeling with data assimilation

*Futoshi Takahashi[1], Shin ya Nakano[2], Takuto Minami[3], Hinami Taniguchi[4], Ryosuke Nakashima[4], Masaki Matsushima[5], Hisayoshi Shimizu[6], Hiroaki TOH[7] (1.Faculty of Sciences, Kyushu University, 2.The Institute of Statistical Mathematics, 3.Division of Frontier Planetology, Department of Planetology, Graduate School of Science, Kobe University, 4.Graduate School of Science, Kyushu University, 5.Department of Earth and Planetary Sciences, School of Science, Tokyo Institute of Technology, 6.Earthquake Research Institute, University of Tokyo, 7.Data Analysis Center for Geomagnetism and Space Magnetism, Graduate School of Science, Kyoto University)

[SEM19-P10] Influence of high electrical conductivity heterogeneity at the bottom of the mantle on generation of 2007 geomagnetic jerk

*Hisayoshi Shimizu[1] (1.Earthquake Research Institute, University of Tokyo)

[SEM19-P11] The Elsasser number dependence of core surface flow models and its implications for long-term changes in core dynamics

*Masaki Matsushima[1] (1.Department of Earth and Planetary Sciences, School of Science, Tokyo Institute of Technology)

[SEM19-P12] A modern interpretation of magnetic instability

*Ataru Sakuraba[1] (1.Department of Earth and Planetary Science, University of Tokyo)

Magnetic survey for buried old kilns with paleomagnetic and rock magnetic interpretation

*Tadahiro Hatakeyama[1,2], Yu Kitahara[3], Nobutatsu Mochizuki[4], Yorinao Shitaoka[5], Kenji Kanegae[6], Hirotsugu Matsusaki[7], Naoko Nakamura[8]

1. Information Processing Center, Okayama University of Science, 2. Graduate School of Biosphere-Geosphere Science, Okayama University of Science, 3. Graduate School of Social and Cultural Studies, Kyushu University, 4. Faculty of Advanced Science and Technology, Kumamoto University, 5. Faculty of Geo-Environmental Science, Rissho University, 6. Archaeological Museum, The International University of Kagoshima, 7. Education Board, Ibusuki City, 8. Research Center for Archaeology, Kagoshima University

Magnetic surveys at an old kiln site cluster in Kagoshima Pref., southwest Japan were conducted, and five magnetic anomalies were detected on the hill slopes, based on a Cretaceous sedimentary rocks. A magnetic anomaly map at one of the sites was drawn and an elongated magnetic anomaly zone, along to the upward direction of the slope with 6 to 8 m length, was found. On the other hand, we obtained the paleomagnetic and rock magnetic results for the samples from an excavated old kiln, located nearby the magnetic anomaly site. Assuming the buried source of magnetic anomaly in consideration of paleomagnetic data, the expected magnetic field on the ground surface is calculated and it is well consistent between the observation and the calculation. It can be concluded that the source of the magnetic anomaly is a floor of an old kiln buried 40cm below the surface, northwardly magnetized. This result can indicate that the paleomagnetic and rock magnetic results provide a validated information about the underground objects in the magnetic surveys.

Keywords: Magnetic survey, Paleomagnetism

©2020. Japan Geoscience Union. All Right Reserved.

Paleomagnetic study on the transitionally magnetized volcanic rocks from the Tahaa Island, French Polynesia

*Yuhji Yamamoto[1], Kenneth A Hoffman[2], Myriam Annie Claire Kars[1]

1. Center for Advanced Marine Core Research, Kochi University, 2. California Polytechnic State University

Volcanic rocks collected from the Society Islands, French Polynesia, were systematically investigated in terms of paleomagnetism and geochronology (Yamamoto et al., 2002; Yamamoto and Tsunakawa, 2005; Uto et al., 2007). Some sites were found to be transitionally magnetized, and the follow-up laser-heating $^{40}Ar/^{39}Ar$ dating and additional palaeomagnetic measurements were conducted on samples from these sites in Yamamoto et al. (2007): a lava sequence in the Tahaa Island consisting of the four consecutive lava flows (TA04, 05, 06 and 07) gave the average virtual dipole moments (VDMs) of ~ 5 ZAm2 and the Ar/Ar age of 3.20 +/- 0.03 Ma. This age is consistent with the upper boundary age of the Mammoth reversed subchron in GPTS2012 (3.207 Ma; Ogg et al., 2012).

To further characterize the paleomagnetic behavior recorded in the lava sequence, a follow-up sampling was done in 2014. We collected ~50 new mini-core samples from the sequence, and in addition, 10 new mini-core samples were drilled from a single lava flow of a vicinity lava sequence, which corresponds to the site TA01 in the previous study (K-Ar age of 3.14 +/- 0.06 Ma; Uto et al., 2007). These mini-core samples were cut into specimens and they were subjected to paleomagnetic measurements including the Tsunakawa-Shaw absolute paleointensity experiments. We will report these results together with the previous results which are reanalyzed by a latest scheme.

©2020. Japan Geoscience Union. All Right Reserved.

High resolution paleomagnetic secular variation records from Lake Biwa and its implications on core dynamics

*Hirokuni Oda[1], Yuhji Yamamoto[2], Yoshio Inouchi[3]

1. Institute of Geology and Geoinformation, Geological Survey of Japan, AIST, 2. Kochi University, 3. Waseda University

We have conducted measurements on one of the three piston cores taken from Lake Biwa off Takashima (BWK12-2; length 1633 cm). Sediment comprises of clay intercalated with at least 13 ash layers. Thirteen horizons were dated with 14C using plant pieces giving a maximum age estimate of more than 40 ka. Paleomagnetic cube specimens, u-channel samples and LLchannel samples were taken from the core. Paleomagnetic cube specimens were measured with a SQUID Rock Magnetometer at AF demagnetization steps of 0-80 mT. Results of inclination from the cube samples show an agreement with the paleosecular variation reported by Ali et al. (1999). For example, Inclination show a minimum of ~40 °at 2600 year BP and a maximum of ~58 °at 3400 year BP, both of which can be correlated with a minimum ’h’ at 2400 year BP and a maximum ’i’ at 2900 year BP presented by Ali et al. (1999), respectively. There are reports on "geomagnetic spikes" or "archeomagnetic jerk" from the Near East ca. 980 BC and 890 BC (Ben-Yosef et al., 2009; Shaar et al., 2011). Further, relative paleointensity is estimated from NRM and ARM measurements using discrete and u-channel measurements. Rapid change of paleomagnetic direction and intensity will be discussed in association with the global compilation of paleomagnetic records.

Keywords: archeomagnetic jerk, relative paleointensity, core dyanamics

©2020. Japan Geoscience Union. All Right Reserved.

Paleomagnetism around the Cretaceous-Paleogene boundary in the Pacific red clay

*Yoichi Usui[1], Toshitsugu Yamazaki[2], Junichiro Ohta[3,4,1], Honami Sato[4], Akira Ishikawa[5]

1. Japan Agency for Marine-Earth Science and Technology, 2. Atmosphere and Ocean Research Institute, The University of Tokyo, 3. FRCER, The University of Tokyo, 4. ORCeNG, Chiba Institute of Technology, 5. Department of Earth and Planetary Sciences, Tokyo Institute of Technology

Red clay covers a large portion of the Pacific seafloor. These sediments are expected to be good targets for paleomagnetic and environmental magnetic studies, because magnetic minerals in the oxic environment are not affected by reductive diagenesis. However, paleomagnetic data from red clay are often not straightforward, sometimes attributed to oxic diagenesis. More fundamentally, absolute dating of red clay is difficult, and correlation with polarity timescale remains a challenge. In this presentation, we use newly discovered the Cretaceous-Paleogene (K-Pg) boundary in the red clay around the Minamitorishima Island as a tie-point, and discuss the paleomagnetic data from the sediment. This area has been studied intensively, and we have recovered 71 piston cores (~15 m each). The K-Pg boundary was identified in multiple cores by the age constraints from deep sea agglutinated foraminifera, detailed Iridium measurements, and correlation using magnetic susceptibility. We conducted alternating field and thermal demagnetization on two cores. Both methods yielded characteristic remanence, and polarity patterns consistent between the cores were obtained. Lithological observation and chemical mapping revealed sub-horizontal layering, suggesting minor perturbation due to bioturbation or hiatus. The bottom of the core was estimated to be Late Campanian, while the sedimentation rate in the Cretaceous was estimated to be ~1.5 mm/kyr. The successful magnetostratigraphy in the Mesozoic red clay suggests that oxic diagenesis is not the major factor preventing paleomagnetism. Further studies may constrain the paleogeography of the Pacific plate at around the K-Pg boundary. Besides, the Campanian age at ~15 m depth suggests major hiatus somewhere in the Cenozoic. Indeed, acoustic survey showed that the sediment thickness around the Minamitorishima Island varies significantly. These observations imply that Mesozoic red clay can be recovered from wide area by piston coring or multiple short drillings rather than expensive deep drilling, if one carefully conduct geophysical surveys.

©2020. Japan Geoscience Union. All Right Reserved.

Avalonia, get bent! Paleomagnetism from SW Iberia confirms the Greater Cantabrian Orocline

Bruno Daniel Leite Mendes[2], *Daniel Pastor-Galan[1], Mark J. Dekkers[2], Wout Krijgsman[2]

1. Center for North East Asian Studies, Tohoku University, 2. Paleomagnetic Laboratory 'Fort Hoofddijk', Utrecht University

The amalgamation of Pangea formed the contorted Variscan-Alleghanian orogen suturing Gondwana and Laurussia during Carboniferous. From all swirls of this orogen, a double curve stands out in Iberia, the coupled Cantabrian Orocline and Central Iberian Curve. The Cantabrian Orocline formed subsequent to Variscan orogeny (ca. 315-295 Ma). The mechanisms of formation for this orocline are disputed being the most prominent: 1) An Avalonian (Laurussia) indenter at SW Iberia, that would form the Cantabrian Orocline in a sinistral transpressive orogenic phase. 2) A change in the stress field that buckled the orogen. This change in stress would be potentially far-field and linked to subduction of the Paleo-tethys and/or diachronous collision in the Variscan belt.
In contrast, the geometry and kinematics of the Central Iberian curve are largely unknown. Whereas some authors defend both curvatures are genetically linked, others support they are distinct and formed at different times. Such uncertainty adds an extra layer of complexity into our understanding of the final stages of Pangea amalgamation. We have performed a paleomagnetic analysis of several tectonostratigraphic units in SW Iberiat to solve the late Carboniferous Variscan kinematics. Our results show differential counterclockwise rotations, ranging from 20 degrees and up to 70 degrees at late Carboniferous. These results are coincident with the kinematics expected in the southern limb of the Cantabrian Orocline and discard a concomitant formation of both Cantabrian and Central Iberian curvature. The Avalonian portion of Laurussia rotated with the Cantabrian Orocline at both limbs: the northern one (Ireland, Pastor-Galán et al., 2015) and the southern one (South Portugese Zone, this study). The coherent rotation of Avalonia confirms the Greater Cantabrian Orocline hypothesis and discards the Avalonian indenter as a mechanism of formation for the Cantabrian Orocline. The Greater Cantabrian Orocline extended beyond the Rheic Ocean suture affecting both Laurussia and Gondwana margins and probably formed by a late Carboniferous change in the stress field, due to a still unidentified cause.

Keywords: Orocline, Paleomagnetism, Rock magnetism, Pangea

©2020. Japan Geoscience Union. All Right Reserved.

The Magnetics Information Consortium (MagIC) Data Repository: Status and Future Evolution

*Catherine Constable[1], Nicholas Jarboe[1], Rupert Minnett[2], Anthony A.P. Koppers[3], Lisa Tauxe[1], Lori Jonestrask[1]

1. Scripps Institution of Ocenaography, University of California San Diego, 2. Cogense Inc., 3. Oregon State University

MagIC (earthref.org/MagIC) is dedicated to improving research capacity in the Earth and Ocean sciences by maintaining an open community digital data archive for rock and paleomagnetic data with portals that allow users access to archive, search, visualize, download, and combine versioned datasets. We are a signatory of the Coalition for Publishing Data in the Earth and Space Sciences (COPDESS)'s Enabling FAIR (Findable, Accessible, Interoperable, and Reproducible) Data Commitment Statement and an approved repository for the Nature set of journals. In collaboration with EarthCube's GeoCODES data search portal, we have been adding schema.org JSON-LD headers to our data set landing pages and suggesting extensions to schema.org when needed. Collaboration with the European Plate Observing System (EPOS)'s Thematic Core Service Multi-scale laboratories (TCS MSL) is ongoing with MagIC sending its contributions' metadata to TCS MSL via DataCite records.

Improving and updating our data repository to meet the demands of the quickly changing landscape of data archival, retrieval, and interoperability is a challenging proposition. Most journals now require data to be archived in a "FAIR" repository, but exact specifications for FAIR are still solidifying. Some journals vet and have their own list of accepted repositories while others rely on other organizations to investigate and certify repositories. As part of the COPDESS group at Earth Science Information Partners (ESIP), we have been and will continue to be part of the discussion on the needed and desired features for acceptable data repositories.

We have made continued improvements to MagIC's data validation system and the PmagPy paleomagnetic analysis software suite. Datasets created with PmagPy (earthref.org/PmagPy/cookbook/) or other uploads with the correct method code descriptions can be downloaded from MagIC and viewed using PmagPy. We are actively developing our software and systems to meet the needs of our scientific community. Some current issues are: ensuring coordinated workflows with journals to simultaneously publish the journal article and data in MagIC, sustainability of data repository funding especially in light of the greater demands on repositories due to data policy changes at journals, and how to best share and expose metadata about our data holdings to organizations such as EPOS, EarthCube, and Google.

Keywords: paleomagnetism, rock magnetism, FAIR data, database

©2020. Japan Geoscience Union. All Right Reserved.

Assessing the robustness of long-term field variations in the palaeomagnetic record

*Courtney Jean Sprain[1,2], Andrew J. Biggin[2], Richard K. Bono[2], Chris Davies[3], Greig Paterson[2], Louise Hawkins[2], Lauri J. Pesonen[4], Pavel Doubrovine[5], Toni Veikkolainen[6], Aleksey Smirnov[7], Elisa Piispa[8], Evgeniy Kulakov[5], Siim Ots[9], Luke Fairchild[10]

1. Department of Geological Sciences, University of Florida, Gainesville, FL, USA, 2. Department of Earth, Ocean and Ecological Sciences, University of Liverpool, UK, 3. School of Earth and Environment, University of Leeds, Leeds, UK, 4. Physics Department, University of Helsinki, Finland, FI-00014, Finland, 5. Centre for Earth Evolution and Dynamics, University of Oslo, Norway, 6. Department of Geosciences and Geography, University of Helsinki, Finland, 7. Department of Geological and Mining Engineering and Sciences and Department of Physics, Michigan Technological University, Houghton, MI, USA, 8. School of Earth Sciences, Energy and Environment, Yachay Tech, Ibarra, Ecuador, 9. Department of Geology, University of Tartu, Estonia, 10. Department of Earth and Planetary Sciences, University of California, Berkeley, CA, USA

Deciphering long-term variations in the magnetic field has important implications for elucidating the connection between the magnetic field and deep interior processes. However, long-term field variations are difficult to discern because they require large amounts of data globally distributed in both space and time. Despite these challenges, datasets such as these have been accumulated for periods of time throughout Earth history that are thought to represent distinctive geodynamo regimes including superchrons, and periods of hyper-reversal activity. Potential biasing of palaeosecular variation (PSV) due to imperfect spatial and temporal sampling is challenging to determine robustly. Here, we synthesise the results of a major collaboration in palaeomagnetic field behaviour taking place before, during and after the 2017 Nordic Palaeomagnetic Workshop in Leirubakki, Iceland. Specifically, we employ numerical geodynamo models to ascertain whether our previously claimed long-term variations in Mesozoic palaeomagnetic behaviour are robust. We assess the effects of spatial and temporal data distributions on calculated palaeosecular variation behaviour (specifically, the Model G description of McFadden et al., 1988) by downsampling 42 geodynamo simulations, mimicking the spatial sampling for the Cretaceous Normal Superchron, the Middle Jurassic (both from Doubrovine et al., 2019), and the last 10 Ma (Cromwell et al., 2019), and comparing these results to those from a uniform “yin-yang” grid (Kageyama and Sato, 2004). We find that between different spatial sampling, similar distributions of the Model G *a* (characterising dispersion at the equator, similar to equation used in Doubrovine et al., 2019) and field strength (virtual dipole moment, VDM) can be reproduced, but Model G *b* (latitude-dependent dispersion, similar to equation used in Doubrovine et al., 2019) is less well-determined, especially when mid and high-latitude sites are sparse. For all three spatial grids, calculated Model G *b* values were underestimated compared to the uniform grid. These findings add support to the inverse relationship between field strength and reversal rate, recently reassessed in Kulakov et al. (2019), and additionally suggest that the minimal variation observed between Model G *a* between the CNS, Mid-Jurassic, and past 10 Myr is robust (Doubrovine et al., 2019). Although we can say that Model G *b* is likely underestimated in datasets where mid and high-latitude sites are sparse, it is difficult to know the amount by which it is underestimated. Overall, we find that the most robust parameters for determining changes in field behaviour where data are limited are VDM and Model G *a*. It is important to note that for the three time periods assessed here, we cannot presently distinguish between PSV regimes, unlike for median VDM. This suggests that VDM may be a more powerful proxy for reversal frequency than PSV, with implications for studies of Precambrian field behaviour where precise estimates of reversal frequency may be extremely difficult to obtain.

©2020. Japan Geoscience Union. All Right Reserved.

Keywords: Paleomagnetism, Long-term magnetic field behavior, Geodynamo simulations, Paleosecular variation

©2020. Japan Geoscience Union. All Right Reserved.

Inferring geomagnetic secular variation using MHD/kinematic dynamo modeling with data assimilation

*Futoshi Takahashi[1], Shin ya Nakano[2], Takuto Minami[3], Hinami Taniguchi[4], Ryosuke Nakashima[4], Masaki Matsushima[5], Hisayoshi Shimizu[6], Hiroaki TOH[7]

1. Faculty of Sciences, Kyushu University, 2. The Institute of Statistical Mathematics, 3. Division of Frontier Planetology, Department of Planetology, Graduate School of Science, Kobe University, 4. Graduate School of Science, Kyushu University, 5. Department of Earth and Planetary Sciences, School of Science, Tokyo Institute of Technology, 6. Earthquake Research Institute, University of Tokyo, 7. Data Analysis Center for Geomagnetism and Space Magnetism, Graduate School of Science, Kyoto University

Secular variation (SV) of the Earth's magnetic field is governed by the advection and diffusion processes of the magnetic field within the fluid outer core. The IGRF (International Geomagnetic Reference Field) offers the average SV for the next five years to come, which has been estimated in various methods. In general, forecasting the evolution of a non-linear system like the geodynamo in the Earth's core is an extremely difficult task, because the magnetic field generation processes are controlled by the complex interaction of the core flows and the generated magnetic field. Data assimilation has been a promising scheme forecasting the geomagnetic SV as demonstrated in literatures (Kuang 2010, Fournier et al. 2015), where time dependency is controlled by a numerical dynamo model. While Ensemble Kalman Filter (EnKF) has been a popular method for data assimilation in geomagnetism, we apply a different data assimilation procedure, that is, four-dimensional, ensemble-based variational scheme, 4DEnVar. Applying the 4DEnVar scheme iteratively, we have derived a candidate SV model for the latest version of the IGRF. In evaluating SV, two forecasting strategies are tested, in which core flows are assumed to be steady or time-dependent. The former approach is favored in Fournier et al. (2015), where the magnetic field evolves kinematically by the flows prescribed to be time-independent in the initialization step. On the other hand, we have adopted linear combination of magnetohydrodynamic (MHD) models to construct a candidate as the best forecast (Minami et al. 2020). It is likely that which strategy is more suitable to forecasting SV depends on assimilation scheme and/or numerical dynamo model. However, we have little knowledge on the issue at present. In this study, we investigate results of MHD and kinematic dynamo runs with a 4DEnVar scheme in order to have a grasp of the properties of the scheme in the 5-year forecast process. Also, MHD and kinematic runs are compared to infer internal dynamics responsible for SV in the geomagnetic field.

Keywords: Secular variation, MHD dynamo, Kinematic dynamo, Data assimilation, IGRF

©2020. Japan Geoscience Union. All Right Reserved.

Influence of high electrical conductivity heterogeneity at the bottom of the mantle on generation of 2007 geomagnetic jerk

*Hisayoshi Shimizu[1]

1. Earthquake Research Institute, University of Tokyo

Wavelet transform has been used to analyze geomagnetic jerks, sudden change of second time-derivatives of the geomagnetic field components (e.g., [1]). A ridge in wavelet transform allows us to identify a possible geomagnetic jerk and its occurrence time. Character of a geomagnetic jerk is quantified by regularity, which is the gradient of the ridge with respect to dilation. Regularity of geomagnetic jerk depends on the geomagnetic field variation at the surface of the Earth's core and the electrical conductivity of the mantle. Regularity distribution obtained for 1969 geomagnetic jerk implies that its regularity at the CMB is 1.55 and electrical conductivity of the bottom 2000 km of the mantle is about 8 S/m [2].
Geomagnetic jerks somewhat localized in the south Atlantic region were observed around 2003 and 2007 (e.g. [3]). Superposition of fast equatorial Rossby waves at the top of the core [4] and Alfvén wave excited by buoyancy heterogeneity at some depth in the core [5] are proposed as possible cause of the localized geomagnetic jerks. An alternative of the cause is outcome of interaction between sudden variation of the toroidal magnetic field at the CMB and electrical conductivity heterogeneity in the D" region [6].
Regularity of 2007 geomagnetic jerk is expected to provide a clue for discussing the involvement of high electrical conductivity heterogeneity since it would results in higher regularity than the other geomagnetic jerks but different from that due to magnetohydrodynamic waves.
Estimated regularities of magnetic field eastward component at M'Bour (MBO, Senegal) and Chambon la Forêt (CLF, France) around 2007 geomagnetic jerks are larger than that for 1969 geomagnetic jerk at both stations. This is compatible with the scenario of the generation of 2007 geomagnetic jerk by interaction between toroidal field variation and high electrical conductivity heterogeneity while 1969 geomagnetic jerk is purely due to the poloidal field from the core. It seems that the variations are not from simple sinusoidal wave which should result in higher regularity.

Reference:
1. M.M. Alexsandrescu et al., J. Geophys. R., 100, 12,557-12,572 (1995)
2. M.M. Alexsandrescu et al., J. Geophys. R., 104, 17,735-17,745 (1999)
3. A. Chulliat et al., Geophys. Research Lett., 37, L0730 (2010)
4. A. Chulliat et al., Geophys. Research Lett., 42, 3321-3329 (2015)
5. J. Aubert and C. Finlay, Nature Geoscience, 12, 393-398 (2019)
6. T. Koyama et al., Phys. Earth Planet, Int., 129, 99-116 (2002)

Keywords: geomagnetic jerk, D" region, electrical conductivity heterogeneity

©2020. Japan Geoscience Union. All Right Reserved.

The Elsasser number dependence of core surface flow models and its implications for long-term changes in core dynamics

*Masaki Matsushima[1]

1. Department of Earth and Planetary Sciences, School of Science, Tokyo Institute of Technology

Fluid flow in the Earth's metallic liquid core drives dynamo action that generates the Earth's intrinsic magnetic field. The pattern of core flow is likely to influence generation process of the geomagnetic field as well as its spatial and temporal variation. Inversely, information on core flow can be provided by geomagnetic field data. Hence, core flow near the core-mantle boundary (CMB) can be derived from geomagnetic field models. Geomagnetic secular variations at the CMB are assumed to be caused by magnetic diffusion only due to the no-slip boundary condition imposed for the flow there. Inside the viscous boundary layer at the CMB, it is assumed that motional induction, advection and magnetic diffusion contribute to temporal variations of geomagnetic field, and that the viscous force plays an important role in force balance. Below the viscous boundary layer, it is assumed that magnetic diffusion can be neglected as in the frozen-flux approximation, and that core flow is in a tangentially magnetostrophic state.

The effect of core electrical conductivity on core flow modeling has been investigated. It turns out that the ratio of mean toroidal flow to mean poloidal flow decreases with increase of core electrical conductivity. This results from the Lorentz force proportional to core electrical conductivity. This can be extended to investigating the effect of the Elsasser number, which is a non-dimensional measure of relative importance between the Lorentz force and the Coriolis force in the Navier-Stokes equation, on core flow models. The Elsaser number is proportional to core electrical conductivity and inversely proportional to the rotation rate of the Earth and core density. It is conceivable that the rotation rate of the Earth has been decreasing due to tidal friction with the Moon, whereas the core electrical conductivity has been increasing with decrease of core temperature after the core formation. This suggests that the Elsasser number in the past was smaller than the present value; that is, core flow could be more tangentially geostrophic than the present state.

Keywords: core flow, geomagnetic field, Elsasser number

©2020. Japan Geoscience Union. All Right Reserved.

A modern interpretation of magnetic instability

*Ataru Sakuraba[1]

1. Department of Earth and Planetary Science, University of Tokyo

Linear analysis was a basic and tractable methodology in the early stage of planetary dynamo researches. One of such linear problems was a kinematic dynamo in which time development of a small-amplitude magnetic field perturbation was analyzed in the presence of an arbitrary steady fluid motion. This helped us to understand what type of flow structure was effective in magnetic field amplification, what type of magnetic field structure naturally grew, and of course to confirm an MHD dynamo was possible. Another linear study was magnetic instability in which time development of small-amplitude magnetic and velocity perturbations were analyzed in the presence of an arbitrary static toroidal magnetic field. In general, a toroidal field confined in a rotating fluid sphere becomes unstable if the field intensity is strong enough. Early theoretical studies revealed the conditions for ideal instability without electric resistance (e.g. Acheson 1972). However, it is found that addition of a finite but not high resistivity enhances instability (e.g. Fearn 1984). The controlling parameter of the resistive instability is the Elsasser number. The critical Elsasser number is generally about O(10), implying that this gives an upper bound for planetary magnetic field intensity because a higher magnetic field intensity rather destroys the dynamo due to magnetic instability (Zhang and Jones 1994).

These linear studies seem to be inactive in the recent 25 years during which nonlinear self-consistent dynamo simulations become easy. However, we cannot neglect those classical studies because they elucidate fundamental physical processes underlying a complex planetary dynamo. Here I present an idea that magnetic instability plays an important, positive role in the dynamo process. First, the number of convective rolls (the azimuthal wavenumber) in the core is determined by the critical wavenumber of magnetic instability, which is the optimal wavenumber at which the magnetic field and velocity perturbations grow fastest and effectively transport internal heat to the mantle. Second, the growth rate of magnetic instability controls the magnetic field saturation in the core. Magnetic instability is, in some sense, an energy transport process from the axisymmetric to non-axisymmetric parts. Therefore, the energy flow to smaller scales is balanced by the opposite energy flow creating the axisymmetric magnetic field due to dynamo action. There is a possibility that equating two linear growth rates of magnetic instability and a kinematic dynamo gives a relation between the Elsasser number and the magnetic Reynolds number that is the control parameter of a kinematic dynamo problem. I will give a detailed explanation based on my recent numerical results of magnetic instability of axisymmetric toroidal field confined in a rotating inviscid fluid sphere.

©2020. Japan Geoscience Union. All Right Reserved.

[E] Poster | S (Solid Earth Sciences)：S-EM Earth's Electromagnetism

[S-EM20] Electric and Electromagnetic survey technologies and the scientific achievements: Recent advances

convener:Kiyoshi Baba(Earthquake Research Institute, The University of Tokyo), Tada-nori Goto(Graduate School of Life Science, University of Hyogo), Toshihiro Uchida(National Institute of Advanced Industrial Science and Technology), Toru Mogi(Faculty of Science, Tokyo Institute of Technology)

Detailed subsurface images by electric and electromagnetic (EM) surveys are indispensable to investigate the electrical features of the interior of the Earth both for academic and commercial purposes. The technologies, techniques, and methods for surveys, data analysis, and interpretation involve many common aspects that should be solved by scientists and engineers in cooperation since the studies cover a broad range of targets in various spatial-time scales and places on land and seafloor, e.g., natural resource explorations, environment and hazard evaluations, and the crustal and mantle tectonics and dynamics. And the knowledge should be shared in the international community for further development of this field. The session invites papers on recent advances in the electric and EM survey technologies and techniques including instrumentations, the data analysis methods including modeling, inversion, and imaging techniques, and the scientific achievements including novel way of interpretations, from the world.

[SEM20-P01] A tensor measurement with simultaneously transmitted Electromagnetic Accurately Controlled, Routinely Operated Signal System: utilization of distortionless response tensor

*Kuo Hsuan Tseng[1], Yasuo Ogawa[2] (1.Tokyo Institute of Technology, 2.Volcanic Fluid Research Center, Tokyo Institute of Technology)

[SEM20-P02] Pseudo 3-D resistivity model for Geomagnetic Induced Current (GIC) based on 3-D seismic velocity structure

*Tada-nori Goto[1], Kota Hori[1] (1.Graduate School of Life Science, University of Hyogo)

[SEM20-P03] Sensitivity of local electromagnetic response functions from Sq field to the electrical conductivity in the upper mantle

*Xiaoli WAN[1,2], Hisayoshi Shimizu[2], Hisashi Utada[2] (1.Tongji Univ., 2.Earthquake Research Institute, the Univ. of Tokyo)

[SEM20-P04] The sparse inversion of the magnetic data to recover subsurface blocky structures.

*Mitsuru Utsugi[1] (1.Aso Volcanological Laboratory, Institute for Geothermal Sciences, Graduate School of Science, Kyoto University)

[SEM20-P05] Understanding Unzen volcano magmatic system by broadband Magnetotelluric observation

*Agnis Triahadini[1], Koki Aizawa[2], Keita Chiba[2], Kanta Miyano[1], Yuto Yamamoto[1], Kazunari Uchida[2], Tasuku Hashimoto[1] (1.Department of Earth and Planetary Sciences Graduate School of Science Kyushu University, 2.Institute of Seismology and Volcanology Faculty of Science Kyushu University)

A tensor measurement with simultaneously transmitted Electromagnetic Accurately Controlled, Routinely Operated Signal System: utilization of distortionless response tensor

*Kuo Hsuan Tseng[1], Yasuo Ogawa[2]

1. Tokyo Institute of Technology, 2. Volcanic Fluid Research Center, Tokyo Institute of Technology

The Electromagnetic Accurately Controlled, Routinely Operated Signal System (EM-ACROSS) is a specially designed system for controlled source electromagnetic investigation. The EM-ACROSS combines with a stable transmitter system and at least one receiver for obtaining the electric and magnetic field at the observation site. The core purpose of this system is a specifically designed signal which is repeatedly transmitted with high accuracy and precision to against the noise.

For obtaining a tensor measurement to solve the galvanic distortion issue, two independent signals were transmitted respectively by the different grounded sources for tensor electromagnetic fields. Two signals were specially designed for different antennas with specifically chosen frequency sets. Which were detectable in the data processing due to its accurately controlled properties. This system provided vector source current at the transmitter and the vector electric field measurements at an observation site without interference, leading to the observation of a “source-current” to “electric-field” tensor response. As the source was precisely controlled, the receiver could get a high signal-to-noise ratio data from the data stacking process.

A forward modeling code was developed for this system by utilizing the finite element method with tetrahedral unstructured meshes. For comparing the calculated electric fields from the forward modeling with those observed, the local distortion effect due to the near surface inhomogeneities was addressed by a new tensor function, which dived out the distortion effect.

This distortionless tensor function was utilized to verify the temporal change in the inversed resistivity models with magnetotelluric (MT) data at Kusatsu-Shirane volcano, Japan. To evaluate the detectability by this tensor system, two 3D resistivity models were prepared. One is the 3D inverted model which inverted from a 2001-2005 MT dataset, and the other is the 3D inverted model from a 2017-2018 MT dataset. For the respective two inverted resistivity models the numerical responses from forward modeling and the observed EM-ACROSS responses (in 2017-2018) were compared by utilizing the distortion-removed electric field tensors. The EM-ACROSS data (2018-2018) fit better with the 3D modeling response using the 2017-2018 MT data than to that using 2001-2015 MT data.

This study provided an alternative method to verify the temporal changes in a volcanic hydrothermal

©2020. Japan Geoscience Union. All Right Reserved.

system with joint time-lapse MT monitoring and controlled source electromagnetic observation. The developed system provides a solution for the environmental noise issue and distortion effect. The final product could be the new conception in future exploration and monitoring in the volcanos.

Keywords: magnetotelluric, geophysical prospecting, geophysical techniques, controlled-source electromagnetics

©2020. Japan Geoscience Union. All Right Reserved.

Pseudo 3-D resistivity model for Geomagnetic Induced Current (GIC) based on 3-D seismic velocity structure

*Tada-nori Goto[1], Kota Hori[1]

1. Graduate School of Life Science, University of Hyogo

Geomagnetic Induced Current (GIC) is a natural hazard due to a huge geomagnetic storm, whose large current amplitude makes severe troubles on the electric power grid, pipe lines and other metallic elongated infrastructure. For prevention of this new-typed disaster, three-dimensional (3-D) resistivity structure of the crust and mantle is necessary for evaluation of degree of GIC. Magnetotelluric (MT) survey is effective for obtaining such deep resistivity structures. However, artificial noise around highly populated areas restrict the MT survey and no resistivity structures are obtained. Other geophysical information such as 3-D seismic velocity structures has been obtained in such populated areas. If the relationship between the crustal/mantle seismic velocity and resistivity can be found, the subsurface resistivity structure can be inferred from the 3-D velocity structure.

In this study, an integrated analysis of the subsurface resistivity structure and seismic velocity structure is attempted to find the correlation between these two physical properties and to promote quantitative understanding of the deep crust and the uppermost mantle. The target region is the east Hokkaido, where the GIC was observed together with the geomagnetic storm. The two-dimensional (2-D) resistivity structure by MT survey (Sato et al., 2001) and the 3-D seismic velocity structure deduced by seismic tomography (Matsubara et al., 2019) are used in this study. We first focus on the correlation between two different physical property with cross-plots, and approximately express the correlation at each geological area. We found a positive correlation of resistivity and P-wave velocity at the mantle depths. Based on a rock physics model, the feature can be interpreted with porosity distribution with fluid (magmatic material). On the other hand, negative correlations are often found at the crustal depths. It cannot be well fitted by the simple-pore model, but could be explained by the presence of conductive minerals such as graphite. Although the relationship between resistivity and seismic velocity is not simple, we try to construct a pseudo-resistivity model based on 3-D seismic velocity distribution. Finally, we compare the predicted GIC at the eastern Hokkaido area with the observed one.

Keywords: GIC, Magnetotellurics, Seismic Tomography

©2020. Japan Geoscience Union. All Right Reserved.

Sensitivity of local electromagnetic response functions from Sq field to the electrical conductivity in the upper mantle

*Xiaoli WAN[1,2], Hisayoshi Shimizu[2], Hisashi Utada[2]

1. Tongji Univ., 2. Earthquake Research Institute, the Univ. of Tokyo

Solar quiet daily variations of the Earth’ s magnetic field, Sq field variations, are composed of externally inducing electric current system in the ionosphere and internally induced current system within conductive Earth. Spherical harmonic analysis of magnetic field on quiet days showed that dominant spherical harmonic modes are those with spherical harmonic degree n=p+1 and order m=p for a period 24/p hours up to p=4. Schmucker (1999a) named them as the principal modes of Sq. It is possible to separate the scalar magnetic field potential at each of these periods into external and internal parts by spectral and spherical harmonic analyses, and the responses obtained from them may be used to study the electrical conductivity in the upper mantle. Ratios of the internal to external coefficients, q-response, of the spherical harmonic expansion, global responses, may be useful when Earth is radially symmetric. However, for a realistic three-dimensional (3-d) Earth, one external spherical harmonic mode generates various internal modes due to lateral heterogeneities like land-ocean distribution and heterogeneity in the upper mantle, and each internal term has to be related to all existing external terms. This implies that a global response such as the q-response is difficult to apply for estimating 3-d structure (Schmucker, 1999b). In this study, we consider local electromagnetic responses such as Bz/Bx, Bz/By, magnetotelluric (MT), and corresponding quantities, where x, y and z are northward, eastward and vertically downward components, respectively. We investigate the sensitivity of these responses with respect to the electrical conductivity of the upper mantle by forward modeling of electromagnetic field.

Here theoretical responses were evaluated at the depth of seafloor in order to apply the results on the electromagnetic field observed there. We first examine the sensitivity of the response functions for 1-d radially symmetric conductivity structure modified according to Olsen (1998). The responses for the Sq's principal modes are calculated using a method based on Banks (1969). In addition to showing the responses have sensitivity to 1-d structure, apparent resistivity calculated from Ex/By and Ey/Bx due to the principal modes are compared with those calculated assuming source field with spherical harmonic mode of n=1 and m=0 to discuss the influence of source field that has spatial structure. Then, we evaluate the influence of 3-d conductivity structure on the responses using forward modeling code by Uyeshima and Schultz (2000). Influence of land-sea conductivity contrast on the responses are shown. Also, sensitivity of the responses to a rectangular heterogeneous body (in a spherical coordinate) in the upper mantle is discussed by evaluating the responses by changing the size, depth, and conductivity of the heterogeneous body.

References

Banks, R. J., 1969. Geomagnetic variations and the electrical conductivity of the upper mantle. Geophys. J. R. astr. Soc. 17, 457-487.

Olsen, N., 1998. The electrical conductivity of the mantle beneath Europe derived from C-response from 3 to 720 hr. Geophys. J. Int. 133, 298-308.

Schmucker, U., 1999a. A spherical harmonic analysis of solar daily variations in the years 1964-1965: response estimates and source fields for global induction—I. Methods. Geophys. J. Int., 136, 439-454.

©2020. Japan Geoscience Union. All Right Reserved.

Schmucker, U., 1999b. A spherical harmonic analysis of solar daily variations in the years 1964-1965: response estimates and source fields for global induction—I. Results. Geophys. J. Int., 136, 455-476.
Uyeshima, M. and Schultz, A., 2000. Geoelectromagnetic induction in a heterogeneous sphere: a new 3-D forward solver using a staggered-grid finite difference method, Geophys. J. Int., 140, 636-650.

©2020. Japan Geoscience Union. All Right Reserved.

The sparse inversion of the magnetic data to recover subsurface blocky structures.

*Mitsuru Utsugi[1]

1. Aso Volcanological Laboratory, Institute for Geothermal Sciences, Graduate School of Science, Kyoto University

Magnetic inversion is one of the popular method to obtain information about the subsurface structure. However, this method has a serious problem, that is, the linear equations to be solved become ill-posed, under-determined, and thus, the uniqueness of the solution is not guaranteed. As a result, several different models fit the observed magnetic data with the same accuracy. To reduce the non-uniqueness of the model, conventional studies introduced regularization method based on the quadratic solution norm. However, these regularization methods impose a certain level of smoothness, and as the result, the resultant model is likely to be blurred.

To obtain a focused magnetic model, Utsugi (2019) introduced a combination of the conventional L2 norm penalty (which is equivalent to the first order Tihkonov penalty) and L1 norm penalty. As is widely known, L1 norm regularization promotes sparseness of the model. Utsugi (2019) showed that, by introducing the L1-L2 norm penalty into the magnetic inversion, a model which is not overly blurred, and not excessively concentrated can be derived.

To facilitate the model interpretation, some of recent inversion studies focused on to recover the sharp boundary and block structure. However, L2 norm penalty is very simple and favorable because of its convexity, the ability to recover the sharp boundaries seems to be not enough when it is used with L1 norm penalty. Therefore, in this study, I tried some variations of the penalties which is used as the combination with the L1 norm penalty, such as fused-lasso penalty (Tibshirani, 2005), TSV (Total Squared Variation) penalty (Kuramochi et al.,2018), and will discuss about the best combination of the penalty which has good ability to recover the blocky structure, and is easy to implement.

Keywords: 3D magnetic inversion, sparse regularization, L1 norm regularization

©2020. Japan Geoscience Union. All Right Reserved.

Understanding Unzen volcano magmatic system by broadband Magnetotelluric observation

*Agnis Triahadini[1], Koki Aizawa[2], Keita Chiba[2], Kanta Miyano[1], Yuto Yamamoto[1], Kazunari Uchida[2], Tasuku Hashimoto[1]

1. Department of Earth and Planetary Sciences Graduate School of Science Kyushu University, 2. Institute of Seismology and Volcanology Faculty of Science Kyushu University

The magma system of Unzen volcano are believed to be sourced from under Chijiwa bay, 15 km west of Shimabara Peninsula, Nagasaki. Most of the magma chamber models of Unzen are derived from ground deformation measurement, i.e Kohno et al (2008) who used deformation data before and several years after 1991-1995 eruption. According to them, four pressure source models are proposed which located below the intensive smarm zone before eruption reported by Umakoshi et al (2001). Among the pressure sources, the most intensive sources are pressure source D which situated about 15 km under Chijiwa bay and pressure source C is located 5-6 km west of the active dome (Fugendake and Heisei-shinzan) at about 6 km depth. The D source explains why in the surround area underwent ground uplifting after the eruption ceased while the C source experienced deflation during eruption. After considering petrology data by Sugimoto et al (2005), these pressure sources are later concluded as deep basaltic magma reservoir and shallow crust dacite chamber respectively. Thus, more than one magma chambers related to Unzen volcano are expected below Shimabara Peninsula. During December 2019, we installed 23 MT sites consisted of 7 sites to record both E-field and B-field and 16 sites for E-field only. The sites were distributed across Minami-Shimabara and Obama area, around the suspected area of D and C pressure source. The distance of each sites are approximately 2-4 km where the recording period is 4-14 days depends on the site. Our purpose of study is to determine magmatic system of Unzen in correlation with pressure sources D and C. If they are existed than they are possibly detectable using MT. Because MT method is highly sensitive to conductive zone such as fluid rich zone or melt rich magma. Currently, we are processing the acquired data. At glance, the phase tensor and tipper at longer period > 100s are roughly aligned toward Southwest direction. For the inversion, we will include the MT data from several stations located in 2 km west of the summit, previously obtained by Triahadini et al (2019). Thus, we will present more complete analysis of the resistivity structure in the JPGU meeting.

Keywords: Unzen, Shimabara Peninsula, Magma Chamber, MT, Resistivity

©2020. Japan Geoscience Union. All Right Reserved.



MT observation sites of Shimabara Peninsula. Figure was made using Google Earth

©2020. Japan Geoscience Union. All Right Reserved.

[E] Poster | S (Solid Earth Sciences)：S-IT Science of the Earth's Interior & Techtonophysics

[S-IT23] Property and role of liquids inside terrestrial planets

convener:Tatsuya Sakamaki(Department of Earth Science, Tohoku University), Yoichi Nakajima(Kumamoto University, Priority Organization for Innovation and Excellence)

Liquids of silicates and metals inside of terrestrial planets play important role in the physical, chemical, and thermal evolutions of planets. This session aims at understanding the physical and chemical properties of liquids from shallower to deep parts of terrestrial planets, which are strongly related to the long history of those planets from the planetary accretion to the present-day dynamics. In addition, we call for presentations by researchers from various backgrounds of geochemical, experimental, theoretical/computational, and seismic/geodynamical ones, who investigate the physical and chemical properties of liquids and the behaviors and roles inside of terrestrial planets. Relevant topics include, but are not limited to, partial melting and melt extraction, liquid-solid partitioning, high pressure experiments on melts, and seismic detections of mantle melts and outer core anomaly.

[SIT23-P03] Effect of water on the structure of sodium silicate melts under pressure

*Tomonori Ohashi[1], Tatsuya Sakamaki[1], Ken-ichi Funakoshi[2], Miki Muranushi[1], Chikara Shito[1,3], Osamu Ikeda[1], Yuki Shibazaki[4], Akio Suzuki[1] (1.Tohoku Univ., 2.CROSS, 3.Univ. Tokyo, 4.NIMS)

[SIT23-P04] Nitrogen in the core from sound velocity measurements of liquid Fe-N at high pressure

*Asaki Iwamoto[1], Yoichi Nakajima[1,2], Daisuke Kinoshita[1], Yasuhiro Kuwayama[2,3], Kei Hirose[3], Daisuke Ishikawa[2,4], Alfred Q.R. Baron[2] (1.Kumamoto University, 2.RIKEN MDL, 3.The University of Tokyo, 4.JASRI)

[SIT23-P05] Sound velocity of liquid Fe-P alloy at high pressure

*Yoichi Nakajima[1,2], Daisuke Kinoshita[3], Yasuhiro Kuwayama[4], Kei Hirose[5,4], Asaki Iwamoto[3], Daisuke Ishikawa[6], Alfred Q.R. Baron[2] (1.POIE, Kumamoto Univ., 2.RIKEN MDL, 3.Grad. School Sci. Tech., Kumamoto Univ., 4.Dept. Earth Planet. Sci., Univ. Tokyo , 5.ELSI, Tokyo Tech. , 6.JASRI)

Effect of water on the structure of sodium silicate melts under pressure

*Tomonori Ohashi[1], Tatsuya Sakamaki[1], Ken-ichi Funakoshi[2], Miki Muranushi[1], Chikara Shito[1,3], Osamu Ikeda[1], Yuki Shibazaki[4], Akio Suzuki[1]

1. Tohoku Univ., 2. CROSS, 3. Univ. Tokyo, 4. NIMS

Behavior of high-pressure silicate melts, which is controlled by their physico-chemical properties, is crucial to understand the magmatism in the deep Earth. Particularly, the H_2O content significantly affects the properties, such as density (e.g., Matsukage et al. 2005; Sakamaki et al. 2006) and viscosity (e.g., Poe et al. 2006; Suzuki et al. 2011). Since such physical properties can be largely determined by the atomic structure, there are considerable interests in revealing how the structure changes with increasing pressure.

Here, structures of dry Na_2O-8/3SiO_2 (NS8/3) melts and hydrous ones with 5 wt% (NS8/3-H5) and with 9 wt% H_2O (NS8/3-H9) were determined under high pressure and temperature by means of the in-situ X-ray diffraction (XRD). The in-situ XRD study was carried out using a cubic-type multi-anvil apparatus MAX80, which is installed at the AR-NE5C beamline of Photon Factory, KEK at Tsukuba, Japan. The experimental *P*-*T* conditions were about 1.4–6.7 GPa and 900–1060 ˚C, respectively.

The obtained total structure factors, *S*(*Q*) of dry NS8/3 and NS8/3-H5 melts show that the position of the first sharp diffraction peaks (FSDP) monotonically shift to higher-*Q* with pressure. In contrast, the pressure dependence of the FSDP for NS8/3-H9 melt has a minimum around 4 GPa. This minimum indicates the intermediate-range order structure of the melt extends up to 4 GPa and shrinks at higher pressure. The reduced radial distribution functions, *G*(*r*) of NS8/3-H9 melt indicate different pressure evolutions in the average Na-O bond lengths, showing a sharp elongation between 3 and 4 GPa. This implies an enlargement of the -Na-O-Na- domain (Greaves 1985; Noritake 2017), and so this elongation can explain the decrease of the FSDP position up to 4 GPa. With increasing pressure,the O-O and Si-Si lengths in NS8/3-H9 melt remains constant, whereas these lengths in dry NS8/3 melt monotonically decrease. The difference in this behavior to the pressure increase can be explained that the Si-O-Si angle dominantly bends in polymerized melts with increasing pressure, while modifier cations mainly work as a cushion and the Si-O-Si angle does not shrink accordingly in depolymerized melts (Wang et al. 2014).

Keywords: hydrous silicate melt, liquid structure, synchrotron X-ray diffraction, high pressure and temperature

©2020. Japan Geoscience Union. All Right Reserved.

Nitrogen in the core from sound velocity measurements of liquid Fe-N at high pressure

*Asaki Iwamoto[1], Yoichi Nakajima[1,2], Daisuke Kinoshita[1], Yasuhiro Kuwayama[2,3], Kei Hirose[3], Daisuke Ishikawa[2,4], Alfred Q.R. Baron[2]

1. Kumamoto University, 2. RIKEN MDL, 3. The University of Tokyo, 4. JASRI

The Earth’ s liquid outer core is mainly of iron, alloying with ~5wt.% nickel and ~10wt.% some light elements [1]. Geochemical observations show that the silicate mantle is depleted in nitrogen relative to primordial meteorites which are believed to have similar composition of the bulk earth. This indicates that a large portion of nitrogen in bulk earth can be stored in the core [2,3]. In order to examine the possibility of nitrogen in the core, it’ s benefit to compare the sound velocity of liquid Fe-N alloy under high-pressure and –temperature corresponding to the core conditions with seismological observations. In this study, we have performed inelastic X-ray scattering (IXS) measurements to determine the longitudinal velocity of the liquid Fe-N alloy under high-pressure and –temperature conditions.
We carried out IXS measurements up to 76 GPa and 2200 K, using a laser-heated diamond-anvil cell (LH-DAC) at the RIKEN Quantum NanoDynamics beamline BL43LXU of SPring-8 [4]. We used a Fe80N20 foil as a starting sample and single crystal Al2O3 discs as thermal insulator. We judged the sample melting based on X-ray diffraction measurements during heating, and then measured IXS of the liquid sample. The IXS spectra was collected in a momentum transfer range of 3-5.7 nm-1 with an energy resolution of ~2.8 meV at 17.94 keV. The longitudinal sound wave (P-wave) velocity of liquid Fe80N20 was determined from the dispersion relation of the longitudinal acoustic phonon mode of the sample. We fit the P-wave velocity data for liquid Fe80N20 with an equation of state, which enabling to extrapolate the present velocity date to core pressures and also calculate the destiny and bulk modulus under high pressure conditions . Compared with pure Fe [5], the P-wave velocity of liquid Fe80N20 is faster by ~10% and the density is lower by ~8% in the present experimental conditions. By extrapolating the present results to the Earth’ s outer core conditions and then comparing with seismological observations, we found that the upper limit of nitrogen is ~3.3 wt% in the outer core.
[1] Stevenson, Science 214, 611-619 (1981).
[2] Marty, Earth Planet. Sci. Lett. 313-314, 56-66 (2012).
[3] Li et al., Earth Planet. Sci. Lett. 377-378, 311-323 (2013).
[4] Baron, SPring-8 Inf. Newsl. 15(1), 14-19 (2010).
[5] Anderson and Ahrens, J. Geophys. Res. 99(B3), 4273-4284 (1994)

Keywords: Outer core, Sound wave velocity, High pressure

©2020. Japan Geoscience Union. All Right Reserved.

Sound velocity of liquid Fe-P alloy at high pressure

*Yoichi Nakajima[1,2], Daisuke Kinoshita[3], Yasuhiro Kuwayama[4], Kei Hirose[5,4], Asaki Iwamoto[3], Daisuke Ishikawa[6], Alfred Q.R. Baron[2]

1. POIE, Kumamoto Univ., 2. RIKEN MDL, 3. Grad. School Sci. Tech., Kumamoto Univ., 4. Dept. Earth Planet. Sci., Univ. Tokyo , 5. ELSI, Tokyo Tech. , 6. JASRI

The compositions and physical properties of planetary cores are of great importance to understand the core formation processes, the thermal and chemical evolutions, and the present-day core dynamics. Terrestrial planets such as Mercury, Mars, as well as Earth are believed to have molten cores that consist of Fe alloys with lighter components such as hydrogen, carbon, nitrogen, oxygen, silicon, phosphorous, and sulfur [1]. Therefore, the physical property of liquid Fe alloys with possible lighter elements at high pressure relevant to the core conditions is key to understanding the planetary cores. Phosphorous is one of the candidates for the light elements in planetary cores because iron phosphorous alloys such as schreibersites (Fe_3P) and allabogdanite (Fe_2P) are often found in chondrites and iron meteorites [2,3]. Here we report the P-wave velocity of liquid Fe-P up to 96 GPa based on inelastic X-ray scattering (IXS) measurements.

We performed IXS measurements at the Quantum NanoDynamics beamline (BL43LXU) [4] of the RIKEN SPring-8 Center. The sample of $Fe_{75}P_{25}$ together with single crystal Al_2O_3 thermal insulators was compressed by a diamond-anvil cell (DAC), and then melted using the laser-heating system installed at the beamline. The longitudinal acoustic phonon mode of the liquid was measured in a momentum transfer range of 3-6 nm^{-1}. The P-wave velocity of liquid $Fe_{75}P_{25}$ was determined up to 96 GPa based on the phonon dispersion relation obtained at each pressure condition. Based on the P-wave velocity determined at high pressures, we constructed the equation of state for liquid $Fe_{75}P_{25}$. We found that the influence of phosphorous on the sound velocity of liquid Fe [5] is almost negligible under the present experimental pressure conditions, while the phosphorous reduces the bulk modulus and density of liquid Fe.

References:
[1] D.J. Stevenson, Science **214** 611–619 (1981).
[2] R. Skála and I. Císařova. Phys. Chem. Miner. **31**, 721-732 (2005).
[3] S.N. Brítvin et al., Am. Mineral. **87**,1245-1249 (2002).
[4] A.Q.R. Baron SPring-8 Inf. Newsl. **15**, 14–19 (2010). http://user.spring8.or.jp/sp8info/?p=3138
[5] W.W.Anderson and T.J. Ahrens, J. Geophys. Res. **99**, 4273–4284 (1994).

Keywords: Planetary cores, Liquid Fe alloys, Sound velocity, High pressure

©2020. Japan Geoscience Union. All Right Reserved.

[E] Poster | S (Solid Earth Sciences)：S-IT Science of the Earth's Interior & Techtonophysics

[S-IT24] MAGMA AND FLUID TRANSPORT IN THE EARTH'S INTERIOR

convener:Bjorn Mysen(Geophysical Laboratory, Carnegie Inst. Washington), Eiji Ohtani(Department of Earth and Planetary Materials Science, Graduate School of Science, Tohoku University), Dapeng Zhao(Department of Geophysics, Tohoku University), Michihiko Nakamura(Division of Earth and Planetary Materials Science, Department of Earth Science, Graduate School of Science, Tohoku University)

The principal mass and energy transport agents in the Earth's interior are magma and fluids. The objective of the proposed session is to combine experimental data, observations, and theoretical modeling to describe the transport properties and processes.
Melting, crystallization, and devolatilization occur across temperature intervals within which the distribution of mass between melts, fluids, and crystals is established. Element partitioning between melts, crystals, and fluids is needed to describe these processes. Physical properties of melts and fluids are controlled by their chemical composition, temperature, and pressure. The mass transfer processes depend on the property information. Magma aggregation at depth and ascent toward the surface are direct functions of density contrasts and permeability and depends on temperature, pressure, chemical composition and concentration of volatile components.
The mass transfer processes are imaged globally and locally by geophysical observations such as seismic tomography and electrical conductivity profiles. Magma sources in the deep mantle and the crust are also imaged by these geophysical tools. The mass transfer to the surface can be observed as the volcanic eruption in which phase separation of magma and fluid, and crystallization during the magma ascent control the type of eruptions. These are processes imaged with geophysical methods with which a three-dimensional structure of magma and fluid plumbing systems can be described, and in the geological records of earlier phenomena.
The proposed session will focus on those phenomena including laboratory experiments, numerical modeling, and observations using geophysical, seismological and geochemical approaches. These include physical and chemical properties and process of magma and fluid, near surface processes of volcanic eruptions, and geophysical imaging of various scales from locally to globally. Contributions to any of these subjects are encouraged.

[SIT24-P01] Viscosity of silicate network phase-separating from aqueous fluid

*Takehito Koyama[1] (1.Institute of Industrial Science, the University of Tokyo)

[SIT24-P02] Structure and density of H_2O-rich Mg_2SiO_4 melts at high pressure from *ab initio* simulations

*Gerd Steinle-Neumann[1], Liang Yuan[1,2], Akio Suzuki[2] (1.Bayerisches Geoinstitut, Universitaet Bayreuth, 2.Department of Earth Science, Tohoku University)

[SIT24-P03] A three-dimensional electrical conductivity model of the crust beneath the southern Tohoku district, NE Japan

Aoi Motoyama[1], *Masahiro Ichiki[1], Yasuo Ogawa[2], Makoto Uyeshima[3], Koichi Asamori[4], Toshihiro Uchida[5], Takao Koyama[3], Shin'ya Sakanaka[3,6], Hideaki Hase[3,8], Koki Aizawa[3,7], Yusuke Yamaya[3,5] (1.Graduate School of Science, Tohoku University, 2.School of Science, Tokyo Institute of Technology, 3.Earthquake Research Institute, The University of Tokyo, 4.Tono Geoscience Center, Japan Atomic Energy Agency, 5.National Institute of Advanced Industrial Science and Technology, 6.Graduate School of International Resource Science, Akita University, 7.Graduate School of Science, Kyushu University, 8.Geothermal Energy and Development Co. Ltd.)

[SIT24-P04] **Experimental constraint on the fluid connectivity in an olivine–H_2O–CO_2–NaCl system in subduction zones**

*Yongsheng HUANG[1], Takayuki Nakatani[1], Michihiko Nakamura[1], Catherine McCammon[2] (1.Graduate School of Science, Tohoku University, 2.Bayerisches Geoinstitut, University of Bayreuth)

[SIT24-P05] **Anomalous structural dynamics of basaltic melt at mantle conditions: Implications for superplumes and magma oceans**

*Arnab Majumdar[1], Min Wu[2,1], Yuanming Pan[1], Toshiaki IITAKA[3], John S Tse[1] (1.University of Saskatchewan, 2.Zhejiang University of Technology, 3.RIKEN)

Viscosity of silicate network phase-separating from aqueous fluid

*Takehito Koyama[1]

1. Institute of Industrial Science, the University of Tokyo

Silicates and aqueous fluids are fundamental to multi-spatiotemporal-scale geodynamics on Earth. An important phenomenon of their mixtures is phase separation or phase demixing (Hack et al., 2007), creating different liquid phases; This is significant for magma differentiation (Kawamoto et al., 2012) as similar as crystallization, for magmatic dynamics from the crustal deep to the surface (Allabar and Nowak, 2018), and maybe, for crustal activities (Koyama, JpGU [2012, 2019]). To these time-consuming processes, viscous dynamics of the silicate phase slower than that of the aqueous one is crucial, but almost unknown. We have to consider the thermodynamic relations between the components in the non-equilibrium process, when using usual flow mechanism as the base.

This mechanism in melt silicate network, although still debated, can basically be interpreted as the conformation change through diffusion of the formers, Si, bridging O, Al, etc. (Mysen & Richet, 2005, Stebbins, 2016). In mixing hydrous melts, the increasing H_2O drastically lowers the viscosity; The modifier H with its non-bridging O makes the network variable through the dissociation and polymerization as the terminal OH and free H_2O, and through the inter-strand hopping as the OH (ibid.). However, these softening actions of H (OH & H_2O) through the reactive former-modifier collisions must be realized under the entropic mixing. Then, in coexisting melts of silicate network (formers) and aqueous fluid (modifiers) under SiO_2-H_2O demixing, are the actions of H the same as that in the mixing or not? Here, I expect to be not, or rather to be the opposite. This is because that the enthalpic demixing, overcoming the entropic mixing with the “both-like-both” one, leads to the “likes-like-likes” situation for both groups; The H_2O and OH, favoring themselves more than the network, must prevent the dissociation but promote the polymerization. Under this preferential polymerization the network shrinks with the strand tension instead of the fracturing to demix from the fluid. The tension must suppress the strand vibration creating the inter-strand collision for the OH hopping and for the network-former diffusion itself. Thus, these “inert” actions of H on the network in the demixing must be the hardening or the viscosity and solidity increasing, even in the highly hydrous situation, contrasted with the softening in the mixing. This state must be transient under the intense demixing in the early stage (transient gel: Tanaka, 2017; Koyama & Tanaka, 2018). Further, the hardening will be assisted by the actions of other modifiers, Na, K, Mg, etc., similar to that of H and by the enthalpy overwhelming the entropy in lower temperature and pressure.

Although having to be verified theoretically and experimentally, these qualitative results of the asymmetric behaviors of the silicate network and aqueous fluid in thier demixing will connect to magmatic and seismic processes: the convection suppression due to the elastic resistance of the demixing network in the chamber and the explosive eruption to the surface through the brittle fructuring of the network under rapid volatile expansion; a hypothetic phase-separating continental lower crust of the shrinking-network and diffusing-fluid for compressive and fluid-concerned intracrustal seismicity (Koyama, JpGU [2012, 2019]).

Keywords: phase separation or phase demixing, silicate network, aqueous fluid, viscosity

©2020. Japan Geoscience Union. All Right Reserved.

Structure and density of H_2O-rich Mg_2SiO_4 melts at high pressure from *ab initio* simulations

*Gerd Steinle-Neumann[1], Liang Yuan[1,2], Akio Suzuki[2]

1. Bayerisches Geoinstitut, Universitaet Bayreuth, 2. Department of Earth Science, Tohoku University

Water has a strong effect on silicate melt properties, yet its dissolution mechanism in depolymerized melts, typical for mantle composition, remains poorly understood. Here we report results of first-principles molecular dynamics simulations of hydrous Mg_2SiO_4 melts with 6 wt.%, 16 wt.% and 27 wt.% H_2O at pressure and temperature conditions relevant to the upper mantle and mantle transition zone. The results show that hydrogen not only bonds to network-forming cations Si, but also to network-modifying cation Mg which - nevertheless - remains the most important network modifier. There is no evidence to support the hypothesis inferred from experimental data that water may cause an increase in the melt polymerization for ultramafic magmas; the ratio of non-bridging oxygens per Si increases with the addition of the oxygen from H_2O. The partial molar volume of water is independent on concentration in our simulations which allows us to examine the density of hydrous melt systemmatically. The critical water content - at which melts are neutrally buoyant compared to the surrounding mantle - is ~4 wt.% H_2O for a pyrolite melt, much lower than the high water content (>10 wt.%) observed in petrological experiments and estimated thermodynamically for low-degree partial melts formed in the vicinity of the mantle transition zone.

Keywords: mantle transition zone, water in silicate melts

©2020. Japan Geoscience Union. All Right Reserved.

A three-dimensional electrical conductivity model of the crust beneath the southern Tohoku district, NE Japan

Aoi Motoyama[1], *Masahiro Ichiki[1], Yasuo Ogawa[2], Makoto Uyeshima[3], Koichi Asamori[4], Toshihiro Uchida[5], Takao Koyama[3], Shin'ya Sakanaka[3,6], Hideaki Hase[3,8], Koki Aizawa[3,7], Yusuke Yamaya[3,5]

1. Graduate School of Science, Tohoku University, 2. School of Science, Tokyo Institute of Technology, 3. Earthquake Research Institute, The University of Tokyo, 4. Tono Geoscience Center, Japan Atomic Energy Agency, 5. National Institute of Advanced Industrial Science and Technology, 6. Graduate School of International Resource Science, Akita University, 7. Graduate School of Science, Kyushu University, 8. Geothermal Energy and Development Co. Ltd.

This study reports a three-dimensional electrical resistivity distribution model in the crust beneath the onshore southern Tohoku district, NE Japan. The southern Tohoku district here contains southern Yamagata prefecture, southern Miyagi prefecture, eastern Niigata prefecture, and northern Fukushima prefecture. This resistivity analysis aims three-fold. (1) To delineate fluid distribution in the crust beneath the onshore forearc of southern Tohoku district: The seismic swarm beneath around Iwaki city has been active since the 2011 off the Pacific coast of Tohoku Earthquake. The seismicity is interpreted as being induced by fluid migration from the deep crust. We investigate if conductive body in the crust elongates northwards from beneath Iwaki city. (2) To detect whether outstanding crustal fluid distributes beneath the onshore backarc. (3) To reveal a finer three-dimensional crustal conductivity distribution model beneath Ou-backbone range in southern Tohoku district, which we expect to give the interpretation of genesis of the volcanoes and of another seismic swarm occurring beneath around Yonezawa-city.

We compile the magnetotelluric (MT) and geomagnetic transfer function (GDS) data which were acquired by Uchida (2004), Umeda et al. (2008), Asamori et al. (2011), Uyeshima (private comm.) and Ogawa (private comm). The 118 observation sites locate in the study area. Both MT and GDS frequency response is used to model three-dimensional resistivity distribution. The period range is 0.03 to 652 second.

The resultant resistivity model reveals no conductor beneath the onshore forearc in Fukushima prefecture. The model rather shows resistor there with over several-thousand Ωm, which corresponds to the Abukuma batholiths. Thus, our model indicates that the area only around Iwaki-city is peculiar forearc, where fluid migrates upward from deep crust. Neither exists an outstanding conductor beneath backarc of the study area. However, a few local shallow conductors (down to 5 km depth) lie beneath the backarc. The bottom boundary of one of the conductors around Iide-Mountain area clearly bounds the local seismicity there. Although the cut-off depth of seismicity shows distinct undulation beneath regional backarc of the study area, the resistivity distribution shows no correspondence to the cut-off depth undulation. The outstanding crustal conductors are found beneath Ou-backbone range in the study area. We find the clear correspondence between deep low frequency events (20-40 km depth) and the conductor beneath Bandai-Azuma volcanoes. This image is similar with the relation of low velocity and deep low frequency event (Niu et al., 2018; Chen et al., 2019). The conductor beneath Ou-backbone range delineates the hot-finger image. The conductor branches at about 20 km depth.

Keywords: Electrical conductivity/resistivity

©2020. Japan Geoscience Union. All Right Reserved.

Experimental constraint on the fluid connectivity in an olivine–H_2O–CO_2–NaCl system in subduction zones

*Yongsheng HUANG[1], Takayuki Nakatani[1], Michihiko Nakamura[1], Catherine McCammon[2]

1. Graduate School of Science, Tohoku University, 2. Bayerisches Geoinstitut, University of Bayreuth

In subduction zones, the circulation of slab-derived aqueous fluid through a mantle wedge plays a key role in arc magma genesis and global material cycling. Their presence can be detected by geophysical observations because of their remarkable influence on the physical properties of overlying plate. Recently, high electrical conductors have been detected by magnetotelluric observations beneath some fore-arcs and are believed to store voluminous slab-derived fluids. This implies that the mantle wedge at fore-arc depths is permeable for aqueous fluids. At high temperature and high pressure condition, dihedral angle is an important parameter to control the fluid connectivity in a fluid-bearing rock. The subduction zone fluid is now gradually recognized as a multicomponent fluid that is composed of the H_2O, salt (NaCl), nonpolar gas (CO_2) and dissolved solid components. However, the effect of multicomponent fluid on dihedral angle is still unclear, which restricts our understanding for realistic fluid circulation model in subduction zones. In this study, we experimentally constrain the dihedral angle in olivine–H_2O–NaCl–CO_2 systems at 1–4 GPa and 800–1100 ˚C to understand the combined effect of salt and nonpolar gas on the connectivity of aqueous fluids in the mantle wedge. Results in H_2O–CO_2 system show that CO_2, contrast to NaCl, tends to increase the dihedral angle at 1 GPa and 800–1100 ˚C, and 2 GPa and 1100 ˚C. However, it can reduce the dihedral angle even below 60˚ at relatively high pressure and low temperature conditions where olivine partly reacts with CO_2 to form magnesite and orthopyroxene. Results in the multicomponent system suggest that the effect of NaCl on dihedral angle is much more significant than that of CO_2. In addition, strikingly, the dihedral angles in the multicomponent system are the smallest among all investigated systems and much smaller than 60˚ under the presence of magnesite and orthopyroxene. Therefore, the multicomponent fluid can infiltrate into the forearc mantle wedge through the interconnected fluid network, which can account for the high electrical conductivity anomalies detected in the forearc region. This work was supported by the JSPS Japanese-German Graduate Externship.

Keywords: Subduction zone, Multicomponent fluid, Fluid connectivity, Dihedral angle

©2020. Japan Geoscience Union. All Right Reserved.

Anomalous structural dynamics of basaltic melt at mantle conditions: Implications for superplumes and magma oceans

*Arnab Majumdar[1], Min Wu[2,1], Yuanming Pan[1], Toshiaki IITAKA[3], John S Tse[1]

1. University of Saskatchewan, 2. Zhejiang University of Technology, 3. RIKEN

Transport properties such as diffusivity and viscosity of melts determined the evolution of the early Earth’ s magma oceans. They also govern many present-day processes of the Earth, from mantle convection to plate tectonics, magma migration and volcanic activity. Unfortunately, carrying out experimental measurements of melt diffusivity and viscosity at most mantle conditions are rendered impossible due to technical challenges. In this theoretical work we report the structure, density, diffusivity, electrical conductivity, and viscosity of a model basaltic ($Ca_{11}Mg_7Al_8Si_{22}O_{74}$) melt. The calculations have been performed using first-principles molecular dynamics simulations at temperatures from 2200 K (0 to 80 GPa) to 3000 K (40-70 GPa) and 4000 K (120 GPa). There is good agreement between our results on the melt structure and viscosity at low pressure with that of experiments and previous theoretical predictions. A significant finding is that, although the density and coordination numbers around Si and Al increase with pressure, however, the Si-O and Al-O bonds become more weak and ionic. The temporal atomic interactions at high pressure are fluxional and fragile. Thus, making the atoms more mobile and reversing the trend in transport properties at pressures close to 50 GPa. The reversed melt viscosity under lower mantle conditions allows new constraints on the timescales of the early Earth’ s magma oceans. It also provides the first tantalizing explanation for the horizontal deflections of superplumes at ~1000 km below Earth’ s surface.

Keywords: ab-initio molecular dynamics, basalt, viscosity reversal

©2020. Japan Geoscience Union. All Right Reserved.

[E] Poster | S (Solid Earth Sciences)：S-IT Science of the Earth's Interior & Techtonophysics

[S-IT25] Structure and Dynamics of Earth and Planetary Mantles

convener:Takashi Yoshino(Institute for Planetary Materials, Okayama University), Takashi Nakagawa(Department of Earth Sciences, The University of Hong Kong), Dapeng Zhao(Department of Geophysics, Tohoku University)

Interdisciplinary approach can lead to a better understanding of the dynamics and evolution of the deep interiors of the Earth and planets. We welcome any submissions of recent results in observational, theoretical and experimental studies on seismology, geomagnetism, mineral physics, dynamics of deep interiors, and any other relevant fields from researchers in many countries. The integration of such results is also welcome. In particular, we encourage any contributions focusing on "plate and mantle dynamics in Earth and terrestrial planets". This session will be organized as the main session of the SEDI-J group in the Solid Earth Section of JpGU. We encourage all participants concerning the deep planetary interior to submit this session.

[SIT25-P01] **Origin** of **Plate Tectonics**,Why did Plate Tectonics occur **only on Earth**?
Why is there a Deep Ocean Floor and Seawater **only on Earth**?
Mystery (**Driving Force** and **Origin of Pacific Rim Back-Arc Basin**).
we challenge Them All !

*Akira Taneko[1] (1.SEED SCIENCE Lab.)

[SIT25-P02] The viscosity structure of the low-viscosity zone of the Moon derived from the tidal response

*Yanxia Tan[1], Yuji Harada[1] (1.State Key Laboratory of Lunar and Planetary Sciences, Macau University of Science and Technology)

[SIT25-P05] 2D Visco-elasto-plastic numerical modeling of buckling and uplift on passive margin under compression: implications for topography of SE Korea and the East Sea (Japan Sea)

*Seok-Hyeon Do[1] (1.Kangwon National University)

[SIT25-P06] **Development of 3-D Lagrangian Free Subduction Model: Implications for Surface Process of the Earth**

*Jae-Yoon Keum[1], Byung-Dal So[1] (1.Kangwon National University)

[SIT25-P07] **Application of Parker-Oldenburg Algorithm to map Moho Discontinuity using Gravity Data in Western North America Cordillera**

*Mohammad Shehata[1,2], Hideki Mizunaga[2] (1.Department of Geology, Faculty of Science, Port Said University, Egypt, 2.Department of Earth Resources Engineering, Faculty of Engineering, Kyushu University, Japan)

[SIT25-P08] Multi-mode surface wave phase speed distribution in North America

*Hitoshi Matsuzawa[1], Kazunori Yoshizawa[2], Fan-Chi Lin[3] (1.Graduate School of Science, Hokkaido University, 2.Faculty of Science, Hokkaido University, 3.The University of Utah)

[SIT25-P09] Mapping azimuthal anisotropy in the Australasian upper mantle with multi-mode surface waves

*Kazunori Yoshizawa[1,2], Yuka Nishimura[2] (1.Faculty of Science, Hokkaido University, 2.Graduate School of Science, Hokkaido University)

[SIT25-P10] **Upper mantle anisotropy beneath Sri Lanka region using shear-wave splitting analysis**

*Shivam Chandra[1] (1.Undergraduate student member)

[SIT25-P11] Lattice preferred orientation of akimotoite deformed in the D111 Kawai-type multianvil apparatus

*Longli Guan[1], Daisuke Yamazaki[1], Noriyoshi Tsujino[1] (1.Institute for Planetary Materials, Okayama University, Misasa, Japan)

[SIT25-P12] Mantle discontinuities oceanward of the Krile - Honshu slab

*Masayuki Obayashi[1], Junko Yoshimitsu[1], Yoshio Fukao[1] (1.Japan Agency for Marine-Earth Science and Technology)

[SIT25-P13] Tomography Model Using Singular Value Decomposition

*Jun Su[1,2], Christine Houser[2], John William Hernlund[2] (1.Department of Earth and Planetary Sciences, Tokyo Institute of Technology, 2.Earth-Life Science Institute)

[SIT25-P14] **Whole-mantle P-wave tomography beneath East Asia**

*Yu Katayama[1], Dapeng Zhao[1], Genti Toyokuni[1] (1.Research Center for Prediction of Earthquakes and Volcanic Eruptions, Graduate School of Science, Tohoku University)

[SIT25-P15] **Seebeck coefficient measurement of olivine by dual heating system and its application to the redox kinetics of the subducted slabs**

*Ran Wang[1], Takashi Yoshino[1] (1.Institute for Planetary Materials, Okayama University)

[SIT25-P16] High-pressure generation to 150 GPa in multianvil apparatus using the 6-8-2 system with nano-polycrystalline diamond anvils.

*Takehiro Kunimoto[1], Masayuki Nishi[1], Tetsuo Irifune[1] (1.Geodynamics Research Center)

Origin of Plate Tectonics,Why did Plate Tectonics occur only on Earth? Why is there a Deep Ocean Floor and Seawater only on Earth? Mystery (Driving Force and Origin of Pacific Rim Back-Arc Basin). we challenge Them All !

*Akira Taneko[1]

1. SEED SCIENCE Lab.

Why is"***Multi-Impact Hypothesis***" Origin of "Moon"?,
But also Origin of "Deep Ocean Floor of Earth"and"Plate Tectonics"?
Origin of "Seven Seas of Earth"and"Plate Boundary"and"Returned Pacific Arc Archipelago,Back Arc Basin, Solitary Trench",Origins of "***Extreme Extinction of Species***"and"Asteroid Belts and Differentiated Meteorites"and "Jupiter Great Red Spot", and Origins of "Pluto"and"Core-rich Venus", Origins of "Rotation Axis Inclination", "Rapid Change of Plate Moving Direction"and"Kimber light pipe"and Origin of "Moon" is ***all Result of a Series of Solar System Evolutions.***

Orbit of Differentiated Mars-sized protoplanet CERRA formed at the Ceres position according to Bode's law changed to an Elliptical Orbit due to Perturbation of Mssive Jupiter Gas Planet. At Position where Gravity of Sun and Jupiter are balanced, CERRA ruptures and Orbits in a Row as Train-Mantle-Ruptured Asteroids like Comet Shoemaker-Levy Ninth. At Intersection with Earth's Orbit, a Collision chance occurs at each meeting cycle. This Train Mantle Fragment caused Multi-Impact. Core and Mantle Fragments of CERRA became a Molten Sphere, and Velocity and Angular Momentum were reduced by Law of Equal Energy distribution, which became Origin of Core-Rich Venus. Collision Speed and Angle were calculated theoretically, and V=12.4km/s and Φ=36.45 degrees were obtained. Projectile in Earth's Mantle could explain Lunar Orbit Rm ≒ 60×Re, which was slightly less than Secondary Space Velocity of 11.2 km/s. Ejected ***Earth Mantle is eccentric*** and rotates around Common center of Gravity, so that Heavier one(front side = Basalt rich) ***always faces Earth.*** Moon was covered with Molten Crust, but under Impact of Heavy Bombardment of Meteorite, Underground Basalt(black) expanded and flowed out, forming LunarSea. Component of Asteroid belt (fragment of CERRA) is Andesitic mantle.On Back-side of Moon(surface component of Earth=Andesitic),even if it collides, it becomes Same breccia and Craters,***but Basalt sea is not formed.***

"Why does ***only*** *Earth* have Deep Ocean Floor and Seawater?" Mystery ***can be explained below.***
One hundred years ago,when Wegener ***proposed Theory of Continental Drift (Origin of Plate Tectonics)***, he also ***pointed out Mystery of Frequency of two peaks at Earth's altitude***. It is a Mystery that Seafloor with an Average Depth of about 4 km(1/1000 *Radius of 6,400 km.*) has formed about 70% of Earth's Surface.

In "Multi-Impact Hypothesis"
is ***Lunar Origin Hypothesis***, but also Origin of Great Extinction of Species such as Ocean Floor and Plate Tectonics ***in Collisions.***Orbit of Differentiated CERRA turned into an Elliptical orbit to Jupiter by Subsequent perturbation of Giant planet Jupiter.CERRA's Orbital flattening took about 600 million years, and Earth and CERRA were completely differentiated and solidified.
At a position where Gravitation was equal between Sun and Jupiter, Tension exceeded Strength of CERRA and ***Tidal Rupture occurred.*** Like Comet Shoemaker, Levi and Ninth in 1997, it became Train &CERRA's mantle fragment intermittently ***collided with Earth*** instead of Jupiter.

©2020. Japan Geoscience Union. All Right Reserved.

Defect was isostatic and formed a **Deep Ocean Floor** with an **Average Dpth of 4 km. Surrounding Plate** collapsed to form **Return Pacific Concave Back Arc Basin. High-latitude Collision** toward Antarctic position stopped when **Tethys Sea** and **Indian Ocean, Earth Tilt** and **Antarctic Continent** moved to **Rotation Axis Position.**

Instead of **God making Land in Sea**, ***Dent was created by Collision on land, and connected to form Ocean Floor.***
During **First launch of Moon**, ***Earth's Mantle cracked*** and ***became a Plate Boundary.***
Collision of Mantle Fragment with Hawaiian location resulted in **Ejection of Moon** and **Origin of Kimberlite Pipe.**

"Why did **Plate Tectonics** occur ***only on Earth***?"
It is ***inevitable*** that **Tragedy of CERRA** born **inside Giant Mass Jupiter** and **Collision of Train Mantle Fragment**.
Driving Force is a couple that Minimizes Moment of Inertia, and **when Plates begin to overlap**, Convex Plate goes under Concave Plate.**Origins of Asteroid belt** and **Jupiter's Great Red Spot** can be explained ***without Contradiction.***

Clinging to **Thermal Convection Hypothesis** cannot explain **Sudden Change in Direction of Plate movement**, ***Does Not reach*** **Truth.**

Assuming **Correct Model**, **Theory** ***can verify Collision Speed and Angle by Abduction***, **Re-Verification** ***through*** **Experiments and Observations** is **desired.**

But Giant Impact Hypothesis is **Accidental Collision** of Mars-sized Tia gives only **3×Re Orbital Energy.**
Furthermore, Mechanism of Accelerating Up to **60×Re(=Moon Energy)** is not shown.
It is *a Plan to simulate a* ***mantle-only Moon*** but not to explain its **Feeding Zone**.

It will also be released in**M-IS22,**M-ZZ56(May 24),U-02(**May26AM2**),S-IT25(**26AM1***)

Keywords: Origin of Plate Tectonics, Why did Plate Tectonics occur only on Earth?, Why is there a Deep Ocean Floor and Seawater only on Earth? , Challenge Mystery of all origins ! Will be revealed in M-IS22 session!, Origin of Plate Tectonics can be explained by the same Origin, as Origin of Moon and Origin of Earth's Deep Ocean Floor, Multi-Impact Hypothesis can explain Origins of Moon, Earth, Earth's Ocean, and Living things.

©2020. Japan Geoscience Union. All Right Reserved.

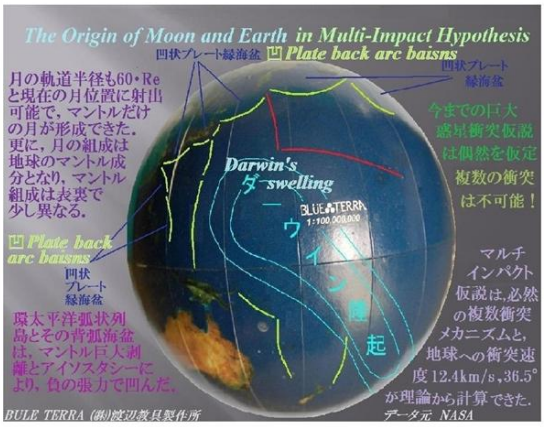
6.地球 Abduction

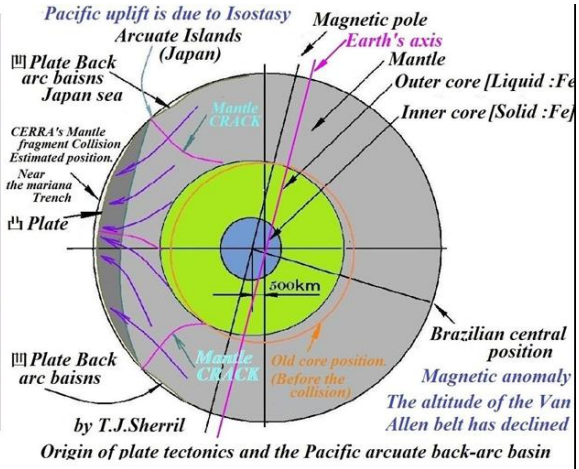
①環太平洋弧状列島の起源,

②深海洋底の起源とアイソスタシーによる凹プレートの形成メカニズム

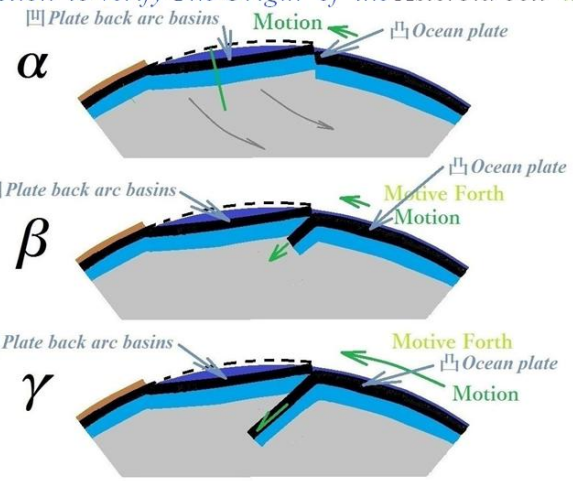
③プレート相互の重なり始めのメカニズム

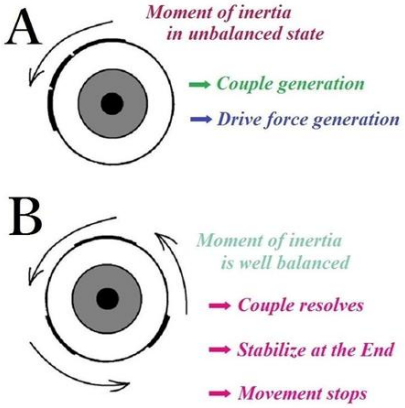
④駆動力(偏芯慣性モーメント)





Abduction to verify The Origin of the Asteroid belt in Multi-Impact Hypothesis .





©2020. Japan Geoscience Union. All Right Reserved.

The viscosity structure of the low-viscosity zone of the Moon derived from the tidal response

*Yanxia Tan[1], Yuji Harada[1]

1. State Key Laboratory of Lunar and Planetary Sciences, Macau University of Science and Technology

The effect on the tidal response of the low-viscosity zone at the deep interior of the Moon is investigated, in particular from the viewpoint of its possible viscosity structure on a few simple assumptions of some hypothetical temperature profiles. Based on the Love number theory, the tidal parameters are computed numerically in order to demonstrate their structure dependences on the low-viscosity zone as well as the frequency dependence. Unlike the earlier consideration, the viscosity structure of the low-viscosity zone here is not assumed to be fully uniform any longer but linked with either a couple of temperature profiles, namely, the thermal boundary layer model or the convective layer model. The calculations show that the latest observational ranges of the frequency-dependent quality factors can be satisfied only by the convective layer model with some viscosity value for the interlayer but not by the thermal boundary layer model for any structure. The approximate viscosity solution is estimated to be 3.3×10^{16} Pa s. If considering also the observational ranges of the Love numbers together with those of the quality factors, the solution of the outer radius of the low-viscosity zone is approximately 560 km. These solutions are almost identical to those based on the previous uniform model. It is concluded that in the Maxwell model the thermal state of the bottom layer of the lunar mantle is predicted to be mainly controlled by the local convection, and possibly maintained by the energy balance between convective cooling and tidal heating, as previously suggested.

This work was financially supported by the Research Funding Projects (No. 007/2016/A1, No. 119/2017/A3, and No. 187/2017/A3) at the Science and Technology Development Fund, the Macau Special Administrative Region.

Keywords: Geophysics, Interior, Moon, Tides, Solid body

©2020. Japan Geoscience Union. All Right Reserved.

2D Visco-elasto-plastic numerical modeling of buckling and uplift on passive margin under compression: implications for topography of SE Korea and the East Sea (Japan Sea)

*Seok-Hyeon Do[1]

1. Kangwon National University

The continental margin, which shows prominent topographical structures such as buckling, uplift, and fault, is categorized into the active and passive margins. Although the passive margins are considered geophysically stable, it is likely to be reactivated into the active margins such as subduction zone due to external forces and its own gravitational weight. Previous studies, based on geophysical observations (e.g., seismic reflection, tomography, gravity anomaly, and marine terrace uplift), suggested that the EW compression exerting on SE Korean Peninsula induced a buckling structure with ~60-70 km wavelength and uplift rate of ~0.3 m/ky. In this study, we reproduced the Korean passive margin associated with buckling and uplift structures, and found the clear correlation between the strength of oceanic lithosphere and wavelength of buckling structure. We developed the passive margin model with 2D visco-elasto-plastic finite element method in the Lagrangian manner. Due to the lack of available geophysical data for inferring rheological structure beneath the Korea Peninsula and the East Sea (Japan Sea), we performed a parametric numerical simulation with a wide range of rheology. In the reference model, the domain composed of the mantle, oceanic and continental (upper and lower) crusts is compressed horizontally by constant velocity boundary condition (i.e., ~3-6 cm/yr). The reference model exhibits a buckling structure with ~200 km wavelength on oceanic crust and uplift rate of ~0.6 m/ky on continental crust. We experimented with varying the variables using the strength of oceanic lithosphere as a variable. Our model showed that different strength of oceanic lithosphere caused the buckling with different amplitude to that of the reference model. The stronger strength of oceanic lithosphere, the buckling structure becomes bigger. We suggest that the Korea passive margin with buckling and uplift structure has developed due to the combination of young oceanic lithosphere and EW compression.

Keywords: Korean Peninsula, buckling, uplift, East Sea (Japan Sea), visco-elasto-plastic

©2020. Japan Geoscience Union. All Right Reserved.

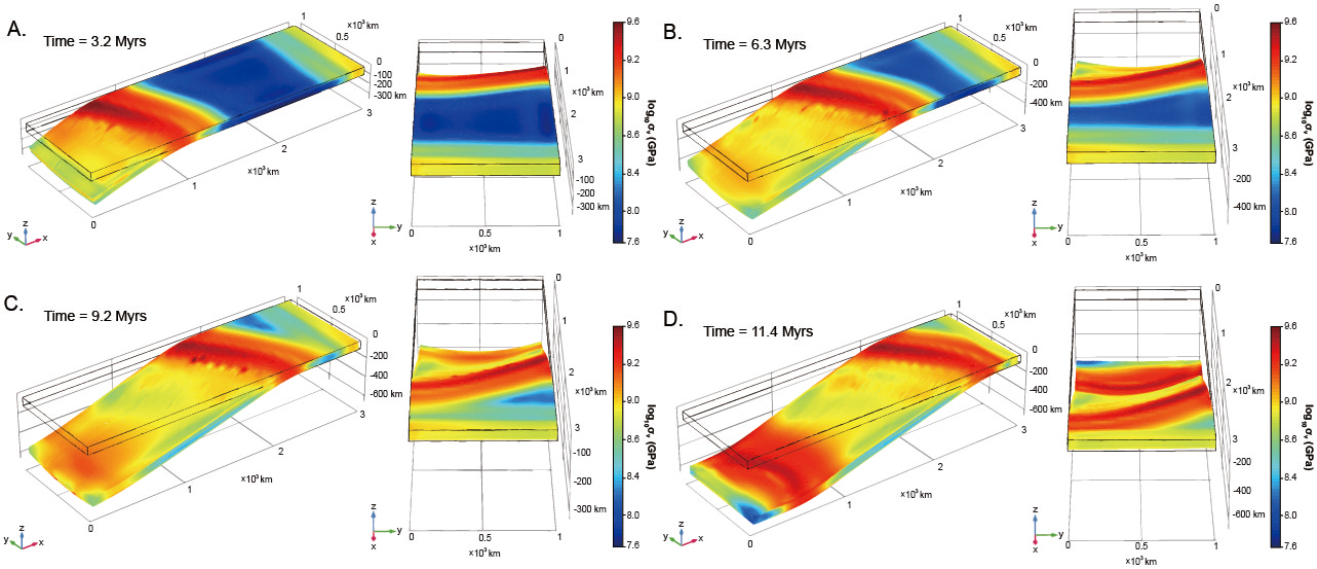
Development of 3-D Lagrangian Free Subduction Model: Implications for Surface Process of the Earth

*Jae-Yoon Keum[1], Byung-Dal So[1]

1. Kangwon National University

Variation of surface curvature along trench which is geodetically observed is ubiquitous in modern subduction zones on Earth. Global reference frame suggested differential trench motion in the one subduction zone. Its resultant trench shape has been explained by tectonic mechanism such as heterogeneities in ages of the plate at trench, slab width and overriding plate. However, relationship between the trench motion and sedimentation which is fundamental surface process of the Earth (e.g, climate, eustatic sea level change, amount of supply and erosion due to vertical topography change) relatively has been poorly understood. In this study, we developed 3-D thermo-mechanical free subduction model using viscoelastic material based on Lagrangian finite element method. We quantitatively evaluated relationship between trench shape along strike direction and sediment thickness by implementing realistic rheology including brittle, diffusion, and dislocation creep. We suggest that if sedimentary accumulation vary gradually along trench axis, differential trench rollback rates could be obtained and various trench shpae including oblique subduction could occur. Our results, including the geodynamic implication that the Earth’ s surface process contributes to subduction physics, are expected to improve the understanding of the structure of deep subduction.

Keywords: Subduction zone, Numerical model, Trench infill material



©2020. Japan Geoscience Union. All Right Reserved.

Application of Parker-Oldenburg Algorithm to map Moho Discontinuity using Gravity Data in Western North America Cordillera

*Mohammad Shehata[1,2], Hideki Mizunaga[2]

1. Department of Geology, Faculty of Science, Port Said University, Egypt, 2. Department of Earth Resources Engineering, Faculty of Engineering, Kyushu University, Japan

Parker–Oldenburg algorithm was applied to airborne gravity data in the western USA to map the Moho discontinuity. F-H Parasnis method was also applied to the gravity data to estimate the Bougeur reduction density for calculation of the Bougeur gravity anomaly. The inversion process uses the Oldenburg equation (Oldenburg, 1974), which is a rearrangement of Parker’ s equation (Parker, 1973), to estimate the depth to the undulating interface from the gravity anomaly by means of an iterative process. These formulas are shown as follows,

The resulted Moho depth map shows depths ranging from 9 km to 50 km. Moho anomalies showed good spatial correlation with the major physiographic provinces in the study area. The subduction trench of the Farallon remnants (Juan de Fuca and Gorda) was mapped at the north of the Mendocino Triple Junction (MTJ). The subducting plates show north-east dipping direction with low dipping angle. The effect of the subduction appears in the structure at the northern part (i.e. Cascade Mountain, Walla-Walla plateau and Northern Rocky Mountains), whereas the southern part is affected by the transform movement of the Pacific Plate yielding a set of basins (Central Valley, Great Basin and Wyoming Basin). Results of this research, in conjunction with other information of the area, provide a new information for the analysis of the tectonic framework of the western North-America.

References

Oldenburg, D.W., 1974. The inversion and interpretation of gravity anomalies. *Geophysics* **39** (4), 526–536.

Parker, R.L., 1973. The rapid calculation of potential anomalies. *Geophysical Journal of the Royal Astronomical Society* **31**, 447–455

Keywords: Parker–Oldenburg algorithm, Moho Discontinuity, Airborne Gravity Data, Northern America Cordillera

©2020. Japan Geoscience Union. All Right Reserved.

Multi-mode surface wave phase speed distribution in North America

*Hitoshi Matsuzawa[1], Kazunori Yoshizawa[2], Fan-Chi Lin[3]

1. Graduate School of Science, Hokkaido University, 2. Faculty of Science, Hokkaido University, 3. The University of Utah

The recent deployment of high-density broadband seismic networks in continental regions enables us to investigate the detailed seismic images of the continental upper mantle using seismic surface waves. Making the most of such seismic arrays, we have recently developed two-step array-based methods for (1) the multi-mode phase speed measurements based on a *f-k* analysis with a long-linear array, and (2) the modal waveform decomposition for the centroid location of array, based on the linear Radon transform (Matsuzawa & Yoshizawa, GJI, 2019). Such array-based multi-mode phase speed measurements are expected to be of help in enhancing the vertical resolution of 3-D S-wave speed models.

We applied the method (1) to an extensive data set from the Transportable Array stations of USArray, and mapped phase speed distributions in North America (Matsuzawa & Yoshizawa, AGU Fall Meeting 2018). We could obtain preliminary phase speed maps of the fundamental-mode and the first four higher-mode surface waves. Although the large-scale anomalies (i.e., fast phase speeds in cratons in the stable eastern US., slow phase speeds in the tectonically active western US.) could be identified, the lateral resolution of the phase speed maps was limited, compared with earlier tomography models using inter-station and single-station measurements. This suggests that the small-scale tectonic features tend to be blurred and averaged out due to the long linear array (2000–4000 km).

To overcome this problem, we apply the inter-station dispersion analysis (Hamada & Yoshizawa, GJI, 2015) and the eikonal tomography method (Lin *et al.*, GJI, 2009) to the decomposed modal waveforms of the fundamental-mode derived from the method (2). In the eikonal tomography, the phase speed distributions can be retrieved by calculating the gradient of the phase traveltime field without any inversion processes.

The resultant fundamental-mode phase speed maps of Rayleigh and Love waves exhibit enhanced lateral resolution, showing some small-scale tectonic features in the inland of the US. The results indicate that the decomposed modal waveforms at the centroid of the linear array represent the average phase speeds in a relatively small area of several-hundred kilometers, which is equivalent to the wavelength of the fundamental-mode surface waves. Such decomposed fundamental-mode seismograms can be further used to enhance the quality of higher-mode measurements through the mode-stripping of the fundamental-mode from the observed seismogram.

Keywords: surface wave, higher mode, tomography, array-based analysis

©2020. Japan Geoscience Union. All Right Reserved.

Mapping azimuthal anisotropy in the Australasian upper mantle with multi-mode surface waves

*Kazunori Yoshizawa[1,2], Yuka Nishimura[2]

1. Faculty of Science, Hokkaido University, 2. Graduate School of Science, Hokkaido University

Azimuthal anisotropy in the upper mantle from seismic surface waves provides us with the information of mantle dynamics, such as the present-day mantle flow and the remnant of past deformation in the lithosphere. The Australian plate is currently the fastest-moving tectonic plate including a large continent, encompassed by the intensive seismicity, particularly in its north (Indonesia) and east (Tonga-Kermadec to New Zealand). Thus, the entire continent can be covered by dense ray paths utilizing broad-band seismic stations deployed throughout the continent. This unique tectonic setting of the Australian plate allows us to reconstruct high-resolution tomography models in the Australasian region.

In this study, we construct azimuthally anisotropic phase speed maps of multi-mode surface waves incorporating azimuthal anisotropy, which are then used to construct three-dimensional S wave models with azimuthal anisotropy. We employ the database of path-specific multi-mode phase speeds for the fundamental mode and up to the fourth-higher modes surface waves by Yoshizawa (2014), which has been measured by using the non-linear waveform fitting method (Yoshizawa & Ekstrom, 2010).

The results suggest that the fast-axis of azimuthal anisotropy in the upper mantle is nearly parallel to the absolute plate motion (APM) in the oceanic area, but is more complicated in the continental area. The azimuthal anisotropy beneath the Australian continent above 150 km depth reflects the past deformation frozen in the lithosphere, which is characterized by the E-W oriented anisotropy. However, below 150 km depth, azimuthal anisotropy tends to represent the present-day shear flow in the asthenospheric mantle beneath the cratonic lithosphere, which moves to the north. Beneath the Tasman Sea between New Hebrides Trench and New Zealand, we can see the circular pattern of azimuthal anisotropy, especially at a shallower depth above 200 km.

The thickness of the Australian lithosphere becomes thinner toward the eastern margin of the continent, which is well reflected in the cross-sections of the azimuthally anisotropic S wave model. The agreement between APM and azimuthal anisotropy can be observed at the depth below the lithosphere-asthenosphere transition estimated from the isotropic S wave speed model, indicating the effects of mantle flow under the fast drifting Australian continent.

Keywords: azimuthal anisotropy, surface wave, upper mantle, Australia

©2020. Japan Geoscience Union. All Right Reserved.

Upper mantle anisotropy beneath Sri Lanka region using shear-wave splitting analysis

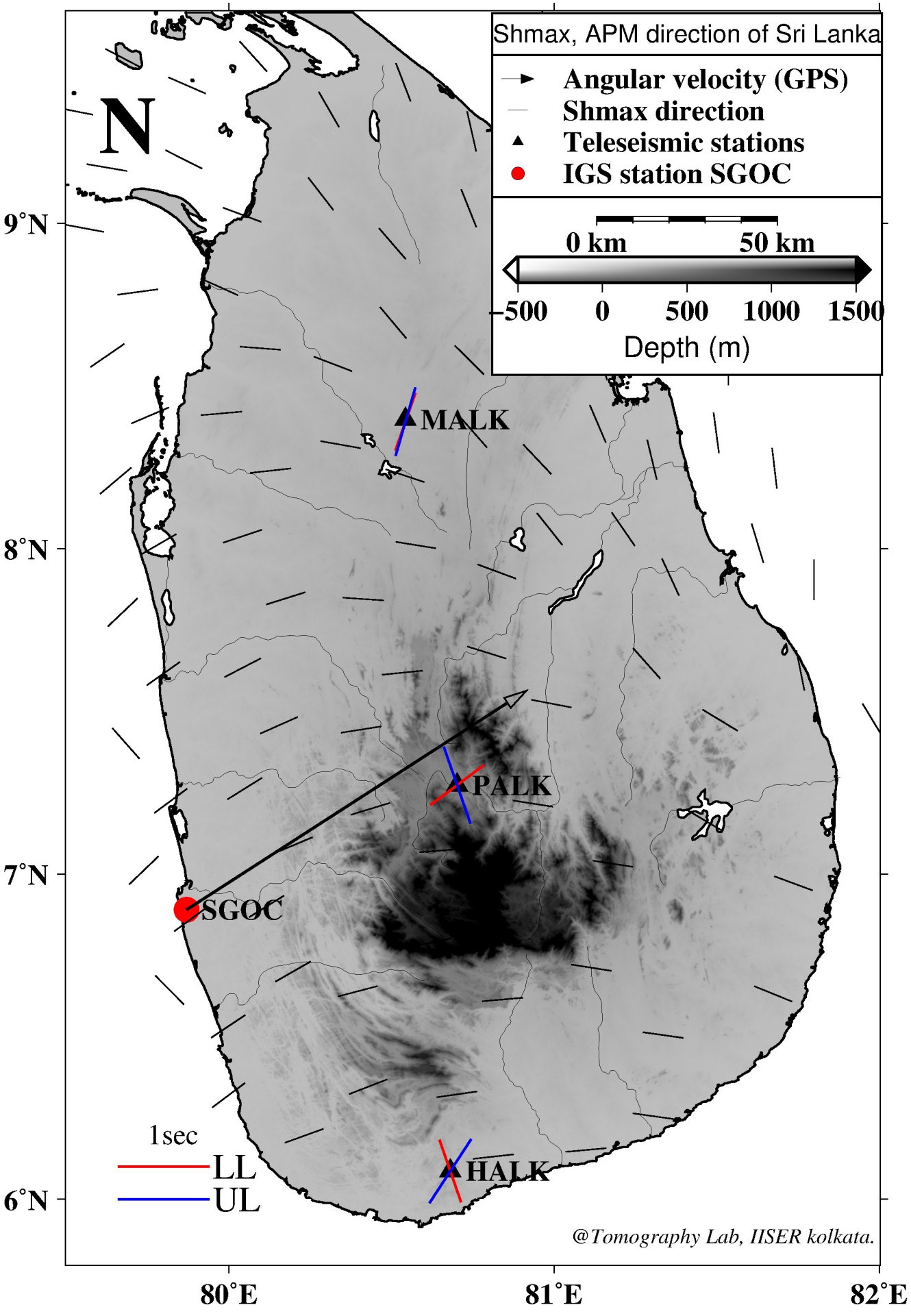
*Shivam Chandra[1]

1. Undergraduate student member

Anisotropy in the Earth’ s upper mantle is a signature of past and present deformation. Seismic anisotropy beneath a seismic station can be inferred by analyzing core-refracted (SK(K)S, PK(K)S) seismic phases. In this study, upper mantle anisotropy is investigated using shear wave splitting of SK(K)S phases at 3 stations in Sri Lanka. Sri Lanka consist of four main lithological units, viz., the Highland Complex (HC), the Wanni Complex (WC), the Vijayan complex (VC) and the Kadugannawa complex (KC). Shear wave splitting measurements were done for ~30 high-quality waveforms recorded in the region, using rotational correlation (RC), minimum energy (SC) and eigenvalue techniques. The result of the shear-wave splitting measurement shows the presence of two anisotropic layers in the upper mantle, viz., the upper layer with fast polarization direction (Φ): NW-SE and delay time (δt): 0.4-0.5 s, and the lower layer with Φ: NE-SW and δt: 0.6-0.8 s. Our study suggests that fast axis direction of lower layer with an average delay time of 0.6 s depicts a ~67 km thick anisotropic layer with 4% anisotropy beneath Sri Lanka region. Comparison of Absolute Plate Motion (APM) direction with fast directions infer that the Simple Asthenospheric Flow (SAF) model prevails in this region. On the other hand, Comparison of Maximum Horizontal stress (S_{hmax}) and the Global Positioning System (GPS) with the fast direction infer that there is partial contribution from lithospheric mantle. So, the anisotropy in Sri Lanka is mainly governed by asthenospheric flow, and partially due to lithospheric mantle.

Keywords: Shear wave splitting, Fast direction, Asthenospheric flow, Anisotropy

©2020. Japan Geoscience Union. All Right Reserved.



©2020. Japan Geoscience Union. All Right Reserved.

Lattice preferred orientation of akimotoite deformed in the D111 Kawai-type multianvil apparatus

*Longli Guan[1], Daisuke Yamazaki[1], Noriyoshi Tsujino[1]

1. Institute for Planetary Materials, Okayama University, Misasa, Japan

Seismic anisotropies are one of the key factors for understanding the mantle dynamic and have been observed near Tonga subducted slabs in the mantle transition zone and the uppermost lower mantle (mid-mantle) (e.g. Chen & Brudzinski, 2003; Vavryčuk, 2006; Nowacki et al.,2015). Spatial variation of seismic anisotropy in the Tonga subduction zone was reported by Vavryčuk. (2006). The stagnant slab above 660 km of northern segment shows that *P*-waves propagate more slowly in the direction normal to slab interface, while they propagate more slowly along the slab sinking direction in the penetrated slab below the 660 km of southern segment. The seismic anisotropy, in general, can be often caused by lattice preferred orientation (LPO) of elastically anisotropic minerals. LPO of akimotoite (ilmenite-structured (Mg, Fe) SiO_3) is plausible to interpret these seismological observations because it has a strong elastically anisotropic feature and it is one of main constituting mineral at the mantle transition zone and the uppermost lower mantle. Although pioneer works investigated the slip system of akimotoite (Cordier, 2002; Shirashi et al., 2008), it has not been fully determined yet. In this study, therefore, we conducted well-controlled deformation experiments at high pressure and temperature to observe LPO of akimotoite developed during deformation. The starting material of akimotoite aggregates was synthesized from $MgSiO_3$ glass at ~21 GPa and 1400℃, in the Kawai-type multianvil apparatus. Subsequent deformation experiments were conducted on the akimotoite aggregates at 21-23 GPa and 900-1200℃ by using high-pressure deformation apparatus, so-called D111 type apparatus, installed at Institute for Planetary Materials, Okayama University. Total strain and average strain rate were determined to be 0.08-0.19 and 2.63×10^{-5}-5.76×10^{-6} s^{-1}, respectively for the uniaxially deformed sample and 0.4-2.1 and 1.06×10^{-5} -6.03×10^{-5} s^{-1}, respectively for the sheared sample. All LPO patterns at experimental temperature ranged from 900 to 1200℃ indicate the c-axis of akimotoite is preferentially sub-parallel to the compression direction, suggesting a dominant slip plane on (0001). The variation of *P*-waves anisotropy observed in Tonga subduction zones at depths of the mid-mantle can be explained in terms of the LPO of akimotoite induced by different stress field between northern and southern slab segments. The LPOs of northern and southern slabs are mainly caused by the simple shear deformation with σ_2 perpendicular to the advance direction (slip direction) and along the slab and uniaxially compression with σ_1 parallel to the downdip direction, respectively. Our preliminary conclusion is consistent with geophysical observations (Bonnardot et al., 2009).

Keywords: akimotoite, lattice preferred orientation, mantle transition zone, subduction slabs, seismic anisotropy

©2020. Japan Geoscience Union. All Right Reserved.

Mantle discontinuities oceanward of the Krile - Honshu slab

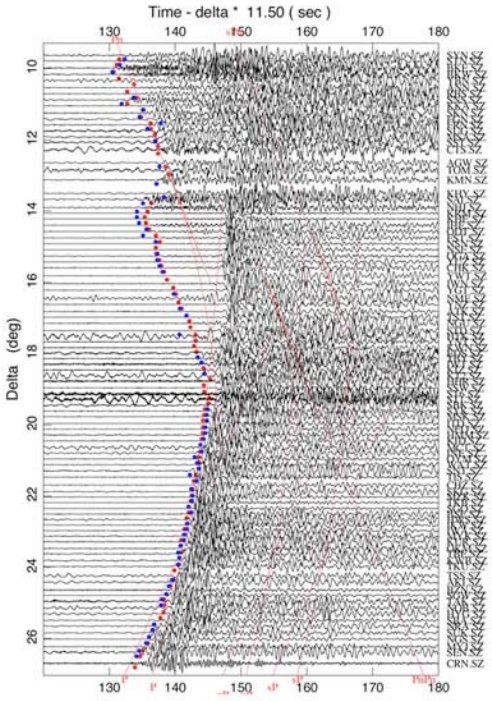
*Masayuki Obayashi[1], Junko Yoshimitsu[1], Yoshio Fukao[1]

1. Japan Agency for Marine-Earth Science and Technology

Triplication waveforms of the 410-km discontinuity (the 410) and 660-km discontinuity (the 660) recorded on Hi-net (High Sensitivity Seismograph Network in Japan) from Kuril earthquakes are analyzed to investigate seismic structures of the discontinuities. The first P-waves of which ray paths bottom depths well above the 410 arrive much earlier than expected by any standard spherical velocity model because they propagate through the dipping Pacific fast slab. However, such fast arrivals are well predicted by our tomography model GAP_P4 (Obayashi et al., 2013) (Figure 1). On the other hand, the later phases of the mantle discontinuity triplication are less affected by the dipping slab. Figure 2 shows the region of interest indicated by the ray paths grazing the discontinuities located oceanward the Kurile-Honshu slab. Figure 3 shows the square of envelope waveforms stacked for 11 earthquakes after equalizing the focal depths to a common depth of 120 km. This equalization was made using a representative slowness value of 11.5 or 9.7 (sec/deg) to emphasize the retrograde branch of the 410 or 660 triplication. The retrograde branches of the 410 and the 660 are clearly observed as shown by yellow thick lines in Figure 3. The retrograde branch for the 660 is consistent with the theoretical travel time predicted by IASP91 model. However, the retrograde branch for the 410 arrives later by 2 or 3 seconds and its slowness is larger than the prediction, suggesting slow anomalies atop of the 410. We will show a spherical model that explains the characteristics described above.

Keywords: mantle discontinuity, slab, triplication

©2020. Japan Geoscience Union. All Right Reserved.



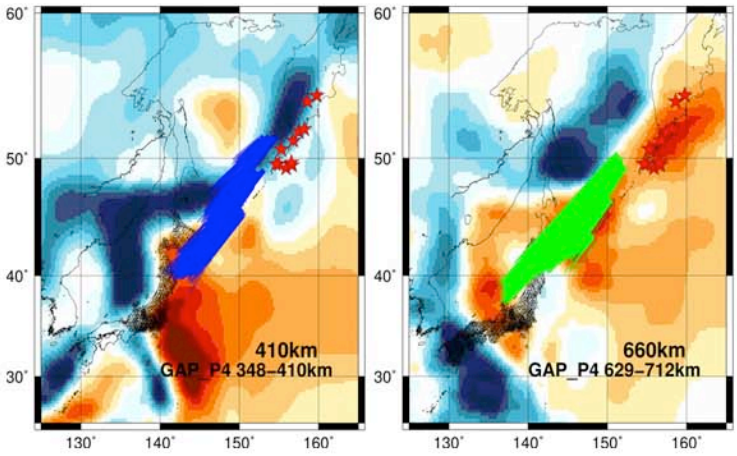


Figure 2. ray paths grazing the 410 (left) and the 660 (right) superimposed on GAP_P4 3D velocity model.

Figure 1. Vertical compornent Hinet seismograms for the Kuril earthquake on Oct. 16, 2012 aligned with increasing epicentral distance. Onset times manually picked (blue) and predicted by GAP_P4 (red) are shown by dots.

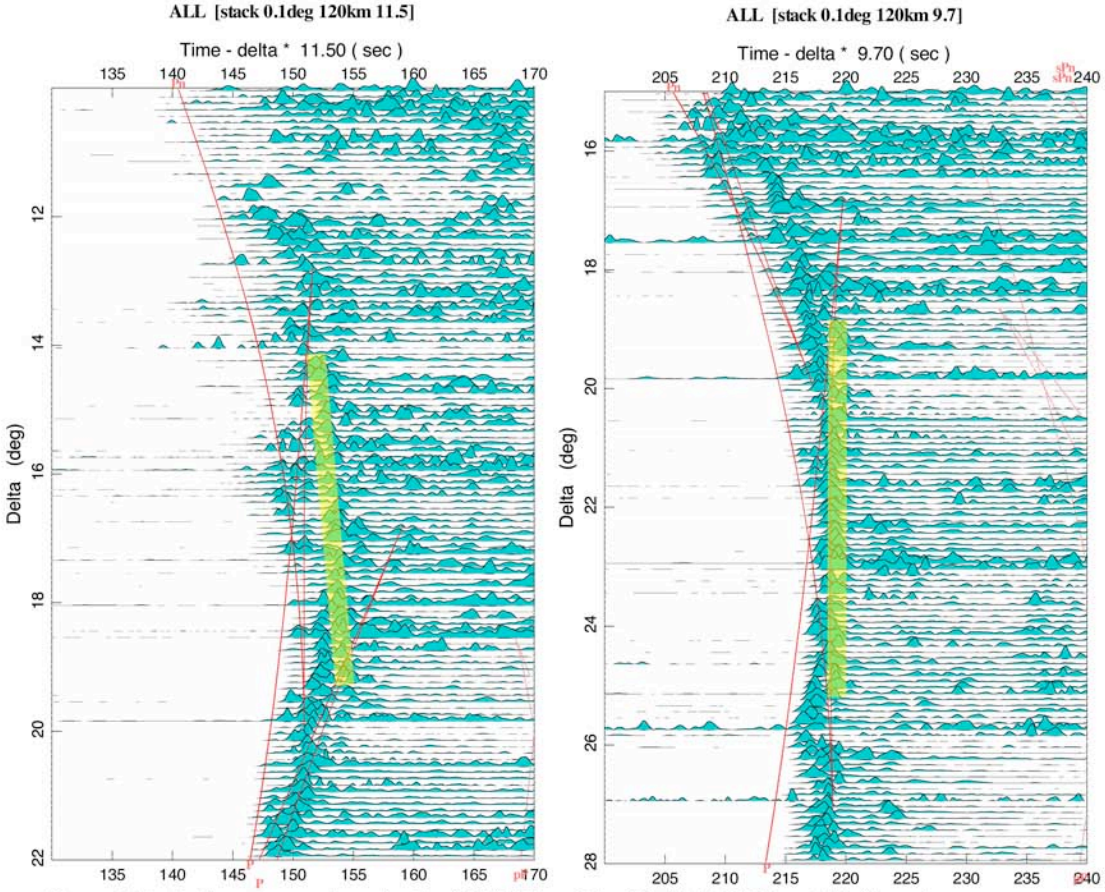


Figure 3 Stacked square envelope for the 410 (left) and the 660 (right) Yellow thick lines show the reterograde brances of the triplication that we focus on in this study.

©2020. Japan Geoscience Union. All Right Reserved.

Tomography Model Using Singular Value Decomposition

*Jun Su[1,2], Christine Houser[2], John William Hernlund[2]

1. Department of Earth and Planetary Sciences, Tokyo Institute of Technology, 2. Earth-Life Science Institute

We apply a singular value decomposition (SVD) solution for the inverse problem in tomography and compares model results with a least-squares (LSQR) method which uses first difference radial and lateral smoothing parameters for regularization. Taking advantage of the increased computing power and efficient algorithms, we are now able to introduce the SVD method to solve a non-sparse matrix inversion like three-dimensional global mantle tomography. This study finds the k value for truncated SVD can serve as a unique regularization parameter and produce models with similar spectral power to the LSQR solutions.

We examine the SVD method using the same dataset as the tomographic model HSML06: long-period travel time residuals downloaded from the Incorporated Research Institutions for Seismology Data Management Center from 1976 to 2005. When employing a least-squares inversion, changing the smoothing parameters requires an entire re-calculation of inversion. However, the SVD solution provides a less computationally expensive way to regularize tomographic models by increasing or decreasing the number of singular values that contribute to the solution. Structures of small scale and fluctuations of short wavelength contribute smaller singular values and correspond to the later part of the singular matrix according to its descending property. We evaluate the SVD tomographic models to determine the necessary contribution of the smaller singular values to retain seismic structure resolved using the least-squares technique. The SVD solutions are desirable since they require negligible computation time and the resulting resolution operator provides a quantitative means for comparing tomography with geodynamics models.

Keywords: SVD, Tomography, Inverse Problem

©2020. Japan Geoscience Union. All Right Reserved.

Whole-mantle P-wave tomography beneath East Asia

*Yu Katayama[1], Dapeng Zhao[1], Genti Toyokuni[1]

1. Research Center for Prediction of Earthquakes and Volcanic Eruptions, Graduate School of Science, Tohoku University

The geological structure and tectonics of East Asia are characterized by the India-Asia collision in the southwest and subduction of the Pacific plate and the Philippine Sea plate from the east. The Pacific slab exists as a stagnant slab in the mantle transition zone, which is closely related to intraplate volcanism in NE Asia. Volcanoes in mainland China, such as those in Changbai, Datong, Ashikule and Hainan are intraplate volcanoes, which are quite different from the volcanoes in subduction zones and mid-ocean ridges. The origin of magmatic fluids associated with the formation of the intraplate volcanoes and causal mechanism of large earthquakes in the continental region have been investigated by many previous tomographic studies (e.g., Zhao et al., 2011; Ma et al., 2019). However, the detailed crustal and mantle structures under the intraplate volcanoes and the slab structures are still not very clear. In this study, we investigate these issues by conducting whole-mantle P-wave tomography beneath the East Asian region.

We use a large number of P-wave arrival time data of earthquakes selected from the ISC-EHB catalog and Annual Bulletin of Chinese Earthquakes. The events are relocated using depth phase data. To select a best set of earthquakes, we divided the crust and mantle into small cubic blocks and only selected an event in each block that had the maximum number of arrival-time data and the smallest error in the hypocentral location. The events are selected so that they have a uniform distribution in the study region.

We use the multiscale global tomography method (Zhao et al., 2013, 2017), which can prevent the over-dense grid nodes arranged at higher latitudes. A denser 3-D grid is arranged in East Asia, whereas a coarser 3-D grid is arranged in the surrounding whole globe.

Our new tomographic model shows the following features.

(1) Low-velocity anomalies are generally revealed in the whole mantle under the Hainan region, which may reflect the whole-mantle Hainan plume.

(2) Very heterogeneous structures are revealed under the Tibetan region, which may reflect the complex subduction of the Indian plate beneath the Eurasian plate.

(3) Slab tear is revealed under the marginal seas, which is consistent with the recent result obtained by Ma et al. (2019).

References

©2020. Japan Geoscience Union. All Right Reserved.

Ma, J., Y. Tian, D. Zhao, C. Liu, T. Liu (2019). Mantle dynamics of Western Pacific and East Asia: New insights from P-wave anisotropic tomography. *Geochem. Geophys. Geosyst.* 20, 3628-3658.
Zhao, D., S. Yu, E. Ohtani (2011). East Asia: Seismotectonics, magmatism and mantle dynamics. *J. Asian Earth Sci.* 40, 689-709.
Zhao, D., Y. Yamamoto, T. Yanada (2013). Global mantle heterogeneity and its influence on teleseismic regional tomography. *Gondwana Res.* 23, 595-616.
Zhao, D., M. Fujisawa, G. Toyokuni (2017). Tomography of the subducting Pacific slab and the 2015 Bonin deepest earthquake (Mw 7.9). *Scientific Reports* 7, 44487, doi:10.1038/srep44487.

Keywords: Seismic tomography, East Asia, Hainan plume

©2020. Japan Geoscience Union. All Right Reserved.

Seebeck coefficient measurement of olivine by dual heating system and its application to the redox kinetics of the subducted slabs

*Ran Wang[1], Takashi Yoshino[1]

1. Institute for Planetary Materials, Okayama University

Subduction plays an important role in the plate tectonics of the Earth and is closely related to many activities such as water transport, volcanism and mantle convection. In addition, the subducted slabs can also influence the redox state of the Earth’ s interior because the descending slabs are always colder and more oxidized compared with the surrounding mantle. Since thermal boundary layer is likely to develop around the cold slab, the heat conduction could produce the electrical potential gradient by the Seebeck effect. The Seebeck coefficient is a parameter to define the type of the dominant charge carrier inside the materials under thermal gradient. Positive value of seebeck coefficient means the charge carriers have positive valence such as electron holes (small polarons) and protons. When the value is negative, electrons or metal vacancy are potential charge carriers.

To determine the Seebeck coefficient under high pressure, we established the cell design with dual heating systems on the 6-axis apparatus. Two disk TiB_2 heaters were placed in the octahedral cell to make two insulated heating systems. Temperature differences were produced on the two sides of the sample by dual heaters and the temperatures were measured by separated thermocouples on each side of the sample. In addition, the electromotive force (voltage difference) of the sample was measured by high resolution multimeter. Therefore, we could easily obtain the seebeck coefficient from the formula, $S = \Delta V / \Delta T$. To check the reliability of the method, we use two types of P-type silicon single crystals with different boron doping concentrations as the test materials. The results are quite consistent with previous experimental and calculation results obtained at ambient pressure.

In order to better understand the redox kinetics of the subduction zones, olivine, the dominant phase in the upper mantle, is the most important mineral to control the redox condition. We measured the Seebeck coefficient of olivine under high pressure. The Seebeck coefficient of the sintered Fo_{90} aggregates was measured at 5 GPa. The Seebeck coefficient is positive and decreases with increasing temperature. The positive to negative transition of the charge carrier occurred at around 1100-1200℃. Thus, we can assume that the temperature of the overlying mantle at about 150 km is above 1350℃, and then olivine would behave as N-type semiconductors. In contrast, olivine in the cold slab behaves as P-type semiconductor, suggesting that the cold slab will be oxidized itself by the Seebeck effect.

Keywords: Seebeck coefficient, redox kinetics, subducted slab, thermal boundary layer, charge carrier, olivine

©2020. Japan Geoscience Union. All Right Reserved.

High-pressure generation to 150 GPa in multianvil apparatus using the 6-8-2 system with nano-polycrystalline diamond anvils.

*Takehiro Kunimoto[1], Masayuki Nishi[1], Tetsuo Irifune[1]

1. Geodynamics Research Center

The pressures available in Kawai-type multianvil apparatus (KMA), using second-stage anvils of tungsten carbide (WC) or sintered diamond (SD), have been limited to about 30 GPa and 60 GPa, respectively [e.g.1,2]. Recent efforts in introductions of new WC and SD materials and improvements in cell assemblies significantly expanded these limits to 60 GPa for WC anvils and 120 GPa for SD anvils [3,4,5]. An attempt has also been made to the harder nano-polycrystalline diamond (NPD) as the second-stage anvils demonstrated the potential importance of this noted ultra-hard material for KMA, but the available pressures have been limited to ~90 GPa because of the limitation in the size of the NPD anvils [6].

Kunimoto and Irifune (2010) introduced a newly-designed cell assembly for 6-8-2 type cell with NPD as third-stage anvils, and reported generation of pressures up to 125 GPa [7], but it was difficult to produce further higher pressures. So, we have been trying to improve the cell assembly for the 6-8-2 system to generate the pressure equivalent to the Earth’ s core-mantle boundary (CMB), for better understanding of this heterogeneous region using advantages of KMA over competing diamond anvil cell.

In situ X-ray experiments were conducted using the KMA (SPEED-Mk.II) at SPring-8, BL04B1. We used sintered polycrystalline $MgSiO_3$-perovskite (Pv) synthesized in a KMA as a starting material. Generated pressures were determined from the unit cell volumes of Au and MgO using adequate equation of state [8,9]. Upon compression, the X-ray diffraction profile showed the $MgSiO_3$-Pv changed to an amorphous-like phase above ~70 GPa at the room temperature. Eventually, we reached pressures of about 150 GPa in two independent runs, which are the highest pressure ever reported in KMA, although we were unable to identify the crystal structure of the sample due to amorphization. The pressure achieved in these runs completely cover the entire D” region (approx. 125-135 GPa), and some attempts have also been made to produce high temperatures under such pressures.

References

[1] K. Litasov, A. Shatskiy, P. N. Gavryushkini, S. Sharygin, P. I. Dorogokupets, A. N. Dymshits, E. Ohtani, Y. Higo, K. Funakoshi. P-V-T equation of state of siderite to 33 GPa and 1673 K. Phys Planet Earth Inter., 224, 83-87 (2013).

[2] E. Ito, *Multianvil cells and high-pressure experimental methods, in Treatise on Geophysics*, G. Schubert ed., Elsevier, Amsterdam, Vol.2, 197-230 (2007).

[3] T. Kunimoto, T. Irifune, Y. Tange, and K. Wada, Pressure generation to 50 GPa in Kawai-type multianvil apparatus using newly-developed tungsten carbide anvils, High Pres. Res., 36, 97-104 (2016).

[4] D. Yamazaki, E. Ito, T. Yoshino, N. Tsujino, A. Yoneda, H. Gomi, J. Vazhakuttiyakam, M. Sakurai, Y. Zhang, Y. Higo, and Y. Tange, High-pressure generation in the Kawai-type multianvil apparatus equipped with tungsten-carbide anvils and sintered-diamond anvils, and X-ray obserbation on $CaSnO_3$ and $(Mg,Fe)SiO_3$, C. R. Geoscience, 351, 253-259 (2019).

©2020. Japan Geoscience Union. All Right Reserved.

[5] T. Ishii, D. Yamazaki, N. Tsujino, F. Xu, Z. Liu, T. Kawazoe, T. Yamamoto, D. Druzhbin, L. Wang, Y. Higo, Y. Tange, T. Yoshino, and T. Katsura, Pressure generation to 65 GPa in Kawai-type multianvil apparatus with tungsten carbide anvils, High Press. Res., 37, 507-515 (2017).

[6] T. Irifune, T. Kunimoto, T. Shinmei, and Y. Tange, High pressure generation in Kawai-type multianvil apparatus using nano-polycrystalline diamond anvils, C. R. Geoscience, 351, 260-268 (2019).

[7] T. Kunimoto, and T. Irifune, Pressure generation to 125 GPa using 6-8-2 type multianvil apparatus with nano-polycrystalline diamond anvils, J. Phys. Conf. Ser., 215, 012190 (2010).

[8] T. Tsuchiya, First principle prediction of the P-V-T equation of state of gold and the 660-km discontinuity in Earth’ s mantle, J. Geophys. Res., 108, 2462 (2003).

[9] Y. Tange, Y. Nishihara, and T. Tsuchiya, Unified analysis for P-V-T equation of state of MgO: A solution for pressure-scale problems in high P-T experiments, J. Geophys. Res., 114, B03208 (2009).

Keywords: nano-polycrystalline diamond, high-pressure generation, multi anvil apparatus

©2020. Japan Geoscience Union. All Right Reserved.

[E] Poster | S (Solid Earth Sciences)：S-IT Science of the Earth's Interior & Techtonophysics

[S-IT26] Interaction and Coevolution of the Core and Mantle in the Earth and Planets

convener:Kenji Ohta(Department of Earth and Planetary Sciences, Tokyo Institute of Technology), Tsuyoshi Iizuka(University of Tokyo), Kenji Kawai(Department of Earth and Planetary Science, School of Science, University of Tokyo), Taku Tsuchiya(Geodynamics Research Center, Ehime University)

Recent observational and experimental investigations have significantly advanced our understanding of the structure and constituent materials of the deep Earth. Yet, even fundamental properties intimately linked with formation and evolution of the planet, such as details of the chemical heterogeneity in the mantle and light elements dissolved in the core, remain unclear. Seismological observations have suggested a vigorous convection in the lower mantle, whereas geochemistry has suggested the presence of stable regions there that hold ancient isotope signatures. The amounts of radioactive isotopes that act as heat sources and drive dynamic behaviors of the deep Earth are also still largely unknown. We provide an opportunity to exchange the achievements and ideas, and encourage persons who try to elucidate these unsolved issues of the core-mantle evolution using various methods, including high-pressure and high-temperature experiments, high-precision geochemical and paleomagnetic analyses, high-resolution geophysical observations, geo-neutrino observations, and large-scale numerical simulations. Papers stimulating an interdisciplinary collaboration relating to establishment of the Japan-SEDI community are also welcomed.

[SIT26-P01] Density of Fe^{3+}-bearing magma at high pressure

Rintaro Ban[1], *Akio Suzuki[1], Tatsuya Sakamaki[1] (1.Department of Earth Science, Graduate School of Science, Tohoku University)

[SIT26-P02] Quantitative evaluation of the geochemical correlation length within the single granitic body, toward the error estimation of geoneutrino flux from the Japanese crust

*Kenta Ueki[1], Minami Kazuki[2], Akimichi Taketa[2], Tsuyoshi Iizuka[3], Sanshiro Enomoto[4], Nozomu Takeuchi[2], Hiroyuki Tanaka[2] (1.Japan Agency for Marine-Earth Science and Technology, 2.Earthquake Research Institute, the University of Tokyo, 3.Department of Earth and Planetary Science, The University of Tokyo, 4.University of Washington, Department of physics)

[SIT26-P03] Re-evaluation of thermal data in the Japanese Islands for better estimation of the temperature structure in the crust

*Makoto Yamano[1], Akiko Tanaka[2], Hideki Hamamoto[3], Shusaku Goto[2], Takumi Matsumoto[4] (1.Earthq. Res. Inst., Univ. Tokyo, 2.Geol. Surv. Japan, AIST, 3.Center Environ. Sci. Saitama, 4.Nat. Res. Inst. Earth Sci. Disaster Resilience)

[SIT26-P04] Outer core flows and dynamo induced by heterogeneous growth of the inner core of the Earth

*Shin-ichi Takehiro[1], Youhei SASAKI[2] (1.Research Institute for Mathematical Sciences, Kyoto University, 2.Department of Architecture/Institute of Fundamental Sciences, Setsunan University)

[SIT26-P05] Seismic structure near the inner core boundary in the north polar region

*Toshiki Ohtaki[1], Satoru Tanaka[2], Satoshi Kaneshima[3], Weerachai Siripunvaraporn[4,5], Songkhun Boonchaisuk[5,6], Sutthipong Noisagool[4,5], Kenji Kawai[7], Taewoon Kim[2], Yuki Suzuki[7], Yasushi Ishihara[2], Koji MIYAKAWA[8], Nozomu Takeuchi[8], Hitoshi Kawakatsu[8] (1.Geological Survey of Japan, National Institute of Advanced Industrial Science and Technology (AIST), 2.Japan Agency for Marine-Earth Science and Technology (JAMSTEC), 3.Department of Earth and Planetary Sciences, Faculty of Sciences, Kyushu University, 4.Faculty of Science, Mahidol University, Kingdom of Thailand, 5.ThEP Center, Commission on Higher Education, Kingdom of Thailand, 6.Geoscience Program, Mahidol University, Kingdom of Thailand, 7.Graduate School of Science, University of Tokyo, 8.Earthquake Research Institute, University of Tokyo)

[SIT26-P06] Deformation experiments of lower mantle minerals using D111 type press

*Noriyoshi Tsujino[1], Daisuke Yamazaki[1], Yu Nishihara[2] (1.Institute for Planetary Materials, Okayama University, 2.GRC, Ehime University)

[SIT26-P07] **Chromium isotopes of basalts from the Ontong Java Plateau and Samoan Ocean Islands: Implications for the core-mantle interaction**

*Yuki Hibiya[1], Tsuyoshi Iizuka[2], Katsuhiko Suzuki[1], Shigekazu Yoneda[3] (1.Japan Agency for Marine-Earth Science and Technology, 2.The University of Tokyo, 3.National Museum of Nature and Science)

[SIT26-P08] The tungsten isotopic compositions of kimberlites: constraints on material circulation in the deep Earth

*Otaro Kobayashi[1], Tsuyoshi Iizuka[1], Hatsuki Enomoto[1] (1.Department of Earth and Planetary Science, Graduate School of Science, The University of Tokyo)

[SIT26-P09] In situ X-ray and neutron diffraction studies of hcp iron hydride

*Sho Kakizawa[1,2], Hiroyuki Kagi[2], Chikara Shito[2], Hiroyuki Saitoh[3], Yuji Higo[4], Yoshinori Tange[4], Asami Sano-Furukawa[5], Takanori Hattori[5], Katsutoshi Aoki[2] (1.Hiroshima University, 2.Geochemical Research Center, The University of Tokyo, 3.National Institutes for Quantum Radiological Science and Technology, 4.Japan Synchrotron Radiation Research Institute, 5.J-PARC center, Japan Atomic Energy Agency)

[SIT26-P10] ***Ab initio*** **lattice thermal conductivity of (Mg,Fe)O ferropericlase at the deepest mantle**

*Haruhiko Dekura[1], Taku Tsuchiya[1] (1.Geodynamics Research Center, Ehime University)

[SIT26-P11] Soft Core-Mantle Boundary: A Mechanism for Chemical Interactions Between the Core and Mantle

*Kang Wei Lim[1], Irene Bonati[1], Scott D Hull[2], John W Hernlund[1] (1.Earth-Life Science Institute, Tokyo Institute of Technology, 2.Earth and Environmental Sciences, University of Rochester)

[SIT26-P12] **Electrical conductivity measurement of water-bearing bridgmanite using an externally heated diamond anvil cell**

*Yoshiyuki Okuda[1], Kenji Ohta[1], Yu Nishihara[2], Hiroyuki Kagi[3], Kei Hirose[3,4] (1.Tokyo Institute of Technology, 2.Ehime University, 3.University of Toyko, 4.Earth-Life Science Institute)

[SIT26-P13] Mechanisms of the post-perovskite transformation in $NaNiF_3$

Koyumi Yamashita[1], *Tomoaki Kubo[1], Yoshinori Tange[2], Yuji Higo[2] (1.Kyushu Univ., 2.JASRI)

Density of Fe^{3+}-bearing magma at high pressure

Rintaro Ban[1], *Akio Suzuki[1], Tatsuya Sakamaki[1]

1. Department of Earth Science, Graduate School of Science, Tohoku University

Previous studies indicate the high concentration of Fe_2O_3 in the lower mantle. Even though the partial molar volume of Fe_2O_3 has become essential for discussing the magma in the deep mantle, there is no data of partial molar volume of Fe_2O_3 at high pressure and temperature. This study is aimed to obtain partial molar volume of Fe_2O_3 in silicate melts under high pressure. Fe^{3+}-rich starting material was compressed by a Kawai-type multi-anvil apparatus at high pressure of above 4 GPa and high-temperature of above 1800 ˚C. We determined the third-order Birch-Murnaghan equation of state of melts from results of sink-float method. By combining the compression curves of melts and the equation of state of silicate melts proposed in Wakabayashi and Funamori (2013), partial molar volumes were yielded between 8 and 22 GPa and 1800 ˚C. These results indicate that compressibility of Fe_2O_3 is much higher than that of FeO within the range of 8 GPa to 22 GPa.

Keywords: magma, partial molar volume, density, mantle, high pressure

©2020. Japan Geoscience Union. All Right Reserved.

Quantitative evaluation of the geochemical correlation length within the single granitic body, toward the error estimation of geoneutrino flux from the Japanese crust

*Kenta Ueki[1], Minami Kazuki[2], Akimichi Taketa[2], Tsuyoshi Iizuka[3], Sanshiro Enomoto[4], Nozomu Takeuchi[2], Hiroyuki Tanaka[2]

1. Japan Agency for Marine-Earth Science and Technology, 2. Earthquake Research Institute, the University of Tokyo, 3. Department of Earth and Planetary Science, The University of Tokyo, 4. University of Washington, Department of physics

Geoneutrino observation at anti-neutrino observatory "KamLAND" (Kamioka, Hida City, Gifu Prefecture) allows us to estimate the total abundance of Uranium and Thorium in the deep Earth. By subtracting the crustal contribution from the KamLAND observation, it is possible to estimate the flux of mantle-derived geoneutrino. As ~50% of the observed geoneutrino flux at KamLAND is derived from the nearby Japan crust, precise estimations of geoneutrino flux from the Japan crust and its error are essential to estimate the flux of mantle-derived geoneutrino accurately. For this purpose, we have established a stochastic estimation method for crustal chemical composition. Based on the stochastic compositional model, we have calculated the geoneutrino flux from the Japan crust. At present, the estimated values of geoneutrino flux from the Japanese crust exhibit a considerable uncertainty because of the difficulty in handling spatial correlations (in other words, compositional similarities within each geological unit).
In this study, dense sampling was performed in a single granite body (Inada granite, Kasama City, Ibaraki prefecture) to quantitatively understand the spatial correlation of rock chemical composition. By analyzing the compositional differences between samples at various distances, the spatial correlation length of the compositions was evaluated. Based on the analysis, the "typical composition of a km-scale rock body," which excludes small (cm-m) spatial-scale composition variations, was estimated with an uncertainty. Under this proper correlation modeling, geoneutrino flux estimation errors from the Japan crust would be reduced. We also discuss the magmatic processes that derived the geochemical variations of granite, based on the differences in spatial correlation depending on the elemental species.

Keywords: Geoneutrino, Granite, Geochemical modeling

©2020. Japan Geoscience Union. All Right Reserved.

Re-evaluation of thermal data in the Japanese Islands for better estimation of the temperature structure in the crust

*Makoto Yamano[1], Akiko Tanaka[2], Hideki Hamamoto[3], Shusaku Goto[2], Takumi Matsumoto[4]

1. Earthq. Res. Inst., Univ. Tokyo, 2. Geol. Surv. Japan, AIST, 3. Center Environ. Sci. Saitama, 4. Nat. Res. Inst. Earth Sci. Disaster Resilience

For investigation of the structure and composition of crust, we need to combine various geophysical data with estimated subsurface temperature stricture as well as geological and petrological information, since physical properties of rocks depend on temperature. Surface heat flow is the most fundamental data for estimation of subsurface temperature structure. However, published heat flow data on land in the Japan have been rather sparse and not evenly distributed owing to the limitation of boreholes available for temperature measurement.

Borehole temperature profiles have been measured in observation wells for the Hi-net seismograph network, which are densely and evenly distributed over the Japanese Islands. Temperature measurements have been conducted in groundwater monitoring wells located in and around large cities as well. Although these data can be valuable sources of new heat flow data, the most of the wells are shallow, 50 to 150 m, and subject to influence of ground surface temperature (GST) variation. We selected temperature profile data in relatively deep wells, over 150 m, in the central part of Honshu and attempted to evaluate the influence of GST variation on subsurface temperature structure.

After eliminating data apparently affected by groundwater flow, we reconstructed GST history in the past at each well through inversion analysis of the temperature profile data, taking account of the layered subsurface structure based on borehole lithological column information. GST histories for the last 300 years were successfully reconstructed at several sites in Kanto and Tokai regions and the obtained GST variations are similar to each other. It suggests that we may be able to determine an average GST history for each region in Japan, which can be used for analysis of shallow well temperature data in the region.

For determination of heat flow values, we need to know thermal conductivity of formations through which temperature gradient is measured. At many stations, however, it is difficult to obtain rock/sediment samples for thermal conductivity measurement. Aiming for better evaluation of surface heat flow, we have been conducting measurement of thermal conductivity of core samples collected from Hi-net wells and boreholes drilled for volcano observation. We used an optical scanning instrument, TCS (Thermal Conductivity Scanner), which enables nearly continuous measurement along the core, as well as a conventional box-type probe, QTM (Quick Thermal Conductivity Meter). High-density data with TCS provide valuable information on small-scale heterogeneity in thermal conductivity. For most of the samples we measured, the average of values obtained with TCS is consistent with the value with QTM.

A new version of database "Thermal Data Collection in and around Japan" was released by Geological Survey of Japan in March 2019. It contains updated compilations of heat flow data in the northwest Pacific area (0 to 60 ˚N, 120 to 160 ˚E) and geothermal gradient data in and around Japan, and a new collection of thermal conductivity values measured on rock samples from boreholes in Japan. These datasets, in combination with data from Hi-net boreholes and groundwater monitoring wells, would serve as a basis for modeling thermal structure of subduction zones around the Japanese Islands.

©2020. Japan Geoscience Union. All Right Reserved.

Keywords: temperature structure, heat flow, thermal conductivity, borehole temperature, ground surface temperature, database

©2020. Japan Geoscience Union. All Right Reserved.

Outer core flows and dynamo induced by heterogeneous growth of the inner core of the Earth

*Shin-ichi Takehiro[1], Youhei SASAKI[2]

1. Research Institute for Mathematical Sciences, Kyoto University, 2. Department of Architecture/Institute of Fundamental Sciences, Setsunan University

Recent seismological observations suggest longitudinal heterogeneity of seismological wave velocity of the inner core of the Earth, which stimulates a discussion that phase change at the inner core boundary (ICB) does not occur uniformly in the horizontal directions. One of the mechanism explaining heterogeneous growth of the inner core, is that hydrodynamic instability of the inner core surrounded by the phase boundary causes translational motion inside the inner core. The expected amplitude of the motion is 5e-10 m/s,
which is one order of magnitude larger than that of the velocity of uniform growth of the inner core. This suggests that heterogeneous component of the inner core growth dominates the uniform one if this mechanism actually operates in the core of the Earth, However, almost numerical simulations of geodynamo performed so far assume homogeneous buoyancy condition at ICB. In this study, we investigate the characteristics of outer core flows and dynamo action when the inner core grows heterogeneously. By performing numerical experiments of MHD rotating spherical dynamo, the effects of heterogeneous buoyancy condition at ICB are examined, as well as those of the rotation of the inner core. The governing equations of the numerical model is those for MHD Boussinesq fluid. The radius ratio of the inner and outer spherical boundaries is fixed to 0.35, the Ekman number is 1e-4, compositional and magnetic Prandtl numbers are 1, the modified Rayleigh number is 0.075. The compositional boundary conditions at ICB is
either uniform or Y_1^1 spherical harmonics type. The inner core either co-rotates with the mantle, rotates faster than the mantle, or slower. The results of time integrations show that the magnetic field is maintained when the inner core is co-rotating while it decays when the inner core is rotating faster or slower than the mantle. The obtained the magnetic field is dipolar in the case of uniform compositional boundary condition, whereas the magnetic field localizes in the case of Y_1^1 type ICB condition.

Keywords: Heterogeneity, Inner core, Core Mantle boundary

©2020. Japan Geoscience Union. All Right Reserved.

Seismic structure near the inner core boundary in the north polar region

*Toshiki Ohtaki[1], Satoru Tanaka[2], Satoshi Kaneshima[3], Weerachai Siripunvaraporn[4,5], Songkhun Boonchaisuk[5,6], Sutthipong Noisagool[4,5], Kenji Kawai[7], Taewoon Kim[2], Yuki Suzuki[7], Yasushi Ishihara[2], Koji MIYAKAWA[8], Nozomu Takeuchi[8], Hitoshi Kawakatsu[8]

1. Geological Survey of Japan, National Institute of Advanced Industrial Science and Technology (AIST), 2. Japan Agency for Marine-Earth Science and Technology (JAMSTEC), 3. Department of Earth and Planetary Sciences, Faculty of Sciences, Kyushu University, 4. Faculty of Science, Mahidol University, Kingdom of Thailand, 5. ThEP Center, Commission on Higher Education, Kingdom of Thailand, 6. Geoscience Program, Mahidol University, Kingdom of Thailand, 7. Graduate School of Science, University of Tokyo, 8. Earthquake Research Institute, University of Tokyo

The upper inner core of the Earth has quasi-hemispherical heterogeneity [Tanaka and Hamaguchi, JGR 1997]. A region that occupies a smaller area, called as 'East', has higher P-wave velocity and attenuation and smaller anisotropy compared with the rest, which is called as 'West'. To determine the boundary between these two regions at high latitudes, we analyze waveforms from Central America earthquakes observed at temporal broadband seismic network in Thailand (Thai Seismic Array; TSAR) [Tanaka et al., *Bull. Earthq. Res. Inst. Univ. Tokyo*, 2019]. Rays from C. America earthquakes to the network pass in the inner core, and have their turning points near 180˚E in the north polar region, which is close to the supposed boundary by several seismic studies. We pick differential traveltimes between PKPbc, which turn in the lower outer core, and PKIKP, which turn in the inner core, on the waveforms, and obtain differential residuals relative to ray-theoretical values predicted by PREM. The observed residuals are compared with those for global models and regional inner core models which represent 'East', 'West', and the South Pole. The residuals are also compared with residuals of South America earthquakes observed in Japan, which sample the 'western' upper inner core.

Keywords: P-wave velocity, inner core, heterogeneity

©2020. Japan Geoscience Union. All Right Reserved.

Deformation experiments of lower mantle minerals using D111 type press

*Noriyoshi Tsujino[1], Daisuke Yamazaki[1], Yu Nishihara[2]

1. Institute for Planetary Materials, Okayama University, 2. GRC, Ehime University

One dimensional viscosity models of the Earth’s mantle proposed by geophysical observations suggested that the lower mantle had the largest viscosity in the Earth’s mantle. In order to understand mantle dynamics in the Earth’s interior, it is important to know the viscosity of the Earth’s lower mantle. However, there are large variations of viscosity in the lower mantle between suggested models because of limitation of locations for geophysical observations. Therefore, it is important to determine viscosity of lower mantle minerals by high pressure experiments in order to discuss mantle dynamics. Bridgmanite would be the most abundant mineral in the lower mantle. This mineral could dominate the lower mantle viscosity at low strain conditions. In addition, ferropericlase, which would be the second abundant mineral in lower mantle and considered to softer than bridgmanite, might dominate the lower mantle viscosity with large shear strain condition. In this study, we conducted in-situ stress-strain measurements of uniaxial deformation experiments of bridgmanite aggregate and shear deformation experiments of post-spinel phase using D-111 type high pressure apparatus.

In-situ measurements were conducted using MAX III with D111 type guide block at PF-AR NE7A beam line. Mg-pure bridgmanite aggregates and Mg-pure post-spinel phase aggregates, which is bridgmanite and periclase mixture with 1:1 molar ratio, were used as starting material for uniaxial and shear deformations experiments, respectively. Experimental conditions are 1473-1673 K and 24-27 GPa. WC second cubic anvils with cone (6°) to take 2D X-ray diffraction, was used along X-ray path. Largest strain ε of uniaxial deformation experiments of bridgmanite reached approximately 0.3. We changed strain rate and/or temperature conditions within one uniaxial deformation experiment to determine stress-strain relationship and temperature effect precisely, respectively. Based on obtained stress exponent n and activation enthalpy H^* in this study, dominant deformation mechanisms would be dislocation creep. At normalized strain (10^{-5} /s), the creep strength of bridgmanite in this study is the largest in constituent mantle minerals reported by D-DAI apparatus. At shear deformation experiments, maximum shear strain reached around 1, which was much larger than the strain at which the hint of strain weakening of bridgmanite was observed in Girard et al. (2016) while stress of bridgmanite were almost constant until maximum strain. The obvious stress weakening of bridgmanite was not observed until shear strain ~ 1 in this study.

Keywords: rheology, viscosity, Lower mantle

©2020. Japan Geoscience Union. All Right Reserved.

Chromium isotopes of basalts from the Ontong Java Plateau and Samoan Ocean Islands: Implications for the core-mantle interaction

*Yuki Hibiya[1], Tsuyoshi Iizuka[2], Katsuhiko Suzuki[1], Shigekazu Yoneda[3]

1. Japan Agency for Marine-Earth Science and Technology, 2. The University of Tokyo, 3. National Museum of Nature and Science

Introduction: Basaltic rocks from large igneous provinces (LIPs) and from ocean islands (OIBs) are thought to be derived from the deep-rooted mantle upwelling. Recent studies have shown that some of these rocks, including OIBs from Samoa and Hawaii, are characterized by ^{182}W deficits that are well resolved from the ambient upper mantle [1, 2]. This negative ^{182}W signature has recently been proposed to originate from the outer core which has a μ^{182}W of −220 [3-5]. If so, the ^{182}W anomaly may be accompanied by deficits of ^{53}Cr, a decay product of a short-lived radionuclide ^{53}Mn, because Cr is more siderophile than Mn at high temperature [6, 7]. However, the Cr isotope variations of LIPs and OIBs are still poorly known. Here, we report the mass independent Cr isotopic data for basaltic rocks from the Ontong Java plateau (OJP) and Samoan OIBs, to further examine the core-mantle interaction that can cause the systematic isotopic variability between LIPs and OIBs.

Results & Discussion: We prepared OJP drill core samples provided by the Ocean Drilling Program and basalt samples from the Samoan Island of Tutuila. The chemical separation and purification of Cr from the samples were made following the procedure described by [8]. The recoveries of Cr were 90-100% for all samples. We have measured Cr stable isotope compositions of the samples processed through the separation scheme by thermal ionization mass spectrometry (TIMS). The external reproducibilities achieved here were ±5 ppm and ±11 ppm for ^{53}Cr and ^{54}Cr, which are markedly smaller than isotope variation among planetary materials (^{53}Cr ~1 ε ; ^{54}Cr ~2 ε). The Cr isotope analyses so far yielded ε^{53}Cr = 0.03 ±0.05, ε^{54}Cr = 0.02 ±0.10 (2SE) for the OJP basalts, and ε^{53}Cr = 0.03 ±0.05, ε^{54}Cr = −0.03 ±0.11 ~ 0.05 ±0.11 for the Samoan basalts. The results for both the OJP and Samoan basalts reveal that there is no resolvable $^{53, 54}$Cr excess or deficit in their source. Our results suggest that there' s no systematical contribution to Cr isotope signatures in the source of OJP and Samoan islands from the material with the anomalous Cr isotope compositions. Therefore, the chemical interaction between the core and the LIPs and OIBs sources is not detectable in terms of the Cr isotopes. This implies that, unlike W, the difference in the Cr concentrations of the core and the mantle might not be so large, or that Cr in the core does not necessarily diffuse in the mantle.

[1] Mundl et al. (2017) *Science,* **356,** 66-69, [2] Willbold et al. (2011) *Nature,* **477,** 195-199, [3] Rizo et al. (2019) *GRL,* **11,** 6-11, [4] Mundl et al. (2017) *Science,* **356,** 66-69. [5] Kleine et al. (2009) *GCA,* **73,** 5150-5188, [6] McDonough et al. (2003) *ToG2,* **568,** 559-575, [7] Chabot and Agee (2003) *GCA,* **67**, 2077−2091, [8] Hibiya et al. (2019) *GGR,* **43,** 133-145.

Keywords: Chromium isotope, core-mantle interaction, LIPs, OIBs

©2020. Japan Geoscience Union. All Right Reserved.

The tungsten isotopic compositions of kimberlites: constraints on material circulation in the deep Earth

*Otaro Kobayashi[1], Tsuyoshi Iizuka[1], Hatsuki Enomoto[1]

1. Department of Earth and Planetary Science, Graduate School of Science, The University of Tokyo

The short-lived ^{182}Hf-^{182}W isotopic system (^{182}Hf $\rightarrow$ ^{182}W + β -) has been widely used to probe early differentiation events (*e.g.*metal-silicate segregation and silicate differentiation). Since ^{182}Hf has a short half-life of 8.9 Myr (Vockenhuber *et al.*, 2004), it decayed into ^{182}W during the first 60 Myr of the solar system's history. Given that W is moderately siderophile, it preferentially partitioned into the Earth's core during its segregation. Hf, in contrast, is lithophile and is retained in the silicate portion of the Earth. As a result, the ^{182}W/^{184}W ratio of the Earth's core is estimated to be ~220 ppm lower than the terrestrial mantle (Touboul *et al.*, 2012). In addition, early silicate differentiation could have also created the variation in ^{182}W/^{184}W ratios. Since W is more incompatible than Hf, an "early depleted reservoir" may have an excess in ^{182}W and, in contrast, its complementary "early enriched reservoir" (EER) may have a deficit in that value.

Mundl *et al.* (Mundl *et al.*, 2017) reported negative μ^{182}W (deviations in ppm from the ^{182}W/^{184}W isotopic composition of the terrestrial standard) values in oceanic island basalts (OIB) which negatively correlate with ^{3}He/^{4}He. This result suggests that there exist early-differentiated reservoirs in the present-day deep mantle, since OIB are considered to have their sources in the lower mantle. Several processes have been proposed to explain the deficits in ^{182}W, for example, core-mantle interaction and the contribution from the EER. However, none of the hypothesis can satisfy geochemical constraints. This study provides new constraints on this issue by investigating plume-derived rocks, kimberlites.

In this study, we performed ^{182}W isotope analysis of kimberlites from South Africa, China and Brazil with MC-ICP-MS (*Thermo Fisher Scientific* Neptune Plus). Kimberlites are ultrabasic rocks that are presumed to have their origin deep in the Earth like OIB. On the other hand, globally distributed kimberlites have relatively undifferentiated isotopic compositions close to those of bulk silicate Earth (BSE), whereas OIB have relatively differentiated values. From these results, kimberlites are considered to originate from an isotopically primordial reservoir like the Earth's primitive mantle (Woodhead *et al.*, 2019).

All measured ^{182}W/^{184}W values of kimberlites were within analytical error of a terrestrial standard, which is considered to have the value of the modern accessible mantle. The present result indicates that the depletion of the present-day upper mantle in incompatible elements has occurred after ^{182}Hf was no longer extant, as there is no difference in ^{182}W values between the primordial mantle and the already depleted mantle. In addition, given that OIB show μ^{182}W negative anomalies (Mundl *et al.*, 2017), whereas kimberlites didn't show any anomalies, the source mantle of OIB is considered to be more strongly affected by the core-mantle interaction or the EER than that of kimberlites.

Keywords: tungsten isotope, kimberlite

©2020. Japan Geoscience Union. All Right Reserved.

In situ X-ray and neutron diffraction studies of hcp iron hydride

*Sho Kakizawa[1,2], Hiroyuki Kagi[2], Chikara Shito[2], Hiroyuki Saitoh[3], Yuji Higo[4], Yoshinori Tange[4], Asami Sano-Furukawa[5], Takanori Hattori[5], Katsutoshi Aoki[2]

1. Hiroshima University, 2. Geochemical Research Center, The University of Tokyo, 3. National Institutes for Quantum Radiological Science and Technology, 4. Japan Synchrotron Radiation Research Institute, 5. J-PARC center, Japan Atomic Energy Agency

The internal structure of the Earth can be divided into a” rock mantle” and a “metallic iron core”. The mantle is mainly composed of silicate minerals, but experimental studies suggested the presence of metallic iron in the Earth’s mantle [e.g., Frost et al., 2004; Rohrbach et al., 2007]. Metallic iron has been discovered as an inclusion in diamond and peridotite originating from the deep Earth [Jones et al., 2008; Ishimura et al., 2009]. Therefore, considering that there is a metallic core below the mantle, metallic iron exists all over the deep Earth. In addition, one of the major features of the Earth is the presence of water. Water is thought to exist not only as surface seawater but also as OH ions in the deep Earth minerals. Hydrogen can be partition into metallic iron than silicate minerals [e.g., Shibasaki et al., 2009]. Therefore, it is expected that metallic iron existing the deep Earth is hydrogenated.

The phase diagram changes abruptly when pure metallic iron is hydrogenated. In the case of pure metallic iron, fcc (face-centered cubic) or hcp (hexagonal closed packing) phase can be present under deep Earth conditions. On the other hand, fcc or dhcp (double hexagonal close packing) phase appear in the case of iron hydride. The hcp phase of iron hydride is a metastable phase. Conventional phase diagram of iron hydride has been determined only in experiments under hydrogen saturated conditions. However, our recent studies have revealed that hcp iron hydride is stable under low-concentration hydrogen condition [e.g., Machida et al., 2019]. Therefore, experiments under low-concentration hydrogen condition are important to discuss iron hydride under the deep Earth.

We conducted in-situ neutron diffraction experiments under high pressure and high temperature at J-PARC MLF BL11 to determine hydrogen-induced volume expansion coefficient of hcp-FeD_x. Deuterated Ammonia borane (ND_3BD_3) was used as hydrogen source This material decomposed to D_2 and BN at high pressure and high temperature conditions. The experimental conditions were 10-12 GPa, 300-900 K. Hydrogen content was controlled to D/Fe = 0.45. In addition, we conducted in-situ X-ray diffraction experiment under high pressure and high temperature at SPring-8 BL04B1 and BL14B1 to determine P-T-x phase diagram, especially maximum hydrogen content of hcp-FeH_x at a high pressure and high temperature condition. The experimental conditions were 3-16 GPa, 300-1100 K. Hydrogen content was controlled to D/Fe =0.5-0.8.

In the in-situ X-ray experiments, we observed coexistence of hcp and fcc-FeH_x. The hydrogen content is x = 0.4 and 0.7 for hcp and fcc-FeH_x at 15 GPa and 700 K, respectively. There is an immiscibility gap between hcp and fcc-FeH_x. In this presentation, we will discuss hcp iron hydride based on the results of neutron diffraction experiments.

Keywords: iron hydride, hexagonal closed packing phase, X-ray, neutron

©2020. Japan Geoscience Union. All Right Reserved.

Ab initio lattice thermal conductivity of (Mg,Fe)O ferropericlase at the deepest mantle

*Haruhiko Dekura[1], Taku Tsuchiya[1]

1. Geodynamics Research Center, Ehime University

Determination of lattice thermal conductivity (κ_{lat}) of lower mantle (LM) minerals is a key to understanding the dynamics and evolution of the earth’ s deep interior. (Mg, Fe)O Ferropericlase (Fp) is believed to be the second most abundant LM mineral after (Fe, Al) bearing $MgSiO_3$ bridgmanite and postpervskite (PPv). Recent experimental and theoretical studies under LM pressures showed that κ_{lat}) of MgO is substantially reduced by Fe incorporation (Ohta *et al.*, 2017; Hsieh *et al.*, 2018; Song *et al.*, 2019). However, the temperature condition is limited to a low temperature of 300 K, which is far from the actual LM condition. Therefore, the role of FP on the heat transport at the deepest mantle is still poorly understood. In this study, we determined κ_{lat} of FP at the LM pressure and temperature conditions, based on the *ab initio* anharmonic lattice dynamics techniques with fully solving the phonon Boltzmann transport equation (Dekura and Tsuchiya, 2017; 2019) combined with the internally consistent LDA+*U* technique for more precisely describing the Fe-O bond (Wang *et al.*, 2015). Calculations demonstrate strong negative solid solution effects (~-70-80% for ~13-19 mol% FeO) of low-spin Fe on κ_{lat} of MgO owing to decreases both in phonon group velocity and lifetime. An effective κ_{lat} of the lowermost mantle is then estimated for pyrolytic aggregate (FP+PPv) with pyrolytic ratio to be ~4 $Wm^{-1}K^{-1}$, which produces a net heat flow from the core to mantle ~6-7 TW. This value is more than ~50% smaller than that estimated from the core with high thermal conductivity of iron (~15 TW). This discrepancy could be reconciled by the thermally or chemically stratified layer at the top of the outer core observed seismologically (Helffrich and Kaneshima, 2010) if subadiabatic temperature gradient exists there.

Keywords: Lowermost mantle, Lattice thermal conductivity , Ferropericlase, Ab initio calculations

©2020. Japan Geoscience Union. All Right Reserved.

Soft Core-Mantle Boundary: A Mechanism for Chemical Interactions Between the Core and Mantle

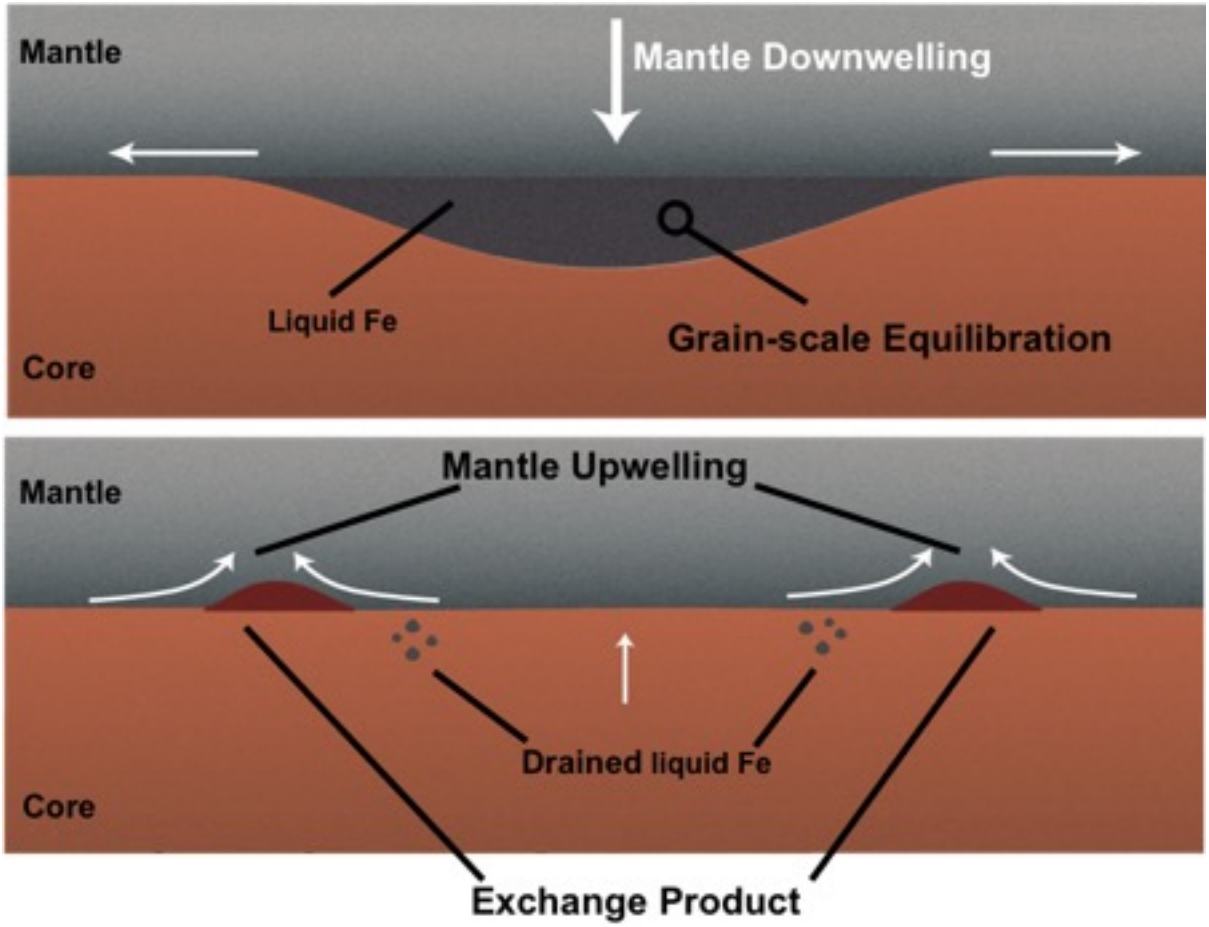
*Kang Wei Lim[1], Irene Bonati[1], Scott D Hull[2], John W Hernlund[1]

1. Earth-Life Science Institute, Tokyo Institute of Technology, 2. Earth and Environmental Sciences, University of Rochester

A recent study measuring global isotopic compositions in ocean island basalts (OIBs) combined with geochemical mixing models suggested that to explain the negative correlations between μ^{182}W values with $^{3}He/^{4}He$ values, there should be at least three mantle reservoirs present, two of which are primordial and preserved in the deep mantle. One of the primordial mantle reservoirs is hypothesized to contain material at the core-mantle boundary (CMB) that is chemically and isotopically equilibrated with the core, such that it records core-like isotopic signatures. Although there have been discussions on the possibility of core metal being entrained in mantle material, there is a lack of evidence of correlated enrichment in siderophile elements in OIBs. This raises doubts as to whether the unique isotopic signatures are a manifestation of interactions between the core and lowermost mantle. We propose a mechanism involving metal intrusion to explain how it is possible for mantle rock to obtain core-like isotopic signatures without the presence of metal itself: In the vicinity of mantle downwellings, deviatoric stresses at the CMB deform the boundary to produce a dynamic topography that depresses into the liquid core. At the high pressure-temperature conditions, the metal intrudes between the solid grains and “wets” the grain boundaries. Combining with the excess fluid pressure head induced in topographic lows, this drives intrusion of metal into the basal mantle rock. The intrusion of metal rheologically weakens the metal-rock mixture, promoting lateral gravitational spreading which draws additional material downwards. This enhances the circulation into the mixed layer and “softens” the lower boundary condition for mantle convection. During lateral spreading, liquid metal is squeezed out of pore spaces due to viscous compaction and falls back into the core. This can allow dense, reacted rocks to accumulate away from downwelling flows that contain isotopic signatures from the core without any trace of siderophile elements. As a first order approximation, we assume that the infiltration of metal into submerged rock occurs on timescales much shorter than the residence time of mantle rocks at the CMB, and the subsequent compaction of the mixture and expulsion of metal occurs on similarly short timescales. Next, we assume that the intruded layer is sufficiently thin such that the thin-layer approximation for a viscous fluid can be applied. To obtain a rough idea of the dynamics involving the rock-metal mixture, we incorporate the thin-layer approximation at regions with negative dynamic topography in a numerically simulated 2D Cartesian mantle convection model. This model assumes that the mantle is an isoviscous, incompressible, Boussinesq fluid. The addition of the thin layer at the CMB generates a boundary-driven flow which superimposes on the buoyancy-driven one in the mantle. Initial results show that the viscosity contrast between the submerged layer and reference mantle has a significant effect on which flows dominate: for the thin layer at sufficiently low viscosities, the boundary-driven flows dominate the dynamics and impede the movement of downwellings. This is accompanied by the increase in temperature of the mantle from the bottom-up as the secondary flow field spreads warm material from the CMB towards the top, thereby reducing the heat flux through the CMB. In addition, we observe that as Rayleigh number increases, the average amplitude of the dynamic topography and gain (the ratio between the flux of material into the layer due to the boundary-driven flow to that of the buoyancy-driven one) decreases.

©2020. Japan Geoscience Union. All Right Reserved.

Keywords: Core-mantle boundary, Core-mantle interaction, Dynamic topography, Isotopic signatures



©2020. Japan Geoscience Union. All Right Reserved.

Electrical conductivity measurement of water-bearing bridgmanite using an externally heated diamond anvil cell

*Yoshiyuki Okuda[1], Kenji Ohta[1], Yu Nishihara[2], Hiroyuki Kagi[3], Kei Hirose[3,4]

1. Tokyo Institute of Technology, 2. Ehime University, 3. University of Toyko, 4. Earth-Life Science Institute

The presence of water strongly affects the structure, phase relation and physical properties of the Earth's deep mantle minerals (Chen et al., 2020; Chang et al., 2017). Since electrical conductivity is sensitive to the water content of minerals, the electrical conductivity inferred from the analysis of electromagnetic induction brings the spatial distribution of water in the Earth's interior. Previous studies have estimated the actual water content of the Earth's upper mantle and the mantle transition zones by comparing the geophysically inferred electrical conductivity with the experimentally measured water content dependence of the electrical conductivity of mantle minerals (e.g., Karato, 2011). However, so far, the water content dependence of the electrical conductivity of lower mantle minerals have never been reported. Bridgmanite is the most abundant mineral in the Earth's lower mantle. Its water solubility is yet controversial, which varies from 5~4000 ppm (Litasov et al., 2003; Murakami et al., 2002), implying that studies on water solubility of bridgmanite is not sufficient to constrain the actual water distribution in the lower mantle. Here we measured the electrical conductivity of $Mg_{0.88}Fe_{0.14}Al_{0.11}Si_{0.91}O_3$ bridgmanite containing 500 ppm H_2O at high *P-T* conditions using an externally heated diamond anvil cell. We used a quasi-four terminal method for electrical conductivity measurements. Water content of our sample was estimated by Fourier transform infrared spectrometer (FTIR). From our results, we will discuss the water content of the Earth's lower mantle.

References

Chen, H. *et al.* Possible H_2O storage in the crystal structure of $CaSiO_3$ perovskite. *Phys. Earth Planet. Inter.* **299**, 106412 (2020).

Chang, Y. Y. *et al.* Hydration-reduced lattice thermal conductivity of olivine in Earth's upper mantle. *Proc. Natl. Acad. Sci. U. S. A.* **114**, 4078–4081 (2017).

Karato, S. I. Water distribution across the mantle transition zone and its implications for global material circulation. *Earth Planet. Sci. Lett.* **301**, 413–423 (2011).

Litasov, K. *et al.* Water solubility in Mg-perovskites and water storage capacity in the lower mantle. *Earth Planet. Sci. Lett.* **211**, 189–203 (2003).

Murakami, M. *et al.* Water in Earth's Lower Mantle. **295**, 1885–1888 (2002).

Keywords: lower mantle, bridgmanite, water, electrical conductivity

©2020. Japan Geoscience Union. All Right Reserved.

Mechanisms of the post-perovskite transformation in $NaNiF_3$

Koyumi Yamashita[1], *Tomoaki Kubo[1], Yoshinori Tange[2], Yuji Higo[2]

1. Kyushu Univ., 2. JASRI

Strong seismic anisotropy has been observed in the D" layer at the bottom of the lower mantle. This is possibly attributed to lattice preferred orientation (LPO) of bridgmanite (pv) and/or post-perovskite phase (ppv) induced by mantle flow, however their interpretations are still under debate. In particular, the ppv transformation exhibits topotaxy (having crystallographic relationship between pv and ppv) at least a certain condition in analogue material ($NaNiF_3$), which may cause LPO transition, and thus should be considered when interpreting seismic anisotropy (Dobson et al., 2013). However, topotaxy in the ppv transformation has been found in the single crystalline sample only at large overpressure and low temperature condition that is far from the equilibrium boundary. It is likely that the transformation proceeds near the equilibrium boundary in the D" region, where incoherent grain-boundary nucleation and growth mechanism may be dominant without topotaxy. In this study, we conducted the ppv transformation experiments in polycrystalline $NaNiF_3$ to investigate the dominant transformation mechanisms in the D" layer.

The starting material is equi-granular polycrystalline $NaNiF_3$ pv (~5-10 μm grain size) that was synthesized from a powder mixture of NiF_2 and NaF at 2 GPa and 750-800℃ for 40-60 min using a DIA-type high-pressure apparatus (MAX 90D) at Kyushu University. Transformation experiments were carried out by using Kawai-type high-pressure apparatus with the quenching method at Kyushu University (QDES) and with in-situ X-ray observation method at BL04B1 of SPring-8 (SPEED 1500). In the latter case, the phase transition was observed by time-resolved X-ray diffraction measurement using the energy dispersive method. Au was used as a pressure marker, and the overpressure (dP) of the phase transition was estimated based on the equilibrium boundary determined by Shirako et al. (2012). Transformation textures in the recovered samples were examined by SEM and EBSD.

In the case of the in-situ X-ray observation, we observed the transformation during the isothermal pressurization (~2.8 GPa/h) at 400˚C, 600˚C, 800˚C, and 1000˚C. The dP needed for the initiation of the transformation drastically increases with decreasing temperature. For example, the transformation started at dP of 1.5 GPa and 1000℃, however it did not occur even at the dP of 15 GPa and 400℃. Dobson et al. (2013) reported the intracrystalline lamellar nucleation of ppv phase in single crystalline pv with having crystallographic relationships at 700℃ and dP of ~9 GPa. Our study demonstrated that the ppv transformation can proceeds at much smaller dP conditions. We observed lamellar textures implying topotaxy in the recovered samples even at such small dP conditions. This is a typical feature for the ppv transition that is not seen in the olivine-spinel and post-garnet transformations. This may suggest that topotaxy generally occurs in the D" region. On the other hand, the lamellar spacing and width drastically increases with decreasing dP. We found that, after the nucleation stage at high T and small dP conditions, the ppv phase largely grow in the a-axis direction outside the parental pv grain, resulting in the formation of large rod-like crystal over the parental grains. The fast growth by rod-like ppv crystals likely occurs by the migration of incoherent interface, which may erase the texture induced by topotaxy.

Keywords: post-perovskite transformation, topotaxy, seismic anisotropy

©2020. Japan Geoscience Union. All Right Reserved.

[E] Poster | S (Solid Earth Sciences)：S-IT Science of the Earth's Interior & Techtonophysics

[S-IT27] Oceanic lithosphere and asthenosphere

convener:Nozomu Takeuchi(Earthquake Research Institute, University of Tokyo), Ban-Yuan Kuo(Institute of Earth Sciences, Academia Sinica), Rob L Evans(Woods Hole Oceanographic Institution), Younghee Kim(Seoul National University)

The oceanic lithosphere/asthenosphere system (LAS) is one of the most fundamental features of plate tectonics. In recent years, the elucidation of the oceanic lithosphere/asthenosphere system has become one of the hot topics in solid earth science. New data from the ocean floor are being extensively obtained under the Pacific Array initiative (http://eri-ndc.eri.u-tokyo.ac.jp/PacificArray/) and others, and a great variety of views are proposed and discussed. In this session, we will discuss on observation technologies, views of the oceanic lithosphere/asthenosphere system, the strategies for interpretation of the observations (including seismic and/or electrical conductivity anisotropy), constraints/ideas on the role and abundance of water/melt in the mantle (including the transition zone), and other related topics for elucidating this enigmatic system. We call for contributions from diverse fields, including but not limited to seismology, magnetotellurics, petrology/mineralogy, dynamical modelling, and mineral physics.

[SIT27-P01] The Oldest Array: Japan-Korea Pacific Array collaboration to study the lithosphere-asthenosphere system below the oldest part of the Pacific Ocean

*Hajime Shiobara[1], Hisashi Utada[1], Seung-Sep Kim[2], YoungHee Kim[3], Kiyoshi Baba[1], Takehi Isse[1], Hogyum Kim[3], HyeJeong Kim[1], Hiroko Sugioka[4], Nozomu Takeuchi[1], Yuki Kawano[1], Hitoshi Kawakatsu[1], Sang-Mook Lee[3], Onboard scientists of 2018/2019 Oldest cruises (1.Ocean Hemisphere Research Center, Earthquake Research Institute, University of Tokyo, 2.Chungnam National University, 3.Seoul National University, 4.Kobe University)

[SIT27-P02] The Electrical Conductivity Structure of The Oldest Pacific: Preliminary Results from Magnetotelluric Observation Data of Pacific Array, Oldest-1

*Hogyum Kim[1], Kiyoshi Baba[2], Hisashi Utada[2], Sang-Mook Lee[1], Hitoshi Kawakatsu[2], YoungHee Kim[1] (1.School of Earth and Environmental Sciences, Seoul National University, 2.Earthquake Research Institute, The University of Tokyo)

[SIT27-P03] P Velocity Heterogeneities in the Upper Mantle beneath the Northwestern Pacific

*Nozomu Takeuchi[1], Hitoshi Kawakatsu[1], Hajime Shiobara[1], Takehi Isse[1], Hiroko Sugioka[2], Aki Ito[3], Hisashi Utada[1] (1.Earthquake Research Institute, University of Tokyo, 2.Kobe University, 3.JAMSTEC)

[SIT27-P04] Seismic velocity structure beneath the oldest region of the Pacific ocean basin from multiscale finite-frequency traveltime tomography

*Hyunsun Kang[1], Younghee Kim[1], Shu-Huei Hung[2], Pei-Ying Patty Lin[3], Takehi Isse[4], Hajime Shiobara[4], Hitoshi Kawakatsu[4], Sang-Mook Lee[1], Hisashi Utada[4], Nozomu Takeuchi[4] (1.Seoul National University, 2.National Taiwan University, 3.National Taiwan Normal University, 4.Earthquake Research Institute, The University of Tokyo)

The Oldest Array: Japan-Korea Pacific Array collaboration to study the lithosphere-asthenosphere system below the oldest part of the Pacific Ocean

*Hajime Shiobara[1], Hisashi Utada[1], Seung-Sep Kim[2], YoungHee Kim[3], Kiyoshi Baba[1], Takehi Isse[1], Hogyum Kim[3], HyeJeong Kim[1], Hiroko Sugioka[4], Nozomu Takeuchi[1], Yuki Kawano[1], Hitoshi Kawakatsu[1], Sang-Mook Lee[3], Onboard scientists of 2018/2019 Oldest cruises

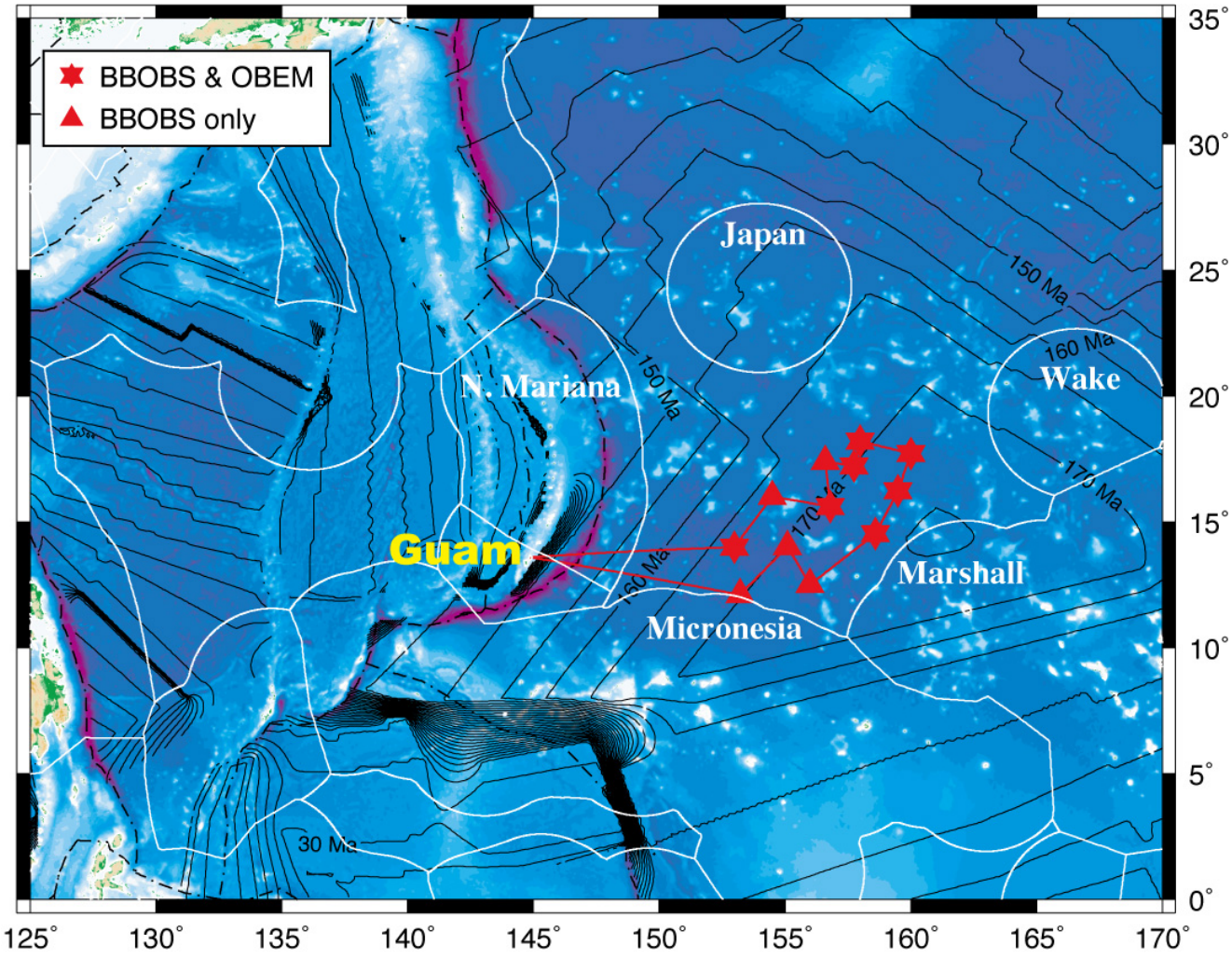
1. Ocean Hemisphere Research Center, Earthquake Research Institute, University of Tokyo, 2. Chungnam National University, 3. Seoul National University, 4. Kobe University

There remain a lot of unresolved problems that limit our understanding of the physical nature of the lithosphere-asthenosphere system (LAS), although nearly 60 years have passed since the concept of plate tectonics was born. In-situ measurement of the physical property distributions in the mantle by seafloor geophysical array observations in all over the age will be one of the keys to reveal these problems, and the Pacific Array concept has been proposed. The Pacific Array has been launched in 2018, by deployments of two seafloor arrays, one by a US group and the other by a Japan-Korea collaboration. In this presentation, the scientific perspective and the observation report of the latter are shown. We selected the oldest part (the mean age of about 170 Ma) of the Pacific Basin for the first deployment of the Pacific Array. In the study area, the seafloor isochron suggested by magnetic lineations is seen to converge to a small triangle which shows the shape of the Pacific plate when it was born in the middle Jurassic. One of the scientific purposes of this Oldest array is to reveal the early evolution of the Pacific LAS by estimating the anisotropic seismic structure from analysis of the BBOBS data. We also intend to examine the relation between the seafloor depths and mantle geotherms that might be recorded in the mantle to answer the long-lasting question why older seafloors are flat.

The deployment cruise was conducted from October 30 to November 9, 2018, by R/V Isabu (Korea Institute of Ocean Science and Technology: KIOST), started from and returned to Guam, USA. 12 sets of broad-band ocean bottom seismometers (BBOBSs) and 7 sets of ocean bottom electro-magnetometers (OBEMs) were deployed in the study area. The recovery cruise was performed between October 26 and November 9, 2019, by using another KIOST’ s R/V Onnuri, with the same route of the deployment. Although the weather and sea condition during the recovery cruise was severe, all BBOBSs and OBEMs were recovered with healthy data, except one BBOBS that was troubled in the deployment with the broadband sensor unit and recorded the DPG data only. Preliminary analysis results both of seismic and electro-magnetic data are individually presented in this meeting by Takehi Isse and Hogyum Kim, respectively.

Keywords: lithosphere-asthenosphere system, Pacific Array, ocean floor array observation, BBOBS, OBEM

©2020. Japan Geoscience Union. All Right Reserved.



©2020. Japan Geoscience Union. All Right Reserved.

The Electrical Conductivity Structure of The Oldest Pacific: Preliminary Results from Magnetotelluric Observation Data of Pacific Array, Oldest-1

*Hogyum Kim[1], Kiyoshi Baba[2], Hisashi Utada[2], Sang-Mook Lee[1], Hitoshi Kawakatsu[2], YoungHee Kim[1]

1. School of Earth and Environmental Sciences, Seoul National University, 2. Earthquake Research Institute, The University of Tokyo

With the complex regional history from the creation between Izanagi-Farallon-Phoenix plates system to the oldest crust of the Pacific over 180 Ma, the west Pacific basin between Northern Mariana, Marshall Islands, and Micronesia has been considered as an ideal place to study the anisotropy structure related with the crustal evolution and the thermal history of oceanic lithosphere-asthenosphere system (LAS). As an element of the international collaboration Pacific Array project, which aims to deploy “array of arrays” over the entire Pacific, a joint research group of Japan-Korea scientists conducted in-situ ocean bottom geophysical observation of the Oldest-1 region for a year from 2018 to 2019. 12 ocean bottom seismometers and 7 ocean bottom electromagnetometers (OBEMs) provided by Earthquake Research Institute, The University of Tokyo, has been deployed and recovered on vessels (RV Isabu and RV Onnuri, respectively) of Korea Institute of Ocean Science and Technology (KIOST).

Here we report the preliminary analysis of magnetotelluric data from 7 OBEMs of the Oldest-1 array. After the initial processing to correct anomalous peaks in time series, shift of internal clocks, and the effect from bathymetry/land-sea distribution, we estimated a 1-D regional mean profile of electrical conductivity. In the context of the thermal evolution process of oceanic LAS, the 1-D electrical structure represents the oldest end member of the Pacific basin.

Keywords: Pacific Array, Lithosphere-Asthenosphere System, Ocean Bottom Electromagnetometer, Marine Magnetotellurics

©2020. Japan Geoscience Union. All Right Reserved.

P Velocity Heterogeneities in the Upper Mantle beneath the Northwestern Pacific

*Nozomu Takeuchi[1], Hitoshi Kawakatsu[1], Hajime Shiobara[1], Takehi Isse[1], Hiroko Sugioka[2], Aki Ito[3], Hisashi Utada[1]

1. Earthquake Research Institute, University of Tokyo, 2. Kobe University, 3. JAMSTEC

We previously conducted waveform inversion of P waveforms recorded by our BroadBand Ocean Bottom Seismometers (BBOBSs) deployed in the Northwestern Pacific. We could reveal the depth profile of the P velocity of the oceanic upper mantle, which has not been well resolved by previous surface wave or receiver function analysis. The resulting P model shows higher and lower velocities in the lithosphere and the asthenosphere, respectively, and the velocity contrast was approximately 2/3 of that in the previous S models. However, the observed waveforms appear to show regional variations, and the validity to discuss using 1-D models was not very clear.

In this study, we investigated to reveal regional variations of P structures within the Northwestern Pacific. We defined two data bins so that the raypaths belonging to each bin sample similar regions with similar azimuths. The observed waveforms of each bin are coherent, which shows plausibility to compare obtained 1-D models. The preliminary results showed significant differences both in the lithosphere and the asthenosphere. The observed differences in the lithosphere (~4%) are consistent to the azimuthal anisotropy in the uppermost mantle reported by previous exploration studies. However, the differences in the asthenosphere (~2%) are unlikely to be explained by azimuthal anisotropy by olivine LPO because the angles to the plate motion direction are similar. This may suggest some mechanism to produce larger-scale (~1000 km) lateral heterogeneities in the asthenosphere.

Keywords: seismology, mantle, lithosphere, asthenosphere

©2020. Japan Geoscience Union. All Right Reserved.

Seismic velocity structure beneath the oldest region of the Pacific ocean basin from multiscale finite-frequency traveltime tomography

*Hyunsun Kang[1], Younghee Kim[1], Shu-Huei Hung[2], Pei-Ying Patty Lin[3], Takehi Isse[4], Hajime Shiobara[4], Hitoshi Kawakatsu[4], Sang-Mook Lee[1], Hisashi Utada[4], Nozomu Takeuchi[4]

1. Seoul National University, 2. National Taiwan University, 3. National Taiwan Normal University, 4. Earthquake Research Institute, The University of Tokyo

The 12 broadband ocean-bottom seismometers (BBOBS) and 7 electro-magnetometers (OBEM) were deployed in Oct-Nov 2018 for a duration of 12 months on the 7˚x7˚ area of the oldest (~170 Ma) Pacific basin, where the mantle structure below is poorly constrained (Becker et al., 2014). This experiment (Pacific Array) was conducted as a collaboration between South Korea and Japan to investigate an early evolution of the Pacific lithosphere-asthenosphere system. In this study, we perform multiscale finite-frequency traveltime tomography to elucidate the lithospheric-scale seismic structure from the 12 BBOBS data. We extract teleseismic waveforms with earthquake magnitudes greater than 5.5 within an epicentral distance of 30-98 degrees from the array, and measure relative traveltime residuals of P waves in high-frequency (8-16 s) and low-frequency (16-32 s) bands by multichannel cross-correlation method (VanDecar and Crosson, 1990). The relative traveltimes measured at the two different frequency bands are sensitive to seismic velocity structures with different length scales and allow better recovery of the velocity perturbations in tomographic models (Hung et al., 2004). We apply data adaptive, multiscale parameterizations based on wavelet transforms, which can account for variability in data coverage and provide a tomographic model with spatial-varying resolutions (Hung et al., 2010). We plan to show preliminary P-wave velocity structure of the upper mantle below the Pacific Array region with the checkerboard resolutions test results to confirm the reliability of the obtained tomographic images.

Keywords: Pacific Array, broadband ocean-bottom seismometer (BBOBS), Pacific basin, multiscale finite-frequency traveltime tomography, lithosphere-asthenosphere system

©2020. Japan Geoscience Union. All Right Reserved.

[E] Poster | S (Solid Earth Sciences)：S-IT Science of the Earth's Interior & Techtonophysics

[S-IT28] Mantle dynamic from thermochemical imaging from observable to numerical modeling

convener:Walid Ben Mansour(Macquarie University), Yosuke Aoki(Earthquake Research Institute, University of Tokyo)

Mantle plays a key role on the present-day topography. If the temperature is one of the key parameters, the chemical composition of the mantle is also very important. In the last 20 years, different approaches tried to bring new information on the thermochemical structure of the mantle. The development of high-performance computational infrastructures (HPCI) and new algorithms to manage the processing of big data brings new opportunities to produce high-resolution images and better understanding of mantle dynamics. This session wishes to bring together contributions from experimental geophysics and computational geochemistry to large scale geodynamics, which are aimed at imaging and modeling thermochemical structure on different time scales. Presentations of new methods combining multiple observations of geophysical and geochemical datasets with regional to global geophysical modeling are particularly encouraged.

[SIT28-P01] Constraints on the composition of LLSVPs from seismic properties of lower mantle minerals

*Kenny Vilella[1], Thomas Bodin[2], Charles-Edouard Boukare[3], Frederic Deschamps[4], James Badro[5], Maxim Ballmer[6], Yang Li[7] (1.Hokkaido University, 2.Laboratoire de Geologie de Lyon, 3.Ecole Polytechnique Federale de Lausanne, 4.Institute of Earth Sciences, Academia Sinica, 5.Institut de Physique du Globe de Paris, 6.ETH Zurich, 7.Institute of Geology and Geophysics, Chinese Academy of Science)

Constraints on the composition of LLSVPs from seismic properties of lower mantle minerals

*Kenny Vilella[1], Thomas Bodin[2], Charles-Edouard Boukare[3], Frederic Deschamps[4], James Badro[5], Maxim Ballmer[6], Yang Li[7]

1. Hokkaido University, 2. Laboratoire de Geologie de Lyon, 3. Ecole Polytechnique Federale de Lausanne, 4. Institute of Earth Sciences, Academia Sinica, 5. Institut de Physique du Globe de Paris, 6. ETH Zurich, 7. Institute of Geology and Geophysics, Chinese Academy of Science

Seismic observations have suggested the presence of two LLSVPs in the lowermost mantle. These two reservoirs are likely to be chemically distinct from the ambient mantle and to influence the dynamics of the whole Earth. Several studies have tried to constrain the compositions explaining their seismic properties with the hope that it may help to identify their formation mechanism. In particular, compositions enriched in iron (10 wt%) and bridgmanite (Bm, 90 vol%) are good candidates. These compositions are somewhat consistent with the reservoirs produced by the solidification of a primitive magma ocean, except that the iron enrichment (>20 wt%) is much larger. Here, we provide a reappraisal of the potential compositions for LLSVPs based on an improved mineralogical model including, for instance, the effect of alumina and spin state transition. We have also investigated systematically the effects of six parameters: FeO and Al_2O_3 content, proportion of $CaSiO_3$ and Bm, oxidation state and temperature contrast between ambient mantle and LLSVPs. From the 81 millions cases studied, only 166 thousands cases may explain the seismic observations. Nevertheless, these successful cases involve a large range of parameters with, for instance, FeO and Al_2O_3 content between 12–28 wt% and 5–19 wt%, respectively. A principal component analysis (PCA) is then applied to our results. The PCA has highlighted two robust results:
(i) the proportion of ferropericlase (Fp) should be low (<6 vol%);
(ii) the formation of Fe^{3+}-bearing Bm is much more favorable than other iron-bearing phases.
Following these results, we have identified two end-member compositions: one Bm-rich and one CaPv-rich. Each end-member can then be associated with various temperature contrasts, although a low temperature contrast (<500 K) is more favorable, and various FeO contents, provided a certain proportion between oxidation state, FeO and Al_2O_3 content is maintained. As a last step, we discussed different scenarios for the formation of LLSVPs. In particular, the solidification of a magma ocean may produce reservoirs with FeO and Al_2O_3 content similar to the ones we found but their proportion of Fp is too large. From a broader perspective, constraints on the mineral proportion of LLSVPs are probably the best to discriminate between different formation mechanisms.

Keywords: LLSVP, Composition, Lower Mantle, Mineral Physics, Seismic observations, Earth

©2020. Japan Geoscience Union. All Right Reserved.

[E] Poster | S (Solid Earth Sciences)：S-IT Science of the Earth's Interior & Techtonophysics

[S-IT29] New perspectives on East Asia geodynamics

convener:Jonny Wu(University of Houston), Asuka Yamaguchi(Atomosphere and Ocean Research Institute, The University of Tokyo), Kyoko Okino(Atmosphere and Ocean Research Institute, The University of Tokyo), Timothy B Byrne(University of Connecticut)

East Asia is one of the most tectonically active regions on Earth and includes the Eurasian continental margin, the western Pacific subduction zones and many of Earth's marginal seas. The region has a long history of subduction, collision, backarc basin opening and closing, and other plate boundary interactions. In recent years, a wide range of new observations have been collected from the land, oceans and Earth interior, including detailed geologic data, zircon age spectra, earthquakes, high resolution crustal to mantle imaging, and Big Data. These new data show the detailed space-time evolution of subduction zones, mountain building, slab stagnation, crustal deformation, continental dynamics, backarc spreading, and other East Asian geodynamics cannot be fully explained by classic theories; new perspectives are needed. Here we seek to share new insights on the geologic history, paleomagnetism, and geophysical character of East Asia since the Paleozoic. We also invite geodynamic models that integrate diverse datasets into a more holistic view of this dynamic environment.

[SIT29-P02] Early Miocene zircon U-Pb ages in the Hidaka Supergroup of the Tomuraushi area, Hokkaido : Ridge subduction or marginal basin magmatism?

*Michiru Inoue[1], Hayato Ueda[1] (1.Department of Geology, Niigata University)

[SIT29-P03] Subduction and exhumation history of the early metamorphic rocks of southern Kamuikotan Zone, Hokkaido, Japan.

*Yuki Furukawa[1], Hayato Ueda[1], Megumi Ozawa[2] (1.Niigata University, 2.Asano Taiseikiso Engineering Corporation)

[SIT29-P04] Examination of hiterland based on clastic rock composition and zircon U-Pb age in the Nikoro Group, Tokoro Belt

*Komei Nara[1], Yuta Akutsu[2], Hayato Ueda[1] (1.Niigata University, 2.Kowa co.Ltd)

[SIT29-P05] Zircon U-Pb ages and felsic volcanic clasts in the Lower Cretaceous Rebun Group, Hokkaido

*Nozomu Suzuki[1], yusuke Sugiyama, Hayato Ueda[1] (1.Niigata University)

[SIT29-P06] Paleozoic accretionary complex in the Khangai-Khentei belt, central Mongolia, and stratigraphy of Devonian chert

*Tomohito Nakano[1], Yukio Isozaki[2], Uyanga Bold[2], Otgonbaatar D[3], Yukiyasu Tsutsumi[4] (1.Department of Earth and Planetary Science, The University of Tokyo, 2.Department of Earth Science and Astronomy, Multi-disciplinary Sciences - General Systems Studies, Graduate School of Arts and Sciences, The University of Tokyo, 3.Institute of Paleontology and Geology, Mongolian Academy of Science, 4.Department of Geology and Paleontology, National Museum of Nature and Science)

[SIT29-P07] Tectono-depositional evolution of the Mio-Pleistocene forearc basin on the Boso Peninsula, central Japan

*Nana Kamiya[1], Yuzuru Yamamoto[2], Masayuki Utsunomiya[3], Feng Zhang[4], Weiren Lin[1] (1.Graduate School of Engineering, Kyoto University, 2.Kobe University, 3.AIST, 4.Nagoya Institute of Technology)

[SIT29-P08] Preliminary Study on the Crustal Deformation along Sagaing Fault in Myanmar by using GNSS data

*Tha Zin Htet Tin[1,2], Takuya NISHIMURA[3], Manabu Hashimoto[3], Eric Lindsey[4], Myo Thant[2,5] (1.Graduate School of Science, Kyoto University, 2.Department of Geology, University of Yangon, Myanmar, 3.Disaster

Prevention Research Institute, Kyoto University, 4.Earth Observatory of Singapore, Nanyang Technological University, Singapore, 5.Myanmar Earthquake Committee)

[SIT29-P09] Evidence for Late Mesozoic intraoceanic subduction offshore NE Asia from mantle convection and geoid models

*Lorenzo Colli[1], Jonny Wu[1], Yi-An Lin[1] (1.University of Houston)

[SIT29-P10] Brittle-Plastic Structures Provide Constraints on the Rapid Exhumation of the Central Range: Taiwan

*Lauren Donati[1], Lindsey Aman[1], Susan Adams[1], Jonathan C Lewis[1] (1.Indiana University of Pennsylvania)

[SIT29-P11] Where are the proto-South China Sea slabs? SE Asian plate tectonics and mantle flow history from global mantle convection modeling

*Yi-An Lin[1], Lorenzo Colli[1], Jonny Wu[1] (1.University of Houston)

Early Miocene zircon U-Pb ages in the Hidaka Supergroup of the Tomuraushi area, Hokkaido : Ridge subduction or marginal basin magmatism?

*Michiru Inoue[1], Hayato Ueda[1]

1. Department of Geology, Niigata University

Abstract

The Hidaka Supergroup in central Hokkaido has been regarded as a Paleogene accretionary complex. It consists mainly of deformed sedimentary rocks, and is also known to contain MORB lavas and dolerites, which erupted on and intruded in unconsolidated trench sediments (in situ MORB). It has thus been considered to suggest ridge subduction in the Paleogene period. Tomuraushi area is one of the most typical localities of the in situ MORB in the Hidaka Belt. However, limited and indirect age data have been so far available for the age of MORB eruption.

Based on field mapping, we divided the Hidaka Supergroup in the Tomuraushi area into six lithological units in structurally ascending order as unit A (black mudstone), unit B (muddy turbidites), unit C (basalts and dolerites with black mudstones) , unit D (red, green and black mudstone), unit E (sandy turbidites) , and unit F (black mudstone). Successions from units A to C and from D to E are regarded as conformable, and the boundaries between units C and D, and between E and F as reverse faults. Therefore, the Hidaka Supergroup in this area consists of at least three thrust sheets.

We determined detrital zircon U-Pb ages for six samples of sandstone and tuff collected from units B, C, and E. Zircons from each tuff sample shows a single age cluster with weighted mean of 18-20 Ma. Zircon U-Pb ages from sandstone samples showed the youngest clusters about 22-26 Ma.

Based on the results above, sedimentary ages of units B and C is considered as 18-20 Ma, and of unit E younger than 22 Ma. The age of N-MORB eruption is contemporaneous with the unit C deposition in the Early Miocene, significantly younger than the timing of subduction of the Izanagi-Pacific Ridge along the Eurasian margin assumed in 50-60 Ma (Seton et al., 2015; Wu & Wu, 2019). Instead, the ages are coeval with zircon U-Pb ages of granulite facies metamorphism (Usuki et al., 2006) and of MORB-type gabbro (Kemp et al., 2007) in the Hidaka Metamorphic Belt to the south of the Tomuraushi area. Because the Oligocene-Early Miocene Hidaka intrusive and metamorphic events are attributed to back-arc rifting and spreading of the Kuril and Japan basins by these authors, the Tomuraushi in situ MORB could also be formed along with the same events.

References

Kemp, A. I. S., Shimura, T. and Hawkesworth, 2007, Linking granulites, silicic magmatism, and crustal growth in arcs: Ion microprobe (zircon)U–Pb ages from the Hidaka metamorphic belt, Japan. Geology, 35, 807–810

Seton, M., Flament, N., Whittaker, J., Müller, R. D., Gurnis, M. and Bower, D. J., 2015, Ridge subduction sparked reorganization of the Pacific plate-mantle system 60–50 million years ago. Geophysical Research Letters, 42(6), 1732-1740

Usuki T., Kaiden H., Misawa K. and Shiraishi K., 2006, Sensitive high-resolution ion microprobe U-Pb ages of the Latest Oligocene-Early Miocene rift-related Hidaka high-temperature metamorphism in Hokkaido, northern Japan. Island Arc, 15, 503-516

Wu, Tsung-Jui, J. and Wu, J., 2019, Izanagi-Pacific ridge subduction revealed by a 56 to 46 Ma magmatic gap along the northeast Asian margin. Geology, 47, 953-957

©2020. Japan Geoscience Union. All Right Reserved.

Keywords: zircon, U-Pb age, Neogene, Miocine, Hidaka belt

©2020. Japan Geoscience Union. All Right Reserved.

Subduction and exhumation history of the early metamorphic rocks of southern Kamuikotan Zone, Hokkaido, Japan.

*Yuki Furukawa[1], Hayato Ueda[1], Megumi Ozawa[2]

1. Niigata University, 2. Asano Taiseikiso Engineering Corporation

The Kamuikotan Zone is a Cretaceous to Paleogene low-temperature and high-pressure metamorphic belt that extends from north to south in the central part of the Sorachi-Yezo belt in Hokkaido. The Iwashimizu Complex in the southern part of the Kamuikotan Belt is considered as a Lower Cretaceous accretionary complex, in which the Pirashuke Unit near the structural top show the oldest metamorphic age in the belt as well as amphibolite blocks in serpentine melanges. It is expected that these rocks tell us the timing, thermal structure, and its temporal change just after the subduction initiation. Therefore, we focus on the Pirashuke Unit and surrounding rocks in the Iwashimizu complex.
In the Shizunai-Niikappu area, the Pirashuke Unit is subdivided into units 1 (basalt), 2 (chart, siliceous mudstone, sandstone), 3 (basalt, chert), 4 (lapilli tuff), and 5 (chert) in structurally ascending order, and the top parts are covered by mid-Cretaceous and younger sediments.
Based on equilibria of pumpellyite (P), actinolite (A), alkali pyroxene (N), epidote (E), and sodic amphibolite (R), rocks in this area are classified into PAN type and PNR type. The PAN type rocks occur in the northeastern and southwestern parts, and also locally in the northwestern parts as a wedge. The PNR type rocks occur as a zone between the PAN type rocks from the northwest to the southeast. The PAN type rocks are considered to lie in the structurally higher horizons than PNR type rocks. The Schreinemarker’ s bundle analysis suggests that the PAN type quilibrium are formed in lower pressure or higher temperature than the PNR type. In the further east (structurally lower), lawsonite-bearing assemblages instead of epidote occurs suggesting lower temperature than both PAN and PNR types.
U-Pb ages were measured for detrital zircons extracted from a sandstone and tuffeceous siliceous mudstone. In the sandstone, the youngest peak peak of ~127 Ma was found in a cluster ranging 120-150 Ma as the older limit of its sedimentary age. Pi-129 zircons showed a single peak with the weihted mean age of 123 Ma as a sedimentary age. Time interval from the sedimentary ages to the metamorphism (~25 km at 125 Ma) for the Pirashuke Unit was no greater than 2 m.y., leading a estimate of the vertical velocity of subduction faster than 10 mm/y. Assuming the minimum slab dip as 45 degrees based on the destance from the Kamuikotan Zone to the eastern margin of the Idonnappu Zone (as the trench site), the subduction velocity of >14 mm/y can also be estimated. The time interval from metamorphism at ~125 Ma to surface erosion with unconformity at 110-105 Ma suggests an exhumation rate of 1–2 mm/y. In the structurally lower Shizunai Unit, vertical subduction rate of ~1 mm/y vertical subduction rate is estimated based on the youngest sedimentary age (~125 Ma) and the metamorphic depth and ages (15-20 km at 110 Ma). The Pirashuke Unit rocks were subducted with a velocity as fast as general plate velocity, while the Shizunai Unit rocks were subducted at a velocity one order of magnitude slower. Therefore, the Pirashuke rocks were probably underplated after subduction together with the slab, while the Shizunai rocks were detached from the slab at shallow levels and then slowly subducted.
Occurrences of higer-temperature PAN-type rocks structurally overlying the PNR type suggest that the hanging-wall wedge mantle was still hot immediately after the subduction initiation. Hornblende cryustals in amphibolite blocks of serpentinite melange in adjacent area are commonly mantled by actinolite and rimmed by sodic amphibole. This zoning can be correlated with the map-scale zonation of PAN and PNR types. Taking occurrences of lawsonite also into account, the subduction zone was probably deastically refrigerated from amphibolite-grade to lawsonite-grade temperatures in a short period contemporaneously with accretionary growth of the Iwashimizu subduction complex.

©2020. Japan Geoscience Union. All Right Reserved.

Keywords: Kamuikotan Zone, Hokkaido, metamorphic rock, Subduction Zone, Adduct, Zircon U-Pb dating

©2020. Japan Geoscience Union. All Right Reserved.

Examination of hiterland based on clastic rock composition and zircon U-Pb age in the Nikoro Group, Tokoro Belt

*Komei Nara[1], Yuta Akutsu[2], Hayato Ueda[1]

1. Niigata University, 2. Kowa co.Ltd

The Tokoro Belt in eastern Hokkaido consists of accretionary complexes of the Cretaceous Nikoro Group and the Paleogene Yubetsu Group, and the overlying forearc basin sediments of the Late Cretaceous Saroma Group. It is widely accepted that the Tokoro belt rocks were formed along the southern margin of the Sea of Okhotsk. Although the Sea of Okhotsk occupies a large portion of NW Pacific and is important to make a comprehensive oceanic plate reconstruction, component and origin of its submerged crust has not been well understood. In this paper we present clastic composition and detrital zircon age of the Nikoro Group clastic rocks, which were supplied from the crust of the Sea of Okhotsk.
The Nikoro Group consists of basalt, chert, limestone, red mudstone and volcanolithic sandstone. We divided the group in western parts of the belt into clastic-dominant Unit I and basalt-dominant Unit II. Unit I is an imbricate stack of sedimentary sequences from chert to mudstone and sandstone. Unit II is a structural pile dominantly of basalt and chert.
Sandstones in the Nikoro Group are lithic wacke composed of volcanic rock fragments as well as plagioclase and clinopyroxene particles. Both chemical composition of volcanic rock fragments and detrital clinopyroxene suggest clastic supply from a volcanic arc.
Zircons extracted from a trachyte yielded ~152 Ma[u1] age suggesting the age of subducted oceanic crust. Detrital zircons from sandstone range from 80 to 154 Ma. A tonalite lens in sheared red mudstone yielded zircons of ~147 Ma, implying that the adjacent crust was juvenile rather than cratonic.
Precambrian zircons first appear in the Paleocene sandstone of the Yubetsu Group. In the Nikoro Group and Saroma Group sandstones, detrital zircons are quite scarce, and no Paleozoic or Precambrian zircon is so far found.
The clastic composition and detrital zircons ages are in general agreement with dredged volcanic and plutonic rocks from the Sea of Okhotsk floor. Since no zircons older than Jurassic are found, and no dredged rocks older than Triassic has been reported, the Sea of Okhotsk crust probably originated from Mesozoic island arc rather than a continental arc or rifted continental margin.

Keywords: Tokoro belt, accretionary complexes, Nikoro Group, Okhotsk

©2020. Japan Geoscience Union. All Right Reserved.

Zircon U-Pb ages and felsic volcanic clasts in the Lower Cretaceous Rebun Group, Hokkaido

*Nozomu Suzuki[1], yusuke Sugiyama, Hayato Ueda[1]

1. Niigata University

The Rebun - Kabato Belt, is characterized by Early Cretaceous arc volcanic and volcaniclastic rocks. The belt extends to the Harachiyama Formation of NE Honshu (Kitakami Mountains) in the south and Moneron Island offshore Sakhalin in the north. The Rebun –Kabato belt has been assumed to be a clastic source for the Sorachi Group, which comprise an accreted or trapped ocean basin in central Hokkaido. Thus, history and composition of volcanic activity in the Rebun-Kabato Belt is important to reconstruct oceanic plate configuration offshore Japan in the Early Cretaceous. This study examines stratigraphy, age, and clastic composition of the Rebun Group in Rebun Island and discusses on the cryptic basement on which the arc volcanic activity occurred.

We divided the Rebun Group into seven stratigraphic units (J, US1, and UN1 to UN5). The lowermost unit J is composed of thin-bedded volcaniclastic turbidites and massive volcaniclastic conglomerates, The overlying units are composed of volcaniclastic sandstone and conglomerate, and partly with tuff breccia and lapilli tuff. US1 unit consists both of conglomerate and sandstone. UN1, UN3 and UN5 unit are gravelly, and the UN2 and UN4 units are dominated by sandstone.

Bulk-rock silica contents of 26 volcanic clasts were diverse ranging from basaltic andesite to rhyolite, in spite that no felsic rocks have been known to occur in the Rebun Group. All the volcanic clats are subalkaline and tholeiitic. They can be subdivided into high-Ti and low-Ti groups. The high-Ti group show a typical tholeiite trend with evidently increasing TiO2 and FeO along with differentiation. The low-Ti group show increasing SiO2 and decreasing TiO2 and FeO somewhat similar to calc-alkaline rocks. The felsic clasts are metaluminous.

We obtained zircon U-Pb ages from a tuff bed in unit J. Concordant ages ranging from 110-142 Ma shows a skewed peak of probability density suggesting a mixture of two age groups averaging 123 Ma and 136 Ma. The younger and more dominant 123 Ma group is considered to represent the sedimentary age. The older group zircons probably originated either from xenocrysts inherited in the magma chamber or accidental grains involved during eruption and/or transportation. In both cases, the older zircons suggest an age of the host crustal rocks in which the felsic magma developed and erupted.

Occurrences of felsic rock clasts from the lowermost unit of Rebun Group imply that the underlying crust had already been more or less mature until 123 Ma. The crust was probably dominated by juvenile igneous rocks because of metaluminous composition of rhyolites and the absence of old inherited zircons in the tuff. The underlying crust could be oceanic because the belt neighbors the Sorachi-Yezo Belt in the east, where oceanic basalts are also overlain by arc-derived detritus. On the other hand, felsic magma in the Harachiyama Formation as a southern extension of the Rebun –Kabato Belt is considered to have developed within the underlying Jurassic accretionary complex of Eurasian margin, because some rhyolites are peraluminous and contain inherited zircons of Precambrian ages presumably originated from the host sandstone. These contrasting occurrences suggest that the Rebun-Kabato-Harachiyama arc was formed crosscutting previous plate boundary between Eurasia and the Sorachi ocean basin.

©2020. Japan Geoscience Union. All Right Reserved.

©2020. Japan Geoscience Union. All Right Reserved.

Paleozoic accretionary complex in the Khangai-Khentei belt, central Mongolia, and stratigraphy of Devonian chert

*Tomohito Nakano[1], Yukio Isozaki[2], Uyanga Bold[2], Otgonbaatar D[3], Yukiyasu Tsutsumi[4]

1. Department of Earth and Planetary Science, The University of Tokyo, 2. Department of Earth Science and Astronomy, Multi-disciplinary Sciences - General Systems Studies, Graduate School of Arts and Sciences, The University of Tokyo, 3. Institute of Paleontology and Geology, Mongolian Academy of Science, 4. Department of Geology and Paleontology, National Museum of Nature and Science

The Khangay-Khentei belt (KKB) in central Monglia is composed of Devonian-Carboniferous accretionary complexes (ACs), which were formed in one of the convergent plate boundaries within the Paleo-Asian ocean (PAO) between Siberia and North China continental blocks. This belt extends for more than 1200 km in NE-SW and 300 km wide in central Mongolia, of which main distribution is located in the Khangai Mtns. Preliminary researches were sporadically performed for basic mapping, and radiolarian dating. Nonetheless, vast areas still remain unmapped/undated. In order to document the essential characteristics of AC, i.e., ocean plate stratigraphy, we conducted detailed field mapping and sample collection of bedded cherts and sandstones in three areas; i.e., Arvaikheer, Bayankhongor, and the upper reach of the Orkhon River, along the southern margin of the Khangai Mountains. Cherts are for microfossil (radiolarians + conoodnts) dating, whereas sandstones are for U-Pb dating of detrital zircons. We collected 30 samples of chert, and 3 samples of sandstone. This presentation reports the first results of microfossil dating and U-Pb zircon geochronology for these three areas.

Keywords: Devonian, accretionary complex, Mongolia, deep-sea chert, Zircon, Radiolaria

©2020. Japan Geoscience Union. All Right Reserved.

Tectono-depositional evolution of the Mio-Pleistocene forearc basin on the Boso Peninsula, central Japan

*Nana Kamiya[1], Yuzuru Yamamoto[2], Masayuki Utsunomiya[3], Feng Zhang[4], Weiren Lin[1]

1. Graduate School of Engineering, Kyoto University, 2. Kobe University, 3. AIST, 4. Nagoya Institute of Technology

The Boso Peninsula, central Japan is located near a plate boundary between North America Plate, Philippine Sea Plate and Pacific Plate. The peninsula consists of accretionary prisms and a forearc basin fills, which indicates it developed with subduction of Sagami Trough. The forearc basin in the Boso Peninsula has developed with plate subduction and has a large-scale geological structure, the Kurotaki Unconformity. Variations of geological structure and lithology involved in the Kurotaki Unconformity has been confirmed, however detail of evolution such as paleotemperature and maximum burial depth are unclear. In this study, geological and engineering analyses were performed to investigate an evolution history of the Mio–Pleistocene forearc basin correlated to the plate subduction in the Boso Peninsula, central Japan.

Integrating the results of the geological, paleo-thermal and consolidation analyses, an evolution history of the Boso forearc basin were suggested. In the western part, major differences above and below the Kurotaki Unconformity were identified in the distributions of geologic bodies and their structures, paleotemperatures, and consolidation characteristics. These variations probably relate to a change in the convergence direction of the Philippine Sea Plate at ~3 Ma. Uplift and erosion of the Miura Group during the formation of the unconformity, and compression parallel to the direction of plate-subduction apparently caused the variations in the attitudes of geologic bodies. In the eastern part, the distribution of the consolidation yield stress appears to indicate that the burial process of the forearc basin occurred regardless of the development of the Kurotaki Unconformity, as ascertained from the patterns of consolidation yield stress for the Kazusa and Miura groups above and below the unconformity, respectively. Vitrinite reflectance corresponding to paleotemperature also shows no break in trend or values across the Kurotaki Unconformity. Because this feature is similar to the characteristics of the consolidation yield stress trend, any difference in vitrinite reflectance across the unconformity is thought to have disappeared because of the burial process. The uninterrupted trends in vitrinite reflectance and consolidation trend in the eastern part between the Miura and the Kazusa groups can be explained by the greater subsidence of the eastern part of the Boso forearc basin compared with the western part since ~2.3 Ma. Considering a possibility that a subsidence and uplift rate around the Boso Peninsula had been dependent on the way of subduction, the investigated variation of evolution between the western and eastern part of the Boso forearc basin contribute to determining the way of subduction.

Keywords: Forearc basin, Boso Peninsula, Vitrinite reflectance, Consolidation test

©2020. Japan Geoscience Union. All Right Reserved.

Preliminary Study on the Crustal Deformation along Sagaing Fault in Myanmar by using GNSS data

*Tha Zin Htet Tin[1,2], Takuya NISHIMURA[3], Manabu Hashimoto[3], Eric Lindsey[4], Myo Thant[2,5]

1. Graduate School of Science, Kyoto University, 2. Department of Geology, University of Yangon, Myanmar, 3. Disaster Prevention Research Institute, Kyoto University, 4. Earth Observatory of Singapore, Nanyang Technological University, Singapore, 5. Myanmar Earthquake Committee

Background

The plate tectonic motion between India, Eurasia, Sunda and Burma plates is responsible for the major geological processes in Myanmar. Among them, earthquakes are important mechanism responsible for geohazards in Myanmar. Currently, relative motion between the India and Sunda plates is about 35 mm/yr (Socquet et al,2006) and the rate of subduction of Indian plate beneath the Burma plate is about 12 - 24 mm/yr (Mallick et al.,2019). Due to this subduction and convergence between the India-Eurasia and Burma plates, fold and thrust belts are developed in the western part of Myanmar. Another major active geological structure in Myanmar is the 1200km long Sagaing Fault, a right-lateral strike slip fault, north-south trending along central Myanmar with slip rate of 18 –20 mm/yr. Most of the major cities in Myanmar, including Yangon, Mandalay, Nay Pyi Taw, Bago, Sagaing, Taungoo, Meiktila, etc., lie near-by and along the Sagaing Fault. Many large earthquakes have struck along this fault, resulting in many hundreds of casualties and significant damages in Myanmar over the past century.

GPS Measurement and Data Processing

A GPS network was constructed under the collaboration between Earth Observatory of Singapore (EOS), Myanmar Earthquake Committee (MEC) and Department of Meteorology and Hydrology, Myanmar (DMH) in Myanmar since 2012. 17 continuous GPS stations were instslled along 3 transect perpendicular to the Sagaing Fault from upper to lower Myanmar. To improve coverage in the Indo- Myanmar (Burma) Ranges in the west and Eastern Highland in the east, additional campaign measurements have been conducted since 2016. We possessed more than 113 campaign stations and 17 continuous stations to enable an estimate of crustal deformation across Myanmar. We estimated site velocities for the 17 permanent stations since 2012 and 41 campaign stations since 2016. We included RINEX data from nearby permanent IGS network stations in our processing to improve the accuracy of site positions and define a consistent reference frame in our research area. Daily coordinate positions for permanent and campaign stations in the International Terrestrial Reference Frame 2014 (ITRF2014) were computed using GIPSY-OASIS ver 6.4 software from Jet Propulsion Laboratory (JPL). Ocean tide loading was calculated using FES2014b model by the Onsala Space Observatory (http://holt.oso.chalmers.se/loading/) with respect to the joint mass center of solid Earth and ocean combined.

Result

We confirmed that the present-day relative motion and the direction of movement between the GNSS stations are consistent with the dextral strike slip of this fault system. The stations on the eastern side of the Sagaing Fault show smaller velocities with respect to the Sunda plate than those on the western side of the Sagaing Fault. The western stations still have significant motion with respect to the India plate. This result implies that the eastern part of Myanmar is generally experiencing less internal deformation than

©2020. Japan Geoscience Union. All Right Reserved.

the western side. The velocities in the Mandalay area show an additional WSW-ward movement due to the effect of clockwise rotation of the Eastern Himalayan Syntaxis from the north.

Keywords: GNSS, Sagaing Fault, Burma plate, Indo-Myanmar Ranges, Eastern Himalayan Syntaxis

©2020. Japan Geoscience Union. All Right Reserved.

Evidence for Late Mesozoic intraoceanic subduction offshore NE Asia from mantle convection and geoid models

*Lorenzo Colli[1], Jonny Wu[1], Yi-An Lin[1]

1. University of Houston

The existence of the Izanagi plate is well established both from magnetic lineations and fracture zones in the western Pacific and from tomographic imaging of the deep mantle underneath East Asia. But its spatial extent, position and motion through time remain poorly known.

A common scenario envisages the Izanagi as a large and long-lived plate extending from central Panthalassa to the eastern margin of Eurasia. In this scenario the Izanagi plate is conjugate to the Farallon and Phoenix plates before the inception of the Pacific plate and it subducts continuously beneath East Asia during the Mesozoic (e.g. Müller et al., 2016). But more complex scenarios, entailing the existence of additional plates and subduction zones, have been proposed based on both geologic evidence from the East Asian margin and tomographic images of mantle seismic structure.

Here we explore four kinematic plate motion models of increasing complexity, starting with a maximum-size Izanagi plate and introducing in steps a number of additional plates and intraoceanic subduction zones in accordance with geologic evidence along the East Asian margin. We assimilate these kinematic plate motion models in geodynamic models of global mantle convection in the form of a time-dependent velocity boundary condition at the Earth’ s surface. Their implications for the evolution of mantle structure in East Asia during Mesozoic time up to present-day are presented and discussed, focusing in particular on how well the modeled present-day state can match tomographic images of the mantle and the geoid.

Keywords: Panthalassa, Arc accretion, Oku-Nikapu complex, Mainitskiy terrane

©2020. Japan Geoscience Union. All Right Reserved.

Brittle-Plastic Structures Provide Constraints on the Rapid Exhumation of the Central Range: Taiwan

*Lauren Donati[1], Lindsey Aman[1], Susan Adams[1], Jonathan C Lewis[1]

1. Indiana University of Pennsylvania

Taiwan records some of the highest late Cenozoic exhumation rates in the world as the result of the collision between the Luzon volcanic arc and the passive margin of Eurasia. To understand how such rapid exhumation is accommodated, we focus on late-stage plastic and early brittle structures in river outcrop exposures along the eastern Central Range. We specifically focus on the youngest metamorphic fabric in these outcrops documented as S3, syn-kinematic veins, and crosscutting well developed joint sets. We suggest that veins document the bridge between the plastic and brittle regime, as mm-scale veins are locally cut by S3, while others cross-cut the outcrop. The geometry of these structures shows relative consistency. S3 is a shallow-dipping fabric that is locally well developed in cm- and mm-scale folds of older metamorphic fabrics. The veins and joints mostly strike NW-SE and dip nearly vertically. We focus on the details of these geometries over >100 km along strike, and in strike-normal transects along the Chingsui, Hongye, and Xinwulu/Dalun rivers. We see slight variation in the sub-horizontal orientation of S3 from N to S, with the biggest deviation occurring along the Chingsui River near where high-pressure rocks have been discovered. Joints show small changes in dip angle, however consistency in strike, with again, the greatest change in dip along the Chingsui River. Overall the veins are sub-parallel to the joints and show similar along-strike variations, with one exception in the area of the Chingsui River where the veins show more variation in strike. In the strike-perpendicular transects, S3 shows some variation in orientation, while veins and joints seem to change mostly in dip steepness. The patterns we see in the S3, veins, and joints provide constraints in the plastic-to-brittle transition in 3 dimensions. We suggest that S3, as the oldest structure, records the greatest variation in geometry and this reflects post-S3 processes. Similarly, the younger veins and joints show consistent strike and slight dip variation along strike. We suggest that the veins and joints formed in a uniform stress field and were differentially rotated passively in response to gradients in uplift rate and/or magnitude.

Keywords: Veins, Joints, Central Range

©2020. Japan Geoscience Union. All Right Reserved.

Where are the proto-South China Sea slabs? SE Asian plate tectonics and mantle flow history from global mantle convection modeling

*Yi-An Lin[1], Lorenzo Colli[1], Jonny Wu[1]

1. University of Houston

In this study we explored the contrasted plate tectonic reconstructions proposed for the proto-South China Sea and SE Asia, including Philippine Sea plate tectonics near Japan. We implemented four different end-member plate models into global geodynamic models to test their predicted mantle structure against tomography. All models reproduced the Sunda slabs beneath Peninsular Malaysia, Sumatra and Java and the proto-South China Sea (PSCS) slabs beneath present Palawan, northern Borneo, and offshore Palawan; some models also predicted slabs under the southern South China Sea. PSCS slabs generated from double-sided PSCS subduction and earlier Borneo rotation generated a slightly better fit to tomography but pure southward PSCS subduction was also viable. A smaller Philippine Sea plate (PSP) with a short ~1000 km restored northern slab (i.e. Ryukyu slab) was clearly superior to a very long >3000 km slab. Our preferred model had a smaller PSP overriding a vanished ocean south of Japan; this model produced slab anomalies south of the Ryukyu trench at ~400-800 km depth that best match seismic tomography.

The following plate model variants were assimilated in the geodynamic models: (1) southward vs. double-sided PSCS subduction; (2) early Borneo counterclockwise rotations during the Oligocene to Early Miocene vs. later rotations (mid- to Late Eocene and Early Miocene); (3) a smaller Philippine Sea plate restored with a shorter ~1000 km northern slab vs. a longer >3000 km slab. This study assimilates four different plate models into the numerical model TERRA (Bunge et al., 1998). We digitally re-built in GPlates (Boyden et al., 2011) the implemented the plate models as a set of continuously closing plates in order to generate a global self-consistent velocity field to be assimilated into the convection models. The temperature fields were converted to seismic velocities assuming a Pyrolite composition and equilibrium mineralogy. We quantify the correlation between our geodynamic models and seismic tomography within SE Asia. For the tomography models S40RTS and LLNL-G3Dv-JPS we explicitly accounted for their finite resolution (Ritsema et al., 2011; Simmons et al. 2019).

Keywords: Geodynamic model, Southeast Asian plate tectonics, proto-South China Sea plate model, Philippine Sea plate model

©2020. Japan Geoscience Union. All Right Reserved.

[E] Poster | S (Solid Earth Sciences)：S-IT Science of the Earth's Interior & Techtonophysics

[S-IT30] Tectonic collision systems in continents and oceans

convener:Ling Bai(ITP Institute of Tibetan Plateau Research, Chinese Academy of Sciences), James Mori(Earthquake Hazards Division, Disaster Prevention Research Institute, Kyoto University), Xiaodong Song(University of Illinois at Urbana-Champaign), Yuzo Ishikawa(The National Institute of Advanced Industrial Science and Technology)

Collisions between continental plates and between continental and oceanic plates resulted in the formation of significant orogen and subduction systems worldwide, including the deepest trough and highest mountain in East Asia. The tectonic structures and seismic hazards associated with the collision processes have long been studied in order to understand fundamental features in these different tectonic environments. We invite contributions from scientists working across various temporal and spatial scales on problems related to lithosphere and mantle dynamics and surface processes for the collision zones. This session will provide a platform to encourage collaborations in all related disciplines, including geomorphology, paleoseismology, structural geology, tectonics, seismology, geodesy, and modeling.

[SIT30-P01] Upper mantle deformation of the Terror Rift and northern Transantarctic Mountains in Antarctica: Insight from P-wave anisotropic tomography

★Invited Papers

*heng zhang[1] (1.Institute of Tibetan Plateau Research, Chinese Academy of Sciences)

[SIT30-P02] Source parameters of the 2019 Ms6.3 Medog earthquake in the southeastern Tibetan plateau and its tectonic implications

*Guohui Li[1,2], Ling Bai[1], Lin Ding[1], Bowen Song[1,3,4], Yong Jiang[1,4] (1.Key Laboratory of Continental Collision and Plateau Uplift, Institute of Tibetan Plateau Research, Center for Excellence in Tibetan Plateau Earth Sciences, Chinese Academy of Sciences, 2.Institute of Earthquake forecasting, China Earthquake Administration, 3.Geophysical Exploration Center , China Earthquake Administration, 4.University of Chinese Academy of Sciences)

[SIT30-P03] Crustal and mantle velocity structures of the Sulawesi Island from multi-scale seismic tomography.

*Bagus Adi Wibowo[1,2], Ling Bai[2], Supriyanto Rohadi[1], Muzli -[1], Andry Syaly Sembiring[1], Rahmat Triyono[1], Muhamad Sadly[1], Suko Prayitno Adi[1] (1.Meteorological, Climatological, and Geophysical Agency, Indonesia, 2.ITP Insitute of Tibetan Plateau Research, Chinese Academy of Sciences, China)

[SIT30-P04] Forearc basin development at the Northern Andes – southern boundary transform fault: Progreso basin, SW Ecuador

*Carlos Alberto Aizprua Luna[1,2,3], Cesar Witt[2] (1.Department of Geosciences and Petroleum, Norwegian University of science and Technology (NTNU), Trondheim, Norway , 2.Univ. Lille, CNRS, Univ. Littoral Côte d'Opale, UMR 8187, LOG, Laboratoire d'Océanologie et de Géosciences, F 59000 Lille, France, 3.Facultad de Ingeniería en Ciencias de la Tierra, Escuela Superior Politécnica del Litoral, Campus Gustavo Galindo – km 30.5 vía perimetral, Guayaquil, Ecuador)

[SIT30-P05] Seismic anisotropy in the deep continental upper mantle beneath Tibetan Plateau

*Cheng-Chien Peng[1,2], Ban-Yuan Kuo[2], Eric Debayle[3], Ling-Yun Chiao[1] (1.IONTU Institute of Oceanography National Taiwan University, 2. Institute of Earth Sciences Academia Sinica, 3.Laboratoire de Géologie de Lyon, Université Claude Bernard Lyon 1)

[SIT30-P06] Shear velocity structure of the crust and lithospheric mantle beneath Taiwan from teleseismic Rayleigh-wave tomography

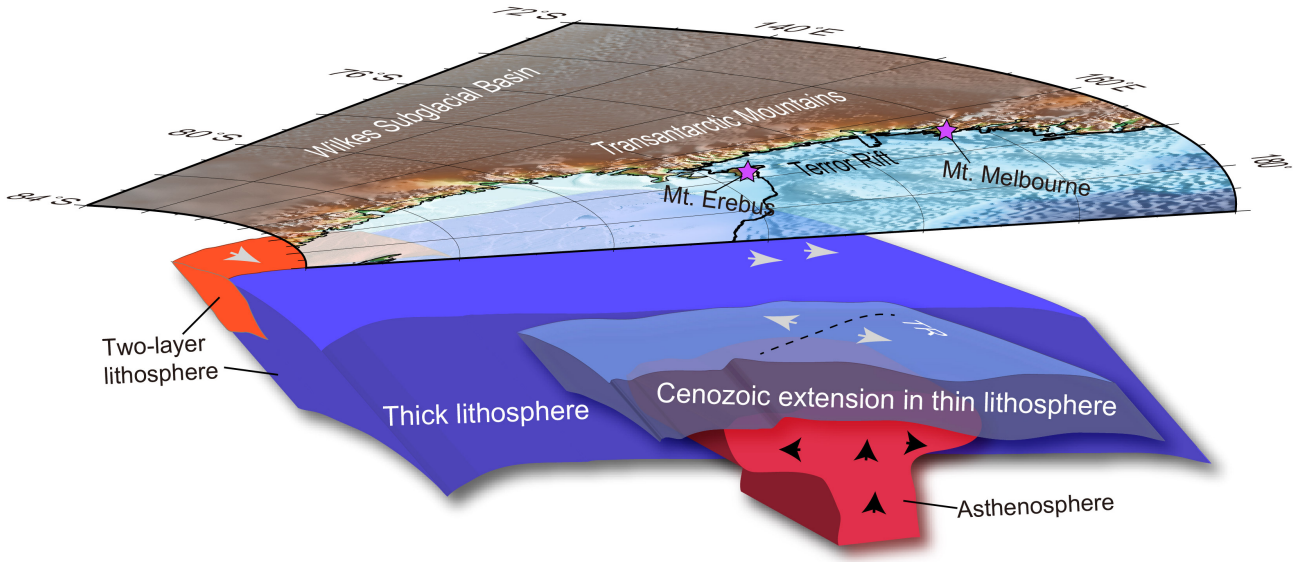
*Ayush Goyal[1], Shu-Huei Hung[1] (1.Department of Geosciences, National Taiwan University)

Upper mantle deformation of the Terror Rift and northern Transantarctic Mountains in Antarctica: Insight from P-wave anisotropic tomography

*heng zhang[1]

1. Institute of Tibetan Plateau Research, Chinese Academy of Sciences

A large number of teleseismic travel-time data are used to determine the first P-wave radial anisotropy tomography beneath the Terror rift, the northern Transantarctic Mountains (NTAM) and the Wilkes Subglacial Basin (WSB) in Antarctica. Our results show that variations of radial anisotropy occur in both horizontal and vertical directions. In the NTAM, a high-velocity zone with positive radial anisotropy is revealed at shallower depths, which reflects the lithospheric deformation pattern formed during the Ross Orogeny. In contrast, negative radial anisotropy appears at depths > 200 km under the NTAM, which is caused by the characterization of olivine fabric rather than foundering lithosphere. Beneath the western WSB, a two-layer lithosphere exists that contains rift-induced cracks. To the east of the NTAM, asthenospheric upwelling occurs at shallow depths beneath the Terror rift. Then the upwelling asthenosphere flows northward to Mt. Melbourne and southward to Mt. Erebus.



©2020. Japan Geoscience Union. All Right Reserved.

Source parameters of the 2019 Ms6.3 Medog earthquake in the southeastern Tibetan plateau and its tectonic implications

*Guohui Li[1,2], Ling Bai[1], Lin Ding[1], Bowen Song[1,3,4], Yong Jiang[1,4]

1. Key Laboratory of Continental Collision and Plateau Uplift, Institute of Tibetan Plateau Research, Center for Excellence in Tibetan Plateau Earth Sciences, Chinese Academy of Sciences, 2. Institute of Earthquake forecasting, China Earthquake Administration, 3. Geophysical Exploration Center , China Earthquake Administration, 4. University of Chinese Academy of Sciences

An Ms6.3 earthquake occurred at Medog County, Nyingchi City, Tibet at Beijing time 04:15 on 24 April 24 2019. This earthquake is located in the northeast corner of the Himalaya orogenic belt where the Indian plate underthrusts beneath the Eurasian plate. Here the crustal shortening and the tectonically rotated deformation is the strongest with respect to other areas along the Himalayan orogenic belt.

Based on the waveforms recorded by the local broadband seismic stations we deployed at the eastern Himalaya syntaxis, and the waveform and traveltime data obtained from Chinese and international seismic networks, we determined the earthquake location, focal mechanism and rupture process.

The resulting epicenter of this earthquake is (94.56±0.01˚E, 28.41±0.01˚N) and the focal depth is 13.3± 1.6 km below the surface (or 11.5±1.6 km beneath the sea level). The focal mechanism solution strike/dip/slip is 202˚/17˚/20˚. The large rupture is mainly concentrated about 5 km to the NNE of the initial rupture area. Combined with other previous geophysical and geological studies, we infer that the earthquake occurred at the rapid turning area where the Main Himalayan thrust suddenly rotated nearly 90˚. The major tectonic feature for this area is the west-dipping subduction and northward thrust of the Sang syntaxis with respect to the Namche Barwa syntaxis.

Keywords: Eastern Himalaya syntaxis, 2019 Ms6.3 Medog earthquake, arthquake relocation, Focal mechanism solution, Source rupture process

©2020. Japan Geoscience Union. All Right Reserved.

Crustal and mantle velocity structures of the Sulawesi Island from multi-scale seismic tomography.

*Bagus Adi Wibowo[1,2], Ling Bai[2], Supriyanto Rohadi[1], Muzli -[1], Andry Syaly Sembiring[1], Rahmat Triyono[1], Muhamad Sadly[1], Suko Prayitno Adi[1]

1. Meteorological, Climatological, and Geophysical Agency, Indonesia, 2. ITP Insitute of Tibetan Plateau Research, Chinese Academy of Sciences, China

We did multi-scale seismic tomography in and around the Sulawesi Island, Indonesia, to acquire better seismic velocity structures and to discuss its tectonic implications of the area. We used a regional-scale double-difference tomography method to invert the body wave (P and S-wave) phases of earthquakes from InaTEWS' (Indonesia' s Tsunami Early Warning System) earthquake catalog from 2017 to 2018. The data included some important seismic events occurred in this time period, such as The Palu Earthquake, the West Sulawesi (Mamasa) swarm earthquake and other seismic activity related to tectonic setting among research area.

From Vp and Vs velocity anomalies, we found signs of magmatic activity below volcanoes along the Northern Arm of Sulawesi, the activity of the left-lateral strike-slip fault of Palu-Koro, and signs of upward tectonic activity between lower crust and upper mantle boundary that may have caused the West Sulawesi (Mamasa) earthquake swarm. These findings explained the implication to local tectonic conditions after these significant seismic events and added a more critical understanding of tectonic interaction in lithosphere beneath the Sulawesi Island.

Keywords: Sulawesi Island, seismic tomography, earthquake swarm, volcanoes

©2020. Japan Geoscience Union. All Right Reserved.

Forearc basin development at the Northern Andes –southern boundary transform fault: Progreso basin, SW Ecuador

*Carlos Alberto Aizprua Luna[1,2,3], Cesar Witt[2]

1. Department of Geosciences and Petroleum, Norwegian University of science and Technology (NTNU), Trondheim, Norway , 2. Univ. Lille, CNRS, Univ. Littoral Côte d’ Opale, UMR 8187, LOG, Laboratoire d’ Océanologie et de Gé osciences, F 59000 Lille, France, 3. Facultad de Ingeniería en Ciencias de la Tierra, Escuela Superior Politécnica del Litoral, Campus Gustavo Galindo –km 30.5 vía perimetral, Guayaquil, Ecuador

It has been recognized that obliquity between convergent plates along active margins results in strain partitioning, both normal and parallel to the trench. Such active margins may develop large scale strike-slip faults that can be prolonged for hundreds of kilometers, commonly located along the volcanic arc, and bounding different forearc crustal slivers. The mechanisms proposed for the development of such large-scale faults have been discussed and well documented in regions such as the western North America, where the accretion of allochthonous terranes may have played a great role in the observed deformation styles. However, less is known along the area linking the large strike-slip faults and the actual trench, and how this may have controlled the forearc tectonic-stratigraphic evolution along the area. Few studies, like the Eocene Tyee forearc basin in Oregon, discuss the formation of sedimentary basins along a plate boundary transform fault, in connection to a system developed along the suture of an allochthonous oceanic terrane accreted to the continental margin. In the Northern Andes, a Late Cretaceous oceanic plateau sliver underlies the forearc region of SW Ecuador, with its southern limit interacting with the continental basement of South America. The great Progreso Basin is located along and across the inferred suture zone, and its study has provided us with an insight on the fault termination styles of large-scaled strike-slip faults, their associated tectonic elements, their link to the trench, and their influence on the stratigraphic record. Based on multi-channel seismic profiles, industrial borehole data, surface exposures, and recent radiometric age results, we attempt to make a paleogeographic reconstruction of the early stages of forearc basin evolution at the southern boundary of the Northern Andes sliver. The geological record of rapid shallowing of the forearc from deep marine deposits into fluvio-deltaic successions by Oligocene time, and restricted conditions of the forearc region through the development of perched extensional sub-basins, suggest a more complex systems than a simple transtensional strike-slip regime at the fault termination area. We suggest that the inherited configuration following the collision and accretion of an oceanic crustal sliver accompanied by the development of a local and thick accretionary wedge by Paleocene time, and the post-Oligocene transtensional regime along the southern boundary transform fault of the North Andean Sliver better explain the observed basin configuration at this region.

Keywords: Forearc basin, outer forearc high, strike-slip faults, accretionary wedge, tectonic scape

©2020. Japan Geoscience Union. All Right Reserved.

Seismic anisotropy in the deep continental upper mantle beneath Tibetan Plateau

*Cheng-Chien Peng[1,2], Ban-Yuan Kuo[2], Eric Debayle[3], Ling-Yun Chiao[1]

1. IONTU Institute of Oceanography National Taiwan University, 2. Institute of Earth Sciences Academia Sinica, 3. Laboratoire de Géologie de Lyon, Université Claude Bernard Lyon 1

Multimode Rayleigh wave tomography (Pandey et al., 2015) shows a depth-dependent azimuthal anisotropy in the Tibetan Plateau which may involve different stress field orientations in the lithosphere and the underlying mantle. The azimuthal anisotropy model could explain some characteristics of SKS splitting, but fails to predict the large delay time in central Tibet, probably owing to the lack of sensitivity of Rayleigh waves in the deep upper mantle. To reconcile the discrepancy in delay time between the model prediction and the SKS data, we search for new anisotropy parameters of the upper mantle layer (200~250 km) of the model to fit the SKS observations. In this process, we fix the upper layers of the Rayleigh model assuming they were well constrained. The best fit result shows that changing orientation slightly (<30˚) and increasing anisotropy intensity to ~10% in the upper mantle layer can improve the SKS data fitting remarkably. Because 10% anisotropy intensity is unlikely within the 50 km thickness layer, we suggest that this anisotropy layer extends to deep upper mantle (>250 km) beneath the Tibetan plateau. This modified region is roughly beneath the north of the Bangong-Nujiang suture zone that coincides with the northern front of the underthrusted Indian lithosphere. The mechanisms that may cause this thick anisotropy layer in the mantle is under investigation.

Keywords: seismic anisotropy, upper mantle, Tibetan Plateau, Rayleigh wave tomography

©2020. Japan Geoscience Union. All Right Reserved.

Shear velocity structure of the crust and lithospheric mantle beneath Taiwan from teleseismic Rayleigh-wave tomography

*Ayush Goyal[1], Shu-Huei Hung[1]

1. Department of Geosciences, National Taiwan University

The interaction of two opposite-verging subduction systems of the Eurasian Plate (EP) and Philippine Sea Plate (PSP) and consequent collision between the Luzon arc of the PSP and Eurasian continental margin resulted in a lithotectonically complex orogen in Taiwan. To reveal its structural complexity associated with the plausible orogenic process and dynamic mechanism, numerous tomographic studies of crustal structures beneath Taiwan and the surrounding region have been conducted extensively. However, the crust-mantle boundary (Moho) and lithospheric mantle structure which potentially provide clues to unravel the tectonic model responsible for the Taiwan orogeny remains less explored. In this study, we analyze vertical-component Rayleigh wave data from teleseismic earthquakes recorded by a totally ~160 broadband on-land and ocean-bottom seismometer stations distributed across Taiwan and offshore islands and at seafloor offshore eastern Taiwan during the years of 2007-2017. A wavelet-based, two-station method that properly characterizes the time-varying spectral properties of earthquake signals is employed to measure dispersive phase velocities or travel times of fundamental-mode Rayleigh waves propagating between station pairs in the periods of 13-81 s. The obtained frequency-dependent traveltimes are then used to invert for a 3-D shear-wave velocity model. The preliminary resulting model indicates that the crust is thickest beneath the mid-western flank of the Western Central Range or Backbone Range Slate Belt and shallowest beneath the Huatung basin (HB) under the oceanic PSP. More detailed and robust features of shear velocity heterogeneities will be explored through the advanced probability inversion technique.

Keywords: phase velocity, Rayleigh wave , two-station method, Taiwan orogen, subduction zone

©2020. Japan Geoscience Union. All Right Reserved.

[E] Poster | S (Solid Earth Sciences)：S-IT Science of the Earth's Interior & Techtonophysics

[S-IT31] Planetary cores: Structure, formation, and evolution

convener:Hidenori Terasaki(Faculty of Science, Okayama University), Eiji Ohtani(Department of Earth and Planetary Materials Science, Graduate School of Science, Tohoku University), Gerd Steinle-Neumann(Bayerisches Geoinstitut, Universitaet Bayreuth), William F McDonough(Department of Earth Science and Research Center for Neutrino Science, Tohoku University, Sendai, Miyagi 980-8578, Japan)

There are fundamental links between the formation and evolution of planets and their satellites to that of their cores both in terms of magnetic field generation and chemical and physical structure. Defining physical and chemical properties of the cores and core materials of these terrestrial bodies are therefore fundamental for understanding their internal structures and thermal profile. Recent advances in experimental and theoretical studies provide new insights into the Earth's cores and other terrestrial bodies, including the role of light elements in the early history of planets and at current times. Recent, current and future space missions have and will continue to obtain data on the internal structure of terrestrial planets (e.g., Mars and Mercury) and planet-satellite systems. We anticipate presentations on recent advances on the physical and chemical properties of cores and discussions regarding the latest views of their formation and evolution. We welcome contributions from mineral/rock physics, geophysics, geochemistry, geodynamics, and planetary science.

[SIT31-P01] Sound velocity measurement of Fe-Ni-Si alloys at high pressure and high temperature

*Daijo Ikuta[1], Eiji Ohtani[1], Hiroshi Fukui[2,3], Hiroshi Uchiyama[4], Satoshi Tsutsui[4], Baron Alfred[3] (1.Department of Earth Science, Tohoku University, 2.Department of Material Science, University of Hyogo, 3.RIKEN, 4.JASRI)

[SIT31-P02] Mercury core size constrained from elastic properties of Fe-Ni-S-Si liquid

Iori Yamada[1], *Hidenori Terasaki[1], Ryo Tsuruoka[1], Asaka Kamiya[1], Tadashi Kondo[1], Yoshinori Tange[2], Yuji Higo[2] (1.Graduate School of Science, Osaka University, 2.JASRI)

[SIT31-P03] Metal-silicate partitioning of carbon at the core formation

*Yutaro Tsutsumi[1], Naoya Sakamoto[2], Kei Hirose[3], Shunpei Yokoo[1], Shoh Tagawa[4], Hisayoshi Yurimoto[5] (1.The University of Tokyo, 2.Creative Research Institution, Hokkaido University, 3.Earth-Life Science Institute, Tokyo Institute of Technology, 4.Department of Earth and Planetary Science, The University of Tokyo, 5.Department of Natural History Sciences, Hokkaido University)

[SIT31-P04] Thermodynamic analysis of density of Fe-Ni-S melts at high pressure

*Satoru Urakawa[1], Hidenori Terasaki[2], Akihiko Machida[3] (1.Department of Earth Sciences, Okayama University, 2.Department of Earth and Space Science, Osaka University, 3.QST)

[SIT31-P05] Possibility of percolation of Fe-S melts in asteroids

*Takumi Miura[1], Hidenori Terasaki[1], Tadashi Kondo[1] (1.Department of Earth and Space Science, Graduate School of Science, Osaka University)

[SIT31-P06] Effect of Isostatic Rebound on Lithosphere in the Discrete Element Method Simulation

*Soojung An[1] (1.Kangwon National University)

Sound velocity measurement of Fe-Ni-Si alloys at high pressure and high temperature

*Daijo Ikuta[1], Eiji Ohtani[1], Hiroshi Fukui[2,3], Hiroshi Uchiyama[4], Satoshi Tsutsui[4], Baron Alfred[3]

1. Department of Earth Science, Tohoku University, 2. Department of Material Science, University of Hyogo, 3. RIKEN, 4. JASRI

The Earth's core has supposed to be constituted by iron-nickel alloys containing about 10% nickel as the main constituent and some light elements. The candidates of light element are sulfur, oxygen, carbon, hydrogen, and silicon. Among them, silicon is one of the most convincing light elements. The structure, physical properties and its chemical compositions of the Earth's core has been discussed with the seismic structure model of the Earth such as preliminary reference Earth model (PREM) based on seismic wave velocity observations. Constraints on the chemical composition of the Earth's core have been discussed by comparing the model with the physical properties of the Fe-Ni-X alloys that are candidates for the composition of the Earth's core. For the physical properties, a sound velocity and a density of materials are directly related to the knowledge obtained from seismic wave velocity observations. Therefore, the information of sound velocity and density for Fe-Ni-X system are important to understand the properties of the Earth's core and to restrict its chemical compositions. However, for the Fi-Ni-Si system, which is considered to be a promising candidate for the constituents of the Earth's core, were not well studied especially high pressure and high temperature conditions.
In this study, we measured the sound velocity and density of the Fi-Ni-Si system under high pressure and high temperature conditions, and discuss the composition of the Earth's core through comparison with the results and PREM.

Keywords: Fe-Ni-Si system, sound velocity, high pressure

©2020. Japan Geoscience Union. All Right Reserved.

Mercury core size constrained from elastic properties of Fe-Ni-S-Si liquid

Iori Yamada[1], *Hidenori Terasaki[1], Ryo Tsuruoka[1], Asaka Kamiya[1], Tadashi Kondo[1], Yoshinori Tange[2], Yuji Higo[2]

1. Graduate School of Science, Osaka University, 2. JASRI

Surface on Mercury is found to contain 1–4 wt% of sulfur from X-ray spectroscopy of the MESSENGER spacecraft (Nittler et al. 2011). The S content on the surface suggests that certain amounts of S and Si are likely to be contained in the Mercury core based on partitioning of S and Si between metal and silicate melts (Chabot et al. 2014).

In this study, we measured the V_P of liquid Fe–Ni–S–Si up to 17 GPa and investigated the effect of pressure and alloying of S+Si on the V_P to constrain the radius of Mercury core. High pressure experiments were performed using 1500 ton Kawai-type multianvil press at BL04B1 beamline, SPring-8 synchrotron facility. The P-wave velocity was measured using the pulse-echo overlap method.

The V_P of Fe-Ni-S-Si liquids of this study locate in between reported V_P of Fe-Ni-S and Fe-Ni-Si. Thus, there is an offset between S and Si effects on the V_P. Based on the obtained elastic properties of liquid Fe-Ni-S-Si, we estimated the Mercury core radius which satisfies the observed total mass and moment of inertia of Mercury and discuss possible core composition.

Keywords: Mercury, Sound velocity, iron-alloy, Core

©2020. Japan Geoscience Union. All Right Reserved.

Metal-silicate partitioning of carbon at the core formation

*Yutaro Tsutsumi[1], Naoya Sakamoto[2], Kei Hirose[3], Shunpei Yokoo[1], Shoh Tagawa[4], Hisayoshi Yurimoto[5]

1. The University of Tokyo, 2. Creative Research Institution, Hokkaido University, 3. Earth-Life Science Institute, Tokyo Institute of Technology, 4. Department of Earth and Planetary Science, The University of Tokyo, 5. Department of Natural History Sciences, Hokkaido University

Carbon has been considered to be one of the possible major light elements in the Earth’s core. While carbon is known to be strongly siderophile (iron-loving) at relatively low pressures, its metal-silicate partitioning under high pressure and temperature (*P*-*T*) conditions, typical for those of core segregation from silicate (~50 GPa, 3500 K), has been least examined yet. Here we performed melting experiments on Fe metal + MORB glass at such high *P*-*T* conditions in a laser-heated diamond-anvil cell (DAC). The metal-silicate partitioning of carbon was examined by using two different sets of starting materials; carbon was included in Fe in one set of experiments, and it was contained as CO_2 in silicate glass in another set. After melting at high *P*, samples were recovered from a DAC, and their cross sections were prepared with a focused ion beam (FIB). Textural and compositional characterizations were made by electron microprobes. Subsequently carbon concentrations in coexisting molten iron and silicate melt were obtained by using a high-resolution imaging technique with secondary ion mass spectrometry (SIMS). These experimental results and the possible concentration of carbon in the core will be discussed at the meeting.

Keywords: Outer core, Light elements, Melting experiments, Carbon, Hydrogen

©2020. Japan Geoscience Union. All Right Reserved.

Thermodynamic analysis of density of Fe-Ni-S melts at high pressure

*Satoru Urakawa[1], Hidenori Terasaki[2], Akihiko Machida[3]

1. Department of Earth Sciences, Okayama University, 2. Department of Earth and Space Science, Osaka University, 3. QST

Density of liquid Fe-alloy is one of the important physical properties to understand dynamics of planetary liquid core. However, we have only limited information on the pressure, temperature and composition dependency of density of liquid Fe-alloy. We have focused on Fe-Ni-S alloy, which are thought to be universally present as core constituents of planets and satellites, and measured their densities at high-temperatures and pressures by X-ray absorption technique. Here we report the results of thermodynamic analysis of the density of liquid Fe-Ni-S alloy. Density (molar volume) of liquid Fe-Ni-S alloy measured at 3 GPa was analyzed by associated solution model assuming the associated compounds, Fe, FeS, NiS and Ni. We evaluated the molar volume and the thermal expansivity of each associated compound as well as the interaction parameters between associated compounds. As a result, we can express the temperature and composition dependence of the density of liquid Fe-Ni-S alloy at 3 GPa. We found a negative excess volume between Fe-FeS and FeS-NiS and a positive excess volume between Ni-NiS. We will also discuss the pressure evolution of the phase relationships of the Fe-FeS.

Keywords: density, molar volume, thermal expansion, liquid Fe alloy

©2020. Japan Geoscience Union. All Right Reserved.

Possibility of percolation of Fe-S melts in asteroids

*Takumi Miura[1], Hidenori Terasaki[1], Tadashi Kondo[1]

1. Department of Earth and Space Science, Graduate School of Science, Osaka University

Many asteroids and planetesimals have been reported to compose of metallic cores surrounded by silicate mantles (Barrat et al., 2015). Due to negligible accretional heating in asteroids, percolation of liquid iron alloy through solid silicates is likely to be one of the plausible core formation process in asteroids. It is important for understanding asteroid core formation process to clarify whether or not liquid iron alloy percolates through solid silicate matrix. In previous percolation experiments, the dihedral angle between olivine and Fe-S melts is reported to be less than 60˚ below 2-3 GPa depending on olivine composition at oxidized conditions, indicating that the Fe-S melt can percolate through crystalline olivine (Terasaki et al., 2008). To understand core formation process in asteroids, it is important to measure the dihedral angel between Fe-S melts and orthopyroxene (opx) which is one of the major mantle mineral of asteroid as with olivine.

In this study, percolation experiments were performed at 2.5 GPa and 1863 K using cubic multi-anvil devices. Annealing durations range from 15 to 60 min at target temperatures. Starting material was natural opx powder (Fe#=0.29) and Fe-S (S=40, 50 at%). Fe-S layer was set between orthopyroxene layers. Textures of recovered samples were observed using scanning electron microscope. We observed that FeS did not percolate in solid opx, while $Fe_{60}S_{40}$ percolated in opx. In the percolated region, opx was turned into olivine by chemical reaction during experiment. Based on these results (texture, measured dihedral angle, and chemical compositions), we will discuss a possible process of percolation of Fe-S melt in opx solid.

Keywords: Percolation, Asteroid, Core formation

©2020. Japan Geoscience Union. All Right Reserved.

Effect of Isostatic Rebound on Lithosphere in the Discrete Element Method Simulation

*Soojung An[1]

1. Kangwon National University

Mass redistribution of the lithosphere due to imposed or removed loads, so-called isostatic rebound, makes the surface to rise or sink. Loads may consist of continental shelves, ice, large lakes, thrust sheets, sediment, and volcanoes. Until the isostatic equilibrium is reached, the rising or sinking of the lithosphere will continue. When surface settings are being unloaded (i.e., melting of ice, sediment erosion), the new stress would be given continuously at existing fractures, inducing extension of the length of the microfracture. Also, it would trigger an earthquake arisen from stress releases which can induce rock failures suppressed by loads. A lot of numerical analysis method is being used to modeling this problem. Finite element method which considers the model a continuum-based has been widely used to analyze various phenomena of the earth’ s tectonic systems. However, since the finite element method considers the model a continuum-based, when it comes to observing surface extensional fractures on rifting regions along the basins being expanded, it is not suitable enough to study the rock failure mechanism. In this study, we simulated a time-dependent isostatic rebound with brittle failure of surface bedrock due to the removal of loads using DEM (discrete element method). The discrete element method is introduced by Cundall and Strack (1979), which can deal with the complex behavior of the material as a result of interactions between discrete particles. We used the open-source discrete element analysis software package YADE which holds good maintainability and expandability due to command scripting system using python.

Keywords: discrete element method, iso-static rebound, earthquake

©2020. Japan Geoscience Union. All Right Reserved.

[E] Poster | S (Solid Earth Sciences)：S-IT Science of the Earth's Interior & Techtonophysics

[S-IT32] Do plumes exist?

convener:Hidehisa Mashima(Center for Obsidian and Lithic Studies, Meiji University), Gillian R Foulger(Durham University), Dapeng Zhao(Department of Geophysics, Tohoku University)

The debate regarding whether anomalous volcanic areas on Earth's surface are fed by deep-mantle plumes is widely considered to be the most significant debate currently ongoing in Earth science. Not only does the debate touch on a fundamental aspect of how Earth works dynamically, but the subject is extraordinarily cross-disciplinary to an extent that probably few scientists fully realize. Sub-disciplines that can contribute to efforts to resolve the debate include sedimentology, palaeontology, tectonophysics, geochronology, volcanology, petrology, geochemistry, geothermal research, seismology, geodesy, electromagnetics and many others.
In addition to the disciplines of Earth science, the plume debate provides a remarkable and thought-provoking subject for scientific philosophy and reflections on correct scientific methodology: (1) What exactly is a plume? People often change their definition of a plume a posteriori in order to fit their observations. (2) How can the plume- or the plate hypothesis be falsified? (3) Do Earth scientists tend to present only one possible interpretation of their data, or do papers reflect all possible interpretations? Unfortunately, the former is often the case. (4) Are published interpretations consistent with other data from the subject field area? Often they are not, and the inconsistencies are not sufficiently highlighted nor discussed. These issues are particularly useful for inducting students into correct scientific working. In summary, the debate provides enormously fertile ground for new, fundamental questions and cross-disciplinary research.
This session welcomes studies of melting anomalies on Earth from the point of view of any sub-discipline. We also welcome studies of geological phenomena which are attributed to mantle plumes, such as back-arc extension, plate motion, sedimentary basin formation and lithospheric uplift, and any other work that bears on this fascinating and challenging geological debate.

[SIT32-P02] **Origin of the Caroline Plateau/Seamount Chain from a short lived mantle plume**

*Guoliang Zhang[1,3], Ji Zhang[1,2], Shuai Wang[1,2] (1.Institute of Oceanology, Chinese Academy of Sciences, 2.University of Chinese Academy of Sciences, 3. Center for Ocean Mega-Science, Chinese Academy of Sciences)

[SIT32-P03] Meteorite Impact Origin of ***Mantle Plumes*** Growing Downward by ***Mantle Depletion of Volatiles*** Not Convection From CMB

*Hermann G. W. Burchard[1] (1.Oklahoma State University)

[SIT32-P04] Genesis of high-Ni olivine phenocrysts of the Dali picrites in the Central Emeishan large igneous province

★Invited Papers

*Wenchang Cai[1], Zhaochong Zhang[1], Jiang Zhu[2], M. Santosh[1,3], Ronghao Pan[1] (1. China University of Geosciences, Beijing, China, 2.Yunnan Institute of Geological Sciences, Kunming,, China, 3.Department of Earth Sciences, University of Adelaide, Australia)

[SIT32-P05] Continental crust in the ocean

*Gillian R Foulger[1] (1.Durham University)

[SIT32-P06] The magma system beneath Changbaishan Volcano, China: an insight from magnetotellurics imaging

*Wule Lin[1], Xiangyun Hu[1], Bo Yang[1] (1.Hubei subsurface Multi-Scale Imaging Key Laboratory, Institute of Geophysics and Geomatics, China University of Geosciences)

[SIT32-P07] Evidence for the strike-slip opening of the Japan Sea

*Hidehisa Mashima[1] (1.Center for Obsidian and Lithic Studies, Meiji University)

Discussion

[SIT32-P08] **Genesis of high-Ni olivine phenocrysts of the Dali picrites in the Emeishan large igneous province, SW China.**

*Wenchang Cai[1], Zhaochong Zhang[1], Jiang Zhu[1,2], M. Santosh[1,3], Ronghao Pan[1] (1. China University of Geosciences, Beijing, China, 2.Yunnan Institute of Geological Sciences, Kunming, China, 3.Department of Earth Sciences, University of Adelaide, Australia)

Origin of the Caroline Plateau/Seamount Chain from a short lived mantle plume

*Guoliang Zhang[1,3], Ji Zhang[1,2], Shuai Wang[1,2]

1. Institute of Oceanology, Chinese Academy of Sciences, 2. University of Chinese Academy of Sciences, 3. Center for Ocean Mega-Science, Chinese Academy of Sciences

The genesis of an oceanic plateau bears important information on the mantle dynamics and mantle compositions. The Caroline Rise (or Caroline ridges) has played an important role in the tectonic frame of the western Pacific, however, the nature and origin of the Caroline Rise has long been unclear. In this study we first confirmed that it represents an oceanic plateau formed as a large igneous province based on seafloor sampling program. The Caroline Plateau is connected to the east with the Caroline Seamount Chain that is considered to have been formed by a deep-rooted hotspot. To investigate the mantle source nature of the Caroline Plateau and its genetic relationship with the Caroline Seamount Chain, we age-dated and analyzed the geochemistry (major and trace elements and Sr-Nd-Pb-Hf isotopes) of the basalt samples from the Caroline Plateau. The basalt samples are classified into two groups, the alkali and the tholeiite groups. The results of age-dating indicate older ages for the tholeiite group than the alkali group. Thus, the tholeiite group basalts are apparently older than the Caroline Islands and are close to the basalts of Ontong Java Plateau in trace element patterns. We suggest that the tholeiite group basalts represent the main stage volcanism and the alkali group basalts represent the late stage volcanism of the Caroline Plateau. The alkali group basalts show trace element and isotope compositions similar to those of the Caroline Islands to the east. The tholeiitie group basalts can be formed by mixing between the alkali group basalts and the depleted Caroline plate basalts based on Sr-Nd-Pb-Hf isotope compositions, suggesting involvement of depleted upper mantle components in the mantle source. The MORB-like depleted geochemical nature of the tholeiite group basalts indicates formation of the Caroline Plateau under the thin Caroline plate lithosphere. The Caroline Plateau/Seamount volcanic chain could be explained by the Caroline hotspot based on their formation ages of and tectonic reconstruction. The Caroline Plateau/Islands volcanic system shows increasing alkalinity and Sm/Yb ratio of basalts with time, which implies for decreasing activities of a short-lived mantle plume. This work was financially supported by the National Natural Science Foundation of China (91858206, 41876040).

Keywords: alkali basalt, age-date, geochemistry, hotspot, mantle plume, Caroline plateau

©2020. Japan Geoscience Union. All Right Reserved.

Meteorite Impact Origin of ***Mantle Plumes*** Growing Downward by ***Mantle Depletion of Volatiles*** Not Convection From CMB

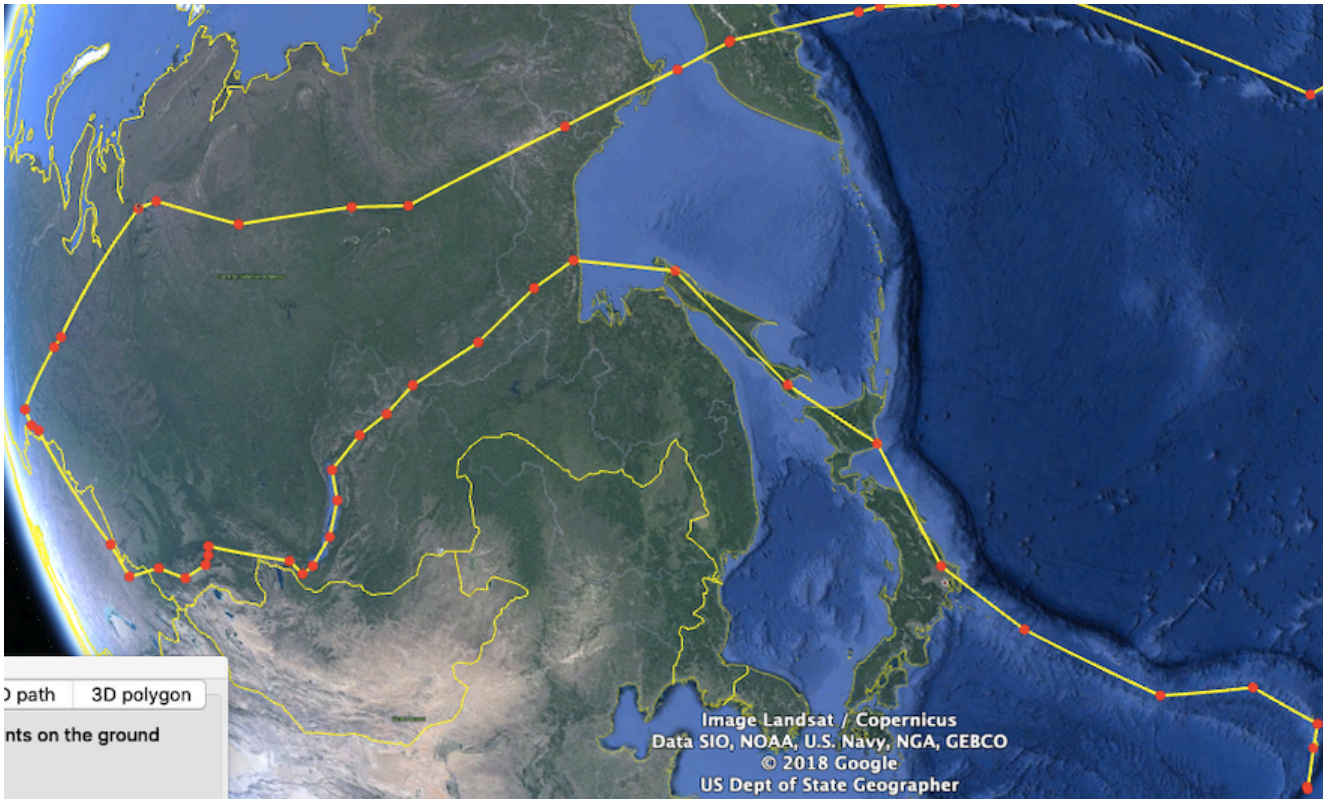
*Hermann G. W. Burchard[1]

1. Oklahoma State University

The origin of ***Mantle Plumes*** has remained uncertain until now. Here, we present evidence of ***meteorite impact*** origin, based upon our prime example, the Yellowstone ***hotspot*** and Columbia River Basalt ***large igneous province*** LIP. The hotspot is shallow, only 200 km deep, invalidating a theory of mantle plume origin. The hotspot track runs from the Yellowstone National Park in NW Wyoming, back in time, to the volcanic Modoc Plateau in NE California. We present evidence of apparent remnants of an impact crater existing in the Modoc, a large multi-ring structure at least 160 km diameter. Much of this complex crater has become obliterated by later Cascadia and Sierra orogenies. The crater has a tall 4,100 foot non-igneous central uplift cone, locally known as Chalk Mountain, consisting of diatomaceous earth, presumably the rebound cone of a thin-crust meteorite impact at the Miocene cratonic margin. This falsifies a theoretical prohibition of cosmic impact volcanism. Based on recent insights into explosive volcanism a ***plausible mechanism based upon mantle depletion of dissolved volatiles*** is proposed for how meteorite impacts can lead to resurgent calderas of the Yellowstone type and apparent LIP origin from ***thin crust ET impacts***, invalidating theoretical constructs of mantle plumes. Another example of cardinal importance for planet Earth biosphere endurance and survival is a pair end-Permiian comet impacts in the South Kara Sea and the West Siberian basin, apparently fragments of the same giant comet or Edgeworth–Kuiper belt object. Very possibly other fragments of the same body have impacted at times near the Permo-Triassic transition, as the Emeishan LIP in Sichuan, China. The reason is that comets have a fragile nature, being weakly consolidated by gravitational accretion around metal cores, as seen in the Norilsk nickel mine, exploiting the metal core of the S Kara Sea impactor, analogous to the Sudbury, Ontario astrobleme. A hotspot track results from the initial magma chamber, excavated by teraton or even petaton TNT equivalent impact explosions, with deep mantle pentration by tens of km in thin oceanic crust. Here, the S Kara Sea impact initiated the continental extension of the Emperor-Hawaii sea mount chain, Mt Kilauea atop the remnant hotspot. The analogous W Siberian plane hotspot track exits mainland Asia at Sachalin Island, and continues on through Japan to the Marianas ending at the Challenger Deep, Fig. 1. In this case, unlike the S Kara Sea-Hawaii hotspot track, where the metal core remained in the crust at or near the impact site, the core penetrated the crust completely and sank into the mantle. The great depth of the Challenger Deep is due to the large weight of the metal core mass, still sinking deeper now, as can be seen from the GPS continental drift directions world-wide converging upon the Pacific region near Guam. For a continental impact such as Chicxulub on the Yukatan peninsula, the impact may excavate only to the Moho, with a plutonic ***warmspot*** as the result instead of a volcanic hotspot. The Greater Antilles mark the warmspot track by their granitic basements beneath Tertiary limestones, except in terminal Virgin Gorda, where granite rocks famously form the popular "Baths" at the surface, the warmspot having joined the volcanic arc of the Lesser Antilles.

Keywords: Yellowstone Hotspot, Impact Volcanism , Volatile Depletion, Siberian hotspot tracks, Challenger Deep, Warmspot

©2020. Japan Geoscience Union. All Right Reserved.



©2020. Japan Geoscience Union. All Right Reserved.

Genesis of high-Ni olivine phenocrysts of the Dali picrites in the Central Emeishan large igneous province

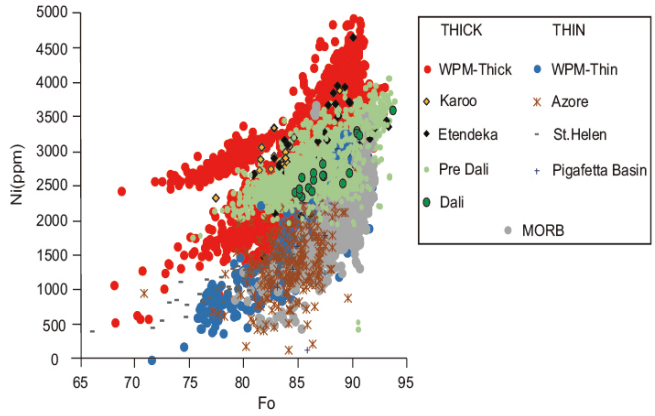
*Wenchang Cai[1], Zhaochong Zhang[1], Jiang Zhu[2], M. Santosh[1,3], Ronghao Pan[1]

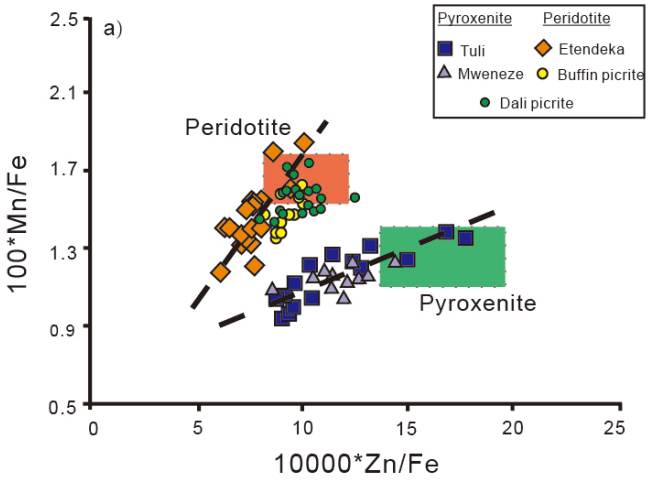
1. China University of Geosciences, Beijing, China, 2. Yunnan Institute of Geological Sciences, Kunming,, China, 3. Department of Earth Sciences, University of Adelaide, Australia

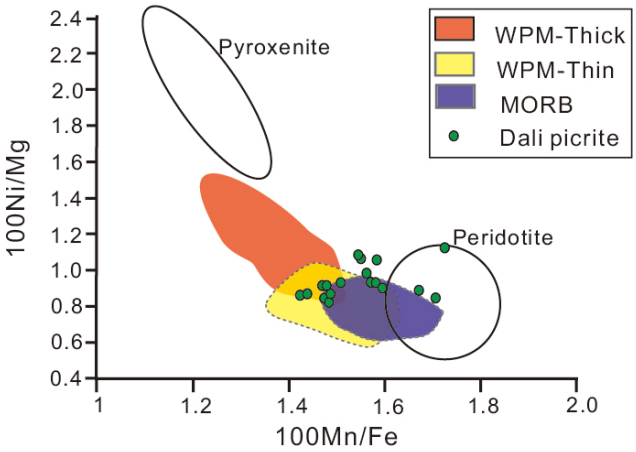
The Emeishan Large Igneous Province (ELIP) is considered as one of the typical mantle plume-derived LIPs. The picrites formed at relatively high temperatures in this ELIP provide one of the important lines of argument for the role of mantle plume. Here we report trace element data on olivine phenocrysts in the Dali picrites from the ELIP. The olivines are Ni-rich, and characterized by high (>1.4) 100*Mn/Fe value and low (<13) 10000*Zn/Fe value, indicating a peridotite dominated source. Since olivine-melt Ni partition coefficient ($K_D Ni^{ol/melt}$) will decrease at high temperature and pressure, the picrites derived from peridotite melting at high pressure and which crystallized olivines at lower pressure can generate high concentrations of Ni in olivine phenocrysts, excluding the necessity of a metasomatic pyroxenite contribution. Based on the Al-in-olvine thermometer, olivine crystallization temperature and mantle potential temperature (T_P) were calculated at ~1491℃ and ~1559℃ respectively. Our results are ~200℃ higher than that of the normal asthenospheric mantle, and are consistent with the role of mantle thermal plume for the ELIP.

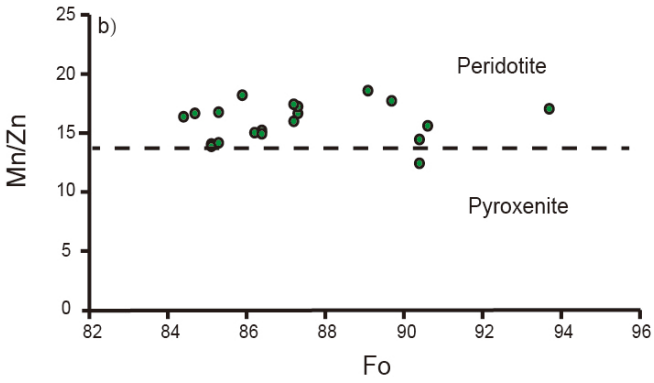
Keywords: Emeishan large igneous province, Picrite, Olivine, Trace element geochemistry, Mantle plume

©2020. Japan Geoscience Union. All Right Reserved.









©2020. Japan Geoscience Union. All Right Reserved.

Continental crust in the ocean

*Gillian R Foulger[1]

1. Durham University

Conventional plate tectonics envisages simple continental breakup with clean splitting of supercontinents and subsequent orderly widening of oceans by seafloor spreading about a central ridge. No sooner was this paradigm proposed when the clear, first-order misfit of intraplate and large-volume volcanism was highlighted. That was quickly accommodated by adding an additional degree of freedom into the theory of Earth dynamics, i.e., ad hoc mantle plumes. Although this simple picture was adequate in the early years of plate tectonics, the subsequent rapid accumulation of vast datasets of ever-more-precise observations has rendered a theory of such simplicity no longer tenable. Simple plate tectonics can now serve only as a basic canvas on which the complexities of the real world must be painted. There is no better region for illustrating this than the Northeast Atlantic Realm which illustrates the full range of complexities. After a history of tectonic unrest spanning several 100 Myr true continental breakup, involving fracture of the entire lithosphere and ocean widening via sea-floor spreading, finally proceeded. However, geological complications are on at least an equal level to features arguably amenable to description by simple plate tectonics. Spreading ridges developed by propagation through continental lithosphere comprising a collage of cratons separated by orogenic belts. Where these propagators met insurmountable barriers the extension demanded by local kinematics could only be accommodated by diffuse continental extension. Continual changes occurred in the direction of regional extension and these resulted in local tectonic instabilities manifest in lateral ridge migrations, jumps, and parallel-ridge-pair extension. Extreme, magma-assisted continental extension, together with intense volcanism, formed lava-capped transitional crust. As a consequence the true extent of continental crust under the oceans is unclear. The geophysical characteristics of transitional crust are ambiguous in terms of physical properties. This presents a challenge to mapping continental material in the oceans, a problem that can be mitigated by joint interpretation with gravity, heatflow and geochemical data. Known continental blocks in the ocean include the array of blocks west of the British continental shelf (the Hatton-, George Bligh-, Lousy-, Bill Bailey’ s- and Faroe Bank Highs, and Wyville-Thompson- and Fugløy Ridges), the Jan Mayen Microplate Complex, the Greenland-Iceland-Faroe Ridge and likely others that remain to be found. All of the above complexities in the solid Earth have profoundly affected the natural environment in the region, especially the oceans and the biosphere, and must be taken into account in predictions of future evolution of the natural environment.

Keywords: continent, hotspot, crust

©2020. Japan Geoscience Union. All Right Reserved.

The magma system beneath Changbaishan Volcano, China: an insight from magnetotellurics imaging

*Wule Lin[1], Xiangyun Hu[1], Bo Yang[1]

1. Hubei subsurface Multi-Scale Imaging Key Laboratory, Institute of Geophysics and Geomatics, China University of Geosciences

The largest intraplate volcanic system in northeast Asia is the Changbaishan Volcanic Field in the Western Pacific Volcanic Belt approximately 1400 km from the Japan Trench, where the Pacific plate subducts beneath the Eurasian plate. The Changbaishan Volcanic Field is located on the northern edge of the Sino-Korean Craton, above a big mantle wedge. This stratovolcano is composed of an old basaltic shield, a young trachytic-to-rhyolitic cone, and a summit caldera. One of the two most violent eruptions in recorded human history occurred here between 920 and 960 AD and is known as the ‘Millennium Eruption’. The volcanic field experienced its most recent eruption in 1903 AD, followed by periods of unrest between 2002 and 2005. Concerns about increased activity made Changbaishan the focus of study for potential geologic hazards. Using magnetotelluric data collected from 2012 to 2014, we created a nearly linear N-S directional profile of the region across the Tianchi caldera in order to investigate the subsurface structure. A resistive crustal body is visible in the south part of the Changbaishan area in our three-dimensional model. Two successive magmatic conductors are beneath the Tianchi caldera less than 20 km from the surface. Petrologic analysis of comendite-trachyte from the Millennium Eruption indicates a formation from two different magmas and the double magmatic conductors are consistent with the geochemical model. Assuming the outermost resistivity of the magma body nearest to the surface is 25 Ω·m then it is located at a depth of 2 to 6 km and maybe responsible for recent volcanic earthquake events and ground deformation. Beneath the near surface magma chamber is a larger conductive magma body centered at an approximate depth of 15 km. This larger magma body maybe the main supply for the shallow magma system.

Keywords: Changbaishan Volcanic field, magnetotellurics, magma chamber

©2020. Japan Geoscience Union. All Right Reserved.

Evidence for the strike-slip opening of the Japan Sea

*Hidehisa Mashima[1]

1. Center for Obsidian and Lithic Studies, Meiji University

The opening tectonics of the Japan Sea is important for our understanding of the evolution and dynamics of East Asia. An appropriate model of the opening tectonics of the Japan Sea is the double door opening model based on paleomagnetic declinations observed in the Japan Arcs. The model assumes that SW Japan arc would have 40-60° clockwise rotated and NE Japan would have 40° anticlockwise rotated during the Japan Sea opening. Structural features of the Japan Arcs, the Japan Sea and their vicinities indicate that the Japan Sea would have opened south-southwestward as a strike-slip matter using the Tsushima-Goto Fault, Sakhalin-Central Hokkaido and the Japan Trench as master faults.

Faults oriented to an NNE-SSW direction formed in the Cretaceous are developed both in north Kyushu and SE Korea. Faults oriented to NNW-SSE to NW-SE directions are developed in the Paleogene north Kyushu sedimentary basin and the Paleogene East China Sea Shelf Basin. Pre-Paleogene strata continues with same direction from north Kyushu to the western Chugoku district. The Tsushima-Goto Fault striking between the Japan Sea and the East China Sea disconnects the north Kyushu sedimentary basin and the East China Sea Shelf basin. These structural features indicate that north Kyushu-the western Chugoku district would have migrated along the Tsushima-Goto Fault during the Japan Sea opening.

Echelon faults oriented to an NNW-SSE direction are developed in NE Japan. Rapid subsidence was occurred during the Japan Sea opening at the bending points of the NNW-SSE faults where the faults turn anticlockwise their directions from north to south. The eccentrically-subsidence indicates that the NE Japan would have carried out sinistral deformation using the Japan Trench as the master fault. Along Sakhalin-central Hokkaido, the boundary between the JS and the Okhotsk Sea, the Cretaceous Yezo Supergroup characterizing flysch is distributed as a narrow band. Dextral structures developed there in early Miocene, which would have been caused by the extending of the Kuril Basin. The Japan Sea is composed of basins and continental fragments bounded by faults oriented to NNE-SSW to N-S directions and faults oriented to an E-W direction.
These lines of evidence indicate that the Japan Sea would have opened as a strike-slip matter rather than the double-door matter. Paleomagnetic declinations observed in Japan would be the results of rotations of small faulted-blocks rather than those of coherent arcs. The brittle/ ductile transition zone in the crust beneath Japan would have been shallow under the high geothermal condition, which are represented by the submarine green tuff volcanism during the Japan Sea opening. The shallow brittle/ ductile transition would have made block rotation easy.

Keywords: the Japan Sea, opening tectonics , strike-slip

©2020. Japan Geoscience Union. All Right Reserved.

Genesis of high-Ni olivine phenocrysts of the Dali picrites in the Emeishan large igneous province, SW China.

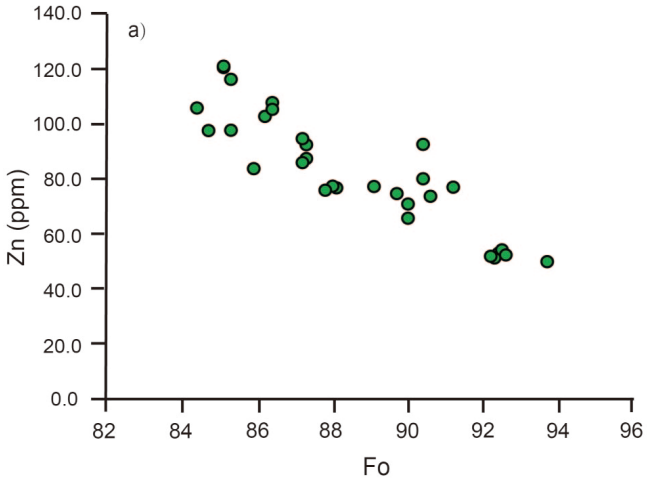
*Wenchang Cai[1], Zhaochong Zhang[1], Jiang Zhu[1,2], M. Santosh[1,3], Ronghao Pan[1]

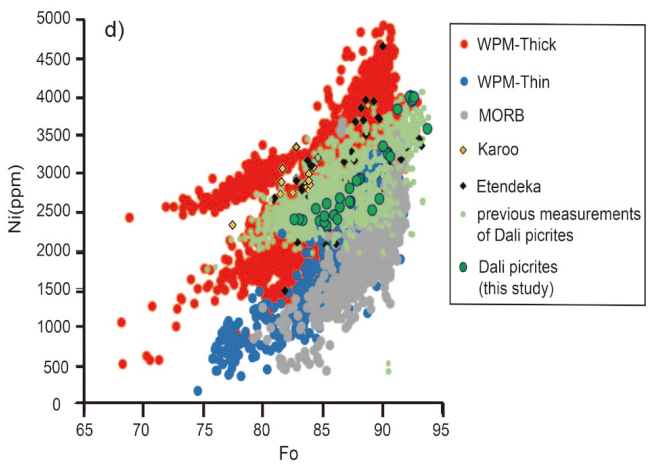
1. China University of Geosciences, Beijing, China, 2. Yunnan Institute of Geological Sciences, Kunming, China, 3. Department of Earth Sciences, University of Adelaide, Australia

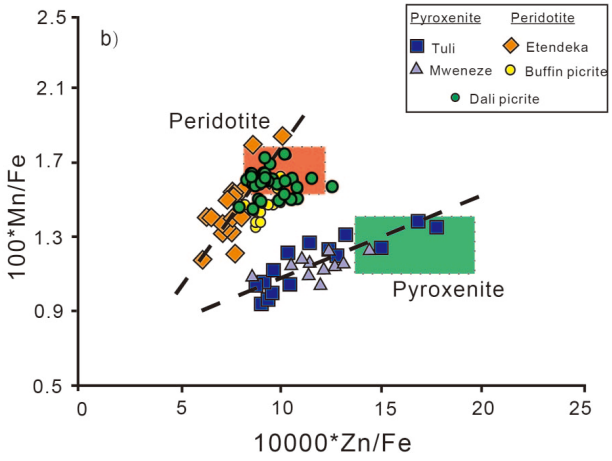
The Emeishan Large Igneous Province (ELIP) in SW China is considered as one of the typical mantle plume-derived LIPs. The picrites formed at relatively high temperatures in the ELIP provide one of the important lines of argument for the role of mantle plume. Here we report trace element data on olivine phenocrysts in the Dali picrites from the ELIP. The olivines are Ni-rich, and characterized by high (>1.4) 100*Mn/Fe value and low (<13) 10000*Zn/Fe value, indicating a peridotite dominated source. Since olivine-melt Ni partition coefficient ($K_D Ni^{ol/melt}$) will decrease at high temperature and pressure, the picrites derived from peridotite melting at high pressure and which crystallized olivines at lower pressure can generate high concentrations of Ni in olivine phenocrysts, excluding the necessity of a metasomatic pyroxenite contribution. Based on the Al-in-olvine thermometer, olivine crystallization temperature and mantle potential temperature (T_P) were calculated at ~1491 ℃ and ~1559 ℃ respectively. Our results are ~200 ℃ higher than that of the normal asthenospheric mantle, and are consistent with the role of mantle thermal plume for the ELIP.

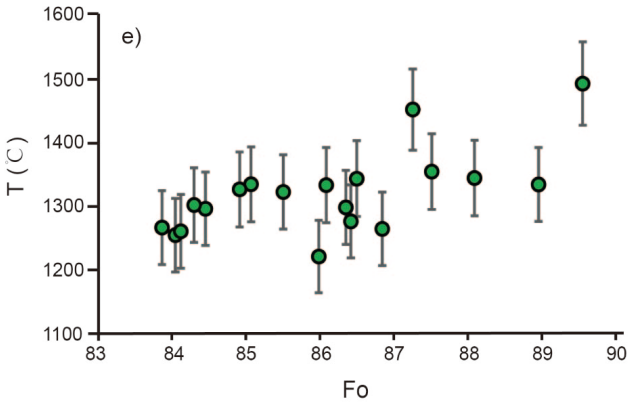
Keywords: Emeishan large igneous province, Picrite, Olivine, Trace element geochemistry, Mantle plume

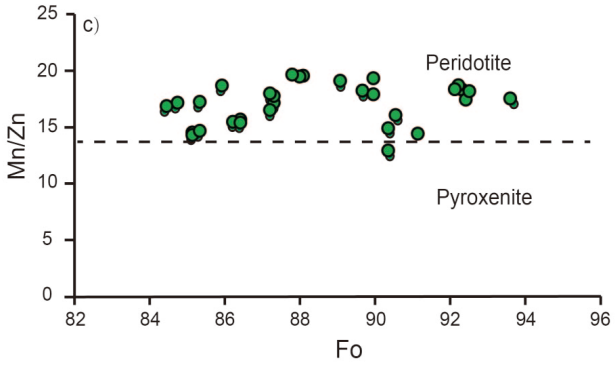
©2020. Japan Geoscience Union. All Right Reserved.











©2020. Japan Geoscience Union. All Right Reserved.

[E] Poster | S (Solid Earth Sciences)：S-GL Geology

[S-GL33] Geologic structure and tectonic history of East Asia and Japanese Islands

convener:Jun Hosoi(Geological Survey of Japan, Institute of Geology and Geoinformation, AIST), Makoto Otsubo(Geological Survey of Japan, Research Institute of Earthquake and Volcano Geology)

The main aim of this session is to discuss geologic structure and tectonic history of East Asia, especially of Japanese Islands, on the basis of the recent results of geology and other earth sciences.

[SGL33-P01] Deformation characteristics and metamorphic temperature of the high-pressure terrace of the Taiwan orogeny

*Han Chun Lin[1], Yuan Hsi Lee[1], Lucas Manuel Ortinez Mesalles[1], Jian Cheng Lee[2] (1.Department of Earth and Environmental Sciences, National Chung-Cheng University, Taiwan, 2.Institute of Earth Sciences, Academia Sinica, Taiwan)

[SGL33-P02] Zircon U-Pb Ages from sandstones of the Muro Accretionary sequence in the Shimanto Superbelt, Kii Peninsula, Southwestern Japan

*Takanori Bessho[1], Hiroyuki Suzuki[2], Toshiya Yamamoto[3], Tohru Danhara[4], Hideki Iwano[4], Takafumi Hirata[5] (1.Department of Geosciences Osaka City University, 2.Nanki Kumano Jeopark Center, 3.Tanabe Highschool, 4.Kyoto Fissin-Track Co., Ltd., 5.Tokyo University)

[SGL33-P03] Geochemical characteristics of metamorphic and igneous rocks from the Hida belt: whole-rock major and trace elements, and multiple S isotope compositions

*Raiki Yamada[1], Shinnosuke Aoyama[2], Ouchi Wataru[1], Toshiro Takahashi[1], Satish Kumar M.[1] (1.Niigata University, 2.Yokohama National University)

[SGL33-P04] Identification of the source caldera for the Pliocene pyroclastic flow deposit in NE Japan based on apatite trace-element compositions

*Reishi Takashima[1], Haruka Kusakawa[2], Yuji Orihashi[3], Hiroshi Nishi[1] (1.Tohoku University, 2.Chichibu Taiheiyo Cement Co. Ltd. , 3.Hirosaki University)

[SGL33-P05] New age constraints and tectonic significance of the early Miocene sediments in the Hidaka Belt around Tomuraushi area, central Hokkaido, Japan

*Futoshi Nanayama[1,2], Mahito Watanabe[1], Toru Yamasaki[1], Hideki Iwano[3], Tohru Danhara[3], Takafumi Hirata[4] (1.Geological Survey of Japan, AIST, 2.CWMD, Kumamoto University, 3.Kyoto Fission-Track Co. Ltd, 4.The University of Tokyo)

[SGL33-P06] Provenance of the Yezo forearc basin in Northeast Japan from detrital zircon U–Pb age spectra

*Koh Kubomi[1], Shin-ichi Sano[2], Minami Murakami[3], Hiroto Ota[1], Mitsuhiro Nagata[1], Koshi Yamamoto[4], Shigeru Otoh[2] (1.Graduate School of Science and Engineering, University of Toyama, 2.Academic Assembly, Faculty of Sustainable Design, University of Toyama, 3.OYO Corporation, 4.Graduate School of Environmental Studies, Nagoya University)

[SGL33-P07] Tectonics of the Miocene Median Tectonic Line in the west of Ina-Valley, central Japan

*Akira Ono[1] (1.None)

[SGL33-P08] On the paleocurrent of the Miocene Goto Group in Fukue Island, Nagasaki Prefecture

*Yuta Ikebata[1], Shoichi Kiyokawa[1] (1.Department of Earth and Planetary Sciences, Graduate School of Science, Kyushu University)

[SGL33-P09] **North-South extension and compression juring the Japan Sea opening in the Amakusa, western Kyushu, Japan**

*Kentaro Ushimaru[1], Atsushi Yamaji[1] (1.Division of Earth and Planetary Sciences, Graduate School of Science, Kyoto University)

[SGL33-P10] Visualization of a high-strain shear zone based on a field survey for minor faults: A case study of southern Kyushu, Japan

*Akira Goto[1], Koji Shimada[1], Masakazu Niwa[1], Shuji Terusawa[2] (1.Japan Atomic Energy Agency, 2.OYO Corporation)

[SGL33-P11] Structural position of the Akiyoshi Limestone in the Permian accretionary complex of the Akiyoshi Belt, Southwest Japan

*Koji Wakita[1], Hokuto Obara[2], Takanori Nakagawa (1.Yamaguchi University Community Future Center, 2.Mine Akiyoshidai Karst Plateau Geopark Promotion Council)

[SGL33-P12] **Deformation characteristics and metamorphic temperature of the high-pressure terrace of the Taiwan orogeny**

*Han Chun Lin[1], Yuan Hsi Lee[1], Lucas Mesalles[1], Jian Cheng Lee[2] (1.Department of Earth and Environmental Sciences, National Chung-Cheng University, 2.Institute of Earth Sciences, Academia Sinica, Taiwan)

Deformation characteristics and metamorphic temperature of the high-pressure terrace of the Taiwan orogeny

*Han Chun Lin[1], Yuan Hsi Lee[1], Lucas Manuel Ortinez Mesalles[1], Jian Cheng Lee[2]

1. Department of Earth and Environmental Sciences, National Chung-Cheng University, Taiwan, 2. Institute of Earth Sciences, Academia Sinica, Taiwan

Different mechanisms have been proposed about how the subduction-related high-pressure terrane exhumates to the Earth’ s surface that might come from different tectonic settings. Taiwan orogeny results from arc-continental collision since 6-7Ma and recent studies show that high-pressure Yuli belt is associated with this process. The high-pressure terrane has been buried to ca. 50 km in-depth, and the surrounding terrane is ca. 12-20 km in depth. How the different terrane exhumed to the surface and what kind of structures are developed during the subduction to exhumation process? Here we collect the samples from low to high metamorphic and pressure terrane around the southern Central Range and use the RSCM methods, structural analysis, and zircon fission-track dating to reveal the possible exhumation process.

Three-stage foliations have been observed in eastern Central Range. The S1 is parallel to S0 associated with well-growth mica which is related to the highest metamorphism. The S2 is high-angle dipping foliation with fine-grain mica growth associated with tight to isoclinal folding. The S3 is shallow dipping foliation associated with small to mesoscale recumbent folding. The S3 results from the vertical force, which is strongly related to the recent exhumation process.

The RSCM results show the metamorphic temperature increases from ca. 340°C (low-grade slate) to ca. 500°C (high-pressure belt) in short distances that might infer a high shear zone; however, the zircon fission-track ages are similar in 0.7-1Ma and the eastern Central Range accelerate exhumation since ca. 2Ma simultaneously indicating the different metamorphic terranes have been merged before 2Ma. We suggest that the later stage foliation S2-S3 is related to this rapid exhumation process and the S1 is associated with the highest metamorphism suggesting it could be related to the subduction process.

Keywords: Raman Spectroscopy of Carbonaceous Material, fission track dating, structural analysis, high-pressure Yuli Belt, Taiwan orogeny

©2020. Japan Geoscience Union. All Right Reserved.

Zircon U-Pb Ages from sandstones of the Muro Accretionary sequence in the Shimanto Superbelt, Kii Peninsula, Southwestern Japan

*Takanori Bessho[1], Hiroyuki Suzuki[2], Toshiya Yamamoto[3], Tohru Danhara[4], Hideki Iwano[4], Takafumi Hirata[5]

1. Department of Geosciences Osaka City University, 2. Nanki Kumano Jeopark Center, 3. Tanabe Highschool, 4. Kyoto Fissin-Track Co., Ltd., 5. Tokyo University

The depositional ages of Shimanto Accretionary Prism in the Kii Peninsula, Southwestern Japan, have been mainly determined by radiolarian fossils. But recently, the fission track and U-Pb ages of detrital zircon in the sandstone have been reported (Ohira et al, 2016; Tokiwa et al 2016, 2017). However, these reports are confined to Cretaceous and early Paleogene System. Zircon U-Pb dating of three specimens of sandstone from the later Paleogene Muro Accretionary Sequence (AC) was carried out by using LA-ICP-MS. The consideration on the difference of radiolarian ages and U-Pb ages of detrital zircon has been done. Moreover, the cause of increasing supply from East Asia Precambrian detritus after Middle Eocene were examined. Muro AC is subdivided into three tectonostratigraphic units (TU) by thrusts, i.e., the Notake, the Ohkamidawasan, the Ichikano and the Susami TU from north to south. The Radiolarian fossil age of Notake TU shows Middle Eocene. The one of the Ichikano TU are assigned to range from later Middle Eocene to Late Eocene and the one of the Susami TU range from later Middle Eocene to Early Oligocene.As for the zircon U-Pb age, the Notake TU dated at 72.0±0.2 Ma, the Ichikano TU at 36.1±1.9 Ma and Susami TU at 59.6±1.0 Ma respectively deduced from the weighted mean of the youngest cluster.The value of the zircon U-Pb age from Notake and Susami TU are clearly older than the radiolarian fossil age. These gaps are presumed to be due to influence of Magmatic hiatus. The zircon U-Pb age from Ichikano TU is concordant with the radiolarian fossil age. The part of the zircon being included in Ichikano TU is thought to be derived from contemporaneous igneous rocks. Paleo-Proterozoic zircons (1600-2500 Ma) have been slightly found in all samples and Almost of these zircons are rounded. Therefore, these zircons are thought to be recycled grains. As it becomes more abundant in the younger TU, i.e., Susami TU, the supply from the Precambrian clastics of East-Asia continent is presumed to be increased. These Precambrian clastics are well exemplified by containing rounded zircon, purple zircon, Ig2-type garnet (Teraoka et al., 1998; Bessho,2012) and Orthoquartzite (Tokuoka,1970; Tokuoka and Bessho, 1980). Furthermore, the increasing of Precambrian zircon will support this hypothesis. As for the cause of increasing of East Asia Precambrian detritus, three assumptions will be suggested. In the first place, igneous activity was poor in the deposition time of Muro AS. In the second place, subaerial erosion became intense because of the fall of sea level by glacial eustacy (Bickert and Heinrich, 2011). Furthermore, large submarine fan composing Muro AS grew up in the trench basin.This study was supported by a grant from the Nanki Kumano Geopark Promotion Council.

Keywords: Zircon U-Pb dating, Paleogene Muro Accretionary Sequence, Shimanto Superbelt, Kii Peninsula

©2020. Japan Geoscience Union. All Right Reserved.

Geochemical characteristics of metamorphic and igneous rocks from the Hida belt: whole-rock major and trace elements, and multiple S isotope compositions

*Raiki Yamada[1], Shinnosuke Aoyama[2], Ouchi Wataru[1], Toshiro Takahashi[1], Satish Kumar M.[1]

1. Niigata University, 2. Yokohama National University

The Hida belt is one of the Japanese basement units, indicating relationships with the North China block [1] and/or the South China block [2]. Some studies consider that these metamorphic rocks were formed during the collision between the North and South China blocks [3]. Accordingly, the formation history and the origin of the Hida belt will be of great significance to understand establishment of the eastern Asia continent and processes of continental growth. We collected samples of metamorphic rocks and granitoids from the Hida belt for geochronological and geochemical analyses. In this abstract, we present some geochemical data of the Hida granites including multiple S isotope compositions.

The Hida belt consists of the Hida metamorphic rocks, the Unazuki metamorphic rocks and the Hida granites [4]. The Hida metamorphic rocks, composed mainly of orthogneisses, paragneisses, amphibolite and marble, were formed by several times of metamorphism, and the last regional metamorphism occurred in the eastern margin of the Eurasian continent during Early to Middle Triassic period (250–235 Ma; [5]). The Metamorphic grade reached from amphibolite to granulite facies, with eclogitic rocks [6]. Protolith of the Unazuki metamorphic rocks derived from late Paleozoic sediments, limestone and acidic volcanic rocks was also metamorphosed around 250 Ma at medium P/T conditions [7, 8]. The Hida granites consists of the Triassic Hida older granites and the Jurassic Hida younger granites [4]. We already reported 240 Ma and 190–180 Ma of ^{238}U–^{206}Pb weighted mean ages from the older and younger Hida granites, respectively [9].

SiO_2 content of the Hida granites ranges from 52.7 wt.% to 75.1 wt.%. Both of the older and younger Hida granites show I-type granitic trends in $_2$–ASI diagram and have intermediate composition between sub-alkaline and alkaline series [10]. All samples are plotted in volcanic arc field of tectonic discrimination diagrams for granitoids (Nb+Y–Rb [11] and Rb/30–Hf–Ta*3 diagrams [12]). Additionally, many samples of the Hida granites have adakitic composition (high Sr/Y ratio) and show depleted patterns toward HREE in REE pattern diagram. Negative anomalies of Nb and Ta in trace element patterns suggest that their origins are related to subduction zone magmatism. The Hida granites exhibit small variations in $\delta^{34}S$ ranging from −2.1‰ to +5.2‰ and $\Delta^{33}S$ from −0.02‰ to +0.00‰, suggesting sulfur was mainly derived from the mantle and subsequent high temperature mass-dependent processes. Our results of whole-rock geochemistry are consistent with the idea that the Hida granites were generated by melting of the mafic lower continental crust under high pressure environment where garnet coexists [13, 14]. It is considered that non-adakitic granites resulted from crustal melting under relatively low-pressure. Moreover, geochemical characteristics of the Hida granites suggest that the continental crust had grown in subduction zone of the margin of the eastern Eurasian continent.

[1] Horie et al., 2018. Chem. Geol., 484, 148–167.
[2] Wallis et al., 2020. Island Arc, DOI: 10.1111/iar.12339.
[3] Kunugiza et al., 2010. J. Geol. Soc. Japan, 116, 83–101.
[4] Takahashi et al., 2010. Gond. Res., 17, 102–115.

©2020. Japan Geoscience Union. All Right Reserved.

[5] Takahashi et al., 2017. Island Arc, DOI: 10.1111/iar.12220.
[6] Suzuki, 1973. J. Japan Assoc. Mineral. Petrol. Econ. Geol., 68, 372–382.
[7] Hiroi, 1978. J. Geol. Soc. Japan, 84, 521–530.
[8] Hiroi, 1983. Contrib. Mineral. Petrol., 82, 334–350.
[9] Yamada et al., 2019. Ann. Meet. Geol. Soc. Japan, abstr., 66–66.
[10] Miyashiro, 1978. Contrib. Mineral. Petrol., 66, 91–104.
[11] Pearce et al., 1984. Jour. Petrol., 25, 956–983.
[12] Harris et al., 1986. Collision Tectonics, Geol. Soc. Spec. Pub. 19, 67–81.
[13] Arakawa and Shinmura, 1995. Chem. Geol., 124, 217–232.
[14] Ishihara, 2005. Bull. Geol. Surv. Japan, 56, 117–126.

Keywords: Hida belt, geochemistry, Sulfer isotope

©2020. Japan Geoscience Union. All Right Reserved.

Identification of the source caldera for the Pliocene pyroclastic flow deposit in NE Japan based on apatite trace-element compositions

*Reishi Takashima[1], Haruka Kusakawa[2], Yuji Orihashi[3], Hiroshi Nishi[1]

1. Tohoku University, 2. Chichibu Taiheiyo Cement Co. Ltd. , 3. Hirosaki University

It is known that a lot of calderas were formed on the Northeast Japan during Pliocene period. Such dense caldera-forming volcanic activity resulted in frequent intercalations of volcaniclastic deposit in the Pliocene sedimentary strata and deep-sea cores around Northeast Japan. However, most of these Pliocene volcaniclastic deposits have not been identified their source volcanoes. The Hirosegawa Tuff Member, consisting of a pair of Pliocene pyroclastic fall and flow deposits, is known as the widely traceable volcaniclastic deposits in the eastern part of central Northeast Japan. The source volcano of the member remains being not identified because of the poorly preservation of volcanic glass of the member in some locations as well as sporadic distributions of the member attributed to the tectonic uplift and erosion since Pliocene. Trace-element compositions of apatite phenocrysts are useful in tephrochronology because they change in response to various conditions of magma when they crystalize. In addition, apatite is highly tolerant to burial diagenesis and welding processes, its trace-element compositions are powerful tool for correlation of pre-Quaternary tephra, although this method has not become widely used so far. Here we analyzed trace-element compositions of apatite and U-Pb ages of zircon for the Hirosegawa Tuff Member and pyroclastic flow deposits of the Pliocene Calderas around Sendai, and demonstrate that the Hirosegawa Tuff Member mapped in previous studies is different volcanic ejecta depending on areas. Furthermore, these analyses identify the source volcano of the Hirosegawa Tuff Member at the type section to be the Shiroishi Caldera located 50km south of the type section.

Keywords: Apatite, zircon, tephrochronology, Pliocene, pyroclastic flow deposits

©2020. Japan Geoscience Union. All Right Reserved.

New age constraints and tectonic significance of the early Miocene sediments in the Hidaka Belt around Tomuraushi area, central Hokkaido, Japan

*Futoshi Nanayama[1,2], Mahito Watanabe[1], Toru Yamasaki[1], Hideki Iwano[3], Tohru Danhara[3], Takafumi Hirata[4]

1. Geological Survey of Japan, AIST, 2. CWMD, Kumamoto University, 3. Kyoto Fission-Track Co. Ltd, 4. The University of Tokyo

In the Hidaka Supergroup of the Tomuraushi region, there was known alternated beds of sandstone and mudstone named the Chikapupetsu Formation, which has a slightly unconsolidation from the surrounding strata. In this study, the depositional age of the Chikapupetsu Formation was constrained by two methods. Two zircon U-Pb ages of 22.5 ±0.7 Ma and 19.5 ±0.1 Ma were obtained for the maximum depositional age of the formation based on the minimum age of detrital zircon grains from turbiditic sandstone and acidic tuff by the LA-ICP-MS method. In addition, presence of diatom fossils in the formation indicates an early Miocene age for the depositional age of the formation. Because the depositional age of the Hidaka Supergroup has been considered as the Paleocene to early Eocene, the Chikapupetsu Formation should be excluded from the Hidaka Supergroup. Instead it can be correlated with the upper members of the Tsubetsu and Kawakami groups on the basis of their depositional age. We already reported late Oligocene Tatsuushi and Erimo formations in the Hidaka Belt, which has been active as a right-lateral strike-slip fault since the late Oligocene. The Chikapupetsu Formation is considered to be a marine deposit formed between the Kamishiyubetsu Formation on middle Miocene and the Tatsuushi and Erimo formations on late Oligocene along with the activity of the Kamishiyubetsu tectonic zone.

This work was supported by JSPS KAKENHI Grant Number JP19K04025.

Keywords: Depositional age, Zircon U-Pb age, LA-ICP-MS, Chikapupetsu Formation, Hidaka Belt, Early Miocene

©2020. Japan Geoscience Union. All Right Reserved.

Provenance of the Yezo forearc basin in Northeast Japan from detrital zircon U–Pb age spectra

*Koh Kubomi[1], Shin-ichi Sano[2], Minami Murakami[3], Hiroto Ota[1], Mitsuhiro Nagata[1], Koshi Yamamoto[4], Shigeru Otoh[2]

1. Graduate School of Science and Engineering, University of Toyama, 2. Academic Assembly, Faculty of Sustainable Design, University of Toyama, 3. OYO Corporation, 4. Graduate School of Environmental Studies, Nagoya University

Introduction

In Hokkaido, the Cretaceous to Paleogene Yezo Group narrowly extends in the north direction, and the Upper Cretaceous Futaba and Nakaminato groups sporadically occur in the Pacific side of Northeast Japan[1)]. They are thought to have been deposited in the forearc basin along the East Asian active continental margin, called the "Yezo forearc basin" [1)]. The modal composition of sandstones[2),3)] of the Yezo Group, and the detrital zircon age spectra[4)] suggested that its provenance is the East Asian continental margin. However, we have not been able to identify the specific provenance of each formation of the Yezo Group and its equivalents. In this presentation, we discuss the provenance of the Yezo forearc basin from the detrital zircon age spectra of sandstone samples and the database of the age and distribution of igneous rocks in East Asia.

Geological Setting

The Yezo Group consists mainly of black mudstone and sandstone. It is subdivided into the Shuparogawa (Srs), Hikagenosawa (Hgs), Mikasa (Mks), Haborogawa (Hbs), and Hakobuchi formations (Hks1, Hks2), in ascending order[5)]. The Futaba Group, consisting mainly of sandstone and mudstone, unconformably covers the granites of the Abukuma Belt. The group comprises the Ashizawa (Aos), Kasamatsu, and Tamayama formations (Tys), in ascending order[6)]. The Nakaminato Group consists mainly of turbidite and is subdivided into the Hiraiso and Isoai formations (Is8), in ascending order[7)]. The codes for the nine sandstone samples analyzed in this study are in the parentheses.

Analytical Method

We separated detrital zircons from each sandstone sample, measured their U/Pb isotopic ratios with LA-ICPMS, and calculated the U–Pb ages. YC is the weighted mean of the youngest zircon $^{206}Pb/^{238}U$ age and the other ages with the error bar ($\pm 2\sigma$) overlapping with the youngest age.

Result

Figure 1 summarizes the result of our measurements of the Yezo, Futaba, and Nakaminato groups.

Discussion

Samples Srs, Hgs, and Mks have zircons crystallized during the magmatic hiatus in Korea[8)] (158–138 Ma), 230–210 Ma, and 2400–1800 Ma zircons. The database indicates that igneous rocks of these ages are widely exposed in South China[9)]. In addition, paleomagnetic studies[10)] suggested that the Hikagenosawa and Takinosawa formations of the Yezo Group was deposited at 10°N and moved to the north during the Cretaceous. Thus, the provenance of the Yezo Group was probably South China during the Aptian to Cenomanian.

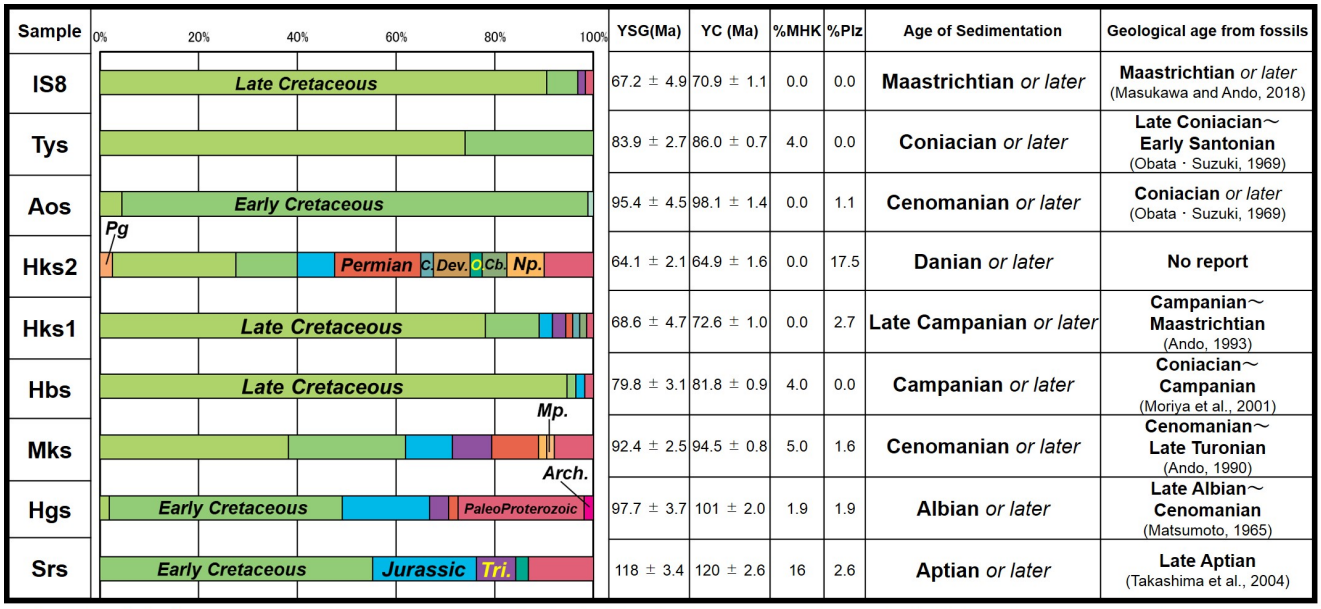
The detrital zircons from sample Aos are mostly 120–100 Ma in age and likely originated from the 120–100 Ma granites in the Abukuma Belt[11)]. 96–83 Ma zircons occupy more than 70% of the detrital zircons from sample Tys and likely originated from the ca. 90–80 Ma igneous rock bodies in the Inner

©2020. Japan Geoscience Union. All Right Reserved.

Zone of Southwest Japan[12].
About 95% of the detrital zircons from sample Hbs are 100–80 Ma. Thus, coeval, 100–80 Ma igneous rocks of an active igneous belt must have occupied the hinterland of sample Hbs.
From the Hakobuchi Formation of the Yezo Group, sample Hks1 has 250–203 Ma, 310 Ma, and 490 Ma detrital zircons, and about 18% of the detrital zircons from sample Hks2 are Paleozoic (excluding Permian) ones (Fig. 1). Sample Is8 has 210 Ma and 1800 Ma zircons. 500–400 Ma and 300 Ma igneous rock bodies widely crop out in Far East Russia[13]. The provenance of the Yezo and Nakaminato groups in the latest Cretaceous was probably Far East Russia. These lines of evidence strongly suggest that the provenance of the Yezo forearc basin continuously changed from south to north.

Reference 1) Ando, 2003: *J. Asian Earth Sci.*, **21**, 921–; 2) Kiminami, 1986: *J. Sediment. Soc. Japan*, **4**, 1–; 3) Takashima et al., 2001: *J. Geol. Soc. Japan*, **107**, 359–; 4) Murakami et al.,2016: *2016JpGU*: SGL37-P01; 5) Takashima et al., 2004: *Cretaceous Res.*, **25**, 365–; 6) Ando et al., 1995: *J. Geol.*, **104**, 284–; 7) Masukawa and Ando, 2018: *Cretaceous Res*, **91**, 362–; 8) Lee et al., 2010: *Isl. Arc*, **19**, 647–; 9) Wang et al., 2013: *Gondwana. Res.*, **23**, 1273–; 10) Tamaki and Itoh, 2008: *Isl. Arc,* **17**, 270–; 11) Tsuchiya et al.,2013: *J. Geol. Soc. Japan.*, **119**, 154–; 12) Iida et al., 2015: *Isl. Arc*, **24**, 205–; 13) Bi et al., 2014: *J. Asian Earth Sci.*, **96**, 301–.

Keywords: Cretaceous, Detrital Zircon, Yezo forearc basin, Yezo Group, Futaba Group, Nakaminato Group



Sample	YSG(Ma)	YC (Ma)	%MHK	%Plz	Age of Sedimentation	Geological age from fossils
IS8	67.2 ± 4.9	70.9 ± 1.1	0.0	0.0	**Maastrichtian** *or later*	**Maastrichtian** *or later* (Masukawa and Ando, 2018)
Tys	83.9 ± 2.7	86.0 ± 0.7	4.0	0.0	**Coniacian** *or later*	**Late Coniacian～ Early Santonian** (Obata・Suzuki, 1969)
Aos	95.4 ± 4.5	98.1 ± 1.4	0.0	1.1	**Cenomanian** *or later*	**Coniacian** *or later* (Obata・Suzuki, 1969)
Hks2	64.1 ± 2.1	64.9 ± 1.6	0.0	17.5	**Danian** *or later*	**No report**
Hks1	68.6 ± 4.7	72.6 ± 1.0	0.0	2.7	**Late Campanian** *or later*	**Campanian～ Maastrichtian** (Ando, 1993)
Hbs	79.8 ± 3.1	81.8 ± 0.9	4.0	0.0	**Campanian** *or later*	**Coniacian～ Campanian** (Moriya et al., 2001)
Mks	92.4 ± 2.5	94.5 ± 0.8	5.0	1.6	**Cenomanian** *or later*	**Cenomanian～ Late Turonian** (Ando, 1990)
Hgs	97.7 ± 3.7	101 ± 2.0	1.9	1.9	**Albian** *or later*	**Late Albian～ Cenomanian** (Matsumoto, 1965)
Srs	118 ± 3.4	120 ± 2.6	16	2.6	**Aptian** *or later*	**Late Aptian** (Takashima et al., 2004)

Fig. 1 Detrital zircon-age of the Yezo Group (Srs～Hks2), the Futaba Group (Aos, Tys), and, the Nakaminato Group (Is8). YSG and YC denote the age of the youngest zircon and the youngest cluster (the weighted mean of the youngest zircon $^{206}Pb/^{238}U$ age and the other ages with the error bar ($\pm 2\sigma$) overlapping with the youngest age), respectively, of each sandstone sample. %MHK and %Plz are the percentages of zircons during the magmatic hiatus in Korea, and the Paleozoic zircons excluding the Permian ones, respectively.

©2020. Japan Geoscience Union. All Right Reserved.

Tectonics of the Miocene Median Tectonic Line in the west of Ina-Valley, central Japan

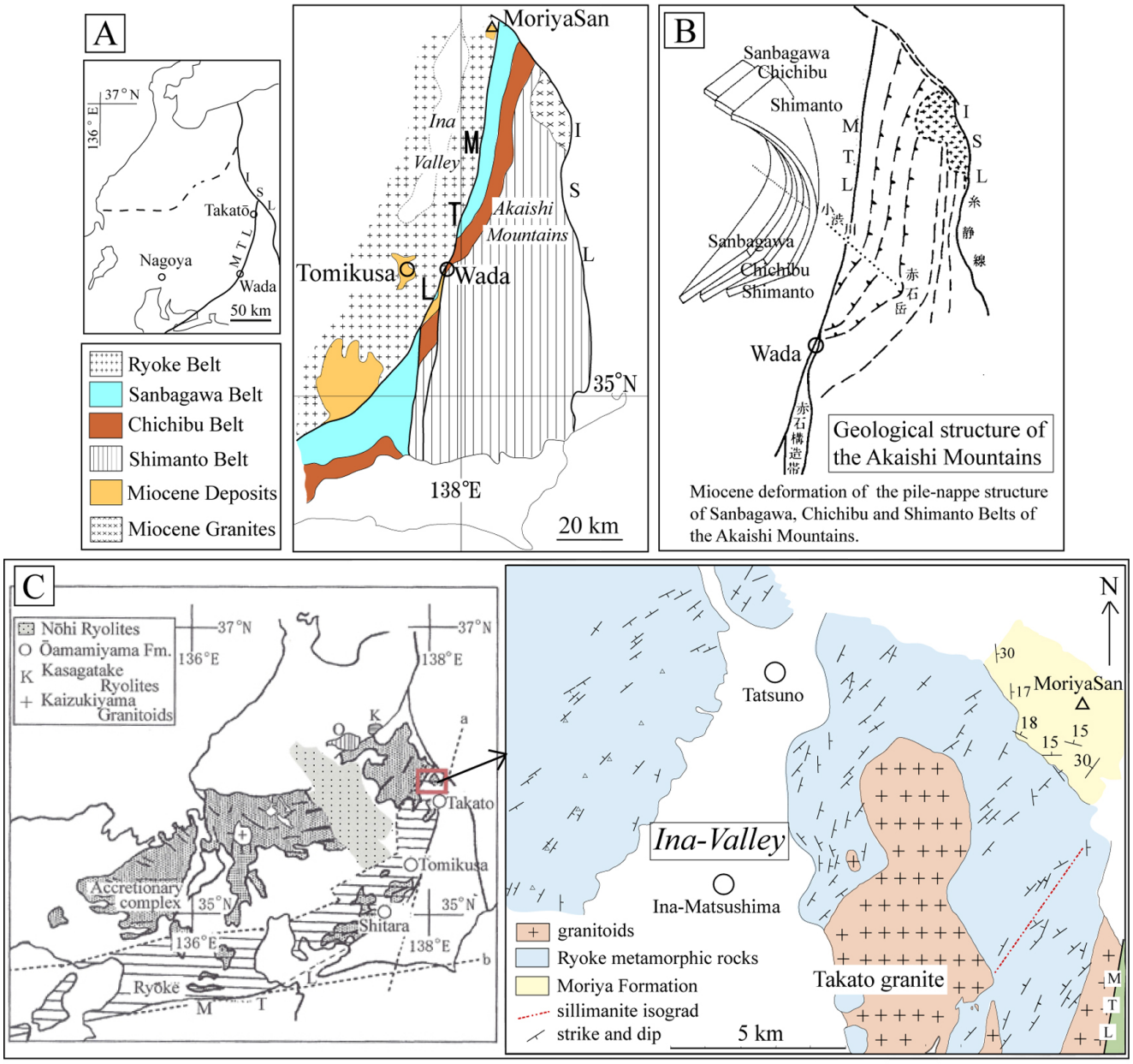
*Akira Ono[1]

1. None

Consider the tectonics of geological bodies A and B which are in contact with a fault in a shallow crust. Rotation of the geological body B occurs with respect to A. The rotation axis is assumed to be vertical or horizontal, but in either case, overlap and void of the geological bodies occur at the boundary between the geological bodies A and B. This virtual overlap and void are actually eliminated by the tectonic movement and deformation of geological bodies around the boundary fault. A tectonic zone is formed between the geological bodies A and B after the rotation.
It is reasonable to assume that geological body A is the inner zone of the Ina-Valley area and geological body B is the Akaishi Mountains of the outer zone in view of the geology and tectonics of these areas. Figure A is a schematic geological map of the area in question. Bedding planes of the Miocene Moriya and the Tomikusa basins are dipping gently below 20˚. On the other hand, the Miocene Wada Formation of the Akaishi Mountains is highly deformed and bedding planes are steeply tilted. The marked tilting of the bedding planes can be regarded as a rotating motion with the almost horizontal rotation axis.
The geological structure of the Akaishi Mountains is not a layered structure of gently inclined geological bodies that is found in the Kanto and Kii Mountains. Various geological bodies of the Akaishi Mountains are complexly deformed as shown in Figure B, and many geological units are partially missing. This complex geological structure was formed during the expansion period of the Sea of Japan. Moreover the Akaishi Mountains greatly rotated counterclockwise with respect to the inner zone of the Kinki region. The rotation axis was vertical and lateral movements in the N-S direction were also very intense.
In the western edge of the Mino belt and the northwestern edge of the Ryoke belt, i.e. the Ina-Valley area, the strikes of bedding planes are about N45˚E (Figure C). In these areas, the rotational motion around the vertical axis is estimated to be almost the same everywhere. According to the paleomagnetic study of the Miocene andesite dike swarm in the eastern part of Takayama City, Gifu Prefecture, located at the west end of the problem area, the paleomagnetic data are almost the same as those of the inner zone of the Kinki district. In the opening period of the Sea of Japan, the Takayama and the Ina-Valley areas suffered no counterclockwise rotational movement relative to the inner zone of the Kinki region.
Considering the large differences in the Miocene tectonics mentioned above, a tectonic zone may be formed between the Ina-Valley area and the Akaishi Mountains during the opening period of the Japan Sea. It is reasonable to consider large-scale horizontal and vertical movements of geological bodies in the tectonic zone. However, this kind of tectonic zone has hardly been confirmed. This contradiction can be resolved by assuming that most of the geological bodies in the tectonic zone were transported toward the earth surface. The missing geological bodies may be found as clastic materials in Miocene subduction zone. The current eastern border of the Ryoke belt near the Akaishi Mountains may have suffered similar tectonics during the formation of the Miocene Median Tectonic Line. In this area, narrow geological units elongated in N-S directions are found, and this is evidence for the missing tectonics.

Keywords: Miocene tectonics, Median Tectonic Line, Ina-Valley, Akaishi Mountains, Missing tectonic zone

©2020. Japan Geoscience Union. All Right Reserved.



©2020. Japan Geoscience Union. All Right Reserved.

On the paleocurrent of the Miocene Goto Group in Fukue Island, Nagasaki Prefecture

*Yuta Ikebata[1], Shoichi Kiyokawa[1]

1. Department of Earth and Planetary Sciences, Graduate School of Science, Kyushu University

The Goto Islands are located about 60 km west of Kyushu and consist of five major islands and more than 200 islands around them. This region is located at the western edge at the Sea of Japan expansion period (around 15Ma) and occupies an important position to record tectonics that shift from land arcs to island arcs at the edge of the continental edge of East Asia. In the Goto Islands, The Goto Group (Ueda, 1961) consisting of Miocene sedimentary rocks is distributed throughout. Rhyolites (Matsui and Kawata, 1986) and granites (Kawata et al., 1994) are intruding into it. In addition, the entire structure and detailed stratigraphy of the Goto Group has been clarified (Yamamoto, 2006MS; Hasegawa 2008MS; Yasunaga et al., 2005MS). In particular, the Goto Group exposed to Fukue Island consists of the Tachiya layer consisting of tuff breccia, the Okuura formation (Kawada, 1994) consisting of alternation of sandstone and mudstone, the toraku formation consisting of alternation of sandstone and mudstone, and hotokezaki formation consisting of sandstone, which is rich in charcoal products and develops a large cross bedding from the bottom. The Okuura Formation is further divided into three parts: lower, middle and upper. The lower part consists of alternation of fine to medium sandstone and dark gray shale to siltstone. The middle part consists of alternation of about 20 m thick medium-grained sandstone and 1-2 m thick mudstone. The upper part coarsens from the lower part into alternation of fine-grained white sandstone and black sandstone, alternation of medium-grained sandstone and mudstone, and medium-grained sandstone. In this study, we focused on the thick sandstone layer in the Goto Group, determined the paleocurrent mainly in the cross bedding and investigated the changes in each stratigraphy and regional flow from the time of the formation of the Goto group.
In this study, a total of 158 paleocurrent data were obtained in Fukue Island, including the Okuura formation (60 pieces), the Toraku formation (94 pieces), and the Hotokezaki formation (4 pieces). It was found that the paleocurrent obtained for each stratigraphy changed from the lower, northeast to south, and then again to the north, and changed to indicate various flows at the top level. In addition, it was found that paleocurrent showed the different direction flow even in the same layer level as by region, and it was remarkable especially in the upper part of the Okuura formation and the toraku formation. In the future, I will collect data at the bottom and middle part of the Goto Group, which has a small number of data. In addition, I conduct surveys on islands other than FukueIsland and collect data from a wide area.

Keywords: Miocene rocks, paleocurrent

©2020. Japan Geoscience Union. All Right Reserved.

North-South extension and compression juring the Japan Sea opening in the Amakusa, western Kyushu, Japan

*Kentaro Ushimaru[1], Atsushi Yamaji[1]

1. Division of Earth and Planetary Sciences, Graduate School of Science, Kyoto University

The opening of theJapan Sea in the early to middle Miocene was believed to be accompanied by compressional tectonics at its southwestern margin, i.e., northern and western Kyushu, Japan; and the compression resulted in the folds in Tsushima Island between Korea and Kyushu and in Amakusa Islands, western Kyushu (Ishikawa and Tagami, 1991; Sakai, 1993). Eocene formations are folded with NNE-trending axes in Amakusa. In the present work, we collected orientation data from planar intrusive bodies in Amakusa-Shimoshima Island to test their hypothesis.

We observed altered andesite intrusions, i.e., 50 dikes and 18 sills. Their ages are loosely constrained to be 14–20 Ma by the radiometric ages of intrusive bodies in Amakusa (Nagao et al., 1992; Hamasaki, 1996) The method of Yamaji and Sato (2011), which fits a mixed Bingham distribution to the orientations of planar intrusions, was applied to the 68 data. As a result, we obtained normal-faulting and reverse-faulting stress regimes, indicating N-S extensiona and N-S compression. The latter is oblique to the fold axes, so that the previous researchers' hypothesis about the folding accompanied by the Japan Sea opening is improbable. A few NNE-trending rhyolitic dikes in the island led Yamamoto (1991) to suggest horizontal maximam stress in the trend. The rhyolitic dikes may have been accompanied by the first phase rifting in the Okinawa Trough to the southwest of the island.

Keywords: stress, Japan Sea opening, dike, Kyushu, Okinawa Trough

©2020. Japan Geoscience Union. All Right Reserved.

Visualization of a high-strain shear zone based on a field survey for minor faults: A case study of southern Kyushu, Japan

*Akira Goto[1], Koji Shimada[1], Masakazu Niwa[1], Shuji Terusawa[2]

1. Japan Atomic Energy Agency, 2. OYO Corporation

Owing to a nationwide GNSS network installed since mid-1990s, several high-strain shear zones defined as concentrated regions of strain rates have been recognized in Japanese Islands (Sagiya et al., 2000, PAGEOPH). The high-strain shear zone with a sinistral strike-slip was identified also in southern Kyushu (Nishimura and Hashimoto, 2006, Tectonophysics; Wallace et al., 2009, Geology). There have had large earthquakes in this area such as the 1997 Northwestern Kagoshima Earthquake (Faculty of Science, Kagoshima Univ., 1997, Report of CCEP), however, any seismogenic faults associated with these earthquakes or active faults with strike-slip tectonic landforms had not been previously recognized at the surface.

In this study, we focused on existing minor faults to clarify a geological evidence of the shear zone suggested by geodetic studies. Basement rocks in the study area are mostly composed of sandstone and mudstone of the Shimanto accretionary complex, and are with a minor exposure of the Miocene Shibi-san Granodiorite (Yoneda and Iwamatsu, 1987, J. Geol. Soc. Japan). Mesoscale fault zones with clayey gouge and cataclasite are rare in the study area. Instead, minor faults cutting bedding planes and deformation structures subparallel to the bedding (such as mélange fabric), suggesting the formation clearly after the accretion of the Shimanto accretionary complex, are commonly observed. Slip directions can be examined from striations along the minor faults. Striations are also often identified along joints in the massive sandstone. Based on orientation data of these striations, we applied stress tensor inversion techniques (Yamaji, 2000, J. Struct. Geol.; Yamaji and Sato, 2012, Comp. Geosci.) to elucidate stress states. Our field survey in northwestern Kagoshima (22 ×16 km) revealed an occurrence of the E-W trending zone of ~2 km wide showing a stress state consistent with the sinistral high-strain shear zone (NE-SW compression and NW-SE extension). This zone largely overlaps the aftershock distribution of the 1997 Northwestern Kagoshima Earthquake. This study can contribute to one of helpful approaches to examine potential future activities of faults (or shear zones) without clear tectonic landforms.

This study was funded by METI, Japan as part of its R&D program supporting development of technology for geological disposal of HLW.

Keywords: high-strain shear zone, stress tensor inversion, minor faults, southern Kyushu

©2020. Japan Geoscience Union. All Right Reserved.

Structural position of the Akiyoshi Limestone in the Permian accretionary complex of the Akiyoshi Belt, Southwest Japan

*Koji Wakita[1], Hokuto Obara[2], Takanori Nakagawa

1. Yamaguchi University Community Future Center, 2. Mine Akiyoshidai Karst Plateau Geopark Promotion Council

Akiyoshi Limestone of the Akiyoshi Belt yields well preserved fusulinids, and its detailed stratigraphy and geological structure have been studied nearly for 100 years. The characteristic feature is the overturned structure of the limestone beds. The mechanism of the overturned structure has been discussed as the Akiyoshi Orogeny, but recently the limestone collapse model has been widely accepted. However, the limestone collapse model in the Japan Trench has some problems. Daiichi Kashima Seamount on the Pacific Plate has collapsed in the trench. However, the collapsed materials are never accreted into the continental margin along the Japan Trench, where the tectonic erosion occur. On the other hand, in the Nankai Trough, which is the accretionary boundary along the Southwest Japan, seamounts never collapse at the trench. As the hard seamount advances by pushing away the soft accretionary prism, and the accretionary wedge is deformed instead.
The most probable case is the limestone part on the seamount offscraping in the deep part of the accretionary wedge. After the offscraping, the limestone fragment moved upward, and appeared at the outer forearc high. The limestone fragment collapses and accumulates into forearc basin and/or trench slope basin. The purpose of this study is to reveal the accretionary process of the Akiyoshi limestone, which was offscraped from the top of the seamount and incorporated into the accretionary prism in the Permian period. Present analog of the Permian accretionary complex of the Akiyoshi Belt is the accretionary prism formed along the Java Trench near the Sulawesi Island, western Indonesia. In the presentation, new tectonic model of Akiyoshi limestone is proposed using analog of the Java accretionary wedge.

Keywords: Akiyoshi, Limestone, Permian, accretionary complex

©2020. Japan Geoscience Union. All Right Reserved.

Deformation characteristics and metamorphic temperature of the high-pressure terrace of the Taiwan orogeny

*Han Chun Lin[1], Yuan Hsi Lee[1], Lucas Mesalles[1], Jian Cheng Lee[2]

1. Department of Earth and Environmental Sciences, National Chung-Cheng University, 2. Institute of Earth Sciences, Academia Sinica, Taiwan

Different mechanisms have been proposed about how the subduction-related high-pressure terrane exhumates to the Earth’ s surface that might come from different tectonic settings. Taiwan orogeny results from arc-continental collision since 6-7Ma and recent studies show that high-pressure Yuli belt is associated with this process. The high-pressure terrane has been buried to ca. 50 km in-depth, and the surrounding terrane is ca. 12-20 km in depth. How the different terrane exhumed to the surface and what kind of structures are developed during the subduction to exhumation process? Here we collect the samples from low to high metamorphic and pressure terrane around the southern Central Range and use the RSCM methods, structural analysis, and zircon fission-track dating to reveal the possible exhumation process.

Three-stage foliations have been observed in eastern Central Range. The S1 is parallel to S0 associated with well-growth mica which is related to the highest metamorphism. The S2 is high-angle dipping foliation with fine-grain mica growth associated with tight to isoclinal folding. The S3 is shallow dipping foliation associated with small to mesoscale recumbent folding. The S3 results from the vertical force, which is strongly related to the recent exhumation process.

The RSCM results show the metamorphic temperature increases from ca. 340°C (low-grade slate) to ca. 500°C (high-pressure belt) in short distances that might infer a high shear zone; however, the zircon fission-track ages are similar in 0.7-1Ma and the eastern Central Range accelerate exhumation since ca. 2Ma simultaneously indicating the different metamorphic terranes have been merged before 2Ma. We suggest that the later stage foliation S2-S3 is related to this rapid exhumation process and the S1 is associated with the highest metamorphism suggesting it could be related to the subduction process.

Keywords: Raman Spectroscopy of Carbonaceous Material, fission track dating, structural analysis, high-pressure Yuli Belt, Taiwan orogeny

©2020. Japan Geoscience Union. All Right Reserved.

[E] Poster | S (Solid Earth Sciences)：S-RD Resources, Mineral Deposit & Resource Exploration

[S-RD35] Mineral Resources for Society: Ore deposit formation and exploration

convener:Yasushi Watanabe(Faculty of International Resource Sciences, Akita University), Kotaro Yonezu(Deaprtment of Earth Resources Engineering, Faculty of Engineering, Kyushu University)

Mineral resources are fundamental to Society, particularly for a modern way of life, as they are used in every facet of life, from housing and transport to low-C energy sources to mobile phones. Metals and non-metals are mined from surface or underground ore deposits. The largest production - aside from industrial minerals - is iron ore from iron formations, 2,400 million tonnes (Mt) yearly (USGS), and P2O5 (263 Mt). This is followed by Al (60 Mt), Cr (30 Mt), Cu (20 Mt), Zn + Pb (19 Mt) and Ni (2 Mt); Mo and Sn (each 290 kilotonnes, kt), REEs (130 kt), Co (111 kt), Li (43 kt) and Ag (25 kt). Smaller amounts of essential metals include In (720 t), Ga (300 t) and Ge (126 t). Reserves (i.e., amounts proven by drilling to be economically feasible to mine) for many elements are 2-3+ decades, with known Resources typically up to 100 years or more (e.g., Fe, P), at present consumption rates.

Future global mineral resources depend on the consumption rate minus the recycling rate for given elements; shortfalls need to be made up over time by discovery of new resources. Discovery occurs by exploration; although technology assists this task, geologists must still work in the field and map, assess alteration and geochemical anomalies, and test these plus geophysical anomalies by drilling. Few anomalies ever reach a feasibility study, and many deposits with a feasibility study eventually are not mined for economic, social, environmental, political or other reasons. In order to be geologically successful at exploration, geologists must understand the characteristics of the ore deposit style sought, and appreciate the variations that occur within the deposit style they are seeking. This requires understanding how ore deposits form, and how characteristics may vary depending on different geologic settings. This session invites presentations on ore deposits and features that assist their discovery.

[SRD35-P01] Heavy mineral sands ore deposits in Somaliland (Southern Gulf of Aden) coastal areas

*Awul Mohamud Ibrahm[1], Mohammed Ali[2] (1.Burao University, 2.Khalifa University of Science and Technology)

[SRD35-P02] **Economic potential of red earth deposits in the north and northwestern coastal belt of Sri Lanka**

*W.L.A.C.I. Weedagama [1,2], N.W.B. Balasooriya[2], Atula Senaratne[2], Bhathiya Athurupana[2], Rohana Chandrajith[2], Nadeesha H. Koralegedara[2] (1.Post Graduate Institute of Science, University of Peradeniya, Peradeniya, Sri lanka, 2.Department of Geology, University of Perdeniya, Peradeniya, Sri Lanka)

[SRD35-P03] Mineralogy and sulfur isotopic compositions of the Mowana vein-type copper deposit, Northeastern, Botswana

*AMOGELANG KOOGANNE[1], Akira Imai[2], Ryohei Takahashi[1], Andrea Agangi[1] (1.Akita University, 2.Kyushu University)

[SRD35-P04] Potential for Iron Oxide-Apatite Deposit and Iron Oxide-Copper-Gold Deposit in Japan: A new paradigm beyond current metallogeny

*Hiroyasu Murakami[1], Atsushi MIYASHITA[2] (1.Waseda University, 2.Seikei University)

Heavy mineral sands ore deposits in Somaliland (Southern Gulf of Aden) coastal areas

*Awul Mohamud Ibrahm[1], Mohammed Ali[2]

1. Burao University, 2. Khalifa University of Science and Technology

Heavy mineral enriched samples along the Somaliland coast were analysed using X-ray Fluorescence, X-ray Diffraction and SEM-EDS techniques. This study reveals that a considerable amount of heavy minerals is present along the Somaliland coast and confirms the presence of high concentration titanium and iron bearing minerals. The titanium detected in geochemical analysis occurs in the form of ilmenite, rutile, titanite and taniferous magnetite. Also, present in minor or trace amounts, are garnet, zircon and monazite.

Heavy mineral accumulations in the east and west of Somaliland have different mineralogical assemblages. The east of Somaliland is dominated by quartz with moderate concentration of plagioclase, K-feldspar, magnetite, hematite and titanium bearing minerals, whereas in the west of Somaliland, the dominant minerals are quartz, K-feldspar and plagioclase with variable proportions of ilmenite, rutile, mica, amphibole and pyroxene. These variations in mineral assemblages suggest different composition of the catchment areas that supply sediment to these deposits. The catchment area in the east of Somaliland consists mainly of Proterozoic crystalline basement of the Qabri Bahar complex, Gabbro-Synenite belt and granitic intrusions that outcrop in Hudiso, Tulo Dibijo and surrounding areas. The primary sources of heavy minerals in the west of Somaliland comprise of high-grade metamorphic rocks of the Mora and Qabri Bahar complexes as well as the Miocene volcanics that outcrop in Laferug and Hagabo areas.

The heavy mineral sand deposits observed along the Somaliland coast have the potential to provide commercially important heavy minerals, in particular ilmenite.

Keywords: Heavy mineral sands deposits, Ilmenite, Rutile, Titanium Oxide

©2020. Japan Geoscience Union. All Right Reserved.

Economic potential of red earth deposits in the north and northwestern coastal belt of Sri Lanka

*W.L.A.C.I. Weedagama [1,2], N.W.B. Balasooriya[2], Atula Senaratne[2], Bhathiya Athurupana[2], Rohana Chandrajith[2], Nadeesha H. Koralegedara[2]

1. Post Graduate Institute of Science, University of Peradeniya, Peradeniya, Sri lanka, 2. Department of Geology, University of Perdeniya, Peradeniya, Sri Lanka

Massive layers of red earth formations that belong to the Quaternary age is found along the northwestern coastal belt of Sri Lanka. The deposit is overlaying the Miocene limestone beds, covering approximately 40 sq. km with an average thickness of 20 m. At present the material is wasted and used only as a land filling material. Therefore, the present study aims to evaluate the economic importance and also assess the spatial distribution of economically important minerals in the red-earth deposit. Red earth samples were collected from 2 to 3 m depths from selected locations along the deposit. Sieve analyses, isodynamic separation followed by XRD analyses and ICP-MS techniques were used to determine the particle size distribution, mineralogy and geochemical composition of collected samples. The main constituents of red earth were quartz, clay- and iron oxide minerals such as magnetite and hematite. Zircon and monazite are also present in minor quantities. The granulometric data showed that southern part of the deposit is well sorted (CC<4) sand compared to the northern part (CC>4). The content of Rare Earth Elements (REEs) were significantly higher in the southern part compared to the northern part. Among the REEs, cerium (499 mg/kg), lanthanum (255 mg/kg), and neodymium (205 mg/kg) were dominated. Even though the REEs concentrations were proportionally increased with the depth, some intermediate layers were found with a lower content of REEs. The lateral distribution of opaque minerals such as magnetite and ilmenite showed a similar trend where 2 to 3% of such minerals were recorded. Kaolinite was the most abundant clay mineral in the deposits. The clay content significantly decreased towards the northern part of the deposit. The red earth also showed a potential of removing toxic elements such as Pb, As and Cr from industrial waste water.

Keywords: Red earth, rare earth elements (REE), water treatment potential, Miocene limestone

©2020. Japan Geoscience Union. All Right Reserved.

Mineralogy and sulfur isotopic compositions of the Mowana vein-type copper deposit, Northeastern, Botswana

*AMOGELANG KOOGANNE[1], Akira Imai[2], Ryohei Takahashi[1], Andrea Agangi[1]

1. Akita University, 2. Kyushu University

The Mowana deposit is located in the southern part of the Zimbabwe Craton which extends into the north of Botswana. It contains approximately 72.000 kt of measured and indicated mineral resources at 0.8% average copper grade and 0.25 % cut off grade. The deposit has since discovery received little study and documentation. Therefore, this study presents the preliminary documentation of the mineralization and associated alteration characteristics on the basis of petrography and sulfur isotopic analyses.

The Mowana copper deposit is hosted within the north-northeast striking and nearly vertical dipping sliver known as the Bushman Lineament of carbonaceous and argillaceous metasediments of the Paleoproterozoic Matsitama Metasedimentary Group formed in a large sedimentary basin in the Southern African Shield. The Matsitama Metasedimentary Group is enclosed within foliated granitoids of the Mosetse Complex. The contact between the granite-gneiss and the overlying sediments is tectonic. These units are overlain by the Phanerozoic Karoo Supergroup sequence of conglomerates and siltstones.

The Cu mineralization occurs in quartz ±calcite ±alkali feldspar vein and breccias which are near or in contact with the silicified limestone and argillite host rocks. Moreover, appreciable amounts of galena and sphalerite are hosted in the quartz ±calcite ±fluorite veins. The granitic gneisses occur as country rocks. The graphitic schists occur as irregularly distributed lenses or patches between the mineralized breccia and carbonate rocks as well as the mineralized breccia and the argillite. The host rocks are characterized by silicification, chloritization, epidotization, sericitization, and carbonate alterations. The principal metallic minerals are chalcopyrite, pyrite, galena, and sphalerite. Supergene mineralization is categorized by the significant presence of chalcocite, native copper and bornite. The upper part of the deposit is oxidized as indicated by the presence of supergene malachite and chrysocolla. Gangue minerals are mainly quartz, calcite, sericite, epidote, and chlorite.

Sulfur isotopic ratios were determined on the sulfides; chalcopyrite and pyrite from the mineralized quartz veins. The $d^{34}S$ of five chalcopyrite samples from the mineralized veins range from -0.8 to +3.3‰ while the $d^{34}S$ of two pyrite samples are higher, +15.4 and +18.0 ‰. The contrasting sulfur isotopic ratios from the chalcopyrite and pyrite suggest different sulfur sources for the two minerals. The high $d^{34}S$ of pyrite can be attributed to closed system reduction of seawater sulfate of the Paleoproterozoic era.

©2020. Japan Geoscience Union. All Right Reserved.

Potential for Iron Oxide-Apatite Deposit and Iron Oxide-Copper-Gold Deposit in Japan: A new paradigm beyond current metallogeny

*Hiroyasu Murakami[1], Atsushi MIYASHITA[2]

1. Waseda University, 2. Seikei University

The Naka-Osaka Mine in Shimonita, Gunma Prefecture, Japan, is the geosite of the Shimonita Geopark. This mine is also an industrial heritage site where iron manufacturing was carried out in the early Meiji era in Japan. It was produced high-grade magnetite ore. In the Naka-Osaka deposite, fine-grained euhedral apatite is commonly observed as inclusions of magnetite ore. The apatite containing chlorine has similar chemical property as the altered minerals associated with magnetite, which suggests that apatite has the same origin to magnetite. Magnetite with apatite in a neutral to alkaline alteration zone at high temperatures above 500˚C in close to the large-scale tectonic line. These features of the Naka-Osaka mine strongly suggests that the magnetite ore deposit belongs to the iron oxide-apatite (IOA or Kiruna) type.

In addition to current results from the Naka Osaka deposit showing the probability of IOA (Iron-Oxide Apatite or Kiruna) type deposits in Japan, based on that iron oxide type (IOA and IOCG) deposits were discovered around the world from the Precambrian to the Mesozoic ages, therefore, we will reconsider a potential iron oxide type deposits (IOA and IOCG) among magnetite -bearing hydrothermal deposits in Japan. In the vicinity of the Naka-Osaka Mine, there are magnetite ores with gold-containing skarn at the Nakatsu deposit in the Chichibu Mine, and magnetite ores with gold-containing skarn and loellingite at the Kobushi Mine. The origin of these ore deposits needs to reconsider whether an iron oxide-copper-gold type (IOCG).

Iron oxide (IOA and IOCG) deposits, which is occasionally attracting attention as rare earth resources, have recently been explained by a hydrothermal origin with high-temperature iron-chloride fluid penetrating tectonic zone, which is becoming more convincing than an igneous origin related to solidification of iron oxide melt (so-called magnetite lava). Adding to the result from Naka-Osaka deposit, we will propose a new metallogeny based on identifying the presence of apatite in the magnetite ore and their chemical compositions by expanding a scope of magnetite bearing hydrothermal deposits including Kamaishi and Ashio. We also explore a possibility of discovery for a giant copper deposit in Japan by reviewing the formation temperature, pressure (depth) as well as Cu / Au ratio of these deposits.

Keywords: Hydrothermal Magnetite deposit, Iron Oxide-Copper-Gold deposit, Iron-Oxide Apatite deposit, Copper resources, Shimonita Geopark, Naka-Osaka Mine

©2020. Japan Geoscience Union. All Right Reserved.

[E] Poster | S (Solid Earth Sciences)：S-MP Mineralogy & Petrology

[S-MP36] Physics and Chemistry of Minerals

convener:Seiji Kamada(Frontier Research Institute for Interdisciplinary Sciences, Tohoku University), Masahiro KAYAMA(Department of General Systems Studies, Graduate School of Arts and Sciences, The University of Tokyo)

In this session, we will discuss the physics and chemistry of the Earth and planetary materials (including amorphous and melts) based on the results obtained from various experimental methods such as X-ray diffraction, FT-IR, Rman spectroscopy, electron microscopic observations, and computer simulations.

[SMP36-P01] Chemical and optical evaluation of zircon synthesized by Li-Mo flux method

*Masahiro KAYAMA[1], Das Kaushik[2], Yuta Tsuchiya[3] (1.Department of General Systems Studies, Graduate School of Arts and Sciences, The University of Tokyo, 2.Department of Earth and Planetary Systems Science, Hiroshima University, 3.Department of Biosphere-Geosphere Science, Okayama University of Science)

[SMP36-P02] Geological study around Strontian mine considered from zeolite and galena.

*Yuki Inoue[1], Mana Yasui[2], Hiroshi Hagiya[1], Atsushi Yamazaki[3] (1.Tokyo City University , 2.Waseda Research Institute for Science and Engineering, 3.Department of Resources and Environmental Engineering, School of Creative Science and Engineering, Waseda University)

[SMP36-P03] The influence of OH content on elastic constants of single-crystal topaz studied via sphere-resonance method

*Kako Aradachi[1], Tohru Watanabe[1], Morihisa Hamada[2] (1.University of Toyama, 2.Japan Agency for Marine-Earth Science and Technology)

[SMP36-P04] Structural changes of diatomaceous earth by heat treatment

*Naoya Sasaki[1,2], Akane Arasuna[1], Masayuki Okuno[1] (1.Kanazawa University, 2.Industrial Research Institute of Ishikawa)

[SMP36-P05] Density and elastic properties of liquid gallium using externally heated diamond anvil cell

*Ryo Tsuruoka[1], Hidenori Terasaki[1], Seiji Kamada[2,3], Fumiya Maeda[3], Tadashi Kondo[1], Iori Yamada[1], Satoru Urakawa[4], Akira Yoneda[5], Naohisa Hirao[6], Saori I. Kawaguchi[6], Akihiko Machida[7] (1.Department of Earth and Space Science, Graduate School of Science, Osaka University, 2.Frontier Research Institute for Interdisciplinary Sciences, Tohoku University, 3.Department of Earth and Planetary Materials Science, Graduate School of Science, Tohoku University, 4.Department of Earth Sciences, Okayama University, 5.Institute for Planetary Materials, Okayama University, 6.JASRI, 7.QST)

[SMP36-P06] Nano-polycrystalline diamond synthesized through the decomposition of stearic acid under high pressure and high temperature condition

*Hideaki Kawamura[1], Hiroaki Ohfuji[1] (1.Geodynamics Research Center, Ehime University)

[SMP36-P07] The magnetite-maghemite-hematite transformation

*Ibuki Kinebuchi[1], Atsushi Kyono[1], Yoshinari Sano[1] (1.University of Tsukuba)

[SMP36-P08] Effect of pressure on the band gap and the Seebeck coefficient of silicon

*Hitoshi Gomi[1], Ran Wang[2], Takashi Yoshino[2] (1.Tokyo Institute of Technology, 2.Okayama University)

[SMP36-P09] Density measurement of magmas under high pressure by the sink/float method

*Akio Suzuki[1] (1.Department of Earth Science, Graduate School of Science, Tohoku University)

[SMP36-P10] Twinning in wadsleyite

Nobuyoshi Miyajima[1], Johannes Buchen[1,2], *Takaaki Kawazoe[1,3] (1.Bayerisches Geoinstitut, University of Bayreuth, 2.Division of Geological and Planetary Sciences, California Institute of Technology, 3.Department of Earth and Planetary Systems Science, Hiroshima University)

[SMP36-P11] Melting experiments in the system $MgSiO_3$-SiO_2 at 13 GPa

*Takuya Moriguti[1], Akira Yoneda[1], Eiji Ito[1] (1.Institute for Planetary Materials, Okayama University)

Chemical and optical evaluation of zircon synthesized by Li-Mo flux method

*Masahiro KAYAMA[1], Das Kaushik[2], Yuta Tsuchiya[3]

1. Department of General Systems Studies, Graduate School of Arts and Sciences, The University of Tokyo, 2. Department of Earth and Planetary Systems Science, Hiroshima University, 3. Department of Biosphere-Geosphere Science, Okayama University of Science

Zircon, $ZrSiO_4$ phase occurring in various types of terrestrial and extraterrestrial rocks, is an important mineral to interpret the geological history. Crystallization, metamorphic, and sedimentary ages of zircon in the rocks can be determined by the radioactive elements. The zoning textures and Ti content in zircon reflect the thermal history of the magmatic and metamorphic processes. Furthermore, the elementary and structural features of zircon easily change during hydrothermal alteration. Natural zircon shows a decrease of the crystallinity, finally leading to amorphization, as a process of metamictization by radiations from radioactive elements in geological time. Zircon in impactite and meteorites often records an impact event of the host body as the shock-induced microstructure and texture. Such useful information on igneous, metamorphic and sedimentary processes have been obtained from microanalyses (e.g., electron microscope, SHRIMP, LA-ICP-MS, and Raman spectroscopy) of zircon. Synthetic zircon has been available as a standard material for accurate microanalyses, e.g., highly-pure synthetic zircon for checking sample background and a starting material for high-pressure and -temperature experiments to reproduce the metamorphic process and hydrothermal alteration in the geological events. Therefore, in this study, zircon was synthesized by the Li-Mo flux method reported by (Hanchar et al. 2001) using a heating furnace under various conditions.

Synthetic ZrO_2 and SiO_2 powder samples and Li_2SiO_3, Li_2MoO_4 and, MoO_3 flux were put into an unwelded platinum crucible (100 cc) in the heating furnace at room temperature (RT) and ambient pressure. Temperature in the heating furnace rose initially from RT to 1250 ˚C for 18 h, then kept at 1250 ˚C for 10 h, decrease from 1250 to 1000 ˚C for 500, 125, 63, 32, and 12 h (cooling rate of 0.5, 2.0, 4.0, 7.8, and 20.8 ˚C/h, respectively), and finally dropped from 1000 ˚C to RT for 25 h. All the recovered samples were measured by the optical and scanning electron microscopes, cathodoluminescence (CL) microscopy, and Raman spectroscopy. WDS analysis by EPMA and LA-ICP-MS measurements were performed for only zircon synthesized at a cooling rate of 0.5 ˚C/h.

All of the zircon grains synthesized at each cooling rate show a large amount of euhedral single crystals with inherent crystal planes and a few to several hundreds of micrometer size under an optical microscope. The crystal grain size seems to decrease with the cooling rate from 4.0 to 20.8 ˚C/h and show almost no change below 4.0 ˚C/h, implying that all of the dissolved SiO_2 and ZrO_2 were separated completely from the flux above 4.0 ˚C/h to form $ZrSiO_4$ crystals. CL microscopy revealed that there are oscillatory and sector zoning textures in all of the synthetic zircon, of which the shapes are corresponding to crystal planes of the zircon (that is, outer rims) observed in an optical microscope. WDS analyses of the major chemical composition of the zircon at 0.5 ˚C/h show SiO_2, ZrO_2, HfO_2 contents of 33.02, 66.46, and 1.79 wt%, respectively. Chemical compositions of these elements are homogeneous within the single crystals. As a result of WDS analyses of the zircon, trace elements of Y_2O_3, Al_2O_3, ThO_2, P_2O_5, Yb_2O_3, CaO, Nb_2O_5, UO_2, and Sc_2O_3 are below 0.005 wt% in content or undetected. LA-ICP-MS analyses of the zircon indicate that Y and Nb contents reach 2.6 and 1.0 ppm, and La, Ce, Pr, Nd, Sm, Eu, Gd, Tb, Dy, Ho, Er, Tm, Yb, Lu, Pb, Th, and U were below 1 ppm or detection limit. Raman spectroscopy of the synthetic zircon at

©2020. Japan Geoscience Union. All Right Reserved.

0.5 ˚C/h calibrated using a Kr bright line exhibits pronounced peaks at 974 and 1008 cm^{-1}, both of which the peak positions are corresponding to theoretical values of zircon unaffected by radiations, that is, metamictization. These facts imply that zircon crystals synthesized here are high quality and is expected to be used as a standard material for various microanalyses and experimental replication.

Keywords: Zircon, Synthesis, Li-Mo flux

©2020. Japan Geoscience Union. All Right Reserved.

Geological study around Strontian mine considered from zeolite and galena.

*Yuki Inoue[1], Mana Yasui[2], Hiroshi Hagiya[1], Atsushi Yamazaki[3]

1. Tokyo City University , 2. Waseda Research Institute for Science and Engineering, 3. Department of Resources and Environmental Engineering, School of Creative Science and Engineering, Waseda University

The Strontian mine is located approximately 170 km northwest of Edinburgh in Scotland. The Strontian mine had been produces lead and zinc since the 18th century, and barium in the 20th century. Not only mineral ore but zeolites containing Sr and Ba have been reported(Green et, 2008).

Utada (1995) reports that there is no relationship between host rock and zeolite in the Izu Peninsula, but in recent years Fujita et al.(2016) have closely related host rocks and zeolite as their composition in the Ogasawara Islands. The purpose of this study is to compare the composition of zeolite from the Strontian mine with the host rock and another rocks and to examine the formation and neighboring geologic relationships of zeolite.

This study investigated ore formation centered on zeolite. Zeolite was found at the Strontian mine. They were analyzed using SEM-EDS and XRF, XRD. The zeolite and rocks produced at The Strontian mine were analyzed using SEM-EDS and XRF and XRD. Three types of zeolite produced at the Strontian mine, harmotome, brewsterite, and heulandite-Sr, were confirmed by XRD and SEM-EDS. From the symbiotic relationship of these minerals, the temperature during zeolite formation was estimated at 65-85 ℃. Zeolite from the Strontian mine is rich in bivalent cations. Also, they contain a lot of Sr and Ba. The granodiorite around the mine is rich in Sr and Ba. Sr and Ba were the most abundant in plagioclase. Observation of granodiorite with a polarizing microscope and SEM-EDS revealed that Ca and K of plagioclase were replaced and became sericite.

The age of formation of the lead mine was estimated using galena isotopes. The Strontian mine was estimated at 430 Ma, considering a two-stage evolution from 2670 Ma Lewis gneiss. This age was consistent with the age of titanium and zircon granodiorite.

From the analysis results of these zeolite and galena, Pb, Sr and Ba derived from granodiorite formed the Strontian deposit at the Strontian mine by hydrothermal circulation accompanying the intrusion of the 430 Ma Strongian granodiorite. Finally, it is considered that the hydrothermal activity contained in the veins formed zeolite as the temperature of the series of hydrothermal activity circulation decreased.

Keywords: zeolite, Strontian mine, Pb isotope ratio, galena

©2020. Japan Geoscience Union. All Right Reserved.

The influence of OH content on elastic constants of single-crystal topaz studied via sphere-resonance method

*Kako Aradachi[1], Tohru Watanabe[1], Morihisa Hamada[2]

1. University of Toyama, 2. Japan Agency for Marine-Earth Science and Technology

Transport of ocean floor sediments by plate motions might play an important role in the circulation of materials within the Earth. Imaging subducted sediments through seismological observations requires a thorough understanding of elastic properties of sediment origin hydrous minerals. Topaz is a hydrous mineral with ideal chemical formula $Al_2SiO_4(F_{2-x},OH_x)$, which can be formed from subducted sediment at high pressures. Although elastic constants of topaz have been reported, experimentally determined values show no systematic relationship between elastic constants and OH molar content. Moreover, there are significant differences between experimental and theoretical values. To understand the influence of OH content on elastic constants, we have studied elastic constants of three single crystals of topaz with different OH contents (x=0.28, 0.45, 0.66) by the sphere-resonance method.
Sphere samples (D=2.6~6.5 mm) were made from single crystals of natural topaz by the two-pipe method. Lattice parameters were determined and orthorhombic symmetry was confirmed by XRD. Resonant frequencies were measured with different specimen-holding forces. Extrapolating to the specimen-holding force of zero, we obtained frequencies of "free" oscillation. Elastic constants were determined by comparing measured and calculated resonant frequencies. The xyz algorithm (Visscher et al., 1991) was employed to calculate resonant frequencies of the sphere samples. At an ambient temperature, Our determined elastic constants C_{11}, C_{22}, C_{44}, C_{66}, C_{12}, C_{23} and C_{31} increase with increasing OH molar content, while C_{33} and C_{55} decrease. These changes are similar to those seen in theoretical values (Ulian and Valdre, 2017) except for C_{11}, though there are significant differences between experimental and theoretical values.

Keywords: Topaz, Elastic constants, Water

©2020. Japan Geoscience Union. All Right Reserved.

Structural changes of diatomaceous earth by heat treatment

*Naoya Sasaki[1,2], Akane Arasuna[1], Masayuki Okuno[1]

1. Kanazawa University, 2. Industrial Research Institute of Ishikawa

In this study, the structural changes in the diatomaceous earth from U.S.A (Grade D110, Celite Co.) by heat treatment up to 1200˚C were investigated using XRF, XRD, ATR-IR and Raman spectroscopy. These results provide important information to elucidate the structure of fossilized diatom shell that has been rarely reported and the characteristic of structural change by heat treatment comparing the previous result for diatom.
The results of chemical analysis show this sample included of 93.1 mass% SiO_2 due to diatom shells and also containing a small amount of Al_2O_3, Fe_2O_3, MgO and CaO from clay minerals. Observed TG curve of this sample shows it contains about 12 mass% of H_2O molecules and OH. The diatomaceous earth samples were heat-treated at 200, 400, 600, 800, 900, 1000, 1100 and 1200˚C.
The XRD patterns for samples up to 800˚C show broad amorphous phase peaks at around 2θ=22˚ and weak diffraction peaks at around 2θ=19˚ due to clay minerals. The XRD patterns for heat-treated samples at 900 and 1000˚C showed amorphous phases. This means clay minerals amorphized at 900˚C due to dehydration. At 1100˚C and 1200˚C, cristobalite phase were observed. The positions of broad peaks for amorphous phase show the samples have 6-membered rings of SiO_4 tetrahedra as the basic structural unit. On the other hand, previous results for thermal change of diatom show crystallization above 800˚C.
ATR-IR spectrum for non-treated sample is similar with that of diatom except sharp O-H band at around ν=3620cm^{-1}, this band could be attributed to OH of clay minerals. On the other hand, the broad band ν=2800-3700cm^{-1} could be attributed H_2O molecules in amorphous SiO_2 phase. se bands disappeared by heating at 900˚C. This result is consistent with that of XRD measurement. bands at ν=800 and 1020cm^{-1}, which are attributed to the Si-O-Si bending vibration and the Si-O stretching mode show not large thermal change up to 1000˚C. Over 1000˚C, these bands shift their position and become sharp by crystallization of cristobalite.
Raman spectrum at ν=200-800cm^{-1} of non-treated sample is also similar with that for diatom of the previous work. This mean the basic structure of diatomaceous earth composed 6-membered rings of SiO_4 tetrahedra. Because, the intensity around ν=450cm^{-1} is strong, which band could be attributed symmetric stretching band of Si-O-Si. By increasing treated temperature up to 1000˚C, the intensities around at ν=450, 490 and 600cm^{-1} increase. This means 6-membered rings of SiO_4 tetrahedra are largely increased and 4- and 3-membered rings appear and the nanostructure becomes similar to the spectrum SiO_2 glass by heat treatment. This Raman spectrum change is not similar with that of diatom. Furthermore, the structural changes of diatomaceous earth by heat treatment show a different tendency from the diatom that have been reported so far. Now, we can guess that the difference of temperature change in XRD between diatom and diatomaceous earth can be probably due to the small quantity of clay minerals and fossilization process diatom to diatomaceous earth.

©2020. Japan Geoscience Union. All Right Reserved.

Density and elastic properties of liquid gallium using externally heated diamond anvil cell

*Ryo Tsuruoka[1], Hidenori Terasaki[1], Seiji Kamada[2,3], Fumiya Maeda[3], Tadashi Kondo[1], Iori Yamada[1], Satoru Urakawa[4], Akira Yoneda[5], Naohisa Hirao[6], Saori I. Kawaguchi[6], Akihiko Machida[7]

1. Department of Earth and Space Science, Graduate School of Science, Osaka University, 2. Frontier Research Institute for Interdisciplinary Sciences, Tohoku University, 3. Department of Earth and Planetary Materials Science, Graduate School of Science, Tohoku University, 4. Department of Earth Sciences, Okayama University, 5. Institute for Planetary Materials, Okayama University, 6. JASRI, 7. QST

It is important to measure density of liquid metals at high pressure and high temperature for understanding compression behavior and elastic properties of liquid metals. Since gallium (Ga) has a low melting temperature, Ga can become liquid state easily under high pressure. The densities of liquid Ga have been reported by X-ray tomography (Li et al. 2014), by sound velocity (Ayrinhac et al. 2015), by reverse Monte Carlo simulations combined with X-ray scattering data (Yu et al. 2012). However these densities were not consistent with each other. X-ray absorption method is effective to measure liquid density directly. In this study, the densities of liquid gallium were measured using X-ray absorption method combined with an externally heated diamond anvil cell (DAC).

In X-ray absorption method, density of liquid Ga was obtained from measured incident and transmitted X-ray intensities of the samples using Lambert-Beer law (Takubo et al. 2019). Ga sample and two reference materials (RbBr, KBr, or Fe) were loaded into each hole drilled on a pre-indented Re gasket. The Re gasket was coated with Al_2O_3 to avoid a reaction between the Ga sample and the gasket. High pressure was generated using a symmetric DAC with a lever-arm frame. High temperature was generated using external heaters composed of Pt-Rh wires with a ZrO_2 insulator. X-ray absorption measurements were conducted with monochromatic X-ray of 30 keV at BL10XU and BL22XU beamlines in SPring-8.

The density of liquid Ga were measured up to 10 GPa and 533 K. The elastic properties (bulk modulus (K_{T0}), its pressure derivative (K')) of liquid Ga were calculated by fitting the density data with equations of state (EOSs) and obtained 45.8(4) GPa, 6.1(2) from third-order Birch-Murnaghan EOS at 500 K, respectively. In lower pressure region, the compression curve is consistent with the density calculated from sound velocity data reported by Ayrinhac et al. (2015). However, our results show that density variation is smaller than Ayrinhac et al. (2015) in higher pressure (e.g. 1% smaller at 10 GPa).

Keywords: gallium, diamond anvil cell, X-ray absorption method

©2020. Japan Geoscience Union. All Right Reserved.

Nano-polycrystalline diamond synthesized through the decomposition of stearic acid under high pressure and high temperature condition

*Hideaki Kawamura[1], Hiroaki Ohfuji[1]

1. Geodynamics Research Center, Ehime University

Nano-polycrystalline diamond (NPD) synthesized by the direct conversion of graphite under high pressure and high temperature conditions (15-25 GPa, 2000-2500℃) has an ultra-high hardness and superior mechanical properties and is therefore widely used for various industrial and scientific applications. In the present study, we found a novel route for synthesizing NPD using stearic acid ($C_{18}H_{36}O_2$) as a starting material. The temperature condition required for the synthesis of transparent NPD from stearic acid is as low as 1000℃ at 13 and 17 GPa, which is surprisingly lower (by ~1000℃) than those for the conventional NPD synthesis using graphite and related carbon sources such as glassy carbon. We also characterized the microtexture and crystallographic feature of the products recovered from a wide range of temperature and pressure conditions using TEM and discussed the formation mechanism from stearic acid at significantly lower temperatures. The samples recovered from 13 and 17 GPa are transparent NPD composed of extremely fine diamond crystals with grain sizes smaller than 20 nm. In contrast, those synthesized at 10 GPa are composed exclusively of graphite, whose crystallinity and grain size clearly change from almost amorphous like to platy crystals up to 100 nm with heating temperature.

Our study suggests that the amorphous-like, extremely poorly crystalline carbon produced by the thermal decomposition of stearic acid provides preferential nucleation sites for diamond and significantly lower the activation energy for diamond formation. The removal of volatile components such as H_2O generated through the stearic acid decomposition from the system is also important to obtain pore-free transparent NPD. Our finding would open up new possibilities for further sizing-up of NPD samples (at present 1 cm both in diameter and height at maximum) at moderate temperature and pressure, which will be essential for new and advanced applications of NPD in both scientific and industrial fields.

Keywords: Nano-polycrystalline diamond (NPD), High Pressure, C-H-O fluid, TEM

©2020. Japan Geoscience Union. All Right Reserved.

The magnetite-maghemite-hematite transformation

*Ibuki Kinebuchi[1], Atsushi Kyono[1], Yoshinari Sano[1]

1. University of Tsukuba

Magnetite (Fe_3O_4), which is ubiquitous in the crust, is transformed into hematite (α-Fe_2O_3) by the oxidation of Fe^{2+} to Fe^{3+}. In this oxidation process, maghemite (γ-Fe_2O_3) is formed as an intermediate phase, which is isomorphous as magnetite. Maghemite has a part of the octahedral site in magnetite that is vacancy. Elucidation of the oxidation mechanism of magnetite will lead to elucidation of magnetic susceptibility changes during weathering of igneous and sedimentary rocks, but continuous changes in local structure of magnetite are largely unknown. In this study, in order to elucidate the mechanism of the phase transition from magnetite to hematite via maghemite, X-ray absorption fine structure (XAFS) and X-ray diffraction (XRD) measurements were used to determine the area around Fe in the oxidation process of magnetite. We investigated the continuous local structural change of, and the change of long-range structure of the whole crystal.
XANES showed that the proportion of Fe^{3+} increased with increasing heating temperature and heating time, and finally all Fe became Fe^{3+}. From the radial structure function of EXAFS, it was found that the peak depending on the presence of Feoct in magnetite attenuated as the heating temperature increased, and then changed to a function indicating the structure of hematite. From the XRD, as the heating temperature increases and the heating time increases, first, octahedral vacancies have characteristic peaks in ordered maghemite, and then magnetite and maghemite peaks decrease, and hematite peaks appear and increase. From the above results, in the oxidation of magnetite, the Fe-O bond of some octahedral site is broken first, and Fe diffuses to become maghemite. Then, the rearrangement of Fe and O in the octahedral site with a vacancy at the center and the Fe-O4 tetrahedral site is thought to cause a phase transition to a hematite consisting entirely of octahedra.

Keywords: Magnetite, Maghemite, Hematite, XRD, XAFS

©2020. Japan Geoscience Union. All Right Reserved.

Effect of pressure on the band gap and the Seebeck coefficient of silicon

*Hitoshi Gomi[1], Ran Wang[2], Takashi Yoshino[2]

1. Tokyo Institute of Technology, 2. Okayama University

Many physical properties of semiconductors and insulators are characterized by their band gap energy, which is the energy difference between the valence band minimum (VBM) and the conduction band maximum (CBM). The pressure dependence of the band gap energy of Si is unique among the group 14 elements, which form the diamond-type crystal structure. The other three semiconductors (C, Ge and Sn) have positive pressure coefficient of the band gap energy, i.e. the band gap energy increases with increasing pressure whereas Si has negative pressure coefficient (Wei & Zunger, 1999; Angilella et al., 2008). The Seebeck coefficient is one of the important physical properties that closely related with the band gap energy (Goldsmid & Sharp, 1999; Ricci et al., 2017). However, measurements of the Seebeck coefficient under high pressure are very limited for both metallic (e.g. Getting & Kennedy 1970; Nishihara et al., 2019) and non-metallic (Yoshino et al., submitted) samples. Therefore, we conducted first-principles calculations of Si-I (diamond structure) by using the Quantum ESPRESSO package. The structure relaxation was performed at 0, 5 and 10 GPa pressures with PBE-PAW potential. To calibrate the bandgap, we also computed the quasi-particle self-consistent GW (QSGW) calculation with the ecalj package. The calculated bandgap values are $E_{g,PBE}$ = 0.609 and $E_{g,GW}$ = 1.465 eV for PBE-PAW and QSGW, respectively at 0 GPa, whereas the literature value is 1.11 eV. The bandgap energy decreases with increasing pressure. Note that most of the exchange correlation functionals such as PBE underestimate the bandgap energy, whereas the GW approximation tends to overestimate it. Because the Seebeck coefficient critically depends on the bandgap energy, we empirically corrected it as $E_g = 0.4*E_{g,PBE} + 0.6 * E_{g,GW}$. The Seebeck coefficient was calculated by using the BoltzTraP package. The effect of impurity is represented within the rigid band model. The absolute value of the Seebeck coefficient decreases with carrier (impurity) concentration. Our calculation at 0 GPa and 300 K underestimated the literature values with the impurity concentration lower than ~10^{19} (cm^3). This is due to the phonon drag effect (Weber and Gmelin, 1991). Our calculation considered the diffusion term only, but the actual Seebeck coefficient should be sum of the diffusion term and phonon drag term. Note that the phonon drag becomes negligible at high temperature and/or high carrier concentration. The absolute value of the Seebeck coefficient decreases with increasing pressure, because the bandgap decreases with pressure. Similarly, it decreases with decreasing carrier concentration at high temperature. Therefore, pressure (and hence the bandgap energy) and impurity concentration have competing effects on the Seebeck coefficient of Si.

Keywords: band gap, Seebeck coefficient, silicon, GW approximation

©2020. Japan Geoscience Union. All Right Reserved.

Density measurement of magmas under high pressure by the sink/float method

*Akio Suzuki[1]

1. Department of Earth Science, Graduate School of Science, Tohoku University

Density of magmas (silicate melts) is an important property, which controls its transportation in the Earth’ s interior. Therefore, various studies have been carried out under high pressure. We have engaged in the density measurement under the static compression. By the measurement of the X-ray absorbance, we can determine the density. However, the synchrotron X-ray beam is essential for high pressure experiments. The density of melt under high pressure can be restricted by observing the sinking and the flotation of the buoyancy markers in the melt. This sink/float experiments can be conducted without the synchrotron beam. Using the sink/float method we have measured various compositions of magmas (silicate melts). The buoyancy marker is selected with considering the following requirements. (1) The marker crystal does not react with the melt. (2) Its equation of state is accurately determined under high pressures and high temperatures to calculated the density of the marker. In the experiments, initially the marker crystal is loaded at the center of the sample container, and it is surrounded by the sample powder. At high pressure the sample was heated to be molten. If the heating duration is sufficient, the marker crystal sinks or floats depending on the density difference between the surrounding melt and the marker. The sample is quenched under high pressure to hold the position of the marker crystal. The recovered sample is cut to confirm the position of the marker. In the presentation, we demonstrate the recent development of the density measurement of magmas (silicate melts) by the sink/float method.

Keywords: magma, density, sink/float method, high pressure, mantle

©2020. Japan Geoscience Union. All Right Reserved.

Twinning in wadsleyite

Nobuyoshi Miyajima[1], Johannes Buchen[1,2], *Takaaki Kawazoe[1,3]

1. Bayerisches Geoinstitut, University of Bayreuth, 2. Division of Geological and Planetary Sciences, California Institute of Technology, 3. Department of Earth and Planetary Systems Science, Hiroshima University

Twinning was discovered in wadsleyite, which is the most abundant mineral at the upper part of the mantle transition zone. Wadsleyite crystals were synthesized from a powder of San Carlos olivine with distilled water at a pressure of 15 GPa and a temperature of 1670 K for 3 h using a multi-anvil apparatus. The wadsleyite twin was found based on change in color at a twin boundary due to strong pleochroism of wadsleyite by observing a thin section of the twin by optical microscopy. A thin foil perpendicular to the twin boundary was cut by focused iron beam (FIB) and was observed by transmission electron microscopy (TEM). The TEM observation revealed that twin domains make a 180˚ rotation about an axis perpendicular to the {101} plane in the pseudo-cubic system (cf. ringwoodite). Moreover, the composition plane of the twin domains is the {101} plane in the pseudo-cubic system. The wadsleyite twinning may be important in phase transformation, growth and deformation.

Keywords: mantle transition zone, wadsleyite, twinning, twin, twin boundary, high pressure

©2020. Japan Geoscience Union. All Right Reserved.

Melting experiments in the system $MgSiO_3$-SiO_2 at 13 GPa

*Takuya Moriguti[1], Akira Yoneda[1], Eiji Ito[1]

1. Institute for Planetary Materials, Okayama University

Melting behavior of silicates is essentially important to assess the chemical differentiation in a deep magma ocean in an early stage of the Earth. Therefore, melting relations of the system MgO-SiO_2 have been extensively studied since a pioneer work by Bowen and Anderson [1]. Furthermore, many scenarios of chemical differentiation in the deep magma ocean has been proposed based on the results of high pressure melting experiments (e.g. [2]). However, almost all of these works have been carried out on limited range of compositions from MgO to $MgSiO_3$, assuming that the bulk mantle composition is peridotitic or close to that derived from CI chondrite. Recently, enstatite chondrite (E-chondrite) has been favored as the source material of bulk earth [3], because the isotope systematics of the Earth and Moon are nearly identical to those of E-chondrite over O, N, Mo, Re, Os, and Cr. In E-chondrite, the silicate composition is characterized by $SiO_2/(SiO_2+MgO)$ = 0.53 ~ 0.58 (molar ratio: SiO_2[M]) [4], which is substantially higher than that of the peridotitic mantle (~0.43).

In order to understand the mantle differentiation in the E-chondrite earth model, it is indispensable to clarify the melting relations in the system $MgSiO_3$-SiO_2 at high pressures. Moreover, it also enables us to constrain the chemical composition of the crust formed in the early Earth. Nevertheless, there have been only limited works on the melting behavior of the system $MgSiO_3$–SiO_2 under high pressures. Information regarding phase relations in the system has been so far limited to 5 GPa based on the experiments using the multi anvil apparatus (MAA) [5], Using a diamond anvil cell (DAC), on the other hand, melting experiments on the system MgO-SiO_2 were carried out at pressures from 24 to 139 GPa in phase equilibrium studies in order to determine eutectic melting curves and examine eutectic compositions [6, 7]. Compared with DAC, MAA has remarkable advantages of larger sample volume under stable and homogenous temperature conditions (e.g. [8]). In this study, therefore, we are precisely determining the melting relations in the system $MgSiO_3$–SiO_2 at pressures between 5 and 25 GPa using the Kawai-type multi anvil apparatus; we would present the results obtained at 13 GPa in the presentation.

In the system $MgSiO_3$–SiO_2, SiO_2[M] values of eutectic point were 0.56 (1620 ºC) [9] and 0.60 (1920 ºC) [5] at 1 and 5 GPa, respectively, showing increase of SiO_2[M] with increasing temperature and pressure. In this study at 13 GPa, eutectic composition was 0.60 of SiO_2[M] at 2300 ºC, which is same as that at 5 GPa and showing systematic increase in eutectic temperature with increase of pressure. If source material of Earth is enstatite chondrite, therefore, composition of melts formed at magma ocean (up to ~3000 ºC and ~30GPa) in the early Earth show chemical homogeneity to ~400 km depth from the surface.

In this study, we also examined temperature effect on the experimental pressure up to 2500 ºC based on the phase boundary between stishovite–coesite (SiO_2), showing that the pressure at 2500 ºC was almost 3 GPa higher than that at room temperature. We conclude that this difference is caused by thermal expansion of specimens in the cell during heating.

References

[1] Bowen and Anderson (1914) Am. J. Sci. 4th ser. 37, 487-500.
[2] Ito and Katsura (1992) Am. Geophys. Union Monogr. 67, 315-322.
[3] Javoy et al. (2010) Earth Planet. Sci. Lett. 293, 259-268.

©2020. Japan Geoscience Union. All Right Reserved.

[4] Wasson and Kallemeyn (1988) Phil. Trans R. Soc. Lond. A325, 535-544.
[5] Dalton and Presnall, 1997 Dalton and Presnall (1997) Geochim. Cosmochim. Acta 61, 2367-2373.
[6] Baron et al. (2017) Earth Planet. Sci. Lett. 472, 186-196.
[7] Ozawa et al. (2018) Geophys. Res. Let. 10.1029/2018GL079313.
[8] Ito et al. (2007) Treatise on geophys. 2, 197-230.
[9]Hudon et al. (2005) J. Petrol. 46, 1859-1880.

Keywords: enstatite chondrite, melting relation, magma ocean, mantle differentiation, high pressures

©2020. Japan Geoscience Union. All Right Reserved.

[E] Poster | S (Solid Earth Sciences)：S-MP Mineralogy & Petrology

[S-MP37] Supercontinents and crustal evolution

convener:Madhusoodhan Satish-Kumar(Department of Geology, Faculty of Science, Niigata University), Krishnan Sajeev(Centre for Earth Sciences, Indian Institute of Science), Tomokazu Hokada(National Institute of Polar Research), Yasuhito Osanai(Division of Evolution of Earth Environments, Faculty of Social and Cultural Studies, Kyushu University)

Supercontinent formation and dispersion has been enigmatic in the Earth's history. Eurasia is one such current supercontinent and incredible progress in the understanding of its geological evolution has been achieved in the past decades. Earlier supercontinents in
the Earth's history such as Gondwana (0.5 Ga), Rodinia (1.0 Ga), Columbia/Nuna (2.0 Ga), Kenorland (2.5 Ga) and Vaalbara (3.1 Ga), have been the focus of several studies, however limited information on older supercontinents has restricted in understanding their tectonic evolution. Several important unsolved issues remain, such as how, when and where these supercontinents formed and how long they remained as such before breaking apart. Additional questions arise on the processes that triggered the fragmentation and unification of continents. In this session, we invite authors around the world to present original new
data as well as review results on the continental scale crustal processes and tectonic evolution that are associated with supercontinent formation events in Earth's history. The well-studied Eurasia and Gondwana supercontinents are of particular focus. Topics of interest include, but not restricted to, extremes in metamorphism, P-T-d-t evolution, magmatism, and the role of fluids. We hope to provide a platform for scientific discussions that will enlighten our understanding of the physical and chemical processes in the continental crust that records episodes of orogenesis that contributed to the formation and evolution of supercontinents.

[SMP37-P01] Subdivision of the Lützow-Holm Complex in East Antarctica

*Tomokazu Hokada[1,2], Daniel J. Dunkley[1], Kazuyuki Shiraishi[1,2], Yoshikuni Hiroi[3,1], Yoichi Motoyoshi[1,2] (1.National Institute of Polar Research, 2.The Graduate University for Advanced Studies, SOKENDAI, 3.Chiba University)

[SMP37-P02] Detrital zircon geochronology of the Limpopo Complex, southern Africa: Implications for Neoarchean to Paleoproterozoic collisional events

Taeko Uehara[1], *Toshiaki Tsunogae[1,2], Thembiso Otladisang Basupi[1], Yukiyasu Tsutsumi[3] (1.The University of Tsukuba, 2.University of Johannesburg, 3.National Museum of Nature and Science)

[SMP37-P03] Multiple sulfur isotope geochemistry of the Precambrian mafic dyke swarms in the Dharwar craton, South India.

*Silpa Ammini Sasidharan[1], Madhusoodhan Satish-Kumar[1] (1.Department of Geology, Faculty of Science, Niigata University)

[SMP37-P04] Signatures of poly-phase deformation and an upper amphibolite metamorphism from garnet bearing schists of Askot Klippe, Kumaun Himalayas

*Prakash Chandra Arya[1], Krishnan Sajeev[1] (1.Indian Institute of Science)

[SMP37-P05] Sr-Nd isotopic evidence for juvenile components and extensively reworked ancient crustal materials in the Vijayan Complex, Sri Lanka

*M A Sanjeewa P K Malaviarachchi[1], Madhusoodhan Satish-Kumar[2], Toshiro Takahashi[2] (1.Department of Geology, Faculty of Science, University of Peradeniya, Sri Lanka, 2.Department of Geology, Faculty of Science, Niigata University, Japan)

[SMP37-P06] Geochemical characteristics of mafic and felsic igneous rocks (1.9-1.75 Ga) in the Lesser Himalaya: Regional variation and its implications for tectonic setting

*Ryuichi Shinjo[1], Tomoki Amuro[1], Kohei Oura[1], Kazuya Oshiro[1], Shiro Tahara[1], Harutaka Sakai[2] (1.Department of Physics and Earth Sciences, University of the Ryukyus, 2.Department of Geology and Mineralogy, Kyoto University)

[SMP37-P07] A Tarim-North India connection in northern Gondwana related to final closure of the Proto-Tethys Ocean: Constraints from provenance of early Paleozoic sedimentary rocks in the Altyn Tagh orogen

*Qian Liu[1,2], Toshiaki Tsunogae[2,3], Guochun Zhao[4,5] (1.JSPS, 2.Tsukuba Univ. , 3.Johannesburg Univ. , 4.HKU, 5.Northwest Univ.)

[SMP37-P08] Native iron and serpentinization of peridotite, Oshika Village, Nagano Prefecture, Japan

*Yuya Takeda[1], Seiichiro Uehara[2] (1.Department of Earth and Planetary Science, Graduate School of Science, Kyushu University, 2.Department of Earth and Planetary Science, Faculty of Science, Kyushu University)

Subdivision of the Lützow-Holm Complex in East Antarctica

*Tomokazu Hokada[1,2], Daniel J. Dunkley[1], Kazuyuki Shiraishi[1,2], Yoshikuni Hiroi[3,1], Yoichi Motoyoshi[1,2]

1. National Institute of Polar Research, 2. The Graduate University for Advanced Studies, SOKENDAI, 3. Chiba University

Neoproterozoic to early Paleozoic geologic evolution of East Antarctica is key for understanding of the final amalgamation of Gondwana supercontinent. The Lützow-Holm Complex in eastern Dronning Maud Land of East Antarctica is located within the Neoproterozoic-Cambrian suture zones continuing from India through Sri Lanka. All these areas experienced high-grade metamorphism at ~600-520 Ma (e.g., Shiraishi et al., 2008).

In this presentation, we summarize the currently available U-Pb ages of this area (see Table and Figure attached in this abstract), and propose the subdivisions of the Lützow-Holm Complex based on the protolith ages as follows (from southwest to northeast);
- Inhovde Unit (INH; 1070-1040 Ma),
- Rundvag Unit (RVG; 2520-2470 Ma),
- Skallevik Unit (SKV; 1830-1790 Ma),
- Langhovde Unit (LHV; 1100-1050 Ma),
- East Ongul Unit (EOG; 630 Ma), and
- Akarui Unit (AKR; 970-750 Ma).

As discussed in Shiraishi et al. (2008), one important issue of this area is Cape Hinode that is geographically located within Akarui Unit of the Lützow-Holm Complex. The rocks in Cape Hinode experienced the high-grade metamorphism at ~960 Ma that is significantly older than the surrounding Lützow-Holm rocks (~600-520 Ma). Cape Hinode is, therefore, independent (exotic) to the surrounding Lützow-Holm Complex, and is defined as “Hinode Block”. The boundary between Hinode Block and the surrounding Akarui Unit of the Lützow-Holm Complex is not clear. Further study is required to interpret Kasumi Rock and Niban Iwa either belonging to Akarui Unit or Hinode Block.

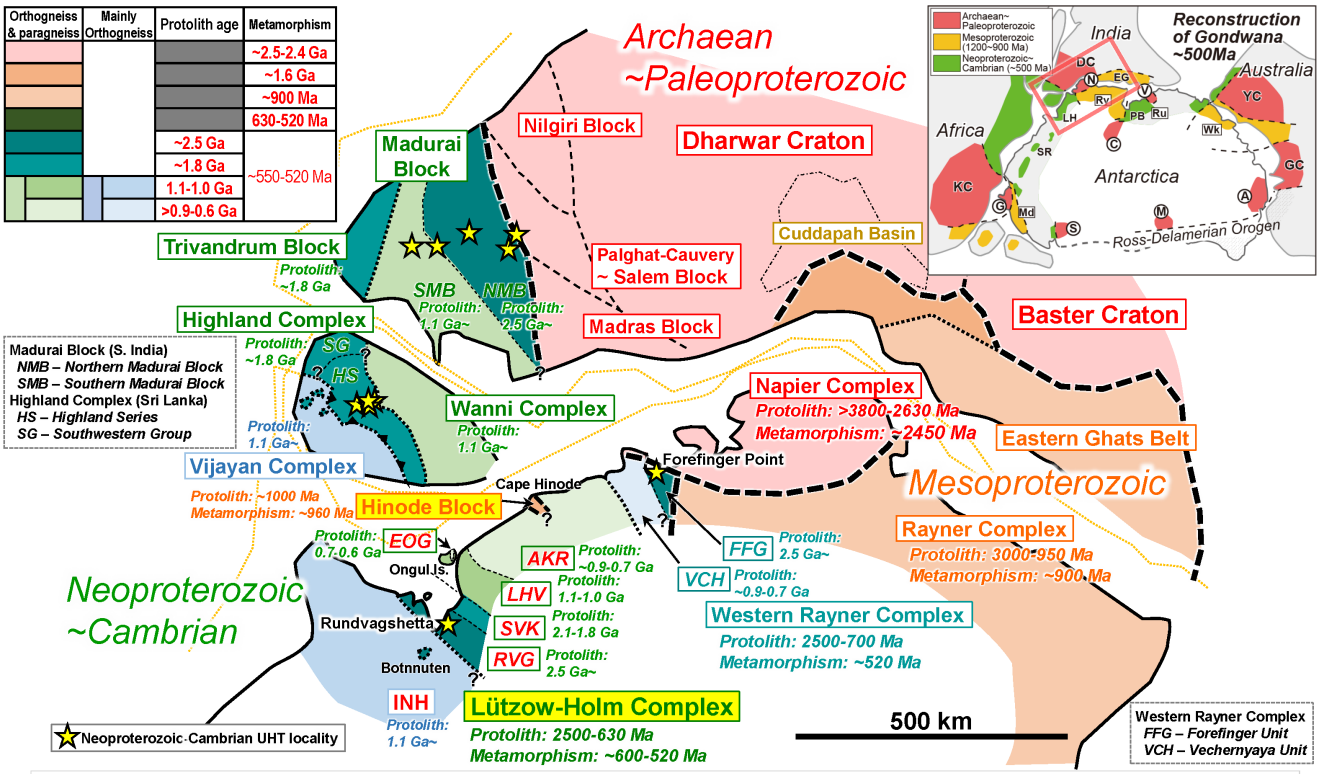
Although this presentation does not intend to do the correlation between Antarctica and Sri Lanka-India, the earlier correlation proposed by Shiraishi et al. (1994) requires only minor modification. Lithological and geochronological similarities imply some broad picture on the correlation among each geologic units in Antarctica, Sri Lanka and India (see Figure). For example, Botnnuten located in the southernmost part of the Lützow-Holm Complex is one isolated mountain exposed in the ice sheet, and is possibly klippe belonging to Rundvag Unit as like several isolated klippes (Highland Complex) located within the Vijayan Complex, Sri Lanka.

Figure: Regional geology, and the subdivision of the Lützow-Holm Complex.

Table: Summary of the published U-Pb ages for the Lützow-Holm Complex. Pink: metamorphic rocks (igneous origin), blue: metamorphic rocks (sedimentary origin), gray: intrusive rocks (syn/post-tectonic).

Keywords: East Antarctica, Lützow-Holm Complex, Gondwana, U-Pb age

©2020. Japan Geoscience Union. All Right Reserved.



Lützow-Holm Complex, Metamorphism >600-520 Ma, Protolith 2500-630 Ma (detrital 3300-630 Ma)

Skallevik Unit (SKV), Protolith 1850-1790 Ma (detrital 3300-1800? Ma)

Locality	Protolith	Protolith (igneous/detrital) age	Metamorphic age	rock type	Ref.
Telen	Igneous	2126, 1830+/-10	621+/-6, 600, 554	felsic gneiss	Th18
Telen	Dyke	1838, 554+/-7		metagranite dyke	D14
Telen(※)	Sedimentary	(2500-2000)	532+/-6	pelitic gneiss	S94-03
Telen	Sedimentary	3300-1800	571+/-4, 639+/-5	pelitic gneiss	D14
Skallen	Igneous	1795	675, 612-598	mafic granulite	Th18
Skallen (x4)	Sedimentary		650-580, 560-500	pelitic gneiss	H06
Skallevikshalsen (x7)	Igneous	2129, 1846, 1845, 1841, 1834, 1831	630-520, 595+/-9, 541+/-12	orthogneiss / charnockite	D14
Skallevikshalsen	Igneous	1785	617, 569+/-4, 531	felsic gneiss	Th18
Skallevikshalsen	Sedimentary	2800-1800	610-530, 538+/-4	pelitic gneiss	D14
Skallevikshalsen (x3)	Sedimentary		600-530, 576+/-9, 564+/-10	pelitic gneiss	D14
Skallevikshalsen	Sedimentary		595+/-11, 524+/-7	Grt-Sil gneiss	Kw16
Skallevikshalsen	Sedimentary	2796-1971	606-545	quartzite	Tm18
Skallevikshalsen	Dyke	1857	590-550	metagranite dyke	D14
Skallevikshalsen (x3)	Dyke	628, 608, 586	620-530	metadyke, pod. granite	D14

(※) this sample was probably inccorectly listed as "West Ongul" in Shiraishi et al., 1994, 2003

Rundvag Unit (RVG), Protolith 2520-2470 Ma (detrital 3200-2400? Ma)

Locality	Protolith	Protolith (igneous/detrital) age	Metamorphic age	rock type	Ref.
Sudare Rock	Igneous	2510+/-12		charnockite	D14
Sudare Rock	Igneous	(2510)	(550)	charnockite	T16
Sudare Rock	Sedimentary	(2290)	723, 637, 610, 586-507	pelitic gneiss	Tm18
Berrodden	Intrusive	534+/-5		granodiorite	D14
Rundvagshetta	Igneous	2518+/-24		felsic gneiss	D14
Rundvagshetta	Igneous	2501+/-9		charnockite	D14
Rundvagshetta	Igneous		555+/-3.5	felsic gneiss	T16
Rundvagshetta	Sedimentary	(2500-2300)	521+/-9	pelitic gneiss	S94-03
Rundvagshetta	Sedimentary		517+/-9	leucosome	F00
Rundvagshetta	Sedimentary	3200-2400	594+/-6, 540+/-9	quartzite	D14
Rundvagshetta	Sedimentary	3000-2400		pelitic gneiss	D14
Rundvagshetta	Sedimentary		619-486	quartzite	Tm18
Rundvagshetta	Dyke		534+/-7, 518+/-6	pyroxene vein	D14
Rundvagshetta	Intrusive	607+/-6	535+/-9	orthogneiss	D14
Vesleknausen	Igneous	2506+/-15	620-540	pyroxene granulite	T14
Vesleknausen	Igneous	(2490)	(550)	charnockite	T16
Botnnuten	Igneous	2472+/-20		charnockite	D14
Botnnuten	Sedimentary	2800-2400	590-550, 583+/-5	pelitic gneiss	D14
Botnnuten	Intrusive	587+/-3		metagranite	D14
Austhovde	Igneous		605, 551+/-7	charnockite	Th18
Austhovde	Igneous	2517, 2495, 1819+/-19	864, 722, 627+/-28	Bt gneiss	Th18
Austhovde	Sedimentary		533+/-9	pelitic gneiss	S94-03
Austhovde	Sedimentary	2632-2313	591, 587, 563	quartzite	Tm18
Austhovde	Dyke	(2519), 543-522		metagranite dyke	D14

Inhovde Unit (INH), Protolith 1070-1040 Ma

Locality	Protolith	Protolith (igneous/detrital) age	Metamorphic age	rock type	Ref.
Inhovde	Igneous	(1000)	550+/-12	Hbl-Bt gneiss	S94-03
Inhovde	Igneous	1065+/-17	565-518	orthogneiss	D14
Inhovde	Igneous	1041+/-23		orthogneiss	D14
Inhovde	Igneous	981+/-18	574+/-10	Hbl-Bt gneiss	T15
Inhovde	Intrusive	1084, 544+/-11		metagranite	D14
Inhovde	Intrusive	529+/-6		granite dyke	D14
Futatsu Iwa	Igneous	1071+/-26	551-516	orthogneiss	D14
Futatu-Iwa	Igneous	999+/-6		charnockite	T15

Langhovde Unit (LHV), Protolith 1100-1050 Ma (detrital 2100-1000? Ma)

Locality	Protolith	Protolith (igneous/detrital) age	Metamorphic age	rock type	Ref.
Langhovde	Sedimentary	1827, 1283-839	579-521	pelitic gneiss	Tm18
Skarvsnes	Igneous	1102+/-27		charnockite	D14
Skarvsnes	Igneous	1072+/-6		felsic gneiss	D14
Skarvsnes	Sedimentary	2100-1000	530	pelitic gneiss	D14
Kjuka	Igneous	1054+/-17		orthogneiss	D14
W. Ongul (x4)	Igneous	1096, 1084, 1069, 1060	550-520, 554+/-11, 552+/-4	orthogneiss	D14
W. Ongul	Sedimentary	1199-697	618, 555, 524	pelitic gneiss	Tm18
W. Ongul (※)	Sedimentary	1006+/-21	532+/-8	pelitic gneiss	S94-03
E. Ongul	Igneous	1058+/-12	540	orthogneiss	D14
E. Ongul	Sedimentary	1100-620	540	pelitic gneiss	D14

(※) this sample was probably inccorectly listed as "Telen" in Shiraishi et al., 1994, 2003

East Ongul Unit (EOG), Protolith 630 Ma (detrital 630 Ma)

Locality	Protolith	Protolith (igneous/detrital) age	Metamorphic age	rock type	Ref.
E. Ongul	Igneous	633+/-4	550-540	orthogneiss / charnockite	D14
E. Ongul	Igneous	630+/-4	580-540	orthogneiss / charnockite	D14
E. Ongul	Igneous	633+/-6	590, 548+/-4	orthogneiss / charnockite	D14
E. Ongul	Igneous	630, 587+/-5	580-530	orthogneiss / charnockite	D14
E. Ongul	Sedimentary	634+/-21	530	pelitic gneiss	D14

Akarui Unit (AKR), Protolith 970-750 Ma (detrital 2000-700? Ma)

Locality	Protolith	Protolith (igneous/detrital) age	Metamorphic age	rock type	Ref.
Sinnan Rocks	Sedimentary		553+/-6	pelitic gneiss	S94-03
Niban Iwa	Igneous	964, 940+/-6		orthogneiss	D14
Niban Iwa	Dyke	1100-900, 551+/-11		metagranite dyke	D14
Kasumi Rock	Igneous	984+/-7		Hbl-Bt gneiss	T15
Tenmondai Rock	Sedimentary	2018, 1627, 1468, 1141-701	608-528	pelitic gneiss	Tm18
Tenmondai	Dyke	581+/-7	540+/-7	sil dyke	D14
Akarui Point	Igneous	950-750 (847+/-8)		felsic orthogneiss	Kz16
Akarui Point	Sedimentary		518+/-12	pelitic gneiss	S94-03
Akarui Point	Sedimentary	1212-631	607-510	quartzite	Tm18
Tama Point	Igneous	965+/-8, 826+/-19	582+/-11	Hbl-Bt gneiss	T15

Metamorphic rock (igneous origin)
Metamorphic rock (sedimentary origin)
Intrusive rock (syn/post-tectonic)

References of U-Pb ages:
S94-03: Shiraishi et al., 1992, 1994, 2003, Polar Geosci., 16, 76-99.
F00: Fraser et al., 2000, J. Metamorphic Geol., 18, 441-454.
H06: Hokada & Motoyoshi, 2006, Polar Geosci., 19, 118-151.
D14: Dunkley et al., 2014, Abst. 7th SHRIMP Workshop, 116-121.
T14: Tsunogae et al., 2014, Geosci. Frontiers, 5, 167-182.
T15: Tsunogae et al., 2015, Precamb. Res., 266, 467-489.
Kw16: Kawakami et al., 2016, J. Min. Petr. Sci., 111, 129-143.
Kz16: Kazami et al., 2016, J. Asian Earth Sci., 130, 206-222.
T16: Tsunogae et al., 2016, Lithos, 263, 239-256.
Tm18: Takamura et al., 2018, Geosci. Frontiers, 9, 355-375.
Th18: Takahashi et al., 2018, J. Asian Earth Sci., 157, 245-268.

Hinode Block, Metamorphism 970-960 Ma, Protolith 1020 Ma (detrital 3300-1000? Ma)

Locality	Protolith	Protolith (igneous/detrital) age	Metamorphic age	rock type	Ref.
Cape Hinode	Igneous	1017+/-13		metatrondjemite	S94-03
Cape Hinode	Igneous	1020+/-7	960	metatrondjemite	D14
Cape Hinode	Sedimentary	3300-1000	970	pelitic gneiss	D14

©2020. Japan Geoscience Union. All Right Reserved.

Detrital zircon geochronology of the Limpopo Complex, southern Africa: Implications for Neoarchean to Paleoproterozoic collisional events

Taeko Uehara[1], *Toshiaki Tsunogae[1,2], Thembiso Otladisang Basupi[1], Yukiyasu Tsutsumi[3]

1. The University of Tsukuba, 2. University of Johannesburg, 3. National Museum of Nature and Science

We report new detrital zircon ages of quartzites from the Central Zone of the Limpopo Complex, which corresponds to the collisional suture within the Kalahari Craton. The Central Zone has been subdivided into several units: Beit Bridge Complex, Phikwe Complex, and Motloutse Complex. The Beit Bridge Complex occupies the dominant part of the Central Zone in Zimbabwe and South Africa, and is composed of supracrustal rocks including pelitic gneiss, meta-BIF, marble, quartzite, and metabasites that underwent high- to ultrahigh-temperature metamorphism (e.g., Tsunogae and van Reenen, 2011). Cores of detrital zircons from quartzites show magmatic ages of 3.6-3.0 Ga, suggesting that the zircons were probably derived from proximal sources such as the basement gneisses in the Zimbabwe Craton and the Kaapvaal Craton. The ages are also comparable with the inferred collision age of the Zimbabwe and Kaapvaal Cratons (ca. 2.7 Ga), suggesting that the quartzites deposited between 3.0 and 2.7 Ga.

In contrast, detrital zircon ages of the Phikwe and Motloutse Complexes in Botswana are significantly younger (2.9-2.4 Ga), suggesting that the quartzites from the complexes deposited after 2.4 Ga. Therefore, although Beit Bridge, Phikwe, and Motloutse Complexes are correlated based on the occurrence of similar supracrustal lithologies, the quartzites in the Botswanan side of the Central Zone might have formed after the Neoarchean “Limpopo Orogeny”. The timings of protolith formation and high-grade metamorphism in the Phikwe and Motloutse Complexes could be related to the Magondi Orogeny that affected the western part of the Zimbabwe Craton at ca. 2.0 Ga.

References

Tsunogae, T. and van Reenen, D.D. (2011) High-pressure and ultrahigh-temperature granulite-facies metamorphism of Precambrian high-grade terranes: Case study of the Limpopo Complex. Geological Society of America Memoir, 207, 107-124.

Keywords: Limpopo Complex, detrital zircon geochronology, metamorphism, Magondi Belt

©2020. Japan Geoscience Union. All Right Reserved.

Multiple sulfur isotope geochemistry of the Precambrian mafic dyke swarms in the Dharwar craton, South India.

*Silpa Ammini Sasidharan[1], Madhusoodhan Satish-Kumar[1]

1. Department of Geology, Faculty of Science, Niigata University

Archean rock units are perfect tracers of various events occurred in the early Earth systems. The records of the anoxic atmosphere in the Archean and the interaction of the lithosphere-hydrosphere and atmosphere has been recorded in these units as Mass Independent Fractionation (MIF) of sulfur isotopes until about 2.4 Ga. The recycling of these Archean materials in the mantle leads to the occurrence of sulfur isotopic composition with Mass independent fractionation in the mantle-derived rocks. However, isotope fractionation can also occur in high-temperature high-pressure conditions, possibly associated with deep mantle dynamics. As per the cosmochemical records, a prime share of the Earth’s sulfur is present at the core [1]. This implies that the magma reservoirs in the deep mantle should also have fractionated sulfur isotopes although it has been considered to have chondritic sulfur isotopic ratio. In the mantle, sulfur is found predominantly in the form of sulfides [2]. Significant equilibrium isotopic fractionation occurs in the deep Earth under the higher pressure-temperature conditions, however, recently recycling of surface sulfur has been considered as well using multiple sulfur isotope signatures [3].
In the current study, the mafic dyke swarms in the Dharwar craton are considered. A detailed geochemical characterization of the dykes were carried out, including Sr and Nd isotopic composition. The results indicate a prominent enriched mantle component in younger paleoproterozoic dykes, whereas older Archean dykes preserve primitive mantle signatures [4]. Reconnaissance analysis of representative dyke of various ages have been carried out for the multiple sulfur ($\delta^{34}S$, $\Delta^{33}S$ and $\Delta^{36}S$) isotope composition. $\delta^{34}S$ for all the samples were negative, whereas $\Delta^{33}S$ and $\Delta^{36}S$ shows only nominal, but distinct variations. The samples are showing a scattered distribution in the variation diagrams of both $\delta^{34}S$ versus $\Delta^{33}S$ and $\Delta^{33}S$ versus $\Delta^{36}S$ and are suggesting a mantle signature in most cases. The distribution of the multiple sulfur isotope and their relative abundances in the form of $\Delta^{33}S$, $\delta^{34}S$, and $\Delta^{36}S$ leads to a better understanding of the Archean sulfur reservoirs and the possible isotopic fractionation in the deep earth. Further detailed studies are ongoing, and we present a comprehensive evaluation of recycling vs. mantle components in the Archean to Paleoproterozoic lithospheric mantle beneath the Dharwar craton.

References

[1] Sakai, H., Marais, D., Ueda, A. and Moore, J., 1984. Concentrations and isotope ratios of carbon, nitrogen and sulfur in ocean-floor basalts. Geochim. Cosmochim Acta, 48, 2433-2441.
[2] Dreibus, G. and Palme. H. 1996. Cosmochemical constraints on the sulfur content in the Earth’s core. Geochim. Cosmochim. Acta, 60 (7), pp. 1125-1130.
[3] Farquhar, J. and Jackson, M. 2016. Missing Archean sulfur returned from the mantle. PNAS, 113, 12893-12895.
[4] Silpa, A.S. and Satish-Kumar, M. 2018. Dyke Swarms in the Dharwar Craton: A Key to Understanding the Late Archean to Early Proterozoic Cratonic Correlations. J. Indian Inst. Sci., 98(4), 365-378.

Keywords: Archean, Sulfur isotopes, Mafic dyke swarms, Mass Independent Fractionation (MIF)

©2020. Japan Geoscience Union. All Right Reserved.

©2020. Japan Geoscience Union. All Right Reserved.

Signatures of poly-phase deformation and an upper amphibolite metamorphism from garnet bearing schists of Askot Klippe, Kumaun Himalayas

*Prakash Chandra Arya[1], Krishnan Sajeev[1]

1. Indian Institute of Science

Askot klippe, a detached mass from the main crystallines of the Himalayas, lies in the lesser Himalayan sedimentary zone of the eastern Kumaun Himalayas, it is known for its occurrence of polymetallic mineralization within the schist and gneisses. The present work is focused on microtextural studies and computation of the thermal gradients of the garnet bearing schists of Askot klippe, these schists preserves signatures of poly phase deformation in their microstructure related to tectonic transportation and deformational histories of Himalayan orogeny. The micro-texture of these schists shows three distinct stages of deformation (D1, D2, and D3) with syn-tectonic garnet growth. The Thermal gradients have been computed by using Fe-Mg exchange between garnet and biotite. The X_{Mg} values for garnet and biotite are X_{Mg} (grt) ~ 0.06 and X_{Mg} (bt) ~ 0.85 respectively. The computed temperatures (~590 ^{o}C) suggests that the garnet bearing schists of Askot klippe has undergone a peak metamorphic conditions upto upper amphibolite facies.

Keywords: Kumaun Himalayas, klippe, geothermobarometry

©2020. Japan Geoscience Union. All Right Reserved.

Sr-Nd isotopic evidence for juvenile components and extensively reworked ancient crustal materials in the Vijayan Complex, Sri Lanka

*M A Sanjeewa P K Malaviarachchi[1], Madhusoodhan Satish-Kumar[2], Toshiro Takahashi[2]

1. Department of Geology, Faculty of Science, University of Peradeniya, Sri Lanka, 2. Department of Geology, Faculty of Science, Niigata University, Japan

The Vijayan Complex (VC) of Sri Lanka comprises a significantly large volume of calc-alkaline amphibolitic and granitic orthogneises (biotite gneiss, hornblende-biotite gneiss and granitoids) of ages known as ~1-1.1 Ga. A considerable volume of basic and felsic to intermediate magmatic intrusions also occur concordant with the main amphibolitic-granitic suite. In the present study, we present major and trace elements and Sr-Nd isotope systematics of a range of orthogneisses from the Vijayan Complex of Sri Lanka. Two groups of samples were recognized geochemically; (1) rocks having OIB-like trace and rare earth element composition with less-radiogenic 87Sr/86Sr isotope ratios (Depleted Group) and (2) rocks having MORB-like composition with extremely high-radiogenic 87Sr/86Sr ratios (Enriched Group). The majority of the samples in both groups show depleted mantle-model ages (TDM) in the range of 1.4-3.3 Ga, which is considerably older than the published magmatic crystallization age (~1 Ga) of the VC. High and variable Sr initials and negative epsilon Nd values of > +4 are compatible with their derivation by melting of older basement rocks with a long crustal residence history. The rest of the samples have model ages in the range of 0.9-1.1 Ga, nearly-coeval with the crystallization age of the VC, indicating their separation from the mantle as juvenile inputs. Therefore, protolith sources of the majority of these rocks could be mixtures of distinctive components formed much earlier than the time of predominant magmatism (~1 Ga) in the VC. Hence, we envisage that the VC constitutes a collage of juvenile components and extensively reworked ancient crustal materials in variable proportions within the main amphibolitic-granitic suite.
Acknowledgement: First Author acknowledges the visiting fellowship offered by the Niigata University (2017-2018) for promotion of International Collaborative Research

Keywords: Sr-Nd isotopes, Juvenile vs. recycled, Vijayan Complex

©2020. Japan Geoscience Union. All Right Reserved.

Geochemical characteristics of mafic and felsic igneous rocks (1.9-1.75 Ga) in the Lesser Himalaya: Regional variation and its implications for tectonic setting

*Ryuichi Shinjo[1], Tomoki Amuro[1], Kohei Oura[1], Kazuya Oshiro[1], Shiro Tahara[1], Harutaka Sakai[2]

1. Department of Physics and Earth Sciences, University of the Ryukyus, 2. Department of Geology and Mineralogy, Kyoto University

The major and trace element and Nd-Hf isotopic compositions of Proterozoic meta-igneous rocks from the lower part of Lesser Himalayan sequence provide insights into the nature of their source mantle and its tectonic setting. We observed bimodal (basaltic and rhyolitic) magmatic feature in these rocks; this type of volcanism generally occurs in areas of extensional tectonics, particularly rifts. Two types of mafic rocks are identified: within-plate-type (OIB or more specially E-MORB like) rocks and Nb-Ta-depleted, continental arc like rocks. Within-plate type mafic rocks are dominated in the eastern Nepal, but similar rocks are also found in the western Nepal. Although models for the tectonic setting of these igneous rocks remain controversial (e.g., passive margin, continental arc, continental rift with possible hotspot), our new geochemical data supports the rift model associated with mantle plume activity, which evolved to the passive margin. The Nb-Ta depleted, arc-like rocks have lower eNd (t) and eHf (t) than within-plate type rocks; we consider that this type of magmas formed by interaction of mantle-derived magmas with crustal components. The felsic rocks have similar or slightly lower eNd (t) and eHf (t) values relative to arc-like mafic rocks, suggesting relatively limited crustal interaction. They are derived from juvenile crust of underplated mafic magmas. Most of felsic rocks have remarkably low Nb/Ta ratios (<5), suggesting modification on their chemical composition by intensive sub-solidus magmatic-hydrothermal alteration.

Keywords: Lesser Himalaya, Kuncha Formation, tectonic setting

©2020. Japan Geoscience Union. All Right Reserved.

A Tarim-North India connection in northern Gondwana related to final closure of the Proto-Tethys Ocean: Constraints from provenance of early Paleozoic sedimentary rocks in the Altyn Tagh orogen

*Qian Liu[1,2], Toshiaki Tsunogae[2,3], Guochun Zhao[4,5]

1. JSPS, 2. Tsukuba Univ. , 3. Johannesburg Univ. , 4. HKU, 5. Northwest Univ.

Evolution of the northern margin of Gondwana, especially to the north of India and Australia, remains enigmatic. The primary reason for this enigma is complex amalgamation of northern Gondwana involving a wealth of present-day East Asian blocks associated with consumption and closure of the Proto-Tethys Ocean during early Paleozoic time. Compared to considerable progress on configuration of some other Asian blocks in northern Gondwana (e.g., South China, North China, and Lhasa, etc.), much controversy still concerns when and where the Tarim craton was amalgamated with northern Gondwana due to final closure of the North and South Altyn Oceans (two branches of the Proto-Tethys Ocean between southeastern Tarim and northern Gondwana).

Provenance tracing of sedimentary rocks based on detrital zircon U-Pb-Hf isotopes has been widely applied to constrain paleotectonic relationships among major tectonic units. This forms the justification of this study, which focused on systematic field-based zircon U-Pb dating and Hf isotopic analyses for early Paleozoic sedimentary rocks in the Altyn Tagh orogen, southeastern Tarim. New dating results reveal depositional ages from ca. 494 to 426 Ma. Provenance tracing indicates the ca. 494-477 Ma samples dominantly sourced from local Altyn Tagh to the south of the North Altyn Ocean, whereas an augmented supply of detritus from Tarim to the north of the North Altyn Ocean characterizes the ca. 465-449 Ma samples based on remarkable increase of ca. 840-780 Ma, 2.0-1.7 Ga, and 2.7-2.4 Ga detrital zircons. This change indicates a major provenance shift from a single to multiple source regions between ca. 477 and 465 Ma, marking the timing of final closure of the North Altyn Ocean. Zircon U-Pb-Hf isotopic data from the ca. 444-426 Ma samples resemble those from the ca. 465-449 Ma samples, suggesting local sediment recycling related to a post-collisional regime. Together with ophiolitic, (ultra)high-pressure metamorphic, and magmatic records in the region, final closure of the North Altyn Ocean can be constrained to occur in the Middle Ordovician, slightly later than final closure of the South Altyn Ocean during latest Cambrian-Early Ordovician time. Considering the other branches of the Proto-Tethys Ocean, we infer that the entire Proto-Tethys Ocean might have been progressively closed at ca. 500-420 Ma, leading to amalgamation of most East Asian blocks with northern Gondwana. Detrital zircon U-Pb-Hf isotopic comparison indicates that Tarim shares a closer affinity to North India than to other tectonic units located further to the east of Australia or west of Arabia-Iran along the northern margin of Gondwana. This work would be a significant contribution towards understanding configuration of Gondwana associated with evolution of the Proto-Tethys Ocean.

This study was financially supported by a National Natural Science Foundation of China Project (grant 41730213), a Grant-in-Aid for Scientific Research from Japan Society for the Promotion of Science (JSPS) to Dr. Qian Liu (No. 19F19020), and a Hong Kong Research Grants Council General Research Fund (grant 17307918). JSPS International Research Fellowship is also much appreciated.

Keywords: Provenance tracing, Early Paleozoic, Tarim, Northern Gondwana

©2020. Japan Geoscience Union. All Right Reserved.

©2020. Japan Geoscience Union. All Right Reserved.

Native iron and serpentinization of peridotite, Oshika Village, Nagano Prefecture, Japan

*Yuya Takeda[1], Seiichiro Uehara[2]

1. Department of Earth and Planetary Science, Graduate School of Science, Kyushu University, 2. Department of Earth and Planetary Science, Faculty of Science, Kyushu University

Serpentinization is a reaction to form serpentine from peridotite and hot water, and Fe^{2+} becomes Fe^{3+} since magnetite is formed from Fe^{2+} in forsterite. At that time, hydrogen is generated, and a more reducing environment is formed iron, awaruite (Ni_2Fe-Ni_3Fe) (Frost, 1985).
Peridotite in Oshika Village, Shimoina-gun Nagano Prefecture is located mainly in Irisawai and Ogawara, and iron formed by serpentinization is reported for the first time in Japan (Okamoto et al., 1981; Sakai & Kuroda, 1983). Serpentine veins have three stages. Iron is found in veins composed chrysotile-2M_{c1} and brucite in the 2nd stage of serpentine veins. In this study, the peculiar serpentine vein was reexamined for the purpose of the elucidation of the formation of iron and awaruite.
Obtained samples were analysed by powder X-ray diffraction (XRD) to determine the constituent serpentine species.The selected samples were analyzed by optical microscope, scanning electron microscope (SEM) with energy dispersive spectrometer (EDS), electron microprobe analyzer (EPMA) and transmission electron microscope (TEM). Experimental devices was Ultima IV and Rint Rapid II (XRD), JSM-7001 (SEM), JMS-8530FF (EPMA). TEM observation was carried out at 300kV using JEM 3200FSK at the Ultramicroscopy Research Center at Kyushu university.
The peridotite is composed of forsterite and chromite, linear serpentine veins ranging from a few cm to 10 of μm in width. There were up to 4 directions of the vein. Serpentinization was made to be 4 stages from the anteroposterior relation of the vein by the observation by the slice. The vein of these 4 stages was made to be serpentine veins I, II, III, IV from the early one. The serpentine veins consisted lizardite, chrysotile-2M_{c1}, brucite, magnetite, iron, and awaruite. The serpentine veins are characterized in Table 1. Serpentine vein IV have elliptical and striated areas rich in brucite. Iron has irregular shapes, and some change to magnetite. Awaruite is a minute crystal, and it is unevenly distributed in the vein. The chemical compositions of serpentine and brucite in the veins were measured by SEM-EDS, and #Mg=Mg/ (Mg + Fe) was obtained. The serpentine of veins I and II was #Mg=0.94, that of veins III and IV was #Mg=0.96, and that of brucite was #Mg=0.66~0.79 0.77~0.86.
Iron is in serpentine veins III and IV, ranging in size from 1 μm to 100 μm, and contains up to 3.2% Ni and 3.1% Co. Iron of serpentine vein III was arranged in the position in which the long axis of the ellipse was perpendicular to the serpentine vein, and the iron of serpentine vein IV was irregularly shaped. Native iron was also found in the serpentine veins, which were not linear. Awaruite is found in all serpentine veins and most of them are in the range of 50 nm to several 100 nm, and many of them are automorphic crystal. Awaruite consists of $Ni_{0.79}Fe$ to $Ni_{2.55}Fe$ and is rich in iron.

Keywords: serpentinization, iron

©2020. Japan Geoscience Union. All Right Reserved.

表1 蛇紋石脈の特徴

	蛇紋石脈Ⅰ	蛇紋石脈Ⅱ	蛇紋石脈Ⅲ	蛇紋石脈Ⅳ
脈の幅	2，3 ㎜～ 数100 ㎛	2，3 ㎜～ 数100 ㎛	10 ㎛～ 100 ㎛	200 ㎛～ 300 ㎛
脈の色	黒（肉眼） 黒褐色（薄片）	緑黒色（肉眼） 褐色（薄片）	灰緑色（肉眼） 白色（薄片）	緑褐色（肉眼） 褐色＋白色（薄片）
蛇紋石の＃Mg	0.94	0.94	0.96	0.96
ブルース石の＃Mg	0.66～0.79	0.66～0.79	0.77～0.86	0.77～0.86
自然鉄	無し	無し	1～100 ㎛ 楕円形をしている。	不規則な形
アワルワ鉱	50～数100 ㎚少量	50～100 ㎚の結晶が全体的に多く含む	50～数100 ㎚ 脈の中心と縁に見られる。	部分的に小さい結晶が集まっている。
磁鉄鉱	ほとんど見られない	不規則な形	自然鉄の自体が磁鉄鉱化している	不規則な形をしたものが多く見られる。

Table 1. The characteristics of serpentine vein

serpentine vein	Ⅰ	Ⅱ	Ⅲ	Ⅳ
Vein width	2，3 ㎜～ several 100 ㎛	2，3 ㎜～ several 100 ㎛	10 ㎛～ 100 ㎛	200 ㎛～ 300 ㎛
Vein color (naked eye) (flakes)	black dark brown	green-brack brown	grayish green colorless	green brown brown and colorless
＃Mg of serpentine	0.94	0.94	0.96	0.96
＃Mg of blucite	0.66～0.79	0.66～0.79	0.77～0.86	0.77～0.86
Iron	none	none	1～100 ㎛ elliptical shape	irregularly shape
Awaruite	50～several 100 ㎚ Small amount	50～100 ㎚	50～several 100 ㎚	Small crystals are unevenly distributed.
Magnetite	Small amount	irregularly shape	Iron are surrounded by magnetite.	irregularly shape

©2020. Japan Geoscience Union. All Right Reserved.

[E] Poster | S (Solid Earth Sciences)：S-MP Mineralogy & Petrology

[S-MP38] Deformed rocks, Metamorphic rocks and Tectonics

convener:Yoshihiro Nakamura(Geological Survey of Japan, National Institute of Advanced Industrial Science and Technology), Yumiko Harigane(Geological Survey of Japan, National Institute of Advanced Industrial Science and Technology (AIST))

We invite all researchers who aim to understand the dynamics of the earth's crust and mantle at the plate boundaries, to discuss the latest results from various viewpoints. The scope will include contributions through petrology and structural geology as well as various techniques including rheology and transformation of heat and mass.

[SMP38-P01] Metamorphism and geochronology of garnet amphibolite from the Beishan Orogen, southern Central Asian Orogenic Belt: Constraints from P-T path and zircon U-Pb dating

*Wenbin Kang[1], Wei Li[1] (1.State Key Laboratory of Continental Dynamics, Department of Geology, Northwest University, Xi'an 710069, China)

[SMP38-P02] Field evidence and mineral assemblage of eclogite from the Khungui zone, Zavkhan terrane, Western Mongolia

*Manzshir Bayarbold[1], Atsushi Okamoto[1], OTGONBAYAR DANDAR[1], Masaoki Uno[1], Noriyoshi Tsuchiya[1] (1.Graduate School of Environmental Studies, Tohoku University)

[SMP38-P03] Eclogite-to-granulite transition in the Ufipa Complex (Tanzania): Pressure—Temperature—time paths of a Pan-African continental collision zone

*Morita Isamu[1], Tatsuki Tsujimori[1], Nelson Boniface[2], Kennet E Flores[3], Shogo Aoki[4], Kazumasa Aoki[4] (1.Tohoku University, 2.University of Dar es Salaam, 3.Brooklyn College of the City University of New York, 4.Okayama University of Science)

[SMP38-P04] **Geochemistry, Pressure-Temperature conditions and tectonic setting of the amphibolite from the southern part of Motloutse Complex, eastern Botswana**

*Thembiso Otladisang Basupi[1], Toshiaki Tsunogae (1.Graduate of Life and Environmental Sciences, University of Tsukuba)

[SMP38-P05] **Crystal Preferred Orientation Development of Secondary Olivine Formed by Hydration of Orthopyroxene: Implication to Anisotropy of Shallow Mantle Wedge during Initiation Stage of Subduction**

*OTGONBAYAR DANDAR[1], Atsushi Okamoto[1], Takayoshi Nagaya[2], Masaoki Uno[1], Noriyoshi Tsuchiya[1] (1.Graduate School of Environmental Studies, Tohoku University, 2.Graduate School of Science, University of Tokyo)

[SMP38-P07] **Crustal fracturing and brecciation processes in middle crust associated with granitoid intrusions in Sør Rondane Mountains, East Antarctica**

*Tatsuya Takemori[1], Masaoki Uno[1], SATISH KUMAR[2], Noriyoshi Tsuchiya[1], Atsushi Okamoto[1] (1.Tohoku University, 2.Niigata University)

[SMP38-P08] Multiple timings of high-grade garnet-forming metamorphism from Sør Rondane Mountains, East Antarctica

*Fumiko Higashino[1], Tetsuo Kawakami[2], Shuhei Sakata[3], Takafumi Hirata[3] (1.Faculty of Science, Okayama University of Science, 2.Kyoto University, 3.The University of Tokyo)

[SMP38-P09] **Thermal modeling for "Hot-on-cold" thrusting: Thermal structure during orogenic movement at the western boundary of Eastern Ghats Belt, India**

*Fumihiko Sato[1], Tomoeki Nakakuki[1], Kaushik Das[1] (1.Hiroshima University)

[SMP38-P10] Fluid-rock interaction and formation of high-grade metamorphic rocks in the Trivandrum Block, southern India

*Nishi Ayumi[1] (1.Faculty of Life and Environmental Sciences, University of Tsukuba)

[SMP38-P11] Structural geology of Hidaka Metamorphic Belt in the Mt.Nozuka and Mt.Rakko area, Hokkaido,JAPAN -Growth process and mechanism of the Cenozoic continental crust-

*Moeko Kanno[1], Tsuyoshi Toyoshima[2], Hayato Ueda[2] (1.Graduate school of Science and Technology, Environmental Science and Technology,Earth science, 2.Niigata University, Faculty of Science,Department Geology)

[SMP38-P13] **Raman carbonaceous material thermometry applied to mapping the thermal structure of contact metamorphic domains in the Hongusan area, central Japan incorporating the effects of widespread detrital carbonaceous material**

*Ken Yamaoka[1], Simon Richard Wallis[1], Akira Miyake[2], Yui Kouketsu[3] (1.The University of Tokyo, 2.Aichi University of Education, 3.Nagoya University)

[SMP38-P14] Raman parameters of carbonaceous material estimated from fully-automatic spectral fitting method and their relation to vitrinite reflectance

*Shunya Kaneki[1], Yoshihiro Nakamura[2], Yui Kouketsu[3], Hideki Mukoyoshi[4] (1.Disaster Prevention Research Institute, Kyoto University, 2.Geological Survey of Japan, National Institute of Advancecd Industrial Science and Technology, 3.Graduate School of Environmental Studies, Nagoya University, 4.Graduate School of Science and Engineering, Shimane University)

[SMP38-P15] Raman spectroscopy of quartz eclogite in the Sanbagawa metamorphic belt: Potential of Raman geobarometry using kyanite-quartz system

*Yuki Tomioka[1], Yui Kouketsu[1], Tomoki Taguchi[2] (1.Nagoya University, 2.Kyoto University)

[SMP38-P16] The R.G. Coleman Cazadero Collection: A preliminary sample description for systematic curation

*Oka Hiroki[1], Tatsuki Tsujimori[1] (1.Tohoku University)

[SMP38-P17] The Microstructure and Composition of Picrolitic Antigorite Veins in Serpentinites from the High-P Metamorphic Yuli Belt in Eastern Taiwan

*Ilona Talvikki Sakaguchi[1], Yui Kouketsu[1], Chin-Ho Tsai[2], Dominikus Deka Dewangga [2], Katsuyoshi Michibayashi[1] (1.Nagoya University, 2.National Dong Hwa University)

[SMP38-P18] Estimation of P-T history of amphibolite tectonic blocks in serpentinite mélange of Kamuikotan metamorphic rocks

*Yuto Kimura[1], Toru Takeshita[1] (1.Department of Natural History Sciences, Graduate School of Science, Hokkaido University)

[SMP38-P19] Datolite in the high-pressure marble from the Eastern Iratsu body of the Sanbagawa metamorphic belt

*Kenta Yoshida[1], Sota Niki[2], Hikaru Sawada[1,2], Ryosuke Oyanagi[1] (1.Japan Agency for Marine-earth Science and Technology, 2.Geochemical Research Center, The University of Tokyo)

[SMP38-P20] The occurrence of jadeite in the ultramafic body discovered in the Sanbagawa belt, Shibukawa region, central Japan

*Hikaru Shioya[1], Katsuyoshi Michibayashi[1], Yui Kouketsu[1], Masaki Enami[1] (1.Nagoya University)

[SMP38-P21] Geochronology of the Yorii metamorphic rocks on the Kanto Mountains - Extension of the Abukuma metamorphic rocks to Southwest Japan.

Shota Matsunaga [2], *Atsushi MIYASHITA[1], Tatsuki Tsujimori[2], Kazumasa Aoki[3], Shogo Aoki[3] (1.Seikei University, 2.Tohoku University, 3.Okayama University of Science)

[SMP38-P22] Geology, deformation, and metamorphism of high-grade Shimanto accretionary complex in Kerama Islands, Okinawa, Ryukyu arc

*Ippei Yamamoto[1], Kenichiro Tani[2], Yui Kouketsu[3], Rina Fukuchi[1], Hiroaki Koge[4], Asuka Yamaguchi[1] (1.Atmosphere and Ocean Research Institute, The University of Tokyo, 2.National Museum of Nature and Science, 3.Nagoya University, 4.National Institute of Advanced Industrial Science and Technology)

Metamorphism and geochronology of garnet amphibolite from the Beishan Orogen, southern Central Asian Orogenic Belt: Constraints from P-T path and zircon U-Pb dating

*Wenbin Kang[1], Wei Li[1]

1. State Key Laboratory of Continental Dynamics, Department of Geology, Northwest University, Xi'an 710069, China

Numerous lenses of garnet amphibolite occur in the garnet-bearing biotite-plagioclase gneiss belt in the Baishan area of the Beishan Orogen, which connects the Tianshan Orogen to the west and the Mongolia-Xing'an ling Orogen to the east. The study of metamorphism in Beishan area is of great significance to explain the tectonic evolution of Beishan orogen. According to the microstructures, mineral relationships, and geothermobarometry, we identifed four stages of mineral assemblages from the garnet amphibolite sample: (1) a pre-peak stage, which is recorded by the cores of garnet together with core-inclusions of plagioclase (Pl_1); (2) a peak stage, which is recorded by the mantles of garnet together with mantle-inclusions of plagioclase (Pl_2) + amphibole (Amp_1) + Ilmenite (Ilm_1) + biotite (Bt_1), developed at temperature-pressure (P-T) conditions of 818.9–836.5 ˚C and 7.3–9.2 kbar; (3) a retrograde stage, which is recorded by garnet rims + plagioclase (Pl_3) + amphibole (Amp_2) + orthopyroxene (Opx_1) + biotite (Bt_2) + Ilmenite (Ilm_2), developed at P-T conditions of 796.1–836.9 ˚C and 5.6–7.5 kbar; (4) a symplectitic stage, which is recorded by plagioclase (Pl_4) + orthopyroxene (Opx_2) + amphibole (Amp_3) + biotite (Bt_3) symplectites, developed at P-T conditions of 732 ±59.6 ˚C and 6.1 ±0.6 kbar. Moreover, the U-Pb dating of the Beishan garnet amphibolite indicates an age of 301.9 ±4.7 Ma for the protolith and 281.4 ±8.5 Ma for the peak metamorphic age. Therefore, the mineral assemblage, P-T conditions, and zircon U-Pb ages of the Beishan garnet amphibolite defne a near-isothermal decompression of a clockwise P-T-t (Pressure-temperature-time) path, indicating the presence of over thickened continental crust in the Huaniushan arc until the Early Permian, then the southern Beishan area underwent a process of thinning of the continental crust.

Keywords: Beishan Orogen, Garnet amphibolite, P-T-t path, Zircon U-Pb dating

©2020. Japan Geoscience Union. All Right Reserved.

Field evidence and mineral assemblage of eclogite from the Khungui zone, Zavkhan terrane, Western Mongolia

*Manzshir Bayarbold[1], Atsushi Okamoto[1], OTGONBAYAR DANDAR[1], Masaoki Uno[1], Noriyoshi Tsuchiya[1]

1. Graduate School of Environmental Studies, Tohoku University

Eclogite and blueschist complexes are the most important indicators of the tectonic evolution of the folded system such as the Central Asian Orogenic belt (CAOB), the largest orogenic belt in the world. One of the most important features of the CAOB is a widespread occurrence of high pressure (HP) and ultrahigh pressure (UHP) eclogites and blueschist facies rocks in many tectonic belts. The UHP-HP rocks related to the mostly ophiolite sequences, show the suture zone between Paleo Asian-ocean and small cratons. These suture zones are represented by Muya in eastern Siberia, Gorni Altai in southern Siberia, Northern Mongolia, Kokechetav in Central Kazakhstan, Chandman in western Mongolia. However, relationship between these occurrences is still unclear. In addition, only one occurrence of the HP rocks has been reported in Mongolia (Chandman). Therefore, in order to constrain tectonic evolution of Paleo Asian-ocean (PAO), it is important to study UHP-HP rocks in CAOB. In this study, we investigated occurrences and petrology of eclogite, and amphibolite in the Khungui zone, Zavkhan terrane, western Mongolia, and discuss its metamorphic evolution and significance in the CAOB.

Zavkhan terrane in western Mongolia represents a northwest segment of CAOB. Zavkhan terrane is a Proterozoic cratonic fragment and divided into three subzones, which are the Urgamal, Hutul and Khungui zones from west to east. Khungui zone is dominated by gneiss, quartzite, and amphibolite of Paleoproterozoic Buduun metamorphic formation, the basement of Zavkhan cratonal terrane.

We focus on 5 garnet amphibolites collected from Buduun formation of Khungui zone, Zavkhan terrane. Bulk composition of amphibolites shows on average 50.7 % SiO_2, 9.3% CaO, 2.5% Na_2O and 0.84% K_2O, trace-elements patterns are similar to those of N-MORB, except for the element of Th. All amphibolites shows schistosity and have garnet (Grt), amphibole (Amp), quartz (q), clinopyroxene (Cpx), rutile, epidote (epi), plagioclase (Pl), muscovite (mus). It is noted that omphacite occurs as Grt inclusions in the most of samples.

Grts occur as two types: euhedral grain and aggregate. Compositionally, garnets can be divided into three types: garnet 1 (Grt1), garnet 2 (Grt2), and transitional garnet (TGrt). Grt1 is observed as cluster (400 μm) of garnet grains but its composition shows one garnet grain. Grt1 contains few inclusions (omphacite and q) and has composition zoning from core ($Alm_{60.8}Grs_{28.2}Prp_{9.6}Sps_{1.4}$) to rim ($Alm_{57.53}Grs_{32.75}Prp_{8.89}Sps_{0.82}$). Omphacite is observed in rim of Grt1. Grt2 (190 μm) contains numerous inclusions (core: q, amphibole, epi, and rarely mus, and rim: omphacite) and has composition zoning from core ($Alm_{51.3}Grs_{34.17}Sps_{8.62}$, $Prp_{5.84}$) to rim ($Alm_{57.0}Grs_{35.91}Prp_{5.69}Sps_{1.32}$). TGrt1 (40-210 μm) has very rare inclusions (q and rarely amp) and homogenous composition ($Alm_{59.26}Grs_{32.07}Prp_{7.43}Sps_{1.22}$). Cpx (omphacite) occurs in matrix (Xjd=0.32-0.38) and as inclusion (Xjd=0.34-0.44) of Grt rim (Grt1 and Grt 2). Cpx is replaced by Pl, amp, and q forming symplectite. Calcic to sub calcic amp occur in matrix and as inclusions of garnets. In matrix, amp has compositional zoning from barroisite at core to hornblende at rim whereas amp in grt has hornblendic composition.

The Grt amphibolites from Buduun formation, Khungui zone, Zavkhan terrane were suffered from eclogite

©2020. Japan Geoscience Union. All Right Reserved.

facies metamorphism. Based on minerology and mineral chemistry, 3 metamorphic stages can be determined: pre-Peak (M1), Peak (M2), and retrograde (M3). M1 is marked by inclusions (Amp (calcium), Epi, Mus, and q) in Grt2 core. M2 is represented by omphacite (in Grt1 and Grt2 rims) and composition of Grt1 (402-466 ˚C) and Grt2 (411-525 ˚C) rims. M3 (retrograde) is traced by transformation of omphacite into amp-Pl-q symplectite and hornblende. The new point of eclogite facies rocks is important to reconstruct tectonic evolution of PAO, especially from the Chandman area to northern Mongolia.

Keywords: Garnet, Eclogite, Buduun formation, Central Asian Orogenic Belt

©2020. Japan Geoscience Union. All Right Reserved.

Eclogite-to-granulite transition in the Ufipa Complex (Tanzania): Pressure—Temperature—time paths of a Pan-African continental collision zone

*Morita Isamu[1], Tatsuki Tsujimori[1], Nelson Boniface[2], Kennet E Flores[3], Shogo Aoki[4], Kazumasa Aoki[4]

1. Tohoku University, 2. University of Dar es Salaam, 3. Brooklyn College of the City University of New York, 4. Okayama University of Science

Eclogites and eclogite-facies rocks in most high pressure–ultrahigh pressure (H*P*–UH*P*) metamorphic complexes have generally experienced retrograde metamorphism. In collision zones, deeply subducted continental crust rocks undergo recrystallization/overprinting throughout exhumation. During crustal stabilization of H*P*–UH*P* rocks after a collisional event, granulite- and/or upper amphibolite-facies often obliterates the records of prograde and/or metamorphic peak. Pressure-temperature-time paths often expressed these metamorphic histories in several complex such as the Western Gneiss Region, Eastern Himalaya, and North Qinling. We conducted petrological and geochronological research for partially granulitized eclogite and associated metamorphic rocks of the Neoproterozoic Ufipa Complex (Southwestern Tanzania). We distinguished at least three metamorphic stages, an eclogite stage (M1), a granulite stage (M2), and a retrograde amphibolite stage (M3). Mineral assemblages and geothermobarometry revealed *P*–*T* conditions of 2.4–2.6 GPa and 920–960℃ for the M1 eclogite stage, and 1.3–1.6 GPa and 900–940℃ for the M2 granulite stage. *In-situ* zircon LA-ICP-QMS U–Pb dating and REE geochemistry combined with inclusion mineralogy on polished thin-section yielded an eclogite-facies stage at 588 ±3 Ma. H*P* granulite-facies recrystallization zircons yielded 562 ±3 Ma. These new data suggest a time interval Δt between eclogite facies peak and retrograde H*P* granulite-facies recrystallization of ~26 Mry. Based on these estimations, a clockwise *P*–*T* path was constructed and exhumation rate was yields ~1.0–1.6 km/Mry. This data is consistent with the results of one-dimensional numerical modelling for double thickened crust that assumes that the *P*–*T* path was attributed to tectonic thermal perturbation and relaxation. This model also suggest a clockwise *P*–*T*–*t* path, followed by strong isothermal decompression, which similar to the thermobarometric calculations on the Ufipa eclogites. This model also support high exhumation rate of ~1.0-1.6 km/Mry.

Keywords: eclogite, granulitization, Neoproterozoic, heat transfer, P-T-t path

©2020. Japan Geoscience Union. All Right Reserved.

Geochemistry, Pressure-Temperature conditions and tectonic setting of the amphibolite from the southern part of Motloutse Complex, eastern Botswana

*Thembiso Otladisang Basupi[1], Toshiaki Tsunogae

1. Graduate of Life and Environmental Sciences, University of Tsukuba

Amphibolites constitute prominent rock types in Archean high-grade terranes in eastern Botswana and these include the Motloutse and Phikwe Complex terranes (Aldiss, 1991; Carney et al., 1994). Phikwe Complex is considered part of the larger Limpopo Complex high-grade terrane between the Archean Kaapvaal and Zimbabwe cratons. Available studies indicate polymetamorphic amphibolite- to granulite-facies conditions from metasedimentary rocks of the Phikwe Complex (McCourt et al., 2004). Unlike the Phikwe Complex, no granulite-facies conditions or polymetamorphism has been reported so far from the Motloutse Complex, which occurs to the SW of the Zimbabwe Craton (Smith and Phofuetsile, 1985; Aldiss, 1991). In spite of this, there has been no study in modern literature on the amphibolite rocks belonging to Motloutse complex. This study is to focus on the geochemistry, pressure-temperature (*P-T)* condition and tectonic setting of mafic rocks (amphibolites) of the Motloutse Complex and amphibolites from Phikwe Complex are introduced for comparison.
The field survey conducted indicated amphibolites occupying prominent hills in the respective areas surrounded by granitoids. Available geochronological data indicate that the granitoids in both areas are Neoarchean (ca 2.65 Ga). Therefore, the mafic rocks must be older than ca 2.65 Ga. Overprint events (e.g., partial melting) were observed in amphibolites.
The field description shows that the amphibolites are made up of plagioclase, hornblende, biotite and quartz. Petrographic images of the amphibolites shows slight alteration of plagioclase to sericite and triple junction texture of the hornblende-plagioclase (plagioclase as an indication of deformation). Alignment of minerals is a common feature. Hornblende + plagioclase + quartz + sericite + ilmenite + magnetite dominates the composition.
Metamorphic temperature estimates for amphibolites from Maope area using hornblende-plagioclase geothermometry of Holland and Blundy (1994) ranges from 650 to 780 ˚C. The geothermobarometry *P-T* condition estimates using the hornblende-plagioclase of Schmidt (1992) and Anderson and Smith (1995) recorded 572 to 670˚C at 3.5 to 7 kbar and 450 to 670˚C at 3.7 to 7.3 kbar. These results estimate bracket the Maope amphibolites on the upper amphibolite to lower granulite facies metamorphic condition.
Whole-rock geochemical analysis indicates that the amphibolites are characterised by high SiO_2 (45.40–54.82 wt.%) and MgO (4.40–10.25 wt.%) contents, some are comparable with boninites. The TAS plot characterise the amphibolites of Maope area and Phikwe area as basaltic to basaltic andesite composition. The primitive mantle elements normalised and chondrite-normalised REE pattern indicate that they are likely to have been derived from the same parental magma. The positive Pb, Sr, and Eu anomalies reflect plagioclase accumulation on the magma during fractionation. The tectonic setting plots show volcanic arc basalts in an oceanic arc environment. The results also show hydrated magma of tholeiitic composition due to subduction that lead to boninites like mafic rocks. We therefore suggest that the protolith of the Maope amphibolites formed by subduction as boninites like mafic rocks in an oceanic arc environment. Based on field evidence and results of geothermobarometry, we suggest that the amphibolites were later exposed to peak metamorphism due to partial melting that is believed to have been the only Paleoprotezoic (2.06 Ga) overprint in Motloutse Complex (Zeh eta al., 2009). The source of

©2020. Japan Geoscience Union. All Right Reserved.

the overprint remains unknown.

Keywords: Amphibolites, amphibolite facies, granulite facies, boninites, plagioclase accumulation.

©2020. Japan Geoscience Union. All Right Reserved.

Crystal Preferred Orientation Development of Secondary Olivine Formed by Hydration of Orthopyroxene: Implication to Anisotropy of Shallow Mantle Wedge during Initiation Stage of Subduction

*OTGONBAYAR DANDAR[1], Atsushi Okamoto[1], Takayoshi Nagaya[2], Masaoki Uno[1], Noriyoshi Tsuchiya[1]

1. Graduate School of Environmental Studies, Tohoku University, 2. Graduate School of Science, University of Tokyo

Crystal preferred orientation (CPO) of olivine (Ol) provides significant effects on physical properties of the upper mantle, and the comparison of the Ol CPO analyses and observations of seismic anisotropy make it possible to simulate the flow pattern of upper mantle. The CPO analyses on naturally or experimentally deformed Ol samples have shown the relationship between deformation conditions (stress, temperature and H_2O content) and CPO patterns produced by the plastic deformation [e.g. 1]. In contrast, some studies have suggested specific topotactic relationships between Ol and serpentine minerals [e.g. 2, 3]. Therefore, the metamorphic reactions provide crucial controls on the physical properties of mantle. However, our understanding on their effects for mantle wedge anisotropy is still limited. In this study, we show the characteristic features of CPO of secondary olivine (S-Ol) formed after orthopyroxene (Opx) in metaharzburgite from the Naran massif, the Khantaishir ophiolite, western Mongolia and discuss seismic anisotropy of S-Ol-bearing mantle wedge during initiation stage of subduction.

Metaharzburgite in the Naran massif is composed of primary olivine (P-Ol), S-Ol, antigorite, and Cr-Spinel. S-Ol mainly occurs as mm-scale aggregates. S-Ol aggregate is composed of 10-50 μm Mg-rich olivines, magnetite, and sub-parallel bands of antigorite (B-Atg). Our previous study revealed that these S-Ol+B-Atg formed by pseudomorphic replacement of Opx during hydration of mantle wedge although primary Opx was not preserved [4]. P-Ol, S-Ol and B-Atg, and antigorite in matrix (M-Atg) show contrasting CPOs, respectively. P-Ol CPO shows the strong concentration of the *b*- and *c*-axes normal to the foliation and parallel to the lineation. It suggests plastic deformation by dislocation creep under relatively low stress and high-water condition. CPOs of M-Atg and P-Ol reveal clear crystallographic relationships between Atg and P-Ol: the concentrations of the *a*-, *b*- and *c*-axes of M-Atg are sub-parallel to the *b*-, *c*- and *a*-axes of P-Ol, respectively (topotactiv growth of M-Atg after P-Ol). In contrast to P-Ol, S-Ol aggregate does not show a strong CPO in an entire thin section, but the weak CPOs are developed in individual S-Ol aggregates. This indicates that the S-Ol CPO was developed not by deformation processes but was affected by the orientation of pre-exisiting Opx grains. The distribution of B-Atg in S-Ol aggregates could represent the cleavage of P-Opx, and the (001) plane of B-Atg is oriented sub-normal to the P-Opx cleavage. Assuming that Atg bands present the cleavage of P-Opx, the *c*- and *b*-axes of Atg are likely to be sub-parallel and normal to the Opx cleavages, respectively. These features suggest that high-T hydration of mantle wedge of the Naran massif proceeded without intense deformation and anisotropy development during initial stage of subduction zone development.

References:

1. Karato et al., 2008, Annu. Rev. Earth Planet. Sci. **36**, 59-95
2. Boudier et al., 2010, J. Petrol. **51**, 495–512
3. Nagaya et al., 2014, EPSL, **387**, 67–76
4. Dandar et al., 2019, CMP, **174**, 86

©2020. Japan Geoscience Union. All Right Reserved.

Keywords: Metamorphic reaction, Secondary olivine CPO, Topotactic growth, Khantaishir Ophiolite, Subduction zone

©2020. Japan Geoscience Union. All Right Reserved.

Crustal fracturing and brecciation processes in middle crust associated with granitoid intrusions in Sør Rondane Mountains, East Antarctica

*Tatsuya Takemori[1], Masaoki Uno[1], SATISH KUMAR[2], Noriyoshi Tsuchiya[1], Atsushi Okamoto[1]

1. Tohoku University, 2. Niigata University

Recent geophysical observations, such as seismic tomography and magnetotellurics methods, have shown that there is a correlation between the distribution of magma, H_2O-CO_2 fluid and hypocenters (Asamori et al., 2010). On the other hand, the observations of magmatic/hydrothermal deposits have revealed that granitic magmas and carbonate mineral veins are closely related to crustal failures (Oliver et al., 2006). In order to clarify these relationships, understanding of the dynamic fracturing processes, such as flow velocity, fluid pressure, etc. is necessary. In this study, we clarify the crustal fracturing processes by elucidating the origin and velocity of fluid in crustal fracturing and brecciation associated with granitic magma.

The survey area is Balchenfjella, Sør Rondane Mountains, East Antarctica, located within the collision zone during the formation of the Gondwana continent, where the middle and lower crustal materials of the granulite facies are exposed (Ishikawa et al., 2012). The host rock granulite is intruded by breccia dyke with a matrix of carbonate rock (hereinafter, referred to as carbonate breccia dyke) and granitic dyke that are more than 100 m wide, which captures carbonate rock, granite, gneiss as tens of cm to tens of meters of clasts. For two dykes, we estimated the temperature and pressure conditions at the time of intrusion, the origin of the fluid forming two dykes, created a model of the fracturing processes, and finally, estimated the fluid velocity during fracturing.

The results indicate that, the temperature and pressure conditions at the time of intrusion were P = 200 (MPa) and T = 580 to 700 (° C), which is equivalent to pyroxene-hornfels facies, indicating a crustal fracturing in the middle crustal conditions. Based on the carbon-oxygen isotope ratio and trace element composition, the matrix of carbonate breccia dyke has originated from sedimentary carbonate rock (metalimestone) and reacted with the magmatic fluid. Based on the bulk composition, the granitic dyke is syn-collisional granite. The particle size distribution of the captured clasts is 8~102 (m) for carbonate dyke and 17~61 (m) for granitic dyke. By using the Ergun equation, the minimum fluidization rate was calculated to be 190 (km/h) and 40 (km/h), respectively.

This suggests that five stages of magma/fluid activity and two types of brecciation had occurred. In particular, regarding brecciation, as magmatic fluid flows into the metalimestone layer during the intrusion of granite, CO_2 is released due to the decarbonation, and the fluid pressure exceeds the lithostatic pressure, disrupts the crust, rises at a flow velocity of over c. 200 km/h, and forms carbonate breccia dyke. Subsequently, the granitic magma intruded at c.40 km/h, forming granitic dyke.

From these observations, it is clarified that the decarbonation of carbonate rock caused by the intrusion of granite causes explosive crustal destruction and can move through the crust at velocities exceeding 200 km/h.

©2020. Japan Geoscience Union. All Right Reserved.

Keywords: breccia, decarbonation, crust fracturing

©2020. Japan Geoscience Union. All Right Reserved.

Multiple timings of high-grade garnet-forming metamorphism from Sør Rondane Mountains, East Antarctica

*Fumiko Higashino[1], Tetsuo Kawakami[2], Shuhei Sakata[3], Takafumi Hirata[3]

1. Faculty of Science, Okayama University of Science, 2. Kyoto University, 3. The University of Tokyo

In high-grade metamorphic rocks, U-Pb geochronology of zircon is a powerful tool to understand metamorphic events. This is because zircon represents relatively high closure temperature of U-Pb system and its atomic structure remains stable over long periods of geological time. Since zircon could record various metamorphic stages of high-grade metamorphism (e.g., Harley et al., 2007), the appropriate interpretation of their ages is significant. The REE pattern of distribution coefficient between zircon and garnet ($D_{REE(z/g)}$) has been used as a useful tool to establish the link between zircon geochronology and timing of garnet formation. A considerable issue is that the REE patterns of $D_{REE(z/g)}$ have been reported to become positive with decreasing temperature, increasing pressure, or increasing X_{Ca} in garnet (e.g., Harley et al., 2001; Rubatto, 2002; Hokada and Harley, 2004; Buick et al., 2006; Rubatto and Hermann, 2007). In spite of these uncertainty, traditional REE patterns of $D_{REE(z/g)}$ have been used to understand whether the garnet was formed in equilibrium with zircon or not. The typical way that experimental D_{REE} data sets are used to evaluate empirical data, is to overlay them on natural data sets and gauge their similarity. The flat REE pattern of $D_{REE(z/g)}$ is often interpreted to represent equilibrium between these two phases.

In order to handle empirical data sets in a practical manner, Taylor et al. (2017) proposed to use array plot whose slope from $D_{Yb(z/g)}/D_{Gd(z/g)}$ is plotted against $D_{Yb(z/g)}$ values. An advantage of the new array plot is usages of two key parameters which together can represent the slope of the REE pattern and REE abundance of the traditional REE partitioning plot. It is noted that more than one garnet and zircon generation may be formed by recrystallization and a degree of chemical re-equilibration varies in terranes that have undergone polymetamorphism.

In the Sør Rondane Mountains (SRM), East Antarctica, Late Proterozoic to Cambrian granulites are widely exposed (e.g., Jacobs and Thomas, 2004; Shiraishi et al., 2008; Osanai et al., 2013; Kitano et al., 2016). In the SRM, each metamorphic event has been correlated to the different zircon age groups, mainly using Th/U ratio of the dated zircon domains (e.g., Shiraishi et al., 2008). Limited number of previous studies have investigated REE patterns of zircon and garnet in the SRM (e.g., Hokada et al., 2013). Therefore, in this study, *in situ* U-Pb dating of zircon included in garnet and the $D_{REE(z/g)}$ values are evaluated using the array plot, in order to determine the timing(s) of garnet-forming metamorphism in selected regions of the SRM.

In situ U-Pb dating of zircon and quantitative analysis of REE in garnet and zircon have been performed using LA-ICPMS on seven mafic and pelitic gneisses collected from Perlebandet, Brattnipene, Pilten, Mefjell, and Balchenfjella in the SRM. The rims of zircon inclusions in garnet from seven samples gave U-Pb ages of ~560 Ma (Pilten and Balchenfjella), ~580 Ma (Perlebandet and Mefjell) and ~610-620 Ma (Balchenfjella and Brattnipene). Each sample gave a single peak age distribution for the zircon rim dating. Using the traditional $D_{REE(z/g)}$ pattern plots and the array plot, five samples are evaluated to be in equilibrium between host garnet and the dated zircon domain. Zircon rims included in garnet from the other two samples, on the other hand, were not in equilibrium with the host garnet. In summary, the five equilibrium samples could reveal the multiple timing of garnet formation in different regions of the SRM; Perlebandet (~580 Ma), Brattnipene (~610-620 Ma), Pilten (~580 Ma), and Balchenfjella (~560 Ma and ~610 Ma). The details of garnet-forming metamorphism will be discussed.

©2020. Japan Geoscience Union. All Right Reserved.

Keywords: REE, LA-ICPMS, high-temperature metamorphic rock

©2020. Japan Geoscience Union. All Right Reserved.

Thermal modeling for "Hot-on-cold" thrusting: Thermal structure during orogenic movement at the western boundary of Eastern Ghats Belt, India

*Fumihiko Sato[1], Tomoeki Nakakuki[1], Kaushik Das[1]

1. Hiroshima University

The boundary areas between the orogenic belts and pre-existing cratons preserve important information regarding the growth and evolution of old continents. The boundary areas experienced multiple phases of metamorphism, deformation, activities of crustal fluids, these hold the important key to understand continental evolutions. Regarding the orogenesis and its thermal structure, it is important to validate the petrogenetic evidence from rock records by computer simulation.
The Eastern Ghats granulite Belt (EGB) is a Proterozoic orogenic belt that extends ~1000km in the northeast-southwest direction along the east coast of India. Archean Baster craton (BC) is located just west of it. From the detailed structural geological, petrological and geochronological works, it is understood that “Hot-on-cold” thrusting occurred between the deep crust of EGB and the shallow crust of BC.
The present study area is north-western EGB, i.e. between the Phulbani domain and 10 km away from the boundary thrust. Monazite U-Th-total Pb (EPMA) dating and petrological data on the corundum + spinel + garnet-bearing granulite of this domain revealed that this area had undergone peak ultra-high temperature metamorphism in the deep crust during 1000-900 Ma. Following that the youngest thermal event is documented at approximately 650-500 Ma from the felsic gneiss. This youngest age was found inside EGB only within a few kilometers on both sides of the boundary, but most prominent close to the boundary.
We consider this age and its geographic spread is related to the final “Hot-on-cold” thrusting during the final amalgamation of EGB crust with the Indian continent. This thermal overprinting was up to the amphibolite facies. In order to understand the cooling process of after peak, we set this age distribution on the present erosional surface as the boundary condition of the thermal structure model and considered computer simulation of thrusting.
In this study, we present the results of the 2D/3D numerical simulations of “Hot-on-cold” thrusting and comparing it with the metamorphic rock records. The numerical model is carried out by computer calculation using the temperature equation obtained by discretizing the thermal advection and convection equations by finite volume method with progress in time.

Keywords: 2D/3D Thermal modeling, Hot-on-cold thrusting, Orogen-boundary shear zone, EGB, India

©2020. Japan Geoscience Union. All Right Reserved.

Fluid-rock interaction and formation of high-grade metamorphic rocks in the Trivandrum Block, southern India

*Nishi Ayumi[1]

1. Faculty of Life and Environmental Sciences, University of Tsukuba

Infiltration of supercritical fluids from external sources into lower crustal rocks probably plays an important role on the formation and the stability of various high-grade metamorphic rocks. Generally, introduction of high-H2O activity fluids (such as pure H2O fluid) in the lower crust will enhance hydration or partial melting, whereas low-H2O activity fluids (such as CO2-rich fluid) will give rise to dehydration reactions to form anhydrous mineral assemblages (such as orthopyroxene-bearing granulite-facies assemblages). As a case study in southern India, this study evaluates the petrogenesis of a white-colored (bleached) hydration vein and a dark-colored dehydration vein associated with granulites from Parakkani and Marthandam in the Trivandrum Block, southern India. The Trivandrum Block is a granulite block formed by a Neoproterozoic to Cambrian (ca. 600-510 Ma) high-grade metamorphism probably related to a series of collisional events during the assembly of Gondwana supercontinent. The bleached vein occurring parallel to the foliation of the matrix anhydrous charnockite body (orthopyroxene + quartz + plagioclase + K-feldspar + biotite) is characterized by a hydrous mineral assemblage of garnet + biotite + quartz + plagioclase + K-feldspar. In contrast, the dark-colored vein occurring perpendicular to the foliation of the matrix garnet-biotite gneiss (garnet + biotite + quartz + plagioclase + K-feldspar) has an anhydrous mineral assemblage of orthopyroxene + quartz + plagioclase + K-feldspar + biotite. The field occurrences and the mineral assemblages in the host-vein rocks indicate possible effects of fluid migration in the lower crust for the formation of the two types of vein. It is important to note that the two veins occur in the same area around Marthandam. The preliminary results of this study thus suggest complex fluid migration history during the formation of granulites in the Trivandrum Block.

Keywords: charnockite, garnet-biotite gneiss, fluid-rock interaction, Trivandrum Block, Southern India, vein

©2020. Japan Geoscience Union. All Right Reserved.

Structural geology of Hidaka Metamorphic Belt in the Mt.Nozuka and Mt.Rakko area, Hokkaido,JAPAN -Growth process and mechanism of the Cenozoic continental crust-

*Moeko Kanno[1], Tsuyoshi Toyoshima[2], Hayato Ueda[2]

1. Graduate school of Science and Technology, Environmental Science and Technology,Earth science, 2. Niigata University, Faculty of Science,Department Geology

Hidaka metamorphic belt (HMB) of the southwestern part of Hidaka belt, Hokkaido, northern Japan, was regarded as an island¬−arc type crustal slab formed by prograde metamorphism up to granulite-facies and voluminous partial melting during early Eocene (e.g. Osanai et al., 1992). However, Shimura et al. (2015) and Takahashi et al. (2017, 2018) recently proposed that HMB consists of two different metamorphic belts formed during 40–30 and 19 Ma respectively and there is the former on the latter. Shimura et al. (2018) also showed 40–30 Ma metamorphic rocks suffered 19 Ma metamorphism. Moreover, Jahn et al. (2014) reported granites were generated during 45–46 and 37 Ma in the northern part of Hidaka belt. From these new zircon ages, the necessary of reconstruction of tectonics of HMB was drawn.

We carried out structural analysis and zircon U–Pb geochronology of the Hidaka metamorphic and plutonic rocks from the Niobetsu River and Menasyunbetsu River regions, in order to discuss tectonics of HMB.

In the study area, HMB consists mainly of S-Type tonalite (Grt tonalite and Grt-Bt tonalite), I-Type tonalite (Hbl-Bt tonalite), Niobetsu complex (Owada et al., 2004), amphibolite and pelitic and psammitic gneisses. Niobetsu complex, consists of gabbro and diorite. Metamorphic inclusions are observed in S-Type tonalite and Niobetsu complex. Metamorphic rocks in the study area are of zones III and IV (Osanai et al., 1992). Metamorphic inclusions are also of zones III and IV. Most of the rocks align along a NW–SE trend except for N–S trending Niobetsu complex.

Newly obtained zircon U-Pb ages reveal three magmatic stages, two in Eocene at about 45 Ma (S-type tonalite), and about 33 Ma (I-type tonalite), and one in Miocene at about 19 Ma (diorite of Niobetsu complex) in HMB of the study area. Because these plutonic rocks are accompanied by migmatites and metamorphic inclusions, it is possible that three stages of magmatism went with metamorphism and HMB was formed by three stages of metamorphism.

Asymmetrical magmatic flow structure like S-C-C' fabric of mylonite is observed in margins of Niobetsu complex, indicating a normal sense of shear. The asymmetrical structure suggests that Niobetsu complex intrusion and magmatic flow occurred under extensional conditions.

In the study area, three stages of mylonitization are recognized: Dm1, Dm2, and Dm3 stages. Dm1, Dm2, and Dm3 mylonitizations were caused by dextral to dextral-normal sense, dextral to dextral-reverse sense, and dextral−sense of shear respectively. Mineral lineation in Dm1 mylonite plunges gently toward the southeast. Dm3 mylonitization is concentrated in rocks near the Hidaka Main Thrust.

Dm1 mylonitization showing dextral to dextral-normal sense of shear occurred under dextral transtensional conditions. In the northern− central parts of HMB, mylonitization of basal−lower S-type tonalites occurred under dextral transpressional conditions (Toyoshima et al., 1997). Basal−lower S-type tonalites in the northern and central parts of HMB are the products of 19 Ma magmatism (Kemp et al., 2007), while S-type tonalites in the study area are the products of 45 Ma magmatism. Therefore, it is possible that the dextral transtension and dextral transpression occurred during different deformation stages. Another possibility is when the dextral transtension and dextral transpression occurred during the

©2020. Japan Geoscience Union. All Right Reserved.

same deformation stage (Dm1). In this possibility, Dm1-mylonitizaton caused pivotal movement, rotation of shear plane, and the difference in type of fault between the northern–central and southern parts.

Keywords: Structural geology, Hokkaido, Hidaka Metamorphic Belt, crust, mylonit

©2020. Japan Geoscience Union. All Right Reserved.

Raman carbonaceous material thermometry applied to mapping the thermal structure of contact metamorphic domains in the Hongusan area, central Japan incorporating the effects of widespread detrital carbonaceous material

*Ken Yamaoka[1], Simon Richard Wallis[1], Akira Miyake[2], Yui Kouketsu[3]

1. The University of Tokyo, 2. Aichi University of Education, 3. Nagoya University

Raman carbonaceous material thermometry (RCMT) can be applied to a wide range of lithologies and over a wide temperature range of 150–655 ˚C. The utility of this method opens the possibility of determining the thermal structure of metamorphic domains with unprecedented spatial resolution. RCMT is based on averages of numerous measurements in a single sample and a potential complicating factor is the presence of detrital carbonaceous material that can bias the average values. Such detrital grains are commonly recognized as grains of highly crystalline CM (close to graphite) amongst grains of lower crystallinity. Recent studies in the Himalayas and Taiwan have shown that the material cycling process in convergent plate margins leads to the storage of highly crystalline CM in sediment because it is relatively resistant to weathering and erosion processes. The existence of detrital CM needs to be assessed to estimate appropriate temperatures and errors using the RCMT. However, there are few studies where the effects of detrital material have been quantitatively studied. Application of RCMT to relatively low-grade metamorphic rocks (< ~400 ˚C) can easily detect the presence of detrital CM because of a crystallinity gap between weathering-resistant high-grade CM and lower-grade metamorphic CM. However, it is unknown whether detrital and metamorphic CM can be clearly distinguished in higher-grade metamorphic domains. It is also not clear whether detrital grains of CM with crystallinity less than graphite can also be present. In the Hongusan area of Aichi Prefecture, two distinct types of thermal structures can be recognized: firstly one associated with the regional high-*T/P* type Ryoke metamorphism, and secondly later overprinting contact metamorphism recognized around two separate granitic intrusions. Application of the RCMT to 100 metamudstone samples in the study area reveals that several samples show multimodal crystallinity of CM which indicates the existence of a large amount of detrital CM grains including both fully crystallized graphite and lower crystallinity metamorphic CM grains. A new procedure was developed to filter out the effects of detrital CM and assist in determining the metamorphic thermal structure. The results clearly show the distinct thermal structures related to regional and contact metamorphism with a high spatial resolution that can be used to determine the extent of the contact metamorphism. The estimated temperatures show good agreement with a more limited data set obtained using silicate equilibria models. Spatial changes in the distributions of the metamorphic and detrital CM clearly show that as the maximum temperature increases, CM with low crystallinity progressively transforms to graphite and multiple crystallinity peaks gradually merge to one at a high grade. These results show RCMT can be used to derive detailed and reliable temperature estimates even if the original metasedimentary rock contains a significant amount of detrital CM. The recognition of detrital CM can be used to infer the grade of metamorphic rocks present in the hinterland that supplied the detritus of the Mino–Tanba belt. This approach can be added to the tools used in the provenance analysis of sedimentary rocks. The contact aureole around the Shinshiro tonalite in this area is remarkably thick and may reflect the tectonic setting during magma emplacement or the cooling process of magma. The formation process may be constrained by considering the thermal model and the obtained Raman CM temperature.

©2020. Japan Geoscience Union. All Right Reserved.

Keywords: Raman carbonaceous material thermometry, Detrital carbonaceous material, Metamorphic temperature mapping, Ryoke metamorphic belt

©2020. Japan Geoscience Union. All Right Reserved.

Raman parameters of carbonaceous material estimated from fully-automatic spectral fitting method and their relation to vitrinite reflectance

*Shunya Kaneki[1], Yoshihiro Nakamura[2], Yui Kouketsu[3], Hideki Mukoyoshi[4]

1. Disaster Prevention Research Institute, Kyoto University, 2. Geological Survey of Japan, National Institute of Advancecd Industrial Science and Technology, 3. Graduate School of Environmental Studies, Nagoya University, 4. Graduate School of Science and Engineering, Shimane University

Carbonaceous material (CM) is widely distributed in sedimentary and metamorphic rocks, and its thermal maturity and crystallinity have been used as an indicator of burial and metamorphic temperature history. The relationship between maturity and temperature history of CM has been documented by various analytical techniques, including X-ray diffraction measurements, vitrinite reflectance measurements, transmission electron microscopy, infrared spectroscopy, and Raman spectroscopy. Among these, Raman spectroscopy is increasingly being used because of its rapidness and usefulness, as well as it is normally non-destructive technique (Henry et al., 2019).

A typical Raman spectrum of CM exhibits two distinct peaks of D (around 1350 cm^{-1}) and G bands (around 1580 cm^{-1}) (Tuinstra & Koenig, 1970). Various spectral parameters, which is associated with the thermal maturity of CM, are reported; e.g., intensity ratio and full-width at half maximum (FWHM) of D and G bands. Importantly, there are mainly two types in these spectral parameters: (1) parameters calculated from raw data, or (2) parameters calculated by performing spectral fitting. One of the representative parameters of the latter was proposed by Beyssac et al. (2002). Because it is argued that their R2 ratio (area of G band / area of D1+D2+G bands) is closely related to the CM maturity, numerous studies adopted the R2 ratio as a representative parameter of Raman spectra of CM (e.g., Kouketsu et al., 2014). On the other hand, Henry et al. (2018) suggested that spectral fitting should not be performed because it leads to unnecessary errors, and recommended to focus on the parameters that can be calculated from the raw spectrum without spectral fitting.

In the light of these backgrounds, the final goal of this study is to investigate whether spectral fitting of Raman spectra of CM is useful to evaluate its thermal maturity. As a first step toward this purpose, we developed a Python script that automatically perform spectral fitting of Raman spectra of CM. Analytical procedures of the script mainly consist of 5 parts: (i) smoothing by Savitzky-Golay filtering method, (ii) background correction with 1^{st} or 3^{rd} order polynomial function, (iii) normalization, (iv) setting of initial spectral parameters, and (v) non-linear spectral fitting with pseudo-Voigt function. We analyze the published data of Raman spectra of CM by Kouketsu et al. (2014), Mukoyoshi et al. (2018), and Nakamura et al. (2019), and compared the calculated parameters with the reported values of vitrinite reflectance. We will show preliminary results of our attempts in this presentation.

Keywords: Carbonaceous material, Raman spectroscopy, Spectral fitting, Vitrinite reflectance

©2020. Japan Geoscience Union. All Right Reserved.

Raman spectroscopy of quartz eclogite in the Sanbagawa metamorphic belt: Potential of Raman geobarometry using kyanite-quartz system

*Yuki Tomioka[1], Yui Kouketsu[1], Tomoki Taguchi[2]

1. Nagoya University, 2. Kyoto University

The pressure–temperature conditions of metamorphic rocks have been estimated by using thermodynamic models based on the chemical equilibrium between coexisting minerals. Recently, the development of a new method called “Raman geothermobarometer” has been progressing. It applies Raman spectroscopy and focuses on the residual pressure of the inclusion minerals. In particular, “garnet-quartz Raman barometer” using quartz inclusions in garnet has been proposed as a useful technique, which estimates residual pressure from peak shift of Raman spectrum and converts to metamorphic pressure (Enami et al., 2007_AM; Kouketsu et al., 2014_AM). On the other hand, the host garnet forms a solid solution, and each end member has different physical parameters. Therefore, theoretical errors occur between the actual measurement value and the numerical calculation assuming garnet as an end member. In this study, we verified a new Raman geobarometer using kyanite instead of garnet. Neither kyanite nor quartz forms a solid solution, and kyanite is stable under a wide pressure and temperature range. Hence, the kyanite-quartz system may be applicable to various high-pressure metamorphic rocks.

The samples used in this study are quartz eclogites from the Gongen region in the Sanbagawa metamorphic belt, central Shikoku, southwest Japan. The peak metamorphic pressure–temperature condition of the Gongen quartz eclogite was estimated to be 2.3–2.4 GPa/675–740 ℃, which is the highest pressure in the Sanbagawa metamorphic belt in central Shikoku (Miyamoto et al., 2007_JMPS). In this study, five quartz eclogite samples were collected from one location on the ridge of Mt. Gongen and two locations along the Tokonabedani valley. Two quartz eclogite samples described by Miyamoto et al. (2007) were also analyzed. For each sample, Raman spectroscopic analyses were performed on thick sections (about 100 μm thick) and only quartz inclusions completely encapsulated in kyanite were analyzed. All Raman spectra of 237 quartz inclusions in kyanite showed a peak shift toward higher wavenumber sides indicating compressive stress. residual pressure values calculated from the peak shift showed a wide range of 0.16–0.89 GPa. In order to evaluate the factor of the variation in residual pressure, the inclusion diameter was measured, but no significant correlation was found with the residual pressure. Raman mapping was performed to confirm the distribution of the residual pressure inside the inclusion, but it is homogeneous except grain boundary. Therefore, the following possibilities are considered as the factors of the variation in residual pressure: (1) quartz inclusions were trapped in kyanite at wide pressure–temperature range, (2) effect of healed crack in host kyanite during exhumation.The peak metamorphic condition was calculated based on the maximum residual pressure of 0.89 GPa using a numerical model, and the result shows in good agreement with previously estimated range by using the thermodynamic modeling (Miyamoto et al., 2007). This result suggests that kyanite had been growing during the Sanbagawa peak metamorphic condition. Additionally, calculations using the maximum values at each sampling locations also show good agreement with the metamorphic range reported by the previous study, and thus Gongen quartz eclogite is thought to have subducted extensively to the deepest depth of the Sanbagawa metamorphism.

©2020. Japan Geoscience Union. All Right Reserved.

This study indicates that kyanite can be used as a host mineral like garnet, and the kyanite-quartz system can estimate the peak pressure–temperature condition. However, some unverified points remain such as the effect of the elastic anisotropy of kyanite and quartz, and the possibility of underestimating the metamorphic conditions by selecting the highest value from the few measurement results. In the future, research will be conducted toward the development of a highly reliable geothermobarometer based on these improvements.

Keywords: Raman spectroscopy, geobarometer, high-pressure, kyanite, quartz

©2020. Japan Geoscience Union. All Right Reserved.

The R.G. Coleman Cazadero Collection: A preliminary sample description for systematic curation

*Oka Hiroki[1], Tatsuki Tsujimori[1]

1. Tohoku University

The Ward Creek near Cazadero is one of the most classic blueschist localities in California Coast Ranges. The area is also known as a difficult place to sample due to private property concerns. In 2019, one of the authors (T. Tsujimori) received a collection-donation from Professor Robert G. Coleman; the rock collection include various metamorphic rocks from Cazadero (e.g., Coleman et al. 1965) and other areas[DPG1] . The aim for the donation was not only reuse and re-investigate the precious samples but also to curate the collection for future generations.

The RGC Cazadero Collection includes up to 222 rock samples (~40 kg), seventy-seven mineral separates, 126 petrographic thin-sections, field notes, maps, and photos. All rock samples were collected by Professor Coleman from 1950’s to early 1990’s. Both rocks and thin-sections are labeled with two or three-digit numbers indicating samples, abbreviation of collector's name, and two-digit numbers representing the year collected (e.g., 102-RGC-58). The labeling allows us to correlate among samples, thin-sections, notes, and maps. Some labels in the collection correspond to samples described in classic articles; we confirmed five samples in Coleman and Lee (1962), twenty-five samples in Coleman and Lee (1963), four samples in Coleman et al. (1965), four samples in Coleman and Papike (1968), and one sample in Coleman and Lanphere (1971). Thus far, we have examined all 126 petrographic thin-sections. Based on the preliminary petrographic observations using optical microscope, the samples can be grouped as metabasalt, metachert, and meta-ironstone. Hundred-eighteen thin-sections contains glaucophanic amphibole, and further forty-six glaucophane-bearing samples are characterized by the glaucophane + garnet mineral assemblage, indicating higher-grade metamorphism. Furthermore, five garnet- and glaucophane-bearing samples are eclogitic, containing mainly of garnet and omphacite. Notably one eclogite, 62-RGC-58 in Coleman et al. (1965), contains porphyroblastic lawsonite. All glaucophane-bearing samples show textbook-quality, spectacular microtexture with various color. Meta-ironstones and mtacharts also exhibit spectacular microtextures of dark-blue riebeckitic amphibole with numerous garnet, stilpnomelane, and rare deerite.

For the systematic curation, we are also attempting 'digitally archiving' paper materials. In this poster presentation, we will introduce our preliminary descriptions of the RGC Cazadero Collection, and will show potential for future petrologic and geochemical studies.

Keywords: Franciscan Belt, Blueschist, Eclogite

©2020. Japan Geoscience Union. All Right Reserved.

The Microstructure and Composition of Picrolitic Antigorite Veins in Serpentinites from the High-P Metamorphic Yuli Belt in Eastern Taiwan

*Ilona Talvikki Sakaguchi[1], Yui Kouketsu[1], Chin-Ho Tsai[2], Dominikus Deka Dewangga [2], Katsuyoshi Michibayashi[1]

1. Nagoya University, 2. National Dong Hwa University

Fluid activity plays a key role in many subduction zone processes such as in melt formation and elemental cycling. Serpentinite is an important component of the subducting oceanic lithosphere as well as the mantle wedge and the hydration and dehydration reactions of serpentine minerals have a major impact on the hydrodynamics of the subduction zone. Recently, it has also been suggested that fluids released from serpentine minerals could be the cause for seismicity occurring in subduction zones at intermediate depths (~50-300 km).

In order to study the nature of fluid flow in the subduction zone, we collected and analyzed serpentinite samples from Yuli belt, which is a high pressure metamorphic belt in eastern Taiwan. Yuli belt is mainly composed of pelitic, psammitic and chloritic schists, but also contains various other lithologies including several occurrences of serpentinites and meta-mafic rocks. The samples presented in this study were collected from the Juisui area, which is known for hosting several occurrences of glaucophane-bearing rocks suggesting that these rocks represent a relatively deep section of the subduction zone with peak metamorphic pressures around 10–13 kbar. Based on field observations, such as intensive quartz veining in the pelitic schist and Na-metasomatism in the contact of the pelitic schist and the serpentinites, it appears that the rocks in the Juisui area have been subject to widespread fluid infiltration.

Our study focuses on describing the microstructure and composition antigorite veins, which occur in the serpentinite bodies. Because antigorite is a high temperature serpentinine mineral, we interpret that the veins represent fluid flow occurring in the deeper parts of the subduction zone. The picrolitic antigorite veins have a fibrous appearance but are in fact composed of elongated splintery antigorite. The thickness of the veins ranges from a few millimeters to several centimeters. Various vein structures have been observed, including syntaxial and crack-seal veining. We also discovered several generations of cross-cutting antigorite veins suggesting multiple pulses of fluid flow. Unlike the matrix, the veins do not contain any magnetite. However, dolomite is often associated with the picrolitic antigorite veins and cross-cutting relationships imply that the CO_2-rich fluid entered the serpentinite around the same time that the antigorite veins formed. We will discuss the composition of the antigorite veins and the possible nature of the fluids that created them further in this presentation.

Keywords: Yuli belt, Serpentinite, Picrolitic antigorite veins, Subduction zone fluid flow

©2020. Japan Geoscience Union. All Right Reserved.

Estimation of P-T history of amphibolite tectonic blocks in serpentinite mélange of Kamuikotan metamorphic rocks

*Yuto Kimura[1], Toru Takeshita[1]

1. Department of Natural History Sciences, Graduate School of Science, Hokkaido University

Serpentinite mélange is a geological body which contains fragments(these are called tectonic blocks)of metamorphosed oceanic crust and sedimentary rocks.The tectonic blocks in serpentinite mélange have experienced various pressure and temperature conditions in the subduction channel.Serpentinite mé lange of the Kamuikotan metamorphic belt which is distributed in the central part of Hokkaido.According to Ishizuka and Imaizumi(1983),the estimated P-T histories are such ones where prograde metamorphism at intermediate-pressure conditions occur first,which are followed by retrograde metamorphism at high-pressure conditions based on the compositional zoning of minerals.However,Okamoto(2016)and Ando(2018)reported that many types of amphibolites are distributed in the area and compositional zoning of these minerals were found to be varied.This presentation describes new findings about tectonics and thermal evolution in the subduction zonebased on the P-T histories of the amphibolite blocks.The study area,Dainuppu river is located at c.30km northwest of Asahikawa city.Many types of amphibolite blocks occur in this area.Garnet-epidote-amphibolite show the mineral assemblage,Grt+Ep+Ca-Amp+Na-Amp+Ttn+Rt±Chl±Ms± Op,epidote-amphibolite,Ep+Ca-Amp+Na-Amp+Ttn±Rt±Chl+Ms+Qtz±Op and Chlorite rich epidote amphibolie,Ep+Ca-Amp+Ttn+Chl+Ms+Qtz±Op.The protolith of these samples is thought to derive from mafic rocks.P-T history of these samples were estimated by compositional zoning of minerals.In particular,P-T conditions of garnet-epidote-amphibolites are estimated by THERIAK-DOMINO(de Capitani and Petrakakis, 2010).As a result of these analysis,garnets recorded incleasing temperature path as shown by decresing Mn content from core to rim.Peak metamorphism of garnet-epidote-amphibolites were predicted from THERIAK-DOMINO,T=650℃,P=9.5kbar.Pistacite content($Ps=Fe^{3+}/(Fe^{3+}+Al)\times 100$)indicates decreasing temperature path as shown by increasing the ratio from core to rim(Ps=9.5 to~ 30)for all of matrix epidote.In particular, pistacite content of garnet-epidote-amphibolites recorded greater decreasing temperature than other samples.Almost all amphiboles indicate retrograde metamorphism from core to rim.Except chlorite rich epidote amphibolite,the Na-amphiboles overgrew hornblende~barroisite,shown by the drastic increases of the $^{(B)}Na$(~0.5p.f.u in core to 1.5-2.0p.f.u in rim).On the other hand,$Al^{(IV)}$ decrease 1.8-1.0 p.f.u.This retrograde metamorphism can be divided into two stages:the first where $^{(B)}Na$ remains almost unchanged at 0.55p.f.u and $Al^{(IV)}$ gradually decreases from 1.9 to 1.0-1.5p.f.u from core to rim,second which is characterized by drastic decreasing $Al^{(IV)}$ and increasing $^{(B)}Na$ (0.4-0.6p.f.u to 1.4-1.8p.f.u)in outer rim.Garnet-epidote-amphibolites and epidote amphibolite recorded both of the retrograde stages.The tectonics infered from estimated P-T history from tectonic blocks in Dainuppu river area are summerized as followed(1)Garnet-epidote amphibolites subducted at relatively warmer geotherm about 25-30℃/km(2)Subducted garnet-epidote amphibolites and epidote amphibolite were stagnated and subduction channel cooled down at least 15℃/km(3)Garnet-epidote amphibolites and epidote amphibolite were inferred to further experience retrograde metamorphism leading to the overgrowth of Na-amphiboles.The scheme of P-T history can be explain by the model of Gerya(2002) that the tectonic blocks showing clock wise and counter clock wiseP-T path which subduct earlier and later respectively, are juxtaposed at a deeper part and exhumed together,which Okamoto(2016)observed for tectonic blocks in Kamuikotan metamorphic belt.Similar P-T histories of the tectonic schemehave been inferred in eclogite from western-Iratsu body in Sambagawa belt Endo et al,(2012) and amphibolite from Nagal ophiolite complex in India Bhowmik and Ao,(2016).

©2020. Japan Geoscience Union. All Right Reserved.

Keywords: Serpentinite mélange, Metamorphic P-T history, Tectonic blocks

©2020. Japan Geoscience Union. All Right Reserved.

Datolite in the high-pressure marble from the Eastern Iratsu body of the Sanbagawa metamorphic belt

*Kenta Yoshida[1], Sota Niki[2], Hikaru Sawada[1,2], Ryosuke Oyanagi[1]

1. Japan Agency for Marine-earth Science and Technology, 2. Geochemical Research Center, The University of Tokyo

Datolite [$CaBSiO_4(OH)$] was newly found from an eclogite-facies marble collected from the Eastern Iratsu body, where the eclogite-facies metamorphism has been recognized (e.g., Takasu & Kohsaka, 1987), in the Sanbagawa metamorphic belt of central Shikoku. The investigated marble is composed of calcite-dominated matrix and quartz pool, the latter of which contains datolite as an inclusion mineral in garnet. The matrix mainly consists of calcite, diopside, and garnet. Weak foliation is defined by the elongation of coarse and deformed grains of calcite. Garnet in the matrix contains omphacite, epidote, quartz, phengite, and albite as inclusions. Quartz pool occurs concordantly with the main foliation and is composed of quartz, garnet, calcite, and diopside with trace amount of pyrite and titanite. Garnet in the quartz pool shows patchy texture with the almost pure grossular part ($Grs_{98}Adr_2$) occurring as dark cores in back-scattered electron images (BSI) and the surrounding andradite-rich part ($Grs_{90}Adr_{10}$) recognized as bright part in BSI, the latter of which contains datolite.

The formation conditions of the datolite-bearing bright part of the garnet were estimated using quartz-Raman barometry (Kouketsu et al., 2014a) and thermodynamic calculation. Quartz grains occurring in the bright part were carefully selected and measured by a Raman micro-spectrometer (RAMANtouch, NanoPhoton), yielding $\Delta\omega_1$ values of ~5. Based on the mineral assemblage, the following temperature-dependent reactions were considered in the system of CASH-CO_2 using Perple_X (Connolly, 2005). The lack of zoisite and wollastonite in the quartz pool indicates a temperature range of approximately 500-600 ºC under the assumption of X_{CO2} ~ 0.01:

zoisite + quartz + calcite = grossular + CO_2 + H_2O

calcite + quartz = wollastonite + CO_2

Consequently, the formation conditions of the datolite-bearing bright part of the garnet were estimated as ~550 ºC and 1.1-1.3 GPa, which coincide with the peak temperature conditions of surrounding non-eclogite unit of the Besshi district (Kouketsu et al., 2014b).

In the Sanbagawa metamorphic belt, the most common phase of borosilicate is tourmaline that is formed both in prograde stage and retrograde stage. Datolite is reported only as vein-filling minerals that is considered to be retrograde origin in the Sanbagawa belt (Kato et al., 1957; Minagawa and Nishio, 2002). Both datolite and tourmaline can be stable under the pressure-temperature conditions of the Sanbagawa metamorphic belt including prograde through peak to most of retrograde stage. However, datolite is generally stable under the alkaline conditions (Yang and Rosenberg, 1995) where tourmaline is not (Morgan and London, 1989). The finding of datolite instead of tourmaline indicates the strong alkaline conditions during the formation of quartz pool. Model calculations of Galvez et al. (2015) indicated that the aqueous fluids equilibrated with a metapelite under the expected P-T conditions would be alkaline conditions if carbon is not incorporated in the model. According their calculation, the alkalinity of the fluid equilibrated with the rock would decrease during the exhumation. Therefore, tourmalines recognized in the retrograde stages of the Sanbagawa metamorphic belt becomes stable due to such decrease of

©2020. Japan Geoscience Union. All Right Reserved.

alkalinity.

References: Connolly (2005) 10.1016/j.epsl.2005.04.033; Galvez et al. (2015) 10.1016/j.epsl.2015.06.019; Kato et al. (1957) 10.2465/ganko1941.41.198; Kouketsu et al. (2014a) 10.2138/am.2014.4427; Kouketsu et al. (2014b) 10.1111/iar.12075; Minagawa & Nishio (2002) Mem. Fac. Sci. Ehime Univ. 8, 11-17.; Morgan & London (1989) 10.1007/BF00373721; Takasu & Kohsaka (1987) 10.5575/geosoc.93.517; Yang and Rosenberg (1995) 10.2138/am-1995-5-616

Keywords: datolite, deep fluid, grossular, Sanbagawa metamorphic belt, borosilicate mineral

©2020. Japan Geoscience Union. All Right Reserved.

The occurrence of jadeite in the ultramafic body discovered in the Sanbagawa belt, Shibukawa region, central Japan

*Hikaru Shioya[1], Katsuyoshi Michibayashi[1], Yui Kouketsu[1], Masaki Enami[1]

1. Nagoya University

The Sanbagawa belt is a representative high-pressure metamorphic belt of southwestern Japan. Shibukawa region is located along the border of Aichi and Shizuoka prefectures and consists of the Sanbagawa crystalline schist group and the Mikabu greenstone group. The Sanbagawa group consists of pelitic, psammitic and siliceous schists and the Mikabu group consists dominantly of greenstones with hornblendite, metagabbro and ultramafic bodies. Both groups occur alternatively in the region. The blueschist phase indicators such as jadeite, glaucophane and lawsonite have been reported previously. In particular, jadeite occurs in metagabbroic rocks surrounded by ultramafic rocks or lawsonite-bearing schists(Seki, 1960; Seki et al., 1960). From our field observation, we discovered jadeite-bearing veinlet was discovered in a dunite block of the Shibukawa ultramafic body. The veinlet cut through the dunite block and occur ~5mm in width. The veinlet consists of diopside, grossular garnet, chlorite and relict olivine in addition to jadeite, and minor euhedral magnetite. Jadeite grains occur as anhedral patches in the grossular grains and their grain sizes are less than 100 μm. The major element compositions of jadeite are rich in Na and Al (Na_2O=14.7–15.4 wt.%; Al_2O_3=24.3–25.5 wt.%) and poor in Ca (CaO=0.4–1.3 wt.%). Jadeite values (=(Na-Fe^{3+})/(Na+Ca)x100) are 92–97%. In this study, we present the occurrence and chemical compositions of jadeite in detail and discuss how this high-pressure mineral has been taken place in the Shibukawa region.

References

Seki, Y., 1960, Jadeite in Sanbagawa crystalline schists of central Japan. *Am. J. Sci.*, **258**, 505-715.
Seki, Y., Aiba, M. and Kato, C., 1960, Jadeite and minerals of meta-gabbroic rocks in the sibukawa district, central Japan. *Am. Min.*, **45**, 668-679.

Keywords: Sanbagawa belt, Ultramafic, Jadeite, Rodingite

©2020. Japan Geoscience Union. All Right Reserved.

Geochronology of the Yorii metamorphic rocks on the Kanto Mountains - Extension of the Abukuma metamorphic rocks to Southwest Japan.

Shota Matsunaga [2], *Atsushi MIYASHITA[1], Tatsuki Tsujimori[2], Kazumasa Aoki[3], Shogo Aoki[3]

1. Seikei University, 2. Tohoku University, 3. Okayama University of Science

In the Pacific type orogen, non-metamorphic accretionary complexes (AC) and high *P/T* metamorphic rocks as deeper facies of AC, often exist in pairs, for example as the Shimanto belt and Sanbagawa belt. Jurassic AC is widely distributed in Japan arc. On Northneast Japan, part of the deep facies of the Jurassic AC are thought to be the Abukuma metamorphic belt (Hiroi, 1998). On Southwest Japan, the Oshima metamorphic rocks in the Shikoku region and the Higo metamorphic rocks in the Kyushu region are corresponding to the Abukuma belt, but it's not distributed widely (Takagi and Arai, 2003).
Tiny metamorphic rock masses are distributed in the low angle faults of the base of Atogura Nap in the Yorii area, the Kanto Mountains. These metamorphic rocks are called the Yorii metamorphic rocks (Takagi, 1991). The Yorii metamorphic rocks have been pointed out to be similar to the Abukuma metamorphic rocks on the basis of the Sr isotope initial values of the accompanying granites, but the sedimentary age and the metamorphic age of the original rocks have not been clarified.
In this study, the zircons U-Pb ages in pelitic gneisses of the Yorii metamorphic rocks were determined by LA-ICPMS. These ages are close to the zircon U-Pb ages and fossil ages of the Abukuma Belt, and it's indicates that the Yorii metamorphic rocks are probably an extension of the Abukuma Belt to Southwest Japan.

Hiroi Y et. al., 1998, J. Metamorphic Geol., 16, 67-81.
Takagi, H. (1991), Gakujutsu Kenkyu (Scientific Res.), School of Education, Waseda Univ., Ser. Biol. Geol., 40, 9-25.
Takagi H. and Arai H., (2003),Gondowana Res., 6, 657-668.

Keywords: Yorii Metamorphic Rocks, Abukuma Metamorphic Belt, Zircon U-Pb age

©2020. Japan Geoscience Union. All Right Reserved.

Geology, deformation, and metamorphism of high-grade Shimanto accretionary complex in Kerama Islands, Okinawa, Ryukyu arc

*Ippei Yamamoto[1], Kenichiro Tani[2], Yui Kouketsu[3], Rina Fukuchi[1], Hiroaki Koge[4], Asuka Yamaguchi[1]

1. Atmosphere and Ocean Research Institute, The University of Tokyo, 2. National Museum of Nature and Science, 3. Nagoya University, 4. National Institute of Advanced Industrial Science and Technology

The along-arc distribution of accretionary complexes in the Japanese Islands is extended to the Ryukyu arc. Kerama Islands is located at the southwestern edge of the Cretaceous to Paleogene Shimanto belt, 30 km away from Naha, Okinawa. Geology of Kerama Islands was reported until 1980s (Kashima and Takahashi, 1978; Kizaki and Yamamoto, 1985). Previous study shows that mineral composition of greenstone (epidote + actinolite) suggests high-*T* metamorphic condition and geochemical features of greenstone correspond to N-MORB (Chinen *et al.*, 2004). However, neither depositional age nor deformation structures of Kerama Islands has not been analyzed yet. In this study, we report lithology, deformation structure, depositional and metamorphic age, and peak paleotemperature of Kerama Islands to reconstruct formation history of accretionary complex. Implication of tectonic background in this area will be presented in “New perspectives on the geodynamics of East Asia” (S-IT29) session of this meeting.

In agreement with previous studies (Kashima and Takahashi, 1978; Kizaki and Yamamoto, 1985), our new geological map shows that the bedrock of Kerama Islands is made up of a pile of three lithological units, greenstone, metasandstone, and pelitic schist in ascending order. Metasandstone unit is characterized by massive metasandstone including psammitic schist layers. Dynamically recrystallized quartz grains are commonly observed under a microscope. Pelitic schist unit, which often consists of alternation of pelitic and psammitic schist, shows well-defined schistosity and overlies metasandstone unit with conformity boundary. Detailed observation of the contact between the top of greenstone unit and the bottom of sedimentary rock layer shows that the boundary records intrusion of basaltic lava, the protolith of the greenstone. In contrast, bottom of the greenstone unit is characterized by “conglomerate mylonite” originated from gravel sandstone, which records evidence of ductile shear deformation along an estimated thrust forming duplication of greenstone and metasediments.

Foliation of green, pelitic, and psammitic schists is parallel to bedding plane and dips SW in general. Stretching lineations and fibers of layer-parallel quartz veins on the foliation exhibit NW-SE trend. Axes of asymmetric folds observed in pelitic schist unit show NE-SW trend, suggesting top-to-SE shear. The fold axes are perpendicular to stretching lineations. High-angle normal faults branching from low-angle normal fault are found in pelitic schist unit. These deformation features are classified into three deformation stages: D1 (underthrusting), D2 (underplating) and D3 (exhumation), respectively.

U-Pb ages of detrital zircon grains obtained from metasandstone in Kerama Islands were carried out using LA- ICP-MS installed at the National Museum of Nature and Science. The youngest age of zircon is 104-110 Ma (early Cretaceous) and no zircon grains with late Cretaceous age is obtained.

We examined peak metamorphic temperature of pelitic schist and conglomerate mylonite. Raman spectra of carbonaceous materials in thin section of the samples are obtained using a Raman spectrometer with a 532 nm Nd-YAG laser (system installed at Nagoya University). The result shows that the bedrock of

©2020. Japan Geoscience Union. All Right Reserved.

Kerama Islands suffered 470-525˚C, which is consistent with the temperature range of metamorphic facies proposed in the greenstone.

The depositional age of the protolith of Kerama metamorphic rock is ˜100 Ma, corresponds to that of the northern part of the Shimanto belt. However, metamorphic temperature of the metamorphic rock in Kerama Islands is definitely higher than any reported temperatures in the Shimanto belt. Based on protolith age and metamorphic condition, Kerama metamorphic rock would be correlated to Sanbagawa belt in SW Japan (Itaya *et al.*, 2011; Aoya and Endo, 2017), Nagasaki metamorphic rock (Kouchi *et al.*, 2011), or Tananao schist belt in Taiwan (Chen *et al.*, 2016).

©2020. Japan Geoscience Union. All Right Reserved.

[E] Poster | S (Solid Earth Sciences)：S-MP Mineralogy & Petrology

[S-MP39] Oceanic and Continental Subduction Processes

convener:REHMAN Hafiz Ur(Department of Earth and Environmental Sciences, Graduate School of Science and Engineering, Kagoshima University), Tatsuki Tsujimori(Tohoku University), Kazuaki Okamoto(Faculty of Education, Saitama University)

This session aims at bringing earth scientists from Japan and overseas to present their research related to the processes of oceanic and continent subduction, continent-continent collisions, metamorphism of crustal rocks, formation of the oceanic/continental arcs, and accretion/ tectonic erosion of material along subduction boundaries.

Topics such as role of the fore- and back-arcs in the subduction zones, process of accretion of volcaniclastic and terrigenous sediments along the subduction/collision boundaries, deformation and metamorphism of subducted crust, and exhumation will be the main focus of the session.

Exchange of ideas among geoscientists applying different approaches on problems related to the theme of the session are most welcome.

[SMP39-P01] Deeply subducted Jurassic ridge hydrothermal ore deposit -case study from the Sanbagawa eclogite-amphibolite-blueschist-

Yuki Wakabayashi[1], *Yukari Otsuka[1], Kazuaki Okamoto[1] (1.Saitama University)

[SMP39-P02] Metasomatic and metamorphic signature of the MORB in the Shimanto belt

*Yuka Mikami[1], Kazuaki Okamoto[1] (1.Saitama University)

[SMP39-P03] New titanite U–Pb age of so-called 'Inishi-type' calcareous rock from the Hida Belt: Constraints on timing of the carbonate–silicate rock interaction during a collision

*Hironobu Harada[1], Tatsuki Tsujimori[1], Shogo Aoki[2], Kazumasa Aoki[2] (1.Tohoku Univesity, 2.Okayama Univerity of Science)

[SMP39-P04] Stable isotope study of carbonate associated with antigorite serpentinite: O–C isotope characterization of a textually zoned calcite rock from the Itoigawa–Omi area, Japan

*Toshiaki Komata[1], Tatsuki Tsujimori[1], Hideko Takayanagi[1], Yasufumi Iryu[1] (1.Tohoku University)

[SMP39-P07] The Miocene Kaikomagatake granitoid pluton in the Izu collision zone, central Japan: its petrogenesis, emplacement depth and exhumation history

*Satoshi SAITO[1] (1.Graduate School of Science and Engineering, Ehime University)

[SMP39-P08] Whole-rock chemical composition of the granitoids in Ryoke belt, Takanawa Peninsula, northwest Shikoku, southwest Japan

*Kazuya Shimooka[1], Satoshi SAITO[1], Kenichiro Tani[2], Toshiro Takahashi[3] (1.Graduate School of Science and Engineering, Ehime University, 2.National Museum of Nature and Science, 3.Graduate School of Science and Technology, NiigataUniversity)

[SMP39-P09] Pressure-to-depth conversion models for metamorphic rocks: review and application

*Arthur Bauville[1], Philippe Yamato[2] (1.Center for Mathematical Science and Advanced Technology, JAMSTEC, 2.University of Rennes 1, France)

[SMP39-P10] Late Paleozoic-early Mesozoic magmatism in Delgerkhaan region, Central Mongolia: constraints from the zircon U-Pb age and geochemistry

*Ariuntsetseg Ganbat[1], Tatsuki Tsujimori[1,2], Chimedtseren Anaad[3], Munkhtsengel Baatar[3], Inna Safonova[4,5] (1.Department of Earth Science, Graduate School of Science, Tohoku University, Sendai, Japan, 2.Center for Northeast Asian Studies, Tohoku University, Sendai, Japan, 3.Mongolian University of Science and Technology, Ulaanbaatar, Mongolia , 4.Novosibirsk State University, Novosibirsk, Russia, 5.Sobolev Institute of Geology and Mineralogy, SB RAS, Novosibirsk, Russia)

Deeply subducted Jurassic ridge hydrothermal ore deposit -case study from the Sanbagawa eclogite-amphibolite-blueschist-

Yuki Wakabayashi[1], *Yukari Otsuka[1], Kazuaki Okamoto[1]

1. Saitama University

Subduction of cold oceanic plate transports water down to mantle although most amount of water is released by dehydration process. The dehydration reaction and fluid chemistry are fixed by P, T, and redox state. High P/T metamorphic rocks are exhumed from the paleo-subduction zone. Therefore, dehydration process was recorded in the high P/T rocks. The sanbagawa metamorphic rocks suffered high P/T metamorphism at Cretaceous. It is notice that the Besshi-type ore deposit (Volcanogenic massive sulfide) is included in the Sanbagawa metamorphic rocks. origin of the Besshi ore deposit was related to Jurassic global deep-sea hydrothermal activity. Presence of the Bessi-type ore deposit in subducting plate might have controlled the redox state of blueschist-eclogite transformation. Field observation and sample collection were done from eclogite, amphibolite and blueschist outcrops from the Besshi area. In the Besshi area, the metamorphic rocks dips northward in general. Therefore, from north to south, the structural succession is traceable. From the north, metabasite-metachert association overlies the Tonaru eclogite mass, and amphibolite-blueschist succession underlies. The origin of the metabasite-association is ascribed as MORB and deep-sea sediment. Protolith of the Tonaru eclogite is considered as subducted oceanic Island Arc (Aoki et al., 2019). Under the microscope observation these rocks never contain considerable amount of sulfides. Underlying amphibolite and blueschist have mine drifts in each lithologies with certain sulfides. Bulk chemistry suggests that the protoliths are MORB and OIB. It suggests that the Sanbagawa amphibolite-blueschist has brought the ridge hydrothermal material beneath the stacked oceanic Island arc material in deep subduction zone at Cretaceous. Thus, subducted Jurassic-deep-sea-hydrothermal material was stored beneath the stacked Oceanic Island Arc in Cretaceous mantle.

Keywords: Subduction, Sanbagawa

©2020. Japan Geoscience Union. All Right Reserved.

Metasomatic and metamorphic signature of the MORB in the Shimanto belt

*Yuka Mikami[1], Kazuaki Okamoto[1]

1. Saitama University

Subduction and accretion history of Pacific plate is well reconstructed in the orogenic belt in SW Japan (e.g. Maruyama et al.,1997). Shimanto belt is composed of accretion complex from Cretaceous to Tertiary (e.g. Kimura et al.,2013). It distributes from the Kanto to Kyushu area extending over 800 km. Protoliths of the Shimanto belt is mainly composed of terrigenous sandstone and pelitic rocks and minor amount of limestone, chert and basalt. Origin of the Cretaceous basalt has been considered as either in-situ MORB due to ridge-subduction or accreted MORB due to the ridge subduction (e.g. Onishi and Kimura.1995). Recently Nozaki et al. (2018) have shown that the ridge hydrothermal ore deposit is associated the MORB in the Shimanto belt. To testify the extent of the hydrothermal alteration, we investigated the outcrops from Gobo area, in western Kii district. and Makimine area, Nobeoka district. From the Gobo area, the MORB outcrop is included as pillowed basalt in the sandstone mélange. The pillow margin suffered cataclastic deformation with alteration. In the Makimine area, there is a porphyry granite intruding the sandstone, and suffered contact metamorphism. Surrounding layers also suffered mylonitic deformation with metamorphism. Presence of large ring-dike (Okureyama dike) and Miocene granite are considered as overriding accreted margin on the subducting ridge due to back-arc rifting at 15 Ma. Contribution of the melt and heating effect from the hanging wall side of the Nobeoka thrust (the out-of-sequence thrust) might be greater than fluid facilitation of the thrust movement.

Keywords: MORB, contact metamorphism, the out-of-sequence thrust

©2020. Japan Geoscience Union. All Right Reserved.

New titanite U–Pb age of so-called 'Inishi-type' calcareous rock from the Hida Belt: Constraints on timing of the carbonate–silicate rock interaction during a collision

*Hironobu Harada[1], Tatsuki Tsujimori[1], Shogo Aoki[2], Kazumasa Aoki[2]

1. Tohoku Univesity, 2. Okayama Univerity of Science

Titanite ($CaTiSiO_5$) is a widespread accessory mineral in calcareous gneiss that can contain small amount of uranium in its lattice. Because of relatively high closure temperature of Pb in titanite (~600–700˚C), it has a potential for direct dating of titanite-forming metamorphic reaction using the U–Pb isotopic system. We conducted titanite LA-ICPMS U–Pb dating for so-called 'Inishi-type' calcareous rock from the Hida Belt. The calcareous rock has also known as clinopyroxene-bearing migmatite, which is characterized by the presence of coarse-grained diopside–hedenbergite series clinopyroxene and titanite. It has been thought that the 'Inishi-type' calcareous rock had formed by the interaction between marble and amphibolite that might have occurred at a period of anatexis of lower to middle crust accompanying regional deformation and felsic magma intrusion. The investigated sample is pegmatitic calcareous rock that contains the mineral assemblage plagioclase ($An_{>25}$) + orthoclase + quartz + clinopyroxene + titanite ±calcite. The abundant occurrence of orthoclase suggests an effect of mixing of anatectic melt with a syenitic composition.

LA-ICPMS analyses of coarse-grained titanites show highly variable $^{238}U/^{206}Pb$ ratio (15.0–24.0) and $^{207}Pb/^{206}Pb$ ratio (0.172–0.419). The scattered trend defines an isochron line with a lower intercept at 225.4 ±2 Ma. This age was also supported by U–Pb age (222 ±3 Ma) of metamorphic zircon formed in marble. Our new titanite age is slightly younger than the inferred timing of peak metamorphism of the Hida Belt (~240 Ma). However, the result clearly indicates that 'Inishi-type' calcareous rock was formed by the post-collisional event, possibly anatectic event accompanying intrusion of syenitic magma into the calcareous rock. The timing of these events consistent with the age of post-collisional migmatite and syenite from the Sulu–Dabie ultrahigh-pressure metamorphic belt. Although zircon geochronology is not simple in orthogneiss-dominant polymetamorphosed metamorphic complex like the Hida Belt, titanite U–Pb dating for reaction rock formed via carbonate–silicate rock interaction would be effective to interpret timing of specific event

Keywords: titanite, U-Pb dating, Hida Belt

©2020. Japan Geoscience Union. All Right Reserved.

Stable isotope study of carbonate associated with antigorite serpentinite: O–C isotope characterization of a textually zoned calcite rock from the Itoigawa–Omi area, Japan

*Toshiaki Komata[1], Tatsuki Tsujimori[1], Hideko Takayanagi[1], Yasufumi Iryu[1]

1. Tohoku University

In order to understand carbon behavior in forearc serpentinite, we investigated a textually zoned metasomatic calcite rock associated with antigorite serpentinite of the Non-eclogitic Unit of the Omi area, Japan (Tsujimori, 2004 [doi:10.5575/geosoc.110.591]; Yamada et al., 2019 [doi:10.2465/jmps.190726]). The investigated calcite rock (~ 10 cm in size) occurs in 'blackwall'-like outcrop of chlorite-tremolite rock containing decimeters-size blocks of amphibolite and partially-carbonated antigorite serpentinites. The presence of antigorite and feritchromite in serpentinites and the lack of glaucophanitic amphibole rim in the hornblende of amphibolite suggest that the calcite rock had formed at the amphibolite-facies condition. The calcite-rich rock shows a concentric zoning that subdivided into three layers based on mineral assemblages. In the core part, a pseudomorph consisting of microcrystalline calcites with polycrystalline fine-grained talc aggregates suggest the presence of precursor dolomite. The transition of the mineral assemblage calcite + talc + quartz at the core to the assemblage calcite + talc + tremolite + quartz in the middle layer can be explained by decreasing X_{CO2} and/or increasing temperature.

Despite the zoned texture and the different mineral assemblage, systematic stable carbon and oxygen isotope analyses using by micro-sampling technique found no clear core-to rim change. $\delta^{13}C$ (‰ VPDB) and $\delta^{18}O$ (‰ VSMOW) values are from −5.0 to −4.1‰ (average −4.4‰ [n = 34]) and +15.6 to +16.4‰ (average 16.1‰ [n = 34]), respectively. It is noteworthy that $\delta^{13}C$ of zoned calcite rock is significantly higher than the $\delta^{13}C$ values of graphite (−8.6 to −7.9‰) in jadeitite in the Omi area (Ogawara and Akai, 2014 [doi:10.2465/jmps.131125a]) and also dolomite nodule (−13.4 to −13.6‰; this study) associated with lizardite serpentinite in the Franciscan Complex. Although there are a few possible carbon sources for the calcite rock, the $\delta^{13}C$ close to −5‰ might have reflected a mantle-derived carbon. On the other hand, relatively high $\delta^{18}O$ values suggest that the calcite-rock-forming aqueous fluids were in equilibrium with metasedimentary rocks.

Keywords: antigorite serpentinite, metasomatic rock, carbon isotope, oxygen isotope, amphibolite-facies

©2020. Japan Geoscience Union. All Right Reserved.

The Miocene Kaikomagatake granitoid pluton in the Izu collision zone, central Japan: its petrogenesis, emplacement depth and exhumation history

*Satoshi SAITO[1]

1. Graduate School of Science and Engineering, Ehime University

The Miocene Kaikomagatake pluton is one of the Neogene granitoid plutons exposed in the Izu collision zone, where the juvenile Izu-Bonin oceanic arc is colliding against the mature Honshu arc. The pluton intrudes discordantly into the Cretaceous to Paleogene Shimanto accretionary complex of the Honshu arc along the Itoigawa-Shizuoka Tectonic Line, which is the collisional boundary between the two arcs. The pluton consists mainly of hornblende–biotite-bearing granodiorites and biotite-bearing granite. Zircon U-Pb age of 13.8 –12.4 Ma were reported (Sueoka et al., 2017), interpreted as the crystallization age of the pluton.

The Kaikomagatake pluton has SiO_2 contents of 68–75 wt%. It has high-K series compositions and its incompatible element abundances are comparable to the average upper continental crust. Major and trace element compositions of the pluton show well defined chemical trends. The trends can be interpreted with a crystal fractionation model involving the removal of plagioclase, biotite, hornblende, quartz, apatite and zircon from a potential parent magma with a composition of ~68 wt% SiO_2. The Sr isotopic compositions, together with the partial melting modeling results, suggest that the parent magma is derived by ~53 % melting of a hybrid lower crustal source comprising ~70 % K-enriched basaltic rocks of the Izu-Bonin arc and ~30 % Shimanto metasedimentary rocks of the Honshu arc. The petrogenetic model of the Kaikomagatake pluton suggests that the contribution of the metasedimentary component is required to produce incompatible element-rich granitoid magma with compositions comparable to the average upper continental crust (Saito et al., 2012).

The emplacement depth of the Kaikomagatake pluton estimated by the Al-in-hornblende geobarometer is ~2.2 –2.4 kbar (Watanabe et al., under revision). Combined with low-temperature thermochronological data reported by Sueoka et al. (2017), the magma emplaced and solidified at the upper to middle crustal depth (~9 –8 km depth) at 14 –12 Ma and is situated at the depth for a period of ~10 million years, and then uplifts rapidly after ~3.3 Ma with the exhumation rate of ~4 mm/year. The early stage of the collision between the Izu-Bonin and the Honshu arcs contributed little to exhumation of the collision zone crust at the Kaikomagatake pluton area.

References:
Saito et al. (2012) Contributions to Mineralogy and Petrology, 163, 611–629.
Sueoka et al. (2017) Journal of Geophysical Research: Solid Earth, 122, doi:10.1002/2017JB014320.
Watanabe et al. (under revision) Submitted to Journal of Metamorphic and Petrological Sciences.

Keywords: Granitoid, Kaikomagatake pluton, Izu collision zone

©2020. Japan Geoscience Union. All Right Reserved.

Whole-rock chemical composition of the granitoids in Ryoke belt, Takanawa Peninsula, northwest Shikoku, southwest Japan

*Kazuya Shimooka[1], Satoshi SAITO[1], Kenichiro Tani[2], Toshiro Takahashi[3]

1. Graduate School of Science and Engineering, Ehime University, 2. National Museum of Nature and Science, 3. Graduate School of Science and Technology, NiigataUniversity

Mesozoic to Early Cenozoic granitic rocks are widely distributed along the Circum-Pacific continental margins. The Cretaceous –Paleogene granitic rocks in southwest Japan are a part of huge igneous belts that developed along the continental margin of East Asia. The granitic rocks in southwest Japan have been divided into three arc-parallel provinces including the Ryoke, San-yo, and San-in Belts based on their lithologies and geochemical characteristics, associated ore deposits, and formation ages (Ishihara, 1971). The Ryoke Belt is the type locality for the low-P/high-T metamorphic facies series defined by Miyashiro (1961), and consists of metamorphic rocks and Cretaceous ‘I-type’ and ilmenite-series granitoids (Takahashi et al., 1980). It has been suggested that a transect from the San-yo to Ryoke Belt represents a crustal cross section of the Cretaceous Asian continental margin down to mid-crustal depths (12–14km), and the Ryoke Belt represents the deep crust (Nakajima, 1994, 1996). Therefore, understanding the petrological processes of granitoid formation in the Ryoke Belt would contribute to understanding deep crustal processes along the continental margin (e.g., Akasaki et al., 2015).

We carried out whole-rock and Sr-Nd isotope analysis of the Ryoke granitoids exposed in the Takanawa Peninsula to indicate their petrological characteristic. Takanawa Peninsula located in northwest Shikoku island, southwest Japan. Multiple granitoids are distributed on the Takanawa Peninsula. The granitoids are mainly comprised of tonalitic rocks, granodioritic rocks, and granitic rocks. These show different SiO_2 content : 61-68 wt% for tonalitic rocks, 67-76 wt% for granodioritic rocks, 70-80 wt% for granitic rocks. And these show multiple trends on Harker diagram. Sr-Nd isotope composition of granitoids shows equivalent contents between SrI: 0.70669-0.70793 and NdI: 0.51217-0.51234. The multiple trends on Harker diagram suggest this area’s granitoids were comprised multiple magma. Similar SrI and NdI contents in granitoids suggest the same source of granitoids. Kagami et al. (1985; 2000) and Kodama et al. (2019) showed mafic rocks around this area had similar SrI (0.70654-0.70657) and NdI (0.51173-0.51241) composition to granitoids. Our results suggest that mafic rocks are a source material of granitoids in Takanawa Peninsula.

Reference: Akasaki et al. (2015) Lithos 230, 82 91. Ishihara (1971) Jour. Geo. Soc. Japan 77, 441–452. Kagami et al. (1985) Geochem. J. 19, 237-243. Kagami et al. (2000) Island Arc 9, 3-20. Kodama et al. (2019) Jour. Minral. Petrol. Sci. 114, 99-104. Miyashiro (1961) Jour. Petrol. 2, 277–311. Nakajima (1994) Lithos 33, 51–66. Nakajima (1996) Transactions of the Royal Soc. Edinburgh: Earth Sciences 87, 183–91. Ochi (1982) Geo. Soc. Japan 88, 511-522. Shimooka et al. (2019) Jour. Minral. Petrol. Sci. 114, 284-289. Takahashi (1980) Mining Geology, Special Issue 88, 13–28.

Keywords: Granitoids in Ryoke belt, Whole-rock chemical composition , Sr-Nd isotope, Takanawa Peninsura

©2020. Japan Geoscience Union. All Right Reserved.

Pressure-to-depth conversion models for metamorphic rocks: review and application

*Arthur Bauville[1], Philippe Yamato[2]

1. Center for Mathematical Science and Advanced Technology, JAMSTEC, 2. University of Rennes 1, France

Pressure estimated from metamorphic rocks is one of the main tools for geodynamic reconstructions. The pressure-temperature path of UHP metamorphic rocks typically shows a linear increase of P and T followed by a rapid drop of Pressure at near-constant temperature. The geological history can be reconstructed by using the metamorphic pressure as a proxy for depth. Researchers often base their geodynamic reconstruction on a simple linear mapping of pressure to depth, by considering that the pressure is the weight of the overlying column of rock or lithostatic pressure. In recent years, an increasing corpus of evidence demonstrates that rocks can experience pressures that deviate from the lithostatic state on the order of GPa. These deviations can be at the scale of the orogen (Petrelli and Podladchikov, 2002), the outcrop (Jamtveit et al., 2018; Luisier et al., 2019); or even at the grain-scale (Tajcmanova, 2015). Thus, these studies raise the concern that metamorphic pressures may not be reliable proxies for depth, and therefore could not be used for geodynamic reconstructions. The objective of this contribution (1) to review the various models proposed in the literature for metamorphic pressure, (2) to formulate analytical models with simple assumptions that can be used to convert metamorphic pressure to depth even in the case where pressure deviates significantly from the lithostatic pressure. We use our pressure-to-depth conversion models to estimate the depth of ~60 samples from various orogens worldwide. The prediction of the different models varies widely. Some models predict depth as deep as 160km for specific samples, while other models predict depth <75 km (i.e. deepest depth of the Moho) for all data points. We discuss the limits of applicability and the geodynamic implications of each model.

Keywords: metamorphism, overpressure, pressure-to-depth

©2020. Japan Geoscience Union. All Right Reserved.

Late Paleozoic-early Mesozoic magmatism in Delgerkhaan region, Central Mongolia: constraints from the zircon U-Pb age and geochemistry

*Ariuntsetseg Ganbat[1], Tatsuki Tsujimori[1,2], Chimedtseren Anaad[3], Munkhtsengel Baatar[3], Inna Safonova[4,5]

1. Department of Earth Science, Graduate School of Science, Tohoku University, Sendai, Japan, 2. Center for Northeast Asian Studies, Tohoku University, Sendai, Japan, 3. Mongolian University of Science and Technology, Ulaanbaatar, Mongolia , 4. Novosibirsk State University, Novosibirsk, Russia, 5. Sobolev Institute of Geology and Mineralogy, SB RAS, Novosibirsk, Russia

Investigating geochemical characteristics and crystallization age of igneous rocks is necessary to understand their petrogenesis and relation of orogenic belts formed in place of former oceans. The Mongol-Okhotsk orogenic belt is the youngest segment of the world’ s largest Central Asian orogenic belt. It formed by the suturing of the Mongol-Okhotsk Ocean and subsequent collision of the Siberian and North China cratons in late Paleozoic to Mesozoic time. The general geology and numerous intrusions of mafic to felsic igneous rocks younging from west to east along the Mongol-Okhotsk suture suggest that the ocean closed in a scissor-like manner, from the late Carboniferous to the Permian in central Mongolia and/or until the Triassic–early Jurassic in southeastern Transbaikalia. However, the robust time of its closure remains debatable. There are numerous large volcano-plutonic fields of late Paleozoic to late Mesozoic ages distributed over a huge territory from Russian Transbaikalia to northern and central Mongolia. The volcano-plutonic belts host abundant granitoid intrusions, both small to medium size plutons and huge batholiths. We studied igneous rock complexes in the Delgerkhaan region of the Khangay-Khentey turbidite basin, Central Mongolia, in order to understand the tectonic evolution of the western Mongol-Okhotsk belt. The study area hosts several granitoid plutons of diorite, granodiorite, monzodiorite, monzogranite and alkaline granite distinguished as Avdrant, Delgerkhaan and Batkhaan granitoid complexes, which intrude Devonian-Carboniferous sediments of the Khangay-Khentey turbidite basin. The zircons separated from seven representative intrusions have euhedral-subhedral shapes, oscillatory magmatic zoning, and Th/U values of 0.38-1.3, indicating their magmatic origin. The zircons of Batkhaan granitoids (2 samples) yielded U-Pb ages of 274±1 Ma and 282±3 Ma (~ Early Permian). The U-Pb ages of zircons of Delgerkhaan and Avdrant granitoids (5 samples) show the time of their emplacement between 240±3 Ma and 220±1 Ma (~Late-Middle Triassic). Chemically, the Early Permian intrusions and coeval rhyolitic lavas show typical geochemical affinities to A-type granites, i.e. high silica, alkalis and high-field strength elements (HFSE), element (REE) spectra. In tectonic discrimination diagrams, their compositions all plot in the fields of A-type granites. On the contrary, the Late-Middle Triassic intrusions are characterized by a wider range of major oxides matching the normal and high-K subalkaline series and indicating their affinity to I-type granites. In addition, they are enriched in light REE and large ion lithophile elements, depleted in heavy REE and HFSE, and show no or minor negative Eu anomalies. The Late-Middle Triassic intrusions are compositionally similar to igneous rocks formed in an active continental margin setting. According to the previous studies, island arc magmatism and double-sided subduction of the oceanic crust of the Mongol-Okhotsk Ocean started in early Carboniferous time followed by the deposition of the turbidite basin. The A-type geochemical features of the Early Permian granites and rhyolites allow us to conclude that they formed by low-degree partial melting of a crustal source in an extensional setting, which was triggered by slab break-off during subduction of the Mongol-Okhotsk oceanic plate.

©2020. Japan Geoscience Union. All Right Reserved.

Keywords: Late Paleozoic–early Mesozoic magmatism, Geochronology, Geochemistry, Mongol-Okhotsk Ocean

©2020. Japan Geoscience Union. All Right Reserved.

[E] Poster | S (Solid Earth Sciences)：S-MP Mineralogy & Petrology

[S-MP40] Thermal structure of subduction zones: modeling and the rock record

convener:Simon Richard Wallis(The University of Tokyo), Takayoshi Nagaya(Graduate School of Science, The University of Tokyo), Shoichi Yoshioka(Research Center for Urban Safety and Security, Kobe University)

The thermal structure of subduction zones is key to understanding the origin of magma,
the cycling of rocks and volatiles and the distribution of earthquakes in these regions. In recent years there have been many recent advances in thermal modeling of subduction zones and most are in broad general agreement. However, different approaches and different assumptions about boundary conditions mean that significant differences remain. The rock record of subduction-type metamorphism has the potential to provide useful additional constraints on the conditions of otherwise inaccessible regions. However, with few exceptions this record has not been closely considered in developing models. Recent studies have highlighted differences between the range of subduction conditions preserved in the rock record and those predicted for modeling of modern subduction zones. However, the reasons for such differences are unclear. Key remaining questions are how to improve the consistency between the modeling and rock record, and the most effective use of the rock record to constrain the boundary conditions for modeling. We invite contributions from subduction zone modelers and researchers of subduction-type metamorphic rocks. The aim of this session is to explore how best to combine these two approaches to estimate conditions along subduction zones and to improve our understanding of these geologically important regions.

[SMP40-P01] Brucite as a major phase in the shallow mantle wedge

*Takayoshi Nagaya[1], Simon Richard Wallis[1], Kazuhiro Kawahara[2], Shunsuke Endo[3], Hiroshi Mori[4], Yoshihiro Asahara[5] (1.Graduate School of Science, The University of Tokyo, 2.Japan Oil, Gas and Metals National Corporation, 3.Shimane University, 4.Shinshu University, 5.Nagoya University)

[SMP40-P02] Development of high fluid pressure at the base of the shallow mantle wedge due to presence of an antigorite shear zone

*Simon Richard Wallis[1], Mari Yokota[1,2] (1.The University of Tokyo, 2.Nagoya University)

[SMP40-P03] Mineralogy and structure of the shallow mantle wedge: evidence from seismic anisotropy in the Ryukyu Arc and structural petrological studies

*Takayoshi Nagaya[1], Simon Richard Wallis[1], Andrew Walker[2], James Wookey[3], Kazuhiko Ishii[4], Michael Kendall[5] (1.Graduate School of Science, The University of Tokyo, 2.University of Leeds, 3.University of Bristol, 4.Osaka Prefecture University, 5.University of Oxford)

[SMP40-P04] Low-pressure type metamorphic rocks from No-jima Island, Yamaguchi Prefecture

*ZEJIN LU[1] (1.Graduate School of Science and Engineering for Innovation, Yamaguchi University)

Brucite as a major phase in the shallow mantle wedge

*Takayoshi Nagaya[1], Simon Richard Wallis[1], Kazuhiro Kawahara[2], Shunsuke Endo[3], Hiroshi Mori[4], Yoshihiro Asahara[5]

1. Graduate School of Science, The University of Tokyo, 2. Japan Oil, Gas and Metals National Corporation, 3. Shimane University, 4. Shinshu University, 5. Nagoya University

The shallow part of the mantle wedge in convergent margins is relatively low temperature and influx of water from the subducting slab will cause peridotite mantle to become serpentinized. If this serpentinization affects olivine-rich mantle and proceeds under low SiO2 activity, brucite can be a major phase where temperatures are <450˚C. However, only very few natural examples have been documented mostly from blocks witin serpentinite diapirs associated with subduction along the Izu-Bonin arc and the proportion and distribution of this mineral in the mantle wedge is not well known. The formation of brucite is generally thought to be suppressed by the supply of silica in excess of that present in olivine, either by the break down of pyroxene or the inflow of SiO2 in aqueous solution. The presence of brucite causes a drastic lowering of the strength of serpentinite even at proportions of a few per cent and determining its distribution and proportion is a key issue in developing physical models for the shallow mantle wedge. The subduction-type Sanbagawa metamorphic belt contains a large number of units derived from the wedge mantle. One of the largest of these units is the Shiraga metaserpentinite body. Brucite is present in two types (brucite I and II) that can be distinguished by their chemical zonation and microstructure. Brucite I shows clear reaction microstructures with antigorite to form olivine. In contrast, brucite II shows no reaction relationships with antigorite and is interpreted as a retrograde product. The original amount of brucite I was estimated based on both thermodynamic modeling combined with bulk rock composition and point counting of constituent minerals combined with metamorphic reactions. The results of the two techniques show the original fully hydrated shallow parts of the Sanbagawa mantle wedge contained ~10–15 vol.% brucite before the onset of exhumation of the Shiraga body and before peak metamorphic conditions. A distinct zone of brucite-free essentially monomineralic antigorite serpentinite occurs limited to a 100-m thick marginal zone of the body. This indicates a limited degree of Si-metasomatism by slab-derived fluids in the shallow mantle wedge. The presence of brucite may strongly affect the H2O budget and mechanical properties of serpentinite, these should be taken into consideration when examining the behavior of the shallow mantle wedge.

Keywords: Brucite, Shallow forearc mantle, Si metasomatism, Serpentinite, Antigorite, Sanbagawa metamorphism

©2020. Japan Geoscience Union. All Right Reserved.

Development of high fluid pressure at the base of the shallow mantle wedge due to presence of an antigorite shear zone

*Simon Richard Wallis[1], Mari Yokota[1,2]

1. The University of Tokyo, 2. Nagoya University

Deep slow earthquakes in subduction zones are concentrated at the base of the wedge mantle, but the reasons for this relationship are not well understood. High fluid pressures are thought to be an essential component of slow earthquakes, enabling slip at low shear stresses characteristic of slow earthquakes and compatible with recorded high vp/vs ratios. One of the prerequisites for high fluid pressure is the presence of a cap rock that can trap fluid in a limited region. Quartz precipitated from slab-derived fluids has been proposed as important component to forming cap rocks at the base of the overriding crust. However, quartz is not stable in the mantle wedge and in this region a different mechanism is required. In the cool mantle wedge, the addition of SiO2 through the influx of aqueous fluids will cause the development of serpentine and the presence of this serpentine may also affect the permeability. Experimental evidence shows foliated antigorite serpentinite has a strong permeability anisotropy with very slow flow perpendicular to the foliation. A laterally continuous layer of foliated antigorite serpentinite could act as a cap rock but its presence is not widely recognized. The subduction-type Sanbagawa metamorphic belt preserves numerous blocks of former mantle wedge and the boundary with the surrounding slab-derived schists represents the paleo subduction boundary. Units that formed at depths of ~35-45 km similar to that shown by deep slow earthquakes show a 100 m-wide strongly-foliated zone of antigorite schist followed by narrow zone of actinolite and talc-bearing lithologies along the boundary with slab-derived metapelite. A estimate of the amount of fluid flow can be derived by using the amount of added silica needed to make the serpentinite compared to the original mantle lithology and the solubility of SiO2 at the recorded metamorphic temperatures. These calculations show good agreement with estimates based on modelling of slab dehydration reactions. A comparison with experimentally determined fluid permeability suggests that the presence of an antigorite shear zone will cause high fluid pressures to develop at around 35-45 km depth. The presence of an antigorite shear zone along the base of the mantle wedge may control the depth of deep slow earthquakes.

Keywords: Antigorite, Shear zone, Subduction zone, Fluid flow, Sanbagawa belt

©2020. Japan Geoscience Union. All Right Reserved.

Mineralogy and structure of the shallow mantle wedge: evidence from seismic anisotropy in the Ryukyu Arc and structural petrological studies

*Takayoshi Nagaya[1], Simon Richard Wallis[1], Andrew Walker[2], James Wookey[3], Kazuhiko Ishii[4], Michael Kendall[5]

1. Graduate School of Science, The University of Tokyo, 2. University of Leeds, 3. University of Bristol, 4. Osaka Prefecture University, 5. University of Oxford

The dynamics of hydrated mantle in subduction zones is a key part of understanding recycling of materials from the Earth’ s surface into the deep interior. Antigorite is the main hydrous phase in the forearc mantle and the amount, distribution and alignment of antigorite are essential to understanding anisotropy, strength and fluid transport in this region. Seismic velocities are commonly used to identify antigorite-rich domains. However, antigorite is highly-anisotropic and depending on the seismic ray path, its properties can be very difficult to distinguish from non-hydrated olivine-rich mantle. Here, we utilize this anisotropy and show how an analysis of seismic anisotropy that incorporates measured ray path geometries in the Ryukyu arc can constrain the distribution, orientation and amount of antigorite. The Ryukyu arc is associated with very large s-wave splitting of around 1 s for both local slab and teleseismic events. These observations show the main source of anisotropy is within the mantle wedge. The size of the mantle wedge is insufficient to account for the large delay times by olivine alone and several previous workers have suggested that presence of aligned antigorite is the main cause of the anisotropy. We show that to account for the large delay times requires the presence of foliated antigorite-rich domains with an alignment that changes from vertical to slab-parallel. This orientation change suggests the presence of convective flow in the hydrated forearc mantle, a new insight into this zone that is traditionally considered to rigid block. Our modelling also allows quantitative estimates of the amount and distribution of the antigorite in the forearc. These estimates incorporate various sources of uncertainty including: variations in strength of natural antigorite CPO patterns, the degree of anisotropy caused by the crust, differences due to the method used to estimate seismic anisotropy from rock texture, and the model used to estimate anisotropy from the recorded seismicity. We find more than 54 % of the wedge must consist of antigorite. In addition, shear wave splitting analysis in several other subduction zones indicates large-scale serpentinization and forearc mantle convection are likely to be more widespread than generally recognized.

Keywords: Anisotropy, Hydrous forearc mantle, Antigorite, Shear wave splitting, Ryukyu, Crystallographic preferred orientation

©2020. Japan Geoscience Union. All Right Reserved.

Low-pressure type metamorphic rocks from No-jima Island, Yamaguchi Prefecture

*ZEJIN LU[1]

1. Graduate School of Science and Engineering for Innovation, Yamaguchi University

No-jima island is located in the Seto Inland Sea, Yamaguchi Prefecture. It is a region that underwent Cretaceous low-pressure type regional metamorphism (Ryoke metamorphism). No-jima island is underlain by crystalline schists and metabasalts. Metabasalts show the geochemical character similar to the within plate basalts, for instance the green stones in the Mino-Tamba belt. Moreover, the metamorphic grade of the schists corresponds to the biotite zone of the Yanai region of the Ryoke belt, but the petrological character of the rocks from No-jima island has been unclear. In addition, the geological correlation with the neighboring area, Kasado-jima island, the Oshima peninsula, and Ohtsu-jima island has not been understood yet. Therefore, the aim of this study, based on the mineral paragenesis of the pelitic schists, is to discuss the metamorphism of the rocks from No-jima island, and also to unravel the thermal structure of the low-pressure type metamorphism, the Ryoke belt, in this region.

The metabasalts are mainly exposed on the northeastern part of the island but occur rarely in the west coast of the island. They are included in the schists of sedimentary origin as blocks. The metamorphic rocks are composed mainly of the pelitic schist and metamorphosed chert with bedded structure (siliceous schist hereafter) with trace amounts of calc-silicate schist as thin layers or lenses. The pelitic and siliceous schists are intermittently distributed on the western and southeastern coast of the island. Fold structures such as close folds often develop in the southern part of the island. Granite dikes with 1–2 m width intrude the schists on the western coast.

The metabasalt is porous and has a prominent pillow structure and often shows the amygdaloidal texture. Phenocryst minerals of igneous origin are of clinopyoroxene and plagioclase with minor amounts of amphibole. It contains recrystallized fibrous amphiboles partially coexisting with biotite. Calcite locally fill the amygdules and occurs as veins. The pelitic and siliceous schists show the repidoblastic texture, and are composed of Bt+Ms+Pl+Qtz±Grt±Chl. The pelitic schist locally involves Crd. The calc-silicate schist is composed of Bt+Cal+Qtz. The mineral assemblage of the pelitic schists changes from north to south of the island; Bt+Ms+Chl+Pl+Qtz in the north and Bt+Ms+Grt+Pl+Chl+Qtz±Kfs in the south. On the other hand, the mineral assemblage of siliceous schist is mainly Ms+Bt+Grt+Pl+Qtz. The island can, therefore, be divided into the biotite zone in north and the garnet zone in south in terms of the mineral paragenesis of the pelitic schists.

The chemical compositions of garnet from the pelitic and siliceous schists show XFe > XMn and XFe < XMn, respectively. The XMg values of the pelitic and siliceous schists are less than 0.035. The XCa values of the pelitic and siliceous schists are of less than 0.05 and more than 0.1, respectively. The garnet of pelitic schist and siliceous schist shows a normal zoning with reduced spessartine toward the rim, probably formed during prograde metamorphism. The geothermobarometers for garnet-biotite (Ferry and Spear, 1978) and garnet-pagioclase-biotite-quartz (Hoish, 1990) are adapted to the pelitic schist. As a result, the peak metamorphic temperature and pressure conditions are estimated to be 480–530 ℃ and 180–300 MPa, respectively. According to the result, the thermal structures around the Seto Inland Sea region are discussed.

©2020. Japan Geoscience Union. All Right Reserved.

Keywords: Ryoke metamorphism, Low-pressure type, Garnet isograd

©2020. Japan Geoscience Union. All Right Reserved.

[E] Poster | S (Solid Earth Sciences)：S-VC Volcanology

[S-VC41] Timescales of magmatism: from genesis to eruption

convener:Chamberlain Katy Jane(University of Derby), Iona McIntosh(Japan Agency for Marine-Earth Science and Technology), Kenichiro Tani(Department of Geology and Paleontology, National Museum of Nature and Science), Akihiko Tomiya(Geological Survey of Japan, National Institute of Advanced Industrial Science and Technology)

Magmatic processes are known to operate across a range of timescales: from thousands to millions of years' residence and evolution within a magmatic plumbing system, through to the hours to minutes prior to eruption. Understanding the timescales of these magmatic processes, including accumulation, ascent, eruption, and final cessation of activity is vital for interpreting and responding to future magmatic activity. Together with thorough dating of deposits that reveal timing and frequency of past eruptions, this knowledge provides the foundation for improved hazard management in volcanic regions. By using a range of petrological, geophysical, geochemical and geochronological tools, increasingly detailed timescale constraints can be placed on past eruptive episodes.

In this session we invite submissions that examine magmatism and volcanism across a variety of timescales; from residence and rejuvenation within the crustal column, to eruptive triggering mechanisms and syn-eruptive processes, and their relation to the long-term timing and frequency of repeated activity.

[SVC41-P01] **Magma mixing triggering eruption of deep rhyolite at Ascension Island, south Atlantic**

*Katy Jane Chamberlain[1], Jenni Barclay[2], Katie Preece[3], Richard J Brown[4], Iona McIntosh[5], E IMF[6] (1.ESRC, School of Environmental Sciences, University of Derby, Derby, DE22 1GB, UKUniversity of Derby, 2.School of Environmental Sciences, University of East Anglia, Norwich, NR4 7TJ, UK, 3.Department of Geography, College of Science, Swansea University, Swansea, SA2 8PP, UK., 4.Department of Earth Sciences, Durham University, Durham, DH1 3LE, UK, 5.Institute for Marine Geodynamics, Japan Agency for Marine Earth Science and Technology, Yokosuka 237-0061, Japan, 6.Edinburgh Ion Microprobe Facility, University of Edinburgh, Edinburgh, EH9 3FE, UK)

[SVC41-P02] The August 2019 Eruption of Volcano 0403-091: timescales of pumice raft formation and evolution during dispersal

*Iona McIntosh[1], Isobel Yeo[2], Scott Bryan[3], Matthew Dunbabin[3], Kenichiro Tani[4], Patrick Collins[5] (1.Japan Agency for Marine-Earth Science and Technology, 2.National Oceanography Centre Southampton, UK, 3.Queensland University of Technology, Australia, 4.National Museum of Nature and Science, Japan, 5.Queens University Belfast, UK)

[SVC41-P03] Magma plumbing system at Zao volcano, NE Japan: time scales of magmatic processes revealed by chemical zoning in orthopyroxene phenocrysts

*Motohiro Sato[1], Masao Ban[1] (1.Graduate School of Science and Technology, Yamagata University)

[SVC41-P04] Discovery of Quaternary volcanism in southern Sakhalin

*Kenichiro Tani[1], Hiroshi Kawabata[2], Osamu Ishizuka[3], Takashi Sano[1], Alexey Yu. Martynov[4] (1.National Museum of Nature and Science, 2.Kochi University, 3.Geological Survey of Japan/AIST, 4.Far East Geological Institute, Russian Academy of Sciences)

[SVC41-P05] Timescales of magmatic processes related to the AD 2000 eruptions at Miyakejima, Japan

*Chris Conway[1], Nobuo Geshi[1], Yumiko Harigane[1], Genji Saito[1], Akihiko Tomiya[1] (1.Geological Survey of Japan)

[SVC41-P06] **Boninite ascent rates constrained using chromite crystal chemistry: Observations of experimental products applied to the extrusive sequence of the Troodos Ophiolite**

*Daniel Coulthard[1], Georg F Zellmer[1], Sebastien Jego[2], Akihiko Tomiya[3] (1.Volcanic Risk Solutions, Massey University, Palmerston North, New Zealand, 2.Institut des Sciences de la Terre d'Orleans, Centre

National de la Recherche Scientifique, Universite d'Orleans, Orleans, France, 3.Geological Survey of Japan, Advanced Institute of Science and Technology, Tsukuba, Japan)

[SVC41-P07] Novel approach for olivine-hosted melt inclusion corrections and its application to northern Japan tephras.

*Raimundo Brahm[1], Georg F Zellmer[1], Takeshi Kuritani[2], Naoya Sakamoto[3], Daniel Coulthard[1], Mitsuhiro Nakagawa[2], Eiichi Sato[4], Hisayoshi Yurimoto[3] (1.VRS, Massey Univ., 2.Grad. School of Sc., Hokkaido Univ., 3.IIL, CRI, Hokkaido Univ., 4.Hokkaido Univ. of Educ.)

Magma mixing triggering eruption of deep rhyolite at Ascension Island, south Atlantic

*Katy Jane Chamberlain[1], Jenni Barclay[2], Katie Preece[3], Richard J Brown[4], Iona McIntosh[5], E IMF[6]

1. ESRC, School of Environmental Sciences, University of Derby, Derby, DE22 1GB, UKUniversity of Derby, 2. School of Environmental Sciences, University of East Anglia, Norwich, NR4 7TJ, UK, 3. Department of Geography, College of Science, Swansea University, Swansea, SA2 8PP, UK., 4. Department of Earth Sciences, Durham University, Durham, DH1 3LE, UK, 5. Institute for Marine Geodynamics, Japan Agency for Marine Earth Science and Technology, Yokosuka 237-0061, Japan, 6. Edinburgh Ion Microprobe Facility, University of Edinburgh, Edinburgh, EH9 3FE, UK

Ocean island volcanoes which erupt effusively and explosively, with magmatic compositions ranging from basalt to rhyolite present challenging environments for forecasting of future eruptive activity. Ascension Island, in the south Atlantic, is one of these ocean island volcanoes, with a ~1 million year history of subaerial eruptive activity [1], but with the most recent eruption occurring only ~500 years ago [2]. Studies of the range of compositions erupted from Ascension Island have highlighted the importance of relatively closed-system fractional crystallisation in generating the evolved melts erupted, with low magmatic fluxes assigned to being responsible for clear spatial separation of mafic and felsic magmas at the surface [3]. Yet, identification of a mingled eruption has potential to further understand the origins of felsic melts at Ascension Island, and to provide greater constraints both on crustal structure and ascent rates of magmas.

In this contribution we present field observations, whole rock geochemical data, in situ mineral and melt inclusions analyses and textural characterisation of this unique mingled fall deposit from Ascension Island. This data is used to test the importance of fractional crystallisation vs. anatexis in generating the rhyolitic end-member of the mingled fall deposit, given that high water concentrations in melt inclusions are suggestive of formation at or near the Moho. Petrological data are used to infer multiple magmatic origins for the crystals. Glass and crystal compositional data is combined with textural observations to infer relatively short mingling to eruption timescales, on the order of days. The location of magma storage regions, and potential unrest timescales are particularly important on the populated Ascension Island where the nearest inhabited land mass is 1600 km away.

[1] Jicha, B.R., Singer, B.S. and Valentine, M.J., 2013. 40Ar/39Ar geochronology of subaerial Ascension Island and a re-evaluation of the temporal progression of basaltic to rhyolitic volcanism. Journal of Petrology, 54(12), pp.2581-2596.

[2] Preece, K., Mark, D.F., Barclay, J., Cohen, B.E., Chamberlain, K.J., Jowitt, C., Vye-Brown, C., Brown, R.J. and Hamilton, S., 2018. Bridging the gap: 40Ar/39Ar dating of volcanic eruptions from the ‘Age of Discovery’. Geology, 46(12), pp.1035-1038.

[3] Chamberlain, K.J., Barclay, J., Preece, K.J., Brown, R.J. and Davidson, J.P., 2019. Lower Crustal Heterogeneity and Fractional Crystallization Control Evolution of Small-volume Magma Batches at Ocean Island Volcanoes (Ascension Island, South Atlantic). Journal of Petrology, 60(8), pp.1489-1522.

Keywords: Magma mixing, Ocean island volcano, Crustal melting

©2020. Japan Geoscience Union. All Right Reserved.

The August 2019 Eruption of Volcano 0403-091: timescales of pumice raft formation and evolution during dispersal

*Iona McIntosh[1], Isobel Yeo[2], Scott Bryan[3], Matthew Dunbabin[3], Kenichiro Tani[4], Patrick Collins[5]

1. Japan Agency for Marine-Earth Science and Technology, 2. National Oceanography Centre Southampton, UK, 3. Queensland University of Technology, Australia, 4. National Museum of Nature and Science, Japan, 5. Queens University Belfast, UK

A new eruption of Volcano 0403-091 (30 km NW of Vava’u, northern Tonga) occurred without warning on the 7th August 2019 following 18 years of dormancy. The eruption produced a >200 km2 pumice raft that was intercepted by two boats, causing navigational problems and hull abrasion. Rafts pose a range of potential hazards for marine traffic and infrastructure, yet their formation processes and evolution during dispersal are poorly understood. The 7th August raft was imaged by satellites almost daily, so its source and path are well-constrained. This eruption therefore provides a unique opportunity to sample both rafted pumice with known float times and sunken pumice at the vent, as well as a rare chance to study vent structure, hydrothermal activity and marine life interactions immediately following an explosive, shallow marine eruption.

Here we present the first results from a rapid response survey of the submarine vent site, conducted 6 months after the eruption. The vent was investigated using a small Remotely Operated Vehicle (ROV), a small Autonomous Underwater Vehicle (AUV) and a surface glider, alongside a grab sampler and mini-dredge designed for operation from a small vessel. Video transects, bathymetry and sampling together enable characterisation of the seafloor eruption products, post-eruptive vent morphology, and the recovery of seafloor ecosystems 6 months after an explosive shallow submarine volcanic eruption.

In addition, we compare the proximal seafloor deposits with a suite of samples from the floating pumice raft that experienced different float times, enabling us to compare the change in physical characteristics of pumice during its lifetime in the raft. These samples include pumice collected by a boat that intersected the raft shortly after eruption (floated for 1 week), and pumice subsequently collected from the shores of some Fijian Islands (floated for > 1 month). Physical, geochemical and textural (including high resolution X-ray computed tomography) analyses of these different pumice types from a single well-constrained eruption will help to determine the controls on pumice raft formation and their potential hazards for marine shipping and infrastructure.

Keywords: pumice raft, submarine eruption

©2020. Japan Geoscience Union. All Right Reserved.

Magma plumbing system at Zao volcano, NE Japan: time scales of magmatic processes revealed by chemical zoning in orthopyroxene phenocrysts

*Motohiro Sato[1], Masao Ban[1]

1. Graduate School of Science and Technology, Yamagata University

[Introduction]

Understanding of magma plumbing system is fundamentally the most important issue for the volcanic disasters mitigation. The youngest activity of Zao volcano (NE Japan) repeated phreato-magmatic eruptions in "Okama crater" (ca. AD1200 to present) and precursory phenomena, such as volcanic tremors and earthquakes has been observed since 2013. Recent advance of volcanic petrology allows us to reveal the magma plumbing system more in detail. The detailed analysis of textures and chemical zoning of phenocrystic minerals can provide useful information of the magma pluming system. Moreover, using the elemental diffusion chronometry applied to compositionally zoned crystals, we can know the time scales of complex magma dynamics. Here, we present and discuss pre-eruptive processes of Okama crater eruption products (Okp) by using zoning profiles of orthopyroxene phenocrysts.

[Mineral compositions and end-member magmas]

Juvenile bomb samples are medium-K and calc-alkaline series basaltic andesite to andesite (56-57% SiO2), including plagioclase, orthopyroxene, clinopyroxene and magnetite as phenocryst. Plagioclase phenocrysts show wide range of compositions between $An_{60\text{-}92}$ and broad peaks were identified ($An_{65, 75, 88}$). Orthopyroxene compositions range between 56-76 Mg# with two peaks (66, 74 Mg#). Clinopyroxene compositions range between 63-77 Mg# with a single peak (68 Mg#). These various crystals are made by magma mixing between low-T end-member magma (L-magma) with low An and Mg#, and high-T end-member magma (H-magma) with high An and Mg#. Physicochemical conditions of end-member magmas were constrained by using the rhyolite-MELTS algorithm. The optimum conditions for each end-member magmas are as follows, H-magma: >76 Mg#, 52-53% SiO_2, >1040˚C, 200-250 MPa, 5.0% H_2O, and L-magma: 64-66 Mg#, 60% SiO_2, 950-970˚C, 200 MPa, 3.0% H_2O.

[Zoning profiles of orthopyroxene phenocrysts]

The opx phenocrysts can be divided low-(opx-A, 64-66 Mg#), high- (opx-B, >72 Mg#), and extremely low-(opx-A’, <63 Mg#) Mg types based on core composition. Based on compositional zoning of rim (inside from outermost rim), opx-A are subdivided into -A1 to -A4. A1 show no zoning, while A2 to A4 have Mg rich rims (>70 Mg#). In the Mg rich rim, Al is high, but Cr is low in A2, Al and Cr are high in A-3, and Al and Cr are low in A4. Type B is subdivided into B1, which has normal zoned rim, and B2, which shows skeletal texture. Core compositions of opx-A are equilibrium in L-magma, and reverse zoned rim compositions of opx-A3 and core compositions of opx-B1 and -B2 are in equilibrium with H-magma. Outermost rims (66-67 Mg#, almost high-Al content) are observed in many of the phenocrysts, which were formed in the mixed magma. The composition of the mixed magma is estimated to be similar to that of the groundmass.

[Mixing processes and the time scales]

Based on above zoning profiles of Mg#, Al, and Cr in orthopyroxene phenocrysts, low-T and modified high-T magmas mixing is recognized other than low- and high-T magmas mixing. The modified high-T magma (Mm magma) was formed by incorporation of the mixed magma into the high-T magma when the

©2020. Japan Geoscience Union. All Right Reserved.

latter injected into the former. We estimated the residence time of both cases of mixing by Fe-Mg diffusion modeling applied to the Mg# zoning of orthopyroxene phenocrysts. The estimated timescales are mostly a few decades for low- and high-T magma mixing and a few days to decades for low-T and the Mm magma mixing.

The pre-eruptive processes of the Okp are proceeded as follows. The injection of the high-T magma and mixed with the low-T magma (a few decades before the eruption), resulted in the formation of the mixed magma. The injection of the high-T magma into the mixed magma formed the Mm magma tentatively, that mixed with the L-magma (a few decades to a few days before the eruption).

Keywords: Plumbing system, Magma mixing, Residence time, Orthopyroxene, Rhyolite-MELTS, Zao volcano

©2020. Japan Geoscience Union. All Right Reserved.

Discovery of Quaternary volcanism in southern Sakhalin

*Kenichiro Tani[1], Hiroshi Kawabata[2], Osamu Ishizuka[3], Takashi Sano[1], Alexey Yu. Martynov[4]

1. National Museum of Nature and Science, 2. Kochi University, 3. Geological Survey of Japan/AIST, 4. Far East Geological Institute, Russian Academy of Sciences

Cenozoic tectono-magmatic processes in the western Pacific margins and their precise timings are critical in comprehending the behaviors of the Pacific Plate motion and associated back-arc basin formation, such as those in the Philippine Sea Plate and the Eurasia margin during formation of the Sea of Japan.

Compared to the other parts of the western Pacific region, records of magmatism in the northwestern Pacific margin, including those in Sakhalin and Kamchatka, Russian Far East, are still not well studied.

The southern part of Sakhalin sporadically exposes Oligocene (~30 Ma) to Miocene (~5 Ma) basaltic to andesitic lavas and dikes along the western coast (Okamura et al., 1998; Shimazu et al., 1992; Takeuchi, 1997). Geochemical studies have suggested a change in magma generation occurred from older Oligocene-Miocene arc magmatism to younger Mid-Late Miocene alkaline and subalkaline intraplate-magmatism (Okamura et al., 2005). The largest occurrence of volcanic rocks in Sakhalin is in the Lamanon area, where basaltic lava and volcanic breccia are exposed in a wide (~40 km E-W and ~60 km N-S) zone. Furthermore, the Lamanon area is characterized by the presence of more than ten conspicuous cones, varying in size from ~1 to ~5 km in diameter. Erokhoev and Shilov (1971) documented one of the cones, Mt. Ichara, located at the western end, to be a dacite lava dome. But due to their difficult accessibility, no further research has been conducted on these cones.

We conducted a reconnaissance survey of the Lamanon cones in 2017, visiting three of the cones, Mts. Ichara, Krutaya, and Krasnova. Our survey confirmed that all of the cones are mono-lithologic, dacite lava dome. A recovered sample yielded a Pleistocene (<1 Ma) Ar-Ar plateau age, indicating the occurrence of Quaternary volcanism in Sakhalin for the first time. Furthermore, the whole-rock compositions of the Lamanon dacites show elevated Sr/Y ratios, and enrichment in Mg and Ni, which are consistent with geochemical affinities similar to those of adakite.

Since the slab depth of the Pacific Plate beneath the Lamanon area is deeper than 600 km, it is unlikely that dacite magma generation was related to the subducting slab. Instead, given that the Lamanon area is located at the northeastern continuation of the rift system within the Sea of Japan, we propose that deep crustal melting associated with the rifting may have generated the dacite magma.

Keywords: Sakhalin, Quaternary, Volcanism

©2020. Japan Geoscience Union. All Right Reserved.

Timescales of magmatic processes related to the AD 2000 eruptions at Miyakejima, Japan

*Chris Conway[1], Nobuo Geshi[1], Yumiko Harigane[1], Genji Saito[1], Akihiko Tomiya[1]

1. Geological Survey of Japan

Integrating the petrological and geophysical records of magmatism is necessary to improve our understanding of the types and timescales of processes that precede volcanic eruptions. Studies of recent eruptions in Japan provide opportunities for this improvement, due to the high-resolution network of monitoring equipment installed for active volcanoes. We present results from a diffusion chronometry case study of pyroclasts from an explosive eruption at Miyakejima on 18 August, 2000. Previous petrological studies have shown that this eruptive event was preceded by magma mixing, which makes it a suitable candidate for testing whether the timescales determined from crystal zoning patterns can aid the interpretation of geophysical data.
Timescales for magma mixing were calculated by modelling diffusion profiles in normally zoned olivine crystals, which record a late-stage magma hybridization event. Mineral chemistry and orientation data were collected by electron probe microanalysis (EPMA) and electron backscatter diffraction (EBSD) techniques, respectively. Utilization of multiple elements and correction for diffusion anisotropy ensured that the calculated timescales incorporated recent methodology developments in this field. The new and existing petrological constraints were compared with the time series of monitoring data during the eruptive episode. These comparisons highlight the difficulty of definitively attributing geophysical signals to magma recharge events where complex volcano-magmatic processes occur.

Keywords: magma mixing, diffusion timescales, volcanic eruption

©2020. Japan Geoscience Union. All Right Reserved.

Boninite ascent rates constrained using chromite crystal chemistry: Observations of experimental products applied to the extrusive sequence of the Troodos Ophiolite

*Daniel Coulthard[1], Georg F Zellmer[1], Sebastien Jego[2], Akihiko Tomiya[3]

1. Volcanic Risk Solutions, Massey University, Palmerston North, New Zealand, 2. Institut des Sciences de la Terre d'Orleans, Centre National de la Recherche Scientifique, Universite d'Orleans, Orleans, France, 3. Geological Survey of Japan, Advanced Institute of Science and Technology, Tsukuba, Japan

Boninites are rare high magnesium andesites that often contain trace chromites that form early. These melts continue to crystallize a significant volume of silicate minerals. Magmatic differentiation drives chromite out of equilibrium with the residual melt with respect to both divalent and trivalent cation proportions. To simulate this process, we have performed internally heated pressure vessel experiments, providing insights into the processes of crystal-melt re-equilibration through time. While Fe-Mg exchange equilibrates the tetrahedrally coordinated divalent cations in chromite in < 6 hours, equilibration of trivalent cations in octahedral coordination with residual melts is slow. Our experimental results show chromite Al concentrations are ubiquitously lower, and Fe^{2+}/Fe^{3+} values are ubiquitously higher than modelled equilibrium values, indicating that there was insufficient time for significant Al and Fe^{3+} incorporation to occur at the expense of Cr. Similar observations can be made for natural chromite compositions in the extrusive sequence of the Troodos ophiolite. Based on a simple model of diffusive equilibration, we estimate that the core of a microphenocrystic chromite 60 μm in diameter (size of natural microphenocrysts: 50-500 μm; Cameron, 1985) may take up to 500 years to equilibrate under conditions analogous to the physiochemical state of melt at the time of eruption. For the extrusive sequence, this implies an ascent rate of boninites greater than 16 m/year for disequilibrium textures and compositions to be preserved.

Cameron, W.E., 1985. Petrology and origin of primitive lavas from the Troodos ophiolite, Cyprus. Contributions to Mineralogy and Petrology 89, 239-255.

Keywords: Boninite, Chromite, Ascent, Petrology, Disequilibrium, Analogue

©2020. Japan Geoscience Union. All Right Reserved.

Novel approach for olivine-hosted melt inclusion corrections and its application to northern Japan tephras.

*Raimundo Brahm[1], Georg F Zellmer[1], Takeshi Kuritani[2], Naoya Sakamoto[3], Daniel Coulthard[1], Mitsuhiro Nakagawa[2], Eiichi Sato[4], Hisayoshi Yurimoto[3]

1. VRS, Massey Univ., 2. Grad. School of Sc., Hokkaido Univ., 3. IIL, CRI, Hokkaido Univ., 4. Hokkaido Univ. of Educ.

Olivine-hosted melt inclusions (MIs) are widely used as a tool to study the early stages of magmatic evolution. There are a series of processes after MI trapping that affect MI composition, including post-entrapment crystallization (PEC) of the host mineral at the MI boundaries, exsolution of volatile phases into a “shrinkage bubble” and diffusive exchange between the MI and his host. Classical correction schemes applied to olivine-hosted MIs include PEC correction through addition of olivine back to the melt until it reaches equilibrium with the host composition and “Fe-loss” correction for Fe-Mg diffusive exchange as described by Danyushevsky et al. (2000). These two corrections rely on the assumption that the original host composition is preserved. Usually, studies focus on high forsterite melt inclusion (>Fo80), where the degree of correction is small and the olivine host composition is assumed to be preserved.

In this study we develop a novel MI correction scheme that is applicable to more evolved (< Fo80) melt inclusions where the original host crystal composition has not been preserved. The new scheme allows correction of MI compositions from antecrystic hosts with long and varied temperature histories. The correction relies on fitting a set of MIs compositions to modelled liquid lines of descent (LLD) through fractional crystallization (FC). A Matlab® script iterates FC simulations using alphaMELTS (Asimow and Ghiorso, 1998; Ghiorso and Sack, 1995) starting from the most primitive MI composition of a set. A grid of initial conditions with variable P, H_2O, fO_2, olivine addition and MgO/FeO_t of the first MI are selected to simulate the possible magmatic conditions and the effects of PEC and Fe-Mg exchange on the first MI.

After the generation of the FC simulations, each MI is fitted to the modelled LLDs by addition of olivine to the MI composition. The best fit for each MI is obtained by minimizing the compositional distance between the corrected MI and the LLD. We use the definition of the Aitchison distance for a compositional space geometry (Aitchison, 1986) to quantitively compare similarity between two compositions. The combination of the minimum Aitchison distance of the set of melt inclusion to each LLD is a measure of “good of fitness” of each FC model to the corrected set of MI compositions. Statistical analysis of the models shows that the best fit results for basic MI compositions converges on a particular mineral proportion of the FC path (olivine:pyroxene:plagioclase).

Application of this methodology to MI sets provides estimations of original compositions and magmatic conditions during MI entrapment. Two sets of MIs hosted in olivine antecrysts (Fo76-78) from basaltic tephras from Hakkoda and Akita-Komagatake volcanoes were processed using this methodology. Hakkoda MIs are enriched in Fe compared to whole rock trends, caused by Fe-gain through diffusive equilibration during storage, whereas most MIs in the Akita sample loss suffered of Fe during storage. Using the new correction methodology, we estimate that crystallization of the host crystals in Hakkoda occurred at <1.5 kb and c. 1.5 H_2O wt%, whereas in Akita it occurred at <1.0 kb and c. 1.0 H_2O wt%.

©2020. Japan Geoscience Union. All Right Reserved.

Aitchison, J., 1986. The statistical analysis of compositional data. Chapman and Hall, London; New York.

Asimow, P.D. and Ghiorso, M.S., 1998. Am. Mineral., 83(9): 1127-1132.

Danyushevsky, L.V., Della-Pasqua, F.N. and Sokolov, S., 2000. Contributions to Mineralogy and Petrology, 138(1): 68-83.

Ghiorso, M.S. and Sack, R.O., 1995. Contributions to Mineralogy and Petrology, 119: 197-212.

Keywords: Melt inclusions, Post-entrapment crystallization, Antecrysts, Arc magmatism

©2020. Japan Geoscience Union. All Right Reserved.

[E] Poster | S (Solid Earth Sciences)：S-VC Volcanology

[S-VC42] Dynamics of volcanic eruptions and their physical and chemical processes

convener:Atsuko Namiki(Graduate School of Integrated Arts and Sciences, Hiroshima University), Christian Huber(Brown University), Michael Manga(University of California Berkeley), Yujiro Suzuki(Earthquake Research Institute, The University of Tokyo)

A Volcanic eruption is a hazardous phenomenon that results from a sequence of coupled processes, including storage in the subsurface and ascent to the surface. The volcanic gas exsolving from the ascending magma generates bubbles, which influence both the potential energy of the magma (density) and its resistance to flow (viscosity). Bubbles can sometimes deform and/or fragment the surrounding magma, leading up to explosive eruptions that develop volcanic plumes and/or pyroclastic flows. A broad range of approaches is required to tackle these processes and better understand the factors that govern the physics of explosive eruptions. We welcome contributions from interdisciplinary approaches, including, geophysical observations of active/quiet volcanoes, geochemical measurements of eruptive products, theoretical approaches, and numerical simulations, and laboratory experiments designed to explore the fundamental processes underlying explosive volcanism.

[SVC42-P01] A Model Experiment of Fracture Induced Long-Period Events: Injection of Pressurized Gas Into a Viscoelastic Rock Analog

*Atsuko Namiki[1], Makoto Takahashi[1], Ryo Tsutsui[1] (1.School of Integrated Arts and Sciences, Hiroshima University)

[SVC42-P02] Multi-parameter observations at Shikabe geyser and unique changes in interval between eruptions

*Ayuta Tsuge[1], Hiroshi Aoyama[1], Masayoshi Ichiyanagi[1] (1.Institute of Seismology and Volcanology, Faculty of Science, Hokkaido University)

[SVC42-P03] A new model of buoyancy-driven bubble coalescence with deformation effect

*Takafumi Maruishi[1], Atsushi Toramaru[2] (1.Department of Earth and Planetary Sciences, Graduate School of Sciences, Kyushu University, 2.Department of Earth and Planetary Sciences, Faculty of Sciences, Kyushu University)

[SVC42-P05] Experimental validation of a two-layer model for pyroclastic density currents

*Hiroyuki A. Shimizu[1], Takehiro Koyaguchi[2], Yujiro J. Suzuki[2], Brosch Ermanno[3], Gert Lube[3] (1.National Research Institute for Earth Science and Disaster Resilience, 2.Earthquake Research Institute, The University of Tokyo, 3.Massey University)

[SVC42-P06] **Numerical simulation of ballistic trajectories based on wind tunnel experiments**

*Kae Tsunematsu[1] (1.Yamagata University)

[SVC42-P07] Excitation of airwave by a bubble bursting in particle-bearing fluids : regime transitions and implications for basaltic volcanic eruptions

*Ikuro Sumita[1], Kana Hashimoto[2] (1.Geosciences and Civil Engineering, Institute of Science and Engineering, Kanazawa University, 2.Graduate School of Natural Science and Technology, Kanazawa University)

[SVC42-P08] Ash fall observation using 2D-Video Disdrometer

*Eiichi Sato[1], Masato Iguchi[2] (1.Meteorological Research Institute, 2.Kyoto Univ.)

[SVC42-P09] An attempt at quantification of starting eruption cloud at Sakurajima volcano

*Taishi Yamada[1], Masato Iguchi[1], Eisuke Fujita[2] (1.Sakurajima Volcano Research Center, Disaster Prevention Research Institute, Kyoto University, 2.National Research Institute for Earth Science and

Disaster Resilience)

[SVC42-P10] Temperature dependence of titanomagnetite composition in a titanohematite-free silicic magma

*Naoki Araya[1], Michihiko Nakamura[1] (1.Department of Earth Science, Graduate School of Science, Tohoku University)

[SVC42-P11] **STRATIGRAPHY AND CHARACTERISTICS OF CALDERA II DEPOSITS, BATUR VOLCANIC COMPLEX, BALI, INDONESIA**

*Rahajeng Ardinni Noor[1], Atsushi Toramaru[1], Agung Harijoko[2,3], Haryo Edi Wibowo[2], Tomoharu Miyamoto[1], Mitsuru Okuno[4] (1.Department of Earth and Planetary Sciences, Faculty of Sciences, Kyushu University, 2.Department of Geological Engineering, Universitas Gadjah Mada, Indonesia, 3.Disaster Studies Center, Universitas Gadjah Mada, Indonesia, 4.Department of Earth System Science, Faculty of Science, Fukuoka University, Japan)

[SVC42-P12] Factors affecting the sequence of the Plinian eruption inferred from rock texture and physical properties - an example of the 1783 eruption, Asama volcano, Japan

*Tatsuki Mizuno[1], Fukashi Maeno[1], ATSUSHI YASUDA[1] (1.Earthquake Research Institute, Department of Earth and Planetary Science, University of Tokyo)

[SVC42-P13] Thermal history of pyroclasts reflecting the structure of eruption clouds: Application of textural analysis of pyrrhotite oxidation

*Keiko Matsumoto[1] (1.Geological Survey of Japan, The National Institute of Advanced Industrial Science and Technology)

[SVC42-P14] Intermittent ascent of aphyric andesitic melts revealed by cryptic micro-antecryst textures

*Charline Lormand[1], Georg F Zellmer[1], Naoya Sakamoto[2], Geoff Kilgour[3], Teresa Ubide[4], Hisayoshi Yurimoto[2], Alan Palmer[5], Karoly Nemeth[1], Yoshiyuki Iizuka[6], Anja Moebis[5] (1.School of Agriculture and Environment, Volcanic Risk Solutions, Massey University, PO Box 11222, Palmerston North 4442, New Zealand, 2.Isotope Imaging Laboratory, Natural History Sciences, Hokkaido University, Sapporo 060-0810, Japan, 3.GNS Science, Wairakei Research Centre, Private Bag 2000, Taupo 3352, New Zealand, 4.School of Earth and Environmental Sciences, The University of Queensland, Brisbane, QLD 4072, Australia , 5.School of Agriculture and Environment, Department of Soil Science, Massey University, PO Box 11222, Palmerston North 4442, New Zealand , 6.Institute of Earth Sciences, Academia Sinica, 128 Academia Road Sec. 2, Nankang, Taipei 11529, Taiwan)

A Model Experiment of Fracture Induced Long-Period Events: Injection of Pressurized Gas Into a Viscoelastic Rock Analog

*Atsuko Namiki[1], Makoto Takahashi[1], Ryo Tsutsui[1]

1. School of Integrated Arts and Sciences, Hiroshima University

Low-frequency seismic waves are frequently observed in volcanic areas. To understand the source mechanism of such low-frequency signals, we conducted model experiments simulating the volcanic gas injection into a rock. The rocks heated by the ascending magma and hydrothermal fluid may be very hot and damaged, such that their shear wave velocities are low. Similarly, solidifying magmas should have a low shear wave velocity. Our experiments show that the injection of pressurized air into such soft rocks creates multiple cracks and causes pulse-like seismic signals. When the rock analog is further softened, only high-frequency oscillation appears. These results suggest that the low-frequency component observed in the volcanic area before the initiation of eruptions may be the result of crack generation.

Reference:
Namiki, A., Takahashi, M., and Tsutsui, R. (2019), A model experiment of fracture induced long-period events: Injection of pressurized gas into a viscoelastic rock analog. Geophysical Research Letters, 46, 11906-11914.

Keywords: LP, crack propagation, rheology

©2020. Japan Geoscience Union. All Right Reserved.

Multi-parameter observations at Shikabe geyser and unique changes in interval between eruptions

*Ayuta Tsuge[1], Hiroshi Aoyama[1], Masayoshi Ichiyanagi[1]

1. Institute of Seismology and Volcanology, Faculty of Science, Hokkaido University

Geyser is a hot spring characterized by periodical spouting of superheated water together with steams or non-condensed gases. Since the physical processes of eruption of steam and hot water are similar to those of volcanic eruption, geysers have been studied as an analogy of volcanic eruption.

One of the major features of geyser phenomena is Interval between eruptions (IBE). IBEs are different for each geyser and have a wide range from a few minutes to several hours. Furthermore, a geyser sometimes has more than one constant IBE. For example, El Cobreloa geyser in El Tatio, Chile, repeats several small eruptions approximately every 14 minutes and followed by large eruptions lasting about one hour with a repeating period of about four hours (Namiki et al., 2014), and some geysers in Yellowstone National Park, United States, have changed the IBEs for long periods, which seem to be influenced by precipitation and river discharge (Hurwitz et al., 2008). However, there are few quantitative studies focusing on the mechanism of such IBE changes.

The Shikabe geyser in southern Hokkaido was discovered through the development of hot springs in 1952. It is a large geyser erupting more than 10m and haves a relatively short IBE about 12 minutes After the field experiments conducted by Otani in 1961 (Otani, 1961), any physical observation had not been carried out to this day although the eruption characteristics, such as IBE, eruption height and discharge volume, might have changed since then. Therefore, in this study we started multi-parameter observations using some physical monitoring instruments at the Shikabe geyser in order to obtain new knowledge on the phenomena associated with the geyser eruption and to understand the mechanism of IBE change. Since IBE of the Shikabe geyser is about 12 minutes, we can collect a lot of field data of spouting events. Moreover, an iron pipe conduit of a known diameter might be an advantage to constrain the geyser’s geometry.

The monitoring contents are video camera, thermal infrared camera, micro-barometer, acoustic sensor, tiltmeter, seismometer, and thermometer. The acoustic sensor and micro-barometer were placed at the same position about 4m from the vent, and the seismometer and tiltmeter were placed at the same position about 6m from the vent. The thermometer has a sensor attached to the vent and measures the temperature of the water when the hot water overflows from the nozzle. Observation started on November 25, 2019, and continuous data recording were made on five instruments except video camera and thermal infrared camera.

©2020. Japan Geoscience Union. All Right Reserved.

We confirmed regular pattern of signals corresponding to eruption and quiescence in the observed data. Micro barogram and acoustic signal show high frequency waves associated with eruption. Temperature signal captured successfully the timing of overflow and recorded the maximum temperature of hot water higher than 100℃. The seismogram contains a quite high frequency component associated with eruption. However, since it greatly exceeds the frequency band widely reported in the observation of volcanoes and geysers, we must check the seismic data carefully. The ground tilt in the transverse direction indicates changes clearly that seem to correspond to inflation and deflation of the reservoir. However, no clear change was observed in the radial direction, which suggests that the aquifer may have a complex geometry.

Our data show that IBE of the Shikabe geyser was not always constant but rather showing characteristic change in time. The average of IBE is about 12 to 13 minutes. IBE sometimes becomes 2-3 minutes longer than the mean interval, and the next IBE is certainly about 1 minutes shorter than the average. Compering the long IBE event with short one, both the quiescence period and the discharge period in one eruption cycle were long in the long IBE event, while both were short in the short one. The occurrence frequency of this characteristic IBE change varies day by day. As a next step, we would like to discuss the cause of this IBE change quantitatively, taking its relationship with weather conditions into account.

Keywords: Geyser, Observation, Interval between eruptions

©2020. Japan Geoscience Union. All Right Reserved.

A new model of buoyancy-driven bubble coalescence with deformation effect

*Takafumi Maruishi[1], Atsushi Toramaru[2]

1. Department of Earth and Planetary Sciences, Graduate School of Sciences, Kyushu University, 2. Department of Earth and Planetary Sciences, Faculty of Sciences, Kyushu University

In low viscosity magma like basalts, a buoyant force can no longer be ignored. Bubbles move upward by buoyant force and approach each other. They coalesce when approached sufficiently and become larger. The large bubbles move upward quickly and release their gas contents to the surface. It relates to episodic activities observed in Hawaiian and Strombolian eruptions.

Moving bubbles drive flow around them and make near bubbles deform. In Manga and Stone (1995), they reported that the deformed bubbles attract near bubbles due to their hydrodynamic interaction. The attracting effect significantly changes coalescence dynamics but there are no theoretical models to predict their behavior.

Firstly, we drive equations describing bubble trajectory based on the theory which deals with two-body interaction taking bubble deformation into account. The equations allow us to calculate the relative movement of two bubbles. We assume that the liquid surrounding bubbles is viscous fluid and the deformation of the bubbles is small enough.

Relative trajectory is controlled by two dimensionless parameters, bond number (the ratio of viscous force driven by buoyancy and surface tension) and the size ratio of the two bubbles. The viscosity of the liquid effect only changes the time scale but doesn’t change the coalescence behavior. The calculation by the equations can reproduce the two-bubble trajectories reported in Manga and Stone (1995). Almost the same equations have already been derived and solved in the same paper but contain some errors and failed to reproduce the experimental data.

Secondly, we determine the critical conditions whether two bubbles coalesce or not. We have the critical initial separation as a function of bond number and size ratio of two bubbles. Coalescence efficiency is directly calculated from the critical separation. We compare the results of our calculation with experimental data in which coalescence efficiency in terms of critical separation of as a function of size ratio (Kushner et al., 2001; Manga and Stone, 1995). Coalescence efficiency increases linearly with bond number and reaches a constant value. This is caused by effective deformation for the large bond number. Our results agree well with the experiments. For small bond number (small bubble size), the coalescence efficiency decreases with increasing the size contrast. For large bond number (large bubble size), the calculation gives larger efficiency than the experimental data. The discrepancy is because of a limit of the approximation. The coalescence efficiency nearly constants for the large bond number in the experiments. So, we can treat efficiency as a constant for large bond number.

Our simple model can reproduce such a complex attracting behavior reported in the previous experiments. With our new method, we can calculate the evolution of bubble size distribution including bubble coalescence driven by buoyancy. It is noteworthy that the bubble interaction with the deformation effect show quite different behavior from rigid spheres case. For instance, the coalescence efficiency for the larger bubbles (larger than 5mm in silicate melts) considerably 10 times larger than rigid spheres case.

©2020. Japan Geoscience Union. All Right Reserved.

Keywords: Bubble deformation, Bubble coalescence, Viscous fluid

©2020. Japan Geoscience Union. All Right Reserved.

Experimental validation of a two-layer model for pyroclastic density currents

*Hiroyuki A. Shimizu[1], Takehiro Koyaguchi[2], Yujiro J. Suzuki[2], Brosch Ermanno[3], Gert Lube[3]

1. National Research Institute for Earth Science and Disaster Resilience, 2. Earthquake Research Institute, The University of Tokyo, 3. Massey University

During explosive volcanic eruptions, a hot mixture of volcanic particles and gas is ejected from the volcanic vent and can flow along the ground surface as a pyroclastic density current (PDC). A PDC is generally characterized by a strong density stratification; it is composed of a dilute current (particle volume fractions $\Phi < 10^{-2}$) over a dense basal current ($\Phi \sim 10^{-1}$). The dynamics of such strongly stratified PDCs can be investigated by a two-layer depth-averaged model (Shimizu et al., 2019, J. Volcanol. Geotherm. Res., 381, 168-184). In this study, we have validated our two-layer model by comparison with two experiments: (1) the pyroclastic-flow eruption large-scale experiment (PELE; Lube et al., 2015, J. Geophys. Res., 120, 1487-1502) and (2) a granular-flow experiment (GFE; Girolami et al., 2008, J. Geophys. Res., 113, B02202).

In the PELE, an experimental current is generated by the controlled gravitational collapse of a hot aerated suspension of particles and air from an elevated hopper into an instrumented inclined channel. A well-defined dataset has been newly obtained from the PELE for the purpose of validation and benchmarking. In the experiment, a strongly stratified current (consisting of a dilute turbulent suspension flow and a basal bedload region) flowed into the inclined channel and the distal horizontal channel, and it produced the deposits by progressive aggradation of particles at the base during flowing. Numerical simulations using our two-layer model were conducted under the same condition of the experiment. The numerical results for the upper dilute current (e.g., front position and thickness) agree well with the experimental data for the dilute suspension flow. The numerical results for the dense basal current and the deposits also agree with the experimental data, when the volume fraction in the dense basal current (Φ_b) is set to the value observed in the experiments (the time-averaged value for the bedload at an upstream point; i.e., $\Phi_b = 0.02$) and the constant deposition speed at the base of the dense current (D) is tuned to 3.7×10^{-4} m/s.

In the GFE, a stationary fluidized mixture in the rectangular-lock domain was released at time $t = 0$, flowed into the horizontal channel, and produced the deposits by progressive aggradation during flowing. Numerical simulations using the basal-layer model in our two-layer model were conducted under the same condition of the experiment. The numerical results agree well with the experimental data for the flow-front position as a function of time and the final deposit distribution, when Φ_b is set to the initial value measured in the experiment (i.e., $\Phi_b = 0.42$) and D is tuned to 1.7×10^{-2} m/s.

The above two results ($D = 3.7 \times 10^{-4}$ m/s and $\Phi_b = 0.02$ for the PELE; $D = 1.7 \times 10^{-2}$ m/s and $\Phi_b = 0.42$ for the GFE) imply that the physics is different between the bedload region observed in the PELE and the granular flow observed in the GFE. The value of D for the GFE can be quantitatively explained by the hindered-settling model for $\Phi_b = 0.42$. That for the PELE, on the other hand, is substantially smaller than the value predicted by the hindered-settling model ($D \sim 10^{-2}$ m/s for $\Phi_b = 0.02$). The small deposition speed (i.e., $D = 3.7 \times 10^{-4}$ m/s) and the small particle volume fraction (i.e., $\Phi_b = 0.02$) in the PELE are consistent with the qualitative observation that saltating/rolling/sliding of particles occur in the bedload region owing to a complicated combination of deposition and erosion processes (i.e., some particles do

©2020. Japan Geoscience Union. All Right Reserved.

not simply settle to the bottom) in this experiment. These results indicate that the dynamics and sedimentation processes of the dense basal layer depend on the source condition and/or the presence of the slope. A sophisticated dynamical model considering the combination of deposition and erosion processes may reproduce the experimental data both for the bedload region in the PELE and the granular flow in the GFE.

Keywords: Pyroclastic density current, Ignimbrite, Numerical simulation, Experimental validation, Two-layer model, Granular flow

©2020. Japan Geoscience Union. All Right Reserved.

Numerical simulation of ballistic trajectories based on wind tunnel experiments

*Kae Tsunematsu[1]

1. Yamagata University

Ballistic projectiles are large (>10 cm) pyroclasts, ejected from erupting volcanoes, that draw parabolic trajectories without being influenced by the flow of the gas and solid mixture (e.g. Taddeucci et al., 2017). Transport dynamics of ballistic projectiles are studied by observing real volcanic eruptions or numerical simulations. The largest unknown factor of ballistic transport is aerial drag, which is hard to estimate by observation.

There are many examples of drag measurements for artificial shapes such as cylinders and cubes, but only a few examples of drag measurements using real volcanic rocks. Therefore, wind tunnel experiments were implemented using a block obtained from Zao volcano, which erupted in 1895 (Kochibe, 1896). In order to clarify the size effect we used blocks of the same shape but different sizes. The results of these experiments were (1) the drag coefficient depends on the Reynolds number (when the block rotates more than three times per second) and the cross-sectional shape, (2) the lift coefficient of the block is very low compared to the drag coefficient when the block is rotating.

Numerical simulations were conducted using the drag and lift coefficients obtained from the wind tunnel experiments. Based on the numerical simulation results we show how the drag and lift coefficients affect the transport of ballistic blocks with and without rotation, and the condition of the blocks that travel furthest, by varying the block size, the ejection angle, and the rotation status.

Keywords: Ballistic projectiles, Wind tunnel experiments, Drag coefficient, Lift coefficient

©2020. Japan Geoscience Union. All Right Reserved.

Excitation of airwave by a bubble bursting in particle-bearing fluids : regime transitions and implications for basaltic volcanic eruptions

*Ikuro Sumita[1], Kana Hashimoto[2]

1. Geosciences and Civil Engineering, Institute of Science and Engineering, Kanazawa University, 2. Graduate School of Natural Science and Technology, Kanazawa University

Basaltic magma becomes more viscous, solid-like (i.e., elastic-like) and non-Newtonian (shear-thinning, possessing yield stress), as its crystal content increases. However their effects on bubble bursting and airwave excitation are poorly understood. Here we conduct laboratory experiments to investigate these effects by injecting a bubble with a volume V into a suspension consisting of non-Brownian particles (volumetric fraction phi) and a Newtonian liquid. We match the refractive indices of the particles and liquid, so that the subsurface bubble is visualized. We show that depending on phi and V, airwaves with diverse waveforms are excited, covering a broad frequency band of f of the order of 10-10^4 Hz. In a suspension of phi <= 0.3, the bubble bursts after forming a hemispherical cap at the surface and excites a high-frequency (HF) - wave (f = 1 - 2 x 10^4 Hz) having an irregular waveform. However in a suspension of phi = 0.4, when the bubble V is above critical, it bursts as soon as it protrudes above the surface and excites Helmholtz resonance with f of the order of 10^3 Hz. Superimposed on the waveform is a HF-wave component excited upon bursting, and a low frequency (f of the order of 10 Hz) air flow which vents out when the aperture grows. This transition of bubble bursting style and airwave excitation mechanism can be explained by bubble film being stretched above a critical strain rate such that the film rutpures by brittle failure. We also study the case where the fluid level is lowered such that an air column (length L) resonance is excited in addition to Helmholtz resonance. When L exceeds critical, air column resonance continues longer than the Helmholtz resonance, because the decay rate of the former becomes smaller than that of the latter. Our experiments indicate that whenever Helmholtz resonance is excited, we may use the frequency and decay rate to constrain the bubble volume and aperture radius, and also to infer the change of magma rheology.

Keywords: crystal-bearing magma, viscoelasticity, non-Newtonian rheology, bubble bursting, airwave, resonance

©2020. Japan Geoscience Union. All Right Reserved.

Ash fall observation using 2D-Video Disdrometer

*Eiichi Sato[1], Masato Iguchi[2]

1. Meteorological Research Institute, 2. Kyoto Univ.

Meteorological Research Institute (MRI) conducts ash fall observation using two-dimensional video disdrometers (2DVDs) in Sakurajima, Kagoshima. 2DVD is a ground-based instrument that originally observes precipitation particles, and is used for verification of dual-polarization radar observation. 2DVD can obtain particle size distribution, three-dimensional shape, and fall velocity of the targets by using an optical method. It is expected that it enable us to observe ash fall precisely, however, there are some drawbacks. One of the drawbacks is lowness of the ashfall capture rate, because it performs an "in situ" observation at a fixed point. In addition, the instrument is so sensitive that frequent maintenance is required.
On October 14, 2019, ash fall was successfully captured using a 2DVD in Kurokami, Sakurajima. As a result, it was found that a group of small and flat particles existed in the volcanic ash. It is known that a polarimetric parameter called differential reflectivity increases after secession of large particles from volcanic ash plume, and the observation result using 2DVD can be the evidence of this parameter change. In this presentation, the outline of the observation method using 2DVD and some observation results will be shown.

Keywords: 2D-Video Disdrometer, Sakurajima volcano, ash fall, dual-polarization/polarimetric radar, volcanic eruption plume/cloud

©2020. Japan Geoscience Union. All Right Reserved.

An attempt at quantification of starting eruption cloud at Sakurajima volcano

*Taishi Yamada[1], Masato Iguchi[1], Eisuke Fujita[2]

1. Sakurajima Volcano Research Center, Disaster Prevention Research Institute, Kyoto University, 2. National Research Institute for Earth Science and Disaster Resilience

Behavior of eruption cloud has a variety corresponding each stage in a sequence of an eruption. An eruption cloud (or column) during continuous ash emission is often modeled as a steady flow (e.g., Woods, 1988). Contrary, behavior of an eruption column in its starting stage is characterized as expansion and ascending, because the eruption cloud ascends into atmosphere with entraining surrounding air (e.g., Woods and Kienle, 1994). Ishihara et al. (1983) revealed that starting eruption cloud emerges from the crater rim with vertical velocity of promotional to altitude to the power of -3. After the cloud reached certain height, the velocity turns to a constant value of 21-28 m/s. Such a sequence is often explained by transition of driving force of starting eruption cloud. Eruption cloud emerges from the vent with gas thrust. As the eruption column ascend, the cloud obtains alternative driving force of the buoyancy with entraining surrounding air (Patrick, 2007).
The starting stage of an eruption cloud is also accompanied with considerable geophysical signals, such as strain change (Iguchi, 2009), seismic (Tameguri et al., 2002), and infrasound (Yamada et al., 2017). These previous studies examined source process of each geophysical signals, but few study focus on the relationship between the source dynamics of starting eruption cloud and the signals. Our goal in here is to understand how the source process of each geophysical signals can be connected to the dynamics of starting eruption cloud, and propose a method to constrain the behavior of stating eruption cloud with geophysical data. In this poster, some characteristics of starting eruption cloud revealed by still images at Sakurajima volcano are presented.
We installed a visual camera of DFKZ12GX236 with a resolution of 1920x900 pixels and an interval of 4 fps at station KUR (Sakurajima Volcano Research Center, Disaster Prevention Research Institute, Kyoto University) where about 5 km away from active Minamidake vents of Sakurajima volcano. Each pixel location is converted vertical- horizontal plane crossing the vent following a method by Terada et al (2003). Following this conversion, observed still images cover apparent height of 2.5 km above the crater rim, where about 0.9 km above the sea level. The location of KUR does not provide direct view of crater bottom of the Minamidake vents, where is located at 250 m beneath the Source-West crater rim on October 2018 (MLIT, 2018). We also refer data of radial extensometer and vertical short period seismometer at Arimura observation tunnel, and an infrasound microphone at station HAR.
To understand fundamental characteristics of starting eruption cloud, we examined time history of the top height of eruption column as a representative eruption cloud velocity of 12 events since October 2018. Most (10) events have a constant ascending velocity of 5-20 m/s during its ascending stage. Contrary, two events emerge from the crater rim with faster ascending velocity of 50-100 m/s. Velocity decrease to 20-40 m/s following 20 seconds. Radial strain change and the maximum value of seismic and infrasound records of the latter two events (65-122 nano strain, 71-84 μm/s, 57.8-72.2 Pa) are greater than that of events having a constant ascending velocity (38-63 nano strain, 0.3-86 μm/s, <48.9 Pa). In case of an event having the maximum ascending velocity (December 24, 2018), the radial strain and volume change rate estimated with infrasound signal (e.g., Oshima and Maekawa, 2000) have time history that well correlated with that of ascending velocity.
Those characteristics suggest that certain relation can exist between the excitation of the geophysical signals and gas thrust region of eruption cloud. Hence, the behavior of staring eruption cloud can be

©2020. Japan Geoscience Union. All Right Reserved.

constrained with analyzing enough number of events.
Acknowledgement: Strain and seismic data at Arimura tunnel is provided by the Osumi Office of River and National Highway, MLIT.

Keywords: Eruption cloud, Eruption dynamics, Sakurajima volcano

©2020. Japan Geoscience Union. All Right Reserved.

Temperature dependence of titanomagnetite composition in a titanohematite-free silicic magma

*Naoki Araya[1], Michihiko Nakamura[1]

1. Department of Earth Science, Graduate School of Science, Tohoku University

Titanomagnetite ($Fe_{3-X}Ti_XO_4$, X=0–1) is a common mineral in volcanic rocks. Due to the fast elemental diffusion in this phase and the sensitivity of its composition to temperature and oxygen fugacity, titanomagnetite has been used to probe pre-eruptive magmatic processes. When titanomagnetite coexists with titanohematite ($Fe_{2-X}Ti_XO_3$, X=0–1), the temperature and oxygen fugacity dependence of titanomagnetite composition is well known, and solid solution composition of the Fe-Ti oxides can be used as a thermo-oxybarometer. However, titanohematite-free magmas are common for mafic to intermediate systems, and the effect of magmatic parameters such as temperature, pressure, oxygen fugacity, and melt composition on titanomagnetite composition in a titanohematite-free system is poorly understood. To expand the applicability of titanomagnetite composition to probe pre-eruptive magmatic processes, it is necessary to determine the titanomagnetite–melt partitioning as a function of the above parameters in a titanohematite-free system. Thus, we conduct high-pressure and high-temperature experiments at 925–1050 ˚C, 50–150 MPa, and an oxygen fugacity at the Re–ReO_2 buffer (~ΔNNO +1.8). Matrix glass of the pumices from the Sakurajima 1914 Plinian eruption (SiO_2 ~70 wt%) was used as a starting material, and crushed titanomagnetite phenocrysts from the same eruption (ulvöspinel content 36 mol%) or pure magnetite crystals from Lovers Hole (New York, USA) were added as seed crystals. Experimental charges reproduced both titanohematite-free and titanohematite-bearing systems. When oxygen fugacity is buffered, the ulvöspinel content of titanomagnetite in titanohematite-free charges decreases with increasing temperature. This change is described as an exchange reaction of the magnetite component and the ulvöspinel component between titanomagnetite and silicate melt. The correlation between temperature and ulvöspinel content of titanomagnetite in a titanohematite-free system is opposite to that in a titanohematite-bearing system.

Keywords: titanomagnetite, partitioning experiments, pre-eruptive magmatic processes

©2020. Japan Geoscience Union. All Right Reserved.

STRATIGRAPHY AND CHARACTERISTICS OF CALDERA II DEPOSITS, BATUR VOLCANIC COMPLEX, BALI, INDONESIA

*Rahajeng Ardinni Noor[1], Atsushi Toramaru[1], Agung Harijoko[2,3], Haryo Edi Wibowo[2], Tomoharu Miyamoto[1], Mitsuru Okuno[4]

1. Department of Earth and Planetary Sciences, Faculty of Sciences, Kyushu University, 2. Department of Geological Engineering, Universitas Gadjah Mada, Indonesia, 3. Disaster Studies Center, Universitas Gadjah Mada, Indonesia, 4. Department of Earth System Science, Faculty of Science, Fukuoka University, Japan

Batur Volcanic Complex (BVC) consists of two overlaying calderas, namely Caldera I and Caldera II, with several post-caldera cones within the calderas. The previous study correlated the Caldera I and II to Ubud Ignimbrite (23 k.a) and Gunungkawi Ignimbrite (20 k.a), respectively. Those ignimbrites cropped out at Ubud area of about 20 km on the southern of BVC. More recent study reported the younger (5.2 k.a) thick deposit of caldera-forming eruption cropped out inside the rim of Caldera I and surrounding the BVC. The deposit consists of Penelokan pumice fall of plinian phase deposit and Batur Ignimbrite. These deposits interpreted as the youngest caldera-forming eruption product of Caldera II instead of Gunungkawi Ignimbrite. This study intended to describe and report the stratigraphy and characteristic of the deposits in order to interpret the dynamic of caldera-forming eruption of Caldera II.

The juvenile materials of the deposits are composed of white, grey, and banded pumices and/or scoria. Analyses done in a total of 13 bulk samples from Penelokan Fall and Batur Ignimbrite, including Grain Size Distribution (GSD) in the size range of phi -5 to 1, componentry analysis in the size of phi -2 to -4, density analysis in juveniles in the size of phi -3 to -4 around 100 grains in each sample, x-ray fluorescence (XRF), thin section, and scanning electron microscope (SEM).

GSD data show that the deposits of Plinian fall and matrix of PDC have unimodal distribution. In the proximal area, Plinian fall dominated by coarse materials (phi -3 and -4) of pumice and/or scoria, whereas, the PDC dominated by fine materials (phi >1). The coarse materials in PDC mostly composed of lithic. The bulk density of white pumice range from 0.5-0.8 gr/cm^3, grey pumice 0.5-1.1 gr/cm^3 and scoria 0.9-1.1 gr/cm^3. Based on petrographic and SEM analysis, the vesicularity of juvenile deposits are 47.40-58.09% and mostly phenocryst poor (0.47-2.88%). Phenocryst are composed of plagioclase, orthopyroxene, and clinopyroxene. The occurrence of phenocrysts and microlites in white pumice are rare, in contrast, common in grey pumice and abundance in scoria. The XRF data show that the deposits are grouped into trachy-andesite to trachyte, and classified as sub-alkaline series. The PDC deposits have a wider range in SiO_2 content (61.95-68.05 wt %). However, Plinian falls relatively narrow (61.98-63.67 wt %) with LOI number 1.28-3.33.

The eruption of Caldera II of the Batur Volcanic Complex occurs from the Plinian eruption produces the Plinian-fall, and the unsteady column produced intra-plinian PDC. On the other hand, the collapse of the column deposited the ignimbrite. Most of the sequence deposited within the Caldera I floor, however when the eruption intensity increase, the deposit could reach the distal area up to 17 km from the Caldera I rim. Lithic rich content and basal lag breccia are suggesting the vent opening process occurs. After several continuous eruptions, the proximal area started to collapse due to the emptying of the magma chamber. The variation of juveniles and range of density generate by variation in physical characteristics primarily for crystal and microlite content.

©2020. Japan Geoscience Union. All Right Reserved.

Keywords: Volcanism, Caldera-forming Eruption, Batur Caldera, Stratigraphy, Characteristic

©2020. Japan Geoscience Union. All Right Reserved.

Factors affecting the sequence of the Plinian eruption inferred from rock texture and physical properties - an example of the 1783 eruption, Asama volcano, Japan

*Tatsuki Mizuno[1], Fukashi Maeno[1], ATSUSHI YASUDA[1]

1. Earthquake Research Institute, Department of Earth and Planetary Science, University of Tokyo

Plinian-style eruption is characterized by a large-scale column formed by an explosive magma rising. It often shows variation of eruptive style such as pyroclastic flows and lava flows, and the eruption styles change complicatedly in the same series of activity. Determining the factors controlling the eruptive style and its change is important for predicting the sequence of the eruption. In this study, we focus on the 1783 eruption of Asama volcano in order to understand the magma ascent process and factors controlling eruptive style through analysis of chemical composition and observation of rock texture. In the climactic phase of the 1783 eruption, a large column was established and pumice-fall deposits were formed at first, then the eruptive style changed to pyroclastic flows. Magma composition in the pyroclastic flow phase changed to be lower SiO_2. Pumice-fall deposits are divided into 16 layers. Upper half of the deposits were formed in climactic phase. In the middle level of deposits, there are some red ash layers which may have formed by pyroclastic flows before climactic phase. The main units of pyroclastic flow deposits include gray scoriaceous juvenile clasts. The bottom layer of pyroclastic flows contains juvenile pumice clasts, so the changes of chemical composition and eruptive style was not simultaneous.

Pumice clasts from fallout and pyroclastic flow deposits were chosen for measurement of density, microscopy, and chemical analyses. The apparent density ranges 0.6-0.9 g/cm^3 in fall deposits, 0.7-0.95 g/cm^3 in pumiceous pyroclastic flow deposits, and 0.7-1.2 g/cm^3 in scoriaceous pyroclastic flow deposits. The ratio of the connected vesicles ranges 87-96% in fall deposits, 83-98% in pumiceous pyroclastic flow deposits, and 91-95% in scoriaceous pyroclastic flow deposits. The ratio of connected vesicles ranges widely in pumiceous clasts, pyroclastic flow deposits have lower ratio than fall deposit. Scoriaceous clasts have higher ratio than pumiceous clasts. Phenocryst types are plagioclase, orthopyroxene, clinopyroxene, and Fe-Ti oxide, and olivine is rare. SiO_2 content of groundmass glass shows bimodal distribution around 67wt% and 72wt%. Pyroclastic flow deposits contain abundant low-SiO_2 clasts than pumice-fall deposits. Magma temperature and water content are estimated from chemical composition of plagioclase and matrix glass (Putirka, 2008; Waters and Lange, 2015), then SiO_2= 67 wt%, T=1060-1100℃, H_2O=0.8-1.0 wt% and SiO_2=72 wt%, T=1000-1015℃, H_2O=1.2-1.4 wt%. Vesicles in pyroclasts in the upper units are more connected and elongated. Clast types in pyroclastic flows are similar to the lower part of fallout units, but scoriaceous ones have thick bubble wall glass. We analyzed crystal and vesicle textures by using the shareware program ImageJ and CSD correction (Higgins, 2006). Crystallinity range 7-14% and poor in microlite. The average vesicularity of each layer ranges around 75% in pumice-fall deposit, excepting middle level, and 65-67% in middle level fall deposit and pyroclastic flow deposit. Bubble number density (BND) ranges 2.0-4.0×10^{13} m^{-3}, then the flow deposits show higher in BND than the fall deposits. Decompression rate for each layer can be estimated from BND, SiO_2 content, water content, and temperature (Toramaru, 2006). It was calculated at 3.2-4.7×10^7 (Pa/s) in fall deposits, 5.0×10^7 (Pa/s) in pumice flow deposit, and 1.0×10^8 (Pa/s) in scoriaceous flow deposit.

The change of the decompression rate has a correlation with changes of the eruptive style from column formation to pyroclastic flow generation. Fall deposits accompanied by red ash in the middle layer, which

©2020. Japan Geoscience Union. All Right Reserved.

indicates simultaneous generation of pyroclastic flows, show high decompression rate. Based on these results, it is suggested that the increase of magma decompression rate is densely related to generation of pyroclastic flows during the climactic phase of the 1783 eruption.

Keywords: Asama Volcano, eruptive style, magma ascent process, textural analyses

©2020. Japan Geoscience Union. All Right Reserved.

Thermal history of pyroclasts reflecting the structure of eruption clouds: Application of textural analysis of pyrrhotite oxidation

*Keiko Matsumoto[1]

1. Geological Survey of Japan, The National Institute of Advanced Industrial Science and Technology

Entrainment of air in eruption clouds causes rapid oxidation of pyroclasts due to an increase of oxygen fugacity at a high temperature. Oxidation texture of sulfide minerals (pyrrhotite) in pyroclasts can be an indicator for the process of air entrainment and temperature change in eruption clouds as it forms via interaction with air. To demonstrate the contrast of air entrainment and thermal disequilibrium processes of Plinian and Vulcanian eruption columns, oxidation texture of pyrrhotite in four andesitic pyroclastic eruptions of Asama and Sakurajima volcanoes was investigated. Although pyrrhotite and oxidized pyrrhotite crystals were commonly observed in the pumice clasts of these four eruptions, the component proportions and degree of oxidation of the pyrrhotite crystals were significantly different between Plinian and Vulcanian fall-deposits. Component proportions of oxidized pyrrhotite crystals were high for pumice deposits of the Asama 1783 and the Sakurajima 1914 Plinian eruptions than those of the Asama 2004 and the Sakurajima 2010 Vulcanian eruptions. These results indicate that the temperature of pumice clasts was kept above the closure temperature of pyrrhotite oxidation in the Plinian eruption clouds for a long time, while they dropped quickly in the Vulcanian one. The high temperature maintenance in Plinian clouds probably reflects (i) multiple mixing of an eruption cloud due to the continuous nature of Plinian flow and (ii) heat retainment in a pumice clast in the buoyant plume of the Plinian cloud. Thus, textural analysis of oxidized pyrrhotite can be a new approach for constraining the duration of high temperatures of an eruption cloud from fall-deposits, thereby reflecting the eruption dynamics.

Keywords: eruption cloud, pyrrothite, oxidation, Sakurajima volcano, Asama volcano

©2020. Japan Geoscience Union. All Right Reserved.

Intermittent ascent of aphyric andesitic melts revealed by cryptic micro-antecryst textures

*Charline Lormand[1], Georg F Zellmer[1], Naoya Sakamoto[2], Geoff Kilgour[3], Teresa Ubide[4], Hisayoshi Yurimoto[2], Alan Palmer[5], Karoly Nemeth[1], Yoshiyuki Iizuka[6], Anja Moebis[5]

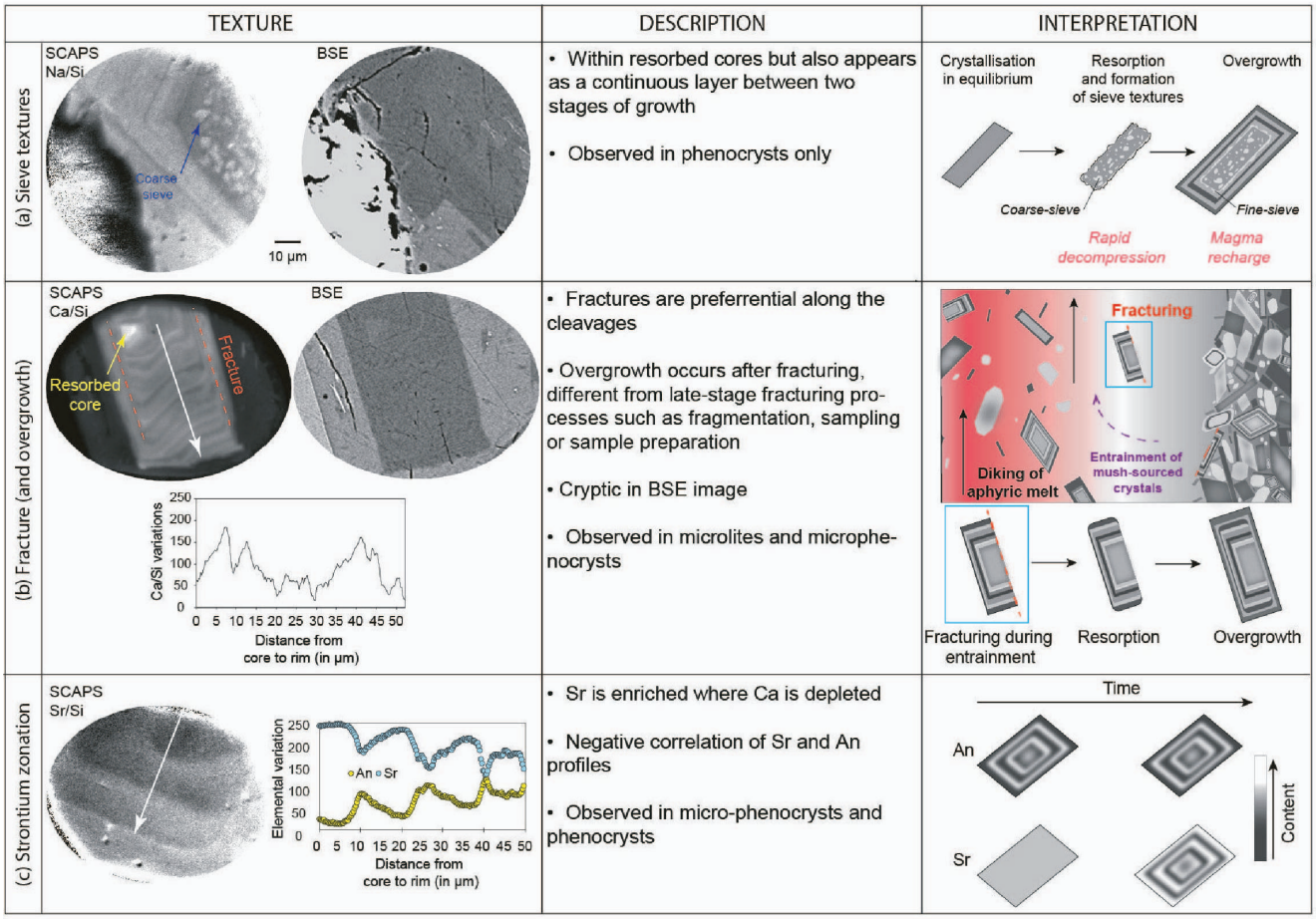
1. School of Agriculture and Environment, Volcanic Risk Solutions, Massey University, PO Box 11222, Palmerston North 4442, New Zealand, 2. Isotope Imaging Laboratory, Natural History Sciences, Hokkaido University, Sapporo 060-0810, Japan, 3. GNS Science, Wairakei Research Centre, Private Bag 2000, Taupo 3352, New Zealand, 4. School of Earth and Environmental Sciences, The University of Queensland, Brisbane, QLD 4072, Australia , 5. School of Agriculture and Environment, Department of Soil Science, Massey University, PO Box 11222, Palmerston North 4442, New Zealand , 6. Institute of Earth Sciences, Academia Sinica, 128 Academia Road Sec. 2, Nankang, Taipei 11529, Taiwan

Crystal cargoes transported by arc magmas upon eruption often consist of complexly zoned phenocrysts with diverse histories. While these crystals record the early stage of magma formation and evolution, they are not ideal recorders of ascent processes, which are the keys to useful constraints for adequate volcano monitoring. Conversely, microlites and micro-phenocrysts, frequently associated with decompression-induced degassing or cooling, are relevant recorders of late-stage ascent processes. Our study focusses on the active Tongariro Volcanic Centre (TgVC), located at the southern end of the Taupo Volcanic Zone; an active volcanic complex that has produced a wide range of explosive eruption styles fed by intermediate magmas. Scoriae from these volcanoes contain glassy and nearly-aphyric tephras, carrying microlites of plagioclase and pyroxene (mostly orthopyroxene). Major element analyses, combined with textural information, are used to assess equilibrium between the microlites/micro-phenocrysts and the groundmass glass. Chemical disequilibrium of some plagioclase and pyroxene crystals with the surrounding glass is common in most tephras. To investigate this further, we mapped plagioclase and pyroxene phenocrysts, micro-phenocrysts and microlites at submicron resolution for major and trace element distributions via chemical mapping and SIMS-SCAPS imaging. From a total of 105 images, six plagioclase textural patterns are noted: resorption and overgrowth, oscillatory zoning, single compositional jump, sieve textures, fractures, and strontium zonation; while in pyroxene microlites the following textures are found: resorption and overgrowth, calcium-rich rims, magnesian core and calcic rims, fractures, and aluminium zonation. Microlite textures are observed down to <30 μm in most tephras from TgVC, and interpreted in the context of an interplay of magmatic processes involving multiple events of magma recharge/mixing, pressure fluctuations, fracturing, and rapid cooling and crystal growth. Since TgVC is located in an extensional tectonic setting, we envision a vertically oriented magma plumbing system, where short-lived and nearly-aphyric magma pulses accommodate crustal extension through dyking. Explosive eruptions occur when a hot magma batch fractures through previous intrusions, recycling a variety of small crystals grown under diverse physico-chemical conditions and stored in rapidly cooled, previously intruded dykes. Thus, textures cryptic to conventional imaging indicate that a significant proportion of the microlitic and micro-phenocrystic mineral cargo is of antecrystic origin (i.e. hence referred as “micro-antecrysts”) and cannot be attributed to late-stage nucleation and growth at the onset of volcanic eruptions.

Keywords: microlites, micro-phenocrysts, zonations, Tongariro Volcanic Centre, magma ascent

©2020. Japan Geoscience Union. All Right Reserved.

Some textures and zonations observed in plagioclase microlites, micro-phenocrysts and phenocrysts of the Tongariro Volcanic Centre andesitic tephras: (a) sieve textures resulting from rapid decompression; (b) fracture (and overgrowth) triggered by entrainment of crystals from a crystal-mush-like environment; (c) strontium zonation associated with a negative correlation with An suggesting recycling of old crystals. Ca, Si, Sr, Na, BSE and An respectively stand for calcium, silica, strontium, sodium, back-scattered electron and



©2020. Japan Geoscience Union. All Right Reserved.

[E] Poster | S (Solid Earth Sciences)：S-VC Volcanology

[S-VC43] Magma crystallization, fragmentation, and their roles on volcanic eruption

convener:Takahiro Miwa(National research institute for earth science and disaster prevention), Satoshi Okumura(Division of Earth and Planetary Materials Science, Department of Earth Science, Graduate School of Science, Tohoku University), Pranabendu Moitra(University of Arizona)

Crystallization of magma during magma ascent in the conduit has a large impact on the dynamics of volcanic eruptions. Magma viscosity and brittleness increase with crystallization. This change of rheological properties may cause brittle fragmentation of low-viscosity basaltic magma during highly explosive subplinian and Plinian eruptions. On the other hand, crystallization may form rigid crystal frameworks, causing efficient outgassing through the interaction between the crystal frameworks and growing gas bubbles in ascending magma, resulting in effusive eruptions. This session aims to integrate information of elementary processes to develop physical models of multiphase magma ascent and eruption. In this view, we welcome innovative and multidisciplinary contributions from experimental volcanologists, numerical modelers, petrologists, and also geophysicists who develop and extend techniques to explore crystallization and bubble-crystal interactions, and their effects on fragmentation and outgassing of multiphase magma during effusive and explosive eruptions.

[SVC43-P01] Estimating the parameter to determine bubble - crystal interaction styles

*Ikeda Kyoko[1], Atsushi Toramaru[1] (1.Kyushu University, Department of Earth and Planetary Science)

[SVC43-P02] Effects of equilibrium crystallization on conduit flow dynamics during the 1986 eruption at Izu-Oshima volcano

*Tomofumi Kozono[1], Hidemi Ishibashi[2], Satoshi Okumura[3], Takahiro Miwa[4] (1.Department of Geophysics, Graduate School of Science, Tohoku University, 2.Department of Geoscience, Faculty of Science, Shizuoka University, 3.Department of Earth Science, Graduate School of Science, Tohoku University, 4.National Research Institute for Earth Science and Disaster Resilience)

[SVC43-P03] Experimental study on groundmass crystallization of the Izu-Oshima 1986 B basaltic andesite magma during conduit ascent

Ryoya Oida[2,3], *Hidemi Ishibashi[1], Akihiko Tomiya[3], Masashi Ushioda[3], Natsumi Hokanishi[4], Atsushi Yasuda[4] (1.Faculty of Science, Shizuoka University, 2.Graduate School of Integrated Science and Technology, Shizuoka University, 3.GSJ, AIST, 4.Univ. Tokyo, ERI)

[SVC43-P04] Effect of superheating on decompression-induced crystallization of hydrous rhyodacite magma: An experimental study

*Kazuhisa Matsumoto[1], Satoshi Okumura[1], Akihiko Tomiya[2] (1.Division of Earth and Planetaly Materials Science, Department of Earth Science, Graduate School of Science, Tohoku University, 2.Geological Survey of Japan, National Institute of Advanced Industrial Science and Technology)

[SVC43-P05] Analog experiment on vesiculation by crystallization with H_2O-KCl-CO_2

*Shiho Fujimura[1], Atsushi Toramaru[1] (1.Kyushu University)

[SVC43-P06] Deep Crystallization of Tholeiitic Melt: Insights from Manguao Basalt, Palawan, Philippines

*James Cesar Avisado Refran[1], Tsukasa Ohba[1], Carlo Arcilla, Takashi Hoshide[1], Ma. Ines Rosana Balangue-Tarriela (1.Akita University)

[SVC43-P07] Relationship between the change of eruption style and the rock texture of ejecta during the Shinmoe-dake 2018 eruption, Kirishima, Japan

*Sayaka Shohata[1], Fukashi Maeno[2], Yuki Suzuki[3], ATSUSHI YASUDA[2], Natsumi Hokanishi[2] (1.Department of Earth and Planetary Science, School of Science, The University of Tokyo, 2.Earthquake Research

Institute, The University of Tokyo, 3.Faculty of Education and Integrated Arts & Sciences, Waseda University)

[SVC43-P08] Stratigraphy and Unit Determination of Ranau Tuff in Sumatra, Indonesia

*Rachmi Mustika Pertiwi Putri Gunawan[1], Atsushi Toramaru[1], Tomoharu Miyamoto[1] (1.Department of Earth and Planetary Sciences, Kyushu University, Fukuoka, Japan)

[SVC43-P09] 3D crystal size distributions of pyroxene nanolites based on nanoX-ray CT analyses

*Shota Okumura[1], Mayumi Mujin[2], Akira Tsuchiyama[3,4], Akira Miyake[1] (1.Department of Geology and Mineralogy, Graduate School of Science, Kyoto University, 2.Division of Earth and Planetary Materials Science, Department of Earth Science, Tohoku University, 3.Research Organization of Science and Technology, Ritsumeikan University, 4.Guangzhou Institute of Geochemistry, Chinese Academy of Sciences)

[SVC43-P10] Pre-eruptive Magma Condition of Tondano Caldera I: Domato Tuff, Minahasa, NE Sulawesi, Indonesia

*Tabegra Disando[1], Atsushi Toramaru[1] (1.Department of Earth and Planetary Sciences, Kyushu University, Fukuoka, Japan)

[SVC43-P11] **Magma fracturing, oxidation and nanolite crystallization processes during silicic magma eruption: Implication from textural and chemical analyses on oxidized obsidian**

*Kyohei Sano[1], Eiichi Sato[2] (1.Graduate School of Regional Resource Management, University of Hyogo, 2.Faculty of Liberal Arts and Sciences, Osaka Prefecture University)

[SVC43-P12] Redox state and nanolite crystallization of erupting magma during ash forming eruption at Bromo Volcano, Indonesia

*Takahiro Miwa[1], Hidemi Ishibashi[2], Masato Iguchi[3], Genji Saito[4], ATSUSHI YASUDA[5], Natsumi Hokanishi[5] (1.National research institute for earth science and disaster resilience, 2.Shizuoka University, 3.DPRI, Kyoto University, 4.AIST, 5.ERI, University of Tokyo)

Estimating the parameter to determine bubble - crystal interaction styles

*Ikeda Kyoko[1], Atsushi Toramaru[1]

1. Kyushu University, Department of Earth and Planetary Science

In the magma, the interaction between suspended crystals and the rising bubble made by buoyancy is important because the interaction can be expected to control the chemical evolution of magma chamber and their stratification through the rheological properties and bulk densities. Beline et al (2010) showed that there are three interaction styles with changing bubble diameter and viscosity of the liquid by laboratory experiments using an analog material: a single plastic cube and a controlled single bubble in viscous liquid. However, the crystal - bubble interaction is still poorly understood since the factors to make a difference among the three interaction styles are not explained enough. In order to solve this problem, we give some constraint on the controlling parameters to determine three interaction styles by analogue experiments.
The experiments are performed in the tank filled with viscous liquid (analog material of silicate melt)and prepared three different viscosity(0.29 Pa・s, 6.46 Pa・s, 19.1 Pa・s). The plastic cube (analog material of crystal) with 10 mm is suspended in liquid by a rod. The bubble is injected into the liquid from 11cm below the plastic cube from a syringe connected to a motor controlled by the PC program by which we can change the initial bubble size. We examine the probability of occurrence of three styles of interaction: "stuck", "pass", and "split"; "stuck" in which a bubble stays under the solid cube, "pass" in which a bubble moves around the cube and "split" in which a bubble separated into two bubbles. To determine the probabilities, we did the repetition of 10 times for the same condition of initial bubble radii and viscosity.
In our experiments, we observed two styles of the interaction of "stuck" and "pass" and not "split". It is found that the smaller bubble tends to “stuck”, on the other hand, the probability of “pass” became higher as the bubble radii are larger. To reveal the boundary of “stuck” and “pass”, we use Bound number which is a dimensionless number representing the ratio of bubble relaxation time and the bubble rising time per their radius. From the results of the examination using the size ratio between solid cube and the final attached bubble, and Bond number, it is suggested that there are two regimes in the mechanism of interaction styles. These two different regimes are caused by Reynolds number which is the ratio of inertia force and viscous resistance. In low Reynolds number regime is controlled by the final maximum bubble diameter which resulted from mechanical interaction between bubble and cubes in the higher viscosity. For example, if the deformed bubble diameter is larger in the horizontal length than the cube width, the bubble path throws the cube. In high Reynolds number regime is controlled by inertia force. The probability of occurrence of “pass” is higher as the bubble radius becomes larger with inertia force.
Thus, we found that there are two regimes in the bubble-crystal interaction style; one is a static regime (low Re) controlled by the geometrical relation in the horizontal sizes including static deformation, another is a dynamic regime (high Re) controlled by the inertia of a rising bubble by buoyancy.

©2020. Japan Geoscience Union. All Right Reserved.

Keywords: analog experiment, bubble-crystal interaction

©2020. Japan Geoscience Union. All Right Reserved.

Effects of equilibrium crystallization on conduit flow dynamics during the 1986 eruption at Izu-Oshima volcano

*Tomofumi Kozono[1], Hidemi Ishibashi[2], Satoshi Okumura[3], Takahiro Miwa[4]

1. Department of Geophysics, Graduate School of Science, Tohoku University, 2. Department of Geoscience, Faculty of Science, Shizuoka University, 3. Department of Earth Science, Graduate School of Science, Tohoku University, 4. National Research Institute for Earth Science and Disaster Resilience

A diversity of eruption styles has been mainly studied in silicic volcanism, in which the competition between vesiculation of hydrous magma and gas escape from the magma in conduit flow is one of the main factors controlling eruption styles (explosive or effusive). In basaltic magmatism, diverse eruption styles are also been observed especially in island arc volcanoes with hydrous magma. In this study, we investigated the origin of the diverse eruption styles during the 1986 eruption of Izu-Oshima volcano, Japan, using a 1-D steady conduit flow model. Ishibashi and Oida (2018) proposed that a variety of equilibrium crystallization paths during magma ascent caused by a difference in magma temperature is a key factor controlling the eruption styles which range from lava flow to sub-Plinian eruptions. We assessed the effects of the equilibrium crystallization on conduit flow dynamics during the 1986 Izu-Oshima eruptions. In the conduit flow model, magmatic properties of the Izu-Oshima eruptions were properly set based on petrological observations and thermodynamic modeling. We also applied various models for magma fragmentation (expansion, shear-induced, and stress) and gas escape (permeable flow and bubble segregation) because information about these processes in basaltic magma is limited. We obtained two distinct patterns of conduit flow depending on equilibrium crystallization path and magma temperature as expected in the previous study: a low (or high) temperature and high (or low) crystallinity magma induces a flow with high (or low) magma viscosity. When a shear-induced or stress fragmentation is applied, the flow with high viscosity leads to fragmentation and explosive eruption, whereas that with low viscosity leads to effusive eruption without fragmentation. We also found that expansion fragmentation is promoted for the flow with high viscosity when gas escape due to bubble segregation is applied because the high viscosity prevents the bubble segregation. Our results revealed that due to the above relationship between the crystallinity or viscosity and the explosivity of basaltic eruptions, there exist the conduit flow solutions corresponding to the lava flow and sub-Plinian eruptions at Izu-Oshima volcano. Although crystallization kinetics has been recognized as an important process controlling the eruption dynamics, our results indicate that the equilibrium crystallization process is also strongly controlling the eruption styles in basaltic volcanism.

Keywords: Basaltic eruption, Conduit flow, Eruption style, Crystallization, Fragmentation, Gas escape

©2020. Japan Geoscience Union. All Right Reserved.

Experimental study on groundmass crystallization of the Izu-Oshima 1986 B basaltic andesite magma during conduit ascent

Ryoya Oida[2,3], *Hidemi Ishibashi[1], Akihiko Tomiya[3], Masashi Ushioda[3], Natsumi Hokanishi[4], Atsushi Yasuda[4]

1. Faculty of Science, Shizuoka University, 2. Graduate School of Integrated Science and Technology, Shizuoka University, 3. GSJ, AIST, 4. Univ. Tokyo, ERI

Melting and crystallization experiments were performed for H_2O-saturated basaltic andesite magma of the Izu-Oshima 1986 B eruption at 0.1-200 MPa pressure conditions, to constrain the pre-eruptive pressure condition and to simulate crystallization process during conduit ascent of the magma. The 1986 B eruption was sub-Plinian and erupted almost aphyric (<1 vol.% phenocrysts of plagioclase), microlite-rich basaltic andesite magma with bulk SiO_2 content of ~54.5 wt.%. Powdered samples of the basaltic andesite were used for the starting materials of our experiments. We performed high-temperature phase equilibrium experiments at 0.1 MPa and high-pressure conditions (1010-1200ºC and 20-200MPa), using the fO_2-controlled electric furnace and the internally heated pressure vessel (KOBELCO Dr. HIP) at GSJ, AIST, respectively. In both experiments, the samples were heated at experimental temperatures for 3 hours and then quenched. Redox conditions were controlled at Ni-NiO buffer during the experiments at 0.1 MPa, whereas the high-P experiments were performed under more oxidized conditions because fO_2 was not controlled. The quenched samples were processed to polished thin sections for microprobe analyses. BSE image observations and chemical analyses of microlites and glasses were done using FE-EPMA (JEOL JXA-8530FPlus) and EPMA (JEOL-8800R) at ERI, University of Tokyo, respectively.
First, H_2O-saturated liquidus of the basaltic andesite magma was experimentally constrained and formulated as a function of pressure as $10000/T = 8.5 + 0.0027P + 0.049P^{0.5}$. Assuming the magma was at 1070-1100 ºC (Fujii et al., 1988) and saturated with H_2O and plagioclase in its magma chamber, the pre-eruptive pressure is estimated to be ~70-115 MPa; the pressure corresponds to the depth of ~2.8-4.6 km, which is consistent with previous geophysical result (Ida, 1995).
Secondly, phase equilibrium experiments were performed at 1080 ºC, the eruptive temperature of the magma, and various pressure conditions from 75 MPa to 0.1 MPa, to simulate crystallization during conduit ascent of the magma. Plagioclase and Fe-Ti oxide are found in all samples, whereas pyroxene crystallized at pressure lower than 35 MPa. As pressure decreases, plagioclase content increases from 2.5 vol.% at 75 MPa to 42.5 vol.% at 0.1 MPa. At 20 MPa, plagioclase and total crystal contents are ~20 vol.% and ~40 vol.%, respectively, which are similar to those in the natural scoria samples. Considering the effects of fO_2 and crystallization kinetics on crystallinity, the results suggest that the pressure at which crystallization ended during conduit ascent of the magma was lower than 20MPa, corresponding to the depth < ~1km. We infer that fragmentation occurred at the depth because the crystallinity of >~40 vol.% corresponds to the critical crystallinity at which viscous-brittle transition occurs for melt-crystal-bubble system with bubble content of <30-50 vol.%.
Lastly, the effect of temperature on crystallinity was examined at 20MPa. As temperature increases from 1080 ºC to 1110 ºC, total crystal contents drastically decrease from ~40vol.% to ~5 vol.%. The result indicates that decreasing temperature facilitates viscous-brittle transition and fragmentation due to increase of crystallinity. Therefore, temperature is a critical factor controlling eruption style of mafic magma. We think that the difference of eruption styles between A and B magmas of the Izu-Oshima 1986 eruption was essentially caused by the difference of magmatic temperature.

©2020. Japan Geoscience Union. All Right Reserved.

Keywords: crystallization, microlite, mafic magma, Izu-Oshima, eruption style

©2020. Japan Geoscience Union. All Right Reserved.

Effect of superheating on decompression-induced crystallization of hydrous rhyodacite magma: An experimental study

*Kazuhisa Matsumoto[1], Satoshi Okumura[1], Akihiko Tomiya[2]

1. Division of Earth and Planetaly Materials Science, Department of Earth Science, Graduate School of Science, Tohoku University, 2. Geological Survey of Japan, National Institute of Advanced Industrial Science and Technology

Decompression experiments have been applied to determine decompression rates during magma ascent to the surface (e.g., Hammer and Rutherford, 2002). The texture of crystals in pyroclasts also records the pressure at magma fragmentation level during explosive eruption (e.g., Okumura et al., 2019). Comparison between the texture of crystals in natural pyroclasts and that in experimental products enables us to estimate the decompression rate and magma fragmentation pressure. This is a powerful method to estimate the processes of magma ascent; however, it has been thought that an experimentally reproduced texture of crystals depends on superheating before decompression. Indeed, two decompression experiments performed at the similar experimental condition but different superheating (Brugger and Hammer, 2010; Riker et al., 2015) show large difference in the number density of crystals.

In this study, we carried out a series of decompression experiments to investigate the effect of superheating on the number density and size of crystals and total crystallinity. We used powdered pumice sample of the 1977 sub-Plinian eruption of Usu volcano, Japan as a starting material. The liquidus temperature of this magma was estimated to be ~920˚C (Ohnishi and Tomiya, 2018). For the decompression experiments, we prepared four types of starting materials synthesized (annealed) at the same pressure (130 MPa) and temperature (900˚C), corresponding to the magma chamber condition (Ohnishi and Tomiya, 2018), but preheated at temperatures of 900, 940, 970, and 1300˚C (different degree of superheating) using a cold seal pressure vessel (CSPV) at Tohoku Univ and internally heated pressure vessel at GSJ/AIST. The durations of preheating and annealing are 2 to 48 h and 48 to 138 h, respectively. In the synthesized samples, no plagioclase was found when the sample was preheated at 1300˚C, and the number density of plagioclase increases with the decrease in preheating temperature although total crystallinity is not different. Decompression experiments were isothermally conducted at a temperature of 900˚C using CSPV, with continuous decompression from 130 to 30 MPa and decompression rates of 100, 20 and 5 MPa h^{-1}. After decompression, the sample was rapidly quenched, and the number density and size of crystals and total crystallinity were investigated.

Our results clearly indicate that the degree of superheating influences the number density and size of crystal. The number densities of plagioclase in the products preheated at 1300 and 970˚C are much lower than those at 940 and 900˚C . Under high decompression rate (100 MPa h^{-1}), no plagioclase was found in the product preheated at 1300˚C. The size of plagioclase is large in the products preheated at 1300 and 970˚C under decompression rate of 20 and 5 MPa h^{-1}.

We also observed the dependence of the number density on the decompression rates. The maximum number density of plagioclase was found at 20 MPa h^{-1} in the products preheated at 940 and 900℃. On the other hand, the number density in the product preheated at 970˚C shows only small variation with decompression rate. This indicates that the number density depends on decompression rate when crystallization is dominated by nucleation rather than growth.

On the basis of these results, we conclude that the degree of superheating controls the number density

©2020. Japan Geoscience Union. All Right Reserved.

and size of crystal as well as decompression rate. This is probably because the superheating determines the number density of clusters smaller than the critical nuclei size (Sato, 1995). When the number density of the cluster is high, the nucleation controls the relaxation of effective undercooling, while the undercooling is relaxed by the growth process under low number density of the cluster. Therefore, the effect of superheating must be considered when the decompression experiment and the resultant number density is applied to determine decompression rate and fragmentation pressure.

Keywords: volcanic eruption, Usu volcano, decompression expriments, decompression-induced crystallization, superheating, number density

©2020. Japan Geoscience Union. All Right Reserved.

Analog experiment on vesiculation by crystallization with H_2O-KCl-CO_2

*Shiho Fujimura[1], Atsushi Toramaru[1]

1. Kyushu University

Volatile components such as H_2O and CO_2 are dissolved in the magma chamber under the volcano. These volatile components cause the bubble formation in the magma leading to the volcano eruptions.

One type of bubble formation in the magma chamber is induced by cooling and crystallization (so called “second boiling”). Crystals formation due to cooling by the host rock reduces the melt volume, and the volatile components that cannot be dissolved in the crystals concentrate in the melt.

Yoshigai (2011) investigated this process by an analog system using carbonated water. The carbonated water was used as the analog material of the melt, and the CO_2 as the volatile component in the melt. When the solution was cooled below freezing point, the crystallization of ice, the bubble formation ,and the pressure increase were observed. However, since the ice has larger molar volume than the solution, it was unclear whether the pressure increase was due to the generation of bubbles or the formation of the ice.

Therefore, the purpose of this study was to reproduce the cooling crystallization and the bubble formation by analog experiments without pressure increase due to the ice formation. In order to do that, we use the system H_2O-KCl-CO_2, taking the advantage of the crystallization of KCl.

From the H_2O-KCl phase equilibrium diagram, assuming the room temperature of 20 ℃, the 25 wt% KCl solution is thought to be just saturated at 20 ℃. When the solution of that concentration is cooled, it can be expected that KCl crystals gradually crystallize and bubble formation occurs.

The acrylic cylindrical container(the diameter: 5 cm, the height: 5 cm) was used in the experiment. Only the lower bottom (aluminum plate) of the container was cooled by using a Peltier device throughout the experiment. During the experiment, the temperature was measured by thermo-couples(both K type) at the top and bottom in the container and the pressure inside the container was measured by the pressure-transduce(made by KISTLER). The video image was taken by GoPro (HERO 7 BLACK).

The experimental results above the eutectic point of H_2O-KCl binary system show that the crystallization of KCl was observed, but no CO_2 bubble was generated. This can be interpreted that the concentration rate of CO_2 by the KCl crystallization is smaller than the solubility increasing rate by cooling, from the calculation.

In the experiments below the eutectic point -10 ℃ the total volume of H_2O and KCl crystals is expected to increase until the totally crystallized and to change depending on the amount of heat loss compensating the release of latent heat. We also examine the effect of surrounding temperature by controlling the variable temperature of used incubator where the container of solutions and sensors are set.

In the experiments performed at 10 ℃ and 16 ℃ of surrounding temperature, KCl was crystallized first, and below the eutectic point, ice and KCl crystals formed, and bubbles formed only near the inner side wall of the cylindrical container. However, in the experiment kept at 3 ℃, no bubbles formed even after

©2020. Japan Geoscience Union. All Right Reserved.

the solution nearly totally crystallized.

Bubbles were generated only around the crystals. It is suggested that, the crystals were thick and the gap between the crystal and the container was large. When the experiment performed above the eutectic point, no bubble was observed. The reason is considered that in the initial concentration performed in this experiment, the amount of crystals generated during cooling is insufficient. The calculation for silicate systems shows that the concentration of H_2O by crystallization dominates or is similar to the solubility increase of H_2O by cooling. So, in the silicate system, the crystallization can induce the volatile concentration and lead to the bubble formation.

Keywords: magma, crystallization, analog experiment

©2020. Japan Geoscience Union. All Right Reserved.

Deep Crystallization of Tholeiitic Melt: Insights from Manguao Basalt, Palawan, Philippines

*James Cesar Avisado Refran[1], Tsukasa Ohba[1], Carlo Arcilla, Takashi Hoshide[1], Ma. Ines Rosana Balangue-Tarriela

1. Akita University

Manguao Basalt is a basalt-basaltic andesite lava flow field found on the northeast end of Palawan Island, Philippines. The relatively-stable nature of the Palawan Continental Block seemingly contradicts the presence of the geomorphologically-young lava flow field. This study investigates the occurrence and origin of Manguao Basalt, and its relation to evolution of the Palawan microcontinent.

Good exposures of the Manguao Basalt lava flow field are found nearshore; with flow structures and features (i.e. levees, channels, and tumuli) still intact and observable in several locations. The lava flow is generally blocky and vesicular, with perceptible phenocrysts and chert xenoliths. Macroscopic observations of obtained samples show identifiable olivine and pyroxene phenocrysts. Petrographic observations show olivine dominance in phenocryst and plagioclase dominance in groundmass. Pyroxenes are found both in phenocryst and groundmass assemblages. Mineral textures observed from petrography shows precedence of pyroxene phenocrysts from olivine. Plagioclase laths in groundmass also show precedence from anhedral groundmass pyroxenes. Volcanic glass fills the interstices between plagioclase and pyroxene; forming intersertal textures. A general overview of the crystallization sequence (pyroxenes àolivine àplagioclase àgroundmass pyroxenes), from petrography, is presented.

Major element chemistry from bulk-rock compositions characterizes the Manguao Basalt as subalkaline and tholeiitic. Bivariate diagrams show fractionation in ferromagnesians (i.e. olivine and pyroxenes) but limited fractionation in later-formed minerals (i.e. plagioclase). Total iron over magnesium (FeOt/MgO) versus silica (SiO_2) plots (Miyashiro, 1974) of Manguao Basalt shows 'straddling' tholeiite and calc-alkaline character. AFM ternary plots show diagnostic early iron enrichment, reflecting a tholeiitic trend. Trace element chemistry confirms the early ferromagnesian fractionation from nickel, chromium, and cobalt trends. Tectonic discrimination diagrams of Manguao Basalt show resemblance with different basalts from other known tectonic settings (i.e. continental flood basalts, island-arc basalts, continental-arc basalts, and within-plate basalts). However, association of Manguao Basalt with ocean-island basalts (OIB) or mid-ocean ridge basalts (MORB) appears inconclusive; plotting outside MORB-OIB array defined by Pearce (2008). These inconsistencies that accompany trace element discrimination diagrams have been pointed out by Li et al. (2015). Nevertheless, their utility is in constraining possible tectonic processes that influence melt generation and evolution. Trace element patterns in MORB- and OIB-normalized spider diagrams show enriched melt character of Manguao Basalt (i.e. more enriched than any MORB, but depleted compared to OIB). Characteristic Nb-Ta depletion is absent for Manguao Basalt, indicating possible non-subduction influence. Positive anomalies in continent-derived trace elements (e.g. K, Th, and Ba) are observable and consistent in any spider diagram presented (MORB-, NMORB-, EMORB-, and OIB-normalized).

Mineral chemistry data (olivine, orthopyroxene, clinopyroxene, and plagioclase) confirm crystallization sequence inferred from petrography. The most magnesian mineral species are orthopyroxene and clinopyroxene phenocrysts (Mg# > 80). Calculations using orthopyroxene barometer shows highest pressure (~5 kbar) and thermometers (i.e. opx-liquid) show highest temperatures (~1260 ˚C). Obtained

©2020. Japan Geoscience Union. All Right Reserved.

pressure and temperature conditions were used as benchmarks for simulations of source melting and crystallization.

Simulations of melting of different mantle sources (e.g. fertile and depleted mantle) were done using the MELTS program. Equilibrium and fractional melting from depressurization (15 kbar à5 kbar) of any mantle source produce liquids that are saturated in pyroxene components. Subsequent crystallization of melt, while being at equilibrium with source and at elevated pressures (~5 kbar) produce orthopyroxenes with similar compositions to orthopyroxenes in Manguao Basalt. The formation of olivine and the rest of the groundmass requires significant evolution of melt prior to its removal; as both components show 'evolved' melt origin. The model for magmatic underplating is presented here as a possible setup for the origin of Manguao Basalt.

Keywords: MELTS Program, Crystallization, Tholeiitic Melt

©2020. Japan Geoscience Union. All Right Reserved.

Relationship between the change of eruption style and the rock texture of ejecta during the Shinmoe-dake 2018 eruption, Kirishima, Japan

*Sayaka Shohata[1], Fukashi Maeno[2], Yuki Suzuki[3], ATSUSHI YASUDA[2], Natsumi Hokanishi[2]

1. Department of Earth and Planetary Science, School of Science, The University of Tokyo, 2. Earthquake Research Institute, The University of Tokyo, 3. Faculty of Education and Integrated Arts & Sciences, Waseda University

The amount of crystals and crystal size distributions (CSD) in the groundmass reflect the history of crystal nucleation and crystal growth responding to processes of magma decompression and cooling. Recent eruptive events are well observed directly in detail, so there is a possibility to advance understanding the main factor which decide eruptive style by analyzing groundmass texture. Shinmoe-dake volcano, Japan, erupted in 2011 and 2018. The 2011 eruption was characterized by three sub-plinians and lava dome effusion, but the 2018 was only lava dome effusion. This difference is important to understand the eruptive style branching factor. However, discussion based on the detail analysis of ejecta is not enough. The purpose of this study is to compare the texture of different types of rocks erupted from the 2018 eruption and reveal the magma process, and to compare with the 2011 eruption which has been already studied (Suzuki et al., 2018) and discuss the cause of different eruptive style. The samples of the 2018 products are classified into four groups. Pumice ejected from the early stage eruption (P1), pumice ejected from the latter eruption (P2), lava effused from the summit crater after the P1 eruption (L), and ballistic ejecta that the eruption date is unidentified but after P1 (B). The samples were analyzed with EPMA and FE-EPMA. Chemical composition data analyzed by EPMA were used to calculate the crystallinity of groundmass based on mass balance. High magnification photos and element mapping data were processed and used for quantitative textural analysis. In quantitative analysis, plagioclase microlite number density and CSD were calculated mainly using the method of Higgins (2000). According to the analyzed composition data, the magma is almost the same as the 2011. However, there were textural differences for each type and it reflects different effective undercooling. L has the highest groundmass crystallinity, followed by P1 and B, and P2 has the lowest. Plagioclase number density of P1 was the largest, L and B had almost the same value, and P2 was the smallest. The CSD peak value of P2 was the highest, P1 was the second and near to the P2, L was the third, and B was the lowest. These results suggest the condition which crystallization occurred. L showed smaller number density than P1 and P2, but the highest crystallinity, so I presumed it experienced crystal growth effectively. B showed the smallest number density and steep slope in CSD. This means nucleation rate was larger than L. P1 had highest number density and CSD peak, it was formed under the highest nucleation rate. P2 showed the steepest slope in CSD so that it was formed under the lowest growth rate. The relationship between nucleation/ crystal growth rate and effective undercooling shows a bell-shaped. According to the result this time and comparison with the 2011 eruption, it can be arranged in ascending order, L, B, P1, P2 in terms of effective undercooling. Effective undercooling has a positive correlation with magma ascending rate. It can be presumed to reflect the slowest and constant ascent rate for the lava dome. Ballistic product rose slowly as lava but ejected with high speed from shallower conduit. At the early phase, pumice ascended slowly above the lava-forming magma. In contrast, latter phase pumice ascended quickly. Additionally, CSD value is higher than 2011, the features of P2 and 2011 sub plinian pumice, B and 2011 ballistic ejecta were similar. This can be interpreted that the 2018 eruption had lower magma discharge rate than 2011, and changing during the eruption. It was presumed that lava dome grew at a constant rate from the data of time-sequence observation (NIED), but textural analysis results suggest the speed of lava effusion

©2020. Japan Geoscience Union. All Right Reserved.

was not constant.

Keywords: Shinmoe-dake volcano, Crystal size distribution

©2020. Japan Geoscience Union. All Right Reserved.

Stratigraphy and Unit Determination of Ranau Tuff in Sumatra, Indonesia

*Rachmi Mustika Pertiwi Putri Gunawan[1], Atsushi Toramaru[1], Tomoharu Miyamoto[1]

1. Department of Earth and Planetary Sciences, Kyushu University, Fukuoka, Japan

Ranau Tuff is a thick massive ignimbrite produced by a large caldera-forming eruption at ±33 ky ago. The deposit covers about 70 km around its vicinity with an approximate bulk volume of 173 km^3. The remnant edifice of Ranau has an unusual shape of caldera, which is thought to be caused by the combination of pull-apart basin and caldera formation. Active tectonic setting and volcanism in the area affected the process in the magma chamber and influenced the products, especially pumice clast in ignimbrite. Although it has a huge deposit, there are only limited studies about Ranau Tuff. Therefore, this study tries to characterize the pumice by classifying them into several types and clarify the stratigraphy to obtain an insight into the magma chamber condition.

We clarified the stratigraphy of nine locations around Ranau Lake by fieldwork. For non-welded deposits, we did the grain size analysis for dried samples from each layer by sieving tools. We did the component analysis for the grains larger than 2 mm by grouping into pumice, lithic, and free-crystal with the hand-picking method. For pumice grains with the selected size range (4-8 mm and 8-16 mm), we conducted the 3D volume measurement using Medit Solutonix D700 3D scanner and read the files by Hira 3D viewer to determine the bulk density. To know the major and trace element compositions of the pumice samples, we used the X-Ray Florescence (XRF) method.

From the fieldwork, it is found that Ranau Tuff mostly shows massive and non-welded ignimbrite with no evidence of the precursory Plinian phase. We observed thin fall deposit layers (5-10 cm) within the non-welded ignimbrite layers in Location 2 (9.2 km NE from caldera rim). Component analysis and mineralogy observation for the thin sections show three dominant pumice types of the ignimbrites; type A (pyroxene-bearing), type B (quartz-bearing), and type C. The lithic components are similar in all samples. Otherwise, the free-crystal of quartz, feldspar, biotite, and quartz-biotite aggregate are found in all locations except that in location 6 (type A pumice) and less than 5% in the lower part of location 9 (type C pumice). Qualitatively, the size of vesicle and phenocryst in pumice type A and C is smaller than that in type B. Besides, bubble-bearing and hourglass melt inclusions identified only in quartz phenocryst of pumice B. Major and trace element variation diagrams also show distinct trends among these pumice types. Therefore, we call the unit with each dominant pumice type by unit A (pumice type A), unit B (pumice type B), and unit C (pumice type C). Most of the deposits we found around Ranau Lake are unit B, only location 6 (36 m NE from caldera rim) is unit A and lower part of location 9 (15.6 km NE from caldera rim) is unit C which deposited before unit B.

A different system of magma in each unit is represented by the relation between its chemical trend and the pumice occurrence. Unit A (pyroxene-bearing) has less silica and potassium content than unit B (quartz-bearing) and C. The alkali-silica diagram of unit B does not show a clear trend which possibly affected by potassium content from biotite crystal in the whole-rock samples. However, there is a clear gap among the units in the incompatible trace elements-silica variation diagram such as Zr, Ba, K, Nb and does not show a linear relationship. This fact suggests different magma batches system formed prior to Ranau caldera-forming eruption.

©2020. Japan Geoscience Union. All Right Reserved.

Keywords: Ranau Tuff, Caldera-forming eruption, Component analysis, Pumice types

©2020. Japan Geoscience Union. All Right Reserved.

3D crystal size distributions of pyroxene nanolites based on nanoX-ray CT analyses

*Shota Okumura[1], Mayumi Mujin[2], Akira Tsuchiyama[3,4], Akira Miyake[1]

1. Department of Geology and Mineralogy, Graduate School of Science, Kyoto University, 2. Division of Earth and Planetary Materials Science, Department of Earth Science, Tohoku University, 3. Research Organization of Science and Technology, Ritsumeikan University, 4. Guangzhou Institute of Geochemistry, Chinese Academy of Sciences

Groundmass texture of pyroclasts, such as crystal shapes and population density, reflects physical condition during crystallization and thus is important to understand ascent conditions in conduits. For instance, Castro et al. (2003) have confirmed crystal elongation with decreasing size, which means a change of physical condition. Besides, crystal size distributions (CSDs), which are the numbers of crystals per volume per each size-range, are used to infer magma dynamics, such as mixing and syneruptive ascent (e.g., Marsh, 1998). However, most of these studies are based on 2D analyses (SEM observations): CSDs are acquired through stereological corrections from 2D to 3D (Higgins, 2000). On the other hand, some researches have aimed to acquire true 3D texture through serial sectioning, X-ray computed tomography with pixel size of 3–30 μm (Jerram et al., 2018), and optical transmission microscopy (e.g., Castro et al., 2003). However, few 3D observations for pyroclasts have spatial resolution of smaller than μm-scale necessary for analyses of groundmass crystals; that is, their 3D dataset is insufficient. It is necessary to present their true 3D data and test accuracy of the stereological corrections of 2D data for CSDs. We aimed to infer the ascent conditions based on the true 3D data.

Recent researches on extraterrestrial samples have used synchrotron radiation-based X-ray computed nanotomography (SR-nanoXCT) at BL 47XU of SPring-8, a synchrotron radiation facility in Japan, with effective spatial resolution of ~100 nm (e.g., Tsuchiyama et al., 2012; Matsumoto et al., 2019). We applied this SR-nanoXCT to pyroxene nanolites (< 1 μm in width; Mujin et al., 2017) in pumices and acquired their 3D data and directly measured CSDs (CT-CSDs). We analyzed two pumices from the 2011 eruption of Shinmoedake, the Kirishima volcano: one is from a sub-Plinian eruption and the other is from a Vulcanian explosion. Two equant specimens (ca. 25 μm on a side) for the SR-nanoXCT were extracted from each pumice using a focused ion beam system (Quanta 200 3DS, FEI). We also acquired CSDs of pyroxene crystals in 2D with a field-emission SEM (JSM-7001F, JEOL) (SEM-CSDs) in addition to the CT-CSDs.

We found that the shapes of pyroxene nanolites exhibit different features between the two pumice samples, although the degree of elongation varies greatly from crystal to crystal even in each specimen: elongate prisms with swallowtail ends in the sub-Plinian pumice, and slightly thicker prisms with flat ends in the Vulcanian pumice. In the sub-Plinian pumice, smaller nanolites tend to become more elongate. However, such a tendency is not found in the Vulcanian pumice. As for CSDs, the CT-CSDs and the SEM-CSDs correspond well with each other. They show a log-linear figure for the Vulcanian pumice. On the other hand, for the sub-Plinian pumice, the SEM-CSD exhibits a kink at 1 μm of crystal width and a steeper slope in the finer size-range, and the CT-CSD also exhibits such a steep slope.

Because crystals become elongated with large undercooling (Shea and Hammer, 2013), the difference in degree of crystal elongation indicates that the sub-Plinian magma batch has undergone larger undercooling than the Vulcanian one. Besides, this elongation can affect figures of CSDs. There are cases where elongated small crystals generate a falsely-high population density of the small crystals (e.g., Castro

©2020. Japan Geoscience Union. All Right Reserved.

et al., 2003). For the sub-Plinian pumice, however, this effect appears to be insignificant, although the small nanolites become elongated. The concave upward curvature of the CSD is interpreted as an accelerated increase in population density and nucleation rate of small crystals, which results from increasing undercooling. These results are considered to reflect a difference in ascent rate for the eruption styles: the sub-Plinian magma batch ascended acceleratedly but the Vulcanian one was in a steady condition in the shallow conduit.

Keywords: X-ray CT, CSD, pyroxene, nanolite, Shinmoedake

©2020. Japan Geoscience Union. All Right Reserved.

Pre-eruptive Magma Condition of Tondano Caldera I: Domato Tuff, Minahasa, NE Sulawesi, Indonesia

*Tabegra Disando[1], Atsushi Toramaru[1]

1. Department of Earth and Planetary Sciences, Kyushu University, Fukuoka, Japan

Tondano Caldera Complex (TCC) marked an important historical record of volcanism in the NE Sulawesi region. Domato Tuff was produced from Tondano Caldera I, on 2.0±0.4 Ma ($^{40}Ar/^{39}Ar$ isotopes), by the first event in TCC, with the widest distribution of dacitic to rhyolitic ignimbrites (~17 km^3 DRE). Aim of this study is to characterize Domato deposit and reveal the pre-eruptive magma condition shortly before the caldera-forming eruption occurred.

We conducted sample description, weight sieving for Grain Size Distribution (GSD), component analysis of grain, and bulk density measurement. To know the pumice texture and ash morphology, we carried out image analysis by optical microscope, SEM-EDS TM3030 Plus, and FOAMS version 1.0.4. Measurement of mineral and glass composition is conducted by FE-EPMA JEOL-JXA-8530F.

We found several layers of pyroclastic deposits with light to light brown pumice, fine to medium bubble, and poor crystal. GSD Data indicated a different characteristic on each layer which is classified into a pyroclastic fall unit showing grain-supported characteristics and two pyroclastic flows unit showing matrix-supported characteristics. Fall product comprises <10% of volcanic lithic (altered rock abundance) whereas in each flow product has 5-25% and 25-70% of various types of volcanic lithics (all deposits have <5% banded pumice and <1% single crystal). All of pumice has 0.6-0.9 g/cm^3 (0.7-0.8 g/cm^3 of mode) of bulk density; 60-74% of vesicularity; 20-32% of glass; and consists of phenocryst plagioclase; pyroxene; hornblende; and opaque mineral which increases the content up to 10% on flow unit.

By combining fieldwork data and laboratory analyses, we identified three units deposit as Plinian fall (P1), Ignimbrites (P2), and Lithic-rich Ignimbrite (P3). P1 and P2 have An_{41}-An_{54} of plagioclase; 72-78% of SiO_2 glass and An_{41}-An_{58} of plagioclase; 76%-81% of SiO_2 in glass while on P3 has lower An content (An_{32}-An_{49}) of plagioclase; higher silica content 77-81% of glass. The common texture on plagioclase is found as oscillatory zoning, patchy zoning, and glomeroporphyritic.

After synthesizing deposits characters observed all locations, these three units correspond to three phases from the Plinian eruption (P1); PDC (P2); then Lithic-rich PDC (P3) during evacuating of the magma chamber. Presence of precursory Plinian (P1) suggests an internal magmatism-triggered caldera-forming eruption. Abundance of altered rock in P1 proposes a volcanic cone which exists before the caldera formation. Production on the same type of volcanic lithic in higher abundance in P2 and P3 are enhanced by higher eruption intensity accompanying conduit widening in the single vent. The dominant oscillatory zoning plagioclase suggests a convection perturbation at the melt-crystal interface during fractional crystallization. Moreover, evolved compositions of magmatic glass from P1, P2, to P3 with time might be related to the shift of eruption style during caldera-forming eruption.

Keywords: Tondano Caldera, Domato Tuff, Caldera-forming Eruption

©2020. Japan Geoscience Union. All Right Reserved.

Magma fracturing, oxidation and nanolite crystallization processes during silicic magma eruption: Implication from textural and chemical analyses on oxidized obsidian

*Kyohei Sano[1], Eiichi Sato[2]

1. Graduate School of Regional Resource Management, University of Hyogo, 2. Faculty of Liberal Arts and Sciences, Osaka Prefecture University

Silicic volcanism ranges from explosive to effusive. Understanding what controls in such activity is an important issue to explain the explosive-effusive transition. Especially, a recent study revealed that oxygen fugacity affects the melt viscosity (Genova et al., 2017). Thus, it is important to characterize the microlite and/or nanolite as the indicator of magma fracturing, crystallization and oxidation processes on silicic magma eruption. At the Akaishiyama obsidian lava on Shirataki, northern Hokkaido, Japan, we can observe the red-colored oxidized obsidian mingled with black-colored obsidian on the surface of lava. The mingled obsidian shows various contrasts and distributions on the hand specimen, and we can consider that such various oxidation and fracturing textures reflect the different mechanisms of fracturing, outgassing, and oxidation during the eruption. In this study, we performed textural and chemical analyses on oxidized obsidian by using Field Emission Electron Probe Micro Analyzer (FE-EPMA) at Osaka Prefecture University to describe the textural variation relating to the magma fracturing and oxidation. Our analyses using FE-EPMA revealed that microlite and nanolite crystalized on oxidized and fractured texture. On this texture, we could also observe the chemical heterogeneity of FeO and CaO on glass chemical compositions. In this presentation, we describe the relation between nanolite crystallization and magma fracturing, oxidation texture and finally discuss the formation process of heterogeneous magma fracturing, crystallization and oxidation textures during the eruption.

Keywords: obsidian, oxidation, nanolite, magma fracturing

©2020. Japan Geoscience Union. All Right Reserved.

Redox state and nanolite crystallization of erupting magma during ash forming eruption at Bromo Volcano, Indonesia

*Takahiro Miwa[1], Hidemi Ishibashi[2], Masato Iguchi[3], Genji Saito[4], ATSUSHI YASUDA[5], Natsumi Hokanishi[5]

1. National research institute for earth science and disaster resilience, 2. Shizuoka University, 3. DPRI, Kyoto University, 4. AIST, 5. ERI, University of Tokyo

We discusses a vent-conduit process during ash forming eruption at Bromo volcano, Indonesia, based on the observation of microstructure and redox variation of volcanic glass. The volcanic ash particles were collected in 24th March 2011 by real-time sampling from ongoing activity. The activity was characterized by strombolian eruption and emission of gray-brown ash plume with shock wave, showing magma head ascended to near the ground surface. The volcanic glass of the ash forming eruption comprises brown and black glasses under the stereoscopic microscope. Although both of volcanic glasses exhibits glassy appearance and identical chemical composition, observation of microstructure by Field-Emission Electron Micro Probe Analyzer (FE-EPMA) showed that the black glass contains nanolites (Mujin and Nakamura, 2014) in its matrix glass. The Fe-K edge μ-XANES (micro X-ray Absorption Near Edge Structure) spectra demonstrate that brown glass ($Fe^{3+}/\Sigma Fe$ = 0.20-0.26) is more reduced than black glass ($Fe^{3+}/\Sigma Fe$ = 0.32-0.60). From combination of the glass composition, the measured $Fe^{3+}/\Sigma Fe$ ratio and 1060 degree C of temperature, the oxygen fugacities are estimated to be NNO which is similar with that of magmatic gas from Bromo (Aiuppa et al. 2015) for brown glass and NNO+4 for black glass. Moreover we found that the oxygen fugacity becomes higher in nanolite-developed region around the edge or vesicle wall in a single black glass. These suggest close relationship between oxidation and nanolite crystallization. Vigorous recycling of eruptive material from repetitive eruptions can cause oxidation of volcanic glass and nanolite crystallization.

Keywords: Volcanic ash, Redox state, Nanolite

©2020. Japan Geoscience Union. All Right Reserved.

[E] Poster | S (Solid Earth Sciences)：S-GC Geochemistry

[S-GC48] Volatiles in the Earth - from Surface to Deep Mantle

convener:Takeshi Hanyu(Japan Agency for Marine-Earth Science and Technology, Research Institute for Marine Geodynamics), Gray E Bebout(Lehigh University), Hirochika Sumino(Department of Basic Science, Graduate School of Arts and Sciences, The University of Tokyo), Yuji Sano(Division of Ocean and Earth Systems, Atmosphere and Ocean Research Institute, University of Tokyo)

Volatiles play an important role in the dynamical and chemical processes in the Earth. The presence of volatiles drastically changes mineral stability and rheological behavior of the rocks. Chemical fractionation, such as partial melting, hydration, and dehydration are controlled by volatiles in the rocks. Volatiles enhance the production of magmas and drive their ascent and volcanic eruption. The atmosphere and hydrosphere have been generated by variety of degassing events from the mantle through volcanism. Some volatiles in the Earth's surface have been suggested to be recycled back into the mantle beyond subduction zones. Although the significance of volatiles in the Earth's evolution has been recognized, each of these processes is poorly constrained. We therefore welcome contributions from experimental, observational, and modeling studies that help shed light on the behavior, chemical/physical characteristic, and flux/budget of volatiles, such as hydrogen, carbon, nitrogen, noble gases, halogens, and sulfur. We encourage studies linking the behavior of multiple volatile elements and their isotopic compositions. Studies investigating the linkage between volatile and solid geochemical tracers, the phase equilibria of volatile-bearing mantle assemblages, and the effect of volatiles on the physical properties of the mantle are also welcome.

[SGC48-P01] Helium isotopic signature of the plate boundary suture in an active arc-continent collision

*Ai-ti Chen[1,2], Yuji Sano[1], Timothy B Byrne[3], Naoto Takahata[1], Tsanyao Frank Yang[2], Yunshuen Wang[4], Chuan-Chou Shen[2] (1.Univ. of Tokyo, 2.National Taiwan Univ., 3.Univ. of Connecticut, 4.Central Geological Survey)

[SGC48-P02] ^{4}He/U-Th dating of pore waters from Quaternary sediments of the Swiss Midland

★Invited Papers

*Yama Tomonaga[1], Edith Horstmann[1], Gaudenz Deplazes[2], Rolf Kipfer[1] (1.Swiss Federal Institute of Aquatic Science and Technology (Eawag), 2.National Cooperative for the Disposal of Radioactive Waste (Nagra))

[SGC48-P03] Noble gas composition in hot spring gas in Shikine Island, Izu–Bonin volcanic arc, Japan

*Kotaro Toyama[1], Hirochika Sumino[1], Muga Yaguchi[2], Takeshi Ohba[3], Takashi Toyofuku[4], Shigeki Wada[5] (1.The University of Tokyo, 2.Meteorological Research Institute, 3.Tokai Univ., 4.JAMSTEC, 5.Shimoda Marine Research Center, University of Tsukuba)

[SGC48-P04] Helium and CO_2 fluxes in Wakamiko caldera

*Ma. Teresa Escobar[1], Naoto Takahata[1], Kotaro Shirai[1], Takanori Kagoshima[1], Kentaro Tanaka[1], Hajime Obata[1], Yuji Sano[1] (1.Atmosphere and Ocean Research Institute University of Tokyo)

[SGC48-P05] Noble gas isotope compositions of mafic phenocrysts in the Stage 3 lavas of Kusatsu-Shirane Volcano

★Invited Papers

*Nobuko Kametani[1,2], Hirochika Sumino[3], Kenta Ueki[4], Morihisa Hamada[4], Yasuo Ishizaki[5] (1.Graduate School of Science and Engineering, University of Toyama, 2.Mount Fuji Research Institute Yamanashi Prefectural Government, 3.Department of Basic Science, Graduate School of Arts and Sciences, The University of Tokyo, 4.Research Institute for Marine Geodynamics, Japan Agency for Marine-Earth Science and Technology, 5.Faculty of Sustainable Design, University of Toyama)

[SGC48-P06] **The complex melt–fluid–rock interaction history of a dismembered cumulate dunite from eastern Singhbhum Craton, India**

*Tushar Mouli Chakraborti[1], Arijit Ray[2], Gautam Kumar Deb[2] (1.Hiroshima Univ., 2.Presidency Univ.)

[SGC48-P07] SIMS sensitivity factors of ^{2}H and $^{16}O^{2}H$ relative to ^{18}O in spinel-structured oxides

*Georg F Zellmer[1], Naoya Sakamoto[2], Minami Kuroda[3], Isao Sakaguchi[4], Hisayoshi Yurimoto[2,5] (1.Massey University, 2.Hokkaido University, 3.AIST, 4.National Institute of Material Sciences, 5.Japan Aerospace Exploration Agency)

Helium isotopic signature of the plate boundary suture in an active arc-continent collision

*Ai-ti Chen[1,2], Yuji Sano[1], Timothy B Byrne[3], Naoto Takahata[1], Tsanyao Frank Yang[2], Yunshuen Wang[4], Chuan-Chou Shen[2]

1. Univ. of Tokyo, 2. National Taiwan Univ., 3. Univ. of Connecticut, 4. Central Geological Survey

We report new noble gas signatures of groundwaters, hot springs, and bedrock samples from two major fault system that form the plate boundary suture between the Eurasian and the Philippines Sea Plates. In the south, the east-dipping Eurasian Plate is associated with a relatively simple plate boundary fault as suggested by a well-defined cluster of earthquakes related to the active, east-dipping Chihshang Fault zone, which is the main conduit for mantle helium. In the north, as the subduction direction flips from the east-dipping Eurasian Plate to the north-dipping Philippine Sea Plate, the plate boundary fault is represented by a more complex system of east and west dipping structures. Clear signals of mantle contamination, as evidenced in helium isotopes, are also reduced in this area. We propose that as the subduction direction flips from south to north along strike, the tortuosity of the fault-related conduits increases, reducing the flow and limiting the release of mantle-derived gases.

Keywords: 2018 Mw 6.4 Hualien Earthquake, noble gas, Chihshang Fault , Taiwan

©2020. Japan Geoscience Union. All Right Reserved.

^{4}He/U-Th dating of pore waters from Quaternary sediments of the Swiss Midland

*Yama Tomonaga[1], Edith Horstmann[1], Gaudenz Deplazes[2], Rolf Kipfer[1]

1. Swiss Federal Institute of Aquatic Science and Technology (Eawag), 2. National Cooperative for the Disposal of Radioactive Waste (Nagra)

Dating based on the ^{4}He/U-Th method can be used to estimate the residence time of pore waters in very low-permeable rocks and consolidated sediments. The residence time is inferred from the time necessary to accumulate radiogenic ^{4}He measured in the pore water being produced by the decay of U and Th in the sediment matrix [1].

In the Jurassic Opalinus Clay, the pore water still contains the signature of the original marine formation water that was entrapped during sediment deposition. The pore water composition was altered only by diffusive processes [2,3]. The fact that even ~100-Ma-old water signatures can be preserved in their original pore space suggests that such preservation might also be possible in much younger dense glacial deposits. The ^{4}He concentrations measured in the pore waters of glacial tills were translated into mean residence times of 15-25 kyrs [4] that agree rather well with the expected depositional ages of 25-31 kyrs [5]. These observations, as well as evidence from lacustrine sediments [6,7], suggest that, if the solute transport in the pore space is sufficiently attenuated, even unconsolidated sediments can "store" and host "old" pore waters.

In the present work we investigate if the ^{4}He/U-Th dating of pore waters can be used as a novel tool to complement other dating tools (e.g., optically-stimulated luminescence) for unconsolidated Quaternary sediments. We applied the ^{4}He/U-Th method to date pore waters in the time range of 10 to 100 thousands of years which covers the age range of the sedimentary depositions targeted by the Quaternary drillings (QBO) managed by the National Cooperative for the Disposal of Radioactive Waste (Nagra) in Switzerland. In particular, we focus on fine-grained lacustrine sediment layers that might provide low-permeability conditions suitable for the preservation of radiogenic ^{4}He concentrations in the pore space.

We report the preliminary results of the ^{4}He/U-Th dating based on the measurements conducted in sediment samples from selected QBO, highlighting potential and challenges of the method with respect to the studied glaciofluvial sediments of the Swiss Midland.

References

[1] Torgersen, T., Clarke, W.B. (1985). Helium accumulation in groundwater, I: an evaluation of sources and the continental flux of crustal ^{4}He in the Great Artesian Basin, Australia. *Geochim. Cosmochim. Acta 49*, 1211–1218
[2] Gimmi T., Waber H. N., Gautschi A., Rübel A. (2007). Stable water isotopes in pore water of Jurassic argillaceous rocks as tracers for solute transport over large spatial and temporal scales. *Water Resour. Res. 43*(4).
[3] Mazurek, M., Alt-Epping, P., Bath, A., Gimmi, T., Niklaus Waber, H., Buschaert, S., et al. (2011). Natural tracer profiles across argillaceous formations. *Appl. Geochem. 26*(7), 1035–1064.
[4] Hendry, M. J., Kotzer, T. G., Solomon, D. K. (2005). Sources of radiogenic helium in a clay till aquitard

©2020. Japan Geoscience Union. All Right Reserved.

and its use to evaluate the timing of geologic events. *Geochim. Cosmochim. Acta 69*(2), 475–483.
[5] Wassenaar L.I., Hendry M.J. (2000). Mechanisms Controlling the Distribution and Transport of ^{14}C in a Clay-Rich Till Aquitard. *Groundwater 38*(3), 343–349.
[6] Tomonaga, Y., Brennwald, M. S., Meydan, A. F., Kipfer, R. (2014). Noble gases in the sediments of Lake Van - Solute transport and palaeoenvironmental reconstruction. *Quat. Sci. Rev. 104*, 117–126.
[7] Tomonaga, Y., Brennwald, M. S., Kipfer, R. (2015). Attenuation of noble-gas transport in laminated sediments of the Stockholm Archipelago. *Limnol. Oceanogr. 60*(2), 497–511.

Keywords: radiogenic He, fluid transport, glaciofluvial sediments, age estimation

©2020. Japan Geoscience Union. All Right Reserved.

Noble gas composition in hot spring gas in Shikine Island, Izu–Bonin volcanic arc, Japan

*Kotaro Toyama[1], Hirochika Sumino[1], Muga Yaguchi[2], Takeshi Ohba[3], Takashi Toyofuku[4], Shigeki Wada[5]

1. The University of Tokyo, 2. Meteorological Research Institute, 3. Tokai Univ., 4. JAMSTEC, 5. Shimoda Marine Research Center, University of Tsukuba

Shikine island is located on the rear-arc side of the northern part of the Izu–Bonin arc, and is a rhyolite-dominated volcano which erupted in ca. 8000 years ago. Recently, the CO_2-rich emission were found in coastal area of southern Shikine island (Agostini et al., 2015 RSMS). It is considered that its gas is volcanic gas.

Geochemical features of volcanic gas provide important information on both the current status of cooling magma batches intruding the upper crust and interaction processes taking place between rising fluids and hosting rocks. Especially, noble gases have great potential as tracers for mantle sources and fingerprinting of geothermal reservoirs (Pinti et al., 2013, JVGR), because the noble gases in the gas are derived from three potential sources: the crust, the mantle, and the atmosphere. We report noble gas composition of hot spring free gases collected from 2 sites (Mikawa-bay and Jinata-hot spring) in coastal area of southern Shikine island during 2016 to 2019.

The measured $^{3}He/^{4}He$ ratios were corrected for atmospheric contamination based on $^{4}He/^{20}Ne$ ratios. The air-corrected $^{3}He/^{4}He$ ratios ranged from 7.8 to 8.0 Ra, where 1 Ra denotes atmospheric $^{3}He/^{4}He$ ratio of 1.4×10^{-6} (Ozima and Podosek, 2002, Noble Gas Geochemistry). This value is similar to that (8±1 Ra) of the upper mantle estimated from mid-ocean ridge basalts (MORB). The $^{20}Ne/^{22}Ne$ and $^{21}Ne/^{22}Ne$ ratios of the samples ranged from 9.86 to 9.93 and from 0.0292 to 0.0294, respectively, which are totally similar to the atmospheric component (9.80 for $^{20}Ne/^{22}Ne$ and 0.0290 for $^{21}Ne/^{22}Ne$; Ozima and Podosek, 2002). The $^{38}Ar/^{36}Ar$ ratios or 0.187–0.189 were also atmospheric (0.188; Ozima and Podosek, 2002). In contrast, the $^{40}Ar/^{36}Ar$ ratios ranging from 297 to 300, were slightly higher than that of the atmosphere component (296.0; Nier, 1950, Physical Review), suggesting that they reflect the gas source. Noble gas relative abundances are given using the F-value notation (Ozima and Podosek, 2002) in which measured abundances are normalized to the air abundance with ^{36}Ar as the reference isotope, i.e., $F(i)=(i/^{36}Ar)_{sample} / (i/^{36}Ar)_{atmosphere}$. Some researchers suggested that the relative abundances in fumaroles and hot-spring gases in geothermal area reflect elemental fractionation during boiling and steam separation at hydrothermal temperatures (Pinti et al., 2013 JVGR). The condensation temperature in the present area is estimated as about 150˚C adopting the model of batch fractionation using an initial air saturated seawater end-member at 25˚C to the observed $F(^{20}Ne)$ and $F(^{132}Xe)$.

Keywords: Noble gas composition, Sikine Island, Hot spring gas

©2020. Japan Geoscience Union. All Right Reserved.

Helium and CO_2 fluxes in Wakamiko caldera

*Ma. Teresa Escobar[1], Naoto Takahata[1], Kotaro Shirai[1], Takanori Kagoshima[1], Kentaro Tanaka[1], Hajime Obata[1], Yuji Sano[1]

1. Atmosphere and Ocean Research Institute University of Tokyo

Wakamiko caldera is part of the active volcanic arc system situated in Kagoshima Bay. It is closely being monitored because it has the potential for a destructive eruption. In this study, we collected seawater and sediment pore water samples within Wakamiko caldera and nearby sites around Kagoshima Bay in 2015. Helium isotopes, which are good geochemical tracers for sources of fluids, were measured to know the composition and origin of the hydrothermal effluents. Gas composition, including carbon and nitrogen isotopes, was also analyzed to understand the provenance of the dissolved gases in the pore water. This is the first report on the dissolved gases in sediment pore water in Wakamiko caldera.

Helium isotopic ratios in both seawater and sediment pore water show a mixture of air saturated seawater (~1Ra) and magma source with ~7Ra. This means the origin of excess helium-3 in bottom water is same as that in sediment. This trend is similar to previous studies in 2010 and 2014, which indicate that hydrothermal activity is stable in this period. The ^3He and ^4He fluxes derived from this study are 13.7 - 18.4 atoms/cm^2s and 1.51 - 1.54 x10^6 atoms/cm^2s, respectively. These estimates reflect background diffusion of helium in the Wakamiko caldera. Measurement of gas composition showed that the pore waters are CO_2 rich and stable carbon isotope analysis revealed that the CO_2 in the system is a mixture of biogenic sources and magmatic volatiles similar to that of Mt. Sakurajima. Finally, the estimated average magmatic CO_2 flux from the submerged caldera is 1.41 x 10^5 mol/yr.

Keywords: Helium Isotopes, Carbon Dioxide, Hydrothermal Vents

©2020. Japan Geoscience Union. All Right Reserved.

Noble gas isotope compositions of mafic phenocrysts in the Stage 3 lavas of Kusatsu-Shirane Volcano

*Nobuko Kametani[1,2], Hirochika Sumino[3], Kenta Ueki[4], Morihisa Hamada[4], Yasuo Ishizaki[5]

1. Graduate School of Science and Engineering, University of Toyama, 2. Mount Fuji Research Institute Yamanashi Prefectural Government, 3. Department of Basic Science, Graduate School of Arts and Sciences, The University of Tokyo, 4. Research Institute for Marine Geodynamics, Japan Agency for Marine-Earth Science and Technology, 5. Faculty of Sustainable Design, University of Toyama

Kusatsu-Shirane Volcano is an active volcano, composed of two composite pyroclastic cones (Mt. Shirane and Mt. Motoshirane). Typical eruptions at Kusatsu-Shirane during the last 140 years were phreatic eruptions, and the first historic phreatic eruption at Mt. Motoshirane occurred on 23 January, 2018. The chemical and isotopic compositions of volcanic gases can be useful indicator of volcanic activity because it can be a geochemical tracer for the contributions of various components such as magma, crust and atmosphere, and the degree of magma degassing. The air-corrected $^{3}He/^{4}He$ ratio of Sessho-gawara fumarole, located on 2 km east of the 2018 phreatic vent, had been constant at 7.0-7.5 Ra during 2014 and 24 January 2018, and dropped to 6.5 Ra on 13 February 2018 [1]. Therefore, Toyama et al. [1] expected that the low $^{3}He/^{4}He$ ratios observed after the 2018 eruption may reflect relative increase of the contribution of gas supplied from the Mt. Motoshirane hydrothermal reservoir which may have low $^{3}He/^{4}$ He ratio. However, the relationship of noble gas isotopic compositions between possible end-member components such as volcanic gas and evolved crustal magma and mantle-derived mafic magma, which is the possible source of hydrothermal fluid, is poorly understood. In order to obtain information on the noble gas isotopic ratios of mafic and evolved crustal magmas, we analyzed mafic phenocrysts in lavas erupted during the Stage 3 (after 16 ka [2]).

We report the noble gas (He, Ne, Ar) isotopic ratios of mafic phenocrysts (ol, opx, cpx) in the andesitic lavas of Kusatsu-Shirane Volcano. The lavas analyzed in this study were Kagusa Lava erupted from Mt. Shirane, and Sessho Lava and Furikozawa Lava both erupted from Mt. Motoshirane. After fragmentation of these lavas using SELFRAG Lab (High-voltage pulsed power selective fragmentation system) installed at JAMSTEC, about 100 mg each phenocryst was separated by hand picking. Noble gas (He, Ne, Ar) isotope analysis was conducted using a mass spectrometer installed at the University of Tokyo. In-vacuo crushing method was used for extraction of noble gases [3].

The preliminary $^{3}He/^{4}He$ ratios were as follows: cpx in Furikozawa Lava was 6.0 ±0.9 Ra; ol in Furikozawa Lava was 11.0 ±2.6 Ra; and ol in Sessho Lava was 8.3 ±0.5 Ra. These values are similar to the $^{3}He/^{4}He$ ratio of volcanic gases such as Kitagawa fumaroles on the northern flank of Mt Shirane (average 7.6 Ra) and Sessho-gawara fumaroles (average 7.2 Ra) [1]. The $^{4}He/^{40}Ar^{*}$ ratios (Ar* denotes non-atmospheric ^{40} Ar) were as follows: ol and cpx in Furikozawa Lava were 0.14 and 0.62, respectively; opx in Kagusa Lava was 0.22; and ol in Sessho Lava was 0.65. In contrast, Kitagawa fumaroles were 9.4 and Sessho-gawara fumaroles were 3.9. Because He is more soluble than Ar within silicate melt, $^{4}He/^{40}Ar^{*}$ ratio of magma would increase as it degasses. Using $^{4}He/^{40}Ar^{*}$ ratios as the index for the degree of magma degassing, Sessho Lava was slightly more degassed than Furikozawa Lava and Kagusa Lava. In contrast, the values observed in current fumaroles suggest that volcanic gas is derived from magma that is significantly degassed compared to magmas that have crystallized mafic minerals. These results suggest that $^{4}He/^{40}$ Ar* ratio of volcanic gas has a potential to be a good indicator to monitor degassing stage of magma and/or replenishment of undegassed primitive magma to a shallow magma chamber. As the

©2020. Japan Geoscience Union. All Right Reserved.

above-mentioned data are preliminary, we will discuss more in details by analyzing more samples.

References: [1] Toyama et al., JpGU2019, SVC38-P07, 2019. [2] Takahashi et al., *Proc. Inst. Nat. Sci. Nihon Univ.* 2010. [3] Sumino *et al.*, *J. Mass Spectrom. Soc. Jpn.* 2001.

Keywords: noble gas, isotope ratio, Kusatsu-Shirane Volcano

©2020. Japan Geoscience Union. All Right Reserved.

The complex melt–fluid–rock interaction history of a dismembered cumulate dunite from eastern Singhbhum Craton, India

*Tushar Mouli Chakraborti[1], Arijit Ray[2], Gautam Kumar Deb[2]

1. Hiroshima Univ., 2. Presidency Univ.

Serpentinized Cr–spinel bearing dunite to cpx–dunite rocks are found as a dismembered N–S trending unit within multiply deformed metasedimentary rocks of Mid–Proterozoic belonging to the North Singhbhum Mobile Belt, in the eastern margin of Archaean Singhbhum Craton, India. The elongated, lenticular unit occurs close to the Bangriposi Shear Zone. The northern part of the unit is significantly more serpentinized than the southern part, where serpentinization is restricted to veins. The unusual mineral assemblages and reaction relationships observed in these rocks can be grouped into three types– Type 1 assemblage is made up of relict olivine + diopside + apatite ±clinochlore + ferrichromite + serpentine + magnetite ±metal sulphides–oxides and is from the southern part. Type II assemblage consists of diopside + hydrous augite + clinochlore + Ca–amphiboles + ferrichromite ±apatite + serpentine + magnetite ±metal sulphides–oxides, and Type III is hydrous augite + clinochlore + Ca–amphiboles + ferrichromite + serpentine + magnetite ±metal sulphides–oxides. Relict olivines from Type I are zoned (core– $Fo_{82–84}$ & rims– $Fo_{76–80}$) and have unusually high NiO and MnO. They display cumulus textures and are accompanied in places by inter–cumulus diopside (Mg no. 87–93) having very low Al_2O_3, TiO_2, Cr_2O_3 and Na_2O. Diopsides from Type II have similar compositions except lower Mg no. (76–80). Augites from Type II and III contain high OH with low TiO_2, Cr_2O_3, Na_2O and variable Al_2O_3. They occur as aggregates enveloping serpentine pseudomorphs accompanied by interstitial Fe–rich clinochlore (Mg no. 74–88). Ca–amphiboles (Edenite and pargasite) occur exclusively with hydrous augite. Serpentines from Type I have higher Mg no. than Type II and III. Fe–Ni sulphides and Mn–oxides occur as accessories, more frequently in Type II and III. Bulk–rock chemistry of these rocks shows high LOI and FeO. Also, a significant enrichment in LREE is observed. Apart from the effects of serpentinization (serpentine growth, magnetite formation and Cr–spinel recrystallization) there are additional textural and chemical evidences of prior fluid–melt–rock interactions. The NiO and MnO rich olivines from the relict areas suggest secondary enrichment via a metal–rich fluid phase, which could’ ve been responsible for the metal–rich accessory phases. Textural evidence suggests that clinochlore and hydrous augite formed simultaneously, and along with formation of Ca–amphiboles, indicates involvement of a hydrated melt–fluid. Bulk–rock LREE enrichment without conspicuous enrichment in LILEs also point towards an enriched melt–fluid phase. Interstitial apatite requires infiltration of a Ca–rich melt–fluid. Single clinopyroxene thermobarometry yields almost similar temperature but varying pressure ranges for the three assemblage types– Type I: 0.3–0.7 GPa & 1140–1240 ˚C, Type II: 1–1.2 GPa & 1275–1300 ˚C, and Type III: 0.6–1.1 GPa & 1270–1330 ˚C. Ca–amphiboles from Type II and III yield average P–T ranges of 0.9 GPa & 1000 ˚C. The discussed evidences paint a very complex history of melt–fluid–rock interaction of these rocks. However, some facts and constrains can be established– (i) The protolith was a cumulate dunite to cpx–dunite unit possibly from the lower crust, (ii) The rocks experienced high–T melt–fluid–rock interaction either in a single or multiple stage leading to formation of hydrous silicates, Ni and Mn enrichment of olivines and bulk–rock LREE enrichment, and (iii) Serpentinization was the final event to affect these rocks, possible during their transport and emplacement. Considering lower oceanic crustal heritage of these rocks, possible sources of the melt–fluid of the high–T event could’ ve been high–T hydrothermal fluids or melt–fluids from rising from the mantle. This study highlights the importance of deciphering the melt–fluid–rock interaction histories of Precambrian ultramafic rocks.

©2020. Japan Geoscience Union. All Right Reserved.

Keywords: Melt-fluid-rock interaction, Cumulate dunite, Ni-rich olivine, Hydrous silicate

©2020. Japan Geoscience Union. All Right Reserved.

SIMS sensitivity factors of ^{2}H and $^{16}O^{2}H$ relative to ^{18}O in spinel-structured oxides

*Georg F Zellmer[1], Naoya Sakamoto[2], Minami Kuroda[3], Isao Sakaguchi[4], Hisayoshi Yurimoto[2,5]

1. Massey University, 2. Hokkaido University, 3. AIST, 4. National Institute of Material Sciences, 5. Japan Aerospace Exploration Agency

Spinel-structured oxides ("spinels") are a group of nominally anhydrous minerals characterized by a wide range of solid solution. To allow the analysis of hydrogen in spinels by ion microprobe, Relative Sensitivity Factors (RSFs), which are typically matrix-dependent, need to be determined. For this work, we have selected five natural spinels from the Mg-Al-Fe-Ti-Cr-Mn-Zn compositional space. We present an approach to estimate spinel density on basis of bulk chemical composition determined by electron microprobe. Densities in our samples range from 3.7 to 5.1 g cm^{-3}. Samples were implanted with a fixed dose of deuterium (1 x 10^{15} atoms cm^{-2}) using an ion energy of 40 keV. Subsequently, we performed depth profiling using a Cs^{+} primary beam on the Cameca ims-1270 ion microprobe at Hokkaido University, monitoring secondary ion counts of ^{2}H and ^{18}O, and at high mass-resolution $^{16}O^{2}H$, $^{17}O^{1}H$, and ^{18}O, until the implanted ion counts dropped below background levels. From the reduced data, we calculated the RSFs for secondary ions of atomic ^{2}H and molecular $^{16}O^{2}H$ relative to ^{18}O as matrix element. RSFs for ^{2}H are similar for all spinels at 1.11 ±0.32 (2 σ) x 10^{22} atoms cm^{-3}, indicating a small matrix effect for ^{2}H despite the large compositional range of spinels studied. In contrast, RSFs for $^{16}O^{2}H$ relative to ^{18}O decrease with spinel density from 2.65 ±0.36 (2 σ) x 10^{21} atoms cm^{-3} at 3.7 g cm^{-3} to 3.41 ±0.73 (2 σ) x 10^{20} atoms cm^{-3} at > 4.5 g cm^{-3}, indicating a strong matrix effect on secondary dimer production during processes of ion sputtering and secondary ionization. Our data imply that the analysis of water in natural spinels may be undertaken through measurement of H or OH, but that spinel densities must be well-determined in the case of OH measurement. Mineral density effects on RSF values will have to be evaluated prior to analysis of water in other nominally anhydrous solid solution minerals.

Keywords: spinel-structured oxides, relative sensitivity factors, secondary ion mass spectrometry, hydrogen analysis, nominally anhydrous minerals

©2020. Japan Geoscience Union. All Right Reserved.

[E] Poster | S (Solid Earth Sciences)：S-TT Technology & Techniques

[S-TT50] Synthetic Aperture Radar and its application

convener:Yohei Kinoshita(University of Tsukuba), Yu Morishita(Geospatial Information Authority of Japan), Shoko Kobayashi(Tamagawa University), Takahiro Abe(Earth Observation Research Center, Japan Aerospace Exploration Agency)

ALOS-2 and Sentinel-1, which have highly enhanced capacity compared to previous SAR satellites, were launched in 2014, and their utilization has been widely expanding as data have accumulated for approximately five years. Other long-operating SAR satellites like TerraSAR-X and Cosmo-SkyMed also contribute to expanding the SAR utilization. Now we are facing a new and abundant era of the satellite SAR, along with a worldwide trend to an open and free data policy of satellite data, under the situation of next-generation advanced and/or constellated SAR satellite plans by both public agencies (e.g. ALOS-4 and NISAR) and private sectors. In addition, SAR technologies with other platforms, such as ground-based SAR with high temporal resolution and UAV (Unmanned Aerial Vehicle) SAR with flexible operability, have also been developed and used for various targets. These facts indicate that the SAR utilization has become widespread in both basic researches (e.g., earth science) and diverse applications (e.g., disaster prevention and forest monitoring). In this session, we would like to invite various kinds of research and application results with regard to SAR, sharing our knowledge and having a discussion for the advancement of the SAR utilization.

[STT50-P01] Development of InSAR tropospheric phase delay correction system at MRI (4th report)

*Satoshi Okuyama[1], Shinobu Ando[1], Toshiki Shimbori[1] (1.Meteorological Research Institute)

[STT50-P02] Progress for detecting surface displacement associated with 2018 Boso SSE by ALOS-2 ScanSAR interferometry

*Yohei Kinoshita[1] (1.University of Tsukuba)

[STT50-P03] Interseismic crustal deformation along the Xianshuihe Fault System, Western China, detected by ALOS-2 ScanSAR interferometry

*XUEMEI WANG[1], Youichiro Takada[2] (1.Department of Natural History Sciences, Graduate School of Science, Hokkaido University, 2.Department of Earth and Planetary Sciences, Hokkaido University)

[STT50-P04] Estimation of crustal deformation at Azumayama volcano during Aug. 2014 – Oct. 2019 by using InSAR in comparison with GNSS

*Takehiro Arai[1], Yoshiko Ogawa[1], Yasuhiro Hisada[1], Hirohide Demura[1], Taku Ozawa[2], Satoshi Miura[3] (1.The University of Aizu, 2.Graduate school of Science and Faculty of Science, Tohoku Univeristy, 3.National Research Institute for Earth Science and Disaster Resilience)

[STT50-P05] Extraction of topographic changes associated with the 2018 eruption and tsunami of Krakatau volcano using time-series SAR

*Daiki Inano[1], Hodaka Okazaki[1], Masanobu Shimada[1] (1.Tokyo Denki University)

[STT50-P06] Land subsidence prediction in Beijing plain using machine learning methods

*Yuyi Wang[1], Yun Pan[1] (1.Capital normal university)

[STT50-P07] Estimation of velocity distribution of Shirase Glacier derived from SAR data obtained by ERS-1/2 tandem mission (2)

*Koichiro Doi[1,2], Yuichi Aoyama[1,2], Kazuki Nakamura[3], Tsutomu Yamanokuchi[4], Kazuo Shibuya[1] (1.National Institute of Polar Research, 2.The Graduate University for Advanced Studies, SOKENDAI, 3.College of Engineering, Nihon University, 4.Remote Sensing Technology Center)

[STT50-P08] Evaluation of inundation area extraction method for the 2018 Western Japan heavy rainfall using PALSAR-2

*Hasatani Ryuta[1], Hiroto Nagai[2] (1.Waseda Univ School of Creative Science and Engineering, 2.Waseda Univ School of Education)

[STT50-P09] Integration of ALOS PALSAR and Landsat-7 ETM+ data for buried lineaments extraction at the Farafra Oasis, Egypt

*Noha Ismail Medhat[1,2], M.-Y Yamamoto[1], K. Mansour[2], A.M Abbas[2], M. Abdel Zaher[2] (1.Kochi University of Technology, 185, Miyanokuchi, Tosayamada, Kami, Kochi, 782-8502, Japan, 2.National Research Institute of Astronomy and Geophysics, Helwan, Cairo 11421, Egypt)

[STT50-P10] Development of multi-type portable radar interferometer for volcano observation

Taku Ozawa[1], *Yuji Himematsu[1] (1.National Research Institute for Earth Science and Disaster Resilience)

[STT50-P11] An Open-Source InSAR Time Series Analysis Package LiCSBAS and Its Application

*Yu Morishita[1,2], Milan Lazecky [2], Tim J. Wright [2], Jonathan R. Weiss [3,2], Yasser Maghsoudi [2], John R. Elliott [2], Andy Hooper [2] (1.Geospatial Information Authority of Japan, 2.University of Leeds, 3.University of Potsdam)

Development of InSAR tropospheric phase delay correction system at MRI (4th report)

*Satoshi Okuyama[1], Shinobu Ando[1], Toshiki Shimbori[1]

1. Meteorological Research Institute

Introduction

SAR Interferometry is a technique which utilize the phase information of the SAR images to detect surface displacement which took place between two observations. However, its result contains the effect of medium between the antenna and the target such as tropospheric delay. To correct the tropospheric delay, method which utilizes numerical weather model has been proposed (Hobiger et al., 2008; Ozawa and Shimizu, 2010). We have been developing a tropospheric delay correction system since 2018 and obtained good result (Okuyama et al., 2019). This version, hereinafter called “version 1”, had problem in computation efficiency. We have improved the efficiency by replacing the coordinate system for calculation of the tropospheric delay.

Changes

Version 1 calculates tropospheric delay in ECEF coordinate system for the best accuracy. However, SAR interferograms is in geographic coordinate system, while numerical weather model we used, NuSDaS-format JMA-MA (Meso-Analysis), is a gridded data in Lambert conformal conic (LCC) projection. The difference of coordinate system of the input data forced us to calculate numerous times of coordinate transformation. Our new version, “Version 2” computes tropospheric delay in LCC projection. This reduce the number of coordinate transformation to just once per point. As a result, computation time reduced greatly, from 5 hours to 3 minutes. Calculation in LCC projection assumes flat Earth and may result in inaccurate estimation, however, the difference between Version 1 and 2 is around 1.5mm. This is small enough compared to the phase stability of the interferograms.

Future direction

Version 2 calculates tropospheric delay at the ground surface by extrapolating values from bottom 2 planes. We will introduce Land Surface data to eliminate extrapolation.

Acknowledgement

PALSAR-2 level 1.1 data are shared among PIXEL (PALSAR Interferometry Consortium to Study our Evolving Land surface) and provided from JAXA under a cooperative research contract with ERI, Univ, Tokyo. The ownership of PALSAR-2 data belongs to JAXA.

Keywords: SAR Interferometry, tropospheric delay, delay correction

©2020. Japan Geoscience Union. All Right Reserved.

Progress for detecting surface displacement associated with 2018 Boso SSE by ALOS-2 ScanSAR interferometry

*Yohei Kinoshita[1]

1. University of Tsukuba

The slow slip event (SSE) is known to release accumulated strain energy with no or slight seismic wave radiation. The SSE is usually detected by highly accurate geophysical measurements such as the Global Navigation Satellite System (GNSS) and seismometers because of very small surface deformation on the order of millimeters to centimeters, and small ground oscillation (named as a tremor). Until now, several papers reported SSEs at Tokai area (e.g. Yamamoto et al. 2005, EPS; Ozawa et al. 2016, EPS), Cascadia (e.g. Dragert et al. 2004, EPS; Hawthorne and Bartlow 2018, JGR), and Nankai Trough (Kobayashi 2017, EPS; Ozawa 2017, EPS). The area around Boso Peninsla is also a location where SSEs have occuered with intervals of several years (Fukuda 2018, JGR). However, most of the reffered papers here used GNSS observations that have a limitation of low spatial resolution (Usually a few tens of kilometers between ground stations). In the previous presentation (Kinoshita et al., JpGU2019), we reported that the surface displacement of the 2018 Boso SSE could be detected by the stacking method of Sentinel-1 SLCs with an atmospheric delay correction based on the Japan Meteolorogical Agency Meso-Scale Model (MSM). In this study we performed the InSAR analysis using ALOS-2 ScanSAR data for the purpose of complementing the results derived from Sentinel-1 InSAR.
We performed the InSAR analysis using the RINC software version 0.41 to interfere 14 ScanSAR images. The ScanSAR data used here spans from January 2016 to September 2019. The path and frame are 17 and 2900, respectively. Topographic phase contributions were modeled and removed by the use of the SRTM4 30m DEM. All the interferograms were phase-unwrapped with the SNAPHU software. Since interferograms were to some extent contaminated by the phase noise due to ionospheric disturbances, we applied the Split Spectrum Method for all the interferograms to remove this.
Most of processed interferograms showed significant coherence to recover the SSE displacement, although the non-dispersive atmospheric delay signal was also significant. The ionospheric contribution that is the dispersive component of the atmospheric delay could be effectively removed by the Split Spectrum Method.
By the presentation, I will perform the time series analysis and the atmospheric delay correction to mitigate the non-dispersive atmospheric contribution and to detect the SSE signal. I will present the progress of this study in the presentation.

Keywords: InSAR, slow slip event, atmospheric delay

©2020. Japan Geoscience Union. All Right Reserved.

Interseismic crustal deformation along the Xianshuihe Fault System, Western China, detected by ALOS-2 ScanSAR interferometry

*XUEMEI WANG[1], Youichiro Takada[2]

1. Department of Natural History Sciences, Graduate School of Science, Hokkaido University, 2. Department of Earth and Planetary Sciences, Hokkaido University

The Xiansuihe fault system (XFS) is a large-scale strike slip fault running eastern part of the Tibetan plateau. Its western part lies high altitude and dry area, while eastern part runs mountainous area partly covered by vegetation. Although we know XSF hosts many historical earthquakes, it is difficult to grasp its current activity mainly because it is too large and too remote to be equally covered by ground based observations like GNSS. Therefore, Interferometric Synthetic Aperture Radar (InSAR) is suitable technique to make a detailed map of current fault activities. Wang et al. (2009) reported strain concentration at the western part of XSF using C-band satellites (ERS-1/2 and Envisat), which suffered from low coherence. Also, their study area is very limited (> 100 km). Zhang et al. (2019) also reported interseismic strain localization along XSF using Sentinel-1 interferograms. But their results include strong oscillation probably affected by tropospheric disturbances.
In this study, we use ALOS-2 ScanSAR images to grasp overall interseismic crustal deformation along XFS. All the interferograms are processed by GAMMA software suite (Wegmüller and Werner, 1997). The SAR images we used are acquired from descending orbit, which is more sensitive to the XSF motion than those taken from ascending orbit. We processed three interferometric pairs with temporal baseline ranging from 3 to 4 years. The coherence of those interferograms are high in summer along all the fault traces, while it decreases in winter only in eastern section. Almost all the interferograms are covered by strong long wave-length noise, possibly resulting from ionospheric and tropospheric perturbations. Assuming that GNSS data are correct, we estimated the InSAR error at each GNSS station, and interpolated the errors into all the pixels to remove the long-wavelength noise (Fukushima and Hooper, 2011; Takada et al., 2018). The GNSS velocity field used for correction has been estimated by Liang et al., (2013). The interferograms thus corrected indicate strain rate concentration along the whole trace of XSF, which is much wider than previous studies. We are currently applying the time-series analysis and the split spectrum method (Gomba et al., 2015; Furuya et al., 2017) to remove ionospheric effects before the GNSS correction.

Keywords: ALOS-2, ScanSAR, GNSS

©2020. Japan Geoscience Union. All Right Reserved.

Estimation of crustal deformation at Azumayama volcano during Aug. 2014 –Oct. 2019 by using InSAR in comparison with GNSS

*Takehiro Arai[1], Yoshiko Ogawa[1], Yasuhiro Hisada[1], Hirohide Demura[1], Taku Ozawa[2], Satoshi Miura[3]

1. The University of Aizu, 2. Graduate school of Science and Faculty of Science, Tohoku Univeristy, 3. National Research Institute for Earth Science and Disaster Resilience

Azumayama volcano is one of the active volcanoes in Fukushima prefecture. Azumayama had been issued the volcanic alert level 2 during winter 2014 - fall 2016 and fall 2018 - spring 2019. It is the most active volcano in the Fukushima Pref. We have been working on to clarify time-series of crustal deformation at Azumayama volcano [1].

In this study, InSAR (Interferometric Synthetic Aperture Radar) analysis was conducted using the data of Advanced Land Observing Satellite 2 (ALOS2) / Phased Allay type L-band Synthetic Aperture Radar 2 (PALSAR2). The crustal deformation was estimated around Azumayama volcanobased on the 12 analysis pairs of InSAR. The numerical weather model MSM (Meso Scale Model) [2] was used to correct atmospheric delay. Then new InSAR results and GNSS [3] data were compared for consistent understanding of crustal deformation in the time series.

As the results, atmospheric delays in InSAR were mitigated for most analysis pairs by introducing numerical weather model (MSM). On the other hand, MSM atmospheric correction often did not work well for the InSAR pairs where the weather condition of either of the 2 observation dates was changing rapidly, such as the approach of a cold front or a typhoon. Temporary uplift and subsidence were observed in the north of the Oana crater and a sharp uplift was observed in the west of the crater the period from fall 2018 to spring 2019. The center of crustal movement was considered to had moved to the west of Oana crater from 2014 to 2019.

[1] Abe. K, et al., 2019, JpGU, “Mitigation of atmospheric delay in InSAR for fair estimate of crustal deformation at Azumayama volcano”

[2] MSM, https://www.jma.go.jp/jma/kishou/know/whitep/1-3-6.html

[3] Miura, Tohoku University, The report of 131th the Coordinating Committee for Prediction of Volcanic Eruption

Keywords: Azumayama, volcano, crustal deformation, synthetic aperture radar, numerical weather model, InSAR

©2020. Japan Geoscience Union. All Right Reserved.

Extraction of topographic changes associated with the 2018 eruption and tsunami of Krakatau volcano using time-series SAR

*Daiki Inano[1], Hodaka Okazaki[1], Masanobu Shimada[1]

1. Tokyo Denki University

Synthetic aperture radar (SAR) has the advantage of being able to observe over a wide area without being affected by the weather or day and night. Because SAR passes through clouds and smoke, changes in the island immediately after the eruption can be clearly seen even if the eruptions and volcanic ash erupt from the crater. Then, in order to classify land and sea from the images observed by SAR, consider the definition of land and sea. The land area is a place where the altitude is 0 m or more, and the scattered signal is generally larger than that of the sea area. On the other hand, the sea area is a zone where the altitude is 0 meters, and the reflected signal is generally small. Since the signal in the land area is larger than that in the sea area, it appears bright in the amplitude image.

In this study, we used the time-series SAR data to extract changes in island area for topographic changes associated with the eruption of Anak Krakatau Island in 2018. We analyzed the image data from January 22, 2018 to May 21, 2019, and calculated the area change by two methods for three scenes in which the terrain changed significantly.

The first is a histogram method. From the amplitude image, histograms of the land area and the sea area are created, and an optimum threshold at which both distribution functions intersect is determined. Then, the area where the backscattering coefficient was larger than the sea was defined as land, and the area was calculated by multiplying the number of pixels in the land area by the image cell size. This method works with high accuracy when the island is clearly brighter than the sea. However, when the sea surface is rough and the scattering coefficient is high as in this study, it may be difficult to make clear identification.

The second is a shoreline extraction method. The pixel value of the amplitude image is forcibly set to 0 based on the threshold value obtained by the histogram method. Then, the coastline displayed brightly is extracted (manual operation), and the inside of the extracted closed curve is included in the land area. Similar to the histogram method, the number of land pixels was multiplied by the image cell size. The shoreline extraction method is considered to be a method that can calculate the area with higher accuracy than the histogram method without being affected by backscatter on the sea.

As a result, the area of Anak Krakatau Island was 2.88 square kilometer before the eruption, 3.07 square kilometer after the eruption, and 3.06 square kilometer several months after the eruption. As for the amount of change, the island area increased by 0.18 square kilometer before and several months after the eruption. It is said that it is difficult to analyze an island surrounded by the sea on all sides using the interferometric SAR method. The method in this study is considered to be very effective in the area where the coastline is clear even in the analysis of such islands.

©2020. Japan Geoscience Union. All Right Reserved.

Land subsidence prediction in Beijing plain using machine learning methods

*Yuyi Wang[1], Yun Pan[1]

1. Capital normal university

Land subsidence is usually difficult to be predicted due to its complex regulating processes, especially in the metropolitan environment, such as Beijing, where both natural and anthropogenic factors exist. This study aims to investigate the potential and limitations of machine learning methods in predicting land subsidence of a metropolitan area with a case study in Beijing, where significant land subsidence has been reported since early 1950s. The SAR image data of Radarsat-2 was collected, and the SBAS-InSAR (Small Baseline InSAR) interferometry was used to monitor the spatial distribution of land subsidence in the Beijing Plain from 2012 to 2015, while five machine learning methods (random forest algorithm, decision tree algorithm, extra tree algorithm, Boosting algorithm, neural network algorithm) were used to establish the models for prediction, with a focus on the driving factors of precipitation, groundwater level changes (unconfined water level and confined water level), distance from the fault, elevation, compressible layer thickness, and land use. The results shown that: (1) the extra tree method had the best performance (94.03%), followed by the boosting algorithm (93.91%) and decision tree (90.50%), in contrast to a degraded performance by the neural network (79.8%) and boosting algorithm (67.4%). (2) based on data mining methods of machine learning algorithms, the factor contribution rate of diving factors to land subsidence in Beijing plain was obtained, which showed that precipitation has the highest influence, followed by compressible layer thickness, confined water level change, unconfined water level change, distance from fault zone, altitude, and land use; (3) future development of land subsidence was simulated with varying groundwater level rise scenarios. The results demonstrated a good potential of machine learning methods in predicting and understanding the land subsidence in the metropolitan area towards a sustainable groundwater resources management.

Keywords: land subsidence, Machine learning, InSAR technology, Beijing

©2020. Japan Geoscience Union. All Right Reserved.

Estimation of velocity distribution of Shirase Glacier derived from SAR data obtained by ERS-1/2 tandem mission (2)

*Koichiro Doi[1,2], Yuichi Aoyama[1,2], Kazuki Nakamura[3], Tsutomu Yamanokuchi[4], Kazuo Shibuya[1]

1. National Institute of Polar Research, 2. The Graduate University for Advanced Studies, SOKENDAI, 3. College of Engineering, Nihon University, 4. Remote Sensing Technology Center

Shirase Glacier is one of the fastest flowing ice streams in Antarctica flowing into the southernmost of Lü tzow-Holm Bay in Dronning Maud Land, East Antarctica. It is important to clarify the spatial flow rate distribution with a high-resolution to investigate causes of the fast flow and the temporal flow rate changes. In order to make a high-resolution flow velocity map, we can apply a usual interferometric Synthetic Aperture Radar (InSAR) technique to an InSAR pair data. However, since flowing velocity of the ice stream is greater than 2 km/year (Nakamura et al., 2007, Aoyama et al., 2016), it is difficult to estimate the flow velocity by applying the InSAR technique to the ordinal repeat cycle SAR mission data.

Tandem mission by European Satellite of Remote sensing (ERS)-1/2 was conducted in 1996 and 1999. In this tandem mission, ERS-2 had flown after ERS-1 in the same orbit with an interval of one day, and many InSAR pairs with one day temporal baseline were obtained through the mission.

We successfully obtained three SAR interferograms over Shirase Glacier using this tandem mission InSAR pairs acquired at 1996/06/02-1996/06/03, 1999/11/14-1999/11/15 and 1999/12/19-1999/12/20. We estimated surface displacements along range direction (direction of radar illumination) by applying differential InSAR (DInSAR) with a TanDEM-X 90m DEM (Rizzoli et al., 2017) to remove topographic phase. We also estimated displacements along azimuth direction (direction perpendicular to range direction) by applying a split beam interferometry (SBI) (Bechor and Zebker, 2006) technique to the three InSAR pairs. By combining the range and azimuth displacements, spatial flow velocity distributions can be derived with a high-resolution. Since displacements obtained by the DInSAR and SBI techniques contain artificial displacements due to some interferometric phase trends, we estimated the artificial displacement trends from displacements over outcrop rock areas under an assumption that no crustal displacements occurred there for one day, and the trends were eliminated. We show an example of surface ice displacement over Shirase Glacier obtained from the pair 1999/11/14-1999/11/15 in the figure.

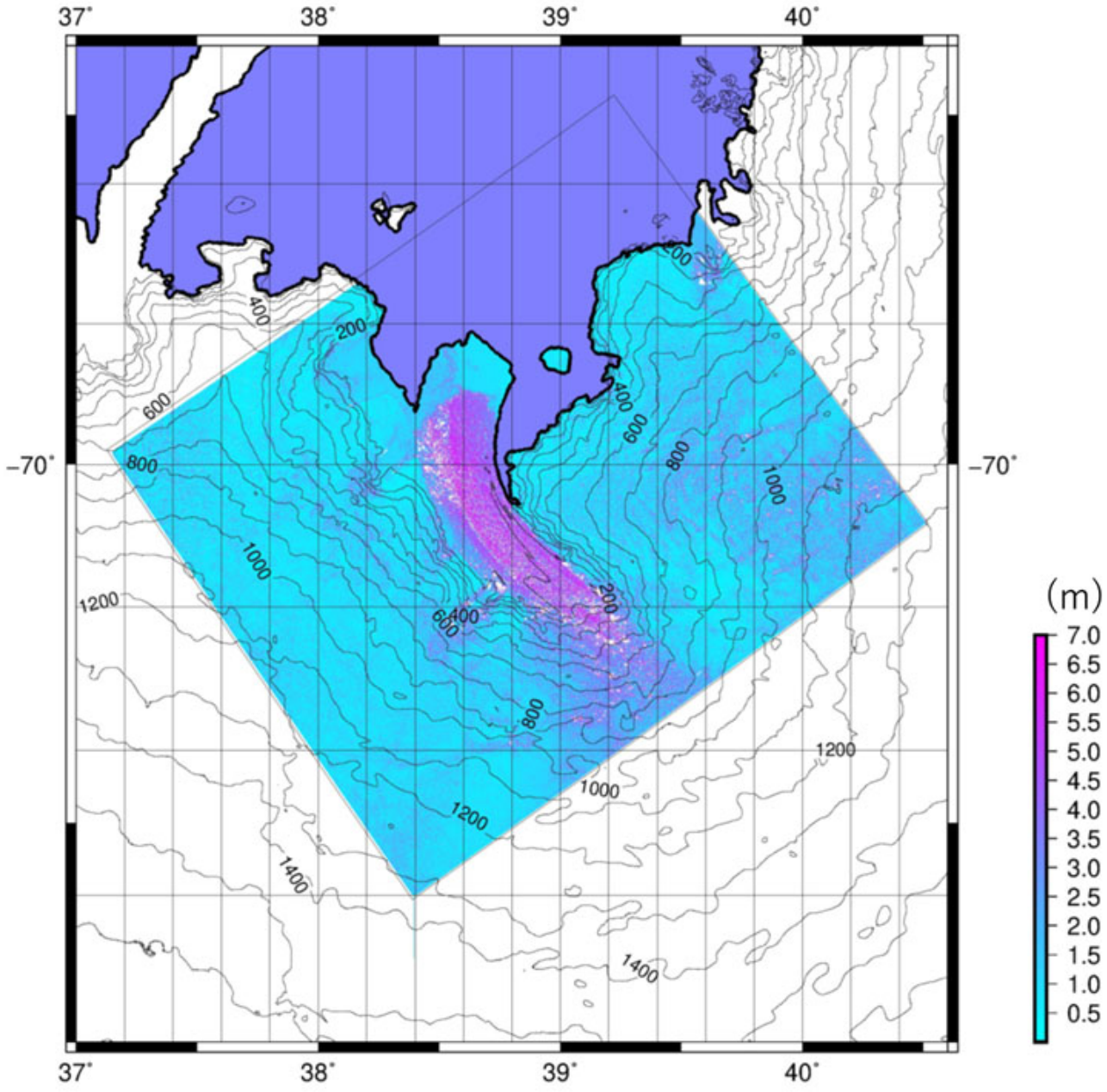
We can evaluate accuracies of the obtained ice surface displacements from the displacements over outcrop rock areas after the artificial trends for each pair. The averages standard deviations of the three pairs observed over the outcrop rock areas are 4 cm in range direction and 123 cm in azimuth direction.

We also compared the flow rates and directions with in-situ GNSS measurements situated on a downstream site in Shirase Glacier observed for three years from 2015 to 2017. We found mean differences between the two observations (DInSAR −GNSS) of -0.691 (m/day) in flow rate and 15.7 (deg.) in flow direction.

In the presentation, we will show two-dimensional flow velocity maps with a resolution of approximately 20 m at the three periods and discuss spatial and temporal velocity changes.

Keywords: Shirase Glacier, flow velocity map, ERS-1/2 tandem mission, DInSAR, SBI

©2020. Japan Geoscience Union. All Right Reserved.



©2020. Japan Geoscience Union. All Right Reserved.

Evaluation of inundation area extraction method for the 2018 Western Japan heavy rainfall using PALSAR-2

*Hasatani Ryuta[1], Hiroto Nagai[2]

1. Waseda Univ School of Creative Science and Engineering, 2. Waseda Univ School of Education

In recent years, due to global warming, there are many opportunities to use SAR (Synthetic aperture rader) mounted on earth observation satellites for emergency observation of typhoons and heavy rains and for measuring damage over a wide area. Many methods for extracting the inundation areas from SAR have been proposed, but most of them are methods that perform threshold processing of the backscatter coefficient from the intensity information. However, a method of extracting the inundation area by combining the intensity information and the phase information has not been established yet, and there are few examples(Ohki et al., 2016).

In this study, PALSAR-2 satellite is used. From the intensity information, One is a normalized backscattering intensity change index image (NoBADI) (Nagai et al., 2017)is created. It is possible to display unusual inundation area using multiple images before inundation, And the other is a single image of the backscattering intensity was created. From the phase information, two types of images are created a pair immediately before and after the disaster: γ_{pre} (observation interval width: about 3 months) and a pair before and after the disaster: γ_{summer} (observation interval width: about 2 years). The verification area in this study is the inundation area of Kurashiki City and Soja City in Okayama validation prefecture, which was flooded by heavy rains on 2018, and the area 3 km around it. From the intensity information, Inundation areas were extracted by classifying land cover, paddy areas, upland areas, and building areas. From the topological information, Extract the inundation area in the building area. The κ coefficient was used as the index of inundation area extraction accuracy.

As a result of the inundation area extraction, it was found that the paddy field area and upland field area showed a higher value of κ coefficient when the backscattering intensity single image was used regardless of the presence of the speckle noise filter. It was confirmed that when the filter window size was enlarged, a high κ coefficient was shown. The urban area showed the highest value of the κ coefficient when the coherence image of the phase information was used. As for the κ coefficient of the phase information, γ pre: $\kappa = 0.397$ γ summer: $\kappa = 0.037$ was calculated.It is necessary to consider the observation period when creating interference pairs.

Next steps we will propose an optimal method for extracting the inundation area according to the geographical features, And Determine the optimal filter window size from the viewpoint of maintaining high resolution images.

Reference :
Ohki, M., Watanabe, M., Natsuaki, R., Motohka, T., Nagai, H., Tadono,T.,Suzuki, S., Ishii, K., Itoh, T., Yamanokuchi, T., Shimada, M., : FloodArea Detection Using ALOS-2 PALSAR-2 Data for the 2015 HeavyRainfall Disaster in the Kanto and Tohoku Area, Journal of The Remote Sensing Society of Japan, VOL36, No4pp. 348-359, 2016
Nagai, H., Ohki, M., Abe,T., : Robust flood area detection using a L-band synthetic aperture radar: Preliminary application for Florida, the U.S. affected by Hurricane Irma, AGU, 2017

©2020. Japan Geoscience Union. All Right Reserved.

Keywords: SAR, NoBADI, Coherence analysis, Flood area extraction

©2020. Japan Geoscience Union. All Right Reserved.

Integration of ALOS PALSAR and Landsat-7 ETM+ data for buried lineaments extraction at the Farafra Oasis, Egypt

*Noha Ismail Medhat[1,2], M.-Y Yamamoto[1], K. Mansour[2], A.M Abbas[2], M. Abdel Zaher[2]

1. Kochi University of Technology, 185, Miyanokuchi, Tosayamada, Kami, Kochi, 782-8502, Japan, 2. National Research Institute of Astronomy and Geophysics, Helwan, Cairo 11421, Egypt

In the last few years, ALOS/PALSAR (L-band) (HH, HV, VH and VV) images have been widely used due to its ability to penetrate the surface in certain conditions for example of low moisture or dry friable sandy soil. Images from ALOS-1 sensor have been applied to delineate subsurface structures. Optical images such as Landsat-7 ETM+ data are used to discriminate between scatterings from earth surface and subsurface materials. Thus, Farafra desert is an optimal environment for L-band microwave penetration. Therefore, this research involves mapping and interpretation of lineaments, surface and subsurface structures. The interested four spots at Farafara sand sheets display many structures that not have been traced in the Egyptian official geological maps.

Speckle noise is found in radar images due to many reasons, for example, when an object strongly reflected between itself and the spacecraft causing noise. Refined LEE Filter (RLF) is applied for speckle noise reduction; speckle noise near strong edges is not strongly filtered, leaving the center of the pixel unfiltered, so, this procedure is an essential step in processing of polarimetric data to improve the accuracy of the data and enhance resolution. ALOS/PALSAR data are processed into circular polarization for providing the best viewing of morphological and subsurface lineaments. The ellipse shape governed by two axes; semi-major axis ‘a’ and semi-minor axis ‘b’. Orientation angle(ψ) is measured from positive horizontal axis X counter clockwise direction, orientation angle range from 0° to 180°. Ellipticity (χ) is a shape parameter defined by the degree of oval shape, defined by $\chi = arctan b/a$ and can take values between -45° to $+45^{\circ}$. As, the circular polarization yielded best outputs of subsurface structure in different trends, full polarimetric ALOS/PALSAR images (PLR) are transformed into circular polarization, by changing both angles into orientation angle $\psi = 0^{\circ}$ and elliptical angle $\chi = 45^{\circ}$. Full polarimetric images are represented in Pauli RGB. Landsat-7 ETM+ data are freely uploaded with the same date and location of ALOS/PALSAR images. Bands 1, 2, 3, 4, 5 and 7 are merged together, then bands (R:2, G:4, B:7) are changed to obtain best spatial resolution. Landsat-7 images have some gap areas, which is essentially be filled with Landsat-7 data acquired at the same time of the year by histogram matching technique to fill the missed pixels of the interested target scenes according to Landsat 7. The obtained rose diagram shows two trends of dominant and secondary; the most dominant direction is North West (NW 330˚), while the secondary trend is North (North 10°). This result is confirmed by the field survey. The dominant direction of lineaments extracted from ALOS/PALSAR images is well fitted with the secondary direction of the geological structure in the study area.

This work represents a stage of achievement in detecting buried lineaments covered by sand sheets by using ALOS/PALSAR and Landsat-7 ETM+. Surface and subsurface lineaments that can be extracted in Farafra formations. May be due to its geological nature and spatial resolution that well fit to ALOS/PALSAR radar wave. Extracted orientation of the lineaments; especially in sand sheets proved great correlation with the secondary trend of the geological structure at Farafra map. Ground penetrating radar can easily support confirmation of ALOS/PALSAR result at the traced interested spots; alternatively, consuming time and budget in exploring the whole area. In addition, parameter analysis of soil samples from field survey will be carried out, if possible.

©2020. Japan Geoscience Union. All Right Reserved.

Keywords: ALOS/PALSAR , Landsat-7 ETM+, subsurface lineaments

©2020. Japan Geoscience Union. All Right Reserved.

Development of multi-type portable radar interferometer for volcano observation

Taku Ozawa[1], *Yuji Himematsu[1]

1. National Research Institute for Earth Science and Disaster Resilience

Recent advances in spaceborne SAR and its analysis techniques have enabled us to detect volcano deformation in a detailed. As a result, spaceborne SAR has been used as a useful tool in the evaluation of volcanic activity and the study of mechanisms. However, the frequency of spaceborne SAR observation is limited to the recurrence period satellite, and therefore, it is difficult to detect volcano deformation that its distribution changes greatly within a short time. Then, we are developing “multi-type portable radar interferometer” for detecting volcano deformation in the task B sub-theme 2 of the “Next Generation Volcano Research” project. It transmits radar wave from the ground, and then, can detect volcano deformation with high temporal resolution. By this sensor, we want to be able to observe a wide area as frequently as once a day by repeat observations. For this purpose, it is necessary to use a system that does not cause a decrease in coherence due to vegetation. Therefore, in this sensor, we adopted an L-band radar wave with high permeability to vegetation, and fabricated an experimental sensor. We carried out an experiment measurement within 1-hour by its sensor in the Asama-yama for 1 hour, and it was confirmed that high coherence was obtained. Furthermore, a phase change considered to be an atmospheric delay was detected (Ozawa and Himematsu, 2019).
Since it is necessary to carried out repeat observation in this system, it is necessary to confirm whether appropriate coherence can be obtained by the repeat path observation. Therefore, we carried out experiment measurements at the southwestern foot of the Tsukuba-san on October 16 and October 17, 2019. The slant distance to the summit is about 4 km. In this experiment, the rail was installed on the concrete part of the riverside of the Sakura-gawa, and the observation by the ground-based type was performed. Applying SAR interferometry to a data pair that observation interval was one day, a high coherence was obtained in the region where strong scattering intensity was obtained. At the summit, a phase change of about half a cycle is detected, which may be an atmospheric delay component. From this result, it was confirmed that the repeat path observation by the multi-type portable radar interferometer for volcano observation can be applied successfully. Furthermore, in order to investigate the continuity of coherence, a measurement experiment at the Tsukuba-san was performed every about once a month. High coherence was obtained in the result of data pair with an observation interval of one month. However, decorrelation became remarkable in the result of the data pair with the observation interval of 2 months, and in that with the observation interval of 3 months, the area where coherence was obtained was limited to around the summit where the vegetation was relatively sparse. From the above, it can be said that the continuity of coherence for the present version of experimental sensor is about two months. Tsukuba-san is covered by relatively dense vegetation, it may have caused such short continuity of coherence. However, its improvement is necessary, because longer continuity of coherence is preferable for volcano observation. Significant noise sometimes superimposes on the SAR image obtained from the current experimental sensor, and it may cause decorrelation. Now, we are improving hardware and software to solve this problem, and we will investigate whether these improvements can improve the continuity of coherence in the future.

©2020. Japan Geoscience Union. All Right Reserved.

An Open-Source InSAR Time Series Analysis Package LiCSBAS and Its Application

*Yu Morishita[1,2], Milan Lazecky [2], Tim J. Wright [2], Jonathan R. Weiss [3,2], Yasser Maghsoudi [2], John R. Elliott [2], Andy Hooper [2]

1. Geospatial Information Authority of Japan, 2. University of Leeds, 3. University of Potsdam

For the past five years, C-band Sentinel-1 and L-band ALOS-2 have provided abundant and useful Synthetic Aperture Radar (SAR) data, which have the potential to reveal global ground surface deformation at high spatial and temporal resolutions. However, for most users, fully exploiting the large amount of associated data is challenging, especially over wide areas. Whereas Geospatial Information Authority of Japan (GSI) has been monitoring surface deformations over Japan areas using ALOS-2 data, a sophisticated time series analysis technique has not been implemented for the nationwide scale.

To help address these challenges, we have developed LiCSBAS (https://github.com/yumorishita/LiCSBAS, https://doi.org/10.3390/rs12030424), an open-source SAR interferometry (InSAR) time series analysis package that integrates with the automated Sentinel-1 InSAR processor (LiCSAR). LiCSBAS utilizes freely available LiCSAR products, and users can save processing time and disk space while obtaining the results of InSAR time series analysis. In the LiCSBAS processing scheme, interferograms with many unwrapping errors are automatically identified by loop closure and removed. Reliable time series and velocities are derived with the aid of masking using several noise indices. The easy implementation of atmospheric corrections to reduce noise is achieved with the Generic Atmospheric Correction Online Service for InSAR (GACOS).

Using case studies in southern Tohoku and the Echigo Plain, Japan, we demonstrate that LiCSBAS applied to LiCSAR products can detect both large-scale (>100 km) and localized (~km) relative displacements with an accuracy of <1 cm/epoch and velocities of ~2 mm/yr with ~60 observations over 2 years. We detect displacements with different temporal characteristics, including linear, periodic, and episodic, in Niigata, Ojiya, and Sanjo City, respectively.

LiCSBAS and LiCSAR products facilitate greater exploitation of globally available and abundant SAR datasets and enhance their applications for scientific research and societal benefit.

Interferograms from satellites other than Sentinel-1 and generated using a variety of software packages can also be processed by LiCSBAS. The software will enable GSI to improve its monitoring capability and realize robust continuous nationwide monitoring of surface deformation exploiting ALOS-2 and coming ALOS-4 data.

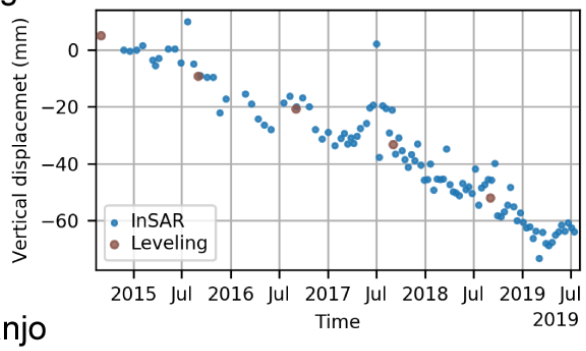
We also present applications of LiCSBAS and LiCSAR products to all major urban areas in Japan and continental-scale Alpine Himalayan Belt in this presentation.

Keywords: InSAR, Sentinel-1, time series analysis, deformation monitoring, subsidence, automatic processing

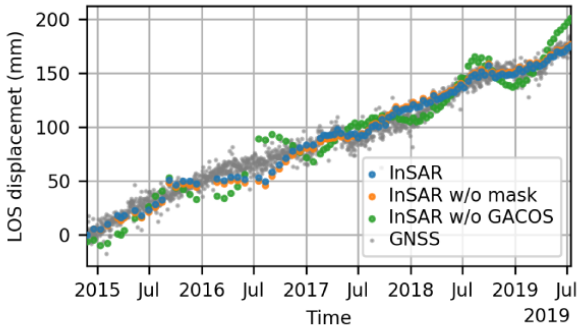
©2020. Japan Geoscience Union. All Right Reserved.

Processed by LiCSBAS using LiCSAR products

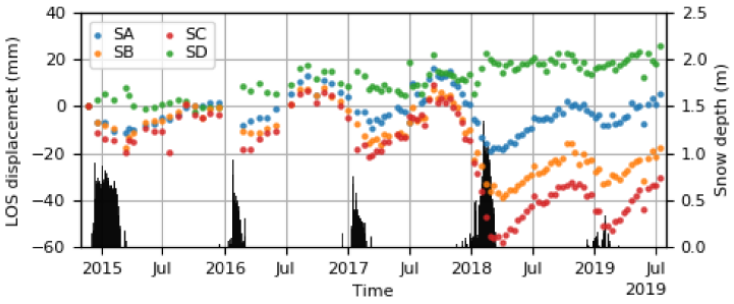
Niigata



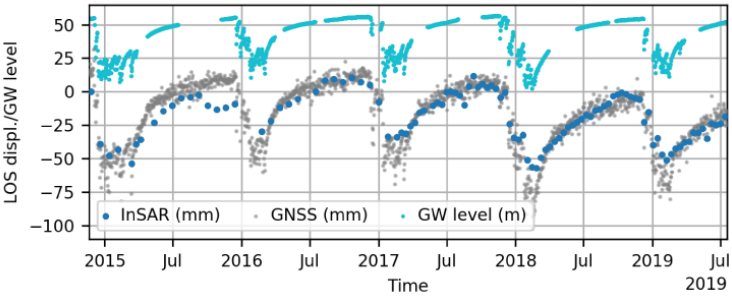
GNSS 950179

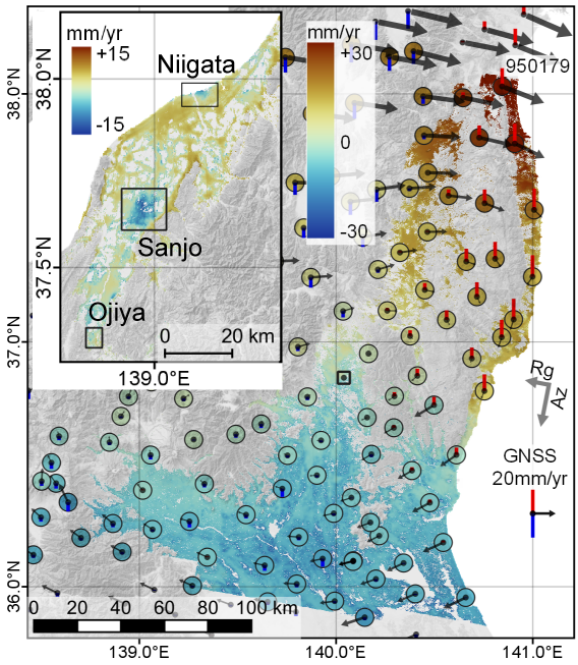


Sanjo



Ojiya





©2020. Japan Geoscience Union. All Right Reserved.

[E] Poster | S (Solid Earth Sciences)：S-TT Technology & Techniques

[S-TT51] seismic monitoring and processing system

convener:Takahiro Maeda(National Research Institute for Earth Science and Disaster Resilience)

This session covers scientific and technical issues in seismic monitoring or data processing systems for earthquakes or explosions observation. This includes development or improvement of seismic observation networks, innovative techniques in observation and monitoring, cutting-edge data acquisition and processing techniques in geophysical explorations. Other topics related to geophysical observation are also welcome.

[STT51-P01] Acquisition and application of offshore W-VSP in deep gas field in East China Sea basin

*Shunli Gao[1], Senqing Hu[1], Jun Zhao[1] (1.China National Offshore Oil Corporation (CNOOC), China Limited-Shanghai)

[STT51-P02] Study on the cause of the misalignment of the incidence azimuth of the air gun signal at the S-net station estimated from particle motion

*Ryoichi Iwase[1] (1.National Research and Development Agency, Japan Agency for Marine-Earth Science and Technology)

[STT51-P03] Analysis of Seismic Waves from Continuous and Controlled Seismic Signal System in Kyushu Area

*Ryosuke Matsuura[1], Tatsunori Ikeda[2,3], Takeshi Tsuji[1,2,3], Koshun Yamaoka[4] (1.Cooperative Program for Resources Engineering, Kyushu University, 2.Department of Earth Resources Engineering, Kyushu University, 3.International Institute for Carbon-Neutral Energy Research (I2CNER), Kyushu University, 4.Earthquake and Volcano Research Center, Graduate School of Environmental Studies, Nagoya University)

[STT51-P04] Development of seismic waveform monitor application by JAVA

*Masayoshi Ichiyanagi[1], Hiroaki Takahashi[1] (1.Institute of Seismology and Volcanology, Graduate School of Science, Hokkaido University)

[STT51-P05] Yet another module for reading WIN format data in ObsPy

*Shigeki Nakagawa[1], Aitaro Kato[1] (1.Earthquake Research Institute, the University of Tokyo)

[STT51-P07] Calibration of broadband seismographs based on the teleseismic records

*Takeshi Kimura[1] (1.National Research Institute for Earth Science and Disaster Resilience)

[STT51-P09] DEVELOPMENT OF CLOUD-TYPE MICROTREMOR OBSERVATION SYSTEM

*Shigeki Senna[1], Atsushi Wakai[1] (1.National Research Institute for Earth Science and Disaster Resilience)

[STT51-P10] Development of underground structure information analysis cloud system

*Shigeki Senna[1] (1.National Research Institute for Earth Science and Disaster Resilience)

Acquisition and application of offshore W-VSP in deep gas field in East China Sea basin

*Shunli Gao[1], Senqing Hu[1], Jun Zhao[1]

1. China National Offshore Oil Corporation (CNOOC), China Limited-Shanghai

Offshore Walkaway &walkaround VSP(W-VSP) is one of the borehole seismic. Compared with towing cable seismic method, borehole seismic has less absorption and attenuation of high-frequency information because of less propagation paths, so it is an innovation attempt of seismic technology for deep gas fields in East China Sea.

Oil and Gas exploration in East China Sea basin reveals some special geological conditions: deep reservoir, complex structure and reservoir anisotropy which cause many problems in conventional streamer seismic acquisition and processing, such as multiple, low signal-to-noise ratio and low resolution.

The W-VSP test area is fully covered by 3D towing cable seismic data and the local structure is a small faulted anticline trap with nose structure background under the control of basement high. The main target layer is sand-shale interbedded deposited in the braided river delta of Eocene and the drilling shows that the trap is rich in gas in channel reservoir below 4000m.

After selecting the test well, making acquisition simulation design, optimizing the acquisition mode and parameters, W-VSP acquisition was conducted by placing geophone in the borehole and shooting around by seismic vessel. The 2D walkaway was conducted with the same survey line direction as the existing 3D survey to ensure the optimal data quality and matching with the existing data. Shot point range is 6000m for inline and crossline, and 3.0 km and 4.5 km for loop line. Shot interval is 25m. Time sampling rate is 1ms. Record length is 7000ms. The source is 4210in.cu^3 (single source) with 4 subarrays and 6m sinking depth.

Good results of field and processing data are obtained from W-VSP, which improves the interpretation accuracy of the structure and reservoir around the wellbore. In the deep layer below 4300m, band width of W-VSP data is 0-80 Hz, main frequency is 45 Hz, far higher than the 25 Hz of the streamer 3D seismic data.

By extracting suitable seismic processing parameters, such as attenuation factor and multiple models, well-driven streamer 3D processing is carried out, and we obtained high quality 3D seismic data with enhanced resolution and signal-to-noise ratio. The test shows that the seismic image can be effectively improved by this technology, which is good for sand tracing and gas reservoir description in offshore deep gas fields.

Well-driven 3D seismic processing mainly uses key technologies to obtain well-driven processing parameters from Z-VSP and W-VSP data, including: (1) true amplitude recovery factor TAR; (2) absorption attenuation factor Q; (3) corridor stack section; (4) anisotropic parameters; (5) time-depth relationship and velocity. Well-driven are mainly from the following aspects. Firstly, wavelet processing, ghost suppression technology and anti-Q filter technology and other offshore wide-band processing technologies are adopted to improve resolution and broaden the frequency band. Secondly, shallow

©2020. Japan Geoscience Union. All Right Reserved.

water multiple suppression, tau-p domain deconvolution, SRME, high-precision radon transform and other techniques are used to suppress various multiples step by step, focusing on the fidelity of de-noising process, to improve the signal-to-noise ratio. Finally, high precision velocity analysis, grid tomography modeling and pre-stack depth migration are applied to improve the imaging accuracy.
According to the analysis of well-driven 3D seismic processing results, due to the enhancement of deep energy and the effective removal of multiples, the results is improved in seismic events, having higher signal-to-noise ratio and better continuity. The sand distribution of the main gas reservoirs in deep layer are consistent with drilling results. Through tracking and interpretation of sand at 4600 m depth, the gas reservoir was revealed as a structural and lithological composite type, with the faulted anticline area of 0.54 km^2 at the high position. However, due to the lateral change of sand, the area of sand inclined stratigraphic trap is 0.38 km^2. The reserves calculated according to the fine description of this sand are consistent with the developed reserves of gas fields.

Keywords: Walkaway &walkaround VSP, Well-driven 3D seismic processing, true amplitude recovery factor TAR, absorption attenuation factor Q, anisotropic parameters, improved seismic data quality

©2020. Japan Geoscience Union. All Right Reserved.

Study on the cause of the misalignment of the incidence azimuth of the air gun signal at the S-net station estimated from particle motion

*Ryoichi Iwase[1]

1. National Research and Development Agency, Japan Agency for Marine-Earth Science and Technology

The author estimated the orientation of the Ocean Bottom Seismometer (OBS) and seismic wave velocities in the sediment of seafloor surface at 12 stations of the large cabled observatory ” S-net” (Seafloor observation network for earthquakes and tsunamis along the Japan Trench), consisting of 150 stations in a vast area in the Pacific Ocean on the east coast of Japan from off Hokkaido to Boso Peninsula, which was installed by National Research Institute for Earth Science and Disaster Resilience (NIED). The result of the estimated orientation of the OBSs is consistent with Takagi et al. (2019). P-wave velocity is estimated to be around 1.8 km/s at most stations, and S-wave velocity is estimated to be less than 0.4 km/s at stations on landward slope and 0.3–0.7 km/s at those on the seaward slope of the trench.
However, the estimated incident azimuth of the air gun signal based on the particle motion does not always coincide with the actual azimuth of the air gun (ship azimuth) in time series, and misalignment is recognized. Some are caused by local seafloor topography such as a nearby seamount having a large relative height. On the other hand, however, misalignments are observed at some stations where such seafloor topography does not exist. Regarding the misalignment of the sound source azimuth, it was observed that in the sound source localization of an air gun using OBS off Kamaishi City in Iwate Prefecture the misalignment was up to approximately 9 degrees (Iwase, 2016).
The topographic feature common to the stations installed in the Japan Trench area is the slope. Therefore, the effect of the case where the fluid-solid interface is inclined was examined. However, the observed value cannot be explained by the inclination angle estimated from the 500 m mesh seafloor topographic data published by JODC of the Japan Coast Guard. Also, the slope estimated from the particle motion of the surface wave observed in the air gun signal is roughly equivalent to the seafloor topographic data.
When the relationship between the X-axis of the OBS and the azimuth misalignment was examined, the misalignment tends to be smaller in the azimuth of the X-axis of the OBS. This suggests the influence of the seismometer installation orientation and the coupling state with the seafloor.
I would like to thank and National Research Institute for Earth Science and Disaster Prevention (NIED), Earthquake Research Institute (ERI), The University of Tokyo, and Japan Oceanographic Data Center (JODC), Japan Coast Guard, for providing data.

References
R. Iwase, Jpn. Jour. App. Phys, 55, 07KG01, 2016.
R. Takagi et al., SRL, 90(6), 2175-2187, 2019.

Keywords: S-net, particle motion, transmitted wave

©2020. Japan Geoscience Union. All Right Reserved.

Analysis of Seismic Waves from Continuous and Controlled Seismic Signal System in Kyushu Area

*Ryosuke Matsuura[1], Tatsunori Ikeda[2,3], Takeshi Tsuji[1,2,3], Koshun Yamaoka[4]

1. Cooperative Program for Resources Engineering, Kyushu University, 2. Department of Earth Resources Engineering, Kyushu University, 3. International Institute for Carbon-Neutral Energy Research (I2CNER), Kyushu University, 4. Earthquake and Volcano Research Center, Graduate School of Environmental Studies, Nagoya University

One of the methods to continuously monitor the underground is to use Accurately Controlled Routinely Operated Signal System (ACROSS). By mechanically spinning a weight, this apparatus continuously emits artificial seismic waves, which allows us to know the precise seismic velocity change between the ACROSS and seismometers. By monitoring the difference, underground movements such as earthquakes and volcanic activities can be linked to velocity change, which leads to prediction of such disasters. In this research, we focused on observing P-waves and S-waves which arrived the seismometers located around the ACROSS. Using weight stacking, we stacked maximum 119 days of data to distinguish ACROSS signal from random noises, weighing the signal according to the quantity of noise. By taking the motion of certain direction from the transfer function, different types of waves can be separated, making it easier to analyze in detail. We also investigated signal to noise ratio to clarify how far the signal travels. The result indicates that seismic waves from small-sized ACROSS in Kuju area can be observed 50-100 km far away, and seismic waves becomes clear enough to detect velocity change with 20 days of stacking in stations 10-30 km away. The results of ray tracing demonstrated that observed P-waves can be used to image and monitor the geothermal reservoir and the crustal seismic structure in Kyushu Island.

Keywords: Artificial seismic source, ACROSS, velocity change, SNR

©2020. Japan Geoscience Union. All Right Reserved.

Development of seismic waveform monitor application by JAVA

*Masayoshi Ichiyanagi[1], Hiroaki Takahashi[1]

1. Institute of Seismology and Volcanology, Graduate School of Science, Hokkaido University

Aftershock activity, earthquake swarm and volcanic earthquakes occur continuously. Easy waveform monitoring system is required for real time monitoring everywhere during field work. We have developed an application system that can display continuous seismic waveforms in real time. This system was developed in JAVA language and does not depend on the operating system of computer system. It can run, therefore, on any laptop computers (Windows, Mac OS, etc.).
Waveform data recorded at seismic station are sent every second to data center at universityby WIN binary format (Urabe, 1994). Next, every minute binary data file is created using every second data packet. Finally, every minute binary data is converted to text format and stored to file server system. Our system can read simple text data because it can be applicable for any binary format.
By starting this system on the client personal computer, data is automatically downloaded from the file server and a continuous seismic waveform is displayed on screen.Data is updated automatically every minute by accessing to data file server. Waveforms of two stations can be displayed simultaneously on one JAVA window screen. Seismic station can be selected with the mouse from the selection screen. It is also possible to change the amplitude of the seismic waveform, and to display re-scaled waveform for the previous 30 minutes.
This system can also display long term data, e.g. crustal deformation data such as strain, tilt meter and tide gauges. Display time can be extended up to 48 hours. Simultaneous display of seismic and crustal deformation data on a screen is easily realized. In addition, any text format time series data can be applicable to this system.
Our new system provides easy real-time monitor tool in seismic activity, volcano activity, tsunami waveform, etc. Real-time earthquake monitoring is very important and necessary for risk management in the dangerous field work of earthquake and volcano observation. Our system is in operation stably in field observation and daily earthquake monitoring in Hokkaido University.

Keywords: Seismic waveform, Monitor, JAVA

©2020. Japan Geoscience Union. All Right Reserved.

Yet another module for reading WIN format data in ObsPy

*Shigeki Nakagawa[1], Aitaro Kato[1]

1. Earthquake Research Institute, the University of Tokyo

The ObsPy (Beyreuther *et al*., 2010) is one of the common tools for processing seismic data. This tool can treat various formats of seismic data, of course including the WIN format. However, the original module for reading the WIN format data has some issues. The issues are: 1) bugs in decoding 0.5 bytes and 3 bytes compression data, 2) not treated properly with missing data and variable sampling rates, and 3) too slow. The third issue is a very serious problem reading large volume waveform datasets. For example, it takes 80 seconds to read a WIN format file containing 3000 channels data with one minute length. Major cause of these issues is that this original module was created by pure Python. Therefore, we have implemented yet another module for reading WIN format data. Features of our new module are: 1) reading the WIN format data and outputs the ObsPy Stream object, and 2) resolves above three issues in the original module. Calling shared libraries from Python is a typical technique to wrap the native libraries and improve execution times. Uehira *et al*. (2010) introduced shared libraries into the WIN system. The "libwinsystem.so" shared library provides various functions for reading or writing the WIN format data. Using this library for decoding the WIN compressed data in our module was effective in solving the first and third issues. To deal with second issue, when the gap of time stamps or sampling rates was found, our module separates waveform data properly. Reading a WIN format file using our module is about 8 times faster than the original module. We are planning to open our module to the public.

References:
1) Beyreuther, M., R. Barsch, L. Krischer, T. Megies, Y. Behr and J. Wassermann (2010), ObsPy: A Python Toolbox for Seismology, SRL, 81(3), 530-533.
2) Uehira, K., T. Urabe, T. Tsuruoka and S. Nakagawa (2010), 64-bit compatibility of WIN system, SSJ Fall Meeting, C11-08.

Acknowledgements: This study was partially supported by the MEXT of Japan, under its The Second Earthquake and Volcano Hazards Observation and Research Program (Earthquake and Volcano Hazard Reduction Research), and by JST CREST Grant Number JPMJCR1763, Japan.

Keywords: WIN system, ObsPy

©2020. Japan Geoscience Union. All Right Reserved.

Calibration of broadband seismographs based on the teleseismic records

*Takeshi Kimura[1]

1. National Research Institute for Earth Science and Disaster Resilience

Broadband seismometer data are essential for the development of seismological studies such as those investigating earthquake sources and the Earth’ s structure. However, previous studies [e.g., Kimura eta l., 2015] have revealed that the metadata describing these data can possibly be contaminated by instrumentation response errors that are often difficult to recognize from visual waveform checks. Herein, we report on the development of a method to calibrate the instrumentation responses from recording ground motions in observation networks whose station intervals are smaller than 200 km.

The method is based on comparisons between teleseismic surface wave records at a target station and those at multiple surrounding reference stations, from which we estimate the corner period, damping factor and sensitivity in the instrumentation response at the target station. We applied the method to F-net broadband seismometers in Japan.

For STS-1 seismometer of vertical component at TMR station, we could not recognize obvious errors in the corner period and sensitivity. However, the damping factor had increased gradually since 2005 and reached about 2.0 in 2011. After the leveling of the seismometer in November 2011, the damping factor returned to about 0.7. For STS-2 seismometer of vertical component at SHR station, the sensitivity had been about half of the normal value from start of the observation to September 2012. After the replacement of the host-box, the sensitivity settled at normal value.

The estimated calibration values will be useful for the various research using the broadband seismometer data.

Keywords: broadband seismograph, calibration, quality-control

©2020. Japan Geoscience Union. All Right Reserved.

DEVELOPMENT OF CLOUD-TYPE MICROTREMOR OBSERVATION SYSTEM

*Shigeki Senna[1], Atsushi Wakai[1]

1. National Research Institute for Earth Science and Disaster Resilience

1. Introduction

In order to sophisticate seismic hazard maps, it is essential to construct highly accurate subsurface structure models. However, in addition that it costs immensely on boring surveys and seismic reflection surveys, it is very difficult to collect subsurface structure data in wide area although those efforts have ever been made. On the other hand, microtremor observations have been conducted in recent years, by which seismic period characteristics and subsurface velocity structure can be estimated in accuracy to some extent except earthquake observations. A microtremor observation is a greatly useful geophysical exploration method to construct subsurface structure models for earthquake ground motion prediction. For the purpose of obtaining dynamic characteristics on ground, it is necessary to make observations of microtremor, PS logging and surface wave. However, on especially PS loggings and surface wave surveys, it is not expectable to make a lot of observations due to a lot of costs, observers skills and difficulty of interpretation for analysis results. To get over these problems, we have ever developed an analysis method, equipment and a system with which we can make a great number of observations with quality of microtremor data kept.

2. Development of the Observation System

We made a system of a process from observation to analysis so that we can efficiently make use of the analysis methods described above. The system consists of ① a microtremor meter as an observation instrument, ② a mobile device, mainly a tablet device, which can transfer data from the spot to analysis system, ③ a cloud-type analysis system which can analyze data in real-time and can deliver analysis results, ④ a database and a data format which can manage data and analysis results etc.

3. Cloud-type Analysis System

Data registered in a database need to be automatically quality checked and analyzed, and then S wave velocity structure obtained from analysis results need to be delivered and checked with map information by using WEBGIS etc. Also, in order to confirm data quality check and analysis results on sites, it is necessary to analyze data transferred to a database in nearly real time and to make it possible to browse analysis results.

For realizing these requirements, it is our challenge to create an application for a smartphone and a &sbquocloud-type analysis system&sbquo which can rapidly conduct quality check and analysis of microtremor data. An application for a smartphone enables us to receive data in real time and to conduct quality check of data such as wave, spectra check and simple SN ratio management of microtremor, by using functions of &sbquoiBidou&sbquo. While, a cloud analysis system enables to conduct detailed analysis and quality check for received data, to estimate S wave velocity structure using the conventional analysis method almost automatically and to deliver analysis results within a few minutes. It is expected that this cloud system enables us to obtain analysis results from twenty to ten hundred times more rapidly than the normal system.

4. Conclusion

This system has a mechanism that human errors decrease on registration of location information, photos,

©2020. Japan Geoscience Union. All Right Reserved.

observation data, raw observed records and analyzed results because data registration and analysis etc. are completed on sites. By the mechanism, we can lend most of national institutes, which cannot conduct a research in spite of their willingness to observations due to expensive seismometers and beginners in the observation. In the future, increase of observer base, homogenization of data and acquisition of so many data can be the basis to create more accurate seismic hazard maps or earthquake susceptibility maps across the country.

Keywords: Microtremors, S wave velocity structure, Cloud system, Array observation

©2020. Japan Geoscience Union. All Right Reserved.

Development of underground structure information analysis cloud system

*Shigeki Senna[1]

1. National Research Institute for Earth Science and Disaster Resilience

NIED has been constructing shallow and deep integrated ground models of 250m mesh units in 11 prefectures in the Kanto, Tokai and Kumamoto regions. Construction of a ground model requires a huge amount of data collection and model creation time, and it is difficult to create and verify a wide-area model without an efficient mechanism for modeling. In constructing this ground model, the following items are considered to be the most important items.

① Collection of basic ground data for building a ground model

② Standardization of ground data format and creation of database

③ Establishment of ground modeling method that can be automated and mechanism of automatic generation

④ Verification and correction of the created ground model

These four items do not function if they exist independently. By systematizing the four items as one system, it becomes possible to efficiently construct a ground model that can reproduce the same model no matter who models it. Also, it is difficult to model a wide area even if one of the above items is missing. In order to construct a nationwide ground model, NIED has constructed an underground structural information analysis cloud system that systematically organizes the above four items.

This cloud system uses a standard format of digital data related to the construction of ground models such as boring data, microtremor observation / analysis result data, ground models created based on local government earthquake damage assumptions, land use maps, seamless geological maps, and DEM data. It is possible to construct a ground model such as a 250m mesh or a 50m mesh based on the ground model construction method authorized by the earthquake headquarters. Modeling can also be verified from the constructed ground model and seismic and microtremor observation records (S-wave velocity and dominant period).
In the future, in order to further improve this system, we plan to promote the use of AI so that high-quality models can be constructed from a small amount of data.

Keywords: Underground structure model, Cloud type system, Geological survey data

©2020. Japan Geoscience Union. All Right Reserved.

[E] Poster | S (Solid Earth Sciences)：S-TT Technology & Techniques

[S-TT52] Seismic Big Data Analysis Based on the State-of-the-Art of Bayesian Statistics

convener:Hiromichi Nagao(Earthquake Research Institute, The University of Tokyo), Aitaro Kato(Earthquake Research Institute, the University of Tokyo), Keisuke Yano(The University of Tokyo, Graduate School of Information Science and Technology), Takahiro Shiina(Earthquake Research Institute, The University of Tokyo)

Recently, a big seismic database has been being constructed that collects data of vibrators implemented in such as buildings, lifelines and smartphones, in addition to seismic data of the conventional continuous/temporal dense seismic observation arrays. Development of methodologies and algorithms, which are inadequate at this moment, optimized to comprehensively analyze the seismic big data is essential in order to utilize the big database as much as possible for prevention/mitigation of earthquake disasters and clarification of earthquake phenomena. On the other hand, recent progress of Bayesian statistics is significant, which is the mathematical basis of various methodologies, such as machine learning, especially deep learning, to extract valuable information from big data. The state-of-the-art of Bayesian statistics is expected to substantially advance seismic big data analyses.
This session mainly accepts presentations that focus on analyses of seismic big data, especially related to analysis methods based on Bayesian statistics such as machine learning, sparse modeling and data assimilation, and their applications to real seismic data. Presentations related to mathematical or statistical theories beneficial to data analyses, feasibility studies of algorithms eventually applicable to real seismic data, and the current status of seismic observations and analysis results are also highly welcome.

[STT52-P01] Comprehensive analysis of deep low-frequency earthquakes in 52 regions all over Japan

*Ryo Kurihara[1], Kazushige Obara[1] (1.Earthquake Research Institute, The University of Tokyo)

[STT52-P02] An application of reversible-jump MCMC method for simultaneous determinations of 1-D velocity structures and hypocenters around a fault (I): Formulation

*Masayuki Kano[1], Takahiro Shiina[2] (1.Graduate school of science, Tohoku University, 2.Earthquake Research Institute, The University of Tokyo)

[STT52-P03] An application of reversible-jump MCMC method for simultaneous determinations of 1-D velocity structures and hypocenters around a fault (II): Synthetic analyses

*Takahiro Shiina[1], Masayuki Kano[2] (1.Earthquake Research Institute, The University of Tokyo, 2.Graduate School of Science, Tohoku University)

[STT52-P04] A Bayesian seismic tomography adapted to discontinuities

*Sumito Kurata[1], Naoya Takakura[1], Keisuke Yano[1], Fumiyasu Komaki[1] (1.Graduate School of Information Science and Technology, The University of Tokyo)

[STT52-P05] Multi-mode surface wave tomography with trans-dimensional hierarchical Bayesian inversion: application to Australia

*Kazunori Yoshizawa[1,2], Toru Taira[2] (1.Faculty of Science, Hokkaido University, 2.Graduate School of Science, Hokkaido University)

[STT52-P06] Twin Experiment of 4DVar Capable of Uncertainty Quantification Based on Seismic Wavefield Propagation

*Hiromichi Nagao[1,2], Shin-ichi Ito[1,2], Masayuki Kano[3], Mitsuru Matsumura[4] (1.Earthquake Research Institute, The University of Tokyo, 2.Graduate School of Information Science and Technology, The University of Tokyo, 3.Graduate School of Science, Tohoku University, 4.CJS Inc.)

[STT52-P07] On the Optimum Solutions of Bayesian Inversions

*Daisuke Sato[1], Yukitoshi Fukahata[1] (1.Disaster Prevention Research Institute, Kyoto University)

[STT52-P08] Towards application of data-driven sparse sensor placement technique developed in fluid mechanics to seismology

*Takayuki Nagata[1], Keigo Yamada[1], Yuji Saito[1], Taku Nonomura[1], Keisuke Asai[1] (1.Tohoku University)

Comprehensive analysis of deep low-frequency earthquakes in 52 regions all over Japan

*Ryo Kurihara[1], Kazushige Obara[1]

1. Earthquake Research Institute, The University of Tokyo

In the most volcanic regions all over Japan, deep low-frequency (DLF) earthquakes occur at depths of 10–50 km in which regular crustal earthquakes rarely occur. The dominant frequencies of DLF earthquakes are about 1–10 Hz, which is lower than those of regular earthquakes with similar magnitudes. DLF earthquakes near volcanoes are considered to be affected by fluid in the lower crust because they often occur in or around of low-velocity anomalies (e.g. Hasegawa et al., 2005). However, generating mechanism of DLF earthquakes and relationship with the surrounding structure are still unknown because hypocenters of DLF earthquakes do not have a good resolution due to their weak signals. Kurihara et al. (2019 SSJ) analyzed DLF earthquakes all over Japan based on relocation analysis using network correlation coefficient method (Ohta and Ide, 2011), classification using waveform correlation, and detection using matched filter technique. In results, for example in Hijiori, northeastern Japan, we showed that hypocenters of DLF earthquakes concentrate into some small isolated groups with separations of several kilometers in the vertical direction. Temporal activity patterns of DLF earthquakes are different in each group; in other words, there are both groups in which DLF earthquakes constantly occur and episodically occur. As like Hijiori, discrete distributions of groups of DLF earthquakes were also observed in many other volcanoes.

In this study, as for quantifying temporal activity patterns of DLF earthquakes, we defined an index “swarm ratio (SR)” for each group of all regions which show the ration of swarm DLF earthquakes and generally classified the activity patterns in 52 regions all over Japan. SR means the ratio of swarm DLF earthquakes out of all DLF earthquakes in the groups. Swarm DLF earthquakes were defined as the DLF earthquakes. Swarm DLF earthquakes are defined when 10 or more earthquakes occur with the shorter interval from the former earthquake than the expected interval time of the group.
In many regions especially in Tohoku district, only the groups of DLF earthquakes with SR lower than 0.7 in which DLF earthquakes constantly occur were observed. On the other hand, 12 regions, such as Yakedake and Ontake, included groups with high SR values over 0.7 that shows episodic occurrences of DLF earthquakes. In addition, magnitude-frequency distributions show that groups with episodic DLF earthquakes have high b-value in Gutenberg-Richter law compared to groups with constant DLF earthquakes. These results suggest that episodic DLF earthquakes may repeatedly occur in the concentrated same smaller-scale sources and constant DLF earthquakes may occur in some different sources.

Keywords: Deep low-frequency earthquakes

©2020. Japan Geoscience Union. All Right Reserved.

An application of reversible-jump MCMC method for simultaneous determinations of 1-D velocity structures and hypocenters around a fault (I): Formulation

*Masayuki Kano[1], Takahiro Shiina[2]

1. Graduate school of science, Tohoku University, 2. Earthquake Research Institute, The University of Tokyo

Locations of earthquakes are one of the fundamental information in seismology. To determine hypocenters, a one-dimensional (1-D) velocity model, such as the JMA2001 1-D velocity model [Ueno et al., 2002], is routinely used. In the case of local seismic swarm activities, such as aftershocks of a large earthquake, a local 1-D velocity model is often constructed. Although a single 1-D velocity model was conventionally adopted for the source area of the swarm, it was reported that two or more 1-D velocity models can accurately estimate location of hypocenters when earthquakes occur at around a structural boundary [e.g., Sakai et al., 2004]; that is, seismic velocities change across the source area. Since such structural boundary often act as a slip plane of a large earthquake, preliminary understandings for the earthquake and monitoring of its aftershocks will improve by utilizing several local 1-D velocity models.

A 1-D velocity model is generally constructed based on seismological and/or geological knowledge [e.g., Sakai et al., 2004]. Three-dimensional analyses, i.e., tomographic inversion, would detect those heterogeneous structures if a large amount of seismological observations were obtained. In other words, with small dataset of seismic records, it is difficult to know a presence of structural boundary and velocity structures of each seismological/geological unit around a fault without obvious surface exposure of them. Therefore, in our series of presentation (this study and Shiina and Kano [this meeting]), we propose a Bayesian-based approach for simultaneous determination of hypocenters of earthquakes and 1-D velocity structures around a fault. Additionally, our approach assigns each station to a specific velocity model.

This study uses a reversible-jump Markov chain Monte Carlo (rj-MCMC) method to estimate 1-D velocity models and hypocenters of earthquakes. In an analysis of seismic velocity structure of Earth’s interior, the rj-MCMC method can change a number of discrete units, i.e., grid, block, or layer, and investigate P- and S-wave velocities of the discrete units. Bodin and Sambridge [2013] adopted this method to estimate a two-dimensional velocity structure. Based on their formulation, we developed the rj-MCMC approach; layered velocity structures and hypocenters are simultaneously determined when given a number of 1-D velocity models.

In this presentation, we will summarize formulations of the developed method in detailed. An application of this method for synthetic data sets will be summarized by Shiina and Kano [this meeting].

©2020. Japan Geoscience Union. All Right Reserved.

An application of reversible-jump MCMC method for simultaneous determinations of 1-D velocity structures and hypocenters around a fault (II): Synthetic analyses

*Takahiro Shiina[1], Masayuki Kano[2]

1. Earthquake Research Institute, The University of Tokyo, 2. Graduate School of Science, Tohoku University

Our series of presentation (this study and Kano and Shiina [this meeting]) proposes an approach that can simultaneously estimate one-dimensional (1-D) velocity models and hypocenters based on a reversible-jump Markov chain Monte Carlo (rj-MCMC) method. A location of earthquake is routinely determined by using locally optimized 1-D velocity model, such as the JMA2001 1-D velocity model [Ueno et al., 2002]. Meanwhile, two or more 1-D velocity model can improve estimation accuracy of hypocenters of which earthquakes occur at around structural boundary [e.g., Sakai et al., 2004].
As described in Kano and Shiina [this meeting], we developed the rj-MCMC method for determining hypocenters and structures when a number of 1-D velocity models is given. In this presentation, therefore, we evaluate the developed method by using synthesized data sets that derived from two 1-D velocity models. Since the rj-MCMC requires only travel times between an earthquake and a receiver, we employ fast-marching method [e.g., Sethian and Popovici, 1999; Rawlinson and Sambridge, 2004] for travel time calculations. Note that a rj-MCMC-based estimations of 1-D velocity model and hypocenters had been suggested [e.g., Ryberg and Haberland, 2019]. However, the previous studies for the 1-D case mainly handled earthquakes which widely distributed in the targeted area. We thus discuss advantages and shortenings of the rj-MCMC method to simultaneous determinations of hypocenter and single 1-D velocity model for concentrated hypocenters, i.e., seismic swarms and aftershocks of a large earthquake.

Keywords: Hypocenter, 1-D velocity structure, rj-MCMC

©2020. Japan Geoscience Union. All Right Reserved.

A Bayesian seismic tomography adapted to discontinuities

*Sumito Kurata[1], Naoya Takakura[1], Keisuke Yano[1], Fumiyasu Komaki[1]

1. Graduate School of Information Science and Technology, The University of Tokyo

Seismic tomography is an analysis method to estimate subsurface structures of the Earth using arrival times of earthquakes. In this study, we introduce two procedures to estimate velocity structures under western North America on the basis of arrival times of P-waves.
We divide subsurfaces into meshes with different seismic velocities. We consider associations among the meshes in the estimation of velocity parameters. Velocity structures are broadly continuous but change drastically along the discontinuity such as Moho and Conrad. In addition, they change largely along the boundary between land and sea. Therefore, we first adopt Bayesian estimation with the prior distribution accommodating such information.
We second introduce a regularization to estimate behavior of velocity structures around discontinuities more sharply. We apply a network Lasso-type regularization to estimate velocity parameters. We use the regularization term which penalizes difference of velocity parameters among adjacent meshes. With this effect, similar velocities will be smoothed, on the other hand, sharp changes of velocity will be emphasized.
The resulting velocity structure can capture change points of velocities more clearly. We compare our procedure with the existing tomography through numerical studies.

Keywords: Seismology, Seismic tomography, Bayesian statistics

©2020. Japan Geoscience Union. All Right Reserved.

Multi-mode surface wave tomography with trans-dimensional hierarchical Bayesian inversion: application to Australia

*Kazunori Yoshizawa[1,2], Toru Taira[2]

1. Faculty of Science, Hokkaido University, 2. Graduate School of Science, Hokkaido University

Seismic surface waves are primary information sources for three-dimensional mapping of the crust and upper mantle. Most of the structural mapping for shear wave speed models in the crust and upper mantle has been based primarily on the linearized inversions of surface wave dispersion data. Such linearized inversions, however, involve intrinsic limitations, such as the influence of *a priori* constraints and the entrapment into local minima. With the increasing computational power, a fully nonlinear approach based on the model parameter search with the Markov chain Monte Carlo method is now feasible.

In this study, we employ the trans-dimensional hierarchical Bayesian (TDB) inversion to construct a new 3-D radially anisotropic S wave model in the Australian upper mantle, which requires almost no subjective *a priori* information. We use multi-mode phase speed maps in Australia by Yoshizawa (2014), and the local dispersion curves of multi-mode Love and Rayleigh waves are inverted for extracting the probability density functions of radially anisotropic S wave model. This process is repeated for all the grid points in our target region, which eventually produce a 3-D shear wave model.

The TDB approach requires significant computational power compared with the classical linearized inversions, i.e., several thousand times more CPU time is required in our case to evaluate more than a million models. Still, it enables us to flexibly parameterize the model parameters (i.e., the number of layers in this case, and data uncertainties can also be handled properly through the hierarchical Bayesian approach.

Through the comparisons of our new 3-D model from TDB approach with our earlier 3-D model from a conventional linearized inversion, we have found that the large-scale features are mostly consistent between these models. However, our new TDB model shows the enhanced strength of heterogeneity and well-resolved spatial distribution of seismic anisotropy, which well reflects the past and current tectonics of the continental upper mantle. In particular, the vertical change in shear wave speeds can be well constrained in the TDB model by the use of the trans-dimensional parameterization, and the data fit to dispersion curves are improved by the use of the hierarchical Bayes approach.

Keywords: surface wave, tomography, Bayesian inversion, anisotropy, Australia

©2020. Japan Geoscience Union. All Right Reserved.

Twin Experiment of 4DVar Capable of Uncertainty Quantification Based on Seismic Wavefield Propagation

*Hiromichi Nagao[1,2], Shin-ichi Ito[1,2], Masayuki Kano[3], Mitsuru Matsumura[4]

1. Earthquake Research Institute, The University of Tokyo, 2. Graduate School of Information Science and Technology, The University of Tokyo, 3. Graduate School of Science, Tohoku University, 4. CJS Inc.

The four-dimensional variational method (4DVar) is a data assimilation technique widely used especially in the case of a massive numerical simulation model such as weather forecasting. The conventional 4DVar only optimizes parameters and initial conditions of time series but never evaluates their uncertainties. We proposed a new 4DVar that evaluated the uncertainties after obtaining the optima [Ito, Nagao et al., Phys. Rev. E, 2016]. The key technique in the new 4DVar is the second-order adjoint method, which obtains the product of a Hessian matrix and a given vector avoiding a direct computation of the Hessian matrix.

We verify this new 4DVar by applying it to an issue of seismic wave propagation in the two-dimensional field. The forward computation based on the wave equation is done by the finite volume method in space and the velocity Verlet method in time, which conserves the total energy during the time evolution. The periodic boundary conditions are assumed for the both horizontal boundaries of the computational domain, and the fixed boundaries are assumed for the top and bottom of the domain. The set of adjoint models is solved by a time integrator that enables an exact computation of Hessian-vector product without any discretization errors [Ito et al., 2019].

We report the result of this verification through a twin experiment that checks whether the new 4DVar properly estimates true values of parameters assumed in advance and quantifies their uncertainties.

Keywords: data assimilation, seismic wave propagation, uncertainty quantification, adjoint method

©2020. Japan Geoscience Union. All Right Reserved.

On the Optimum Solutions of Bayesian Inversions

*Daisuke Sato[1], Yukitoshi Fukahata[1]

1. Disaster Prevention Research Institute, Kyoto University

Geophysical inversions are frequently built on the Bayesian inferences. Bayesian inferences provide the posterior probability distribution function (pdf) from 1) the observation equation to relate the data and model parameters and 2) the prior distribution of the model parameters, via Bayes' theorem. The more extended approach, called fully Bayesian inference, serves a joint posterior pdf in terms of model parameters and hyperparameters, by further considering the hyperprior distribution: the prior for the hyperparameters.

The posterior pdf requires criteria for informational reductions to obtain the most reliable (optimum) model parameters. The best way of reduction is nontrivial, and the criteria can be summarized into three groups. The first is the probability maximum of the posterior pdf (maximum a posteriori, MAP). This is the most intuitive way. Another is using the probability maximum in the marginalized posterior in terms of hyperparameters, by integrating the posterior pdf over the model parameters. The optimum model parameters are then evaluated as the ordinary weighted least squares given by the selected hyperparameters. This is exactly the Akaike Bayesian information criterion (ABIC), and has been adopted in the wide classes of geophysical inversions (Yabuki & Matsu'ura, 1996). The other is using the marginalized posterior pdf in terms of model parameters, by integrating the posterior over the hyperparameters. It contains, for example, the average, the median, and the most frequent values (the mode). The last group of indices has been common for the previous fully Bayesian inferences, such as Fukuda & Johnson (2008). Therefore, we call these as fully Bayesian inferences, in contrast to MAP and ABIC.

MAP, ABIC, and previous fully Bayesian inferences give similar results in most case (e.g., Fukuda & Johnson, 2008). However, we report a clear discrepancy between them for the case of large numbers of model parameters.

First, we derived the analytic expressions of the solutions for MAP and previous fully Bayesian inferences, as well as their uncertainty represented by covariances, in the problem where the observation equation is linear in terms of model parameters. The obtained solutions clarified that any kind of the previous fully Bayesian inferences (averages, modes, medians, and so on) almost surely gives the same estimate value as the MAP estimate in the asymptote of large numbers of model parameters, for wide classes of hyperprior like the uniform distribution. The solutions of MAP and the previous fully Bayesian inferences are further shown to be different from the solution of ABIC.

Next, we employed the synthetic test to clarify the difference between ABIC and other estimates, with using the small roughness as a prior (Yabuki & Matsu'ura, 1992). The numerical investigation clarified that distribution of MAP estimates (that is the posterior pdf itself) converged to the overfitted solution for given data and the prior is neglected unfairly, as we improve the resolution of models by increasing the number of model parameters. Meanwhile, the estimate of ABIC did not induce the aforementioned problem and provided the significantly closer estimates to the true solutions than MAP estimates with fine discretization.

©2020. Japan Geoscience Union. All Right Reserved.

These are counterintuitive from the standard view where ABIC is regarded as a tractable approximation to assess the joint posterior pdf in terms of model parameters and hyperparameters (Gelman et al., 2013). The accuracy deterioration due to the overfitting in the case of the higher resolution with fewer discretization errors can be a crucial problem in the inversions for real data, where the true parameters are intrinsically unknown. Our results suggest the way of improving the ordinary fully Bayesian inferences along the way of ABIC, and warn the potential risks hidden behind the MAP and previous fully Bayesian inferences.

Keywords: Fully Bayesian Inferences, Inversion Validations

©2020. Japan Geoscience Union. All Right Reserved.

Towards application of data-driven sparse sensor placement technique developed in fluid mechanics to seismology

*Takayuki Nagata[1], Keigo Yamada[1], Yuji Saito[1], Taku Nonomura[1], Keisuke Asai[1]

1. Tohoku University

Reduced-order modeling gathers a lot of attention in fluid mechanics for fluid analysis and flow control. Proper orthogonal decomposition (POD)[1] is one of the effective methods to decompose the high-dimensional fluid data into significant modes. The dimension of the flow field data can be reduced by reconstructing the data using several selected significant modes. In addition, if the data can be effectively expressed by a limited number of POD modes as shown in Fig. 1, the limited sensor placed at appropriate positions gives us the approximated full state information as follows[2]:

$\boldsymbol{y} = \boldsymbol{HUx}$, (1)

where $\boldsymbol{y} \in \mathbf{R}^p$, $\boldsymbol{H} \in \mathbf{R}^{p \times n}$, $\boldsymbol{U} \in \mathbf{R}^{n \times r}$, and $\boldsymbol{x} \in \mathbf{R}^r$ are the observation vector, the sparse sensor location matrix, the spatial POD modes, and the POD mode amplitude, respectively. Here, p, n, and r are the number of the sensor location, degree of freedom of the spatial POD modes, and the rank for truncated POD, respectively.

Schematic diagram of Eq. (1) is illustrated in Fig. 2. This problem is considered to be one of the sensor selection problems when the POD mode $\boldsymbol{U}$ and the strength x are assumed to be a sensor-candidate matrix and the latent state variables, respectively. Obtaining $\boldsymbol{H}$ matrix corresponds to the computation for the sensor selection, and the convex approximation method[3] and the QR-based greedy algorithm[2] have been used. In our group, data-driven sparse sensor selection algorithms for the data obtained in experimental fluid dynamics have been developed. The data in the fluid dynamics is noisy high-dimensional multi-component data so that a fast and robust sensor selection algorithm is necessary to realize a real-time on-line measurement and flow control. We proposed three algorithms recently.

Fast Greedy sensor selection algorithm for the scalar data

The computational cost is a critical problem for high-dimensional data analysis. We extended the previous QR-based greedy algorithm and reduced the computational cost. In our method, the objective function of the problem was redefined to be the maximization of the determinant of the matrix appearing in pseudo-inverse matrix operation. The procedure for the maximization of the determinant of the corresponding matrix is the same as that of the previous QR-based greedy method when the number of sensors less is less than or equal to that of state variables. When the number of sensors greater than that of state variables, new sensors are calculated by a proposed determinant-based greedy method which is accelerated by both determinant formula and matrix inversion lemma.

Fast Greedy sensor selection algorithm for the vector data

The multi-component data such as velocity distributions in x and y directions frequently appear in the fluid data. The sparse sensor selection using the convex approximation algorithm for the vector data was valid, but it requires long computational time to analyze high-dimensional data due to its expensive computational cost. Therefore, we extended our determinant-based greedy algorithm, which is a much lower computational cost compared to convex approximation, for vector data.

Fast greedy sensor selection in measurement with correlated noise

The noise-robust greedy sparse-sensor-selection method based on the determinant maximization was proposed. Optimization is conducted by maximizing the determinant of the matrix which corresponds to

©2020. Japan Geoscience Union. All Right Reserved.

the inverse matrix appearing in the Bayesian estimation operator. The computational cost is slightly larger than that of the previous methods, but the estimation accuracy is much improved. We will apply and improve these methods to seismic research with the seismic research group.

References

[1] Berkooz *et al. Annu. Rev. Fluid Mech.* **25**, 539-575 (1993).
[2] Manohar *et al. IEEE cont. sys. Mag.* **38**(3), 63-86 (2018).
[3] S. Joshi and S. Boyd, *IEEE Trans. Sig. Proc.* **57**(2), 451-462 (2009).
[4] Sito *et al.*, arXiv:1911.08757 (2019).
[5] Saito *et al.*, arXiv:1906.00778 (2019).
[6] Yamada *et al.*, arXiv:1912.01776 (2019).

Keywords: data-driven science, sparse sensor

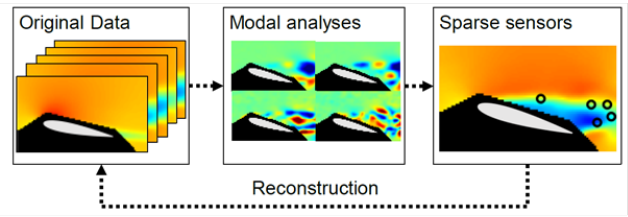


Figure 1 Schematic diagram of the present study.

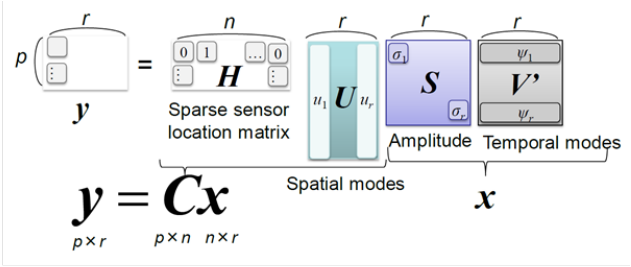


Figure 2 Schematic diagram of the sensor placement problem.

©2020. Japan Geoscience Union. All Right Reserved.

[E] Poster | S (Solid Earth Sciences)：S-TT Technology & Techniques

[S-TT53] Airborne surveys and monitoring of the Earth

convener:Shigekazu Kusumoto(Graduate School of Science and Engineering for Research, University of Toyama), Takao Koyama(Earthquake Research Institute, The University of Tokyo), Yuji Mitsuhata(AdvancedIndustrial Science and Technology), Shigeo Okuma(Geological Survey of Japan, National Institute of Advanced Industrial Science and Technology (AIST))

Airborne surveys are useful to better understand the whole and/or the detailed structures of the Earth and their variations. They can be implemented from a traditional manned and newly-developed unmanned aircraft to efficiently map very large or remote areas with difficult access. We invite studies on theory, instrumentation, processing, modeling or inversion and applications of airborne surveys.

[STT53-P01] Repeated droneborne magnetic survey in Iwoyama, Kirishima volcano

*Takao Koyama[1], Atsushi Watanabe[1], Takayuki Kaneko[1], Takao Ohminato[1], Yoshiaki HONDA[2] (1.Earthquake Research Institute, The University of Tokyo, 2.Center for Environmental Remote Sensing, Chiba University)

[STT53-P02] Utilization of Beta Angle for Detecting Edges in Potential Field Methods

*Tamer Mahmoud Ragab Farag[1,2], Remon Aziz[3,2], Hidiki Mizunaga[1] (1.Exploration Geophysics lab, Earth Resources Engineering Department, School of Engineering, Kyushu University, 2.Exploration Sector, Nuclear Materials Authority, 3.Center for Northeast Asian Studies, Tohoku University)

[STT53-P03] Three Dimensional Geophysical Inversion of Airborne Magnetic Data from the Yellowstone National Park (YNP), Western North America

*Mohammad Shehata[1,2], Hideki Mizunaga[2] (1.Department of Geology, Faculty of Science, Port Said University, Egypt, 2.Department of Earth Resources Engineering, Faculty of Engineering, Kyushu University, Japan)

[STT53-P04] Development of a multiband uncooled infrared cameras system for imaging volcanic sulfur dioxide (SO_2) gas

*Tetsuya Jitsufuchi[1] (1.National Research Institute for Earth Science and Disaster Resilience)

[STT53-P05] Topographic changes in Kirishima Iwo-yama volcanic area obtained by UAV photogrammetry

*Yuichi Iwasa[1], Takeshi Matsushima[2] (1.department of earth and planetary sciences, graduate school of sciences, Kyushu University, 2.Institute of Seismology and Volcanology, Faculty of Sciences, Kyushu University)

Repeated droneborne magnetic survey in Iwoyama, Kirishima volcano

*Takao Koyama[1], Atsushi Watanabe[1], Takayuki Kaneko[1], Takao Ohminato[1], Yoshiaki HONDA[2]

1. Earthquake Research Institute, The University of Tokyo, 2. Center for Environmental Remote Sensing, Chiba University

In Mt. Iwoyama, Kirishima, volcanic tremors have occurred since the end of 2013, and then some fumaroles are observed. A small phreatic eruption has occurred in the south of the edifice on 19th April 2018, in which the last eruption has occurred about 250 years ago. According to geodetic deformation measurements, inflation of the edifice was detected. The pressure source location is inferred at about 1km below the surface. Also, according to MT surveys, a clay layer is detected in the shallow area due to hydrothermal alteration. Therefore, the phreatic explosion may have happened due to vaporization of volcanic fluid through cracks of the clay layer (Tsukamoto et al., 2018). It is important to observe thermal change and gas emission at such a crack prior to explosions in order to understand the process of the phreatic explosion.

We have conducted high-resolution aeromagnetic survey by drone in Iwoyama in last May. In our survey, the DJI Matrice 600 Pro multicopter is used and Geometrics G-858 cesium optical pumping magnetometer is installed on it. The magnetic sensor is hung down at 5m from the drone. A GNSS receiver with barometric altimeter is also installed in order to correct the time and measure the position. It totally flew more than 15 km by 10 flights in a half of days. The flight courses were programmed prior to flights, and thus they can be reused again in the future surveys, and retrieve geomagnetic data along the same course.

We have carried out flights in 50 m and 100 m above the surface. In the west of survey area, geomagnetic total intensity anomaly by 750 nT at 50 m above and 500 nT at 100 m above were found. In the east, which is just above the Mt. Iwoyama, the anomalies are 400 nT at 50 m above and 100 m above. It indicates that demagnetization is occurred beneath the Mt. Iwoyama as inferred.

We conducted survey again in last December on the same flight courses which are programmed in a drone, in order to detect the temporal variation of magnetic intensity of the edifice. It, however, does not show significant changes, and it indicates that thermal condition beneath Iwoyama is not activated recently.

Droneborne survey has a potential to be a powerful tool to monitor a thermal condition beneath the volcano.

Keywords: aeromagnetic survey, drone, Iwoyama, Kirishima volcano

©2020. Japan Geoscience Union. All Right Reserved.

Utilization of Beta Angle for Detecting Edges in Potential Field Methods

*Tamer Mahmoud Ragab Farag[1,2], Remon Aziz[3,2], Hidiki Mizunaga[1]

1. Exploration Geophysics lab, Earth Resources Engineering Department, School of Engineering, Kyushu University, 2. Exploration Sector, Nuclear Materials Authority, 3. Center for Northeast Asian Studies, Tohoku University

Gravity and magnetic methods are potential field methods in exploration geophysics. Gravity method measure lateral variation in densities whereas magnetic method measures the lateral variation in magnetic susceptibility. One of the complications of interpretation of magnetic data is the displacement or skewness as a result that the geomagnetic field is not vertical in general. Depth, lateral variation of physical property, dipping angle, thickness and magnetic field inclination are important parameters affecting the shape and orientation of the anomalies. They make the qualitative interpretation specially for regional scale surveys (marine or airborne) very difficult. The magnetic anomaly over the causative body depends on latitude because of the dipolarity nature of the geomagnetic field in addition to the remnant magnetization of every magnetic source. Sources and edges detection is the first and one of the most important qualitative interpretation step of potential field methods in geophysics. A lot of methods were developed to delineate the edge of the subsurface bodies cause anomalies in gravity and magnetic based on the derivative in X, Y and Z directions. Total horizontal derivative, analytical signal and TDX revels the maximal of the source body edges. Whereas tilt angle and theta angle were developed to detect the maxima of the causative body. Beta angle has been developed to detect the source body and its edges depending on the derivatives in X, Y and Z directions. Beta angle is the angle between the analytical signal and the derivative in Z direction. It is narrower than tilt angle and marks the body edges sharper. Beta angle shows the magnetic anomalies with sharp edges. Beta angle has a range from $-\pi/2$ to $\pi/2$. Beta angle has been applied to airborne magnetic data and the result compared with THD, AS, Tilt angle, TDX and theta map. Beta angle map can delineate the different magnetic anomalies sources with sharp edges

Keywords: Edge detection, Potential field, Beta Angle, Magnetic, Gravity

©2020. Japan Geoscience Union. All Right Reserved.

Three Dimensional Geophysical Inversion of Airborne Magnetic Data from the Yellowstone National Park (YNP), Western North America

*Mohammad Shehata[1,2], Hideki Mizunaga[2]

1. Department of Geology, Faculty of Science, Port Said University, Egypt, 2. Department of Earth Resources Engineering, Faculty of Engineering, Kyushu University, Japan

Yellowstone National Park (YNP) displays numerous and extensive hydrothermal features. Airborne Total Magnetic Intensity (TMI) data of the area was acquired from the USGS. TMI data was processed and Reduce-to-Pole (RTP) map was produced. Analytic Signal (ASA) and Theta map filters were applied to the magnetic data to delineate the structural Lineaments of the magnetic sources. Three dimensional geophysical inversion was applied to the magnetic data using the algorithms of Li and Oldenburg (1996), the inversion reveals the 3-D distribution of the magnetic susceptibility for a depth of few kilometers which delineate the alteration zones of the geothermal system in the area. The inversion parameters were selected to fit both the resolution of subsurface model and calculation capacity of the running computer. The boundary of Yellowstone caldera was delineated efficiently from the ASA and Theta maps. Inversion results show that the hydrothermal zones coincide with magnetic lows observed in aeromagnetic surveys, which suggests a strong demagnetization of both the shallow and deep substratum within these areas associated with the removal of magnetic minerals by hydrothermal alteration processes over a thickness of a few hundred meters in hydrothermal areas at YNP, and that the maximum degree or maximum thickness of demagnetization correlates closely with the location of hydrothermal activity and mapped alteration.

References

Li, Y., and Oldenburg, D. W. (1996). 3-D inversion of magnetic data. *Geophysics*, **61**(2), 394-408

Keywords: Yellowstone National Park YNP, magnetic inversion, hydrothermal alteration

©2020. Japan Geoscience Union. All Right Reserved.

Development of a multiband uncooled infrared cameras system for imaging volcanic sulfur dioxide (SO_2) gas

*Tetsuya Jitsufuchi[1]

1. National Research Institute for Earth Science and Disaster Resilience

National Research Institute for Earth Science and Disaster Resilience (NIED) launched the “Development of Remote Sensing Techniques for Surface Phenomena of Volcano” under the “Promotion Project for Next Generation Volcano Research Theme B subtheme 2 subtopic 2-2” in October 2016. The objective of this project is to develop a surface phenomenon imaging camera (SPIC), which combines the advantages of current airborne spectral imaging systems, visible-light cameras, and infrared cameras so that it can be used for both on-ground and oblique observations from helicopters. Under this project, we are planning to develop a new observation device called a surface phenomena imaging camera with uncooled infrared camera (SPIC-UC). In this study, we present first results of the development for SPIC-UC prototype. The SPIC-UC is planned to realize a highly cost-effective device used to measure the temperature and SO_2 gas concentration distributions by selecting an uncooled microbolometer focal plane array (FPA) to measure the long wave infrared regions (LWIR, 8000–14000 nm). To realize SPIC-UC, we prototyped a multiband uncooled infrared cameras system by adopting an uncooled VGA camera sensor (uncooled microbolometer) with built-in spectral filters. The prototyped cameras constitute a twin-lens camera system (capable of synchronous measurement) consisting of Camera 1 and Camera 2, with the following specifications: filters built in Camera 1 will have a transmission bandwidth for wavelengths of 9000 nm or more and those built in Camera 2 will have a transmission bandwidth for wavelengths between 8370 and 8920 nm, which much to the infrared light absorption region of SO_2 gas. The performance evaluations for the prototyped camera system revealed that it can achieve a NETD of approximately 0.6 K for blackbody temperatures of 0–81 ˚C in the ambient temperature range of -10 to 50 ˚C and that they can detect SO_2 gas concentration distributions of 1 to 2 ppmv or more at normal temperature in the background conditions of 50 ˚C or more. These results indicate that the proposed cameras can be a prototype SPIC-UC system.

Keywords: uncooled infrared camera, SO2 gas, volcano observations

©2020. Japan Geoscience Union. All Right Reserved.

Topographic changes in Kirishima Iwo-yama volcanic area obtained by UAV photogrammetry

*Yuichi Iwasa[1], Takeshi Matsushima[2]

1. department of earth and planetary sciences, graduate school of sciences, Kyushu University, 2. Institute of Seismology and Volcanology, Faculty of Sciences, Kyushu University

Aerial photogrammetry using UAV(Unmanned Aerial Vehicle) is a speedier, cheaper, and safer method than conventional topographic surveying methods, and has been spread rapidly in recent years. This can be utilized in active volcano observation, but there are still few examples.

In this study, We conducted mission flight by UAV in Kirishima Iwo-yama located Ebino city, Miyazaki prefecture before and after the phreatic eruption in April 2018. Then, the eruption area was three-dimensional modeled by aerial photogrammetry.

While the model before the eruption was successfully constructed, in the constructed model after eruption, a gap has occurred due to the effect of the fumarole. This is one of problems of UAV photogrammetry in active volcano. In this study, to resolve this problem, adding to the conventional nadir photography, the oblique photography from the low altitude was carried out again in November 2019. As a result, the model after the eruption could be constructed without the gap.

By comparing the model before and after the eruption, it was suggested that the local uplift detected by InSAR may be observed in the central part of survey area. In the erupted area, large topographic changes due to crater formation that could not be observed by InSAR were observed. From the measurement results, volume changes due to topographic changes before and after the eruption, which were not measured until now, could be estimated.

These results indicate that UAV photogrammetry is a simple and effective method for detecting topographic changes in active volcanic observation.

This work was partly supported by MEXT under Integrated Program for Next Generation Volcano Research and Human Resource Development, and under Earthquake and Volcano Hazards Observation and Research Program. Also it was supported by ERI, The University of Tokyo under Joint Usage Program.

Keywords: UAV, photogrammetry, volcano, Iwo-yama

©2020. Japan Geoscience Union. All Right Reserved.

[E] Poster | S (Solid Earth Sciences)：S-TT Technology & Techniques

[S-TT54] Creating future of solid Earth science with high performance computing (HPC)

convener:Takane Hori(R&D Center for Earthquake and Tsunami, Japan Agency for Marine-Earth Science and Technology), Yuji Yagi(Graduate School of Life and Environmental Sciences, University of Tsukuba, Tsukuba), Katsuhiko Shiomi(National Research Institute for Earth Science and Disaster Resilience)

Due to the development in computer science and computational science, large-scale or many times forward simulations and/or inversion analyses have become available recently. In solid Earth science, large-scale seismic wave propagation and crustal deformation with high fidelity models based on high resolution observation data have been demonstrated; uncertainty in crustal deformation caused by material properties and structures can be investigated based on many-time calculations for different material properties and structures; fault slip inversion analyses for non-Gaussian error distribution, etc. Thus, we will invite researchers who are applying HPC technology in forward simulations and inversion analyses and discuss how to improve more the collaboration between computer & computational sciences and solid Earth science not only in Japan but also from US and/or Europe. We are welcome submission by the researchers who are interested in this scope, especially students and young researchers.

[STT54-P01] Python based finite element code development for fluid geodynamics using JIT compiler and benchmark test

*Sangjin Park[1] (1.Kangwon National University)

[STT54-P02] Hybrid parallelization of Discrete Element Method (DEM): Toward a large-scale geotechnical HPC applications

*Mikito Furuichi[1] (1.Japan Agency for Marine-Earth Science and Technology)

[STT54-P03] Elastic Green's function library based on subduction zone models of high fidelity using the finite element method

*Takane Hori[1], Ryoichiro Agata[1], Tsuyoshi Ichimura[2], Kohei Fujita[2], Takuma Yamaguchi[2], Takeshi Iinuma[1] (1.Research Institute for Marine Geodynamics, Japan Agency for Marine-Earth Science and Technology, 2.ERI, The University of Tokyo)

Python based finite element code development for fluid geodynamics using JIT compiler and benchmark test

*Sangjin Park[1]

1. Kangwon National University

Python has very high productivity by supporting intuitive grammar and various libraries, but as an interpreted language, it is relatively slower than compiled languages such as c. Many attempts have been made to overcome working process of Python code which executes source code written by high-level language and translates to machine language simultaneously, including development of JIT (Just In Time) Compiler. Jit caches functions defined within the Python script by translating them into machine language. Since it omits the translation process to the machine language when reusing the cached function, Python using JIT compiler may show computational speed equal to the compiled language. We developed a Python-based finite element code for geodynamics equipped with JIT compiler, improving computational speed and keeping its good maintainability. Our code simulates the thermal convection within the coupled system between the time-dependent heat equation and the steady-state Stokes equation. It affords various simulations such as the boundaries between multiphase-fluid and large deformation of materials in Eulerian mesh with particle-in-cell method. In this study, we benchmarked various tests to assess the reliability of the code. Not only we successfully made simple mantle convection model but also we added a lot of geometries and sticky-air approach into test models using PIC (particle-in-cell) method.

Keywords: Python, Finite element method, Numerical geodynamics

©2020. Japan Geoscience Union. All Right Reserved.

Hybrid parallelization of Discrete Element Method (DEM): Toward a large-scale geotechnical HPC applications

*Mikito Furuichi[1]

1. Japan Agency for Marine-Earth Science and Technology

Discrete element method (DEM) is one of the standard simulation methods originally developed for granular physics and it has been recently extended to multi-physics simulations with advanced interaction models of visco-elasto-plastic rheologies and thermo-chemical reactions. Recently, DEM has been extensively utilized in various fields of studies such as geotechnics, geoscience, civil engineering, industry, and disaster prevention problems. This study presents the implementation and performance demonstration of parallel DEM simulation based on an iterative load balancer. The proposed techniques were verified by the reproducibility test. The numerical sandbox and slump tests with certain DEM particles demonstrated the efficiency of the large-scale DEM to capture the multi-scale events in the granular media. The visualization of the stress chains from the large-scale DEM simulation reveals the existence of arcuate stress structures that may control accretionary prism formation, which is an important scientific discovery

Keywords: DEM, Granular material, HPC

©2020. Japan Geoscience Union. All Right Reserved.

Elastic Green’s function library based on subduction zone models of high fidelity using the finite element method

*Takane Hori[1], Ryoichiro Agata[1], Tsuyoshi Ichimura[2], Kohei Fujita[2], Takuma Yamaguchi[2], Takeshi Iinuma[1]

1. Research Institute for Marine Geodynamics, Japan Agency for Marine-Earth Science and Technology, 2. ERI, The University of Tokyo

Green’s functions (GFs) for elastic deformation due to unit slip on the fault plane is an essential tool to estimate earthquake rupture processes and their preparation processes underground. Because these estimation results are often applied to creating socially important information such assessments of seismic and tsunami hazards, the dependence of these estimation results on the numerical models used for calculating GFs should be minimized to maintain the reproducibility of the estimations, which is essential to the reliability of the assessment. One solution is that the same GFs, which are calculated using numerical simulation models with high fidelity to a database of underground structures and the definitions of the coordinate systems to which many people agree, are used in various studies of estimating the underground processes. Here, we calculated an elastic Green’s function library based on subduction zone models of high fidelity using the finite element (FE) method, which is open to the public on a web server. We targeted two well-known subduction zones in Japan, the Nankai Trough and the Japan Trench subduction zones. The library was calculated based on the 3D heterogeneous elastic property of “Japan integrated velocity structure model version 1”, proposed for earthquake hazard assessments conducted by the Japanese government. In the FE meshes used for the calculation, the resolution of the layer boundaries in the underground structure is the same as that of the original database. The ellipsoidal shape of the earth, which is often approximated with a projected plane or a spherical shape, was also incorporated by faithfully following the definitions of the coordinate systems in Geodetic Reference System 1980 adopted by the International Union of Geodesy and Geophysics and the Japanese Geodetic Datum 2000. We expect the use of this library in estimating underground processes regarding earthquakes helps to minimize the variability of the estimation results depending on the settings of the numerical simulation model to calculate GFs, which should eventually contribute to the increase the reliability of seismic and tsunami hazard assessments. Furthermore, the library should also help researchers introduce a more realistic earth model in their analyses without laborious numerical model construction, numerical simulations and data processing.

Keywords: heterogeneous structure, Green's function, crustal deformation

©2020. Japan Geoscience Union. All Right Reserved.

[E] Poster | S (Solid Earth Sciences)：S-CG Complex & General

[S-CG55] Petrology, Mineralogy & Resource Geology

convener:Yu Nishihara(Geodynamics Research Center Ehime University), Koichi Momma(National Museum of Nature and Science), Tatsuo Nozaki(Submarine Resources Research Center, Research Institute for Marine Resources Utilization, Japan Agency for Marine-Earth Science and Technology), Nobutaka Tsuchiya(Department of Geology, Faculty of Education, Iwate University)

We widely invite presentations in the fields of petrology, mineralogy and resource geology. Especially description of minerals and rocks, investigation of their origin and evolution by field investigation and/or laboratory experiments, and development of new methods are accepted.

[SCG55-P01] Generation of mafic and felsic magmas of the Iwanoyama-Iyuzan volcanic chain in the Higashi-Izu Monogenetic Volcano Field, Izu-Bonin arc, Japan

*Yoji Arakawa[1], Hiromichi Kani[2], Soichiro Ueno[3], Taro Shinmura[4], Kei Ikehata[1] (1.Earth Evolution Sciences, Faculty of Life and Environmental Sciences, University of Tsukuba, 2.Sabo and Landslide Technical Center, 3.College of Geosciences, School of Life and Environmental Sciences, 4.Faculty of Economics, Kumomoto Gakuen University)

[SCG55-P02] Redox paths of granitic magma in Chiquicamata, northern Chile.

*Tetsuichi Takagi[1] (1.Research Institute for Geo-Resources and Environment, National Institute of Advanced Industrial Science and Technology)

[SCG55-P04] Anatomy of the Cretaceous Shaku-dake High-Mg diorite (HMD) intrusion, north Kyushu, SW Japan: Sheet on sheet model, and its genesis

*Keisuke Eshima[1], Masaaki Owada[1], Atsushi Kamei[2] (1.Yamaguchi University Graduate school of sciences and technology for innovation, 2.Shimane University Department of earth science, interdisciplinary faculty of science and engineering)

[SCG55-P05] Formation process of pegmatitic pyroxenite in the western limb of Bushveld Igneous Complex, South Africa

Shuhei Yoshida[1], *Takuya Echigo[1], Yasushi Watanabe[1] (1.Graduate School of International Resource Sciences, Akita University)

[SCG55-P06] **Ilmenite-series granitoids of the Peninsular Ranges batholith of southern and Baja California and the inner zone batholith of southwestern Japan**

*Mia Flores[1] (1.Stanford University)

[SCG55-P07] Whole-rock chemical composition analysis of granitic rocks in the Goto Islands, southwestern Japan

*Kazuhiro Koga[1], Motohiro Tsuboi[1], Ryunosuke Ikeda[1], Misaki Kubo[1] (1.Kwansei Gakuin University)

[SCG55-P08] Geochemical constraints on origin and formation of the Mikabu–Sorachi Plateau

*Naoto Kimura[1,2], Yuji Ichiyama[3], Takashi Miyazaki[2], Bogdan S. Vaglarov[2], Qing Chang[2], Takeshi Hanyu[2], Jun-Ichi Kimura[2] (1.Graduate School of Science and Engineering, Chiba University, 2.Japan Agency for Marine–Earth Science and Technology, 3.Graduate School of Science, Chiba University)

[SCG55-P09] Gesis of vesiculation in basalt sills of the Shimokawa ophiolite in the northern Hidaka belt, Hokkaido with influence on basalt sill of the Ab-Kfs vein

*Kato Satomi[1], Sumio Miyashita[2] (1.Graduate school of science and technology, Niigata university, 2.Hokkaido Research Center of Geology)

[SCG55-P10] Siliceous concretion in Miocene diatomaceous muddy rock, northeastern Noto Peninsula, central Japan

*Seika Oto[1], Kosei Komuro[1], Masaaki Shimizu[2], Hisatada Akahane (1.Toyama University, 2.Hokuriku Polytechnic College)

[SCG55-P11] Spectral Analysis of Cathodoluminescence of Barite

*Tomita Makiko[1], Shin Toyoda[1], Hirotsugu Nishido[1] (1.Okayama university of science)

[SCG55-P13] Mineralogical study on bur-shaped pyrite in SK050 volcanic ash in Uonuma Groupe, Niigata Prefecture

*Hiroaki Ohfuji[1], Akinori Matsuda[1], Takeshi Kakegawa[2] (1.Geodynamics Research Center, Ehime University, 2.Graduate School of Science, Tohoku University)

[SCG55-P14] Multi-photon luminescence measurement of natural and treated diamonds

*Shoko Odake[1], Hiroaki Ito[2], Hiroshi Takahashi[3], Shingo Ono[2] (1.GIA Tokyo Godokaisha, 2.Nagoya Institute of Technology, 3.Gemological Institute of America)

[SCG55-P15] Study for development of geothermal exploration technique using thermoluminescence of feldspar

*Takahiro Sato[1], Nobuo Hirano[1], Noriyoshi Tsuchiya[1], Atsushi Okamoto[1] (1.Tohoku University)

[SCG55-P16] Synthesis of highly dense and fine-grained crustal and mantle mineral aggregates by spark plasma sintering (SPS) technique

*Sanae Koizumi[1], Takehiko Hiraga[1] (1.Earthquake Research Institute,The University of Tokyo)

[SCG55-P17] Development of simultaneous measurement system of viscosity and permeability for highly accurate evaluation of groundwater under high pressure and high temperature condition

*Tomoya Muramoto[1] (1.National Institute of Advanced Industrial Science and Technology)

[SCG55-P18] **Evaluation of the influence of particle size on characteristics of particle shape using an automated particle image analysis**

*AIKO HAYAUCHI[1], Daisuke Sasakura[1] (1.Malvern Panalytical division of Spectris Co., Ltd)

[SCG55-P19] Genesis of the low-Sr Granitoid in the northern Kyushu

*Yayoi Muraoka[1], Masaaki Owada[2], Teruyoshi Imaoka[2], Atsushi Kamei[3], Kazuhiro Miyazaki[1] (1.Advanced Industrial Science and Technology, 2.Yamaguchi Univ., 3.Shimane Univ.)

Generation of mafic and felsic magmas of the Iwanoyama-Iyuzan volcanic chain in the Higashi-Izu Monogenetic Volcano Field, Izu-Bonin arc, Japan

*Yoji Arakawa[1], Hiromichi Kani[2], Soichiro Ueno[3], Taro Shinmura[4], Kei Ikehata[1]

1. Earth Evolution Sciences, Faculty of Life and Environmental Sciences, University of Tsukuba, 2. Sabo and Landslide Technical Center, 3. College of Geosciences, School of Life and Environmental Sciences, 4. Faculty of Economics, Kumomoto Gakuen University

The Higashi-Izu Monogenetic Volcano Field (HIMVF) comprises more than 70 subaerial monogenetic volcanoes on the eastern Izu Peninsula and 50 submarine volcanoes in the eastern offshore of the northern Izu-Bonin volcanic arc. Some of the volcanoes are arranged along a NW-SE trends, suggesting fissure eruptions. Petrological studies of the HIMVF have focused on the mafic volcanic rocks (e.g., Hamuro et al., 1983; Umino and Koyama, 1991; Takahashi et al., 2002; Nichols et al., 2012), whereas the felsic volcanic rocks have been investigated mainly to clarify the generation processes of felsic magmas (e.g., Miyajima, 1990; Suzuki et al., 2000; Kanai et al., 2013). In the present study, we investigated volcanic rocks from the Iwanoyama-Iyuzan chain, which represent the most recent subaerial eruptions (2.7 ka). These eruption products are bimodal in composition, comprising dacite and basaltic andesite. The dacites contain phenocrysts of orthopyroxene (Opx), plagioclase (Pl), and minor hornblende and clinopyroxene (Cpx), whereas the basaltic andesites and andesites contain Opx, Pl, Cpx, and olivine. Disequilibrium assemblages of phenocryst minerals and xenocrysts (quartz) are observed in the dacites and andesites.

Bimodal chemical compositions are apparent in Pl anorthite content (An mol. %) of An85-95 and An40-70, and in Opx Mg number (Mg#) of 76-80 and 68-72 in both the dacites and basaltic andesites. These bimodal compositions, as well as disequilibrium assemblages of phenocryst minerals and textures strongly suggest that both the mafic and felsic magmas underwent magma mixing and/or mingling. Whole rock major and trace element characteristic also show bimodality. Rare-earth element (REE) patterns differ between the felsic and mafic rocks; the dacites show enrichment in light REEs and concave down patterns of middle - heavy REEs, whereas the basaltic andesites display slightly inclined patterns from light to heavy REEs. $^{87}Sr/^{86}Sr$ ratios of the rocks show a small range (0.70328-0.70348), but differ slightly among volcanic units, indicating distinct sources for the parental magmas of each volcano.

The parental mafic magmas were probably basaltic andesite in composition, but with slight spatial variations in composition. The mafic magmas are inferred to have formed by mixing of lower crustal materials with primary basaltic magmas or by assimilation and fractional crystallization of the primary basaltic magmas. In contrast, the felsic magmas are interpreted to have been dacitic magmas, similar to the Iwanoyama and Ananoyama dacites. The parental magmas that formed these dacites may have been generated by partial melting of middle- to upper- crustal materials with some variations in $^{87}Sr/^{86}Sr$ ratios. The mafic and felsic magma types likely mixed and/or mingled to a degree and were then erupted in different locations along the fissure within a limited time interval.

Keywords: Higashi-Izu Monogenetic Volcano Field, Iwanoyama-Iyuzan Volcanic Chain, Bimodal volcanism, Northern Izu-Bonin volcanic arc

©2020. Japan Geoscience Union. All Right Reserved.

Redox paths of granitic magma in Chiquicamata, northern Chile.

*Tetsuichi Takagi[1]

1. Research Institute for Geo-Resources and Environment, National Institute of Advanced Industrial Science and Technology

The western cordillera of South America is one of the largest-scale magnetite-series granitic terranes in the world. The granitoids consist mainly of granodiorite to quartz diorite in Cretaceous, and often contain copper porphyries that were mineralized under highly oxidized magmatic conditions. To investigate the redox paths of granitic magma of this terrane, petrography of granitic rocks in the Chiquicamata area of northern Chile has been conducted using the rock collection by Dr. Shunso Ishihara. The rock specimens 79CHU7 and 79CHU3 (Ishihara et al., 1984 Bull GSJ, 35, 503-536) were selected from the collection because they are the least hydrothermally altered. 79CHU7 is a bt-cpx-opx quartz monzodiorite with a magnetic susceptibility of 14.5 x 10^{-3} SI units. In the rock, maghemite occurs as subhedral grains without ilmenite lamellae, whereas magnetite or martite could not be found. Ilmenite occurs as composite grains with maghemite and discrete grains. The Fe-Ti oxides occur with/within pyroxenes, biotite, and as fine-grained inclusions in calcic plagioclase. The compositions of cpx-opx pairs yield 910 to 862 ˚C by two-px geothermometer (Putirka, 2008 RiMG, 69, 61-120). 79CHU3 is a bt-hbl granodiorite with a magnetic susceptibility of 13.5 x 10^{-3} SI units. Maghemite occurs as subhedral grains without ilmenite lamellae similarly to 79CHU7, whereas magnetite could not be found. Mn-rich ilmenite is found with maghemite, but is mostly replaced by rutile/hematite aggregates or titanite. The Fe-Ti oxides and titanite occur mostly with hornblende and biotite. Hornblende occurs as subhedral to euhedral and homogeneous grains, and shows the compositions of magnesiohornblende (Si= 7.2-7.4 apfu, O=23). The compositions of hbl-pl pairs yield 689 to 588 ˚C by hbl-pl geothermometer (Holland and Blundy, 1994 CMP, 116. 433-447). The petrography above mentioned indicates the following crystallization sequence: 1) magnetite crystallization began in the early magmatic stage, and continued to the late magmatic stage. 2) magnetite was oxidized to maghemite in the late magmatic to subsolidus stages under relatively dry conditions. In 79CHU3, ilmenite was decomposed by further oxidation. These phenomena are attributable to the Chiquicamata magma containing enough sulfuric gas to maintain fO_2 along the H_2S-SO_2 gas buffer (Takagi and Tsukimura, 1997 Econ Geol, 92, 81-86). Throughout the magmatic to subsolidus stages, the magma/rock were continuously oxidized by SO_2 during cooling.

Keywords: granite, magnetite, Chile, Chuquicamata, sulfur

©2020. Japan Geoscience Union. All Right Reserved.

Anatomy of the Cretaceous Shaku-dake High-Mg diorite (HMD) intrusion, north Kyushu, SW Japan: Sheet on sheet model, and its genesis

*Keisuke Eshima[1], Masaaki Owada[1], Atsushi Kamei[2]

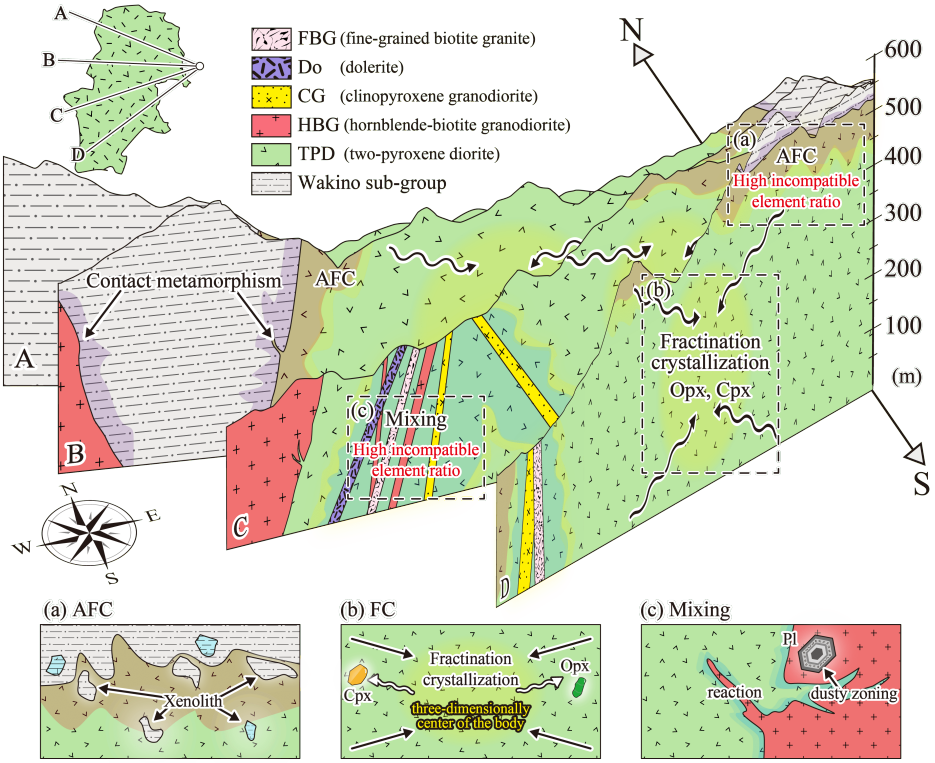
1. Yamaguchi University Graduate school of sciences and technology for innovation, 2. Shimane University Department of earth science, interdisciplinary faculty of science and engineering

The formation of plutons has fundamental implications for the geological linkage between volcanism and plutonism (e.g., Lipman, 2007; Macdonald et al., 2014), and ultimately for our understanding of the growth and evolution of the Earth’ s crust (e.g., Bachl et al., 2001; Annen, 2011; Menand et al., 2011). Much of the research on magmatic intrusions has focused on the mechanics and dynamics of dikes, which are the main agent for the vertical transport of magma through the crust (e.g., Lister and Kerr, 1991; Rubin, 1995; Menand and Tait, 2002). In comparison, that on sills has been discussed mainly on the mechanical and dynamical aspects of the propagation of sills, and on the deformation induced by sill intrusions (Pollard, 1973; Pollard and Holzhausen, 1979; Fialko et al., 2001; Malthe-Sørenssen et al., 2004). In recent years, however, the supply and emplacement mechanism of sills have been clarified from both of the detailed field research and experimental works using gelatin as natural analogs (Kavanagh, 2006; Menand, 2008, 2011). They stressed that such an emplacement mechanism gives an important role in the crustal evolution. Therefore, we performed the geological and petrological investigations and clarified a petrological character of magmatic processes, plumbing system, and growth process of the Shaku-dake high-Mg diorite (HMD) intrusion from the Cretaceous northern Kyushu batholith, Southwest Japan. It can contribute to the elucidation of large-scale igneous activity in northern Kyushu during the Cretaceous.

The granodiorites, the main constituent rock type of the Cretaceous batholiths from northern Kyushu, show the zircon U–Pb ages of 104 –102 Ma, and are accompanied coevally by fine-grained gabbro to diorite (e.g., Adachi et al., 2012; Tiepolo et al., 2012). Recently, the gabbro to diorite with the high-Mg andesite (HMA) compositions, referring to high-Mg diorite (HMD), has been reported (e.g., Kamei et al., 2004; Yuhara and Uto, 2007; Eshima and Owada, 2018; Eshima et al., 2019). The mantle-derived mafic magma is strongly involved in the origin of granitic magma as a parent magma and/or a heat source of crustal melting. The geology of Mt. Shaku-dake is composed of two-pyroxene diorite (TPD) and various dikes that intrude the Wakino sub-group as the host rock. The dikes are divided into five types; dolerite (Do), porphyritic fine-grained tonalite (PFT), clinopyroxene granodiorite (CG), hornblende-biotite granodiorite (HBG), and fine-grained biotite granite (FBG). In addition, the TPD intrudes into the host rock (Wakino sub-group) as the sheet converted from the vertical dike; thereby, suggesting the feeder dike. The TPD shows lithological variations on the metric and centimeter scales with different mineral mode and grain size. These field occurrences suggest that there were multiple injections of magma through the feeder dike before the TPD intrusion was fully consolidated. That is to say, the TPD intrusion is considered to be grown by the loading of sills and to bring to various compositional changes.

Keywords: sheet on sheet model, 3D model, high-Mg diorite (HMD), magma process

©2020. Japan Geoscience Union. All Right Reserved.



©2020. Japan Geoscience Union. All Right Reserved.

Formation process of pegmatitic pyroxenite in the western limb of Bushveld Igneous Complex, South Africa

Shuhei Yoshida[1], *Takuya Echigo[1], Yasushi Watanabe[1]

1. Graduate School of International Resource Sciences, Akita University

In the western limb of Bushveld Igneous Complex, South Africa, there are several discordant ultramafic intrusive rocks which cut the layered sequence of mafic-ultramafic plutonic rocks. We investigated the crystal growth process of the intrusive rock in Tweefontein area within southern part of the eastern Bushveld Igneous Complex. This intrusive rock is located in the upper critical zone in Rustenburg Layered Suite. The outcrop at Tweefontein is well-exposed and pegmatitic (grain size is greater than 2mm) pyroxenite intruded into the host rock, anorthosite. At the boundary between pyroxenite and anorthosite, grain size of the pyroxene is greater than the pyroxene at the core part of the intrusive rock. The pyroxenite consists of clinopyroxene (>80%), orthopyroxene (<10%) and other minor minerals such as plagioclase, hornblende, biotite and chlorite. It is notable that hornblende is present only in the course-grained clinopyroxene. SEM-EDS analysis showed that the end-member proportions of clinopyroxene are 46-47% wollastonite, 43-44% enstatite, and 9-10% ferrosilite and has no chemical zoning between their rim and core. Crystal size distributions (CSDs) of the clinopyroxenes showed linear trend and no local maximum. These trends reflect crystal growth process and absence of local maximum indicates that those clinopyroxenes grew by relatively simple process and neither Ostwald ripening nor annealing occurred. The CSD of coarse-grained pyroxenite has concave up curve and suggests that this trend resulted from crystal coarsening. Cawthorn et al. (2000) reported the ratios of Sr and O isotopes of this ultramafic intrusive rock at Tweefontein and concluded that there is no contribution of external fluid or assimilation of sedimentary rocks. These results suggest that hornblende in the course- grained pyroxenite crystallized as primary phase from the mafic-ultramafic magma which was enriched in water. The viscosity of hydrous silicate melt is much lower than anhydrous one and crystal growth of clinopyroxene can be promoted in the low viscosity magma.

Keywords: Bushveld Igneous Complex, Pegmatitic pyroxenite, Crystal size distribution, Viscosity

©2020. Japan Geoscience Union. All Right Reserved.

Ilmenite-series granitoids of the Peninsular Ranges batholith of southern and Baja California and the inner zone batholith of southwestern Japan

*Mia Flores[1]

1. Stanford University

Belts of juxtaposed oxidized and reduced granitoids in continental margin batholiths around the circum-Pacific have been characterized primarily by striking differences in magnetic susceptibility. Oxidized belts display high magnetic susceptibility, which is proportional to magnetite content. The reduced rocks tend to be magnetite-poor and lack Fe-oxide minerals in general. Fundamentally, Fe-oxide mineralogy and abundance is a function of oxygen fugacity. The oxidized belts were termed “magnetite-series” and the reduced belts were termed “ilmenite-series” by Dr. Shunso Ishihara. The best examples of this juxtaposition are in the Peninsular Ranges batholith (PRB) of southern and Baja California as well as the inner zone batholith of southwestern Japan, in which 100s of km-long boundaries between magnetite-series and ilmenite-series granitoids exist. Specifically, the well-studied ilmenite-series granitoids of the Ryoke and San’yo belts of Japan act as comparisons to better understand the petrogenesis of the ilmenite-series La Posta belt of the PRB. Hornblende-biotite monzogranite of the San’yo belt were collected from quarries in Okayama prefecture. The Ushigaura tonalite and Ushigaura granite were sampled from exposures of the Ryoke belt on Shōdoshima Island. The Sierra San Pedro Martí r and Laguna Juarez plutons of the La Posta belt were sampled by previous researchers from San Diego State University. Both plutons are zoned from hornblende-biotite tonalite in the rim, to a zone of hornblende-biotite granodiorite, and to a two mica monzogranite in the core. Plutons of the La Posta belt commonly include titanite, unlike the San’yo and Ryoke belts, which may indicate relative differences in oxygen fugacity. Biotite and amphibole compositions, which are sensitive to pressure, temperature, water fugacity and oxygen fugacity, may provide more information about the conditions that ilmenite-series plutons cool under. Characterization of biotite and amphibole are a first step towards more detailed Tl isotope analyses as well as Fe3+/(Fe2++Fe3+) quantification.

Keywords: Ilmenite-series, Granitoids

©2020. Japan Geoscience Union. All Right Reserved.

Whole-rock chemical composition analysis of granitic rocks in the Goto Islands, southwestern Japan

*Kazuhiro Koga[1], Motohiro Tsuboi[1], Ryunosuke Ikeda[1], Misaki Kubo[1]

1. Kwansei Gakuin University

The Goto Islands in Nagasaki Prefecture are located on the western end of the Kyushu district, and on the southern end of the Sea of Japan. The Goto Islands consists of five main islands, Nakadori, Wakamatsu, Naru, Hisaka and Fukue islands from northeast to southwest. Some small islands distribute around main islands. Geology of the Goto islands consists of sedimentary rocks of the Goto group, tuffs, Goto granitic rocks, rhyolite and basalt (Kawada et al., 1994). Goto granitic rocks consist of granodiorite, granodiorite porphyry, and granophyre, and the ages of these rocks are reported c. 15 Ma (Ishikawa & Tagami, 1991). This age is related to the time of the opening of the Sea of Japan, and there is a possibility that the magmatism of these granitic rocks is related to the opening tectonics of the Sea of Japan. In this study, we analyzed whole-rock chemical composition of granitic rocks in the middle eastern part of Fukue Island, the northern part of Hisaka Island, and the northern part of Nakadori Island, and discuss their petrogenesis.

Granodiorite porphyry, granodiorite and granite occur in the middle eastern part of Fukue Island. The northern part of Hisaka Island is mainly composed of granodiorite and granite, and there are some outcrops where the leucocratic rocks and melanocratic rocks sharply border each other. Basic intrusive rocks are also identified. Granodiorite porphyry, granodiorite and granite with intermediate enclaves are identified in the northern part of Nakadori Island. There are also some outcrops where the melanocratic granitic rocks are included into the leucocratic granitic rocks. Granodiorite porphyry, granodiorite and granite from Fukue Island, granodiorite, granite and basic intrusive rocks from Hisaka Island, and granodiorite porphyry, granodiorite, granite and intermediate enclaves from Nakadori Island were sampled. The major elements and trace elements were analyzed with X-ray fluorescence spectrometry, and rare earth elements (REE) were analyzed with inductively coupled plasma mass spectrometry.

The content of SiO_2 ranges from 65.3 to 72.7 wt.% for granodiorite porphyry, from 62.4 to 75.9 wt.% for granodiorite and granite, 48.8 and 48.9 wt.% for basic intrusive rocks, and from 58.2 to 64.5 wt.% for intermediate enclaves. Onthe granodiorite porphyry, the content of Fe_2O_3, MnO, TiO_2 and P_2O_5 decreases, and K_2O and Al_2O_3 content increases with increasing SiO_2 content. On the granodiorite and granite, the content of Fe_2O_3, MnO, TiO_2, CaO, P_2O_5, Al_2O_3 and MgO decreases, and K_2O content increases with increasing SiO_2 content. On the SiO_2–FeO*/MgO diagram, the granodiorite porphyry shows calc-alkaline series composition. The other granitic rocks are divided into the high–FeO*/MgO group which shows extremely high FeO*/MgO ratio, and the low–FeO*/MgO group which shows tholeiitic series composition.

The geochemical discrimination diagram of trace elements (Pearce et al., 1984) shows that granodiorite porphyry and low-FeO*/MgO group granitic rocks have the characteristics of volcanic arc granite (VAG), and high-FeO*/MgO group granitic rocks have the characteristics of volcanic arc granite (VAG) to within-plate granite (WPG).

The REE patterns show that the samples are rich in light-REE and poor in heavy-REE. Both positive and negative Eu anomalies are observed in the REE patterns of the granitic rocks. Some samples show Ce

©2020. Japan Geoscience Union. All Right Reserved.

anomalies, probably due tothe weathering.

The chemical composition analysis reveals that the granitic rocks in the Goto Islands may have multiple origins.

Reference

Ishikawa, N. and Tagami, T., 1991, *J. Geomag. Geoelectr.*, **43**, 229–253.

Kawada, K., Kamada, Y., Matsui, K., 1994, Geology of Fukue district. With Geological Sheet Map at 1: 50,000, *Geol. Surv. Japan*, 47p.

Pearce, J. A., Harris, N. B. W., Tindle, A. G., 1984, *Jour. Petrol.*, **25**, 956–983.

Keywords: granitic rocks, Goto Islands, whole-rock chemical composition

©2020. Japan Geoscience Union. All Right Reserved.

Geochemical constraints on origin and formation of the Mikabu–Sorachi Plateau

*Naoto Kimura[1,2], Yuji Ichiyama[3], Takashi Miyazaki[2], Bogdan S. Vaglarov[2], Qing Chang[2], Takeshi Hanyu[2], Jun-Ichi Kimura[2]

1. Graduate School of Science and Engineering, Chiba University, 2. Japan Agency for Marine–Earth Science and Technology, 3. Graduate School of Science, Chiba University

It is generally accepted that mantle plume upwelling had been active in the Pacific Ocean during the Cretaceous period based on the thorough studies of Cretaceous oceanic plateaus (e.g., Larson, 1991; Coffin and Eldholm, 1994). The presence of the Izanagi–Farallon–Pacific triple junction in the Paleo–Pacific Ocean has been proposed based on the geometry of paleomagnetic anomalies (Sager et al., 1988, 1999; Nakanishi et al., 1989, 1999). An Early Cretaceous mantle plume arrival beneath the triple junction constructed the Shatsky Rise with its high degrees of melting (Sano et al., 2012). This plume also possibly formed several oceanic plateaus on the Izanagi and Farallon plates, and parts of them have been considered to be preserved as accreted fragments in continental margins (Sager et al., 1988; Larson, 1991; Kimura et al., 1994; Ichiyama et al., 2014).

The Mikabu and Sorachi–Yezo Belts are Cretaceous terrains distributed in Japan and contain voluminous greenstones as ophiolitic members, which are metamorphosed picrite, basalt, and gabbro. The Mikabu and Sorachi picrites have extremely magnesian olivine phenocrysts (up to $Fo_{93.5}$), and the mantle potential temperatures of more than 1600℃ are estimated (Ichiyama et al., 2012, 2014). The greenstones have been considered to be fragments of an oceanic plateau in the Jurassic–Cretaceous Pacific Ocean (Mikabu–Sorachi Plateau; MSP), and some scientists believe that this plateau was formed with the Shatsky Rise on the Izanagi–Pacific ridge (Kimura et al., 1994; Ozawa et al., 1999; Sakakibara et al., 1999; Ichiyama et al., 2012, 2014; Sawada et al., 2019). However, the zircon U–Pb dating of the Mikabu mafic rocks and sandstones shows igneous ages of ca. 155 Ma (Sawada et al., 2019; Endo and Yokoyama, 2019) and an accretion age of ca. 130 Ma (Endo and Wallis, 2017), respectively, implying that the MSP emerged on an intraplate (i.e., Izanagi plate) rather than on a plate boundary (i.e., Izanagi–Pacific ridge) because estimated travel time of the Izanagi plate would take ~80 Myr from the ridge to the trench (Müller et al., 2016).

Miyazaki et al. (2015) proposed that an isotopic boundary between the Indian and Pacific mantle types is present beneath the Pacific Ocean and has been stationary, at least, from Cretaceous to present. Recently, Aoki et al. (2019, 2020) suggested that metagabbro and mafic gneiss in the eclogite unit of the Sanbagawa Belt were formed in an island arc setting within the Pacific Ocean in 200–180 Ma. If this is a case, it would be expected that the Mikabu–Sorachi (ca. 155 Ma) greenstones record mantle isotopic heterogeneity beneath the Paleo–Pacific Ocean.

In this presentation, we will provide new geochemical and isotopic data of the Mikabu and Sorachi greenstones (picrite, gabbro, and alkali basalt). These data will enable us to constrain the source material and tectonic setting of the MSP in the Jurassic Pacific Ocean.

Keywords: Mikabu Belt, Sorachi–Yezo Belt, Matle plume, Paleo–Pacific Ocean, Indian–Pacific mantle boundary

©2020. Japan Geoscience Union. All Right Reserved.

©2020. Japan Geoscience Union. All Right Reserved.

Gesis of vesiculation in basalt sills of the Shimokawa ophiolite in the northern Hidaka belt, Hokkaido with influence on basalt sill of the Ab-Kfs vein

*Kato Satomi[1], Sumio Miyashita[2]

1. Graduate school of science and technology, Niigata university, 2. Hokkaido Research Center of Geology

Vesiculation of magma depends on volatile components in the magma and the eruption depth. Basaltic rocks with N-MORB features from the Shimokawa ophiolite generally show poor vesiculation. However some of massive basalts are vesiculated up to 10 vol. %. Miyashita (1999) proposed that the high vesiculation is caused by an interaction between sediments and intruding magmas. We present new finding of Ab-Kfs veins, size distribution and bulk composition of the vesiculated massive basalt sills. We discuss how Ab-Kfs vein affects massive basalt sills.

The Shimokawa ophiolite is exposed in the northern part of central Hokkaido. Serpentinized harzburgite and gabbro occur at the lowest part. The lower part of the main body consists of alternation of dolerite and sediments, the upper part consists of pillow lava, and the middle part shows intermediate features between the upper and lower parts. (Miyashita and Watanabe, 1988). High vesicular massive basalt sills interlayered between sediments are found from three locations. The sediments are silicified along the contacts.

Massive basalt sill 1 about 22 m thick occurs at the lowest horizon in the vesiculated massive basalt sills. This sill contains many irregular shaped xenoliths of sediments, indicating that the sill intruded into unsolidified sediments.

The Shimokawa ophiolite shows typical N-MORB signatures (Zr/Nb>17). High vesicular basalts tend to be high LIL elements contents than poorly vesiculated basalts. REE ratios exhibits that there are two types in the Shimokawa ophiolite, about 0.8 La/Yb ratios with N-MORB patterns (sill 2, most of sill 3, most of pillow lava), and about 1.2 La/Yb ratio with T-MORB patterns (sill 1, some sill 3, some pillow lava). However, HFS elements that are immobile during alteration processes reveal N-MORB features. Therefore, LIL elements and light REE are probably modified from the primary compositions.

The Ab-Kfs veins are >2 mm width and thicker than later calcite veins. The border of the Ab-Kfs vein is not straight and waves. It is noted that the Ab-Kfs veins do not cut primary igneous crystals. We measured vesicularities of 22 samples from the massive basalt sill 1. The marginal part within 50 cm from the contact is not vesiculated. Vesicularities increase upward until about 18 m from the lower contact. But basalts containing Ab-Kfs veins show high vesicularity. Plagioclase number densities (PND) show a systematic variation. The margin shows a high value (40 number/mm^2) and inside shows low values (4-6 number/mm^2), implying that the margin is fine-grained and inside is coarse-grained. The PND of basalt containing the Ab-Kfs vein is higher than surrounding rocks (15 number/mm^2), indicating fine-grained than surrounding basalts. Cr_2O_3%(cpx) shows that inside of sill 1 is evolved (Cr_2O_3% (cpx) 0.25%), but surrounding Ab-Kfs vein is less evolved (Cr_2O_3% (cpx) 0.8%) as similar with those of the margin. Above facts suggest that the Ab-Kfs veins were formed before the solidification of the sills.

When magma intruded into thick unsolidified sediments, neighboring sediments are rapidly dehydrated

©2020. Japan Geoscience Union. All Right Reserved.

and solidified due to heating by magmas. Expelled hydrothermal fluids from the sediments could not escape from the sills because of sealing effects of overlying solidified sediments, leading mixing with magmas.

The Ab-Kfs veins were formed before the solidification of magma, as described above. Surrounding basalts of the Ab-Kfs veins are highly vesiculated and fine-grained. Furthermore pyroxene compositions of neighboring basalts are less evolved. Therefore, the Ab-Kfs veins affect cooling rate, volatile components and differentiation of injected magmas. Silicified sediments release H_2O, LIL elements such as K_2O and Rb, and CO_2 due to dissolution of organic carbon. The released elements are entrained in the intruding magma via the Ab-Kfs veins, resulting in high vascularity of magma.

[1]Miyashita and Watanabe, 1988. [2]Miyashita, 1999.

Keywords: vesiculation, MORB, northern Hidaka belt

©2020. Japan Geoscience Union. All Right Reserved.

Siliceous concretion in Miocene diatomaceous muddy rock, northeastern Noto Peninsula, central Japan

*Seika Oto[1], Kosei Komuro[1], Masaaki Shimizu[2], Hisatada Akahane

1. Toyama University, 2. Hokuriku Polytechnic College

Siliceous concretions called as "Koburi-ishi" are embedded in the diatomaceous muddy rocks from the Iizuka Formation of middle Miocene, the northeastern Noto Peninsula, central Japan. They have platy to ellipsoidal forms with 1-5 cm in diameter, are embedded in specific horizons or in association with faults, in the host diatomaceous muddy rocks which contain a large number of microfossils mainly of marine diatoms with radiolarians and sponge spicules. Here we describe the siliceous concretions mineralogically, and discuss their formative processes and environment.

Microscopic observation clarify that the siliceous concretions contain microfossils with hard matrices of siliceous phases and have concentric growth structure. This indicates that hard matrices phases were precipitated from interstitial solution. The XRD analysis for siliceous phases after the elimination of clay fraction indicates that both siliceous concretions and the host diatomaceous muddy rocks are composed of opal-A and opal-CT. The peak fitting assuming Gaussian distribution reveals that siliceous concretions contain more opal-CT than the host diatomaceous muddy rocks. The cristobalite in opal-CT from siliceous concretions has 4.121 ~ 4.137 Å, which is wider d-spacing of (101) than that from the host diatomaceous muddy rocks of 4.073 ~ 4.083 Å.

Original sediments of the host rocks from the Iizuka Formation were deposited under shallow marine environment. They were buried up to about 500 meters in depth of sedimentary sequences. Biogenic opal-A of diatoms in diatomaceous muddy sediments from the Iizuka Formation changed to opal-CT by the diagenetic phase transformation responsible for the burial depth. It is known that the sequences were uplifted repeatedly to the present location. The wider d-spacing of (101) of siliceous concretions suggests they were formed under shallower burial environment than host rocks. Considering that the solubility of silica in seawater is higher than that in meteoric water due to the contribution of Na-Si complex, the inflow of meteoric water by upheaval triggered the formation of the siliceous concretions. As the meteoric water invaded into a series of the sequences along permeable horizons or fault planes, mixing of interstitial seawater of the host diatomaceous muddy rocks and meteoric water took place at the permeable horizons or fault planes. As a result, dissolved silica in interstitial seawater was precipitated along the horizons or planes to form siliceous concretions.

Keywords: opal-CT, concretion, diagenesis, diatomite

©2020. Japan Geoscience Union. All Right Reserved.

Spectral Analysis of Cathodoluminescence of Barite

*Tomita Makiko[1], Shin Toyoda[1], Hirotsugu Nishido[1]

1. Okayama university of science

Cathodoluminescence (CL), luminescence following electron excitation, in minerals varies in emission color, intensity, and spectrum, gives information on impurity compositions and structural lattice defects. In the present study, CL of barite (BaSO4) was investigated, which had not been studied in detail. Although CL in many minerals has similarity with photoluminescence (PL), excited by UV, and radioluminescence (RL), excited by X-rays, it was found that barite is not the case.
Twenty-five natural barite samples, which show PL of various colors, were examined in the present study. SEM-CL analysis was conducted using an SEM (JEOL: JSM-5410) combined with a grating monochromator (Oxford: Mono CL2) in the range from 300 to 800 nm in 1 nm steps with a temperature-controlled stage from -190 to 25 ℃. The wavelength dependent photomultiplier response was corrected with a standard light source to have correct CL spectra. They were then converted to the ones according to photon energy in eV and then deconvoluted into Gaussian components with using OriginPro 9J.
Color CL images with blue emissions were obtained only from five samples while other samples show no CL, although most samples examined here exhibit various luminescent colors of blue, beige, yellow, white and magenta under a UV lamp.
As the result of the spectral analysis with deconvolution, the spectra with the strong and weak blue emissions have a broad band around 370 nm in UV-blue region, but no clear emission in red region. In previous studies, luminescence peaks were reported due to an intrinsic center of SO_4^{2-} and to an impurity center of Pb-ion or Eu-ion [1,2]. The peak position of the present result was found to be close to these previous studies.
With EPMA and LA-ICP-MS analysis, Pb contents were obtained in the samples. It was found that those with Pb content of 23.8 wt% or more show strong CL and that those with 500 ppm or less show weak CL, while those with no CL do not contain any impurity elements. The temperature-controlled CL measurements reveled that the peak position of blue CL of strong emission (hence larger Pb content) did not change with temperature, whereas the emission intensity of the sample, containing Pb of 0.5 wt% or less, increase with temperature.
Therefore, the blue CL emissions found in barite might be composed of an impurity center of Pb-ion activator or sensitizer, and the 3.28 eV component may be composed of SO_4^{2-}defect centers.

[1] Marshall, J. (1988) Cathodoluminescence of geological materials, Unwin Hyman, 1-146.
[2] Hirotsugu, N. et al. (2004) Temperature effect on cathodoluminescence of anhydrite.

Keywords: Barite, Cathodoluminescence, emission mechanism

©2020. Japan Geoscience Union. All Right Reserved.

Mineralogical study on bur-shaped pyrite in SK050 volcanic ash in Uonuma Groupe, Niigata Prefecture

*Hiroaki Ohfuji[1], Akinori Matsuda[1], Takeshi Kakegawa[2]

1. Geodynamics Research Center, Ehime University, 2. Graduate School of Science, Tohoku University

Sedimentary pyrite shows a variety of morphologies and textures from euhedral crystals to framboidal, radiating and colloform aggregates depending on the formation environments. Here we report a very unique case of pyrite morphology, “bur-shaped” aggregate, found in microscopic pyrite occurring in SK050 volcanic ash, which is one of the many tephra layers intercalated in the Uonuma formation, Niigata Prefecture.

SK050 volcanic ash and the under- and overlying muddy sediment samples collected from the outcrop along the Shibanomata River in Oguni Town contain microscopic pyrite which can be divided into three types by morphology, (1) framboidal, (2) polyframboidal, and (3) bur-shaped aggregates. Framboidal and polyframboidal aggregates occur in all the sediment samples collected, while bur-shaped aggregates are found exclusively within the SK050 volcanic ash, where the relative proportion of framboidal aggregates is very low. Bur-shaped pyrite is characterized by spheroidal shape with a number of spines and shows a normal size distribution ranging from 20 to 60 μm in diameter, which is more or less larger than that of framboidal pyrite (10-50 μm). SEM observation on the cross-sections through the core prepared by FIB revealed that bur-shaped pyrite always has a framboidal pyrite in its core from which columnar pyrite crystals grew in a radiating manner. Each columnar crystal is terminated by a pyramidal apex, which corresponds to the spines observed on the outer surface of bur-shaped pyrite. These observations suggest that bur-shaped pyrite is a unique product of pyrite overgrowth around a framboidal pyrite core. Sulfur isotope analysis of the SK050 volcanic ash containing bur-shaped pyrite showed very heavy isotopic ratios ($\delta^{34}S$= ca. +20 ~ +25‰), which are clearly distinct from those of the under- and overlying sediments containing framboidal pyrite (ca. 0 ~ +15‰). It seems that bur-shaped pyrite formed as a result of an extensive overgrowth of pre-existing framboidal pyrite when a fluid highly saturated with pyrite penetrated into the SK050 volcanic ash layer which has a much higher permeability than the under- and overlying sediments.

Keywords: Pyrite, Framboidal pyrite

©2020. Japan Geoscience Union. All Right Reserved.

Multi-photon luminescence measurement of natural and treated diamonds

*Shoko Odake[1], Hiroaki Ito[2], Hiroshi Takahashi[3], Shingo Ono[2]

1. GIA Tokyo Godokaisha, 2. Nagoya Institute of Technology, 3. Gemological Institute of America

Treatments are widely used to modify diamond’ s body color to improve it's value as a gem. Typical examples of treatments are annealing in high-temperature and high-pressure (HPHT) environment to remove brownish color from diamonds and irradiation with an electron beam to add bluish color. To distinguish between natural and treated diamonds, spectroscopic measurements are used. The spectroscopic measurements currently used are limited to the surface and the area near the surface of the diamond. In order to accurately and quickly distinguish between natural and treated diamonds, a method for evaluating the defect distribution inside the diamond is needed. In this study, distribution of defects in natural and treated diamonds were evaluated three-dimensionally by using multi-photon luminescence measurements.
The measurements were performed on natural untreated, HPHT treated (type I and type IIa), and electron beam irradiated diamonds. The measurement of multi-photon luminescence is widely used for biological research, and is a method capable of measuring three-dimensional defects inside a sample with nondestructive and high spatial resolution. A multi-photon laser-scanning microscope (Olympus, FV1200MPE) was used for the measurement. In a multi-photon laser-scanning microscope, excitation light from a femtosecond laser is reflected by a mirror and focused and irradiated to a sample using an objective lens. By using a galvanometer mirror, excitation light is moved in the XY direction, and the objective lens is moved in the optical axis direction, and scanning is performed in the Z direction, thereby enabling three-dimensional scanning. The multi-photon luminescence generated from the samples were collected using the objective lens, and the multi-photon luminescence intensity was measured using a photomultiplier tube. Band pass filters were used to isolate defects in specific wavelength ranges.
As a result, in natural diamonds the differences of the color center in different growth planes were visualized three-dimensionally. In treated diamonds, distribution of 1-micron size defects in HPHT were visualized. In irradiated diamonds, irradiation-related defects were observed only in the surface area. In this presentation, we will discuss details about differences between conventional methods and multi-photon luminescence measurements.

Keywords: Diamond, Multi-photon luminescence, Treatment

©2020. Japan Geoscience Union. All Right Reserved.

Study for development of geothermal exploration technique using thermoluminescence of feldspar

*Takahiro Sato[1], Nobuo Hirano[1], Noriyoshi Tsuchiya[1], Atsushi Okamoto[1]

1. Tohoku University

Japan has abundant geothermal resources, and geothermal development is important in energy strategies, but its development is not progressing. This is because geothermal power development costs are expensive, and lead times are long. As a solution to these problems, a simple geothermal exploration method using mineral thermoluminescence has been proposed. Thermoluminescence (TL) is a phenomenon in which energy is accumulated inside a mineral crystal by radiation, and this energy is released as luminescence by thermal stimulation. Light emission due to energy accumulated by natural radiation is called as natural thermoluminescence (NTL), and light emission due to energy accumulated by irradiation of artificial radiation is called as artificial thermoluminescence (ATL). Tsuchiya et al. (2000) and Saito et al. (2017) showed that Geothermal exploration using TL of quartz has effectiveness. Feldspar also emits TL like quartz, but few studies have been conducted on geothermal exploration methods using TL of feldspar. Feldspar is a ubiquitous mineral at the crust, if a geothermal exploration method using feldspar TL can be developed, TL geothermal exploration can be applied to areas without quartz. In addition, it is thought that the accuracy of the geothermal exploration method using the TL can be improved by using it in combination with the quartz TL. In this study, the basic properties of TL of feldspar were studied.

The geothermal exploration method using TL of quartz utilizes the difference in NTL intensity due to geothermal influence. This utilizes the property that accumulated energy is released by heat and utilizes the phenomenon that the intensity of light emission (NTL) decreases as it approaches the heat source, that is, as the geothermal temperature increases. An isothermal decay experiment was performed using K-feldspar in pegmatite to examine whether the same method can be applied to feldspar. As the heating environment conditions, three patterns were prepared: a sample only heated, a sample immersed in acidic water (Tamagawa hot spring water) and heated, and a sample immersed in neutral water (distilled water). These samples were reacted at temperature of 90, 125, 150, 200 and 250 ºC, and 24, 168 and 672 hours. The total number of samples is 45. To evaluate thermoluminescence, first observe the glow curve. Glow curve is obtained by subtracting background luminescence intensity (mainly infrared radiation from heater) from thermo luminescence intensity of mineral crystals. After that, integrate the glow curve from 50ºC to 350ºC and define that integrated value as the TL intensity. Regarding the relationship between the TL intensity and the heating temperature/time, the decay of TL intensity was observed as the heating temperature was higher and the heating time was longer. Regarding the relationship between the TL intensity and the heating environment, no change was observed in the tendency of the TL intensity decay even when the heating environment was changed. Therefore, it is considered that the decay of TL intensity depends more on the influence of temperature than on the influence of hydrothermal alteration. These results of the TL intensity decay were kinetically interpreted, and fitting was performed assuming a fifth-order reaction. As a result, the apparent activation energy was 1.25 eV. This value is in good agreement with the quartz results calculated in previous studies, indicating the possibility of geothermal exploration using NTL of feldspar.

In the poster presentation, feldspars collected from rocks such as tuff and granite will also be discussed.

©2020. Japan Geoscience Union. All Right Reserved.

Keywords: thermoluminescence, feldspar, geothermal exploration

©2020. Japan Geoscience Union. All Right Reserved.

Synthesis of highly dense and fine-grained crustal and mantle mineral aggregates by spark plasma sintering (SPS) technique

*Sanae Koizumi[1], Takehiko Hiraga[1]

1. Earthquake Research Institute,The University of Tokyo

We will present the synthesis of various types of the upper mantle and crustal mineral aggregates including mono-phase aggregates of Fe–free and Fe--bearing olivine, enstatite ($MgSiO_3$) and anorthite ($CaAl_2Si_2O_8$), two-phase composites of olivine + spinel, olivine + diopside ($CaMgSiO_6$), olivine + enstatite and anorthite + diopside and three-phase composites of olivine + enstatite + diopside. We prepared mineral powders through solid state reaction of source powders at high temperature (Koizumi et al. 2010). They are densified by spark plasma sintering, which results in obtaining highly dense and fine-grained aggregates. In SPS, it is essential to use proper starting powders and sintering conditions such as temperature, duration time and heating rate. At low temperature of 1130 - 1250˚C, short duration of 20 min and low heating rate of 10˚C/min, we could obtain aggregates with grain size of 0.2 μm in minimum.

Keywords: Sintering, Mantle mineral, Crustal mineral

©2020. Japan Geoscience Union. All Right Reserved.

Development of simultaneous measurement system of viscosity and permeability for highly accurate evaluation of groundwater under high pressure and high temperature condition

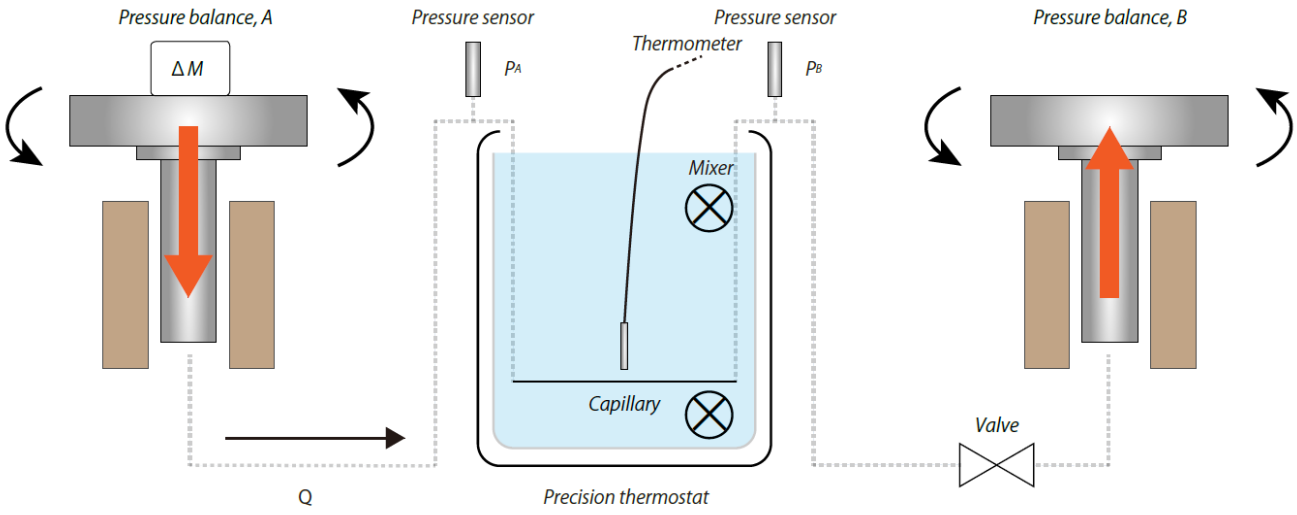
*Tomoya Muramoto[1]

1. National Institute of Advanced Industrial Science and Technology

In predicting the flow behavior of groundwater, the viscosity of groundwater in the ground under high pressure and high temperature is very important. According to Darcy’s law, the volumetric flow rate of groundwater is determined by the balance between “Mobility” and “Driving Force”. Here, in order to determine “Mobility”, the viscosity of the fluid is required. From this, it can be said that the viscosity of the fluid is very important for accurately predicting the underfround flow field.

We developed a new method for the high-pressure viscosity measurement of a fluid using two pressure balances. In this method, the concept of a capillary method used in a viscosity measurement and cross-float technique are applied. We evaluated the pressure dependency of the viscosity of dioctyl sebacate. On comparing our results with the those in the literature, it was confirmed that the result showing the pressure dependence of viscosity was similar to that mentioned in literature. Thus, we confirmed that the measurement system developed in this study could accurately evaluate the pressure dependence of viscosity. In the future, focusing on the similarity between flow field descriptions based on Darcy’s law used for permeability measurements and Hagen-Poiseulle’s law used for highly accurate viscosity measurements by capillary method, we will develop simultaneous measurement system of viscosity and permeability at high temperature and high pressure. The measurement system to be developed in this study makes it possible to determine the permeability based on the national measurement standard, and to accurately evaluate of the permeability and mass transport characteristics of groundwater.

Keywords: High-pressure, Darcy flow, Viscosity



©2020. Japan Geoscience Union. All Right Reserved.

Evaluation of the influence of particle size on characteristics of particle shape using an automated particle image analysis

*AIKO HAYAUCHI[1], Daisuke Sasakura[1]

1. Malvern Panalytical division of Spectris Co., Ltd

1. Introduction

In many fields dealing with geology, the relation between particle morphology in the soils and various phenomena is widely studied. Particle morphology indicates particle size, particle shape and various other characteristics. In particular, size and shape are complementary relationship. As a previous research, we reported the results of particle shape evaluation of volcanic ash whose particle size was evaluated using a sieve, and clarified that particle size evaluation using a sieve is affected by the particle shape. [1]. Notable aspect of size and shape distribution matters are its having inversed relationship qualitatively. Typically, in soil, the finer particle are relatively more circular shape than the coarse particle. This is because, for example, finer particles are presumed to be provided by abrasion fracture when falling from a rock surface due to ground distortion and/or rising. Therefore, the simultaneously integrated investigation between size and shape is important.

The existing technology to investigate size and shape matter are the microscopic technics, sieving, sedimentation and laser diffraction analysis. Challenges of existing technologies on above are that it is each independent technic to investigate between size and shape. Especially, microscopic analysis is the near impossibility of measuring a statistically significant number of several ten thousand number of particles as recommended in ISO 13322-1,2 and quantitatively information. Recent advances in computer technology have allowed for a new automated particle image analysis (APIA) approach.

We reported and discuss about capability of APIA method was useful to resolve these issues on the model soil samples considerd fracture processes as one of realistic ground mechanics process.

2. Material and method

Sea sand, 300~600um(30~50mesh) (FUJIFILM Wako Pure Chemical Corporation) was used for this study. A part of the sample was milled with a ball mill (Mini Mill 2, FRITSCH).

As APIA system, Morphologi 4 (Malvern Instruments) was used for evaluation of particle size and shape. The observation mode was diascopic mode (Transmittance mode) and magnification was 125x in total magnification. The sample was dispersed with SDU (Sample Dispersion Unit) which attached Morphologi 4. Number of measured particles is over than 2,000 and parameter filter function on software was used based on shape and pixel number of particle image.

3. Result

Mean value of Circularity for original sea sand and 5 minutes milled sea sand is shown in Table 1. All particle circularity of original sea sand is smaller than all particle circularity of 5 minutes milled sea sand. For particles larger than 150um, circularity both original sea sand and 5 minutes milled sea sand are almost same. Particle of the same size as before milling, that is, particles of a large size, were simply particles that were not milled. Therefore, it is considered that these particles maintain their shape.

Focusing on the small particle size, it was confirmed that the trend was the same as the trend of all particle. In particular, the circularity of particles smaller than 20um was almost the same as the circularity of the whole particles. This is a simple result comes from the number ratio of particles smaller than 20um is highest (Percentage of particles by particle size is shown in Table 2).

These data will discuss in detail on that day.

©2020. Japan Geoscience Union. All Right Reserved.

4. Conclusions

It was confirmed that particle shape changes according to particle size with APIA method. The particle shape results from the shape of the particles in numerical majority. It is also revealed that it is necessary to use a number-based particle size distribution device to understand the number of particles by particle size.

[1] Aiko Hayauchi, Daisuke Sasakura. “An evaluation of sieving effect of volcanic ash fine particles by a statistical particles image analysis” JPGU2013 Abstract.

Keywords: Particle shape, Particle size, Maprticle morphology

Classification by particle size(um)	Circularity Mean		
	Original	5 minutes milled	⊿(original/5 minutes milled)
All	0.75	0.82	0.07
CED>=150um	0.74	0.75	0.01
150um>CED>=74um	0.71	0.76	0.05
74um>CED>=38um	0.73	0.78	0.05
38um>CED>=20um	0.75	0.80	0.05
20um>CED	0.76	0.83	0.07

Table 1: Mean value of circularity for original sea sand and 5 minutes milled sea sand

Classification by particle size(um)	Count based ratio(%)		Volume based ratio(%)	
	Original	5 minutes miilled	Original	5 minutes miilled
CED>=150um	22	0.059	99.9	12
150um>CED>=74um	4.3	1.1	0.11	39
74um>CED>=38um	6.4	6.0	0.023	31
38um>CED>=20um	11	18	0.0045	13
20um>CED	56	75	0.0027	6.0

Table 2: Percentage of particles by particle size

©2020. Japan Geoscience Union. All Right Reserved.

Genesis of the low-Sr Granitoid in the northern Kyushu

*Yayoi Muraoka[1], Masaaki Owada[2], Teruyoshi Imaoka[2], Atsushi Kamei[3], Kazuhiro Miyazaki[1]

1. Advanced Industrial Science and Technology, 2. Yamaguchi Univ., 3. Shimane Univ.

The Cretaceous granitoids are widely exposed on the northern Kyushu, Southwest Japan. These granitoids were distinguished between the low-Sr and high-Sr granitoids by their Sr contents (Izawa et al., 1990). The boundary of these is the Kokura-Tagawa Tectonic Line (KTT). In the east side of KTT, the low-Sr granitoids are distributed. On the other hand, the high-Sr granitoids are exposed on the west side of KTT. The Hirao granodiorite and related granite dike are exposed on the east side of KTT. The Hirao granodiorite occurs as a stock with 16 km N-S and 4 km E-W, and has Sr contents of 213-291 ppm. In this study, the authors discussed the magmatic processes of the Hirao granodiorite and petrogenesis of the low-Sr granitoids by comparing the Ushikiri-yama granodiorite (high-Sr granitoid, details reported by Eshima et al., 2019).

The Hirao granodiorite and the granite dike have similar mineral assemblage, consisting mainly of plagioclase, quartz, K-feldspar, biotite and hornblende. In addition, the granodiorite and the granite dike geochemically resemble each other; for instance, their REE patterns and Sr-Nd isotopic values. The result of mass balance calculation reveals that the granite dike magma can be formed by subtraction of plagioclase and hornblende from the Hirao granodiorite magma.

The different Sr contents between the high- and low-Sr granitoids in this region can be explained by the following magmatic processes; magma mixing, assimilation of host rock, degree of fractional crystallization or partial melting, and composition of source materials. The magma mixing and assimilation of the host rocks were ruled out in terms of field occurrence. The geochemical study including trace elements and Sr-Nd isotopic compositions revealed that the Hirao granodiorite and the Ushikiri-yama granodiorite were shared with similarity source materials. Moreover, the magmatic processes of the both granodiorite were similar regarding the degree of fractionation and partial melting. Considering geochemical characteristics combined with melting experiments, the Hirao granodiorite representative of the low-Sr granitoid magma can be produced by relatively low-pressure melting rather than the high-Sr granitoid; thereby, leaving plagioclase as the residual phase at the source region.

Keywords: North Kyushu, Granitoids

©2020. Japan Geoscience Union. All Right Reserved.

[E] Poster | S (Solid Earth Sciences)：S-CG Complex & General

[S-CG56] ICDP Oman Drilling Project: Oman to Oceanic Lithosphere to Island Arc Formation and Beyond

convener:Eiichi TAKAZAWA(Department of Geology, Faculty of Science, Niigata University), Katsuyoshi Michibayashi(Department of Earth and Planetary Sciences, Nagoya University), Sayantani Chatterjee(Niigata University, Department of Geology, Faculty of Science)

The on-going Oman Drilling Project has drilled numerous hard-rock cores of ancient oceanic lithosphere and the underlying subduction zone of the Samail ophiolite in Oman, with support from ICDP, IODP, the Sloan Foundation's Deep Carbon Observatory, and Japanese, US, and European research agencies. In this session, we invite presentations on the scientific results of Oman Drilling Project. We also invite related studies of on-land geological investigations of Oman ophiolites and experimental studies. The session is intended to be interdisciplinary, including the fields of geophysics, geochemistry, petrology, engineering, and biology.

[SCG56-P01] Numerical prediction of effect of olivine content for proceeding of serpentinization

*Kazuki Yoshida[1], Atsushi Okamoto[1], Ryosuke Oyanagi[2], Hiroyuki Shimizu[3], Noriyoshi Tsuchiya[1], Oman Drilling Project Phase 2 Science Party (1.Tohoku university, 2.Japan Agency for Marine-Earth Science and Technology, 3.Kajima Corporation)

[SCG56-P02] Variable occurrences of magnetite and iron mobility during serpentinization: insights from samples from CM1A of Oman Drilling Project

★Invited Papers

*Ryosuke Oyanagi[1], Kazuki Yoshida[2], Yasuhiro Niwa[3], Yasuo Takeichi[3], Masao Kimura[3], Kenta Yoshida[1], Atsushi Okamoto[2], Oman Drilling Project Phase 2 Science Party (1.Japan Agency for Marine-Earth Science and Technology (JAMSTEC), 2.Graduate school of environmental studies, Tohoku University, 3.High Energy Accelerator Research Organization (KEK))

[SCG56-P04] Crack aspect ratio in the serpentinized peridotites inferred from onboard ultrasonic data by the Oman Drilling Projects

★Invited Papers

*Ikuo Katayama[1], Natsue Abe[2], Keishi Okazaki[3], Kohei Hatakeyama[1], Yuya Akamatsu[1], Katsuyoshi Michibayashi[4], Marguerite Godard[5], Peter B Kelemen[6], Phase 2 Science Party The Oman Drilling Project (1.Department of Earth and Planetary Systems Science, Hiroshima University, 2.Mantle Drilling Promotion Office, MarE3, JAMSTEC, 3.Kochi Institute for Core Sample Research, JAMSTEC, 4.Department of Earth and Planetary Sciences, Nagoya University, 5.Géosciences Montpellier, CNRS, Université de Montpellier, 6.Lamont Doherty Earth Observatory, Columbia University)

[SCG56-P05] Pore geometry in diabase collected by the Oman DP inferred from elastic wave velocity

*KUMPEI NAGASE[1], Ikuo Katayama[1], Kohei Hatakeyama[1], Yuya Akamatsu[1], Keishi Okazaki[2], Natsue Abe[3], Katsuyoshi Michibayashi[4] (1.Department of Earth and Planetary Systems Science, Graduate School of Science, Hiroshima University, 2.Japan Agency for Marine-Earth Science Technology, 3.Mantle Drilling Promotion Office, MarE3, Japan Agency for Marine-Earth Science and Technology, 4.Department of Earth and Planetary Sciences, Graduate School of Environmental Studies, Nagoya University)

[SCG56-P06] Water Content in Nominally Anhydrous Mineral of Crust/Mantle Boundary Recovered by International Oman Drilling Project

*Muhamad Asyraf Aminuddin[1], Tomoaki Morishita[1,2], Juan Miguel Ramirez Guotana[1,2], Keita Itano[1], Kenji Shimizu[3], Takayuki Ushikubo[3] (1.Kanazawa University Graduate School Natural Science and Technology, 2.Oman Science Party, 3.Kochi Institute for Core Sample Research,JAMSTEC)

[SCG56-P08] Microstructures, bulk and mineral chemistry of the gabbro cores of Holes GT1A and GT2A drilled in the Oman Drilling Project – Melt distribution in the subaxial lower crust
★Invited Papers

*Susumu Umino[1,3], Takahiro Fudai[1], Osamu Ishizuka[2], Yuki Kusano[2] (1.Kanazawa University, 2.Geological Survey of Japan, 3.JAMSTEC)

[SCG56-P09] Trace element and Sr isotopic compositions of gabbros and peridotites at the CM1A drilling site of Wadi Tayin block in the Oman ophiolite

*Masako Yoshikawa[1], Tomoaki Morishita[2], Ryoko Senda[3], Tomoyuki Shibata[1] (1.Department of Earth and Planetary systems Science, Hiroshima University, 2.Faculty of Geosciences and Civil Engineering, Kanazawa University, 3.Faculty of Social and Cultural Studies, Kyushi University)

[SCG56-P10] **First geochemical and mineralogical results of Oman Crust-Mantle transition: holes CM1A and CM2B characterization aboard DV-Chikyu_ Oman Drilling Project, Phase 2 Leg3**

*Fatma Kourim[1], Mathieu Rospabé[2], Sayantani Chatterjee[3], Manolis Giampouras[4], Keisuke Ishii Ishii[3], Akihiro Tamura[5], Nick Dygert[6], Ryosuke Oyanagi[2], Kou-Lung Wang[1,7], Marguerite Godard [8], Mathieu Benoit[9], Damon A-H Teagle[10], Eiichi Takazawa Takazawa[11,3], Peter Kelemen[11], Jude Coggon[10], Oman Drilling Project Phase 2 Science Party (1.Institute of Earth Sciences, Academia Sinica, 2.Research Institute for Marine Geodynamics, JAMSTEC, 3.Nigata University, 4.University of Granada, 5.Kanazawa University, 6.The university of Tennessee, 7.National Taiwan University, 8.University of Montpellier, 9.Toulouse university, 10. Southampton University, 11.Columbia University)

[SCG56-P11] Petrological study of the crust-mantle boundary using CM2B cores from the ICDP Oman Drilling Project.

*Natsuki Oyanagi[1], Eiichi TAKAZAWA[1,2], Sayantani Chatterjee[1], Oman Drilling Project Phase 2 Science Party (1.Faculty of Science, Niigata University, 2.VERC, IMG, JAMSTEC)

[SCG56-P12] Mantle-melt reaction recorded in the ICDP Oman Drilling Project Hole CM2B in Wadi Tayin massif of the Samail ophiolite

*Eiichi TAKAZAWA[1,2], Natsuki Oyanagi[1], Sayantani Chatterjee[1], Fatma Kourim[3], Katsuyoshi Michibayashi[4], Oman Drilling Project Phase 2 Science Party (1.Department of Geology, Faculty of Science, Niigata University, 2.VERC, IMG, JAMSTEC, 3.Institute of Earth Sciences, Academia Sinica, 4.Graduate School of Environmental Studies, Nagoya University)

[SCG56-P13] **High resolution X-ray computed tomography and scanning electron microscopy studies of inclusions in Oman podiform chromitite: implications for rapid cooling in Moho Transition Zone**

*Yuan YAO[1], Eiichi TAKAZAWA[2,3], Sayantani CHATTERJEE[2], Antonin RICHARD[4], Christophe MORLOT[4], Laura CRÉON[5], Salim AL-BUSAIDI[6], Katsuyoshi MICHIBAYASHI[7] (1.Graduate School of Sciences & Technology, Niigata University, 2.Department of Geology, Faculty of Science, Niigata University, 3.Volcanoes and Earth's Interior Research Center, Research Institute for Marine Geodynamics, Japan Agency for Marine-earth Science and Technology, 4.Université de Lorraine, CNRS, GeoRessources lab, France, 5.Sorbonne Université, nstitut de Minéralogie, de Physique des Matériaux et de Cosmochimie (IMPMC), France, 6.Maadin Enterprises LLC, Oman, 7.Department of Earth & Planetary Sciences, Graduate School of Environmental Studies, Nagoya University)

[SCG56-P14] **Silicate inclusions in dispersed chromites at the mantle-crust transition zone: the link between dunite and chromitite formations**

*Mathieu Rospabe[1], Georges Ceuleneer[2], Mathieu Benoit[2], Mary-Alix Kaczmarek[2] (1.Research Institute for Marine Geodynamics (IMG), Japan Agency for Marine-Earth Science and Technology, 2.Géosciences Environnement Toulouse (GET), Observatoire Midi-Pyrénées, Université de Toulouse, CNRS, IRD)

[SCG56-P15] **Mantle petrological mapping in the Oman ophiolite reveals large scale heterogeneities possibly in relation with mantle source variation**

Tomoya Suzuki[1], *Marie Python[1], Main Tokinaga[1], Masako Yoshikawa[2], Georges Marie Ceuleneer[3], Shoji Arai[4] (1.Hokkaido University Department of Natural History Science Division of Earth and Planetary Systems Sciences, 2.Department of Earth and Planetary systems Science, Hiroshima University, 3.Université Paul Sabatier, GET, OMP, Toulouse, 4.Department of Earth Sciences, Faculty of Science, Kanazawa University)

[SCG56-P16] Peridotites beneath the ophiolite: Petrology and chemistry of peridotite bodies located below the metamorphic sole of the Oman ophiolite

Main Tokinaga, Marie Python, Georges Ceuleneer, Tomoya Suzuki and Jean-Paul Breton

*Tokinaga Main[1] (1.Hokkaido University Department of Natural History Science Division of Earth and Planetary Systems Sciences)

[SCG56-P17] Evolution of Island Arc Volcanoes: Ankaramite-Andesite-Basalt (ANANBA) Model

*Yoshihiko Tamura[1], Tomoki Sato[1], Osamu Ishizuka[1], Yasuhiro Hirai[1], Takashi Miyazaki[1] (1.Research Institute for Marine Geodynamics, Japan Agency for Maine-Earth Science and Technology)

Numerical prediction of effect of olivine content for proceeding of serpentinization

*Kazuki Yoshida[1], Atsushi Okamoto[1], Ryosuke Oyanagi[2], Hiroyuki Shimizu[3], Noriyoshi Tsuchiya[1], Oman Drilling Project Phase 2 Science Party

1. Tohoku university, 2. Japan Agency for Marine-Earth Science and Technology, 3. Kajima Corporation

The extent and progress of serpentinization within the oceanic lithosphere is a key to understanding global water circulation within the Earth's interior and seismicity at subduction zone. However, the mechanism to control the serpentinization rate of the oceanic lithosphere is still unclear. In this study, we reveals the importance of modal abundance of olivine grains on the feedback among fluid flow, fracturing and reaction based on the analyses of natural rocks and numerical modeling by distinct element method (DEM). The analyzed rocks are taken from Oman Drilling Project hole CM1A which through the crust-mantle transition zone. The analyzed rocks are olivine-gabbro, troctolite, dunite and wehrlite which show a large variation of the amounts of olivine. In troctolite and olivine gabbros, characteristic fracture patterns are observed: mesh-like texture within olivine grains and radial cracking around the olivine grains. Serpentine was observed along these fractures in olivine grains, it is suggesting that these fracture was a main fluid pathway during serpentinization. Moreover, a positive relationship was found between moral abundance of olivine and the extent of serpentinization.

The numerical simulation based on two-dimensional distinct element method (DEM) combining fluid advection and reaction (Shimizu and Okamoto., 2016) was conducted to examine the effect of amount of olivine grains to unreacted matrix. We consider a simple volume increasing hydration reaction (150% volume increase), and the rock model consist of reactive part (olivine) and unreactive part (plagioclase and pyroxene). We conducted five conditions varying distance between each olivine grains. As the result, the olivine grains made connected fracture network, which increase in permeability and reaction progress. However, when too low olivine content, it could not make enough fracture for reaction proceeding. In the other hands, when too much olivine amount condition, the permeability and bulk reaction progress become less because volume expansion caused fracture clogging which inhibited further fluid infiltration to fresh olivine grains.

These results suggest that (1) an increase of olivine amount results in development of fracture network to percolate fluids, but (2) too much olivine amounts prevent the fluid flow as volume-expansion close the fractures which obstruct fluid penetration. The discrepancy between natural observation and numerical modeling for dunite suggest the importance of other fluid pathways such as nano-scale pores in serpentine for complete serpentinization.

Shimizu, H., Okamoto, A., 2016. The roles of fluid transport and surface reaction in reaction-induced fracturing, with implications for the development of mesh textures in serpentinites. Contributions to Mineralogy and Petrology, 171, 73.

Keywords: Serpentinization, Discrete Element Method, Oceanic lithosphere

©2020. Japan Geoscience Union. All Right Reserved.

Variable occurrences of magnetite and iron mobility during serpentinization: insights from samples from CM1A of Oman Drilling Project

*Ryosuke Oyanagi[1], Kazuki Yoshida[2], Yasuhiro Niwa[3], Yasuo Takeichi[3], Masao Kimura[3], Kenta Yoshida[1], Atsushi Okamoto[2], Oman Drilling Project Phase 2 Science Party

1. Japan Agency for Marine-Earth Science and Technology (JAMSTEC), 2. Graduate school of environmental studies, Tohoku University, 3. High Energy Accelerator Research Organization (KEK)

Serpentinization of the oceanic lithosphere provides significant impacts on biological activities at seafloors, as oxidation of Fe^{2+} in olivine results in a reduction of water to produce hydrogen and hydrocarbons. In serpentinized peridotites, Fe^{3+} is mostly contained in magnetite. However, the distribution of magnetite is not always uniform but commonly concentrated along veins. In addition, serpentine, which is the main constituent mineral of serpentinized peridotite, also can be a host phase for Fe^{3+}. Therefore, the behaviors of iron such as partitioning, mobility, and redox conditions, and their relation to hydrogen production during serpentinization are still poorly constrained. In this contribution, we report the preliminary results of micro- to nano-scale observation of magnetite and iron distribution within wehrlite and dunite at the crust-mantle boundary of the Samail ophiolite, recovered from the Oman Drilling Project hole CM1A. The synchrotron-based multi-scale X-ray CT images were taken by the beamline NW2A, PF-AR at KEK, Japan.

The wehrlite sample (CM1A-144Z-4-66-68) is partly serpentinized and olivine grains show mesh texture composed of mesh rim and veins. Mesh rim is composed of serpentine (Mg#~94) with minor brucite and magnetite. The vein in mesh texture is composed of serpentine (Mg#~95) + magnetite. Magnetite shows two types of occurrence: the first type of magnetite with a size of 1-2 μm occurs as planar aggregate at the center of the mesh veins. The second type of magnetite occurs in the mesh rim. The CT image reveals that the second type of magnetite accompanies pore with a size of ~0.5 μm, and seems to align. Within unreacted olivine mesh core, magnetite accompanying pore is also observed, which is similar to the second type of magnetite. Such occurrence suggests that the second type of magnetite was formed within fluid inclusions of olivine, and micro- to nano-scale pores were not collapsed during serpentinization although it essentially involves volume-increasing reactions.

In contrast to wehrlite, dunite (CM1A-90z) is completely serpentinized and cut by the later serpentine veins, which is a common feature of dunite samples from CM1A. In the matrix, magnetite uniformly occurs in size less than 5 μm, and does not show the evidence of mesh texture. The detailed observation revealed that later veins are composed of Fe-poor serpentine (Mg#~98) with reaction zones with plenty amount of magnetite. In the reaction zone, the euhedral magnetite with size in 10-30 μm was concentrated within the reaction zone. These occurrences suggest that magnetite was formed during serpentinization, iron could move by dissolution and precipitation processes in response to the infiltration of external fluids.

Keywords: serpentinization, hydrothermal alteration, Ferric iron, Magnetite

©2020. Japan Geoscience Union. All Right Reserved.

Crack aspect ratio in the serpentinized peridotites inferred from onboard ultrasonic data by the Oman Drilling Projects

*Ikuo Katayama[1], Natsue Abe[2], Keishi Okazaki[3], Kohei Hatakeyama[1], Yuya Akamatsu[1], Katsuyoshi Michibayashi[4], Marguerite Godard[5], Peter B Kelemen[6], Phase 2 Science Party The Oman Drilling Project

1. Department of Earth and Planetary Systems Science, Hiroshima University, 2. Mantle Drilling Promotion Office, MarE3, JAMSTEC, 3. Kochi Institute for Core Sample Research, JAMSTEC, 4. Department of Earth and Planetary Sciences, Nagoya University, 5. Géosciences Montpellier, CNRS, Université de Montpellier, 6. Lamont Doherty Earth Observatory, Columbia University

To assess pore geometry in the highly altered peridotites collected by the Oman Drilling Projects, we analyzed ultrasonic velocity of the serpentinized dunites and harzburgites from mantle sections at Holes BA1B, 3A, and 4A. First, we estimated serpentine fraction based on grain density to obtain the porosity-free reference velocity, suggesting a nearly complete serpentinization at shallow depth but decrease of hydration at deeper depth. We assumed that the difference between reference and measured velocity attributes to pores with spheroidal shape that are embedded in the samples. Application of effective medium theory to onboard P-wave and porosity data indicates that pore aspect ratio mostly lies between 0.1 and 0.01 and crack density is ranging from 0.58 to 0.02. We found a positive relationship between aspect ratio and serpentine fraction, suggesting a change in pore shape controlled mainly by the dissolution–precipitation processes during hydration, consistent with microstructural observations. The relatively high aspect ratio and hence high fluid flux at shallow depths also agree with the present-day hydration processes that are inferred from the borehole fluid chemistry. The inversion of ultrasonic data provides a series of elastic moduli, and we can estimate Poisson’ s ratio, which is a key physical property to interpret geophysical observations in the oceanic lithosphere.

Keywords: pore geometry, serpentinite, Oman ophiolite

©2020. Japan Geoscience Union. All Right Reserved.

Pore geometry in diabase collected by the Oman DP inferred from elastic wave velocity

*KUMPEI NAGASE[1], Ikuo Katayama[1], Kohei Hatakeyama[1], Yuya Akamatsu[1], Keishi Okazaki[2], Natsue Abe[3], Katsuyoshi Michibayashi[4]

1. Department of Earth and Planetary Systems Science, Graduate School of Science, Hiroshima University, 2. Japan Agency for Marine-Earth Science Technology, 3. Mantle Drilling Promotion Office, MarE3, Japan Agency for Marine-Earth Science and Technology, 4. Department of Earth and Planetary Sciences, Graduate School of Environmental Studies, Nagoya University

Geophysical survey observed anomalous low Vp/Vs ratio in oceanic upper crust (Spudich and Orcutt 1980). Although, it is previously explained by felsic rock such as trondhjemite is one of interpretation for such low Vp/Vs. Occurrence of trondhjemite is highly localized in ophiolite complexes (Christensen and Smewing 1981). Another possibly to explain is thick pore with large aspect ratio (shearer 1988). In this study, we measured physical properties of diabase collected from the Oman ophiolite, and we investigate pore aspect ratio from simultaneous measurement of velocity and porosity.
We developed simultaneous measurement system of elastic wave velocity and porosity under hydrostatic pressure, using Intra-vessel deformation and fluid flow apparatus at Hiroshima University. Elastic wave velocity and porosity were measured under confining pressure up to 200 MPa at fluid-saturated condition. Elastic wave velocity was measured by a pulse transmission method using both P- and S-wave piezoelectric transducers with a resonant frequency of 2 MHz. Porosity was calculated by initial porosity measured by pycnometer before compaction, and volume change of pore fluid after compaction using syringe pump. We used porous altered diabase with various porosity collected from the Oman Drilling project.
The experimental result shows that both P-wave and S-wave velocities increase with decreasing of porosity due to closing of pore. Sample with low porosity shows an increasing of Vp/Vs with increasing porosity whereas, sample with high porosity shows a decreasing of Vp/Vs with porosity. And then, we investigate pore aspect ratio from measured velocities and porosities based on application of effective medium theory by Kuster and Toksoz (1974). As a result, this implies that different aspect ratio in these samples, pore aspect ratio is more than an order of magnitude higher in the high porosity diabase. This implies that there is possibility that anomalous low Vp/Vs observed in the oceanic upper crust might be explained by the presence of pore with large aspect ratio.

Keywords: Oceanic crust, Ophiolite, Vp/Vs ratio, Aspect ratio

©2020. Japan Geoscience Union. All Right Reserved.

Water Content in Nominally Anhydrous Mineral of Crust/Mantle Boundary Recovered by International Oman Drilling Project

*Muhamad Asyraf Aminuddin[1], Tomoaki Morishita[1,2], Juan Miguel Ramirez Guotana[1,2], Keita Itano[1], Kenji Shimizu[3], Takayuki Ushikubo[3]

1. Kanazawa University Graduate School Natural Science and Technology, 2. Oman Science Party, 3. Kochi Institute for Core Sample Research,JAMSTEC

The presence of water in the Earth’ s mantle has been to have a prominent role in the volatile cycle of Earth’ s mantle but measuring water flux into the mantle proved to be difficult and not fully constraint. Nevertheless, measuring water content in the mantle have its importance. It is known that some portion of water can be stored in nominally anhydrous mineral (NAM) like olivine and pyroxene which support the presence of water in the deep mantle. The significance of water retained in such minerals are that it can cause deformation to the minerals such as olivine which is the most abundant mineral in the mantle. Measuring water content in the oceanic plate specifically in the crust-mantle section is the most practical as water retained in the oceanic plate should be nearly zero due to the upwelling of the asthenosphere causing partial melting to occur extracting water into the melt. Therefore, the objective of this study is to measure water content in the oceanic crust specifically in the crust-mantle boundary.

As direct sample from the crust-mantle section is unattainable, ophiolite is used for this water content analysis as samples with the idea of measuring water content in oceanic plate as ophiolite is tectonically originated from mid-ocean ridge. However, some studies showed ophiolite might be affected by a later subduction zone tectonic setting (Lippard *et al.,* 1986) where second stage magmatism occurred at the subduction zone during obduction process. Thus, a high-water content could prove that ophiolite might be affected by subduction metasomatism. Ophiolite samples were from core samples recovered by International Oman Drilling Project in Samail Ophiolite, Oman. The core recovered reached about 400m depth and consists of layered gabbro (160 m), dunite (150 m) and harzburgite (75 m) with a compositionally gradational zone of 15m between dunite and harzburgite. Samples from each sequence (gabbro, dunite and harzburgite) of the core were used for water content analysis.

Secondary Ion Mass Spectrometry (SIMS) is used for water content analyses (Shimizu et al., 2017). SIMS have its disadvantage like high hydrogen background in low-concentration phases, but improved technique and procedure established by Hauri (Hauri et al., 2002; Koga et al., 2003: Shimizu et al., 2017) contributing for more reliable quantifications of low-level volatiles. Improved sample preparation technique and analytical sensitivity (Koga, 2003) are done like use of indium metal as embedment material instead of epoxy to limit the hydrogen background (Koga et al., 2003: Shimizu et al., 2017). IMS-1280HR of SIMS instrument is used which are installed in the Kochi Institute for Core Sample Research, JAMSTEC with 20 keV of Cs^+ ion beam bombarded to the sample surface with diameter 10-15 micrometer. Negative secondary ions of $^{12}C^-$, $^{16}OH^-$, $^{19}F^-$, $^{30}Si^-$, $^{32}S^-$ and ^{35}Cl signals will be collected from the center of analysis spot. The internally corrected data using ^{30} Si signal intensity were calibrated by the analyses of glass and olivine standard materials with known H2O concentrations.

Based on the result, $^{16}OH/^{30}Si$ signal intensities value on the layered gabbro sample are consistent with no significant changes of value on the rims and core of olivine. In contrast, $^{16}OH/^{30}Si$ signal intensities value on the dunite and harzburgite showed uncertainties where high hydrogen background occurred due to the presence of serpentine in the sample that prevent water to be completely removed during

©2020. Japan Geoscience Union. All Right Reserved.

degassing process prior analysis. Despite that, we can certain that the water content measured in gabbro sample is 34 ppm on average and the water content measured in dunite and harzburgite are on the range of 30-50 ppm. When comparing the value to the previous study of water content of olivine in natural peridotites obtained by Secondary Ion Mass Spectrometry (Kurosawa et. al., 1997, Warren & Hauri, 2014), the water content in olivine are significantly high. The explanation of high-water content of olivine is related to hydrous melting. Hydrous melting is where the presence of water in the mantle lower the solidus temperature allowing melts to be formed. The hydrous melting occurred in ophiolite support that subduction metasomatism might happened in ophiolite.

Keywords: Ophiolite, Nominally anhydrous minerals, Oman, Olivine, Secondary Ion Mass Spectrometry (SIMS)

©2020. Japan Geoscience Union. All Right Reserved.

Microstructures, bulk and mineral chemistry of the gabbro cores of Holes GT1A and GT2A drilled in the Oman Drilling Project –Melt distribution in the subaxial lower crust

*Susumu Umino[1,3], Takahiro Fudai[1], Osamu Ishizuka[2], Yuki Kusano[2]

1. Kanazawa University, 2. Geological Survey of Japan, 3. JAMSTEC

The lower crustal section of the Oman Ophiolite was drilled in the Oman Drilling Project in 2016 to 2017 and recovered 400 m long cores each from Hole GT1A and GT2A in Wadi Gideah, north of Ibra. The purpose of this research is to correlate the microstructures and the amount of trapped melt of the gabbro samples and to understand the conditions of magmatic and hypersolidus deformation that operated in the lower crust beneath the Oman paleoridge axis.

Cored samples are predominantly olivine gabbros consisting of anhedral olivine, anhedral to subhedral clinopyroxene and subhedral to euhedral plagioclase. Deformed olivine aggregates and clinopyroxene with quarter structures are embedded in plagioclase with equilibrium granoblastic textures and large euhedral plagioclases with resorbed turbid cores. Considering these textures combined with the mechanical strength of the three constituent minerals, these gabbros suffered deformation under the presence of melt, which assisted complete recovery of strain through recrystallization of fine-grained plagioclase and overgrowth of euhedral rims around magmatic plagioclase cores. Poikilitic and ophitic clinopyroxene occur sporadically throughout the holes, which are commonly present in the upper gabbros. Hypersolidus deformation structures are present irrespective to depth.

The whole-rock Mg#s of gabbro core samples from stratigraphically lower and higher sections (Hole GT1A and GT2A) range in 72-83 and 68-79, respectively. The lowest Mg#s of 72-74 overlap those of the spreading-stage sheeted dikes. The whole-rock Al_2O_3 versus MgO plots indicate the whole-rock compositions are mainly controlled by accumulated plagioclase, olivine, clinopyroxene associated with a small amount of primitive melts. The whole-rock Mg# and incompatible elements (REEs and HFSEs) are lower and higher in GT2A, suggesting larger amounts of trapped melt at higher levels in the lower crust. Clinopyroxene preserve cores with higher Mg# than the rims and surrounding smaller clinopyroxenes. Lower Ti in the core and jumps in Ti concentration define the core-rim boundary of clinopyroxenes, through which Mg# gradually changes. In addition to this, olivine grains are almost homogeneous and consistently lower in Mg# than the clinopyroxenes with reversed rims in contact with olivines, indicating diffusive Fe-Mg exchange between olivine and clinopyroxene during cooling.

The amounts of trapped melt between cumulus phases were estimated by two ways. First one is to determine La and Ce concentrations in the core of clinopyroxenes with LA-ICP-MS. Second one assumes La and Ce concentrations of trapped melts to be equivalent to those of the sheeted dikes, and estimates the sheeted dike compositions by using an Fe-Mg partition coefficient of 0.275 (Putirka, 2003) between clinopyroxene and the melt. Mass balance calculations yield the amount of trapped melt in gabbros to be 5 to 10 mass% in general and 25 mass% at most.

Poorly developed modal layering, evidence of common hypersolidus deformation, ubiquitous presence of zoned cumulus minerals and common ophitic clinopyroxenes as well as the amount of trapped melt >5 mass% are all characteristics of foliated gabbros. In addition to this, field observations of the gabbros

©2020. Japan Geoscience Union. All Right Reserved.

along Wadi Gideah, including the Site GT1A and GT2A show that the gabbroic rocks poorly develop modal layering but foliation defined by shape-preferred orientation of clinopyroxenes in the most stratigraphic levels, including both GT1A and GT2A holes. Layered gabbros with well-developed modal layering are only present in the lowermost levels in the crust just above the Moho Transition Zone.

We concluded that both GT1A and GT2A sampled the thick foliated gabbros in Wadi Gideah section, which crystallized on the axial melt lens floor and were transported downward in the lower crust.

Keywords: Oman ICDP, GT1A, GT2A, Lower oceanic crust, Gabbro glacier, Foliated gabbro

©2020. Japan Geoscience Union. All Right Reserved.

Trace element and Sr isotopic compositions of gabbros and peridotites at the CM1A drilling site of Wadi Tayin block in the Oman ophiolite

*Masako Yoshikawa[1], Tomoaki Morishita[2], Ryoko Senda[3], Tomoyuki Shibata[1]

1. Department of Earth and Planetary systems Science, Hiroshima University, 2. Faculty of Geosciences and Civil Engineering, Kanazawa University, 3. Faculty of Social and Cultural Studies, Kyushi University

Detailed petrological structure of the oceanic plate, which covers around 70% of the earth's surface, is still a debate due to difficulty in obtaining samples directly. Petrological section of the oceanic plate and its physical and chemical characteristics have been suggested from detailed observations of ophiolite, as ophiolites are believed to be fragments of the oceanic plate obducted to the surface by tectonic thrusting. However, it has been pointed out that geochemical signature of constituent rocks of ophiolite has often been affected by weathering and metamorphism during/after obduction which have severely changed their original elemental and isotopic compositions (e.g., Pearce & Cann, 1971).

The Oman ophiolite is one of the best preserved sections of oceanic plate (oceanic crust and upper mantle) worldwide, and consists of multiple blocks that lie along more than 400 km of the Arabian coast (eg, Nicolas et al., 1988). The Oman Drilling Project by the International Scientific Drilling Program was proceeded at multiple sites in the Oman ophiolite. We study samples of the CM1A site that penetrates the crustal-mantle boundary of the Wadi Tayin block in the southern Oman ophiolite.

The core sample is 404.15 m in length, composed mainly with olivine gabbro in the upper 160 m (Layered Gabbro sequence), with massive dunite from 160 m to 310 m (Crust-Mantle Transition sequence), and with deeper harzburgite (Mantle sequence)(Takazawa et al., 2019). Geochemical and isotopic compositions of these samples are expected to provide a continuous chemical composition of the oceanic plate, including the crustal-upper mantle boundary without chemical modification by surface weathering and metamorphism.

We analyzed trace element compositions of two gabbro samples and a dunite sample from Layered Gabbro sequence, three dunite samples from Crust-Mantle Transition sequence, and a harzburgite sample from Mantle sequence. Trace element concentrations generally decrease from the gabbros in Layered Gabbro sequence to the dunites in Crust-Mantle Transition sequence through the dunite in Layered Gabbro sequence and the harzburgite in the Mantle sequence. Multi-elemental patterns of samples, that is trace element concentrations normalized to mid-ocean ridge basalt, show following signatures; (1) the gabbros have gently convex shape at medium rare earth elements (REEs) with positive anomalies of Ba, Pb, Sr and Eu and negative anomalies of Th and U relative to neighboring REEs, (2) multi-element patterns of the dunite in Layered Gabbro sequence share depleted pattern from heavy REEs to medium REEs with positive anomalies of Sr and Eu of the harzburgite in Mantle sequences. The dunite, however, shows depleted pattern from middle REEs to light REEs, while the harzburgite shows enriched pattern with incompatible elements compared to middle REEs, and (3) the dunite samples in Crust-Mantle Transition sequence show U-shaped patterns, and extensive positive anomalies of Pb and Sr relative to surrounding elements.

We will report Sr isotopic compositions of these samples by comparing to the data from the Oman

©2020. Japan Geoscience Union. All Right Reserved.

outcrop samples.

References

Nicolas et al., Tectonophysics, 1989; Pearce & Cann, EPSL, 1971; Takazawa et al., Abs of JpGU, 2019

Keywords: Oman Drilling Project, gabbro, peridotites, trace elements, Sr isotopic ratios

©2020. Japan Geoscience Union. All Right Reserved.

First geochemical and mineralogical results of Oman Crust-Mantle transition: holes CM1A and CM2B characterization aboard DV-Chikyu_ Oman Drilling Project, Phase 2 Leg3

*Fatma Kourim[1], Mathieu Rospabé[2], Sayantani Chatterjee[3], Manolis Giampouras[4], Keisuke Ishii Ishii[3], Akihiro Tamura[5], Nick Dygert[6], Ryosuke Oyanagi[2], Kou-Lung Wang[1,7], Marguerite Godard [8], Mathieu Benoit[9], Damon A-H Teagle[10], Eiichi Takazawa Takazawa[11,3], Peter Kelemen[11], Jude Coggon[10], Oman Drilling Project Phase 2 Science Party

1. Institute of Earth Sciences, Academia Sinica, 2. Research Institute for Marine Geodynamics, JAMSTEC, 3. Nigata University, 4. University of Granada, 5. Kanazawa University, 6. The university of Tennessee, 7. National Taiwan University, 8. University of Montpellier, 9. Toulouse university, 10. Southampton University, 11. Columbia University

The transition from the crust to the mantle of Oman ophiolite was drilled at Holes CM1A and CM2B (Wadi Tayin Massif) during Phase 2 of the Oman Drilling Project (Nov. 2017-Jan. 2018). The 400m-long Hole CM1A core crosses from the lower crust, through the crust-mantle transition zone, into residual upper mantle peridotites. The 300m-long Hole CM2B core samples the crust-mantle transition zone and underlying residual mantle peridotites. The main logged lithological units are olivine gabbro, gabbro, dunite, harzburgite and wehrlite, associated with minor gabbronorite, troctolite, websterite, anorthosite, and chromitite. During Oman-DP Phase 2 Leg 3 (ChikyuOman; July-Aug. 2018), 95 and 67 samples of core from CM1A and CM2B, respectively, were analyzed for whole-rock major and minor elements (XRF) as well as CO_2 and H_2O concentrations (CHNS). XRD measurements were performed on the 69 onsite samples. Furthermore, whole-rock (pressed powder pellets) and mineral trace element contents were determined for selected samples onboard the D/V Chikyu, using the NewWave Research UP-213 Nd:YAG deep UV (213 nm) laser ablation system coupled with an Agilent 7500ce quadrupole ICP-MS.

Samples from holes CM1A and CM2B have a large petrological and chemical variability, mainly reflecting the different rock types, especially across the crust-mantle transition. CM1A and CM2B volatile element contents reflect extensive serpentinization linked to interaction with H_2O-rich fluids, and abundant carbonate veins downhole, suggesting an association between CO_2-rich fluids and serpentinization. Whole-rock and ortho- and clinopyroxene trace element abundances are similar to Oman ophiolite compositions described in previous studies. All gabbroic domains display nearly parallel REE patterns with a strong depletion in HFSE relative to REE. Dunites display variable trace element contents and REE patterns, negative or positive anomalies in Eu and commonly moderate to strong positive anomalies in U, Pb, Sr and Ti. The variation of REE concentrations and patterns observed in Oman dunites could be explained by melt-rock reactions leading to dunite formation, after the dissolution of orthopyroxene in harzburgite and interaction with interstitial melt.

Keywords: Oman crust-mantle transition, gabbros, dunite, harzburgite, Oman ophiolite, XRF, XRD, ICP-MS, LA-ICP-MS, Chikyu_OmanDP

©2020. Japan Geoscience Union. All Right Reserved.

Petrological study of the crust-mantle boundary using CM2B cores from the ICDP Oman Drilling Project.

*Natsuki Oyanagi[1], Eiichi TAKAZAWA[1,2], Sayantani Chatterjee[1], Oman Drilling Project Phase 2 Science Party

1. Faculty of Science, Niigata University, 2. VERC, IMG, JAMSTEC

In this study, a petrological and geochemical study was carried out on the origin of the crust-mantle boundary using the cores from Hole CM2B drilled by ICDP Oman Drilling Project in the Wadi Zeeb of the Wadi Tayin massif, southern Oman ophiolite. Many studies have been done on the origin of the crust-mantle transition zone (MTZ) in the Oman ophiolite, and various models have been proposed [1-9]. However, the process that created the boundary between the MTZ dunite and the mantle harzburgite has not been understood yet. This study aims to investigate the petrographic characteristics and mineral compositions of the cores from Hole CM2B, and to clarify the process forming the boundary between the MTZ and the mantle section.

Analytical results of mineral compositions revealed the presence of dunite with NiO content of olivine below the range of the olivine mantle array [10], indicating reactional fractional crystallization of olivine from a melt. There is also a dunite with a lower olivine Fo value than the range of olivine spinel mantle array (OSMA) [11], indicating the possibility of cumulus olivine crystallized from the melt. Furthermore, TiO_2 and Na_2O contents of clinopyroxene increased near the boundary between the MTZ dunite and the mantle harzburgite. Furthermore, clinopyroxenes in the dunites and harzburgites near the boundary between the MTZ and the mantle section are highly enriched in incompatible elements including rare earth elements (REEs).

We consider that the enrichment of incompatible elements at the boundary as a result of the zone melting of mantle harzburgite. The boundary between the MTZ and the mantle harzburgite is a kind of active reaction front where the dissolution of orthopyroxene (Opx) and precipitation of olivine continuously proceed to make dunitic MTZ thicker. For most of the incompatible elements the partition coefficients between Opx and melt are greater than those between olivine and melt. If the dissolution of Opx and precipitation of olivine continued for a long time to create a thick MTZ, the melt at the boundary becomes highly enriched in incompatible elements. This phenomenon is consistent with the presence of harzburgite, which has high spinel Cr# (=atomic Cr/[Cr + Al] ratio) and low olivine Fo value at the top of the mantle section.

On the other hand, the decrease in spinel Cr# in harzburgite at a depth of 260 m may be the result of a reaction with a melt flowing from the outside because of high Al_2O_3, TiO_2 and Na_2O contents and enrichment in REEs in the clinopyroxene at the corresponding depth compared to the surroundings.

[1] Pallister and Hopson, 1981, *J. Geophys. Res.*, **86**, 2593-2644.
[2] Kelemen et al., 1995, *Nature*, **375**, 747-753.
[3] Korenaga and Kelemen, 1997, *J. Geophys. Res.*, **102**, 27729-27749.
[4] Koga et al., 2001, *G-cubed*, **2**, 2000GC000132.
[5] Collier and Kelemen, 2010, *J. Petrol.*, **51**, 1913-1940.
[6] Abily and Ceuleneer, 2013, *Geol.*, **41**, 67-70.
[7] Rospabé et al., 2017, *Geol.*, 2017139.

©2020. Japan Geoscience Union. All Right Reserved.

[8] Rospabé et al., 2018, *Geochem. Cosmochim. Acta*, **234**, 1-23.
[9] Rospabé et al., 2019, *Earth Planet. Sci. Lett.*, **516**, 108-121.
[10] Takahashi and Uto, 1986, *Bull. Vol. Soc. Japan*, Sec. Ser., **30**, S17-S40.
[11] Arai, 1994, *Chem. Geol.*, **113**, 191-204.

Keywords: Oman ophiolite, crust-mantle boundary, Moho transition zone, mantle section, ICDP Oman Drilling Project

©2020. Japan Geoscience Union. All Right Reserved.

Mantle-melt reaction recorded in the ICDP Oman Drilling Project Hole CM2B in Wadi Tayin massif of the Samail ophiolite

*Eiichi TAKAZAWA[1,2], Natsuki Oyanagi[1], Sayantani Chatterjee[1], Fatma Kourim[3], Katsuyoshi Michibayashi[4], Oman Drilling Project Phase 2 Science Party

1. Department of Geology, Faculty of Science, Niigata University, 2. VERC, IMG, JAMSTEC, 3. Institute of Earth Sciences, Academia Sinica, 4. Graduate School of Environmental Studies, Nagoya University

At the crust - mantle boundary of the Oman ophiolite, there is a dunite dominant layer of dozens to hundreds of meters in thickness called the crust-mantle transition zone (MTZ) [1]. The formation of MTZ dunite can be attributed to the accumulation of olivine crystallized from MORB melt [2] and the reaction of orthpyroxene-undersaturated MORB melt with harzburgite [3-6], and the involvement of fluid [7-10]. The ICDP Oman Drilling Project carried out onshore drilling of the crustal-mantle boundary of the Oman ophiolite in order to clarify the formation process of the MTZ and its relation to the oceanic Mohorovicic discontinuity.

The drilling site is located in the Wadi Zeeb of Wadi Tayin massif in the southern Oman ophiolite. Hole CM1A (UTM: 40Q 637000E, 2533870N) and Hole CM2B (UTM: 40Q 637000E, 2534270N) were drilled, and 404.15m and 300.00m cores were collected at 100% recovery rate, respectively. In the summer of 2018, the detailed core description was carried out on the deep-sea science drilling vessel "Chikyu", and measurements of chemical and physical properties of the cores were performed using various instruments.

In this study we report the downhole variations of whole rock major and trace element compositions in Hole CM2B with special attention to the boundary between MTZ dunite and mantle harzburgite. Across this boundary orthopyroxene (Opx) disappears in the MTZ dunite. Whole rock CaO wt% decreases from 0.7-0.9 wt% in the harzburgite to 0.3-0.6 wt% in the dunites of the lower part of MTZ to less than 0.2 wt% in the dunites of the upper part of MTZ. The existence of intermediate dunite in the lower part of MTZ, often with thin layers of gabbro and plagioclase wehrlite, may impose constraints on the origin of the MTZ dunite.

In the chondrite-normalized pattern of rare earth elements (REEs) in whole rock, most of the harzburgites show a spoon-shaped pattern depleted in middle rare earth elements, while the harzburgite at the contact to the MTZ dunite shows a convex upward pattern with enrichment in middle to heavy rare earth elements. A similar tendency is also observed in the clinopyroxenes in dunite and harzburgite. Clinopyroxenes in the harzburgites near the boundary between MTZ dunite and mantle harzburgite are most enriched in incompatible elements including REE.

The harzburgites and dunites at the boundary between MTZ dunite and mantle harzburgite are most strongly influenced by the reaction with the melt that formed MTZ dunite by the dissolution of opx and precipitation of olivine [3]. The top of the mantle harzburgite is thought to have been a reaction front where harzburgite reacts with the melt and converts it to dunite. It is considered that the MTZ became thicker as the reaction front moved deeper. In the process of dissolving Opx and crystallizing olivine, it is possible that a similar mechanism to zone melting was activated at the reaction front, causing the concentration of incompatible elements in the melt. The equilibrium with such a melt has made peridotites enriched in incompatible elements at the boundary.

©2020. Japan Geoscience Union. All Right Reserved.

[1] Boudier and Nicolas (1995) *J. Petrol.*, **36**, 777-796.
[2] Pallister and Hopson, 1981, *J. Geophys. Res.*, **86**, 2593-2644.
[3] Kelemen et al., 1995, *Nature*, **375**, 747-753.
[4] Korenaga and Kelemen, 1997, *J. Geophys. Res.*, **102**, 27729-27749.
[5] Collier and Kelemen, 2010, *J. Petrol.*, **51**., 1913-1940.
[6] Abily and Ceuleneer, 2013, *Geol.*, **41**, 67-70.
[7] Koga et al., 2001, *G-cubed*, **2**, 2000GC000132.
[8] Rospabé et al., 2017, *Geol.*, 2017139.
[9] Rospabé et al., 2018, *Geochem. Cosmochim. Acta*, **234**, 1-23.
[10] Rospabé et al., 2019, *Earth Planet. Sci. Lett.*, **516**, 108-121.

Keywords: Oman ophiolite, mantle section, mantle-melt reaction, crust-mantle transition zone, Mohorovicic discontinuity

©2020. Japan Geoscience Union. All Right Reserved.

High resolution X-ray computed tomography and scanning electron microscopy studies of inclusions in Oman podiform chromitite: implications for rapid cooling in Moho Transition Zone

*Yuan YAO[1], Eiichi TAKAZAWA[2,3], Sayantani CHATTERJEE[2], Antonin RICHARD[4], Christophe MORLOT[4], Laura CRÉON[5], Salim AL-BUSAIDI[6], Katsuyoshi MICHIBAYASHI[7]

1. Graduate School of Sciences & Technology, Niigata University, 2. Department of Geology, Faculty of Science, Niigata University, 3. Volcanoes and Earth's Interior Research Center, Research Institute for Marine Geodynamics, Japan Agency for Marine-earth Science and Technology, 4. Université de Lorraine, CNRS, GeoRessources lab, France, 5. Sorbonne Université, nstitut de Minéralogie, de Physique des Matériaux et de Cosmochimie (IMPMC), France, 6. Maadin Enterprises LLC, Oman, 7. Department of Earth & Planetary Sciences, Graduate School of Environmental Studies, Nagoya University

High-Cr# (= atomic Cr/[Cr + Al]) chromite has been observed as the lining of inclusions within the host chromite, and has been proposed to have originated as early crystallizing microcrystals[1]. These high-Cr# chromite lining, however, cannot be explained by the host chromite–melt reactions, and consequently its origin remains controversial. Moreover, the genesis and the evolution of the inclusions are poorly understood. In this study, we used high resolution x-ray computed tomography (HRXCT) combined with scanning electron microscope (SEM) to obtain 3D and 2D images of inclusions within chromites from the Samail ophiolite to investigate the evolution of melt inclusions within chromite.

The 3D HRXCT and SEM images showed the spatial distributions of inclusions and the skeletal morphology of the host chromite. Under the rapid cooling, the host chromites grew skeletal crystals to trap melt inclusions [2]. After trapping melt inclusions, the host chromite continued to grow on the inner wall of the inclusions [3]. This overgrowth may be recognized as a high-Cr# chromite lining. Many previous studies of the inclusions in chromites have ignored the influence of the formation of lining [4]. The initial Cr content of the melt inclusions should have been much higher than previously estimated, suggesting that the parental melt for the chromitite may have been highly enriched in Cr, being supersaturated in chromite. Moreover, the 3D distribution of inclusions in host chromite with skeletal morphology implies that the formation of inclusions depended on the cooling rate of chromite-forming melt, implying that the parental melt of the chromitite was rapidly cooled in the Moho Transition Zone.

References

[1] Borisova, A. Y., Ceuleneer, G., Kamenetsky, V. S., Arai, S., Béjina, F. and Abily, B. (2012). A New View on the Petrogenesis of the Oman Ophiolite Chromitites from Microanalyses of Chromite-hosted Inclusions. Journal of Petrology, 53, 2411–2440.

[2] Prichard, H. M., Barnes, S. J. and Godel, B. (2018). A mechanism for chromite growth in ophiolite complexes: evidence from 3D high-resolution X-ray computed tomography images of chromite grains in Harold's Grave chromitite in the Shetland ophiolite. Mineralogical Magazine, 82, 457–470.

[3] Roedder, E. (1984). Fluid inclusions (Vol. 12). pp. 25–44, Reviews in Mineralogy, Mineralogical Society of America, Washington, D.C., 49-60

[4] Rollinson, H., Mameri, L. and Barry, T. (2018). Polymineralic inclusions in mantle chromitites from the

©2020. Japan Geoscience Union. All Right Reserved.

Oman ophiolite indicate a highly magnesian parental melt. Lithos, 310–311, 381–391.

Keywords: Chromitite, Melt inclusion, Samail ophiolite, Oman Drilling Project

©2020. Japan Geoscience Union. All Right Reserved.

Silicate inclusions in dispersed chromites at the mantle-crust transition zone: the link between dunite and chromitite formations

*Mathieu Rospabe[1], Georges Ceuleneer[2], Mathieu Benoit[2], Mary-Alix Kaczmarek[2]

1. Research Institute for Marine Geodynamics (IMG), Japan Agency for Marine-Earth Science and Technology, 2. Géosciences Environnement Toulouse (GET), Observatoire Midi-Pyrénées, Université de Toulouse, CNRS, IRD

Melt-rock reactions have a significant impact on the mineralogical and chemical composition of mantle peridotite. Observations in ophiolites and more patchy data from oceanic drilling show that below oceanic spreading centres, MORB-peridotite interaction at the transition between the mantle and the oceanic crust leads to the formation of a thick dunitic layer hosting chromitites ore bodies. Dunite and chromitite appear then to be two companion products of a common melt-peridotite reaction.

The petrological processes that originate the dunitic mantle-crust transition zone (DTZ) can be studied in the Maqsad area (Oman ophiolite) where is exposed a paleo-mantle diapir that fed the former spreading centre with MOR-like melts. The DTZ reaches more than 300 m in thickness atop the central part of the paleo-diapir. Interstitial melt suffered crystallization during its migration, comprising mainly plagioclase, clinopyroxene, but also orthopyroxene and pargasitic amphibole. The presence of such minerals witness migration of a hydrous melt that is restricted to this level and does not reach deeper levels in the mantle section. It was tentatively attributed to a parent melt hybrid between the MORB generated by the deep partial melting of the mantle and a hydrated fluid fraction coming from above, likely seawater in origin (Rospabé et al., 2017, *Geology*).

The presence of orthopyroxene and amphibole, together with mica, enclosed in chromite grains (scattered in dunites and in chromitites) strongly suggests that this hybrid melt was involved early in both the formation of dunite and the re-mobilization of chromium at the Maqsad mantle-crust transition zone (Borisova et al., 2012, *Journal of Petrology*; Rospabé et al., 2017, *Geology*). By the detailed and systematic study of the silicate inclusions enclosed in the chromite grains dispersed in the DTZ, we show they are an excellent target to make the link between the dunite and the chromitite ore bodies of higher grade. Our results suggest that the ore genesis processes involved in the formation of chromitites are not restricted to the ore bodies themselves but operated on the much larger scale of the whole DTZ. It leads to consider the entire DTZ as an ore deposit. In this spirit, the DTZ dunites may be regarded as low grade dispersed ore.

Keywords: Oman ophiolite, dunitic mantle-crust transition zone, chromite, silicate inclusions, fluid-melt-rock reactions

©2020. Japan Geoscience Union. All Right Reserved.

Mantle petrological mapping in the Oman ophiolite reveals large scale heterogeneities possibly in relation with mantle source variation

Tomoya Suzuki[1], *Marie Python[1], Main Tokinaga[1], Masako Yoshikawa[2], Georges Marie Ceuleneer[3], Shoji Arai[4]

1. Hokkaido University Department of Natural History Science Division of Earth and Planetary Systems Sciences, 2. Department of Earth and Planetary systems Science, Hiroshima University, 3. Université Paul Sabatier, GET, OMP, Toulouse, 4. Department of Earth Sciences, Faculty of Science, Kanazawa University

Long debate have been hold about the tectonic setting of the Oman ophiolite. Some researcher outlining the MORB affinity of most magmatic features in favour of a mid-ocean ridge setting and other insisting on the ultra-depleted nature of the mantle and the petrological and chemical characteristics of the metamorphic sole as support for a supra-subduction zone setting. Recent studies have suggested that the tectonic settings may have switched from an open ocean to a subduction zone, explaining most of the characteristics of the ophiolite as well as that of the metamorphic sole.

Magmatic dykes present within the mantle section show that several type of magma may have circulated in the Oman ophiolite: a MORB-like end-member melt and more a more depleted end-member melt, richer in Si with possible andesitic affinity. Only little mixing between these two end-members is observed in the mantle dykes and the geographical distribution is non random with MORB-like melts concentrating in the South-eastern massifs while andesitic melts are dominant in the north-western massifs. The same distribution can be observed for other ophiolitic features, like the chemistry of chromitite pods, the chemistry of chromian-spinels in pyroxenite dykes (richer in Ti and lower in Cr in the south-eastern massifs for both features), and the presence or absence of pyroxene-rich concordant layers in the mantle (abundant only in the north-western massifs).

In this study, we put an additional piece to this edifice by showing that the mantle chemistry, in particular its chromian spinel chemistry show basically the same type of variation. If the silicate chemistry was mostly buffered by mantle processes and do not show any significant difference all along the ophiolite, Cr# in Cr-pinels is on average 15% lower in the south-eastern massifs, in particular the Wadi Tayin massif, than in the north-western ones. This could suggest that the melting degree was significantly lower (about 4%) in the Wadi Tayin massif compared to the north-western part of the ophiolite, however the structure of the Wadi Tayin massif is in contradiction with this hypothesis. A partial melting degree about 4% lower would lead to a 10 to 20% decrease in the magma amount and then in a significantly thinner crustal section, which is not the case in the Oman ophiolite where all the massif a a similar crustal thickness.

On the other hand, Cr# in mantle Cr-spinel could be influenced by other processes than only partial melting and possibly reflects other petrographical properties. It is reasonable to think that the Wadi Tayin mantle melted at the same degree than in the other massifs of the Oman ophiolite. The lower Cr# can be explained in the frame of mantle heterogeneities and mantle sources variations. All well studied magmatic features showed that melts were richer in Al, Ti and lower in Cr, Si in the south-eastern massifs compared to the north-western part of the ophiolite. We conclude then that the mantle below the ophiolite presented large scale (70 to 150 km wide) heterogeneities and that mantle sources were basically different in the various part of the ophiolite. Crust and mantle dykes chemistry was strongly influenced by their mantle sources and cannot be interpreted only in the frame of tectonic settings. Our study cannot bring any definitive answer about the tectonics settings of the Oman ophiolite but show that the presence

©2020. Japan Geoscience Union. All Right Reserved.

of certain petrographical or chemical characteristics have to be considered with great caution.

Keywords: Oman ophiolite, Mantle heterogeneity, Mantle source

©2020. Japan Geoscience Union. All Right Reserved.

Peridotites beneath the ophiolite: Petrology and chemistry of peridotite bodies located below the metamorphic sole of the Oman ophiolite

Main Tokinaga, Marie Python, Georges Ceuleneer, Tomoya Suzuki and Jean-Paul Breton

*Tokinaga Main[1]

1. Hokkaido University Department of Natural History Science Division of Earth and Planetary Systems Sciences

The Oman ophiolite is a large slab of Tethyan ocean floor obducted onto the Arabic peninsula. It comprises one of the largest pieces of exposed lithospheric peridotites and is a wonderful natural laboratory for mantle science. The emplacement of the ophiolite resulted from intraoceanic subduction in North-northeast direction followed by a period of continental subduction leading to the Oman margin burying. High pressure metamorphic rocks in the northern most Saih Hatat suggest a depth of about 40 km, lower grade metamorphism at the southern border of this massif as well as in Jebel Akhdar show that the subduction slope was rather steep (Breton et al., 2004).

The Oman ophiolite is the last of several nappes thrusted onto the autochtonous units (Saih Hatat and Jebel Akhdar), and then the highest in the general stratigraphic column of Oman (Béchennec, 1989). Although some melange do exist at the base of the ophiolite, with serpentine blocks interbedded within the Hawasina units, tectonic inversion was not observed in Oman up to now.

In this study, we describe the petrological characteristics of several relatively small peridotites bodies found in direct contact with the cretaceous limestones from the Arabic platform and located stratigraphically below the Hawasina units and the metamorphic sole. Those peridotite bodies are mostly located at the northern border of Jebel Akhdar, more rarely at the southern border of Saih Hatat. They crop out as a few meters to a few kilometers-wide massifs, most of the time highly serpentinised or carbonated and deformed. They are characterized by the absence of magmatic veins and dykes, their stratigraphic location below the amphibolite from the metamorphic sole, and when found as ophiolitic melange, by the inclusion of limestone blocks. In these 3 points, they differ from the ophiolite mantle main body, which is located above the Hawasina units and metamorphic sole, contains ubiquitously magmatic dykes and veins, and when observed as ophiolitic melange, contains blocks of amphibolite and/or pelagic sediment from the Hawasina nappes. One of the largest of these peridotites is located near a small village called Taww at the northeastern most border of Jebel Akhdar, so that by contrast to the ophiolite peridotites, we will call these peridotites the Taww peridotites. In order to understand the petrogenesis of the Taww peridotites, we sampled several peridotite bodies from both locations below and above the metamorphic sole and Hawasina units. Only one of our samples taken near Ibra had an unclear stratigraphic position (this sample is called “Ibra” in the present study).

The ophiolitic peridotites are all from the lowermost ophiolite, taken a few meters to a few tens of meter above the metamorphic sole. Their petrological characteristics are similar to what was described for basal peridotite by other researchers: they are mostly high depleted harzburgites containing 1 to 7% of Cpx with granular and porphyroclastic textures. The Taww peridotites seem to contain slightly less Cpx and more Opx but their textures are basically very similar to the usual ophiolite peridotites.

©2020. Japan Geoscience Union. All Right Reserved.

The mineral chemistry shows that the Taww peridotites as well as the ophiolite peridotites are residual harzburgites. However, the Taww peridotites, instead more depleted in Cpx than the ophiolite peridotites, show lower Cr-spinel Cr# and higher Al content in Opx, suggesting a possible lower melting degree than in the ophiolite but also a relatively Al-rich chemical environment. Cpx chemistry in Oman peridotites are difficult to interpret as refertilisation and melt trapping widely occurred during the magmatic history. In our study, Cpx in ophiolite lherzolites and Cpx-rich harzburgites (2 to 5% Cpx) show a Na and Ti-rich chemistry showing that they are mainly from trapped melts and refertilisation processes. By contrast, ophiolite harzburgites and the Taww peridotites, independently of their lithology, show a very depleted chemistry suggesting that they are mostly melting residue.

Keywords: Oman ophiolite peridotite, metamorphic sole, Degree of partial melting

©2020. Japan Geoscience Union. All Right Reserved.

Evolution of Island Arc Volcanoes: Ankaramite-Andesite-Basalt (ANANBA) Model

*Yoshihiko Tamura[1], Tomoki Sato[1], Osamu Ishizuka[1], Yasuhiro Hirai[1], Takashi Miyazaki[1]

1. Research Institute for Marine Geodynamics, Japan Agency for Maine-Earth Science and Technology

Nishinoshima, a submarine andesitic volcano in the Ogasawara (Bonin) Arc, ~ 1 000 km south of Tokyo, Japan, suddenly erupted in November 2013, after 40 years of dormancy. Olivine-bearing phenocryst-poor andesites found in older submarine lavas from the flanks of the volcano have been used to develop a model for the genesis of andesitic lavas from Nishinoshima (Tamura et al., 2019). In this model, primary andesite magmas originate directly from the mantle as a result of shallow and hydrous melting of plagioclase peridotites. Andesites erupted from Nishinoshima that were produced in the recent history of the volcano have been generated by olivine fractionation of primary andesitic magmas.
Primary (high Mg#) andesite is produced only when the crust is thin, and consequently only in oceanic arcs. Active examples include boninites erupted in the northern Tonga arc and reararc (Cooper et al., 2010; Resing et al., 2011).
To further examine this hypothesis, we have dived Doyo Seamount by using manned submersible SHINKAI 6500 to sample primitive magmas from the volcano, which is located about 50 km north of Nishinoshima and is underlain by thinner curst (15 km) compared to Nishinoshima. Doyo Seamount is located approximately 900 km south of Tokyo at 27˚41’ N, 140˚48’ E in the Ogasawara Arc. There is a small satellite cone about 11 km east of the summit of Doyo Seamount at the depth of ~3,000 m. A ridge extends on the flank of the volcano from the summit in the ENE direction to the depth of ~2,400 m. Thus, we tried to sample this satellite cone and the deeper part of the ridge. Interestingly, 13 samples out of all 21 samples, which we have recovered during this dive 6K#1519, are olivine-clinopyroxene basalts containing 20-40 % of very coarse clinopyroxene phenocrysts, which could be called ankaramite. Ankaramites are strongly vesiculated and their blocks have rough and rugged surface, which are different from smooth surface of basaltic pillow lavas. Some of ankaramite magmas might have had explosive eruptions at the depth of 2,000~3,000 m, which have resulted in volcaniclastic cones or brecciated lava flows.
Similar primitive and phenocryst-rich ankaramitic basalts were recovered from the old submarine knolls near Nishinoshima (Tamura et al., 2019) and Kibblewhite volcano in the Kermadec arc (Hirai, PhD thesis 2020). We suggested that lithospheric mantle was thicker before the development of Nishinoshima volcano and other oceanic arcs. Primary basaltic magmas could have been generated at depth beneath the thicker lithospheric lid, and these magmas might have interacted with the lithospheric uppermost mantle during their ascent and have resulted in the unique ankaramite magmas. The temperature of the upper part of the mantle wedge increases with frequent passage of magmas through it, and continuous subduction beneath it will drench the whole mantle wedge, thus, the thickness of the lithosphere will decrease and approach the thickness of the curst in mature arcs. Doyo Seamount could represent the early stage of Nishinoshima volcano, and thus, ankaramite magma is deemed to be a precursor of andesitic magmas. We present here the evolution model of oceanic arc volcanoes, which start from ankaramites through andesites to basalts (ANANBA model).

Keywords: andesite, ankaramite, basalt

©2020. Japan Geoscience Union. All Right Reserved.

[E] Poster | S (Solid Earth Sciences)：S-CG Complex & General

[S-CG57] New perspectives of subduction zone earthquake dynamics through experiments across-scales

convener:Masataka Kinoshita(Earthquake Research Institute, University of Tokyo), Yoshio Kono(Geodynamics Research Center, Ehime University), Eiichiro Araki(Japan Agency for Marine-Earth Science and Technology), Hiroko Kitajima(Texas A&M University College Station)

Knowledge on subduction zone earthquake phenomena has considerably increased in the last decade. On the other hand, there are limits to seismological approach alone to comprehensively elucidate the earthquake mechanism in which phenomena that differ by 10 orders of magnitude in space and time, from earthquake nucleation/growth processes to its driving force. Steps to enable scientific earthquake forecasting should include; monitoring regional seismic/tectonic activity using networked observatories, sampling of and insitu measurement in seismogenic faults and plate materials through ultra-deep drilling, and reproduction/insitu-observation of fracture nucleation processes by high-pressure quantum-beam experiments. Through a close collaboration, we challenge a dynamic imaging of earthquake processes. Based on the proposal submitted as a Large Research Master Plan 2020 of the Science Council of Japan, we will deepen the interdisciplinary discussion on subduction-zone earthquakes and the state & property of lithosphere. We welcome, but not limited to, presentations from fields of ocean and land networks observation, seismogenic zone drilling, rock mechanical & quantum beam experiments, fracture process theory, etc.

[SCG57-P01] Spatiotemporal variation in frictional behavior within the Nankai accretionary prism

*Hanaya Okuda[1], Matt J Ikari[2], Alexander Roesner[2], Katja Stanislowski[2], Andre Hüpers[2], Asuka Yamaguchi[1], Achim J Kopf[2] (1.Atmosphere and Ocean Research Institute, University of Tokyo, 2.MARUM – Center for Marine Environmental Sciences, University of Bremen)

[SCG57-P02] Changes in frictional properties of mud gouge with depth in the Nankai Trough accretionary prism

*Kyuichi Kanagawa[1], Takuma Ogawa[2], Tomoya Funaki[2], Tomoya Nakanishi[3], Sayumi Sagano[3], Junya Fujimori[3], Michiyo Sawai[1] (1.School of Science, Chiba University, 2.Faculty of Science, Chiba University, 3.Graduate School of Science and Engineering, Chiba University)

[SCG57-P03] Frictional properties of greenstone: Effects of the seamount subduction on faulting at the subduction zone

*Michiyo Sawai[1], Junya Fukaumi[1], Miki Takahashi[2], Yasutaka Hayasaka[3], Kyuichi Kanagawa[1] (1.Chiba University, 2.Geological Survey of Japan, AIST, 3.Hiroshima University)

[SCG57-P04] Mechanical weakness of the Nankai accretionary prism: Insights from a correlation between Vp and strength of cuttings

*Manami Kitamura[1], Takehiro Hirose[2] (1.National Institute of Advanced Industrial Science and Technology , 2.Japan Agency for Marine-Earth Science and Technology, Kochi Instutute for Core Sample Research)

[SCG57-P05] Structural analyses of inner accretionary wedge in the Nankai trough based on borehole resistivity image

*Yohei Hamada[1], Takehiro Hirose[1], Yoshinori Sanada[2] (1.Japan Agency for Marine-Earth Science and Technology Kochi Institute for Core Sample Research, 2.Japan Agency for Marine-Earth Science and Technology Institute for Marine-Earth Expolaration and Engineering)

[SCG57-P06] Dynamic strain energy as new evaluation item of a seismogenic fault

*Arito Sakaguchi[1], Masato Ichiki[2], Kikka Takiguchi[1] (1.Yamaguchi Univ., 2.SANO TAISEIKISO ENGINEERING Co.Ltd)

[SCG57-P07] Depth dependent spatial variation of pore size distribution for sediments at Nankai accretionary prism

Kouku Inoue[2], *Wataru Tanikawa[1], Yoshitaka Hashimoto[2], Osamu Tadai[4], Manami Kitamura[5], Yohei Hamada[1], Takehiro Hirose[1], Weiren Lin[3] (1.Japan Agency for Marine-Earth Science and Technology, Kochi Instutute for Core Sample Research, 2.Kochi University, 3.Kyoto University, 4.Marine Works Japan LTD., 5.AIST)

[SCG57-P08] Reconstruction of splay fault activity based on integrated subsurface geological data of the slope basin on the Nankai accretionary prism off Muroto

*Yuichi Okuma[1,2], Asuka Yamaguchi[1], Rina Fukuchi[3], Hiroaki Koge[4], Juichiro Ashi[2,1] (1.Atmosphere and Ocean Research Institute, the University of Tokyo, 2.Department of Natural Environmental Studies, Graduate School of Frontier Science, the University of Tokyo, 3.DIA CONSALTANTS COMPANY LIMITED., 4.The National Institute of Advanced Industrial Science and Technology)

[SCG57-P10] Subduction of Kyushu-Palau Ridge can cause local thermal disturbance, as estimated from new heat flow data in the forearc in the eastern Kyushu, Japan

*Masataka Kinoshita[1], Rie Nakata[1], Yoshitaka Hashimoto[2] (1.Earthquake Research Institute, University of Tokyo, 2.Kochi University)

Spatiotemporal variation in frictional behavior within the Nankai accretionary prism

*Hanaya Okuda[1], Matt J Ikari[2], Alexander Roesner[2], Katja Stanislowski[2], Andre Hüpers[2], Asuka Yamaguchi[1], Achim J Kopf[2]

1. Atmosphere and Ocean Research Institute, University of Tokyo, 2. MARUM –Center for Marine Environmental Sciences, University of Bremen

Nankai Trough is one of the most active earthquake zones on the planet and has been focused for many years. Samples were collected from many drilling sites of the International Ocean Drilling Project drilled as a part of the Nankai Trough Seismogenic Zone Experiment project to explore the earthquake mechanisms within the Nankai Trough subduction zone system. We report the experimental results of frictional behavior for samples recovered at different locations in the Nankai subduction zone. Our findings will help to describe (1) the spatiotemporal variation in frictional behavior during the accretion process, (2) the potential for seismic activities along the décollement and splay faults, and (3) the evolution of the accretionary prism.

In this study, three drilling sites were selected which are located in sediments approaching subduction seaward of the trench (Site C0011), in young accreted sediments in the prism toe (Site C0006), and in older accreted sediments in the inner prism (Site C0002). We selected the samples based on the comparability of lithology and clay content. All samples from Site C0011 were Shikoku Basin sediments and samples from Site C0006 included both accreted trench deposits and accreted Shikoku Basin sediments. Laboratory shear experiments on intact samples were performed in a single-direct shear device at in-situ effective normal stresses, calculated assuming a hydrostatic pore fluid pressure, with samples saturated with 3.5% simulated salt water as pore fluid. Intact samples were trimmed from core samples into cylindrical shapes to fit the experimental cell (~20 mm height, ~25 mm diameter). Shear velocities were set to be 10 μm/s for a displacement of 5 mm as a “run-in” process before the velocity was stepped from 0.01 –0.03 –0.1 –0.3 –1 –3 –10 –30 μm/s for 700 μm displacement at each velocity. Friction data obtained from the measured shear stress normalized to the normal stress at each velocity step was fit to a rate- and state-dependent friction law to quantitatively investigate the potential for frictional instability.

Measured steady-state friction coefficients showed inverse correlations with clay content, but no clear relation with smectite content. Because this trend was observed at all three sites, frictional strengths could be primarily controlled by lithological composition: sandy trench deposits exhibit high friction coefficients whereas lower values are seen for clayey hemipelagic sediments. Samples from the prism toe generally showed higher friction coefficients than those from both other sites for the entire range of clay content. This could be because these currently overthrusted sediments at the prism toe may be highly overconsolidated due to lateral compression near the frontal thrust. Negative friction-velocity dependence, a prerequisite of unstable slip, was observed for the input and inner prism sediments even when the samples showed low friction coefficients. Prism toe material had both a negative and positive velocity dependence on friction.

Our measurements of friction velocity-dependence suggest that input sediment and old accreted sediment could be frictionally unstable and therefore favorable for seismic slip, whereas young accreted sediment may resist earthquake slip. Ongoing work on the sample from the deep part of old accreted

©2020. Japan Geoscience Union. All Right Reserved.

sediments is expected to provide further information on the slip partitioning between décollement and megasplay fault near the seismogenic zone, as well as fault activities and structural evolution within the Nankai accretionary prism.

Keywords: Nankai Accretionary Prism, Friction Experiment

©2020. Japan Geoscience Union. All Right Reserved.

Changes in frictional properties of mud gouge with depth in the Nankai Trough accretionary prism

*Kyuichi Kanagawa[1], Takuma Ogawa[2], Tomoya Funaki[2], Tomoya Nakanishi[3], Sayumi Sagano[3], Junya Fujimori[3], Michiyo Sawai[1]

1. School of Science, Chiba University, 2. Faculty of Science, Chiba University, 3. Graduate School of Science and Engineering, Chiba University

In order to investigate the changes in frictional properties of mud gouge with depth in the Nankai Trough accretionary prism, we conducted triaxial friction experiments on gouge of a mud sample cored from 2183.6 mbsf (meters below seafloor) at IODP Site C0002, at three conditions supposed at depths of 1000, 3000 and 5000 mbsf there. We conducted two series of friction experiments; slide-hold-slide experiments for static friction data and rate-stepping experiments for dynamic friction data. In the former series of friction experiments, sliding at an axial displacement rate of 1 μm/s was held for periods ranging from 10s to 10^4s, after which sliding was resumed at the same rate. In the latter series of friction experiments, axial displacement rate was changed stepwise among 0.1, 1 and 10 μm/s.

The slide-hold-slide experiments show that the coefficient of static friction μ_s decreases from 0.37–0.38 at the 1000 mbsf condition to 0.30–0.31 at the 3000 mbsf condition, while it increases to 0.33–0.36 at the 5000 mbsf condition. Healing $\Delta\mu$ (increase in friction coefficient upon resuming sliding after a holding time t_h) was not noticeable at $t_h \leqq 1000$s during the 3000 mbsf condition experiment, while $\Delta\mu$ was recognized at $t_h \geqq 100$s during the other experiments. $\Delta\mu$ increases logarithmically with t_h, which was more prominent at the 5000 mbsf condition. Dehydration of smectite at the 3000 mbsf condition where temperature was 100˚C possibly increased pore pressure in the impermeable gouge layer, which was responsible for the minimum μ_s and non-healing effect at $t_h \leqq 1000$s at this condition. While lithification of gouge particles by pressure solution was possibly responsible for increasing μ_s and $\Delta\mu$ with t_h at the 5000 mbsf condition where temperature was 150˚C.

The rate-stepping experiments show that the steady-state friction coefficient μ_{ss} also decreases from 0.32–0.35 at the 1000 mbsf condition to 0.29–0.31 at the 3000 mbsf condition, while it increases to 0.32–0.33 at the 5000 mbsf condition. The minimum μ_{ss} at the 3000 mbsf condition is also attributable to dehydration of smectite as in the case of μ_s. a–b value (rate dependence of μ_{ss}) decreases with depth from 0.0018–0.0062 at the 1000 mbsf condition to −0.0005–0.0017 at the 5000 mbsf condition, suggesting that a transition from aseismic faulting to seismic faulting occurs around the depth of 5000 mbsf at IODP Site C0002. Thus the megathrust supposed to be present at ≈5200 mbsf there is likely at a seismogenic condition. Dependence of a–b value not only on temperature but also on displacement rate suggests that thermally activated pressure solution is relevant to this change in frictional stability.

Keywords: frictional properties, mud gouge, Nankai Trough accretionary prism

©2020. Japan Geoscience Union. All Right Reserved.

Frictional properties of greenstone: Effects of the seamount subduction on faulting at the subduction zone

*Michiyo Sawai[1], Junya Fukaumi[1], Miki Takahashi[2], Yasutaka Hayasaka[3], Kyuichi Kanagawa[1]

1. Chiba University, 2. Geological Survey of Japan, AIST, 3. Hiroshima University

Subducting seamounts are thought to generate large earthquakes by increasing the normal stress on the subduction interface and to act as asperities (e.g., Cloos, 1992). There is also a possibility that they act as barriers for rupture propagation due to the large resistance (e.g., Kodaira et al., 2000). On the other hand, since a seamount near the southern end of the Japan Trench has been mostly aseismic over the 80 years while many earthquakes have occurred in its adjacent areas, Mochizuki et al. (2008) suggested that the interplate coupling is weak there. In spite of many studies on subducting seamounts, frictional properties of seamount materials are still poorly understood. In this study, we conducted friction experiments to reveal the frictional strength of seamounts and investigate how the seamounts act at subduction zones.

We conducted friction experiments on gouges of a greenstone from the Akiyoshi terrane in Yamaguchi, where a huge seamount with Carboniferous to Permian limestone accreted during the Permian time (e.g., Sano, 2006). Thin layer of greenstone underlying the limestone is distributed over 10 km along a fault. Experiments were performed at slip velocities of 0.0013 to 1.3 m/s, normal stresses of 0.7 to 4.0 MPa, and wet but drained conditions, using a rotary-shear apparatus installed at AIST.
At a slip velocity of 1.3 m/s, typical slip-weakening behavior was observed; friction coefficient μ rapidly increased at the onset of sliding and then progressively decreased to ~0.1 with displacement. Steady-state friction coefficient μ_{ss} at this velocity clearly decreases with increasing normal stress. μ_{ss} is high up to ~0.7 at low velocities, and decreases to ~0.1 at a seismic slip velocity of 1.3 m/s. The sample deformed at this high velocity shows a clear localized shear zone, whereas the sample deformed at a low velocity does not. μ_{ss} of the Akiyoshi greenstone is higher than μ_{ss} of typical subduction zone materials especially at low velocities; μ_{ss} of sediments at the Tohoku subduction zone is <0.2 (Sawai et al., 2014) and μ_{ss} of those at the Nankai Trough is <0.4 (Tsutsumi et al., 2011). Hence a seamount possibly acts as a barrier for rupture propagation due to its high frictional strength.

Keywords: seamount, frictional strength, greenstone

©2020. Japan Geoscience Union. All Right Reserved.

Mechanical weakness of the Nankai accretionary prism: Insights from a correlation between Vp and strength of cuttings

*Manami Kitamura[1], Takehiro Hirose[2]

1. National Institute of Advanced Industrial Science and Technology , 2. Japan Agency for Marine-Earth Science and Technology, Kochi Instutute for Core Sample Research

The elastic wave velocity (Vp) and unconfined compressive strength (C0) of sedimentary rocks are key parameters needed to address the stress state at depth in subduction zones. However, a correlation between Vp and C0, particularly for active accretionary prism sediments, is unknow because samples from active offshore prisms have been limited to depths shallower than 1 km. We thus measure Vp on intact cuttings collected from 980 meters below seafloor (mbsf) to 3040 mbsf, the Nankai accretionary prism at Site C0002, Integrated Ocean Drilling Program (IODP) Expedition 348. Vp at room temperature and pressure gradually increases with depth from 2.2 - 2.5 km/s at 980 - 1180 mbsf to 2.5 - 3.2 km/s at 2910 - 3040 mbsf. Previous studies investigated that Vp for the Nankai accretionary prism sediments increases with increasing effective pressure, and provided the values of pressure correction of 0.02 –0.04 km/s per MPa (e.g., Raimbourg et al., 2010; Hashimoto et al., 2010; 2011). We thus use the value of pressure correction of 0.02 km/s per MPa to estimate the in-situ Vp. The in-situ Vp increases from 2.4 - 2.6 km/s at 980 - 1180 mbsf to3.2 - 3.8 km/s at 2910 - 3040 mbsf. Our estimated in-situ Vp are consistent with Vp measured on cores under in-situ pressure conditions by laboratory experiments (Raimbourg et al., 2010; Hashimoto et al., 2011) and Vp for logging while drilling (LWD) (Expedition 315 Scientists, 2009; Strasser et al., 2014; Tobin et al., 2015). Finally, we compare the relationship between our estimated Vp and C0 (reported by Kitamura et al., 2019) at the Nankai accretionary prism with the global empirical Vp-C0 relationships (e.g., Chang et al., 2006). The global empirical relationships are based on the data on onshore sedimentary rock samples all over the world. Our provided Vp-C0 relationship suggested that the Nankai accretionary prism sediments are weaker in strength (C0) than those of global trend at any given Vp.

Keywords: Nankai Trough, IODP Expedition 348, Elastic wave velocity, Drill cuttings

©2020. Japan Geoscience Union. All Right Reserved.

Structural analyses of inner accretionary wedge in the Nankai trough based on borehole resistivity image

*Yohei Hamada[1], Takehiro Hirose[1], Yoshinori Sanada[2]

1. Japan Agency for Marine-Earth Science and Technology Kochi Institute for Core Sample Research, 2. Japan Agency for Marine-Earth Science and Technology Institute for Marine-Earth Expolaration and Engineering

The present geological structure of the inner accretionary wedge beneath forearc basin sediments records the history of the developing processes of the accretionary prism and the plate subduction zone. The macro scale structure of the inner wedge, however, is not well illustrated by seismic reflection due to poor contrast in acoustic impedance of the deep accretionary prism sediments. Consequently, the relationship between the development of the accretionary prism and its structural history is still unclear. We here analyze the logging data acquired in the IODP Nankai trough drilling project in order to clarify the geological structure of the inner wedge and to estimate the transition of strain direction of the Nankai trough.

In the Nankai Trough Drilling Project Exp. 314, 338 and 348, forearc basin and underlying accretionary prism were penetrated at site C0002 located in Kumano Basin. Continuous logging data are acquired from surface to approximately 3000 meter-below-seafloor (mbsf). Based on the collected resistivity image, gamma-ray, and sonic logs, we recognized and measured beddings and fractures and their strike and dip angles. Over 2000 beddings are found in the accretionary prism to be inclined in both NNW and SSE directions at high angles of 60-90˚. The fractures and faults are found at 300 locations. A fracture-concentrated zone was observed around 2600-2700 mbsf, however, the fracture and faults do not show any clear trends. Although these descriptions were approximately the same as the cruise reports and previous research (Boston et al. 2016), “eye spots” were newly identified on the resistivity image. This is considered to be a closed bedding around a fold axis, because the inclination direction of the formation changes significantly above and below the eye spot. The direction of the fold axis is considered to be given by the direction orthogonal to this eye spot and to be ENE–WSW.

The depth distribution of the fold was estimated based on the depth change of azimuth and dip of the bedding. The fold properties such as fold axis, axial plane, interlimb angle, and the wavelength are calculated from the beddings at inflexion points assuming that the fold can be regarded as a concentric fold. As a result, the folds are classified mainly as open-folds with large interlimb angle of 150˚ to 170˚, and the axis azimuths are ENE–WSW direction, which was consistent with the direction obtained from the eye spot. However, the plunges change greatly with 0-70 degrees, and it cannot be regarded as a single fold structure. These folding axes show a girdle distribution on a stereo plot suggesting that these folds were deformed secondarily by another folding having an axis in the NNW-SSE direction.

Our investigations revealed that the inner wedge of the Nankai accretionary prism consists of high-angle beddings and open-folds in two stages. Since the primal fold axes indicate the ENE-WSW direction with horizontal axial planes, it is considered that these primal folds were formed in outer wedge before tilting by accretion. During or after the tilting, the second folds have developed along the NNW-SSE direction. The direction of these primal- and second folds are consistent with the stress direction analysis using the borehole breakouts and the strike-slip fault movement in the vicinity of the giant branch fault (megasplay fault). The meso- and macro scale structure in the inner wedge, revealed in this research, can indicate the history of change in stress orientation during developing in accretionary prism.

©2020. Japan Geoscience Union. All Right Reserved.

Keywords: NanTroSEIZE, inner accretionary wedge, logging-while-drilling

©2020. Japan Geoscience Union. All Right Reserved.

Dynamic strain energy as new evaluation item of a seismogenic fault

*Arito Sakaguchi[1], Masato Ichiki[2], Kikka Takiguchi[1]

1. Yamaguchi Univ., 2. SANO TAISEIKISO ENGINEERING Co.Ltd

Since earthquake is stress response of the crust, the stress-strain record of the host rock around the fault tell us significant clue of the seismic mechanism. During inter-seismic period, host rock around the asperity deformed elastically to cause the earthquake. Immediately before the earthquake, a rupture propagates from deep nucleation point, and high stress must concentrate at tip of the fracture. This stress concentration causes elastic strain momentary in host rock of the fault, and high stress area moves with rupture propagation.

The strain energy of these event can be estimated from paleo-stress distribution around the fault. It is expected that the highest peak of stress must be appeared at fault center, and stress level will decrease with distance from the fault. The area under the stress decay curve in the stress-distance graph indicates strain energy of the host rock.

Paleo-stress of ancient fault rock can be estimated from elastic rebounded rock using calcite twin method (Sakaguchi et al., 2011).

The Okitsu Fault in Shimanto accretionary complex, southwest Japan is ancient seismogenic fault of plate subduction zone. This fault involves pseudotachylyte and can be observed more than 10 km along the strike of the fault. Higher stress than the background stress of regional Shimanto accretionary complex was found around the Okitsu Fault. This may be due to dynamic stress concentration during rupture propagation. The value of estimated dynamic strain energy is approximately 390 MJm^-2 at eastern tip of the Okitsu Fault. The strain energy along the strike of the fault decreases toward west and disappears at 2 km from the eastern tip. The strain energy along the fault increases again to several MJm^-2 at 9 km from the eastern tip. This strain energy variation may show existence of some locked asperities along the strike of the fault.

Keywords: stress, subduction zone, seismogenic fault

©2020. Japan Geoscience Union. All Right Reserved.

Depth dependent spatial variation of pore size distribution for sediments at Nankai accretionary prism

Kouku Inoue[2], *Wataru Tanikawa[1], Yoshitaka Hashimoto[2], Osamu Tadai[4], Manami Kitamura[5], Yohei Hamada[1], Takehiro Hirose[1], Weiren Lin[3]

1. Japan Agency for Marine-Earth Science and Technology, Kochi Instutute for Core Sample Research, 2. Kochi University, 3. Kyoto University, 4. Marine Works Japan LTD., 5. AIST

Sediment porosity at accretionary prism varies with burial depth mainly due to mechanical compaction. Elastic wave velocity and thermal conductivity that are primary governed by porosity thus increase with depth. On the other hand, influence of depth and compaction on pore size distribution is not well known. Permeability is related with not only porosity but also pore size distribution. Therefore depth variation of permeability can be estimated from that of pore size distribution by understanding the fundamental physical process that causes the depth variation. In this study, porosity and pore size distribution were measured on cuttings and core samples obtained by NantroSEIZE project, IODP Expedition 348 (Site C0002).

Sediment at site C0002 is mainly composed by silty sediment. 44 cuttings and 7 core samples were used in this study. At the beginning, samples were washed by sea water, then dried using vacuum pump. Then, porosity and grain density were measured by using a gas pycnometer. Finally, porosity and pore size distribution of the same samples used for the gas pycnometer measurements were measured by a mercury intrusion porosimeter. 3D X-ray microscope was used to visualize internal microstructures of samples, and XRD analysis was performed to evaluate mineral composition.

Our results show a porosity ranges from 20 to 55 % for the gas pycnometer method, and 15 to 50 % at 878-2825mbsf, and 2 to 5 % at 2830-3200mbsf for the mercury injection method. Both porosities deceased gradually with depth. However, at depth around 2200 mbsf, porosity was fluctuated at around 15 to 34%, which were deviated from depth reduction curve. On the whole, porosity measured by the gas pycnometer is relatively higher than that measured by the mercury porosimeter. Pore size distribution at depth shallower than 2000 mbsf show clear single peak, which represents model of pore size, and mode gradually decreased with depth. On the contrary, at depth greater than 2000 mbsf, pore size distribution shows broad and it is difficult to determine the mode.
3D X-ray microscopic images for samples at around 2200 mbsf show variation of amount of coarse grain particles and the fractures developed parallel to preferred orientation of sediment particles. XRD data shows variation of clay mineral compositions among samples. Therefore, fluctuation of porosity and pore size distribution around at 2200 mbsf is explained by the lithological variation and fracture formations. The average pore size decreases with depth, therefore, the permeability probably decreases with depth at Site C0002.

Keywords: Nankai Trough, Porosity, Pore size distribution, IODP Expedition 348, Permeability

©2020. Japan Geoscience Union. All Right Reserved.

Reconstruction of splay fault activity based on integrated subsurface geological data of the slope basin on the Nankai accretionary prism off Muroto

*Yuichi Okuma[1,2], Asuka Yamaguchi[1], Rina Fukuchi[3], Hiroaki Koge[4], Juichiro Ashi[2,1]

1. Atmosphere and Ocean Research Institute, the University of Tokyo, 2. Department of Natural Environmental Studies, Graduate School of Frontier Science, the University of Tokyo, 3. DIA CONSALTANTS COMPANY LIMITED., 4. The National Institute of Advanced Industrial Science and Technology

Estimating activity of a splay fault is important to understand the long-term formation process of an accretionary prism as well as a pattern of coseismic slip propagation. Splay faulting causes local uplift in an accretionary prism, which would be recorded in a slope basin.
In this study, we conducted interpretation of subsurface structures of a slope basin located at the hanging wall of a splay fault to reconstruct activity of the splay fault on the off-Muroto area of the Nankai accretionary prism. 3-D seismic volume obtained during R/V *Ewing 9907/9908* cruise (Bangs et al., 2004) and high-resolution cross-section images obtained by deep towed subbottom profiler on the R/V Hakuho-maru KH-16-5 cruise were used in this study. This basin is located at 80 kilometers to the southwest of the Cape Muroto and a depth of 3000 m, and 8 kilometers long in northwest-southeast and 6.5 kilometers long in northeast-southwest forming an ellipse shape. Cores from Site 1175 and Site 1176 obtained by Ocean Drilling Program (ODP) Leg 190 were also reanalyzed to constrain lithology, structures and age.
As a result of seismic interpretation, three structural units and two splay faults were confirmed. They were named as Unit A, Unit B and Unit C from top to bottom, and landward and seaward splay faults as Splay Fault Y and Splay Fault Z, respectively. Unit A is characterized by tilted reflectors that getting steep with depth. The age of the bottom of this unit is estimated to be ~0.5 Ma, which means the tilting had started ~0.5 Ma due to the activity of Splay Fault Z. The high-resolution cross-section obtained by subbottom profiler (SBP) combined with tephra age results from Site 1175 core shows that activities of minor faults at the southern edge of slope basin, subsidiary formed by Splay Fault Z, decreased at ~105 ka, and stopped at ~28 ka. Considering these results, we constrained changes the activity of Splay fault Z: faulting started at ~0.5 Ma, gradually decreased at ~105 ka and stopped at ~28 ka.

Keywords: slope basin, High resolution sub-bottom profiler, Nankai accretionary prism, Ocean Drilling Program, Splay faults

©2020. Japan Geoscience Union. All Right Reserved.

Subduction of Kyushu-Palau Ridge can cause local thermal disturbance, as estimated from new heat flow data in the forearc in the eastern Kyushu, Japan

*Masataka Kinoshita[1], Rie Nakata[1], Yoshitaka Hashimoto[2]

1. Earthquake Research Institute, University of Tokyo, 2. Kochi University

In the Hyuga-nada forearc region off eastern Kyushu, weaker degree of plate coupling is inferred from frequent seismicity and the slow slips inferred from seafloor geodetic data. This exhibits a clear contrast against the strong coupling in the Nankai Trough region to the east. Based on 3D numerical simulation and the low heat flow values, Yoshioka (2007) suggested that the weaker coupling in Hyuga-nada is attributed to the lower temperature in the seaward side of the plate boundary. However, the tectonics around Hyuga-nada is much complicated from plate-scale to sub-km-scale, In a reginal scale, a colder and probably rough-surface crust (west Philippine Basin; ~60 Ma) is subducting with steeper dip angle at depth, in contrast to the young, smoother Shikoku Basin to the east. Along the old/young boundary, the Kyushu-Palau Ridge (KPR; trending N60W) is obliquely subducting toward N30W since several Ma B.P., possibly scraping off the overlying forearc block westward.

Here we present heat flow data including new ones obtained along JAMSTEC seismic lines to discuss how the heat flow is affected by these tectonic/morphological disturbances.

The heat flow marks a sharp boundary across KPR; it is 50-100mW/m2 to the east and 25-40mW/m2. The transition from high to low heat flow occurs in only 20 km across KPR. Higher heat flows of 100 mW/m2 to the east are located near the axis of Nankai Trough, similar to those reported off Muroto. It is attributed to the fluid discharge along decollement. The lack of such high heat flow to the west may simply the lack of measurement in the corresponding area.

We performed a simple 3D thermal modeling, considering the subduction of old and young crusts (age difference of 20 Ma) neighboring to each other. Both orthogonal and oblique azimuth of subduction are tested. Due to thermal exchange between the neighboring crusts the width of thermal transition becomes wider with time, but not much difference along subducting direction, probably because of rapid subduction. Calculated heat flow profile is generally in good agreement with the observed heat flow trend, consistent with Yoshioka (2007) results.

A closer inspection of heat flow and the morphological feature, however, reveals a coincidence between heat flow minimum and the location of subducted KPR (as supported by the magnetic anomaly) and the location of flow-frequency tremors. Seamount subduction is inferred to cause a local stress anomaly and an elevated pore pressure, which is associated to heat flow anomalies. We will discuss this local effect as well.

Keywords: Kyushu-Palau Ridge, Heat flow, Slow earthquake

©2020. Japan Geoscience Union. All Right Reserved.

[E] Poster | S (Solid Earth Sciences)：S-CG Complex & General

[S-CG58] Science of slow earthquakes: Toward unified understandings of whole earthquake process

convener:Satoshi Ide(Department of Earth an Planetary Science, University of Tokyo), Hitoshi Hirose(Research Center for Urban Safety and Security, Kobe University), Kohtaro Ujiie(Graduate School of Life and Environmental Sciences, University of Tsukuba), Takahiro Hatano(Department of Earth and Space Science, Osaka University)

Accumulating observational studies on various types of slow deformation events, such as tectonic tremors, very low frequency events, and slow slip events, portrays some universal characteristics in generally complex behavior, including interaction among events and influence by various outer loadings. Some of these phenomena seem to have causal relation with the occurrence of very large earthquakes. A unified understanding of these slow and fast earthquake processes requires an approach integrating geophysics, seismology, geodesy, geology, and non-equilibrium statistical physics. We welcome presentations based on, but not limited to, geophysical observation, data analysis, analytical theory, numerical simulation, field study, and laboratory experiments.

[SCG58-P01] CMT inversion of offshore earthquakes along the Nankai Trough: Separated distributions of slow and regular earthquakes on the plate boundary

*Shunsuke Takemura[1], Ryo Okuwaki[2], Tatsuya Kubota[3], Katsuhiko Shiomi[3], Takeshi Kimura[3], Akemi Noda[3] (1.Earthquake Research Institute, the University of Tokyo, 2.University of Tsukuba, 3.National Research Institute for Earth Science and Disaster Resilience)

[SCG58-P02] **Understanding of temporal change in slow earthquake migration speed**

*Keisuke Ariyoshi[1], Roland Burgmann[2], Jean-Paul Ampuero[3] (1.Japan Agency for Marine-Earth Science and Technology, 2.University of California, Berkeley, 3.Université Côte d'Azur)

[SCG58-P03] One-hour-duration SSEs found during a Short-term SSE in the Tokai region.

*Kazuki Miyaoka[1], Akio Katsumata[2], Satoshi Itaba[3] (1.Japan Meteorological Agency, 2.Meteorological Research Institute, 3.National Institute of Advanced Industrial Science and Technology)

[SCG58-P04] Activities of low frequency tremors in Sanriku-Oki before the 2011 Tohoku-Oki earthquake

*Hidenobu Takahashi[1], Ryota Hino[1], Naoki Uchida[1], Kazuaki Ohta[2], Masanao Shinohara[3], Ryosuke Azuma[1], Susumu Kawakubo[1] (1.Graduate school of Science Tohoku University , 2.National Research Institute for Earth Science and Disaster Resilience, 3.Earthquake Research Institute, the University of Tokyo)

[SCG58-P05] Detailed Spatial Slip Distribution for Short-term Slow Slip Events along the Nankai Subduction Zone, Southwest Japan

*Masayuki Kano[1], Aitaro Kato[2] (1.Graduate school of science, Tohoku University, 2.Earthquake research institute, The University of Tokyo)

[SCG58-P06] Fist detection of shallow tremor at the Guerrero gap, Mexico.

*Raymundo Omar Plata Martinez[5], Satoshi Ide[1], Naoto Mizuno[1], Masanao Shinohara[2], Tomoaki Yamada[3], Allen Husker[4], Jorge Real[4], Victor Cruz-Atienza[4], Yusuke Yamashita[5], Akiko Toh[1], Yoshihiro Ito[5] (1.Department of Earth an Planetary Science, University of Tokyo, 2.Earthquake Research Institute, University of Tokyo, 3.Japan Meteorological Agency, 4.Institute Geophysics, UNAM, 5.Disaster Prevention Research Institute, Kyoto University)

[SCG58-P07] Depth profile of frictional properties inferred from cuttings obtained at the Nankai trough C0002 drilling site

*Riho Fujioka[1], Ikuo Katayama[1], Takehiro Hirose[2], Manami Kitamura[3] (1.Hiroshima Univercity, 2.Kochi Institute for Core Sample Research, Japan Agency for Marine-Earth Science and Technology, 3.National Institute of Advanced Industrial Science and Technology)

[SCG58-P08] Slip rate dependence of dynamic water permeability for low permeable fault and the role of fluid

*Wataru Tanikawa[1] (1.Japan Agency for Marine-Earth Science and Technology, Kochi Instutute for Core Sample Research)

[SCG58-P09] Gouge friction on a meter-scale laboratory fault

*Futoshi Yamashita[1], Eiichi Fukuyama[2,1], Akihiro Shimoda[2], Shun Watanabe[3] (1.National Research Institute for Earth Science and Disaster Resilience, 2.Graduate School of Engineering, Kyoto University, 3.Faculty of Engineering, Kyoto University)

[SCG58-P10] Spatio-temporal correlations in tremor activity in south-west Japan

*Anca Opris[1], Takahiro Hatano[1] (1.Department of Science, Osaka University)

[SCG58-P11] On 3-D resistivity structure in the SW part of Shikoku-Island, SW Japan, and sensitivity of the Network-MT responses to the structure

*Makoto Uyeshima[1], Ryoukei Yoshimura[2], Maki Hata[1], Hiroshi Ichihara[3], Koki Aizawa[4] (1.Earthquake Research Institute, The University of Tokyo, 2.Disaster Prevention Research Institute, Kyoto University, 3.Graduate School of Environmental Studies, Nagoya University, 4.Graduate School of Science, Kyushu University)

[SCG58-P12] Variations of scaling relationships for shallow tremor; implications from the probabilistic cell automaton model

*Masaru Nakano[1], Suguru Yabe[2] (1.Japan Agency for Marine-Earth Science and Technology, 2.Geological Survey of Japan, AIST)

[SCG58-P13] High Fluid Pressure Patch beneath the Décollement as a Potential Source of Slow Earthquakes at the Nankai Trough

*Takehiro Hirose[1], Yohei Hamada[1], Wataru Tanikawa[1], Nana Kamiya[2], Yuzuru Yamamoto[3], Takeshi Tsuji[4], Masataka Kinoshita[5] (1.Kochi Institute for Core Sample Research, Japan Agency for Marine-Earth Science and Technology, 2.Graduate School of Engineering, Kyoto University , 3.Japan Agency for Marine-Earth Science and Technology, 4.Department of Earth Resources Engineering, Kyushu University, 5.Earthquake Research Institute, the University of Tokyo)

[SCG58-P14] The November 11, 2018 long-period-monotonic big earthquake occuring near Mayotte island off East Africa and seismic activity observed by the Iranian broadband seismic stations

*Sadaomi Suzuki[1], Hossein Sadeghi[2] (1.Tono Research Institute of Earthquake Science, Association for the Development of Earthquake Prediction, 2.Department of Geology, Faculty of Science, Ferdowsi University of Mashhad, Iran)

[SCG58-P15] Dense broadband seismic campaign for deep very low frequency earthquakes in Shikoku, Kii and Tokai regions in the Nankai subduction zone

*Akiko Takeo[1], Kazushige Obara[1] (1.Earthquake Research Institutute, the University of Tokyo)

[SCG58-P16] **Fluid flow patterns in fluid injection into swelling gel particles**

*Kojiro Otoguro[1], Yutaka Sumino[1] (1.Department of Applied Physics, Faculty of Science Division I, Tokyo University of Science)

[SCG58-P17] Seismic reflection profiling across deep low-frequency tremor zone in western Shikoku, southwestern Japan

*Eiji Kurashimo[1], Kimihiro Mochizuki[1], Takashi Iidaka[1], Kazushige Obara[1] (1.Earthquake Research Institute, the University of Tokyo)

[SCG58-P18] Long-term Viscoerastic Relaxation and Spatially Inhomogeneous Viscosity Structure

*Yusaku Tanaka[1] (1.Earthquake Research Institute, University of Tokyo)

[SCG58-P19] A physical model of tremor response to periodic external stresses in poroelastic medium

*Ryunosuke Sakamoto[1], Yoshiyuki Tanaka[1] (1.University of Tokyo Graduate School of Science)

[SCG58-P20] The radial pattern of brittle viscoelastic fluids between rotating parallel plates

*Tatsuya Nishikubo[1], Hiroki Ishikawa[1], Shoma Kato[1], Yutaka Sumino[1] (1.Department of Applied Physics, Faculty of Science Division I, Tokyo University of Science)

[SCG58-P21] Offshore surveys of seismic structures and seismicity of regular and low-frequency earthquakes around Amami islands

*Tsutomu Takahashi[1], Ayako Nakanishi[1], Yojiro Yamamoto[1], Yasushi Ishihara[1], Aki Ito[1], Ryuta Arai[1], Seiichi Miura[1], Shuichi Kodaira[1], Yoshiyuki Kaneda[2] (1. Japan Agency for Marine-Earth Science and Technology, 2.Kagawa Univ.)

[SCG58-P22] Slip distributions of short-term slow slip events in the northern Kii Peninsula based on NIED Hi-net tilt measurements

*Chujo Naoya[1], Hitoshi Hirose[2,1,3], Takeshi Kimura[3] (1.Department of Planetology, Graduate School of Science, Kobe University, 2.Research Center for Urban Safety and Security, Kobe University, 3.National Research Institute for Earth Science and Disaster Resilience)

[SCG58-P23] Trial detection of deep low frequency tremor using analog seismograms of Kanto-Tokai Observation Network in 1988-1990

*Takanori Matsuzawa[1], Tetsuya Takeda[1] (1.National Research Institute for Earth Science and Disaster Resilience)

[SCG58-P24] Estimation of the spatial distribution of Qs values beneath the Kii Peninsula, Japan by the twofold spectral ratio method

*Kodai Sagae[1], Hisashi Nakahara[1], Takeshi Nishimura[1], Kazutoshi Imanishi[2] (1.Solid Earth Physics Laboratory,Department of Geophysics,Graduate School of Science,Tohoku University, 2.National Institute of Advanced Industrial Science and Technology (AIST))

[SCG58-P25] 3-D thermal modeling of generation mechanisms for short-term slow slip events and low-frequency earthquakes along the Ryukyu trench

*Nobuaki Suenaga[1], Shoichi Yoshioka[1,2] (1. Research Center for Urban Safety and Security, Kobe University, 2.Department of Planetology, Graduate School of Science, Kobe University)

[SCG58-P26] Spatio-temporal evolution of long- and short-term slow slip events in the Tokai region, central Japan estimated from a very dense GNSS network, during 1997-2017

*Hiromu Sakaue[1], Takuya NISHIMURA[2], Jun'ichi Fukuda[3], Teruyuki Kato[4] (1.Graduate School of Science, Kyoto University, 2.Disaster Prevention Research Institute Kyoto University, 3.Earthquake Research Institute,The University of Tokyo, 4.Hot Springs Research Institute of Kanagawa Prefectural Government)

[SCG58-P27] Repeating activity of shallow low-frequency tremor in Hyuga-nada

*Yusuke Yamashita[1], Masanao Shinohara[2], Hiroko Sugioka[3], Aki Ito[4], Tsutomu Takahashi[4], Daisuke Suetsugu[4] (1.Disaster Prevention Research Institute, Kyoto University, 2.Earthquake Research Institute, the University of Tokyo, 3.Graduate School of Science, Kobe University, 4.Japan Agency for Marine-Earth Science and Technology)

[SCG58-P28] Shallow low-frequency tremor in the Japan Trench subduction zone

*Sachiko Tanaka[1], Takanori Matsuzawa[1], Youichi Asano[1] (1.National Research Institute for Earth Science and Disaster Resilience)

[SCG58-P29] Shallow low-frequency tremor activity off Erimo, Hokkaido from 2006 to 2007 revealed from pop-up type ocean bottom seismometers

*Susumu Kawakubo[1], Ryosuke Azuma[1], Ryota Hino[1], Hidenobu Takahashi[1], Kazuaki Ohta[2], Masanao Shinohara[3] (1.Graduate School of Science, Tohoku University, 2.National Research Institute for Earth Science and Disaster Resilience, 3.Earthquake Research Institute, University of Tokyo)

[SCG58-P30] High-velocity frictional behavior of fault gouges in the presence of pore fluid

*Akito Tsutsumi[1] (1.Graduate School of Science, Kyoto University)

[SCG58-P31] Detection of low-frequency aftershocks of the 2019 Ridgecrest earthquake sequence

*Ayako Tsuchiyama[1], Taka'aki Taira[2], Junichi Nakajima[1], Roland Bürgmann[3] (1.Earth and Planetary Sciences at Tokyo Institute of Technology, 2.Berkeley Seismological Laboratory, 3.Earth and Planetary Science, University of California, Berkeley)

[SCG58-P32] Structural characteristics of the Nankai trough subduction zone off Kii channel revealed from densely obtained seismic reflection profiles

*Yasuyuki Nakamura[1], Shuichi Kodaira[1], Tetsuo No[1], Yuka Kaiho[1], Kazuya Shiraishi[1], Gou Fujie[1], Seiichi Miura[1], Koichiro Obana[1] (1.Japan Agency for Marine Earth Science and Technology)

[SCG58-P34] Long-Term Activity Changes of Very Low Frequency Earthquakes in the Ryukyu Trench

*Mamoru Nakamura[1] (1.Faculty of Science, University of the Ryukyus)

[SCG58-P35] Seismic Velocity Mapping of the Plate Boundary Structures in the Slow Earthquake Gap Zone off Western Kii Peninsula, Nankai Trough

*Yanfang Qin[1], Gou Fujie[1], Shuichi Kodaira[1], Yasuyuki Nakamura[1], Yuka Kaiho[1], Tetsuo No[1], Koichiro Obana[1], Seiichi Miura[1] (1.JAMSTEC Japan Agency for Marine-Earth Science and Technology)

[SCG58-P36] Distribution of very low-frequency earthquakes in the Miyako Strait, central Ryukyu Trench

*Hiromu Furugen[1], Mamoru Nakamura[1] (1.Graduate School of Engineering and Sience, Univercity of the Ryukyus)

[SCG58-P38] Spatiotemporal evolution of interplate slip in the Hyuganada and the Bungo Channel from 1996 to 2000 based on GNSS data

*Sawako Teshiba[1], Hitoshi Hirose[1,2] (1.Department of Planetology, Graduate School of Science, Kobe university, 2.Research Center for Urban Safety and Security, Kobe University)

[SCG58-P39] An estimation of stress changes based on earthquake swarm seismicity accompanied by Boso slow slip events

*Tomoki Ukawa[1], Hitoshi Hirose[2,1] (1.Department of Planetology, Graduate School of Science, 2.Research Center for Urban Safety and Security, Kobe University)

[SCG58-P40] Spatial heterogeneity of shallow tremor activity near the Japan Trench

*Shukei Ohyanagi[1], Kazuaki Ohta[2], Yoshihiro Ito[3], Ryota Hino[4], Yusaku Ohta[4], Ryosuke Azuma[4], Masanao Shinohara[5], Kimihiro Mochizuki[5], Toshinori Sato[6], Yoshio Murai[7] (1.Kyoto University, Graduate School of Science, 2.National Research Institute for Earth Science and Disaster Resilience, 3.Kyoto University, Disaster Prevention Research Institute, 4.Tohoku University, 5.Tokyo University, Earthquake Research Institute, 6.Chiba University, 7.Hokkaido University)

[SCG58-P41] Can crack-seal veins record recurrence intervals of slow earthquakes?

*Naoki Nishiyama[1], Kohtaro Ujiie[1], Masayuki Kano[2] (1.University of Tsukuba, 2.Tohoku University)

[SCG58-P42] Complementary Distribution between Very Low Frequency Earthquakes and Interplatecoupling area in the southwestern Ryukyu Trench

*Ren Yakabu[1], Mamoru Nakamura[1] (1.University of the Ryukyus)

[SCG58-P43] Different deformation styles in the source regions of the 2019 Yamagata-oki earthquake and the 1964 Niigata earthquake

*Taku Ueda[1], Lina Yamaya[1], Yosihiko Ogata[2], Aitaro Kato[1] (1.Earthquake Research Institute, the University of Tokyo, 2.The Institute of Statistical Mathematics)

[SCG58-P44] Uncovering complex characteristics of earthquake time series using complex network analysis

*Sumanta Kundu[1], Anca Opris[1], Takahiro Hatano[1] (1.Department of Earth and Space Science, Osaka University.)

[SCG58-P45] Exploring slow slip events and their scaling in 3D simulations of fault slip

*Luca Dal Zilio[1], Nadia Lapusta[1], Jean-Philippe Avouac[1] (1.Seismological Laboratory, California Institute of Technology, Pasadena, CA)

[SCG58-P46] Nature of the Lithosphere in Alternating Regions of Slow Earthquakes in South America

*POUSALI MUKHERJEE[1], Yoshihiro Ito[1], Takuo Shibutani[1], Emmanuel Soliman M Garcia[1], Raymundo Omar Plata Martinez[1] (1.Disaster Prevention Research Institute, Kyoto University)

CMT inversion of offshore earthquakes along the Nankai Trough: Separated distributions of slow and regular earthquakes on the plate boundary

*Shunsuke Takemura[1], Ryo Okuwaki[2], Tatsuya Kubota[3], Katsuhiko Shiomi[3], Takeshi Kimura[3], Akemi Noda[3]

1. Earthquake Research Institute, the University of Tokyo, 2. University of Tsukuba, 3. National Research Institute for Earth Science and Disaster Resilience

Due to complex three-dimensional (3D) heterogeneous structures, conventional one-dimensional (1D) analysis techniques using onshore seismograms can yield incorrect estimation of earthquake source parameters, especially dip angles and centroid depths of offshore earthquakes. Indeed, detail analysis of 2016 southeast off the Kii Peninsula earthquake revealed that observed seismic and tsunami record could be explained by low-angle thrust faulting on the plate boundary (e.g., Kubota et al., 2018; Takemura et al., 2018; Wallace et al., 2016) but regional 1D moment tensor analysis showed high-angle reverse faulting mechanism.

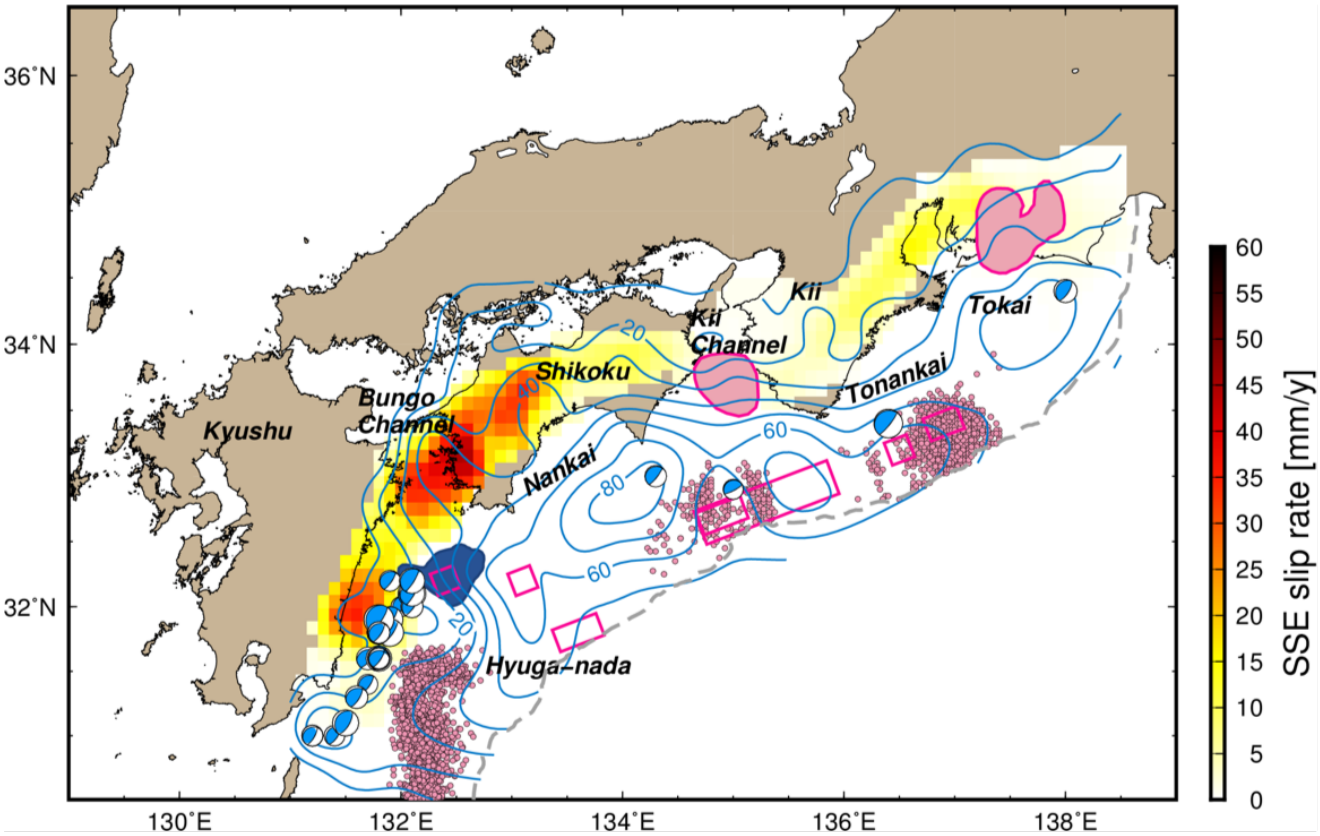
Combining long-term onshore seismic observations and numerical simulations of seismic wave propagation in a 3D model, we conducted centroid moment tensor (CMT) inversions of earthquakes along the Nankai Trough. Green’s functions for CMT inversions of moderate earthquakes were evaluated via OpenSWPC (Maeda et al., 2017) using the Japan Integrated Velocity Structure Model (Koketsu et al., 2012). We re-analyzed moderate (*Mw* 4.3-6.5) earthquakes listed in the F-net catalog (Fukuyama et al., 1998; Kubo et al., 2002) that occurred from April 2004 to August 2019. By introducing the 3D structures of the low-velocity accretionary prism and the Philippine Sea Plate, our CMT inversion method provided better constraints of dip angles and centroid depths for offshore earthquakes. These two parameters are important for evaluating earthquake types in subduction zones.

Our 3D CMT catalog of offshore earthquakes and published slow earthquake catalogs (e.g., Kano et al., 2018) along the Nankai Trough depicted spatial distributions of slip behaviors on the plate boundary. The regular and slow interplate earthquakes were separately distributed, with these distributions reflecting the heterogeneous distribution of effective strengths on the plate boundary. By comparing the spatial distribution of seismic slip on the plate boundary with the slip-deficit rate distribution (Noda et al., 2018), regions with strong coupling were identified.

Acknowledgments
We used F-net waveform data and the F-net MT catalog (https://doi.org/10.17598/NIED.0005). Our CMT catalog and CMT results of assumed source grids for each earthquake are available from https://doi.org/10.5281/zenodo.3661116. The FDM simulations of seismic wave propagation were conducted on the computer system of the Earthquake and Volcano Information Center at the Earthquake Research Institute, the University of Tokyo. This study was supported by the Japan Society for the Promotion of Science (JSPS) KAKENHI Grant Numbers 17K14382 and 19H04626.

Keywords: Nankai Trough, CMT inversion, offshore earthquake, 3D heterogeneous structure

©2020. Japan Geoscience Union. All Right Reserved.



Spatial distribution of slip behaviours on the plate boundary along the Nankai Trough. Plotted focal mechanisms are low-angle thrust faulting solutions at depths around the plate boundary. The coseismic slip area of the 1968 *Mw* 7.5 Hyuga-nada earthquake (Yagi *et al.* 1998) is shaded in dark blue. SSE slip rates were evaluated from the combined SSE catalogues (Nishimura *et al.* 2013, Takagi *et al.* 2016, 2019). The pink circles indicate the epicentres of the shallow LFTs of the Hyuga-nada and the shallow VLFEs in the Tonankai region referred from Yamashita et al. (2015) and Takemura, Noda, et al. (2019). The pink shaded and enclosed areas indicate the large slip areas of long-term SSEs (Kobayashi 2014, Miyazaki *et al.* 2006) and shallow SSEs (Yokota & Ishikawa 2020), respectively. The blue contour lines indicate the slip-deficit rates [mm/yr] on the plate boundary by Noda *et al.* (2018) .

©2020. Japan Geoscience Union. All Right Reserved.

Understanding of temporal change in slow earthquake migration speed

*Keisuke Ariyoshi[1], Roland Burgmann[2], Jean-Paul Ampuero[3]

1. Japan Agency for Marine-Earth Science and Technology, 2. University of California, Berkeley, 3. Université Côte d'Azur

Recent observations show evidence of propagation of postseismic slip, which may contain information about the mechanical properties of faults. Ariyoshi et al. (2019) develop a new analytical relationship between the propagation speed of aseismic slip transients and fault frictional properties, modeled by a rate- and state-dependent friction law. In the paper, we identify systematic dependencies of afterslip propagation speed on effective normal stress σ and frictional properties (the coefficients a and a-b which quantify the instantaneous and the steady-state velocity-dependence of friction, respectively, and the characteristic slip distance L of fault state evolution). Lower values of the parameter $A=a\sigma$ cause faster propagation in areas where the passage of the postseismic slip front induces large shear stress changes $\Delta\tau$ compared to A, which are typically located near the mainshock rupture. In areas where $\Delta\tau/A$ is small, typically more distant from the mainshock, afterslip propagation speed is more sensitive to $(a\text{-}b)\sigma$. The propagation speed is proportional to initial slip velocity and, under the condition that loading span is significantly shorter than the passage of postseismic slip, inversely proportional to L. In this presentation, we extend our relationship to slow earthquake migration process by comparing our analytical solution with simulated results in previous model (Ariyoshi et al., 2012). The result can explain the reason why slow earthquake migration speed increases in the preseismic stage of megathrust earthquake because of increasing the initial slip velocity for small asperity ongoing chain reaction, which might be applicable to the observed slow earthquake activity in the preseismic stage of the 2011 Tohoku earthquake.

Keywords: rate- and state-dependent friction law, subduction zones, megathrust earthquakes

©2020. Japan Geoscience Union. All Right Reserved.

One-hour-duration SSEs found during a Short-term SSE in the Tokai region.

*Kazuki Miyaoka[1], Akio Katsumata[2], Satoshi Itaba[3]

1. Japan Meteorological Agency, 2. Meteorological Research Institute, 3. National Institute of Advanced Industrial Science and Technology

The Short-term Slow Slip Events (s-SSE) occur repeatedly several times per year in the deeper than the seismogenic zone of the Nankai Trough area southwestern Japan. These s-SSEs have moment magnitude equivalent to about 5.5 - 6.0 and duration of approximately a week.
Japan Meteorological Agency (JMA) operates borehole strain-meter network and analyses the s-SSE activities by using an hourly resampled data of them.
Recently, Katsumata et al, (2020) found a small change with extremely shorter duration than usual s-SSEs in time series data of laser extensometers installed in the Aichi and Shizuoka prefectures. We confirmed the existence of the small change in the one minute resampled strain-meter data in February 2019 Tokai s-SSE. Here, we report the analysis of the small rapid change.

A Mw6.0 s-SSE (hereafter parent-SSE) occurred from 3 to 11 February, 2019 in Aichi prefecture and evident changes of strain-meter data with intense tremor activity were observed.
In 5 February which is the most active period of the parent-SSE, smaller but faster changes were observed from 15:30 to 16:30 in the some stations around Aichi prefecture.
So, we performed analysis to infer the fault plane assuming a plate boundary slow slip. Result, a small slip equivalent to Mw5.0 with 1 hour duration was calculated.
Furthermore, two other similar changes were found in the parent-SSE with a careful data checking, Mw 4.8 small slip on the plate boundary with duration of 50 minutes and Mw4.8 one with 45 minutes were also calculated.
As well as the known s-SSE, these events were also accompanied with transient intense tremor activity.

We guessed them to be an unknown Slow Slip Event, faster than the known SSE occurred in the same tectonic mechanism on the plate boundary.

Ide et al. (2007) proposed a Moment-Duration scaling law for slow earthquakes and demonstrated that the various kind of slow earthquakes observed throughout the world are on the scaling law.
And Ide et al. (2007) pointed out a possibility of existence of Mw4-5 events with tens minutes to 1 hour in which no events have been observed. The new event presented in this work are exactly the predicted ones.

Keywords: short-term SSE, One hour duration SSE, Tokai

©2020. Japan Geoscience Union. All Right Reserved.

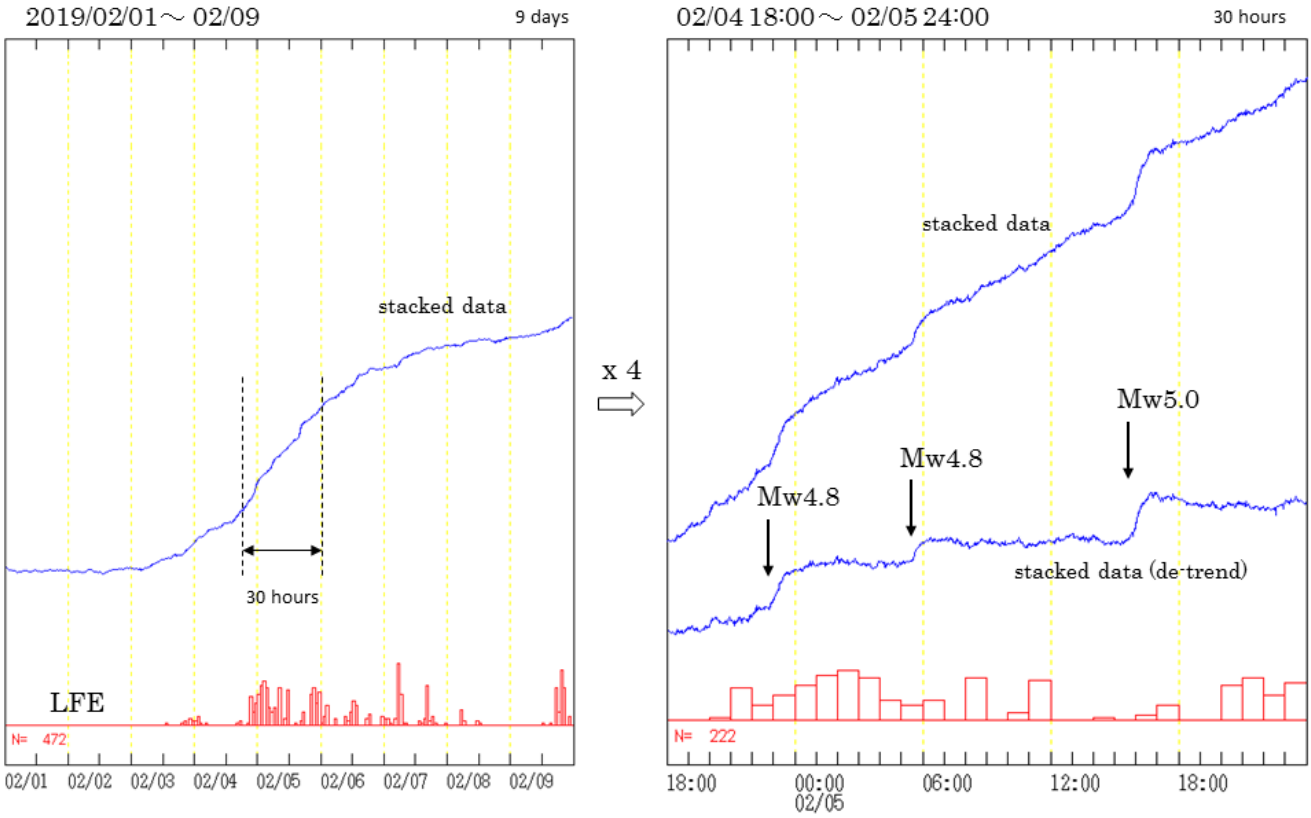


Fig. Stacked strain-meter time-series data

©2020. Japan Geoscience Union. All Right Reserved.

Activities of low frequency tremors in Sanriku-Oki before the 2011 Tohoku-Oki earthquake

*Hidenobu Takahashi[1], Ryota Hino[1], Naoki Uchida[1], Kazuaki Ohta[2], Masanao Shinohara[3], Ryosuke Azuma[1], Susumu Kawakubo[1]

1. Graduate school of Science Tohoku University , 2. National Research Institute for Earth Science and Disaster Resilience, 3. Earthquake Research Institute, the University of Tokyo

Recently, slow earthquakes have been discovered in Tohoku-oki by using the Seafloor Observation Network for Earthquakes and Tsunamis along the Japan Trench (S-net) (Tanaka et al., 2019). These activities differ from those in Nankai Trough (Obara and Kato, 2016), where sources of slow earthquakes and megathrust are clearly separated, and slow earthquakes are continuously distributed along the deeper and shallower side of the seismogenic zone, whereas those show complex spatial distribution along the Japan Trench (Nishikawa et al., 2019).

In northern Sanriku-Oki region between 39˚N and 40.7˚N, low frequency tremors (LFTs) frequently occur as well as very low frequency earthquakes (VLFEs) (Matsuzawa et al., 2015), but their activities are significantly lower in the southern Sanriku-Oki regions (~39˚N). Since the southern LFT cluster is located within the coseismic slip zone of the 2011 Tohoku-Oki earthquake (Iinuma et al., 2012), it is probable that the occurrence of the massive coseismic slip affects the LFT activities after the Tohoku-oki earthquake.

Here, we report the activities of LFTs in Sanriku-Oki before the 2011 Tohoku-Oki earthquake. We used 46 short-period ocean bottom seismograms (OBSs) deployed from Oct. 2007 to May 2008. The envelope correlation method (e.g. Obara, 2002, Ohta et al., 2019) is applied to the OBS seismograms, with almost the same parameter settings as the study by Nishikawa et al. (2019) using the S-net data. As a result, we detected 448 and 168 tremors in northern and southern Sanriku-Oki regions, respectively. In the northern region, LFTs show evident along-strike migration during multiple episodes, each of which has ~1 week duration. The migration speed is ~ 20 km/day, which is comparable to that observed in the deep LFTs in the western Shikoku of Nankai (Obara, 2002).

The S-net observation for two years after the 2011 Tohoku-Oki earthquake detected 2894 events in the northern region, while only 17 in the southern region. Our result using the OBS data in 2007 and 2008 suggests that the LFTs in the southern Sanriku-Oki was much more active before the Tohoku-Oki earthquake and the change in the LFT activity reflects the change of the behavior of the plate boundary caused by the massive interplate earthquake.

Keywords: Slow earthquake, Ocean bottom seismometer

©2020. Japan Geoscience Union. All Right Reserved.

Detailed Spatial Slip Distribution for Short-term Slow Slip Events along the Nankai Subduction Zone, Southwest Japan

*Masayuki Kano[1], Aitaro Kato[2]

1. Graduate school of science, Tohoku University, 2. Earthquake research institute, The University of Tokyo

Short-term slow slip events (S-SSEs) with a duration of days to weeks have intensively occurred at the transition zone at depths of ~ 35 km along the Nankai subduction zone, southwest Japan. Because crustal deformation due to a single S-SSE is small, the source fault has been often represented as a single planar uniform slip model, resulting to little constraint on the spatial heterogeneity in amount of slip. Here, to comprehensively investigate the detailed cumulative spatial distribution of S-SSEs in the whole Nankai subduction, we adopted a stacking approach of GNSS data by referencing low-frequency earthquakes which are assumed to be accompanied by S-SSEs. We have successfully extracted cumulative displacements due to a series of S-SSEs occurred from 2004 to 2009, showing coherent signals that are almost opposite to the direction of plate subduction. Then, we inverted these surface displacements to fault slip along the plate interface. The estimated slip indicates significant slip patches laterally elongated along the transition zone at the depths of ~30–35 km, and small patches on the shallow portion of ~15 km depth in eastern Shikoku and Tokai as well as in western Shikoku inferred by Kano et al. (2019). The two shallow patches locate on the downdip edge of the coseismic slip area in 1946 Nankai earthquake, while the Tokai small slip is located on the shallower side of the anticipated source area of the magnitude 8 class earthquake. In addition, the large slip patches of S-SSEs are possibly complementary to the spatially dense low-frequency earthquake areas; the number of low-frequency earthquakes is low in major slow-slip areas. This spatial dependence of fault slip style even within the transition zone provides new insights of generation mechanism of slow earthquakes.

Keywords: slow slip events, Nankai subduction zone, low-frequency earthquakes

©2020. Japan Geoscience Union. All Right Reserved.

Fist detection of shallow tremor at the Guerrero gap, Mexico.

*Raymundo Omar Plata Martinez[5], Satoshi Ide[1], Naoto Mizuno[1], Masanao Shinohara[2], Tomoaki Yamada[3], Allen Husker[4], Jorge Real[4], Victor Cruz-Atienza[4], Yusuke Yamashita[5], Akiko Toh[1], Yoshihiro Ito[5]

1. Department of Earth an Planetary Science, University of Tokyo, 2. Earthquake Research Institute, University of Tokyo, 3. Japan Meteorological Agency, 4. Institute Geophysics, UNAM, 5. Disaster Prevention Research Institute, Kyoto University

The Guerrero gap, located at the Mexican subduction zone, is a seismic gap which has not had any significant earthquake (M>7) in almost 119 years. Furthermore, slow earthquakes like tectonic tremors and slow slip events are frequent in the down dip portion of the gap at approximately 40 km depth. Even when slow earthquakes in the Guerrero gap are well documented, until now there has been no confirmation of slow earthquake activity at the shallow portion of the gap close the trench. With no offshore instrumentation, it has been a difficult task to collect enough evidence to prove that tremors or slow slip take place near the trench. For this reason, a seven stations array of Ocean Bottom Seismometers (OBS) was deployed inside the Guerrero gap. One-year data was analyzed in search of shallow tremors using a modified envelope correlation method. Over 130 tremors were detected close to the trench. Tremors do not show any migration, but small burst of tremors show recurrence periods of approximately one and three months. Seismic signals of these tremors have duration between 10-100 sec, they show no clear arrivals both of P and S wave, are efficient at a frequency band between 2 and 8 Hz and are deficient at frequencies above 10 Hz, attenuating rapidly. More analysis is being done to understanding the nature of these tectonic tremors and their connection with seismicity. By comparing other seismic and geodetic data, such as ocean bottom pressure gauges, GPS/acoustic measurements and high-resolution bathymetry, we are now trying to explain tremor influence in the seismic hazard associated to the shallow portion of the GG.

Keywords: Slow earthquake, Guerrero gap, Shallow tremor

©2020. Japan Geoscience Union. All Right Reserved.

Depth profile of frictional properties inferred from cuttings obtained at the Nankai trough C0002 drilling site

*Riho Fujioka[1], Ikuo Katayama[1], Takehiro Hirose[2], Manami Kitamura[3]

1. Hiroshima Univercity, 2. Kochi Institute for Core Sample Research, Japan Agency for Marine-Earth Science and Technology, 3. National Institute of Advanced Industrial Science and Technology

Nankai megathrust earthquakes has occurred repeatedly, and has caused great damage historically (e.g., Ando et al., 1975). To understand the process of Nankai megathrust earthquakes, Nankai Trough Seismogenic Zone Excavation Project (NanTroSEIZE) has been conducted as part of the IODP since 2007 to 2019. Friction experiments were performed using core samples collected at the Nankai Trough Seismogenic Zone Excavation Project (Ikari and Saffer, 2011 and Takahashi et al., 2014), however, depth variations were limited in these previous experiments because cores were retrieved from limited depth intervals. In order to make a continuous depth profile of frictional properties, we carried frictional experiments using cuttings samples collected at every 50 m over the interval from 860 to 3000 mbsf in the ultra-deep riser hole, Site C0002 .

Frictional tests were conducted by biaxial frictional machine at Hiroshima university under saturated conditions (brine,0.5 mol/L) at in-situ effective normal stress (σe = 9–34 MPa). The cuttings samples were ground and the grain size was adjusted to less than 106 μm. The gouge sample was sandwiched by gabbro blocks in double–direct configuration. After slip behavior reached a steady state at 3 μm/s, velocity was changed stepwise between 0.3, 3, and 33 μm/s. In this test, frictional coefficient at a steady state and the velocity dependence defined by the rate- and sate-dependent friction constitutive law were examined. All tests were conducted in water tank filled with brine. The relationship between friction properties and clay minerals were investigated by comparing the total clay mineral content and smectite content of cuttings samples reported by the IODP 348 Expedition data report.

Frictional coefficient at the drilling Site C0002N are ranging from 0.472 to 0.575. There is no relationship between depth and frictional coefficient. Frictional coefficient was slightly decrease with increasing smectite content, which is consistent with the pervious study (Takahashi et al., 2014). The smectite content of samples collected at a deeper depth decrease, and therefore we expect future increasing coefficient of friction of these samples in the future measurements of deeper samples. Velocity dependence of friction(a-b) were ranging from -0.009 to 0.020. In most cases, velocity strengthening was observed, but the neutral of velocity-dependence was characteristically appeared at depths around 1100–1800 mbsf. Although Takahashi et al. (2014) has reported velocity strengthening in all experiments at the Site C0002, velocity dependence might be influenced by effective normal stress. Since the occurrence of slow earthquake is possibility related to a neutral sate of velocity dependence (e.g., Ikari and Saffer, 2011), the observed neutral dependence might attribute to the shallow very low-frequency earthquakes observed in the Nankai accretionary prism.

Keywords: friction, Nankai trough, clay minerals, accretionary prism

©2020. Japan Geoscience Union. All Right Reserved.

Slip rate dependence of dynamic water permeability for low permeable fault and the role of fluid

*Wataru Tanikawa[1]

1. Japan Agency for Marine-Earth Science and Technology, Kochi Instutute for Core Sample Research

Evolution of fluid transport and mechanical properties of faults by frictional sliding is key to control slow earthquake and dynamic fault rupture. In this study, change of water permeability of simulated faults (granite and dolerite) by frictional sliding at slow (0.1 mm/s) to fast (1 m/s) slip rate with long slip displacements (~1 m) were investigated in laboratory experiments. Rotary shear apparatus was used in the laboratory tests at 2 MPa of normal stress. Elix pure water was used as pore fluid to measure permeability. Water permeability suddenly increased by sliding to achieve to steady state values. After slip stopped, permeability decreased gradually to initial permeability or below initial values in several ten minutes. Both dynamic permeability and friction coefficient show slip rate dependence that both permeability enhancement and reduction of friction is significant at high velocity sliding. Velocity step change tests confirmed the positive slip rate dependence of permeability. The slip rate dependence is explained by dilation of hydraulic aperture due to frictional heating because pore pressurization and thermal expansion of pore spaces on slip plane are effectively induced by thermal pressurization at high slip rate. The change of water viscosity by frictional heat in part explains the apparent permeability recovery after sliding. The lower dynamic permeability and lower friction of granite than those of dolerite is explained by rich in quartz minerals that polish slip surface strongly to reduce hydraulic apertures.
The laboratory results suggest the importance of permeability evolution on slow to fast earthquake processes; coseismic fault slip induces significant permeability enhancement that fail to occurrence of pore pressurization, whereas temporal small permeability change during slow slip suggests the difficulty in large pore pressure drop.

Keywords: permeability, friction coefficient, roughness, slow earthquake, thermal pressurization, slip rate dependence

©2020. Japan Geoscience Union. All Right Reserved.

Gouge friction on a meter-scale laboratory fault

*Futoshi Yamashita[1], Eiichi Fukuyama[2,1], Akihiro Shimoda[2], Shun Watanabe[3]

1. National Research Institute for Earth Science and Disaster Resilience, 2. Graduate School of Engineering, Kyoto University, 3. Faculty of Engineering, Kyoto University

National Research Institute for Earth Science and Disaster Resilience (NIED) has been conducting friction experiments with meter-scale rock specimens using a large-scale shaking table. We have presented a result that the work rate at which the meter-scale rock friction starts to decrease is one order of magnitude smaller work rate than that of the centimeter-scale one (Yamashita et al., 2015, Nature). Mechanical, visual and material observations suggested that the difference of frictional properties between centimeter and meter scale is caused by slip-evolved heterogeneous stress concentration on gouge bumps generated with the frictional slip. We confirmed that numerical simulation based on the observations is fully consistent with the experimental results. However, it should be noted that the natural fault zone generally involves gouge layer in it. Therefore, it is crucial to investigate which the scale dependence of frictional property can be seen or not under such a condition. To answer this question, we conducted meter-scale gouge friction experiments using the large-scale shaking table. We used metagabbro blocks from India as driver blocks. The contacting area was 1.5 m long and 0.1 m wide. As the simulated gouge, we ground metagabbro blocks by the jet mill, so that the average diameter of the gouge particle is approximately 10 μm and the maximum diameter of that is less than 200 μm. We roughened the fault surface by sandblasting after polishing the surface so that the fault surface can grip the gouge particles. We distributed the simulated gouge with a thickness of 3 mm on the fault and then sheared at a constant or step-change velocity after applying normal stress up to 6.7 MPa at maximum. We will present basic experimental results at the meeting.

Keywords: Frictional property, Gouge, Large-scale laboratory experiment

©2020. Japan Geoscience Union. All Right Reserved.

Spatio-temporal correlations in tremor activity in south-west Japan

*Anca Opris[1], Takahiro Hatano[1]

1. Department of Science, Osaka University

Tremor activity is known to exhibit temporal episodic behaviour (burst-type activity followed by periods of inactivity), as well as spatial migration. Previous studies have investigated the temporal (Idehara et al., 2014) or the spatial clustering (Obara et al., 2010) of tremor activity in south-west Japan. We propose to investigate the correlations in tremors, based on the space-time combined correlation integral (Tosi et al., 2008). Thus, we are considering a simultaneous analysis of the interdistance among events in both space and time coordinates.
In previous studies, three distinct areas of tremor occurrence have been identified, with two seismicity gaps in between. Some explanations have been proposed for the phenomena, but no clear evidence can yet explain the presence of these seismically inactive regions. We aim to get some insight by modelling the spatial distribution and intermittent activation of the Shikoku, Kii and Tokai areas in respect to the Nankai and Tokai locked area. We analyse the local slope of time correlation dimension (d_t) as a function of time interval (σ) and hypocentral distance (r), using two different catalogues, retrieved from the World Tremor Database and a recently improved catalogue, respectively (Mizuno et al, 2019). We compare the obtained results for the two catalogues and discuss the overall implications on statistics of the different methods of detecting the tremor activity.

©2020. Japan Geoscience Union. All Right Reserved.

On 3-D resistivity structure in the SW part of Shikoku-Island, SW Japan, and sensitivity of the Network-MT responses to the structure

*Makoto Uyeshima[1], Ryoukei Yoshimura[2], Maki Hata[1], Hiroshi Ichihara[3], Koki Aizawa[4]

1. Earthquake Research Institute, The University of Tokyo, 2. Disaster Prevention Research Institute, Kyoto University, 3. Graduate School of Environmental Studies, Nagoya University, 4. Graduate School of Science, Kyushu University

In the Bungo channel region at the western margin of the Nankai megathrust rupture zones, the long-term slow slip events (SSE) repeatedly occurred about every 6 or 7 years and we are now having the most recent event. The SSE also activate deeper episodic tremors and slips (ETS) on the plate interface. In order to examine mechanism of the SSE and/or concurrent ETS activities, especially to clarify influence of interstitial fluids on occurrence of the events, or to detect movement of the fluids associating with the events, we have started the Network-MT survey in the western part of the Shikoku Island facing the Bungo channel since April, 2016.

We use metallic telephone line network of the Nippon Telegraph and Telephone Corp. to measure the electrical potential difference with long baselines of from several kilometers to 10 and several kilometers. We selected 17 areas in the western part of the Shikoku Island and installed 3 or 4 electrodes in the respective areas. The electrical potential differences measured in this way are known to be less affected by small scale near-surface lateral resistivity heterogeneities (e.g. Uyeshima, 2007). We also measure the geomagnetic field at two stations in the target region. With the aid of the BIRRP code (Chave and Thomson, 2004), we could estimate the frequency-domain response functions of good quality. After applying the 3-D DASOCC inversion code (Siripunvaraporn et al., 2004), which directly invert the Network-MT response between the voltage difference on each dipole and the magnetic field, we could obtain the 3-D resistivity structure in the target region. Data from Apr. to May, 2016 are used. Site (dipole) and period numbers are respectively 53 and 10 (from about 20 s to 10,000 s). Grid sizes of the model are 60 (NS), 57(EW) and 45 (vertical). We started from an initial model of uniformly 100 Ohm-m in land portion and sea water is fixed to be 0.3 Ohm-m. The initial RMS was 12. We got a model with RMS 2.42 on 5% error floor.

First, cross sections along lines in NNW-SSE with and without the slow slip events are examined. The most remarkable low resistivity anomalies are detected in the middle crust of the hanging wall of the subducting Philippine Sea slab in all the cross-sections. As was often pointed out in the previous studies (e.g. Hata et al., 2018; Ichihara et al., 2014), earthquakes also in this region tend to occur in the resistive area avoiding those low resistivity anomalies. Due to existence of this shallower crustal conductive anomalies, however, it was difficult to resolve resistivity distribution along the subducting slab. No remarkable conductive anomaly could be imaged in both of the areas with and without the slow slip events. In order to clarify the relationship between the resistivity structure and the slow slip area, plan view conductivity distributions parallel to the slab surface are examined and compared with the seismic Qp structures (Kita and Matsubara, 2016). Some positive correlation between both parameters can be detected. Mantle wedge above the slab with the slow slip event is relatively resistive and high Qp. On the other hand, mantle wedge above the slab without the slow slip event is relatively conductive and low Qp. The resistive and high Qp layer may indicate an impermeable layer which confine the fluids along the subducting slab. The confined fluids may cause slow slip events, although the fluids could not be explicitly imaged as the conductive anomaly. We also want to show temporal variation of the Network-MT responses.

As was written above, significant slow slip event occurred recently. Then, we want to show how the Network-MT responses are sensitive to temporal resistivity change along the slab. In a test model, 10 km

©2020. Japan Geoscience Union. All Right Reserved.

thick conductive layer is assigned just beneath the top surface of the slab. The resistivity is set to be 20 Ohm-m (thus 500 S anomaly). RMS of the best fit model was 2.42, whereas 3.65 for the test model. Decrease of the apparent resistivity and increase of the phase value in the relatively higher frequency range can be detected.

This study is supported by JSPS KAKENHI Grand Number JP16H06475 in Scientific Research on Innovative Areas "Science of Slow Earthquakes". It is also partly supported by the Ministry of Education, Culture, Sports, Science and Technology (MEXT) of Japan, under its Earthquake and Volcano Hazards Observation and Research Program. We acknowledge staffs of the Nippon Telegraph and Telephone WEST Corporation and associated companies for their cordial support in the survey. We also thank H. Abe, A. Takeuchi and Y. Suwa in ERI for their help in preparing and installing instruments.

Keywords: slow slip event beneath the Bungo Channel, 3-D resistivity structure, Network-MT observation, sensitivity

©2020. Japan Geoscience Union. All Right Reserved.

Variations of scaling relationships for shallow tremor; implications from the probabilistic cell automaton model

*Masaru Nakano[1], Suguru Yabe[2]

1. Japan Agency for Marine-Earth Science and Technology, 2. Geological Survey of Japan, AIST

Scaling relationships of seismic phenomena is one of keys to understand the source processes. In our previous study, the event size distribution of shallow tremor that occurred along the Nankai trough was well fitted by the tapered Gutenberg-Richter (TGR) (Kagan 2002 GJI) distribution (Nakano et al. 2019 GRL). In that study, the cutoff magnitude (Mc) of TGR, above which the event size distribution is well fitted by an exponential law, and the b-value (slope of the size distribution in logarithmic scales smaller than Mc) varied in each activity period. Detailed analysis showed that both Mc and the b-value temporally changed DURING activities in 2016 off Kumano and 2018 off Muroto (Nakano et al. 2019 JpGU). To clarify the factors that control the event size distribution may help our understandings of slow earthquake source mechanisms. In this study, we try to explain the observed changes in the event size distribution based on the 2D probabilistic cell automaton (PCA) model proposed by Ide and Yabe (2018 PAG), which well explains the statistical properties of the broadband slow earthquakes including event size distributions.

In the 2D PCA model, each cell has two states: “stop” and “slip”, which probabilistically alternates according to the states of neighboring cells. The controlling parameters of the 2D PCA model would be: the source size in x and y directions (Nx and Ny), the transition probability of the cell status (pb), ignition of fault slip (pl), and energy dissipation during slip (pv).

Our simulations show that the source size (Nx and Ny) and pb changes Mc without significantly affecting the b-value as already shown by Ide and Yabe (2018) (their Figure 4). On the other hand, increasing the excess stopping probability (pv) due to energy dissipation systematically reduces Mc while increases the b-value, namely smaller-size events predominate due to the suppression of event growth. The effects of ignition (pl), or loading, is small compared to pv, but further detailed studies are necessary because these parameters would affect the system in a similar way.

The observed changes in Mc and the b-value in the shallow tremor showed negative correlations in these parameters. In the 2016 off Kumano activity, Mc decreased in the end 5 days of the activity synchronized with the b-value increase and event number decrease. In the 2018 off Muroto activity, decreases in Mc was observed in the middle 30 days and end 30 days during 4 months activity, synchronized with the b-value increases and event number decreases. The observed changes in the size distributions can be explained by increase in the excess stopping probability (pv) during the lower activity periods.

In this study, we showed that the changes in pv systematically explains the observed temporal changes in the event size distributions of the shallow tremor, but its physical meaning is not clarified yet. Temporal changes in the stopping probability of cell movement in PCA may correspond to changes in the frictional properties along the causative fault. Further careful investigations based on experimental and/or theoretical studies to clarify materials that control the frictional properties on a fault, which changes could occur in a several to ten days, is necessary.

Acknowledgments: This research was supported by JSPS KAKENHI Grant Number JP18K13639 and

©2020. Japan Geoscience Union. All Right Reserved.

16H06477 in Scientific Research on Innovative Areas “Science of Slow Earthquakes”

Keywords: DONET, Nankai trough, earthquake size distributions, slow earthquakes

©2020. Japan Geoscience Union. All Right Reserved.

High Fluid Pressure Patch beneath the Décollement as a Potential Source of Slow Earthquakes at the Nankai Trough

*Takehiro Hirose[1], Yohei Hamada[1], Wataru Tanikawa[1], Nana Kamiya[2], Yuzuru Yamamoto[3], Takeshi Tsuji[4], Masataka Kinoshita[5]

1. Kochi Institute for Core Sample Research, Japan Agency for Marine-Earth Science and Technology, 2. Graduate School of Engineering, Kyoto University , 3. Japan Agency for Marine-Earth Science and Technology, 4. Department of Earth Resources Engineering, Kyushu University, 5. Earthquake Research Institute, the University of Tokyo

Pore fluid pressure is important for understanding generation of both megathrust and slow earthquakes at subduction zones. However, its occurrence and quantitative constraints are quite limited. Here, we report the estimate of pore pressure by the analysis of transient upwelling flow from the borehole, that was observed while drilling the underthrust sediments in the Nankai Trough off Cape Muroto during IODP Expedition 370. In order to interpret the observed velocity and duration of the flow, we have solved a radial diffusion equation to estimate pore pressure before penetrating an aquifer. The calculation yields that the pore pressure exceeded ~3 MPa above hydrostatic and the size scale of the aquifer is several hundred meters, in case of an aquifer permeability of 10^{-13} m^2. Our result suggests that the underthrust sequence is currently composed of patchily-distributed high-pressure aquifers.

In the neighborhood of the drilling site, very low frequency (VLF) earthquakes have been reported (e.g., Obara and Kato, 2016). Seismic survey has suggested a possible linkage between high pore pressure zone and the distribution and generation of slow earthquakes (e.g., Kodaira et al., 2004). Furthermore, high temperature and pressure friction experiments by Sawai et al. (2016) suggested that a transition from stable to unstable slip behavior appears with increasing pore fluid pressure that is a prerequisite for the generation of slow earthquakes. Our result implies that the slow earthquakes at off Cape Muroto can be attributed with slip behaviors along not only décollement but also the patchily distributed high-pore-pressure aquifers in the underthrust sediments.

Keywords: fluid pressure, slow earthuake, Nankai Trough

©2020. Japan Geoscience Union. All Right Reserved.

The November 11, 2018 long-period-monotonic big earthquake occuring near Mayotte island off East Africa and seismic activity observed by the Iranian broadband seismic stations

*Sadaomi Suzuki[1], Hossein Sadeghi[2]

1. Tono Research Institute of Earthquake Science, Association for the Development of Earthquake Prediction, 2. Department of Geology, Faculty of Science, Ferdowsi University of Mashhad, Iran

The 11 November 2018 Mayotte event (SEQ) was first introduced in the media by Maya Wei-Haas (2018) on National Geographic Magazine as a strange earthquake of which seismic waves were recorded by instruments around the world, but unusually nobody felt them. The Mayotte event in the absence of body waves caused long-duration, long-period surface waves traveling around the globe. Cesca et al. (2020) by analyzing regional and global seismic and deformation data suggested drainage of a deep magma reservoir. Tono Research Institute of Earthquake Science recorded the data with the broadband seismometer (STS-1) and gravimeter (gPhone) installed in Mizunami, Japan (Murakami et al., 2019). The records by Iranian broadband stations clearly showed the longperiod seismic signals around 10 (UTC) on November 11, 2018 (Figure 1). We studied records by 26 stations distributed throughout the country. The stations are operated by National Center of Broadband Seismic Network of Iran, International Institute of Earthquake Engineering and Seismology (IIEES). Since the frequency content of Fourier amplitude spectra appeared the signal of the surface waves as a peak around 0.06 Hz, we applied a bandpass filter of 0.05-0.07 Hz to the waveform data. To separate Rayleigh from love in surface waves, the filtered horizontal components were rotated to the radial and transverse components based on an assumed epicenter location at the latitude of 12.7S and longitude of 45.4E degrees. The stations considered as an array and the investigation was carried out in two ways. First, the position of each station was taken as the reference point of the array coordinate, and arrival delay times at the other stations relative to the reference were calculated. The phase velocity and the back-azimuth of each station were estimated through the least-square regression method. The estimated back azimuths were within 13 degrees from the back azimuths from the assumed epicenter. The average phase velocity for Rayleigh and Love phases are calculated as 2.97 and 3.31 km/sec, respectively. Second, we applied semblance analysis to six stations with the shortest spacing distances. However, the distance between the adjacent stations relative to the signal wavelength was not enough short to prevent spatial aliasing. Nevertheless, the interesting was that the semblance results were different for radial and transverse components. We calculated surface-wave magnitude (Ms) for the event and a number of recorded earthquakes occurring in the Mayotte area from May 13 to June 1, 2018. Linear regression was used to define relationships between the calculated Ms and the USGS body-wave magnitude (mb) and the local magnitude by BRGM catalog (Bertil et al. , 2019), and the moment magnitude (Mw) from the CMT solutions of HRVD and USGS.

Keywords: Mayotte island, very-long-period monotonic signal, Iranian broadband seismic stations

©2020. Japan Geoscience Union. All Right Reserved.

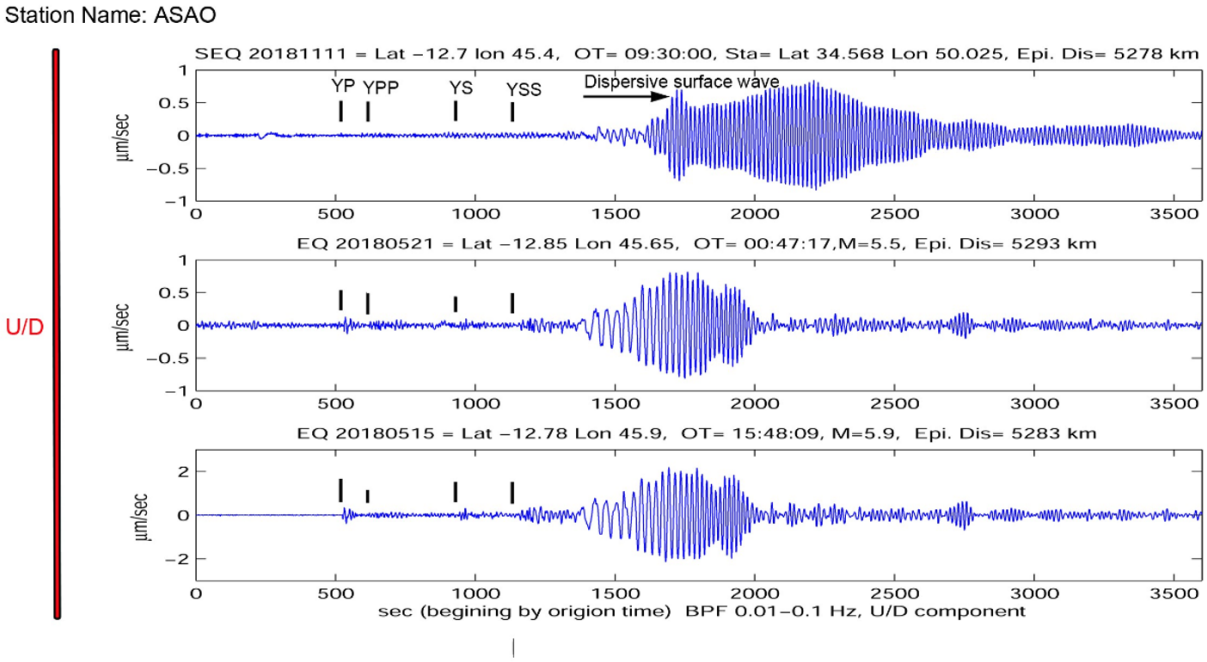


Figure 1. Comparison of the seismic waveforms of SEQ and two regular earthquakes, May-21 and May-15, 2018 observed by ASAO station in Iran. The seismic waves are filtered in the band 0.01 to 0.1 Hz. ↵

©2020. Japan Geoscience Union. All Right Reserved.

Dense broadband seismic campaign for deep very low frequency earthquakes in Shikoku, Kii and Tokai regions in the Nankai subduction zone

*Akiko Takeo[1], Kazushige Obara[1]

1. Earthquake Research Institutute, the University of Tokyo

Very low frequency earthquake (VLFE) is one type of slow earthquakes observed by broadband seismometers at a period range around 20-50 s at the plate interfaces of subduction zones. The signal of deep VLFEs at the down-dip side of seismogenic zone tends to be small compared to that of shallow VLFEs at the up-dip side near the trench. To observe deep VLFEs, we have installed broadband seismometers in the Nankai subduction zone in three different stages.

In the first stage, we deployed three stations in the Shikoku island in 2015 by the earthquake and volcano hazards observation and research program. In the second stage, we deployed two stations in the Shikoku island and one station in the Kyushu island in 2017 as a part of “Science of Slow Earthquakes” project. The seismometers are either CMG-3T (120 s) of the Guralp or the Trillium QA/PA (120 s) of the Nanometrics. The recorders are LF-1100/2100 of the Hakusan. The data is in WIN format and is transferred to Earthquake Research Institute, the University of Tokyo in almost real time. These stations are called “BC series” because their target is the Bungo Channel region where various types of slow earthquakes have been observed. By analyzing these datasets, we have detected and determined centroid moment tensor and its uncertainty for 324 events from 2018 to early 2019.

In the third stage, in this study, we have installed 11 stations and will install 4 more stations from 2019 to 2020 as a part of “Science of Slow Earthquakes” project. The numbers of stations are 7 in the Shikoku, 4 in the Kii and 4 in the Tokai regions. We chose the locations in the Shikoku region near the active area of low frequency tremor but less active area of VLFEs to detect small events. The stations in the Kii and Tokai regions are located near the active area of VLFEs to analyze broadband (10-100 s) spectrum of each event. The seismometers are CMG-3T (120 and 100 s) tested in the Nokogiriyama observatory of Earthquake Research Insititute for one week. The recorder is RT130 of the Reftek. The data is in SEED-STEIM2 format and transferred to newly constructed virtual server on the Sakura VPS service by VPN connection (NXR mobile router and DTI SIM). We will continue monitoring these datasets and determine detailed source parameters of VLFEs to understand the dynamics of interplate slip in the future.

Keywords: Slow earthquake, Southwest Japan, Very low frequency earthquake

©2020. Japan Geoscience Union. All Right Reserved.

Fluid flow patterns in fluid injection into swelling gel particles

*Kojiro Otoguro[1], Yutaka Sumino[1]

1. Department of Applied Physics, Faculty of Science Division I, Tokyo University of Science

Frequency of slow slip events varies by pore-fluid pressure, and further, pore-fluid pressure varies by permeability change caused by silica dissolution [1]. It is important for comprehensive understanding of earthquake mechanism to understand not only how permeability change in various situations but also how fluid flows with such variation of permeability. For this purpose, we explore the fluid flow in varying permeability by an analogue injection experiment.

In this study, we tried to imitate a fluid flow in thin fracture. Thus, we used a thin 2-dimensiohnal cell made of two acrylic plates. The gap between the plates was set as 1 mm to imitate fracture. We initially filled the gap with samples, gel particle, made of sodium polyacrylate. This gel particle is so called ionic gel, and can swell to be 1000 times in its volume when pure water is added. Furthermore, we can tune the swelling rate, as well as final swelled volume by changing the salinity of water [2]. We used the gel particle whose typical radius 350 μm in dry condition. After we filled the cell with the sample, we tapped 10 times so as to have particle packed well [3]. We then injected an aqueous phase, an aqueous solution of sodium chloride, into the cell from the bottom of the 2-dimensional cell. As a control parameter, we have changed the concentration of sodium chloride Cs, and injection rate Q. The schematic illustration of experimental setup is shown in Fig. 1.

Fig.2 is the obtained phase diagram. In the diagram, particles are displaced by fluid flow in white areas, and fluid penetrates in deep black areas. At high Q and C_s, the gel particle did not swell significantly, and the injection front steadily expanded circularly without the interruption of fluid flow. On the other hand, at low Q and C_s, due to the swelling of gel particles, fluid flow was blocked, and the injection front branched. These behavior, the transition from branching to circular injection front, can be considered with a simple mathematical model.

[1] P. Audet and R. Burgmann, *Nature* **510**, 389-392(2014).

[2] T. Tanaka*, From gels to life, University of Tokyo Press* (2002).

[3] M. Suzuki, *J. Soc. Powder Technol., Japan*, **40**, 348-354(2003)

Keywords: Injection of fluid, Pattern dynamics, Swelling gel particle

©2020. Japan Geoscience Union. All Right Reserved.

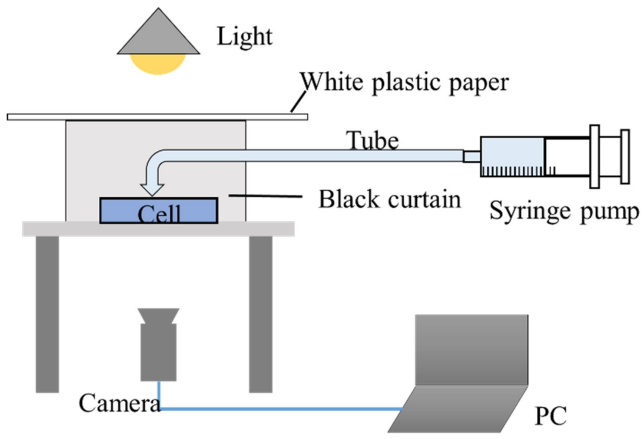


Fig.1 Schematic representation of experiment setup

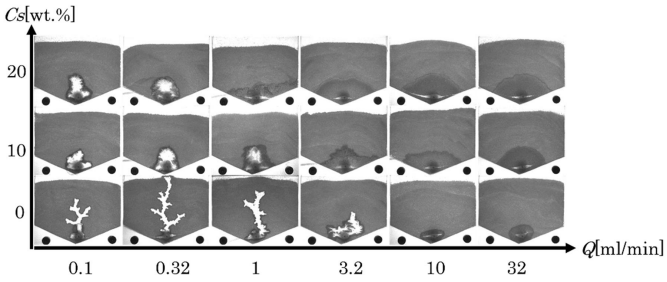


Fig.2 Phase diagram of injection behavior

©2020. Japan Geoscience Union. All Right Reserved.

Seismic reflection profiling across deep low-frequency tremor zone in western Shikoku, southwestern Japan

*Eiji Kurashimo[1], Kimihiro Mochizuki[1], Takashi Iidaka[1], Kazushige Obara[1]

1. Earthquake Research Institute, the University of Tokyo

The Nankai trough region, where the Philippine Sea Plate (PHS) subducts beneath SW Japan arc, is a well-known seismogenic zone of interplate earthquakes. In recent years, various slip motions with different time scales, including episodic tremors and very low-frequency earthquakes have been recognized in neighboring regions of the seismogenic zone (e.g., Obara and Kato, 2016). A narrow zone of nonvolcanic tremor has been found in SW Japan fore-arc, along strike of the arc (Obara, 2002). The spatial distribution of the tremor is not homogeneous in a narrow belt but concentrated forming clusters. Revealing structural factors that control the fault slip behavior is important to understand the subduction dynamics. The fluid pressure on a plate interface is one of the key factors to understand the fault slip behavior (e.g., Saffer and Tobin, 2011). Seismic reflection characteristics can provide important information on the fluid-related heterogeneity of structure around plate interface. A series of active seismic experiments were undertaken in 2008 and 2014 to obtain a structural image beneath the western part of Shikoku, southwestern Japan (Takeda et al., 2008, 2015). Takeda et al. (2015) provided the geometry of the subducting PHS. To investigate the lateral variation of reflection characteristics along tremor zone, we conducted active seismic experiment in the western part of Shikoku in November 2019. Our seismic experiment had two survey lines. One was carried out along a 80-km-long seismic line between Seiyo and Kumakogen (S-K line) in the east-west direction and the other was carried out along a 50-km-long seismic line between Ozu and Shimanto (O-S line) in the north-south direction. Six hundred seismic stations were deployed with about 200 m spacing for the S-K line and about 250 m spacing for the O-S line. Six explosive shots with charge size of 200 kg were fired on our survey lines. We obtained high signal-to-noise ratio explosion data along the entire length of the profile. The most remarkable feature of the record sections is that high amplitude reflections, probably from the top of the subducting PHS, are recognized. To obtain the detailed structure image, we applied the seismic reflection technique to explosion data. The stacked image shows several features of the deeper part of the hanging wall and the northward dipping plate boundary at 8-10 sec in two-way travel time.

Keywords: Deep low-frequency tremor, Seismic reflection profiling, Philippine Sea plate

©2020. Japan Geoscience Union. All Right Reserved.

Long-term Viscoerastic Relaxation and Spatially Inhomogeneous Viscosity Structure

*Yusaku Tanaka[1]

1. Earthquake Research Institute, University of Tokyo

Activities of very low-frequency earthquakes after mega-thrust earthquakes can be related to afterslips (e.g., Baba et al., 2020 JGR) but estimation of the spatiotemporal distribution of afterslip is difficult. For instance, GNSS observation can detect the signal of crustal deformation by afterslip + viscoelastic relaxation and their simultaneousness makes it hard to separate those signals.

One method for the separation is to use very long-term data. Time constant of afterslip is relatively short compared to that of viscoelastic relaxation, so the data obtained long after the earthquake do not include the signal of afterslip. By estimating viscoelastic relaxation based on those data and removing its contribution in the whole time series, we can gain the data mainly reflecting afterslip. This concept is very simple and today most of researches attempting to separate afterslip and viscoelastic relaxation are more or less related to it. However, it has one unignorable problem, namely, spatial inhomogeneousness of viscosity structure.

Suito (2017 EPS) suggested that three dimentional rheological heterogeneity is necessary for interpreting viscoelastic relaxation caused by the 2011 Tohoku-Oki earthquake based on GNSS data including ocean bottom stations and also showed that the viscosity of oceanic mantle can be higher than that of mantle wedge. However, it is still unclear if similar phenomena can be observed in different earthquakes and in different places.

In this presentation, I report that spatial inhomogenous viscosity structure is decisively important to interpret GNSS + satellite gravimetry observation results about post-seismic phenomena of the 2004 Sumatra-Andaman earthquake, the 2006-2007 doublet Kuril earthquakes, the 2009 Samoa-Tonga earthquake, the 2010 Maule earthquake, the 2011 Tohoku-Oki earthquake, and the 2012 Indian-Ocean earthquake. I also show the viscosity structure can possibly be even more complex than expected.

Keywords: viscoelastic relaxation, Burgers rheology, crustal deformation, GNSS, GRACE, GRACE-FO

©2020. Japan Geoscience Union. All Right Reserved.

A physical model of tremor response to periodic external stresses in poroelastic medium

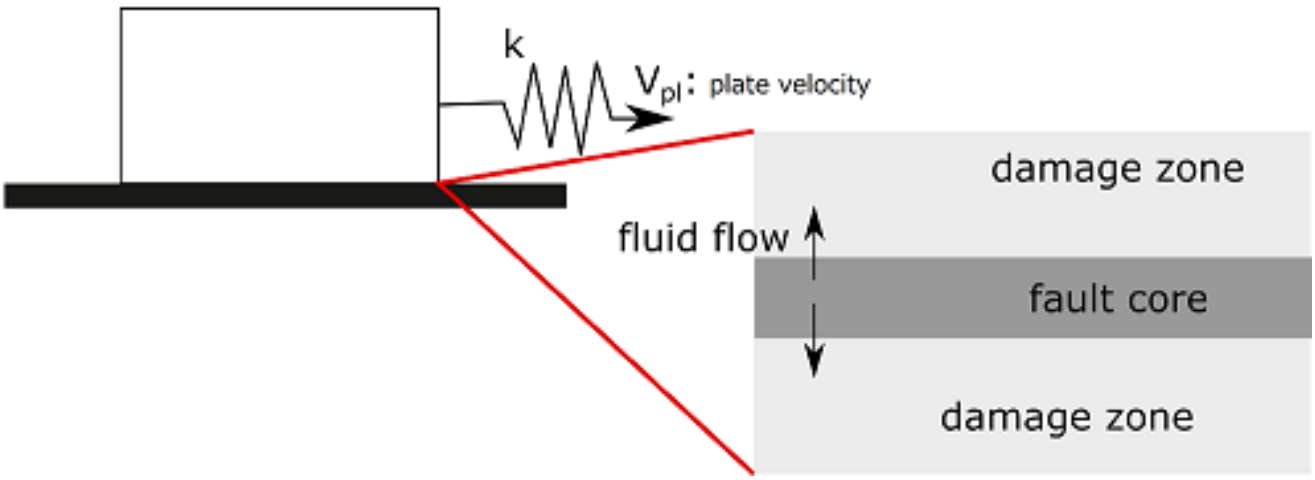
*Ryunosuke Sakamoto[1], Yoshiyuki Tanaka[1]

1. University of Tokyo Graduate School of Science

It is known that tectonic tremors are generated by the rupture of small rata-weakening asperities which is caused by slow slip on the surrounding plate interface. In most cases, tectonic tremors occur in areas where the pore fluid pressure is higher. Because high-pressure fluids reduce the effective normal stress significantly, tectonic tremors can be triggered by weak perturbing external stresses such as tidal stresses. Previous studies show that the rate for tremor occurrences exponentially changes [e.g., 1]. Other studies show that the peak of the tremor occurrence rate advances/delays relative to the peak of tidal stresses [2 & 3].So far, no model has been constructed that could explain all of the above observations with realistic fault parameters. Most of tidal response models did not take the presence of pore fluids into account. In this study, we reveal how the pore fluids behave under periodic external stresses by considering fluid pressure change due to dilatancy within fault core (fig) and show that this model could explain the observations reported above [1-3].In addition, we will discuss which kinds of material parameters affect the tidal sensitivity based on our model. Furthermore, we will investigate how the behavior of the system changes under multiple periodic perturbations.

[1] S. Yabe, Y. Tanaka, H. Houston and S. Ide, J. Geophys. Res. Solid Earth, 120, 7587–7605 (2015)
[2] R. Nakata, N. Suda and H. Tsuruoka, Nature Geosci. 1, 676-678 (2008)
[3] Thomas, A. M., R. Bürgmann, D. R. Shelly, N. M. Beeler, and M. L. Rudolph, J Geophys Res. 117, (2012)

Keywords: tremor, poroelastic medium, spring-slider model



©2020. Japan Geoscience Union. All Right Reserved.

The radial pattern of brittle viscoelastic fluids between rotating parallel plates

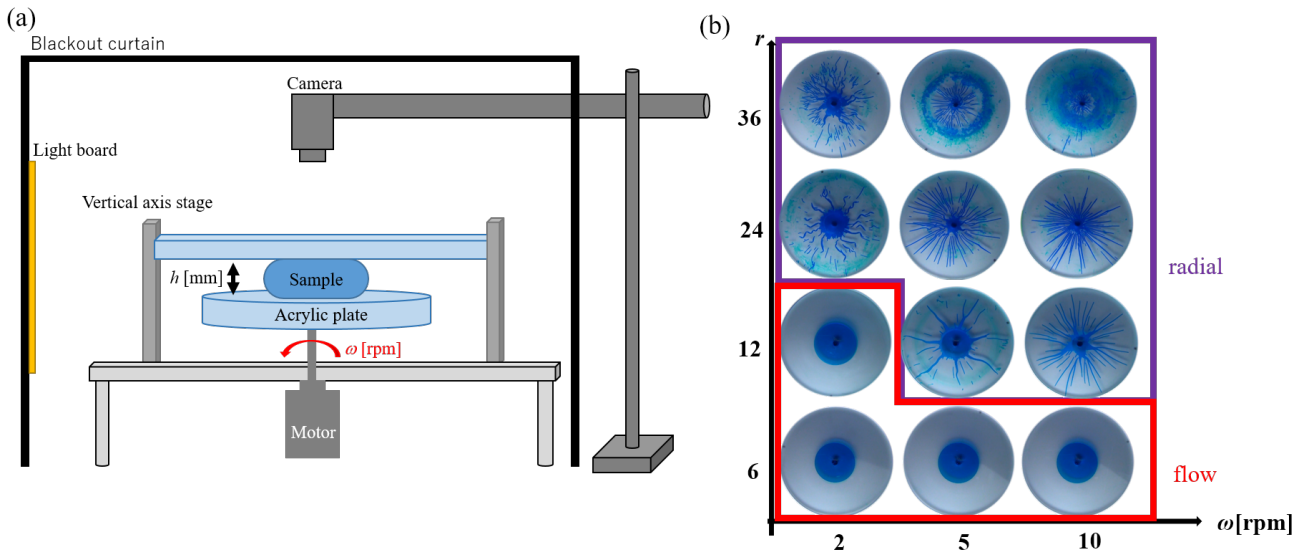
*Tatsuya Nishikubo[1], Hiroki Ishikawa[1], Shoma Kato[1], Yutaka Sumino[1]

1. Department of Applied Physics, Faculty of Science Division I, Tokyo University of Science

Slow earthquake occurs at marginal region between seismogenic and steady sliding zones[1]. At the seismogenic zone, a subducting plate can be recognized as brittle elastic solid, whereas the plate can be recognized as ductile viscous liquids at the steady sliding zones. For this reason, we assume that the marginal material behavior, viscoelasticity, can be relevant to general slow earthquakes. Here we report the analogue experimental system with viscoelastic fluids under continuous shear with rotating plates.
As a viscoelastic fluids, we used a gel, which is mixture of micro emulsion with telechelic polymer, so called bridged emulsion. One reason for using this sample for the present experiment is that the gel is known to behave as an ideal Maxwell fluids with single relaxation time under linear oscillatory shear. Another reason for the choice of this gel is, in nonlinear rheological regime, the gel behaves as brittle solid with low fracturing energy at the shear rate higher than the inverse of the relaxation time. The gel is made from the mixture of cetylpyridinium chloride(CPCl), octanol, decane,0.2M NaCl aq, and poly (ethylene glycol) distearate as telechelic polymer, which has hydrophilic main chain with hydrophobic ends[2]. As a parameter, we changed the concentration of bridging telechelic polymer, which determined the shear modulus and relaxation time.
In order to observe long term behavior of sample under shear, we used rotating plates as an experimental geometry as shown in Fig. (a). A plate is rotated with fixed angular velocity on the other plate. The gap between the plates was kept as 1 mm. The angular velocity was used as the other parameter. The typical behavior of the sample is shown in Fig. (b). We found that the sample showed radial pattern when the angular velocity was large enough, whereas the radial pattern is absent for the small angular velocity. This transition of pattern was controlled by the characteristic shear rate which is determined by the relaxation time of the samples. Indeed, we observed the coexistence of flow and the radial patterns when the angular velocity was marginal. Such behavior can be understood due to the liquid and elastic nature of the sample depending on the shear rate.

[1] K. Obara, A. Kato, Science 353, 253-257 (2016).
[2] M. Filali and J. Appell, J. Phys. Chem. B 103, 7293-7301 (1999).

©2020. Japan Geoscience Union. All Right Reserved.



©2020. Japan Geoscience Union. All Right Reserved.

Offshore surveys of seismic structures and seismicity of regular and low-frequency earthquakes around Amami islands

*Tsutomu Takahashi[1], Ayako Nakanishi[1], Yojiro Yamamoto[1], Yasushi Ishihara[1], Aki Ito[1], Ryuta Arai[1], Seiichi Miura[1], Shuichi Kodaira[1], Yoshiyuki Kaneda[2]

1. Japan Agency for Marine-Earth Science and Technology, 2. Kagawa Univ.

Ryukyu arc, southwestern Japan, shows high activities of various slow earthquakes such as slow slip events (e.g., Heki & Kataoka 2008; Nishimura 2014) and shallow low frequency tremors (e.g.,Yamashita et al. 2015). We conducted passive and active source surveys around Amami islands to elucidate detailed activities of regular and slow earthquakes and seismic structures. For the passive source survey, we deployed 30 short-period ocean bottom seismographs (OBSs) and 5 temporal onshore stations at 25~40 km interval. Deployed OBS recorded ground motion from Mar. 2019 to July or Aug. 2019. As a part of active source surveys, we conducted wide-angle OBS and multichannel seismic (MCS) reflection surveys along a survey line between Amami-Oshima and Tokunoshima islands by the R/V Kaimei of Japan Agency for Marine-Earth Science and Technology (JAMSTEC). This survey line is almost perpendicular to the Ryukyu trench. We laid out 30 OBSs at 6km interval along this survey line for the refraction survey.

Seismic data of the passive survey observed many regular earthquakes and several sequences of low frequency earthquakes (LFEs). We relocated a few hundred earthquakes (M>2) listed in the earthquake catalog by the Japan Meteorological Agency (JMA) by using OBS and onshore stations' data. We also estimated epicenters of about 200 LFEs by envelope correlation method. LFEs distribute between Amami islands and Ryukyu trench, and distance from the Ryukyu trench is about 20-80km. One of the LFE sequences locates at off west of the Amami plateau. Source area of this sequence shows relatively high activity of regular earthquakes. While, the source area of another LFE sequence off the southeast of Amami-Oshima island shows quite low activity of regular earthquakes. Our seismic section of active source survey crosses the latter LFE area. MCS reflection data shows strong reflection with negative polarity from the plate boundary beneath this LFE area. This spatial coincidence of reflective plate boundary and LFEs is similar with the southern Ryukyu arc (Arai et al. 2016). Power spectra and duration times of these LFEs are also resemble with those observed at southern Ryukyu arc. Bathymetry of the Philippine sea plate implies different geometrical properties of subducting plate between these two areas. Similarities of LFEs in these areas would become an important constraint for source and structure models at Ryukyu subduction zone.

Acknowledgement: This study is supported by "Research Project for Compound Disaster Mitigation on the Great Earthquakes and Tsunamis around the Nankai Trough Region" of the Ministry of Education, Culture, Sports, Science and Technology (MEXT) of Japan. We are grateful for Amami-city, Tokunoshima-town, Amagi-town, China-town and Toshima-village for their kind corporation for onshore seismic observations.

©2020. Japan Geoscience Union. All Right Reserved.

Slip distributions of short-term slow slip events in the northern Kii Peninsula based on NIED Hi-net tilt measurements

*Chujo Naoya[1], Hitoshi Hirose[2,1,3], Takeshi Kimura[3]

1. Department of Planetology, Graduate School of Science, Kobe University, 2. Research Center for Urban Safety and Security, Kobe University, 3. National Research Institute for Earth Science and Disaster Resilience

In the southwest Japan subduction zone, short-term slow slip events (SSEs) with nonvolcanic tremor (Episodic Tremor and Slip: ETS, Rogers and Dragert, 2003) which last for several days to weeks occur repeatedly. Because the short-term SSEs occur at the downdip extension of a megathrust earthquake rupture zone, the SSEs are one of the key factors for stress buildup processes of the megathrust earthquakes (e.g., Obara and Kato, 2016)[h1] . Therefore, detailed slip distributions of short-term SSEs are important for understanding the strain accumulation and release at the ETS zone. In the northern Kii Peninsula, short-term SSEs have been detected by[h2] previous studies, but their fault motions have been modeled with uniform slip on a rectangular fault (e.g., Hirose and Obara, 2006).[h3] This may introduce a bias in the estimation of amount of slip.
Here we apply an inversion method which can express a spatial slip distribution to tilt step measurements in the northern Kii Peninsula and estimate detailed slip distributions of nine[h4] short-term SSEs from November 2004 to October 2009. We also discuss the classification of the short-term SSE source areas[h5] by analyzing multiple short-term SSEs in the northern Kii Peninsula.
We used time-series records of a high-sensitivity accelerometer (tiltmeter) installed at NIED Hi-net stations located in the Kii Peninsula and Tokai areas. We applied the BAYTAP-G (Tamura et al., 1991) program together with atmospheric pressure records observed at the Tsu Local Meteorological Observatory to the tilt records in order to remove tidal components and an atmospheric pressure response. We measured a tilt change (tilt step) due to an SSE after detrending. Although tilt steps of the analyzed SSEs have already been determined in previous studies (e.g., Hirose and Obara, 2006; Sekine et al, 2010), we redetermined them from the original tilt records to improve station coverage for an SSE and to obtain a more reliable tilt step dataset. We estimated a slip distribution that explains the tilt step dataset for an SSE by a conventional inversion method by Hirose and Kimura (submitted).
As a result, a spatial slip distribution for a short-term SSE in the northern Kii Peninsula is estimated based on tilt records for the first time. The estimated moment magnitudes of the nine SSEs range from 5.5 to 6.1. The obtained tilt steps, and main locations and magnitudes of the estimated slip are basically consistent with the previous studies (e.g., Hirose and Obara, 2006). A comparison of these slip distributions shows that the slip areas are roughly classified to two groups: one is that the center of a slip distribution is located mainly onshore (corresponding to the Shima Peninsula part of the tremor belt), and the other is that that is located offshore in the Ise Bay area (corresponding to the Ise Bay part of the tremor belt). This suggests that there are two “SSE patch” regions where SSEs of the similar size repeatedly occur on the plate interface.
Longer study period and more comprehensive detection of short-term SSEsmay improve our understandings of the relationship between recurrence intervals and magnitudes of SSEs, and the strain accumulation and release processes in the northern Kii Peninsula.

Acknowledgments: This work was supported by JSPS KAKENHI Grant Number JP16H06474.

Keywords: southwest Japan subduction zone, megathrust earthquake, inversion method, plate interface

©2020. Japan Geoscience Union. All Right Reserved.

©2020. Japan Geoscience Union. All Right Reserved.

Trial detection of deep low frequency tremor using analog seismograms of Kanto-Tokai Observation Network in 1988-1990

*Takanori Matsuzawa[1], Tetsuya Takeda[1]

1. National Research Institute for Earth Science and Disaster Resilience

Slow earthquakes (i.e. low frequency tremor (LFT), very low frequency earthquakes and slow slip events (SSEs)) have been vigorously studied since the discovery of deep low frequency tremor (LFT) in the Nankai region (Obara, 2002). However, the past activity of LFT is not clear, as these events were not well known in 20th century and continuous seismic data in this period is rare due to the cost of data storage. Therefore, only analog seismograms are available source to reveal the LFT activity in such period. In terms of the crustal deformation, Kobayashi et al. (2006) revealed the activity of short-term SSEs in the Tokai region since 1984, using a strain meter of JMA. On the other hand, as the data volume of seismic data is much larger than that in geodetic observations, it is not easy to keep the recordings for a long time. Fortunately, NIED has stored the paper recordings of seismograms of the Kanto-Tokai Observation Network, which started since late 1970s. In our previous study, we have reported the tentative result of LFT detection in the Tokai region from 1980 to 1987, using this data (Matsuzawa and Takeda, 2019). In this study, we report the tentative result from 1988 to 1990, in which occurrence of a long-term SSE is reported (Kobayashi and Yoshida, 2004).

We visually examined waveforms at Shimoyama (SMY) seismograph in the Kanto-Tokai Observation Network by NIED, to detect active episodes of LFT, as in our previous study. The waveforms are identified as tremor-like signal lasts for several minutes and is repeatedly found within several days, even if a single station is used. When the number of low frequency signal is small within several hours, we discard the event, as it is not clear whether the signal is caused by a regular earthquake or a small LFT episode. This feature was also confirmed using simulated analog seismogram and current LFT catalog (Matsuzawa and Takeda, 2019). After visual inspection of the waveforms from 1988 to 1990, we found possible LFT episodes, for example, in Apr. 1988, Oct. 1988, Feb. 1989, Oct. 1989, Jun. 1990, and Sept. 1990. In addition, possible triggered tremor by a far field earthquake is found, for example, after an M7.7 earthquake in Philippines on Jul. 16, 1990.

In our studied period, six tremor episodes are detected, while short-term SSEs are reported in Apr. 1988, Oct. 1988, and Oct. 1989, which correspond to our detected episodes. In our previous study, we reported four tremor episodes in 1980-1985, and three episodes in 1986-1987. Combining our new result, our results suggests that tremor was active in 1986-1990. Tremor episode were active in 2003-2004 during a long-term SSE in 2000-2005. The activation of tremor in late 1980s is similar to the activation during a long-term SSE in 2000-2005. However, the active period of tremor precedes the period of the long-term SSE in this case. Therefore, the long-term SSE in late 1980s may start close to the deep LFT region and propagated to shallower part. Further study, including location of tremor episodes, might reveal the details and variety of slip process in long-term SSE events.

Keywords: Low Frequency Tremor, Analog Seismogram, Slow Earthquakes

©2020. Japan Geoscience Union. All Right Reserved.

Estimation of the spatial distribution of Qs values beneath the Kii Peninsula, Japan by the twofold spectral ratio method

*Kodai Sagae[1], Hisashi Nakahara[1], Takeshi Nishimura[1], Kazutoshi Imanishi[2]

1. Solid Earth Physics Laboratory,Department of Geophysics,Graduate School of Science,Tohoku University, 2. National Institute of Advanced Industrial Science and Technology (AIST)

Evaluation of radiation energies of tremors is important to understand the generation mechanism. Previous studies estimated the radiation energy assuming a spatially uniform S-wave attenuation quality factor, Qs value, over the area of interest (e.g. Maeda and Obara, 2009). However, when we discuss a regionality of the tremor generation, the spatial changes of Qs values are important. The objective of this study is to estimate the spatial distribution of Qs values beneath the Kii Peninsula by using the twofold spectrum ratio method (e.g. Matsuzawa et al., 1989).

We use a dense seismic array (39 three-component velocity sensors, array aperture:1.5 km) installed by AIST at the Kii Peninsula. We also use seismograms recorded at a Hi-net station (N.HYSH) that is located close to the seismic array. We analyze the data for 2 years from July 2012 to July 2014, referring to the tremor catalog determined by Sagae et al. (2019 JpGU) in which 27,066 events are listed for the 2 years. For tremors recorded at the stations, we calculate velocity amplitude spectra and estimate their slopes at a frequency range of 2.0-4.0 Hz. Outliers are removed by setting a threshold of 4.4 times Median Absolute Deviation of the spectral slopes at each station. Totally, 18,330 events are selected for the following analysis.

We create horizontal blocks of 0.1×0.1˚ within a region of 136˚E to 137˚E and 34˚N to 35˚N. The twofold spectral ratio method is applied when the number of tremor events in a block is more than 100. We calculate twofold spectral ratios for two events locating in the block, when their separations are more than 5 km. Qs value is estimated by the twofold spectral ratio method. In this method, a logarithm of a twofold spectral ratio that is corrected for the geometrical spreading (log TSR) is linearly proportional to a twofold differential travel time (TDTT); The slopes is $-\pi f/Qs$, and an intercept is a term about the radiation pattern. However, the intercept is expected to be close to 0 when focal mechanisms of tremors occurring in a block are similar. At each narrow frequency band (2.0-4.0 Hz, 2.8-5.6 Hz, 4.0-8.0 Hz), we assume that Qs value of the structure along the ray paths from hypocenters to the seismic array and the Hi-net station is constant. Then, we estimate the slope ($-\pi/Qs$) and the intercept at each frequency band.

Estimated Qs values are summarized as follows; Qs values are in a range of 63-458, 58-896, and 66-2044 at 2.0-4.0 Hz, 2.8-5.6 Hz, and 4-8 Hz, respectively. Qs values estimated at the high frequency band tend to be larger. However, at the high frequency band, the number of blocks for which the Qs value is estimated to be a negative value increases. The intercepts are confirmed to be close to 0 (-0.03 ~ 0.008) in blocks for which Qs values are estimated to be a positive. This suggests that focal mechanisms of tremors occurring within the same block are similar.

Keywords: Deep low frequency tremor, Twofold spectrum ratio method, Qs value, Kii Peninsula

©2020. Japan Geoscience Union. All Right Reserved.

3-D thermal modeling of generation mechanisms for short-term slow slip events and low-frequency earthquakes along the Ryukyu trench

*Nobuaki Suenaga[1], Shoichi Yoshioka[1,2]

1. Research Center for Urban Safety and Security, Kobe University, 2. Department of Planetology, Graduate School of Science, Kobe University

Interplate seismicity, such as short-term slow slip events (S-SSEs) and low-frequency earthquakes (LFEs), has been identified in the Ryukyu Trench, southwest Japan. As one of the specific characteristics of these events, the depths where S-SSEs take place at the plate interface beneath Okinawa Island are approximately 10 km shallower than those beneath the Yaeyama Islands. In this study, we constructed a three-dimensional parallelepiped thermal convection model associated with subduction of the Philippine Sea (PHS) plate beneath the Amurian (AM) plate at the Ryukyu subduction zone. We applied the subduction history of the PHS plate in the model region, referring to the plate rotation model and the trench motion model. Then, we performed a time-dependent numerical simulation for the last 15 Myr to elucidate the relationships among the calculated thermal structure, dehydration from the subducting plate, and interplate seismic events. To constrain the calculated thermal structure, we used observed heat flow data. As a result, the interplate temperatures where S-SSEs occur are estimated to range from 350℃ to 450℃ beneath both Okinawa Island and the Yaeyama Islands, although the latter are approximately 50-100℃ higher than the former. This temperature range corresponds well with that of the transition zone from unstable sliding to stable sliding. On the other hand, LFEs occur in a temperature range of 300 to 400℃ beneath both Okinawa Island and the Yaeyama Islands in our model, which is roughly within the temperature range of the transition zone, although it is approximately 50℃ lower than that in the region where S-SSEs occur. Using phase diagrams for hydrous minerals of the oceanic crust and the slab mantle, we estimated the water content distribution and dehydration gradient per unit distance in the subduction direction of the PHS plate. Near the S-SSE fault planes, a dehydration gradient of 0.05 wt%/km is identified beneath Okinawa Island associated with the phase transformation from blueschist to lawsonite blueschist within hydrous minerals of the oceanic crust. In contrast, dehydration gradients of 0.13 wt%/km and 0.12 wt%/km are identified beneath the Yaeyama Islands associated with the phase transformation from lawsonite blueschist to amphibole eclogite within the oceanic crust and from brucite to antigorite within the slab mantle, respectively. Further, there are no specific dehydration gradients in the LFE occurrence region beneath both Okinawa Island and the Yaeyama Islands in our model, although there is a possibility that dehydration fluid materials in the S-SSE occurrence region are transported to the LFE occurrence region, considering the migration feature of LFEs and the synchronicity of activity between S-SSEs and LFEs. Therefore, we conclude that both the interplate temperature and dehydration gradient play key roles in the occurrences of S-SSEs and LFEs and that the larger dehydration gradient beneath Yaeyama Island than beneath Okinawa Island is the main reason for the depth difference in S-SSEs.

©2020. Japan Geoscience Union. All Right Reserved.

Spatio-temporal evolution of long- and short-term slow slip events in the Tokai region, central Japan estimated from a very dense GNSS network, during 1997-2017

*Hiromu Sakaue[1], Takuya NISHIMURA[2], Jun'ichi Fukuda[3], Teruyuki Kato[4]

1. Graduate School of Science, Kyoto University, 2. Disaster Prevention Research Institute Kyoto University, 3. Earthquake Research Institute,The University of Tokyo, 4. Hot Springs Research Institute of Kanagawa Prefectural Government

We analyzed Global Navigation Satellite System (GNSS) data from 1997 to 2017 for the Tokai region of tne Nankai subduction zone, in order to investigate long- and short-term slow slip events (SSEs) on the subduction interface. The GIPSY-OASIS II software (version 6.1) was used to estimate daily coordinates of continuous GNSS stations operated by GSI and temporary GNSS stations operated by JUNCO (the Japanese University Consortium for GPS Research). It is well known that GNSS time series have many systematic signals and noises that do not result from SSEs. They include, for example, seasonal variations, co- and post-seismic deformation of the 2004 southeast off Kii Peninsula earthquakes (M_j 7.1/7.4), the 2008 Ibaraki-ken-oki earthquake (M_j 7.0), the 2008 Fukushima-ken-oki earthquake (M_j 6.9), the 2010 Fukushima-ken-oki earthquake (M_j 6.7), and the 2011 Tohoku-oki earthquake (M_w 9.0), and crustal deformation of volcanic activity on the northern Izu Islands in 2000. After removing them, we applied a modified Network Inversion Filter (NIF) [Fukuda et al., 2008] to estimate daily slip and slip rate on the subduction plate interface. Our results showed a long-term SSE from 2000 to 2005 involved two slip phases/subevents. The slip peak of the first phase was estimated at a depth of 20 km from the end of 2000 to the end of 2001. Another long-term slow slip with slower slip rates was estimated around this slip peak from 2013 to 2015. The slip peak of the second phase estimated at a depth of 30 km from the end of 2002 to the beginning of 2005. The slip area of the second phase was extended/migrated to the down-dip tremor area, and the recurrence period of tremor became short during this period. Our results show spatio-temporal distribution for not only those long-term SSEs in 2000-2005 and 2013-2015, but also short-term SSEs (M_w <6.1). The maximum estimated daily slip rates for short-term SSEs are an order of magnitude larger than those of the long-term SSE, and peak slip for short-term SSEs migrates along strike with LFTs synchronously.

Keywords: slow slip event, Tokai region, GNSS

©2020. Japan Geoscience Union. All Right Reserved.

Repeating activity of shallow low-frequency tremor in Hyuga-nada

*Yusuke Yamashita[1], Masanao Shinohara[2], Hiroko Sugioka[3], Aki Ito[4], Tsutomu Takahashi[4], Daisuke Suetsugu[4]

1. Disaster Prevention Research Institute, Kyoto University, 2. Earthquake Research Institute, the University of Tokyo, 3. Graduate School of Science, Kobe University, 4. Japan Agency for Marine-Earth Science and Technology

In the Hyuga-nada region, since the first observation of shallow tremor in 2013, ocean bottom seismological observations have been carried out in the focal area of the shallow tremor since 2014. From March 2017, ocean bottom seismological and geodetical observation have been conducted by the "Science of Slow Earthquakes", JSPS KAKENHI Grant-in-Aid for Scientific Research on Innovative Area, MEXT, Japan. During the first observation period, the ocean bottom seismometers (OBSs) were retrieved from January to February 2019, and good seismic records were obtained. From December 2017 to January 2018 during the observation period, shallow slow earthquake activity was documented from off east Tanegashima Island to Hyuga-nada, and shallow tremors and VLFE activity were recorded on the OBS network. The epicenter of shallow tremor was determined by almost same method as Yamashita *et al*. [2015]. The depth of the tremor source was fixed to the plate boundary model by Nakanishi *et al*. [2018], and the S-wave velocity structure was a uniform structure of Vs = 3.5km/s. For the analysis, the hypocenter was determined by a total of 18 OBSs, including 10 OBSs from another project (the research project for compound disaster mitigation on the great earthquakes and tsunami around the Nankai trough region, the MEXT of Japan) that had been conducting observations in the off east Tanegashima Island at the same time. As a result of the hypocenter determination, it was found that the epicenter distribution of shallow tremor almost coincided with the focal area up to the point where the epicenter distribution turned eastward in the area of the 2013 activity. This distribution is consistent with the first migration area of the two migrations seen in the 2013 activity. In the 2017-2018 activity, a clear migration from south to north direction was confirmed and the end point of the migration are almost the same as the first migration in the 2013 activity. The region where the migration has stopped is considered to be the region where the Kyushu Palau Ridge is subducted. According to the estimation results of the released seismic energy rate by Watanabe [2019], it is located in the region where the released seismic energy rate is relatively low. It is suggested that the heterogeneity of the structure around the plate boundary greatly affects the tremor activity region and the generation process of the shallow tremor. Our new result of the almost same hypocenter distribution and activity characteristics as in 2013, it has become clear for the first time that the shallow tremor activity occurs repeatedly in the same place and has similar activity characteristics in this region. Although no significant pressure change has been observed by ocean bottom pressure gauges at this moment and the expected short-term slow slip event has not been directly observed, its size was assumed to be not larger than Mw~6. The all equipment for second observation will be retrieved from spring to summer 2020.

Acknowledgments: This study is supported by the JSPS KAKENHI Grant Number JP16H06471, JP17K01328, and the research project for compound disaster mitigation on the great earthquakes and tsunami around the Nankai trough region, the MEXT of Japan.

Keywords: shallow tremor, Hyuga-nada, Ocean bottom observation

©2020. Japan Geoscience Union. All Right Reserved.

Shallow low-frequency tremor in the Japan Trench subduction zone

*Sachiko Tanaka[1], Takanori Matsuzawa[1], Youichi Asano[1]

1. National Research Institute for Earth Science and Disaster Resilience

In the regions off Tokachi and Sanriku, we have identified shallow low-frequency tremor using the records from the Seafloor observation network for earthquakes and tsunamis along the Japan Trench, S-net (Tanaka et al., 2019). It occurs between the 10- and 25-km depth contours of the plate interface, and its characteristics including duration (half a day to a few weeks) and recurrence time (one month to one year) vary with location along the trench. In the present study, we extend our analysis to a wider offshore area from Hokkaido to Boso Peninsula. The data we used are the continuous three-component velocity seismograms recorded at 125 S-net stations (S1-S5) for the period from 2017 to 2019. We constructed root mean square (RMS) envelopes of the seismograms band-pass filtered between 2 and 10 Hz, and searched tremor sources every one minute using overlapping two-minute time windows by the method of Tanaka et al. (2019) based on an envelope correlation analysis (Obara, 2002) and an event clustering scheme (Frohlich and Davis, 1990). In addition to the regions off Tokachi and Sanriku, clusters of tremor were located in the regions off Fukushima and Ibaraki. These clusters also lie within a narrow zone between the 10- and 25-km depth contours of the plate interface. As is the case with the tremor off Tokachi and Sanriku, the tremor off Fukushima occurs at similar locations to the very low frequency (VLF) earthquakes detected using seismic data from onshore networks (Matsuzawa et al., 2015). About 20 episodes of tremor were observed in this region, and some were coincident with the VLF earthquakes. In the region off Ibaraki, tremor episodes were detected less frequently (six in the three years), with each lasting for half a day to a day, although these were located in a smaller area than previously reported by Nishikawa et al. (2019). On the other hand, no tremor was found in the large slip area of the 2011 Mw 9.0 Tohoku earthquake as was shown by Nishikawa et al. (2019). The locations of tremor and the variations of its properties show strong lateral heterogeneities of the slip behavior at the shallow plate interface in the Japan Trench subduction zone.

Keywords: shallow low-frequency tremor, Japan Trench, S-net

©2020. Japan Geoscience Union. All Right Reserved.

Shallow low-frequency tremor activity off Erimo, Hokkaido from 2006 to 2007 revealed from pop-up type ocean bottom seismometers

*Susumu Kawakubo[1], Ryosuke Azuma[1], Ryota Hino[1], Hidenobu Takahashi[1], Kazuaki Ohta[2], Masanao Shinohara[3]

1. Graduate School of Science, Tohoku University, 2. National Research Institute for Earth Science and Disaster Resilience, 3. Earthquake Research Institute, University of Tokyo

The shallow part of the plate boundary around the Kuril and Japan Trench junction, off Erimo, Hokkaido, is known as the place where slow earthquakes are comparatively active along the Japan island arc. In this region, VLFEs (Very Low Frequency Earthquakes) have been observed since the 2003 Tokachi-Oki Earthquake (Asano et al., 2008). On the other hand, LFTs (Low Frequency Tremors) were firstly discovered in 2016 based on the inspection of the seismograms obtained by the Seafloor observation network for earthquakes and tsunamis along Japan Trench (S-net) (Tanaka et al., 2019; Nishikawa et al., 2019). One of the important discoveries by the S-net is that the LFT activity off Erimo usually precede the VLFE activity by 0.5–4 days (Tanaka et al., 2019). The correlation between the LFTs and VLFEs persistence of the VLFEs activity before and after the 2011 Tohoku-oki Earthquake (Asano et al., 2008; Tanaka et al., 2019), it is expected that the LFT activity would exist before the S-net deployment and before the occurrence of the 2011 Tohoku-oki earthquake off Erimo region. This study aims to clarify the LFT activity in the region by analyzing the OBS records obtained in the development from 2006 to 2007.

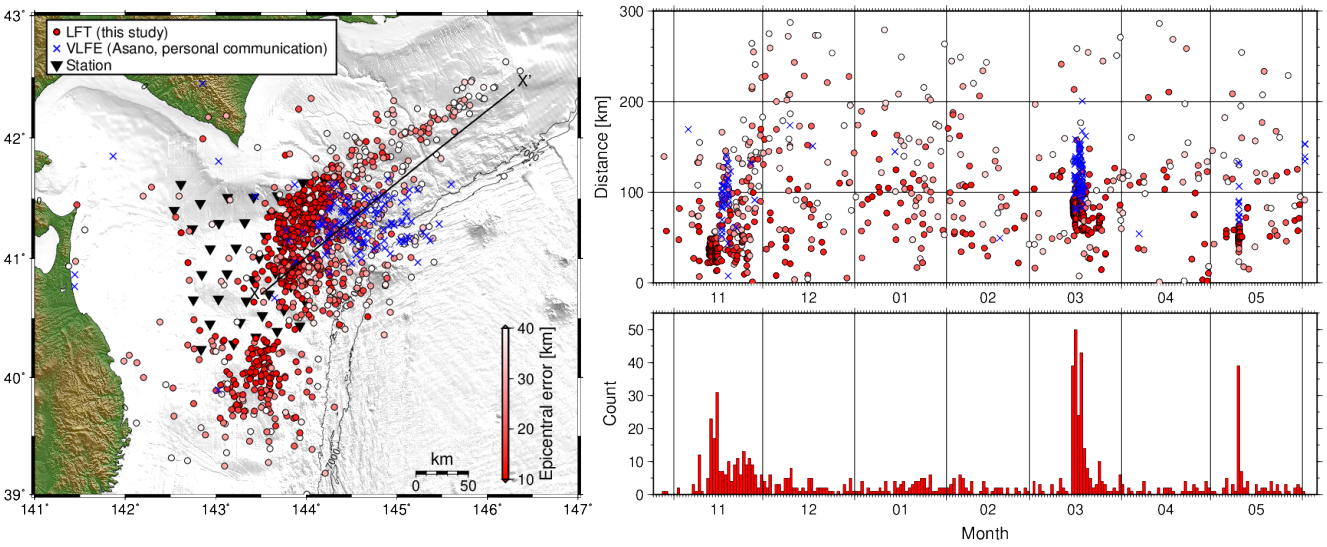
In this study, we detect LFTs from the records of 42 pop-up type ocean bottom seismometers from October 25, 2006 to June 5, 2007. For detection of seismic events and determination of their hypocenters, we use the envelope correlation method (Ide, 2010). We defined an event as an earthquake if a maximum cross-correlation (CC) value exceeds 0.6 for more than 10 station-pairs. Then, we determined its hypocenter by using lag-times maximizing the CCs at the station pairs, as arrival time difference of S-waves from the source. For discrimination of LFTs from other type of events, we selected events with duration larger than 20 sec and of magnitude less than 3 as LFTs. After the first screening, we excluded the events having large epicenter errors and large time residuals. As a result, 989 LFTs were identified out of 10,445 events firstly detected. The detected LFTs were distributed at a certain distance from the trench axis and the LFTs with focal depth errors less than 10 km are distributed near the plate boundary.

During the analysis period, we found three major LFTs activities with VLFEs activities. During the first period (2006/11/12–19), the LFTs activity showed migration towards northeast by 16–23 km/day though detectivity of LFTs may be degraded by the pronounced aftershocks following the middle Kuril Trench earthquake on November 15, 2006. The LFTs during the second period (2007/3/15–19) also migrated but was directed towards southwest by 25–30 km/day. On the other hand, the last activity occurred in the narrower area than others and converged just one day on May 10, 2007, and the migration like previous periods was not recognized.

We found that every LFT swarm activity preceded the known VLFEs (Asano et al., 2008). The VLFEs detected 0.5–4.5 days after the onset of the LFTs swarm occasion. Similar relationship between the LFT and the VLFEs is reported for the current activities in the region (Tanaka et al., 2019). The locations of the swarm almost coincide with the LFT distribution located by the S-net data (Nishikawa et al., 2019). These common points between the LFT/VLFE activities at present and in 2006-2007 indicate that the shallow plate boundary off Erimo does not change in their behavior in terms of the slow-slip activity through the period containing the 2011 Tohoku-oki earthquake happened.

©2020. Japan Geoscience Union. All Right Reserved.

Keywords: Shallow low-frequency tremor, Ocean bottom seismometer, Kuril Trench



©2020. Japan Geoscience Union. All Right Reserved.

High-velocity frictional behavior of fault gouges in the presence of pore fluid

*Akito Tsutsumi[1]

1. Graduate School of Science, Kyoto University

Recent observations of slow earthquakes in the vicinity of high pore-fluid pressure suggest that variation in pore-fluid pressure plays a role in the underlying mechanism of the slow earthquakes. However, little is known of the frictional properties of subduction-zone materials in the presence of pore-fluids. To study the effect of pore-fluid on the seismic faulting process in subduction-zones, we performed friction experiments on the sediments entering to the Costa Rica subduction zone. Rotary-shear friction experiments were conducted on the input biogenic ooze material collected at reference sites U1381A during IODP Exp. 334 (Vannucchi et al., 2012) at normal stresses of 2.0–5.0 MPa and at various slip velocities V of 0.3–130 mm/s. The collected samples were oven dried at 60 degree Celsius for 24 hours, and gently disaggregated using a pestle to be used as the experimental gouges. We prepared two types of experimental conditions: impermeable and permeable conditions. Impermeable conditions consist of a pair of gabbro cylinders (25.0 mm in diameter) with an intervening thin layer of gouge (0.5 g). For permeable conditions we used a permeable sandstone (Berrea sandstone) instead of using gabbro for one side of the rock-cylinder pair. On both permeability conditions, distilled water (0.8–1.0 ml) was added to prepare pore-fluid saturated condition of the gouge initially. Under impermeable conditions, experiments performed at higher slip velocities (>3 mm/s) show a dramatic decrease in frictional coefficient values upon the initial shear loading. The value of the friction is as high as ~0.6 at the onset of sliding, following which it rapidly decreases to attain a value as low as ~0.1. The decreased friction value is constant at the lowered level for duration of slip as long as 100s, then it increases gradually to attain roughly steady-state value of ~0.6. Under permeable conditions, such a dramatic decrease and the following increase in frictional strength is not observed. The frictional behavior of the gouges under permeable conditions is similar to the behavior observed at the lowest slip velocity (0.3 mm/s) under impermeable conditions when friction is plotted against elapsed time. We suggest that the slip weakening and the following strengthening behavior observed at high velocity test under impermeable conditions is likely attributed to a transient change in fluid pressure inside of the fault zone during the shearing of the gouge. Magnitude of the pore-fluid pressure change should depend on the degree of pore-space change and the compressibility of the fluid filled gouge material. The experimental results suggest importance of studying how pore-fluid pressure evolves during faulting process to understand the frictional behavior of faults in subduction zones.

Keywords: gouge friction, pore pressure, slip weakening, slip strengthening

©2020. Japan Geoscience Union. All Right Reserved.

Detection of low-frequency aftershocks of the 2019 Ridgecrest earthquake sequence

*Ayako Tsuchiyama[1], Taka'aki Taira[2], Junichi Nakajima[1], Roland Bürgmann[3]

1. Earth and Planetary Sciences at Tokyo Institute of Technology, 2. Berkeley Seismological Laboratory, 3. Earth and Planetary Science, University of California, Berkeley

Low-frequency earthquakes generally have relatively stronger spectral components in the lower frequency range, compared to what is expected based on their magnitude. This type of earthquakes has been considered to be generated in some specific environments, such as volcanic regions and subduction zones that are also generating slow slip events and tremors. They usually occur in deeper regions below ~15km; however, some recent studies show that they can also be observed among aftershocks of large inland earthquakes in Japan (i.e., Niigata in 2004, Iwate-Miyagi in 2008, Kumamoto in 2016) with very shallow depth (~5km). Here, we attempt to detect such ‘low frequency aftershocks’ associated with a very recent earthquake sequence that occurred in Ridgecrest in California in 2019 on the source of waveform data from Plate Boundary Observatory Borehole Networks and nearby instruments archived at NCEDC, SCEDC and IRIS. We are considering The Frequency Index (FI) as a way to identify candidate events. FI is defined as: FI = log10(AH/AL), where AH and AL represent the mean spectral amplitude within the high-frequency band (e.g., 10-15 Hz) and low-frequency band (e.g., 2-5 Hz), respectively. We will discuss our results and the methods used to identify low frequency aftershocks from their spectra.

Keywords: Low-frequency earthquakes, aftershocks

©2020. Japan Geoscience Union. All Right Reserved.

Structural characteristics of the Nankai trough subduction zone off Kii channel revealed from densely obtained seismic reflection profiles

*Yasuyuki Nakamura[1], Shuichi Kodaira[1], Tetsuo No[1], Yuka Kaiho[1], Kazuya Shiraishi[1], Gou Fujie[1], Seiichi Miura[1], Koichiro Obana[1]

1. Japan Agency for Marine Earth Science and Technology

Shallow very low frequency events (SVLFEs) activity has been recently investigated using offshore and onshore stations in the Nankai Trough. SVLFEs have been active off the Kumano basin, off Kii channel and Cape Muroto, but not active off the western Kii peninsula. To explore possible structural factors relevant to the SVLFE activity, we conducted seismic surveys in the Nankai trough between off Cape Shionomisaki and Cape Muroto. Two seismic reflection surveys were conducted in November –December 2018 and December 2019 –January 2020 using R/V Kaimei and R/V Kairei. In total, 44 seismic reflection profiles across the trough axis were acquired with 4km separation. In addition, eight profiles along the trough axis were obtained. Pre-stack time migrated profiles from the data collected in the 2018 survey and post-stack time migrated profiles from the data obtained in the 2019 –2020 survey were interpreted to map the structural features, e.g., top of the subducting oceanic crust, decollement, thrust faults. We observed the thickness of the sediments above the subducting oceanic crust is constant along the trough axis in the shallow most part of the Nankai subduction zone off the western Kii peninsula, where the SVLFE activity has been low. On the other hand, the thickness is variable off the Kii channel to Cape Muroto, where the SVLFE activity has been reported. The variation could be originated from the past subduction of the seamount and could be related to the local undulation of the subducting oceanic crust. Interpreted decollement in the shallow megathrust has positive polarity off the western Kii peninsula but shows negative off western Kii channel to Cape Muroto. We also recognized that the depth of the subducting oceanic crust could be greater in the landward portion of the survey area off the western Kii peninsula. Another local deep part of the subducting oceanic crust was detected around 32.7˚N, 135˚E where the SVLFE activity was reported to be lower.

Keywords: Nankai Trough, seismic imaging

©2020. Japan Geoscience Union. All Right Reserved.

Long-Term Activity Changes of Very Low Frequency Earthquakes in the Ryukyu Trench

*Mamoru Nakamura[1]

1. Faculty of Science, University of the Ryukyus

Very-low frequency earthquakes (VLFEs) have been occurring regularly along the Ryukyu Trench. Their activities are concentrated in the south of the Yaeyama Islands, off the south of Okinawa Island, and near Amami Island. The VLFEs occur every two to three months in each region. A single activity lasts about 1 to 3 days. Although there are several clusters of activities between Miyako Island and Okinawa Island, the activity of the VLFEs is low in this region. The long-term variation of the activity of VLFEs in the plate interface reflects the temporal variation of the degree of strain accumulation and strain release in the plate interface. Therefore, I investigated the long-term changes in the activity of VLFEs in each region. The data are based on the VLFEs catalog obtained by the method denoted by Nakamura and Sunagawa (2015). The arrival time of maximum amplitude of the VLFE was picked from the vertical waveform with a bandpass filter of 0.02-0.05 Hz, and the epicenter was determined using the arrival time of the maximum amplitude at each seismic station. The VLFEs whose magnitudes were 3.5 were used in the analysis. The used period is from 2002 to 2019.

As a result, the activity of the VLFE in the Yaeyama Islands has been gradually decreasing since 2002. In the Yaeyama Islands, a series of M_J 7.0 (March 26, 2002) and M_J 6.9 (March 31, 2002) inter-plate earthquakes occurred in 2002, and seismic activity with magnitudes of 6.0 or more temporarily increased in 2002. The changes in the regular earthquakes activity and VLFE activity would reflect the process in which the strain in the plate interface is temporarily partially released due to the change in the coupling rate at the plate interface in the southwestern part of the Ryukyu Trench.

On the other hand, in the vicinity of Okinawa Island, the activity of the VLFEs has been rapidly increasing since 2015. On the other hand, there was no increase in activities around Amami-Oshima Island during this period. During this period, earthquake swarms occurred in the subducting slab near the trench axis of the central Ryukyu Trench. This suggests that the change of the activity of the VLFEs and seismicity would reflect the release of the strain with the progress of the slow earthquake on the plate interface.

Keywords: very low frequency earthquake, Ryukyu Trench, seismicity

©2020. Japan Geoscience Union. All Right Reserved.

Seismic Velocity Mapping of the Plate Boundary Structures in the Slow Earthquake Gap Zone off Western Kii Peninsula, Nankai Trough

*Yanfang Qin[1], Gou Fujie[1], Shuichi Kodaira[1], Yasuyuki Nakamura[1], Yuka Kaiho[1], Tetsuo No[1], Koichiro Obana[1], Seiichi Miura[1]

1. JAMSTEC Japan Agency for Marine-Earth Science and Technology

Recently many slow earthquakes have been observed along the Nankai trough subduction zone, where the Philippine Sea plate underthrusts the Amur plate. These events show along strike variations, especially in the central part of the Nankai trough, they were observed off Kii channel and Shinomisaki, but not reported in the area between them, off western Kii peninsula. Slow earthquakes are considered to be the key to understand the nature of subducting plate boundary and its seismic coupling. In November and December 2018, an active source seismic survey was conducted by the Japan Agency for Marine-Earth Science and Technology (JAMSTEC) using R/V KAIMEI in Nankai subduction zone off Kii channel to Shonomisaki to investigate the structural features and its possible relationship to the slow events.

The cruise carried out 34 dense gridded multichannel seismic (MCS) reflection profiles to obtain a 3D overview of the fault distribution and deformation of the sediments. At the same time, a 2D refraction seismic survey was also implemented, with air gun shooting at the interval of 100 m, recorded by 96 high resolution ocean bottom seismometers (OBS) that were spaced 1 km apart, covered from the seaward side of the subduction trench to the accretionary prism. The data quality is good and we can trace first arrivals up to ~80 km, it allow us to reveal seismic velocity structure within the overlying plate and the crust of the subducting plate. We applied travel time tomography to the OBS data, the seismic velocity and seismic reflection image show the depth of décollement and the volume of materials between dé collement and the top of oceanic crust are diverse from Kumano area (e.g., Park et al, 2010; Kamei et al. 2013), where there are many slow earthquakes occurred. On the other hand, the toe of the accretionary prism is more homogeneous than that in the Kumano Basin, which could be due to the topography of the subducting oceanic crust, leading to different seismogenic structures.

Keywords: Nankai Trough, slow earthquake gap zone, seismic velocity model

©2020. Japan Geoscience Union. All Right Reserved.

Distribution of very low-frequency earthquakes in the Miyako Strait, central Ryukyu Trench

*Hiromu Furugen[1], Mamoru Nakamura[1]

1. Graduate School of Engineering and Sience, Univercity of the Ryukyus

Very low-frequency earthquake (VLFE) constantly occur in the Ryukyu Trench. This activity is low in the region where the mega-tsunami occurred in the past (Nakamura and Sunagawa, 2015), which suggests that the activity would correlate inversely to the occurrence of large earthquakes. The VLFEs also occur in the Miyako Strait, which is between Okinawa Island and Miyako Island. The VLFE activity in this region is low and their distribution is scattered. However, the detection ability of the VLFE in this region would be low because this area is far from the F-net stations of the NIED, and also the error of epicentral determination would be large. In this study, we conducted epicentral determination of the VLFEs including the data of temporary stations in order to reveal where the VLFEs occur in this region.

As a waveform of the broadband earthquake, we used the F-net stations of the NIED and the temporary stations (Hateruma, Tarama, Miyako, Kume, and Okinoerabu) which were set by Association for The Development of Earthquake Prediction (ADEP). The waveforms were band-pass filtered at the frequency range of 0.05–0.1Hz for seismogram of top and bottom, using the Seismic Analysis Code (SAC). Next, we searched the VLFE swarms which occurred between the Okinawa island to Miyako island from the VLFE catalog that is computed for the method of (Nakamura and Sunagawa, 2015), and we adopted the most remarkable events to the template. Next, we conducted the detection of the VLFE swarms which occurred in 5 October 2017 and epicentral determination.

Three VLFE events were detected and their hypocenters were determined during this period. The epicenters were located near 25.227N and 126.415E with a radius approximately 20 km. This position is almost the same as that obtained by Nakamura and Sunagawa (2015) and is distributed within a narrower area compared with the results of Nakamura and Sunagawa (2015). Although the accuracy of the location from the trench is poor because the seismic stations are parallel to the island arc, it indicates that the cluster of the VLFE in the region occur in a narrow area.

Keywords: Very Low Frequency Earthquake, Ryukyu Trench, Seismic

©2020. Japan Geoscience Union. All Right Reserved.

Spatiotemporal evolution of interplate slip in the Hyuganada and the Bungo Channel from 1996 to 2000 based on GNSS data

*Sawako Teshiba[1], Hitoshi Hirose[1,2]

1. Department of Planetology, Graduate School of Science, Kobe university, 2. Research Center for Urban Safety and Security, Kobe University

The Philippine Sea plate is subducting beneath the Amurian plate along the Nankai trough in southwestern Japan. In the western end of this area, the Bungo Channel and Hyuganada, it is known that afterslip and slow slip events (SSEs) occur on the plate interface. For example, in the Hyuganada region, afterslip follows two M 6.7 earthquakes in 1996 (e.g., Yagi et al., 2001) and repeating SSEs occur in the afterslip area (Yarai and Ozawa 2013), and SSEs repeatedly occur in the Bungo Channel (e.g., Hirose et al., 1999). Previous studies analyzed spatial and temporal slip history of a part of these events. For example, Yagi et al. (2001) showed the spatial slip distribution of the afterslip and Ozawa et al. (2007) studied the afterslip and an SSE around the Bungo Channel around 1997. However, few studies estimate the spatiotemporal slip history in the entire region between 1996 and 2000, the time period for which these slip events took place. Therefore, the purpose of this study is to estimate aseismic slip evolution in Hyuganada and the Bungo Channel , and to propose the occurrence of an SSE in 1998 in the afterslip area.

We use daily coordinates of GEONET GNSS stations processed by Geospatial Information Authority of Japan (GSI) (F3 solutions; Nakagawa et al., 2009). Coordinate time-series data at 47 stations in Kyusyu, Shikoku and Chugoku areas for the period between September 1, 1996, and June 1, 2000 are analyzed. We estimate a common-mode time-series that is calculated by 21 stations for the same period to remove noise of 47 stations. After remove common-mode, a secular liner component of these stations estimated by the period from October 1, 1998 to June 1, 2000, coseismic jumps and artificial steps caused by station maintenances are removed from these stations. We assume a geometry of the plate interface on the subducting Philippine Sea plate estimated by Shiomi et al. (2008) and Nakanishi et al. (2018), and the interface geometry is represented by 11 ×21 small square subfaults whose area is 13 ×13 *km2* for each. We apply a time-dependent inversion method (Hirose et al., 2014) to the preprocessed data to estimate a spatiotemporal slip evolution on the plate interface.

Three slip events are resolved. First event is a slip around Hyuganada started from around September 1996 and continued to October 1997. Second event is a slip around Bungo Channel continued from around January, 1997 to March, 1998. Third event is a slip around Hyuganada continued from around May in 1998 to March in 1999. First event corresponds to the afterslip of the two Hyuganada earthquakes. However, although the first earthquake in Hyuganada occurred on October 19, 1996, this event began from around September 1996. Probably, this is because the inversion contains temporal smoothness. Second event corresponds to the 1997 Bungo Channel SSE. We can divide the slip into three region spatially that are southwestern Shikoku, northeastern Bungo Channel and southwestern Bungo Cannel, because the slip distribution and the development of seismic moment show migrations of SSE two times. Seismic moment of the slip around southwestern Shikoku increased from around January to April in 1997, and the slip migrated to southwest after April. The slip around northeastern Bungo Channel started from around May in 1997 and seismic moment continued to increase until around November in 1997. The slip of this region expanded and migrated to southwest for the period of increasing seismic moment. Seismic moment of the slip around southwestern Bungo Cannel increased for

©2020. Japan Geoscience Union. All Right Reserved.

the period between around September and December in 1997. Third event is smaller area than the afterslip of Hyuganada in 1996 but almost same location. The slip of this event is about 10cm. Seismic moment of the slip is 6.0×10^{18} N/m (Mw=6.5). Yarai and Ozawa (2013) detected repeating SSEs in this region after 2005, hence the detected slip in 1998 is a likely predecessor of the Hyuganada SSEs.

We estimate the spatiotemporal evolution of aseismic slip in Hyuganada and the Bungo Channel, especially the afterslip of the two Hyuganada earthquakes and the Bungo Channel SSE in 1997 and an SSE in the afterslip area. We found that (1) slip migrations of the Bungo Channel SSE two times; and (2) an SSE occurrence in 1998, which is a predecessor of the reported Hyuganada SSEs after 2005 (Yarai and Ozawa, 2013).

Acknowledgments: GNSS data were provided by GSI and this work was supported by JSPS KAKENHI Grant Number JP16H06474.

Keywords: slow slip event

©2020. Japan Geoscience Union. All Right Reserved.

An estimation of stress changes based on earthquake swarm seismicity accompanied by Boso slow slip events

*Tomoki Ukawa[1], Hitoshi Hirose[2,1]

1. Department of Planetology, Graduate School of Science, 2. Research Center for Urban Safety and Security, Kobe University

In off the coast of Boso peninsula, the occurrence of slow slip events (SSEs) are reported (e.g., Ozawa et al., 2003). SSE does not cause seismic motion and tsunami in itself, but in the northern part of the SSE area, earthquake swarm activity arises concurrently with SSE. A previous study stated that earthquake swarm were triggered by SSE (Hirose et al., 2014), so it is expected that an SSE affects a stress field in the area of earthquake swarm, but the quantitative relationship is poorly known. In this study, we estimate a stress change before and after each of the Boso SSEs by using the method of Dieterich et al. (2000) based on seismicity rate of the earthquake swarm.

We used JMA unified Hypocenter catalog from 1997/10/01 to 2015/12/31. And analysis domain in this study was approximately 60 km×60 km square and depth of 10 km~35 km. This domain contains almost entire areas of the earthquake swarm areas accompanied by the Boso SSEs. Because there was a possibility that detection ability of earthquakes have changed during the analysis periods, we assessed a completeness magnitude, and we selected earthquakes larger than or equal to M1.5.

To calculate the time series of stress changes, we applied seismicity rates to the equation (3) in Dieterich et al. (2000). The values of parameters required to the calculation are set as follows ;

A, a dimensionless fault constitutive parameter, is 0.005, that is the value used in Dieterich et al., 2000; normal stress is 340 MPa, that equals to the overburden pressure less hydrostatic pore-fluid pressure in a depth of 20 km; reference stressing rate is 0.05 MPa/yr . That was calculated under the assumption that the amount of one SSE’s stress drop (Hirose et al., 2012) was recovered in an average SSE’s recurrence interval. r , steady-state seismicity rate at the reference stressing rate, is 0.123 /day, we assume the seismicity is in steady-state from 2003/1/1 to 2006/12/31.

Consequently, stress changes in the SSEs, 2002SSE, 2007SSE, 2011SSE, and 2014SSE were +0.1 MPa, +0.5MPa, +0.5MPa, -0.7MPa, respectively. Their interval were changed 77mo.→58mo(2002SSE), 58mo.→50mo. (2007SSE), 50mo.→26mo.(2011SSE), and 26mo.→54mo. (2014SSE). That is the recurrence interval was shorten in cases with a positive stress change, and prolonged in negative stress change’s case. In the cases of 2002SSE and 2014SSE that the amount of stress increase was small or negative, the duration of the SSEs are about twice as long as other cases (Fukuda, 2018). This suggests that the duration and the complexity of a source process of an SSE may contribute to the stress change.

Keywords: recurrence interval, Coulomb stress, Dieterich

©2020. Japan Geoscience Union. All Right Reserved.

Spatial heterogeneity of shallow tremor activity near the Japan Trench

*Shukei Ohyanagi[1], Kazuaki Ohta[2], Yoshihiro Ito[3], Ryota Hino[4], Yusaku Ohta[4], Ryosuke Azuma[4], Masanao Shinohara[5], Kimihiro Mochizuki[5], Toshinori Sato[6], Yoshio Murai[7]

1. Kyoto University, Graduate School of Science, 2. National Research Institute for Earth Science and Disaster Resilience, 3. Kyoto University, Disaster Prevention Research Institute, 4. Tohoku University, 5. Tokyo University, Earthquake Research Institute, 6. Chiba University, 7. Hokkaido University

The Japan Trench subduction zone hosts various types of seismic activities, such as Mw 9.0 Tohoku Oki megathrust event, tectonic tremors, and VLFEs. Recent development of S-Net (cabled network of OBSs) and intense free-fall type OBS observations near the trench revealed very frequent activity of shallow tremor along the whole subduction margin [Nishikawa et al., 2019; Ohta et al., 2019; Tanaka et al., 2019]. The tremor identified in these studies have poor resolution in their depth, since they located the tremor with the envelope cross correlation method. From 2016 to 2017, we had deployed an array of 3 dense OBS arrays near the trench axis of offshore Fukushima region. Taking advantage of the array analysis, we have shown that the shallow tremor observed in the offshore Fukushima region is predominantly occurring at the plate interface [Ohyanagi et al., 2019 JpGU]. However, in this research, epicenter of the tremor is located solely based on arrival direction of tremor wave estimated at 3 arrays. Due to limitation of the method, tremor cannot be located in some area within the array of arrays network. Thus, distribution of tremor hypocenters has spatial gap which may caused by methodological issues.
Here, we updated hypocenters of ambient tremors and dynamically triggered tremors using the Multi Beam Back-Projection method [Ghosh et al., 2009; 2012] to verify if tremors are occurring at the spatial gap. Ghosh et al. (2009; 2012) does not evaluate uncertainty of located tremor explicitly. In our study, we evaluate uncertainty of located hypocenters following a method proposed in Arnadottir and Segall (1994). Succeeded in locating the tremors, we estimated their energy rate. The site amplification factor of each OBS is corrected between 2Hz –8Hz by the coda normalization method (e.g., Sato and Fehler, 1998). After the site amplification factor is corrected for each OBS, we evaluate seismic energy of the tremors at each array. At certain array, time delay is applied to waveforms of the tremors according to their slowness and arrival direction acquired through beamforming. The delayed traces are stacked to suppress ambient noise. The stacked traces at each array is then collected for geometrical spreading and intrinsic attenuation to estimate seismic energy at the source. At last, the estimated energy is divided by duration of the tremor to convert to the energy rate.
The updated location still shows spatial heterogeneity within a shallow tremorgenic region. The ambient tremor activity is more frequent in the up-dip part of the region, and less frequent in the down-dip part. Although spatial distribution of the energy rate of the tremors is more or less homogeneous within the whole region, some of the tremors occuring up-dip have about 2 order larger energy rate than others. The frequent and potential of high energy rate activity of the tremor in the up-dip part may be related to the crustal deformation observed near the trench axis in offshore Fukushima [Iinuma et al., 2016; Tomita et al., 2017].

Acknowledgements: This study is supported by JSPS KAKENHI (19H05596).

Keywords: tremor, Japan Trench, array analysis, OBS

©2020. Japan Geoscience Union. All Right Reserved.

Can crack-seal veins record recurrence intervals of slow earthquakes?

*Naoki Nishiyama[1], Kohtaro Ujiie[1], Masayuki Kano[2]

1. University of Tsukuba, 2. Tohoku University

The repeated slow earthquakes down-dip of the seismogenic zone may trigger megathrust earthquakes by transferring stress to the locked seismogenic zone. Recent geodetic study in the Nankai subduction zone suggested that recurrence interval of slow slip event has decreased from >5 years to ~1 year toward next megathrust earthquake. Repeated brittle thrusting near the downdip limit of the seismogenic zone was recorded in quartz-filled, crack-seal shear veins in the Makimine mélange of the Late Cretaceous Shimanto accretionary complex, southwest Japan. The crack-seal texture in the veins is defined by phyllosilicate inclusion bands subparallel or oblique to the vein margins. The geometry of inclusion bands in the veins indicates temporal order of crack-seal events. The measurement of the thickness of inclusion bands in shear veins show that there are three patterns of temporal change in inclusion band thickness: monotonous decrease or increase in band thickness or decrease and then increase in band thickness. We estimated the minimum time interval between crack-seal events by using a kinetic model of quartz precipitation. We assume fluid pressure drop from lithostatic to hydrostatic values at each crack-seal event, which is supported by large variations in fluid/vapor ratio of two-phase fluid inclusions between inclusion bands. The results show that the minimum time interval between crack-seal events decreased from 3–8 years to 0.2–0.5 years during 50–100 years, which is comparable to the temporal change in recurrence interval of slow slip toward next megathrust earthquake. If repeated brittle thrusting coincided with slow slip events (i.e., episodic tremor and slow slip), the crack-seal veins may be geological indicators for identifying past temporal change in slow slip recurrence interval. The progressive increase in recurrence interval of crack-seal events may reflect an increase in recurrence interval of slow slip after megathrust earthquake, while decreased and increased band thickness may represent the change in recurrence time of slow slip events before and after megathrust earthquake.

Keywords: crack-seal vein, recurrence interval

©2020. Japan Geoscience Union. All Right Reserved.

Complementary Distribution between Very Low Frequency Earthquakes and Interplatecoupling area in the southwestern Ryukyu Trench

*Ren Yakabu[1], Mamoru Nakamura[1]

1. University of the Ryukyus

No thrust earthquake of moment magnitude (Mw) > 8.0 has occurred in the past 300 years in the Ryukyu Trench, which is located in the northwestern boundary of the Philippine Sea Plate [Ando et al., 2009]. Thus, interplate coupling has been assumed to be low in the Ryukyu trench. However, a mega tsunami with the run-up height up to 30 m struck Ishigaki Island on April 24th , 1771. Very low frequency earthquakes (VLFEs) are very active along the Ryukyu Trench (Nakamura and Sunagawa, 2015). The clusters of the VLFE activities are distributed around Amami Island, Okinawa Island, and the Yaeyama Islands. In the Southwest Ryukyu trench, the locked zone is distributed to the west from 123 degrees (Hsu et al., 2012 GRL), and the source area of the 1771 Yaeyama tsunami is located around 125 degrees. The VLFE cluster near the Yaeyama Islands are complementary to the coupled area and tsunami source area. (Nakamura and Sunagawa, 2015). Nevertheless, since the hypocenter of the VLFEs was determined using the Fnet observation network, the accuracy of the hypocenter determination was poor at the western edge of the observation network, and it was difficult to determine the western extent of the VLFEs cluster areas. Then we analyzed the distribution of VLFEs in the southwestern edge of the Ryukyu Trench by integrating the data of Japan's Fnet observation network and Taiwan's broadband earthquake observation network (BATS). We used 3 F-net stations and 6 BATS stations from 2005 to 2018. The seismograms of the vertical component was 0.02-0.05 Hz band-pass filtered, and the waveforms at neighbor 2 or 3 stations were computed by the semblance analysis to determine the hypocenter. As a result, In the southwestern Ryukyu trench, the VLFEs was distributed to the east of the south-southwest offshore of Yonaguni Island. The cluster did not overlap with the coupled zone (Hsu et al. 2012) near Taiwan, indicating that the clusters of VLFEs and the coupled zones are distributed complemental.

Keywords: slow earthquake, very low frequency earthquake, Ryukyu Trench

©2020. Japan Geoscience Union. All Right Reserved.

Different deformation styles in the source regions of the 2019 Yamagata-oki earthquake and the 1964 Niigata earthquake

*Taku Ueda[1], Lina Yamaya[1], Yosihiko Ogata[2], Aitaro Kato[1]

1. Earthquake Research Institute, the University of Tokyo, 2. The Institute of Statistical Mathematics

On June 18, 2019, a Mj6.7 earthquake occurred at Yamagata-oki. The source region of this earthquake is adjacent to that of the Mj7.5 earthquake which occurred on June 16, 1964, and in this region, there are few aftershocks right after the 1964 earthquake, and the seismicity rate in recent years is extremely low (Earthquake Research Committee, 2019). This observation suggests that the source region of the 2019 Yamagata-oki earthquake was not ruptured by the Niigata earthquake, but the cause has not been revealed. In order to elucidate the relationship between these two areas, this study compared the characteristics of seismicity between the two areas.

We used the JMA catalog constructed by Japan Meteorological Agency (the Preliminary Determination of Epicenters). We applied HIST-ETAS (Hierarchical Space Time Epidemic Type Aftershock Sequence) model (e.g., Ogata, 2004) considering the spatial dependence of each parameter of the Space Time ETAS model (e.g., Ogata, 1998), to the hypocenter catalog (M1.8) from 1998 through 2019 in order to estimate the spatial distribution of background seismicity rate μ and number of aftershock occurrences K. As a result, we find that μ-value is higher and K-value is lower in the source region of Yamagata-oki earthquake than in that of Niigata earthquake.

In addition to these differences, we find that the b-value, which is one of the characteristics of the seismicity, is lower in the source region of Yamagata-oki earthquake than in that of Niigata earthquake. Moreover, comparing the seismic wave velocity structure obtained by Matsubara et al. (2019), the P wave velocity is lower in the source region of Yamagata-oki earthquake than in that of Niigata earthquake. The difference in seismic wave velocity and characteristics of seismicity between these two areas suggests that the macroscopic behavior in the source region of Yamagata-oki earthquake is more ductile than in that of Niigata earthquake. In more ductile area, microfracture is likely to proceed and it decreases seismic wave velocity. In addition, background seismicity rate (μ) decreases in more ductile area because of low brittleness. Moreover, the results of rock experiments and numerical simulation by Amitrano (2003) imply the increase in aftershock productivity (K) and the decrease in b-value in more ductile area. Focusing on the short-wavelength component of the linear strain rate distribution in the east-west direction (Meneses-Gutierrez and Sagiya , 2016), the different response for the 2011 off the pacific coast of Tohoku earthquake between the source regions of Yamagata-oki earthquake and Niigata earthquake is appeared. These differences may reflect different deformation styles between the two regions.

Keywords: the 2019 Yamagata-oki earthquake, HIST-ETAS model, brittle-ductile

©2020. Japan Geoscience Union. All Right Reserved.

Uncovering complex characteristics of earthquake time series using complex network analysis

*Sumanta Kundu[1], Anca Opris[1], Takahiro Hatano[1]

1. Department of Earth and Space Science, Osaka University.

A detailed analysis has been performed by mapping the time series of seismic data into a complex network consisting of nodes and links. Each seismic event is considered as a node and the links are determined between pairs of nodes based on the criteria of visibility graph, which is found to be a useful tool in extracting the non-trivial characteristics of a time series. We have investigated both earthquake magnitude time series and inter-event time (IET) series for three different categories of earthquakes, namely, ordinary earthquakes, earthquake swarms, and tremors. Our analysis of the degree distribution of the associated network suggests that the magnitudes of the events for all types of earthquakes are statistically uncorrelated whereas, the inter-event time series show long-range correlations. In connection with the 1/f type noises, the IET series of tremors are found to have distinctly different behavior than the other two types of earthquakes. We also find that the associated networks for both the time series display small-world behavior, high clustering and hierarchical organization. Furthermore, our findings based on the assortativity coefficient reveal that the swarms are more intermittent in nature compared to the tremors.

Keywords: Earthquake time series, Visibility graph

©2020. Japan Geoscience Union. All Right Reserved.

Exploring slow slip events and their scaling in 3D simulations of fault slip

*Luca Dal Zilio[1], Nadia Lapusta[1], Jean-Philippe Avouac[1]

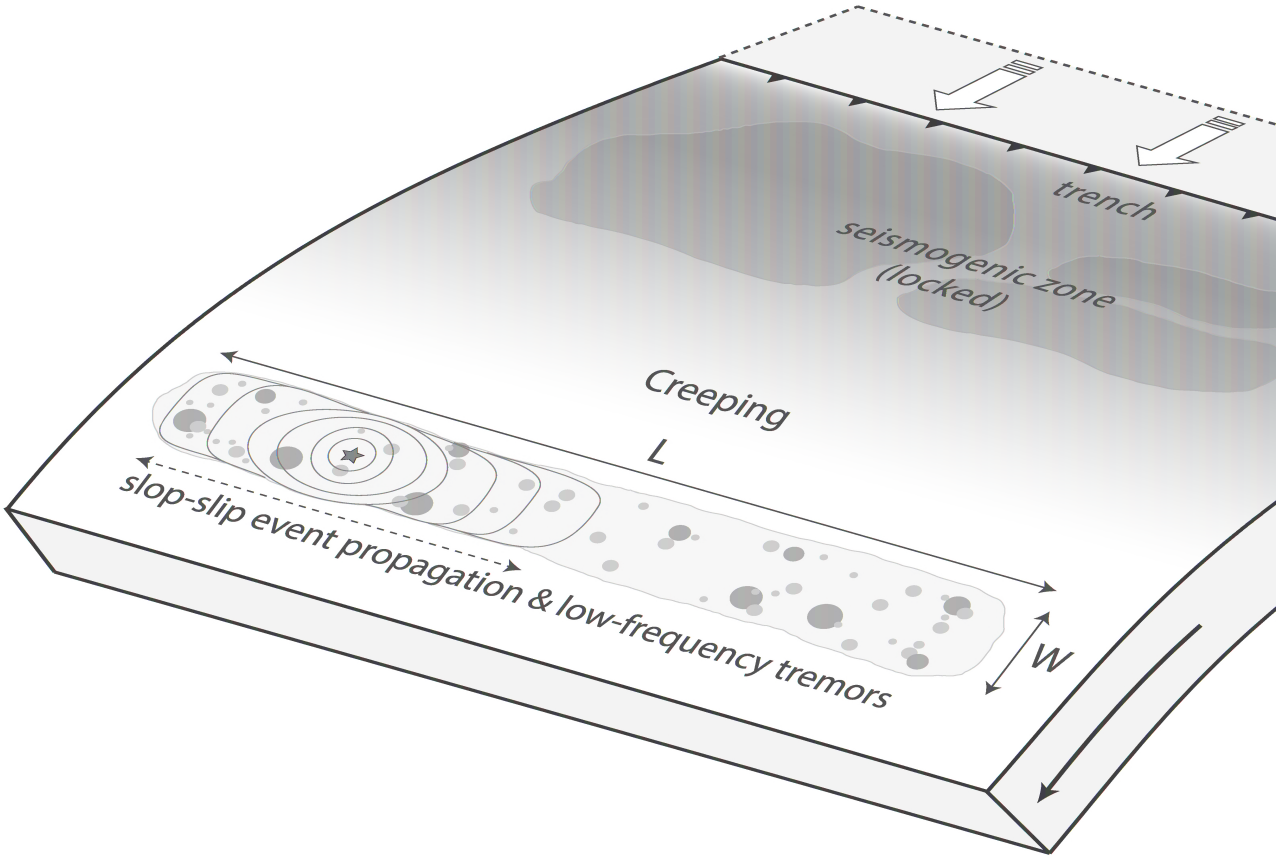
1. Seismological Laboratory, California Institute of Technology, Pasadena, CA

Tectonic faults accommodate a wide spectrum of slip modes, ranging from earthquakes to slow slip events (SSEs). While regular earthquakes are events with rupture velocities governed by inertial stress transfer with elastic wave speeds, the physical mechanisms responsible for underlying slow fault slip phenomena are less understood. In particular, key questions remain about how SSEs nucleate and propagate and whether they follow different scaling laws from ordinary earthquakes. Observations have shed light on these issues. However, due to significant noise in the time series and uncertainties related to the relatively short observational timespan, there is no unique way to interpret observations and determine the underlying mechanism of such SSEs. To overcome this limitation and to investigate synthetic data of longer timescales, here we apply a rate-and-state friction law and dilatancy effects to a three dimensional model of a subduction megathrust. By testing a wide spectrum of frictional properties, we investigate under which conditions sliding instability develops into sustained slow slip events. In particular, we study the processes that control variations in slip velocity, propagation speed, stress drop, as well as the aspect ratio of individual uni- and bi-directional SSEs.

Our model explains the earthquake-like cubic moment-duration scaling of SSEs recently observed in Cascadia subduction zone. Our results suggest that regular earthquakes and SSEs are both the result of frictional stick-slip motion. The pulse-like propagation, along-strike segmentation, and frequency-magnitude distribution of our simulated SSEs are remarkably similar to those observed on the Cascadia subduction zone. However, in contrast to the traditional assumptions, the cubic moment-duration scaling of SSEs arises not because the average rupture velocity and the stress drop of SSEs are magnitude-invariant, but rather because they increase with the increasing SSE magnitude. These results not only illuminate the dynamics of SSEs but also demonstrate that the same scaling can arise for different underlying reasons. The traditional circular crack model with magnitude-invariant rupture velocities and stress drops, which is the standard explanation for the cubic moment-duration scaling, does not apply to SSEs. This finding raises the question whether this traditional model and its assumptions hold even for regular earthquakes.

Keywords: Slow-slip events, Cascadia subduction zone, Scaling Properties

©2020. Japan Geoscience Union. All Right Reserved.



©2020. Japan Geoscience Union. All Right Reserved.

Nature of the Lithosphere in Alternating Regions of Slow Earthquakes in South America

*POUSALI MUKHERJEE[1], Yoshihiro Ito[1], Takuo Shibutani[1], Emmanuel Soliman M Garcia[1], Raymundo Omar Plata Martinez[1]

1. Disaster Prevention Research Institute, Kyoto University

Subduction zones host some of the greatest megathrust earthquakes in the world. Slow earthquakes have been also discovered around the subduction zones of the Pacific rim very close to megathrust earthquakes in several subduction zones in Chile, Cascadia, Mexico, Alaska, and New Zealand (Obara and Kato, 2016). Investigating the lithosphere of the slow earthquake area versus non slow-earthquake areas in subduction zones is crucial in understanding the role of the internal structure to control slow earthquakes. Deep transient slow slip had been detected in the Atacama region in Chile (Klein et al., 2018). Socquet et al. (2017) suggested that aseismic slow slip is one of the potential precursors of the 2014 M_w8.1 2014 Iquique earthquake. In this study, we investigate the lithospheric structure beneath stations in and around the slow earthquake area in Atacama and Iqueque. We also study the non slow-earthquake areas in the South America subduction zone using receiver function analysis and inversion method using teleseismic earthquakes. Here we focus on, especially the Vp/Vs ratios from both the slow and non slow earthquake areas, because the Vp/Vs ratio is sensitive to the fluid distribution in the lithosphere; the fluid distribution possibly controls the potential occurrence of slow earthquakes. Additionally, the nature of the slab can also play a crucial factor. At the boundary of the slab, the Vp/Vs results show variation in the slow earthquake area, and far off from the slow earthquake area. The Vp/Vs ratio results across depth shows significantly higher value in the deeper oceanic slab region beneath the stations in the slow earthquake areas with higher contrast at the boundary. The stations very close to the slow earthquake areas also preserves high Vp/Vs contrast at the boundary of the slab. On the other hand, the Vp/Vs contrast at the slab boundary significantly reduces for the stations in the non slow earthquake area.

Keywords: Receiver function, Vp/Vs ratio, fluids, slow earthquake, slab, South America

©2020. Japan Geoscience Union. All Right Reserved.

[E] Poster | S (Solid Earth Sciences)：S-CG Complex & General

[S-CG59] Evolution and movement of the crustal surface and application of geo- and thermochronology

convener:Noriko Hasebe(Institute of Nature and Environmental Technology, Kanazawa University), Shigeru Sueoka(Japan Atomic Energy Agency), Frederic Herman(University of Lausanne), Takahiro Tagami(Graduate School of Science, Kyoto University)

The terrestrial earth surface is the habitat of humans and undergoes drastic changes caused by endogenic and exogenic processes. Establishing the chronology of the past changes/episodes is a key to understanding ongoing processes and to predict future physical environments. This session aims at comprehensive understanding of dynamics of the earth's surface, including crustal movements, uplift-denudation processes, and subsequent landform development occurred in various spatio-temporal scales. In addition to the thermochronological approach, it welcomes interdisciplinary studies based on, e.g., tectonic geomorphology, structural geology, geodetic observation, cosmogenic nuclides, numerical calculations, and analogue experiments.

[SCG59-P01] Thermochronology on the fore-arc side of Northeast Japan Arc

*Yuya Kajita[1], Shigeru Sueoka[2], Shoma Fukuda[1], Noriko Hasebe[3], Akihiro Tamura[4], Tomoaki Morishita[4], Barry P. Kohn[5], Takahiro Tagami[1] (1.Graduate School of Science, Kyoto University, 2.Japan Atomic Energy Agency, 3.Institute of Nature and Environmental Technology, Kanazawa University, 4.Department of Sciences, Kanazawa University, 5.School of Earth Sciences, University of Melbourne)

[SCG59-P02] AFT thermochronology of Cretaceous granites from the northern part of the NE Japan Arc: estimating thermal/denudation histories based on thermal inverse modeling

*Shoma Fukuda[1,2], Shigeru Sueoka[2], Noriko Hasebe[3], Akihiro Tamura[4], Tomoaki Morishita[4], Takahiro Tagami[1] (1.Graduate School of Science, Kyoto University , 2.Japan Atomic Energy Agency, 3.Institute of Nature and Environmental Technology, Kanazawa University, 4.Department of Earth Sciences, Kanazawa University)

[SCG59-P03] Izu-Bonin arc collision and mountain formation of the South Fossa Magna region: New insights from low-temperature thermochronology

*Yumi Kobayashi[1], Shigeru Sueoka[2], Shoma Fukuda[1], Barry P. Kohn[3], Tatsunori Yokoyama[2], Noriko Hasebe[4], Akihiro Tamura[5], Tomoaki Morishita[5], Takahiro Tagami[1] (1.Division of Earth and Planetary Science, Graduate School of Science, Kyoto University, 2.Tono Geoscience Center, Japan Atomic Energy Agency, 3.School of Earth Sciences, University of Melbourne, 4.Institute of Nature of Environmental Technology, Kanazawa University, 5.Department of Earth Science, Faculty of Science, Kanazawa University)

[SCG59-P05] Analyses of Sag Pond Stratigraphy to Assess the Disaster History along Lembang Fault, West Java, Indonesia

Januar Ridwan[2], *Noriko Hasebe[1], Eko Yulianto[2], Nandang Supriatna[2], Amar Amar[2] (1.Institute of Nature and Environmental Technology, Kanazawa University, 2.Research Center for Geotechnology, Indonesian Institute of Science)

[SCG59-P06] Dating marine terraces by terrestrial cosmogenic nuclides: applicability and limitations

★Invited Papers

*Yuki Matsushi[1], Tetsuya Komatsu[2], Shigeru Sueoka[2], Yusuke Yonaga[2], Yumi Ogawa[2], Natsuko Fujita[2], Yoko Saito-Kokubu[2] (1.Disaster Prevention Research Institute, Kyoto University, 2.Japan Atomic Energy Agency)

[SCG59-P07] Constraining thermal/denudation histories in the last 0.1 Myr using multi-OSL-thermochronometry applied to samples from deep boreholes

*Manabu Ogata[1], Georgina King[2], Frédéric Herman[2], Shigeru Sueoka[1], Ryuji Yamada[3], Kentaro Omura[3] (1.Tono Geoscience Center, Japan Atomic Energy Agency, 2.Institute of Earth Surface Dynamics, University of Lausanne, 3.National Research Institute for Earth Science and Disaster Prevention)

[SCG59-P08] Thin section etching of zircon for micro thermochronology by fission track method: A trial

Hiroaki Koyama[2], *Noriko Hasebe[1] (1.Institute of Nature and Environmental Technology, Kanazawa University, 2.Department of Earth Sciences, Kanazawa University)

Thermochronology on the fore-arc side of Northeast Japan Arc

*Yuya Kajita[1], Shigeru Sueoka[2], Shoma Fukuda[1], Noriko Hasebe[3], Akihiro Tamura[4], Tomoaki Morishita[4], Barry P. Kohn[5], Takahiro Tagami[1]

1. Graduate School of Science, Kyoto University, 2. Japan Atomic Energy Agency, 3. Institute of Nature and Environmental Technology, Kanazawa University, 4. Department of Sciences, Kanazawa University, 5. School of Earth Sciences, University of Melbourne

Northeast (NE) Japan is one of the best regions to study tectonics of island arc, because NE Japan has comparatively obvious island arc components of fore-arc, volcanic front, back-arc and back-arc basin. Therefore, there are many studies on the tectonic evolution of NE Japan (e.g. Amano and Sato, 1989; Sato, 1992; Nakajima, 2013). Ota (2010) says that the mountains in NE Japan are uplifted by compression across arc (i.e east-west compression). However, there are a few quantitative investigations of the mountain uplift and denudation histories which are important factors estimating island tectonics.

As a technique for measuring uplift or denudation rates, some are known (e.g. GPS survey, elevation of terraces, thermochronology etc.), but in regard to million-year-scale mountain uplift and denudation rates, it can be said that thermochronology is the most appropriate method. Thermochronology can reconstruct the time-temperature relationship of rock/mineral samples, based on radiometric ages and closure temperatures specific to the combination of radiometric dating methods and target minerals. Furthermore, some assumptions enable discussion of mountain uplift and denudation histories. At overseas massive orogenic zones thermochronology has been applied since 1970s (Hermam et al., 2013). At NE Japan there are, today, some studies that discuss differences of uplift/denudation history between fore-arc, Ou backbone range and back-arc using thermochronology (e.g. Sueoka et al., 2017; Fukuda et al., 2019; Fukuda et al., in review). However, in these preceding studies, it is not sufficient to discuss a respective and more particular thermal and denudation history about arc component units. Therefore, in this study, we focus on fore-arc side of NE Japan, Kitakami Mountains and Abukuma Mountains and then to estimate detail thermal and denudation history we apply thermochronology there.

We adopt apatite fission-track (AFT), apatite (U-Th-Sm)/He (AHe) analyses as thermochronological methods. AFT ages are 139.4-78.6 Ma at Kitakami, 61.0-40.5 Ma at Abukuma. AHe ages are 51.2-36.1 Ma at Kitakami, 75.9-60.1 Ma at Abukuma. With our results and ages which preceding studies provide we discuss age trend and denudation history respectively.

At Kitakami Mountains, AFT ages become younger gradually (140-80 Ma) from the most eastern locality to around 141.6 degrees longitude locality. On the other hand, all AHe ages are about 50-40 Ma except for the most western locality of which the AHe age is 90 Ma. However, at the most western locality the AHe age is older than the AFT age which usually indicates older ages because of the different closure temperature, so a local thermal event like hydrothermal activity possibly affect the ages of this locality.

At Abukuma Mountains, AFT age trend changes at Hatagawa fault zone (HFZ), which AFT ages tend to be younger in the west side of HFZ than in the east side. AHe age trend also seems to change at HFZ like AFT age trend, but considering the error bars it is not obvious. And at the most eastern locality the AFT age is comparatively young. Because the AFT age is younger than the AHe age at this locality, perhaps, there was a local thermal event like Kitakami Mountains.

©2020. Japan Geoscience Union. All Right Reserved.

Then we calculated the average denudation rate using the AFT ages. As the result of calculation, at every locality in Kitakami Mountains and Abukuma Mountains the average denudation rate is <0.10 mm/yr. Therefore, both mountains are stable at 10^{7-8} year time scale. However, this result does not suggest that the denudation rate is continuously <0.10 mm/yr, so to construct more detail denudation histories we have to apply new thermochronological method which is available at shorter time scale.

As future subjects, ①improvement of accuracy and precision by further analyzing ②increasing number of sampling localities and employing another thermochronological method (e.g. cosmogenic nuclides analysis) ③applying new thermochronological methods (e.g. thermal inverse modeling by AFT; Electron Spin Resonance thermochronometry) to estimate more detail thermal and denudation histories ④ discussion of geothermal gradient, uplift model and tectonics model at Kitakami Mountains and Abukuma Mountains.

Acknowledgements: This study was carried out under a contract with METI (Ministry of Economy, Trade and Industry) as part of its R&D supporting program for advanced research on long-term stability of geological environment. This study was also supported by the Grant-in-Aid for Scientific Research on Innovative Areas (KAKENHI No. 26109003) from the Ministry of Education, Culture, Sports, Science and Technology (MEXT).

Keywords: Kitakami Mountains, Abukuma Mountains, Thermochronology, Fission-track

©2020. Japan Geoscience Union. All Right Reserved.

AFT thermochronology of Cretaceous granites from the northern part of the NE Japan Arc: estimating thermal/denudation histories based on thermal inverse modeling

*Shoma Fukuda[1,2], Shigeru Sueoka[2], Noriko Hasebe[3], Akihiro Tamura[4], Tomoaki Morishita[4], Takahiro Tagami[1]

1. Graduate School of Science, Kyoto University , 2. Japan Atomic Energy Agency, 3. Institute of Nature and Environmental Technology, Kanazawa University, 4. Department of Earth Sciences, Kanazawa University

Northeast (NE) Japan Arc is located at the subduction zone on the Pacific plate, which is known as a typical island arc because of having the inland linear topographic alignments and the island arc units. The tectonic history of the NE Japan Arc has been investigated by geologic and geomorphic researches so far. In particular, the evolution of the NE Japan arc after the opening of the Sea of Japan since ca. 15 Ma was well-understood (e.g., Sato, 1992, Jour. Geophys. Res.; Nakajima, 2013, INTECH; Yoshida et al., 2013, Geol. Soc. Lond. Spec. Pub.). Recently, the multidisciplinary project entitled “Crustal Dynamics” has successfully discovered a lot of geoscientific implications based on geodesy, geomorphology, and geology (Iio et al., 2018, EPS). As one of the disciplines in this project, thermochronology aimed at reconstructing vertical movements of the shallow crust over long-term timescales (>10^6 yr) in the unit of an island arc, and has contributed to revealing thermal/denudation histories coeval with the intense E-W compressive stress field since the Quaternary.

Thermochronology is a discipline which generally uses radiometric ages obtained from radiometric dating methods, and closure temperatures specific to the combinations of applied dating methods and these targeting minerals (namely, thermochronometers). Thus, thermal histories of rock bodies can be revealed, and moreover, denudation histories of them can also be estimated under the assumption of geothermal structure. Low-temperature thermochronology is useful for understanding upper crustal mountain building processes, which includes (U-Th)/He and fission-track (He and FT, respectively) methods for apatite and zircon. However, thermochronometric approaches directly measure cooling processes of rock bodies. Therefore, it is noteworthy that uplift histories require some assumptions, such as appropriate geothermal gradients and dynamic equilibrium between denudation and uplift (see the principle and application of thermochronology in Sueoka et al., 2016, Geosci. Fron.; Sueoka and Tagami, 2019, Jour. Geogr.).

Research findings by thermochronology of the NE Japan Arc are introduced here. We collected the Cretaceous-Paleogene granitic samples across the southern part of the NE Japan Arc, which is called as the S-traverse, and applied apatite and zircon He (namely, AHe and ZHe) methods (Sueoka et al., 2017, EPS), and apatite FT (AFT) methods (Fukuda et al., 2019, JAES:X) into island arc provinces, i.e., the Abukuma mountains, the Ou Backbone Range (OBR), and the Iide and Asahi mountains. These studies uncovered the contrasts of thermal and denudation histories between each tectonic unit. In the latest research, we have applied He methods into the northern part of the NE Japan Arc, namely, the Kitakami mountains, the OBR, and the Shirakami and Taihe mountains as the N-traverse (Fukuda et al., in press, EPS). This study attempted to reveal the overall trend of thermal and denudation histories along the NE Japan Arc. Consequently, estimated the similar contrasts of them along the S-traverse, which quantitatively provided that the landform development of arc-along direction is probably controlled by the E-W compressive stress field. In this presentation, we report the results of AFT dating and thermal

©2020. Japan Geoscience Union. All Right Reserved.

inverse modeling along the N-traverse in order to improve the thermal/denudation histories obtained by He thermochronometers.

We obtained AFT ages ranging from 138.0–2.0 Ma, which were consistent with the age contrasts between island arc provinces based on the He methods. In addition, thermal inverse modeling using by HeFTy (Ketcham, 2005, RiMG) provided high-accuracy thermal/denudation histories. On the fore-arc side, slow cooling patterns were estimated since the Cretaceous-Paleogene, while in the OBR and on the back-arc side, rapid cooling patterns were inferred since few Ma as last cooling episodes. Such last cooling episodes perhaps reflected the intense compressive stress field after the Quaternary, which indicated comparable to Fukuda et al. (2019, JAES:X). These observations implied that the S- and N-traverses have probably similar trends of thermal and denudation histories based on AFT methods as well as He thermochronometers. For enhancing the spatial-temporal resolutions of data, some future works will involve applying the application of lower-temp. thermochronometers (e.g., ESR or OSL methods), and extending our study area by increasing the number of sampling localities. Now, we have been conducting ongoing researches around the Kitakami, Abukuma mountains, and the OBR. Further investigations are desirable.

Keywords: Thermochronology, Northeast Japan Arc, Fission-track method, Island arc, Mountain building process

©2020. Japan Geoscience Union. All Right Reserved.

Izu-Bonin arc collision and mountain formation of the South Fossa Magna region: New insights from low-temperature thermochronology

*Yumi Kobayashi[1], Shigeru Sueoka[2], Shoma Fukuda[1], Barry P. Kohn[3], Tatsunori Yokoyama[2], Noriko Hasebe[4], Akihiro Tamura[5], Tomoaki Morishita[5], Takahiro Tagami[1]

1. Division of Earth and Planetary Science, Graduate School of Science, Kyoto University, 2. Tono Geoscience Center, Japan Atomic Energy Agency, 3. School of Earth Sciences, University of Melbourne, 4. Institute of Nature of Environmental Technology, Kanazawa University, 5. Department of Earth Science, Faculty of Science, Kanazawa University

The South Fossa Magna region is one of the unique regions in the world, being situated at an active arc-arc collision zone. It is thought that up to four crustal blocks of the Izu-Bonin arc have collided with this area since the middle Miocene, resulting in crustal modification of the Honshu arc side (e.g. Amano et al., 1999; Kano, 2002). However, the timing and effect of these blocks are still debatable.
Horizontal deformation such as the rotation of the collided blocks has been studied mainly by paleomagnetism. In this study, in order to reveal the vertical deformation, low-temperature thermochronometry was performed on basement granites. The uplift and denudation history were estimated and compared with the collision events.
Apatite fission track (AFT) ages obtained in this study were significantly younger than the granite formation ages and are consistent within an uncertainty of $\pm 2\sigma$ at all localities. The apatite (U-Th)/ He (AHe) ages were younger or consistent within an error than the AFT ages and previously reporter ages. Using this data inverse thermal history modeling using the HeFTy software (Ketcham, 2005) was carried out. Results indicate that the last cooling started at about 1 Ma in the northern and central parts of the Kofu granites in the Kanto Mountains, and at about 5 Ma in the southern part. Considering only the timing for the onset of the last cooling, these ages are in accord with the collision ages previously reported for the Izu block and the Tanzawa block, respectively.
The average denudation rates in the South Fossa Magna region were estimated from the age and temperature of the onset of the last cooling and these are consistent with average uplift rates over the last 0.1 Ma estimated from the elevation of fluvial terraces (Fujiwara et al., 2005). This suggests that vertical deformation such as uplift of the Honshu arc side has continued at a constant rate from the time of collision of the Izu block to the present.
In summary, our results suggest that collisions between the crustal blocks affected uplift of the mountains. However, considering that cooling rates in the Tanzawa Mountains, which are closest to the Izu block, did not increase due to the collision of the Izu block (Yamada and Tagami, 2008), the collision of the Izu block might not have directly influenced the uplift and denudation of the Tanzawa Mountains. For further discussion on the tectonic history of the crustal blocks, thermal inversion analysis at more localities in the Kanto Mountains and Misaka Mountains, which are located northwest of the Izu block, are required.

References:
1. Amano et al., 1999, *Structural Geology*, **43**, 11-20
2. Kano, 2002, *Bull. Earthq. Res. Inst. Univ. Tokyo*, **77**, 231-248
3. Ketcham, 2005, *Reviews in Mineralogy & Geochemistry*, **58**, 275-314
4. Fujiwara et al., 2005, *Journal of Nuclear Fuel Cycle and Environment*, **11(2)**, 113-124
5. Yamada and Tagami, 2008, *Journal of Geophysical Research*, 10.1029/2007JB005368

©2020. Japan Geoscience Union. All Right Reserved.

Keywords: low-temperature thermochronology, South Fossa Magna, apatite fission track

©2020. Japan Geoscience Union. All Right Reserved.

Analyses of Sag Pond Stratigraphy to Assess the Disaster History along Lembang Fault, West Java, Indonesia

Januar Ridwan[2], *Noriko Hasebe[1], Eko Yulianto[2], Nandang Supriatna[2], Amar Amar[2]

1. Institute of Nature and Environmental Technology, Kanazawa University, 2. Research Center for Geotechnology, Indonesian Institute of Science

Sag pond stratigraphy studies have a potential for the assessment of Lembang fault activity. Previous results have showen some indication of the earthquake-related process in the sag pond sedimentation record, but the level of confidence is uncertain especially for the events revealed by the recent Paleoseismological studies. This research conducted using the diatom analysis to see the fluctuation of sag pond water level and change in depositional environment, which is controlled by the Lembang fault movement. We analyzed Cihideung sag pond deposit from the playground in Graha Puspa Estate area, Lembang, Indonesia, which also used in the previous sag pond stratigraphy research. The diatom analysis was carried out combined with sediment characterizations, including water content, grain size measurement, organic matter, carbonate concentration, and biogenic silica analysis. We also provide radiocarbon ages to open the correlation with the estimated great earthquakes by present paleoseismology research of Lembang fault. We recognized the stratigraphy of ~5m core and classified into five sedimentary units which represent the sedimentation history of the Cihideung sag pond. We interpret sedimentation changes that could represent the earthquake-related process and classified based on the level of confidence. The event with highest level of confidence include three events that related to the humic sag pond formation and two great earthquake event in 15th Century and 1771-1537 BCE. However, this assessment still need improvement with better resolution and other additional analyses in the future to enhance the confidence in the reconstruction of paleoseismological events.

Keywords: Sag pond, Lembang fault activity

©2020. Japan Geoscience Union. All Right Reserved.

Dating marine terraces by terrestrial cosmogenic nuclides: applicability and limitations

*Yuki Matsushi[1], Tetsuya Komatsu[2], Shigeru Sueoka[2], Yusuke Yonaga[2], Yumi Ogawa[2], Natsuko Fujita[2], Yoko Saito-Kokubu[2]

1. Disaster Prevention Research Institute, Kyoto University, 2. Japan Atomic Energy Agency

This study overviews methodology for application of terrestrial cosmogenic nuclides for dating marine terraces. Accumulation of in-situ produced cosmogenic nuclides in near-surface bedrock reflects several factors such as exposure duration, sedimentation, and denudation of the landform. For cases of uplifted coastal surfaces, inheritance accumulated under pre-emergence erosional environment also affects the age accuracy, which can be inferred from the nuclide concentration of a representative modern wave-cut bench. We simulated evolution of subsurface depth profiles of cosmogenic ^{10}Be concentration in quartz in terrace bedrock emerged at marine isotope stages (MIS) 1, 5e, 7, 11, and 13 with different parameter settings. Applicability and limitation of this method were then tested by comparing those model curves to actual depth-concentration profiles measured using boring cores extracted at two uplifted marine terraces in Muroto Peninsula, southern-east Shikoku, Japan, elevated to ~160 m above the present sea level.

Acknowledgements: This study was carried out under a contract with METI (Ministry of Economy, Trade and Industry) as part of its R&D supporting program for developing geological disposal technology.

Keywords: terrestrial cosmogenic nuclide, marine terrace, exposure dating, uplift rate

©2020. Japan Geoscience Union. All Right Reserved.

Constraining thermal/denudation histories in the last 0.1 Myr using multi-OSL-thermochronometry applied to samples from deep boreholes

*Manabu Ogata[1], Georgina King[2], Frédéric Herman[2], Shigeru Sueoka[1], Ryuji Yamada[3], Kentaro Omura[3]

1. Tono Geoscience Center, Japan Atomic Energy Agency, 2. Institute of Earth Surface Dynamics, University of Lausanne, 3. National Research Institute for Earth Science and Disaster Prevention

Constraining the denudation history is necessary for evaluating change of the Earth’s surface. Terrestrial cosmogenic nuclide (^{10}Be, ^{26}Al) dating is used to evaluate denudation rates averaged over a few meters at 10^2-10^4 year timescales, whereas low-temperature thermochronology, such as fission-track and (U-Th)/He methods, is applied to estimate denudation histories over a few to several kilometers in the last 10^6-10^8 years. However, the method of constraining the middle-term (10^4-10^5 years) denudation history remains challenging.
Recently, optically stimulated luminescence (OSL) thermochronometry has been proposed as a tool that offers potential for tight constraint of cooling histories in the low-temperature domain (30-100 ℃) over 10^4-10^5 year timescales. This method consists of determining the timing and rate at which electrons are trapped and thermally released in minerals, in response to in situ radiation and rock cooling. Luminescence signals can be converted into a rock cooling rate, or denudation history, by constraining the kinetic parameters that describe electron trapping and detrapping.

Application of OSL-thermochronometry is currently limited to regions that have experienced denudation rates higher than 5 mm/year (assuming a general geothermal gradient in Japan, which is ~0.03 ℃/m); luminescence signals saturate before the rocks are exhumed to the surface in slowly-denuding regions. However, constraining the slow cooling histories may be possible if unsaturated samples are obtained from within deep boreholes. Here we apply multi-OSL-thermochronometry to deep borehole cores drilled at the Tono and Rokko regions, southwest Japan, that have experienced slow (~0.1 mm/year) and moderate (~0.5 mm/year) denudation rates, respectively. We used the MIZ-1 core at Tono region, Gifu, and the Kabutyama core (National Research Institute for Earth Science and Disaster Resilience) at Rokko Mountains, Hyogo. In this presentation, we will present the preliminary results of the analyses.

This study was carried out under a contract with METI (Ministry of Economy, Trade and Industry) as part of its R&D supporting program for advanced research on long-term stability of geological environment.

Keywords: Luminescence

©2020. Japan Geoscience Union. All Right Reserved.

Thin section etching of zircon for micro thermochronology by fission track method: A trial

Hiroaki Koyama[2], *Noriko Hasebe[1]

1. Institute of Nature and Environmental Technology, Kanazawa University, 2. Department of Earth Sciences, Kanazawa University

Zircon is a mineral commonly used for fission track dating. However, since it is an accessary mineral, it is generally used for analysis after the mineral separation. With the conventional methods, rocks are crushed and important information on the mineral occurrence is lost. If we could develop etching method of zircon in the thin sections, the interaction between coexisting minerals, the relationship between zircon occurrence and its age can be studied. Thin section dating could contribute micro thermochronology on samples with potential paleotemperature difference among a narrow zone, e.g., a fault gouge, an archeological vase, or archeological furnace sites, etc. The analyses without Teflon sheet mounting, which sometimes suffer electrostatic disturbance, may be useful for observation by, for example, AFM or SEM. To avoid the destruction of a thin section during the etching by high temperature alkali eutectic etchant, pinpoint etching only on zircon was tried. In order to perform pinpoint etching, a pipette tip made of polypropylene or Teflon was tried, but dropping of the etchant on the sample was impossible, because of the rapid solidification during the experiment. Dropping the etchant using a Teflon coated spoon on a sample was possible, but the control in amount of etchant was difficult. A photosetting resin was used as a material for bonding the rock and the slide glass. As a result of trial with several etchants, it was found that rocks came off with an etching solution at 160℃ or higher. The KOH:NaOH eutectic mixture used in the conventional zircon fission track method was found to be unsuitable because it had a melting point of about 170℃. On the other hand, the KOH:NaOH:LiOH eutectic mixture used as an alternative etchant has a melting point of about 140℃ and has higher etching efficiency than the KOH:NaOH eutectic mixture. Zircon in thin section was able to be etched using a KOH:NaOH:LiOH eutectic mixture at 150℃.

Keywords: Fission Track, etching, zircon

©2020. Japan Geoscience Union. All Right Reserved.

[E] Poster | S (Solid Earth Sciences)：S-CG Complex & General

[S-CG60] Toward Discoveries in Solid Earth Sciences by Machine Learning

convener:Takahiko Uchide(Research Institute of Earthquake and Volcano Geology, Geological Survey of Japan, National Institute of Advanced Industrial Science and Technology (AIST)), Yuki Kodera(Meteorological Research Institute, Japan Meteorological Agency), Hisahiko Kubo(National Research Institute for Earth Science and Disaster Resilience)

The recent development of the machine learning techniques including the deep learning is leading innovations in various fields. The applications of these techniques, for example, the classification, the pattern recognition, and the regression of data, to solid earth sciences are also now under development. On the other hand, there are concerns on the human-interpretability of the deep learning.
This session will provide an opportunity to share the application studies to various fields in solid earth science and inspire each other. In particular, we encourage contributions which made discoveries in solid earth sciences. We also look forward to studies addressing the black box issue of the deep learning.

[SCG60-P02] Detection of seismic signals under low SNR condition using an artificial neural network: Toward development of dense low cost citizen seismic network in Yokohama

*Ahyi KIM[1], Hiroki UEMATSU[1], Gakuto NAKAO[1] (1.Yokohama City University)

[SCG60-P03] Earthquake detection based on deep learning

Junyu Yu[1,2], *Takahiko Uchide[2], Yuji Yagi[1] (1.Graduate School of Life and Environmental Sciences, University of Tsukuba, 2.Geological Survey of Japan, AIST)

[SCG60-P04] Large-scale matched-filter analysis with similarity search

*Naoto Mizuno[1], Satoshi Ide[1] (1.Department of Earth and Planetary Science, The University of Tokyo)

Detection of seismic signals under low SNR condition using an artificial neural network: Toward development of dense low cost citizen seismic network in Yokohama

*Ahyi KIM[1], Hiroki UEMATSU[1], Gakuto NAKAO[1]

1. Yokohama City University

We have developed a community based low cost seismic network in Yokohama, Japan, called Citizen Seismic Network (CSN), to monitor local scale strong motion which is closely linked to community’ s life. Each sensor unit composed of 12 bit MEMS accelerometer and Raspberry Pi.

Since the units are supposed to be installed under high-noise condition such as inside of house where spiky noise made by human activities often misinterpreted as seismic signal, it is difficult to discriminate the seismic signals from other noises. In such condition, applying conventional detection method using amplitude ratio (e.g. STA/LTA) is problematic. To overcome the issue, we employed an artificial neural network (ANN) that utilizes pattern recognition to retrieve seismic signals. To make the ANN work, we trained it using numerical data set produced by seismic records obtained from conventional seismometer adding CSN sensor noise. As the network input, vector modulus of three component of accelerogram are used.

Firstly we explore the optimum number of input units and training data. Secondly, using the trained ANN, we tried to identify the numerical seismic signals which are not used in the training process. As a result, 95% of the P-wave is successfully detected. The comparison with the performance of STA/LTA using real data observed by our sensor indicates that our method reduce the false detection significantly.

Detection is further improved with multiple stages training: noise data detected as “seismic signal” is included in the next training process as “noise”. The ANN trained with multiple stages stably detects P-wave for Japan Meteorological Agency seismic intensity scale above 3. It indicates that our method can make low cost MEMS sensor not only as reasonable strong motion detector but also as P-wave detector for the intensity above 3. It means our sensor network can be used as a complementary of the conventional seismic network for earthquake early warning.

Keywords: artificial neural network, citizen seismic network, MEMS sensor

©2020. Japan Geoscience Union. All Right Reserved.

Earthquake detection based on deep learning

Junyu Yu[1,2], *Takahiko Uchide[2], Yuji Yagi[1]

1. Graduate School of Life and Environmental Sciences, University of Tsukuba, 2. Geological Survey of Japan, AIST

Earthquake detection, identifying the presence of an earthquake and determining its hypocenter, is challenging, because it requires the correct detection and association of seismic phases across different seismographs while also precisely picking the arrivals of P and S waves. Yet, this effort is essential for producing the earthquake catalog that provides important insights into many studies of observational seismology, such as the spatiotemporal distribution of Gutenberg-Richter's *b*-value, the geometry of faults, and foreshock behavior. Better catalog also enables us to use more event data for the determination of source parameters, such as focal mechanisms.

Despite several separating automatic methods are continuously developed to resolve each step of earthquake detection, seismic analysts still strive to identify earthquakes or calibrate the result proposed by automatic method manually for the superior accuracy and reliability of expert-made estimation. Accompanying with the explosion of seismic waveform data caused by the development of high sensitivity seismograph network, however, comprehensively identifying earthquakes from such massive data is becoming increasingly difficult, especially for earthquakes which are small yet dominate the overwhelming majority of earthquakes.

We integrate earthquake detection procedures into an efficient, sensitive, and coherently end-to-end framework. The framework extends Mask R-CNN, which is the de-facto standard method for instance segmentation in deep learning, by training it on multi- and single-seismograph waveform data separately to construct a detector branch in parallel with a picker branch, and afterwards both branches are concatenated together. The detector branch efficiently detects the time spans in which seismic phases originating from a common causative earthquake are included in a 120-second multi-seismograph waveform window while segmenting the preliminary tremors (waveforms from P- to S-arrivals) observed at each seismograph roughly. The picker branch subsequently generates high-quality segmentation masks that covers preliminary tremors further precisely to pick P- and S-wave arrival times. The framework, in addition, predicts confidence scores of distinguishing seismic phases from ambient noise for each earthquake and each preliminary tremor respectively, which can be used as the criterion of monitoring the quality of earthquake identification and phase picking.

We evaluate the framework on an unseen test dataset of 3,591 discrete earthquakes accompanying with the target labels of expert-picked P- and S-wave arrival time from Japan Meteorological Agency (JMA) earthquake catalog. After discarding some prediction scored with low confidence, the framework has successfully recalled and relocated 97.61% of the test earthquakes with small errors both in the phase arrival times and the hypocenter location, showing a near-human-level detection accuracy and great generality. We then apply the framework to a set of one-month continuous waveform data that have been

©2020. Japan Geoscience Union. All Right Reserved.

recorded by a temporary seismograph network operated by Geological Survey of Japan, National Institute of Advanced Industrial Science and Technology (AIST) in northern Ibaraki, Japan. While trained on the seismic waveform data from a different seismic network, the framework generalizes well and has identified more microearthquakes beyond JMA earthquake catalog over the certain area around the temporary network, which allows us to demonstrate its robustness and detection sensitivity.

We hope our effective approach will serve as a general automatic method of earthquake detection to help ease monitoring earthquake activities and provide new information to facilitate further researches in seismology.

Keywords: Deep learning, Neural network, Instance segmentation, Earthquake catalog, Time-series analysis, Computational seismology

©2020. Japan Geoscience Union. All Right Reserved.

Large-scale matched-filter analysis with similarity search

*Naoto Mizuno[1], Satoshi Ide[1]

1. Department of Earth and Planetary Science, The University of Tokyo

The matched-filter analysis (Gibbons and Ringdal, 2006) is one of the essential tools in modern seismology. It detects events by calculating the cross-correlation between the template waveforms and the observed waveforms. In both ordinal and low-frequency earthquakes, this algorithm improves the number of detections of small events (e.g., Shelly et al., 2007a; Peng and Zhao, 2009; Kato et al., 2012; Ross et al., 2019). The matched-filter analysis is based on the assumption that the cross-correlation of two events should be high when their locations and mechanisms are similar. Because of this assumption, the detections are limited to similar events to the templates. To prevent missing events, we need to use a large number of templates to cover an analysis region. Ross et al. (2019) used nearly 284,000 earthquakes listed in the Southern California Seismic Network catalog as templates to detect small earthquakes and created a new catalog, which is almost complete for earthquakes of $M > 0.3$. Previous studies used parallel processing to manage massive computation, which is efficient to perform template matching (e.g., Chamberlain et al., 2018; Beaucé et al., 2018; Senobari et al., 2019; Zimmerman et al., 2019; Liu et al., 2020). Even with these improvements in algorithms, large-scale computation has been necessary.

In this study, we develop a new algorithm for the matched-filter analysis with a large number of template waveforms. Instead of using massive computational resources, our method improves the computation complexity with similarity search and efficiently handles over 100,000 templates by a single workstation. We reduce the formulation of the matched-filter analysis to the nearest neighbor search and introduce approximations to reduce the computational cost. Our algorithm is efficient for parallel processing on the graphics processing unit and manages the increase of templates using the approximations. The computation speed is remarkably improved and achieves over 100 times faster than the ordinary matched-filter analysis.

Keywords: Matched-filter analysis, Similarity search, Machine learning

©2020. Japan Geoscience Union. All Right Reserved.

[E] Poster | S (Solid Earth Sciences)：S-CG Complex & General

[S-CG61] The Japan Trench: Learning from the 2011 M=9 Tohoku-Oki earthquake, a decade later

convener:Takeshi Iinuma(National Research and Development Agency Japan Agency for Marine-Earth Science and Technology), Asuka Yamaguchi(Atomosphere and Ocean Research Institute, The University of Tokyo), Aitaro Kato(Earthquake Research Institute, the University of Tokyo), Tianhaozhe Sun(Pacific Geoscience Centre, Geological Survey of Canada)

The 2011 Tohoku-Oki earthquake (M=9) and its devastating tsunami triggered numerous new studies of earthquake processes in the northeast Japan subduction zone and worldwide. Multidisciplinary data in great quality and quantity have been collected across the shoreline during and since the earthquake. Important offshore observations include seafloor mapping, sub-seafloor geophysical imaging, coring, logging, and laboratory measurements associated with ocean drilling, GNSS-acoustic measurements of crustal deformation in and beyond the rupture area at an increasing number of sites, and multi-dataset geophysical observations by the newly established cabled seafloor monitoring network (the S-net) that covers the entire offshore area of the margin. Many geophysical and geological studies such as seismological and geodetic analyses, field surveys on fault-zone, regional and margin-wide structures, laboratory experiments on fault-zone and wall rock properties, and the associated numerical modeling have been conducted to investigate the preparation and generation of the M=9 rupture, its postseismic deformation, and its impacts on the general margin geodynamics. Today, approaching a decade from the earthquake, we need to synthesize these results to summarize what we have learned, what is still unknown, and what new studies should be conducted in the future. In this session, we welcome presentations on all aspects of the 2011 Tohoku-Oki earthquake and the seismogenic processes in the Japan Trench and other subduction margins based on, but not limited to, geophysical and geological field observations, laboratory experiments, and modeling studies.

[SCG61-P01] Vertical deformation style along the Sanriku coast inferred from coastal geology examined after the Tohoku earthquake

*Yuichi Niwa[1], Toshihiko Sugai[2] (1.Faculty of Science and Engineering, Chuo University, 2.Department of Natural Environmental Studies, Graduate School of Frontier Sciences, The University of Tokyo)

[SCG61-P02] Trial of the crustal deformation detection accompanied with the tremor activities in Fukushima-Oki deduced from the ocean bottom pressure gauge data

*Hideto Otsuka[1], Yusaku Ohta[1], Ryota Hino[1], Kazuaki Ohta[2] (1.Research Center for Prediction Earthquakes and Volcanic Eruptions, Graduate School of Science, Tohoku University, 2.National Research Institute for Earth Science and Disaster Resilience)

[SCG61-P03] Seafloor Displacement along the Japan Trench Caused by the 2011 Tohoku-Oki Earthquake Examined by Repeated Bathymetric Surveys

★Invited Papers

*Toshiya Fujiwara[1,9], Shuichi Kodaira[1], Gou Fujie[1], Yuka Kaiho[1], Toshiya Kanamatsu[1], Takafumi Kasaya[2], Yasuyuki Nakamura[1], Tetsuo No[1], Tsutomu Takahashi[1], Takeshi Sato[3], Narumi Takahashi[4,1], Yoshiyuki Kaneda[5,1], Katharina Bachmann[6], Christian dos Santos Ferreira[6], Gerold Wefer[6], Michael Strasser[7], Tianhaozhe Sun[8] (1.Research Institute for Marine Geodynamics, Japan Agency for Marine-Earth Science and Technology, 2.Research Institute for Marine Resources Utilization, Japan Agency for Marine-Earth Science and Technology, 3.Sapporo Regional Headquarters, Japan Meteorological Agency, 4.National Research Institute for Earth Science and Disaster Resilience, 5.Kagawa University, 6.MARUM, University of Bremen, 7.Institute of Geology, University of Innsbruck, 8.Pacific Geoscience Centre, Geological Survey of Canada, 9.Kochi University)

[SCG61-P04] Modelling of spontaneous and periodic slow slip in the northern part of the Japan Trench

*Ryoko Nakata[1,2], Takane Hori[1], Ryota Hino[2] (1.Japan Agency for Marine-Earth Science and Technology, 2.Graduate School of Science, Tohoku University)

[SCG61-P05] Structural-morphological and sedimentary features of forearc slope off Miyagi, NE Japan: implications for development of forearc basins and plumbing systems

*Jih-Hsin Chang[1], Jin-Oh Park[2], Tzu-Ting Chen[3], Asuka Yamaguchi[2], Tetsuro Tsuru[4], Yuji Sano[2], Ho-Han Hsu[3], Kotaro Shirai[2], Takanori Kagoshima[2], Kentaro Tanaka[2], Chiori Tamura[2] (1.Geological Survey of Japan, National Institute of Advanced Industrial and Science Technology., 2.Atmosphere and Ocean Research Institute, The University of Tokyo., 3.Institute of Oceanography, National Taiwan University., 4.Tokyo University of Marine Science and Technology.)

[SCG61-P06] Structural variation in the shallowest part of the Japan Trench subduction zone and its correlation with shallow megathrust slip and tsunamigenesis

*Yasuyuki Nakamura[1], Toshiya Fujiwara[1], Shuichi Kodaira[1], Seiichi Miura[1], Koichiro Obana[1] (1.Japan Agency for Marine Earth Science and Technology)

Vertical deformation style along the Sanriku coast inferred from coastal geology examined after the Tohoku earthquake

*Yuichi Niwa[1], Toshihiko Sugai[2]

1. Faculty of Science and Engineering, Chuo University, 2. Department of Natural Environmental Studies, Graduate School of Frontier Sciences, The University of Tokyo

Along the Sanriku coast, northeast Japan, discrepancies in crustal movement have been reported between uplift on a timescale of 10^5 years estimated from presence of flat surface previously recognized as Pleistocene marine terrace (Koike and Machida, 2001) and subsidence on a timescale of 10^1 –10^2 years from geodetic record (Kato, 1983; Ozawa et al., 2011). Some hypothetical models, which explain these discrepancies, are proposed in relation to megathrust earthquake cycle (e.g., Nishimura, 2014). These models assume that crustal movement style is same within whole part of the Sanriku coast, and show that amount of accumulation of uplift exceeds that of subsidence during one earthquake cycle. However, because of lack of reliably identified MIS5 (ca. 125ka) marine terrace with age data along the Sanriku coast except for northernmost of the coast (Miyazaki and Ishimura, 2018), and of putative marine terrace along the southern part of the Sanriku coast (Koike and Machida, 2001), spatial distribution of crustal movement cannot be estimated on the basis of only feature of Pleistocene marine terrace.

After the 2011 earthquake, we have examined Holocene sedimentary successions of alluvial plains distributed along the Sanriku coast in order to obtain data on millennial-scale crustal movements, which help to solve the problem about the temporal inconsistency of crustal movement. Recent studies have reported millennial-scale subsidence in central to southern parts of the coast (e.g., Niwa et al., 2014; Niwa et al., 2017), but only one comparable dataset is available for the northern part of the coast (Niwa et al., 2019). To obtain a comprehensive understanding of millennial-scale crustal movements along the Sanriku coast, we obtained well-dated Holocene sediment cores from the Kuji plain in the northern part of the coast.

These cores record a transgressive barrier-lagoon system from ca. 9500 to 8000 cal BP, a regressive prodelta to delta front from ca. 8000 to 6500 cal BP, and a subsequent wave-influenced shallow marine and fluvial environment. Relative sea-levels in the Kuji plain are higher than −20.1 m, higher than −4.3 m, higher than −4.8 m, and higher than −5.9 m on the basis of sediments deposited under the sea-level dated to 9000 to 8730 cal BP, 7580 to 7470 cal BP, 6940 to 6740 cal BP, and 6400 to 6260 cal BP. These sea-levels are higher than that in the Tsugaruishi plain, central Sanriku coast, where millennial-scale subsidence was previously estimated (Niwa et al., 2017). This discrepancy indicates that the Kuji plain has uplifting trend relative to the Tsugaruishi plain on a millennial-scale. By the addition of relative uplifting trend of the Omoto plain (Niwa et al., 2019), millennial-scale crustal movements along the Sanriku coast are best characterized as subsidence along the central to southern parts and relative uplift along the northern Sanriku coast. Spatial distribution of millennial-scale crustal movements accords with marine terrace distribution that uplifting trend during the past 100ka is confirmed only in northernmost of the Sanriku coast (Miyazaki and Ishimura, 2019). This agreement suggests a continuous southward tilting trend along the Sanriku coast since ca. 100 ka.

Kato (1983) Tectonophysics, 97, 183-200. Koike and Machida (2001) The University of Tokyo Press, p105. (in Japanese with English abstract) Miyazaki and Ishimura (2018) J. Geogr. (Chigaku-zasshi), 127,

©2020. Japan Geoscience Union. All Right Reserved.

735-757 (in Japanese with English abstract). Nishimura (2014) J. Disaster Res., 9, 294-302. Niwa et al. (2014) Quat. Res. (Dai-yonki kenkyu), 53, 311-312 (in Japanese with English abstract). Niwa et al. (2017) Quat. Int., 456, 1-16. Niwa et al. (2019) Quat. Int., 519, 10-24. Ozawa et al. (2011) Nature, 475, 373-377.

Keywords: alluvial plain, coastal geology, millennial-scale crustal movements, Sanriku coast

©2020. Japan Geoscience Union. All Right Reserved.

Trial of the crustal deformation detection accompanied with the tremor activities in Fukushima-Oki deduced from the ocean bottom pressure gauge data

*Hideto Otsuka[1], Yusaku Ohta[1], Ryota Hino[1], Kazuaki Ohta[2]

1. Research Center for Prediction Earthquakes and Volcanic Eruptions, Graduate School of Science, Tohoku University, 2. National Research Institute for Earth Science and Disaster Resilience

Recently, various phenomena of the slow slip events (SSEs) were detected in the Japan Trench. For example, Ohta et al. (2019) have detected low-frequency tremor activities in the Fukushima-Oki deduced from the Ocean Bottom Seismometer (OBS). They found the five tremor episodes with recurrence intervals of ~60 days which slow migration behavior and shear mechanisms consistent with plate subduction. They estimated the slip amount caused by these episodes based on the cumulative apparent moment of the tremor events as proposed by Hiramatsu et al. (2008). The apparent moment of the tremor was calculated on the basis of the ground displacement of the tremor seismograms and then converted to the seismic moment of the SSEs with an empirical scaling factor (Hiramatsu et al., 2008). The cumulative slip amount was roughly 1.5cm to 2.0cm. During the OBS observation, Tohoku University also developed the five Ocean Bottom Pressure-gauge (OBP) to detect the crustal deformation phenomena. In this study, we try to detect the crustal deformation accompanied with the tremor activities in this region.

Firstly, we assess the expected vertical displacement amount in the OBP sites. We assumed the fault model based on the results from Ohta et al. (2019). The fault area covered the area of the tremor activity, and the fault slip amount was assumed as 2cm which was based on the result of Ohta et al. (2019). The expected vertical displacement was approximately less than 1cm. This amount, however, may have the uncertainty because the slip amount may be affected by the value of the scaling factor which control the relationship between the seismic amount and apparent moment.

The obtained OBP time series will contain not only the crustal deformation but also the other contribution such as tidal component, non-tidal component, and specific sensor drift. Ocean tides were accounted for by harmonic analysis using the BAYTAP-G model of Tamura et al. (1991) and removed from the OBP time series. The model by Inazu et al. (2012) were applied to remove the non-tidal component. We fitted the drift model (Watts and Kontoyiannis, 1990) to each of the observed time series to estimate the drift function of individual sensors and removed from the time series.

Based on the obtained time series, we tried to detect the crustal deformation accompanied with the tremor activities. However, no significant displacement was detected from the OBP time series. This suggests that no crustal deformation has occurred beyond the current detectable accuracy of OBP. The current detectable accuracy of OBP is approximately ~1cm. If the 1cm displacement occurred at the OBP sited, roughly 5.7cm interplate slip is required. This is about 3.5 times slip amount suggested by Ohta et al. (2019).

Keywords: Ocean Bottom Pressure-gauge, Seafloor crustal deformation, Fukushima-Oki, Episodic tremor and slip, scaling

©2020. Japan Geoscience Union. All Right Reserved.

Seafloor Displacement along the Japan Trench Caused by the 2011 Tohoku-Oki Earthquake Examined by Repeated Bathymetric Surveys

*Toshiya Fujiwara[1,9], Shuichi Kodaira[1], Gou Fujie[1], Yuka Kaiho[1], Toshiya Kanamatsu[1], Takafumi Kasaya[2], Yasuyuki Nakamura[1], Tetsuo No[1], Tsutomu Takahashi[1], Takeshi Sato[3], Narumi Takahashi[4,1], Yoshiyuki Kaneda[5,1], Katharina Bachmann[6], Christian dos Santos Ferreira[6], Gerold Wefer[6], Michael Strasser[7], Tianhaozhe Sun[8]

1. Research Institute for Marine Geodynamics, Japan Agency for Marine-Earth Science and Technology, 2. Research Institute for Marine Resources Utilization, Japan Agency for Marine-Earth Science and Technology, 3. Sapporo Regional Headquarters, Japan Meteorological Agency, 4. National Research Institute for Earth Science and Disaster Resilience, 5. Kagawa University, 6. MARUM, University of Bremen, 7. Institute of Geology, University of Innsbruck, 8. Pacific Geoscience Centre, Geological Survey of Canada, 9. Kochi University

After the 11 March 2011 Tohoku-oki earthquake, we have conducted multibeam bathymetric surveys. The bathymetric data were collected along the same tracks obtained before the earthquake. These selected tracks were crossing the trench and extending from the landward to seaward trench slopes. We examined seafloor displacement on the landwardrelative to the seaward by means of the difference in multibeam bathymetry before and after theearthquake. Up until the present, we have evaluated several tracks from off-Fukushima to off-Sanriku, thus the seafloor displacement distributionalong the Japan Trench.

Along the off-Miyagi tracks near the epicenter, crossing the trench at 38˚05'N,the landward slope was largely elevated, the seafloor displacement extended to the trench, and there was sharp bathymetric changes at the trench axis [Fujiwara et al., Science 2011]. The conclusive result suggests fault rupture and slip extending to a shallow part of the subduction zone reached the trench axis. We estimated the coseismic horizontal displacement using the horizontal bathymetric offset. The horizontal displacement was very large about 50 m to the trenchward direction.

Notably, on the outermost landward slope, the 40 km wide area between the slope break and the trench axis, the seafloor was more than 10 m shallower on average. The observed seafloor elevation change on the outermost landward slope corresponds to a sum of vertical displacement and additional uplift for the sloping seafloor due to horizontal displacement. This uplift was likely an important factor contributing to the generation of the massive pulsating pattern of tsunami waves.

The method described in the Fujiwara et al. [2011] paper implicitly assumed the seafloor moved as a block unit. Sun et al. [Nat. Commun. 2017] evaluated the fault slip distribution over the most near-trench 40 km zone. The slip gently increased towards the trench and peaked at the trench axis. The slip was determined to be about 60 m.Quantitative information on the shallow slip is of critical importance to understand the rupture mechanism and the generation of the ensuring devastating tsunami.

Upward and downward changes in seafloor elevation of ±50 m are evident at the axial seafloorat 38˚05'N. Seismic data showed deformation of the sediment layer within the trench.The result is further evidence of the rupture propagation through the sediment layer [Kodaira et al., Nat. Geosci. 2012; Strasser et al., Geology 2013]. This bathymetric deformation is confined to an area extending 13 and 7 km along and across the trench directions, respectively. Currently, similar prominent bathymetric deformation is not found in any other places.

©2020. Japan Geoscience Union. All Right Reserved.

Large seafloor displacements suggesting coseismic slips to the trench were consistent in survey tracks in the off-Miyagi area, as far as the track at 38˚35'N. While, smaller seafloor displacements were observedalong the off-Fukushima track crossing the trench at 37˚25'N and along the off-Sanriku track crossing the trench at 39˚05'N, therefore the large coseismic slip to the trench is considered to be limited to the off-Miyagiarea near the epicenter.

We acquired three off-Sanriku survey trackscrossing the trench at 39˚10'N, 39˚20'N, and 39˚30'Nbecause maximum tsunami height caused by the earthquakewas observed at the coast of Sanriku.The evaluated seafloor displacements were relatively small, less than about 20 m in trenchward horizontal displacement and several meters in vertical displacement. Thus localized very large fault slip or very large submarine landslide is unlikely at least on the three survey tracks. There were coherent relative differences in the seafloor elevation on the landward trench slopes, which suggests the outermost lower slope was uplifted and the middle slope and the mid-slope terrace subsided along the trench axis [Fujiwara et al., GRL 2017].

Relatively small displacements less than 20 m in horizontal displacement and several meters in vertical displacement, these values are within ranges of error of the analysis [Fujiwara et al., MGR 2015]. Thus, quantitative discussion is rather difficult as values of the seafloor displacements are concerned about burying in the ranges of error. Additionally, in our analysis, data quality of the bathymetric data before the earthquake was major problem because the usage of repeated bathymetric survey for detection of seafloor displacement was not foreseen at that time. For the future, repeated acquisition of high resolution and accuracy bathymetric data using state-of-the-art technology at the present time of survey is important in the tectonically active regions.

Keywords: 2011 Tohoku-Oki Earthquake, Seafloor Displacement, Japan Trench, Multibeam Bathymetry, Tsunami

©2020. Japan Geoscience Union. All Right Reserved.

Modelling of spontaneous and periodic slow slip in the northern part of the Japan Trench

*Ryoko Nakata[1,2], Takane Hori[1], Ryota Hino[2]

1. Japan Agency for Marine-Earth Science and Technology, 2. Graduate School of Science, Tohoku University

In our previous studies, we focused the afterslip of the 2011 Tohoku-Oki earthquake, and conducted numerical simulation of earthquake generation cycles along the Japan Trench. We reflected trench-parallel remarkable difference of fault structure between the central and southern part based on marine survey and observations to spatial distribution of friction parameters of M~9 coseismic and postseismic areas. As a result, we could explain longer duration of postseismic slip in the southern part of the Japan Trench. However, we did not modeled slips in the northern part of the Japan Trench, where large coseismic slip of the Tohoku-Oki earthquake did not propagated, and slow-slips and tsunami earthquakes occur. Here, we modeled spontaneous and periodic slow slip in the northern part of the Japan Trench by using the same method. We will discuss roles of these slow slip during interseismic periods of a massive earthquake to understand physical conditions for generating a massive earthquake.

©2020. Japan Geoscience Union. All Right Reserved.

Structural-morphological and sedimentary features of forearc slope off Miyagi, NE Japan: implications for development of forearc basins and plumbing systems

*Jih-Hsin Chang[1], Jin-Oh Park[2], Tzu-Ting Chen[3], Asuka Yamaguchi[2], Tetsuro Tsuru[4], Yuji Sano[2], Ho-Han Hsu[3], Kotaro Shirai[2], Takanori Kagoshima[2], Kentaro Tanaka[2], Chiori Tamura[2]

1. Geological Survey of Japan, National Institute of Advanced Industrial and Science Technology., 2. Atmosphere and Ocean Research Institute, The University of Tokyo., 3. Institute of Oceanography, National Taiwan University., 4. Tokyo University of Marine Science and Technology.

Multibeam (MB) and subbottom profile (SBP) data along the forearc slope off Miyagi, Japan, are combined to investigate structural-morphological and sedimentary structures along the forearc slope of the Japan Trench subduction zone. In addition to dip-oriented slope gullies, the MB data image a nearly dip-perpendicular slope trough bounded by a fault scarp landward of the trench-slope break. Seaward of the trench-slope break, the subbottom mostly contains normal faults that dip in opposite direc- tions. The SBP data show not only unconformity and sliding surfaces, but also underfilled (forearc trough) and filled structures that may reflect the most recent forearc subsidence and basin filling. We propose these forearc trough and associated filling structures may indicate the earliest developments of modern isolated basins. Thus, a model of forearc basin development from slope gully to slope trough, isolated basins and forearc basin, transferred by active structures, could be proposed. Observed seafloor liquefaction in the SBP data may represent a near-surface seep structure of a plumbing system that enables hydrosphere- mantle fluid migration plausibly activated by earthquake cycles.

Keywords: forearc slope, isolated basin, forearc trough, liquefaction

©2020. Japan Geoscience Union. All Right Reserved.

Structural variation in the shallowest part of the Japan Trench subduction zone and its correlation with shallow megathrust slip and tsunamigenesis

*Yasuyuki Nakamura[1], Toshiya Fujiwara[1], Shuichi Kodaira[1], Seiichi Miura[1], Koichiro Obana[1]

1. Japan Agency for Marine Earth Science and Technology

The shallow megathrust slip to the vicinity of the trench is one of the key features of the 2011 Tohoku earthquake. Understanding the detailed structure in the shallowest portion of the Japan Trench subduction zone is indispensable to investigate the nature of the shallow slip. We have conducted seismic reflection surveys using a “compact” seismic system to map the seismic structural characters in the Japan trench axis region. Differential bathymetry estimation provided strong evidence with which to examine the shallow megathrust slip to the trench. Seismic sections in areas with large horizontal displacement estimated from differential bathymetry display folds and thrust faults, whereas ones in areas without large displacement display chaotic acoustic structures in the trench axis without any clearly imaged thrust faults or folding deformation. We suggest that the thrust faults clearly imaged in the trench axis acted as the shallowest plate boundary megathrust during the Tohoku earthquake and caused the displacement observed by the differential bathymetry. The trench axis around the 39.5˚N where the tsunami source was proposed, the seismic sections and bathymetric data indicate the past slope failures. The differential bathymetry estimates suggested no large trench-ward displacement during the Tohoku earthquake in this region. Taking into account the slope failures imaged in the seismic profiles in this region, we speculate that small-scale slope failure might have contributed to tsunamigenesis during the Tohoku earthquake. In the north of 40˚N where neither large displacement nor tsunami generation was supposed during the Tohoku earthquake. In this region, the seismic sections show a well-developed thrust-and-fold structure not only within the vicinity of the trench axis but beneath the lower landward slope 10 –20 km landward from the trench axis. This area is proposed as the tsunami source area of the 1896 Meiji Sanriku earthquake together with the area of slope failure around 39.5˚N. The Meiji Snariku earthquake and tsunami might be generated by a combination of the slope failure and thrust faults imaged.

Keywords: Japan Trench, seismic imaging, shallow megathrust slip, slope failure

©2020. Japan Geoscience Union. All Right Reserved.

[E] Poster | S (Solid Earth Sciences)：S-CG Complex & General

[S-CG62] Investigation of inputs to subduction zones: Influence of tectonic processes on the incoming plate

convener:Makoto Yamano(Earthquake Research Institute, the University of Tokyo), Tomoaki Morishita(School of Geoscience and Civil Engineering, College of Science and Technology, Kanazawa University), Gou Fujie(Japan Agency for Marine-Earth Science and Technology)

Various tectonic processes occur on the seaward side of the trench associated with bending of the incoming oceanic plate, e.g., fracturing of oceanic crust, infiltration of water, and intraplate volcanism. Investigation of these processes and their influence on the incoming plate provides important information on the boundary condition at the trench, inputs to subduction zones. Variation in inputs should significantly affect geophysical/geological phenomena around the plate interface and geochemical cycles in subduction zones. We welcome contributions from a broad range of earth science (geophysics, geology, petrology, and so on) discussing topics related to inputs to subduction zones such as occurrence of tectonic processes due to bending of the incoming plate, modification of the incoming plate by the processes, relationship between the processes and the inherited structure of the incoming plate, and influence of the processes on the subduction plate interface. We hope discussions are made on studies of a variety of subduction zones, including the Japan Trench and the Nankai Trough, and comparative studies among different subduction zones.

[SCG62-P01] Incoming Plate Faulting at the Outer Slope of the Middle America Trench offshore Mexico

*Emmanuel Soliman M Garcia[1], Yoshihiro Ito[1] (1.Disaster Prevention Research Institute, Kyoto University)

[SCG62-P02] Analysis of the variations in topographic features around the outer-rise of Japan trench

*Tomoko Hanyu[1], Jin-Oh Park[2], YUE SUN[2], Ehsan Jamali Hondori[2], Yukari Kido[3] (1.Kobe Ocean-Bottom Exploration Center, Kobe University, 2.Atmosphere and Ocean Research Institute, The University of Tokyo, 3.Japan Agency for Marine-Earth Science and Technology)

[SCG62-P03] Drift sediments recording bottom current history in NW Pacific

*Kiichiro Kawamura[1], Tomoka Adachi[1], Maki Suzukawa[1] (1.Yamaguchi University)

[SCG62-P04] Effects of lithology on the mechanical properties of the input materials at the Hikurangi margin

*Alexi Kristina Allen[1], Hiroko Kitajima[1] (1.Texas A and M University)

[SCG62-P05] Subduction initiation at active spreading mid-ocean ridge indicated by ultrahigh temperature slab melting

*Chiou-ting Lin[1], Kuei-Chih Feng[2], Masaki Enami[3], Hou-Chun Liu[4], Ji-Hao Zhu[6], Ron Harris[5], Wei-Dong Sun[1] (1.Center of Deep Sea Research, Institute of Oceanology, Chinese Academy of Sciences, 2.Department of Mechanical Engineering, Ming Chi University of Technology, 3.Institute for Space–Earth Environmental Research, Nagoya University, 4.Department of Earth Science, National Cheng Kung University, 5.Department of Geology, Brigham Young University, 6.State Oceanic Administration, Second Institute of Oceanography, Ministry of Natural Resources)

Incoming Plate Faulting at the Outer Slope of the Middle America Trench offshore Mexico

*Emmanuel Soliman M Garcia[1], Yoshihiro Ito[1]

1. Disaster Prevention Research Institute, Kyoto University

At the northern segment of the Middle America subduction zone, the Cocos Plate subducts underneath the North America Plate. Seaward of the trench, the seafloor contains horsts and grabens. These structures are typically associated with normal faulting, but their orientation with respect to the trench are mostly parallel or sub-parallel, which suggests that they are reactivated abyssal hills faults. At other subduction zones, such as at the Kuril and the Alaska-Aleutian, the reactivation of these normal faults formed at the spreading ridge is typically attributed to bending of the incoming plate. However, compared with the outer rise at these other subduction zones, the flexural deformation of the incoming Cocos Plate offshore Mexico is less prominent. This is expected if the elastic thickness is dependent on age, since the seafloor age in this region is less than 30 Ma. Furthermore, the characteristics of the trench outer slope faults vary across the segments of the subduction zone offshore Mexico. At the northwest portion which is offshore Guerrero, the fault scarps are mostly lower than 100 meters and have strikes that tend to be parallel to the trench. Meanwhile, at the southeast portion which is offshore Chiapas, the fault scarps are a few hundred meters in height and have strikes that are slightly oblique to the trench. To better understand the connection between lithospheric flexure and the observed normal faulting at the trench outer slope, we calculated the stresses due to elastic bending, which is linearly related to the curvature of the plate. Deriving the curvature from bathymetry can be challenging because of the presence of rough seafloor topography such as seamounts. Thus, to minimize effects from the bathymetric noise, we set up a regularized parameter estimation problem to solve for the bending curvature. Our results suggest that the higher plate curvatures at the Chiapas segment compared with the Guerrero segment are consistent with the differences in observed faulting and seismicity between the two regions.

Keywords: bend faults, lithospheric flexure, subduction zones

©2020. Japan Geoscience Union. All Right Reserved.

Analysis of the variations in topographic features around the outer-rise of Japan trench

*Tomoko Hanyu[1], Jin-Oh Park[2], YUE SUN[2], Ehsan Jamali Hondori[2], Yukari Kido[3]

1. Kobe Ocean-Bottom Exploration Center, Kobe University, 2. Atmosphere and Ocean Research Institute, The University of Tokyo, 3. Japan Agency for Marine-Earth Science and Technology

The 1933 Showa-Sanriku earthquake which was caused by a shallow and near-trench earthquake-fault on the outer-rise of the northern part of Japan Trench occurred 37 years after the 1896 Meiji-Sanriku tsunami earthquake. Precise location of earthquake-fault of the 1933 earthquakes have not yet been obtained (e.g. Obana et al., 2018).
For identifying the earthquake-fault around the outer-rise of Japan trench, it is necessary to determine the mechanism by which the topographic features of the outer-rise are formed. Most of the previous studies about flexural modeling identify only the deformed shape of the subducting plate without considering the features unrelated to flexural bending, such as earthquake-faults, seamounts, and volcanic ridges. Sparse topographic and gravity data make it difficult to estimate the elastic thickness distribution of the local area adjacent to the faults. To solve this problem, we aim to calculate the "non-isostatically-compensated topography (non-isostatically topography)" by using the method of Zhang et al. (2014). The non-isostatically topography was calculated by removing from the observed bathymetry (1) the effects of sediment loading, (2) isostatically-compensated topography based on gravity modeling, (3) age-related lithospheric thermal subsidence, and (4) flexural model of the bending plate. Fine scale bathymetry data set, which was compiled and provided by JCG and JAMSTEC (after Kido et al., 2011), was used for the analysis. The Matlab toolbox TAFI (Jha et al., 2017) was applied for modeling flexural deformation of the bending plate. The plate flexural bending model was estimated by every 0.05 degrees for latitude perpendicular to the subduction.
We will discuss the non-isostatically topographic features and elastic thickness in the local area of the outer-rise of Japan Trench.

References

Jha, S., et al. (2017). Toolbox for Analysis of Flexural Isostasy (TAFI)—A MATLAB toolbox for modeling flexural deformation of the lithosphere. *Geosphere*, 13(5), 1555-1565.
Kido, Y., et al. (2011). Bathymetric feature around Japan Trench obtained by JAMSTEC multi narrow beam survey. *Japan Geoscience Union Meeting 2011*, MIS036-P58.
Obana, K., et al. (2018). Seismicity in the source areas of the 1896 and 1933 Sanriku earthquakes and implications for large near-trench earthquake faults. *Geophysical Journal International*, 212(3), 2061-2072.
Zhang, F., et al. (2014). Variations in oceanic plate bending along the Mariana trench. *Earth and Planetary Science Letters*, 401, 206-214.

Keywords: Japan trench, outer rise, topography, non-isostatically topography, plate bending model

©2020. Japan Geoscience Union. All Right Reserved.

Drift sediments recording bottom current history in NW Pacific

*Kiichiro Kawamura[1], Tomoka Adachi[1], Maki Suzukawa[1]

1. Yamaguchi University

We reported in detail deep-sea drift sediments collected from on an abyssal plain in NW Pacific. Four sediment core samples were collected using a 4-m piston corer system during the cruise KH-18-5; HFPC01–04. The sediment samples are composed of mostly diatomaceous silty clay layers with sandy layers. The sediment layers are interbedded with a volcanic ash layer. There are two lines of evidence on drift sediments on the basis of sedimentological and magnetical analyses as follows.
First, we counted sedimentary grains of 63–128 μm in diameter in 2 cm intervals. The sedimentary grains consist of quarts, pumice, volcanic glass, diatom, radiolaria and so on. Two types of pumice grains could be observed as dirty grains with mud cover and clear grains. The clear pumice and volcanic glass would be associated with volcanic eruption, whereas the dirty pumice has no correlation with those grains. There were spike peaks of dirty pumice grains cyclically throughout the core sediments. We consider that the dirty pumice might be washed out of surface sediments and transported with long-term flows as re-sedimentation processes.
Second, we measured magnetic properties in the sediment core samples; anisotropy of magnetic susceptibility (AMS) and paleomagnetism. In general, the AMS demonstrates the alignment patterns of magnetic grains in specimens. These anisotropy can be represented by magnetic ellipsoids with three magnetic axes; maximum, intermediate and minimum susceptibilities (hereafter Kmax, Kint, Kmin, respectively). Kmax generally indicates the alignment direction of the magnetic grains. In this case, sediment core samples were rotated during sampling operation, so that we could not understand the north direction of the samples. In order to determine the north direction, we measured paleomagnetic directions in the core samples. We used remenent magnetization data under the 200G alternating field demagnetization conditions. Thus, we measured alignments of magnetic grains using two magnetic methods. As a result, the Kmax direction of these sediment core samples were mostly E-W indicating sub-parallel to the present bottom current directions as shown in Fujio and Yamamoto (2005).
As mentioned above, the the magnetic grains in the sediment core samples in NW Pacific were alinged sub-parallel to the present bottom current directions. This indicates that these sediments were transported and deposited by the bottom currents as drift sediments and/or contourite deposits. At least, the sediments were closely related to the bottom currents. These sediments contained dirty pumice grains indicating probably a re-working process.

Keywords: Contourite, Bottom current, Anisotropy of magnetic susceptibility

©2020. Japan Geoscience Union. All Right Reserved.

Effects of lithology on the mechanical properties of the input materials at the Hikurangi margin

*Alexi Kristina Allen[1], Hiroko Kitajima[1]

1. Texas A and M University

Subduction zones are known to produce large, damaging earthquakes, but they can also experience slow-slip events which cannot be felt by humans. Understanding the mechanisms that influence this variation in slip rate is crucial for better assessing how the subduction zones will act in the future. While the seafloor sediments make up a small portion of the subducting oceanic plate, they can have a noticeable impact on its ability to produce both large earthquakes and slow-slip events. Here, we report the mechanical properties of sediments and rocks that are subducting in the Hikurangi Margin. The International Ocean Discovery Program (IODP) Expedition 375 recovered input sediments and basement rocks at Sites U1520 and U1526. We compared shipboard physical properties with the chemical composition determined using the X-ray fluorescence (XRF) scanner at the Gulf Coast Repository. We also analyzed drilling data and conducted deformation experiments on volcaniclastic materials from Site U1520. By integrating the XRF data with porosity, p-wave velocity, and drilling parameters, as well as lab tests to determine the strength of these rocks, we can evaluate how the composition of the sediments affects their physical and mechanical properties. The preliminary results show a strong correlation between calcium content, porosity, and p-wave velocity for the volcaniclastic cores. There is also evidence to suggest that the torque on bit during drilling is an indication of rock strength as it increases sharply when the calciferous-volcaniclastic boundary is reached. Triaxial compression tests in the lab should confirm and quantify the rock strength of the volcaniclastic materials. This investigation into the subducting sediments properties builds onto pre-existing studies into the effects of seamounts on subduction and the factors that influence the slip rate at subduction zones.

Keywords: Subduction zones, Hikurangi Margin, laboratory experiments

©2020. Japan Geoscience Union. All Right Reserved.

Subduction initiation at active spreading mid-ocean ridge indicated by ultrahigh temperature slab melting

*Chiou-ting Lin[1], Kuei-Chih Feng[2], Masaki Enami[3], Hou-Chun Liu[4], Ji-Hao Zhu[6], Ron Harris[5], Wei-Dong Sun[1]

1. Center of Deep Sea Research, Institute of Oceanology, Chinese Academy of Sciences, 2. Department of Mechanical Engineering, Ming Chi University of Technology, 3. Institute for Space–Earth Environmental Research, Nagoya University, 4. Department of Earth Science, National Cheng Kung University, 5. Department of Geology, Brigham Young University, 6. State Oceanic Administration, Second Institute of Oceanography, Ministry of Natural Resources

The initiation of plate subduction is the last piece of the jigsaw puzzle of the plate tectonic theory. How the subduction of small oceanic plates commenced, and the magmatism of the subduction initiation has been particularly controversial. Here we report a new type of calc-alkaline andesite/dacite associated with initiation of subduction. The *Lichi andesite/dacite (LAD)* has typical geochemical features of slab melting, but abnormally displays relative enrichments in Nb-Ta and depletion in Ti and Pb. The *LAD* mineral assemblage consists mostly of plagioclase and two-pyroxenes with rare hornblende and biotite. No quartz or K-feldspar phenocrysts are observed. The presence of cristobalite in the matrix of the dacite and geochemical relations indicate slab melting occurs at an ultrahigh temperature and relatively low pressure environment, which is consistent with subduction initiation of an active spreading ridge along a transform fault.

Keywords: Subduction Initiation, Ridge Subduction, Slab Melting, Manila Trench, South China Sea, Lichi Mélange

©2020. Japan Geoscience Union. All Right Reserved.

[E] Poster | S (Solid Earth Sciences)：S-CG Complex & General

[S-CG63] Dynamics in mobile belts

convener:Yukitoshi Fukahata(Disaster Prevention Research Institute, Kyoto University), Ray Y Chuang(Department of Geography, National Taiwan University), Toru Takeshita(Department of Natural History Sciences, Graduate School of Science, Hokkaido University), Hikaru Iwamori(Earthquake Research Institute, The University of Tokyo)

The dynamic behaviors of mobile belts are expressed across a wide range of time scales, from the seismic and volcanic events that impact society during our lifetimes, to orogeny and the formation of large-scale fault systems which can take place over millions of years. Deformation occurs on length scales from microscopic fracture and flow to macroscopic deformation to plate-scale tectonics. To gain a physical understanding of the dynamics of mobile belts, we must determine the relationships between deformation and the driving stresses associated with plate motion and other causes, which are connected through the rheological properties of the materials. To understand the full physical system, an integration of geophysics, geomorphology, geology, petrology, and geochemistry is necessary, as is the integration of observational, theoretical and experimental approaches. In particular, rheological properties, which are physically affected by fluids in the crust and chemical reactions assisted by fluids, can be resolved only through such an interdisciplinary approach. After the 2011 great Tohoku-oki earthquake, large-scale changes in seismic activity and regional scale crustal deformation were observed, making present-day Japan a unique natural laboratory for the study of the dynamics of mobile belts. This session welcomes presentations from different disciplines, such as seismology, geodesy, tectonic geomorphology, structural geology, petrology, geochemistry and hydrology, as well as interdisciplinary studies, that relate to the dynamic behaviors of mobile belts.

[SCG63-P01] Seismic potential along the Caribbean subduction zone northwestern Colombia revealed by GPS data

*Sindy Carolina Lizarazo[1], Takeshi Sagiya[2], Hector Mora-Paez[3] (1.Graduate School of Environmental Studies - Nagoya University, 2.Disaster Mitigation Research Center - Nagoya Univesity, 3.Geological Survey of Colombia - GeoRED Project)

[SCG63-P02] New Megathrust Locking Model for the Southern Kurile Subduction Zone Incorporating Viscoelastic Relaxation and Non-uniform Compliance of Upper Plate

*Yuji ITOH[1], Takuya NISHIMURA[2], Kelin WANG[3], Jiangheng HE[3] (1.Graduate School of Science, Kyoto University, 2.Disaster Prevention Research Institute, Kyoto University, 3.Pacific Geoscience Centre, Geological Survey of Canada)

[SCG63-P03] Occurrence of normal-type earthquakes and stress loading model under Boso Peninsula, Japan

*Akinori Hashima[1], Hiroshi Sato[1], Toshinori Sato[2] (1.Earthquake Research Institute, University of Tokyo, 2.Graduate School of Science, Chiba University)

[SCG63-P04] 3-D Numerical Simulation of Island Arc Deformation Due to Steady Plate Subduction

*Yutaro Mori[1], Yukitoshi Fukahata[2] (1.Graduate School of Science, Kyoto University, 2.Disaster Prevention Research Institute, Kyoto University)

[SCG63-P05] Cause of the horizontal deformation of the Philippine Sea plate subducting beneath southwestern Japan

*Kazuki Miyazaki[1], Junichi Nakajima[1] (1.Department of Earth and Planetary Sciences, Tokyo Institute of Technology)

[SCG63-P06] Modeling strain concentration zones in Kyushu Island considering heterogeneous rheological structure

*Bunichiro Shibazaki[1] (1.International Institute of Seismology and Earthquake Engineering, Building Research Institute)

[SCG63-P07] Estimation of inelastic strain rate in the lower crust based on GNSS and seismic data and its implication for dynamics in Kyushu, southwest Japan

*Yuhei Yuasa[1], Satoshi Matsumoto[2] (1.Department of Earth and Planetary Sciences, Graduate School of Science, Kyushu University, 2.Institute of Seismology and Volcanology, Faculty of Science, Kyushu University)

[SCG63-P08] Tectonic development along the Hinagu fault zone, Kumamoto Prefecture, Japan

*Kenta Kobayashi[1], Keiji Ogashiwa[1] (1.Department of Geology, Faculty of Science, Niigata University)

[SCG63-P09] Physical modeling of postseismic deformation following the 2008 Iwate-Miyagi Nairiku Earthquake

*Yoshiki Takei[1], Youichiro Takada[2], James Daniel Paul Moore[3], Mako Ohzono[4] (1.Department of Natural History Sciences, Hokkaido University, 2.Faculty of Science, Hokkaido University, 3.Earth Observatory of Singapore, Nanyang Technological University, 4.Institute of Seismology and Volcanology, Graduate School of Science, Hokkaido University)

[SCG63-P10] Spatial change of extension direction detected by paleostress analysis in the Miocene Tanabe Group, Southwest Japan

*Noriaki Abe[1], Katsushi Sato[1] (1.Division of Earth and Planetary Science, Graduate School of Science, Kyoto University)

[SCG63-P11] Non-double-couple earthquake in the focal area of the 2000 Western Tottori earthquake by “0.1 manten” hyperdense seismic observation and spatial distribution of non-double-couple components

*Yuto Hayashida[1], Takumi Motokoshi[1], Satoshi Matsumoto[2], Yoshihisa Iio[3], Shin'ichi Sakai[4], Aitaro Kato[4], Group for "0.1 manten" hyperdense seismic observation Group registration (1.Department of Earth and Planetary Sciences, Graduate School of Science, Kyushu University, 2.Institute of Seismology and Volcanology, Faculty of Sciences, Kyushu University , 3.Disaster Prevention Research Institute, Kyoto University, 4.Earthquake Research Institute, University of Tokyo)

[SCG63-P12] **Driving stress of the 2013 M_W5.8 Awaji Island earthquake, Japan, inferred from well-constrained focal mechanisms and its seismotectonic implication**

*Kazutoshi Imanishi[1], Makiko Ohtani[2], Takahiko Uchide[1] (1.Geological Survey of Japan, AIST, 2.Earthquake Research Institute, The University of Tokyo)

[SCG63-P13] A systematic investigation of rupture directivity, stress drop, fault geometry, and radiation efficiency of small inland earthquakes in Japan

*Keisuke Yoshida[1] (1.Tohoku University)

[SCG63-P14] Modeling Internal Deformation Due to Inelastic Sources Under Inhomogeneous Structures

*Daisuke Sato[1], James Daniel Paul Moore[2] (1.Disaster Prevention Research Institute, Kyoto University, 2.Earth Observatory of Singapore)

[SCG63-P15] Combined inversion technique to determine stress condition and friction coefficient from fault orientation

*Katsushi Sato[1] (1.Division of Earth and Planetary Sciences, Graduate School of Science, Kyoto University)

[SCG63-P16] **Correlation between physical and hydraulic properties of rock fractures constrained by surface geometry: Digital rock physics approach**

*Kazuki Sawayama[1], Takuya ISHIBASHI[2], Fei Jiang[3], Takeshi Tsuji[4], Yasuhiro Fujimitsu[4] (1.Graduate school of engineering, Department of Earth Resources Engineering, Kyushu University, 2.Fukushima Renewable Energy Institute, National Institute of Advanced Industrial Science and Technology, 3.Department of Mechanical Engineering, Faculty of Engineering, Yamaguchi University, 4.Department of Earth Resources Engineering, Faculty of engineering, Kyushu University)

[SCG63-P17] The evolution of cataclastic rocks and their implication on the development of the Median Tectonic Line fault architecture, Japan

*Thomas Jing Yi Yeo[1], Toru Takeshita [1], Wencheng Huang[1] (1.Department of Natural History Sciences, Graduate School of Science, Hokkaido University)

[SCG63-P18] Development history of the mylonite zone distributed along the Mie Prefecture Median Tectonic Line

*Huang Wencheng[1], toru Takeshita[1], Thomas Jing Yi Yeo [1], Jun-Ichi Ando[2] (1.Department of Natural History Sciences, Graduate School of Science, Hokkaido University, 2.Department of Earth and Planetary Systems Science, Graduate School of Science, Hiroshima University)

[SCG63-P19] **Extensional stress conditions determined from the orientations of Middle Miocene dikes in the Kumano area**

*Toshiki Haji[1,2], Atsushi Yamaji[1] (1.Graduate School of Science, Kyoto University, 2.Institute of Geology and Geoinformation, AIST)

[SCG63-P20] Syn-orogenic extrusion of HP-LT blueschists in the northern Tyrrhenian Sea (northern Apennines, Italy)

*Samuele Papeschi[1], Eric Ryan[2], Hans Joachim Massonne[3,4], Giovanni Musumeci[5,6], Francesco Mazzarini[6], Giulio Viola[7] (1.Japan Agency for Marine Earth-Science and Technology, Kochi, Japan, 2.Department of Geoscience and Petroleum, Norwegian University of Science and Technology, Trondheim, Norway, 3.School of Earth Sciences, China University of Geosciences, Wuhan, P.R. China, 4.Fakultät Chemie, Universität Stuttgart, Stuttgart, Germany, 5.Dipartimento di Scienze della Terra, Università di Pisa, Pisa, Italy, 6.Istituto Nazionale di Geofisica e Vulcanologia, Pisa, Italy, 7.Dipartimento di Scienze Biologiche, Geologiche e Ambientali, Università di Bologna, Bologna, Italy)

[SCG63-P21] **Elastic wave velocities and electrical conductivity in a brine-saturated granitic rock with single fracture**

*Tohru Watanabe[1], Arina Tomioka[1] (1.University of Toyama)

[SCG63-P22] Hydraulic monitoring results during SIMFIP injection experiments through Shionohira fault zones in Fukushima Prefecture, Japan

*Kazuhiro Aoki[1], Hiroshi Wakahama[2], Haruka Nojo[2], Etuo Iwasaki[2], Masao Kametaka[2], Yukumo Tanaka[1], Takumi Yoshida[1], Kazuyoshi Seshimo[1] (1.Japan Atomic Energy Agency, 2.Dia Consultants)

[SCG63-P23] Change in electrical conductivity in a brine-saturated granite under uni-axial compression

*Yui Aikawa[1], Tohru Watanabe[1] (1.University of Toyama)

[SCG63-P24] Grain shape and connevtivity of pores in granular materials

*Katazakai Haruka[1], Tohru Watanabe[1] (1.Toyama University)

[SCG63-P25] Grain shape and pressure sensitivity of transport properties in granular materials

*Maremichi Abe[1], Tohru Watanabe[1] (1.Toyama University)

Seismic potential along the Caribbean subduction zone northwestern Colombia revealed by GPS data

*Sindy Carolina Lizarazo[1], Takeshi Sagiya[2], Hector Mora-Paez[3]

1. Graduate School of Environmental Studies - Nagoya University, 2. Disaster Mitigation Research Center - Nagoya Univesity, 3. Geological Survey of Colombia - GeoRED Project

Colombia is characterized by the complex interaction among the Caribbean, Nazca and South American plates, as well as the North Andean and Panama blocks. This setting causes intense seismicity and faulting along the collision and subduction regions whose natures are not well understood. Under these conditions, the current GPS network becomes an important tool to study the regional kinematics, understand the observed crustal deformation and evaluate the seismic potential in the country.

We analyzed data from 87 continuous GPS stations during the period 2008-2017 obtained by the GeoRED project from the Geological Survey of Colombia and the COCONet project (Continuously Operating Caribbean GPS Observational Network).Daily coordinates of the GPS sites were calculated using the GAMIT/GLOBK software v.10.7 under the ITRF2014 reference frame. Then, average displacement rates were calculated by using HECTOR software considering seasonal components and offsets due to instrumental changes (Bos et al., 2013). Finally, a geodetic inversion analysis following Yoshioka et al. (1993) was performed in order to evaluate the interplate coupling and the seismic potential along the Caribbean subduction zone.

Along the Caribbean subduction zone, we identified an isolated fully locked patch south of the city of Cartagena extending from 5km to 20km depths. The origin of this asperity is enigmatic and it allows us to propose two possible interpretations. The first one is elastic deformation able to generate a Mw 8.2 earthquake. We obtained a seismic moment accumulation rate of assuming an average slip deficit rate of 9.9 mm/yr and consequently, we estimate an average recurrence interval of ~540 years. Although there is no record of giant earthquakes in this area, we cannot reject this scenario because the historical record is too short to register the past event. The second one is that the whole deformation is inelastic. Estimates of long-term shortening based on seismic cross sections do not support this hypothesis because it is too small compared with the geodetic rate. However, still this possibility holds since there is a possibility of an accelerated deformation during the last 1 Ma. To discern between both scenarios, it is essential to conduct a careful geological investigation to identify recent evidence of crustal shortening or paleotsunami along northwestern Colombia.

Keywords: Seismic potential, Interplate coupling, Caribbean subduction zone, GPS data, Colombia

©2020. Japan Geoscience Union. All Right Reserved.

New Megathrust Locking Model for the Southern Kurile Subduction Zone Incorporating Viscoelastic Relaxation and Non-uniform Compliance of Upper Plate

*Yuji ITOH[1], Takuya NISHIMURA[2], Kelin WANG[3], Jiangheng HE[3]

1. Graduate School of Science, Kyoto University, 2. Disaster Prevention Research Institute, Kyoto University, 3. Pacific Geoscience Centre, Geological Survey of Canada

In the southern Kurile subduction zone, many megathrust earthquakes have occurred, including a M 9 tsunamigenic event in the 17th century. Current locking state of the megathrust has been inferred from land GNSS data before the 2003 M_w 8.0 Tokachi-oki earthquake in many previous studies using either elastic or viscoelastic models. The previous locking models exhibit physically unreasonable features such as slip deficit rates exceeding the plate convergence rate and/or high a degree of locking at large depths where stick-slip behavior is not expected. We think the cause of the problems is the assumption of a mechanically uniform upper plate. In order to improve the locking model, we have constructed a subduction zone model that includes variations in the elastic compliance of the upper plate in the margin-normal direction, consistent with the thermal regime of the subduction zone.
We construct a 3D viscoelastic model using the Finite Element Method. In our model, the rigidity values in the backarc, volcanic arc, and forearc regions are 48 GPa, 16 GPa, and 48 GPa, respectively. The elastic thicknesses of the three areas are 10 km, 7.5 km and 25 km, respectively, except for a portion of the forearc that has a greater thickness to account for the presence of a “cold nose” of the mantle wedge. For comparison, we also construct a model in which the upper plate rigidity and elastic thickness are uniformly 48 GPa and 25 km, respectively. We generate interseismic viscoelastic Green’s functions using these structures and derive megathrust locking distributions by inverting GNSS velocities prior to the 2003 earthquake.
In the model of non-uniform upper plate, full locking of the megathrust is limited to depths shallower than the downdip rupture limits of the 2003 mainshock and the 1973 M_w 7.8 Nemuro-oki earthquake in the northeastern neighbor region. Similar results in which parts of past megathrust rupture areas are not fully locked during the interseismic period have been reported for the Tohoku-oki and Kamchatka regions. It is consistent with the shrinking of megathrust locked zone during the interseismic period and/or the invasion of dynamic rupture into low-locking areas predicted by numerical simulations with a rate-and-state friction laws. However, sensitivity tests using forward modeling show that full locking covering the 2003 rupture area can also reasonably fit the horizontal GNSS data. To constrain spatiotemporal changes in megathrust locking during the interseismic period in future studies, we will need a much longer observational time window which requires additional conventional geodetic data prior to the GNSS era. In our preferred model, the near-trench part of the megathrust is fully locked. A model in which the near-trench part is forced to creep can fit the land GNSS velocities equally well. Therefore, even after incorporating the non-uniform compliance and interseismic viscoelastic relaxation, the locking state of the megathrust near the trench cannot be resolved by the land data only. Nevertheless, we infer locking near the trench axis of the Nemuro-oki region because no tremor is detected with the seafloor observation network S-net.

Keywords: Megathrust Locking, Viscoelastic Relaxation, Earthquake Cycle, The Southern Kurile Subduction Zone

©2020. Japan Geoscience Union. All Right Reserved.

©2020. Japan Geoscience Union. All Right Reserved.

Occurrence of normal-type earthquakes and stress loading model under Boso Peninsula, Japan

*Akinori Hashima[1], Hiroshi Sato[1], Toshinori Sato[2]

1. Earthquake Research Institute, University of Tokyo, 2. Graduate School of Science, Chiba University

Boso Peninsula, Japan, was formed by the interaction of the Philippine Sea, Eurasian and Pacific plates around the trench-trench-trench Boso triple junction. Normal-type earthquakes are persistently observed in the subducting Philippine Sea slab under the peninsula at depth of ~30 km, including a recent (2019) Mw4.9 earthquake which caused shaking throughout the Kanto region (greater Tokyo). Such shallow intra-plate earthquakes are potentially hazardous to this heavily populated region, yet their mechanism is poorly understood, compared with the outer rise earthquakes or intermediate deep earthquakes within slabs. In the previous study, we modeled long-term deformation due to steady subduction of the Pacific and Philippine Sea plates (Hashima et al., Tectonophysics, 2016). Here, we calculate stress rates in the Philippine Sea slab and the surrounding area, using our subduction model, to explain the generation of the regional stress field and its effect on earthquake occurrence.

In our model, the subduction of the Pacific and Philippine Sea plate is expressed by the steady slip (dislocation) on the plate interfaces. The collision of the Izu Peninsula is expressed by slip-rate deficit. The area of the slip-rate deficit is determined to satisfy the long-term deformation data obtained by geological and geomorphological methods. Then, slip-rate deficit turned out to be distributed on the northwest side of the Izu Peninsula.

Using this optimum model, we obtained all-around horizontal extensional stress rates under Boso Peninsula both above and below the Eurasian-Philippine Sea plate interface. In broader view, the stress rates are northwest-southeast compression in the collision zone around Izu Peninsula, strike-slip type in the Philippine Sea plate to the south, and horizontal extension in the Eurasian plate north of Boso Peninsula.

We apply our calculated stress rates to the nodal planes of the observed earthquakes to calculate the Coulomb failure function (ΔCFF). These calculated ΔCFFs are generally positive on normal-type earthquakes under Boso. This result indicates that modeled intra-plate stress pattern is consistent with earthquake occurrence as the stress release process. The ΔCFFs are also consistent with earthquakes in adjacent seismically active areas: the Izu collision zone, the interior of the Philippine Sea plate, and in seismic swarms in the Eurasian plate northeast of Boso Peninsula, which further supports our stress loading model.

To reveal the individual contributions of the Philippine Sea and Pacific subduction and the Izu collision, we decomposed the calculated stress rates. The collision effect is negligible on Boso Peninsula. The subduction of the Pacific plate creates east-west extension, while that of the Philippine sea plate creates north-south extension. Both subduction together creates the characteristic all-around extension under Boso Peninsula.

Keywords: Boso Peninsula, Stress loading, Coulomb stress, Plate subduction, Philippine Sea Plate

©2020. Japan Geoscience Union. All Right Reserved.

3-D Numerical Simulation of Island Arc Deformation Due to Steady Plate Subduction

*Yutaro Mori[1], Yukitoshi Fukahata[2]

1. Graduate School of Science, Kyoto University, 2. Disaster Prevention Research Institute, Kyoto University

Island arc-trench system is characterized by a pair of anomalies in topography and free-air gravity, which is high in the island arc and low around the trench. Although this feature is observed without exception in the world, physical mechanism of the formation of this feature has not been well understood. Fukahata and Matsu'ura (2016) calculated deformation of the island-arc lithosphere due to steady plate subduction for a 2-D problem and explained the deformation mechanism based on the combination of lithospheric rotation and gravity. However, 3-D geometry of the plate interface may have an important effect on lithospheric deformation. For example, a large negative gravity anomaly is observed around a bend of a trench axis (Sandwell and Smith, 1997). This feature has been well reproduced by a numerical model (Hashimoto et.al., 2008), but the physical mechanism of the formation has not been clarified yet.

In this study, we develop a 3-D numerical model based on elastic-viscoelastic dislocation theory and compute lithospheric displacement rates in the island arc-trench system caused by steady slip on a plate interface, which has a convex bend toward the island arc along the trench axis. Computed results show that the island arc lithosphere significantly subsides around the bend, where horizontal extension parallel to the trench axis is observed. This result suggests that the slip vectors that have the direction away from the bend along the trench in the overriding plate results in mass deficit around the bend and subsidence of the island-arc lithosphere.

Keywords: island-arc trench system, steady plate subduction, free-air gravity anomaly

©2020. Japan Geoscience Union. All Right Reserved.

Cause of the horizontal deformation of the Philippine Sea plate subducting beneath southwestern Japan

*Kazuki Miyazaki[1], Junichi Nakajima[1]

1. Department of Earth and Planetary Sciences, Tokyo Institute of Technology

The Philippine Sea plate subducting in southwestern Japan shows an interesting feature that it undergoes horizontal deformation after subduction. However, the cause of the significant deformation remain poorly understood. Therefore, this study investigates the horizontal deformation of the Philippine Sea plate in terms of the geometrical interaction with the Pacific plate.

First, we confirm that the observed eastern limit of the Philippine Sea plate beneath Kanto can be well reproduced with the subduction of the Philippine Sea plate onto the Pacific plate at dip angles of 12º down to a depth of 40 km and 40º at greater depths. Next, we apply the method that can expand a deformed plane surface to an undeformed geometry using lattice points assigned on the subducted Philippine Sea plate. Based on the two analyses, we conclude that the deformation of Philippine Sea plate is controlled by the shape of Pacific plate.

Keywords: Philippine Sea Plate, Pacific Plate

©2020. Japan Geoscience Union. All Right Reserved.

Modeling strain concentration zones in Kyushu Island considering heterogeneous rheological structure

*Bunichiro Shibazaki[1]

1. International Institute of Seismology and Earthquake Engineering, Building Research Institute

Recent large intra-plate earthquakes in Japan have occurred in strain concentration zones which have been revealed by the analysis of dense GNSS data. For example, the 2016 Kumamoto earthquake occurred in a strain concentration zone in Kyushu Island (Nishimura et al., 2016) and the 2016 Central Tottori earthquake occurred in the Sanin strain concentration zone (Nishimura and Takada, 2017). It is thought that strain concentration zones are caused by heterogeneous rheological structures that are the result of heterogeneous thermal structures and distributions of water content and preexisting geological structures. This study models the Kyushu strain concentration zones to understand the generation processes of large intraplate earthquakes by considering the heterogeneous rheological structure.

Geothermal gradients according to data obtained from Hi-net (Matsumoto et al. 2007) and from the Geological Survey of Japan (Tanaka et al. 2004) indicate high geothermal anomalies in the Beppu–Shimabara graben zone, in particular, regions that include the Kujyu and Aso volcanoes and the Beppu region. Geothermal gradients are also high in the regions of the Kirishima and Sakurajima volcanoes. The distribution of the geothermal gradient is similar to that of the cut-off depth of the seismicity obtained by Matsumoto et al. (2016).

This study models strain concentration zones by considering the heterogeneous rheological structure using the finite element method (Shibazaki et al., 2007), with nonlinear viscoelasticity and Mohr–Coulomb plasticity. From the observed geothermal gradient distribution, we assume that temperature increases with depth. We set the boundary conditions as extensional in the N–S direction and compressional in the E–W direction. We reproduce the strain concentration zone along the Futagawa fault, where the 2016 Kumamoto earthquake occurred. However, we cannot reproduce the strain concentration zone along the Hinagu fault. Therefore, we include the low-strength region around the Hinagu fault zone considering the existence of an ancient accretional complex, and the low-strength region in the northern part of the Okinawa Trough. By considering these low-strength regions, we can reproduce the strain concentration zones along the Futagawa and Hinagu fault zones, the pattern of which is similar to the observed one.

Keywords: strain concentration zone, Kyushu, finite element method, thermal structure, Okinawa Trough

©2020. Japan Geoscience Union. All Right Reserved.

Estimation of inelastic strain rate in the lower crust based on GNSS and seismic data and its implication for dynamics in Kyushu, southwest Japan

*Yuhei Yuasa[1], Satoshi Matsumoto[2]

1. Department of Earth and Planetary Sciences, Graduate School of Science, Kyushu University, 2. Institute of Seismology and Volcanology, Faculty of Science, Kyushu University

It is considered that localization of inelastic deformation due to viscous inhomogeneity in the lower crust results strain concentration zone in island arc, and estimation of the inelastic strain rate in the lower crust is being performed. On the other hand, while the inelastic strain rate and the deviatoric stress are related by the flow rule, the information on the estimated deviatoric stress field has not been taken much care in the previous studies. In this study, we proposed a new method for estimating the inelastic strain rate in the lower crust, which incorporates the information of deviatoric stress field. Furthermore, since the subduction of the plate is an important factor for the crustal deformation process in island arc, we also attempted simultaneously to estimate the distribution of locking at the interface of the subducting slab with the inelastic strain rate in the lower crust.

We adopted back slip model (Savage, 1983) for the coupling of the interface and the box-shaped source (Barbot et al., 2017) for inelastic deformation in the lower crust. Using the ground surface strain rate estimated from GNSS observations as data, the inelastic strain rate in the lower crust and the slip deficit rate at the plate boundary were estimated. We applied two constrains in the scheme: 1) the smoothing of the slip deficit rate distribution and 2) the direction of the inelastic strain rate followed the deviatoric stress (flow rule). The strength of these constraints is determined by minimizing the Akaike Bayesian information criterion (Akaike, 1980).

The results showed that high inelastic strain rate (~1×10^{-6} /yr) were obtained around Central and southwestern Kyushu. These areas correspond to the areas with high seismic activity. We found that the seismicity was induced by the inelastic deformation in the lower crust by calculating the stress change due to the inelastic deformation in the lower crust. In addition, these areas have high geothermal gradients in Kyushu (Tanaka et al., 2004), and the seismic velocity at depth 20 km is low velocity anomalies (Saiga et al., 2010). The results suggest that the lower crust in these region is in a high temperature / wet environment, and that the viscosity of the rocks is low. Therefore, the estimated high inelastic strain rate can be interpreted as an inelastic deformation concentration zone in the low viscosity lower crust. Also, the estimated the distribution of slip deficit rate is 10 - 25 mm/yr around the Bungo Channel, while the Hyuga-Nada is hardly locked. The stress change due to locking between plates are smaller than one due to inelastic deformation in the lower crust. Therefore, it is considered that the inelastic deformation in the lower crust plays an important role in seismic activity and crustal deformation in inland Kyushu.

Keywords: Kyushu, inelastic, Inland Earthquakes

©2020. Japan Geoscience Union. All Right Reserved.

Tectonic development along the Hinagu fault zone, Kumamoto Prefecture, Japan

*Kenta Kobayashi[1], Keiji Ogashiwa[1]

1. Department of Geology, Faculty of Science, Niigata University

The Futagawa and the Hinagu fault zones were activated at the time of the 2016 Kumamo earthquake. To understand how fault zones have developed over a long period of time, it is necessary to observe fault zone structures at the macro to microscope scales. We carried out field surveys in the aftershock area of the earthquake, and analyzed the meso-structures of the brittle fault rock zones and porphyry dikes. Paleo-stress field and K-Ar age of the porphyry were determined.
NNE-SSW striking remarkable brittle shear zone was recognized in the Hinagu Formation (Early Cretaceous), indicated dextral-normal slip sense (2nd stage). On the other hand, outsides of the shear zone, indicated sinistral slip sense (1st stage). The shear zone was intruded by porphyry dikes, and cut by NNW striking sinistral and E-W striking dextral minor faults (3rd stage). Based on the slip sense of the 2nd stage faults and geometry of the dikes, paleo-stress field was determined as strike slip to normal type. The K-Ar age of the porphyry was dated as 21.78±0.56Ma.
Brittle fault rock zones were also distributed in the Higo metamorphic rocks. The macroscale fault zone in the aftershock area has a long history of deformation and complicated structure. Parts of them were selected, and activated at the time of the aftershocks.

Keywords: Kumamoto Prefecture, Hinagu fault, active fault, fault rocks

©2020. Japan Geoscience Union. All Right Reserved.

Physical modeling of postseismic deformation following the 2008 Iwate-Miyagi Nairiku Earthquake

*Yoshiki Takei[1], Youichiro Takada[2], James Daniel Paul Moore[3], Mako Ohzono[4]

1. Department of Natural History Sciences, Hokkaido University, 2. Faculty of Science, Hokkaido University, 3. Earth Observatory of Singapore, Nanyang Technological University, 4. Institute of Seismology and Volcanology, Graduate School of Science, Hokkaido University

The Iwate-Miyagi Nairiku Earthquake (hereafter IMNE) occurred on June 14, 2008 (Mw 6.8). Fault models of the mainshock have been proposed from GNSS survey (Ohta et al., 2008; Iinuma et al., 2009), InSAR analysis (Takada et al., 2009; Abe et al., 2011), and seismographs (Suzuki et al., 2010). The fault models proposed from GNSS and seismographs consist of west-dipping reverse faults with maximum slip exceeding 6 meters. On the other hand, InSAR and offset measurement of SAR intensity images clearly indicate the existence of east-dipping fault along the western side of the hypocentral area.

Large postseismic deformation following the mainshock also have been detected by GNSS and InSAR (e.g., Iinuma et al., 2009; Ohzono et al., 2011; Takada et al., 2011). The interferograms taken from descending orbit (2008/7/16 - 2010/7/22) indicate the LOS displacements ~10 cm away from the satellite at hanging-wall side of the west-dipping faults, and ~15 cm toward the satellite around the northern part of Mt. Kurikoma.

Two physical models of the postseismic deformation of IMNE have been proposed previously. Iinuma et al. (2009) estimated the after-slip distribution from GNSS data near the fault traces for a month after the mainshock. They found cumulative afterslip on the coseismic faults as well as nearby active fault named the Dedana Fault (DF). The viscoelastic relaxation of this earthquake was calculated by Ohzono et al. (2011). They modeled crust-mantle system as an elastic layer overlying a viscoelastic substratum, and successfully explained the far-field displacements. In these studies, (1) only GNSS data were used, and (2) mutual interaction between the afterslip and viscoelastic relaxation has not been considered.

In this study, we construct a physical model of the postseismic deformation following IMNE on the basis of half analytic solution, named Unicycle (Barbot et al., 2017; Moore et al., 2017). With Unicycle, we consider (1) mutual interaction between the afterslip and the viscoelastic relaxation, (2) afterslip following the rate-and-state friction law (e.g., Dieterich, 1979; Ruina, 1983), and (3) horizontal heterogeneity of rock rheology with nonlinear power-law creep predicted from room experiments (e.g., Kirby, 1983). We started from simple model with the rheological structure proposed by Ohzono et al. (2011) and the coseismic slip distribution proposed by Iinuma et al. (2009).

In our calculation, large afterslip on DF is not triggered unlike Iinuma et al. (2009). The calculated postseismic displacement field well explains far-field GNSS data, which is consistent with Ohzono et al. (2011). In addition, our calculation explains the near-field GNSS data in the eastern side of the faults. Large discrepancies between the calculated and the observed displacements along the western side of hypocentral area are, possibly due to lack of the east-dipping fault in the current coseismic slip model. Thus, we have to consider the conjugate fault system proposed by Takada et al. (2009) and Abe et al. (2013) to explain both GNSS and InSAR data.

©2020. Japan Geoscience Union. All Right Reserved.

Keywords: Iwate-Miyagi Niariku Earthquake, Modeling of postseismic deformation

©2020. Japan Geoscience Union. All Right Reserved.

Spatial change of extension direction detected by paleostress analysis in the Miocene Tanabe Group, Southwest Japan

*Noriaki Abe[1], Katsushi Sato[1]

1. Division of Earth and Planetary Science, Graduate School of Science, Kyoto University

Stress state in forearc basin is considered to reflect deformations along the underlying plate boundary fault and of basement such as accretionary prism. Lin et al. (2010) reported spatial difference of stress in the Kumano Basin, present-day forearc basin offshore the Kii Peninsula (Lin et al., 2010). Extension direction is perpendicular to trench near outer-arc high, whereas it becomes perpendicular to subduction direction as distance from outer-arc high increases. The spatial resolution, however, is not enough to reveal whether the difference reflects local deformations or regional stress change related to plate subduction or deformation of basement. Onland paleoforearc basin sediments, as an analog to present basin, are suitable for bring out spatial variety of stress. This study performed a series of paleostress analyses by using outcrop-scale structures in the Miocene Tanabe Group, paleoforearc basin sediments. The study area extends roughly 10 km along the coastal area of the Shirahama Formation, the upper part of the Tanabe Group, the Kii Peninsula, southwest Japan. The measured structures consist of outcrop-scale faults and mineral veins. Fault displacements range from about several mm to 1 m. The thicknesses of veins are about several mm. In total, 159 faults and 245 veins have been observed. They have been analyzed by the stress inversion methods (Sato, 2006; Yamaji and Sato, 2011), which can detect multiple stress conditions from a dataset.
As the result, normal and strike-slip faulting stress regimes were detected. The horizontal extension direction was spatially variable. It trends roughly N-S in southern area, rotates clockwaise and trends E-W in northern area. The change of extension direction is not consistent with the frequency of map-scale faults. Extension normal to the outer-arc high at the southern end of the Kumano Basin can be considerd to reflect rising of outer-arc high. The change of extension direction in the Tanabe Group may be reflect the same tectonics at the pereiod.

References
Lin, W., M. L. Doan, J. C. Moore, L. McNeill, T. B. Byrne, T. Ito, D. Saffer, M. Conin, M. Kinoshita, Y. Sanada and others, 2010, Geophysical Research Letters, 37.
Sato, K., 2006, Tectonophysics, 421, 319-330.
Yamaji, A., Sato, K., 2011, Journal of Structural Geology, 33, 1148-1157.

Keywords: forearc basin, stress analysis, fault-slip analysis, mineral vein

©2020. Japan Geoscience Union. All Right Reserved.

Non-double-couple earthquake in the focal area of the 2000 Western Tottori earthquake by “0.1 manten” hyperdense seismic observation and spatial distribution of non-double-couple components

*Yuto Hayashida[1], Takumi Motokoshi[1], Satoshi Matsumoto[2], Yoshihisa Iio[3], Shin'ichi Sakai[4], Aitaro Kato[4], Group for "0.1 manten" hyperdense seismic observation Group registration

1. Department of Earth and Planetary Sciences, Graduate School of Science, Kyushu University, 2. Institute of Seismology and Volcanology, Faculty of Sciences, Kyushu University , 3. Disaster Prevention Research Institute, Kyoto University, 4. Earthquake Research Institute, University of Tokyo

Non-double-couple (NDC) earthquakes are defined as a faulting of ordinary double-couple (DC) earthquake on a fault associated with additional rupture at the hypocenter. They have been mainly observed in volcanic zones and interpreted as faulting related to fluid effects in the hypocentral region. Study on NDC earthquakes is important for understanding the faulting process and provides an opportunity to obtain new information on stress and strength of the Earth’s crust.

We had installed 1,000 temporary seismic stations in and around the source region of the 2000 Western Tottori Earthquake during the period from April 2017 to April 2018. This observation is called “0.1 manten” hyperdense seismic observation. We determined hypocenters using the data of the seismic network of both the “0.1 manten” and Hi-net by NIED. We manually picked the arrival times and P wave polarities. We found that the observational polarity distribution was slightly different from that expected by a DC source model at certain areas. Especially, we observed positive polarities at the stations where the DC model suggested to be negative polarities on and around the null-axis and nodal planes. In this study, we attempted to estimate the precise moment tensor solution to explain the observed polarity for the NDC event. We adopted the tensile-shear model and searched optimal model by performing a grid search and correlation analysis of S/P wave amplitude ratio.

We revealed that most of the events were modeled as DC earthquake or DC earthquake with an opening crack. In addition, we found the trend that the events with large NDC components were located around the large co-seismic slip zone and the northern part of the aftershock area where we observed a branched fault zone. These results suggest that pressurized fluid or a weak tensile crack might exist along the rupture zone of the Western Tottori earthquake.

Keywords: non-double-couple, the 2000 Western Tottori earthquake, focal mechanism, tensile crack

©2020. Japan Geoscience Union. All Right Reserved.

Driving stress of the 2013 M_w5.8 Awaji Island earthquake, Japan, inferred from well-constrained focal mechanisms and its seismotectonic implication

*Kazutoshi Imanishi[1], Makiko Ohtani[2], Takahiko Uchide[1]

1. Geological Survey of Japan, AIST, 2. Earthquake Research Institute, The University of Tokyo

A driving stress of the 2013 M_w5.8 reverse-faulting Awaji Island earthquake was investigated using well-constrained focal mechanism solutions. The stress tensor inversion and the slip tendency analysis revealed that the stress field within the source region deviates from the surrounding area, in which the stress field locally contains a reverse-faulting component with NNW–SSE compression. This local fluctuation in the stress field is indispensable to produce the reverse-faulting earthquake. The existing knowledge on regional-scale stress (tens to hundreds of km) could not predict the occurrence of the Awaji Island earthquake, emphasizing the importance of estimating local-scale (< tens of km) stress information. We suggest that the local-scale stress heterogeneity has been formed by local tectonic movement, i.e., the formation of flexures in combination with recurring deep aseismic slips. The coseismic Coulomb stress change induced by the disastrous 1995 M_w6.9 Kobe earthquake increased along the fault plane of the Awaji Island earthquake, while the postseismic one was negative. We concluded that the gradual stress buildup due to the interseismic plate locking along the Nankai trough overcame the postseismic stress reduction in a few years, pushing the Awaji Island earthquake fault over its failure threshold in 2013. The observation that the earthquake occurred in response to the interseismic plate locking has an important implication in terms of seismotectonics in southwest Japan, facilitating further research on the causal relation between the inland earthquake activity and the Nankai trough earthquake. Furthermore, this study highlighted that the dataset before the mainshock may not have sufficient information to reflect the stress field in the source region due to the lack of earthquakes in that region, because the earthquake fault is generally locked prior to the mainshock. Further research is needed for estimating the stress field in the vicinity of an earthquake fault via pre-mainshock seismicity alone.

Keywords: 2013 Awaji Island earthquake, stress, seismotectonics

©2020. Japan Geoscience Union. All Right Reserved.

A systematic investigation of rupture directivity, stress drop, fault geometry, and radiation efficiency of small inland earthquakes in Japan

*Keisuke Yoshida[1]

1. Tohoku University

Stress drops of small earthquakes have been estimated under the priori assumption that the rupture propagates symmetrically within a circular fault. However, recent studies have observed directivity effects on seismic waves even for small earthquakes. In this study, the rupture directivity was investigated systematically for small to moderate-sized earthquakes (M 3.5-5.5) beneath inland Japan from 2004 to April 2019. The apparent moment rate functions were determined, and their corner frequencies were inverted using the rupture parameters of 1,463 earthquakes. The results indicate that most of the analyzed earthquakes (1,335 of 1,463) are characterized by a significantly asymmetrical rupture propagation. The rupture tends to propagate to the direction along the fault-strike both for dip-slip and strike-slip earthquakes. The stress drop for the earthquakes were estimated by considering the asymmetrical rupture propagation. The average value of the stress drop is 16.8 MPa, which is almost two times larger than that based on the commonly used symmetrical rupture model. Spatial distribution of stress drop correlates well with the maximum shear strain rate in central and eastern Japan where strain rate probably contributed to the accumulation in the background stress field. Estimated stress drop increases with depth. These observations are consistent with the hypothesis that stress drop reflects the absolute values of shear stress and fault strength.

Keywords: Rupture directivity, stress drop, crustal earthquakes

©2020. Japan Geoscience Union. All Right Reserved.

Modeling Internal Deformation Due to Inelastic Sources Under Inhomogeneous Structures

*Daisuke Sato[1], James Daniel Paul Moore[2]

1. Disaster Prevention Research Institute, Kyoto University, 2. Earth Observatory of Singapore

Available geodetic/seismological data and inelastic crustal deformations such as fault motions, volcano deformation, and asthenospheric deformation have been tied by the modeling of the elastic deformations incurred in the crust (Yabuki & Matsu'ura, 1992; Ide & Takeo, 1997). However, theoretical Green's functions (observation equations) for the inversions of these inelastic sources are currently available only for the simple elastic properties of 1D or homogeneous structures. 3D modeling of the elastic inhomogeneity is already achieved with finite-element and finite-difference methods (e.g., Hashima et al., 2016) but still computationally expensive.

In this study, we present a suite of analytical and semianalytical solutions of Green's functions for the displacements, strains, and stress due to localized (faulting) and distributed (volumetric) inelastic deformation in an elastically inhomogeneous full- and half-space. Variations in elasticity are treated as piecewise constant elastically homogeneous regions. We prove the equivalence between the boundary traction integral equations with those for displacement or volumetric inelastic strain, which have known analytic forms. With this equivalence, we are able to express the traction balance on the boundaries between elastic regions with contrasting elastic parameters, by a corresponding virtual fault displacement or volumetric strain.

We demonstrate this approach with computer programs that evaluate these expressions free of major singular points. These expressions represent a powerful tool for the analysis of deformation data applicable to many primary geophysical applications.

Keywords: faulting and volcano deformations, velocity structure, integral equation methods

©2020. Japan Geoscience Union. All Right Reserved.

Combined inversion technique to determine stress condition and friction coefficient from fault orientation

*Katsushi Sato[1]

1. Division of Earth and Planetary Sciences, Graduate School of Science, Kyoto University

Stress condition and friction coefficient of fault control the brittle deformation in earth's upper crust. Since shear zone materials cannot preserve their physical properties at the time of activation over the geological time scale, it is difficult to estimate the friction coefficients of ancient geological faults.
This study proposes to simultaneously estimate the friction coefficient of faults and the stress condition which activated them by the following procedure. Stress tensor inversion using fault-slip data can calculate principal stress axes and a stress ratio, which allows us to draw a normalized Mohr's circle. Assuming that the faults have a common value of friction coefficient, the frequency of fault orientation is expected to have a peak at the tangential point between the Mohr's circle and the friction envelope and to decrease according to the distance from the envelope. This model was combined with the Wallace-Bott hypothesis that a fault slips along the shear stress vector to compose the objective function of inversion to determine the stress condition and frictional coefficient.
The method was applied to some examples of natural outcrop-scale faults. The first example is from the Pleistocene Kazusa Group, central Japan, which filled a forearc basin of the Sagami Trough. Stress inversion analysis showed WNW-ENE trending tensional stress with a low stress ratio. The friction coefficient was calculated to be about 0.7, which is typical value for sandstone.
Another example is from an underplated tectonic mélange in the Cretaceous to Paleogene Shimanto accretionary complex in southwest Japan along the Nankai Trough. The stress condition was determined to be an axial compression perpendicular to the foliation of shale matrix. The friction coefficient ranges from 0.1 to 0.3, which is extremely low indicating a weak plate boundary under the accretionary wedge.

Keywords: stress tensor inversion, fault-slip analysis, friction coefficient, fault instability

©2020. Japan Geoscience Union. All Right Reserved.

Correlation between physical and hydraulic properties of rock fractures constrained by surface geometry: Digital rock physics approach

*Kazuki Sawayama[1], Takuya ISHIBASHI[2], Fei Jiang[3], Takeshi Tsuji[4], Yasuhiro Fujimitsu[4]

1. Graduate school of engineering, Department of Earth Resources Engineering, Kyushu University, 2. Fukushima Renewable Energy Institute, National Institute of Advanced Industrial Science and Technology, 3. Department of Mechanical Engineering, Faculty of Engineering, Yamaguchi University, 4. Department of Earth Resources Engineering, Faculty of engineering, Kyushu University

Fracture flow and fracture aperture distribution are of great interest to evaluate the mechanism of earthquake and fractured reservoirs. To predict and image the subsurface fluid-flow behavior, geophysical observations, such as seismic and electromagnetic methods, and classical rock physical models have been broadly applied. However, there is no established rock physical model to estimate the fluid-flow behaviors (e.g., permeability) in the fracture from resistivity or elastic wave velocity, and thereby fluid-flow behavior in the fracture are difficult to be precisely interpreted by geophysical data. To reveal the fluid-flow behavior in the fractured zone, we need to establish the rock physical model for the fracture. In this study, to establish the rock physical model which can correlate fracture aperture, fracture permeability, elastic wave velocity and resistivity, we measured and calculated them by using real rock and digitalized rock fractures.

We conducted laboratory fluid-flow test by using fractured Inada granite (50 mm in a diameter, 80 mm in a length) which have single tensile fracture with different roughness. For the numerical model, we digitalized this real rock fracture (0.1 mm grid resolution) to calculate fluid-flow, resistivity and elastic wave velocity under the same condition with experiment. A series of 3D fracture flow simulations was revealed by using Lattice Boltzmann method and we applied finite element analysis to calculate resistivity and elastic wave velocity after this fluid-flow simulation.

As the results of experiments and simulations, we clarify the changes in fracture aperture, fracture permeability, elastic wave velocity and resistivity associated with increasing effective normal stress. Moreover, changes in the permeability and the resistivity were not affected by the roughness, whereas velocity change shows roughness dependency. This roughness dependence of velocity change can be explained by the distribution of asperities. We also correlate the changes in permeability, resistivity and elastic wave velocity. The relationship between permeability and resistivity can be modeled regardless of the roughness, while the relationship between permeability and elastic wave velocity change depend on the roughness. Our results suggest that the resistivity survey is effective for estimating the change in permeability, whereas elastic wave velocity may need to be modeled in consideration of the asperities. As the results of further studies using synthetic fracture, fracture geometry (e.g., asperity) affects these relationships.

Keywords: digital rock physics, elastic wave velocity, resistivity, permeability, fracture flow, Lattice Boltzmann Method

©2020. Japan Geoscience Union. All Right Reserved.

The evolution of cataclastic rocks and their implication on the development of the Median Tectonic Line fault architecture, Japan

*Thomas Jing Yi Yeo[1], Toru Takeshita [1], Wencheng Huang[1]

1. Department of Natural History Sciences, Graduate School of Science, Hokkaido University

The Median Tectonic Line (MTL) is a long-lived crustal scale fault that experienced a long history of movement. Beginning from the Late-Cretaceous period, the MTL has been an active strike slip fault, directly related to the formation of the mylonites in the southern marginal shear zone of the Ryoke granitoid belt (e.g. Hara et al., 1980) and was later superposed by cataclasite at the core region during exhumation. During the early Paleocene (c.60Ma), large scale north dipping normal faulting occurred which led to the juxtaposition of the Ryoke granitoids against the Sanbagawa metamorphic rocks. (Kubota & Takeshita, 2008)

Field observations in the Ryoke granitoids of the MTL fault zone in Mie Prefecture, SW Japan, show that the mylonitic rocks originated from two main protoliths namely tonalite and granite located at the southern and northern part respectively, both of which are extended in the E-W direction (Bui, 2019). We for the first time found that the two bodies were separated by a north dipping normal fault which we named Akaiwadani fault. The granitic body are mainly mylonites with bands of ultramylonites at the proximal region of the Akaiwadani fault. The tonalitic body mainly consists of protomylonite with bands of mesomylonites and also utramylonites at the core region of the MTL.

The purpose of our study is to characterise the types of cataclasites found in the MTL region and relate them to their deformation mechanism and conditions. Methods applied include SEM-EBSD analysis for quartz CPOs, XRD analysis for bulk mineralogy, and image analysis of microstructures were preformed. Analysis done includes shaped preferred orientations (SPOs), clast sizes, orientations, etc.

The cataclasites overprint the core region of both fault zones, evidenced by the occurrence of ultramylonite clasts. The cataclasites can be roughly divided into foliated and non-foliated ones. Non-foliated cataclasites only exist near the fault core of the MTL, whereas foliated cataclasites are found in abundance. All foliated cataclasites have a various degree of alteration to phyllosilicates, potentially indicating the degree of maturity, coinciding with the phyllonites described by Jefferies et. al (2006). XRD results indicate a significant drop in the percentage of K-feldspars in the Akaiwadani fault cataclasites and also a reduction of plagioclase in cataclasites of the MTL core zone. This may be contributed by the enhancement of fluid flow during cataclasis causing albitisation and pressure solution. We also first observed that some of the phyllonites have undergone poly-cataclasis. The SPO of clasts within a poly-cataclasites suggests that the smaller older clast (G_1) is randomly orientated whereas the larger younger clast (G_2) shows a stronger preferred orientation. This implies that the rock experienced multiple cycles of brittle deformation and consolidation during the prolonged fault movement.

Such study holds significance in characterising the spatiotemporal strain distributions in the MTL fault zone in relation to the changes in slip rate of the MTL. Phyllonites are found to formed with the presence of phyllosilicates as a result of pressure solution or alteration associated with the aseismic slip of the MTL. Such mechanism was first described by Spry (1969) as phyllosilicate creep and Niemeijer & Spiers (2005)

©2020. Japan Geoscience Union. All Right Reserved.

stated that phyllosilicate creep occurs with slow slip velocity <0.5 μms^{-1}. Moreover, the poly-cataclasites may potentially indicate the evidences of both generation of earthquake and phyllosilicate creep, which are associated with their respective palaeo-seismic and aseismic slip periods.

References

Hara, et. al, 1980. *Memoirs of the Geol. Soc. Japan* 18, 27–49.
Kubota & Takeshita, 2008. *Island Arc* 17, 129–151.
Bui, 2019. PhD Diss. Hokkaido Uni, Japan.
Jefferies, et. al, 2006. *J Struct Geol* 28, 220–235.
Niemeijer & Spiers, 2005. *Geol. Soc., London* 245, 303–327.
Spry. 1969. *Metamorphic Textures*.

Keywords: Median Tectonic Line, Phyllonites, Poly-cataclasites, Fault Architecture, Ryoke Granitoids, Multiphase deformation

©2020. Japan Geoscience Union. All Right Reserved.

Development history of the mylonite zone distributed along the Mie Prefecture Median Tectonic Line

*Huang Wencheng[1], toru Takeshita[1], Thomas Jing Yi Yeo [1], Jun-Ichi Ando[2]

1. Department of Natural History Sciences, Graduate School of Science, Hokkaido University, 2. Department of Earth and Planetary Systems Science, Graduate School of Science, Hiroshima University

The Median Tectonic Line (MTL) is the longest fault in Japan over 800 km and is an excellent place to study rock deformation. Both the brittle and plastic deformation associated with the fault zone is crucial for the understanding of fault development. A ductile shear zone with sinistral sense was first developed at the end of the Cretaceous period (74-67 Ma, Shimada, et al., 1998) at the north block of the Median Tectonic Line where the Ryoke granite is located. During Early Paleogene (63-58 Ma, Kubota and Takeshita, 2008), it joined together with the Sanbagawa belt located in the southwestern outer zone, forming the current of MTL. In this study, the localization of deformation was described for the plastically deformed Ryoke granites, and their development is also discussed.

In recent years, studies on the plastic deformation of mylonites at the Median tectonic line has been actively conducted. According to Dong (2019), based on the c-axis fabric of quartz microstructure, the mylonites could be categorized as tonalitic protomylonite zone (distance from Median tectonic line, 0-350m), granitic mylonite zone with S-type quartz texture (350-500m) and granitic mylonite zone with P-type quartz texture (500-800m). The definition of the S-type and P-type quartz microstructures are based on Masuda and Fujimura (1981). In the S-type mylonite zone, a Y-maxima c-axis fabric (estimated deformation temperature: 400-500 degrees, e.g. Takeshita, 1996) and a type II cross girdle c-axis fabric(300-400 degrees) was developed. By comparing the mylonite zone with P-type quartz microstructure with the mylonite zone with S-type quartz microstructure, the grain size of quartz grains has been reduced from 140 microns to 20-30 microns, where the quartz grains are becoming finer. In the mylonite zone with a P-type quartz microstructure, only the Y-maximum c-axis fabric develops as it experiences a relatively higher deformational temperature. Based on the above-mentioned results, first, a mylonite zone with a P-type quartz microstructure was formed, and then the deformation stopped at a distance of more than 500 m north of the MTL. The deformation continued at a distance of 350-500 m as the temperature decreased. Thus, a localization model for the deformation that forms the S-type mylonite zone was proposed (Dong, 2019).

In this study, we conducted field surveys and analyzed the microstructure of the Tsukide region over an area of 2km width and 1km north from the MTL. To analyze the deformational characteristics of K-feldspar, the K-feldspars are stained with sodium cobaltinitrite. The following new findings were obtained from the study. (1) The K-feldspar phenocrysts in the mylonite zone with S-type quartz microfabric located at 350-500 m are weakly deformed and not damaged. The K-feldspar is plastically deformed in the mylonite zone with P-type quartz microfabric located at 500-900 m. (2) The K-feldspar in the mylonite zone with S-type quartz microfabric has a smaller grain size, and it was observed to be associated with the development of the EW trending fault. Grain size reduction was seen at the northern block of the fault, but it was not observable in the southern block.

Based on the above results, the following considerations were made on the development of the MTL structure. In the mylonite zone with S-type quartz microfabric, K-feldspar is not altered and maintains the original phenocryst texture, therefore it cannot be fully interpreted by the progressive the deformational

©2020. Japan Geoscience Union. All Right Reserved.

process as proposed by Dong (2019). One of the possible explanations is that the mylonite zones with P-type and S-type quartz microfabric have different source rocks and are formed under different conditions, and they may have been juxtaposed together by the possible presence of faults.

Keywords: Median Tectonic Line, strain localization, mylonite, quartz c-axis fabric pattern, quartz dynamic recrystallization

©2020. Japan Geoscience Union. All Right Reserved.

Extensional stress conditions determined from the orientations of Middle Miocene dikes in the Kumano area

*Toshiki Haji[1,2], Atsushi Yamaji[1]

1. Graduate School of Science, Kyoto University, 2. Institute of Geology and Geoinformation, AIST

We deny the established theory about the compressional stress in the SW Japan arc in the Middle Miocene after 15 Ma that terminated the Japan Sea opening. The orientations of dikes with such ages in the Kumano area, southern Kii Peninsula, are considered to evidence the compression (e.g., Tsunakawa, 1986; Yamamoto, 1991). A few tens of dikes in the area were considered to make a NNW trending parallel dike swarm, and the E-W trending folds of the strata that hosted the dikes were thought of as the evidence for the compression during the dike intrusion. However, it is uncertain when the formation was folded. In addition, previous researchers assumed that dikes were formed more or less perpendicular to the axis of maximum horizontal compression. This is not always true: Overpressured magma can intrude into fractures with various orientations. Consequently, the arguments about the timing of folding and the stress condition for the dike intrusion has been circular.

In the Kumano area, we observed 14 felsic dikes in the Early to early Middle Miocene Kumano Group and 151 mafic dikes in the early Middle Miocene Shionomisaki Igneous Complex. The uppermost part of the group interfingers with the basal part of the complex. The orientations of the dikes were inverted by fitting mixed Bingham distributions (Yamaji and Sato, 2011) to reveal the stress regime during their intrusions. The method determines three principal stress axes, stress ratio and non-dimensional magma pressure only from dike orientations. The method can determine one or a few stresses from non-parallel dikes.

As a result, the normal faulting stress regime with the ENE-WSW trending σ_3-axis and a stress ratio of 0.14 was determined from the felsic dikes. The magma pressure was relatively low. The mafic ones had various trends, but those with NW trends were dominant. The normal faulting stress regime with NE-SW trending σ_3-axis and a stress ratio of 0.50 was determined from the mafic dikes. The magma pressure was relatively high. We obtained the zircon fission-track ages of 14.5 ±1.4 Ma and 13.9 ±1.4 Ma from two felsic dikes. The microfossil and fission-track ages (Ikebe et al., 1975; Hoshi et al., 2003) indicate that both types of dikes intruded from 14.5 to ~13 Ma. Therefore, the area was affected by NE-SW to ENE-WSW extensional stress after 15 Ma. The folding probably postdated the magmatism.

Keywords: fission-track age, tectonic stress, forearc magmatism

©2020. Japan Geoscience Union. All Right Reserved.

Syn-orogenic extrusion of HP-LT blueschists in the northern Tyrrhenian Sea (northern Apennines, Italy)

*Samuele Papeschi[1], Eric Ryan[2], Hans Joachim Massonne[3,4], Giovanni Musumeci[5,6], Francesco Mazzarini[6], Giulio Viola[7]

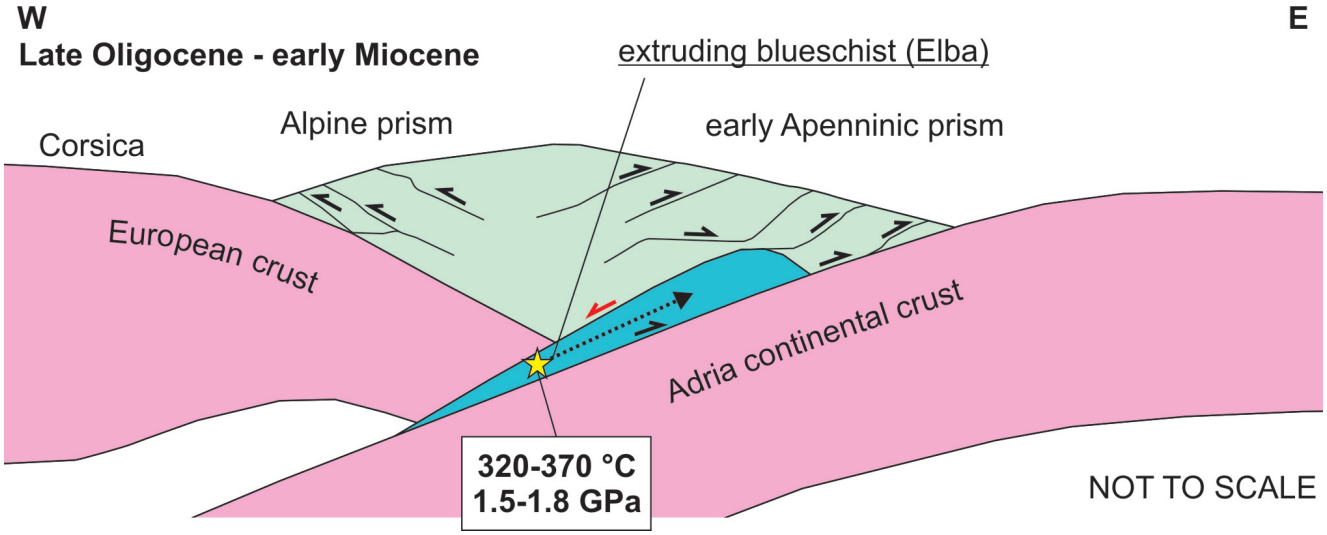
1. Japan Agency for Marine Earth-Science and Technology, Kochi, Japan, 2. Department of Geoscience and Petroleum, Norwegian University of Science and Technology, Trondheim, Norway, 3. School of Earth Sciences, China University of Geosciences, Wuhan, P.R. China, 4. Fakultät Chemie, Universität Stuttgart, Stuttgart, Germany, 5. Dipartimento di Scienze della Terra, Università di Pisa, Pisa, Italy, 6. Istituto Nazionale di Geofisica e Vulcanologia, Pisa, Italy, 7. Dipartimento di Scienze Biologiche, Geologiche e Ambientali, Università di Bologna, Bologna, Italy

High pressure-low temperature (HP-LT) rocks, such as blueschists and eclogites, help us to understand deep processes that shape collisional zones during underplating, accretion, and exhumation. A key question in geoscience is which processes drive the exhumation of deep-seated, underplated rocks. To answer this question, we studied glaucophane- and lawsonite-bearing metabasites, calcschists, and marbles, which are exposed on the Island of Elba (Italy) in the northern Tyrrhenian Sea. These rocks record HP-LT metamorphism, which is related to the Oligocene –Early Miocene continental collision in the northern Apennines. The HP rocks on Elba are characterized by a top-to-the-west mylonitic deformation that is related to their exhumation within a pile of west-dipping and east-verging nappes. Detailed analyses of bulk rock and minerals and phase equilibria modeling of metabasites from Elba constrain peak metamorphic conditions to 1.5-1.8 GPa and 320-370 ˚C and indicate nearly isothermal exhumation to greenschist-facies conditions at 0.2 GPa. During exhumation, peak metamorphic assemblages were overprinted and partially obliterated by epidote-blueschist and, subsequently, albite-greenschist facies metamorphic assemblages. Geochronological data indicate that exhumation occurred over a period of time of 15 Ma between the early Miocene (20-19 Ma) and the late Miocene (6 Ma) with exhumation rates around 2.5-3.7 km/Ma.

Based on this study, we propose that continental units were brought to greater depths than previously reported for the northern Apennines. We show that syn-orogenic extrusion acted as the main exhumation mechanism for continental and oceanic units during early continental collision in this orogenic section.

Keywords: exhumation, extrusion, blueschist, phase equilibria modeling, northern Apennines, Mediterranean Sea

©2020. Japan Geoscience Union. All Right Reserved.



©2020. Japan Geoscience Union. All Right Reserved.

Elastic wave velocities and electrical conductivity in a brine-saturated granitic rock with single fracture

*Tohru Watanabe[1], Arina Tomioka[1]

1. University of Toyama

Geophysical mapping of fluids is critical for understanding crustal processes. Interpretation of seismic velocity and electrical resistivity structures requires a thorough understanding of the pore structure that governs physical properties under high pressures. Watanabe et al. (2019) showed that wide aperture parts in cracks remain open to govern physical properties under high pressure. In the crust, there should be cracks with various sizes: from grain boundary to large faults. In order to understand the role of a fracture as a conduction path under high pressure, we have made measurements of elastic wave velocities and electrical conductivity in a brine-saturated granitic rock with single fracture. A cylindrical rock sample (D=26 mm, L=30 mm) with single fractures was cored from a block (20 cm x 20 cm x 20 cm) of Aji granite from Kagawa Prefecture, which was artificially fractured. The fracture goes through the sample from top to bottom. The sample was filled with 0.1 M KCl aqueous solution, and velocity and conductivity were simultaneously measured by using a 200 MPa hydrostatic pressure vessel. The pore-fluid was electrically insulated from the metal work by using plastic devices. Compressional and shear wave velocities were measured in the direction subperpendicular to the fracture, while electrical conductivity in the axial direction.

A preliminary experiment was conducted up to 40 MPa. Compressional and shear wave velocities increase with increasing confining pressure. At 40 MPa, the compressional wave velocity was almost the same as that in intact Aji granite samples, while the shear wave velocity was significantly lower than that in intact samples. The electrical conductivity at the atmospheric pressure was around one order of magnitude higher than that in intact samples. It greatly decreased from 0.1 MPa to 5 MPa, then showed a gradual decrease to 40 MPa. The conductivity at 40 MPa is also around one order of magnitude higher than that in intact samples. The average aperture of fracture at 40 MPa is estimated to be 2 micro meters. However, the fracture should be segmented under high pressure. X-ray CT observation will be conducted to understand the pore structure under high pressure.

Keywords: seismic velocity, electrical conductivity, fluid

©2020. Japan Geoscience Union. All Right Reserved.

Hydraulic monitoring results during SIMFIP injection experiments through Shionohira fault zones in Fukushima Prefecture, Japan

*Kazuhiro Aoki[1], Hiroshi Wakahama[2], Haruka Nojo[2], Etuo Iwasaki[2], Masao Kametaka[2], Yukumo Tanaka[1], Takumi Yoshida[1], Kazuyoshi Seshimo[1]

1. Japan Atomic Energy Agency, 2. Dia Consultants

The Shionohira fault caused the April 11, 2011 Fukushima ken Hamadori Earthquake of Mw 6.7 which occurred one month after the Tohoku-Oki earthquake of Mw 9.0. Co-seismic surface ruptures trending NNW-SSE allowed to estimate a normal slip faulting with a 2 m maximum displacement. The authors have been conducting a series of studies at the Shionohira fault and its southern extensions in order to develop a fault activity evaluation method.
The fault slip injection tests using a SIMFIP (Step-Rate Injection Method for Fracture In-situ Properties) probe have been performed at the Shionohira and Minakamikita sites (Aoki, et al., 2019 and Watanabe, et al., 2019). This report gives the hydraulic monitoring results obtained from a borehole located about 3m distance from the injection hole during the injection tests conducted at both sites.

In the fault slip injection tests, double packers were placed above and below the underground fracture and high pressure water was injected from the surface to artificially trigger a slip in the fracture in order to measure the three dimensional deformation in micrometer to millimeter units (Guglielmi et al., 2013). Pore pressure was monitored in a monitoring hole located about 3 meters from the injection hole in order to check the continuation of a fracture zone and to obtain hydro-mechanical data.

Significant increase in pore pressure was measured in the intervals of fault fracture zone corresponding to the increase of water inflow at both Shionohira and Minakamikita sites, suggesting that water flow pass had been created from the injection interval to the monitoring boreholes through fracture plane. Backflow of the injected water from the open fracture back into the interval was also observed. Permeability in fault plane will be discussed at the conference.

At Shionohira site, a vertical injection borehole of 30m length was drilled at 7.3m from the top of the fault escarpment (S70W) perpendicular to the strike of Shionohira fault (N20W). A vertical monitoring borehole of 30m length was drilled in the direction of S70W at 7.3m from the top of the fault escarpment perpendicular to the strike of the fault. The distance between the two boreholes was 3.3m running nearly parallel to the fault at N8W. Pore pressure was monitored with a single packer set at depths of GL.-12.20m to GL.-13.20m in the monitoring borehole. Test 1 was conducted between depths 7.0m and 11.5m isolated with upper and lower packers and pressurized above the recently activated fault zone in the unfaulted sandstone layers. Test 2 was conducted between depths 12.8m and 17.3m across the recently activated fault zone. Test 3 was held at depths between 17.0m and 21.4m to assess the ancient fault activation zones in the metamorphic green schist. A significant increase in pore pressure was measured in Test 2.

At Minakamikita site, the target fault has an N-S strike with a dip of 80 degrees to the west. Because of the limitation in study area, injection and monitoring boreholes were drilled at 50 degrees to the east from the surface, of 30m lengths each. The distance between the two boreholes was 3.5m. Pore pressure was monitored with double packers set at depths of GL.-17.0m to GL.-18.0m and GL.-25.0m to GL.-25.9m in the monitoring borehole.

©2020. Japan Geoscience Union. All Right Reserved.

Injection tests were performed at the following four intervals: (1) fracture zone 1 (G.L.-19.75 to -21.70m); (2) fracture zone 2(G.L.-21/65 to -23.60m); (3) sandstone layer G.L.-17.85 to -19.80m); and (4) greenschist (G.L.-23.29 to -25.24m). A significant increase in pore pressure was measured at interval (2).

Keywords: Shionohira fault, SIMFIP experiment, Hydraulic monitoring, Injection experiment

©2020. Japan Geoscience Union. All Right Reserved.

Change in electrical conductivity in a brine-saturated granite under uni-axial compression

*Yui Aikawa[1], Tohru Watanabe[1]

1. University of Toyama

Geophysical observations have shown that fluids exist pervasively within the crust. Fluids fill intergrain cracks (open grain boundaries) and intra-grain cracks at the upper and middle crust conditions. Since the opening of cracks strongly depends on the stress state, electrical conductivity should be anisotropic under a stress state. We have conducted uni-axial compression tests on a brine-saturated granitic rock and studied the change in electrical conductivity in the directions parallel and perpendicular to the compression.

The loading system is composed of a hand press (Maximum load: 20 kN), a load cell and stainless steel end-pieces. A fine grained (100-500 mm) biotite granite (Aji, Kagawa Pref., Japan) was selected as a rock sample for its small grain size and textural uniformity. A cube sample with the edge length of 25 mm was filled with 0.1 M KCl aqueous solution and loaded up to 20 MPa. Electrical impedance was monitored during a compression test with two-electrode method (Ag-AgCl electrodes). Separate compression tests were made for measuring electrical impedance in two directions.

Electrical conductivity decreased with increasing axial stress in the directions parallel and perpendicular to the compression. When the axial stress was increased from 0 MPa to 10 MPa, the magnitude of decrease in conductivity was 5% both in the direction parallel and perpendicular to the compression. The decrease in conductivity was much smaller than that observed in hydrostatic compression tests (e.g., Watanabe and Higuchi, 2015). The decrease in conductivity must be caused by the closure of cracks, which were perpendicular or subperpendicular to the compression. Electrical conduction paths in the direction parallel and perpendicular to the compression are both composed of these cracks. Electrical conductivity in two directions thus shows similar changes. A differential stress will not lead to an anisotropy in electrical conductivity.

Keywords: electrical conductivity, crack, fluid, stress, anisotropy

©2020. Japan Geoscience Union. All Right Reserved.

Grain shape and connevtivity of pores in granular materials

*Katazakai Haruka[1], Tohru Watanabe[1]

1. Toyama University

Connectivity of pores controls transport properties in granular materials and strongly depends on grain shape (Friedman, 2005). When the porosity is identical, electrical conductivity of a brine-filled granular material is significantly higher for spherical grains than for oblate spheroidal grains. However, connectivity of pores in granular materials has not been fully understood. In order to understand the influence of grain shape on the connectivity of pores, we conducted electrical conductivity measurements on brine-filled granular materials. Various types of sand were employed. The structure of pores and grain shape were characterized through analyses of X-ray CT images. Measurements were conducted on granular materials composed of spherical glass beads for comparison. The influence of grain shape on the connectivity of pore will be discussed in our presentation.

Keywords: Pore, Conductivity, Particle shape

©2020. Japan Geoscience Union. All Right Reserved.

Grain shape and pressure sensitivity of transport properties in granular materials

*Maremichi Abe[1], Tohru Watanabe[1]

1. Toyama University

The connectivity of pores is a key factor in controlling transport properties of rocks. Even in porous rocks, it is sensitive to the confining pressure. Electrical conductivity in brine-saturated Berea sandstone (porosity~20%) decreased by ~22% as the confining pressure was increased to 40 MPa, while the pore-fluid pressure was kept at the atmospheric pressure. From the volumetric strain measurement, the change in porosity should be less than 1%. The observed relatively large decrease in conductivity must be caused by a significant reduction of the connectivity of pores under pressure. In order to understand the influence of pressure on the connectivity of pores, we conducted compression tests on granular materials: spherical glass beads and oblate quartz sand. Compressional wave velocity increases with increasing pressure similarly in both materials, while electrical conductivity decreases significantly only in quartz sand. This suggest the important role of grain shape in governing the pressure sensitivity of connectivity of pores. X-ray micro CT images of granular materials impregnated with epoxy resin were analyzed to study the structure of pores. Changes in electrical conductivity under pressure and the structure of pores will be presented for different grain shapes.

Keywords: granular materials, pore, electrical conductivity

©2020. Japan Geoscience Union. All Right Reserved.

[E] Poster | S (Solid Earth Sciences)：S-CG Complex & General

[S-CG64] Crust-mantle connections

convener:Yoshihiko Tamura(Research Institute for Marine Geodynamics, Japan Agency for Maine-Earth Science and Technology), Osamu Ishizuka(Geological Survey of Japan, AIST)

The western portion of the Pacific Plate, the oldest oceanic plate in the world, has been drilled several times and, based on Ocean Drilling Program (ODP) Site 801, an understanding of its layers, from pelagic clay through chert to alkali basalts and tholeiitic mid-ocean ridge basalts (MORB), has been established. This oldest oceanic plate is experiencing a renaissance and we propose a strategy to drill the most suitable three sites to recover specific parts of the plate to continue its renaissance. This submitted IODP preproposal is entitled The Renaissance of the Oldest Oceanic Plate: REY (Rare Earth elements and Yttrium) rich Mud, Radiolarite of Jurassic-Cretaceous Boundary (JKB), and Jurassic Oceanic Crust without Moho. The drilling sites, MM, MAT, and MINA, target (1) the most complete sedimentary sequence of pelagic clay including REY-rich mud, (2) newly found outcrops of the Jurassic-Cretaceous boundary (JKB), and (3) MORB tholeiites without Moho, respectively. This session invite scientists who are interested in these exciting drillings.
It is common knowledge that the Moho is the boundary between the crust and the Earths mantle, discovered by and named after the Croatian seismologist Andrija Mohorovicic. The oceanic Moho is defined by seismic reflection images, but seismic profiles generally show that Moho reflections are not universal. Where the Moho can be detected clearly the crust is thicker. A good example is the profile from Kaneda et al. (2010) near Minami-Tori Shima, which is the main motivation for drilling at Site MINA. The session also seeks to explore the crust-mantle connections among ophiolites, at divergent and convergent plate boundaries and ocean island settings based on petrology, geochemistry, geophysics, geochronology, and geodynamics studies.

[SCG64-P01] Temporal evolution of proto-Izu-Bonin-Mariana arc volcanism over 10 Ma: Constraints from statistical analysis of melt inclusion compositions

★Invited Papers

*Morihisa Hamada[1], Hikaru Iwamori[1,2,3], Philipp A. Brandl[4], Takayuki Ushikubo[1], Kenji Shimizu[1], Motoo Ito[1], He Li[5], Ivan P. Savov[6] (1.Japan Agency for Marine-Earth Science and Technology, 2.Department of Earth and Planetary Sciences, Tokyo Institute of Technology, 3.Earthquake Research Institute, University of Tokyo, 4.GEOMAR Helmholtz Centre for Ocean Research Kiel, 5.Institute of Oceanology, Chinese Academy of Sciences, 6.School of Earth and Environment, University of Leeds)

[SCG64-P02] Evolution of Rear Arc Magmas following backarc basin formation behind the Izu arc: Site U1437, IODP Exp. 350

*Takashi Miyazaki[1], J B Gill[2], C Hamelin[3], S M DeBari[4], Tomoki Sato[1], Yoshihiko Tamura[1], Jun-Ichi Kimura[1], Bogdan Stefanov Vaglarov[1], Qing Chang[1], Ryoko Senda[5], Satoru Haraguchi[6] (1.Research Institute for Marine Geodynamics, Japan Agency for Marine-Earth Science and Technology, 2.University of California, Santa Cruz, 3.University of Bergen, 4.Western Washington University, 5.Kyushu University, 6.University of Tokyo)

[SCG64-P03] The earliest stage of Izu rear-arc volcanism revealed by drilling at Site U1437, IODP Expedition 350

Tomoki Sato[1], Takashi Miyazaki[1], *Yoshihiko Tamura[1], James B Gill[2], Martin Jutzeler[3], Ryoko Senda[4], Jun-Ichi Kimura[1] (1.Research Institute for Marine Geodynamics, Japan Agency for Maine-Earth Science and Technology, 2.Department of Earth and Planetary Science, University of California Santa Cruz, Santa Cruz, California, USA, 3.School of Natural Sciences and Centre for Ore Deposit and Earth Sciences, University of Tasmania, Tasmania, Australia, 4.Faculty of Social and Cultural Studies, Kyushu University, Fukuoka, Japan)

[SCG64-P04] The origin of fertile plagioclase lherzolite in the Upper Zone of the Horoman peridotite complex

★Invited Papers

*Yumeto KOGURE[1], Eiichi TAKAZAWA[1,2] (1.Department of Geology, Faculty of Science, Niigata University, 2.VERC, IMG, JAMSTEC)

[SCG64-P05] Water-saturated solidus and second critical endpoint of peridotite determined by textures and chemistry of the quenched liquid

*Jintuan Wang[1], Eiichi Takahashi[1] (1.Guangzhou Institute of Geochemistry, Chinese Academy of Sciences)

Temporal evolution of proto-Izu-Bonin-Mariana arc volcanism over 10 Ma: Constraints from statistical analysis of melt inclusion compositions

*Morihisa Hamada[1], Hikaru Iwamori[1,2,3], Philipp A. Brandl[4], Takayuki Ushikubo[1], Kenji Shimizu[1], Motoo Ito[1], He Li[5], Ivan P. Savov[6]

1. Japan Agency for Marine-Earth Science and Technology, 2. Department of Earth and Planetary Sciences, Tokyo Institute of Technology, 3. Earthquake Research Institute, University of Tokyo, 4. GEOMAR Helmholtz Centre for Ocean Research Kiel, 5. Institute of Oceanology, Chinese Academy of Sciences, 6. School of Earth and Environment, University of Leeds

International Ocean Discovery Program (IODP) Expedition 351 “Izu–Bonin–Mariana (IBM) Arc Origins” drilled Site U1438, situated in the north-western region of the Philippine Sea. Here volcaniclastic sediments and the igneous basement of the proto-IBM volcanic arc were recovered. To gain a better understanding of the magmatic processes and evolution of the proto-IBM arc, we studied melt inclusions hosted in fresh igneous minerals and sampled from 30- to 40-Ma-old deposits, reflecting the maturation of arc volcanism following subduction initiation at 52 Ma. We performed a novel statistical analysis on the major element composition of 237 representative melt inclusions selected from a previously published dataset, covering the full age range between 30 and 40 Ma. In addition, we analysed volatiles (H_2O, S, F and Cl) and P_2O_5 by Secondary Ion Mass Spectrometry (SIMS) for a subset of 47 melt inclusions selected from the dataset. Based on statistical analysis of the major element composition of melt inclusions and by considering their trace and volatile element compositions, we distinguished five main clusters of melt inclusions, which can be further separated into a total of eight subclusters. Among the eight subclusters, we identified three major magma types: (1) enriched medium-K magmas, which form a tholeiitic trend (30–38 Ma); (2) enriched medium-K magmas, which form a calc-alkaline trend (30–39 Ma); and (3) depleted low-K magmas, which form a calc-alkaline trend (35–40 Ma). We demonstrate that (1) the eruption of depleted low-K calc-alkaline magmas occurred prior to 40 Ma and ceased sharply at 35 Ma; (2) the eruption of depleted low-K calc-alkaline magmas, enriched medium-K calc-alkaline magmas and enriched medium-K tholeiitic magmas overlapped between 35 and 38–39 Ma; and (3) the eruption of enriched medium-K tholeiitic and enriched medium-K calc-alkaline magmas became predominant thereafter at the proto-IBM arc. Identification of three major magma types are distinct from the previous work, in which enriched medium-K calc-alkaline magmas and depleted low-K calc-alkaline magmas were not identified. This indicates the usefulness of our statistical analysis as a powerful tool to partition a mixture of multivariable geochemical datasets, such as the composition of melt inclusions in this case. Our data suggest that a depleted mantle source had been replaced by an enriched mantle source due to convection beneath the proto-IBM arc from >40 to 35 Ma. Finally, thermodynamic modelling indicates that the overall geochemical variation of melt inclusions assigned to each cluster can be broadly reproduced either by crystallisation differentiation assuming P = 50 MPa (about 2-km deep) and 2 wt % H_2O (almost saturated H_2O content at 50 MPa) or P = 300 MPa (about 15-km deep) and ~6 wt % H_2O (almost saturated H_2O content at 300 MPa). Assuming oxygen fugacity (f_{O2}) of log f_{O2} equal to +1 relative to nickel-nickel oxide (NNO) buffer best reproduces the overall geochemical variation of melt inclusions, but assuming a more oxidising conditions (log f_{O2} = +1 to +2 NNO) likely reproduces the geochemical variation of enriched medium-K and calc-alkaline melt inclusions (30–39 Ma).

Keywords: Izu-Bonin-Mariana arc, Volatiles, Melt inclusion, Amami Sankaku Basin, International Ocean DIscovery Program, Statistical analysis

©2020. Japan Geoscience Union. All Right Reserved.

©2020. Japan Geoscience Union. All Right Reserved.

Evolution of Rear Arc Magmas following backarc basin formation behind the Izu arc: Site U1437, IODP Exp. 350

*Takashi Miyazaki[1], J B Gill[2], C Hamelin[3], S M DeBari[4], Tomoki Sato[1], Yoshihiko Tamura[1], Jun-Ichi Kimura[1], Bogdan Stefanov Vaglarov[1], Qing Chang[1], Ryoko Senda[5], Satoru Haraguchi[6]

1. Research Institute for Marine Geodynamics, Japan Agency for Marine-Earth Science and Technology, 2. University of California, Santa Cruz, 3. University of Bergen, 4. Western Washington University, 5. Kyushu University, 6. University of Tokyo

IODP Site U1437 is located in the Izu rear-arc region, at 31.790 N, 139.026 E. The recovered core consists of seven lithologic units. The oldest four (Units IV through Unit VII) that include volcaniclastics and hyaloclastites with coarse lava clasts as well as tuff and lapilli-tuff, and have ages of about 6–15 Ma [1, 2] is focused to investigate the evolution of that mantle soon after Shikoku back arc basin opened between 24-15 Ma. Recent geochemical studies clarified that the previous stage of N-Izu rear arc volcanism was not consistently same to current form [3, 4, 5]. To test and constrain these hypotheses in detail, we investigated the early N-Izu rear-arc magmatism using our new Sr-Nd-Hf-Pb isotope data and the Arc Basalt Simulator v. 4 (ABS4) coded by [6]. Like to the classification of [5], three types of volcaniclastic sediments characterized the Izu reararc at Site 1437 from 15 to 6 Ma, based on our new Sr-Pb-Nd-Hf isotope and trace element ratios. They are RASC (Rear Arc Seamount Chains), Rift, and VF (Volcanic Front)-types. Rift-type sediments dominate from 15 to 9 Ma, and RASC-type from 9 to 6 Ma. Both are from proximal sources. VF-derived sediments are less common and randomly distributed. The models of ABS4 for mafic Unit VII samples show the magma genesis that are similar to those for basalts in the modern rift environment indicating the addition of ~1% of a melt-rich slab component generated at ~125 km to a Philippine Sea Plate ambient mantle that was more depleted than DMM. The magma source and tectonic implications of this evolution will be discussed.
[1] Tamura et al. (2015) Proc. IODP, Exp. 350. [2] Schmitt et al. (2018) Int. Geol. Rev. 60, 956-976. [3] Gill et al. (2018) G3 19, 1217-1243. [4] Sato et al. (2020) Island Arc e12340. [5] Heywood et al. (2020) G3 e2019GC008353. [6] Kimura et al. (2014) Geochem. Geophys. Geosyst. 15, 691-739.

Keywords: Subduction zone, Geochemistry, Izu rear-arc

©2020. Japan Geoscience Union. All Right Reserved.

The earliest stage of Izu rear-arc volcanism revealed by drilling at Site U1437, IODP Expedition 350

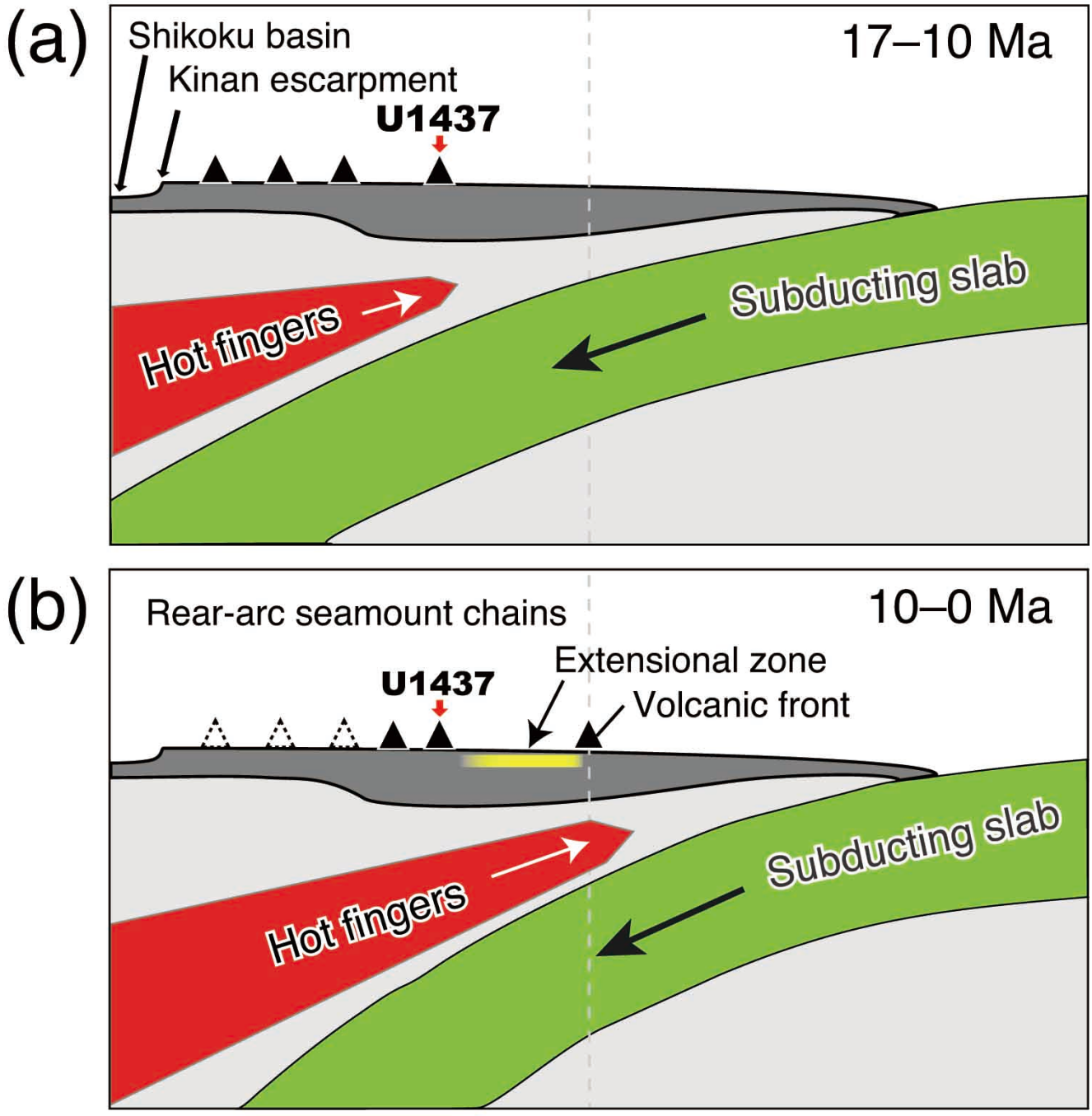
Tomoki Sato[1], Takashi Miyazaki[1], *Yoshihiko Tamura[1], James B Gill[2], Martin Jutzeler[3], Ryoko Senda[4], Jun-Ichi Kimura[1]

1. Research Institute for Marine Geodynamics, Japan Agency for Maine-Earth Science and Technology, 2. Department of Earth and Planetary Science, University of California Santa Cruz, Santa Cruz, California, USA, 3. School of Natural Sciences and Centre for Ore Deposit and Earth Sciences, University of Tasmania, Tasmania, Australia, 4. Faculty of Social and Cultural Studies, Kyushu University, Fukuoka, Japan

International Ocean Discovery Program Expedition 350 drilled between two Izu rear-arc seamount chains at Site U1437 and recovered the first complete succession of rear-arc rocks. The drilling reached 1,806.5 m below seafloor. In-situ hyaloclastites, which had erupted before the rear-arc seamounts came into existence at this site, were recovered in the deepest part of the hole (~15-16 Ma). Here we show that the composition of the oldest rocks recovered do not have rear-arc seamount chain geochemical signatures, but instead show affinities with volcanic front or some of the extensional zone basalts between the present volcanic front and the rear-arc seamount chains. We infer that following the opening of the Shikoku back-arc basin, Site U1437 was a volcanic front or a rifting zone just behind the volcanic front, and was followed at ~9 Ma by the start of rear-arc seamount chains volcanism. This geochemical change records variations in the subduction components with time, which might have followed eastward moving of hot fingers in the mantle wedge and deepening of the subducting slab below Site U1437after the cessation of Shikoku back-arc basin opening.

Keywords: Izu-Ogasawara arc, subduction zone, slab

©2020. Japan Geoscience Union. All Right Reserved.



©2020. Japan Geoscience Union. All Right Reserved.

The origin of fertile plagioclase lherzolite in the Upper Zone of the Horoman peridotite complex

*Yumeto KOGURE[1], Eiichi TAKAZAWA[1,2]

1. Department of Geology, Faculty of Science, Niigata University, 2. VERC, IMG, JAMSTEC

The Horoman periodite complex is a 2,800m thick orogenic lherzolite complex inter-layered along the Hidaka Main Thrust. Although much research has been done on the Horoman complex, the origin of the layered structure is still being discussed. The Upper Zone structurally occupies the upper 800-meter-thick section and has recorded a thermal history about max 200˚C higher than the Lower Zone [1]. In the Horoman peridotite complex, small amounts of mafic layers of a centimeter to a meter thick are often found in peridotites. Relatively thick mafic layers (tens of centimeters to a meter) are thought to have formed as cumulates that crystallized from melts at various depths (i.e., garnet- or plagioclase-stability field) [2] [3]. On the other hand, the plagioclase lherzolite is often accompanied by a thin mafic layer of a few centimeters. Malaviarachchi et al. (2010) [4] concluded that the thin mafic layers alternated with thin peridotites in the Horoman river have been formed from a Pacific-type MORB melt of about 300 Ma. Investigating the origin of the other thin mafic layers is important in studying the layered structure of the Horoman complex. Therefore, we selected a continuous section in the Upper Zone (Fumo section) for this study and examined variations of whole rock major and trace element compositions along lithological sequences.

The Fumo section has a thickness of 263m, which is about one third of the thickness of the Upper Zone and consists of plagioclase lherzolite (51%) and harzburgite (49%) with minor amount of mafic rocks. The lower 190 meters are dominated by plagioclase lherzolite and locally form banding with harzburgites of several centimeters to several meters thick. The upper 73 meters consist of 70 m thick single harzburgite layer and become plagioclase lherzolite at the top. In the Fumo section, 1 to 3 centimeters-thick mafic layer appears locally concentrated in plagioclase lherzolite. Amphibole is included in the mafic layer and its surrounding plagioclase lherzolite, but not in plagioclase lherzolite and harzburgite far from the mafic layers. In many cases, plagioclase and spinel form fine-grained granular seams, whereas in the neighbor of the mafic layer, lenticular shaped plagioclase-rich pools with a thickness of several centimeters are also observed.

The plagioclase lherzolite and harzburgite show a linear trend in the whole rock major elements vs. MgO diagrams, and the mafic layer is plotted on this extension, suggesting the possibility of mixing two end members. Among the plagioclase lherzolites, those with lower MgO and enrichments in melt components such as Al, Ca, Na than DMM [5] are distributed near the mafic layer in the Fumo section. Thus, the melt infiltrated to peridotite to form both mafic layer and fertile plagioclase lherzolite. The presence of amphiboles only in the mafic layer and its surrounding plagioclase lherzolite suggests that the melt forming the mafic layer may have been a hydrous melt.

On the other hand, plagioclase lherzolites, which are located far from the mafic layer in the Fumo section, have composition similar to DMM or more depleted in melt components. They may have the original composition of peridotite before the intrusion of mafic layer-forming melt. The plagioclase lherzolites near the boundary with harzburgite is depleted in melt components relative to other plagioclace lherzolites, and their composition is comparable to that of the lower zone lherzolite. Since the Upper Zone has a higher temperature history than the Lower Zone, it indicates that the subsolidus reaction in which spinel,

©2020. Japan Geoscience Union. All Right Reserved.

Opx and Cpx become plagioclase and olivine was promoted in the Upper Zone even with the same composition. This suggests that there were two different origins of plagioclase in the Upper Zone.

[1]Ozawa, 2004, J. *Petrol.*, **45**, 253-273.
[2] Shiotani and Niida, 1997, *Memoir. Geol. Soc. Japan.*, **47**, 123–137.
[3] Takazawa et al., 1999, *J. Petrol.*, **40**, 1827-1851.
[4] Malaviarachchi et al., 2010, *J. Petrol.*, **51**, 1417-1445.
[5] Workman and Hart, 2005, *Earth Planet. Sci. Lett.*, **231**, 53-72.

Keywords: Horoman Peridotite, mantle, mafic layer, orogenic lherzolite, Hidaka Metamorphic Belt

©2020. Japan Geoscience Union. All Right Reserved.

Water-saturated solidus and second critical endpoint of peridotite determined by textures and chemistry of the quenched liquid

*Jintuan Wang[1], Eiichi Takahashi[1]

1. Guangzhou Institute of Geochemistry, Chinese Academy of Sciences

Water-saturated (‘wet’) solidus of mantle peridotite defines the initial melting temperature of Earth’s mantle under water-saturated conditions and the second critical endpoint (SCEP) marks the end of the wet solidus. However, the location of the wet solidus remains an outstanding issue for over 50 years and the position of the SCEP is hotly debated. Published wet solidus shows a difference of 200–600˚C at given pressures, meanwhile, reported SCEP ranges from < 4 to > 6 GPa. Using a large-volume multi-anvil apparatus SAKURA-2500 at Guangzhou Institute of Geochemistry, we investigated the water-saturated melting behavior of a fertile peridotite (at 3–6 GPa, 950–1200 ˚C) and obtained well-preserved quenched liquid. Based on the texture and chemistry of the quenched liquid, we successfully determined the wet solidus and the SCEP of peridotite (Fig A, bold red curve). Experiments were carried out with 25mm edge MgO octahedron (25M) with $LaCrO_3$ heater of 9mm OD and 6mm ID. Staring material was a mixture of glass and $Mg(OH)_2$ with the bulk chemical composition equivalent to a fertile peridotite KLB-1 + 10 wt% H_2O.

At 3 GPa, the quenched fluids exhibit fragile fibres at 950 ℃ and spherule–fibre mixtures at > 1000 ℃ (Fig. B&C). While the quenched hydrous melt appears as a felt-like mass or as dendritic crystallites and coexists with the fluids (Fig. C). We interpreted the presence of spherule–fibre mixtures as evidence for aqueous fluid above the solidus and fragile fibres as evidence for aqueous fluid below the solidus. Thus, the occurrence of quenched melt and spherule–fibre mixtures indicate that the wet solidus lies between 950 and 1000 ℃ at 3 GPa and that 3 GPa is lower than the critical pressure. The most important textural difference between the run products at 3 GPa and those at other pressures (4 and 6 GPa) is the presence of aqueous fluids in the former (Fig. B&C) and the absence of which in the latter (Fig. D&E). The spherule–fibre mixtures were not found in the 4 and 6 GPa run products. Liquids quenched from 4 and 6 GPa run products are homogeneous (SCF supercritical fluid), suggesting that Pc is lower than 4 GPa.

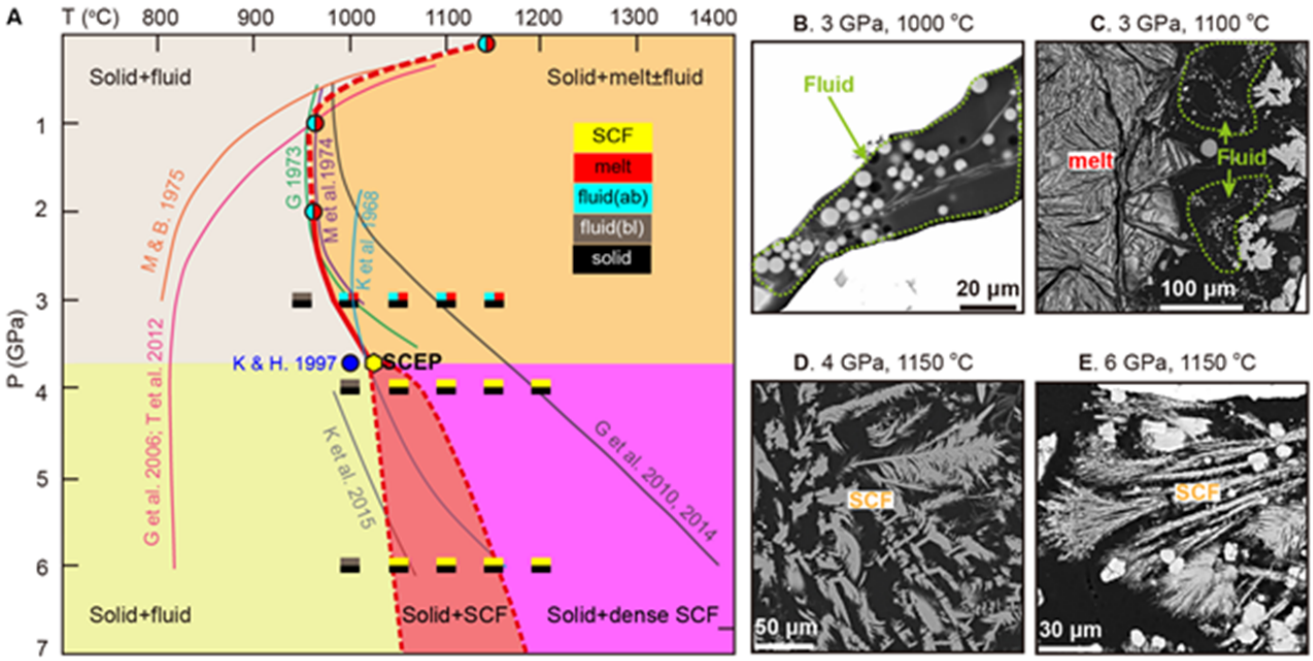
Compositions of the liquids were analyzed by averaging broad area using EDS. We find that the liquid compositions become more deficient in silica and richer in olivine components with increasing pressures. In conjunction with previous studies, the compositions of silicate melts or SCFs change regularly with pressure: andesitic at 1 GPa, boninite-like at 3 GPa, picritic at 4 GPa, and kimberlite-like at pressures > 5 GPa. These results propose that ultra-basic magmas can be formed in subduction zones at low temperatures, high pressure, and H_2O rich conditions. On the basis of present experiments and detailed observation on the cross section of north Japan based on seismology and petrology, we propose a new magma genesis model in subduction zone (Takahashi & Wang, JpGU2020, S-CG64).

Reference:

The water-saturated solidus and second critical endpoint of peridotite: Implications for magma genesis within the mantle wedge, Jintuan Wang, Eiichi Takahashi, Xiaolin Xiong, Linli Chen, Li Li, Toshihiro Suzuki and Michael Walter (2020) J. Geophys. Res.: Solid Earth, Vol.125, in press.

©2020. Japan Geoscience Union. All Right Reserved.

Keywords: wet solidus, peridotite, second critical endpoint



©2020. Japan Geoscience Union. All Right Reserved.

[E] Poster | B (Biogeosciences)：B-BC Biogeochemistry

[B-BC03] Earth and Planetary Science Frontiers for Life and Global Environment

convener:Yoshinori Takano(Japan Agency for Marine-Earth Science and Technology (JAMSTEC)), Yohey Suzuki(Graduate School of Science, The University of Tokyo), Shingo Kato(RIKEN), Keisuke Fukushi(Institute of Nature & Environmental Technology, Kanazawa University)

Earth and planetary science is currently capable of sampling from three frontiers: space, deep ocean and deep underground for the study of the origin and evolution of life. Next generation sequencing technology of nucleic acids and nanotechnology driven innovation of solid characterizations are very powerful to expand our understanding of many fields of earth and planetary sciences. It is also important for us to be aware of global warming and climate change that dramatically affect biodiversity, biological activities and elemental cycling. The aim of this session is to cross the border of science sections to explore the frontiers of earth and planetary science.

[BBC03-P01] Radiocarbon and noble gas isotope study to constrain origin of methane in Hakuba Happo serpentinite-hosted hot spring

*Konomi Suda[1], Takahiro AZE[2], Yosuke Miyairi[1], Yusuke Yokoyama[2], Yohei Matsui[2,3], Hisahiro Ueda[3], Takuya Saito[3], Tomohiko Sato[4], Yusuke Sawaki[2], Ryosuke Nakai[1], Hideyuki Tamaki[1], Hiroshi A Takahashi[1], Noritoshi Morikawa[1] (1.National Institute of Advanced Industrial Science and Technology, 2.The University of Tokyo, 3.Japan Agency for Marine-Earth Science and Technology, 4.Tokyo Institute of Technology)

[BBC03-P02] Deep Microbial Colonization in Saponite-Bearing Fractures in Aged Basaltic Crust: Implications for Subsurface Life on Mars

*Yuri Sueoka[1], Seiya Yamashita[1], Mariko Kouduka[1], Yohey Suzuki[1] (1.Graduate School of Science, The University of Tokyo)

[BBC03-P03] Trace element chemistry of deep-sea corals from different oceanic regions

*Kazuko Saruwatari[1], Makoto Miura[1], Nozomu Iwasaki[2] (1.GIA Tokyo Godo Kaisha, 2.Rissho University)

[BBC03-P04] Verification of ice-mineralization process: formation of authigenic carbonates in alkaline lakes during freezing condition in south Mongolia.

*TAKUMA KITAJIMA[1], Keisuke Fukushi[2,1], Baasansuren Gankhurel[1], Yasuhito Sekine[4], Masahiro Yoda[3,4], Davaadorj Davaasuren[5] (1.kanazawa university, 2.Institute of Nature and Environmental Technology Kanazawa University, 3.the university of Tokyo, 4.Earth-Life Science Institute, 5.National University of Mongolia)

[BBC03-P05] The rediscovery of diversity of archaeol derivative in halophilic archaea especially living in high salt concentration

*Noriaki YAMAUCHI[1] (1.Department of Earth and Planetary Sciences, Faculty of Sciences, Kyushu University)

[BBC03-P06] China's terrestrial ecosystem carbon balance during the 20th century: An analysis with a process-based biogeochemistry model

*Yanyu Lu[1], Wei Sun[2], Dongyan He[1], Hanqing Deng[1], Hong Tian[1], Biwen Wu[1] (1.Anhui Climate Center, Anhui Meteorological Administration, 2.Anhui Public Meteorological Service Center, Anhui Meteorological Administration)

[BBC03-P07] Adsorption behavior of molybdenum on ferrihydrite :dynamics analysis of Mo in Erdenet river, Mongolia

*Akihiro Okuyama[1], Solongo Tsetsgee[1], Keisuke Fukushi[2] (1.Kanazawa University , 2.Institute of Nature and Environmental Technology)

[BBC03-P08] Genomic and geochemical characterization of antimony-reducing microbial consortium obtained from mine tailing soil

*Okubo Tomotaka[1], Daisuke Yamashita[1], Hiroyuki Kashima[2], Satoshi Mitsunobu[3], Natsuko Hamamura[1]
(1.Kyushu University , 2.JAMSTEC, 3.Ehime University)

Radiocarbon and noble gas isotope study to constrain origin of methane in Hakuba Happo serpentinite-hosted hot spring

*Konomi Suda[1], Takahiro AZE[2], Yosuke Miyairi[1], Yusuke Yokoyama[2], Yohei Matsui[2,3], Hisahiro Ueda[3], Takuya Saito[3], Tomohiko Sato[4], Yusuke Sawaki[2], Ryosuke Nakai[1], Hideyuki Tamaki[1], Hiroshi A Takahashi[1], Noritoshi Morikawa[1]

1. National Institute of Advanced Industrial Science and Technology, 2. The University of Tokyo, 3. Japan Agency for Marine-Earth Science and Technology, 4. Tokyo Institute of Technology

Serpentinite-hosted systems attract more interest from the perspective of studying the origin of life. High concentrations of methane (CH_4) and higher hydrocarbons (C_{2+}) are commonly observed in serpentinite-hosted systems (e.g., Schrenk et al., 2013; Etiope and Sherwood-Lollar, 2013). Previous studies have suggested that stable hydrogen and carbon isotopic compositions of hydrocarbons are compatible with abiotic formation via polymerization process (Proskurowski et al., 2008; Suda et al., 2017). However, little is known about when and where the hydrocarbon synthesis occurs. Our purpose is to constrain both the time and place for methane production by analyzing radiocarbon isotope (^{14}C) and noble gas isotopes (^{3}He, ^{4}He, ^{20}Ne) in the serpentinite-hosted hot spring in Hakuba Happo, Japan. Hakuba Happo hot spring lies on a serpentinized ultramafic rock body in the Shiroumadake area, which belongs to the Hida Marginal Tectonic Belt in central Japan. Hyperalkaline hot spring water (ca. 50˚C, pH = 10.6) rich in H_2 and CH_4 gas is pumped from two borehole wells; Happo #1 and Happo #3 (Homma and Tsukahara, 2008; Suda et al., 2014). Sample collection was conducted between 2015 and 2018. In the same manner as Suda et al. (2017), gas and water samples were obtained from two borehole wells. Pipe-scale carbonate samples of the Happo #1 borehole well were collected at the timing of when the old water-pumping pipes were replaced with new pipes in 2016. For the ^{14}C measurements of CH_4, a sample preparation step of CH_4 combustion to CO_2 was conducted at JAMSTEC by using the custom-built flow-through vacuum line system, which was based on Pack et al. (2015). Radiocarbon contents of purified CO_2 samples were determined at the University of Tokyo by using the graphitization system (Yokoyama et al., 2007) and the Accelerator Mass Spectrometry (AMS). The sample preparation and ^{14}C-AMS measurement for carbonate samples were conducted at the University of Tokyo by using an automated sample preparation system, which is composed of an elemental analyzer and a glass vacuum line based on Kato et al. (2014). Noble gas isotope abundances were measured with a noble gas mass spectrometer at GSJ, AIST. The concentration of dissolved inorganic carbon (DIC) in spring water was measured by using GasBench/IRMS system at GSJ, AIST.

We found that ^{14}C contents in CH_4 were close to the detectable limit, whereas pipe-scale carbonates which precipitated from hot spring water contained the detectable ^{14}C. Radiocarbon evidence rules out a modern carbon (e.g., atmospheric CO_2, organics in surface soil) as the carbon source for CH_4, suggesting that Hakuba Happo CH_4 is derived from old carbon source in deep crust or mantle. In Hakuba Happo hot spring, CO and CO_2 were below detection limit (<0.0005 vol.%). DIC concentration was <28 μmol/L (upper values because of suspicion of air contamination during sampling), which was lower than dissolved CH_4 concentration (124-664 μmol/L; Suda et al., 2014). If CH_4 production occurs under on-site condition, the inorganic carbon compounds (CO, CO_2 and DIC) are not likely to be a carbon source for CH_4. The high helium isotope ratio ($^{3}He/^{4}He$) was observed in both well sites, indicating that a major portion of He is mantle derived. In Shiroumadake area, the $^{3}He/^{4}He$ ratios tend to decrease with distance from Norikura Volcanic Chain, suggesting volcanic gases are dissolved in groundwater and then brought to surrounding hot spring. The $CH_4/^{3}He$ ratios of Hakuba Happo samples were one order of magnitude higher than those of other hot springs which are not directly related to serpentinite rocks. Exceptionally

©2020. Japan Geoscience Union. All Right Reserved.

high $CH_4/^3He$ ratio can not be explained by simple influx of mantle-derived CH_4. Another CH_4 source different from mantle-CH_4 may be required. Based on the ^{14}C and noble gas results, we suggest that a major portion of CH_4 at Hakuba Happo is produced in deep crust rather than shallow and modern groundwater.

Keywords: Serprntinite, hyperalkaline hot spring, methane, radiocarbon, noble gas isotope

©2020. Japan Geoscience Union. All Right Reserved.

Deep Microbial Colonization in Saponite-Bearing Fractures in Aged Basaltic Crust: Implications for Subsurface Life on Mars

*Yuri Sueoka[1], Seiya Yamashita[1], Mariko Kouduka[1], Yohey Suzuki[1]

1. Graduate School of Science, The University of Tokyo

One of the most promising planetary bodies that might harbor extraterrestrial life is Mars, given the presence of liquid water in the deep subsurface. The upper crust of Mars is mainly composed of > 3.7-billion-year-old basaltic lava where heat-driven fluid circulation is negligible. Earth’ s oceanic crust composed of basaltic lava is recognized as the analogous crustal environment to the Martian subsurface. The basaltic crust tends to cool down for 10–20-million-years after formation. However, microbial life in old cold basaltic lava is unknown in large part even in the Earth’ s oceanic crust, because of the lack of vigorous circulation preventing sampling of pristine crustal fluid from boreholes. Alternatively, investigation of deep microbial life using pristine drill cores obtained from basaltic lava is important. We investigated a basaltic rock core sample with mineral-filled fractures drilled during Integral Ocean Drilling Project Expedition 329 that targeted 104-million-year-old oceanic crust. It was revealed that fractures/veins were filled with Mg-rich smectite called saponite and calcium carbonate by mineralogical characterizations of fracture-infilling minerals. The organic carbon content from the saponite-rich clay fraction in the core sample was 23 times higher than that from the bulk counterpart, which appears to be sufficient to supply energy and carbon sources to saponite-hosted life. Furthermore, our method developed newly to detect microbial cells in a thin-section of the saponite-bearing fracture revealed the dense colonization of SYBR-Green-I stained microbial cells spatially associated with saponite. These results imply that the presence of saponite in old cold basaltic crust is favorable for microbial life. In addition to carbonaceous chondrite, saponite is a common product of low-temperature reactions between water and mafic minerals on Earth and Mars. Therefore, it is expected that deep saponite-bearing fractures could host extant life and/or the past life on Mars.

Keywords: water-rock interactions, Fe, Mg-smectite

©2020. Japan Geoscience Union. All Right Reserved.

Trace element chemistry of deep-sea corals from different oceanic regions

*Kazuko Saruwatari[1], Makoto Miura[1], Nozomu Iwasaki[2]

1. GIA Tokyo Godo Kaisha, 2. Rissho University

Deep-sea corals belong to Octocorallia subclass animal known to live up to 1500 meters depth, which is different from reef corals of Hexacorallia subclass living near shallow oceans. Mineralogically, these corals are high magnesium calcite containing about 10% magnesium. Red-pink-white corals among them are, especially, called as precious corals and organic gemstones. Its major habitats are the eastern Atlantic Ocean from the Mediterranean to Africa, the western Pacific Ocean from Japan and Vietnam, and the North Pacific Ocean from Midway to Hawaii. The trace element composition of these three deep sea corals is analyzed by Laser Ablation Inductively Coupled Plasma Mass Spectrometry (LA-ICP-MS). As a result similar to previous studies (1-2), differences in lead and barium concentrations were observed, suggesting that they correlate with the seawater composition of the habitat.

1) Hasegawa et al. (2012) Trace elements in Corallium spp. as indicators for origin and habitat, Journal of Experimental Marine Biology and Ecology

2) Vielzeuf et al. (2018) Growth kinetics and distribution of trace elements in precious corals. Frontiers in Earth Science.

Keywords: deep-sea coral, trace element chemical composition, LA-ICP-MS

©2020. Japan Geoscience Union. All Right Reserved.

Verification of ice-mineralization process: formation of authigenic carbonates in alkaline lakes during freezing condition in south Mongolia.

*TAKUMA KITAJIMA[1], Keisuke Fukushi[2,1], Baasansuren Gankhurel[1], Yasuhito Sekine[4], Masahiro Yoda[3,4], Davaadorj Davaasuren[5]

1. kanazawa university, 2. Institute of Nature and Environmental Technology Kanazawa University, 3. the university of Tokyo, 4. Earth-Life Science Institute, 5. National University of Mongolia

Alkaline lakes have functions of absorption of atmospheric CO_2 to natural water and fixation of dissolved carbonate by mineralization. Therefore, it has been considered that alkaline lakes located in arid area inside the continents play important roles in carbon cycle on the earth surface (Finley et al., 2015; Fukushi and Matsumiya, 2018). Generally, formation of carbonate minerals was caused by evaporation of lake water under dry environment. However, alkaline lakes in cold inland area are frozen in winter. Frozen lakes cannot evaporate because it is isolated from the air.

Freezing of lake water causes the increase of the ion concentrations because almost most of the ions are excluded from ice to solution. Inland closed lakes don’ t have inflow and outflow rivers of which situation is almost same with evaporation. Therefore, the mineralization can be also caused by freezing process.

In this study, we have examined “ice-mineralization” process in the alkaline lakes from the observations of water chemistry from summer to winter in Mongolia.

Keywords: carbonate, alkaline lake, mineralization

©2020. Japan Geoscience Union. All Right Reserved.

The rediscovery of diversity of archaeol derivative in halophilic archaea especially living in high salt concentration

*Noriaki YAMAUCHI[1]

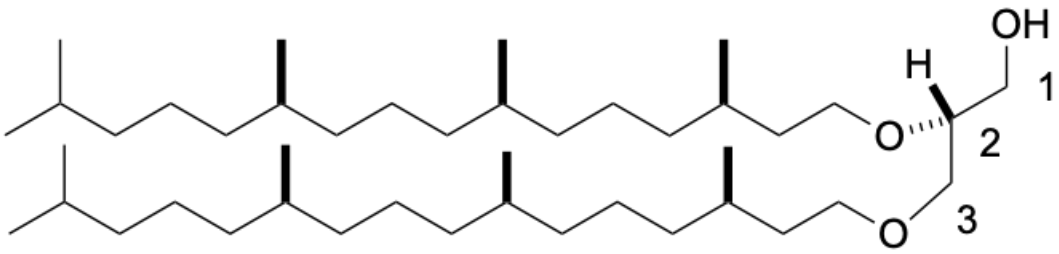
1. Department of Earth and Planetary Sciences, Faculty of Sciences, Kyushu University

Archaea has a characteristic lipid-core, archaeol(**1**). Further, a characteristic diether lipid-core (C_{20}-C_{25} diether (**2**), extended archaeol) which is constructed from one C_{25} and one C_{20} isoprenoid is produced by halophilic archaea[1]. Recently, Dawson et al. showed the existence of several unsaturated isoprenoid diethers in the lipid-core of several halophilic archaea isolated from very high salt concentration[2]. On the other hands, existence of regioisomer **3** were shown in halite from Spain[3].
In my study, chemically synthesized unsaturated diether were different from those of Dawson’s unsaturated diether, the existence of the regioisomeric mixture were strongly suggested[4]. And the chemical synthesis of **2** and **3** revealed diether in halite is the mixture of **2** and **3**[5].
Until now, **2** have been the only isomer from a cultured microorganic origin. On the other hand, **2** and **3** were existed in halite. Further, the comparison of chemical synthetic unsaturated diether and microorganic samples, diversity of unsaturation in archaeol and extended archaeol were observed in perliminary study. The search of **3**, and the analysis of diversity of unsaturation of archaeol and extended archaeol were conducted in each microorganisms, the halophilic archaea especially living in a high salt concentration. The comprehensive analysis of lipid core obtained from the type cultures in Riken BRC, isolated from high salt concentration field, or from halite were incubated, and the lipid-core analysis were executed. The progress of this study is presented.
About the the preparation of lipid core, alkaline hydrolysis of polar head group used by the preparation ofhydroxyarchaeol[6] were adopted instead of acid hydrolysis usually performed. Thus, the divirsity of unsaturtion of archaeol derivative in each halophilic archaea species. And the exsitence of extended archaeol isomer **3** from the *Halorhabus utahensis* (JCM 11049) with its unsaturated derivative were proved. So far, the archaeol derivative were only discussed in **1**, **2** and its unsatutaed isomers. However, the relatively large diversity in each species in extremely halophilic archaea exists. Further studies from the comprehensive analysis is in progress.

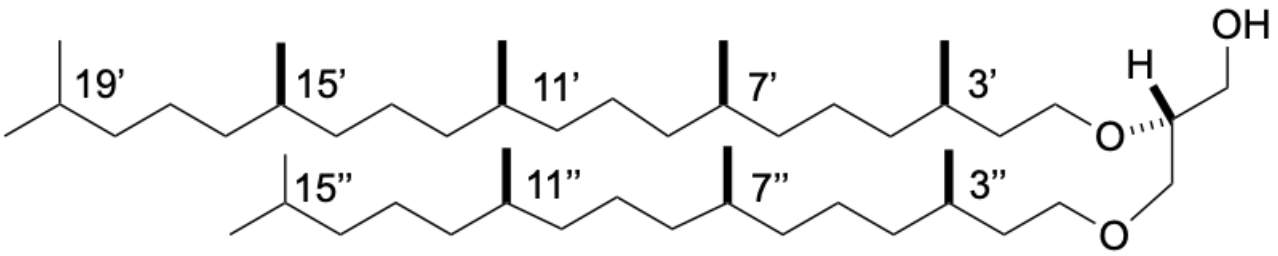
[1] De Rosa et al., J. Gen Microbiol (1982) 265: 343. [2] Dawson et al., Org Geochem (1982) 48: 1. [3] Teixidor *et al.,* Geochem Cosmochim Acta (1993) 57: 4479. [4] Yamauchi, Res Org Geochem (2019) 35: 1. [5] Yamauchi, (2019) JpGU meeting 2019, BBG02-P03. [6] Sprott et al., J Biol Chem (1990) 265: 13735.

Keywords: halophilic archaea, archaeol, diversity, ether lipid

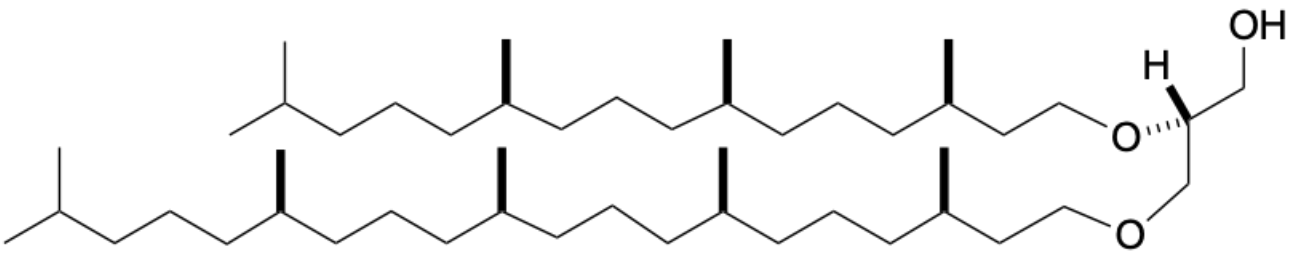
©2020. Japan Geoscience Union. All Right Reserved.



1



2



3

©2020. Japan Geoscience Union. All Right Reserved.

China’s terrestrial ecosystem carbon balance during the 20th century: An analysis with a process-based biogeochemistry model

*Yanyu Lu[1], Wei Sun[2], Dongyan He[1], Hanqing Deng[1], Hong Tian[1], Biwen Wu[1]

1. Anhui Climate Center, Anhui Meteorological Administration, 2. Anhui Public Meteorological Service Center, Anhui Meteorological Administration

China’s terrestrial ecosystems play a pronounced role in the global carbon cycle. Here we combine spatially-explicit information on vegetation, soil, topography, climate and land use change with a process-based biogeochemistry model to quantify the responses of terrestrial carbon cycle in China during the 20th century. We find that that the regional soil thermal and moisture regimes have dramatically changed. Specifically, evapotranspiration increased due to rising temperature and soils were drying in the last two decades of the 20th century. At a century scale, China’s terrestrial ecosystems have acted as a carbon sink averaging at 0.09 Pg C yr^{-1}, with large inter-annual and decadal variabilities. The regional sink has been enhanced due to the rising temperature and CO_2 concentration, with a slight increase trend in carbon sink strength along with the enhanced net primary production in the century. Meanwhile, the heterotrophic respiration increased in response to warming. The spatial and temporal variabilities of carbon balance in China are due to multiple controlling factors including temperature and precipitation and changing atmospheric CO_2 concentrations. Land-use changes including reforestation and afforestation during the late 20th century partially contributed to the increase in carbon sink at the national scale.

Keywords: China, Terrestrial Ecosystem Model, Carbon cycle, Climate change, Land use, Hu Huanyong line

©2020. Japan Geoscience Union. All Right Reserved.

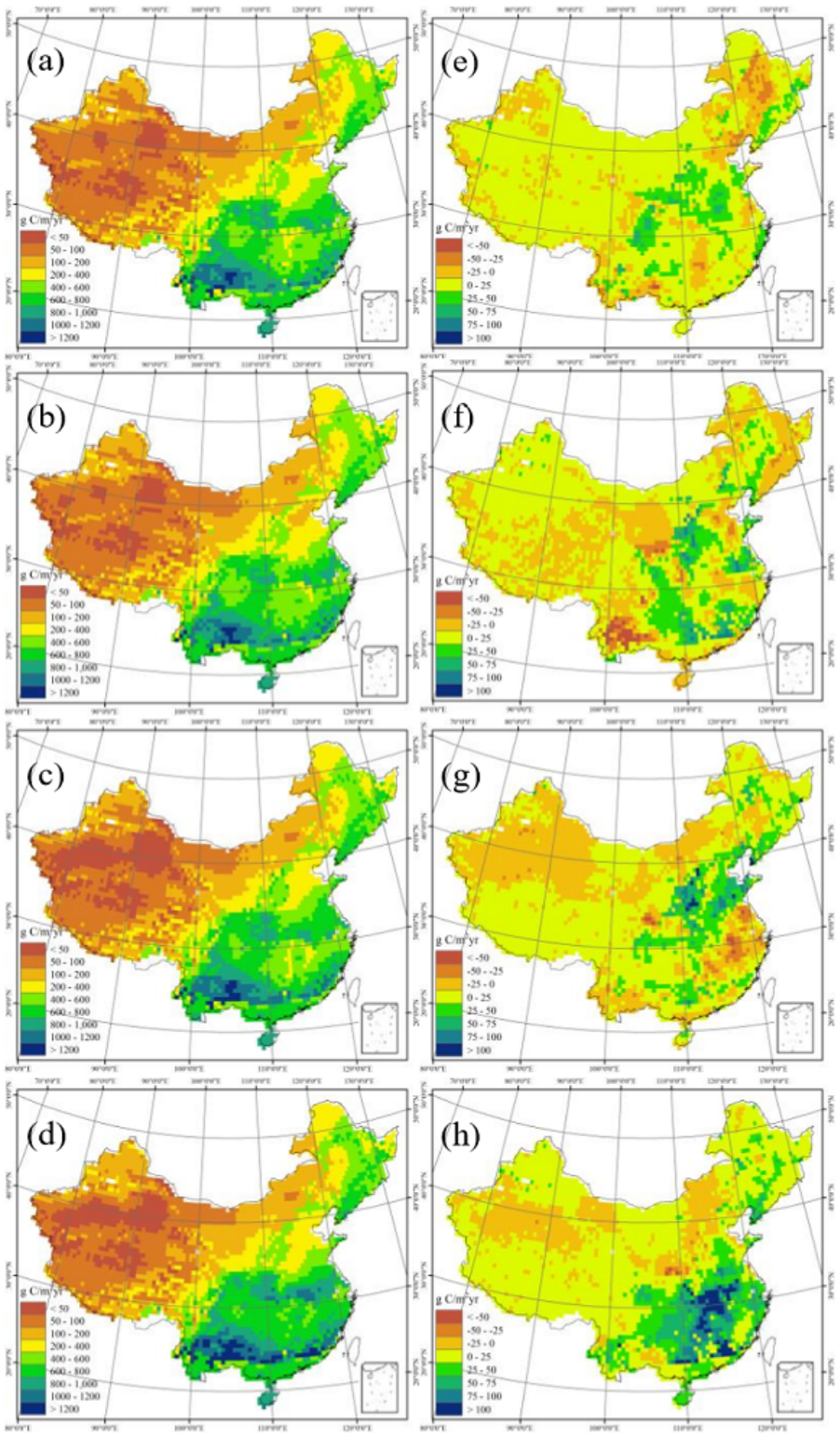


Figure. Spatial patterns of annual net primary production (NPP, a ~ d) and net ecosystem production (NEP, e ~ h) during the1900s (a, e), 1930s (b, f), 1960s (c, g), and 1990s (d, h) in China.

©2020. Japan Geoscience Union. All Right Reserved.

Adsorption behavior of molybdenum on ferrihydrite :dynamics analysis of Mo in Erdenet river, Mongolia

*Akihiro Okuyama[1], Solongo Tsetsgee[1], Keisuke Fukushi[2]

1. Kanazawa University , 2. Institute of Nature and Environmental Technology

Changes of molybdenum concentration in rivers in the Erdenet region of Mongolia may be caused by the adsorption and desorption reactions of molybdenum on ferrihydrite. In this study, we conducted molybdenum adsorption experiments on ferrihydrite and constructed the predictive model which can predict the adsorption behaviors of molybdenum by surface complex modeling. The result of the adsorption experiment showed that the adsorption was almost complete up to pH 7 at acidic condition, but desorption over pH 7, and almost completely desorbed at pH 10. The adsorption data was parameterized using an extended triple layer model, a submodel of surface complex modeling. We used one outer sphere complex ($>SOH_2^+_HMoO_4^-$) and two inner sphere complexes ($>S(OH)_2MoO_3(H_2O)$, $>S(OH)_2MoO_3OH^-$). These complexes were consistent with spectroscopic results of molybdenum adsorption on ferrihydrite. The distribution coefficient K_d was calculated to compare with the measured value observed in the river-sediment system in Erdenet area. The comparison showed that the trends of the change of the observation can be captured by the theoretical model. This study suggests that the environmental behavior of molybdenum in rivers in the Erdenet region may be affected by the adsorption/desorption of molybdenum by ferrihydrite.

Keywords: molybdenum, ferrihydrite, surface complexation modeling

©2020. Japan Geoscience Union. All Right Reserved.

Genomic and geochemical characterization of antimony-reducing microbial consortium obtained from mine tailing soil

*Okubo Tomotaka[1], Daisuke Yamashita[1], Hiroyuki Kashima[2], Satoshi Mitsunobu[3], Natsuko Hamamura[1]

1. Kyushu University , 2. JAMSTEC, 3. Ehime University

Antimony (Sb) is a naturally occurring toxic element. Although the concentrations of Sb in soils are generally low, elevated levels of Sb have been released via mining and other anthropogenic activities. Antimony is commonly associated with arsenic (As) in the polluted environments, and both elements have similar chemistry and toxicity. Antimony and arsenic are mainly found in two oxidation states, trivalent (III) and pentavalent (V). The pentavalent form, Sb(V), is the stable species over a wide redox range and is often found to be strongly adsorbed with hydrous Fe(III) oxide in natural soils.
Although we have just began to unveil the full diversity of microbial-Sb interactions, microorganisms are likely to play important roles in Sb redox transformations in the environment. Recently, we have obtained various bacterial isolates and enrichment cultures capable of Sb transformations. In this study, we characterized Sb(V)-reducing anaerobic consortium by using physiological, geochemical, and genomic approaches. An anaerobic consortium was enriched from antimony mine tailing soil by its ability to reduce Sb(V) with lactate. As previously reported with a dissimilatory Sb(V)-reducing bacterium [1], the precipitation of Sb(III) as antimony trioxide was also confirmed in this consortium by X-ray absorption near-edge structure (XANES) analysis. In addition to Sb(V), other electron acceptors such as As(V), Fe(III) citrate, and anthraquinone-2,6-disulfonate (AQDS) were reduced in the presence of lactate. Microbial reduction of Fe(III) can release toxic metalloids bound to Fe(III) oxides, potentially influencing mobility of Sb and As in the contaminated soils. The ability of this consortium to utilize solid-state electrode as an electron donor was also indicated by using a bioelectrochemical system. Phylogenetic analysis of this consortium showed the predominant presence of Firmicutes and α-Proteobacteria-related populations. Draft genome sequence of this consortium was also determined. Majority of the sequences (>90%) were assigned to Firmicutes, and 79% of sequences belonged to the genus *Desulfitobacterium.* Functional genes associated with arsenic resistance, nitrate reduction, nitrogen fixation, polysulfide reductase, and putative reductive dehalogenase were found in the genome, indicating metabolic versatility of this consortium. Collectively, our study showed that the Sb(V)-reducing microbiota may influence mobility of Sb by direct reduction of Sb(V) and indirectly by the reduction of Fe(III), and its potential to facilitate bioremediation of other environmental pollutants indicated by the genomic content.

[1] Abin C.A., Hollibaugh J.T. Environ. Sci. Technol. 48, 681-688. (2014)

Keywords: Antimony, Arsenic, bioreduction, dissimilatory Fe(III) reduction

©2020. Japan Geoscience Union. All Right Reserved.

[E] Poster | B (Biogeosciences)：B-PT Paleontology

[B-PT04] Biomineralization and Geochemistry of Proxies

convener:Takashi Toyofuku(Japan Agency for Marine-Earth Science and Technology (JAMSTEC)), Jelle Bijma(Alfred-Wegener-Institut Helmholtz-Zentrum für Polar- und Meeresforschung), Hiroshi Kitazato(Tokyo University of Marine Science and Technology (TUMSAT)), Kotaro Hirose(Faculty of Science and Engineering, Waseda University)

In order to reconstruct the Earth climate system, marine paleoclimatologists resort to transfer functions or geochemical proxies, which are produced or affected by organisms. The relationships used for reconstructions are generally based on field calibrations or derived from laboratory experiments. The danger of these so-called empirical relationships is that they may be valid only within the restricted parameter space of their calibration. Application of proxy relationships to very different environmental settings (e.g. high vs. low latitude or glacial vs. interglacial) requires a mechanistic understanding of these relationships. Much progress can be expected by a better understanding of the biomineralization mechanisms and the incorporation of proxy signals.
In this session we facilitate contributions related to the biomineralization, calibration and validation of marine proxies from field study, laboratory culture experiment and paleo-environmental reconstruction.

[BPT04-P01] Variation of geochemistry in sea urchins cultured under the long-term acidification experiment

Riki Miyai[1], Hideki Takami[2], Daisuke Muraoka[2], Atsushi Suzuki[3], Yukihiro Nojiri[4], *Mayuri Inoue[1] (1.Department of Earth Sciences, Okayama University, 2.Tohoku National Fisheries Research Institute, 3.Geological Survey of Japan, AIST, 4.Faculty of Science and Technology, Hirosaki University)

[BPT04-P02] Relationship between anthropogenic pollution and spatiotemporal change in element composition contained in the bottom sediments from Tokyo Bay, Japan.

*Sumika Yoneto[1], Kotaro Hirose[1], Hideo Yamazaki[2], Kazuo Kamura[1] (1.Faculty of creative science and engineering of the department of resources and environmental engineering, Waseda University, 2.Department of Life Science, School of Science and Engineering, Kindai University)

[BPT04-P03] Morphologic changes of a calcareous nannofossil group, *Reticulofenestra* group, from Eocene to Miocene in the Atlantic Ocean

*Doi Nobuhiro[1], Koji Kameo[2] (1.Division of Earth and Environmental Sciences, School of Science and Engineering, Chiba University, 2.Department of Earth Sciences, Faculty of Sciences, Chiba University)

[BPT04-P04] The formation process of axial internode skeletons in deep-sea isidid octocorals inferred from crystal orientation

*Yukiko Kozaka[1], Katsuyoshi Michibayashi[2], Yui Kouketsu[2], Yuki Tokuda[3], Hiroshi Sato[4] (1.Institute for Space-Earth Environmental Research, Nagoya University, 2.Department of Earth & Planetary Sciences, Graduate School of Environmental Studies, Nagoya University, 3.Faculty of Environmental Studies, Tottori University of Environmental Studies, 4.School of Business Administration, Senshu University)

[BPT04-P05] A challenge to 3D morphological analysis of diatom cells

*Megumi Saito-Kato[1], Yukiko Nagai[1,2], Hayato Yokoyama[3] (1.Department of Geology and Paleontology, National Museum of Nature and Science, 2.Japan Agency for Marine-Earth Science and Technology, 3.RC Gear)

[BPT04-P06] The cell dynamics of sexual reproduction in foraminifera *Spirillina vivipara*

*Yukiko Nagai[1,2], Remi Tsubaki[3], Nanami Kishigami[2], Takashi Toyofuku[2,4] (1.National Museum of Nature and Science of Tokyo, 2.Japan Agency for Marine-earth Science and Technology , 3.The University Museum, The University of Tokyo, 4.Tokyo University of Marine Science and Technology)

[BPT04-P07] Foraminifera: either biological organs or chemical factories

*Hiroshi Kitazato[1] (1.Tokyo University of Marine Science and Technology (TUMSAT))

[BPT04-P08] Identification of factors affecting partitioning of rare arth elements between calcite and seawater

*Kana Fujimori[1], Hirotaka Nishino[1], Tasuku Akagi[1] (1.Department of Earth and Planetary Sciences, Faculty of Sciences, Kyushu University)

Variation of geochemistry in sea urchins cultured under the long-term acidification experiment

Riki Miyai[1], Hideki Takami[2], Daisuke Muraoka[2], Atsushi Suzuki[3], Yukihiro Nojiri[4], *Mayuri Inoue[1]

1. Department of Earth Sciences, Okayama University, 2. Tohoku National Fisheries Research Institute, 3. Geological Survey of Japan, AIST, 4. Faculty of Science and Technology, Hirosaki University

Since the Industrial Revolution, ocean acidification (OA) is expected to adversely affect marine ecosystems, especially carbonate organisms. In this study, we investigate the effects of OA on the chemical composition and structure of the shell and spines of sea urchins, *Mesocentrotus nudus* and *Strongylocentrotus intermedius*, whose main components are calcite. In addition, the potential of sea urchins as paleoenvironmental proxies is also examined.
In this study, sea urchins were raised under the following five carbon dioxide partial pressures (pCO_2, μ atm): (i) 2000, (ii) 1000, (iii) 700, (iv) 350 (controlled setting), (v) 250. The conditions from (i) to (iii) were adjusted by addition of CO_2 and that of (v) was adjusted chemically. For the culture experiment, 5 to 7 sea urchins were placed in individual bottles at each setting. The shell length and the body weight were measured monthly, and one spine from individual sea urchin was also collected at this time. Oxygen and carbon isotope ratios ($\delta^{18}O$, $\delta^{13}C$) contained in the spines of *M. nudus* were measured with a stable isotope ratio mass spectrometer (IsoPrime). The Mg/Ca ratio contained in the spines of both sea urchins, the shell and the lantern (chewing part) of *S. intermedius* were measured with an inductivity coupled plasma optical emission spectrometer (Agilent 720). The observation of the surface structure of both sea urchins was performed by a scanning electron microscope (JEOL, JSM-5500G).
As the result of culture experiments, the shell length and the body weight decreased with increasing pCO_2. The spine Mg/Ca ratios of both sea urchins showed positive relations against pCO_2. Since it has been reported that calcites with higher Mg contents have higher solubility, spines of sea urchins would become vulnerable under the projected OA conditions. The SEM observations of surface structures of spines showed that spines reared under higher pCO_2 conditions were disordered compared to those reared at controlled setting. For the results of $\delta^{18}O$ and $\delta^{13}C$ measurements on the spines of *M. nudus*, variation of $\delta^{13}C$ showed a clear negative correlation without temperature effect. On the other hand, $\delta^{18}O$ in the spines showed a seasonal change which is probably related to variation of seawater temperature during the rearing period with negligible effects from differences of pCO_2. Therefore, $\delta^{18}O$ and $\delta^{13}C$ in the spines of *M. nudus* would have potential for environmental proxies of water temperature and seawater pCO_2, respectively.

Keywords: sea urchin, ocean acidification, culture experiment

©2020. Japan Geoscience Union. All Right Reserved.

Relationship between anthropogenic pollution and spatiotemporal change in element composition contained in the bottom sediments from Tokyo Bay, Japan.

*Sumika Yoneto[1], Kotaro Hirose[1], Hideo Yamazaki[2], Kazuo Kamura[1]

1. Faculty of creative science and engineering of the department of resources and environmental engineering, Waseda University, 2. Department of Life Science, School of Science and Engineering, Kindai University

Elucidating temporal variations using sediment records from the hydrosphere is an effective methodto evaluate the historical trends of environmental loads and the resulting effect to aqueous ecosystems.

The watershed of Tokyo Bay is widespread in Kanto Plain including large cities in capital district such as Tokyo and Yokohama, where approximately 30 million people live (1/4 of that of Japan). Especially, industrial and residential districts with urban infrastructures are located along the coasts, and 25,000 ha of water area are reclaimed. Therefore, history of the effects of such anthropogenic modifications are considered to be recorded in the bottom sediments in Tokyo bay as a temporal variations of element components.

Matsumoto (1983) investigated the elemental composition for the last 100 years up to 1981 in Tokyo Bay, and evaluated the manifestation and peak of artificial alteration. However, the spatiotemporal distribution after the peak, especially trace metal elements such as rare metals are not enough clarified. Therefore, we investigated the temporal distribution of each elements for the last 70 years in two surface cores TB12B-38 (c.l. 82 cm) and TB15-68 (c.l. 58.5 cm) recently drilled in Tokyo Bay by using ICP-MS. We also investigated surface sediments collected at 14 sites in Tokyo Bay to evaluate the horizontal distribution of each elements and the factor of the concentration to the bottom sediment.

Temporal distributions of many elements, including Cu, Pb, Zn which are the general indicators for industries, rapidly increased from 1950’s to 1970’s, then decreased to core surface (2010’s). These trends are considered to be the effects of the historical change of anthropogenic loads, such as the high economic growth after the World War II and later effluent control for the severe environmental problem. More specific trends in each element due to their emission source and sedimentation trend will be discussed on the presentation.

Reference: Matsumoto. E. (1983), Sediment environment in Tokyo Bay (review)

Keywords: anthropogenic pollution, human induced environmental change, element compositions, trace metal, Tokyo Bay

©2020. Japan Geoscience Union. All Right Reserved.

Morphologic changes of a calcareous nannofossil group, *Reticulofenestra* group, from Eocene to Miocene in the Atlantic Ocean

*Doi Nobuhiro[1], Koji Kameo[2]

1. Division of Earth and Environmental Sciences, School of Science and Engineering, Chiba University, 2. Department of Earth Sciences, Faculty of Sciences, Chiba University

Coccolithophores, uniceller marine phytoplankton, produce calcite plates called coccolith, consisting of two elliptical discs arranged a lot of tiny, tabular calcite plates (e.g., Young et al., 1992). The *Reticulofenestra* group, composed of a genus *Reticulofenstra* and its related taxa, is one of the major coccoliths during the Cenozoic. Specimens have been classified by their shape and central structures of a coccolith. Size variations during the Miocene and Pliocene have been studied (Young, 1990; Kameo and Bralower, 2000) because frequent size reductions can be considered to correlate globally. Changes in size and morphologic characters of *Reticulofenestra* group have been studied mainly in the Neogene and Quaternary, and a few in the Paleogene to the Early Miocene. So, we applied biometric measurements to *Reticulofenestra* group in the Paleogene to the Early Miocene in order to clarify evolutionary trend of this taxon.

In this study, we investigated morphologic characters and sequential size variations of *Reticulofenestra* group during the Eocene–Miocene based on the scanning electron microscope (SEM) observation. Samples from Ocean Drilling Program (ODP) Leg 208 in the South Atlantic Ocean were used. The ages of the core used here range from ~42 Ma to ~10 Ma. One hundred specimens of *Reticulofenestra* group were examined and morphometric analysis (measurements of diameters of overall coccolith and its central part) were done using a software ImageJ.
Specimens in the *Reticulofenestra* group can be divided into three genera, *Cyclicargolithus*, *Dictyococcites*, and *Reticulofenestra* based on their morphologic characters. Moreover, dominated ranges of larger forms of each genus were clearly different; *Reticulofenestra* in the Eocene–lower Oligocene, *Dictyococcites* in the Oligocene–lower Miocene, and *Cyclicargolithus* in the lower Oligocene–lower Miocene, respectively. The size of the central opening of *Cyclicargolithus* can be a good morphologic character to separate it from other forms of *Reticulofenestra* group. After the middle Miocene, another abundant occurrence of large forms of *Reticulofenestra* are observed with some morphologic changes. Detailed observations will enable us to clarify specific characters of each *Reticulofenestra*.

[Reference]
Kameo, K. and Bralower, T. J., 2000. Neogene calcareous nannofossil biostratigraphy of Sites 998, 999, and 1000, Caribbean Sea. In Proceedings of the Ocean Drilling Program, Scientific Results, 165, 3-17. College Station TX.
Young, J. R., 1990. Size variation of Neogene Reticulofenestra coccoliths from IndianOcean DSDP cores. Journal of Micropaleontology, 9, 71–86
Young, J. R., Didymus, J. M., Brown, P. R., Prins, B., & Mann, S., 1992. Crystal assembly and phylogenetic evolution in heterococcoliths. Nature, 356, 516-518.

Keywords: Calcareous nannofossil, Morphologic change, Scaning electronic microscope

©2020. Japan Geoscience Union. All Right Reserved.

The formation process of axial internode skeletons in deep-sea isidid octocorals inferred from crystal orientation

*Yukiko Kozaka[1], Katsuyoshi Michibayashi[2], Yui Kouketsu[2], Yuki Tokuda[3], Hiroshi Sato[4]

1. Institute for Space-Earth Environmental Research, Nagoya University, 2. Department of Earth & Planetary Sciences, Graduate School of Environmental Studies, Nagoya University, 3. Faculty of Environmental Studies, Tottori University of Environmental Studies, 4. School of Business Administration, Senshu University

Isidid octocorals (Bamboo coral), which are cosmopolitan in distribution and occur to 4850 m in depth, have bamboo-like jointed axis consisting of elongated calcitic internodes with hollow structures in its center. These are joined by short nodes consisting of dark scleroprotains. The calcareous internode grows both vertically and horizontally, and show concentric growth layers in transverse section. To understand the formation process of their skeletons, previous studies have only focused the histology, cytology, and the observations using SEM. However, the hypotheses of the formation process are not consistent with each other.

The previous study suggested a rejuvenation near the center part of the calcareous internode by using radio carbon dating methods. The causes of the rejuvenation are considered (1) the changes of the age of water mass or (2) the secondary infilling of the hollow structure of internode (Farmer et al., 2015). On the other hand, the histological study of the precious red coral (*Corallium rubrum*) suggested that the formation of concentric layers of calcitic axial skeleton were secreted by skeletogenic epithelium on its outer surface (Grillo et al., 1993). Based on the histological study, the process of the infilling of the inner hollow part of axial skeleton may not be suitable for isidid octocorals.

To ascertain whether the infilling of the center part of internodes occurs in the isidid octocorals, we analyze the crystal orientation of the calcitic internodes. The different formation processes considered to makes different crystal structures. The isidid octocorals samples are collected by dredge during KH-10-7 from the Conrad Rise, Indian sector of the Southern Ocean. Our EBSD data of both the horizonal and vertical lines show that (1) the internodes are not composed by the fiber crystals but the very fine grains, (2) the directions of the c axis of the calcitic internodes are almost parallel to vertical growth line, (3) the crystal structure of the internodes is almost uniformed. These results support that the formation of the calcitic internodes occurs only on the outermost part of internodes by the skeletogenic epithelium. This clarification of the formation process makes the isidid octocorals available for paleoceanographic research.

Keywords: Deep-sea coral, Bamboo coral, Conrad Rise

©2020. Japan Geoscience Union. All Right Reserved.

A challenge to 3D morphological analysis of diatom cells

*Megumi Saito-Kato[1], Yukiko Nagai[1,2], Hayato Yokoyama[3]

1. Department of Geology and Paleontology, National Museum of Nature and Science, 2. Japan Agency for Marine-Earth Science and Technology, 3. RC Gear

3D images of diatom cells

Keywords: diatom, 3D image, photogrammetry, FIB-SEM

©2020. Japan Geoscience Union. All Right Reserved.

The cell dynamics of sexual reproduction in foraminifera *Spirillina vivipara*

*Yukiko Nagai[1,2], Remi Tsubaki[3], Nanami Kishigami[2], Takashi Toyofuku[2,4]

1. National Museum of Nature and Science of Tokyo, 2. Japan Agency for Marine-earth Science and Technology , 3. The University Museum, The University of Tokyo, 4. Tokyo University of Marine Science and Technology

Foraminifera performs both asexual and sexual reproduction. In asexual reproduction, it has been reported that the cytoplasm of one foraminifer into 10 to more than 1000 individuals and proliferates. However, foraminifera proliferated many cases by only asexual reproduction in culture experiments. Therefore, information about sexual reproduction is limited. In sexual reproduction, many foraminifers form zoospores and release them to the outside. It has been reported that the released zoospores cross each other and become new individuals. In other benthic foraminifera, there are known species in which 2 to 3 foraminiferal cells are mixed and sexually reproduced.
In this study, we observed cell dynamics of sexual reproduction in the foraminifer *Spirillina vivipara*. This species grows a tubular spirally shell with cytoplasmic growth. It is known that *S. vivipara* grows rapidly and changes generation rapidly enough to divide from the mother cell and become reproductive in a few days (Myers, 1936). In our observations, it was observed that the generation changes while repeating asexual reproduction and sexual reproduction in about 5 to 14 days, so in this study, we described cell dynamics of the sexual reproduction of *S. vivipara* in detail.

Keywords: Foraminifera, Culture biology, Cell biology, Imaging

©2020. Japan Geoscience Union. All Right Reserved.

Foraminifera: either biological organs or chemical factories

*Hiroshi Kitazato[1]

1. Tokyo University of Marine Science and Technology (TUMSAT)

Foraminifers are eukaryotic microorganisms that roots have been traced back to pre-Cambrian Era. The organism adapts to ambient environments with rapid evolutionary rates. Recently, foraminifers are used as quite sensitive proxy organisms for Earth's environments. But, why ? We need to know foraminifers both from biological organs and chemical factories. During my presentation, I would like to figure out natural history of foraminifers. the view points should make clear foraminifers as chemical factories.

Keywords: foraminifer, eukaryotic micro-organisms, natural history, chemical factory

©2020. Japan Geoscience Union. All Right Reserved.

Identification of factors affecting partitioning of rare arth elements between calcite and seawater

*Kana Fujimori[1], Hirotaka Nishino[1], Tasuku Akagi[1]

1. Department of Earth and Planetary Sciences, Faculty of Sciences, Kyushu University

[Introduction]

Concentrations of 14 rare earth elements (REEs) in carbonates are considered to reflect that of seawater via partitioning coefficients, which may be controlled by chemical conditions of seawater. Therefore, partitioning coefficients could be used as a proxy of either REE composition of seawater or chemical conditions. However, the reported partitioning coefficients of rare earth elements are inconsistent, and it has not been certain whether it could be applied to an actual seawater column. In the ocean, carbonate particles are supplied at the surface layer and absorb dissolved elements during settling through a column. In this study, we devised an experimental system mimicking a natural seawater column, where carbonate particles were introduced to carry out partitioning. We have identified several factors that affect the partitioning.

[Method]

Calcite particles of various sizes were added to seawater in a reaction vessel, and were left to partition REEs for a certain period under slightly saturated conditions with respect to calcite by modulating carbon dioxide partial pressure in bubbling air. The calcite particles in half of the seawater were size-separated by elutriation and analyzed for REEs and Ca using ICP-MS and ICP-OES (Stage 1). The calcite particles in another half the seawater were further subjected to the partitioning under an unsaturated condition with respect to calcite by increasing the carbon dioxide partial pressure in bubbling air (Stage 2). They were treated in the same manner as in Stage 1. The partitioning coefficient under each condition was determined by analyzing the relationship between particle size and Ln/Ca.

[Results]

Thermodynamic analysis of the system using pH and calcium concentration data revealed that the presence of REEs significantly inhibits the dissolution of calcium carbonate. REEs have been reported to inhibit calcium carbonate growth, but inhibition of dissolution has not been reported. The partitioning pattern was significantly affected by the addition of iron, but it was found that Mn in seawater had little effect. Also, iron appeared to form an independent hydroxide phase. In addition, it was found that the overall pattern sensitively changes depending on pH of seawater. We also conducted experiments with a fairly small amount of REEs added. Partitioning values higher than most of the reported values were obtaine.

Keywords: Rare earth elements, Calcite, seawater, partitioning experiments

©2020. Japan Geoscience Union. All Right Reserved.

[E] Poster | B (Biogeosciences)：B-PT Paleontology

[B-PT05] Biotic History

convener:Isao Motoyama(Faculty of Science, Yamagata University), Takao Ubukata(Division of Geology & Mineralogy, Department of Earth & Planetary Sciences, Kyoto University), Kazuyoshi Moriya(Department of Earth Sciences, Faculty of Education and Integrated Arts and Sciences, Waseda University)

The Biotic History session covers all aspects of ancient life and the history of biosphere through the geologic time. The study of ancient life is essential for unveiling mysteries of our planet earth. It also provides evidence for evolution of oceans, continents and island arcs. Modern progress in this field has been enhanced by interdisciplinary collaboration with allied sciences, such as paleoceanography and evolutionary biology. Our session intends to be a hub of communication amongst all earth scientists studying the biosphere; we welcome biological and biogeochemical approaches toward the understanding of the history of life.

[BPT05-P01] Chemostratigraphy and paleoenvironmental reconstruction of the Ediacaran-Cambrian section in Khubsugul Group, northern Mongolia

*Hatena Osawa[1], Tatsuo Oji[1], Hideko Takayanagi[2], Pedro J. Marenco[3], Koichi Mimura[1], Sersmaa Gonchigdorj[4], Kano onodera[1] (1.Nagoya University, 2.Tohoku University, 3.Bryn Mawr College, 4.Mongolian University of Science and Technology)

[BPT05-P02] Planktic foraminiferal biostratigraphy across the mid-Cretaceous Oceanic Anoxic Events

Soichi Shirakawa[3], Ryo Nakanishi[2], *Kazuyoshi Moriya[1] (1.Department of Earth Sciences, Faculty of Education and Integrated Arts and Sciences, Waseda University, 2.Department of Earth Sciences, School of Education, Waseda University, 3.Department of Earth Sciences,Resources and Environmental Engineering, Graduate School of Creative Science and Engineering, Waseda University)

[BPT05-P03] Organic carbon isotope stratigraphy across the Cenomanian/Turonian boundary at northern Atlantic

Yasuko Miyakura[2], *Kazuyoshi Moriya[1], Akiko S. Goto[3], Takashi Hasegawa[3] (1.Department of Earth Sciences, Faculty of Education and Integrated Arts and Sciences, Waseda University, 2.Department of Earth Sciences,Resources and Environmental Engineering, Graduate School of Creative Science and Engineering, Waseda University, 3.Faculty of Earth Science and Civil Engineering, Institute of Science and Engineering, Kanazawa University)

[BPT05-P04] The analysis of periostracum on Ammonoid shells from Cretaceous Yezo Group

*Hideharu Kohno[1], Haruyoshi Maeda[1] (1.Kyushu University)

[BPT05-P05] A functional-morphospace analysis of allometrically growing ammonoids

*Takao Ubukata[1] (1.Department of Geology & Mineralogy, Kyoto University)

[BPT05-P06] Phylogenetic aspect of ontogenetic trajectory of whorl shape in ammonoids

*Takao Ubukata[1], Fumitaka Katsuno[1] (1.Department of Geology & Mineralogy, Kyoto University)

[BPT05-P07] Evaluation of the metabolic status in extant Amniota based on nasal structures

*Seishiro Tada[1], Takanobu Tsuihiji[1,2] (1.Department of Earth and Planetary Science, Graduate School of Science, The University of Tokyo, 2.Department of Geology and Paleontology, National Museum of Nature and Science)

Chemostratigraphy and paleoenvironmental reconstruction of the Ediacaran-Cambrian section in Khubsugul Group, northern Mongolia

*Hatena Osawa[1], Tatsuo Oji[1], Hideko Takayanagi[2], Pedro J. Marenco[3], Koichi Mimura[1], Sersmaa Gonchigdorj[4], Kano onodera[1]

1. Nagoya University, 2. Tohoku University, 3. Bryn Mawr College, 4. Mongolian University of Science and Technology

According to the fossil record, the early evolution of multicellular animals occurred during the late Ediacaran and early Cambrian. However, detailed timing and process of the evolution are unclear partially due to the scarceness of fossil record and appropriate research site. Moreover, paleoenvironmental reconstruction of marine environment during the Ediacaran-Cambrian and its relationship with the early animal evolution are still unclear on the global scale. This study focuses on the Khubsugul Group in northern Mongolia as a prospective research site for paleontological and paleoenvironmental studies.

Ediacaran and Cambrian Khubsugul Group consists of three formations: Ongoluk, Khesen and Erkhelnur Formations in upward sequence. Recent fossil discovery of “Doushantuo-type” microfossils from the group as well as the occurrence of relatively large-sized trace fossils from the coeval formations of adjacent Dzabkhan terrane also implies that the Khubsugul Group is potentially important for future paleontological study. Nevertheless, very few geochronological or paleoenvironmental studies have been done for the Khubsugul Group. Therefore, carbon isotope and geochemical analyses of this group, the former for the correlation of the group, and the latter for the marine environmental study have been conducted.

New $\delta^{13}C$ data from the Ongoluk and Khesen Formations showed two negative excursions, one in the upper part of Ongoluk Formation and the other in the upper part of Khesen Formation. The Ediacaran-Cambrian boundary could be assigned to either of the two horizons in the group considering the world-wide existence of a conspicuous negative excursion (BACE excursion) at the boundary.

The results of total sulfur (TS) and total organic carbon (TOC) analysis both showed high concentrations in the calcareous shale in the lower part of the Khesen Formation. This result could be explained by either of the two scenarios: one is that the redox variation had driven the changes in TS and TOC, and the other is related to the biotic activity. The former, redox variation scenario stands on the understanding that carbonate rocks would record high TS and TOC values if the seawater is anoxic and record low values if oxic. The measured values may indicate that the seawater changed to relatively anoxic during the deposition of the Khesen Formation. The latter, biotic scenario is inferred from the result that increase of TS and TOC coincides with the increase of siliciclastic components and concentrations of metal elements (aluminium, iron, manganese, vanadium, thorium, and molybdenum). According to these increases, a scenario can be proposed that the terrestrial weathering and input of siliciclastics and other metal elements into the marine environment during this period promoted enhanced production by marine organisms.

Keywords: Khubsugul Group, carbon isotope, PC-C boundary, paleoenvironmental reconstruction

©2020. Japan Geoscience Union. All Right Reserved.

Planktic foraminiferal biostratigraphy across the mid-Cretaceous Oceanic Anoxic Events

Soichi Shirakawa[3], Ryo Nakanishi[2], *Kazuyoshi Moriya[1]

1. Department of Earth Sciences, Faculty of Education and Integrated Arts and Sciences, Waseda University, 2. Department of Earth Sciences, School of Education, Waseda University, 3. Department of Earth Sciences,Resources and Environmental Engineering, Graduate School of Creative Science and Engineering, Waseda University

Massive deposition of carbon-rich black shales in the mid-Cretaceous is widely known as Oceanic Anoxic Event (OAE). OAE is identified as a negative feedback cooling mechanism at the Cretaceous thermal maximum. In fact, a sudden temperature drop and southward migration of Boreal fauna have been reported just after the beginning of the OAE at the Cenomanian/Turonian boundary (OAE2). Distinctive faunal turnovers in pelagic taxa, such as calcareous nannofossils, planktic foraminifers, radiolarians, etc., have also been found at OAE2. Among these taxa, planktic foraminifers show an interesting pattern in extinction. Deep dwelling species went extinct at the beginning of the OAE2, followed by the extinction of thermocline dwelling species. The rest of mixed layer dwelling species survived. These observations have been reported from rather expanded outcrops distributed around North Atlantic, and possibly indicate shoaling of the top depth of the oxygen minimum zone in a water column.

In this study, we report planktic foraminiferal biostratigraphy from the Cenomanian through the Campanian at Newfoundland margin to identify planktic foraminiferal diversity change against some environmental perturbations in this age. Samples were recovered by Integrated Ocean Drilling Program Expedition 342. Semi-glassy preserved individuals with open-aperture occurred throughout the sequences analyzed. We found two intervals showing faunal turnover in planktic foraminifers. The first, lower interval is correlated to the Cenomanian/Turonian boundary. Sediment of this interval is composed of black shale, which indicates that this faunal turnover represent the extinction event at OAE2. The second, upper interval can be correlated to the Santonian/Campanian boundary or lower Campanian. At this interval, fluxes of both benthic and planktic foraminiferal individuals become almost zero. Sediments trun into darker in color, but no sign of black shale. On the other hand, abundant foraminiferal test fragments have been found in smear slides. These facts indicate planktic foraminifers did inhabit within a water column, but their test were not well preserved in sediments, implying bottom water acidification at this interval. We possibly found two different types of biotic response against the environmental perturbations in the mid- to late Cretaceous.

Keywords: Cretaceous, planktic foraminifers, Stratigraphy

©2020. Japan Geoscience Union. All Right Reserved.

Organic carbon isotope stratigraphy across the Cenomanian/Turonian boundary at northern Atlantic

Yasuko Miyakura[2], *Kazuyoshi Moriya[1], Akiko S. Goto[3], Takashi Hasegawa[3]

1. Department of Earth Sciences, Faculty of Education and Integrated Arts and Sciences, Waseda University, 2. Department of Earth Sciences,Resources and Environmental Engineering, Graduate School of Creative Science and Engineering, Waseda University, 3. Faculty of Earth Science and Civil Engineering, Institute of Science and Engineering, Kanazawa University

Carbon cycle is one of the important drivers/regulators of Earth's climate system. In the modern world, increasing atmospheric carbon dioxide concentration produces global warming which we should deal with. It is suspected that climate-carbon cycle feedback in near future would become positive feedback. As a result, obviously, global warming would be accelerated. On the other hand, in geological history, climate-carbon cycle feedback may act as negative feedback. One of those examples is Oceanic Anoxic Event (OAE) in the mid-Cretaceous. OAE is defined as stratigraphically restricted deposition of carbon-rich sediment in the world ocean. The deposition of massive amount of carbon on the global seafloor decreases atmospheric carbon dioxide, resulting in global cooling.

Since OAE is the global event, a carbon cycle perturbation at OAE can be found in global sediments. On the other hand, precise age, i.e. stratigraphic position, of carbon-rich black shale is significantly different from site to site. For example, black shale occurs throughout the Cenomanian/Turonian transition in the Equatorial Atlantic, while it is restricted to the upper Cenomanian in British coast. In this study, we present new records of organic carbon isotope stratigraphy at Newfoundland margin, mid-latitude western Atlantic. Samples were recovered by Integrated Ocean Drilling Program Expedition 342. Although upper half of the Cenomanian/Turonian transition were within a core gap and not recovered, the first buildup, trough, second buildup intervals of carbon isotope stratigraphy are clearly identified. Interestingly, black shale only occurs the trough and second buildup intervals, which can be correlated to the upper half of the Plenus Marls Member in British coast. This observation implies that productivity and ocean circulation in mid-latitude western Atlantic (Newfoundland) were different from those of mid-latitude eastern Atlantic (British coast).

Keywords: Cretaceous, Oceanic Anoxic Event, Carbon isotope stratigraphy

©2020. Japan Geoscience Union. All Right Reserved.

The analysis of periostracum on Ammonoid shells from Cretaceous Yezo Group

*Hideharu Kohno[1], Haruyoshi Maeda[1]

1. Kyushu University

Molluscs are animals belonging to the phylum Mollusca in the taxonomic class of creature. Its features are (1) the body is bilaterally symmetric, (2) the mantle (membrane covering the internal organs) is maintained, and (3) the calcium carbonate shell is formed. Among them, the shells of molluscs that form shells are covered with an organic film called periostracum. Its thickness and fine shape differ depending on the species.

The periostracum surface of modern bivalves (e.g. Unionidae, Lternulidae) has been shown to retain microprojections, and the microprojections on the periostracum itself help protect the shell from friction between the water stream and the shell. It is suggested that it is possible. In addition, molluscan periostracum is known to contain pigments (mainly melanin, carotenoids, tetrapyrrole) and to exhibit various colors. Heretofore, it has been considered that the color of the periostracum is a complex one that varies greatly depending on the side chain of the pigment compound and the type of binding protein. However, recent spectroscopic studies suggest that the structure of the polyenes that make up the carotenoids can determine the color. The color and color band of the periostracum formed by polyenes play important ecological roles, such as identifying the same species and camouflaging the predator's eyes.

On the other hand, organic periostracum is easily decomposed and hardly remain in fossils. However, a closer examination reveals that even the fossil of Ammonoids may still have periostracum. For example, *Owenites* cf. *koeneni* from the Triassic has a dark color band on the periostracum. This band is considered to be the original pattern when it was alive because (1) it had a radial pattern and (2) the pattern was interrupted at the damaged part of the shell. Color bands and shells are also known from *Protexanites*, *Tetragonites*, and *Gaudryceras* from the Cretaceous Yezo Group. However, its substance (function, color of the time when Ammonoid alive, etc.) has not yet been clarified because it was difficult to extract the pigment. In this study, we clarify substance of the periostracum preserved in Ammonoid shells from the Cretaceous Yezo Group.

To clarify the substance of the periostracum, *Gaudryceras*, which is known to have a large number from the upper Albian to Maastrichtian and known to have a better periostracum quality of preservation than other individuals, was selected. The surface and cross-section microstructure of periostracum were observed by SEM. Observation of the surface confirmed a clear structural difference between the shell and the periostracum that was presumed to coat on it. The former has a structure in which the crystals constituting the shell are layered. The latter had many microprojections (1-5 μm in diameter) as seen in the shells of modern bivalves.

Keywords: Ammonoid, Periostracum, Gaudryceras

©2020. Japan Geoscience Union. All Right Reserved.

A functional-morphospace analysis of allometrically growing ammonoids

*Takao Ubukata[1]

1. Department of Geology & Mineralogy, Kyoto University

Theoretical morphology allows us to generalize the relationship between geometries and functional properties of biological form by constructing a functional landscape on a theoretical morphospace. Functional-morphospace analyses have been widely performed particularly for planispiral ammonoids using Raup’s theoretical morphologic model. However, such studies have largely omitted any exploration of the potential effects of allometry because Raup’s model is designed to simulate isometric growth. Here I propose a novel theoretical morphologic model which mimics allometric shell growth commonly observed in ammonoids to represent ontogenetic trajectories of morphological traits as well as shell shape itself. I tried to generalize the relationship between the shape change trajectories and hydrostatic and hydrodynamic properties using the newly introduced model.
The present model approximates shell shape by a planispiral conical tube with elliptic cross-section just as Raup’s model. However, the parameters are defined referring to a hypothetical spiral passing through the center of the elliptic generating curve unlike Raup’s parameters. They are defined using four dimensions, i.e., the lengths of a pair of radius vectors of the spiral parted by p (r_q, r_{q-p}), and radii of the elliptic generating curve in the radial and bilateral directions (h_q, b_q), that are functions of the revolving angle of the generating curve around coiling axis. The present model is based on the allometric relations of r_{q-p}, h_q, and b_q to r_q, and is defined by a total of six allometric coefficients (two for each allometry): degree of whorl involution, relative whorl height, relative whorl breadth, and their scaling exponents. A biometric analysis using more than 100 ammonoid species shows that ontogenetic change in shell shape can fairly be approximated by the present allometric model in most species examined.
A functional morphospace analysis was performed using the present allometric model. A time series of functional landscapes was constructed on a morphospace with reference axes representing the allometric coefficients. Hydrostatic inefficiency of shell shape was assessed by the specific surface area of the totally produced shell. Hydrodynamic inefficiency of shell shape at high Reynolds number was estimated by the projected area of the shell in the direction of movement per unit volume. Hydrodynamic inefficiency of shell shape at low Reynolds number was evaluated by the surface area of the exposed shell portion per unit volume. The results of the analyses revealed the followings: 1) Hydrostatic efficiency highly depends on allometry of whorl involution (or whorl expansion) rather than on allometry of whorl cross-sectional shape. 2) A positive allometry of whorl involution produces hydrostatically inefficient shell shape in a large individual. 3) Allometry of whorl cross-sectional shape dominantly influences hydrodynamic efficiency either at high or low Reynolds number. 4) When the whorl is depressed, a positive allometry of whorl height seems to compromise the three functional properties in a large individual, while a negative allometry of whorl height tends to minimize both hydrostatic and hydrodynamic efficiencies. The results suggest that a negative allometry of umbilical width commonly observed in many ammonoid lineages is advantageous for nektonic or nekton-benthic mode of life.

Keywords: theoretical morphology, allometry, functional-morphospace analysis

©2020. Japan Geoscience Union. All Right Reserved.

Phylogenetic aspect of ontogenetic trajectory of whorl shape in ammonoids

*Takao Ubukata[1], Fumitaka Katsuno[1]

1. Department of Geology & Mineralogy, Kyoto University

Ontogenetic changes in shell geometry commonly observed in ammonoids have long attracted much attention among paleontologists from both phylogenetic and functional morphologic points of view. Many authors have tried to extract phylogenetic information from their ontogenetic trajectories using traditional morphometrics or theoretical morphology. However, morphological variation in ammonoid shell form cannot be fully encompassed in a few ratios of dimensions. Geometric morphometrics developed in decades allows us to utilize thoroughly multidimensional information contained in morphological data. Here we use geometric morphometrics as an exploratory tool to compare ontogenetic trajectories of cross-sectional shape of ammonoid whorl. In order to assess phylogenetic signals in the whorl shape and its ontogeny, a relative warp analysis, a principal components analysis of partial warp scores, was performed after Procrustes superimposition of landmarks and semi-landmarks recorded along the outline of the whorl cross section.
As a result of the analysis using ten Cretaceous species, we found phylogenetic signals in morphometric data obtained from radial cross sections of ammonoid shells. The shape variation distinguishing each superfamily was summarized in three principal components that represent, respectively, relative whorl height, development of the ventrolateral shoulder, and shape of the lateral flanks. The shape change trajectories depicted in the size–shape space fairly separate higher taxa, even though many species commonly show a dorsoventral elongation of the whorl with growth. The rate of the dorsoventral elongation was different not only among superfamilies but also between genera within the same superfamilies. The results revealed that non-uniform morphological variation as well as the uniform component has important phylogenetic information in ammonoids. The ontogenetic trajectories of some non-uniform components tend to show complicated patterns in the size–shape space, and we found a diagnostic fluctuation pattern of the shape change trajectories characterizing desmoceratoid species. The present study indicates that relative warp analysis is useful for extracting phylogenetic signals from morphometric variables collected from ammonoid shells if we focus on ontogenetic variation. Further analyses using larger numbers of species are required to identify features in ontogenetic trajectories that characterize each phylogeny.

Keywords: ontogenetic trajectory, ammonoids, geometric morphometrics

©2020. Japan Geoscience Union. All Right Reserved.

Evaluation of the metabolic status in extant Amniota based on nasal structures

*Seishiro Tada[1], Takanobu Tsuihiji[1,2]

1. Department of Earth and Planetary Science, Graduate School of Science, The University of Tokyo, 2. Department of Geology and Paleontology, National Museum of Nature and Science

Dinosaurs are one of the best known, most intensively studied and most successful clades of tetrapods. Since they were recognized as a distinct lineage of vertebrates in the 19th Century, one of the main research focuses on dinosaurs has been their physiology, especially concerning the question “Were dinosaurs warm-blooded (endotherm) or cold-blooded (ectotherm)?” Endothermic animals regulate their body temperature by internal heat production, whereas ectotherms depend on external heat sources. Deciphering the metabolic status of dinosaurs would help improve our understanding of their ecology and evolutionary changes leading to extant birds.

One potential “Rosetta stone” for thermal physiology is the nasal turbinate. It is a scroll-like structure in the nasal cavity and is present only in endotherms (birds and mammals) among extant tetrapods. This structure increases the surface area and volume of the nasal cavity for efficient heat and water exchanges between the respiratory mucosa and inhaled- and exhaled-air, thus compensating for extra heat and water losses caused by efficient lung ventilation in endotherms. Because the degree of development of the nasal cavity is expected to be correlated with the form and size of the nasal cavity, characteristics of the latter are potentially informative in evaluating the metabolic status of amniote animals, especially fossil forms.

Before tackling the question on dinosaur metabolism, it is necessary to establish a quantitative relationship between the metabolic condition and size of the nasal structure in extant amniotes so that could be applied to extinct species.

In the present study, heads of more than 40 extant species were CT-scanned and their nasal cavities were digitally reconstructed three-dimensionally based on the scanned data. The surface area and volume of the nasal cavity were then measured as size parameters of this structure. These values were plotted against the skull volume for comparison between endotherms and ectotherms.

The result shows a clear difference in the slope of the regression lines between endotherms and ectotherms. As expected, endotherms have significantly larger nasal cavities than ectotherms, likely reflecting the existence of the nasal turbinates. In contrast, however, there is no significant difference detected in the slope of the regression lines between them when those size parameters of the nasal cavity was plotted against the whole body weight. One possible explanation for such a difference is that, because the head region houses the brain, an organ metabolically highly consumptive, and endotherms tend to have a relatively larger brain than ectotherms, so the skull volume may be more tightly correlated with metabolic conditions than the body weight. The body weight also tends to have a lager margin of the error than the skull volume because the former sometimes needs to be estimated rather than being directly measured (e.g., cases of alcohol-preserved specimens).

These results suggest that it may be possible to infer metabolic conditions of amniotes based on the size of the nasal cavity. Applying the above relationship to the fossil record of non-avian dinosaurs will

©2020. Japan Geoscience Union. All Right Reserved.

contribute to clarifying the evolutionary changes in metabolism toward fully endothermic extant birds.

Keywords: Metabolism, Evolution, Dinosauria, Amniota

©2020. Japan Geoscience Union. All Right Reserved.

[E] Poster | B (Biogeosciences)：B-CG Complex & General

[B-CG06] Decoding the history of Earth: From Hadean to the present

convener:Tsuyoshi Komiya(Department of Earth Science & Astronomy Graduate School of Arts and Sciences The University of Tokyo), Yasuhiro Kato(Department of Systems Innovation, Graduate School of Engineering, University of Tokyo), Katsuhiko Suzuki(Submarine Resources Research Center, Japan Agency for Marine-Earth Science and Technology), Kentaro Nakamura(Department of Systems Innovation, School of Engineering, University of Tokyo)

The latest results of Earth's evolution and geological processes through 4.6 billion year
s from Hadean to Modern, based on various approaches including fieldworks, chemical
analyses, experiments and computer simulation, will be presented. In this session, we ai
m to discuss and understand causal relationships and interplay among the evolution of
Earth's deep interior, changes in the surface environments, and development and evolut
ion of life. Wide-ranging topics are accepted.

[BCG06-P01] Ocean oxidation and microbial activity just after the Marinoan Snowball Earth

*Tsuyoshi Komiya[1], Miyuki Anzai[1], Teruyuki Maruoka[2], Yohei Matsui[3], Manabu Nishizawa[3], Yusuke Sawaki[1] (1.Department of Earth Science & Astronomy Graduate School of Arts and Sciences The University of Tokyo, 2.Faculty of Life and Environmental Sciences, University of Tsukuba, 3.Japan Agency for Marine-Earth Science and Technology)

[BCG06-P02] Alkaline magmatism in a fore-arc region: igneous activity in relation to the Ashizuri igneous complex, SW Japan

Takumi Matsumoto[1], *Kazumasa Aoki[1] (1.Department of Applied Science Okayama University of Science)

[BCG06-P03] Feedback mechanism of solid earth system on glacial-interglacial climate cycles: Constraints from osmium isotopic mass-balance in the ocean

★Invited Papers

*Yusuke Kuwahara[1], Kazutaka Yasukawa[2,1,3], Koichiro Fujinaga[3,2], Tatsuo Nozaki[4,2,5,3], Junichiro Ohta[2,3,6], Honami Sato[3,4], Jun-Ichi Kimura[6], Kentaro Nakamura[1], Yasuhiro Kato[2,1,3,4] (1.Department of Systems Innovation, School of Engineering, The University of Tokyo, 2.Frontier Research Center for Energy and Resources, School of Engineering, The University of Tokyo, 3.Ocean Resources Research Center for Next Generation, Chiba Institute of Technology, 4.Submarine Resources Research Center, Japan Agency for Marine-Earth Science and Technology, 5.Department of Planetology, Graduate School of Science, Kobe University, 6.Volcanos and Earth’s Interior Research Center, Research Institute for Marine Geodynamics, Japan Agency for Marine-Earth Science and Technology)

[BCG06-P04] Geochemical constraints on the Earth environment after the Lomagundi Event;The Cape Smith belt, Canada

★Invited Papers

*Kento Motomura[1], Shoichi Kiyokawa[1], Minoru Ikehara[2], Takashi Sano[3], Kentaro Tanaka[4], Tsubasa Miki[4], Yuji Sano[4] (1.Kyushu Univ., 2.Kochi Univ., 3.National Museum of Nature and Science, 4.Univ. of Tokyo)

[BCG06-P05] Occurrence, petrography and chemical compositions of black shale in the Isua supracrustal belt: A potential to decode surface environmental conditions on the early Earth

*Suzuki Akiko[1], Yusuke Sawaki[2], Tsuyoshi Komiya[2] (1.The University of Tokyo , Graduate School of Science, 2.Department of Earth Science & Astronomy Graduate School of Arts and Sciences The University of Tokyo)

[BCG06-P06] U-Pb chronology and geochemistry of detrital monazites from major North American rivers

*Kazumi Yoshiya[1], Keita Itano[2], Tsuyoshi Iizuka[1], Shigenori Maruyama[3] (1.The University of Tokyo, Department of Earth and Planetary Science, 2.Kanazawa University, 3.Tokyo Institute of Technology, Earth-Life Science Institute)

[BCG06-P07] Variations of burial rates of organic carbon in terrestrial and marine environments during the Phanerozoic

*Kazuhiro Aoyama[1], Eiichi Tajika[1], Kazumi Ozaki[2] (1.Department of Earth and Planetary Science, Graduate School of Science, The University of Tokyo, 2.Toho University)

[BCG06-P08] New morphotypes, cell-wall structures, and elemental distribution of the Gunflint microfossils

*Kouhei Sasaki[1], Akizumi Ishida[1], Naoto Takahata[2], Yuji Sano[2], Takeshi Kakegawa[1] (1.Department of Earth Science, Graduate school of Science, Tohoku University, 2.Atmosphere and Ocean Research Institute, The University of Tokyo)

[BCG06-P09] Modelling the behaviors of marine carbon isotopic composition after Neoproterozoic snowball Earth event

*Akari Miki[1], Eiichi Tajika[1], Kazumi Ozaki[2] (1.Department of Earth and Planetary Science, Graduate School of Science, The University of Tokyo, 2.Toho University)

[BCG06-P10] Paleoecological variations reconstructed by organic matter derived from lichens and fungi across the Cenomanian/Turonian boundary in the Tomamae area, northern Hokkaido, Japan

*Masashi A. Ikeda[1], Ken Sawada[2], Takuto Ando[3], Hideto Nakamura[4], Reishi Takashima[5], Hiroshi Nishi[5] (1.Graduate School of Science, Hokkaido University, 2.Department of Earth and Planetary Sciences, Faculty of Science, Hokkaido University, 3.Estuary Research Center, Shimane University, 4.Faculty of Science, Osaka City University, 5.The Center for Academic Resources and Archives, The Tohoku University Museum, Tohoku University)

[BCG06-P11] Petrography of magnesite-orthopyroxene-olivine veins in the Ujaragssuit Nunât layered ultramafic body terrane, southern West Greenland

*Toma Takahashi[1], Tomoaki Morishita[1], Tomoyuki Mizukami[1], Akihiro Tamura[1], Keita Itano[1], Juan Miguel Guotana[1], Ikuya Nishio[1], Kanta Takahashi[1], Kristoffer Szilas[2] (1.Kanazawa university, 2.University of Copenhagen)

[BCG06-P12] Palynomorph assemblage in sedimentary rocks of the Mesoproterozoic Qaanaaq Formation from northwestern Greenland.

*Yuki Hara[1], Takuto Ando[3], Ken Sawada[2] (1.Graduate School of Science, Hokkaido University, 2.Department of Earth and Planetary Science, Faculty of Science, Hokkaido University, 3.Estuary Research Center, Shimane University)

[BCG06-P13] Pb-Pb chronology of Fe-Ti oxides

*Ito Kengo[1], Tsuyoshi Iizuka[1] (1.The University of Tokyo)

Ocean oxidation and microbial activity just after the Marinoan Snowball Earth

*Tsuyoshi Komiya[1], Miyuki Anzai[1], Teruyuki Maruoka[2], Yohei Matsui[3], Manabu Nishizawa[3], Yusuke Sawaki[1]

1. Department of Earth Science & Astronomy Graduate School of Arts and Sciences The University of Tokyo, 2. Faculty of Life and Environmental Sciences, University of Tsukuba, 3. Japan Agency for Marine-Earth Science and Technology

The Marinoan Snowball Earth event is one of the most severe environmental changes, and occurred about 650 million years ago in the Cryogenian. It is widely considered that the Earth was completely covered with ice, and that bioactivity significantly collapsed during that event. On the other hand, many fossils including acritarchs, Metazoan eggs and embryos, and algae were found after the Marinoan Snowball Earth event, indicating the bioactivity was completely recovered and organisms quite rapidly evolved in the Ediacaran. However, recovery and extent of bioactivity just after the event is still obscure. Therefore, we tried to estimate the biological activity just after the Snowball Earth event based on geological and geochemical studies of the Cap Carbonate deposited right after the event.

We analyzed aggregate of organic matter, carbonate rocks and pyrites in the Cap Carbonate of the Siduping section, South China. The Cap Carbonate is subdivided into 3 parts: C1, C2 and C3 in an ascending order. The C1 part consists of a stromatactis structure, which forms network structures of many quartz veins, and contains many domains rich in organic materials and pyrite within cavities of the stromatactis structure. The rims of veins comprise quartz, which suggests that carbonate has been silicified and replaced by silica minerals simultaneously or immediately after deposition. Generally speaking, the silicification of carbonate is due to organic acid formed by heterotrophs. Most of the central parts of the veins or cavities of the stromatactis structures contain aggregate of organic matter and pyrite, suggesting active microbial activity within pore water of conduits and among minerals. We call the organic matter as stromatactis organic matter hereafter. The C2 and C3 parts comprise layered dolostone, and the C3 part contains more detrital materials than the C2 part. No stromatactis structure is present in the C2 and Ce parts. We examined the stromatactis organic matter and organic matter within carbonate parts of the carbonate rocks from the C1 to C3 parts in order to estimate the microbial activity in the ocean and sediment.

The isotope ratios of organic carbon within the carbonate parts in the C2 and C3 parts range from -28 to -24‰, corresponding to photosynthesis by cyanobacteria. The carbon isotope ratios of organic matter within the carbonate parts in the C1 part is characterized by a wide range of the values (-34~-22‰), possibly due to mixing between photosynthetic carbon fixation and methane-related processes. In addition, carbon isotope ratios of the stromatactis organic matter are significantly low, ranging from -35 to -30%, possibly due to the methane-related processes. Methanogen and anaerobic methanotrophic Archaea possibly produced the organic matter with the low carbon isotope values. In addition, there are many pyrite grains occur together with the stromatactis organic matter, which also suggests active sulfate reduction together with the anaerobic methanotrophic activity. We try to prove the microbial combination based on sulfur isotopes.

Nitrogen isotope ratios range from -2 to +7‰. The nitrogen isotope values of the stromatactis organic matter in the C1 part ranges from -1 to +1‰, whereas those of carbonate parts abruptly increase from -1~+1‰ in the lower part to +7‰ at the top of the C1 part. The low values around -1 to +1‰ indicate that

©2020. Japan Geoscience Union. All Right Reserved.

nitrogen fixation was dominant after the Snowball Earth event. On the other hand, the high nitrogen isotope values indicate that the nitrification and denitrification restarted at that time possibly because seawater became oxic enough to form nitrate. On the other hand, it is considered that nitrogen fixation by methanogen was also active within the sediment because nitrogen isotope values of organic matter formed in seawater increased to +7‰, but the nitrogen isotope values of the stromatactis organic matter formed within sediment were consistently around 0‰.
Carbon and nitrogen isotope values of the stromatactis organic matter and organic matter in the carbonate parts in the Cap Carbonate suggest that ocean and subseafloor environments shared common biological activity just after the Marinoan Snowball Earth event, and that the ocean was very quickly recovered to oxic and nitrate-rich environment. The rapid recovery probably became a prelude to biological evolution of emergence of the Metazoan.

Keywords: Marinoan Snowball Earth, Carbon isotope chemistry, Nitrogen isotope chemistry, Ediacaran, Recovery of biological activity and evolution of life, Sulfur isotope chemistry

©2020. Japan Geoscience Union. All Right Reserved.

Alkaline magmatism in a fore-arc region: igneous activity in relation to the Ashizuri igneous complex, SW Japan

Takumi Matsumoto[1], *Kazumasa Aoki[1]

1. Department of Applied Science Okayama University of Science

A-type granitic rocks are basically developed in anorogenic tectonic setting and relatively alkaline composition (e.g. Cremens et al., 1986; Bonin, 2007 and references therein). These rocks are volumetrically insignificance compared with the vast amounts of I- and S-type rocks exposed in various parts of the world, but their genesis plays one of important roles in understanding of evolution of granitic rocks through Earth’ s history because the granite rocks exist in only the Earth within the Solar system that may represent the specificity of the Earth.

Ring igneous complex exposed in Shikoku is called Ashizuri igneous complex (Murakami et al., 1983; 1989), and is composed mainly of felsic lithology with subordinate amount of alkaline gabbro and dolerite (Murakami et al., 1983; 1989; Stein et al., 1996). The felsic rocks are classified into the A-type granite. They are a close genetic relation with the opening of Japan Sea and the commencement of subduction of the young and hot Shikoku Basin of the Philippine Sea plate during the Neogene period (e.g. Kimura et al., 2005; Shinjoe et al., 2010; 2019). Thus, identifying the formation process of Ashizuri igneous complex leads to a greater understanding of the alkaline magmatism in arc-trench systems. A lot of studies for the genesis of the Ashizuri igneous rocks have been reported so far, however, there are no unified views on this issue (e.g. Kimura et al., 2005; Shinjoe et al., 2010; Yoshikura, 2012).

Igneous zircon is one of powerful tools to elucidate the origin of the parental magmas because the trace elements of zircons could vary depending on the parent melt compositions controlled by some physicochemical processes such as crystallization, differentiation and dehydration (e.g. Grimes et al., 2007; 2015; Yang et al., 2012). Moreover, U–Pb dating of igneous zircons can be used to constrain the timings of igneous activity. In this study, we report new U–Pb and geochemical data of the zircons separated from three granitic and two gabbroic rocks in the Ashizuri igneous complex by the using laser ablation ICP mass spectrometry. Moreover, zircon data from sandstone sample in the Paleogene Shimizu Formation intruded by the Ashizuri igneous complex is also reported. Finally, we would like to discuss the origin of the alkaline magmatism in fore-arc regions as illustrated by a case study of the Ashizuri igneous complex, based on our new data integrated with previous geological and geochemical data reported by other researchers.

©2020. Japan Geoscience Union. All Right Reserved.

Feedback mechanism of solid earth system on glacial-interglacial climate cycles: Constraints from osmium isotopic mass-balance in the ocean

*Yusuke Kuwahara[1], Kazutaka Yasukawa[2,1,3], Koichiro Fujinaga[3,2], Tatsuo Nozaki[4,2,5,3], Junichiro Ohta[2,3,6], Honami Sato[3,4], Jun-Ichi Kimura[6], Kentaro Nakamura[1], Yasuhiro Kato[2,1,3,4]

1. Department of Systems Innovation, School of Engineering, The University of Tokyo, 2. Frontier Research Center for Energy and Resources, School of Engineering, The University of Tokyo, 3. Ocean Resources Research Center for Next Generation, Chiba Institute of Technology, 4. Submarine Resources Research Center, Japan Agency for Marine-Earth Science and Technology, 5. Department of Planetology, Graduate School of Science, Kobe University, 6. Volcanos and Earth's Interior Research Center, Research Institute for Marine Geodynamics, Japan Agency for Marine-Earth Science and Technology

Solid earth has affected and responded to changes in the global carbon cycle and climate. Volcanic degassing of carbon dioxide (CO_2) and silicate chemical weathering consuming atmospheric CO_2 are believed to have regulated the carbon budget of Earth's surface system on a geologic timescale (>10^6 yr). However, characteristics of the solid earth response against shorter (<10^5 yr) fluctuations such as the Quaternary glacial-interglacial cycles, are still controversial. In order to constrain the response of the solid earth to glacial-interglacial climate changes, we employed the marine Os isotopic ratios ($^{187}Os/^{188}Os$) as a proxy of solid earth response. The marine Os isotopic ratio reflects the relative intensity of two dominant influxes to the ocean: radiogenic continental materials ($^{187}Os/^{188}Os$ = 1.0–1.4) and unradiogenic mantle-like materials (i.e. hydrothermal fluids and cosmic dust) ($^{187}Os/^{188}Os$ = ~0.12). Owing to the contrasting $^{187}Os/^{188}Os$ values between these two influxes, and short residence time of Os in the ocean (~10^4 yr), the variability in $^{187}Os/^{188}Os$ of seawater can constitute a sensitive tracer for mantle and continental inputs into the marine environment on a glacial-interglacial timescale. Here we show a high-resolution record of the marine osmium isotopic composition ($^{187}Os/^{188}Os$) as a proxy of solid earth's response during the past 300,000 years. We demonstrate that the seawater $^{187}Os/^{188}Os$ has varied associating with glacial-interglacial cycles. Based on a marine Os isotopic mass-balance simulation, the observed $^{187}Os/^{188}Os$ fluctuation cannot solely be explained by the change of global chemical weathering rate synchronized with glacial-interglacial climate changes. Instead, the fluctuation can be reproduced by a combination of two short-term processes: (1) inputs of radiogenic Os derived from the intense weathering of glacial-till during deglaciation, and (2) inputs of unradiogenic Os derived from enhanced seafloor hydrothermalism during glacials. Our results constitute the first evidence that the solid earth system involving chemical weathering of glacial-till and seafloor magmatism systematically and repetitively responded to the glacial-interglacial cycles on <10^5 yr timescales.

Keywords: Glacial-Interglacial cycles, Seawater Osmium isotopic ratio, Carbon cycle

©2020. Japan Geoscience Union. All Right Reserved.

Geochemical constraints on the Earth environment after the Lomagundi Event; The Cape Smith belt, Canada

*Kento Motomura[1], Shoichi Kiyokawa[1], Minoru Ikehara[2], Takashi Sano[3], Kentaro Tanaka[4], Tsubasa Miki[4], Yuji Sano[4]

1. Kyushu Univ., 2. Kochi Univ., 3. National Museum of Nature and Science, 4. Univ. of Tokyo

The beginning of the Paleoproterozoic era (ca. 2.5–1.6 Ga) is characterized by Great Oxidation Event (GOE: ca. 2.5–2.3 Ga) and subsequent positive carbon isotope excursion event (Lomagundi Event: ca. 2.2–2.0 Ga). These events represent dynamic changes between the Archean and Proterozoic Earth environment including the primary production, oceanic sulfate level, and redox structure (e.g. Lyons et al., 2014). Last two decades, several studies have cleared the Earth environment during ca. 2.5–2.0 Ga, however, aftermath of the events is poorly constrained. In this study, we measured organic carbon isotope ($\delta^{13}C_{org}$) of black shales deposited ca. 1.96 Ga and estimated Earth environment after the Lomagundi Event.

Two core samples consisting of sandstone–black shale alternations were drilled at the Cape Smith belt, Canada (4G8069 and 718.3333). These two drilling points are 10 km off each other. Sedimentary sequences composing a part of 4G8069 and 718.3333 are regarded as Povungnituk Group sediments which were deposited on the continental margin of the Superior at about 1.96 Ga (St-Onge & Lucas, 1990). Komatiitic lava overlying the sandstone–black shale sequence is observed at the top of the 4G8069 core. 718.3333 core also contains komatiitic lava, but the lava is observed ~100 m above our sampling intervals. Microscopic observation revealed that the black shales are rich in organic matter and pyrrhotite which origin is likely to sedimentary pyrite generated by bacterial sulfate reduction.

$\delta^{13}C_{org}$ values of the 4G8069 core range from −32.0 ‰to −29.5 ‰and show systematic changes. Two carbon isotope excursions (CIEs) are identified from the 4G8069 core: CIE 1) the gradual increase from bottom of the sequence (−32.0 ‰) to 45 m point (−29.5 ‰), CIE 2) the gradual decrease between 45 m and 50 m (−32.1 ‰), and subsequent increase toward the top (−31.0 ‰). CIE is also observed in the 718.3333 core, which shows gradual decrease from −30.6 ‰to −33.2 ‰, and subsequent increase toward −31.9 ‰.

CIE 1 of the 4G8069 core could be comparable with CIE of the 718.3333 core based on ~100 m distance from the komatiitic lava. Therefore, it is plausible that CIEs occurred at least twice after the Lomagundi Event. There are two possibilities for the trigger of the CIEs: (1) volcanic activities or (2) oxidative weathering could cause CIEs.

References

Lyons, TW, Reinhard, CT, and Planavsky, NJ, 2014, The rise of oxygen in Earth’ s early ocean and atmosphere: Nature, v. 506, p.307-315.

St-Onge, MR, and Lucas, SB, 1990, Evolution of the Cape Smith Belt: Early Proterozoic continental underthrusting, ophiolite obduction and thick-skinned folding. In The Early Proterozoic Trans-Hudson Orogen of North America, v. 37, p. 313-351.

©2020. Japan Geoscience Union. All Right Reserved.

Keywords: Paleoproterozoic, Organic carbon isotope

©2020. Japan Geoscience Union. All Right Reserved.

Occurrence, petrography and chemical compositions of black shale in the Isua supracrustal belt: A potential to decode surface environmental conditions on the early Earth

*Suzuki Akiko[1], Yusuke Sawaki[2], Tsuyoshi Komiya[2]

1. The University of Tokyo , Graduate School of Science, 2. Department of Earth Science & Astronomy Graduate School of Arts and Sciences The University of Tokyo

The Earth is the only planet, which has been covered with H_2O-ocean throughout the geologic time, in the Solar System. Therefore, it is very important to understand the origin and evolution of the Earth's oceans. Generally speaking, there are two ways to decipher the Earth's early evolution. The first is numerical calculation, and the second is the analysis of geological samples. The numerical calculations provide general solutions that may have occurred on Earth, but may not provide specific events that have occurred only on Earth. Therefore, this study adopts the latter method. In particular, to estimate the surface environment of the early Earth, it is essential to examine sedimentary rocks formed on the early Earth, and it is important to find sedimentary rocks such as black shale, that are suitable for the estimation, from the Eoarchean geological terrains. There will be.

One of the significant events on the early Earth was the Late Heavy Bombardment (LHB). It is considered that the event occurred 4.2 to 3.8 Ga based on age-distribution of the moon's craters, and that the event caused significant impacts of a large number of meteorites on the earth. However, no evidence is, so far, found from terrestrial materials so that it is still controversial whether the event really took place. It is generally known that meteorite impacts leave anomalous signatures of a platinum element group in abyssal sedimentary rocks. However, the concentration of Ir in the banded iron formations (BIFs) in the Isua supracrustal belt has been analyzed, but no significant anomaly has been found. Generally speaking, it is regarded that the BIFs was slowly deposited, analogous to modern deep-sea pelagic sediments such as chert. On the other hand, it is widely known that the banded iron formation is derived from intermittent hydrothermal activity. It is more important to study sedimentary rocks with a low sedimentation rate, such as black shale.

Relatively, less metamorphosed supracrustal rocks, under the amphibolite facies or less conditions, are present in the Isua area in southern West Greenland. In 2016, we conducted a geological survey of the Isua Supracrustal Belt, and discovered new black shale outcrops. Black shale, rich in organic matter, has been reported in the western part of the Isua Superficial Rock Zone (Rosing, 1999), but no black shale has been reported in the northeastern part In addition, the previous report did not show detailed description of the geological occurrence such as accompanied lithology and detailed lithostratigraphy. This presentation reports the geological occurrence, mineralogical description, major and minor chemical compositions of the black shale, and discusses its significance.

The Isua Supracrustal Belt (ISB) is located approximately 150 km northeast of Nuuk, and has an arcuate shape. The ISB is composed of ultramafic rocks, basalts with pillow structures, BIFs, chert, carbonate, and clastic sedimentary rocks such as conglomerate, sandstone and pelitic rocks. It is intruded by the Eoarchean (3.7 to 3.8 Ga) granitic gneiss (Itsaq gneiss). Although they have undergone metamorphism under the greenschist to amphibolite facies conditions, we mention the rocks as rock names of the estimated precursors hereafter. The northeastern part consists of piles of about 10 fault-bounded

©2020. Japan Geoscience Union. All Right Reserved.

subunits, which have similar lithostratigraphy of basaltic layer, chert and clastic sedimentary rocks in an ascending order to each other. The lithostratigraphy is similar to modern ocean plate stratigraphy. The existence of the imbricate structure and oceanic plate stratigraphy suggests that the belt was an accretionary complex.

Black shale occurs mainly in two regions of the northeastern part of the ISB; the northern black shale has been previously described as mafic sedimentary rocks (Komiya et al., 1999) or chert (Nutman & Friend, 2009). The black shale stratigraphically underlies the BIFs. It is considered that the BIFs in the ISB belong to the Algoma-type because it is regarded that all of them occur on basaltic lava so far. However, this work presents another occurrence of the BIFs, which were deposited on black shale. In addition, the discovery may allow us to detect the LHB signatures from the Eoarchean sedimentary rocks because black shale, generally speaking, is deposited quietly slowly in open ocean.

In this study, microscopic observation and chemical analysis were performed in addition to the geological observation. The northern black shale contains quartz, calcite and chlorite, whereas the southern black shale consists of quartz, amphibolite and biotite. We will also discuss the results of chemical analysis.

Keywords: Black shale, The early Earth, Late Heavy Bombardment

©2020. Japan Geoscience Union. All Right Reserved.

U-Pb chronology and geochemistry of detrital monazites from major North American rivers

*Kazumi Yoshiya[1], Keita Itano[2], Tsuyoshi Iizuka[1], Shigenori Maruyama[3]

1. The University of Tokyo, Department of Earth and Planetary Science, 2. Kanazawa University, 3. Tokyo Institute of Technology, Earth-Life Science Institute

The North American continent formed through collisions of Archean cratons which surrounded by Proterozoic orogenic belts, and the outermost parts are enclosed by Phanerozoic orogens. Detrital minerals in river sands have been eroded from basement rocks along rivers, and transported to the river mouth areas. Monazite, one of the robust minerals, is a light rare-earth element phosphate which can be precisely dated by the uranium-thorium-lead method. Monazite occurs as an igneous mineral in low-Ca peraluminous felsic rocks and as a metamorphic mineral in a wide range of metamorphic rocks. Previous monazite chronology and geochemistry revealed that detrital monazites from the African rivers recorded orogenic metamorphic events more accurately than detrital zircons (Itano et al., 2016). In this study, we extend the application of monazite chronology and geochemistry to large rivers of the North American continent in order to better understand orogenic metamorphic events in the continent. To constrain the timing and nature of major orogenic events that formed the continent, we analyzed U-Pb ages and geochemical compositions of 178 detrital monazite grains from the Mississippi (83 grains) and Mackenzie Rivers (95 grains). The U-Pb age distribution of detrital monazite from the Mackenzie River shows large four peaks at 0.15-0.2, 1.8-1.9, 2.0, 2.6 Ga and small peaks at 0.45 and 2.5 Ga. On the other hand, that from the Mississippi River shows large three peaks at 1.45, 1.7, 2.65 Ga and small peaks at 0.4, 1.1, 1.65, 1.85 Ga. Some of the monazite age peaks are not observed in the U-Pb age histograms of detrital zircons from the same rivers (Iizuka et al., 2005; Rino etal., 2004; 2008), suggesting that the age peaks reflect the timing of major metamorphic events. Comparison with geological events, 0.15-0.2 Ga peak of the Mackenzie River reflects contributions from the Cordilleran orogen (Gehrels et al., 2002). Other large peaks around 1.8-2.0 Ga of the Mackenzie River may reflect contributions from the Thelon, Wopmay and Trans-Hudson orogens. The largest peak for monazite from the Mississippi River is observed around 1.4 Ga. It may reflect contributions from anorogenic magmatism (Nyman et al., 1994) or early stage of the Grenville Orogeny (Windley, 1993). The second large peak around 1.7 Ga of the Mississippi River may reflect contributions from the Penoken, Trans-Hudson, and Yavapai-Mazatzal orogens.

Keywords: monazite, U-Pb geochronology, REE

©2020. Japan Geoscience Union. All Right Reserved.

Variations of burial rates of organic carbon in terrestrial and marine environments during the Phanerozoic

*Kazuhiro Aoyama[1], Eiichi Tajika[1], Kazumi Ozaki[2]

1. Department of Earth and Planetary Science, Graduate School of Science, The University of Tokyo, 2. Toho University

Emergence and evolution of land plants had a large effect on atmospheric O_2 and CO_2 levels through carbon geochemical cycle, especially an increase in an efficiency of chemical weathering of soils, and an increase in a rate of organic carbon burial on land. However, there are few studies which evaluate influence of the rise of land plant and relative contribution of organic carbon burial in terrestrial and marine environments to the carbon geochemical cycle and to the climate through geologic time.

In this research, we modified a model for combined cycles of carbon and sulfur (GEOCARBSULF) to consider this problem. We estimated ratios of global organic carbon and pyrite burial rates (C/S ratio) from the model with marine carbon and sulfur isotopic records. We used compiled data of C/S ratio from sediments deposited in freshwater, oxygenated and euxinic seawater environments to distinguish the burial rates of organic carbon in terrestrial and marine environment.

As a result, it was indicated that, as inferred from the previous studies of carbon cycle by Robert Berner, the burial rate of organic carbon in terrestrial environment had increased greatly in the Late Paleozoic (Carboniferous) owing to advent of vascular plants which produces microbially resistant organic matters such as lignin. In contrast, it was also shown that terrestrial burial rate had been virtually zero before the Silurian when there were no vascular plants on land, and decreased largely at the Devonian/Carboniferous, Permian/Triassic and Triassic/Jurassic mass extinction boundaries. We will discuss influence of Ocean Anoxic Events (OAEs) on the burial rate of organic carbon and pyrite through the Phanerozoic time.

Keywords: carbon cycle, C/S ratio, land plant, Phanerozoic

©2020. Japan Geoscience Union. All Right Reserved.

New morphotypes, cell-wall structures, and elemental distribution of the Gunflint microfossils

*Kouhei Sasaki[1], Akizumi Ishida[1], Naoto Takahata[2], Yuji Sano[2], Takeshi Kakegawa[1]

1. Department of Earth Science, Graduate school of Science, Tohoku University, 2. Atmosphere and Ocean Research Institute, The University of Tokyo

Precambrian microfossils have been studied by previous investigators for decades to constrain their microbial activity, while their ultrastructure and chemical composition have been poorly understood. Since microbial metabolism is performed on the cell surface, the elemental compositions, ultrastructure and coexisting minerals of microfossils can be a strong clue to understand their microbial metabolisms. In the present study, in situ analysis on individual microfossils by high spatial resolution Secondary Ion Mass Spectrometry (NanoSIMS) was performed together with other standard geochemical and mineralogical methods on the Gunflint microfossils, well known as great preservation, occurred in the 1.9 Ga Gunflint Formation, Canada.

Morphological observation revealed that some new morphotypes of microfossils having morphological affinities to cyanobacterial akinete (*archeaoellipsoides*), eukaryotes and fungi, which had not been reported in this age. Bilayered cell-wall structures were also newly discovered in thick-wall spherical microfossils. Having multi-layered wall structure are essential for modern-style microbial life, such as cyanobacteria, to promote complex metabolism and the storage of organelles. These findings indicate that advanced microbes and modern-style cell wall structures had already evolved in the Paleoproterozoic ocean, earlier than thought in previous studies.

Secondary ion mapping for 12C-, 12C14N-, and 32S- were newly obtained on 30 individual Gunflint microfossils with 10 morpho-types. They showed mostly similar elemental distribution patterns among different morpho-types. A unique elemental distribution was observed in globular type microfossils, showing that heterogeneous N and S distribution between the cell wall and inner structure. This indicates that this type of microfossil possibly had a special function, such as production of baeocytes during cell differentiation like modern cyanobacteria (e.g., Pleurocapsales).

Outer parts (i.e., walls) and inner parts of examined microfossils often showed contrast chemistries. Inside organic matter contained microcrystals of iron-bearing minerals and trace amounts of Ca or Mo. They imply that successful detection of minerals and elements, which are possibly related to cyanobacterial enzyme. Outer parts were generally depleted in N and enriched in S. In addition, Na, K, and Cl were often detected from cell wall indicating deposition of chloride crystals with organic matter of microfossils, which were suggested that the Gunflint microbiota were active in the evaporitic environment.

This research does not only constrain the microbial activities indicating the early rise of advanced microbes and modern like biological functions in the Gunflint ocean, but also provides new keys to understand the evolution of early life and their living environments in the Paleoproterozoic era.

Keywords: microfossils, Paleoproterozoic, NanoSIMS

©2020. Japan Geoscience Union. All Right Reserved.

Modelling the behaviors of marine carbon isotopic composition after Neoproterozoic snowball Earth event

*Akari Miki[1], Eiichi Tajika[1], Kazumi Ozaki[2]

1. Department of Earth and Planetary Science, Graduate School of Science, The University of Tokyo, 2. Toho University

The atmospheric oxygen level is thought to have increased soon after the snowball Earth events in the early and late Proterozoic, leading to the modern oxygen-rich environment from a completely anoxic environment [e.g. 1-5]. A biogeochemical cycle model [6] predicts that an extremely hot climate immediately after the snowball Earth event should cause intense continental weathering and supply a large amount of nutrients into the ocean, leading to increases of primary productivity in the surface ocean and global organic carbon burial, which, in turn, results in an inevitable rise of the atmospheric oxygen level. However, since the massive organic carbon burial removes a large amount of light carbon isotopes from the environment, a positive excursion of marine carbon isotope ratio is predicted, which contradicts the marine carbon isotope record in the snowball Earth events in the Neoproterozoic. Here, we report an investigation of the behavior of marine carbon isotope ratio just after the snowball Earth event. We propose a possible scenario for explaining the negative excursion of carbon isotope ratio with a new idea that a temperature dependence of a rate of microbial decomposition of organic matter may explain an apparent negative anomaly of the carbon isotope ratio in seawater. We will compare this new scenario with various other scenarios proposed so far and discuss the possible scenario, with a marine biogeochemical carbon cycle model coupled with an atmospheric photochemical model.
[1] Rye and Holland (1998) Am. J. Sci., 298, 621-672. [2] Bekker and Holland, (2012) Earth Planet. Sci, Lett. 317-318, 295-304. [3] Och and Shields-Zhou (2012) Earth Sci. Rev., 110, 26-57. [4] Lyons et al. (2014) Nature, 506, 307-315. [5] Kirschvink et al. (2000) Proc. Natle. Acad. Sci., 97, 1400-1405. [6] Harada et al. (2015) Earth Planet. Sci. Lett., 419, 178-186.

Keywords: snowball Earth event, atmospheric oxygen, carbon isotopic composition, biogeochemical cycle

©2020. Japan Geoscience Union. All Right Reserved.

Paleoecological variations reconstructed by organic matter derived from lichens and fungi across the Cenomanian/Turonian boundary in the Tomamae area, northern Hokkaido, Japan

*Masashi A. Ikeda[1], Ken Sawada[2], Takuto Ando[3], Hideto Nakamura[4], Reishi Takashima[5], Hiroshi Nishi[5]

1. Graduate School of Science, Hokkaido University, 2. Department of Earth and Planetary Sciences, Faculty of Science, Hokkaido University, 3. Estuary Research Center, Shimane University, 4. Faculty of Science, Osaka City University, 5. The Center for Academic Resources and Archives, The Tohoku University Museum, Tohoku University

The Cretaceous period is known as the extreme greenhouse period due to active magmatism caused by superplume. Especially in the mid-Cretaceous, the Oceanic Anoxic Events (OAEs) occurred in several times, and had a great impact on marine and terrestrial ecosystems. Moreover, many animals and plants in the terrestrial ecosystem likely have undergone rapid diversification since the mid-Cretaceous (e.g. Dilcher, 2000; Meredith et al., 2011). Noticeably, the lichens have acquired strong light tolerance and undergone rapid diversification, and fungi have gained new symbiotic relations with trees through the appearance of ectomycorrhizal fungi since the mid-Cretaceous (e.g. Gaya et al., 2015; Taylor et al., 2011). However, these researches are limited to molecular phylogenetic analysis and numerical simulations, and few fossil records have been reported. In the present study, we analyzed biomarkers and organic fossils (palynomorph) derived from the lichen and fungi in the sediments deposited across the Cenomanian/Turonian boundary (CTB) from the northern Hokkaido, Japan to evaluate paleoecology during environmental disturbance event.

We analyzed sedimentary rocks across the CTB in the Saku Formation, Yezo Group, were collected from the Omagari-zawa sections of the Tomamae area, northern Hokkaido, Japan. The sediments used correspond to the OAE2 intervals (1st build-up, Trough, 2nd build-up and Plateau phases), determined by $\delta^{13}C$ stratigraphy (Omatsu et al., 2014). For the biomarker analysis, lipids were extracted from freeze-dried sediments, subsequently fractionated using silicagel column, and analyzed by GC-MS. For palynomorph analysis, kerogens were separated by HCl and HF from the extraction residue, and observed under a fluorescent light microscope.

Based on sterane and hopane ratios, we confirmed the high contribution of terrigenous matter input and low maturity of organic matter (vitrinite reflectance ca. 0.4% level; lignite to subbituminous coal rank) in the Omagari-zawa section. Recently, a perylene is thought to be fungal biomarker. In our study, we tentatively defined that the ratio of perylene to plant-derived aromatic terpenoids is useful as indicator of fungal biomass in terrestrial flora i.e. fungal activity. On the other hand, it has known that the lichens produce dibenzofuran (DBF). In particular, we suggested that specific isomers of alkyl DBF such as 1-methyl DBF are useful for the lichen biomarkers. Here, we established the ratio of 1-methyl DBF to plant wax *n*-alkanes (C_{27}-C_{31}), and it assumed to reflect relative contribution of lichens among terrestrial plants. These results implied that the fungi constantly flourished, and their activities declined during environmental disturbances such as before and after the 1st build-up and before the 2nd build-up stages. On the other hand, the variations in lichen-derived biomarker index are synchronous with those of the angiosperm/gymnosperm ratio (ar-AGI), indicating that the lichen increased during the angiosperm expansion period. The coniferous vegetation index such as Higher Plant Parameter (HPP) increased during the 1st build-up and 2nd build-up stages, implying that the conifer has expanded under arid

©2020. Japan Geoscience Union. All Right Reserved.

condition. However, the HPP values declined during the Trough and Plateau stages. These results suggest that, in the eastern margin of the Asian continent during the CTB, fungal activity was affected by arid/humid fluctuation, while lichen contribution on terrestrial ecosystem was greatly affected by angiosperm/gymnosperm vegetation changes.

Keywords: paleoecology, lichen, fungi, biomarker, palynomorph, Cretaceous

©2020. Japan Geoscience Union. All Right Reserved.

Petrography of magnesite-orthopyroxene-olivine veins in the Ujaragssuit Nunât layered ultramafic body terrane, southern West Greenland

*Toma Takahashi[1], Tomoaki Morishita[1], Tomoyuki Mizukami[1], Akihiro Tamura[1], Keita Itano[1], Juan Miguel Guotana[1], Ikuya Nishio[1], Kanta Takahashi[1], Kristoffer Szilas[2]

1. Kanazawa university, 2. University of Copenhagen

Researches on Hadean-Archean terranes are essential to reconstruct the geologic past of the early Earth, which is believed to be different from the present plate tectonics. Southern West Greenland preserves a wide exposure of Archean geologic units. This study reports magnesite-bearing veins in the Ujaragssuit Nunât layered ultramafic body, southern West Greenland.

Ultramafic rocks are transformed into serpentinite and carbonated rocks when they react with H_2O-CO_2 fluids under low temperature conditions. Carbonated ultramafic rocks from the Archean geological unit might provide information on impact of carbonatization of peridotite on atmospheric and water chemistry in Archean.

The studied magnesite-bearing veins occur in amphibole harzburgite. The magnesite-bearing veins contain coarse grained olivine and orthopyroxene, anthophyllite and talc, with minor amounts of phlogopite, chlorite, Cr-spinel and Fe-Ni sulfide. Magnesite contain anthophyllite and olivine. Anthophyllite is radial in shape. The Mg# (Mg/(Mg+Fe) atomic ratio) is 0.927-0.941 for magnesite, 0.862-0.882 for anthophyllite, 0.893-0.901 for coarse-grained orthopyroxene, 0.974-0.984 for talc, respectively. Orthopyroxene sometimes contains magnesite as inclusion, and micro-veins mainly composed of talc. Fine-grained olivine with minor amount of magnetite occurs in the micro-veins. The Mg# is 0.893-0.901 for coarse-grained orthopyroxene, 0.974-0.984 for talc, and 0.872-0.889 for fine-grained olivine. The Mg# of fine-grained olivine in talc micro-veins (0.872-0.889) are distinctively lower than coarse-grained olivine and olivine inclusions in magnesite (0.882-0.905).

The carbonate veins were formed as follows: 1) coarse-grained orthopyroxene was formed by the reaction between olivine in the host and CO2-bearing fluid

Mg_2SiO_4 (P1) + CO_2 (fluid) = $MgCO_3$ + $MgSiO_3$ (1),
whereas coarse-grained olivine and anthophyllite were formed by reaction with low-CO_2 activity fluids, such as

$5MgSiO_3 + H_2O = Mg_2SiO_4$ (secondary) + $Mg_3Si_4O_{10}(OH)_2$ (2),
and the fine-grained olivine in talc veins in large grained orthopyroxene was formed by the reaction
$9MgSiO_3 + H_2O$ (fluid) = $Mg_7Si_8O_{22}(OH)_2 + Mg_2SiO_4$ (3).

Keywords: Ancient Carbonation, Ultramafic rocks, West Greenland

©2020. Japan Geoscience Union. All Right Reserved.

Palynomorph assemblage in sedimentary rocks of the Mesoproterozoic Qaanaaq Formation from northwestern Greenland.

*Yuki Hara[1], Takuto Ando[3], Ken Sawada[2]

1. Graduate School of Science, Hokkaido University, 2. Department of Earth and Planetary Science, Faculty of Science, Hokkaido University, 3. Estuary Research Center, Shimane University

The evolutions of cyanobacteria and eukaryotic algae have been thought to be promoted by expansion of shallow ocean environment under long-term climatic warming by volcanic activity during the Mesoproterozoic, which is reconstructed by the analyses of sedimentary rocks deposited the delta-submarine fan system formed during the Grenville orogeny (Taira, 2007). Molecular biological researches supported that the pronounced promotion of eukaryote evolution was possibly occurred during the Mesoproterozoic (Philippe and Adoutte, 1998). In paleontological studies of the Mesoproterozoic fossils, organic microfossils such as acritarchs were used as strong indicators for reconstructing the marine organisms. The acritarchs is one of organic microfossils (palynomorphs) that are insoluble by acid and alkali treatments, and cannot be assigned to known group of organisms while they are thought to be cysts and sporangia of eukaryotic organisms. Morphology of the acritarchs became various and complicated after the Phanerozoic, especially during the Paleozoic, so that the acritarch fossils were used for paleontological and paleoenvironmental reconstructions after the Paleozoic. However, there are few studies for evolutional history and paleoecology including the biological response against environmental changes of the acritarchs during the Precambrian. In the present study, we performed the morphological observation of the acritarch fossils in the Mesoproterozoic sediments from northwestern Greenland to identify and examine their species (kinds) and to reconstruct the paleoecology of the marine organism during the Mesoproterozoic.

The samples used were greyish shales of the Qaanaaq Formation belonging to the Dundas Group, collected from the Thule Basin in northwestern Greenland during July-August 2018 and 2019. These expeditions were supported by MEXT (Japanese Ministry of Education, Culture, Sports, Science and Technology) through Arctic Challenge for Sustainability (ArCS) the Arctic region research project. The kerogens were separated by HCl and HF treatments of the sediments, and observed under a fluorescent light microscope.
We could identify 8 kinds of acritarchs such as *Leiosphaeridia* sp., *Synsphaeridium* sp., *Satka* sp., *Navifusa majensi*, *Simia* sp., *Lophosphaeridium* sp., *Schizofusa* sp., *Tasmanites* sp. and filamental microfossils. *Leiosphaeridia* sp. is the most abundant in all horizons of the Qaanaaq Formation in our study, and their diameters tend to increase upwards of the horizons. The *Leiosphaeridia* sp. fossils include several species and cannot distinguish with the broken and isolated colonial cells because their cells have simple structure (Samuelsson et al., 1999). From this fact, the increasing of the fossil sizes observed in our study was presumably affected by the mixture and shift of the several species morphologically identified as *Leiosphaeridia*. *Synsphaeridium* sp. and *Satka* sp. are distinctive features in the aggregates of cellular structures (colonial species), and the relative abundances of these two acritarchs in all assemblage tend to increase in total acritarchs assemblages in the upper horizons. These results indicate that such acritarchs were important for increasing cell size of the eukaryotic algae, and moreover, these evolved to multicellular organisms.

Keywords: Acritarchs, Mesoproterozoic, Palynomorph, Greenland

©2020. Japan Geoscience Union. All Right Reserved.

©2020. Japan Geoscience Union. All Right Reserved.

Pb-Pb chronology of Fe-Ti oxides

*Ito Kengo[1], Tsuyoshi Iizuka[1]

1. The University of Tokyo

Fe-Ti oxides appear in a wide range of igneous and metamorphic rocks. These minerals have been widely used for investigating the temperature and oxidation state of igneous and metamorphic processes. In addition, their potential as a U–Pb chronometer was demonstrated: Burton and O’ Nions (1990) reported Pb isotope compositions of Fe-Ti oxides in amphibolite- and granulite-facies orthogneisses in Sri Lanka, whereas Noyes et al. (2011) presented Fe-Ti oxide Pb isotope analysis of the Monastery kimberlite in South Africa. The results of these previous studies illustrated that the potential utility of Fe-Ti oxides as a reliable U-Pb chronometer due to having high U/Pb value and high closure temperature of Pb (~ 800 ℃). Nevertheless, the application of Fe-Ti oxide chronology remains highly limited. This is mainly because Fe-Ti oxides generally have only moderately high U contents (~0.1 ppm) so that the presence of small amounts of contaminant Pb degrades the age precision and accuracy. In this study, we utilized the acid leaching technique to improve the precision and accuracy of Fe-Ti oxide chronometer.

We analyzed Fe- Ti oxides from the anorthosite FC1 in the Duluth complex, which yields the widely used zircon U-Pb standard (1,099 ±0.6 Ma : Paces & Miller. (1993)). We evaluated the resistance of Fe-Ti oxides to acid leaching using SEM observation. In addition, we analyzed acid washed Fe-Ti oxides for Pb isotopes by MC-ICPMS. The results show that Fe-Ti oxides have high U/Pb ratio (> 189) compared with the whole rock fraction (3.29) and yield a reliable Pb–Pb age (1107 ±102 Ma: MSWD = 15).

Recently, we have applied Fe-Ti oxide Pb-Pb chronology to an amphibolite in the Acasta Gneiss Complex, Canada. The Acasta Gneiss Complex is an Archean terrane containing the oldest known rocks (Bowring & Williams. (1999)) and is composed of felsic orthogneisses and amphibolites. Although the formation and metamorphic ages of the felsic gneisses have been extensively investigated, no reliable chronological data have been obtained from the amphibolites. We are in the process of determining Pb–Pb ages of Fe-Ti oxides from the amphibolites in an attempt to get the reliable chronological information.

Keywords: Pb-Pb chronology, Fe-Ti oxides, Acasta Gneiss Complex, mafic rocks

©2020. Japan Geoscience Union. All Right Reserved.

[E] Poster | B (Biogeosciences)：B-CG Complex & General

[B-CG07] Phanerozoic biodiversity change: radiation and extinction

convener:Yukio Isozaki(Department of Earth Science and Astronomy, Multi-disciplinary Sciences - General Systems Studies, Graduate School of Arts and Sciences, The University of Tokyo), Yusuke Sawaki(The University of Tokyo)

This session explores the latest progress in the paleobiodiversity studies, particularly about the final 500 m.y.-long history of life during the Phanerozoic. All paleo-environmental, stratigraphic, and paleotological studies are welcome.

[BCG07-P01] Investigation on the internal texture of demospongiae fossil in meta-tuff from the Cambrian Akazawa Formation, Hitachi district

*Michio Tagiri[1], Katsutoshi Hanawa[2], Akira Oikawa[2], Noriaki Watanabe[3] (1.Hitachi City Museum, 2.Geonet Hitachi, 3.Graduate School of Environmental Studies, Tohoku Univ.)

[BCG07-P02] **Re-evaluating acid digestion for the analysis of organic carbon and nitrogen contents and stable isotope ratios in geological reference materials**

*Wataru Fujisaki[1], Yohei Matui[1] (1.Japan Agency for Marine-Earth Science and Technology)

[BCG07-P03] Taxonomy of Silurian conodonts from the Yokokurayama Group, Kurosegawa tectonic zone, distributed in Kochi Prefecture

*Akifumi Ito[1], Sachiko Agematsu[1], Yuichi Fukushima[1] (1.University of Tsukuba)

[BCG07-P04] **Devonian ostracods from the Fukuji area, Takayama City, Gifu Prefecture, central Japan**

*Mai Harashima[1], Sachiko Agematsu[1] (1.University of Tsukuba)

Investigation on the internal texture of demospongiae fossil in meta-tuff from the Cambrian Akazawa Formation, Hitachi district

*Michio Tagiri[1], Katsutoshi Hanawa[2], Akira Oikawa[2], Noriaki Watanabe[3]

1. Hitachi City Museum, 2. Geonet Hitachi, 3. Graduate School of Environmental Studies, Tohoku Univ.

We already reported the occurrence of demospongiae fossil from Cambrian meta-tuffs in the Hitachi Paleozoic formation, the southmost Abukuma Mountains. We investigate the internal texture of these sponges by means of stereoscopic microscope, polarized microscope and X-ray CT scan instrument. Deformed bubble-shaped globe of 1mm diameter are packed in the fossil, and those link with each other by fine tube. These globes consist of internal and external walls with reticulation. The globe with these walls may be a choanocyte of sponge. In the poster presentation, we will show this internal texture of sponge fossil by means of the animation of CT scan photographs and of the 3D shaping,

The stromal tissue of sponge fossil is occupied by very fine-grained silicate material, in which the sponge spicule-like texture develops, but this texture is completely replaced by fine acicular amphiboles. The sponge spicule did not remain in these fossils. However, whitish siliceous and micro-bubble bearing sponge texture still remains. Demospongiae fossil was formed by silicification in tuff.

Keywords: Cambrian formation, meta-tuff, demospongiae fossil, X-ray CT scan, cell form, recrystallized spicule

©2020. Japan Geoscience Union. All Right Reserved.

Re-evaluating acid digestion for the analysis of organic carbon and nitrogen contents and stable isotope ratios in geological reference materials

*Wataru Fujisaki[1], Yohei Matui[1]

1. Japan Agency for Marine-Earth Science and Technology

The accurate and precise determination of the total nitrogen (TN) and organic carbon (TOC) abundances and its isotopic compositions ($\delta^{15}N_{TN}$ and $\delta^{13}C_{org}$) in sedimentary rocks have been considered as important proxies for our interpretation of paleoenvironmental and paleoclimate processes. For the carbon and nitrogen analyses, the following acid digestion techniques have conventionally been employed: (1) acidification followed by sequentially rinsing with deionized water (rinse method), (2) acidification by exposure to an acid vapor (fumigation method), and (3) acidification in silver capsules (capsule method). Among these methods, acidification by the rinse method using hydrochloric acid has been widely used and is the standard treatment method for the elemental and isotopic analyses of both nitrogen and carbon in sedimentary rocks. However, some researchers have reported that the acid strength and heating during the decalcification in the rinse method could lead to a change in the TN and TOC contents and its isotopic compositions. Additionally, previous works showed that the TN and $\delta^{15}N_{TN}$ values of HCl acidified samples had changed compared with that of untreated samples. In this study, we systematically compared the effect of acidified and non-acidified samples (in rinse method) on the reliability of TN and TOC abundances and $\delta^{15}N_{TN}$ and $\delta^{13}C_{org}$ values by using geological reference materials (GRMs) issued by the GSJ and USGS: marine sediments (JMs-1, JMs-2, and SBC-1), stream sediments (JSd-3 and JSd-4), and lake sediment (JLk-1).

The TN and TOC concentrations and $\delta^{15}N_{TN}$ and $\delta^{13}C_{org}$ values were measured with a Flash EA1112 elemental analyzer coupled to a Thermo-Finnigan DELTA plus advantage isotope ratio mass spectrometer interfaced with a ConFlo IV at JAMSTEC. Acidified and untreated samples were prepared in three batches to ensure accuracy and precision in the analytical data and evaluate the procedural error. Approximately 200–500 mg of powdered samples was weighted in a 15mL glass tube and acidified in 8 mL 2M or 6M HCl at room temperature or at 70 ℃ in a thermostatic bath for 24 hours, respectively. Subsequent to acidification, the residue was sequentially rinsed three times with Milli-Q water, and dried at 80 ℃ for 48 hours in a closed oven with a light Al foil cover. Aliquots of the acid-treated and untreated samples were weighted into a tin capsule (9 ×10 mm, Lüdi) for the carbon and nitrogen analyses. The analytical reproducibility of the TN and TOC concentrations was evaluated by repeated analyses of reference materials (USGS40 and USGS41); the reproducibilities were better than ±1.8 % and ±1.0 %, respectively. The $\delta^{15}N_{TN}$ and $\delta^{13}C_{org}$ values are represented in ‰relative to atmospheric N_2 and the Vienna Peedee Belemnite (V-PDB) standard, respectively. The uncertainties in the $\delta^{15}N_{TN}$ and $\delta^{13}C_{org}$ values were within ±0.13‰ and ±0.09‰, respectively, as determined by the repeated analyses of reference materials.

Our results show that the average values of TN contents in the rinse method of all GMR samples are lower than that of untreated samples by up to 70 %. Additionally, the $\delta^{15}N_{TN}$ ratios of acid-treated samples, except for SBC-1, were decreased to 2.1‰ in maximum as compared with untreated samples. The magnitudes of the negative shift of TN and $\delta^{15}N_{TN}$ values were larger when the samples were acidified in 6M HCl and heated at 70 ℃. Loss of ^{15}N has previously reported during the acidification and was attributed to small losses of acid-soluble proteins and amino acids via the volatilization of oxidized

©2020. Japan Geoscience Union. All Right Reserved.

nitrogenous organic compounds. However, the $\delta^{15}N_{TN}$ values of SBC-1 are almost stable under the acidified and non-acidified conditions, probably indicating that the organic matter composition in SBC-1 was significantly different from the other GMS samples. On the other hand, as similarly to the nitrogen analysis, the magnitudes of the negative shift of TOC and $\delta^{13}C_{org}$ values were larger when acidification by 6M HCl and heating at 70 ℃ of GMR samples. It suggests that the decalcification with 2M HCl was unsatisfied with obtaining accurate results probably because of the poorly-soluble minerals, such as siderite and dolomite that were retained during the acidification. Overall, we propose that the analysis of nitrogen and carbon contents and its isotopic compositions should be separately measured, i.e., non-acidified sample for nitrogen analysis and 6M HCl acidified and heated samples for carbon analysis.

©2020. Japan Geoscience Union. All Right Reserved.

Taxonomy of Silurian conodonts from the Yokokurayama Group, Kurosegawa tectonic zone, distributed in Kochi Prefecture

*Akifumi Ito[1], Sachiko Agematsu[1], Yuichi Fukushima[1]

1. University of Tsukuba

Paleozoic sedimentary rocks distributed around Mt. Yokokurayama, Kochi Prefecture, are classified into the Yokokurayama Group consisting of the Gomi, Fukata, Ichiyama, Joryu, Nakahata, and Ochi formations, in ascending order. Although there have been sporadic reports and descriptions on trilobites, corals, and others macrofossils, the area is one of the best known Paleozoic fossil localities in Japan. Based on these paleontological studies, the depositional age of the Yokokurayama Group has been thought to be Silurian to Devonian. The authors are recently conducting reviews and taxonomic reexaminations of Paleozoic conodonts in Japan. In this presentation, we show a result of the study on the Yokokurayama Group.

The group is mainly made up of clastic sedimentary rocks, except for the Fukata Formation composed of carbonate rocks. The Fukata Formation, which is about 200 m in thickness, consists of light grey, massive limestones and limestone conglomerates. Kuwano (1974) reported several Ordovician and Silurian conodonts from the formation (The Ordovician specimens are thought to be a reworked assemblage). The massive limestone comprises lime mudstone an wackestone, under a microscope, and contains macrofossil fragments and very fine-sized quartz grains. Three conodont species belonging to three genera are identified from the formation: *Ozarkodina* sp., *Panderodus unicostatus*, and *Wurmiella excavata*. These species indicate that the Fukata Formation was deposited during middle to late Silurian.

Keywords: Silurian conodonts, limestone

©2020. Japan Geoscience Union. All Right Reserved.

Devonian ostracods from the Fukuji area, Takayama City, Gifu Prefecture, central Japan

*Mai Harashima[1], Sachiko Agematsu[1]

1. University of Tsukuba

Ostracods are one of the most long-ranging group of crustaceans from the Ordovician to present day. Ostracods occur in every aquatic environment and their fossils are important indicator as a palaeoenvironment. In addition, most of the Palaeozoic ostracods are benthonic or nektobenthonic. Thus, Palaeozoic ostracods have been used for analysis of palaeogeography. In Japan, while Cenozoic ostracods are well known, much less work has been done on Paleozoic ostracods. This study focuses on ostracods from the Lower Carbonate Member of the Lower Devonian Fukuji Formation, and discusses their palaeobiogeogpahy.
The Fukuji Formation located in the Fukuji area, Takayama city, Gifu Prefecture, central Japan. Fossiliferous black bedded limestone and gray massive limestone are mainly distributed in this area. These limestones are divided into four lithofacies; coral rudstone, bioclastic pack/wackestone, micrite and peloidal grainstone. Quartz grains are also included in limestones, consequently the Fukuji Formation was deposited under sallow marine near coral reefs along a continental magin. Using the method called Hot-acetolysis, 11 ostracod species belonging to 15 genera are obtained from limestone of the Lower Carbonate Member. Most of the ostracods are classified into Palaeocopida or Podocopida, thus relevant to shallower-water ostracod assemblage. In addition, the ostracods from the Fukuji Formation share species-level links with those of South China and Russia, indicating palaeogeographical relationships with those areas.

Keywords: Devonian, Hida-Gaien Belt, Fukuji Formation, ostracoda, palaeobiogeography

©2020. Japan Geoscience Union. All Right Reserved.

[E] Poster | G (General)：General

[G-01] Amazing technologies and capabilities that contribute to STEAM

convener:Day Brian Hamilton(NASA Ames Research Center), Emily Law(Jet Propulsion Laboratory), Go Murakami(Institute of Space and Astronautical Science, Japan Aerospace Exploration Agency), Kristen J Erickson(NASA Headquarters)

NASA, JAXA, and other agencies play an essential role in Education and Communication to inspire, engage and educate in the disciplines of Science, Technology, Engineering, Art, and Math (STEAM). The remarkable science discoveries, knowledge, and research are shared with audiences through a variety of technologies such as web portals, mobile apps, VR/AR applications, citizen science/crowdsourcing applications, and the serving of data as commodities for use by advanced visualization facilities including planetariums. This contributes to improving teaching and learning, increasing scientific literacy of the general public, and enriching STEAM efforts. This session seeks talks and demonstrations that: describe existing capabilities, technologies, tools and facilities that contribute to Education, Engagement and Communication; exciting projects and programs in development; and what other awesome technology ideas that will greatly benefit Education, Engagement and Communication, and STEAM. This has been an ongoing, successful session at the AGU Fall Meeting for the past 5 years and we look forward to expanding it to JpGU.

[G01-P01] Dagik Earth: 3-D digital globe for STEAM education in schools and museums

*Akinori Saito[1], Takuya Tsugawa[2], Takahito Kazama[1], Noriyuki Nishi[3], Yoshisuke Kumano[4] (1.Department of Geophysics, Graduate School of Science, Kyoto University, 2.National Institute of Information and Communications Technology, 3.Faculty of Science, Fukuoka Universtiy, 4.Graduate School of Science and Technology, Graduate School of Education, Shizuoka University)

[G01-P02] Increasing the understanding of abstract chemical concepts using VR programming

Garrison Penzo[1], Dante H Delgado[1], *Colleen M Knight[1] (1.College of Coastal Georgia)

[G01-P03] **STEAM Engagement with NASA's Solar System Treks**

*Brian Hamilton Day[1], Emily Law[2], NASA Solar System Treks Team -[2] (1.NASA Ames Research Center, 2.NASA Jet Propulsion Laboratory)

Dagik Earth: 3-D digital globe for STEAM education in schools and museums

*Akinori Saito[1], Takuya Tsugawa[2], Takahito Kazama[1], Noriyuki Nishi[3], Yoshisuke Kumano[4]

1. Department of Geophysics, Graduate School of Science, Kyoto University, 2. National Institute of Information and Communications Technology, 3. Faculty of Science, Fukuoka Universtiy, 4. Graduate School of Science and Technology, Graduate School of Education, Shizuoka University

Dagik Earth is a project to utilize a portable 3-D digital globe for STEAM education in schools and museums. 3-D digital globe is an attractive device to present scientific data of the Earth and planets, and now widely used in science museums. Geo-cosmos is a large one with 6-m diameter in Mirai-kan, Japan. Science On a Sphere (SOS) is developed by NOAA, and installed in more than 150 science museums all over the world. Dagik Earth is much simpler than these systems with much lower cost. It consists of a spherical screen, a PC projector and a PC or tablet. No special equipment is required. The software is freely available for education and science. It is used in classroom from elementary schools to universities, science museums, and science events. The flexibility of the system enables to use the 3-D digital globe in various occasions even outdoors. A join event with music concert was held in Kyoto national museum in August, 2019. The outline of the system, its usage examples and the future plan of the development will be introduced in the presentation.

Keywords: digital globe, 3-D presentation, STEAM, science education, science and music, public outreach

©2020. Japan Geoscience Union. All Right Reserved.

Increasing the understanding of abstract chemical concepts using VR programming

Garrison Penzo[1], Dante H Delgado[1], *Colleen M Knight[1]

1. College of Coastal Georgia

Chemical concepts such as the structure of the atom or the inner workings of nuclear chemistry are often difficult to convey to students. The main setback for students is the inability to visualize structures at the subatomic level. In a true interdisciplinary project, undergraduate mathematics majors teamed up with a chemistry professor to develop two programs within the Oculus platform. One program allows students to visualize the actual behavior of electrons in an atom. The other program allows users to create a theoretical nucleus and watch that nucleus undergo nuclear decay to reach the next stable nucleus. The output to the user identifies the new nucleus, and a list of decays allows the user to follow the path of decay to a stable nucleus. Both of these programs increased the understanding of chemical concepts to the undergraduate students who programmed the applications and can also serve as valuable tools to make abstract concepts more accessible in the classroom and beyond.

Keywords: Virtual Reality, Nuclear Chemistry, Atomic Structure, Undergraduate Research, Chemistry

©2020. Japan Geoscience Union. All Right Reserved.

STEAM Engagement with NASA’s Solar System Treks

*Brian Hamilton Day[1], Emily Law[2], NASA Solar System Treks Team -[2]

1. NASA Ames Research Center, 2. NASA Jet Propulsion Laboratory

NASA's Solar System Treks (https://trek.nasa.gov) online portals provide web-based suites of interactive visualization and analysis tools to enable mission planners, planetary scientists, students, and the general public to access mapped data products from past and current missions for a growing number of planetary bodies. These portals are being used for site selection and analysis by NASA and its international and commercial partners supporting upcoming missions. The portals offer great benefits for science, technology, engineering, art, and math (STEAM) education and public outreach, providing access to data from a wide range of instruments aboard a variety of past and current missions. As a component of NASA's Science Activation Infrastructure, they are available as resources for NASA STEAM programs, and to the greater STEAM community. As new missions are planned to a variety of planetary bodies, these tools facilitate public understanding of the missions and engage the public in the process of identifying and selecting where these missions will land.

During the past year, significant changes have been made to The Solar System Treks suite. New portals have been added and portals for a range of additional bodies are now in development. New visualization and analysis tools are being integrated. New data products have been ingested and new means of generating specific data products including image mosaics and DEMs have been implemented.

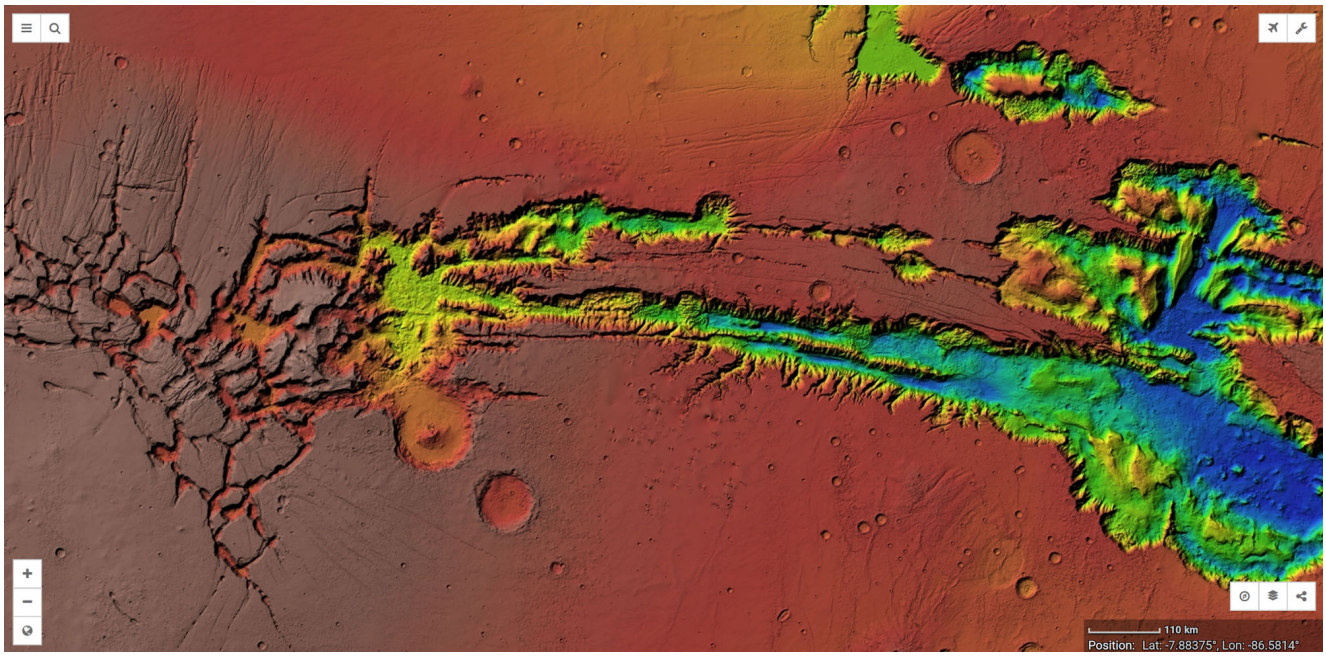
As of early 2020, there are seven web portals in the program available to the public. This expanded list includes portals for the Moon, Mars, Vesta, Ceres, and Titan. Icy Moons Trek features seven of Saturn’s smaller icy moons. The latest addition is the new Mercury Trek portal, developed in collaboration with JAXA in support of its role in the BepiColombo mission. Two new portals are scheduled for release this spring and will be showcased at JpGU: Ryugu Trek supports JAXA’s Hayabusa2 mission and Bennu Trek supports NASA’s OSIRIS-REx mission. In addition, Phobos Trek, focusing on Mars’ larger moon, is currently under development in support of JAXA’s planned MMX mission. Interfaces for the Mercury, Ryugu, and Phobos portals are being internationalized with main interface controls offered in both English and Japanese. All of the portals are unified under a new project home site with supporting content. As web-based toolsets, the portals do not require users to purchase or install any software beyond current web browsers.

The portals provide analysis tools for measurement and study of planetary terrain, allowing data to be layered and adjusted to optimize visualization. Visualizations are easily stored and shared. The portals provide interactive 3D visualization capabilities, allowing users to fly over the terrains of other worlds. Users have the ability to select terrain for generation of STL/OBJ files that can be directed to 3D printers. Such 3D prints are valuable tools in museums, public exhibits, and classrooms - especially for the visually impaired. Particularly popular is the ability for users to draw any path they want across a planetary surface using the browser interface. The system returns a QR code which the user scans into their smartphone, places their phone in an inexpensive pair of Cardboard-compatible goggles, and flies whatever path they drew in virtual reality. The program supports additional clients, web services, and APIs facilitating dissemination of planetary data to external applications and venues such as planetariums. NASA challenges and hackathons also provide members of the software development community opportunities to participate in tool development and leverage data from the portals.

©2020. Japan Geoscience Union. All Right Reserved.

While we are expanding the number of worlds covered by the project, we are paying special attention to the Moon and enhancing Moon Trek’ s capabilities supporting upcoming human and robotic missions to the Moon.

Keywords: STEAM, Education, Outreach, Planetary Science, NASA, JAXA



©2020. Japan Geoscience Union. All Right Reserved.

[E] Poster | M (Multidisciplinary and Interdisciplinary)：M-IS Intersection

[M-IS01] Tsunami deposit

convener:Daisuke Ishimura(Department of Geography, Tokyo Metropolitan University), Takashi Chiba(Faculty of Bioresource Sciences, Akita Prefectural University), Masaki Yamada(Department of Geology, Faculty of Science, Shinshu University), Takashi Ishizawa(International Research Institute of Disaster Science, Tohoku University)

The 2011 off the Pacific coast of Tohoku Earthquake and tsunami have an influence on the development of tsunami deposit research. After the tsunami, a lot of findings have been reported on various research fields. However, it is still uncertain how to use the tsunami deposit in the estimation of tsunami size and source and the risk assessment. In this session, we welcome researches from all aspect of sedimentary records of modern and paleo tsunamis both onshore and offshore, and numerical and experimental modeling studies for risk assessment. In addition, we also welcome other event deposits, such as flooding and storm surge, that they are considered to be important for discrimination of tsunami deposit.

[MIS01-P01] Distribution of tephra and tsunami deposits in Shikotan Island: Outline of the Japan-Russia joint research in 2019

*Yuichi Nishimura[1], Alexander Shishkin[2], Yasuhiro Takashimizu[3], Daisuke Sugawara[4], Takashi Ishizawa[5], Koichiro Tanigawa[6] (1.Graduate School of Science, Hokkaido University, 2.Institute of Marine Geology and Geophysics, Russian Academy of Sciences, 3.Faculty of Education, Niigata University, 4.Museum of Natural and Environmental History, Shizuoka, 5.International Research Institute of Disaster Science, Tohoku University, 6.The National Institute of Advanced Industrial Science and Technology)

[MIS01-P02] Facies description of 15 valley-filled tsunami deposits observed in Lake Tokachi-Chobushi for the past 2500 years and evaluation of their recurrence intervals

*Kiyoyuki Shigeno[1], Futoshi Nanayama[2,5], Kazuaki Watanabe[2], Masayuki Ishii[3], Keita Fukatsu[4] (1.Meiji consultant co.,Ltd., 2. Geological Survey of Japan, AIST, 3.Ishii Professional Engineer Office, 4.Notsuke Peninsula Nature Center, 5.CWMD,Kumamoto Univ.)

[MIS01-P03] Relationship between facies of tsunami deposits and paleo sedimentary environment which were reconstructed from plant macro fossils in peat

*Takashi Ishizawa[1], Yuichi Nishimura[2] (1.International Research Institute of Disaster Science, Tohoku University, 2.Institute of Seismology and Volcanology, Hokkaido University)

[MIS01-P04] Ages and distribution of paleo-tsunami deposits since 6 ka at Koyadori, Yamada Town, Iwate Prefecture, northeast Japan

*Daisuke Ishimura[1], Keitaro Yamada[2] (1.Department of Geography, Tokyo Metropolitan University, 2.Research Organization of Science and Technology, Ritsumeikan University)

[MIS01-P05] Machine-learning for correlation of tsunami deposits using geochemical proxy

*Kamiya Tomohisa[1], Kazuhisa Goto[2], Takashi Ishizawa[1], Hiroshi Tetsuka[1], Erick Velasco R.[1], Daisuke Ishimura[3], Kenta Satoh[1] (1.Tohoku University, 2.University of Tokyo, 3.Tokyo Metropolitan University)

[MIS01-P08] Numerical study of the formation process of sandy deposit formed by the 2011 Tohoku-oki tsunami

*wataru nakamura[1], Kazuhisa Goto[2], MASASHI WATANABE[3] (1.Tohoku University, 2.The University of Tokyo, 3.Chuo University)

[MIS01-P09] Reduction Effect of Tsunami Sediment Transport by Coastal Forest: Numerical Simulation of the 2011 Tohoku Tsunami on Sendai Plain, Japan

*Satoshi Kusumoto[1], Kentaro Imai[1], Aditya Gusman[2], Kenji Satake[3] (1.JAMSTEC, 2.GNS Science, 3.ERI, The University of Tokyo)

[MIS01-P10] Temporal change in sedimentological and geochemical characteristics of the 2011 Tohoku-oki tsunami deposits in the northeastern region of Fukushima Prefecture

*Kentaro Izumi[1], Ikuro Narayama[1], Tomoya Abe[2] (1.Faculty & Graduate School of Education, Chiba University, 2.Geological Survey of Japan, National Institute of Advanced Industrial Science and Technology)

[MIS01-P11] Flow reflection of onshore tsunami and features of the deposits

*Yasuhiro Takashimizu[1], Hibiki Saito[1] (1.Niigata University)

[MIS01-P12] Numerical estimation of paleotsunami size at southern part of Japan Trench based on geological records

*Hokuto Higaki[1], Kazuhisa Goto[2], Hideaki Yanagisawa[3], Daisuke Sugawara[4] (1.Tohoku University, 2.Department of Earth and Planetary Science, The University of Tokyo, 3.Department of regional Management, Faculty of Liberal Arts, Tohoku Gakuin University, 4.Museum of Natural and Environmental History, Shizuoka)

[MIS01-P13] Detailed analysis of tsunami deposits made by large-scale laboratory experiments

*Takumi Yoshii[1], Shiro Tanaka[1], Masafumi Matsuyama[1] (1.Central Research Institute of Electric Power Industry)

Distribution of tephra and tsunami deposits in Shikotan Island: Outline of the Japan-Russia joint research in 2019

*Yuichi Nishimura[1], Alexander Shishkin[2], Yasuhiro Takashimizu[3], Daisuke Sugawara[4], Takashi Ishizawa[5], Koichiro Tanigawa[6]

1. Graduate School of Science, Hokkaido University, 2. Institute of Marine Geology and Geophysics, Russian Academy of Sciences, 3. Faculty of Education, Niigata University, 4. Museum of Natural and Environmental History, Shizuoka, 5. International Research Institute of Disaster Science, Tohoku University, 6. The National Institute of Advanced Industrial Science and Technology

Historical and prehistorical tsunami deposits in Shikotan Island, the Northern Territories, were studied as parts of visa-free exchange programs of Japan and Russia. The reconnaissance survey was conducted from July 5th to 15th in 2019 in Horobetsu, Anama, Matakotan, Chiboi, and Inemoshiri. And candidates of tsunami deposits and volcanic tephra were examined at 32 sites by using a handy geoslicer and a peat sampler. As a result, In Inemoshiri, 6 candidates of tsunami deposit and 4 tephras were traced inland up to 530m from the coast. In Horobetsu, 1 candidate of tsunami deposit and 3 tephras were traced inland up to 350m from the coast. In Shikotan Island, it is reported that tephra from volcanoes of Hokkaido, such as Ko-c1 (1856), Ta-a (1739), Ko-c2 (1694), Ta-b (1667), Ma-b (10th Century) and Ta-c (2,700 BP) are deposited (Razzhigaeva et al., 2016). With these volcanic deposits as the key layer, we can estimate the age of the candidates of tsunami deposits. Our study was mainly conducted in the peatland developed in a valley facing the sea, as there are no wide and flat wetlands on the island. We needed to distinguish sandy layers caused by slope collapse and river flood from tsunami deposits based on a detailed survey of their distribution and sedimentary facies at each site.

Keywords: Shikotan Island, tsunami deposit, volcanic tephra

©2020. Japan Geoscience Union. All Right Reserved.

Facies description of 15 valley-filled tsunami deposits observed in Lake Tokachi-Chobushi for the past 2500 years and evaluation of their recurrence intervals

*Kiyoyuki Shigeno[1], Futoshi Nanayama[2,5], Kazuaki Watanabe[2], Masayuki Ishii[3], Keita Fukatsu[4]

1. Meiji consultant co.,Ltd., 2. Geological Survey of Japan, AIST, 3. Ishii Professional Engineer Office, 4. Notsuke Peninsula Nature Center, 5. CWMD,Kumamoto Univ.

It is known that M8-class trench-type earthquakes occur every 100 to several decades in the eastern Pacific coast of Hokkaido. In addition to this, it has been clarified that interlocking giant earthquakes of Mw 8.5-9 class with the epicenters off Tokachi and Nemuro offshore occur repeatedly at intervals of 300 to 500 years (Nanayama et al., 2003; Nanayama, 2020). It can be considered that the giant tsunami trace stratigraphy between Tokachi coast and Nemuro coast has been almost established by the research results of the past 20 years. However, the estimated tsunami size and recurrence period are not clear because the number of tsunami deposits differs depending on the area, even if the interval between giant tsunamis is about 300 to 500 years. In particular, the number of tsunami deposits recorded is regulated by topography and sedimentary environment. In previous studies, tsunami deposits were found to occur more frequently in sediments filling the valley topography than in the surrounding marsh environment.

Lake Tokachi-Chobushi is a brackish lake with a width of about 1.8 km and a maximum depth of about 1.5 km. It is known that a tidal inlet emerges at the southwestern edge of the lake due to the seasonal break of the sand bar. On the southern shore of this tidal inlet, large cliffs of sea cliffs of about 9 m in height appear continuously. Here, there are two fissured valleys with a width of about 50 to 100 m that erode the Upper Pliocene to Pleistocene long nodule (diatomaceous silt deposit). This valley is filled with a Holocene peat layer of about 3.5 m thickness. The fifteen tsunami-originated event sand layers are sandwiched in this peat layer. The fifteen event sand layers consist mainly of fine-grained sand to silty sand, with a thickness of several centimeters to several tens of centimeters. The base may have a sub-round to sub-angular gravels and these diameters are 1 to 2 cm. From the degree of sorting, sand particles are assumed to originate from marine sand.

Four clear Holocene tephras were interposed in the peat layer, and the top tephra was found to be Ta-b (AD 1667 eruption from Tarumai Volcano), the tephra at the bottom is assumed to be Ta-c (2.5 cal kyr BP eruption from Tarumai Volcano). Using the ages obtained from these tephras, the recurrence interval of the event sand layer for the last 2500 years is estimated to be about 150 years. This value is significantly lower than the 300-500 years thought to have been caused by the tsunami associated with the giant earthquake. In this case, it is suggested that the tsunami caused by the M8 class interplate earthquake that occurred every 100 to tens of years in the Kuril Trench is also preserved. However, it is difficult to determine the magnitude of the earthquake or tsunami that caused each event deposit by at least outcrop observation alone.

References

Nanayama, F., Satake, K., Furukawa, R., Shimokawa, K., Shigeno, K., Atwater, B.F., August 2003, Unusually

©2020. Japan Geoscience Union. All Right Reserved.

large earthquakes inferred from tsunami deposits along the Kuril Trench. Nature, 424, 660–663.

Nanayama, F., 2020, Evidence of giant earthquakes and tsunamis of the 17th-century type along the southern Kuril subduction zone, eastern Hokkaido, northern Japan: A review. (SP501) CHARACTERIZATION OF MODERN AND HISTORICAL SEISMIC–TSUNAMIC EVENTS, AND THEIR GLOBAL–SOCIETAL IMPACTS, Geol. Soc. London, DOI: 10.1144/SP501-2019-99.

Keywords: valley-filled tsunami deposit, Kuril Trench, giant earthquake, 500-year interval earthquake, Hokkaido, Pacific coast

©2020. Japan Geoscience Union. All Right Reserved.

Relationship between facies of tsunami deposits and paleo sedimentary environment which were reconstructed from plant macro fossils in peat

*Takashi Ishizawa[1], Yuichi Nishimura[2]

1. International Research Institute of Disaster Science, Tohoku University, 2. Institute of Seismology and Volcanology, Hokkaido University

Correlation of tsunami deposits is important to assess inundation area by paleotsunami. In general, correlation of tsunami deposits is conducted using facies of tsunami deposits and age marker (tephra or ^{14}C dating). However, even though some tsunami deposits were formed by same tsunami, the facies of tsunami deposits often vary due to paleo sedimentary environment. Herein, we show facies variations of tsunami deposit which were formed by same tsunami but were preserved in different sedimentary environment. Our study area is Kiritappu wetland, Hokkaido. We surveyed about 40 m^2 area of the wetland and focused on 17th and 12-13th century tsunami deposits which were already correlated in the wetland by tephrochronology. Sedimentary environment was reconstructed by analysis of plant macro fossils in peat. Our results showed that tsunami deposits formed at water place (characterized by reeds within peat) were thicker than the tsunami deposits formed at relatively dried wetland. Moreover, tsunami deposits formed at water place showed bluish color and had clear sedimentary structures such as lamina and grading. Our results indicate that correlation by tsunami deposit facies is not preferable unless sedimentary environment is discussed. Such findings were important to discuss correlation of tsunami deposits at wetland.

Keywords: tsunami deposit, subduction zone earthquakes, correlation

©2020. Japan Geoscience Union. All Right Reserved.

Ages and distribution of paleo-tsunami deposits since 6 ka at Koyadori, Yamada Town, Iwate Prefecture, northeast Japan

*Daisuke Ishimura[1], Keitaro Yamada[2]

1. Department of Geography, Tokyo Metropolitan University, 2. Research Organization of Science and Technology, Ritsumeikan University

Long-term paleo-seismic history is significant for the understanding of earthquake mechanisms and the assessment of earthquake and related hazards (e.g., tsunami). Especially, tsunami deposits research progressed after the devastating large tsunamis (e.g., the 2004 Indian Ocean earthquake and 2011 Tohoku-oki earthquake) and paleo-tsunami deposits have been identified all over the world. In the terrestrial environment, it is generally difficult to find an appropriate site for revealing the long-term paleo-tsunami history and such appropriate sites were limited due to landform development and artificial modification. It is true along the Pacific coast area in the Tohoku region, northeast Japan. However, the authors found the most appropriate site for the reconstruction of long-term paleo-tsunami history on the Sanriku Coast. This is the Koyadori site, where organic fine sediments accumulated continuously since Towada-Chuseri (To-Cu) tephra (ca. 6 ka; Mclean et al., 2018) and sediments supply from surrounding are small except for tsunami deposits. In this study, we show the ages of paleo-tsunami deposits since 6 ka and their subsurface distribution in Koyadori lowland based on dense and many excavation and drilling surveys.

From 2012 to 2015, we conducted trench excavation survey (Ishimura and Miyauchi, 2015), outcrop survey (Ishimura and Miyauchi, 2015), drilling survey (Ishimura et al., 2014), short Geoslicer survey (Ishimura et al., 2015), and long Geoslicer survey from 200 m to 400 m distance from the coastline and used these samples to this study. In the laboratory, we conducted the radiocarbon dating, tephra analysis, μXRF analysis, and gravel roundness analysis for lateral correlations of sediments. In this study, we mainly used five long Geoslicer samples. All samples reached To-Cu tephra and, that is, they record a continuous 6 thousand years history. From these samples, we confirmed that there are 14 tsunami deposits including the 2011 event after To-Cu tephra and the average recurrence interval is estimated to be 300-400 years.

Subsurface distribution of them was revealed by sedimentary facies, geochemical signature, gravel roundness, and radiocarbon dates of long Geoslicer, short Geoslicer, and drilling cores. As a result, the most appropriate site in Koyadori for tsunami deposits research is limited only 300 m to 350 m area distance from the coastline. On the other hand, in the seaside area behind the 5-m-high beach ridge (200 m to 300 m distance from the coastline), large erosion occurred a few times after To-Cu tephra and these erosions were not expected from the present topography. This indicates that we need to care buried topography and to conduct a multi drilling survey. Takeda et al. (2018) pointed out a similar thing.

This study gives us clues for tsunami deposits identification and accurate lateral correlation of sediments. Dense drilling surveys and/or continuous outcrops tell us an accurate number of tsunami deposits. Tephra layers give us robust ages and correlative layers in sediments. A geochemical signature can be used to correlate background sediments and gravel roundness is useful to identify tsunami deposits and correlate them. Radiocarbon dating gives us confirmation of the lateral correlation of sediments. We thought that this is an efficient procedure for paleo-tsunami deposits research.

©2020. Japan Geoscience Union. All Right Reserved.

Keywords: Tsunami deposits, Sanriku Coast, Towada-Chuseri (To-Cu) tephra, Roundness, Itrax, Lateral correlation of tsunami deposits

©2020. Japan Geoscience Union. All Right Reserved.

Machine-learning for correlation of tsunami deposits using geochemical proxy

*Kamiya Tomohisa[1], Kazuhisa Goto[2], Takashi Ishizawa[1], Hiroshi Tetsuka[1], Erick Velasco R.[1], Daisuke Ishimura[3], Kenta Satoh[1]

1. Tohoku University, 2. University of Tokyo, 3. Tokyo Metropolitan University

Correlation of tsunami deposits is very important to assess local tsunami size and frequency. In general, paleotsunami researchers conduct coring at several sites and correlate tsunami deposits in each core based on lithology and chronology. However, it is difficult to correlate tsunami deposits based only on lithology if the coring points are separated. Also, measuring numerous ^{14}C age is costly. Herein, we propose a methodology to correlate tsunami deposits based on geochemical features together with machine learning technique. As geochemical proxy, we measured elements of tsunami deposits by using a core scanner that can conduct non-destructive and high-resolution XRF analysis. To correlate tsunami deposits based on elemental data quantitatively, we used SVM (support vector machine), machine learning technique for classification. We compare the results of correlations by machine learning and that by conventional approach based on lithology and chronology. As a result, we found that machine learning is useful to find the possible way of correlation while it is difficult to correlate tsunami deposits based only on machine learning. Therefore, machine learning is useful for correlation of tsunami deposits as a supplementary tool of other methods, and it is beneficial for us to decrease the number of samples for dating and to enhance reliability of correlation.

Keywords: Tsunami deposits, machine learning

©2020. Japan Geoscience Union. All Right Reserved.

Numerical study of the formation process of sandy deposit formed by the 2011 Tohoku-oki tsunami

*wataru nakamura[1], Kazuhisa Goto[2], MASASHI WATANABE[3]

1. Tohoku University, 2. The University of Tokyo, 3. Chuo University

For modeling of tsunami sediment transport, grain size is generally assumed as single grain size or multiple grain size. Although there are some studies that conducted modeling under the multiple grain size condition, most studies have been performed under the single grain size. However, in the single grain size condition, we cannot calculate lateral and horizontal variations of grain size distribution of tsunami deposits, so we cannot confirm whether the model can reproduce landward and upward fining features that are commonly observed in the tsunami deposits. In this study, we simulated the sediment transport during the 2011 Tohoku-oki tsunami in order to evaluate the reproducibility of the modeling and to clarify the sedimentation process of the tsunami deposit.

Our study area is around the right bank of the Nanakita River mouth in Sendai, Japan. In this area, a detailed field survey was carried out by Abe et al. (2012), and we set a transect along their transect B. Delft3D, which is developed by deltales, was used in this study. Based on the 2011 Tohoku-oki tsunami modeling results using a source model proposed by Imamura et al. (2012), we extracted a wave profile at 2 km offshore of the transect. Then, this wave pattern was set as an incident wave for the calculation. We assumed 5 m thick movable bed uniformly from the bottom of the sea to the Teizan canal as in Watanabe et al. (2018), while landward from the canal was assumed as fixed bed. Normal distribution was assumed as grain size distribution at the movable bed based on Takashimizu et al. (2012) and Szczuciński et al. (2012); then four particle size was chosen for the multiple grain size modeling. We carried out calculations under multiple and single grain conditions (sediment 1 to 4) plus single grain size at mode diameter (354 μm) and compared each result. Manning's roughness coefficient was assumed based on a distribution map of Sugawara et al. (2014). Modeling results showed that inundation distance, flow depth and distribution of the tsunami deposit were generally consistent with those measured by Abe et al. (2012), although there were some discrepancy in the flow depth near the shoreline. Fining landward trend was not changed to the coarsening trend through the calculation. Although landward coarsening trend was locally and temporally formed, it was then changed to the fining trend through time. As a whole, our modeling results reproduced landward thinning and fining trends. Actually, the modeling results using both single mode diameter and the multiple grain size were almost similar. This is probably because normal distribution of grain size was assumed in this study and the percentage of around mode diameter is high.

Keywords: tsunami numerical simulation, multiple grain size, the 2011 Tohoku-oki tsunami

©2020. Japan Geoscience Union. All Right Reserved.

Reduction Effect of Tsunami Sediment Transport by Coastal Forest: Numerical Simulation of the 2011 Tohoku Tsunami on Sendai Plain, Japan

*Satoshi Kusumoto[1], Kentaro Imai[1], Aditya Gusman[2], Kenji Satake[3]

1. JAMSTEC, 2. GNS Science, 3. ERI, The University of Tokyo

The reduction effect of the energy of tsunami waves during their passage through coastal forest has been recognized since the 1998 Papua New Guinea tsunami and the 2004 Indian Ocean tsunami (e.g., Dengler and Preuss, 2003, PAGEOPH; Nandasena et al., 2008, JSCE). Numerical simulations conducted to investigate the effects of coastal forest on tsunamis (e.g., Shuto, 1987, Coastal Engineering in Japan; Harada and Imamura, 2005, Advances in Natural and Technological Hazards Research) have showed that tsunami height, inundation distance and flow velocity are markedly reduced by the presence of coastal forest. However, the reduction effect of coastal forest on the transport of tsunami sediments has not been evaluated. In this study, we examined the contribution of coastal forest to tsunami sediment movement by using the numerical simulation of tsunami sediment transport on Sendai plain, Japan, during the 2011 Tohoku tsunami.

To account for varying roughness coefficient in areas of coastal forest, the composite equivalent roughness coefficient was used (e.g., Aburaya and Imamura, 2002, JSCE; Imai et al., 2013, JSCE). Tree occupancy and trunk width are given as 1 %, and 0.15 m, respectively, on the basis of the previous studies (e.g., Harada et al., 2000, JSCE; Imai et al., 2009, JSCE). The area of coastal forest was determined from aerial photographs and land use maps compiled before the 2011 Tohoku earthquake.

Our results revealed that the simulated mean sediment concentration, wave height, flow velocity, and inundation limit were abruptly reduced by the presence of coastal forest. The volumes of net deposition and erosion were reduced to 52-85% of those in the simulation without coastal forest; these reductions were particularly remarkable for fine sand. The maximum extent and thickness of sand layer are also reduced. This evidence of the inhibition of sediment transport by coastal forest suggests that land use conditions and the vegetation environment at the time of a tsunami should be considered in evaluations of historical tsunamis on the basis of geological evidences.

Keywords: tsunami simulation, sediment transport modeling, coastal forest, composite equivalent roughness coefficient

©2020. Japan Geoscience Union. All Right Reserved.

Temporal change in sedimentological and geochemical characteristics of the 2011 Tohoku-oki tsunami deposits in the northeastern region of Fukushima Prefecture

*Kentaro Izumi[1], Ikuro Narayama[1], Tomoya Abe[2]

1. Faculty & Graduate School of Education, Chiba University, 2. Geological Survey of Japan, National Institute of Advanced Industrial Science and Technology

To evaluate how sedimentological and geochemical characteristics of tsunami deposits temporally change, we collected samples of the 2011 Tohoku-oki tsunami deposits and the underlying and overlying deposits at several sites in northeastern region of Fukushima Prefecture. In this study, thickness, grain size, sedimentary structures and organic-matter content of the tsunami deposits were observed and analyzed. As a result, thicknesses of the tsunami deposits do not show significant temporal change from at least 2014 to 2019. In addition, soft-X observations show that laminae are observed in tsunami deposits at several sites, suggesting that original sedimentary structures have been preserved in the past nearly 8 years. On the other hand, grain-size and organic-matter analyses of the tsunami and underlying deposits revealed that at least some portions of the tsunami deposits have been transported into the underlying deposits, resulting in sediment homogenization. It is assumed that this sediment homogenization has been caused by bioturbation mainly of meiobenthos whose body size is similar to sediment grain size.

Keywords: tsunami deposits, temporal change, Fukushima Prefecture

©2020. Japan Geoscience Union. All Right Reserved.

Flow reflection of onshore tsunami and features of the deposits

*Yasuhiro Takashimizu[1], Hibiki Saito[1]

1. Niigata University

This study aims to obtain features of the onshore tsunami deposit indicated-flow reflections based on the analyses of a block sample of the 2011 Tohoku-oki tsunami deposits in the Odaka region of Minami-Soma city, Japan. Sampling site U-07 was located 1.75 km from coastline and surrounded by artificial embankments of an approximately 3 to 4 m height in the southern and western parts. In previous studies, the flow direction of the tsunami inverted and the inflow tsunami was changed to outflow after the collision of the runup tsunami with the embankments.
According to the results of the analyses, the U-07 sample was composed of three units, namely, Units 1, 2, and 3 in ascending order. Unit 2 was further subdivided to 6 units, namely, a, b, c, d, e, and f in ascending order. Unit 1 was composed of coarse-grained sandy sediments with mud clasts by runup flow, Unit 2 of alternating beds of sand (Units 2b, d, and e) and mud (Units 2a, d, and f) from the flow inversion and outflow, and Unit 3 of the mud accumulated from suspended loads in stagnating seawater after the tsunami. Mud layers in Unit 2 were interpreted as mud drapes under water stagnation by the tsunami collision with the artificial embankments. On the other hand, sand layers in Unit 2 were the deposits from complicated flow by the tsunami collisions and outflow after the collisions.

Keywords: mud drape, 2011 Tohoku-Oki tsunami

©2020. Japan Geoscience Union. All Right Reserved.

Numerical estimation of paleotsunami size at southern part of Japan Trench based on geological records

*Hokuto Higaki[1], Kazuhisa Goto[2], Hideaki Yanagisawa[3], Daisuke Sugawara[4]

1. Tohoku University, 2. Department of Earth and Planetary Science, The University of Tokyo, 3. Department of regional Management, Faculty of Liberal Arts, Tohoku Gakuin University, 4. Museum of Natural and Environmental History, Shizuoka

In the coastal area facing to the northern and central Japan Trench, many researchers have conducted paleotsunami surveys to estimate the size and frequency of tsunamis in the past several thousand years. In contrast, the area facing to the southern part of Japan Trench has poorly been studied due to the coastal urbanization. Therefore, the elucidation of tsunami size and frequency in the southern part of Japan Trench has not been well understood in comparison with the northern and central Japan Trench. It is reported that deposits in Kobatake-ike pond in Choshi City, Chiba Prefecture, record three large tsunami events during past three thousand years; tsunami were probably triggered by the subduction zone earthquakes at southern part of Japan Trench (Yanagisawa et al., 2016). The thickness and grain size of these tsunami deposits have different in characteristics and may be important factors for constraining the tsunami size in the southern part of Japan Trench. This study applies coupled tsunami hydrodynamic and sediment transport modeling to paleotsunami deposits at Kobatake-ike pond in order to estimate the fault parameters of earthquakes and tsunamis in the southern part of Japan Trench. Source parameters of each paleotsunami events were investigated by comparing numerical simulations with thicknesses of tsunami deposits in the Kobatake-ike pond in addition to historical records of tsunami inundation, if available. Numerical simulation results revealed that the tsunami caused by the earthquake with the fault slip of 11 to 16 m and Mw of 8.34 to 8.43 repeatedly and constantly occurred in the southern part of Japan Trench. Sediment transport modeling results suggest that modeled thicknesses of the tsunami deposits in the Kobatake-ike pond sensitively reflect changes of the grain size of deposit and the fault slips. Therefore, the thickness and grain size of the tsunami deposits may provide the effective constraints for estimating fault parameters of the historic/prehistoric tsunami which has no detailed historical records.

Keywords: tsunami deposits, sediment transport modelling, southern part of Japan Trench

©2020. Japan Geoscience Union. All Right Reserved.

Detailed analysis of tsunami deposits made by large-scale laboratory experiments

*Takumi Yoshii[1], Shiro Tanaka[1], Masafumi Matsuyama[1]

1. Central Research Institute of Electric Power Industry

The characteristics of tsunami deposits can reflect the hydraulic parameters of tsunami which made the tsunami deposits. However, considerable variation of tsunami deposits in the field makes it difficult to estimate the scale of tsunami from the resulting deposits. Thus, the authors have conducted the large-scale laboratory experiment on tsunami deposits and succeeded in reproducing the deposits (Yoshii et al., 2017, 2018). In these previous studies, the hydrodynamic conditions and the resulting deposits were investigated by using bulk samples.

In this presentation, we will present detailed analysis of tsunami deposits made by these flume experiments and discuss the reproducibility of the deposits in the flume. Okazaki et al.,(2017a,b) have already indicated that the se flume tsunami deposits has the complex structures and Okazaki el al.,(2018) have discussed the similarity to the tsunami deposits in the field. Based on these results, we analyzed the structure of these flume deposits by using core samples and peer samples. The result will provide useful information for future field investigation and interpretation of tsunami deposits.

(Reference)

Yoshii, T., Tanaka S., Matsuyama M.: Tsunami deposits in a super-large wave flume, Marine Geology 391, 98–107, 2017.

Yoshii, T., Tanaka S., Matsuyama M.: Tsunami inundation, sediment transport, and deposition process of tsunami deposits on coastal lowland inferred from the Tsunami Sand Transport Laboratory Experiment (TSTLE), Marine Geology 400(1), 107–18, 2018.

Okazaki, H., Yoshii, T., Miyata, Y.: Analysis of morphology and grain fabric for Tsunami experimental deposits, The 124th Annual Meeting of the Geological Society of Japan, 2017.

Okazaki, H., Yoshii, T., Akiyama, D.: Three-dimensional analysis with high-frequency ground penetrating radar of tsunami experiment deposits, JpGU-AGU Joint Meeting, 2017.

Okazaki, H., Yoshii, T., Miyata, Y.: Tsunami deposits in a large wave flume and the 2011 Tohoku-oki tsunami, Annual meeting of the Sedimentological Society of Japan (SSJ), 2018.

Keywords: Tsunami deposit, Laboratory experiment, Sedimentary structure

©2020. Japan Geoscience Union. All Right Reserved.

[E] Poster | M (Multidisciplinary and Interdisciplinary)：M-IS Intersection

[M-IS02] Environmental, socio-economic and climatic changes in Northern Eurasia

convener:Pavel Groisman(NC State University Research Scholar at NOAA National Centers for Environmental Information, Asheville, North Carolina, USA), Shamil Maksyutov(National Institute for Environmental Studies), Evgeny P Gordov(Institute of Monitoring of Climatic and Ecological Systems SB RAS), Akiyo Yatagai(Hirosaki University)

We invite presentations on the biogeochemical cycles, the surface energy budget and water cycle, and climate and ecosystem interactions in Northern Eurasia (land-cover/land-use change, atmospheric aerosols, soil, and permafrost changes that affect and are being affected by climate and ecosystem change), human dimension, and tools to address the Northern Eurasia studies.

In environmental studies, our Session foci are on the permafrost changes in Siberia, Asian Mountains, and the Arctic coastal regions and on the carbon cycle of Northern Eurasia.

In the regional water cycle studies, our Session foci are on the changing distribution of precipitation intensity, frequency, form (solid versus liquid) and on the pattern and seasonal cycle changes of runoff.

In the human dimension studies, our Session foci are on assessments of impact of the ongoing environmental changes in Northern Eurasia on the human well-being and on mitigation strategies development in response to harmful consequences of these changes.

The particular foci of this Session will be the studies of changes that impacts regional sustainable development in Eurasian Arctic and the Drylands of Northern Eurasia.

We invite also early career scientists associated with (or interested in) the Northern Eurasia Earth Science Partnership Initiative and its continuation, Northern Eurasia Future Initiative (http://nefi-neespi.org/NEFI-WhitePaper.pdf).

[MIS02-P01] BIOAVAILABILITY OF METALS DEPENDING ON THEIR SPECIATION IN NORTHERN LOW-SALINE WATER

*Tatyana I Moiseenko[1], Marina I Dinu[1] (1.Russian)

[MIS02-P02] Divergent responses of ecosystem water-use efficiency to extreme droughts over Northern Eurasia

*Mengtian Huang[1], Panmao Zhai[1] (1.Chinese Academy of Meteorological Science)

[MIS02-P03] Homogeneity analysis of air temperature and wind speed records of the Azov-Black sea region

*Natalia Alexandrovna Lemeshko[1], Vladislav P. Evstigneev[2,3], Maxim P. Evstigneev[2], Pavel Ya. Groisman[4] (1.SPBU, 2.IPTS, 3.SevSU, 4.IORAS)

[MIS02-P04] Soil response to sub centennial climate change

*Natalia Alexandrovna Lemeshko[1], Vladislav P. Evstigneev[2,3], Alexey V. Rusakov[1], Pavel Groisman[4] (1. SPBU , 2.IPTS , 3.SevSU, 4.IORAS)

[MIS02-P05] Climate change impacts on seed quality and distribution of light-needled *Pinus sylvestris* and *Larix* spp. in Northern Eurasia in a warming climate

*Nadezhda Tchebakova[1], Elena I. Parfenova[1], Elena V. Bazhina[1], Nina A. Kuzmina[1], Pavel Y. Groisman[2] (1.Institute of Forests, Siberian Branch, Russian Academy of Sciences, 2.NC State University Research Scholar)

[MIS02-P06] Northern Eurasia Future Initiative (NEFI), Update

*Pavel Groisman[1,2,3] (1.NC State University Research Scholar at NOAA National Centers for Environmental Information, Asheville, North Carolina, USA, 2.Shirshov Institute of Oceanology, Russian Academy of Sciences, Moscow, Russia , 3.Hydrology Science and Services Corporation, Asheville, North Carolina, USA)

BIOAVAILABILITY OF METALS DEPENDING ON THEIR SPECIATION IN NORTHERN LOW-SALINE WATER

*Tatyana I Moiseenko[1], Marina I Dinu[1]

1. Russian

The bioavailability and ecotoxicity of metals are determined by their speciation, which in their turn depend on the parameters of the aqueous environment: the content of calcium, humic acids, pH, temperature and a combination with other metals. The paper highlights metal speciation calculating model which is based on mathematical modeling of the chemical reactions in natural waters. Metal concentrations (Hg, Cd, Pb, Ni, Cu, Al, Sr) were determined and their speciation in water was calculated for 22 research areas in the Kola region. At these same points, the accumulation of metals in various systems of the fish was studied (as exemplified by whitefish). It is shown that the biogeochemical activity of metals determines the ratio of labile and unlabele speciation in water. In the zones of distribution of the non-ferrous industry effluents, metal aqua-ions of the studied metals prevail; during the distribution, the ratio changes in accordance with the metals activity. The bioavailability of metal speciation is estimated depending on the aqueous geochemical conditions and, accordingly, the speciation of metals (*in situ)* based on the results of original studies in the lakes of the Kola North of Russia. The connection between the metal contents in fish and metal content in water have been identified using multidimensional scaling and RDA-techniques.

Keywords: metals, accumulation, speciation

©2020. Japan Geoscience Union. All Right Reserved.

Divergent responses of ecosystem water-use efficiency to extreme droughts over Northern Eurasia

*Mengtian Huang[1], Panmao Zhai[1]

1. Chinese Academy of Meteorological Science

Water, as one of the most basic environmental factors of terrestrial ecosystems, is of significant importance for the thermal acclimation and metabolism of terrestrial vegetation. Water availability is a major limitation to the distribution and productivity of terrestrial vegetation. At the ecosystem scale, water-use efficiency (WUE) is generally defined as the ratio of annual gross primary productivity (GPP) and annual evapotranspiration (ET). It indicates the coupling of the carbon and water gross fluxes exchanged between ecosystem and the atmosphere, and monitors the adaptability of an ecosystem to variable climate conditions. Previous researches have concluded a significant positive trend in WUE in most areas of terrestrial ecosystems over the globe, as a result of the increasing CO_2 concentration and climate change during the past several decades. At the same time, extreme climatic events, such as heat waves, drought etc., occurred across the globe. These changes have likely altered the ecological functioning of terrestrial ecosystems, as well as the structure of plant communities. Nevertheless, how terrestrial ecosystem WUE responds to extreme climatic events is still poorly understood.

In this study, we examine the impacts of extreme drought events on ecosystem WUE during 1948-2008, with a particular focus on distinguishing response of different biomes over Northern Eurasia. The responses of ecosystem WUE to extreme droughts differed among different regions. For northern high latitudes (north of 50˚N), hot days and increasing solar radiation were usually concurrent with droughts, which to some extent eliminate the limitations of low temperature and insufficient light on photosynthesis. In this case, vegetation productivity was potentially enhanced, with higher ecosystem WUE during drought years than during normal years. By contrast, for biomes in relatively arid climate conditions, extreme drought years tended to aggravate the water stress for vegetation growth. Consequently, in these regions, vegetation photosynthesis was largely suppressed with significantly lower ecosystem WUE observed. Our results, therefore, highlight that background climate is a crucial factor determining drought impacts on terrestrial carbon-water interactions. Further increases in baseline aridity could therefore exacerbate the impact of punctuated droughts on terrestrial ecosystems.

Keywords: water-use efficiency, droughts, terrestrial ecosystems

©2020. Japan Geoscience Union. All Right Reserved.

Homogeneity analysis of air temperature and wind speed records of the Azov-Black sea region

*Natalia Alexandrovna Lemeshko[1], Vladislav P. Evstigneev[2,3], Maxim P. Evstigneev[2], Pavel Ya. Groisman[4]

1. SPBU, 2. IPTS, 3. SevSU, 4. IORAS

In the study a homogeneity of long-term hydrometeorological data series of monthly air temperature and wind speed was tested using routine observations at thirteen sea coast stations of the Azov-Black Sea region for the whole period. Test for time-series homogeneity was carried out by method introduced by Wang et al. who used penalized maximal t - and F-tests to detect mean value shifts in the data with lag-1 autocorrelation. The method is implemented as a recursive testing algorithm within RHtestsV3 package for R software environment for statistical computing and graphics. Detection of inhomogeneity by means of RHtestsV3 was carried out in the mode “with a reference series” for monthly air temperature and in the mode “without a reference series” for monthly wind speed. As a result, inhomogeneity shifts supported by metadata were detected and adjusted. The main sources of heterogeneity of meteorological observations are as follows: meteorological site relocation, changes in instrument exposure due to urbanization, changes in instrument mounting and sheltering, changes in type of the instrument and terms of observations. Only 3 among 13 stations have homogeneous data series both for air temperature and wind speed. For all the rest stations, only homogeneous data series more accurately reflect climate change dynamics general for the Azov-Black Sea region. Therefore, application of adjusted climatic data series instead of initial one is reasonable for inference making about climatic tendencies in the region under study and is necessary stage of climate treatment. The validity of ready-to-use algorithm was confirmed enabling RHtestsV3 introduction into climatological datasets processing.

This work was supported by the RFBR project No. 18-05-01073

Keywords: data series inhomogeneity , climatological data series treatment, climatological inhomogeneity adjustment

©2020. Japan Geoscience Union. All Right Reserved.

Soil response to sub centennial climate change

*Natalia Alexandrovna Lemeshko[1], Vladislav P. Evstigneev[2,3], Alexey V. Rusakov[1], Pavel Groisman[4]

1. SPBU , 2. IPTS , 3. SevSU, 4. IORAS

The most inertial object of the climate system is the lithosphere, including soil. To study the impact of modern climate change on agricultural soils, which are currently under wild cenoses, a special technique is being developed. For its development, the vast territory of the Yaroslavl Volga region was selected, for which we have data on the morphological and genetic properties of agricultural soils for more than 40 years. In order to obtain a climate-dependent response of soils to the current scale of global warming, data on the evolution of soils, parent rocks, vegetation, and also the intensity of anthropogenic impact are used. The methodology is based on a comparison of the climatic component for two periods - 1961-1990 and 1991-2018. The analysis of the variability of air temperature, precipitation, temperature totals of more than 10 ˚C and agroclimatic indices for these periods. A joint analysis of changes in soil properties and climatic indicators will allow us to evaluate the speed of soil processes and soil fertility and become the basis for modeling soil climate for the future.

This work was supported by the RFBR project No. 19-29-05243.

Keywords: global warming, climate indicators, soil climate

©2020. Japan Geoscience Union. All Right Reserved.

Climate change impacts on seed quality and distribution of light-needled *Pinus sylvestris* and *Larix* spp. in Northern Eurasia in a warming climate

*Nadezhda Tchebakova[1], Elena I. Parfenova[1], Elena V. Bazhina[1], Nina A. Kuzmina[1], Pavel Y. Groisman[2]

1. Institute of Forests, Siberian Branch, Russian Academy of Sciences, 2. NC State University Research Scholar

Global simulations have demonstrated the potential for profound effects of climate change on the distribution of terrestrial ecosystems and individual species at all hierarchical levels. We modeled progressions of potential forest types, dominant tree species and their seed zones (climatypes) in Siberia during the 21st century. We developed and used large-scale bioclimatic models and statistical seed models to predict forest types and seed crops in a warming climate. All simulations were run for the baseline period 1961-1990 and for the mid- and end of the century. We ran twenty global circulation models from CMIP5 (AR5) and used two climate change scenarios RCP 2.6 (less warming) and RCP 8.5 (greater warming) to provide a range of warming. Ecological-bioclimatic modeling projects substantial vegetation changes: biomes shift northwards; area of conifer forest decreases and grasslands increases. The zone at risk of forest loss in Siberia would extend northwards. To minimize negative consequences and benefit from climate change in Siberian forests potential adaptive measures may be introduced depending on management goals. A genetic approach is to assist trees and forests to adapt to new climates by transferring seed to locations that are suitable to the seed zones of future climates. A bioclimatic model of *Pinus sylvestris* seed quality and productivity that relates seed weight and climates ($R^2 = 0.74$) was used to map the seed weight distributions in new CMIP5 RCP 2.6 and RCP 8.5 climates. Seed weight isolines would shift northwards in a warming climate: as far as 500 km in the moderate scenario and up to 1000 km in the extreme scenario. In the cold climate of Siberia pine and larch seed production may benefit from climate warming and would favor to expanding areas of productive forests.

The study was supported by RFBR grant # 20-05-00540.

Keywords: Climate change , Boreal forest, Seed zones , Seed quality and distribution, Pinus sylvestris and Larix spp. , Northern Eurasia

©2020. Japan Geoscience Union. All Right Reserved.

Northern Eurasia Future Initiative (NEFI), Update

*Pavel Groisman[1,2,3]

1. NC State University Research Scholar at NOAA National Centers for Environmental Information, Asheville, North Carolina, USA, 2. Shirshov Institute of Oceanology, Russian Academy of Sciences, Moscow, Russia , 3. Hydrology Science and Services Corporation, Asheville, North Carolina, USA

NEFI was conceived in 2015 as a successor of the Northern Eurasia Earth Science Partnership Initiative (NEESPI; ***http://neespi.org***). In 2016, a NEFI White Paper was posted at ***http://nefi-neespi.org/***. This White Paper was converted and expanded into two peer-reviewed programmatic NEFI Science Plan papers (Monier et al. 2017; Groisman et al. 2017). Being focused on the same region, the difference between two Initiatives stems from their major Science Questions: (1) NEESPI: How do Northern Eurasia' s terrestrial ecosystems dynamics interact with and alter the biosphere, atmosphere, cryosphere, and hydrosphere of the Earth? (2) NEFI: How to provide in Northern Eurasia a sustainable societal development (economy well-being, activities, health, and strategic planning) in changing climate, ecosystems, and societies? In other words, while NEESPI foci were on understanding of the processes that have and will be occurred over Northern Eurasia, NEFI foci are to answer questions about what should be done for the human well-being in the changing natural and social environments of the region. Currently, NEFI includes 30 international projects devoted to the Arctic, Eurasian boreal forest zone, and the Dry Land Belt of Northern Eurasia. Each year, the NEFI active organizes three or more dedicated NEFI Sessions at the AGU, JpGU and SCERT Conferences. NEFI Special Issue of the *Environ. Res. Lett.* is being published (currently, the Issue has 35 papers accepted and 23 manuscripts are in the review process). The deadline for the article submissions is June 30, 2020. Incomplete list of NEFI publications in 2018-2019 includes about 50 per-reviewed papers and book chapters. NEFI is open for joining of other research groups.

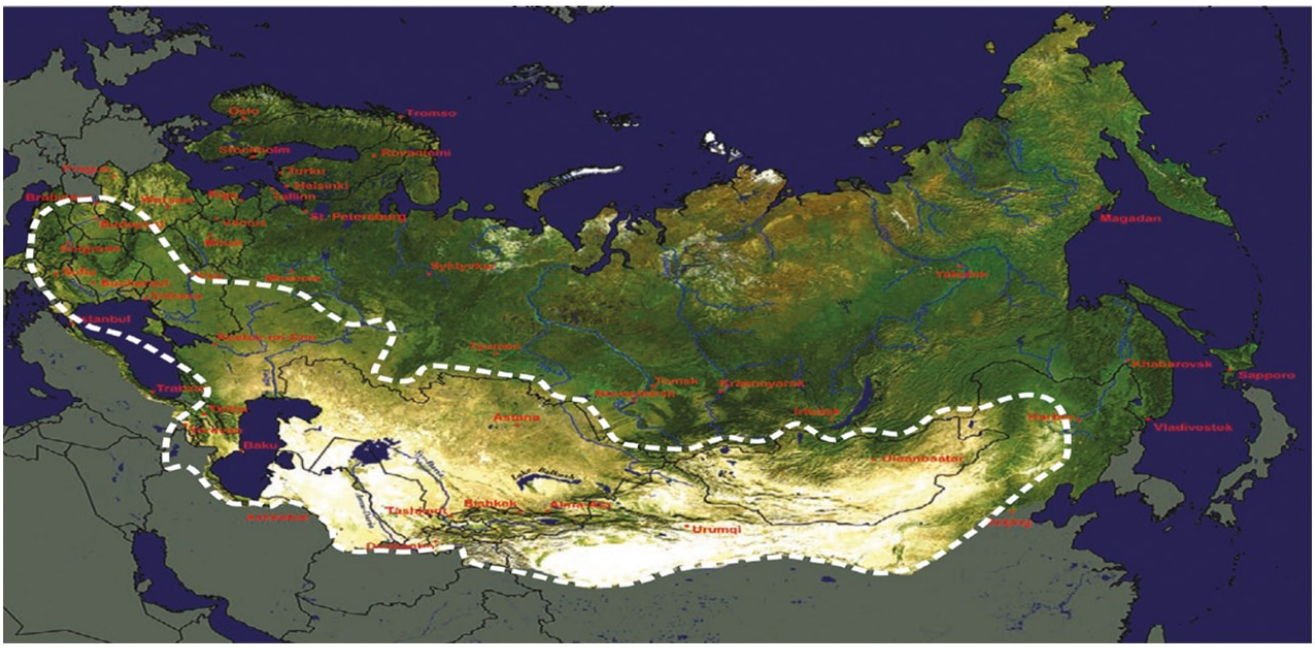
References:

Groisman et al. 2017: Northern Eurasia Future Initiative (NEFI): Facing the challenges and pathways of global change in the twenty-first century. *Progress in Earth and Planetary Science*, **4**:41.

Monier et al. 2017: A Review of and Perspectives on Global Change Modeling for Northern Eurasia. *Environ. Res. Lett.*, **12**: 083001.

Keywords: Northern Eurasia, Environment and socio-economic changes, Climate change

©2020. Japan Geoscience Union. All Right Reserved.



©2020. Japan Geoscience Union. All Right Reserved.

[E] Poster | M (Multidisciplinary and Interdisciplinary)：M-IS Intersection

[M-IS03] Structure and deformation in the overlying plate due to subduction and related feedbacks

convener:Hiroshi Sato(Earthquake Prediction Research Center, Earthquake Research Institute, The University of Tokyo), David A Okaya(University of Southern California), Eh Tan(Institute of Earth Sciences, Academia Sinica), Masahiro Ishikawa(Graduate School of Environment and Information Sciences Yokohama National University)

Subduction over time modifies the overriding plate by fractionation, accretion, and tectonic deformation. This can lead to processes such as tectonic shortening (orogeny), regional uplift, weakening by back-arc spreading and volcanism, basin formation, and/or destabilization of the lithosphere. In turn, the composition, strength, and morphology of the overlying plate, which may be the product of a long geological history and have significant along-strike variations, can affect current large-scale subduction dynamics such as slab dip, and ultimately broad-scale plate kinematics in two and three dimensions. Examples of geological settings that bear witness to these processes are found along the Pacific Rim, including Japanese arcs, Taiwan, Hikurangi, northwestern North America, and Tethys margin, including Himalaya and the Mediterranean mobile belt. We seek contributions from all geoscience disciplines that document the structure and tectonic evolution of overlying plate deformation and their feedbacks onto subduction processes. We welcome studies on topics such as: geologic and tectonic geomorphological deformation of the overlying plate and its relation to the subduction; geodetic deformation of the overlying plate; active and passive imaging of the overlying plate and crustal structure; rheological features obtained by laboratory and earthquake seismology; basin development and mountain building processes; numerical geodynamical modeling of overlying plate deformation; and backarc opening proceses. Comparisons of the Nankai and Japan Trench subduction systems to other global subduction zones are of particular interest. This session is supported by ILP (International Lithosphere Program).

[MIS03-P01] Three-dimensional seismic velocity model of the Nankai Trough subduction zone considering marine seismic reflection and onshore seismic data

*Ayako Nakanishi[1], Minako Katsuyama[1], Narumi Takahashi[1,2], Hiromi Kamata[1], Katsuhiko Shiomi[2], Shuichi Kodaira[1], Yoshiyuki Kaneda[1,3] (1.Japan Agency for Marine-Earth Science and Technology, 2.National Research Institute for Earth Science and Disaster Resilience, 3.Kagawa University)

[MIS03-P02] Deformation of the seismogenic zone in the northeastern part of the Izu Peninsula, Japan, inferred from GNSS observations

*Ryosuke Doke[1], Ryou Honda[1], Masatake Harada[1], Kazuki Miyaoka[2], Teruyuki Kato[1], Mikio Satomura[3] (1.Hot Springs Research Institute of Kanagawa Prefecture, 2.Japan Meteorological Agency, 3.Shizuoka University)

[MIS03-P03] Shift in provenance composition of Cretaceous Japan arc: from Jurassic granitoids/accretionary complex to Cretaceous granitoids

*Ryo Hasegawa[1], Yukio Isozaki[1], Atsushi Yamamoto[3], Yukiyasu Tsutsumi[2] (1.The University of Tokyo, 2.National Museum of Nature and Science, 3.Kindai University)

[MIS03-P04] High-resolution seismic profiles in the Shonai plain and Yamagata basin, northern Honshu, Japan

*Naoko Kato[1], Tatsuya Ishiyama[1], Hiroshi Sato[1], Shin Koshiya[2], Taro Koike[3], Katsuya Noda[3] (1.Earthquake Research Institute,University of Tokyo, 2.Faculty of science and engineering, Iwate University, 3.Geosys, Inc.)

[MIS03-P05] Seismic transect across the central part of Northern Honshu, Japan

*Hiroshi Sato[1], Tatsuya Ishiyama[1], Hirokazu Ishige[2], Naoko Kato[1], Masanao Shinohara[1], Takaya Iwasaki[1,6], Eiji Kurashimo[1], Hidehiko Shimizu[2], Shinji Kawasaki[2], Susumu Abe[2], Makoto MATSUBARA[3], Shin Koshiya[4], Tetsuo No[5], Shuichi Kodaira[5], Naoshi Hirata[1] (1.Earthquake Prediction Research Center,

Earthquake Research Institute, The University of Tokyo, 2.JGI, Inc., 3.National Research Institute for Earth Science and Disaster Resilience, 4.Iwate University, 5.Japan Agency for Marine-Earth Science and Technology, 6.Association for the Development of Earthquake Prediction)

Three-dimensional seismic velocity model of the Nankai Trough subduction zone considering marine seismic reflection and onshore seismic data

*Ayako Nakanishi[1], Minako Katsuyama[1], Narumi Takahashi[1,2], Hiromi Kamata[1], Katsuhiko Shiomi[2], Shuichi Kodaira[1], Yoshiyuki Kaneda[1,3]

1. Japan Agency for Marine-Earth Science and Technology, 2. National Research Institute for Earth Science and Disaster Resilience, 3. Kagawa University

Three-dimensional seismic velocity model must be necessary for forecasting earthquakes and tsunami events more reliably as well as determination of hypocenters with high-resolution around the Nankai Trough. Although Nakanishi et al. (2018) first constructed the three-dimensional seismic velocity model, it was mainly based on results of marine seismic refraction survey. To construct more realistic model, results of marine seismic reflection surveys must be also considered into the three-dimensional model that will be able to explain the seismic reflection data. In this study, we try to upgrade the three-dimensional model by integrating the results of marine seismic reflection surveys. In particular, seismic interfaces interpreted by both seismic refraction and reflection surveys are all adjusted in the time domain. Precise velocity structure of the shallow sediments estimated by using seismic reflection data are preferentially used to construct the three-dimensional model. Geometry of the plate interface beneath the Shikoku island estimated by receiver function analysis by using onshore seismic observation give more well-determined and reliable information for deep structure. In this presentation, we show an upgraded three-dimensional model considering marine seismic reflection and onshore seismic data.
This study is part of 'Research project for compound disaster mitigation on the great earthquakes and tsunamis around the Nankai trough region' and the project 'Comprehensive evaluation of faults information on offshore Japan' funded by Ministry of Education, Culture, Sports, Science and Technology, Japan.

Keywords: Three-dimensional seismic velocity model

©2020. Japan Geoscience Union. All Right Reserved.

Deformation of the seismogenic zone in the northeastern part of the Izu Peninsula, Japan, inferred from GNSS observations

*Ryosuke Doke[1], Ryou Honda[1], Masatake Harada[1], Kazuki Miyaoka[2], Teruyuki Kato[1], Mikio Satomura[3]

1. Hot Springs Research Institute of Kanagawa Prefecture, 2. Japan Meteorological Agency, 3. Shizuoka University

The Izu collision zone, which is characterized by the collision between the Izu-Bonin arc and the Honshu arc, is located in the northernmost part of the Philippine Sea Plate. Particularly in the northeastern margin of the zone, numerous large earthquakes have occurred throughout history. To clarify the convergent tectonics of this zone related to the occurrence of these large earthquakes, in this study we collected and analyzed Global Navigation Satellite System (GNSS) observation data from the Izu collision zone.

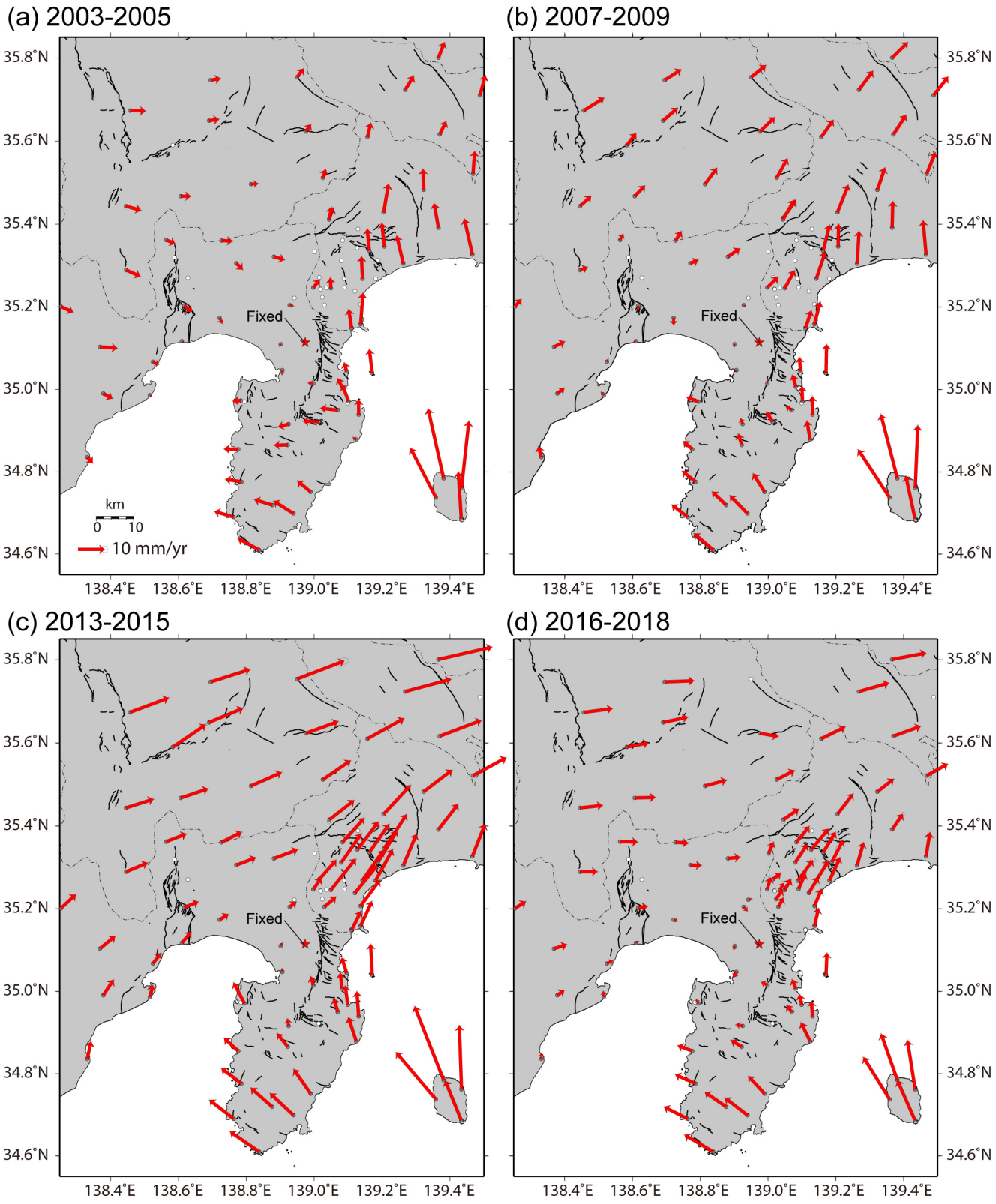
We used observation data from our GNSS sites, as well as other sites, to calculate the velocity vectors and strain rate fields of the region in and around the Izu Peninsula in central Japan. Our calculations provided the following results:
•The GNSS velocity vectors in the eastern and western parts of the Kita-Izu Fault Zone are different; in particular, the sites located farther east have larger northward velocities in the area between the fault zone and the Ashigara Plain.
•There is a shear deformation zone in the area extending from the northeastern part of the Izu Peninsula to south of the Tanzawa Mountains, with maximum shear directions that agree with the left-lateral slip direction of the Kita-Izu Fault Zone.
•Seismic activities in the Tanzawa Mountains and the northeastern part of the Izu Peninsula were correlated. This might suggest that both areas are affected by temporal changes in stress accumulation due to the subduction of the Philippine Sea Plate.
•The deformation rate obtained by GNSS data is almost the same as or twice the geologically determined deformation rate. This fact is important when considering the relationship between the accumulation process of deformation in the shear zone and the occurrence of large earthquakes at the West Sagami Bay Fracture or the Sagami Trough.
•The shear zone can be regarded as the transition zone between plate collision and subduction zones: that is, the northeastern part of the Izu Peninsula is being dragged by the relative motion between the separated Izu Peninsula and the North American Plate, which is coupled to the rigid portion of the Philippine Sea Plate.
•We assumed the existence of a weakly coupled detachment zone beneath the shear deformation zone. This can explain both the northward velocities in the shear zone and the divergent displacement and dyke intrusion in the Higashi-Izu Monogenetic Volcano Group.

Reference

Ryosuke Doke, Ryou Honda, Masatake Harada, Kazuki Miyaoka, Teruyuki Kato, Mikio Satomura (2020) Deformation of the seismogenic zone in the northeastern part of the Izu Peninsula, Japan, inferred from GNSS observations, *Geological Society, London, Special Publications*, 501, https://doi.org/10.1144/SP501-2019-104

Keywords: Izu collision zone, Crustal deformation, GNSS, Shear deformation, Plate motion, Seismic activity

©2020. Japan Geoscience Union. All Right Reserved.



©2020. Japan Geoscience Union. All Right Reserved.

Shift in provenance composition of Cretaceous Japan arc: from Jurassic granitoids/accretionary complex to Cretaceous granitoids

*Ryo Hasegawa[1], Yukio Isozaki[1], Atsushi Yamamoto[3], Yukiyasu Tsutsumi[2]

1. The University of Tokyo, 2. National Museum of Nature and Science, 3. Kindai University

U-Pb dating of detrital zircons in shallow marine/fluvial sandstones is effective in reconstructing distributary pattern of terrigenous clastics within ancient active continental margins, e.g., the differentiation of fore-arc, intra-arc, and back-arc basins. The Japan segment of Cretaceous arc-trench system in East Asia experienced an episodic formation of crustal rocks, such as arc granitoids, accretionary complexes, and blueschists; nonetheless, details in secular change of arc-related sedimentary basins and their provenance were not fully clarified. This study investigated detrital zircon chronology of the Late Jurassic and Early Cretaceous fore-arc sandstones (18 samples) in SW Japan from Kyushu to Kii peninsula, central Japan. We obtained the following results. 1) During the Late Jurassic to Valanginian (163-133 Ma), pre-Cretaceous (with Proterozoic) zircons were supplied steadily to the fore-arc domain, 2) after the Hauterivian, their abundance started to decrease, and 3) after the Albian, Cretaceous zircons predominated in the fore-arc, whereas pre-Cretaceous ones became almost absent throughout the Late Cretaceous. In contrast, in intra-arc and back-arc domains, older zircons were constantly supplied till the end-Cretaceous. This major change in provenance likely reflected the emergence of a major topographic relief composed of Cretaceous arc granitoids that performed as a significant barrier for older grain flux to the fore-arc domain. The significant arc magmatism and emplacement of voluminous arc-granitoids during the Cretaceous may have first induced surface erosion of the overlying Jurassic accretionary complexes (sandstones with abundant Proterozoic and Paleozoic detrital zircons) that were intruded by the Cretaceous granitoids primarily in mid-shallow crustal levels, and then the erosion of arc granitoids *per se*.

Keywords: U-Pb age, provenance, detrital zircon, fore-arc, SW Japan, Cretaceous

©2020. Japan Geoscience Union. All Right Reserved.

High-resolution seismic profiles in the Shonai plain and Yamagata basin, northern Honshu, Japan

*Naoko Kato[1], Tatsuya Ishiyama[1], Hiroshi Sato[1], Shin Koshiya[2], Taro Koike[3], Katsuya Noda[3]

1. Earthquake Research Institute,University of Tokyo, 2. Faculty of science and engineering, Iwate University, 3. Geosys, Inc.

Understanding the relationship between active fault and seismic source fault with more detailed structural data on source faults is crucial to estimate seismic hazards, . For this purpose, we carried out seismic reflection profiling to illuminate geometry of blind thrusts in the Shonai plain and Yamagata basin, Northeast Japan. Three seismic lines (Yuza, Nakanomata and Amarume) are located across the central to eastern margin of the Shonai plain to image underlying blind thrust structures, and Sagae line crosscuts the western margin of Yamagata plain to image fault-related folds above a west-dipping thrust. The length of seismic line is 6-12 km. In seismic data collection, we used vibrator trucks as a seismic source and deployed 10 Hz geophones at 10 m interval covering whole seismic line. Seismic shots with sweep frequencies of 5-100Hz were provided at all midpoints of receivers and corresponding seismic signals were recorded by fixed 600-1000 channels of seismic recorders. The obtained seismic data were processed using conventional common midpoint (CMP) reflection methods. All of seismic sections successfully illuminate subsurface images down to 2 seconds in two-way travel time, and depth converted seismic sections show detailed structures of fault-related folds above blind thrust faults and east-dipping reflectors in 1.5km depth in the Amarume and Nakanomata seismic line.

©2020. Japan Geoscience Union. All Right Reserved.

Seismic transect across the central part of Northern Honshu, Japan

*Hiroshi Sato[1], Tatsuya Ishiyama[1], Hirokazu Ishige[2], Naoko Kato[1], Masanao Shinohara[1], Takaya Iwasaki[1,6], Eiji Kurashimo[1], Hidehiko Shimizu[2], Shinji Kawasaki[2], Susumu Abe[2], Makoto MATSUBARA[3], Shin Koshiya[4], Tetsuo No[5], Shuichi Kodaira[5], Naoshi Hirata[1]

1. Earthquake Prediction Research Center, Earthquake Research Institute, The University of Tokyo, 2. JGI, Inc., 3. National Research Institute for Earth Science and Disaster Resilience, 4. Iwate University, 5. Japan Agency for Marine-Earth Science and Technology, 6. Association for the Development of Earthquake Prediction

Northern Honshu, Japan, is known as a classic example of compressive island arc forming a trench-arc-backarc basin. To understand the crustal deformation and the mechanisms devastative earthquakes in the overriding plate, construction of numerical model is needed. To construct an advanced numerical model, the information of lithospheric structure is essential. We conducted a seismic profiling across the central part of Northern Honshu using controlled sources in summer of 2019. The seismic line crosses the epicentral area of the 2011 Tohoku-oki earthquake (M9). For constructing a numerical model on crustal deformation the structural investigation whole lithosphere is required. We aimed two step approach to obtain total lithospheric structure; one is using a controlled source and the other is by passive recording. Here we describe the results of onshore seismic reflection profile the crustal structure obtained by deep seismic reflection profiling. The length of onshore seismic line is 160 km within the total 850-km-long seismic line from Japan trench to the Yamato bank. The air-gun shots in the forearc and backarc sides were recorded by onshore seismic line using 1616 fixed channels. Onshore seismic sources were four vibroseis trucks and three dynamite shots. To obtain the deep crustal image, we used low-frequency signals. The produced sweep frequency by vibroseis trucks was 3 to 40 Hz and seismic signals were recorded by 4.5 and 5 Hz geophones. Sets of 150 stationary vibroseis sweeps were produced at about 10 km interval along the seismic line. Conventional CMP reflection processing and refraction tomography revealed the crustal structure down to 10 km. Together with the velocity structure obtained by earthquake tomography (Matsubara et al., 2019). Lithospheric structure is estimated by velocity structure obtained from active and passive sources, and geological data. With seismic reflection profiles in the forearc (Miura et al., 2005) and backarc (No et al., 2014), the onshore seismic section portrays the first image of the seismic reflection profile across the Northern Honshu arc from the trench to the backarc basin. The basic structure of the overlying plate were formed by the rifting of backarc opening stage. Most of the active faults inherited from the Miocene normal faults. The formation of backarc basins were achieved by the development of multi-rift systems. An axial part of failed rift within a continental crust is marked by a higher P-wave velocity lower crust, thick post-rift sediments underlaid by thick basalts. The failed rift is bounded by faults dipping to the outward of rift axis associated with mafic intrusion in a rift axis. The reverse faulting of the rift-bounding faults produced a fold-and-thrust belt in the post-rift Neogene basin fill. Judging from the tectonic geomorphological and geological features, these faulting and fault-related folding are active in late Quaternary. Detachment in this fold-and-thrust belt commonly accommodates in over pressured mudstone units in the rift basin. The major style of deformation of backarc is basement involved normal faults. Reactivation as reverse fault concentrated along the backarc continental failed rift.

Keywords: Trench-arc-backarc system, Deep Seismic reflection profiling, Seismogenic source faults, Backarc rifting, Northern Honshu

©2020. Japan Geoscience Union. All Right Reserved.

[E] Poster | M (Multidisciplinary and Interdisciplinary)：M-IS Intersection

[M-IS04] An asteroid impact in SE Asia at 0.8 Ma and its effect on the environment and biota

convener:Ryuji Tada(Department of Earth and Planetary Science, Graduate School of Science, The Univeristy of Tokyo), Paul A Carling(University of Southampton), Wickanet Songtham(Nakhon Ratchasima Rajabhat University, Thailand), Kerry Sieh(Nanyang Technological University)

The impact of a small celestial body in Indochina Peninsula at 0.79 Ma, known as Australasia Tektite event (AATE), has been known for more than half a century due to the wide-spread distribution of tektite. Yet, the source crater of the tektite is not yet found inspite of the probable large size (>30 km in diameter) of crater, its relatively young age, and intensive search by many researchers. However, the situation is changing rapidly during the last several years and the area for the location of the crater is gradually narrowed down. Also, the evidence of environmental perturbation and possible relation with local extinction and migration of hominid and animals has been suggested recently.
In addition, because its timing is close to the Matsuyama/Brunhes paleomagnetic reversal event and in the middle of glacial lowstand during MIS 20, precise age of AATE and its relation with glacio-eustatic sea level changes should have a significant implication to Quaternary chronostratigraphy.
For these reasons, we propose a special interdisciplinary session on the location, mode, magnitude, and exact timing of the AATE impact and its possible effect on the environment and biota
The topic should be of major interest to geologists, sedimentologists, planetary scientists, paleontologists, paleoclimatologists, anthropologists, and so on, especially to those working in SE Asia. Thus adequate topic for JpGU-AGU joint meeting.

[MIS04-P01] Discovery of Australasian microtektites in the hemipelagic sediments of the Japan Sea: It's significance and implications

*Ryuji Tada[1,2,3], Toshihiro Tada[3], Jumpei Yoshioka[4] (1.Geo-Cosmology Center, Chiba Institute of Technology, 2.Research Center for Earth System Science, Yunnan University, 3.Department of Earth and Planetary Science, the Univeristy of Tokyo, 4.Atmospheric and Ocean Research Institute, the University of Tokyo)

[MIS04-P02] Ejection behavior after hypervelocity oblique impacts in an atmosphere

*Kosuke Kurosawa[1], Ryota Moriwaki[1], Kojiro Suzuki[2], Takafumi Matsui[1] (1.Planetary Exploration Research Center, Chiba Institute of Technology, 2.Department of Advanced Energy, Graduate School of Frontier Sciences, The University of Tokyo)

[MIS04-P03] Shock-induced vitrification affected on cathodoluminescence of quartz: possibility as a shock barometer and its potential application to natural impact samples

*Yu Chang[1], Masahiro KAYAMA[2], Eiichi Tajika[1], Yasuhito Sekine[3], Toshimori Sekine[4], Hirotsugu nishido[5], Takamichi Kobayashi[6] (1.Department of Earth and Planetary Science, Graduate School of Science, The University of Tokyo, 2.Department of General Systems Studies, Graduate School of Arts and Sciences, The University of Tokyo, 3.Earth-Life Science Insitute, Tokyo Institute of Technology, 4.Center for High Pressure Science and Technology Advanced Research, 5.Research Institute of Natural Science, Okayama University of Science, 6.National Institute for Materials Science)

[MIS04-P04] Evaluation of shock deformation of the basement sandstone around the probable impact site of Australasian Tektite Event using synchrotron X-ray diffraction analysis

★Invited Papers

*Toshihiro Tada[1], Masahiro KAYAMA[2], Yu Chang[1], Akira Miyake[3], Yohei Igami[4], Ryuji Tada[1,5,6], Paul A Carling[7], Wickanet Songtham[8], Eiichi Tajika[1] (1.Department of Earth and Planetary Science, The University of Tokyo , 2.Department of Multi-Disciplinary Sciences, The University of Tokyo , 3.Division of Earth and Planetary Sciences, Kyoto University , 4.Institute of Materials and Systems for Sustainability, Nagoya University, 5. Planetary Exploration Research Center, Chiba Institute of Technology, 6.Research Center for Earth System Science, Yunnan University, 7.Geography and Environmental Science, University of Southampton, 8. Northeastern Research Institute of Petrified Wood & Mineral Resources, Nakhon Ratchasima Rajabhat University)

[MIS04-P05] Quaternary stratigraphy and occurrence of the Australasian tektites in Thailand, Laos PDR, and Cambodia: implication of the impact location

*Wickanet Songtham[1], Ryuji Tada[2], Paul A Carling[3], Toshihiro Tada[2], Praphas Chansom[1] (1.Nakhon Ratchasima Rajabhat University, Thailand , 2.The University of Tokyo, Japan, 3.The University of Southampton, United Kingdom)

[MIS04-P06] Assessment for BPCA method as biomass burning proxies and their application to meteorite impact event

*Song Lu[1], Youhei Yamashita[2], Tomohisa Irino[2], Toshihiro Tada[3], Ryuji Tada[3] (1.Graduate School of Environmental Science, Hokkaido University , 2.Faculty of Environmental Earth Science, Hokkaido University, 3.Department of Earth and Planetary Science , Graduate School of Science, The University, of Tokyo)

[MIS04-P07] Converging lines of evidence for burial of the Australasian impact crater within the Bolaven volcanic field, Southern Laos

*Kerry Sieh[1], Jason Herrin[1], Dayana Schonwalder Angel[1], Vanpheng Sihavong[2], Brian Jicha[3], Brad Singer[3], Weerachat Wiwegwin[4], James Daniel Paul Moore[1], Paramesh Banerjee[1], Tawachai Chualaowanich[4], Punya Charusiri[5] (1.Earth Observatory of Singapore, Nanyang Technological University, 639798 Singapore, 2.Department of Geology and Mines, Ministry of Energy and Mines, Vientiane, Lao People's Democratic Republic, 3.Department of Geoscience, University of Wisconsin–Madison, Madison, WI 53706, 4.Department of Mineral Resources, Ministry of Natural Resources and Environment, Ratchatewi, 10400 Bangkok, Thailand, 5.Department of Geology, Chulalongkorn University, Khet Pathumwan, 10330 Bangkok, Thailand)

Discovery of Australasian microtektites in the hemipelagic sediments of the Japan Sea: It’s significance and implications

*Ryuji Tada[1,2,3], Toshihiro Tada[3], Jumpei Yoshioka[4]

1. Geo-Cosmology Center, Chiba Institute of Technology, 2. Research Center for Earth System Science, Yunnan University, 3. Department of Earth and Planetary Science, the Univeristy of Tokyo, 4. Atmospheric and Ocean Research Institute, the University of Tokyo

Tektite is a glass material formed from terrestrial debris ejected during a meteorite impact. (Sub)millimeter-scale tektites are called microtektites. Tektites occur in four strewn fields and Australasian strewn field is the youngest (ca. 0.8 Ma) and the largest (>10% of the Earth surface) of them. Previous studies revealed asymmetric distribution of the Australasian microtektites with the most distant distribution toward the southeast from southeast Asia to Antarctica. Although the exact location of the impact has not yet been identified, recent studies suggest the location as in southern Laos. Because location and magnitude of the impact can be estimated based on distribution of microtektites, to precisely define the distribution of microtektites is important.

During IODP Expedition 346, Tada et al. (2015) found possible microtektites at site U1422 in the northern part of the Japan Sea from the horizon immediately below the Matsuyama-Brunhes boundary. Here we report the occurrence of microtektites from this horizon at site U1422 and the equivalent horizon at U1426. Microtektites are mostly spherical with some teardrop and dumbbell forms of ca. 100 mm in diameter, transparent and pale olive green in color. Major element composition of microtektite agree well with that of Australasian microtektites reported in previous literatures. The Quaternary hemipelagic sediments of the Japan Sea are characterized with millennial-scale alternations of dark and light layers that can be traced throughout the deeper part of the sea, and the microtektite horizons at the two sites shows parallel relationship with dark layers immediately above and below it, suggesting they are synchronous, supporting primary ejecta origin.

Discovery of Australasian microtektite at site U1422 extends northeastward distribution of Australasian microtektite by ca. 2500 km, almost double the extent in northeastward direction. Microtektite flux to site U1426 is >500 particles/cm^2, which is much larger than expected. It is possible that previous studies overlooked microtektites of less than 125 mm because they used >125 mm fraction to look for microtektites. The result of this study suggests that distribution of Australasian microtektites could be much larger than previously suggested. It is possible that Australasian microtektite horizon can be distributed widely in northwest Pacific.

Keywords: Australasian tektite, microtektite, IODP Expedition 346, the Japan Sea, site U1422, site U1426

©2020. Japan Geoscience Union. All Right Reserved.

Ejection behavior after hypervelocity oblique impacts in an atmosphere

*Kosuke Kurosawa[1], Ryota Moriwaki[1], Kojiro Suzuki[2], Takafumi Matsui[1]

1. Planetary Exploration Research Center, Chiba Institute of Technology, 2. Department of Advanced Energy, Graduate School of Frontier Sciences, The University of Tokyo

It is believed that the Australasian strewn field is an outcome after an hypervelocity oblique impact. The impact must occur in a thick Earth’ s atmosphere, resulting in an intense interaction between ejected materials and the surrounding atmosphere. Here, we report about a new experimental apparatus to investigate the impact outcomes after hypervelocity impacts under an atmosphere. The system has been installed to a hypervelocity impact laboratory at Planetary Exploration Research Center of Chiba Institute of Technology. The system is consist of a two-stage light gas gun, a vacuum chamber with a gas inlet and with two glass view ports that face each other, a high-speed video camera, and a pulsed-diode laser-light source. In addition, we constructed a Schlieren imaging optics between the light source and the camera to visualize the flow field driven by an downrange moving ejecta plume. We could capture Schlieren images with the time resolution of 0.2 microsecond. By using the system, we conducted a series of hypervelocity oblique-impact experiments with polycarbonate projectiles 4.8 mm in diameter. The impact velocity was ranged from 2.7 km/s to 6.9 km/s. The impact angle was fixed at 45 degrees measured from the target surface. Three different targets, which are made of polycarbonate, aluminum, and copper, were used to examine the effects of the shock impedance of the target materials on the ejection behavior. After the air in the chamber was evacuated, we introduced N_2 or Ar gas into the chamber up to 6.0 kPa. We observed a downrange moving ejecta plume and an intense atmospheric interaction with the surrounding gas as a strong self-emission in the visible range. We found that the morphology of the ejecta plume depends on both impact velocity and the target materials. In the poster presentation, we will discuss about possible environmental perturbations after the hypervelocity oblique impact.

Keywords: The Australasian strewn field, Hypervelocity oblique impacts, atmospheric interaction

©2020. Japan Geoscience Union. All Right Reserved.

Shock-induced vitrification affected on cathodoluminescence of quartz: possibility as a shock barometer and its potential application to natural impact samples

*Yu Chang[1], Masahiro KAYAMA[2], Eiichi Tajika[1], Yasuhito Sekine[3], Toshimori Sekine[4], Hirotsugu nishido[5], Takamichi Kobayashi[6]

1. Department of Earth and Planetary Science, Graduate School of Science, The University of Tokyo, 2. Department of General Systems Studies, Graduate School of Arts and Sciences, The University of Tokyo, 3. Earth-Life Science Insitute, Tokyo Institute of Technology, 4. Center for High Pressure Science and Technology Advanced Research, 5. Research Institute of Natural Science, Okayama University of Science, 6. National Institute for Materials Science

Impact cratering is a ubiquitous process on terrestrial planets and asteroidal bodies in the solar system. Many researches focus on impact craters on the Earth to reveal details of planetary-scale shock metamorphism. In particular, quantification of shock pressure that minerals in meteorites and impactites have experienced leads to a clue to understanding a partition of the impact energy and cratering mechanism on Earth as well as terrestrial planet and asteroids. Quartz, which is one of the most abundant and widely distributed rock-forming minerals on the Earth’ s crust, has been widely used to evaluate shock pressure on the impactite. However, the conventional shock barometer based on the mineralogical features of quartz, such as observation of planer deformation features (PDFs), are no more than a qualitative approach. Hence, it is required for a more detailed and accurate evaluation of shock pressure to develop a new advanced method using quartz.

Recently, we clarified the drastic change of cathodoluminescence (CL) features of quartz due to shock metamorphism [1]. The blue CL emission intensity (450-460 nm) of quartz increases drastically with the experimentally shock-induced pressure and reaches up to 100 times as large as that of the starting materials. The mechanism for the increase in the blue CL intensity can be explained by a combination of Dauphine twin generation and shock-induced vitrification. Because of the monotonical response to shock pressure, the blue CL intensity of the shocked quartz could be used as a new shock barometer [1]. In this study, we measured natural samples of quartz in impactite from the Chicxulub Crater drill core (YAX-1) in order to verify its application as shock barometer using CL for the natural crater samples.

The two core samples named Unit 1 (ejecta from impact-produced tsunami deposit) and Unit 5 (impact melts) were extracted from the YAX-1 core and selected for CL analyses. The extracted quartz grains form these samples were measured by microphotography of the PDFs orientation and the qualitatively estimated shock pressures of the quartz grains are < 15 Gpa for Unit 1, and 25 - 40 GPa for Unit 5 [2].

Quartz samples from Chicxulub crater exhibit similar CL profile to shock experimental quartz samples. Both natural samples show two peaks; CL spectra of Unit 1 samples consist of a pronounced peak at ~440 nm and a broad peak at ~630 nm. On the other hand, Unit 5 samples have a weak peak at ~440 nm and the peak at ~630 nm with relatively high CL intensity. As Unit 5 samples originate from impact melt which have experienced a high-temperature effect, post-impact annealing could affect the original blue CL emission of the quartz samples. Unit 1 samples, ejecta from the tsunami deposit, would have experienced lower degree of post-impact annealing than Unit 5 samples. These facts suggest that blue CL emission could be used as a shock barometer for natural impact samples which were not strongly affected by post-shock annealing. The quantitative pressure estimation and applicable scope of CL to natural impact samples will be also discussed.

©2020. Japan Geoscience Union. All Right Reserved.

[1] Chang et al., (2016) JpGU Meeting, PSS11-P21.

[2] Chang et al., (2018) MAPS 53, 7, 1323-1340.

Keywords: Shocked quartz, cathodoluminescence, shock metamorphism

©2020. Japan Geoscience Union. All Right Reserved.

Evaluation of shock deformation of the basement sandstone around the probable impact site of Australasian Tektite Event using synchrotron X-ray diffraction analysis

*Toshihiro Tada[1], Masahiro KAYAMA[2], Yu Chang[1], Akira Miyake[3], Yohei Igami[4], Ryuji Tada[1,5,6], Paul A Carling[7], Wickanet Songtham[8], Eiichi Tajika[1]

1. Department of Earth and Planetary Science, The University of Tokyo , 2. Department of Multi-Disciplinary Sciences, The University of Tokyo , 3. Division of Earth and Planetary Sciences, Kyoto University , 4. Institute of Materials and Systems for Sustainability, Nagoya University, 5. Planetary Exploration Research Center, Chiba Institute of Technology, 6. Research Center for Earth System Science, Yunnan University, 7. Geography and Environmental Science, University of Southampton, 8. Northeastern Research Institute of Petrified Wood & Mineral Resources, Nakhon Ratchasima Rajabhat University

Shocked quartz has been the most commonly used mineral as a barometer of shock metamorphism in the terrestrial impact structures, because of its abundance, durability, and tendency to develop striking and unique deformation features depending on the degree of shock pressure. Various methods have been developed to evaluate the shock pressure that the minerals experienced, such as optical and electron microscope, Raman and cathodoluminescence spectroscopy, and X-ray diffraction (XRD) analyses. However, it is still difficult to quantitatively evaluate the degree of shock metamorphism under the lower range (5–15 GPa) of shock pressure.

Quartz powder samples highly compressed above 25 GPa by shock experiments are known to exhibit lattice expansion that is detected by laboratory powder XRD analyses. However, the lattice expansion of quartz shocked below 25 GPa could not be monitored by a laboratory X-ray diffractometer, resulting in the impossibility of determination of shock pressure in the lower range. In this study, we applied synchrotron XRD analysis, with quite higher energy resolution and X-ray beam intensity than the laboratory instrument, in order to detect a change of lattice constants of quartz in the wide range of shock pressure from 5 to 40 GPa. The experimentally shocked quartz samples, not grinded, were subject to the synchrotron XRD analysis using a high-resolution diffractometer with a multidetector system on beamline BL4B2 at the Photon Factory in the High Energy Accelerator Research Organization (KEK PF). Synthetic Si powder was selected for a standard material for wave energy calibration, leading to monitoring a change of lattice constants at $0.001^\circ\theta$ resolution.

The result of the synchrotron XRD analysis revealed that with increasing shock pressure, the lattice constants of quartz slightly increase in the low shock pressure range of 5–15 GPa and drastically in the high range of 20–30 GPa. Quartz samples shocked above 35 GPa show no XRD signals, indicating that the amorphization has been completed. Similar drastic changes of the lattice constants in the pressure range of 20–30 GPa and absence of XRD signals above 35 GPa have been reported in the previous laboratory XRD analyses. The lattice expansion recognized in the low shock pressure range of 5–15 GPa is up to 0.00059(6) Å (0.01%) for the constant *a*, 0.0003(1) Å (0.006%) for the constant *c* and 0.034(6) $Å^2$ (0.03%) for the cell volume *V*. All of the values cannot be explained by the above-mentioned sample and analytical errors. As this pressure range is corresponding to appearances of mechanical twins and planar deformation features (PDFs), this slight lattice expansion might be caused by a change of quartz structure due to these low-grade shock-induced microtextures. This result indicates that the measurement of lattice constants of quartz by synchrotron XRD analysis is useful to evaluate lower (5–15 GPa) range of shock deformation.

©2020. Japan Geoscience Union. All Right Reserved.

Then we applied this technique to the basement Mesozoic sandstones around the probable impact site of Australasian Tektite Event. The basement sandstone samples were taken from 18 sites in northeastern Thailand and southern Laos. The synchrotron XRD analysis of quartz extracted from the sandstone samples by chemical treatments was conducted to determine the values and distribution of shock pressure around the probable impact site.
The result of the synchrotron XRD analysis demonstrated that the lattice constants of quartz increase eastward, from northeastern Thailand to the southern part of the Thailand-Laos border. The lattice expansion is up to 0.00028(6) Å (0.006%) for the constant *a*, 0.0003(1) Å (0.005%) for the constant *c* and 0.018(6) $Å^2$ (0.02%) for the cell volume *V*. This spatial variation of the lattice constants of quartz in the basement Mesozoic sandstone indicates that the degree of shock deformation increase to the Thailand-Laos bordar and that the impact took place somewhere in the area around the border.

Keywords: Australasian Tektite, Shocked metamorphism, synchrotron X-ray diffraction analysis

©2020. Japan Geoscience Union. All Right Reserved.

Quaternary stratigraphy and occurrence of the Australasian tektites in Thailand, Laos PDR, and Cambodia: implication of the impact location

*Wickanet Songtham[1], Ryuji Tada[2], Paul A Carling[3], Toshihiro Tada[2], Praphas Chansom[1]

1. Nakhon Ratchasima Rajabhat University, Thailand , 2. The University of Tokyo, Japan, 3. The University of Southampton, United Kingdom

Quaternary sediments and stratigraphy in northeastern Thailand, southern Laos PDR, and northeastern Cambodia have been investigated and studied. A 0.8 Ma tektite-bearing sedimentary layer was recognized in association with basal breccia sediments ranging in sizes from pebbles to granules regarding as a key bed layer representing a 0.8 Ma marker. The tektites were mainly splash-form with some Muong Nong-type, layered, at some places. They were mainly discovered as floated specimens on ground surface but some tektites were on site as in situ occurrence at a certain stratigraphic position mostly along the interface between the basement and the key bed layer generally coated by iron oxide as ferricreted layers. These in situ tektites were widely discovered in Thailand, Laos PDR, and Cambodia. The basements supporting the key bed layer are gravel and sand deposits with petrified woods in general as well as the Mesozoic sandstone bedrocks. Some gravel deposits overlay the Cenozoic basalt flows whereas some basalt gravels are also of constitution of the gravel deposits. Whereas, the sediments over the tektite-bearing key bed are widely distributed over the region characterized by structureless reddish orange fine-sand deposits with basal breccia granules and pebbles in association with some in situ tektites regarding as ejecta materials. The stratigraphic succession over the key bed were vertically and laterally varied over the region. In Thailand and Cambodia, they were characterized as tektite-bearing fine sand deposits that is clearly visible in northeastern Thailand designated as some soil series by the Land Development Department with thickness ranging from 3 to 5 meters. The basal part of the ejecta deposits varied into pebbles of sandstone fragments in Laos clearly visible in some areas of Salavan Province. This type of sediments is probably hidden under the younger basalt flows in the areas of the Bolaven Plateau. This Quaternary stratigraphic succession and the occurrence of the Australasian tektites can be speculated that the impact location is highly reliable that it is at a location within the southern Laos PDR around 0.8 Ma.

Keywords: Australasian tektites, basal breccia, impact location, Indochina

©2020. Japan Geoscience Union. All Right Reserved.

Assessment for BPCA method as biomass burning proxies and their application to meteorite impact event

*Song Lu[1], Youhei Yamashita[2], Tomohisa Irino[2], Toshihiro Tada[3], Ryuji Tada[3]

1. Graduate School of Environmental Science, Hokkaido University , 2. Faculty of Environmental Earth Science, Hokkaido University, 3. Department of Earth and Planetary Science , Graduate School of Science, The University, of Tokyo

Behavior of black carbon (BC) is crucial for the earth surface environment because it could cause global warming by absorbing sunlight in the atmosphere. BC is originated from incomplete combustion of biomass or fossil fuels. Combustion in natural processes is incomplete due to local limitation of oxygen during the fire, which leads to the formation of organic fire residues. Robustness of BC to degradation in the natural environment enables us to use BC as a proxy to study the driving force of frequency and burning temperatures of past wildfire events. But the previous fire researches did not discuss the BC archives of fire remnants caused by meteorite impact.

Objective of this study is to reconstruct the thermal field during Australasian Tektite Event (AATE) and its impact on climate change. For these purposes, the burning temperatures were estimated for ejecta deposits and charcoal samples through measurement of composition of benzene polycarboxylic acids (BPCAs), molecular markers of fire residues, determined with High Performance Liquid Chromatography (HPLC).

It has been suggested that the location of the impact crater is in eastern part of Indochina peninsula. Surge and air-fall deposits were sampled from the outcrop at Huai Om section site (HO), in NE Thailand. HO section consists of Units1, 2, and 3 in ascending order. Unit1 consists of alternating beds of granular fine-medium sand and silt with red shale fragment. Unit2 is characterized by inversely graded granular to pebbly sand. Unit3 is homogenous fine-medium sand with granules. Plant debris were also collected in Ban Tha Chang, which may have undergone pyrolysis during the AATE event.

The concentration of BPCA in Units2 and 3 sediments are 5 times higher than sediments from Unit1 in HO site. The fire temperature estimated from B6CA (%) indicate that the charcoal in Units2 and 3 sediments experienced a fire above 500 ˚C, while those in Unit1 were burnt by a fire of only 400 ˚C. We speculate that the charcoal in sediments formed by surge and air-fall contains charcoals from different environments of burning temperature.

The concentration of BPCA in plant debris samples are about 10 mg/g, all of them from low temperature fires (< 400℃). The estimated burning temperature for two plant debris samples from Ban Tha Chang show higher BPCA concentrations and higher fire temperatures than one sample from Ban tha Chang and the other from NR1 site. Although all the sampling sites are closely located, the BPCA compositions showed that the bark and core of these plant debris experienced different pyrolysis temperatures.

Keywords: Biomass burning, Benzene polycarboxylic acid, Australasian Tektite Event

©2020. Japan Geoscience Union. All Right Reserved.

Converging lines of evidence for burial of the Australasian impact crater within the Bolaven volcanic field, Southern Laos

*Kerry Sieh[1], Jason Herrin[1], Dayana Schonwalder Angel[1], Vanpheng Sihavong[2], Brian Jicha[3], Brad Singer[3], Weerachat Wiwegwin[4], James Daniel Paul Moore[1], Paramesh Banerjee[1], Tawachai Chualaowanich[4], Punya Charusiri[5]

1. Earth Observatory of Singapore, Nanyang Technological University, 639798 Singapore, 2. Department of Geology and Mines, Ministry of Energy and Mines, Vientiane, Lao People's Democratic Republic, 3. Department of Geoscience, University of Wisconsin–Madison, Madison, WI 53706, 4. Department of Mineral Resources, Ministry of Natural Resources and Environment, Ratchatewi, 10400 Bangkok, Thailand, 5. Department of Geology, Chulalongkorn University, Khet Pathumwan, 10330 Bangkok, Thailand

Physical and chemical characteristics of the Australasian tektites suggest that they originated within the Thai-Lao Khorat Plateau, and more specifically within the 100,000 km^2 inner strewnfield of Muong Nong-type tektites. The lack of an obvious crater and very low rates of erosion in this region imply that the crater must lay buried. Several converging lines of evidence imply that indeed the 0.8-Ma impact crater is buried beneath the 350-m thick summit flows of the 5,000-km^2 Bolaven volcanic field in southern Laos. Chemical compositions of the tektites indicate the presence of a weathered basaltic component that had accumulated mostly during the few million years before the impact. Accordingly, ^{40}Ar-^{39}Ar dates from distal lava flows can be traced uphill to weathered pre-impact basalts now buried beneath younger flows of the summit impact region. Also as predicted by the hypothesis, all ^{40}Ar-^{39}Ar dates from exposed flows at and near the impact region post-date the impact. Moreover, a gravity anomaly there may reflect the presence of a buried ~15 km wide elliptical crater with low-density fill. We interpret a thick deposit of crudely layered, bouldery sandstone and mudstone breccia in two outcrops 10–20 km from the center of the impact crater to be part of the proximal ejecta blanket. Fractured quartz grains within these boulder clasts lend support to this interpretation of an impact origin of these peculiar deposits. A pebbly, cobbly layer that extends and thins for more than 100 km from the impact site, almost everywhere containing angular muong nong tektites, comprises the more distal part of the ejecta blanket. Commonly, atop this layer is a massive, meters-thick coarse-silty to fine-sandy layer that we interpret to be partially or largely comprised of fallout of fine debris driven and convected into the atmosphere during and immediately following the impact. In this talk, we will present available physical and geochronologic evidence for the Bolaven impact as the source for the Australasian tektite strewnfield. In an accompanying contribution, we will present correlative geochemical evidence.

©2020. Japan Geoscience Union. All Right Reserved.

[E] Poster | M (Multidisciplinary and Interdisciplinary) : M-IS Intersection

[M-IS05] Cenozoic Evolution of the Asian Monsoon and the Indo-Pacific Paleoclimates

convener:Masanobu Yamamoto(Faculty of Environmental Earth Science, Hokkaido University), Steven C Clemens(Brown University), Hongbo Zheng(Research Center for Earth System Science, Yunnan University), Ryuji Tada(Department of Earth and Planetary Science, Graduate School of Science, The Univeristy of Tokyo)

The Asian monsoon (AM) and the El Nino-Southern Oscillation (ENSO) are dominant atmospheric-ocean phenomena on the Earth and affect the climates of Asia, Oceania and circum-Pacific regions. During the Cenozoic, the climate of these areas changed drastically, but the behaviors of the Asian monsoon and the tropical ocean-atmosphere interactions like the ENSO were not fully understood. From July 2013 to December 2016, IODP conducted a series of expeditions such as 346 (Asian Monsoon), 353 (Indian Monsoon Rainfall), 354 (Bengal Fan), 355 (Arabian Sea Monsoon), 356 (Indonesian Throughflow), 359 (Maldives Monsoon and Sea Level), 361 (Southern African Climate), and 363 (Western Pacific Warm Pool) that are related to the AM and tropical Pacific climate evolution and its interaction with global climate system in NW and tropical Pacific and Indian Ocean regions, and exciting results are coming out. We believe it is timely to start synthesizing the results of these cruises and update and exchange information and ideas to promote our understanding of the AM and tropical Pacific evolution, variability, their controlling factors, and their interaction with global climate system during the Cenozoic. On orbital and millennial timescales, studies on the response of the AM and the ENSO to climate forcing are intensively studied using various archives such as sediments, speleothems, corals, etc., during the last decade. Presentations and discussions on the above topics from various backgrounds (proxy and modeling studies) are highly welcome.

[MIS05-P01] Isotope analysis of Neogene marine sediment from Maldives

*Yuka Tatera[1], Katsuyuki Yamashita[1], Tsuyoshi Ishikawa[2], Mayuri Inoue[1] (1.Okayama University, 2.Kochi Institute for Core Sample Research, JAMSTEC)

[MIS05-P02] Human activities during last 700 years as recorded in the concentrations of polycyclic aromatic hydrocarbons and pentacyclic triterpene methyl ethers in sediment cores from Lake Suigetsu

*Masaya Inagaki[1], Hideto Nakamura[2], Masanobu Yamamoto[1], Takeshi Nakagawa[3] (1.Graduate School of Environmental Science, Hokkaido University, 2.Faculty of Science, Osaka City University, 3.Research Center for Palaeoclimatorogy, Ritsumeikan University)

[MIS05-P03] Reconstruction of paleoclimate changes in the region where the Okhotsk culture flourished over the past 2,700 year

*Ryuichi Seto[1], Osamu Seki[2], Masanobu Yamamoto[3], Takuya Itaki[4] (1.Graduate School of Environmental Science, Hokkaido University, 2.Institute of Low Temperature Science, Hokkaido University, 3.Facility of Environmental Earth Science, Hokkaido University, 4.Geological Survey of Japan, AIST)

[MIS05-P04] Fluvio-sedimentary response to late Quaternary climate at the Himalayan frontal thrust, central Nepal

*Mari Hamahashi[1], Judith Hubbard[1], Samuel Haines[1], Rafael Almeida[2], Edgardo Latrubesse[1], Sanjita Mishra[3], Lewis Owen[4], Soma Nath Sapkota[3] (1.Earth Observatory of Singapore, Nanyang Technological University, 2.Yachay Technical University, Ecuador, 3.Department of Mines and Geology, National Seismological Center, Nepal, 4.North Carolina State University, USA)

[MIS05-P05] Tropical western Pacific hydrology during the last 6000 years based on charcoal records from Borneo

*Masanobu Yamamoto[1], Takafumi Kikuchi[1], Hiromichi Sakurai[1], Ryoma Hayashi[2], Osamu Seki[1], Takafumi Omori[3], Abdullah Sulaiman[4], Hasrizal Shaari[5], Lulie Melling[6] (1.Faculty of Environmental Earth Science, Hokkaido University, 2.Lake Biwa Museum, 3.The University of Tokyo, 4.Minerals and Geoscience Department Malaysia, 5.Universiti Malaysia Terengganu, 6.Tropical Peat Research Institute)

Isotope analysis of Neogene marine sediment from Maldives

*Yuka Tatera[1], Katsuyuki Yamashita[1], Tsuyoshi Ishikawa[2], Mayuri Inoue[1]

1. Okayama University, 2. Kochi Institute for Core Sample Research, JAMSTEC

The South Asian Monsoon (SAM) is one of the most intense climatic elements mainly affecting around India. Betzler et al. (2016) suggested that the SAM was established around 12 Ma from the presence of drift sediment, but it has not yet been clarified in detail when and how it developed. In this study, we analyzed Pb and Sr isotope ratios in marine sediments from the Maldives in order to understand the variation of wind direction and its relation to the development of the SAM. Lead has four naturally occurring stable isotopes, and when the lead mineral is formed, the lead isotope is sequestered from the parent nuclide, at which point the change in the lead isotope ratio stops. Lead is not subject to significant physical and chemical isotope fractionation, making lead isotope a potential tool to determine the origin of lead bearing minerals. In addition, since the ocean tends to have a uniform Sr isotope composition in terms of dissolved Sr, it is possible to estimate the input balance of the region such as inflow of Sr from the continent based on the measurements of Sr isotope ratios.
In this study, the core of Site U-1468 (4 ˚56′N, 73 ˚4′E) drilled during the cruise of the International Ocean Discovery Program Exp.359, which has an age from ~25 to 10 Ma, was used for the analysis of Pb and Sr isotope ratios. The core is characterized by coral reefs around it with dead bodies piled up and rich in carbonate components. Therefore, the sample was chemically separated into carbonate and non-carbonate components and Pb and Sr were purified on each type of sample. The isotope ratios were analyzed using TIMS (Finnigan MAT262) for both Pb and Sr and MC-ICP-MS (NEPTUNE) for Pb, and the contents of Pb and Sr in 5% of the sample were measured by ICP-MS (Aglient 7700x).
As a result of the measurement of Pb isotope ratio of Maldives sediment, both carbonate component and non-carbonate component show a trend in which the ^{206}Pb / ^{204}Pb increases from around 13 Ma when the drift sediment was developed. In this study, the carbonate component has a systematically higher Pb isotope ratio than that of the non-carbonate component which is similar to that reported from the Himalayas (Wilson et al., 2015). For the Sr isotope ratios, $^{87}Sr/^{86}Sr$ in the carbonate components has a value close to that of seawater, that may reflect the influence of the surrounding seawater. On the other hand, variation of $^{87}Sr/^{86}Sr$ in the non-carbonate components behaves differently from that in seawater before 13 Ma, suggesting another input of Sr around this age.

©2020. Japan Geoscience Union. All Right Reserved.

Human activities during last 700 years as recorded in the concentrations of polycyclic aromatic hydrocarbons and pentacyclic triterpene methyl ethers in sediment cores from Lake Suigetsu

*Masaya Inagaki[1], Hideto Nakamura[2], Masanobu Yamamoto[1], Takeshi Nakagawa[3]

1. Graduate School of Environmental Science, Hokkaido University, 2. Faculty of Science, Osaka City University, 3. Research Center for Palaeoclimatorogy, Ritsumeikan University

Polycyclic aromatic hydrocarbons (PAHs) are formed by burning of biomass or fossil fuel. Pentacyclic triterpene methyl ethers (PTMEs) are biomarkers that typically derive from graminoid plants. The presence of these compounds indicates human activities, for example, industrial burning, agriculture, and so on. In this study, we analyzed PAHs and PTMEs in sediment cores (SG06 and SG17 LIMNOS cores) from Lake Suigetsu in Fukui Prefecture. The concentration of PAHs peaks around 1945 C.E., indicating intense biomass burning near the study site. We suppose that this reflects the structural fires caused by air-attacks in the neighboring cities such as Tsuruga and Maizuru. The ratio of specific PAHs changed during the studied period, suggesting changes in the usage of biomass and fossil fuels. The relative amount of PTMEs, i.e., Sawamilletin and Miliacin, changed in 1320 C.E. and 1530 C.E. This suggests a change in graminoid vegetation around the study site, which might be related to historical shifts in cropping system.

©2020. Japan Geoscience Union. All Right Reserved.

Reconstruction of paleoclimate changes in the region where the Okhotsk culture flourished over the past 2,700 year

*Ryuichi Seto[1], Osamu Seki[2], Masanobu Yamamoto[3], Takuya Itaki[4]

1. Graduate School of Environmental Science, Hokkaido University, 2. Institute of Low Temperature Science, Hokkaido University, 3. Facility of Environmental Earth Science, Hokkaido University, 4. Geological Survey of Japan, AIST

The Okhotsk Culture, which is characterized by marine hunting lifestyle, is different from the culture peculiar to other regions of Japan, and thus is wrapped in many mysteries. Okhotsk culture was transformed into Tobinitai Culture around A.D. 10 century and ended. Climate change has been proposed to be one of the reasons for the demise of the culture (Onishi, 1996). However, the relationship between climate change and Okhotsk culture is not well understood because of the lack of detailed paleoclimate records in the region where Okhotsk culture prospered. In this study, we generate high-resolution paleoclimate records in the northern Hokkaido and south Okhotsk Sea over the past 2,700 years based on organic and isotope geochemical techniques in order to better understand the causal relationship between the regional climate and Okhotsk culture.

Terrestrial paleoclimate is reconstructed from a peat core collected from Sarufutsu wetland in northern Hokkaido while a paleoceanographic change in the Okhotsk Sea is derived from a marine sediment core taken from off the coast of Shari, Okhotsk Sea. We apply the hydrogen isotope ratio of plant leaf wax, as well as the mineral content to estimate the change in the hydrological cycle in terrestrial realm where the Okhotsk culture has flourished. On the other hand, SST is reconstructed from TEX_{86} temperature proxy, while sea ice change is reconstructed from the stable carbon isotope ratio of phytoplankton derived C_{16} fatty acid. TEX_{86} based SST record shows that long-term cooling trend over the past 2,700 years with the rapid cooling around 800 years ago, which corresponds to the late stage of Medieval Climate Anomaly. In this presentation, we discuss the regional climatic impact on Okhotsk culture based on multiple paleoclimate records obtained from terrestrial and marine paleoclimate achieves.

Keywords: Okhotsk Culture

©2020. Japan Geoscience Union. All Right Reserved.

Fluvio-sedimentary response to late Quaternary climate at the Himalayan frontal thrust, central Nepal

*Mari Hamahashi[1], Judith Hubbard[1], Samuel Haines[1], Rafael Almeida[2], Edgardo Latrubesse[1], Sanjita Mishra[3], Lewis Owen[4], Soma Nath Sapkota[3]

1. Earth Observatory of Singapore, Nanyang Technological University, 2. Yachay Technical University, Ecuador, 3. Department of Mines and Geology, National Seismological Center, Nepal, 4. North Carolina State University, USA

Indo-Asian monsoonal fluctuations throughout the late Quaternary have likely altered the depositional environment in the frontal Himalaya. The Indian summer monsoon is responsible for more than 80% of the annual rainfall in the subtropical regions of the Himalayan foreland to the Indo-Gangetic-Bengal basin, significantly impacting river discharge and sediment flux in the system. The effect of monsoon on sedimentation (deposition vs incision), however, exhibit regional variabilities. While downstream variations may be explained by sediment supply tapering off downstream and increased effect of sea-levels on rivers, variations among other areas in the frontal foreland are not well understood, and are likely due to the differences in the size of the river/catchment, the distance downstream, and the amount of tectonic activity.

To reconstruct the late Quaternary evolution of the fluvio-sedimentary environment at the frontal foreland of central Nepal, we study the sedimentary facies and chrono-stratigraphy over the last 50 ky from ten boreholes across the Main Frontal Thrust there, using optically stimulated luminescence and radiocarbon dating. Previous seismic survey along the riverbed imaged ~100 m thick sediments above the incised bedrock, and onlap of strata onto folded strata, implying recent enhanced effect of sedimentation and changes in river base-levels (Almeida et al. 2018). Drilling penetrated 50-100 m of these sediments below the surface. We observe three types of facies along the depth: (a) poorly-sorted gravels with silt to sand, interpreted to be coarse-grained braided channel facies, (b) moderately-sorted silt to sand with gravels sandwiched by thin floodplain silts, interpreted to be fine-grained braided channel facies, and (c) massive, well-sorted clayey silt with bioturbation, alternating redox state and occasional sand beds, interpreted to be fluvio-lacustrine facies. Facies (c) likely deposited in a depocenter formed by the damming of the river due to the uplift on the thrust anticline. A major transition from facies (b) and (c) to facies (a) occurred at the early Holocene to latest Pleistocene (~12-13 ka, or slightly younger), inferred from preliminary age results, in which sediments were finer prior to this period, and coarser afterwards.

Given the sediment age range and the observed variations in <~40 ky timescales, the most relevant features comparable are likely to be monsoonal climate variations. The observed facies transition around the early Holocene likely coincide with the strengthened monsoon that is reported at ~15-12 ka and ~10-6.5 ka from cave speleothems in northern India (Sinha et al. 2005; Dutt et al. 2015), correlating with the time the northern hemisphere summer solar insolation increased towards the peak, around the Bolling-Allerod interstadial and/or across the last glacial to interglacial boundary. We interpret that strengthened monsoon have led to increased river discharge and advance of coarse bedload-dominant braided channels. Weak monsoon periods, in contrast, decreased river discharge and formed finer-grained channel environment with high lateral mobility.

Further age results from the samples will enable to constrain the variations in deposition rates, and the timing of incision and on-lap surfaces imaged in the seismic section. Deposition rates infer rates of aggradation and/or progradation, reflecting sediment supply, which is not necessarily dependent on river

©2020. Japan Geoscience Union. All Right Reserved.

discharge. Monsoon have likely affected the base-levels through varying river discharge and sediment supply.

Understanding the large-scale processes that govern sediment supply and base-levels in the foreland will allow us to generalize the processes elsewhere and help in interpreting various rates from sediment age including tectonic deformation. Study of sedimentary processes and the effect of climate in these depositional fan systems will impact our overall understanding of sediment fluxes within this large system.

Keywords: Himalayan foreland basin, Indian monsoonal climate, Main Frontal Thrust

©2020. Japan Geoscience Union. All Right Reserved.

Tropical western Pacific hydrology during the last 6000 years based on charcoal records from Borneo

*Masanobu Yamamoto[1], Takafumi Kikuchi[1], Hiromichi Sakurai[1], Ryoma Hayashi[2], Osamu Seki[1], Takafumi Omori[3], Abdullah Sulaiman[4], Hasrizal Shaari[5], Lulie Melling[6]

1. Faculty of Environmental Earth Science, Hokkaido University, 2. Lake Biwa Museum, 3. The University of Tokyo, 4. Minerals and Geoscience Department Malaysia, 5. Universiti Malaysia Terengganu, 6. Tropical Peat Research Institute

Borneo is one of the islands between the tropical Pacific and Indian Oceans. The climate is tropical, and both temperature and precipitation are high year-round. The precipitation is influenced by both the Asian winter monsoon the El Niño-Southern Oscillation (ENSO). Today, the ENSO regulates the frequency of forest fires in Borneo. In El Nino years, the frequency of forest fires is significantly higher, due to low precipitation and dry environments.
In this study, we generated 6200-year long charcoal records from Borneo peats to understand changes in hydrology in the western Pacific region on centennial and millennial timescales and what regulated precipitation in Borneo. Charcoal in sediments is a good proxy of forest fires. We retrieved peat cores from five different sites in northwestern Borneo.
In each site, charcoal abundance show large fluctuation. The peaks are correlated between five different locations. This correspondence suggests that charcoal abundance reflect regional environmental changes rather than local factors. The abundance peak of charcoal in Borneo peats appeared every several hundred years, showing a 560-year periodicity, reflecting regional dry-wet cycles in Borneo. Higher charcoal abundance corresponded to higher solar irradiance and El Niño (Moy et al., 2002) from about 4000 to 1000 years BP, but the relationship was not clear and even reverse in other periods. The variation is consistent with stalagmite δ18O records from inland China and central India. This suggests a linkage of tropical climatic dynamics and the Asian summer monsoon on multi-centennial timescale.

Keywords: fire history, Borneo, Charcoal, Holocene

©2020. Japan Geoscience Union. All Right Reserved.

[E] Poster | M (Multidisciplinary and Interdisciplinary)：M-IS Intersection

[M-IS06] Dust

convener:Ishizuka Masahide(Kagawa University), Yasunori Kurosaki(Arid Land Research Center, Tottori University), Thomas Sekiyama(Meteorological Research Institute), Kana Nagashima(Japan Agency for Marine-Earth Science and Technology, Research and Development Center for Global Change)

Mineral dust is generated from the ground surface by strong winds, and it transports long distance over the earth. In the process, cloud formation and absorption and scattering of solar radiation cause weather and climate changes. Also, when deposited in the ocean, feeding nutrients to phytoplankton, promoting photosynthesis, and when deposited on snow and ice causes albedo change. This is known as the yellow dust (Asian dust) phenomenon in Asia region including Japan. In order to understand this, integration in a wide range of academic areas is necessary.
 In the emission process, the amount of dust changes greatly depending on the surface conditions in dryland area, and in order to know the effect, it is necessary to deal with broad areas such as soil, topography, vegetation, precipitation, desertification and soil deterioration. In the transport process, we deal with areas such as weather, atmospheric aerosol, radiation. In the deposition process, we deal with areas such as ocean, snow ice, health to people and livestock. Drying and changes in vegetation also have social scientific aspects such as national policies, management of livestock, and population increase. In addition, dust and sand dunes are common phenomena not only in the Earth but also in other planets such as Mars and Saturn. In this way, it is impossible to understand the dust phenomenon only from one field, it is important for researchers in many areas to discuss and share information through this session, and advance exchange of researchers.

[MIS06-P01] Detection of aeolian dust in a sedimentary sequence at Tsujita Site

*Haranosono Daichi[1], Shin Toyoda[1], Kenji Nagai[2], Toshirou Naruse (1.Okayama Univesity of Science, 2.Aichi Gakuin University)

[MIS06-P02] Effect of stone on threshold friction velocity in Tsogt-Ovoo, Mongolia: Observation and Model simulation

*Batjargal Buyantogtokh[1], Yasunori Kurosaki[1], Masahide Ishizuka[3], Tsuyoshi T Sekimaya[2], Taichu Y Tanaka[2], Atsushi Tsunekawa[1], Mitsuru Tsubo[1] (1.Arid Land Research Center, Tottori University, 2.Japan Meteorological Agency, Meteorological Research Institute, 3.Faculty of Engineering and Design, Kagawa University, Japan)

[MIS06-P03] Monitoring dry-season vegetation mass at a dust hotspot (Tsogt-Ovoo) in the northern Gobi Desert

*Jing Wu[1], Yasunori Kurosaki[1], Ganatsetseg Batdelger[2], Adrian Chappell[3], Ishizuka Masahide[4], Batjargal Buyantogtokh[1] (1. Arid Land Research Center, Tottori University, 2.Information and Research Institute of Meteorology, Hydrology and Environment, Mongolia, 3.School of Earth and Ocean Science, Cardiff University, UK, 4.Faculty of Engineering and Design, Kagawa University)

[MIS06-P04] Wind tunnel experiment on sand saltation splash by using a high-speed camera

*Ishizuka Masahide[1], Yasunori Kurosaki[2], Hiroaki Hagino[3], Kazuki Nanko[4], Gantsetseg Batdelger[5], Yukio Yasuda[4], Satoru Suzuki[6] (1.Kagawa University, Faculty of Engineering and Design, 2.Tottori University, Arid land research center, 3.Forestry and Forest Products Research Institute, Tohoku Research Center, 4.Forestry and Forest Products Research Institute, Department of Disaster Prevention, Meteorology and Hydrology, 5.Information and Research Institute of Meteorology Hydrology and Environment, Mongolia, 6.Forestry and Forest Products Research Institute, Center for Forest Damage and Risk Management)

Detection of aeolian dust in a sedimentary sequence at Tsujita Site

*Haranosono Daichi[1], Shin Toyoda[1], Kenji Nagai[2], Toshirou Naruse

1. Okayama Univesity of Science, 2. Aichi Gakuin University

The Tsujita site is located in Yahata Nishi-ku, Kitakyuushu City, Fukuoka. This site was excavated to clarify the historical dynamics of human migration to Japanese Islands during the late Pleistocene. Total of 9 sedimentary layers have been recognized by the conducted excavations. The observations that Layer 4 is underlaid by the primary Aso-4 pyroclastic flow deposition (Layer 5) and AT was found in the middle of Layer 2 would indicate that Layers 2 to 4 correspond to the last interglacial to glacial climate change. If this is the case, Layer 2 should be composed of loess, Layer 3 of paleosol, and Layer 4 of loess. Burnt rock fragments was found from the lowest part of the Layer 3 to the uppermost part of Layer 4.
The number of oxygen vacancies in quartz measured by ESR (electron spin resonance) correlate with the ages of granitic rocks. Using this feature, there are several works that discussed the origin of the aeolian dust brought to the Japanese Islands from China. The present study aimed to find the change of the amount of aeolian dust from China deposited in the sedimentary sequence of Tsujita site.
From Layers 2 to 5 at the Babayama part of Tsujita site, 22 sediment samples were collected with every 5 cm interval. The sediment samples were treated with hydrochloric acid and hydrogen peroxide followed by grain size separation with the Stokes method into 2 to 20, 20 to 50, and 50 to 125 μm. The samples were then treated with hexafluorosilicic acid to extract quartz. By XRD analysis with calibration with silicon, the quartz content in the sample was estimated. After giving γ rays to a dose of 2.5 kGy, the extracted quartz was heated at 300 ˚C for 15 minutes before ESR measurement.
The number of oxygen vacancies was obtained as the signal intensity of the E_1' center in a unit of 1.3×10^{15} spins/g for the 2~20μm grain size fractions. As the first order approximation, it was assumed that the number of oxygen vacancies in aeolian dust from China is 20 unit and the local dust is 0 in order to estimate the fraction of the aeolian component in the measured sample, from the obtained number of oxygen vacancies. Finally using that, we calculated the mass of quartz of the aeolian dust component from China and the mass was divided by the initial mass of the sediment to obtain the concentration ranging from 0 to 1800 ppm. The concentration of aeolian dust quartz component from China was found to be higher in Layer 1 and 3 while lower in Layer 2 and 4 confirming the correlation with the estimated climate change.

Keywords: Aeolian dust , Electron spin resonance

©2020. Japan Geoscience Union. All Right Reserved.

Effect of stone on threshold friction velocity in Tsogt-Ovoo, Mongolia: Observation and Model simulation

*Batjargal Buyantogtokh[1], Yasunori Kurosaki[1], Masahide Ishizuka[3], Tsuyoshi T Sekimaya[2], Taichu Y Tanaka[2], Atsushi Tsunekawa[1], Mitsuru Tsubo[1]

1. Arid Land Research Center, Tottori University, 2. Japan Meteorological Agency, Meteorological Research Institute, 3. Faculty of Engineering and Design, Kagawa University, Japan

In arid areas, surface roughness is mainly controlled by inert non-erodible elements such as rocks, stone, gravel, and green and senescent vegetation. They affect the erosion threshold in two ways. First, the elements cover part of the surface and thus protect it from the Aeolian erosion. Secondly, they consume part of the wind momentum that will not be available to initiate particle motion (Marticorena et al., 1997). Although the effect of stone and gravel on sand flux is studied by mainly a field wind tunnel measurement, there are few reports on the simulation of threshold friction velocity and field observation with the stone effect of the Gobi Desert. We will show the results of the threshold friction velocity and sand flux by observation and simulation around Tsogt-Ovoo located in the northern part of the Gobi Desert, Mongolia. Simulations were conducted with two conditions which are with and without stone effects. We made measurements of stone coverage, sand saltation count, and meteorological parameters at 11 sites during 31 April –5 May 2018 and 25 April –10 May 2019. Threshold friction velocities were estimated from sand saltation count data observed at 30-seconds intervals. Vertically integrated sand saltation flux for each dust event was estimated from saltation amount data observed by passive samplers installed at 10 cm, 30 cm, 50 cm, and 100 cm heights. We used the dust emission scheme of Shao (2004). Figure 1 shows that simulation results are improved very well at sites by an installation of stone effects except for the Main site and the site of 2019Sub14A in 2019. Regarding the Main site and the site of 2019Sub14A, we are thinking the senescent vegetation and soil crust suppressed the sand saltation, but we don’ t have quantitative data about them.

Keywords: saltation, stone, roughness, erosion threshold, Gobi Desert

©2020. Japan Geoscience Union. All Right Reserved.

Monitoring dry-season vegetation mass at a dust hotspot (Tsogt-Ovoo) in the northern Gobi Desert

*Jing Wu[1], Yasunori Kurosaki[1], Ganatsetseg Batdelger[2], Adrian Chappell[3], Ishizuka Masahide[4], Batjargal Buyantogtokh[1]

1. Arid Land Research Center, Tottori University, 2. Information and Research Institute of Meteorology, Hydrology and Environment, Mongolia, 3. School of Earth and Ocean Science, Cardiff University, UK, 4. Faculty of Engineering and Design, Kagawa University

Accurate prediction of dust emission is of significance to prevent its eco-environmental and social-economic damaging effects on not only source regions but also down-wind regions. However, due to insufficient observation data of erodibility factors (especially at source regions) and a lack of understanding of how and to what extent they affect dust emission, the model simulation of dust is not behaving well. As one of the important erodibility components, effects of vegetation on dust emission have been widely investigated. Most previous studies analyzed green vegetation during growing season, while the period for green vegetation is short in the Gobi Desert. Early studies pointed out green vegetation in summer remained as dead leaves till next spring, and suppresses dust emission. However, few studies have dealt with monitoring of dry-season vegetation mass in the northern Gobi Desert. The present study aims to estimate dry-season vegetation mass by using remote sensing data (e.g., MODIS) at Tsogt-Ovoo (TsO), Mongolia.

Soil Tillage Index (STI), which is the ratio of band 6 (1.6 μm) and band 7 (2.1 μm) derived from MODIS Nadir BRDF-Adjusted Reflectance products, is a potential index to estimate dry-season vegetation mass. STI in September 2019 around TsO was tested against field measurement of aboveground biomass (AGB). We found a significant correlation between STI and AGB (R^2=0.49, $p<0.05$). In addition, STI in April was compared with an estimated shear stress (U_s*) scaled by the freestream wind speed (U_h) during the period of 2001-2018. The estimated U_s^*/U_h reflects the aerodynamic roughness and shelter based on albedo. We also found a highly negative relationship between STI and U_s^*/U_h (R^2=0.59, $p<0.01$). Abundant dead leaves result in high values of STI, as well as increase roughness and decrease wind momentum at the soil surface, thus resulting low values of U_s^*/U_h.

The results imply that STI can be applied to monitor dry-season vegetation mass in the Gobi Desert and potentially in large-scale dust simulation models.

Keywords: Soil Tillage Index (STI), MODIS, BRDF, albedo

©2020. Japan Geoscience Union. All Right Reserved.

Wind tunnel experiment on sand saltation splash by using a high-speed camera

*Ishizuka Masahide[1], Yasunori Kurosaki[2], Hiroaki Hagino[3], Kazuki Nanko[4], Gantsetseg Batdelger[5], Yukio Yasuda[4], Satoru Suzuki[6]

1. Kagawa University, Faculty of Engineering and Design, 2. Tottori University, Arid land research center, 3. Forestry and Forest Products Research Institute, Tohoku Research Center, 4. Forestry and Forest Products Research Institute, Department of Disaster Prevention, Meteorology and Hydrology, 5. Information and Research Institute of Meteorology Hydrology and Environment, Mongolia, 6. Forestry and Forest Products Research Institute, Center for Forest Damage and Risk Management

Saltation is one of the process for sand and dust transportations. Sand movement makes geomorphological changes in not only desert and coastal area but other planets. In this study, we focus on the saltation splash. When saltation sand particles hit grounds, not only dust but other sands are newly emitted to the atmosphere. The new sand emission from grounds induced by saltation is known as ″ splash″. The splash particles receive energy from impacting saltation particles and can move as creeping or new saltation. The emitted new sand particles (splash particles) directly get energy from wind and accelerate the particle velocity. Then, they might behave as new impacting (saltation) particles. By repeating saltation and splash, large amount of sand and dust are supplied to the atmosphere more and more.
In order to clarify the mechanism of splash, wind tunnel experiments are conducted in Forestry and Forest Products Research Institute, Tsukuba, Japan. Toyoura sand is used as saltation particle and three soils are used as a target soil, 1) Mongol soil which has both finer and larger particles (Loam) sampled at Tsogt-Ovoo in the northern Gobi Desert, Mongolia, 2) Toyoura sand, and 3) Kasaoka clay. Sand splash is measured by using a high-speed camera. The frame rate is set to 30000 fps in order to capture particles as clearly as possible. PTV (Particle Tracking Velocimetry) method is used to analyze the particles motion. As a result, when the velocity of saltation particle is about 7.0 m s^{-1}, the mean velocity of splashing particles is 2.8 m s^{-1}. A reduction of kinetic energy of saltation particle is evaluated after hitting the ground surface. These findings are fundamental for elucidating the process of saltation and will link to improve dust forecasting accuracy of atmospheric dust transport models.

Keywords: Asian dust, KOSA, dryland, kinetic energy, PTV analysis, Gobi Desert

©2020. Japan Geoscience Union. All Right Reserved.

[E] Poster | M (Multidisciplinary and Interdisciplinary)：M-IS Intersection

[M-IS07] Aqua planetology

convener:Yasuhito Sekine(Earth-Life Science Insitute, Tokyo Institute of Technology), Hidenori Genda(Earth-Life Science Institute, Tokyo Institute of Technology), Keisuke Fukushi(Institute of Nature & Environmental Technology, Kanazawa University), Tomohiro Usui(Japan Aerospace Exploration Agency)

This proposed session covers a wide range of topics related to chemical reactions and dynamics involving water on planetary bodies; for instance, water-rock-organics interactions within planetesimals, distribution of water in the early Solar system, hydrological and biogeochemical processes on Earth and terrestrial planets, geochemical cycles, redox-pH gradients, and habitability on early Mars and icy moons, and theory to understand how to build habitable aquaplanets.

[MIS07-P01] Isotopic fractionation of methane gas with clathrate hydrate formation under the condition of ice crust / internal ocean boundary in icy satellite

*Kushi Kudo[1], Atsushi Tani[1], Keita Yamada[2], Naohiro Yoshida[2,3] (1.Department of Human Environmental Science, Graduate School of Human Development and Environment, Kobe University, 2.Department of Chemical Science and Engineering, School of Materials and Chemical Technology, Tokyo Institute of Technology, 3.Earth–Life Science Institute, Tokyo Institute of Technology)

[MIS07-P02] Observation of the interface between ice and water under high pressure with gas as a simulation of the bottom of ice crust in icy bodies

*Kenshiro Moriyama[1], Atsushi Tani[1] (1.Department of Human Environmental Science, Graduate School of Human Development and Environment, Kobe University)

[MIS07-P03] H_2-rich hydrothermal environment in the Enceladus' subsurface ocean

*Takazo Shibuya[1], Sota Numaho[1,2], Hisahiro Ueda[1], Sakiko Kikuchi[1], Yutaro Takaya[3], Takuya Saito[1], Mariko Abe[1], Masaru Tomita[2], Ken Takai[1] (1.Japan Agency for Marine-Earth Science and Technology, 2.Keio University, 3.Waseda University)

[MIS07-P04] Abiotic nitrate reduction in hydrothermal environments and nitrogen cycle in early earth

*Manabu Nishizawa[1], Takuya Saito[1], Akiko Makabe[1], Takazo Shibuya[1], Ken Takai[1] (1.Japan Agency for Marine-Earth Science and Technology)

[MIS07-P05] Experimental study of phosphorus dissolution from hydroxyapatite in liquid CO_2

*Kaito Seo[1,2,3], Takazo Shibuya[3], Fujishima Kosuke[4], Ken Takai[3], Masaru Tomita[1,2] (1.Graduate School of Media & Governance, Keio Univ., 2.Inst. Adv. Biosci., Keio Univ., 3.X-Star, JAMSTEC, 4.ELSI, Tokyo Tech)

[MIS07-P06] Effects of minerals on the formose reaction: implication for the potential ribose formation on ancient Mars

*Chinatsu Ono[1], Takeshi Kakegawa[1], Yoshihiro Furukawa[1] (1.Graduate School of Science, Tohoku University)

[MIS07-P07] **Hydrogen generation by water-rock reactions on the early Mars**

*Hisahiro Ueda[1], Takazo Shibuya[1] (1.JAMSTEC)

[MIS07-P08] Impact-generated hydrothermal systems that can promote organic synthesis: Implications for the origin of life

*Kazumu Kaneko[1], Yasuhito Sekine[2], Takazo Shibuya[3], Hisahiro Ueda[3], Natsumi Noda[2,4] (1.Department of Earth and Planetary sciences, School of science, Tokyo Institute of Technology, 2.Earth-Life Science Institute, Tokyo Institute of Technology, 3.Japan Agency foe Marine-Earth Science and Technology, 4.Department of Earth and Planetary science, Graduate School of science, The University of Tokyo)

[MIS07-P09] Clumped isotope signatures of abiotic methane formed via Fischer-Tropsch catalysis and their implications

*ZHANG NAIZHONG[1], YASUHITO SEKINE[1], MAYUKO NAKAGAWA[1], NAOHIRO YOSHIDA[1] (1.Earth-Life Science Institute, Tokyo Institute of Technology)

[MIS07-P10] **Development of novel characterization method for extraterrestrial clay mineral**

*Kosuke Inoue[1], Keisuke Fukushi[2], Koki Morida[3], Hiroki Suga[4], Yoshio Takahashi[4] (1.Kanazawa University , 2.Institute of Nature and Environmental Technology, 3.Graduate School of Science, The University of Kanazawa, 4.Graduate School of Science, The University of Tokyo)

[MIS07-P11] Evolution of aqueous environment on Early Mars inferred from reconstructed water chemistry at Gale

*Keisuke Fukushi[1], Yasuhito Sekine[2,1] (1.Institute of Nature & Environmental Technology, Kanazawa University, 2.Earth-Life Science Institute, Tokyo Institute of Technology)

[MIS07-P12] Effective formation of Al-rich surface clays through acidic water activity on early Mars

*Mitsuteru Sugiuchi[1], Yasuhito Sekine[2], Shuya Tan[2,3], Natsumi Noda[2,3], Yoshio Takahashi[3], Ramses M Ramirez[2] (1.Department of Earth and Planetary Science, School of Science, Tokyo Institute of Technology, 2.Earth-Life Science Institute, Tokyo Institute of Technology, 3.Department of Earth and Planetary Science, Graduate School of Science, The University of Tokyo)

[MIS07-P13] **The Preparation for Return Sample from Asteroid Ryugu by STXM at KEK-PF**

*Hiroki Suga[1,2], Sakiko Kikuchi[3], Shuya Tan[1,4], Shohei Yamashita[2], Yasuo Takeichi[2], Daisuke Wakabayashi[2], Masao Kimura[2], Yoshio Takahashi[1,2], Yasuhito Sekine[4] (1.Graduate School of Science, The University of Tokyo., 2.Institute of Materials Structure Science, High Energy Accelerator Research Organization (KEK)., 3.Institute for Extra-cutting-edge Science and Technology Avant-garde Research (X-star), Japan Agency for Marine-Earth Science and Technology (JAMSTEC)., 4.Earth-Life Science Institute (ELSI), Tokyo Institute of Technology.)

[MIS07-P14] Clustering analysis of Ryugu spectral data obtained by NIRS3 infrared spectrometer onboard Hayabusa2 spacecraft

*Moe Matsuoka[1], Hikaru Iwamori[2], Deborah Lolin Domingue[3], Tomohiro Usui[1], Kohei Kitazato[4], Takahiro Iwata[1] (1.ISAS/JAXA, 2.Earthquake Research Institute, the University of Tokyo, 3.Planetary Science Institute, 4.University of Aizu)

[MIS07-P15] Recognition and classification of Martian chaos terrains using imagery machine learning

*Hiroki Shozaki[1], Yasuhito Sekine[2], Nicholas Guttenberg[2,3] (1.Tokyo Institute of Technology, School of Science, Dept. of Earth and Planetary Sciences, 2.Earth-Life Science Insitute, Tokyo Institute of Technology, 3.Cross Compass Ltd.)

[MIS07-P16] Reactive iron supply control dominant sulfur species in the limestones of Ediacaran Doushantuo and Dengying Formations

*Fumihiro Matsuura[1], Ryoichi Nakada[2], Yuichiro Ueno[3,2], Yusuke Sawaki[4], Masafumi Saitoh[5], Kajitani Iori[4], Tomohiro Usui[1] (1.JAXA, 2.JAMSTEC, 3.Tokyo Tech, 4.The University of Tokyo, 5.University of Lausanne)

[MIS07-P17] New sulfur isotopes 1-D photochemical model for revealing early earth's atmosphere

*Yoshiaki Endo[1,2], Mark W. Claire[2], Chester E. Harman[2,3], Laura Crick[2] (1.Tokyo Institute of Technology, 2.University of St Andrews, 3.NASA Ames Research Center)

[MIS07-P18] Retrieval of vertical structure in the Martian atmosphere during 2007 global dust storm by OMEGA/MEx limb observation

*Risei Kogure[1], Arnaud Mahieux[2,3], Hiromu Nakagawa[1], Shohei Aoki[2], Yasumasa Kasaba[1], Nao Yoshida[1] (1.TOHOKU University, 2.Belgian Institute for Space Aeronomy (BIRA-IASB), 3.University of Texas at Austin, USA)

[MIS07-P19] Numerical experiments of climate of early Mars by the use of DCPAM

*Masaki Ishiwatari[1], Yoshiyuki O. Takahashi[2], George L. Hashimoto[3], Kiyoshi Kuramoto[1], Yoshi-Yuki Hayashi[2] (1.Department of Cosmosciences, Graduate school of Science, Hokkaido University, 2.Department of Planetology, Graduate School of Science, Kobe University, 3.Department of Earth Sciences, Faculty of Science, Okayama University)

[MIS07-P20] Habitable zone for a planet with a small amount of water on its surface

*Takanori Kodama[1], Hidenori Genda[2], Ryouta O'ishi[3], Ayako Abe-Ouchi[3] (1.University of Bordeaux, 2.Earth-Life Science Institute, Tokyo Institute of Technology, 3.Atmosphere and Ocean Research Institute, University of Tokyo)

[MIS07-P21] Formation region of volatile-rich asteroids inferred from nucleosynthetic isotope variations in carbonaceous chondrites

*Ryota Fukai[1], Sota Arakawa[2] (1.Japan Aerospace Exploration Agency, 2.National Astronomical Observatory of Japan)

Isotopic fractionation of methane gas with clathrate hydrate formation under the condition of ice crust / internal ocean boundary in icy satellite

*Kushi Kudo[1], Atsushi Tani[1], Keita Yamada[2], Naohiro Yoshida[2,3]

1. Department of Human Environmental Science, Graduate School of Human Development and Environment, Kobe University, 2. Department of Chemical Science and Engineering, School of Materials and Chemical Technology, Tokyo Institute of Technology, 3. Earth–Life Science Institute, Tokyo Institute of Technology

Icy satellites have capability of having extra biota due to eruption of plume, which is consisted by sea ice particles including organic matter. The observation using Cassini clarified that this plume included hydrogen molecule (H_2), CO_2, methane (CH_4) and organic matter (e.g. Porco et al. 2006; Waite et al. 2006, 2009, 2017). Especially in plume gas species, methane (CH_4) is regarded as one of the candidate of signature of biological activity due to CH_4 formation reaction by methanogen. However CH_4 gas in plume is consisted of not only microbial origin but also primitive and/or hydrothermal origin and this fact does not let CH_4 detection is sufficient for conclusion for existence of biological activity by microbe. Therefore, we consider that evaluation of the elementary process of CH_4 isotopic fractionation ($\delta^{13}C$ and δD of CH_4) via room experiment is important for isotopic observation of icy satellite in nearly future.

In this study, we focus on CH_4 hydrate which is reservoir to produce the plume (Kieffer et al. 2006) and plan to evaluate isotopic fractionation with its formation. Isotopic fractionation with hydrate formation has been found at only δD of CH_4 (~10‰) at the Earth condition (P: ~6 MPa) (e.g. Hachikubo et al. 2007, 2015; Lapham et al. 2012). In the case of condition of icy satellites and icy planets, the pressure range is wider than of the Earth, and therefore we need to estimate isotopic fractionation (P: 5–50 MPa).

We formed clathrate hydrate samples using hydrate formation equipment under the extreme environments, which can hold until 50 MPa. We lowered cell temperature from room temperature to 276 K, and then stirred CH_4 gas and pure water at 85 or 400 RPM stirring rotation speed to form hydrate sample. We inserted CH_4 gas at slightly higher pressure than the previous studies (5, 10 MPa). We collected gas samples of primitive gas from CH_4 gas cylinder and remained gas samples from the high pressure cell after hydrate formation, and then we measured stable isotopic ratio ($\delta^{13}C$ and δD of CH_4) using GC-IRMS equipment at Tokyo Tech.
Results in isotopic measurements show that the $\delta^{13}C$ value of remained gas phase was slight lower (less than 1‰) than of primitive gas phases and became lower at higher pressure. This suggest that 1) $^{13}CH_4$ and $^{12}CH_4$ easily condensed into gas phase in hydrate and remained gas phase (plume) with clathrate hydrate formation, respectively, and 2) this condensation became stronger at higher pressure. Furthermore, the $\delta^{13}C$ value of remained gas phase became lower at faster stirring rotation speed. Since Wijayanti (2018) reported that hydrate formation rate, stability and storage capacity became higher at higher stirring rotation speed, the above tendency of stronger isotopic fractionation at higher stirring rotation speed is acceptable. We found slight isotopic fractionation unlike in the previous reports. As the isotopic fractionation easily occurs by pressure, we plan to proceed the experiment at higher pressure. These tendencies indicate that isotopic fractionation of CH_4 with clathrate hydrate formation in icy satellites may depend on pressure and stirring rotation speed in internal ocean water–CH_4 gas mixing.

Keywords: methane gas, icy satellite, clathrate hydrate, isotopic fractionation, pressure dependence, stirring rotation speed

©2020. Japan Geoscience Union. All Right Reserved.

©2020. Japan Geoscience Union. All Right Reserved.

Observation of the interface between ice and water under high pressure with gas as a simulation of the bottom of ice crust in icy bodies

*Kenshiro Moriyama[1], Atsushi Tani[1]

1. Department of Human Environmental Science, Graduate School of Human Development and Environment, Kobe University

Gas hydrates are clathrate compounds where hydrogen-bonded water cages include a guest gas molecule. Methane hydrate is one of famous gas hydrates because it is naturally found in deep-sea and permafrost sediments on the Earth. Gas hydrates would exist in icy bodies as well. One of the candidates is Pluto where the presence of subsurface ocean is suggested. Gas hydrates may exist between the ice shell and the subsurface ocean and play an important role as insulator to keep warm inside. The presence of subsurface ocean is also suggested in some icy satellites like Enceladus. INMS (Ion and Neutral Mass Spectrometer) aboard the Cassini orbiter has investigated composition of the plumes there that includes H2O (< 90 %), CH4, CO2, NH3, and other various organic materials. These results could reflect the composition of the subsurface ocean and imply the presence of clathrate hydrates in the ocean. Density of gas hydrates depends on guest gas molecules. For example, methane hydrate is lighter than the water, whereas CO2 hydrate is heavier. If CO2 hydrate forms at the bottom of the icy shell, the average density may become large and the ice (water ice + CO2 hydrate) may start to sink locally. If the size of each gas hydrate become small and granular gas hydrates exist in subsurface ocean, heat can be transferred by not only thermal conduction but also convection. This means that icy bodies may be cooled faster. To elucidate how gas hydrates form in the subsurface ocean in icy bodies, we developed the observation system of gas hydrate formation and dissociation below the ice sheet. The observation system was set in the thermostatic cooling bath after it was filled with water. As temperature in the cell degreased, water ice was formed in the lower part of the cell and high pressure gas was supplied. In this study, we used CF4 gas to increase the pressure in the system to form CF4 hydrate. It is heavier than water and should sink in the water cell, if it is formed. After several experiments, we found that the surface of water ice slightly changed to hold CF4 gas on the ice surface.

Keywords: icy bodies, ice crust, subsurface ocean, gas hydrate

©2020. Japan Geoscience Union. All Right Reserved.

H_2-rich hydrothermal environment in the Enceladus' subsurface ocean

*Takazo Shibuya[1], Sota Numaho[1,2], Hisahiro Ueda[1], Sakiko Kikuchi[1], Yutaro Takaya[3], Takuya Saito[1], Mariko Abe[1], Masaru Tomita[2], Ken Takai[1]

1. Japan Agency for Marine-Earth Science and Technology, 2. Keio University, 3. Waseda University

Saturn's icy moon Enceladus has a global ocean beneath the icy crust and is presently discharging water-vapor plume from its south pole. The discovery of silica nanoparticles derived from the plume strongly suggested the presence of ongoing seafloor hydrothermal activities hosted by chondritic rocky core (Hsu et al., 2015; Sekine et al., 2015). Furthermore, the Cassini spacecraft detected molecular hydrogen (H_2) from the plume, which pointed to the energetic habitability of H_2-utilizing living forms sustained by the hydrothermal serpentinization of the rocky core (Waite et al., 2017). In this work, we conducted a hydrothermal experiment using synthetic metal-free chondrite and alkaline fluids at 200 ˚C, 200 bars to assess (1) whether the serpentinization of rocky core has the potential to satisfy the observed hydrogen flux from the subsurface ocean to the space and (2) the habitability of H_2-utilizing living forms based on the H_2 concentration of potential hydrothermal fluid generated in the seafloor hydrothermal systems.

The results show that the H_2 concentration in the fluid increased up to 14.6 mmol/kg 5,760 hours after the beginning of the experiment, which indicates that water-chondrite reactions likely generate H_2-rich hydrothermal fluid. 3D tidal heating simulations indicates that more than 10 GW of heat can be generated by tidal friction and that water transport in the tidally heated permeable core can also generate hotspots (1–5 GW) at the seafloor in the south pole region (Choblet et al., 2017). If it is assumed that the heat flux of hotspots is totally carried by 200-degree C hydrothermal venting, the H_2 flux at the south pole seafloor is estimated to be 5.2×10^8–2.6×10^9 mol/year, corresponding to 10–260 % of the H_2 flux (1–5×10^9 mol/year) observed by Cassini spacecraft. Therefore, the observed H_2 flux can be partially or completely explained by hydrothermal activities near the south pole hotspots. Of course, if lower-temperature but global hydrothermal activities are present, the seafloor water-chondrite reactions would sufficiently account for the observed H_2 flux.

The high H_2 concentration of fluid in the experiment corresponds to those of peridotite-hosted seafloor hydrothermal systems on Earth. Considering that hydrogenotrophic methanogens certainly exist in most of the terrestrial peridotite-hosted hydrothermal systems, the results suggest that the hydrothermal systems on Enceladus are capable of sustaining hydrogenotrophic methanogenesis if temperature of venting hydrothermal fluids is close to 200 degrees C. Further water-chondrite experiments at temperatures lower than 200 degrees C would provide more constraints on the temperature of hydrothermal systems and the habitability of H_2-utilizing living forms within Enceladus.

©2020. Japan Geoscience Union. All Right Reserved.

Abiotic nitrate reduction in hydrothermal environments and nitrogen cycle in early earth

*Manabu Nishizawa[1], Takuya Saito[1], Akiko Makabe[1], Takazo Shibuya[1], Ken Takai[1]

1. Japan Agency for Marine-Earth Science and Technology

Nitrogen is an essential element for life as a major component of biomolecules and a substance for energy metabolism. Currently, nitrogen cycle in surface environments is mainly driven by biological processes including nitrogen fixation, nitrification and denitrification. In contrast, little is known about nitrogen cycle in the pre-biotic Earth and its relation to chemical evolution. This study focuses on nitrate chemistry during water-rock interaction in deep-sea hydrothermal environments to understand the fate of atmospherically-derived nitrate in the Hadean ocean. In this study, artificial seawater with nitrate was reacted with synthetic komatiite at i) 250°C and 500 bar or ii) 350°C and 500 bar, using a closed system hydrothermal reactor reaction cell. To unravel the pathway and kinetics of nitrate reduction, time course measurements of chemical and nitrogen isotopic composition of fluid samples were conducted during the ongoing experiments. Our experiments show multi-step reduction of nitrate to ammonium and dinitrogen and temperature-dependence on the molar ratio of final products (NH_4^+/N_2). The experimental results imply that the Hadean deep-sea hydrothermal vents may have been favorable for chemical evolution in that both electron acceptor for energy metabolism (nitrate) and reduced nitrogen for organic synthesis (ammonium) were continuously supplied to the hydrothermal fluid-seawater mixing zone.

Keywords: Nitrogen, pre-biotic earth

©2020. Japan Geoscience Union. All Right Reserved.

Experimental study of phosphorus dissolution from hydroxyapatite in liquid CO_2

*Kaito Seo[1,2,3], Takazo Shibuya[3], Fujishima Kosuke[4], Ken Takai[3], Masaru Tomita[1,2]

1. Graduate School of Media & Governance, Keio Univ., 2. Inst. Adv. Biosci., Keio Univ., 3. X-Star, JAMSTEC, 4. ELSI, Tokyo Tech

Phosphorus (P) is known as one of the essential elements for life. It is incorporated in various macromolecules like DNA and RNA, phospholipids that forms cell membrane, as well as the energy currency and cofactors including but not limited to ATP, Acetyl-CoA and NADPH [1]. In the biogeochemical P cycle, oceanic content is far less than that on land, due to low solubility of phosphate minerals in seawater [2]. On Earth, major mineral that contains P is apatite [$Ca_5(PO_4)_3$-(F,Cl,OH)] in which, over 95% of P in the crust is included [3]. Few studies suggest additional supply sources of P through meteorites or other terrestrial minerals but their contribution to early chemical evolution is still under debate[4]. Under the ocean floor near hydrothermal vent sites, pool of liquid carbon dioxide (CO_2) was found [5,6]. Liquid CO_2 has unique property as a solvent, which can dissolve various hydrophobic chemical compounds including alcohols, carboxylic acids, phenol, esters, amides, etc., that are in many cases insoluble in water [7,8]. It is plausible that such liquid CO_2 reservoirs likely existed on hadean Earth, due to higher CO_2 concentration in the atmosphere [9] and deeper ocean compared to today. Apatite is known for their insoluble nature in seawater, however it has been shown to dissolve in CO_2 rich brines [10]. Hence, in this study, we performed dissolution of P from the powder of hydroxyapatite in liquid CO_2 saturated system with aqueous solution and analyzed the P concentration in both liquids.

[1] Leslie EO. 2004. [2] Van Cappellen P and Ingall ED.1996. [3] Paytan A and McLaughlin K. 2007. [4] Pasek MA, *et al.* 2013. [5] Lupton J, *et al.* 2006. [6] Konno U, *et al.*, 2006. [7] Hyatt JA.1984. [8] Said-Galivev IV *et al.* 2004. [9] Sleep NH. 2010.[10] Toner JD and Catling D. 2020.

Keywords: origin of life, P, phosphorus mineral, liquid CO2, apatite

©2020. Japan Geoscience Union. All Right Reserved.

Effects of minerals on the formose reaction: implication for the potential ribose formation on ancient Mars

*Chinatsu Ono[1], Takeshi Kakegawa[1], Yoshihiro Furukawa[1]

1. Graduate School of Science, Tohoku University

DNA, RNA, and proteins work together to support the essential system of the present life. RNAs catalyze biological reactions as well as have nucleotide sequence transcribed from DNA. Therefore, abiotic RNA formation has been regarded as an essential step of the origin of life. Ribose is an essential constituent of RNA and is known to form in the formose reaction in which a series of condensation and polymerization of formaldehyde under alkaline condition forms many sugar molecules. Thus, formose reaction on prebiotic Earth has been investigated intensively. On the other hand, chemical evolution might have happened on the other planets in some extent. Mars, one of the candidates of past habitable planet, is shown to have liquid water on the surface and/or subsurface and had CO_2-rich atmosphere. Thus, photochemical formaldehyde formation would have been possible on ancient Mars. However, ribose formation on ancient Mars has not been investigated. Therefore, this study investigates effects of ancient Martian environments to the formose reaction and evaluated potential ribose synthesis on ancient Mars. In particular, this study investigates effects of minerals potentially presented on ancient Mars. Phyllosilicates such as saponite distribute widely in Noachian sediments. Carbonates such as magnesite, siderite, and calcite have been found from sediments close to the Noachian phyllosilicate-rich sediment. The Gale crater sediments suggests a neutral pH of the lake water on Noachian Mars. On the other hand, sulfides such as jarosite and gypsum were known to present in Hesperian sediments and suggest the presence of acidic aquatic environments on Hesperian Mars.

The formose reaction experiments were conducted with formaldehyde and glycolaldehyde with minerals. Ribose formation was accelerated in neutral solution with several minerals. The residual amount of formaldehyde was decreased with increasing reaction. Ribose formation was not seen in acidic solution (pH: ~4) with/without minerals, although tetroses were formed.

These results suggest that ribose was spontaneously formed from formaldehyde and glycolaldehyde in neutral aquatic environments implying that ancient Mars promoted sugar-forming chemical evolution.

Keywords: ribose, formose reaction, ancient Mars

©2020. Japan Geoscience Union. All Right Reserved.

Hydrogen generation by water-rock reactions on the early Mars

*Hisahiro Ueda[1], Takazo Shibuya[1]

1. JAMSTEC

Clay minerals such as serpentine and chlorite was observed in Mars' s Noachian terrains, which are interpreted as evidence for early weathering, hydrothermal activity, and diagenetic aqueous environments (Ehlmann et al., 2011; Mcsween et al., 2016). This indicates that serpentinization occurred and possibly hydrogen was generated. The H_2 is an important molecule as one of energy sources for hydrogenotrophic chemotrophs and as a reducing agent in the Mars' surface environment.

Olivine is commonly exposed in Mars' s crustal rocks such as Gusev basalt and meteorite and its Fe content is higher than that in the Earth (Ehlmann and Edwards, 2014; Morris et al., 2010). Because thermodynamic calculations suggest that potential for the H_2 generation by olivine hydration becomes higher with increasing Fe content in olivine (Klein et al., 2013b), a larger amount of H_2 production via water-rock interactions is expected on the early Mars. However, it has not revealed how SiO_2 and Al_2O_3 contents affect H_2 generation during reactions between Gusev basalt and fluid, as discussed for terrestrial equivalents by reported Frost and Beard., (2007) and Shibuya et al., (2015). Furthermore, since in addition to presence of Mg-Fe-Ca carbonate minerals in the surface (Niles et al., 2013), atmospheric CO_2 level on the early Mars could be high (Kurokawa et al., 2018; Ramirez et al., 2014), the serpentinization and H_2 generation on the early Mars is also possibly limited by incorporation of Fe into carbonate minerals during alteration (Ueda et al., 2016).

In this study, we conducted two hydrothermal experiments to examine the amount of H_2 generated by reactions between synthetic Gusev basalt and CO_2-free and -rich fluids at 300 ˚C, 200 bars, respectively. The synthetic Gusev basalt includes olivine, Cr-spine and glass, and shows spinifex texture as observed for terrestrial komatiites.

The results of the experiment under the CO_2-rich condition show that ΣCO_2 concentration in the fluid decreased from about 400 mmol/g to 90-100 mmol/kg, which suggests formation of carbonate minerals. The H_2 concentration in the fluid increased up to ~2 mmol/kg under the CO_2-rich condition and up to about 1.4 mmol/kg under the CO_2-free condition, approximately 2500 hours after the beginning of the experiment. The observed trend that H_2 concentration in the fluid generated under CO_2-rich condition is higher than that under CO_2-free condition is inconsistent with the previous experiments using terrestrial komatiites (Ueda et al., 2016). This is possibly because the experiments have not yet reached a steady state and /or because the precipitated carbonate minerals have not included Fe as ferrous iron. The results suggest that H_2 generation potential of hydrothermal alteration of Gusev basalt, regardless of CO_2 -free or -rich condition, is greater than normal basalts and less than ultramafic rocks (peridotite) in the Earth (e.g., Seyfried et al., 2007). Thus, the results imply that the water-rock reactions on the ancient Mars provide the amount of H_2 enough to maintain life' s ecosystem.

Keywords: early Mars, Serpentinization, Carbonation, hydrogen

©2020. Japan Geoscience Union. All Right Reserved.

Impact-generated hydrothermal systems that can promote organic synthesis: Implications for the origin of life

*Kazumu Kaneko[1], Yasuhito Sekine[2], Takazo Shibuya[3], Hisahiro Ueda[3], Natsumi Noda[2,4]

1. Department of Earth and Planetary sciences, School of science, Tokyo Institute of Technology, 2. Earth-Life Science Institute, Tokyo Institute of Technology, 3. Japan Agency foe Marine-Earth Science and Technology, 4. Department of Earth and Planetary science, Graduate School of science, The University of Tokyo

Understanding of geological processes responsible for prebiotic organic synthesis on Hadean Earth is critical for the origin of life. Hydrothermal systems are suggested to be a promising emergence place of life given both of the presences of early chemoautotrophs in current hydrothermal vents and chemical gradients (e.g., Martin et al., 2008). However, organic synthesis, such as CH_4 formation, through reduction of CO_2 are considered to be inhibited even high abundances of H_2 without metallic catalysts (e.g., Shibuya et al., 2013, McCollom, 2016). On the other hand, life would have emerged on Earth at least in 3.95 billion years ago, which is coincident with the end of the late heavy bombardment period. Recent studies suggest that impacts of differentiated bodies (e.g., metallic small bodies) would have provided Fe-Ni alloy into the impact craters (e.g., Kendall and Melosh, 2016), where hydrothermal systems could have been subsequently induced due to impact heating (e.g., Osinski et al., 2013). Here, we perform both hydrological modelling and hydrothermal experiments to examine the possibilities of prebiotic organic synthesis within an impact crater of differentiated bodies on early Earth.

Using the hydrological model, we reproduce hydrothermal groundwater circulations emerged within an impact crater with diameter of ~200 km. Our model results show that a large-scale hydrothermal circulation occurs within whole of the crater when the heat source is 200ºC beneath the crater. In this large-scale circulation, upwelling of hydrothermal groundwater occurs mainly at the crater floors where the altitudes are lowest. In contrast, our results also indicate that multiple circulation cells appear within the crater when the heat source is 300ºC. In the small-scale circulations, groundwater experiences temperatures up to ~200ºC and, then, rapidly upwells into the crater cavity. Our results suggest that hydrothermal circulations would be closed within the crater cavity if the heat source is 200ºC or greater. The experienced temperature would be ~200ºC in the hydrothermal circulations.

We conducted hydrothermal experiments using a $^{13}CO_2$-containing (99.99 % ^{13}C), NaCl solution and a powder mixture of synthesized basaltic rocks and Fe-Ni alloy at temperatures of 200ºC and 300ºC and a pressure of 300 bars. Although almost initial CO_2 (~ 90 %) is fixed as carbonate mineral, we find the formation of $^{13}CH_4$, $^{13}C_2H_6$, and HCOOH (or $HCOO^-$) from CO_2 in fluid samples collected during the experiments. C_3H_8 is also found in the experiment of temperature of 200ºC. Hydrothermal alterations of basaltic rocks control fluid pH as alkaline (pH ~8–9) (Shibuya et al., 2013), where reactive HCO_3^- is stable and is reduced to form $HCOO^-$ using H_2 in fluids. Metallic Fe-Ni alloy would be a catalyst to hydrogenate $HCOO^-$ to CH_4. Based on the low H_2 concentrations in the fluids, the rate limiting reaction of CH_4 formation is highly likely H_2 production due to oxidation of metallic Fe. Given the low activation energy of oxidation of metallic Fe (30 kJ/mol: Grosvenor et al., 2005), CH_4 formation proceeds effectively even at low temperatures, such as 200ºC.

Combining these results, we suggest that impacts of differentiated bodies would have provided hydrothermal environments, where reduced organic molecules are effectively provided. Produced CH_4 and other hydrocarbons could be converted to prebiotic organics, such as HCN or HCHO, through

©2020. Japan Geoscience Union. All Right Reserved.

photochemical reactions. The formation process of CH_4 from CO_2 is similar to the carbon fixation of anaerobic chemoautotrophs, such as methanogen; namely, methyl branch of acetyl CoA pathway. Our results imply that impact-generated hydrothermal systems could provide a promising place where early life could have acquired metabolic pathways on Earth.

Keywords: Early Earth, Organic synthesis, Hydrological modelling, Hydrothermal experiment, Origin of life

©2020. Japan Geoscience Union. All Right Reserved.

Clumped isotope signatures of abiotic methane formed via Fischer-Tropsch catalysis and their implications

*ZHANG NAIZHONG[1], YASUHITO SEKINE[1], MAYUKO NAKAGAWA[1], NAOHIRO YOSHIDA[1]

1. Earth-Life Science Institute, Tokyo Institute of Technology

The isotopic compositions of CH_4, such as $^{13}C/^{12}C$ and D/H ratios ($\delta^{13}C$ and δD, respectively), are widely used as a tracer for identifying the CH_4 formation processes. However, obvious defects are existent, such as partly overlapping of isotopic signatures for different CH_4 sources, difficulty in constraining CH_4 generated from two or more sources, and so on (Douglas et al., 2017). Very recently, CH_4 clumped isotope signatures has been considered as a helpful constraint to provide more information on origins of natural CH_4 (e.g. Douglas et al., 2017; Young et al., 2017).

The clumped isotope refers to molecules substituted by two or more rare stable isotopes, e.g. $^{13}CH_3D$ and $^{12}CH_2D_2$, whose abundance relative to a random distribution is temperature dependent (Stolper et al., 2014). Therefore, the formation temperatures of CH_4 can be obtained if the reactions are in isotopic equilibrium. On the other hand, kinetic effect will introduce disequilibrium clumped isotope values, which can be used in identifying specific process/mechanism (Stolper et al., 2015). Overviewing the literature of CH_4 clumped isotope, almost all of the studies focused on the microbial and thermogenic CH_4 samples so far, while limited abiotic data has been reported by Young et al. (2017) and Wang et al. (2018) only. Two preliminary results of low-temperature Fischer-Tropsch Type (FTT) reaction (Sabatier reaction) using ruthenium (Ru) as catalyst presented strongly disequlibrated clumped isotope signals, which was considered to be caused by quantum tunneling effect (Young et al., 2017). On the other hand, lack of clumped isotope data from other FTT reaction with different catalyst and reactant, limiting this technique as a tool to identify the pathways of natural abiotic CH_4 formation.

In this study, we will present the clumped isotopic signatures of laboratory produced abiotic CH_4 via gaseous FTT reactions, using various experimental parameters and catalysts, such as Ni, Fe, Ru and Co. Both $\Delta^{13}CH_3D$ and $\Delta^{12}CH_2D_2$ values are analyzed using a 253 Ultra High Resolution Isotope Ratio Mass Spectrometer established in Earth-Life Science Institute (ELSI), Tokyo Institute of Technology, following the similar procedures described in Eldridge et al. (2019). We will discuss the controlling factors of clumped isotopic signatures in laboratory produced abiotic CH_4, and try to apply these results in clarifying the producing mechanism of natural abiotic CH_4 gases, which might provide more information to illustrate the early earth environment and life origin, as well as other planet with abiotic CH_4 existent.

References: Douglas et al., 2017, Organic Chemistry; Eldridge et al., 2019, ACS Earth Space Chem.; Stolper et al., 2014, Geochim. Cosmochim. Acta.; Stolper et al., 2015, Geochim. Cosmochim. Acta.; Wang et al., 2018, Geochim. Cosmochim. Acta.; Young et al., 2017, Geochim. Cosmochim. Acta.

Keywords: Methane, Clumped isotope, Catalyst

©2020. Japan Geoscience Union. All Right Reserved.

Development of novel characterization method for extraterrestrial clay mineral

*Kosuke Inoue[1], Keisuke Fukushi[2], Koki Morida[3], Hiroki Suga[4], Yoshio Takahashi[4]

1. Kanazawa University , 2. Institute of Nature and Environmental Technology, 3. Graduate School of Science, The University of Kanazawa, 4. Graduate School of Science, The University of Tokyo

Clay minerals, a kind of hydrous minerals that may be included in meteorites, are generated in the presence of liquid water. There are a wide variety of clay mineral species depending on their mineral content and coordination positions. The mineral species of clay minerals are related to their formation environment (e.g., the cation compositions and/or the Eh-pH condition). Therefore, the characterization of clay mineral species can reveal the water environment of extraterrestrial material such as meteorite when they were formed. In this study, we focused on the “scanning transmission X-ray microscope (STXM)” as a new tool for analyzing meteorite samples containing clay mineral species. The purpose of this study is to collect X-ray absorption spectra of the major elements from various standard clay minerals on the earth for the construction of a database for the identification of clay minerals species in the actual meteorite samples such as Martian meteorite.

Keywords: Clay Mineral, STXM, XAFS, Meteorite

©2020. Japan Geoscience Union. All Right Reserved.

Evolution of aqueous environment on Early Mars inferred from reconstructed water chemistry at Gale

*Keisuke Fukushi[1], Yasuhito Sekine[2,1]

1. Institute of Nature & Environmental Technology, Kanazawa University, 2. Earth-Life Science Institute, Tokyo Institute of Technology

There is a wealth of geomorphological and mineralogical evidence indicating the presence of liquid water on early Mars. The NASA rover Curiosity has conducted a geological survey of the successive lacustrine and eolian sediments from Gale crater, a former lake on Mars, and provided mineralogical and geochemical data of the sediments. We developed a methodology for quantitative estimation of the water chemistry of the pore water in the sediments based on exchangeable cation compositions in the smectite and the salt mineralogy (Fukushi et al 2019). We applied the methodology to the lacustrine sediments from Yellowknife Bay formation, the lowermost layer of Gale crater observed by Curiosity, and found that the water chemistry was of Na-Cl type with moderate salinity (0.1-0.5 mol/kg) and circumneutral pH (Fukushi et al 2019). The Curiosity has obtained the mineralogical and geochemical data from the several lacustrine sediments from Murray formation, the upper layer of Gale crater, and showed the presence of smectite and some authigenic minerals in the sediments. In present study, we applied the methodology to the sediments from the Murray formation. The environmental condition to produce the water chemistry in the Murray formation and the evolution of water environment at Gale will be discussed in this presentation.

Reference:
Fukushi, K., Sekine, Y., Sakuma, H., Morida, K. and Wordsworth, R., 2019, Semiarid climate and hyposaline lake on early Mars inferred from reconstructed water chemistry at Gale. *Nature Communications*, **10;** 4896; doi:10.1038/s41467-019-12871-6.

Keywords: Early Mars, Authigenic minerals, Evolution of water chemistry

©2020. Japan Geoscience Union. All Right Reserved.

Effective formation of Al-rich surface clays through acidic water activity on early Mars

*Mitsuteru Sugiuchi[1], Yasuhito Sekine[2], Shuya Tan[2,3], Natsumi Noda[2,3], Yoshio Takahashi[3], Ramses M Ramirez[2]

1. Department of Earth and Planetary Science, School of Science, Tokyo Institute of Technology, 2. Earth-Life Science Institute, Tokyo Institute of Technology, 3. Department of Earth and Planetary Science, Graduate School of Science, The University of Tokyo

Remote sensing observations have revealed a widespread occurrence of weathering profiles in the low-latitude regions of Mars (e.g., Bishop et al., 2008, Murchie et al., 2009). The weathering profiles consist of Al-rich clays and sulfate minerals in the upper part and Mg/Fe-rich clay minerals in the lower part (Murchie et al., 2009; Bishop et al., 2008). These secondary minerals would have been formed through water-rock reactions between basement rocks and infused surface water on early Mars (Zolotov and Mironenko, 2016, Bishop et al., 2018). The previous geochemical model suggests that Al-rich clays may have formed due to water-rock reactions near pH 8 in a prolonged warm period (~10^6 years) (Bishop et al., 2018). Although the timescale may be consistent with a proposed formation time of valley networks, the spatial distribution of the weathering profiles on Mars does not always agree with that of valley networks. This may imply that the formation of Al-rich clays may not be simply formed as a result of the same water activity that formed valley networks.

In the present study, we perform laboratory experiments of chemical weathering using a newly-developed flow-through type reactor, in which solution is continuously infused into Martian soil analogues. We used two types of solution: One is pure water in dissolution equilibrium with 1 bar of CO_2 (pH ~ 4) and the other is sulfuric acid solution in dissolution equilibrium with 1 bar of CO_2 (pH ~ 1). Our experimental results using pure water in equilibrium with CO_2 show that pH values near the top of the reaction vessel are 4–5 owing to high levels of dissolved CO_2; whereas, in the lower part of the reaction vessel, pH are 6–7 owing to pH buffer by carbonate mineral. Under this weakly acid to circumneutral pH conditions, a supply of Al and Si into pore water is limited owing to slow dissolution of plagioclase. Since olivine dissolves effectively in this pH range, Mg carbonate forms in the reaction vessel. On the other hand, our experimental results using acidic sulfuric solution show that pH at the top of the reaction vessel becomes 2–3 owing to pH buffer by sulfate mineral. In the lower part of the reaction vessel, pH becomes 5–6 owing to cation supply by dissolution of primary minerals. At the top of the reaction vessel with pH 2–3, Al, Si and Mg are effectively supplied to the pore water owing to rapid dissolution of both plagioclase and olivine. Since the pore water including these ions is infused into the lower part with pH 5–6, Al-rich clay mineral, montmorillonite, precipitates in the reaction vessel. After consumption of Al and Si in pore water due to deposition of Al-rich clays, Mg-rich clay mineral, Mg saponite, forms subsequently in the lower part of the reaction vessel. The formation order of the secondary minerals in the experiment using acidic sulfuric solution is consistent with the weathering profiles observed on Mars. Based on the measured Al contents in the pore water, we suggest that Al-rich clay deposits of the weathering profiles can be generated rapidly (~10^3 years) by infusion of acidic surface water enriched in sulfuric acid. The weathering profiles may have formed upon transient warming at locations where sulfuric acids accumulated on early Mars; whereas, valley networks would have formed at locations where precipitation rates were high.

Keywords: Early Mars, Secondary minerals, Laboratory experiment, Chemical weathering, Surface environment

©2020. Japan Geoscience Union. All Right Reserved.

©2020. Japan Geoscience Union. All Right Reserved.

The Preparation for Return Sample from Asteroid Ryugu by STXM at KEK-PF

*Hiroki Suga[1,2], Sakiko Kikuchi[3], Shuya Tan[1,4], Shohei Yamashita[2], Yasuo Takeichi[2], Daisuke Wakabayashi[2], Masao Kimura[2], Yoshio Takahashi[1,2], Yasuhito Sekine[4]

1. Graduate School of Science, The University of Tokyo., 2. Institute of Materials Structure Science, High Energy Accelerator Research Organization (KEK)., 3. Institute for Extra-cutting-edge Science and Technology Avant-garde Research (X-star), Japan Agency for Marine-Earth Science and Technology (JAMSTEC)., 4. Earth-Life Science Institute (ELSI), Tokyo Institute of Technology.

Hayabusa2 mission aimed at conducting sample return from a C-type asteroid named Ryugu, which is considered to be the parent body of the carbonaceous chondrite. As for the formation process of the Ryugu, the following hypotheses have been considered (i) internal heating case by short-lived radionuclide, (ii) impact heating case, (iii) incipient aqueous alteration case, and (iv) masking case by darker organic matter contributing to the low reflectance of Ryugu. If we can extract the information about the past collision and the water environment from the organic matter and secondary minerals in the actual Ryugu return sample, the scenarios above can be determined. In 2019, we analyzed the organic and inorganic simulated samples using a new Scanning Transmission X-ray Microscope (STXM) installed at BL-19A of Photon Factory.

As for the analog of the extraterrestrial organic matter, recovered samples of organic simulants of planetary bodies (OSPBs) from impact experiment described in [Sekine et al., 2018, MAPS] was used. STXM measurement was performed for the shock experienced OSPBs which recovered from shock wave with 0, 2, 5, 10, and 12 GPa. On the other hand, synthesized secondary saponite which was described in [Kikuchi and Shibuya, 2019, Asteroid Science 2019, #2049] was used. After the 100 days synthesized experiment, the newly formed fibrous minerals were notably observed at the surface of the original olivine, these minerals were identified as a saponite by the lattice fringes using TEM. Both of these samples were dropped on the Formvar-membrane supported Cu-mesh grid before the STXM measurement. The exposure time of clay sample to the atmosphere was less than 3 min before it was mounted on the STXM to prevent oxidation of Fe(II) in saponite. STXM stack measurement was conducted to C K-edge of OSPBs and Fe L_{III}-edge of synthesized saponite. Several grains were measured to guarantee the reproducibility. In addition, repeated stack measurement (9 times) was conducted to confirm the X-ray irradiation damage.

The C-XANES feature of shock-recovered OSPBs above about 7 GPa and 400 ˚C, which would be achieved in a typical asteroid belt collision, showed that the aromatic and graphite peaks are dominant with broad shape. From these results, we can summarize that (i) the aromatic and graphite peaks were not remarkable in the unheated sample, (ii) the aromatic and graphite peaks were confirmed but broad in the collision experienced sample, and (iii) the aromatic and graphite peaks become sharp and remarkable in the long-term heating sample. It is indicated that to distinguish between short-term heat event by collision and long-term heating event by radioactive elements is possible by C-XANES features.

Even if saponite is a common product of the low-temperature water-rock reaction between water and mafic minerals on Earth, Fe(II)-saponite is easily oxidized to Fe(III)-saponite under the atmospheric condition. In this study, the Fe(II) in the saponite is obviously detected by the minimized oxidation. Besides, we checked the beam damage on the Fe(II)-saponite oxidation by repeating measurements in the same field of view, the peak intensity of Fe(III) did not increase clearly shown. These results suggested that

©2020. Japan Geoscience Union. All Right Reserved.

STXM is better enough to identify the Fe(II)-saponite, and the best measurement condition of the extraterrestrial secondary minerals is an air-isolated system throughout the sample preparation to the analysis.

Throughout this study, the C-XANES analysis results of OSPBs gave us the evaluation criteria to determine the Ryugu formation scenarios. The synthesized redox-sensitive clay minerals analysis by STXM-XANES also contribute to the detailed identification of clay mineral species and its related water redox condition, which is also useful to determine scenarios of Ryugu alteration.

Keywords: Hayabusa2, Ryugu, STXM, Organic Matter, Saponite, Synchrotron Radiation

©2020. Japan Geoscience Union. All Right Reserved.

Clustering analysis of Ryugu spectral data obtained by NIRS3 infrared spectrometer onboard Hayabusa2 spacecraft

*Moe Matsuoka[1], Hikaru Iwamori[2], Deborah Lolin Domingue[3], Tomohiro Usui[1], Kohei Kitazato[4], Takahiro Iwata[1]

1. ISAS/JAXA, 2. Earthquake Research Institute, the University of Tokyo, 3. Planetary Science Institute, 4. University of Aizu

The Near-infrared Spectrometer (NIRS3) onboard the Hayabusa2 spacecraft obtained near-infrared (NIR) reflectance spectra of C-type asteroid 162173 Ryugu at an altitude of ~20 km from July 10-12 2018 with a spatial resolution of ~40 m (Box-A). The NIRS3 data, ranging from 1.8–3.2 μm with a spectral sampling resolution of 18 nm [1], show a 2.72-μm OH stretching absorption and a low reflectance which are globally homogeneous and similar to moderately-heated or shocked carbonaceous chondrite spectra [2, 3].

This study performs cluster analysis of Ryugu's NIR spectral data using a new statistical method [4] based on combinations of k-means cluster analysis (KCA), principal component analysis (PCA), and independent component analysis (ICA) for the seven channels ranging from 1.8 to 3.0 μm with ~200 nm interval and one channel at 2.72 μm of NIRS3 Box-A data. We performed three-step cluster analysis: (1) standardization and whitening of the original data using PCA, (2) dimension reduction of the data by selecting principal components (PCs) with significant eigenvalues and the corresponding scores of the individual data, and (3) performing KCA (and ICA) [4]. Whitening is essential to extract the independent features hidden in the data, which is not possible only by standardization.

The preliminary result of KCA and PCA using photometric-corrected Box-A global data obtained on July 11th 2018 shows that the data variation can be characterized with three significant PCs. We performed KCA using the values of these three PCs as the whitened and dimension-reduced data. To find the optimal number of clusters (k), k was varied from five to eight. The case with k = 6 (Fig.1) best captures the spectral properties. Regional heterogeneity is observed, even in the northern equatorial region which displays homogeneous morphologies in the Optical Navigation Camera Telescope (ONC-T) images [3].

All the clusters have a common OH-absorption at 2.72 μm with similar depths, yet they have differences in albedo and slope. The brightest average spectra are distributed around the equatorial ridge and in the Southern hemisphere around 150 to 300 degrees in longitude. The reddest spectra are located in the Southern region around 90 to 150 degrees in longitude. Interestingly, the spectra of the pole regions are grouped into the same clusters as those distributed in other areas. In addition to global thermal alteration, more plausible causes producing this NIR feature differences possibly reflecting variations in; (a) carbon content, (b) opaque material abundance, (c) grain size and porosity, and (d) space weathering maturation across the surface of Ryugu. A previous clustering study [5] suggest that NIR clusters indicate hydrous mineral contents variation. Our study further proposes a possible grain size and porosity variation to explain the spectral reddening.
In this study we found that the clustering results indicate NIR spectra would have a heterogeneity depending on location. For further study, we will perform KCA, PCA, and ICA analyses using photometric-corrected NIR data of lower altitude observations.

Figure 1. A NIRS3 spectral cluster map using data obtained on July 11th 2018 at ~20 km altitude. The six

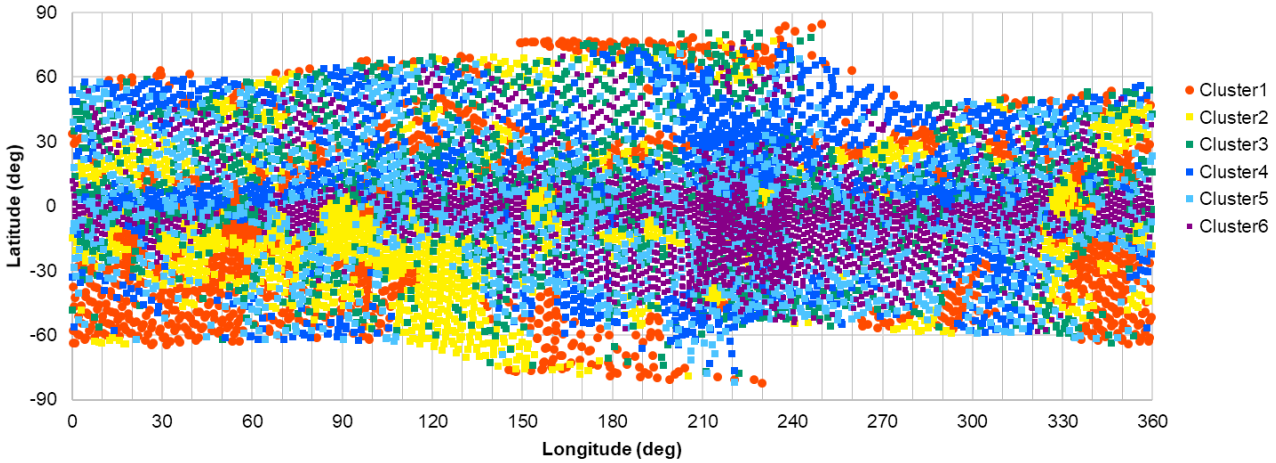
©2020. Japan Geoscience Union. All Right Reserved.

clusters are separately distributed possibly reflecting the geomorphology and/or surface mineralogical/physical properties.

References: [1] Iwata, T. et al. (2017) Space Sci. Rev., 208, 317-337. [2] Kitazato, K. et al. (2019) Science, 364, 272. [3] Sugita, S. et al. (2019) Science, 364, 252. [4] Iwamori, H. et al. (2017) Geocham. Geophys. Geosyst., 18, 994-1012. [5] Barucci, A. et al. (2019) Astron. Astrophys., 629, A13.

Acknowledgements: We appreciate support from the Japan Society for the Promotion of Science (JSPS) Core-to-Core Program "International Network of Planetary Sciences”, and JSPS Grant-in-Aid for Scientific Research on Innovative Areas (Aqua Planetology, No.17H06459). D. Domingue was supported by the NASA Hayabusa2 Participating Scientist Program (NNX16AL34G), and the Solar System Exploration Research Virtual Institute 2016 (SSERVI16) Cooperative Agreement (NNH16ZDA001N) SSERVI-TREX.

Keywords: Reflectance spectra, Hayabusa2, Hydrous minerals



©2020. Japan Geoscience Union. All Right Reserved.

Recognition and classification of Martian chaos terrains using imagery machine learning

*Hiroki Shozaki[1], Yasuhito Sekine[2], Nicholas Guttenberg[2,3]

1. Tokyo Institute of Technology, School of Science, Dept. of Earth and Planetary Sciences, 2. Earth-Life Science Insitute, Tokyo Institute of Technology, 3. Cross Compass Ltd.

Chaos terrains on Mars are irregular to circular fractured areas that consist of jumbled knobs and polygonal flat-topped blocks (e.g. Pedersen et al., 2014) . The blocks of the chaos terrains vary in size (kilometers to tens of kilometers) and shape depending on locations (e.g. Pedersen et al., 2014) . The blocks are surrounded by depressions with altitude difference of typically 1–2 km (e.g. Warner et al., 2011) . Chaos terrains locate primarily in Valles Marineris, with the numbers of ~470 individual terrains, on Mars. Based on the preservation of the original surface structures on the fractured blocks, some chaos terrains are interpreted to be collapsed terrains due to discharge of groundwater upon melting of ice (e.g. Zegers et al., 2010) . This can be supported by the fact that chaotic terrains are often associated with outflow channels (e.g. Pedersen et al., 2014) . On the other hand, others propose that based on the geomorphologic features, other chaos terrains may have been formed through different formation processes, including magma excavation (Sharp, 1973) , degradation of ground ice (e.g. Zegers et al., 2010) , and clathrate destabilization (e.g. Rodriguez et al., 2006) . Owing to high resolution images on Mars, a number of chaos terrains have been found thus far. However, only limited numbers of chaos terrains are investigated to interpret the formation mechanisms. In addition, the interpretations of the observations vary depending on the locations. This implies that there are significant differences in the morphology and possibly formation mechanisms among the chaos terrains.

In the present study, we perform imagery machine learning for the chaos terrains on Mars with aims at for recognition and classification. We used the fine-tuning VGG19 model, which was constructed by Visual Geometry Group with convolutional layer depth of 19. We prepare total 3300 images of chaotic terrains on Mars, including 1100 visible images taken with the Context Camera, CTX, in grayscale, 1100 images of thermal inertia map taken with the Thermal Emission Imaging System, THEMIS, and colored 1100 images of Mars Orbiter Laser Altimeter (MOLA) High-Resolution Stereo Camera (HRSC) blended digital elevation model (DEM) taken by Mars Global Surveyor, MGS and Mars Express, MEX. Among the chaos terrains, we define two types of chaos terrains: Ones were probably formed through the discharge of groundwater based on the previous studies (e.g. Zegers et al., 2010; Roda et al., 2014; Rodriguez et al., 2005) (221 images) , and the others were probably generated in association with magma excavation and tectonic tiles based on the previous studies (Sharp, 1973; Bamberg et al., 2014) (151 images) . We also collect 200 images of non-chaotic features, such as valley networks and impact craters, on Mars to construct the classifier.

Our preliminary results show that using THEMIS images, we can classify chaotic terrains with 83% accuracy. The constructed classifier is useful to find new chaos terrains on Mars and other planets, such as Earth. However, the accuracy to recognize whether they formed through discharge of groundwater or magma excavation is low. This means that the formation mechanisms may not be able to suggest based on only the morphology.

Keywords: Mars, Chaotic terrains, Machine learning

©2020. Japan Geoscience Union. All Right Reserved.

©2020. Japan Geoscience Union. All Right Reserved.

Reactive iron supply control dominant sulfur species in the limestones of Ediacaran Doushantuo and Dengying Formations

*Fumihiro Matsuura[1], Ryoichi Nakada[2], Yuichiro Ueno[3,2], Yusuke Sawaki[4], Masafumi Saitoh[5], Kajitani Iori[4], Tomohiro Usui[1]

1. JAXA, 2. JAMSTEC, 3. Tokyo Tech, 4. The University of Tokyo, 5. University of Lausanne

C-S-Fe systematics in modern and ancient sedimentary systems have been intensively investigated from 1970s. The availability of reactive iron limits pyrite formation in both euxinic and non-euxinic marine sediments where sufficient metabolizable organic matter is supplied. The dominant sulfur species in the most sedimentary carbonate rocks is pyrite, though organic sulfur, a second significant sink for sulfur during early diagenesis, can be a major sulfur species exceeding the content of pyrite. Relative contribution of organic sulfur on total sulfur is controlled by the supply of reactive iron. The limestones in the Ediacaran Dengying Formation, South China have minor amount of carbonate associated iron (Fe_{carb}) concomitant with low pyrite concentration compared to the limestones and dolostones in the preceding Ediacaran Doushantuo Fm.. Given the adequate TOC content in the limestones of the Dengying Fm., pyrite content is controlled by sulfate concentration or reactive iron supply. Here we investigated species and concentration of sulfur distributed within the matrix of the limestones of the Shibantan Member in the Dengying Fm. and the Member 3 of Doushantuo Fm. by μ-XRF and S K-edge X-ray absorption near edge structure (XANES) analyses. The XANES spectra of Dengying limestone show peaks corresponding to the organic sulfur and carbonate associated sulfate (CAS), whereas the XRF analyses suggests that the organic sulfur occurs in the matrix of limestones with concentrations exceeding 100 ppm. In contrast, the XANES spectra of Doushuntuo limestone indicate that the S dominantly occurs as CAS. The different characteristics observed in XANES spectra of samples collected from two Fms. suggest that sulfur cycle during the deposition of Doushantuo and Dengying Fms. were dominated by different mechanism. The abundant organic sulfur preserved in the Dengying limestone may be resulted from intense sulfurization of organic matter owing to the iron limitation during deposition. The speciation μ-XRF mapping showed that the distribution of CAS in the matrix of limestone is different between Doushntuo and Dengying limestones. The average CAS concentrations within the matrix of the two Dengying limestones are 199 ± 153 ppm and118 ±112 ppm with eliminating the outlier to make normal distribution. On the other hand, the average CAS concentrations within the matrix of the two Doushantuo limestones are 173 ±37 ppm and 199 ±53 ppm. The standard deviation of CAS concentration within the matrix of limestone in Doushantuo Fm. is much smaller than that of Dengying Fm, which shows the CAS in the limestone of the Doushantuo Fm. are distributed with small heterogeneity compared to that of the Dengying Fm. We suggest isotopic composition of a fluid possibly ocean water can be reconstructed from the limestone, in which CAS is distributed with relatively small heterogeneity, with dodging secondary vein and intense elimination of soluble sulfate.

Keywords: Doushantuo Formation, Dengying Formation, μ-XRF and S K-edge XANES, carbonate associated sulfate

©2020. Japan Geoscience Union. All Right Reserved.

New sulfur isotopes 1-D photochemical model for revealing early earth's atmosphere

*Yoshiaki Endo[1,2], Mark W. Claire[2], Chester E. Harman[2,3], Laura Crick[2]

1. Tokyo Institute of Technology, 2. University of St Andrews, 3. NASA Ames Research Center

Constraining the atmospheric composition of planets is essential to understanding habitability. However, the chemical composition of the early Earth's atmosphere is poorly understood. Here, mass-independent fractionation of sulfur isotopes (MIF-S) in pre-2.4 Ga sedimentary rocks provide a hint of atmospheric composition at that time. For the early Earth, it is believed that partial pressure of O_2 was very low and atmosphere was reducing. Recently, our sulfur dioxide (SO_2) photochemical experiments under carbon monoxide (CO) atmosphere reproduced the $\Delta^{36}S/\Delta^{33}S$ slope from the Archean (~−1), which is the most basic character of Archean MIF-S (Endo et al. 2016). Moreover, it was found that the MIF-S trend depends on total pressure, indicating that MIF-S is sensitive to absorption spectral shape of SO_2 via SO_2' s own UV absorption (Endo et al. 2019). We synthesized SO_2 isotopologues absorption spectra which reproduce the MIF-S of photochemical experiments (Endo et al. 2019). Therefore, we can predict MIF-S produced in various atmospheric compositions using the SO_2 isotopologues absorption spectra and irradiative UV spectra, and the resulting MIF-S depends on altitude. Here, we develop a 1-D (vertical) photochemical model including 4 sulfur isotopes (^{32}S, ^{33}S, ^{34}S, and ^{36}S) and very high resolution SO_2 absorption spectra (~0.0004 nm). This new model is based on previous models including sulfur isotopes and low wavelength resolution SO_2 absorption spectra (Claire et al. 2014; Izon et al. 2017). We will present preliminary results and discuss the meaning of MIF-S in Early Earth rocks and modern atmospheric sulfates, if possible, Martian meteorites.

Keywords: Earth's Early atmosphere, Sulfur isotope

©2020. Japan Geoscience Union. All Right Reserved.

Retrieval of vertical structure in the Martian atmosphere during 2007 global dust storm by OMEGA/MEx limb observation

*Risei Kogure[1], Arnaud Mahieux[2,3], Hiromu Nakagawa[1], Shohei Aoki[2], Yasumasa Kasaba[1], Nao Yoshida[1]

1. TOHOKU University, 2. Belgian Institute for Space Aeronomy (BIRA-IASB), 3. University of Texas at Austin, USA

Recent studies have revealed an unexpected high abundance of water vapor in the middle atmosphere that supposedly drives the enhancement of the atomic hydrogen escape (Chaffin et al., 2017; Fedorova et al., 2018, 2020, Heavens et al., 2018; Vandaele et al., 2019; Aoki et al., 2019). However, it is unclear how to extract water vapor from the lower atmosphere and place it in the middle atmosphere since water vapor is limited in its vertical propagation by the cold trap of its condensation level. The cold trap leads to water freezing out, confining water in the lower atmosphere. It has been proposed that an inflation of the lower atmosphere due to the sunlight absorbed by the upsurge of dust associated with intensified meridional circulation can transport water vapor effectively into the middle atmosphere (Aoki et al., 2019; Neary et al., 2019). A comprehensive picture of the water transport and the background atmospheric condition in the middle atmosphere is yet to be established. Two-dimensional local distribution of physical parameters can contribute to clarify the transient phenomena, such as rocket dust storm (Spiga et al., 2013).

In this study, we aim to present the 2D vertical structures of water vapor, dust opacity, and CO_2 non-LTE emission in the periods of 2007 global dust storm (Ls = 265-305) using the OMEGA limb observation onboard Mars Express. The indexes of water-vapor, dust opacity are obtained from the wavelength ratio between 2.50 and 2.64 micron (Maltaliati et al., 2011), and the radiance at 2.70 micron (Fouchet et al., DPS, 2004), respectively. CO_2 non-local thermal equilibrium (LTE) emission is detected at 4.3 micron (Piccialli et al., 2016). From the slope of the observed spectrum between 0.5 and 3.0 micron, the effective radius of aerosol particles can be estimated. As the reference, observations during the global dust storm in orbit#4483 (Ls = 268) and orbit#4621 (Ls = 292) is compared with that at clear-sky season in orbit#291 (Ls = 17) and orbit#685 (Ls = 68).

We show a significant increase of water vapor up to ~60 km altitude during the global dust storm, as reported by recent studies (Vandaele et al., 2019; Aoki et al., 2019; Fedorova et al., 2020). Our result suggests the concentration of water vapor in 40-60 km altitudes. This is totally different from that at orbit#685 at clear-sky season, which shows the confined water vapor up to ~40 km altitude.

The slopes of observed spectra suggest larger particle size during the global dust storm at orbit#4483 (~1.0 micron) than that in the clear-sky at orbit#291 (~0.4 micron). This is comparable with previous studies (Oliva et al., 2018; Clancy et al., 2019). We find that such large aerosols reach into the mesosphere.

We confirmed that the CO_2 non-LTE emission peaks at higher altitudes (100-120 km) during the global dust storm in orbit#4483 (The statistical analysis can be found in Piccialli et al. (2016)). This result basically suggests about 20 km increase of peak altitudes comparing with that in the clear-sky at orbit#291. This can be explained by the heating by absorption of incoming sunlight via suspended dust particles.

©2020. Japan Geoscience Union. All Right Reserved.

We intend to discuss the physical parameters, such as water vapor amount, dust opacity etc by using JACOSPAR (Iwabuchi and Yang, 2011; Iwabuchi et al., 2016), which is a multiple scattering radiative transfer code that uses the backward-propagating Monte Carlo method, and the dependent sampling approach in order to reduce the computation time.

Keywords: Mars, Dust storm, vertical profile, OMEGA

©2020. Japan Geoscience Union. All Right Reserved.

Numerical experiments of climate of early Mars by the use of DCPAM

*Masaki Ishiwatari[1], Yoshiyuki O. Takahashi[2], George L. Hashimoto[3], Kiyoshi Kuramoto[1], Yoshi-Yuki Hayashi[2]

1. Department of Cosmosciences, Graduate school of Science, Hokkaido University, 2. Department of Planetology, Graduate School of Science, Kobe University, 3. Department of Earth Sciences, Faculty of Science, Okayama University

We have been performing one- and three-dimensional numerical experiments of early Mars. In order to do those, we have developed a radiation model for a thick CO_2 atmosphere, and implemented that into our general circulation model, DCPAM. The radiation model includes advances on radiative transfer calculations which were reported by our groups. The DCPAM is an atmospheric GCM, which uses primitive equation system, and a number of parameterizations, such as radiation, turbulent diffusion, surface energy budget, and condensation processes.

Numerical experiments of one-dimensional radiative convective equilibrium of pure CO_2 atmosphere without radiative effects of cloud shows surface pressure dependence of surface temperature which is similar to that reported by a previous study. That is, surface temperature is highest at a surface pressure of several bars. But, the highest surface temperature is far below the freezing point.

Three-dimensional numerical experiments are also performed by the use of the general circulation model, DCPAM, with the radiation model. In the experiments, we assumed both cases with and without radiative effects of cloud. In experiments without radiative effects of cloud, global mean surface temperatures are similar to those obtained by one dimensional radiative convective equilibrium experiments. But, surface temperature increases with increasing the surface pressure. Further, in experiments with radiative effects of cloud, surface temperature is higher than freezing point. The behavior is different from that reported by previous study.

We will check the energy budget, circulation structures, and atmospheric structures obtained by the models in order to consider the difference of results between ours and previous study's.

Keywords: early Mars, radiative transfer, general circulation model, radiative convective equilibrium

©2020. Japan Geoscience Union. All Right Reserved.

Habitable zone for a planet with a small amount of water on its surface

*Takanori Kodama[1], Hidenori Genda[2], Ryouta O'ishi[3], Ayako Abe-Ouchi[3]

1. University of Bordeaux, 2. Earth-Life Science Institute, Tokyo Institute of Technology, 3. Atmosphere and Ocean Research Institute, University of Tokyo

Some of the detected exoplanets are expected to be Earth-sized rocky planets. Habitable exoplanets seem to be significant targets for observation of exo-terrestrial planet and exo-life. Liquid water evaporates entirely when planets receive the insolation above a certain critical value, which is called the runaway greenhouse threshold. If planets receive very weak insolation, on the other hand, such planets lapse into the snowball state where the insolation is called the complete freezing threshold. Most of studies for habitable exo-terrstrial planet have been discussed introducing the habitable zone, in which planets can maintain liquid water on their surface for a long term.

We call a planet with a small amount of water on its surface, a land planet. Land planets have less water amount in its atmosphere and can radiate stronger planetary radiation than that for aqua planets, which have a large amount of water on its surface. Thus, a planet with a small amount of water on its surface has a wider habitable zone than that for a planet with a large amount of water on its surface [Abe et al., 2011; Kodama et al., 2018; 2019]. Here, we investigate the relationship between the width of the habitable zone and the surface water distribution using 3D GCM(General Circulation Model). We confirm that the habitable zone strongly depends on the surface environment. In this presentation, we summarize the climates and habitability for exo-land planets.

Keywords: Exoplanet, Habitable Planet, Climate

©2020. Japan Geoscience Union. All Right Reserved.

Formation region of volatile-rich asteroids inferred from nucleosynthetic isotope variations in carbonaceous chondrites

*Ryota Fukai[1], Sota Arakawa[2]

1. Japan Aerospace Exploration Agency, 2. National Astronomical Observatory of Japan

Describing the comprehensive evolutionary scenario for asteroids (i.e., meteorite parent bodies) is the key issue to explain the various physical processes of the Solar System, such as migration of giant planets and late accretion of volatile elements to rocky planets. In this study, we tried to determine the formation region of asteroids by utilizing the nucleosynthetic Cr isotopic variation ($^{54}Cr/^{52}Cr$) in bulk-scale carbonaceous chondrites (CCs) that possibly record the information of the protoplanetary disk. Numerical calculations are conducted to track the temporal evolution of isotopically different (solar and presolar) dusts and $^{54}Cr/^{52}Cr$ values for mixed materials with disk radius. Our results suggest that nucleosynthetic isotopic variations in CCs were predominantly caused by the spatial heterogeneities of dusts. The formation region of B-, Ch-, D-, and K-type asteroids could be determined using the profile of $^{54}Cr/^{52}Cr$ and the accretional ages of CCs. Among these asteroids, B-type asteroids formed in the outermost region, which is apparently inconsistent with the present population of asteroids showing that D-type asteroids are generally located beyond most of the C-complex asteroids. Both the initial and present orbits of asteroids can be explained by the scatter attributed to the inward–outward gas-drag migration of Jupiter and Saturn.

Keywords: asteroid, chondrite, isotopic heterogeneity

©2020. Japan Geoscience Union. All Right Reserved.

[E] Poster | M (Multidisciplinary and Interdisciplinary)：M-IS Intersection

[M-IS08] Paleoclimatology and paleoceanography

convener:Yusuke Okazaki(Department of Earth and Planetary Sciences, Graduate School of Science, Kyushu University), Benoit Thibodeau(University of Hong Kong), Akitomo Yamamoto(Japan Agency for Marine-Earth Science and TechnologyAtmosphere and Ocean Research Institute), Hitoshi Hasegawa(Faculty of Science and Technology, Kochi University)

Past environmental changes and events at multi-decadal to tectonic timescale toward an understanding of Earth climate system by an integration of terrestrial and marine proxy studies and numerical modeling will be discussed. This session includes a special series of presentations on the ocean circulation under climate change in the past, present and future relating to MOC, ventilation and hypoxia. We welcome a variety of paleo-environmental studies from a wide range of background. We hope that this session will provide an opportunity to promote communication between participants from multidisciplinary field.

[MIS08-P01] Reconstruction of the climate condition in the Carnian from bedded chert by using a new index of chemical weathering

*Tenichi Cho[1] (1.Waseda University)

[MIS08-P02] Response of Climate and Water Cycle to Atmospheric CO2; Cretaceous vs. Modern

*Taro Higuchi[1], Ayako Abe-Ouchi[1], Wing-Le Chan[1] (1.Atmospheric and Ocean Research Institute, the University of Tokyo)

[MIS08-P03] Enhanced dinoflagellate productivity by ocean stratification and eutrophication in the Anthropocene, Miocene, and Cretaceous

★Invited Papers

*Takuto Ando[1], Ken Sawada[2] (1.Estuary Research Center, Shimane University, 2.Faculty of Science, Hokkaido University)

[MIS08-P04] Study on productivity feedback during the recovery phases of early Eocene hyperthermals: Comparison between the central North Pacific Ocean and southern Indian Ocean

★Invited Papers

Koshiro Sato[1], *Kazutaka Yasukawa[1,2], Junichiro Ohta[1,2], Keishiro Azami[1], Kentaro Nakamura[1], Koichiro Fujinaga[2,1], Minoru Ikehara[3], Yasuhiro Kato[1,2] (1.School of Engineering, The University of Tokyo, 2.ORCeNG, Chiba Institute of Technology, 3.Center for Advanced Marine Core Research, Kochi University)

[MIS08-P05] Sulfur isotope ratios in co-occuring barite and carbonate from Eocene sediments: A comparison study

*Kotaro Toyama[1], Adina Paytan[2], Ken Sawada[3], Takashi Hasegawa[4] (1.The University of Tokyo, 2.UCSC, 3.Hokkaido Univ., 4.Kanazawa Univ.)

[MIS08-P06] Late Eocene travertine in the SE Tibet and cyclical change in its isotopic composition implying the monsoon climate

*Aki Sakuma[1], Hirokazu Kato[1], Yoshihiro Kakizaki[1], Akihiro Kano[1], Ryuji Tada[2,3], Hongbo Zheng[2] (1.Department of Earth and Planetary Science, School of Science, the University of Tokyo, 2.Yunnan University, 3.Chiba Institute of Technology)

[MIS08-P07] **Reconciling marine influences in the Eastern Siwaliks through the use of biomarkers and reconstructing the Miocene-Pliocene closure of Himalayan Foreland Basin**

*Biswajit Roy[1], Sohom Roy[1], Sambit Ghosh[1], Prasanta Sanyal[1] (1.Indian Institute of Science Education Research Kolkata)

[MIS08-P08] The paleo ocean temperature recorded in carbonate clumped isotope of early Pleistocene fish otolith fossils from the Dainichi Formation of the Kakegawa Group, Shizuoka

*Hirokazu Kato[1], Shota Amekawa[1], Akihiro Kano[1] (1.Department of Earth and Planetary Science, The University of Tokyo)

[MIS08-P09] **Orbital–scale paleoceanographic changes around the Pacific side of Japan in Early Pleistocene based on calcareous nannofossil records**

*Daisuke Kuwano[1], Koji Kameo[1], Yoshimi Kubota[2], Kanako Mantoku[2], Masayuki Utsunomiya[3], Makoto Okada[4] (1.Chiba University, 2.National Museum of Nature and Science, 3.Geological Survey of Japan, AIST, 4.Ibaraki Uviversity)

[MIS08-P10] Sea-ice history in the central Okhotsk Sea based on diatom assemblages during the Middle Pleistocene Transition

Araki Eisuke[1], *Yusuke Okazaki[1], Lo Li[2] (1.Department of Earth and Planetary Sciences, Graduate School of Science, Kyushu University, 2.Department of Geosciences, National Taiwan University)

[MIS08-P11] Millennial-scale hydrographic changes in the northwestern Pacific during marine isotope stage 19: Teleconnections with ice melt in the North Atlantic

★Invited Papers

*Yuki Haneda[1], Makoto Okada[2], Yoshimi Kubota[3], Yusuke Suganuma[1] (1.National Institute of Polar Research, 2.Department of Earth Science, College of Science, Ibaraki University, 3.National Museum of Nature and Science)

[MIS08-P12] Influence of Southern Ocean Intermediate water on the South Pacific's thermocline during the last ~500 Ka

*RAUL TAPIA[1,3], Sze Ling Ho[1], Nele Meckler[2], Dirk Nürnberg[3] (1. Institute of Oceanography, National Taiwan University, Taipei, Taiwan, 2.Bjerknes Centre for Climate Research and Department of Earth Science, University of Bergen, Norway, 3.GEOMAR – Helmholtz Centre for Ocean Research Kiel, Kiel, Germany)

[MIS08-P13] Simulating selected time intervals during the Quaternary using MIROC-ES2L earth system model in comparison with paleo-proxy data

★Invited Papers

*Rumi Ohgaito[1], Akitomo Yamamoto[1], Tomohiro Hajima[1], Manabu Abe[1], Hiroaki Tatebe[1], Michio Kawamiya[1], Ayako Abe-Ouchi[2,3,1] (1.Japan Agency for Marine-Earth Science and Technology, 2.U. Tokyo, AORI, 3.NIPR)

[MIS08-P14] Fossil diatom records from IODP Exp. 382 Sites U1536 and U1538 (preliminary results)

*Yuji Kato[1], Michael E. Weber[2], Maureen E. Raymo[3], Trevor Williams[4], - The IODP Expedition 382 Scientists (1.Center for Advanced Marine Core Research, Kochi University, 2.University of Bonn, Germany, 3.Lamont-Doherty Earth Observatory of Columbia University, USA, 4.International Ocean Discovery Program, Texas A&M University, College Station, USA)

[MIS08-P15] Variations of the North and South Pacific Subtropical Gyres over the past 400 kyrs

*Furukawa Keisuke[1], Osamu Seki[2] (1.Graduate School of Environmental Science, Hokkaido University, 2.Institute of Low Temperature Science, Hokkaido University)

[MIS08-P16] Paleovegetation and paleoenvironmental changes in the northern Mongolia since MIS 3 (preliminary results)

*Ryosuke Imaoka[1], Koji Shichi[2], Hitoshi Hasegawa[1], Niiden Ichinnorov[3], Nagayoshi Katsuta[4], Davaasuren Davaadorj[5], Masafumi Murayama[1], Miho Sasaoka[1], Masao Iwai[1] (1.Kochi University, 2.Forestry and Forest

Products Research Institute, 3.Mongolian Academy of Sciences, 4.Gifu University, 5.National University of Mongolia)

[MIS08-P17] Constraining the magnitude and spatial pattern of low-to-mid latitudes western Pacific ocean temperature changes in the past 25 kyr

*Sze Ling Ho[1], Sicheng Le[1], Ren Yi Ooi[1], RAUL TAPIA[1], Da-Cheng Lin[2], Min-Te Chen[2], Yuan-Pin Chang[3], Masanobu Yamamoto[4], Liang-Jian Shiau[2,5], Chuan-Chou Shen[6], Pai-Sen Yu[7] (1.Institute of Oceanography, National Taiwan University, Taipei, Taiwan., 2.Institute of Applied Geosciences, National Taiwan Ocean University, Keelung, Taiwan, 3.Department of Oceanography, National Sun Yat-sen University, Kaohsiung, Taiwan, 4.Faculty of Environmental Earth Science, Hokkaido University, Sapporo, Japan, 5.Exploration and Development Research Institute, CPC Corporation, Miaoli, Taiwan, 6.High-Precision Mass Spectrometry and Environment Change Laboratory (HISPEC), Department of Geosciences, National Taiwan University, Taipei, Taiwan, 7.Taiwan Ocean Research Institute, NARLabs, Kaohsiung, Taiwan)

[MIS08-P18] Changes in oceanic carbon and oxygen cycle during Heinrich event

*Akitomo Yamamoto[1], Ayako Abe-Ouchi[2] (1.Japan Agency for Marine-Earth Science and TechnologyAtmosphere and Ocean Research Institute, 2.Atmosphere and Ocean Research Institute, The University of Tokyo)

[MIS08-P20] Stalagmite evidence for ^{18}O-depleted surface water of Japan Sea during the last glacial

*Shota Amekawa[1], Kenji Kashiwagi[2], Masako Hori[3], Tomomi Sone[4], Hirokazu Kato[1], Tomoyo Okumura[5], Tsai-Luen Yu[6], Chuan-Chou Shen[6,7,8], Akihiro Kano[1] (1.Graduate School of Science, The University of Tokyo, 2.Department of Environmental Biology and Chemistry, Faculty of Science, University of Toyama, 3.Division of Natural Sciences, Osaka Kyoiku University, 4.Marine Works Japan LTD., 5.Center for Advanced Marine Core Research, Kochi University, 6.High-precision Mass Spectrometry and Environment Change Laboratory (HISPEC), Department of Geosciences, National Taiwan University, 7.Global Change Research Center, National Taiwan University, 8.Research Center for Future Earth, National Taiwan University)

[MIS08-P21] Biogenic opal changes at the Kamchatka Strait in the Bering Sea since the last glaciation

*Koshiro Matsuo[1] (1.Department of Earth and Planetary Sciences, Graduate School of Science, Kyushu University)

[MIS08-P22] Intermediate water formation in the Bering Sea since the last glacial maximum based on *Cycladophora davisiana* abundances.

*Kento Ogata[1], Yusuke Okazaki[1] (1.Kyushu university Earth and Planetary sciences)

[MIS08-P23] Analysis from Benthic foraminifera populations of expansion and intensify of the northwestern Pacific oxygen minimum zone during the last deglaciation

*Keisuke Sakai[1], Ken'ichi Ohkushi[1], Akihiko Shibahara[2] (1.Graduate School of Human Development and Environment, Kobe University, 2.Fukui Prefectural University Institute of Dinosaur Research)

[MIS08-P24] Changes in carbon and oxygen isotopes of benthic foraminifera in the East China Sea since the last glacial maximum

*Miki Muranaka[1], Yusuke Okazaki[2], Yoshimi Kubota[3] (1.Department of Earth and Planetary Sciences, Kyushu University, 2.Department of Earth and Planetary Sciences, Graduate School of Science, Kyushu University, 3.National Museum of Nature and Science)

[MIS08-P26] **Southward Migration of Inter-Tropical Convergence Zone (ITCZ) during Mid-Late Holocene: New Evidence from Sri Lanka**

*Kasun Gayantha[1], Patrick Roberts[2], Joyanto Routh[3], Achim Brauer[4], Rohana Chandrajith[5], Oshan Wedage[2], Florian Ott[2], Gerd Gleixner[1] (1.Max Planck Institute for Biogeochemistry, Jena, Germany, 2.Max Planck Institute for the Science of Human History, Jena, Germany, 3.TEMA-M, Linköping University, Linköping, Sweden, 4.GFZ, Potsdam, Germany, 5.Department of Geology, University of Peradeniya, Sri Lanka)

[MIS08-P27] Diatom and Chrysophyceae Assemblages from the Holocene Alluvial Core Sediments at Southern and Western Coasts of Korea Peninsula

*Kaoru Kashima[1], Yu Fukumoto[3], Sangheon Yi[2], Dong-Yoon Yang[2], Min Han[2] (1.Department of Earth and Planetary Sciences, Kyushu University, 2.Korea Institute of Geoscience & Mineral Resources (KIGAM) , 3.Ritsumeikan University)

[MIS08-P28] Correlation between stable isotope ratio of pollen and climate, as well as its possible application for paleoclimatology

*Yamasaki Akiteru[1], Keitaro Yamada[2], Takayuki Omori[3], Ikuko Kitaba[2], Takeshi Nakagawa[2] (1.Fukui Prefectural Satoyama-Satoumi Reserch Institute, 2.Research Centre for Palaeoclimatology, Ritsumeikan University, 3.The University museum, The University of Tokyo)

[MIS08-P29] Uncertainty of tree-ring based temperature reconstruction: Effects of soil moisture environment and air pollution on reconstruction records

*Shunsuke Tei[1], Shinya Takano[1], Teppei J Yasunari[1] (1.Arctic Research Center, Hokkaido University)

[MIS08-P30] Horizontal distribution of diatoms in the western Bering Sea surface waters

*Aika Yamamoto[1], Yusuke Okazaki[2] (1.Department of Earth and Planetary Sciences, Kyushu University, 2.Department of Earth and Planetary Sciences, Graduate School of Science, Kyushu University)

[MIS08-P31] Spatio-temporal variations in fossil coral assemblages in late Middle Pleistocene limestones of the Minatogawa Formation, southern Okinawa-jima, Japan

*Riho Tomatsu[1], Marc Humblet[1], Kazuhiko Fujita[2], Yui Kouketsu[1], Yasufumi Iryu[3] (1.Graduate School of Environmental Studies, Nagoya University, 2.Department of Physics and Earth Sciences, University of the Ryukyus, 3.Institute of Geology and Paleontology Graduate School of Science Tohoku University)

Reconstruction of the climate condition in the Carnian from bedded chert by using a new index of chemical weathering

*Tenichi Cho[1]

1. Waseda University

Reconstruction of paleoclimate during the Triassic Period is important for the understanding of the Earth system operated during the super-continent and super-ocean, polarized surface landform condition. In the early Late Triassic, an abrupt warming/humidification event, so-called Carnian Pluvial Episode emerged, which was considered to be triggered by the eruption of LIP and increasing atmospheric CO_2. Previous studies regarding the Carnian Pluvial Episode were mainly performed in the western Tethys realm, while the global impact of the Carnian Pluvial Episode is not well understood. This study newly presents the reconstruction of continental chemical weathering intensity through the Carnian from the pelagic deep-sea sediment, which is preserved as bedded chert in the accretionary complex in Japan. In this study, to unravel the hinterland chemical weathering variation from bedded chert, a new weathering index was introduced. The new index was derived from the multivariate statistical analysis (Independent component analysis) using major element compositions of fresh igneous rock and their weathering profiles. The concentrations (wt. %) of TiO_2, Al_2O_3, Fe_2O_3, MgO, Na_2O, K_2O were used to extract the chemical weathering variation which should be independent from the source rock composition. The newly developed index has two features; (1) It retains the advantage of W index (e.g., applicable to a wide range of rock types; less sensitive to specific element concentrations; Ohta and Arai, 2007). (2) It does not require the SiO_2 and CaO concentration data, and thus applicable to samples with contamination of silica, apatite, or calcite. This new index enables the quantitative reconstruction of chemical weathering not only in bedded chert but also in shallow sea or terrestrial sediments that contain diagenetically derived calcite or biogenic apatite fragment. To investigate the climate of the continental region in the Carnian, more than 80 mudstone samples were successively collected from the bedded chert sequence of Section R, Q, Inuyama area, Mino terrain, which cover the whole Carnian Stage (Sugiyama, 1997, Nakada et al., 2014, Yamashita et al., 2018). After washing in an ultrasonic bath to remove the weathered part of the rock surface, major elements were analyzed by XRF (ZSX Primus II , Rigaku Co., Ltd.). The new chemical weathering index demonstrates a clear increase at the Lower Carnian/Upper Carnian boundary, and this high weathering condition continues about 1.3 million years. Then, the weathering intensity decrease suddenly at the boundary of TR5A and TR5B radiolarian biozones (Tuvalian substage). The onset timing of this high weathering period matches with that of the Carnian Pluvial Episode in Tethys. This result suggests that, in the middle of the Carnian, the prolonged warming/humid period lasted for about 1.3 million years in the broad area of the continental region related to the Carnian Pluvial Episode. This increasing of continental weathering intensity and the changes in fossil assemblage suggest that the Carnian Pluvial Episode was a global phenomenon and this environmental disturbance affected biological evolution not only in the Tethys realm but also in the whole Panthalassa. Thanks go to Prof. Tohru Ohta of Waseda University for kind advice and fruitful discussions. Dr. Kazutaka Yasukawa of the University of Tokyo is thanked for his guidance of Independent component analysis. This study was supported by the National Science Foundation of China (Grant No. 41888101; D. Kemp).

Keywords: Carnian Pluvial Episode, Deep-sea sediments, Continental weathering, Inuyama, W index, Triassic

©2020. Japan Geoscience Union. All Right Reserved.

Response of Climate and Water Cycle to Atmospheric CO2; Cretaceous vs. Modern

*Taro Higuchi[1], Ayako Abe-Ouchi[1], Wing-Le Chan[1]

1. Atmospheric and Ocean Research Institute, the University of Tokyo

The study of paleoclimate during warm periods using climate models is important for the understanding of the Earth system under greenhouse conditions and for verifying model performance.
The Cretaceous is known as one of the warmest periods in the Phanerozoic due to intense volcanic activity and increased levels of greenhouse gases. In particular, the mid-Cretaceous is the warmest during that period, and terrestrial proxy data (e.g., climatically sensitive sediment) from that time show a marked change in the water cycle. For example, mid-Cretaceous strata distributed throughout the low latitudes of Asia include desert deposits or evaporites, indicating aridification during the mid-Cretaceous. It is thought that the cause of the change in the water cycle is the result of increased atmospheric CO2, because within the Cretaceous, mid-Cretaceous CO2 concentration in the atmosphere was especially high. If the water cycle change during the mid-Cretaceous is due to increased atmospheric CO2, then it should be comparable with that associated with global warming predictions as suggested by climate models. However, the water cycle changes in the Asian region are quite different. Thus, it is not obvious whether the change in the water cycle during the mid-Cretaceous can be attributed to increased atmospheric CO2. Even if it can be, it is still not clear why the responses of the water cycle to increased CO2 differ during present day and the Cretaceous.
To resolve this issue, simulations of the Cretaceous climate with different CO2 levels are carried out in this study using the atmosphere-ocean general circulation model MIROC4m. The aim is to investigate the response of the climate and water cycle to increased atmospheric CO2 for a Cretaceous paleogeography and to compare results with Cretaceous proxy data and a present-day warming experiment.
The precipitation change due to increased CO2 in the Cretaceous experiment is consistent with the water cycle change during the mid-Cretaceous, as indicated by geological evidence. With increased atmospheric CO2, the precipitation in the low latitude regions of Asia decreases in the Cretaceous experiment, while it increases in the present-day experiment. The precipitation decreases in southern Europe, but increases in the mid-latitude regions of Asia and North America. This result implies that the water cycle change during the mid-Cretaceous can be explained as a response to increased atmospheric CO2.
Water budget analysis indicates that the difference in the water cycle changes is attributed to the different summer atmospheric circulation responses in Asia. In the Cretaceous experiment, the updraft in the continental interior weakens due to increased atmospheric stability with global warming, resulting in a decrease in the precipitation. On the other hand, in the present-day experiment, it does not fully weaken because diabatic heating over the Tibetan plateau enhances the atmospheric circulation. As a result, the increase in moisture flux due to increased atmospheric moisture overcomes the effect of the atmospheric circulation weakening, resulting in increased precipitation with increased atmospheric CO2.
Additionally, ‘No-Tibet’ experiments, eliminating the Tibetan plateau, are carried out in order to investigate the role of the Tibetan plateau on the water cycle change due to increased atmospheric CO2. In the No-Tibet experiments, the precipitation decreases in low latitude regions of Asia with global warming, which is comparable to the results of the Cretaceous experiment. The summer updraft in Asia becomes weaker than that in the present-day experiment, resulting in decreased precipitation. These results indicate that, in the low latitude regions of Asia, the difference between the precipitation changes of the present day and the Cretaceous is attributed to the Tibetan plateau. This study shows that the

©2020. Japan Geoscience Union. All Right Reserved.

water cycle change due to increased CO2 is strongly dependent on the geographical conditions.

Keywords: paleoclimate, Cretaceous, AOGCM

©2020. Japan Geoscience Union. All Right Reserved.

Enhanced dinoflagellate productivity by ocean stratification and eutrophication in the Anthropocene, Miocene, and Cretaceous

*Takuto Ando[1], Ken Sawada[2]

1. Estuary Research Center, Shimane University, 2. Faculty of Science, Hokkaido University

Dinoflagellate is one of the main marine organisms causing red-tide near coastal region. Red-tide, especially harmful algal bloom (HAB), impact on not only fishery but also human health, and therefore, the prediction of red-tide/HAB are important for understanding variability in marine ecosystem in the future. Red-tide events are also related to the expansion of nutrient-rich water. For example, dinoflagellate bloom caused by eutrophication near the coastal area of Japan during high economic growth period (~Anthropocene). Summer stratification is the other factor to enhance occurrence of red-tide. A large number of marine organisms near the coast of Florida are actually killed by the blooming of toxic dinoflagellate (*Karenia brevis*) owing to oceanic stratification during summer in 2018 (Weisberg et al., 2019, *JGR Oceans*). These obvious changes in marine ecosystem in the present gain on importance to reveal relationship between dinoflagellate bloom and climate change. Dinosterol is biosynthesized by dinoflagellate and used as dinoflagellate biomarker in the sediments/sedimentary rocks. Triaromatic dinosteroid is applicable dinoflagellate biomarker for mature sedimentary rocks. In this presentation, we focus on the Anthropocene, late Miocene and mid-Cretaceous OAEs, and compare the variation in dinosteroid percentage with the paleoclimatological /paleoceanological proxies.
We collected the sediment/sedimentary rock samples from Seto Inland Sea (Japan, Anthropocene), Andaman Sea (IODP Exp.353, site U1447, late Miocene), Hokkaido (Yezo Group, Japan, the mid-Cretaceous OAE2) and Vocontian Basin (south eastern France, the mid-Cretaceous OAEs).
Dinosterol are main dinosteroid among the samples collected from Seto Inland Sea and Andaman Sea. We defined DSIP (Dinosteroid index for polar fraction; %) as the percentage of dinosterol/dinostanol among the sterols without C_{29} sterols mostly originated from terrestrial plants. The values of DSIP are higher in the surface sediments deposited near the coast in Seto Inland Sea compared with the samples collected from Pacific Ocean and Yodo River flowing into Osaka Bay. Especially, DSIP is the highest value in the Sea of Harima which is characterized by stratified and eutrophic water in summer season. On the other hand, DSIP values increased from ~7 Ma in the sediment core samples collected from Andaman Sea. Holbourn et al (2018, *Nature Commun.*) suggested that the cooling event in Andaman Sea after 7 Ma was related to strengthening of the dry and cold East Asian winter monsoon. Winter monsoon enhance the North Equatorial Current and the East Indian Current which transport nutrient-rich water from the Strait of Malacca into the Andaman Sea (Brewer et al., 2015, *CSIRO Oceans and Atmosphere*). It is likely that dinoflagellate productivity is also higher under eutrophic condition during the late Miocene.
Triaromatic dinosteroids are main identifiable dinosteroids in the Cretaceous sedimentary rocks collected from Hokkaido and SE France. TADS (Triaromatic dinosteroid index %; Ando et al., 2017a, *Org. Geochem.*), which indicates the productivity of dinoflagellate, were higher in the samples from the mid-Cretaceous OAE1b and 2 levels in Vocontian Basin, SE France. The marine environment in Vocontian Basin during OAE1b and 2 were characterized by eutrophic and stratified condition due to wet and warm climate (Herrle 2003, *Mar. Micropaleontol.*; van Helmond et al., 2014, *Geology*). However, there is no obvious change in TADS values in the samples of OAE2 level collected from the Yezo Group, Hokkaido. The biomarker-based redox indicated the timing of oceanic anoxia in Hokkaido are different from OAE2 in the Tethys and Atlantic regions (Ando et al., 2017b, *Island Arc*). These results imply that dinoflagellate bloom was mainly related to ocean stratification and eutrophication during the Anthropocene, Miocene, and Cretaceous.

©2020. Japan Geoscience Union. All Right Reserved.

Keywords: dinoflagellate, ocean stratification, eutrophication, red-tide

©2020. Japan Geoscience Union. All Right Reserved.

Study on productivity feedback during the recovery phases of early Eocene hyperthermals: Comparison between the central North Pacific Ocean and southern Indian Ocean

Koshiro Sato[1], *Kazutaka Yasukawa[1,2], Junichiro Ohta[1,2], Keishiro Azami[1], Kentaro Nakamura[1], Koichiro Fujinaga[2,1], Minoru Ikehara[3], Yasuhiro Kato[1,2]

1. School of Engineering, The University of Tokyo, 2. ORCeNG, Chiba Institute of Technology, 3. Center for Advanced Marine Core Research, Kochi University

The Paleocene-Eocene Thermal Maximum (PETM) at 56 Ma was the most serious and well-studied hothouse in the Cenozoic era, characterized by a rapid global warming by 5 to 8˚C, severe ocean acidification, and a distinct negative carbon isotope ($\delta^{13}C$) excursion both in the marine and terrestrial realms [1]. These features suggest a massive injection of ^{13}C-depleted greenhouse gas(es) to the ocean-atmosphere system. Moreover, during the early Eocene period (ca. 56-52 Ma), multiple PETM-like transient global warming episodes, called hyperthermals, have also been recognized over the past dozen years [2].

A previous study using the ODP legacy cores drilled in the southern Indian Ocean indicated that an enhanced biological pump efficiently sequestered the excess carbon in the recovery phases of the PETM and other modest hyperthermals, regardless of the magnitude of the events [3]. However, it remains uncertain whether this productivity feedback is a globally general response of the Earth system to a rapid warming.

Here we newly analyzed deep-sea sediment samples collected from ODP Site 1215A in the central North Pacific Ocean, in which multiple hyperthermal events including the PETM, Eocene Thermal Maximum (ETM) 2 and ETM3 are recorded [4]. We constructed a multi-elemental dataset of major- and trace-element contents, $\delta^{13}C$, $\delta^{18}O$, and $CaCO_3$ content for bulk sediment. Based on the dataset, we estimated the abundance of Ba associated with the biological productivity. In the presentation, we will compare the results in the central North Pacific Ocean and southern Indian Ocean, and discuss their relationships with the multiple hyperthermal events.

[1] McInerney and Wing (2011) *Ann. Rev. Earth Planet. Sci.* **39**, 489-516.
[2] Zachos et al. (2010) *Earth Planet. Sci. Lett.* **299**, 242-249.
[3] Yasukawa et al. (2017) *Sci. Rep.* **7**, 11304.
[4] Leon-Rodriguez and Dickens (2010) *Palaeogeogr. Palaeoclimatol. Palaeoecol.* **298**, 409-420.

Keywords: PETM, hyperthermals, climate change, deep-sea sediment, biological productivity, Earth system

©2020. Japan Geoscience Union. All Right Reserved.

Sulfur isotope ratios in co-occuring barite and carbonate from Eocene sediments: A comparison study

*Kotaro Toyama[1], Adina Paytan[2], Ken Sawada[3], Takashi Hasegawa[4]

1. The University of Tokyo, 2. UCSC, 3. Hokkaido Univ., 4. Kanazawa Univ.

The marine sulfur cycle over geologic timescales is closely linked to the redox state of the Earth's surface environments due to the burial of redox-sensitive sulfur species. Fluctuations in the $\delta^{34}S_{sw}$ record have been related to a wide range of global environmental changes, such as oxygenation of the biosphere, bacterial evolution, and mass extinctions. In order to investigate the utility of bulk carbonate as a recorder of seawater sulfate sulfur isotope ratios ($\delta^{34}S_{sw}$), co-existing pelagic barite and bulk carbonate in Eocene sediments from the Equatorial Pacific Ocean (IODP Exp. 320/321 Sites U1331 to U1333) were analyzed for their sulfur isotope ratios ($\delta^{34}S$). The $\delta^{34}S$ from both minerals showed parallel fluctuation throughout the Eocene with carbonate associated sulfate (CAS) values about 0.8‰ heavier than those of barite. A similar offset was observed in CAS $\delta^{34}S$ obtained using species-specific cleaned planktonic foraminifers (Rennie et al., 2018). The consistent results from two distinct minerals suggest that the original $\delta^{34}S_{sw}$ can be derived from bulk CAS analysis, if post deposition carbonate recrystallization is minimal.
Our $\delta^{34}S_{barite}$ data added an important data set in middle Eocene (Lutetian, 47.8 to 41.2 Ma). The data set combined with previous studies showed a ~5‰ increase of $\delta^{34}S_{sw}$ during the Eocene (from 53 Ma to 36 Ma) with the majority of the shift within 7 myr between 53 and 46 Ma. This change is more gradual than previously reported. The timing of this $\delta^{34}S_{sw}$ shift coincides with extensive pyrite burial in the Arctic Ocean, supporting the hypothesis that the 5‰ increase in Eocene $\delta^{34}S_{sw}$ has been caused by ^{34}S-enriched water outflow from the Arctic Ocean as suggested in the previous study.

Keywords: Sulfur isotope, Carbonate associated sulfate, Barite, Eocene

©2020. Japan Geoscience Union. All Right Reserved.

Late Eocene travertine in the SE Tibet and cyclical change in its isotopic composition implying the monsoon climate

*Aki Sakuma[1], Hirokazu Kato[1], Yoshihiro Kakizaki[1], Akihiro Kano[1], Ryuji Tada[2,3], Hongbo Zheng[2]

1. Department of Earth and Planetary Science, School of Science, the University of Tokyo, 2. Yunnan University, 3. Chiba Institute of Technology

The Asian monsoon is the most dominant monsoon system in the world but when and how it was established is still under the debate. Recently, its onset during the late Eocene was suggested (Licht et al., 2014) but little geological evidence in the low-latitude region hinder the reliable evaluation of the past climate pattern. In this study, we investigated the sedimentary environment of the late Eocene limestone in the Jianchuan basin by the microfacies and carbon and oxygen isotope analyses. We identified six lithofacies (laminated bindstone, oncoidal grainstone, calcareous conglomerate, wackestone, lime-mudstone, and bafflestone) and the limestone appears regular lamination and encrusted waterweed, which are unique features of travertine. The high $\delta^{13}C$ and low $\delta^{18}O$ values strongly support the travertine origin and disagree with the previous interpretation of lacustrine carbonate. The high $\delta^{13}C$ values resulted from a large proportion of isotopically depleted fraction from endogenic CO_2. Furthermore, high-resolution isotopic analysis for the laminated travertine confirms a seasonal pattern that is consistent with the laminated texture observed in the modern travertine. The isotopic pattern of the travertine also indicates humid summer and dry winter in the late Eocene, which are the same as the modern monsoonal climate regime.

Keywords: travertine, late Eocene, Asian monsoon, Jianchuan basin

©2020. Japan Geoscience Union. All Right Reserved.

Reconciling marine influences in the Eastern Siwaliks through the use of biomarkers and reconstructing the Miocene-Pliocene closure of Himalayan Foreland Basin

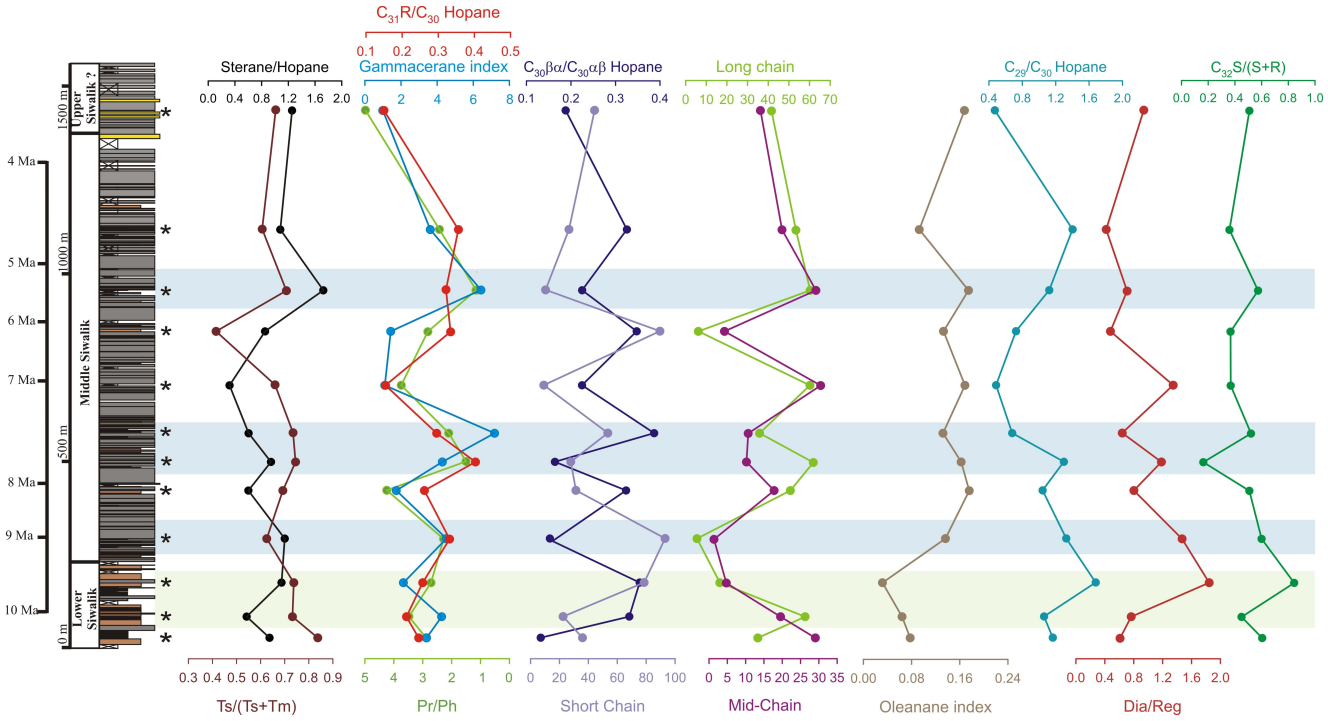
*Biswajit Roy[1], Sohom Roy[1], Sambit Ghosh[1], Prasanta Sanyal[1]

1. Indian Institute of Science Education Research Kolkata

The Siwalik group of rocks archives an essential part of the Himalayan foreland basin evolution. These east-west laterally extended foreland sedimentary packages were previously thought to have been deposited by fluvial alluvial fan settings. However, recent studies on ichnofossils, leaf macrofossils, pollens, and sedimentary architectures provided contradicting evidence from the Miocene-Pliocene Eastern Siwalik suggesting a depositional exclusively of marine dominated environment setting. The marine signatures suggest openness of the foreland basin to marine influences that were supposed to have closed after the retreating of Eocene sea. However, most of these signatures are qualitatively known from the Eastern Siwalik. To validate the marine influences more quantitatively, an alternate perspective, molecular-level characterization of these Eastern Siwalik sedimentary sequences has been attempted to re-evaluate the organic matter (OM) origin and paleo-depositional conditions. The *n*-alkane profiles show a bimodal distribution, with a relatively higher abundance of long-chain *n*-alkanes, Pristane/*n*-C_{17} and Phytane/*n*-C_{18} cross-plot, and relative abundance of C_{27}-C_{28}-C_{29} steranes suggesting major OM contributions from the terrigenous source. The temporal increase in the oleanane index also demarcates an increase in contribution from higher-plants with age. Redox-sensitive parameters like Pristane/Phytane and C_{30}-norhopane/C_{30}-hopane ratios indicate fluctuations between highly oxic to suboxic conditions typical for the terrestrial dominated environment. Interestingly, an increased abundance of gammacerane, high regular sterane/17a-hopane ratios, and high $d^{13}C$ values of bulk OM during the suboxic phases suggests water-column stratification and deposition in hyper-saline/brackish water or marine conditions. Our data, therefore, indicate a mixture of the terrestrial, lacustrine and open bay/estuarine type, suggesting a fluctuating near-shore depositional condition during Siwalik deposition. Throughout the depositional period of the Eastern Siwaliks, marine influences (high $C_{31}R/C_{30}$ hopane and Gammacerane index) were observed mostly during the deposition of the older deposits, which then subsided and allowed the domination of the fluvial signatures (higher Oleanane and long-chain n-alkane abundance) with minor marine influx during forced transgression stage. However, Late Miocene-Pliocene tectonics in the hinterland areas subsequently uplifted the foreland basin and drove back the paleo-Bay of Bengal Sea leading to complete closure of the Himalayan foreland basin and allowed the deposition of fluvial sedimentary packages.

Keywords: Hopane and Sterane, Siwaliks, Foreland Basin

©2020. Japan Geoscience Union. All Right Reserved.



©2020. Japan Geoscience Union. All Right Reserved.

The paleo ocean temperature recorded in carbonate clumped isotope of early Pleistocene fish otolith fossils from the Dainichi Formation of the Kakegawa Group, Shizuoka

*Hirokazu Kato[1], Shota Amekawa[1], Akihiro Kano[1]

1. Department of Earth and Planetary Science, The University of Tokyo

The Dainichi Formation of Kakegawa Group distributed in southwestern Shizuoka Prefecture is shallow sea sediment of early Pleistocene (~2 Ma) and contains various marine fish otoliths. Otolith is calcium carbonate structure in the inner ear of vertebrates and used as balance indicator. Otolith of teleost fish especially grows large and many of them weigh over ~10 milligrams. They often keep firm structure in stratums. We analyzed the bulk and clumped isotopes of fossil and modern otoliths of several species including *Sillago* sp. *Nibea* sp. *Apogonichthys* sp. in order to examine their potential for the ancient temperature archive.

The carbonate clumped isotopes thermometry is a technique to reconstruct the temperature of mineral precipitation without the isotopic information of the parent water. The abundance anomaly of $^{47}CO_2$ (Δ_{47}) generated by acid digestion of calcite is an index of temperature (Ghosh *et al.* 2006). There are few studies about otolith Δ_{47} value although its rigid microstructure is tolerant against diagenetic alternation. The temperature calibration of fish otolith Δ_{47} value by Ghosh et al. (2007) is marginally different from the original calibration of Ghosh et al. (2006). The small discrepancy might reflect a vital effect, or systematic error in temperature estimation of fish growth (Eiler, 2011). We used temperature calibration depending on synthetic calcites developed by Kato et al. (2019).

The Δ_{47} values were 0.709–0.723‰ (13.0–17.4˚C) for fossil *Sillago*, 0.717–0.719‰ (14.0–14.7˚C) for fossil *Nibea* and 0.724‰ (12.4˚C) for fossil *Apogonichthys* with typical measurement error of ±0.01‰. While the modern otoliths yield Δ_{47} temperatures well reproducing the modern ocean temperature. The result of paleo temperature reconstruction is ~5˚C colder than Δ_{47} temperatures from modern otoliths. The paleo water $\delta^{18}O$ value reconstructed from fossil otolith $\delta^{18}O$ corrected by Δ_{47} temperature was –1–−2‰VSMOW. This value is significantly lower than present ocean $\delta^{18}O$ and may indicate strong influence of fresh water in the depositional setting of the lower Pleistocene Dainichi Formation.

References;

Eiler (2011) *Quat. Sci. Rev.* 30, 3575–3588.

Ghosh et al. (2006) *Geochim. Cosmochim. Acta* 70, 1439–1456.

Ghosh et al. (2007) *Geochim. Cosmochim. Acta* 71, 2736–2744.

Kato et al. (2019) *Geochim. Cosmochim. Acta* 244, 548–564.

©2020. Japan Geoscience Union. All Right Reserved.

Keywords: Pleistocene, Fish otolith, Paleo ocean temperature, Carbonate clumped isotope

©2020. Japan Geoscience Union. All Right Reserved.

Orbital-scale paleoceanographic changes around the Pacific side of Japan in Early Pleistocene based on calcareous nannofossil records

*Daisuke Kuwano[1], Koji Kameo[1], Yoshimi Kubota[2], Kanako Mantoku[2], Masayuki Utsunomiya[3], Makoto Okada[4]

1. Chiba University, 2. National Museum of Nature and Science, 3. Geological Survey of Japan, AIST, 4. Ibaraki Uviversity

The Mid-Pleistocene Transition (MPT) is the well-known interval that the dominant periodicity of earth's climate cycles shifted from 41 to 100 ky rhythms (e.g., Elderfield et al., 2012). This study will discuss paleoceanographic changes during the Early Pleistocene before the MPT around the central part of the Pacific side of Japan based on calcareous nannofossil assemblages. We studied the Kiwada Formation in the Kazusa Group, distributed the Boso Peninsula. Two different counting techniques were used to clarify biostratigraphic and paleoceanographic events based on calcareous nannofossils. The age model for this section was proposed by Kuwano et al. (2019a, b). Investigaed ages is Marine Isotope Stage (MIS) 41 to 36. Spectral analyses using the PAST3 software were also applied in order to extract paleocanographic signals from nannofossils.
At least 13 species and 13 genera of calcareous nannofossils were identified in the examined section. *Umbilicosphaera sibogae*(Kuroshio water index) increased at the glacial-interglacial boundaries, *Florisphaera profunda* (stratified, warm offshore water index) and *Helicosphaera* spp. (freshwater inflow index) increased in the interglacial period. On the other hand, *Calcidiscus leptoporus* (cool offshore water index) and very small *Gephyrocapsa* spp. (eutrophic freshwater index) increased during the glacial period. In particular, *Coccolithus pelagicus* (eutrophic cool water index) abundant at the end of the glacial period. The power spectra of *F. profunda*, *U. sibogae*, very small *Gephyrocapsa* spp., and *C. leptoporus* show 55-57 kyr periodicity, which also appeared in benthic foraminiferal $\delta^{18}O$. The periodicity of 22-23 kyr was recognized from relative abundances of *F. profunda*, *U. sibogae*, and *Helicosphaera* spp. Those sequential fluctuations of nannofossils indicate that northward/southward of the Kuroshio and Subarctic Front around the Pacific side of Japan. It can be presumed that oceanic front movements linked East Asian monsoon variations because paleoceanographic records in this study corresponded with Chinese loess-paleosol records (Sun et al., 2010).

[Reference]
Elderfield et al., 2012, *Science*, **337**, 704-709., Kuwano et al., 2019a, *The 126th Annual Meeting of the Geological Society of Japan, Abstract*, R23-P2., Kuwano et al., 2019b, *The 1st Asian Palaeontological Congress, Abstract*, P64., Sun et al., 2010, *Earth and Planetary Science Letters*, **297**, 525-535.

Keywords: Calcareous nannofossil, Kazusa Group, Kiwada Formation, Paleocenography, East Asian monsoon

©2020. Japan Geoscience Union. All Right Reserved.

Sea-ice history in the central Okhotsk Sea based on diatom assemblages during the Middle Pleistocene Transition

Araki Eisuke[1], *Yusuke Okazaki[1], Lo Li[2]

1. Department of Earth and Planetary Sciences, Graduate School of Science, Kyushu University, 2. Department of Geosciences, National Taiwan University

The Okhotsk Sea is the second largest marginal sea in Pacific Ocean. One of the most notable features of the Okhotsk Sea is the seasonal sea-ice cover from late autumn to early spring, constituting the southernmost sea-ice covered area in the northern hemisphere. Recent climate changes have significantly impact in the sea-ice covered area in Okhotsk Sea, however, geological timescale sea-ice evolution histories is still unknown in this region due to the lack of long paleoclimatic records. During the period between 1.25 and 0.75 Ma known as the Mid-Pleistocene Transition (MPT), the glacial/interglacial (G/IG) cycles has modulated from 41-kyr to 100-kyr. The first deep glaciation appeared in the Marine Isotope Stage (MIS) 16, between 0.68 and 0.62 Ma. To reveal sea-ice history in the Okhotsk Sea during the MPT period, diatom floral assemblages in a giant piston core obtained from the central Okhotsk Sea (MD01-2414; 53°11.77’ N; 149°34.80’ E; water depth 1123 m) were investigated. Age model of MD01-2414 was established based on magneto-stratigraphy as well as orbital-tunings of element concentrations and sediment color, yielding the bottom age as ~1.6 Ma. Diatom abundance (No. valves g-1 dry sediment) between 1.2 and 0.6 Ma showed cyclic patterns along with G/IG cycles: increased (decreased) abundances by 1 or 2 orders of magnitude during cold (warm) periods, vice versa. A total of 18 genus 21 species were identified in MD01-2414 core. Main diatom species were Actinocyclus curvatulus, Paralia marina/sulcata, Rhizosolenia hebetata forma hiemalis, Shionodiscus trifultus, and S. oestrupii. Sea-ice related species such as Bacterosira bathyomphala, Fragilariopsis cylindrus, F. oceanica were less than 10% throughout the MPT except for MIS 26, 18, and 16. The MIS 26 peak was temporal whereas the MIS 18 to MIS 16 peaks continued for tens of thousands years. This suggests that the onset of major sea-ice cover was since MIS 18, ~0.75 Ma in the central Okhotsk Sea.

Keywords: Okhotsk Sea, Sea-ice, Diatom assemblages, Middle Pleistocene Transition

©2020. Japan Geoscience Union. All Right Reserved.

Millennial-scale hydrographic changes in the northwestern Pacific during marine isotope stage 19: Teleconnections with ice melt in the North Atlantic

*Yuki Haneda[1], Makoto Okada[2], Yoshimi Kubota[3], Yusuke Suganuma[1]

1. National Institute of Polar Research, 2. Department of Earth Science, College of Science, Ibaraki University, 3. National Museum of Nature and Science

Marine isotope stage (MIS) 19 has been suggested as one of the best orbital analogs for present interglacial, because of the similarity of the orbital configurations between both interglacial periods. Therefore, paleoenvironmental reconstructions of MIS 19 will provide valuable knowledge to evaluate the anthropogenic impacts for present and future climate changes. Additionally, the abrupt climate changes associated with the iceberg melting in the North Atlantic are globally documented in the paleoceanographic and paleoclimatic records during the MIS 20–19 transition and late MIS 19, suggesting global climatic teleconnection during the periods. The Kuroshio Current, the largest western boundary current of the North Pacific ocean, transports a large amount of heat and water poleward strongly influences the East Asian climate, however, responses of the Kuroshio Current to the ice melting in the North Atlantic remains unknown. Here, we reconstruct detailed paleoceanographic variations in the northwestern Pacific during MIS 19 using stable oxygen isotope ($\delta^{18}O$) records from the Chiba composite section (CbCS), central Japan. Spectral and wavelet analyses were conducted in order to assess periodicity of our new $\delta^{18}O$ records. Vertical water temperature structure and their gradient (ΔT) exhibit latitudinal displacements of the Kuroshio Extension Front (KEF) on multi-millennial scale across the MIS 20–19 transition and during late MIS 19 (MIS 19b to 19a). Results of the spectral and wavelet analyses for the $\delta^{18}O$ records show periodicities of approximately 3,000–6,000 year during late MIS 19. Similarities of timing and periodicity between paleoceanographic records from the CbCS and North Atlantic indicate that disruption of the Atlantic meridional overturning circulation due to freshwater discharge into the North Atlantic caused the southward displacements of the KEF via atmospheric dynamic. A power of the 9,700 year-periodicity in surface planktonic $\delta^{18}O$ and ΔT is stronger during MIS 19c, which probably originates from tropics caused by equatorial insolation at equinoxes with the orbital perihelion. This result indicates the seasonality of the insolation at low-latitudes paced the sea surface condition at the CbCS throughout MIS 19 and this low-latitude influence became larger especially when the North Atlantic forcing by freshwater discharges and AMOC variability was low.

Keywords: marine isotope stage 19, oxygen isotope, climatic teleconnection, foraminifera, Kuroshio Extension Front, Chiba composite section

©2020. Japan Geoscience Union. All Right Reserved.

Influence of Southern Ocean Intermediate water on the South Pacific’ s thermocline during the last ~500 Ka

*RAUL TAPIA[1,3], Sze Ling Ho[1], Nele Meckler[2], Dirk Nürnberg[3]

1. Institute of Oceanography, National Taiwan University, Taipei, Taiwan, 2. Bjerknes Centre for Climate Research and Department of Earth Science, University of Bergen, Norway, 3. GEOMAR –Helmholtz Centre for Ocean Research Kiel, Kiel, Germany

The Southern Ocean Intermediate Waters (SOIWs), such as Subantarctic Mode Water and Antarctic Intermediate Water, transport climatic signals from high to low latitudes and ventilate the thermocline in the Southern Hemisphere Gyres. Reconstructions of the SAMW-AAIW in the South Pacific suggest substantial spatial variability in their advection to lower latitudes during the last glacial, but the SOIWs’ impact on the South Pacific Gyre’ s thermocline beyond the last glacial cycle is largely unknown.

Here, we present ~500 ka multiproxy records of Mg/Ca ratios, clumped isotopes and stable oxygen isotope, measured on sea surface and thermocline-dwelling planktic foraminifera from the center of the SPG. The local salinity and Mg/Ca-temperature at the sea surface is relatively stable (~10 ºC) throughout the record. However, the dual proxy-based thermocline temperature records show two distinct climatic intervals. Prior to 300 ka, the conditions were cold and fresh, with average temperatures of ~4 ºC. Thereafter (<300 ka), the thermocline of the SPG became warmer and saltier, with average temperatures of ~8 ºC.

The SOIWs variability in the Pacific basin have been traditionally linked to the Southern Westerlies Winds. However, the evolution of the subsurface-temperature and -salinity substantially differs from the glacial-interglacial variability (position and/or intensity) of the Southern Westerlies Winds. We discuss several possible mechanisms that could lead to this enigmatic shift in our thermocline temperature and salinity records.

Keywords: Mg/Ca, Planktic Foraminifera, Intermediate waters, Stable isotopes

©2020. Japan Geoscience Union. All Right Reserved.

Simulating selected time intervals during the Quaternary using MIROC-ES2L earth system model in comparison with paleo-proxy data

*Rumi Ohgaito[1], Akitomo Yamamoto[1], Tomohiro Hajima[1], Manabu Abe[1], Hiroaki Tatebe[1], Michio Kawamiya[1], Ayako Abe-Ouchi[2,3,1]

1. Japan Agency for Marine-Earth Science and Technology, 2. U. Tokyo, AORI, 3. NIPR

Simulating paleoclimate is a valuable opportunity to evaluate climate models on simulating climate change significantly different from the present day. We performed numerical experiments targeting several time periods during the Quaternary, Last Glacial Maximum (LGM, 21,000 years before present), mid-Holocene (6ka) and the last millennium (LM) using an earth system model, MIROC-ES2L.
MIROC-ES2L is an earth system model (ESM) (Hajima et al. 2019) which was developed to simulate future climate projection and to contribute Coupled Model Intercomparison Project phase 6 (CMIP6).
In this presentation, we describe how we simulated the paleoclimate experiments, compare the output with paleo-proxy data and discuss the agreements and discrepancies between them. The reference experiment is pre-industrial control (PI), which was submitted to CMIP6 as “piControl”.
We performed the experiments following protocol of Paleoclimate Modelling Intercomparison Project (PMIP) phase 4 (PMIP4, Kageyama et al. 2017). For LGM, we began a spin-up experiment using the physical core of MIROC-ES2L. An experiment is branched from PI and the greenhouse gas levels (GHGs) are changed to the LGM values. After integration for 2,640 years, the other LGM conditions are applied step by step manner and the total spin-up reached 6,760 model years. The initial conditions at the 6,760th year of the spin-up experiment were used to initiate an experiment using MIROC-ES2L. Finally, the length of the integration reached 9,060 years from the beginning of the spin-up and the last 100 year climatology was submitted to PMIP4/CMIP6. Tropical temperature cooling of LGM relative to PI is -2.0 degree Celsius. This is comparable with paleo-proxy archives (Bartlein et al. 2011, MARGO project members 2009). The temperature anomaly over the mid to high latitudes varies more than in the tropics. For the central Greenland, the cooling of the LGM experiment resulted -11.1 degree Celsius relative to PI, which is about the half of the estimate by ice core data (Johnsen et al. 1995, Dahl-Jensen et al. 1998). The large discrepancy would be attributed to the difficulty of the realization of ocean thermohaline state in the model experiment.
6ka is known from the warming of the northern hemisphere and from associated strengthen of the boreal summer monsoons. We branched the simulation from PI and gave the orbit and GHGs of 6ka condition (Otto-Bliesner et al. 2017), and extended 1500 model years. The climatology of the last 100 year was used for the analyses and was submitted to CMIP6/PMIP4. The temperature anomaly during boreal summer showed the warming as expected from the radiation anomaly. Strengthen of boreal summer monsoons were simulated in the experiment, consistent with proxy data qualitatively, but quantitatively underestimated. This is persistent tendency of modelling studies under PMIP model configurations. We would either need further components of model or improve experimental conditions.
The initial state of LM is obtained by an experiment forced with 850 CE condition constantly for 200 model years. LM was started from the end of this experiment. LM is a time varying experiment for 1000 years from 850 CE until 1850 CE, conducted in the same manner with historical experiments following Jungcluas et al. (2017). The resulting time series of the northern hemisphere mean temperature revealed repeating clear cooling responses to huge volcanic eruptions. The responses to the other forcing were not clear. Further investigations and sensitivity experiments would be necessary but the other forcing supposed to be too weak compared to the internal variabilities. The LM is followed by a historical experiment (HIST) until 2014 CE. HIST experiment represented multi-decadal climate variabilities during

©2020. Japan Geoscience Union. All Right Reserved.

the industrial era as well as the other standard historical experiments submitted for CMIP6.

Keywords: PMIP, earth system model

©2020. Japan Geoscience Union. All Right Reserved.

Fossil diatom records from IODP Exp. 382 Sites U1536 and U1538 (preliminary results)

*Yuji Kato[1], Michael E. Weber[2], Maureen E. Raymo[3], Trevor Williams[4], - The IODP Expedition 382 Scientists

1. Center for Advanced Marine Core Research, Kochi University, 2. University of Bonn, Germany, 3. Lamont-Doherty Earth Observatory of Columbia University, USA, 4. International Ocean Discovery Program, Texas A&M University, College Station, USA

As the Southern Ocean plays a significant role in global climate system, there has been a great discussion about paleoceanographic changes in the Southern Ocean. Of these, fossil diatoms preserved in sediments have been treated as useful paleoenvironmental indicators for reconstructing past ocean conditions over geological timescales.

International Ocean Discovery Program (IODP) Expedition 382 (from March to May 2019) obtained several high-resolution sediment cores from Scotia Sea (Atlantic sector of the Southern Ocean), which covers Plio-Pleistocene ages. Of these, Site U1536 (59.44ºS, 41.06ºW, water depth 3220 m, Dove Basin) and Site U1538 (57.44ºS, 43.36ºW, water depth 3131 m, Pirie Basin), which are located in the vicinity of modern winter sea-ice limit, are likely to contain robust paleoceanographic information such as sea-ice history and SST changes. In the current presentation, we will present preliminary results of diatom assemblage analysis extending past ca. 0.5 myrs and discuss their paleoceanographic and biostratigraphic significance.

Keywords: diatom, Southern Ocean, paleoenvironment, IODP

©2020. Japan Geoscience Union. All Right Reserved.

Variations of the North and South Pacific Subtropical Gyres over the past 400 kyrs

*Furukawa Keisuke[1], Osamu Seki[2]

1. Graduate School of Environmental Science, Hokkaido University, 2. Institute of Low Temperature Science, Hokkaido University

The gyre in the ocean is thought to play an important role in the climate system as meridional heat and material transports between low and high latitudes. In late Pleistocene paleoceanographic study, previous study revealed that the large variation of intensity of North Pacific Subtropical Gyre (NPSG) associated with glacial-interglacial cycles with 23 kyr cycle (Yamamoto et al., 2008), suggesting a precession control on intensity of NPSG circulation. However, the mechanism driving the long-term variability of the subtropical gyre and its role in global climate change are still remains uncertain.
In this study, we reconstructed and analyze mid sea surface temperature (SST) records in the western and eastern sides in the NPSG and South Pacific Subtropical Gyre (SPSG) for the past 400 kyrs to investigate evolution of those gyres. We reconstructed intensity of the gyre circulation from ΔSST difference between west and eastern sides of the gyres. The west-east ΔSST record in SPSG show orbital scale variations over the past 400 kyrs. Spectral analysis suggests predominance of 23 and 41 kyr cycles, suggesting precession and obliquity control on SPSG.

Keywords: Sea surface temperature, South Pacific Subtropical Gyre, Paleoceanography

©2020. Japan Geoscience Union. All Right Reserved.

Paleovegetation and paleoenvironmental changes in the northern Mongolia since MIS 3 (preliminary results)

*Ryosuke Imaoka[1], Koji Shichi[2], Hitoshi Hasegawa[1], Niiden Ichinnorov[3], Nagayoshi Katsuta[4], Davaasuren Davaadorj[5], Masafumi Murayama[1], Miho Sasaoka[1], Masao Iwai[1]

1. Kochi University, 2. Forestry and Forest Products Research Institute, 3. Mongolian Academy of Sciences, 4. Gifu University, 5. National University of Mongolia

We present results of paleovegetation and paleoenvironmental analysis for new lake sediment record of Sangiin Dalai lake in the northern Mongolia. We took a surface sediment core in August 2016 (16SD02; 84 cm length), and five boring cores in March 2019 (19SD01~05; totally ca. 16 m length) from Sangiin Dalai lake, a large permanent hard water lake. The studied lake is located in the southern margin of Siberian continuous permafrost zone, and surrounded by forest-steppe vegetation dominated by Larix Sibirica. In order to reconstruct paleoenvironmental and paleovegetation change, we conducted palynological analysis and high-resolution elemental composition analysis using μXRF core scanner (Cox, Itrax) at Center for Advanced Marine Core Research, Kochi University. We also performed ^{14}C and OSL age dating. On the basis of palynological analysis and biome reconstruction (Tarasov et al., 2000), marked vegetation changes from steppe-desert in last glacial to steppe-taiga in the Holocene were reconstructed. We also note the periodic lithological change indicating drastic lake environmental change during MIS 3. Further palynological analysis for reconstructing variations in paleovegetation and paleoenvironment in the northern Mongolia since MIS 3, and comparison with palynological record in surrounding area (e.g., Kotokel lake in southern Siberia: Shichi et al., 2009; and Orog lake in southern Mongolia: Yu et al., 2019) are now ongoing.

References

Shichi, K., Takahara, H., Krivonogov, S. K., Bezrukova, E. V., Kashiwaya, K., Takehara, A., & Nakamura, T. (2009). Late Pleistocene and Holocene vegetation and climate records from Lake Kotokel, central Baikal region. Quaternary International, 205, 98-110.

Tarasov, P. E., Volkova, V. S., Webb III, T., Guiot, J., Andreev, A. A., Bezusko, L. G., et al. (2000). Last glacial maximum biomes reconstructed from pollen and plant macrofossil data from northern Eurasia. Journal of Biogeography, 27, 609-620.

Yu, K., Lehmkuhl, F., Schlütz, F., Diekmann, B., Mischke, S., Grunert, J., et al. (2019). Late Quaternary environments in the Gobi Desert of Mongolia: Vegetation, hydrological, and palaeoclimate evolution. Palaeogeography, Palaeoclimatology, Palaeoecology, 514, 77-91.

Keywords: pollen analysis, paleovegetation, global warming

©2020. Japan Geoscience Union. All Right Reserved.

Constraining the magnitude and spatial pattern of low-to-mid latitudes western Pacific ocean temperature changes in the past 25 kyr

*Sze Ling Ho[1], Sicheng Le[1], Ren Yi Ooi[1], RAUL TAPIA[1], Da-Cheng Lin[2], Min-Te Chen[2], Yuan-Pin Chang[3], Masanobu Yamamoto[4], Liang-Jian Shiau[2,5], Chuan-Chou Shen[6], Pai-Sen Yu[7]

1. Institute of Oceanography, National Taiwan University, Taipei, Taiwan., 2. Institute of Applied Geosciences, National Taiwan Ocean University, Keelung, Taiwan, 3. Department of Oceanography, National Sun Yat-sen University, Kaohsiung, Taiwan, 4. Faculty of Environmental Earth Science, Hokkaido University, Sapporo, Japan, 5. Exploration and Development Research Institute, CPC Corporation, Miaoli, Taiwan, 6. High-Precision Mass Spectrometry and Environment Change Laboratory (HISPEC), Department of Geosciences, National Taiwan University, Taipei, Taiwan, 7. Taiwan Ocean Research Institute, NARLabs, Kaohsiung, Taiwan

Upper ocean (0–200 m) temperature reflects large scale ocean circulations and the atmospheric-ocean heat exchange. It is therefore a useful metric in characterizing paleoclimate, including the roles played by the East Asian Monsoon and the Indo-Pacific Warm Pool in driving the hydroclimate of East Asia. Geochemical proxies are widely used to reconstruct past ocean temperature, but may yield discrepant estimates due to chemical and ecological differences. This uncertainty in reconstructions can be constrained by a multiproxy approach. However, most existing paleoclimate studies in East Asia are inferred from single paleotemperature proxy. Consequently, the multiproxy discussion in this region is in fact based largely on different proxies from different sites, rendering it challenging to disentangle the effect of local climate from proxy discrepancy. In this study, we aim to characterize the magnitude and spatial pattern of the upper ocean temperature change in the western Pacific using an integrative multiproxy, multisite approach. Our sediment core sites span the South China Sea, Indo-Pacific Warm Pool and Kuroshio region. We generate a multiproxy paleotemperature database by combining newly generated data with published data. For all these sites, we obtain paleotemperature records inferred from three proxies, each based on vastly different source organisms, namely planktic foraminifera-based Mg/Ca, haptophyte-based UK’ 37, and archaea-based TEX86. As all proxies have their own pros and cons, this approach allows us to take advantage of the strengths of proxies to constrain the uncertainty of the others, thereby improving the robustness of paleoclimate reconstructions. As well as providing a constraint to the magnitude and spatial pattern of temperature change, this multiproxy database allows mapping of the ocean temperature change between distinct climate periods such as the Holocene and Last Glacial, which are often used to benchmark climate models. We envisage that this systematic multiproxy approach will refine our understanding of past changes in the oceans surrounding East Asia.

Keywords: South China Sea, Multiproxy, Sea surface temperature, East Asian Monsoon

©2020. Japan Geoscience Union. All Right Reserved.

Changes in oceanic carbon and oxygen cycle during Heinrich event

*Akitomo Yamamoto[1], Ayako Abe-Ouchi[2]

1. Japan Agency for Marine-Earth Science and TechnologyAtmosphere and Ocean Research Institute, 2. Atmosphere and Ocean Research Institute, The University of Tokyo

Weakening of the Atlantic Meridional Overturning Circulation (AMOC) during Heinrich events was often accompanied by the atmospheric CO_2 increase of 10-20 ppm over 1000 years. Previous modeling studies display conflicting atmospheric CO_2 response to an AMOC shut down. On the other hand, recent paleoproxy records suggest that dwindling iron fertilization by dust in the Southern Ocean can contribute millennial-scale CO_2 oscilations (Martínez-García et al., 2014). However, the effect of changes in iron cycle has not been considered in the previous modeling studies.
In this study, we investigate the response of atmospheric CO_2 to changes in ocean circulation and dust-bone iron supply using numerical models. In associate with the AMOC weakening from 26 Sv to 6 Sv, the atmospheric CO_2 decreases by 2 ppm over 1000 years. Combining AMOC weakening and decrease in dust-bone iron supply, the atmospheric CO_2 increases more than 10 ppm. Reduction in export production associated with dwindling iron supply in the Southern Ocean release carbon from the deep sea, contributing to the increase in the atmospheric CO_2. Reduction in export production simultaneously increases dissolved oxygen in the Antarctic Bottomo Water, which is consistent with proxy records. Our results show the significant contribution of changes in dust-bone iron supply to the millennial CO_2 change in the glacial periods.

Keywords: Ocean carbon cycle, dissolved oxygen, Ocean iron cycle, Heinrich event

©2020. Japan Geoscience Union. All Right Reserved.

Stalagmite evidence for ^{18}O-depleted surface water of Japan Sea during the last glacial

*Shota Amekawa[1], Kenji Kashiwagi[2], Masako Hori[3], Tomomi Sone[4], Hirokazu Kato[1], Tomoyo Okumura[5], Tsai-Luen Yu[6], Chuan-Chou Shen[6,7,8], Akihiro Kano[1]

1. Graduate School of Science, The University of Tokyo, 2. Department of Environmental Biology and Chemistry, Faculty of Science, University of Toyama, 3. Division of Natural Sciences, Osaka Kyoiku University, 4. Marine Works Japan LTD., 5. Center for Advanced Marine Core Research, Kochi University, 6. High-precision Mass Spectrometry and Environment Change Laboratory (HISPEC), Department of Geosciences, National Taiwan University, 7. Global Change Research Center, National Taiwan University, 8. Research Center for Future Earth, National Taiwan University

In East Asia monsoonal realm, stalagmites generally record lower $\delta^{18}O$ during warm humid interglacials and higher $\delta^{18}O$ in the cold dry glacials. Here, we present an unusual trend in stalagmite $\delta^{18}O$ between the last glacial interval and Holocene from Fukugaguchi Cave, Niigata Prefecture, where a major moisture source is the East Asian winter monsoon (EAWM) carrying vapor from the warm surface of the Japan Sea. The $\delta^{18}O$ profile of this stalagmite overall exhibits low $\delta^{18}O$ values; the mean sampled glacial $\delta^{18}O$ is distinctly lower than the mid-Holocene mean of another stalagmite (Sone et al., 2013) from the same cave. An interpretation assuming greater vapor transportation than mid-Holocene from the intensified EAWM during the last glacial contradicts marine carbonate records indicating that the entrance of the Tsushima Warm Current into the Japan Sea was interrupted because of lowered sea level. Additionally, our model indicates that the amount effect of winter meteoric water was insignificant. Low $\delta^{18}O$ in the stalagmite dated to glacial intervals in Fukugaguchi Cave most likely resulted from low-salinity and ^{18}O-depleted surface water, which developed in the isolated Japan Sea. This is the first terrestrial evidence indicating ^{18}O depletion and salinity of the Japan Sea surface water during the last glacial.

Keywords: stalagmite, East Asian winter monsoon, the last glacial period, Japan Sea

©2020. Japan Geoscience Union. All Right Reserved.

Biogenic opal changes at the Kamchatka Strait in the Bering Sea since the last glaciation

*Koshiro Matsuo[1]

1. Department of Earth and Planetary Sciences, Graduate School of Science, Kyushu University

The subarctic Pacific is known as a high biological productivity region mainly by diatoms. Particularly the central and eastern parts of the subarctic Pacific are high nutrient low chlorophyll (HNLC) regions. In the HNLC regions, lack of micronutrients such as iron regulate phytoplankton productivity despite of macronutrient availability such as nitrate, phosphate and silicate. Modern oceanographic observation has revealed dissolved iron transportation from the Okhotsk Sea to the western subarctic Pacific thorough intermediate water. Biological productivity in the subarctic Pacific was markedly low during the last glacial. Since the last glacial termination, the productivity in the subarctic Pacific increased but considerable regional differences were observed. In this study, biogenic opal content in KST-2A-PC obtained from the Kamchatka Strait was measured to understand changes in diatom production in the western Bering Sea. The biological opal content in KST-2A-PC showed gradual increase since the last glaciation without deglacial peak. This pattern was not similar to the central and eastern Bering Sea but similar to the Okhotsk Sea. The peaks of biological productivity at the southern, eastern, and northern Bering Sea and north open Pacific during the last deglaciation were influenced by increasing of supply in macronutrients which came from deep water and/or from continental shelves following the rise of sea level. However, Macronutrients had been consumed completely before reaching the western Bering Sea, so, in the last deglaciation, there were no peak of biological productivity at the western Bering Sea and in the Okhotsk Sea. Since Holocene, supply of macronutrients from deep sea and dissolved Fe from the Okhotsk Sea transported by intermediate water was increased, which caused increasing of biological productivity in the north Pacific marginal seas. Changes of utilization efficiency in macronutrients indicate that it was in the period from the last deglaciation to Holocene that macronutrients as regulatory factor of biological productivity were replaced with dissolved Fe, thus HNLC regions ware formed.

Keywords: The Bering Sea, The last glaciation, Biological productivity

©2020. Japan Geoscience Union. All Right Reserved.

Intermediate water formation in the Bering Sea since the last glacial maximum based on *Cycladophora davisiana* abundances.

*Kento Ogata[1], Yusuke Okazaki[1]

1. Kyushu university Earth and Planetary sciences

Radiolarians are marine zooplankton with biogenic opal skeleton living in surface to deep ocean. Radiolarian microfossil assemblages in deep-sea sediments are used as paleoceanographic indicators and stratigraphic markers. Cycladophora davisiana is a radiolarian species dwelling in intermediate water with low temperature, high oxygen concentration, and rich in organic carbon. Therefore, increase and decrease in C. davisiana abundance in marine sediments suggests the presence of ventilated intermediate water. The Bering Sea, a marginal sea located in the North Pacific, is to be a source region of well-ventilated intermediate water in the glacial North Pacific. Here we show changes of C. davisiana abundances in sediment core obtained from the Kamchatka Strait, the largest strait in the Bering Sea, to reconstruct intermediate water formation change since last glaciation. KST-2A piston core sample was obtained from the Kamchatka Strait during Mu18 cruise by R/V Prof. Multanovskiy (56°11’ N;165°1’ E; water depth 3545 m; core long 454 cm). KST-2A-PC recorded past 20 kyrs (since the last glacial maximum, LGM) based on radiocarbon dating of planktic foraminifera and calcium concentration patterns. Two types of microslides were prepared for light microscopic observation by sieved through screens with different mesh opening sizes (>63 μm and >45 μm). Total radiolarian abundances (No. skeleton g-1) have gradually increased for the past 20 kyrs. Cycladophora davisiana abundances (No. skeleton g-1) fluctuated with peaks during deglacial warming periods. Although the total radiolarian and C. davisiana abundances (No. skeleton g-1) were significantly low during LGM, relative abundances (%) of C. davisiana were high during LGM as well as the deglacial warming periods. These C. davisiana abundance patterns suggest that intermediate water formation was active in the Bering Sea during the deglaciation. Total radiolarian abundances (No. skeleton g-1) estimated by using >45 μm were much higher than those of >63 μm. However, there was no significant difference in %C. davisiana patterns between >45 μm and >63 μm samples.

Keywords: intermediate water, Cycladophora davisiana, Bering Sea

©2020. Japan Geoscience Union. All Right Reserved.

Analysis from Benthic foraminifera populations of expansion and intensify of the northwestern Pacific oxygen minimum zone during the last deglaciation

*Keisuke Sakai[1], Ken'ichi Ohkushi[1], Akihiko Shibahara[2]

1. Graduate School of Human Development and Environment, Kobe University, 2. Fukui Prefectural University Institute of Dinosaur Research

During the last deglaciation, the oxygen minimum zone (OMZ) at 1 km water depth in the northwestern Pacific Ocean intensified. However, time-series fluctuations of the upper layer of the OMZ are poorly understood. Fossil benthic foraminifera are useful indicators of historic deoxygenation at the seafloor due to their specific patterns of adaptation to dysoxic environments. Thus, we studied benthic foraminifera assemblages in a sediment core taken from a water depth of 777 m off of Hokkaido, North Japan, to reconstruct changes in the upper layer of the OMZ during the last deglaciation. The results suggested that dysoxic species such as Brizalina seminuda and Buliminella tenuata increased rapidly during the Bølling/Ållerød warming event, implying severe oxygen depletion. Similar dysoxic assemblages were recorded at 1 km water depth in this region. We concluded that the upper limit of the OMZ in the northwestern Pacific expanded during the last deglaciation, due to an increase in biological production and decrease in intermediate water ventilation.

Keywords: Benthic foraminifera, last deglaciation, oxygen minimum zone, northwestern Pacific, Bølling/Ållerød

©2020. Japan Geoscience Union. All Right Reserved.

Changes in carbon and oxygen isotopes of benthic foraminifera in the East China Sea since the last glacial maximum

*Miki Muranaka[1], Yusuke Okazaki[2], Yoshimi Kubota[3]

1. Department of Earth and Planetary Sciences, Kyushu University, 2. Department of Earth and Planetary Sciences, Graduate School of Science, Kyushu University, 3. National Museum of Nature and Science

The continental shelves shallower than 200 m water depths occupies more than 70 % of the area of East China Sea (ECS). During the last glacial maximum (LGM), sea-level dropped by 120 m. Therefore, vast area of the ECS continental shelves were aerially exposed. Here we present carbon and oxygen isotopes of benthic foraminifera in sediment core from the Danjo Basin, northern ECS (KY07-04-PC01, 31˚38.35’ N, 128˚56.64’ E, 758 m water depth). Foraminiferal shells are composed of calcite ($CaCO_3$). Carbon isotope ratio ($\delta^{13}C$) of benthic foraminifera is used as a proxy for nutrient concentrations Therefore, benthic foraminiferal $\delta^{13}C$ is useful for reconstructing past water mass structures. Oxygen isotope ratio ($\delta^{18}O$) of benthic foraminifera is used as a proxy for ice volume and water temperature. Two benthic foraminiferal taxa *Uvigerina* spp. and *Hyalinea balthica* were picked up from KY07-04-PC01 sample and were used for $\delta^{13}C$ and $\delta^{18}O$ measurements. The $\delta^{13}C$ of *Uvigerina* spp. during LGM was ~2 ‰heavier than those of Holocene. This offset can be explained by oscillation of two water masses in ECS: cold and nutrient-rich Chinese coastal water was prevailing in glacial semi-closed ECS; warm and nutrient-depleted Kuroshio water increased since deglaciation with sea-level rise. The $\delta^{18}O$ of *Uvigerina* spp. gradually decreased from 3.76 ‰during LGM to 2.39 ‰during late Holocene. The 1.36 ‰ $\delta^{18}O$ offset is caused by ice volume and water temperature. Because the ice volume effect for benthic $\delta^{18}O$ between LGM and present is estimated to be 1.1 ‰, the residual 0.27 ‰is equivalent to water temperature change of 1 ℃. This suggests intermediate water temperature in northern ECS has risen by 1 ℃ since LGM. There are two morphology in *Uvigerina* spp., with more spiny and less spiny. Because offsets of $\delta^{13}C$ and $\delta^{18}O$ between the two morphologic types, it is desirable to measure separately. *Hyalinea balthica* showed ~1 ‰lighter $\delta^{13}C$ and $\delta^{18}O$ values than those of *Uvigerina* spp. In addition, it was time-consuming for cleaning *Hyalinea balthica* shells. Thus, *H. balthica* is not a proper benthic foraminiferal species for $\delta^{13}C$ and $\delta^{18}O$ measurements.

©2020. Japan Geoscience Union. All Right Reserved.

Southward Migration of Inter-Tropical Convergence Zone (ITCZ) during Mid-Late Holocene: New Evidence from Sri Lanka

*Kasun Gayantha[1], Patrick Roberts[2], Joyanto Routh[3], Achim Brauer[4], Rohana Chandrajith[5], Oshan Wedage[2], Florian Ott[2], Gerd Gleixner[1]

1. Max Planck Institute for Biogeochemistry, Jena, Germany, 2. Max Planck Institute for the Science of Human History, Jena, Germany, 3. TEMA-M, Linköping University, Linköping, Sweden, 4. GFZ, Potsdam, Germany, 5. Department of Geology, University of Peradeniya, Sri Lanka

Southward migration of the mean latitudinal position of the Inter-Tropical Convergence Zone (ITCZ) as a response to decreasing solar insolation in the Northern hemisphere during the Mid and Late Holocene is discussed widely (Haug et al. 2001; Broccoli et al. 2006; Fleitmann et al. 2007). This hypothesis is supported by the millennial-scale continuous weakening trend of the Indian summer monsoon (ISM) and Asian summer monsoon (ASM) within the core monsoon domains in the Indian sub-continent (Gupta et al. 2003), East Asia (Wang and Tsonis 2008), Middle East (Fleitmann 2003) and South America (Maslin and Burns 2000). However, in contrast to this hypothesis, some studies suggest an abrupt weakening of the ISM and ASM between ~ 4.5 and 5.0 ka BP (Morrill et al. 2003 and references therein). This forms a question of whether the ISM and ASM weakening occurred gradually related to orbital forcing or abruptly due to variations in other components of the climatic system, that is important to know for developing general and regional climate models that help to predict future climate trends.

The South Asian region is directly impacted by the ISM and retreating Indian winter monsoon (IWM) and the agriculture-based economy in this region is strongly dependent on the seasonal precipitation. However, very limited well-dated and continuous paleoclimate archives, especially in the southern parts of the Indian sub-continent that is fed by both summer and winter monsoon rainfalls creates a significant knowledge gap to understand the behavior of Indian monsoon system. So far, our understanding of millennial-scale ITCZ fluctuations depends on the ISM records and evidence from the retreating IWM are still scarce.

The geographical location of Sri Lanka, lying in the center of the seasonal ITCZ migration path and the rain shadow effect due to the central highlands, allows us to study the summer and winter monsoon rainfall variations separately. The position of ITCZ is directly impacting the duration of both monsoon seasons (Fig 1). Therefore, a multi-proxy analysis was conducted on three sediment cores retrieved from the summer monsoon-fed wet zone (South Bolgoda Lake and Horton Plains) and winter monsoon-fed dry zone (Panama lagoon) of Sri Lanka. Together with ^{14}C based age models, rainfall variations in the regions were traced based on compound-specific carbon and hydrogen isotopes of leaf wax *n*-alkane (*n*-C_{33} and C_{31}) and detrital elemental ratios (Zr/Rb and Zr/Al) related to grain size variation.

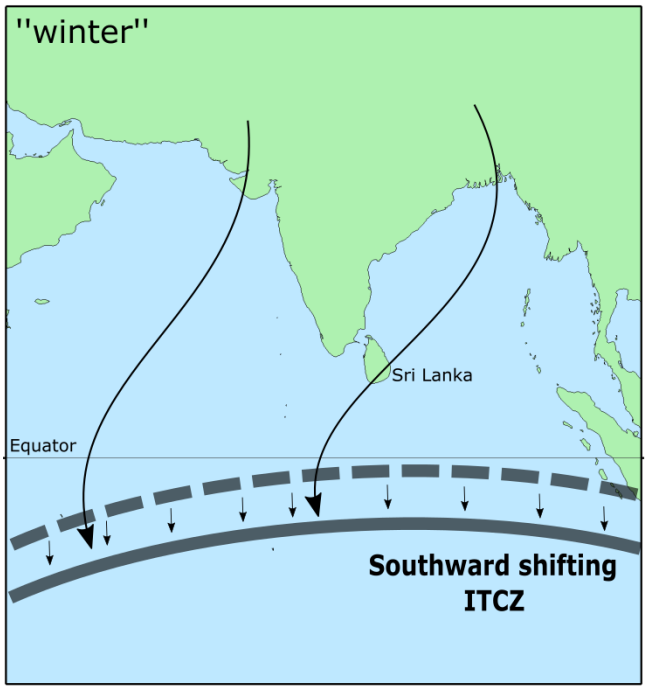
The increasing trend of δD and $\delta^{13}C$ values of leaf wax *n*-alkane of ISM influenced South Bolgoda Lake and Horton Plains showed a gradually decreasing trend of the rainfall over last ~6 ka BP despite few short-term abrupt events. This trend is also supported by the gradual decreasing trend of detrital element ratios (Zr/Rb and Zr/Al) supporting less continental erosion from declining rainfall. In contrast to these trends observed in the wet zone, retreating IWM influenced Panama lagoon located in the dry zone showed inverse results indicating a more gradual increase in winter precipitation during the same period. This inverse relationship between ISM and IWM rainfall can be explained by the concept of southward migration of the mean latitudinal position of ITCZ during the mid and late Holocene that occurred as a

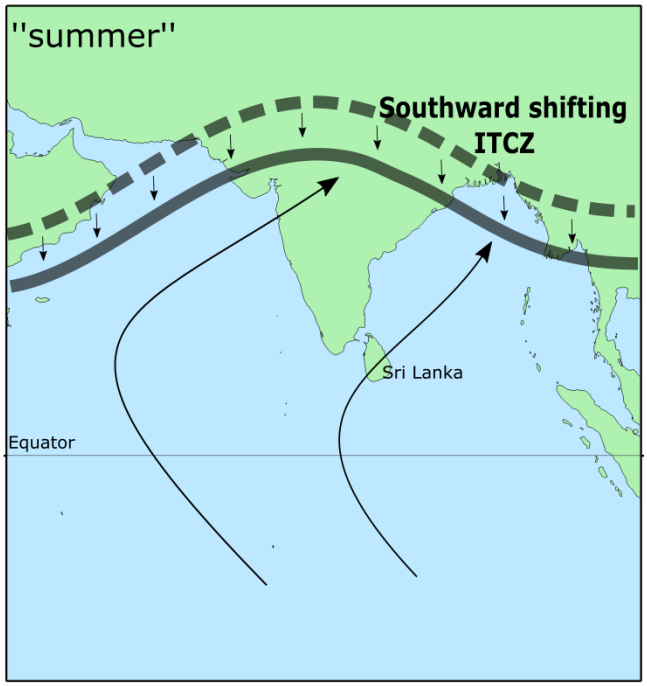
©2020. Japan Geoscience Union. All Right Reserved.

response of solar insolation variations in the Northern and Southern

Hemispheres. When the southern and northernmost positions of ITCZ gradually shift southward, the duration of IWM rainfall can increase resulting in relatively higher rainfall in the dry zone of Sri Lanka. Meantime, the inverse effect on the ISM can be expected in the wet zone. Our results indicate that the annual precipitation of Sri Lanka shifting towards a winter monsoon dominant system from summer monsoon dominant system over last ~ 6 ka BP, as a result of the solar-induced shift of ITCZ.

Keywords: Paleoclimate, ITCZ, Monsoon, Sri Lanka, Holocene





©2020. Japan Geoscience Union. All Right Reserved.

Diatom and Chrysophyceae Assemblages from the Holocene Alluvial Core Sediments at Southern and Western Coasts of Korea Peninsula

*Kaoru Kashima[1], Yu Fukumoto[3], Sangheon Yi[2], Dong-Yoon Yang[2], Min Han[2]

1. Department of Earth and Planetary Sciences, Kyushu University, 2. Korea Institute of Geoscience & Mineral Resources (KIGAM) , 3. Ritsumeikan University

The Holocene alluvial sediments kept traces of the abrupt Holocene climatic events in coastal area. Park et al (2019) presumed at 8.2 ka, 4.2ka and 2.8 ka BP events using drilling cores at south and west coast of Korea Peninsula by Pollen analysis, C14 dating and chemical analyses.

We selected the three cores along the western and southern coasts of Korea Peninsula for the analysis of diatom and Chyrysophyceae assemblages. All cores presumed to insert marine clay within the core by their lithological observation. The diatom assemblages showed the marine transgressive process at the lowland according to the Holocene marine transgression, the closing bay and lagoon forming processes, marine regressions and land forming processes clearly. Diatoms also showed the erosional stages by the sudden changes of their assemblage compositions when we could not find the erosional structures in the deltaic sediment. For discussing of the ancient sailing rout, to detect the erosional surface by tidal currents was necessary to presume the ancient water depth.

Chrysophyceae is one of the single cell algae, generally called as Golden Algae. It forms hard silicate cist (Statospore) at the resting period of its life cycle. Although soft bodies of Chrysophyceae were not able to be kept in the sediments, their statospores were well kept in the sediments. They were reported not only from freshwater lake and pond sediments, but also from oceanic drilling cores. The Statospores taken from the cores of this paper might be freshwater alkaline favorite ones by their shapes and size. The possibility for the tools of paleo-environmental reconstructions has been under discussing.

In this presentation, we will discuss the Diatom and Chrysophyceae Assemblages from STP17-13 core, southern coast of Korea Peninsula, STP16-01 core, south-western coast of Korea Peninsula and DSE18-06 core at western coast of Korea Peninsula. All of them were taken undisturbed core samples until the base of the Holocene, and lithological and microfossil assemblages (Pollen) presumed the Holocene climatic events at 8.2 ka, 4.2ka and 2.8ka in the cores. Diatom and Chrysophyceae Assemblages shifted to be corresponded to those climatic events.

Keywords: Chrysophyceae, Diatom, Holocene, Korea, Sea level change, Climatic change

©2020. Japan Geoscience Union. All Right Reserved.

Correlation between stable isotope ratio of pollen and climate, as well as its possible application for paleoclimatology

*Yamasaki Akiteru[1], Keitaro Yamada[2], Takayuki Omori[3], Ikuko Kitaba[2], Takeshi Nakagawa[2]

1. Fukui Prefectural Satoyama-Satoumi Reserch Institute, 2. Research Centre for Palaeoclimatology, Ritsumeikan University, 3. The University museum, The University of Tokyo

Introduction

Obtaining detailed paleoclimate information on terrestrial realms is essential for understanding the interaction between the atmosphere and the ocean. In particular, climate in mid- latitudinal land is closely related to the human’ s life.
Fossil pollen analysis in lacustrine sediments is a widely used method for examining the paleoclimate on land (e.g. Tarasov et al., 2011; Kigoshi et al., 2014).
Quantitative reconstruction of paleoclimate using pollen data has also been attempted (Guiot, 1991; Nakagawa et al. 2002). However, direct correlation between pollen records and other high-quality data sets, such as ice core and ocean records, is not straightforward because of the response time of vegetation (Williams et al., 2002).
To solve this problem, the possibility of reconstructing paleoclimate using pollen isotope data has been pointed out (Loader and Hemming, 2004). Recently developed method of efficient high purity pollen extraction (Yamada et al.,2019, INQUA) made it realistic.
We aim at quantitative reconstruction of paleoclimate based on pollen isotope data. In this study, we evaluated the response of pollen isotope to climate using live arboreal pollen.

Method

Studies on the relationship between pollen stable isotope ratios and climate in Europe suggests a correlation between hydrogen isotope ratio and precipitation. However, the data size is too small to use the results for application. In this study, we measured oxygen isotope ratio of cedar pollen that were collected from 125 sites across Japan. The measurement was made using TC/EA (thermo Scientific Co., Ltd.) of the University Museum, the University of Tokyo.
As the meteorological observation data, we used mesh agricultural meteorological data from National Agriculture and Food Research Organization (NARO). he mesh dataset has 1km resolution and was generated from AMeDAS weather observation records, taking into account temperature lapse rate, topography and other relevant factors (Kiyono, 1993; Ono et al., 2016).

Results and discussion

The 125 sites that we could include in this study covered an area with an average annual temperature of 12-17 ˚C, precipitation of 1600-4000mm, altitude of 0-1000m, and latitude of 32-39 ˚.A strong correlation between pollen oxygen isotope ratio the mean annual temperature was found (r = 0.66).On the other hand, there was a systematic drift in isotope ratio according to the altitude of the pollen sampling point.
This study confirms that the oxygen isotope ratio of pollen responds to temperature.
In the future, although we still have to understand the isotope fractionation process of pollen and apply correction against altitude, it is possible to use the pollen oxygen isotope data for quantitatively reconstructing temperature.

©2020. Japan Geoscience Union. All Right Reserved.

Keywords: pollen, stable isotope, paleoclimate

©2020. Japan Geoscience Union. All Right Reserved.

Uncertainty of tree-ring based temperature reconstruction: Effects of soil moisture environment and air pollution on reconstruction records

*Shunsuke Tei[1], Shinya Takano[1], Teppei J Yasunari[1]

1. Arctic Research Center, Hokkaido University

Since global observation records only cover for the last 120 years, the paleoclimate reconstruction using proxy records is indispensable to fully understand past climate change on a multi-decadal/century time scale. Tree rings have long been used to be an excellent proxy for temperature. However, since the latter half of the 20th century, the correlation between the tree ring parameters (width and density) and temperature has been significantly weakened in several areas in the northern high latitudes, which likely reduces credibility of the reported tree-ring based temperature reconstructions. While the temperature records indicate a substantial warming trend in the late 20th century, tree rings in such areas do not display a corresponding change. Although some hypotheses on explaining the inconsistency have been suggested, the best mechanism for fully understand it has not been obtained yet.

The purpose of our study is to identify the environmental factors responsible for the influencing the relationship between tree-ring parameters and temperature in the northern high latitudes by using available datasets for tree ring parameters and environmental variables. We focus on two environmental factors: 1) soil moisture environment; 2) air pollution, both of which might affect plant carbon uptake processes through adjustment of stomatal openness. We clarify the effects of these environmental factors on tree ring parameters. In this presentation, we intend to show the preliminary results on this, especially for the possible impact of the air pollution on the tree ring parameters.

Keywords: Temperature reconstruction, Tree ring, Air pollution

©2020. Japan Geoscience Union. All Right Reserved.

Horizontal distribution of diatoms in the western Bering Sea surface waters

*Aika Yamamoto[1], Yusuke Okazaki[2]

1. Department of Earth and Planetary Sciences, Kyushu University, 2. Department of Earth and Planetary Sciences, Graduate School of Science, Kyushu University

Diatoms are phytoplankton with biogenic opal ($SiO_2 \cdot nH_2O$) frustules. A variety of diatom species live in various aquatic environments sensitively responding to environmental change. Diatom’ s reproduction rate is notably rapid due to their reproductive cycle by combining asexual cell division and sexual reproduction to restore the cell size. Diatoms are major primary producer in the present hydrosphere. The Bering Sea is a margin sea of North Pacific with northern continental shelves and southern basin. The Bering Sea is characterized by high productivity mainly by diatoms. In particular, pronounced high productivity area called the Bering Sea Green Belt is distributed along the edge of the continental shelves. Productivity in the Bering Sea has strong seasonality with primary spring peak and secondary fall peak due to insolation and nutrient availability in the euphotic zone. Purpose of this study is to clarify the horizontal distribution of diatom assemblages in western Bering Sea. Surface water samples were collected at 30 stations in the western Bering Sea during Mu18 cruise by *R/V Multanovskiy* in summer 2018. The seawater samples were filtered onboard. After disembarking, scanning electron microscopic observation for diatom assemblages was performed using the filter samples. A total of 15 genus 9 species were identified. Clear differences of diatom assemblages were found between basin and continental shelf stations. Major diatom taxa in basin stations were *Nitzschia* spp., *Fragilariopsis* spp., and *Neodenticula seminae.* On the other hand, major diatom taxa in continental shelf stations were *Nitzschia* spp., *Thalassiosira* spp., and *Arcocellulus* spp. Most of *Fragilariopsis* spp. encountered in this study were markedly small probably proliferated by asexual reproduction. Among *Thalassiosira* spp., *T.* cf. *oceanica* were commonly found at most of the shelf stations except for stations with low temperature and high salinity where *T. nordenskioeldii* and *T. pacifica* were abundant.

©2020. Japan Geoscience Union. All Right Reserved.

Spatio-temporal variations in fossil coral assemblages in late Middle Pleistocene limestones of the Minatogawa Formation, southern Okinawa-jima, Japan

*Riho Tomatsu[1], Marc Humblet[1], Kazuhiko Fujita[2], Yui Kouketsu[1], Yasufumi Iryu[3]

1. Graduate School of Environmental Studies, Nagoya University, 2. Department of Physics and Earth Sciences, University of the Ryukyus, 3. Institute of Geology and Paleontology Graduate School of Science Tohoku University

Quaternary reef-complex deposits crop out extensively in the Ryukyu Islands, southwestern Japan, providing a unique record of reef growth history close to the northern limit of modern coral reef distribution. The late Middle Pleistocene Minatogawa Formation (<0.4 Ma) is exposed along the coast of southern Okinawa Island and on nearby islets. The Minatogawa Formation is 20 m thick in the study area and is composed of four units (in ascending order: Unit 1–4) separated by unconformities. The main lithologies are coral-rich limestone (coral boundstone and rudstone) and well-sorted detrital limestone (mainly foraminifer-rich grainstone). In this study, we examine the taxonomic compositions and the spatio-temporal distribution of fossil coral assemblages in the Minatogawa Formation to achieve the following goals: (1) to clarify the depositional history of the Minatogawa Formation and (2) to reconstruct relative sea-level changes and their impact on coral communities. To reach these objectives, field work was carried out in a large quarry in southern Okinawa Island. Results reveal six distinct coral assemblages in Unit 2 and 3, each indicating a particular reef environment, from shallow (<5 m) exposed and protected settings to deeper (up to 25–30 m) reef-slope settings. The coral assemblage found in Unit 2 suggests that the coral boundstone and well-sorted detrital limestone in this unit formed concomitantly in a lower reef slope setting, or perhaps, a shallower but turbid environment. In contrast, the analysis of coral assemblages of Unit 3 and of the boundary between the coral boundstone and adjacent well-sorted detrital limestone in this unit suggest a relative sea-level history more complex than previously thought, as attested by the occurrence of a subaerial exposure surface between the coral boundstone and adjacent well-sorted detrital limestone. Temporal (vertical) variations in coral assemblages within Unit 3 reflect the various stages of reef growth, from reef initiation at the base of the unit to reef demise at the top due to exposure during relative sea-level fall. In addition, crustal movements have influenced reef growth during the deposition of the Minatogawa Formation. A syn-depositional fault intersecting the boundary between Unit 2 and 3 attests of small-amplitude sea-level changes caused by tectonic activity. Ongoing efforts are being made to constrain the age of the Minatogawa Formation in order to clarify the relationship between its depositional history and global eustatic sea-level changes.

Keywords: fossil coral communities, late middle Pleistocene, environmental and sea level changes, tectonic uplift, Minatogawa Formation, Okinawa-jima

©2020. Japan Geoscience Union. All Right Reserved.

[E] Poster | M (Multidisciplinary and Interdisciplinary)：M-IS Intersection

[M-IS09] Interdisciplinary studies on pre-earthquake processes

convener:Katsumi Hattori(Department of Earth Sciences, Graduate School of Science, Chiba University), Dimitar Ouzounov(Center of Excellence in Earth Systems Modeling & Observations (CEESMO) , Schmid College of Science & Technology Chapman University, Orange, California, USA), Jann-Yenq LIU(Department of Space Science and Engineering, National Central University, Taiwan), Qinghua Huang(Peking University)

This session expands the interdisciplinary discussions on preparation process of earthquake and earthquake predictability by presenting the latest progress in studying the physically based pre-earthquake phenomena. New observations from space and ground have provided evidences, which may enhance better understanding of tectonic activity. The session anticipates talks that include but not limited to observations and analyses of seismic, electrical, electromagnetic, electro-chemical and thermodynamic processes related to stress changes in the lithosphere along with their statistical and physical validation. Presentations on the latest observational results associated with major earthquakes obtained by different methodologies are welcomed. The topics of the session are as follows but not limited.

 -General discussion on earthquake preparation process and the physics of pre-earthquake signals
 - Theory, modeling, laboratory experiments, computational simulation for generation and propagation of pre-earthquake signals and their connection with seismic cycle
 - Multi-parameter observations, detection, and validation of pre-earthquake signals
 - Cross-disciplinary studies, practical and technical approaches for better understanding of earthquake preparation processes and their connection with seismicity

[MIS09-P01] FORMOSAT-7/COSMIC-2 observing seismo-ionospheric precursors of the 14 November 2019 M7.1 Indonesia Earthquake

*JANN-YENQ Liu[1,2], CHIYEN LIN[1,2], FU-YUAN CHANG[1,2], Yuh-Ing Chen[3] (1.Center for Astronautical Physics and Engineering, National Central University, Taiwan, 2.Department of Space Science and Engineering, National Central University, Taiwan, 3.Graduate Institute of Statistics, National Central University, Taiwan)

[MIS09-P02] Statistical Analysis of Pre-Seismic Ionospheric Anomalies and their Characteristic

*Sanaka Saito[1], Chie Yoshino[1], Katsumi Hattori[1] (1.Chiba University)

[MIS09-P03] **Pre-earthquake early-warning signals of ULF geoelectric data and their earthquake forecasting probability: A case of Kakioka, Japan**

★Invited Papers

*Hong-Jia Chen[1], Katsumi Hattori[1], Ryo Takahira[1] (1.Chiba University)

[MIS09-P04] Numerical simulation of ULF electromagnetic wave propagation in the lithosphere associated with earthquakes by using the WLP-FDTD method

*Ryota Kimura[1], Yoshiaki Ando[1], Katsumi Hattori[2] (1. The University of Electro-Communications, 2.Chiba University)

[MIS09-P05] **Geomagnetic *Sq* equivalent currents variation characters in the 210°mm meridian region**

*Xiaocan Liu[1], Katsumi Hattori[2,3], Huaran Chen[1], Peng Han[4], Chie Yoshino[2], Xudong Zhao[1] (1.Institute of geophysics China Earthquake Administrition, 2.Graduate School of Science, Chiba University, Chiba, Japan, 3.Center for Environmental Remote Sensing, Chiba University, Chiba, Japan, 4.Department of Earth and Space Sciences, Southern University of Science and Technology, ShenZhen, China)

[MIS09-P06] Measurement of vertical distribution of environmental radiation using a drone at Choshi

*Tohru Okabayashi[1], Kiyotaka Ninagawa[2], Isao Yamamoto[2], Nobuhiro Maeda (1.Chiba Institute of Science, 2.Okayama University of Science)

[MIS09-P07] Ground Rn flux anomaly and crustal activity around Asahi station, Boso Peninsula, Japan

*Haruna Kojima[1], Chie Yoshino[1], Katsumi Hattori[1], Michikuni Shimo[2], Toshiharu Konishi[3], Ryuichi Furuya[4] (1.Chiba University, 2.Fujita Health University, 3.OHYO KOKEN KOGYO Co.,Ltd, 4.COM SYSTEM Inc.)

[MIS09-P08] **The Study of Sq Equivalent Current during the Solar Cycle**

*Xudong Zhao[1] (1.Institute of Geophysics, China Earthquake Administration)

[MIS09-P09] Development of 3D self-potential tomography and electro-kinetic effects

*ayaka ishikawa[1], Katsumi Hattori[1] (1.chiba university)

[MIS09-P10] Application of Multi-channel Spectrum Analysis (MSSA) in noise reduction to MT data observed at Boso Peninsula in Japan

*Shu Kaneko[1], Katsumi Hattori[2], Toru Mogi[2], Chie Yoshino[2] (1.Chiba University Graduate School of Science and Engineering, 2.Chiba University Graduate School of Science)

[MIS09-P11] Development of Ionospheric Electron density tomography using linear regularization.

*Sanaka Saito[1], Rui Song[1], Katsumi Hattori[1] (1.Chiba University)

FORMOSAT-7/COSMIC-2 observing seismo-ionospheric precursors of the 14 November 2019 M7.1 Indonesia Earthquake

*JANN-YENQ Liu[1,2], CHIYEN LIN[1,2], FU-YUAN CHANG[1,2], Yuh-Ing Chen[3]

1. Center for Astronautical Physics and Engineering, National Central University, Taiwan, 2. Department of Space Science and Engineering, National Central University, Taiwan, 3. Graduate Institute of Statistics, National Central University, Taiwan

FORMOSAT-7/COSMIC-2 (F7/C2), with the mission orbit of 550 km altitude, 24-deg inclination, and a period of 97 minutes, was launched on 25 June 2019. Tri-GNSS Radio occultation System (TGRS), Ion Velocity Meter (IVM), and RF beacon onboard F7/C2 six small satellites allow scientists to observe the plasma structure and dynamics in the mid-latitude, low-latitude, and equatorial ionosphere in detail. F7/C2 TGRS sounds ionospheric RO (radio occultation) electron density profiles, while F7/C2 IVM probes the ion density, ion temperature, and ion velocity at the satellite altitude. The F7/C2 electron density profiles and the ion density, ion temperature, and ion velocity, as well as the global ionospheric map (GIM) of the total electron content (TEC) derived from global ground-based GPS receivers are used to detect seismo-ionospheric precursors (SIPs) of the 14 November 2019 M7.1 Indonesia Earthquake. The GIM TEC and F7/C2 RO NmF2 significantly increase specifically over the epicenter on 25-26 October, which indicates SIPs of the 14 November 2019 M7.1 Indonesia Earthquake being detected. The F7/C2 RO electron density profiles upward motions suggest that the eastward electric fields have been enhanced during the SIP days of the 2019 M7.1 Indonesia earthquake. The seismo-generated electric fields of the 2019 M7.1 Indonesia earthquake are 0.34-0.64 mV/m eastward. The results demonstrate that F7/C2 can be employed to detect SIPs in the ionospheric plasma, which shall shed some light on earthquake prediction/forecast.

Keywords: FORMOSAT-7/COSMIC-2, radio occultation, seismo-ionospheric precursor

©2020. Japan Geoscience Union. All Right Reserved.

Statistical Analysis of Pre-Seismic Ionospheric Anomalies and their Characteristic

*Sanaka Saito[1], Chie Yoshino[1], Katsumi Hattori[1]

1. Chiba University

Recently, many papers show various electromagnetic phenomena preceding earthquakes. For example, anomalous changes in ionospheric electrons observed by GNSS satellites (GNSS-TEC) have been reported worldwide. [Kon et al., 2011] performed statistical analysis on pre-seismic anomalies of the total electron contents (TEC) over Japan. Their results showed that significant positive anomalies appear 1-5 days before the earthquake.
On the other hand, GNSS-TEC data exist after the late 1990s. In this study, we focused on the ionosonde which is a ground-based ionosphere monitoring instrument that has long-term data (1958-) over Japan. We performed statistical correlation analysis between a sizeable earthquake and an anomaly in the ionospheric maximum electron density (NmF2) and its altitude (hmF2). The method of statistical analysis is Superposed Epoch Analysis (SEA). From the results of SEA.

We take 15 days backward median and its IQR for the definition of anomalies. If the observed data exceeds median+1.5IQR or median-1.5IQR, we define it shows anomaly.

Since ionospheric disturbances are also caused by geomagnetic storms, it is necessary to remove these effects. We checked the characteristics of ionospheric anomalies caused by geomagnetic storms in statistically and removed those effects based on the magnitude of storm and its generation time in local time.
We select earthquakes occurred within 1000 km and 350 km radius from the ionosonde station, and M >= 6 and D <= 40 km.

The results of SEA show that there are significant positive anomalies in NmF2 for 6-10 days before the earthquake within a radius of 1000 km and for 1-10 days within a radius of 350 km. On the other hand, no clear anomalies were found for hmF2.

Further, Molchan's Error Diagram (MED) analysis was performed to assess the precursory of NmF2. We applied MED analysis for the most significant anomalies such as 6-10 days in 5-day count and 7 days in 1-day count before the earthquake. As a result, MED showed a precursor to the earthquake in both cases.

©2020. Japan Geoscience Union. All Right Reserved.

Pre-earthquake early-warning signals of ULF geoelectric data and their earthquake forecasting probability: A case of Kakioka, Japan

*Hong-Jia Chen[1], Katsumi Hattori[1], Ryo Takahira[1]

1. Chiba University

As laboratory rock experiments and field data analyses show, electromagnetic phenomena are believed to be candidates for the short-term prediction of large earthquakes. Moreover, among previous studies for the field data analyses, ULF electromagnetic signals are one of the most promising precursor methods due to deep skin depth observation. However, the previous studies were carried on through case-study analyses or one-phase optimizations (i.e., a training phase). Before the earthquake forecasting, the first intermediate step is to test relationships between the prescribed anomalies and an earthquake catalog. This is what machine learning scientists refer to as "the training phase". Once detecting anomalies of any earth science data, we have to define a specific algorithm relying on a limited set of unambiguous parameters, which associates those anomalies within a target space-time-magnitude window relative to an impending earthquake. This is the only way to quantify the skill of the tested model and its sensitivity to input parameters. After the training phase, true forecasts can be proposed, which consist in selecting the optimal model parameters and applying them to an independent dataset (i.e., a testing phase). In this study, we verify the relationship between electromagnetic anomalies and earthquakes through the two-phase optimization (i.e., a training phase and a testing phase). First, we analyze ULF geoelectric data at Kakioka, Japan each day and calculate three statistical moments (i.e., variance, skewness, and kurtosis) based on the early-warning signal theory (Scheffer, 2009). Second, we estimate the thresholds for variance, skewness, and kurtosis for the N- and E-components of the geoelectric data and define the anomalies for the three statistical moments of both components. Third, we set up a predictive model and optimize this model within a training phase. Fourth, we select the optimal model parameters and test those parameters within a forecasting phase following the training phase. Results show that the model performance for the forecasting phase has significance, implying that the pre-earthquake electromagnetic anomalies are true earthquake precursors, although the mechanism remains unclear. The present study is therefore intended to make contributions to the establishment of correctly examining correlations between anomalies of earth science data and earthquake catalogs.

Keywords: ULF geoelectric data, statistical moment, earthquake forecast

©2020. Japan Geoscience Union. All Right Reserved.

Numerical simulation of ULF electromagnetic wave propagation in the lithosphere associated with earthquakes by using the WLP-FDTD method

*Ryota Kimura[1], Yoshiaki Ando[1], Katsumi Hattori[2]

1. The University of Electro-Communications, 2. Chiba University

For decades, many papers reported that the Ultra Low Frequency (ULF) radiations associated with earthquakes were observed by magnetometers installed at the Earth’ s surface. Those mainly focused on detection of anomalies exceeding noises, or anomalous characteristics extracted from noises via signal processing. However, observed signals involve information of not only their source intensity, but also losses of media in which the ULF waves propagate, which should be taken into account. For this reason, numerical simulation of ULF propagation in the lithosphere is of importance.

In this study, we develop numerical simulation of the ULF propagation by using the weighted Laguerre polynomial finite-difference time-domain (WLP-FDTD) method with considering electrical properties of lithosphere, and investigate correlation between magnitude of earthquakes and the source current intensity of ULF radiation which is deduced from the numerical simulation.

The WLP-FDTD method solves electromagnetic fields by expanding solutions into weighted Laguerre polynomial series, discretizing computational region in space, and reducing the Maxwell equations into linear equations. This method is not a marching-on-time, but a marching-on-degree scheme, so that we can obtain more precise solutions by iteration even for responses over long time duration. The WLP-FDTD method showed several ten times less computational time than the conventional FDTD method.

We adopt Loma Prieta earthquake as a standard because the observation was performed over wide range of frequency bands so that frequency characteristics of the source current can be deduced. The conductivity distribution around the epicenter was obtained by the magnetotelluric measurement and it is implemented in the WLP-FDTD simulation.

Next, we calculate the source current intensity of earthquakes, such as Spitak EQ (1988), Biak EQ (1996), and Alum Rock EQ (2007), under the assumption that the frequency dependence of the source current is the same as one of Loma Prieta EQ. Especially, in Biak EQ the ULF signals are not detected directly, but the polarization analysis showed an anomaly associated with EQ. Therefore, we deduce that the Signal-to-Noise ratio of Biak EQ is approximately -3dB because the ULF wave at the observation point is less than noises, but is not much less. The conductivity is also taken into consideration in the simulation in each EQ, using MT measuments and bathymetry data.

From the above analyses, it is found that the relative intensity of source currents grows exponentially with the magnitude of EQs.

Keywords: Ultra Low Frequency electromagnetic wave, Weighted Laguerre Polynomial FDTD, Seismo-electromagnetics

©2020. Japan Geoscience Union. All Right Reserved.

Geomagnetic *S*q equivalent currents variation characters in the 210° mm meridian region

*Xiaocan Liu[1], Katsumi Hattori[2,3], Huaran Chen[1], Peng Han[4], Chie Yoshino[2], Xudong Zhao[1]

1. Institute of geophysics China Earthquake Administrition, 2. Graduate School of Science, Chiba University, Chiba, Japan, 3. Center for Environmental Remote Sensing, Chiba University, Chiba, Japan, 4. Department of Earth and Space Sciences, Southern University of Science and Technology, ShenZhen, China

Abstract When solar-terrestrial disturbances are absent, daily variations of the geomagnetic field are called *S*q (solar quiet) [Campbell, 1989; Yamazaki, 2009]. It is well known that the amplitude of *S*q variation shows annual changes [Chapman and Bartels, 1940; Chapman, 1951, Kane, 1976], well as the intensity and morphology of the equivalent *S*q current system, and the position of the vortex centers of the current system have an annual variation in the local time and latitude [Matsushita and Maeda, 1965; Takeda, 1999,2002; Olsen, 1997; Yamashita and Iyemori,2002; Xu W.Y., 1992, 1993,2003,2004; Zhao X.D. et.al, 2008, 2010,2014]. Most of these studies are based on global geomagnetic observations, so there is lack of researches on regional *S*q variation changes, Yamazaki (2009) analyzed the spatial distribution of the annual and semiannual *S*q variations by using 19 stations along 210°mm during 1996 to 2007, but the external and inner parts of Sq equivalent current system were not be separated in his work. So, in present work, we use different stations along 210° mm to investigate the variation characteristics of the external and inner two parts of *S*q equivalent current systems respectively during 2009 to 2013 in Japan- Australia region.

We use 20 geomagnetic observatories distributing at both the Northern hemisphere and the Southern hemisphere along with the 210°magnetic meridian(mm) from 2009 to 2013, which include 10 observatories in Japan, and investigate the variation characters of *S*q equivalent external and inner currents in D season(January, February, October, December, namely winter season) E season(March, April, September, November namely equinox season) and J season (May, June, July, August, namely summer season), here we use three currents parameters to analyze, as the local time (LT), latitude (Lat) and current intensity(J) of current vortexes center, as the result, both external and inner current parameters demonstrate significant seasonal variation respectively. There are also special case, as each hemisphere have one vortex in northern and southern, we find Lat parameter in northern vortex of external current and southern vortex of inner current almost have non-seasonal variations. Then, we analysis more detail variation characters in each season, like J parameter in D season is lowest, have values about 50kA to 100kA, however the values are about 100kA to 150kA in other seasons of external currents. And we also get some asymmetric variation characters for northern and southern hemisphere, for example, in J season, LT of Southern hemisphere vortex center is about 1400LT, but in northern hemisphere vortex center is about 1030LT at the same time, here, obvious LT time shift and asymmetric activity between two hemispheres appear.

Keywords: Sq equivalent current, variation characters, external current, inner current, seasonal variation, asymmetric variation

©2020. Japan Geoscience Union. All Right Reserved.

Measurement of vertical distribution of environmental radiation using a drone at Choshi

*Tohru Okabayashi[1], Kiyotaka Ninagawa[2], Isao Yamamoto[2], Nobuhiro Maeda

1. Chiba Institute of Science, 2. Okayama University of Science

Increases of radon density in atmosphere [1] and in groundwater [2] at the southern part of Hyogo Prefecture Earthquake in 1995 were reported, respectively. In the case of Tohoku Region Pacific Coast Earthquake, the data obtained the exhaust air monitor that peak duration was long and the peak decreased rapidly before earthquake has been reported at the radiation facility of Fukushima Medical College in Fukushima [3]. An anomalous increase in radon concentration was measured at the Nakaizu observatory on the Izu Peninsula prior to the 2011 Thohoku earthquake [4].

We have reported continuous measurements of atmospheric radon density on the ground at Okayama for three years, Kochi, Choshi and Kiyosumi for two years, to predict earthquakes. In these measurements, we usually measured daily variations of the radon density. A model of the daily variations was proposed by Yoshioka [5].

This time, we tried to measure the vertical distribution of environmental radiation in atmosphere by using a drone (DJI MAVIC2 PRO) with a gamma ray detector, Radi (PA-1100, HORIBA). Preliminary measurement was done at Choshi (N35.71˚, E140.84˚), inside Chiba Institute of Science (CIS) from 12:06 to 12:17 on Feb. 15, 2020. We observed radiations of 0.056 micro-Sv/h (43m of altitude), 0.05 (56.6m), 0.054 (60.5m), 0.043 (79.5m), 0.036 (101.5m), 0.032 (112.5m), 0.033 (124m), 0.034 (141m) and 0.022 (151.2m). Environmental radiation dose trended to decrease in increase of altitude. Further measurements of vertical distribution of environmental radiation around CIS will be presented.

[1] Igarashi G., Saeki S., Takahata N., Sumikawa K., Tasaka S., Sasaki Y., Takahashi M. and Sano Y. : Ground-water radon anomaly before the Kobe earthquake in Japan, Science, 269, 60-61, 1995.

[2] Yasuoka, Y. and Shinogi, M.: Anomaly in atmospheric radon concentration: a possible precursor of the 1995 Kobe, Japan, earthquake. Health Physics, 72, 759-761, 1997.

[3] Nagahama H., Yasuoka Y., Suzuki T., and Homma Y.: Radon Variation in the Air before the 2011 Tohoku Earthquake (Mw =9.0), Programme and Abstracts, A32-09, The Seismological Society of Japan. 2011, Fall Meeting. (Japanese)

[4] Tsunomori F. and Tanaka H.: Anomalous change of groundwater radon concentration monitored at Nakaizu well in 2011. Radiation Measurements, 60, 35-41, 2014.

[5] Yoshioka K.: Atmospheric Diffusion Process Based on Time Change of ^{222}Rn vertical Profile, Journal of aerosol research, 17 (4), 267-275, 2002. (Japanese)

Keywords: radon, atmosphere, earthquake predictability

©2020. Japan Geoscience Union. All Right Reserved.

Ground Rn flux anomaly and crustal activity around Asahi station, Boso Peninsula, Japan

*Haruna Kojima[1], Chie Yoshino[1], Katsumi Hattori[1], Michikuni Shimo[2], Toshiharu Konishi[3], Ryuichi Furuya[4]

1. Chiba University, 2. Fujita Health University, 3. OHYO KOKEN KOGYO Co.,Ltd, 4. COM SYSTEM Inc.

In recent years, there are many studies reported on electromagnetic phenomena preceding earthquakes such as geomagnetic, ionospheric, and atmospheric anomalous changes. Ionospheric anomalies preceding large earthquakes are most of the promising phenomena. Lithosphere-Atmosphere-Ionosphere Coupling (LAIC) model has been proposed to explain earthquake-related atmospheric and ionospheric phenomena. In this study, to evaluate the possibility of chemical channel of LAIC by observation, we have installed sensors for atmospheric electric field (AEF), atmospheric ion concentration (AIC), atmospheric Rn concentration (ARC), ground Rn concentration (GRC), and weather elements at Asahi station, Boso Peninsula, Japan. Because the atmospheric electricity parameters could be mainly influenced by weather factors, it is necessary to remove these influences as much as possible. In this sense, we apply the MSSA (Multi-channel Singular Spectral Analysis) to remove these influences from the GRC variation and estimate the ground Rn flux (GRF). We investigated the correlations between GRF and crustal activity such as earthquakes and deformation.

For earthquakes within an epicenter distance of 50 km from the station, it is found that the correlation between Rn flux and regional cumulative seismic moment and/or Es index, which indicates the daily local seismic energy received at the station. These earthquakes had the characteristics they occurred directly underneath the station in the boundary of the Pacific Plate and the North American Plate and they are reverse fault type components.

We investigated the relationship between stress change and GRF to consider the model of fluctuation of the GRF. In this study, we calculated the dilatation using the F3 solution published by the Geospatial Information Authority of Japan. As a result, the GRF increased with compression and decreased with expansion. The result suggests that GRF has the sensitivity to stress changes and can be an indicator of large earthquakes that have pre-slip and slow slip events.

Keywords: Lithosphere-Atmosphere-Ionosphere Coupling, atmospheric electric field, atmospheric ion concentration, ground Rn concentration, atmospheric Rn concentration

©2020. Japan Geoscience Union. All Right Reserved.

The Study of Sq Equivalent Current during the Solar Cycle

*Xudong Zhao[1]

1. Institute of Geophysics, China Earthquake Administration

The Sq current relates to the solar very closely. The activities of solar directly affect the Sq current. In this paper, the geomagnetic data from INTERMAGNET and Geomagnetic Network Center of China Earthquake Administration in 23rd solar cycle (1996~2006) have been used to analyze the variation of external and internal source Sq equivalent current. The method we adopted is the spherical harmonics analysis. The strength of the Sq equivalent current has a good correlation to the spot number of the sun. The intensity of the current is larger during the solar maximum years than that during the solar minimum years. The latitude of the current focus is not affected significantly by the solar activities. There is an evident difference between the seasonal change of current intensity during the solar maximum years and solar minimum years. During the solar maximum years, the peak value of current intensity occurs near the equinoxes, while during the solar minimum years, the peak value of current intensity occurs near the solstices.

Keywords: external and internal Sq current, the spherical harmonics analysis, solar activity

©2020. Japan Geoscience Union. All Right Reserved.

Development of 3D self-potential tomography and electro-kinetic effects

*ayaka ishikawa[1], Katsumi Hattori[1]

1. chiba university

Visualization of the dynamics of underground fluid is important to investigate geothermal resources and study earthquake generation physics. Conventionally, potential as a resource and physical characteristics of the epicenter have been estimated and interpreted using snapshots from MT and electrical exploration. If a dynamic image of underground flow could be visualized, its understanding would be further advanced. Therefore, in this paper, we tried to visualize underground flow by constructing three-dimensional self-potential tomography using sandbox experiments. Specifically, we have constructed a three-dimensional self-potential tomography algorithm for numerical simulation of self-potential generation due to groundwater flow (electro-kinetic effect) and for estimation of groundwater dynamics (pressure head and direction of water flow) using self-potentials. It was also verified by actual experiments of water injection. In the water injection experiment, the box was filled with homogeneous sand and water was injected from the lower part of the tank on the one side, which is simulating the groundwater flow. The parameters of the sand in the box, such as the permeability coefficient and the interface conductivity coefficient, were measured in another experiment, and are constant in the box. So, realistic values are used.
First, the reconstruction results of pore water pressure (pressure head) and water flow from the self-potential changes by the numerical simulation of the injection experiment and those by the reconstruction using the developed tomography are consistent. It suggests that the developed tomographic algorithm are confirmed effective. Furthermore, the dynamics of underground flow were investigated by applying the developed algorithm to the actual experimental data. Details will be shown in the presentation.

©2020. Japan Geoscience Union. All Right Reserved.

Application of Multi-channel Spectrum Analysis (MSSA) in noise reduction to MT data observed at Boso Peninsula in Japan

*Shu Kaneko[1], Katsumi Hattori[2], Toru Mogi[2], Chie Yoshino[2]

1. Chiba University Graduate School of Science and Engineering, 2. Chiba University Graduate School of Science

Near the Boso Peninsula, there are triple junctions where the Pacific Plate, the Philippine Sea Plate, and the North American Plate gather, and crustal deformation is very active. Off the coast of Boso is the epicenter of the Enpo earthquake, and the southern Boso area is the epicenters of the 1702 Genroku Kanto earthquake and the 1923 Taisho Kanto earthquake. Recently, slow slip events have been confirmed off Katsuura every 5-6 years. In 2014-2016, Chiba University conducted a wide-area MT survey in the Boso Peninsula to investigate the source structure of the past major earthquake and the resistivity structure of the plate boundary. The observations were made at 12 long-term observation points at 1 Hz sampling using U43 and 41 short-term observation points at 2400, 150 and 15 Hz using MTU-5 and MTU-5A. However, in the Boso Peninsula, the influence of artificial noise included in the acquired MT data is extremely large due to leakage current from a DC train, factories, or power lines running around/in the peninsula. A conventional remote reference method using geomagnetic 1 Hz data at Memambetsu station operated by Japan Meteorological Agency was applied to the Boso MT data, but the effect of noise reduction was insufficient. Therefore, in this study, we applied the noise removal of time series data using Multi-channel Singular Spectrum Analysis (MSSA) as preprocessing of MT analysis. MSSA parameters include window length, data length, and principal component grouping. By changing these parameters, the effect of noise removal on Boso MT data was investigated in detail. This time, we will report mainly on the effect of noise removal by parameters.

Keywords: noise reduction, Multi-channel Singular Spectrum Analysis, MT method

©2020. Japan Geoscience Union. All Right Reserved.

Development of Ionospheric Electron density tomography using linear regularization.

*Sanaka Saito[1], Rui Song[1], Katsumi Hattori[1]

1. Chiba University

The physical mechanisms of pre-seismic ionospheric anomalies are still not wel-known. In order to clarify the physical mechanism, it is essential to understand the three-dimensional distribution of ionospheric electrons. [Hirooka et al., 2012] developed and operated ionospheric tomography by using GEONET data. However, their method has a drawback that the estimation of the ionospheric structure becomes unstable because the SN ratio falls during the night. Therefore, it is necessary to continuously reconstruct the three-dimensional structure of the ionospheric electron density. We tried to develop ionospheric tomography which can be applied in the nighttime. In this study, we developed a 3D tomography using the Phillips-Tikhonov regularization. In order to evaluate the performance, we used simulated data with International Reference Ionosphere (IRI) model for reconstruction. The results are not so bad and will be shown in the presentation.

©2020. Japan Geoscience Union. All Right Reserved.

[E] Poster | M (Multidisciplinary and Interdisciplinary)：M-IS Intersection

[M-IS10] Coupling between the atmosphere, ionosphere and magnetosphere above thunderstorms

convener:Pasko Victor P(Pennsylvania State University Main Campus), Yukihiro Takahashi(Department of Cosmosciences, Graduate School of Science, Hokkaido University), Mitsuteru Sato(Department of Cosmoscience, Hokkaido University), Teruaki Enoto(RIKEN)

This session will cover all aspects of coupling between lightning, sprites, jets, elves and the atmosphere/ionosphere/magnetosphere system. This includes observations of transient luminous events, associated radio and electromagnetic effects (ULF-VHF), energetic radiation (X ray and gamma ray) effects, and theoretical results on these topics. This includes also studies about the impact of these phenomena at a local or global scale.

[MIS10-P01] Thunder Cloud Project : Ground-based multipoint radiation measurement campaign of high-energy atmospheric phenomena

*Teruaki Enoto[1], Yuuki Wada[2,1], Takayuki Yuasa, Yuko Ikkatai[2], Kazuhiro Nakazawa[3], Shohei Hisadomi[3], Yuna Tsuji[3], Harufumi Tsuchiya[4,1], Takeshi Morimoto[5], Yoshitaka Nakamura[6], Masashi Kamogawa[7], Yousuke Sato[8] (1.RIKEN, 2.The University of Tokyo, 3.Nagoya University, 4.Japan Atomic Energy Agency, 5.KINDAI Univeristy , 6.Kobe City College of Technology , 7.University of Shizuoka, 8.Hokkaido University)

[MIS10-P02] The Contribution of Lightning and Precipitation Currents to the Global Atmospheric Electric Circuit

Bandholnopparat Kittanapat[1], *Mitsuteru Sato[1], Yukihiro Takahashi[1], Kamogawa Masashi[2] (1.Department of Cosmoscience, Hokkaido University, 2.Global Center for Asian and Regional Research, Univ. of Shizuoka)

[MIS10-P03] Photodetachment of electrons at sprite altitudes by molecular nitrogen emissions as a mechanism of initiation of sprite streamers

*Victor P Pasko[1], Reza Janalizadeh[1] (1.Pennsylvania State University Main Campus)

Thunder Cloud Project : Ground-based multipoint radiation measurement campaign of high-energy atmospheric phenomena

*Teruaki Enoto[1], Yuuki Wada[2,1], Takayuki Yuasa, Yuko Ikkatai[2], Kazuhiro Nakazawa[3], Shohei Hisadomi[3], Yuna Tsuji[3], Harufumi Tsuchiya[4,1], Takeshi Morimoto[5], Yoshitaka Nakamura[6], Masashi Kamogawa[7], Yousuke Sato[8]

1. RIKEN, 2. The University of Tokyo, 3. Nagoya University, 4. Japan Atomic Energy Agency, 5. KINDAI Univeristy , 6. Kobe City College of Technology , 7. University of Shizuoka, 8. Hokkaido University

In winter, we frequently observe low-altitude thunderstorms and powerful lightning discharges in the coastal area along the Sea of Japan. Since 2006, the Gamma-Ray Observation of Winter THunderclouds (GROWTH) collaboration has been measuring gamma-ray glows, high-energy radiation from thunderstorms, in this area. Recently, we are expanding this project to a multi-point radiation measurement network at the Kabazawa city, which was named ‘Thunder Cloud Project’, and being collaborated with ground-based radio monitoring of lightning discharges. We also developed several versions of handy radiation detectors. Every winter, this new observation campaign has been detecting not only many gamma-ray glows from thunderstorms but also photonuclear reactions triggered by lightning discharges. In 2020, we are working to make our observation network a new citizen-supporting program, in which citizen supporters will deploy our handy detectors in their home. Here we summarize our recent progress and future prospect of the Thunder Cloud Project.

©2020. Japan Geoscience Union. All Right Reserved.

The Contribution of Lightning and Precipitation Currents to the Global Atmospheric Electric Circuit

Bandholnopparat Kittanapat[1], *Mitsuteru Sato[1], Yukihiro Takahashi[1], Kamogawa Masashi[2]

1. Department of Cosmoscience, Hokkaido University, 2. Global Center for Asian and Regional Research, Univ. of Shizuoka

Thunderstorms and electrified rain/shower clouds are the main current sources in the global atmospheric electric circuit (GEC). These current sources generate the upward current to the ionosphere and maintain the electrical potential gap of ~250 kV between the ionosphere and the Earth' s surface. However, the contribution of the global lightning and precipitation activities to the GEC is still poorly understood due to the difficulty of estimating the occurrence number of cloud-to-ground (CG) and intracloud (IC) discharges. In addition, it is difficult to quantitatively estimate the contribution of the global precipitation current to the GEC due to the difficulty of identifying the precipitation volume and its global distribution. This study aims to investigate the contribution of lightning and precipitation currents to the GEC. First, the global map of the IC/CG ratio (Z-ratio) estimated by the JEM-GLIMS data and the CG lightning data obtained by the WWLLN were combined to estimate the global occurrence number of the IC discharges with the time resolution of 5 minutes and with the spatial resolution of 0.2º×0.2º. Then, the estimated occurrence number of the IC and CG discharges and the precipitation data provided by the global precipitation measurement (GPM) project and the tropical rainfall measuring mission (TRMM) were used as the input parameters in the 3-dimensional model of the GEC, which we have newly developed. In this model, the average column resistance including the influence of the cloud coverage was assumed. Using this model, we estimated the fair weather electric field at the Syowa station in Antarctica, Reading station in UK, and Kakioka station in Japan. It was found that the lightning and precipitation currents in the GEC were ~80 A and ~1200 A, respectively. It was also found that the average fair weather electric field is ~ 70 V/m. The absolute value of the estimated fair weather electric field is almost consistent with the observational data. From these results, the role of lightning and precipitation current in the GEC is quantitatively evaluated, and we found that the upward current to the ionosphere generated by lightning discharges is only 6% while that induced by the precipitation is 94%.

Keywords: Lightning, Global Electric Circuit

©2020. Japan Geoscience Union. All Right Reserved.

Photodetachment of electrons at sprite altitudes by molecular nitrogen emissions as a mechanism of initiation of sprite streamers

*Victor P Pasko[1], Reza Janalizadeh[1]

1. Pennsylvania State University Main Campus

Modeling and experimental findings indicate that the presence of plasma irregularities is a necessary condition for initiation of sprite streamers [e.g., Lang et al., JGR, 116, A10306, 2011; Qin et al., JGR, 116, A06305, 2011; GRL, 40, 4777, 2013; Nat. Comm., 5, 3740, 2014]. Sprite streamers are often preceded by a relatively low intensity diffuse glow discharge referred to as sprite halo [Barrington-Leigh et al., JGR, 106, 1741, 2001]. Janalizadeh and Pasko [Abstracts AE21A-08; AE21B-3132; presented at 2018 Fall Meeting, AGU, Washington DC, 10-14 Dec., 2018] introduced a framework allowing investigation of sprite streamer initiation as a result of electron impact ionization (due to lightning induced electric field) and photoionization (due to halo emissions) of small traces of metallic species deposited by meteoric trails. Furthermore, Janalizadeh and Pasko [Abstract AE31B-3105; presented at 2019 Fall Meeting, AGU, San Francisco CA, 9-13 Dec., 2019] have recently expanded this framework to studies of photodetachment of electrons from O-, O2-, OH- and NO3- ions. In the present work we expand on initial results reported at 2019 Fall AGU Meeting. In particular, we investigate streamer initiation from O2- ions, which possess the lowest electron affinity (i.e., 0.45 eV) among negative ions mentioned above [e.g., Phelps, Can. J. Chem., 47, 1783,1969; Pavlov, Surv. Geophys., 35, 259, 2014]. We also consider sequential sprite streamer initiation as a result of photodetachment from O- ions in more detail. Note that O- is the most abundantly produced negative ion in sprite streamers [Sentman et al., JGR, 113, D11112, 2008; Gordillo-Vazquez, J. Phys. D: Appl. Phys., 41, 234016, 2008] and may provide relatively long-lasting seeds for sequential initiation of sprite streamers. In addition to the first positive N2, second positive N2, first negative N2+, and Lyman-Birge-Hopfield (LBH) N2 band systems that have already been documented in sprites [e.g., Liu et al., GRL, 33, L01101, 2006, and references therein] and for which photodetachment has already been modeled [Janalizadeh and Pasko, Abstract AE31B-3105; presented at 2019 Fall Meeting, AGU, San Francisco CA, 9-13 Dec., 2019], we also consider photodetachment from aforementioned negative ions due to N2 band systems in the extreme ultraviolet spectral region, that has previously been discussed in the context of O2 photoionization in air [e.g., Zheleznyak et al., High Temp. 20, 357, 1982; Janalizadeh and Pasko, PSST, 28, 10, 105006, 2019].

©2020. Japan Geoscience Union. All Right Reserved.

[E] Poster | M (Multidisciplinary and Interdisciplinary)：M-IS Intersection

[M-IS11] Expedition Earth: discovering our planet's past and future through scientific drilling

convener:Junichiro Kuroda(Department of Ocean Floor Geoscience, Atmosphere and Ocean Research Institute, the University of Tokyo), Katsuyoshi Michibayashi(Department of Earth and Planetary Sciences, Nagoya University), Kohtaro Ujiie(Graduate School of Life and Environmental Sciences, University of Tsukuba), Clive Robert Neal(University of Notre Dame)

This multidisciplinary session encourages presentations of various scientific researches that uses samples and data obtained through scientific drilling projects such as the International Ocean Discovery Program (IODP) and the International Continental Scientific Drilling Project (ICDP). We organize several subsessions on the basis of scientific themes to effectively convey achievements and information to the audiences. These scientific themes include "Resilient and Dynamic Earth" (geohazard, climate change and natural resources), "Terrestrial to Extraterrestrial" (plate tectonics, planetary structure, asteroid impacts, and deep biosphere/astrobiology), and "Innovative Science and Technology" (subseafloor observatories, drilling technology development and data science). This session will invite lectures that summarize recent achievements and highlights in each field, and encourages presentations on recently implemented ICDP projects and IODP expeditions. We also aim to provide information on upcoming ICDP projects or IODP expeditions, and we welcome contributions on state-of-the art technological developments related to scientific drilling. The principal goal of this session is to provide a place where participants can efficiently acquire substantial information related to scientific drilling.
Also please visit the J-DESC event page for more details on this session;
J-DESC event page

[MIS11-P01] Monsoon-influenced variations in calcareous and siliceous plankton community structure and upper- water column stratificatio of the western Bay of Bengal during the past 80 kyr

★Invited Papers

*Yuki Ota[1], Hodaka Kawahata[2,3,1], Junichiro Kuroda[2,3], Atsushi Suzuki[1], Toyoho Ishimura[4] (1.National Institute of Advanced Industrial Science and Technology, 2.Atmosphere and Ocean Research Institute, The University of Tokyo, 3.Department of Earth and Planetary Science, The University of Tokyo, 4.National Institute of Technology, Ibaraki College)

[MIS11-P02] Preliminary results of IODP Exp. 382: Iceberg Alley and Subantarctic Ice and Ocean Dynamics

*Yuji Kato[1], Osamu Seki[2], Mutsumi Iizuka[2], Masanobu Yamamoto[3], Michael E. Weber[4], Maureen E. Raymo[5], Victoria L. Peck[6], Trevor Williams[7], - The IODP Expedition 382 Scientists (1.Center for Advanced Marine Core Research, Kochi University, 2.Institute of Low Temperature Science, Hokkaido University, 3.Faculty of Environmental Earth Science, Hokkaido University, 4.University of Bonn, Germany, 5.Lamont-Doherty Earth Observatory of Columbia University, USA, 6.British Antarctic Survey, UK, 7.International Ocean Discovery Program, Texas A&M University, College Station, USA)

[MIS11-P03] Osmium isotopic composition and platinum group element abundances of Cretaceous-Paleogene boundary section at Site U1514C on the Mentelle Basin, SW Australia

Hayu Ota[1], *Junichiro Kuroda[2,3], Maria Luisa Tejada[3], IOPD Exp 369 Shipboard Science Party (1.University of Tsukuba, 2.AORI, University of Tokyo, 3.JAMSTEC)

[MIS11-P04] Short-term environmental disturbance of early Turonian (Cretaceous) in southern high latitude : Insights from organic geochemistry

*Yusuke Takagi[1], Yukina Takeda, Kengo Sadami, Akiko S. Goto[2], Takashi Hasegawa[2] (1.Earth Science Course School of Natural System, College of Science and Engineering, Kanazawa University, 2.Faculty of Geoscience and Engineering, Institute of Science and Engineering, Kanazawa University)

[MIS11-P05] Neogene Kuroshio variability and evolution of the North Pacific subtropical gyre

*Yusuke Okazaki[1] (1.Department of Earth and Planetary Sciences, Graduate School of Science, Kyushu University)

[MIS11-P06] SCORE Drilling: Preliminary results of Expedition 912-Leg 1 at Tokai, Nankai Trough, southwest Japan

*KanHsi Hsiung[1], Toshiya Kanamatsu[1], Ken Ikehara[2], Io Miura[3], Juichiro Ashi[3], Shuichi Kodaira[1], Kohsaku Arai[2], Natsumi Okutsu[1], Kan Aoike[1] (1.Japan Agency for Marine-Earth Science and Technology, 2.Institute of Geology and Geoinformation, National Institute of Advanced Industrial Science and Technology, 3.The Atmosphere and Ocean Research Institute, The University of Tokyo)

[MIS11-P07] Analytical method of noble gases using cuttings to understand distribution and origin of noble gases in accretionary prism in precise -

*Tomohiro Toki[1], Shugo Kurahashi[1], Naoto Takahata[2], Yuji Sano[2,3] (1.Faculty of Science, University of the Ryukyus, 2.Atmosphere and Ocean Research Institute, The University of Tokyo, 3.Institute of Surface-Earth System Science, Tianjin University)

[MIS11-P08] Variation of pore water geochemistry across the mass transport deposits off Cape Erimo, Hokkaido, Japan

*Sara Fujiwara[1], Hitoshi Tomaru[1] (1.Chiba University)

[MIS11-P09] 3.1Ga Banded Iron Formation drilling: DXCL drilling project in the coastal Pilbara terrane in Australia

*Shoichi Kiyokawa[1], Takashi Ito[2], Minoru Ikehara[3], Kosei E. Yamaguchi[4], Kohei Ishikawa[1], Mami Takehara[5], Kenji Horie[5] (1.Department of Earth and Planetary Sciences Faculty of sciences, Kyuushu University, 2.Faculty of Education, Ibaraki University , 3.Center for Advanced Marine Core Research, Kochi University, 4. Toho University and NASA Astrobiology Institute, 5.National Institute of Polar Research)

[MIS11-P10] In-situ crustal stress measurement in inland Japan - Applications of DCDA method to rock core samples from NIED seismic observation wells -

*Kentaro Omura[1], Akio Funato[2], Takatoshi Ito[3] (1.National Research Institute for Earth Science and Disaster Resilience, 2.Fukada Geological Institute, 3.Institute of Fluid Science, Tohoku University)

[MIS11-P11] Rock magnetic properties, grain size, and layer thickness of turbidites at the northern Hikurangi margin, New Zealand: Results from IODP Exp. 375, Site U1520

*Atsushi Noda[1], Annika Greve[2] (1.National Institute of Advanced Industrial Science and Technology, 2.Department of Earth Sciences, Utrecht University, The Netherlands)

[MIS11-P13] An attempt to integrate 3D seismic and borehole datasets: construction of a 3D geomechanical model at the Nankai Trough, SW Japan.

*Yasuhiro Yamada[1,2,3], Adam Wspanialy[1], Kazuya Shiraishi[1] (1.Japan Agency for Marine-Earth Science and Technology (JAMSTEC), 2.Kochi University, 3.Royal Holloway University of London)

[MIS11-P14] A Perspective of the Mantle Drilling and Observatory Initiative

*Nan XIAO[1], Natsue Abe[1], Yasuhiro Yamada[1], Fumio Inagaki[1] (1.Japan Agency for Marine Earth Science and Technology)

[MIS11-P15] **Learning Lessons is Key to the Success in Future Scientific Ocean Drilling**

*KYAW MOE[1] (1.Japan Agency for Marine-Earth Science and Technology)

[MIS11-P16] **The upcoming IODP Japan Trench Paleoseismology Expedition: New perspectives from tracking past earthquakes in the sedimentary record**

*Michael Strasser[1], Ken Ikehara[2], Carol J. Cotterill[3], Lena Maeda[4] (1.University of Innsbruck, Austria, 2.Institute of Geology and Geoinformation, National Institute of Advanced Industrial Science and Technology, Japan, 3.British Geological Survey, U.K., 4.JAMSTEC Japan Agency for Marine-Earth Science and Technology)

Monsoon-influenced variations in calcareous and siliceous plankton community structure and upper- water column stratificatio of the western Bay of Bengal during the past 80 kyr

*Yuki Ota[1], Hodaka Kawahata[2,3,1], Junichiro Kuroda[2,3], Atsushi Suzuki[1], Toyoho Ishimura[4]

1. National Institute of Advanced Industrial Science and Technology, 2. Atmosphere and Ocean Research Institute, The University of Tokyo, 3. Department of Earth and Planetary Science, The University of Tokyo, 4. National Institute of Technology, Ibaraki College

To enhance understanding of the forcing factors of marine biological community structure in the Bay of Bengal, we studied proxies for biogenic carbonate and silicate production in the western Bay of Bengal and compared them with proxies for upper-ocean stratification and strength of the Indian summer monsoon (ISM). Specifically, we investigated the record in a sediment core in the western Bay of Bengal that extended to approximately 80 kyr before the present. The records of Globigerinoides ruber sensu stricto $\delta^{18}O$ minus Neogloboquadrina dutertrei $\delta^{18}O$($\Delta\delta^{18}O_{r-d}$) were used to investigate changes in upper-ocean stratification. In addition, mass accumulation rates (MARs) of $CaCO_3$ and biogenic silica were used as proxies of calcareous and siliceous productivities. Greater difference between Globigerinoides ruber sensu stricto $\delta^{18}O$ and Neogloboquadrina dutertrei $\delta^{18}O$ during the marine isotope stage (MIS) 1 and 5a indicate intervals with less saline and more stratified conditions. In contrast, the relatively small difference between both planktic foraminiferal $\delta^{18}O$ during MIS 2 and 4 indicates diminished stratification during these periods. Elevated carbonate production during MIS 2 and 4, demonstrated by the increase in $CaCO_3$ MAR, could have been driven by lower freshwater influx to the western Bay of Bengal resulting from lower ISM precipitation, and thus the increased mixing and upwelling of deep nitrate into the photic zone. The relative increase in BSi MAR during periods of high ISM precipitation and decreased salinity of surface waters suggests a limited recovery in biological siliceous production under interglacial conditions, possibly due to enhanced fluvial SiO_4 delivery to the ocean. Fluctuations of $\Delta\delta^{18}O_{r-d}$ during MIS 3 indicate that freshwater stratification was moderate and insufficient to restrict upwelling. This might have induced moderate biogenic silica and carbonate productions during this period.

Keywords: Sediment record, Biogeochemical data, Bay of Bengal, Planktonic δ18O

©2020. Japan Geoscience Union. All Right Reserved.

Preliminary results of IODP Exp. 382: Iceberg Alley and Subantarctic Ice and Ocean Dynamics

*Yuji Kato[1], Osamu Seki[2], Mutsumi Iizuka[2], Masanobu Yamamoto[3], Michael E. Weber[4], Maureen E. Raymo[5], Victoria L. Peck[6], Trevor Williams[7], - The IODP Expedition 382 Scientists

1. Center for Advanced Marine Core Research, Kochi University, 2. Institute of Low Temperature Science, Hokkaido University, 3. Faculty of Environmental Earth Science, Hokkaido University, 4. University of Bonn, Germany, 5. Lamont-Doherty Earth Observatory of Columbia University, USA, 6. British Antarctic Survey, UK, 7. International Ocean Discovery Program, Texas A&M University, College Station, USA

We collected sediment cores from five sites in Atlantic sector of the Southern Ocean during International Ocean Discovery Program (IODP) Expedition 382, which took place from March to May 2019. The recovered material includes continuously deposited Plio–Pleistocene sediments. Our primary aim is to reconstruct the past history and variability in Antarctic Ice Sheet (AIS) mass loss and associated paleoceanographic changes. The drilling sites include two sites (Site U1534 and U1535) at the northern edge of the Scotia Sea and three sites (Sites U1536–U1538) in the southern Scotia Sea. The materials from Sites U1534 and U1535, which are located in the vicinity of Subantarctic Front, will be used to reconstruct how ocean circulation responds to climate changes. The principal object of Sites U1536–U1538 is to study the flux of icebergs through “Iceberg Alley,” the main pathway along which icebergs calved from the margin of the AIS travel. In the current presentation, we will present an overview of the expedition with a special focus on biostratigraphic results and preliminary results of TEX86 derived sea surface temperature records in Sites U1537 and U1538 during the Plio-Pleistocene.

Keywords: IODP, Antarctic Ice Sheet, Iceberg Alley, Southern Ocean, paleoceanography

©2020. Japan Geoscience Union. All Right Reserved.

Osmium isotopic composition and platinum group element abundances of Cretaceous-Paleogene boundary section at Site U1514C on the Mentelle Basin, SW Australia

Hayu Ota[1], *Junichiro Kuroda[2,3], Maria Luisa Tejada[3], IOPD Exp 369 Shipboard Science Party

1. University of Tsukuba, 2. AORI, University of Tokyo, 3. JAMSTEC

During IODP Expedition 369, Cretaceous and Paleogene sediments were recovered at Site U1514 in the Mentelle Basin, off SW Australia. Shipboard micropaleontological investigation revealed that Cretaceous–Paleogene boundary (K–Pg boundary, 66.0 Ma) is located at 369-U1514C-23R-2, 2-3 cm interval, at 393.52 m depth (core depth from seafloor, CSF-A). Here, uppermost Maastrichtian light gray chalk is overlain by Paleocene greenish gray claystone with a heavily bioturbated contact. In this study, we analyzed abundances of platinum group elements (PGEs)—including Ru, Pd, Os, Ir and Pt—and the radiogenic isotopic composition of Os ($^{187}Os/^{188}Os$) for the sediments across the K–Pg boundary section. According to the shipboard studies on bio- and magnetostratigraphy, applying ages from the Geologic Time Scale 2012, our samples cover a time interval from 68.1 Ma (Maastrichtian) to 65.9 Ma (Danian). Our data show a clear peak in Ru (4.8 ng g^{-1}), Os (1.4 ng g^{-1}) and Ir (5.3 ng g^{-1}) concentrations at 393.52 m CSF-A, with values two orders of magnitude higher than background concentrations during the Maastrichtian. Abundances of PGEs of the sample from 393.52 m CSF-A show a flat pattern when normalized to CI chondrite values, while the other samples show patterns similar with the upper continental crust. The sample from 393.52 m CSF-A also marks a clear drop in the $^{187}Os/^{188}Os$ value of 0.18. Our data on the PGE abundances and Os isotopes clearly shows that the sediment at 393.52 m CSF-A contains PGEs from an extraterrestrial source, most likely associated with the well-known bolide impact at the K–Pg boundary.

The $^{187}Os/^{188}Os$ values in the uppermost Maastrichtian interval show two [LKO1] gradual decreases from 0.6 to 0.4 and 0.4 to 0.2, while those in the lowermost Danian interval show a gradual increase from 0.2 to 0.4. The gradual variation in Os isotopic composition suggests that sediment was deposited continuously without significant hiatus. The decreasing trends of $^{187}Os/^{188}Os$ values in the Maastrichtian interval is slightly different from those reported from other sites previously, which may be attributed to either 1) heavy bioturbation or 2) some local or regional volcanic events at this site.

Keywords: Os isotope, PGE, K-Pg boundary

©2020. Japan Geoscience Union. All Right Reserved.

Short-term environmental disturbance of early Turonian (Cretaceous) in southern high latitude : Insights from organic geochemistry

*Yusuke Takagi[1], Yukina Takeda, Kengo Sadami, Akiko S. Goto[2], Takashi Hasegawa[2]

1. Earth Science Course School of Natural System, College of Science and Engineering, Kanazawa University, 2. Faculty of Geoscience and Engineering, Institute of Science and Engineering, Kanazawa University

An environmental change of the Early Turanian, Cretaceous was investigated using the samples from IODP Exp. 369, U1512. A stable carbon isotope stratigraphy based on bulk rock analysis showed a positive 3 ‰ carbon isotope excursion (CIE) within the lower Turonian. Based on this high isotopic value and the biomarker composition, phytoplankton blooming is interpreted to be a factor that caused the CIE.

During Turonian (93.9-89.8±0.3Ma), which is the target of this study, temperature as warm as ~30℃ was suggested by some previous studies and physical simulation even in the high latitude regions. Turonian is an age of recovery from major environmental changes after the disturbance of the carbon cycle by Oceanic Anoxic Event 2 (OAE2: Cenomanian/Turonian boundary event). Site U1512, in Great Australia Bight, was located around the paleolatitude about 60 ˚S during Early Turonian. The site is expected to provide new paleoenvironmental information and add important geologic records of paleoenvironments. In this study, a positive 3‰ carbon isotope excursion (CIE) in the lower Turonian is investigated as it should be a signal of paleoenvironmental change and perturbation.
Additional denser samples were taken across the CIE to obtain the exact magnitude and duration of the CIE. It emerged that the time interval of the CIE was about 4-20 thousand years. Compound-specific carbon isotope analyses were also performed on selected samples across the CIE. The carbon-isotopic profile of *n*-alkanes did not replicate that of the bulk organic carbon indicating the CIE observed with the bulk analyses is not comparable to that of OAE2, and rather ascribed to a change in origin of organic matters and their mixing rate. Biomarker analysis at the CIE horizon revealed that compounds from marine plankton (C_{27}diacholentenes, ≦ *n*-C_{18} *n*-alkane) dominated relative to the terrestrial ones. Higher isotopic value of bulk organic carbon in the CIE horizon can be ascribed to smaller carbon isotopic fractionation of phytoplankton during blooming. Based on these results, phytoplankton blooming is interpreted to be a most plausible factor for the CIE.

Keywords: Organic geochemistry, Cretaceous, International Ocean Discovery Program

©2020. Japan Geoscience Union. All Right Reserved.

Neogene Kuroshio variability and evolution of the North Pacific subtropical gyre

*Yusuke Okazaki[1]

1. Department of Earth and Planetary Sciences, Graduate School of Science, Kyushu University

The Kuroshio Current is a western boundary current located on the western edge of the North Pacific subtropical circulation. It transports numerous amounts of heat and materials from the equatorial Pacific to the mid-latitudes of the North Pacific. Changes in the Kuroshio Current flow path and strength under different climate must had a pronounced impact on the climate and environments in the North Pacific and surrounding regions. The Mid-Miocene Climatic Optimum (MMCO) is the one of the most remarkable Neogene warming event prolonged from 16 to 14 Ma. During MMCO, The Kuroshio Current flowed much more northward, which leaded marked expansion of subtropical circulation in the North Pacific, evidenced by terrestrial geologic records from the NW Pacific margin. Unfortunately, complete sedimentary sequence of MMCO in the western North Pacific has not yet obtained due to hiatuses distributed widely in the western North Pacific. We have re-established DSDP 296 biostratigraphy (calcareous nannofossils, planktic foraminifera, and radiolaria) and chemostratigraphy (strontium isotope ratios, and stable carbon and oxygen isotope ratrios) from the northern Kyushu-Palau Ridge near the Kuroshio Current flow path to reveal almost continuous sedimentation for the past 20 Myrs although the several drilling gaps. Re-drilling at site DSDP 296 will provide us a chance to recover complete sedimentary sequence including MMCO. Since late Miocene, earth’s climate has cooled down, intensification of the glaciation in the Northern Hemisphere during Pliocene, and leaded to an initiation of glacial-interglacial cycles. However, long-term Kuroshio Current variability responding to the above major climatic events are still poorly understood mainly due to lack of appropriate marine sediment samples. We would like to fill the gap by drilling new sediment cores along the western North Pacific margin such as the Benham Rise, Okinawa Trough besides the DSDP 296 site.

Keywords: Kuroshio, North Pacific subtropical gyre, Neogene

©2020. Japan Geoscience Union. All Right Reserved.

SCORE Drilling: Preliminary results of Expedition 912-Leg 1 at Tokai, Nankai Trough, southwest Japan

*KanHsi Hsiung[1], Toshiya Kanamatsu[1], Ken Ikehara[2], Io Miura[3], Juichiro Ashi[3], Shuichi Kodaira[1], Kohsaku Arai[2], Natsumi Okutsu[1], Kan Aoike[1]

1. Japan Agency for Marine-Earth Science and Technology, 2. Institute of Geology and Geoinformation, National Institute of Advanced Industrial Science and Technology, 3. The Atmosphere and Ocean Research Institute, The University of Tokyo

Chikyu Shallow Core Program (SCORE) is a short and shallow ocean drilling program, providing opportunities for scientific ocean drilling test and project which can complete in a short period of time by using the ocean drilling vessel (D/V) Chikyu except for IODP expedition period. The title of Expedition 912-Leg 1 is “Enigmatic recurrence pattern of Tokai earthquake in the Nankai Trough, southwest Japan: the link between great earthquakes and ridge subduction”. The objective of our program is to investigate the past earthquake occurrence from a continuous sedimentary sequence at a local tectonic basin (i.e., Kanasunose Trough) in the Nankai Trough. The target of this drilling program is to find an enigmatic recurrence pattern of Tokai earthquake in the Nankai Trough, southwest Japan. Hydraulic Piston Coring System (HPCS) of the D/V Chikyu can provide an opportunity to obtain an excellent long and continuous sedimentary record to unravel the earthquake recurrence pattern of this study area.

Expedition 912 was conducted by D/V Chikyu sailing from Shimizu to Sasebo, Japan from 4 January - 15 January 2020. The Leg 1 of Expedition 912 was cored Hole A and B in Site C9035. The penetration depth at site C9035 is 80.19 meters with HPCS drilled from 5 January to 8 January 2020. The site of Hole A is at 34°5.7000’ N, 138°8.0300’ E with 2413.5 meters of water depth in the Kanasunose Trough, the Nankai Trough. Because mud line cannot be identified in Hole A, Hole B was drilled in 10-m southeast to Hole A. Hole B is at 34°5. 6962’ N, 138°8.0346’ E with 2414.0 meters of water depth. The cores including 9.5 m thick of Hole A and 80.0 m thick of Hole B was retrieved. Core recoveries are 105.3% and 104.7% of Hole A and Hole B, respectively. The shipboard measurements of whole-round cores involved X-ray CT scan and multisensory core logger (MSCL). After splitting, we conduct measurements including visual core description, smear slides, split surface image, paleomagnetic measurement by superconducting rock magnetometer, penetration strength, and moisture and density measurements, and Vane shear test.

The sedimentary succession is dominated by silty sediments with numerous coarse-grained (coarse silt–very fine sand) layers and some volcanic ash layers and spots. Two lithological units (Unit I and II) can be distinguished based on sedimentary facies. Unit I (0 –42.1 m) consists of bioturbated silt and layered coarse silt–very fine sand with massive silt. Three ashes were founded in Unit I and will provide good age control. Layered coarse silt–very fine sand beds with fining upward pattern can be regarded as turbidite beds. Unit II (42.1 m –80.19 m) is characterized by matrix-supported gravelly mud–muddy gravel and angular mudstone gravel. In the downhole variation changes in around 42 m also can be observed in the GRA density, Natural Gamma radiation, and Electric resistivity. The future work will focus on the significant turbidite beds which could be related to earthquakes, and to evaluate the recurrence intervals of earthquakes in Unit I. After integration of post-cruise measurements, the relationship between great earthquakes and ridge subduction of Tokai earthquake in the Nankai Trough will be expected.

©2020. Japan Geoscience Union. All Right Reserved.

Keywords: Turbidite, Paleoseismology, Tokai earthquake, Nankai Trough

©2020. Japan Geoscience Union. All Right Reserved.

Analytical method of noble gases using cuttings to understand distribution and origin of noble gases in accretionary prism in precise -

*Tomohiro Toki[1], Shugo Kurahashi[1], Naoto Takahata[2], Yuji Sano[2,3]

1. Faculty of Science, University of the Ryukyus, 2. Atmosphere and Ocean Research Institute, The University of Tokyo, 3. Institute of Surface-Earth System Science, Tianjin University

In this study, we measured noble gases from cuttings crushed in a vacuum, and obtained a data set of noble gases free from air contamination. As a result, the contribution rate of air-saturated interstitial water could be determined, and the helium isotope ratio released from the slab of the Philippine Sea Plate could be determined accurately. In addition, mantle-derived helium laterally would be supplied from wedge mantle around 1503 mbsf. Based on the lithology and hydrocarbons distribution, the sandstone layer distributed between 1000 and 1500 mbsf could play a role as flow path of deep-rooted gas from great depths. To obtain more accurate in-situ information than gas analysis using mud gas, we propose gas analysis using cuttings as an international standard for exploration of noble gas distribution during drilling.

Keywords: cuttings, noble gas, analytical method, accretionary prism

©2020. Japan Geoscience Union. All Right Reserved.

Variation of pore water geochemistry across the mass transport deposits off Cape Erimo, Hokkaido, Japan

*Sara Fujiwara[1], Hitoshi Tomaru[1]

1. Chiba University

Marine pore water geochemistry is often constrained by the redox potential and microbial activities in shallow sediment and also receives dissolved elements from minerals under high temperature/pressure environment in deep sediment. The concentration gradients of these elements therefore reflect the gradual change of physicochemical environment in the sediment column, which characterize basic material migration system in surface area. However, the sediment environment is disturbed and becomes discontinuous when a drastic environmental change such as submarine landslide occurs. The pore water in the mass transport deposit (MTD) can be also disturbed and changes thereafter to stabilize again under the given new condition. This may significantly disrupt the material circulation system via pore water at the Earth's surface, however, the relationship between these phenomena and the distribution of MTD has not been sufficiently discussed. In this study, we analyzed geochemical composition of pore waters collected across the MTD and investigated how the pore water geochemistry responded to the disturbance of sediment environment.

Pore waters were collected from sedimentary sequences intercalated with MTDs down to ~100 mbsf off Cape Erimo, Hokkaido, Japan during the Chikyu Shallow Core Program (SCORE) by D/V Chikyu in 2017. The pore water geochemistry shallower than sulfate-methane interface (SMI) rapidly changes due to anaerobic methane oxidation, decomposition of organic matter, methane production from organic matter, precipitation of carbonates etc. On the other hand, below the SMI, the pore water composition was changed mainly by the mineral alterations in high temperature environments and the diffusion of components which released into or removed from the pore water due to decomposition of biogenic sedimentary rocks and organic matter. In particular, the concentration gradients of iodine and magnesium become smaller around the upper boundary of the MTD, unlike the gradual changes in concentration through the entire drilling depth. In addition, barium and lithium showed a curve-like concentration change with minimum values at the upper boundary of the MTD. The radioisotopic analysis of iodine showed significantly high value in the MTD, reflecting seawater component dominates in the interval. These changes were caused by trapping, migrating, and accumulating shallow pore water in the deeper sediments, pore water geochemistry can be modified along with the development of the MTD.

Keywords: Chikyu SCORE, Mass transport deposit, 129I, Iodine geochronology, Pore water

©2020. Japan Geoscience Union. All Right Reserved.

3.1Ga Banded Iron Formation drilling: DXCL drilling project in the coastal Pilbara terrane in Australia

*Shoichi Kiyokawa[1], Takashi Ito[2], Minoru Ikehara[3], Kosei E. Yamaguchi[4], Kohei Ishikawa[1], Mami Takehara[5], Kenji Horie[5]

1. Department of Earth and Planetary Sciences Faculty of sciences, Kyuushu University, 2. Faculty of Education, Ibaraki University , 3. Center for Advanced Marine Core Research, Kochi University, 4. Toho University and NASA Astrobiology Institute, 5. National Institute of Polar Research

The Dixon Island –Cleaverville Drilling Project (DXCL) was successfully completed at Cleaverville Beach, northwestern Pilbara Craton, at August 2007, 2012. The drilling provided ‘fresh’ samples (free of recent, near-surface weathering effects) of Archean banded iron-formation (BIF) and black carbonaceous shale. The formations drilled were the Cleaverville Formation, Dixon Island Formation, and Port Robinson Basalt (new name), all interpreted as belonging to a Mesoarchean immature island-arc succession at three drilling site, DX, CL1, CL2 and CL3. Drilling revealed that although modern weathering at Cleaverville Beach extends to depths of 50 m and the drill core is suitable for petrologic, geochemical, and isotopic investigations. Here we focus CL3 core (200m long) which focus the Cleaverville Formation with BIF. The BIF in this area is well exposed along the coast area.

The Cleaverville Formation was subdivided by the Black Shale and BIF members. The Black Shale Member formed organic rich black shale which formed 10-20 cm thick beds and with thin silt- very fine sandstone lamination. The fine grain is mostly related volcanic origin plagioclase. These volcaniclastic laminations have well preserved cross laminations and identified as younging direction. The thin very fine sandstone laminations are increase to the top. The BIF Member formed three units, 1) Siderite BIF unit which formed fine laminated greenish shale/white chert and massive chlorite rich greenish shale, 2) Magnetite BIF unit which formed fine lamina of magnetite/white chert and massive chlorite rich greenish shale, and 3) Black shale-siderite unit which formed fine laminated black shale and greenish siderite.

In detail observation, the BIF Member not contains detrital grains such as volcaniclastics origin fine sandstone. Bedded thickness in Siderite BIF and Magnetite BIF is resembles about 10-20 cm in each bed, also massive greenish shale beds are resembled each unit. The greenish massive greenish shale is very homogenous. These beds are corelated red and white beds in outcrop, which have lateral variation of thickness from 50 –100m wide. Some these beds are more than 80 cm in thickness to change 10 cm in thickness.

In addition, magnetite laminations are only formed in fine lamina of greenish shale portion in the Siderite BIF. The most BIF Member contains overgrowth siderite crystals especially in white chert lamination. Most place of Siderite BIF and Magnetite BIF are not containing early stage sedimentation evidence. Only black shale-siderite unit contains organic rich wavy laminations. It might be preserved primary sedimentation evidence during deposition of iron material. These very thin wavy laminations suggest that the microbial (Iron oxidized bacteria) activity might be occurred on the ocean floor surface. However, it is still unknown of the origin of homogenous greenish shales as sedimentary muds or diagenetic beds.

Keywords: BIF, greenstone belt, Archean, siderite, magnetite

©2020. Japan Geoscience Union. All Right Reserved.



©2020. Japan Geoscience Union. All Right Reserved.

In-situ crustal stress measurement in inland Japan - Applications of DCDA method to rock core samples from NIED seismic observation wells -

*Kentaro Omura[1], Akio Funato[2], Takatoshi Ito[3]

1. National Research Institute for Earth Science and Disaster Resilience, 2. Fukada Geological Institute, 3. Institute of Fluid Science, Tohoku University

In-situ crustal stress is an important factor to understand earthquake mechanism and tectonic activities. However, the reliable in-situ crustal stress data seems to still be poor, because complicated procedures are necessary for measure the in-situ crustal stress in a borehole. We tried to apply DCDA (Diametrical Core Deformation Analysis) method for in-situ crustal stress measurement using boring core rock samples. DCDA method measures the circumferential diameter variation and elastic constants of core sample if we have recovered the core sample from the borehole. We expect the method can be applied to old-time boring core samples from NIED (National Research Institute for Earth Science and Disaster Resilience) seismic observation wells, and we may collect global in-situ crustal stress data in Japan island.
We used recovered hard rock core samples from 7 Hi-net observation wells of NIED (more than 10 years ago) from the depth about 100m - 200m (one is from the depth of 2000m). The circumferential core diameter variation was measured by an especially designed apparatus that consists of an optical micrometer, a pair of motor-driven rollers and a data processing system (Funato and Ito, 2017, IJRMMS). We got the sine curves of circumferential diameter variation of some of the core samples associated with stress relief. The data suggest that the DCDA method is applicable to boring core samples from shallow seismic observation wells.
To decide the value of stress, we need elastic constants of the core samples; Young's modulus and Poisson's ratio. We tried to use the data of rock mass P and S wave velocities by means of P-S logging at the time of boring. Assuming the value of densities, we calculated the elastic constants of the core samples. Assuming 2.5 g/cm3 as a representative value of various kind of rocks composing the crust, the differential stresses are around 10 MPa. Those results suggest the in-situ crustal stresses are measured by DCDA method in global area of inland Japan with existing core rock samples. In the next step, we will apply laboratory rock tests to measure the elastic constants of core samples directly.

Keywords: DCDA method, in-situ crustal stress, rock core, inland Japan

©2020. Japan Geoscience Union. All Right Reserved.

Rock magnetic properties, grain size, and layer thickness of turbidites at the northern Hikurangi margin, New Zealand: Results from IODP Exp. 375, Site U1520

*Atsushi Noda[1], Annika Greve[2]

1. National Institute of Advanced Industrial Science and Technology, 2. Department of Earth Sciences, Utrecht University, The Netherlands

Environmental magnetism is the study of the fine magnetic minerals in sediments. Differences in type, abundance, magnetic grain-size, and diagenetic state allow to draw conclusions about the sediment source regions, transport and depositional conditions. Here we present the results of detailed rock magnetic investigations conducted on turbidites deposited within the trough sediments at IODP site U1520, Exp. 375, northern Hikurangi Margin, New Zealand. The study encompassed the measurement of rock magnetic properties and grain size on a total 67 turbidites in the upper part (Lithological Units 1–3, 0–510 mbsf) of the hole U1520D.

Discrete paleomagnetic samples were collected from cores by pushing standard 7-cm^3 plastic cubes into the sediment near the basal part of turbidites. The cubes were subjected to magnetic analysis at JAMSTEC. Low-field, mass-dependent magnetic susceptibility (χ) and AMS were measured using an AGICO Kappabridge KLY-4S. AFD and ARM acquisition experiments were conducted using a horizontal 2G cryogenic passthrough magnetometer with an in-build degausser. ARM was imparted in a peak alternating field of 80 mT (AF), and a 100-μT biasing field along +z. Subsequently we imparted an IRM along +z using an ASC Impulse Magnetizer and a field of 1.2 T. Remanence was subsequently measured and the same procedure repeated by applying reverse fields of 0.1 and 0.3 T. Magnetic hysteresis parameters (B_c, B_{cr}, M_s, M_{rs}) were measured using a MicroMag Vibrating Sample Magnetometer. As final step, grain-size analyses were conducted using a laser diffraction/scattering particle size distribution analyzer.

The magnetic susceptibility (χ), SIRM (here: $IRM_{1.2T}$), NRM and M_s are sensitive to the concentration of magnetic minerals within the turbidites. and are parameters to indicate the magnetic grain-size. The S-ratios are calculated using and , respectively. S-ratios help to distinguish between the contributions of magnetically hard and soft remanence carriers (e.g. magnetite vs. hematite). The ratios of the hysteresis parameters M_{rs}/M_s and $B_{cr}/B_c$are indicative for the magnetic domain and thus grainsize. We applied the K-means cluster analysis for these magnetic properties to characterize the turbidites into the three units which have distinct magnetic properties.

Samples in cluster 1 have relatively low values of χ, SIRM, S-ratios and SIRM/χ, and intermediate values of M_{rs}/M_s and B_{cr}/B_c. The majority of the turbidites sampled in Unit 2 and parts of Unit 3 were classified into cluster 1. Samples from cluster 2 show low values of B_{cr}/B_c, intermediate values of χ, and high values of SIRM, S-ratios and SIRM/χ, and high values of M_{rs}/M_s. These samples can be found throughout Units 1–3. Cluster 3 is represented by high χ, S-ratios, intermediate SIRM and B_{cr}/B_c, and low M_{rs}/M_s and SIRM/χ values. This cluster was recognized only in Unit 1. Most of the thick and coarse-grained turbidites belong into Cluster 3. One of the major differences between cluster 3 and the other clusters is that the SIRM is weaker than in cluster 2, while χ is higher than cluster 2. The other difference is a very low M_{rs}/M_s and high B_{cr}/B_c ratios, indicating cluster 3 is dominated by multidomain (MD)-sized grains.

©2020. Japan Geoscience Union. All Right Reserved.

There are two viable interpretations for this dataset: The distribution of the clusters may reflect on different source regions of the turbidity currents. A major difference exists between the rock magnetic properties of lithological units 1 and 2. This may indicate a major change in the dominant sediment provenance and transport direction. Alternatively, the differences in the rock magnetic properties may also be caused by differing diagenetic state through the sequence (e.g. magnetite–greigite–pyrite). These differences may be affected by depositional conditions such as submarine landslides or turbidity currents.

Keywords: IODP, Hikurangi Trough, New Zealand

©2020. Japan Geoscience Union. All Right Reserved.

An attempt to integrate 3D seismic and borehole datasets: construction of a 3D geomechanical model at the Nankai Trough, SW Japan.

*Yasuhiro Yamada[1,2,3], Adam Wspanialy[1], Kazuya Shiraishi[1]

1. Japan Agency for Marine-Earth Science and Technology (JAMSTEC), 2. Kochi University, 3. Royal Holloway University of London

Data integration is vital to explore subsurface. One of the reasons is that a variety of different geophysical methods are used to acquire data from subsurface and the reality can hardly be expressed by a single data source. The sparsity of the subsurface data and limited quality, because of the indirect measurement, may also be included in the reasons as well. Once we can drill a borehole, then we could get much more data. Such borehole data, however, have a huge scale gap to the exploration geophysics data and the integration is a key technique to fill the gap by all means.

As one of such initiatives, we used 3D seismic data and well data acquired at the Nankai Trough offshore Kii Peninsula, Japan, where extensive scientific drilling and geophysical surveys performed by the International Ocean Drilling Programme (IODP) and JAMSTEC, to construct a geomechanical model. The technique has been utilized for commercial purpose by the oil and gas industry to optimize production / well placement in the existing fields and to avoid borehole failure, but rarely used for scientific purposes. In this presentation, we are going to report some updates of the modelling, and discuss how such approach is useful for future scientific drilling.

Keywords: scientific drilling, data integration, nankai tough

©2020. Japan Geoscience Union. All Right Reserved.

A Perspective of the Mantle Drilling and Observatory Initiative

*Nan XIAO[1], Natsue Abe[1], Yasuhiro Yamada[1], Fumio Inagaki[1]

1. Japan Agency for Marine Earth Science and Technology

Over the past half century, there has been a desire in geoscience to explore the entire sequence of Earth’s oceanic crust and to reach the upper mantle beneath the Mohorovičić discontinuity (also termed the “Moho”). Scientists have common knowledge that the mantle as the largest layer of Earth’s interior, makes up to about 83% in volume and 67% in weight of our planet; however, nobody has ever seen the pristine mantle. To comprehensively understand the plate tectonics, earth dynamics, and evolution of the our planet, drilling through the “Moho” to the mantle, offers an unprecedented opportunity to all the science community of truly integrated scientific approaches toward a better understanding of the ocean, atmosphere, and biosphere on Earth.
The mantle beneath the oceanic crust can ONLY be accessed through scientific ocean drilling. Over the past 50 years, scientific ocean drilling has been a great success to expand our knowledge of the ocean-Earth-life system and provided new insights into the essence of planetary habitability. After years from the first try of mantle drilling in 1950s, the *Chikyu* was built in 2005 as a new generation of scientific ocean drilling vessel. *Chikyu* was born to meet the strong demand that human can know better about our planet by penetrating the oceanic crust down to Earth’s upper mantle where is the deepest accessible limit for today’s drilling technology.
The challenge into the upper mantle will also provide an excellent opportunity of and potential for the long-term observatory of the mantle and the crustal behaviors. To date, large gaps in our understanding of the Earth’s dynamism and the interactions between multi-spheres remain to be filled. Continued international and transdisciplinary collaborations among the scientific ocean drilling community will help all scientists to illuminate the Earth’s activities of the planetary system, from deep time to the present, and to the future. NOW is the time to build up the mantle-dedicated scientific ocean drilling program and its initiative for future observatory. In this presentation, the Mantle Drilling Promotion office (MDP), newly established in JAMSTEC in April 2019, will share the concept and perspective of the mantle drilling and observatory initiative.

Keywords: mantle, ocean drilling, chikyu

©2020. Japan Geoscience Union. All Right Reserved.

Learning Lessons is Key to the Success in Future Scientific Ocean Drilling

*KYAW MOE[1]

1. Japan Agency for Marine-Earth Science and Technology

Most of scientific ocean drilling (IODP, ODP) expeditions fall in deep (>300 m water depth) and ultra deepwater (>1500 m) environments which are designated in oil and gas industry as most complex and high risk areas to operate and cost three times more than shallower water depths. Three key factors play in deepwater project management- time, cost and quality and hence those programs drill fewer wells while maximizing well information extraction.

Over five decades of deepwater drilling experience, scientific ocean drilling pioneered in offshore drilling technology ahead of oil industry at the beginning, however industry progressed later in offshore exploration and production with bigger rewards from higher oil prices and long term production. In 2005, D/V Chikyu was built in hope of overcoming seismogenic zone drilling challenges with riserless drilling. Key lessons learnt from the 12 years of operations include deep seismic imaging, operation under high current, borehole instability and geomechanics, operation efficiency with best use of technology, coring in faster rate and better quality, clean sampling for microbiology analysis.

While IODP operators are struggling with drillship maintenance and operating cost, oil and gas industry has been transforming in speed into digitalization and developing new technologies to maximize efficiency in time and cost as well as for safety. Within the limits, IODP operators developed and tested new or better tools and techniques in imaging, sampling, measurement and analyses and drilling optimization. To continue challenging into the ultra deepwater targets, IODP needs to work closely not only with International Continental Drilling Program but also with industry R&D portfolio in exchange of deepwater experience.

Keywords: IODP, ICDP, Deepwater Drilling Technology and Challenges

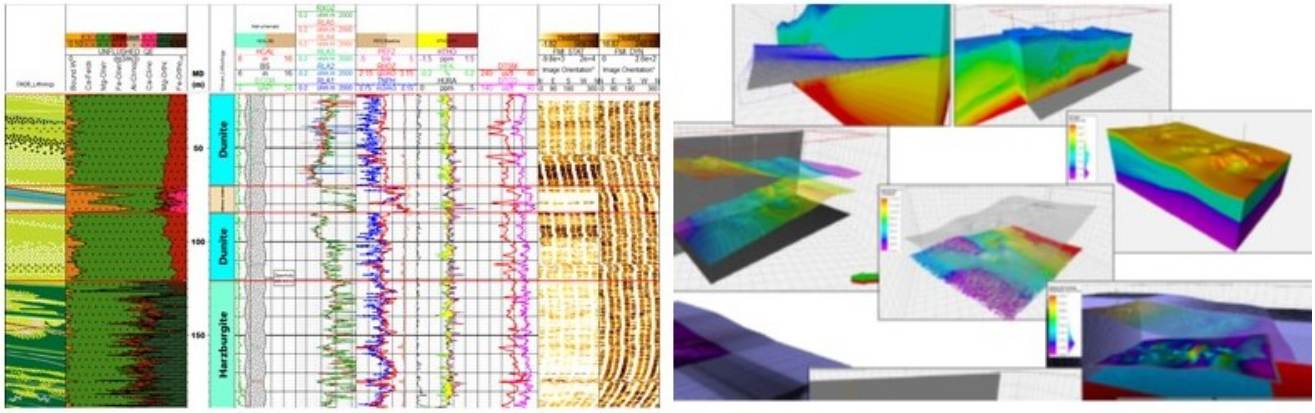


Figure. Use of new technology from industry in scientific drilling, elemental wireline logging data compared with core analyzed XRF and XRD (left) and 3D Geophysical and geomechanical modeling (right).

©2020. Japan Geoscience Union. All Right Reserved.

The upcoming IODP Japan Trench Paleoseismology Expedition: New perspectives from tracking past earthquakes in the sedimentary record

*Michael Strasser[1], Ken Ikehara[2], Carol J. Cotterill[3], Lena Maeda[4]

1. University of Innsbruck, Austria, 2. Institute of Geology and Geoinformation, National Institute of Advanced Industrial Science and Technology, Japan, 3. British Geological Survey, U.K., 4. JAMSTEC Japan Agency for Marine-Earth Science and Technology

Short historical and even shorter instrumental records limit our perspective of earthquake maximum magnitude and recurrence and thus are inadequate to fully characterize Earth’s complex and multiscale seismic behavior and its consequences. Examining prehistoric events preserved in the geological record is essential to reconstruct the long-term history of earthquakes and to deliver observational data that help to reduce epistemic uncertainties in seismic hazard assessment for long return periods. “Submarine paleoseismology” is a promising approach to investigate deposits from the deep sea, where earthquakes leave traces preserved in the stratigraphic succession. However, at present we lack the comprehensive data sets and long-term records that allow for conclusive distinctions between quality and completeness of the paleoseismic archives.

Motivated by the mission to fill the gap in long-term records of giant (Mw 9 class) earthquakes, International Ocean Discovery Program (IODP) Expedition 386, Japan Trench Paleoseismology, aims at testing and developing submarine paleoseismology in the Japan Trench. We will implement a multicoring approach by Mission Specific Platform shallow subsurface (40 m) giant piston coring to recover the continuous upper Pleistocene to Holocene stratigraphic successions of trench-fill basins along an axis-parallel transect of the 7–8 km deep trench. The cores from 18 proposed primary (and/or 13 alternate) sites will be used for multimethod applications to characterize event deposits for which the detailed stratigraphic expressions and spatiotemporal distribution will be analyzed for proxy evidence of earthquakes.

Sediment remobilization related to the 2011 Mw 9.0 Tohoku-Oki earthquake and the respective deposits are preserved in trench basins formed by flexural bending of the subducting Pacific plate. These basins are ideal study areas for testing event deposits for earthquake triggering because they are poorly connected for sediment transport from the shelf and experience high sedimentation rates and low benthos activity (and thus high preservation potential) in the hadal environment. Results from conventional coring covering the last ~1,500 y reveal good agreement between the sedimentary record and historical documents. Subbottom profile images are consistent with basin-fill successions of episodic muddy turbidite deposition and thus define clear targets for paleoseismologic investigations on longer timescales accessible only by IODP coring.

We will apply, further refine, and implement new methods for establishing event stratigraphy in the deep sea and for recognizing giant versus smaller earthquakes versus other driving mechanisms. Our results can potentially produce a fascinating record that unravels an earthquake history that is 10–100 times longer than currently available information. This would contribute to a tremendous advance in the understanding of the recurrence pattern of giant earthquakes and earthquake-induced geohazards globally and provide new constraints on sediment and carbon flux of event-triggered sediment mobilization to a deep-sea trench and its influence on the hadal environment.

©2020. Japan Geoscience Union. All Right Reserved.

This JpGU online presentation will introduce the scientific motivation and background (including latest results from recent research leading up to this upcoming IODP expedition), scientific objective and perspective of this upcoming IODP expedition jointly implemented by ECORD and JAMSTEC-MarE3

Keywords: Earthquake History, Event Stratigraphy, Hadal Trenches, IODP



©2020. Japan Geoscience Union. All Right Reserved.

[E] Poster | M (Multidisciplinary and Interdisciplinary)：M-IS Intersection

[M-IS12] Developments and applications of XRF-core scanning techniques in natural archives

convener:Huang Jyh-Jaan Steven(Institute of Geology, University of Innsbruck), Atsuko Amano(National institute of Advanced Industrial Science and Technology), Masafumi MURAYAMA(Faculty of Agriculture and Marine Science, Kochi University), Liang-Chi Wang(National Chung Cheng University)

X-ray fluorescence (XRF) core scanning techniques have revolutionized element proxy-based paleo-researches over the last decade and now becomes an indispensable tool for many research area. However, despite being fast, non-destructive and providing records of elemental variations at submillimeter resolution, science applications of XRF-core scanning results also encounter numerous challenges due to its intrinsically semi-quantitative and ultra-high resolution nature, such as the influences of down-core physical and organic variations, parameter optimizations of machinery, as well as quantitative calibrations and evaluations of the voluminous and complex scanning data. Therefore, the implications of shifts and trends in the elemental data remain difficult to interpret in many settings.
It is therefore considered timely to bring together international specialists using high-resolution XRF-core scanners in all fields of science to present new research, to stimulate new collaborations and discussions, as well as to propose new technological developments.

[MIS12-P01] Reconstruction of variations in South Pacific westerly jet path during the last glacial

★Invited Papers

*Hitoshi Hasegawa[1], Fuyu Nagaya[1], Kana Nagashima[2], Nagayoshi Katsuta[3], Masafumi MURAYAMA[1], Naomi Harada[2] (1.Kochi University, 2.JAMSTEC, 3.Gifu University)

[MIS12-P03] The chemical composition and temporal change of varve-like sediment in Beppu Bay.

*Yoshiaki Suzuki[1], Michinobu Kuwae[2], Ken Ikehara[1], Kazuno Arai[3], Masafumi MURAYAMA[3] (1.National Institute of Advanced Industrial Science and Technology, 2.Ehime Univ., 3.Kochi Univ.)

[MIS12-P04] Change of depositional environment in Lake Tazawa estimated by X-ray fluorescence core scanner

*Yoko Ishiyama[1], Daizo Ishiyama[1], Kazuyoshi Yamada[2], Masafumi MURAYAMA[3], Takeshi Hayashi[4] (1.Graduate School of International Resource Sciences, Akita University, 2.Museum of Natural and Environmental History, Shizuoka, 3.Center for Advanced Marine Core Research, Kochi University, 4.Faculty of Education and Human Studies, Akita University)

[MIS12-P05] **Multiproxies applied on sediment core for revealing the environmental changes and natural disaster events in Lake Kitaura, central Japan**

Huei-Fen Chen[1], Jun-You Wu[1], *Liang-Chi Wang[2], Hao-Yang Lee[3], Jyh-Jaan Steven Huang[4], Nobuyoshi Yamashita[5], Tomonori Naya[6] (1.Institute of Earth Sciences, National Taiwan Ocean University, Taiwan, R.O.C, 2.Department of Earth and Environmental Sciences, National Chung Cheng University, Taiwan, R.O.C., 3.Institute of Earth Sciences, Acedemia Sinica, Taiwan, R.O.C., 4.Department of Geology, University of Innsbruck, Austria, 5.Research Institute for Environmental Management, AIST, Japan, 6.Institute of Geology and Geoinformation, Geological Survey of Japan, AIST, Japan)

[MIS12-P06] Detecting the seismo-turbidites of off Kumano, the Nankai Trough using ITRAX profile

*Natsumi Okutsu[1], Juichiro Ashi[2], Rina Fukuchi[3], Asuka Yamaguchi[2] (1.Japan Agency for Marine-Earth Science and Technology, 2.Atmosphere and Ocean Research Institute, The University of Tokyo, 3.Dia consultants Ltd.)

[MIS12-P07] **Multivariate statistical and multi-proxy constraints on earthquake-triggered sediment remobilization processes in the central Japan Trench**

Tobias Schwestermann[1], *Jyh-Jaan Steven Huang[1,5], J. Konzett[2], A. Kioka[3], G. Wefer[4], Ken Ikehara[5], J. Moernaut[1], T.I. Eglinton[6], M. Strasser[1,4] (1.Institute of Geology, University of Innsbruck, 2.Institute of Mineralogy and Petrography, University of Innsbruck, 3.Department of Earth Resources Engineering, Kyushu University, 4.MARUM – Center for Marine Environmental Sciences, University of Bremen, 5.Geological Survey of Japan, National Institute of Advanced Industrial Science and Technology (AIST), 6.Geological Institute, ETH Zürich)

[MIS12-P09] Comparison of element profiles obtained from Itrax-XRF core scanner in evaluating data quality among laboratories used by geological reference material.

*Atsuko Amano[1], Jyh-Jaan Steven Huang[2], Ken Ikehara[1], Masafumi MURAYAMA[3], Takuya Matsuzaki[3] (1.National institute of Advanced Industrial Science and Technology, 2.University of Innsbruck, 3.Kochi University)

Reconstruction of variations in South Pacific westerly jet path during the last glacial

*Hitoshi Hasegawa[1], Fuyu Nagaya[1], Kana Nagashima[2], Nagayoshi Katsuta[3], Masafumi MURAYAMA[1], Naomi Harada[2]

1. Kochi University, 2. JAMSTEC, 3. Gifu University

We present results of XRF core scanner analysis on a marine sediment core (MR16-09 PC02) obtained from coastal southern Chile (46S, 76W, 2793 m depth). The study site is located near the boundary of present-day South Pacific summer and winter westerly jet path. Thus, the compositional change of studied core thought to record latitudinal changes of Southern westerly that influence rainfall patterns and water discharges of southern Chile. XRF core scanner (Cox, Itrax) were conducted at Center for Advanced Marine Core Research, Kochi University. Using method of Katsuta et al. (2019), water content-corrected X-ray fluorescence intensities of wet sediment cores were converted to elemental concentrations. Based on the obtained elemental composition, we reconstructed multi-millennial-scale variations in terrestrial detrital inputs, that likely record variations in westerly jet path during the last glacial.

Keywords: Westerly jet path, last glacial

©2020. Japan Geoscience Union. All Right Reserved.

The chemical composition and temporal change of varve-like sediment in Beppu Bay.

*Yoshiaki Suzuki[1], Michinobu Kuwae[2], Ken Ikehara[1], Kazuno Arai[3], Masafumi MURAYAMA[3]

1. National Institute of Advanced Industrial Science and Technology, 2. Ehime Univ., 3. Kochi Univ.

In Beppu Bay, Pref. Oita (central Japan), we aimed to reveal the way to record events such as anthropogenic activities and hazards into the sediment. For this purpose, we obtained several surface sediment cores using G.S.-type surface sediment sampler (Ashura) and gravity core sampler in 2017 and 2019. These sediment cores were CT-scanned and analyzed by the micro XRF scanner (ITRAX). We also measured radioactivities of ^{137}Cs and excess ^{210}Pb by 4cm intervals for age determination.

We investigated 4 points in the bay and checked the depth distribution of the sediment in 2017. At the deepest part of Beppu Bay, 70m depth, we found laminated semi-pelagic sediment with clear lamination with 6-7mm thickness. In the shallower area of the bay, we cannot find lamination. Based on the result of ITRAX measurement and Soft-X images, it is revealed that lamination is caused by the change in the amount of detrital material. The amount and composition of detrital material also show several positive spikes. Some of them can be observed by naked eyes as light gray or reddish-brown colored thin layers (minor event layers), suggesting that they were supplied from different provenance than usual. These layers are considered to be caused by the occurrence of floods, earthquakes, or eruption. The results of Pb and Cs measurements agree with the age of Ev-1a, which is considered to be caused by the Hyuga-Nada earthquake in 1968 (Kuwae et al., 2013). Counting of lamination also agrees with Pb and Cs based age model when unclear lamination is interpolated by the average thickness of laminations.

In the survey on Sep. 2019, we aimed to verify newly deposit sediments in the last two years. We also aimed to obtain the core with sufficient length from the sediment-water interface to the horizon below the ^{210}Pb would be attenuated. Using Ashura sediment sampler with 120 cm-long acrylic pipes, we could obtain the cores with 90cm length. Based on the correlation of the cores of 2019 and 2017, we found newly deposited sediment with 2 cm thickness at the top part of the 2019 core. This accumulation rate agrees with the thickness of laminations found in both cores. These results strongly suggest that lamination at the bottom of Beppu Bay is annual lamination, varve. The inflow of detrital material by heavy seasonal rain could be the generation factor of varve. Lamina preservation becomes clear gradually after around 1960. there is a possibility that the submarine stratified structure has been strengthened by the change of a marine environment with economic growth. We are conducting the measurement of Cs and Pb isotopes of the 2019 core.

Keywords: Beppu Bay, annual lamination, varves, event layers

©2020. Japan Geoscience Union. All Right Reserved.

Change of depositional environment in Lake Tazawa estimated by X-ray fluorescence core scanner

*Yoko Ishiyama[1], Daizo Ishiyama[1], Kazuyoshi Yamada[2], Masafumi MURAYAMA[3], Takeshi Hayashi[4]

1. Graduate School of International Resource Sciences, Akita University, 2. Museum of Natural and Environmental History, Shizuoka, 3. Center for Advanced Marine Core Research, Kochi University, 4. Faculty of Education and Human Studies, Akita University

Lake Tazawa, located in eastern part of Akita Prefecture, is caldera lake formed at 1.7 Ma (Kano et al., 2008 & 2020). The lake is the deepest lake in Japan (432 m in depth). Researches on sediments of Lake Tazawa are few because of difficulty of sampling caused by the depth. Four sediment cores were collected from Lake Tazawa in 2015. The age of sediments at the bottom of the cores is estimated to be 7,000 years ago (Matsuoka, 2016). In this study, TZW15-4 core sample, which is located at the point near caldera wall in southwest part in Lake Tazawa, was investigated. The distance between edge of Lake Tazawa and sampling point of TZW15-4 is 1.0 km. This study presents results of variation of facies of sediments, grain size distribution, density, mineral assemblage and chemical composition determined by X-ray fluorescence (XRF) core scanner, Itrax regarding TZW15-4 core sample and estimates events in Lake Tazawa from 7000 years ago to present.

Total length of TZW15-4 core is 340 cm. The sediment core is composed of silt, sandy silt, diatom earth and tephra. The dominant sediment is silt in the core. Thirty-eight (38) sandy silt layers, 9 diatom earth layers and 2 tephra layers are intercalated in the silt. The tephra layers are Towada Chuseri and Towada-a tephra (Matsuoka, 2016). The sediment is classified into three parts from lower to upper parts from 340 to 185 cm, 185 to 13 cm and 13 to 0 cm by observation by naked eyes. The lower part is characterized by presence of lamina of sandy silt. The part from 185 to 13 cm is characterized by dominance of silt. The part from 13 to 0 cm is also characterized by discolored silt. The relative density of sediments of the core samples was measured by Computed Tomography (CT) scan. The part of silt and sandy silt correspond to low density and high density, respectively.

Fe, As, Ca, Sr, Cu, Pb and Zn concentrations of the core samples were measured by XRF core scanner. The positions having high intensity of Ca and Sr (peaks of Ca and Sr) in the Ca and Sr spectra correspond to sandy silt. Based on the number of peaks of Ca in the core sample, number of emplacements of sandy silt in silt can be clarified clearly.

Age of sediments of TZW15-4 was estimated by ^{14}C radiometric method (Matsuoka, 2016). Based on the age data and number of peaks of Ca (number of sandy silt layers), frequency of emplacement of sandy silt layers was estimated. The frequency is different in the part from 340 to 185 cm and the part from 185 to 13 cm. The frequency of sandy silt layers in the part from 340 to 185 cm is 6.1 times/1000 years, on the other hand, the frequency of sandy silt layers in the part from 185 to 13 cm is 1.7 times/1000 years. Particle size distribution also shows that sandy silt layers in the parts from 340 to 185 cm and 185 to 13 cm is rich and poor in sand component, respectively. Lake Tazawa does not have large river flowing into Lake Tazawa. Source of sediment materials is thought to be derived from the somma of lake Tazawa. Under the warmer condition, amount of precipitation at catchment area of Lake Tazawa is thought to be increased. Amount and frequency of inflow of sediment materials was increased due to the increase of amount of precipitation. This mechanism corresponds to bottom part (340 to 185 cm). On the other hand, the upper part was estimated to be sediments that was formed under small precipitation in colder period because the low frequency of inflow of sandy silt layer and low abundance of sand in sandy silt layers. Based on the ^{14}C radiometric age data (Matsuoka, 2016, Fukumoto et al., 2019), the boundary between the part from 340 to 185 cm and part from 185 to 13 cm corresponds to the age of climate

©2020. Japan Geoscience Union. All Right Reserved.

change around 4,700 BP. The age accord with the age of the starting of climate cooling in Japan around 5,000 BP (Komoto, 2008; Fukumoto et al., 2019).

Keywords: Lake Tazawa, Lake sediment, Depositional environment, X-ray fluorescence core scanner, Holocene

©2020. Japan Geoscience Union. All Right Reserved.

Multiproxies applied on sediment core for revealing the environmental changes and natural disaster events in Lake Kitaura, central Japan

Huei-Fen Chen[1], Jun-You Wu[1], *Liang-Chi Wang[2], Hao-Yang Lee[3], Jyh-Jaan Steven Huang[4], Nobuyoshi Yamashita[5], Tomonori Naya[6]

1. Institute of Earth Sciences, National Taiwan Ocean University, Taiwan, R.O.C, 2. Department of Earth and Environmental Sciences, National Chung Cheng University, Taiwan, R.O.C., 3. Institute of Earth Sciences, Acedemia Sinica, Taiwan, R.O.C., 4. Department of Geology, University of Innsbruck, Austria, 5. Research Institute for Environmental Management, AIST, Japan, 6. Institute of Geology and Geoinformation, Geological Survey of Japan, AIST, Japan

Lake Kitaura is located in the northeast area of Tokyo, facing the Pacific Ocean. We pay more attention to the natural disaster records of this lagoon. Previous studies indicate that the Lake Kitaura recorded twice volcano eruption events, one is A.D. 1707 (Fuji-Hoei), and the other is A.D. 1783 (Asama-a). We drilled two sediment cores here in A.D. 2017 to use multiproxies for interpreting the environmental changes and natural disaster events. First, according to the magnetic susceptibility scan by MSCL, we defined volcanic eruption events in the position of peaking magnetic susceptibility. Our results reveal 6 layers of the volcanic eruption in the lake based on historical records. Those are eruptions from Mt. Fuji in A.D. 1707 and Mt. Asama in A.D. 1783, 1973, 1983, 2004, 2009. The composition of volcanic glass was determined by EDS and LA-ICP-MS for analyzing the SiO_2 content and ratio of Rb/Y and Rb/Sr.

We found that the grain size of sediments was influenced by the volcanic eruption, typhoon, and tsunami events. Br/Ti and S/Ti ratio from Itrax core scanner gives us the information of environmental changes between marine and freshwater, and also indicate that the lagoon formed after about A.D. 1200. After the Mt. Fuji eruption in A.D. 1707, the river brought a lot of sediment accumulation at that time to cause the Br/Ti and S/Ti signals decreasing and forming a more closed brackish environment. We also can judge the duration of salt damage before the Hitachi River locks in A.D. 1975. The sediment cores may record the tsunami event of A.D. 1707, and frequent storm tides between A.D.1275-1340 closed to the time of Kamikaze typhoon in historical records.

Keywords: Lake Kitaura, sediment core, volcanic, disaster, Itrax

©2020. Japan Geoscience Union. All Right Reserved.

Detecting the seismo-turbidites of off Kumano, the Nankai Trough using ITRAX profile

*Natsumi Okutsu[1], Juichiro Ashi[2], Rina Fukuchi[3], Asuka Yamaguchi[2]

1. Japan Agency for Marine-Earth Science and Technology, 2. Atmosphere and Ocean Research Institute, The University of Tokyo, 3. Dia consultants Ltd.

Paleoseismic studies using turbidite have been performed in various sea regions including off the west coast of North America. The characteristics and sedimentation process of turbidite may vary depending on the composition of sediments, the scale of seismic motion, and the seafloor topography. Therefore, for estimating the seismic history using turbidite, it is important to compile characteristics on sedimentary structures, physical properties, chemical compositions, etc. and extract features in each sea region. This study focuses on obtaining the fundamental data of fine-grained turbidites, and apply it to reconstruct the seismic history in the off Kumano, the Nankai subduction zone.

We analyzed multi-cores and piston cores collected from off Kumano, the Nankai Trough. Main samples are obtained from small slope-basins with pin-point accuracy. Based on its sedimentary structure and magnetic susceptibility, fine-grained turbidites are identified. We will mainly report its chemical characteristics based on XRF core scanner, ITRAX.

The first feature of fine-grained turbidite off Kumano is the stratigraphic change of Mn content. McHugh et al. (2016) show a sharp positive peak in Mn just below turbidite, which is different from the trend observed in this study. They suggest that it is due to the shift of the redox boundary just below turbidite. On the other hand, in this study Mn shows the minimum in the mud layer just below the turbidite and starts increasing from the base of the turbidite. High Mn value continues to the high CT value horizon. In the low CT value horizon above it, Mn decreases upward to the base of the next turbidite. The possible scenario for this Mn variation is as follows: when turbidite is deposited, the lower layers below turbidite are separated from the sea floor. This makes deposits reductive and decrease of Mn. On the other hand, the turbidite upper surface must be in contact with oxic seawater for a long time.

The second feature is the stratigraphic change of Ca and Fe. Coarse silt layer (hereinafter, this is called KLa unit), silt layer (KLb) and a thick homogeneous clay layer from the bottom to the top of the upper unit can be identified as fine-grained turbidites. More specifically, KLa unit shows low CT value, which cannot be shown in X-ray CT image and has Fe peak in ITRAX profile. KLb unit shows high CT value and has Ca positive peak in XRF core scanner profile. Although X-ray CT image can be useful tool to identify the fine-grained turbidites, it may lead to misunderstanding the basement of fine-grained turbidites. C-14 radiocarbon dating of the foraminifera, the individual sediment layer interval is 160 years, which is almost consistent with past earthquake recurrence intervals. Moreover, some C-14 ages agree with historical earthquake ages.

Keywords: turbidite, the Nankai Trough

©2020. Japan Geoscience Union. All Right Reserved.

Multivariate statistical and multi-proxy constraints on earthquake-triggered sediment remobilization processes in the central Japan Trench

Tobias Schwestermann[1], *Jyh-Jaan Steven Huang[1,5], J. Konzett[2], A. Kioka[3], G. Wefer[4], Ken Ikehara[5], J. Moernaut[1], T.I. Eglinton[6], M. Strasser[1,4]

1. Institute of Geology, University of Innsbruck, 2. Institute of Mineralogy and Petrography, University of Innsbruck, 3. Department of Earth Resources Engineering, Kyushu University, 4. MARUM –Center for Marine Environmental Sciences, University of Bremen, 5. Geological Survey of Japan, National Institute of Advanced Industrial Science and Technology (AIST), 6. Geological Institute, ETH Zürich

Understanding the impact of earthquakes on subaqueous environments is key for submarine paleoseismological investigations seeking to provide long-term records of past earthquakes that allow assessing seismic and tsunami hazards on relevant time scales. In the central Japan Trench, three event deposits (i.e., turbidites) linked to past major earthquakes over the last 1,500 years have been identified and stratigraphically correlated across several isolated basins along the trench. However, their spatio-temporal petrographic and geochemical fingerprints have not yet been established, limiting our knowledge about sediment source and the underlying remobilization processes induced by these past earthquakes. In this study, we show that the existing event-stratigraphic correlation can be significantly enhanced by employing a multivariate statistical correlation of X-ray fluorescence core scanning, magnetic susceptibility, and wet bulk density data from cores taken along the central Japan Trench. Such statistical correlation is confirmed by heavy mineral analysis of the turbidite sands and further combined with new erosion model based on previously reported bulk organic carbon ^{14}C dates. We find that surficial sediment remobilization, a process where strong seismic shaking remobilizes just the upper few centimeters of slope sediment, is the predominant remobilization process during strong earthquakes at the Japan Trench. This finding sheds light on source-to-sink processes in hadal trenches during earthquakes and helps to assess the completeness of the turbidite paleoseismic record. We further suggest that shallow-buried tephra on the slope might significantly influence the volume and the geochemical and petrographic fingerprints of remobilized sediment.

©2020. Japan Geoscience Union. All Right Reserved.

Comparison of element profiles obtained from Itrax-XRF core scanner in evaluating data quality among laboratories used by geological reference material.

*Atsuko Amano[1], Jyh-Jaan Steven Huang[2], Ken Ikehara[1], Masafumi MURAYAMA[3], Takuya Matsuzaki[3]

1. National institute of Advanced Industrial Science and Technology, 2. University of Innsbruck, 3. Kochi University

The non-destructively and high-resolution X-ray fluorescence (XRF) core scanner have become a useful tool for paleoenvironmental research as well as in many other fields. In Japan, two Itrax-XRF core scanner (Itrax) produced by Cox Analytical Systems, equipping different generations of XRF detectors, were set up at Center for Advanced Marine Core Research in Kochi University (CMCR, CS-38, first generation) at 2014 and National Institute of Advanced Industrial Science and Technology (AIST, CS-49, third generation) in 2019, respectively. In order to understand data quality of these two Itrax, six geological reference materials from different sedimentary environments (lake, marine and fluvial sediments produced in Geological Survey of Japan) were measured.
The reference materials were firstly filled in 2.2×2.2 cm sample cube and covered by a thickness of 1.4 μm PET film. These samples were measured in 100, 30, 15, 5, 1 seconds of exposure times using Molybdenum (Mo) and Chromium (Cr) X-ray tubes at 0.2 mm intervals, respectively. All the XRF spectra were reevaluated by the Q-Spec software (Cox Analytical Systems, version 15.1) to obtain individual element peak area. The continuous 50 measurements in the central part of scanning were selected and averaged to avoid possible edge error. These results (Al, Si, S, K, Ca, Ti, Mn, Fe, Ni, Cu, Zn, Rb, Sr, Ba, Pb) were further compared with the absolute concentrations of six reference materials and calculated the correlation coefficients (R^2) with each exposure times and X-ray tubes.
Beside the results using Mo X-ray tube at AIST (failed to measure due to the machine failure), we compare our results with the data using first generation XRF detector in National Taiwan University (NTU, CS-16 in 2009) that reported by Huang et al. (2016). The correlation coefficients of Si, S, K, Ca, Ti, Mn, Fe, Ni, Cu, Zn, Rb and Ba show high (R^2>0.90) among all the laboratories in all machine setting, while Al shows low (R^2<0.80). Therefore, we confirm that (1) the influence of different exposure times is insignificant for the accuracy of the scanning results; (2) Al is difficult to measure by Itrax due to its low detectability, even advanced XRF detectors in CMCR and AIST were used. More detailed discussion will be made once we obtain the Mo tube data of AIST.

Keywords: Itrax-XRF core scanner, data quality, geological reference material

©2020. Japan Geoscience Union. All Right Reserved.

[E] Poster | M (Multidisciplinary and Interdisciplinary)：M-IS Intersection

[M-IS13] Integrated Analysis of Geoscience Observations from the Floor to Surface of the Ocean

convener:Keisuke Ariyoshi(Japan Agency for Marine-Earth Science and Technology), Joan S Gomberg(USGS Earthquake Science Center), Narumi Takahashi(National Research Institute for Earth Science and Disaster Resilience), Motoyuki Kido(International Research Institute for Disaster Science, Tohoku University)

Sea bottom pressure data contains various components such as crustal deformation, ocean oscillation, tidal variability, atmospheric change, and instrumental drift. So far, seismologists have treated the ocean oscillation as noise, and ocean physicists have done vice versa (considering crustal deformation as noise). Such problems apply to ongoing undersea acoustic distance measuring and other types of ocean observations. In this session, wewelcome contribution on various topics focusing on the complementary relationship between seismology, ocean physics, meteorology, tsunami technology, and other related fields.

[MIS13-P01] Launch of GNSS-Acoustic observation for horizontal and vertical movements off Nemuro using a triangular PXP array with an optional centered-PXP.

*Yukiho Kimura[1], Motoyuki Kido[2], Yusaku Ohta[1], Chie Honsho[1], Fumiaki Tomita[3] (1.Graduate School of Science, Tohoku University , 2.International Research Institute of Disaster Science, Tohoku University, 3.JAMSTEC)

[MIS13-P02] A study on the effects of sea surface height and density of sea water on bottom pressure off the southeastern coast of Hokkaido, Japan after El Nino events using a high-spatial-resolution ocean assimilation data

*Takuya Hasegawa[1,2], Akira Nagano[1], Keisuke Ariyoshi[1], Toru Miyama[1], Hiroyuki Matsumoto[1], Masahide Wakita[1] (1.JAMSTEC, 2.Tohoku University)

[MIS13-P03] Bottom Pressure Variation in Association with the 2017-Present Large-meander of the Kuroshio South of Japan

*Akira Nagano[1], Yusuke Yamashita[2], Keisuke Ariyoshi[1], Takuya Hasegawa[1,4], Hiroyuki Matsumoto[1], Masanao Shinohara[3] (1.JAMSTEC Japan Agency for Marine-Earth Science and Technology, 2.Kyoto University, 3.The University of Tokyo, 4.Tohoku University)

Launch of GNSS-Acoustic observation for horizontal and vertical movements off Nemuro using a triangular PXP array with an optional centered-PXP.

*Yukiho Kimura[1], Motoyuki Kido[2], Yusaku Ohta[1], Chie Honsho[1], Fumiaki Tomita[3]

1. Graduate School of Science, Tohoku University , 2. International Research Institute of Disaster Science, Tohoku University, 3. JAMSTEC

Recent studies on tsunami deposit revealed that M9-class huge earthquakes repeatedly occur along the Kuril trench. This suggests that the seismicity gap found in the shallow portion of the off-Nemuro subduction zone shall not be a stably sliding area but an interseismic locking area, which causes destructive tsunamis at the time of a huge earthquake like as the off-Miyagi region. Then the research groups in Tohoku and Hokkaido universities and JAMSTEC have started integrated geodetic and seismic surveys on July 2019 to reveal the interplate locking condition off Nemuro. In this talk, we focus on GNSS-Acoustic (GNSS-A) observation among the whole surveys.

Three GNSS-A sites were newly constructed along the survey line nearly perpendicular to the trench axis off Nemuro. They are G21 (four PXPs (Precision Transponders), ~100 km from the trench, 2920 m in depth) and G22 (four PXPs, ~35 km from the trench, 6242 m in depth) on the land-side slope, and G23 (three PXPs, ~30 km from the trench, 6700 m in depth) on the Pacific plate. The layout of G21 and G22 has a unique feature with a centered-PXP in the triangular PXP array, which can “resolve vertical motions even only by point survey” as well as horizontal motion. Thus, this layout will be useful for employing autonomous surface platforms which are not suited for moving survey. Different emission angles to PXPs are required to distinguish vertical motions from sound speed variation. The DOP (Dilution of Precision) based evaluation in geometrical strength [e.g., Imano, 2020] showed that putting a centered-PXP produced sufficiently different angles when dimension of the array (circumradius) to the site depth is larger than 0.7; in the viewpoint of detecting vertical motions, this four-PXP layout results in favorable geometry than our pre-existing six-PXP sites (consisting of large and small concentric triangles) which are specialized to solve horizontal gradients of sound speed structure.

In this campaign cruise, both moving and point surveys were conducted at each site for determination of array geometry and position of the array. In this talk, we firstly report on the positioning of the individual PXPs to determine the array geometries because of the first campaign survey. Reference sound velocity profile was calculated from concurrently-measured CTD or XCTD cast. We expressed temporal variation of the sound velocity by NTD (Nadir Total Delay) that consists of B-spline curves every 250 s. Then, we simultaneously solved NTDs and the 3-D position of three or four PXPs in a single array. The positions were successfully determined with accuracies of 4.9–13.8 cm in horizontal and 9.9–13.2 cm in vertical with RMSs in traveltime residuals of 0.070–0.085 ms. Significant positive bias in NTD by ~3.0 ms was obtained at the time of CTD casts, which should be zero in definition because of the reference velocity. This bias indicates that the true sound velocity is ~0.9996 of that calculated using our employed formula by Chen & Millero (1977).

The next survey is scheduled in May 2020 and tentative array displacements will be obtained after that. Now we try to analyze time variation of apparent vertical motions of the array during the point survey of this campaign, which can be a rough indication of the accuracy in the estimate of inter-campaign vertical

©2020. Japan Geoscience Union. All Right Reserved.

displacement. We will also report on this issue in the talk.

Acknowledgements
The data used were obtained during the Shinsei-maru KS-19-12 cruise. PXPs are owned by Hokkaido University and Tohoku University partially funded by “Earthquake and Volcano Hazards Observation and Research Program (Second)” and “activity of the Core Research Cluster of Disaster Science in Tohoku University (a Designated National University)”.

Keywords: GNSS-A, off Nemuro, seafloor crustal deformation

©2020. Japan Geoscience Union. All Right Reserved.

A study on the effects of sea surface height and density of sea water on bottom pressure off the southeastern coast of Hokkaido, Japan after El Nino events using a high-spatial-resolution ocean assimilation data

*Takuya Hasegawa[1,2], Akira Nagano[1], Keisuke Ariyoshi[1], Toru Miyama[1], Hiroyuki Matsumoto[1], Masahide Wakita[1]

1. JAMSTEC, 2. Tohoku University

To investigate the effects of sea surface height (SSH) and sea water density on bottom pressure (BP) off the southeastern coast of Hokkaido, Japan after El Nino events, a state-of-the-art high-spatial-resolution (1/12 degree) ocean assimilation data of the JCOPE2M for the period of 2001-2018 are analyzed. On year-to-year timescale, after the weak El Nino events occurring in 2004/05, 2006/07 and 2009/10, positive SSH anomalies less than 0.15 m appear off the southeastern coast of Hokkaido, while stronger SSH anomalies greater than 0.2 m exist after the very strong El Nino event of 2015/16. The result shows that although such positive SSH anomalies have effect of increase of BP, density changes of sea water from the sea surface to the ocean bottom (i.e., steric effect), in general, cancel out the effect of SSH anomalies on BP change. In offshore area (i.e., area with bottom depth of deeper than 1000 m), roughly 90 % of the effect of the SSH anomaly is cancelled out by the density change of sea water, and roughly 80 % in near-coastal area with bottom depth from 500 m to 1000 m. In the area very close to the coast with bottom depth less than 500 m, density change of sea water cannot cancel adequately the SSH anomalies as compared to the offshore area; for example, from 20 % to 50 % in the area with bottom depth of around 100 ~ 200 m. Thus, it can be said that oceanic isostasy is generally well established especially in the offshore area, as contrast to the shallow area.To check further the strength of the oceanic isostasy, oceanic isostasy anomaly (OIA) is newly introduced in this study. The OIA is defined as a sum of SSH anomalies and geopotential distance (GPD) anomalies from bottom to sea surface. If value of OIA is zero, it means that oceanic isostasy is perfectly established; if OIA is positive (negative), oceanic fluid can lead increase (decrease) of BP. The value of OIA ranges from -0.025 to +0.025 m for both weak and strong El Nino events. For example, at PG1, OAI shows 0.003 m in July 2015, then becomes to 0.015 m in July 2016, showing a change rate of roughly +0.01 m/year during this period. OIA again becomes to be a small value (0.003 m) in July 2017, showing roughly -0.01 m/year change rate of OIA from July 2016 to July 2017. It is also shown that spatial pattern of OIA is not same for each El Nino event. This means that effect of oceanic fluid on BP change shows a spatio-temporal change in association with El Nino events at year-to-year timescale. The present results indicate that effect of oceanic fluid due to both SSH and sea water density changes on BP change cannot be neglected when BP change (or change rate of BP) should be evaluated with order of 1 cm (or 1 cm/year) at year-to-year scale. Therefore, to better take the year-to-year scale BP changes due to crustal deformation related to such as long-term slow slip events (SSEs) or plate convergence, OIA should be removed from the total value of BP.

Acknowledgements: This work was partly supported by the Japan Society for the Promotion of Science (JSPS), Grant-in-Aid for Scientific Research (15H04228, 15H02835, 17K05660).

Keywords: ocean bottom pressure, sea surface height, sea water density, oceanic isostasy, El Nino

©2020. Japan Geoscience Union. All Right Reserved.

©2020. Japan Geoscience Union. All Right Reserved.

Bottom Pressure Variation in Association with the 2017-Present Large-meander of the Kuroshio South of Japan

*Akira Nagano[1], Yusuke Yamashita[2], Keisuke Ariyoshi[1], Takuya Hasegawa[1,4], Hiroyuki Matsumoto[1], Masanao Shinohara[3]

1. JAMSTEC Japan Agency for Marine-Earth Science and Technology, 2. Kyoto University, 3. The University of Tokyo, 4. Tohoku University

In the region off the southern coast of Japan, the Kuroshio alternatively takes large-meander (LM) and non-large-meander (NLM) paths on interannual to decadal time scales. An LM path is greatly displaced southward associated with a large cyclonic eddy off the southern coast of Japan. Meanwhile, an NLM path flows near the coast. Further, there are two types of LM path in terms of the stability of the current path. An LM path formed in August 2004 and continued until July 2005 is an example of the stable type. The LM path was formed from a nearshore NLM path, which flows through the channel north of Miyake-jima Island. Meanwhile, another LM path occurred in September 2017 and continued at present is an example of the unstable type. The LM path changed from an offshore NLM path, which passes through the channel south of Hachijo-jima Island. In addition, the meandering trough of the LM was observed to be more shifted to the east and to be frequently located on the Izu-Ogasawara Ridge. To obtain the mechanisms of the two types of LM path, we performed a detailed comparison between the 2004-2005 and 2017-present LM paths using hydrographic, acoustic surface-bottom round-trip time, sea surface height (SSH), and bottom pressure (BP) data. While, associated with the formation of the stable type (2004-2005 LM) , BP varies vigorously owing to the passage of a deep cyclonic eddy, BP before the formation of the unstable type (2017-present LM) is invariable. In this study, using bottom pressure data collected in the area east of Hyuga-nada, Kyushu, from March 2014 to April 2019, we examine the variation during the LM period.

Keywords: Kuroshio, Large meander, Sea surface height, Bottom pressure

©2020. Japan Geoscience Union. All Right Reserved.

[E] Poster | M (Multidisciplinary and Interdisciplinary)：M-IS Intersection

[M-IS14] Evolution of Pelagic Realm

convener:Atsushi Matsuoka(Department of Geology, Faculty of Science, Niigata University), Toshiyuki Kurihara(Graduate School of Science and Technology, Niigata University), Tetsuji Onoue(Department of Earth and Planetary Sciences, Faculty of Science, Kyushu University), XIN LI(State Key Laboratory of Palaeobiology and Stratigraphy, Nanjing Institute of Geology and Palaeontology, Chinese Academy of Sciences)

This session focuses on the evolution of ecosystem in the pelagic realm,
including discussions on all aspects of pelagic biota covering biostratigraphy,
biochronology, evolution, and biogeography, which are important to the
reconstruction of the spatio-temporal framework in the pelagic realm.
Reconstructions of plate configuration through time are included in the scope of
 this session. Biological, geochemical, sedimentological approaches to the
pelagic environments are welcomed.

[MIS14-P01] **Preservation of Permian–Triassic boundary section in the Jurassic accretionary complex of the Lake Hamana, Central Japan**

*Wang Ding[1], Kohtaro Ujiie[1], Katsuo Sashida[1] (1.University of Tsukuba)

[MIS14-P02] Outreach activities for radiolarian science since the InterRad 15 in Niigata, 2017

*Atsushi Matsuoka[1] (1.Department of Geology, Faculty of Science, Niigata University)

[MIS14-P03] **Phyletic evolution and paleogeographic distribution of the Early Cretaceous radiolarian *Turbocapsula***

*XIN LI[1], Matsuoka Atsushi[2] (1.State Key Laboratory of Palaeobiology and Stratigraphy, Nanjing Institute of Geology and Palaeontology, Chinese Academy of Sciences, 2. Department of Geology, Faculty of Science, Niigata University)

[MIS14-P04] New tectonostratigraphic unit of the Ashio terrane in the Ashio Mountains, central Japan

*Tsuyoshi Ito[1] (1.Geological Survey of Japan, National Institute of Advanced Industrial Science and Technology)

Preservation of Permian–Triassic boundary section in the Jurassic accretionary complex of the Lake Hamana, Central Japan

*Wang Ding[1], Kohtaro Ujiie[1], Katsuo Sashida[1]

1. University of Tsukuba

The Permian-Triassic (P–T) boundary has been received extensive attention, because it recorded the largest mass extinction event in Earth’ s history. However, the entire P-T section has been rarely preserved in the pelagic sedimentary rocks. We examined the lithostratigraphy and deformation structures of the accreted pelagic rocks in Lake Hamana, Central Japan, based on a detailed field mapping and the radiolarian ages. The constructed lithostratigraphy is composed of Late Permian gray chert, black chert, black claystone with a high carbon content of 4.86%–6.78%, siliceous claystone, black chert, and middle Triassic gray chert, in the ascending order. The symmetry in the lithostratigraphy and the change in the radiolarian ages with respect to black carbonaceous claystone are presumed to represent a deep-sea anoxic event that occurred across the P–T boundary. The P–T boundary black carbonaceous claystone suffered from an intense shear, resulting in blocks of siliceous claystone in the scaly black claystone matrix. In places, the sheared terrigenous rocks composed of sandstone blocks in the mudstone matrix are intercalated into the pelagic rocks, possibly representing complex mélange forming processes during the development of the Jurassic accretionary complex.

Keywords: P–T boundary, black carbonaceous claystone, Lake Hamana

©2020. Japan Geoscience Union. All Right Reserved.

Outreach activities for radiolarian science since the InterRad 15 in Niigata, 2017

*Atsushi Matsuoka[1]

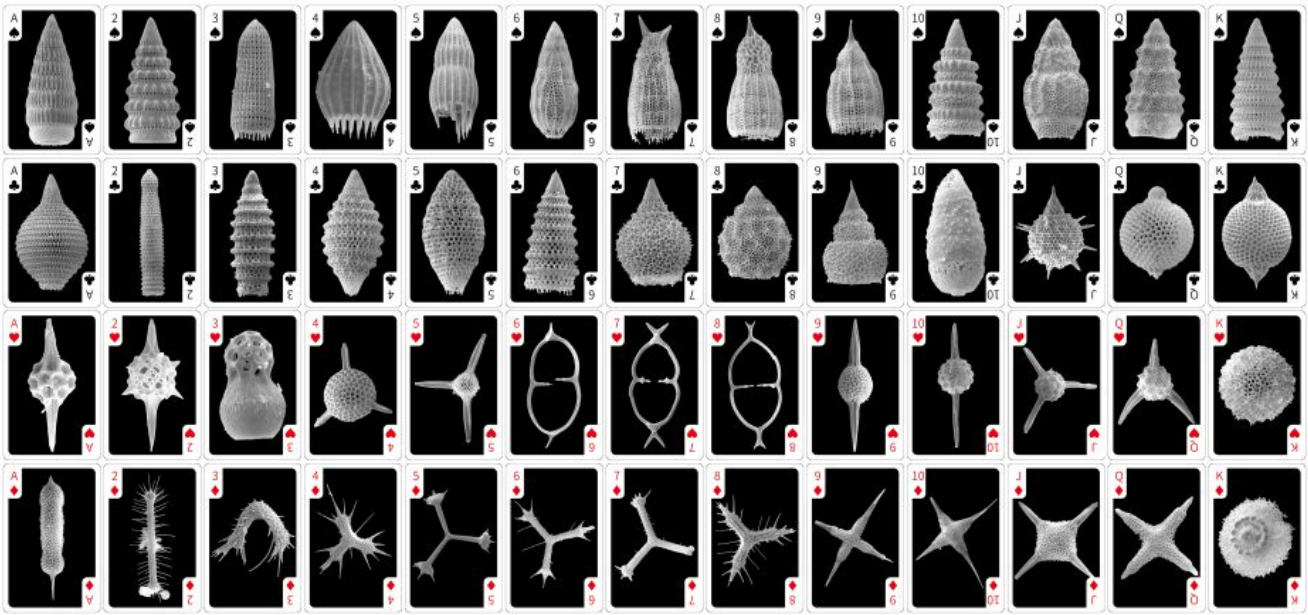
1. Department of Geology, Faculty of Science, Niigata University

Calendars for the year of 2019 and 2020 were produced for enhancing a degree of social recognition of radiolarians. Images for the 2019 calendar come from radiolarian specimens taken from a single rock sample of earliest Cretaceous (Berriasian) tuffaceous clayey radiolarite collected during a dive of the submersible "Shinkai 6500" along the outer slope of the Mariana Trench. Color images of living radiolarians for the 2020 calendar come from radiolarian specimens in the surface water of the East China Sea near Okinawa Island.

A set of playing cards using scanning electron microscope (SEM) images of radiolarian specimens in the same sample as that for the 2019 calendar. The sample contains more than 400 radiolarian species. Candidates of marker taxa defining the Jurassic-Cretaceous boundary can be found in the fauna.

A picture book including SEM images of the above-mentioned Maria radiolarians was published in collaboration with a writer and a book producer. Photo exhibitions were organized in relation to this publication in Tokyo, Osaka, Niigata and other cities in Japan.

Keywords: radiolaria, calendar, card game, picture book



©2020. Japan Geoscience Union. All Right Reserved.

Phyletic evolution and paleogeographic distribution of the Early Cretaceous radiolarian *Turbocapsula*

*XIN LI[1], Matsuoka Atsushi[2]

1. State Key Laboratory of Palaeobiology and Stratigraphy, Nanjing Institute of Geology and Palaeontology, Chinese Academy of Sciences, 2. Department of Geology, Faculty of Science, Niigata University

A radiolarian biostratigraphic study ranging from the latest Barremian to the Aptian of a pelagic sequence (section BB1) near Babazhadong in southern Tibet revealed phyletic relationships of species belonging to the genus *Turbocapsula*. Three species and two subspecies are included in this genus: *Turbocapsula tetras* LI & MATSUOKA, *T. fugitiva* O'DOGHERTY, and *T. costata* (*T. costata* (WU) *multicostata* LI & MATSUOKA, and *T. costata* (WU) *costata*). *Turbocapsula fugitiva* appears to have arisen from *T. tetras* by losing the septa between the third and the fourth segments. *Turbocapsula fugitiva* seems to have given rise to *T. costata* multicostata following the development of thicker costae between its two to five rows of pores. With the decrease in the number of the costae and the development in the costae, *T. costata multicostata* evolved into *T. costata costata*. The phyletic evolution of the genus *Turbocapsula* has a high stratigraphic value.An overview of localities where *Turbocapsula costata* (Wu) has been reported and lithology, depositional setting, associated fossil records, Paleomagnetic data from these localities are summarized. All these data lead to the conclusion that locations of known *T. costata*-bearing strata are restricted to the low to mid-latitude Mediterranean and eastern Tethys. This indicate that the zonation established by the phyletic evolution of the genus *Turbocapsula* cannot be utilized for Early Cretaceous zonal correlations between the Pacific, the Atlantic and other regions.

Keywords: Early Cretaceous, radiolarian, Turbocapsula , Phyletic evolution, paleogeographic distribution

©2020. Japan Geoscience Union. All Right Reserved.

New tectonostratigraphic unit of the Ashio terrane in the Ashio Mountains, central Japan

*Tsuyoshi Ito[1]

1. Geological Survey of Japan, National Institute of Advanced Industrial Science and Technology

The Ashio terrane, a Jurassic accretionary complex, is distributed over the Ashio Mountains of Gunma and Tochigi prefectures, central Japan. Previously, the Ashio terrane is divided into three tectonostratigraphic unit, namely the Kurohone–Kiryu, Omama and Kuzu complexes. The author has recognized new tectonostratigraphic unit (tentative name: Complex A) from the Ashio terrane. The characteristics of Complex A are described here.

Complex A is distributed over mainly the Hachioji hills and Mt. Gyodosan in Tochigi and Gunma prefectures. This complex overlies tectonically the Kuzu Complex and consisits mainly of muddy mixed rock and chert with minor amounts of blocks of sandstone and siliceous mudstone. Early–middle Permian, Triassic and Middle Jurassic radiolarians were obtained from chert. Middle Jurassic radiolarians were extracted from siliceous mudstone and mudstone.

The presence of the Permian chert without basalt and carbonate is the notable characteristic for the comparison with other terrane such as the Tamba and Mino terranes. Although some tectonostratigraphic units of the Tamba and Mino terranes possess Permian chert, these generally include abundant basalt and carbonate as well. Meanwhile, Complex A has no basalt nor carbonate. The comparison indicates the uniqueness of Complex A, suggesting that the complex has unusual geologic history.

Keywords: radiolaria, Permian chert, Ashio terrane, Jurassic accretionary complex, Ashio Mountains

©2020. Japan Geoscience Union. All Right Reserved.

[E] Poster | M (Multidisciplinary and Interdisciplinary)：M-IS Intersection

[M-IS15] Global climate change driven by the Southern Ocean and the Antarctic Ice Sheet

convener:Osamu Seki(Institute of Low Temperature Science, Hokkaido University), Akira Oka(Atmosphere and Ocean Research Institute, The University of Tokyo), Yoshifumi Nogi(National Institute of Polar Research), Robin Elizabeth Bell(Lamont Doherty Earth Observatory)

The Southern Ocean and Antarctic ice sheet, which are the giant reservoirs of heat, water, and materials, have a potential to play central roles in long-term global climate change. This system is composed of the following sub-systems; ice shelf which is a place of the interaction of ice sheet and ocean, flowing iceberg, seasonal sea ice zone, Antarctic bottom water which drives the thermohaline circulation, active biological production and Antarctic Circumpolar Current. These sub-systems are interacted with each other and have significant impact on changes in the global environmental system. This session aim to summarize recent observational and simulation studies from various fields relating to the past and present changes in the Antarctic Ice sheet and Southern Ocean, which are essential elements for unraveling the changes in the global climate system. Further, future science plans for understanding of the environmental changes of the Antarctic Cryosphere is also discussed.

[MIS15-P02] Inflows of offshore-origin warm water toward Totten Ice Shelf region, East Antarctica

*Daisuke Hirano[1], Kohei Mizobata[2], Takeshi Tamura[3], Masato Ito[1], Kaihe Yamazaki[1], Yoichiro Koh[1], Masaaki Kiuchi[4], Hiroto Murase[2], Hiroko Sasaki[5], Shigeru Aoki[1] (1.Institute of Low Temperature Science, Hokkaido University, 2.Tokyo University of Marine Science and Technology, 3.National Institute of Polar Research, 4.Fisheries Sciences, Hokkaido University, 5.National Research Institute of Far Seas Fisheries)

[MIS15-P03] Changes of Antarctic Bottom Water off the Wilks Land coast of the Australia-Antarctic Basin

*Taiyo Kobayashi[1] (1.Japan Agency for Marine-Earth Science and Technology)

[MIS15-P04] Preliminarily results from numerical modeling of chlorofluorocarbons (CFCs) and sulfur hexafluoride (SF_6) in the Southern Ocean

*Yoshihiko Ohashi[1], Michiyo Yamamoto-Kawai[1], Kazuya Kusahara[2] (1.Tokyo University of Marine Science and Technology, 2.Japan Agency for Marine Earth Science and Technology)

[MIS15-P05] Dense water production and downslope flow off Cape Darnley reproduced by a realistic numerical model

*Vigan Mensah[1], Yoshihiro Nakayama[1], Masakazu Fujii[2], Yoshifumi Nogi[2], Kay I. Ohshima[1] (1.Institute of Low Temperature Science, 2.National Institute of Polar Research)

[MIS15-P06] Modeling Ice-shelf ocean interactions of West Antarctic and East Antarctic ice shelves

*Yoshihiro Nakayama[1], Hong Zhang[2], Vigan Mensah[1], Shigeru Aoki[1], Dimitris Menemenlis[2] (1.Institute of Low Temperature Science, Hokkaido University, 2.NASA Jet Propulsion Laboratory, California Institute of Technology)

[MIS15-P08] Geological evidences for Cape Darnley Bottom Water in the Wild Canyon, Antarctica: Preliminary results of R/V Hakuho-maru KH-20-1 cruise

*Minoru Ikehara[1], Hiroshi Sato[2], Masakazu Fujii[3], Keiko Takehara[4] (1.Center for Advanced Marine Core Research, Kochi University, 2.Senshu University, 3.National Institute of Polar Research, 4.Soka University)

[MIS15-P09] Boulder, cobble, pebble, and granule of continental crust rocksfrom the Wild Canyon, off Cape Darnley, East Antarctica: Preliminary results of dredged samples during KH-20-1 cruise, R/V Hakuho-maru

*Hiroshi Sato[1], Masakazu Fujii[2], Minoru Ikehara[3], Keiko Takehara[4] (1.School of Business Administration, Senshu University, 2.National Institute of Polar Research and SOKENDAI, 3.Center for Advanced Marine Core Research, Kochi University, 4.SOKA University)

[MIS15-P11] **Revising the Dome Fuji ice core chronology**

*Ikumi Oyabu[1], Kenji Kawamura[1,2,3], Kyotaro Kitamura[1], Frédéric Parrenin[4], Anais Orsi[5], Christo Buizert[6] (1.National Institute of Polar Research, Research Organization of Information and Systems, 2.The Graduate University of Advanced Studies (SOKENDAI), 3.Japan Agency for Marine Science and Technology (JAMSTEC), 4.Institut des Géosciences de l'Environnement, 5.Laboratoire des sciences du climat et de l'environnement, 6.Oregon State University)

[MIS15-P12] Carbonaceous aerosol records in Domu Fuji ice core over the past 160 kyrs

Haruki Honda[2], *Osamu Seki[1], Kaori Ono[1], Yoshinori Iizuka[1] (1.Institute of Low Temperature Science, Hokkaido University, 2.Graduate School of Environmental Science, Hokkaido University)

[MIS15-P13] **CO_2 sensitivity experiments to study the climate of the mid-Pliocene Warm Period: results from Antarctica and the Southern Ocean**

*Wing-Le Chan[1], Ayako Abe-Ouchi[1,2] (1.Atmosphere and Ocean Research Institute, The University of Tokyo, 2.National Institute for Polar Research)

[MIS15-P14] Glacial ocean carbon cycle changes caused by enhanced stratification in the Southern Ocean and iron fertilization from glaciogenic dust

*Hidetaka Kobayashi[1], Akira Oka[1], Akitomo Yamamoto[2], Ayako Abe-Ouchi[1] (1.Atmosphere and Ocean Research Institute, The University of Tokyo, 2.Japan Agency for Marine-Earth Science and Technology)

[MIS15-P15] **Incorporation of grounding line parameterizations in the three-dimensional ice sheet model SICOPOLIS**

*Takashi Obase[1], Ayako Abe-Ouchi[1,2], Fuyuki SAITO[3], Ralf Greve[4] (1.Atmosphere and Ocean Research Institute, the University of Tokyo, 2.National Institute of Polar Research, 3.Japan Agency for Marine-Earth Science and Technology, 4.Institute of Low Temperature Science, Hokkaido University)

[MIS15-P16] Modeling the evolution of the Antarctic ice sheet driven by basal melting using the three-dimensional ice sheet model SICOPOLIS

*Kaho Harada[1], Ayako Abe-Ouchi[1,2], Takashi Obase[1], Fuyuki SAITO[3], Ralf Greve[4] (1.Atmosphere and Ocean Research Institute, The University of Tokyo, 2.National Institute of Polar Research, 3.Japan Agency for Marine-Earth Science and Technology, 4.Institute of Low Temperature Science, Hokkaido University)

[MIS15-P17] **Antarctic ozone and precipitation variability in the Southern Hemisphere**

*Alessandro Damiani[1], Raul Cordero[2], Pedro Llanillo[3], Sarah Feron[4], Hitoshi Irie[1], Shingo Watanabe[5] (1.Chiba University, Japan, 2.Santiago University, Chile, 3.AWI, Germany, 4.Stanford University, USA, 5.JAMSTEC, Japan)

[MIS15-P18] Position of grounding line at outlet glacier.

*Chiyuki Narama[1], Tsutomu Yamanokuchi[2], Shin Sugiyama[3] (1.Program of Field Research in the Environmental Sciences, Niigata University, , 2.RESTEC, 3.Institute of Low Temperature Science, Hokkaido University)

[MIS15-P19] Acceleration and retreat of Langhovde Glacier, East Antarctica, after the breakup of land-fast sea ice in 2016

*Ken Kondo[1,2], Shin Sugiyama[2] (1.Graduate School of Environmental Science, Hokkaido University, 2.Institute of Low Temperature Science, Hokkaido University)

[MIS15-P20] **Flow velocity and ice sheet elevation of Shirase Glacier and Totten Glacier from SAR and Laser altimetry**

*Shotaro Ohkawa[1], Koichiro Doi[2], Kazuki Nakamura[3], Hiroto Nagai[1] (1.WASEDA University, 2.National Institute of Polar Research, 3.Nihon University)

[MIS15-P21] Summary of the 3rd Year Activities of the Project on the Interaction of the solid Earth and the
Antarctic Ice Sheet

*Yoichi Fukuda[1], Jun Nishijima[2], Takahito Kazama[1], Kazuki Nakamura[3], Koichiro Doi[4], Yusuke Suganuma[4], Jun'ichi Okuno[4], Akito Araya[5], Heitaro Kaneda[6], Yuichi Aoyama[4], Hideki Miura[4] (1.Department of Geophysics, Graduate School of Science, Kyoto University, 2.Graduate School of Engineering, Kyushu University, 3.Faculty of Engineering, Nihon University, 4.National Institute of Polar Research, 5.ERI, University of Tokyo, 6.Graduate School of Science, Chiba University)

[MIS15-P22] **Dependences of GIA model parameters on the geodetic data in East Antarctica**

*Jun'ichi Okuno[1,2], Koichiro Doi[1,2], Akihisa Hattori[2], Yoichi Fukuda[3] (1.National Institute of Polar Research, 2.The Graduate University for Advanced Studies, 3.Kyoto Univ.)

[MIS15-P23] Antarctic ice sheet dynamics during the Last Interglacial

*Mutsumi Iizuka[1], Osamu Seki[1], Keiji Horikawa[3], Tina van de Flierdt[2], Tomohisa Irino[1], Masanobu Yamamoto[1], Takuya Itaki[4], Saiko Sugisaki[4], Minoru Ikehara[5], Yusuke Suganuma[6] (1.Hokkaido university, 2.Imperial College London, 3.University of Toyama, 4.Geological Survey of Japan, 5.Center for Advanced Marine Core Research, Kochi University, 6.National Institute of Polar Research)

[MIS15-P24] **East Antarctic meltwater influx from the Wilkes Subglacial Basin since the Last Glacial Maximum as determined by beryllium isotopes**

*Bethany Behrens[1,2], Yosuke Miyairi[1], Adam David Sproson[1], Masako Yamane[3], Yusuke Yokoyama[1,2,4] (1.Atmosphere and Ocean Research Institute, University of Tokyo, 5-1-5 Kashiwanoha, Kashiwa, Chiba 277-8564, Japan, 2.Graduate Program on Environmental Science, University of Tokyo, Komaba, Meguro, Tokyo 153-0041, Japan, 3.Institute for Space-Earth Environmental Research, Nagoya University, Furocho, Chikusa, Nagoya, Aichi, 464-8601, Japan, 4.Department of Earth and Planetary Science, Graduate School of Science, University of Tokyo, Hongo, Bunkyo, Tokyo 113-8654, Japan)

[MIS15-P25] Geophysical and geological signatures of submarine canyons off Cape Darnley, Antarctica

*Masakazu Fujii[1,2], Minoru Ikehara[3], Hiroshi Sato[4], Keiko Takehara[5], Takuya Itaki[6], Yoshifumi Nogi[1,2], Yasuyuki Nakamura[7] (1.National Institute of Polar Research, 2.The Graduate University for Advanced Studies, SOKENDAI , 3.Center for Advanced Marine Core Research, Kochi University, 4.Senshu University, 5.SOKA University, 6.Geological Survey of Japan, AIST, 7.Japan Agency for Marine Earth Science and Technology)

[MIS15-P26] Structure across the South Shetland Trench from the incoming plate to the back-arc basin

*Hiroaki Koge[1], Masakazu Fujii[2], Jinyu ZHOU[3], Kyoko Okino[3], Minoru Ikehara[4], Asuka Yamaguchi[3], Taichi Sato[1] (1.GSJ, AIST, 2.NIPR, 3.AORI, UTokyo, 4.Kochi University)

[MIS15-P27] Preliminary results of the JARE 61 geomorphological survey at Langhovde in Lutzow Holm Bay, East Antarctica

*Takeshige Ishiwa[1], Yuki Tokuda[2], Takuya Itaki[3], Satoshi Sasaki[4], Yusuke Suganuma[1], Shintaro Yamasaki[5] (1.National Institute of Polar Research, 2.Tottori University of Environmental Studies, 3.National Institute of Advanced Industrial Science and Technology, 4.Shimane University, 5.Disaster Prevention Research Institute, Kyoto University)

[MIS15-P28] Changes in oxygen and CFC concentrations in AABW along 115°E from 1990s to 2010s

*Michiyo Yamamoto-Kawai[1], Narimi Baba[1], Yoshihiko Ohashi[1] (1.Graduate School of Marine Science and Technology, Tokyo University of Marine Science and Technology)

Inflows of offshore-origin warm water toward Totten Ice Shelf region, East Antarctica

*Daisuke Hirano[1], Kohei Mizobata[2], Takeshi Tamura[3], Masato Ito[1], Kaihe Yamazaki[1], Yoichiro Koh[1], Masaaki Kiuchi[4], Hiroto Murase[2], Hiroko Sasaki[5], Shigeru Aoki[1]

1. Institute of Low Temperature Science, Hokkaido University, 2. Tokyo University of Marine Science and Technology, 3. National Institute of Polar Research, 4. Fisheries Sciences, Hokkaido University, 5. National Research Institute of Far Seas Fisheries

The Antarctic ice sheet is the largest freshwater reservoir on the Earth surface. Mass loss from the Antarctic ice sheet results directly in global sea-level rise and Southern Ocean freshening. Recent observational and modeling studies have demonstrated that ice shelf basal melting, resulting from the inflow of warm water onto the Antarctic continental shelf, plays a key role in the ice sheet’s mass balance. In recent decades, warm ocean-cryosphere interaction in the Amundsen and Bellingshausen Seas (ABS) has received a great deal of attention. In contrast, East Antarctic continental shelves are primarily occupied by “cold waters” (Schmidtko et al., 2014), with ice shelves typically having cold ice cavities. An exception is Totten Ice Shelf (TIS) which experiences the highest basal melt rates in East Antarctica (>10 m/yr) comparable with those for the ABS ice shelves. Although comprehensive hydrographic observations from ice front to continental shelf and slope regions are indispensable for understanding ice-ocean interaction beneath the TIS, so far, the observations in these regions are quite sparse. The only one observation has been done by Australia in January 2015 and has revealed relatively warm, modified CDW inflows into TIS cavity (Rintoul et al., 2016; Silvano et al., 2017).

In this presentation, we show the characteristics of offshore-origin warm water distribution at the TIS ice front and continental slope regions, using the hydrographic data obtained by Icebreaker *Shirase* in March 2018 (59th Japanese Antarctic Research Expedition) and R/V *Kaiyo-maru* in February 2019 (multidisciplinary ecosystem survey in the eastern Indian sector of the Antarctic with a focus on Antarctic krill, Fisheries Agency). The offshore-origin modified Circumpolar Deep Water (mCDW, up to 0.3°C) is found in deep glacial troughs near the TIS ice front, which is ~0.7°C warmer than that observed at the almost same position in January 2015 (Rintoul et al., 2016). This suggests a seasonal or interannual variation in inflowing ocean heat flux into TIS cavity. Along the continental slope, warmer mCDW (>1°C) lies at subsurface layer (~300-500 dbar), and particularly warm cores (1.2-1.4°C) is found around the eastern limb of cyclonic eddies, indicating a possible role of cyclonic eddies on a poleward transport of offshore warm water. Various processes from offshore to ice front regions would consequently result in the variations in the ocean heat flux into TIS cavity (i.e., the magnitude of basal melting) with various time scales.

Keywords: offshore warm water, eddy transport , ice-ocean interaction, Totten Ice Shelf, East Antarctica

©2020. Japan Geoscience Union. All Right Reserved.

Changes of Antarctic Bottom Water off the Wilks Land coast of the Australia-Antarctic Basin

*Taiyo Kobayashi[1]

1. Japan Agency for Marine-Earth Science and Technology

Changes of Antarctic Bottom Water (AABW) off teh Wilks Land coast (near 115˚E) of the Australia-Antarctic Basin were examined mainly with historical hydrographic datasets and recent observations of reasearch vessels and deep floats. From climatological views, AABW (denser than γ^n = 28.30) has decreased its thickness since around 1970 by the rate of about 15 m yr^{-1} at the “hypothetical” station of 60˚S 115˚E. The freshening of AABW began before 1960 in the region and it was accelerated in time. These climatological features are fairly consistent with those that had been reported on the AABW changes in the other regions in the Australia-Antarctic Basin.

After around 2010, however, the changes in AABW seemed to have modulated from these climatological trends. The thickenss of AABW was kept at almost the same level until around 2015, and then it has decreased rapidly (by about 50-100 m yr^{-1}). The isothermal salinity decreased rapidly by more than -1.0×10^{-3} yr^{-1} for the period of 2010-2015, and then the freshening seemed to be halted.

The recent modulations of the AABW changes off the Wilks Land coast are similar to the recent changes in AABW off the Adélie/George V Land coast (around 140˚E) (Kobayashi, 2018) at many points. Meanwhile they have several differences; the former modulations probebly began about 4 years later of the latter occureances, and and the former changes were more gradual than the latters. These feasures would suggest that the recent modulations of the AABW changes off the Wilkes Land coast were derived from the arrival of the modified AABW from the east and ultimately attributed to the collapse of Mertz Glacier Tongue in February 2010.

Keywords: AABW, Deep Argo

©2020. Japan Geoscience Union. All Right Reserved.

Preliminarily results from numerical modeling of chlorofluorocarbons (CFCs) and sulfur hexafluoride (SF_6) in the Southern Ocean

*Yoshihiko Ohashi[1], Michiyo Yamamoto-Kawai[1], Kazuya Kusahara[2]

1. Tokyo University of Marine Science and Technology, 2. Japan Agency for Marine Earth Science and Technology

Antarctic Bottom Water (AABW) forms in the Southern Ocean and spreads throughout the global ocean. The time scale of AABW spreading has not been understood in detail. To quantitatively understand its time scale, it is effective to use transient tracers such as chlorofluorocarbons (CFCs) and sulfur hexafluoride (SF_6). We carry out numerical experiments of CFCs and SF_6 in the Southern Ocean using a coupled ocean-sea ice-ice shelf model and investigate the relationship between partial pressure of CFC-12 (pCFC-12) and partial pressure of SF_6 (pSF_6) in AABW. The concentrations of pCFCs in the model are significantly high near formation regions of the AABW (Ross Sea, Weddell Sea, off the Cape Darnley, and off the Adelie Land). This horizontal distribution is consistent with observational results. The linear relationship between pCFC-12 and pSF_6 are found near formation regions of the AABW, indicating that a strong mixing of waters with different ages. The transit time distribution (TTD) method using pCFC-12 and pSF_6 provides information about mean age and age distribution of a water parcel. In the presentation, we will reveal the TTD in the model and estimate the water mass age using the TTD and observed multi-transient tracers.

Keywords: Antarctic Bottom Water , Transient tracer, Numerical modeling

©2020. Japan Geoscience Union. All Right Reserved.

Dense water production and downslope flow off Cape Darnley reproduced by a realistic numerical model

*Vigan Mensah[1], Yoshihiro Nakayama[1], Masakazu Fujii[2], Yoshifumi Nogi[2], Kay I. Ohshima[1]

1. Institute of Low Temperature Science, 2. National Institute of Polar Research

The ability of the Massachusetts Institute of Technology general circulation model (MITgcm) to reproduce dense water production and its downslope outflow through a complex topography is evaluated through a series of simulations at different horizontal and vertical resolutions. The study domain is the region off Cape Darnley in East Antarctica, where intense sea ice production from March to October leads to the formation of Dense Shelf Water, previously observed to outflow periodically as a downslope current. Our experiments are based on a hydrostatic parametrization, using a coupled ocean-ice-atmosphere model for realistic forcing and sea ice production. Different vertical and horizontal resolutions are used to evaluate the relative importance of the model vertical grid and of the topography on the production of dense water and its outflow, and the model output is compared with the mooring observation data for evaluation purposes. The bottom topography data around the main canyon (Wild Canyon) are based on multibeam echo-sounder observations. While the outflow of dense shelf water is seen in the model outputs at the mooring location for each vertical and horizontal resolution, increasing the horizontal resolution leads to a start of the outflow and a periodicity more consistent with the observations. This suggest the dominant role of horizontal resolution for the accurate reproduction of dense shelf water production and outflow. We then proceed to determine the optimal setting allowing for reproduction of these phenomena at the lowest possible computational cost.

Keywords: Ocean-ice modelling, East Antarctica, Dense Water production, Sea ice

©2020. Japan Geoscience Union. All Right Reserved.

Modeling Ice-shelf ocean interactions of West Antarctic and East Antarctic ice shelves

*Yoshihiro Nakayama[1], Hong Zhang[2], Vigan Mensah[1], Shigeru Aoki[1], Dimitris Menemenlis[2]

1. Institute of Low Temperature Science, Hokkaido University, 2. NASA Jet Propulsion Laboratory, California Institute of Technology

In the Amundsen and Bellingshausen Seas (ABS), modified Circumpolar Deep Water (mCDW) intrudes into ice shelf cavities of West Antarctic Ice Sheet (WAIS), causing high ice shelf melting near the ice sheet grounding lines, accelerating ice flow, and controlling the pace of future Antarctic contributions to global sea level (~0.3mm/y). On the other side of Antarctica, recent studies are pointing out that the ice shelves of East Antarctic Ice Sheet (EAIS) may be beginning to shrink, which is crucial as the EAIS contains marine-based ice equivalent to 19 m of global sea-level rise. Recent oceanographic observations evidenced the inflow of mCDW (~-0.4ºC) into the Totten ice shelf cavity.

Using MITgcm, we have conducted various regional ocean simulations for ice shelves in the ABS and off Sabrina coast with a focus on Pine Island,/Thwaites ice shelves and Totten ice shelf, respectively. Our ABS domain extends from the Antarctic Continent to 65ºS and from 140ºW to 65ºW and our East Antarctic domain extends from the Antarctic Continent to 60ºS and from 90ºE to 150ºE. Detailed comparison between model and observations are conducted. Pathways of mCDW towards grounding lines, temporal and spatial variabilities of ice shelf melt rates, mechanisms of simulated and observed interannual variabilities, etc., have been investigated.

In this presentation, we will summarize key findings and model capabilities from available ocean configurations. We introduce our various existing model outputs focusing on the eastern Amundsen Sea as an example, and demonstrate how to access these outputs and plot basic variables. We hope that these model outputs can be utilized for different aspects of oceanographic researches including observational planning, boundary conditions for ocean and ice sheet models, and data analysis for physical, biological and biogeochemical oceanography.

Keywords: Ice shelf ocean interaction, West Antarctica, East Antarctica, Ocean modeling

©2020. Japan Geoscience Union. All Right Reserved.

Geological evidences for Cape Darnley Bottom Water in the Wild Canyon, Antarctica: Preliminary results of R/V Hakuho-maru KH-20-1 cruise

*Minoru Ikehara[1], Hiroshi Sato[2], Masakazu Fujii[3], Keiko Takehara[4]

1. Center for Advanced Marine Core Research, Kochi University, 2. Senshu University, 3. National Institute of Polar Research, 4. Soka University

The Cape Darnley Bottom Water (CDBW) produced in the Cape Darnley polynya (CDP) descends down Wild Canyon (Ohshima et al., 2013). According to the mooring observations (Ohshima et al., 2013), significant signals of CDBW was found at the center of Wild Canyon just off the CDP. Two months after the onset of active sea-ice production, a colder, less saline, and denser signal appeared and became dominant after June. However, there are no direct evidence for sedimentary processes in the Wild Canyon. We have conducted marine geological survey in Wild Canyon during the KH-20-1 cruise by R/V Hakuho-maru in 2020 austral summer. We obtained sediment samples at two sites using multiple corer with deep-sea camera at the bottom of the Wild Canyon. For site CAD-5 (2660m water depth), small amount of sands was recovered. Based on deep-sea camera observation, sea-floor is covered by sand and rocks. Short sediment cores were recovered at the site St16 (3347 m water depth), which is located at downstream area from CAD-5. Sediments were composed of sandy silt in the canyon, and current ripple are observed on the seafloor in the canyon, which is main stream of the CDBW.

Keywords: Southern Ocean, Anatactic Bottom Water, paleoceanography, deep-sea camera

©2020. Japan Geoscience Union. All Right Reserved.

Boulder, cobble, pebble, and granule of continental crust rocksfrom the Wild Canyon, off Cape Darnley, East Antarctica: Preliminary results of dredged samples during KH-20-1 cruise, R/V Hakuho-maru

*Hiroshi Sato[1], Masakazu Fujii[2], Minoru Ikehara[3], Keiko Takehara[4]

1. School of Business Administration, Senshu University, 2. National Institute of Polar Research and SOKENDAI, 3. Center for Advanced Marine Core Research, Kochi University, 4. SOKA University

The Cape Darnley Bottom Water (CDBW), which is produced in the Cape Darnley polynya (CDP), descends down the Wild Canyon (Ohshima et al., 2013). According to the mooring observations by Ohshima et al. (2013), significant signals of CDBW were found at the center of the Wild Canyon just off the CDP. Two months after the onset of active sea-ice production, a colder, less saline, and denser signal appeared and became dominant after June. However, there is no direct evidence for the transportation processes of geological materials in the Wild Canyon.

Dredge operation was performed during KH-20-1 cruise at the bottom of Wild Canyon. Approximately 170 kg of granitoid and metamorphic rocks that are consist of continental crust were recovered. They contain boulder, cobble, pebble, and granule size of granitoid and metamorphic rocks. Furthermore, they show subangular to subrounded shape. Based on deep-sea camera observation, sea-floor is covered with soft sediments and scattered boulders.

Lithology and petrological characteristics of continental crust rocks will reveal not only transportation and sedimentary processes at the Wild Canyon but also (tectonic) development history of both the Wild Canyon and East Antarctica.

Keywords: East Antarctica, Cape Darnley Bottom Water, Granitoid, Metamorphic rock

©2020. Japan Geoscience Union. All Right Reserved.

Revising the Dome Fuji ice core chronology

*Ikumi Oyabu[1], Kenji Kawamura[1,2,3], Kyotaro Kitamura[1], Frédéric Parrenin[4], Anais Orsi[5], Christo Buizert[6]

1. National Institute of Polar Research, Research Organization of Information and Systems, 2. The Graduate University of Advanced Studies (SOKENDAI), 3. Japan Agency for Marine Science and Technology (JAMSTEC), 4. Institut des Gé osciences de l'Environnement, 5. Laboratoire des sciences du climat et de l'environnement, 6. Oregon State University

Precise chronology is essential for paleoclimate proxies to examine the sequences, durations and phasing of the climate records, as well as for numerical simulations, both for their input and validation data to better understand the transient behaviors of climate and ice sheet. The chronology of the Dome Fuji ice core over the last 340 kyr was constructed by synchronizing variations in the O_2/N_2 ratio of occluded air with local summer insolation (Kawamura et al., 2007) with stated uncertainty of less than ~2.5 kyr in general. The accuracy of the chronology is generally supported by the comparison with a radiometric (U-Th) dating of Chinese speleothem records (Cheng et al., 2009), but relatively large errors were recently found around the last interglacial period (Fujita et al., 2015). Here, we revise the Dome Fuji chronology using newly acquired O_2/N_2 ratio (summer insolation proxies), new densification models and 1-D ice flow model (PaleoChrono), and discuss the timing of penultimate deglaciation from atmospheric records of CH_4 concentrations and $\delta^{18}O$ of O_2 in the Dome Fuji ice core.

References

Fujita, S. et al. (2015), *Clim. Past.*, 11, 1395-1416 .
Kawamura, K., et al. (2007), *Nature*, 448, 912-916.
Cheng, H. et al. (2009), *Science*, 326, 248-252.

Keywords: chronology, ice core, Dome Fuji

©2020. Japan Geoscience Union. All Right Reserved.

Carbonaceous aerosol records in Domu Fuji ice core over the past 160 kyrs

Haruki Honda[2], *Osamu Seki[1], Kaori Ono[1], Yoshinori Iizuka[1]

1. Institute of Low Temperature Science, Hokkaido University, 2. Graduate School of Environmental Science, Hokkaido University

Carbonaceous aerosols influence climate via direct and indirect effects on radiative balance and are thought to have a potential to substantially affect global climate. Although numerous studies have been conducted to better understand chemical and physical properties, source, transport and fate of carbonaceous aerosols in the atmosphere, significance of carbonaceous aerosol for global scale climate still remains uncertain. This is mainly due to difficulty to evaluate net radiative effects of carbonaceous aerosol. In this study, we reconstructed changes in terrestrial and marine derived biogenic carbonaceous aerosols during the glacial-interglacial cycle (over the past 160 kyrs) based on analysis of organic molecular tracers in Antarctic ice core, Dome Fuji, in order to evaluate substantial role and impact of biogenic carbonaceous aerosol on glacial-interglacial scale climate. The fluxes of both terrestrial and marine derived organic molecular tracers show large variations over the past 160 kyrs with low and high during the glacial and deglacial to interglacial periods, respectively. Their variation patterns are consistent with biomass changes in the aerosol source regions; high latitude regions of the South America and South Atlantic Ocean. This correspondence suggests emissions of the biogenic carbonaceous aerosols are primary controlled by biomass of aerosol sources. Comparison of the organic molecular tracers and surface air temperature records in the Dome Fuji ice core and sea surface temperature in the water vapor source revealed that the emission of biogenic carbonaceous aerosol does not correlate with Antarctic and Southern Ocean temperatures. The observed decoupling of high latitude temperature in the southern hemisphere and biogenic carbonaceous aerosol indicates that carbonaceous aerosol does not play an important role in affecting large scale climate change and thus, that net radiative effect of carbonaceous aerosols is almost negligible.

Keywords: carbonaceous aerosol, ice core

©2020. Japan Geoscience Union. All Right Reserved.

CO_2 sensitivity experiments to study the climate of the mid-Pliocene Warm Period: results from Antarctica and the Southern Ocean

*Wing-Le Chan[1], Ayako Abe-Ouchi[1,2]

1. Atmosphere and Ocean Research Institute, The University of Tokyo, 2. National Institute for Polar Research

The mid-Pliocene Warm Period (mPWP), 3.3-3 million years ago, was a period of sustained warmth before global cooling occurred and a shift to repeated glacial cycles. It was also the most recent time in the history of Earth when atmospheric carbon dioxide levels were similar to those of present day. The study of this period is thus of much importance, given the growing concerns over future climate change associated with anthropogenic emissions of greenhouse gases. Recently, an increasing number of climate models have been used to investigate the mPWP climate, most contributing to the Pliocene Model Intercomparison Project (PlioMIP), while a large collection of proxy data from both terrestrial and marine sources have been made available. Reconciling model results and proxy data remains an important issue.

In our study, we use the mid-resolution MIROC4m coupled atmosphere-ocean general circulation model and apply ice sheet configuration, land-sea mask, orography and biome distribution from PRISM data sets, as set forth in the second phase of PlioMIP. We conduct a series of experiments which include a range of atmospheric carbon dioxide levels given the spread in values suggested by different sources of proxy data and show how various aspects of the climate in the southern polar region respond. We also compare sea surface temperature anomalies with proxy values derived from PRISM data sets.

Keywords: climate modeling, Pliocene, Antarctica, Southern Ocean, paleoclimate

©2020. Japan Geoscience Union. All Right Reserved.

Glacial ocean carbon cycle changes caused by enhanced stratification in the Southern Ocean and iron fertilization from glaciogenic dust

*Hidetaka Kobayashi[1], Akira Oka[1], Akitomo Yamamoto[2], Ayako Abe-Ouchi[1]

1. Atmosphere and Ocean Research Institute, The University of Tokyo, 2. Japan Agency for Marine-Earth Science and Technology

The glacial-interglacial variation of atmospheric carbon dioxide concentration (pCO_2) is recognized to mainly arise from changes in the ocean carbon cycle, but the detailed mechanism behind this change is not clarified. This study conducts an ocean carbon cycle simulation using a global-scale three-dimensional ocean general circulation model considering the enhanced stratification in the Southern Ocean and the iron fertilization from glaciogenic dust during the glacial periods and shows the glacial change of atmospheric pCO_2 by about 80 ppm. Considering these processes also improves simulating the ocean inventory and distribution of dissolved oxygen, carbonate ion, $\delta^{13}C$, and radiocarbon ages. We show that the effective biological pump under the enhanced stratification and increased ocean alkalinity inventory due to carbonate compensation, which are not appropriately considered in previous OGCM studies, are important to sequester carbon to the deep ocean under the constraints of proxy data during glacial periods.

Keywords: ocean carbon cycle, glacial-interglacial cycle, Southern Ocean, iron fertilization, carbonate compensation

©2020. Japan Geoscience Union. All Right Reserved.

Incorporation of grounding line parameterizations in the three-dimensional ice sheet model SICOPOLIS

*Takashi Obase[1], Ayako Abe-Ouchi[1,2], Fuyuki SAITO[3], Ralf Greve[4]

1. Atmosphere and Ocean Research Institute, the University of Tokyo, 2. National Institute of Polar Research, 3. Japan Agency for Marine-Earth Science and Technology, 4. Institute of Low Temperature Science, Hokkaido University

Understanding the nature, stability and climatic thresholds of the Antarctic ice sheet is important for projecting future sea level change. Flow of Antarctic ice sheet is commonly represented with Shallow Ice Approximation (SIA) and Shallow Shelf Approximation (SSA). However, under coarse horizontal resolution (~10km) that is feasible for long-term simulation of Antarctic ice sheet of glacial cicyles, combined SIA/SSA model has limited utility in the migration of grounding lines (Pattyn et al. 2012). Recent Antarctic Ice Sheet models utilize sub-grid parameterization of grounding line migrations to represent large-scale grounding line migration of Antarctic marine ice sheets during glacial cycles. Here, a sub-grid grounding line parameterization is incorporated to the 3-dimensional ice sheet model SICOPOLIS. We present the results of model evaluations under both of idealized topography and realistic Antarctic topography.

Keywords: Antarctic ice sheet, ice sheet model

©2020. Japan Geoscience Union. All Right Reserved.

Modeling the evolution of the Antarctic ice sheet driven by basal melting using the three-dimensional ice sheet model SICOPOLIS

*Kaho Harada[1], Ayako Abe-Ouchi[1,2], Takashi Obase[1], Fuyuki SAITO[3], Ralf Greve[4]

1. Atmosphere and Ocean Research Institute, The University of Tokyo, 2. National Institute of Polar Research, 3. Japan Agency for Marine-Earth Science and Technology, 4. Institute of Low Temperature Science, Hokkaido University

The Antarctic ice sheet is the largest fresh-water storage at present, whose geometry and volume have changed in response to climate changes like glacial-interglacial cycles. These changes are controlled by the surface and basal mass balance of the Antarctic ice sheet, which also affect grounding line migration. The basal melting beneath ice shelves is one of the dominant drivers for mass loss from the Antarctic ice sheet as it causes ice shelves to thin and reduce their buttressing effect on the upstream grounded ice, which leads to accelerated ice drainage and thus mass loss. However, the relative importance of basal melting on the response of the Antarctic ice sheet to climate change is still not clear.

In this study, we use the three-dimensional ice sheet model SICOPOLIS to investigate steady states of the Antarctic ice sheet with various basal melting rates beneath ice shelves, starting from the present-day ice sheet as initial condition. We analyze the response of the whole Antarctic ice sheet as well as that of specific areas, namely the Siple Coast, Wilkes, Aurora and Recovery subglacial basins. Siple Coast is located in West Antarctica, at the east side of the Ross Ice Shelf, while the other basins are located in East Antarctica. All areas have large ice shelves, so that they are highly sensitive to the basal melting beneath ice shelves. We also investigate steady states of the Antarctic ice sheet at various sea levels relative to the present to take into account the influence of glacial-interglacial cycles.

Keywords: Antarctic ice sheet, ice shelf, basal melting, ice sheet model

©2020. Japan Geoscience Union. All Right Reserved.

Antarctic ozone and precipitation variability in the Southern Hemisphere

*Alessandro Damiani[1], Raul Cordero[2], Pedro Llanillo[3], Sarah Feron[4], Hitoshi Irie[1], Shingo Watanabe[5]

1. Chiba University, Japan, 2. Santiago University, Chile, 3. AWI, Germany, 4. Stanford University, USA, 5. JAMSTEC, Japan

Although Antarctic ozone depletion occurs mostly in spring, the consequent reduction in shortwave heating lasts long into the summer, accelerating the stratospheric zonal winds and causing negative geopotential height anomalies at high latitudes. Such changes propagate from the stratosphere to the troposphere, affecting winds, precipitation, pressure, and temperature and result in a modulation of the trend of the Southern Annular Mode (SAM), especially during the austral summer. Nevertheless, Antarctic ozone can also potentially affect the climate at an interannual timescale due to its significant interannual springtime variability. On the other hand, ozone anomalies can be considered a proxy for variability in polar vortex strength. In this study, we investigated the interannual connection among ozone, SAM, and precipitation, exploring the possibility of using springtime Antarctic ozone as a predictor of summertime precipitation. Observations were compared with simulations of the present and future climate from a coupled climate model with interactive atmospheric chemistry. Then, in an attempt to identify the regions where ozone variations could improve seasonal predictions, we focused on areas where previous studies found a connection between surface climate and the ozone hole. Overall, we suggest that including ozone variations in models could enhance seasonal predictions.

Keywords: Antarctica, precipitation, ozone

©2020. Japan Geoscience Union. All Right Reserved.

Position of grounding line at outlet glacier.

*Chiyuki Narama[1], Tsutomu Yamanokuchi[2], Shin Sugiyama[3]

1. Program of Field Research in the Environmental Sciences, Niigata University, , 2. RESTEC, 3. Institute of Low Temperature Science, Hokkaido University

To identify a grounding line at the Langhovde Glacier in East Antarctica, "double differential interferometric SAR (DDInSAR) analysis" is performed using ALOS-2 / PALSAR-2 microwave data. By comparing the vertical component obtained by DDInSAR with the field survey data, we estimated position of a grounding line at the Langhovde Glacier.

Keywords: outlet glacier, grounding line, Langhovde Glacier, DDInSAR

©2020. Japan Geoscience Union. All Right Reserved.

Acceleration and retreat of Langhovde Glacier, East Antarctica, after the breakup of land-fast sea ice in 2016

*Ken Kondo[1,2], Shin Sugiyama[2]

1. Graduate School of Environmental Science, Hokkaido University, 2. Institute of Low Temperature Science, Hokkaido University

The Antarctic ice sheet drains ice into the ocean through floating ice shelves and outlet glaciers, which play key roles in the mass balance of the Antarctic ice sheet. Since iceberg calving and ice shelf basal melting are major ablation processes of the ice sheet, understanging the dynamics of floating ice is important. Land-fast sea ice affects the stability of ice shelves by exerting battressing force on the ice front. For example, previous studies reported glacier front retreat, disintegration of ice shelves and ice flow acceleration after breakup of sea ice in front of glaciers (e.g. Miles et al., 2017). Lützow-Holm Bay located in East Antarctica is usually covered with land-fast sea ice all year round, but a large portion of sea ice broke up in April 2016 (Aoki et al., 2017). In order to investigate the impact of the sea ice break up on outlet glaciers in the region, we carried out satellite observations on Langhovde Glacier, one of the outlet glaciers terminating in Lützow-Holm Bay. Glacier terminus position was deliniated from 2000 to 2020, using Landsat 7 Enhanced Thematic Mapper Plus (ETM+) and Landsat 8 Operational Land Imager (OLI) imagery. Changes in glacier surface area near the calving front were devided by the width of the calving front to obtain mean retreat/advance distance. Ice flow velocity field from 2014 to 2020 was measured, by applying a feature tracking method (Sakakibara and Sugiyama, 2014) to Landsat 8 OLI image pairs.

Terminus position has been relatively stable from 2000 to 2012, with only small fluctuations within a range of 200 m. The glacier then advanced by 400 m from 2012 to 2016. After 2016, the year of the land-fast sea ice break up, the terminus retreated rapidly by 720 m by 2020 as a result of large calving events in 2016 and 2019. The glacier front reached the most retreated position since 2000. After the sea ice breakup, ice speed increased from 110 m a^{-1} in 2017 to 135 m a^{-1} in 2019. The results of this study suggest the glacier had been stabilized by the land-fast sea ice by 2016. Rapid retreat and acceleration after the breakeup indicate significant influence of sea ice on the dynamics of outlet glaciers in Antarctica.

References

Miles, B.W.J. and Stokes, C.R. and Jamieson, S.S.R (2017), Simultaneous disintegration of outlet glaciers in Porpoise Bay (Wilkes Land), East Antarctica, driven by sea ice break-up, *The Cryosphere*, **11**, 427-442.

Aoki, S. (2017), Breakup of land-fast sea ice in Lützow-Holm Bay, East Antarctica, and its teleconnection to tropical Pacific sea surface temperatures, *Geophys. Res. Lett.*, **44**, 3219–3227.

Sakakibara, D., and S. Sugiyama (2014), Ice-front variations and speed changes of calving glaciers in the Southern Patagonia Icefield from 1984 to 2011, *J. Geophys. Res. Earth Surf.*, **119**, 2541–2554.

Keywords: Antarctic, Ice sheet, Glacier, Sea ice

©2020. Japan Geoscience Union. All Right Reserved.

Flow velocity and ice sheet elevation of Shirase Glacier and Totten Glacier from SAR and Laser altimetry

*Shotaro Ohkawa[1], Koichiro Doi[2], Kazuki Nakamura[3], Hiroto Nagai[1]

1. WASEDA University, 2. National Institute of Polar Research, 3. Nihon University

The whole area of Antarctica ice mass balance has already calculated by previous studies (eg. Rignot et al., 2019). However, Antarctic glaciers have various flow rates, which might be related to their responses to climate change, therefore present flow dynamics observation at high spatial and temporal resolutions is necessary.

This study estimates two glaciers' ice flow velocity and ice elevation profiles in available parts. Two glaciers which are Totten Glacier and Shirase Glacier in the East Antarctica were chosen in this study. Previous studies found out that Totten Glacier has been melted rapidly (Li et al., 2016; Rignot et al., 2013), whereas Shirase Glacier is one of the fastest ice streams in Antarctica (Nakamura et al., 2010; Rignot et al., 2011). We estimated the ice flow velocities using Synthetic Aperture Radar (SAR) images corrected by C-band SAR onboard Sentinel-1A/-1B in 2018 to 2019 and the Phased Array L-band SAR-2 (PALSAR-2) onboard Advanced Land Observing Satellite-2 (ALOS-2) in 2017 to 2018.

The Geoscience Laser Altimeter System (GLAS) on the Ice, Cloud, and land Elevation Satellite (ICESat) and the Advanced Topographic Laser Altimeter System (ATLAS) instrument onboard ICESat-2 provide accurate global elevation data. ICESat-2 was launched on September 15, 2018, which is the newest laser altimeter satellite at this time. ICESat data is available from 2003 to 2009 and ICESat-2 data are available from 2018 to 2019. Laser altimetry data are combined with the existing digital surface models (DSM) like the Reference Elevation Model of Antarctica (REMA) and ALOS World 3D-30m (AW3D30) which have some data missing. Laser altimetry data was used to fill some data missing of DSM.

In the presentation, we will estimate ice volume change and ice flux from glacier to compare with the past results using flow velocity data and elevation data. We will also try to cover some data missing in the DSMs using the elevation data. DSMs are necessary for using estimating flow velocities from other SAR data processing techniques like InSAR.

This study was partially supported by JSPS KAKENHI Grant No. 17H06321.

Keywords: Totten glacier, Shirase glacier, Sentinel-1, ICESat-1/2, flow velocity

©2020. Japan Geoscience Union. All Right Reserved.

Summary of the 3rd Year Activities of the Project on the Interaction of the solid Earth and the Antarctic Ice Sheet

*Yoichi Fukuda[1], Jun Nishijima[2], Takahito Kazama[1], Kazuki Nakamura[3], Koichiro Doi[4], Yusuke Suganuma[4], Jun'ichi Okuno[4], Akito Araya[5], Heitaro Kaneda[6], Yuichi Aoyama[4], Hideki Miura[4]

1. Department of Geophysics, Graduate School of Science, Kyoto University, 2. Graduate School of Engineering, Kyushu University, 3. Faculty of Engineering, Nihon University, 4. National Institute of Polar Research, 5. ERI, University of Tokyo, 6. Graduate School of Science, Chiba University

A five years research project funded by JSPS (Japan Society for the Promotion of Science) has been started in July 2017. The title of the project is "Giant reservoirs of heat/water/material: Global environmental changes driven by Southern Ocean and Antarctic Ice Sheet" and is aiming to establish a new research area for Antarctic environmental system science. The project consists of 7 research topics, including Antarctic ice sheet and Southern ocean sciences, new observation methodology, modeling and other interdisciplinary topics, and we are involved in the topic, "Interaction of the solid Earth and the Antarctic Ice Sheet".

The Antarctic ice sheet is an essential element of the Earth system for predicting the future environment changes. Thus many studies have been conducted by means of geomorphological, geological, geodetic surveys, as well as satellite observations. For these studies, one of the largest uncertainties is the effects of GIA and the main reason of the uncertainties come from insufficient in-site observations. Thus we planned to conduct geomorphological, geological and geodetic surveys in the outcrop areas and the coastal areas in East Antarctica. Combining these new observations with other in-site data, various satellite data and numerical modeling, we aim to estimating a precise GIA model, constructing a reliable ice melting history after the last glacial maximum and obtaining the viscoelastic structure of the Earth's interior.

As the third year activities, we conducted absolute gravity measurements in Korean Jang Bogo station and Itarian Marrio Zucchelli station, boring core sampling and geomorphological surveys near Indian Maitri Station as well as several data analyses, numerical modeling, and other related studies.

In this presentation, we report these activities and the results so far obtained, and the observation/research plans in 2020 as well.

This study was partially supported by JSPS KAKENHI Grant No. 17H06321.

Keywords: Glacial Isostatic Adjustment, Ice sheet changes, Sea level rise, East Antarctica

©2020. Japan Geoscience Union. All Right Reserved.

Dependences of GIA model parameters on the geodetic data in East Antarctica

*Jun'ichi Okuno[1,2], Koichiro Doi[1,2], Akihisa Hattori[2], Yoichi Fukuda[3]

1. National Institute of Polar Research, 2. The Graduate University for Advanced Studies, 3. Kyoto Univ.

Recent global warming has accelerated the melting of both the Greenland and Antarctic ice sheets and has resulted in global sea-level rise, which has become a social concern. The recent melting of the Antarctic Ice Sheet (AIS), the largest freshwater reservoir on Earth, has been detected by various observations. In particular, time series of gravity changes by GRACE, which launched in 2002, described in detail the movement and change of mass in Antarctica. However, the observation of gravity fields such as GRACE includes not only the change of ice mass but also the change of mass caused by the deformation of the solid Earth called Glacial Isostatic Adjustment (GIA). For this reason, an accurate estimate of the solid Earth deformation is required to prescribe the recent ice mass balance by gravity observations.
Furthermore, the current deformation rate of the solid Earth also includes the component induced by the melting of the AIS since the Last Glacial Maximum (ca. 20kyr before present). Therefore, the estimates of the deglaciation history of the AIS on a time scale over 10,000 years derived from geomorphic and geological observations are also required. In the GIA modeling study, the development of numerical methods simulating the Earth's response due to surface load has been continued with the inference of the melting history of the continental ice sheets simultaneously. At present, several scenarios of the AIS deglaciation history based on geomorphic and geological data have been proposed and are still being debated. In this study, we discuss the GIA-derived gravity change and crustal deformation in the East Antarctic region using the previously published AIS deglaciation models and the GIA modeling code currently under development. GIA is highly dependent not only on surface load variations such as the changes of ice and seawater volume but also on the structure of the Earth's interior (mainly viscosity structure of the mantle). Therefore, to discuss the recent ice mass change in detail, we will conduct the numerical experiments with the extensive GIA model parameters and show the effects of the GIA-induced geodetic signals on the estimates of current ice mass fluctuations quantitatively.

Keywords: Glacial Isostatic Adjustment, Antarctic Ice Sheet, gravity change, viscosity structure of the Earth's mantle

©2020. Japan Geoscience Union. All Right Reserved.

Antarctic ice sheet dynamics during the Last Interglacial

*Mutsumi Iizuka[1], Osamu Seki[1], Keiji Horikawa[3], Tina van de Flierdt[2], Tomohisa Irino[1], Masanobu Yamamoto[1], Takuya Itaki[4], Saiko Sugisaki[4], Minoru Ikehara[5], Yusuke Suganuma[6]

1. Hokkaido university, 2. Imperial College London, 3. University of Toyama, 4. Geological Survey of Japan, 5. Center for Advanced Marine Core Research, Kochi University, 6. National Institute of Polar Research

Ongoing global warming could cause various problems in the future. One of the serious concerns potentially caused by the global warming is a sea level rise due to the melting of ice sheet. Antarctic ice sheet, which hold a massive amount of fresh water, was considered to be stable even if global warming progresses in a future. However, recent studies have shown that Antarctic ice sheet is more sensitive to global warming than previously thought. Therefore, it is an important to better understand extent to which Antarctic ice sheet sensitive to global warming.

Study of past warm period provides a useful insight into the prediction of sea level rise in a future. In particular, the last interglacial (MIS 5e), which was ~1˚C warmer than that of the preindustrial, is receiving increased attention, since sea level in the period is estimated to be several meters higher than that of the present. This suggests substantial loss of Antarctic ice sheet during MIS 5e. However, variability of Antarctic ice sheet during MIS 5e has been poorly understood. In this study, we generate high resolution records of mineral composition, Nd isotope and iceberg rafted debris (IBRD) in GC1407 collected from near the Wilkes Basin, East Antarctica (130.518˚E, 63.74˚S) in order to better understand Antarctic ice sheet dynamics during the warmer than the present climate condition.

The two episodic IBRD increase events are found to be recognized during MIS 5e in GC1407, suggesting that increases in icebergs transport occurred during MIS 5e. Nd isotope and mineral composition records in GC1407 suggest that icebergs originated from area with relatively higher eNd, possibly either Wilkes Land Basin or West Antarctica ice sheets. The iceberg discharge events happened when Antarctic air temperature was warmer than that of preindustrial era, suggesting a link between Antarctic warming and increase in iceberg discharge. Furthermore, the timings of iceberg

©2020. Japan Geoscience Union. All Right Reserved.

discharge events are simultaneous with the onsets of sea level rises estimated from geological record in Western Australia. The correspondence between the sea level and Antarctic ice sheet records suggests substantial contribution of Antarctic ice mass loss to the sea level rises during MIS 5e.

Keywords: Antarctic Ice Sheet, Last interglacial, Nd isotope

©2020. Japan Geoscience Union. All Right Reserved.

East Antarctic meltwater influx from the Wilkes Subglacial Basin since the Last Glacial Maximum as determined by beryllium isotopes

*Bethany Behrens[1,2], Yosuke Miyairi[1], Adam David Sproson[1], Masako Yamane[3], Yusuke Yokoyama[1,2,4]

1. Atmosphere and Ocean Research Institute, University of Tokyo, 5-1-5 Kashiwanoha, Kashiwa, Chiba 277-8564, Japan, 2. Graduate Program on Environmental Science, University of Tokyo, Komaba, Meguro, Tokyo 153-0041, Japan, 3. Institute for Space-Earth Environmental Research, Nagoya University, Furocho, Chikusa, Nagoya, Aichi, 464-8601, Japan, 4. Department of Earth and Planetary Science, Graduate School of Science, University of Tokyo, Hongo, Bunkyō, Tokyo 113-8654, Japan

The West Antarctic Ice Sheet (WAIS) and East Antarctic Ice Sheet (EAIS) contain an amount of ice equivalent to 3-5 m and 53 m sea level rise, respectively (1). The WAIS, as a largely marine-based ice sheet, is susceptible to changes in ocean temperatures and prone to retreat. Recent research has revealed that areas of the EAIS situated below sea level are also very sensitive to atmospheric and oceanic temperature changes and vulnerable to retreat (2, 3). The two largest subglacial basins in East Antarctica, the Wilkes and Aurora subglacial basins, hold a total ice mass equivalent to 28 m sea level rise (4), demonstrating that even a partial collapse of the EAIS would have a major effect on global sea level.

To investigate the response of these vulnerable areas to a warming ocean and atmosphere, we have evaluated beryllium isotope concentrations from Adélie Basin, located on the continental shelf offshore the Wilkes Subglacial Basin. Our record covers the most recent period of major Holocene ice sheet retreat, sea level rise, and increased atmospheric CO_2since the Last Glacial Maximum ice sheet retreat (5). The beryllium isotope data suggest oceanic or climatic changes occurred at ca. 9.8 ka, ca. 6.3 ka, and from ca. 4.1 ka. From prior research, we can conclude our high meteoric ^{10}Be values at ~9.8 ka and ~6.3 ka are attributed to an open marine environment created by the retreat of grounded ice along with an increased influx of meltwater (6-8). The elevated concentration and frequency variation of meteoric ^{10}Be values starting from ~4.1 ka indicates a change in regime, possibly linked to changes in climate.

(1) Wilson DJ, Bertram RA, Needham EF, van de Flierdt T, Welsh KJ, McKay RM, et al. Nature. 2018;561(7723):383-6.

(2) Hansen MA, Passchier S. Geo-Marine Letters. 2017;37(3):207-13.

(3) DeConto RM, Pollard D. Nature. 2016;531:591.

(4) Shen Q, Wang H, Shum C, Jiang L, Hsu HT, Dong J. Scientific reports. 2018;8(1):4477.

(5) Yokoyama Y, Esat TM, Thompson WG, Thomas AL, Webster JM, Miyairi Y, et al. Nature. 2018;559(7715):603-7.

(6) Yokoyama Y, Anderson JB, Yamane M, Simkins LM, Miyairi Y, Yamazaki T, et al. Proceedings of the National Academy of Sciences. 2016;113(9):2354.

(7) Valletta RD, Willenbring JK, Passchier S, Elmi C. Paleoceanography and Paleoclimatology. 2018;33(9):934-44.

©2020. Japan Geoscience Union. All Right Reserved.

(8) Behrens B, Miyairi Y, Sproson AD, Yamane M, Yokoyama Y. Journal of Quaternary Science. 2019;34(8):603-8.

Keywords: East Antarctica, beryllium isotopes, Holocene, ice sheet instability, Wilkes Subglacial Basin

©2020. Japan Geoscience Union. All Right Reserved.

Geophysical and geological signatures of submarine canyons off Cape Darnley, Antarctica

*Masakazu Fujii[1,2], Minoru Ikehara[3], Hiroshi Sato[4], Keiko Takehara[5], Takuya Itaki[6], Yoshifumi Nogi[1,2], Yasuyuki Nakamura[7]

1. National Institute of Polar Research, 2. The Graduate University for Advanced Studies, SOKENDAI , 3. Center for Advanced Marine Core Research, Kochi University, 4. Senshu University, 5. SOKA University, 6. Geological Survey of Japan, AIST, 7. Japan Agency for Marine Earth Science and Technology

The Antarctica continental slope off Cape Darnley is known as a major pathway of colder, less saline, and denser bottom water, which is produced in the Cape Darnley polynya and known as the Cape Darnley Bottom Water (CDBW). The mooring observations showed that significant signals of CDBW occurs at the center of the Wild Canyon (Ohshima et al., 2013). Intensive erosion and material transports from shallow regions to deep ocean can be expected here, but the relationship between submarine canyons and bottom water is still debated. Here we present new observations from large networks of submarine canyons off Cape Darnley. We conducted underway geophysical mapping, multichannel reflection seismic survey, bottom rock samplings and bottom sediment coring in this region during the R/V Hakuho-maru KH-19-1 and KH-20-1 cruises. Underway geophysical mapping was widely conducted in the area 60 ×90 miles. Multibeam bathymetry, sub-bottom profiler, total and vector magnetic fields, and gravity data were acquired. New bathymetric map compiled with previous survey data (e.g., Japanese Antarctic Research Expedition 51–55) clearly reveals that a large channel network of submarine canyons exists in the pathway of the CDBW. Sub-bottom and multichannel seismic reflection profile clearly show sub-seafloor structure of submarine canyons and surrounding sedimentary layers. Based on collected rocks, cored sediments, and deep-sea camera observations, it is shown that seafloor surface is covered with angular clast and sand in the shallower part of the channel. Furthermore, it is observed that sandy silt with current ripple morphology is deposited in the deeper part of the channel. These results imply that a main stream of the CDBW strongly contribute to erosion, transportation, and sedimentation at the submarine canyons, shaping the seafloor off Cape Darnley continental slope. This finding provides new insight into the ice-ocean-seafloor connection and indicates the distribution of the Cape Darnley Bottom Water, which is potentially linked to material transports from continent and/or continental margin into the deep ocean.

Keywords: East Antarctica, Submarine canyon, Cape Darnley Bottom Water, Marine geology and geophysics

©2020. Japan Geoscience Union. All Right Reserved.

Structure across the South Shetland Trench from the incoming plate to the back-arc basin

*Hiroaki Koge[1], Masakazu Fujii[2], Jinyu ZHOU[3], Kyoko Okino[3], Minoru Ikehara[4], Asuka Yamaguchi[3], Taichi Sato[1]

1. GSJ, AIST, 2. NIPR, 3. AORI, UTokyo, 4. Kochi University

How are back-arc basins (BABs) formed in the continental crust? It is little known because active BABs are rare. Bransfield Strait in the South Shetland Trench system, Antarctica, and Okinawa Trough in Ryukyu Island Arc are considered the limited active continental back-arc basins which going on opening without a large strike-slip. Therefore, the researches of both areas are the key to the question. The formation of BABs is also expected to affect the formation of accretionary prisms through the changes in convergence rate and/or the sediment supply system from the continent.

We conducted the geophysical observations in the Antarctic Sea using R/V Hakuho-maru in December 2019 (KH-19-6 leg4 cruise)., We successfully obtained the data along the lines across the South Shetland Trench from the incoming plate to the back-arc basin. The collected data include; multi-narrow beam echo sounder (MBES) bathymetry data, shipborne vector magnetic fields data, shipboard gravimeter data, sub-bottom profiles (SBP), and XCTD profiles.

We describe the area of the South Shetland Islands in 65°W / 55°W / 62°40’ S / 58°S and show the preliminary report of these data on the point of the structures.

In this area, we had three XCTD casts to obtain the seawater sound velocity profile in which seawater conductivity (equivalent to salinity), temperature, and depth. The profile of XCTD #1 (58°20.974’ S, 65° 18.237’ W) showed higher velocity near sea surface than those of the profiles of XCTD #2 (61° 03.815’ S, 57°56.977’ W) and XCTD #3 (61°58.998’ S, 62°19.352’ W). XCTD #2 and #3 showed the almost similar sound velocity profile. All of the data was used for the sound velocity correction of the MBES data.

The bathymetric grid is created with noise removal processing using Caris HIPS and SIPS. The slope angle map is also created from the bathymetric map. We described the geomorphological features across the lines of the South Shetland Trench from the incoming plate to the back-arc basin with respect to the seafloor morphology, slope angle map, and SBP profiles.

On the incoming plate of the South Shetland Trench, the lineaments trending NE-SW direction are well-developed on the seafloor. Most of these lineaments are considered to be formed during seafloor spreading process of the former Phoenix-Antarctic Spreading Ridge, because they are almost parallel to the direction of the ridge. In addition, several dome-shaped structures can be seen near 58°40’ S, 64° 20’ W on the incoming plate. Based on the SBP profiles, the relative height was approximately 700 m, however, any internal structures were not recognized due to the strong reflection at the surface of the structure.

In the South Shetland Trench, there is a depth difference between the east and west ("west in King George island ", "strait between Smith Island and Snow Island"); the depth of the east side is approximately -5300m, on the west side the depth is approximately -4700m. The bottom of the trench is relatively flat, therefore it can be expected to fill with sediments. In the operation of the piston core, we could recover the samples with almost full recovery. However, SBP profiles do not have enough resolution to confirm a clear sedimentary structure.

In the landward slope in the arc-trench system, on the east side, the motif of the slope looks uniform angle from the bottom to the 500m below the sea surface, and gradually rises to a depth of 300m from there. In the western slope, at our bathymetry data, the sedimentary environment may be different from that on the

©2020. Japan Geoscience Union. All Right Reserved.

east, since he lamina-like linear structure was observed in the westside upper position.
At the JpGU, we will show magnetic features calculated from vector magnetic data to further describe the structures.

Keywords: Antarctica, back-arc spreading, tectonics

©2020. Japan Geoscience Union. All Right Reserved.

Preliminary results of the JARE 61 geomorphological survey at Langhovde in Lutzow Holm Bay, East Antarctica

*Takeshige Ishiwa[1], Yuki Tokuda[2], Takuya Itaki[3], Satoshi Sasaki[4], Yusuke Suganuma[1], Shintaro Yamasaki[5]

1. National Institute of Polar Research, 2. Tottori University of Environmental Studies, 3. National Institute of Advanced Industrial Science and Technology, 4. Shimane University, 5. Disaster Prevention Research Institute, Kyoto University

The mass loss of the Antarctic Ice Sheet due to the global climate changes will largely contribute to global sea-level rise. The information of present ice-sheet mass balance is required to achieve an accurate projection of Antarctic Ice Sheet changes. The timing and amplitude of Antarctic Ice Sheet change during the Last Deglaciation is essential to assess a glacial isostatic adjustments effect on the present ice-sheet mass balance. However, the difficulty of access to Antarctica makes it challenging to obtain field-based evidence of ice-sheet and sea-level change during the Last Deglaciation. In the 61st Japanese Antarctic Research Expedition (JARE61), the geomorphological survey was carried out in Langhovde and West Ongul Island in Lutzow Holm Bay, East Antarctica. We will report the preliminary results of JARE 61 such as the bathymetry data, CTD profiles, and sampling locations in shallow water and Lake Nurume of Langhovde. These data will be used to obtain the geological evidence of paleoenvironmental changes due to sea-level and ice-sheet fluctuation in future studies.

Keywords: Japanese Antarctic Research Expedition , Antarctic Ice Sheet Change, Geomorphological Survey

©2020. Japan Geoscience Union. All Right Reserved.

Changes in oxygen and CFC concentrations in AABW along 115°E from 1990s to 2010s

*Michiyo Yamamoto-Kawai[1], Narimi Baba[1], Yoshihiko Ohashi[1]

1. Graduate School of Marine Science and Technology, Tokyo University of Marine Science and Technology

Antarctic Bottom Water (AABW) is formed by a mixing of old deep water with newerly ventilated shelf water. This process has important implications for the transport of heat, freshwater, oxygen and carbon into deep ocean. Recent studies suggest reduction of AABW formation due to surface warming and freshening. In order to investigate changes in ventilation rate and properties of AABW, we have compared CFCs, oxygen and other water properties between observations made in 2016/2017 and 1995/1996 in the Australian sector of the Southern Ocean. Results showed increases in apparent oxygen utilization (AOU) and CFC age, indicating reduced ventilation of AABW in 20 years. We compare results with model simulation to discuss possible mechanisms of the reduction as well as quantitative implication of the reduction.

Keywords: AABW, CFC, Oxygen

©2020. Japan Geoscience Union. All Right Reserved.

[E] Poster | M (Multidisciplinary and Interdisciplinary)：M-IS Intersection

[M-IS16] Rift-related tectonics, magmatism, mineralization, and paleoceanographic effects

convener:Luisa Tejada Maria(Volcano and Earth Interior Research Center, Institute for Marine Geodynamics, Japan Agency for Marine-Earth Science and Technology), Eun Young Lee(Chonnam National University), Erik Wolfgring

The session will focus on various types of rift-related magmatism and associated mineralization that forms during different stages of development from rifting to breakup. It will focus on various tectonic mechanisms resulting in either passive or active margins, effusion of both mafic and felsic volcanic rocks or their intrusive equivalents, and paleoceanographic perturbations. The session may include various topics relating to tectonic models and interpretations, magma generation and evolution, lithospheric interaction, intrusive mechanism, eruption mechanisms, and associated mineralization. In addition, contributions regarding the possible link of hotspots or mantle plumes with continental rifting and contemporaneous paleoceanographic perturbations are most welcome. Both oral and poster presentations are desired.

[MIS16-P01] Rift-related volcanism at Naturaliste Plateau, Indian Ocean

*Maria Luisa Tejada[1], Eun Young Lee[2], Hans-Jurgen Brumsack[3], Bernhard Schnetger[3], Dennis Harry[4], Seong Soo Chun[2], Jun-Ichi Kimura[1] (1.Volcano and Earth Interior Research Center, Institute for Marine Geodynamics, Japan Agency for Marine-Earth Science and Technology, 2.Faculty of Earth System and Environmental Sciences, Chonnam National University, Gwangju, Republic of Korea, 3.Institut für Chemie und Biologie des Meeres (ICBM), Carl von Ossietzky Universität Oldenburg, Oldenburg, Germany, 4.Department of Geosciences, Colorado State University, Fort Collins, CO, USA)

[MIS16-P02] Qualitative Assessment of the Transition and Noble Metal Enrichment in Hydrothermally Altered Volcanic Sequence Using a Portable X-ray Fluorescence Spectrometer

*Xandr Neal Borja Uboan[1], Maria Luisa Tejada[2], Eun Young Lee[3], Wataru Tanikawa[4] (1.National Institute of Geological Sciences, University of the Philippines Diliman, Philippines, 2.Institute for Marine Geodynamics (IMG), Japan Agency for Marine-Earth Science and Technology, Yokosuka, Kanagawa 237-0061 Japan, 3.Faculty of Earth and Environmental Science, Chonnam National University, Gwangju, Republic of Korea, 4.Kochi Institute for Core Sample Research, Japan Agency for Marine-Earth Science and Technology, Nankoku 783-8502 Japan)

[MIS16-P03] Petrophysical characteristics of the volcanic succession at IODP Site U1513: Implications for stratigraphy and alteration

*Eun Young Lee[1], Maria Luisa Tejada[2], Seung Soo Chun[1], Insun Song[3], Erik Wolfgring [4] (1.Faculty of Earth Systems and Environmental Sciences, Chonnam National University, Gwangju, Rep. Korea, 2.Institute for Marine Geodynamics (IMG), Japan Agency for Marine-Earth Science and Technology, Yokosuka, Kanagawa, Japan, 3.Korea Institute of Geoscience and Mineral resources, Daejeon, Rep. Korea, 4.Department of Geodynamics and Sedimentology, University of Vienna, Vienna, Austria)

[MIS16-P04] Paleoenvironments of a Cretaceous marginal ocean basin - the Turonian to Santonian of the Australo-Antarctic Gulf, IODP Site U1512

*Erik Wolfgring [1], Michael Anthony Kaminski[2], Anna Waśkowska[3] (1.University of Vienna, Geodynamics and Sedimentology, Althanstrasse 9, 1090 Vienna, Austria, 2.King Fahd University of Petroleum and Minerals (KFUPM), Earth Sciences Department, Geosciences, Dhahran, SaudiArabia, 3.Faculty of Geology, Geophysics and Environmental Protection, AGH University of Science and Technology, Mickiewicza St. 50, Cracow, Poland)

[MIS16-P06] The facies architecture of felsic subaqueous volcanoes in “Green Tuff” Formation in the Katakai field, Niigata, Japan

*Miyuki Nonaka[1,2], Masahiko Yagi[1], Yasuo Yamada[1], Susumu Umino[3] (1. Japan Petroleum Exploration Co.,Ltd., 2.Graduate School of Natural Science & Technology, Kanazawa University, 3.Department of Earth

Sciences, Kanazawa University)

Rift-related volcanism at Naturaliste Plateau, Indian Ocean

*Maria Luisa Tejada[1], Eun Young Lee[2], Hans-Jurgen Brumsack[3], Bernhard Schnetger[3], Dennis Harry[4], Seong Soo Chun[2], Jun-Ichi Kimura[1]

1. Volcano and Earth Interior Research Center, Institute for Marine Geodynamics, Japan Agency for Marine-Earth Science and Technology, 2. Faculty of Earth System and Environmental Sciences, Chonnam National University, Gwangju, Republic of Korea, 3. Institut für Chemie und Biologie des Meeres (ICBM), Carl von Ossietzky Universität Oldenburg, Oldenburg, Germany, 4. Department of Geosciences, Colorado State University, Fort Collins, CO, USA

Seismic reflection and dredging data indicate that extensive volcanism on and around the Naturaliste Plateau accompanied Early Cretaceous rifting between Australia-Antarctica and Greater India during the breakup of Eastern Gondwana. However, no direct stratigraphic evidence for this was available until International Ocean Discovery Program drilled into the volcanic sequence at Site U1513. We report petrological, petrophysical, paleomagnetic, and geochemical data from this volcanic sequence and discuss their: (1) petrogenesis and emplacement history; (2) lithostratigraphy; and (3) relationship with onshore and previously dredged basalts in Australia and the Naturaliste Plateau, respectively. The volcanic sequence consists of interlayered lava flows and volcaniclastic flows, cut by multiple intrusions. Baked and depositional contacts suggest that at least five phases of eruption took place, possibly in response to episodic rifting events. Petrological and textural evidence suggest subaerial to shallow water eruption. Primary magma composition derived from the most primitive basalts (high MgO, Ni, and Cr) could be parental to most of the flows and, by extension, to dredged basalts and onshore Bunbury Basalt based on geochemical similarity. Petrogenetic modeling indicates origin from magmas generated by ~20% partial melting at 1.5 GPa and a mantle potential temperature of 1398℃, indicating a more fertile than normal ocean ridge mantle source, which corroborates chemical affinities with basalts generated by the Kerguelen plume. Magnetrostratigraphy of overlying volcaniclastic-rich sedimentary unit indicates contemporaneous emplacement of Site U1513 basalts with the oldest Bunbury Basalt flows and the reported age of the earliest seafloor magnetic anomalies in the Perth Abyssal Plain. Available evidence indicates that Site U1513 were erupted near sea level during the last stages of extension on this part of the southwest Australian margin, after seafloor spreading had begun on the Perth Abyssal Plain but before the onset of seafloor spreading west of Naturaliste Plateau. The timing of emplacement and the relatively fertile source derived from petrogenetic modeling suggest an influence of a thermal anomaly during rifting.

Keywords: Naturaliste Plateau basalts, East Gondwana breakup, Kerguelen plume, IODP Site U1513

©2020. Japan Geoscience Union. All Right Reserved.

Qualitative Assessment of the Transition and Noble Metal Enrichment in Hydrothermally Altered Volcanic Sequence Using a Portable X-ray Fluorescence Spectrometer

*Xandr Neal Borja Uboan[1], Maria Luisa Tejada[2], Eun Young Lee[3], Wataru Tanikawa[4]

1. National Institute of Geological Sciences, University of the Philippines Diliman, Philippines, 2. Institute for Marine Geodynamics (IMG), Japan Agency for Marine-Earth Science and Technology, Yokosuka, Kanagawa 237-0061 Japan, 3. Faculty of Earth and Environmental Science, Chonnam National University, Gwangju, Republic of Korea, 4. Kochi Institute for Core Sample Research, Japan Agency for Marine-Earth Science and Technology, Nankoku 783-8502 Japan

IODP Expedition 369 recovered the first stratigraphically constrained volcanic sequence at Site U1513 on the Naturaliste Plateau, comprising basalt flows interlayered with volcaniclastic beds and intruded by dikes. Dike intrusions may be responsible for the widespread hydrothermal alteration. We used portable X-ray fluorescence (pXRF) to measure the elemental composition and assess any metal enrichment trends associated with hydrothermal alteration. Most major elements (Si, Ti, Fe, Mg, Ca, P) and some trace elements (Sr, Y, Cr, Zn, Cu, Ru, Pd, Ag) measured by pXRF have ≦10% precision. Concentrations measured by both pXRF and XRF plotted with depth show a similar trend for most elements but with some discrepancies. The matches and differences can be explained by the type of material measured by pXRF (i.e., clast/vein/matrix/groundmass vs. whole rock). Concentration plots of transition metals with depth show a notable enrichment at ~688, ~695, and ~697 meters below seafloor (mbsf) for Hole U1513E and ~700, ~710, and ~750 mbsf for Hole U1513D. Enrichment of Fe concentration coincides with the presence of hematite, goethite, and dickite associated with the alteration of the glassy matrix, groundmass, and Fe-Ti oxides during hydrothermal alteration. Spikes in the concentration of Cu reflect the occurrence of native copper as vein or dissemination near the dike intrusions or within the volcaniclastic units. For the noble metals, apparent depletion of Ru and Pd is notable at ~700 and ~750 mbsf, and enrichment of Ag at ~700 and ~750 mbsf. Apparent depletion or enrichment of the elements may be associated with their mobility and immobility during hydrothermal alteration. The pXRF measurement can be used for qualitative assessment of the enrichment or depletion of elements during hydrothermal alteration and as a preliminary tool to identify sample points for further studies of alteration and mineralization associated with the volcanic sequence.

Keywords: X-ray Fluorescence, Hydrothermal Alteration, Naturaliste Plateau

©2020. Japan Geoscience Union. All Right Reserved.

Petrophysical characteristics of the volcanic succession at IODP Site U1513: Implications for stratigraphy and alteration

*Eun Young Lee[1], Maria Luisa Tejada[2], Seung Soo Chun[1], Insun Song[3], Erik Wolfgring [4]

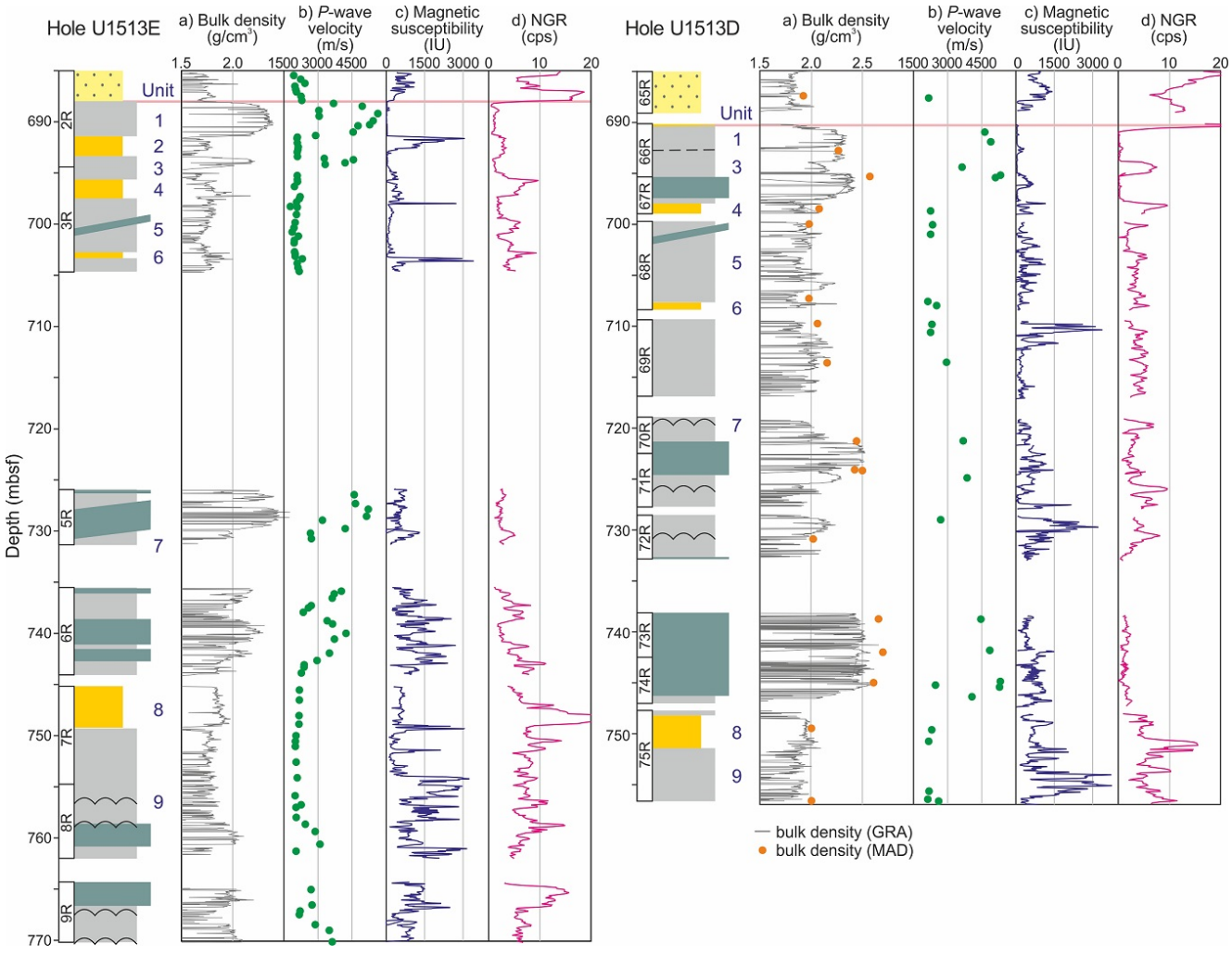
1. Faculty of Earth Systems and Environmental Sciences, Chonnam National University, Gwangju, Rep. Korea, 2. Institute for Marine Geodynamics (IMG), Japan Agency for Marine-Earth Science and Technology, Yokosuka, Kanagawa, Japan, 3. Korea Institute of Geoscience and Mineral resources, Daejeon, Rep. Korea, 4. Department of Geodynamics and Sedimentology, University of Vienna, Vienna, Austria

International Ocean Discovery Program (IODP) Expedition 369 recovered the volcanic rocks at Site U1513 on the eastern flank of the Naturaliste Plateau, offshore southwest Australia. The volcanic succession (Lithostratigraphic Unit VI) is defined as the syn-rift volcanic rocks emplaced during the Valanginian breakup between Greater India and Australia-Antarctica. Based on a total cored thickness of 82.2 m, it is subdivided into nine lithologic units: Units 1, 3, 5, 7 and 9 are classified as basaltic flows, and Units 2, 4, 6 and 8 as volcaniclastic flows. Dolerite dikes and hydrothermal veins intruded the whole volcanic succession. During the expedition, the excellent correlation between physical properties and the lithologic units in Hole U1513D was used as a guide to correlate the lithologic boundaries in Hole U1513E. We define that the variation in the petrophysical datasets correspond to the lithologic boundaries and mineralogical composition of/within the units in Holes U1513D and U1513E. We present the physical properties, lithologic descriptions as well as XRF data, acquired during and after the expedition, and demonstrate the good correspondence between lithologic/mineralogical and petrophysical characteristics. In both holes, the top of the volcanic succession is characterized by sharp increases in bulk density and *P*-wave velocity and a drop in Natural Gamma Ray (NGR) values. Within the succession, intervals of low bulk density, low *P*-wave velocity and high porosity, with coinciding spikes in NGR, define the volcaniclastic units, and correspond well to highly altered basalts. The increase of alteration degree in basaltic units contributes to a decrease in bulk density, *P*-wave velocity and an increase in porosity, NGR values. Comparatively high bulk density, high *P*-wave velocity and low porosity are associated with dikes. Magnetic susceptibility in the succession is high, and varies downhole with occasional sharp increases that are attributed to alteration by iron-bearing minerals and paramagnetic clay minerals. Our results show that systematic acquisition and assessment of physical properties in the volcanic succession can be used to discriminate lithologic boundaries, mineralogical composition, and alteration type and degree. Such correlation can be a useful tool for drilling and core description strategies in future ocean drilling expeditions.

Tejada, M.L.G., Lee, E.Y., Chun, S.S., Harry, D.L., Riquier, L., Wainman, C.C., 2020. Data report: petrology and volcanic stratigraphy at Site U1513, IODP Expedition 369. Proceedings of the International Ocean Discovery Program, 369. IODP, College Station, TX.

Keywords: petrophysics, volcanic stratigraphy, alteration, IODP Site U1513

©2020. Japan Geoscience Union. All Right Reserved.



©2020. Japan Geoscience Union. All Right Reserved.

Paleoenvironments of a Cretaceous marginal ocean basin - the Turonian to Santonian of the Australo-Antarctic Gulf, IODP Site U1512

*Erik Wolfgring [1], Michael Anthony Kaminski[2], Anna Waśkowska[3]

1. University of Vienna, Geodynamics and Sedimentology, Althanstrasse 9, 1090 Vienna, Austria, 2. King Fahd University of Petroleum and Minerals (KFUPM), Earth Sciences Department, Geosciences, Dhahran, SaudiArabia, 3. Faculty of Geology, Geophysics and Environmental Protection, AGH University of Science and Technology, Mickiewicza St. 50, Cracow, Poland

IODP Expedition 369 (Australia Cretaceous Climate and Tectonics) drilled an approximately 700 m thick Santonian to Turonian succession (nannofossil zones CC 17-CC 10) at Site U1512 in the Great Australian Bight (Fig. 1). Site U1512 was drilled aiming at understanding the paleoceanographic evolution of the Southern Australian realm during the final stages of the breakup of Eastern Gondwana and to help document the Late Cretaceous climate evolution in the Southern High Latitudes (SHL).

The formation of the Australo-Antarctic gulf is characterized by rapid subsidence from the Albian onwards. Restricted accommodation space and a marginal marine setting that is affected by the discharge of a vast continental river system to the North are factors that seriously influenced the paleoecologic setting recovered in the Great Australian Bight.

Material recovered at IODP Site U1512 presents an unique record of a deep water agglutinated foraminifera community from the Southern High Latitudes. The highly diverse assemblages yield many new taxa that are yet to be described.

Calcareous benthic foraminifera are generally rare or absent, as well as planktonic taxa. Calcareous benthic foraminifera are frequently recovered from the early to mid-Turonian as well as Santonian strata. Hole U1512A yields highly abundant radiolaria from the mid Turonian onwards - the share of radiolarian of the total microfossil assemblage often exceeds 50% in the younger strata of U1512. The stratigraphic framework is based on calcareous nannofossil biostratigraphy and assigns the succession to calcareous nannofossil zones CC16/17-CC10c.

Preliminary results show a diverse foraminiferal assemblage: 180 taxa were identified (126 agglutinated and 54 calcareous). The most common elements of the deep-water agglutinated foraminifera assemblage are tubular (i.e., *Kalamopsis grzybowski*, *Bathysiphon* spp, *Ammodiscus* spp…) and planispiral forms (i.e., *Haplophragmoides* spp., *Buzasina* sp., *Labrospira* spp…). The Turonian strata yield highly abundant *Bulbobacculites problematicus* and *Spiroplectammina navarroana*. The presence of *Uvigerinammina* provides a tie-point to the Tethyan deep-water agglutinated foraminifera biozonation of Geroch & Nowak (1984).

The total abundance of tubular agglutinated taxa that show an epifaunal habitat preference in relation to the entire assemblage peaks just before we record an increase in the abundance of radiolaria in the mid Turonian. Generally, the abundance of tubular agglutinated foraminifera and radiolaria correlates negatively through Hole U1512A.

The assessment of foraminiferal assemblages together with the evolution of other fossil groups (Radiolaria in particular) indicates unstable conditions at Site U1512 during the early Turonian-Santonian.

©2020. Japan Geoscience Union. All Right Reserved.

Preliminary results from the quantitative analysis of the benthic foraminiferal assemblages could indicate either changes in paleobathymetry or instable patterns in ocean circulation creating a restricted paleoenvironmental regime during Late Cretaceous times. The prominent increase in the abundance of radiolaria during the mid-Turonian coincides with a previous peak in the abundance of tubular epifaunal foraminifera. This could either indicate an increase in bathymetry (and associated changes in ocean chemistry) that would roughly correspond to the Turonian sea level highstand. As high latitudes reflect climatic change more directly, changes in the microfossil assemblage could furthermore reflect a subtle recovery of the mid Turonian SHL temperature regime after the Cretaceous thermal maximum.

Keywords: Cretaceous , Australia, Antarcrica

©2020. Japan Geoscience Union. All Right Reserved.

The facies architecture of felsic subaqueous volcanoes in “Green Tuff” Formation in the Katakai field, Niigata, Japan

*Miyuki Nonaka[1,2], Masahiko Yagi[1], Yasuo Yamada[1], Susumu Umino[3]

1. Japan Petroleum Exploration Co.,Ltd., 2. Graduate School of Natural Science & Technology, Kanazawa University, 3. Department of Earth Sciences, Kanazawa University

Interpretation of the mechanism of subaqueous volcanic activity related to “Green Tuff” is important since it greatly contributes to clarifying the formation process of the island arc and active subaqueous volcanoes all over the world. Also, “Green Tuff” is necessary from the viewpoint of energy resources because it is bearing and producing a large amount of gas especially in the Northeast part of Japan. In this study, we constructed a facies model of the subaqueous basin in which a variety of volcanic facies are intercalated with sedimentary facies to clarify a series of volcanic activity styles in the unrevealed “Green Tuff” field located in the Niigata Chuetsu district.

The Katakai field is located 10km southwest of Nagaoka-city and consists of an anticline 5km long and 1.5km wide extending in the NNE - SSW direction. “Green Tuff” was produced by subaqueous volcanic activity during back-arc rifting in early to middle Miocene. After the activity, Nanatani and Teradomari Mudstone as source rock overly the “Green Tuff” formation in late Miocene. Finally, the compressive tectonic movement created the current anticline in the field. The top of “Green Tuff” Formation is deeper than 4,000m, its thickness is more than 1,000m and its lower limit is unidentified.

We observed cuttings and core samples from more than a dozen wells in the field analyzed major elements in the cutting samples and trace elements of the core samples with the information of electricity well logging and FMI image data.

The Formation is the succession of volcanic materials which consist mainly of felsic rocks (from rhyolite to dacite) and accompanied with mafic rocks (from basalt to basaltic andesite). The stratigraphic classification characterized by rock types, textures, occurrences, and distribution is below:

The lower part of the formation at least several tens meters thick is distributed only in the south of the field. It is dominated by pumice clasts and glassy rhyolite lava. They are considered as carapace pumice breccia which surrounds lava dome. The middle part several hundred meters thick is distributed over the whole area in the field. It has a wide variety of rhyolite, including massive lava, breccia, tuff breccia, tuff, and perlite. They are considered as the complexes of lava domes which consist of coherent lava facies, block lava facies and resediment facies one to several hundred meters thick and several hundred to one thousand meters wide. The complex in the north of the field is dominated by glassy rhyolite lava with flow band and breccia. The upper part about several hundred meters thick is distributed over the whole area of the field. It consists of dacite pumice, tuff breccia, and tuff. The uppermost part is distributed from the central area to the south area of the field and consists of massive lava, breccia, and tuff breccia.
From the bottom to upper part, massive basalt lavas several tens to a hundred meters thick bearing intersertal textures are observed. They are considered to the succession of sheet flows during the bimodal volcanic activity.

From their distribution, the transition of the eruption style throughout the subaqueous volcanic activity is

©2020. Japan Geoscience Union. All Right Reserved.

indicated. The formation was composed of the successions of felsic the lava domes and mafic sheet flows by the bimodal volcanic activity. In the early stage, the lava domes associated with carapace pumice breccia formed under the deep marine environment. As the increment of the supply rate of magma, large-scale volcanic complexes were created from south to central part of the field. On the other hand, the north of the field had the source of lava which formed the complex(es) of relatively glassy lava domes. In the late stage, after the dacite pyroclastic material was provided over the whole area under the shallow marine environment, the magma changed its composition to rhyolite and provided a volcanic complex.

Keywords: Green Tuff, back-arc rifting, Miocene, volcanic facies, lava dome

©2020. Japan Geoscience Union. All Right Reserved.

[E] Poster | M (Multidisciplinary and Interdisciplinary)：M-IS Intersection

[M-IS17] Astrobiology

convener:Hikaru Yabuta(Hiroshima University, Department of Earth and Planetary Systems Science), Seiji Sugita(Department of Earth and Planetary Science, Graduate School of Science Sciece, The University of Tokyo), Misato Fukagawa(National Astronomical Observatory of Japan), Fujishima Kosuke(Tokyo Institute of Technology, Earth-Life Science Institute)

Twenty years have passed since when the field of Astrobiology, which aims to unveil the origins, evolution, and habitability of life by integrating multidisciplinary fields, was established. Individual themes related to Astrobiology, such as chemical evolution in the early Solar System, formation of planetary system, prebiotic chemistry in the early Earth, evolution of life in the Earth's history, extremophile, and habitable planetary environments, has been studied by the knowledge and methods from the multiple fields, which has enabled us to explain "Where we came from" in some ways. However, despite an overwhelming number of investigations and discussions through gathering of the scientists from different fields, there has remained the long-standing unsolved question: How did abiotic materials gain biological function in the Earth and elsewhere in universe? There is still a large gap between prebiotic organic chemistry and biochemistry toward Origins of Life and planetary habitability. Therefore, the JpGU Astrobiology session focuses on pathfinding of "integration of astronomy, geoscience, and biochemistry", which will face an increasing need for the future Astrobiology. In order to enhance our understanding of "What is life", we propose to discuss the biochemical events linked with planetary systems, which is beyond the knowledge in a test tube, by an integration of exoplanets and molecular biology, etc. Through this approach, we will lead the discussions and developments of life-detection strategies for the future exploration of life in universe.

[MIS17-P01] Stability of Amino Acids and Amino Acid Precursors in Space: Approaches Through Space Experiments (Tanpopo and Tanpopo 2) and Ground Simulation Experiments

*Kensei Kobayashi[1], Tomohito Sato[1], Takuya Yokoo[1], Itsuki Sakon[2], Kazumichi Nakagawa[3], Hajime Yano[4], Miki Nakayama[5], Hajime Mita[5], Hirofumi Hashimoto[4], Shin-ichi Yokobori[6], Akihiko Yamagishi[4,6], Satoshi Yoshida[7], Isao Yoda[8], Hitoshi Fukuda[8], Yoshiyuki Oguri[8], Kazuhiro Kanda[9], Hiromi Shibata[3], Jun-ichi Takahashi[1], Yoko Kebukawa[1] (1.Yokohama National Univ., 2.Univ. Tokyo, 3.Osaka Univ., 4.JAXA/ISAS, 5.Fukuoka Inst. Tech., 6.Tokyo Univ. Pharm. Life Sci., 7.QST, 8.Tokyo Inst. Tech., 9.Univ. Hyogo)

[MIS17-P02] Radiation transfer simulation of circular polarization at the NIR/UV wavelengths

*Hajime Fukushima[1], Hidenobu Yajima[1], Masayuki Umemura[1] (1.Center for Computer Sciences, University of Tsukuba)

[MIS17-P03] Analysis of nucleic acid bases formed from simulated interstellar media

*Kotomi Sugaya[1], Kensei Kobayashi[1], Yoko Kebukawa[1], Yoshiyuki Oguri[2], Hitoshi Fukuda[2] (1.Yokohama National University, 2.Tokyo Institute of Technology)

[MIS17-P04] Astronomical detections of prebiotic molecules with the next generation Very Large Array

*Misato Fukagawa[1], Daisuke Iono[1], Munetake Momose[2] (1.National Astronomical Observatory of Japan, 2.Ibaraki University)

[MIS17-P05] Evaluation of the aldononitrile acetate ester derivatization method for aldose analysis in products from chemical evolution experiments

*Shunpei Abe[1], Yoko Kebukawa[1], Kensei Kobayashi[1] (1.Yokohama National University)

[MIS17-P06] **Polycyclic aromatic hydrocarbons in Jbilet Winselwan carbonaceous CM chondrite: Novel molecular proxies for thermal metamorphism of asteroids**

Hiroki Kato[1], *Hikaru Yabuta[1] (1.Hiroshima University, Department of Earth and Planetary Systems Science)

[MIS17-P07] Relationship between visible reflectance at 550 nm and carbon contents in carbonaceous chondrites: At-tempt to estimate the bulk carbon contents of asteroid Ryugu's surface

*Hikaru Yabuta[1] (1.Hiroshima University, Department of Earth and Planetary Systems Science)

[MIS17-P08] Minerals and their catalytic effects on amino acid formations in environments simulating asteroids

*Walaa Elmasry[1], Yoko Kebukawa[1], Kensei Kobayashi[1] (1.Yokohama national university, graduate school of Engineering Science)

[MIS17-P09] The Surviving Rate of Organic Materials after the Cometary Impacts

*Taiki Suzuki[1,2], Takashi Shibata[2], Natsuki Hosono[3] (1.Astrobiology Center, 2.National Astronomical Observatory of Japan, 3.Japan Agency for Marine-Earth Science and Technology)

[MIS17-P10] **Supercritical fluids in the search for origins-of-life in Earth and beyond**

*CANER AKIL[1], Kosuke Fujishima[1] (1.Earth-Life Science Institute)

[MIS17-P11] Estimation of the fraction of life-bearing planets that evolve intelligence f_i in the Drake equation by the terrestrial extinction history

*KOHJI TSUMURA[1] (1.Department of Natural Science, Faculty of Science and Engineering, Tokyo City University)

[MIS17-P12] The safety assessments of reaction vessels used for the space exposure experiments in order to synthesize nucleotide by UV irradiation

*Madoka Shiromizu[1], Kazumichi Nakagawa[2], Yoshitaka Bessho[3], Hajime Mita[1] (1.Fukuoka Institute of Technology, 2.Osaka University, 3.Academia Sinica, Institute of Biological Chemistry)

Stability of Amino Acids and Amino Acid Precursors in Space: Approaches Through Space Experiments (Tanpopo and Tanpopo 2) and Ground Simulation Experiments

*Kensei Kobayashi[1], Tomohito Sato[1], Takuya Yokoo[1], Itsuki Sakon[2], Kazumichi Nakagawa[3], Hajime Yano[4], Miki Nakayama[5], Hajime Mita[5], Hirofumi Hashimoto[4], Shin-ichi Yokobori[6], Akihiko Yamagishi[4,6], Satoshi Yoshida[7], Isao Yoda[8], Hitoshi Fukuda[8], Yoshiyuki Oguri[8], Kazuhiro Kanda[9], Hiromi Shibata[3], Jun-ichi Takahashi[1], Yoko Kebukawa[1]

1. Yokohama National Univ., 2. Univ. Tokyo, 3. Osaka Univ., 4. JAXA/ISAS, 5. Fukuoka Inst. Tech., 6. Tokyo Univ. Pharm. Life Sci., 7. QST, 8. Tokyo Inst. Tech., 9. Univ. Hyogo

Amino acids have been detected in water extracts of carbonaceous chondrites (CCs) [1], which suggests that extraterrestrial organics could be sources for the first life on the Earth. The fact that amino acids extracted from CCs increased after acid-hydrolysis [1] showed that not only free amino acids but also amino acid *precursors* were present in them. Experiments simulating interstellar environments showed that amino acid *precursors*, rather than free amino acids, were formed [2]. Though extraterrestrial *amino acid precursors* have not been well-identified, aminonitriles and hydantoins could be candidates. Beside such *simple* amino acid precursors, *complex* amino acid precursors were found in the product after proton irradiation of interstellar media analogue [3]. If extraterrestrial amino acids were delivered to the primitive Earth, they should survived in space environments against various types of energetic particles and photons. We investigated the stability of amino acids and their precursors against heavy ions, gamma-rays, UV, soft X-rays, etc. In addition to these laboratory simulations, we exposed amino acids and their precursors in the Exposed Facility of Kibo, ISS in the Tanpopo mission (2015-2019) [4] and the Tanpopo 2 mission (2019-2020).

Ground Experiments: Samples used were glycine (Gly), aminoacetonitrile (AAN), hydantoin (Hyd) and CAW (products of proton irradiation of a mixture of CO, NH_3 and H_2O [3]). *Heavy ions irradiation*: Aqueous solution of each molecule, frozen in liquid nitrogen, was irradiated with 290 MeV/u carbon ions from HIMAC (NIRS, Japan). *γ -Rays irradiation*: Aqueous solution of each target molecule was irradiated with γ -rays (5-15 kGy) from a ^{60}Co source (Tokyo Tech, Japan). *UV irradiation*: Each sample was UV irradiated from a xenon (Ushio), a deuterium (Hamamatsu Photonics) or an eximer lamp (Ushio) after dried in pits of an aluminum plate. *Soft X-rays irradiation*: Each sample was on the Al plate was irradiated with soft X-rays from a BL-6 of NewSUBARU. *Hydrothermal reaction*: Aquous solution of each sample was heated at 150℃ for 6-24 hours in an ETTAS Hightemp oven. Amino acid analysis: all the target materials were acid-hydrolyzed (6 M HCl, 110℃, 24 h), and were determined with an amino acid analyzer (Shimadzu UHPLC NEXERA).

The Tanpopo Mission: Alminum exposure panels with small pits were used. Gly, Hyd and CAW were put in the pits and covered with hexatriacontane (HTC). Five plates were prepaired: (i) The space-exposed with a MgF_2 window, (ii) the space-exposed with a SiO_2window, (iii) the dark control that was space-exposed behind other panels, (iv) the cabin control, stored in the ISS cabin and (v) stored in a ground laboratory (the ground control). Three sets of the plates were launched in 2015, and each set of the plates returned to the Earth in 2016, 2017 or 2018.

The Tanpopo 2 Mission: Gly, Hyd and CAW with different thickness of HTC were prepaird by using the

©2020. Japan Geoscience Union. All Right Reserved.

same kind of aluminum plate. Besides them, Gly and CA (products of proton irradiation of a mixture of CO and NH_3) were directly evaporated onto silicon plates. The silicon plates with and without windows were prepared. Space exposure of the aluminum and the silicone plates with the target organics started in August 2019, and will returned to the Earth in 2020.

RESULTS AND DISCUSSION Recovery was discussed by glycine amount since glycine was major compound after acid-hydrolysis of the products (with the exception of Ival and EMHyd). Among Gly, Hyd, AAN and CAW, Gly showed the lowest recovery against gamma-rays, and AAN showed the lowest recovery in hydrothemal reaction, while Hyd showed the lowest recovery after space exposure of the Tanpopo Mission. In the case of UV irradiation, relative stability differed by the kinds of light sources: Gly was more stable than CAW in the Xe-lamp experiment, but CAW showed higher recovery than Gly in the D_2-lamp experiment and the soft X-ray experiment. Thus space experiments are importance to test stability in actual space environment. Overall, space UV would be fatal to all the organics tested, so that they should be protected by shielding with minerals or other materials to survive in space for a long period. CAW, complex precursor of amino acids, showed to be more stable against charged particles, soft X-rays, VUV and heat than free amino acids and simple precursors. The Tanpopo 2 would give further information on stability of organics in space.

[1] K. Kvenvolden et al., Nature, **228**, 923-926 (1970).

[2] T. Kasamatsu et al., *Bull. Chem. Soc. Jpn.*, **70**, 1021 (1996).

[3] Y. Takano *et al.*, *Appl. Phys. Lett.*, **84**, 1410-1412 (2004).

[4] A. Yamagishi *et al.*, *ISTS Web Paper Archive*, **2013-k-49**, 1-7 (2013).

Keywords: Amino acids, Amino acid precursors, Space experiments, Origins of life, Ultraviolet light, Cosmic dusts

©2020. Japan Geoscience Union. All Right Reserved.

Radiation transfer simulation of circular polarization at the NIR/UV wavelengths

*Hajime Fukushima[1], Hidenobu Yajima[1], Masayuki Umemura[1]

1. Center for Computer Sciences, University of Tsukuba

Circular polarization (CP) at the ultraviolet (UV) wavelength induces the enantiomeric excesses. It is suggested that they initially cause the biomolecular chirality of amino acids. The excesses of L-acids are also discovered in meteorites, and it is proposed that the CP light in the interstellar medium is related to biologically homochirality. In the star-forming regions, the high degree of CP (>20%) at the near-infrared (NIR) wavelength induced by aligned dust grains is observed, but it is not known that it exists at the UV wavelength. In this study, we develop the radiative transfer code with the Monte Carlo technic, which follows a change of Stokes parameters in scattering/absorption processes by dust grains. We find that the high degree of the CP at the NIR wavelength is realized when the micron-size dust grains exist in the interstellar medium, and the CP degree of the UV light reaches 20% with sub-micron sized dust grains. We will discuss the relations of the CP degree between the NIR and UV wavelength.

Keywords: circular polarization, non-spherical dust grains, star-forming regions

©2020. Japan Geoscience Union. All Right Reserved.

Analysis of nucleic acid bases formed from simulated interstellar media

*Kotomi Sugaya[1], Kensei Kobayashi[1], Yoko Kebukawa[1], Yoshiyuki Oguri[2], Hitoshi Fukuda[2]

1. Yokohama National University, 2. Tokyo Institute of Technology

1. Introduction
In the course of chemical evolution, it is necessary to supply nucleic acid bases which are major constituents of DNA and RNA. Since nucleic acid bases are detected in the meteorite, it is considered to be generated in space environments such as in molecular clouds.
In this study, first, we considered analytical methods for nucleic acid bases in mixtures with complicated compositions. Second, in order to verify the generation of nucleic acid bases in interstellar media, proton beam simulating cosmic ray was irradiated to the interstellar media analogs, and we investigated possible generation of nucleic acid bases and related compounds. From these experiments, we considered the possibility that nucleic acid bases essential for the generation of life could be supplied from out of the Earth.
2. Experimental
(1)Nucleic acid bases analysis
Twelve nucleic acid bases standard reagents [adenine (Ade), guanine(Gua), cytosine(Cyt), uracil (Ura), thymine(Thy), pirimidine(Pyr), hypoxanthine(Hyp), xanthine(Xan), purine(Pu), barbituric acid(BA), isoguanine(Iso-Gua), isocytsine(Iso-Cyt)] were first fractionated by gel filtration chromatography (GFC) and then each fraction was analyzed by reversed-phase HPLC (RP-HPLC), where a novel core-shell column (SunShell RP-AQUA) was used.
(2)Proton irradiation experiment
As a simulated interstellar media, a mixed gas of CO and NH_3 (350 Torr each) and 5 mL of ultrapure water were enclosed in a Pyrex glass tube, and 2 mC of 2.5 MeV proton beam was irradiated to the gas mixture by using Tandem accelerator at Tokyo Institute of Technology. The resulting product is hereafter referred to as “CAW.”
Irradiated products were injected into GFC and sorted in three compartments of retention time 15-30min (CAW1), 30-45min (CAW2), 45-60min (CAW3).
Each fractionated CAW was injected to RP-HPLC, and the nucleic acid bases were identified. For the comparison, the products were analyzed directly by RP-HPLC without fractionation by GFC.
3. Results and Discussion
(1)Nucleic acid bases analysis
In RP-HPLC, comparing the standards separation with the SunShell RP-AQUA column with a previously-used Capcell Pak C18 column, it was found that separation with SunShell RP-AQUA superior separation for each base to conventional reversed-phase columns. Therefore, in the separation / analysis of nucleic acid bases by using RP-HPLC, it was found that more accurate analysis can be performed by using SunShell RP-AQUA column.
(2)Proton irradiation experiment
BA, Cyt, Ade were detected from CAW1, Iso-Cyt was detected from CAW2, and Gua was detected from CAW3. Since Ura and Cyt were predominant in past experiments, it was suggested that Cyt and Ura are easily generated from interstellar media. In addition, BA that are considered as a candidate for non-canonical proto-RNA system, was clearly detected. It was suggested that BA is a molecule that is likely to be produced in the interstellar environment.
Compared with the RP-HPLC chromatograms of without pre-fractionation with GFC, RP-HPLC

©2020. Japan Geoscience Union. All Right Reserved.

chromatograms after fractionated with GFC looked better since huge peak of polymer-like products appeared at 1-4 min are removed, and it facilitated the identification of nucleic acid bases whose retention time was 1-4 min. In addition, it was found that nucleic acid bases with less yields could be more clearly detected. It was found that pre-fractionation of the nucleic acid bases by GFC made it possible to loaded less amount of samples on the column of RP-HPLC and the analysis of nucleic acid bases could be performed more accurately.

4. Conclusions

In this experiment, it was found that the separation using the SunShell RP-AQUA column is useful for analysis of nucleic acid bases in RP-HPLC, compared with conventional Capcell Pak C18 column. In addition, it was found that in complex mixtures, nucleic acid bases can be more accurately by pre-fractionation with GFC in the separation of nucleic acid bases.

In proton beam irradiation experiments, Ade, Gua, Cyt, Ura, which are components of RNA, were generated from simulated interstellar media, together with non-canonical bases such as Iso-Cyt and BA, which are considered to be components of proto-RNA.

From these facts, it was suggested that various nucleic acid bases and analogs whose structures were similar to them could be generated in interstellar environments.

©2020. Japan Geoscience Union. All Right Reserved.

Astronomical detections of prebiotic molecules with the next generation Very Large Array

*Misato Fukagawa[1], Daisuke Iono[1], Munetake Momose[2]

1. National Astronomical Observatory of Japan, 2. Ibaraki University

The next generation Very Large Array (ngVLA) is the ground-based cm/mm-wave radio telescope, and one of the future astronomy projects led by US for the next decade. The dedicated study group for ngVLA has recently been launched in the National Astronomical Observatory of Japan to seek for the eventual Japanese participation in this project. The telescope will be composed of 214 18-m antennas with the baselines up to 9000 km (extending from Hawaii to the US Virgin Islands), providing the unprecedented sensitivity and angular resolution. The ngVLA will cover the cm/mm-wave range, which will become a great advantage to detect complex prebiotic molecules that are free from line blending. In fact, one of the key science goals of ngVLA is "Probing the Initial Conditions for Planetary Systems and Life with Astrochemistry". The simulations on biogenic molecules such as Glycine and Glyceraldehyde (McGuire et al. 2018) show that the lines from those molecules are below the detectability of the existing telescopes but will be discovered with ngVLA, enabling transformational science on the chemical building blocks of life.

©2020. Japan Geoscience Union. All Right Reserved.

Evaluation of the aldononitrile acetate ester derivatization method for aldose analysis in products from chemical evolution experiments

*Shunpei Abe[1], Yoko Kebukawa[1], Kensei Kobayashi[1]

1. Yokohama National University

Introduction

Sugars and sugar derivatives play important roles in biological processes on the Earth. Sugars such as ribose, a component of RNA, are essential compounds for the origin of life. Since some sugars have been found in meteorites [1, 2], there is a possibility that some sugars made in space brought to the early Earth by meteorites. As a prebiotic sugar formation reaction, “formose reaction” have been attacked attention [3].

Since there are so many kinds of sugars and sugar derivatives, GC/MS is a promising technique to identify them, but a suitable derivatization technique is required for it. One of the derivatization methods for sugars is aldononitrile acetate ester derivatization. This method is very effective for aldoses [4]. However, previous studies have mainly focused on pentoses [2], and other sugars have not been widely discussed. In this research, we verified the usefulness of the aldononitrile acetate ester derivatization for aldoses other than pentose. In addition, verification of whether sugars were formed or not in products by “formose-like reaction” simulating the interior of meteorite parent bodies.

Experimental

Standard reagents of aldose (C3-C6: glyceraldehyde, erythrose, threose, ribose, lyxose, arabinose, xylose, allose, glucose, galactose) were derivatized by aldononitrile acetate ester derivatization. Then resulting sugar derivatives were analyzed by GC/MS. Limits of detection of all the aldoses were examined.

In order to simulate reactions in the meteorite parent bodies, a mixture of H2O, HCHO and NH3 (molar ratios were 100:5:5, 100:5:1, 100:5:0 and 100:10:0) were prepaird. 200 mL each of the mixture was heated at 150℃ for 3 days. An aliquot of each product was derivatized by the present method, and analyzed by GC/MS.

Result and Discussion

Retention time and major m/z of each aldose were obtained with authentic standards: The retention time (major m/z’s) were as follows. Triose: 9.7 min (m/z 86, 103), tetroses: 17.7-18.0 min (m/z 103, 145), pentoses: 24.8-26.0 min (m/z 103, 115, 145), and hexoses : 31.0-33.0 min (m/z 103, 115, 145).There is a correlation between the carbon number and the retention time. The carbon number increases by 1, then the retention time increases by about 7 minutes.

Although varied by the number of carbon, limits of detection of the aldoses were about 2~50 mM.

By comparing the analysis results of aldose standard reagents and the products of the “formose-like reaction” simulating the interior of meteorite parent bodies, peaks similar to those of tetroses and hexoses were detected in all the products. In the 100:5:1 product, pentoses were tentatively detected in addition to tetroses and hexoses. It was suggested that, in the products of 100:5:5, 100:5:0 and 100:10:0, glyceraldehyde (C3) generated in the initial stage of formose-like reaction reacted with unreacted formaldehyde (C1) to form tetroses (C4), or reacted with other glyceraldehyde to form hexoses (C6). The other possibility is that the glycolaldehyde (C2) generated in the initial stage of formose-like reaction reacts with other glycolaldehyde to form tetroses, and this tetroses reacts with glycolaldehyde to form hexoses. In the sample of 100:5:1, slightly added ammonia might act as a catalyst, which promoted

©2020. Japan Geoscience Union. All Right Reserved.

the formation of pentoses. Further experiments are required to verify such hypotheses.

References

[1] G. Cooper et al. (2001) *Nature*, 414, 879-883.
[2] Y. Furukawa et al. (2019) *PNAS*, 116, 24440-24445.
[3] H. J. Cleaves II (2008) *Precambrian Res.*, 164,111-118.
[4] K. Kobayashi et al. (1989) Bunseki Kagaku, 38, 608-612.

Keywords: sugar

©2020. Japan Geoscience Union. All Right Reserved.

Polycyclic aromatic hydrocarbons in Jbilet Winselwan carbonaceous CM chondrite: Novel molecular proxies for thermal metamorphism of asteroids

Hiroki Kato[1], *Hikaru Yabuta[1]

1. Hiroshima University, Department of Earth and Planetary Systems Science

Introduction: On June 27, 2018, Hayabusa2 spacecraft arrived at the C-type asteroid Ryugu (Watanabe et al. 2019). The surface of Ryugu is thought to have experienced thermal metamorphism, according to the remote sensing observations (Kitazato et al. 2019). Therefore, it is important to investigate the chemical compositions of thermally metamorphosed CM chondrites for understanding the surface process of asteroid Ryugu. Although the extents of thermal metamorphism of CM chondrites have been evaluated by elemental and molecular compositions of insoluble organic matter (IOM) (Naraoka et al. 2004; Yabuta et al. 2005), molecular-level evolution of IOM is still unknown. Soluble organic molecules from the thermally metamorphosed CM chondrites have not been quantified (Shimoyama et al. 1989). Therefore, in this study, we analyzed polycyclic aromatic hydrocarbons (PAHs) in Jbilet Winselwan CM chondrite, which is a thermally metamorphosed CM chondrite and show similar reflectance spectrum to that of asteroid Ryugu (Sugita et al. 2019), for precise evaluation of parent body thermal metamorphism. The relative abundances of the hydrocarbons were compared with those of Murray CM chondrite and Allende CV3 chondrite.

Samples and Methods: Powdered samples of Jbilet Winselwan (CM2), Murray (CM2), and Allende (CV3) meteorites (0.2-0.4g) were extracted with dichloromethane/methanol (9:1) by sonication. The extracts were applied to a silica gel column. From the column, aliphatic hydrocarbons were eluated with hexane and then PAHs were eluated with dichloromethane. The hexane and dichloromethane eluates were concentrated to 100 μl individually under a nitrogen flow for analysis by a GC-MS. Identification and quantification of compounds were made by comparison of peak retention times on mass chromatograms and mass spectra, and peak areas, respectively, with those of standard compounds. For compounds without standard compounds, identification was made by comparison of mass spectra with library data.

Results and discussion: Total concentration of PAHs from Jbilet Winselwan meteorite (0.22 μg/g meteorite) was 350 times lower than those from Murray meteorite (74.0 μg/g meteorite). Di- and trimethylnaphthalenes, fluorene, phenanthrene, pyrene, fluoranthene, methylbiphenyl (0.002-0.036 μg/g meteorite) were identified from Jbilet Winselwan, while low molecular weight PAHs, such as naphthalene, methylnaphthalene, and acenaphthene, and cata-condensed PAHs, such as anthracene, benz[a]anthracene, chrysene, were not detected. Thus, highly volatile and/or structurally unstable PAHs in Jbilet Winselwan meteorite were preferentially lost during thermal metamorphism. On the other hand, biphenyl-type PAHs, such as biphenyl (BIP), methylbiphenyls (MBP), diphenylamine, benzophenone, fluorenone, dinenzofuran, oxibisbenzene, are relatively abundant in Jbilet Winselwan compared to those in Murray and Allende. In order to evaluate the thermal metamorphism on the parent body of Jbilet Winselwan meteorite, we have applied several organic geochemical molecular thermal indicators: (i) a

©2020. Japan Geoscience Union. All Right Reserved.

ratio of fluorene to 2-methylbiphenyl (FLU/2-MBP) and (ii) methylphenanthrene (MP) isomer ratio ([2-MP+3-MP]/[1-MP+4-MP+9-MP]). The ratio of FLU/2-MBP for Jbilet Winselwan was one order of magnitude higher than Murray, indicating that cyclisation reaction of 2-MBP to give FLU prpbably occured during thermal metamorphism of the Jbilet Winselwan parent body. Also the MP isomer ratio for Jbilet Winselwan was three times higher than Murray, indicating that methyl rearrangement of methylphenanthrene isomers probabaly occured during thermal metamorphism of the Jbilet Winselwan parent body. Applying the ratios to the kinetic parameters of these two reactions obtained by organic geochemical studies (Alexander et al. 1988; Sanpei et al. 2004), it was estimated that Jbilet Winselwan meteorite experienced 410 –428 degrees Celcius for one week, or 387-397 degrees Celcius for one month.

Keywords: Carbonaceous chondrites, PAHs, Thermal metamorphism

©2020. Japan Geoscience Union. All Right Reserved.

Relationship between visible reflectance at 550 nm and carbon contents in carbonaceous chondrites: At-tempt to estimate the bulk carbon contents of asteroid Ryugu’ s surface

*Hikaru Yabuta[1]

1. Hiroshima University, Department of Earth and Planetary Systems Science

Remote sensing observations of asteroid Ryugu by Hayabusa2 mission has revealed that Ryugu is one of the darkest bodies in the Solar System (Watanabe et al. 2019). It is of great interest to identify the darkening agent of Ryugu’ s surface. In the preliminary investigation, it was reported that there was a correlation between the reflectance at 550 nm of primitive carbonaceous chondrites and the insoluble organic matter (IOM) contents of the meteorites. Their result suggests that the bulk carbon contents of asteroid Ryugu are potentially estimated by the visible re-flecntance acquired by optical navigation camera (ONC) of Hayabusa2 spacecraft. On the other hand, it is challeng-ing to estimate IOM contents from meteorites, due to the mass loss during the purification process by acid treat-ment and/or due to its static electricity. In this regard, total carbon contents can be estimated more accurately rather than IOM contents. Therefore, in this study, the reflectance spectra and total carbon contents of the same meteorite samples were measured in this study for increasing the accuracy of correlation.
As the samples, three primitive carbonaceous CM/CI chondrites (Murchison, Murray, and Yamato 980115), five thermally metamorphosed CM/CI chondrites (Jbilet Winselwan, Yamato 982086, Yamato 793321, Belgica 7904, and Yamato 86720), and three carbonaceous chondrites (Murchison, LAP 04721, and Tagish Lake) experimentally heated at different temperatures (300, 400, 500, 600 and 900˚C) for 50 hrs, and a simulant of Phobos were used. Their grain sizes and/or porosity were made constant. Reflectance spectra of the meteorites were analyzed by VERTEX 70v, Bruker (Tohoku Univ.). Total carbon contents of the meteorites were analyzed by a CHN elemental analyzer (Flash EA1112) (Kochi Univ.).
For the primitive CM/CI chondrites and thermally metamorphosed CM/CI chondrites, roughly linear correla-tions were observed between total carbon contents and reflectance at 550 nm (R(550)) and 390 nm (R(390)). Thus, the meteorites with higher carbon contents show lower reflectance. However, some meteorites (Murchison, Murray, Y-982086, Jbilet Winselwan, Y-793321) with similar carbon contents showed variations in reflectance. This is probably due to the difference in chemical compositions between primitive CM/CI chondrites and thermally meta-morphosed CM/CI chondrites. The thermally metamorphosed CM/CI chondrites containing IOM with higher aro-maticity (Yabuta et al. 2005) show lower reflectance compared to the primitive CM/CI chondrites. Based on the relationship, asteroid Ryugu, whose mean R(550) is 0.019, may contain higher than 3% of carbon.
In the correlation plots between total carbon contents and R(550) and R(390) for the experimentally heated car-bonaceous chondrites, overall, meteorites with higher carbon contents show lower reflectance. However, individual meteorites showed different behaviors during heating. For instance, the reflectance values of Murchison were low-ered while the total carbon contents of Murchison did not change during heating up to 400˚C. During heating at 500 - 600˚C, the reflectance values of Murchison were raised again while the total carbon contents of Murchison decreased only slightly. At 900˚C, the total carbon contents of Murchison suddenly decreased with increasing reflec-tance. These variations in reflectance are related to not only total carbon contents but also chemical change of IOM with increasing temperature, such as aromatization, pyrolytic degradation, and gasification. LAP 04721 and Tagish Lake showed similar trends, but their variations in reflectance differed depending on their original carbon contents and compositions. Based on the relationship, R(550) of Ryugu is the most similar to those of the

©2020. Japan Geoscience Union. All Right Reserved.

heated Tagish Lake at 400-600˚C or heated Murchison at 400˚C. The result appears to be consistent with the conclusion obtained by the near infrared spectral pattern of the surface of Ryugu (Kitazato et al. 2019).

©2020. Japan Geoscience Union. All Right Reserved.

Minerals and their catalytic effects on amino acid formations in environments simulating asteroids

*Walaa Elmasry[1], Yoko Kebukawa[1], Kensei Kobayashi[1]

1. Yokohama national university, graduate school of Engineering Science

Extraterrestrial delivery of organic compounds including amino acids to the early Earth during the late heavy bombardment (3.8-4.5 billion years ago) may have been important for the origin of life. Recently, it is suggested that chondritic organic matter was produced through reactions of interstellar formaldehyde, followed by condensation, and carbonization probably during hydrothermal alteration on chondritic asteroids (Cody et al 2011). Furthermore, Kebukawa et al. (2013, 2015) illustrated that the presence of ammonia significantly enhances the yields of IOM from formaldehyde via formose reaction at 150 ˚C, producing amino acids. Meteorites serve as delivery systems for extraterrestrial phyllosilicate minerals to Earth. Phyllosilicates may act as absorbents and catalysts for the reactions of organic precursor molecules in the early solar system (Pearson et.al 2002). In the current research, we are studying formations of amino acid at 150 ˚C and reveal the expected role of minerals, namely, montmorillonite, olivine and serpentine for amino acid productions in water-bearing planetesimals.

We synthesized organic compounds using a mixture of water, formaldehyde and ammonia (H2O, H2CO, NH3) in a ratio of 100:7:1 with adding minerals (10 g/ L) by simulating primordial materials in comets and asteroids. Aqueous solutions were heated at 150 ˚C for 24, and 72 hours. The resulted products were divided into two parts, the first part analyzed using a FT/IR, and GFC, while the other one was acid hydrolyzed, desalted, and subjected to amino acid analysis using an HPLC.

In HPLC analysis, considerable amounts of various amino acids including glycine and alanine were detected. Moreover, presence of non-protein amino acids (β-Ala, γ-ABA) is considered as an evidence for extraterrestrial origin and against terrestrial contamination. Our preliminary results showed that the obtained amount of amino acids was elevated with the presence of minerals. FT/IR spectra of samples with minerals showed more spectral intensities than samples without minerals due to synthesis of more organic compounds. GFC showed that high molecular weight organic compounds were formed which may be characterized as amino acid precursors that maintain stable at high temperature and longer durations giving various kinds of amino acids after acid hydrolysis. These results suggested that various amino acids could be formed abiotically via a mixture of formaldehyde, ammonia, and water, as well as, the associated minerals act as catalysts to produce amino acid precursors during aqueous activities in the planetesimals.

References:
Cody, G. D. et al. PNAS 108, 19171–19176 (2011).
Kebukawa, Y., David Kilcoyne, A. L. & Cody, G. D. The Astrophysical Journal 771, 19 (2013).
Kebukawa, Y. & Cody, G. D. Icarus 248, 412–423 (2015).
Pearson, V. K. Meteoritics & Planetary Science 37, 1829–1833 (2002).

Keywords: Metrorite, Formaldehyde, Olivine, Serpentine

©2020. Japan Geoscience Union. All Right Reserved.

The Surviving Rate of Organic Materials after the Cometary Impacts

*Taiki Suzuki[1,2], Takashi Shibata[2], Natsuki Hosono[3]

1. Astrobiology Center, 2. National Astronomical Observatory of Japan, 3. Japan Agency for Marine-Earth Science and Technology

While it is widely accepted that the first life has emerged through the chemical evolution with simple organic materials on the early Earth, the origin of organic materials is still controversial. On the early Earth, a large amount of material is believed to have been delivered by comets/meteorites, providing the starting materials for the origin of life. Despite the importance, the large objects would not have been decelerated by the atmosphere and subjected to compression heating. The numerical studies discussed the possibility of molecular surviving during the cometary impact (e.g., Chyba et al. 1990; Blank et al. 1997; Pierazzo & Chyba 1999). These studies suggested that the extreme pressure and the obliqueness of the impact may increase the surviving rate of the organic molecules.

However, the previous numerical studies employed the simple method by reducing the dimension to 2D, or by assuming the relationship between the obliqueness and the temperature. In the poster, we present the latest result of the 3D simulation of oblique impacts utilizing DISPH (Density Independent Smoothed Particle Hydrodynamics) code. A supercomputer named XC50 and the Framework for Developing Particle Simulators (FDPS) enabled us to solve the three-dimensional impacts without any assumption for the obliqueness. The comet and the sea are composed of the 8200 and eight million particles, respectively. The cometary radius is fixed to be 1 km, and the dependency of the temperature on the obliqueness and the initial velocity are investigated. During the simulation, the physical parameters of all particles are traced through five seconds after the impacts. We name the particles with the peak temperature less than 1200 K as the low-temperature particles, where the organic materials may survive. As the results of our calculation, the percentage of the low-temperature particles is almost zero if the obliqueness is more than 70 degrees. Still, it increases along with the increase of the obliqueness.

In addition to the percentage of low-temperature particles for the different obliqueness, we consider the probability of impacts with different obliqueness to obtain the surviving rate for the organic materials. Then, we estimated the surviving rate of the organic materials to be 2 percent. If this is the case, comets could have provided organic materials more efficiently than the interstellar dust particles and other formation processes on the early Earth. Our result suggests that cometary impact may have been the primary source to provide organic materials to the early Earth.

Keywords: origin of life, comet, organic materials

©2020. Japan Geoscience Union. All Right Reserved.

Supercritical fluids in the search for origins-of-life in Earth and beyond

*CANER AKIL[1], Kosuke Fujishima[1]

1. Earth-Life Science Institute

The origins of life is unresolved. The path leading to a self-sustainable complexed chemical system is yet unknown, and at the core of this system exists a two-biopolymer (nucleic acids and proteins) system conserved in all life forms on Earth. This system is supported by an aqueous condition maintained by water. In this context, water has been considered as a sign for habitable environment on Earth and beyond where life can emerge. However, the abiotic synthesis of biopolymers is thermodynamically unfavorable in water. The paradox behind the water prone biopolymer and the water as a biosolvent bring into question whether alternative solvents existed on early Earth to drive chemical reactions leading to more complexed molecules including biopolymers.

In this study, we aim to investigate the effect of supercritical carbon dioxide ($scCO_2$) upon chemical reactions that are difficult to occur in aqueous conditions. $scCO_2$ has been known for its use in the industry as a ‘green’ solvent, however it has also found in deep-sea environments in modern ocean and more likely to be present in Hadean Earth which could have served as the key matrix to promote other different chemistry from aqueous chemical reactions. We will focus on two fundamental steps towards the formation of biopolymers 1) Non-enzymatic synthesis of nucleotides (from nucleobase, sugar and phosphate), 2) Condensation of nucleotides and amino acids towards abiotic synthesis of the two-biopolymer architecture.

Keywords: supercritical carbon dioxide, chemical evolution, astrobiology

©2020. Japan Geoscience Union. All Right Reserved.

Estimation of the fraction of life-bearing planets that evolve intelligence f_i in the Drake equation by the terrestrial extinction history

*KOHJI TSUMURA[1]

1. Department of Natural Science, Faculty of Science and Engineering, Tokyo City University

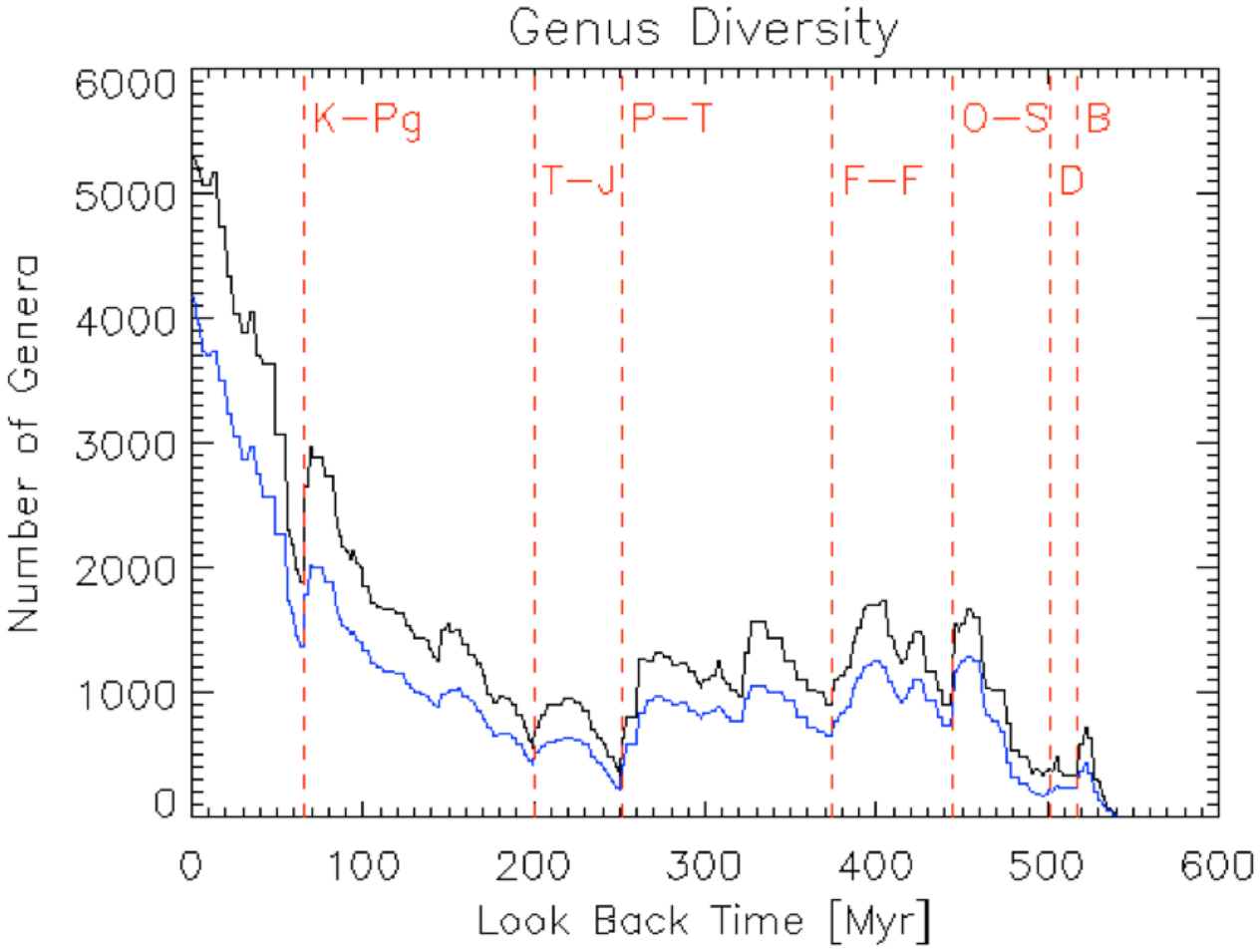
The Drake equation is a simple algebraic expression for quantifying the number of communicative civilizations in our Galaxy. Although some factors in the Drake equation can be reliably estimated by recent astronomical observations, remaining other factors are largely or entirely based on conjecture. One of such conjectural factors in the Drake equation is f_i, which is the fraction of planets with life on which an intelligent civilization emerges. The previous estimates of f_i range from pessimistic (f_i ~0) to optimistic (f_i ~1).

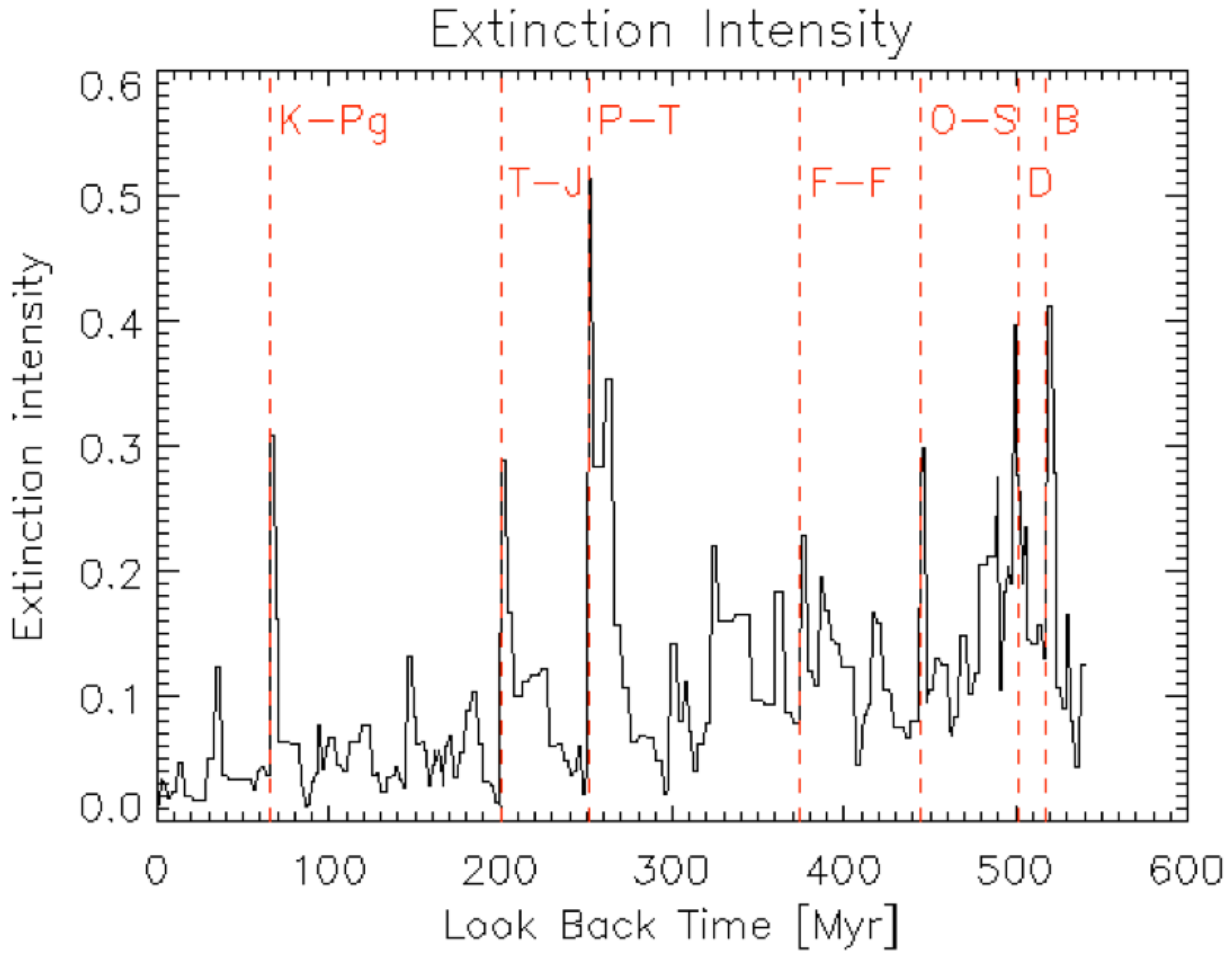
In this presentation, a new approach to estimate f_i is introduced based on the terrestrial extinction history, which is our only available data. Since its birth, life on the Earth has gone through any magnitudes of extinction due to various external factors such as the changes in the environment or the impacts of meteorites. In this study, f_i was calculated as a probability that we have continued to "win the lottery of extinction" since the birth of life, assuming that the intensity of extinction is determined by a probability density function, and also assuming that complex life essentially always becomes intelligent if it does not become extinct first like the terrestrial evolution history. The probability density function of extinction was deduced from the histogram of extinctions in the Phanerozoic eon of the Earth, covering from 540 Myr ago to present with 3 Myr resolution (Rohde & Muller 2005).

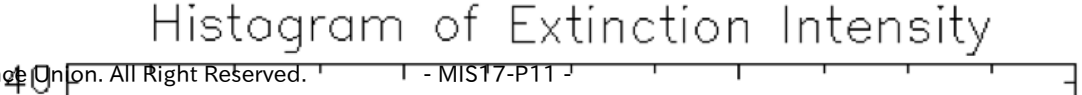
The histogram of the extinction intensity in the Phanerozoic eon was fitted by a log-normal function very well (reduced chi-squared of the fitting is ~1). The choice of the log-normal distribution function is supported by the statistical principle that a random multiplicative process converges to a log-normal distribution owing to the Central Limit Theorem. Because the terrestrial extinctions were basically caused by random events such as volcanic activities of the Earth or asteroid impacts, it can be justified that the terrestrial extinction intensity is expressed by the log-normal probability distribution as a result of the random multiplicative process. Assuming that the fitted log-normal function is a probability density function of the extinction intensity of terrestrial life, the survival probability for a unit time (3 Myr), p, is calculated as $p = 0.9985^{+0.0012}_{-0.0058}$. The factor f_i in the Drake equation can be expressed as $f_i = p^{T/\Delta T}$, where T is the evolution time of intelligent life and ΔT is the time resolution of the probability distribution function (ΔT = 3 Myr in this case). Recent geological evidences suggest that the first life on the Earth occurred 3.7-4.1 Gyr ago. Assuming that the obtained probability distribution function of extinction can be extended to this era, the evolution factor f_i can be calculated as $f_i = 0.13^{+0.52}_{-0.13}$ (99% confidence level) for 4.1 Gyr. This is the first data-based estimation of f_i. Because f_i is the two-parameter function of p and T, this method can be extended to the other life-bearing exoplanets by estimating these two parameters in some way, although this estimation is still based on the one-sample statistic of the Earth.

Keywords: Drake equation, SETI, mass extinction

©2020. Japan Geoscience Union. All Right Reserved.







©2020. Japan Geoscience Union. All Right Reserved.

©2020. Japan Geoscience Union. All Right Reserved.

The safety assessments of reaction vessels used for the space exposure experiments in order to synthesize nucleotide by UV irradiation

*Madoka Shiromizu[1], Kazumichi Nakagawa[2], Yoshitaka Bessho[3], Hajime Mita[1]

1. Fukuoka Institute of Technology, 2. Osaka University, 3. Academia Sinica, Institute of Biological Chemistry

1. Introduction

Nucleotides are constituents of DNA and RNA, the process of nucleotide synthesis in the primitive Earth is one of the most important processes in the origin of life.
In the previous studies, nucleobases and sugars have been found in the carbonaceous chondrites and the simulated primitive Earth experiments. Thereby, source materials of nucleotides would be existed in the primitive ocean. And, molecular oxygen and ozone didn’t exist in the atmosphere of the primitive Earth. This suggests that the short wavelength (≦280 nm) UV lights, which is interrupted at the surface of the present Earth, reached to the surface and worked as an important energy source for the chemical reactions at that time. Therefore, we proposed a hypothesis that nucleotides would be synthesized by the UV irradiation in the primitive ocean.
In order to verify this hypothesis, nucleotide synthesis experiments using the Japanese exposure facility on the International Space Station (ISS) as a similar UV environment to the primitive Earth are proposed in the part of the “TANPOPO 4” mission. “TANPOPO” is series name of the astrobiology experiments in Japan using the ISS. In the previous "TANPOPO" mission, films or powdered organic compounds were exposed to the space environment. But this nucleotide synthesis would be performed under aqueous solution. Then, new apparatus those are able to used in the space exposure experiment should be required. The exposure facility on the ISS is in environment of ultra-high vacuum and rapid temperature changes. The reaction vessel containing the aqueous solution should be sealed completely and the seal should withstand the drastic temperature changes in ultrahigh vacuum. Therefore, we developed vessels that can expose the aqueous solution to UV rays by improving the cells used in the TANPOPO experiments.
In this paper, nucleotide synthesis experiments by UV irradiation and the preliminary safety assessments of new developed reaction vessels those are based on the previous TANPOPO mission were performed.

2. Experimental method

Equimolar solution of nucleobases and ribose-5-phosphate (R5P) were mixed and irradiated with UV light (172 nm) for 4 days. This irradiation is equivalent to approximately one year of irradiation on the ISS orbit. After irradiation, irradiated solutions were analyzed by high-resolution LC/MS in order to confirm the synthesized nucleotides.
The reaction vessel was placed in ultra-high vacuum environment where the temperature changes drastically and left for several months. The changes in degree of vacuum and mass were observed, and it was tested whether the solution leaked from the reaction vessel.

3. Result

Five kind of nucleotides were synthesized by UV irradiation. Adenylic acid was the highest yield and thymidylic acid was not found after irradiation. Furthermore, it was found that the addition of Ni^{2+} ions increased the yield of adenylic acid. The conformational analysis of the synthesized nucleotide will be performed.

©2020. Japan Geoscience Union. All Right Reserved.

We improved the structure-assessed cells used in the TANPOPO experiments and construced the reaction vessels for UV exposure that can seal the aqueous solution (Figure). Since the surface temperature of the ISS changes from 30 to -40 ℃, the solution freezes and melts repeatedly. A little air was admitted into the reaction vessel to prevent the MgF_2 glass from breaking due to volume expansion when water was frozen. The sealing test under ultra high vacuum and repeatedly temperature change conditions showed that the reaction vessel did not break and did not leak solution. In addition, this reaction vessels withstood the maximum vibration at launch and landing on water in the random vibration test. In the future, we will investigate the strength change of the O-ring inside the reaction vessel by UV irradiation and temperature change.

Keywords: astrobiology, origin of life, nucleotide, UV irradiation



©2020. Japan Geoscience Union. All Right Reserved.

[E] Poster | M (Multidisciplinary and Interdisciplinary)：M-IS Intersection

[M-IS19] Conservation of geoparks, natural geosites, and cultural heritage: weathering and damage assessment

convener:Luigi Germinario(Saitama University), Celine Schneider(University of Reims-Champagne-Ardenne), Chiaki T. Oguchi(Institute for Environmental Science and Technology, Graduate School of Science and Engineering, Saitama University), Tetsuya Waragai(Graduate School of Science and Engineering, Nihon University), Miguel Gomez-Heras(Universidad Autonoma de Madrid), Patricia Vazquez(GEGENAA EA 3795 University of Reims Champagne-Ardenne), Magdalini Theodoridou(Cardiff University), Wonsuh Song(Waseda University)

Geoparks, geosites, World Heritage Sites, and historical structures represent an important natural and/or cultural heritage. They have been exposed to weathering in the geological and human time scale, so that the rocks and other geological materials they are made of, may often face severe deterioration. In order to preserve those sites, conservation measures should be considered. Several studies were carried out on this topic, involving a wide range of research fields: geomorphology, engineering geology, geoarchaeology, conservation science, geoconservation, materials science, petrophysics, geochemistry, geotechnical engineering, etc. However, our knowledge on many aspects is still limited. This session welcomes contributions presenting original research, discussions, as well as case studies, on documentation, measurement and monitoring techniques, experimental procedures, predictive models, damage assessment, etc. Papers from all the research fields dealing with the broad topic of geosites and cultural heritage are invited.

[MIS19-P01] Development of magnetic resonance surface scanners for the nondestructive in-situ measurement of water fractions in cultural heritages

*Yoshito Nakashima[1] (1.National Institute of Advanced Industrial Science and Technology)

[MIS19-P02] Effect of temperature and humidity changes on salt weathering: Verification by rock surface moisture content and color measurements

Masaki Oi[1], *Masato Sato[2], Tsuyoshi Hattanji[3] (1.Graduate School of Life and environmental Sciences, University of Tsukuba, 2.National Research Institute for Earth Science and Disaster Resilience, 3.Faculty of Life and Environmental Sciences, University of Tsukuba)

[MIS19-P03] Study on relationship between water content, NIR absorbance and colour values of various stones and cement mortars

*Chiaki T. Oguchi[1], Keni'chiro Tanaka[2] (1.Institute for Environmental Science and Technology, Graduate School of Science and Engineering, Saitama University, 2.Department of Engineering, Saitama University)

[MIS19-P04] Surface morphology representations at different scales for rock art characterisationSurface morphology representations at different scales for rock art characterisation

Mohammad Hafez Seada[1,3], *Miguel Gomez-Heras[1], Laura Lopez-Gonzalez[2], Ayman Hamed[3] (1.Universidad Autonoma de Madrid, 2.Art Fabrik, 3.Suez University)

[MIS19-P05] THERMOGRAPHIC ANALYSIS AS AN NON DESTRUCTIVE TECHNIQUE FOR AN EARLY DETECTION OF BIOCOLONISATION ON BUILDING STONE

*Stephanie Eyssautier Eyssautier[1], Kamel Mouhoubi Mouhoubi[2], Fany Reffuveille Reffuveille[3], jean-luc Bodnar Bodnar[2] (1.GEGENAA EA 3795 UFR Sciences Exactes et Naturelles – 2, Esplanade Roland Garros, France, University of Reims Champagne-Ardenne (URCA), 51100 cedex, Reims, France, 2.ITHEMM, UFR Sciences Exactes et Naturelles, BP 1039, Reims Cedex 02, 51687, France, University of Reims Champagne-Ardenne (URCA), Moulin de la Housse BP 1039, 51687 Reims, France, 3.BIOS EA 4691, U.F.R. Pharmacie, 51, rue Cognacq Jay, University of Reims Champagne-Ardenne (URCA), 51095 Reims Cedex, France)

[MIS19-P06] Effectiveness of waterproofing protection coating on salt weathering experiment using building stones

*Chiaki T. Oguchi[1], Akimune Sasaki[2] (1.Institute for Environmental Science and Technology, Graduate School of Science and Engineering, Saitama University, 2.Department of Engineering, Saitama University)

[MIS19-P07] Integration of durability parameters of cultural heritage building stones using by integrated geomatic methodologies

*Sebastien LARATTE[1], Céline THOMACHOT-SCHNEIDER[1], Gilles FRONTEAU[1], Alexandra GUILLANEUF [1], Patricia VAZQUEZ[1] (1.University of Reims-Champagne-Ardenne)

Development of magnetic resonance surface scanners for the nondestructive in-situ measurement of water fractions in cultural heritages

*Yoshito Nakashima[1]

1. National Institute of Advanced Industrial Science and Technology

Nondestructive measurement techniques are essential for the maintenance and investigation of cultural heritages. Water is often responsible for the degradation of the outdoor cultural heritages, such as walls and pavements made of stones, plasters, clays, and bricks. Portable scanners that allow the nondestructive quantification of water contents are needed for the in-situ investigation of porous wet walls and pavements. I am developing such scanners to measure the water volume fraction of outdoor cultural heritages. The principle of the scanners is based on the low-field time-domain proton magnetic resonance (i.e. NMR) relaxometry employing a single-sided magnetic circuit [1]. Water protons in a static magnetic field produced by the single-sided permanent magnets are excited by the radio-frequency coil, and the resultant proton transverse relaxation signals are acquired as raw data, which can be translated into water volume fractions, and pore-size distributions and permeabilities of the wet porous media. The investigation depth (distance from the coil to the sensed region) is several to several tens of millimeters, depending on the magnet size. A surface scanner with an investigation depth of 30mm constructed for a different purpose [2] was as heavy as 50 kg, which is not a hand-held type. Thus I am constructing a new scanner employing a smaller magnet (4 kg in weight) as shown in the figure, which allows hand-held use and increase the operationability. The current status and future perspective of the new scanner being developed would be presented.

Reference

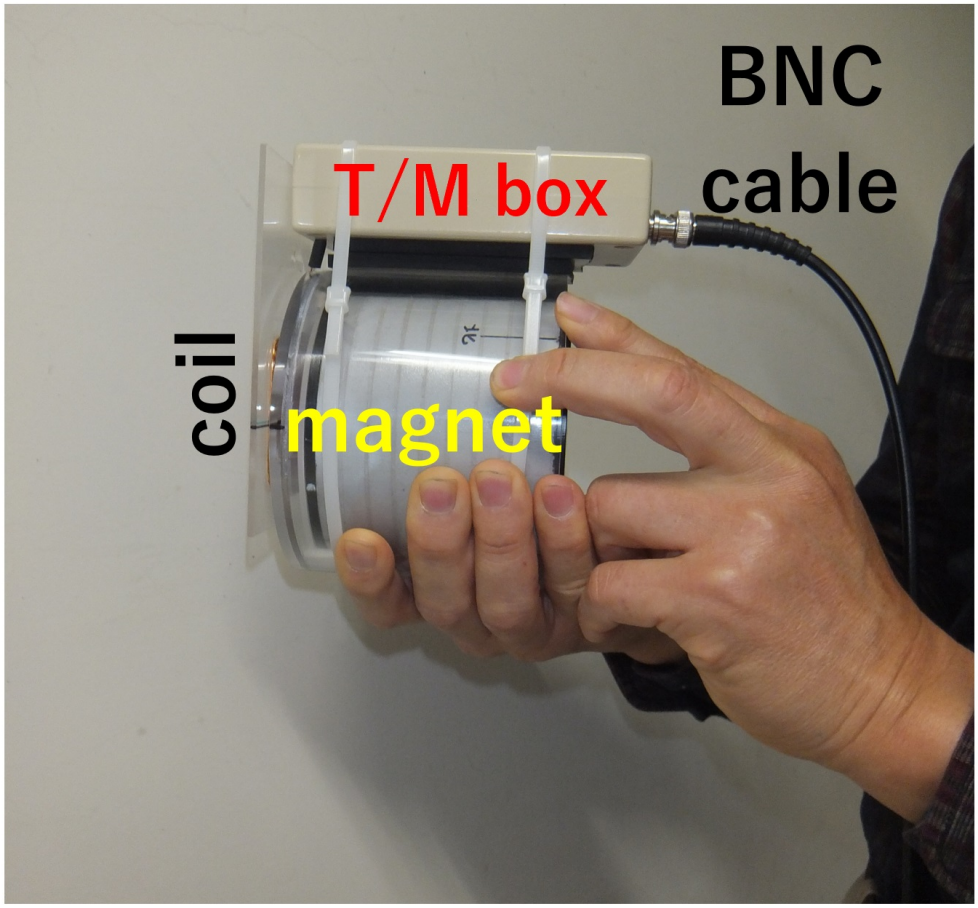
[1]: Nakashima, Y. et al. (2020) Nondestructive quantification of moisture in powdered low-rank coal by a unilateral nuclear magnetic resonance scanner. International Journal of Coal Preparation and Utilization (in press). https://doi.org/10.1080/19392699.2020.1722656

[2]: Nakashima, Y. (2019) Non-Destructive Quantification of Lipid and Water in Fresh Tuna Meat by a Single-Sided Nuclear Magnetic Resonance Scanner. Journal of Aquatic Food Product Technology 28, 241-252. https://doi.org/10.1080/10498850.2019.1569742

Keywords: nondestructive test, NMR, porous media

©2020. Japan Geoscience Union. All Right Reserved.

Sensor unit consisting of a magnet and a coil with a tuning/matching box.



©2020. Japan Geoscience Union. All Right Reserved.

Effect of temperature and humidity changes on salt weathering: Verification by rock surface moisture content and color measurements

Masaki Oi[1], *Masato Sato[2], Tsuyoshi Hattanji[3]

1. Graduate School of Life and environmental Sciences, University of Tsukuba, 2. National Research Institute for Earth Science and Disaster Resilience, 3. Faculty of Life and Environmental Sciences, University of Tsukuba

This study investigates weathering processes using porous rocks with three types of salts in field environments where water supply is limited to vapor in air. The experiments were performed using three types of rocks (Oya tuff, Ubara sandstone and Kominato mudstone). Each rock sample was cut into a cylinder having a diameter of 5 cm and a height of 5 cm. The shaped rock was immersed in a saturated salt solution of NaCl, Na_2SO_4, or $MgSO_4$ for 48 hours, then oven-dried at 110˚C. After these treatments, the rock cylinders were placed in a box on a field for 51 days in winter or summer season. The two types of boxes were used in the experiment; one has a transparent roof penetrating solar radiation and another has a roof shielding solar radiation. The roofs prevent rainwater into the two boxes, then water supply is limited to water vapor in air.

The experimental results are summarized as follows: (1) Rocks containing salt weathered during the daytime with low humidity. (2) Rock weathering in summer were greater than those in winter. (3) Weathering rates of rocks with sodium chloride were largest when exposed to solar radiation, while they were smallest without solar radiation.

Moisture content and color of rock surface indicated that the salt deliquesced and turned into a solution during high-humidity term at night, and recrystallized during the daytime with low humidity. As a result, detachment progressed during the daytime. Temperature and humidity observation suggested that the deliquescence in summer was longer and more frequent than that in winter. In actual field environments such as stone heritage, cave wall and tafone, the seasonal contrast in weathering rates would be occurred by the difference in temperature and humidity conditions for deliquescence.

Keywords: deliquescence, crystallization, hydration, infrared optical moisture meter, visible microspectrometer, field weathering experiment

©2020. Japan Geoscience Union. All Right Reserved.

Study on relationship between water content, NIR absorbance and colour values of various stones and cement mortars

*Chiaki T. Oguchi[1], Keni'chiro Tanaka[2]

1. Institute for Environmental Science and Technology, Graduate School of Science and Engineering, Saitama University, 2. Department of Engineering, Saitama University

This study examined the relationships between water content, absorbance, and color values in various building stones and mortar cements. The rocks used are; Shirahama sandstone, Oya tuff, Savonnierre limestone, Shirakawa welded tuff, Tago sandstone, while cement mortars used are sulfate resistant Portland cement (SRPC) and normal Prtland cement (NPC), NPC mixed with silica fume (SF) and fly ash (FA). Those rocks and mortars are cut into rectangle with the size of 5 cm-5 cm-15 cm. Firstly, the specimens were dried at 110 degrees for 24 hours, and then, they were immersed in distilled water in 24 hours. Then, they were taken from the distilled water and weighed to calculate water content and porosity. By using moisture measurement apparatus (JE-130, JE Engineering Co. Ltd.) with near infrared ray (NIR), absorbance values were measured and weight with elapsed time. In the same way, L* values were also measured by using colorimeter (CM-700d, Minolta Co. Ltd.) with elapsed time. The relationship among water content, absorbance values, L* was compared for each specimen. As a result, it is turned out that the values of absorbance increase with increasing water content, whereas the values of L* increase with decreasing water content.

Keywords: near infrared ray (NIR), water content, colour measurement

©2020. Japan Geoscience Union. All Right Reserved.

Surface morphology representations at different scales for rock art characterisationSurface morphology representations at different scales for rock art characterisation

Mohammad Hafez Seada[1,3], *Miguel Gomez-Heras[1], Laura Lopez-Gonzalez[2], Ayman Hamed[3]

1. Universidad Autonoma de Madrid, 2. Art Fabrik, 3. Suez University

Rock art is one of the oldest evidences of cultural transmission and probably one of the most sensitive to decay. Rock art is often found in shelters and outcropping rocks in areas where they are difficult to protect both again natural weathering agents and vandalism. In this scenario, surface morphology representations serve for the quantification of rock weathering or any change caused by human hands. Surface morphology is also an excellent tool for archaeological studies, particularly in rock art in the form of engravings, as micro-topographic measurements may be of substantial importance for the interpretation of the tools used for engraving. This communication deals with a set of Palaeolithic petroglyphs in Domingo Garcia (Segovia, Spain). This set of petroglyphs, which includes a variety of engraving techniques, is found across a wide area in a very rural setting that makes it very difficult to manage in terms of conservation. This communication explores different techniques for surface morphology acquisition at different scales, discussing their use for conservation and site management.
[This work was supported by Top Heritage (P2018/NMT-4372) programmes from the Regional Government of Madrid (Spain)].

Keywords: Rock art, Weathering characterisation, Photogrammetry, Conservation management



©2020. Japan Geoscience Union. All Right Reserved.

THERMOGRAPHIC ANALYSIS AS AN NON DESTRUCTIVE TECHNIQUE FOR AN EARLY DETECTION OF BIOCOLONISATION ON BUILDING STONE

*Stephanie Eyssautier Eyssautier[1], Kamel Mouhoubi Mouhoubi[2], Fany Reffuveille Reffuveille[3], jean-luc Bodnar Bodnar[2]

1. GEGENAA EA 3795 UFR Sciences Exactes et Naturelles –2, Esplanade Roland Garros, France, University of Reims Champagne-Ardenne (URCA), 51100 cedex, Reims, France, 2. ITHEMM, UFR Sciences Exactes et Naturelles, BP 1039, Reims Cedex 02, 51687, France, University of Reims Champagne-Ardenne (URCA), Moulin de la Housse BP 1039, 51687 Reims, France, 3. BIOS EA 4691, U.F.R. Pharmacie, 51, rue Cognacq Jay, University of Reims Champagne-Ardenne (URCA), 51095 Reims Cedex, France

Life on stones as microbial communities colonized substrates freshly exposed to the atmosphere where climatic conditions as sunlight, temperature and water availability are the key factors to the micro-organisms growth. The micro-organisms colonization is a widely recurring phenomenon which can lead to irreparable damage and the loss of unique cultural monuments. Besides the biological weathering, biofilms induce fouling that changes the visual aspect of monuments and statues. Biocolonisation is a major concern for conservators who face the endless maintenance of buildings which reach a notable economic costs.

Microbial communities composing biofilms spread thanks to nutritive elements found in the components of stone, and favour the anchorage of other micro-organisms such as fungi, algae, moss and lichen which deteriorate the materials by minerals dissolution and penetration of hyphae and roots driving to chemical and mechanical damage. In this respect, the early biofilm growth on stone walls must be taken into account to limit stones damage and financial costs. The colour measurement is currently used in cultural heritage as a non-destructive technique (NDT) to assess the biofilm spreading on a stone wall through its colour change. Nevertheless, other factors inducing colour variations are not driven by micro-organisms such as urban pollution, humidity degree and natural ageing of patina over time. Accordingly, the tracking of pioneer micro-organisms on stones is not always easy by this method and an earlier detection of biocolonisation should be more profitable than a visual one. In this study, infrared thermography (IRT) has been investigated in first assays in order to assess the sensitivity of this NDT to track down the biocolonisation earlier than colourimetry. It is an evaluation tool commonly used in monitoring and maintenance of buildings. The stone surfaces and subsurfaces are tested by analysis of thermal emissions. It is a powerful technique for art analysis thanks to its non-contact imaging application. This work analyzed thermal responses of biocolonised stones after a stimulation by a heating pulse (active IRT). Two natural limestones have been selected for their use in many buildings in Eastern France (Courville and Savonnières stones). Samples have been previously exposed six months in a garden where biofilms grew, then compared to non-exposed samples. The experiment has been set up in laboratory condition in order to avoid external artefacts. Recorded thermograms have been analysed by using post-processing calculations as SVD (Singular Value Decomposition) thanks to IR Explorer software and temperature variation of surfaces have been measured from them. First results displayed that SVD highlighted a net variation between stones without biofilm and stones with biofilm. Moreover, after a flash stimulation the maximum temperature was higher on the stone surface with biofilm than without it in dry and damp conditions for both types of stones. This study showed that active IRT could detect thermal variations on stones due to the biofilm settlement. This technique is thus able to highlight weak variations of energy for the detection of early biofilm.

©2020. Japan Geoscience Union. All Right Reserved.

Keywords: stone, biofilm, thermography

©2020. Japan Geoscience Union. All Right Reserved.

Effectiveness of waterproofing protection coating on salt weathering experiment using building stones

*Chiaki T. Oguchi[1], Akimune Sasaki[2]

1. Institute for Environmental Science and Technology, Graduate School of Science and Engineering, Saitama University, 2. Department of Engineering, Saitama University

Salt damage impact on buildings and cultural properties and developing various coating materials on waterproofing protection were obtain investigated recently. However, there are few studies on its effectiveness under severe condition of saline solution immersion to building stones. In the present study, continuous partial immersion experiment were performed by using 4 types of specimens of Oya tuff and Savonierre sandstone blocks to be found the effectiveness of waterproofing protection coat. From the experiment, the following findings were obtained regarding the effectiveness of the protection coating for salt weathering: 1) preventing salt solution from absorbing water; 2) suppression of rock surface degradation by filling gaps in rock surface; 3) increase the strength of rock surface; and 4) causeing a certain damage under conditions that allow water absorption.

Keywords: building stone, waterproofing protection coating, salt weathering

©2020. Japan Geoscience Union. All Right Reserved.

Integration of durability parameters of cultural heritage building stones using by integrated geomatic methodologies

*Sebastien LARATTE[1], Céline THOMACHOT-SCHNEIDER[1], Gilles FRONTEAU[1], Alexandra GUILLANEUF [1], Patricia VAZQUEZ[1]

1. University of Reims-Champagne-Ardenne

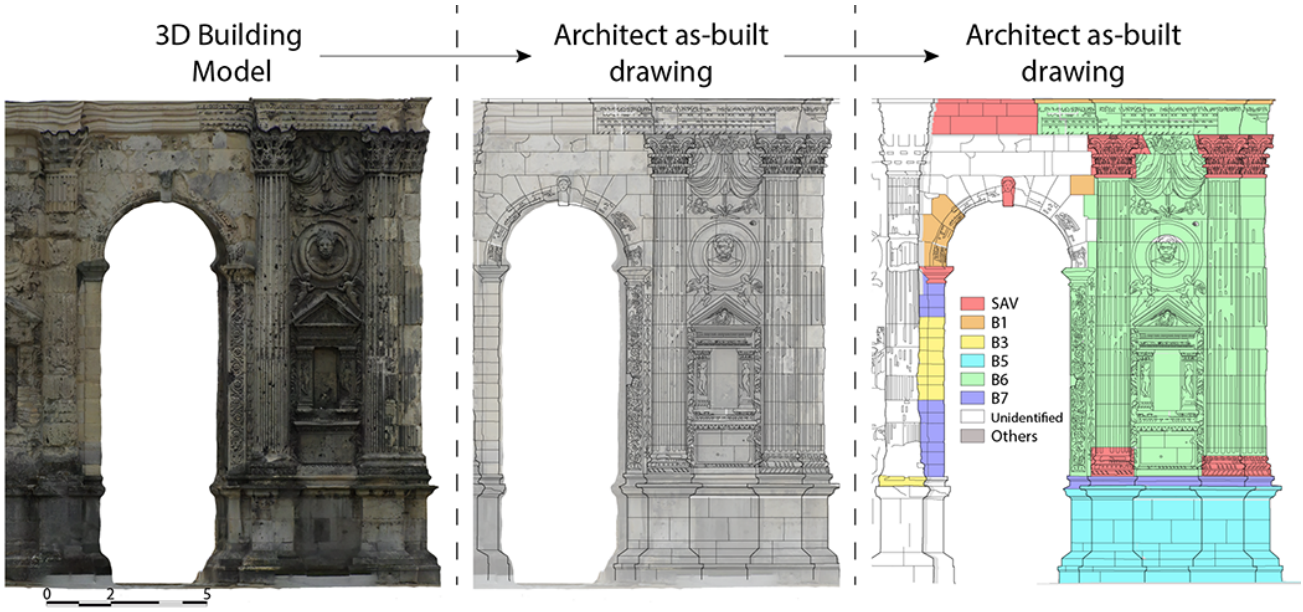
The “Porte de Mars”, is one of the most emblematic ancient monuments of the city of Rheims. This three-bay roman arch rises at the northern end of former *Durocortorum,* capital of *Gallia Belgica* province. Its construction dates from the mid 2nd to early 3rd c. AD. It was then integrated into the Late Roman rampart of the city. Encased, from 1162 to 1856, in the medieval city wall and then in the castle of the city's archbishops, it was completely cleared and restored during the 19th century. During this period, it was barely saved from being dismantled after the ruin of the archbishops' castle and its complete dismantling by the town's population. It is considered the largest "arch" of the Roman Empire north of Roma. It is 32.35 m long, 6.45 m wide and 12 m high today. Since its rediscovery and until today, the “Porte de Mars” is located in the centre of Rheims, at the crossroads of major traffic axis.

A photogrammetric survey was carried out using a total of 370 high-resolution photos. For this, a camera with a 20.3 Megapixel sensor was used, taking care to work with a single focal length. The upper part of the monument was treated in a second step thanks to the presence of an aerial lift. Part of the photos were taken by fixing the camera on a pole and using a tablet as a means of preview, georeferencing and remote control. After a quality control; the photographs were processed with the Agisoft Metashape software which allows to carry out all the operations of the photogrammetry calculation chain (Structure fFrom Motion - SfM method). This method allows the reconstruction of 3D objects from 2D data. The technique is based on an algorithm that automatically matches points in a set of photos. These points are then treated as remarkable points and repositioned in space in the manner of the perception of volumes by biological eyes. The spatial coordinates of the points are on the one hand calculated by the software and on the other hand provided by the georeferencing data of the images. The distances between 125 key points on the monument are measured with a laser range distance meter (Leica Disto D2) in order to scale the model to its final dimensions. The software allows the extraction of orthophotographs from the 3D mesh according to the chosen orientations.

The modelled datas and orthophotos are injected into a geographic information system (GIS) implemented under QGis 3.4 because of the interoperability of the formats considered. Its data is then used as the basis for plan and volume plots on the one hand and an attribute database on the other. These data are both qualitative (nature of the stone, petrography, assumed origin, restoration phase, etc.) and quantitative (chemical composition, mineralogy, porosity, capilarity, etc.). The methodology will also make it possible to discretize continuous information such as thermal data at the stone scale.
This non-destructive approach to the monument built from an integrated geomatics chain of operations allows the cross-referencing of data of various origins (geological, environmental, archaeological...). Interoperability of the database is essential so that this tool can represent a transversal interest and be used in the framework of building conservation. This approach allows the construction of thematic maps of the monument, such as material maps, stone compatibility maps or prospective parameter maps such as the durability of materials. In addition, the use of photogrammetry has considerably lightened the process of acquisition and calculation of the model, making the construction of the information system much easier.

©2020. Japan Geoscience Union. All Right Reserved.

Keywords: Photogrammetry, GIS, 3D model



©2020. Japan Geoscience Union. All Right Reserved.

[E] Poster | M (Multidisciplinary and Interdisciplinary)：M-GI General Geosciences, Information Geosciences & Simulations

[M-GI33] Data assimilation: A fundamental approach in geosciences

convener:Shin ya Nakano(The Institute of Statistical Mathematics), Yosuke Fujii(Meteorological Research Institute, Japan Meteorological Agency), Takemasa Miyoshi(RIKEN), SHINICHI MIYAZAKI(Graduate School of Science, Kyoto University)

Data assimilation is an inversion approach to estimate the evolution of a system by utilizing a constraint given by a dynamical simulation model. Data assimilation is now widely used not only in meteorology and oceanography but also other fields of geosciences such as hydrology, solid earth science, and space science. This session aims at providing
an opportunity for discussion on data assimilation studies among researchers of various field of geosciences. We encourage contributions addressing novel methods and theoretical developments of data assimilation. Contributions dealing with useful applications of data assimilation are also welcome.

[MGI33-P01] Oceanic iron distribution of the global ocean estimated by data assimilation approach

★Invited Papers

*Toshimasa Doi[1], Satoshi Osafune[1], Shuhei Masuda[1], Hajime Obata[4], Kazuhiro Misumi[3], Jun Nishioka[2] (1.Japan Agency for Marine-Earth Science and Technology, 2.Hokkaido University, 3.Central Research Institute of Electric Power Industry, 4. The University of Tokyo)

[MGI33-P02] Enhanced correlations between SST and precipitation in the weather time scale represented by a coupled atmosphere-ocean data assimilation system

*Yosuke Fujii[1], Chiaki Kobayashi[1], Ichiro Ishikawa[1], Takaya Yuhei[1] (1.Meteorological Research Institute, Japan Meteorological Agency)

[MGI33-P03] Non-Gaussian statistics in global atmospheric dynamics with a 10240-member ensemble Kalman filter experiment using an intermediate AGCM

★Invited Papers

*Keiichi Kondo[1,2], Takemasa Miyoshi[2] (1.Meteorological Research Institute, 2.RIKEN Center for Computational Science)

[MGI33-P04] Data assimilation of lightning observation data for global numerical weather prediction

*Toshiyuki Ishibashi[1] (1.Meteorological Research Institute/Japan Meteorological Agency)

[MGI33-P05] Development of a "multilingual" data assimilation library

*Shin ya Nakano[1], Genta Ueno[1], Shunichi Nomura[1], Daisuke Murakami[1] (1.The Institute of Statistical Mathematics)

[MGI33-P06] Observation impact study in global numerical weather prediction

*Toshiyuki Ishibashi[1] (1.Meteorological Research Institute/Japan Meteorological Agency)

Oceanic iron distribution of the global ocean estimated by data assimilation approach

*Toshimasa Doi[1], Satoshi Osafune[1], Shuhei Masuda[1], Hajime Obata[4], Kazuhiro Misumi[3], Jun Nishioka[2]

1. Japan Agency for Marine-Earth Science and Technology, 2. Hokkaido University, 3. Central Research Institute of Electric Power Industry, 4. The University of Tokyo

Information on the distribution of dissolved iron (*dFe*) concentrations in many parts of the ocean has been provided by recent ocean observation programs. However, a knowledge is still limited concerning the rates of processes that control the concentrations and cycling of *dFe* in the ocean. In this study, we constructed a three-dimensional gridded dataset of oceanic *dFe* concentrations by using both observations and a simple model of the iron cycle. The fluxes of *dFe* from the sea surface associated with the falling aeolian dust and from the dissolution of sediments on the seafloor of the continental shelves were set as the external flux. We used a Green's function approach to integrate the observations and a simple model. The control variables, in addition to model parameters, were the flux of *dFe* from the dissolution of sediments on the seafloor of the continental shelves. The three-dimensional distribution of *dFe* that we obtained was in basic agreement with observations. These estimates imply large differences in the cycling of *dFe* between the two basins that would need to be taken into consideration in projections of future scenarios. Although there is some uncertainty in our estimates, global estimates of iron cycle characteristics based on this approach can be expected to enhance understanding of the iron cycle process in the ocean.

Keywords: oceanic iron, data assimilation

©2020. Japan Geoscience Union. All Right Reserved.

Enhanced correlations between SST and precipitation in the weather time scale represented by a coupled atmosphere-ocean data assimilation system

*Yosuke Fujii[1], Chiaki Kobayashi[1], Ichiro Ishikawa[1], Takaya Yuhei[1]

1. Meteorological Research Institute, Japan Meteorological Agency

The Meteorological Research Institute (MRI) of the Japan Meteorological Agency has developed a weakly-coupled atmosphere-ocean data assimilation system, MRI-CDA1, and coupled reanalysis experiments based on MRI-CDA1 are conducted for the period from November 2013 to December 2015. Then we examined the relationship between sea surface temperature (SST) and atmospheric elements in the one-to-ten-day time scale which is the typical time scale for weather variation. In the coupled reanalysis, the variation of SST is positively correlated with the variation of precipitation with one-day lag, and the variation of precipitation is negatively correlated with the variation of SST with one-day lag, particularly in the tropics. High SST, thus, induces atmospheric convection and the convection induces low SST in turn. These lagged correlations mostly disappear between precipitation and prescribed SST data in an uncoupled atmospheric reanalysis. When the prescribed SST is replaced by the SST in the ocean data assimilation system forced by the atmospheric reanalysis, the lagged correlations are recovered but weaker than those in the coupled reanalysis. Thus, the lagged correlations are enhanced with coupled data assimilation. In addition, correlations become weaker also when the prescribed SST is replaced by the SST in the coupled reanalysis, which means that the precipitation field in the coupled reanalysis is changed in order to adjust to the SST field driven by the coupled model. This is contrastive to the longer (intraseasonal) time scale in which the atmospheric field in the coupled reanalysis is mostly unchanged from the conventional atmospheric reanalysis but SST filed is adjusted to the atmospheric fields. This effect of coupled data assimilation enhancing the correlations between SST and precipitation may cause improvement of the precipitation field over the uncoupled atmospheric analysis.

Keywords: Coupled Data Assimilation, Coupled Reanalysis, Air-Sea Interaction, Sea Surface Temperature, Precipitation

©2020. Japan Geoscience Union. All Right Reserved.

Non-Gaussian statistics in global atmospheric dynamics with a 10240-member ensemble Kalman filter experiment using an intermediate AGCM

*Keiichi Kondo[1,2], Takemasa Miyoshi[2]

1. Meteorological Research Institute, 2. RIKEN Center for Computational Science

In our previous work, we performed local ensemble transform Kalman filter (LETKF) experiments with 10240 ensemble members using an intermediate atmospheric general circulation model (AGCM) known as the SPEEDY (T30/L7) model. The previous study reported that the improvement in the tropics was relatively small by increasing the ensemble size up to 10240. We hypothesize that these small improvements be related to convectively dominated tropical dynamics. In this study, we found that the non-Gaussian probability density functions (PDFs) appeared in the regions with large analysis error, mainly in the tropics and storm track regions. The non-Gaussian PDFs are mainly generated by convective parametrization in the tropics and by the instability associated with advection in the storm track regions.

Acknowledgements: This study was partly supported by JST CREST (JPMJCR1312), JST AIP (JPMJCR19U2), JSPS KAKENHI (JP16K17806), and Post-K priority issue 4 of Japan Agency for Marine-Earth Science and Technology, which was promoted by the Ministry of Education, Culture, Sports, Science and Technology, Japan. Part of the results was obtained using the K computer at the RIKEN R-CCS through proposal numbers ra000015 and hp150019.

Keywords: ensemble data assimilation, non-Gaussian PDF

©2020. Japan Geoscience Union. All Right Reserved.

Data assimilation of lightning observation data for global numerical weather prediction

*Toshiyuki Ishibashi[1]

1. Meteorological Research Institute/Japan Meteorological Agency

To improve the accuracy of global numerical weather prediction (NWP), it is necessary to assimilate more observation data with a data assimilation system (DAS). Lightning observation data is new valuable observation data including information on the deep part of cumulonimbus clouds. Lightning observation from satellites has been ongoing since the 1990s. The third generation geostationary meteorological satellites are equipped with lightning sensors and have high spatiotemporal resolution and wide observation coverage. However, to assimilate the lightning observation data adequately, there are some basic difficulties, which are the nonlinearity of the lightning observation operator, shortage of forecast accuracy for water substances, and water substance error statistics. In this research, we first summarize lightning observations and observation operators, and then describe our initial results such as forward calculation of lightning. We also consider next steps of the data assimilation of lightning observations.

Keywords: data assimilation, numerical weather prediction, lightning

©2020. Japan Geoscience Union. All Right Reserved.

Development of a "multilingual" data assimilation library

*Shin ya Nakano[1], Genta Ueno[1], Shunichi Nomura[1], Daisuke Murakami[1]

1. The Institute of Statistical Mathematics

Data assimilation is now applied in various fields not limited to geophysical researches. There are several documents and textbooks for data assimilation methods, and some free data assimilation codes are also available. These materials have been helping researchers of various research areas who want to use data assimilation techniques. However, it is sometimes time-consuming to implement a data assimilation method for a practical simulation code after reading the documents and the public assimilation codes. In particular, if one can not find any data assimilation codes written in his/her familiar language, it would take trouble to development a data assimilation code. We aim to provide a data assimilation program library in a variety of programming language which is easy for various researches to try to apply. As a pilot work, we developed a library of the particle filter based on Python which was reported last year, and it have been provided for several researchers. Now we are developing a similar framework in different languages such as R and Matlab which help researchers to develop a data assimilation system with the ensemble Kalman filter or the particle filter. We will introduce our data assimilation library and discuss future prospects.

Keywords: Data assimilation software, ensemble Kalman filter, particle filter

©2020. Japan Geoscience Union. All Right Reserved.

Observation impact study in global numerical weather prediction

*Toshiyuki Ishibashi[1]

1. Meteorological Research Institute/Japan Meteorological Agency

To improve the accuracy of global numerical weather prediction (NWP), it is necessary to assimilate more observation information with a data assimilation system (DAS). To know impact of each assimilated observation on analyses and forecasts is essential for this. In this study, we estimate observation impacts using the adjoint based impact estimation method, which used an adjoint operators of a DAS and a NWP model. Various properties of observation impact such as nonlinearity, probabilistic nature, system dependency are also considered.

Keywords: data assimilation, observation impact, adjoint operator

©2020. Japan Geoscience Union. All Right Reserved.

[E] Poster | M (Multidisciplinary and Interdisciplinary)：M-GI General Geosciences, Information Geosciences & Simulations

[M-GI34] Near Surface Investigation and Modeling for Groundwater Resources Assessment and Conservation

convener:Jui-Pin Tsai(National Taiwan University, Taiwan), Hwa-Lung Yu(National Taiwan University), Makoto Taniguchi(Research Institute for Humanity and Nature), Ping-Yu Chang(National Central University)

Groundwater resources serve as a vital source for regional water supply under the climate change condition. However, improper use of the available groundwater resources leads to serious environmental disasters such as land subsidence or seawater intrusion. Therefore, groundwater management is a key issue for groundwater resources conservation. Before applying any management practice, it is essential to accurately assess the groundwater system in multi-scales. In this session, we focus on the issues associated with the application of near-surface investigation and modeling on groundwater resources assessment. We welcome studies related to numerical modeling, spatiotemporal modeling, data fusion, and field investigation using hydrogeological approaches, geophysical approaches, geochemical approaches, and remote sensing. We also welcome the studies associated with groundwater contamination transport and remediation, geothermal energy exchange, groundwater microorganisms, hot spring, volcanic hydrology, and environmental disasters evaluation and prevention. We especially encourage the pilot groundwater management studies that solve multi-scale and interdisciplinary problems.

[MGI34-P01] Digital water level analysis based on well tide and air pressure effect

*feng he ding[1] (1.Earthquake Administration of Ningxia Hui Autonomous Region)

[MGI34-P02] Applying Independent Component Analysis and Wavelets Analysis to Explore the Response of Groundwater Level to Surface Hydrology

*Chin Wei Huang[1], Liang Cheng Chang[1], Chin Tsai Hsiao[2], Wan Chung Lu[3], Tzu Hua Lai[3] (1.Department of Civil Engineering, National Chiao-Tung University, Hsinchu, Taiwan 30010, R.O.C., 2.Department of Landscape Architecture, Chung Chou University of Science and Technology, Changhua County, Taiwan, 510, R.O.C, 3.Central Geological Survey, MOEA, Taiwan 235, R.O.C)

[MGI34-P03] Optimal Artificial-Recharge Planning to Raise the Groundwater Level of Land Subsidence Area

*Ming-Sheng Wang[1], Liang Cheng Chang[1], Wan Chun Lu[2], Yun Shuen Wang[2] (1.Department of Civil Engineering, National Chiao-Tung University, Hsinchu, Taiwan, 30010, R.O.C, 2.Central Geological Survey, MOEA, Taiwan 235, R.O.C)

Digital water level analysis based on well tide and air pressure effect

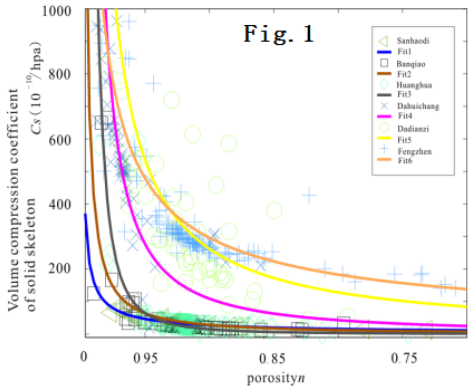
*feng he ding[1]

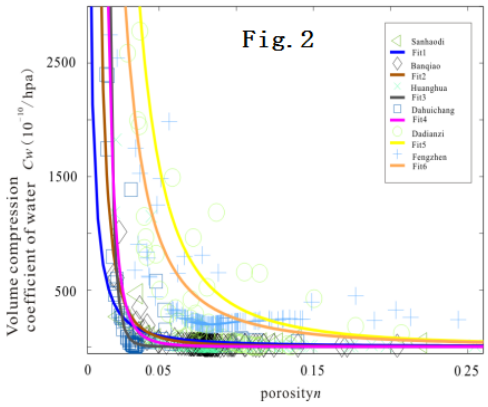
1. Earthquake Administration of Ningxia Hui Autonomous Region

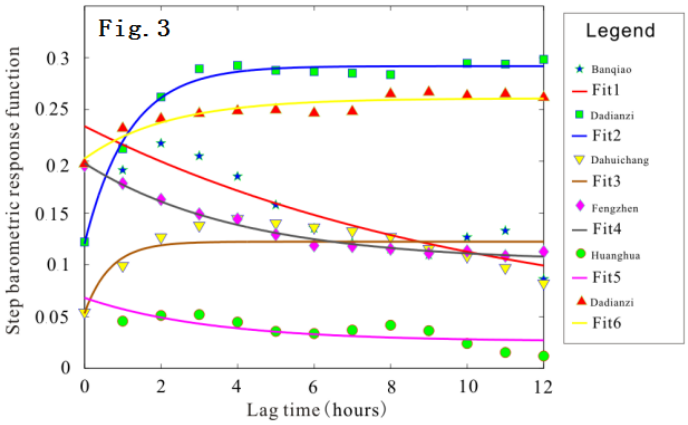
In this paper, the porosity, the volume compression coefficient of solid skeleton and the volume compression coefficient of water in the aquifer are studied by using the air pressure coefficient and tide factor from Dahuichang Well, Banqiao Well, Huanghua Well, Dadianzi Well, Fengzhen Well and Sanhaodi Well in the north of North China.
The results show that there is an obvious power function relationship between porosity and volume compression coefficient of solid skeleton and that of water in aquifer.(1)In the first quadrant, the volume compression coefficient of aquifer solid skeleton increases with the increase of porosity.This is due to the fact that when the pore pressure increases, the volume of water decreases. When the external stress remains unchanged, the skeleton stress decreases, the skeleton volume increases, and the pore volume increases together.Therefore, with the decrease of skeleton stress and the increase of skeleton volume (expansion), the volume change (or rate of change) is also larger (easy to compress). The compression coefficient of skeleton volume increases with the increase of porosity.(2)When the pore pressure increases, the volume of water decreases, and the smaller the volume change (or change rate), the smaller the volume compression coefficient of water. At the same time, this process is the process of porosity increase. Therefore, the volume compression coefficient of water decreases with the increase of porosity.(3)The elastic deformation of water decreases with the increase of porosity. This is because the compression coefficient of water is smaller and smaller, and the volume change is smaller and smaller, so the water is more difficult to compress. At the same time, the solid skeleton is easy to compress and elastic deformation becomes stronger.(4)The relationship between the volume compression coefficient of the water in the aquifer and the solid skeleton satisfies the quadratic polynomial of one variable, and the volume compression coefficient of the water in the aquifer is larger than the volume compression coefficient of the solid skeleton, so the water is easier to be compressed.
In addition, combined with the step response function of water level to air pressure in convolution regression method, the results of groundwater type determination of the aquifer system of these six Wells show that there is an obvious exponential function form with e as the bottom between the lag time of water level to air pressure and the step response function of water level to air pressure in each of the six Wells. The positive and negative coefficient a before the base number e determines the underground water of the Well aquifer system Type of water. For pressure Wells, the step response function of water level to air pressure increases with the increase of lag time of water level to air pressure, while for non pressure Wells and semi pressure Wells, it is the opposite.

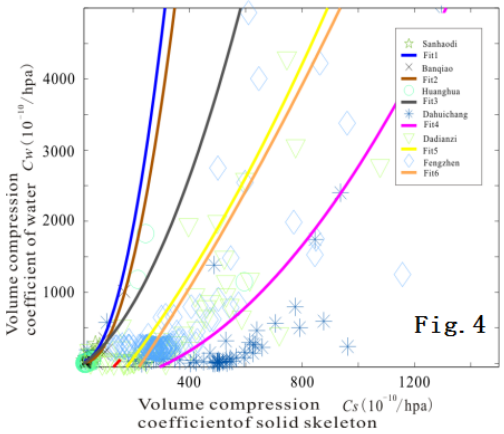
Keywords: Well water level, Well tide effect, Barometric response

©2020. Japan Geoscience Union. All Right Reserved.









©2020. Japan Geoscience Union. All Right Reserved.

Applying Independent Component Analysis and Wavelets Analysis to Explore the Response of Groundwater Level to Surface Hydrology

*Chin Wei Huang[1], Liang Cheng Chang[1], Chin Tsai Hsiao[2], Wan Chung Lu[3], Tzu Hua Lai[3]

1. Department of Civil Engineering, National Chiao-Tung University, Hsinchu, Taiwan 30010, R.O.C., 2. Department of Landscape Architecture, Chung Chou University of Science and Technology, Changhua County, Taiwan, 510, R.O.C, 3. Central Geological Survey, MOEA, Taiwan 235, R.O.C

The groundwater is a component of the global hydrology cycle. For an aquifer system, the responses of the external forces such as rainfall, river flow, groundwater pumping and earth tide etc. were mixed in the groundwater level. This study applies the Independent Component Analysis (ICA) and the Wavelets Analysis to decompose the signals of groundwater level, rainfall and river water-level in time and frequency domain. The decomposition facilitates exploring the response of groundwater level to the surface hydrology. The independent components (ICs) of groundwater level and external forces are examined by their cross-correlations and the associated wavlets transform. The proposed method was applied to the Taichung Basin based on the data collected during 2009-2017. The study identified a pair of groundwater level ICs to rainfall ICs with a high correlation coefficient value (0.85) and a similar pattern of wavelets transform. A river water-level ICs with correlation coefficient 0.69 to groundwater level ICs was also identified. The result demonstrates that the rainfall has a significant influence on the groundwater level, and the river water-level has a moderate impact on the groundwater system in Taichung Basin. Besides examing the impact of surface hydrology to groundwater level, the proposed methodology can obtain a clean signal pair of impact-to-response and that is valuable to more advanced study.

Keywords: Fourier Transform, Groundwater, Independent Component Analysis, Wavelet Transform

©2020. Japan Geoscience Union. All Right Reserved.

Optimal Artificial-Recharge Planning to Raise the Groundwater Level of Land Subsidence Area

*Ming-Sheng Wang[1], Liang Cheng Chang[1], Wan Chun Lu[2], Yun Shuen Wang[2]

1. Department of Civil Engineering, National Chiao-Tung University, Hsinchu, Taiwan, 30010, R.O.C, 2. Central Geological Survey, MOEA, Taiwan 235, R.O.C

The alluvial fan of the Zhuoshui River in Taiwan has rich groundwater resources. However, the groundwater over-pumping to supply the agricultural and aquaculture water demand in early year induced drawdown of groundwater level significantly, and caused land subsidence problems. To mitigate the land subsidence problem, raising the groundwater level is the most effective method.
Therefore, this study develops an optimal planning model for regional groundwater recharge planning and applies the model to the Zhuoshui River alluvial fan. The optimal planning model integrated a genetic algorithm with a surface water allocation model and a groundwater simulation model. To reduce the computational complexity, the optimal planning model is formulated as a sequential optimization model instead of a global optimal one. The model computes the optimal recharge plan step by step. For each step, three consecutive time steps optimal was considered. To further increase the computational efficiency, a response matrix model is used to surrogate the groundwater numerical simulation model, MODFLOW. However, before creating a response matrix, a groundwater simulation model (MODFLOW) needs to be built. The optimal planning model was applied to compute the optimal recharge plain in the Zhuoshui River alluvial fan. The retired water treatment plants are the candidate sides to be selected as injection sites. The simulation results demonstrated that the optimal recharge plan can indeed raise the groundwater level significantly. The principle of the proposed methodology can be applied to other land subsidence areas, and the result is a valuable reference for mitigating the land subsidence problem

©2020. Japan Geoscience Union. All Right Reserved.

[E] Poster | M (Multidisciplinary and Interdisciplinary)：M-GI General Geosciences, Information Geosciences & Simulations

[M-GI36] Open Science in Progress: Data Sharing, e-Infrastructure, and Transparency in International Contexts

convener:Yasuhisa Kondo(Research Institute for Humanity and Nature), Baptiste Cecconi(LESIA, Observatoire de Paris, CNRS, PSL Research University), Yasuhiro Murayama(Strategic Program Produce Office, National Institute of Information and Communications Technology), Shelley Stall(American Geophysical Union)

Open Science is widely accepted as a new research paradigm to accelerate scientific innovation. Deployed by ICSU-WDS (2008), G8 Open Data Charter (2013), deployment of Research Data Alliance (2013), OECD Global Science Forum's research projects (2016), and G7 Science Ministers' Communique (2017), it commonly refers to the top-down policies making results of publicly-funded research freely available and accessible. Open Science also refers to the participatory bottom-up approaches such as citizen science, crowdfunding, and transdisciplinary research (Kitamoto 2016). It is noted that both approaches envision the transformation of research process to more findable, accessible, interoperable, and reusable one (Wilkinson et al. 2016).
Followed by the JpGU-AGU Great Debate "Role of open data and open science in Geoscience" at JpGU Annual Meeting 2018, follow-up sessions at the AGU Fall Meetings 2018 and 2019, and JpGU 2019, this session reviews the current broad spectrum of Open Science in international contexts. The session welcomes a wide range of papers and posters covering (but not limited to) open research data, open source licenses, data papers and journals, data repository, e-infrastructures and platforms for sharing data, citizen science, crowdsourcing, crowdfunding, transdisciplinary research, capacity building, international networking, and deployment in earth and planetary sciences.

[MGI36-P01] Research Data: Emerging Challenges and Opportunities in International Research Collaborations

★Invited Papers

*Kamata Takehito[1] (1.Sophia University)

[MGI36-P02] Data Management and Computing Services for the NenuFAR Telescope

*Baptiste Cecconi[1,2], Loh Alan[1,2], Evangelia Tremou[1], Julien N Girard[3], Brice Lamire[4], Philippe Hamy[4], Albert Shih[4], Pierre Le Sidaner[4], Cédric Viou[2], Emmanuel Thétas[2], Philippe Zarka[1,2], Laurent Denis[2] (1.LESIA, Observatoire de Paris, CNRS, PSL Research University, France, 2.Station de radioastronomie de Nançay, CNRS/Observatoire de Paris - PSL - Université d'Orléans/OSUC, France, 3.AIM/CEA Paris-Saclay, Université de Paris, CNRS, Gif-sur-Yvette, France, 4.DIO, Observatoire de Paris, CNRS, PSL Research University, France)

[MGI36-P03] Open data action to publish the GNSS-A seafloor geodetic data

*Tadashi Ishikawa[1], Yusuke Yokota[2], Shun-ichi Watanabe[1] (1.Hydrographic and Oceanographic Department, Japan Coast Guard, 2.Institute of Industrial Science, the University of Tokyo)

[MGI36-P04] Sample management in JAMSTEC: Cooperation-based management of diverse samples

★Invited Papers

*Takayuki Tomiyama[1], Tohru Iseto[1], Yasumi Toyoda[1], Miki Morioka[1], Makoto Ito[1] (1.Japan Agency for Marine-Earth Science and Technology)

[MGI36-P05] Improving the Reusability of Data and Sample Obtained JAMSTEC's Research Vessels and Submersibles

*Kazuyo Fukuda[1], Hajime Kawakami[1], Hiroki Horikawa[1], Tomoki Sasaki[1], Takako Sato[1], Takayuki Tomiyama[1], Makoto Ito[1], Yasumi Toyoda[1], Hideaki Saito[1], Chizuru Saito[1] (1.Japan Agency for Marine-Earth Science and Technology)

[MGI36-P06] Activities toward research data management at NIES/CGER

*Yoko Fukuda[1], Chisato Wada[1], Yasuhiro Tsukada[1], Jiye Zeng[1], Tomoko Shirai[1] (1.National Institute for Environmental Studies)

Research Data: Emerging Challenges and Opportunities in International Research Collaborations

*Kamata Takehito[1]

1. Sophia University

Researchers and professionals from different academic backgrounds share diverse types of information, knowledge, and data to study interconnected complex global issues. Their collaborations yield new knowledge that can create innovations around the world, and interdisciplinary teams of specialists work together to conduct flexible research collaborations in analyzing large amounts of data, information, and samples.

Research data governance policies regarding international research vary across academic disciplines, professions, and nations. Researchers, professionals, and all related stakeholders need to understand emerging challenges and opportunities in integrating research data with their collaborators across nations. This study introduces emerging challenges and opportunities in integrating data across nations.

Anderson (2010) identified the four dimensions of national research system, the organization of the research system, the legal and regulatory systems, the oversight related to research integrity, and the training of graduate students and postdoctoral fellows as potential challenges when promoting research and support in international research collaboration. Dealing with challenges at the appropriate organizational levels is key to pursuing successful international research collaboration.

There are many education and research systems around the world, and the affiliated systems influence researchers' engagement and involvement differently. In addition, each individual's academic, professional, and cultural experience determines and reflects the attitudes, behaviors, characteristics, objectives, and values of an organization or institution. It is crucial to recognize differences in trained individuals' knowledge, skills, research integrity and ethics, as well as other research-related training (National Research Council, 2011).

Different legal and regulatory systems pose challenges for international research collaboration. Some government agencies and international organizations have more complex hierarchies than others, and some nations are strict on spending their public funds in particular research fields. Recognizing differences among organizations, sectors, and nations will be significant to establish effective collaboration and communication platforms to deal with emerging challenges in international research collaborations.

The increase of data storage capacity and the development of information technology infrastructure have enabled researchers and professionals to integrate data and samples through international research collaborations. Although each academic discipline has different data sharing principles and practices, it is the shared responsibility among the stakeholders to improve data integration infrastructure in data management and governance in international research collaborations.

National funding agencies or oversight organizations do not have the clear authority and function to assess the various risks and threats associated with data sharing in international research collaboration. Elsevier started offering to store the research data that underlie the papers published in its journals;

©2020. Japan Geoscience Union. All Right Reserved.

however, it did not consider the cost of doing so (National Research Council, 2018). Researchers must work with their collaborators to recognize research integrity principles, understand government regulations, follow legal guidelines, spend allocated funds appropriately, satisfy other requirements, and ensure public trust in research (Kaye, 2015).

Incorporating multiple data integration perspectives and practices will be significant to eliminate potential challenges and create responsible research data governance policies in international research collaborations. Based on the definitions of internationalization, this study examines the organizational responsibilities and functions of the research data governance at the institutional, sector, national, and international levels.

Keywords: International research collaborations, Research data integration, Data governance

©2020. Japan Geoscience Union. All Right Reserved.

Data Management and Computing Services for the NenuFAR Telescope

*Baptiste Cecconi[1,2], Loh Alan[1,2], Evangelia Tremou[1], Julien N Girard[3], Brice Lamire[4], Philippe Hamy[4], Albert Shih[4], Pierre Le Sidaner[4], Cédric Viou[2], Emmanuel Thétas[2], Philippe Zarka[1,2], Laurent Denis[2]

1. LESIA, Observatoire de Paris, CNRS, PSL Research University, France, 2. Station de radioastronomie de Nançay, CNRS/Observatoire de Paris - PSL - Université d' Orléans/OSUC, France, 3. AIM/CEA Paris-Saclay, Université de Paris, CNRS, Gif-sur-Yvette, France, 4. DIO, Observatoire de Paris, CNRS, PSL Research University, France

NenuFAR is a new radioastronomy instrument located in Nançay (France) operating in the 10–85 MHz frequency band. It is a SKA (Square Kilometre Array) Pathfinder at low frequency at the last stages of its construction, currently in early science phase. The instrument will produce up to 2 PB of data per year in its standalone imager mode. We are now setting up a local data center in order to pre-process the raw data. An e- or physical infrastructure is under development and will allow for, e.g., data transfer/storage/archive, user access and computing time allocation management, scientific analysis platform deployment with preconfigured radio astronomy software suites.

Keywords: Radioastronomy, Data center

©2020. Japan Geoscience Union. All Right Reserved.

Open data action to publish the GNSS-A seafloor geodetic data

*Tadashi Ishikawa[1], Yusuke Yokota[2], Shun-ichi Watanabe[1]

1. Hydrographic and Oceanographic Department, Japan Coast Guard, 2. Institute of Industrial Science, the University of Tokyo

Seafloor geodetic data are particularly important for monitoring the behavior of undersea inter-plate boundary regions. Since the mid-1990s, Japan Coast Guard have been developing the combined Global Navigation Satellite System-Acoustic ranging (GNSS-A) technique for realizing seafloor geodesy. This technique allows us to collect time series of seafloor crustal deformation. The datasets of time series can be used to investigate several seismological phenomena along the subduction zones around Japan, such as the Nankai Trough and Japan Trench. These regions are globally important places in geodesy and seismology and are also suitable for comparison with other geophysical datasets. Therefore, sharing the datasets in an appropriate way, it is expected to promote further understanding of megathrust zones.

First, we published our datasets on our web site (https://www1.kaiho.mlit.go.jp/KOHO/chikaku/kaitei/sgs/datalist_e.html). However, this is not an appropriate way because the description of the datasets in not sufficient for other researches to use. In addition, our site has not a function to mint DOIs for datasets. To solve this problem, we published our datasets as data paper (Yokota et al. 2018). Data paper is a peer-reviewed paper for descriptions of datasets that advances reuse of the data. Our intention is for data paper to widely share the GNSS-A datasets to promote further advances of seismology and geodesy.

Reference:

Yokota, Y., T. Ishikawa and S. Watanabe (2018): Seafloor crustal deformation data along the subduction zones around Japan obtained by GNSS-A observations, Scientific Data, 5:180182, doi:10.1038/sdata.2018.182.

Keywords: open data, data journal, seafloor geodesy

©2020. Japan Geoscience Union. All Right Reserved.

Sample management in JAMSTEC: Cooperation-based management of diverse samples

*Takayuki Tomiyama[1], Tohru Iseto[1], Yasumi Toyoda[1], Miki Morioka[1], Makoto Ito[1]

1. Japan Agency for Marine-Earth Science and Technology

JAMSTEC[*1] publicly distributes samples and data obtained by JAMSTEC-AORI[*2]-JURCAOS[*3] Cooperative Research Cruises [1], as well as those by JAMSTEC private/open-call cruises, through online database (DB) websites, for additional uses with research/educational purposes. These online DBs are, from a long-term perspective, under a process of reorganization and integration: Public-level information systems for rock and sediment core samples were integrated into DARWIN DB [1] in FY2017. As for marine biological samples, whose information has been mainly distributed through “Marine Biological Sample DB [3], a part of information is already shared with DARWIN to utilize its search/map functions.

DB integration is in progress for not only public-level but also management-level information system, which are operated by sample holders responsible for storage of physical samples. In FY2018, JSDB (JAMSTEC Sample Management Database) is installed for the management of JAMSTEC rock, sediment core and biological samples, and actual data was transferred into this new system in FY2019. For rock and sediment core samples, information forwarding from management-level system (JSDB) to public-level system (DARWIN) is planned to be established in the near future.

JSDB consists of data tables for sample matadata information for onboard sampling activities, sample archive information for status and storage of physical samples, associate data information for various data obtained for samples, literature information for published documents, sample distribution information for service logs for sample requests. User authorization includes group setting, enabling individual sample holders outside Data Management Office to read, create and modify the information in an appropriate manner, although the DB is only accessible from inside JAMSTEC because of security reasons. Associate data information is supposed to include various data types, such as photos/images, text-based descriptions, spread-sheets and URLs etc., and open/close status control and group-setting are available for individual entries. Information for research proposals/projects or other data management issues, which should be associated with multiple samples, can also be managed as associated data information. For the future possibility of involvement with IGSN, sample metadata entries and their vocabulary are reorganized to follow the IGSN Descriptive Metadata [4], as much as possible.

Peoples involved in sample and data management tend to spend much effort for dealing with unusual conditions/situations which are not originally expected. Robustness is important for design/operation of information systems, because lack of flexibility and too much complexity of information systems are frequent causes of such kind of problems.

[*1]Japan Agency for Marine-Earth Science and Technology, [*2]Atmosphere and Ocean Research Institute, the University of Tokyo, [*3]Joint Usage/Research Center for Atmosphere and Ocean Science, *[4]Inernational Geo Sample Number

[1] AORI website for Cooperative Research: https://www.aori.u-tokyo.ac.jp/coop/
[2] JAMSTEC DARWIN website: http://www.godac.jamstec.go.jp/darwin/
[3] JAMSTEC Marine Biological Sample Database: http://www.godac.jamstec.go.jp/bio-sample/

©2020. Japan Geoscience Union. All Right Reserved.

[4] SESAR website; https://www.geosamples.org/metadata

Keywords: Sample, Curation, Database

©2020. Japan Geoscience Union. All Right Reserved.

Improving the Reusability of Data and Sample Obtained JAMSTEC's Research Vessels and Submersibles

*Kazuyo Fukuda[1], Hajime Kawakami[1], Hiroki Horikawa[1], Tomoki Sasaki[1], Takako Sato[1], Takayuki Tomiyama[1], Makoto Ito[1], Yasumi Toyoda[1], Hideaki Saito[1], Chizuru Saito[1]

1. Japan Agency for Marine-Earth Science and Technology

Japan Agency for Marine-Earth Science and Technology (JAMSTEC) has been disseminated information of data and samples obtained by JAMSTEC's research vessels and submersibles via some databases. The core database is the Data and Sample Research System for Whole Cruise Information (DARWIN, http://www.godac.jamstec.go.jp/darwin/e). DARWIN provides information of more than 2000 cruises and 6500 dives, and its related observation data and geological sample. Each cruise or dive information page of DARWIN has links to related contents such as biological sample, deep-sea image, cruise report and data book provided by another databases.

In this poster, we will introduce some examples of efforts to improve the reusability of data and sample described above.

- Assignment of Digital Object Identifier (DOI): DOIs have been assigned to more than 2000 research cruises information from the early 1980s onward to promote data citation. A granularity of DOI is a research cruise information page defined as a cruise ID at this time.

- Specification of Data Policy: DARWIN has been treated data and samples based on only JAMSTEC data policy until FY2018’s research cruises. Currently, the applicable policy is dependent on type of cruise because the cooperative research cruises have been started since FY2019. DARWIN has been updated to display of an applicable policy on each information page clearly. The function is also available to add to another policy in the future.

- Data Rescue: A cruise report is a prompt report that includes the purpose of the cruise, information about what kind of observation was done, how it was done and the results. Cruise reports for past research cruises have been found when moving laboratory and submitted to the Data Management Group. The reports have been scanned and saved as individual PDF to store for long-term and prepare for publication. A part of them with Principle Investigators' consent have been disseminated step by step.

Keywords: data sharing, FAIR data principles

©2020. Japan Geoscience Union. All Right Reserved.

Activities toward research data management at NIES/CGER

*Yoko Fukuda[1], Chisato Wada[1], Yasuhiro Tsukada[1], Jiye Zeng[1], Tomoko Shirai[1]

1. National Institute for Environmental Studies

The Center for Global Environmental Research (CGER), National Institute for Environmental Studies (NIES), has been managing and operating the Global Environmental Database (GED) since May 2014 as a platform for publication and search of data focusing on global environmental research including global warming. DOIs have been assigned to research data sets since 2016, and data have been regularly updated. Nowadays, more and more academic publishers ask authors to publish data used in papers online. Inquiries regarding the publication and DOI minting of evidential data and submissions to data journals are increasing at NIES/CGER. In addition, funding agencies are starting to request researchers to submit a research data management plan that contains policies for storing, managing, and sharing of research data and where to store them when they will be opened. There is an increasing demand to develop a persistent system to store and manage research data.
NIES/CGER has developed a research data management system (RDMS) as a data management platform so that researchers and research assistants can efficiently perform routine research data management and preparation for data publication. The RDMS mainly provides functions to support creating metadata which are essential to search and utilize datasets, versioning, DOI minting and licensing. Research data and metadata registered in the RDMS can be promptly released through GED using a back-end database shared by the RDMS and GED. “Public” or “private” can be set for each data file so that users can also manage private datasets in the RDMS. Access users can also be set for each dataset so that multiple members involved in a project can cooperatively manage their datasets and share update histories. When a user logs in to the RDMS, a list of datasets that the user can access is displayed, and the status indicating the work progress is displayed for each dataset. Moreover, users can visualize research data on a quick plot tool, with which they can set graph types, display parameters, display ranges, and axis titles. In this presentation, we introduce the RDMS and GED currently under development.

Keywords: Research data management, Open science, Open data

©2020. Japan Geoscience Union. All Right Reserved.

[E] Poster | M (Multidisciplinary and Interdisciplinary)：M-GI General Geosciences, Information Geosciences & Simulations

[M-GI37] Integration of Earth Observations and Multiple Use for Earth Science and Benefits to Societies - GEO

convener:Hiroyuki Muraoka(River Basin Research Center), Kentaro Ando(Japan Agency for Marine and Earth Science and Technology), Osamu Ochiai(Japan Aerospace Exploration Agency), Shinichi Sobue(Japan Aerospace Exploration Agency)

Earthquakes and tsunamis, floods and drought, environment deterioration and pollution, global warming and island losing, and ecosystem degradation endanger the security of water, food, energy, health and ecosystem services. To confront these challenges, there is a demand to foster its application capacity and to develop integrated, sharable, and sustained observation systems. Group on Earth Observations (GEO) is a partnership of 107 national governments including Japan and 132 Participating Organizations that envisions a future where decisions and actions for the benefit of humankind are informed by coordinated, comprehensive and sustained Earth observations. There is a unique regional activity focusing on the Asia-Oceania (AO) region which poses big challenges to the society with its large population, various and fast environmental changes and frequent natural disasters. To develop such capacity, it is necessary to promote a regional cooperation on earth observation with various communities. AOGEO aims to foster regional application activities focusing on water security, biodiversity, carbon and greenhouse gas, ocean and islands, and food security, etc. It is also seeking data sharing, Open Data Cube for AO region and user engagement and communication.
This session aims to 1) introduce the current status of data integration efforts in GEO and AOGEO, 2) engage any contributions of similar activities from outside of GEO and AOGEO, and 3) activate GEO and AOGEO activities and its related activities via any submissions and contributions of analysis of earth observations both from integrated data and single unique data on the earth science and societal applications. We seek submissions which include a) scientific researches by use of earth observation data from various platforms including satellite and in-situ, b) development of new data sets for national, regional and global analyses, and c) development of data integration platform and its broad application.

[MGI37-P01] Biodiversity and ecosystem observations by Asia Pacific Biodiversity Observation Network (APBON)

*Hiroyuki Muraoka[1], Yayoi Takeuchi[2], Takehisa Yamakita[3], Yuichi Kano[4], Shin Nagai[3], Sheila Vergara[5], Eun-Shik Kim[6], Tetsukazu Yahara[4,7] (1.Gifu University, 2.National Institute for Environmental Studies, 3.Japan Agency for Marin-Earth Science and Technology, 4.Kyusyu University, 5.ASEAN Centre for Biodiversity, 6.Kookmin University, 7.Kyusyu Open University)

[MGI37-P02] Ocean data networks and its utilization in Asia-Oceania region - challenges in AOGEO

*Kentaro Ando[1], Andy Steven[2], Aidy Mohamed Shawal M Muslim[3], Danling Tang[4], Fumihiko Akazawa[1] (1.Japan Agency for Marine and Earth Science and Technology, 2.Commonwealth Scientific and Industrial Research Organisation, 3.University Malaysian Terenganu, 4.South China Sea Institute of Oceanography)

[MGI37-P03] Multidisciplinary efforts towards regional to global scale CO_2 budget estimation

*Kazuhito Ichii[1], Masayuki Kondo[1], Prabir Patra[2], Nobuko Saigusa[3], Josep Canadell[4] (1.Chiba University, 2.Japan Agency for Marine-Earth Science and Technology, 3.National Institute for Environmental Studies, 4.Commonwealth Scientific and Industrial Research Organisation)

Biodiversity and ecosystem observations by Asia Pacific Biodiversity Observation Network (APBON)

*Hiroyuki Muraoka[1], Yayoi Takeuchi[2], Takehisa Yamakita[3], Yuichi Kano[4], Shin Nagai[3], Sheila Vergara[5], Eun-Shik Kim[6], Tetsukazu Yahara[4,7]

1. Gifu University, 2. National Institute for Environmental Studies, 3. Japan Agency for Marin-Earth Science and Technology, 4. Kyusyu University, 5. ASEAN Centre for Biodiversity, 6. Kookmin University, 7. Kyusyu Open University

The Asia-Pacific (AP) Region encompasses 28 million square kilometers of land area, which is approximately 22 percent of the total global land area, across over different climatic conditions, rich natural resources, and diverse culture. Also, the region contains some of the longest rivers and extensive deltas in the World, the majority of continental and oceanic islands, various coastal ecosystems including mangroves and coral reefs, and large portions of the Pacific Ocean and the Indian Ocean (IPBES 2018). The region account for approximately 54% of global population (UNEP 2016) and hosts 13 of the total 35 biodiversity hotspots and accounts for nearly one third of all the threatened species in the world (CEPF 2015). Having entered the “Asian Millennium,” many countries in AP region are now rapidly growing their economies and social infrastructures. This development is causing the rapid loss of Asian biodiversity, and thus prompting work toward achieving a more sustainable balance between development and conservation is a highly urgent task in the region (IPBES 2018). These circumstances call for interactions and partnerships that will integrate available information, appropriately document those that are being discovered and promote the exchange and use of such information in biodiversity conservation and policy development. Asia is now regarded by many scientists as the most biotically threatened part of the planet, yet to mediate this loss further data is needed to develop baselines on biodiversity and assay patterns of diversity and threat. Science is expected to play a leading role in the area of biodiversity, including characterizing the biodiversity of various areas, clarifying ecosystem services supplied to society, quantifying how rapidly biodiversity is being lost, and justifying needs and identifying possibilities for conservation and sustainable use of biodiversity.

The AP Biodiversity Observation Network (APBON) was established in order to network institutions and research groups in AP region that contribute to and utilize a knowledge resource base for decision making and policy for the conservation of biodiversity and ecosystems. It was launched in 2009, by responding to Biodiversity Observation Network under the Group on Earth Observations (GEO BON) in 2008. Since then, APBON aimed at promoting biodiversity monitoring and contribution to sound decision-making based on scientific knowledge. To do so, APBON facilitates the organization of and periodically convenes a regional network of biodiversity observation institutions to maintain a knowledge base that will support biodiversity conservation. APBON focuses on terrestrial, freshwater and marine systems to develop the observations and ecosystem service assessment.

In this paper we review how APBON has achieved developing networks; we have facilitated the communication and interaction opportunities inter-/intra- researchers and stakeholders through workshops and publications. APBON successfully developed as a network of biodiversity scientists belonging to many institutes of AP region (Yahara et al. 2014). APBON has also contributed to networking biodiversity-related bodies and programs including CBD, GBIF, IUCN, International Long-Term Ecological Research–East Asia–Pacific Regional Network (ILTER-EAP) and Asia Oceania GEO (AOGEO). The multidisciplinary efforts in APBON also contributed to develop a strategy for the Earth observation for biodiversity monitoring by connecting in-situ and satellite observations. We also developed tools for data

©2020. Japan Geoscience Union. All Right Reserved.

collection, sharing, analysis, and synthesis for further observations and capacity building. Contributions to carrying out assessments such as IPBES, which contributed to improving ecosystem management and sustainable use of biodiversity, are also highlighted.

Keywords: biodiversity, climate change, ecosystem services, forest loss, landuse change

©2020. Japan Geoscience Union. All Right Reserved.

Ocean data networks and its utilization in Asia-Oceania region - challenges in AOGEO

*Kentaro Ando[1], Andy Steven[2], Aidy Mohamed Shawal M Muslim[3], Danling Tang[4], Fumihiko Akazawa[1]

1. Japan Agency for Marine and Earth Science and Technology, 2. Commonwealth Scientific and Industrial Research Organisation, 3. University Malaysian Terenganu, 4. South China Sea Institute of Oceanography

Ranging from the mountaintops of the Himalaya to small atoll nations in the Pacific Ocean, the Asia-Oceania (AO) region encompasses two-thirds of the world's population, that live in more than 60 countries that vary in size, economy, development status and environmental condition. With continuing development, particularly urbanization, the AO region is subject to rapid and widespread environmental changes that result in environmental deterioration, habitat and biodiversity loss and pollution that even reaches to the farthest waters for the Pacific. Sustainable development must therefore be based on a comprehensive assessment of disaster and environmental risks, along with their potential ramifications for environmental security and human well-being.

Thus, the Group of Earth Observation (GEO) has developed a new regional initiative, Asia Ocean GEO (AOGEO), that seeks to exploit coordinated access to earth observations to support sound decision-making at local, national and regional scales.

Under the AOGEO, the “Ocean, Coasts and Islands Task” promotes better access to marine data through: interoperability of data such as catalogues of state owned-data; standardization of in situ and satellite data through the development and application of standards including Analysis Ready Data (ARD), that provide confidence and consistency, and to better validate satellite based marine and coastal products by applying in-situ observation for calibration, validation and algorithm processing. OCI continues to build upon its user-engagement activities with Oceania states to provide capacity building and training, develop regionally-specific best-practice EO methods and products that are useful to these communities in addressing climate, environment and livelihood issues.

Keywords: Group on Earth Observation, Asia-Oceania GEO, earth observation data

©2020. Japan Geoscience Union. All Right Reserved.

Multidisciplinary efforts towards regional to global scale CO_2 budget estimation

*Kazuhito Ichii[1], Masayuki Kondo[1], Prabir Patra[2], Nobuko Saigusa[3], Josep Canadell[4]

1. Chiba University, 2. Japan Agency for Marine-Earth Science and Technology, 3. National Institute for Environmental Studies, 4. Commonwealth Scientific and Industrial Research Organisation

The estimation of greenhouse gas (GHG) emissions and removals from the country to the global scales is essential to assess progress towards the goals of the Paris Agreement. The “global stocktake”, specifically aiming to track such progress, provides an important opportunity for the scientific community to contribute towards the development of key indices and measures. The development of country-scale CO2 budgets are one of such measures. In the Asia-Oceania GEO (AO-GEO) framework, Taskgroup-3: Carbon and GHG Monitoring is expected to contribute to the development of greenhouse gases budgets.

In this presentation, we will show the current activities on this Task group. In particular, we will report on the refinements of both top-down and bottom-up estimate approaches, high-level syntheses , and application of recently available new observation datasets to better understand and constrain carbon budgets at the country, continental, and global scales.

Keywords: Carbon cycle, Synthesis, Paris Agreement

©2020. Japan Geoscience Union. All Right Reserved.

[E] Poster | M (Multidisciplinary and Interdisciplinary)：M-AG Applied Geosciences

[M-AG42] CTBT IMS Technologies for Detecting Nuclear Explosion and Their Applications to Earth Science

convener:Ozel Nurcan Meral(Comprehensive Nuclear-Test-Ban Treaty Organization), Hiroyuki Matsumoto(Japan Agency for Marine-Earth Science and Technology), Noriko Kamaya(Earthquake Research Institute, The University of Tokyo), Yosuke Naoi(Japan Atomic Energy Agency)

The Comprehensive Nuclear-Test-Ban Treaty Organization (CTBTO) was founded in 1996 in response to the adaption of the Treaty in 1996 by the United Nations General Assembly, which bans nuclear explosions on the Earth's surface, in the atmosphere, underwater and underground. The Treaty has a unique and comprehensive verification regime to make sure that nuclear explosion goes detected. The regime is supported by International Monitoring System (IMS) composed of the four state-of-the-art technologies; 1) Seismic, 2) Hydroacoustic, 3) Infrasound, and 4) Radionuclide, by the International Data Centre (IDC), and by the On-Site Inspections (OSI).
IMS will, when complete, consists of 337 facilities worldwide to monitor the planet for signs of nuclear explosion. Around 90 % of the facilities are operational and sending the data to the IDC in Vienna, Austria.
The huge amount of data collected by the IMS network can be used for other purposes such as civil and scientific applications in addition to detecting nuclear explosions. For example, they can provide Tsunami Warning centers with near real-time information about an underwater earthquake. The data could also help better understand of earthquakes, volcanoes, oceans, climate change, and other issues on our planet.
This session will provide the overview of the IMS, the scientific discussion on each technology, and its outcomes. The session strongly welcomes young scientists and engineers who are interested in four IMS technologies.

[MAG42-P01] Overview of Integrated Operational Exercise conducted under CTBT national operational system in Japan.

*RYOHEI EMURA[1], Takayuki Otsu[1], Masashi Motohashi[1], Toyomi Sakamoto[1], Soshi Iwata[1], Takanari Fujii[1], Mami Nogami[1], Makiko Iwakuni[1] (1.Japan Weather Association)

[MAG42-P02] Contribution of the hydroacoustic hydrophone stations of the International Monitoring System to natural disaster mitigation

*Hiroyuki Matsumoto[1], Mario Zampolli[2], Georgios Haralabus[2], Jerry Stanley[2], Nurcan Meral Özel[2] (1.Japan Agency for Marine-Earth Science and Technology (JAMSTEC), 2.Comprehensive Nuclear-Test-Ban Treaty Organization (CTBTO))

[MAG42-P03] Detection of hydroacoustic signals associated with the 2015 Torishima volcanic tsunami earthquake

*Hiroko Sugioka[1], Natsuo Nemoto[1] (1.Kobe University)

[MAG42-P04] **Noble Gas Joint Measurement Project regarding CTBT**

*Yuichi Kijima[1], Yoichi Yamamoto[1], Yutaka Tomita[1] (1.Japan Atomic Energy Agency)

Overview of Integrated Operational Exercise conducted under CTBT national operational system in Japan.

*RYOHEI EMURA[1], Takayuki Otsu[1], Masashi Motohashi[1], Toyomi Sakamoto[1], Soshi Iwata[1], Takanari Fujii[1], Mami Nogami[1], Makiko Iwakuni[1]

1. Japan Weather Association

Japan Weather Association (JWA) is working as the Comprehensive Nuclear-Test-Ban Treaty (CTBT) National Data Centre-1 (NDC-1) of Japan. JWA is in charge of analysis on waveform data, operation and maintenance of seismic and infrasound stations in Japan as for Station Operator (SO).
NDC-1 has two main roles of 1: Collect and analyze waveform data related to seismic and infrasound waves and provide advice from a technical perspective and 2: Operation and maintenance of monitoring facilities of the International Monitoring System (IMS) (8 sites in Japan)
As a part of the provisional operation at NDC-1, in cooperation with the Secretariat and NDC-2, integrated operation exercises with continuous monitoring for one week are conducted a few times per a year. The purpose of these exercises is to contribute to the training of analysts, as well as to catch up issues and problems in automatic seismic wave monitoring system operation and manual analysis operation. It also aims to verify the analysis results by an automatic system and by analysts.
Assuming a nuclear test monitoring activity during the full operation of NDC-1, the test operation of the automatic seismic wave monitoring system is performed, and if the occurrence of an event is suggested within the preset monitoring target areas, the analyst conducts a detailed analysis and closely examines the location and characteristics of the event (whether or not it is an explosion event). In addition, we summarize exercises results, verify analysis results, and extract issues after ending integrated operational exercise.
Furthermore, in order to address the issues and problems that became apparent through the integrated operation exercises, monitoring techniques and analysis methods have been improved. The results of studies on improvement and advancement of monitoring technology and analysis methods will be reflected in the various systems in operation. It will be verified through the next integrated operation exercise.
In this presentation, we will also introduce the approaches including cooperation with the Secretariat and NDC-2.

Keywords: CTBT, National Data Centre, seismic, waveform analysis, event discrimination analysis

©2020. Japan Geoscience Union. All Right Reserved.

Contribution of the hydroacoustic hydrophone stations of the International Monitoring System to natural disaster mitigation

*Hiroyuki Matsumoto[1], Mario Zampolli[2], Georgios Haralabus[2], Jerry Stanley[2], Nurcan Meral Özel[2]

1. Japan Agency for Marine-Earth Science and Technology (JAMSTEC), 2. Comprehensive Nuclear-Test-Ban Treaty Organization (CTBTO)

In-situ data recorded by the water-column hydrophones of the hydroacoustic (HA) stations of the International Monitoring System (IMS) of the Comprehensive Nuclear-Test-Ban Treaty (CTBT) are examined. The main objective of this study is to share the knowledges and understand how the IMS HA facilities contribute to natural disaster mitigation through the examination of in-situ data of the IMS hydrophones. The first part of the presentation is focusing on the detectability of tsunami by the IMS hydrophones. Data of the IMS hydrophones station HA11, Wake Island (U.S. Territory) at the Tohoku, Japan earthquake in 2011 are examined. The HA11 station which is about 3100 km southeast from the source area could detect tsunami signals in addition to T-phase associated with the main shock. It is evidenced that the theoretical dispersion curve of surface gravity wave follows the dispersive feature recorded at the frequency range less than 10^{-2} Hz. The similar result could be obtained at HA03, Juan Fernandez Islands during the Chile earthquake in 2015. These instances suggest that the tsunami signals can be identified by the water-column hydrophones at the time when tsunami propagates over the IMS hydrophone stations. The second part of the study is focusing on the hydroacoustic signals originated from the submarine eruptions of Ioto, a volcanic island of Japan. Cross-correlation analysis is applied to the hydrophone triplet data of HA11, about 2700 km away from the volcano to estimate the direction-of-arrival (DOA) of hydroacoustic signals of the entire period of September in 2018. Volcanic seismicity based on the on-site observation had become higher than usual, and discolored waters and a splash were observed nearshore by a local flyover during this period. Although hydroacoustic signals associated with seismic activities in the Pacific region are usually apparent, it is possible to discriminate between Ioto volcanic activity and other seismic activities based on the DOA. Our analysis suggests that about three-fourth of detectable hydroacoustic signals were associated with the submarine eruptions of Ioto. The analysis of hydroacoustic data recorded at the IMS hydrophone station HA11 shows that the remote hydrophones appear to be capable of detecting and identifying signals from submarine volcanic eruptions at distances of 1000’s of kilometers.

©2020. Japan Geoscience Union. All Right Reserved.

Detection of hydroacoustic signals associated with the 2015 Torishima volcanic tsunami earthquake

*Hiroko Sugioka[1], Natsuo Nemoto[1]

1. Kobe University

On 2015 May 2, a submarine earthquake occurred underneath the Smith Caldera near Torishima on the Izo-Bonin arc, Japan. The occurrence of such earthquakes is quasi-regular, approximately every 10 years, always accompanying anomalously large tsunamis. The focal mechanism is always a type of non–double couple known as compensated linear vector dipole (CLVD) with the vertical T axis. The moment magnitude is always 5.6 to 5.7. Most CLVD earthquakes with a vertical T (or P) axis have been reported at active volcanoes on land or on an island but not under the sea. The Torishima earthquakes are unique in that they are submarine CLVD events accompanying anomalously large tsunamis (Satake and Kanamori, 1991; Kanamori et al., 1993) and successive T-wave trains (Sugioka et al., 2000). Its mechanism of the 2015 earthquake was estimated as a CLVD with vertical opening of the shallow horizontal tensile fault (Fukao et al., 2018).

We calculated the autocorrelation function of data recorded on hydrophones of the Dense Oceanfloor Network system for Earthquakes and Tsunamis system (DONET) to improve the noise to signal ratios. We extracted significant hydroacoustic signals at the frequency of around 1.3 Hz associated with the 2015 Torishima volcanic tsunami earthquake.

Keywords: volcanic tsunami earthquake, CLVD, hydroacoustic

©2020. Japan Geoscience Union. All Right Reserved.

Noble Gas Joint Measurement Project regarding CTBT

*Yuichi Kijima[1], Yoichi Yamamoto[1], Yutaka Tomita[1]

1. Japan Atomic Energy Agency

The Japan Atomic Energy Agency has been conducting the measurement of radioxenon using the transportable xenon laboratories (TXLs) at Horonobe, Hokkaido and Mutsu, Aomori since 2018, as part of the noble gas joint measurement project with CTBTO, which is aimed at contribution in better understandings of the measurement data obtained at the CTBT International Monitoring System (IMS) Takasaki radionuclide station. The comparison among the measurement results of radioxenons at 3 measuring points (Horonobe, Mutsu and Takasaki) since 2018, and the analyses results by atmospheric transport modelling (ATM) on estimation of emission source of radioxenon detected will be reported.

©2020. Japan Geoscience Union. All Right Reserved.

[E] Poster | M (Multidisciplinary and Interdisciplinary)：M-AG Applied Geosciences

[M-AG43] The Application Usability Level (AUL): A Standard Measure of Progress to Benefit Space Research

convener:Jeffrey Klenzing(NASA Goddard Space Flight Center), Adam C Kellerman(University of California Los Angeles), Brett A Carter(RMIT University), Tam Dao(Geospatial Center, RMIT University)

As space physics becomes both more interdisciplinary and more intertwined with commercial and government operations, there has risen a need for improved communication between different groups, and a system for tracking the progress of a project towards the specific application for a given user. The Application Usability Level (AUL) framework was developed precisely for this task, and in addition, encourages publication of instrument-like papers for delivering and publicizing AULs to help the community quantify the progress of successful applications, metrics, and validation efforts.

In a given project within the AUL framework, there is typically a diverse eco-system of individuals necessary to ultimately produce a useful space weather product or productive research collaboration. For example, in the case of non-academic fields, users and researchers alike may benefit from a translator, i.e. a broker, who may help with the effective transition from research to operations. Independent validators are another essential player for validation efforts and comparing like products for a specified application. In many cases the different players throughout the process will act in multiple roles as well as act in different roles for different projects and AUL pathways.

We invite papers to this session that show projects which are using the AUL framework, have found new research and applications through transdisciplinary interactions, or describe how a project moves through this eco-system and the players involved.

[MAG43-P01] HF-START web tool

★Invited Papers

*Kornyanat Hozumi[1], Ryo Nakao[2], Hiroyuki Nakata[2], Susumu Saito[3], Takuya Tsugawa[1], Chihiro Tao[1], Hidekatsu Jin[1], Masato Nagahara[1], Mamoru Ishii[1] (1.National Institute of Information and Communications Technology (NICT), Tokyo, Japan, 2.Graduate School of Engineering, Chiba University, Chiba, Japan, 3.National Institute of Maritime, Port and Aviation Technology, Electronic Navigation Research Institute (ENRI), Tokyo, Japan)

[MAG43-P02] On the assessment of daily Equatorial Plasma Bubble occurrence modeling and forecasting

*Brett A Carter[1], Julie Currie[1], Tam Dao[1], Endawoke Yizengaw[2], John Retterer[3], Michael Terkildsen[4], Keith Groves[3], Ronald Caton[5] (1.RMIT University, 2.Aerospace, 3.Boston College, 4.Bureau of Meteorology, 5.Air Force Research Laboratory)

[MAG43-P03] The sami2py ionospheric model: a Phase 1 AUL project

*Jeffrey Klenzing[1], Jonathon Smith[1,2], Alexa Jean Halford[1], Michael Hirsch[3], Joe Huba[1,4] (1.NASA Goddard Space Flight Center, 2.Catholic University of America, 3.Boston University, 4.Symtek)

HF-START web tool

*Kornyanat Hozumi[1], Ryo Nakao[2], Hiroyuki Nakata[2], Susumu Saito[3], Takuya Tsugawa[1], Chihiro Tao[1], Hidekatsu Jin[1], Masato Nagahara[1], Mamoru Ishii[1]

1. National Institute of Information and Communications Technology (NICT), Tokyo, Japan, 2. Graduate School of Engineering, Chiba University, Chiba, Japan, 3. National Institute of Maritime, Port and Aviation Technology, Electronic Navigation Research Institute (ENRI), Tokyo, Japan

To improve communication between space weather research groups and radio propagation users, the radio propagation subgroup was started in the A01 group (Space Weather Forecast System) under the PSTEP (Project for Solar-Terrestrial Environment Prediction) umbrella in early 2016. Day-to-day bottom side variation of ionosphere has great influence on availability and integrity of radio waves in high frequency (HF, 3-30 MHz) band. We, therefore, developed the HF propagation simulator that is capable with the realtime realistic ionospheric information. The simulator name is HF-START (HF Simulator Targeting for All-users' Regional Telecommunications).

Recently, the HF-START web tool has been being prepared for public users. We have been working toward a development of a near realtime service. No prerequisite on space weather knowledge is required to use the HF-START web tool. The HF-START web tool will have a closed test service within NICT from March 2020. Its service will be opened to the public later. We open for international collaboration to gain global competitiveness on the service.

Keywords: HF-START, Radio Propagation Simulator, Space Weather, Ionosphere, HF

©2020. Japan Geoscience Union. All Right Reserved.

On the assessment of daily Equatorial Plasma Bubble occurrence modeling and forecasting

*Brett A Carter[1], Julie Currie[1], Tam Dao[1], Endawoke Yizengaw[2], John Retterer[3], Michael Terkildsen[4], Keith Groves[3], Ronald Caton[5]

1. RMIT University, 2. Aerospace, 3. Boston College, 4. Bureau of Meteorology, 5. Air Force Research Laboratory

The prediction of Equatorial Plasma Bubbles (EPBs) on a daily basis is an ongoing scientific challenge, despite decades of observations and research. Various methods for predicting the onset of EPBs have now been developed, however the research community is yet to investigate the methods for which these prediction models and techniques can be meaningfully evaluated and compared. Various assessment metrics, including percentage correct (PC), the Heidke Skill Score (HSS) and the True Skill Statistic (TSS), have been reported for space weather predictions, but the validity of their use for the purpose of EPB prediction assessment has yet to be investigated. In this study, 12 months of co-located GPS and UHF scintillation observations from locations spanning South America, Atlantic/Western Africa, Southeast Asia and Pacific sectors is used to evaluate the Generalized Rayleigh-Taylor (R-T) plasma instability growth rates calculated from the Thermosphere Ionosphere Electrodynamics General Circulation Model (TIEGCM). As part of this analysis, the limitations and caveats in using various assessment metrics are explored. In particular, the impact of employing significance testing on skill scores as a means of selecting thresholds is demonstrated. The sensitivity of the HSS, TSS and the Odds Ratio Skill Score (ORSS) to dataset type (i.e., GPS versus UHF) and dataset size (30, 50, 60 and 90 days/events) is also investigated, and it is shown that when a minimum of 50 days is used then the resulting TSS and ORSS values are similar. Further, it is shown in this analysis that to achieve statistically significant TSS and ORSS values 50 days/events are required. To investigate methods for conducting model-model comparisons, the TIEGCM R-T growth rate is compared to the ‘persistence’ forecast using the ORSS, but it is shown that the levels of 95% significance do not clearly indicate which model/method is higher quality. To that end, the concept of forecast ‘sufficiency’ is used as a direct comparison between the TIEGCM R-T growth rate the persistence forecast, and the results were found to be mixed across the different stations and EPB seasons. Importantly, throughout most of the datasets, these EPB prediction techniques were found to be of comparable quality (i.e., ‘insufficient for each other’). In this analysis, a valuable lesson learned is that it is important that the observation dataset exhibits an appropriate level of daily EPB variability in order to be used as a valid model/technique evaluation. The UHF observations from South America tended to show little daily variability in this analysis, therefore preventing any conclusive model-model comparison. Recommendations for how to meaningfully use skill scores and ‘sufficiency’ to track EPB forecast model/technique progress are given.

Keywords: Equatorial Plasma Bubbles, Ionospheric scintillations, Forecast assessment

©2020. Japan Geoscience Union. All Right Reserved.

The sami2py ionospheric model: a Phase 1 AUL project

*Jeffrey Klenzing[1], Jonathon Smith[1,2], Alexa Jean Halford[1], Michael Hirsch[3], Joe Huba[1,4]

1. NASA Goddard Space Flight Center, 2. Catholic University of America, 3. Boston University, 4. Symtek

Sami2py is a python module that runs the SAMI2 ionospheric model, as well as archives, loads and plots the resulting modeled values. SAMI2 is a model developed by the Naval Research Laboratory to simulate the motions of plasma in a 2D ionospheric environment along a dipole magnetic field [Huba et al, 2000]. SAMI2 solves for the chemical and dynamical evolution of seven ion species in this environment (H^+, He^+, N^+, O^+, N_2^+, NO^+, and O_2^+). The python implementation allows for additional modifications to the empirical models within SAMI2, including reduction of the exospheric temperature in the NRLMSIS thermosphere and the input of custom ExB ion drifts.

The code is open source and available to the community on github. As part of the Application Usability Level (AUL) framework, we will discuss the usability of this code in terms of simple ionospheric applications, including as a core dependence of the “growin” project.

Keywords: ionosphere, model, space weather

©2020. Japan Geoscience Union. All Right Reserved.

[E] Poster | M (Multidisciplinary and Interdisciplinary) : M-AG Applied Geosciences

[M-AG45] Satellite Land Physical Processes Monitoring at Medium/High/Very High Resolution

convener:Jean-Claude Roger(University of Maryland College Park), Shinichi Sobue(Japan Aerospace Exploration Agency), Eric Vermote(NASA Goddard Space Flight Center), Ferran Gascon(European Space Agency)

We solicit papers on the land physical processes monitoring. In particular, it will include the inversion and use of land products from medium, high, and very high spatial resolution. For the last years, medium, high, and very high resolutions became a useful and a powerful toll for Earth studies. Topics of interest mainly include (not limited to):- New developments for data processing, including atmospheric correction and cloud screening;- Analysis and correction of directional effects in land surface reflectances;- Use of time series of surface reflectances for land monitoring, including land cover classification and crop yield prediction (including data integration and data harmonization);- Development and use of new vegetation indices (i.e. red edge) and other products for agriculture applications;- Theoretical studies for sensors capabilities enhancements to future sensors at high/medium resolutions;- Use of products in agricultural monitoring applications (such as crop area, crop type, crop growing, yield estimation and prediction, damage assessment);- Agriculture monitoring algorithm description;- Evaluation or validation of potential products with ground measurements, official statistics;- International initiative to enhance Earth-Observing-based agricultural information.Depending on outcome, we think about a special issue.

[MAG45-P01] Toward a Consistent Data Records from Coarse, Medium and High Spatial Resolution Earth Observation Satellites

*Eric Vermote[1], Sergii Skakun[1,2], Jean-Claude Roger[1,2] (1.NASA Goddard Space Flight Center, 2.University of Maryland, Dept. of Geographical Sciences)

[MAG45-P02] Mapping and analysis of irrigation water quality index of Hisar district Haryana, India by using Surfer Software

*shilpa singh[1], Amit Kumar[1], Yogesh Pandey[1], JAHANGEER -[2] (1.SKUAST- Kashmir, 2.University of Nebraska)

[MAG45-P03] Aerosol models for satellite atmospheric corrections.

*Jean-Claude Roger[1,2], Eric Vermote[2], Sergii Skakun[1,2], William Rountree[1,2], Andres Santamaria Artigas[1,2], Natacha Kalecinski[1,2], Oleg Dubovik[4], Brent Holben[3] (1.University of Maryland College Park, Departement of Geographysical Sciences, College Park, MD 20742, USA, 2.Nasa Goddard Space Flight Center, Code 619, Greenbelt, MD 20771, USA, 3.Nasa Goddard Space Flight Center, Code 618, Greenbelt, MD 20771, USA, 4.Laboratoire d'Optique Atmospherique, University of Lille, Villeneuve d'Ascq, 59655, France)

[MAG45-P04] AVHRR LTDR product cloud and snow mask using Support Vector Machines

*Jose Luis Villaescusa[1,2], Eric Vermote[2], Jean-Claude Roger[1,2], Belen Franch[3,1], Sergii Skakun[1,2] (1.University of Maryland College Park, 2.NASA Goddard Space Flight Center, 3.Universitat de Valencia)

[MAG45-P05] Winter wheat yield assessment from Landsat 8 and Sentinel-2 data

*Sergii Skakun[1,2], Eric Vermote[2], Belen Franch[1,3], Jean-Claude Roger[1,2] (1.University of Maryland College Park, 2.NASA Goddard Space Flight Center, 3.University of Valencia)

[MAG45-P06] INDICATORS OF HIGH VARIABILITY COVER LAND with Landsat-8 and Sentinel-2

*Natacha kalecinski[1,2], Sergii Skakun[1,2], Jean-Claude Roger[1,2], Eric Vermote[2] (1.Department of Geographical Sciences, University of Maryland College Park, USA, 2.NASA Goddard Space Flight Center, Greenbelt, USA)

[MAG45-P07] CAMSIS: An Automated System for the Validation of Surface Reflectance from High Spatial Resolution Sensors

Eric Vermote[2], Joel McCorkel[3], *Andrés Eduardo Santamaría-Artigas[1,2], William Henry Rountree[1,2], Sergii Skakun[1,2], Belen Franch[4,1], Jean-Claude Roger[1,2] (1.University of Maryland, College Park, 2.NASA Goddard Space Flight Center Code 619, 3.NASA Goddard Space Flight Center Code 618, 4.Universitat de Valencia, Spain)

Toward a Consistent Data Records from Coarse, Medium and High Spatial Resolution Earth Observation Satellites

*Eric Vermote[1], Sergii Skakun[1,2], Jean-Claude Roger[1,2]

1. NASA Goddard Space Flight Center, 2. University of Maryland, Dept. of Geographical Sciences

Surface reflectance is one of the key products used in developing several higher-order land products, such as Vegetation Indices, Albedo and LAI/FPAR, it is therefore seminal to detecting trends in the biosphere and land surface and has been classed by NOAA as a “Fundamental Climate Data Record (FDCR) for Land”. Building a long-term surface reflectance data record of climate quality implies combining different instruments, sensors and satellites, accounting for different spatial resolutions and spectral characteristics, assuring consistent calibration, and correcting for atmospheric and directional effects. As the spatial resolution issue is addressed by aggregating the original data to a resolution still suitable for climate studies (e.g. 0.05 degree latitude, longitude), the instrument calibration becomes the first major hurdle one has to go through before being able to proceed any further.

In this work, we are using robust reflectance data records and inter-comparison methods that we have developed over the past several years (consisting of atmospheric correction, directional effect correction and spectral normalization) to establish and verify the inter-consistency of the reflectance products from the AVHRR sensors on-board NOAA 7, 9, 11, 14, 16, 17 and 18, the MODIS sensors on-board Aqua and Terra and the VIIRS sensors on-board Suomi-NPP and JPSS1 as well as OLCI/SLSTR from Sentinel 3. These approaches are also applied to high spatial resolution dataset from Sentinel 2A and 2B and Planet Lab.

Keywords: surface reflectance

©2020. Japan Geoscience Union. All Right Reserved.

Mapping and analysis of irrigation water quality index of Hisar district Haryana, India by using Surfer Software

*shilpa singh[1], Amit Kumar[1], Yogesh Pandey[1], JAHANGEER -[2]

1. SKUAST- Kashmir, 2. University of Nebraska

An investigation is carried out to analyze the underground water quality of 26 villages in Hisar for their quality parameters and comprehensively arriving at a single water quality index. The irrigation water samples were collected manually from the bore wells which are approximately equally distributed all over 26 villages of Hisar. The samples were analyzed using standard procedures in the laboratory (APHA, 1985). The parameters analyzed during the analysis are pH, EC, Chlorides, Calcium, Magnesium representation of irrigation water quality attributes using SURFER 7.0 for individual as well as weighted water quality index. From the investigation, it is clearly evident that the groundwater of the area needs some degree of treatment before consumption. Based on the investigations carried out, it is observed that Saharwa, Kanwari, Lakhpul, Kinala, Adampur, Chanotl and Bhaganal villages contain water quality very poor for irrigation purpose due to over salt accumulation. Necessary measures are to be taken to gain safe irrigation and drinking water to the people living in the villages. Total hardness was found to be very high in Kanwari and Lakhpul villages. Very high concentrations of chloride, calcium and magnesium were found in Mangali, Sisai , Salemgarh and Balaws villages. The water quality is good in Lawda, Bagla, Madha, Parba, Sarsod, Rajli, Siswal, and Dahima villages based on water quality index. The qater quality was found moderately food in Sundawas, Moth Rangran, Parbhuwala, Lohari Ragho and Masudpur villages.

Keywords: Water quality index, Irrigation, Concentration, Total hardness

©2020. Japan Geoscience Union. All Right Reserved.

Mapping and analysis of irrigation water quality index of Hisar District, Haryana , India by using Surfer Software

Shilpa Singh[1], Amit Kumar[2] , Yogesh Pandey[1], Jahangeer [3]
[1]Department of Soil and Water Engineering , COAE&T, SKUAST-K, Srinagar
[2]Department of Farm Power and Machinery , COAE&T, SKUAST-K, Srinagar
[3] Nebraska Water Center, University of Nebraska-Lincon

An investigation is carried out to analyze the underground water quality of 26 villages in Hisar for their quality parameters and comprehensively arriving at a single water quality index. The irrigation water samples were collected manually from the bore wells which are approximately equally distributed all over 26 villages of Hisar. The samples were analyzed using standard procedures in the laboratory (APHA, 1985). The parameters analyzed during the analysis are pH, EC, Chlorides, Calcium, Magnesium representation of irrigation water quality attributes using SURFER 7.0 for individual as well as weighted water quality index. From the investigation, it is clearly evident that the groundwater of the area needs some degree of treatment before consumption. Based on the investigations carried out, it is observed that Saharwa, Kanwari, Lakhpul, Kinala, Adampur, Chanotl and Bhaganal villages contain water quality very poor for irrigation purpose due to over salt accumulation. Necessary measures are to be taken to gain safe irrigation and drinking water to the people living in the villages. Total hardness was found to be very high in Kanwari and Lakhpul villages. Very high concentrations of chloride, calcium and magnesium were found in Mangali, Sisai , Salemgarh and Balaws villages. The water quality is good in Lawda, Bagla, Madha, Parba, Sarsod, Rajli, Siswal, and Dahima villages based on water quality index. The qater quality was found moderately food in Sundawas, Moth Rangran, Parbhuwala, Lohari Ragho and Masudpur villages.

Keyword: water quality index, irrigation, concentration, Total hardness.

©2020. Japan Geoscience Union. All Right Reserved.

Aerosol models for satellite atmospheric corrections.

*Jean-Claude Roger[1,2], Eric Vermote[2], Sergii Skakun[1,2], William Rountree[1,2], Andres Santamaria Artigas[1,2], Natacha Kalecinski[1,2], Oleg Dubovik[4], Brent Holben[3]

1. University of Maryland College Park, Departement of Geographysical Sciences, College Park, MD 20742, USA, 2. Nasa Goddard Space Flight Center, Code 619, Greenbelt, MD 20771, USA, 3. Nasa Goddard Space Flight Center, Code 618, Greenbelt, MD 20771, USA, 4. Laboratoire d'Optique Atmospherique, University of Lille, Villeneuve d’Ascq, 59655, France

The land surface reflectance is a fundamental climate data record at the basis of the derivation of other climate data records (Albedo, LAI/Fpar, Vegetation indices) and has been recognized as a key parameter in the understanding of the land-surface-climate processes.

This work relies on a generic approach developed to derive surface reflectance over land from a variety of sensors. The approach is based on the inversion of the radiative transfer equation in the Lambertian case, with no adjacency effects, that account for a simplified coupling of the absorption by atmospheric gases and scattering by molecules and aerosols as implemented in the 6SV radiative transfer code. The processing code relies on look-up tables generated by 6SV, for which the accuracy (~1%) has been well documented in several papers. The LaSRC code uses ancillary data such as pressure and gas concentrations but relies on a per pixel inversion of the aerosol properties to assure the best possible accuracy for the surface reflectance, as aerosols can be highly variable both in space and time. This new aerosol inversion builds on the extensive dataset acquired by the Terra platform, combining MODIS and MISR to derive an explicit and dynamic map of band ratio’s between blue and red channels and is a refinement of the operational approach used for MODIS and LANDSAT over the past 15 years. The aerosol inversion is generic and applicable to a variety of sensors. We use this basic approach to derive Landsat 8 and Sentinel 2 surface reflectance products for medium, high and very high spatial resolution (MODIS, VIIRS, LANDSAT, SENTINEL-2, WORLD VIEW 3…). The validation scheme is based on using aerosol models developed for each AERONET sites. We will present here the methodology to get these models. We will also show comparison of surface reflectance products with field measurements done by an instrument developed by us.

Finally, we will presents performances of LaSRC inter-compared with other operational approaches in the framework of the CEOS-ACIX (Atmospheric Correction Intercomparison eXercise) Calibration Validation Task co-Lead by ESA and NASA.

Keywords: Aerosol, Surface reflectance, Validation, Atmospheric corrections

©2020. Japan Geoscience Union. All Right Reserved.

AVHRR LTDR product cloud and snow mask using Support Vector Machines

*Jose Luis Villaescusa[1,2], Eric Vermote[2], Jean-Claude Roger[1,2], Belen Franch[3,1], Sergii Skakun[1,2]

1. University of Maryland College Park, 2. NASA Goddard Space Flight Center, 3. Universitat de Valencia

The Advanced Very High Resolution Radiometer (AVHRR) sensors aboard the different NOAA satellites provide a unique global remote sensing dataset that ranges from the 1980s to the present. Using these data, the NASA funded Long Term Data Record (LTDR) project aims to develop a quality and consistent Climate Data Record (CDR) of AVHRR data with the use of the Moderate Resolution Imaging Spectrometer (MODIS) instrument as a reference. The current product uses a simple climatology approach using the red band to mask clouds from land and has no internal algorithm to discern cloud from snow. Previous studies using AVHRR data make use of MODIS climatology or multispectral threshold techniques. In this study we aim to use both approaches to better detect clouds and snow. We do this by assigning a probability of belonging to each class according to the distance of each pixel to the average climatology MODIS pixel, and to the multispectral clusters obtained using MODIS bands analogous to AVHRR. These distances are then treated as independent variables in an SVM classification that best selects the threshold to increase the separability of the classes. First, this approach is tested on MODIS data, and then applied to AVHRR. The main objective is to increase the overall accuracy of the classification, since errors in the cloud/snow mask have a significant impact on accurately determining global long-term trends of level-2 parameters such as surface albedo and have a direct impact on the Earth’ s radiative forcing.

Keywords: AVHRR, LTDR, Cloud Mask, Snow detection, SVM

©2020. Japan Geoscience Union. All Right Reserved.

Winter wheat yield assessment from Landsat 8 and Sentinel-2 data

*Sergii Skakun[1,2], Eric Vermote[2], Belen Franch[1,3], Jean-Claude Roger[1,2]

1. University of Maryland College Park, 2. NASA Goddard Space Flight Center, 3. University of Valencia

Combination of data acquired by Landsat 8 and Sentinel-2 remote sensing satellites can provide high temporal resolution globally (3-5 days) (Li & Roy, 2017), which is critical for various applications requiring dense data time series. Previously, such (or better) high temporal resolution at global scale was available mainly for remote sensing sensors, which acquire daily data over Earth’ s surface, but at coarser spatial resolution (> 250 m) (Justice et al., 1998, 2013). The latter, for example, includes space-borne remote sensing sensors, such as MODIS, VIIRS, AVHRR, SPOT-VEGETATION. Taking into account an increased frequency of observations at moderate spatial resolution (<30 m), the assumption is that methods and models developed for generating products for coarse spatial resolution sensors can be ported to moderate spatial resolution sensors (Landsat 8/OLI, Sentinel-2/MSI). However, the practice shows that such transition is not always straightforward due to larger data gaps because of clouds and uneven coverage, sensor characteristics and increased spatial resolution (at least at the order of 10, when going from 250 m to 30 m).

Consider a crop yield assessment/forecasting application (Becker-Reshef et al., 2010a). The hypothesis is that satellite-based features, such as vegetation indices (VIs) or biophysical parameters derived at a single date or accumulated over some time period, can be correlated to crop yields (Johnson 2016, Meroni et al., 2016). Since the reference data on crop yields are mainly available at regional scale, the corresponding empirical models are built by averaging satellite-based features over those regions and correlating these derived variables to crop yields (Becker-Reshef et al. 2010b, Franch et al., 2015; Kogan et al., 2013). It is assumed that there is a homogeneity within the region in terms of crops grown and agricultural practices applied and, therefore, the averaging should be performed for satellite data acquired at the same (or approximately the same) stages of crop growth, meaning that the data are normalized. This is usually the case for coarse spatial resolution remote sensing sensors, which enable high likelihood of obtaining cloud-free data over the Earth’ s surface (Whitcraft et al., 2015a, 2015b). This is also evidenced by multiple successful applications of applying coarse spatial resolution satellite data to crop yield assessment and forecasting (Becker-Reshef et al. 2010b, Franch et al., 2015; Johnson 2016; Kogan et al., 2013; Kolotii et al., 2015; López-Lozano et al., 2015; Mkhabela et al., 2011).

However, this is not the case for moderate spatial resolution satellite data (<30 m). Irregular spatial coverage, when the area in question is covered by several “stripes” sensed at different times, and high revisit cycles lead to discrepancies in dates of cloud-free observations. Therefore, satellite data should be normalized for the further processing. Though a combination of Landsat 8 and Sentinel-2 offers high frequency of observations, discrepancies in available cloud-free data, however, will still exist. With more and more applications transitioning to a higher spatial resolution, it is important to explore and analyze the effect of those discrepancies on the quality of the resulting products. In the case of crop yield assessment, one of the important questions is as follows: How do discrepancies in dates of satellite observations influence the performance of empirical crop yield models at regional scale? The present study aims to address this question by documenting results of the study on building empirical models for winter wheat yield assessment with Landsat 8 and Sentinel-2 data in Ukraine. Through simulation modelling and analysis of real datasets, we show that satellite data normalization is critical in building robust crop yield models. Not performing satellite data normalization may lead to poorer performance of

©2020. Japan Geoscience Union. All Right Reserved.

the empirical crop yield model, which would be attributed not to the lack of correlation with satellite-derived variables, but rather to observation irregularities.

©2020. Japan Geoscience Union. All Right Reserved.

INDICATORS OF HIGH VARIABILITY COVER LAND with Landsat-8 and Sentinel-2

*Natacha kalecinski[1,2], Sergii Skakun[1,2], Jean-Claude Roger[1,2], Eric Vermote[2]

1. Department of Geographical Sciences, University of Maryland College Park, USA, 2. NASA Goddard Space Flight Center, Greenbelt, USA

In the actual context of constant increase in human population and climate warming, the land use is more than ever important for agriculture with issues like food production, irrigation, crop yield and fertilization. It is also important for forestry including various issues such as parasites spread, long term CO_2 storage or natural spaces near or inside large towns. The use of active and passive remote sensing from space allows us to have a better understanding of what is going on. The increase in satellite’s spatial and temporal resolutions offers an incredible tool which can be of great interest to study parameters at a national or continental scale.

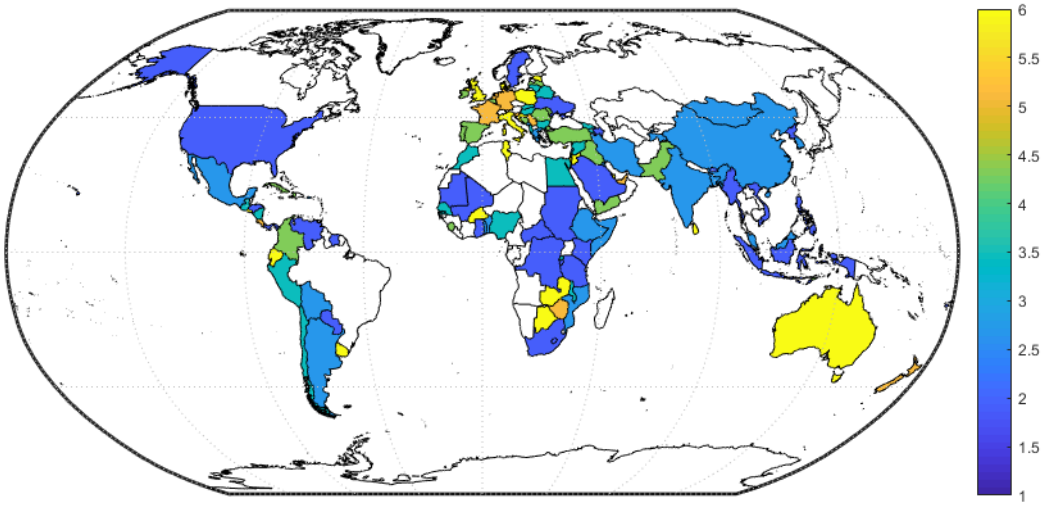
The aim of this study is to find indicators of drastic change of agriculture land cover over the globe in the first step and for particular countries in a second step.

We propose a study to link key parameters of agriculture land cover modifications from human activity and meteorological events. Even if it is difficult to quantify the quantity of earth change in land use, different database were developed like the one from Food and Agriculture Organization (FAO). We defined significant proxies and parameters to identify drastic changes as a marker of social changes for different countries during these 10 past years. The proxies used are trend, ramp rate, ramp amplitude of area, production, yield and importation/exportation. We can define a number of drastic events in agricultural cover for each country. The study is concentrated around the grass feet for a part and the crop land in the other part with the 6 majors crop: Soybean, Wheat, Maize, Rice, Millet, Sunflower.

To study high variability at the country’s scale, we combined the use of Sentinel-2 and Landsat-8 normalized difference vegetation index (NDVI). In complement to satellites dataset, ground base dataset such as meteorological stations helps us to better understand key parameters which can be related to actual land cover. Several approaches as high urbanization area, stability versus conflicts, deforestation and meteorological hazards are explored to provide a wide field of vision of actual and future agricultural practice.

Keywords: land cover, crop land, FAOSTAT, Sentinel-2 Landsat-8

©2020. Japan Geoscience Union. All Right Reserved.



©2020. Japan Geoscience Union. All Right Reserved.

CAMSIS: An Automated System for the Validation of Surface Reflectance from High Spatial Resolution Sensors

Eric Vermote[2], Joel McCorkel[3], *Andrés Eduardo Santamaría-Artigas[1,2], William Henry Rountree[1,2], Sergii Skakun[1,2], Belen Franch[4,1], Jean-Claude Roger[1,2]

1. University of Maryland, College Park, 2. NASA Goddard Space Flight Center Code 619, 3. NASA Goddard Space Flight Center Code 618, 4. Universitat de Valencia, Spain

We present CAMSIS, an automated system for the validation of satellite surface reflectance products. The system is currently installed 120 meters above ground on a TV tower at the Chequamegon National Forest, WI, USA, and captures imagery in Blue (470nm), Green (550nm), Red (650nm) and Near-Infrared (850nm) wavelengths every 15 minutes. Raw imagery from the camera is calibrated to surface reflectance values using a 50% reflectance calibration target mounted on a motorized arm, which permits to protect the reference target while not in use. The calibrated imagery is georeferenced using very-high spatial resolution imagery from an aerial sensor and resampled to match the satellite data spatial resolution and grid. In this work, we present the comparison between CAMSIS calibrated data and 10 meter Sentinel-2 atmospherically corrected reflectance, derived by the LaSRC (Land Surface Reflectance Code) processor. Results for the Blue, Green, and Red bands show Coefficient of Determination (R2) values higher than 0.90 and Root Mean Square Error (RMSE) values close to 0.01. However, the NIR band show worse results with an R2 of 0.18 and an RMSE of 0.11, which suggests stronger Bidirectional Reflectance (BRDF) effects for this band that still need to be fully accounted for, especially for the pixel of forest areas. Results for the NDVI also show good agreement between S2 and CAMSIS, with an R2 of 0.86 and RMSE of 0.05. These initial results show that CAMSIS provides valuable information for continuous validation of high spatial resolution surface reflectance. Future research will focus on developing and implementing BRDF correction methods based on CAMSIS data.

Keywords: Surface Reflectance, Camera System, Automated Validation

©2020. Japan Geoscience Union. All Right Reserved.

[E] Poster | M (Multidisciplinary and Interdisciplinary)：M-SD Space Development & Earth Observation from Space

[M-SD46] Effects of lightning, severe weather and tropical storms

convener:Mitsuteru Sato(Department of Cosmoscience, Hokkaido University), Yoav Yair(Interdisciplinary Center Herzliya), Xiushu Qie(Institute of Atmospheric Physics, Chinese Academy of Sciences), Yukihiro Takahashi(Department of Cosmosciences, Graduate School of Science, Hokkaido University)

Thunderstorms are markers of deep convection and severe weather, producing heavy precipitation, hail and strong winds that lead to significant natural hazards, especially in coastal and urban areas. Huge economic damages and loss of human lives often result from such events. As the intensity and frequency of thunderstorms is projected to increase in the future - when the atmosphere and oceans become warmer - the need for detecting and nowcasting thunderstorms and lightning on local and regional scales becomes crucial.
We invite contributions dealing with thunderstorms and lightning and their atmospheric effects. We seek contributions focusing on convective storm evolution, forecasting of thunderstorms and lightning using regional and global detection networks as well as other sensors. Also, works on global lightning patterns in an era of climate change, satellite-based studies of thunderstorms and other remote-sensing technologies, as well as urban effects on lightning and public safety from lightning danger.

[MSD46-P01] Modelling of streamer ignition and propagation in the system of two approaching hydrometeors

★Invited Papers

*Victor P Pasko[1], Jaroslav Jansky[2] (1.Pennsylvania State University Main Campus, 2.Department of Mathematics and Physics, University of Defense, Brno, Czechia)

[MSD46-P02] Estimation of cloud base altitude using cloud images captured by all-sky camera

*Atsuya Nemoto[1], Hiroyo Ohya[2], Alessandro Damiani[3], Tamio Takamura[3], Toshiaki Takano[2], Hiroyuki Nakata[2] (1.Graduate School of Science and Engineering, Chiba University, 2.Graduate School of Engineering, Chiba University, 3.Center for Environmental Remote Sensing, Chiba University)

[MSD46-P03] Variation of Phase Relation Between OLR in Western Pacific Warm Pool and the Equator

*Kambiz Torabi[1], Yukihiro Takahashi (1.Department of Cosmosciences, Hokkaido University)

[MSD46-P04] An observational study on thunder cloud activities over Tama, Tokyo based on atmospheric electrostatic field measurements - Case study for the hail storm event in May 4, 2019 -

★Invited Papers

*Jun-Ichi Hamada[1], Jun Matsumoto[1], Tomoshige Inoue[1], Masashi Kamogawa[2], Yukihiro Takahashi[3] (1.Faculty of Urban Environmental Sciences, Tokyo Metropolitan University, 2.Global Center for Asian and Regional Study, University of Shizuoka, 3.Department of Cosmosciences, Graduate School of Science, Hokkaido University)

[MSD46-P05] Relation between Lightning Activities Measured by the V-POTEKA Network and Intensity Development of Western North Pacific Typhoons

*Mitsuteru Sato[1], Loren Joy Estrebillo[1], Yukihiro Takahashi[1], Hisayuki Kubota[1], Shunsuke Niwa[1], Glenn Vincent Lopez[2], Joel Marciano[2] (1.Department of Cosmoscience, Hokkaido University, 2.ASTI, DOST)

Modelling of streamer ignition and propagation in the system of two approaching hydrometeors

*Victor P Pasko[1], Jaroslav Jansky[2]

1. Pennsylvania State University Main Campus, 2. Department of Mathematics and Physics, University of Defense, Brno, Czechia

The lightning initiation in low thundercloud fields represents an unsolved problem in lightning discharge physics. One of the initial conditions required for formation of a hot leader channel is initiation of non-thermal streamer discharges. Streamers can be initiated from electron avalanches, however, the problem of existence of an electric field strong enough for streamer initiation in thunderclouds is still open. The maximum electric field in thunderstorms measured by balloons is typically ~3-4 kV/cm/atm, that is significantly smaller than the breakdown electric field needed for avalanche multiplication of electrons Ek=28.7 kV/cm/atm. One of the possible explanations for the streamer corona initiation is that hydrometeors greatly intensify the local electric field by at least an order of magnitude to initiate an electron avalanche. It was suggested that a particle pair or chain create more favorable conditions for initiation of lightning discharge than a single precipitation particle in low electric fields. Recently, Cai et al. [GRL, 44, 5758-5765, 2017] and Cai et al. [JGR, 123, 7050-7064, 2018] analyzed the ignition conditions for two hydrometeors of same and different radii. In the present work we use first principles plasma fluid model to study streamer initiation scenarios in a system of two hydrometeors with typical radii on the order of several millimeters under thunderstorm conditions (i.e., at an elevated location in the Earth's atmosphere corresponding to half of air density at ground level and at applied electric field approximately half of that required for avalanche multiplication of electrons in air). It is demonstrated that UV photons produced by the electrical discharges developing due to the electric field enhancement in the gap between two hydrometeors and resultant photoionization in the discharge volume lead to much less stringent conditions for conversion of these discharges to a filamentary streamer form than in the case not accounting for the effects of photoionization. It is also demonstrated that this photoionization feedback [Naidis, JPD, 38, 2211-2214, 2005; Liu et al., JASTP, 80, 179-186, 2012] is critical for understanding and correct description of the subsequent streamer discharges developing on the outer periphery of two hydrometeors whose potential is equalized due to the electrical connection established by the initial streamer discharge between them. The initial streamer ignition between the hydrometeors can be preceded by the corona development, that can have detrimental effect on the ignition. However, it is demonstrated that for hydrometeors approaching with a speed of 10 m/s the effect of this onset corona is small.

©2020. Japan Geoscience Union. All Right Reserved.

Estimation of cloud base altitude using cloud images captured by all-sky camera

*Atsuya Nemoto[1], Hiroyo Ohya[2], Alessandro Damiani[3], Tamio Takamura[3], Toshiaki Takano[2], Hiroyuki Nakata[2]

1. Graduate School of Science and Engineering, Chiba University, 2. Graduate School of Engineering, Chiba University, 3. Center for Environmental Remote Sensing, Chiba University

Clouds may significantly affect the radiation budget and water cycles of the Earth by altering their various properties. Besides the cloud microphysical properties, the cloud base height, which is one of the important cloud macrophysical structures, is of particular significance for the infrared radiation at the surface. The cloud base height is also extremely important for air safety, airborne military activities, and surveillance operations [Vislocky and Fritsch, 1997]. Thus, an accurate method for estimating cloud base height may further improve our understanding for the impact of clouds on the Earth's radiation budget and provide useful information for improvement of aviation safety. Ground-based instruments, such as radars and lidars, can help obtain relatively accurate the cloud base height locally [Takano and Takamura, 2014]. However, they cannot provide the cloud base height information in wide area. The advantage of satellites is that high-resolution, two-dimensional distributions of the microphysical and macrophysical properties of clouds may be retrieved on a global scale [Huang et al., 2006]. However, the retrieval of the cloud base height is considerably complex and not directly available from satellite observations. Wilheit and Hutchison [2000] also proposed a method to retrieve the cloud base height by combining passive microwave brightness temperature and infrared cloud top temperature. However, these methods work mainly for special cloud types (e.g., relatively thin, stratiform, or convective clouds). In this study, we propose an estimation method of the cloud base height using a pair of cloud images observed by all-sky imagers at two sites. The advantage of all-sky imagers is to be cheaper than radars and lidars. The two all-sky imagers were installed on the roofs of Engineering Research Building 1 (35.6246N, 140.1037E) and 2 (35.6266N, 140.1040E) in Nishi-Chiba campus in Chiba University, Japan. The distance between the two all-sky imagers is 216 m. The all-sky imagers have equisolid angle projection method that cloud amount can be estimated with high accuracy. The estimation method of the cloud base height is described below. When the cloud base height is assumed in the range of 500-3000 m with step of 10 m, the two cloud images are projected to each map. Then we calculate cross-correlation between the two maps. When the cross-correlation coefficients take the maximum in the all cases, the cloud base height is determined. As a result, the cloud base heights were estimated to be 1330 m and 1370 m at 13:03:12 LT and 13:06:12 LT on 27 August, 2018, respectively. The cloud base height was observed to be 1830 m by a lidar installed by the National Institute for Environmental Studies (NIES) in the same campus in Chiba University at 12:45:00 LT. The difference of the cloud base height (about 500 m) could be caused by the time difference of observations (18-21 minutes). In addition, we estimated the cloud base height for two isolated clouds at 13:29:53 LT on 16 November, 2018. The cloud base heights were estimated to be 1950 m and 1850 m, respectively. The lidar measured a reflection altitude of 2160 m at 13:30:00 LT on the same day. There was a difference of about 200-300 m between them, because the cloud themselves observed by the all-sky imagers might be different from those observed by the lidar. In the session, we will compare between the cloud base height estimated by cloud images and that observed by the 95-GHz FMCW cloud radar FALCON-I that was originally developed by our group.

©2020. Japan Geoscience Union. All Right Reserved.

Variation of Phase Relation Between OLR in Western Pacific Warm Pool and the Equator

*Kambiz Torabi[1], Yukihiro Takahashi

1. Department of Cosmosciences, Hokkaido University

Linkage between the 11-year solar activity based on sunspot number and climate change of the Earth has been suggested by monthly or yearly averaged data, even though short periodic variation could modulate longer periodic phenomena. In pervious study, 27-day variation of Outgoing Longwave Radiation (OLR) during solar maximum year was found by Takahashi et al. (2010). Moreover, anti-phase relation between lightning around Marine Continent and OLR around Western Pacific Warm Pool region was found by Sanmiya et al. (2013).

Motivation of this study is that clarifying the phase relation of about one-month periodic variation of OLR in Western Pacific Warm Pool and the equator. We have performed cross correlation analysis between OLR in Western Pacific Warm Pool and the equator by using interpolated OLR data from NOAA. Western Pacific Warm Pool is known as correlating negatively with lightning around Marine Continent and typhoon-rich area. The equator is known as correlating positively with lightning around Marine Continent and typhoon-pool area. We will discuss about characteristics of variation of phase relation from 1974 to 2018 which includes 21st to 24th of solar cycle.

Keywords: OLR, WPWP, teleconnection

©2020. Japan Geoscience Union. All Right Reserved.

An observational study on thunder cloud activities over Tama, Tokyo based on atmospheric electrostatic field measurements - Case study for the hail storm event in May 4, 2019 -

*Jun-Ichi Hamada[1], Jun Matsumoto[1], Tomoshige Inoue[1], Masashi Kamogawa[2], Yukihiro Takahashi[3]

1. Faculty of Urban Environmental Sciences, Tokyo Metropolitan University, 2. Global Center for Asian and Regional Study, University of Shizuoka, 3. Department of Cosmosciences, Graduate School of Science, Hokkaido University

In order to monitor lightning activities and development of thunder clouds, we have established an observational network with electromagnetic and electrostatic field measurements over the Tokyo metropolitan area since 2016. In the early summer and summer seasons of 2019, we observed atmospheric electrostatic field with the electric field monitor (BOLTEK ELF-100) at Hachioji campus of Tokyo Metropolitan University and the surrounding area. In the afternoon of May 4, 2019, hail and heavy rainfall were observed in a wide area including the observational sites. Form the X-band Multi-Parameter radar observation, thunder clouds had developed with the height of 10 km or more near the observational site at around the time of hail was observed. The electrostatic field measurement detected frequent lightning around the peak of hail events and the electrostatic field fluctuations due to developing/approaching of the thunder clouds. At the meeting, we will discuss the relationship between atmospheric electrostatic field variations and thundercloud development processes more detail.

This study was supported by TMU Strategic Research Fund (President Selected) of Tokyo Metropolitan University and Japan Science and Technology Agency (JST) and Japan International Cooperation Agency (JICA) under SATREPS.

Keywords: Thunder cloud, Heavy rainfall, Atmospheric electrostatic field

©2020. Japan Geoscience Union. All Right Reserved.

Relation between Lightning Activities Measured by the V-POTEKA Network and Intensity Development of Western North Pacific Typhoons

*Mitsuteru Sato[1], Loren Joy Estrebillo[1], Yukihiro Takahashi[1], Hisayuki Kubota[1], Shunsuke Niwa[1], Glenn Vincent Lopez[2], Joel Marciano[2]

1. Department of Cosmoscience, Hokkaido University, 2. ASTI, DOST

Lightning activity is a good proxy representing the precipitation and updraft intensities in thunderclouds. Recent studies suggest that the monitoring of the lightning activities has a high potential to predict the maximum wind speed and minimum sea-level pressure of the tropical cyclone by one or two days before, though the prediction error of typhoon intensities by the recent meteorological model is getting worse in the past 30 years. Many countries in the western north Pacific region suffer from the attack of tropical cyclone (typhoon) and have a strong demand to predict the intensity development of typhoons by means of a cost-effective way. Thus, we have developed a new automatic lightning observation system (V-POTEKA) and installed this system in the Philippines, Guam, Palau, Jakarta, Okinawa, and Sapporo since September 2017. Using the V-POTEKA data, lightning locations are estimated by using the time-of-arrival geolocation software. We have compared the relation between the lightning activities measured by the V-POTEKA network and the intensity variation of the western north Pacific typhoons in 2018 and 2019. In 2018 and 2019, a total of 29 and typhoons occurred, respectively. As for the 2018 typhoons, we selected 11 of 29 typhoon events and conducted cross-correlation analysis between lightning activities and typhoon intensities. We confirmed that the time variations of the detected lightning event numbers and typhoon intensities (maximum wind speed and center pressure) are highly correlated. Especially, there is clear time lag (~1.5 days) between lightning activities and typhoon intensities in the category 1-3 typhoons, that is, the peak of lightning activity comes first, then the peak of the typhoon intensity comes next. However, as for the super typhoons (category 5 typhoons), this relation is not always clear. At the presentation, we will also show the detailed results derived from this cross-correlation analysis between lightning activities and intensity development of the 2019 typhoons.

Keywords: Lightning activity, Typhoon, Intensity prediction

©2020. Japan Geoscience Union. All Right Reserved.

[E] Poster | M (Multidisciplinary and Interdisciplinary)：M-TT Technology & Techniques

[M-TT48] Cryoseismology - A new proxy for detecting surface environmental variations of the Earth -

convener:Masaki Kanao(National Institute of Polar Research), Seiji Tsuboi(JAMSTEC, Center for Earth Information Science and Technology), Genti Toyokuni(Research Center for Prediction of Earthquakes and Volcanic Eruptions, Graduate School of Science, Tohoku University), Yoshihiro Hiramatsu(School of Geosciences and Civil Engineering, College of Science and Engineering, Kanazawa University)

In high latitude and elevation regions, the Earth's glaciers, ice sheets, sea ice, permafrost, and snowpacks are undergoing rapid change. Fortunately, many of the cryospheric processes of interest produce ground vibrations. Analysis of these seismic signals can yield insight into the relationship between environmental forcing and the response of ocean-cryosphere-solid earth system.
Ice-related seismic motions for small magnitude events are generally named ice-quakes and can be generated by glacially related dynamics. Such kinds of cryoseismic sources are classified into the movements of ice sheets, sea-ice, oceanic tide-cracks, icebergs and the calving fronts of ice caps. Cryoseismic waves are likely to be influenced by variations in environmental conditions, and the continuous study of their time-space variability provides indirect evidence of climate change. As glacial earthquakes are the most prominent phenomena found recently in polar regions particularly around Greenland, the new innovative studies from seismology are expected by long-term monitoring under extreme conditions in the Earth's environment.
Taking these issues into account, the conveners are willing to invite many contributions to a special session on "Cryoseismology", which cover recent topics on glacial related seismic events and associated phenomenon. It is particularly encouraged to have contributions based on seismic signals involving the dynamics of ice sheets, sea-ice, icebergs and glaciers. Although the glacial earthquakes are the most prominent evidence found recently in polar regions, all related topics involving polar seismology are welcome, such as studies of crust and mantle structure, comparison of tectonic and glacier-related seismicity, recent triggered earthquakes and active volcanoes, glacial isostatic adjustment (GIA), harmonic tremor associated with cryoseismic events.

[MTT48-P01] Seismic observations in Greenland by a joint USA and Japanese GLISN team (2011–2019)

*Genti Toyokuni[1], Masaki Kanao[2], Seiji Tsuboi[3] (1.Research Center for Prediction of Earthquakes and Volcanic Eruptions, Graduate School of Science, Tohoku University, 2.NIPR, 3.JAMSTEC)

[MTT48-P02] Estimation of seismic source location around East Ongul Island, East Antarctica, by using two seismic arrays

*Manami Nakamoto[1], Masaki Kanao[2] (1.Association for the Development of Earthquake Prediction, 2.National Institute of Polar Research)

[MTT48-P03] Progress in Cryoseismology – A review of Japanese contribution -

*Masaki Kanao[1] (1.National Institute of Polar Research)

[MTT48-P04] Characteristic multi-sphere interaction in the coastal and marine environment inferred from infrasound observation at Terra Nova Bay, Antarctica

*Takahiko Murayama[1], Masaki Kanao[2] (1.Japan Weather Association, 2.National Institute of Polar Research)

Seismic observations in Greenland by a joint USA and Japanese GLISN team (2011–2019)

*Genti Toyokuni[1], Masaki Kanao[2], Seiji Tsuboi[3]

1. Research Center for Prediction of Earthquakes and Volcanic Eruptions, Graduate School of Science, Tohoku University, 2. NIPR, 3. JAMSTEC

The Greenland Ice Sheet (GrIS) is a huge storehouse of water on Earth, and has the potential to raise the global sea level by approximately 7 m if completely melted. Although researchers have been mainly studying the GrIS surface snowmelt as a response to climate warming, recent progress in ice-core drilling, remote sensing, and theoretical analyses has turned a spotlight on its basal conditions. However, the traditional observation techniques, such as ice-core drilling and ice-penetrating radar, provide only discontinuous information in both time and space.

Seismic observation is now drawing widespread attention as an alternative method for monitoring the GrIS. The Greenland Ice Sheet Monitoring Network (GLISN), an international project between 11 countries that began in 2009, now provides broadband, continuous, and real-time seismic data from 35 stations in and around Greenland. Japan is a partner country from when the GLISN project was launched, and has been sending an expedition team every year since 2011. In 2011, a joint USA and Japanese GLISN team installed the dual seismic–GPS station ICESG-GLS2 in the middle of the GrIS. During 2012–2018, we conducted maintenance of three stations on the GrIS (station codes: ICESG-GLS2, DY2G-GLS1, and NEEM-GLS3), and three stations on bedrock in coastal areas (NUUK, DBG, and SOEG). We had succeeded in real-time transmission of broad-band and continuous seismic waveform data from the three ice stations. It was the first time in the world that the seismic data with such a high sampling rate are transferred from the ice sheet. The data is now open to public and available from the IRIS Data Management Center (http://www.iris.edu/ds/nodes/dmc/). This presentation will summarize our field activities for 2011–2019, and introduce the future field plans.

Acknowledgments: The Japanese GLISN team has been supported by research grants from JSPS (24403006, 18K03794).

Keywords: GLISN project, Greenland Ice Sheet (GrIS), Seismic observation

©2020. Japan Geoscience Union. All Right Reserved.

Estimation of seismic source location around East Ongul Island, East Antarctica, by using two seismic arrays

*Manami Nakamoto[1], Masaki Kanao[2]

1. Association for the Development of Earthquake Prediction, 2. National Institute of Polar Research

In the polar region, various vibration phenomena are exited in association with physical interactions between the solid earth, atmosphere, ocean, and cryosphere systems. These phenomena can be observed as seismic and infrasonic waves, and the relationship between their occurrence and environmental variations was pointed out in the Lützow-Holm Bay region, East Antarctica (e.g., Murayama et al. 2017; Tanaka et al. 2019). To monitor environmental changes, it is important to reveal their characteristics and generation processes. Although several seismic and infrasound stations have been deployed in and around East Ongul Island, East Antarctica, it is not sufficient to detect small seismic events such as local icequakes and tremors because of the sparsity of the stations in the existing seismic network. One of the useful methods for estimating source locations is the array analysis, which uses data obtained by a dense seismic network. Hence, we carried out a special experiment using two seismic arrays in East Ongul Island during the summer of 2017-2018. These two arrays consisted of seven three-component seismometers and six vertical seismometers, respectively, with a spacing of about 100m. First, we picked 93 short-duration seismic events based on the short-term-average to long-term-average (STA/LTA) ratio from continuous waveforms with a high signal-to-noise ratio (SNR). Contamination caused by strong winds, as well as long-duration signals from the ice-breaker ship and helicopters, were carefully filtered out. Then, we estimated the direction of arrival of these signals by applying semblance analysis. As a result, we found that some of their epicenters existed around East Ongul Island. These events can be considered as icequakes because the sea-ice condition around the Lützow-Holm Bay had been changing dramatically during the observation period. We further investigate the relationship between these signals and the sea-ice distribution in this area.

Keywords: seismic array observation, antarctic

©2020. Japan Geoscience Union. All Right Reserved.

Progress in Cryoseismology –A review of Japanese contribution -

*Masaki Kanao[1]

1. National Institute of Polar Research

Majority areas of Antarctica and Greenland are under the thick ice sheet and characterized by evolving cryosphere surroundings. In the polar region, associated with the recent trend on climate change such as global warming, glacier relating earthquakes are increasing during this 21st century. In this paper, a decade of progress in “Cryoseismology” at bi-polar regions will be demonstrated by focusing on the contribution from Japanese researches. In particular, specific cryoseismic events are treated, which occurred in the coastal area of East Antarctica, around the Lutzow-Holm Bay, together with the coast and whole inland area of Greenland. Harmonically frequency-overtone signals are explained by a constant source, suggesting inter-glacial asperities that generate characteristic cryoseismic tremors.

©2020. Japan Geoscience Union. All Right Reserved.

Characteristic multi-sphere interaction in the coastal and marine environment inferred from infrasound observation at Terra Nova Bay, Antarctica

*Takahiko Murayama[1], Masaki Kanao[2]

1. Japan Weather Association, 2. National Institute of Polar Research

Characteristic features of infrasound waves observed in the Antarctic reveal physical interaction involving surface environments around the continent and Southern Ocean. An infrasound array (100 m spacing) by using three sensors (Chaparral Physics Model 25, with a detectable frequency range of 0.1-200 Hz), together with a broadband barometer (Digiquartz Nano-Resolution Model 6000-16B Barometer, with a detectable frequency range of 0-22 Hz) were installed at Jang Bogo Staion, Tera Nova Bay, West Antarctica in December 2015 by the Korea Arctic and Antarctic Research Program (KAARP). The initial data recorded by the broadband barometer include several signals originated surrounding surface environment, in addition to the local wind noises such as katabatic signals. Clear signals from background oceanic origin (the "microbaroms") are continuously recorded at the austral summer on mid-December with predominant frequency around 5 s. Variations of their frequency context and strength appeared in Power Spectral Density are affected by evolution of the sea-ice surrounding the Tera Nova Bay.

©2020. Japan Geoscience Union. All Right Reserved.

[E] Poster | M (Multidisciplinary and Interdisciplinary)：M-TT Technology & Techniques

[M-TT49] GEOSCIENTIFIC APPLICATIONS OF HIGH-DEFINITION TOPOGRAPHY AND GEOPHYSICAL DATA IN THE ANTHROPOCENE

convener:Yuichi S. Hayakawa(Faculty of Environmental Earth Science, Hokkaido University), Shigekazu Kusumoto(Graduate School of Science and Engineering for Research, University of Toyama), Christopher A Gomez(Kobe University Faculty of Maritime Sciences Volcanic Risk at Sea Research Group)

Recent technical developments have enabled us to acquire high-definition topographic and geophysical data for geoscientific research, including land surface processes, subsurface structures, submarine and aerial environments, and geo-ecological interactions. Such high-definition or high-resolution data are particularly useful for studies on relatively short-term, i.e., decadal to millennial time scales, and for future predictions using numerical modelings. In this session, we expect submissions on topics challenging the issues in the Anthropocene, the most recent geological era of the Earth considerably affected by human activities. A range of topics would fit the session framework, such as theoretical works, improvements in the data acquisition, extensive data preservation and archiving, pre- and post-processing, statistical analysis, physical modeling, and numerical simulation for any kind of geoscientific research in the Anthropocene. The methodological approaches may include, but not limited to, laser scanning, SfM-MVS photogrammetry, GNSS precise positioning, SAR interferometry, multi-beam sonar, ground-penetrating radar, geomagnetic and electromagnetic sensors, based on terrestrial (fixed or mobile) and aerial (UAV or manned airborne) platforms.

[MTT49-P01] **A Study of Slope Displacement Monitoring with PSInSAR Technique**

*Chin-jen Lin[1], Shen Yu Hsiao[1] (1.National Chung Hsing University)

[MTT49-P02] Monitoring Soil Erosion Changes by SBAS-InSAR Technology

*Yu-Chi Hsieh[1], Shen Yu Hsiao[1] (1.National Chung Hsing University)

[MTT49-P03] Spatiotemporal analysis of topography and vegetation in check dams using RTK-UAV and SfM-MVS photogrammetry

*Masato Hayamizu[1], Yasutaka Nakata[1], Satoshi Hasui[1], Hajime Sato[1], Yu Nagasaka[1], Akiko Nagasaka[1] (1.Hokkaido Research Organization Forestry Research Institute)

[MTT49-P04] A new method to measure in situ soil density using SfM-MVS photogrammetry

*Christopher A Gomez[1] (1.Kobe University Faculty of Maritime Sciences Volcanic Risk at Sea Research Group)

[MTT49-P05] **Comparison of wide-range topographic data derived from UAV-SfM and airborne lidar: a case study at Taal Volcano, the Philippines**

*Yuichi S. Hayakawa[1], Shigekazu Kusumoto[2], Takuro Ogura[3,5], Toshiyasu Nagao[4], Paul Karson B. Alanis[6] (1.Faculty of Environmental Earth Science, Hokkaido University, Japan, 2.Graduate School of Science and Engineering for Research, University of Toyama, Japan, 3.Graduate School of Frontier Science, The University of Tokyo, Japan, 4.Institute of Oceanic Research and Development, Tokai University, Japan, 5.Graduate School of Environmental Science, Hokkaido University, Japan, 6.Philippine Institute of Volcanology and Seismology (PHIVOLCS), Department of Science and Technology, The Philippines)

A Study of Slope Displacement Monitoring with PSInSAR Technique

*Chin-jen Lin[1], Shen Yu Hsiao[1]

1. National Chung Hsing University

This research is aimed at slope displacement monitoring on Taiwan mountainous areas in 2019 using Persistent Scatterer Interferometric Synthetic Aperture Radar (PSInSAR) technique. The radar satellite images used in this study are from Sentinel-1 mission developed by the European Space Agency (ESA). The software for data processing is based on Stanford Method for Persistent Scatterers (StaMPS). The surface displacement of each observation ground point is computed by six satellite images with different observation times. The weather and atmosphere conditions affecting observations are precisely corrected in the procedure of data processing. The results from PSInSAR will be well compared to those from the optical images and the GPS stations. With this research, the slope activities on Taiwan mountainous areas can be monitored. This research also can provide effective information on disaster risk assessment.

Keywords: PSInSAR, slope displacement, Sentinel-1

©2020. Japan Geoscience Union. All Right Reserved.

Monitoring Soil Erosion Changes by SBAS-InSAR Technology

*Yu-Chi Hsieh[1], Shen Yu Hsiao[1]

1. National Chung Hsing University

This study uses the Synthetic Aperture Radar (InSAR) technique to analyze the soil erosion mass changes in the past 7 years at four major reservoir areas in Taiwan. Four major reservoirs include Shimen, Tseng-Wen, Techi, and Nanhua reservoirs where are averagely distributed in northern, central, and southern Taiwan. The method for deriving soil erosion changes is based on Small Baseline Set Algorithm (SBAS). The radar satellite data used in this study is from the missions of Sentinel and ALOS PALSAR. The software for data processing is GMTSAR. The changes of the soil erosion monitored by SBAS-InSAR will be mutually verified with those measured by the erosion pins. It is expected that with this study, the erosion degree of the slopes of the four reservoir areas can be accurately calculated to provide important references in the fields of hydraulic engineering, and soil and water conservation.

Keywords: SBAS-InSAR, Soil Erosion, Erosion Pin

©2020. Japan Geoscience Union. All Right Reserved.

Spatiotemporal analysis of topography and vegetation in check dams using RTK-UAV and SfM-MVS photogrammetry

*Masato Hayamizu[1], Yasutaka Nakata[1], Satoshi Hasui[1], Hajime Sato[1], Yu Nagasaka[1], Akiko Nagasaka[1]

1. Hokkaido Research Organization Forestry Research Institute

In the world mountain and forest streams, the construction of soil erosion control dams (also called check dams or Chisan-dams; hereinafter called “Chisan-dam”) has been widely applied to stabilize the sediment movement of the river basin. Despite the number of constructed Chisan-dam more than 35000 in Hokkaido (Tamate & Hayajiri 2008), there are few reports of quantitative evaluation of whether the topography changed as planned or how the forest vegetation changed after the establishment. Therefore, it is needed to conduct an efficient survey of many Chisan-dams and assess whether the topography and vegetation are changing as planned.

Unmanned Aerial Vehicle (UAV) photogrammetry and structure-from-motion multi-view stereo (SfM-MVS) photogrammetry are widely applied due to the advantage of obtaining Digital Surface Model (DSM) at relatively low cost. Whereas, the accuracy of the model varies because it is difficult to set Ground Control Points (GCPs) uniformly such as small forest basin. In October 2018, the DJI Phantom 4 RTK unmanned aerial vehicle (RTK-UAV) was launched with direct integration of the Real Time Kinematic - Global Navigation Satellite System (RTK-GNSS). The aerial images of RTK-UAV records highly accurate position information via RTK-GNSS, and it is possible to acquire high-precision DSM without installing GCPs even in forest areas with many undulations and obstruction (Nakata et al. in press).

The aim of this study was to measure the change of longitudinal gradient before and after the construction of a Chisan-dam constructed in 1985. After restoring the vertical slope before construction from the design drawing of 1985, a vertical survey using a total station was conducted at the same site in August 2019. In addition, we verified the possibility of construction of a high-resolution DSM model without GCPs using the RTK-UAV.

As a field survey using total station, the riverbed 34 years after the Chisan-dam construction was equal to the height of the sedimentary surface, and it was achieved the planned gradient. On the other hand, the riverbed below the Chisan-dam was scoured by about 1 m more than before its construction. Result of investigating the flight conditions of the RTK-UAV, a DSM model with a resolution of 2.67 cm / pix was constructed without using GCP. In the presentation, the validity of the RTK-UAV survey will be discussed by comparing the data obtained from the field survey with the data extracted from the DSM.

Keywords: check dam, UAV-SfM, RTK-UAV, topography, vegetation

©2020. Japan Geoscience Union. All Right Reserved.

A new method to measure in situ soil density using SfM-MVS photogrammetry

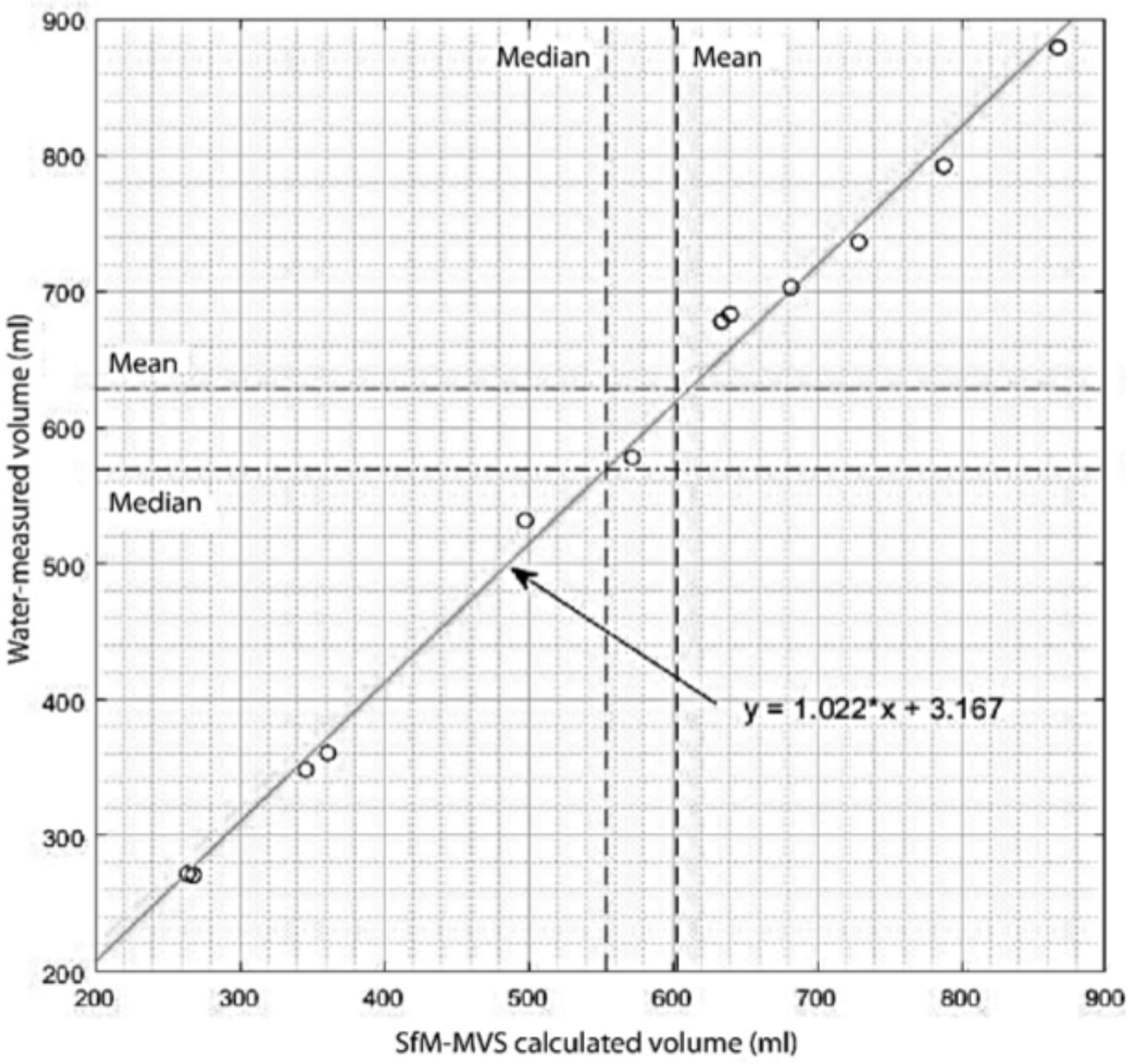
*Christopher A Gomez[1]

1. Kobe University Faculty of Maritime Sciences Volcanic Risk at Sea Research Group

The measure of soil density in the field has been relying traditionally on the sand-cone method, the balloon method or the radioactive method. All those methods require heavy equipment, are not appropriate for non-horizontal surfaces, and do not provide control over the methodological error in the field, that is very site-dependent.
To solve this issue, the author has developed a new (or adapted other methods from different fields) method to measure the soil density using photogrammetry based on SfM-MVS, so that the method can be used in irregular soils that are coarse grains, and with limited equipment transported in the field. Furthermore, the method the author proposes can be used along outcrops vertically and on horizontal surfaces, whereas a perfectly horizontal surface was necessary up to present.
Results show good agreement between the water-measured hole volume and the SfM-MVS data, with the best linear fit correlation line of y=1.022*x+3.167, where x is the SfM-MVS calculation and y represents the water measurement. The water-measures are thus slightly higher than the volumes calculated using SfM-MVS. The RMSE of the upper 50% of the data is ~5 and the lower 50% displays an RMSE of 2.6 (about half of the top 50%). The author interpreted this result as being a function of the small crannies that are filled with water and that can’ t be calculated from SfM-MVS, which had a millimeter-scale infra-millimeter (after software calculation). Therefore the discrepancy between the two datasets can be potentially linked to the size of the surface of the hole walls and the roughness of the grains.
The photogrammetric-based method to measure field density proves to be a reliable method with a control on the potential error (error control from the photogrammetric method), providing a more reliable method of field density measure and calculation. At present, the author is preparing further result presentation with full-scale field data, showing the usability and reducing the weight of the equipment carried in the field.

Keywords: SFM-MVS photogrammetry, soil density, field measurement, unconsolidated soils

©2020. Japan Geoscience Union. All Right Reserved.



©2020. Japan Geoscience Union. All Right Reserved.

Comparison of wide-range topographic data derived from UAV-SfM and airborne lidar: a case study at Taal Volcano, the Philippines

*Yuichi S. Hayakawa[1], Shigekazu Kusumoto[2], Takuro Ogura[3,5], Toshiyasu Nagao[4], Paul Karson B. Alanis[6]

1. Faculty of Environmental Earth Science, Hokkaido University, Japan, 2. Graduate School of Science and Engineering for Research, University of Toyama, Japan, 3. Graduate School of Frontier Science, The University of Tokyo, Japan, 4. Institute of Oceanic Research and Development, Tokai University, Japan, 5. Graduate School of Environmental Science, Hokkaido University, Japan, 6. Philippine Institute of Volcanology and Seismology (PHIVOLCS), Department of Science and Technology, The Philippines

Frequent acquisition of topographic data for a wide area is fundamental for studies on volcanoes because volcanic activities often cause changes in topography, and other properties, including gravitational anomalies, needs to be calibrated based on the topographic data. Airborne laser scanning (ALS) by a crewed aircraft is a standardized approach to acquire topographic data in a wide area, but its high cost limits its frequent applications. Measurements using an unmanned aerial vehicle (UAV)-based structure-from-motion (SfM) photogrammetry is becoming more popular in recent years for geoscientific studies, but its accuracy is often found to be relatively low particularly if ground control points (GCPs) are unable to be set in the areas of interest. However, the use of low-accuracy data can still be beneficial for some specific research purposes such as geomorphological mapping and gravity mapping. To validate the usefulness of low-accuracy data, we compare ALS-derived and UAV-SfM-derived topographic data of the island of the Taal volcano in the Philippines. Although the UAV-based data shows significant inaccuracies and errors, the data can be instantly obtained at a low cost and is found to be enough for a rough geomorphological mapping and calibration of gravitational data for the wide area. Further assessments and compilation of acceptable resolution and accuracy of various topographic data are encouraged.

Keywords: digital elevation model, airborne laser scanning, unmanned aerial vehicle

©2020. Japan Geoscience Union. All Right Reserved.

[E] Poster | M (Multidisciplinary and Interdisciplinary)：M-TT Technology & Techniques

[M-TT50] Distributed Fiber Optic Sensing for Geophysical Applications

convener:Matthew Becker(California State University Long Beach), Xiangfang Zeng(Institute of Geodesy and Geophysics, Chinese Academy of Sciences), Ziqiu Xue(Research Institute of Innovative Tech for the Earth), Herbert F Wang(University of Wisconsin Madison)

Distributed fiber optic sensing has generated tremendous excitement with applications including seismology, seismic imaging, hydrology, petroleum development, carbon dioxide sequestration, and geothermal energy. Distributed Temperature Sensing (DTS) became widely accessible about a decade ago. DTS can measure temperature along a fiber optic cable at sub-meter intervals, over distances of kilometers, and at sampling frequencies of 0.1 Hz or less. Distributed Acoustic Sensing (DAS) is a more nascent technology that is only now being tested for geophysical applications. DAS can acquire dynamic strain at sub-meter intervals, over distances of kilometers, and at sampling frequencies of 100 kHz or less. Both technologies can use standard telecommunication fiber optic cables for measurement. DAS, for example, has been used to sense earthquake movements in unused (dark) buried fiber optic communication networks. We invite presentations that discuss novel applications of distributed fiber optic sensing, interpretation of results of monitoring, and advancements in processing of data streams. This session will bring together practitioners from many disciplines to discuss opportunities, share experience, and suggest solutions to technical challenges.

[MTT50-P01] Advances in Distributed Acoustic Sensing for Applications in the Earth Sciences

*Thomas Coleman[1], Tom Parker[1], Sergey Shatalin[1], Jack Maxwell[1], Mahmoud Farhadiroushan[1], Michael Mondanos[1] (1.Silixa Ltd.)

[MTT50-P02] Lessons learned from dark fiber distributed arrays in a large urban campus

*Dante Fratta[1], Herbert F Wang[1], Neal Lord[1], Shreeshrita Patnaik[1], Agatha Podrasky[2], Alexander Malamet[1], Paul Barford[1] (1.University of Wisconsin Madison, 2.Silixa Ltd.)

[MTT50-P03] Combining DAS and air-gun: a cost-effective medium change monitoring system

*Xiangfang Zeng[1], Baoshan Wang[2], Jun Yang[3], Yuansheng Zhang[4], Zhenghong Song[2,1], Xiaobin Li[4], Rongbin Lin[1], Manzhong Qin[4], Congxin Wei[4] (1.State Key Laboratory of Geodesy and Earth's Dynamics, Innovation Academy for Precision Measurement Science and Technology, Chinese Academy of Sciences, 2.School of Earth and Space Sciences, University of Science and Technology of China, 3.Earthquake Agency of Yunnan Province, 4.Earthquake Agency of Gansu Province)

[MTT50-P04] DAS Research Coordination Network in Geosciences and Engineering

*Herbert F Wang[1], Robert Woodward[3], Robert Detrich[3], Scott Tyler[2] (1.University of Wisconsin Madison, 2.University of Nevada, Reno, 3.Incorporated Research Inst Seismology)

[MTT50-P05] **Distributed Acoustic Sensing (DAS) as a Distributed Hydraulic Sensor**

*Matthew Becker[1], Thomas I Coleman[2], Christopher Ciervo[1] (1.California State University Long Beach, Long Beach California, 2.Silixa LLC, Houston, USA)

Advances in Distributed Acoustic Sensing for Applications in the Earth Sciences

*Thomas Coleman[1], Tom Parker[1], Sergey Shatalin[1], Jack Maxwell[1], Mahmoud Farhadiroushan[1], Michael Mondanos[1]

1. Silixa Ltd.

Over the past decade, distributed acoustic sensing (DAS) has evolved from a novel to established tool in the earth sciences with still ever-expanding applications. The adoption of DAS for geophysical investigations has been facilitated by advanced optoelectronic architectures with amplitude and phase coherent, broadband measurement capability over a few tens of kilometers. The development of high precision engineered sensing fiber and associated DAS systems has allowed DAS system noise for an individual sensing channel to match that of point sensors. The inherent capabilities of DAS for monitoring and characterization of earth processes have generated an increasing level of interest in retrofitting DAS to existing optical fiber infrastructure to create vast terrestrial sensing arrays. A suite of methods has been recently developed that further expand sensor range and coverage, offering a significant capability and economic improvement for both retrofit and new infrastructure installations. The application of range extending methods for interrogation of dark fiber networks is discussed. Based on these developments, the next few years are expected to mark an era of rapidly expanding adoption of DAS, with exciting opportunities and challenges on the horizon for maximizing value from spatially and temporally expansive data.

Keywords: Distributed Sensing, Distributed Acoustic Sensing, DAS, Fiber Optic, Dark Fiber

©2020. Japan Geoscience Union. All Right Reserved.

Lessons learned from dark fiber distributed arrays in a large urban campus

*Dante Fratta[1], Herbert F Wang[1], Neal Lord[1], Shreeshrita Patnaik[1], Agatha Podrasky[2], Alexander Malamet[1], Paul Barford[1]

1. University of Wisconsin Madison, 2. Silixa Ltd.

We have deployed a distributed acoustic sensing (DAS) array using dark fiber across the urban campus of the University of Wisconsin-Madison. During two weeks, a Silixa iDAS interrogator was used to target campus traffic, railway activity, commercial movements across busy thoroughfares, sporting events, and a carillon concert. These events were captured on the DAS array and used to assess the performance of dark fiber for the deployment in city-wide and regional monitoring systems. This deployment faced challenges related to the mapping of the cable, the coupling of the optic fiber to conduits and near-surface ground, and multiple sources from different locations acting simultaneously. The lessons learned from these studies can be used to develop a better sensing array and make greater use of existing communication infrastructure.

Keywords: distributed acoustic sensing, geophysics

©2020. Japan Geoscience Union. All Right Reserved.

Combining DAS and air-gun: a cost-effective medium change monitoring system

*Xiangfang Zeng[1], Baoshan Wang[2], Jun Yang[3], Yuansheng Zhang[4], Zhenghong Song[2,1], Xiaobin Li[4], Rongbin Lin[1], Manzhong Qin[4], Congxin Wei[4]

1. State Key Laboratory of Geodesy and Earth's Dynamics, Innovation Academy for Precision Measurement Science and Technology, Chinese Academy of Sciences, 2. School of Earth and Space Sciences, University of Science and Technology of China, 3. Earthquake Agency of Yunnan Province, 4. Earthquake Agency of Gansu Province

The large-volume air-gun systems have been installed in serval water reservoirs to excite high similar signal. The air-gun signal can be detected up to 150 km that make it possible to monitor medium change at large scale. The deployment cost of monitoring system can be significantly reduced with the low-cost DAS system. Two DAS air-gun experiments were conducted at two sites with different settings. A telecommunication fiber-optic cable in urban area was used in the first experiment. After stacking, the air-gun signal emerges on the 30-km DAS array at about 9 km epicentral distance. A 5-km cable was deployed starting from the air-gun source to about 2 km away. About 800-m cable was frozen into the ice above the air-gun and provided clear single-shot signals. The rest cable was lay on the road and the part across a fault is cemented. On the stacking multiple shots' records, the wavefield in fault zone emerges too. These two experiments demonstrate the feasibility of using various fiber-optic cables as dense array to acquire air-gun signal in different environments.

Keywords: medium change, air-gun, distributed acoustic sensing

©2020. Japan Geoscience Union. All Right Reserved.

DAS Research Coordination Network in Geosciences and Engineering

*Herbert F Wang[1], Robert Woodward[3], Robert Detrich[3], Scott Tyler[2]

1. University of Wisconsin Madison, 2. University of Nevada, Reno, 3. Incorporated Research Inst Seismology

A DAS Research Coordination Network (RCN) is being formed under a National Science Foundataion award to advance the applications of Distributed Acoustic Sensing (DAS) in geosciences and engineering. The RCN will also strive to bring together DAS researchers and users from a diverse international base of research organizations, industry, technology companies, and government agencies to exploit synergies and enhance efficient utilization of resources in DAS development and applications. The RCN activities will be focused around multi-day workshops and short courses, and topical webinars. Working Groups will be formed in major areas of DAS applications, data management, and technology. Guidance and direction for the community activities will be by the principal investigators and a multidisciplinary steering committee. Early-career scientists and graduate students are the target audience for activities.

Keywords: distributed acoustic sensing, geophysics

©2020. Japan Geoscience Union. All Right Reserved.

Distributed Acoustic Sensing (DAS) as a Distributed Hydraulic Sensor

*Matthew Becker[1], Thomas I Coleman[2], Christopher Ciervo[1]

1. California State University Long Beach, Long Beach California, 2. Silixa LLC, Houston, USA

Distributed Acoustic Sensing (DAS) instruments were originally intended to measure oscillatory strain (vibration) at frequencies of 1 Hertz or more. Recently, the ability to measure much lower frequencies has opened the possibility of using DAS as a strain sensor in boreholes. A fiber optic cable that is mechanically coupled to a geologic formation will strain in response to hydraulic stresses in pores and fractures. Because DAS measures dynamic strain along the entire length of a fiber optic cable, it is capable of both locating hydraulically active features and quantifying the hydraulic stress in the formation. We present field experiments in which a fiber optic cable was mechanically coupled to a crystalline rock borehole. The formation was stressed hydraulically at a second well using alternating injection and pumping. The DAS instrument measured oscillating strain at the location of a fracture zone known to be hydraulically active. The experiment was repeated in two wells using multiple periods of hydraulic stressing. Nanostrain was measured in response to head changes as small as 2 mm of water. These results suggest that fiber optic cable embedded in geologic formations may be used to map hydraulic connections in three dimensions. A great advantage of this approach is that strain and, therefore, hydraulic stress can be measured without beforehand knowledge of the fracture network. The technology has obvious applications in oil and gas, geothermal energy, and remediation of groundwater in fractured bedrock.

Keywords: distributed acoustic sensing, borehole geophysics, fractured bedrock, geothermal, rock strain

©2020. Japan Geoscience Union. All Right Reserved.

[E] Poster | M (Multidisciplinary and Interdisciplinary) : M-ZZ Others

[M-ZZ53] Availability of earth science data in renewable energy field

convener:Hideaki Ohtake(National Institute of Advanced Industrial Science and Technology), Fumichika Uno(Nihon University, College of Humanities and Sciences), Teruhisa Shimada(Graduate School of Science and Technology, Hirosaki University), Daisuke Nohara(Central Research Institute of Electric Power Industry)

Renewable energy penetration is increasing dramatically in the world. Renewable energy power generations have become a strong presence in grid operations. However, it is a challenge for renewable energy to be stable power sources due in part to natural variability of renewable energy and its uneven distribution. For effective use of renewable energy, a combinational use of various power resources and energy storage technologies (e.g., pumped-storage power generation, storage battery system, electric vehicles) should be desired. Therefore, we need to understand the amount of renewable resources, causes of variation, and the predictability of power output. Then, observation and forecast information from earth science field should be analyzed and applied to power energy field to achieve easy use of earth science databases.
 Recently, observation databases from remote sensing technology and/or forecasts from numerical models have become essential for both renewable energy and electric power system fields. Impacts of both earth science data and optimization are essential to economic evaluation of grid operations.
This proposed session needs your presentation from the whole of renewable energy fields (such as, wind power, solar power, geothermal power, tidal power, wave power and biomass power generations). Our goal of this session is to exchange views with various researchers between renewable energy field and earth science field (e.g., usage-trends of earth science datasets for renewable energy field, earth science datasets availability, integrated studies, renewable energy resources in future climate system, and a request from renewable energy field to earth science field).
The proposed session features contribution of general interest within earth sciences community.

[MZZ53-P01] Geothermal exploration of the Iwaki Volcano using the Br/Cl ratio in river, spring, and hot spring waterGeothermal exploration of the Iwaki Volcano using the Br/Cl ratio in river, spring, and hot spring water

*Seiichiro Ioka[1], Kazuyoshi Asai[2], Kazumi Asai[2], Ayako Mikami[3], Sachi Wakasa[1] (1.Institute of Regional Innovation, Hirosaki University, 2.Geo Science Laboratory, 3.Aomori Prefectural Kizukuri Senior High School)

[MZZ53-P02] Machine learning based prediction of solar power generation by utilizing all-sky camera

*Masataka Imai[1], Toru Kouyama[1], Hideaki Ohtake[1], Takashi Oozeki[1], Mitsuteru Sato[2] (1.National Institute of Advanced Industrial Science and Technology, 2.Hokkaido University)

[MZZ53-P03] Probabilistic Wind Power Prediction Based on Ensemble Weather Forecasting

*Daisuke Nohara[1], Masamichi Ohba[1], Takeshi Watanabe[1], Shinji Kadokura[1] (1.Central Research Institute of Electric Power Industry)

[MZZ53-P04] Improvement of prediction of wind power generation output for an area and its sub-area by using monitoring data

*Shinji Kadokura[1], Daisuke Nohara[1], Masamichi Ohba[1], Atsushi Hashimoto[1], Hiromaru Hirakuchi[1] (1.Central Research Institute of Electric Power Industry)

[MZZ53-P05] Detectability of large forecast error on surface solar radiation using grand ensemble method considering atmospheric circulation patterns

*Fumichika Uno[1,4], Mio Matsueda[2], Takashi Oozeki[3], Hideaki Ohtake[3,4], Yoshinori Yamada[4] (1.Atmoshere and Ocean Research Institute, The University of Tokyo, 2.University of Tsukuba, 3.National Institute of Advanced Industrial Science and Technology, 4.Japan Meteorological Agency, Meteorological Research Institute)

Geothermal exploration of the Iwaki Volcano using the Br/Cl ratio in river, spring, and hot spring waterGeothermal exploration of the Iwaki Volcano using the Br/Cl ratio in river, spring, and hot spring water

*Seiichiro Ioka[1], Kazuyoshi Asai[2], Kazumi Asai[2], Ayako Mikami[3], Sachi Wakasa[1]

1. Institute of Regional Innovation, Hirosaki University, 2. Geo Science Laboratory, 3. Aomori Prefectural Kizukuri Senior High School

Promising geothermal resource exploration areas in the vicinity of the Iwaki Volcano include the area around Dake and Hyakuzawa. Since 2011, three geothermal resource exploration drillings have been conducted around the Dake area. However, no promising geothermal power site has been found. Therefore, this study attempts to identify signs of such a site from the Br/Cl ratio of river, spring, and hot spring water samples collected from various locations around the entire area of the Iwaki Volcano.

We used 10 spring water, 18 stream water, and 27 hot spring water (Onsen) samples. We analyzed sample for Li^{+}, Na^{+}, NH_4^{+}, K^{+}, Mg^{2+}, Ca^{2+}, F^{-}, Cl^{-}, Br^{-}, NO_3^{-}, SO_4^{2-}, Fe, Mn, Sr, Ba, B, Si, alkalinity, $\delta^{18}O$, and δD.

The analysis of Br/Cl in the hot spring water samples using the Cl vs. Br concentration diagram from Angcoy and Arnórsson (2015) revealed that they were relatively clearly divided into having seawater or magmatic (geothermal signature) origins. From the Br/Cl ratio of the hot spring water samples, it was determined that any geothermal signature in the river and spring waters would be detected by the Br/Cl ratio of those samples.

The results of the analysis of the Br/Cl ratio of these river and spring water samples indicated that they were not magmatic in origin with the exception of two rivers flowing around the Dake and Hyakuzawa areas. However, hot spring water flows into these. Thus, no promising geothermal resource exploration areas were found outside the Dake and Hyakuzawa areas.

Keywords: Iwaki Volcano, Br/Cl ratio, Geothermal exploration

©2020. Japan Geoscience Union. All Right Reserved.

Machine learning based prediction of solar power generation by utilizing all-sky camera

*Masataka Imai[1], Toru Kouyama[1], Hideaki Ohtake[1], Takashi Oozeki[1], Mitsuteru Sato[2]

1. National Institute of Advanced Industrial Science and Technology, 2. Hokkaido University

In recent years, the installed capacity of the global solar photovoltaic (PV) represents exceeds 500 GW and that meets 2.6% of world electricity demand at the end of 2018 (the new 2019 Edition of the IEA PVPS report: 2019 Snapshot of Global PV Markets). Because of the awareness of climate change rises, increasing the renewable energy sources must be crucial and solar PV is regarded as the largest component of the renewable energy source. The cost of solar panels continues to decline, and the growth of PV is expected to continue as their strongest increase in five years.

The long-term average power output of solar PV is well characterized by diurnal and seasonal changes in solar insolation. However, short-term (minutes and hours) PV output is much harder to predict due to meteorological volatility, especially cloud coverage. At the current stage, the electric demands still depend on the other sources (e.g. fossil fuels). Therefore, it is desired to control the production and distribution of electricity more efficiently (smart grid), and the precise prediction of solar PV power generation is one of the important tasks to minimize the waste of other resources and to establish the efficient energy system as well as increasing the total capacity of solar PV. The state-of-the-art short-term predictions of PV output are poor, with a root mean square error (RMSE) of order 200–400 W m^{-2} for ~10 minute level predictions in partly cloudy conditions. Recently, the machine learning technique becomes popular prediction methods for the solar PV power generation. Several studies utilized all-sky images to predict the power generation assessing images correlate with contemporaneous PV output. One of the issues to develop such kind of machine-based prediction model is preparing the dataset. Ideally, the all-sky camera should be installed at the close place of PV panels located, and the data was collected for several years considering the seasonal weather change.

In this study, we used over 5 years of all-sky images obtained at Nayoro Observatory, Faculty of Science, Hokkaido University. Solar irradiance and other meteorological measurements (e.g. temperature, humidity, wind speed and direction, and precipitation) are recorded every 1 minute at the same time of image acquisition. We developed a multi-layered 3D convolutional network model with fully connected layers, where we input five sequent images with reduced size of 100 x 100 pixels and tested to predict solar irradiance at the next time step (1 minute later). Our model can predict the solar irradiance within the RMSE of 10% when the weather is fine. As for the partially cloudy condition, our model results showed spiky variations of the irradiance Although the absolute precision is worse in such sky condition, large variability in the solar irradiance (PV power generation) could be predicted by our model. In order to increase the total performance of our model we now developing other RNN (Recurrent Neural Network) based model to enable to learn the temporal feature in the sequent sky condition change. Additionally, we are preparing additional input information of other weather information. In this presentation, we will demonstrate our latest results for predicting the solar power generation by utilizing the all-sky images obtained at an astronomical observatory.

Keywords: Solar power , Deep learning, All-sky camera

©2020. Japan Geoscience Union. All Right Reserved.

Probabilistic Wind Power Prediction Based on Ensemble Weather Forecasting

*Daisuke Nohara[1], Masamichi Ohba[1], Takeshi Watanabe[1], Shinji Kadokura[1]

1. Central Research Institute of Electric Power Industry

Despite the growing popularity of renewable (e.g., wind and solar) energy usage, the volatility of the corresponding sources, partially due to the natural variability of weather conditions, hinders their further commercialization and necessitates the development of cost-effective and easily implementable predictive models such as those simulating power generation. Despite the recent increase in the accuracy of numerical weather prediction models, most of them still face problems such as the poor predictability of wind ramp event intensity, location, and timing, which can be addressed through the use of probabilistic modeling. Herein, we present a probabilistic wind power prediction method based on a numerical weather prediction model, using a power curve empirically estimated from the relationship between area-averaged wind speed and area-integrated wind power generation to project wind power and accounting for the inherent uncertainty associated with the above curve. The established probabilistic prediction method exhibits high statistical consistency and reliably captures the confidence interval of wind power variability, thus being well suited for ramp event prediction.

Keywords: Probabilistic prediction, Wind power , Ramp events

©2020. Japan Geoscience Union. All Right Reserved.

Improvement of prediction of wind power generation output for an area and its sub-area by using monitoring data

*Shinji Kadokura[1], Daisuke Nohara[1], Masamichi Ohba[1], Atsushi Hashimoto[1], Hiromaru Hirakuchi[1]

1. Central Research Institute of Electric Power Industry

Introduction of power generation by renewable energy such as photovoltaics(PV) and wind power (WT) is worldwidely progressing. Since PV and WT power generation are markedly fluctuated due to the change of the wheather, there is concern about the stability of the electric power system. Therefore, we have been developing a prediction method of wind power generation output to contribute for the stabilization of electric power system.
In this method, the numerical forecast value provided by the Japan Meteorological Agency is downscaled using the weather model WRF and CFD model to predict the wind speed at the wind turbine, and the power output is predicted using the power curve. By adding the generated power output for each wind turbine obtained, the total output of the area is obtained.
In this study, we evaluated the accuracy by simulating the power generation output for each sub-area divided into eight in the Tohoku area and the total. It was confirmed that the accuracy was improved by performing the correction using the relationship between the past observational and prediction power generation output data. However, when the correction is performed on the basis of the observational data of the wind speed and the power output of each windmill, it is suggested that the accuracy is further improved, therefoe the more detailed measurement is still important.

Keywords: Wind power output prediction, wind power generation, Weather forecast, Monitoring data

©2020. Japan Geoscience Union. All Right Reserved.

Detectability of large forecast error on surface solar radiation using grand ensemble method considering atmospheric circulation patterns

*Fumichika Uno[1,4], Mio Matsueda[2], Takashi Oozeki[3], Hideaki Ohtake[3,4], Yoshinori Yamada[4]

1. Atmoshere and Ocean Research Institute, The University of Tokyo, 2. University of Tsukuba, 3. National Institute of Advanced Industrial Science and Technology, 4. Japan Meteorological Agency, Meteorological Research Institute

Forecasting of surface solar radiation (SSR) using numerical weather prediction (NWP) models usually use at several hours to several days forecast. Large forecast errors (forecast busts) for SSR and therefore photovoltaic power generation may lead to either a shortage of power supply or production of excessive surplus power. This study assessed the hit rate and false alarm rate of forecast busts event using lognormal ensemble spread (standard deviation of ensemble forecast). This study used the lognormal ensemble spread on the four NWP centers (Japan Meteorological Agency: JMA, European Centre for Medium-Range Weather Forecasts: ECMWF, National Centers for Environmental Prediction: NCEP, United Kingdom Met Office: UKMO). Also, we evaluated the a multi-center grand ensemble (MCGE), which calculated weighted average of the esemble forecast on 4 NWP center.
The study period is January 2014 to May 2017 in five winter months (January, February, May, November, December), and forecast lead time is from 24 to 144 hour every 24hours. The forecast busts were defined as the top 5, 10, 15, 20 absolute forecast error. The atmospheric circulation patterns are categorized Winter monsoon (WM), Winter Pacific (WP), High Pressure (HP), Low Pressure (LP), Southerly Flow (SF) using 500hPa height. As the results, the proposed method in this study indicate higher detectability of forecast bust than the non-categorized detection (previous study) method. The values of Youden index improved of considering the flow patterns. Moreover, the improvement assessed by the false alarm rate under perfect hit rate (FPR) was indicated in all cases. The FPR is smallest when top 5% forecast busts cases, The FPRs of MCEG in 6 forecast lead time are 0.52, 0.44, 0.50, 0.44, 0.41, 0.53 respectively. The improvement not only the detection method using MCGE but also the method using single NWP center ensemble forecast.

Keywords: Ensemble forecast, Detection of large forecast error, Surface solar radiation, Renewable energy

©2020. Japan Geoscience Union. All Right Reserved.

[E] Poster | M (Multidisciplinary and Interdisciplinary) : M-ZZ Others

[M-ZZ54] Communicating Hazard and Risk: What do we know about how to make this information understandable?

convener:Danijel Schorlemmer(GFZ German Research Centre for Geosciences), Alexandra Freeman(Winton Centre for Risk and Evidence Communication, University of Cambridge), Sarah Dryhurst(University of Cambridge), Naoshi Hirata(National Research Institute for Earth Science and Disaster Resilience)

There is no point modelling hazards and risks if that information is of no use to decision makers (at individual and policy levels including the scientific community, the public, governmental institutions, engineers, policy makers, emergency and resilience managers). We therefore have to ensure that we are providing the information focusing on the needs of these stakeholders, in a format and time frame that is of use to them, minimizing the possibility of misunderstanding or misperception.

In this session we aim at addressing the problems surrounding communicating hazard and risk of natural catastrophes. Important questions include: who are the key stakeholders for each kind of information? What information does each require? How do we balance the trade-off between restricting the information provided to improve comprehension versus the ethics of withholding information? How do we approach the boundary between providing information and providing advice? How do we communicate the different uncertainties (both epistemic and aleatory)? What can be learned about the communication of geospatially- and temporally-dynamic data from other fields (such as meteorology, military defence etc.) and how should we communicate in ongoing crises, in particular during unexpected changes in the development of catastrophic events? How do we ensure our communications are trustworthy? What are the metrics of success in such communications?

We will be considering all time frames and stages of hazard assessment from long-term maps and planning to emergency warning and rapid loss assessment when an event occurs. This includes all possible communication channels (e.g. scientific publications, public or press announcements, social networks, TV, radio, newsletters) and/or content types (e.g. text, video, graphics).

We solicit contributions from all fields with the aim of bringing together a variety of researchers to share their experiences from their respective fields.

[MZZ54-P01] An Integrated GIS and Big Data Platform for Meteorological Disaster Risk Management and its Application

*YING LI[1] (1.Beijing Climate Center)

[MZZ54-P02] Emergency flood detection using multiple information: Integrated analysis of natural hazard monitoring and social media data

*Kikuko Shoyama[1] (1.National Research Institute for Earth Science and Disaster Resilience)

[MZZ54-P03] Global Dynamic Exposure and the OpenBuildingMap - Communicating Risk and Involving Communities

*Danijel Schorlemmer[1], Naoshi Hirata[2], Kuo-Fong Ma[3], Karsten Prehn[1], Cecilia Nievas[1], Thomas Beutin[1], Fabrice Cotton[1], Max Wyss[4] (1.GFZ German Research Centre for Geosciences, Potsdam, Germany, 2.National Research Institute for Earth Science and Disaster Resilience, Tsukuba. Japan, 3.Earthquake-Disaster & Risk Evaluation and Management (E-DREaM) Center, National Central University, Taiwan, 4.International Centre for Earth Simulation Foundation, Geneva, Switzerland)

[MZZ54-P04] Tokyo Metropolitan Resilience Project, from CSR to CSV

*Takashi Furuya[1], Keiko Tamura[2], Danijel Schorlemmer[3], Naoshi Hirata[1] (1.National Research Institute for Earth Science and Disaster Resilience, Tsukuba, Japan, 2.Niigata University, Risk Management Office, Niigata, Japan, 3.GFZ German Research Center for Geosciences)

An Integrated GIS and Big Data Platform for Meteorological Disaster Risk Management and its Application

*YING LI[1]

1. Beijing Climate Center

Under the background of global changes, the frequency and intensity of various meteorological disasters are increasing, which poses a great challenge to the risk management worldwide. The Sendai Framework was put forward by the third world conference on disaster reduction, providing a roadmap for the international community to respond to disaster risks. In recent years, China has stepped up its implementation of disaster risk reduction actions, but there has been no systematic platform to supply professional services of meteorological disaster risk reduction for decision makers. In order to effectively reduce the risk of meteorological disasters and meet the urgent need in service, Beijing Climate Center of China developed a Meteorological disaster risk management platform (MDRMP), which integrates the technology of big data management, scientific achievements transformation and spatiotemporal multidimensional visualization, under a unified highly intensified framework. Through three years of hard work, MDRMP was initially built and has been put into operation, providing professional services for decision makers and other stakeholders with realtime disaster monitoring, early warning, impact analysis and risk assessment. The main functions of MDRIMP include hazard identification, risk prediction, risk regionalization, warning service, information inquiry, online analysis, etc.

MDRMP contains four subsystems, namely, Big Data Application Center, Model and Algorithm Center, Online Analysis Center and Operation Center. Big Data Application Center include 12 major categories, more than 600 million various pieces of information. Based on the Cloud-terminal and GIS technology, the multisource and heterogeneous data is jointed in horizontal direction and correlated in vertical direction with its spatial attributes, forming the core database of the whole system. Model and Algorithm Center integrated more than 100 models of the algorithm related to disaster risk analysis. The algorithm library realizes the unified scheduling, management and real-time monitoring through registration, classification and execution monitoring technologies. MDRMP has already been applied nationwide based on a Cloud terminal, and support unified access, personalized configuration and service customization of users in provinces, cities and counties in China. This paper provides an overview, functions and the current status of the MDRMP. It will also describe how services are made available to the end user via various channels in addition to the productions of MDRMP in routine operations.

Keywords: disaster risk, GIS, big data

©2020. Japan Geoscience Union. All Right Reserved.

Emergency flood detection using multiple information: Integrated analysis of natural hazard monitoring and social media data

*Kikuko Shoyama[1]

1. National Research Institute for Earth Science and Disaster Resilience

Nowadays the extreme weather events occur more frequently due to climate change. In October of 2019, the eastern japan was hit by a large and high-speed typhoon, Hagibis (no.19). This unprecedented typhoon caused the evacuation of 237 thousand people, the casualties of over 300 people, and the house damage of over 94,000 households throughout the affected area. Flood is one of the most devastating natural disasters thus providing effective early warning is critical to reducing disaster impacts as preparing for such extreme weather events. Current warning against rainfall-induced disasters is issued based on the rainfall threshold, which varies depending on the disaster type. For example, the amount of 1.5 hours-effective rainfall and the river water level have been used as relevant criteria for flood hazards. However, warning based on only natural hazard monitoring is not enough to detect areas subject to disaster. Integrated analysis natural hazard monitoring and social media data could improve the warning system to enhance awareness for disaster managers and citizens about the emergency event. We analyzed time-series data including rainfall, effective rainfall, river water level monitoring data, and Twitter data relating to disaster events during 5 days from 11 to 15 October, focusing on the most affected area around the watershed of Abukuma-river and Chikuma river in Japan. The analysis using 47,520 tweet samples revealed that spatial and temporal resolution and extent of these monitoring data influence to detect the emerging change and spatial deviation relate to the flood events. Thus, the design of monitoring system should meet the criteria for emergency detection.

Keywords: flood, emergency detection, effective rainfall, Twitter

©2020. Japan Geoscience Union. All Right Reserved.

Global Dynamic Exposure and the OpenBuildingMap - Communicating Risk and Involving Communities

*Danijel Schorlemmer[1], Naoshi Hirata[2], Kuo-Fong Ma[3], Karsten Prehn[1], Cecilia Nievas[1], Thomas Beutin[1], Fabrice Cotton[1], Max Wyss[4]

1. GFZ German Research Centre for Geosciences, Potsdam, Germany, 2. National Research Institute for Earth Science and Disaster Resilience, Tsukuba. Japan, 3. Earthquake-Disaster & Risk Evaluation and Management (E-DREaM) Center, National Central University, Taiwan, 4. International Centre for Earth Simulation Foundation, Geneva, Switzerland

The substantial reduction of disaster risk and live losses, a major goal of the Sendai Framework by the United Nations Office for Disaster Risk Reduction (UNISDR) requires a clear understanding of the dynamics of the built environment and how it affects, in case of natural disasters, the life of communities, represented by local governments and individuals. These dynamics are best understood and captured by local communities, following two of the guiding principles UNISDR formulated: "empowerment of local authorities and communities" and "engagement from all of society". Moreover, communities that participate in risk assessments increase their understanding of efficient risk mitigation measures.

Our Global Dynamic Exposure model and its technical infrastructure build on the involvement of communities in a citizen-science approach. We are employing a crowd-sourced exposure capturing based on OpenStreetMap (OSM), an ideal foundation with already more than 375 million building footprints (growing daily by ~150,000), and a plethora of information about school, hospital, and other critical facilities. We are harvesting this dataset with our OpenBuildingMap system by processing the information associated with every building in near-real-time. We are enriching this dataset in a truly big-data approach by including built-up area detection from remote sensing with satellite and radar imagery combined with different sources of road networks, as well as various open datasets and aggregated exposure models that provide relevant additional information on buildings and land use. With this approach, we increase the resolution of existing exposure models from aggregated exposure information to building-by-building vulnerability. Additionally, we include available open datasets to further improve our indicator assessment.

We expect the quality of near-real-time estimates of the extent of natural disasters to increase by an order of magnitude, based on the data we are collecting. We envision authorities and first responders greatly benefitting form maps pinpointing the greatest trouble spots in disasters and from detailed quantitative estimates of the likely damage and human losses. With our tools, interested communities can capture their exposure and analyze how natural disaster may affect them. It helps communicating risks down to the community level and helps educating community members in the risks they are facing, how they can mitigate risks, and how they can prevent losses of lives.

Keywords: Exposure, Risk, Communication, Earthquakes, Loss, Big data

©2020. Japan Geoscience Union. All Right Reserved.

Tokyo Metropolitan Resilience Project, from CSR to CSV

*Takashi Furuya[1], Keiko Tamura[2], Danijel Schorlemmer[3], Naoshi Hirata[1]

1. National Research Institute for Earth Science and Disaster Resilience, Tsukuba, Japan, 2. Niigata University, Risk Management Office, Niigata, Japan, 3. GFZ German Research Center for Geosciences

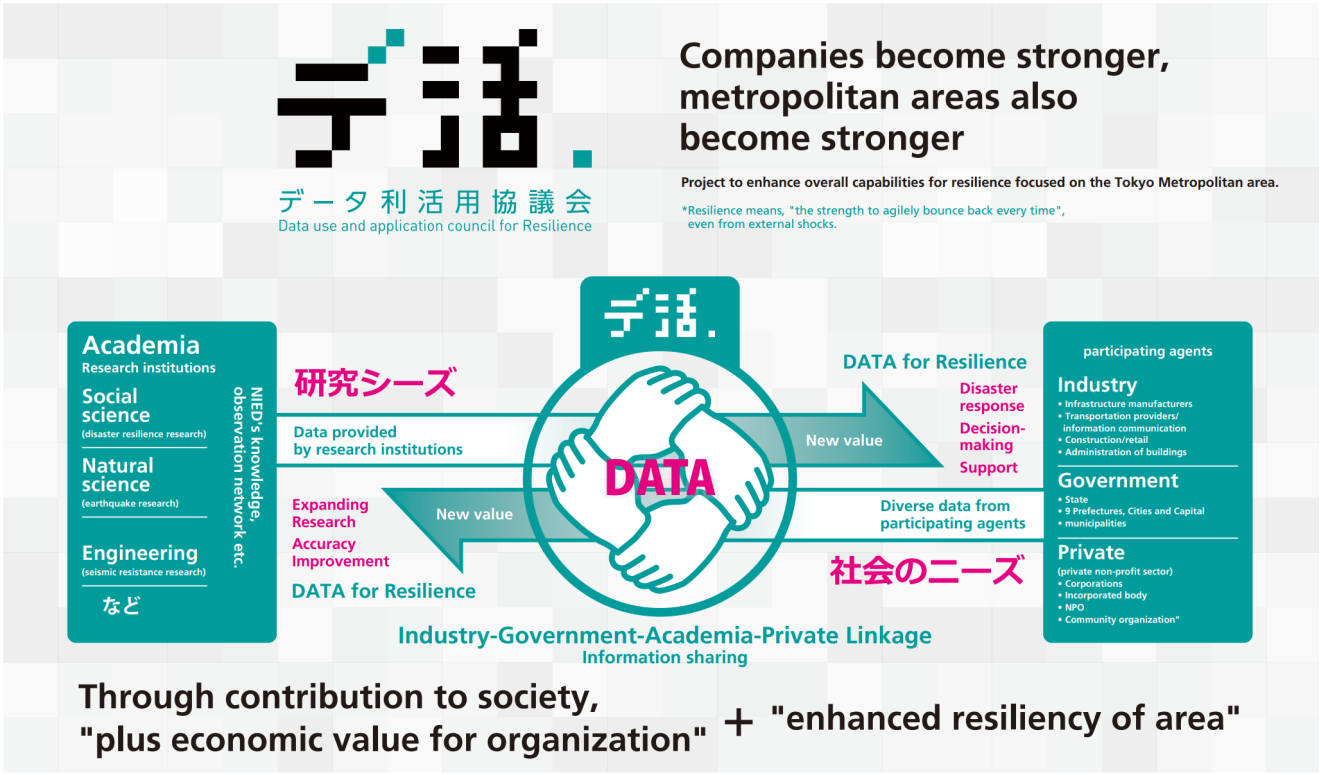
The Tokyo metropolitan area will likely be hit in the future by a major earthquake of magnitude 7 or larger. Such an earthquake will create a serious disaster due to the extraordinary exposure and a population of more than 35M. To reduce potential losses, it is necessary to improve the disaster resilience of Tokyo, its building stock, economy and society. For this purpose, in April 2017 the “Tokyo Metropolitan Resilience Project” started to integrate multi-disciplinary research of social sciences, seismology, and earthquake engineering. Furthermore, to improve disaster management capabilities, we founded a Data Use and Application Council for Resilience (named DEKATSU) among four Japan-wide sectors; industry, government, NPO/NGOs, and academia. They are intended to collaborate to contribute improved resilience capabilities, currently mainly in the Tokyo metropolitan area by following the strategy of holding public symposia, organizing private thematic panels, and implementing data disclosure policies. We develop activities from CSR(Corporate Social Responsibility) to CSV(Creating Shared Value).

DEKATSU has members from 53 private companies, 3 municipalities, 9 NPO/NGOs (as of 11 February, 2020). Eight thematic panels*, consisting of the consortium members with common interests and issues, were established within DEKATSU. "Academics" is providing research results for solving problems of companies and organizations in the field of disaster/disaster prevention techniques and measures. "Industries" is providing information and data. "Government" is providing guidance, regulation, and information. "NPO/NGOs" is providing information about local needs and connecting the consortium to the public.

The National Research Institute for Earth Science and Disaster Resilience (NIED), Japan, is the core institute of the project. And we aim to gather and consolidate data effective for the overall business continuity and disaster response capabilities of government and private sector, as well as for disaster resilience activities of individuals.

Keywords: Disaster Resillience, integrated multi-disciplinary research, Data Use and Application Council for Resilience(“DEKATSU”), Industry-Government-Academia-Private Linkage, Tokyo Metropolitan, CSV(Creating Shared Value)

©2020. Japan Geoscience Union. All Right Reserved.



©2020. Japan Geoscience Union. All Right Reserved.